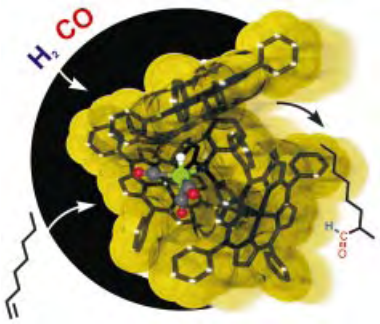
ANGEWANDTE CHEMIE
INTERNATIONAL EDITION
A Journal of the Gesellschaft Deutscher Chemiker
2001
40/22
Pages 4109–4308

COVER PICTURE

The cover picture shows a rhodium catalyst (green) that is encapsulated by three porphyrin molecules (black; the van der Waals radii are shown in yellow). The hemispherical assembly is obtained by a self-assembly process using readily available pyridylphosphane and zinc-porphyrin building blocks. Its exclusive formation is based on selective coordination of the nitrogen atom to the zinc atom and the phosphane group to the rhodium center. The catalyst assemblies show a higher activity than the free rhodium catalyst in the rhodium-catalyzed hydroformylation of 1-octene, and the branched product is now the main product. In a similar way, the assembly of porphyrin building blocks to pyridylphosphane can regulate the performance of palladium catalysts in the Heck reaction. Further details about these catalyst assemblies can be found in the article by Reek et al. on p. 4271 ff.

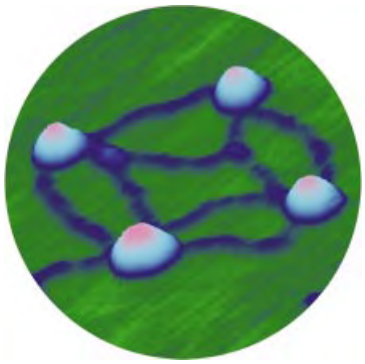


REVIEW

Contents

At the crossroads of biotechnology, nanoscience, and materials research lies a new interdisciplinary research area, in which the use of evolutionary optimized biomolecules for the development of advanced materials and analytical procedures is investigated. As an example, nanoparticles can be interconnected with DNA to generate nanostructured hybrid materials (see scanning force microscopy image).

Angew. Chem. **2001**, *113*, 4254–4287



C. M. Niemeyer* 4128–4158

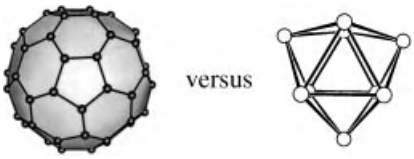
Nanoparticles, Proteins, and Nucleic Acids: Biotechnology Meets Materials Science

Keywords: analytical methods · biotechnology · materials science · nanostructures · supramolecular chemistry

 © WILEY-VCH Verlag GmbH, D-69451 Weinheim, 2001 1433-7851/01/4022-4111 $ 17.50+.50/0

MINIREVIEW

Contents



There is a common feature between the two recently synthesized polymers $^{1}_{\infty}\{C_{70}^{2-}\}$ and $^{1}_{\infty}\{[Ge_9]^{2-}\}$: The successful linking of homoatomic anions into one-dimensional polymers opens up fantastic opportunities for the design and construction of nanostructures. A comparison between these structural modules (see schematic representation) shows that Zintl ions, which have been known for more than a hundred years, are in no way inferior to the fullerenes.

Angew. Chem. **2001**, *113*, 4289 – 4293

T. F. Fässler* ..... 4161 – 4165

Homoatomic Polyhedra as Structural Modules in Chemistry: What Binds Fullerenes and Homonuclear Zintl Ions?

Keywords: cage compounds · fullerenes · polymers · Zintl ions

ESSAY

Reality, or through the looking-glass? In 1951 two important advances in structural chemistry were made: Pauling formulated the α-helix as an important structural element in proteins, and Bijvoet solved the problem of determining absolute configuration. This essay covers events binding these two discoveries.

Angew. Chem. **2001**, *113*, 4295 – 4301

J. D. Dunitz* ..... 4167 – 4173

Pauling's Left-Handed α-Helix

Keywords: biographies · history of science · stereochemistry · structure elucidation

VIPs

The following communications are "Very Important Papers" in the opinion of two referees. They will be published shortly (those marked with a diamond will be published in the next issue). Short summaries of these articles can be found on the *Angewandte Chemie* homepage at the address http://www.angewandte.com

Origin of Ferromagnetism in Cyano-Bridged Compounds Containing d^1 Octacyanometallates — L. F. Chibotaru,* V. S. Mironov, A. Ceulemans ◆

Lewis Acid/Base Stabilized Phosphanylalane and -gallane — U. Vogel, A. Y. Timoshkin, M. Scheer* ◆

Towards the Understanding of Solid-State Structures: From Cubic to Chain-like Arrangements in Group 11 Halides — T. Söhnel, H. Hermann, P. Schwerdtfeger* ◆

Homogeneous Reactions in Supercritical Carbon Dioxide by Using a Catalyst Immobilized in a Microporous Silica Membrane — L. J. P. van den Broeke,* E. L. V. Goetheer, A. W. Verkerk, E. de Wolf, B.-J. Deelman, G. van Koten, J. T. F. Keurentjes ◆

Design and Synthesis of a Peptide that Binds Specific DNA Sequences through Simultaneous Interaction in the Major and in the Minor Groove — M. E. Vázquez, A. M. Caamaño, J. Martínez-Costas, L. Castedo, J. L. Mascareñas*

Cesiumauride Ammonia (1/1: $CsAu \cdot NH_3$)—A Crystalline Analogue of Alkali Metals Dissolved in Ammonia? — A.-V. Mudring, M. Jansen,* J. Daniels, S. Krämer, M. Mehring, J. P. Ramalho, A. H. Romero, M. Parrinello

Enantiopure Double-Helical Acetylenic Cyclophanes — D.-L. An, T. Nakano, A. Orita, J. Otera*

Supramolecular Cluster Catalysis: A Case Study of Benzene Hydrogenation Catalyzed by a Cationic Triruthenium Cluster under Biphasic Conditions — G. Süss-Fink,* M. Faure, T. R. Ward

 © WILEY-VCH Verlag GmbH, D-69451 Weinheim, 2001 1433-7851/01/4022-4112 $ 17.50+.50/0

HIGHLIGHT

Contents

From genome data to a successful drug: Many companies are eager to make this journey in the future, though roadmaps are still scarce. We comment on a novel method that promises to make the trip from gene to drug (see schematic representation) shorter and more effective by predicting protein functions from their three-dimensional structure.



Angew. Chem. **2001**, *113*, 4303 – 4305

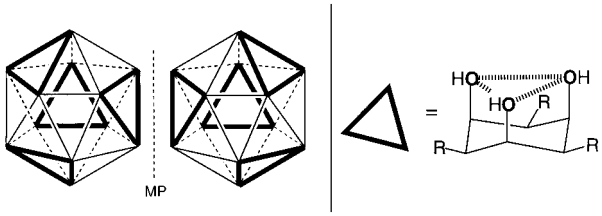
G. Folkers,* C. D. P. Klein ... 4175 – 4177

Computational Methods Facilitate the Assignment of Protein Functions

Keywords: bioinformatics · drug research · functional genomics · molecular modeling · proteome analysis

COMMUNICATIONS

A homoleptic metal complex with four tripodal tridentate ligands can have chiral tetrahedral *T* symmetry. An example of such a complex has been prepared, and the proposed highly symmetric, but chiral structure (see schematic representation, MP = mirror plane, R = $NHCH_2PH$) has been confirmed.



Angew. Chem. **2001**, *113*, 4307 – 4310

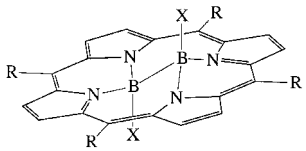
J. Sander, K. Hegetschweiler,* B. Morgenstern, A. Keller, W. Amrein, T. Weyhermüller, I. Müller 4179 – 4182

T-Symmetrical Icosahedra: A New Type of Chirality in Metal Complexes

Keywords: chelates · chirality · group theory · structure elucidation · tripodal ligands

---

Fitting B_2 bridges in porphyrins (see picture) can be achieved by reaction of dilithiated porphyrins with B_2Cl_4 as well as by reductive elimination from diborylporphyrins. Coordination takes place under rectangular distortion of the porphyrin framework.



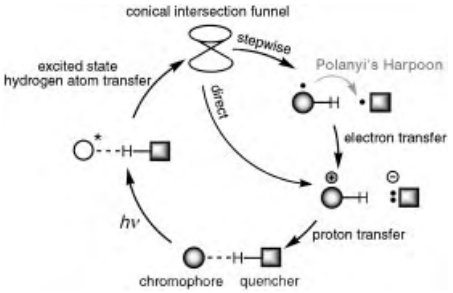
Angew. Chem. **2001**, *113*, 4311 – 4313

A. Weiss, H. Pritzkow, P. J. Brothers,* W. Siebert* ..... 4182 – 4184

Coordinated B_2 Bridges in Porphyrins—Unexpected Formation of a Diborane(4)- from a Diborylporphyrin

Keywords: boron · diboranes · N ligands · porphyrinoids

Radical-pair disproportionation through sequential electron – proton transfer (Polanyi's harpoon) is one efficient mechanism leading to quenching fluorescence of n,π*-excited states by hydrogen donors. This mechanism is demonstrated by ab initio MS-CASPT2 calculations and experimental investigations (photoproduct studies and EPR spin-trapping experiments) on the quenching of singlet-excited azoalkanes by chlorinated hydrocarbons.



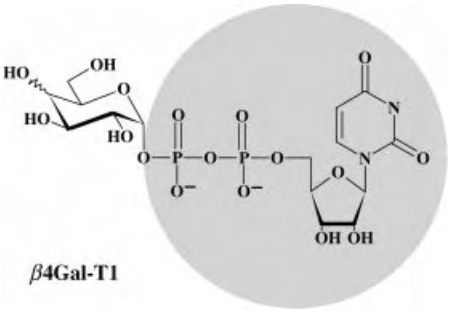
Angew. Chem. **2001**, *113*, 4313 – 4318

A. Sinicropi, R. Pogni,* R. Basosi, M. A. Robb, G. Gramlich, W. M. Nau,* M. Olivucci* ..... 4185 – 4189

Fluorescence Quenching by Sequential Hydrogen, Electron, and Proton Transfer in the Proximity of a Conical Intersection

Keywords: ab initio calculations · conical intersections · electron transfer · fluorescence quenching · proton transfer

Saturation transfer difference (STD) NMR experiments reveal the binding epitopes of UDP-Gal and UDP-Glc bound to the glycosyltransferase β4Gal-T1 (see picture). Whereas the enzyme recognizes the galactose residue in UDP-Gal, it does not make any close contacts with the glucose residue in UDP-Gal, it does not make any close contacts with the glucose residue in UDP-Glc. This observation explains why β4Gal-T1 binds to UDP-Glc but is unable to transfer glucose to an acceptor substrate.



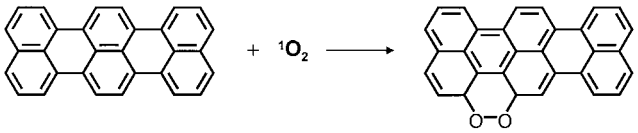
Angew. Chem. **2001**, *113*, 4320 – 4323

T. Biet, T. Peters* ..... 4189 – 4192

Molecular Recognition of UDP-Gal by β-1,4-Galactosyltransferase T1

Keywords: carbohydrates · glycoproteins · molecular recognition · NMR spectroscopy · transferases

The photooxidation of single dye molecules (see scheme) can be followed by confocal fluorescence microscopy. The self-sensitized reaction with singlet oxygen leads to a suite of products, which may be differentiated spectrally. Tentative structures for certain photoproducts have been obtained from quantum-chemical calculations.



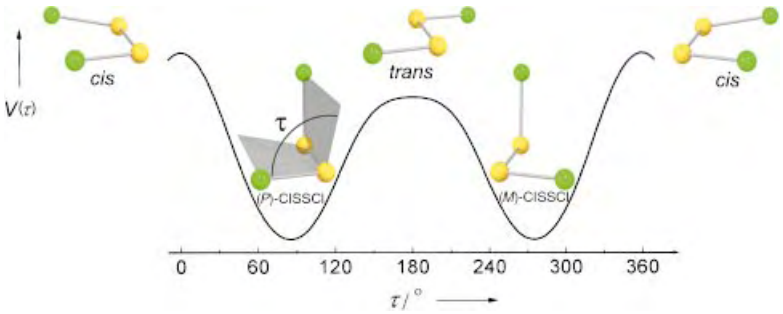
Angew. Chem. **2001**, *113*, 4323 – 4326

T. Christ, F. Kulzer, P. Bordat, T. Basché* ..... 4192 – 4195

Watching the Photo-Oxidation of a Single Aromatic Hydrocarbon Molecule

Keywords: fluorescence spectroscopy · photochemistry · single-molecule spectroscopy

Meaninglessly small would be the effects from parity violation according to the traditional point of view on the structure and dynamics of chiral molecules; enantiomers would thus exist as symmetry-related structures, which are de facto stable because of very long tunneling times. With ClSSCl as the first example, electroweak and tunneling dynamics calculations demonstrate that the de lege asymmetry arising from the parity-violating energy difference ΔE_{pv} between the two enantiomers ((*P*)- and (*M*)-ClSSCl, the figure shows the torsional potentials) dominates by far over the tunneling splitting in the symmetrical case. These results are of fundamental interest for our concept of molecular chirality.



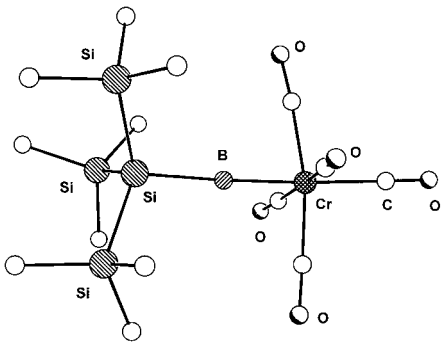
Angew. Chem. **2001**, *113*, 4342 – 4345

R. Berger, M. Gottselig, M. Quack,* M. Willeke ..... 4195 – 4198

Parity Violation Dominates the Dynamics of Chirality in Dichlorodisulfane

Keywords: ab initio calculations · chirality · electroweak interactions · parity violation · torsional tunneling splitting

An extremely low-field shifted ^{11}B NMR signal at $\delta = 204.3$ and a very short Cr–B distance of 187.8 pm characterize the title compound $[(OC)_5Cr=B-Si(SiMe_3)_3]$ (see structure), which is the first borylene complex in which the boron atom is both coordinatively and electronically unsaturated.



Angew. Chem. **2001**, *113*, 4327 – 4329

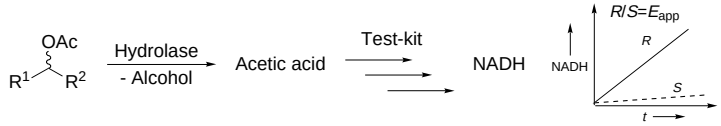
H. Braunschweig,* M. Colling, C. Kollann, K. Merz, K. Radacki ..... 4198 – 4200

$[(OC)_5Cr=BSi(SiMe_3)_3]$: A Terminal Borylene Complex with an Electronically Unsaturated Boron Atom

Keywords: B ligands · boron · borylene complexes · chromium

 © WILEY-VCH Verlag GmbH, D-69451 Weinheim, 2001 1433-7851/01/4022-4114 $ 17.50+.50/0

A rapid and reliable test for the determination of hydrolase activity and enantioselectivity comprises the conversion of acetic acid released from acetates to NADH by using a commercially available enzymatic test-kit (see scheme). The NADH is spectrophotometrically quantified in a microtiter plate format.



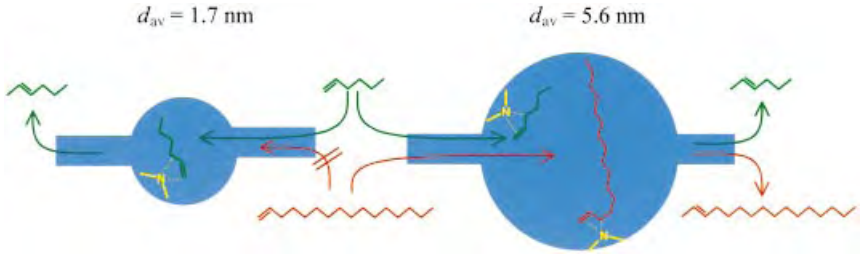
Angew. Chem. **2001**, *113*, 4329 – 4333

M. Baumann, R. Stürmer, U. T. Bornscheuer* ..... 4201 – 4204

A High-Throughput-Screening Method for the Identification of Active and Enantioselective Hydrolases

Keywords: biotransformations · enantioselectivity · enzyme catalysis · high-throughput screening · molecular evolution

High specific surface areas and adjustable pore sizes are outstanding characteristics of nanoporous silicon nitride based materials prepared by using oxygen-free molecular precursors in a novel template-assisted sol – gel approach. The nitrides represent a new class of shape-selective superbase catalysts (see, for example, the schematic representation of alkene isomerization).



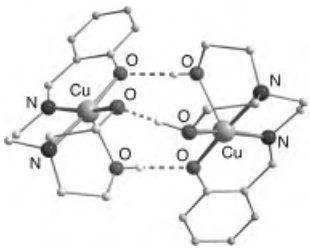
Angew. Chem. **2001**, *113*, 4336 – 4339

D. Farrusseng, K. Schlichte, B. Spliethoff, A. Wingen, S. Kaskel,* J. S. Bradley, F. Schüth ..... 4204 – 4207

Pore-Size Engineering of Silicon Imido Nitride for Catalytic Applications

Keywords: heterogeneous catalysis · microporous materials · nitrides · silicon · solid-state reactions · superbases

The self-complementary coordination unit $[Cu(H_2sabhea)]^+$ with a pentadentate amino alcohol as ligand enables the synthesis of the first triply hydrogen-bridged dinuclear copper(II) complex (see picture). Proton transfer allows the reversible transformation between this triply and the corresponding doubly hydrogen-bridged form. Despite the very short hydrogen bond found for the triply bridged complex, its exchange coupling constant is much smaller than that for the doubly bridged complex. $H_3sabhea$ = *N*-salicylidene-2-(bis(2-hydroxyethyl)amino)ethyl amine.



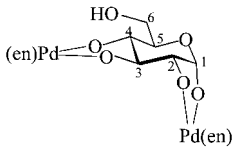
Angew. Chem. **2001**, *113*, 4333 – 4336

W. Plass,* A. Pohlmann, J. Rautengarten ..... 4207 – 4210

Magnetic Interactions as Supramolecular Function: Structure and Magnetic Properties of Hydrogen-Bridged Dinuclear Copper(II) Complexes

Keywords: copper · density functional calculations · hydrogen bonds · magnetic properties · supramolecular chemistry

The most important monosaccharide—and not a single structurally characterized transition metal complex. That is the actual situation regarding basis data for understanding or designing metal-catalyzed reactions of D-glucose. This oversight is remedied with a palladium(II) complex and a structural analysis (see picture, en = ethylenediamine).



Angew. Chem. **2001**, *113*, 4356 – 4358

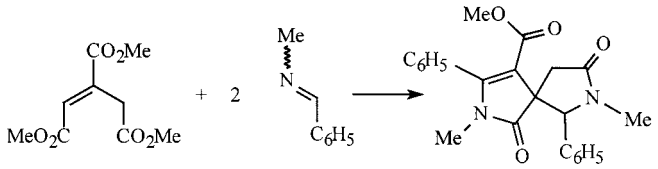
P. Klüfers,* T. Kunte ..... 4210 – 4212

A Transition Metal Complex of D-Glucose

Keywords: carbohydrates · glucose · palladium · structure elucidation

 © WILEY-VCH Verlag GmbH, D-69451 Weinheim, 2001 1433-7851/01/4022-4115 $ 17.50+.50/0

The multitalented synthetic reagent trimethyl aconitate (**1**) is a renewable raw material with a high density of functional groups that up to now has only been scarcely used as a C_6 building block. Domino reactions with **1** consisting of imine additions and intramolecular acylations provide simple access to heteropolycycles in one-pot reactions. For example, **1** reacts with *N*-methylbenzylidenamine (**2**) to give the spiro[pyrrolidinone-3,3′-dihydropyrrolinone] **3** in 40% yield (see scheme).



1 **2** **3**

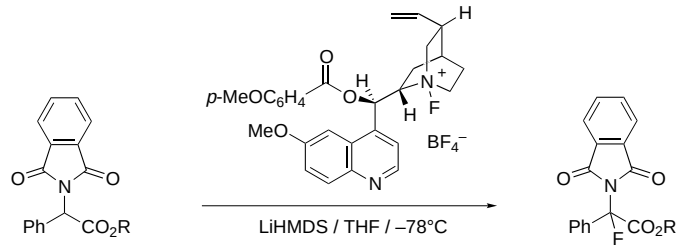
Angew. Chem. **2001**, *113*, 4354 – 4356

D. Witthaut, R. Fröhlich, H. J. Schäfer* ..... 4212 – 4214

Heterocycles through Domino Reactions with Trimethyl Aconitate, a Versatile Synthetic Building Block

Keywords: acylation · domino reactions · imines · nitrogen heterocycles · spiro compounds

A decisive step forward: A one-step fluorination on modified cinchona alkaloids produced a new range of enantiopure fluorinating agents that display high enantioselectivities in electrophilic fluorination. The first enantioselective synthesis of *N*-protected α-fluorophenylglycine derivatives was achieved with an enantiomeric excess up to 94% [Eq. (a); R = Et, CN; HMDS = hexamethyldisilazanide].



(a)

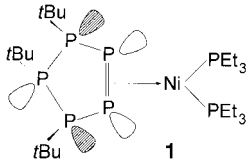
Angew. Chem. **2001**, *113*, 4339 – 4341

B. Mohar, J. Baudoux, J.-C. Plaquevent, D. Cahard* ..... 4214 – 4216

Electrophilic Fluorination Mediated by Cinchona Alkaloids: Highly Enantioselective Synthesis of α-Fluoro-α-phenylglycine Derivatives

Keywords: alkaloids · amino acids · asymmetric synthesis · fluorination · fluorine

Forming a phosphorus envelope: The first structurally characterized cyclooligophosphanide ion [*cyclo*-(P_5tBu_4)]$^-$ to be obtained by a targeted synthesis reacts with [$NiCl_2(PEt_3)_2$] by loss of a *t*Bu group to give (η^2-3,4,5-tri-*tert*-butylcyclopentaphosphene)bis(triethylphosphane)nickel(0) (**1**). The previously unknown cyclopentaphosphene ring in **1** has an envelope conformation in solution and in the solid state, and the *t*Bu groups adopt an *all-trans* configuration.



1

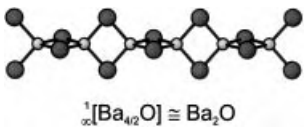
Angew. Chem. **2001**, *113*, 4345 – 4348

A. Schisler, P. Lönnecke, U. Huniar, R. Ahlrichs, E. Hey-Hawkins* ..... 4217 – 4219

Sodium Tetra-*tert*-butylcyclopentaphosphanide: Synthesis, Structure, and Unexpected Formation of a Nickel(0) Tri-*tert*-butylcyclopentaphosphene Complex

Keywords: nickel · phosphorus heterocycles · P ligands

Linear $^1_\infty$[$Ba_{4/2}O$] chains (see picture) of edge-sharing Ba_4O tetrahedra are separated by sodium atoms in the crystal structure of the new sodium barium suboxide $NaBa_2O$. The metal-rich compound is held together by a combination of ionic and metallic bonding according to the formulation $Na^+(Ba^{2+})_2O^{2-}\cdot 3e^-$.



Angew. Chem. **2001**, *113*, 4348 – 4351

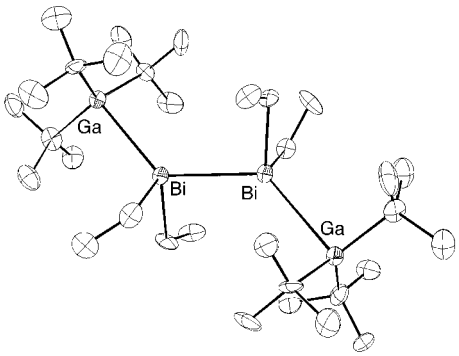
G. V. Vajenine, A. Simon* .. 4220 – 4222

$NaBa_2O$: A Fresh Perspective in Suboxide Chemistry

Keywords: barium · sodium · suboxides · subvalent compounds

 © WILEY-VCH Verlag GmbH, D-69451 Weinheim, 2001 1433-7851/01/4022-4116 $ 17.50+.50/0

Functioning as a bidentate ligand toward Lewis acids, dibismuthane forms bisadducts of the type $[R_3M]_2[Bi_2R'_4]$ with $R_3M = tBu_3Al$ (**1**) and tBu_3Ga (**2;** structure depicted; $R' = Et$), which were characterized by single-crystal X-ray diffraction.



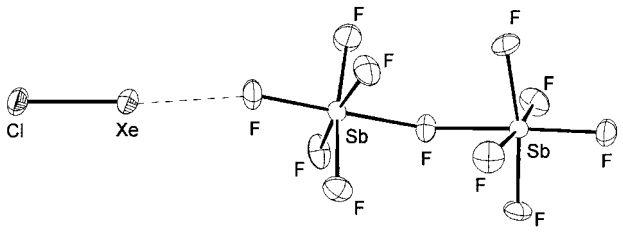
Angew. Chem. **2001**, *113*, 4351 – 4353

A. Kuczkowski, S. Schulz,* M. Nieger ..... 4222 – 4225

Reactions of Et_4Bi_2 with tBu_3M (M = Al, Ga)—Synthesis of Complexes with a Bidentate Dibismuthane Ligand

Keywords: adducts · aluminum · bismuth · gallium

Chlorine – fluorine exchange in XeF^+ leads to the orange crystalline salt $[XeCl]^+[Sb_2F_{11}]^-$ (see structure), which is stable below $-10^\circ C$. Thus, the number of known noble gas monohalogen cations is now three and, as calculations show, is approaching the theoretically possible limit. The synthesis of other such compounds—with the exception of ArF^+, which remains a formidable task—seems unlikely.



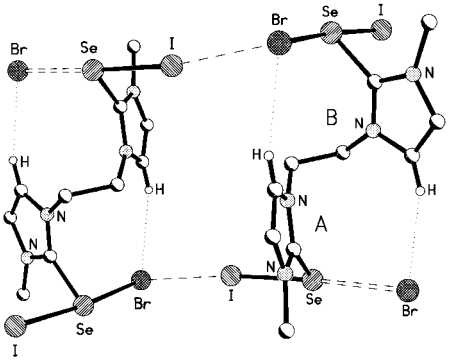
Angew. Chem. **2001**, *113*, 4318 – 4320

S. Seidel, K. Seppelt* ..... 4225 – 4227

The $XeCl^+$ Ion: $[XeCl]^+[Sb_2F_{11}]^-$

Keywords: ab initio calculations · chlorine · noble gas compounds · structure elucidation · xenon

Almost linear I-Se-Br groups with $d(Se{-}Br) > d(Se{-}I)$ occur in $\mathbf{1} \cdot 2IBr$ (see structure), the first "T-shaped" Se adduct with IBr, which was synthesized by the oxidative addition of IBr to 1,2-bis(3-methylimidazoline-2-selonyl)ethane (**1**) in MeCN. Density functional theory calculations indicate the intramolecular Br···H interactions as being responsible for the peculiar structural features of the I-Se-Br groups.



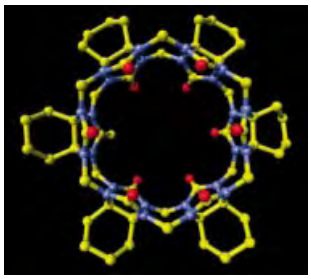
Angew. Chem. **2001**, *113*, 4359 – 4362

M. C. Aragoni, M. Arca, A. J. Blake, F. A. Devillanova,* W.-W. du Mont, A. Garau, F. Isaia, V. Lippolis,* G. Verani, C. Wilson ..... 4229 – 4232

1,2-Bis(3-methyl-imidazolin-2-ylium iodobromoselenanide)ethane: Oxidative Addition of IBr at the Se Atom of a >C=Se Group

Keywords: density functional calculations · donor – acceptor systems · halogens · hypervalent compounds · Se ligands

Reminiscent of the ringed planet Saturn, new cucurbit[*n*]uril (CB[*n*]) derivatives CB*[5] and CB*[6] have rings decorating the "equator". The rings in this case are five- and six-fused cyclohexane rings, respectively (the structure of CB*[6] is shown). The remarkable solubility of the new CB[*n*] derivatives in water and organic solvents allows not only their unusual binding properties toward metal and organic ions in neutral water but also their applications in ion-selective electrodes to be studied.



Angew. Chem. **2001**, *113*, 4363 – 4365

J. Zhao, H.-J. Kim, J. Oh, S.-Y. Kim, J. W. Lee, S. Sakamoto, K. Yamaguchi, K. Kim* ..... 4233 – 4235

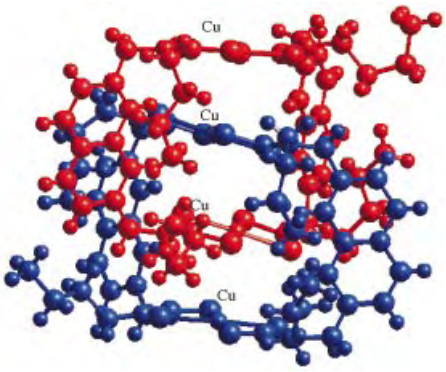
Cucurbit[*n*]uril Derivatives Soluble in Water and Organic Solvents

Keywords: cucurbituril · host – guest systems · ion-selective electrodes · molecular recognition · supramolecular chemistry

 © WILEY-VCH Verlag GmbH, D-69451 Weinheim, 2001 1433-7851/01/4022-4117 $ 17.50+.50/0

Chemical oxidation of two preformed dinuclear copper(II) dithiocarbamate macrocycles leads to the formation of a novel mixed-valence tetranuclear copper(II)/copper(III) dithiocarbamate [2]catenane in near quantitative yield. Structural (see X-ray crystal structure), magnetic susceptibility, electrospray mass spectrometry, and electrochemical studies all support the formation of a $Cu^{II}Cu^{III}Cu^{II}Cu^{III}$ tetranuclear catenane dication.

Angew. Chem. **2001**, *113*, 4365 – 4369



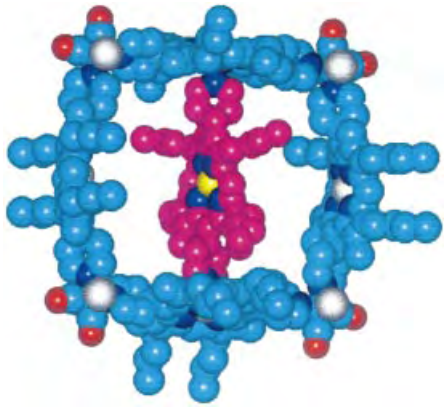
M. E. Padilla-Tosta, O. D. Fox, M. G. B. Drew, P. D. Beer* .. 4235 – 4239

Self-Assembly of a Mixed-Valence Copper(II)/Copper(III) Dithiocarbamate Catenane

Keywords: catenanes · copper · mixed-valent compounds · redox chemistry · self-assembly

Supramolecular complex formation imparts stability and substrate selectivity to a simple manganese-porphyrin-based epoxidation catalyst. Lewis acid/Lewis base directed assembly was used to encapsulate the epoxidation catalyst within a supramolecular square structure to form an enzyme-like catalyst system. The "molecular square" (see picture) takes on the functions of the protein superstructure in an enzyme: it spatially protects the catalytic core from decomposition and induces reaction selectivity.

Angew. Chem. **2001**, *113*, 4369 – 4372



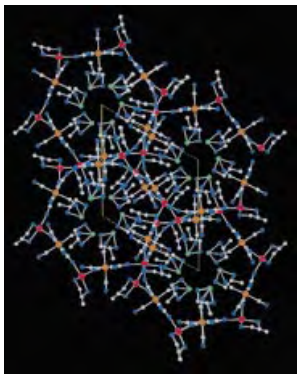
M. L. Merlau, M. del Pilar Mejia, S. T. Nguyen,* J. T. Hupp* .. 4239 – 4242

Artificial Enzymes Formed through Directed Assembly of Molecular Square Encapsulated Epoxidation Catalysts

Keywords: epoxidation · homogeneous catalysis · host – guest systems · self-assembly · supramolecular chemistry

The transparent, double bridged-(*R*)-spiral three-dimensional polymeric complex $K_{0.4}[Cr(CN)_6]$-[Mn(*S*)-pn](*S*)-pn$H_{0.6}$ ((*S*)-pn = (*S*)-1,2-diaminopropane) has been synthesized and characterized (see X-ray structure; Cr: brown, Mn: red, C: gray, N: blue, K: green). Magnetic measurements on the complex show that the Mn^{II} and Cr^{III} ions interact ferrimagnetically and magnetic transition occurs at 53 K (Curie temperature).

Angew. Chem. **2001**, *113*, 4372 – 4375



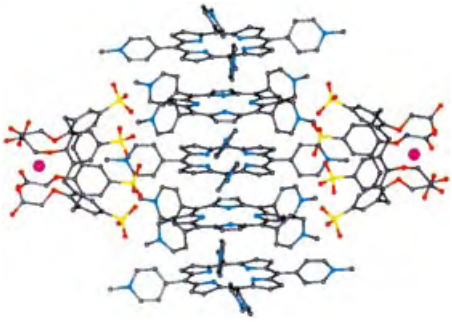
K. Inoue,* H. Imai, P. S. Ghalsasi, K. Kikuchi, M. Ohba, H. Ōkawa, J. V. Yakhmi ..... 4242 – 4245

A Three-Dimensional Ferrimagnet with a High Magnetic Transition Temperature (T_C) of 53 K Based on a Chiral Molecule

Keywords: chirality · chromium · helical structures · magnetic properties · manganese

Self-aggregation of water-soluble pyridinium-substituted porphyrins with functionalized calixarenes leads to well-defined pH-tunable stoichiometries. Two assemblies with different porphyrin:calixarene ratios that crystallized at pH 2 and 6 (see structure) have been structurally characterized. The Job plots of Soret band broadenings indicate that these structures are also preserved in solution.

Angew. Chem. **2001**, *113*, 4375 – 4377



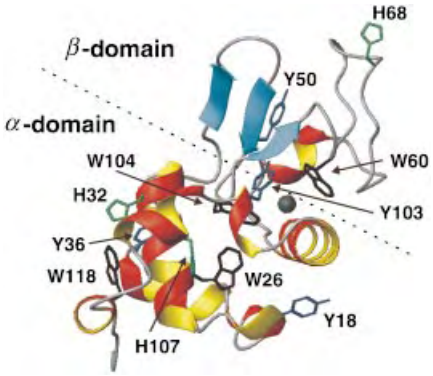
L. Di Costanzo, S. Geremia, L. Randaccio,* R. Purrello,* R. Lauceri, D. Sciotto,* F. G. Gulino, V. Pavone ..... 4245 – 4247

Calixarene – Porphyrin Supramolecular Complexes: pH-Tuning of the Complex Stoichiometry

Keywords: calixarenes · host – guest systems · porphyrinoids · self-assembly · supramolecular chemistry

 © WILEY-VCH Verlag GmbH, D-69451 Weinheim, 2001 1433-7851/01/4022-4118 $ 17.50+.50/0

Aspects of the structure of the intermediate populated after 200 ms in the Ca^{2+}-induced refolding of α-lactalbumin have been derived by time-resolved photo-CIDNP NMR methods. Refolding at constant denaturant concentration was initiated by laser-induced ion release from photolabile chelators. The NMR data demonstrated that part of the polypeptide chain in the β-domain of α-lactalbumin samples adopt non-native conformations while a hydrophobic core of the α-domain is already formed (see picture).



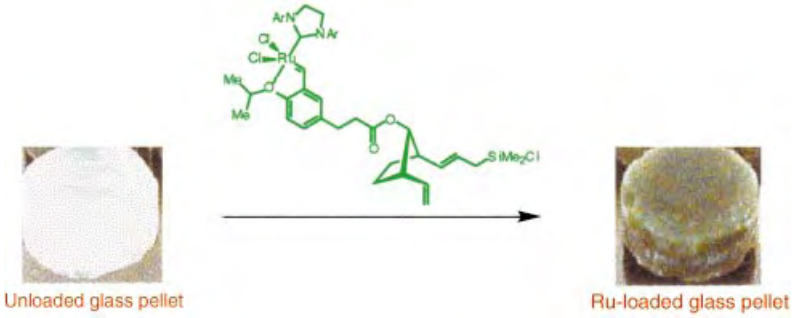
Angew. Chem. **2001**, *113*, 4378 – 4381

J. Wirmer, T. Kühn, H. Schwalbe* ..... 4248 – 4251

Millisecond Time Resolved Photo-CIDNP NMR Reveals a Non-Native Folding Intermediate on the Ion-Induced Refolding Pathway of Bovine α-Lactalbumin

Keywords: calcium · NMR spectroscopy · protein folding · structure elucidation

Glass-bound Ru-based catalysts! Ru-containing glass pellets (see picture) efficiently promote olefin metathesis reactions and are easily employed in syntheses of compound libraries. These robust catalysts are active in air and commercially available solvents, can be recycled up to 16 times, and removed from reaction mixtures with a simple pair of tweezers (minimal solvent waste).



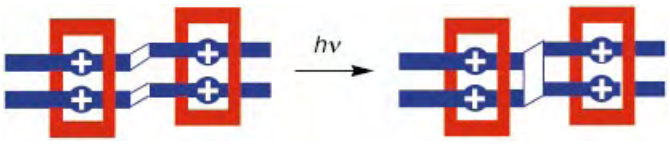
Angew. Chem. **2001**, *113*, 4381 – 4386

J. S. Kingsbury, S. B. Garber, J. M. Giftos, B. L. Gray, M. M. Okamoto, R. A. Farrer, J. T. Fourkas,* A. H. Hoveyda* ..... 4251 – 4256

Immobilization of Olefin Metathesis Catalysts on Monolithic Sol – Gel: Practical, Efficient, and Easily Recyclable Catalysts for Organic and Combinatorial Synthesis

Keywords: combinatorial chemistry · immobilization · metathesis · ruthenium · supported catalysts

A bis(dialkylammonium ion)-substituted stilbene derivative cocrystallizes with bisparaphenylene[34]crown-10 to form, in the solid state, a 2:2 host – guest complex wherein the stilbene double bonds are aligned with a relative geometry suitable for a stereospecific photochemical [2+2] cycloaddition. When irradiated with white light, this crystalline complex forms a single diastereoisomer of the corresponding cyclobutane derivative (see schematic presentation), the stereochemistry of which has been determined unambiguously in the solid state by X-ray crystallography to be *syn-anti-syn*.



Angew. Chem. **2001**, *113*, 4386 – 4391

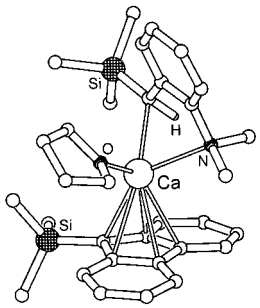
D. G. Amirsakis, M. A. Garcia-Garibay,* S. J. Rowan, J. F. Stoddart,* A. J. P. White, D. J. Williams* ..... 4256 – 4261

Host – Guest Chemistry Aids and Abets a Stereospecific Photodimerization in the Solid State

Keywords: photochemistry · pseudorotaxanes · self-assembly · solid-state reactions · template synthesis

 © WILEY-VCH Verlag GmbH, D-69451 Weinheim, 2001 1433-7851/01/4022-4119 $ 17.50+.50/0

Tackling tacticity: The first well-defined heteroleptic benzylcalcium complex (see structure) initiates the living polymerization of styrene. Chain-end control results in a polymer enriched in syndiotactic sequences. Stereo errors arise from fast inversion of the chiral carbanionic chain end. Increasing the styrene concentration accelerates the insertion and leads to a considerable reduction of the stereo errors.



Angew. Chem. **2001**, *113*, 4391 – 4394

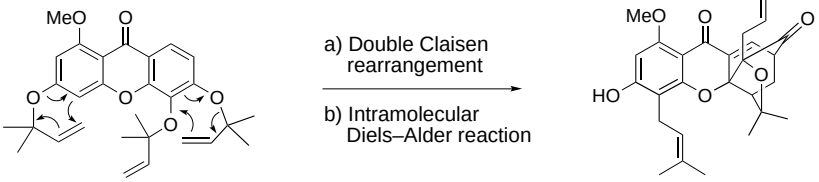
S. Harder,* F. Feil, K. Knoll 4261 – 4264

Novel Calcium Half-Sandwich Complexes for the Living and Stereoselective Polymerization of Styrene

Keywords: calcium · carbanions · homogeneous catalysis · polymerization · polystyrene

---

A further demonstration of the value of "biomimetically" inspired synthetic strategies toward natural products is provided by the title reactions that were developed for the construction of 4-oxatricyclo[4.3.1.0]decan-2-one systems from prochiral aromatic precursors. This biomimetic cascade was applied to the synthesis of 1-*O*-methylforbesione (**2**) from the prenylated xanthone **1** in one pot.



1 **2**: 1-*O*-methylforbesione

Angew. Chem. **2001**, *113*, 4394 – 4398

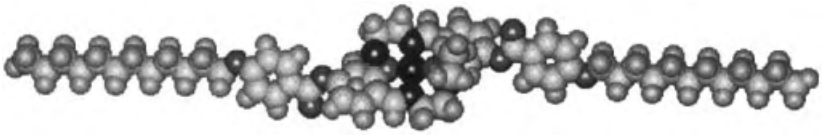
K. C. Nicolaou,* J. Li ..... 4264 – 4268

"Biomimetic" Cascade Reactions in Organic Synthesis: Construction of 4-Oxatricyclo[4.3.1.0]decan-2-one Systems and Total Synthesis of 1-*O*-Methylforbesione via Tandem Claisen Rearrangement/Diels – Alder Reactions

Keywords: cascade reactions · cycloaddition · natural products · rearrangement · total synthesis

---

The rodlike Fe^{III} complex of an *N*-alkyloxysalicylidenyl-*N*′-ethyl-*N*-ethylenediamine ligand, shown as a computer model in the picture, is the first compound in which spin-crossover (SC) and liquid-crystalline (LC) properties coexist. This synergy should allow the magnetic and optical properties of SC compounds to be combined with the sensitivity of the LC state to electromagnetic fields.



Angew. Chem. **2001**, *113*, 4399 – 4401

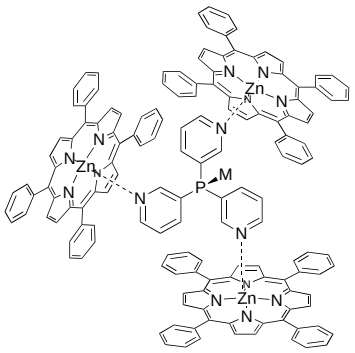
Y. Galyametdinov,* V. Ksenofontov, A. Prosvirin, I. Ovchinnikov, G. Ivanova, P. Gütlich,* W. Haase ..... 4269 – 4271

First Example of Coexistence of Thermal Spin Transition and Liquid-Crystal Properties

Keywords: iron · liquid crystals · metallomesogens · spin crossover

---

Enforced ligand dissociation as a result of steric interactions between Zn^{II} porphyrin units and the N atoms of pyridylphosphane ligands determines the catalytic properties of the encapsulated transition metal complexes (see picture). These assemblies show increased catalytic activity in the palladium-catalyzed Heck reaction and rhodium-catalyzed hydroformylation. M = transition metal catalyst.



Angew. Chem. **2001**, *113*, 4401 – 4404

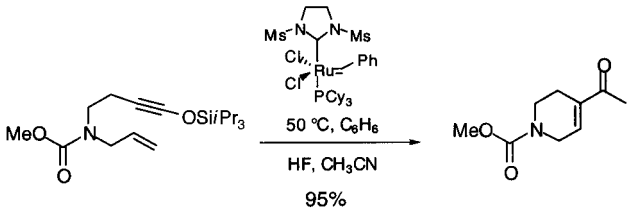
V. F. Slagt, J. N. H. Reek,* P. C. J. Kamer, P. W. N. M. van Leeuwen .... 4271 – 4274

Assembly of Encapsulated Transition Metal Catalysts

Keywords: homogeneous catalysis · porphyrinoids · self-assembly · supramolecular chemistry

 © WILEY-VCH Verlag GmbH, D-69451 Weinheim, 2001 1433-7851/01/4022-4120 $ 17.50+.50/0

Mechanistically intriguing participation of siloxyalkynes occurs in the intramolecular Ru-catalyzed metathesis with terminal alkenes (see scheme; Ms = methanesulfonyl). Combined with efficient protodesilylation, this process resulted in the development of a new method for the synthesis of highly functionalized enones starting from readily accessible acyclic precursors. Heterocyclic and polycyclic compounds were prepared efficiently, which illustrates the generality of this novel method.



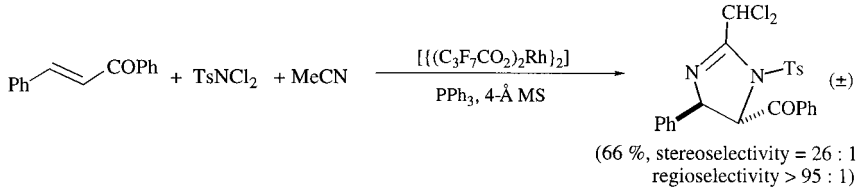
Angew. Chem. **2001**, *113*, 4404 – 4407

M. P. Schramm, D. S. Reddy, S. A. Kozmin* ..... 4274 – 4277

Siloxyalkyne – Alkene Metathesis: Rapid Access to Highly Functionalized Enones

Keywords: enones · homogeneous catalysis · metathesis · siloxyalkynes · synthetic methods

A three-component electrophilic reaction transforms olefins into imidazoline and diamine derivatives (see scheme). Rhodium(II) heptafluorobutyrate dimer (2 mol %) was utilized as the catalyst and *N*,*N*-dichloro-*p*-toluenesulfonamide ($TsNCl_2$) and acetonitrile as the nitrogen sources. Modest to good yields (45 – 82 %) and high regio- and stereoselectivity were achieved.



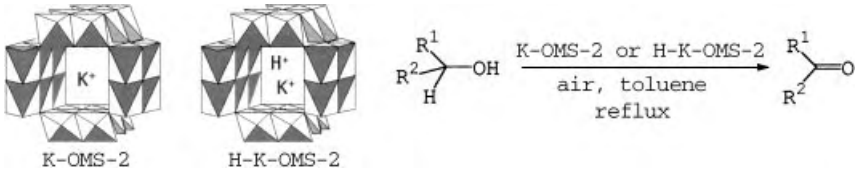
Angew. Chem. **2001**, *113*, 4407 – 4410

G. Li,* H.-X. Wei, S. H. Kim, M. D. Carducci ..... 4277 – 4280

A Novel Electrophilic Diamination Reaction of Alkenes

Keywords: amination · electrophilic additions · homogeneous catalysis · nitrogen heterocycles · rhodium

Mixed-valent manganese octahedral molecular sieves K-OMS-2 and H-K-OMS-2 are used to oxidize a wide range of alcohols with 100 % selectivity and 90 – 100 % conversion in most cases. The reaction (see scheme) is aerobic, catalytic, mild, efficient, stable, inexpensive, selective, and environmentally friendly.



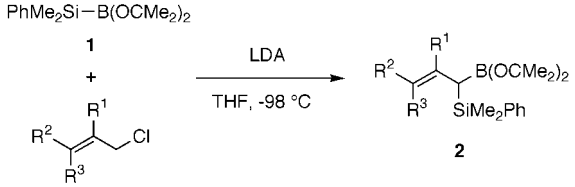
Angew. Chem. **2001**, *113*, 4410 – 4413

Y.-C. Son, V. D. Makwana, A. R. Howell, S. L. Suib* ..... 4280 – 4283

Efficient, Catalytic, Aerobic Oxidation of Alcohols with Octahedral Molecular Sieves

Keywords: alcohols · heterogeneous catalysis · manganese · mixed-valent compounds · oxidation

Silylboryl reagents for organic synthesis: 1-silyl-1-boryl-2-alkenes (**2**) were prepared efficiently by *gem*-silylborylation of α-chloroallyllithium compounds from (dimethylphenylsilyl)(pinacolato)borane (**1**; see scheme, LDA = lithium diisopropylamide) and were demonstrated to allylate acetals and aldehydes in the presence of a Lewis acid to produce (*E*)-4-alkoxy-alkenylboronates. Heating the reagents with aldehydes in the absence of Lewis acid afforded (*Z*)-4-hydroxy-alkenylsilanes stereospecifically.



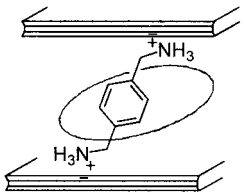
Angew. Chem. **2001**, *113*, 4413 – 4416

M. Shimizu,* H. Kitagawa, T. Kurahashi, T. Hiyama* ..... 4283 – 4286

1-Silyl-1-boryl-2-alkenes: Reagents for Stereodivergent Allylation Leading to 4-Oxy-(*E*)-1-alkenylboronates and 4-Oxy-(*Z*)-1-alkenylsilanes

Keywords: alkenes · allylation · boron · carbenoids · silicon

As an alternative to the rotaxane method, an organoclay can be used as a template for the efficient formation of macrocycles (ring in schematic representation) which are easily extracted from the clay interlayer space. The four-step synthesis involved preparation of a pillared clay from the dihydrochloride salt of *p*-xylylenediamine, insertion of neutral *p*-xylylenediamine into the pillared structure, reaction of the neutral *p*-xylylenediamine in the layers with isophthaloyl chloride and formation of the tetramide macrocycle, and extraction of the product from the clay.



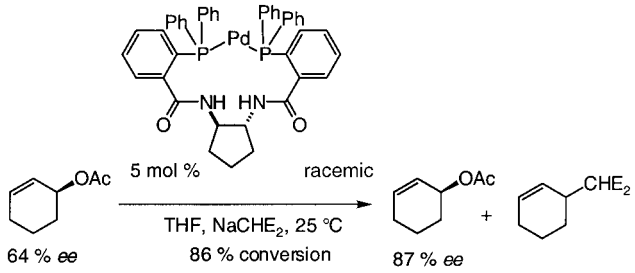
V. Georgakilas, D. Gournis, D. Petridis* ..... 4286 – 4288

Organoclay Derivatives in the Synthesis of Macrocycles

Angew. Chem. **2001**, *113*, 4416 – 4418

Keywords: clays · macrocycles · supramolecular chemistry · template synthesis · through-bond interactions

An even-handed approach: by use of an enantiomerically enriched substrate and study of the changes in enantiomer ratio of substrate under pseudo zero-order conditions, racemic catalysts may be employed to determine whether the enantiomerically pure catalyst would be effective for kinetic resolution of the racemic substrate (see scheme; E = CO_2Me).



B. Dominguez, N. S. Hodnett, G. C. Lloyd-Jones* ..... 4289 – 4291

Testing Racemic Chiral Catalysts for Kinetic Resolution Potential

Angew. Chem. **2001**, *113*, 4419 – 4421

Keywords: allylation · asymmetric catalysis · kinetic resolution · palladium

Supporting information on the WWW (see article for access details).

* Author to whom correspondence should be addressed

The cover picture was designed by Erik Zuidema and Vincent Slagt.

BOOKS

Sciences of Synthesis, Houben-Weyl Methods of Molecular Transformations — E. Jim Thomas — *J. Mulzer* 4293

Carbohydrates in Chemistry and Biology — Beat Ernst, Gerald W. Hart, Pierre Sinaÿ — *H. S. Conradt* 4294

Electron Transfer in Chemistry — Vincenzo Balzani — *S. R. Waldvogel, C. Mück-Lichtenfeld* 4295

The Amide Linkage — Arthur Greenberg, Curt M. Breneman, Joel F. Liebman — *T. Lectka* 4297

High-Throughput Synthesis — Irving Sucholeiki — *J. Rademann* 4298

NMR Imaging of Materials — Bernhard Blümich — *K. Momot* 4298

 © WILEY-VCH Verlag GmbH, D-69451 Weinheim, 2001 1433-7851/01/4022-4122 $ 17.50+.50/0

WEB SITES

http://www.vuw.ac.nz/~teespitt/essentials/, http://www.mhhe.com/physsci/chemistry/carey/, http://www.whfreeman.com/stryer4/ Companion Sites for Textbooks *R. Breinbauer* 4301

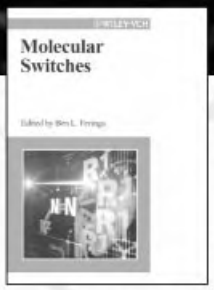
SERVICE

- **VIPs** 4112
- ***Angewandte's* Sister-Journals** 4303
- **Events** 4125, 4126
- **Vacancies** A133
- **Keywords** 4306
- **Authors** 4307
- **Preview** 4308

Don't forget all the Tables of Contents from 1998 onwards may be still found on the WWW under: http://www.angewandte.com

Issue 21, 2001 was published online on October 31

Switch to new horizons



B. L. FERINGA, (Ed.) University of Groningen, The Netherlands

Molecular Switches

2001. XVI, 464 pages. Hardcover.
DM 268.00 / £ 85.00
ISBN 3-527-29965-3

Every day we use switches to turn electric appliances on and off and no computer could function without them. Molecular switches work in the same way, changing from state one to another depending on environmental influences. However, as opposed to normal switches, molecular switches are extremely tiny and their application in nanotechnology, biomedicine and computer chip design opens up whole new horizons.

In this manual, the editors and authors describe molecular switches made of catenates and rotaxanes, dihydroazulenes, fulgides, liquid crystals and polypeptides. The spectrum of topics discussed ranges from chiropticene switches via multifunctional systems to molecular logical switches.

A wealth of information for chemists and materials scientists in industry and academia interested in one of the most innovative branches of their discipline.

From the Contents:

- Introduction on molecular switches
- Photoswitching of diarylalkenes
- Fulgide based photoswitches
- Azulenes
- Electrooptical switches
- Electron transfer photoswitching
- Metallo-based photoswitches
- Photoswitches of liquid crystals
- Photoresponsive polymers, monolayers and thin films
- Supramolecular switches
- Metallo-rotaxanes and catenanes
- Supramolecular switches;
- Molecular shuttles
- Switchable molecular receptors and recognition processes
- Biomolecular switches.

0357_0102_4_vi

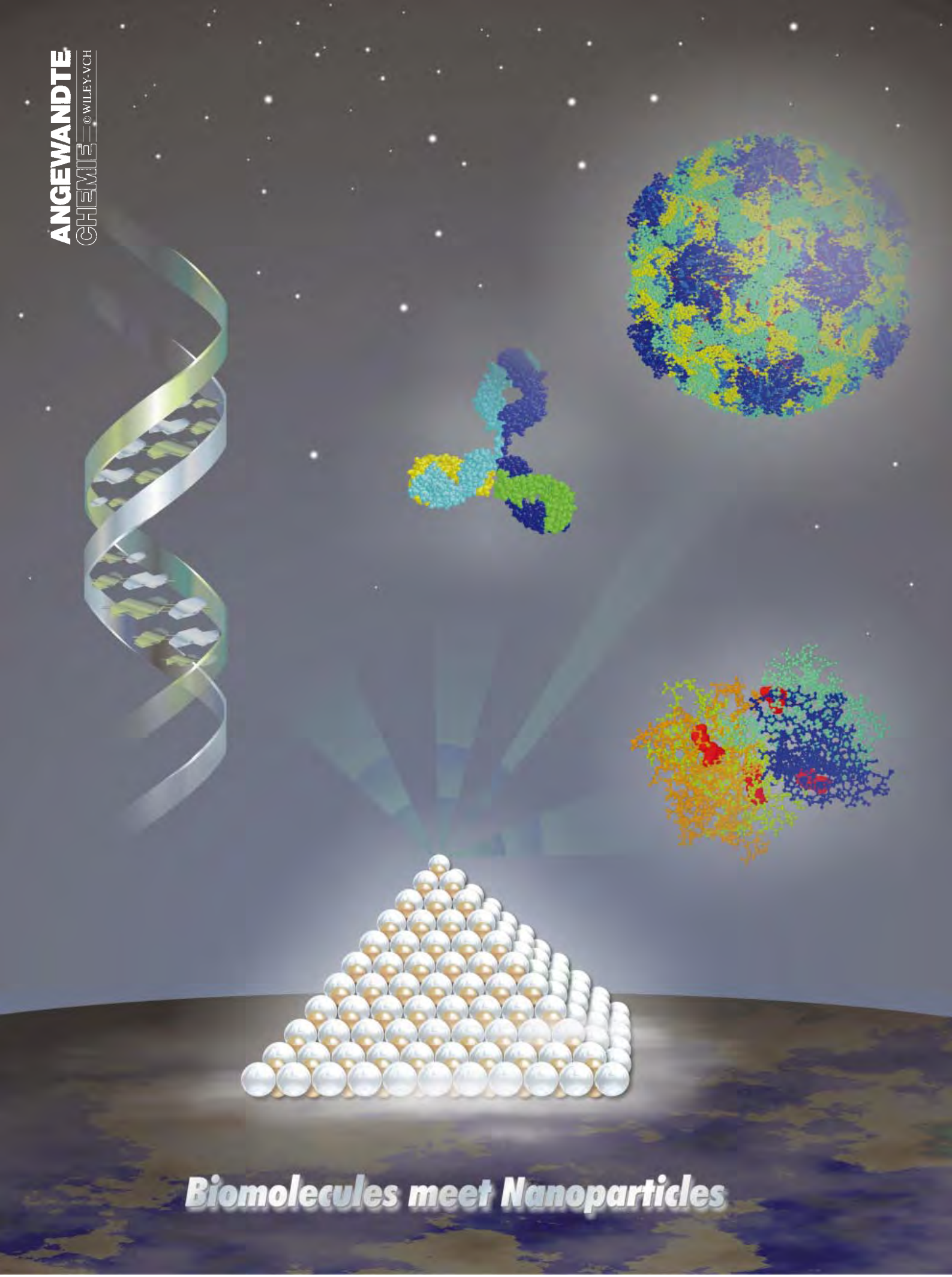
WILEY

WILEY-VCH, P.O. Box 10 11 61, 69451 Weinheim, Germany
Fax: +49 (0) 62 01-60 61 84 • e-mail: service@wiley-vch.de • www.wiley-vch.de

WILEY-VCH

 © WILEY-VCH Verlag GmbH, D-69451 Weinheim, 2001 1433-7851/01/4022-4123 $ 17.50+.50/0

ANGEWANDTE CHEMIE © WILEY-VCH



Nanoparticles, Proteins, and Nucleic Acids: Biotechnology Meets Materials Science

Christof M. Niemeyer*

Based on fundamental chemistry, biotechnology and materials science have developed over the past three decades into today's powerful disciplines which allow the engineering of advanced technical devices and the industrial production of active substances for pharmaceutical and biomedical applications. This review is focused on current approaches emerging at the intersection of materials research, nanosciences, and molecular biotechnology. This novel and highly interdisciplinary field of chemistry is closely associated with both the physical and chemical properties of organic and inorganic nanoparticles, as well as to the various aspects of molecular cloning, recombinant DNA and protein technology, and immunology. Evolutionary optimized biomolecules such as nucleic acids, proteins, and supramolecular complexes of these components, are utilized in the production of nanostructured and mesoscopic architectures from organic and inorganic materials. The highly developed instruments and techniques of today's materials research are used for basic and applied studies of fundamental biological processes.

Keywords: analytical methods · biotechnology · materials science · nanostructures · supramolecular chemistry

1. Introduction

"The essence of chemical science finds its full expression in the words of that epitome of the artist–scientist Leonardo da Vinci: *'Where Nature finishes producing its own species, man begins, using natural things and with the help of this nature, to create an infinity of species.'*" Nobel laureate Jean-Marie Lehn used these words to give an outlook on the future and perspectives of supramolecular chemistry.[1] In a highly interdisciplinary effort, the pioneering work of Pedersen, Cram, and Lehn on supramolecular aggregates held together by weak noncovalent interactions has developed over the past 30 years into a well-established discipline. Supramolecular chemistry concerns the investigation of nature's principles to produce fascinating complex and functional molecular assemblies, as well as the utilization of these principles to generate novel devices and materials, potentially useful for sensing, catalysis, transport, and other applications in medicinal or engineering science.[1–3] Another example of modern technical achievements concerns the development of advanced, functional, and even "smart" materials for applications in highly integrated mechanical, optical, and electronic devices, sensors, or catalysts. The enormous advance attained in this area so far is illustrated impressively by comparing materials used in last centuries electrical devices such as millimeter-sized copper wires to today's (sub)micrometer-sized optical and electronical parts, comprised of modern conducting and electroluminescent organic polymers.[4]

Similar advances have been made in the biological sciences. Natural evolution has led to highly functional assemblies of proteins, nucleic acids, and other (macro)molecules which perform complicated tasks that are still daunting for us to try to emulate. As an example, the 20 nm ribosome particle is an effective supramolecular machine which spontaneously self-assembles from more than 50 individual protein and nucleic acid building blocks, thereby impressively demonstrating the power of biologically programmed molecular recognition.[5] Starting with the discovery of the double helix structure of DNA, biology has grown from a purely descriptive and phenomenological discipline to a molecular science. Recombinant DNA technology brought insights into the basic principles of many biochemical processes, and it has also opened the door to modern biotechnology. Today we are able to genetically engineer relatively simple bacterial cells, and we are on our way towards tailoring complex organisms. In view of such revolutionary developments, it seems particularly challenging to fuse biotechnology with materials science (Figure 1). Merging these disciplines will allow us to take advantage of the improved evolutionary biological components to generate new smart materials and, conversely, to

[*] Priv.-Doz. Dr. C. M. Niemeyer
Biotechnologie und Molekulare Genetik
Universität Bremen, FB2–UFT
Leobener Strasse, 28359 Bremen (Germany)
Fax: (+49) 421-218-7578
E-mail: cmn@uni-bremen.de

 © WILEY-VCH Verlag GmbH, D-69451 Weinheim, 2001 1433-7851/01/4022-4129 $ 17.50+.50/0

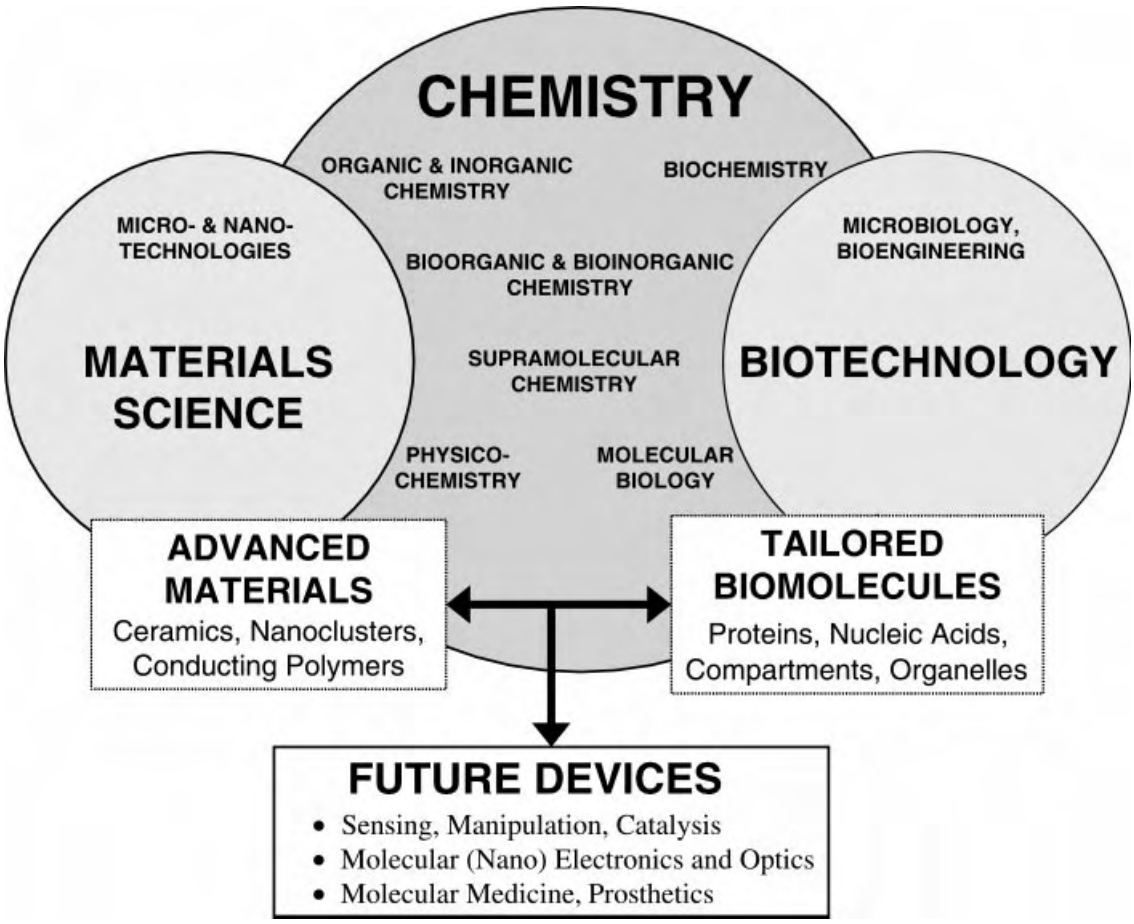


Figure 1. Chemistry is the central science for the development of applied disciplines such as materials research and biotechnology. Materials science, which is based on classic chemical research fields and engineering technologies, has led to enormous advances in tailoring advanced modern materials.

apply today's advanced materials and physicochemical techniques to solve biological problems.

Both biotechnology and materials science meet at the same length scale (Figure 2). On the one hand, biomolecular components have typical size dimensions in the range of about 5 to 200 nm. To exploit and to utilize the concepts administered in natural nanometer-scale systems, the development of nanochemistry is crucial.[6] On the other hand, commercial requirements to produce increasingly miniaturized microelectronic devices strongly motivate the elaboration of nanoscale systems. The structural dimensions of computer microprocessors are currently in the range of about 200 nm. They are only just available by conventional top-down processes (miniaturization processes) such as photolithography, but for the foreseeable future, such technologies hardly allow the large-scale production of parts that are significantly smaller than 100 nanometers. "There is plenty of room at the bottom," as Nobel physicist Richard Feynman pointed out more than 40 years ago,[7] and thus today's nanotechnology research puts a great emphasis on the



Christof M. Niemeyer studied chemistry at the Philipps Universität in Marburg (Germany), and worked in the group Prof. M. T. Reetz on enantioselective aldol reactions with chiral boron reagents. During his doctoral studies with Prof. Reetz at the Max-Planck Institut für Kohlenforschung in Mülheim an der Ruhr (Germany), his research interests focused on the development of organometallic receptors and their supramolecular host–guest complexes. During his post-doctoral visit in the laboratories of Prof. Charles R. Cantor at the Center for Advanced Biotechnology in Boston, MA, his main interests shifted towards biomolecular recognition systems. In mid-1994, he joined the group of Prof. Dietmar Blohm at the University of Bremen (Germany), and in November 2000 he completed his habilitation in organic chemistry. He received the 1999 DECHEMA habilitation prize for biotechnology. His research interests lie in the synthesis and characterization of semisynthetic DNA–protein and nanoparticle conjugates and their applications in molecular biotechnology.

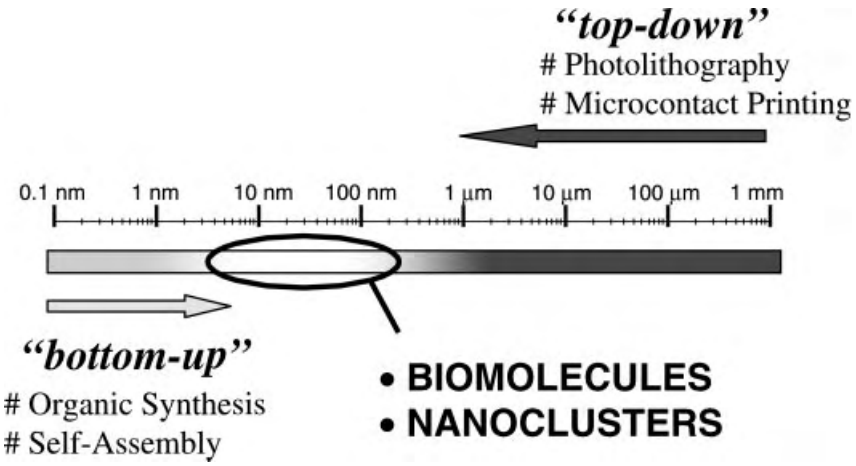


Figure 2. A gap currently exists in the engineering of small-scale devices. Whereas conventional top-down processes hardly allow the production of structures smaller than about 200 – 100 nm, the limits of regular bottom-up processes are in the range of about 2 – 5 nm. As a result of their own dimensions, two different types of compounds appear to be suited for addressing that gap: 1) biomolecular components, such as proteins and nucleic acids, and 2) colloidal nanoparticles comprised of metal and semiconductor materials.

development of bottom-up strategies (enlargement strategies), which concern the self-assembly of (macro)molecular and colloidal building blocks to create larger, functional devices.[8] The individual components to be employed in self-assembling processes should fulfill some basic requirements. First, distinct intrinsic functionality, such as steric, optical, electronic, or catalytic properties are desired to allow the particular applications envisaged. Second, the modules need to be programmable through their specific constitution, configuration, conformation, and dynamic properties to enable specific recognition for self-assembly. Third, the building blocks should have an appropriate size to bridge the gap between the submicrometer dimensions that are reachable by classical top-down engineering and the dimensions that are addressable by classical bottom-up approaches, such as chemical synthesis and supramolecular self-assembly (Figure 2).

Inorganic nanoparticles are particularly attractive building blocks for the generation of larger superstructures.[9–16] Such nanoparticles can be prepared readily in large quantities from various materials by relatively simple methods. The dimensions of the nanoparticles can be controlled from one to about several hundred nanometers, with a fairly narrow size distribution. Most often, the particles are comprised of metals, metal oxides, and semiconductor materials, such as Ag_2S, CdS, CdSe, and TiO_2. The nanoparticles have highly interesting optical, electronic, and catalytic properties, which are very different from those of the corresponding bulk materials and which often depend strongly on the particle's size in a highly predictable way. Examples include the wavelength of the light emitted from semiconductor nanocrystals which can be utilized for biolabelling[17, 18] or in lasers,[19] as well as the external magnetic field required to switch a magnetized particle, which is highly relevant in magnetotactic bacteria[20] and in hard disk drives.[21] Moreover, certain types of nanoparticles can be considered as "artificial atoms"[22] since they are obtainable as highly perfect nanocrystals, which can be used as building blocks for the assembly of larger two- and three-dimensional structures.[23]

A number of outstanding monographs and reviews already deal with the rapidly increasing area of fundamental and applied nanoparticle research.[9–15] This article is intended to summarize approaches which go beyond the questions of pure materials science. These approaches currently emerge at the intersection of materials science and molecular biotechnology.[24–26] This novel field of research is closely associated with the surface chemistry and the physical properties of inorganic nanoparticles, the topics of bioorganic and bioinorganic chemistry, and the various aspects of molecular biology, recombinant DNA technology, recombinant protein expression, and immunology. In particular, this article describes the utilization of nucleic acids and proteins as programmable recognition units to modify and improve the nanoparticle's assembly capabilities, and thus, to allow for nanostructured and mesoscopic supramolecular hybrid architecture. Moreover, recent efforts to utilize nanoparticles as tools for fundamental and applied studies on biomolecular interaction are summarized.

2. Coupling of Nanoparticles and Biomolecules

Bioorganic and bioinorganic chemistry are the interdisciplinary fields which provide the basis for joining biotechnology with materials science. For instance, bioorganic model systems have long been elaborated to provide tools for probing the mechanisms of biological principles, as well as to develop chemical means for the handling and manipulating biological components.[27, 28] Analogously to the interactions that are abundant in many reaction centers of enzymes between the amino acid side chains and the metal centers, the interaction between organic ligands and the surface of an inorganic nanoparticle paves the way for the coupling of biomolecular recognition systems to generate novel materials. Although inorganic nanoparticles can be prepared from various materials by several methods,[9, 10, 13–15] the coupling and functionalization with biological components has only been carried out with a limited number of chemical methods. Some examples are summarized in Table 1.

Typically, the wet-chemical preparation of the nanoparticles is carried out in the presence of stabilizing agents (often citrate, phosphanes, or thiols) which bind to the atoms exposed at the surface of the nanoparticles. This capping leads to a stabilization and prevents uncontrolled growth and aggregation of the nanoparticles. In the case of a labile capping layer such as citrate, biomolecules can be linked directly with the metal particle by exchange reactions with stronger binding ligands (Figure 3). This method is usually applied in the coating of colloidal gold with thiol-containing

Table 1. Coupling of inorganic nanoparticles and biomolecules.

Particle	Linker	FG	Biomolecule	Reference
Au	–	HS-Cys	immunoglobulins, serum albumins	[34, 152]
Au	citrate	H_2N-Lys[a]	proteins	[156, 217]
Au	streptavidin	biotin-$(CH_2)_6$-	immunoglobulins, serum albumins	[218]
Au	**3**		immunoglobulin, streptavidin	[42]
Au	streptavidin	biotin-$(CH_2)_6$-	DNA	[148e, 219]
Au	–	HS-$(CH_2)_6$-	DNA	[77, 82]
Au	–	$(HS\text{-}PO_3R_2)_5$-	DNA	[30, 31]
Au	**2**		DNA	[33]
Au	**4**	HOOC-Glu	proteins	[43]
Au	**5**	HS-Cys	proteins	[158]
Ag	citrate	H_2N-Lys[a]	heme proteins, immunoglobulins	[35, 36, 166]
ZnS		HS-Cys	gluthathione	[47]
CdS		HS-Cys	peptides	[46]
CdS	Cd^{2+}, HS-$(CH_2)_2$-OH[a]		DNA	[39, 41]
CdSe/ZnS[b]		HS-$(CH_2)_6$-	DNA	[79]
CdSe/CdS/SiO_2[b]	**6**	NHS – biotin	streptavidin	[17]
CdSe/ZnS[b]	HS-(CH_2)-COOH	H_2N-Lys	immunoglobulin, transferrin	[18]
CdSe/ZnS[b]	**1**	H_2N-Lys[a]	leucine zipper fusion proteins	[32]
SnO_2, TiO_2	HOOC-$(CH_2)_n$-NH_2	HOOC-Glu	proteins[c]	
GaAs, InP	phosphoramide ε-NH_2	HOOC-Glu	proteins[c]	[220]

Examples of chemical interactions used for the coupling of nanoparticles with biological macromolecules (FG = functional coupling group, see Figure 3). [a] Adsorption through Coulombic interactions. [b] Core/shell nanoparticles. [c] Proposed from related studies of nanoparticle binding to analogously modified solid substrates.

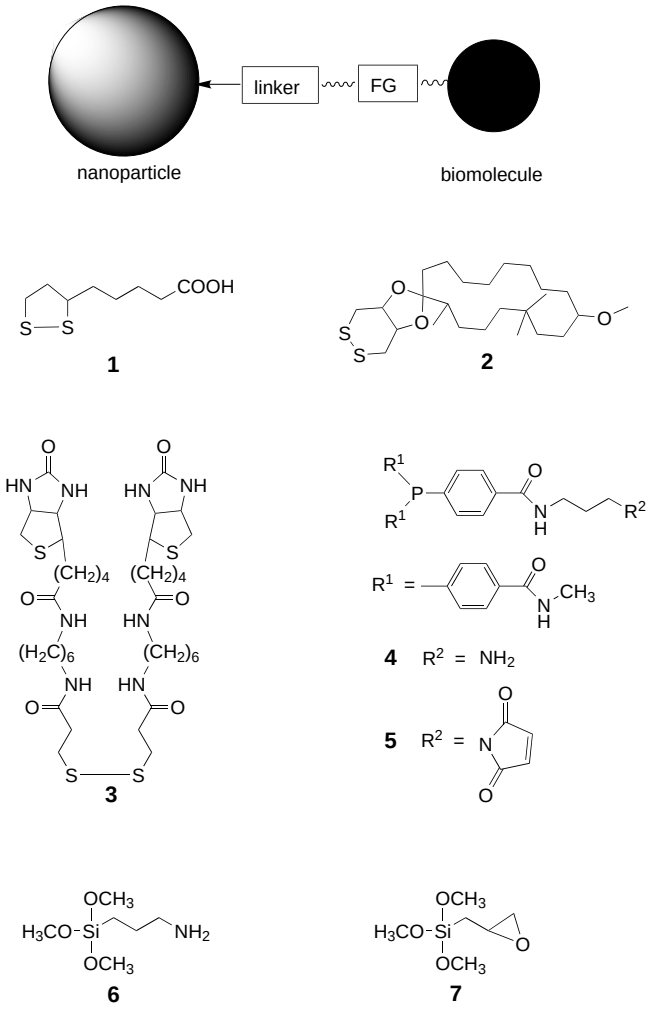


Figure 3. General schematic representation of methods to couple inorganic nanoparticles and biomolecules (FG = functional coupling group). Representative structures of typical linkers are listed beneath (see also Table 1).

proteins, for example, immunoglobulins (IgG) and serum albumins, which have cysteine residues that are accessible for the heterogeneous interphase coupling. If no such residues are available in the native proteins, thiol groups can be incorporated by chemical means (e.g. with Traut's reagent (2-iminothiolane))[29] or by genetic engineering. Similarly, DNA molecules can be synthesized with alkylthiol groups at the 3′- or 5′-ends by using appropriate phosphoramidite precursors in a solid-phase synthesis. The *n*-alkylthiolated DNA has been used extensively in the preparation of DNA-functionalized gold and semiconductor nanoparticles (Table 1). As an interesting alternative, DNA oligonucleotides that contain several adenosyl phosphothioate residues at their ends have been used to interact directly with the metal surface of nanoparticles.[30, 31] The use of cyclic disulfide linkers such as **1**[32] and **2**[33] (Figure 3) leads to nanoparticle cappings, which are more stable towards ligand exchange than the corresponding conjugates prepared with the conventional reagents that contain a single thiol group or acyclic disulfide units. The greater stability is likely a result of the anchoring of the ligands to the nanoparticles through two sulfur atoms.[33]

In the case of nanoparticles that are stabilized by anionic ligands such as citrate or lipoic acid (**1**), the biomolecules are often coupled through noncovalent electrostatic interactions. For instance, gold and silver nanoparticles, which are produced by the citrate method, have been functionalized with IgG molecules at high pH values that are slightly above the isoelectric point of the citrate ligand.[34] This allows an effective binding between the positively charged amino acid side chains of the protein and the negatively charged citrate groups of the colloids. The optimal coupling ratio can be determined by means of a flocculation assay. The addition of electrolytes to gold and silver nanoparticles causes flocculation as a result of the shielding of the repulsive double-layer charges which normally stabilize them. The aggregation can be conveniently monitored photometrically by the decrease

and/or red shift of the plasmon absorption band at about 520 nm.[35] Protein adsorption stabilizes the metal particle and the steric repulsion of the particles prevents flocculation. The amount of stabilizer needed to prevent flocculation is determined by increasing the concentration of electrolyte in various nanoparticle preparations, previously coated with distinct amounts of proteins. The amount often corresponds to a single monolayer of proteins attached to the surface of the nanoparticle. Other examples of protein coating through electrostatic interactions include the directed adsorption of heme-containing redox enzymes at citrate-stabilized silver nanoparticles,[36–38] and the binding of basic leucine zipper proteins to semiconductor particles that are stabilized with lipoic acid (**1**).[32] Similarly, the adsorption of DNA molecules to positive or neutral CdS nanoparticles has been studied in detail.[39–41] A different approach, which takes advantage of a combination of various noncovalent interactions, employs specific receptor–ligand binding for the coupling of nanoparticles and biomolecules. For instance, chemisorption of disulfide **3** (Figure 3) to colloidal gold particles provides ligands that are specifically recognized and bound by the complementary receptors (strept)avidin and antibodies that are directed against the biotin moiety.[42]

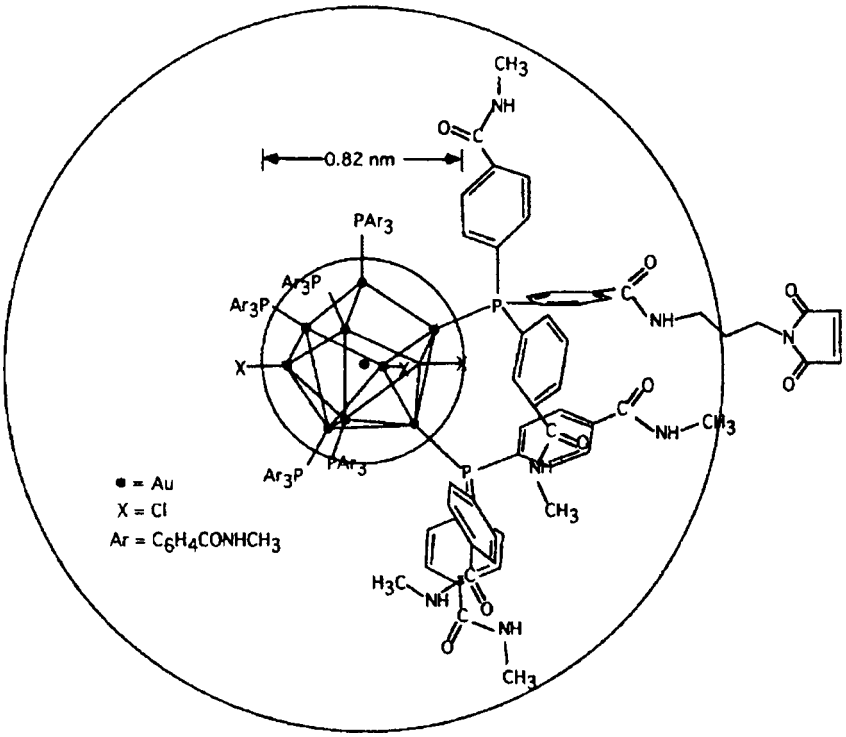


Figure 4. Molecular structure of an undecagold cluster, which is stabilized with phosphane ligands. A single maleimido group is attached per gold cluster to allow chemical coupling of thiolated components. Reproduced from http://www.nanoprobes.com.

Another approach is based on thiols or disulfides, and phosphane ligands (**1**, **4**, and **5**; Figure 3), which contain terminal carboxy, amino, or maleimide groups. These can be used for the coupling of biological components by means of carbodiimide-mediated esterification and amidation, or reaction with thiol groups. To prepare gold conjugates as probes for histological applications, this strategy is routinely used in the coupling of proteins with well-defined 0.8-nm undecagold nanoclusters, stabilized with arylphosphanes and ligand **5** (Figure 4).[43] Furthermore, the monomaleimido gold clusters have been coupled with thiolated DNA oligomers to synthesize probes for homogeneous nucleic acid analyses[44] and to prepare nanocrystal molecules (Section 3.2.2).[45]

Various syntheses of semiconductor colloids in the presence of thiol ligands,[9–16] and in special cases the biosynthesis of cysteine- or gluthathione-protected CdS and ZnS colloids,[46, 47] or the efficient gram-quantity colloid production of water-soluble ZnS nanocrystal powders[48] have been reported. Mercaptoacetic[*] acid stabilized CdTe nanoparticles have been coupled with the ε-amino groups of the biotin-binding protein streptavidin through covalent amide bonding.[49] In the case of silica-coated Cd/chalcogen nanoparticles, the hydroxy groups at the surface can be used for the covalent coupling of biomolecules by using a variety of commercially available silanes such as **6** and **7** (Figure 3). This method is commonly applied in the biofunctionalization of larger, SiO_2-based microspheres and has been used to couple SiO_2-coated core (CdSe)/shell (CdS) particles to biomolecules.[17] When the inorganic nanoparticles are covered with a bioorganic matrix, such as the polypeptide core in remineralized ferritin (Section 4.3), the entire spectrum of protein-modification chemistry can be applied for further functionalization and coupling steps.

The above examples demonstrate that some chemical means have already been explored for the physical linkage of inorganic and biological materials. However, there is still a great demand for alternative methods to allow for compensation of typical problems that arise in the biofunctionalization of inorganic nanoparticles. In particular, harsh reaction conditions often lead to the degradation and inactivation of sensitive biological compounds, and ligand-exchange reactions that occur at the colloid surface often hinder the formation of stable bioconjugates. Moreover, the synthesis of stoichiometrically defined nanoparticle–biomolecule complexes is a great challenge, and is particularly important from a molecular engineering point of view to generate well-defined nanoarchitectures.

3. Biomolecule-Directed Nanoparticle Organization

Many approaches have been described for the formation of two- and three-dimensional arrays of metal and semiconductor nanoparticles,[11–13, 15] for example, random inclusion of the particles into gel and glassy matrices, deposition of the

[*] In this review, the commonly used prefix "mercapto-" is used rather than the IUPAC-recommended "sulfanyl-".

particles on structured surfaces, or chemical coupling in solution by means of bivalent crosslinker molecules. An example of the latter is the alkyldithiol-directed aggregation of gold colloids,[50] which leads to extended networks of cross-linked nanoparticles. Similarly, biomolecules can also be used as cross-linkers (Figure 5). Initially, the two sets of nanoparticles are functionalized with individual recognition groups that are complementary to each other, or else are complementary to a molecular linker (Figures 5 A and B, respectively). Driven by the biospecific interaction, the two particle batches assemble to form extended nanoparticle networks, which in some cases can grow to the size of macroscopic materials. Rather than just exploring novel, unconventional coupling systems, the major motivation for this approach is based on the unique properties of biomolecular linkers, which promise new applications such as tunable and/or switchable materials. In particular, the tremendous recognition capabilities of biomolecules, and their potential to be addressed and manipulated through biochemical procedures that use designed tools such as enzymes, should provide the basis for entirely novel routes to construct advanced materials rationally.

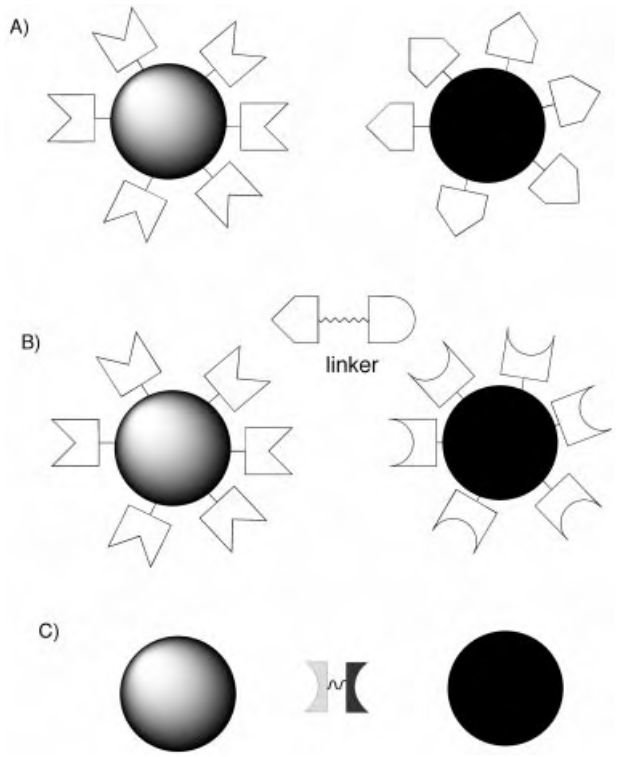


Figure 5. Solution-phase chemical coupling with biomolecular recognition elements. A) Two sets of nanoparticles are functionalized with individual recognition groups that are complementary to each other. B) The particle-bound recognition groups are not complementary to each other, but can be bridged through a bispecific linker molecule. C) A bivalent linker that directly recognizes the surfaces of the nanoparticles is used for aggregation.

3.1. Protein-Based Recognition Systems

The coupling approaches depicted in Figure 5 have been experimentally realized by using protein-based recognition systems. One of the first examples took advantage of the specific interaction between antibodies and low molecular weight organic compounds, the so-called hapten groups.[34] The latter can be used to cross-link nanoparticles, which are previously coated with antibody molecules that specifically recognize the hapten group (Figure 6). Shenton et al. functionalized gold and silver nanoparticles with immunoglobulins of class G and E (IgG and IgE, respectively), which had a specificity directed against either the D-biotin or the dinitrophenyl (DNP) group.[34] To allow the cross-linking of the IgG-functionalized nanoparticles, bivalent linkers that contained two terminal hapten groups were synthesized. The monospecific linker **8**, which is comprised of two DNP moieties, and the bispecific linker **9** were used (Figure 6) to induce the directed assembly of homo-oligomeric or heterodimeric aggregates, respectively. The precipitate formed was characterized by transmission electron microscopy (TEM) and large disordered 3D networks of discrete nanoparticles were found. In the case of the bimetallic Ag–Au networks, however, the degree of integration was not as high as expected for an oligomerization process that is regulated by highly specific biomolecular recognition. This suggests that further progress will require a more sophisticated engineering of the antibody–antigen interface.[34]

Other approaches to using protein-based recognition systems to organize inorganic nanoparticles made use of the unique interaction between the biotin-binding protein streptavidin (STV) and its low molecular weight ligand D-biotin.[42, 51] The remarkable biomolecular recognition of the water-soluble biotin (vitamin H) by the homotetrameric protein STV is characterized by the extraordinary affinity constant of the STV–biotin interaction of about 10^{14} $dm^3 mol^{-1}$, which makes it the strongest ligand–receptor interaction currently known.[52] Another great advantage of STV is its extreme chemical and thermal stability. Biotinylated materials are often commercially available or can be prepared by using a variety of mild biotinylation procedures, and thus biotin–STV conjugates form the basis of many diagnostic and analytical tests.[53]

Connolly and Fitzmaurice have used the STV–biotin interaction to organize gold colloids that were functionalized by chemisorptive coupling to the disulfide biotin analogue **3**.[42] According to the generalized principle depicted in Figure 5 B, the subsequent cross-linking was achieved by the addition of STV as a linker. The immediate change of the sol from red to blue was indicative of the formation of oligomeric networks. This process was also monitored by dynamic light scattering (DLS), which showed that the average hydrodynamic radius of all particles in solution rapidly increased upon STV-directed assembly (Figure 7 A). TEM images revealed networks with an average of 20 interconnected particles that were separated by about 5 nm, which correlates with the diameter of an STV molecule. Since the deposition of the colloid aggregates on the graphite substrate used for TEM characterization might affect aggregation or alteration of existing structures, small angle X-ray scattering (SAXS) was employed to probe the solution structure of the networks (Figure 7 B). The angular dependence of the intensity of the scattered X-ray radiation is quantitatively related to the size

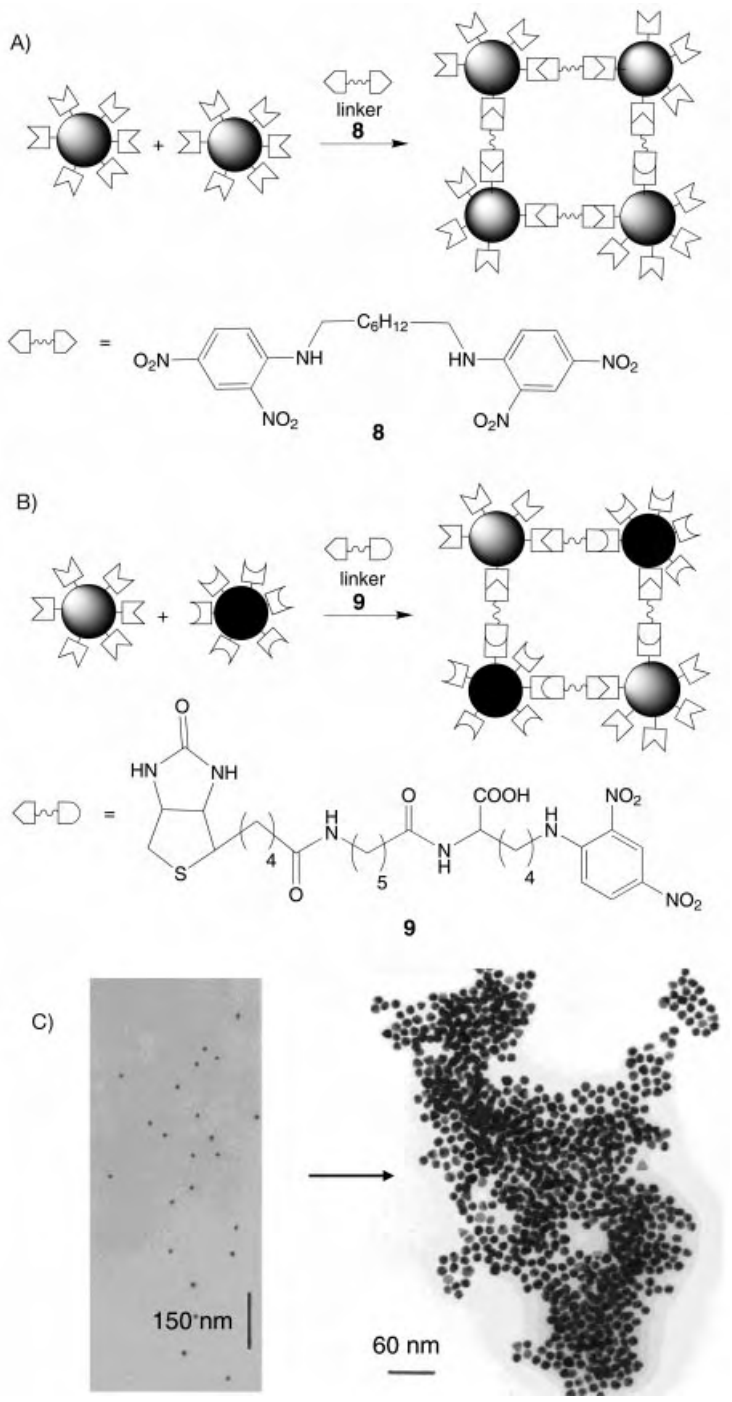


Figure 6. Cross-linking of Ag and Au nanoparticles functionalized with IgG molecules. Bivalent linkers with two terminal hapten groups, either monospecific **8** or bispecific **9**, allow the directed assembly of homo-oligomeric (A) or heterodimeric (B) aggregates, respectively. The TEM images (C) were obtained from colloidal Au/antibody aggregates before (left) and after (right) the addition of linker **8**. (Reproduced, with permission, from ref. [34].)

and shape of the assemblies measured. Thus the pair–distance distribution function (PDDF), which describes the number of pairs of scattering centers as a function of their separation, can be calculated. SAXS of nonaggregated samples showed a single maximum in the PDDF which is indicative of dispersed particles. In the case of STV-coupled nanoparticles, however, SAXS indicated the presence of trimers of 16-nm-diameter hard spheres (the gold colloids), separated by a minimum distance of 4 nm.[42]

In agreement with earlier studies,[51] the above findings suggest that the STV–biotin system is versatile for developing novel strategies for assembling nanoparticles in solution or on a substrate. The applicability of the STV–biotin system for generating supramolecular aggregates is enhanced by the availability of various biotin analogues[54, 55] and recombinant STV mutants.[56–61] A wide range of rate and equilibrium constants can be used to allow the fine-tuning of the dynamic and structural properties of colloidal hybrid materials. It was suggested that extensive use of protein-based assembly could lead to a "factory of the future", in which the nanoproduction of spatially defined aggregates takes place by means of the bottom-up assembly of nanoparticles, directed by multiple highly specific biomolecular recognition elements.[62] Such a scenario would dramatically benefit from the advances in modern biotechnology, providing us with the technical skills for tailoring novel protein components by means of directed evolution strategies. Recombinant DNA technology has already led to the development of high-affinity artificial linker systems, such as antibodies that are specific against digoxigenin and fluorescein haptens,[63, 64] or short peptides, such as the 9-mer FLAG-sequence.[65, 66] These coupling systems have proven their applicability in various diagnostic assays, and it seems likely that they are also convenient for generating inorganic nanoparticle networks.

The power of today's biotechnological methods was recently applied to generate de novo protein linker units that directly recognize distinct surfaces of semiconductor materials, thereby avoiding the necessity of previous chemical functionalization of the particles (Figure 5C). Belcher and co-workers used phage-display techniques to select 12-mer peptides with a binding specificity for distinct semiconductor surfaces.[67] Based on a combinatorial library of about 10^9 random 12-mer peptides, phage clones were selected for their specific binding capabilities to one of five different single-crystal semiconductors: GaAs(100), GaAs(111)A, GaAs(111)B, InP(100), and Si(100). These substrates were chosen to allow the systematic evaluation of peptide–substrate interactions. Specific peptide binding was found that is selective for the crystal composition (for example, binding to GaAs, but not to Si) and crystal face (for example, binding to GaAs(100), but not to GaAs(111)B). As shown in Figure 8, the clone G12-3 specifically binds to a GaAs pattern, but not to the SiO_2 regions on the same substrate. This clone was even capable of differentiating between two zinc-blend crystal structures, GaAs and AlAs, which have almost identical lattice constants of 5.66 Å and 5.65 Å, respectively. Binding occurred specifically to the GaAs substrate.

The basis for this selectivity, whether it is chemical, structural, or electronic, is still under investigation. The

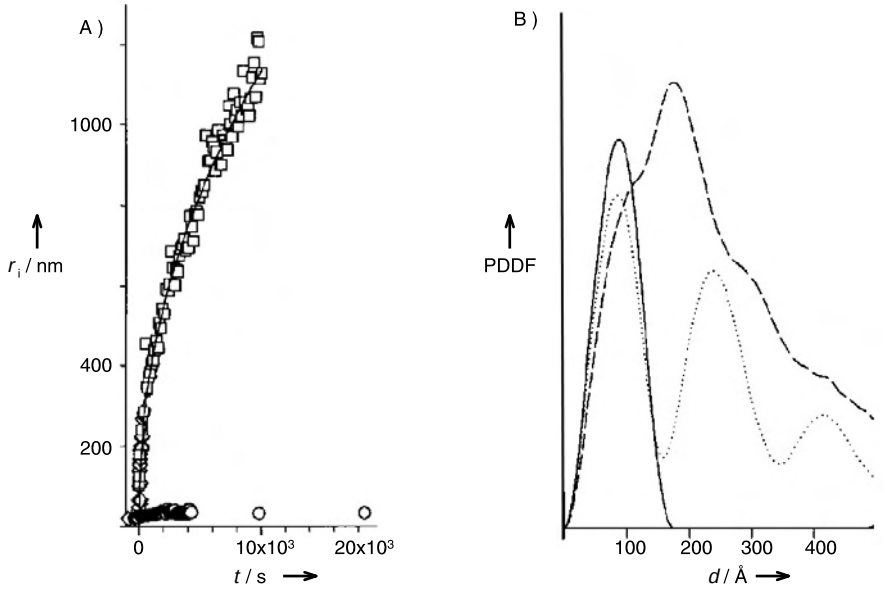


Figure 7. Characterization of streptavidin-mediated cross-linking of Au nanoparticles functionalized with disulfide **3**. A) DLS measurement to determine the average hydrodynamic radius (r_i) of all particles in solution. The rapid increase upon the addition of STV is indicative of the aggregation of particles modified with **3** (squares). The control reaction (circles) with unmodified nanoparticles confirms that the increase in r_i is a result of the proposed specific biotin–STV interactions. B) Small-angle X-ray scattering (SAXS) allows the solution structure of the networks to be probed. Shown are the pair–distance distribution functions (PDDF) under three different conditions. A single maximum is obtained for dispersed Au colloids (continuous line). For STV-induced aggregation (dotted line), the maxima correspond to 16-nm gold spheres separated by 4 nm (consistent with the diameter of STV), whereas for salt aggregation (dashed line) the maxima correspond to touching spheres (data reproduced, with permission, from ref. [42]).

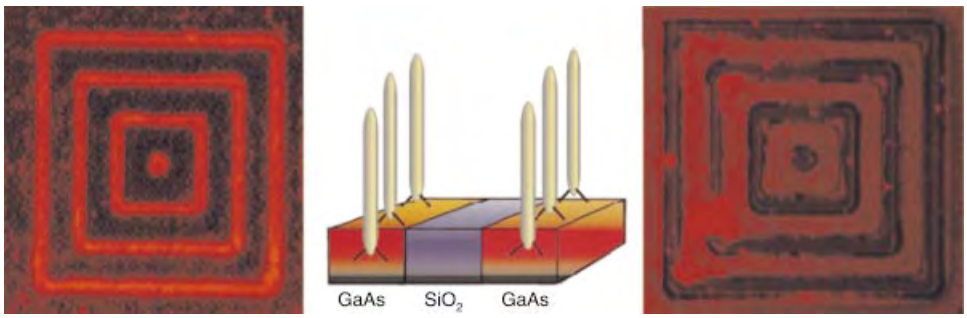


Figure 8. Recognition of an inorganic semiconductor surface by a bacteriophage, selected by phage display of a combinatorial pool of polypeptides. The diagram in the middle depicts the specific binding of the phage to the 1-μm lines of GaAs separated by 4-μm SiO_2 spacers. The phage binding was visualized with a fluorophor-labeled antibody, leading to fluorescent illumination of the GaAs lines (left). In the control experiment, no phage was present, but staining reactions were carried out (right) (adapted from ref. [67], with permission).

various substrates offer individual chemical reactivities and thus the phage selectivity is not particularly surprising. Even in the case of different GaAs surfaces, the composition of surface oxide layers is expected to be different, which in turn might also influence the peptide-surface interaction. However, the sequence analysis of various clones has revealed the presence of an average of about 40% polar functional groups and about 50% Lewis base functional groups. The statistical abundance of the latter is only 34%, which suggests that the interactions between peptide Lewis bases and Lewis acid sites on the substrates are important for specific recognition.[68] The evolved peptides may be applied to the generation of bispecific linker molecules with the ability to bind to two different semiconductor or metal surfaces (Figure 5C), thereby paving the way for novel bottom-up approaches for producing complex nanoparticle heterostructures.[67] Furthermore, this work also has implications for the understanding of the fundamental processes of biomineralization, in which protein components control the formation of materials by specifically interacting with growing crystallites (Section 5.4.2).

Mechanical hybrid elements comprised of nanostructured inorganic components and biomolecular devices were constructed from DNA[69] and recently from motor proteins.[70] The latter was produced from a recombinant F_1-ATPase motor protein, immobilized on 80-nm diameter Ni columns and coupled with a nanopropeller of approximately 1000 nm length. The ATPase molecule, which is capable of producing about 100 pN nm of rotary torque by the hydrolysis of ATP,[71] rotates the propeller with a velocity of about 5 rps.

3.2. DNA-Based Nanoparticle Aggregates

The use of biomolecules for developing nanotechnology devices was already envisioned by early researchers, who suggested the use of biological macromolecules as components of nanostructured systems.[72–74] DNA is particularly suitable to serve as a construction material in nanosciences.[75, 76] Despite its simplicity, the enormous specificity of the adenine–thymine (A–T) and guanine–cytosine (G–C) Watson–Crick hydrogen bonding allows the convenient programming of artificial DNA receptors. The power of DNA as a molecular tool is enhanced by our ability to synthesize virtually any DNA sequence by automated methods, and to amplify any DNA sequence from microscopic to macroscopic quantities by means of polymerase chain reaction (PCR). Another very attractive feature of DNA is the great mechanical rigidity of short double helices, so that they behave effectively as a rigid rod spacer between two tethered functional molecular components on both ends. Moreover, DNA displays a relatively high physicochemical stability. Finally, nature provides a complete toolbox of highly specific biomolecular reagents, such as endonucleases, ligases, and

other DNA-modifying enzymes, which allow for the processing of DNA material with atomic precision and accuracy on the Ångström level. No other (polymeric) material offers these advantages, which are ideal for molecular constructions in the range of about 5 nm up to a few micrometers. The following section (3.2.1) will focus on the use of DNA as a construction material for the production of nanoparticle assemblies.

3.2.1. DNA-Directed Oligomerization of Nanoparticles

Mirkin and co-workers have used DNA hybridization to generate repetitive nanocluster materials (Figure 9). Following the generalized scheme in Figure 5B, two noncomplementary oligonucleotides were coupled in separate reactions

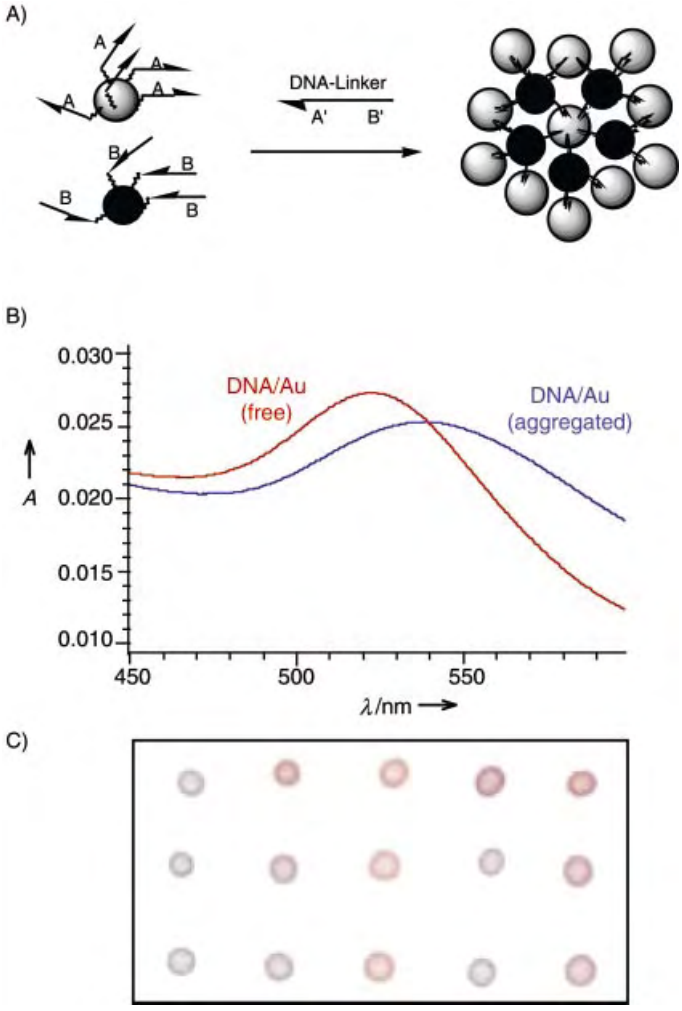


Figure 9. Assembly of gold colloids by using DNA hybridization. A) Two batches of gold particles are derivatized with noncomplementary oligonucleotides, either through 5′- or 3′-thiol groups. The nanoparticles are oligomerized by using a single-stranded nucleic acid linker molecule. Network formation leads to a characteristic change in the plasmon absorption (B). The color change can be used to macroscopically detect DNA hybridization by using an assay in which DNA/Au conjugates and a sample with potential target DNA is spotted on a hydrophobic membrane (C). Red spots indicate the absence of fully matched DNA, whereas blue spots are indicative of complementary target DNA. (Data in C are reproduced, with permission, from ref. [89]. Copyright 1999 American Chemical Society.)

with 13-nm gold particles by means of thiol adsorption.[77] A DNA duplex molecule that contains a double stranded region and two cohesive single-stranded ends, which are complementary to the particle-bound DNA, was used as a linker. The addition of the linker duplex to a mixture of the two oligonucleotide-modified colloids led to the aggregation and slow precipitation of a macroscopic DNA-colloid material. The reversibility of this process was demonstrated by the temperature-dependent changes of the UV/VIS spectroscopic properties. Since the colloids contained multiple DNA molecules, the oligomerized aggregates were well-ordered and three-dimensionally linked, as deduced from the TEM analysis. Images of two-dimensional, single-layer aggregates revealed close-packed assemblies of the colloids with uniform particle separations of about 6 nm, which corresponds to the length of the DNA linker duplex.[77]

More recent work by the Mirkin group concerns the generation of binary networks. For example, two types of gold clusters of either 40- or 5-nm diameter were modified with individual 12-mer oligonucleotides, and were assembled by using a complementary 24-mer oligonucleotide linker.[78] As a result of the specificity of Watson–Crick base-pairing, only heterodimeric A–B composites with alternating particle sizes are formed (Figure 9). In the case of an excess of one particle, satellite-like aggregate structures were generated and characterized by means of TEM. In a similar approach, oligonucleotide-functionalized CdSe/ZnS quantum dots and gold nanoparticles were incorporated into binary nanoparticle networks.[79] TEM analysis revealed that the hybrid metal/semiconductor assemblies adopted the expected A–B-structure, and fluorescence and electronic absorption spectroscopy indicated cooperative optical and electronic phenomena within the network materials. The oligomerization of DNA-coated gold nanoparticles depicted in Figure 9 can also be mediated by conjugates comprised of oligonucleotides and the STV protein. Interestingly, the thermodynamically most stable oligomeric networks are only formed upon heating the kinetically controlled adducts produced initially.[80]

Further studies of DNA-linked gold nanoparticle assemblies concerned the influence of the DNA spacer length on the optical[81] and electrical[82] properties of the networks. The experiments provided evidence that the linker length kinetically controls the size of the aggregates, and that the optical properties of the nanoparticle assemblies are governed by the size of the aggregate.[81] In contrast, it was found that the electrical properties of dried DNA–nanoparticle aggregates are not influenced by the length of the linker. Although SAXS clearly indicated that distances between particles in solution are related to the length of the linker, the networks collapse upon drying, thereby forming bulk materials comprised of nanoparticles covered with an insulating film of DNA. These materials show semiconductor properties that are not influenced by the linker lengths.[82]

Despite these advances, very little is known about the manipulation and tailoring of such nanoparticle networks, for instance, on ways to influence the structure and topography of the DNA hybrid materials subsequent to their formation by self-assembly. Within the context of fundamental studies on DNA-linked nanoparticle networks, the oligomeric aggre-

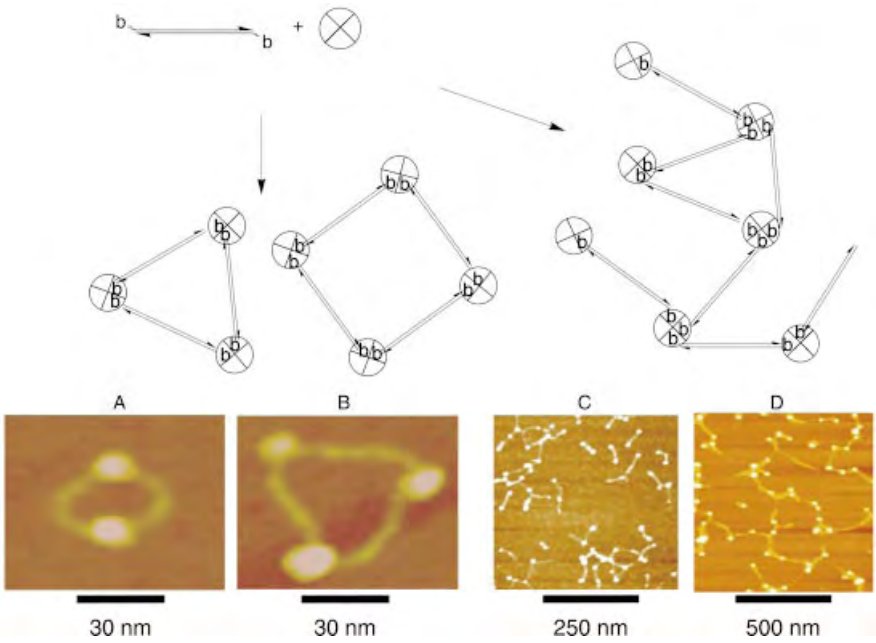


Figure 10. Synthesis of nanoparticle networks by using dsDNA as spacer groups. The dsDNA fragments contain two binding sites (b) attached to the two 5′-ends of the dsDNA. The binding sites are either biotinyl groups that allow cross-linking of the biotin-binding protein streptavidin as a model nanoparticle (A – C), or thiol groups that allow the connection of 5-nm gold colloids (D). Adapted in part from reference [86], with permission.

gates generated from bioorganic streptavidin (STV) particles and bisbiotinylated dsDNA are suitable model systems to gain insight into the properties of complex particle networks (Figure 10). The STV functions as a 5-nm model particle that can undergo a limited number of interconnections to other particles within the network. Either one, two, three, or four biotinylated DNA fragments can be conjugated with STV by means of the high-affinity STV – biotin interaction. This simplifies the complexity of the supramolecular particle networks, and thus allows the convenient analysis of effects that occur from variations, for example, in the immobilization parameters. Furthermore, the size of the dsDNA linker fragments, which are typically about 30 to 170 nm in length, allow convenient direct observation by means of scanning force microscopy (SFM; Figure 10).[83–86] These findings are convenient for both disciplines involved: the use of SFM allows insight into biomolecular structure and assembly dynamics; in turn, the well-defined and clearly distinguishable DNA – STV nanostructures can be used as calibration standards for soft materials in the detailed study of tip-convolution effects and of the influence of measuring parameters in SFM analyses.[87, 88]

3.2.2. Individual Nanoscaled Particle Assemblies

The work of Mirkin and co-workers described above leads to novel hybrid materials with promising electronic and optical properties, potentially useful for applications in materials science,[24, 89, 90] and the results also have a tremendous impact on immediate diagnostic applications, in particular, DNA microarray-based nucleic acid analyses (Section 5.2.2). As a result of the enormous potential of these novel compounds, it is partiuclarly important to overcome limitations which may result from the lack of stoichiometric control during the assembly process. To control the architecture of nanomaterials, spatially defined arrangements of molecular devices are required. For example, to organize metal and semiconductor nanocrystals into ultra-small electronic devices one may consider a linear aggregate of several individual components (Figure 11 A). Similarly, as initially demonstrated for proteins,[91] gold nanoclusters that contain a single nucleic acid moiety,[45, 92] have been rationally assembled into stoichiometrically defined nanoscale aggregates (Figure 11 B).

To control the stoichiometry and architecture of nanomaterials, Alivisatos and co-workers synthesized well-defined monoadducts from commercially available 1.4-nm gold clusters that contain a single reactive maleimido group and thiolated 18-mer oligonucleotides.[45, 92] Subsequent to purification, these conjugates allowed the rational construction of well-defined nanocrystalline molecules by means of DNA-directed assembly with a single-stranded template that contains the complementary sequence stretches (Figure 11 B).

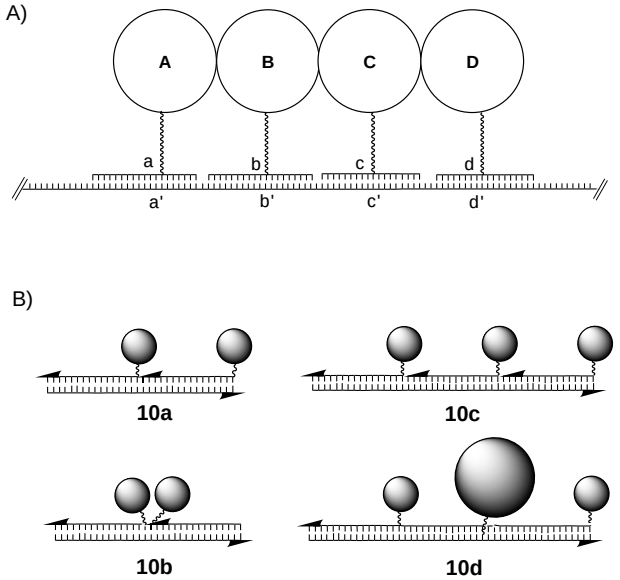


Figure 11. A) DNA-directed assembly of four different nanoscaled building blocks to form a stoichiometrically and spatially defined supramolecular aggregate. B) Self-assembly of nanocrystal molecules by means of DNA hybridization.[45] Conjugates from gold particles (shaded spheres) and 3′- or 5′-thiolated oligonucleotides allowed the formation of head-to-head (**10a**) or head-to-tail (**10b**) homodimers. A template that contains the complementary sequence in triplicate effects the formation of the trimer **10c**. The concept described by A) has also been used in the DNA-directed assembly of proteins,[91] β-galactosyl carbohydrates,[215] and organometallic compounds.[216]

Depending on the template, the DNA-nanocluster conjugates were assembled to generate the head-to-head (**10a**) and head-to-tail (**10b**) homodimeric target molecules in approximately 70% purity, as determined by TEM analysis. Consistent with model calculations, the center-to-center distances observed in the two isomers were about 3–10 nm and 2–6 nm in **10a** and **10b**, respectively. TEM images also confirmed the structure of trimeric molecules **10c**. More recently, multiple gold nanocrystal aggregates were generated by DNA-directed assembly.[92] The preparations, which contain up to three nanoclusters of different sizes organized in several ways, were then purified by electrophoresis. TEM characterization indicated that the nanocrystal molecules have a high flexibility when the DNA backbone is nicked (e.g. **10c**), whereas an unnicked double helix (e.g. **10d**) significantly lowers the flexibility. UV/VIS absorbance measurements indicated changes in the spectral properties of the nanoparticles as a consequence of the supramolecular organization.[92]

The concept of using DNA as a framework for the precise spatial arrangement of molecular components was carried out originally with the covalent conjugates of single-stranded DNA oligomers and STV protein.[91] The STV–DNA conjugates **11** were used as model systems for a variety of important fundamental studies on the DNA-directed assembly of macromolecules.[85] In addition to their model character, the covalent DNA–STV conjugates are also convenient as versatile molecular adapters in the nanoproduction of supramolecular assemblies. The covalently attached oligonucleotide moiety supplements the four native biotin-binding sites of STV with a specific recognition domain for a complementary nucleic acid sequence. This bispecificity allows the use of the DNA–STV conjugates as adapters for the assembly of basically any biotinylated compound along a nucleic acid template.[85] As an example, the strong biotin–STV interaction and the specific hybridization capabilities of the DNA–STV conjugates **11** were used to organize gold nanoclusters (Figure 12).[51] In this work, 1.4-nm gold clusters that contain a single amino substituent were derivatized with a biotin group, and the biotin moiety was used subsequently to organize the nanoclusters into the tetrahedral superstructure, defined by the geometry of the biotin-binding sites of the STV. Subsequently, the nanocluster-loaded proteins self-assemble in the presence of a complementary single-stranded nucleic acid carrier molecule, thereby generating novel biometallic nanostructures such as **12** (Figure 12). Since the DNA–STV conjugates can be used as a molecular construction kit, this approach even allows the combined assembly of inorganic and biological components to produce functional biometallic aggregates such as **13**, which contain an immunoglobulin molecule (Figure 12). Aggregate **13** was produced from STV conjugates **11a**–**11e** as well as from conjugates of **11f** and biotinylated antibodies, which were previously coupled in separate reactions. The functionality of the antibody in this aggregate allows the targeting of the biometallic nanostructures to specific tissues, substrates, or other surfaces. This approach impressively demonstrates the applicability of protein–ligand interaction and DNA hybridization for the nanoconstruction of novel inorganic/bioorganic hybrid systems.[51]

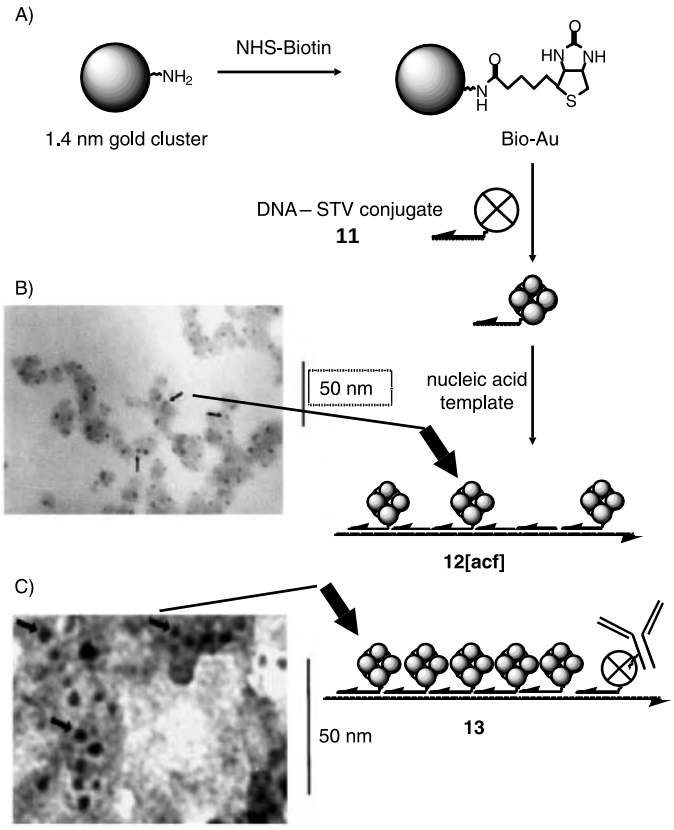


Figure 12. A) DNA-directed assembly of biotinylated gold (Bio–Au) nanoclusters with DNA–STV conjugates **11** as molecular adapters. Specific nucleic acid hybridization leads to biometallic aggregates **12**. TEM images of B) the biometallic aggregate **12[acf]** (the letters in brackets indicate the protein components bound to the carrier) and C) an antibody-containing biometallic construct **13**. Data from reference [51], with permission.

3.3. Biomimetic Systems

Analogously to the biomolecule-based oligomerization of nanoparticles (Figure 5), reversible abiotic recognition systems have been applied to the supramolecular organization of nanoparticles. For example, Fitzmaurice and co-workers have reported the heterosupramolecular generation of novel inorganic materials.[93] Semiconducting titanium dioxide particles (22 nm) were stabilized with a modified pyridine substituent, which can specifically recognize a uracil derivative that is covalently linked with the electron-acceptor viologen. Hydrogen bonding of the uracil–viologen conjugate to the nanoparticles led to the formation of a heterosupramolecular inorganic–organic hybrid. Band–gap excitation of the self-assembled donor–acceptor system induces electron transfer from the donor (TiO_2 nanocrystallite) to the acceptor (viologen).[93] More recently, gold[94] and silver[95] nanoparticles, stabilized with a monolayer comprised of ω-undecylthiol and an alkane thiol **14** that contains a dibenzo-18[crown]-8 moiety, were aggregated by pseudorotaxane assembly. Bis(dibenzylammonium) cations **15** were used as linker units (Figure 13). As indicated from NMR spectroscopic and DLS measurements, the extent of nanocrystal aggregation can be controlled by the relative amount of linker

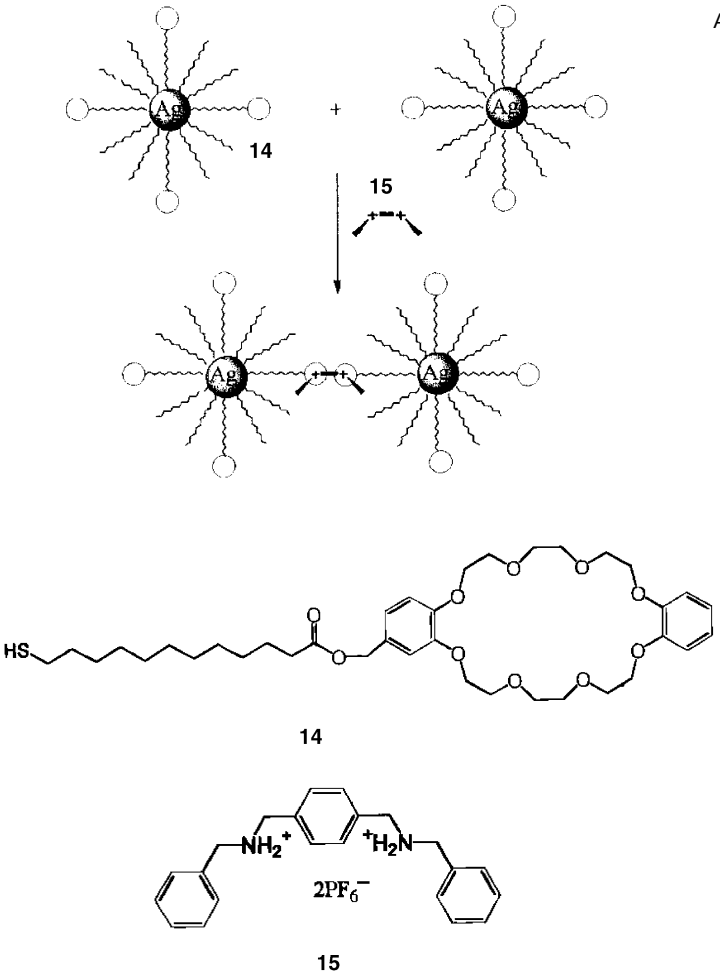


Figure 13. Silver nanocrystals stabilized with a monolayer of an alkyl thiol and **14**, aggregated through pseudorotaxane formation in the presence of bis-dibenzylammonium cations **15** as linker units. Reproduced in part from ref. [95], with permission. Copyright 2000 American Chemical Society.

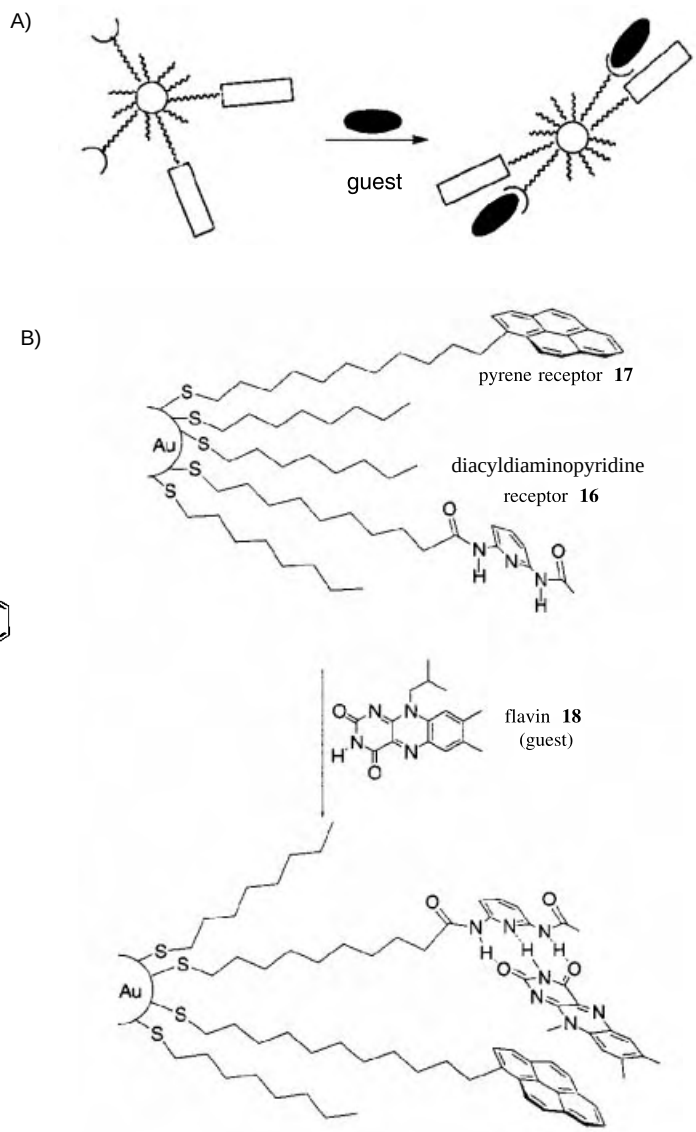


Figure 14. Supramolecular template formation of a polyvalent binding site on SAM-stabilized gold colloids that contain the receptor groups **16** and **17**. Adapted from ref. [96d], with permission. Copyright 2000 American Chemical Society.

15, or by the addition of inhibitors such as free dibenzo-18[crown]-8.[95]

In general, the above self-assembled monolayer (SAM) functionalized gold colloids (SAM-colloids)[96] provide a versatile platform for the production of multivalent receptors. In these systems, the number of functional ligands can be controlled during particle formation or displacement reactions,[96b] and the mobility of thiol ligands on the surface of the gold colloids can be utilized to create environmentally responsive systems.[96d] To this end, gold nanoparticles were coated with a mercaptooctanol SAM that contained two receptor groups: diacyldiaminopyridine **16** and pyrene **17** (Figure 14). The exposure of flavin **18** to the doubly functionalized colloids induced a guest-templated surface rearrangement of the two receptor groups, thereby forming a self-optimized, bivalent binding site for the flavin. Although the imprinted formation of binding sites on two-dimensional planar gold surfaces has previously been reported,[97] the nanoparticle-based receptors open novel ways to generate diffusible probes for the recognition of biomolecular protein and cell surfaces.[96d] Moreover, this approach should be expandable to catalytically and optically active chemical groups,[98] as well as to SAM-bound biomolecules, such as enzymes, receptors, and antibodies,[99] thereby providing novel tools for immunoassays, biosensors, and model systems for the study of membrane diffusion processes.

4. Biotemplating

The electrostatic and topographic properties of biological macromolecules and their derived supramolecular complexes can be used for the synthesis and assembly of organic and inorganic components. In this biological templating approach, regular two-dimensional lattices of bacterial cell surface proteins, nano- and micrometer-sized nucleic acid components, as well as hollow biomolecular compartments such as virus particles, have already been exploited for the generation of nanoparticles and supramolecular architecture.

4.1. Bacterial Surface Layers

Crystalline cell surface layers, S-layers, are the most abundant structures in procaryotic organisms. S-layers consist of multiple copies of a single polypeptide, which spontaneously forms highly regular nanoporous superlattices of varying symmetry (Figure 15). As a result of their extraordinary

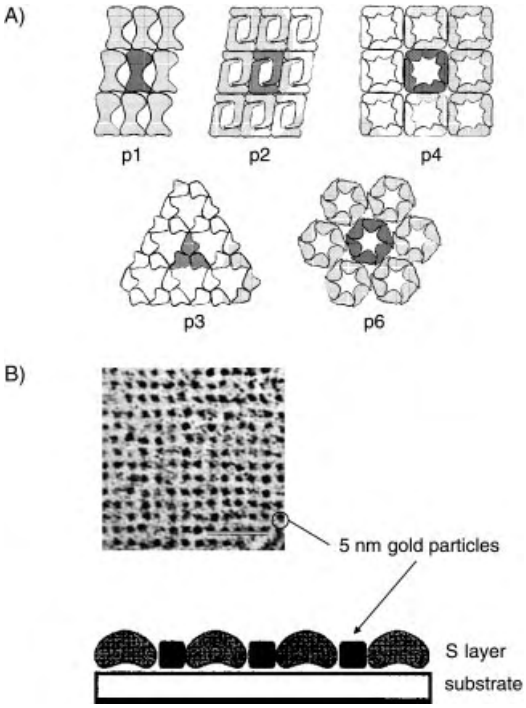


Figure 15. Bacterial surface layers (S layers). A) Different types of S layers with a diagonal (p1, p2), square (p4), or hexagonal (p3, p6) symmetry. B) TEM image of a gold superlattice prepared by using a square S layer lattice mounted on a substrate. Data from ref. [100], with permission.

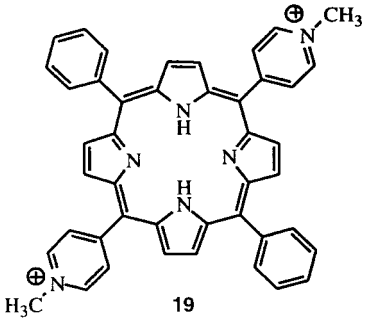
regularity, S-layers are unique systems to study structure, genetics, and dynamic self-assembly processes of biomolecular components. Furthermore, isolated native and chemically or genetically engineered S-layers offer a broad range of applications ranging from biotechnology, diagnostics, and vaccines to molecular nanotechnology.[100] The regular pores within the two-dimensional protein crystals of S-layers have been used as templates for the generation of nanoparticle arrays. Shenton et al. described the synthesis of CdS superlattices by using recrystallized S-layers from *Bacillus stearothermophilus* on electron microscope slides.[101] The immobilized S-layer was mineralized by incubation in a $CdCl_2$ solution, and subsequent treatment with H_2S. TEM analyses showed that the monodisperse 5-nm CdS nanocrystals grown were organized in a regular array, located within the nanopores of the protein matrix.

Dieluweit et al. produced a square superlattice of uniform 4–5 nm gold particles with a repeat distance of about 13 nm, by using an S-layer lattice of *Bacillus sphaericus* that was chemically modified to contain thiol groups within the individual protein building blocks.[102] For this purpose, a solution of tetrachloroauric(III) acid was used to generate a thin gold coating of the S-layer. Electron irradiation during TEM investigation of the samples led to the formation of the 5-nm gold particles (Figure 15). Mertig et al. prepared a highly oriented 2-nm platinum nanocluster array by means of biomolecular templating with an S-layer of *Sporosarcina ureae*.[103] In contrast to the above approaches, the cluster array was prepared in homogenous solution by treating a suspension of the S-layer with a solution of K_2PtCl_4 and subsequent reduction using NaN_3. As indicated by TEM analysis, the Pt clusters have clear metallic character, and the lateral p4-symmetric cluster arrangement is defined by the underlying protein crystal.[103]

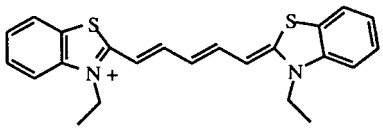
Recently, Hall et al. reported the precipitation of preformed gold colloids by using a hexagonally packed intermediate (HPI) S-layer of *D. radiourans*.[104] The HPI layer has a periodic structure of hexameric units and each forms a hollow cone-shaped protrusion with a positively charged cavity with a width of about 2 nm. Exposure of surface-mounted HPI layers to an aqueous solution of citrate-stabilized 5- and 10-nm gold colloids led to the formation of micrometer-sized arrays of regularly spaced nanoparticles, hexagonally organized with center-to-center spacings of about 18 nm, which are have the same pattern as the underlying S-layer lattice. In competition experiments with a 1:1 mixture of the 5- and 10-nm particles, the HPI layer exhibited exclusive binding of the 5-nm colloids. The binding of the 10-nm particles led to a preferential adsorption of particles with an average diameter of 8.0 ± 1.3 nm, which is significantly smaller than the mean particle diameter of 9.7 ± 2.2 nm. No long-range periodicity was observed for the adsorption of 20-nm particles or of positively charged 5-nm particles. These results demonstrate that the shape and electrostatic properties of a biotemplate can be used to control the spatial arrangement of micrometer-sized arrays of inorganic nanoparticles. Future developments of this approach are particularly promising since the engineering of only a single gene is required for tailoring the topographical and chemical properties of the S-layer.[105]

4.2. DNA-Templated Assembly

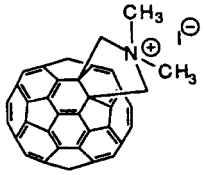
The electrostatic and topographic properties of the DNA molecule can also be used for the templated synthesis of supramolecular aggregates of inorganic and organic building blocks. An early example of this approach was reported by Gibbs et al.,[106] who demonstrated that porphyrin derivatives that contain cationic side chains (e.g. **19**), form long-range structures on a DNA template. These supramolecular porphyrin assemblies have the same helical sense as the nucleic acid template. Further studies gave more insight into the kinetic and thermodynamic properties of the DNA–porphyrin assemblies.[107, 108] The use of DNA as a nanotemplate for the spontaneous assembly of cationic cyanine dye **20** to form supramolecular aggregates was reported by Armitage and co-workers.[109, 110] Dye **20** dimerizes in the presence of dsDNA that contains alternating A/T residues. Strikingly, the dimer binding is highly cooperative. The binding of the first dimer greatly facilitates the binding of a second dimer, leading



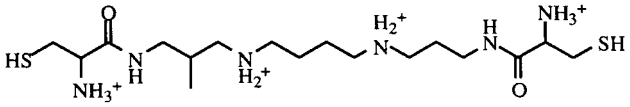
19



20



21



22

to the formation of an extended helical cyanine dye aggregate in the case of longer DNA templates. Thus, the DNA structure precisely controls the spatial dimensions of the supramolecular aggregate.

Tour and co-workers have used DNA to congregate macromolecular C_{60} fullerene molecules **21**, which were modified with an *N*,*N*-dimethylpyrrolidinium iodide substituent.[111] The electrostatic binding of **21** to the phosphate backbone of DNA could be directly imaged by TEM without the need for heavy metal shadowing or other staining techniques. TEM analysis of the DNA fullerene hybrid materials revealed that the complexation had significantly altered the structure of the DNA. In the case of circular plasmid DNA templates, it was found that the diameter of the hybrid complexes were condensed about fivefold, whereas the thickness of the double helix ranged between 15 and 30 nm, instead of 2 nm for native DNA. This condensation (shortening and thickening) of the dsDNA is probably a consequence of extensive hydrophobic interactions between the fullerene moieties attached to the DNA. Similar condensation effects are well know from polyamines, such as spermine and spermidine, which induce a significant packing of DNA structures. The dynamics of such DNA condensates at the solid–liquid interface have been studied recently by SFM.[112] The spermine-induced packing of DNA to generate calibrated bioorganic particles of nanometer-sized dimensions was reported by Blessing et al.[113] They used the polymerizable cation **22**, which can bind to the minor groove of B-DNA. The air-induced thiol/disulfide oligomerization of **22** in the presence of a plasmid DNA led to the physical collapse of the DNA, together with the formation of 50 ± 15 nm particles. Such nanometric monomolecular DNA particles are potentially useful for gene delivery.[114]

Pioneering work on the DNA-templated generation of metal and semiconductor nanoparticle arrays was carried out by Coffer and coworkers.[115–118] They used the negatively charged phosphate backbone of the DNA double helix to accumulate Cd^{2+} ions, which were subsequently treated with Na_2S to form CdS nanoparticles. For this, solutions of calf thymus DNA and Cd^{2+} ions were mixed, and subsequently, molar amounts of Na_2S initiated the formation of CdS nanoparticles. TEM analysis indicated that the particles were fairly monodisperse with an average diameter of about 5.6 nm.[115] Since the actual role of the DNA was vague from this study, later experiments investigated the potential influence of the sequence of the DNA template on the particle binding.[116] The adenine content of the DNA particularly affects the size of the nanoparticles, thereby providing indirect evidence for the suggested template mechanism. Subsequent studies concerned the synthesis of surface-bound mesoscopic nanoparticle aggregates.[117, 118] For this purpose, the 3455 base pair circular plasmid DNA pUCLeu4 was used as a template, forming a circle with a diameter of about 375 nm. The DNA was mixed with Cd^{2+} ions in solution, and subsequently, the Cd^{2+}-loaded DNA was adsorbed on an amino-modified glass substrate. CdS nanostructures were formed by treatment with H_2S.[117] TEM analysis revealed that CdS particles with a diameter of about 5 nm had developed, which were assembled close to the circular DNA backbone. A measurement of its circumference indicated the intactness of some of the DNA molecules. However, various other aggregates with irregular shapes were also observed.

In addition to its use as a nanotemplate, DNA can also be employed to produce micrometer-scaled elements, which are potentially useful in microelectronics. Braun et al. described an example in which a 16-μm λ-DNA molecule, which contained two cohesive ends, was used to bridge the ≈12–16 μm distance between two gold microelectrodes, prepared by standard photolithography (Figure 16).[119] Subsequent to the functionalization of the electrodes with individual capture oligonucleotides, the DNA fragment was allowed to hybridize. Successful interconnection of the electrodes was confirmed by optical microscopy of the fluorescent labeled λ-DNA. Next, the sodium ions bound to the phosphate backbone of the λ-DNA were exchanged with Ag^+ ions, and the latter were chemically reduced by hydroquinone. The small silver aggregates formed along the DNA backbone were then used as catalysts for further reductive deposition of silver, eventually leading to the formation of a silver nanowire. This micrometer-sized element with a typical width of 100 nm had a granular morphology, as determined by SFM (Figure 16). Two terminal electrical measurements of the Ag nanowire revealed non-linear, history-dependent $I-V$ curves, possibly a result of polarization or corrosion of the individual 30–50 nm Ag grains that comprised the wires.[119]

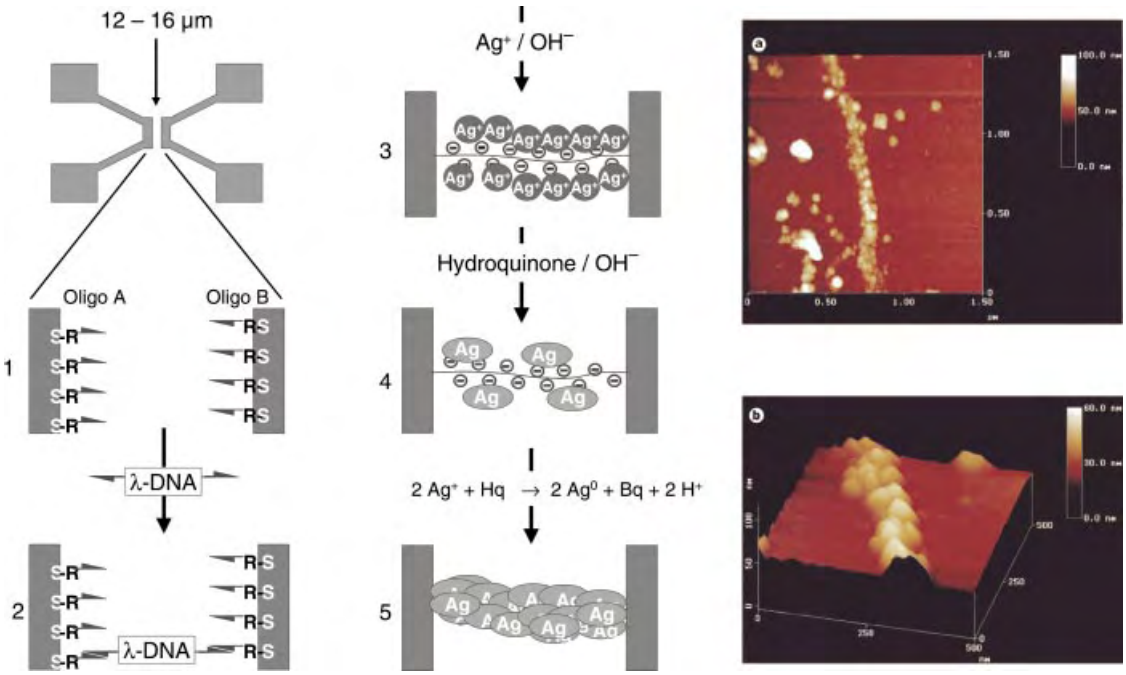


Figure 16. DNA-templated synthesis of a conducting silver wire. SFM images revealed the granular structure of the wire. Reproduced from ref. [119], with permission.

Richter et al. reported the use of λ-DNA for the templated growth of Pd clusters.[120] This was achieved by activation of the DNA with palladium acetate and subsequent reduction of the DNA-bound Pd ions with a sodium citrate/lactic acid/dimethylamine borane solution. This led to the formation of DNA-associated one- and two-dimensional arrays of well-separated 3–5 nm Pd clusters.[120] Subsequent work has focused on the preparation of highly conductive nanowires by using DNA templates[121] as well as on the mechanism of the initial nucleation of the metal clusters.[122] The DNA-templated production of mesoscale structures from preformed, positively charged 3-nm CdS particles with a thiocholine-modified surface was reported by Torimoto et al.[123] As a result of the electrostatic interaction between positively charged nanoparticle surfaces and the phosphate groups of DNA, the particles were found to be assembled into chains, as determined by TEM analysis. The CdS nanoparticles were arranged in a quasi-one-dimensional dense packing, which revealed interparticle distances of about 3.5 nm, correlating with the height of one helical turn of the DNA double strand.[123] The electrostatic assembly of lysine-stabilized gold particles on DNA was also reported.[124]

The examples described above give initial impressions of how DNA can be utilized as a template in the synthesis of nanometric and mesoscopic aggregates. However, the studies emphasize the importance of fundamental research on how the interaction between DNA and the various binders, such as metal and organic cations, influences the structure and topology of the nucleic acid components involved. Potential applications include the use of DNA strands[119] and networks[125] to prepare microelectronic devices, or the use of DNA circles[84, 126–130] to produce nanoscaled Aharonov–Bohm rings.[131]

4.3. Bio-Nanoreactors

Nature has developed a variety of protein components that function as carriers or storage devices for metal components. Of these systems, the iron-storage protein ferritin is probably the most intensively studied and best understood.[132] Ferritin consists of a central core of hydrated iron(III)oxide encapsulated with a multisubunit protein shell. During formation, the protein shell self-assembles in the first step to form a hollow cage of about 8 nm in diameter. As a consequence, subsequent inorganic mineralization leads to spatially confined nanoparticles of an antiferromagnetic iron oxide similar to the mineral ferrihydrite.[133] Because of the pores within the polypeptide shell, the mineral can be removed by reductive dissolution, leading to the formation of a demetallated protein, termed apoferritin.[134] It has long been known that apoferritin can be remineralized by chemical procedures,[135] and the reconstitution of the ferrihydrite core in ferritin has served to investigate the catalytic properties of the apoferritin with respect to iron(II) oxidation and nucleation of ferrihydrite within the protein compartment.[136]

In the early 1990's, Mann and co-workers began to explore the use of ferritin as a nanometer-sized bioreactor for producing metal particles other than the natural ferrihydrite (Figure 17). Horse spleen apoferritin was used as a nanometer-sized reaction vessel to generate manganese oxide and uranyl oxyhydroxide crystals.[137] As an example, nanoparticles were synthesized by basic hydrolytic polymerization of uranyl acetate, leading to the formation of uniform 6-nm uranyl oxyhydroxide particles within the spatially confined supramolecular protein cages. Later work concerned the production of magnetic proteins by reconstituting apoferritin with the ferrimagnetic minerals magnetite (Fe_3O_4)[138] and

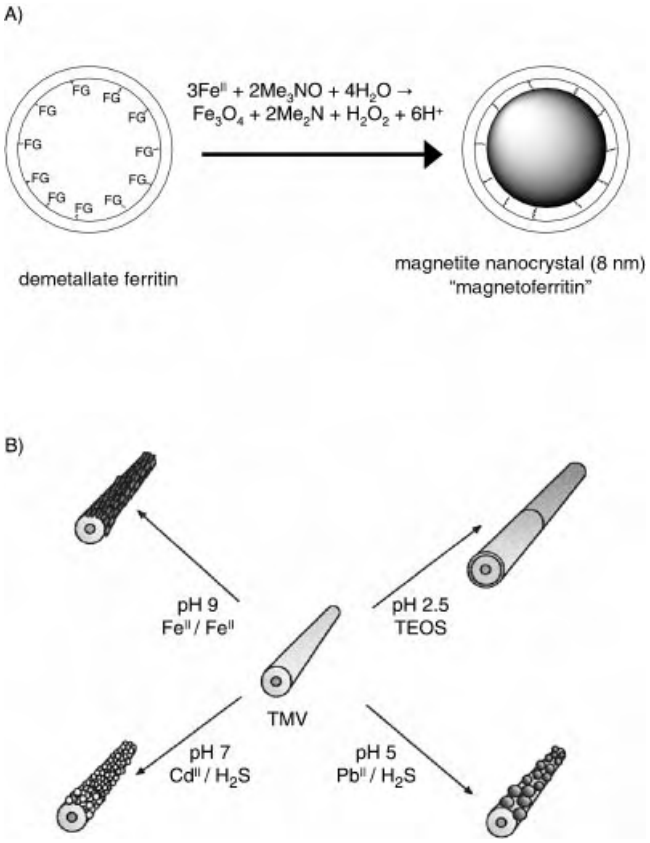


Figure 17. A) Hollow protein cages used as spatially confined bioreactors for the growth of inorganic nanoparticles (FG = functional group, which acts as a nucleation site for biomineralization). B) Synthesis of nanotube composites by using TMV templates. (TEOS = tetraethoxysilane). Reproduced from ref. [144], with permission.

magnetite/maghemite (Fe_3O_4/γ-Fe_2O_3).[139] As a result of the inner diameter of the nanoreactors, about 6–7 nm diameter crystaline inorganic particles were formed, as determined by TEM. The magnetite/maghemite particles were generated by oxidation of apoferritin with trimethylamino-*N*-oxide, which was loaded with various amounts of iron(II) ions. The magnetic properties were studied by using SQUID magnetometry, and an approximately linear dependence of the superparamagnetic blocking temperature on iron loading was found.[138] The monodisperse magnetic proteins might be utilized in biomedical imaging, cell labeling, and separation procedures (Section 5.3). Moreover, the coupling of biotin recognition groups to the ferritin allowed the assembly of the bioinorganic particles with streptavidin connectors (see Section 3.1) to form oligomerized superstructures.[140]

In a recent contribution, 15-nm lumazine synthase capsid particles, comprised 60 polypeptide subunits in the form of an ≈8-nm hollow cage, were used as a nanobioreactor to produce iron oxide nanoparticles.[141] Virus particles are another type of biological structure that can be applied as a template for biomineralization. Virus particles typically consist of several hundred to thousands of protein molecules that assemble in the form of a hollow compartment, which holds the viral nucleic acid. The self-assembly of the tobacco mosaic virus (TMV) is the most comprehensively understood system of biological self-assembly.[142, 143] TMV is a stable virion and can withstand temperatures of up to 60 °C and pH values between 2 and 10. It is made up of 2130 identical protein building blocks, arranged in a helical motif around the viral RNA to form a hollow tube of 300×18 nm in size with a central channel with a diameter of 4 nm. The internal and external surfaces of the supramolecular protein assembly consists of a repeated pattern of charged amino acid residues such as glutamate, aspartate, arginine, and lysine, which should offer a variety of nucleation sites for surface-controlled biomineralization. This assumption led Shenton et al. to use TMV particles as a template to generate inorganic–organic nanotube composites by means of template mineralization.[144] As indicated in Figure 17B, several routes were explored for the synthesis of nanotube composites that use TMV templates. The sol–gel condensation of TEOS led to the formation of electron-absorbing SiO_2 rods, which were identified as TMV particles covered with a uniform 3-nm silica shell. Coprecipitation of TMV and $CdCl_2$ or $Pb(NO_3)_2$ and H_2S led to the production of hybrid materials in which disordered aggregates of CdS (5 nm) or PbS (30 nm) nanoparticles, respectively, were adsorbed on the external surface of the TMV template. Similar CdS nanoparticles had previously been synthesized by using a ferritin nanoreactor.[145] The TMV particles were also subjected to iron oxide mineralization by adding NaOH to an acidic dispersion of iron(II)/iron(III) that contained the virions. This led to a poorly crystalline ferrihydrite deposition on the external surface of the protein template. In contrast, slow aerial oxidation of TMV in anaerobic iron(II) solution yielded virions covered with an even 2 nm thick iron oxide film.[144]

Spherical virus protein cages were used for the host–guest encapsulation of inorganic and organic materials. Douglas and Young used well-defined cowpea chlorotic mottle virus (CCMV) particles, obtained from in vitro assembly of purified viral-coat protein subunits (Figure 18).[146, 147] Each protein

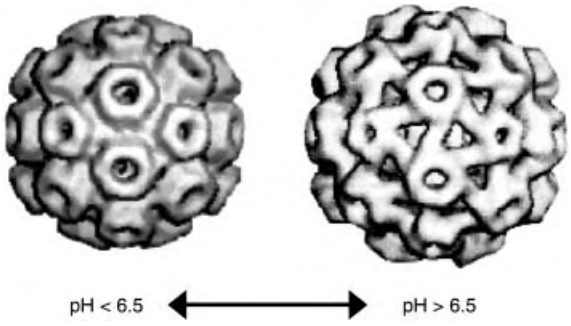


Figure 18. Cryoelectron microscopy and image reconstitution of the CCM virus. The structure in an unswollen condition at low pH values (left) and in a swollen condition at high pH values (right). Swelling results in the formation of 60 pores with a diameter of 2 nm. Reproduced from ref. [146], with permission.

building block has nine basic amino acid residues (arginine or lysine), which point into the interior of the ≈18-nm cavity. Thus, the positively charged inner compartment of the ≈28-nm diameter CCMV particles provides a suitable interface for inorganic crystal nucleation, such as the growth of polyoxometalate species, paratungstate and decavanadate.

For this purpose, a pH-dependent gating mechanism of the CCMV virions was used. At pH values greater than 6.5, CCMV particles swell up by about 10%. This leads to the formation of 60 separate 2-nm pores, which allow free molecule exchange between the cavity and the bulk medium. In contrast, no exchange of large molecules occurs at pH values lower than 6.5. Therefore, empty virions were incubated with inorganic molecular tungstate (WO_4^{2+}) at pH 6.5, concentrated and subsequently washed at pH 5, at which point the pores in the protein shell close and the tungstate ions oligomerize. The latter process is a crystallization that yields uniform 6.7-nm diameter nanocrystals. Besides the polyoxometalate species, organic polymer nanobeads have also been produced within the spatially constrained virions. The pH-dependent encapsulation of an anionic polymer (polyanetholsulfonic acid) was carried out at pH 7.5, and the subsequent lowering of the pH to 4.5 resulted in the formation of polymer-loaded virus particles of uniform size distribution, as determined by TEM analysis.[146]

The above examples demonstrate that biomolecular compartments are suitable in applications for the formation of nanophase materials as well as for supramolecular encapsulation strategies. It is safe to assume that future developments will focus on the generation of altered protein building blocks for the self-assembly of novel improved biological reaction compartments using today's powerful techniques of molecular biology. Based on the native proteins, rational or random mutagenesis will allow us to design recombinant proteins that have optimized recognition capabilities for the assembly of distinctively shaped superstructures and possess appropriate amino acid residues for the effective nucleation of organic and inorganic nanomaterials.

5. Applications

From a biotechnological point of view, the term application is strictly associated with commercial products that (at least potentially) address significant markets. With respect to this stringent definition, real applications of the bioinorganic hybrid materials described above are rare at the present time. However, the fusion of biotechnology with materials science has great potential for generating advanced materials, and in turn, today's advanced materials and devices, as well as modern physicochemical techniques can be applied to solve biological problems. Thus, bioanalytical applications are currently the most practical outcome of the interdisciplinary work. Biological sciences greatly benefit from the refinement of analytical techniques, originally developed for material and physicochemical sciences.

5.1. Physicochemical Techiques

The most prominent physical characterization method for biological systems is scanning force microscopy (SFM). SFM has become a tremendously useful tool to map biological surfaces with high spatial resolution. In particular, the application of functionalized tips enables biospecific chemical force microscopy.[148] Moreover, SFM allows biomolecules to be stretched, and thus brings novel insight into the exploration of nucleic acid conformation and protein folding.[149]

Surface plasmon resonance (SPR) spectroscopy is another advancing technique which contributes to the comprehensive understanding of biomolecular structure and dynamics.[150] The surface-sensitive optical technique of SPR imaging is used to characterize ultrathin organic and biopolymer films at metal interfaces in a spatially resolved manner, for example, at the boundary between a gold layer and a liquid phase. Because of its high surface sensitivity and its ability to measure in real time the interaction of unlabeled biological molecules with arrays of surface-bound species, SPR imaging has been successfully implemented in the characterization and monitoring of biomolecular interactions, such as heterogeneous antibody–antigen binding at surfaces, and the study of solid-phase DNA hybridization.

The extensive studies of interfacial processes between biomolecules and metal surfaces have also led to the refinement of distinguished spectroscopic methods, in particular, surface-enhanced Raman scattering (SERS). In SERS, molecules adsorbed on roughened gold or silver surfaces exhibit vibrational spectral intensities that are enhanced up to 100000-fold.[151] Since the SERS method only detects principally the first monolayer adsorbed on the enhancing substrate, this technique allows the elucidation of specific interactions that occur between solid substrates and adsorbed biomolecules. For example, citrate-reduced silver colloids demonstrate excellent SERS enhancements and good biocompatibility. Thus, this substrate has been used for detailed studies of adsorbed proteins, which indicated that several enzymes such as chlorocatechol dioxygenase,[36] cytochrome c (Cc),[37] and several cytochromes P450,[38] retain their activity while adsorbed on this type of metal surface. However, since colloidal Ag preparations are often obtained as a heterogeneous population of different particle sizes and shapes, this leads to poorly reproducible optical properties and protein aggregation characteristics. On the other hand, although methods for preparing monodisperse protein-coated gold nanoparticles are well developed,[152] Au colloids unfortunately reveal significantly lower SERS enhancement factors with visible excitation, and thus SERS intensities of biomolecule/Au colloid conjugates are relatively weak.

Natan and co-workers reported a solution to this problem: the small heme-containing redox enzyme Cc can be used as a model system which adsorbs to citrate-stabilized gold surfaces in an oriented fashion through its lysine-rich heme pocket.[35] Au nanoparticles with a diameter of 12 nm were coated with Cc, and the resulting conjugates were used to deliver the protein to colloidal Ag for SERS measurements (Figure 19). SERS spectra of the Ag/Cc/Au sandwich aggregates indicated that the protein retains its native conformation. The advantage of this approach is that the Ag/Cc/Au sandwich can be made at the well-defined concentration of the Au carrier particles, and the SERS measurement can be made at another concentration of the Ag colloids (which may be less defined). Moreover, this approach allows one to overcome the normal dependence of SERS intensity on increasing distance from the Ag substrate by positioning the analyte between two metal

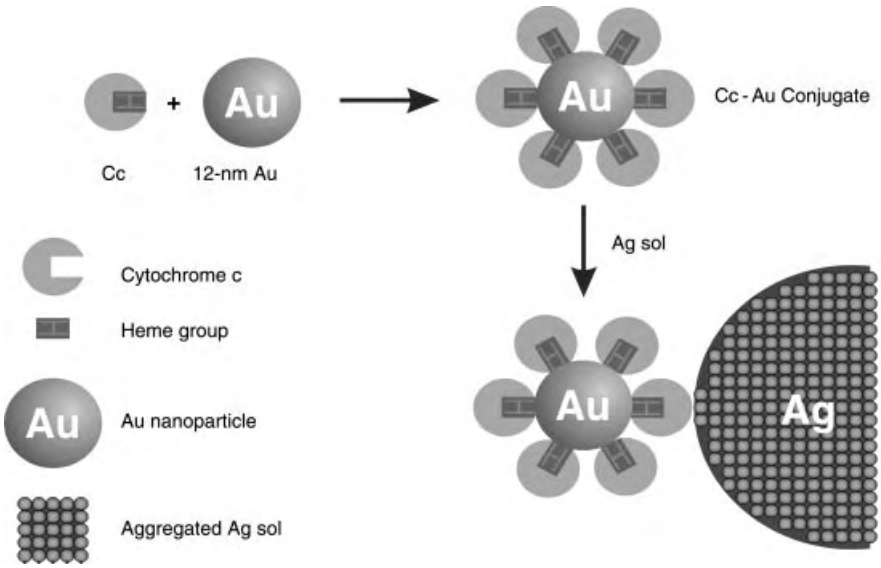


Figure 19. Formation of a metal–Cytochrom c (Cc) metal sandwich for SERS. The heme-containing redox enzyme Cc adsorbs to citrate-stabilized gold particles in an oriented fashion through its lysine-rich heme pocket. The resulting conjugates are used to deliver the protein to colloidal Ag for SERS measurement. Adapted from ref. [35].

surfaces.[35] It was observed that the metal/protein/metal sandwich conjugates revealed significantly higher electromagnetic fields between the particles.[153] The strong interparticle electromagnetic coupling was deduced from the wavelength-dependent SERS enhancement ratios, and the presence of wavelength-shifted single-particle surface-plasmon bands. Thus, such studies are important for experimental verification of theoretically predicted electromagnetic effects between closely spaced metal nanoparticles.[153] In addition to basic studies, the SERS technique also has the potential for the development of analytical methods, for example, as a structure-specific detection method for capillary electrophoresis,[154] or for quantifying dsDNA in bioanalytical assays.[155]

5.2. Nanoparticles as Biolabels

5.2.1. Protein-Coated Particles

Gold nanoparticles that are functionalized with proteins have long been used tools in the biosciences.[156] For instance, antibody molecules adsorbed on colloidal gold (10–40 nm) are routinely used in histology, thus allowing the biospecific labeling of distinguished regions of tissue samples and subsequent TEM analysis. More advanced small gold clusters with a diameter of 0.8 or 1.4 nm can be used for the site-specific labeling of biological macromolecules (Figure 4).[43, 157, 158] These labels have a number of advantages over colloidal probes, including better resolution, stability, and uniformity. Moreover, their small size improves the penetration and more quantitative labeling of antigenic sites. The 1.4-nm particles are the smallest gold clusters that can be seen directly under a conventional electron microscope, allowing a spatial resolution of about 7 nm when covalently attached to antibody fragments. The visibility of the clusters can be improved by a wet-chemical silver enhancement step for use in electron or light microscopy for histological purposes, or to detect picogram amounts of antigens in immunoblots.[159]

The silver enhancement can also be applied for the electrical sensing of biological binding events, for instance, through the short circuiting of microelectrodes (Figure 20). Gold nanoparticles are immobilized in the gaps of microelectrodes through biospecific interactions such as immunosorption of antibodies.[160] The colloids serve as catalytic cores for the reductive deposition of a conducting layer of silver, which short circuits the two electrodes. The resulting decrease in ohmic resistance is used as a positive signal for the sensing of the biospecific interaction to be detected. Other approaches used electrode-immobilized layers of gold colloids for the adsorption of the redox enzyme horse-radish peroxidase to prepare biosensors for the electrocatalytic detection of hydrogen peroxide.[161–163] Gold nanoparticles can also be applied to enhance detection limits in SPR-based real-time biospecific interaction analysis (Figure 21).[164, 165] The dramatic enhancement of SPR biosensing with colloidal Au was initially observed in a sandwich immunoassay in which Au nanoparticles were coupled to a secondary antibody. The latter was used to detect a primary antibody bound through specific immunosorption to the antigen immobilized on the gold sensor surface. The immunosorptive binding of the colloidal gold to the sensor surface led to a large shift in plasmon angle, a broadened plasmon resonance, and an increase in minimum reflectance, thereby allowing picomolar detection of the antigen.[164] Similarly, an improvement in sensitivity by about 1000-fold was obtained in nucleic acid hybridization analysis, when a colloidal gold/oligonucleotide conjugate was used as a probe (Figure 21).[165] These results suggest that the detection limit of SPR[150] now begins to approach that of traditional fluorescence-based DNA hybridization detection.

The use of colloidal silver plasmon-resonant particles (PRPs) as optical reporters in biological assays has recently been described.[166] PRPs can readily be observed individually with a microscope configured for dark-field microscopy, with standard white-light illumination. The use of PRPs, whose surfaces are coated with bioactive ligands, was illustrated in a model sandwich immunoassay for goat anti-biotin antibody. Because PRP labels are nonbleaching and bright enough to be identified and counted rapidly, they might soon be applicable in ultrasensitive assay formats based on single-target molecule detection.[166]

Semiconductor nanoparticles are also powerful fluorescent probes, which can be used for the labeling of biological components.[17, 18, 32, 167] The quantum dots have several advantages over conventional fluorescent dyes. Their fluorescence

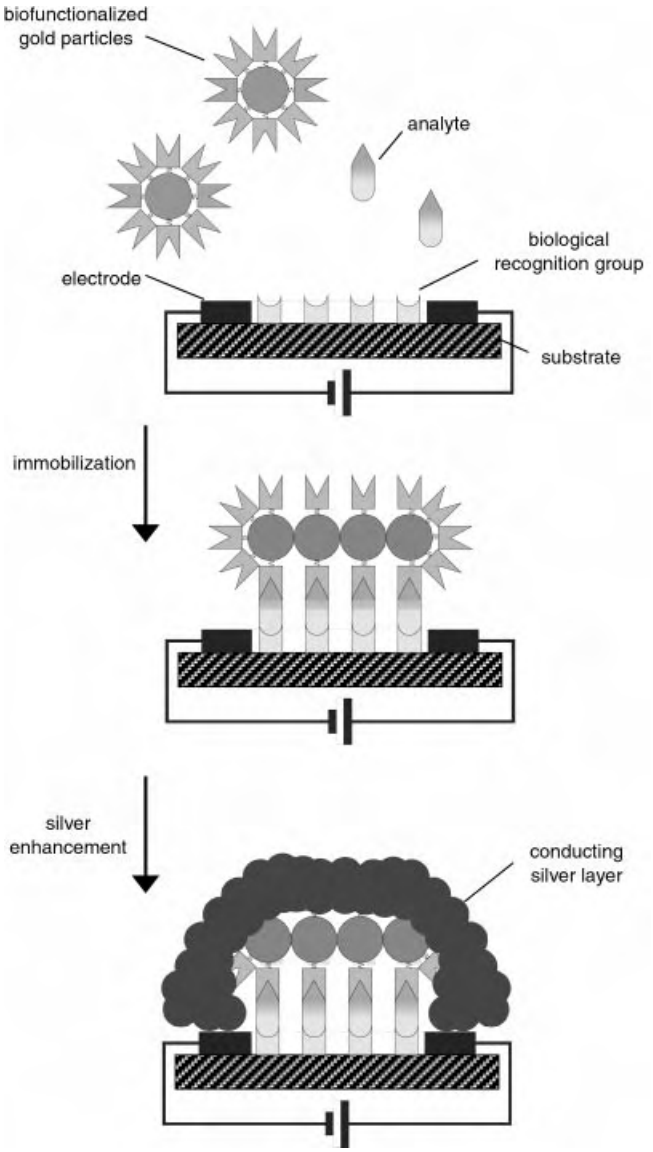


Figure 20. Electrical detection of biorecognition processes. Receptor groups such as antibodies or DNA oligomers are immobilized in the gap between two microelectrodes and used as a capture agent to bind complementary target molecules specifically. In a sandwich-type assay, the captured analyte is tagged with colloidal gold by a second biological recognition unit. Subsequent reductive deposition of silver leads to the formation of a conducting metal layer which short-circuits the two electrodes.

absorption and emission are conveniently tunable by their size and material composition, and the emission peaks have a narrow spectral linewidth (Figure 22). Typically, emission widths are 20–30 nm (full-width at half-maximum, FWHM), which is only one third of the emission linewidth of a conventional organic dye. The high quantum yields often range from 35–50% for core (CdSe)–shell (ZnS) nanoparticles. Moreover, quantum dots are about 100 times as stable against photobleaching as organic dyes, and they often reveal a long fluorescence lifetime of several hundred nanoseconds. This allows time-delayed fluorescence measurements, which can be used to suppress the autofluorescence of biological matrices.[168]

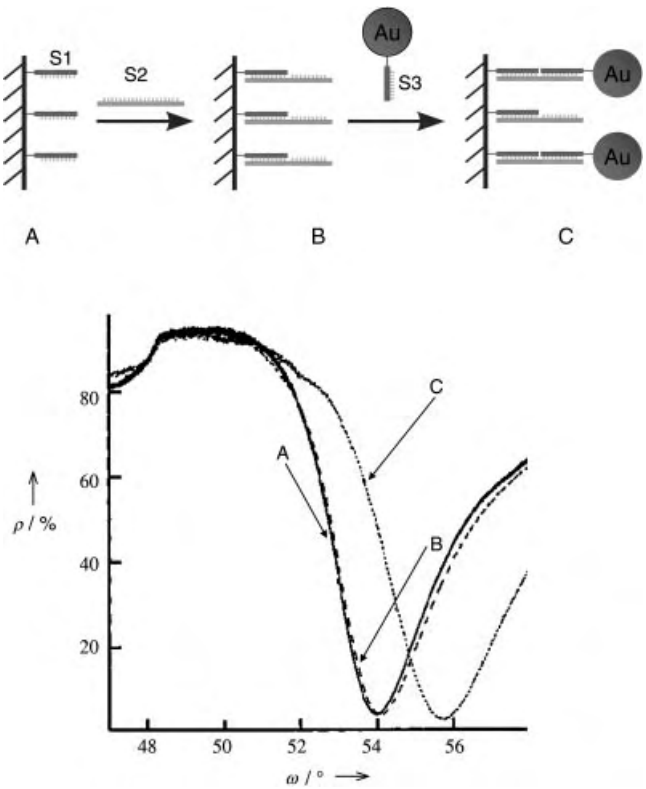


Figure 21. Sensing of DNA hybridization by means of SPR. A gold sensorchip functionalized with capture oligonucleotides S1 (A), is used to bind complementary target DNA S2 specifically (B). Introduction of a colloidal gold–oligonucleotide conjugate S3 allows the detection of the surface-immobilized complementary target (C). The corresponding SPR curves (reflectance ρ as a function of the SPR angle ω) show the large increase in ω in the transition from B to C, compared to that from A to B. Data from ref. [165], with permission. Copyright 2000 American Chemical Society.

Bruchez, Jr. et al. used core (CdSe)–shell (CdS) nanoparticles that were coated with an additional layer of silica for biolabeling.[17] The silica layer makes the nanoparticles water soluble and also allows covalent coupling of functional groups by means of organosilane chemistry. To demonstrate this principle, mouse fibroblast cells were labeled with two different sizes of nanocrystals. Green, 2-nm particles that were coated with methoxysilylpropyl urea and acetate groups were found to bind specifically to the cell nucleus by electrostatic interactions. Red, 4-nm biotinylated nanocrystals were used to label F-actin filaments, owing to the biotin–STV interaction. The surface of the nanocrystal was covalently modified with biotin groups, and the biotinylated nanoparticles were used for the specific staining of the actin filaments, previously labeled with phalloidin—biotin conjugate and STV. The dual labeled fibroblast were imaged with a conventional wide-field confocal fluorescence microscope, using a mercury lamp as a light source with a fluorescein isothiocyanate excitation filter and a single long-pass detection filter. Despite this simple setup, both colors were clearly visible simultaneously, and the green and red labels could be distinguished with the naked eye (Figure 22).[17]

Chan et al. used 4.2-nm ZnS-protected CdSe quantum dots, stabilized with a layer of mercaptoacetic acid.[18] The latter

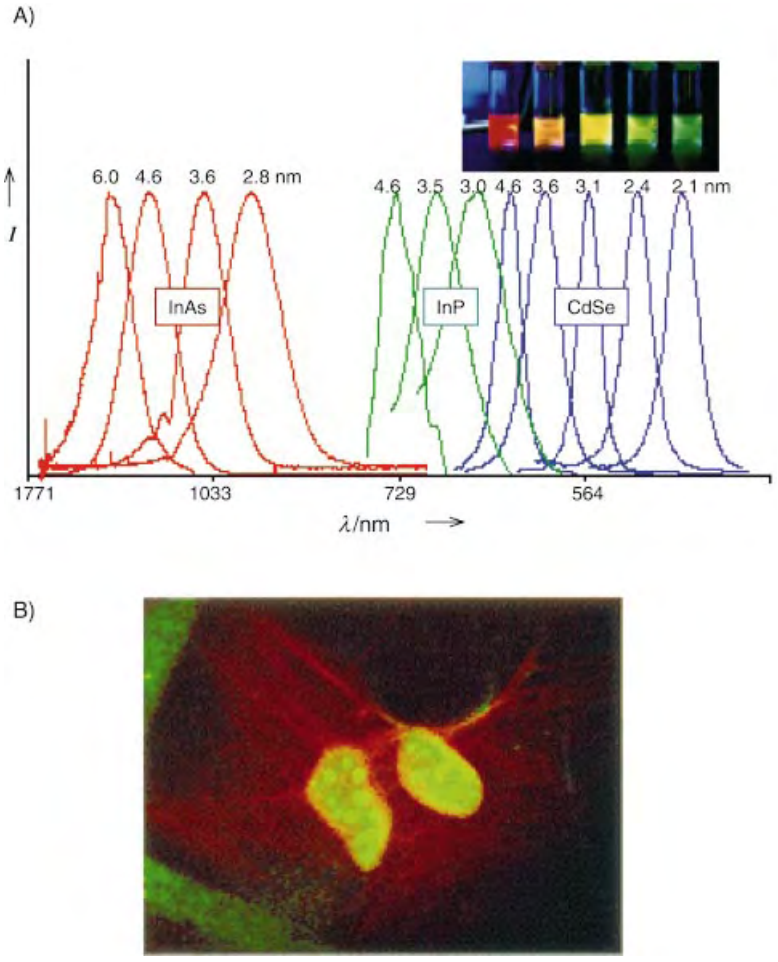


Figure 22. A) Fluorescence emission spectra of semiconductor quantum dots; B) cross-section through dual-labeled mouse fibroblasts. The actin fibers are stained red. The nonspecific labeling of the nuclear membrane by both the red and the green probes results in a yellow color. Reproduced from ref. [17], with permission. Copyright 1998 American Association for the Advancement of Science.

improved the water solubility of the nanoparticles, and the carboxy groups also allowed the covalent coupling to various biomolecules by cross-linking to reactive amino groups. The quantum dots were coupled with transferrin, a protein that induces receptor-mediated endocytosis.[169] A HeLa cell culture was incubated with the resulting nanoparticle–protein conjugates, and confocal microscopy revealed that the conjugates were transported into the cell. (HeLa cells are epithelial cells; they were isolated from a cervix carcinoma of a patient, *He*nrietta *La*cks, and were the first human cells from which a permanent cell culture was established.) In another example, the suitability of the nanocrystals for sensitive immunoassays was investigated. Conjugates with IgG molecules were prepared and subjected to immunoprecipitation by using a complementary antibody with a binding specificity for the particle-bound proteins. The extensive aggregation observed in this simple experiment clearly indicated that the attachment of nanocrystals does not harm the functionality of the biomolecule.[18] In a recent continuation of this work, micrometer-sized polymer particles were tagged with various quantum dots to achieve an optical "barcode" for biomolecules.[170]

Mattoussi et al. recently described a novel approach to the coupling of biomolecules with semiconductor quantum dots.[32] They prepared a recombinant protein linker that contained a basic leucine zipper motif, which induces a net positive charge, thereby allowing electrostatic binding to negatively charged semiconductor quantum dots (Figure 23). Functional proteins, such as bioactive enzymes or binding proteins can be attached to the leucine zipper motif through the flexible linker chain by means of genetic engineering. The use of a model fusion protein which consists of the maltose binding protein (MBP) allowed the preparation of biofunctionalized 4-nm CdSe/ZnS quantum dots that containing about 19 protein molecules per nanoparticle. The conjugates had the full biological functionality of the MBP as well as the undisturbed photoluminescent properties of the quantum dots. Moreover, it was observed that the binding of the leucine zipper is beneficial to the stability of the nanoparticle stability in aqueous solutions.[32] Stable, water-soluble oligonucleotide conjugates were recently prepared from hydroxy-capped quantum dots.[171] These nanoparticles can be used as labels in FISH (fluorescence in situ hybridization).

Besides problems of solubility, physicochemical stability, and quantum efficiency of the semiconductor nanocrystals, which still remain to be solved, the routine application of such nanoparticles as biolabels is still controversial, particularly because of general environmental concerns regarding the use of highly toxic cadmium compounds in biomedical diagnostics. As a result of

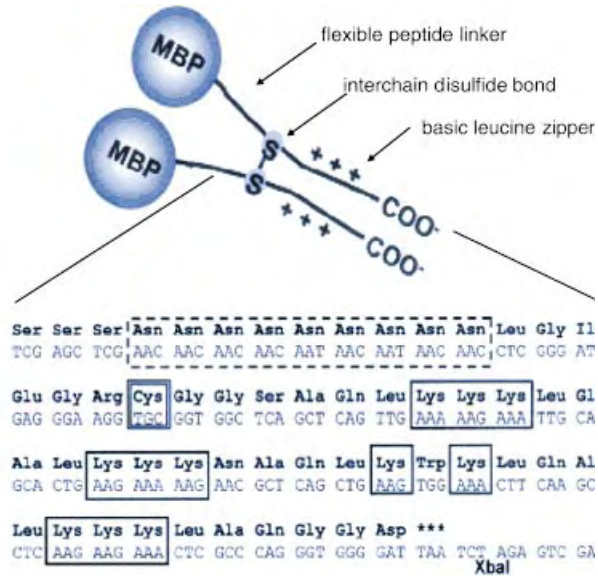


Figure 23. Recombinant protein linker which contains a functional protein moiety,MBP, and a basic leucine zipper motif. The primary amino acid sequence indicates the flexible peptide linker (boxed with dashed lines), the cysteine residue for covalent interchain linking (double boxed), and the lysine residues, which contribute to the net positive charge of the leucine zipper (single boxed). Reproduced from ref. [32], with permission. Copyright 2000 American Chemical Society.

their lower toxicity, colloids made up of other materials such as the chemically stable, highly luminescent, and less toxic $LaPO_4$:Ce,Tb nanocrystals[172] might provide a solution to this problem.

5.2.2. Nucleic Acid Coated Particles

Whereas protein-coated gold colloids have long been used in bioanalytical techniques, applications of DNA-functionalized Au particles were only introduced five years ago by Mirkin and co-workers.[77, 89] The DNA-directed nanoparticle aggregation depicted in Figure 9 can be used for simple and economically viable sensors in biomedical diagnostics, for example, for the detection of nucleic acids from pathogenic organisms. Although detailed studies of the optical phenomena associated with the supramolecular colloid assembly are still in progress,[81] several analytical applications that allow the detection of nucleic acids in homogenous solutions have already been reported.[44, 89, 173] Furthermore, the use of DNA-functionalized nanoparticles in the heterogeneous nucleic acid hybridization with capture oligonucleotides attached to solid supports have recently attracted much attention. Mirkin and co-workers[174] as well as other groups[175–180] have reported the DNA-directed immobilization of gold nanoparticles to form supramolecular surface architecture. The specific nucleic acid mediated immobilization of gold nanoparticles can be utilized for the topographic labeling of surface-bound DNA targets. This readily allows the highly sensitive scanometric detection of nucleic acids in DNA chip analyses.[181] The latter approach is based on the reduction of silver ions in the presence of gold particles (Figure 24) and allows a 100-fold increase in sensitivity over conventional fluorescent DNA detection.[182] The size-selective light scattering of Au nanoparticles with diameters of 50 and 100 nm has been used for the two-color labeling of oligonucleotide arrays.[183]

The use of colloidal gold nanoparticles also allows a signal enhancement in the DNA hybridization detection by means of a quartz crystal microbalance,[31, 184–186] angle-dependent light scattering,[187] and surface-plasmon resonance (Figure 21).[165] Willner and co-workers recently reported the use of DNA-functionalized 2.6-nm CdS nanoparticles for the photoelectrochemical detection of nucleic acid hybridization. An array of quantum dots was assembled at the surface of an electrode by using the specific hybridization of complementary DNA fragments. Upon irradiation, a photocurrent is generated which is proportional to the amount of target DNA.[188]

DNA-tagged proteins can also be readily immobilized on DNA-coated gold nanoparticles.[99] This approach has several advantages over the conventional methods to adsorb proteins on colloidal gold. Not only do the biofunctionalized nanoparticles retain the undisturbed recognition properties of the proteins immobilized, but they also reveal an extraordinary stability that even allows the regeneration of the DNA/Au particles. The bioinorganic hybrid components have been used as reagents in a sandwich immunoassay for the detection of proteins. A silver development technique promoted by gold particles was used to analyze fmol-amounts of antigens, and can also be used in the spatially-addressable detection of chip-immobilized antigens.[99]

5.3. Therapeutic Applications

Gold particles are well-established carriers for the delivery of dsDNA in the so-called gene-gun technology.[189] In this

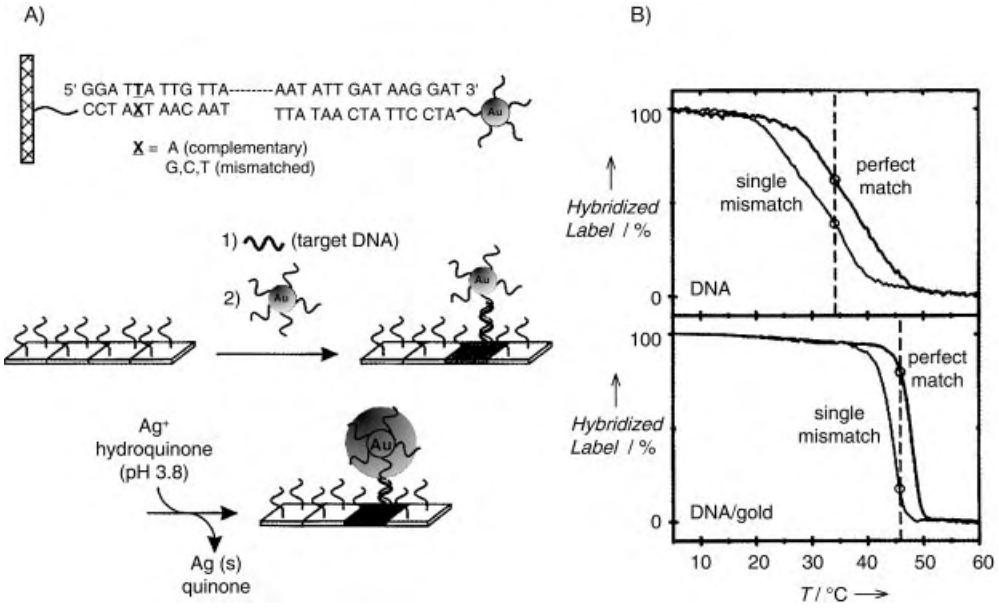


Figure 24. Scanometric detection of nucleic acids in DNA chip analyses. Capture oligonucleotides are immobilized on glass slides and used for the specific binding of target nucleic acids. Oligonucleotide-functionalized gold nanoparticles are employed as probes in solid-phase DNA hybridization detection. Subsequent to a silver enhancement step, the immobilization of the colloidal gold probe is detected by scanning the glass substrate with a conventional flatbed scanner. The extraordinary sharp melting point of the immobilized DNA–nanoparticle networks (see melting curves on the right) allows single-mismatches to be detect by means of this method. Reproduced from ref. [181], with permission. Copyright 2000 American Association for the Advancement of Science.

method, plasmid DNA with a typical length of several 1000 base pairs is adsorbed on Au or tungsten colloids with a typical size of about 500 nm to several micrometers. The DNA- or RNA-coated particles are loaded into a gun-like device in which a low pressure helium pulse delivers the particles into virtually any target cell or tissue. An advantage of this technique is that cells do not have to be removed from the tissue to transform cells. The particles penetrate the cells and release the DNA, which is diffused into the nucleus and, for example, incorporated into the chromosomes of the organism. Since its development in the mid-1980s, the gene gun technology has led to numerous examples of the tremendous potential of this method for "biolistic" transfection of organisms[189] as well as for DNA immunization.[190] The latter technique, also known as DNA vaccination, or genetic immunization, is a vaccine technology that can be used to stimulate protective immunity against many infectious pathogens, malignancies, and autoimmune disorders in animal models. Plasmid DNA, which encodes a polypeptide antigen, is introduced into the host cell (e.g. by means of gene gun particle bombardment), where it serves as a template for the highly efficient translation of its antigen. This leads to an immune response that is mediated by the cellular and/or humoral immune system and is specific for the plasmid-encoded antigen.[190]

Paramagnetic nanoparticles are currently being investigated for biomedical applications in the treatment of cancer.[191] Biocompatible dextran- or silane- coated superparamagnetic magnetite nanoparticles can be incorporated into malignant cells by means of endocytosis. The intracellular magnetic fluids are excited with alternating magnetic fields, thus leading to an increase in the local temperature, thereby inducing hyperthermia. It has been demonstrated that magnetic fluid hyperthermia (MFH) affects mammary carcinoma cells in vitro and in vivo.[191]

5.4. Nanoparticles as Model Systems

Two general aspects of metal and semiconductor nanoparticles make them suitable model systems for the study of fundamental biological phenomena. On the one hand, their size matches the macromolecular components employed in living systems. Proteins, nucleic acid fragments and their supramolecular complexes such as the nucleosome, the various complexes involved in DNA replication and transcription, and the ribosome, have typical dimensions in the range of 2 – 200 nm. On the other hand, nanoparticles of inorganic materials are essential building blocks in biomineralization, a fundamental biological process in which nature chemically generates morphology by means of genetic instructions. It is thus not surprising that the current advances in the study of metal and semiconductor nanoparticles has led to their consideration as model systems for the study of the interactions between proteins and nucleic acids and also for the understanding of the fundamental principles of biomineralization.

5.4.1. DNA – Protein Interaction

Besides using semiconductor and metal nanoparticles for tagging antibody and oligonucleotide probes, the nanoparticles themselves can also be used as probes for studying biological processes. They have an appropriate size similar to that of proteins and their ligand sphere can be adjusted readily with a variety of chemical groups. Thus, they can be considered as inorganic model proteins to investigate nonspecific DNA – protein interactions.[39–41] The protein-induced bending and wrapping of DNA by proteins is particularly important on the scale of a few base pairs up to about 150 base pairs, which corresponds to lengths of about 1 – 50 nm.[192] The most prominent example of sequence-independent binding and bending of DNA by proteins is the wrapping of about 150 base pairs of DNA around the nucleosome particle (diameter ≈11 nm), which consists of eight basic histone proteins (Figure 25).[193] Recent studies suggest that the histones, which

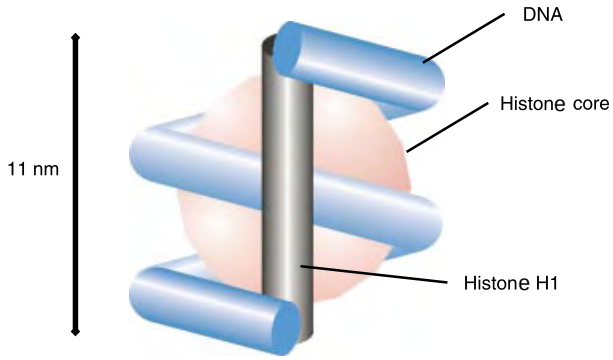


Figure 25. Model of the nucleosome particle: eight basic proteins make up the histon core, which serves as a carrier to bind 165 base pairs of dsDNA, which is wrapped around the protein core in 1.8 turns of a left-handed DNA superhelix. An additional histone molecule H1 locks the nucleosome, thus leading to a particle with a diameter of about 11 nm.

for a long time have been considered as passive structural substrates for DNA binding, might indeed influence gene expression by competing with transcription factors for DNA binding.[194] Thus, a detailed understanding of the nonspecific DNA – protein interactions and protein-induced DNA bending is important for the elucidation of the fundamental biological processes of DNA storage and processing.

Murphy and co-workers developed an unconventional way to study the adsorption of DNA onto protein-sized quantum dots.[39–41] The nanoparticle mimics a protein-like surface in terms of size and surface groups with the additional benefit of a spectroscopic probe to monitor DNA – nanoparticle interactions. As an example, if a particular sequence of DNA leads to an unusual shape or flexibility of the molecule, it is likely that these properties affect its binding to the protein-sized nanoparticle. The latter process can be conveniently monitored by photoluminescence quenching titration of the semiconductor nanoparticles. This strategy allows the adsorption of a kinked DNA molecule to 4 nm CdS nanocrystals to be compared with that of a straight DNA molecule (Figure 26). In particular, the self-complementary DNA sequence 5′-GGTCATGGCCATGACC-3′, which has a crystallographic kink of 23^0 at the central GGCC in the presence of magnesium

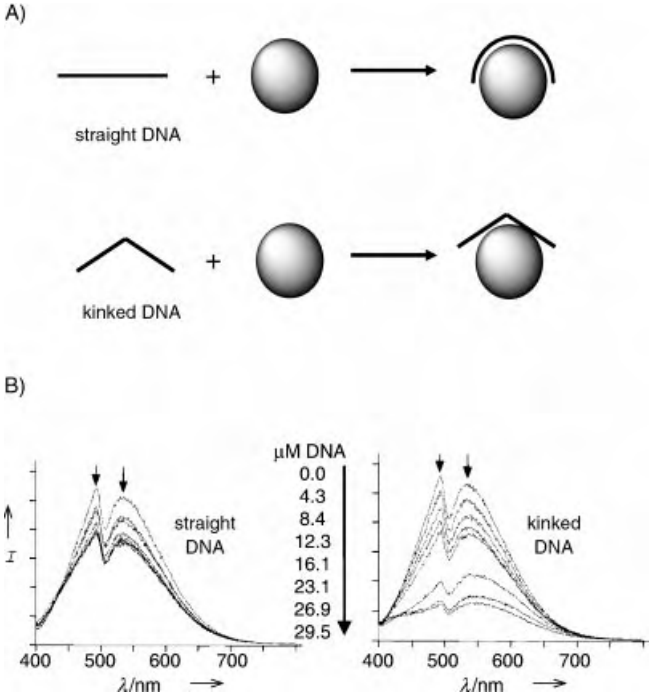


Figure 26. Semiconductor nanoparticles can mimic a protein-like surface. A) Unusual shapes of DNA molecules can affect its binding to protein-sized particles. B) The interaction between a straight and a kinked DNA molecule and a nanoparticle was monitored by photoluminescence quenching titration of 4-nm CdS nanoparticles capped with mercaptoethanol. The concentration-dependent quenching is more efficient for the kinked DNA molecule. Data from ref. [40], with permission. Copyright 1996 American Chemical Society.

ions,[195, 196] is adsorbed on the CdS quantum dots much more readily than the straight 5′-GGGTCCTCAGCTTGCC-3′ and the bent 5′-GGTCCAAAAAATTGCC-3′ oligomer.[39] Studies with neutralized mercaptoethanol-capped CdS particles indicated that magnesium is not essential for the preferred binding of the kinked DNA, whereas the other DNA molecules do not adsorb without a magnesium-enriched surface (Figure 26B).[40]

Recent studies on the temperature- and salt-dependent binding of long calf thymus DNA to 4.5-nm CdS quantum dots by photoluminescence spectroscopy suggest that the adsorption of the DNA is driven by entropy, whereas the enthalpy contribution to the DNA–surface binding is slightly unfavorable. In agreement with the mechanism of nonspecific DNA–protein interactions, the increase in entropy is likely to be a result of the release of solvent and counterions from the interface.[41] These studies demonstrate that semiconductor nanoparticles can be utilized in biological model studies owing to their size, adjustable chemical functionality of the ligand sphere, and their intrinsic fluorescence. Instead of using quantum-dot-based fluorescence-quenching analysis, gold or silver particles may also serve for similar spectroscopic studies with SERS.[197]

5.4.2. Biomineralization

The formation of the biological minerals that make up bones, teeth, or shells, is one of the most intriguing examples of Nature's unique capabilities to program the genesis of macroscopic forms genetically.[198] The power of the process by which nanometer-sized building blocks of mineral crystals are deposited in an organized fashion in the cellular or extracellular matrix of living organisms to build a macroscopic structure is impressively illustrated by the various genera of diatoms, each of which has an individual phenotype (Figure 27).[199] Recent studies suggest that the group-specific morphology of the nanostructured silica diatom cell walls is related to species-specific sets of polycationic peptides, termed silaffins, which have been isolated from diatom cell walls. Silaffins contain covalently modified lysines that bear polyamines consisting of *N*-methylpropylamine units, and ε-*N*,*N*-dimethyllysine groups.[200] The chemical structure of long-chain polyamines, which represent the main organic constituent of the biosilicates, were found to induce silica precipitation rapidly in vitro. Different morphologies of precipitating silica were generated from polyamines of different chain lengths.[201]

Although fundamental research into biomineralization over the past 25 years has brought insight into the mechanisms that control these processes, many questions still persist, in particular, in terms of vertebrate mineralization. For example, the biomineralization of the dental enamel matrix with a carbonated hydroxyapatite mineral is a well-studied system.[198c] Nevertheless, the chemical nature of the first mineral crystals formed in bone and dentin, the factors that lead to the initial deposition of these crystals, and the functions of macromolecules associated with these crystals are not understood. Recent studies on the molecular biology of the ameloblast gene products revealed the primary structures of some principal proteins involved in this extracellular mineralizing system. However, details of the secondary, tertiary, and quaternary structures of amelogenins, tuftelins, ameloblastins, enamelins, and proteinases involved in dental enamel matrix mineralization, their interactions with other matrix and cell surface proteins, and their distinct functions are still largely unknown. However, our current knowledge of these molecules, the probable molecular structure of the enamel matrix, and the functional role of the extracellular matrix proteins is constantly increasing,[198c] which suggests that further research might provide opportunities for the therapeutic manipulation of diseases in which biomineralization is impaired.

Biological antifreezes provide another impressive example of macromolecules with specific recognition capabilities for inorganic structures. The antifreeze proteins (AFPs) and the antifreeze glycoproteins (AFGPs) are a diverse class of proteins which have the ability to inhibit the growth of ice. Antifreezes are consequently found in organisms that live in environments in which sub-zero temperatures are routinely encountered, for instance, in Arctic fish, amphibians, insects, and plants.[202] Although still under active investigation, the molecular basis of the ice growth inhibition mechanism is in principle understood. AFPs have the ability to specifically adsorb to ice, thereby inhibiting its growth. The ice-binding mechanism of the linear alpha-helical type I AFPs has been attributed to their regularly spaced polar residues, which match the ice lattice along a pyramidal plane. As an example, the AFP of winter flounder binds to a specific set of pyramidal

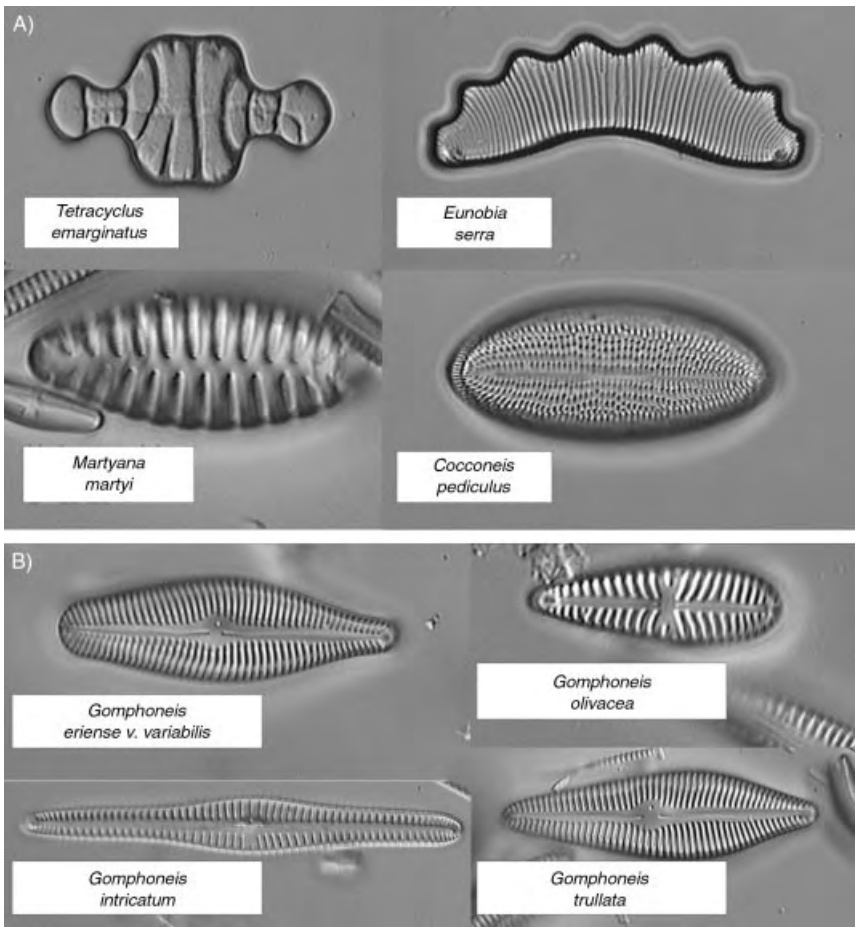


Figure 27. Genera (A) and species (B) of diatoms. Reproduced from: http://www.calacademy.org/research/diatoms/.

surface planes. Four groups of Asp, Asn, and Thr residues in the AFP can interact with the ice surface simultaneously through both hydrogen bonding and van der Waals interactions.[202e] Globular antifreeze proteins such as type III AFP, which lack repeating ice-binding residues, bind to ice with a remarkably flat amphipathic ice-binding site where hydrogen-bonding atoms match two ranks of oxygen atoms on the distinct planes of the ice prism plane.[202f] While some insight into the molecular basis of AFP-mediated ice growth inhibition has already been gained, more studies are required for a comprehensive understanding of the antifreeze action. One of goals is the rational construction of novel antifreezes, which have great potential for commercial applications as food additives to prevent cellular damage and to improve the texture and taste of frozen foods.[202a]

Biomineralization is also important in bacteria. Magnetotactic bacteria, which orient themselves and migrate along geomagnetic field lines, produce intracellular magnetic nanoparticles, the magnetosomes.[203] These comprise nanometer-sized monodisperse crystals of magnetic iron mineral, most often magnetite Fe_3O_4, coated with a magnetosome membrane, which prevents agglomeration (Figure 28). Depending on the bacterial species, the size of the magnetosomes range from 35 to 120 nm, and thus the particles represent a single magnetic domain. The formation of magnetosomes is achieved by means of a biological mechanism that controls the accumulation of iron and the biomineralization of the magnetic crystals with a characteristic size and morphology within membrane vesicles, which consist of protein-containing lipid bilayers. The molecular biology of magnetosome formation is under active investigation, and more than ten different proteins have already been identified to be part of the magnetosome membrane. Bacterial magnetosomes have significant biotechnological potential since they posses advantages over conventional synthetic magnetic particles, in particular their structural perfection and uniformity. Possible applications include the coupling of bioactive compounds, such as nucleic acids, enzymes, and antibodies, which would allows the magnetic manipulation of biocomponents. Moreover, purified and receptor-functionalized magnetosomes have already been used as contrasting agents in the detection of tumors by magnetoresonance tomography.[203]

Early biotechnological applications of bacterial biomineralization processes were described by Dameron et al., who discovered that the yeast *Candida glabrata* produces CdS nanoparticles when cultured in the presence of cadmium salts, which results in the sequestration and detoxification of intracellular cadmium ions.[46, 204, 205] The crystallites are peptide-coated, and the coating peptide varies with the nutrient conditions of the growth medium. When cultured in rich nutrient broth, the yeast forms intracellular CdS particles

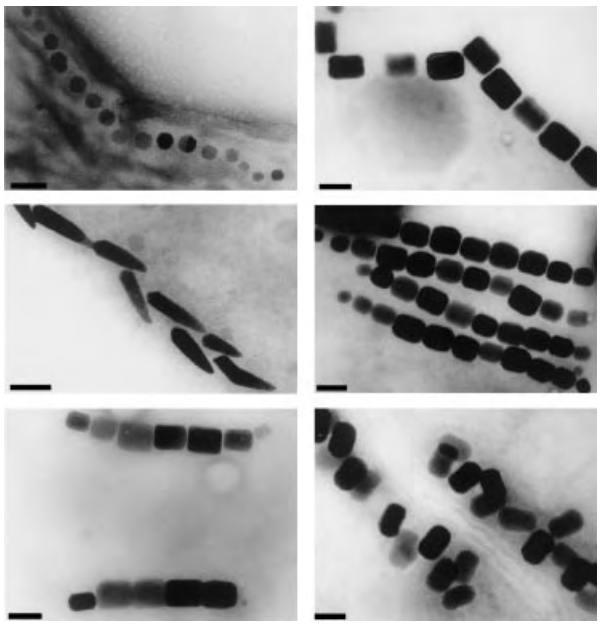


Figure 28. TEM images of magnetosomes obtained from various magnetotactic bacteria. The scale bar corresponds to 100 nm. Reproduced from ref. [203a], with permission.

that are coated with a mixture of glutathione and a γ-glutamylcysteine dipeptide. Cultures in synthetic minimal medium yield particles coated with polymerized peptides of the general structure $(\gamma\text{-Glu-Cys})_n\text{-Gly}$. The biologically produced peptide-coated particles exhibited properties analogous to those of the semiconductor quantum dots, in particular, size-dependent optical properties, photoluminescence, and photoreduction. More recently, a related approach allowed the biological production of ceramic–metal composites, cermets.[206] The silver-accumulating bacterial strain *Pseudomonas stutzeri*, which was originally isolated from a silver mine, was used to produce silver–carbon composite materials, which have the potential to produce optical thin-film coatings.

Besides immediate biotechnological applications, fundamental studies of bacterial nanoparticle formation and the interactions that occur between the organism and the inorganic surfaces[207] are also relevant for a comprehensive understanding of the fundamental material properties of artificial nanoparticles. For example, natural iron oxyhydroxide biomineralization products have recently provided strong evidence for aggregation-based crystal growth and microstructure development.[208] Since it is convenient to prepare perfect nanocrystals in large amounts, the question of whether small nanocrystals can be assembled into pure extended solid structures is of tremendous importance for the development of new optical and electronic materials.[23] For a long time, it seemed that aggregation of preformed nanocrystals assemble to form disordered solids. Recent findings by Banfield et al. suggest that some natural minerals grow by means of an oriented attachment mechanism, which means that a nanoparticle docks to the next in such a way that the two crystals are perfectly aligned.[208] Although there is a strong thermodynamic driving force for aligned attachment since the interface elimination leads to a reduced surface energy, it is still surprising that two crystals fuse together perfectly without getting stuck in any of the almost innumerable misoriented arrangements.[23]

In view of the intriguing power of biological mineralization processes, researchers have started to apply modern advances in molecular biology and biotechnology towards the development of artificial biomineralization approaches. The protein-based recognition of organic and inorganic surfaces has been studied by Addadi and co-workers.[209] They have isolated IgG molecules from animals immunized with crystals of monosodium urate monohydrate, or magnesium urate octahydrate. The antibodies revealed a high specificity and could distinguish between nuclei of crystals with similar molecular and structural characteristics, which suggests that the antibodies bear an imprint of the crystal surface structure in their binding sites. Such antibodies can act as nucleating templates that accelerate crystal formation in vitro.[209a] The generality of this approach was proven by the production of monoclonal antibodies against crystals of 1,4-dinitrobenzene (DNB). The reactivity of the antibodies was specifically directed against the DNB crystals, and they did not interact with molecular DNB conjugated to carrier proteins. Thus, these antibodies are not specific to the DNB molecule but rather to a repetitive motif of molecular moieties exposed at the crystal surfaces.[209b] Similarly, several antibodies were generated which specifically interact with distinct faces of cholesterol monohydrate crystals.[209c] These antibodies, which were raised against the three-dimensional supramolecular antigens, also bind specifically to the two-dimensional geometrically reduced forms of the antigen, such as fluid membranes of cholesterol.[209d,e]

The above results indicate that the binding sites of the antibody recognize a number of molecular moieties that are exposed at the surface in a specific structural organization. Besides serving as a model for the study of antibody recognition and related applications regarding the use of antibodies for targeting defined supramolecular structures in biological systems, the antibody–crystal surface interactions may also pave the way for the development of tailored (semi)synthetic binding proteins for the biomineralization of novel materials. In this context, recombinant DNA technology is a powerful tool for the biological production of novel protein compounds, and the phage-display technique has already allowed the in vitro evolution of protein linkers that directly recognize the surfaces of semiconductor materials (Figure 8).[67] Further research might lead to the development of procedures that enable the genetically coded biological growth of artificial inorganic materials.

6. Conclusions and Perspectives

This article summarizes a young and rapidly increasing research field located at the crossroads of materials research, nanosciences, and molecular biotechnology. An important point concerns the functionalization of inorganic nanoparticles by means of evolutionary optimized biological components. Since the nanoparticles and biomolecules typically meet at the same nanometer length scale, this interdisciplinary approach will contribute to the establishment of a novel field, descriptively termed biomolecular nanotechnology or nanobiotechnology.[76]

Although biomolecules and inorganic materials can be chemically coupled by means of various methods (Section 2), there is still a great demand for mild and selective coupling techniques that allow the preparation of thermodynamically stable, kinetically inert, and stoichiometrically well-defined bioconjugate hybrid nanoparticles. Examples in Nature suggest that enzymatic procedures combined with modern methods of bioorganic syntheses[210] will open novel routes for the generation of well-defined inorganic/biomolecular components, which are useful as building blocks for the bottom-up assembly of sophisticated nanostructured architecture. The first steps in this direction have already been taken by using protein- or nucleic acid based recognition elements (Section 3). In both systems, a large number of complementary binding pairs with a wide variety of free energies of association is available. It therefore remains to be seen whether protein-based conjugation might offer advantages over nucleic acid based assembly.[62] One should expect that nucleic acids are superior for the functionalization of nanoparticles, since the physicochemical properties of a single 20-mer oligonucleotide represents 4^{20} $(=10^{12})$ different recog-

nition elements. The binding strength can be conveniently adjusted by varying the lengths and GC contents of native DNA, or else by using non-natural DNA analogues with altered backbone properties and/or base-pairing specificity. Furthermore, directed evolution, already applied to tailor protein linkers,[67] should also be applicable in the generation of novel nucleic acid based linkers. It seems safe to predict that the tremendous advances in the development of artificial nucleic acid receptors will soon lead to the use of aptamers, which specifically recognize any target structure,[211] in the de novo generation of nucleic acid receptors that are capable of recognizing inorganic surfaces. Consequently, combinations of the two fundamental biological systems, nucleic acids and proteins, are very promising to synergistically cooperate and thus allow novel functions and applications.[85]

Another crossover of biotechnology and materials science concerns the utilization of the chemical and topographical properties of biological components for templating the spatial assembly of organic and inorganic components to form nanometer- and micrometer-sized elements (Section 4). There is still a tremendous need for systematic fundamental research into the interaction between biomolecules and the abiotic components; future perspectives should address these and should also concern the tailoring of the shape and physicochemical properties of the biocomponent by means of genetic engineering and bioconjugate chemistry. Although commercial applications are currently rare, the interdisciplinary work has a great potential for generating advanced materials, which might lead to novel devices for sensing, signal transduction, catalysis, as well as for new biocompatible materials and interfaces, currently being developed for biomedical sciences and tissue engineering.[212] In addition to long term perspectives, today's advanced materials as well as the modern physicochemical techniques originally developed for materials research and physics, are already used in bioanalytical applications or as model systems to solve biological problems (Section 5).

The future development of the joint venture between biotechnology and materials science will profit from the rapid current advances in chemistry as a central science. In addition, the current genome and proteome research will also be beneficial for this field, since it provides data that will allow us to produce even more suitable biocomponents. This might open the door to nanosensors, catalytic and light-harvesting devices, ultrafast molecular switches and transistors, supramolecular mediators between electrical and living systems, and other bio- and optoelectronic parts. Clearly, we are still far from the fabled autonomous nanomachines that heal wounds and perform surgery in a living organism. However, at the beginning of this new century one should remember the dramatic development that total organic synthesis has undergone from the early 1900s to the race for "molecular summits" in the late 1990s.[213, 214] A similar rate of progress in supramolecular sciences at the interface of biotechnology and materials research promises plenty of excitement from future developments.[221]

I wish to thank Dr. M. Adler for critically reading this manuscript, and Prof. D. Blohm for stimulating discussions and generous support. Our work is financially supported by the Deutsche Forschungsgemeinschaft and the Fonds der Chemischen Industrie.

Received: April 2, 2001 [A 464]

[1] J.-M. Lehn, *Supramolecular Chemistry. Concepts and Perspectives*, VCH, Weinheim, **1995**.
[2] F. Vögtle, *Supramolecular Chemistry*, Wiley, Chichester, **1991**.
[3] J. L. Atwood, J. E. D. Davies, D. D. MacNicol, F. Vögtle, *Comprehensive Supramolecular Chemistry*, Elsevier, Oxford, **1996**.
[4] For reviews, see: a) H. Shirakawa, *Angew. Chem.* **2001**, *113*, 2642 – 2648; *Angew. Chem. Int. Ed.* **2001**, *40*, 2574 – 2580; b) A. G. MacDiarmid, *Angew. Chem.* **2001**, *113*, 2649 – 2659; *Angew. Chem. Int. Ed.* **2001**, *40*, 2581 – 2590; c) A. J. Heeger, *Angew. Chem.* **2001**, *113*, 2660 – 2682; *Angew. Chem. Int. Ed.* **2001**, *40*, 2591 – 2611; d) F. Würthner, *Angew. Chem.* **2001**, *113*, 1069 – 1071; *Angew. Chem. Int. Ed.* **2001**, *40*, 1037 – 1039.
[5] The structure of the 50S ribosomal subunit has recently been resolved at a resolution of 2.4 Å: N. Ban, P. Nissen, J. Hansen, P. B. Moore, T. A. Steitz, *Science* **2000**, *289*, 905 – 920. The atomic structures of this subunit and its complexes with two substrate analogues revealed that the ribosome is, in fact, a ribozyme: P. Nissen, J. Hansen, N. Ban, P. B. Moore, T. A. Steitz, *Science* **2000**, *289*, 920 – 930. For reviews on the ribosome structure, see: E. Westhof, N. Leontis, *Angew. Chem.* **2000**, *112*, 1651 – 1655; *Angew. Chem. Int. Ed.* **2000**, *39*, 1587 – 1591; D. M. J. Lilley, *ChemBioChem* **2001**, *2*, 31 – 35.
[6] D. Philp, J. F. Stoddart, *Angew. Chem.* **1996**, *108*, 1242 – 1286; *Angew. Chem. Int. Ed. Engl.* **1996**, *35*, 1154 – 1196.
[7] R. P. Feynman in *Miniaturization* (Ed.: H. D. Gilbert), Reinhold, New York, **1961**, pp. 282 – 296.
[8] G. M. Whitesides, J. P. Mathias, C. T. Seto, *Science* **1991**, *254*, 1312 – 1319.
[9] G. Schmid, *Clusters and Colloids*, VCH, Weinheim, **1994**.
[10] U. Kreibig, *Optical Properties of Metal Clusters*, Springer, New York, **1995**.
[11] H. Weller, *Angew. Chem.* **1996**, *108*, 1159 – 1161; *Angew. Chem. Int. Ed. Engl.* **1996**, *35*, 1079 – 1081.
[12] M. Antonietti, C. Göltner, *Angew. Chem.* **1997**, *109*, 944 – 964; *Angew. Chem. Int. Ed. Engl.* **1997**, *36*, 1079 – 1081.
[13] A. P. Alivisatos, *Science* **1996**, *271*, 933 – 937.
[14] D. L. Feldheim, C. D. Keating, *Chem. Soc. Rev.* **1998**, *27*, 1 – 12.
[15] A. N. Shipway, E. Katz, I. Willner, *ChemPhysChem* **2000**, *1*, 19 – 52.
[16] F. Remacle, R. D. Levine, *ChemPhysChem* **2001**, *2*, 21 – 36.
[17] M. Bruchez, Jr., M. Moronne, P. Gin, S. Weiss, A. P. Alivisatos, *Science* **1998**, *281*, 2013 – 2015.
[18] W. C. W. Chan, S. M. Nie, *Science* **1998**, *281*, 2016 – 2018.
[19] M. Grundmann, *Physica E* **1999**, *5*, 169.
[20] R. E. Dunin-Borkowski, M. R. McCartney, R. B. Frankel, D. A. Bazylinski, M. Posfai, P. R. Buseck, *Science* **1998**, *282*, 1868 – 1870.
[21] S. Sun, C. B. Murray, D. Weller, L. Folks, A. Moser, *Science* **2000**, *287*, 1989 – 1992.
[22] A. Eychmüller, *J. Phys. Chem. B* **2000**, *104*, 6514 – 6528.
[23] A. P. Alivisatos, *Science* **2000**, *289*, 736 – 737.
[24] R. F. Service, *Science* **1997**, *277*, 1036 – 1037.
[25] C. M. Niemeyer, *Angew. Chemie* **1997**, *109*, 603 – 606; *Angew. Chem. Int. Ed. Engl.* **1997**, *36*, 585 – 587.
[26] C. A. Mirkin, T. A. Taton, *Nature* **2000**, *405*, 626 – 627.
[27] H. Dugas, *Bioorganic Chemistry*, Springer, New York, **1989**.
[28] U. Diederichsen, T. K. Lindhorst, B. Westermann, L. A. Wessjohann, *Bioorganic Chemistry*, Wiley-VCH, Weinheim, **1999**.
[29] S. S. Ghosh, P. M. Kao, A. W. McCue, H. L. Chappelle, *Bioconjugate Chem.* **1990**, *1*, 71 – 76.
[30] A. Bardea, A. Dagan, I. Ben-Dov, B. Amit, I. Willner, *Chem. Commun.* **1998**, 839 – 840.
[31] F. Patolsky, K. T. Ranjit, A. Lichtenstein, I. Willner, *Chem. Commun.* **2000**, 1025 – 1026.
[32] H. Mattoussi, J. M. Mauro, E. R. Goldman, G. P. Anderson, V. C. Sundar, F. V. Mikulec, M. G. Bawendi, *J. Am. Chem. Soc.* **2000**, *122*, 12142 – 12150.

[33] R. L. Letsinger, R. Elghanian, G. Viswanadham, C. A. Mirkin, *Bioconjugate Chem.* **2000**, *11*, 289 – 291.
[34] W. Shenton, S. A. Davies, S. Mann, *Adv. Mater.* **1999**, *11*, 449 – 452.
[35] C. D. Keating, K. M. Kovaleski, M. J. Natan, *J. Phys. Chem. B* **1998**, *102*, 9404 – 9413, and references therein.
[36] J. B. Broderick, M. J. Natan, T. V. O'Halloran, R. P. Van Duyne, *Biochemistry* **1993**, *32*, 13771 – 13776.
[37] I. D. G. MacDonald, W. E. Smith, *Langmuir* **1996**, *12*, 706 – 713.
[38] B. N. Rospendowski, K. Kelly, C. R. Wolf, W. E. Smith, *J. Am. Chem. Soc.* **1991**, *113*, 1217 – 1225.
[39] R. Mahtab, J. P. Rogers, C. J. Murphy, *J. Am. Chem. Soc.* **1995**, *117*, 9099 – 9100.
[40] R. Mahtab, J. P. Rogers, C. P. Singleton, C. J. Murphy, *J. Am. Chem. Soc.* **1996**, *118*, 7028 – 7032.
[41] R. Mahtab, H. H. Harden, C. J. Murphy, *J. Am. Chem. Soc.* **2000**, *122*, 14 – 17.
[42] S. Connolly, D. Fitzmaurice, *Adv. Mater.* **1999**, *11*, 1202 – 1205.
[43] D. E. Safer, L. Bolinger, J. S. Leigh, *J. Inorg. Biochem.* **1986**, *26*, 77 – 91.
[44] B. Dubertret, M. Calame, A. J. Libchaber, *Nat. Biotechnol.* **2001**, *19*, 365 – 370.
[45] A. P. Alivisatos, K. P. Johnsson, X. Peng, T. E. Wilson, C. J. Loweth, M. P. Bruchez, Jr., P. G. Schultz, *Nature* **1996**, *382*, 609 – 611.
[46] C. T. Dameron, R. N. Reese, R. K. Mehra, A. R. Kortan, P. J. Carroll, M. L. Steigerwald, L. E. Brus, D. R. Winge, *Nature* **1989**, *338*, 596 – 597.
[47] W. Bae, R. Abdullah, D. Henderson, R. K. Mehra, *Biochem. Biophys. Res. Commun.* **1997**, *237*, 16 – 23.
[48] R. Kho, C. L. Torres-Martinez, R. K. Mehra, *J. Colloid Interface Sci.* **2000**, *227*, 561 – 566.
[49] "Lumineszierende CdTe-Nanoteilchen als Markierungssubstanzen in der klinischen Chemie": K. Hoppe, A. Eychmüller, H. Weller, A. Böttcher, A. Götz, G. Schmitz, poster P146, presented at the 99. Hauptversammlung der Deutschen Bunsengesellschaft für Physikalische Chemie (Würzburg, Germany, June 1 – 3, **2000**).
[50] M. Brust, D. Bethell, D. J. Schiffrin, C. Kiely, *Adv. Mater.* **1995**, *7*, 795 – 797.
[51] C. M. Niemeyer, W. Bürger, J. Peplies, *Angew. Chem.* **1998**, *110*, 2391 – 2395; *Angew. Chem. Int. Ed.* **1998**, *37*, 2265 – 2268.
[52] P. C. Weber, D. H. Ohlendorf, J. J. Wendoloski, F. R. Salemme, *Science* **1989**, *243*, 85 – 88.
[53] M. Wilchek, E. A. Bayer, *Methods Enzymol.* **1990**, *184*, 51 – 67.
[54] B. K. Sinha, C. F. Chignell, *Methods Enzymol.* **1979**, *62*, 295 – 308.
[55] U. Piran, W. J. Riordan, *J. Immunol. Methods* **1990**, *133*, 141 – 143.
[56] T. Sano, M. W. Pandori, X. M. Chen, C. L. Smith, C. R. Cantor, *J. Biol. Chem.* **1995**, *270*, 28204 – 28209.
[57] T. Sano, C. R. Cantor, *Proc. Natl. Acad. Sci. USA* **1995**, *92*, 3180 – 3184.
[58] G. O. Reznik, S. Vajda, C. L. Smith, C. R. Cantor, T. Sano, *Nat. Biotechnol.* **1996**, *14*, 1007 – 1011.
[59] T. G. M. Schmidt, J. Koepke, R. Frank, A. Skerra, *J. Mol. Biol.* **1996**, *255*, 753 – 766.
[60] T. Sano, G. O. Reznik, P. Szafranski, C. M. Niemeyer, S. Vajda, C. L. Smith, C. M. Mello, D. L. Kaplan, M. Rusckowski, D. J. Hnatowich, C. R. Cantor, *Proceedings of the 50th Anniversary Conference of the Korean Chemical Society* (Yonsei University, Seoul, May 24 – 25, **1996**), pp. 359 – 363.
[61] T. Sano, S. Vajda, C. R. Cantor, *J. Chromatogr. B* **1998**, *715*, 85 – 91.
[62] S. Mann, W. Shenton, M. Li, S. Connolly, D. Fitzmaurice, *Adv. Mater.* **2000**, *12*, 147 – 150.
[63] C. Kessler, *Mol. Cell. Probes* **1991**, *5*, 161 – 205.
[64] J. Chevalier, J. Yi, O. Michel, X. M. Tang, *J. Histochem. Cytochem.* **1997**, *45*, 481 – 491.
[65] A. Knappik, A. Plueckthun, *BioTechniques* **1994**, *17*, 745 – 761.
[66] R. G. Chubet, B. L. Brizzard, *BioTechniques* **1996**, *20*, 136 – 141.
[67] S. R. Whaley, D. S. English, E. L. Hu, P. F. Barbara, A. M. Belcher, *Nature* **2000**, *405*, 665 – 666.
[68] Transition metal complexes that contain several cupric ions have been designed to specifically target a complementary histidine pattern on the surface of a protein: M. A. Fazal, C. R. Bidhan, S. Sun, S. Mallik, K. R. Rodgers, *J. Am. Chem. Soc* **2001**, *123*, 6283 – 6290.
[69] For a nanomechanical device based on the ion-dependent B-to-Z conformational transition of a short DNA double helix, see: C. Mao, W. Sun, Z. Shen, N. C. Seeman, *Nature* **1999**, *397*, 144 – 146; for ionic switching of nanoparticles by means of DNA supercoiling, see ref. [86]; an array of cantilevers was used to translate DNA hybridization into a nanomechanical response: J. Fritz, M. K. Baller, H. P. Lang, H. Rothuizen, P. Vettiger, E. Meyer, H. Guntherodt, C. Gerber, J. K. Gimzewski, *Science* **2000**, *288*, 316 – 318; for a DNA molecular tweezer which can be opened and closed by the addition of single-stranded DNA, see: B. Yurke, A. J. Turberfield, A. P. Mills, Jr., F. C. Simmel, J. L. Neumann, *Nature* **2000**, *406*, 605 – 608.
[70] R. K. Soong, G. D. Bachand, H. P. Neves, A. G. Olkhovets, H. G. Craighead, C. D. Montemagno, *Science* **2000**, *290*, 1555 – 1558.
[71] J. K. Lanyi, A. Pohorille, *Trends Biotechnol.* **2001**, *19*, 140 – 144.
[72] K. E. Drexler, *Proc. Natl. Acad. Sci. USA* **1981**, *78*, 5275 – 5278.
[73] N. C. Seeman, *J. Theor. Biol.* **1982**, *99*, 237 – 247.
[74] K. E. Drexler, *Nanosystems: Molecular Machinery, Manufacturing, and Computation*, Wiley, New York, **1992**.
[75] N. C. Seeman, *Trends Biotechnol.* **1999**, *17*, 437 – 443.
[76] C. M. Niemeyer, *Curr. Opin. Chem. Biol.* **2000**, *4*, 609 – 618.
[77] C. A. Mirkin, R. L. Letsinger, R. C. Mucic, J. J. Storhoff, *Nature* **1996**, *382*, 607 – 609.
[78] R. C. Mucic, J. J. Storhoff, C. A. Mirkin, R. L. Letsinger, *J. Am. Chem. Soc.* **1998**, *120*, 12674 – 12675.
[79] G. P. Mitchell, C. A. Mirkin, R. L. Letsinger, *J. Am. Chem. Soc.* **1999**, *121*, 8122 – 8123.
[80] S.-J. Park, A. A. Lazarides, C. A. Mirkin, R. L. Letsinger, *Angew. Chem.* **2001**, *113*, 2993 – 2996; *Angew. Chem. Int. Ed.* **2001**, *40*, 2909 – 2912.
[81] J. J. Storhoff, A. A. Lazarides, R. C. Mucic, C. A. Mirkin, R. L. Letsinger, G. C. Schatz, *J. Am. Chem. Soc.* **2000**, *122*, 4640 – 4650.
[82] S.-J. Park, A. A. Lazarides, C. A. Mirkin, P. W. Brazis, C. R. Kannewurf, R. L. Letsinger, *Angew. Chem.* **2000**, *112*, 4003 – 4006; *Angew. Chem. Int. Ed.* **2000**, *39*, 3845 – 3848.
[83] C. M. Niemeyer, M. Adler, B. Pignataro, S. Lenhert, S. Gao, L. F. Chi, H. Fuchs, D. Blohm, *Nucleic Acids Res.* **1999**, *27*, 4553 – 4561.
[84] C. M. Niemeyer, M. Adler, S. Gao, L. F. Chi, *Angew. Chem.* **2000**, *112*, 3183 – 3187; *Angew. Chem. Int. Ed.* **2000**, *39*, 3055 – 3059.
[85] C. M. Niemeyer, *Chem. Eur. J.* **2001**, *7*, 3188 – 3195.
[86] C. M. Niemeyer, M. Adler, S. Lenhert, S. Gao, H. Fuchs, L. F. Chi, *ChemBioChem* **2001**, *2*, 260 – 265.
[87] S. Gao, L. F. Chi, S. Lenhert, B. Anczykowsky, C. M. Niemeyer, M. Adler, H. Fuchs, *ChemPhysChem* **2001**, *2*, 384 – 388.
[88] B. Pignataro, L. F. Chi, S. Gao, B. Anczykowsky, C. M. Niemeyer, M. Adler, H. Fuchs, *Appl. Phys. A* **2001**, *2*, submitted.
[89] J. J. Storhoff, C. A. Mirkin, *Chem. Rev.* **1999**, *99*, 1849 – 1862.
[90] Polymers that are functionalized with DNA oligomers have been used to prepare nanoparticle aggregates (K. J. Watson, S.-J. Park, J.-H. Im, S. T. Nguyen, C. A. Mirkin, *J. Am. Chem. Soc.* **2001**, *123*, 5592 – 5593), and protein networks (R. B. Fong, Z. Ding, C. J. Long, A. S. Hoffman, P. S. Stayton, *Bioconjugate Chem.* **1999**, *10*, 720 – 725) by means of nucleic acid hybridization.
[91] C. M. Niemeyer, T. Sano, C. L. Smith, C. R. Cantor, *Nucleic Acids Res.* **1994**, *22*, 5530 – 5539.
[92] C. J. Loweth, W. B. Caldwell, X. Peng, A. P. Alivisatos, P. G. Schultz, *Angew. Chem.* **1999**, *111*, 1925 – 1929; *Angew. Chem. Int. Ed.* **1999**, *38*, 1808 – 1812.
[93] L. Cusack, S. N. Rao, D. Fitzmaurice, *Chem. Eur. J.* **1997**, *3*, 202 – 207.
[94] D. Fitzmaurice, S. N. Rao, J. A. Preece, J. F. Stoddart, S. Wenger, N. Zaccheroni, *Angew. Chem.* **1999**, *111*, 1220; *Angew. Chem. Int. Ed.* **1999**, *38*, 1147 – 1150.
[95] D. Fitzmaurice, S. N. Rao, J. A. Preece, J. F. Stoddart, S. Wenger, N. Zaccheroni, *J. Am. Chem. Soc.* **2000**, *122*, 6252 – 6257.
[96] a) M. Brust, M. Walker, D. Bethell, D. J. Schiffrin, R. J. Whyman, *J. Chem. Soc. Chem. Commun.* **1995**, 801; b) R. S. Ingram, M. J. Hostetler, R. W. J. Murray, *J. Am. Chem. Soc.* **1997**, *119*, 9175 – 9178; c) J. Liu, R. Xu, A. E. Kaifer, *Langmuir* **1998**, *14*, 7337 – 7339; d) A. K. Boal, V. M. Rotello, *J. Am. Chem. Soc.* **2000**, *122*, 734 – 735; e) A. K. Boal, F. Ilhan, J. E. DeRouchey, T. Thurn-Albrecht, T. P. Russell, V. M. Rotello, *Nature* **2000**, *404*, 746 – 748; see also refs. [94] and [95].

[97] V. M. Mirsky, T. Hirsch, S. A. Piletsky, O. S. Wolfbeis, *Angew. Chem.* **1999**, *111*, 1191; *Angew. Chem. Int. Ed.* **1999**, *38*, 1108.

[98] a) SAM colloids that contain surface-bound Ru catalysts revealed a combination of homogeneous and heterogeneous properties in ring-opening-metathesis polymerization reactions: M. Bartz, J. Küther, R. Sesharadi, W. Tremel, *Angew. Chem.* **1998**, *110*, 2646 – 2649; *Angew. Chem. Int. Ed. Engl.* **1998**, *37*, 2466 – 2468; b) the photochemical reactivity of stilbene moieties bound to SAM colloids differs from that of stilbene groups attached to planar surfaces: J. Hu, J. Zhang, F. Liu, K. Kittredge, J. K. Whitesell, M. A. Fox, *J. Am. Chem. Soc.* **2001**, *123*, 1464 – 1470; c) 2-nm gold particles that are functionalized with thiolated neoglycoconjugate moieties can be used as model systems for polyvalent carbohydrate interactions: J. M. de la Fuente, A. G. Barrientos, T. C. Rojas, J. Rojo, J. Cañada, A. Fernández, S. Penadés, *Angew. Chem.* **2001**, *113*, 2318 – 2321; *Angew. Chem. Int. Ed.* **2001**, *40*, 2258 – 2261; d) for cyclodextrin-modified nanoparticles, see: J. Liu, S. Mendoza, E. Roman, M. J. Lynn, R. L. Xu, A. E. Kaifer, *J. Am. Chem. Soc.* **1999**, *121*, 4304 – 4305.

[99] C. M. Niemeyer, B. Ceyhan, *Angew. Chem. Int. Ed.* **2001**, *40*, 3685 – 3688; *Angew. Chem.* **2001**, *113*, 3798 – 3801.

[100] U. B. Sleytr, P. Messner, D. Pum, M. Sara, *Angew. Chem.* **1999**, *111*, 1098 – 1120; *Angew. Chem. Int. Ed.* **1999**, *38*, 1034 – 1054.

[101] W. Shenton, D. Pum, U. B. Sleytr, S. Mann, *Nature* **1997**, *389*, 585 – 587.

[102] S. Dieluweit, D. Pum, U. B. Sleytr, *Supramol. Sci.* **1998**, *5*, 15 – 19.

[103] M. Mertig, R. Kirsch, W. Pompe, H. Engelhardt, *Eur. Phys. J.* **1999**, *D9*, 45 – 48.

[104] S. R. Hall, W. Shenton, H. Engelhardt, S. Mann, *ChemPhysChem* **2001**, *2*, 184 – 186.

[105] A genetically engineered alpha-hemolysine membrane protein was functionalized with a DNA oligonucleotide within its 4-nm internal cavity. The resulting DNA-nanopore was used for sequence-specific detection of individual DNA targets: S. Howorka, S. Cheley, H. Bayley, *Nat. Biotechnol.* **2001**, *19*, 636 – 639. Similar nanopores were used to simultaneously accommodate two different cyclodextrin molecules, thereby opening the way for the production of novel multi-analyte sensors: L. Q. Gu, S. Cheley, H. Bayley, *Science* **2001**, *291*, 636 – 640.

[106] E. J. Gibbs, I. Tinoco, Jr., M. F. Maestre, P. A. Ellinas, R. F. Pasternack, *Biochem. Biophys. Res. Commun.* **1988**, *157*, 350 – 358.

[107] R. F. Pasternack, J. I. Goldsmith, S. Szep, E. J. Gibbs, *Biophys. J.* **1998**, *75*, 1024 – 1031.

[108] R. F. Pasternack, E. J. Gibbs, P. J. Collings, J. C. dePaula, L. C. Turzo, A. Terracina, *J. Am. Chem. Soc.* **1998**, *120*, 5873 – 5878.

[109] J. L. Seifert, R. E. Connor, S. A. Kushon, M. Wang, B. A. Armitage, *J. Am. Chem. Soc.* **1999**, *121*, 2987 – 2995.

[110] M. Wang, G. L. Silva, B. A. Armitage, *J. Am. Chem. Soc.* **2000**, *122*, 9977 – 9986.

[111] A. M. Cassel, W. A. Scrivens, J. M. Tour, *Angew. Chem.* **1998**, *110*, 1670 – 1672; *Angew. Chem. Int. Ed.* **1998**, *37*, 1528 – 1531.

[112] M. Y. Ono, E. M. Spain, *J. Am. Chem. Soc.* **1999**, *121*, 7330 – 7334.

[113] T. Blessing, J.-S. Remy, J.-P. Behr, *J. Am. Chem. Soc.* **1998**, *120*, 8519 – 8520.

[114] A. D. Miller, *Angew. Chem.* **1998**, *110*, 1862 – 1880; *Angew. Chem. Int. Ed.* **1998**, *37*, 1768 – 1785.

[115] J. L. Coffer, S. R. Bigham, R. F. Pinizzotto, H. Yang, *Nanotechnology* **1992**, *3*, 69 – 76.

[116] S. R. Bigham, J. L. Coffer, *Colloids Surf. A* **1995**, *95*, 211 – 219.

[117] J. L. Coffer, S. R. Bigham, X. Li, R. F. Pinizzotto, Y. G. Rho, R. M. Pirtle, I. L. Pirtle, *Appl. Phys. Lett.* **1996**, *69*, 3851 – 3853.

[118] J. L. Coffer, *J. Cluster Sci.* **1997**, *8*, 159 – 179.

[119] E. Braun, Y. Eichen, U. Sivan, G. Ben-Yoseph, *Nature* **1998**, *391*, 775 – 778.

[120] J. Richter, R. Seidel, R. Kirsch, M. Mertig, W. Pompe, J. Plaschke, H. K. Schackert, *Adv. Mater.* **2000**, *12*, 507 – 510.

[121] J. Richter, M. Mertig, W. Pompe, I. Monch, H. K. Schackert, *Appl. Phys. Lett.* **2001**, *78*, 536 – 538.

[122] L. C. Ciacchi, W. Pompe, A. De Vita, *J. Am. Chem. Soc.* **2001**, *123*, 7371 – 7380.

[123] T. Torimoto, M. Yamashita, S. Kuwabata, T. Sakata, H. Mori, H. Yoneyama, *J. Phys. Chem. B* **1999**, *103*, 8799 – 8803.

[124] A. Kumar, M. Pattarkine, M. Bhadbhade, A. B. Mandale, K. N. Ganesh, S. S. Datar, C. V. Dharmadhikari, M. Sastry, *Adv. Mater.* **2001**, *13*, 341 – 344.

[125] E. Di Mauro, C. P. Hollenberg, *Adv. Mater.* **1993**, *5*, 384 – 386.

[126] W. Han, S. M. Lindsay, R. E. Dlakic, R. E. Harrington, *Nature* **1997**, *386*, 563.

[127] J. Shi, D. E. Bergstrom, *Angew. Chem.* **1997**, *109*, 70 – 72; *Angew. Chem. Int. Ed. Engl.* **1997**, *36*, 111 – 113.

[128] H. Kuhn, V. V. Demidov, M. D. Frank-Kaminetskii, *Angew. Chem.* **1999**, *111*, 1544 – 1547; *Angew. Chem. Int. Ed.* **1999**, *38*, 1446 – 1449.

[129] M. S. Shchepinov, K. U. Mir, J. K. Elder, M. D. Frank-Kamenetskii, E. M. Southern, *Nucleic Acids Res.* **1999**, *27*, 3035 – 3041.

[130] M. Scheffler, A. Dorenbeck, S. Jordan, M. Wüstefeld, G. v. Kiedrowski, *Angew. Chem.* **1999**, *111*, 3514 – 3518; *Angew. Chem. Int. Ed.* **1999**, *38*, 3312 – 3315.

[131] Y. Aharonov, D. Bohm, *Phys. Rev.* **1959**, *115*, 485.

[132] N. D. Chasteen, P. M. Harrison, *J. Struct. Biol.* **1999**, *126*, 182 – 194.

[133] S. Mann, J. V. Bannister, R. J. P. Williams, *J. Mol. Biol.* **1986**, *188*, 225.

[134] F. Funk, J.-P. Lenders, R. R. Crichton, W. Schneider, *Eur. J. Biochem.* **1985**, *152*, 167 – 172.

[135] I. G. Macara, T. G. Hoy, P. M. Harrison, *Biochem. J.* **1972**, *126*, 151 – 162.

[136] D. M. Lawson, P. J. Artymiuk, S. J. Yewdall, J. M. A. Smith, J. C. Livingstone, A. Treffry, A. Luzzago, S. Levi, P. Arosio, G. Cesareni, C. D. Thomas, W. V. Shaw, P. M. Harrison, *Nature* **1991**, *349*, 541 – 544.

[137] F. C. Meldrum, V. J. Wade, D. L. Nimmo, B. R. Heywood, S. Mann, *Nature* **1991**, *349*, 684 – 687.

[138] F. C. Meldrum, B. R. Heywood, S. Mann, *Science* **1992**, *257*, 522 – 523.

[139] K. K. W. Wong, T. Douglas, S. Gider, D. D. Awschalom, S. Mann, *Chem. Mater.* **1998**, *10*, 279 – 285.

[140] M. Li, K. W. K. Wong, S. Mann, *Chem. Mater.* **1999**, *11*, 23 – 26.

[141] W. Shenton, S. Mann, H. Cölfen, A. Bacher, M. Fischer, *Angew. Chem.* **2001**, *113*, 456 – 459; *Angew. Chem. Int. Ed.* **2001**, *40*, 442 – 444.

[142] L. Stryer, *Biochemistry*, Freeman, New York, **1988**.

[143] G. Stubbs in *The Viruses*, *Vol. 1* (Eds.: A. Mc Pherson, F. Jurnak), Wiley, New York, **1984**, pp. 149 – 202.

[144] W. Shenton, T. Douglas, M. Young, G. Stubbs, S. Mann, *Adv. Mater.* **1999**, *11*, 253 – 256.

[145] K. K. W. Wong, S. Mann, *Adv. Mater.* **1996**, *8*, 928.

[146] T. Douglas, M. Young, *Nature* **1998**, *393*, 152 – 155.

[147] T. Douglas, M. Young, *Adv. Mater.* **1999**, *11*, 679 – 681.

[148] For examples for the SFM characterization of biomolecular systems, see: a) review: H. G. Hansma, *Annu. Rev. Phys. Chem.* **2001**, *52*, 71 – 92; b) enzymatic processing of nucleic acids: S. Kasas, N. H. Thomson, B. L. Smith, H. G. Hansma, X. S. Zhu, M. Guthold, C. Bustamante, E. T. Kool, M. Kashlev, P. K. Hansma, *Biochemistry* **1997**, *36*, 461 – 468; c) mobility of DNA molecules on solid supports: M. Argaman, R. Golan, N. H. Thomson, H. G. Hansma, *Nucleic Acids Res.* **1997**, *25*, 4379 – 4384; d) crystallization of transfer RNA: J. D. Ng, Y. G. Kuznetsov, A. J. Malkin, G. Keith, R. Giege, A. McPherson, *Nucleic Acids Res.* **1997**, *25*, 2582 – 2588; e) characterization of DNA nanostructures: X. Yang, L. A. Wenzler, J. Qi, X. Li, N. C. Seeman, *J. Am. Chem. Soc.* **1998**, *120*, 9779 – 9786; E. Winfree, F. Liu, L. A. Wenzler, N. C. Seeman, *Nature* **1998**, *394*, 539 – 544; for the characterization of synthetic supramolecular DNA-protein conjugates, see refs. [83, 84]; f) improved resolution of the SFM can be attained by using carbon nanotubes as tips: H. Dai, J. H. Hafner, A. G. Rinzler, D. T. Colbert, R. E. Smalley, *Nature* **1996**, *384*, 147 – 151; C. L. Cheung, J. H. Hafner, C. M. Lieber, *Proc. Natl. Acad. Sci. USA* **2000**, *97*, 3809 – 3813. The nanotubes can be functionalized by covalent methods (S. S. Wong, E. Joselevich, A. T. Woolley, C. L. Cheung, C. M. Lieber, *Nature* **1998**, *394*, 52 – 55) to enable the specific chemical and biological discrimination during the imaging, for instance, to detect DNA sequences specifically: A. T. Woolley, C. Guillemette, C. Li Cheung, D. E. Housman, C. M. Lieber, *Nat. Biotechnol.* **2000**, *18*, 760 – 763; g) the functionalization of SFM tips with phospholipase A allows the nanostructured hydrolysis of supported dipalmitoylphosphatidylcholine bilayers: H. Clausen-Schaumann, M. Grandbois, H. E. Gaub, *Adv. Mater.* **1998**, *10*, 949 – 952.

[149] For reviews, see: A. Engel, H. E. Gaub, D. J. Muller, *Curr. Biol.* **1999**, *9*, 133 – 136; A. Janshoff, M. Neitzert, Y. Oberdörfer, H. Fuchs, *Angew. Chem.* **2000**, *112*, 3346 – 3374; *Angew. Chem. Int. Ed.* **2000**, *39*, 3229 – 3355.
[150] For reviews on surface plasmon resonance measurement, see: a) a) J. M. Brockman, B. P. Nelson, R. M. Corn, *Annu. Rev. Phys. Chem.* **2000**, *51*, 41 – 63; b) C. Williams, *Curr. Opin. Biotechnol.* **2000**, *11*, 42 – 46; c) R. L. Rich, D. G. Myszka, *Curr. Opin. Biotechnol.* **2000**, *11*, 54 – 61.
[151] For reviews on SERS, see: a) H. Kneipp, I. Itzkan, R. R. Dasari, M. S. Feld, *Chem. Rev.* **1999**, *99*, 2957 – 2975; b) A. Campion, P. Kambhampati, *Chem. Soc. Rev.* **1998**, *27*, 241 – 250.
[152] M. A. Hayat, *Colloidal Gold: Principles, Methods, and Applications*, Academic Press, New York, **1989**.
[153] C. D. Keating, K. M. Kovaleski, M. J. Natan, *J. Phys. Chem. B* **1998**, *102*, 9414 – 9425.
[154] L. He, M. J. Natan, C. D. Keating, *Anal. Chem.* **2000**, *72*, 5348 – 5355.
[155] X. Dou, T. Takama, Y. Yamaguchi, K. Hirai, H. Yamamoto, S. Doi, Y. Ozaki, *Appl. Opt.* **1998**, *37*, 759 – 763.
[156] J. Kreuter in *Microcapsules and Nanoparticles in Medicine and Pharmacy* (Ed.: M. Donbrow), CRC, Boca Raton, **1992**.
[157] D. E. Safer, J. Hainfeld, J. S. Wall, J. E. Reardon, *Science* **1982**, *218*, 290 – 291.
[158] J. F. Hainfeld, F. R. Furuya, *J. Histochem. Cytochem.* **1992**, *40*, 177 – 184.
[159] J. F. Hainfield, *Proc. Natl. Acad. Sci. USA* **1992**, *89*, 11 064.
[160] O. D. Velev, E. W. Kaler, *Langmuir* **1999**, *15*, 3693 – 3698.
[161] J. Zhao, R. W. Henkens, J. Stonehuerner, J. P. O'Daly, A. L. Crumbliss, *J. Electroanal. Chem.* **1992**, *327*, 109 – 119.
[162] Y. Xiao, H.-X. Ju, H.-Y. Chen, *Anal. Chim. Acta* **1999**, *391*, 73 – 82.
[163] F. Patolsky, T. Gabriel, I. Willner, *J. Electroanal. Chem.* **1999**, *479*, 69 – 73.
[164] L. A. Lyon, M. D. Musick, M. J. Natan, *Anal. Chem.* **1998**, *70*, 5177 – 5183.
[165] L. He, M. D. Musick, S. R. Nicewarner, F. G. Salinas, S. J. Benkovic, M. J. Natan, C. D. Keating, *J. Am. Chem. Soc.* **2000**, *122*, 9071 – 9077.
[166] S. Schultz, D. R. Smith, J. J. Mock, D. A. Schultz, *Proc. Natl. Acad. Sci. USA* **2000**, *97*, 996 – 1001.
[167] A. P. Alivisatos, *Pure Appl. Chem.* **2000**, *72*, 3 – 9.
[168] Europium is often applied as a label in time-resolved immunofluorometric assays. For a review, see: I. Hemmila, S. Dakubu, V. M. Mukkala, H. Siitari, T. Lovgren, *Anal. Biochem.* **1984**, *137*, 335 – 343. The labeling is either achieved by using an Eu-chelate (example: A. Scorilas, A. Bjartell, H. Lilja, C. Moller, E. P. Diamandis, *Clin. Chem.* **2000**, *46*, 1450 – 1455) or -cryptate reagents (G. Mathis, *Clin. Chem.* **1995**, *41*, 1391 – 1397). Time-resolved fluorescence imaging for quantitative histochemistry has recently been described using lanthanide chelates in nanoparticles: V. Vaisanen, H. Harma, H. Lilja, A. Bjartell, *Luminescence* **2000**, *15*, 389 – 397.
[169] E. Smythe, G. Warren, *Eur. J. Biochem.* **1991**, *202*, 689 – 699.
[170] M. Han, X. Gao, J. Z. Su, S. M. Nie, *Nat. Biotechnol.* **2001**, *19*, 631 – 635.
[171] S. Pathak, S. K. Choi, N. Arnheim, M. E. Thompson, *J. Am. Chem. Soc.* **2001**, *123*, 4103 – 4104.
[172] K. Riwotzki, H. Meyssamy, H. Schnablegger, A. Kornowski, M. Haase, *Angew. Chem.* **2001**, *113*, 574 – 578; *Angew. Chem. Int. Ed.* **2001**, *40*, 573 – 576.
[173] The colloidal gold-based detection of nucleic acids in homogeneous solutions can be enhanced by subsequent adsorption of the aggregates on filter membranes: a) R. Elghanian, J. J. Storhoff, R. C. Mucic, R. L. Letsinger, C. A. Mirkin, *Science* **1997**, *277*, 1078 – 1081; b) J. J. Storhoff, R. Elghanian, R. C. Mucic, C. A. Mirkin, R. L. Letsinger, *J. Am. Chem. Soc.* **1998**, *120*, 1959 – 1964; c) R. A. Reynolds, C. A. Mirkin, R. L. Letsinger, *J. Am. Chem. Soc.* **2000**, *122*, 3795 – 3796.
[174] T. A. Taton, R. C. Mucic, C. A. Mirkin, R. L. Letsinger, *J. Am. Chem. Soc.* **2000**, *122*, 6305 – 6306.
[175] J. Reichert, A. Csaki, J. M. Köhler, W. Fritzsche, *Anal. Chem.* **2000**, *72*, 6025 – 6029.
[176] R. Möller, A. Csaki, J. M. Köhler, W. Fritzsche, *Nucleic Acids Res.* **2000**, *28*, E91.
[177] C. M. Niemeyer, B. Ceyhan, S. Gao, L. F. Chi, S. Peschel, U. Simon, *Colloid Polym. Sci.* **2001**, *279*, 68 – 72.
[178] A. Csaki, R. Möller, W. Straube, J. M. Köhler, W. Fritzsche, *Nucleic Acids Res.* **2001**, *29*, E81 – 81.
[179] S. Han, J. Lin, F. Zhou, R. L. Vellanoweth, *Biochem. Biophys. Res. Commun.* **2000**, *279*, 265 – 269.
[180] Particles of different morphology have also been assembled by means of DNA hybridization: a) gold nanowires: J. K. N. Mbindyo, B. D. Reiss, B. R. Martin, C. D. Keating, M. J. Natan, T. E. Mallouk, *Adv. Mater.* **2001**, *13*, 249 – 254; b) gold nanorods: E. Dujardin, L. B. Hsin, C. R. C. Wang, S. Mann, *Chem. Commun.* **2001**, 1264 – 1265.
[181] T. A. Taton, C. A. Mirkin, R. L. Letsinger, *Science* **2000**, *289*, 1757 – 1760.
[182] For reviews on DNA microarray technology, see: a) D. H. Blohm, A. Guiseppi-Elie, *Curr. Opin. Biotechnol.* **2001**,*12*, 41 – 49; b) C. M. Niemeyer, D. Blohm, *Angew. Chem.* **1999**, *111*, 3039 – 3043; *Angew. Chem. Int. Ed.* **1999**, *38*, 2865 – 2869; c) E. M. Southern, K. Mir, M. Shchepinov, *Nat. Genet.* **1999**, *21*, 5 – 9; see also the series of review articles published in this supplement of *Nature Genetics* and in the January issue of *Curr. Opin. Chem. Biol.* **2001**, *5*.
[183] T. A. Taton, G. Lu, C. A. Mirkin, *J. Am. Chem. Soc.* **2001**, *123*, 5164 – 5165.
[184] L. Lin, H. Zhao, J. Li, J. Tang, M. Duan, L. Jiang, *Biochem. Biophys. Res. Commun.* **2000**, *274*, 817 – 820.
[185] S. B. Han, J. Q. Lin, M. Satjapipat, A. J. Baca, F. M. Zhou, *Chem. Commun.* **2001**, 609 – 610.
[186] X. D. Su, S. F. Y. Li, S. J. O'Shea, *Chem. Commun.* **2001**, 755 – 756.
[187] G. R. Souza, J. H. Miller, *J. Am. Chem. Soc.* **2001**, *123*, 6734 – 6735.
[188] I. Willner, F. Patolsky, J. Wasserman, *Angew. Chem.* **2001**, *113*, 1913 – 1916; *Angew. Chem. Int. Ed.* **2001**, *40*, 1861 – 1864.
[189] For reviews on gene-gun technology, see: a) M. T. Lin, L. Pulkkinen, J. Uitto, K. Yoon, *Int. J. Dermatol.* **2000**, *39*, 161 – 170; b) see ref. [156]; c) examples for biolistic transfection: A. Udvardi, I. Kufferath, H. Grutsch, K. Zatloukal, B. Volc-Platzer, *J. Mol. Med.* **1999**, *77*, 744 – 750; S. Kuriyama, A. Mitoro, H. Tsujinoue, T. Nakatani, H. Yoshiji, T. Tsujimoto, M. Yamazaki, H. Fukui, *Gene Ther.* **2000**, *7*, 1132 – 1136; B. Wetterauer, K. Salger, P. Demel, H. Koop, *Biochim. Biophys. Acta* **2000**, *1499*, 139 – 143; V. B. Vassilev, L. H. Gil, R. O. Donis, *Vaccine* **2001**, *19*, 2012 – 2019; d) silica nanoparticles for DNA transfection: C. Kneuer, M. Sameti, U. Bakowsky, T. Schiestel, H. Schirra, H. Schmidt, C. M. Lehr, *Bioconjugate Chem.* **2000**, *11*, 926 – 932.
[190] For reviews on DNA vaccination, see: S. Gurunathan, D. M. Klinman, R. A. Seder, *Annu. Rev. Immunol.* **2000**, *18*, 927 – 974; D. J. Shedlock, D. B. Weiner, *J. Leukocyte Biol.* **2000**, *68*, 793 – 806; E. F. Fynan, R. G. Webster, D. H. Fuller, J. R. Haynes, J. C. Santoro, H. L. Robinson, *Proc. Natl. Acad. Sci. USA* **1993**, *90*, 11 478 – 11 482; overview on delivery systems for gene-based vaccines: T. W. Dubensky, M. A. Liu, J. B. Ulmer, *Mol. Med.* **2000**, *6*, 723 – 732; immunization of mice with peptomers covalently coupled to aluminum oxide nanoparticles: A. Frey, N. Mantis, P. A. Kozlowski, A. J. Quayle, A. Bajardi, J. J. Perdomo, F. A. Robey, M. R. Neutra, *Vaccine* **1999**, *17*, 3007 – 3019.
[191] a) A. Jordan, P. Wust, R. Scholz, B. Tesche, H. Fähling, T. Mitrovics, T. Vogl, J. Cervos-Navarro, R. Felix, *Int. J. Hyperthermia* **1996**, *12*, 705 – 722; b) A. Jordan, P. Wust, R. Scholz, T. Mitrovics, H. Fähling, J. Gellermann, T. Vogl, J. Cervos-Navarro, R. Felix, *Int. J. Hyperthermia* **1997**, *13*, 587 – 605; c) A. Jordan, R. Scholz, P. Wust, T. Schiestel, H. Schmidt, R. Felix, *J. Magn. Magn. Mater.* **1999**, *194*, 185 – 196; d) A. Jordan, R. Scholz, P. Wust, H. Fähling, *J. Magn. Magn. Mater.* **1999**, *201*, 413 – 419.
[192] Examples of sequence-specific binding and bending of DNA by proteins: a) S. Becker, B. Groner, C. W. Muller, *Nature* **1998**, *394*, 145 – 151; b) N. C. Horton, J. J. Perona, *J. Mol. Biol.* **1998**, *277*, 779 – 787; c) D. N. Paolella, Y. Liu, A. Schepartz, *Biochemistry* **1997**, *36*, 779 – 787; d) *DNA – Protein Interactions* (Ed.: D. M. J. Lilley), IRL/Oxford University Press, New York, **1995**.
[193] K. Luger, A. W. Maeder, R. K. Richmond, D. F. Sargent, T. J. Richmond, *Nature* **1997**, *389*, 251 – 260.
[194] J. L. Workman, R. E. Kingston, *Ann. Rev. Biochem.* **1998**, *67*, 549 – 579.

[195] D. S. Goodsell, M. L. Kopka, D. Cascio, R. E. Dickerson, *Proc. Natl. Acad. Sci. USA* **1993**, *90*, 2930 – 2934.
[196] I. Brukner, S. Susic, M. Dlakic, A. Savic, S. Pongor, *J. Mol. Biol.* **1994**, *236*, 26 – 32.
[197] L. A. Gearheart, H. J. Ploehn, C. J. Murphy, *J. Phys. Chem. B* **2000**, submitted.
[198] For reviews, see: a) *Biomineralization: Chemical and Biological Perspectives* (Eds.: S. Mann, J. Webb, R. J. P. Williams), VCH, Weinheim, **1989**; b) S. Mann, *Angew. Chem.* **2000**, *112*, 3532 – 3548; *Angew. Chem. Int. Ed.* **2000**, *39*, 3392 – 3406; c) structural biology of the developing dental matrix: A. G. Fincham, J. Moradian-Oldak, J. P. Simmer, *J. Struct. Biol.* **1999**, *126*, 270 – 299; d) For the biomimetic production of ceramic mesostructures with self-assembled surfactants and polymers, see: D. M. Dabbs, I. A. Aksay, *Annu. Rev. Phys. Chem.* **2000**, *51*, 601 – 622.
[199] F. E. Round, R. M. Crawford, D. G. Mann, *The Diatoms: Biology and Morphology of the Genera*, Cambridge University Press, Cambridge, **1990**.
[200] N. Kroger, R. Deutzmann, M. Sumper, *Science* **1999**, *286*, 1129 – 1132.
[201] N. Kroger, R. Deutzmann, C. Bergsdorf, M. Sumper, *Proc. Natl. Acad. Sci. USA* **2000**, *97*, 14133 – 14138.
[202] a) For a recent review, see: R. N. Ben, *ChemBioChem* **2001**, *2*, 161 – 166; for examples of the molecular structure of antifreeze proteins, see: b) S. P. Graether, M. J. Kuiper, S. M. Gagne, V. K. Walker, Z. Jia, B. D. Sykes, P. L. Davies, *Nature* **2000**, *406*, 325 – 328; c) S. P. Graether, C. I. DeLuca, J. Baardsnes, G. A. Hill, P. L. Davies, Z. Jia, *J. Biol. Chem.* **1999**, *274*, 11842 – 11847; d) W. Gronwald, M. C. Loewen, B. Lix, A. J. Daugulis, F. D. Sonnichsen, P. L. Davies, B. D. Sykes, *Biochemistry* **1998**, *37*, 4712 – 4721; e) A. Cheng, K. M. Merz, *Biophys. J.* **1997**, *73*, 2851 – 2873; f) Z. Jia, C. I. DeLuca, H. Chao, P. L. Davies, *Nature* **1996**, *384*, 285 – 288;.
[203] For reviews, see: a) D. Schüler, R. B. Frankel, *Appl. Microbiol. Biotechnol.* **1999**, *52*, 464 – 473; c) M. Sarikaya, *Proc. Natl. Acad. Sci. USA* **2000**, *97*, 14183 – 14185; c) vertebrate magnetoreceptor: C. E. Diebel, R. Proksch, C. R. Green, P. Neilson, M. M. Walker, *Nature* **2000**, *406*, 299 – 302.
[204] C. T. Dameron, B. R. Smith, D. R. Winge, *J. Biol. Chem.* **1989**, *264*, 17355 – 17360.
[205] C. T. Dameron, D. R. Winge, *Trends Biotechnol.* **1990**, *8*, 3 – 6.
[206] R. Joerger, T. Klaus, C. G. Granqvist, *Adv. Mater.* **2000**, *12*, 407 – 409.
[207] S. K. Lower, M. F. Hochella, Jr., T. J. Beveridge, *Science* **2001**, *292*, 1360 – 1363.
[208] J. F. Banfield, S. A. Welch, H. Zhang, T. Thomson Ebert, R. L. Penn, *Science* **2000**, *289*, 751 – 754.
[209] a) M. Kam, D. Perl-Treves, R. Sfez, L. Addadi, *J. Mol. Recognit.* **1994**, *7*, 257 – 264; b) N. Kessler, D. Perl-Treves, L. Addadi, *FASEB J.* **1996**, *10*, 1435 – 1442; c) D. Perl-Treves, N. Kessler, D. Izhaky, L. Addadi, *Chem. Biol.* **1996**, *3*, 567 – 577; d) D. Izhaky, L. Addadi, *Adv. Mater.* **1998**, *10*, 1009; e) D. Izhaky, L. Addadi, *Chem. Eur. J.* **2000**, *6*, 869 – 874.
[210] D. Kadereit, J. Kuhlmann, H. Waldmann, *ChemBioChem* **2000**, *1*, 145 – 169.
[211] M. Famulok, G. Mayer, M. Blind, *Acc. Chem. Res.* **2000**, *33*, 591 – 599.
[212] *Nat. Biotechnol.* **2000**, *18*, Supplement IT 56 – 58.
[213] R. F. Service, *Science* **1999**, *285*, 184 – 185.
[214] K. C. Nicolaou, D. Vourloumis, N. Winssinger, P. S. Baran, *Angew. Chem.* **2000**, *112*, 47 – 126; *Angew. Chem. Int. Ed.* **2000**, *39*, 44 – 122.
[215] K. Matsuura, M. Hibino, Y. Yamada, K. Kobayashi, *J. Am. Chem. Soc.* **2001**, *123*, 357 – 358.
[216] S. M. Waybright, C. P. Singleton, K. Wachter, C. J. Murphy, U. H. F. Bunz, *J. Am. Chem. Soc.* **2001**, *123*, 1828 – 1833.
[217] J. E. Gestwicki, L. E. Strong, L. L. Kiessling, *Angew. Chem.* **2000**, *112*, 4741 – 4744; *Angew. Chem. Int. Ed.* **2000**, *39*, 4567 – 4570.
[218] K. C. Grabar, J. E. Deutsch, M. J. Natan, *J. Polym. Prepr.* **1995**, 69 – 70.
[219] W.-L. Shaiu, D. D. Larson, J. Vesenka, E. Henderson, *Nucleic Acids Res.* **1993**, *21*, 99 – 103.
[220] S. K. Chopra, J. C. Martin, *Heteroat. Chem.* **1991**, *2*, 71 – 79.
[220] Since the submission of this manuscript, further progress in this rapidly expanding field of research has been published: a) DNA–nanoparticle conjugates: DNA-modified superparamagnetic 3-nm iron oxide particles, which self-assemble in the presence of complementary single-stranded DNA, could be used as magnetic nanosensors: L. Josephson, J. M. Perez, R. Weissleder, *Angew. Chem.* **2001**, *113*, 3304 – 3306; *Angew. Chem. Int. Ed.* **2001**, *40*, 3204 – 3206; patterns of mercaptohexadecanoic acid produced by Dip-Pen nanolithography were chemically modified with DNA oligomers to assemble orthogonally gold nanoparticles, functionalized with complementary oligonucleotides: L. M. Demers, S.-J. Park, T. A. Taton, Z. Li, C. A. Mirkin, *Angew. Chem.* **2001**, *113*, 3161 – 3163; *Angew. Chem. Int. Ed.* **2001**, *40*, 3071 – 3073; DNA-modified core-shell Ag/Au nanoparticles: Y. W. Cao, R. Jin, C. A. Mirkin, *J. Am. Chem. Soc.* **2001**, *123*, 7961 – 7962; DNA transcription is inhibited by cationic mixed monolayer protected gold clusters: C. M. MacIntosh, E. A. Esposito, A. K. Boal, J. M. Simard, C. T. Martin, V. M. Rotello, *J. Am. Chem. Soc.* **2001**, *123*, 7626 – 7629; b) gold nanoparticles functionalized with proteins and biomimetic linker units: characterization of protease-coated colloidal gold: A. Gole, C. Dash, C. Soman, S. R. Sainkair, M. Rao, M. Sastry, *Bioconjug. Chem.* **2001**, *12*, 684 – 690; Lectin-induced association of gold particles modified with α-Lactosyl-ω-mercaptopoly(ethylene glycol): H. Otsuka, Y. Akiyama, Y. Nagasaki, K. Kataoka, *J. Am. Chem. Soc.* **2001**, *123*, 8226 – 8230; gold nanoparticles functionalized with elastin biopolymers: N. Nath, A. Chilkoti, *J. Am. Chem. Soc.* **2001**, *123*, 8197 – 8202; resorcinarene tetrathiols were used as biomimetic linker units to organize large gold nanoparticles: B. Kim, S. L. Tripp, A. Wei, *J. Am. Chem. Soc.* **2001**, *123*, 7955 – 7956; c) SFM cantilever-based nanomechanical sensor devices (ref. [69]) have been applied in the detection of cancer antigens (G. Wu, R. H. Datar, K. M. Hansen, T. Thundat, R. J. Cote, A. Majumdar, *Nat. Biotechnol.* **2001**, *19*, 856 – 860) and single nucleotide polymorphisms (K. M. Hansen, H. F. Ji, G. Wu, R. Datar, R. Cote, A. Majumdar, T. Thundat, *Anal. Chem.* **2001**, *73*, 1567 – 1571). Systematic DNA hybridization experiments revealed that the nanomechanical motion response of the cantilever is caused by changes in configurational entropy and intermolecular energetics induced by specific biomolecular interactions: G. Wu, H. Ji, K. Hansen, T. Thundat, R. Datar, R. Cote, M. F. Hagan, A. K. Chakraborty, A. Majumdar, *Proc. Natl. Acad. Sci. USA* **2001**, *98*, 1560 – 1564.

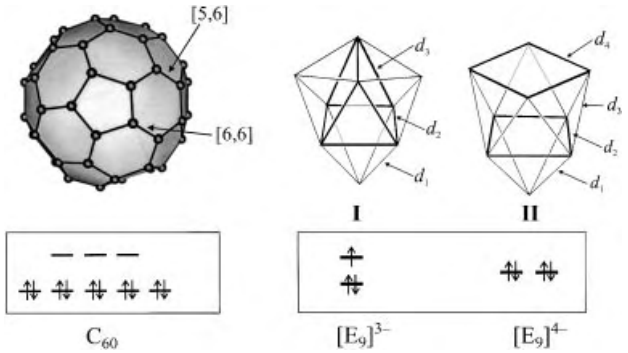
Homoatomic Polyhedra as Structural Modules in Chemistry: What Binds Fullerenes and Homonuclear Zintl Ions?**

Thomas F. Fässler*

Ligand-free homoatomic polyhedra are fascinating, not only because of their aesthetic simplicity but also because of their physical and chemical properties. They serve as electron reservoirs, show structural changes that depend upon the electron count, and can be used as "superatomic" building blocks for the targeted assembly of complex structures. Herein, the increasingly pronounced relationship between the fullerides and the nine-atom Zintl ions, the terels, is considered, even though one class of the compounds can be described as large polyhedra with classical bonds and the other as small clusters with nonclassical bonds (Wade rules). In both classes soluble salts with isolated ions, polymer chains, and binary phases with strong interactions between the ions occur.

The beauty[1] of nine-atom polyhedra E_9 of heavy elements from the carbon subgroup does not pale to the aesthetics of carbon fullerenes. Zintl ions of Group 14 elements and fullerenes are remarkable because they form highly symmetrical homoatomic polyhedral frameworks of varying size (Scheme 1). Polyhedral E_9 clusters have been the subject of intensive investigation for several decades,[2–6] long before the fullerenes were discovered.[7] Along with the boom in fullerene chemistry,[8] which started with the large-scale synthesis of C_{60},[9] recent years have also marked a growing renaissance in the chemistry of homoatomic Zintl ions.[10–13] The parallels between the two fields,[13] rather unnoticed before, have been impressively confirmed with the synthesis of anionic polymeric chains containing connected $^1_\infty\{C_{70}^{2-}\}$[14] and $^1_\infty\{[Ge_9]^{2-}\}$ ions[15] (Figure 1a and b).

Since the discovery of C_{60}, a large number of C_n molecules and C_n anions have been reported; however, only a few were structurally characterized in the solid state. Most of the research was focused on the C_{60} and C_{70} molecules, which are relatively easy to obtain compared to other fullerenes.[16–18] In contrast, a large number of structures have been characterized for E_n polyhedra containing the heavy homologues of carbon (E = Si, Ge, Sn, Pb). Many structures of anions such as $[E_4]^{4-}$, $[E_4]^{6-}$, $[E_5]^{2-}$, $[E_6]^{2-}$, $[E_9]^{3-}$, $[E_9]^{4-}$, and $[E_{10}]^{2-}$ are known from single-crystal X-ray structure analysis. There are also mass spectrometry data for the heavy homologues, confirming the existence of larger cluster anions $[E_n]^-$ and $[AE_n]^-$[19] and cations $[A_mE_n]^+$ (A = alkali metal).[20]



Scheme 1. The structures and degenerate valence orbitals of a) fullerene C_{60} and b) the Zintl ions $[E_9]^{3-}$ and $[E_9]^{4-}$.

Besides the preferred formation of homoatomic polyhedra, the reactivity of fullerenes and fullerene anions also displays remarkable analogy to the chemistry of homoatomic Zintl ions. This parallel is, however, not all that surprising if homoatomic Zintl ions of Group 14 elements are regarded as heavy homologues of the fullerenes. In the fullerene family, the C_{60} and C_{70} molecules are outstanding due to their stability and developed synthetic routes. For homoatomic clusters, E_4 and E_9 frameworks are the most frequent for E = Si to Pb. Anionic E_9 clusters with E = Ge, Sn, and Pb are also stable in solution and thus, like fullerenes and fullerides, can be used for reactions in solution. A controlled arrangement of redox-active polyhedral C_n and E_n units over one, two, or three dimensions opens a new way to the "bottom-up" synthesis of materials with switchable electronic properties. Covalent bonding between polyhedra leads to stable aggregates. In comparison with supramolecular structures based on C_{60} with relatively weak interactions between the units,[21, 22] these covalent aggregates could be retained even upon reduction or

[*] Prof. Dr. T. F. Fässler
Institut für Anorganische Chemie
Technische Universität Darmstadt
Petersenstrasse 18, 64287 Darmstadt (Germany)
Fax: (+49) 6151-166029
E-mail: faessler@ac.chemie.tu-darmstadt.de

[**] This work was supported by the Deutsche Forschungsgemeinschaft.

 © WILEY-VCH Verlag GmbH, D-69451 Weinheim, 2001 1433-7851/01/4022-4161 $ 17.50+.50/0

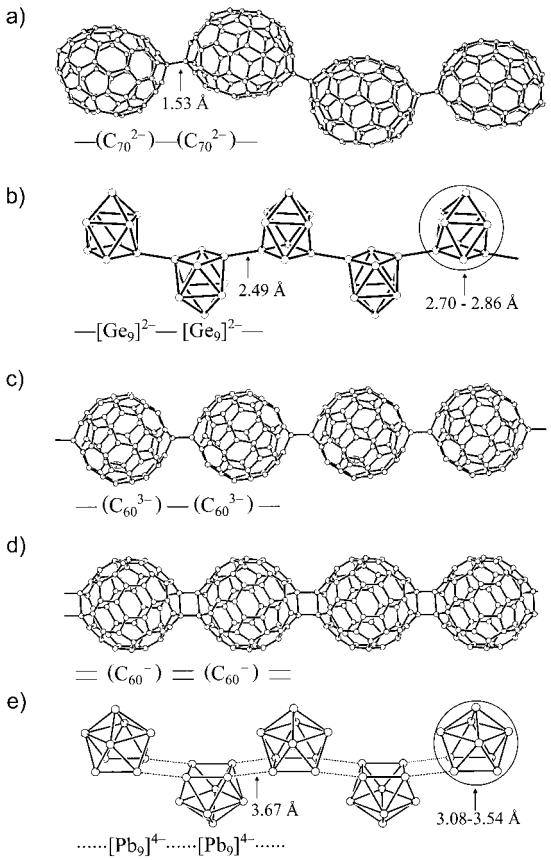


Figure 1. Structural fragments of linear polymers: a) $^1_\infty\{C_{70}^{2-}\}$ in $[Ba(NH_3)_9][C_{70}](NH_3)_7$,[14] b) $^1_\infty\{[Ge_9]^{2-}\}$ in $[K([18]crown-6)]_2[Ge_9](en)$ (en = ethylenediamine),[15] c) $^1_\infty\{C_{60}^{3-}\}$ in Na_2RbC_{60},[36] d) $^1_\infty\{C_{60}^{-}\}$ in RbC_{60},[38] e) the arrangement of $[Pb_9]^{4-}$ ions in K_4Pb_9.[49]

oxidation and, with the proper choice of covalent bridge, could exhibit an electronic interaction between the units.

In the following the close relationship of the C_{60} and C_{70} fullerenes to nine-atom clusters of heavy tetrel elements is discussed on the basis of structural aspects, mostly taking into account the compounds that are unambiguously structurally characterized. All the structures of the E_9 clusters in question are ordered and were determined using X-ray diffraction methods on single crystals. In the case of fullerenes and fullerides, due to the lack of single-crystal data, controversial structural models are also included. Parallels between electronic and magnetic properties are pointed out, when appropriate.

Fullerene carbon cages represent frameworks of strong covalent bonds, which can be described in terms of two-center, two-electron bonds and a conjugated π system. The localization of double bonds leads to different interatomic distances for the [6,6] and [5,5] ring connections (1.38 and 1.45 Å, respectively, Scheme 1). When the fullerenes are reduced to the sixfold negatively charged ions C_{60}^{6-}[23] (Scheme 1, left) and C_{70}^{6-}, their frameworks are preserved.[24] Jahn–Teller distortions, which are expected on the way from neutral cages to the maximally reduced anions in the case of nonsymmetrical population of the degenerate LUMOs of C_{60}, are structurally hardly noticeable.[17, 25, 26] In this respect nine-atom Zintl ions behave very differently. Their frameworks possess structures inbetween the trigonal tricapped prism **I** and the monocapped square antiprism **II** (Scheme 1, right). Structure **I** features three different interatomic distances ($d_2 > d_3 > d_1$), while structure **II** has two ($d_2 > d_1 \approx d_3 \approx d_4$).[27] The expected structure type can be rationalized using the electron counting rules developed by Wade for boranes and carboranes, provided that the B–H and C–H *exo* bonds of homoatomic clusters are substituted by free electron pairs. According to Wade's rules, anions $[E_9]^{2-}$ and $[E_9]^{4-}$ with 38 and 40 valence electrons should possess structures of the *closo* type **I** and *nido* type **II**, respectively. Oxidation of the *nido*-cluster should lead to a distinct change of the structure. Until now, only 39- and 40-electron clusters are unequivocally characterized. In solution and at room temperature the different atomic positions of the $[Sn_9]^{4-}$ and $[Pb_9]^{4-}$ ions are indistinguishable on the NMR timescale. The flexibility of the polyhedra reveals itself in the solid state. A large number of structural investigations of salts containing large counterions (and therefore clusters with only van der Waals type interactions) and binary Zintl phases with strong interactions between the ions have demonstrated that the $[E_9]^{4-}$ polyhedra can undergo strong distortions independant of crystal packing.[13] Many clusters do not strictly obey Wades' rules.

Fullerenes and Zintl ions both form stable radicals. The ESR signals were registered for C_{60}^{x-} ($x = 1-5$) and C_{70}^{-}. The interpretation of the spectra is complex since the energy differences between the possible spin states are small, the effects of disproportionation and dimerization must be taken into account in solution, and samples that are available only in the solid state are often poorly characterized. Magnetic measurements are more reliable; however, up to now they also failed to provide a fully coherent picture.[17, 26] Paramagnetic species $[E_9]^{3-}$ are readily available by oxidation of $[E_9]^{4-}$. The ESR spectra of single crystals and powder suggest the existence of radicals for E = Ge, Sn, and Pb. Magnetic measurements for E = Sn and Pb also indicate that compounds with mixed-valent anions $[E_9]^{2-}/[E_9]^{4-}$ are formed.[28] Distortions of the polyhedra, observed for $[E_9]^{3-}$ ions, may be regarded as a pronounced Jahn–Teller effect (Scheme 1).

In spite of substantial differences in chemical bonding and framework flexibility, fullerides and E_9 clusters equally function as ligands in transition metal complexes. Unsubstituted C_{60} acts as a η^2 ligand (Figure 2a), which is in agreement with limited aromaticity[29] and alternating double and single bonds of [6,6] and [5,5] ring connections. Metal atoms are coordinated by the [6,6] double bond. Substituted fullerenes display η^5 coordination, as the example of $[(\eta^5\text{-}Ph_5C_{60})Tl]$ shows.[30] For E_9 clusters η^4 coordination to the $Cr(CO)_3$ fragment is exclusively observed (Figure 2b; E = Sn, Pb). In salts with $[A^+([18]crown-6)]$ counterions, C_{60}^{3-} and $[E_9]^{4-}$ ions coordinate the alkali metal atoms.[31] In $[K([18]crown-6)]_3[\eta^6,\eta^6\text{-}C_{60}](\eta^3\text{-}C_6H_5CH_3)_2$ two potassium cations sit unsymmetrically above the six-membered rings of the fullerene trianions (Figure 2c), while E_9 polyhedra prefer to coordinate with their triangular faces.[32] However, coordination involving square faces of the polyhedron is also possible (Figure 2d).[33] Finally, there are two-dimensional layers of C_{60}^{2-} ions and one-dimensional arrangements of E_9 clusters in the

 © WILEY-VCH Verlag GmbH, D-69451 Weinheim, 2001 1433-7851/01/4022-4162 $ 17.50+.50/0 *Angew. Chem. Int. Ed.* **2001**, *40*, No. 22

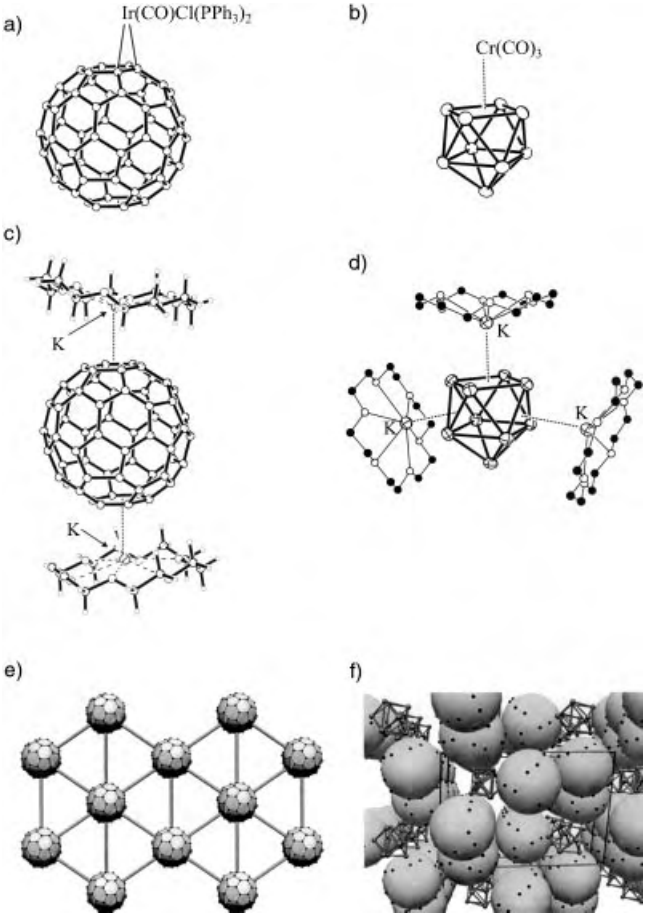


Figure 2. The structures and structural fragments of complexes: a) $[(\eta^2\text{-}C_{60})Ir(CO)Cl(PPh_3)_2]$,[50] b) $[K([2.2.2]crypt)]_4[(CO)_3Cr][\eta^4\text{-}E_9]$ (E = Sn, Pb),[51, 52] c) $[K([18]crown\text{-}6)]_3[\eta^6,\eta^6\text{-}C_{60}](\eta^3\text{-}C_6H_5CH_3)_2$,[26] d) $[K([18]crown\text{-}6)]_4[\eta^3,\eta^3,\eta^4\text{-}Pb_9]$,[33] e) the layer of C_{60}^{2-} ions in $[K([2.2.2]crypt)]_2[C_{60}](C_6H_5CH_3)_4$,[53] f) the arrangement of $[Ge_9]^{3-}$ clusters in $[K([2.2.2]crypt)]_3[Ge_9](en)_{0.5}$[54] (the $[K([2.2.2]crypt)]$ units are shown as large spheres, the carbon atoms as black dots).

salts with $[K^+([2.2.2]crypt)]$ counterions.[34] The distances between the centers of mass of the polyhedra are longer than 12.8 and 8 Å for the examples shown in Figures 2e and 2f, respectively.

Fullerides and E_9 clusters both form binary and ternary phases with alkali metals. Phases of the composition A_3C_{60} and $A_{3-x}A'_xC_{60}$ have been studied with particular intensity[35] due to their superconducting properties. The $Na_2A'C_{60}$ (A′ = K, Rb, Cs)[36, 37] and AC_{60} (A = K, Rb, Cs)[38] phases feature short distances between the C_{60} anions. Although the carbon positions cannot be unambiguously determined from the X-ray powder data, the polymers shown in Figure 1c and 1d are obtained as the best fit of the data using the Rietveld method. The two polymer structures show only small differences in the distances between the centers of the polyhedra (9.36 Å in Na_2RbC_{60}[37] and 9.14 Å in RbC_{60}[38]). The bonds between the anions result from the different orientations of the fullerene molecules. The fit was performed by gradual rotation of the C_{60} molecule and produced only small differences in the *R* factors for both models. In Na_2RbC_{60} the C_{60}^{3-} ions are connected by a C–C single bond. Its length after multiple successive refinement steps was determined to be 1.70 Å. In AC_{60} the bonding between the C_{60}^- ions is analogous to a [2+2] cycloaddition of two bonds. The C_{60}^- ions are connected through [6,6] bonds, which are elongated to the outstanding value of 1.90 Å (Figure 1d), forming the four-membered cycle. The shortest distance between carbon atoms of two neighboring fullerenes is 1.43 Å and thus within the range of a C–C single bond. The phase diagram of alkali metals and C_{60} are complex, and often the quality of the X-ray powder data is insufficient. Therefore, the models shown in Figure 1c and 1d are rather questionable and still the subject of discussion.[39] Noteworthy is a similar linear arrangement of the $[Pb_9]^{4-}$ ions in K_4Pb_9.[40] There are also two relatively short distances between polyanions (Figure 1e).[41] The *exo* bonds are only slightly longer than the interatomic distances in polyhedra and, hence, longer than typical Pb–Pb single bonds. Polymerization of Zintl ions in the solid state is known and was first studied on the example of Ba_3Ge_4 single crystals. Isolated $[Ge_4]^{6-}$ clusters with a butterfly structure of the high-temperature phase β-Ba_3Ge_4 Link into chains $^1_\infty\{[Ge_4]^{6-}\}$ in the α phase at lower temperature.[42]

Successful aggregation of anions in solution into one-dimensional polymers opens new possibilities for the design and construction of nanostructures. This point is proven by the examples of single-crystal analysis from fullerene chemistry and Zintl ion chemistry. By the route known since 1891—namely, reduction of the elements in liquid ammonia[2]—the linear polymer $(C_{70}^{2-})_n$ (Figure 1a) was synthesized from C_{70} and Ba. Extraction of a solidified K/Ge melt with ethylenediamine and subsequent addition of [18]crown-6 provides the polymer $([Ge_9]^{2-})_n$ (Figure 1b). While in the carbon polymers the C–C distances between fullerenes are longer than the intramolecular C–C distances, the polymer containing E_9 clusters features *exo* bonds that are shorter than the intramolecular bonds (see also Figure 3c). The reason for this is the presence of longer, delocalized bonds within the cluster polyhedra, compared to element–element single bonds.

The formation of dimers may be seen as the first step in the synthesis of a polymer. There are only a few such examples among the fullerenes and Zintl ions, nevertheless the parallels are also evident. Tribochemical treatment of the C_{60} with KCN leads to the formation of the dumbbell-shaped dimer C_{60}–C_{60}, in which two C_{60} molecules are bonded through [6,6] ring elements analogous to a [2+2] addition.[43] This is the only example of a compound with linked C_{60} molecules whose structure has been reliably determined from single-crystal data. In contrast to the polymer in Figure 1d, the bonds in the four-membered ring connecting the molecules are almost equal (1.58 and 1.57 Å). On rapid cooling of the alkali metal fullerides of the composition AC_{60} to room temperature, a metastable phase can be obtained that, analogous to the chain shown in Figure 1c, contains $(C_{60}–C_{60})^{2-}$ dimers that are connected by a C–C single bond. The tilting of the $(C_{60}–C_{60})$ units in the polymeric chain would lead to the suggested dimers. The distortion of the chain is only indicated by the appearance of weak superstructure reflections in the X-ray powder pattern.[44] The heavy-element counterpart is the dimer of two connected Ge_9 clusters $([Ge_9]–[Ge_9])^{6-}$.[45] The X-ray single-crystal investigation of the polymer provided the

bonding parameters shown in Figure 1b and proved that the clusters are connected by a Ge–Ge single bond.

Quite surprising is the fact that for the two examples shown in Figure 3a and c there are structures with similar orientations of two C_{60}^{3-} or two $[Sn_9]^{4-}$ ions, but with longer intermolecular distances. In $[K([18]crown\text{-}6)]_3[\eta^6,\eta^6\text{-}C_{60}](\eta^3\text{-}C_6H_5CH_3)_2$ the shortest distances between the carbon atoms of two C_{60}^{3-} ions turn out to be between the [5,6] ring bonds (Figure 3b).[26] Analogous to the germanium dimer, in $[K([18]crown\text{-}6)]Cs_7[Sn_9]_2$ there are two $[Sn_9]^{4-}$ clusters with almost the same orientation with respect to each other and similar coordination of bridging Cs cations (Figure 3d). The distance between the clusters is, naturally, significantly longer than the distances between the atoms within the cluster.[46]

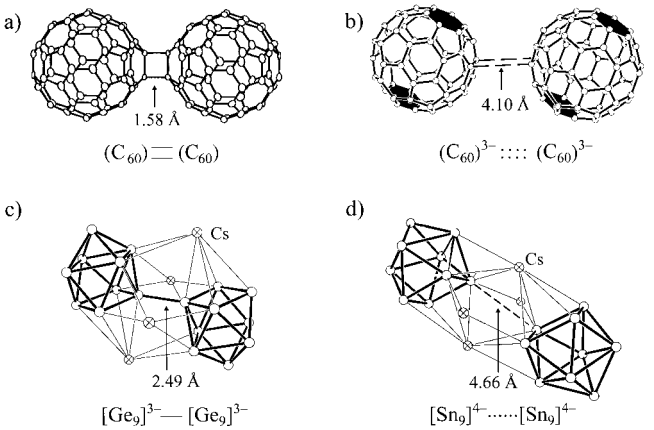


Figure 3. The structures and structural fragments of dimeric polyhedral units: a) $(C_{60})_2$,[43] b) C_{60}^{3-} ion pairs in $[K([18]crown\text{-}6)]_3[\eta^6,\eta^6\text{-}C_{60}](\eta^3\text{-}C_6H_5CH_3)_2$[26] (black shading shows the fragments coordinating potassium atoms, see Figure 2c), c) dimeric unit in $[K([2.2.2]crypt)]_2Cs_4([Ge_9]\text{–}[Ge_9])$[45], d) $[Sn_9]^{4-}$ ion pairs in $[K([18]crown\text{-}6)]Cs_7[Sn_9]_2(en)_4$.[46]

In summary, we can state that in solution fullerenes and fullerides have been better characterized than Zintl ions. Also, in the solid state fullerene compounds feature more interesting properties, such as superconductivity in A_3C_{60}. Since many of the fulleride structures are not unequivocally known, structure–property relationships can only be established in a few cases. In contrast, while the structures of many Zintl ions have been reliably determined, little is known about the physical properties of compounds containing such ions. Successful structural characterization of the $^1_\infty\{C_{70}^{2-}\}$ and $^1_\infty\{[Ge_9]^{2-}\}$ polymers from single-crystal data probably presents a milestone on the way to the controlled arrangement of clusters that may serve as electron reservoirs. We will be waiting with great interest to discover which compound turns out to possess more intriguing properties.

What is to follow? Polymers with mixed structural modules are quite possible, probably upon inclusion of particular bridging atoms between different types of polyhedra. Controlled design of large oligomers and multidimensional polymers? In the field of fullerene chemistry two- and three-dimensional linked systems are being discussed. Carbon-based polymers built from the polyhedral modules are obtained by photochemical reactions or by high-pressure and high-temperature treatment of C_{60} and C_{70}. Indeed, many structures that have been determined for this class of compounds are based on the comparison between various structural models and not on the independent structure refinement.[47] Figure 4a shows the structure of the $^2_\infty[C_{60}]$ polymer resulting from [2+2] cycloaddition. Rietveld analysis indicates that Na_4C_{60} contains a two-dimensional arrangement of C_{60}^{4-} ions, connected by four single bonds (Figure 4b).[48] Two-dimensional polymers consisting of E_9 monomers are yet to be discovered; however, a (supramolecular?) layer framework of Cs^+ and Sn_9^{4-} ions was found between the weakly bonded layers of $[K^+([18]crown\text{-}6)]$ units.[46] Analogous to the formation of the dimer $([Ge_9]\text{–}[Ge_9])^{6-}$ and the one-dimensional polymer $^1_\infty\{[Ge_9]^{2-}\}$ upon oxidative coupling [Eq. (1) and (2)], the next oxidative step would probably lead to the two-dimensional polymer $^2_\infty\{[Ge_9]\}$ [Eq. (3)]. The result

$$2\ [Ge_9]^{4-} \longrightarrow ([Ge_9]—[Ge_9])^{6-} + 2\,e^- \quad (1)$$

$$n/2\ ([Ge_9]—[Ge_9])^{6-} \longrightarrow (—[Ge_9]^{2-}—)_n + n\,e^- \quad (2)$$

$$(—[Ge_9]^{2-}—)_n \longrightarrow \begin{array}{c}|\\(—[Ge_9]—)_n\\|\end{array} + 2n\,e^- \quad (3)$$

would be a neutral, crystalline germanium allotrope built from Ge_9 modules (Figure 4c). It is worth the challenge!

Received: May 28, 2001 [M1515]

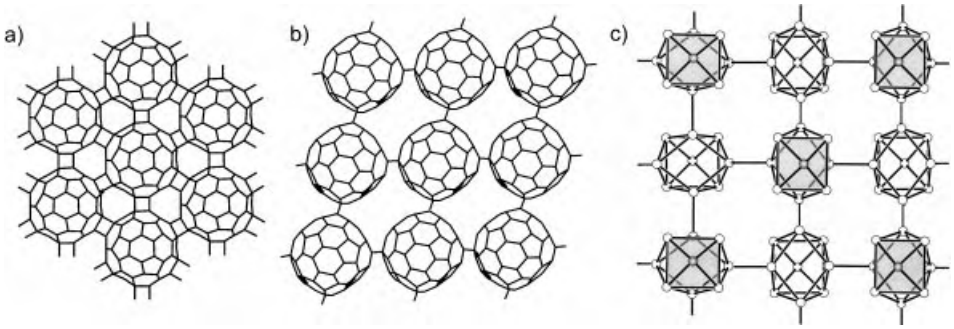


Figure 4. The structural models of a) the polymer $^2_\infty\{C_{60}\}$[47] obtained by high-pressure and high-temperature synthesis and b) the two-dimensional polymer $^2_\infty\{C_{60}^{4-}\}$ in Na_4C_{60}.[48] c) The suggested structure of a germanium allotrope in the form of the two-dimensional polymer $^2_\infty\{[Ge_9]\}$; the type **II** clusters are drawn with their square face alternating up and down.

[1] "The 40e systems Bi_9^{5+}, Sn_9^{4-}, and Ge_9^{4-} form one of the most beautiful clusters known." Quoted from H.-G. von Schnering, *Angew. Chem.* **1981**, *93*, 44–63; *Angew. Chem. Int. Ed. Engl.* **1981**, *20*, 33–51.

[2] A. Joannis, *C. R. Hebd. Seances Acad. Sci.* **1891**, *113*, 795–799.

[3] C. A. Kraus, *Trans. Am. Electrochem. Soc.* **1924**, *45*, 175–186.

[4] E. Zintl, J. Goubeau, W. Dullenkopf, *Z. Phys. Chem. A* **1931**, *154*, 1–46.

[5] L. Diehl, K. Khodadadeh, D. Kummer, J. Strähle, *Chem. Ber.* **1976**, *109*, 3404–3418.

[6] J. D. Corbett, *Chem. Rev.* **1985**, *85*, 383–397.

 © WILEY-VCH Verlag GmbH, D-69451 Weinheim, 2001 1433-7851/01/4022-4164 $ 17.50+.50/0

[7] H. W. Kroto, J. R. Heath, S. C. O'Brien, R. F. Curl, R. E. Smalley, *Nature* **1985**, *318*, 162 – 163.
[8] T. Braun, A. P. Schubert, R. N. Kostoff, *Chem. Rev.* **2000**, *100*, 23 – 37.
[9] W. Krätschmer, L. D. Lamb, K. Fostiropoulos, D. R. Huffman, *Nature* **1990**, *347*, 354 – 358.
[10] C. Belin, M. Tillard-Charbonnel, *Coord. Chem. Rev.* **1998**, *178 – 180*, 529 – 564.
[11] J. D. Corbett, *Struct. Bonding* **1997**, *87*, 157 – 193.
[12] T. F. Fässler in *Metal Clusters in Chemistry* (Eds.: P. Braunstein, L. A. Oro, P. R. Raithby), Wiley-VCH, Weinheim, **1999**, pp. 1612 – 1642.
[13] T. F. Fässler, *Coord. Chem. Rev.* **2001**, *215*, 347 – 377.
[14] H. Brumm, E. Peters, M. Jansen, *Angew. Chem.* **2001**, *113*, 2117 – 2119; *Angew. Chem. Int. Ed.* **2001**, *40*, 2069 – 2071.
[15] C. Downie, Z. Tang, A. M. Guloy, *Angew. Chem.* **2000**, *112*, 346 – 348; *Angew. Chem. Int. Ed.* **2000**, *39*, 337 – 340.
[16] M. S. Dresselhaus, G. Dresselhaus, P. C. Eklund, *Science of Fullerenes and Carbon Nanotubes*, Academic Press, New York, **1996**.
[17] C. A. Reed, R. D. Bolskar, *Chem. Rev.* **2000**, *100*, 1075 – 1119.
[18] A. Hirsch, *Angew. Chem.* **2001**, *113*, 1235 – 1237; *Angew. Chem. Int. Ed.* **2001**, *40*, 1195 – 1197.
[19] T. F. Fässler, H.-J. Muhr, M. Hunziker, *Eur. J. Inorg. Chem.* **1998**, 1433 – 1438.
[20] T. P. Martin, *Angew. Chem.* **1986**, *98*, 197 – 212; *Angew. Chem. Int. Ed. Engl.* **1986**, *25*, 195.
[21] A. M. Cassell, C. L. Asplund, J. M. Tour, *Angew. Chem.* **1999**, *111*, 2565 – 2568; *Angew. Chem. Int. Ed.* **1999**, *38*, 2403 – 2405.
[22] M. Brettreich, S. Burghardt, C. Böttcher, T. Bayerl, S. Bayerl, A. Hirsch, *Angew. Chem.* **2000**, *112*, 1915 – 1918; *Angew. Chem. Int. Ed.* **2000**, *39*, 1845 – 1848.
[23] Q. Xie, E. Perez-Cordero, L. Echegoyen, *J. Am. Chem. Soc.* **1992**, *114*, 3977.
[24] T. Sternfeld, R. E. Hoffman, I. Aprahamian, M. Rabinovitz, *Angew. Chem.* **2001**, *113*, 469 – 471; *Angew. Chem. Int. Ed.* **2001**, *40*, 455 – 457.
[25] K. Himmel, M. Jansen, *Inorg. Chem.* **1998**, *37*, 3437 – 3439.
[26] T. F. Fässler, R. Hoffmann, S. Hoffmann, M. Wörle, *Angew. Chem.* **2000**, *112*, 2170 – 2174; *Angew. Chem. Int. Ed.* **2000**, *39*, 2091 – 2094.
[27] M. Somer, W. Carrillo-Cabrera, E. M. Peters, K. Peters, H. G. von Schnering, *Z. Anorg. Allg. Chem.* **1998**, *624*, 1915 – 1921.
[28] T. F. Fässler, M. Hunziker, M. Spahr, H. Lueken, *Z. Anorg. Allg. Chem.* **2000**, *626*, 692 – 700.
[29] A. Hirsch, Z. Chen, H. Jiao, *Angew. Chem.* **2000**, *112*, 4079 – 4081; *Angew. Chem. Int. Ed.* **2000**, *39*, 3915 – 3917.
[30] A. L. Balch, M. M. Olmstead, *Chem. Rev.* **1998**, *98*, 2123 – 2165.
[31] [18]crown-6 = 1,7,10,13,16-hexaoxacyclooctadecane.
[32] T. F. Fässler, R. Hoffmann, *Angew. Chem.* **1999**, *111*, 526 – 529; *Angew. Chem. Int. Ed.* **1999**, *38*, 543 – 546.
[33] T. F. Fässler, R. Hoffmann, *J. Chem. Soc. Dalton Trans.* **1999**, 3339 – 3340.
[34] [2.2.2]crypt = 4,7,13,16,21,24-hexaoxa-1,10-diazabicyclo-[8.8.8]hexacosane.
[35] A. F. Hebard, M. J. Rosseinsky, R. C. Haddon, D. W. Murphy, S. H. Glarum, T. T. M. Palstra, A. P. Ramirez, A. R. Kortan, *Nature* **1991**, *350*, 600 – 601.
[36] G. M. Bendele, P. W. Stephens, K. Prassides, K. Vavekis, K. Kordatos, K. Tanigaki, *Phys. Rev. Lett.* **1998**, *80*, 736 – 739.
[37] A. Lappas, C. M. Brown, K. Kordatos, E. Suard, K. Tanigaki, K. Prassides, *J. Phys.: Condens. Matter* **1999**, *11*, 371.
[38] P. W. Stephens, G. Bortel, G. Faigel, M. Tegze, A. Jánossy, S. Pekker, G. Oszlanyi, L. Forró, *Nature* **1994**, *370*, 636 – 639.
[39] J. E. Fischer, *J. Phys. Chem. Solids* **1997**, *58*, 1939 – 1947.
[40] V. Quéneau, S. C. Sevov, *Inorg. Chem.* **1998**, *37*, 1358 – 1360.
[41] T. F. Fässler, S. Hoffmann, *Z. Kristallogr.* **1999**, *11*, 722 – 734.
[42] F. Zürcher, R. Nesper, *Angew. Chem.* **1998**, *110*, 3451 – 3454; *Angew. Chem. Int. Ed.* **1998**, *37*, 3314 – 3318. In Ba_3Ge_4 the intermolecular bonds (2.87 Å) are also longer than the intramolecular bonds (2.60 Å).
[43] G.-W. Wang, K. Komatsu, Y. Murata, M. Shiro, *Nature* **1997**, *387*, 583 – 586.
[44] G. Bortel, S. Pekker, L. Gránásy, G. Faigel, G. Oszlányi, *J. Phys. Chem. Solids* **1997**, *58*, 1893 – 1896.
[45] L. Xu, S. C. Sevov, *J. Am. Chem. Soc.* **1999**, *121*, 9245 – 9246.
[46] R. Hauptmann, R. Hoffmann, T. F. Fässler, *Z. Anorg. Allg. Chem.* **2001**, *627*, 2220 – 2224.
[47] Review: B. Sundqvist, *Adv. Phys.* **1999**, *48*, 99 – 116.
[48] G. Oszlányi, G. Baumgartner, G. Faigel, L. Forró, *Phys. Rev. Lett.* **1997**, *78*, 4438 – 4441.
[49] V. Quéneau, S. C. Sevov, *Inorg. Chem.* **1998**, *37*, 1358 – 1360.
[50] A. L. Balch, V. J. Catalano, J. W. Lee, *Inorg. Chem.* **1991**, *30*, 3980 – 3981.
[51] B. W. Eichhorn, R. C. Haushalter, *J. Am. Chem. Soc.* **1988**, *110*, 8704 – 8706.
[52] B. W. Eichhorn, R. C. Haushalter, *J. Chem. Soc. Chem. Commun.* **1990**, 937 – 939.
[53] T. F. Fässler, A. Spiekermann, M. Spahr, R. Nesper, *Angew. Chem.* **1997**, *109*, 502 – 504; *Angew. Chem. Int. Ed. Engl.* **1997**, *36*, 486 – 488.
[54] T. F. Fässler, M. Hunziker, *Inorg. Chem.* **1994**, *33*, 5380 – 5381.

 © WILEY-VCH Verlag GmbH, D-69451 Weinheim, 2001 1433-7851/01/4022-4165 $ 17.50+.50/0

Pauling's Left-Handed α-Helix

Jack D. Dunitz*

On February 28, 1951, his fiftieth birthday, Linus Pauling (Figure 1) submitted to the *Proceedings of the United States National Academy of Sciences* a paper entitled "The Structure of Proteins: Two Hydrogen-Bonded Helical Configurations of the Polypeptide Chain".[1] This paper can be regarded as a milestone in twentieth century science: One of the structures

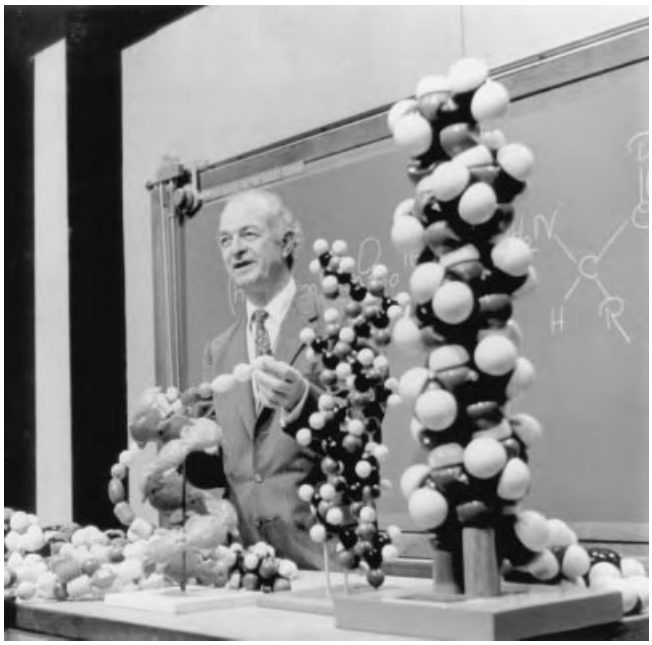


Figure 1. Linus Pauling (1901–1994) surrounded by molecular models, sometime during the 1960s, from the Ava Helen and Linus Pauling Papers, Oregon State University Special Collections.

proposed there was the α-helix. Its formulation was the first and is still one of the greatest triumphs of speculative model building in molecular biology; it is the forerunner of the vast investment in computer-assisted molecular modeling in present-day research in structural chemistry. Nowadays, almost everyone is aware that the α-helix is right-handed (that is to say, if the thumb of the right hand points along the helix axis, then the helix turns in the direction indicated by the fingers of the right hand). Imagine my surprise when, a few months ago, I noticed that in the illustration of the *Proceedings* paper (Figure 2) the helix is drawn left-handed! This is not an error. The choice of a left-handed sense of helicity was made arbitrarily. As written in the paper:

> *"For glycine both the 3.7-residue helix [later named the α-helix] and the 5.1-residue helix [later named the γ-helix] could occur with either a positive or a negative rotational translation; that is, as either a positive or a negative helix, relative to the positive direction of the helical axis given by the sequence of atoms in the peptide chain. For other amino acids with the* L *configuration, however, the positive helix and the negative helix would differ in the position of the side chains, and it might well be expected that in each case one sense of the helix would be more stable than the other. An arbitrary assignment of the R groups has been made in the figures."*

The text speaks of an arbitrary assignment of the R groups, and the modern viewer will recognize that the amino acid residues in the Figure are drawn with the opposite configuration to the natural series. Around each asymmetric carbon atom C(α), the C(α)–N, C(α)–C(O), and C(α)–C(β) bonds are in clockwise sequence when viewed along the C(α)–H bond. In the naturally occurring "laevorotatory" L-amino acids this sequence is anticlockwise.[2] Thus the "arbitrary assignment of the R groups" in the Figure happens to be the incorrect one for

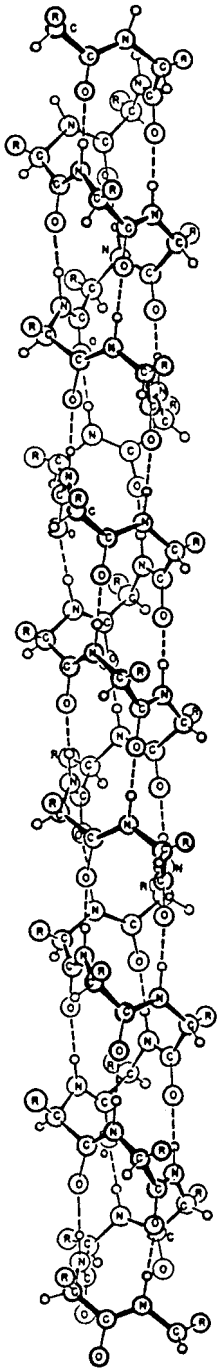


Figure 2. The helix with 3.7 residues per turn (the α-helix), as shown in figure 2 of ref. [1].

[*] Prof. J. D. Dunitz
Organic Chemistry Laboratory
ETH-Hönggerberg, 8093 Zurich (Switzerland)
Fax: (+41) 411-632-1109
E-mail: dunitz@org.chem.ethz.ch

 © WILEY-VCH Verlag GmbH, D-69451 Weinheim, 2001 1433-7851/01/4022-4167 $ 17.50+.50/0

the natural amino acids. Note also that Pauling does not commit himself about the sense of helicity; for a given configuration of the amino acids "one sense of the helix would be more stable than the other" but it is not stated which. Thus the drawing of the α-helix is based on two arbitrary choices: the configuration of the side chains (wrong) and the relative orientation of the side chains in the helix (correct). The structure depicted is the mirror image of the α-helix as it is found in protein structures. Others have certainly noticed this before and possibly drawn their own conclusions about how it came about. The question that intrigues me is this: When Pauling wrote the paper, was he unaware that the absolute configuration of the natural amino acids was already known with a high degree of certainty? It was no longer necessary to make an arbitrary choice. Or was he simply not interested in the question of absolute configuration?

The year 2001 is not only the fiftieth anniversary of the α-helix structure, it also happens to be the fiftieth anniversary of the transformation of stereochemistry from a relative to an absolute basis. This achievement became known to general scientific circles through the paper "Determination of the Absolute Configuration of Optically Active Compounds by Means of X-Rays" published in August 1951 in *Nature* by J. M. Bijvoet, A. F. Peerdeman, and A. J. van Bommel from the University of Utrecht.[3] Essentially the same information had been published by the same authors a few months earlier in the less generally available *Proceedings of the Royal Netherlands Academy of Sciences*.[4] In both papers it is explained how the absolute structure of a chiral crystal can be established from a special type of X-ray diffraction experiment involving the introduction of a phase-lag into the primary scattering process (anomalous scattering); in both papers, as first example of the use of the new method, the absolute structure of the anion in the crystalline double salt rubidium sodium (+)-tartrate (Figure 3) was described. In my student days I had been taught that a chiral crystal and its mirror image yield the same X-ray diffraction pattern, and hence the impossibility of determining the absolute structure of a chiral crystal by means of X-ray diffraction analysis. Yet here it was done! Previous to this, all stereochemical configurations of optically active substances determined by chemical means were assigned relative to an arbitrarily chosen standard. Thus, the assemblage of assigned structures was self-consistent; the individual structures were all, so to speak, consistently on one side of a mirror, but it was left undetermined as to whether these structures correspond to the real world or to a mirror-image world. As it turned out, the absolute configuration found for dextrorotatory tartaric acid (Figure 3) by X-ray diffraction happened to correspond to the one that had been arbitrarily chosen for this substance by Emil Fischer more than a half-century earlier.[5] It was therefore not necessary to rewrite all the stereochemical formulas in the chemistry textbooks. In particular, starting from the newly established (+)-tartaric acid configuration, the absolute configurations of the naturally occurring amino acids could be assigned with reasonable confidence as being the opposite of those depicted in the α-helix paper.[6]

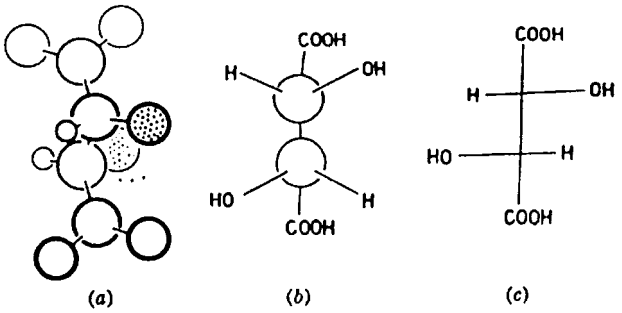


Figure 3. Absolute configuration of natural dextrorotatory tartaric acid. a) As determined by X-rays in sodium rubidium tartrate. b) In a normalized configuration by rotating around single bonds. c) In projection. Reprinted by permission from Nature 1951, *168*, 271–272, ref. [3]. Copyright 1951, Macmillan Magazines Ltd. with original explanatory text.

For those who may be interested in the physics of absolute structure determination using the anomalous scattering method, a few words on these topics may be in order; others may skip this paragraph. Our earlier belief in the "impossibility" of determining the absolute reference frame for describing a crystal structure determined by X-ray analysis had been based on the assumed validity of Friedel's Law, which states that the X-ray diffraction pattern of a crystal is centrosymmetric, whether the crystal itself is centrosymmetric or not. This "law" results from the assumption that phase differences between waves scattered at different points in a crystal depend only on path length differences, which is equivalent to the assumption that any intrinsic phase change connected with the scattering event is the same for all the atoms in the structure. It implies that reflections from opposite faces of a crystal have opposite phase but equal intensity. Since the phase is not observable, the diffraction pattern from a chiral crystal and from its enantiomorph would then be indistinguishable. However, the underlying assumption is not quite correct. When the frequency of the incident X-radiation is such that the radiation is strongly absorbed by one or more of the elements in the crystal, some of the photons scattered by those atom types experience a phase increment of $\pi/2$ with respect to photons scattered by the other atom types—it is *as if* the scattering by a strongly absorbing atom is slightly delayed compared with the others. This is what is called anomalous scattering, and the phase increment, which is independent of path length, leads to small differences in intensity between reflections from opposite crystal faces $\boldsymbol{H}(h, k, l)$ and $-\boldsymbol{H}(\bar{h}, \bar{k}, \bar{l})$ of a chiral crystal, which would otherwise have equal intensity. This is depicted diagramatically in Figure 4, taken from the original paper. Here the anomalous scatterer is rubidium. The resultant vectors $\boldsymbol{F} = \boldsymbol{F}_{\mathrm{Rb}} + \boldsymbol{F}_{\mathrm{rest}}$ for the h,k,l and $\bar{h},\bar{k},\bar{l}$ reflections have equal amplitude and opposite phase. Addition of the anomalous contribution $\Delta\boldsymbol{F}''_{\mathrm{Rb}}$ destroys this equivalence, and the pattern of such differences over many such pairs tells us whether the atomic positions in a right-handed coordinate system correspond to the set $\boldsymbol{X}_{\mathbf{i}}\{x_{\mathrm{i}}, y_{\mathrm{i}}, z_{\mathrm{i}}\}$ or $-\boldsymbol{X}_{\mathbf{i}}\{-x_{\mathrm{i}}, -y_{\mathrm{i}}, -z_{\mathrm{i}}\}$.[7] Indeed, the breakdown of Friedel's Law had been demonstrated twenty years earlier, when Coster, Knol, and Prins utilized it to determine the sense of polarity of zinc sulfide crystals.[8] It was Bijvoet (Figure 5) who realized that polarity is just one-dimensional chirality, and that the

 © WILEY-VCH Verlag GmbH, D-69451 Weinheim, 2001 1433-7851/01/4022-4168 $ 17.50+.50/0

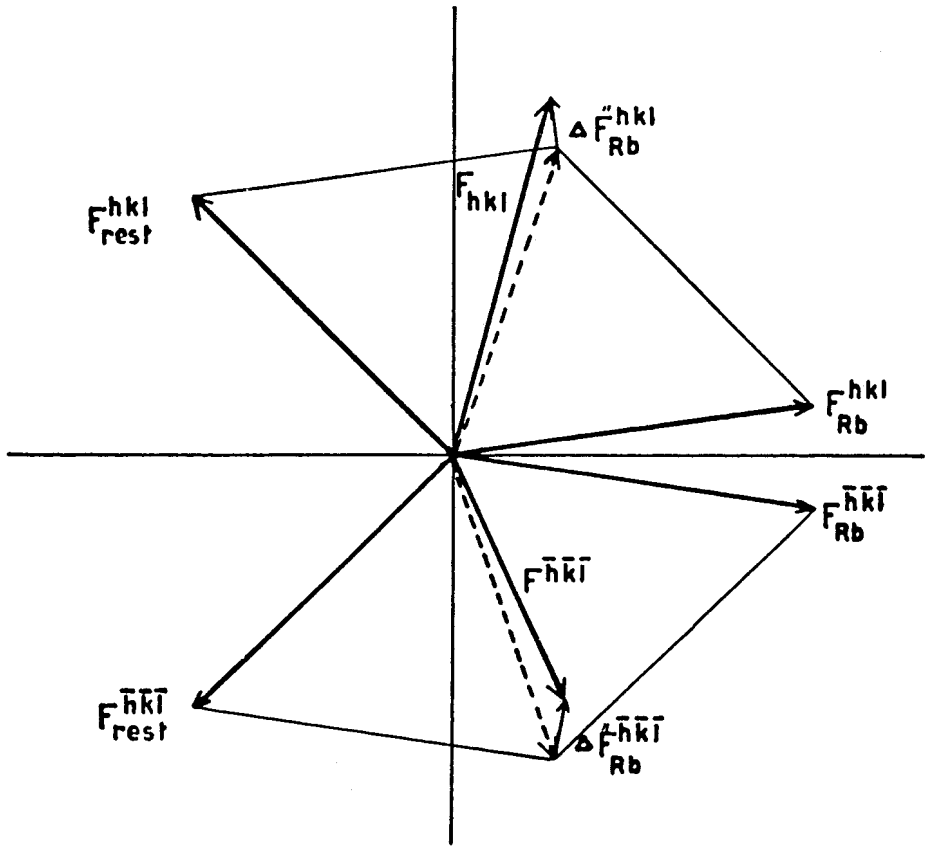


Figure 4. Diagram, reproduced from ref. [4], to illustrate these arguments for the case of sodium rubidium tartrate, where rubidium acts as the anomalous scatterer. The legend to the diagram read: The vectors $\boldsymbol{F}_{Rb}$ and $\boldsymbol{F}_{rest}$ are combined for the reflections hkl and $\bar{h},\bar{k},\bar{l}$ resp. neglecting the imaginary (anomalous) part of the structure factor of Rb. The resultant (dotted) amplitudes are of equal modulus but opposite phase. The introduction of the term $\Delta\boldsymbol{F}''_{Rb}$ with phase increment $\pi/2$ in respect to $\boldsymbol{F}_{Rb}$ is seen to destroy this equality of the resultant modulus.



Figure 5. Johannes M. Bijvoet (1892–1980) taken in 1961 by his son.

determination of the absolute structure of a chiral crystal is no different in principle from the determination of the polarity sense of zinc sulfide. Any residual doubt that may have been entertained about the sign of the phase change involved in the scattering process was effectively eliminated twenty years later by the confirmation of the polarity sense of zinc sulfide by a most unexpected method—noble gas ion reflection mass spectrometry from opposite faces of the crystal.[9] And if even this were not sufficient, an elegant and convincing "chemical" confirmation of the absolute configuration of the α-amino acids was achieved a few year later by the use of "tailor-made additives" in influencing crystal growth by selective molecular recognition and absorption on opposite crystal surfaces.[10]

I have been wondering whether Pauling knew of the result of the Bijvoet experiment when he drew the left-handed helix with the wrong configuration of the amino acid side chains. On the one hand, the Pauling paper was submitted six months before the *Nature* paper appeared and four weeks before publication of the earlier *Proceedings* paper. On the other hand, just down the corridor from Pauling's office at Caltech was the office of John G. Kirkwood (Figure 6), who was then actively investigating the problem of absolute configuration by comparing observed optical rotations of optically active compounds with values derived from his theory of optical rotatory power based on group polarizabilities. Kirkwood, as I shall show, did know about Bijvoet's work and its implications by late 1950, well before the α-helix paper was submitted.

During this period I was a postdoctoral research fellow at Caltech, and although my memory is notoriously fallible, especially about events that took place more than a half-century ago, I have a tenacious recollection that Kirkwood called me into his office one day to show me a letter he had received from a Dutch crystallographer who claimed to have found a method of establishing absolute configuration and to have used this method to determine the absolute configuration of tartaric acid; could I help to explain how this method worked? This, I am sure, was the first I had ever heard about the possibility of using X-ray diffraction to determine absolute configuration. My power to call up the past is inadequate to remember what I thought when I tried to absorb the contents of Bijvoet's letter or what I said to Kirkwood in my attempt to explain the new method. Quite likely I could see that when phase differences between waves

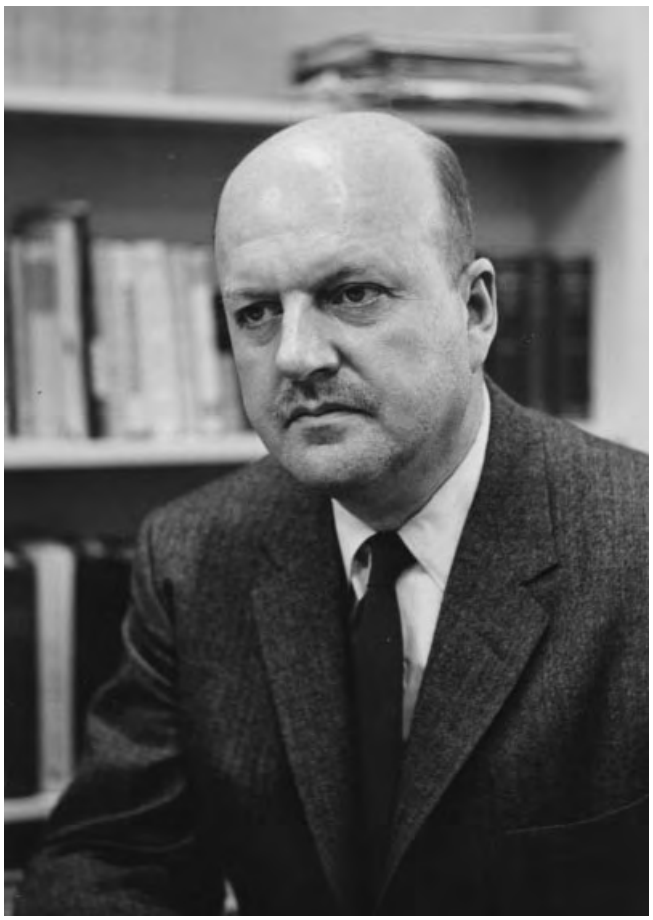


Figure 6. John G. Kirkwood (1907–1959), unknown date. Photographs of individuals maintained by the Office of Public Affairs, Yale University, Manuscripts and Archives, Yale University Library.

scattered from different atoms were no longer determined exclusively by path differences (as in "normal" X-ray diffraction), then, in principle, this would lead to a difference between the intensities of diffracted beams from opposite crystal faces and hence distinguish a chiral structure from its enantiomorph. But I am fairly sure that I could not at the time have been able to derive which enantiomorph was which. That would have been far too complicated for me. It is indeed a complicated matter, and it is easy to get mixed up and obtain the wrong answer by making a "trivial" error in sign—or rather by making an odd number of such errors. Fortunately, nowadays, the software in modern diffractometers and structure analysis and refinement packages makes it almost impossible to make a mistake. I have been able to persuade myself that these conversations with Kirkwood must have taken place sometime in 1950, in any case before Bijvoet wrote the Netherlands Academy *Proceedings* paper.

In July 1951, Kirkwood submitted a paper entitled "The Absolute Configuration of Optically Active Molecules" in which absolute configurations were assigned to the enantiomers of 2,3-epoxybutane and 1,2-dichloropropane from the good agreement between observed and calculated optical rotations.[11] Like the X-ray diffraction experiment, these results again confirmed Fischer's arbitrary assignment as the structurally correct representation of absolute configuration. A similar result was published shortly afterwards by Werner Kuhn.[12] Kirkwood's paper was submitted a month or so before publication of Bijvoet's *Nature* paper, but a footnote states that the result is consistent with that obtained by X-ray diffraction, referring to the Dutch *Proceedings* paper. Symmetrically, a footnote in the *Proceedings* paper states that the authors had learned from Kirkwood that his new calculations of rotatory power and the X-ray result were "concordant as to the assignment of absolute configuration". It is therefore evident that the Bijvoet group in Utrecht and the Kirkwood group at Caltech were in contact and knew about each other's work before the papers were sent off.

To return to Pauling: During the time when he was putting the finishing touches to his helical models of polypeptides, Kirkwood was almost certainly aware of Bijvoet's work on absolute configuration. In any case, Kirkwood was presumably fairly confident that the correctness of Fischer's configurational assignments had been confirmed by his own work.[13] While Fischer's initial assignments had been concerned with the structures of carbohydrates and related substances, the configurational relationships between carbohydrates and other classes of compounds, such as hydroxy acids and amino acids, had recently been settled with reasonable confidence by Christopher Ingold and collaborators.[6] Together with the result of Bijvoet's experiment, this made it highly probable that the natural levorotatory amino acids have the opposite configuration to that depicted in Pauling's paper (Figure 1).

Either Pauling was unaware of these developments when he wrote the α-helix paper, or he knew about them but was uninterested. The first possibility would imply that Kirkwood did not tell Pauling about Bijvoet's achievement or about his own recent work confirming Fischer's assignment and its consequences, or at least failed to draw Pauling's attention to the fact that the amino acids used in construction of the helical models had the incorrect absolute configuration. Since Pauling and Kirkwood spent their days in the same building, had nearby offices, and shared many interests, from quantum mechanics to the structure and properties of proteins, it may seem strange that there was such a lack of scientific contact between them. Although I have no evidence of this and am merely guessing, it seems highly likely that Kirkwood was present at Pauling's seminar in the biology department in the fall of 1950 when the results of the model building work were announced. Following Pauling's theatrical unveiling of his two spiral structures, did Kirkwood notice that the amino acid structural units had the wrong configuration? Possibly not. It is likely that in those days only amino acid specialists had such knowledge immediately at their fingertips, and even among them only the few with a decided inclination towards stereochemistry.[14] Or is it possible that he told Pauling about the discrepancy but in such a way or at such a moment that it made no impression? From conversations with mid-century Caltech survivors I have the impression that the relationship between the two men was not a particularly cordial one, not unfriendly perhaps but remote. Most likely there was too little communication between them.

I tend to believe that when they wrote the paper, or quite possibly even when they made the models, Pauling (or his colleague Robert B. Corey) simply picked one of the two

 © WILEY-VCH Verlag GmbH, D-69451 Weinheim, 2001 1433-7851/01/4022-4170 $ 17.50+.50/0

amino acid configurations (as it happened, the wrong one) to illustrate the helical structures and did not give the problem of absolute configuration much thought. Very likely, neither they nor any of their co-workers were especially interested in this problem or in the various conventions current in organic stereochemistry at the time. Support for this view comes from the fact that the figures in the subsequent papers in the Pauling – Corey series are not self-consistent with respect to the description of the amino acid configuration. In the paper dealing with the helical structures of poly-γ-methyl-L-glutamate and poly-γ-benzyl-L-glutamate fibers,[15] the amino acid residues are depicted (figures 2 and 3 of that paper) with the correct (*S*)-configuration (CIP system). On the other hand, in the paper describing pleated sheet protein structures,[16] the amino acid residues are drawn (figure 3 of that paper) with the (*R*)-configuration. For good measure, in the first paper of the series,[17] atomic coordinates are given for the amino acid residues in the α-helix with the two alternative positions for the C(β) atom, with no indication concerning which position corresponds to the natural series and which to its mirror image. Further support comes from a 1953 paper by Jerry Donohue in which four additional polypeptide helices were proposed, all drawn left-handed in the figures.[18] Inspection of these pictures (and of the accompanying lists of atomic coordinates) reveals that in three of them the amino acid residues have (*R*)-configuration and in the remaining one they have (*S*)-configuration. Donohue, known in his generation as a stickler for exactness in thought and expression, was clearly not interested in the question of absolute configuration of the amino acids and did not consider it important. Only in the mid-1950s were the diagrams drawn to illustrate the α-helix consistently drawn with (S)-configured amino acids.[19] Yet another expression of Pauling's lack of interest in questions of absolute configuration comes from the 1960 3rd edition of his classic "The Nature of the Chemical Bond",[20] where the topic "absolute configuration" is not mentioned in the index and where the name "Bijvoet" occurs only with reference to his early structure determinations of simple inorganic binary compounds such as mercuric bromide.

While the Caltech crystallographers appear to have shown little interest in Bijvoet's determination of absolute configuration, its reception on the other side of the Atlantic Ocean was quite different. Already in the London Chemical Society's 1951 Annual Reports, Dorothy Hodgkin hailed this achievement as the outstanding event in crystallographic research of the year.[21] Similarly, among the crystallographers in the Cavendish Laboratory in Cambridge the Bijvoet experiment was immediately recognized as a major achievement in structural science. Daniel McG. Brown, to whom we owe the establishment of the 3′ – 5′ linkage in nucleic acids, has told me that soon after Bijvoet's result was published, the organic chemists in Cambridge were aware that the conventional configurational formulas for D-sugars and L-amino acids had been shown to be correct and were suitably reassured by this knowledge. Although the method by which this had been achieved was certainly not understood by all and had to be taken on trust by most, its significance was widely perceived. They knew at last on which side of the mirror they stood. In contrast to the uncertainty about the correct handedness of the α-helix structure, there was never any question about the right-handedness of the DNA double-helix structure proposed a couple of years later in 1953.[22] In constructing their models, Watson and Crick used Furberg's "standard configuration" of the β-D-deoxyribofuranose units and its substituents,[23] and found that the model could be built only with a right-handed sense of helicity. Furberg's structure was based on the standard chemical convention, and its correctness is implicitly assumed in the famous *Nature* paper.[22] In the following, more detailed description of the assumptions made in deriving the structure of DNA,[24] the Bijvoet experiment is mentioned in a footnote.

There is also the other question that Pauling left open; even when the configuration of the amino acids in the helix could be settled, "in each case one sense of the helix would be more stable than the other". That is to say, even when the naturally occurring amino acids in the protein chain are given the correct (*S*)-configuration, it is by no means obvious from model building that the α-helix should be right- rather than left-handed. Both models can be constructed and neither is obviously untenable. Referring to the poly-L-glutamate fiber structures, Pauling and Corey wrote: "It seems likely that a poly-L-glutamate helix would be more stable with one screw sense (right-handed or left-handed) than the other, and that helixes (*sic*) of only one kind are formed in significant number in the process of folding",[15] but they did not venture an opinion about which screw sense should be preferred. The main difference between the two structures is that in a right-handed α-helix built from *S*-configured amino acids, the direction of each side chain C(α)–C(β) bond has a component in the direction of the N–H bond, whereas in a left-handed helix the C(α)–C(β) bond points in the direction of the C=O bond. For a polyglycine helix, without the side chains, the left- and right-handed helices are exact mirror images and hence equienergetic. A few months after publication of the Pauling structures, Maurice L. Huggins noted that for amino acids with the correct absolute configuration—he was already aware of the Bijvoet result—a left-handed helix would lead to a C(β)$\cdots$O distance of only 2.64 Å.[25] He concluded that "*levo* polypeptides form right-handed spirals and *dextro* polypeptides left-handed spirals, whichever of these two types of structure is correct". The protein chain is, of course, a "*levo* polypeptide".

During the following decade, the existence of the α-helix as an important structural element of proteins became generally accepted, and there was much, mostly inconclusive discussion about whether it occurred in a left- or right-handed form or even as a mixture of these depending on local conditions. The crude energy estimates available at that time could not lead to any reliable conclusion. The best evidence came perhaps from X-ray diffraction patterns of synthetic polypeptide fibers. For fibers built from the natural series of *S*-configured amino acids, somewhat better agreement with the X-ray patterns was generally obtained with models based on right-handed helices, but the differences were not large and hardly conclusive.[26] As late as 1960, Pauling was apparently still not prepared to make a decision between the two alternatives. In the 3rd edition of his "The Nature of the Chemical Bond", the α-helix is illustrated (ref. [17], figures 12 – 18, p. 500) by drawings of

 © WILEY-VCH Verlag GmbH, D-69451 Weinheim, 2001 1433-7851/01/4022-4171 $ 17.50+.50/0

both right- and left-handed structures built from amino acids with the correct (*S*)-configuration for the natural series, and the question of which helix is preferred is left unanswered—in fact it is not even mentioned.

Indeed, it was only in that year that an answer to the question was provided—by the structure analysis of myoglobin at 2 Å resolution.[27] In this first protein structure at such a high resolution, John Kendrew and his co-workers found that for many stretches of polypeptide chain the observed electron density closely followed that expected for an α-helix with the dimensions given by Pauling and Corey.[17] This was the first direct proof that α-helices are present in proteins. It was also found that the C(β) atoms of the side chains were consistently located in the direction opposite to the C=O bonds of the main chain. As mentioned above, this is the signature of a right-handed helix if the amino acid residues are assigned the correct *S*-configuration.[28] From these arguments, the electron density of the whole myoglobin molecule could be plotted in the correct absolute configuration. All the lengths of α-helix were found to be right-handed. Moreover, in satisfying agreement with this assignment, the molecule as a whole was found to be of the same hand as the four closely similar subunits in hemoglobin, for which the absolute configuration had been determined by anomalous scattering measurements.[29] Since then, α-helices have been recognized as an ubiquitous building element in countless protein structures. They are almost always right-handed, although short stretches (three to five residues) of left-handed α-helix occur occasionally.

I have given reasons for believing that Pauling, around mid-century, was not interested in the problem of absolute configuration or, as we would now put it, in problems of molecular chirality, including biochirality. This may appear surprising in view of Pauling's deep and intuitive grasp of the symmetry aspects of complex crystal structures. We must remember, however, that this was at a time when the word "chirality" had not yet found its way into chemistry, a time many years before we were inundated by conferences, symposia, and journal issues devoted to chiral separation of chiral drugs by chiral chemists using chiral recognition methods.[30] Richard Marsh, one of the few surviving crystallographers from that Golden Age in structural chemistry at Caltech, has explained to me that at that time the Caltech group were interested in details of molecular structure, in bond lengths and bond angles, in interatomic distances, in features that were just as relevant in a left-handed world as in a right-handed one. It was indeed the close attention to such details that allowed Pauling in the first place to build models of polypeptide chains that would satisfy the strict structural requirements that had emerged from such studies. Problems of absolute configuration received little or no attention because there seemed to be no need for them then. Perhaps they were even regarded as a distraction from the task at hand. Sometimes one can focus more clearly by closing one eye.

In collecting information for this article, I have been greatly assisted by correspondence and conversations with many colleagues, especially Richard Marsh at the California Institute of Technology, J. Michael McBride at Yale University, Francis Crick in La Jolla, CA, Daniel McG. Brown in Cambridge, Kurt Mislow at Princeton University, and Frederik Bos on the staff of the Koninklijke Nederlandse Akademie van Wetenschappen.

[1] L. Pauling, R. B. Corey, H. R. Branson, *Proc. Natl. Acad. Sci. USA* **1951**, *37*, 205 – 211.
[2] In the now widely accepted Cahn – Ingold – Prelog (CIP) specification system (R. S. Cahn, C. K. Ingold, V. Prelog, *Experientia* **1956**, *12*, 81 – 94; R. S. Cahn, C. K. Ingold, V. Prelog, *Angew. Chem*. **1966**, *78*, 413 – 447; *Angew. Chem. Int. Ed. Engl*. **1966**, *5*, 385 – 415), the naturally occurring amino acids with anticlockwise sequences as described above are defined as having (*S*)-configuration (except cysteine, where the sulfur linked to the β-carbon of the side chain takes "precedence" over the carbonyl oxygen atom). Those with clockwise sequence have (*R*)-configuration.
[3] J. M. Bijvoet, A. F. Peerdeman, A. J. van Bommel, *Nature* **1951**, *168*, 271 – 272.
[4] A. F. Peerdeman, A. J. van Bommel, J. M. Bijvoet, *Proc. Konink. Neder. Akad. Wetensch. B* **1951**, *54*, 16 – 19.
[5] E. Fischer, *Ber. Dtsch. Chem. Ges.* **1896**, *29*, 1377 – 1683.
[6] The configurational relationships between carbohydrates, hydroxy acids and amino acids were published (P. Brewster, E. D. Hughes, C. K. Ingold, P. A. D. S. Rao, *Nature* **1950**, *166*, 178 – 179) in July 1950, only a few months before submission of the Pauling and Bijvoet papers, but one can assume that this accomplishment rapidly became widely known in stereochemical circles. Soon afterwards, in November 1950, the need for a self-consistent method of specifying molecular configuration was set forth by Cahn and Ingold (R. S. Cahn, C. K. Ingold, *J. Chem. Soc*. **1950**, 612 – 622). The sequence-rule convention proposed in this paper is the forerunner of the CIP specification system (ref. [2]). Although the Cahn – Ingold paper was still based on the then-accepted convention for D-glyceraldehyde as a standard substance, it contains the prescient observation: "The time will come when absolute configuration can be determined with certainty; and the 'standard substance' will be a redundant concept."
[7] Given a right-handed coordinate system to describe the crystal axes, there is never any question about which of the two opposite (*h*, *k*, *l*) faces is which, only the uncertainty about the sense of chirality of the atomic coordinates $\boldsymbol{X}_i$ or $-\boldsymbol{X}_i$. See J. D. Dunitz, *Acta Crystallogr. Sect. A* **1995**, *51*, 588.
[8] D. Coster, K. S. Knol, J. A. Prins, *Z. Phys*. **1930**, *63*, 345 – 369.
[9] H. H. Brongersma, P. M. Mul, *Phys. Lett*. **1973**, *19*, 217 – 220.
[10] L. Addadi, Z. Berkovitch-Yellin, I. Weissbuch, M. Lahav, L. Leiserowitz, *J. Am. Chem. Soc.* **1982**, *104*, 2075 – 2077; Z. Berkovitch-Yellin, L. Addadi, M. Idelson, M. Lahav, L. Leiserowitz, *Nature* **1982**, *296*, 27 – 34.
[11] W. W. Wood, W. Fickett, J. G. Kirkwood, *J. Chem. Phys.* **1952**, *20*, 561 – 568.
[12] W. Kuhn, *Z. Elektrochem.* **1952**, *56*, 506 – 524.
[13] Although mistakes could also happen here! In one of the footnotes of reference [7], several sign errors in an earlier paper (J. G. Kirkwood, *J. Chem. Phys.* **1937**, *5*, 469) are corrected.
[14] I am almost certain that I did not notice at the time! Indeed, I find it most unlikely that I would have been able to identify the conventional spatial arrangement of the natural amino acids then or for many years afterwards.
[15] L. Pauling, R. B. Corey, *Proc. Natl. Acad. Sci. USA* **1951**, *37*, 241 – 250.
[16] L. Pauling, R. B. Corey, *Proc. Natl. Acad. Sci. USA* **1951**, *37*, 251 – 261.
[17] L. Pauling, R. B. Corey, *Proc. Natl. Acad. Sci. USA* **1951**, *37*, 235 – 240.
[18] J. Donohue, *Proc. Natl. Acad. Sci. USA* **1953**, *39*, 470 – 478.
[19] See, for example, figure 4 in B. W. Low, J. T. Edsall, *Aspects of Protein Structure* in *Currents in Biochemical Research* (Ed.: D. W. Green), Interscience, New York, NY, **1956**, p. 398.
[20] L. Pauling, *Nature of the Chemical Bond and the Structure of Molecules and Crystals*, 3rd ed., Cornell University Press, Ithaca, NY, **1960**.
[21] D. C. Hodgkin, *Annual Reports on Progress in Chemistry for 1951*, The Chemical Society, London, **1952**, p. 361.

 © WILEY-VCH Verlag GmbH, D-69451 Weinheim, 2001 1433-7851/01/4022-4172 $ 17.50+.50/0

[22] J. D. Watson, F. H. C. Crick, *Nature* **1953**, *171*, 737 – 738.
[23] S. Furberg, *Acta Chem. Scand.* **1952**, *6*, 634 – 640.
[24] F. H. C. Crick, J. D. Watson, *Proc. R. Soc. London Ser. A* **1954**, *223*, 80 – 96.
[25] M. L. Huggins, *J. Am. Chem. Soc.* **1952**, *74*, 3963 – 3964.
[26] See, for example, for poly-L-alanine fibers A. Elliot, B. R. Malcolm, *Proc. R. Soc. London Ser. A* **1959**, *249*, 30 – 41.
[27] J. C. Kendrew, R. E. Dickerson, B. E. Strandberg, R. G. Hart, D. R. Davies, D. C. Phillips, V. C. Shore, *Nature* **1960**, *185*, 422 – 427.
[28] In the meantime the correctness of the configurations of the natural amino acids as determined by their configurational relationships with other groups of compounds (ref. [6]) had been confirmed by X-ray analysis of L-leucine hydrobromide using the anomalous scattering technique (J. Trommel, J. M. Bijvoet, *Acta Crystallogr.* **1954**, *7*, 703 – 710).
[29] M. F. Perutz, M. G. Rossmann, A. F. Cullis, H. Muirhead, G. Will, A. C. T. North, *Nature* **1960**, *185*, 416 – 421.
[30] The use of the terms "chiral" and "chirality" in chemistry is of fairly recent origin. I first heard the terms in the early 1960s when my Zurich colleagues (Duilio Arigoni, André Dreiding, Albert Eschenmoser, Edgar Heilbronner, Vlado Prelog) used to argue interminably about stereochemical concepts and terminology. When we heard that Kurt Mislow was proposing the term "chiral" from Greek $\chi\varepsilon\iota\rho$ as a multilingually accessible synonym for almost untranslatable "handedness", we unanimously and enthusiastically agreed to use this term at every available opportunity. To the best of my knowledge, its first use in a chemical text is to be found in K. Mislow, *Introduction to Stereochemistry*, Benjamin, New York, NY **1965**, but the term goes back at least to Lord Kelvin (Kelvin, *Baltimore Lectures on Molecular Dynamics and the Wave Theory of Light*, Clay, London, **1904**). See K. Mislow in *Topics in Stereochemistry*, *Vol. 22* (Ed.: S. E. Denmark), Wiley, New York, NY, **1999**, chap. 1 for further details. Following the downfall of parity at the level of the weak force in particle physics, the wider usage of the term "chiral" in a variety of mathematical, physical, chemical, and everyday contexts was urged by L. L. Whyte, *Nature* **1957**, *180*, 513; L. L. Whyte, *Nature* **1958**, *182*, 198.

 © WILEY-VCH Verlag GmbH, D-69451 Weinheim, 2001 1433-7851/01/4022-4173 $ 17.50+.50/0

Computational Methods Facilitate the Assignment of Protein Functions**

Gerd Folkers* and Christian D. P. Klein

A tremendously difficult task will be tackled by biochemists in the next few years: the ever-increasing amount of genomic data has to be put into a functional context. The sequencing of genomes is primarily a logistic challenge for the participating institutions. The throughput of such enterprises can be increased without limits by increasing the available resources. For the time being, the situation is different for the most important ensuing step: The elucidation of the function of the proteins that are encoded by newly identified genes. This area of research has been termed "Functional Genomics".

The DNA sequence immediately leads to the sequence of a protein. Protein sequences have been archived for many years, and thousands of sequences (for proteins whose function is often known) are publicly available.[1] Proteins with a similar sequence often fulfil identical functions; therefore, it is clear that sequence comparisons can lead to the assignment of protein functions. This approach has been pursued for some time,[2] and by continuous improvements of the basic algorithum it has become a valuable tool for geneticists and biochemists. One of the advantages of this method is that it is very fast, and it does not require any three-dimensional structural information. However, it has one fundamental problem: Proteins have evolved in a convergent manner, directed towards their present-day function. This means that proteins which are not evolutionary connected (that is, they do not have a common ancestor), and whose amino acid sequences are not similar, can have a similar or identical function.[3] For example, the enzymes trypsin and subtilisin have a very different amino acid sequence. It would not be possible to recognize their functional similarity by inspecting their primary structure since only about 10% of their sequences are identical. This is not much more than one could expect for a random pair of proteins. However, a certain section of the two enzymes is very similar: it is the region that forms the catalytic center. The amino acids that participate in the catalytic mechanism are neighbors in three-dimensional space, but not on the amino acid chain. It would not be possible to identify these two enzymes as functionally related serine proteases by a sequence-matching technique.

The conservation of the functionally important region is one of the paradigms of protein chemistry. Independent of the primary structure, the physicochemical properties of this region are similar, and in many cases even the participating amino acids are identical.

From Structure to Function

S. Schmitt, M. Hendlich, and G. Klebe have presented a new method for the identification of functional similarity that is based on the conservation of the active site of enzymes and the ligand-binding pocket of receptors.[4] The first step in their approach is to abstract the binding sites of proteins whose function and three-dimensional structure is known. A binding pocket is no longer represented by amino acids, but by the spatial arrangement of certain pseudofunctionalities such as hydrogen-bond donor or acceptor (Figure 1). This data

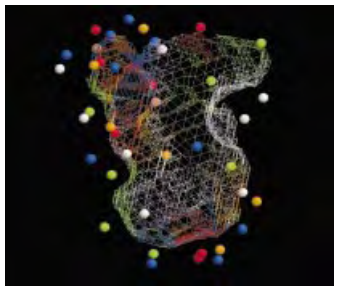


Figure 1. Surfaces and pseudo centers of a binding pocket (from ref. [4]).

reduction allows the construction of a database which is comparably easy to handle but still contains all the relevant information. The (putative) binding pockets of proteins with unknown function are treated analogously and can then be compared to the database. If a similar spatial arrangement of pseudofunctionalities in the binding pocket is found, then the function of the unknown protein can be deduced.

The concept of this method is similar to techniques that are used to identify small-molecule binding partners of proteins such as ligands or inhibitors. Programs that are frequently used in the drug-development process, such as GRID,[5] RELIBASE,[6] and others, may be regarded as "ancestors" of this new approach.

[*] Prof. Dr. G. Folkers, Dr. C. D. P. Klein
Pharmazeutische Chemie
Departement für Angewandte Biowissenschaften
ETH Zürich
Winterthurerstrasse 190, 8057 Zürich (Switzerland)
Fax: (+41) 1-635-6884
E-mail: folkers@pharma.ethz.ch

[**] We would like to thank Dr. H. Rüther, Cologne, Prof. H.-D. Höltje, Universität Düsseldorf, and Prof. Dr. P. A. Schubiger, Paul-Scherrer-Institut, Villingen (Switzerland), for critical comments on the manuscript.

 © WILEY-VCH Verlag GmbH, D-69451 Weinheim, 2001 1433-7851/01/4022-4175 $ 17.50+.50/0

This is not the first attempt to use spatial features of binding pockets for the functional analysis of proteins.[7] The main advantage of the new method is the fact that it does not solely use geometric information (the shape of the pocket), but it also uses the arrangement of physicochemical properties.

It may be surprising for someone experienced in molecular modeling to learn that the method of Schmitt et al. uses only five types of pseudofunctionalities and still gives good results. Programs that are used to determine the intermolecular interaction properties of small molecules use much more sophisticated representations. Electrostatic properties, for example, are ignored (or treated indirectly) by the method of the Klebe research group—which has the advantage that there is no need to calculate such properties before a prediction is made.

The most important prerequisite for the method of Schmitt, Hendlich, and Klebe is that the three-dimensional structure of the protein must be known. It is not sufficient to know the gene or amino acid sequence of the protein. Three-dimensional structures of proteins are usually determined by X-ray crystallography, with NMR spectroscopy gaining importance during the last few years.[8] Both methods, however, are not traditionally known to be fast or easy. The huge commercial potential associated with this field means that attempts are now being made to establish high-throughput methods for the determination of protein structures.[9] Furthermore, theoretical methods are gaining importance,[10] and it is often possible to make predictions that are sufficiently accurate for all practical purposes. Some approaches are based on comparisons of primary structure, whereas others do not need any additional, empirical information.[11]

At the moment, the genomic data that is available for higher organisms appears to contain a considerable amount of errors.[12] If a faulty protein sequence is used to predict the structure and function of a protein, then the abstraction that is made by Schmitt et al. might be advantageous, since the influence of a "false" amino acid on the representation of the binding pocket and on the outcome of the prediction is reduced.

Genes, Proteins, Drugs

The main motivation for the sequencing of genomes is the hope of finding new therapeutic strategies. Drugs are seldomly targeted at the genetic material; intervention is usually made at the protein level. It does not make any sense to select a protein with unknown function as the target for drug development and therapeutic intervention. Figure 2 shows the relevance of genomic data for the development of new drugs: The DNA sequence immediately gives the protein sequence. The three-dimensional structure of the protein can be derived by theoretical methods or is determined experimentally. The next step, the assignment of a function, is critical for the overall success and quite difficult to perform. Genetic engineering techniques are frequently used to generate organisms that lack the gene in question (for example, so-called "knock-out-mice") so that the effect of this mutation on the organism can be studied. It is often difficult (or impossible in the case of humans) to generate such organisms,

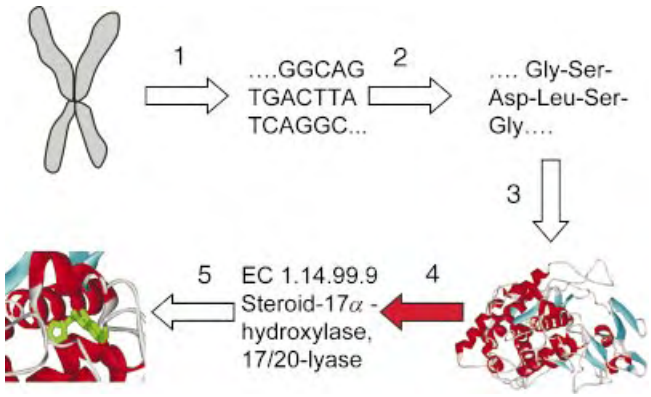


Figure 2. 1: Genome sequencing; 2: translation to primary structure; 3: deduction or determination of 3D structure; 4: functional classification; 5: design of ligands or inhibitors.

and the interpretation of the results can be problematic. Attempts are underway to automatize the experimental procedures for the generation of transgenic animals.[13] Nevertheless, valid theoretical methods can be a very important resource in functional genomics.

The functional analysis is the decisive step when it comes to establish a protein as a target for therapeutic intervention. Once the validity of a target is confirmed, inhibitors or antagonists can be identified or designed using, for example, structure-based design methods.

The database that has been generated by the research group of Klebe could be used for another purpose which is not immediately evident—it might enable us to predict unwanted side-effects. The ideal drug molecule binds exclusively and with high affinity to its target protein. Undesired effects are usually caused by it binding to other proteins. Until now, the only way of assessing such unwanted binding processes is to perform biological tests, which tend to be costly and difficult. Therefore, side-effects are often identified at a later development stage, when considerable investments have been made. The method of the Klebe research group will make it possible to perform a "virtual" search for undesired interaction partners of new drug molecules by searching the database for enzymes or receptors that are prone to bind the candidate molecule. This strategy would be the inversion of a frequently used technique for the search for new ligands, the so-called "virtual screening" (Figure 3 A). One would not look for small

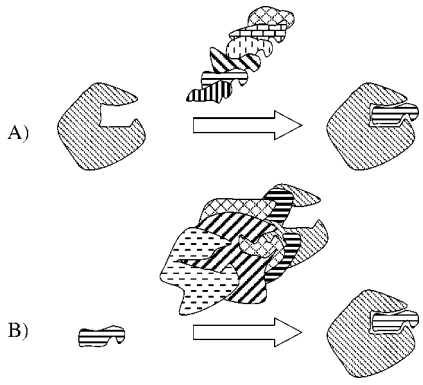


Figure 3. Virtual search for a ligand (A) and a protein (B).

 © WILEY-VCH Verlag GmbH, D-69451 Weinheim, 2001 1433-7851/01/4022-4176 $ 17.50+.50/0

ligands, but for their macromolecular binding partners (Figure 3B). This type of "inverse" virtual screening is not limited to the search for side-effects: For example, one could search for the target protein of biologically active molecules with unknown mechanisms of action.

[1] SWISS-PROT: A. Bairoch, B. Boeckmann, *Nucleic Acids Res.* **1994**, *22*, 3578–3580; http://www.expasy.ch/sprot/, **2001**; BLAST: S. F. Altschul, W. Gish, W. Miller, E. W. Myers, D. J. Lipton, *J. Mol. Biol.* **1990**, *215*, 403–410; http://www.ncbi.nlm.nih.gov/BLAST/, **2001**.

[2] S. B. Needleman, C. D. Wunsch, *J. Mol. Biol.* **1970**, *48*, 443–453; W. R. Pearson, D. J. Lipman, *Methods Enzymol.* **1990**, *183*, 63–98.

[3] A. Fersht, *Structure and Mechanism in Protein Science*, 2nd ed., W. H. Freeman, New York, **1999**.

[4] S. Schmitt, M. Hendlich, G. Klebe, *Angew. Chem.* **2001**, *113*, 3237–3241; *Angew. Chem. Int. Ed.* **2001**, *40*, 3141–3144.

[5] P. J. Goodford, *J. Med. Chem.* **1985**, *28*, 849–857.

[6] M. Hendlich, *Acta Crystallogr. Sect. D* **1998**, *54*, 1178–1182; http://relibase.ebi.ac.uk/, **2001**.

[7] D. Fischer, R. Norel, H. Wolfson, R. Nussinov, *Proteins Struct. Funct. Genet.* **1993**, *16*, 278–292; S. L. Moodie, J. B. Mitchell, J. M. Thornton, *J. Mol. Biol.* **1996**, *263*, 486–500; N. Kobayashi, N. Go, *Eur. Biophys. J.* **1997**, *26*, 135–144; M. Rosen, S. L. Liang, H. Wolfson, R. Nussinov, *J. Mol. Biol.* **1998**, *11*, 263–277; M. Stahl, C. Taroni, G. Schneider, *Protein Eng.* **2000**, *13*, 83–88.

[8] A. Saegusa, *Nature* **1998**, *392*, 219.

[9] Protein Structure Factory (Berlin), http://userpage.chemie.fu-berlin.de/~psf/, **2001**.

[10] P. Bork, D. Eisenberg, *Curr. Opin. Struct. Biol.* **1998**, *8*, 331–332; J. Skolnick, J. S. Fetrow, *Trends Biotechnol.* **2000**, *18*, 34–39; D. Frishman, H. W. Mewes, *Prog. Biophys. Mol. Biol.* **1999**, *72*, 1–17.

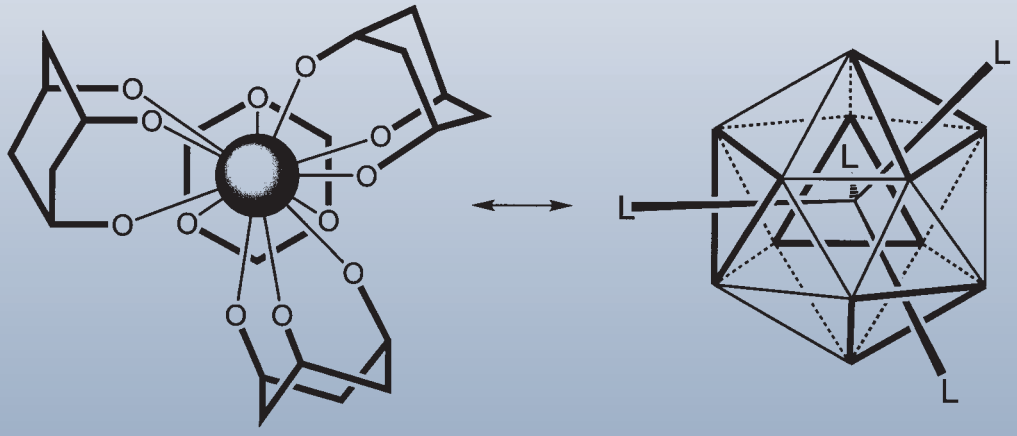
[11] D. J. Osguthorpe, *Curr. Opin. Struct. Biol.* **2000**, *10*, 146–152.

[12] See, for example, S. Karlin, A. Bergman, A. J. Gentles, *Nature* **2001**, *411*, 259–260.

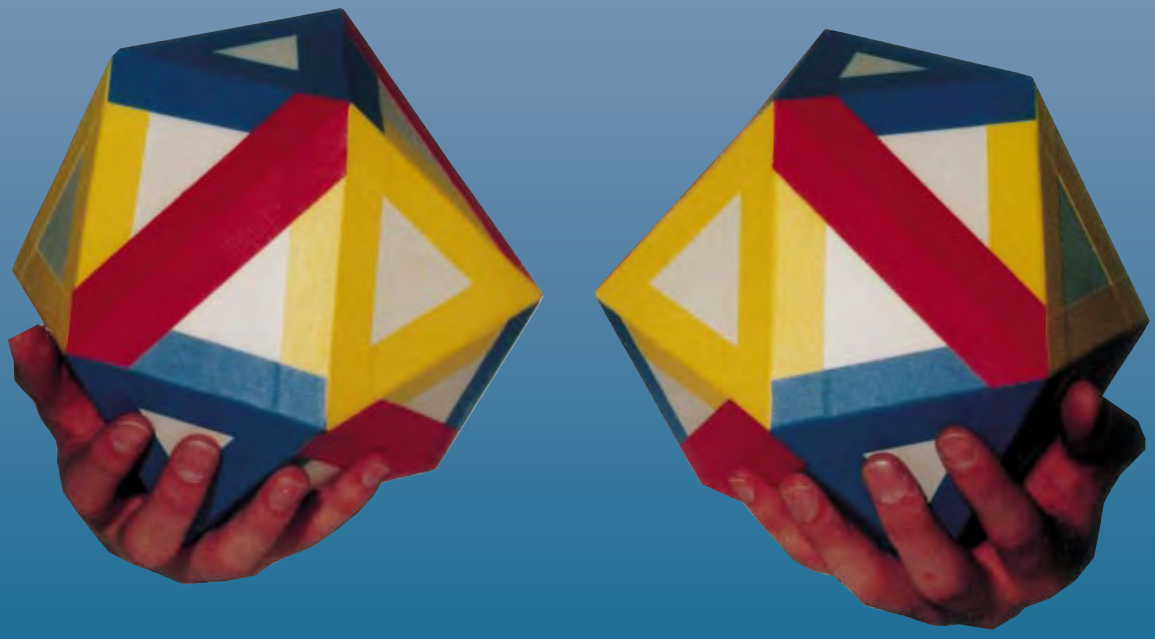
[13] B. P. Zambrowicz, G. A. Friedrich, E. C. Buxton, S. L. Lilleberg, C. Person, A. T. Sands, *Nature* **1998**, *392*, 608–611.

[14] H. J. Böhm, G. Schneider, *Virtual Screening for Bioactive Molecules*, Wiley-VCH, Weinheim, **2000**.

 © WILEY-VCH Verlag GmbH, D-69451 Weinheim, 2001 1433-7851/01/4022-4177 $ 17.50+.50/0



Four equal substituents placed at the vertices of a regular tetrahedron result in a highly symmetric, but chiral, structure if these substituents are tripodal, facedelineated ligands: The resulting icosahedral geometry retains the full rotational symmetry of the tetrahedron.



For more information see the following pages.

 © WILEY-VCH Verlag GmbH, D-69451 Weinheim, 2001 1433-7851/01/4022-4179 $ 17.50+.50/0

T-Symmetrical Icosahedra: A New Type of Chirality in Metal Complexes**

Jürgen Sander, Kaspar Hegetschweiler,*
Bernd Morgenstern, Alice Keller, Walter Amrein,
Thomas Weyhermüller, and Iris Müller

Dedicated to Professor Alan M. Sargeson on the occasion of his 71th birthday

The preparation of metal complexes with a chiral structure has been one of the great challenges in synthetic coordination chemistry within the last 100 years. As early as 1911 Alfred Werner made use of the optical activity of chiral Co^{III} complexes to establish the octahedral geometry of this metal cation.[1] Since this pioneering work, interest in such materials has grown because a variety of important properties, such as enantioselective catalytic activity, specific binding of chiral guests, and optical behavior, depend on chirality.[2, 3] A uniform and undistorted coordination sphere of a metal complex is on its own not chiral, and specific strategies must be used to obtain chiral structures. These include the use of chiral ligands, heteroleptic complexes, or substitution of monodentate ligands L by multidentate analogues.[3] One may elucidate the individual isomers of a metal complex by visualizing with a particular color the corners, edges, or faces of the coordination polyhedron which are occupied by a ligand. A monodentate ligand would represent a colored corner,[4] a bidentate ligand L-L a colored edge,[5] while a C_3-symmetric, tridentate, tripodal ligand L–L–L would represent a colored triangular face. In an edge- or a face-delineated polyhedron containing bi- or tridentate ligands, isomers exist for each configuration in which the colored edges or faces do not meet at any of the vertices. This is rather trivial for coordination numbers up to eight, where only a limited number of solutions exists. The well known octahedral D_3-symmetric tris-chelates $[M(L\text{-}L)_3]$ represent one of the few chiral examples. It would be of particular interest to know whether this concept would allow for the generation of *isometric* chiral structures. Such species would be unique because they are optically active but would not adopt any preferred orientation in space, for example, in an external magnetic or electric field. Only three possible point groups, *T*, *O*, and *I*, account for chiral isometric structures, and corresponding polyhedra would have a minimum of 12, 24, and 60 vertices, respectively.[6] The latter two are outside the range accessible to mononuclear complexes; however, metal complexes with a coordination number of 12 and icosahedral geometry are known.[7, 8] Since the chiral point group *T* is a subgroup of I_h, this strategy should allow for the generation of chiral *T*-symmetric complexes. We performed an exhaustive search for such solutions,[9] and could demonstrate that a total of five isomers,[10] with T_h, D_{3d}, D_3, D_2, and C_2 symmetry, are possible for an icosahedral $[M(L\text{-}L)_6]$ structure. Two of them, namely the T_h and the D_3 isomers have been observed in complexes with bidentate ligands having a sufficiently small bite angle (for example, with NO_3^-).[7, 8] A chiral isometric structure can thus not be achieved by using bidentate ligands. Such a structure is, however, possible by coloring four triangular faces of an icosahedron. If the restriction is applied that the colored faces cannot have common vertices, only one single solution exists (Figure 1); this structure is chiral and retains the full rotational symmetry of the tetrahedron.

A synthetic route to such a complex has been established in our laboratory by testing a series of substituted cyclohexane-1,3,5-triols as possible ligands for Ba^{2+} ions. Since additional binding of H_2O has been observed in the complex formed with the unsubstituted ligand 1,3,5-triamino-1,3,5-trideoxy-*cis*-inositol (taci), namely $[Ba(taci)_2(H_2O)_3]^{2+}$,[11] we used more lipophilic derivatives, such as the tris(benzylamino)- and tris[benzylmethyl)amino] compounds, tbci and tbmci, respectively, for coordination in a non-aqueous medium (Figure 1 d). The hexaalkylated derivative tbmci proved to be too bulky, and the mass spectrum established that only the 1:2 complex $[Ba(tbmci)_2]^{2+}$ formed. For the intermediate tbci, the mass spectrum established the formation of the 1:4 complex $[Ba(tbci)_4]^{2+}$. The NMR data (^1H and ^{13}C) indicated that all four ligand moieties were equivalent, and that the local C_3 symmetry within each ligand was preserved. If a reasonable potential is considered with attractive forces between the cation and the oxygen donors, and repulsion between the individual ligand moieties, the center of gravity of the four ligands should be located on the vertices of a regular tetrahedron (Figure 1 a). Rotation around the threefold axes would generate a variety of different polyhedra such as the truncated tetrahedron, the cuboctahedron, the anticuboctahedron, and the icosahedron (Figure 1 b), with the icosahedral structure being of lowest energy.[7] A crystal-structure analysis of $[Ba(tbci)_4]^{2+}$ did indeed exhibit an almost regular icosahedron for the BaO_{12} sphere (Figure 2).[12]

$[Ba(tbci)_4]Br_2 \cdot 2.5\,MeOH$ crystallizes as a racemate with the two enantiomers related through a center of inversion. The twelve peripheral benzyl moieties encapsulate the central BaO_{12} icosahedron completely, thus generating a lipophilic

[*] Prof. Dr. K. Hegetschweiler, Dr. J. Sander,
Dipl.-Chem. B. Morgenstern
Universität des Saarlandes, Anorganische Chemie
Postfach 15 11 50, 66041 Saarbrücken (Germany)
Fax: (+49) 681-302-2663
E-mail: hegetschweiler@mx.uni-saarland.de
Dipl.-Math. A. Keller
Universität des Saarlandes, Mathematik
Postfach 15 11 50, 66041 Saarbrücken (Germany)
Dr. W. Amrein
Laboratorium für Organische Chemie, ETH-Zentrum
8092 Zürich (Switzerland)
Dr. T. Weyhermüller
Max-Planck-Institut für Strahlenchemie
Postfach 10 13 65, 45413 Mühlheim an der Ruhr (Germany)
Dr. I. Müller
Institut für Analytische Chemie
Postfach 10 21 48, 44721 Bochum (Germany)

[**] Metal Binding of Polyalcohols, Part 7. This work was supported by the Deutsche Forschungsgemeinschaft and the Fonds der Chemischen Industrie. We thank Prof. Dr. E.-U. Gekeler (Saarbrücken), Prof. Dr. W. S. Sheldrick (Bochum), Dr. P. Osvath (Melbourne), and G. W. Hart (Northport, NY; http://www.georgehart.com) for helpful advice and discussion. Part 6: B. Morgenstern, J. Sander, V. Huch, K. Hegetschweiler, *Inorg. Chem.* **2001**, *40*, 5307 – 5310.

Supporting information for this article is available on the WWW under http://www.angewandte.com or from the author.

 © WILEY-VCH Verlag GmbH, D-69451 Weinheim, 2001 1433-7851/01/4022-4180 $ 17.50+.50/0

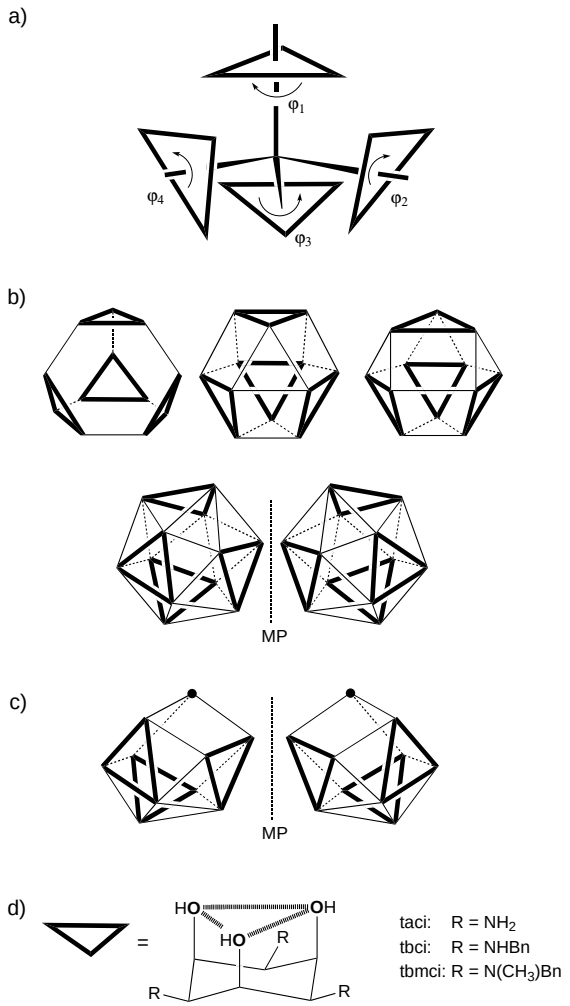


Figure 1. Coordination numbers of 10 and 12: Four tripodal tridentate ligands are arranged around a metal center with their centers of gravity placed on the vertices of a regular tetrahedron (a). Depending on the angles $\varphi_1-\varphi_4$ different coordination polyhedra are obtained. Note that only one two-color solution is possible for each polyhedron and only the icosahedral structure is chiral (b; MP = mirror plane). The highlighted equilateral triangle at the top collapses to a single point (H_2O ligand) giving the chiral C_3-symmetric coordination polyhedron observed for the Sr complex (c). The scheme used for the ligands is shown in (d).

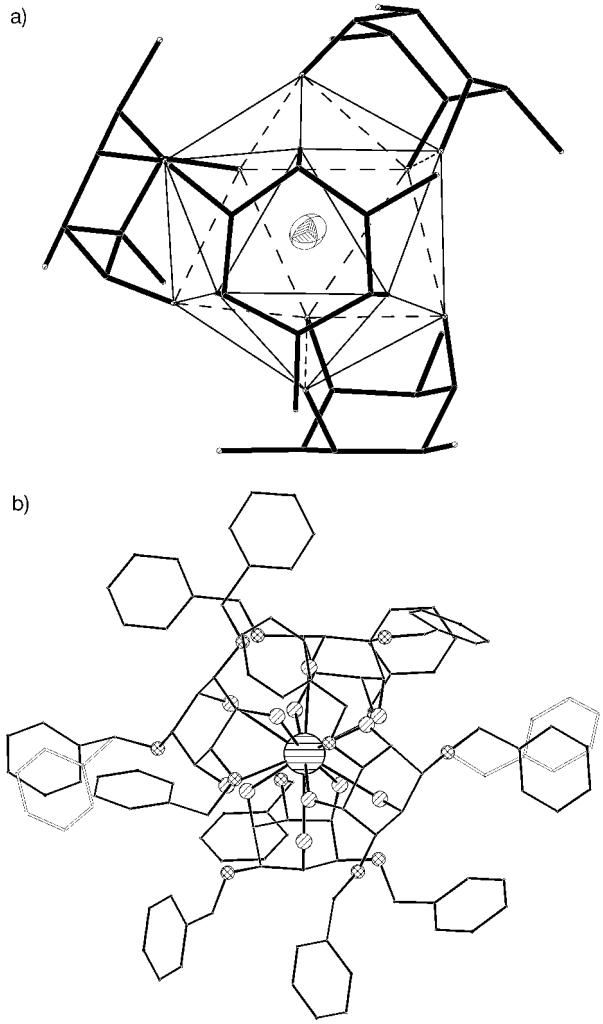


Figure 2. Structure of $[Ba(tbci)_4]^{2+}$ in the crystal. a) The BaO_{12} coordination sphere. b) Ball and stick model of the entire cation showing the disordered phenyl groups. (Ba–O bond lengths: 276(1) – 291(1) pm, mean value: 284 ± 5; O···O distances between adjacent oxygen donor atoms: 285(2) – 340(2) pm, average: 300 ± 12 pm).

molecular surface for the entire cation. The benzyl groups have an asymmetric orientation and the BaO_{12} icosahedron exhibited some minor distortions from full tetrahedral symmetry. However, as shown by the NMR data, the four ligand moieties as well as all the Ba–O bonds are equivalent in solution, and the deviation from true *T* symmetry is clearly the result of crystal packing effects in this particular structure.

Three different types of triangles can be specified in the *T*-symmetric coordination sphere: a) four equilateral triangles defined by the donor set of each ligand, b) twelve irregular triangles with one side derived from the two donors of one ligand and the additional vertex from another ligand, c) four additional equilateral triangles with all three vertices belonging to different ligand entities. Triangles of type a and c lie opposite to each other and are surrounded entirely by triangles of type b. The four threefold axes run through the mid-points of a type a and type c triangle, while the three twofold axes run through the mid-points of the common edges of two adjacent type b triangles.

The high coordination number (12) of $[Ba(tbci)_4]^{2+}$ is clearly a consequence of the large ionic radius of the Ba^{2+} ion. The use of Sr^{2+} and Mg^{2+} result in the formation of $[Sr(tbci)_3(H_2O)]^{2+}$ and $[Mg(tbci)_2]^{2+}$ with coordination numbers of 10 and 6, respectively.[13] The coordination sphere of the Sr complex is closely related to that of the Ba complex: It is obtained if one of the equilateral triangles of the MO_{12} icosahedron collapses to a single point. This point in the Sr complex is occupied by the water ligand. The resulting idealized SrO_{10} polyhedron has chiral C_3 symmetry (Figure 1c). It consists of 10 triangles with an *arachno* structure and three quadrilateral faces (rhombi) having the water oxygen atom as a common vertex. To the best of our knowledge, such a C_3 geometry with a coordination number of 10 is unprecedented. The Mg complex has a simple trigonal antiprismatic (octahedral) coordination.

Molecules with chiral *T* symmetry are scarce, and only a few examples of metal complexes have been reported. In

 © WILEY-VCH Verlag GmbH, D-69451 Weinheim, 2001 1433-7851/01/4022-4181 $ 17.50+.50/0

general they have an oligonuclear structure.[14] A mononuclear complex with *T* symmetry and achiral ligands was hitherto unknown. The structure of $[Ba(tbci)_4]^{2+}$ is further unique in that it represents one of the very few examples of a 12-coordinate complex with exclusive formation of six-membered chelate rings. The facile formation of this complex in non-aqueous media may indicate that lipophilic derivatives of symmetrically substituted *cis*-cyclohexane-1,3,5-triols could serve as building blocks for such complexes if sufficiently large metal centers are used.

Experimental Section

tbci[15] was prepared by the reaction of taci[11] and an excess of benzaldehyde in MeOH, followed by $NaBH_4$ reduction. tbmci was obtained from tbci by an Eschweiler–Clarke-type methylation with formaldehyde and formic acid. Both ligands were characterized by ^1H and ^{13}C NMR spectroscopy as well as positive-ion fast-atom bombardment (FAB^+) MS, and gave correct C,H,N analyses (see Supporting Information).

$[Ba(tbci)_4]Br_2 \cdot 2CH_3OH$: A solution of $BaBr_2 \cdot 2H_2O$ (41 mg) in MeOH (5 mL) was added to a suspension of tbci (220 mg) in MeOH (5 mL). A clear solution was formed from which a crop of colorless crystals deposited within several minutes. Yield: 61 % of the air-dried product. Elemental analysis calcd (%) for $C_{110}H_{140}BaBr_2N_{12}O_{14}$ (2151.57): C 61.41, H 6.56, N 7.81; found: C 61.48, H 6.66, N 7.65; ^1H NMR ($CDCl_3$): $\delta = 2.15$ (3H), 3.70 (6H), 3.80 (3H), 7.23–7.36 (15H); ^{13}C NMR: $\delta = 50.7$, 58.4, 66.7, 125.9, 127.1, 128.5, 140.0; MS (FAB^+, 3-nitrobenzylalcohol) *m/z* (%): 2007.8 (55) $[Ba(tbci)_4Br]^+$, 2005.8 (45) $[Ba(tbci)_3(tbci-H_2)Br]^+$, 1926.3 (7) $[Ba(tbci)_4-H^+]^+$.

Received: June 15, 2001 [Z17289]

[1] A. Werner, *Z. Anorg. Chem.* **1899**, *21*, 145–158; A. Werner, *Ber. Dtsch. Chem. Ges.* **1911**, *44*, 1887–1898.

[2] a) A. Togni, L. M. Venanzi, *Angew. Chem.* **1994**, *106*, 517–547; *Angew. Chem. Int. Ed. Engl.* **1994**, *33*, 497–526; b) C. Piguet, G. Bernardinelli, G. Hopfgartner, *Chem. Rev.* **1997**, *97*, 2005–2062.

[3] a) U. Knof, A. von Zelewsky, *Angew. Chem.* **1999**, *111*, 312–333; *Angew. Chem. Int. Ed.* **1999**, *38*, 302–322; b) A. von Zelewsky, *Stereochemistry of Coordination Compounds*, Wiley, Chichester, **1996**; c) R. E. Ernst, M. J. O'Connor, R. H. Holm, *J. Am. Chem. Soc.* **1967**, *89*, 6104–6113; d) E. L. Muetterties, *J. Am. Chem. Soc.* **1968**, *90*, 5097–5102; e) E. L. Muetterties, *J. Am. Chem. Soc.* **1969**, *91*, 1636–1643.

[4] For an analysis of the colored icosahedron MA_xB_{12-x} with two types of monodentate ligands, see B. K. Teo, H. Zhang, Y. Kean, H. Dang, X. Shi, *J. Chem. Phys.* **1993**, *99*, 2929–2941.

[5] S. V. Jablan, *Z. Kristallogr.* **1995**, *210*, 173–176.

[6] D. Steinborn, *Symmetrie und Struktur in der Chemie*, Wiley-VCH, Weinheim, **1998**.

[7] M. C. Favas, D. L. Kepert, *Prog. Inorg. Chem.* **1981**, *28*, 309–367.

[8] A search of the Cambridge Structural Database revealed a total of 31 hexanitrato complexes with bidentate NO_3^- ligands. A compilation is given in the Supporting Information.

[9] A derivation, based on geometrical and group theory considerations, together with a figure of the five isomers is given in the Supporting Information.

[10] Three of the five possible isomers (T_h, D_3, and D_{3d}) are discussed in ref. [7]; in ref. [5] the total number of possible solutions is erroneously given as six, without specifying the geometry of the individual isomers.

[11] K. Hegetschweiler, R. D. Hancock, M. Ghisletta, T. Kradolfer, V. Gramlich, H. W. Schmalle, *Inorg. Chem.* **1993**, *32*, 5273.

[12] Crystals of composition $[Ba(tbci)_4]Br_2 \cdot 2.5MeOH$ disintegrate rapidly upon exposure to air. A crystal of dimensions $0.30 \times 0.18 \times 0.12$ mm was therefore embedded in a perfluoropolyether and cooled. Data collection was performed at 100(2) K on a SIEMENS SMART-CCD diffractometer, $Mo_{K\alpha}$-radiation ($\lambda = 71.073$ pm): space group $P2_1/n$, $a = 1910.1(5)$, $b = 2650.1(6)$, $c = 2050.1(5)$ pm, $\beta = 95.39(3)^\circ$, $Z = 4$, $V = 10332(4) \times 10^6$ pm^3, $\rho_{calcd} = 1.393$ Mg m^{-3}, $\mu = 1.228$ mm^{-1}, graphite monochromator, numerical absorption correction ($T_{min} = 0.644$, $T_{max} = 0.862$), $2\theta_{max} = 42.0^\circ$. Of 32396 measured reflections, 11083 independent reflections were used for the refinement of 576 parameters, and the structure was solved by direct methods (SHELXS-97). Ba, O, and N atoms were refined with anisotropic displacement parameters (SHELXL-97, full-matrix least-squares calculations on F^2). All other non-hydrogen atoms were refined isotropically. The phenyl groups were modeled as rigid bodies with fixed C–C bond lengths of 1.39 Å and fixed C-C-C angles of 120°. The phenyl groups appeared to be disordered. The disorder could only be partially resolved by using split positions. H(C) atoms were placed at calculated sites (riding model). $R = 0.112$ ($F_o^2 > 2\sigma(F_o^2)$), wR_2 (all data) $= 0.267$. Max/min residual electron density $+1.11/-1.18$ e Å^{-3}.[16]

[13] $[Sr(tbci)_3(OH_2)]Br_2 \cdot 4MeOH$ and $[Mg(tbci)_2]Cl_2 \cdot 10MeOH$ were prepared in an analogous way to the Ba^{2+} complex. Analytical and crystal data,[16] together with a figure showing the molecular structure are given in the Supporting Information.

[14] a) A. Zimmer, D. Kuppert, T. Weyhermüller, I. Müller, K. Hegetschweiler, *Chem. Eur. J.* **2001**, *7*, 917–931; b) A. J. Terpin, M. Ziegler, D. W. Johnson, K. N. Raymond, *Angew. Chem.* **2001**, *113*, 161–164; *Angew. Chem. Int. Ed.* **2001**, *40*, 157–160; c) R. W. Saalfrank, A. Stark, M. Bremer, H.-U. Hummel, *Angew. Chem.* **1990**, *102*, 292–295; *Angew. Chem. Int. Ed. Engl.* **1990**, *29*, 311–315; d) R. G. Raptis, I. P. Georgakaki, D. C. R. Hockless, *Angew. Chem.* **1999**, *111*, 1751–1753; *Angew. Chem. Int. Ed.* **1999**, *38*, 1632–1634.

[15] J. Sander, V. Huch, M. Veith, K. Hegetschweiler, *Z. Kristallogr. New Cryst. Struct.* **2001**, *216*, 105–107.

[16] Crystallographic data (excluding structure factors) for the structures reported in this paper have been deposited with the Cambridge Crystallographic Data Centre as supplementary publication nos. CCDC-164898–164900. Copies of the data can be obtained free of charge on application to CCDC, 12 Union Road, Cambridge CB2 1EZ, UK (fax: (+44) 1223-336-033; e-mail: deposit@ccdc.cam.ac.uk).

Coordinated B_2 Bridges in Porphyrins—Unexpected Formation of a Diborane(4)- from a Diborylporphyrin**

Andre Weiss, Hans Pritzkow, Penelope J. Brothers,* and Walter Siebert*

Dedicated to Professor Max Herberhold on the occasion of his 65th birthday

Free-base porphyrins react with haloboranes to yield diborylporphyrins in which the porphyrin ligands show marked rectangular distortions.[1] The reaction of **1a**-H_2 with $F_3B \leftarrow OEt_2$ in the presence of trace water leads to green **1a**-

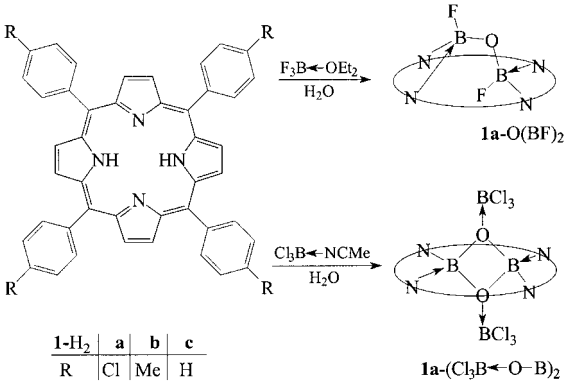
[*] Prof. Dr. W. Siebert, Dipl.-Chem. A. Weiss, Dr. H. Pritzkow
Anorganisch-chemisches Institut der Universität
Im Neuenheimer Feld 270, 69120 Heidelberg (Germany)
Fax: (+49) 6221-54-5609
E-mail: ci5@ix.urz.uni-heidelberg.de

Dr. P. J. Brothers
Department of Chemistry
University of Auckland
Private Bag 92019, Auckland (New Zealand)
Fax: (+64) 9-373-7422
E-mail: p.brothers@auckland.ac.nz

[**] This work was supported by the Deutsche Forschungsgemeinschaft (DFG).

 © WILEY-VCH Verlag GmbH, D-69451 Weinheim, 2001 1433-7851/01/4022-4182 $ 17.50+.50/0

$O(BF)_2$ (Scheme 1), in which each of the boron atoms of the FB−O−BF moiety is connected to two adjacent nitrogen atoms. In contrast **1a**-H_2 reacts with an excess of MeCN →BCl_3 to yield green **1a**-$(Cl_3B \leftarrow O{-}B)_2$, which contains a coordinated four-membered B_2O_2 ring.[2] The distances



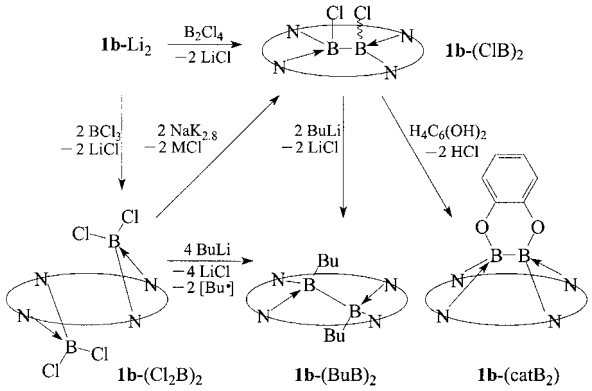
Scheme 1.

between two adjacent nitrogen atoms in the rectangularly distorted porphyrin **1a**-$(Cl_3B \leftarrow O{-}B)_2$ are 2.49 and 3.63 Å ($\Delta = 1.14$ Å). Since this distortion allows the coordination of the two boron atoms in the N_4 plane, we have investigated the synthesis of such compounds. This proved to be possible either by direct insertion of a B−B-bonded fragment into a porphyrin ligand or, surprisingly, by the formation of a B−B bond caused by spontaneous elimination of two butyl radicals from a diborylporphyrin, as we report in the following.

The reaction of **1b**-Li_2[3] with B_2Cl_4 led to dark violet, extremely air- and moisture-sensitive **1b**-$(ClB)_2$ in 80% yield. The ^{1}H NMR spectrum of **1b**-$(ClB)_2$ showed a double set of signals compared to the free porphyrin **1b**-H_2: two singlets for the methyl groups of *para*-tolyl substituents, four doublets, two each for the tolyl *ortho* and *meta* protons, and a typical AB quartet pattern for the pyrrolic protons, consistent with a rectangular distortion of the porphyrin framework and an associated lowering of the symmetry.[2] The ^{11}B signal at $\delta = -12$ is evidence for the tetragonal coordination of the boron atoms. Overall, the spectroscopic data for **1b**-$(ClB)_2$ are consistent with a complex containing a Cl-B-B-Cl fragment in which each B atom is coordinated to two porphyrin nitrogen atoms, and the two chlorine atoms are either *syn* (C_{2v}) or *anti* (C_2) with respect to the porphyrin plane.

Alternatively, **1b**-$(ClB)_2$ can be prepared by the reaction of **1b**-Li_2 with two equivalents of BCl_3 followed by a reductive coupling of the boron atoms (Scheme 2). The first step yields moisture-sensitive green **1b**-$(Cl_2B)_2$ ($\delta(^{11}B) = 5.6$), in which the two Cl_2B moieties are likely to be coordinated on opposite faces of the porphyrin plane for steric reasons.[4] Reduction of **1b**-$(Cl_2B)_2$ with $NaK_{2.8}$ alloy led to **1b**-$(ClB)_2$ in 30% yield.

The reaction of **1b**-$(ClB)_2$ with pyrocatechol (H_2cat) and **1b**-H_2 as auxiliary base gives **1b**-$H_2 \cdot 2HCl$ and the *syn* compound[5] **1b**-$(catB_2)$, whose ^{1}H NMR spectrum shows markedly high-field shifted multiplets at $\delta = 5.3$ (*meta*) and $\delta = 4.1$ (*ortho*) for the catechol aromatic protons, which results from the diamagnetic ring current of the porphyrin



Scheme 2.

system. The synthesis of **1b**-$(catB_2)$ indicates that an inversion of the configuration must take place in the reaction of **1b**-$(ClB)_2$ with an *anti* arrangement (see below) of the Cl atoms.

Treatment of **1b**-$(ClB)_2$ with two equivalents of butyllithium led to the crystalline, olive-green *anti*-dibutyl derivative **1b**-$(BuB)_2$. The ^{1}H NMR signals of the porhyrin protons are slightly shifted in comparison with those of **1b**-$(ClB)_2$ and show the same multiplicity (symmetry). The proton signals of the butyl groups are shifted strongly upfield by the diamagnetic ring current of the porphyrin π system. The methylene protons are observed at $\delta = -5.64$, -3.54, and -1.22, which reflects the increasing distance from the porphyrin core, and the protons of the methyl group appear as a triplet at $\delta = -0.63$. Similar chemical shifts are observed for the butyl groups in the butylmetalloporphyrin complexes **1c**-(BuAl)[6a] and **1c**-(BuGa).[6b]

Surprisingly, we observed the formation of **1b**-$(BuB)_2$ (20% yield in a mixture of products) by treatment of **1b**-$(Cl_2B)_2$ with four equivalents of butyllithium, rather than the expected product **1b**-$(Bu_2B)_2$. We propose that this occurs through the intermediate formation of **1b**-$(Bu_2B)_2$, from which, because of the steric overcrowding, two butyl radicals are eliminated and the two boron atoms are linked. Unidentified products (observed by NMR spectroscopy) might be formed by the reaction of the postulated butyl radicals with **1b**-$(Cl_2B)_2$ and **1b**-$(BuB)_2$. Attempts to react **1b**-Li_2 with Bu_2BCl yielded neither **1b**-$(Bu_2B)_2$ nor **1b**-$(BuB)_2$.

The X-ray structure analyses[7] of single crystals of **1b**-$(BuB)_2$ and **1b**-$(BuB)_2 \cdot CH_2Cl_2$ indicate that the butyl groups are arranged *anti* relative to the porphyrin plane (Figure 1). The boron atoms are located 0.44 Å above and below the N_4 plane, which results in a tetrahedral coordination geometry (angles at B1, and at B1B 104.0–111.9°). The molecule displays an inversion center, the *p*-tolyl rings are almost perpendicular to the porphyrin plane. The B−B distance is 1.77 Å, which is typical for adducts of diborane(4) compounds.[8] As expected, the rectangular distortion of the porphyrin framework is not as marked (distance between adjacent N atoms: 3.28 and 2.49 Å, $\Delta = 0.8$ Å) as in **1a**-$(Cl_3B \leftarrow O{-}B)_2$.

Our results demonstrate both the direct insertion of a $(BCl)_2$ moiety into a porphyrin and also its formation by the reductive dehalogenation of a bis(dichloroboryl)porphyrin.

 © WILEY-VCH Verlag GmbH, D-69451 Weinheim, 2001 1433-7851/01/4022-4183 $ 17.50+.50/0

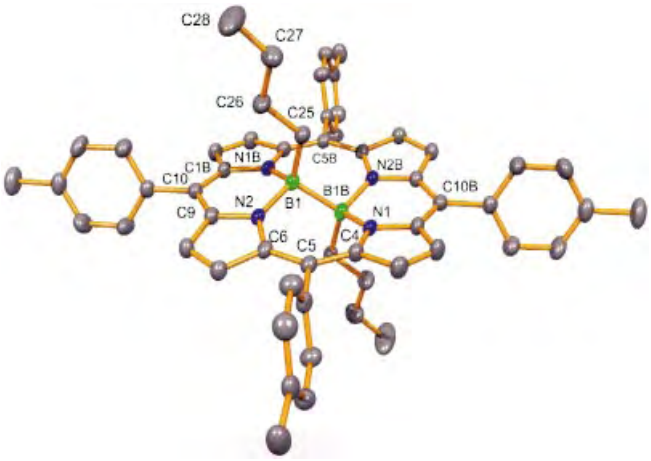


Figure 1. Structure of **1b**-$(BuB)_2 \cdot CH_2Cl_2$ in the crystal. The CH_2Cl_2 molecule and the hydrogen atoms have been omitted for clarity. Selected bond lengths [Å] and angles [°]: B1-B1B 1.769(7), B1-N2 1.584(5), B1-N1B 1.577(4), B1-C25 1.622(5); N1B-B1-N2 104.0(3), C25-B1-B1B 111.9(3), C9-C10-C1B 119.0(3), C4-C5-C6 130.9(3).

The fascinating formation of the diborane(4) derivative **1b**-$(BuB)_2$ from the diborylporphyrin **1b**-$(Cl_2B)_2$ will be further investigated with regard to preparative applications.

Experimental Section

1b-$(ClB)_2$: B_2Cl_4 (290 mg, 1.77 mmol) was condensed onto a suspension of **1b**-Li_2 (940 mg, 1.38 mmol) in hexane (80 mL) at −100 °C. The mixture was allowed to warm to room temperature (3 h) and then stirred for 12 h. This yielded a precipitate which was filtered off, washed with hexane, and extracted with toluene. Yield: 940 mg (80 %) dark violet **1b**-$(ClB)_2 \cdot n$Tol ($n = 0.5-1$). Low-temperature fast atom bombardment (LT-FAB) MS (toluene): *m/z* (%): 760 (1) $[M^+]$, 725 (7) $[M-Cl]^+$, 690 (3) $[M-2Cl]^+$; ^{1}H NMR (200 MHz, CD_2Cl_2): $\delta = 2.71$ (s, 6H; CH_3), 2.76 (s, 6H; CH_3), 7.62 (d, $^3J = 7.9$ Hz, 4H; *meta*), 7.71 (d, $^3J = 7.9$ Hz, 4H; *meta*), 8.14 (d, $^3J = 7.9$ Hz, 4H; *ortho*), 8.22 (d, $^3J = 7.9$ Hz, 4H; *ortho*), 9.16 (AB-q, 8H; β-pyrrole-H); ^{11}B NMR (64 MHz, CD_2Cl_2): $\delta = -12$ (br.); UV/Vis (CH_2Cl_2): λ_{max} (lgε) = 370 (3.78), 425 (4.86), 559 (3.60), 605 nm (3.70).

1b-$(ClB)_2$ was also obtained by treatment of **1b**-$(Cl_2B)_2$ (140 mg, 0.17 mmol) with $NaK_{2.8}$ alloy (0.5 mL) in toluene (20 mL) at −78 °C. After the mixture had been allowed to warm to room temperature (3 h) and stirred for 1 h, it was filtered and the solvent was removed from the filtrate. Yield: 39 mg (30 %) **1b**-$(ClB)_2 \cdot n$Tol (n = 0.5–1).

1b-$(Cl_2B)_2$: BCl_3 (1.00 g, 8.53 mmol) was added to a suspension of **1b**-Li_2 (280 mg, 0.41 mmol) in hexane (80 mL) at −78 °C. The mixture was allowed to warm up and stirred for 14 h at room temperature. The precipitate was removed from the solvent and excess BCl_3 by filtration, then washed with hexane to yield **1b**-$(Cl_2B)_2$ (324 mg; 95 %). ^{1}H NMR (200 MHz, CD_2Cl_2): $\delta = 2.68$ (s, 6H; CH_3), 2.77 (s, 6H; CH_3), 7.72 (d, br, $^3J = 7.4$ Hz, 8H; *meta*), 8.14 (d, br, $^3J = 7.4$ Hz, 8H; *ortho*), 9.34 (m, br, 8H; β-pyrrole-H); ^{11}B NMR (64 MHz, CD_2Cl_2): $\delta = 5.6$ (s); UV/Vis (CH_2Cl_2): at high dilution only decomposition products were detected.

1b-$(BuB)_2$: A 2.5 M *n*BuLi solution (0.3 mL, 0.75 mmol) was added to a suspension of **1b**-$(ClB)_2 \cdot n$Tol (300 mg, 0.35 mmol) in hexane (20 mL) at −78 °C. The reaction mixture was allowed to warm up to room temperature and stirred 16 h. The precipitate was filtered, washed with hexane, and extracted with CH_2Cl_2 to yield olive-green **1b**-$(BuB)_2$ (200 mg, (71 %). LT-FAB-MS (toluene): *m/z* (%): 804 (3) $[M^+]$, 747 (7) $[M-C_4H_9]^+$, 690 (15) $[M-2(C_4H_9)]^+$; ^{1}H NMR (200 MHz, CD_2Cl_2): $\delta = -5.7$ (m, 4H; CH_2), −3.47 (m, 4H; CH_2), −1.13 (m, 4H; CH_2), −0.56 (t, $^3J = 7.3$ Hz, 6H; CH_3), 2.63 (s, 6H; CH_3), 2.67 (s, 6H; CH_3), 7.47 (d, $^3J = 7.4$ Hz, 4H; *meta*), 7.58 (d, $^3J = 7.9$ Hz, 4H; *meta*), 7.93 (d, $^3J = 7.4$ Hz, 4H; *ortho*), 7.99 (d, $^3J = 8.0$ Hz, 4H; *ortho*), 8.34 (AB-q, 8H; β-pyrrole-H); ^{11}B NMR (64 MHz, CD_2Cl_2): $\delta = -6$ (br.); UV/Vis (CH_2Cl_2): λ_{max} (lgε) = 419 (5.28), 443 (4.92), 517 (4.12), 553 nm (4.00).

1b-$(BuB)_2$ was also obtained as one component in a mixture of other, unidentified products from the reaction of **1b**-$(Cl_2B)_2$ with four equivalents of *n*BuLi. Its preparation by this method was confirmed by ^{1}H NMR data (about 20 % yield) and by an X-ray structure analysis.[7]

1b-$(catB_2)$: Pyrocatechol (34 mg, 0.31 mmol) was added to a mixture of **1b**-$(ClB)_2 \cdot$ Tol (260 mg, 0.31 mmol) and **1b**-H_2 (208 mg, 0.31 mmol) in toluene (30 mL) at −78 °C. After the mixture had been allowed to warm to room temperature, it was filtered to remove insoluble **1b**-$H_2 \cdot 2$HCl, and **1b**-$(catB_2)$ (98 mg; 40 %) was isolated from the filtrate. FAB-MS (NPOE: 2-nitrophenyloctylether): *m/z* (%): 798 (10) $[M^+]$, 690 (18) $[M-cat]^+$; ^{1}H NMR (200 MHz, CD_2Cl_2): $\delta = 2.68$ (s, 6H; CH_3), 2.69 (s, 6H; CH_3), 4.15 (m, 2H; $ortho_{cat}$), 5.43 (m, 2H; $meta_{cat}$), 7.48 (d, $^3J = 7.8$ Hz, 4H; *meta*), 7.58 (d, $^3J = 7.9$ Hz, 4H; *meta*), 8.10 (d, br, $^3J = 7.9$ Hz, 8H; *ortho*), 9.10 (AB-q, 8H; β-pyrrole-H); ^{11}B NMR (64 MHz, CD_2Cl_2): $\delta = -15$ (br); UV/Vis (CH_2Cl_2): λ_{max} (lgε) = 370 (3.71), 419 (5.12), 516 nm. (4.23)

Received: July 26, 2001 [Z 17606]

[1] W. J. Belcher, P. D. W. Boyd, P. J. Brothers, M. J. Liddell, C. E. F. Rickard, *J. Am. Chem. Soc.* **1994**, *116*, 8416–8417.

[2] W. J. Belcher, M. Breede, P. J. Brothers, C. E. F. Rickard, *Angew. Chem.* **1998**, *110*, 1133–1135; *Angew. Chem. Int. Ed.* **1998**, *37*, 1112–1114.

[3] H. Brand, J. A. Capriotti, J. Arnold, *Inorg. Chem.* **1994**, *33*, 4334–4337.

[4] Preliminary calculations indicate that a porphyrin complex with two X_2B groups each coordinated through two N atoms on opposite faces of the ligand is a stable energy minumum. W. J. Belcher, PhD thesis, The University of Auckland, **1995**.

[5] Recently the compound 1,2-$(Me_2NB)_2O_2C_6H_4$ was described which is the first example of a six-membered ring formed by a pyrocatecholate and a diborane(4). Usually the formation of five-membered rings by 1,1-connection is preferred.[9]

[6] a) R. Guilard, A. Zrineh, A. Tabard, A. Endo, B. C. Han, C. Lecomte, M. Souhassou, A. Habbou, M. Ferhat, K. M. Kadish, *Inorg. Chem.* **1990**, *29*, 4476–4482; b) K. M. Kadish, B. Boisselier-Cocolios, A. Coutsolelos, P. Mitaine, R. Guilard, *Inorg. Chem.* **1985**, *24*, 4521–4528.

[7] Structural data of **1b**-$(BuB)_2 \cdot CH_2Cl_2$: monoclinic *C*2/c, $a = 25.757$ (2), $b = 8.9382$ (9), $c = 23.314$ (2) Å, $\beta = 114.830(2)^\circ$, $V = 4871.3(8)$ Å^3, $Z = 4$. A total of 14615 independent reflections (4291 observed, $I > 2\sigma(I)$), the measurement was carried out on a Bruker AXS diffractometer SMART 1000 ($Mo_{K\alpha}$ radiation, ω scan, $T = 190(2)$ K), $R1 = 0.066$, $wR2 = 0.215$. The structure was solved by direct methods (SHELXS 86) and refined with all measured reflections against F^2 (SHELXL 97).[10] The structure of **1b**-$(BuB)_2$ (synthesized from **1b**-$(Cl_2B)_2$) was determined as well and showed good agreement. Crystallographic data (excluding structure factors) for the structures reported in this paper have been deposited with the Cambridge Crystallographic Data Centre as supplementary publication no. CCDC-167513 (**1b**-$(BuB)_2 \cdot CH_2Cl_2$) and CCDC-167514 (**1b**-$(BuB)_2$). Copies of the data can be obtained free of charge on application to CCDC, 12 Union Road, Cambridge CB2 1EZ, UK (fax: (+44) 1223-336-033; e-mail: deposit@ccdc.cam.ac.uk).

[8] W. Clegg, M. R. J. Elsegood, F. J. Lawlor, N. C. Norman, N. L. Pickett, E. G. Robins, A. J. Scott, *Inorg. Chem.* **1998**, *37*, 5289–5293.

[9] M. J. G. Lesley, N. C. Norman, A. G. Orpen, J. Starbuck, *New J. Chem.* **2000**, *24*, 115–117, and references therein.

[10] G. M. Sheldrick, SHELXS 86, Universität Göttingen, **1986**; G. M. Sheldrick, SHELXL 97, Universität Göttingen, **1997**.

 © WILEY-VCH Verlag GmbH, D-69451 Weinheim, 2001 1433-7851/01/4022-4184 $ 17.50+.50/0

Fluorescence Quenching by Sequential Hydrogen, Electron, and Proton Transfer in the Proximity of a Conical Intersection**

Adalgisa Sinicropi, Rebecca Pogni,* Riccardo Basosi, Michael A. Robb, Gabriela Gramlich, Werner M. Nau,* and Massimo Olivucci*

The formulation of a general theory for the control of photon energy disposal by interaction with an external additive stands at the basis of the development of novel fluorescence probes and other photoactive materials. We have shown that the fluorescence quenching of n,π*-excited states (X = Y*), like aliphatic azoalkanes and ketones, involves hydrogen atom abstraction from the quencher (R–H).[1–3] This abstraction is not completed on the excited state surface but is "aborted" in the region of a conical intersection (CI)[4] funnel that prompts immediate return to the ground state. This mechanism has recently received support from femtosecond time-resolved experiments in the gas phase.[5]

In this work, we employ high-level quantum chemical computations[6–8] and spectroscopic studies of photochemical intermediates to show that the same CI dominates a region of the potential energy surface with exceptional electronic properties, where hydrogen atom, electron, and proton transfer events are interrelated in an uncommon way. In Salem's correlation diagram for hydrogen abstraction,[9] an n,π*-excited state (ES) correlates with the radical pair (RP) derived from *hydrogen atom* abstraction, and the ground state (GS) correlates with the ion pair (IP) derived from *proton* abstraction. Taking into account our previous results,[1] the originally implicated avoided crossing should be replaced by a CI. The state correlation diagram in Figure 1 is the result. The diagram suggests, implicitly, that a mixture of the ES and GS electronic configurations occurs near the CI where nonadiabatic hops between the ES and GS energy surfaces (vertical dashed arrow in Figure 1) or minute atomic movements on the GS (or ES) energy surface (horizontal dashed arrow) should be accompanied by a sudden change in the electronic configuration from an ES/RP radical-type to a GS/IP covalent/ionic-type wavefunction.

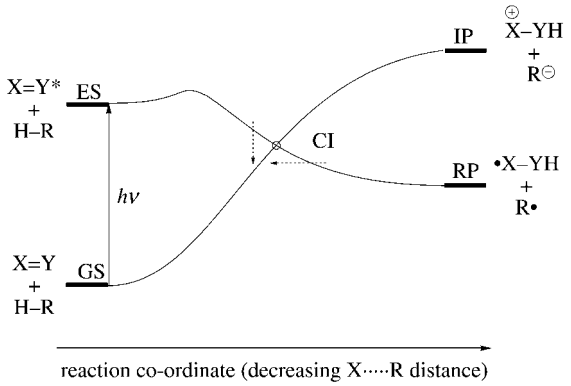
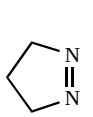


Figure 1. Modified state-correlation diagram of the n,π*-excited state (ES) correlating with the radical pair (RP) derived from hydrogen atom abstraction and the ground state (GS) correlating with the ion pair (IP) derived from proton abstraction. Note the occurrence of a conical intersection (CI).

The present work was once more performed for n,π* singlet-excited azoalkanes, which are known to be quenched by hydrogen donors such as chlorinated hydrocarbons and alcohols.[1, 3] The advantage of azoalkanes is mainly an experimental one, since these chromophores, unlike ketones, do not undergo spontaneous intersystem crossing,[10] which allows a clear-cut assignment of photoreactivity and photoproducts to the singlet-excited state, where CIs come into play (in triplet reactions, the CI is replaced by a singlet–triplet crossing).[11] The pyrazoline/methylene chloride pair was



pyrazoline



DBO

employed as computational model and the 2,3-diazabicyclo[2.2.2]oct-2-ene (DBO)/chloroform as experimental one. For the computations we have employed ab initio CASSCF, CASPT2,[12] and MS-CASPT2[13] calculations to map the minimum-energy paths describing the relaxation from the CI structure and RP disproportionation.[13–18]

As shown in Figure 2, the CI structure features a 2.01 Å interfragment distance, an almost fully formed 1.02 Å N–H bond, and a planar pyrazoline ring. The result of the wavefunction analysis at the CI shows that GS and ES correlate with IP and RP configurations, respectively, as expected from Figure 1. ES can be formally converted to IP by proton abstraction and to RP by hydrogen atom abstraction. The next efforts were devoted to the characterization of the two distinct relaxation paths corresponding to the vertical and horizontal arrows of Figure 1.

The first path corresponds to "direct" GS reconstitution (light arrows in Figure 2). This involves first S_1 decay by partial hydrogen atom transfer. Upon approaching the CI this process is "aborted" through electron transfer to form a transient ion-pair structure ($IP^{\pm}$) with a positively charged

[*] Prof. Dr. R. Pogni, Prof. Dr. M. Olivucci, A. Sinicropi, Prof. Dr. R. Basosi
Dipartimento di Chimica dell'Università di Siena
Gruppo di Chimica e Fotochimica Computazionale
Via Aldo Moro, Siena (Italy)
Fax: (+39) 0577-234278
E-mail: pogni@unisi.it, olivucci@unisi.it
Prof. Dr. W. M. Nau, Dipl.-Chem. G. Gramlich
Departement Chemie der Universität
Klingelbergstrasse 80, 4056 Basel (Switzerland)
Fax: (+41) 61-267-3855
E-mail: Werner.Nau@unibas.ch
Prof. Dr. M. A. Robb
Chemistry Department, Kings College London
Strand London WC2R 2LS (UK)

[**] This work was supported by the Swiss National Science Foundation (project 620-58000.99 for W.M.N. and 2134-62567.00 for G.G.), the Università di Siena (Progetto di Ateneo A.A. 00/02), NATO (CRG 950748), and HFSP (RG 0229/2000-M). We are grateful to Prof. Donati for the use of his monochromator.

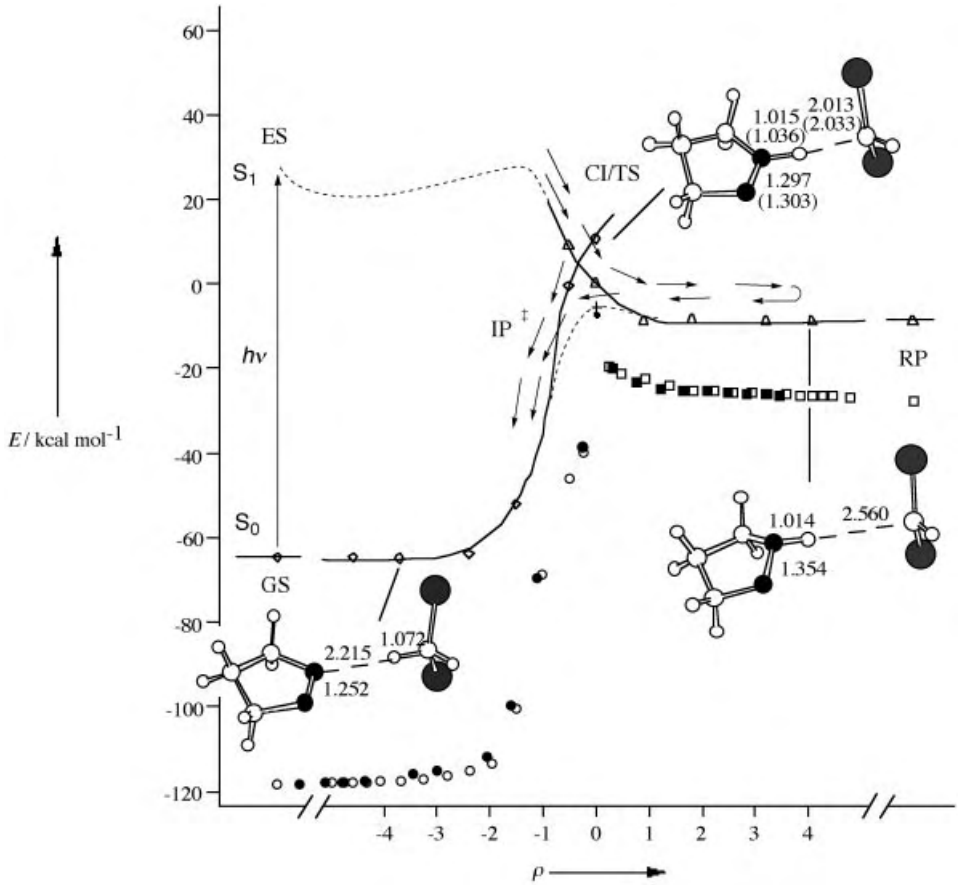
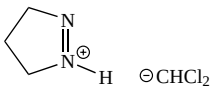
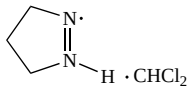


Figure 2. Energy profiles along the CI →GS (CASSCF, ○; CASPT2, ◇) and CI →RP (CASSCF, □; CASPT2, △) relaxation coordinates. The energy profiles of the reactant (CASSCF, ■) and product (CASSCF, ●) branches of the RP →GS reaction coordinate are given together with the corresponding TS energy (CASSCF, ◆; CASPT2, +). The given bond lengths [Å] illustrate the geometric changes occurring along the reaction coordinate ρ [bohr (amu)$^{1/2}$]; values in parenthesis refer to TS. The energy profile along the initial ^{1}n,π*-path (- - - -) is from ref. [1]; this path corresponds to a different reaction coordinate.

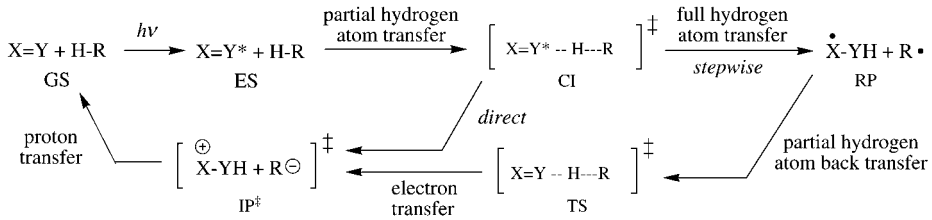




azoalkane fragment (about 0.73 a.u.), 1.1 Å N–H bond, 1.93 Å $CHCl_2\cdots$H-N distance, and 1.29 Å N–N bond (for example at ρ −0.25 in Figure 2). From IP≠, proton transfer occurs to reconstitute GS (Scheme 1). Accordingly, the reaction coordinate connecting CI with GS is dominated by N–H expansion and H···C and N–N compression. In contrast, the second path (full arrows in Figure 2) is dominated by a RP configuration and takes place by a "stepwise" mechanism: radical formation followed by disproportionation to regenerate GS. The corresponding reaction coordinate indicates that RP formation involves an out-of-plane distortion of the azoalkane ring caused by -N-N- expansion and twisting deformation and increased pyramidalization of the N–H center. In detail, the stepwise mechanism can be viewed as a full hydrogen atom transfer followed by a partial hydrogen atom back transfer, an electron transfer (near the CI structure) and, finally, a proton transfer to GS (Scheme 1).

The reaction coordinate for the GS reconstitution by disproportionation of RP has been investigated via a transition-state search on the S_0 potential energy surface. A transition structure (TS) has been located in the strict vicinity of the CI (see geometrical parameters in Figure 2). As reported in Table 1, TS is located about 6 kcal mol^{-1} below the CI and only about 3.5 kcal mol^{-1} (approximately 4.0 kcal mol^{-1} after zero-point energy correction) above RP. Thus RP disproportionation is expected to be a fast process, competitive with diffusion in solution, which is known to exhibit apparent activation energies for solvent viscous flow around 1–3 kcal mol^{-1}.[19]

The close vicinity of the CI and TS structures and the modest S_1-S_0 energy gap at TS (around 20 kcal mol^{-1}) suggest that the stepwise GS reconstitution involves a S_0 intermolecular electron transfer. The S_0 species, namely the RP intermediate, evolves towards a CI/TS region where an electron jump takes place yielding the same IP≠ structure as that generated by a direct surface hop at CI. Formally speaking, radical disproportionation does not occur in a simple hydrogen atom transfer step, that is, ·N–NH + ·R →N=N + HR or RP →GS, but in a stepwise fashion through sequential electron–proton transfer, namely ·N–NH + ·R →[$^+$N–NH + $^-$R]≠ →N=N + HR or RP →IP≠ → GS. This mechanism is consistent with the well-known Polanyi's harpoon model,[20, 21] which is usually applied to simple atom plus diatom gas-phase reactions. In our case the mechanism appears to operate



Scheme 1. Intermediates in the fluorescence quenching of n,π*-excited states (X = Y*) by hydrogen donors (H–R) classified according to their dominant electronic structure and the reaction step. The label ≠ indicates unstable transient entities.

 © WILEY-VCH Verlag GmbH, D-69451 Weinheim, 2001 1433-7851/01/4022-4186 $ 17.50+.50/0

Table 1. Calculated energies for the pyrazoline/methylene chloride chromophore/quencher system.

Structure[a]	CASSCF E [hartree]	CASPT2[b] E [hartree]	CASPT2 ΔE [kcal mol^{-1}]
CI (S_0)	-1183.89476[d]	-1185.03836 (0.73)[c] {-1185.04629}	$\equiv 0.0$
CI (S_1)	-1183.89316[d]	-1185.03768 (0.72)[c] {-1185.02975}	0.7
GS (S_0)	-1183.08361	-1185.14977 (0.75)[c]	-69.9
RP (S_0)	-1183.93902 [0.131][e]	-1185.06053 (0.74)[c]	-13.9
TS (S_0)	-1183.90418[d] [0.132][e]	-1185.05491 (0.72)[c] {-1185.05503}	-10.4
TS (S_1)	-1183.88268[d]	-1185.02138 (0.72)[c] {-1185.02126}	10.7

[a] For abbreviations, see text, Scheme 1, and Figure 1. [b] The MS-CASPT2 energies (in curley brackets) indicate that the general shape of the energy surfaces is not sensitive to wavefunction mixing. However, as reported for other systems,[28] a moderate (about 10 kcal mol^{-1}) energy splitting at CI arises due to differences of the optimized MS-CASPT2 CI geometry. [c] The weight of the CASSCF reference function in the first-order function is given in parentheses. [d] State-averaged value (see ref. [14]). [e] Zero-point vibrational energy in squared brackets.

within a more complex organic RP, where the electron-transfer harpoon triggers the following proton transfer. The involvement of a "harpoon" radical disproportionation in a complex fluorescence quenching and the computational manifestation of this mechanistic detail are unprecedented findings, which may be of importance beyond photochemistry in the field of radical chemistry.

To support this conjecture, we have investigated the topological and electronic structure of the CI/TS region in more detail (Figure 3). Figure 3a provides a three-dimensional representation of the energy profiles given in Figure 2. It is evident that the two S_0 relaxation paths starting at CI and the two branches of the reaction path defined by TS develop along the same energy valleys. This is demonstrated by the resulting prompt convergence of the relaxation and reaction path branches. Furthermore, vibrational frequency computations along the relaxation paths show that the frequencies associated with the $3N-7$ modes orthogonal to the path are all real, thus demonstrating a valley-like structure. To investigate the nature of the S_0 wavefunction in the same region, we have computed the S_1-S_0 energy gap and fragment charges along a small loop centered around CI (see dashed circle in Figure 2) and lying along the plane defined by the two modes that lift the S_1/S_0 energy degeneracy, namely, the branching plane vectors. We start at $\omega = 0^\circ$ with a structure displaced towards IP‡. In Figure 3b we show that the charge distribution of the system undergoes two dramatic events. The first event occurs at about 90° and corresponds to a sudden transfer of one electron from the $CHCl_2$ anion to the pyrazoline cation yielding the RP configuration. The new charge distribution is then maintained up to 270° where a back electron transfer occurs from the pyrazoline radical fragment to the $CHCl_2$ radical. Notice that the wavefunction changes are associated with the two minima in the energy gap diagram (Figure 3c). It is therefore clear that the S_0 energy surface surrounding the CI is divided in two distinct regions with the RP part going from 90° to 270°. Structural analysis reveals that the optimized TS lies on the 90° edge and thus must correspond to the lowest energy critical structure (the bottleneck) for thermal intermolecular electron transfer.

In previous studies[1–3] on the photoreactivity and quenching mechanism, the actual photoproducts and intermediates

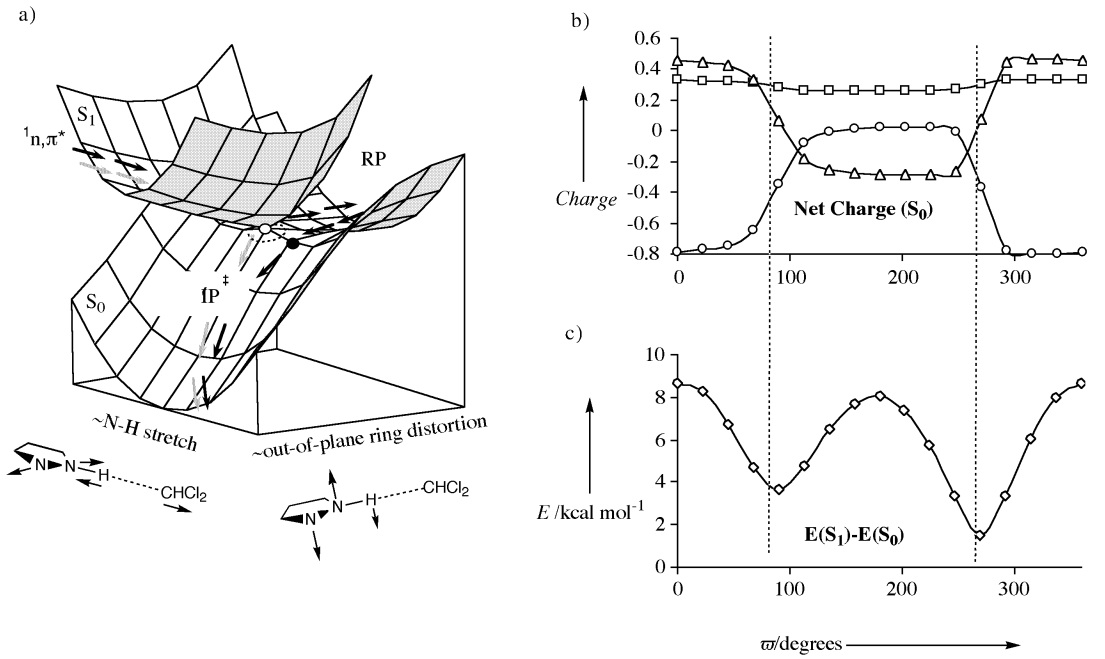


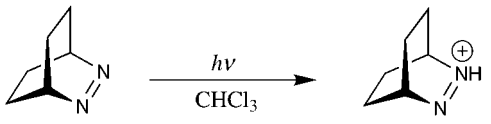
Figure 3. a) Structure of the S_1 and S_0 potential energy surfaces in the CI/TS region (CI, ○; TS, ●). b) S_0 fragment charges [a.u.] along a loop centered around the CI (pyrazoline fragment, △; hydrogen atom, □; $CHCl_2$ fragment, ○). c) CASSCF S_1-S_0 energy gap along the same loop.

 © WILEY-VCH Verlag GmbH, D-69451 Weinheim, 2001 1433-7851/01/4022-4187 $ 17.50+.50/0

were not examined due to the very low photodecomposition quantum yield. However, the above computational findings on the involvement of a metastable RP and a (transient) IP resulting from electron transfer have encouraged a more detailed spectroscopic search for such intermediates. The detection of radicals related to the RP intermediate has been achieved through EPR spectroscopy.[22] A solution of DBO in chloroform was irradiated at room temperature in the presence of the spin-trap reagent *N-tert*-butyl-α-phenylnitrone (PBN). PBN has a high affinity for chlorinated carbon radicals, such as the $^{\bullet}CCl_3$ radical generated by singlet-excited DBO through hydrogen atom abstraction. The magnetic parameters g (2.0061 ± 0.0001), A_H (1.9 ± 0.1), and A_N (14.3 ± 0.1) measured shortly after irradiation compare well with the CCl_3–PBN parameters reported in the literature ($A_H = 1.3$–2.9 and $A_N = 13.4$–15.5), thus supporting production of the $^{\bullet}CCl_3$ radical during photolysis.[23] This radical must derive from hydrogen abstraction with the subsequent formation of the RP intermediate. Although we have provided evidence for the intervention of RP in the photoreaction, no quantitative analysis is possible however, such that we cannot determine to which degree the reconstitution of GS occurs directly through a relaxation from the CI structure (vertical arrow in Figure 1) or through disproportionation of the RP intermediate (horizontal arrow in Figure 1).

In principle, the direct and stepwise pathways for GS reconstitution (see Figure 3a) lead to a *common* unstable $IP^{\pm}$ structure, which regenerates the original GS pair through proton transfer. In contrast to RP, the $IP^{\pm}$ structure resulting from electron transfer is predicted to be unstable, as it immediately accelerates along the proton transfer path. Such a structure cannot be experimentally detected with conventional means. However, our computation neglects the effect of the solvent environment. Solvation could have a significant effect on the shape of the energy surfaces corresponding to the $IP^{\pm}$ state and slow the proton transfer to a degree that ion separation with consequent reactions become competitive.

Circumstantial evidence for the photoinduced formation of ions was indeed obtained. The photolysis of DBO in chloroform[22] gave rise to the formation of the protonated azoalkane DBO-H^+ with a UV absorption at 344 nm [Eq. (1)],[24] consistent with the elimination of HCl from the solvent.



DBO (λ_{max} = 365 nm) DBO–H^+ (λ_{max} = 344 nm) (1)

This characteristic absorption due to DBO-H^+ could be removed, with a concomitant increase in DBO absorption, upon subsequent addition of triethylamine as a base. Control experiments further revealed that HCl is not formed in the direct photolysis of chloroform (or impurities therein), that is, irradiation of this solvent with subsequent addition of DBO did not produce the characteristic DBO-H^+ absorption. We presume that the trichloromethyl anion serves as an initial counterion of DBO-H^+, a process corresponding to a formal proton abstraction. This anion is known to undergo elimination of a chloride anion leading to the overall formation of dichlorocarbene and HCl,[25] which protonates DBO. Unfortunately, a trapping agent that could intercept dichlorocarbene without quenching the excited azoalkane could not be found, and the complexity of the product mixture prevented further analysis.

Various mechanisms can be invoked to account for the formation of DBO-H^+. One must recall that a direct proton abstraction of DBO from chloroform is unlikely in view of its negative pK_a in the excited state[10] and is also in conflict with the correlation diagram, which precludes a direct correlation with an ionic state (Figure 1). Note also that we have presented evidence by means of deuterium isotope effects[1–3] and the study of quenchers with varying acidity,[2] that the quenching is induced by an initial hydrogen atom, and not proton, transfer. We therefore presume, based on the present theoretical findings, that the protonated azoalkane is formed through a sequential hydrogen atom and electron transfer.

In conclusion, the present computational and spectroscopic studies have allowed a detailed mechanistic investigation of the hydrogen abstraction reaction of n,π^*-excited states and the nature of the corresponding conical intersection (CI). This turned out to be unexpectedly rich, since hydrogen atom, electron, and proton transfer all contribute to the same, apparently trivial, quenching process. Most importantly, the disproportionation of the intermediary RP should be better described as a sequential electron–proton transfer (Polanyi's harpooning) in the region of the surface crossing rather than a direct hydrogen transfer. This mechanism, which is inherently related to a surface crossing, may play a role in other radical reactions as well. Also important is the observation that the investigation of electron transfer, which is usually difficult by quantum chemical tools, may become feasible through the investigation of photochemical reaction paths, where mixing of radical- and covalent/ionic-type wavefunctions can be explicitly considered. Recently we have reported examples where different reaction paths for *thermal intramolecular* electron transfer have been successfully mapped.[26, 27] In this contribution we reported the reaction path mapping for both photoinduced and thermal *intermolecular* electron transfer (the two arrows in Figure 1). Remarkably, in all reported cases electron transfer occurs in the strict vicinity of a CI that thus appears to play a key role for both photochemical and thermal electron transfer.

Received: June 22, 2001 [Z17339]

[1] W. M. Nau, G. Greiner, J. Wall, H. Rau, M. Olivucci, M. A. Robb, *Angew. Chem.* **1998**, *110*, 103–107; *Angew. Chem. Int. Ed.* **1998**, *37*, 98–101.
[2] W. M. Nau, G. Greiner, H. Rau, M. Olivucci, M. A. Robb, *Ber. Bunsenges. Phys. Chem.* **1998**, *102*, 486–492.
[3] W. M. Nau, G. Greiner, H. Rau, J. Wall, M. Olivucci, J. C. Scaiano, *J. Phys. Chem. A* **1999**, *103*, 1579–1584.
[4] F. Bernardi, M. Olivucci, M. A. Robb, *Chem. Soc. Rev.* **1996**, *25*, 321–328.
[5] S. De Feyter, E. W.-G. Diau, A. H. Zewail, *Angew. Chem.* **2000**, *112*, 266–269; *Angew. Chem. Int. Ed.* **2000**, *39*, 260–263.

 © WILEY-VCH Verlag GmbH, D-69451 Weinheim, 2001 1433-7851/01/4022-4188 $ 17.50+.50/0

[6] M. J. Bearpark, F. Bernardi, S. Clifford, M. Olivucci, M. A. Robb, B. R. Smith, T. Vreven, *J. Am. Chem. Soc.* **1996**, *118*, 169 – 175.
[7] M. J. Bearpark, F. Bernardi, M. Olivucci, M. A. Robb, B. R. Smith, *J. Am. Chem. Soc.* **1996**, *118*, 5254 – 5260.
[8] P. Celani, M. Garavelli, S. Ottani, F. Bernardi, M. A. Robb, M. Olivucci, *J. Am. Chem. Soc.* **1995**, *117*, 11584 – 11585.
[9] L. Salem, *J. Am. Chem. Soc.* **1974**, *96*, 3486 – 3501.
[10] W. M. Nau, *EPA Newsl.* **2000**, *70*, 6 – 29.
[11] M. Klessinger, *Pure Appl. Chem.* **1997**, *69*, 773.
[12] B. O. Roos, *Acc. Chem. Res.* **1999**, *32*, 137 – 144.
[13] J. Finley, P.-Å. Malmqvist, B. O. Roos, L. Serrano-Andrés, *Chem. Phys. Lett.* **1998**, *288*, 299 – 306.
[14] Geometry optimization and reaction path computations have been carried out at the CASSCF level of theory using a complete active space including twelve electrons in ten orbitals. The orbitals comprise the π and π* N=N orbitals, the four σ and σ* C–N orbitals, the two N lone-pair orbitals of the pyrazoline fragment, and the σ and σ* orbitals of the reactive C–H bond of CH_2Cl_2. To improve the description of the H transfer, the standard 6-31G* basis set (double-ζ plus d-type polarization functions on first- and second-row atoms) has been augmented with p-type polarization and s-type diffuse functions on the methylene chloride hydrogen atoms and with sp-type diffuse functions included in Gaussian 98[15] on the nitrogen centers. Due to wavefunction instability, the S_0 transition state (TS) has been optimized using state-average CASSCF with a S_0 and S_1 weight of 0.5. The relaxation coordinates have been computed according to the following procedure: a) The CI between the excited state (S_1) and ground state (S_0) was optimized using the methodology available in Gaussian 98; b) the S_0 relaxation paths were computed starting from the optimized CI point and using the IRD method described in references [16, 17]. The reaction path branches associated to the optimized TS were computed using the standard IRC method. In order to get a more accurate reaction energetics we re-evaluated the energy along a selected series of relaxation coordinate points using the multireference Møller – Plesset perturbation theory (CASPT2) using MOLCAS-4.[18] The S_1 and S_0 energies at CI and TS, where the energy gap is small, were re-evaluated using the MS-CASPT2 procedure.[13]
[15] *Gaussian 98* (*Revision A.7*), M. J. Frisch, G. W. Trucks, H. B. Schlegel, G. E. Scuseria, M. A. Robb, J. R. Cheeseman, V. G. Zakrzewski, J. A. Montgomery, R. E. Stratmann, J. C. Burant, S. Dapprich, J. M. Millam, A. D. Daniels, K. N. Kudin, M. C. Strain, O. Farkas, J. Tomasi, V. Barone, M. Cossi, R. Cammi, B. Mennucci, C. Pomelli, C. Adamo, S. Clifford, J. Ochterski, G. A. Petersson, P. Y. Ayala, Q. Cui, K. Morokuma, D. K. Malick, A. D. Rabuck, K. Raghavachari, J. B. Foresman, J. Cioslowski, J. V. Ortiz, A. G. Baboul, B. B. Stefanov, G. Liu, A. Liashenko, P. Piskorz, I. Komaromi, R. Gomperts, R. L. Martin, D. J. Fox, T. Keith, M. A. Al-Laham, C. Y. Peng, A. Nanayakkara, C. Gonzalez, M. Challacombe, P. M. W. Gill, B. G. Johnson, W. Chen, M. W. Wong, J. L. Andres, M. Head-Gordon, E. S. Replogle, J. A. Pople, Gaussian, Inc., Pittsburgh, PA, **1998**.
[16] P. Celani, M. A. Robb, M. Garavelli, F. Bernardi, M. Olivucci, *Chem. Phys. Lett.* **1995**, *243*, 1 – 8.
[17] M. Garavelli, P. Celani, M. Fato, M. J. Bearpark, B. R. Smith, M. Olivucci, M. A. Robb, *J. Phys. Chem.* **1997**, *101*, 2023 – 2032.
[18] *MOLCAS*, *Version 4*, K. Andersson, M. R. A. Blomberg, M. P. Fülscher, G. Karlström, R. Lundh, P.-A. Malmqvist, P. Neogrády, J. Olsen, B. O. Roos, A. J. Sadlej, M. Schütz, L. Seijo, L. Serrano-Andrés, P. E. M. Siegbahn, P.-O. Widmark, University of Lund, Lund, Sweden **1997**.
[19] J. Saltiel, P. T. Shannon, O. C. Zafiriou, A. K. Uriarte, *J. Am. Chem. Soc.* **1980**, *102*, 6799 – 6808.
[20] R. D. Levine, R. B. Bernstein, *Molecular Reaction Dynamics and Chemical Reactivity*, Oxford University Press, New York, NY, **1987**.
[21] M. Polanyi, *Atomic Reaction*, Williams and Norgate, London, **1932**.
[22] The photolysis experiments were carried out using a 900 W xenon source and high radiance monochromator (Applied Photophysics Ltd) at $\lambda = 380$ nm. For the EPR experiments, fresh chloroform solutions with the spin trap PBN (3 mM) and DBO (6 mM) were thoroughly deaerated with oxygen-free nitrogen for at least 20 min. EPR spectra were recorded at room temperature on a Bruker 200D SRC instrument equipped with a microwave frequency counter XL (Jagmar). The spectrometer was interfaced with a PS/2 technical instrument hardware computer and the data acquired using the EPR data system CS-EPR (Stelar Inc.). Simulations of the EPR spectra were performed using a home-made program. The irradiation in the absence of DBO led to no detectable signal.
[23] Spin Trap Data Base, NIEHS (National Institute of Environmental Health Sciences) **2001**.
[24] The formation of protonated DBO upon photolysis of DBO in chloroform was also observed by Feth and Greiner (University of Stuttgart-Hohenheim). We are grateful for this information and related fruitful discussions.
[25] J. R. Pliego, Jr., W. B. De Almeida, *J. Phys. Chem.* **1996**, *100*, 12410 – 12413.
[26] L. Blancafort, F. Jolibois, M. Olivucci, M. A. Robb, *J. Am. Chem. Soc.* **2001**, *123*, 722 – 732.
[27] E. Fernández, L. Blancafort, M. Olivucci, M. A. Robb, *J. Am. Chem. Soc.* **2000**, *122*, 7528 – 7533.
[28] M. Garavelli, C. S. Page, P. Celani, M. Olivucci, W. E. Schmid, S. A. Trushin, W. Fuss, *J. Phys. Chem. A* **2001**, *105*, 4458 – 4469.

Molecular Recognition of UDP-Gal by β-1,4-Galactosyltransferase T1**

Thorsten Biet and Thomas Peters*

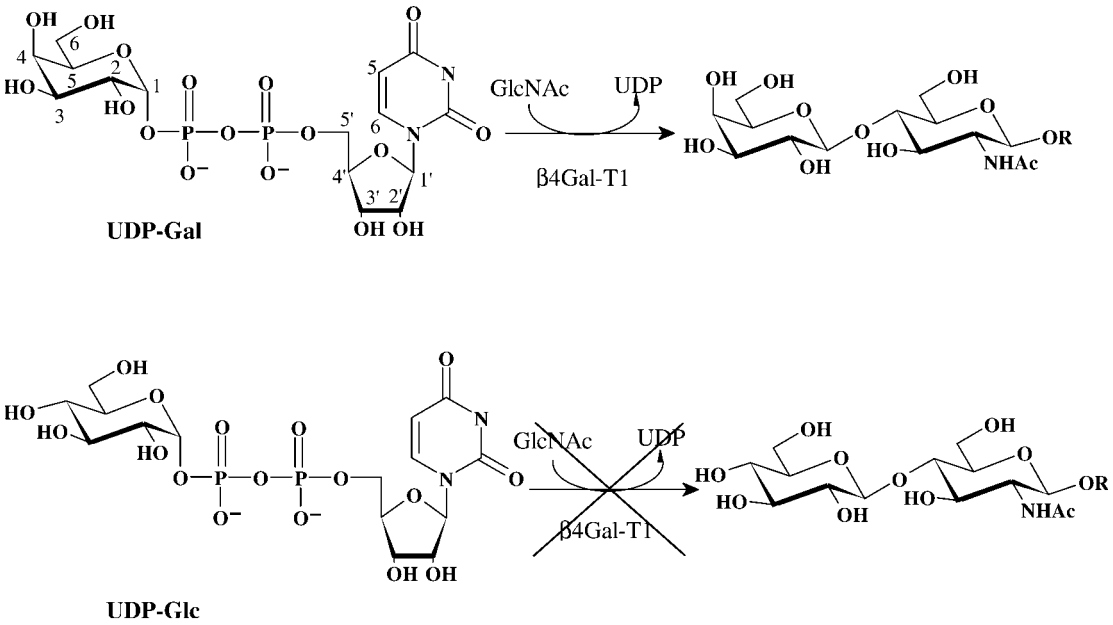
Dedicated to Professor Joachim Thiem on the occasion of his 60th birthday

In mammals, protein – carbohydrate interactions play a crucial role in mediating a variety of biological recognition processes.[1] The enzymes responsible for the biosynthesis of glycan chains are glycosyltransferases, and their malfunction leads to a number of pathological disorders. So far, only limited data are available for the three-dimensional structure of mammalian glycosyltransferases.[2] Recently, an X-ray structure was published of β-1,4-galactosyl-transferase (β4Gal-T1, EC 2.4.1.90/38), a Golgi-resident membrane-bound enzyme, in its free and substrate-bound form.[2c] This transferase is responsible for the transfer of galactose from UDP-Gal (uridine diphospho-D-galactose, Scheme 1) to β-D-*N*-acetylglucosamine residues, furnishing poly-*N*-acetyllactosamine chains found in glycoproteins and glycosphingolipids. The enzyme β4Gal-T1 cocrystallized with the donor substrate UDP-Gal, but the electron density was not sufficient to resolve the terminal galactose residue. Therefore, crucial molecular details of the recognition reaction between β4Gal-

[*] Prof. Dr. T. Peters, Dipl.-Chem. T. Biet
Institut für Chemie, Medizinische Universität zu Lübeck
Ratzeburger Allee 160, 23538 Lübeck (Germany)
Fax: (+49) 451-500-4241
E-mail: thomas.peters@chemie.mu-luebeck.de

[**] This work was supported by the BMBF (FKZ 031161) and the DFG (Teilprojekt B3 of SFB 470). Financial support from the Verband der Chemischen Industrie is gratefully acknowledged. Dr. T. Keller and Dr. G. Wolff (Bruker Analytik GmbH, Rheinstetten) are thanked for excellent support.

Supporting information for this article is available on the WWW under http://www.angewandte.com or from the author.



Scheme 1. β4Gal-T1 transfers D-Galactose from UDP-Gal to D-GlcNAc residues (top reaction). The enzyme is highly specific; for example, it does not process UDP-Glc (bottom reaction) at a significant rate.[8]

T1 and UDP-Gal still must to be revealed. Here we present NMR data that map the binding epitope of UDP-Gal bound to β4Gal-T1 with atomic resolution.

Several NMR experiments are now known for the analysis of protein–ligand interactions. Recently, saturation transfer difference (STD) spectroscopy was introduced for the screening of compound libraries for binding activity towards receptor proteins.[3] The method has proven to be very robust, and requires only small amounts of protein in the μM range.[4] The STD NMR technique is also very useful to map the binding epitope of ligands with atomic resolution.[5] Ligand protons that are in close contact with the protein binding pocket experience a larger fraction of saturation transfer than protons further away. Therefore, protons belonging to the binding epitope of the ligand show larger signal intensities than other ligand protons in the STD NMR spectra. This in turn allows precise definition of the binding epitope.

To study the binding of UDP-Gal to β4Gal-T1[6] we prepared an NMR sample that contained about a 45-fold molar excess of UDP-Gal over β4Gal-T1. To avoid complications from paramagnetic Mn^{2+} we substituted Mn^{2+} by Mg^{2+} in the buffer. This is known to reduce the activity of the enzyme but its functionality is retained.[7] One-dimensional STD NMR spectra were obtained for this sample with saturation times ranging from 0.5–2.0 s. Figure 1b shows the STD spectrum with 2.0 s saturation time; for comparison the 1D ^{1}H NMR spectrum of UDP-Gal is shown in Figure 1a.

From the STD spectra the relative amount of saturation transfer for each individual proton was calculated utilizing a corresponding 1D NMR spectrum as reference (Scheme 2).[5] These values reflect the degree of dipolar interactions of UDP-Gal protons with protons belonging to the active site of the enzyme.

It is clear that the ribose and uracil protons receive the largest amount of saturation transfer. From the ribose residue, the anomeric proton H1′ and the proton H4′ give the most intense STD responses. This is in accordance with the X-ray structure, where the uridine is located in a pronounced binding pocket. Uracil displays a stacking interaction with Phe 226, and as a result H1′ and H4′ of the ribose point towards the interior of the protein, which explains their prominent STD signals. The galactose residue shows smaller STD effects, indicating that this residue is in less intimate contact with the protein surface. Since the galactose residue has to be transferred to an acceptor substrate during the enzymatic reaction, it is reasonable that its contact with the protein's active site is not too tight.

All the protons of the galactose residue show a response in the STD spectrum, indicating that galactose is in direct contact with the enzyme binding pocket. From the galactose protons, H4 and H2 lead to the most prominent STD signals. For comparison, the binding of UDP-Glc (uridine diphospho-D-glucose) to β4Gal-T1 was studied. For UDP-Glc in the presence of β4Gal-T1, STD spectra were obtained also; therefore, binding still occurs. In general, all STD effects were considerably smaller than for UDP-Gal, indicating a much smaller binding affinity (Figure 1). STD effects were only observed for the ribose unit and for uracil; there were no STD responses for the glucose residue. It may be argued that H1 of glucose receives small amounts of saturation, but it was impossible to quantify this effect (Figure 1d). It is concluded that glucose is not in direct contact with the enzyme active site. Apparently, the enzyme does not recognize the glucose residue, and therefore probably fails to properly align the monosaccharide moiety for the transfer. This explains the observation that β4-Gal-T1 does not transfer glucose residues at a significant rate.[8] The finding is also in agreement with the X-ray structure of β4Gal-T1 complexed with uridine diphosphogalactose. An inspection of the orientation of UDP in the binding pocket of β4Gal-T1 shows that a monosaccharide attached to the terminal phosphate of UDP may have a variety of orientations. Therefore, specific interactions with

 © WILEY-VCH Verlag GmbH, D-69451 Weinheim, 2001 1433-7851/01/4022-4190 $ 17.50+.50/0

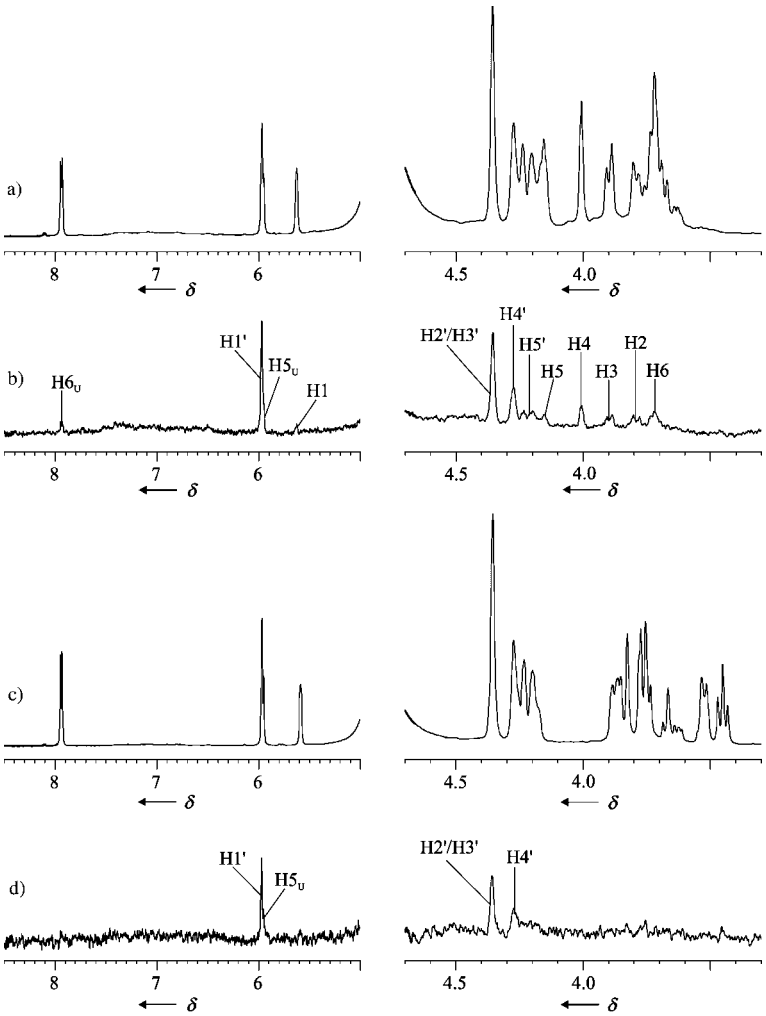
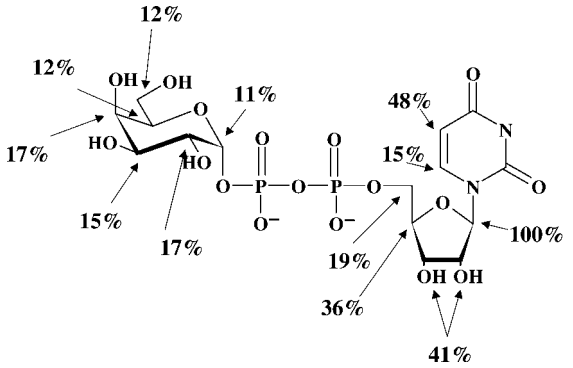


Figure 1. One-dimensional STD NMR (500 MHz) spectra for UDP-Gal (b, 16-fold amplification) and UDP-Glc (d, 32-fold amplification) in the presence of β4Gal-T1 as well as the corresponding ^{1}H NMR reference spectra for free UDP-Gal (a) and UDP-Glc (c). The STD spectra were acquired with selective presaturation at $\delta = 0$ for a duration of 2 s utilizing a cascade of gaussian pulses (duration 50 ms, spacing 1 ms). 2 k scans were recorded for the STD spectra, and 1 K scans for the reference ^{1}H NMR spectra. From the spectra relative STD effects were determined (see Scheme 2).



Scheme 2. Relative STD effects for UDP-Gal bound to β4Gal-T1. The values were calculated by determining the individual signal intensities in the STD spectrum (I_{STD}) and in the reference 1D NMR spectrum (I_0).[5] The ratios of the intensities I_{STD}/I_0 were normalized using the largest STD effect (anomeric proton H1′ of the ribose unit, 100 %) as a reference. The arrows indicate the position of the proton experiencing an STD effect. The value of 41 % corresponds to the cumulative saturation transfer for H2′ and H3′. Likewise, 12 % denotes the sum effect for both protons H6 of the galactose residue. The values for protons H5 and H5′ are estimates only because separate integration of the two signals was difficult.

amino acids will be required to establish binding interactions. We propose that the glucose residue of UDP-Glc protrudes from the binding site, whereas the galactose residue of UDP-Gal is in intimate contact with binding-site protons, as this is reflected by the STD NMR experiments.

The fact that the UDP part of UDP-Glc is bound to the protein is reasonable, as it is known that UMP and UDP as well as their derivatives—for example, UDP-Fuc (uridine diphospho-L-fucose) and UDP-Man (uridine diphospho-D-mannose)—inhibit β4Gal-T1.[9a] The results are consistent with several previous studies where a variety of UDP-Gal derivatives had been synthesized to determine the relative rates of transfer of galactose from UDP-Gal to *N*-acetylglucosamine.[8, 9] It was found that any variation of the galactose moiety reduced the transfer rate. Deoxygenation of the 2-position of galactose only had a minor influence,[9c] but sterically demanding substituents in this position significantly reduced the transfer rate.[8a] The most pronounced effect was observed upon modifying the 4- and the 2-position of galactose in concert; for example, for UDP-GlcNAc (uridine diphospho-*N*-acetyl-D-glucosamine) as a donor substrate no transfer activity was observed. Modification of these two positions lead to almost inactive donor substrates.[8a] This corresponds well with the finding that protons H4 and H2 of galactose receive the largest fraction of saturation transfer (Scheme 2).

Control experiments were performed with UDP-Gal in the presence of two lectins, *Aleuria aurantia* agglutinin (AAA) and *Sambucus nigra* agglutinin (SNA), to exclude the possibility that the effects observed were nonspecific (see the Supporting Information). Lectin AAA specifically recognizes L-fucose moieties,[10] whereas SNA binds to D-galactose, and most tightly to epitopes containing the disaccharide α-D-Neu5Ac-(2,3)-D-Gal.[4b, 11] In the presence of AAA, UDP-Gal showed no STD effects. L-Fucose, which was also present in the same sample, clearly displayed STD signals. In the presence of SNA, UDP-Gal showed strong STD effects for the galactose moiety, and rather weak effects for the rest of the molecule. Thus, individual STD signal patterns were observed upon addition of UDP-Gal for each of the three different proteins, β4Gal-T1, AAA, and SNA, demonstrating that the STD spectra reflect the binding epitope in each case.

Our NMR experiments show that β4Gal-T1 binds to UDP-Gal and to UDP-Glc, albeit with a lower affinity to the latter. Whereas in the case of UDP-Glc only the UDP part of the ligand is in contact with the protein surface, the complete UDP-Gal molecule binds to β4Gal-T1. A quantitative analysis of STD effects allowed definition of the binding epitope of UDP-Gal with atomic resolution. With this technique it will be possible to study the binding of substrates to a variety of glycosyltransferases. Therefore, we are currently applying the method to screen other mammalian glycosyltransferases for which no X-ray data are yet available. The information about

the binding epitopes will be of crucial importance for the design of new selective and potent glycosyltransferase inhibitors.

Experimental Section

All spectra were acquired on a Bruker DRX 500MHz spectrometer with a 5-mm TXI probehead. The STD spectra were measured at 293 K with 2 k scans. The reference spectra were measured with 1 k scans. Saturation tranfer was achieved by using 40 selective gaussian pulses (duration 50 ms, spacing 1 ms). The protein envelope was irridiated at $\delta = 0$ (on-resonance) and $\delta = 40$ (off-resonance). Subsequent substraction was achieved by phase cycling.

The concentrations of β4Gal-T1 were 20 μM and 7 μM for UDP-Gal and UDP-Glc, respectively. Sample volume: 300 μL in a Shigemi tube. The concentration of UDP-Gal was 0.9 mM (UDP-Glc 1 mM). Buffer: 20 mM Tris, 20 mM NaCl, 10 mM $MgCl_2$ ph 7.4 (not corrected).

Received: May 14, 2001 [Z17095]

[1] For an overview, see A. Varki, R. Cummings, J. Esko, H. Freeze, G. Hart, J. Marth, *Essentials of Glycobiology*, Cold Spring Harbor Laboratory Press, Cold Spring Harbor, New York, **1999**.

[2] a) L. N. Gastinel, C. Bignon, A. K. Misra, O. Hindsgaul, J. H. Shaper, D. H. Joziasse, *EMBO J.* **2001**, *20*, 638–649; b) U. M. Unligil, S. Zhou, S. Yuwaraj, M. Sarkar, H. Schachter, J. M. Rini, *EMBO J.* **2000**, *19*, 5269–5280; c) L. N.Gastinel, C. Cambillau, Y. Bourne, *EMBO J.* **1999**, *18*, 3546–3557; d) U. M. Unligil, J. M. Rini, *Curr. Opin. Struct. Biol.* **2000**, *10*, 510–517.

[3] M. Mayer, B. Meyer, *Angew. Chem.* **1999**, *111*, 1902–1906; *Angew. Chem. Int. Ed.* **1999**, *38*, 1784–1788.

[4] a) J. Klein, R. Meinecke, M. Mayer, B. Meyer, *J. Am. Chem. Soc.* **1999**, *121*, 5336–5337; b) M. Vogtherr, T. Peters, *J. Am. Chem. Soc.* **2000**, *122*, 6093–6099; c) H. Maaheimo, P. Kosma, L. Brade, H. Brade, T. Peters, *Biochemistry* **2000**, *39*, 12778–12788.

[5] M. Mayer, B. Meyer, *J. Am. Chem. Soc.* **2001**, *123*, 6108–6117.

[6] Recombinant bovine β4Gal-T1 (M_W 38 kDa) and synthetic UDP-Gal (M_W 610.3 Da) were purchased from Calbiochem.

[7] N. J. Kuhn, S. Ward, W. S. Leong, *Eur. J. Biochem.* **1991**, *195*, 243–250.

[8] a) M. M. Palcic, O. Hindsgaul, *Glycobiology* **1991**, *1*, 205–209; b) L. J. Berliner, R. D. Robinson, *Biochemistry* **1982**, *21*, 6340–6343.

[9] a) T. Endo, Y. Kajihara, H. Kodama, H. Hashimoto, *Bioorg. Med. Chem.* **1996**, *4*, 1939–1948; b) Y. Kajihara, T. Endo, H. Ogasawara, H. Kodama, H. Hashimoto, *Carbohydr. Res.* **1995**, *269*, 273–294; c) G. Srivastava, O. Hindsgaul, M. M. Palcic, *Carbohydr. Res.* **1993**, *245*, 137–144; d) H. Yuasa, O. Hindsgaul, M. M. Palcic, *J. Am. Chem. Soc.* **1992**, *114*, 5891–5892.

[10] a) H. Debray, J. Montreuil, *Carbohydr. Res.* **1989**, *185*, 15–26; b) F. Fukumori, N. Takeuchi, T. Hagiwara, H. Ohbayashi, T. Endo, N. Kochibe, Y. Nagata, A. Kobata, *J. Biochem.* **1990**, *107*, 190–196; c) T. Weimar, T. Peters, *Angew. Chem.* **1994**, *106*, 79–82; *Angew. Chem. Int. Ed.* **1994**, *33*, 88–91.

[11] a) W. F. Broekaert, M. Nsimba-Lubaki, B. Peeters, W. J. Peumans, *Biochem. J.* **1984**, *221*, 163–169; b) E. J. M. Van Damme, A. Barre, P. Rougé, F. Van Leuven, W. J. Peumans, *Eur. J. Biochem.* **1996**, *235*, 128–137.

Watching the Photo-Oxidation of a Single Aromatic Hydrocarbon Molecule**

Thomas Christ, Florian Kulzer, Patrice Bordat, and Thomas Basché*

The ability to observe chemical reactions at the level of single molecules has been demonstrated by fluorescence microscopy.[1] Actually, every optical single-molecule experiment with organic fluorophores under ambient conditions is eventually terminated by a photochemical reaction, which converts the molecule into a state in which it no longer absorbs or fluoresces. Often this photobleaching of organic fluorophores depends on the presence of oxygen, the influence of which on the photophysics and -chemistry of the fluorophores has been elucidated in recent single-molecule experiments.[2] Although photobleaching quite generally is an important mechanism for the degradation of organic dye molecules under ambient conditions, understanding of this process is limited especially for the class of comparatively photo-stable dyes used in single-molecule spectroscopy or for technological applications. For single terrylene molecules in a *p*-terphenyl host crystal, we can unambiguously show that a self-sensitized photo-oxidation is the initial step or directly leads to the terminal photobleaching.

The fluorescence of single terrylene molecules in a *p*-terphenyl host crystal[3] was imaged by confocal microscopy. When following the fluorescence intensity as a function of time (emission time trace) under ambient conditions, various types of intensity changes are observed. Either the fluorescence signal drops to the background level irreversibly after a period of constant emission intensity (Figure 1a) or it jumps to a new level after having dropped to the background level for a short period of time (Figure 1c). As seen in Figure 1c, the latter sequence of events in this case is also terminated by an irreversible drop of the fluorescence signal to the background level. In addition to the time traces, a complete sequence of emission spectra of the molecules under study is recorded simultaneously at regular intervals (5 s). For the molecule, the time trace of which is shown in Figure 1a, all emission spectra are identical until the emission ceases and fully agree with an ensemble spectrum of terrylene in *p*-terphenyl. The spectra in Figure 1d, which belong to the time trace in Figure 1c, shows however that after this molecule resumes emission at ~53 s the spectrum has shifted by 40 nm to the blue. We attribute all the intensity and spectral changes to a photo-oxidation of terrylene or subsequent internal rearrangements of the primary photoproducts.

[*] Prof. Dr. T. Basché, Dipl.-Chem. T. Christ, Dr. F. Kulzer
Institut für Physikalische Chemie
Johannes Gutenberg Universität Mainz, 55099 Mainz (Germany)
Fax: (+49) 6131-3923953
E-mail: thomas.basche@uni-mainz.de

Dr. P. Bordat
Max-Planck-Institut für Polymerforschung
55128 Mainz (Germany)

[**] This work was supported by the Fonds der Chemischen Industrie. We would like to thank R. Schmidt, M. Gudipati, and K. Müllen for very insightful discussions.

 © WILEY-VCH Verlag GmbH, D-69451 Weinheim, 2001 1433-7851/01/4022-4192 $ 17.50+.50/0

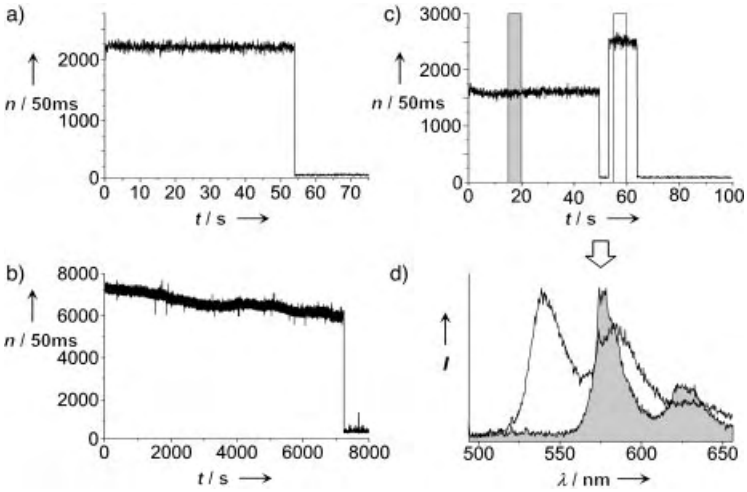


Figure 1. a) Fluorescence intensity of a single terrylene molecule in *p*-terphenyl as a function of time (emission time trace) in air ($\lambda_{exc} = 488$ nm; $I = 53$ kW cm^{-2}; $n =$ number of photo counts). At around 53 s the fluorescence signal irreversibly drops to the background level. b) Emission time trace of a single terrylene molecule in *p*-terphenyl under an argon atmosphere. In this case the emission ceases at around 7200 s after the molecule had emitted 2×10^{10} photons ($I = 53$ kW cm^{-2}). c) Emission time trace of another terrylene molecule in air ($\lambda_{exc} = 488$ nm; $I = 26.5$ kW cm^{-2}). After a dark-state transition the molecules resumes emission at a different intensity level. d) Fluorescence spectra taken during the time periods indicated in c). After the dark-state transition the spectrum is shifted by 40 nm to the blue.

To prove the assumption that photo-oxidation occurs, we have studied several hundred terrylene molecules in air, oxygen, and argon atmospheres at an excitation wavelength of 488 nm. In all cases, approximately 80 % of the molecules showed an irreversible drop of the fluorescence signal while for the remaining number of molecules (20 %) reversible intensity changes and spectral shifts were observed. When analysing the distributions of "on" times in air and oxygen atmospheres before an irreversible signal drop or before a reversible dark state (accompanied by a subsequent spectral shift) occurred, as exemplified in Figures 1 a or 1 c respectively, it is found that the average "on" time becomes much shorter in an oxygen atmosphere. When the measurements are done in a pure argon atmosphere, the "on" times are orders of magnitude longer: For the molecule shown in Figure 1 b the fluorescence signal ceased after $\sim$7200 s, probably due to residual oxygen in the crystal.

The first step in the photo-oxidation of aromatic hydrocarbons is a reaction between electronically excited oxygen in its singlet state [O_2 ($^1\Delta_g$)] and the ground-state aromatic hydrocarbon.[4] Singlet oxygen can be formed by a self-sensitation process through interaction between an electronically excited state (T_1 or S_1) of the hydrocarbon and ground-state oxygen.[4] The self-sensitized photo-oxidation of linear acenes (for example anthracene) in solution is known to yield endoperoxides, which, depending on the illumination wavelength, can either revert to the parent compounds or rearrange through complex mechanisms into different secondary photoproducts.[5] On the other hand, knowledge about photo-oxidation pathways and products of rylenes is rather limited. For perylene in aqueous solution, it has been suggested that the primary reaction with singlet oxygen leads to the formation of either an endo- or an exoperoxide. As major secondary oxidation products 3,10-perylenequinone and 1,12-perylenequinone have been identified.[6]

In case of terrylene, we have performed quantum chemical calculations[7] on a number of possible product structures. Structure **I** in Figure 2 represents the only exoperoxide feasible and structure **II** an endoperoxide formed by attack of the central naphthalene unit. The quantum chemical calculations show that the exoperoxide is stable while they do not converge for the endoperoxide **II**. By computing the $S_0 - S_1$ transitions energies of terrylene and its exoperoxide **I**, we find that the latter is blue shifted by approximately 100 nm. We therefore conclude that the main product (80 %) is structure **I**, which is shifted out of resonance by the fixed excitation wavelength of 488 nm. This shift leads to the irreversible signal drop of the fluorescence signal (see Figure 1 a). It could be argued that the irreversible dark states are due to photoproducts which do not fluoresce rather than being shifted out of resonance. This scenario is highly unlikely because dark photo-oxidation products which absorb light typically rearrange into fluorescent products.[8]

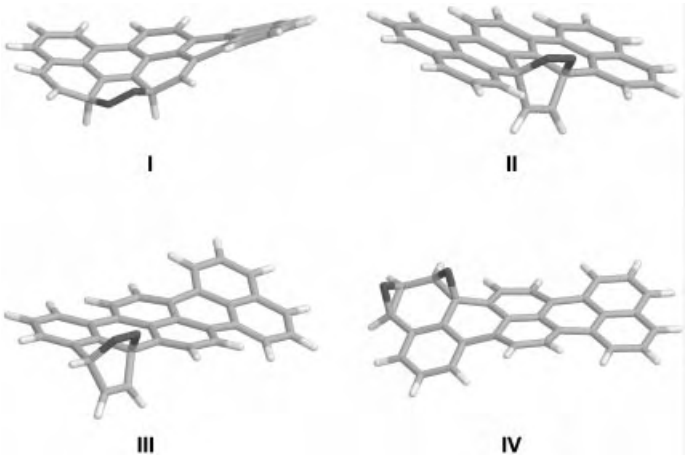


Figure 2. Ground-state structures of the exoperoxide **I**, two endoperoxides **II** and **III**, and a diepoxide **IV** of terrylene as obtained by semiempirical and ab initio quantum chemical calculations in vacuum. The dark segments in the structures indicate the oxygen containing rings. While **I**, **III**, and **IV** are predicted to be stable, this is not true for **II**.

For the molecules in which photo-oxidation led to detectable spectral shifts, the general sequence of events as tracked by the time course of fluorescence intensity and spectra was the same for all molecules investigated (see for example Figure 1 c,d). After a temporary dark state, the molecules resumed emission at a different intensity level and the complete spectrum was shifted. The spectral shifts were not uniform but showed a distribution. Besides the already mentioned 40 nm shift to the blue, stronger (70 nm) or weaker (10 nm) blue shifts and occasionally even red shifts (25 nm) have been observed. These data indicate that the photo-oxidation reaction of terrylene leads to a distribution of

 © WILEY-VCH Verlag GmbH, D-69451 Weinheim, 2001 1433-7851/01/4022-4193 $ 17.50+.50/0

products. In the following, we will limit our discussion to the one shifted by 40 nm to the blue which was the most common product (overall yield: 7.6%) giving rise to a detectable spectral shift.

Endoperoxides of aromatic hydrocarbons are known to be nonfluorescent[8] but can revert into the parent compounds or rearrange into secondary fluorescent products under irradiation. Which of these reactions occur and which secondary products are formed strongly depends on the illumination wavelength.[8] As to the origin of a temporary dark state as exemplified in Figure 1c, we propose the formation of a nonfluorescent terrylene endoperoxide. In our experiments, all detectable temporary dark states were followed by secondary fluorescent photoproducts.

According to our model, the nonfluorescent endoperoxide must still absorb the laser light. This requirement is fulfilled if the endoperoxide is formed in one of the two outer naphthalene rings in the *para*-positions (structure **III**, Figure 2). Quantum chemical calculations[7] indicate that this structure is stable and leads to a blue shift of around 70 nm. (The calculations also have shown that only the *para*-endoperoxide is stable.) At this point, in addition to the quantum chemical calculations in vacuum, we have inserted several product structures into the *p*-terphenyl matrix and performed molecular dynamics (MD) simulations to estimate the solvation shifts. Although these quantities are usually very sensitive to the potentials, the shifts relative to pure terrylene are quite large and we could refer to an optimized model for terrylene in *p*-terphenyl.[9] For oxygen, well-known potentials like OPLS[10] were used. The shift of the endoperoxide **III** relative to terrylene was found between 75 and 100 nm,[11] which is in accordance with the quantum chemical calculations.

Our model is also corroborated by the observation that the Diels–Alder adduct of tetra-*tert*-butylterrylene and acetylenedicarboxylic acid diethylester, which is a structural analogue of **III**, yields an absorption blue shift of 70 nm by conservation of the overall spectral shift.[12] Structure **III** therefore can indeed be expected to still absorb at 488 nm.

In detailed studies by Rigaudy et al.[5], they showed for anthracene and some of its derivatives that the initial step of the photochemical rearrangement of the endoperoxides is the homolytic rupture of the O–O bond. This biradical intermediate rearranges mainly into a diepoxide, which can be stabilized by further subsequent rearrangements. Following these observations, the product shifted by 40 nm to the blue (Figure 1d) could correspond to the diepoxide (**IV**, Figure 2), which is a stable structure according to our calculations. The shifts calculated by quantum chemistry in vacuum[7] and MD[11] in the crystal amount to 70 and 30–55 nm, respectively, which strongly supports our model. While the diepoxide structure seems to be quite reasonable, at present we have no convincing evidence about the chemical structures of the additional secondary fluorescent products mentioned before.

After the secondary fluorescent photoproduct has formed in Figure 1c the emission ceases irreversibly after another 10 seconds, which we attribute to a further photo-oxidation event shifting the product out of resonance with the excitation wavelength. This assumption is based on the observation that the lifetime of any secondary photoproduct becomes, on average, much longer when after its formation the atmosphere is switched immediately to argon or the illumination is blocked.

In some cases, multiple attacks of oxygen could be directly interrogated from intensity and spectral changes. In Figure 3, the formation of the secondary photoproduct, which again exhibits a 40 nm blue shift, is followed by a dark state at ~29 seconds. After the molecule resumes emission, the spectrum is shifted by another 40 nm to give an overall blue shift (compared to terrylene) of about 80 nm. From the spectral shift, we deduce that the second singlet oxygen adds to the same naphthalene unit that was already attacked by the first oxygen molecule (**IV**, Figure 2). After passing a reversible dark state around 43 seconds the absorption is eventually shifted away from the excitation wavelength by what we believe is the addition of a third oxygen molecule.

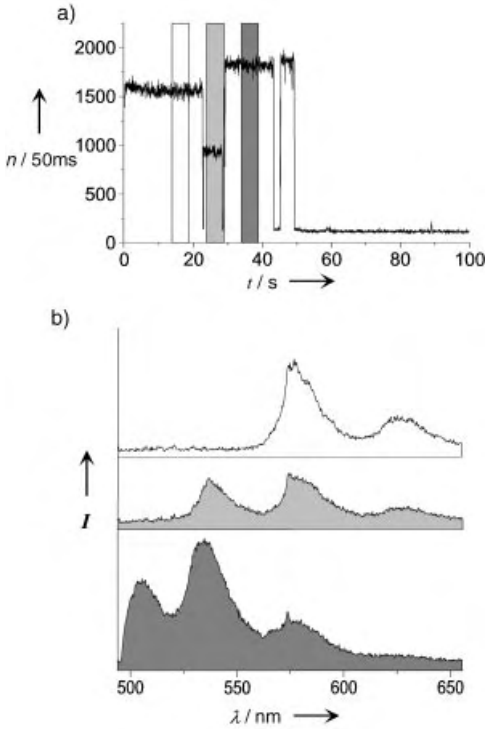


Figure 3. a) Emission time trace of a single terrylene molecule in *p*-terphenyl in air ($\lambda_{exc} = 488$ nm; $I = 26.5$ kW cm^2; n = number of photo counts). After the first two dark states, the molecule resumes emission at different intensity levels. Additionally a reversible dark-state transition occurs around 43 s, which is followed by a final signal drop. b) Fluorescence spectra taken during the time periods indicated in a). After the first dark period the spectrum shifts by 40 nm. The second dark-state transition is followed by a total blue shift of 80 nm. The spectral data below 510 nm are subject to convolution of the emission spectrum with the spectral response of the detection system.

By following fluorescence intensity and spectral changes, we have been able to watch the self-sensitized photo-oxidation of a single fluorophore. We have observed a number of photoproducts and reaction pathways not easily accessible by ensemble experiments, as exemplified by successive photo-oxidation of the same terrylene molecule. These results appear to be an important step towards an

 © WILEY-VCH Verlag GmbH, D-69451 Weinheim, 2001 1433-7851/01/4022-4194 $ 17.50+.50/0

improved understanding of photobleaching and -degradation of aromatic hydrocarbons under ambient conditions. More generally, the study of chemical reactions at the level of single molecules promises novel insights into mechanisms, product distributions, and the reaction kinetics.[1]

Experimental Section

Thin crystalline platelets of *p*-terphenyl doped with terrylene were prepared by cosublimation. In a typical single-molecule experiment first an image ($10 \times 10\ \mu m^2$) was taken with an inverted confocal microscope by raster scanning the sample through the objective focus (numerical aperture: 0.9). Then single molecules were positioned in the focus and fluorescence time traces and spectra were recorded. By using a two-channel detection scheme, the fluorescence light was simultaneously detected by an avalanche photodiode (time traces) and imaged through a spectrograph onto a liquid N_2 cooled CCD (spectra). The microscope allowed the purging of the sample with oxygen, air, or argon.

Received: May 29, 2001 [Z17197]

[1] a) M. M. Collinson, M. R. Wightman, *Science* **1995**, *268*, 1883 – 1885; b) H. P. Lu, L. Xun, X. S. Xie, *Science* **1998**, *282*, 1877 – 1882.

[2] a) O. Panzer, W. Göhde, U. C. Fischer, H. Fuchs, K. Müllen, *Adv. Mater.* **1998**, *10*, 1469 – 1472; b) L. Fleury, B. Sick, G. Zumofen, B. Hecht, U. P. Wild, *Mol. Phys.* **1998**, *95*, 1333 – 1338; c) J. Yu, D. Hu, P. F. Barbara, *Science* **2000**, *289*, 1327 – 1330.

[3] F. Kulzer, F. Koberling, T. Christ, A. Mews, T. Basché, *Chem. Phys.* **1999**, *247*, 23 – 34.

[4] N. J. Turro, *Modern Molecular Photochemistry*, Benjamin/Cummings, Menlo Park, CA, **1978**.

[5] E. Afshari, H. D. Brauer, R. Schmidt, M. Lachgar, J. Rigaudy, *J. Photochem. Photobiol*. **1992**, *63*, 319 – 325.

[6] B. White, M. Nowakowska, J. E. Guillet, *J. Photochem. Photobiol. A* **1989**, *50*, 147 – 156.

[7] Semiempirical (AM1 and MNDO Hamiltonians) and ab initio calculations (4-31G basis) at the restricted Hartree – Fock (RHF) level have been performed for the ground state of photo-oxidation products of terrylene in vacuum with the MOPAC and GAMESS packages. Semiempirical calculations with configuration interaction (including single and double excitations) were employed to calculate electronic transition energies.

[8] R. Schmidt, H. D. Brauer, *J. Photochem*. **1986**, *34*, 1 – 12.

[9] P. Bordat, R. Brown, *Chem. Phys. Lett.* **2000**, *331*, 439 – 445.

[10] W. L. Jorgensen, D. S. Maxwell, J. Tirado-Rives, *J. Am. Chem. Soc.* **1996**, *118*, 11225 – 11236.

[11] To obtain the solvation shifts of the photoproducts by molecular dynamics simulations, in a first approximation we equated the calculated dispersion energy of the electronic ground state of terrylene in *p*-terphenyl with the known experimental solvation shift. This procedure gives us a rescaling factor which we can use to estimate the solvation shifts of the photoproducts (**III**) and (**IV**). (A more complete account of this approach is in preparation.)

[12] K.-H. Koch, PhD thesis, University of Mainz (Germany), **1990**.

Parity Violation Dominates the Dynamics of Chirality in Dichlorodisulfane**

Robert Berger, Michael Gottselig, Martin Quack,* and Martin Willeke

Nearly seventy five years ago, Friedrich Hund contemplated chirality by introducing the quantum mechanical tunnel effect.[1] He explained the origin of molecular chirality as de facto symmetry breaking[2] in relation to the small magnitude of the tunneling splitting $\Delta E_{\pm}$ between the delocalized lowest energy levels of well defined parity (+ and −), an explanation which held prior to the discovery of parity violation in 1956.[3, 4] Now, with electroweak quantum chemistry[5–7] taking the parity-violating nature of the weak interaction into account, we expect a small parity-violating energy difference ΔE_{pv} (about $10^{-13\pm3}\ J\,mol^{-1}$ for molecules consisting of lighter elements) between two enantiomers of a chiral molecule.[5–12] The discovery[6, 7, 10] that ΔE_{pv} is larger by an order of magnitude than previously anticipated has given new impetus to the search for molecular parity violation. Our early results[6, 7] have meanwhile been confirmed by further theoretical calculations.[10–12] For typical, stable chiral molecules with a high energetic barrier against interconversion between enantiomers, $|\Delta E_{pv}|$ should be as a rule much larger than the small tunneling splittings $|\Delta E_{\pm}|$ in the lowest vibrational states. In this case the molecular eigenfunctions have well defined handedness and molecular chirality arises from de lege symmetry breaking. Although this most striking situation is qualitatively predicted,[2, 5] there exists so far no such case for which a quantitative calculation has shown that $\Delta E_{pv} \gg \Delta E_{\pm}$ holds and thus chirality is dominated by de lege parity violation. Here, we present the first such example: dichlorodisulfane (ClSSCl, Figure 1).

Dichlorodisulfane has a chiral C_2-symmetric equilibrium structure with high barriers against interconversion between the *P*- and *M*-enantiomer (Figure 2) and has been previously investigated experimentally and by traditional (parity conserving) quantum chemical calculations on the general series X_2S_2.[13–18] We report here calculations of parity-violating potentials, the corresponding parity-violating energy differences, and the torsional tunneling splitting in the vibrational ground state for ClSSCl, which demonstrate that indeed parity violation dominates the dynamics of chirality in this molecule. Our theoretical findings on dichlorodisulfane and related compounds might prove crucial for experimental

[*] Prof. Dr. M. Quack, M. Gottselig, Dr. M. Willeke
Physical Chemistry
ETH Zürich
8093 Zürich (Switzerland)
Fax: (+41) 1-632-1021
E-mail: Martin@Quack.ch

Dr. R. Berger
Institut für Chemie
TU Berlin
Strasse des 17. Juni 135
10623 Berlin (Germany)

[**] Our work is supported financially by the Schweizerischer Nationalfonds and ETH Zürich (including C^4 and CSCS). We acknowledge discussions with J. Stohner.

 © WILEY-VCH Verlag GmbH, D-69451 Weinheim, 2001 1433-7851/01/4022-4195 $ 17.50+.50/0

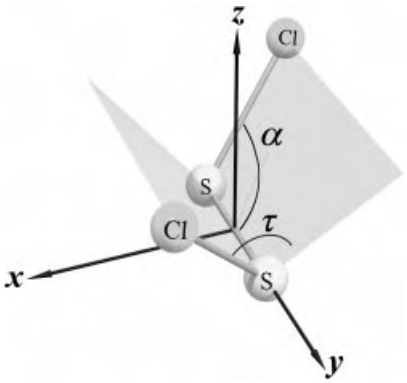


Figure 1. Chiral, C_2-symmetric equilibrium structure and orientation of the *P*-enantiomer of ClSSCl (corresponding to the left minimum in Figure 2) as used in the calculations presented here. It was obtained by a full structure optimization using second-order Møller–Plesset perturbation theory (MP2) in the frozen-core limit with a 6-311 + G(3df) basis set. Our results are consistent with experimental data as well as recent ab initio results.[13, 14, 18] The equilibrium structural parameters are r_e(S–S) = 194.7 pm, r_e(S–Cl) = 205.2 pm, $\alpha = 107.55°$, $\tau = 85.12°$.

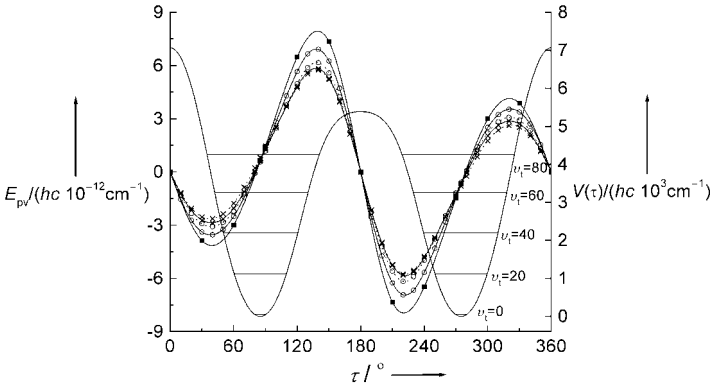


Figure 2. Parity-conserving electronic torsional potential $V(\tau)$ and parity-violating potentials $E_{pv}(\tau)$. $V(\tau)$ (solid line, right axis) was calculated in 10° steps along the torsional coordinate τ employing MP2/6-311 + G(3df). Values of τ between 0° and 180° correspond to the *P*-enantiomer while values of τ between 180° and 360° correspond to the *M*-enantiomer of ClSSCl. $V(\tau = 180°)$ corresponds to the *trans* barrier and $V(\tau = 0°)$ to the *cis* barrier to stereomutation, respectively. $E_{pv}(\tau)$ for different basis sets were calculated along the torsional coordinate in 10° steps (30° for cc-pVTZ-A) and additionally for the equilibrium torsional angle of ClSSCl using MP2/6-311 + G(3df) optimized structures. With an effective one-electron spin–orbit coupling operator,[10] and $Z_{eff}(S) = 12.9$, $Z_{eff}(Cl) = 13.9$ we were able to use a completely decontracted cc-pVTZ basis set additionally augmented with four s- and four p-Gaussian basis functions. The s- and p-like functions added to the sulfur atoms have orbital exponents of $\alpha_{s1}(S) = 2\,497\,000$, $\alpha_{s2}(S) = 16\,670\,000$, $\alpha_{s3}(S) = 111\,200\,000$, $\alpha_{s4}(S) = 742\,400\,000$, $\alpha_{p1}(S) = 2430$, $\alpha_{p2}(S) = 10\,280$, $\alpha_{p3}(S) = 43\,470$, and $\alpha_{p4}(S) = 183\,900$, while those added to chlorine atoms have orbital exponents of $\alpha_{s1}(Cl) = 3\,044\,000$, $\alpha_{s2}(Cl) = 20\,320\,000$, $\alpha_{s3}(Cl) = 135\,600\,000$, $\alpha_{s4}(Cl) = 905\,400\,000$, $\alpha_{p1}(Cl) = 2806$, $\alpha_{p2}(Cl) = 11\,870$, $\alpha_{p3}(Cl) = 50\,210$, and $\alpha_{p4}(Cl) = 212\,400$ (we denote this basis set "cc-pVTZ-A"). The assignment of symbols is as follows: squares and solid line (E_{pv}(RPA/cc – pVTZ – A)); circles and dashed line (E_{pv}(RPA/aug – cc – pVDZ)); crosses and dashed line (E_{pv}(RPA/cc – pVDZ)); circles and solid line (E_{pv}(RPA/6 – 311G(d))); crosses and solid line (E_{pv}(RPA/6 – 31G(d))). Some torsional levels ν_t are indicated.

efforts to directly measure ΔE_{pv} as well as to experimentally discriminate between different theories concerning the physicochemical origin of molecular chirality.[2, 19]

In the present calculations of the parity-violating potentials and the parity-violating energy difference between the *M*- and *P*-enantiomers of ClSSCl, we used our recent multiconfiguration linear response (MC-LR) approach[10] to electroweak quantum chemistry in the limits of the random phase approximation (RPA). Figure 2 shows the results. An important aspect in the present calculations concerns the determination of the very small hypothetical tunneling splittings $\Delta E_{\pm}$ for the parity-conserving, symmetrical potential. The direct variational calculation of the extremely small torsional tunneling splitting in the lowest vibrational states by means, for instance, of the quasiadiabatic channel–reaction path Hamiltonian approach (RPH)[21–23] is not possible due to numerical limitations. Therefore, we use an extrapolation technique to determine the tunneling splitting $\Delta E_{\pm}$. First, we calculated, with the RPH approach, the torsional tunneling splittings $\Delta E_{\pm}(f)$ for various scaled torsional potentials $V(\tau;f) = fV(\tau)$, where τ is the torsional coordinate, f is the scaling factor, and $V(\tau)$ is the unscaled, symmetrical, and thus parity-conserving effective torsional potential with the Born–Oppenheimer electronic potential and the zero-point corrections as the main contributions. The scaling factors were chosen so as to allow accurate numerical computations of the torsional splittings $\Delta E_{\pm}(f)$. Second, we fit the torsional splittings $\Delta E_{\pm}(f)$ with the simple relationship of Equation (1), where P_1, P_2, and P_3 are fit parameters.

$$\lg\left(\frac{\Delta E_{\pm}(f)}{hc\,\mathrm{cm}^{-1}}\right) = P_1 \lg\sqrt{f} + P_2 - P_3\sqrt{f} \qquad (1)$$

Then, we used these parameters and Equation (1) to extrapolate the torsional tunneling splittings $\Delta E_{\pm}(f)$ to $f = 1$. The ground-state torsional tunneling splitting for the original, unscaled torsional potential is thus given by Equation (2).

$$\Delta E_{\pm} = \Delta E_{\pm}(f=1) = (hc)10^{P_2 - P_3}\,\mathrm{cm}^{-1} \qquad (2)$$

Figure 3 displays the calculated torsional tunneling splittings $\Delta E_{\pm}$ as well as the excellent fit with Equation (1). With

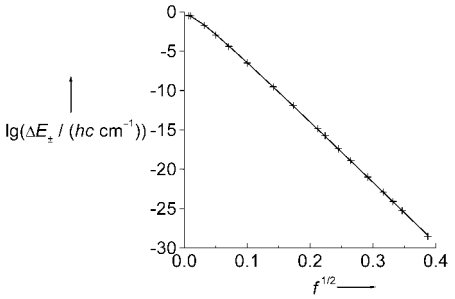


Figure 3. Decadic logarithm of the torsional tunneling splittings $\Delta E_{\pm}(f)$ for differently scaled torsional potentials $V(\tau,f) = fV(\tau)$ calculated with the quasiadiabatic channel–reaction path Hamiltonian approach (+ for RPH) and fit to Equation (1) (line).

the fit parameters $P_1 = 1.16(5)$, $P_2 = 2.59(10)$, and $P_3 = 78.73(24)$, and Equation (1), we obtained $\Delta E_{\pm}/hy \approx 10^{-76}\,\mathrm{cm}^{-1}$ for the ground-state tunneling splitting of ClSSCl. The physical significance of our fit formula can be discussed in terms of a recently presented expression for the ground-state tunneling splitting in a symmetric double-well potential $V(x)$

 © WILEY-VCH Verlag GmbH, D-69451 Weinheim, 2001 1433-7851/01/4022-4196 $ 17.50+.50/0

obtained by the semiclassical Wentzel–Kramers–Brillouin (WKB) theory,[24] Equation (3).

$$\Delta E_{\pm} = 2\hbar\omega\sqrt{\frac{m\omega a^2}{\pi\hbar}}\mathrm{e}^{A}\mathrm{e}^{-S_0/\hbar} \tag{3}$$

The terms S_0 and A are given in Equations (4) and (5), respectively, where ω is the classical angular oscillation frequency of the small amplitude motion around the quadratic wells at $x = a$ and $x = -a$, and m is the reduced mass.

$$S_0 = \int_{-a}^{a}\sqrt{2\,m\,V(x)}\,\mathrm{d}x \tag{4}$$

$$A = \int_{0}^{a}\left[\frac{m\omega}{\sqrt{2\,m\,V(x)}} - \frac{1}{a-x}\right]\mathrm{d}x \tag{5}$$

Scaling of the symmetric double-well potential $V(x;f) = fV(x)$ results in a scaled classical angular harmonic oscillation frequency $\omega(f) = \sqrt{f}\,\omega(f=1)$. Insertion of $V(x;f)$ and $\omega(f)$ into the WKB formula (3) yields the ground-state tunneling splitting as a function of the scaling factor f, which can be written in the form of our fit formula (1) with $P_1 = 3/2$, $P_2 = \lg(2\hbar\omega\sqrt{m\omega a^2/\pi\hbar})\,\mathrm{e}^{A}/J$), and $P_3 = S_0/(\hbar\ln 10)$. In this case of a double-well potential, only one barrier at $x = 0$ is assumed to be finite and contributing to the tunneling dynamics. However, the torsional potential of ClSSCl has two paths with relatively similar barriers that contribute to the torsional tunneling splitting in a six-dimensional tunneling dynamic.[22, 23] Nevertheless, taking P_1, P_2, and P_3 as pure fit parameters we are able to fit the torsional tunneling splittings calculated by RPH for the two-barrier problem. Thus, WKB theory supports our extrapolation scheme. Moreover, we were able to establish good fit results in test calculations for hydrogen peroxide H_2O_2 and various disulfanes X_2S_2 (X = H, D, T) for which accurate experimental and theoretical results are available.[22, 23] In all cases we observe a nearly linear dependence between $\lg(\Delta E_{\pm}(f)/(hc\ \mathrm{cm}^{-1}))$ and $\sqrt{f}$ for large scaling factors. Since $\sqrt{f}$ is proportional to the number of torsional states N, which fit in the harmonic approximation into the well, $\lg(\Delta E_{\pm}(f)/(hc\ cm^{-1}))$ is also proportional to N. The terms $E_{\mathrm{pv}}(\tau)$ and $\Delta E_{\mathrm{pv}} = E_{\mathrm{pv}}(P\text{-enantiomer}) - E_{\mathrm{pv}}(M\text{-enantiomer})$ were obtained using the MC-LR approach to electroweak quantum chemistry in the limit of the random phase approximation.[10] Figure 2 displays $E_{\mathrm{pv}}(\tau)$ calculated with our modified[10] version of the Dalton program[20] for different basis sets. $E_{\mathrm{pv}}(\tau)$ shows the typical dependence on τ with large excursions from negative values for the P-enantiomer (that is, (P)-ClSSCl is stabilized compared to the M-form for $0^\circ < \tau < 80^\circ$), $E_{\mathrm{pv}}(\tau \approx 80^\circ) = 0$ at a chiral geometry,[7] to positive values for the P-enantiomer (namely, (M)-ClSSCl is stabilized), as was also found for H_2O_2 and H_2S_2.[7, 10, 25] Table 1 summarizes ΔE_{pv} for the equilibrium structure of ClSSCl. The values show that (M)-ClSSCl is stabilized compared to (P)-ClSSCl by about $10^{-12}\,\mathrm{cm}^{-1}$. Furthermore, the calculation of the two lowest torsional levels ($\Delta E^{\mathrm{pv}}_{0,1}$) with $E_{\mathrm{pv}}(\tau)$ added to the original effective torsional potential leads to $\Delta E^{\mathrm{pv}}_{0,1}/hc = 1.35 \times 10^{-12}\,\mathrm{cm}^{-1}$ (cc-pVTZ-A, see Figure 2) which is almost equal to $\Delta E_{\mathrm{pv}}/hc = 1.29 \times 10^{-12}\,\mathrm{cm}^{-1}$ for the equilibrium geometry and equal to the expectation values $\langle\Delta E_{\mathrm{pv}}\rangle$ for the localized vibrational states.

Table 1. Parity-violating energy difference $\Delta E_{\mathrm{pv}} = E_{\mathrm{pv}}(P) - E_{\mathrm{pv}}(M)$ for the optimized equilibrium structure of ClSSCl (Figure 1) calculated with different basis sets and MC-LR/RPA.

Method/Basis Set	$\Delta E_{\mathrm{pv}}/hc\ [10^{-12}\,\mathrm{cm}^{-1}]$
RPA/6-31G(d)	1.31
RPA/6-311G(d)	1.29
RPA/cc-pVDZ	1.62
RPA/aug-cc-pVDZ	1.14
RPA/cc-pVTZ-A	1.29

An increase in basis set size lowers the parity-violating energy difference slightly, but it still remains about 64 orders of magnitude larger than the torsional tunneling splitting in the lowest vibrational states, Equation (6).

$$|\Delta E_{\mathrm{pv}}|/hc \approx 10^{-12}\,\mathrm{cm}^{-1} \gg 10^{-76}\,\mathrm{cm}^{-1} \approx |\Delta E_{\pm}|/hc \tag{6}$$

With our RPH approach we accurately calculated a torsional tunneling splitting in the two lowest vibrational states of $10^{-12}\,\mathrm{cm}^{-1}$ for a scaled effective torsional potential of $\sqrt{f} \approx 0.17$ without any extrapolation. Thus, de lege symmetry breaking due to parity violation dominates the dynamics of chirality in ClSSCl independently of the detailed accuracy of the extrapolation procedure. Compared to H_2O_2, H_2S_2, and [N-D_1]aniline, which have been recently theoretically classified as belonging to the group of chiral molecules whose molecular chirality is dominated by de facto symmetry breaking,[21–23, 26] the essential difference is a much higher, effective reduced "tunneling mass"[21] and higher barriers against stereomutation in ClSSCl. Thus, the low energy eigenstates of this molecule have a well defined chirality (P or M). If one generates a superposition state of well defined parity (+ or −) by means of the methods proposed in references [2, 19], the value of ΔE_{pv} in ClSSCl corresponds to a period for parity change of about 30 s. The initial time evolution for parity change in the micro- to millisecond range should be measurable by the technique proposed in reference [19]. Vibrational corrections to ΔE_{pv}[27] are small. The modest relativistic corrections[28] are not expected to change our fundamental conclusions. Collisions and superselection rule effects[2, 30–32] also do not change the conclusions on the *relative* importance of $\Delta E_{\pm}$ and ΔE_{pv} derived here, and could be tested in any case by the same type of experiment.[19] We should draw particular attention also to the superselection rule hypothesis of Pfeiffer and Primas,[30, 33] which tries to explain the stabilization of enantiomers in the high barrier limit *without* invoking parity violation, and thus represents an alternative to the present hypothesis using parity violation. The two approaches would predict quite a different outcome for "Quack's experiment" as referred to by Pfeiffer[30] (see also the critical review in reference [2]). Compared to fluorooxirane[29] and methane derivatives such as methane isotopomers[34] or amino acids important for biology[6, 7, 35–40]—all high barrier limit molecules—dichlorodisulfane has the advantage that in addition to parity violation also the stereomutation dynamics is now well understood, providing a new picture of molecular chirality differing fundamentally from Hund's parity-conserving description.[1, 2]

Received: June 15, 2001 [Z17292]

[1] F. Hund, *Z. Phys.* **1927**, *43*, 805 – 826.
[2] M. Quack, *Angew. Chem.* **1989**, *101*, 588 – 604; *Angew. Chem. Int. Ed.* **1989**, *28*, 571 – 586.
[3] T. D. Lee, C. N. Yang, *Phys. Rev.* **1956**, *104*, 254 – 258.
[4] C. S. Wu, E. Ambler, R. W. Hayward, D. D. Hoppes, R. P. Hudson, *Phys. Rev.* **1957**, *105*, 1413 – 1415.
[5] M. Quack, *Nova Acta Leopold.* **1999**, *81*, 137 – 173.
[6] "Chemical Evolution: Physics of the Origin and Evolution of Life": A. Bakasov, T.-K. Ha, M. Quack in *Proc. 4th Trieste Conf. 1995* (Eds.: J. Chela-Flores, F. Raulin), Kluwer, Dordrecht, **1996**, pp. 287 – 296.
[7] A. Bakasov, T. K. Ha, M. Quack, *J. Chem. Phys.* **1998**, *109*, 7263 – 7285.
[8] R. A. Hegstrom, D. W. Rein, P. G. H. Sandars, *J. Chem. Phys.* **1980**, *73*, 2329 – 2341.
[9] S. F. Mason, G. E. Tranter, *Mol. Phys.* **1984**, *53*, 1091 – 1111.
[10] R. Berger, M. Quack, *J. Chem. Phys.* **2000**, *112*, 3148 – 3158.
[11] P. Lazzeretti, R. Zanasi, *Chem. Phys. Lett.* **1997**, *279*, 349 – 354.
[12] J. K. Laerdahl, P. Schwerdtfeger, *Phys. Rev. A* **1999**, *60*, 4439 – 4453.
[13] B. Beagley, G. H. Eckersley, D. P. Brown, D. Tomlinson, *Trans. Faraday Soc.* **1969**, *65*, 2300 – 2307.
[14] C. J. Marsden, R. D. Brown, P. D. Godfrey, *J. Chem. Soc. Chem. Commun.* **1979**, 399 – 401.
[15] F. M. Bickelhaupt, M. Sola, P. von R. Schleyer, *J. Comput. Chem.* **1995**, *16*, 465 – 477.
[16] D. R. Alleres, D. L. Cooper, T. P. Cunningham, J. Gerratt, P. B. Karadakov, M. Raimondi, *J. Chem. Soc. Faraday Trans.* **1995**, *91*, 3357 – 3362.
[17] P. von R. Schleyer, M. Mauksch, *Angew. Chem.* **2000**, *112*, 2879 – 2881; *Angew. Chem. Int. Ed.* **2000**, *39*, 2756 – 2758.
[18] D. Das, S. L. Whittenburg, *J. Phys. Chem. A* **1999**, *103*, 2134 – 2140.
[19] M. Quack, *Chem. Phys. Lett.* **1986**, *132*, 147 – 153.
[20] T. Helgaker, H. J. Jensen, P. Jørgenson, J. Olsen, K. Ruud, H. Ågren, T. Andersen, K. L. Bak, V. Bakken, O. Christiansen, P. Dahle, E. K. Dalskov, T. Enevoldsen, B. Fernandez, H. Heiberg, H. Hettema, D. Jonsson, S. Kirpekar, R. Kobayashi, H. Koch, K. V. Mikkelson, P. Norman, M. J. Packer, T. Saue, P. R. Taylor, O. Vahtras, *Dalton: An Electronic Structure Program*, Release 1.0 ed., **1997**.
[21] B. Fehrensen, D. Luckhaus, M. Quack, *Z. Phys. Chem. (München)* **1999**, *209*, 1 – 19.
[22] B. Fehrensen, D. Luckhaus, M. Quack, *Chem. Phys. Lett.* **1999**, *300*, 312 – 320.
[23] M. Gottselig, D. Luckhaus, M. Quack, J. Stohner, M. Willeke, *Helv. Chim. Acta* **2001**, *84*, 1846 – 1861.
[24] A. Garg, *Am. J. Phys.* **2000**, *68*, 430 – 437.
[25] A. Bakasov, M. Quack, *Chem. Phys. Lett.* **1999**, *303*, 547 – 557.
[26] B. Kuhn, T. R. Rizzo, D. Luckhaus, M. Quack, M. A. Suhm, *J. Chem. Phys.* **1999**, *111*, 2565 – 2587.
[27] M. Quack, J. Stohner, *Phys. Rev. Lett.* **2000**, *84*, 3807 – 3810.
[28] J. K. Laerdahl, P. Schwerdtfeger, H. M. Quiney, *Phys. Rev. Lett.* **2000**, *84*, 3811 – 3814.
[29] R. Berger, M. Quack, J. Stohner, *Angew. Chem.* **2001**, *113*, 1716 – 1719; *Angew. Chem. Int. Ed.* **2001**, *40*, 1667 – 1670.
[30] "Energy Storage and Redistribution in Molecules": P. Pfeiffer in *Proc. of Two Workshops, Bielefeld, June 1980* (Ed.: J. Hinze), Plenum, New York, NY, **1983**, pp. 315 – 326.
[31] R. A. Harris, L. Stodolski, *J. Chem. Phys.* **1981**, *74*, 2145 – 2155.
[32] M. Simonius, *Phys. Rev. Lett.* **1978**, *40*, 980 – 983.
[33] H. Primas, *Chemistry, Quantum Mechanics and Reductionism*, Springer, Berlin, **1981**.
[34] M. J. M. Pepper, I. Shavitt, P. von R. Schleyer, M. N. Glukhovtsev, R. Janoschek, M. Quack, *J. Comput. Chem.* **1995**, *16*, 207 – 225.
[35] R. Berger, M. Quack, *ChemPhysChem* **2000**, *1*, 57 – 60.
[36] R. N. Zare, W. Bonner, P. Frank in *Chemistry for the 21st Century* (Eds.: E. Keinan, I. Schechter), Wiley-VCH, Weinheim, **2001**, pp. 175 – 208.
[37] "Theories of the Origin of Biomolecular Homochirality": R. Janoschek in *Chirality* (Ed.: R. Janoschek), Springer, Berlin, **1991**, p. 18.
[38] G. E. Tranter, *Mol. Phys.* **1985**, *56*, 825 – 838.
[39] O. Kiyonaga, K. Morihashi, O. Kikuchi, *J. Chem. Phys.* **1998**, *108*, 2041 – 2043.
[40] J. Laerdahl, R. Wesendrup, P. Schwerdtfeger, *ChemPhysChem* **2000**, *1*, 60 – 62.

$[(OC)_5Cr{=}BSi(SiMe_3)_3]$: A Terminal Borylene Complex with an Electronically Unsaturated Boron Atom**

Holger Braunschweig,* Miriam Colling, Carsten Kollann, Klaus Merz, and Krzysztof Radacki

Dedicated to Professor Gerhard E. Herberich on the occasion of his 65th birthday

Stable molecules with both electronically and coordinatively unsaturated boron atoms are extremely rare and restricted to a few methyleneboranes of the type $(Me_3Si)_2C{=}BR$ (R = Me, *t*Bu, 2,3,5,6-tetramethylphenyl, 2,4,6-trimethylphenyl).[1a–e] The chemical and structural properties of such alkyl- and aryl(alkylidene)boranes are decisively determined by the low coordination number and the electron deficiency at the boron center.

A similar bonding situation for boron is found in terminal borylene complexes of the type $[L_xM{=}BR]$ (R = alkyl, aryl, silyl). Owing to their significance[2] for the understanding of metal – boron interactions, alkyl- and arylborylene complexes have been already subject to several theoretical studies.[3a–e] On the basis of ab initio calculations it appears to be generally accepted that these compounds exhibit a stronger metal-to-boron π-backbonding than corresponding borylene complexes $[L_xM{=}B{=}X]$ ($X = NR_2$, F)[4a,b] in which electron deficiency at the boron center is relieved by π interaction with X. Experimental evidence for a complex $[L_xM{=}B{-}R]$ in which R is not a π donor, however, has yet to be reported.

In the course of our investigations on both bridged and terminal borylene complexes,[5a–i] we recently reported on compounds of the type $[(OC)_5M{=}B{=}N(SiMe_3)_2]$ (**1a**, **b**; M = Cr, W). These aminoborylene complexes were obtained either by direct salt elimination reactions[6] or alternatively, in the case of **1a**, by photochemically induced borylene transfer,[7] and represent the only compounds of this type comprising two-coordinate and hence, coordinatively unsaturated boron centers. The boron atom, however, is electronically stabilized by a π-donating amino ligand. Apart from **1a**, **b** only two structurally authentic terminal borylene complexes have been reported, which comprise, however, saturated boron atoms in higher coordination numbers of three and six, respectively.[8, 9]

[*] Dr. H. Braunschweig, Dr. K. Radacki
Department of Chemistry
Imperial College
London SW7 2AY (UK)
Fax: (+44) 20-7594-5900
E-mail: h.braunschweig@ic.ac.uk

M. Colling, Dr. C. Kollann
Institut für Anorganische Chemie der RWTH Aachen
52056 Aachen (Germany)

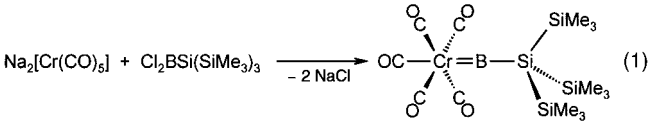
Dr. K. Merz
Ruhr-Universität Bochum, Fakultät für Chemie
Anorganische Chemie I, 44780 Bochum (Germany)

[**] This work was supported by the Deutsche Forschungsgemeinschaft, the Fonds der Chemischen Industrie, EPSRC, and the Royal Society. We are grateful to the Rechenzentrum of the RWTH Aachen for computer time.

 © WILEY-VCH Verlag GmbH, D-69451 Weinheim, 2001 1433-7851/01/4022-4198 $ 17.50+.50/0

Herein we describe the synthesis and structural characterization of $[(OC)_5Cr{=}BSi(SiMe_3)_3]$ (**2**), which is the first borylene complex in which the boron center is both coordinatively and electronically unsaturated.

The title compound **2** was obtained by a salt elimination reaction according to Equation (1) and isolated as yellow crystals in 81% yield. The complex is very soluble in all



(1)

2

common aliphatic or aromatic hydrocarbons and only forms crystals from concentrated solutions at temperatures lower than $-50\,^{\circ}C$. In contrast to its rather stable amino analogue $[(OC)_5Cr{=}B{=}N(SiMe_3)_2]$ (**1a**), the silylborylene complex **2** is extremely sensitive and shows significant decomposition in solution and even in the solid state after several hours at ambient temperature. The enhanced sensitivity of **2** is evidently due to the lack of a ligand-to-boron π interaction, as its steric shielding must be considered equal to or even larger than that in **1a**.

The most striking spectroscopic feature of **2** is the extremely low-field shifted ^{11}B NMR resonance signal at $\delta = 204.3$ in comparison to that for **1a** ($\delta = 92.3$), thus largely extending the known dispersion of the ^{11}B nucleus for classical boranes. Similarly low-field shifted resonances were reported for metal clusters comprising interstitial boron atoms, for example *cis*- and *trans*-$[Fe_4Rh_2(CO)_{16}B]^-$ ($\delta = 211$ and 205).[10a,b] The observed significant difference in the ^{11}B NMR spectroscopic data between **2** and **1a** could be expected for terminal borylene complexes in which the boron center is not part of a boron–ligand π system,[2] particularly if one compares the bridged amino- and alkylborylene complexes of the type $[(\mu\text{-BR})\{(\eta^5\text{-}C_5H_5)Mn(CO)_2\}_2]$ ($R = NMe_2$, $\delta(^{11}B) = 103$; $R = t$Bu, $\delta(^{11}B) = 170$).[5a,b,f] ^1H and ^{13}C NMR spectra of **2** show single sets of signals for all Me and equatorial CO groups, which indicates free rotation about the boron–silicon single bond. Although the structural data support the assumption of a stronger Cr–B π-backbonding in the case of **2** (see below), the CO stretching frequencies are only slightly shifted to higher wavenumbers than those of **1a.**

Single crystals of **2** suitable for an X-ray structure analysis (Figure 1) were grown from hexane at $-78\,^{\circ}C$. The compound crystallizes in the space group $P3_2$ and the molecule adopts C_1 symmetry in the crystal. The molecular structure of **2** reveals some significant differences to that of the aminoborylene complex **1a**, which provides strong evidence for an increased chromium-to-boron π-backbonding. The Cr–B bond in **2** (187.8(10) pm) is 12 pm shorter than that in **1a** (199.6(6) pm), while the axial $Cr{-}C_{ax}$ bond (193.9(10) pm) is 3 pm longer than that in **1a** (190.8(6) pm). This *trans*-effect also becomes evident from the different intramolecular $Cr{-}C_{ax}$ and $Cr{-}C_{eq}$ distances: the $Cr{-}C_{ax}$ distance in **2** is almost 5 pm longer than

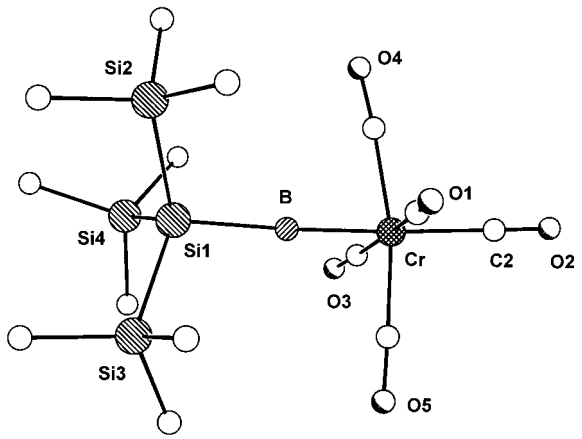


Figure 1. Structure of **2** in the crystal. Selected distances [Å] and angles [°]: Cr-B 1.878(10), B-Si(1) 1.998(10), Cr-B-Si(1) 176.9(5).

the average $Cr{-}C_{eq}$ value of 189.4 pm, while the $Cr{-}C_{ax}$ distance in **1a** resembles the average $Cr{-}C_{eq}$ value of 189.0 pm. A corresponding trend for M–B, $M{-}C_{ax}$, and $M{-}C_{eq}$ bonds was reported for the calculated structures of $[(OC)_4FeBMe]$ and $[(OC)_4FeB(\eta^5\text{-}C_5H_5)]$, which indicated stronger iron-to-boron backbonding in the case of the methylborylene complex.[3a] Additionally, the equatorial CO ligands in **2** show a somewhat stronger umbrella effect than those in **1a** which is indicated by the on average more acute $B{-}Cr{-}C_{eq}$ (**2**: 85°; **1a**: 88°) and $Cr{-}C_{eq}$-O angles (**2**: 176°; **1a**: 179°). Again, calculations on a series of compounds $[L_xM{-}ER]$ (E = B, Al, Ga, In, Tl) showed that a more pronounced umbrella effect indicates a stronger M–E bond.[3b] The aforementioned structural parameters for **2** strongly suggest that the electron deficiency of the boron center demands an enhanced Cr–B π-backbonding. The B–Si and Si–Si distances and the undistorted B-Si-Si angles provide no evidence for hyperconjugation, which is well known to relieve electron deficiency in (silylalkylidene)boranes $(Me_3Si)_2C{=}BR$ by formation of nonclassical $B{-}C{-}Si$ three-center, two-electron (3c–2e) bonds.[1e]

SCF calculations[12] on the parent molecule $[(OC)_5Cr{=}B\text{-}SiH_3]$ (**3**) and on its silane derivative $[(OC)_5Cr{=}BSi(SiH_3)_3]$ (**4**) were performed for staggered and eclipsed conformations of the $Cr(CO)_5$ moiety with respect to the SiR_3 group. For both molecules, the eclipsed form was found to be a minimum, and the staggered one to be a transition state through rotation of the SiR_3 group. The calculated geometries and chemical shifts (by GIAO) of **3** and **4** closely match the experimental data of **2**. The calculated bond lengths are generally slightly longer by 1–4 pm, and the carbonyl umbrella is more opened by 1–2° (Table 1). In particular, the extremely low-field

Table 1. Selected spectroscopic and structural data of **1a**, **2**, **3**, and **4**.

Compound	$\delta(^{11}B)$	$\delta(^{13}C_{ax})$	$\delta(^{13}C_{eq})$	Cr–B [Å]	B–Si/B–N [Å]	$Cr{-}C_{ax}$ [Å]	$Cr{-}C_{eq}$[a] [Å]
1a	92.3	218.0	217.6	1.996(6)	1.353(6)	1.908(6)	1.890
2	204.3	213.3	213.3	1.878(10)	1.998(10)	1.939(10)	1.894
3[b]	196.5	209.8	205.4[a]	1.875	2.026	1.978	1.919
4[b]	195.3	210.5	206.0[a]	1.875	2.026	1.978	1.919

[a] Average value. [b] Calculated values.

 © WILEY-VCH Verlag GmbH, D-69451 Weinheim, 2001 1433-7851/01/4022-4199 $ 17.50+.50/0

shifted ^{11}B NMR resonance signal, the short Cr–B distance, and the *trans*-effect of the silylborylene ligand are reproduced by the calculations. The bonding situation in terms of frontier orbitals follows the known pattern for terminal borylene complexes:[3] the σ donation occurs through the interaction of the HOMO of the $BSiR_3$ ligand with the A_1-symmetric LUMO of the $Cr(CO)_5$ fragment, and the π-backdonation through the corresponding interaction of the doubly degenerate HOMOs of $Cr(CO)_5$ with the LUMO of the borylene unit. Inspection of the MOs in **4** gives no indication for a nonclassical B–Si–Si 3c–2e bond (hyperconjugation), which could relieve the electron deficiency of the boron center. Also, the Wiberg bond indices (WBI) for all three pairs of boron and terminal silicon atoms are close to zero. The WBI for the B–Cr bond (ca. 1) in conjunction with relatively high Mullikan charges on both atoms (B: 0.80; Cr: −1.73) corroborates, as known from other examples, the strongly ionic character of the B–Cr bond.[3]

Experimental Section

2: In analogy to the known synthesis of $Na_2[Cr(CO)_5]$,[13] a solution of $[Me_3NCr(CO)_5]$[14] (0.97 g, 3.86 mmol) in THF (25 mL) was cooled to −78 °C, and a solution of $NaC_{10}H_8$ (46.2 mL, 0.2 M in THF) was added dropwise over a period of 20 min. When the addition was completed all volatile materials were removed under high vacuum (0 °C/0.001 Torr). The remaining yellow solid was treated with Et_2O (50 mL) at 0 °C, filtered, and washed with Et_2O (2 × 10 mL). The light yellow product was dried briefly under high vacuum and subsequently suspended in toluene (30 mL) at −78 °C. A solution of $Cl_2BSi(SiMe_3)_3$[15] (1.05 g, 3.20 mmol) in toluene (5 mL) was added dropwise by a syringe. Within 30 min the suspension was allowed to come to ambient temperature and the color of the reaction mixture turned from orange to dark brown. After the reaction mixture had been stirred for 10 min at ambient temperature, all volatile materials were removed under high vacuum (0.001 Torr). The dark brown residue was treated with hexane (30 mL), filtered, and the remaining solid was washed with hexane (2 × 5 mL). The filtrate was concentrated under vacuum to 10 mL and stored at −80 °C. After 48 h $[(OC)_5Cr{=}BSi(SiMe_3)_3]$ (1.51 g, 2.59 mmol, 80.9 %) was obtained as yellow crystals. All NMR spectra were recorded in $[D_6]$benzene at 25 °C. ^1H NMR (500 MHz, TMS): $\delta = 0.34$ (s; $SiMe_3$); ^{11}B NMR (160 MHz, $Et_2O \cdot BF_3$): $\delta = 204.3$; ^{13}C NMR (126 MHz, TMS): $\delta = 2.6$ ($SiMe_3$), 213.3 (CO); IR (toluene): $\tilde{\nu} = 2066$, 2014, 1982, 1952 cm^{-1} (CO); elemental analysis (%) calcd for $C_{14}H_{27}BCrO_5Si_4$: C 37.32, H 6.04; found: C 36.77, H 5.90.

Received: June 12, 2001 [Z17277]

[1] a) R. Boese, P. Paetzold, A. Tapper, *Chem. Ber.* **1987**, *120*, 1069; b) R. Boese, P. Paetzold, A. Tapper, R. Ziembinski, *Chem. Ber.* **1989**, *122*, 1057; c) M. Pilz, M. Stadler, R. Hunold, J. Allwohn, W. Massa, A. Berndt, *Angew. Chem.* **1989**, *101*, 761; *Angew. Chem. Int. Ed. Engl.* **1989**, *28*, 784; d) M. Pilz, H. Michel, A. Berndt, *Angew. Chem.* **1990**, *102*, 438; *Angew. Chem. Int. Ed. Engl.* **1990**, *29*, 401; e) A. Berndt, *Angew. Chem.* **1993**, *105*, 921; *Angew. Chem. Int. Ed. Engl.* **1993**, *32*, 985.

[2] B. Wrackmeyer, *Angew. Chem.* **1999**, *111*, 817; *Angew. Chem. Int. Ed. Engl.* **1999**, *38*, 771.

[3] a) C. L. B. Macdonald, A. H. Cowley, *J. Am. Chem. Soc.* **1999**, *121*, 12113; b) J. Uddin, C. Boehme, G. Frenking, *Organometallics* **2000**, *19*, 571; c) J. Uddin, G. Frenking, *J. Am. Chem. Soc.* **2001**, *123*, 1683; for reviews see: d) C. Boehme, J. Uddin, G. Frenking, *Coord. Chem. Rev.* **2000**, *197*, 249; and e) G. Frenking, N. Fröhlich, *Chem. Rev.* **2000**, *100*, 717.

[4] For theoretical studies on $[L_xM{=}B{=}X]$ ($X = NR_2$, F) see ref. [3] and a) U. Radius. F. M. Bickelhaupt, A. W. Ehlers, N. Goldberg, R. Hoffmann, *Inorg. Chem.* **1998**, *17*, 1080; b) A. W. Ehlers, E. J. Baerends, F. M. Bickelhaupt, U. Radius, *Chem. Eur. J.* **1998**, *4*, 210.

[5] a) H. Braunschweig, T. Wagner, *Angew. Chem.* **1995**, *107*, 904; *Angew. Chem. Int. Ed. Engl.* **1995**, *34*, 825; b) H. Braunschweig, B. Ganter, *J. Organomet. Chem.* **1997**, *545*, 163; c) H. Braunschweig, M. Müller, *Chem. Ber.* **1997**, *130*, 1295; d) H. Braunschweig, C. Kollann, U. Englert, *Eur. J. Inorg. Chem.* **1998**, 465; e) H. Braunschweig, C. Kollann, K. W. Klinkhammer, *Eur. J. Inorg. Chem.* **1999**, 1523; f) H. Braunschweig, M. Koster, *J. Organomet. Chem.* **1999**, *588*, 213; for reviews see: g) H. Braunschweig, *Angew. Chem.* **1998**, *110*, 1882; *Angew. Chem. Int. Ed. Engl.* **1998**, *37*, 1786; h) H. Braunschweig, M. Colling, *J. Organomet. Chem.* **2000**, *614*, 18; i) H. Braunschweig, M. Colling, *Coord. Chem. Rev.* **2001**, *223*, 1.

[6] H. Braunschweig, C. Kollann, U. Englert, *Angew. Chem.* **1998**, *110*, 3355; *Angew. Chem. Int. Ed.* **1998**, *37*, 3179.

[7] H. Braunschweig, M. Colling, C. Kollann, H. G. Stammler, B. Neumann, *Angew. Chem.* **2001**, *113*, 2359; *Angew. Chem. Int. Ed.* **2001**, *40*, 2298.

[8] A. H. Cowley, V. Lomelí, A. Voigt, *J. Am. Chem. Soc.* **1998**, *120*, 6401.

[9] G. J. Irvine, C. E. F. Rickard, W. R. Roper, A. Williamson, L. J. Wright, *Angew. Chem.* **2000**, *112*, 978; *Angew. Chem. Int. Ed.* **2000**, *39*, 94.

[10] a) A. K. Bandyopadhyay, Rajesh Khattar, J. Puga, T. P. Fehlner, A. L. Rheingold, *Inorg. Chem.* **1992**, *31*, 465; b) C. E. Housecroft, *Coord. Chem. Rev.* **1995**, *143*, 297.

[11] Crystal structure determination of **2**: $C_{14}H_{27}BCrO_5Si_4$, $Mo_{K\alpha}$ radiation ($\lambda = 0.7107$ Å, graphite monochromator), $T = 203(2)$ K, $0.2 \times 0.1 \times 0.1$ mm, trigonal, space group $P3_2$; $a = 9.659(3)$, $b = 9.659(3)$, $c = 23.235(11)$ Å, $V = 1877.5(12)$ Å^3, $Z = 3$, $\rho_{calcd} = 1.195$ g cm^{-1}, $\mu(Mo_{K\alpha}) = 6.66$ cm^{-1}, $F(000) = 708$, 9777 measured reflections ($2.43 < \theta < 25.09$), 4406 independent reflections with $I > \sigma(I)$, 226 variables. Transmission factors: T_{max}: 1.00000, T_{min}: 0.744666. The intensities were measured with a Bruker-axs-SMART diffractometer. The structure was solved by direct methods (SHELXS 97). Refinements were carried out with the SHELXL-97 package. All non-hydrogen atoms were refined with anisotropic temperature factors. The hydrogen atoms were placed in calculated positions and refined isotropically in riding mode (C–H = 98 pm, $U_{iso}(H) = 1.3\ U_{iso}(C)$). All refinements were made by full-matrix least-squares on F^2. $R1$ ($I > 2\sigma(I)$) = 0.0627, $wR2$ (all data) = 0.1596; $GOF = 0.985$. Crystallographic data (excluding structure factors) for the structures reported in this paper have been deposited with the Cambridge Crystallographic Data Centre as supplementary publication no. CCDC-163495. Copies of the data can be obtained free of charge on application to CCDC, 12 Union Road, Cambridge CB2 1EZ, UK (fax: (+44) 1223-336-033; e-mail: deposit@ccdc.cam.ac.uk).

[12] SCF Calculations: The GAUSSIAN 98 package, run on a cluster of workstations was applied for all SCF calculations. The total energies E_h and the ZPVE (in Hartrees, in parentheses) all calculated on B3LYP level with 6-31G(d,p) basis set for nonmetal atoms and CEP-31G for chromium are as follows: $(CO)_5CrBSiH_3$: eclipsed −969.371737 (0.07050), staggered −969.371677 (0.07047); $(CO)_5CrB$-$Si(SiH_3)_3$: eclipsed −1841.480006 (0.122903), staggered −1841.479976 (0.122852); Gaussian 98 (Revision A.7), M. J. Frisch, G. W. Trucks, H. B. Schlegel, G. E. Scuseria, M. A. Robb, J. R. Cheeseman, V. G. Zakrzewski, J. A. Montgomery, R. E. Stratmann, J. C. Burant, S. Dapprich, J. M. Millam, A. D. Daniels, K. N. Kudin, M. C. Strain, O. Farkas, J. Tomasi, V. Barone, M. Cossi, R. Cammi, B. Mennucci, C. Pomelli, C. Adamo, S. Clifford, J. Ochterski, G. A. Petersson, P. Y. Ayala, Q. Cui, K. Morokuma, D. K. Malick, A. D. Rabuck, K. Raghavachari, J. B. Foresman, J. Cioslowski, J. V. Ortiz, B. B. Stefanov, G. Liu, A. Liashenko, P. Piskorz, I. Komaromi, R. Gomperts, R. L. Martin, D. J. Fox, T. Keith, M. A. Al-Laham, C. Y. Peng, A. Nanayakkara, C. Gonzalez, M. Challacombe, P. M. W. Gill, B. G. Johnson, W. Chen, M. W. Wong, J. L. Andres, M. Head-Gordon, E. S. Replogle, J. A. Pople, Gaussian, Inc., Pittsburgh, PA, **1998**..

[13] J. M. Maher, R. P. Beatty, N. J. Cooper, *Organometallics* **1985**, *4*, 1354.

[14] W. Strohmeyer, J. F. Guttenberger, H. Blumenthal, G. Albert, *Chem. Ber.* **1966**, *99*, 3419.

[15] C. Kollan, PhD thesis, RWTH Aachen, Germany, **1999**.

 © WILEY-VCH Verlag GmbH, D-69451 Weinheim, 2001 1433-7851/01/4022-4200 $ 17.50+.50/0

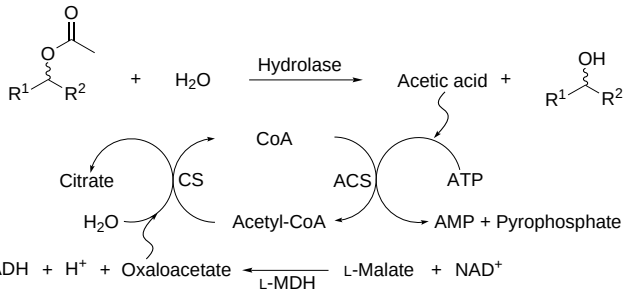
A High-Throughput-Screening Method for the Identification of Active and Enantioselective Hydrolases**

Markus Baumann, Rainer Stürmer, and Uwe T. Bornscheuer*

Hydrolytic enzymes are versatile biocatalysts and find increasing application in organic syntheses.[1] Within this class of enzymes, lipases and esterases are frequently used as they accept a broad range of nonnatural substrates, are usually very stable in organic solvents, and exhibit good to excellent stereoselectivity in the kinetic resolution of racemates or desymmetrization of prostereogenic compounds. Owing to the vast progress in genetic engineering, the number of (commercially) available biocatalysts is rapidly increasing. However, this makes the identification of suitable enzymes by laboratory-scale reactions followed by, for example, GC or HPLC-based determination of optical purities a tedious and time-consuming task. In addition, the recently developed techniques for directed (molecular) evolution[2] require highly sophisticated assays for high-throughput screening (HTS) of large libraries usually containing 10^4–10^6 mutants.

For the rapid determination of enantioselectivity E (also named enantiomeric ratio)[3] several assay formats have been delevoped. Kazlauskas and Janes measured initial rates of hydrolase-catalyzed hydrolysis of *p*-nitrophenyl derivatives of pure chiral carboxylic acids ("Quick E") in the presence of resorufin tetradecanoate to introduce competition yielding more exact E values.[4] Other groups used chromogenic[5] or fluorogenic[6] substrates for the identification of more enantioselective hydrolases. Although measurements with these substances are usually very sensitive, a major disadvantage resides in the presence of bulky groups, which usually differ considerably from the "true" desired substrate, for example an acetate. As a consequence, the risk is high that the identified "suitable" enzymes show different selectivities towards the "true" substrate. To overcome this problem, Kazlauskas and co-workers reported a more general applicable assay in which both acetates of chiral alcohols and esters of chiral carboxylic acids were hydrolyzed in the presence of *p*-nitrophenol, which served as a pH-indicator.[7] A stepwise assay for screening of enantioselective hydrolases by using bromothymol blue as pH-indicator to screen for activity followed by gas chromatography to measure enantioselectivity was reported recently by us.[8] Other methods are based on time-resolved IR-thermographic determination of enantioselectivity[9] or use of "pseudo"-enantiomers in which one form is isotopically labeled in combination with mass spectrometric analysis.[10] The major advantage is that true E values are determined, but the method needs deuterated pure enantiomers and equipment costs are very high. Recently, a "super-HTS" by parallel capillary electrophoresis with chiral cyclodextrins was reported, in which optical purities of fluorescein isothiocyanate (FITC)-labeled amines were measured.[11] So far this system is restricted to amines and also requires investments for expensive equipment.

We now describe a new assay format based on a coupled enzymatic conversion (Scheme 1). First, acetic acid is released by lipase- or esterase-catalyzed hydrolysis from the corresponding chiral ester followed by a cascade of enzymatic reactions (Scheme 1) based on a readily available and cheap test-kit initially developed for food analysis.[12] Thus, acetic acid released in the initial hydrolytic reaction is stoichiometrically "transformed" into NADH, which can be easily quantified by spectrophotometric measurements at 340 nm.



Scheme 1. The hydrolase-catalyzed reaction releases acetic acid, which is converted by acetyl-CoA synthetase (ACS) to acetyl-CoA in the presence of (ATP) and coenzyme A (CoA). Citrate synthase (CS) catalyzes the reaction between acetyl-CoA and oxaloacetate to give citrate. The oxaloacetate required for this reaction is formed from L-malate and NAD^+ in the presence of L-malate dehydrogenase (L-MDH). Initial rates of acetic acid formation can thus be determined by the increase in adsorption at 340 nm due to the increase in NADH concentration. Use of optically pure (*R*)- or (*S*)-acetates allows the determination of the apparent enantioselectivity E_{app}.

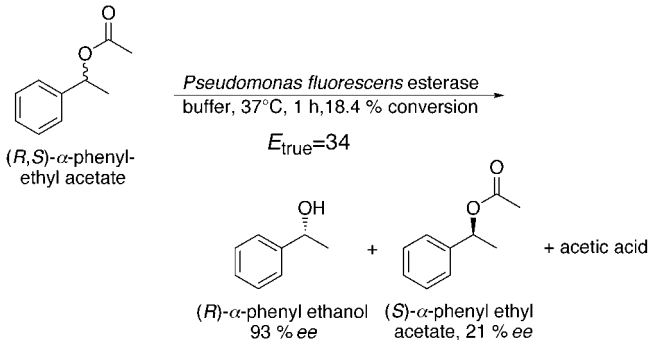
To evaluate this assay format, the hydrolysis of (*R*,*S*)-α-phenyl ethyl acetate (**1**) by a recombinant esterase from *Pseudomonas fluorescens* (PFE)[13a] was chosen as a model reaction (Scheme 2). Earlier results have already shown that PFE converts this substrate with good enantioselectivity.[14]

Preliminary hydrolysis reactions were performed on a mL scale by using lyophilized PFE (1 mg mL^{-1}), 50 mM (*R*,*S*)-**1**, and the acetic acid test-kit as described in the Experimental Section. In addition, conversion and enantiomeric excess were determined by gas chromatographic analysis (Scheme 2). Incubation of (*R*,*S*)-**1** at pH 8.1 in the presence of the test-kit, but in the absence of PFE revealed no NADH formation, thus auto-hydrolysis of **1** can be excluded. Furthermore, neither activity nor enantioselectivity of PFE were affected by

[*] Prof. Dr. U. T. Bornscheuer
Institut für Chemie und Biochemie
Abt. Technische Chemie & Biotechnologie
Universität Greifswald
Soldmannstrasse 16, 17487 Greifswald (Germany)
Fax: (+49) 3834-86-4373
Internet: http://www.chemie.uni-greifswald.de/~biotech
E-mail: bornsche@mail.uni-greifswald.de
M. Baumann
Institut für Technische Biochemie
Universität Stuttgart (Germany)
Dr. R. Stürmer
BASF AG, Abt. Biotechnologie
Ludwigshafen (Germany)

[**] This work was supported by the Ministerium für Wissenschaft, Forschung und Kunst, Baden-Württemberg, Stuttgart, Germany and the BASF AG, Ludwigshafen, Germany. We are especially grateful to Prof. R. D. Schmid (ITB, Universität Stuttgart) for valuable discussions.

 © WILEY-VCH Verlag GmbH, D-69451 Weinheim, 2001 1433-7851/01/4022-4201 $ 17.50+.50/0



Scheme 2. Model reaction for the evaluation of the coupled-enzymatic acetate assay. Under these conditions, the esterase from *Pseudomonas fluorescens* exhibited high *R* selectivity ($E_{true} = 34$) as determined by GC analysis.

test-kit components, as confirmed by control experiments (data not shown). The maximum increase in absorption at 340 nm was about 0.3 per min, which corresponds to the maximum reaction rate that can be determined with the coupled esterase/test-kit system. However, for higher accuracy, a lower rate is recommended. Reactions in microtiter plates (MTP) revealed an almost linear[15] increase in absorbance at 340 nm over 10 min using an esterase concentration of 2 mg mL^{-1} PFE (lyophilized crude cell extract) albeit the concentration of (*R*,*S*)-**1** was varied over a broad range between 5 and 50 mg mL^{-1} (Figure 1). Beside model compound **1**, the assay format is also useful to monitor the

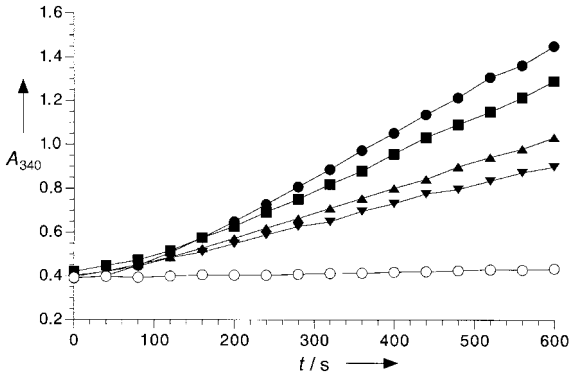
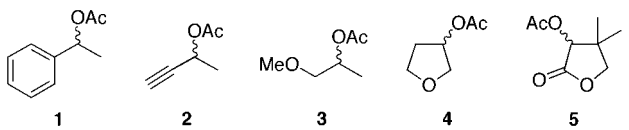


Figure 1. An almost linear increase in NADH concentration with time was observed in the conversion of acetic acid released from PFE-catalyzed hydrolysis of (*R*,*S*)-**1** (none (○), 5 (▼), 10 (▲), 25 (■), 50 mg mL^{-1} (●)). No hydrolysis was observed in the absence of esterase.

conversion of other chiral esters of secondary alcohols (Scheme 3). Here, lipase B from *Candida antarctica* (CAL-B) was chosen as catalyst, as this enzyme represents a frequently used lipase.[16] The coupled conversion of acetates



Scheme 3. Acetates **1**–**5** of secondary alcohols used for evaluation of the assay.

(*R*,*S*)-**2**–(*R*,*S*)-**5** shows that the reaction rates decreased in the order **2** > **3** > **4** > **5** (Figure 2). This observation is consistent with our previous results[8] and also proves that the assay format can be used to identify whether a certain hydrolase is active or not.

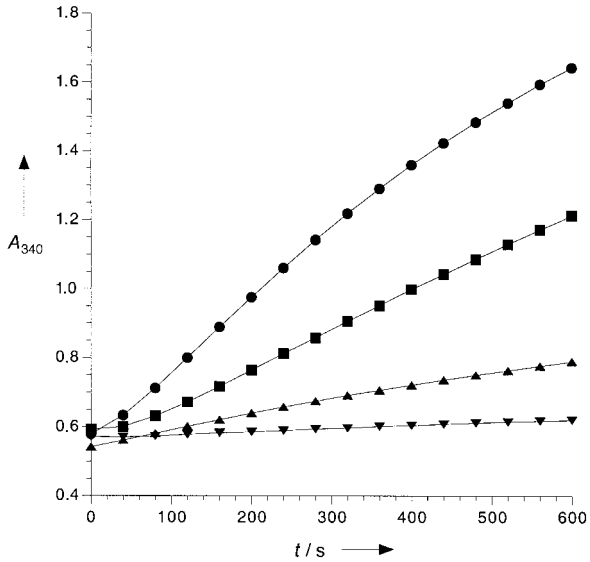


Figure 2. Transfer of the assay format to CAL-B-catalyzed hydrolysis of acetates (*R*,*S*)-**2**–(*R*,*S*)-**5** (0.5 mg mL^{-1}); **2** (●), **3** (■), **4** (▲), **5** (▼).

Measuring initial rates of the acetic acid release from pure enantiomers of (*R*)- or (*S*)-**1** (5 mg mL^{-1}) at an esterase concentration of 1 mg mL^{-1} PFE (lyophilized crude cell extract) in MTP format revealed an almost sole increase in absorption for the *R* enantiomer reflecting the high enantioselectivity of PFE (Figure 3A). The apparent enantioselectivity was calculated to be $E_{app} = 30$,[17] which closely matches the value of $E_{true} = 34$ determined by GC analysis (Scheme 2). Next, a culture supernatant containing PFE was split from one well into two portions to ensure that the same enzyme concentration is used for both enantiomers. In this case, decreased initial rates were observed and a lowered enantioselectivity ($E_{app} = 21$) was calculated (Figure 3B). This can be related to impurities from the cultivation such as cell debris or media components disturbing the determination of released acetic acid. However, it must be emphasized that this test format is useful for the direct determination of hydrolase enantioselectivity in crude cell extracts. This has the advantage that the assay format can be directly transferred to high-throughput screening in libraries obtained by directed evolution. The lowered accuracy of the assay using the crude culture supernatant might be solved by integrating a microtiter plate based purification step, for example, taking advantage of the His_6-tag cloned to the mature PFE. However, this will make the assay more time-consuming and expensive.

Next, we investigated the applicability of the assay format for the determination of *E* values in the resolution of **3** using 16 lipases and esterases. The data in Table 1 show that E_{app} values match closely to the E_{true} values determined by gas chromatography using a chiral column. In accordance to our

 © WILEY-VCH Verlag GmbH, D-69451 Weinheim, 2001 1433-7851/01/4022-4202 $ 17.50+.50/0

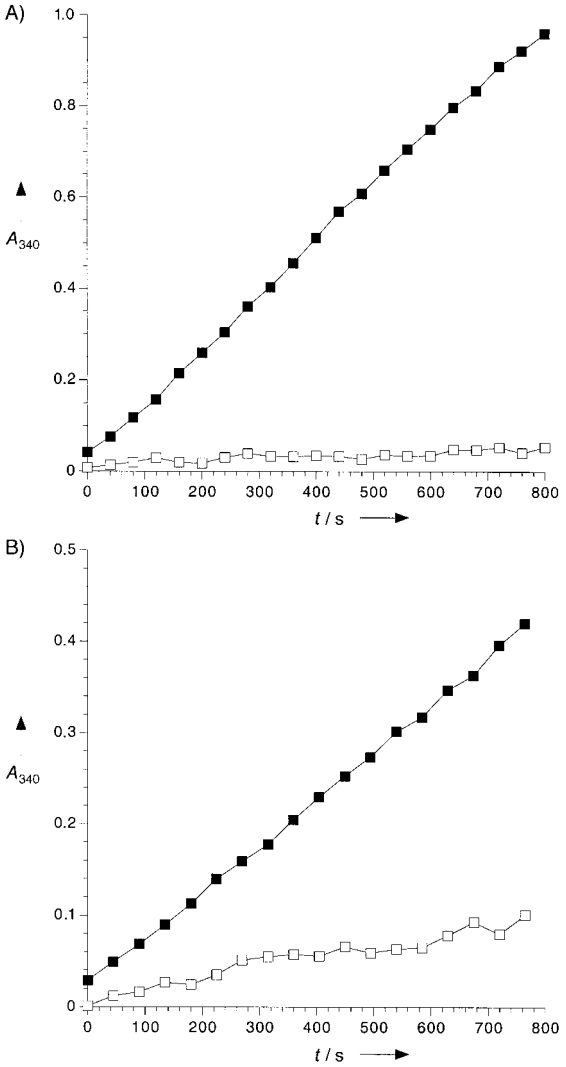


Figure 3. Initial rates determined by using optically pure (*R*)- or (*S*)-**1** (5 mg mL^{-1}; ■ and □, respectively). Reactions were performed by using lyophilized crude cell extract of PFE (A) or a culture supernatant containing PFE (B). Please note the different scaling on the *y* axes.

Table 1. Comparison of enantioselectivity determined by the enzyme cascade method (E_{app}) and by GC analysis (E_{true}) in the kinetic resolution of (*R*,*S*)-1-methoxy-2-propyl acetate by various lipases and esterases.

Enzyme[a]	E_{app} [%]	E_{true} [%]	Configuration[b]
CVL	7.5	4.9	*R*
Chirazyme L6	13.7	12.1	*R*
Chirazyme L10	3.3	2.4	*R*
Chirazyme L12	4.0	5.1	*R*
Chirazyme E1	2.1	2.6	*S*
Chirazyme E2	2.2	1.9	*S*
Chirazyme E3	1.1	1.4	*R*/*S*[c]
Chirazyme E4	2.0	2.3	*R*
PFE	1.4	1.2	*R*
CAL-B	80	100	*R*

[a] CVL = lipase from *Chromobacterium viscosum*; PFE = recombinant esterase from *Pseudomonas fluorescens*;[13a] CAL-B = lipase B from *Candida antarctica*; the following enzymes showed no or very little activity: "acid esterase" (Amano), "acylase" (Amano ACS), lipase from *Aspergillus niger* (Amano A), esterase from *Bacillus stearothermophilus*,[13b] as well as Chirazyme L7 and L8. [b] Configuration of faster reacting enantiomer. [c] *R* selectivity according to MTP assay; *S* selectivity according to GC analysis; note that substrate and product were almost racemic.

previous findings,[8] only CAL-B was found suitable for the efficient resolution of **3**.

As shown in Figure 3, an analysis time of less than 3 – 4 min per assay (plus 1 – 2 min for the pipetting steps) is sufficient to determine enantioselectivities. Thus, in a 96-well plate about 45 enzymes (two wells per biocatalyst, six wells for controls) can be analyzed. This amounts to at least 540 E_{app} values per hour corresponding to about 13000 mutants screened per day.[18] In addition, the assay is rather cheap, as one test reaction costs less than 0.1 € (catalogue price).

Moreover, the method should not be restricted to the measurement of esterase or lipase activity and enantioselectivity. Several other enzyme reactions, which proceed by releasing acetic acid, such as the protease- or amidase-catalyzed hydrolyses of amides should be accessible using the principle described here.

Experimental Section

Materials: Racemic acetates (*R*,*S*)-**1** – (*R*,*S*)-**3** were obtained from commercial suppliers at the highest purity available. Acetates (*R*,*S*)-**4** and -**5** and optically pure (*R*)- and (*S*)-**3** were synthesized from the corresponding alcohols by using standard procedures. Optically pure (*R*)- and (*S*)-**1** were provided by the BASF AG (Ludwigshafen, Germany). All enzymes—except PFE and BSE, which were produced by expression in *E. coli* as described in reference [13]—were obtained from commercial suppliers.

The test-kit for the determination of acetic acid released (initally produced and distributed by Roche Diagnostics, Penzberg, Germany) was purchased from R-Biopharm GmbH (Darmstadt, Germany) and applied in accord with the manufacturers protocol (see also below). Spectrophotometric determination of NADH concentration was performed at 340 nm in the mL-scale on a Ultrospec 3000 photometer (Pharmacia Biotech Ltd., Uppsala, Sweden) and in the µL-scale using a fluorimeter (FLUOstar, BMG LabTechnologies, Offenburg, Germany).

Conversion of racemic substrates for the determination of E_{true} values: For this, enzyme-catalyzed hydrolyses of (*R*,*S*)-**1** and (*R*,*S*)-**3** were performed as described in reference [8]. Conversion and enantiomeric excess (% *ee*) were then determined by GC analysis of samples from the reaction mixture. Enantioselectivities (E_{true} values) were calculated from these according to the method developed by Chen et al.[3]

General procedure for the determination of acetic acid in a MTP assay: A solution of PFE (20 µL, 2 mg mL^{-1}, unless stated otherwise) or CAL-B (2 mg mL^{-1}) was added to a mixture of the test-kit components (150 µL). The reactions were started by adding a solution of **1** – **5** (20 µL, concentrations are indicated in the text and in figure legends as mg mL^{-1}) in sodium phosphate buffer (10 mM, pH 7.3). Mixtures of the test-kit with buffer or cell lysates of noninduced *E. coli* harboring the gene encoding recombinant PFE served as controls. In a similar manner, reaction rates were determined by using optically pure (*R*)- and (*S*)-**1** as well as (*R*)- and (*S*)-**3**. For reactions with crude cell extract, PFE was produced in microtiter plates similar to the published protocol for shake-flask cultivation.[13a] However, the cultivation volume was 200 µL per well and cells were disrupted by two freeze-thaw cycles. Finally, cell debris was removed by centrifugation and the supernatants were used for the assay.

Received: May 21, 2001 [Z17149]

[1] a) R. N. Patel, *Stereoselective Biocatalysis*, Marcel Dekker, New York, **2000**; b) K. Faber, *Biotransformations in Organic Chemistry*, Springer, Berlin, **2000**; c) U. T. Bornscheuer, R. J. Kazlauskas, *Hydrolases in Organic Synthesis—Regio- and Stereoselective Biotransformations*, Wiley-VCH, Weinheim, **1999**.

[2] a) U. T. Bornscheuer, M. Pohl, *Curr. Opin. Chem. Biol.* **2001**, *5*, 137 – 143; b) U. T. Bornscheuer, *Biocatal. Biotransform.* **2001**, *19*, 84 – 96; c) U. T. Bornscheuer, *Angew. Chem.* **1998**, *110*, 3285 – 3288; *Angew.*

Chem. Int. Ed. **1998**, *37*, 3105 – 3108; d) F. H. Arnold, A. A. Volkov, *Curr. Opin. Chem. Biol.* **1999**, *3*, 54 – 59; e) J. D. Sutherland, *Curr. Opin. Chem. Biol.* **2000**, *4*, 263 – 269; f) M. B. Tobin, C. Gustafsson, G. W. Huisman, *Curr. Opin. Struct. Biol.* **2000**, *10*, 421 – 427.
[3] C. S. Chen, Y. Fujimoto, G. Girdaukas, C. J. Sih, *J. Am. Chem. Soc.* **1982**, *104*, 7294 – 7299.
[4] L. E. Janes, R. J. Kazlauskas, *J. Org. Chem.* **1997**, *62*, 4560 – 4561.
[5] M. T. Reetz, A. Zonta, K. Schimossek, K. Liebeton, K.-E. Jaeger, *Angew. Chem.* **1997**, *109*, 2961 – 2963; *Angew. Chem. Int. Ed. Engl.* **1997**, *36*, 2830 – 2832.
[6] a) E. Henke, U. T. Bornscheuer, *Biol. Chem.* **1999**, *380*, 1029 – 1033; b) F. Badalassi, D. Wahler, G. Klein, P. Crotti, J.-L. Reymond, *Angew. Chem.* **2000**, *112*, 4233 – 4236; *Angew. Chem. Int. Ed.* **2000**, *39*, 4067 – 4070.
[7] a) L. E. Janes, A. C. Löwendahl, R. J. Kazlauskas, *Chem. Eur. J.* **1998**, *4*, 2324 – 2331; b) A. M. F. Liu, N. A. Somers, R. J. Kazlauskas, T. S. Brush, F. Zocher, M. M. Enzelberger, U. T. Bornscheuer, G. P. Horsman, A. Mezzetti, C. Schmidt-Dannert, R. D. Schmid, *Tetrahedron: Asymmetry* **2001**, *12*, 545 – 556.
[8] M. Baumann, B. Hauer, U. T. Bornscheuer, *Tetrahedron: Asymmetry* **2000**, *11*, 4781 – 4790.
[9] M. T. Reetz, M. H. Becker, K. M. Kühling, A. Holzwarth, *Angew. Chem.* **1998**, *110*, 2792 – 2795; *Angew. Chem. Int. Ed.* **1998**, *37*, 2647 – 2650.
[10] M. T. Reetz, M. H. Becker, H. W. Klein, D. Stöckigt, *Angew. Chem.* **1999**, *111*, 1872 – 1875; *Angew. Chem. Int. Ed.* **1999**, *38*, 1758 – 1761.
[11] M. T. Reetz, K. M. Kühling, A. Deege, H. Hinrichs, D. Belder, *Angew. Chem.* **2000**, *112*, 4049 – 4052; *Angew. Chem. Int. Ed.* **2000**, *39*, 3891 – 3893.
[12] H.-O. Beutler in *Methods of Enzymatic Analysis*, *Vol. 6*, 3rd ed. (Ed.: H. U. Bergmeyer), Wiley-VCH, Weinheim, **1984**, pp. 639 – 645.
[13] a) N. Krebsfänger, F. Zocher, J. Altenbuchner, U. T. Bornscheuer, *Enzyme Microb. Technol.* **1998**, *21*, 641 – 646; b) Y. Amaki, H. Nakano, T. Yamane, *Appl. Microbiol. Biotechnol.* **1994**, *40*, 664 – 668.
[14] N. Krebsfänger, K. Schierholz, U. T. Bornscheuer, *J. Biotechnol.* **1998**, *60*, 105 – 111.
[15] The assay also yields a linear increase in absorption when increasing concentrations of sodium acetate are used; see also reference [12] and the instructions for use enclosed with the commercial test-kit for accuracy of the method.
[16] E. M. Anderson, K. M. Larsson, O. Kirk, *Biocatal. Biotransform.* **1998**, *16*, 181 – 204.
[17] E_{app} values are the ratio of initial rates determined from the hydrolysis of pure *R* or *S* enantiomers. E_{true} values are derived from resolutions of racemates and therefore also include competition between the two enantiomers for the active site of the enzyme.
[18] More than 50000 mutants can be screened per day, if the analysis time can be reduced to about 1 min per test and faster pipetting steps are possible.

Pore-Size Engineering of Silicon Imido Nitride for Catalytic Applications**

David Farrusseng, Klaus Schlichte, Bernd Spliethoff, Annette Wingen, Stefan Kaskel,* John S. Bradley, and Ferdi Schüth

Microporous and mesoporous materials with high internal surface area and pore volume play a key role in the development of new heterogeneous catalysts and solid membranes.[1] The strategy in the synthesis of materials with well defined pore structure is to direct the networking of molecular or ionic precursors by a templating agent, which can be a molecule, an ion, a polymer, or a supramolecular assembly.[2] Removal of the occluded template produces materials with patterns of characteristic pore size, shape, and structure. Although there is a growing interest in expanding these templating routes to materials other than oxides, only in the case of sulfides and some super-Prussian-blue compounds have micro- and mesoporous inorganic nonoxide materials been synthesized.[3] Nitrido-sodalites with very small pores, probably inaccessible to organic substrates, were obtained from the solid-state reaction of HPN_2 and divalent metal salts.[4]

Several methods for the synthesis of dense silicon nitride starting from elemental silicon, silicon chloride, or even carbodiimide have been reported.[5] However, the first microporous silicon imido nitrides with a mean pore size of 0.7 nm were synthesized by Bradley and Dismukes in pyrolysis reactions of polysilazanes.[6] Mesoporous silicon imido nitride with a narrow pore-size distribution ($d_{av} = 5.6$ nm) and a high specific surface area (up to 1000 $m^2 g^{-1}$) was obtained recently using the ammonolysis of silicon tetrachloride in organic solvents.[7]

We describe herein a template-assisted method which allows, for the first time, tailoring the pore size of microporous silicon nitride materials in a wide range from primary to secondary micropores. In this procedure, tris(dimethylamino)silylamine $[(CH_3)_2N]_3SiNH_2$ **1**[8] is ammonolyzed in a concentrated solution of $CH_3(CH_2)_nNH_2$ ($n = 11 – 17$) in hot acetonitrile. The ammonolysis can be considered as an analogue of silicon oxide manufacture by sol – gel methods using prehydrolyzed tetramethoxysilane and water. After cooling to room temperature, a gel forms which is dried and heated slowly to 823 K in flowing ammonia. According to nitrogen physisorption experiments (Figure 1), such materials prepared using alkylamines of different chain length

[*] Dr. S. Kaskel, Dr. D. Farrusseng, K. Schlichte, B. Spliethoff, Dr. A. Wingen, Dr. F. Schüth
Max-Planck-Institut für Kohlenforschung
Kaiser-Wilhelm-Platz 1, 45470 Mülheim an der Ruhr (Germany)
Fax: (+49) 208-306-2995
E-mail: kaskel@mpi-muelheim.mpg.de
Dr. J. S. Bradley
Department of Chemistry
University of Hull
Cottingham Road, Hull HU6 7RX (UK)

[**] We thank Dr. P. Ågren and U. Specht for helpful discussions on physisorption and precursor syntheses. A Reimar Lüst Fellowship for S.K. was provided by the Max Planck Society.

 © WILEY-VCH Verlag GmbH, D-69451 Weinheim, 2001 1433-7851/01/4022-4204 $ 17.50+.50/0

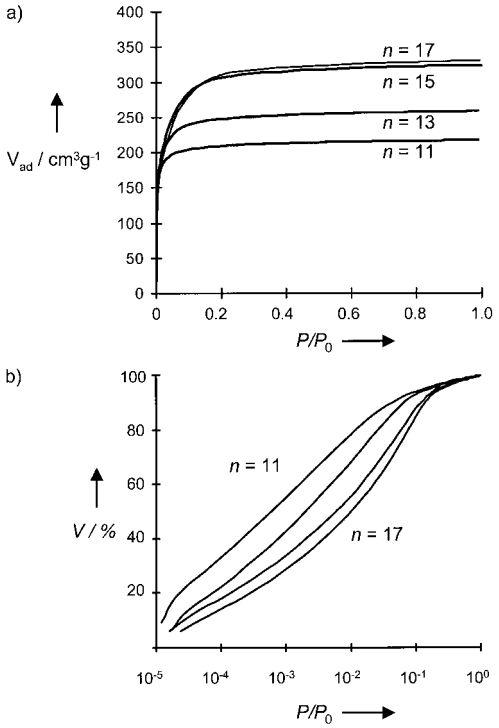


Figure 1. a) Nitrogen physisorption isotherms of microporous silicon imido nitrides prepared using $CH_3(CH_2)_nNH_2$ ($n = 11-17$) as templates, b) logarithmic plot (V = volume adsorbed normalized to volume at $P/P_0 = 1$).

$(CH_3(CH_2)_nNH_2$, $n = 11$, 13, 15, 17) are all microporous and the isotherms are of type I. The micropore volume increases with the length of the amine alkyl chain (Table 1). Logarithmic plots (Figure 1 b) show that for the longer amines used as templates the nitrogen adsorption predominately occurs at

Table 1. Nitrogen physisorption results for high surface-area silicon imido nitrides prepared using linear aliphatic amines $CH_3(CH_2)_nNH_2$ as templates.

Template chain engh n	Micropore volume [cm^3g^{-1}]	Average pore diameter [Å]
11	0.32	11.8
12	0.34	12.4
13	0.37	13.6
14	0.38	13.7
15	0.42	15.7
17	0.48	16.5

higher relative pressures corresponding to secondary micropores. The actual calculation of the pore size using Horvath–Kawazoe or density functional theory (DFT) methods is difficult, since the principal interaction potentials of the adsorbate and the adsorbent are unknown and assumptions have to be made about the pore morphology.[9] The numerical values of the pore diameters calculated from the DFT method (Table 1) are therefore not fully accurate but, more importantly, allow a comparison among members of a class of similar materials which presumably have the same interaction potentials.

The nanometer-sized micropores are easily discerned in high-resolution TEM pictures (Figure 2). They reveal the uniform channel-like pore structure of the air-sensitive nitrides. Crystallization of the inorganic network was neither

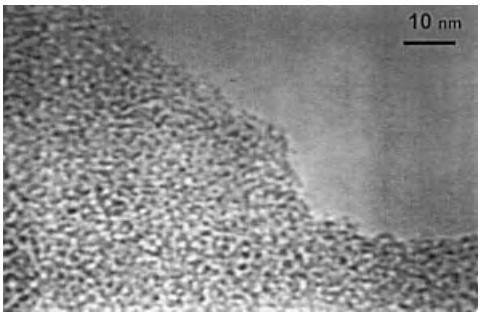


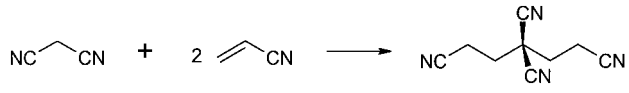
Figure 2. TEM picture of microporous silicon nitride (template: octadecylamine, $d_{av} = 1.7$ nm).

observed in TEM pictures nor in XRD powder patterns even after annealing the gels at 1273 K in a stream of gaseous ammonia. Samples treated thusly maintained their high micropore volume (0.35 cm^3g^{-1}) as well as the pore structure. This surprisingly low sintering tendency is an attractive feature and reveals the promising potential of the material as a support in high temperature catalysis under nonoxidizing conditions.

The pore evolution mechanism is still unknown. The size of the pores is of the same order as the size of the templating molecules, and therefore a micellar templating mechanism—in any case unlikely because of the low dielectric constant of the organic solvent—can be excluded. In fact, we believe that the amines are occluded in the first condensation step and released after thermal consolidation of the network during the heat treatment at about 673 K.

IR spectroscopy of the heat-treated samples was used to identify silicon imido nitride [$\tilde{\nu} = 3408$ (ν(NH)), 1549 ($\delta(NH_2)$), 1182 (δ(NH)), 891 cm^{-1} ($\nu_{as}(Si_2N)$)].[8] The ^{29}Si MAS NMR spectrum consists of a broad line with a maximum at $\delta = -41$ and a shoulder at about $\delta = -50$. The line covers a region between $\delta = -35$ and -55. Such a broadening originates from the amorphous character of preceramic silicon nitride powders, in which various different coordination spheres are present.[10]

Silicon imido nitride with high accessible surface area can be used as a solid base catalyst in Michael addition reactions due to the presence of basic sites. For example, moderately acidic substrates like malononitrile ($pK_a = 11$) are activated to form addition products with substrates like acrylonitrile (Scheme 1).



Scheme 1.

Due to the basicity of the inner surface and its high thermal and chemical stability, silicon nitride can be used as a solid superbase catalyst ($pK_a > 26$) after potassium impregna-

 © WILEY-VCH Verlag GmbH, D-69451 Weinheim, 2001 1433-7851/01/4022-4205 $ 17.50+.50/0

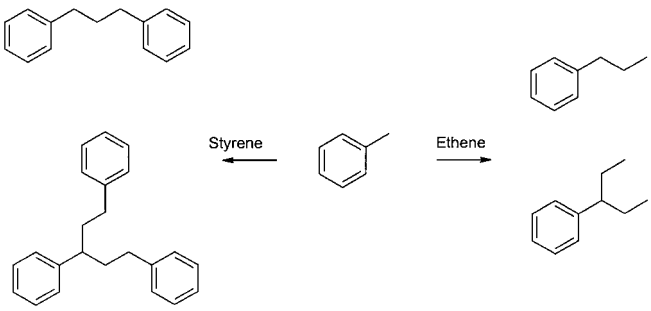
tion.[11] Solid superbases like alkali metal promoted oxides are used in industry for the isomerization of polycyclic alkenes or in side-chain alkylations of alkylbenzenes.[12] In the case of silicon nitride, the covalent network is advantageous to achieve shape selectivity through pore-size engineering, as opposed to nonporous basic oxide supports like MgO or Al_2O_3. Zeolites are less suitable for such reactions due to a high number of acidic sites. However, the catalytic isomerization of 1-butene has been reported over sodium metal clusters located in high-alumina zeolites.[13]

The educt and product selectivity of our nitrides is demonstrated by comparing the performance of microporous ($d_{av} = 1.7$ nm) and mesoporous ($d_{av} = 5.6$ nm) silicon nitride catalysts (Table 2). The side-chain alkylation of toluene with styrene (Scheme 2) proceeds within minutes with the mesoporous catalyst and produces also higher addition products. In

Table 2. Conversion [%] over potassium-promoted micro- and mesoporous silicon imido nitride (reaction time in parentheses).

Reaction	Microporous catalyst ($d_{av} = 1.7$ nm)	Mesoporous catalyst ($d_{av} = 5.6$ nm)
toluene + ethene[a]	74.0 (60 h)[c]	25.0 (96 h)[d]
toluene + styrene[a]	0.0 (48 h)	100.0 (10 min)
1-hexene[b]	99.3 (18 h)	95.5 (2 min)
1-hexadecene[b]	0.0 (18 h)	80.8 (2 min)

[a] Scheme 2. [b] Double bond shift. [c] 30 bar. [d] 20 bar.



Scheme 2.

contrast, the microporous catalyst gives no conversion due to the bulky character of the products. The alkylation reaction with ethene on the other hand (Scheme 2) proceeds smoothly with both catalysts, and at higher ethene pressures (30 bar) the dialkylation product forms even over the microporous catalyst since both propylbenzene and (1-ethylpropyl)benzene fit in the secondary micropores.

Similar differences between micro- and mesoporous nitrides are observed in alkene isomerization reactions. Using the mesoporous catalyst, isomerization of 1-hexene and 1-hexadecene (1:1 mixture) to the more stable alkenes with inner double bonds proceeds within minutes for both substrates. The microporous solid converts instead only the shorter substrate 1-hexene, and the pure 1-hexadecene can be recovered from the mixture. These selectivity differences confirm the results of the nitrogen adsorption measurements. Probably the calculated pore radii are a little to high as compared to the size of the substrates and products, which is due to the limitations of the pore size analysis.

Summarizing, we have demonstrated that pore-size tailoring of silicon imido nitride is possible. The compounds described here represent a new class of shape-selective solid superbase catalysts.

Experimental Section

All operations were performed using an argon-filled glove box or a vacuum line and dry solvents. Alkylamines (Merck, Aldrich) were dried in vacuum prior to use. Tris(dimethylamino)silylamine was prepared according to a procedure previously reported and characterized by GC/MS.[8] Typically, the liquid precursor (1.00 mmol) was added to a solution of $CH_3(CH_2)_nNH_2$ (2 g, $n = 11-17$) in boiling acetonitrile (20 mL, saturated with gaseous ammonia). After 1 h stirring, the reaction mixture was cooled to room temperature and a gel formed at the bottom of the flask. After washing with hot acetonitrile, the gel was dried in vacuum and heated slowly to 823 K in a dynamic ammonia atmosphere (1 bar) to give a yellowish, X-ray amorphous silicon imido nitride powder.

Nitrogen physisorption measurements were performed on a Micromeritics 2000 apparatus. The micropore volume was deduced from the total amount nitrogen adsorbed at $P/P_0 = 0.2$. The Micromeritics DFT program was used to estimate absolute pore sizes.[14] For ^{29}Si MAS NMR experiments, a Bruker Avance 500WB instrument was used. The spectra were recorded using a single-pulse excitation ($\pi/2$, 4.5 μs) with a repetition time of 60 s and a MAS frequency of 5.0 kHz.

The general procedure for potassium promotion is described elsewhere.[11] All test reactions were carried out at 295 K. For alkene isomerizations, 1-hexene and 1-hexadecene were mixed (1:1) and 2 mL of the mixture was added to the catalyst (100 mg). The ethylation was carried out in a 50 mL steel autoclave at a pressure of 20–30 bar loaded with 10 mL toluene. The product composition was analyzed by means of GC/MS and ^{1}H NMR spectroscopy.

Received: June 13, 2001 [Z17285]

[1] J. M. Thomas, W. J. Thomas, *Principles and Practice of Heterogeneous Catalysis*, VCH, Weinheim, **1997**, p. 257.

[2] a) J. Y. Ying, C. P. Mehnert, M. S. Wong, *Angew. Chem.* **1999**, *111*, 58–82; *Angew. Chem. Int. Ed.* **1999**, *38*, 56–77; b) T. J. Barton, L. M. Bull, W. G. Klemperer, D. A. Loy, B. McEnaney, M. Misono, P. A. Monson, G. Pez, G. W. Scherer, J. C. Vartuli, O. M. Yaghi, *Chem. Mater.* **1999**, *11*, 2633–2656; c) G. Oye, J. Sjoblom, M. Stocker, *Adv. Colloid Interface Sci.* **2001**, *89*, 439–466; d) A. Stein, B. J. Melde, R. C. Schroden, *Adv. Mater.* **2000**, *12*, 1403–1419; e) J. Weitkamp, *Solid State Ionics* **2000**, *131*, 175–188; f) U. Ciesla, F. Schüth, *Microporous Mesoporous Mater.* **1999**, *27*, 131–149; g) A. Sayari, P. Liu, *Microporous Mater.* **1997**, *12*, 149–177; h) N. K. Raman, M. T. Anderson, C. J. Brinker, *Chem. Mater.* **1996**, *8*, 1682–1701; i) H. L. Frisch, J. E. Mark, *Chem. Mater.* **1996**, *8*, 1735–1738.

[3] a) S. A. Schunk, F. Schüth in *Molecular Sieves*, *Vol. 1* (Eds.: H. G. Karge, J. Weitkamp), Springer, Heidelberg, **1998**, pp. 229–263; b) A. K. Cheetham, G. Ferey, T. Loiseau, *Angew. Chem.* **1999**, *111*, 3466–3492; *Angew. Chem. Int. Ed.* **1999**, *38*, 3269–3292.

[4] a) W. Schnick, J. Lücke, *Angew. Chem.* **1992**, *104*, 208–209; *Angew. Chem. Int. Ed. Engl.* **1992**, *31*, 213–215; b) W. Schnick, J. Lücke, *Z. Anorg. Allg. Chem.* **1994**, *620*, 2014–2019; c) W. Schnick, *Stud. Surf. Sci. Catal.* **1994**, *84*, 2221–2228; d) W. Schnick, N. Stock, J. Lücke, M. Volkmann, M. Jansen, *Z. Anorg. Allg. Chem.* **1995**, *621*, 987–992; e) J. Weitkamp, S. Ernst, F. Cubero, F. Wester, W. Schnick, *Adv. Mater.* **1997**, *9*, 247–248; f) N. Stock, E. Irran, W. Schnick, *Chem. Eur. J.* **1998**, *4*, 1822–1828.

[5] a) F. L. Riley, *J. Am. Ceram. Soc.* **2000**, *83*, 245–265; b) C. Haluschka, H. J. Kleebe, R. Franke, R. Riedel, *J. Eur. Ceram. Soc.* **2000**, *20*, 1355–1364; c) A. O. Gabriel, R. Riedel, *Angew. Chem.* **1997**, *109*, 371–373; *Angew. Chem. Int. Ed. Engl.* **1997**, *36*, 384–386; d) A. O. Gabriel, R. Riedel, S. Storck, W. F. Maier, *Appl. Organomet. Chem.* **1997**, *11*, 833–841.

 © WILEY-VCH Verlag GmbH, D-69451 Weinheim, 2001 1433-7851/01/4022-4206 $ 17.50+.50/0

[6] a) J. S. Bradley, O. Vollmer, R. Rovai, U. Specht, F. Lefebvre, *Adv. Mater.* **1998**, *10*, 938–942; b) J. S. Bradley, O. Vollmer, R. Rovai, F. Lefebvre, *Mater. Res. Soc. Symp. Proc.* **1999**, *549*, 33–44; c) O. Vollmer, F. Lefebvre, J. S. Bradley, *J. Mol. Catal. A* **1999**, *146*, 87–96; d) J. P. Dismukes, J. W. Johnson, J. S. Bradley, J. M. Millar, *Chem. Mater.* **1997**, *9*, 699–706.
[7] S. Kaskel, D. Farrusseng, K. Schlichte, *Chem. Commun.* **2000**, 2481–2482.
[8] R. Rovai, C. W. Lehmann, J. S. Bradley, *Angew. Chem.* **1999**, *111*, 2073–2076; *Angew. Chem. Int. Ed.* **1999**, *38*, 2036–2038.
[9] a) C. Lastoskie, K. E. Gubbins, N. Quirke, *J. Phys. Chem.* **1993**, *97*, 4786–4796; b) A. Saito, H. C. Foley, *Microporous Mater.* **1995**, *3*, 531–542.
[10] a) E. A. Leone, S. Curran, M. E. Kotun, G. Carrasquillo, R. vanWeeren, S. C. Danforth, *J. Am. Ceram. Soc.* **1996**, *79*, 513–517; b) H. Fujimori, N. Sato, K. Ioku, S. Goto, T. Yamada, *J. Am. Ceram. Soc.* **2000**, *83*, 2251–2254.
[11] S. Kaskel, K. Schlichte, *J. Catal.* **2001**, *201*, 270–274.
[12] a) G. Suzukamo, M. Fukao, T. Hibi, K. Tanaka, M. Minobe, *Stud. Surf. Sci. Catal.* **1997**, *108*, 649–656; b) H. Gorzawski, W. F. Hoelderich, *J. Mol. Catal. A* **1999**, *144*, 181–187.
[13] L. R. M. Martens, P. J. Grobet, P. A. Jacobs, *Nature* **1985**, *315*, 568–570.
[14] DFT (TM) Vers. 1.05, Micromeritics, Norcross, GA, USA. Slit pore model, nitrogen on carbon at 77 K.

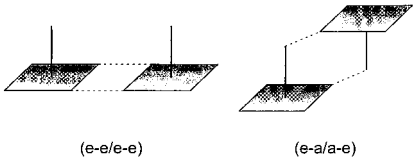
Magnetic Interactions as Supramolecular Function: Structure and Magnetic Properties of Hydrogen-Bridged Dinuclear Copper(II) Complexes**

Winfried Plass,* Axel Pohlmann, and Jens Rautengarten

Dedicated to Professor Ernst-Gottfried Jäger on the occasion of his 65th birthday

Hydrogen bonds play a key role in interactions in biological structures, supramolecular chemistry, and crystal engineering.[1] As such they are also important to understand the properties of relevant magnetic materials.[2] In particular for some copper(II)-containing coordination compounds it has been shown that the variation of possible supramolecular interactions can substantially influence the magnetic properties of related coordination polymers.[3]

Although copper(II) complexes have been widely studied, only two basic patterns of hydrogen bonding have been observed for dinuclear units (Scheme 1). In accord with the preferred square-planar coordination environment for copper(II) ions with the option of one or two additional apical



Scheme 1. Schematic representation for the hydrogen bonding patterns observed for dinuclear copper(II) complexes with square-pyramidal coordination geometry at the copper(II) centers (e: equatorial position, a: apical position).

ligands, these hydrogen bonds can be denoted as either equatorial–equatorial (e–e) or equatorial–apical (e–a) with regard to the position of the involved donor and acceptor atoms. If one considers that the magnetic orbital at each copper(II) ion is defined by the short equatorial bonds, that is basically an orbital of $d_{x^2-y^2}$ type with some possible admixture of d_{z^2} character, a qualitative magneto-structural correlation would predict antiferromagnetic coupling for (e–e/e–e) bridging patterns and weak interactions, which should be of ferromagnetic nature, for (e–a/a–e) bridging patterns. In addition, the magnitude of the magnetic coupling should also be related to the strength of the involved hydrogen bonds. This basic concept is in agreement with the observed structural and magnetic data of relevant systems.[4]

To probe this qualitative magneto-structural relationship we synthesized the copper(II) complex with the trivalent, pentadentate Schiff base ligand *N*-salicylidene-2-(bis(2-hydroxyethyl)amino)ethylamine (H_3sabhea). The resulting self-complementary complex cation $[Cu(H_2sabhea)]^+$ can be isolated as hydrogen-bridged dinuclear complex **1**. Complex **1** can be reversibly deprotonated in aqueous solution yielding **2**, the first triply hydrogen-bridged dinuclear copper(II) complex.

$[\{Cu(H_2sabhea)\}_2](BF_4)_2$ **1**

$[\{Cu(H_2sabhea)\}\{Cu(Hsabhea)\}]BF_4$ **2**

The X-ray crystal structure analyses[5] of the isolated compounds $\mathbf{1}\cdot 0.5\,EtOH\cdot 0.25\,H_2O$ (**1a**) and $\mathbf{2}\cdot H_2O$ (**2a**) reveal the dimeric hydrogen-bridged structure of the cationic copper(II) complexes (Figure 1). The prearranged coplanar configuration for three donor sets of the H_3sabhea ligand (O1, N1, and N2; see Figure 1) defines the orientation of the equatorial plane of the distorted square-pyramidal coordination environment of the copper(II) centers.[6] This is consistent with the observed elongation of the apical Cu–O bonds by about 25–30 pm as compared to the relevant equatorial bonds (see Figure 1). The two hydrogen bonds in **1** involve the equatorially coordinated alcohol group as donor and the phenolate oxygen as acceptor; this leads to a (e–e/e–e) bridging pattern (see Scheme 1). The observed O···O distance of 260 pm is within the range of strong O–H···O hydrogen bonds.[11f] In **1** both apical coordinated alcohol groups are oriented *cis* with respect to the hydrogen bonding

[*] Prof. Dr. W. Plass, Dipl.-Chem. A. Pohlmann, Dipl.-Chem. J. Rautengarten
Fachbereich für Chemie und Biologie, Anorganische Chemie
Universität Siegen
Adolf-Reichwein-Strasse, 57068 Siegen (Germany)
Fax: (+49) 271-740-2555
E-mail: plass@chemie.uni-siegen.de

[**] This work was supported by the Deutsche Forschungsgemeinschaft and the Fonds der Chemischen Industrie. The John von Neumann-Institut für Computing is acknowledged for its generous support with computing time at the supercomputer center of the Forschungszentrum Jülich (Project: Magnetic Interactions in Transition Metal Complexes).

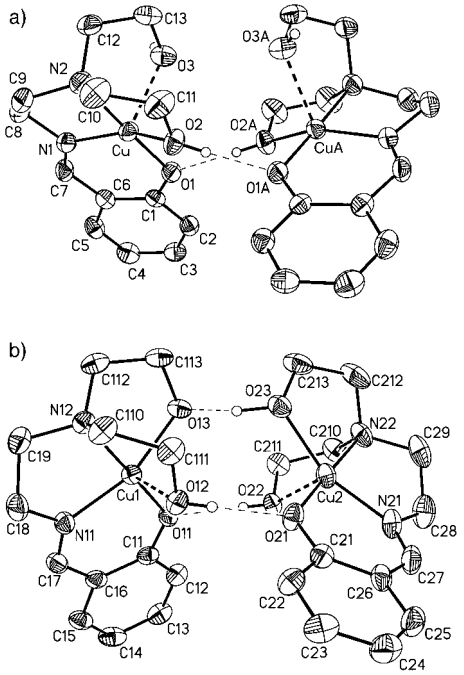


Figure 1. Molecular structure of the hydrogen-bridged cationic complexes **1** (a) and **2** (b) in crystals of **1a** and **2a**, respectively. Thermal ellipsoids of the non-hydrogen atoms are drawn at the 50% probability level. All hydrogen atoms not bound to alcoholic oxygen atoms are omitted for clarity. Solid broken lines indicate bonds to atoms in the apical position of the coordination polyhedron. Hydrogen bonds (thin broken lines) and interatomic distances [pm] and bond angles [°]: **1a**: Cu-O1 189.5(2), Cu-O2 200.5(2), Cu-O3 225.4(2), Cu-N1 192.5(2), Cu-N2 201.9(2); O1 $\cdots$ O2A 259.6(3), O3 $\cdots$ O3A 353.4(3), Cu $\cdots$ CuA 473.6(2); O1-Cu-N2 178.36(9), O2-Cu-N1 151.49(9), O2-Cu-O3 98.26(8), O3-Cu-N1 107.36(9). **2a**: Cu1-O11 192.7(2), Cu1-O12 226.0(2), Cu1-O13 196.3(2), Cu1-N11 193.8(2), Cu1-N12 204.4(2), Cu2-O21 191.8(2), Cu2-O22 227.9(2), Cu2-O23 198.5(2), Cu2-N21 193.1(3), Cu2-N22 203.8(2); O11 $\cdots$ O22 266.4(3), O12 $\cdots$ O21 265.8(3), O13 $\cdots$ O23 244.2(3), Cu1 $\cdots$ Cu2 461.4(2); O11-Cu1-N12 174.50(8), O12-Cu1-N11 101.49(9), O12-Cu1-O13 94.35(8), O13-Cu1-N11 160.36(9), O21-Cu2-N22 176.50(9), O22-Cu2-N21 105.11(9), O22-Cu2-O23 90.44(8), O23-Cu2-N21 159.81(10).

plane, yielding an arrangement that is prepositioned for a third hydrogen bond (interatomic distance between O3 and O3A is 353 pm).

The deprotonation of one of the two apical alcohol groups, as observed in **2**, increases the hydrogen bond acceptor ability of the corresponding oxygen atom and, therefore, enables the formation of the third hydrogen bond between the two copper(II) units. This is accompanied with a conformational alternation of the ethylenediamine chelate ring (N1-C8-C9-N2: δ in **1** and λ in **2**, see Figure 1), which enables the rearrangement of the copper(II) coordination environments in such a way that the equatorial planes now include the newly hydrogen-bonded oxygen atoms O13 and O23 (cf. Figure 1b). The hereby established unique (e–e/e–a/a–e) bridging pattern contains a very short O $\cdots$ O distance of 244 pm (O13 $\cdots$ O23), which is within the range of very strong hydrogen bonds,[1f] whereas the two other hydrogen bonds (O12 $\cdots$ O21 and O11 $\cdots$ O22: 266 pm) are slightly longer than in the protonated complex **1**.

The X-band ESR spectra of microcrystalline powders of **1a** and **2a** recorded at 50 K show broad unstructured bands with no detectable hyperfine structure at $g = 2.09$ (peak to peak separation: 10 mT) and $g = 2.10$ (peak to peak separation: 13 mT), respectively, and a band at half-field from the forbidden $\Delta m_S = 2$ transition at approximately 150 mT. Moreover the temperature dependence of the half-field resonances is consistent with an antiferromagnetic coupling between the two magnetic copper(II) centers. Similar behavior is found for X-band ESR spectra of frozen aqueous solutions of **1** and **2**. In particular the band at half-field transition expected for an exchange-coupled system is observed.

The magnetic susceptibility χ of polycrystalline samples of **1a** and **2a** was measured in a temperature range of 2–295 K using a SQUID susceptometer with an applied field of $H =$ 10 kOe. The temperature dependence of the product $\chi_M T$ is shown in Figure 2. At higher temperatures the susceptibility

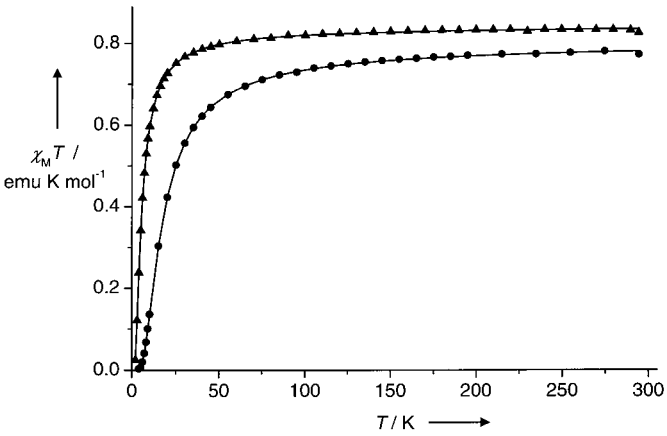


Figure 2. Experimentally determined temperature dependence of $\chi_M T$ for **1a** (●) and **2a** (▲). The solid lines represent the calculated values (see text).

data obeys the Curie–Weiss law and $\chi_M T$ is close to the expected spin-only value for two independent copper(II) centers per molecule. The observed decrease of $\chi_M T$ upon cooling is in accord with the presence of intramolecular antiferromagnetic interactions between the hydrogen-bridged copper(II) centers of **1** and **2**. A quantitative analysis of the magnetic data (corrected for diamagnetic contributions using Pascal constants) assuming an isotropic interaction using the Heisenberg–Dirac–Van Vleck Hamiltonian $\hat{H} = -J\hat{S}_1 \cdot \hat{S}_2$ was used to describe the temperature dependence of the product $\chi_M T$. As shown in Figure 2, good fits to the experimental data were attained for the magnetic parameters $g = 2.07$ and $J = -21$ cm^{-1} for **1a** and $g = 2.12$ and $J = -7$ cm^{-1} for **2a**.

Density functional theory (DFT) calculations were performed to elucidate the electronic structure of the cationic complexes of **1** and **2**.[7] In all calculations split-valence basis sets were used that have been augmented by diffuse functions for the oxygen atoms to enable a proper description of the hydrogen bonds.[8] The geometry optimization was performed with the generalized gradient approximation functional Becke 88/Perdew 91 (B88/PW91).[9] The calculated structural parameters are in good agreement with the values obtained from the X-ray structure analysis. In particular this holds for the coordination environment of the copper(II) centers (calculated structure data for **1**: $\tau = 0.43$; for **2**: Cu1 $\tau = 0.28$, Cu2 $\tau = 0.33$; for X-ray structures see reference [6]) as well as

 © WILEY-VCH Verlag GmbH, D-69451 Weinheim, 2001 1433-7851/01/4022-4208 $ 17.50+.50/0

the hydrogen bonding scheme (calculated structure data for **1**: O1 ··· O2A 259, O3 ··· O3A 355; for **2**: O11 ··· O22 265, O12 ··· O21 265, O13 ··· O23 242 pm; for X-ray structures see. Figure 1).

If the broken-symmetry formalism is utilized, it is possible to express the singlet–triplet gap of exchange-coupled systems with one unpaired electron per center as $J = E_B - E(S=1)$,[10] where E_B is the energy of the broken-symmetry state. This procedure is in keeping with the proposal of Perdew, Savin, and co-workers,[11] who suggested that the broken-symmetry single determinant is the correct solution of the Kohn–Sham equations for the singlet state. The exchange coupling constants calculated with the B88/PW91 functional (**1**: -68 and **2**: -31 cm^{-1}) are too large as compared to the experimental values. This is consistent with the generally observed overestimation of the stabilization of the singlet state relative to the triplet state by DFT methods. The inclusion of Hartree–Fock(HF)-type contributions, which are known to usually overestimate the relative stability of the triplet state, can improve the accuracy of the calculated values.[10] Consequently, calculations with the hybrid method b3lyp[12] yield exchange-coupling constants of -17 and -6 cm^{-1} for **1** and **2**, respectively, which are in excellent agreement with the experimental values.

The magnetic orbitals as derived from the broken-symmetry calculations have basically $d_{x^2-y^2}$ character with contributions from the equatorial oxygen and nitrogen atoms. This is consistent with the observed distorted square-pyramidal coordination geometry at the copper(II) centers. The reduced exchange-coupling constant for **2** as compared to that for **1** indicates that only hydrogen bonds of the (e–e) type are effectively transmitting exchange interactions between the copper(II) centers, that is both the hydrogen donor and the hydrogen acceptor must have contributions to the respective magnetic orbital. Moreover, according to a magneto-structural correlation based on the O ··· O distance of hydrogen-bridged copper(II) complexes that was derived from a theoretical study on the model system[{Cu(OH)$(NH_3)_2$-(H_2O)}$_2$],[13] complexes **1** and **2** should exhibit much larger exchange-coupling constants in the range of -80 to -100 cm^{-1}. This is indicative for the importance of the relative orientation of the magnetic orbitals with respect to each other, which for **1** and **2** is unfavorable as compared to the coplanar orientation of the model system [{Cu(OH)$(NH_3)_2(H_2O)$}$_2$] used for the theoretical study.[13]

In conclusion, we have shown that by utilizing a self-complementary copper(II) coordination unit the first triply hydrogen-bridged dinuclear transition metal complex has been synthesized. This system can be reversibly switched between its triple (**2**) and double hydrogen-bridged (**1**) forms by proton transfer. Their structural and magnetic properties show that a simple magneto-structural correlation based on a hydrogen bond length criterion is not sufficient. On the contrary the key factor is given by the hydrogen bonding pattern. In contrast, the fine tuning of the magnetic properties is related to the hydrogen bonding distances and the relative orientation of the magnetic orbitals of both copper units with respect to the hydrogen bonding pattern.

Experimental Section

The ligand H_3sabhea was synthesized as described in reference [14].

1a: H_3sabhea (0.25 g, 1 mmol) dissolved in ethanol (10 mL) was added to a solution of $Cu(BF_4)_2 \cdot 6H_2O$ (0.34 g, 1 mmol) in ethanol (10 mL) at room temperature. The resulting deep green solution was stirred for 30 min and allowed to stand at room temperature. After a few days green crystals of **1a** formed which were isolated by filtration and washed with ethanol (0.25 g, 61 %). Elemental analysis (%) calcd for $C_{27}H_{41.5}B_2Cu_2F_8N_4O_{6.75}$: C 39.04, H 5.04, N 6.74; found: C 38.93, H 5.06, N 6.81.

2a: A 2N aqueous solution of NaOH (2 mL) was added to H_3sabhea (0.50 g, 2 mmol) dissolved in water (10 mL). To this solution $Cu(BF_4)_2 \cdot 6H_2O$ (0.69 g, 2 mmol) dissolved in water (10 mL) was added. After stirring for 30 min the solution was allowed to stand at room temperature. Within a few days blue crystals of **2a** formed (0.42 g; 57 %). Elemental analysis (%) calcd for $C_{26}H_{39}BCu_2F_4N_4O_7$: C 42.57, H 5.36, N 7.64; found: C 42.57, H 5.16, N 7.41.

Received: April 17, 2001
Revised: August 1, 2001 [Z16956]

[1] a) G. A. Jeffrey, W. Saenger, *Hydrogen Bonding in Biological Structures*, Springer, Berlin, **1991**; b) J. M. Lehn, *Supramolecular Chemistry: Concepts and Perspectives*, VCH, Weinheim, **1995**; c) G. A. Jeffrey, *An Introduction to Hydrogen Bonding*, Oxford University Press, New York, **1997**; d) G. R. Desiraju, *The Crystal as a Supramolecular Entity*, Wiley, Chichester, **1996**; e) D. Braga, F. Grepioni, A. G. Orpen, *Crystal Engineering: From Molecules and Crystals to Materials*, Kluwer, Dordrecht, **1999**; f) G. R. Desiraju, T. Steiner, *The Weak Hydrogen Bond in Structural Chemistry and Biology*, Oxford University Press, New York, **1999**.

[2] *"Magnetism: A Supramolecular Function"*: (Ed. O. Kahn), Kluwer, Dordrecht, **1996**.

[3] a) O. Kahn, Y. Pei, M. Verdaguer, J. P. Renard, J. Sletten, *J. Am. Chem. Soc.* **1988**, *110*, 782–789; b) J. Larionova, S. A. Chavan, J. V. Yakhmi, A. Gulbrandsen Frøystein, J. Sletten, C. Sourisseau, O. Kahn, *Inorg. Chem.* **1997**, *36*, 6374–6381.

[4] a) J. M. Moreno, J. Ruiz, J. M. Dominguez-Vera, E. Colacio, *Inorg. Chim. Acta* **1993**, *208*, 111–115; b) J. A. Bertrand, T. D. Black, P. G. Eller, F. T. Helm, R. Mahmood, *Inorg. Chem.* **1976**, *15*, 2965–2970; c) P. J. van Koningsbruggen, J. G. Haasnoot, R. A. G. de Graaff, J. Reedijk, *Inorg. Chim. Acta* **1995**, *234*, 87–94; d) S. Kotila, *Acta Chem. Scand.* **1994**, *48*, 742–752.

[5] Crystal structure analyses data: **1a**: $C_{27}H_{41.5}B_2Cu_2F_8N_4O_{6.75}$, $M_r = 830.8$, crystal dimensions $0.1 \times 0.2 \times 0.4$ mm, tetragonal, $P\bar{4}2_1c$, $a = 1580.50(7)$, $c = 1350.70(9)$ pm, $V = 3.3740(3)$ nm^3, $Z = 4$, $\rho_{calcd} = 1.636$ g cm^{-3}, $F(000) = 1702$, $T = 183$ K, $\lambda = 71.073$ pm, $\mu(Mo_{K\alpha}) = 1.354$ mm^{-1}, θ range 1.82–27.01°, 19045 measured, 3683 independent reflections ($R_{int} = 0.056$), 237 parameters, $wR_2 = 0.070$, $R_1 = 0.032$ for 2722 reflections with $F > 4\sigma(F)$, Flack parameter $x = 0.52(2)$, max./min. residual electron density in the final difference Fourier map 0.3/-0.3×10^{-6} e pm^{-3}. **2a**: $C_{26}H_{39}BCu_2F_4N_4O_7$, $M_r = 733.5$, crystal dimensions $0.05 \times 0.1 \times 0.5$ mm, monoclinic, $P2_1/c$, $a = 1426.35(7)$, $b = 1838.00(9)$, $c = 1160.78(6)$ pm, $\beta = 94.1310(10)°$, $V = 3.0352(3)$ nm^3, $Z = 4$, $\rho_{calcd} = 1.605$ g cm^{-3}, $F(000) = 1512$, $T = 183$ K, $\lambda = 71.073$ pm, $\mu(Mo_{K\alpha}) = 1.476$ mm^{-1}, θ range 1.43–26.99°, 16338 measured, 6419 independent reflections ($R_{int} = 0.030$), 461 parameters, $wR_2 = 0.085$, $R_1 = 0.039$ for 5015 reflections with $F > 4\sigma(F)$, max./min. residual electron density in the final difference Fourier map $0.4/-0.4 \times 10^{-6}$ e pm^{-3}. The crystallographic data were collected on a Bruker AXS SMART. Lorentz and polarization corrections as well as an empirical absorption correction were performed. The structures were solved by direct methods (SHELXTL) and subsequent full-matrix least-squares refinement against F^2 (G. M. Sheldrick, *SHELXL97*, Universität Göttingen, **1997**). For **1a** the observed systematic absences suggest either of the tetragonal space groups $P\bar{4}2_1c$ and $P4/mnc$. Attempts to solve the structure in the centrosymmetric space group $P4/mnc$ were unsuccessful. This led in agreement with intensity statistics to the noncentrosymmetric tetragonal space group $P\bar{4}2_1c$ as the final choice. The refinement afforded a Flack parameter (H. D.

Flack, *Acta Crystallogr. Sect. A* **1983**, *39*, 876 – 881) of about 0.5, which could not be reduced upon inversion of the parameter set. Therefore the final structure refinement was performed by assuming racemic twinning. All non-hydrogen atoms were refined with anisotropic displacement parameters. The hydrogen atoms attached to alcoholic oxygen atoms were refined isotropically, whereas all other hydrogen atoms were treated by using the appropriate riding model. Crystallographic data (excluding structure factors) for the structures reported in this paper have been deposited with the Cambridge Crystallographic Data Centre as supplementary publication no. CCDC-161491 (**1a**) and CCDC-161490 (**2a**). Copies of the data can be obtained free of charge on application to CCDC, 12 Union Road, Cambridge CB2 1EZ, UK (fax: (+44) 1223-336-033; e-mail: deposit@ccdc.cam.ac.uk).

[6] **1a**: $\tau = 0.45$; **2a**: Cu1, $\tau = 0.24$, Cu2, $\tau = 0.28$. For the definition of τ see: A. W. Addison, T. N. Rao, J. Reedijk, J. van Rijn, G. C. Verschoor, *J. Chem. Soc. Dalton Trans.* **1984**, 1349 – 1356.

[7] High Performance Computational Chemistry Group, *NWChem, A Computational Chemistry Package for Parallel Computers*, Version 4.0.1 (**2001**), Pacific Northwest National Laboratory, Richland, Washington 99352, USA.

[8] a) A. Schäfer, H. Horn, R. Ahlrichs, *J. Chem. Phys.* **1992**, *97*, 2571 – 2577; b) F. Sim, A. St-Amant, I. Papai, D. R. Salahub, *J. Am. Chem. Soc.* **1992**, *114*, 4391 – 4400.

[9] a) A. D. Becke, *Phys. Rev. A* **1988**, *38*, 3098 – 3100; b) J. P. Perdew, J. A. Chevary, S. H. Vosko, K. A. Jackson, M. R. Pederson, D. J. Singh, C. Fiolhais, *Phys. Rev. B* **1992**, *46*, 6671 – 6687.

[10] E. Ruiz, J. Cano, S. Alvarez, P. Alemany, *J. Comput. Chem.* **1999**, *20*, 1391 – 1400.

[11] a) J. P. Perdew, A. Savin, K. Burke, *Phys. Rev. A* **1995**, *51*, 4531 – 4541; b) J. P. Perdew, M. Ernzerhof, K. Burke, A. Savin, *Int. J. Quantum Chem.* **1997**, *61*, 197 – 205.

[12] A. D. Becke, *J. Chem. Phys.* **1993**, *98*, 5648 – 5652.

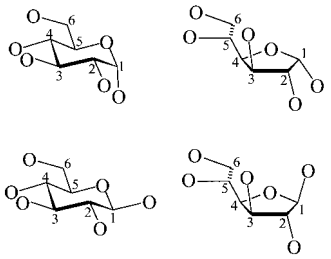
[13] F. Nepveu, S. Gehring, L. Walz, *Chem. Phys. Lett.* **1986**, *128*, 300 – 304.

[14] W. Plass, *Z. Anorg. Allg. Chem.* **1994**, *620*, 1635 – 1644.

A Transition Metal Complex of D-Glucose**

Peter Klüfers* and Thomas Kunte

Special attention is paid to the carbohydrates as the most abundant biogenic raw materials when establishing benign chemical syntheses as a part of sustainable development. In order to overcome the "overfuctionalization" of the carbohydrates, which bear a number of very similar functionalities rather than a large number of functionalities, classical carbohydrate chemistry often uses multistep reaction sequences. Due to by-products and an extensive use of auxiliary agents, carbohydrate chemistry is by no means "green", despite the usage of biogenic raw materials.[1] One approach to solve this problem is reaction steering by metal catalysis. To plan catalysis in a rational way, basic information is needed; in particular, how the substrate reacts with a metal in a specified oxidation state.[2] To what extend the fundamentals are lacking in that area is illustrated by the statement that, to the best of our knowledge, up to now not a single transition-metal complex of D-glucose, as the most important monosaccharide, has been characterized structurally. One of the reasons for this might be the high reactivity of the reducing sugars. Not only the ease of oxidation and their instability in alkaline solution must be accounted for, even the monosaccharides themselves are mixtures in solution. When a coordinating metal moiety is exposed to glucose, for example, it is not predictable whether the sugar will react through its α- or β-furanose, α- or β-pyranose, or a less stable form (Scheme 1; neither open-chain nor septanose forms are considered). For the epimeric D-mannose, it was demonstrated that coordination to a metal can establish β-D-mannofuranose as the main species, although this isomer is unimportant in the normal solution equilibrium of the aldose.[3]



Scheme 1. Oxygen atom pattern of the common α- (top) and β-D-glucose isomers (bottom): Pyranoses with $^4C_1$ conformation (left) and furanoses (right).

Herein, we report on the characterization of a transition metal complex of D-glucose in solution and the solid state. The metal is the good oxidant palladium(II)—oxidation of the aldose, however, could be avoided to such an extent that even crystallization became possible. The starting point of the experiments was the unexpected behaviour of "Pd-en", an aqueous solution of $[(en)Pd(OH)_2]$ (en = ethylenediamine), towards cellulose. Pd-en is a coordinating cellulose solvent, which dissolves the polysaccharide with formation of a metal complex.[4] On investigating largely hydrolyzed cellulose (degree of polymerization approximately 30, compared with about 3000 for native cellulose), our attention was attracted since even with these short chained and hence end-group rich celluloses, there was no enhanced precipitation of palladium(0) due to oxidation of the reducing end groups. Hence monosaccharides—the "pure" reducing end groups—were dissolved in Pd-en and it became apparent that simply cooling the mixtures to about 5 °C suffices to obtain stable solutions without metal precipitation (as expected, no *N*-glycoside formation of the en ligands was observed at the low temperatures applied[5]). Since palladium(II) complexes with an N_2O_2 ligand set are sufficiently inert and diamagnetic, the mixture of isomers can be investigated by NMR spectroscopy in solution. Figure 1 shows the spectrum of a solution with a 3:1 molar ratio of palladium and the sugar. The signals, assigned by $^1H/^{13}C$ correlated spectra, indicated an anomeric mixture made up of two parts α- and one part β-pyranose

[*] Prof. Dr. P. Klüfers, Dipl.-Chem. T. Kunte
Department Chemie der Ludwig-Maximilians-Universität München
Butenandtstrasse 5 – 13, 81377 Munich (Germany)
Fax: (+49) 89-2180-7407
E-mail: kluef@cup.uni-muenchen.de

[**] Polyol – Metal Complexes, Part 37. This work was supported by the Deutsche Forschungsgemeinschaft (Kl624/5). We are indebted to Degussa AG for palladium-based chemicals.—Part 36: K. Benner, P. Klüfers, *Carbohydr. Res.* **2000**, *327*, 287-292.

 © WILEY-VCH Verlag GmbH, D-69451 Weinheim, 2001 1433-7851/01/4022-4210 $ 17.50+.50/0

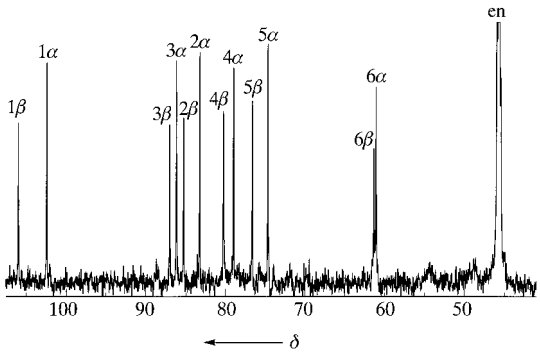


Figure 1. ^{13}C NMR spectra of a solution of D-glucose in Pd-en (see also Table 1). The atom numbering corresponds to Scheme 1 left. Labels α und β relate to the respective anomer of the pyranose form.

Table 1. Signal positions in the ^{13}C NMR spectrum of a 0.35 M solution of D-glucose in 1 M Pd-en. In addition to the chemical shift the coordination-induced shift ($\delta_{Complex} - \delta_{Reference}$)[a] is tabulated. CIS values indicating palladium bonding are printed in bold. The relative amount of the anomers was detected (^1H NMR) as 2:1 in favor of the α form.

	C1	C2	C3	C4	C5	C6
α-D-glucopyranose in Pd-en:						
δ [ppm]	102.6	83.4	86.3	79.1	74.8	61.2
CIS [ppm]	**9.0**	**10.4**	**12.1**	**8.0**	1.9	– 0.9
β-D-glucopyranosein Pd-en:						
δ [ppm]	106.2	85.4	87.2	80.4	76.8	61.5
CIS [ppm]	**8.8**	**9.8**	**10.0**	**9.3**	– 0.6	– 0.8

[a] The reference is an about 0.6 M solution of D-glucose in water.[8]

(compare the 1:2 equilibrium mixture of an aqueous glucose solution). The bonding sites of palladium are indicated by their characteristic "coordination-induced shift" (CIS), which is a downfield shift of about 10 ppm for those carbon atoms that are bonded to metal-coordinating oxygen atoms. As a result, the four oxygen atoms 1 – 4 (for atom numbers see Scheme 1 top left) are bonded to palladium, hence the hemiacetal function is also part of a palladium-coordinating entity. Since the Pd(en) fragment provides a bonding site for one diolato ligand, a binuclear complex should be present with both anomers. The spectra remain the same when the molar ratio of Pd and D-glucose is reduced to 2:1. A further decrease to a 1:1 ratio results in a mixture of monometallated glucoses. The 1,2-metallated species are of particular significance, as may be expected owing to the maximum acidity of the hydroxy group at C1.

We did not succeed in the preparation of crystals of satisfying size. However, a small crystal was obtained from a solution with a 3:1 Pd:D-glucose molar ratio. X-ray analysis[6] proved the crystal to be composed of the main solution species, the α anomer. According to the formula $[(en)_2Pd_2(\alpha\text{-D-Glc}p1,2,3,4H_{-4})]\cdot 7H_2O$ **1** (Glc$p$ = glucopyranose), the spectroscopically determined metal-binding sites were found entirely deprotonated. Figure 2 shows the O1 – O4 deprotonated α-D-glucopyranose tetraanion, which is coordinated as a bis(chelate) ligand to two palladium(II) central atoms. Owing to the weakly scattering crystal it was not possible to locate the hydrogen sites experimentally. However, O–O and O–N distances clearly indicate that all alkoxo oxygen atoms are

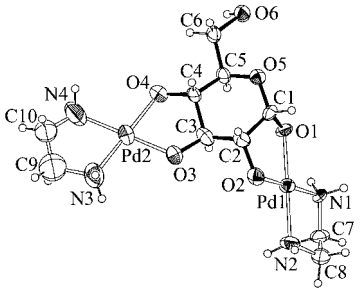


Figure 2. The molecular structure of **1** in the crystal. Thermal ellipsoids are drawn at 40 % probability (C9 and C10 are refined isotropically). Distances [pm]: from Pd1-O1 199.5(11), Pd1-O2 199.9(12), Pd1-N1 202.4(13), Pd1-N2 204.0(14), Pd2-O3 197.6(13), Pd2-N3 200.9(18), Pd2-N4 203(2), Pd2-O4 204.0(13); bonding angles [°]: O1-Pd1-O2 83.5(5), O3-Pd2-O4 84.2(5); torsion angles [°]: O1-C1-C2-O2 43(2), O2-C2-C3-O3 68(2), O3-C3-C4-O4 – 50(2).

acceptors in two hydrogen bonds each, with O–H groups as the donors. N–H functions contribute to the hydrogen bond structure as parts of cooperative chains. With this structural features, the glucose complex fits in the series of polyol complexes with the $(en)Pd^{II}$ fragment.[4]

The oxygen atom pattern of a carbohydrate may match the pattern of free coordination sites of a metal thus forming stable aggregates. With a reducing sugar, the first structure analysis with a transition metal complex—a molybdate(VI) with the β-lyxofuranose ligand[7]—shows that the pentose sugar is able to provide an O_4 rhomb. A later analysis showed that the O_5 pattern provided by β-mannofuranose turned out to be an ideal building block of M_2O_{10} double octahedra of binuclear metallates(III).[3] On the other hand, the oxygen atom patterns of the most important monosaccharide, D-glucose, in any of its hemiacetal forms do not exceed the simple O_2 diol pattern (a consequence is the epimerization reaction of glucose to β-mannofuranose in the presence of trivalent metal ions[3a]). In this work, this steric restriction is taken into account by providing exclusively the $(en)Pd^{II}$ moiety, which is a diol chelator. However, despite the low hapticity, the stability of the complexes is large enough that no signals but those of the doubly metallated species are observed in stoichiometrically composed solutions. Current work is directed towards the issue of making use of the modulated reactivity of the complexed reducing sugars.

Received: April 6, 2001 [Z16918]

[1] *Green Chemistry* (Eds.: P. Tundo, P. Anastas), Oxford University Press, Oxford, **2000**.

[2] For an overview over the field of carbohydrate – metal interactions, including references to further reviews, see: J.-F. Verchère, S. Chapelle, F. Xin, D. C. Crans, *Prog. Inorg. Chem.* **1998**, *47*, 837 – 945.

[3] a) J. Burger, C. Gack, P. Klüfers, *Angew. Chem.* **1995**, *107*, 2950 – 2951; *Angew. Chem. Int. Ed. Engl.* **1995**, *34*, 2647 – 2649; b) A. Geißelmann, P. Klüfers, B. Pilawa, *Angew. Chem.* **1998**, *110*, 1181 – 1184; *Angew. Chem. Int. Ed.* **1998**, *37*, 1119 – 1121.

[4] R. Ahlrichs, M. Ballauff, K. Eichkorn, O. Hanemann, G. Kettenbach, P. Klüfers, *Chem. Eur. J.* **1998**, *4*, 835 – 844.

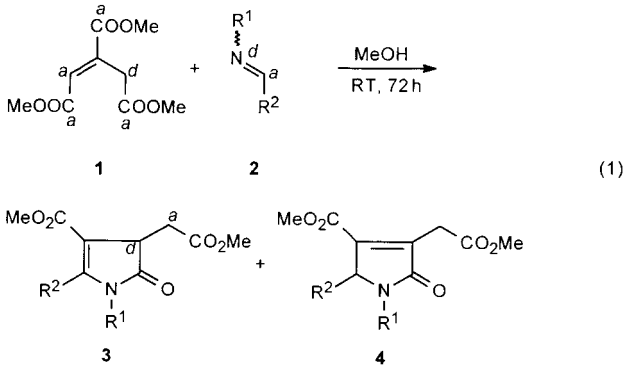
[5] T. Tanase, K. Kurihara, S. Yano, K. Kobayashi, T. Sakurai, S. Yoshikawa, M. Hidai, *Inorg. Chem.* **1987**, *26*, 3134 – 3139; S. Yano, M. Nakagoshi, A. Teratani, M. Kato, T. Onaka, M. Iida, T. Tanase, Y. Yamamoto, H. Uekusa, Y. Ohashi, *Inorg. Chem.* **1997**, *36*, 4187 – 4194.

 © WILEY-VCH Verlag GmbH, D-69451 Weinheim, 2001 1433-7851/01/4022-4211 $ 17.50+.50/0

[6] $C_{10}H_{24}N_4O_6Pd_2 \cdot 7H_2O$, $M_r = 635.27$, yellow rod, $0.09 \times 0.05 \times 0.02$ mm, monoclinic, space group $P2_1$, $a = 8.3451(4)$, $b = 8.8020(5)$, $c = 15.2168(9)$ Å, $b = 93.937(3)^\circ$, $V = 1115.09(11)$ Å^3, $Z = 2$, $\rho = 1.8920(2)$ g cm^{-3}, $2\theta_{max} = 55^\circ$, $Mo_{K\alpha}$, $\lambda = 0.71073$ Å, Stoe IPDS, $T = 200$ K, 8220 reflections, 4283 independent and used in refinement, direct methods (SHELXS), full-matrix least squares against F^2 (SHELXL), 256 parameters, H in calculated positions, $R(F) = 0.180$, $R_w(F^2) = 0.200$, max. difference electron density 1.6 e Å^{-3}, Flack parameter $-0.01(11)$. Crystallographic data (excluding structure factors) for the structures reported in this paper have been deposited with the Cambridge Crystallographic Data Centre as supplementary publication no. CCDC-159804. Copies of the data can be obtained free of charge on application to CCDC, 12 Union Road, Cambridge CB2 1EZ, UK (fax: (+44) 1223-336-033; e-mail: deposit@ccdc.cam.ac.uk).

[7] G. E. Taylor, J. M. Waters, *Tetrahedron Lett.* **1981**, *22*, 1277 – 1278.

[8] M. J. King-Morris, A. S. Serianni, *J. Am. Chem. Soc.* **1987**, *109*, 3501 – 3508.



	R^1	R^2	Yield [%]	**3:4**
a	Benzyl	Phenyl	57	100:0
b	Benzyl	Naphthyl	55	0:100
c	Benzyl	*o*-Hydroxyphenyl	28	38:62
d	2-Furylmethyl	Phenyl	52	100:0
e	Methyl	Phenyl	46	41:59

Heterocycles through Domino Reactions with Trimethyl Aconitate, a Versatile Synthetic Building Block**

Daniel Witthaut, Roland Fröhlich,[+] and Hans J. Schäfer*

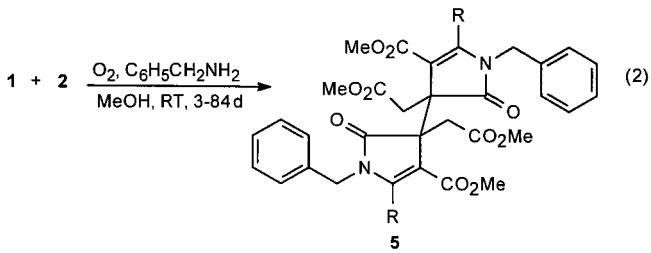
Dedicated to Professor Dieter Hoppe on the occasion of his 60th birthday

Selective C–C bond formations require building blocks of opposite reactivity, that is donors and acceptors. Anionic donors, which are soluble in methanol, simplify thereby the performance of the reaction. Trimethyl aconitate (**1**), a C_6 building block, is of interest in this regard. It possesses five functional groups: one donor, namely the acidic methylene group of a vinylogous malonate and four acceptors, namely the electrophilic double bond and three ester groups. Furthermore aconitic acid is a renewable raw material, which can be extracted from sugar molasses or be obtained by dehydration of citric acid. In spite of these favorable presuppositions **1** has up to now been rarely used in synthesis.[1] First systematic investigations demonstrate that the functional groups in **1** can be used for Michael additions,[2] Diels – Alder cycloadditions,[3] Knoevenagel condensations,[4] and cyclodimerizations.[5] Here we report on domino reactions[6] of the donor(*d*) and acceptor(*a*) groups of **1** with imines.

Stirring equimolar amounts of **1** with the imine **2** in methanol leads to the dihydropyrrolones **3** and **4** [Eq. (1)]. The isomer **4** was shown by AM1 and PM3 calculations to be thermodynamically more stable than **3**. For the product formation the following reaction path appears plausible: **1** reacts with one equivalent of imine in a domino reaction, which consists of a nucleophilic addition, an intramolecular acylation, and a shift of the exocyclic double bond, to form the 2,5-dihydropyrrolone **3**. The subsequent base-catalyzed double bond shift leading to **4** is evidently kinetically controlled by the substituents R^1 and R^2.

2,5-Dihydropyrrolones **3** are components of herbicides[7] and structural motifs of natural products.[8] They are usually prepared by reaction of enaminoesters or imines, respectively, with dialkyl maleates or maleic anhydride leading to N1 – C2 and C4 – C5 connections.[9] The alternative N1 – C2 and C4 – C5 connection established here using **1** and imines allows a simpler variation of the C5 substituent in the dihydropyrrolone.

The reaction of **1** with the imine **2a** in the presence of benzylamine leads to the bisdihydropyrrolone **5a** [Eq. (2)], which is obtained nearly exclusively as the racemate as shown by the crystal structure analysis.



	R	Yield [%]
a	Phenyl	43
b	Naphthyl	35
c	*o*-Hydroxyphenyl	39

As the reaction does not occur when using triethylamine, benzylamine evidently acts as redox-mediator and not as base. Benzylamine is possibly oxidized by air to the cation radical, which is deprotonated to the benzylamino radical. This radical could abstract a hydrogen atom from the simultaneously

[*] Prof. Dr. H. J. Schäfer, Dipl.-Chem. D. Witthaut, Dr. R. Fröhlich[+]
Organisch-chemisches Institut der Universität
Corrensstrasse 40, 48149 Münster (Germany)
Fax: (+49) 251-83-36523
E-mail: schafeh@uni-muenster.de

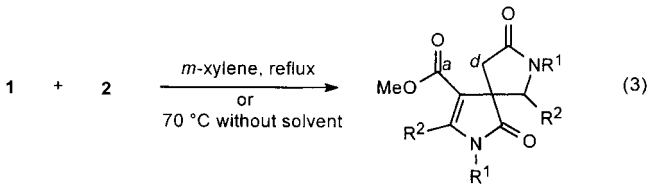
[**] We thank the Bayer AG, Division CH-F fine chemicals for support of this work.

[+] Crystal structure analysis

 © WILEY-VCH Verlag GmbH, D-69451 Weinheim, 2001 1433-7851/01/4022-4212 $ 17.50+.50/0

formed 2,5-dihydropyrolone **3** to form a hydropyrrolone radical which then dimerizes to give product **5a**. The intermediate hydropyrrolone radical is a captodative stabilized[10] allyl radical similar to the stable 4-carbomethoxypyridinyl radical.[11] This domino reaction consisting of an imine addition, an intramolecular acylation, and an oxidative coupling can be transferred to the imines **2b** and **2c**. When used in excess the imines evidently act as redox-mediators themselves making the presence of benzylamine no longer necessary. The bisdihydropyrrolones **5** contain the structural motif of dimer indole alkaloids.[12] They are prepared by 3,3-coupling of appropriate precursors, and in most cases are obtained in low yields due to the steric hindrance associated with forming bonds between the quarternary C3 atoms. An exception is the dimerization of an oxindole enolate with tetraiodomethane, which presumably occurs via an anion-radical mechanism and forms the key step of a folicanthine synthesis.[13]

The spiro[pyrrolidinone-3,3′-dihydropyrrolinone] **6** is obtained in a one-pot reaction from **1** and two equivalents of **2** in refluxing xylene or at 70 °C without solvent [Eq. (3)]. The



(3)

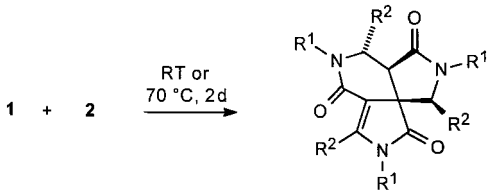
6

2	6	R^1	R^2	Yield [%]	d.r.[18]
e	**a**	Methyl	Phenyl	40	2:1
f	**b**	Methyl	*p*-Methoxyphenyl	41	5:2
g	**c**	Methyl	*p*-Chlorophenyl	44	3:1
h	**d**	Methyl	*o*-Chlorophenyl	38	5:4
i	**e**	Methyl	1*H*-Indol-3-yl	35	5:4
j	**f**	Ethyl	*o*-Chlorophenyl	36	2:1:1

formation of **6** can be explained by a base-catalyzed addition of the intermediate dihydropyrrolone **3** or **4** to the imine and a subsequent intramolecular acylation of the amino group with a second ester group in **1**.[14] Up to now there are only a few routes to the structural motif in **6**.[15] Spiro[pyrrolidine-3,3′-oxindoles] are potential cytostatica,[16a] spiro[succinimide-3,3′-isooxindole] exhibits an antidiabetic activity.[17]

The reaction of **1** with **2g** afforded **6c** in 44 % yield together with the tricyclic spiro compound **7a** in 1 % yield, showing that the remaining reactive acceptor in **6** and the donor of trimethyl aconitate can still react with the imine. When three equivalents of other imines are allowed to react with **1** two further tricyclic spiro compounds are obtained in higher yields [Eq. (4)]. Even though eight diastereomers are conceivable, the crystalline compounds **7b** and **7c** are isolated as one racemic diastereomer in each case (one enantiomer is shown). To our knowledge compounds with the structural motif of **7** have not been described before.

The formation of **7** can be interpreted by a base-catalyzed addition of the intermediate **6** to the imine and subsequent acylation of the amino group by the remaining third ester group. Thus, the C,H-acidic methylene group and the three



(4)

rac-**7**

2	7	R^1	R^2	Yield [%]
g	**a**	Methyl	*p*-Chlorophenyl	1
e	**b**	Methyl	Phenyl	7
k	**c**	Methyl	Pyridin-2-yl	17

ester groups in **1** have been used for product formation. As **7** is formed in a domino reaction that consists of three imine additions with subsequent intramolecular acylation, the yield per step leading to **7c** averages between 70 and 80 %.

Trimethyl aconitate, a cheap renewable raw material that up to now has only been scarcely used as C_6 building unit, has been proved to be a multitalented synthetic building block with its high density of functional groups with donor and acceptor reactivity. It can be used in domino reactions comprising imine additions and intramolecular acylations, which lead in one-pot reactions with **1** to dihydropyrrolones, bisdihydropyrrolones, and spiro[pyrrolinone-3,3′-dihydropyrrolinones]. Furthermore, tricyclic spiro compounds become available using simple reaction conditions.

Experimental Section[19]

3/4: Compound **1** (0.5 g, 2.3 mmol) was dissolved in methanol (5 mL) and after addition of imine (2.3 – 3.5 mmol) the solution was stirred at room temperature for three days. Subsequently the solvent was removed on a rotary evaporator and **3/4** was isolated from the crude product by flash chromatography (petroleum ether/diethyl ether 1/1 (*v*/*v*)).

5a: Compound **1** (2.3 mmol) was dissolved in methanol (5.0 mL) in a 25 mL flask (closed with a fermentation tube filled with paraffin oil). After addition of **2a** (2.3 mmol) and benzylamine (2.3 mmol), the solution was stirred for five days at room temperature. The resulting white precipitate was collected and washed with methanol.

5b, c: Compound **1** (2.3 mmol) and imine (3.5 mmol) were dissolved in methanol (50 mL) in a 250 mL flask (closed with a fermentation tube filled with paraffin oil), stirred for three days at room temperature, and left to stand for 12 weeks. The yellow or white crystals, respectively, were collected and washed with methanol.

6a, **d**: Compound **1** (0.5 g, 2.3 mmol) and imine (4.6 mmol) were dissolved in *m*-xylene (10 mL) and heated for 15 h under reflux. Subsequently the solvent was removed on a rotary evaporator and the residue dissolved in methanol (5 mL). The precipitate, which formed after three days at − 20 °C, was collected and washed with methanol.

6b, c, **e**, **f**: Compound **1** (0.5 g, 2.3 mmol) and imine (4.6 mmol) were stirred without solvent at 70 °C for 48 h and the product was isolated by either flash chromatography or recrystallization from methanol.

7b, c: Compound **1** (0.5 g, 2.3 mmol) and imine (6.9 mmol) were stirred without solvent at 70 °C for 48 h. The resulting dark red or black solid, respectively, was recrystallized from a small volume of methanol.

Received: May 14, 2001
Revised: July 4, 2001 [Z17102]

[1] Applications of trimethyl aconitate reported so far in syntheses: a) J. Mann, S. E. Piper, L. K. P. Yeung, *J. Chem. Soc. Perkin Trans. 1* **1984**, 2081 – 2088; b) L. Birkofer, H. Feldmann, *Justus Liebigs Ann. Chem.*

1964, *677*, 154 – 157; c) J. van Alphen, *Recl. Trav. Chim. Pays-Bas* **1943**, *62*, 334 – 336.
[2] a) Trimethyl aconitate was converted into Michael adducts with C,H-acidic methylene compounds and NaOMe in 70 – 93 % yield (e.g. dimethyl malonate 84 %, methyl acetoacetate 88 %): b) Silke Kratschmer, PhD thesis, Universität Münster, **1998**.
[3] Trimethyl aconitate was converted with dienes to Diels – Alder cycloadducts in 50 – 95 % yield (e.g. cyclopentadiene (toluene, 120 °C) 95 %, cyclohexadiene 50 %, *trans,trans*-1,4-diphenylbutadiene 95 %).[2b]
[4] Reaction of trimethyl aconitate with aromatic and aliphatic aldehydes afforded Knoevenagel condensates in 36 – 93 % yield (e.g. benzaldehyde (toluene, piperidinium acetate, reflux) 56 %, *p*-methoxybenzaldehyde 93 %, cyclohexanecarbaldehyde 60 %).[2b]
[5] S. Kratschmer, H. J. Schäfer, R. Fröhlich, *J. Electroanal. Chem*. **2001**, *507*(1-2), 2 – 10.
[6] a) R. A. Bunce, *Tetrahedron* **1995**, *51*, 13103 – 13159; b) L. F. Tietze, U. Beifuss, *Angew. Chem*. **1993**, *105*, 137 – 170; *Angew. Chem. Int. Ed. Engl*. **1993**, *32*, 131 – 163; c) L. F. Tietze, *Chem. Rev.* **1996**, *96*, 115 – 136; d) L. F. Tietze, F. Haunert in *Stimulating Concepts in Chemistry* (Eds.: M. Shibasaki, J. F. Stoddart, F. Vögtle), Wiley-VCH, Weinheim, **2000**, pp. 39 – 64.
[7] a) B. Bohner, M. Baumann, CH Patent 633678, **1982** [*Chem. Abstr*. **1983**, *98*, 121386]; b) B. Bohner, M. Baumann, DE Patent 2735841, **1978** [*Chem. Abstr*. **1978**, *88*, 152415].
[8] G. D. James, S. Mills, G. J. Pattenden, *J. Chem. Soc. Perkin Trans. 1* **1993**, 2581 – 2584.
[9] a) H. von Dobeneck, E. Brunner, H. Bunke, G. Metzner, R. Schmidt, E. Weil, J. Sonnenbichler, *Liebigs Ann. Chem*. **1981**, 410 – 424; b) J. Barluenga, F. Palacios, S. Fustero, V. Gotor, *Synthesis* **1981**, 200 – 201; c) C. Cavé, A. Gassama, J. Mahuteau, J. d'Angelo, C. Riche, *Tetrahedron Lett.* **1997**, *38*, 4773 – 4776.
[10] H. G. Viehe, R. Merényi, L. Stella, Z. Janousek, *Angew. Chem*. **1979**, *91*, 982 – 997; *Angew. Chem. Int. Ed. Engl*. **1979**, *18*, 917 – 932.
[11] E. M. Kosower, E. J. Poziomek, *J. Am. Chem. Soc.* **1964**, *86*, 5515 – 5516.
[12] G. A. Cordell, J. E. Saxton, *Alkaloids* **1981**, *20*, 10 – 16.
[13] C.-L. Fang, S. Horne, N. Taylor, R. Rodrigo, *J. Am. Chem. Soc*. **1994**, *116*, 9480 – 9486.
[14] When **1** and *N*-benzylidene-*N*-ethylamine were allowed to react at room temperature, the reaction stopped at the imine adduct (R^1: phenyl, R^2: ethyl), which was isolated as one diastereomer in 39 % yield without undergoing the second intramolecular acylation.
[15] To our knowledge no synthesis has been reported to date for the substituted spiro[pyrrolidinone-3,3-dihydropyrrolinone] framework. For an elegant spiro[pyrrolidinone-3,3′-oxindole] synthesis see reference [16a] and references therein. For a spiro[succinimide-3,3′-oxindole] synthesis see reference [16b]. For spiro[pyrrolidinone-3,3′-pyrrolidinone] syntheses starting from dialkyl malonates see reference [16c].
[16] a) P. B. Alper, C. Meyers, A. Lerchner, D. R. Siegel, E. M. Carreira, *Angew. Chem.* **1999**, *111*, 3379 – 3381; *Angew. Chem. Int. Ed. Engl*. **1999**, 3186 – 3189; b) H. Schäfer, *Arch. Pharm. Ber. Dtsch. Pharm. Ges.* **1970**, *303*, 183 – 191; c) C. G. Overberger, D. W. Wang, R. K. Hill, G. R. Krow, D. W. Ladner, *J. Org. Chem.* **1981**, *46*, 2757 – 2764; d) M. A. Casadei, B. D. Rienzo, A. Inesi, F. M. Moracci, *J. Chem. Soc. Perkin Trans. 1* **1992**, 379 – 382.
[17] a) J. Wrobel, A. Dietrich, S. A. Woolson, J. Millen, M. Caleb, *J. Med. Chem*. **1992**, *35*, 4613 – 4627; b) T. Irikura, K. Takagi, S. Fujimori, Y. Hirata, US Patent 4,593,092, **1986** [*Chem. Abstr*. **1986**, *105*, 114900k.
[18] The crystal structures of the main diastereomers of **6a** and **6b** have the (5*S**, 6*R**) configuration at the two stereogenic centers.
[19] Crystal structures of the compounds **3a**, **4e**, **5a** – **c**, **6a**, **6d**, **7a** – **c** have been obtained. Crystallographic data (excluding structure factors) for the structures reported in this paper have been deposited with the Cambridge Crystallographic Data Centre as supplementary publication nos CCDC-163546 (**7c**), CCDC-163547 (**5a**), CCDC-169695 (**3a**), CCDC-169696 (**4e**), CCDC-169697 (**5b**), CCDC-169698 (**5c**), CCDC-169699 (**6a**), CCDC-169700 (**6d**), CCDC-169701 (**7a**), and CCDC-169702 (**7b**). Copies of the data can be obtained free of charge on application to CCDC, 12 Union Road, Cambridge CB2 1EZ, UK (fax: (+44) 1223-336-033; e-mail: deposit@ccdc.cam.ac.uk).

Electrophilic Fluorination Mediated by Cinchona Alkaloids: Highly Enantioselective Synthesis of α-Fluoro-α-phenylglycine Derivatives**

Barbara Mohar, Jérôme Baudoux, Jean-Christophe Plaquevent, and Dominique Cahard*

The discovery of efficient methods for asymmetric fluorination is one of the most fascinating aspects of modern organofluorine chemistry.[1] Indeed, molecules bearing a stereogenic fluorinated carbon atom are of great interest in bio- and medicinal chemistry research. For example, fluorinated amino acids are of special interest for the design of new fluorine-containing peptides with unusual folding patterns, due to H···F bonding, which show interesting biological properties.[2] However, there are to date no reports on the enantioselective synthesis of α-fluoro-α-amino acids.[3]

We recently developed a fundamentally new class of enantioselective electrophilic fluorinating reagents (noted hereafter $[N-F]^+$) derived from cinchona alkaloids.[4] Independently, Shibata and co-workers reported a conceptually similar approach,[5] in which the chiral fluorinating agent was not isolated, but generated in situ. While these studies demonstrated the ability of enantioselective F^+ transfer, further work must be undertaken to reach still higher enantioselectivities. Typical substrates used in both studies were ketones and β-ketoesters for the ease of enolate formation. We report herein the first enantioselective α-fluorination of α-amino acid derivatives. We have carried out extensive studies on the relationship between the structure and enantioselectivity of $[N-F]^+$ cinchona alkaloid derivatives and have discovered that a number displayed very high enantioselectivities. Enantioselection as high as 94 % was attained, exceeding all previous records and indicating that electrophilic fluorination mediated by cinchona alkaloids is a powerful method for the construction of fluorinated chiral centers.

Our successful approach to asymmetric electrophilic fluorination was based upon reacting the preformed ester enolate or nitrile anion with modified *N*-fluoro-cinchona alkaloids. In a first set of experiments, we examined the performance of the first generation of $[N-F]^+$ reagents, namely the four naturally occurring cinchona alkaloids, which have an unprotected hydroxy function. We found that these reagents displayed poor to moderate enantioselective fluorination (7 – 48 % *ee*). We then turned our attention to the structure – enantioselectivity relationship operating in various parts of the *N*-fluoro-

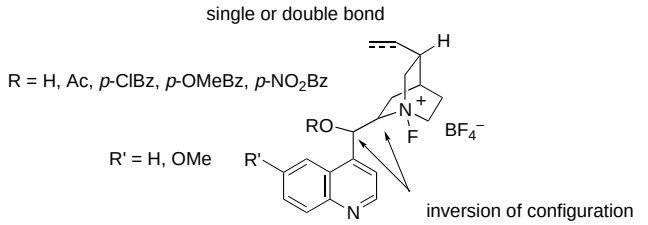
[*] Dr. D. Cahard, B. Mohar, J. Baudoux, J.-C. Plaquevent
Université de Rouen
UMR 6014 de l'IRCOF
76821 Mont Saint Aignan Cedex (France)
Fax: (+33) 2-35-52-29-71
E-mail: dominique.cahard@univ-rouen.fr

[**] This work was supported by Rhodia Organique Fine, France. We thank C. Audouard, Dr. N. Roques, and Dr. J. M. Paris for fruitful discussions.

Supporting information for this article is available on the WWW under http://www.angewandte.com or from the author.

 © WILEY-VCH Verlag GmbH, D-69451 Weinheim, 2001 1433-7851/01/4022-4214 $ 17.50+.50/0

cinchona alkaloids, with a view to improving the enantioselectivity and to pinpointing the factors governing the enantioselection (Scheme 1).

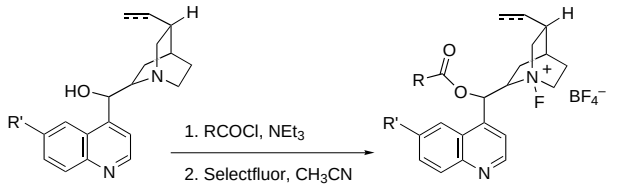


Scheme 1. Structure–enantioselectivity relationship (SER) studies on $[N-F]^+$ cinchona alkaloids.

A new range of $[N-F]^+$ reagents is accessible by capping the hydroxy function of the alkaloid through esterification[6] followed by a transfer-fluorination with Selectfluor (1-(chloromethyl)-4-fluoro-1,4-diazoniabicyclo[2.2.2]octane-bis(tetrafluoroborate); Table 1). Unlike the synthesis of chiral uncharged N–F reagents,[7] we have developed an expeditious synthesis which does not require hazardous fluorine sources.

Various imido-protected (phthaloyl, tetrachlorophthaloyl, succinoyl, dimethylmaleoyl) phenylglycine esters (methyl, ethyl, benzyl), phenylglycinonitrile, and phenylglycine *N*,*N*-diethylamide were prepared and subjected to the α-deprotonation/fluorination sequence. Under the general reaction conditions, amino-protected phenylgycine esters and phenylglycinonitrile yielded the corresponding α-fluorinated compounds in good yields, whereas *N*,*N*-diethyl-*N*-phthaloyl-2-phenylglycinoamide did not react with the $[N-F]^+$ reagents. While the ester function on the substrate exerts no significant effect on the asymmetric induction, the phthaloyl amino protecting group induces a higher degree of enantioselection than the succinoyl and dimethylmaleoyl groups. For subsequent studies, we restricted our work to *N*-phthaloyl-α-aminophenylglycine ethyl ester and phenylglycinonitrile (Table 2).

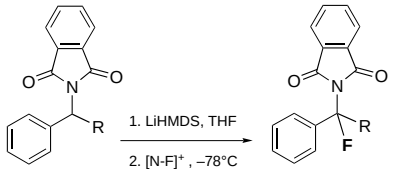
Table 1. Synthesis of $[N-F]^+$ reagents: R′ = H, OMe; R = Me, *p*-ClC_6H_4, *p*-$OMeC_6H_4$, *p*-$NO_2C_6H_4$.



$[N-F]^+$ reagent[a,b]	Yields [%]		$\delta(^{19}F)$[c]	
	esterification	transfer-fluorination	N–F	BF_4
F-AcCD-BF_4	90	95	43.8	−150.4
F-AcCN-BF_4	98	75	37.3	−150.4
F-AcQD-BF_4	96	98	35.7	−149.8
F-AcQN-BF_4	99	96	44.7	−149.8
F-AcDHQD-BF_4	83	83	40.1	−149.6
F-*p*ClBzCD-BF_4	92	90	44.0	−149.7
F-*p*ClBzCN-BF_4	99	87	38.4	−149.7
F-*p*ClBzQD-BF_4	93	89	39.1	−149.7
F-*p*ClBzQN-BF_4	99	97	44.6	−149.7
F-*p*ClBzDHQD-BF_4	80	82	39.5	−149.7
F-*p*ClBzDHQN-BF_4	–[d]	85	45.1	−149.7
F-*p*MeOBzQN-BF_4	95	98	44.4	−149.6
F-*p*NO_2BzQN-BF_4	81	91	44.5	−149.6

[a] The descriptors chosen for $[N-F]^+$ reagent are similar to F-TEDA-BF_4 for Selectfluor. For example, F-*p*ClBzDHQD-BF_4 stands for *O*(9)-*p*-chlorobenzoyl-*N*-fluorodihydroquinidinium tetrafluoroborate. [b] CD = cinchonidine, CN = cinchonine, QD = quinidine, QN = quinine, DHQD = dihydroquinidine, DHQN = dihydroquinine. [c] Measured in $[D_6]$acetone, standard $CFCl_3$. [d] Commercially available.

Table 2. Selected results of the enantioselective electrophilic fluorination of *N*-phthaloylphenylglycine derivatives using various $[N-F]^+$ cinchona alkaloids.



94% *ee*

$[N-F]^+$	R = CO_2Et		R = CN	
	ee [%][a]	Yield [%][b]	*ee* [%][a]	Yield [%][b]
F-CD-BF_4	8	65	36	48
F-AcCD-BF_4	42	87	52	91
F-AcQN-BF_4	76	79	80	88
F-*p*ClBzQN-BF_4	68	73	91	70
F-*p*ClBzDHQN-BF_4	76	86	92	65
F-*p*MeOBzQN-BF_4	66	64	94	56
F-*p*NO_2BzQN-BF_4	60	60	90	58
F-CN-BF_4	26	62	48	68
F-*p*ClBzCN-BF_4	28	67	66	70
F-AcDHQD-BF_4	50	60	75	72
F-*p*ClBzDHQD-BF_4	38	65	82	64

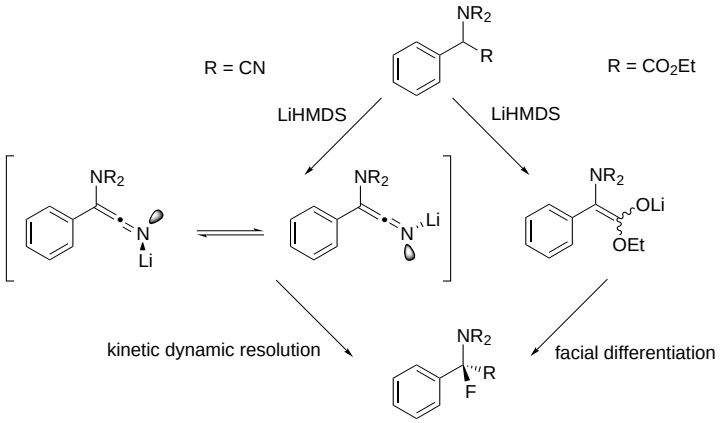
[a] Determined by HPLC analysis using a column Chiralcel OD. [b] Isolated, chromatographically pure material.

Under the usual fluorination conditions, the enantiomeric excesses of *N*-phthaloylphenylglycinonitrile determined by HPLC were consistently higher than those of *N*-phthaloylphenylglycine ethyl ester. Systematically, $[CD-F]^+$ and $[QN-F]^+$ fluorinating agents (for abbreviations see legend to Table 2) gave better enantioselectivities than their corresponding pseudoenantiomers, $[CN-F]^+$ and $[QD-F]^+$, respectively, yielding opposite configurations of the fluorinated compound as confirmed by HPLC analysis. In addition, the enantioselectivity was higher when $[QN-F]^+$ was used rather than $[CD-F]^+$ and when $[QD-F]^+$ was used rather than $[CN-F]^+$, suggesting the participation of the methoxy substituent on the quinoline moiety in the stereoselection.

We have shown that protection of the hydroxy group in the $[N-F]^+$ reagent was crucial to achieve high enantioselectivity. Furthermore, in the ester series, enantioselectivity was higher with acetyl protection than with benzoyl protection. By contrast, in the case of the nitrile derivative, the enantioselectivity was higher with benzoyl protection than with acetyl protection. There was no significant improvement in enantioselectivity by changing the nature of the *para* substituents of the benzoyl protecting group. The best result was obtained with the *O*-(*p*-methoxybenzoyl)-*N*-fluoroquininium tetra-

fluoroborate: an enantiomeric excess of 94% was achieved in the fluorination of *N*-phthaloylphenylglycinonitrile.

The significantly higher enantiomeric excesses observed for the nitrile derivative compared to the ethyl ester derivative could be explained by the different nature of corresponding metalated intermediates. Deprotonation of the ester typically leads to a prochiral sp^2 enolate (mixture of *Z* and *E* isomers), and the asymmetric step consists of a facial enantiodifferentiation. On the other hand, nitrile anions presumably exist as metalated ketenimines bearing axial chirality which undergo racemization rapidly even at low temperature.[8] In this case, enantioselective fluorination results from a kinetic dynamic resolution of the two enantiomers (Scheme 2). We are currently studying this hypothesis, in order to develop models to further rationalize our observations.



Scheme 2. Postulated intermediates in enantioselective fluorination.

In conclusion, we have developed the first enantioselective electrophilic α-fluorination of α-amino acid derivatives using modified *N*-fluoro-cinchona alkaloid reagents. A study of the relationship between structure and enantioselectivity led to a new range of $[N-F]^+$ reagents that display enantiomeric excesses as high as 94% in the synthesis of α-fluoro-*N*-phthaloylphenylglycinonitrile with *O*-(*p*-methoxybenzoyl)-*N*-fluoroquininium tetrafluoroborate.

Experimental Section

Synthetic procedures and spectroscopic data for the $[N-F]^+$ reagents can be found in the Supporting Information.

General procedure for the enantioselective fluorination: LiHMDS (1.06 M in THF, 1.5 equiv; HMDS = hexamethyldilazanide) was added dropwise to a solution of *N*-phthaloylphenylglycine ethyl ester (0.1 mmol, 30.9 mg) at $-78\,^{\circ}C$. After 15 min, *O*-(*p*-chlorobenzoyl)-*N*-fluorodihydroquininium tetrafluoroborate (0.11 mmol, 62.8 mg, 1.1 equiv) was added under nitrogen in one portion. The mixture was stirred at $-78\,^{\circ}C$ for 3 h and then hydrolyzed with H_2O. The mixture was partitioned between CH_2Cl_2 and H_2O, the organic layer dried over $MgSO_4$, and concentrated. For further analyses the crude product was purified by chromatography on preparative silica gel plates with hexane/EtOAc, which yielded α-fluoro-*N*-phthaloylphenylglycine ethyl ester in 86% yield. ^1H NMR (300 MHz): $\delta = 1.31$ (t, $J = 7.1$ Hz, 3H), 4.34 (m, 2H), 7.10–7.90 (m, 9H); ^{13}C NMR (75 MHz): $\delta =$ 13.78, 63.20, 94.33 (d, $J = 220$ Hz), 124.05, 125.65 (d, $J = 8$ Hz), 128.26, 129.51, 131.33, 133.00 (d, $J = 25$ Hz), 134.96, 165.39 (d, $J = 32$ Hz), 166.02 (d, $J = 2$ Hz); ^{19}F NMR (282 MHz): $\delta = -128.8$; HR-MS (EI, 70 eV) for $C_{18}H_{14}FNO_4$ [M^+]: calcd 327.0907, found 327.0908; HPLC: Chiralcel OD, hexane/*i*PrOH (97/3), 1 mL min^{-1}, $t_1 = 23.2$ min, $t_2 = 36.0$ min (76% *ee*); $[\alpha]_D^{20} = +19.0$, $[\alpha]_{578}^{20} = +20.3$ ($c = 4.0$, $CHCl_3$).

Received: June 18, 2001 [Z17311]

[1] K. Muñiz, *Angew. Chem.* **2001**, *113*, 1701–1704; *Angew. Chem. Int. Ed.* **2001**, *40*, 1653–1656.

[2] a) V. P. Kukhar in *Fluorine-Containing Amino Acids, Synthesis and Properties* (Ed.: V. A. Soloshonok), Wiley, Chichester, **1995**; b) K. Uneyama in *Enantiocontrolled Synthesis of Fluoro-Organic Compounds* (Ed.: V. A. Soloshonok), Wiley, Chichester, **1999**.

[3] In previous studies, we explored α-fluorination of *N*-phthaloylphenylglycine ethyl ester under a solid–liquid phase-transfer catalysis with the aid of an achiral fluorinating reagent (*N*-fluorobenzenesulfonimide) and a chiral quaternary ammonium salt (Corey's *O*-allyl-*N*-(9-anthracenylmethyl)ammonium bromide catalysts derived from cinchona alkaloids). The best enantiomeric excess noted was 7% with 60% yield. More details can be found under http://www.mdpi.org/ecsoc-4.htm. α-Fluorinated-α-amino acids derivatives can also be constructed from fluorinated building blocks and resolved through diastereomeric amides (E. Hayashi, H. Fukaya, T. Abe, *J. Fluorine Chem.* **1991**, *52*, 133–147) or esters (Y. Takeuchi, M. Asahina, K. Nagata, T. Koizumi, *J. Chem. Soc. Perkin Trans. 1* **1987**, 2203–2207; Y. Takeuchi, M. Kamezaki, K. Kirihara, G. Haufe, K. W. Laue, N. Shibata, *Chem. Pharm. Bull.* **1998**, *46*, 1062–1064).

[4] a) D. Cahard, C. Audouard, J. C. Plaquevent, N. Roques, *Org. Lett.* **2000**, *23*, 3699–3701; b) D. Cahard, C. Audouard, J. C. Plaquevent, L. Toupet, N. Roques, *Tetrahedron Lett.* **2001**, *42*, 1867–1869.

[5] a) N. Shibata, E. Suzuki, Y. Takeuchi, *J. Am. Chem. Soc.* **2000**, *122*, 10728–10729; b) N. Shibata, E. Suzuki, T. Asahi, M. Shiro, *J. Am. Chem. Soc.* **2001**, *123*, 7001–7009.

[6] H. C. Kolb, P. G. Andersson, K. B. Sharpless, *J. Am. Chem. Soc.* **1994**, *116*, 1278–1291.

[7] a) E. Differding, R. W. Lang, *Tetrahedron Lett.* **1988**, *29*, 6087–6090; b) F. A. Davis, P. Zhou, C. K. Murphy, *Tetrahedron Lett.* **1993**, *34*, 3971–3974; c) F. A. Davis, P. Zhou, C. K. Murphy, G. Sundarababu, H. Qi, R. M. Przeslawski, B. C. Chen, P. J. Carroll, *J. Org. Chem.* **1998**, *63*, 2273–2280; d) Y. Takeuchi, T. Suzuki, A. Satoh, T. Shiragami, N. Shibata, *J. Org. Chem.* **1999**, *64*, 5708–5711; e) Y. Takeuchi, A. Satoh, T. Suzuki, A. Kameda, M. Dohrin, T. Satoh, T. Koizumi, K. L. Kirk, *Chem. Pharm. Bull.* **1997**, *45*, 1085–1088.

[8] a) G. Boche, *Angew. Chem.* **1989**, *101*, 286–306; *Angew. Chem. Int. Ed. Engl.* **1989**, *28*, 277–297; b) D. S. Watt, *J. Org. Chem.* **1974**, *39*, 2799–2800.

 © WILEY-VCH Verlag GmbH, D-69451 Weinheim, 2001 1433-7851/01/4022-4216 $ 17.50+.50/0

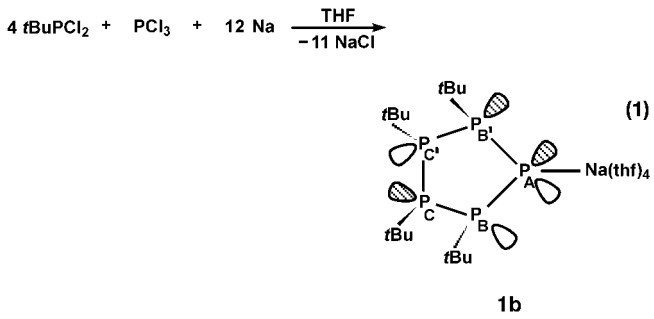
Sodium Tetra-*tert*-butylcyclopentaphosphanide: Synthesis, Structure, and Unexpected Formation of a Nickel(0) Tri-*tert*-butylcyclopentaphosphene Complex**

Andrea Schisler, Peter Lönnecke, Uwe Huniar, Reinhart Ahlrichs und Evamarie Hey-Hawkins*

Dedicated to Professor Hans-Georg von Schnering on the occasion of his 70th birthday

While the first cyclooligophosphanes $(PR)_n$,[1] isolobal to cycloalkanes, were synthesized as early as 1877,[2] the first cyclooligophosphanide ions *cyclo*-$(P_nR_{n-1})^-$ were only described 100 years later,[3, 4] and today the number of such compounds that can be prepared in a targeted manner is still small.[5] The alkali metal compounds K[*cyclo*-(P_3tBu_2)],[3] K[*cyclo*-(P_5Ph_4)],[5] and Li[*cyclo*-(P_ntBu_{n-1})] $(n = 3-5)$[6, 7] could not be isolated as pure compounds and were only characterized by ^{31}P NMR spectroscopy of an inseparable mixture; to date nothing is known about their coordination chemistry. A few complexes with linear oligophosphanide ligands $P_nR_n^{2-}$ are known: metallocene triphosphane-1,3-diyl complexes $[Cp_2M(P_3R_3)]$ (M = Ti, Zr, Hf; R = Me, Et, Ph, *t*Bu),[8] a nickel tetraphosphane-1,4-diyl complex $[Ni(\eta^2\text{-}P_2tBu_2)(P_4tBu_4)]$,[9] and the stannatetraphospholanes $(tBuP)_4SnR_2$ (R = *t*Bu, *n*Bu, Ph) and $(tBuP)_4Sn(Cl)nBu$.[10]

We have shown that the reaction of sodium with $tBuPCl_2$ and PCl_3 in the ratio 12:4:1 in THF gave a product mixture comprising Na[*cyclo*-(P_3tBu_2)],[3, 7] Na[*cyclo*-(P_4tBu_3)],[7] *cyclo*-(P_4tBu_4),[11] $Na_2(P_4tBu_4)$,[3] and sodium tetra-*tert*-butylcyclopentaphosphanide Na[*cyclo*-(P_5tBu_4)] (**1a**). By a systematic variation of the reaction conditions we have now been able to optimize the synthesis of **1a**. Just by warming the reaction mixture to 80 °C for 8 h *cyclo*-(P_4tBu_4) ($\delta(^{31}P) = -58.4$) is formed as the main product; over five days this converts into **1a** and a small amount of the other sodium salts [Eq. (1)]. As *cyclo*-(P_4tBu_4) does not react with Na even on heating for several days in THF, **1a** is probably generated by the direct attack of Na_3P, formed from sodium and PCl_3.[12] As only **1a** and *cyclo*-(P_4tBu_4) are soluble in *n*-pentane, they can be readily separated from the by-products. The separation of *cyclo*-(P_4tBu_4) from **1a** is possible by sublimation; only pure **1a** remains (yield 56%). Recrystallization from THF gives $[Na(thf)_4][cyclo\text{-}(P_5tBu_4)]$ (**1b**). This compound is stable under an inert atmosphere at room temperature and is soluble in ethers and aliphatic and aromatic hydrocarbons.



The $^{31}P\{^1H\}$ NMR spectrum of **1b** shows resonance signals corresponding to an ABB′CC′ spin system.[13] Only one conformational isomer is present. Of the four conformations that correspond to the spectral symmetry[3] and based on the steric requirements of the *tert*-butyl groups the all-*trans* isomer is preferred and this is supported by the coupling constants.[5, 14]

In agreement with the ^{31}P NMR spectrum, the X-ray crystal structure shows an all-*trans* configuration of the *tert*-butyl groups on the phosphorus atoms with an „envelope" conformation[15] of the chiral P_5 ring system (Figure 1).[16] The P1–P5 bond (213.20(11) pm) is noticeably shorter than the other P–P bonds (220.35(12) – 222.92(11) pm). The Na atom has an unusual five-coordinate geometry with four thf molecules and the P_5tBu_4 ring as ligands.[17] The Na–P1 bond of 293.82(15) pm is in the range typical for those reported for sodium phosphanides (277.8(2) – 335.7(2) pm)[18] and the triphosphide $[Na(thf)_4][1,3\text{-}(SitBu_3)_2P_3]$.[19]

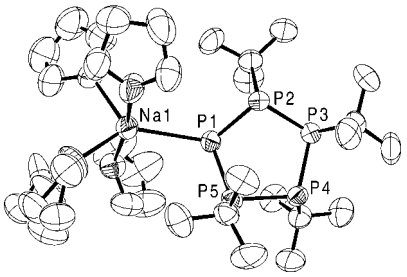
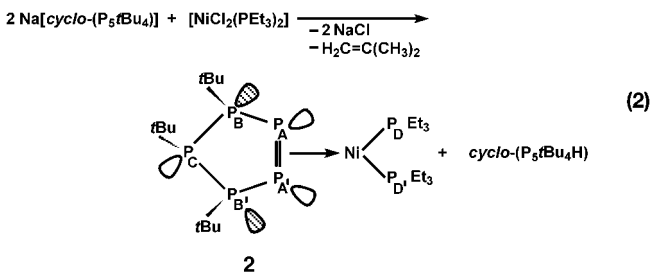


Figure 1. Molecular structure of **1b** (H atoms not shown). Selected bond lengths [pm] and angles [°]: Na-P1 293.82(15), P1-P5 213.20(11), P1-P2 220.35(12), P2-P3 222.92(11), P3-P4 220.81(11), P4-P5 221.11(12), Na-O 235.4(3), 236.6(3), 236.8(3), and 241.2(3); P5-P1-P2 103.74(4), P1-P2-P3 99.97(4), P4-P3-P2 102.56(4), P3-P4-P5 106.34(4), P1-P5-P4 104.99(4) (angle sum 517.6°).

Compound **1a** reacts readily with bis(triethylphosphane)-nickel(II) chloride in polar or nonpolar solvents to give (η^2-3,4,5-tri-*tert*-butylcyclopentaphosphene)bis(triethylphosphane)-nickel(0) (**2**) [Eq. (2)]; *cyclo*-(P_5tBu_4H) is formed as a by-product.[20] Noteworthy in the formation of **2** is the cleavage of



[*] Prof. Dr. E. Hey-Hawkins, Dipl.-Chem. A. Schisler, Dr. P. Lönnecke
Institut für Anorganische Chemie der Universität Leipzig
Johannisallee 29, 04103 Leipzig (Germany)
Fax: (+49) 341-9739319
E-mail: hey@rz.uni-leipzig.de
Dipl.-Phys. U. Huniar, Prof. Dr. R. Ahlrichs
Institut für Theoretische Chemie der Universität Karlsruhe
Kaiserstrasse 12, 76128 Karlsruhe (Germany)

[**] A.S. thanks the Graduiertenförderung des Landes Sachsen for a Ph.D grant.

 © WILEY-VCH Verlag GmbH, D-69451 Weinheim, 2001 1433-7851/01/4022-4217 $ 17.50+.50/0

a *t*Bu group from the anionic *cyclo*-(P_5tBu_4) ring as *t*BuCl with the formation of the previously unknown cyclopentaphosphene ring; however, a few isolobal cyclopentene[21] and 1,2,3-triphospholene complexes[22] are known. Clearly *t*BuCl reacts immediately with **1b** to form *cyclo*-(P_5tBu_4H) and isobutene, as was confirmed by an independent reaction.[23]

In the mass spectrum of [Ni{*cyclo*-(P_5tBu_3)}(PEt_3)$_2$] (**2**), as well as the peak for the molecular ion there is also a peak corresponding to *cyclo*-(P_5tBu_3). Detailed information concerning the structure of **2** is obtained from the $^{31}P\{^1H\}$ NMR spectrum, which shows the typical pattern for an AA′BB′CDD′ spin system.[13] The chemical shifts determined for the five phosphorus atoms (P_A, $P_{A'}$, P_B, $P_{B'}$, P_C) are in the range typical for *tert*-butyl-substituted cyclopentaphosphanes.[24] In this case, as for **1b**, the positions of the lone pairs can be derived from the ^1J and ^2J coupling constants.[5, 14] Thus, as for **1b**, the substituents on the P_5 ring are in an all-*trans* arrangement because of steric constraints. The (negative) coupling constant $^1J_{A,A'}$, which is large in comparison to the other ^1J ring coupling constants, arises from the presence of the multiple bond between the two phosphorus atoms. In good agreement with the NMR data, the X-ray structure of **2** (Figure 2)[16] shows an all-*trans* arrangement of the *t*Bu groups

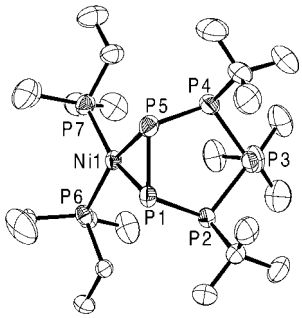


Figure 2. Molecular structure of **2** (H atoms not shown). Selected bond lengths [pm] and angles [°]: Ni1-P7 219.04(9), Ni1-P6 219.69(8), Ni1-P1 223.22(8), Ni1-P5 223.91(8), P1-P5 211.83(11), P1-P2 219.92(10), P2-P3 221.08(11), P3-P4 220.20(11), P4-P5 220.10(12); P6-Ni-P7 108.22(3), P1-Ni1-P5 56.55(3), P1-P5-Ni1 61.56(3), P5-P1-Ni1 61.89(3).

and an envelope conformation[25] of the P_5 ring. The nickel atom is in a distorted square-planar coordination environment, in which the atoms P7, P6, P1, P5 are coplanar and the nickel atom lies 17.73(5) pm out of this plane. At 211.83(11) pm the P1–P5 bond of the P_5 ring clearly has multiple-bond character.[9, 26] The remaining P–P bonds are in the range expected for single bonds.[27] The nickel diphosphene complexes [Ni{η^2-$P_2(SiMe_3)_2$}(PEt_3)$_2$],[28] [Ni(η^2-P_2Ph_2)L] (L = 2,3-bis(diphenylphosphanyl)-*N*-methylmaleinimide),[29] and [Ni(η^2-P_2tBu_2)(P_4tBu_4)][9] have Ni–P bonds (223.6(6) – 225.8(2) pm)[9, 28, 29] that are similar, and P–P bonds that are longer (ca. 214 pm),[28, 29] or of similar length (211.0(5) pm)[9] to those of **2**.

Experimental Section

All procedures were performed under an inert atmosphere of pure argon with the vigorous exclusion of air and moisture. The solvents were saturated with argon and stored over potassium mirrors. $tBuPCl_2$[30] and [$NiCl_2(PEt_3)_2$][31] were prepared by literature methods.

1a, **1b**: PCl_3 (8.29 g, 0.06 mol; 5.3 mL) and Na (17.3 g, 0.75 mol) were carefully added to $tBuPCl_2$ (38.4 g, 0.24 mol) in THF (300 mL). The mixture was heated under reflux for 5 days. After 6 h the initially colorless solution was yellow green, after 5 days, dark brown. The THF was then removed under reduced pressure and the dark brown residue extracted with *n*-pentane (450 mL). The solvent was removed under reduced pressure and the *cyclo*-(P_4tBu_4) separated from **1a** by sublimation (120 °C/10^{-3} Torr). Crystallization from THF at −27 °C gave yellow cubic crystals of [$Na(thf)_4$][*cyclo*-(P_5tBu_4)] (**1b**; m.p. 126.2 – 129.3 °C). On cellulose in air the compound spontaneously ignited. Yield 16.3 g (56 %); ^1H NMR (400 MHz, C_6D_6, 25 °C): $\delta = 1.51$ (d, $^3J(P,H) = 3.0$ Hz, 18 H; *t*Bu), 1.58 (m, $^3J(P,H) = 3.0$ Hz, 18 H; *t*Bu), 1.40 (m, thf), 3.60 (m, thf); $^{13}C\{^1H,^{31}P\}$ NMR (100.6 MHz, C_6D_6, 25 °C): $\delta = 26.26$ (s, thf), 30.71 (s, $C(CH_3)_3$), 31.77 (s, $C(CH_3)_3$), 32.83 (s, $C(CH_3)_3$), 33.32 (s, $C(CH_3)_3$), 68.15 (s, thf); ^{13}C NMR (100.6 MHz, C_6D_6, 25 °C): $\delta = 26.26$ (m, thf), 30.71 (m, $C(CH_3)_3$), 31.77 (q/m, $^1J(C,H) = 123.6$ Hz; $C(CH_3)_3$), 32.83 (m, $C(CH_3)_3$), 33.32 (q/m, $^1J(C,H) = 126.1$ Hz; $C(CH_3)_3$), 68.15 (m, thf); ^{31}P NMR (162 MHz, C_6D_6, 25 °C): $\delta_A = -105.6$, $\delta_B = \delta_{B'} = 82.7$, $\delta_C = \delta_{C'} = 75.0$; $^1J_{A,B} = {}^1J_{A,B'} = -379.2$, $^1J_{B,C} = {}^1J_{B',C'} = -317.3$, $^1J_{C,C'} = -309.4$, $^2J_{A,C} = {}^2J_{A,C'} = -0.1$, $^2J_{B,C'} = {}^2J_{B',C} = -5.4$, $^2J_{B,B'} = -17.2$ Hz.

2: A solution of **1a** (2.24 g, 5.51 mmol) in THF (20 mL) was added dropwise to a vigorously stirred solution of [$NiCl_2(PEt_3)_2$] (1.02 g, 2.79 mmol) in THF (20 mL) at −55 °C. The red solution immediately turned dark brown. After the addition was complete the mixture was stirred for a further 2 h at −55 °C then slowly warmed to room temperature. The solvent was removed under reduced pressure and the brown oily residue treated with *n*-pentane (10 mL) and the solution filtered by cannula. At −27 °C yellow rods of [Ni{*cyclo*-(P_5tBu_3)}(PEt_3)$_2$] (**2**; m.p. 173.2 – 175.9 °C) crystallized, yield 0.92 g (53 %); **2** is soluble in toluene and sparingly soluble in *n*-pentane and *n*-hexane. ^1H NMR (400 MHz, C_6D_6, 25 °C): $\delta = 0.95$ (dt, $^3J(H,H) = 7.6$, $^3J(P,H) = 14.0$ Hz, 18 H; CH_3), 1.46 (d, $^3J(P,H) = 12.0$ Hz, 9 H; *t*Bu), 1.66 (br, 30 H; 2 *t*Bu, CH_2); ^{13}C NMR (100.6 MHz, C_6D_6, 25 °C): $\delta = 9.32$ (t/d/m, $^1J(C,H) = 127.0$, $^2J(C,H) = 4.1$ Hz; CH_3), 19.45 (t/d/m, $^1J(C,H) = 126.8$, $^2J(C,H) = 2.1$, $^1J(C,P) = 21.7$ Hz; CH_2), 32.13 (q/m, $^1J(C,H) = 124.8$ Hz; CH_3 of *t*Bu), 32.97 (q/m, $^1J(C,H) = 123.1$ Hz; CH_3 of *t*Bu), 33.16 (m; $C(CH_3)_3$ of *t*Bu; only one signal observed); ^{31}P NMR (162 MHz, C_6D_6, 25 °C): $\delta_A = \delta_{A'} = 56.6$, $\delta_B = \delta_{B'} = 128.0$, $\delta_C = 98.0$, $\delta_D = \delta_{D'} = 13.5$; $^1J_{A,A'} = -434.6$, $^1J_{A,B} = {}^1J_{A',B'} = -376.6$, $^1J_{B,C} = {}^1J_{B',C} = -332.4$, $^2J_{A,B'} = {}^2J_{A',B} = 18.6$, $^2J_{B,B'} = -26.7$, $^2J_{C,A} = {}^2J_{C,A'} = -11.9$, $^2J_{A,D} = 17.6$, $^2J_{A',D'} = 31.6$, $^2J_{D,D'} = 4.9$, $^3J_{B,D} = 6.3$, $^3J_{B',D'} = -9.9$, $^4J_{C,D} = 0.02$ Hz; MS (EI, 70 eV): *m*/*z* (%): 620.3 (3.4) [M^+], 590.2 (3.4) [$M^+ - P$], 533.0 (5.1) [$M^+ - P$*t*Bu], 502.0 (10.2) [$M^+ - P_2$*t*Bu], 445.0 (15.3) [$M^+ - 2P$*t*Bu], 356.9 (5.1) [$M^+ - 3P$*t*Bu], 327.0 (4.2) [$M^+ - Ni - 2PEt_3 = P_5tBu_3^+$], 294.1 (8.5) [$M^+ - Ni - 2PEt_3 - P = P_4tBu_3^+$], 264 (7.6) [$M^+ - Ni - 2PEt_3 - 2P = P_3tBu_3^+$], 118.1 (44) [$PEt_3^+$] and its decomposition products; molecular ion: found: 620.3/621.3/622.0/623.0; calcd: 620.2/621.2/622.2/623.2; UV/Vis (*n*-pentane): $\lambda_{max}(\varepsilon) = 237$ (5809), 273 sh (2440), 338 (1074), 355 nm (1045).

Density functional calculations: the electronic structures of **1b** and **2** were investigated with the program package Turbomole[33] employing the Becke – Perdew functional B-P86.[32] The calculations for **1b** confirm the structural parameters given in Figure 1 with a P1–P5 bond that is 7 pm shorter than the other P–P bonds. The calculated structure of the free ion [P_5tBu_4]$^-$ gives the same results. As **2** shows almost C_s symmetry (see Figure 2), this was also assumed in the calculation.[34] Starting from the all-*trans*-envelope form of P_5tBu_3, which is energetically most favorable for the free molecule, the structure of **2** was optimized for different conformations of the PEt_3 groups. In the energetically most favorable structure the PEt_3 group has only C_1 symmetry as in Figure 2. The bond lengths of the different conformers differ by only 1 pm; they are up to 5 pm longer than those given in Figure 2 (Ni–P6, Ni–P7 219, Ni–P1, Ni–P5 227, P1–P2 215, remaining P–P bonds 225 pm), the angles given are retained to within 1°.

The electronic structure of **2** clearly shows a singlet wavefunction with formal d^{10} configuration for the Ni center: the Mulliken population analysis[35] gives the occupation Ni $3d^{8.7}4s^{0.8}4p^{0.8}$, which is identical to that of [$Ni(PEt_3)_3$] with a trigonal-planar NiP_3 geometry. The Ni atom functions as an acceptor for the lone pairs of the two PEt_3 ligands and the bonding π molecular orbital (MO) of the P=P bond in P_5tBu_3; it lies in an

 © WILEY-VCH Verlag GmbH, D-69451 Weinheim, 2001 1433-7851/01/4022-4218 $ 17.50+.50/0 *Angew. Chem. Int. Ed.* **2001**, *40*, No. 22

approximately trigonal-planar environment. This interpretation is in agreement with the P=P bond length and the angle of 97° between the planes Ni-P1-P5 and P1-P2-P4-P5.

The UV/Vis spectrum was calculated with time-dependent density functional theory (TDDFT).[36] In spite of the approximate character of this method the calculated spectrum is in good agreement with the measurements. The assignment of the individual peaks is difficult as the molecular orbitals are relatively highly delocalized. The bands all contain an electron transfer from the Ni to P centers.

Received July 16 2001 [Z17521]

[1] M. Baudler, K. Glinka, *Chem. Rev.* **1993**, *93*, 1623 – 1667.
[2] H. Köhler, A. Michaelis, *Ber. Dtsch. Chem. Ges.* **1877**, *10*, 807 – 814.
[3] M. Baudler, C. Gruner, G. Fürstenberg, B. Kloth, F. Saykowski, U. Özer, *Z. Anorg. Allg. Chem*. **1978**, *446*, 169 – 176.
[4] M. Baudler, B. Makowka, *Z. Anorg. Allg. Chem*. **1985**, *528*, 7 – 21.
[5] A. Schmidpeter, G. Burget, *Phosphorus Sulfur* **1985**, *22*, 323 – 336.
[6] G. Fritz, K. Stoll, *Z. Anorg. Allg. Chem*. **1986**, *538*, 78 – 112.
[7] G. Fritz, R. Biastoch, K. Stoll, T. Vaahs, D. Hanke, H. W. Schneider, *Phosphorus Sulfur* **1987**, *30*, 385 – 388.
[8] a) H. Köpf, R. Voigtländer, *Chem. Ber.* **1981**, *114*, 2731 – 2743; b) E. Hey, S. G. Bott, J. L. Atwood, *Chem. Ber.* **1988**, *121*, 561 – 563; c) E. Hey, *Z. Naturforsch. B* **1988**, *43*, 1271 – 1273.
[9] R. A. Jones, M. H. Seeberger, B. R. Whittlesey, *J. Am. Chem. Soc.* **1985**, *107*, 6424 – 6426.
[10] D. Bongert, H.-D. Hausen, W. Schwarz, G. Heckmann, H. Binder, *Z. Anorg. Allg. Chem.* **1996**, *622*, 1167 – 1172.
[11] K. Issleib, M. Hoffmann, *Chem. Ber*. **1966**, *99*, 1320 – 1325.
[12] After briefly heating the mixture the signal for PCl_3 at $\delta = 219.8$ vanishes from the ^{31}P NMR spectrum; S. Berger, S. Braun, H.-O. Kalinowski, *NMR-Spektroskopie von Nichtmetallen*, 1. ed., Thieme, Stuttgart, **1993**, p. 70.
[13] The signs for the coupling constants $^1J_{P,P}$ were set as negative, and the remaining signs and all the other coupling constants were obtained with the program SPINWORKS (K. Marat, SPINWORKS, Version 05.10.2000, University of Manitoba, **2000**).
[14] M. Baudler, D. Koch, *Z. Anorg. Allg. Chem*. **1976**, *425*, 227 – 235; M. Baudler, W. Driehsen, S. Klautke, *Z. Anorg. Allg. Chem*. **1979**, *459*, 48 – 58.
[15] The atom P1 lies − 89.2(1) pm out of the P2-P3-P4-P5 plane; the dihedral angle between the planes P2-P1-P5 and P2-P3-P4-P5 is 41.83(4)°.
[16] Crystal structure data for **1b**: $C_{32}H_{68}NaO_4P_5$, $M_r = 694.70$, orthorhombic, space group *Pbca*, $a = 1790.1(2)$, $b = 2107.3(3)$, $c = 2227.9(3)$ pm; $V = 8.4044(19)$ nm^3, $Z = 8$, $\rho_{calcd} = 1.098$ Mg m^{-3}, $Mo_{K\alpha} = 71.073$ pm, $\mu = 0.258$ mm^{-1}, $2\theta_{max} = 52.8°$, $R = 0.0498$, $Rw = 0.1656$, 47959 measured, 8610 unique reflections, 419 refined parameters, max. residual electron density 0.34 e Å^{-3}. The atoms C25, C26, C27, C28, and O3 (a THF molecule) are disordered. Crystal structure data for **2**: $C_{24}H_{57}NiP_7$, $M_r = 621.20$, monoclinic, space group *C*2/*c*, $a = 4115.8(5)$, $b = 912.65(11)$, $c = 2082.8(3)$ pm, $\beta = 117.831(2)°$; $V = 6.9187(15)$ nm^3, $Z = 8$, $\rho_{calcd} = 1.193$ Mg m^{-3}, $Mo_{K\alpha} = 71.073$ pm, $\mu = 0.896$ mm^{-1}, $2\theta_{max} = 57.8°$, $R = 0.0389$, $Rw = 0.1063$, 21921 measured, 8290 unique reflections, 459 refined parameters, max. residual electron density 0.40 e Å^{-3}. The atoms C19 – C24 (ethyl group on P6) are disordered. The data were collected with a Siemens SMART-CCD diffractometer ($T = 223$ K). The absorption correction was carried out with the program SADABS (G. M. Sheldrick, SADABS, Program for Scaling and Correction of Area-detector Data). Non-hydrogen atoms were localized by direct methods (SHELXS97: G. M. Sheldrick, SHELXS-97, Program for Crystal Structure Solution, Universität Göttingen, **1997**) and the parameters anisotropically refined with Fourier-Syntheses (SHELXL97: G. M. Sheldrick, SHELXL-97, Program for the Refinement of Crystal Structures, Universität Göttingen, **1997**). The hydrogen atoms were calculated for **1b**; for **2** some of the hydrogen atoms could be located and isotropically refined. Crystallographic data (excluding structure factors) for the structures reported in this paper have been deposited with the Cambridge Crystallographic Data Centre as supplementary publication no. CCDC-166890 and -166891. Copies of the data can be obtained free of charge on application to CCDC, 12 Union Road, Cambridge CB2 1EZ, UK (fax: (+44) 1223-336-033; e-mail: deposit@ccdc.cam.ac.uk).
[17] Only one other structurally characterized compound of the type $[Na(thf)_4X]$ has been reported; X = μ_2-oxo-(5,11,17,23-tetra-*tert*-butyl-25,26,27,28-tetraoxycalix(4)arene)niobium(v): A. Caselli, E. Solari, R. Scopelliti, C. Floriani, *J. Am. Chem. Soc*. **1999**, *121*, 8296 – 8305.
[18] Reviews: a) K. Izod, *Adv. Inorg. Chem.* **2000**, *50*, 33 – 107; b) J. D. Smith, *Angew. Chem.* **1998**, *110*, 2181 – 2183; *Angew. Chem. Int. Ed.* **1998**, *37*, 2071 – 2073.
[19] N. Wiberg, A. Wörner, H.-W. Lerner, K. Karaghiosoff, D. Fenske, G. Baum, A. Dransfeld, P. von R. Schleyer, *Eur. J. Inorg. Chem.* **1998**, 833 – 841.
[20] a) W. Hölderich, G. Fritz, *Z. Anorg. Allg. Chem.* **1979**, *457*, 127 – 142; b) M. Baudler, *Angew. Chem.* **1987**, *99*, 429 – 451; *Angew. Chem. Int. Ed. Engl.* **1987**, *26*, 419 – 441.
[21] a) Re complex: M. A. Green, J. C. Huffmann, K. G. Caulton, W. K. Rybak, J. J. Ziólkówski, *J. Organomet. Chem*. **1981**, *218*, C39 – C43; b) Re complex: L. E. Helberg, T. B. Gunnoe, B. C. Brooks, M. Sabat, W. D. Harman, *Organometallics* **1999**, *18*, 573 – 581; c) Pt complex: J. Bordner, D. W. Wertz, *Inorg. Chem.* **1974**, *13*, 1639 – 1643; d) W complex: C. A. Toledano, A. Parlier, H. Rudler, J.-C. Daran, Y. Jeannin, *J. Chem. Soc. Chem. Commun.* **1984**, 576 – 578; e) W complex: R. R. Schrock, S. W. Seidel, N. C. Mösch-Zanetti, D. A. Dobbs, K.-Y. Shih, W. M. Davis, *Organometallics* **1997**, *16*, 5195 – 5208.
[22] I. G. Phillips, R. G. Ball, R. G. Cavell, *Inorg. Chem*. **1987**, *26*, 4074 – 4079.
[23] The reaction of $K_2(P_4tBu_4)$ with *t*BuCl, which produces $H_2P_4tBu_4$ and isobutene, proceeds similarly: M. Baudler, G. Reuschenbach, J. Hellmann, J. Hahn, *Z. Anorg. Allg. Chem*. **1983**, *499*, 89 – 98.
[24] a) J. P. Albrand, J. B. Robert, *J. Chem. Soc. Chem. Commun.* **1974**, 644 – 645; b) L. R. Smith, J. L. Mills, *J. Am. Chem. Soc.* **1976**, *98*, 3852 – 3857; c) M. C. Fermin, S. W. Douglas, *J. Am. Chem. Soc.* **1995**, *117*, *50*, 12645 – 12646; d) K. Diemert, B. Kottwitz, W. Kuchen, *Phosphorus Sulfur* **1986**, *26*, 307 – 320.
[25] The atom P3 lies 41.5(1) pm out of the P1-P2-P4-P5 plane; the dihedral angle between the planes P6-Ni1-P7 and P1-P2-P4-P5 is 78.29(2)°.
[26] V. Caliman, P. B. Hitchcock, J. F. Nixon, *Chem. Commun.* **1997**, 1739 – 1740.
[27] D. E. C. Corbridge, *The Structural Chemistry of Phosphorus*, Elsevier, Amsterdam, **1974**.
[28] B. Deppisch, H. Schäfer, *Acta Crystallogr. Sect. B* **1982**, *38*, 748 – 752.
[29] D. Fenske, K. Merzweiler, *Angew. Chem*. **1984**, *96*, 600 – 602; *Angew. Chem. Int. Ed. Engl*. **1984**, *23*, 635 – 637.
[30] W. Vokusil, J. F. Arens, *Recl. Trav. Chim. Pays-Bas* **1963**, *82*, 302 – 304.
[31] K. A. Jensen, *Z. Anorg. Allg. Chem.* **1936**, *229*, 265 – 281.
[32] a) A. D. Becke, *Phys. Rev. A* **1988**, *38*, 3098 – 3100; b) S. H. Vosko, L. Wilk, M. Nusair, *Can. J. Phys.* **1980**, *58*, 1200 – 1211; c) J. P. Perdew, *Phys. Rev. B* **1986**, *33*, 8822 – 8824.
[33] The geometries were calculated with the Becke – Perdew functional and SVP and TZVP basis sets. Turbomole: a) R. Ahlrichs, M. Bär, M. Häser, H. Horn, C. Kölmel, *Chem. Phys. Lett.* **1989**, *162*, 165 – 169; b) O. Treutler, R. Ahlrichs, *J. Chem. Phys.* **1995**, *102*, 346 – 354 (density functional theory (DFT)); c) K. Eichkorn, O. Treutler, H. Öhm, M. Häser, R. Ahlrichs, *Chem. Phys. Lett.* **1995**, *242*, 652 – 660; K. Eichkorn, F. Weigend, O. Treutler, R. Ahlrichs, *Theo. Chem. Acc.* **1997**, *97*, 119 – 124 (RI/J); d) A. Schäfer, H. Horn, R. Ahlrichs, *J. Chem. Phys.* **1992**, *97*, 2571 – 2577 (SVP); e) A. Schäfer, C. Huber, R. Ahlrichs, *J. Chem. Phys.* **1994**, *100*, 5829 – 5835 (TZVP).
[34] In one case, a frequency calculation gave an imaginary frequency. Reduction to C_1 symmetry only reduces the energy by 3 kJ mol^{-1} and changes the bond lengths by a maximum of 1 pm.
[35] R. S. Mulliken, *J. Chem. Phys.* **1955**, *23*, 1833 – 1840.
[36] The TDDFT[36a,b] excitations were calculated with the SVP basis[33d] and in the RI/J approximation. [33c] The Rydberg excitations are inadequately described with TDDFT, thus the spectrum was only calculated to 240 nm. a) R. Bauernschmitt, M. Haeser, O. Treutler, R. Ahlrichs, *Chem. Phys. Lett.* **1997**, *264*, 573 – 578; b) R. Bauernschmitt, R. Ahlrichs, *Chem. Phys. Lett.* **1996**, *256*, 454 – 464.

$NaBa_2O$: A Fresh Perspective in Suboxide Chemistry**

Grigori V. Vajenine and Arndt Simon*

The 1932 edition of Gmelin's Handbook of Inorganic Chemistry[1] cites several works describing a supposedly metallic suboxide of barium with the composition Ba_2O. This suboxide could, for example, be obtained by treating the metal with BaO at around 1100 °C. In the 1960 complimentary volume on barium[2] the existence of the suboxide is questioned. The solubility of metallic barium in the oxide was cited as a reason for the erroneous reports of Ba_2O. So far no barium suboxides have been reliably characterized.

The chemistry of alkali metal (A) suboxides, on the other hand, was developed in the 1970s[3] following initial reports on cesium suboxides at the beginning of the last century.[4] All of the investigated cesium and rubidium compounds contain oxygen-centered A_6O octahedra of metal atoms that are condensed to larger clusters through face sharing.

The motif of octahedral clusters repeats itself in the still growing family of alkaline earth metal (AE) subnitrides, in which AE_6N clusters or their aggregates form stoichiometric compounds with sodium.[5] The alkali metal suboxides and the alkaline earth metal subnitrides feature a unique combination of ionic bonding within the A_6O or AE_6N clusters and metallic bonding involving the remaining conduction electrons.

Our search for alkaline earth metal suboxides was further stimulated by reports on $M_3Ba_{20}O_5$ (M = Ga, In)[6] and $M_2Ba_{21}O_5$ (M = Si, Ge),[7] which contain $Ba_{18}O_5$ clusters formed by face sharing between five Ba_6O octahedra. These compounds, however, turned out to be oxide hydrides, such as purely ionic $(Ba^{2+})_{21}(Ge^{4-})_2(O^{2-})_5(H^-)_{24}$, when the initially overlooked hydrogen impurity was taken into account.[8, 9]

As Na/K alloy proved to be an excellent flux for the preparation of alkaline earth metal subnitrides, it was also used to prepare a barium suboxide. Additionally, we hoped that a sodium matrix might stabilize the desired suboxide, as in the subnitrides $NaBa_3N$,[13] Na_5Ba_3N,[14] and $Na_{16}Ba_6N$.[15]

First attempts[16] were successful in producing single crystals of a new compound. The crystal structure could be solved and refined based on single-crystal[18] and powder X-ray diffraction data[20] in the stoichiometry $NaBa_2O$,[22] which is the first compound in the Na/Ba/O system.

The most striking feature in the crystal structure of $NaBa_2O$ is the presence of Ba_4O tetrahedra instead of the expected Ba_6O octahedra. Edge sharing between the tetrahedra leads to $^1_\infty[Ba_{4/2}O] \cong Ba_2O$ chains, which are stacked parallel to each other and are separated by sodium atoms (Figure 1), resembling the arrangement of Ba_3N chains in $NaBa_3N$[13] and Na_5Ba_3N.[14] Although the $^1_\infty[Ba_{4/2}O]$ chains in $NaBa_2O$ are analogous to the $^1_\infty[SiQ_{4/2}]$ (Q = S, Se) chains in the silicon dichalcogenides,[23] the packing of the $^1_\infty[Ba_{4/2}O]$ chains and Na atoms results in a new structure type. These chains also determine the preferred direction of crystal growth, resulting in needlelike $NaBa_2O$ crystals. The Ba–O distance of 2.5286(3) Å is significantly shorter than that of 2.76 Å in BaO[24] due to the lower coordination numbers CN = 2 and 4 for Ba and O, respectively, in $NaBa_2O$ compared to those in BaO (CN = 6). The separations between the metal atoms are in the range observed in sodium barium subnitrides and are typical for metallic bonding, which is consistent with the formulation $Na^+(Ba^{2+})_2O^{2-} \cdot 3e^-$.

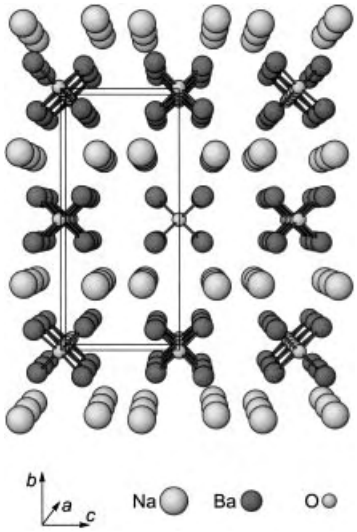


Figure 1. Crystal structure of $NaBa_2O$ as viewed along the linear $^1_\infty[Ba_{4/2}O]$ chains. The orthorhombic unit cell is outlined.

The crystal structure of the suboxide can also be described starting from the body-centered cubic (bcc) packing of the metal atoms, as in elemental Na and Ba. In the first step, Ba and Na atoms are arranged in such a way that every third square layer contains Na atoms, with the remaining positions occupied by Ba atoms according to the $MoSi_2$ structure type.[25] In the second step, half of the tetrahedral holes in the remaining Ba double layers are filled in an ordered fashion by O atoms so that the resulting $^1_\infty[Ba_{4/2}O]$ chains run in the [110] direction of the initial bcc lattice (Figure 2). Full occupation of these voids results in a $ThCr_2Si_2$-type structure.[26] Based on this construction, one would expect an ideal $a:b:c$ ratio of $\sqrt{2}:3:\sqrt{2}$ ($\cong$1:2.12:1) for $NaBa_2O$, which is within 5 % of the 0.95:2.21:1.00 ratio for the observed lattice constants. Incidentally, the value $c/\sqrt{2} = 4.91$ Å lies between the values for the lattice constants of elemental sodium ($a' = 4.29$ Å) and barium ($a' = 5.02$ Å), suggesting that the above-described construction is realistic.

Surprisingly, the crystal volume of $NaBa_2O$ per formula unit ($V = V_{cell}/Z = 175.2$ Å^3) is larger than the sum $V(Na) + 2V(Ba) = 166.3$ Å^3 (Table 1). On first sight it might seem reasonable as the volume of the O atoms adds to that of the metal atoms. However, all suboxides and subnitrides of alkali and alkaline earth metals known so far exhibit crystal volumes

[*] Prof. Dr. A. Simon, Dr. G. V. Vajenine
Max-Planck-Institut für Festkörperforschung
Heisenbergstrasse 1, 70569 Stuttgart (Germany)
Fax: (+49) 711-689-1642
E-mail: simon@sim.mpi-stuttgart.mpg.de

[**] G.V.V. would like to thank the Alexander von Humboldt Foundation and the Max Planck Society for financial support. The authors also thank O. Oeckler for collecting single-crystal diffraction data, W. Röthenbach for temperature-dependent Guinier measurements, and O. Reckeweg for helpful discussions.

 © WILEY-VCH Verlag GmbH, D-69451 Weinheim, 2001 1433-7851/01/4022-4220 $ 17.50+.50/0

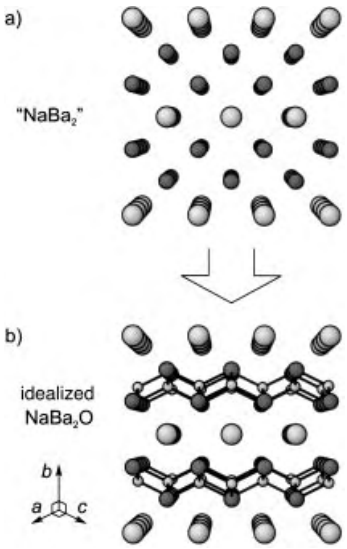


Figure 2. Construction of the crystal structure of $NaBa_2O$ starting from a body-centered cubic lattice as in elemental Na or Ba. Every third layer of the latttice is occupied by Na atoms, with Ba atoms in the remaining layers, corresponding to a hypothetical "$NaBa_2$" alloy (a). The idealized crystal structure of $NaBa_2O$ obtained by filling half of the tetrahedral voids in barium double layers of "$NaBa_2$" by oxygen atoms (b). When this model structure with Ba in (0,0.08333,¼) and Na in (0,¼,¾) is rotated by 45° around the vertical *b* axis and is allowed to relax, the experimentally observed $NaBa_2O$ structure is obtained (see Figure 1).

Table 1. Crystal volumes per formula unit for several Na/Ba/O compounds. The first four lines are identical to Table 5 in ref. [14].

Material	$V = V_{cell}/Z$ [Å^3]	Volume change[a] [%]	Residual per $BaO_{z/y}$ [Å^3][b]	Ref.
Na	39.5	–	–	[31]
Ba	63.4	–	63.4	[31]
Na_2Ba	142.0	−0.3	63.0	[29]
NaBa	102.8	−0.1	63.3	[28]
$NaBa_2O$	175.2	+5.3	67.9	this work
BaO	42.1	−33.6	42.1	[24]

[a] The procentual volume change for $Na_xBa_yO_z$ is defined as $100 \times [V(Na_xBa_yO_z) - xV(Na) - yV(Ba)]/[xV(Na) + yV(Ba)]$. [b] The residual volume for $Na_xBa_yO_z$ is defined as $[V(Na_xBa_yO_z) - xV(Na)]/y$.

corresponding to the sum of the metals, due to dramatic shrinkage of the metal volume upon cation formation. Contractions by $\frac{1}{2}V(Cs_2O) - V(Cs) = -66.1$ Å^3 and $V(BaO) - V(Ba) = -21.3$ Å^3 indicate that the addition of O^{2-} ions to the crystal structures cannot overcompensate the volume reduction due to the formation of Cs^+ and Ba^{2+}. However, there exists an additional effect leading to volume expansion in suboxides and subnitrides, namely, coulombic repulsion between the anions and the remaining conduction electrons. This effect can be quantified by the values $V(NaBa_2O) - V(Na) - V(Ba) - V(BaO) = 30.2$ Å^3 and $V(Cs_{11}O_3) - 5V(Cs) - 3V(Cs_2O) = 83.9$ Å^3, for example, or approximately 30 Å^3 per oxide anion. Such an additional expansion is not enough to overcome the cationic contraction in cesium suboxides ($V(Cs_{11}O_3) = 960.8$ Å^3 is still smaller than $11V(Cs) = 1273.7$ Å^3), but suffices in $NaBa_2O$ because the cationic contraction is significantly weaker for barium than for cesium, as mentioned above.

Additional structural and chemical reasons for the large crystal volume of $NaBa_2O$ include 1) the fact that the metal atoms exhibit no close packing and 2) the long Ba–Ba contacts between the $^1_\infty[Ba_{4/2}O]$ chains ($d_{Ba-Ba} \geq 4.959$ Å) leading to electron confinement and expansion as discussed for Ba_3N.[27] The volume of the Wigner–Seitz cell constructed for Na in the intermetallic phases NaBa[28] ($V(Na) = 38.8$ Å^3) and Na_2Ba[29] ($V(Na) = 39.3$ Å^3) is close to that in metallic sodium ($V(Na) = 39.5$ Å^3), whereas it is significantly larger for $NaBa_2O$ ($V(Na) = 46.8$ Å^3). This finding may be associated with the effect described in (2) or even with a polarization toward anionic sodium.[30]

Relatively large crystal volumes of suboxides and subnitrides suggest that these should decompose under pressure, for example according to Equations (1) and (2). We plan to investigate these reactions. In addition, we will attempt to characterize further compounds which, according to preliminary results, appear to exist in the Na/Ba/O system.

$$NaBa_2O \longrightarrow NaBa + BaO \ (\Delta V_1 = -30.3 \text{ Å}^3 \text{ or } -17.3\%) \quad (1)$$

$$Cs_{11}O_3 \longrightarrow 5Cs + 3Cs_2O \ (\Delta V_2 = -83.9 \text{ Å}^3 \text{ or } -8.7\%) \quad (2)$$

Received: May 16, 2001 [Z17122]

[1] *Gmelins Handbuch der Anorganischen Chemie*, *Band Barium* (Ed.: E. Pietsch), Verlag Chemie, Weinheim, **1932**, pp. 73–74.
[2] *Gmelins Handbuch der Anorganischen Chemie*, *Band Barium* (Ed.: A. Kotowski), Verlag Chemie, Weinheim, **1960**, p. 278.
[3] A. Simon, *Struct. Bonding* **1979**, *36*, 81–127.
[4] E. Rengade, *C.R. Hebd. Seances Acad. Sci.* **1909**, *148*, 1199–1202.
[5] A. Simon, *Coord. Chem. Rev.* **1997**, *163*, 253–270.
[6] C. Röhr, *Z. Kristallogr. Suppl.* **1995**, *9*, 24.
[7] C. Röhr, *Z. Anorg. Allg. Chem.* **1995**, *621*, 1496–1500.
[8] B. Huang, J. D. Corbett, *Inorg. Chem.* **1998**, *37*, 1892–1899.
[9] It is unclear whether another reported suboxide $Ba_{17}Al_3O_7$,[10] which contains $Ba_{17}Al_2O_7$ clusters also composed of condensed oxygen-centered metal octahedra, is contaminated by hydrogen. Attempts to repeat the synthesis of this compound resulted in preparation of another ionic oxide hydride, $(Ba^{2+})_3Al^{3+}(O^{2-})_4H^-$.[11, 12]
[10] C. Röhr, R. George, *Angew. Chem.* **1995**, *107*, 2311–2313; *Angew. Chem. Int. Ed. Engl.* **1995**, *34*, 2115–2116.
[11] B. Huang, J. D. Corbett, *J. Solid State Chem.* **1998**, *141*, 570–575.
[12] M. Zumdick, G. Althoff, C. Röhr, *Acta Crystallogr. Sect. C* **2001**, *57*, 339–340.
[13] P. E. Rauch, A. Simon, *Angew. Chem.* **1992**, *104*, 1505–1506; *Angew. Chem. Int. Ed. Engl.* **1992**, *31*, 1519–1521.
[14] G. J. Snyder, A. Simon, *J. Am. Chem. Soc.* **1995**, *117*, 1996–1999.
[15] G. J. Snyder, A. Simon, *Angew. Chem.* **1994**, *106*, 713–715; *Angew. Chem. Int. Ed. Engl.* **1994**, *33*, 689–691.
[16] The compounds were prepared and handled under purified Ar either in a glove box or on a vacuum line. Samples containing single crystals of $NaBa_2O$ were prepared as follows: Metallic barium (Merck, 99.0%, distilled twice with heating at 1270 K in vacuum to remove hydrogen), BaO_2 (Merck, 93%), and Na/K alloy (Na, Merck, 99% and K, Merck, 98.0%, jointly filtered through a glass filter after being melted in an Ar stream) were mixed in the approximate $Na_{15}K_7Ba_3O$ stoichiometry and sealed in a Ta ampoule under Ar. The latter was sealed in a Duran glass ampoule and treated at 620 K for ten days, followed by cooling to room temperature at 1 K h^{-1}. Needle-shaped single crystals of $NaBa_2O$ were manually selected from the resulting liquid alloy. Single-crystal diffraction studies were carried out on such crystals individually sealed in glass capillaries. Alternatively, small batches of crystals (ca. 50 mg) could be manually gathered for either powder X-ray investigations or elemental analysis. The bulk product, after removal of the liquid alloy in a press, contained about 50 wt% of $NaBa_2O$ according to powder X-ray analysis, contaminated by cubic NaBa and hexagonal Na_2Ba. Bulk $NaBa_2O$, contaminated by NaBa and BaO (ca. 50 wt% $NaBa_2O$), can also be prepared from a mixture of NaBa and Na_2O in a 2:1 molar ratio at 520 K. Single-phase samples

of $NaBa_2O$ could not be prepared; an excess of Na and Ba in the reaction mixture is necessary to stabilize the compound, and this in turn results in the contamination of the product by NaBa and Na_2Ba upon cooling. In a temperature-dependent Guinier measurement[17] pure $NaBa_2O$, obtained from ground single crystals and mixed with powdered glass to reduce absorption effects, begins to decompose to BaO at around 435 K with full decomposition at 490 K. On the other hand, when a sample containing excess Na and Ba is heated, the diffraction lines of $NaBa_2O$ can be observed up to 525 K. However, reaction of the samples with glass could not be excluded under these conditions.

[17] A. Simon, *J. Appl. Crystallogr.* **1971**, *4*, 138 – 145.

[18] Details of the crystal-structure solution and refinement based on single-crystal data: CAD-4 diffractometer, crystal size $0.2 \times 0.15 \times 0.1$ mm, orthorhombic, space group *Cmma* (no. 67), $a = 6.5907(3)$, $b = 15.327(1)$, $c = 6.9385(5)$ Å, Ba in 8*m* (0,*y*,*z*) with $y = 0.08701(2)$ and $z = 0.19869(5)$, Na in 4*g* (0,¼,*z*) with $z = 0.6889(7)$, O in 4*a* (¼,0,0), $V = 700.90(8)$ Å^3, $Z = 4$, $\rho_{calcd} = 2.973$ g cm^{-3}, $2\theta_{max} = 49.94°$, $Ag_{K\alpha}$ radiation, $\lambda = 0.56086$ Å, ω-θ scan, measured at 293 K, 2618 collected and 703 unique reflections ($R_{int} = 0.0216$), absorption correction: ψ-scan, $\mu = 5.877$ mm^{-1}, crystal structure solved using direct methods (SHELXS 97[19]), full-matrix least-squares refinement (anisotropic for all atoms) on F^2 (SHELXL 97[19]), 15 parameters refined, $R1(I > 2\sigma(I)) = 0.0297$, $wR2(I > 2\sigma(I)) = 0.0768$, $R1$(all data) = 0.0309, $wR2$(all data) = 0.0777, GOF = 1.183. Further details on the crystal structure investigation may be obtained from the Fachinformationszentrum Karlsruhe, 76344 Eggenstein-Leopoldshafen, Germany (fax: (+49) 7247-808-666; e-mail: crysdata@fiz-karlsruhe.de), on quoting the depository number CSD-411905.

[19] SHELXTL Version 5.1, Bruker AXS, **1998**.

[20] Powder X-ray diffraction data, collected on samples of ground single crystals sealed in capillaries,[16] was used for full-profile Rietveld refinement; the CSD Package[21] was employed. The atomic positions obtained were consistent with those from the refinement of the single-crystal data, though less accurate. The thermal displacement parameters had to be fixed; the unit cell parameters were refined to $a = 6.5916(3)$ Å, $b = 15.3282(8)$ Å, and $c = 6.9628(4)$ Å with $R_{int} = 0.082$ and $R_{profile} = 0.252$.

[21] "CSD—Universal program package for single crystal and/or powder structure data treatment": L. G. Akselrud, Yu. N. Grin, P. Yu. Zavalij, V. K. Pecharsky, V. S. Fundamenskii, *12th European Crystallographic Meeting*, Moscow, **1989**, *3*, 155 (http://imr.chem.binghamton.edu/zavalij/CSD.html).

[22] Elemental analysis (%) of single-crystal batches: found (calcd): Ba 84.5 and 84.8 (87.6), Na 8.3 and 8.7 (7.3), O 4.1 and 4.2 (5.1), K 1.1 and 1.3 (0); these results are consistent with a small impurity of the Na/K alloy. The metal content was determined using ICP atomic emission spectrometry (TJA IRIS Advantage) after dissolving the samples in aqueous acid. Oxygen was determined as CO by measuring IR absorption after melting the samples with excess graphite (Exhalograph EAO 220, Balzers). The hydrogen content was measured by oxidizing the samples in oxygen at 1320 K and determining the amoung of released water by IR spectroscopy. Analyses of larger bulk samples containing about 50 wt% $NaBa_2O$ yielded 0.008 and 0.012 wt% H. This corresponds to no more than one hydrogen atom per 15 $NaBa_2O$ formula units.

[23] J. Peters, B. Krebs, *Acta Crystallogr. Sect. B* **1982**, *38*, 1270 – 1272.

[24] F. S. Galasso, *Structure and Properties of Inorganic Solids*, Pergamon, Oxford, **1970**, p. 64.

[25] W. H. Zachariasen, *Z. Phys. Chem.* **1927**, *128*, 39 – 48.

[26] Z. Ban, M. Sikirica, *Acta Crystallogr.* **1965**, *18*, 594 – 599.

[27] U. Steinbrenner, A. Simon, *Z. Anorg. Allg. Chem.* **1998**, *624*, 228 – 232.

[28] G. J. Snyder, A. Simon, *J. Chem. Soc. Dalton Trans.* **1994**, 1159 – 1160.

[29] G. J. Snyder, A. Simon, *Z. Naturforsch. B* **1994**, *49*, 189 – 192.

[30] The consideration of the crystal volume of $NaBa_2O$ also provides an additional argument against a possible contamination by hydrogen: Inclusion of hydride would rather decrease the crystal volume. Thus the value of $V(NaH) + V(BaH_2) + V(BaO) = 126.8$ Å^3, an approximation for the crystal volume of hypothetical ionic $Na^+(Ba^{2+})_2O^{2-}(H^-)_3$, is clearly too small.

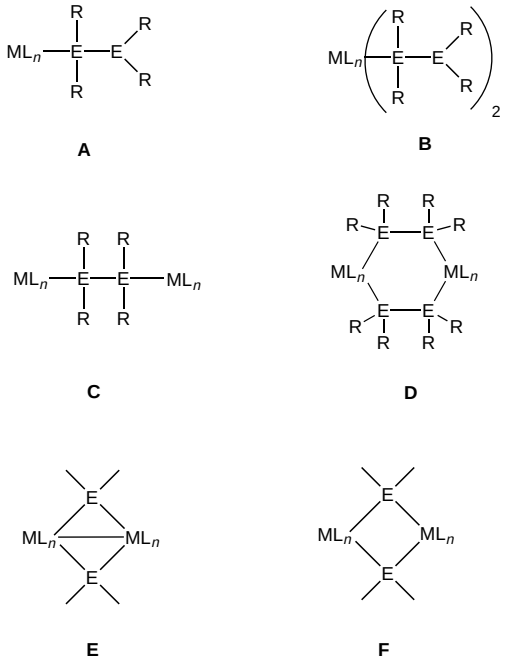
[31] F. S. Galasso, *Structure and Properties of Inorganic Solids*, Pergamon, Oxford, **1970**, p. 28.

Reactions of Et_4Bi_2 with tBu_3M (M = Al, Ga)—Synthesis of Complexes with a Bidentate Dibismuthane Ligand**

Andreas Kuczkowski, Stephan Schulz,* and Martin Nieger

Dedicated to Professor Oskar M. Glemser on the occasion of his 90th birthday

Since Cadet's discovery of the "fuming liquid" in 1757, numerous tetraorganodipnicogens of the type R_4E_2 (E = P, As, Sb) containing a central E–E bond have been synthesized.[1] Detailed investigations on their reactions with transition metal complexes showed their ability to form monodentate (Scheme 1, type A and B) and bidentate complexes (type C and D) under preservation of the central E–E bond. In addition, heterocycles (type E and F) were formed under E–E bond cleavage.[1, 2]



Scheme 1. Coordination modes for transition metal complexes with dipnicogen ligands R_4E_2.

In contrast, reactions with main group metal complexes such as Group 13 trialkyl compounds have been investigated to a far lesser extent. $[Me_4P_2][BH_3]_2$ (type C) was synthesized almost 50 years ago by Nöth and Burg;[3] however, the only structurally characterized compounds known were $Me_4P_2(BH_3)_2$[4] and $Me_4P_2(BH_2Br)_2$[5] prior to our recent

[*] Priv. Doz. Dr. S. Schulz, Dipl.-Chem. A. Kuczkowski, Dr. M. Nieger
Institut für Anorganische Chemie der Universität Bonn
Gerhard-Domagk-Strasse 1, 53121 Bonn (Germany)
Fax: (+49) 228-73-5327
E-mail: sschulz@uni-bonn.de

[**] This work was supported by the Deutsche Forschungsgemeinschaft (DFG), the Fonds der Chemischen Industrie (FCI), the Bundesministerium für Bildung, Wissenschaft, Forschung und Technologie (BMBF), and Prof. E. Niecke, Universität Bonn.

 © WILEY-VCH Verlag GmbH, D-69451 Weinheim, 2001 1433-7851/01/4022-4222 $ 17.50+.50/0

syntheses and X-ray crystal structure determinations of four distibane bisadducts $[Sb_2R_4][MR'_3]_2$ (M = Al, Ga; type C).[6] Distibane bisadducts are stable in the pure form, but readily undergo consecutive reactions in solution under Sb–Sb bond cleavage to give four- and six-membered heterocycles of type F.[6] An analogous reaction pathway was observed by Breunig et al. in the synthesis of the six-membered stibinoindane $[\{(Me_3SiCH_2)_2InSbMe_2\}_3]$ from Me_4Sb_2 and $(Me_3SiCH_2)_3In$.[7]

The low stability of the distibane bisadducts $[Sb_2R_4][MR'_3]_2$ is not surprising, since the stability of the E–E bond in tetraorganodipnicogens R_4E_2 generally decreases with increasing atomic number of the central pnicogen E. Consequently, distibanes and dibismuthanes exhibit the strongest tendency toward disproportionation into the elemental pnicogens E and triorganopnicogens R_3E. As a result only a few stable dibismuthanes have been synthesized and structurally characterized,[8] and, to the best of our knowledge, dibismuthanes have not been reported to serve as a mono- or bidentate ligand. Evidently, both the very weak Bi–Bi bond and the high s character of the lone pairs of electrons limit their potential for further complexation reactions.[9]

In an attempt to gain insight into the reactivity of dibismuthanes toward Group 13 trialkyl compounds, we treated tetraethyldibismuthane Et_4Bi_2 with tri(*tert*)butylalane and -gallane, respectively, in a 2:1 molar ratio [Eq. (1); M = Al (**1**), Ga (**2**)].

$$2\,t\mathrm{Bu_3M} + \mathrm{Bi_2Et_4} \longrightarrow [\mathrm{Et_4Bi_2}][\mathrm{M}t\mathrm{Bu_3}]_2 \qquad (1)$$

Since Et_4Bi_2 is only stable below 0 °C,[8a] the reagents were precooled to −20 °C and combined in a flask in the glovebox. The reaction with $t\mathrm{Bu_3Ga}$ immediately yielded an orange solid, which was recrystallized from *n*-pentane at −30 °C to give orange crystals, while the analogous reaction with $t\mathrm{Bu_3Al}$ resulted in the formation of a dark brown, partially insoluble (metallic) solid. However, if the latter reaction was carried out in *n*-pentane at −78 °C, it yielded a light red solution, which on storage at −60 °C gave yellow crystals after 48 h. Both crystalline products were shown by NMR spectroscopy and single-crystal X-ray diffraction to be the desired dibismuthane bisadducts $[Bi_2Et_4][M t\mathrm{Bu_3}]_2$ (M = Al (**1**), Ga (**2**); type C).

The stability of **1** and **2** both in the pure form and in solution differ significantly. While **2** can be stored at −30 °C in the dark under an inert gas atmosphere without decomposition for weeks, **1** decomposes slowly to give a brown solid. The same tendency was observed in solution. Compound **2** can be dissolved at −30 °C without decomposition, while **1** undergoes consecutive reactions, as was shown by ^{1}H NMR experiments. The signals observed for **2** in [D$_8$]toluene at −30 °C revealed the presence of the organic substituents Et and *t*Bu in a relative intensity ratio of 2:3, clearly indicating the presence of the bisadduct. The resonance signals are shifted to lower field (*t*Bu–M) and higher field (Et–Bi), respectively, as was observed for the corresponding distibane bisadducts $[Sb_2R_4][MR'_3]_2$[6] and the simple Lewis acid–base adducts $R'_3M{-}BiR_3$ (M = Al, Ga).[10] In contrast, the ^{1}H NMR spectrum of **1** recorded at −30 °C shows resonance signals due to the Et and *t*Bu groups in an intensity ratio of 1:1, which is not consistent with the formation of a bisadduct. A spectrum of **1** with the correct signal intensity was finally obtained from a freshly prepared sample, which was dissolved in [D$_8$]toluene and measured at −60 °C.[11]

The stability of **1** and **2** in the gas phase seems to be limited. The mass spectrum of **2** only shows signals for the fragmentation products (Et_4Bi_2 and $t\mathrm{Bu_3Ga}$) of the bisadduct.[12]

Single crystals of **1** and **2** suitable for an X-ray structure determination were obtained from solutions in *n*-pentane at −60 °C.[13] As was observed for the corresponding distibane bisadducts, the substituents bound to bismuth in **1** and **2** adopt staggered conformations. The $Mt\mathrm{Bu_3}$ fragments are arranged *trans*, presumably for steric reasons (Figure 1 and 2). How-

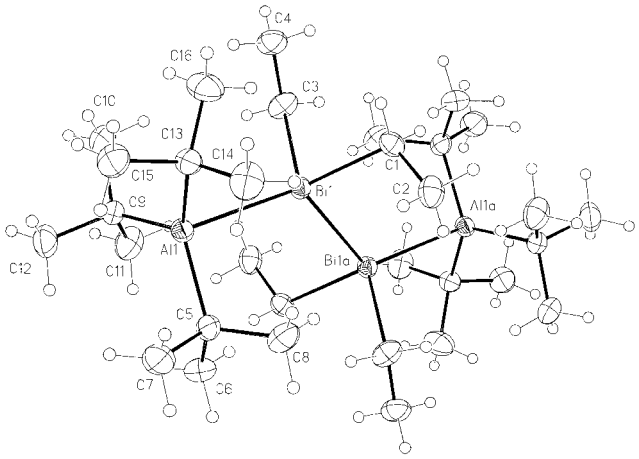


Figure 1. Molecular structure of $[Et_4Bi_2][Al t\mathrm{Bu_3}]_2$ (**1**). Selected bond lengths [Å] and angles [°]: Bi1-Al1 3.084(1), Bi1-Bi1a 2.983(1), Bi1-C1 2.258(3), Bi1-C3 2.275(4), Al1-C5 2.003(4), Al1-C9 2.018(4), Al1-C13 2.026(3); Al1-Bi1-Bi1a 126.7(1), C1-Bi1-C3 94.5(1), C1-Bi1-Bi1a 95.4(1), C3-Bi1-Bi1a 97.8(1), C5-Al1-C9 118.4(2), C5-Al1-C13 116.9(2), C9-Al1-C13 117.5(2).

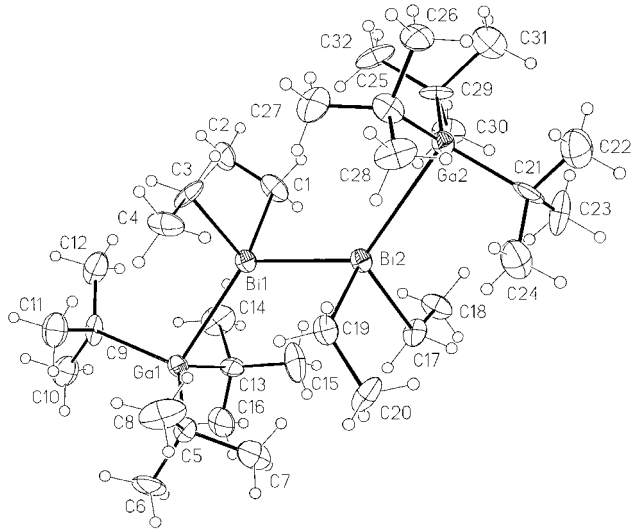


Figure 2. Molecular structure of $[Et_4Bi_2][Ga t\mathrm{Bu_3}]_2$ (**2**). Selected bond lengths [Å] and angles [°]: Bi1-Ga1 3.099(2), Bi2-Ga2 3.114(2), Bi1-Bi2 2.984(1), Bi1-C1 2.274(15), Bi1-C3 2.284(14), Bi2-C17 2.286(14), Bi2-C19 2.286(15), Ga1-C5 2.006(15), Ga1-C9 2.056(17), Ga1-C13 2.045(18), Ga2-C21 2.030(20), Ga2-C25 2.065(17), Ga2-C29 2.029(15); Ga1-Bi1-Bi2 130.2(1), Ga2-Bi1-Bi2 129.7(1), C1-Bi1-C3 93.7(6), C1-Bi1-Bi2 97.5(5), C3-Bi1-Bi2 94.7(5), C17-Bi2-C19 96.6(6), C17-Bi2-Bi1 98.3(4), C19-Bi2-Bi1 96.7(4), C5-Ga1-C9 115.5(6), C5-Ga1-C13 120.1(6), C9-Ga1-C13 118.7(7), C21-Ga2-C25 119.0(8), C21-Ga2-C29 117.5(8), C25-Ga2-C29 116.9(7).

 © WILEY-VCH Verlag GmbH, D-69451 Weinheim, 2001 1433-7851/01/4022-4223 $ 17.50+.50/0

ever, only **1** possesses crystallographic C_i symmetry with the center of symmetry in the Bi–Bi bond. The Bi–Bi bond lengths (2.983(1) (**1**), 2.984(1) Å (**2**)) are almost identical to those of uncomplexed dibismuthanes (Ph_4Bi_2: 2.990, $(Me_3Si)_4Bi_2$: 3.035, $(HC{=}CMe)_2BiBi(MeC{=}CH)_2$: 2.990 Å),[14] despite the increased steric pressure within the adducts. The solid-state structures show no evidence for a Bi–Bi bond weakening.[15] The same tendency was established for the corresponding distibane bisadducts $[Sb_2Et_4][MtBu_3]_2$ (M = Al, Ga).[6] The Al–Bi (3.084(1) Å (**1**)) and Ga–Bi bond lengths (3.099(2) (Ga1–Bi1), 3.114(2) Å (Ga2–Bi2) (**2**)) are comparable to those found in $iPr_3BiMtBu_3$ (3.088(1) (M = Al),[10b] 3.135(1) Å (M = Ga) [10a]), but more than 30 pm longer than the sum of the covalent radii,[16] indicating only weak acid–base interactions. The M–Bi, M–C (average values: 2.016 (**1**), 2.036 (Ga1), 2.041 Å (Ga2) (**2**)), and Bi–C distances (average values: 2.267 (**1**), 2.279 (Bi1), 2.286 Å (Bi2) (**2**)) as well as the sum of the C-Bi-C and C-Bi-Bi bond angles (287.7° (**1**), 285.9° (Bi1), 291.6 (Bi2) (**2**)) in **1** and **2** are almost identical. Compared to the sum of the C-Sb-C and C-Sb-Sb bond angles observed in the distibane bisadducts $[Sb_2Et_4][MtBu_3]_2$ (292.9° (M = Al), 291.1° (M = Ga)), they are slightly decreased. This points to a higher s character of the dative Bi–M bonding electron pairs, as was observed for the simple Lewis acid–base adducts $R'_3M{-}BiR_3$ (M = Al, Ga), and to a higher p character of the Bi–C and Bi–Bi bonding electron pairs compared to those of the stibane bisadducts. Consequently, the sum of the C-M-C bond angles in $[Bi_2Et_4][MtBu_3]_2$ (352.8° (**1**); 354.3°, 353.4° (**2**)) is slightly larger than those found in $[Sb_2Et_4][MtBu_3]_2$ (350.2° (M = Al), 351.1°(M = Ga), indicating Et_4Bi_2 to be a weaker Lewis base than Et_4Sb_2.[17] Currently, we are investigating the nature of the reaction product(s) of **1** and **2** in solution.

Experimental Section

$[Et_4Bi_2][AltBu_3]_2$, **1** ($M = 930.83\ g\,mol^{-1}$): tBu_3Al (2 mmol, 0.40 g) was added at −78 °C to a solution of Et_4Bi_2 (1 mmol, 0.53 g) in *n*-pentane (5 mL). The resulting red solution was stored at −60 °C. After 48 h, yellow crystals of **1** were obtained. Yield: 0.43 g, 0.47 mmol, 47 %. M.p. < −15 °C. NMR data:[18] ^{1}H NMR (300 MHz, [D$_8$]toluene, −60 °C): $\delta = 1.43$ (s, 27 H; *t*Bu), 1.95 (t, $^3J_{H,H} = 7.8$ Hz, 6 H; $MeCH_2$), 2.34–2.55 (m, 4 H; $MeCH_2$); $^{13}C\{^1H\}$ NMR (80 MHz, [D$_8$]toluene, −60 °C): $\delta = 0.7$ ($MeCH_2$), 15.4 ($MeCH_2$), 31.1 (Me_3CAl).

$[Et_4Bi_2][GatBu_3]_2$, **2** ($M = 1016.31\ g\,mol^{-1}$): Precooled (−20 °C) Et_4Bi_2 (1 mmol, 0.53 g) and tBu_3Ga (2 mmol, 0.48 g) were combined in a flask in glovebox. The resulting orange solid was dissolved in cold (−30 °C) *n*-pentane (5 mL) and stored at −30 °C. After 10 h, orange crystals of **2** had formed. Yield: 0.86 g, 0.85 mmol, 85 %. M.p. below −10 °C. NMR data:[18] ^{1}H NMR (300 MHz, [D$_8$]toluene, −30 °C): $\delta = 1.35$ (s, 27 H; *t*Bu), 2.06 (t, $^3J_{H,H} = 7.8$ Hz, 12 H; CH_3CH_2), 2.42–2.62 (m, 8 H; CH_3CH_2); $^{13}C\{^1H\}$ NMR (80 MHz, [D$_8$]toluene, −30 °C): $\delta = 1.4$ (CH_3CH_2), 17.2 (CH_3CH_2), 32.0 (CH_3C); MS (EI, 12 eV): *m*/*z* (%): 57 (100) $[tBu]^+$, 241 (10) $[tBu_3Ga]^+$, 267 (20) $[BiEt_2]^+$.

Received: August 3, 2001 [Z17664]

[1] Cadet's initial studies were continued by Bunsen, who showed this liquid to contain tetramethyldiarsane Me_4As_2, generally known as "cacodyl". For a historical review see: D. Seyferth, *Organometallics* **2001**, *20*, 1488–1498.

[2] a) H. Baumgarten, H. Johannsen, D. Rehder, *Chem. Ber.* **1979**, *112*, 2650–2658; b) R. G. Hayter, *Inorg. Chem.* **1964**, *3*, 711–717; c) J. Chatt, D. A. Thornton, *J. Chem. Soc.* **1964**, 2713; d) I. Bernal, J. D. Korp, F. Calderazzo, R. Poli, D. Vitali, *J. Chem. Soc., Dalton Trans.* **1984**, 1945–1950; e) H. J. Breunig, R. Rösler, *Coord. Chem. Rev.* **1997**, *163*, 33–53.

[3] a) H. Nöth, *Z. Naturforsch. B* **1960**, *15*, 327–329; b) A. B. Burg, R. I. Wagner, *J. Am. Chem. Soc.* **1953**, *75*, 3872–3877; c) A. B. Burg, J. Brendel, *J. Am. Chem. Soc.* **1958**, *80*, 3198–3202; d) A. B. Burg, *J. Am. Chem. Soc.* **1961**, *83*, 2226–2231.

[4] H. L. Carrell, J. Donohue, *Acta Crystallogr. Sect. B* **1968**, *24*, 699–707.

[5] H. Schmidbaur, T. Wimmer, A. Grohmann, O. Steigelmann, G. Müller, *Chem. Ber.* **1989**, *122*, 1607–1612.

[6] A. Kuczkowski, S. Schulz, M. Nieger, P. Saarenketo, *Organometallics* **2001**, *20*, 2000–2006.

[7] H. J. Breunig, M. Stanciu, R. Rösler, E. Lork, *Z. Anorg. Allg. Chem.* **1998**, *624*, 1965–1968.

[8] a) H. J. Breunig, D. Müller, *Angew. Chem.* **1982**, *94*, 448–449; *Angew. Chem. Int. Ed. Engl.* **1982**, *21*, 439–440; b) G. Becker, M. Rössler, *Z. Naturforsch. B* **1982**, *37*, 91–96; c) O. Mundt, G. Becker, M. Rössler, C. Witthauer, *Z. Anorg. Allg. Chem.* **1983**, *506*, 42–58; d) H. J. Breunig, D. Müller, *Z. Naturforsch. B* **1983**, *38*, 125–129; e) A. J. Ashe III, J. W. Kampf, D. B. Puranik, *Organometallics* **1992**, *11*, 2743–2745; f) R. E. von H. Spence, D. P. Hsu, S. L. Buchwald, *Organometallics* **1992**, *11*, 3492–3493; g) A. J. Ashe III, *Adv. Organomet. Chem.* **1990**, *30*, 77; h) O. Mundt, H. Riffel, G. Becker, A. Simon, *Z. Naturforsch. B* **1988**, *43*, 592.

[9] The reaction of Ph_4Bi_2 with $[Re_2Br_2(CO)_6(thf)_2]$ failed to give a stable complex due to disproportionation of Ph_4Bi_2 into Bi and Ph_3Bi: I. Bernal, J. D. Korp, *J. Chem. Soc. Dalton Trans.* **1984**, 1945–1950. Attempts to prepare $[(CO)_5WBi(Ph_2)B(Ph_2)W(CO)_5]$ have been reported but the resulting compound wasn't fully characterized: H. J. Breunig, D. Müller, *J. Organomet. Chem.* **1983**, *253*, C21–C22.

[10] a) A. Kuczkowski, F. Thomas, S. Schulz, M. Nieger, *Organometallics* **2000**, *19*, 5758–5762; b) A. Kuczkowski, S. Schulz, M. Nieger, *Eur. J. Inorg. Chem.* **2001**, 2605.

[11] The proton resonances observed in the NMR spectra of **1** and **2** correspond to an ABX_3 spin system as was shown by simulation. The chemical shifts and coupling constants were determined as follows: **1**: $\delta = 1.95$ (3 H), 2.39 (1 H), 2.50 (1 H); $^3J_{H,H} = 7.1$, 8.6 Hz, $^2J_{H,H} = 18.7$ Hz; **2**: $\delta = 1.06$ (3 H), 2.47 (1 H), 2.56 (1 H); $^3J_{H,H} = 7.2$, 8.5 Hz, $^2J_{H,H} = 17.0$ Hz.

[12] A mass spectrum of **1** could not be obtained due to the thermal instability of **1** at ambient temperature. The same reason accounts for the unsuccessful attempts to obtain reliable elemental analyses of both **1** and **2**. It was not possible to prepare the samples under cold (−20 °C) conditions, which is necessary to avoid significant decomposition of the compounds, in particular of the alane bisadduct **1**.

[13] $[Bi_2Et_4][AltBu_3]_2$ ($C_{32}H_{74}Al_2Bi_2$) **1**, light yellow crystals, crystal dimensions $0.35 \times 0.20 \times 0.10$ mm; $M_r = 930.8$; monoclinic, space group $P2(1)/c$ (no. 14), $a = 8.5064(1)$, $b = 16.1566(3)$, $c = 15.0684(3)$ Å, $\beta = 104.804(1)°$, $V = 2002.2(1)$ Å^3, $Z = 2$, $\lambda(Mo_{K\alpha}) = 0.71073$ Å, $\mu = 8.838\ mm^{-1}$, $\rho_{calcd} = 1.544\ g\,cm^{-3}$, $T = 123(2)$ K, $F(000) = 916$. By using a Nonius Kappa CCD diffractometer, 39642 reflections ($2\theta_{max} = 50°$) were collected (3513 unique, $R_{int} = 0.0839$). The structure was solved by Patterson methods (SHELXS 97)[19] and refined by full-matrix least-squares on F^2 (SHELXL 97).[20] All non-hydrogen atoms were refined anisotropically and hydrogen atoms by a riding model. $R_1 = 0.020$ ($I > 2\sigma(I)$), $wR_2 = 0.034$, 163 parameters, largest max./min. in the final difference Fourier synthesis: 1.017/−0.703 e Å^{-3}. An empirical absorption correction was applied (max./min. transmission 0.4940/0.2109). $[Bi_2Et_4][GatBu_3]_2$ ($C_{32}H_{74}Ga_2Bi_2$) **2**, light orange crystals, crystal dimensions $0.30 \times 0.15 \times 0.10$ mm; $M_r = 1016.3$; monoclinic, space group $P2(1)/n$ (no. 14), $a = 8.5385(7)$, $b = 16.1156(11)$, $c = 29.010(2)$ Å, $\beta = 91.445(2)°$, $V = 3990.6(5)$ Å^3, $Z = 4$, $\lambda(Mo_{K\alpha}) = 0.71073$ Å, $\mu = 10.145\ mm^{-1}$, $\rho_{calcd} = 1.692\ g\,cm^{-3}$, $T = 123(2)$ K, $F(000) = 1976$. By using a Nonius Kappa CCD diffractometer, 9111 reflections ($2\theta_{max} = 50°$) were collected (5222 unique, $R_{int} = 0.0731$). The structure was solved by Patterson methods (SHELXS 97)[19] and refined by full-matrix least-squares on F^2 (SHELXL 97).[20] All non-hydrogen atoms were refined anisotropically and hydrogen atoms by a riding model. $R_1 = 0.062$ ($I > 2\sigma(I)$), $wR_2 = 0.191$, 325 parameters,

 © WILEY-VCH Verlag GmbH, D-69451 Weinheim, 2001 1433-7851/01/4022-4224 $ 17.50+.50/0

largest max./min. in the final difference Fourier synthesis: 2.275/ – 2.815 e Å^{-3}. An empirical absorption correction was applied (max./min. transmission 0.3854/0.1220). Crystallographic data (excluding structure factors) for the structures reported in this paper have been deposited with the Cambridge Crystallographic Data Centre as supplementary publication no. CCDC-164447 (**1**) and CCDC-164446 (**2**). Copies of the data can be obtained free of charge on application to CCDC, 12 Union Road, Cambridge CB21EZ, UK (fax: (+44) 1223-336-033; e-mail: deposit@ccdc.cam.ac.uk).

[14] C. Silvestru, H. J. Breunig, H. Althaus, *Chem. Rev.* **1999**, *99*, 3277 – 3327.

[15] Unfortunately the X-ray crystal structure of Et_4Bi_2 is unknown to date, allowing no comparison of the Bi–Bi bond length between the uncomplexed and complexed form.

[16] The covalent radii of Al (1.25 Å) and Ga (1.26 Å) are almost the same. A. F. Holleman, E. Wiberg, *Lehrbuch der Anorganischen Chemie*, 101. ed., Walter de Gruyter, Berlin, **1995**, p. 1838.

[17] A. Haaland, *Angew. Chem.* **1989**, *101*, 1017 – 1032; *Angew. Chem. Int. Ed. Engl.* **1982**, *28*, 992 – 1007.

[18] The NMR resonance signals are referenced to internal [D_8]toluene (^{1}H NMR: $\delta = 7.20$; ^{13}C NMR: $\delta = 130$).

[19] G. M. Sheldrick, SHELXS-97, Program for Structure Solution, *Acta Crystallogr. Sect. A* **1990**, *46*, 467 – 473.

[20] G. M. Sheldrick, SHELXL-97, Program for Crystal Structure Refinement, Universität Göttingen, **1997**.

The $XeCl^+$ Ion: $[XeCl]^+[Sb_2F_{11}]^-$**

Stefan Seidel and Konrad Seppelt*

XeF_2, XeF_4, and XeF_6 are the only binary noble gas compounds that are thermodynamically stable against decomposition into the elements. $XeCl_2$, however, has only been detected in matrix,[1] not counting the single unreproduced report, in which it was claimed $XeCl_2$ could be prepared by high frequency discharge of Xe, F_2, and $SiCl_4$ or CCl_4 and that it is stable up to 80 °C.[2]

Cocrystallisates of RbCl or CsCl and, XeO_3 are known, however, which have Xe – Cl contact distances of 275(5) to 297(1) pm.[3] Quite recently $(C_6F_5Xe)_2Cl^+$ was prepared from $C_6F_5Xe^+$ and $(CH_3)_3SiCl$. In the solid state it shows contact distances between Xe and Cl of 284.7(1) and 278.4(2) pm and a Xe-Cl-Xe bond angle of 116.96(8)°. Also C_6F_5Xe–Cl has been isolated under very careful conditions starting with $C_6F_5Xe^+$ and the HCl – pyridine adduct 4-$ClC_5H_4N \cdot HCl$. Because of its instability in solution no further detailed structure information is available, but it can be assumed that it contains a real Xe–Cl bond.[4] Since the bond strength is stronger in XeF^+ than in XeF_2, salts with the $XeCl^+$ ion could be the most stable species with a Xe–Cl bond.

[*] Prof. Dr. K. Seppelt, Dipl.-Chem. S. Seidel
Institut für Anorganische und Analytische Chemie
Freien Universität Berlin
Fabeckstrasse 34 – 36, 14195 Berlin (Germany)
Fax: (+49) 30-83853310
E-mail: seppelt@chemie.fu-berlin.de

[**] This work is supported by the Deutsche Forschungsgemeinschaft and the Fonds der Chemischen Industrie

We reacted $[XeF]^+[SbF_6]^-$ in HF/SbF_5 solution with small amounts of $SbCl_5$. Besides the nucleophilic Cl/F exchange [Eq. (1)], oxidation of Cl^- also takes place: An intermediate blue solution is observed, which is stable at room temperature for some time. This blue solution probably contains Cl_4^+, the first oxidation product of chlorine in the liquid phase, which has recently been identified in the form of the blue salt $[Cl_4]^+[IrF_6]^-$.[5] We did not succeed in crystallizing this blue product. After the decomposition into Cl_3^+,[5] the color of the solution changes to green and finally to orange, from which orange crystals were isolated. These melt at about –20 °C under partial decomposition.

$$XeF^+ \text{ (yellow)} + Cl^- \longrightarrow XeCl^+ \text{ (orange)} + F^- \quad (1)$$

The unit cell contains two crystallographically different, but otherwise essentially similar $[XeCl]^+[Sb_2F_{11}]^-$ units (Figure 1, only Molecule I is shown).[6] The Xe–Cl distance is much shorter (230.9(2) pm; Molecule II: 230.4(2) pm) than any

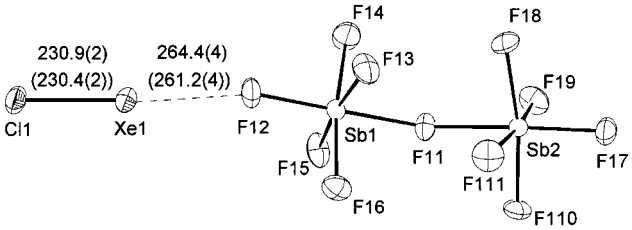


Figure 1. Ion pair $[XeCl]^+[Sb_2F_{11}]^-$ in the crystal (ORTEP representation, 50% probability ellipsoids). Ion pair I is depicted (distances in pm; numbers in parentheses: distances for ion pair II).

Xe–Cl distances measured to date in Xe–Cl compounds and corresponds to a Xe–Cl single bond, as is also predicted by ab initio calculations (230.07 pm, see Table 1). For comparison, isoelectronic ICl has a I–Cl bond length of 230.3 pm in the gaseous state and of 235.1 – 244.0 pm in the solid.[7] Similarly to the XeF^+ and KrF^+ ion,[8, 9] a contact is observed between the $XeCl^+$ ion and an F atom of the $Sb_2F_{11}^-$ ion, which leads to

Table 1. Calculated bond lengths r [pm] for the singlet state and singlet – triplet energy separation ΔE [kJ mol^{-1}] for diatomic noble gas halogen cations; CCSD approximation (numbers in parentheses: MP2 approximation).

Cation	r [pm]	ΔE [kJ mol^{-1}]
ArF^+[a]	168.2 (165.2)	55.8 (76.7)
$ArCl^+$	210.6 (208.1)	– 32.6 (– 30.9)
$ArBr^+$	238.5 (236.4)	– 101.4 (– 112.9)
ArI^+	269.4 (263.4)	– 115.7 (– 128.1)
KrF^+[b]	174.9 (173.5)	99.3 (134.9)
$KrCl^+$	217.7 (215.4)	29.4 (39.4)
$KrBr^+$	238.7 (237.9)	– 27.3 (– 35.8)
KrI^+	261.6 (260.2)	– 57.9 (– 66.5)
XeF^+[c]	189.9 (189.4)	117.9 (154.5)
$XeCl^+$	232.9 (230.7)	74.8 (86.1)
$XeBr^+$	254.4 (253.2)	21.8 (16.4)
XeI^+[d]	276.6 (275.3)	– 13.9 (– 21.7)

[a] See also ref. [12]. [b] 176.5(3) pm in $[KrF]^+[SbF_6]^-$.[9] [c] 188.8(2) pm in $[XeF]^+[SbF_6]^-$.[18] [d] See also ref. [11]. Especially in this combination of two heavy atoms the spin-orbit coupling can strongly influence the values. This is not taken into account.

 © WILEY-VCH Verlag GmbH, D-69451 Weinheim, 2001 1433-7851/01/4022-4225 $ 17.50+.50/0

the formation of an almost linear Cl–Xe···F array with a contact distance of 264.4(4) pm (Molecule II: 261.2(4) pm).

The ^{129}Xe NMR signal (Figure 2) shows strong broadening owing to the quadrupole momentum of the $^{35/37}$Cl isotopes, but also the onset of a splitting due to the ^{129}Xe – $^{35/37}$Cl coupling

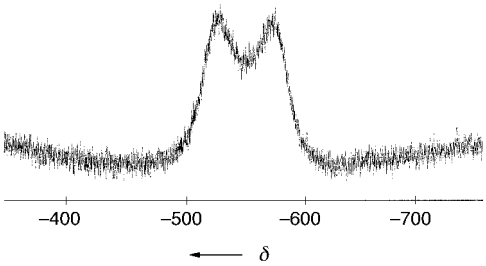


Figure 2. ^{129}Xe NMR spectrum of $[XeCl]^+[Sb_2F_{11}]^-$ in HF/SbF_5.

($I = 3/2$). The Raman spectrum is also in accord with the formula $[XeCl]^+[Sb_2F_{11}]^-$: A Raman band at 391 cm^{-1} (calculated 390.2 cm^{-1}) is clearly attributable to the XeCl vibration frequency, the other bands are typical for the $Sb_2F_{11}^-$ ion.[10] $[XeCl]^+[Sb_2F_{11}]^-$ decomposes at room temperature according to Equation (2).

$$2\,[XeCl]^+[Sb_2F_{11}]^- \longrightarrow Xe + Cl_2 + [XeF]^+[Sb_2F_{11}]^- + 2\,SbF_5 \qquad (2)$$

After the isolation of the new cation $XeCl^+$ the question arose, whether more as yet undetected diatomic noble gas halogen cations could exist. We have calculated all combinations of Ar, Kr, and Xe with F, Cl, Br, and I (Table 1) and the results are as follows: All combinations have a bound $^1\Sigma$ state. But as has been shown already by Klapötke for the XeI^+ ion, a weakly bound $^3\Pi$ state also needs to be considered, which in this case is of lower energy. Thus, the nonexistence of XeI^+ was predicted.[11] Our calculations confirm this special case and predict the same fate for all combinations of the lighter noble gases with the heavier halogens. The singlet – triplet separation is, however, large for the now known cations XeF^+, KrF^+, and $XeCl^+$.

ArF^+, $KrCl^+$, and $XeBr^+$ are undetected combinations to date, but the latter two have such a small singlet – triplet separation that the existence of these cations is unlikely, especially since a lengthening and a further weakening of the bond is expected in the condensed phase.

For the isolation of an ArF^+ salt a counterion is required that can resist the extreme oxidation force and the extreme fluoride ion affinity of ArF^+. Because of the first condition only fluoro-containing anions of elements in their highest oxidation states can be considered. The second condition is equally difficult to meet: Since an ArF_2 molecule is not a bound species according to calculations by various methods,[12] decomposition according to the reaction $[ArF]^+[XF_n]^- \rightarrow Ar + F_2 + XF_{n-1}$ is the problem. We can show that the anions HF_2^-, BF_4^-, and even AsF_6^- will not prevent this spontaneous decomposition because of their F^- donor abilities. Only $[ArF]^+[SbF_6]^-$, $[ArF]^+[AuF_6]^-$, $[ArF]^+[Sb_2F_{11}]^-$, and $[ArF]^+[Au_2F_{11}]^-$ could be isolable, since the fluoride ion affinities of SbF_5 and AuF_5 are large enough

Table 2. Calculated bond lengths r [pm] (MP2-approximation).[16]

	r(F–Ar)	r(Ar···F)
$F–Ar^+\cdots SbF_6^-$	194.9	193.0
$F–Ar^+\cdots AuF_6^-$	184.7	192.9
$F–Ar^+\cdots Sb_2F_{11}^-$ (*cis*)[a]	183.6	191.9
$F–Ar^+\cdots Au_2F_{11}^-$ (*trans*)[a]	173.9	201.6

[a] *cis* and *trans* bridging at the central Sb and Au atom, respectively. The corresponding other isomers are energetically marginally less favorable.

(see Table 2).[13] The calculations of these ion pairs is simplified by the fact that a linear F–Ar···F array can be assumed, also in the crystal, as is found in XeF^+, KrF^+, and $XeCl^+$. Thus, any further interionic interaction of these ion pairs can be neglected in a first approximation. Similar calculations have been presented recently for the KrF^+ ion with various counterions.[9] We interpret the change of the two bond lengths at the argon atom as an increased kinetic stability, that is, $[FAr]^+[SbF_6]^- < [FAr]^+[AuF_6]^- \sim [FAr]^+[Sb_2F_{11}]^- < [FAr]^+[Au_2F_{11}]^-$. But even for the most favorable case $[FAr]^+[Au_2F_{11}]^-$, the decomposition into Ar, F_2, and Au_2F_{10} is exothermic by -231 kJ mol^{-1}. The isolation of an argon compound in the condensed phase, in other words not under matrix or mass spectrometric conditions, remains a formidable task.

Experimental Section

A PFA reaction tube (polyperfluoroethylene-perfluorovinylether-copolymer) with an internal diameter of 6.5 mm was filled in a dry box (< 1 ppm H_2O) with XeF_2 (320 mg, 2 mmol), SbF_5 (2.67 g, 12 mmol), and $SbCl_5$ (60 mg, 0.2 mmol). With the help of a stainless steel vacuum line HF (650 mg, 32.5 mmol) was condensed onto the reaction mixture and the reaction tube was sealed. After brief warming to room temperature a blue solution formed, from which on slow cooling to $-30\,^\circ$C orange crystals deposited. Raman spectrum (1064 nm, $-120\,^\circ$C, solid, cm^{-1}): $\tilde{\nu} = 683$ (62), 672 (100), 649 (55), 614 (82), 493 (16), 391 (50), 383 (sh), 301 (40), 282 (19), 263 (19), 228 (38); ^{129}Xe NMR (HF/SbF_5, 17 °C, $XeOF_4$, 110.45 MHz): $\delta = -551$ (br d, separation: 5165 Hz, $\tau_{1/2} = 8084$ Hz).

Crystal structure determination: A suitable crystal was mounted on a Bruker SMART-CCD-1000 TM diffractometer with help of a special device[14] under cooling and inert gas, and measured.[6] After semiempirical absorption correction by equalizing symmetry-equivalent reflections (SADABS), the structure solution and refinement were carried out with the SHELX programs.[15, 16]

Ab initio calculations: Program Gaussian 98.[16] Møller – Plesset second-order correlation energy correction (MP2) as implemented in the Gaussian program,[17] , as well as coupled-cluster calculation with single and double substitution (CCSD). Basis sets: F, Cl, Ar: 6-311 + G(d,p), as implemented in the Gaussian program, Kr, Xe, Br, I, As, Sb: Relativistically corrected basis sets for the valence electrons and pseudo potentials for the 28 (Kr, Br, As) and 46 (Xe, I, Sb) core electrons.

Further details on the crystal structure investigations may be obtained from the Fachinformationszentrum Karlsruhe, 76344 Eggenstein-Leopoldshafen, Germany (fax: (+49) 7247-808-666; e-mail: crysdata@fiz-karlsruhe.de), on quoting the depository numbers CSD-411897 ($[XeCl]^+[Sb_2F_{11}]^-$) and CSD-411868 ($[XeF]^+[SbF_6]^-$).

Received: June 29, 2001 [Z 17395]

[1] L. Y. Nelson, G. C. Pimentel, *Inorg. Chem.* **1967**, *6*, 1758 – 1759; I. R. Beattie, A. German, H. E. Blayden, S. B. Brumbach, *J. Chem. Soc. Dalton Trans.* **1975**, 1659 – 1662; D. Boal, G. A. Ozin, *Spectrosc. Lett.* **1971**, *4*, 43 – 46; G.-J. Perlow, M. R. Perlow, *J. Chem. Phys.* **1967**, *48*, 955 – 961.

 © WILEY-VCH Verlag GmbH, D-69451 Weinheim, 2001 1433-7851/01/4022-4226 $ 17.50+.50/0

[2] H. Meinert, *Z. Chem.* **1966**, *6*, 71.
[3] R. D. Willet, S. W. Peterson, B. A. Coyle, *J. Am. Chem. Soc.* **1977**, *99*, 8202 – 8208.
[4] H.-J. Frohn, T. Schoer, G. Henkel, *Angew. Chem.* **1999**, *111*, 2751 – 2753; *Angew. Chem. Int. Ed.* **1999**, *38*, 2554 – 2556.
[5] S. Seidel, K. Seppelt, *Angew. Chem.* **2000**, *112*, 4072 – 4074; *Angew. Chem. Int. Ed.* **2000**, *39*, 3923 – 3925.
[6] $[XeCl]^+[Sb_2F_{11}]^-$: orthorhombic, space group $Pna2_1$, $a = 1778.8(3)$, $b = 744.8(1)$, $c = 1708.7(2)$ pm, $V = 2263.9 \times 10^6\,pm^3$, $T = -150\,^\circ C$, $Z = 8$, $Mo_{K\alpha}$ radiation, graphite monochromator, scan width 0.3° in ω, 10 s per frame, 1800 frames, 37397 measured reflections, 6843 independent reflections, 273 parameters, $R(F \geq \sigma(F)) = 0.0365$, $wR_2 = 0.0745$.
[7] R. T. Weigner, *Phys. Rev.* **1947**, *72*, 1268 – 1269; K. H. Bowijk, J. van der Heide, A. Vos, E. H. Wiebenga, *Acta Crystallogr.* **1956**, *9*, 274 – 277; G. B. Carpenter, S. M. Richards, *Acta Crystallogr.* **1961**, *15*, 360 – 364.
[8] V. M. McRae, R. D. Peacock, D. R. Russell, *Chem. Commun.* **1969**, 62 – 63.
[9] J. F. Lehmann, D. A. Dixon, G. J. Schrobilgen, *Inorg. Chem.* **2001**, *40*, 3002 – 3017.
[10] F. O. Sladky, P. A. Bulliner, N. Bartlett, *J. Chem. Soc. A* **1969**, 2179 – 2188; H. Willner, M. Bodenbinder, R. Bröchler, G. Hwang, S. J. Rettig, J. Trotter, B. von Ahsen, U. Westphal, V. Jonas, W. Thiel, F. Aubke, *J. Am. Chem. Soc.* **2001**, *123*, 588 – 602.
[11] T. M. Klapötke, *Heteroat. Chem.* **1997**, *8*, 473 – 478.
[12] S. Frenking, W. Koch, C. A. Dea Kyne, J. F. Liebmann, N. Bartlett, *J. Am. Chem. Soc.* **1989**, *111*, 31 – 33.
[13] K. O. Christe, D. A. Dixon, D. Mc Lemore, W. W. Wilson, J. A. Sheely, J. A. Boatz, *J. Fluorine Chem.* **2000**, *101*, 151 – 153; I.-C. Hwang, K. Seppelt, *Angew. Chem.* **2001**, *113*, 3803 – 3805; *Angew. Chem. Int. Ed.* **2001**, *39*, 3690 – 3693.
[14] H. Schumann, W. Genthe, E. Hahn, M.-B. Hossein, D. von der Helm, *J. Organomet. Chem.* **1986**, *28*, 2561 – 2567.
[15] G. Sheldrick, Program for Crystal Structure Solution, Göttingen, **1986**.
[16] G. Sheldrick, Program for Crystal Structure Refinement, Göttingen, **1993**.
[17] Gaussian 98, M. J. Frisch, G. W. Trucks, H. B. Schlegel, G. E. Scuseria, M. A. Robb, J. R. Cheeseman, V. G. Zakrzewski, J. A. Montgomery, R. E. Stratmann, J. C. Burant, S. Dapprich, J. M. Millam, A. D. Daniels, K. N. Kudin, M. C. Strain, O. Farkas, J. Tomasi, V. Barone, M. Cossi, R. Cammi, B. Mennucci, C. Pomelli, C. Adamo, S. Clifford, J. Ochterski, G. A. Petersson, P. Y. Ayala, Q. Cui, K. Morokuma, D. K. Malick, A. D. Rabuck, K. Raghavachari, J. B. Foresman, J. Cioslowski, J. V. Ortiz, A. G. Baboul, B. B. Stefanov, G. Liu, A. Liashenko, P. Piskorz, I. Komaromi, R. Gomperts, R. L. Martin, D. J. Fox, T. Keith, M. A. Al-Laham, C. Y. Peng, A. Nanayakkara, C. Gonzalez, M. Challacombe, P. M. W. Gill, B. G. Johnson, W. Chen, M. W. Wong, J. L. Andres, M. Head-Gordon, E. S. Replogle, J. A. Pople, Gaussian, Inc., Pittsburgh, PA, **1998**. Ar, Cl, F: basis sets 6-311 + G(d,p) and As, Sb, Kr, Xe, Au: basis sets and pseudo potentials from the Institut für Theoretische Chemie, Universität Stuttgart.
[18] $[XeF]^+[SbF_6]^-$: yellow crystals, obtained from $XeF_2/HF/SbF_5$ solution: $a = 573.8(2)$, $b = 1087.7(2)$, $c = 1095.9(2)$ pm, $\beta = 93.92(2)^\circ$, $V = 639.6 \times 10^6\,pm^3$, $Z = 4$, $P21/c$, $Mo_{K\alpha}$, $Z = 71.069$ pm, $\rho = 4.009\,g\,cm^{-3}$, $2\theta_{max} = 60^\circ$, 2000 measured, 1760 independent reflections ($R_{int} = 0.0144$), absorption correction psi-scan method by measuring seven reflections with $\chi > 80^\circ$ in 36 steps in psi, $T_{max} = 1.0$, $T_{min} = 0.76$, 83 parameters, $R_1 = 0.0189$, $wR_2 = 0.0506$.

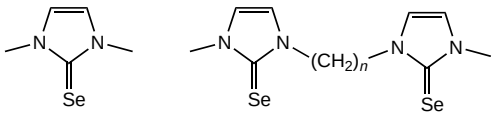
1,2-Bis(3-methyl-imidazolin-2-ylium iodobromoselenanide)ethane: Oxidative Addition of IBr at the Se Atom of a >C=Se Group**

M. Carla Aragoni, Massimiliano Arca, Alexander J. Blake, Francesco A. Devillanova,* Wolf-Walther du Mont, Alessandra Garau, Francesco Isaia, Vito Lippolis,* Gaetano Verani, and Claire Wilson

It is well known that chalcogen(II) halides can be stabilized as adducts of Lewis bases.[1] The most common synthetic approach to such adducts is the reduction of chalcogen(IV) halides in the presence of electron pair donors that may also act as reducing agents.[2] An alternative method to such adducts is the oxidative addition of halogens to chalcogen-containing molecules.[3, 4] As an example, addition of Cl_2 to 1,3-dimethylimidazoline-2-thione[5] gives a stable 10-S-3 hypervalent[6–8] "T-shaped" compound featuring a linear Cl-S-Cl group: the product can also be regarded as an adduct between 1,3-dimethylimidazolin-2-ylidene and SCl_2.[7, 9, 10]

No "T-shaped" S adducts with I_2 have so far been reported, whereas two with Br_2 have been structurally characterized only very recently.[11] On the other hand, analogous Se adducts with Br_2 are numerous,[12b–14] and examples with I_2 have recently been reported.[15, 16] However, the reaction of halogens (X_2) with donor molecules containing the >C=E (E = S, Se) group do not systematically give 10-E-3 hypervalent "T-shaped" compounds, instead a great variety of products can be isolated depending on the identity of the halogen, the chemical environment around the chalcogen carbonyl group and, in some cases, the nature of the solvent and the reaction conditions.[14] In addition to adducts featuring approximately linear E-X-X groups and X-E-X groups, $[>C{-}E{-}E{-}C<]^{2+}$ dicationic species containing a chalcogen–chalcogen bond, and $[>C{-}E{-}X{-}E{-}C<]^{+}$ cations featuring a central X^+ ion linearly coordinated by two chalcogenone molecules have also been described.[14] Compounds belonging to the aforementioned structural archetypes can also be isolated from reactions with interhalogens IX (X = Br, Cl), but surprisingly no "T-shaped" adducts featuring I-E-X (E = S, Se) moieties have been reported so far, indicating a very low tendency of interhalogens to undergo oxidative addition to chalcogen donor atoms and in particular to chalcogen carbonyl >C=E groups.

Recently, we have studied the reactivity of imidazoline-2-selone derivatives **1**–**3** towards I_2[15a] and Br_2.[13a] Hypervalent "T-shaped" compounds containing Br-Se-Br groups were



1 **2** (n = 1) **3** (n = 2)

isolated from the reaction of the three donors with Br_2. Structurally analogous I_2 adducts were isolated only with **1** and **3**, whereas a charge transfer adduct featuring Se-I-I groups was obtained in the case of **2**. We report herein the results of our studies on the reactivity of 1,2-bis(3-methyl-imidazoline-2-selone)ethane (**3**) with IBr.

The reaction of **3** with IBr in MeCN solution in a 1:2 molar ratio gives red-orange crystals of **3**·2IBr after slow evaporation of the solvent. X-ray structure analysis[17] reveals that the compound is the first "T-shaped" selenium adduct featuring I-Se-Br groups (Figure 1). The two I-Se-Br groups are approximately linear; the Se–I bonds are unexpectedly shorter than the Se–Br bonds. Moreover, while the two Se–I bond lengths are similar (2.606(2) in unit A and 2.629(2) Å in unit B, Figure 1), the lengths of the two associated Se–Br bonds differ considerably (2.897(2) in unit A and 2.766(2) Å

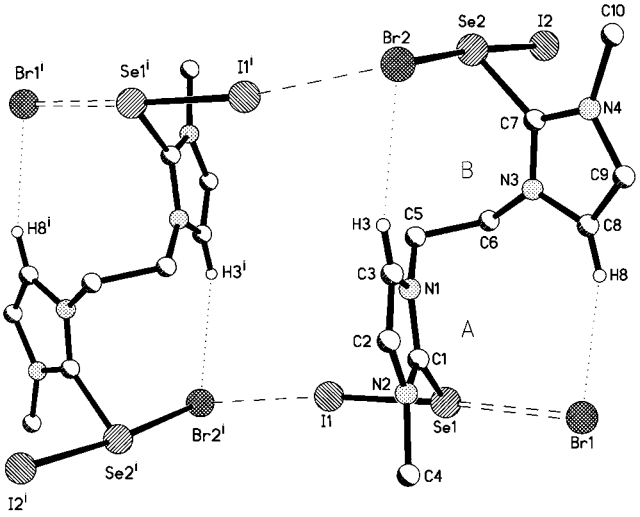


Figure 1. View of a dimeric unit of **3**·2IBr with the numbering scheme adopted. For clarity only those atoms involved in intramolecular hydrogen bonds are shown. A refers to the I-Se-Br system having the longer Se–Br bond (double dashed lines), B to the one with the shorter Se–Br distance. Single dashed and dotted lines denote intermolecular I···Br contacts and intramolecular hydrogen bonds, respectively. Selected bond lengths [Å] and angles [°]: C1-Se1 1.894(9), C7-Se2 1.890(9), Se1-Br1 2.897(2), Se2-Br2 2.766(2), Se1-I1 2.606(2), Se2-I2 2.629(2); C7-Se2-Br2 83.2(3), C1-Se1-I1 95.6(3), C7-Se2-I2 90.6(3), I1-Se1-Br1 175.52(5), I2-Se2-Br2 173.80(5); symmetry code i: $2-x$, $1-y$, $1-z$.

[*] Prof. F. A. Devillanova, Prof. Dr. V. Lippolis, Dr. M. C. Aragoni, Dr. M. Arca, Dr. A. Garau, Dr. F. Isaia, Prof. G. Verani
Dipartimento di Chimica Inorganica e Analitica
The University of Cagliari
S.S. 554 bivio per Sestu, 09042 Monserrato-Cagliari (Italy)
Fax: (+39) 0706754456
E-mail: devilla@vaxca1.unica.it, lippolis@vaxca1.unica.it
Dr. A. J. Blake, Dr. C. Wilson
School of Chemistry, The University of Nottingham
University Park, Nottingham, NG7 2RD (UK)
Prof. Dr. W.-W. du Mont
Institut fur Anorganische und Analytische Chemie der Technischen Universität
38023 Braunschweig (Germany)

[**] This work was supported by the Consiglio Nazionale delle Ricerche (Italy) "Progetto Finalizzato Materiali Speciali per Tecnologie Avanzate II"

Supporting information for this article is available on the WWW under http://www.angewandte.com or from the author.

in unit B (shown as double dashed lines in Figure 1)). The conformation of the molecule is determined by two intramolecular hydrogen bonding interactions (shown as dotted lines in Figure 1) that involve the two bromine atoms (Br1 ··· H8 2.743 Å, Br1 ··· H8-C8 160°; Br2 ··· H3 2.855 Å, Br2 ··· H3-C3 155.1°). Furthermore, two symmetry-related **3**·2IBr adduct units interact through I ··· Br contacts (I1 ··· Br2^{i}, 3.601(2) Å shown as single dashed lines in Figure 1) to form dimeric assemblies. The packing of these dimers is determined by long I ··· I and I ··· Se contacts that range from 3.992(2) to 4.115(3) Å.

Since in **3**·2IBr the order of Se–Br and Se–I bond lengths is reversed with respect to that expected on the basis of the atomic radii, density functional theory (DFT) calculations[20] were carried out on the I_2, Br_2, and IBr, Se-hypervalent adducts of **1** as model compounds and on the cations $[\mathbf{1}\cdot X]^+$ (X = I, Br) to understand the nature of the chemical bond in X-Se-Y systems (X, Y = I, Br) and their donor–acceptor and vibrational properties. On the whole, a very good agreement is found between the optimized geometries of the organic frameworks and the corresponding experimental structural data for $\mathbf{1}\cdot Br_2$,[13b] $\mathbf{1}\cdot I_2$,[15a] $\mathbf{3}\cdot 2Br_2$,[13a] and **3**·2IBr (see Supporting Information for calculated data). The Se–Br bond length calculated for $\mathbf{1}\cdot Br_2$ (2.602 Å) is quite close to the mean value observed in the structure of $\mathbf{1}\cdot Br_2$ (2.575 Å)[13b] and $\mathbf{3}\cdot 2Br_2$ (2.591 Å),[13a] whereas the Se–I bond length calculated for $\mathbf{1}\cdot I_2$ (2.983 Å) is longer than those found in the structures of $\mathbf{1}\cdot I_2$ and $\mathbf{3}\cdot 2I_2$ (mean values 2.812 and 2.821 Å, respectively).[15a] As expected the Se–I distance (2.964 Å) is calculated to be longer than the Se–Br distance (2.794 Å) in **1**·IBr. The Se–X bond lengths calculated for the $[\mathbf{1}\cdot X]^+$ ions (2.539 (X = Br), 2.722 Å (X = I)) are shorter than those calculated for the hypervalent systems, and this shortening is accompanied by an opening of the C-Se-X angle, which increases from 84.3° in $\mathbf{1}\cdot Br_2$ to 97.2° in $[\mathbf{1}\cdot Br]^+$ and from 85.4° in $\mathbf{1}\cdot I_2$ to 98.3° in $[\mathbf{1}\cdot I]^+$. The widening of this angle seems to represent the most sensitive structural variation induced in the Se-hypervalent system upon lengthening of one Se–X bond towards the formation of the $[>C–Se–X]^+$ ion. In this respect unit A in **3**·2IBr (Figure 1), which has a C-Se-I angle of 95.6(3)°, very close to the value of 98.3° calculated for the cation $[\mathbf{1}\cdot I]^+$, can be considered as a $[>C–Se–I]^+$ ion interacting with a Br^- ion through the chalcogen (Se ··· Br 2.897(2) Å). Unit B, which features a shorter Se–Br bond length (2.766(2) Å) and a C-Se-I angle of only 90.6(3)°, can be regarded as being closer to a purely covalent "T-shaped" system.

On passing from the $[\mathbf{1}\cdot X]^+$ ions to the corresponding "T-shaped" adducts the calculated natural bond orbital (NBO) charges (Table 1) on the organic frameworks remain almost unaltered; the selenium atom is partially positively charged in all cases, while the charges on the halogens become considerably negative. In $\mathbf{1}\cdot I_2$ and $\mathbf{1}\cdot Br_2$ the terminal halogen atoms carry a negative charge (−0.393 for $\mathbf{1}\cdot I_2$ and −0.449 e for $\mathbf{1}\cdot Br_2$; see Table 1) equally distributed over the two halogen atoms. In the case of **1**·IBr a negative charge of −0.834 e is unevenly distributed over two halogens with −0.447 e on the more electronegative Br (Table 1). Therefore, the charge distribution calculated on the I-Se-Br moiety in **1**·IBr indicates a more ionic character for the Se–Br bond compared to the Se–I bond.

Table 1. Calculated NBO charges (e) on the N, C, Se, and halogen atoms in **1**, $\mathbf{1}\cdot I_2$, $\mathbf{1}\cdot Br_2$, **1**·IBr, and $[\mathbf{1}\cdot X]^+$ (X = I and/or Br).[a]

	1	$[\mathbf{1}\cdot Br]^+$	$\mathbf{1}\cdot Br_2$	$[\mathbf{1}\cdot I]^+$	$\mathbf{1}\cdot I_2$	**1**·IBr
N	−0.438	−0.376	−0.340	−0.379	−0.392	−0.392/−0.391[b]
C	0.225	0.216	0.224	0.226	0.271	0.275
Se	−0.268	0.355	0.354	0.244	0.212	0.259
I				0.051	−0.393	−0.387
Br		−0.074	−0.449			−0.447

[a] Although the trend in the calculated NBO charges accounts fairly well for the different polar nature of the Se–I and Se–Br bonds, the natural bond orbitals are not well-suited for getting reliable information on Se–X bond orders, since this localized-bond model tends to give limiting ionic forms according to a Lewis formalism. [b] The I-Se-Br moiety is not exactly perpendicular to the ring plane (Br-Se-C-N dihedral angles 97.27 and −81.40°). Therefore a slight difference in the charge on the two nitrogen atoms is observed.

In **3**·2IBr, the intramolecular Br ··· H hydrogen bonding interactions (Figure 1) contribute to a further polarization of the Se–Br bond by stabilizing an increased electronic charge on the Br atom, which leads to the formation of the $[>C–Se–I]^+ \cdots Br^-$ ionic pair. In particular, the two different intramolecular hydrogen bonds stabilize the Br atom at different distances from the selenium atom in units A and B (see Figure 1). In agreement with the calculations, the more ionic the Se–Br bond the shorter the Se–I bond length; in **3**·2IBr the two Br-Se-I groups adopt different intermediate situations between the two limiting cases: purely ionic $[I–Se]^+ \cdots Br^-$ and purely covalent I-Se-Br. In both systems the polarization of the Se–Br bond is such as to reverse the order of the Se–Br and Se–I bond lengths predicted for a purely covalent model.

The intermolecular I ··· Br contacts responsible for the formation of the dimeric units in the crystal structure of **3**·2IBr are consistent either with the calculated charge distribution on the model adducts **1**·IBr (Table 1) or the more ionic character for the Se-hypervalent system in unit A (Figure 1). Indeed, these contacts involve I1, an atom which should carry a small positive charge (see $[\mathbf{1}\cdot I]^+$ ion in Table 1), and Br2^{i}, which belongs to the less ionic Se-hypervalent system of the symmetry-related adduct molecule, an atom which should carry a partial negative charge (see $\mathbf{1}\cdot Br_2$ and **1**·IBr in Table 1). The directionality of these intermolecular I ··· Br contacts (Se2-Br2 ··· I1^{i} 86.84(4)°) can be explained by the nature of the calculated Khon–Sham HOMO and LUMO (Figure 2) on the basis of a donor/acceptor interaction between the π*-HOMO centered on the Se-hypervalent system in unit A of one adduct molecule and the σ*-LUMO centered on the more ionic I-Se-Br system in unit B of the symmetry-related adduct molecule.

Confirmation of the different bonding situations in the two I-Se-Br systems in **3**·2IBr is provided by FT-Raman and FT-IR spectra (300–100 cm^{-1}) of powdered crystals (Figure 3). Owing to the complexity of both spectra, we have calculated the normal vibrational modes for $[\mathbf{1}\cdot I]^+$ and **1**·IBr and simulated the sum of their IR (Figure 4) and Raman spectra to make assignments. In the IR spectrum three main groups of bands, centered at 270, 185, and 130 cm^{-1}, can be identified for

 © WILEY-VCH Verlag GmbH, D-69451 Weinheim, 2001 1433-7851/01/4022-4230 $ 17.50+.50/0 *Angew. Chem. Int. Ed.* **2001**, *40*, No. 22

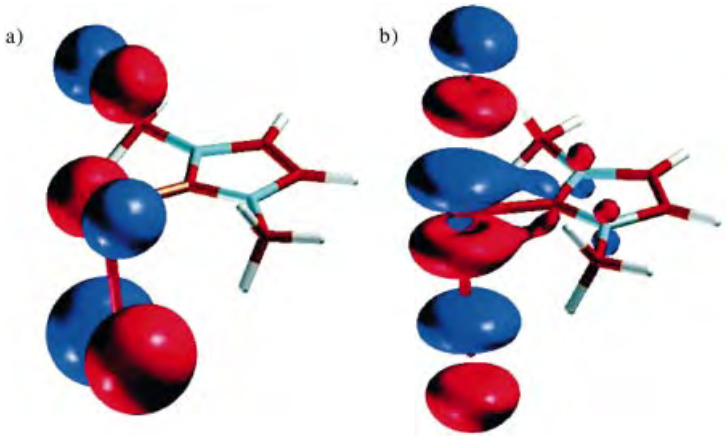


Figure 2. The Kohn–Sham HOMO (a) and LUMO (b) calculated for **1**·IBr. Neither of them contain any contribution from d orbitals of the Se atom. Therefore, from a Lewis point of view, there is no formal octect expansion and both chalcogen–halogen bond orders have to be considered less than one. The same orbital composition is calculated for **1**·Br_2 and **1**·I_2.

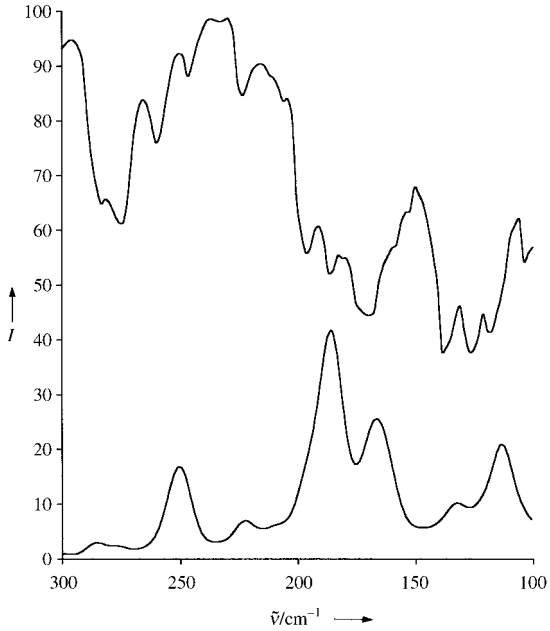


Figure 3. Experimental FT-IR (top) and FT-Raman spectra (bottom) for **3**·IBr in the low frequency region (100–300 cm^{-1}).

both $[\mathbf{1}\cdot I]^+$ and **1**·IBr. The group with the highest frequency can be attributed mainly to a C-Se-I bending mode (279 for $[\mathbf{1}\cdot I]^+$ and 268 cm^{-1} for **1**·IBr). The envelope of very strong bands at about 185 cm^{-1} in the simulated spectrum is due to an N-C-Se bending mode in the imidazoline ring plane (196 cm^{-1}) and to the same vibration coupled to the Se–Br stretch (185 cm^{-1}) for **1**·IBr. The contribution of the N-C-Se bending mode of the cation to this envelope is very small. The two weak bands calculated at 140 and 120 cm^{-1} for $[\mathbf{1}\cdot I]^+$ and **1**·IBr, respectively, are mainly due to rotation of the methyl groups coupled with a stretching vibration of the I-Se-Br moiety for **1**·IBr. Examination of the recorded vibrational spectra for **3**·2IBr (Figure 3) indicates a good correspondence between the IR and Raman bands, with interesting similarities with the simulated spectrum of Figure 4 (red line), thereby confirming the different nature of the bonds in the two I-Se-Br groups. Evidently, an exact match between the calculated and experimental spectra would be unrealistic because the organic frameworks of **1** and **3** are different, and

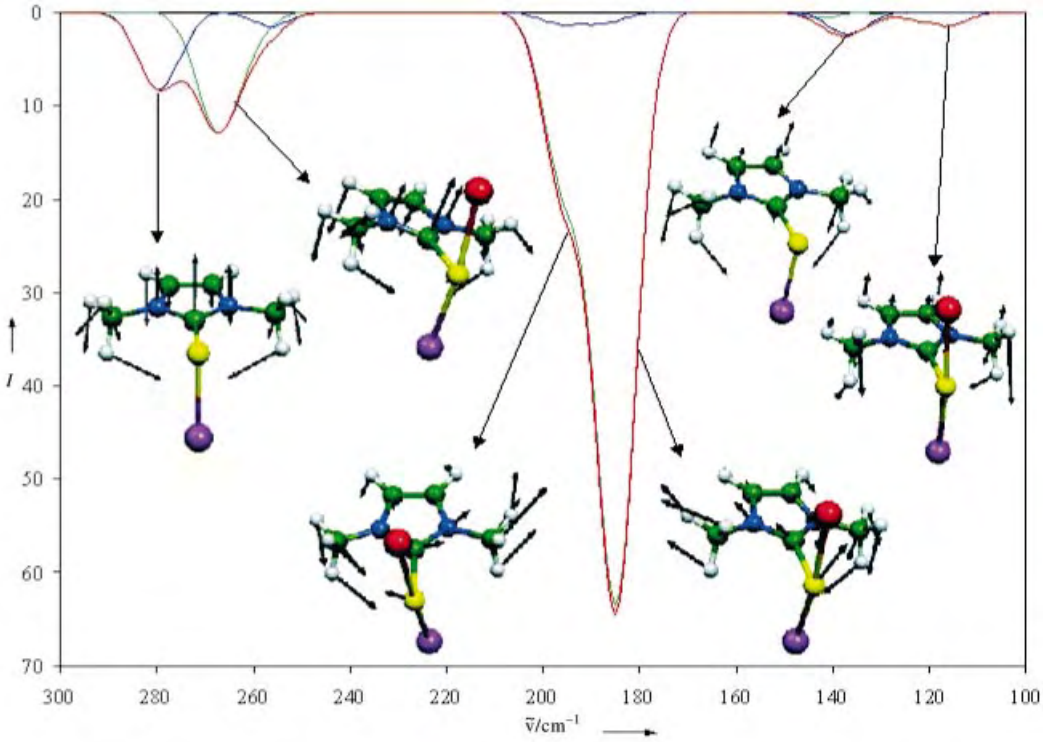


Figure 4. Simulated IR spectrum (100–300 cm^{-1}) based on normal mode DFT calculations for **1**·IBr (green line), $[\mathbf{1}\cdot I]^+$ (blue line), and sum of the two (red line), together with representations of the calculated normal modes.

 © WILEY-VCH Verlag GmbH, D-69451 Weinheim, 2001 1433-7851/01/4022-4231 $ 17.50+.50/0

$[\mathbf{1}\cdot I]^+$ and $\mathbf{1}\cdot IBr$ represent the two extremes in the bond nature of these new "T-shaped" adducts: ionic $[>C\text{-}Se\text{-}I]^+\cdots Br^-$ and covalent I-Se-Br.[29]

Received: May 21, 2001
Revised: August 6, 2001 [Z17146]

[1] K. J. Wynne in *Sulfur Research Trends, Advances in Chemistry Series 110* (Eds.: D. J. Miller, T. K. Wiewiorowski), American Chemical Society, Washington, DC, **1972**, p. 150.
[2] B. Krebs, F.-P. Ahlers, *Adv. Inorg. Chem.* **1990**, *35*, 235.
[3] K. J. Wynne, P. S. Pearson, M. G. Newton, J. Golen, *Inorg. Chem.* **1972**, *11*, 1192.
[4] D. J. Williams, K. J. Wynne, *Inorg Chem.* **1976**, *15*, 1449.
[5] A. J. Arduengo, E. M. Burgess, *J. Am. Chem. Soc.* **1977**, *99*, 2376.
[6] The currently used notation 10-E-3 hypervalent adducts for X-E(R)-X "T-shaped" systems (R = organic framework), proposed by Arduengo et al.,[7] implies that 10 electrons are *formally* associated with E, to which three atoms are bonded. This notation identifies this class of compounds properly and concisely, considering that the term hypervalent not necessary requires the involvement of a d orbital from the central E atom for explaining the bond nature of the X-E(R)-X system.[8]
[7] C. W. Perkins, J. C. Martin, A. J. Arduengo, W. Lau, A. Alegrie, J. K. Kocki, *J. Am. Chem. Soc.* **1980**, *102*, 7753.
[8] *Chemistry of hypervalent compounds* (Ed.: K.-y. Akiba), Wiley-WCH, New York, **1999**.
[9] N. Kuhn, H. Kotowski, T. Kratz, G. Henkel, *Phosphorus Sulfur Silicon Relat. Elem.* **1998**, *136*, 517.
[10] a) A. J. Arduengo III, K. U. R. Dias, R. L. Harlow, M. Kline, *J. Am. Chem. Soc.* **1992**, *114*, 5530; b) A. J. Arduengo III, H. V. Rasila Dias, J. C. Calabrese, *Chem. Lett.* **1997**, 143, and references therein.
[11] a) P. S. Skabara, N. Bricklebank, R. Berridge, S. Long, M. E. Light, S. J. Coles, M. Hursthouse, *J. Chem. Soc. Dalton Trans.* **2000**, 3235; b) M. C. Aragoni, M. Arca, F. Demartin, F. A. Devillanova, A. Garau, F. Isaia, F. Lelj, V. Lippolis, G. Verani, *Chem. Eur. J.* **2001**, *7*, 3122.
[12] a) M. Godfrey, C. A. McAuliffe, R. G. Pritchard, S. Sarwar, *J. Chem. Soc. Dalton Trans.* **1997**, 1031; b) S. M. Godfrey, S. L. Jackson, C. A. McAuliffe, R. G. Pritchard, *J. Chem. Soc. Dalton Trans.* **1998**, 4201.
[13] a) F. Bigoli, P. Deplano, F. A. Devillanova, V. Lippolis, M. L. Mercuri, M. A. Pellinghelli, E. F. Trogu, *Eur. J. Inorg. Chem.* **1998**, 137; b) D. J. Williams, D. Venderveer, B. R. Crouse, R. R. Raye, T. Carter, K. S. Hagen, M. Brewer, *Main Group Chem.* **1997**, *2*, 61.
[14] M. C. Aragoni, M. Arca, F. Demartin, F. A. Devillanova, A. Garau, F. Isaia, V. Lippolis, G. Verani, *Trends Inorg. Chem.* **1999**, *6*, 1, and references therein.
[15] a) F. Bigoli, P. Deplano, F. A. Devillanova, F. Isaia, V. Lippolis, M. L. Mercuri, M. A. Pellinghelli, E. F. Trogu, *Gazz. Chim. Ital.* **1994**, *124*, 445; b) N. Kuhn, T. Kratz, G. Henkel, *Chem. Ber.* **1994**, *127*, 849.
[16] W.-W. du Mont, A. Martens-von Salzen, F. Ruthe, E. Seppälä, G. Mugesh, F. A. Devillanova, V. Lippolis, N. Kuhn, *J. Organomet. Chem.* **2001**, *623*, 14.
[17] Crystals of $\mathbf{3}\cdot 2IBr$ were grown by slow evaporation of a MeCN solution of **3** and IBr in 1:2 molar ratio. Elemental analysis: calcd. for $C_{10}H_{14}Br_2I_2N_4Se_2$: C 15.77, H 1.84, N 7.35; found: C 15.55, H 1.80, N 7.25. Crystal structure analyses: Stoë Stadi-4 four-circle diffractometer, graphite-monochromated $Mo_{K\alpha}$ radiation, $T = 150(2)$ K, $\theta_{max} = 26^\circ$. The structure was solved by using direct methods[18] and all non-hydrogen atoms were located in subsequent difference Fourier syntheses.[19] Hydrogen atoms were placed in calculated positions and were allowed to ride on their parent atoms during refinement. $\mathbf{3}\cdot 2IBr$: $C_{10}H_{14}Br_2I_2N_4Se_2$, $M_r = 761.79$, triclinic, $P\bar{1}$ (no. 2), $a = 7.767(4)$, $b = 9.940(3)$, $c = 13.524(5)$ Å, $\alpha = 96.41(3)$, $\beta = 106.23(3)$, $\gamma = 106.49(4)^o$, $V = 940.4(7)$ Å^3, $Z = 2$, $F(000) = 692$, $\rho_{calcd} = 2.690$ g cm^{-3}, $\mu(Mo_{K\alpha}) = 11.460$ mm^{-1}, dark red trigonal prism ($0.27 \times 0.27 \times 0.16$ mm^3). Numerical absorption corrections ($T_{max} = 0.200$, $T_{min} = 0.0807$), 3693 unique reflections, of which 3124 had $I \geq 2\sigma(I)$. The weighting scheme $w^{-1} = [\sigma^2(F_o^2) + (0.070P)^2 + 15.93P]$, $P = 1/3[MAX(F_o^2,0) + 2F_c^2]$, was applied. At final convergence $R_1 = (I \geq 2\sigma(I)) = 0.0515$, wR_2 (all data) $= 0.1322$ for 183 refined parameters, $S = 1.045$, $(\Delta/\sigma)_{max} = 0.347$, $\Delta\rho_{max} = 1.95$ e Å^{-3} (near heavy atoms). Crystallographic data (excluding structure factors) for the structures reported in this paper have been deposited with the Cambridge Crystallographic Data Centre as supplementary publication no. CCDC-163716. Copies of the data can be obtained free of charge on application to CCDC, 12 Union Road, Cambridge CB2 1EZ, UK (fax: (+44) 1223-336-033; e-mail: deposit@ccdc.cam.ac.uk).
[18] SHELXS-97: G. M. Sheldrick, *Acta Crystallogr. Sect. A* **1990**, *46*, 467.
[19] G. M. Sheldrick, SHELXL-97, Universität Göttingen, Germany, **1997**.
[20] Quantum-chemical calculations on isolated molecules of $\mathbf{1}\cdot I_2$, $\mathbf{1}\cdot Br_2$, $\mathbf{1}\cdot IBr$, and $[\mathbf{1}\cdot X]^+$(X = I, Br) were carried out according to DFT[21] using Gaussian 94,[22a] with the hybrid Becke3LYP functional.[23] The basis sets for the calculations on $[\mathbf{1}\cdot X]^+$, $\mathbf{1}\cdot I_2$, and $\mathbf{1}\cdot IBr$ were the Schafer, Horn, and Ahlrichs pVDZ basis[24] for C, H, N, and Se, while for I and Br we used the Hay–Wadt LANL2DZ basis sets together with effective core potentials.[25] The all-electron former basis set is available for Se and Br but not for the heavier iodine atom. Therefore, in order to be able to compare Se–halogen bonds, the same Hay–Wadt LANL2DZ ECP basis was used for the halogen atoms. In the case of $\mathbf{1}\cdot Br_2$, SCF convergence problems were found, and although several alternative convergence methods were tried, we were able to achieve convergence only with the 6-31G** basis set. Harmonic IR and Raman frequencies were obtained for $\mathbf{1}\cdot I_2$ and $[\mathbf{1}\cdot X]^+$ by using the second derivatives of the DFT energy, computed by numerical differentiation of the DFT energy gradients.[22] Finally, NBO calculations[26] were performed for each molecule using the converged density matrix corresponding to the equilibrium geometries. Molden 3.6[27] was used to investigate the shape of the calculated Kohn–Sham orbitals. Calculated unscaled harmonic frequencies were extracted from the output file and converted into a simulated spectrum with the TABFREQ program, using DFT-calculated intensities and a half bandwidth of 10 cm^{-1}. Analysis and drawings of molecular vibrations were performed with the program Molekel.[28]
[21] a) T. Ziegler, *Can. J. Chem.* **1995**, *73*, 743; b) J. Labanowsky, J. Andzelm, *Density Functional Methods in Chemistry*, Springer, New York, **1991**.
[22] a) M. J. Frisch, G. W. Trucks, H. B. Schlegel, P. M. W. Gill, B. G. Johnson, M. W. Wong, J. B. Foresman, M. A. Robb, M. Head-Gordon, E. S. Replogle, R. Gomperts, J. L. Andres, K. Raghavachari, J. S. Binkley, C. Gonzalez, R. L. Martin, D. J. Fox, D. J. Defrees, J. Baker, J. J. P. Stewart, J. A. Pople, Gaussian 94/DFT, Gaussian, Inc., Pittsburgh, PA, **1994**; b) Gaussian 98 (Revision A.7), M. J. Frisch, G. W. Trucks, H. B. Schlegel, G. E. Scuseria, M. A. Robb, J. R. Cheeseman, V. G. Zakrzewski, J. A. Montgomery, R. E. Stratmann, J. C. Burant, S. Dapprich, J. M. Millam, A. D. Daniels, K. N. Kudin, M. C. Strain, O. Farkas, J. Tomasi, V. Barone, M. Cossi, R. Cammi, B. Mennucci, C. Pomelli, C. Adamo, S. Clifford, J. Ochterski, G. A. Petersson, P. Y. Ayala, Q. Cui, K. Morokuma, D. K. Malick, A. D. Rabuck, K. Raghavachari, J. B. Foresman, J. Cioslowski, J. V. Ortiz, B. B. Stefanov, G. Liu, A. Liashenko, P. Piskorz, I. Komaromi, R. Gomperts, R. L. Martin, D. J. Fox, T. Keith, M. A. Al-Laham, C. Y. Peng, A. Nanayakkara, C. Gonzalez, M. Challacombe, P. M. W. Gill, B. G. Johnson, W. Chen, M. W. Wong, J. L. Andres, M. Head-Gordon, E. S. Replogle, J. A. Pople, Gaussian, Inc., Pittsburgh, PA, **1998**.
[23] a) A. D. Becke, *J. Chem. Phys.* **1993**, *98*, 1372. b) C. Lee, W. Yang, R. G. Parr, *Phys. Rev. B* **1988**, *37*, 785.
[24] A. Schafer, H. Horn, R. Ahlrichs, *J. Chem. Phys.* **1992**, *97*, 2571.
[25] a) P. J. Hay, W. R. Wadt, *J. Chem. Phys.* **1985**, *82*, 299; b) J. V. Ortiz, P. J. Hay, R. L. Martin, *J. Am. Chem. Soc.* **1992**, *114*, 2736.
[26] A. E. Reed, L. A. Curtiss, F. Weinholt, *Chem. Rev.* **1988**, *88*, 899.
[27] G. Schaftenaar, J. H. Noordik, *J. Comput.-Aided Mol. Des.* **2000**, *14*, 123.
[28] S. Potmann, H. P. Lüthi, *Chimia* **2000**, *54*, 766.
[29] In this respect, also the sum of the simulated Raman spectra for $[\mathbf{1}\cdot I]^+$ and $\mathbf{1}\cdot IBr$ agrees reasonably well with the experimental Raman spectrum of $\mathbf{3}\cdot 2IBr$. Details are available from the authors on request.

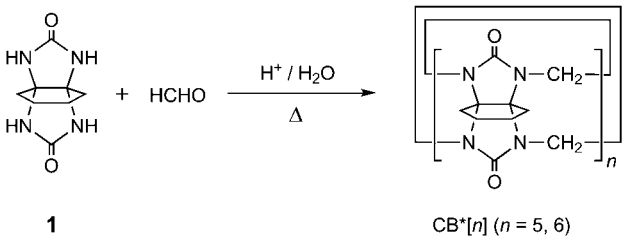
 © WILEY-VCH Verlag GmbH, D-69451 Weinheim, 2001 1433-7851/01/4022-4232 $ 17.50+.50/0

Cucurbit[*n*]uril Derivatives Soluble in Water and Organic Solvents**

Jianzhang Zhao, Hee-Joon Kim, Jinho Oh, Soo-Young Kim, Jae Wook Lee, Shigeru Sakamoto, Kentaro Yamaguchi, and Kimoon Kim*

Cucurbituril (CB[6]), a macrocyclic cavitand comprising six glycoluril units, has a cavity of ~5.5 Å diameter that is accessible through two identical carbonyl-fringed portals.[1] Similar to cyclodextrins (CDs), the cavity can hold small organic molecules through hydrophobic interactions. Unlike CDs, however, the carbonyl groups at the portals allow CB[6] to bind ions and molecules through charge–dipole as well as hydrogen-bonding interactions.[1] The rigid structure and capability of forming complexes with molecules and ions make CB[6] very attractive as a synthetic receptor and as a building block for the construction of supramolecular architectures.[2, 3] Compared to the chemistry of CDs, however, that of CB[6] has developed slowly until recently which may be attributed mainly to its extremely poor solubility in common solvents, and the inability to functionalize these molecules. Our recent synthesis of higher CB homologues cucurbit[*n*]uril (CB[*n*], $n = 7$ and 8) with larger cavities, the dimensions of which are equivalent to those of β- and γ-CDs, respectively, opens up new possibilities in the chemistry of CB[*n*].[4] Nevertheless, the homologues also suffer the same shortcomings as CB[6].[5] Thus, synthesis of CB[*n*] derivatives having substituents at the peripheries that allow them to dissolve in common solvents, and to accept functionalization for further modifications would be a breakthrough in the chemistry of CB[*n*] and enable applications in many areas including separation, transport, and sensors. A straightforward approach to this goal may be condensation of glycoluril derivatives carrying alkyl or aryl groups at the "bridging" positions with formaldehyde, which would produce CB[*n*] derivatives with the corresponding substituents at the "equator". To date, however, the only successful synthesis of CB[*n*] derivatives from this approach (or by any other methods) is for decamethylcucurbit[5]uril (MeCB[5]),[6] synthesized from dimethylglycoluril, which nevertheless still suffers poor solubility in common solvents. After numerous unsuccessful attempts, we have finally succeeded in the synthesis of CB[*n*] derivatives from this condensation approach. Here we report the first CB[*n*] derivatives that are soluble in water as well as organic solvents.

Reaction of cyclohexanoglycoluril (**1**)[7] with formaldehyde in the presence of HCl produces a viscous solution, subsequent treatment of which with H_2SO_4 at 80 °C for 24 h yields a mixture of CB[*n*] derivatives containing *n* cyclohexanoglycoluril units (Scheme 1). The ^1H and ^{13}C NMR spectra reveal that the mixture contains cyclic pentamer ($n = 5$) and hexamer ($n = 6$) as major products (in a ~8:1 ratio), and a small amount of unidentified homologues. After a series of dissolution and fractional crystallizations, the pentamer (CB*[5]) and hexamer (CB*[6]) were isolated from the mixture in 16% and 2% yields, respectively.



Scheme 1. Synthesis of CB*[*n*] ($n = 5$, 6).

The new CB derivatives CB*[5] and CB*[6] have been fully characterized by various methods including X-ray crystallography. Their X-ray analyses[8] reveal the expected structures with five and six fused cyclohexane rings, respectively, decorating the outside of the "equator" of CB[*n*] ($n = 5$, 6; Figure 1). The portal and cavity sizes of CB*[5] and CB*[6] are essentially the same as those of CB[5] and CB[6],

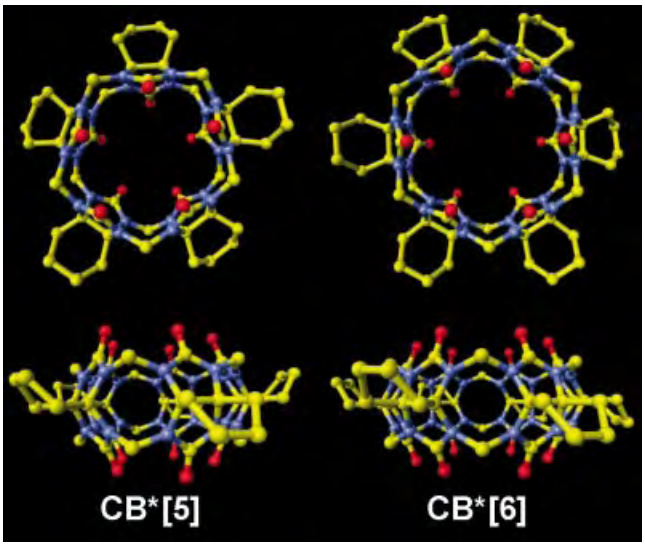


Figure 1. X-ray crystal structures of CB*[5] and CB*[6]. Water molecule(s) encapsulated in the cavities are omitted for clarity. Carbon: yellow, nitrogen: blue, oxygen: red.

[*] Prof. Dr. K. Kim, Dr. J. Zhao,[+] Dr. H.-J. Kim, J. Oh, S.-Y. Kim, Dr. J. W. Lee
National Creative Research Initiative Center for Smart Supramolecules and
Department of Chemistry, Division of Molecular and Life Sciences
Pohang University of Science and Technology
San 31 Hyojadong, Pohang 790-784 (Republic of Korea)
Fax: (+82) 54-279-8129
E-mail: kkim@postech.ac.kr

S. Sakamoto, Prof. Dr. K. Yamaguchi
Chemical Analysis Center, Chiba University
1-33 Yayoicho, Inageku, Chiba 263-8522 (Japan)

[+] Permanent address: Department of Chemistry
Jilin University, Changchun 130023 (P. R. China)

[**] We gratefully acknowledge Creative Research Initiative Program of the Korean Ministry of Science and Technology for support of this work and Brain Korea 21 Program of the Korean Ministry of Education for postdoctoral fellowship to J.Z. and graduate studentships to J.O. and S.-Y.K; $n = 5$ or 6.

Supporting information for this article is available on the WWW under http://www.angewandte.com or from the author.

 © WILEY-VCH Verlag GmbH, D-69451 Weinheim, 2001 1433-7851/01/4022-4233 $ 17.50+.50/0

respectively: the mean cavity and portal diameters, 4.0 and 2.5 Å, respectively, for CB*[5], 5.4 and 4.0 Å, respectively, for CB*[6].

One of the most remarkable properties of these new cucurbituril derivatives CB*[5] and CB*[6] is their high solubility in common solvents such as water, methanol, DMSO, and reasonable solubility in ethanol, DMF, and acetonitrile.[9] Surprisingly, they are both more soluble in water ($\sim 2 \times 10^{-1}$ mol L^{-1}) than in organic solvents ($\sim 3 \times 10^{-2}$ mol L^{-1} or less) despite the presence of the equator-bound fused cyclohexane units. The solubility of CB*[6] in water is comparable to that of α-CD.

The remarkable solubility allowed us now to investigate the host–guest chemistry of CB*[5] and CB*[6] in *neutral* water. For example, a preliminary study on the complex formation of CB*[5] with K^+ ions in neutral water has been carried out using titration calorimetry. CB*[5] binds K^+ ions in a 1:2 stoichiometry with lgK_1 and lgK_2 values of 4.11 ± 0.06 and 2.16 ± 0.03 (pH 6.9), respectively.[10] This result is in contrast to the previous report[11] that MeCB[5] binds K^+ ions (and other alkali metal ions) in a 1:1 stoichiometry with lg$K$ of 3.48 in a 50% formic acid/water solution. The acidic medium has been employed in most binding studies of CB[6] or MeCB[5] because of their poor solubility in neutral water.[1, 11–13] The reported 1:1 binding stoichiometry between MeCB[5] and alkali metal ions in the acidic medium has been attributed to the protonation of one of the receptor portals leaving only the other available for binding a metal ion.[11] The present binding study in neutral water, however, clearly demonstrates that the previously reported 1:1 binding stoichiometry and lower binding constant are a consequence of competition between metal ions and proton for the same binding site in the acidic medium. Comprehensive studies of the binding of CB*[5] and CB*[6] to metal and other ions in neutral aqueous solution are underway.[14]

The utility of water-soluble CB*[6] may be illustrated by the formation in neutral water of a stable 1:1 host–guest complex with acetylcholine, an important neurotransmitter. In the host–guest complex, the acetylcholine trimethylammonium groups are located outside CB*[6] whereas the rest of the molecule resides inside CB*[6] as determined by the NMR chemical shift changes upon complex formation. The formation constant and thermodynamic parameters associated with the inclusion phenomenon have been determined by NMR spectroscopy: lg$K = 3.11$, $\Delta H^0 = -2.7$ kcal mol^{-1}, and $\Delta S^0 = 3.6$ cal mol^{-1} K^{-1}.[15] On the other hand, choline exhibits little interaction with CB*[6] as shown by ^{1}H NMR spectroscopy. CB*[6] therefore behaves as an artificial receptor that can differentiate acetylcholine from choline in neutral water, a property that may find useful applications in neuroscience.

The good solubility of CB*[5] and CB*[6] in organic solvents allowed us to prepare membrane electrodes for ion sensing.[16] In particular, a membrane electrode prepared with CB*[5] was expected to function as an ion-selective electrode (ISE) for Pb^{2+} ions because MeCB[5] had been reported to bind Pb^{2+} ions exceptionally well.[11] A preliminary study revealed that CB*[5] indeed behaves as an ISE for Pb^{2+} ions with good sensitivity and selectivity (Figure 2a; see also Supporting Information). Furthermore, a membrane electrode prepared with CB*[6] is good for detecting acetylcholine with high selectivity over choline and other interfering ions such as Na^+, K^+, and NH_4^+ (Figure 2b), which may be useful in monitoring the neurotransmitter in biological samples.[17] Details of the applications of CB*[5] and CB*[6] in ISEs will be reported separately.

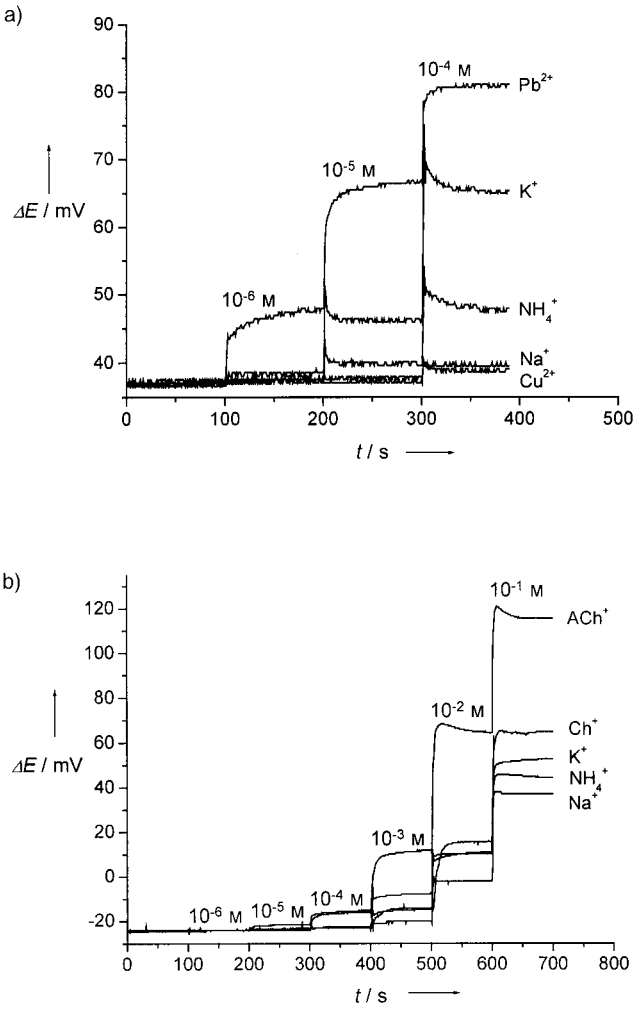


Figure 2. a) Responses of an ISE based on CB*[5] to Pb^{2+} and other ions (pH 4.0 with 1 mM $Mg(OAc)_2$/HCl buffer); b) Responses of an ISE based on CB*[6] to acetylcholine (ACh^+) and other interfering ions including choline (Ch^+) (pH 7.2 with 10 mM Tris buffer). All analytes were used as chloride salts except $Pb(NO_3)_2$ and $Cu(NO_3)_2$. OAc = acetate, Tris = 2-amino-2-(hydroxymethyl)-1,3-propanediol.

In conclusion, we have synthesized the first CB[n] ($n = 5, 6$) derivatives that are soluble in water as well as organic solvents. Their high solubility in common solvents should expand the utilities of CB*[n]. Moreover, it should be possible to introduce other functionalizable substituents at the equator of CB[n] by using the same synthetic method. We may also be able to synthesize other homologues containing higher numbers of substituted glycoluril units.

Experimental Section

CB*[n] ($n = 5, 6$): 37% HCl (0.16 mL) was added to a mixture of **1** (see Supporting Information; 2.0 g, 10.2 mmol) and 30% formaldehyde (1.9 mL, 23.4 mmol). The mixture was stirred and heated to 80 °C to give a purple viscous solution. After concentrated H_2SO_4 (2.5 mL) and water

 © WILEY-VCH Verlag GmbH, D-69451 Weinheim, 2001 1433-7851/01/4022-4234 $ 17.50+.50/0

(5.0 mL) were added, the purple solution was heated at 80 °C for 24 h. The solution was allowed to cool to room temperature, and then diluted with water (10 mL). The solution was poured into acetone (300 mL) to precipitate a solid, which was collected by filtration, and redissolved in water (50 mL). After the solution was neutralized with triethylamine, the solvent was removed under reduced pressure. The remaining solid was suspended in CH_3CN (20 mL) and the suspension filtered. The filter cake contains CB*[5] as a major product whereas the filtrate contains mostly CB*[6]. Recrystallization of the crude products from water produced colorless crystalline products CB*[5] (356.7 mg, 16 %) and CB*[6] (47.8 mg, 2 %). CB*[5]: ^{1}H NMR (300 MHz, D_2O): $\delta = 5.64$ (d, $J = 15.6$ Hz, 10 H), 4.33 (d, $J = 15.8$ Hz, 10 H), 2.20 (s, 20 H), 1.46 (s, 20 H); ^{13}C NMR (75 MHz, D_2O): $\delta = 156.33$, 76.45, 43.51, 23.56, 14.0; IR (KBr): $\tilde{\nu}_{CO}$ 1745 cm^{-1}; MS (ESI): m/z (%): 1123.5 (100) $[M+Na]^+$. CB*[6]: ^{1}H NMR (300 MHz, D_2O): $\delta = 5.73$ (d, $J = 15.9$ Hz, 12 H), 4.32 (d, $J = 16.0$ Hz, 12 H), 2.26 (s, 24 H), 1.49 (s, 24 H); ^{13}C NMR (75 MHz, D_2O): $\delta = 156.43$, 76.51, 44.1, 23.37, 14.07; IR (KBr): $\tilde{\nu}_{CO}$ 1734 cm^{-1}; MS (ESI): m/z (%): 1361.6 (100) $[M+Na+H_2O]^+$. Satisfactory elemental analyses were obtained for CB*[5] and CB*[6].

Received: June 12, 2001
Revised: September 10, 2001 [Z17272]

[1] Reviews on cucurbituril: a) W. L. Mock, *Top. Curr. Chem.* **1995**, *175*, 1; b) P. Cintas, *J. Inclusion Phenom. Mol. Recognit. Chem.* **1994**, *17*, 205; c) W. L. Mock in *Comprehensive Supramolecular Chemistry*, *Vol. 2* (Ed.: F. Vögtle), Pergamon, Oxford, **1996**, p. 477.

[2] a) D. Whang, Y.-M. Jeon, J. Heo, K. Kim, *J. Am. Chem. Soc.* **1996**, *118*, 11333; b) D. Whang, K. Kim, *J. Am. Chem. Soc.* **1997**, *119*, 451; c) D. Whang, K.-M. Park, J. Heo, K. Kim, *J. Am. Chem. Soc.* **1998**, *120*, 4899; d) S.-G. Roh, K.-M. Park, G.-J. Park, S. Sakamoto, K. Yamaguchi, K. Kim, *Angew. Chem.* **1999**, *111*, 672; *Angew. Chem. Int. Ed.* **1999**, *38*, 638; e) E. Lee, J. Heo, K. Kim, *Angew. Chem.* **2000**, *112*, 2811; *Angew. Chem. Int. Ed.* **2000**, *39*, 2699; f) E. Lee, J. Kim, J. Heo, D. Whang, K. Kim, *Angew. Chem.* **2001**, *113*, 413; *Angew. Chem. Int. Ed.* **2001**, *40*, 399; g) J. W. Lee, Y. H. Ko, S.-H. Park, K. Yamaguchi, K. Kim, *Angew. Chem.* **2001**, *113*, 769; *Angew. Chem. Int. Ed.* **2001**, *40*, 746.

[3] a) M. N. Sokolov, A. V. Virovets, D. N. Dybtsev, O. A. Gerasko, V. P. Fedin, R. Hernandez-Molina, W. Clegg, A. G. Sykes, *Angew. Chem.* **2000**, *112*, 1725; *Angew. Chem. Int. Ed.* **2000**, *39*, 1659; b) D. Tuncel, J. H. G. Steinke, *Chem. Commun.* **1999**, 1509; c) C. Meschke, H.-J. Buschmann, E. Schollmeyer, *Polymer* **1999**, *40*, 945.

[4] a) J. Kim, I.-S. Jung, S.-Y. Kim, E. Lee, J.-K. Kang, S. Sakamoto, K. Yamaguchi, K. Kim, *J. Am. Chem. Soc.* **2000**, *122*, 540; b) H.-J. Kim, J. Heo, W. S. Jeon, E. Lee, J. Kim, S. Sakamoto, K. Yamaguchi, K. Kim, *Angew. Chem.* **2001**, *113*, 1574; *Angew. Chem. Int. Ed.* **2001**, *40*, 1526; c) S.-Y. Kim, I.-S. Jung, E. Lee, J. Kim, S. Sakamoto, K. Yamaguchi, K. Kim, *Angew. Chem.* **2001**, *113*, 2177; *Angew. Chem. Int. Ed.* **2001**, *40*, 2119.

[5] CB[*n*] compounds are appreciably soluble in neutral aqueous solutions only when the solutions contain alkali metal ions in high concentrations (> 0.1 M): a) Y.-M. Jeon, J. Kim, D. Whang, K. Kim, *J. Am. Chem. Soc.* **1996**, *118*, 9790; b) D. Whang, J. Heo, J. H. Park, K. Kim, *Angew. Chem.* **1998**, *110*, 83; *Angew. Chem. Int. Ed.* **1998**, *37*, 78.

[6] A. Flinn, G. C. Hough, J. F. Stoddart, D. J. Williams, *Angew. Chem.* **1992**, *104*, 1550; *Angew. Chem. Int. Ed. Engl.* **1992**, *31*, 1475.

[7] IUPAC name: 1*H*,4*H*-3a,6a-butanoimidazo[4,5-*d*]imidazole-2,5(3*H*,6*H*)-dione; G. I. Polozov, I. G. Tishchenko, *Vestsi Akad. Navuk BSSR Ser. Khim. Navuk* **1978**, *3*, 62.

[8] Crystals of CB*[*n*] ($n = 5, 6$) suitable for X-ray work were grown from aqueous solution in a refrigerator. Crystal data of CB*[5]: $[(C_{50}H_{60}N_{20}O_{10})\cdot 25H_2O]$, $M_r = 1551.58$, triclinic, $P\bar{1}$ (No. 2), $a = 15.0886(2)$, $b = 15.7065(1)$, $c = 17.8902(3)$ Å, $\alpha = 101.802(1)$, $\beta = 109.337(1)$, $\gamma = 108.471(1)°$, $V = 3560.49(8)$ Å^3, $Z = 2$, $\rho_{calcd} = 1.447$ g cm^{-3}, $T = 223$ K, $\mu = 1.22$ cm^{-1}. Siemens SMART diffractometer, $Mo_{K\alpha}$ ($\lambda = 0.71073$ Å), all non-hydrogen atoms were refined anisotropically (SHELXL-93). Final refinement on F^2 with all 10651 reflections and 955 variables converged to $R1(>2\sigma(I)) = 0.0925$, $wR2$(all data) = 0.2557, and GOF = 1.094. Crystal data of CB*[6]: $[(C_{60}H_{72}N_{24}O_{12})\cdot 18H_2O]$, $M_r = 1645.70$, $P\bar{1}$ (No. 2), $a = 12.7505(1)$, $b = 15.1302(3)$, $c = 19.3353(4)$ Å, $\alpha = 91.2977(8)$, $\beta = 92.8870(8)$, $\gamma = 92.9115(1)°$, $V = 3719.39(11)$ Å^3, $Z = 2$, $\rho_{calcd} = 1.469$ g cm^{-3}, $T = 223$ K, $\mu = 1.18$ cm^{-1}. Final refinement on F^2 with all 11157 reflections and 1045 variables converged to $R1(I > 2\sigma(I)) = 0.0826$, $wR2$(all data) = 0.2235, and GOF = 1.126. Crystallographic data (excluding structure factors) for the structures reported in this paper have been deposited with the Cambridge Crystallographic Data Centre as supplementary publication no. CCDC-164887 (CB*[5]), and -164888 (CB*[6]). Copies of the data can be obtained free of charge on application to CCDC, 12 Union Road, Cambridge CB2 1EZ, UK (fax: (+44) 1223-336-033; e-mail: deposit@ccdc.cam.ac.uk).

[9] The solubility of CB*[*n*] ($n = 5, 6$) in a solvent was determined by ^{1}H NMR spectroscopy with an internal standard (see Supporting Information). Solubility (mol L^{-1}) of CB*[5] (CB*[6]): 2.6×10^{-1} (1.7×10^{-1}) in D_2O, 3.1×10^{-2} (4.3×10^{-2}) in [D_4]methanol, 1.8×10^{-2} (3.9×10^{-2}) in [D_6]DMSO, 1.3×10^{-3} (6.5×10^{-4}) in [D_6]ethanol, 2.5×10^{-3} (3.4×10^{-3}) in [D_7]DMF, 6.7×10^{-4} (2.1×10^{-3}) in [D_3]acetonitrile.

[10] $\Delta H_1 = -1.49 \pm 0.01$ kcal mol^{-1}, $\Delta S_1 = 13.89$ cal mol^{-1} K^{-1}; $\Delta H_2 = -1.49 \pm 0.04$ kcal mol^{-1}, $\Delta S_2 = 4.98$ cal mol^{-1} K^{-1}.

[11] X. X. Zhang, K. E. Krawowiak, G. Xue, J. S. Bradshaw, R. M. Izatt, *Ind. Eng. Chem. Res.* **2000**, *39*, 3516.

[12] a) H.-J. Buschmann, K. Jansen, C. Meschke, E. Schollmeyer, *J. Solution Chem.* **1998**, *27*, 135; b) H.-J. Buschmann, K. Jansen, E. Schollmeyer, *Thermochim. Acta* **1998**, *317*, 95; c) H.-J. Buschmann, K. Jansen, E. Schollmeyer, *Thermochim. Acta* **2000**, *346*, 33.

[13] R. Hoffmann, W. Knoche, C. Fenn, H.-J. Buschmann, *J. Chem. Soc. Faraday Trans.* **1994**, *90*, 1507.

[14] We performed a preliminary study on the complex formation of CB*[6] with Na^+ ions in neutral water by titration calorimetry, but failed to determine the binding stoichiometry unequivocally as the data can be fitted into 1:2, 1:3, and 1:4 binding models equally well. A further detailed study is needed to establish the binding stoichiometry and affinity.

[15] This inclusion process is accompanied by a positive entropy change, which has been observed in other systems: J. Kang, J. Rebek, Jr., *Nature* **1996**, *382*, 239.

[16] a) E. Bakker, P. Bühlmann, E. Pretsch, *Chem. Rev.* **1997**, *97*, 3083; b) P. Bühlmann, E. Pretsch, E. Bakker, *Chem. Rev.* **1998**, *98*, 1593.

[17] a) P. S. Bates, R. Kataky, D. Parker, *Chem. Commun.* **1993**, 691; b) O. Niwa, T. Horiuchi, R. Kurita, K. Torimitsu, *Anal. Chem.* **1998**, *70*, 1126.

Self-Assembly of a Mixed-Valence Copper(II)/Copper(III) Dithiocarbamate Catenane**

Miguel E. Padilla-Tosta, O. Danny Fox, Michael G. B. Drew, and Paul D. Beer*

During the past few decades the design and high-yielding syntheses of interlocked macrocyclic molecules, the catenanes,[1] have evolved mainly as a result of the elegant and inspirational transition metal and organic templated synthetic

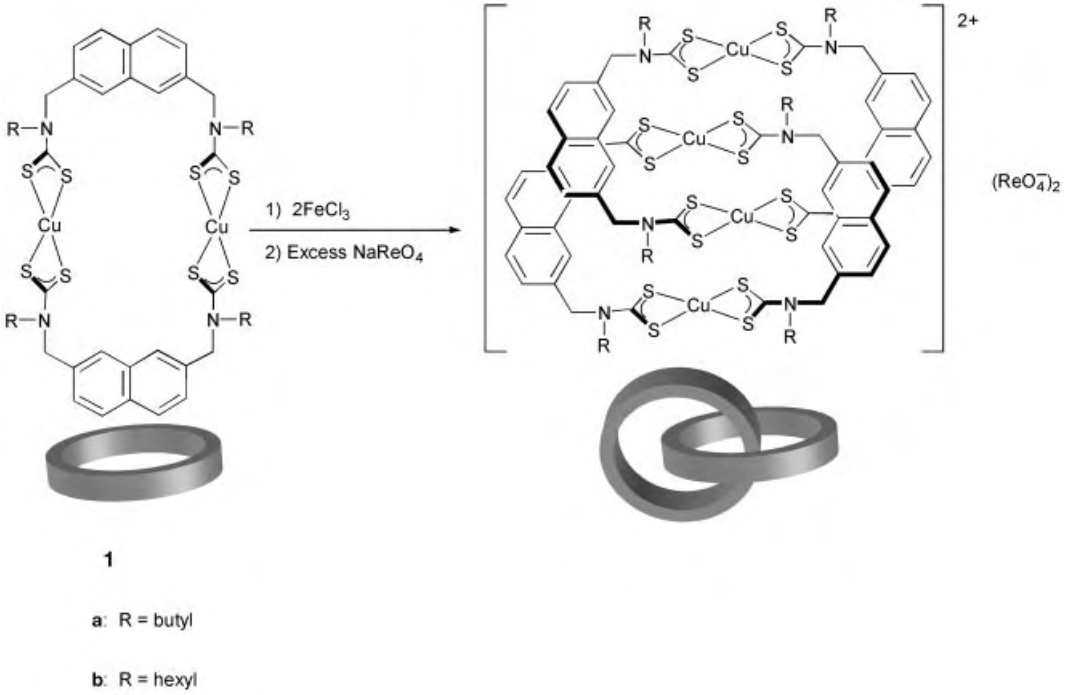
[*] Prof. P. D. Beer, Dr. M. E. Padilla-Tosta, Dr. O. D. Fox
Department of Chemistry
Inorganic Chemistry Laboratory, University of Oxford
South Parks Road, Oxford OX1 3QR (UK)
Fax: (+44) 1865-272690
E-mail: paul.beer@chem.ox.ac.uk
Prof. M. G. B. Drew
Department of Chemistry, University of Reading
Whiteknights, Reading RG6 6AD (UK)

[**] We thank the EPSRC for a postdoctoral fellowship (O.D.F.) and the EPSRC and University of Reading for funds for the crystallographic image plate system.

strategies pioneered by the research groups of Sauvage,[2] Stoddart,[3] and Fujita.[4] In particular, Fujita et al. have demonstrated the quantitative metal-directed self-assembly of [2]catenanes from preformed molecular boxes by using the lability of the palladium(II)/platinum(II)–pyridine coordinate bond in combination with efficient hydrophobic aromatic stacking interactions in aqueous media.[5]

We recently reported on the utility of the dithiocarbamate (dtc) moiety as a coordinating group in the zinc(II), cadmium(II), and copper(II) transition metal directed construction of nanosized resorcarene-based assemblies[6] and macrocycles.[7] The incorporation of redox-active metal–ligand units into the macrocyclic framework of a host introduces the possibility of using the host as an electrochemical sensor for guest substrates,[8] and indeed we have demonstrated the use of the copper(II)/(III)–dtc redox couple as an electrochemical anion-sensing unit in self-assembled dinuclear copper(II) dithiocarbamate macrocycles.[7] The presence of such redox-active metal–ligand moieties also provides an opportunity for switching the lability or inertness of the metal–ligand coordinate bond through a controlled chemical or electrochemically induced redox reaction. We report here the serendipitous synthesis of a novel mixed-valence tetranuclear copper(II)/copper(III) dithiocarbamate [2]catenane by the selective oxidation of two preformed copper(II) dithiocarbamate macrocycles in remarkably high yield.

The addition of two equivalents of iron(III) chloride in MeCN to a solution of the naphthyl-spaced dinuclear copper(II) dithiocarbamate macrocycle (**1a**)[7] in CH_2Cl_2:MeCN (12:1) gave a reaction mixture that was allowed to stand for 12 h at room temperature open to the atmosphere. The addition of excess sodium perrhenate produced crystals of a novel catenane suitable for X-ray structural determination (Scheme 1).



1

a: R = butyl

b: R = hexyl

Scheme 1.

The structure[9] contains discrete cations and ReO_4^- ions and that of the tetranuclear copper catenane $(\mathbf{1a})_2^{2+}$ is shown in Figure 1. All four independent copper atoms have four-coordinate square-planar environments and are bonded to four sulfur atoms from two dithiocarbamate ligands. A search

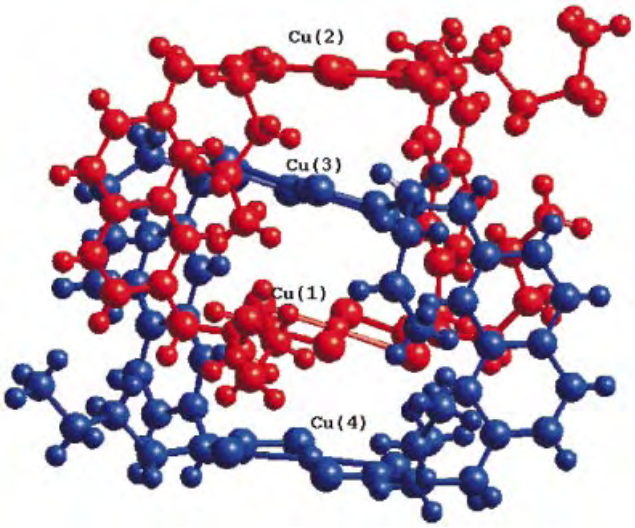


Figure 1. The structure of $(\mathbf{1a})_2^{2+}$ showing the layering of the metal coordination spheres. One link is shown in blue, the other in red.

of the Cambridge Crystallographic Database shows a clear distinction between Cu^{II}–S and Cu^{III}–S bond lengths in these types of complexes, with mean distances of 2.306 Å (76 examples) and 2.210 Å (36 examples), respectively, although both types of copper centers provide square-planar coordination spheres. The bond lengths found in the present structure do not fall clearly into either category (mean bond lengths: Cu(1): 2.233, Cu(2): 2.258, Cu(3): 2.286, Cu(4): 2.300 Å), although it should be noted that the mean bond length of 2.269 Å is intermediate between the mean values for Cu^{II}–S and Cu^{III}–S bonds. It is likely that there is some disorder between the Cu^{II} and Cu^{III} centers, though it is apparent that Cu(1) and Cu(2) have more Cu^{II} character than Cu(3) and Cu(4). Hence, successive copper atoms in the catenane are alternately Cu^{II} and Cu^{III}.

Although each copper center is four coordinate, there are axial contacts, either intra- or intermolecular, from all four copper atoms to two sulfur atoms in adjacent thiocarbamate

 © WILEY-VCH Verlag GmbH, D-69451 Weinheim, 2001 1433-7851/01/4022-4236 $ 17.50+.50/0

ligands; thus the two central copper atoms Cu(1) and Cu(3) in each catenane have two intramolecular Cu ··· S contacts in the range 3.34 to 3.36 Å, while the two outer copper atoms Cu(2) and Cu(4) have only one such contact with distances of 3.18 and 3.27 Å. However, these outer atoms also form axial intermolecular contacts of 3.15 and 3.16 Å to sulfur atoms in adjacent catenanes. Indeed inspection of the crystal packing of the [2]catenane reveals a stacking of catenane units along the b direction that is held together through these intermolecular and intramolecular weak Cu ··· S interactions (Figure 2). Successive coordination spheres of the $[Cu(dtc)_2]$ units, both intra- and intermolecular, are rotated approximately 90° to each other in the chain along the b direction, thus the N-Cu-Cu-N torsion angles range from 90.2 to 100.8° (Figure 1). The adjacent CuS_4 planes within each catenane intersect at angles of 15.4, 16.0, and 15.2°.

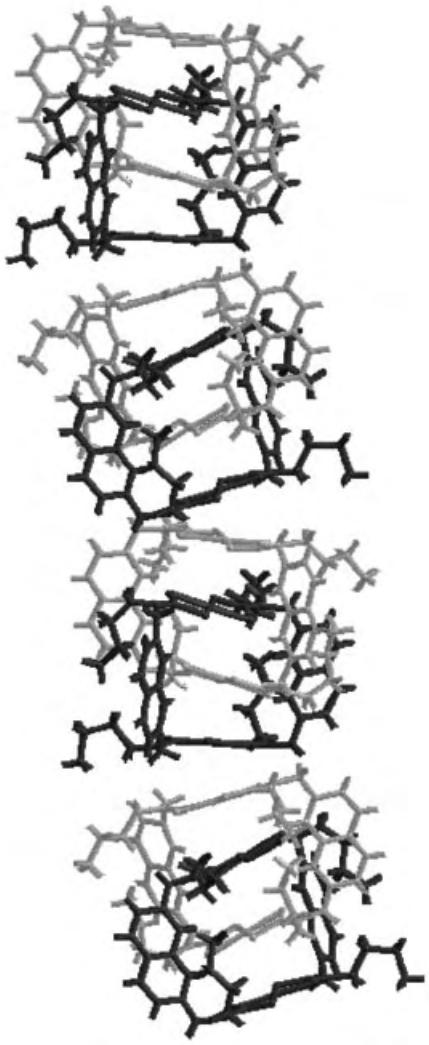


Figure 2. The structure of $(\mathbf{1a})_2^{2+}$ showing the packing of catenanes along the b glide plane. The links are depicted in two shades of gray.

The magnetic susceptibility of **1a** and the catenane was investigated over the temperature range 5 – 300 K. The magnetic susceptibility of **1a** obeys the Curie Law and exhibits a room temperature magnetic moment of 1.76 B.M., which is consistent with the presence of two non-interacting copper(II) ions. The catenane's magnetic susceptibility data also obeys the Curie Law and displays a room temperature magnetic moment (calculated on the basis of two copper(II) d^9 and two low-spin copper(III) d^8 ions) of 2.09 B.M. per copper(II) center. The magnetic moment of the catenane decreases gradually from 2.09 to 1.86 B.M. over the range 75 – 300 K. This magnetic susceptibility data is consistent with the catenane's mixed valency of $Cu^{II}Cu^{III}Cu^{II}Cu^{III}$, and with the copper(II) centers being effectively magnetically isolated at room temperature.[10] The small fall in magnetic moment at lower temperatures is indicative of a weak antiferromagnetic interaction.

Evidence for the existence of the catenane in solution came from electrospray mass spectrometry (ES-MS). Ions corresponding to the dication $\mathbf{1a}^{2+}$ were observed (Figure 3a) following chemical oxidation (using excess $NOBF_4$) of the parent copper(II) – dtc complex. The formation of the catenane was followed by treating a solution of the copper(II) macrocycle in dichloromethane with one equivalent of anhydrous iron(III) chloride, with the solution being allowed to stand (3 h) before being injected into the spectrometer shortly after a small injection of $NOBF_4$. This addition of $NOBF_4$ causes further oxidation of the catenane within the spectrometer and allows for the observation of the trication $(\mathbf{1a})_2^{3+}$ (Figure 3b).[11] Finally, a solution of crystals of $(\mathbf{1})_2(FeCl_4)_2$, synthesized in near quantitative yield, in methanol gave intense ion peaks corresponding to the dication catenanes at m/z: 1024.4 $(\mathbf{1a})_2^{2+}$ and 1136.3 $(\mathbf{1b})_2^{2+}$ together with weaker ion peaks for the mono-charged catenanes at m/z: 2048.8 $(\mathbf{1a})_2^{+}$ and 2273.6 $(\mathbf{1b})_2^{+}$ (Figure 3c).

The electrochemical properties of **1a** and the [2]catenane were investigated in CH_2Cl_2:MeCN (4:1) by using cyclic and square-wave voltammetry with NBu_4BF_4 as the supporting electrolyte. The catenane exhibits two quasi-reversible oxidation waves at 0.07 and 0.25 V (reference Ag/AgCl) whilst, in contrast, the macrocycle (**1a**) displays a single broad quasi-reversible oxidation wave at 0.19 V which is indicative of overlapping waves.[7] It is noteworthy that the first catenane oxidation occurs at a significantly less anodic potential ($\Delta E =$ 120 mV) than that of the macrocycle. This observation suggests that the stabilization of the copper(III) oxidation state is a direct consequence of the unique topological arrangement of the [2]catenane.

In summary a novel mixed-valence tetranuclear copper(II)/copper(III) dithiocarbamate catenane has been prepared by chemical oxidation of two preformed dinuclear copper(II) dithiocarbamate macrocycles. Structural, magnetic susceptibility, electrospray mass spectrometry, and electrochemical studies all support the tetranuclear catenane dication formulation $Cu^{II}Cu^{III}Cu^{II}Cu^{III}$. The mechanism of the catenane's formation may be attributed to the kinetic lability of the copper(III) dithiocarbamate oxidation state[12] which enables the preformed dinuclear copper macrocycle to dissociate on oxidation. By virtue of favorable copper(II)-dithiocarbamate-copper(III)-dithiocarbamate donor – acceptor charge-transfer effects, self-assembly of interlocked macrocycles can then occur to produce the mixed-valence tetranuclear [2]catenane in near quantitative yield.

 © WILEY-VCH Verlag GmbH, D-69451 Weinheim, 2001 1433-7851/01/4022-4237 $ 17.50+.50/0

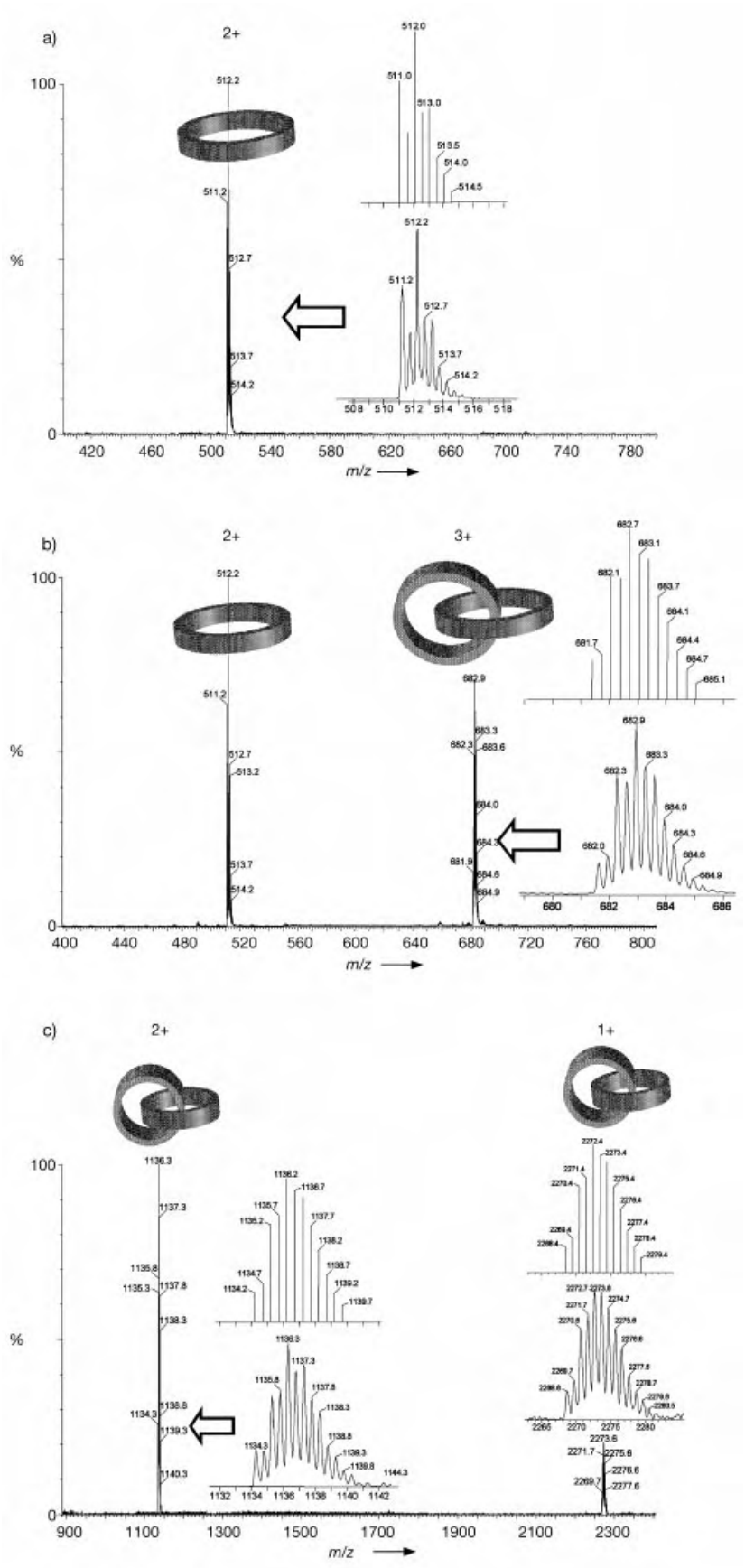


Figure 3. Electrospray mass spectra showing catenane formation. a) Freshly prepared $(\mathbf{1a})^{2+}$. b) Solution of **1a** partially oxidized with $FeCl_3$ after 3 h in the presence of excess $NOBF_4$. c) Crystals of $(\mathbf{1b})_2(FeCl_4)_2$ redissolved in dichloromethane.

Experimental Section

[2]Catenane $(\mathbf{1a})_2(FeCl_4)_2$: A solution of iron (III) chloride (0.049 g, 0.30 mmol) in acetonitrile (3 mL) was added to a solution of **1a**[7] (0.153 g, 0.15 mmol) in dichloromethane (50 mL) and acetonitrile (4 mL). The resulting mixture was allowed to stand at room temperature for 12 h. Removal of the solvent in vacuo and recrystallization from dichloromethane/diethyl ether gave the catenane (0.17 g, 93 %). Elemental analysis calcd for $C_{88}H_{112}N_8S_{16}Cu_4Fe_2Cl_8$: C 43.25, H 4.6, N 4.6 %; found: C 43.3, H 4.5, N 4.8 %. An analogous synthetic procedure was used to prepare $(\mathbf{1b})_2(FeCl_4)_2$ in 94 % yield. Elemental analysis calcd for $C_{104}H_{144}N_8S_{16}Cu_4Fe_2Cl_8$: C 46.8, H 5.4, N 4.2 %; found: C 46.7, H 5.2, N 4.3 %.

Received: July 27, 2001 [Z 17618]

[1] a) *Molecular Catenanes, Rotaxanes and Knots* (Eds.: J.-P. Sauvage, C. Dietrich-Buchecker), Wiley-VCH, Weinheim, **1999**; for recent examples, see b) C. P. McArdle, M. J. Irwin, M. C. Jennings, R. J. Puddephatt, *Angew. Chem.* **1999**, *111*, 3571; *Angew. Chem. Int. Ed.* **1999**, *38*, 3376; D. G. Hamilton, J. E. Davies, L. Prodi, J. K. M. Sanders, *Chem. Eur. J.* **1998**, *4*, 608; c) D. A. Leigh, P. J. Lusby, S. J. Teat, A. J. Wilson, J. K. Y. Wong, *Angew. Chem.* **2001**, *113*, 1586; *Angew. Chem. Int. Ed.* **2001**, *40*, 1538; d) S. L. Castro, O. Just, W. S. Rees, Jr, *Angew. Chem.* **2000**, *112*, 963; *Angew. Chem. Int. Ed.* **2000**, *39*, 933; e) A. Andrievsky, F. Ahuis, J. Sessler, F. Vögtle, D. Gudat, M. Moini, *J. Am. Chem. Soc.* **1998**, *120*, 9712; f) G. A. Breault, C. A. Hunter, P. C. Mayers, *Tetrahedron* **1999**, *55*, 5265.

[2] a) C. O. Dietrich-Buchecker, J.-P. Sauvage, J.-P. Kintzinger, *Tetrahedron Lett.* **1983**, *24*, 5095; b) C. O. Dietrich-Buchecker, J.-P. Sauvage, J.-M. Kern, *J. Am. Chem. Soc.* **1984**, *106*, 3043; c) C. O. Dietrich-Buchecker, J.-P. Sauvage, *Chem. Rev.* **1987**, *87*, 795; d) J.-P. Sauvage, C. O. Dietrich-Buchecker, J.-C. Chambron, *Comprehensive Supramolecular Chemistry*, *Vol. 9* (Ed.: J.-M. Lehn), Pergamon, Oxford, **1995**, chap. 2; e) J. P. Collin, C. O. Dietrich-Buchecker, P. Gavina, M. C. Jimenez-Molero, J.-P. Sauvage, *Acc. Chem. Res.* **2001**, *34*, 477.

[3] a) P. L. Anelli, P. R. Ashton, R. Ballardini, V. Balzani, M. Delgado, M. T. Gandolfi, T. T. Goodnow, A. E. Kaifer, D. Philp, M. Pietraszkiewicz, L. Prodi, M. V. Reddington, A. M. Z. Slawin, N. Spencer, J. F. Stoddart, C. Vicent, D. J. Williams, *J. Am. Chem. Soc.* **1992**, *114*, 193; b) D. B. Amabilino, J. F. Stoddart, *Chem. Rev.* **1995**, *95*, 2725; c) D. Philp, J. F. Stoddart, *Angew. Chem.* **1996**, *108*, 1242; *Angew. Chem. Int. Ed. Engl.* **1996**, *35*, 1154; d) V. Balzani, A. Credi, F. M. Raymo, J. F. Stoddart, *Angew. Chem.* **2000**, *112*, 3484; *Angew. Chem. Int. Ed.* **2000**, *39*, 3348.

[4] a) M. Fujita, K. Ogura, *Coord. Chem. Rev.* **1995**, *148*, 249; b) M. Fujita, K. Ogura, *Bull. Chem. Soc. Jpn.* **1996**, *69*, 1471; c) M. Fujita, *Acc. Chem. Res.* **1999**, *32*, 53.

[5] a) M. Fujita, F. Ibukuro, H. Hagihara, K. *Ogura*, *Nature* **1994**, *367*, 720; b) M. Fujita, F. Ibukuro, K. Yamaguchi, K. Ogura, *J. Am. Chem. Soc.* **1995**, *117*, 4175.

[6] a) O. D. Fox, M. G. B. Drew, P. D. Beer, *Angew. Chem.* **2000**, *112*, 139; *Angew. Chem. Int. Ed.* **2000**,

 © WILEY-VCH Verlag GmbH, D-69451 Weinheim, 2001 1433-7851/01/4022-4238 $ 17.50+.50/0

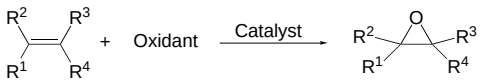
39, 135; b) O. D. Fox, M. G. B. Drew, E. J. S. Wilkinson, P. D. Beer, *Chem. Commun*. **2000**, 391.
[7] P. D. Beer, N. Berry, M. G. B. Drew, O. D. Fox, M. E. Padilla-Tosta, S. Patell, *Chem. Commun*. **2001**, 199.
[8] a) P. D. Beer, P. A. Gale, G. Z. Chen, *J. Chem. Soc. Dalton Trans.* **1999**, 1897; b) P. D. Beer, P. A. Gale, G. Z. Chen, *Coord. Chem. Rev*. **1999**, *185*, 3.
[9] Crystal structure data for $(\mathbf{1a})_2(ReO_4)_2$: $C_{88}H_{112}Cu_4N_8O_8Re_2S_{16}$, $M_r = 2549.37$, monoclinic, space group $P2_1/c$, $a = 16.096(23)$, $b = 26.620(35)$, $c = 32.039(41)$ Å, $\beta = 90.89(1)^\circ$, $V = 13726$ Å^3, $Z = 4$, $\rho_{calcd} = 1.234$ gm cm^{-3}. Data were measured on a Marresearch Image Plate system using $Mo_{K\alpha}$ radiation with the crystal positioned at 70 mm from the Image Plate. 100 frames were measured at 2° intervals with a counting time of 10 mins. 12787 reflections were measured to give 8069 independent reflections (R(int) = 0.0327). Data analysis was carried out with the XDS program.[13] The structure was solved using direct methods with the SHELX86 program.[14] The Re, Cu, and S atoms were refined with anisotropic thermal parameters. The ReO_4 anions had high thermal motion, but no disordered model proved satisfactory. The crystal was twinned (hkl, $hk - l$) with a refined factor of 0.23(2). An absorption correction was introduced using DIFABS.[15] Distance and thermal constraints were used particularly for the alkyl chains. The hydrogen atoms were included in geometric positions and given thermal parameters equivalent to 1.2 times those of the atom to which they were attached. The structure was refined on F^2 using SHELXL.[16] The final R values were $R1 = 0.1094$ and $wR2 = 0.3018$ for 4572 data with $I > 2\sigma(I)$. Crystallographic data (excluding structure factors) for the structure reported in this paper have been deposited with the Cambridge Crystallographic Data Centre as supplementary publication no. CCDC-166825. Copies of the data can be obtained free of charge on application to CCDC, 12 Union Road, Cambridge CB2 1EZ, UK (fax: (+44) 1223-336-033; e-mail: deposit@ccdc.cam.ac.uk).
[10] The observation of a room temperature magnetic moment a little higher than that usually observed for a free copper(II) ion (1.7–1.9 B.M.) may be attributed to either a small quantity of $FeCl_4^-$ co-crystallizing and occupying ReO_4^- sites in the unit cell or incomplete oxidation of the catenane.
[11] We chose to follow the emergence of the tricationic peak because ions arising from the dication catenane (for example, $(\mathbf{1a})_2^{2+}$) overlap with the monocation of the ring (for example, $(\mathbf{1a})^+$), and similarly, the tetracation of the catenane (for example, $(\mathbf{1a})_2^{4+}$) overlaps with the signal for the dication of the ring (for example, $(\mathbf{1a})^{2+}$).
[12] Evidence for the lability of the copper(III) oxidation state in the dithiocarbamate complex comes from the mixing of simple copper(III) alkyldithiocarbamates which leads to global exchange of the alkyldithiocarbamate ligands, as evidenced by electrospray mass spectrometry, see A. M. Bond, R. Colton, A. D. Agostino, J. Harvey, J. C. Traeger, *Inorg. Chem*. **1993**, *32*, 3952.
[13] W. Kabsch, *J. Appl. Crystallogr*. **1988**, *21*, 916.
[14] SHELX86: G. M. Sheldrick, *Acta Crystallogr. Sect. A* **1990**, *46*, 467.
[15] DIFABS: N. Walker, D. Stuart, *Acta Crystallogr. Sect. A* **1983**, *39*, 158.
[16] SHELXL: G. M. Sheldrick, program for crystal structure refinement, University of Gottingen, **1993**.

Artificial Enzymes Formed through Directed Assembly of Molecular Square Encapsulated Epoxidation Catalysts**

Melissa L. Merlau, Maria del Pilar Mejia, SonBinh T. Nguyen,* and Joseph T. Hupp*

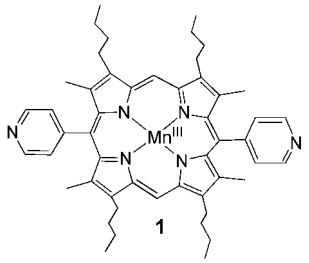
Enzymes are exquisite catalysts for chemical and biochemical reactions: They typically display excellent stability and are highly selective both with respect to the substrates used and the products produced. Most enzymes are comprised of a highly potent catalytic center and a surrounding protein superstructure. In contrast to many, or most man-made, catalysts, naturally occurring enzymes tend to rely upon the superstructure, rather than the catalytic site itself, to achieve substrate selectivity. In addition, the superstructure serves to isolate the catalytic center from other reactive centers, thereby enhancing the center's stability and extending its functional lifetime. Here we describe the artificial enzyme-like induction of stability and selectivity for a simple epoxidation catalyst by a supramolecular coordination chemistry approach. We further show that the selectivity is tailorable through the supramolecular approach. The tailorability permits, in principle, the rapid and systematic optimization of catalytic selectivity for specific substrates.

To demonstrate the utility of the encapsulation concept we targeted the epoxidation of olefins [Eq. (1)] because of its



(1)

relevancy in biooxidation.[1] We stress that our goal here is to demonstrate the utility of directed supramolecular complex formation in manipulating the properties of conventional catalysts rather than to create a competitive analogue of existing epoxidation catalysts.



1

The baseline for comparing catalyst stability was established by using **1**

[*] Prof. Dr. S. T. Nguyen, Prof. Dr. J. T. Hupp, M. L. Merlau, M. del Pilar Mejia
Department of Chemistry and the Institute for Environmental Catalysis
Northwestern University
2145 Sheridan Road, Evanston, IL 60208-3113 (USA)
Fax: (+1) 847-491-7713
E-mail: stn@chem.northwestern.edu
jthupp@chem.northwestern.edu

[**] This work was supported by the National Science Foundation's Partnership in Nanotechnology initiative (NSF grant CHE-9811334) as well as by the EMSI program of the National Science Foundation and the Department of Energy (NSF grant CHE-9810378) at the Northwestern University Institute for Environmental Catalysis. S.T.N. thanks the Alfred P. Sloan Foundation, the Dreyfus Foundation, the DuPont Company, the Beckman Foundation, and the Packard Foundation for support.

(MnDPyP), which was synthesized by the adaptation of published methods.[2, 3] The alkyl groups surrounding the porphyrin framework provide needed solubility in reaction solutions, while the pyridyl groups are essential to the supramolecular assembly process described below. Many variants of simple manganese porphyrins have previously been examined as epoxidation catalysts[4–6] as a result of their high functional and structural similarity to the iron heme moiety comprising the catalytic center of cytochrome P450, a naturally occurring enzyme used in the oxidative metabolism of many biological compounds.[7] The naked manganese porphyrin, like the iron heme mimics, degrades fairly rapidly under catalytic reaction conditions (for example, there is a complete loss of activity after about 50 catalytic cycles). The primary mode of catalyst deactivation under the conditions used is through the formation of an oxo-bridged (Mn-O-Mn) dimer,[8] although some degree of parallel degradation through ligand oxidation cannot be ruled out.

By analogy to the protein superstructure employed by the iron heme in the active cytochrome, we encapsulated catalyst **1** in a supramolecular cavity by using a directed-assembly approach[9] to impart both stability and reaction selectivity (Figure 1). This approach is in contrast to the related method of generating catalyst protection and selectivity enhancement by creating a catalytic cavity using sophisticated and technically challenging covalent chemical modification strategies.[10]

We made use of a large preorganized, porphyrin-derived cavity structure[11] (**2**; itself obtained through coordinative directed assembly) with Lewis acidic receptor sites (Zn^{II}), and a catalytic center (**1**) with peripheral Lewis bases (pyridyl groups; Scheme 1). In the presence of equal or excess amounts of **2**, optimal complex formation is achieved through coordinative directed assembly such that **1** bisects the cavity and doubly binds to the cavity's walls with an association constant of approximately $10^6\,\text{M}^{-1}$ in dichloromethane.[12] Once the catalytic center is encapsulated it cannot attack a similarly encapsulated catalyst or the molecular square framework. At the same time, however, the roughly 9×18 Å "half-cavity" defined by [**1**+**2**] is large enough to permit many olefinic substrates to reach the catalytically active manganese center. In fact, concentration of olefins within the cavity is expected to be high since there is evidence for the preferential binding of aromatic substrates in molecular square cavities.[13, 14] This is thus an ideal scenario for the induction of enhanced catalyst stability, as measured by the increase in catalyst lifetime and by the number of catalytic cycles (turnovers) per manganese reaction center.

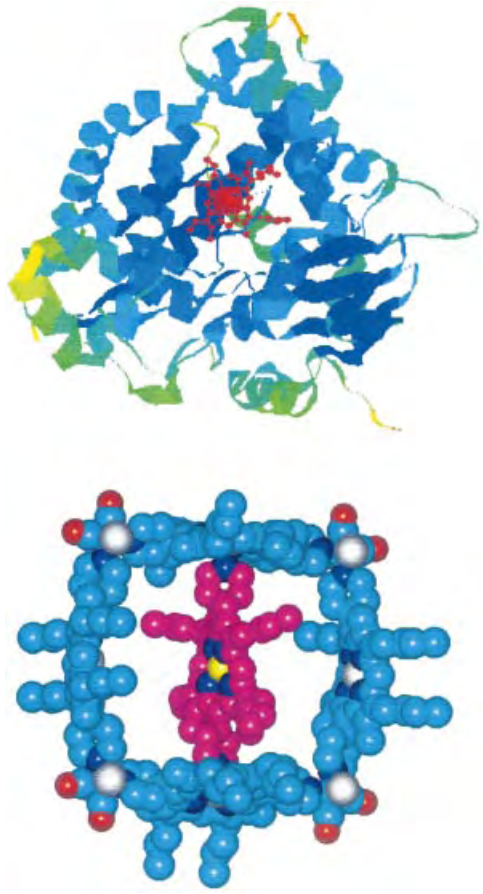
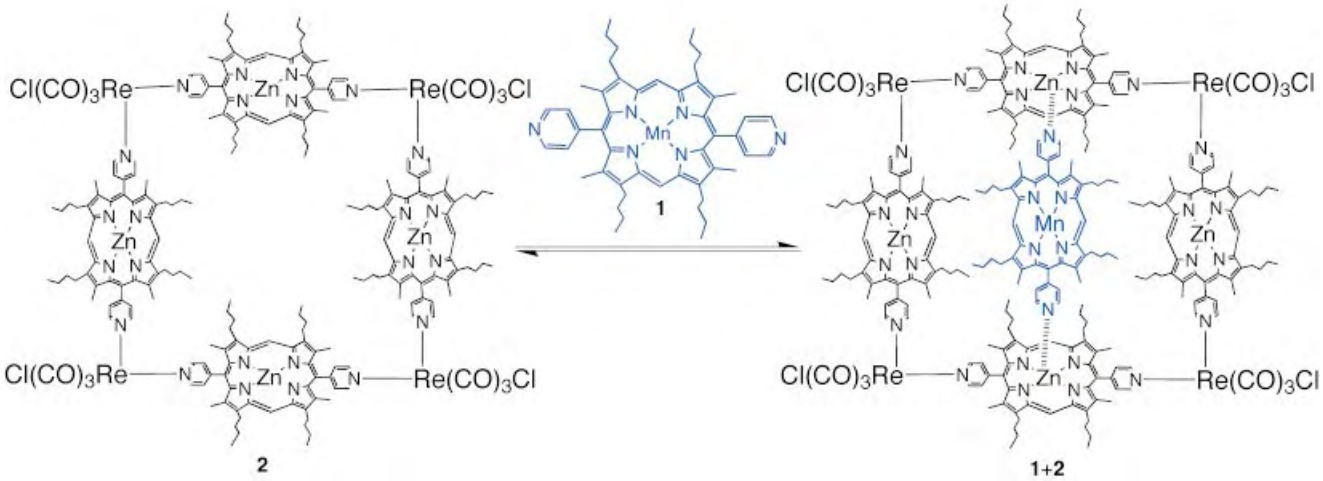


Figure 1. The conceptual topological similarity of cytochrome P450[23] and a supramolecular encapsulated catalyst assembly ([**1**+**2**], see text for more information).

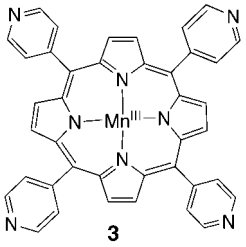
Styrene epoxidation using millimolar solutions of **1** and the supramolecular complex **2** revealed a tenfold increase in the



Scheme 1. Encapsulation of epoxidation catalyst **1** with complex **2** by directed assembly.

 © WILEY-VCH Verlag GmbH, D-69451 Weinheim, 2001 1433-7851/01/4022-4240 $ 17.50+.50/0

turnover number (TON) following complex formation.[15] In addition, the catalyst lifetime under reactive conditions was extended from approximately ten minutes to greater than three hours by protective encapsulation.[16] A quantitative consideration of the formation of the supramolecular complex shows that approximately 3% of the catalyst will remain unbound when millimolar concentrations of catalyst and **2** are used. The dynamic equilibrium between bound and unbound catalyst could account for the observed eventual destruction of all of the catalyst after three hours. Consistent with this interpretation, replacement of **1** by the even more strongly complexed catalyst *meso*-tetra(4-pyridyl)porphinatomanganese(III) chloride (**3**, K_b ca. $10^7\,M^{-1}$) greatly enhances functional stability, and results in TONs of approximately 1500.[17] Conversely, weaker binding complexes result in fewer catalyst turnovers.[8]



3

Since both the above-mentioned catalyst degradation pathways are bimolecular in the catalyst itself, intentional dilution of the catalyst should also enhance its stability. We find that diluting catalyst **1** by a factor of 1000 while retaining the concentration of **2** at the millimolar level (in order to preserve supramolecular association) further improves the stability such that turnover numbers reach nearly 7000 in the case of **2** and 21000 in the case of **3** (Figure 2). Thus, the functional stability of more-or-less conventional catalysts can be enhanced 10- to 100-fold through formation of a supramolecular complex.

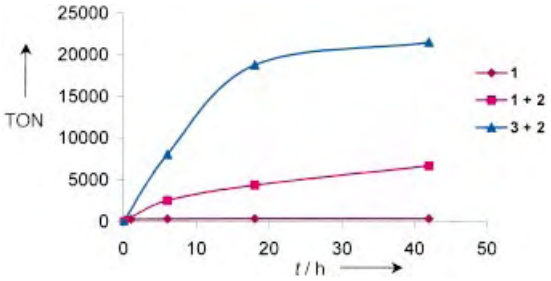
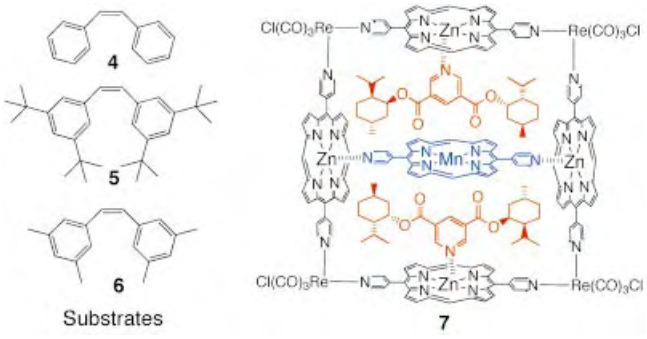


Figure 2. The enhanced stability and enhanced TONs of the catalyst assemblies [**1**+**2**] and [**3**+**2**] compared to the free catalyst **1**.

Formation of the supramolecular complex and catalyst encapsulation also engenders reaction selectivity. For example, competitive epoxidation reactions with both *cis*-stilbene (**4**, Scheme 2) and *cis*-3,3′,5,5′-tetra-*tert*-butylstilbene (**5**) as the substrate showed that the sterically more encumbered **5** is 3.5 times less reactive with [**1**+**2**] than with the naked catalyst. The difference is attributed to partial exclusion of **5** (on the basis of size) from the active-site cavity defined by the encapsulation of **1** by **2**. As illustrated by assembly **7**, the effective cavity size can be further manipulated by incorporating (again, by coordinative directed assembly) up to two additional "ligands". When the cavity-tuning ligands are 3,5-dinicotinic acid dineomenthyl ester, as in **7** (the alkyl groups are not shown for clarity), the reactivity of **5**, again relative to



Scheme 2. Supramolecular complex with a functionalized cavity for enhanced selectivity in catalytic epoxidation.

that of the smaller substrate **4**, is now seven times less with the supramolecular assembly than with the naked catalyst. In addition, the cavity tuning allows for significant (fourfold) differentiation of even very sterically similar substrates, such as **4** and **6**. As expected, changing the size of the cavity-tuning ligand leads to tailorable size selectivity.

Although molecular modeling suggests that **5** should be completely excluded by the modified assembly **7**, we propose that the obtained modest selective exclusion of **5** results from ligand coordination on the outside of the cavity at some of the sites. Since zinc porphyrins can accommodate only one axial substituent,[18, 19] ligation on the outside will preclude ligation on the inside of the square where it can influence the reaction selectivity. More importantly, the walls of the square are fairly free to rotate (around the Re–N bonds) in solution, thus providing a more flexible system than predicted by studies on thin films.[20–22] The preceding argument may also account for an observed lack of enantioselective reaction in cases where optically active cavity-modifying ligands were employed.

In conclusion, the formation of a supramolecular complex imparts stability and substrate selectivity to a simple manganese-porphyrin-based epoxidation catalyst. Additionally, the modular design and synthetic simplicity of the directed-assembly catalyst system is readily tunable and easily modified. The metalloporphyrin catalyst **1** resembles, both structurally and functionally, the catalytic core of cytochrome P450. The encapsulating framework, on the other hand, strongly resembles functionally, if not structurally, the stability- and selectivity-inducing protein superstructure of cytochrome P450 and other enzymes (Figure 1). With appropriate cavity functionalization, the catalyst design concept should enable partial or complete substrate exclusion or inclusion based on other physical or chemical characteristics of the substrate.

Experimental Section

Typical epoxidation procedure: The manganese catalyst **1** or **3** (3 μmol) and molecular square **2** (3 μmol) were combined in dichloromethane (3 mL). Styrene (500 equiv) and octane (14.6 μL, internal GC standard) were added to this solution. Solid iodosylbenzene (100 equiv) was then added every 10 min for 200 min. Additional styrene (500 equiv) was added at 30 min intervals. For studies at high dilution, the manganese catalyst **1** or **3** (3×10^{-9} mol) and molecular square **2** (3 μmol) were combined in dichloromethane (3 mL). Styrene (500000 equiv) and octane (14.6 μL) were added to this solution. PhIO (100000 equiv) was then added in one portion.

 © WILEY-VCH Verlag GmbH, D-69451 Weinheim, 2001 1433-7851/01/4022-4241 $ 17.50+.50/0

Samples (50 μL) were taken periodically and filtered through a silica plug to remove the catalyst. The plug was washed with dichloromethane (3 × 0.5 mL). The filtrates were combined and analyzed by quantitative GLC analysis (HP-5 column, 5° min^{-1} temperature increase, 50 °C initial oven temp, 100 °C final temp). The total turnover number was determined as the total concentration of oxidation products (styrene oxide (ca. 92 %) and phenylacetaldehyde (ca. 8 %)) divided by the initial catalyst concentration.

The epoxidation selectivity experiments were conducted as follows: MnDPyP (3 μmol, 1 equiv) and $[Re(ZnDPyP)]_4$ (1 equiv) were dissolved in dichloromethane (3 mL) followed by the addition of modifying ligands (30 – 300 equiv). *cis*-Stilbene (100 equiv) and **5** or **6** (100 equiv) were added to the mixture. PhIO (100 equiv) was then added. Samples (250 μL) were taken after 10, 20, and 30 min, passed through a neutral alumina plug with pentane eluent (15 mL), and analyzed by HPLC (nitrile column eluted with hexanes). Selectivity is defined as [*cis*-stilbene oxide+*trans*-stilbene oxide]/[sum of epoxides from **5** or **6**] and normalized against MnDPyP.

Received: June 27, 2001 [Z17375]

[1] We emphasize, however, that processes other than epoxidation could equally well have been targeted for study. See for example: M. Nakash, Z. Clyde-Watson, N. Feeder, J. E. Davies, S. J. Teat, J. K. M. Sanders, *J. Am. Chem. Soc.* **2000**, *122*, 5286 – 5293, and references therein.

[2] M. O. Senge, C. J. Medforth, T. P. Forsyth, D. A. Lee, M. M. Olmstead, W. Jentzen, R. K. Pandey, J. A. Shelnutt, K. M. Smith, *Inorg. Chem.* **1997**, *36*, 1149 – 1163.

[3] A. D. Adler, F. R. Longo, F. Kampas, J. Kim, *J. Inorg. Nucl. Chem.* **1970**, *32*, 2443 – 2445.

[4] R. L. Halterman in *Transition Metals in Organic Synthesis*, *Vol. 2* (Eds.: M. Beller, C. Bolm), Wiley-VCH, Weinheim, **1998**, pp. 300 – 306.

[5] L. A. Campbell, T. Kodadek, *J. Mol. Catal. A* **1996**, *113*, 293 – 310.

[6] A. M. D. R. Gonsalves, M. M. Pereira, *J. Mol. Catal. A* **1996**, *113*, 209 – 221, and references therein.

[7] M. J. Guther, P. Turner, *Coord. Chem. Rev.* **1991**, *108*, 115 – 161.

[8] M. L. Merlau, W. J. Grande, S. T. Nguyen, J. T. Hupp, *J. Mol. Catal. A* **2000**, *156*, 79 – 84.

[9] For related reports on noncatalytic directed assembly, see for example: M. D. Levin, P. J. Stang, *J. Am. Chem. Soc.* **2000**, *122*, 7428 – 7429; B. Olenyuk, J. A. Whiteford, A. Fechtenkotter, P. J. Stang, *Nature* **1999**, *398*, 796 – 799; S. Leininger, B. Olenyuk, P. J. Stang, *Chem. Rev.* **2000**, *100*, 853 – 907; N. Takeda, K. Umemoto, K. Yamaguchi, M. Fujita, *Nature* **1999**, *398*, 794 – 796; P. J. Stang, B. Olenyuk, *Coord. Chem. Rev.* **1997**, *30*, 502 – 518.

[10] For selected examples, see J. P. Collman, V. J. Lee, C. J. Kellen-Yuen, X. Zhang, J. A. Ibers, J. I. Brauman, *J. Am. Chem. Soc.* **1995**, *117*, 692 – 703; K. Konishi, K.-I. Oda, K. Nishida, T. Aida, S. Inoue, *J. Am. Chem. Soc.* **1992**, *114*, 1313 – 1317; E. Rose, A. Kossanyi, M. Quelquejeu, M. Soleilhavoup, F. Duwavran, N. Bernard, A. Lecas, *J. Am. Chem. Soc.* **1996**, *118*, 1567 – 1568; Y. Naruta, F. Tani, N. Ishihara, K. Maruyama, *J. Am. Chem. Soc.* **1991**, *113*, 6865 – 6872; D. K. Smith, F. Diederich, *Top. Curr. Chem.* **2000**, *210*, 183 – 227

[11] R. V. Slone, J. T. Hupp, *Inorg. Chem.* **1997**, *36*, 5422 – 5423.

[12] Binding constants were determined by UV/Vis titrimetric methods using the Soret band shift of zinc porphyrins upon coordination of nitrogen bases as an indicator.

[13] Variable substrate (styrene) concentration experiments with catalyst assembly [**1**+**2**] reveal there is Michaelis – Menten kinetic behavior, with values of about 1M for the phenomenological Michaelis constant K_m and about 46 s^{-1} for the kinetic constant k_{cat}.

[14] M. H. Keefe, R. V. Slone, J. T. Hupp, K. F. Czaplewski, R. Q. Snurr, C. L. Stern, *Langmuir* **2000**, *16*, 3964 – 3970.

[15] Control experiments using *fac*-$[Re(CO)_3(pyridine)_2Cl]$ (a surrogate for the corner structures of the square, **2**), ZnDPyP, or H_2DPyP with styrene and iodosylbenzene gave no detectable epoxidation products.

[16] The rate of catalysis with the supramolecular assembly, however, was a factor of three slower than for the naked catalyst. Electronic effects are unlikely to account for the difference, since the strength of the coordination bonds linking **1** to **2** are comparatively weak and since the pyridine groups used by the catalyst to drive directed-assembly are almost certainly oriented out-of-plane with respect to the catalyst's metalloporphyrin core. We tentatively ascribe the rate decrease instead to hindered transport of reactants into the encapsulated active site.

[17] Turnover numbers are approximately 65 for free catalyst **3** (similar to **1**).

[18] C. H. Kirksey, P. Hambright, C. B. Storm, *Inorg. Chem.* **1969**, *8*, 2141 – 2144.

[19] M. Nappa, J. S. Valentine, *J. Am. Chem. Soc.* **1978**, *100*, 5075 – 5080.

[20] S. Belanger, J. T. Hupp, *Angew. Chem.* **1999**, *111*, 2360 – 2362; Angew. *Chem. Int. Ed.* **1999**, *38*, 2222 – 2224.

[21] S. Belanger, J. T. Hupp, C. L. Stern, R. V. Slone, D. F. Watson, T. G. Carrell, *J. Am. Chem. Soc.* **1999**, *121*, 557 – 563.

[22] S. Belanger, K. J. Stevenson, S. A. Mudakha, J. T. Hupp, *Langmuir* **1999**, *15*, 837 – 843.

[23] J. R. Cupp-Vickery, T. L. Poulos, *Nat. Struct. Biol.* **1995**, *2*, 144. Structure obtained from the Protein Database ID: 1OXA.

A Three-Dimensional Ferrimagnet with a High Magnetic Transition Temperature (T_C) of 53 K Based on a Chiral Molecule**

Katsuya Inoue,* Hiroyuki Imai, Prasanna S. Ghalsasi, Koichi Kikuchi, Masaaki Ohba, Hisashi Ōkawa, and J. V. Yakhmi

Investigation of molecule-based magnets, which began in the late 1960s, has led to the successful synthesis of room temperature magnets.[1] Specific features considered in molecule-based magnets include: 1) the ability to design the magnet as well as its structural dimensionality, 2) magnet solubility in water or organic solvents, and, 3) the optical transparency of the magnet.[2] The physical characteristics of greatest interest are the optical properties, particularly with respect to natural optical activity. On the basis of theoretical calculations, new phenomena were expected in optically active magnetic materials.[3] In 1997, Rikken and Raupach observed a small magneto-chiral dichroism (MChD) effect in a chiral paramagnetic material.[4] This effect depends on the

[*] Prof. Dr. K. Inoue, Dr. H. Imai
Department of Applied Molecular Science
Institute for Molecular Science, Okazaki 444-8585 (Japan)
Fax: (+81) 564-54-2254
E-mail: kino@ims.ac.jp
Dr. P. S. Ghalsasi
University of Mumbai, Department of Chemical Technology
Mumbai, 400019 (India)
Prof. Dr. K. Kikuchi
Department of Chemistry, Tokyo Metropolitan University
Hachioji, Tokyo 192-0367 (Japan)
Dr. M. Ohba, Prof. Dr. H. Ōkawa
Department of Chemistry, Graduate School of Science
Kyusyu University, Fukuoka 812-8581 (Japan)
Prof. Dr. J. V. Yakhmi
Chemistry Division, Bhabha Atomic Research Center
Mumbai, 400085 (India)

[**] This work was supported by a program entitled "Research for the Future (RFTF)" of the Japan Society for the Promotion of Science (99P01201).

 © WILEY-VCH Verlag GmbH, D-69451 Weinheim, 2001 1433-7851/01/4022-4242 $ 17.50+.50/0

magnetization of the material, and relatively large effects are expected in the chiral magnets relative to paramagnetic materials. When we construct magnets based on chiral molecules, the chirality must be controlled not only in the molecular structure, but in the entire crystal structure as well. As a consequence of this difficulty few examples of this type of magnet exist.[5, 6]

We have introduced a strategy of using π-conjugated high-spin oligonitroxide radicals as bridging ligands for paramagnetic transition metal ions in order to assemble and align electron spins on a macroscopic scale.[5, 7] In fact, we have succeeded in synthesizing the first chiral magnet by this strategy.[5] These bisnitroxide- or nitronylnitroxide-manganese-based systems are one-dimensional, consequently the transition temperatures required to produce a magnet were low. On the other hand, cyano-bridged dimetallic three-dimensional complexes (Prussian-Blue family) are well known to be promising candidates for producing high transition temperature (T_C) magnetic materials with spontaneous magnetization.[8] Here we report on the crystal structure and physical properties of a 3D chiral ferrimagnet, $K_{0.4}[Cr(CN)_6][Mn(S)\text{-pn}](S)\text{-pnH}_{0.6}$ ((*S*)-pn = (*S*)-1,2-diaminopropane).

The complex $K_{0.4}[Cr(CN)_6][Mn(S)\text{-pn}](S)\text{-pnH}_{0.6}$ was obtained as pale yellow needle crystals by the reaction of $K_3[Cr(CN)_6]$, $Mn(ClO_4)_2$, and (*S*)-1,2-diaminopropane dihydrochloride ((*S*)-pn · 2 HCl) in a 2:3:3 molar ratio in a mixture of methanol and H_2O (1/1; adjusted to pH 7–8 by KOH) under an argon atmosphere. An X-ray structural analysis of a hexagonal crystal of the complex revealed the formation of the chiral 3D network (Figures 1 and 2).[9] In contrast to $[Mn(en)]_3[Cr(CN)_6]_2 \cdot 4H_2O$, only four cyanide groups in the $[Cr(CN)_6]^{3-}$ ion are ligated to Mn^{2+} ions to form the helical dimetallic loops along the *c* axis and to connect the adjacent

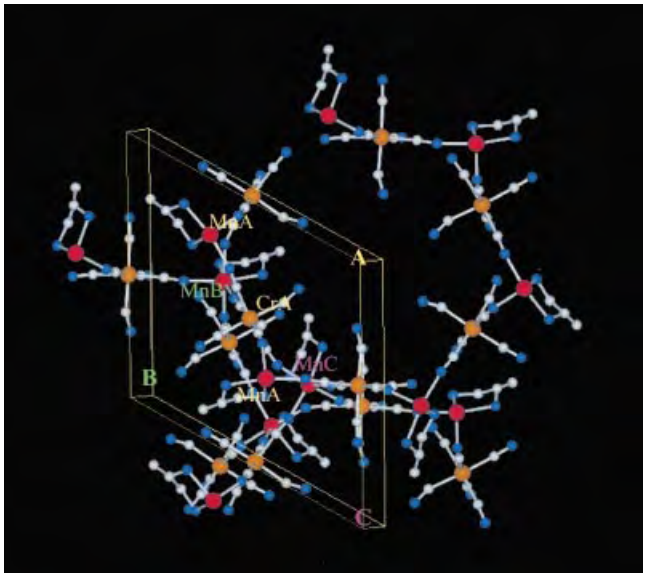


Figure 1. Crystal structure of $K_{0.4}[Cr(CN)_6][Mn(S)\text{-pn}](S)\text{-pnH}_{0.6}$. Views along the *c* axis (A) and of the connection of helical dimetallic loops (B). Some atoms are ommited for clarity. Color scheme: Cr: brown, Mn: red, C: gray, N: blue. CrA in loop A is connected not only to MnA and MnA′ in loop A, but also to MnB and MnC in loops B and C, respectively.

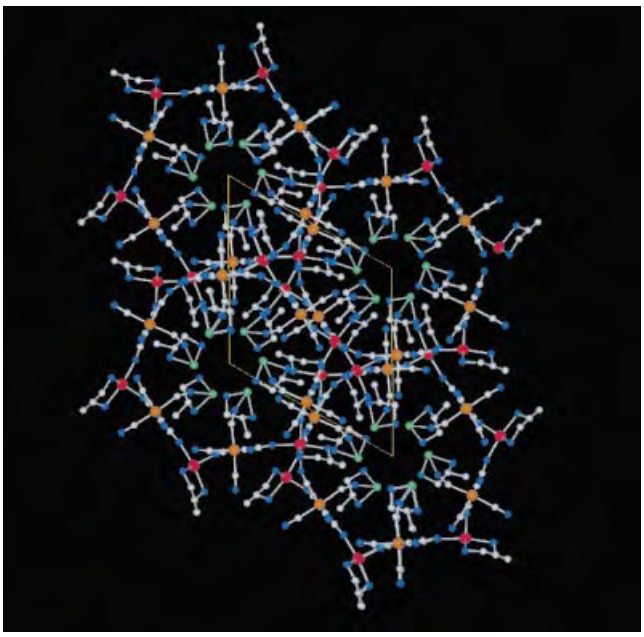


Figure 2. Crystal structure of $K_{0.4}[Cr(CN)_6][Mn(S)\text{-pn}](S)\text{-pnH}_{0.6}$. Views along the *c* axis and showing the connection of the helical dimetallic loops. The same color scheme is used as in Figure 1 and with K atoms shown in green.

loops. The Cr ··· Mn distances (CrA ··· MnA: 5.21 and CrA ··· MnA′:5.28 Å) within a loop are a little shorter than those (CrA ·· MnB: 5.39 and CrA ··· MnC: 5.32 Å) between loops. A single unit possesses two chiral ligands of (*S*)-pn; one is coordinated to a Mn^{2+} ion and the other is located in the cavity of the helical loop and partially coordinated to the K^+ counterion. The site occupancy of the K^+ ion is not unity but 0.4, so about 60% of the latter (*S*)-pn ligand may be protonated to become (*S*)-pnH^+ ions so as to maintain overall neutrality.[10]

The magnetic behavior of the complex was measured on a SQUID susceptometer in the temperature range of 2–300 K and the magnetic field range of 0–5 T. The temperature dependence of the magnetic susceptibility is shown in Figure 3. The $\chi_{mol}T$ value is 4.88 emu K mol^{-1} (6.25 μ_B) at 300 K and decreases with decreasing temperature down to a minimum value of 3.66 emu K mol^{-1} (5.41 μ_B) at 110 K. The

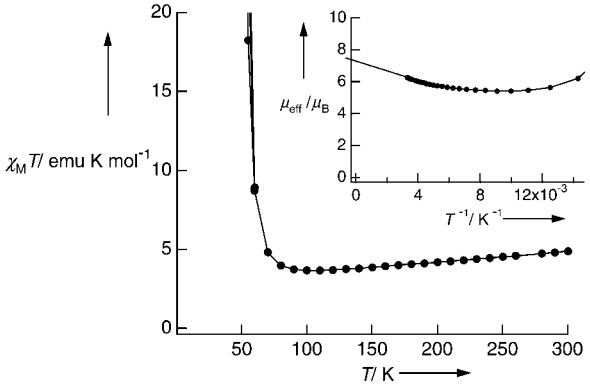


Figure 3. Temperature dependence of $\chi_{mol}T$ values of $K_{0.4}[Cr(CN)_6][Mn(S)\text{-pn}](S)\text{-pnH}_{0.6}$ in the magnetic field of 5000 Oe. Inset: Plot of effective magnetic moment versus 1/*T*.

 © WILEY-VCH Verlag GmbH, D-69451 Weinheim, 2001 1433-7851/01/4022-4243 $ 17.50+.50/0

extrapolated effective magnetic moment value of 7.2 μ_B is in good agreement with the theoretical value at the high temperature limit (Figure 3 inset; calculated with a paramagnetic spin of $5/2 + 3/2 \rightarrow 7.07\ \mu_B$). Upon further cooling the sample, the $\chi_{mol}T$ value increases and diverges. A plot of $1/\chi_{mol}$ versus T in the range from 300 to 110 K obeys the Curie–Weiss law with a Weiss temperature $\theta = -30.9$ K. This value indicates that the antiferromagnetic interaction operates between adjacent Cr^{3+} and Mn^{2+} ions through the cyanide bridges above 110 K. The abrupt increase in the $\chi_{mol}T$ value around 60 K suggests the onset of three-dimensional magnetic ordering.

Both the field cooled (FC) and the zero field cooled magnetization measurements (ZFC) with a low applied field (5 G) in the temperature range from 5 to 100 K show a long-range magnetic ordering below 53 K (Figure 4). The magnetization (M) increases sharply with the applied field and is

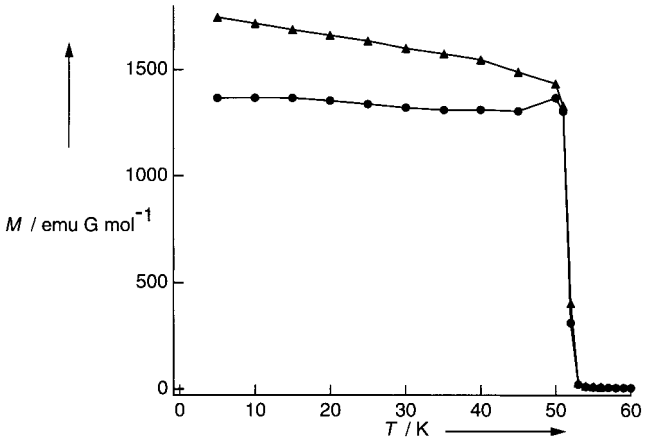


Figure 4. Temperature dependence of the magnetization of $K_{0.4}[Cr(CN)_6][Mn(S)\text{-pn}](S)\text{-pnH}_{0.6}$. The FC (▲) and ZFC (●) magnetization measurements are shown.

saturated rapidly (Figure 5). The saturation magnetization (M_S) is 2 μ_B This value is in good agreement with the theoretical value of antiferromagnetic coupling between Cr^{3+} and Mn^{2+} ions (5/2-3/2 = 2/2). The magnetic hysteresis

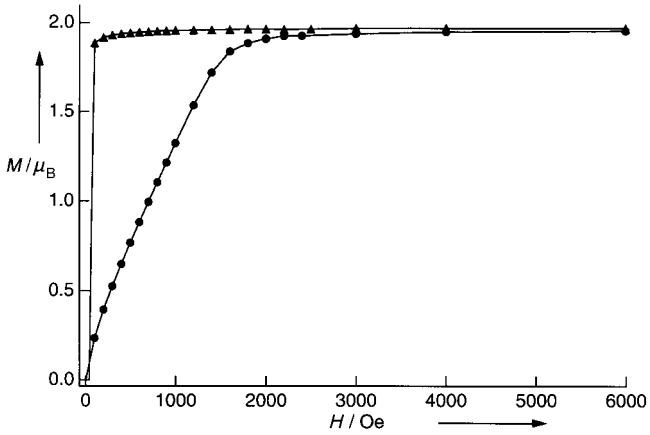


Figure 5. Field dependence of the magnetization at 5 K along the easy axis (c axis, ▲) and the hard axis (perpendicular to c axis; ●).

loop (the remnant magnetization of 30 emu G mol^{-1} and the coercive field of 12 Oe) was observed at 2 K, which shows there is a soft magnetic behavior.

In summary, we have successfully constructed the first novel 3D, fully chiral ferrimagnet; moreover, this ferrimagnet was characterized structurally. Further, the magnetic transition temperature of this complex is relatively high (53 K) for a molecule-based magnet. We believe that this complex is a potential candidate for novel magneto-optical phenomena. In addition to this complex, we have already obtained a few crystals of 3D chiral magnets based on a polymeric cyano-bridged Cr^{3+}-Mn^{2+} compound. It is hoped that these complexes will subsequently lead to the development of a novel group of molecule-based magnets.

Experimental Section

A solution of (*S*)-pn · HCl (0.1 mmol) in water (1 mL) was adjusted to pH 7–8 by the addition of a solution of KOH (0.12 mmol) in water (0.3 mL). A solution of $Mn(ClO_4)_2 \cdot 6H_2O$ (0.1 mmol) in water (0.8 mL) was added to the (*S*)-pn solution under an argon atmosphere. A glass tube (ca. 8 mm diameter, ca. 20 cm long) was charged with this (*S*)-pn and manganese solution, and a mixture of methanol and H_2O (1/2, 1.5 mL) was gently added as an upper layer. A solution of $K_3[Cr(CN)_6]$ (0.07 mmol) in methanol/H_2O (1/1, 1 mL) was added carefully as a third layer under an argon atmosphere, and then the tube sealed. Crystals of the $K_{0.4}[Cr(CN)_6][Mn(S)\text{-pn}](S)\text{-pnH}_{0.6}$ complex grew as pale yellow needles after several weeks.

Received: June 27, 2001 [Z 17372]

[1] J. M. Manriquez, G. T. Yee, R. S. Mclean, A. J. Epstein, J. S. Miller, *Science* **1991**, *252*, 1415; S. Ferlay, T. Mallah, R. Ouahés, P. Veillet, M. Verdaguer, *Nature* **1995**, *378*, 701.

[2] C. Bellitto, P. Day, *J. Chem. Soc. Chem. Commun.* **1978**, 511; "Supramolecular Engneering of Synthetic Metallic Materials Conductors and Magnets": P. Day, *NATO ASI Ser. Ser. C* **1999**, *518*, 253.

[3] G. Wagniere, A. Mejer, *Chem. Phys. Lett*. **1984**, *110*, 546.

[4] G. L. J. A. Rikken, E. Raupach, *Nature* **1997**, *390*, 493.

[5] H. Kumagai, K. Inoue, *Angew. Chem.* **1999**, *111*, 1694; *Angew. Chem. Int. Ed.* **1999**, *38*, 1601.

[6] A. Caneschi, D. Gatteschi, P. Ray, R. Sessoli, *Inorg. Chem*. **1991**, *30*, 3936; M. Hernández-Molina, F. Lloret, C. Ruiz-Pérez, M. Julve, *Inorg. Chem*. **1998**, *37*, 4131; M. Verdaguer, paper presented at the Indo-French Workshop on *Current Trends in Molecular Magnetism* (Bangalore, India), **2000**; E. Coronado, J. R. Galan-Mascaros, C. J. Gomez-Garcia, J. M. Martinez-Agudo, *Inorg. Chem*. **2001**, *40*, 113.

[7] K. Inoue, H. Iwamura, N. Koga, *New J. Chem*. **1998**, *22*, 201; K. Inoue, H. Iwamura, *J. Am. Chem. Soc*. **1994**, *116*, 3173; A. S. Markosyan, T. Hayamizu, K. Inoue, H. Iwamura, *J. Phys. Condens. Mater*. **1998**, *10*, 2323.

[8] M. Ohba, N. Usuki, N. Fukita, H. Okawa, *Angew. Chem.* **1999**, *111*, 1911; *Angew. Chem. Int. Ed.* **1999**, *38*, 1795.

[9] Crystal data for $K_{0.4}[Cr(CN)_6][Mn(S)\text{-pn}](S)\text{-pnH}_{0.6}$: yellow needles, $C_{12}H_{20.6}CrK_{0.4}N_{10}$. $M_r = 397.8877$, crystal dimensions $0.2 \times 0.15 \times 0.10$ mm, hexagonal, space group $P6_1$, $a = 14.7672(4)$, $c = 17.5731(7)$ Å, $V = 3318.75(18)$ Å^3, $\rho_{calcd} = 1.282$ g cm^{-3}, $Z = 6$, $\mu(Mo_{K\alpha}) = 1.282$ mm^{-1}). Data were collected on a Bruker SMART-APEX three-circle diffractometer equipped with a CCD area detector (graphite-monochromated $Mo_{K\alpha}$, $\lambda = 0.71073$ Å, ω-scan mode (0.3° steps), semi-empirical absorption correction on Laue equivalents). The structure was solved by direct methods and refined by full-matrix least-squares refinement against F^2 on all data by using SHELXTL software. Hydrogen atoms were included in their calculated positions but not refined. All non-H atoms, except for C and N atoms in (*S*)-pn that are located in the hole of the helical loop, were refined

 © WILEY-VCH Verlag GmbH, D-69451 Weinheim, 2001 1433-7851/01/4022-4244 $ 17.50+.50/0

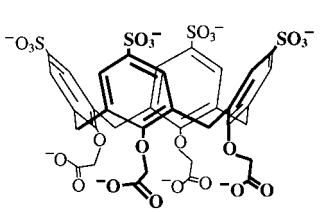
anisotropically. Some disorder in one of the cyanide groups and the (*S*)-pn ligands coordinated to Mn^{2+} ions was also observed. The occupancy of the disordered atoms and the K^+ ion was determined by population anaysis. The refinement converges with $R_1 = 0.0615$ for 2520 data ($I > 4\sigma(I)$), $wR_2 = 0.1371$ for 5405 unique data ($2.81 \le \theta \le 28.33^\circ$), Flack parameter = 0.06(5), max/min residual electron density 0.527/ -0.298 e Å^3. Crystallographic data (excluding structure factors) for the structure reported in this paper have been deposited with the Cambridge Crystallographic Data Centre as supplementary publication no. CCDC-165941. Copies of the data can be obtained free of charge on application to CCDC, 12 Union Road, Cambridge CB2 1EZ, UK (fax: (+44) 1223-336-033; e-mail: deposit@ccdc.cam.ac.uk).

Calixarene – Porphyrin Supramolecular Complexes: pH-Tuning of the Complex Stoichiometry**

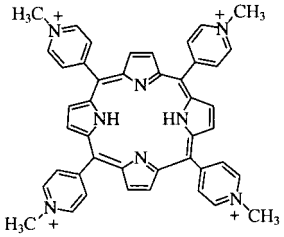
Luigi Di Costanzo, Silvano Geremia, Lucio Randaccio,* Roberto Purrello,* Rosaria Lauceri, Domenico Sciotto,* Fabio Giuseppe Gulino, and Vincenzo Pavone

The rich chemistry of calixarenes and porphyrins as (polytopic) receptors and photoactive species, respectively, as well as the enormous possibility of functionalizing the periphery of these molecules have boosted the synthesis of their covalent conjugates for use as possible molecular devices.[1] It has recently been shown, for example, that covalent porphyrin – calixarene conjugates behave as molecular tweezers when individual specific functions are synergistically exploited.[2] Some preliminary data on the formation of noncovalent complexes have also been reported but, to date, no structural data on such supramolecular species have been presented.[3]

Here we present a spectroscopic and structural study that shows that the cationic porphyrin (H_2T4) and the anionic sulphonated calixarene (C_4TsTc) blocked in a *cone* conformation and bearing carboxylic functions[4] form quite stable supramolecular complexes, both in the solid state and in aqueous solution. Furthermore, the H_2T4:C_4TsTc molar ratio is tuned by the protonation state of the C_4TsTc carboxylate groups.



C_4TsTc



H_2T4

The absorption and fluorescence spectra of H_2T4 are characterized by an intense absorption band at 422 nm (Soret band) and an emission at 650 nm, respectively. C_4TsTc absorbs in the far UV region (about 200 nm) and, at pH 6, emits at 307 and 602 nm. However, at pH 2.2, where the four carboxylic groups of C_4TsTc are all protonated ($pK_{a1} = 3.03$, $pK_{a2} = 3.27$, $pK_{a3} = 3.97$, $pK_{a4} = 4.57$),[5] the emissions are almost completely quenched.

The interaction of H_2T4 with C_4TsTc at pH 6 and $I = 0.05$ M (NaCl) is accompanied by significant hypochromism and broadening of the Soret band (see inset of Figure 1) and remarkable quenching of both the porphyrin and calixarene emissions. The spectroscopic features of H_2T4 at pH 2.2 following complex formation with C_4TsTc ($I = 0.05$ M) are very similar to those observed at pH 6.

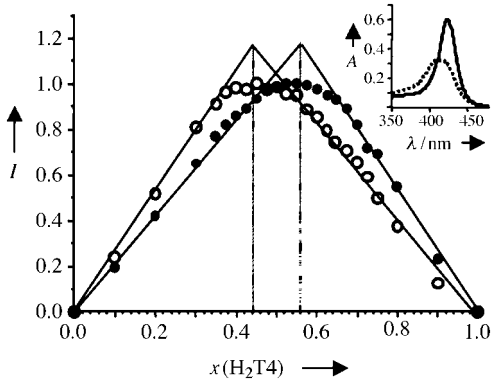


Figure 1. Normalized absorption Job plots at pH 2.2 (○) and 6 (●). The inset shows the absorption spectrum of H_2T4 (2.8 μM) before (——) and after (- - - -) the addition of C_4TsTc (2.2 μM).

However, the Job plots performed at pH 2.2 and 6 show there is a large difference in the ratio of the complex formed (Figure 1). The maximum value at a porphyrin molar fraction of 0.44 at pH 2.2 indicates the formation of species with a 4:3 C_4TsTc:H_2T4 ratio, whereas the maximum value at a porphyrin molar fraction of 0.56 at pH 6 indicates the formation of species with a 4:5 C_4TsTc:H_2T4 ratio. We were able to obtain single crystals of the porphyrin – calixarene complexes at pH ≈ 2 (**1**) and at pH 6 (**2**).

In agreement with the results from the solution study, the H_2T4:(C_4TsTc+H_2T4) molar ratio is 0.43 (2 calixarene moieties, 1.5 porphyrin molecules, and 2 sodium ions) in the asymmetric unit of the crystals obtained at pH ≈ 2 (**1**).[6] Here,

[*] Prof. L. Randaccio, Dr. L. Di Costanzo, Dr. S. Geremia
Centro di Eccellenza di Biocristallografia
Dipartimento di Scienze Chimiche, Università di Trieste
via Licio Giorgieri 1, 34127 Trieste (Italy)
E-mail: randaccio@univ.trieste.it
Prof. R. Purrello, Prof. D. Sciotto, Dr. F. G. Gulino
Dipartimento di Scienze Chimiche
Università di Catania
via Andrea Doria 6, 95125 Catania (Italy)
E-mail: rpurrello@dipchi.unict.it, dsciotto@dipchi.unict.it
Dr. R. Lauceri
ISSN, CNR Valverde, Catania (Italy)
Prof. V. Pavone
Dipartimento di Chimica, Università "Federico II"
Complesso Universitario di Monte S. Angelo
via Cynthia 45, 80131 Napoli (Italy)

[**] This work was supported by the Italian MURST (PRIN MM03185591).

the "central" H_2T4 unit of a trimeric H_2T4 ensemble is arranged on a crystallographic center of symmetry (1/4, 1/4, 0), and each of its methylpyridinium moieties is inserted into a tetra-anionic C_4TsTc molecule from the sulphonate side of the calixarene (Figure 2). The ditopic nature of C_4TsTc allows it

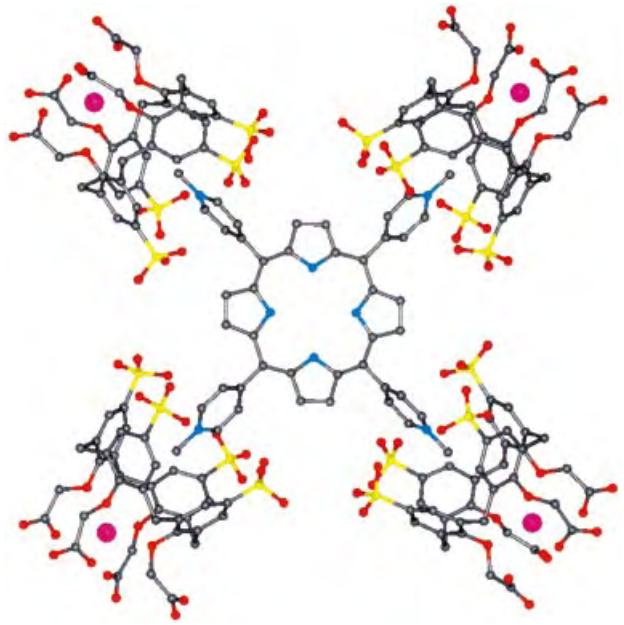


Figure 2. The host–guest interactions in the centrosymmetric unit formed by the central porphyrin cation with calixarene molecules and Na^+ ions (violet circles).

to host one sodium ion on each carboxylate side of the calixarenes. In both **1** and **2** the Na^+ ions are hepta-coordinated by oxygen atoms of the hydroxymethylmethoxy residues at distances in the range of 2.1–2.6 Å. The centrosymmetric unit is sandwiched by two porphyrin rings, which are rotated by 45° with respect to the central one. The resulting neutral supramolecular complex is characterized by a porphyrin mean plane separation of 4.2 Å between the nearly planar porphyrin rings (Figure 3a). The crystal is built up by these supramolecules in such a way as to form large channels (19 × 32 Å; Figure 4), in which the solvent molecules are disordered.

Unlike the crystals obtained at pH 2, the asymmetric unit of the crystals obtained at pH 6[6] contains two hepta-anionic calixarene molecules, three tetracationic porphyrin rings, and two sodium ions, with a H_2T4:(C_4TsTc+H_2T4) molar ratio of 0.6. This value corresponds to a C_4TsTc:H_2T4 molar ratio of 4:6. Seemingly, this result disagrees with the 4:5 ratio obtained in solution. However, a closer look at the structure of **2** readily explains the difference. In fact, the same trimeric ensemble observed in **1**, still arranged on a crystallographic center of symmetry, is also present in **2**, but now, as a result of the deprotonation of the carboxylic groups, the trimeric "core" is staked with two additional porphyrin rings, one above and one below. Each porphyrin ring is rotated by 45° with respect to the external H_2T4 molecules of the trimeric core unit and leads to the 4:5 complex of Figure 3b. The nearly planar five porphyrin rings are separated by a mean plane distance of

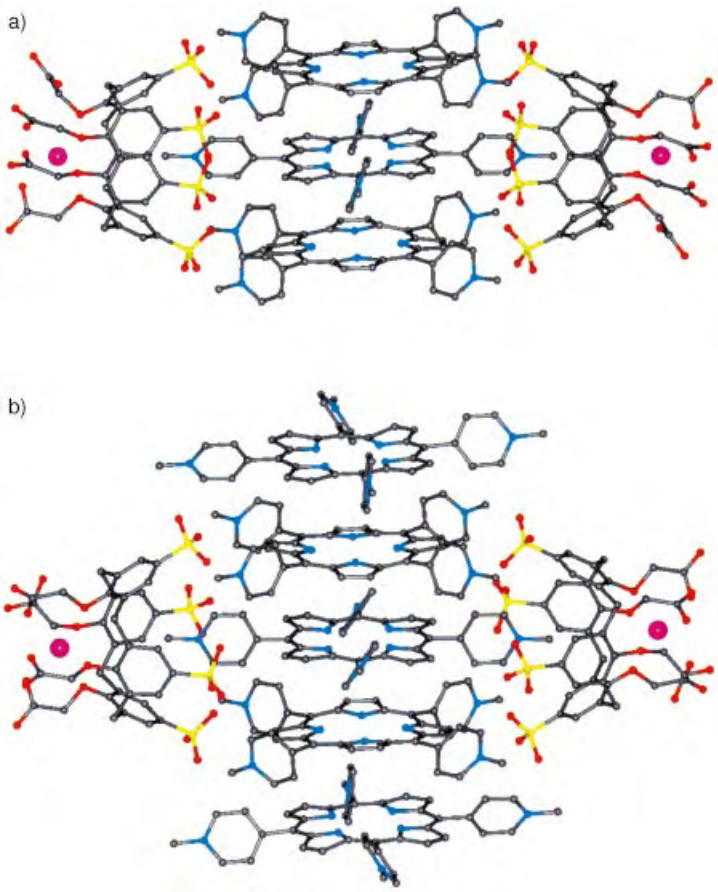


Figure 3. Side views of the neutral supramolecular complex in **1** (a) and the anionic supramolecular complex in **2** (b). In both cases the crystallagraphic centers of symmetry are at the center of the central porphyrin ring. The two calixarene molecules interacting with the central porphyrin ring above and below the plane have been omitted for clarity.

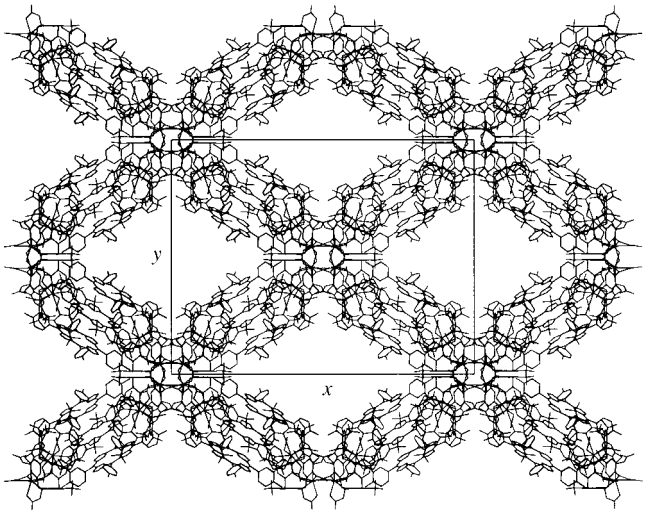


Figure 4. Crystal packing of **1** as viewed along the *z* axis. The channels containing the solvent molecules are shown. The trimeric units are arranged in such a way as to form the walls of the channels.

4.1 Å. The sixth tetracationic H_2T4 unit—arranged on the crystallographic twofold axes—is isolated with respect to the 4:5 core, and essentially balances the charge of the tetra-anionic supramolecule. The isolated porphyrin rings and the

 © WILEY-VCH Verlag GmbH, D-69451 Weinheim, 2001 1433-7851/01/4022-4246 $ 17.50+.50/0

supramolecular anion are packed in such a way as to form two series of interconnected channels which contain the disordered solvent molecules.

Both complexes are stabilized by a synergistic network of noncovalent interactions: 1) electrostatic interactions between the positive residues on the porphyrin rings and the anionic sulphonate groups, 2) stacking interactions between the porphyrin rings, and possibly 3) $CH\cdots\pi$ interactions between the N^+-CH_3 groups and the C_4TsTc molecules. Quite intriguingly, the stoichiometry of the species in the solid state is preserved in solution.

In conclusion, the ditopic nature of C_4TsTc seems to be crucial. The presence of sulphonated and carboxylate groups on the upper and lower rim, respectively, allows for the organization of cationic porphyrins by shielding their like-charge repulsion and providing various sites (the cavity and the anionic groups) for different kinds of weak interactions, as well as the modulation of the number of assembled cationic porphyrins by changing the protonation state of the carboxylic groups.[11] The final result is the formation of stable porphyrin self-aggregates in aqueous solution having a well-defined and tunable stoichiometry. This point is relevant considering that, with few exceptions,[12] porphyrin self-aggregation in water leads to species having ill-defined stoichiometry.

Experimental Section

The supramolecular complexes were prepared and crystallized by the vapor-diffusion method with hanging drops at 18 °C by using Linbro multi-well tissue plates as containers for the reservoir solutions. The stock solutions used were 7 mM C_4TsTc (A) and 14 mM H_2T4Cl_4 (B). Crystals of **1** were obtained in drops formed by mixing solution A (4 μL) with solution B (2 μL) that were set to equilibrate against a reservoir solution of glacial acetic acid (60–70%, 1 mL). The crystals used in the diffraction experiments (typical dimensions $0.4\times0.4\times0.3$ mm) were obtained with 65% glacial acetic acid (pH ≈ 2). Crystals of **2** were obtained in drops formed by mixing solution A (2 μL), solution B (2 μL), and reservoir solution (2 μL) which were set to equilibrate against a reservoir solution (1 mL) containing polyethylene glycol (PEG 300, 30–40% (v/v)) as the precipitant and 0.1M sodium acetate buffer (pH 6.0). The crystals used in the diffraction experiments (typical dimensions $0.6\times0.6\times0.4$ mm) were obtained with 35% PEG 300. Crystals of **1** and **2** deteriorate quickly when left in air. wavelengths of 0.9300 Å for **1** and 0.7100 Å for **2**. The crystals were mounted in loops and frozen to 100 K. The crystal of **1** was cryoprotected by vaseline oil and the crystal of **2** was directly cryocooled. The diffraction data were indexed and integrated using MOSFLM[7] and scaled with SCALA (Collaborative Computational Project, No. 4, 1994). The structures of **1** and **2** were solved by direct methods (SHELXS-97[8]) and refined by full-matrix least-squares methods on F^2 (SHELXL-97[8]). Bond lengths and angles of the porphyrins and calixarenes were restrained. **1**: $C_{276}H_{204}N_{24}O_{96}S_{16}Na_4\cdot 70H_2O$, $M_r=7259$, monoclinic, space group $C2/c$; $a=48.34$, $b=35.47$, $c=25.59$ Å, $\beta=109.03°$, $V=44721$ Å^3, $Z=4$, $\rho_{calcd}=1.078$ g cm^{-3}, $F(000)=15184.0$, $\mu=0.16$ mm^{-1}; 1030 parameters, 501 restraints; max./min. residual electron density 0.84/ − 0.72 e Å^{-3}. Total reflections collected 29111 (resolution 1.20 Å), of which 12420 were unique ($R_{merge}=0.0101$). Final $R_1=0.218$ and $wR_2=0.480$, S(GOF) = 2.9 for 7379 observed reflections ($I>2\sigma(I)$). **2**: $C_{408}H_{312}N_{48}O_{96}S_{16}Na_4\cdot 97H_2O$, $M_r=9775$, monoclinic, space group $C2/c$, $a=52.05$, $b=30.32$, $c=36.10$ Å, $\beta=114.05°$, $V=51986$ Å^3, $Z=4$, $\rho_{calcd}=1.249$ g cm^{-3}, $F(000)=20536$, $\mu=0.16$ mm^{-1}. Total reflections collected 49705 (resolution 1.00 Å), of which 26167 were unique ($R_{merge}=0.0642$). Final $R_1=0.256$ and $wR_2=0.555$, S(GOF) = 3.8 for 16461 observed reflections ($I>2\sigma(I)$); 1402 parameters, 626 restraints; max./min. residual electron density 3.66/ − 0.78 e Å^{-3}. The large values of R_1 and wR_2 are common for supramolecular complexes having very large unit cells[9] and a large number of disordered solvent molecules. Several examples of these structures with values of R_1 of about 0.20 and above have been reported.[10] In addition, the poor quality of the single crystals and the loss of crystallinity during the X-ray exposure did not allow the collection of good diffraction patterns. Crystallographic data (excluding structure factors) for the structures reported in this paper have been deposited with the Cambridge Crystallographic Data Centre as supplementary publication nos. CCDC-167496 (**1**) and -167497 (**2**). Copies of the data can be obtained free of charge on application to CCDC, 12 Union Road, Cambridge CB2 1EZ, UK (fax: (+44) 1223-336-033; e-mail: deposit@ccdc.cam.ac.uk).

Received: July 20, 2001 [Z17548]

[1] a) R. G. Khoury, L. Jaquinod, K. Aoyagi, M. M. Olmstead, A. J. Fisher, K. M. Smith, *Angew. Chem.* **1997**, *109*, 2604–2607; *Angew. Chem. Int. Ed. Engl.* **1997**, *36*, 2497–2500; b) R. Milbradt, J. Weiss, *Tetrahedron Lett.* **1995**, *36*, 2999–3002; c) T. Nagasaki, H. Fujishima, M. Takeuchi, S. Shinkai, *J. Chem. Soc. Perkin Trans. 1* **1995**, 1883–1888.

[2] T. Arimura, S. Ide, H. Sugihara, J. L. Sessler, *New J. Chem.* **1999**, *23*, 977–979.

[3] a) F. G. Gulino, R. Lauceri, R. Purrello, D. Sciotto, *Proceedings 4° Congresso di Chimica Supramolecolare* (Catania, Italy) **1999**, p. 115; b) R. Fiammengo, P. Timmerman, F. de Jong, D. Reinhoudt, *Chem. Commun.* **2000**, 2313–2314.

[4] A. Casnati, Y. Ting, D. Berti, M. Fabi, A. Pochini, R. Ungaro, D. Sciotto, G. G. Lombardo, *Tetrahedron* **1993**, *49*, 9815–9822.

[5] G. Arena, R. Calì, G. G. Lombardo, E. Rizzarelli, D. Sciotto, R. Ungaro, A. Casnati, *Supramol. Chem.* **1992**, *1*, 19–24.

[6] Data collection were performed at the X-ray diffraction beam-line of Elettra Synchrotron, Trieste (Italy) using a MAR345 Image Plate and

[7] W. Kabsch, *J. App. Crystallogr.* **1993**, *24*, 795–800.

[8] G. M. Sheldrick, SHELXS-97 and SHELXL-97, **1997**, University of Göttingen.

[9] F. A. Cotton, C. Lin, C. A. Murillo, *Inorg. Chem.* **2001**, *40*, 575–577.

[10] See for example: H. G. M. Edwards, E. Lawson, M. de Matas, L. Shields, P. York, *J. Chem. Soc. Perkin Trans. 2* **1997**, 1985–1990; D. Whang, K. Kim, *J. Am. Chem. Soc.* **1997**, *119*, 451–452.

[11] R. Purrello, S. Gurrieri, R. Lauceri, *Coord. Chem. Rev.* **1999**, *190–192*, 683–706.

[12] C. Endisch, J. H. Fuhrhop, J. Buschmann, P. Luger, U. Siggel, *J. Am. Chem. Soc.* **1996**, *118*, 6671–6680.

Millisecond Time Resolved Photo-CIDNP NMR Reveals a Non-Native Folding Intermediate on the Ion-Induced Refolding Pathway of Bovine α-Lactalbumin**

Julia Wirmer, Till Kühn, and Harald Schwalbe*

Proteins adopt their native conformation within milliseconds to seconds after the synthesis of the polypeptide chain. This timescale suggests that protein folding follows predetermined folding pathways.[1] Folding intermediates have been detected for a number of proteins along these pathways.[2] Theoretical studies have proposed that folding intermediates may resemble folding traps.[3] The question, therefore, as to whether folding proceeds through well-defined folding intermediates or whether a large number of independent pathways leads to the native structure is of current interest.[4] There are few methods that provide structural insight into folding intermediates with high temporal and site resolution. Herein we report on the kinetic investigation of the Ca^{2+}-induced refolding of α-lactalbumin (α-LA) and NMR characterization at atomic resolution of a folding intermediate populated after 200 ms.

For the calcium binding protein α-LA ($K_D = 2 \times 10^7$ M at 37°C)[5], a partially folded and highly dynamic state of α-LA, the so-called "molten globule", can be stabilized under acidic conditions (pH 2);[6] this molten globule has been proposed to resemble a folding intermediate. Indeed, previous kinetic experiments by Dobson and co-workers revealed a close similarity between the molten globule and a folding intermediate populated during the refolding caused by the dilution from 6 M to 0.54 M guanidinium hydrochloride (GdnCl).[7]

Recently, the application of time-resolved NMR methods to follow protein refolding has gained renewed interest.[8, 9] Comparison of the NMR spectral fingerprint of the aromatic region obtained from NMR refolding experiments of α-LA using time-resolved photo-CIDNP[10] (using tenfold dilution from 6 M GdnCl in the absence of Ca^{2+} ions) suggested a close similarity between the intermediate populated after a few seconds and the static photo-CIDNP spectrum of the acid-stabilized molten globule state of α-LA.[11]

A different approach to the study of refolding of α-LA has been investigated in our research group: Ca^{2+} ions have little effect on the structure of the native state of α-LA,[12] but they stabilize the protein against denaturants such as GdnCl and urea, high temperature, or pressure.[5] The refolding of α-LA can be induced at a constant urea concentration by the addition of Ca^{2+} ions. Figure 1b shows a time–concentration profile of unfolded (U), intermediate (I), and folded (F) states of α-LA derived from kinetic analysis of stopped-flow fluorescence measurements (Figure 1a) of the Ca^{2+}-induced refolding in 2 M urea (α-LA:Ca^{2+} 1:2 final concentrations). When fitted to a three-state model, an intermediate is found to be populated to 70% at $\tau = 350$ ms, as evidenced both by stopped-flow fluorescence (Figure 1a) and CD data. This result is in agreement with the observation of the rise and decay of a non-native NMR signal in the time-resolved experiments discussed below.

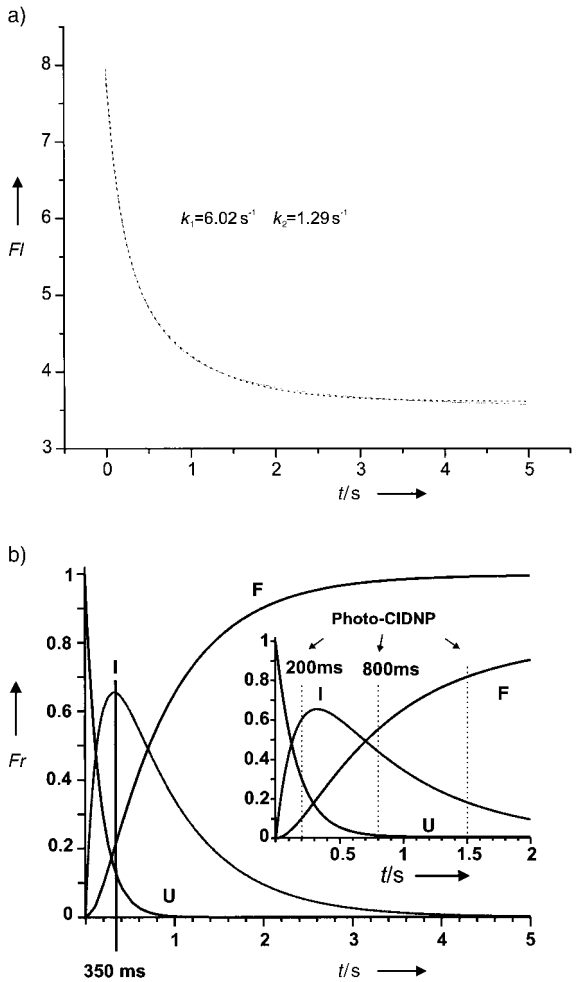


Figure 1. a) Stopped-flow fluorescence data ($\alpha^{exc} = 289$ nm) for the refolding of α-LA in 2 M urea upon the addition of two equivalents of Ca^{2+} ions (Fl = fluorescence, gray line = experimental data, for the exact conditions see the Experimental Section). Data are averages from ten measurements. The urea background was subtracted from the kinetic trace. The fluorescence remains unchanged in blank dilution experiments in the absence of Ca^{2+} ions. The fitting of the data to double exponential decay (assuming three-state kinetics) yields $k_1 = 6.02 \pm 0.06$ s^{-1}, $A_1 = 2.06 \pm 0.02$, $k_2 = 1.29 \pm 0.02$ s^{-1}, $A_2 = 2.15 \pm 0.02$, $R^2 = 0.99993$, and $\chi^2 = 0.00047$ (fit shown as black dots). b) Time–concentration profile of the fraction (Fr) of unfolded (U), folded (F), and intermediate (I) as calculated from k_1 and k_2 by using the software package Maple. The time points at which the kinetic photo-CIDNP NMR spectra have been recorded are indicated in the inset.

[*] Prof. Dr. H. Schwalbe, J. Wirmer, T. Kühn
Department of Chemistry and MIT/Harvard Center for Magnetic Resonance at the Francis Bitter Magnet Laboratory
Massachusetts Institute of Technology
77 Massachusetts Avenue, Cambridge MA 02139 (USA)
Present address: Zentrum für Biologische Magnetische Resonanz
Institut für Organische Chemie
Universität Frankfurt
Marie-Curie-Str. 11
60439 Frankfurt (Germany)
Fax: (+49) 697-9829515
E-mail: schwalbe@nmr.uni-frankfurt.de

[**] We thank the Massachusetts Institute of Technology (start-up funds (H.S.) and Rosenblith stipend (J.W.)), the Karl Winnacker Foundation (H.S.), the Fonds der Chemischen Industrie (H.S., J.W.) and BMBF (J.W.), as well as the DFG (H.S., Schw701/3-1) for financial support. We thank Dr. D. Blechschmidt for helpful discussions. CIDNP = chemically induced dynamic nuclear polarization.

 © WILEY-VCH Verlag GmbH, D-69451 Weinheim, 2001 1433-7851/01/4022-4248 $ 17.50+.50/0

In the NMR experiments reported here, refolding is induced by the release of Ca^{2+} ions from the photolabile chelator DM-Nitrophen (DMN) within 100 ms $< \tau <$ 200 ms at constant denaturant concentration.[8, 13] Our initial studies focused on the characterization of the kinetics for the build-up of the signals corresponding to the methyl groups. The acquisition of the signals for the methyl groups in the native tertiary conformation is a factor of ten slower than the formation of secondary structure of the protein.[8]

Herein refolding of α-LA is studied using time-resolved NMR spectroscopy in conjunction with photo-CIDNP excitation of aromatic residues as pioneered by Hore and coworkers.[11] The experiments described here combine the advantages of photochemical initiation of folding[8] and photo-CIDNP NMR signal detection:[10, 11] namely, the dead-time of the experiment is only governed by the signal-to-noise ratio of the NMR experiment, mixing inhomogeneities are avoided, and the resolution and intensities of aromatic resonances (such as Trp, Tyr, and His) that are in van der Waals contact with CIDNP dyes, such as flavinmononucleotide (FMN), are enhanced.

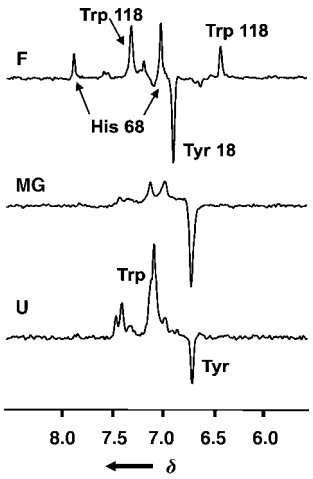


Figure 2. Static photo-CIDNP NMR spectra of the unfolded (U), molten globule (MG), and folded state (F) of bovine α-LA. Spectra are single-scan spectra using 0.5 mM α-LA and 100 ms laser irradiation (sample conditions are given in the Experimental Section). All NMR spectra were analyzed using the software package Felix (MSI).

Figure 2 shows the static photo-CIDNP spectra of the three states of α-LA. Absorptive signals are observed for Trp and His residues; Tyr signals are emissive. For a given amino acid, the signal intensity in the folded state of α-LA can be correlated with the solvent accessibility (SA).[14] In agreement with previous measurements by Hore and coworkers,[11] only Trp 118 (SA = 0.134), Tyr 18 (SA = 0.302), and His 68 (SA = 0.818) lead to a photo-CIDNP effect and contribute to the CIDNP spectrum of folded α-LA. Whereas the spectra of the folded and the unfolded state exhibit sharp lines, broader line widths are characteristic for the molten globule state of α-LA. A distinctive fingerprint for each of the three states can, therefore, be observed using photo-CIDNP spectroscopy.

By applying the combination of ion release and photo-CIDNP, faster ion-induced refolding kinetics can be characterized by NMR spectroscopy with a very small amount (< 0.3 mg, M_r = 14200) of protein, and the changes in the organization of the aromatic core during folding can be monitored with site specificity. The correlation of the photo-CIDNP efficiency may also provide a link to the changes in solvent accessibility during folding.[15]

The experimental setup and the pulse sequence used for these experiments are shown in Figure 3 a and b, respectively.

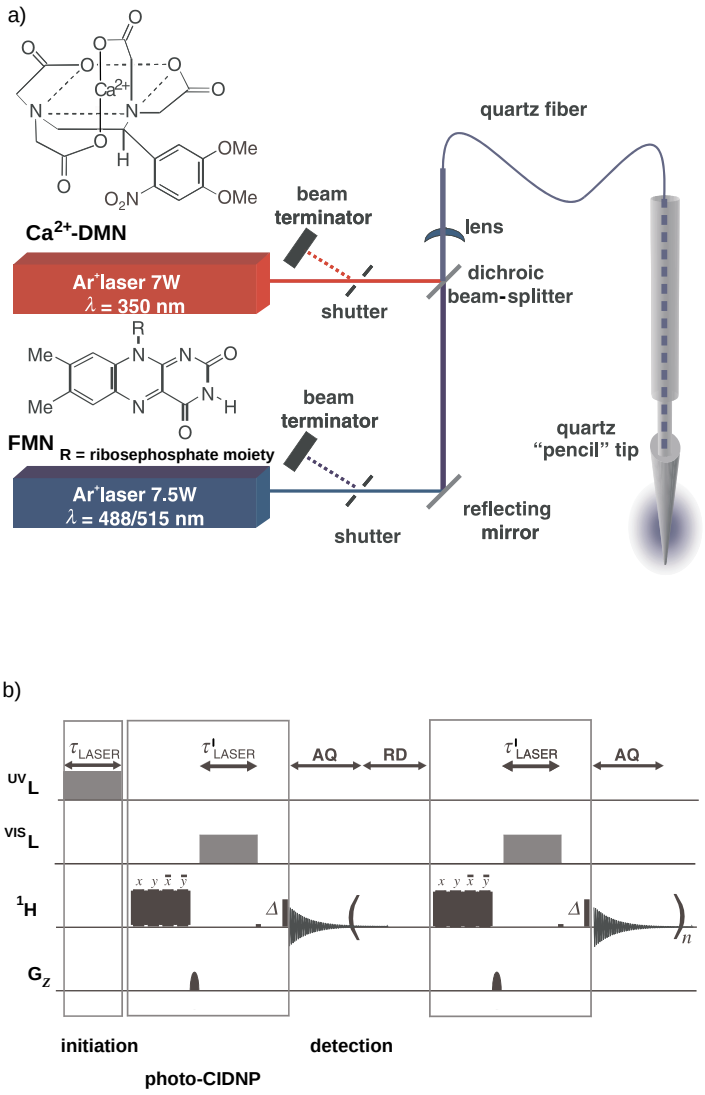


Figure 3. a) Set-up used for laser-NMR coupling. Two argon ion lasers emitting at 350 (7 W) and 488/515 nm (7.5 W) were coupled in the NMR tube through a quartz fiber optic. The coupling efficiency was 70 % for both lasers, as measured by an optical power meter before and after the actual NMR experiment. b) Experimental scheme used for the time-resolved photo-CIDNP experiments. ^{UV}L represents the laser operating at 350 nm for ion release, ^{VIS}L represents the laser operating at 488/515 nm for photo-CIDNP. Equilibrium ^{1}H magnetization is destroyed prior to irradiation with visible light by using trim pulses and a z-gradient (G_z); excitation of the signal and water suppression was done using a jump-return echo pulse sequence. τ_{LASER} = 200 ms, τ'_{LASER} = 100 ms, Δ = 5 ms, AQ = 56 ms, RD = 440 ms or 1140 ms, $\tau_{GRADIENT}$ = 1 ms (50 G cm^{-1}). AQ = aquisition time, RD = relaxation delay.

Ca^{2+} ions were released from DMN inside the NMR spectrometer by irradiation at 350 nm. The accessibility of aromatic side chains was subsequently probed by means of a photochemical reaction (photo-CIDNP). In order to improve the time resolution of the experiment, which is governed by the protein concentration and the metal:α-LA binding constant, a concentration of 0.1 mM (in 160 µL of solution) of α-LA was used. An irradiation time of 200 ms was applied to release 0.2 mM Ca^{2+} ions (of a total of 0.5 mM caged Ca^{2+} ions) to fold the protein. The FMN concentration used in the time-resolved experiments had to be kept low, since higher concentrations were found to suppress ion release.

 © WILEY-VCH Verlag GmbH, D-69451 Weinheim, 2001 1433-7851/01/4022-4249 $ 17.50+.50/0

The results of the time-resolved photo-CIDNP experiments on the ion-induced refolding of α-LA are shown in Figure 4. Native signals of Trp 118 (absorptive signals at $\delta = 6.4$ and 7.42) and Tyr 18 (emissive signal by $\delta = 6.95$) are observed

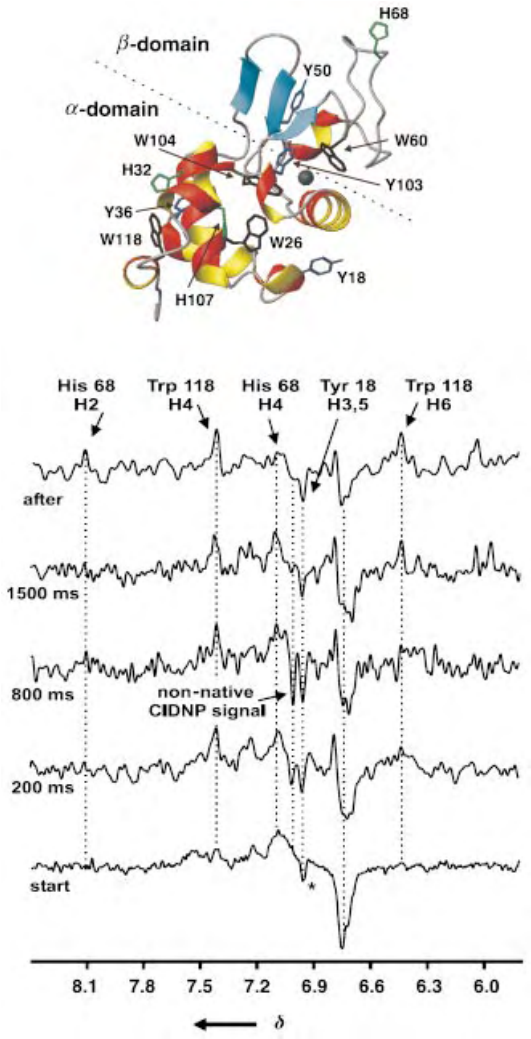


Figure 4. Time resolved photo-CIDNP. The spectra shown are averaged over eight samples. The first and last trace are photo-CIDNP spectra before and after kinetic experiments, respectively; * denotes a native signal present at the start of the experiment. The ribbon representation of the X-ray structure (1HFZ in pdb)[17] of α-LA with tyrosine (blue), tryptophan (black), and histidine (green) residues is indicated. The figure was prepared using the program MOLMOL.[18]

200 ms after initiation of the folding in the first kinetic experiment. Those signals do not significantly change in intensity at later times. A sharp emissive signal at $\delta = 7.05$ arising from one of the three additional Tyr residues in α-LA is present after 200 ms and disappears between 800 and 1500 ms. We assign this signal to the folding intermediate that is also observed in the kinetic analysis of the stopped-flow fluorescence and CD experiments. The chemical shift of the signal does not correspond to any Tyr signal in either the native (F), the unfolded (U), or the molten globule state of α-LA (see Figure 2 and additional NMR data of the native state[16]). It can, therefore, be assigned to an intermediate with a non-native environment.

The assignment of this emissive signal at $\delta = 7.05$ to one of the three remaining Tyr residues (Tyr 36, 50, and 103) cannot be made with certainty. However, the following conclusion can be drawn: It is unlikely that the signal arises from Tyr 36 or Tyr 103 because both Tyr residues are part of hydrophobic clusters formed between Tyr 36 and Trp 118 and between Tyr 103, Trp 60, and Trp 104. Tyr 36 and Tyr 103 are both part of the α-domain in α-LA. In contrast, Tyr 50 is in the β-sheet of the β-domain of α-LA. The assignment of the non-native signal to Tyr 50 would imply that the hydrophobic core in the α-domain of α-LA is locked in its nativelike environment,[7] while parts of the β-domain, maybe those involved in β-sheet formation, would undergo slower structural reorganization.

It is important to note that the emissive Tyr signal seen in the intermediate does not arise from a Tyr residue in a native environment. This result implies that at least part of the polypeptide chain samples non-native conformations during protein refolding. In addition, the emissive signal observed for the folding intermediate populated under the specific experimental conditions has no characteristics of a molten globule. Additional experiments will need to be conducted to further establish the dependence of these observations on the exact folding conditions and to gain further insight into structural aspects of protein folding intermediates at atomic resolution.

Experimental Section

Photo-CIDNP NMR spectroscopy: Two argon lasers (models 2085 and 2017, Spectra Physics) emitting at 350 nm (7 W) and 488/515 nm (7.5 W) were coupled into a 750 MHz home-built NMR spectrometer. The laser beams were guided through an electronic shutter (Uniblitz, Vincent Associates) and combined using a dichroic beam splitter (CVI Laser-optics). The combined laser beam was focused on a multimode silica/silica fiber (1500 μm core, Ceram Optecs). Laser coupling into the NMR spectrometer was performed as described.[8] The overall sample volume used in this setup was 160 μl. Sample conditions were as follows: Kinetic photo-CIDNP: 0.1 mM bovine α-LA, 0.5 mM $CaCl_2$, 0.5 mM DMN, 0.05 mM FMN, 2 M urea, and 50 mM cacodylate buffer in D_2O, pH* 6.7 (pH*: measured in D_2O, uncorrected). The synthesis of DMN and the Ca^{2+} depletion of bovine α-lactalbumin was performed as described.[8] All chemicals were purchased from Fluka.

Static photo-CIDNP: All samples: 0.5 mM α-LA, 0.2 mM FMN, 35 °C in D_2O, U: pH* 2, 8 M urea; MG: pH* 2; F: 50 mM cacodylate, 10 mM $CaCl_2$, pH 6.7.

Stopped-flow fluorescence: Refolding kinetics were acquired using an Applied Photophysics π*-180 stopped-flow spectrometer at 35 °C ($\alpha^{exc} =$ 289 nm, $\alpha^{em} > 320$ nm). Refolding was initiated by mixing 100 μM α-LA against 200 μM $CaCl_2$, both in 2 M urea and 50 mM Tris/HCl at pH 7.0; dead time of the experiment was 1 ms (Tris = tris(hydroxymethyl)aminomethane).

Received: July 5, 2001 [Z 17428]

[1] C. Levinthal in *Mössbauer Spectroscopy in Biological Systems: Proceedings of a meeting held at Allerton House, Monticello, Illinois* (Eds.: J. T. P. DeBrunner, E. Munck), University of Illinois Press, Champaigne, IL, **1969**, pp. 22–24.

[2] a) P. S. Kim, R. L. Baldwin, *Annu. Rev. Biochem.* **1982**, *51*, 459–489; b) P. S. Kim, R. L. Baldwin, *Annu. Rev. Biochem.* **1990**, *59*, 631–660; c) C. M. Dobson, *Curr. Opin. Struct. Biol.* **1992**, *2*, 6–12; d) C. M. Dobson, P. A. Evans, S. E. Radford, *Trends Biochem. Sci.* **1994**, *19*, 31–37.

[3] a) H. S. Chan, K. A. Dill, *J. Chem. Phys.* **1994**, *100*, 9238–9257; b) P. G. Wolynes, J. N. Onuchic, D. Thirumalai, *Science* **1995**, *267*, 1619–1620.

[4] A. Bachmann, T. Kiefhaber, *J. Mol. Biol.* **2001**, *306*, 375–386.

 © WILEY-VCH Verlag GmbH, D-69451 Weinheim, 2001 1433-7851/01/4022-4250 $ 17.50+.50/0

[5] E. A. Permyakov, L. J. Berliner, *FEBS Lett.* **2000**, *473*, 369 – 374.
[6] D. A. Dolgikh, R. I. Gilmanshin, E. V. Brazhnikov, V. E. Bychkova, G. V. Semisotnov, S. Venyaminov, O. B. Ptitsyn, *FEBS Lett.* **1981**, *136*, 311 – 315.
[7] V. Forge, R. T. Wijesinha, J. Balbach, K. Brew, C. V. Robinson, C. Redfield, C. M. Dobson, *J. Mol. Biol.* **1999**, *288*, 673 – 688.
[8] T. Kühn, H. Schwalbe, *J. Am. Chem. Soc.* **2000**, *122*, 6169 – 6174.
[9] a) C. Frieden, S. D. Hoeltzli, I. J. Ropson, *Protein Sci.* **1993**, *2*, 2007 – 2014; b) J. Balbach, V. Forge, N. A. van Nuland, S. L. Winder, P. J. Hore, C. M. Dobson, *Nat. Struct. Biol.* **1995**, *2*, 865 – 870; c) S. D. Hoeltzli, C. Frieden, *Proc. Natl. Acad. Sci. USA* **1995**, *92*, 9318 – 9322; d) J. Balbach, V. Forge, W. S. Lau, N. A. van Nuland, K. Brew, C. M. Dobson, *Science* **1996**, *274*, 1161 – 1163; e) M. Spraul, M. Hoffmann, H. Schwalbe, DE 19548977 C 1 [*Chem. Abstr.* **1997**, *126*: *232572*].
[10] a) J. Bargon, H. Fischer, U. Johnson, *Z. Naturforsch. A* **1967**, *22*, 1551 – 1555; b) P. J. Hore, R. W. Broadhurst, *Prog. Nucl. Magn. Reson. Spectrosc.* **1993**, *25*, 345 – 402; c) R. Kaptein, *Biol. Magn. Reson.* **1982**, *4*, 145 – 191.
[11] K. Maeda, C. E. Lyon, J. J. Lopez, M. Cemazar, C. M. Dobson, P. J. Hore, *J. Biomol. NMR* **2000**, *16*, 235 – 44.
[12] R. Wijesinha-Bettoni, C. M. Dobson, C. Redfield, *J. Mol. Biol.* **2001**, *307*, 885 – 898.
[13] G. C. R. Ellis-Davies, J. H. Kaplan, *J. Org. Chem.* **1988**, *53*, 1966 – 1969.
[14] a) F. M. Richards, *Ann. Rev. Biophys. Bioeng.* **1977**, *6*, 151 – 176; b) B. Lee, F. M. Richards, *J. Mol. Biol.* **1971**, *55*, 379 – 400.
[15] C. Tanford, *Adv. Protein Chem.* **1968**, *23*, 218 – 282.
[16] A. T. Alexandrescu, R. W. Broadhurst, C. Wormald, C. L. Chyan, J. Baum, C. M. Dobson, *Eur. J. Biochem.* **1992**, *210*, 699 – 709.
[17] A. C. Pike, K. Brew, K. R. Acharya, *Structure* **1996**, *4*, 691 – 703.
[18] R. Koradi, M. Billeter, K. Wüthrich, *J. Mol. Graphics* **1996**, *14*, 51 – 55.

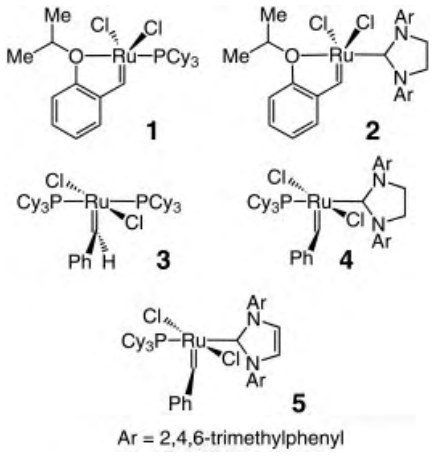
Immobilization of Olefin Metathesis Catalysts on Monolithic Sol – Gel: Practical, Efficient, and Easily Recyclable Catalysts for Organic and Combinatorial Synthesis**

Jason S. Kingsbury, Steven B. Garber, Jonathan M. Giftos, Brian L. Gray, Mariko M. Okamoto, Richard A. Farrer, John T. Fourkas,* and Amir H. Hoveyda*

Environmental issues and recent developments in chemistry and biology have introduced a number of compelling requirements that must be met in the development of practical catalysts. Recyclability is one important attribute. Retrievable catalysts that are recovered inexpensively and without significant waste generation efficiently deliver products of higher purity and lower toxicity. The emerging significance of combinatorial chemistry demands that a catalyst promote reactions efficiently and selectively while being easily adaptable to 96-well and higher density formats; repeated weighing of catalysts or substrates for a library synthesis and subsequent purification of each mixture is costly and time-consuming.

Herein we disclose the synthesis and activity of Ru complexes supported by monolithic (smallest dimension = 1 mm) samples of porous sol – gel glass that effectively promote various olefin metathesis reactions.[1] These catalysts can be easily employed in a library synthesis format without multiple weighings, in air and with undistilled commercial reagent-grade solvents. Catalyst recovery is simply carried out with a pair of tweezers; it does not require filtration and generates minimal solvent waste. The catalyst retains its activity after multiple cycles (>15), affording products that are of high (often analytical) purity without recourse to any purification steps.

Recent reports from our laboratories relate to the chemistry of recyclable monomeric metathesis catalysts (**1** and **2**).[2] A key feature of these systems is the isopropyl styrenyl ether;



this bidentate ligand favors efficient metal recovery for entropic reasons, allowing the promotion of olefin metathesis by a release/return mechanism.[2] These Ru complexes can also offer reactivity and chemo- and stereoselectivity profiles[3] which differ from the alternative catalysts **3**,[4] **4**,[5] and **5**.[6]

Although **1** and **2** are robust and recyclable, catalyst retrieval generates substantial amounts of silica gel and solvent waste. Based on the release/return mechanism, Ru – carbenes **1**,[7] **3**,[8] and **5**[9] were subsequently attached to insoluble cross-linked and monoporous polystyrene polymers as well as to a soluble polyethylene glycol (PEG) resin. However, these supported catalysts typically suffer from one or more of the following shortcomings: 1) There are no reports of catalyst utility in the synthesis of trisubstituted olefins; efficient processes involve only ring-closing metathesis (RCM) reactions with terminal olefin substrates or those that benefit from entropic factors.[7–9a] 2) Diminished

[*] Prof. J. T. Fourkas, Prof. A. H. Hoveyda, J. S. Kingsbury, S. B. Garber, J. M. Giftos, B. L. Gray, M. M. Okamoto, R. A. Farrer
Department of Chemistry
Merkert Chemistry Center
Boston College, Chestnut Hill, MA 02467 (USA)
Fax: (+1) 617-552-1442
E-mail: amir.hoveyda@bc.edu

[**] This research was supported by the NSF (CHE-9905806 to A.H.H., CHE-0073228 to J.T.F., and a predoctoral fellowship to J.S.K.) and Boehringer-Ingelheim. J.M.G. and B.L.G. acknowledge Pfizer for fellowships.

Supporting information for this article is available on the WWW under http://www.angewandte.com or from the author.

activity upon reuse.[7a, 8, 9] 3) Requirement for the addition of solvent during precipitation of the soluble resin[7b] or filtration of nonsoluble ones.[7a, 8, 9] 4) Requirement for alkene additives to ensure reasonable catalyst activity upon reuse.[8, 9a] 5) The need for silica gel chromatography[10] or other purification methods[11] to obtain products with acceptable levels of purity (largely to minimize Ru content). In addition to the above approaches, two systems have been developed which involve permanent attachment to a resin.[12] These variants are either significantly less active than free complexes[12a] or lose substantial reactivity upon recovery.[12b] In all of the above cases, use in a library synthesis would require numerous and deliberate weighing measurements of the catalysts and substrates. If a stock solution of a homogeneous catalyst is used to introduce equal loadings per transformation, the amount of substrate in each well must then be carefully measured. This ultimately leads to higher levels of metal contamination in the products and is equally tedious and time-consuming, since libraries usually contain substrates of varying molecular weights.

In search of an appropriate support, we were attracted to inorganic sol–gels[13] since they offer several advantages: 1) These porous glasses retain a rigid and exposed surface area ($300-1000\ m^2 g^{-1}$), whereas conventional polymer beads typically swell and shrink variably in different media, often resulting in unpredictable effects on catalyst activity. 2) Surface functionalization of a monolithic gel results in a bulk catalyst sample; this obviates the filtration step usually needed for catalyst isolation and minimizes solvent waste. 3) Gelation occurs after a sol is cast into a mold; the gel samples may thus be tailored to a desired size or shape.

For this study, we selected a commercially available (Geltech) glass monolith with an average pore size of 200 Å (Figure 1).[14] Installation of the Ru center on sol–gel and synthesis of an appropriate linker are carried out efficiently in a single vessel (Scheme 1). Treatment of styrene ether **6** with one equivalent of Ru complex **4** and allylchlorodimethylsilane

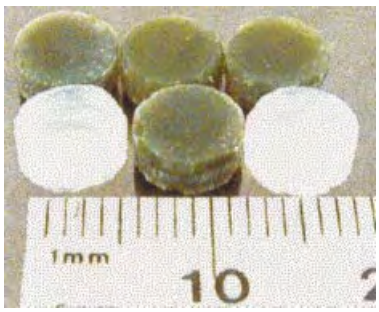


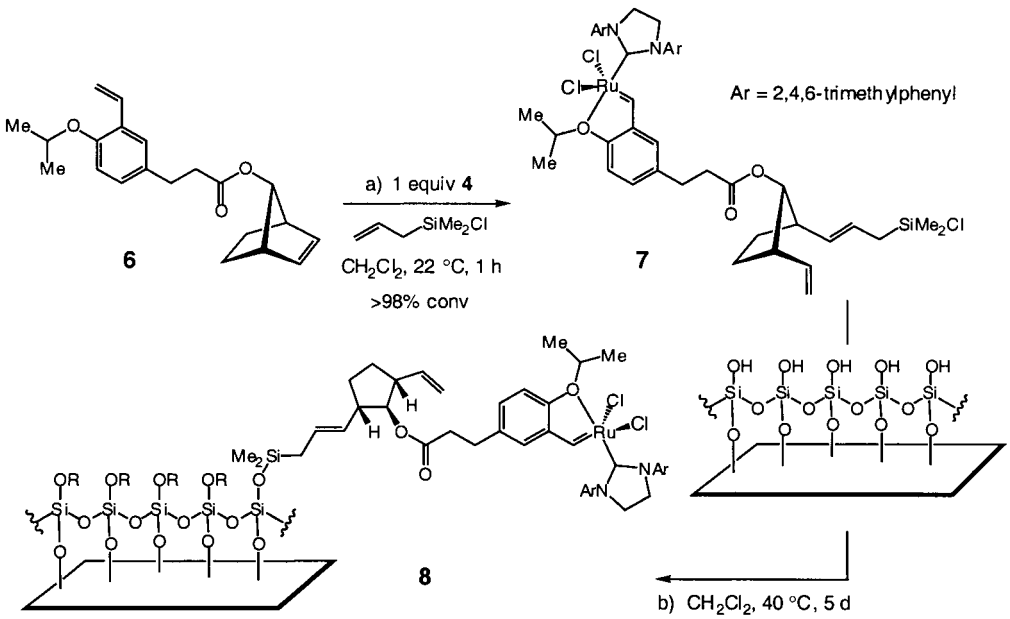
Figure 1. Unfunctionalized (white) and Ru-containing (green) sol–gel monoliths.

(CH_2Cl_2, 22 °C) leads to facile tandem ring-opening metathesis (ROM)/cross metathesis (CM) and subsequent deposition of the Ru center at the bidentate site. Preweighed monolithic sol–gels are added to the solution, and the mixture is allowed to stand at 40 °C for five days[15] to afford loaded dark green glass samples which are washed with CH_2Cl_2 and dried in vacuo (Figure 1). These samples may be stored in air without significant loss of activity.[16] Sol–gel systems **9** and **10** were also prepared by an identical procedure with the corresponding norbornene precursors,[17] and possess similar physical appearance to **8**.

Sol–gel-supported Ru catalysts **8**–**10** provide excellent levels of reactivity for the formation of trisubstituted olefin **12** (see Table 1). There is minimal diminution in reactivity after four cycles (>98% yield in all cases).[18] With purified solvent and under N_2 atmosphere, catalyst **10** was used in the synthesis of **12** for eleven additional rounds (total of fifteen cycles). Although extended times were required for complete conversion,[19] all transformations proceeded to completion (>98% yield). With reagent-grade solvent (used directly from a bottle of Mallinkrodt, AR grade) and under air, the catalyst was employed efficiently three times (>98% conv); however, the reaction did not proceed to completion during the fourth cycle under these conditions.[17]

Glass samples recovered from the fourth cycle (N_2 and purified solvent) were used with different substrates in the ROM/CM process cycle 5 (**13**→**14**). The reaction proceeds to completion, and careful analysis (400 MHz ^{1}H NMR analysis) of the unpurified product shows <2% contamination from the product of the previous RCM (**12**). The same is true for transformations in cycles 6–8: no products or by-products from the previous transformation were detected in any of the unpurified product samples (<2% by 400 MHz ^{1}H NMR spectroscopy).

Several additional issues regarding the data in Table 1 merit mention: 1) In contrast to



Scheme 1. Attachment of Ru complex and linker to glass support in a single vessel.

 © WILEY-VCH Verlag GmbH, D-69451 Weinheim, 2001 1433-7851/01/4022-4252 $ 17.50+.50/0

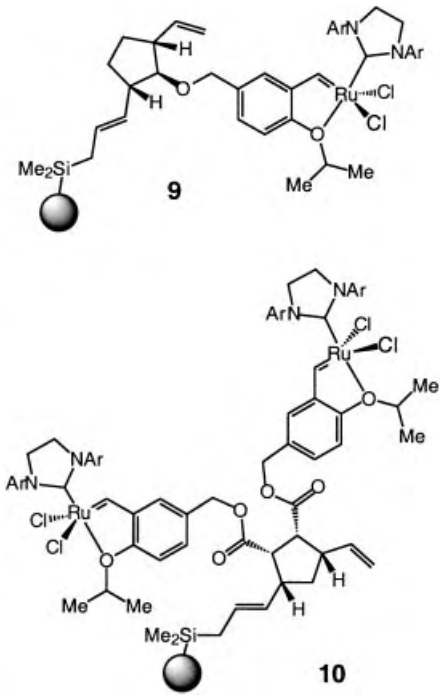
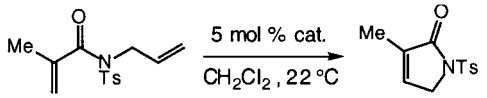
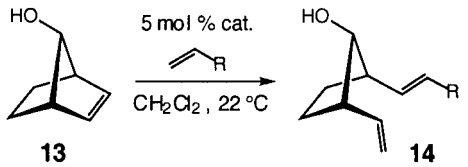


Table 1. Recycling studies with glass-bound metathesis catalysts **8**–**10**.



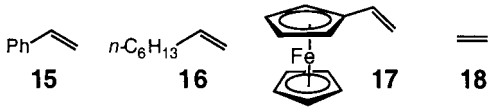
11 **12**

Cycle (*t*)	**8** as catalyst (conv [%]; yield [%])	**9** as catalyst (conv [%]; yield [%])	**10** as catalyst (conv [%]; yield [%])
cycle 1 (3 h)	>98; >98	>98; >98	>98; >98
cycle 2 (3 h)	>98; >98	>98; >98	>98; >98
cycle 3 (3 h)	>98; >98	>98; >98	>98; >98
cycle 4 (3 h)	>98; >98	>98; >98	>98; >98



13 **14**

	(alkene; conv [%])	(alkene; conv [%])	(alkene; conv [%])
cycle 5 (1 h)	15; >98	15; >98	15; >98
cycle 6 (1 h)	16; >98	16; >98	16; >98
cycle 7 (1 h)	17; >98	17; >98	17; >98
cycle 8 (1 h)	18; >98	18; >98	18; >98



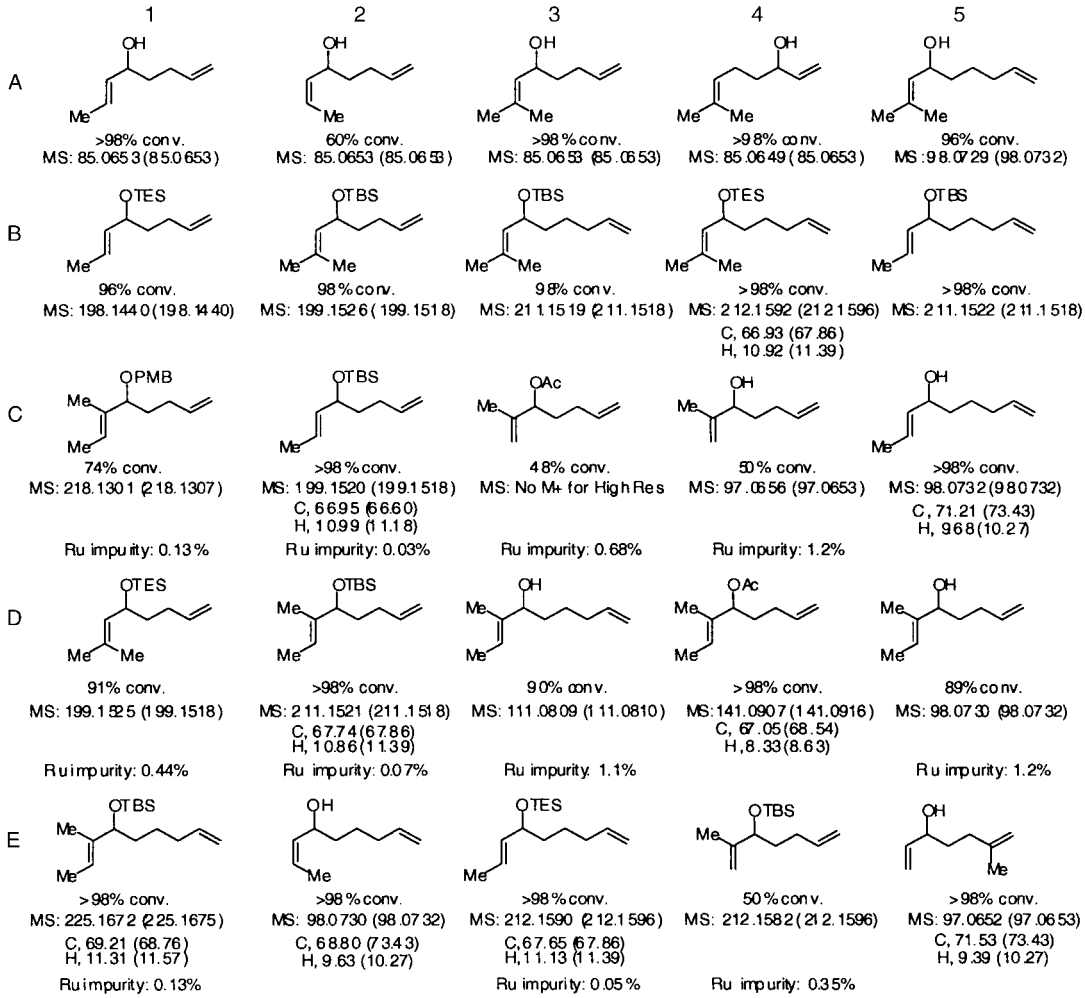
15 **16** **17** **18**

processes run with 5 mol% monomer **2** or **4**, the unpurified reaction mixture (cycles 1–4) in every case consisted of >98% pure cycloolefin, where no catalyst or by-product thereof could be detected (400 MHz ^{1}H NMR spectroscopy). Removal of CH_2Cl_2 in vacuo delivered pure cycloolefin as an off-white solid in >98% yield; silica gel chromatography or distillation was not required. The resulting unpurified materials were determined to be analytically pure (C,H analysis) for all twelve of the experiments in cycles 1–4 of Table 1.[20] Inductively coupled plasma mass spectrometry (ICP-MS) analysis of product samples indicates only 0.04–0.06% (by mass) Ru contamination in the unpurified products, values that are substantially lower than those obtained with homogeneous monomeric catalysts, where all of the catalyst remains in the product mixture which must be purified by silica gel chromatography or distillation. 2) Filtration is not needed for product isolation. The reaction mixture is simply removed with a Pasteur pipette, and the glass sample is rinsed with minimal amounts of CH_2Cl_2. 3) After four rounds of RCM for each supported catalyst, the gel pellets were dried in vacuo and weighed. Highly reproducible mass differences indicated a net 20–25% Ru loss over the four cycles. 4) The functionalized monoliths are physically robust and do not chip or fragment in the presence of small stir bars. Catalytic olefin metathesis can be carried out with supported complexes **8**–**10** without stirring. However, the shortest reaction times are observed with either rotary agitation or magnetic stirring.

Despite the diminution in Ru loading, the catalytic activities of the recycled pellets are still high, as demonstrated by the levels of conversion in the additional cycles. This minor, but steady, loss of active metal content detected after each round of catalysis accounts for the low, but detectable (ICP-MS), levels of Ru in products and the increase in reaction times required for complete conversion during the later rounds.[19] Since the isopropyl styrene ether remains bound to the glass surface during catalysis, it is unavailable to serve as a stabilizing Lewis base for electron-deficient and highly active metal complexes in solution, leading to some Ru–carbene decomposition. It is therefore plausible that small amounts of Ru are released into solution, where the extremely high propagation rate for the metal–carbene gives rise to substantial levels of conversion. The glass-bound catalysts may not be recycled as efficiently when metathesis is performed in the presence of air due to sensitivity of this unstabilized and highly reactive unbound Ru–carbene. Detailed mechanistic studies are underway to rigorously establish whether and to what extent, as observed with monomeric and dendritic variants,[2] any of the released Ru returns to the isopropoxy ligand at the surface of the glass (release/return mechanism).

The practicality of glass-bound Ru complexes in high-throughput synthesis was demonstrated by synthesis of olefin metathesis libraries shown in Schemes 2 and 3 and promoted by glass-supported catalysts **8**–**10**. The first 25-member library (Scheme 2) involved catalytic RCM reactions of a range of dienes with varying levels of alkene substitution. Reactions were carried out for six hours at 22 °C in air with reagent-grade solvent in the presence of one small catalyst pellet within each well. Since the functionalized glass-bound catalyst samples are of uniform size and loading, individual and repetitive weighings of catalyst samples are not needed. An appropriate number of pellets of a given size may be added to a well, depending on the substrate amount. Because the Ru–carbene is released by the available substrate

 © WILEY-VCH Verlag GmbH, D-69451 Weinheim, 2001 1433-7851/01/4022-4253 $ 17.50+.50/0



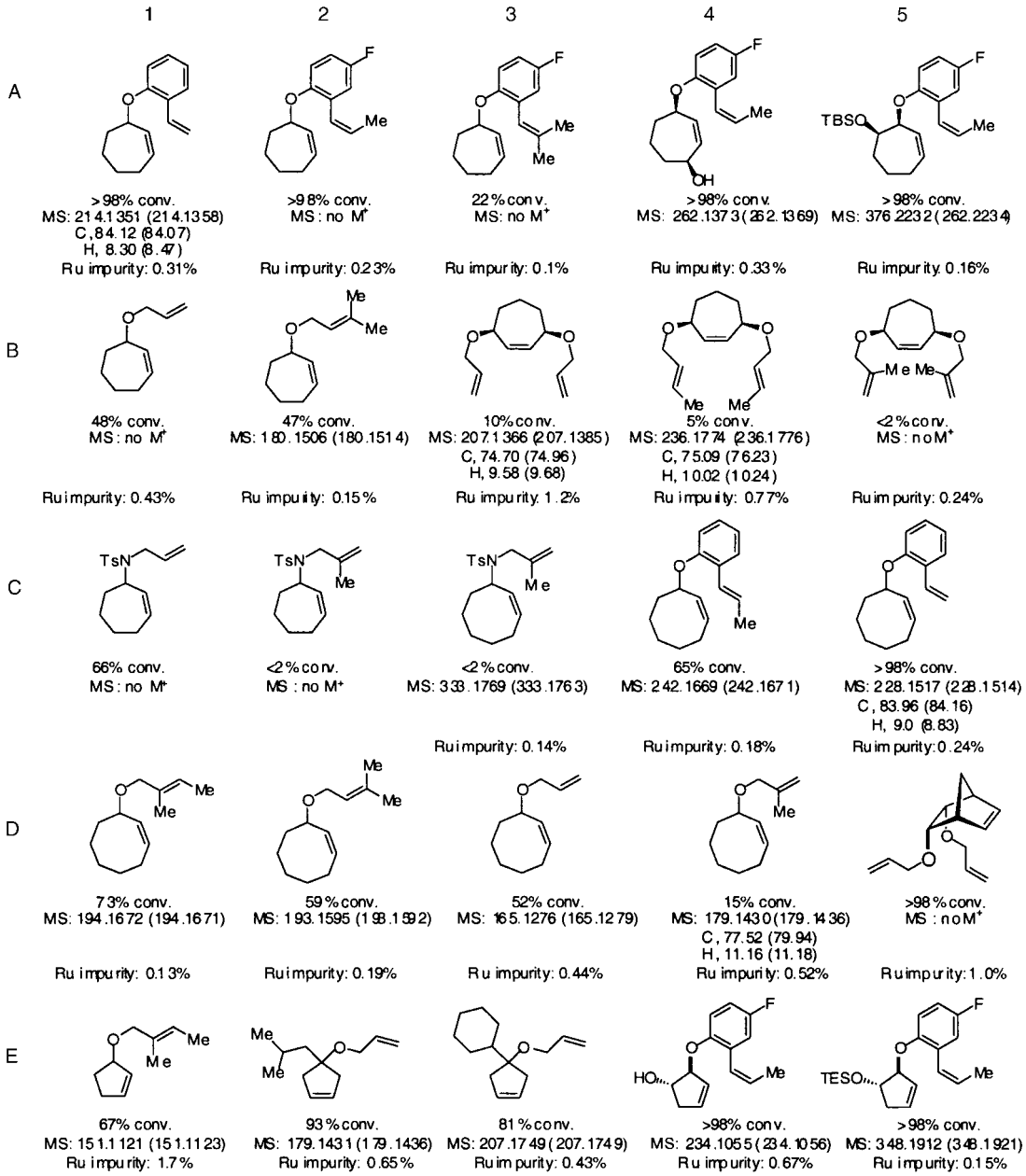
Scheme 2. Library of ring-closing metathesis reactions catalyzed by **8**–**10** (substrates shown only). Conditions: One pellet per well (~5 mol% catalyst available on glass), 0.2 M in CH_2Cl_2, 22 °C, 6 h. Conversions determined by analysis of 400 MHz ^1H NMR spectrum of the reaction mixture. Analysis data obtained from unpurified reaction products after removal of solvent in vacuo. Representative found and calculated values for C, H elemental analyses and high resolution mass spectroscopy are shown below each substrate; calculated values are in parantheses. Level of Ru impurity determined by ICP-MS and shown as percent by mass.

molecules[2] and only small amounts of highly active free Ru–carbene lead to appreciable conversion, larger glass samples or those carrying an excess of catalyst might be used. Most of the Ru remains attached and can simply be recovered by taking away the loaded glass upon completion of the reaction. Workup involves removal of the solutions (pipette), washing of each container and its bound catalysts with CH_2Cl_2 ($3 \times \sim$ 0.5 mL) and evaporation of volatiles in vacuo. As the data in Scheme 2 indicate, all reactions, including those involving trisubstituted olefins, proceeded efficiently. In all but one case (C3), the formation of the desired cyclic adduct was confirmed by high-resolution mass spectrometry. Representative C,H, and ICP-MS analyses show that the products—without any purification—are of high purity and the level of Ru contamination is typically below 1%.

The glass-bound catalysts recovered from the library in Scheme 2 were used to carry out the synthesis of a second library of tandem catalytic ROM/RCM products (Scheme 3). These reactions were allowed to stir in commercial CH_2Cl_2 at 22 °C in air (0.10 mmol substrate as in the first library) and represent a more challenging class of substrates;[1] reactivity is diminished since olefins of higher substitution are involved (e.g., C3 or D2 in Scheme 3). Nevertheless, similar levels of reactivity, as observed with monomeric **2**, were detected in reactions of the second library. Mass spectrometric analysis confirmed the presence of the desired compound in 18 out of 25 cases. Selected elemental analyses indicate products of high purity prior to any purification (e.g., A1 and C5, Scheme 3).

We have thus designed an efficient new strategy for one-pot surface functionalization of monolithic sol–gels that can be effected catalytically or stoichiometrically under mild conditions. Importantly, the strategy for modification of glass surfaces may be readily adapted for immobilization of other catalyst systems. The Ru-based catalysts described herein represent a new class of convenient and practical olefin metathesis catalysts that exhibit high reactivity and can be easily recycled without significant loss of activity or the need for additives or solvents. These catalysts provide products that are of excellent purity before silica gel chromatography or

 © WILEY-VCH Verlag GmbH, D-69451 Weinheim, 2001 1433-7851/01/4022-4254 $ 17.50+.50/0 *Angew. Chem. Int. Ed.* **2001**, *40*, No. 22



Scheme 3. Library of tandem ring-opening/cross metathesis reactions catalyzed by **8**–**10** (substrates shown only). Conditions: One pellet per well (~5 mol% catalyst available on glass), 0.2 M in CH_2Cl_2, 22 °C, 24 h. See legend for Scheme 2 for details on conversion determination and analytical data.

distillation, and can be employed readily in combinatorial synthesis in air and with reagent-grade commercial solvents. The generality and significance of olefin metathesis, together with the chemically and environmentally attractive attributes of the catalysts discussed above, should render these glass-supported Ru-based catalysts of extensive utility in chemistry and all of its related applications.

Receved: August 10, 2001 [Z17703]

[1] a) R. H. Grubbs, S. Chang, *Tetrahedron* **1998**, *54*, 4413–4450; b) A. Furstner, *Angew. Chem.* **2000**, *112*, 3140–3172; *Angew. Chem. Int. Ed.* **2000**, *39*, 3012–3043; c) A. H. Hoveyda, R. R. Schrock, *Chem. Eur. J.* **2001**, *7*, 945–950.

[2] a) J. S. Kingsbury, J. P. A. Harrity, P. J. Bonitatebus, A. H. Hoveyda, *J. Am. Chem. Soc.* **1999**, *121*, 791–799; b) S. B. Garber, J. S. Kingsbury, B. L. Gray, A. H. Hoveyda, *J. Am. Chem. Soc.* **2000**, *122*, 8168–8179.

[3] a) See the Supporting Information in: J. Limanto, M. L. Snapper, *J. Am. Chem. Soc.* **2000**, *122*, 8071–8072; b) S. Gessler, S. Randl, S. Blechert, *Tetrahedron Lett.* **2000**, *41*, 9973–9976; c) S. Randl, S. Gessler, H. Wakamatsu, S. Blechert, *Synlett* **2001**, 430–432; d) J. Cossy, S. BouzBouz, A. H. Hoveyda, *J. Organomet. Chem.* **2001**, *624*, 327–332; for an application of **2** in target-oriented synthesis, see: e) S. BouzBouz, J. Cossy, *Org. Lett.* **2001**, *3*, 1451–1454.

[4] a) P. Schwab, M. B. France, J. W. Ziller, R. H. Grubbs, *Angew. Chem.* **1995**, *107*, 2179–2181; *Angew. Chem. Int. Ed. Engl.* **1995**, *34*, 2039–2041; b) P. Schwab, R. H. Grubbs, J. W. Ziller, *J. Am. Chem. Soc.* **1996**, *118*, 100–110.

[5] M. Scholl, S. Ding, C. W. Lee, R. H. Grubbs, *Org. Lett.* **1999**, *1*, 953–956.

[6] a) M. Scholl, T. M. Trnka, J. P. Morgan, R. H. Grubbs, *Tetrahedron Lett.* **1999**, *40*, 2247–2250; b) J. Huang, E. D. Stevens, S. P. Nolan, J. L. Petersen, *J. Am. Chem. Soc.* **1999**, *121*, 2647–2678; c) L. Ackermann,

A. Furstner, T. Weskamp, F. J. Kohl, W. A. Hermann, *Tetrahedron Lett.* **1999**, *40*, 4787 – 4790.
[7] a) J. Dowden, J. Savovic, *Chem. Commun.* **2001**, 37 – 38; b) Q. Yao, *Angew. Chem.* **2000**, *112*, 4060 – 4062; *Angew. Chem. Int. Ed.* **2000**, *39*, 3896 – 3898.
[8] M. Ahmed, A. G. M. Barrett, D. C. Braddock, S. M. Cramp, P. A. Procopiou, *Tetrahedron Lett.* **1999**, *40*, 8657 – 8662.
[9] a) M. Ahmed, T. Arnauld, A. G. M. Barrett, D. C. Braddock, P. A. Procopiou, *Synlett* **2000**, 1007 – 1009; b) L. Jafarpour, S. P. Nolan, *Org. Lett.* **2000**, *2*, 4075 – 4078.
[10] D. D. Long, A. P. Termin, *Tetrahedron Lett.* **2000**, *41*, 6743 – 6747.
[11] For approaches where Ru impurities are removed by addition of a phosphane, $Pb(OAc)_4$ and a phosphine oxide, respectively, see: a) H. D. Maynard, R. H. Grubbs, *Tetrahedron Lett.* **2000**, *40*, 4137 – 4140; b) L. A. Paquette, J. D. Schloss, I. Efremov, F. Fabris, F. Gallou, J. Mendez-Andino, J. Yang, *Org. Lett.* **2000**, *2*, 1259 – 1261; c) Y. M. Ahn, K. Yang, G. I. Georg, *Org. Lett.* **2001**, *3*, 1411 – 1413.
[12] a) S. T. Nguyen, R. H. Grubbs, *J. Organomet. Chem.* **1995**, 195 – 200; b) S. C. Schürer, S. Gessler, N. Buschman, S. Blechert, *Angew. Chem.* **2000**, *112*, 4062 – 4065; *Angew. Chem. Int. Ed.* **2000**, *39*, 3898 – 3901.
[13] C. J. Brinkler, G. W. Scherer, *Sol-Gel Science: The Physics and Chemistry of Sol-Gel Processing.* Academic Press, San Diego, CA, **1990**.
[14] Each pellet weighs about 50 mg and is about 6 mm in diameter and 3 mm thick.
[15] Extensive optimization studies regarding glass derivatization revealed that shorter reaction times lead to lower loadings of Ru per unit surface area of support. These results suggest that addition of free hydroxy groups on the glass surface to the Si–Cl bond is slow.
[16] Ru loading is calculated from the mass increase which accompanies functionalization of the glass surface. ICP-MS analysis for Ru was also carried out for the supported catalyst. However, the former is more reproducible and reliable.
[17] See the Supporting Information for all experimental details.
[18] Analysis of the 400 MHz ^{1}H NMR spectrum of the unpurified reaction mixtures indicated no difference in reaction efficiency among the three catalysts.
[19] Five hours for cycle 5, six hours for cycles 6 and 7, seven hours for cycle 8, eight hours for cycles 9 and 10, nine hours for cycle 11, ten hours for cycle 12, twelve hours for cycle 13 and fourteen hours for cycles 14 and 15.
[20] Elemental analyses were not obtained for product samples in cycles 5 – 8, since multiple ROCM products are produced in these reactions along with substantial amounts of uncharacterized oligomers (derived from ROMP of **13**). Similar product distributions are obtained by the monomeric **2**.

Host – Guest Chemistry Aids and Abets a Stereospecific Photodimerization in the Solid State**

Dafni G. Amirsakis, Miguel A. Garcia-Garibay,*
Stuart J. Rowan, J. Fraser Stoddart,*
Andrew J. P. White, and David J. Williams*

In memory of Donald J. Cram

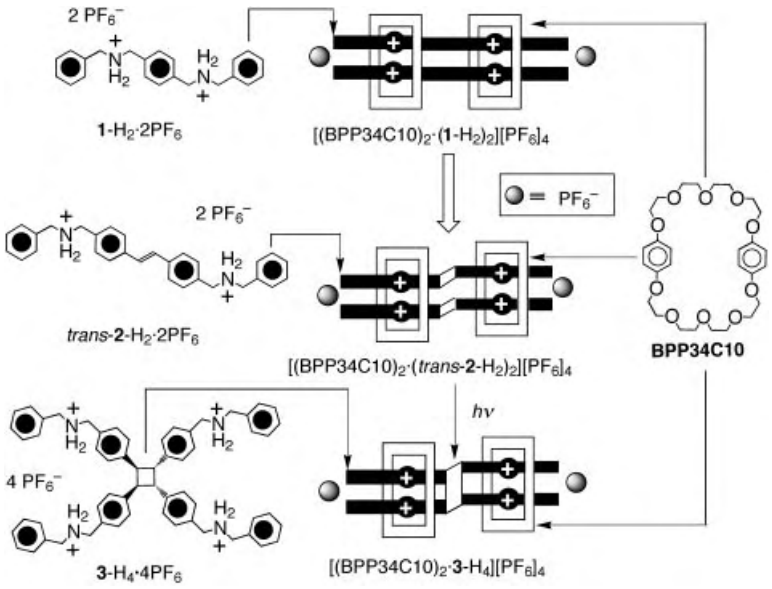
The ability to preorganize olefins for their solid-state photochemical dimerization[1] within a crystalline lattice is a challenging problem.[2] It has been ascertained[3] that, in order for such reactions to occur, the olefinic functions need to be aligned in a parallel manner and to have centroid – centroid separations of about 3.5 – 4.2 Å. The utilization of supramolecular assistance toward the alignment of stilbenes[4] in the solid state offers a potential solution to this problem of preorganization. To date, examples of this methodology include 1) double-stranded complexes of stilbenes bound within the torus of γ-cyclodextrin,[5, 6, 7] 2) the functionalization of the aromatic units of stilbenes to encourage donor – acceptor $\pi-\pi$ stacking interactions,[8, 9] and 3) the incorporation of hydrogen-bond acceptors into a stilbene derivative that are capable of forming a noncovalent macrocycle upon cocrystallization with a hydrogen-bond donor.[10] Herein we demonstrate that cocrystallization of a crown ether with a bis(dialkylammonium) salt—which contains a central *trans*-stilbenoid unit—generates a 2:2 complex within which the two (*E*)-olefinic bonds are aligned in an appropriate geometry that facilitates subsequent stereospecific solid-state photochemical dimerization.

Supramolecular complexes with pseudorotaxane-like architectures that are formed spontaneously from dialkylammonium ions and crown ethers have been studied extensively.[11] It has been demonstrated[12] that the bis(dialkylammonium ion)-containing threadlike dication **1**-$H_2 \cdot 2PF_6$ and the crown ether bis-*p*-phenylene[34]crown-10 (BPP34C10) form a doubly encircled and doubly threaded 2:2 complex $[(BPP34C10)_2 \cdot (\mathbf{1}\text{-}H_2)_2][PF_6]_4$ (Scheme 1) upon cocrystallization in the solid state. This result suggested to us a method for aligning stilbene derivatives in the solid state. By replacing the *p*-phenylene unit of $\mathbf{1}^{2+}$ with a *trans*-stilbenoid unit (namely, producing *trans*-**2**-$H_2 \cdot 2PF_6$) we anticipated that a 2:2 complex $[(BPP34C10)_2 \cdot (\mathbf{2}\text{-}H_2)_2][PF_6]_4$ would form upon cocrystallization in which adjacent *trans*-stilbene olefinic bonds

[*] Prof. M. A. Garcia-Garibay, Prof. J. F. Stoddart, D. G. Amirsakis, S. J. Rowan
Department of Chemistry and Biochemistry
University of California, Los Angeles
405 Hilgard Avenue, Los Angeles, CA 90095-1569 (USA)
Fax: (+1) 310-206-1843
E-mail: mgg@chem.ucla.edu, stoddart@chem.ucla.edu
Prof. D. J. Williams, Dr. A. J. P. White
Chemical Crystallography Laboratory
Department of Chemistry, Imperial College
South Kensington, London, SW7 2AY (UK)
Fax: (+44) 207-594-5835

[**] We thank the National Science Foundation for funding this research.

 © WILEY-VCH Verlag GmbH, D-69451 Weinheim, 2001 1433-7851/01/4022-4256 $ 17.50+.50/0



Scheme 1. The complexation of threads **1**-$H_2 \cdot 2PF_6$ and *trans*-**2**-$H_2 \cdot 2PF_6$ with BPP34C10 generates the 2:2 complexes $[(BPP34C10)_2 \cdot (\mathbf{1}\text{-}H_2)_2][PF_6]_4$ and $[(BPP34C10)_2 \cdot (trans\text{-}\mathbf{2}\text{-}H_2)_2][PF_6]_4$ in the solid state, respectively. Irradiation of $[(BPP34C10)_2 \cdot (trans\text{-}\mathbf{2}\text{-}H_2)_2][PF_6]_4$ in the solid state yields the 2:1 complex $[(BPP34C10)_2 \cdot \mathbf{3}\text{-}H_4][PF_6]_4$.

would be aligned in a manner suitable for a solid-state [2+2] cycloaddition to occur. Depending upon the alignment of the two *trans*-stilbenoid units in the complex, a single diastereoisomer of a tetrasubstituted cyclobutane derivative should be isolable after photochemical irradiation.

The bis(dialkylammonium) salt *trans*-**2**-$H_2 \cdot 2PF_6$ was synthesized by the substitution reaction between *trans*-4,4′-bis(bromomethylstilbene)[6] and benzylamine followed by counterion exchange. Single crystals of the complex $[(BPP34C10)_2 \cdot (trans\text{-}\mathbf{2}\text{-}H_2)_2][PF_6]_4$ were obtained by vapor diffusion of *i*Pr_2O into a solution of an equimolar mixture of *trans*-**2**-$H_2 \cdot 2PF_6$ and BPP34C10 in Me_2CO/CH_2Cl_2. The complex $[(BPP34C10)_2 \cdot (trans\text{-}\mathbf{2}\text{-}H_2)_2][PF_6]_4$ adopts a classic centrosymmetric doubly threaded, doubly encircled [4]pseudorotaxane geometry in the solid state[13, 14] (Figure 1) analogous to that exhibited by those formed between BPP34C10 and, for example, α,α′-bis(benzylammonium)-*p*-xylene[12] and bis(benzylammonium-*p*-toluic acid).[15] The dicationic threads are each hydrogen bonded through their ammonium centers to oxygen atoms in the polyether loops of the crown ether components, the latter having distinctly cupped conformations, with their hydroquinone rings inclined by approximately 51° to one another. The central *trans*-stilbenoid portions of the dicationic threads have near-planar conformations, the torsional twists about the bonds linking the phenyl rings to the central *trans*-olefinic unit being only approximately 3 and 11°, respectively. There are weak interthread π–π stacking interactions between the laterally offset *trans*-stilbene units, with mean interplanar and centroid–centroid separations of 3.57 and 4.33 Å, respectively, between adjacent phenylene rings, and of 3.60 and 4.20 Å, respectively, between the *trans*-olefinic components. Adjacent dumbbell-shaped supermolecules pack end-to-middle (Figure 2). One of the PF_6^- ions is trapped within the cleft formed between the

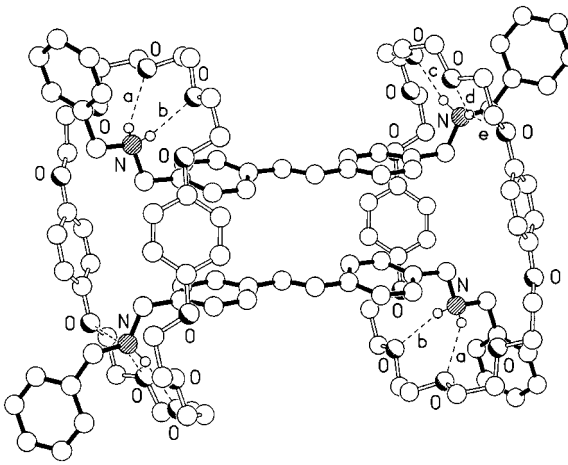


Figure 1. The solid-state supramolecular structure of the doubly threaded, doubly encircled [4]pseudorotaxane $[(BPP34C10)_2 \cdot (trans\text{-}\mathbf{2}\text{-}H_2)_2]^{4+}$. Hydrogen-bonding N···O, H···O distances [Å] and N–H···O angles [°], are a) 2.96, 2.27, 133; b) 3.02, 2.18, 155; c) 2.90, 2.04, 161; d) 2.94, 2.26, 131; and e) 3.17, 2.34, 154.

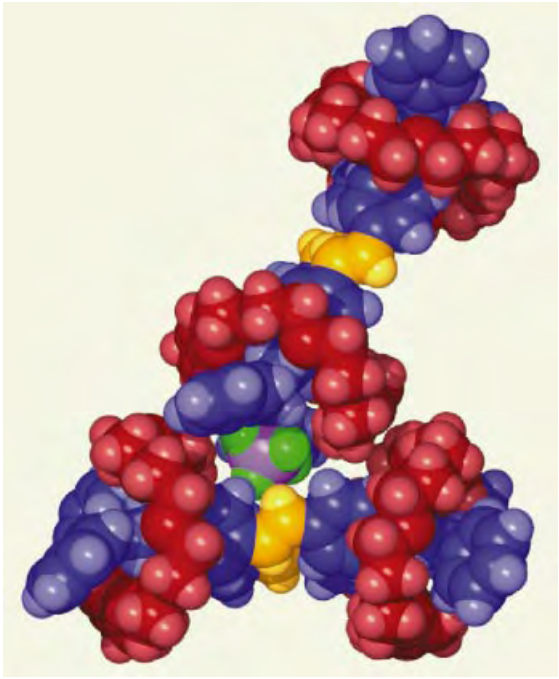


Figure 2. Space-filling representation of the end-to-middle arrangement of adjacent supermolecules of $[(BPP34C10)_2 \cdot (trans\text{-}\mathbf{2}\text{-}H_2)_2]^{4+}$ showing the strategic location of one of the PF_6^- ions (P: purple and F: green) between the two 2:2 complexes (BPP34C10 is shown in red and the *trans*-**2**-H_2^{2+} in blue with the central *trans*-olefinic units highlighted in orange).

outwardly folded pairs of terminal *N*-benzyl units of one supermolecule and the sheared *trans*-stilbenoid units of the other. The shortest associated contact to a fluorine atom is only 2.24 Å from one of the *trans*-stilbene aryl *ortho* hydrogen atoms that is *syn* to the double bond; the associated C···F distance and C–H···F angle are 3.14 Å and 155°, respectively. This positioning of a PF_6^- ion in the cleft formed between the

 © WILEY-VCH Verlag GmbH, D-69451 Weinheim, 2001 1433-7851/01/4022-4257 $ 17.50+.50/0

terminal *N*-benzyl rings and proximal to the NH_2^+ centers of the dications is directly analogous to that observed, for example, in the BPP34C10-based [4]pseudorotaxanes formed with α,α'-bis-(benzylammonium)-*p*-xylene[12] and with bis(benzylammonium-*p*-toluic acid).[15] This packing motif extends in a jigsaw-like manner to form the closely packed sheet illustrated in Figure 3. The upper and lower surfaces of these sheets are essentially hydrophobic, being populated by the hydrogen atoms of the polyether and terminal *N*-benzyl groups. The other unique PF_6^- ion and the included Me_2CO solvent molecules are located in small pockets formed between adjacent sheets.

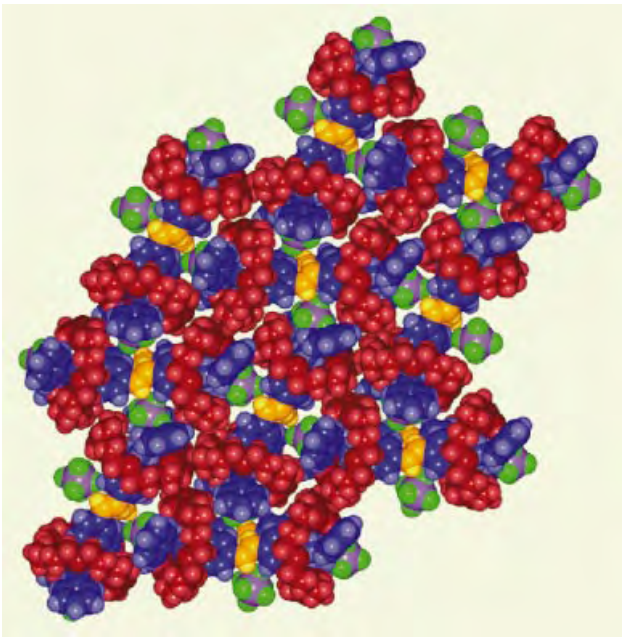


Figure 3. Space-filling representations of the jigsawlike sheets of supermolecules (with strategically located, embedded PF_6^- ions) present in the solid-state supramolecular structure of $[(BPP34C10)_2\cdot(trans\text{-}\mathbf{2}\text{-}H_2)_2]^{4+}$. The color code for the various atoms and components is identical to that described in the caption to Figure 2.

The complexation of two *trans*-$\mathbf{2}^{2+}$ dications with two BPP34C10 crown ethers forces the stilbene threads containing a dialkylammonium ion into a suitable co-conformation for a photochemical [2+2] cycloaddition; that is, the two adjacent stilbene olefin groups of $[(BPP34C10)_2(trans\text{-}\mathbf{2}\text{-}H_2)_2][PF_6]_4$ are aligned in an eclipsed co-conformation with respect to one another and are ideally set up for the solid-state [2+2] photocycloaddition. A powdered crystalline sample (421 mg) of $[(BPP34C10)_2(trans\text{-}\mathbf{2}\text{-}H_2)_2][PF_6]_4$ was irradiated[16] for 30 h with UV light from a Hanovia lamp in a rotating Pyrex tube attached to a Kugelrohr apparatus. A ^{1}H NMR spectrum (400 MHz, CD_3CN) of the irradiated sample is shown in Figure 4b, along with a spectrum (Figure 4a) of the sample prior to irradiation. The spectrum of the photoaddition product reveals the presence of a new singlet at δ 4.58 (which corresponds to the cyclobutane ring protons of $\mathbf{3}\text{-}H_4\cdot 4PF_6$) and the almost complete disappearance of the singlet at δ 7.28 (which corresponds to the alkene protons of

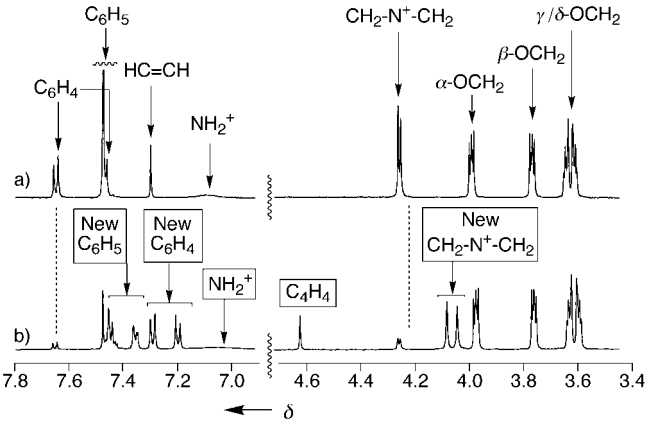
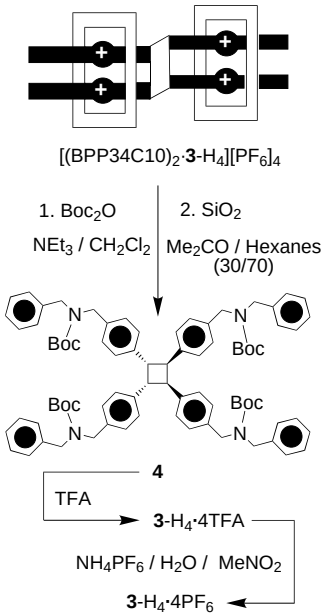


Figure 4. Partial ^{1}H NMR spectra (400 MHz, CD_3CN) obtained a) before and b) after solid-state irradiation of $[(BPP34C10)_2\cdot(trans\text{-}\mathbf{2}\text{-}H_2)_2][PF_6]_4$. The new signal at $\delta = 4.58$ is diagnostic of the *syn-anti-syn* diastereoisomer of $\mathbf{3}\text{-}H_4\cdot 4PF_6$.

trans-$\mathbf{2}\text{-}H_2\cdot 2PF_6$). Integration of peaks associated with the cyclobutane and stilbene derivatives suggests an approximate 80% conversion of *trans*-$\mathbf{2}\text{-}H_2\cdot 2PF_6$ to $\mathbf{3}\text{-}H_4\cdot 4PF_6$. The presence of *only one* new signal corresponding to the cyclobutane methine protons suggested that *only one* diastereoisomer of $\mathbf{3}\text{-}H_4\cdot 4PF_6$ was formed.[17] The irradiated sample of $[(BPP34C10)_2\cdot(trans\text{-}\mathbf{2}\text{-}H_2)_2][PF_6]_4$ was characterized by electrospray ionization (ESI) mass spectrometry where peaks were found at *m*/*z* 837 and 536. These peaks correspond to the $\mathbf{3}\text{-}H^+$ ion of the photodimer and the BPP34C10 crown ether, respectively. No peaks were observed in the gas phase for any complex formed between the photodimer and BPP34C10; this observation is not unexpected, however, since higher order complexes with this crown ether are not always observed.[18]

The cyclobutane derivative $\mathbf{3}\text{-}H_4\cdot 4PF_6$ was separated from the BPP34C10 crown ethers in good yield[19] by a process (Scheme 2) involving: 1) deprotonation of $\mathbf{3}\text{-}H_4\cdot 4PF_6$, followed by protection of the amino groups with di-*tert*-butyldicarbonate to give the Boc-protected derivative **4**, 2) separation of **4** from BPP34C10 by column chromatography on silica gel, 3) removal of the Boc groups from **4** with trifluoroacetic acid (TFA) to give $\mathbf{3}\text{-}H_4\cdot 4TFA$, and 4) counterion exchange with NH_4PF_6 to regenerate $\mathbf{3}\text{-}H_4\cdot 4PF_6$. The free cyclobutane derivative $\mathbf{3}\text{-}H_4\cdot 4PF_6$ was character-



Scheme 2. The isolation of $\mathbf{3}\text{-}H_4\cdot 4PF_6$ from the BPP34C10 crown ethers after photoirradiation of the crystalline complex $[(BPP34C10)_2\cdot(trans\text{-}\mathbf{2}\text{-}H_2)_2][PF_6]_4$ in the solid state. Boc = *tert*-butoxycarbonyl, TFA = trifluoroacetic acid.

 © WILEY-VCH Verlag GmbH, D-69451 Weinheim, 2001 1433-7851/01/4022-4258 $ 17.50+.50/0

ized by ^{1}H NMR and ^{13}C NMR spectroscopies,[20] as well as by ESI mass spectrometry, where the peak of the highest mass (*m*/*z* 1276) corresponded to the cyclobutane derivative having lost one PF_6^- counterion. The *syn-anti-syn* stereochemistry of the cyclobutane derivative was confirmed unambiguously by X-ray crystallographic analysis[14, 21] of **3**-$H_4 \cdot 4$TFA (Figure 5a). This study also showed the tetracation to have inversion symmetry. The four NH_2^+ centers are each involved in N–H···O hydrogen-bonding interactions with the trifluoroacetate anions. Adjacent lattice-translated tetracations are linked by π–π stacking and C–H···π hydrogen-bonding interactions to form tapes (Figure 5b).

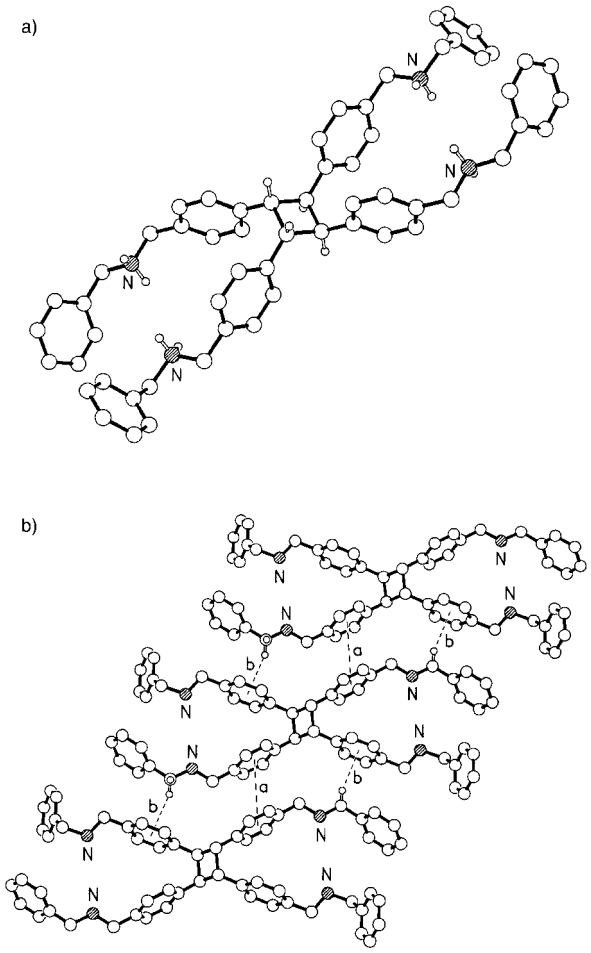


Figure 5. a) The solid-state molecular structure of **3**-H_4^{4+} showing the tetrasubstituted cyclobutane ring with the *syn-anti-syn* configuration. b) Part of one of the tapes present in the solid-state structure of **3**-$H_4 \cdot 4$TFA. The centroid–centroid distance and mean interplanar separation (a) are 4.12 and 3.60 Å, respectively; the C–H···π interaction (b) has H···π 2.78 Å and C–H···π 136°.

In order to demonstrate that the BPP34C10 macrocycles are necessary to achieve the photodimerization, a powdered sample (30 mg) of *trans*-**2**-$H_2 \cdot 2PF_6$ was placed between two Pyrex slides and irradiated for a period of 5 h. No photoproduct was obtained and the only peaks observed in the ^{1}H NMR spectrum of the irradiated material corresponded to *trans*-**2**-$H_2 \cdot 2PF_6$. Photochemical studies conducted in CD_3CN solutions (30 mM) of *trans*-**2**-$H_2 \cdot 2PF_6$—either alone or in the presence of an equimolar amount of BPP34C10—resulted in *trans* to *cis* isomerization of the olefinic unit to yield the *cis*-stilbene derivative[22] *cis*-**2**-$H_2 \cdot 2PF_6$. Irradiation of *trans*-**2**-$H_2 \cdot 2PF_6$ in CD_3OD[23] (20 mM) resulted predominantly in isomerization to *cis*-**2**-$H_2 \cdot 2PF_6$, in addition to the formation of small amounts of the *syn-anti-syn* dimer **3**-$H_4 \cdot 4PF_6$, and the formation of other unidentified products.

We have demonstrated that the solid-state [2+2] photodimerization[24] of the doubly threaded and doubly encircled pseudorotaxane $[(BPP34C10)_2 \cdot (\mathbf{2}\text{-}H_2)_2][PF_6]_4$ proceeds efficiently to yield a single diastereoisomer of **3**-$H_4 \cdot 4PF_6$. The *syn-anti-syn* stereochemistry of the cyclobutane derivative, which is preordained[25] by the solid-state superstructure of the 2:2 complex,[26] was confirmed by X-ray crystallography and ^{1}H NMR spectroscopy. In the future we hope to widen the scope of this technique of solid-state supramolecular assistance by preparing other doubly threaded and doubly encircled pseudorotaxanes (formed between constitutionally asymmetric, olefin-containing dialkylammonium salts and BPP34C10) that might undergo both regiospecific and stereospecific photochemical dimerizations.

Experimental Section

4,4′-Bis(bromomethyl)stilbene[6] (1.98 g, 5.37 mmol) was dissolved in DMF (20 mL) and then benzylamine (1.26 g, 11.8 mmol) was added. The solution was stirred for 1 h and the white precipitate that formed was filtered off and then suspended in Me_2CO (20 mL). Small portions of a saturated aqueous solution of NH_4PF_6 were added until all of the white solid dissolved, and then an excess of H_2O was added to this solution. This process resulted in the formation of a white precipitate, which was filtered off and dried to yield *trans*-**2**-$H_2 \cdot 2PF_6$ (700 mg, 18%). ^{1}H NMR (CD_3CN, 500 MHz, 298 K): $\delta = 4.51$ (s, 8H), 7.15 (s, 2H), 7.32 (s, 10H), 7.43 (d, $J = 8.2$ Hz, 4H), 7.53 (d, $J = 8.2$ Hz, 4H); ^{13}C NMR ($(CD_3)_2CO$, 125 MHz, 298 K): $\delta =$ 51.0, 51.3, 127.0, 128.8, 128.9, 129.3, 130.0, 130.5, 130.7, 131.3, 138.2; MS (FAB): *m*/*z* (%): 565 (50) [*trans*-**2**-$H_2PF_6]^+$, 419 (100) [*trans*-**2**-H]$^+$. Crystals suitable for X-ray cystallography and photochemical irradiation were grown by vapor diffusion of iPr_2O into a solution of a mixture of *trans*-**2**-$H_2 \cdot 2PF_6$ (553 mg, 0.78 mmol) and BPP34C10 (418 mg, 0.78 mmol) in Me_2CO/CH_2Cl_2, (99/1) to yield $[(BPP34C10)_2 \cdot (trans\text{-}\mathbf{2}\text{-}H_2)_2][PF_6]_4 \cdot (Me_2CO)_4$ (960 mg, 90%). These crystals (421 mg, 0.169 mmol) were powdered and then irradiated for 30 h with UV light from a Hanovia lamp in a rotating Pyrex tube attached to a Kugelrohr apparatus. The irradiated solid was suspended in CH_2Cl_2 (20 mL), and then Et_3N (210 mg, 2.07 mmol), di-*tert*-butyldicarbonate (776 mg, 3.56 mmol), and 4-dimethylaminopyridine (DMAP, 1 mg, 8 μmol) were added. The solution was washed after 10 min with H_2O (1 × 30 mL) and 1N HCl (3 × 30 mL), and then the combined aqueous phases were extracted with CH_2Cl_2. The CH_2Cl_2 solutions were combined, dried ($MgSO_4$), filtered, and concentrated. The residue was purified by column chromatography (SiO_2, Me_2CO/hexanes (3/7)) to yield **4** as a clear oil (93 mg, 49%). ^{1}H NMR (CD_2Cl_2, 500 MHz, 298 K): $\delta = 1.46$ (s, 36H), 4.30–4.36 (br m, 16H), 4.51 (s, 4H), 6.95 (br s, 8H), 7.15–7.20 (m, 16H), 7.21–7.52 (m, 12H); ^{13}C NMR ($CDCl_3$, 125 MHz, 298 K): $\delta = 28.0$, 47.2, 49.0, 50.1, 79.6, 127.0, 127.2, 127.6, 128.2, 128.3, 135.7, 138.1, 139.6, 155.6; MS (FAB): *m*/*z* (%): 1137 (20) [**4**-H – *t*Bu – $CO_2]^+$, 1081 (25) [**4**-H – 2*t*Bu – $CO_2]^+$, 1025 (35) [**4**-H – 3*t*Bu – $CO_2]^+$, 925 (40) [**4**-H – 4 *t*Bu – $2O_2]^+$. TFA (2 mL, 26 mmol) was added to a solution of **4** (93 mg, 75 μmol) in CH_2Cl_2 (10 mL). The mixture was evaporated to dryness after 1 h to yield **3**-$H_4 \cdot 4$TFA as a white solid. Crystals suitable for X-ray crystallographic analysis were grown by layer diffusion of hexane into a solution of **3**-$H_4 \cdot 4$TFA (2 mg, 2 μmol) in CH_2Cl_2/TFA (99/1). The remainder of **3**-$H_4 \cdot 4$TFA was suspended in $MeNO_2$ (20 mL) and washed with saturated aqueous NH_4PF_6 (20 mL) and H_2O (2 × 20 mL). The $MeNO_2$ extract was dried ($MgSO_4$), filtered, and

 © WILEY-VCH Verlag GmbH, D-69451 Weinheim, 2001 1433-7851/01/4022-4259 $ 17.50+.50/0

concentrated to yield **3**-$H_4 \cdot 4F_6$ (90 mg, 86%) as a light-brown solid. ^{1}H NMR (CD_3CN, 500 MHz, 298 K): $\delta = 4.03$ (s, 8H), 4.06 (s, 8H), 4.60 (s, 4H), 7.21 (d, $J = 10.2$ Hz, 8H), 7.28 (d, $J = 10.2$ Hz, 8H), 7.38–7.45 (m, 20H); ^{13}C NMR (CD_3CN, 125 MHz, 298 K): $\delta = 46.4$, 50.7, 51.1, 128.1, 128.9, 129.1, 129.7, 129.8, 130.1, 130.3, 141.9; MS (FAB): *m*/*z* (%): 1276 (10) [**3**-$H_4 \cdot 3PF_6$]$^+$, 1129 (27) [**3**-$H_3 \cdot 2PF_6$]$^+$, 983 (35) [**3**-$H_2 \cdot PF_6$]$^+$, 837 (70) [**3**-H]$^+$.

Received: July 9, 2001 [Z17452]

[1] For reviews on solid state photochemistry, see a) M. Hasegawa, *Chem. Rev.* **1983**, *83*, 507–518; b) V. Ramamurthy, K. Venkatesan, *Chem. Rev.* **1987**, *87*, 433–481; c) F. Toda, *Acc. Chem. Res.* **1995**, *28*, 480–486; d) J. N. Gamlin, R. Jones, M. Leibovitch, B. Patrick, J. R. Scheffer, J. Trotter, *Acc. Chem. Res.* **1996**, *29*, 203–209; e) Y. Ito, *Synthesis* **1998**, 1–32; f) A. E. Keating, M. A. Garcia-Garibay in *Organic and Inorganic Photochemistry* (Eds.: V. Ramamurthy, K. S. Schanze), Marcel Dekker, New York, **1998**, pp. 195–248; g) K. Tanaka, F. Toda, *Chem. Rev.* **2000**, *100*, 1025–1074.

[2] a) G. R. Desiraju, C. V. K. M. Sharma, *J. Chem. Soc. Chem. Commun.* **1991**, 1239–1241; b) Y. Ito, B. Borecka, J. Trotter, J. R. Scheffer, *Tetrahedron Lett.* **1995**, *36*, 6083–6086; c) Y. Ito, B. Borecka, G. Olovsson, J. Trotter, J. R. Scheffer, *Tetrahedron Lett.* **1995**, *36*, 6087–6090; d) K. S. Feldman, R. F. Campbell, *J. Org. Chem.* **1995**, *60*, 1924–1925.

[3] a) M. D. Cohen, G. M. J. Schmidt, F. I. Sonntag, *J. Chem. Soc.* **1964**, 2000–2013; b) G. M. J. Schmidt, *J. Chem. Soc.* **1964**, 2014–2021; c) G. M. J. Schmidt, *Pure Appl. Chem.* **1971**, *27*, 647–678.

[4] Unfunctionalized stilbenes are photostable in the solid state because their olefinic groups are generally positioned at a distance greater than 5.0 Å from each other, see G. Kaupp, *Adv. Photochem.* **1995**, *19*, 119–177.

[5] W. Herrmann, M. Schneider, G. Wenz, *Angew. Chem.* **1997**, *109*, 2621–2624; *Angew. Chem. Int. Ed. Engl.* **1997**, *36*, 2511–2514.

[6] W. Herrmann, S. Wehrle, G. Wenz, *Chem. Commun.* **1997**, 1709–1710.

[7] K. S. S. P. Rao, S. M. Hubig, J. N. Moorthy, J. K. Kochi, *J. Org. Chem.* **1999**, *64*, 8098–8104.

[8] M. D. Cohen, R. Cohen, *J. Chem. Soc. Perkin Trans. 2* **1976**, 1731–1735.

[9] G. W. Coates, A. R. Dunn, L. M. Henling, J. W. Ziller, E. B. Lobkovsky, R. H. Grubbs, *J. Am. Chem. Soc.* **1998**, *120*, 3641–3649.

[10] L. R. MacGillivray, J. L. Reid, J. A. Ripmeester, *J. Am. Chem. Soc.* **2000**, *122*, 7817–7818. It is also noteworthy that crystallization of 1,2-*trans*-(4-pyridyl)ethene and $AgBF_4$ in the presence of light results in the formation of a three-dimensional network based upon a cyclobutane–tetrapyridyl ligand with only the *syn-anti-syn* configuration, linked by Ag^I ions; see A. J. Blake, N. R. Champness, S. S. M. Chung, W.-S. Li, M. Schröder, *Chem. Commun.* **1997**, 1675–1676.

[11] a) M. C. T. Fyfe, J. F. Stoddart, *Adv. Supramol. Chem.* **1999**, *5*, 1–53; b) S. J. Cantrill, A. R. Pease, J. F. Stoddart, *J. Chem. Soc. Dalton Trans.* **2000**, 3715–3734.

[12] P. R. Ashton, E. J. T. Chrystal, P. T. Glink, S. Menzer, C. Schiavo, N. Spencer, J. F. Stoddart, P. A. Tasker, A. J. P. White, D. J. Williams, *Chem. Eur. J.* **1996**, *2*, 709–728.

[13] Crystal data for [(BPP34C10)$_2 \cdot$(*trans*-**2**-H_2)$_2$][PF_6]$_4$: [$C_{116}H_{144}N_4O_{20}$][PF_6]$_4 \cdot 4Me_2CO$, $M_r = 2726.5$, monoclinic, space group $P2_1/c$ (no. 14), $a = 17.146(1)$, $b = 20.923(1)$, $c = 19.846(2)$ Å, $\beta = 102.27(1)^\circ$, $V = 6957.3(8)$ Å^3, $Z = 2$ (C_i symmetry), $\rho_{calcd} = 1.302$ g cm^{-3}, $\mu(Cu_{K\alpha}) = 13.5$ cm^{-1}, $T = 293$ K, pale yellow rhombs; 9842 independent measured reflections, F^2 refinement, $R_1 = 0.089$, $wR_2 = 0.253$, 4968 independent observed reflections [$|F_o| > 4\sigma(|F_o|)$, $2\theta \leqslant 120^\circ$], 838 parameters.

[14] Crystallographic data (excluding structure factors) for the structures reported in this paper have been deposited with the Cambridge Crystallographic Data Centre as supplementary publication nos. CCDC-116797 [(BPP34C10)$_2 \cdot$(*trans*-**2**-H_2)$_2$][PF_6]$_4 \cdot$(Me_2CO)$_4$] and -116798 [**3**-$H_4 \cdot$4TFA]. Copies of the data can be obtained free of charge on application to CCDC, 12 Union Road, Cambridge CB2 1EZ, UK (fax: (+44) 1223-336-033; e-mail: deposit@ccdc.cam.ac.uk).

[15] P. R. Ashton, A. N. Collins, M. C. T. Fyfe, S. Menzer, J. F. Stoddart, D. J. Williams, *Angew. Chem.* **1997**, *109*, 760–763; *Angew. Chem. Int. Ed. Engl.* **1997**, *36*, 735–739.

[16] Irradiation of a powdered crystalline sample (30 mg) of [(BPP34C10)$_2 \cdot$(*trans*-**2**-H_2)$_2$][PF_6]$_4$ between two Pyrex slides resulted in a 90% conversion of *trans*-**2**-$H_2 \cdot 2PF_6$ to **3**-$H_4 \cdot 4PF_6$ after 5 h. The solid-state reaction takes longer to reach high conversion on a larger scale because of caking of the solid along the Pyrex tube in addition to less efficient exposure of the UV light.

[17] The chemical shift of this signal at $\delta = 4.58$ is consistent with the *syn-anti-syn* isomer **3**-$H_4 \cdot 4PF_6$ since other *syn-anti-syn* tetraaryl-substituted cyclobutane derivatives have been reported to exhibit resonance of the corresponding ring proton in the range $\delta = 4.10$ to 5.00. In contrast, the *all-trans* tetraaryl-substituted isomer is expected to contain cyclobutane ring protons resonating between $\delta = 3.50$ and 3.80; see a) references [7], [9], and [10]; b) H. Shechter, W. J. Link, G. V. D. Tiers, *J. Am. Chem Soc.* **1963**, *85*, 1601–1605; c) W. H. Laarhoven, T. J. H. M. Cuppen, R. J. F. Nivard, *Tetrahedron* **1970**, *26*, 1069–1083; d) B. S. Green, L. Heller, *J. Org. Chem.* **1974**, *39*, 196–201; e) Y. Ito, T. Kajita, K. Kunimoto, T. Matsuura, *J. Org. Chem.* **1989**, *54*, 587–591.

[18] a) P. R. Ashton, A. N. Collins, M. C. T. Fyfe, P. T. Glink, S. Menzer, J. F. Stoddart, D. J. Williams, *Angew. Chem.* **1996**, *108*, 2058–2061; *Angew. Chem. Int. Ed. Engl.* **1996**, *35*, 1930–1933; b) M. C. Freiters, M. C. T. Fyfe, M.-V. Martínez-Díaz, S. Menzer, R. J. M. Nolte, J. F. Stoddart, P. J. M. van Kan, D. J. Williams, *J. Am. Chem. Soc.* **1997**, *119*, 8110–8120.

[19] Since the photoreaction of [(BPP34C10)$_2 \cdot$(*trans*-**2**-H_2)$_2$][PF_6]$_4 \cdot$(Me_2CO)$_4$ to [(BPP34C10)$_2 \cdot$**3**-H_4][PF_6]$_4 \cdot$(Me_2CO)$_4$ was determined by ^{1}H NMR spectroscopy to have proceeded in an 80% conversion, the overall yield of 42% (that is, 49% for Boc protection and 86% for deprotection and counterion exchange) corresponds to the isolation of 53% of **3**-$H_4 \cdot 4PF_6$.

[20] A ^{1}H NMR chemical shift of $\delta = 4.60$ was observed for the cyclobutane proton of the free **3**-$H_4 \cdot 4PF_6$ after its separation from the crown ethers. This δ value is consistent with the *syn-anti-syn* configuration as described in ref. [17]. The observed ^{13}C NMR chemical shift of $\delta = 46.4$ corresponds to the expected δ value for a cyclobutane carbon atom. A ^1J(C,H) value of 132 Hz, which is consistent with the expected value for this coupling in a cyclobutane ring, was obtained when broad-band decoupling was turned off; see H. Friebolin, *Basic One- and Two-Dimensional NMR Spectroscopy*, VCH, Weinheim, **1993**, p. 95–95.

[21] Crystal data for **3**-$H_4 \cdot$4TFA: [$C_{60}H_{64}N_4$][O_2CCF_3]$_4 \cdot$[HO_2CCF_3]$_4$, $M_r = 1749.3$, triclinic, space group $P\bar{1}$ (no. 2), $a = 10.450(2)$, $b = 12.959(1)$, $c = 15.971(2)$ Å, $\alpha = 77.87(1)$, $\beta = 81.62(1)$, $\gamma = 78.29(1)^\circ$, $V = 2058.6(4)$ Å^3, $Z = 1$ (C_i symmetry), $\rho_{calcd} = 1.411$ g cm^{-3}, $\mu(Cu_{K\alpha}) = 11.9$ cm^{-1}, $T = 193$ K, colorless needles; 6080 independent measured reflections, F^2 refinement, $R_1 = 0.105$, $wR_2 = 0.291$, 3615 independent observed reflections [$|F_o| > 4\sigma(|F_o|)$, $2\theta \leqslant 120^\circ$], 616 parameters.

[22] Prolonged irradiation of these solutions resulted in the production of unidentified by-products, which could correspond to dihydrophenanthrene and phenanthrene derivatives formed by the electrocyclic ring closure of *cis*-**2**-$H_2 \cdot 2PF_6$, see C. O. Parker, P. E. Spoerri, R. E. Buckles, *J. Am. Chem. Soc.* **1955**, *77*, 1040–1041.

[23] Photoirradiation of stilbene derivatives in H_2O or MeOH promotes the formation of dimerized products on account of hydrophobic interactions, see a) reference [17e]; b) M. S. Syamala, V. Ramamurthy, *J. Org. Chem.* **1986**, *51*, 3712–3715.

[24] It must be stressed that this photodimerization is occurring within a supermolecule that exists only in the solid state and involves, not only components that are noncovalently bonded to each other, but also components where mechanical entanglement is present.

[25] The pivotal role of the PF_6^- counterions in determining the formation of the supermolecules in the solid state has been noted previously in related systems, see a) P. R. Ashton, M. C. T. Fyfe, P. T. Glink, S. Menzer, J. F. Stoddart, A. J. P. White, D. J. Williams, *J. Am. Chem. Soc.* **1997**, *119*, 12514–12524; b) P. R. Ashton, M. C. T. Fyfe, S. K. Hickingbottom, S. Menzer, J. F. Stoddart, A. J. P. White, D. J. Williams, *Chem. Eur. J.* **1998**, *4*, 577–589; c) P. R. Ashton, M. C. T. Fyfe, M.-V. Martínez-Díaz, S. Menzer, C. Schiavo, J. F. Stoddart, A. J. P. White, D. J. Williams, *Chem. Eur. J.* **1998**, *4*, 1523–1534; d) P. R. Ashton, S. J.

 © WILEY-VCH Verlag GmbH, D-69451 Weinheim, 2001 1433-7851/01/4022-4260 $ 17.50+.50/0

Cantrill, J. A. Preece, J. F. Stoddart, Z.-H, Wang, A. J. P. White, D. J. Williams, *Org. Lett*. **1999**, *1*, 1917–1920; e) S. J. Cantrill, J. A. Preece, J. F. Stoddart, Z.-H. Wang, A. J. P. White, D. J. Williams, *Tetrahedron* **2000**, *56*, 6675–6681. The present research provides yet another beautiful example of anion-orchestrated self-assembly in the solid state.

[26] The thought processes that led to the design and synthesis of this 2:2 host–guest complex had their origins in the seminal work done by Cram in the 1970s on the face-to-face complexation of crown ethers with primary alkylammonium ions, see a) D. J. Cram, J. M. Cram, *Science* **1974**, *183*, 803–809; b) D. J. Cram, J. M. Cram, *Acc. Chem. Res.* **1978**, *11*, 5–14; c) "Container Molecules and Their Guests": D. J. Cram, J. M. Cram in *Supramolecular Chemistry* (Ed.: J. F. Stoddart, Royal Society of Chemistry, Cambridge, **1994**.

Novel Calcium Half-Sandwich Complexes for the Living and Stereoselective Polymerization of Styrene**

Sjoerd Harder,* Florian Feil, and Konrad Knoll

The many advantages of the anionic living polymerization of styrene (chain-length control, narrow molecular-weight distribution, chain-end functionalization, and particularly block-copolymerization) makes this technique the method of choice in the rational design of new styrene-based polymers.[1] The only disadvantage of this method is the lack of control of the polymers tacticity; control of tacticity offers many advantages in plastic material design.[2] Although stereoregular isotactic polystyrene was made in 1955 by use of classical Ziegler–Natta catalysts,[3] it never found any commercial application because of its extremely slow crystallization rate (crystallization times can be several days!). The discovery of its fast crystallizing syndiotactic form, obtained by polymerization with a titanocene half-sandwich complex, was therefore a revolution in polystyrene chemistry.[4] Syndiotactic polystyrene shows a low glass-transition temperature (104 °C) but high melting point (273 °C) with a high modulus and combines good electrical properties with an excellent solvent resistance.[5] The only disadvantage of stereocontrolled styrene polymerization by titanocene half-sandwiche complexes, however, is the lack of living character.

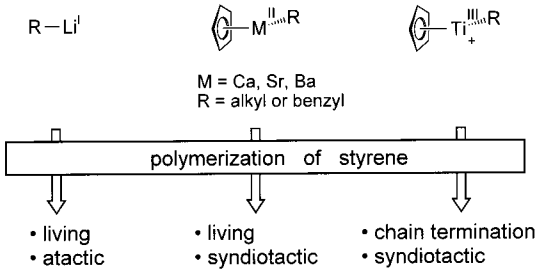
[*] Dr. S. Harder, Dipl-Chem. F. Feil
Fachbereich Chemie
Universität Konstanz
Postfach 5560, M738, 78457 Konstanz (Germany)
Fax: (+49) 7531-883137
E-mail: harder@chemie.uni-konstanz.de
Dr. K. Knoll
Kunststofflaboratorium, BASF AG
67056 Ludwigshafen (Germany)

[**] This work was generously supported by the BASF AG (Ludwigshafen (Germany)) and the university of Konstanz. We would like to acknowledge the following people for numerous discussions: Prof. Dr. H.-H. Brintzinger (Konstanz), Dr. H. Gausepohl, Dr. V. Warzelhan, and Dr. H. Weiss (Ludwigshafen).

Research to combine the favorable properties of anionic living polymerization and stereocontrolled coordination polymerization has come from both sides. Anionic polymerization with *n*BuLi initiators under certain reaction conditions can produce isotactic polystyrene,[6] but traces of water seem to be essential.[7] This observation has led to the use of mixed *n*BuLi/Li-alkoxide initiators; polymerizations, however, have to be carried out in apolar solvents at −30 °C and polymerization times can take up to 5 days with only 50% conversion.[8] Only 15% of the chains are highly isotactic, which indicates the presence of more than one reactive site at the proposed alkoxide initiator cluster. Recently it was discovered that a mixture of living polyisoprenyllithium and LiOH polymerizes styrene with high isotacticity and without atactic parts.[9]

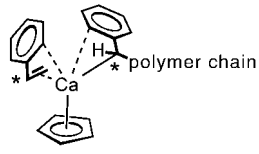
Attempts to make stereocontrolled coordination polymerization living are also under investigation. Under certain conditions, the polymerization of *para*-methylstyrene by titanium half-sandwich complexes shows living features, however, the system was not suitable for the living syndiotactic polymerization of styrene.[10]

Our approach to enable a living and a syndiospecific polymerization of styrene is based on "cross-breeding" the catalysts (RLi) used for classical anionic styrene polymerization and that for coordination polymerization (Scheme 1). A proposed catalytic species for coordination polymerization



Scheme 1.

is a cationic Ti^{III} complex with a cyclopentadienyl spectator ligand and a growing chain. Syndiotactic stereocontrol proceeds through communication of the chiral chain-end and the stereogenic center on the coordinated monomer (**1**). A similar isolobal Group II metal compound could initiate the anionic (living) polymerization of styrene with syndiotactic insertions. We expect the polymerization to be living because of the considerable ionic (alkali metal like) character of the heavier alkaline-earth metals.[11] Syndiotactic insertion is anticipated on the basis of the very similar structure of [CpTiR$^+$] and the proposed Group II species. The use of non- or weak-coordinating solvents is a prerequisite for a coordination polymerization mechanism.

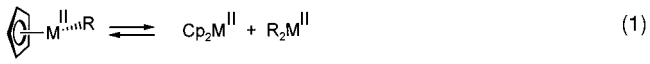


1

The apparent simplicity of the desired catalyst, $CpM^{II}R$ ($Cp = C_5H_5$), is in contrast to the inherent problems associated with this type of compound: a) the synthesis of reactive

 © WILEY-VCH Verlag GmbH, D-69451 Weinheim, 2001 1433-7851/01/4022-4261 $ 17.50+.50/0

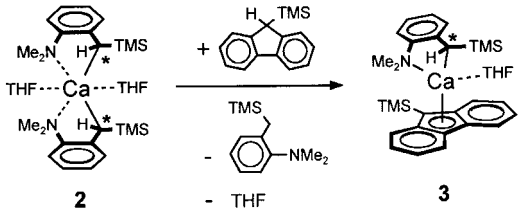
benzyls or alkyls of the heavier alkaline earth metals and b) the Schlenk equilibrium between heteroleptic and homoleptic species [Eq. (1)]: polymerization-active R_2M^{II} species



(1)

cannot be tolerated. We first developed simple synthetic methods for polymerization-active alkaline-earth benzyls.[12, 13] The Schlenk equilibrium can be directed to the heteroleptic side either by using large spectator ligands instead of Cp, this disfavors the homoleptic L_2M species by steric congestion, or by adding an excess of the polymerization-inactive L_2M species to the reaction mixture.

Attempts to polymerize styrene with heteroleptic benzylbarium mixtures were unsuccessful and only atactic polystyrene was obtained.[12] Here we describe our results with the first heteroleptic benzylcalcium compound (**3**), obtained by reaction of the polymerization-active homoleptic benzylcalcium compound (**2**)[13] with 9-Me_3Si-fluorene [Eq. (2); TMS = trimethylsilyl]. The crystal structure of **3** (Figure 1) shows a



(2)

distorted η^5 coordination for the fluorenyl ligand, a C,N bidentate coordination for the benzylic ligand, and coordination of one THF ligand. The NMR spectra of **3** (in benzene) show the exclusive presence of the heteroleptic species. Fast intermolecular ligand exchange processes were not observed on the NMR time scale. The chiral benzylic carbon causes two enantiotopic sides in the fluorenyl ligand: all the hydrogen atoms are unique at room temperature. Fast inversion of the chiral carbanion results in exchange of the two enantiotopic sides and is achieved by raising the temperature ($T_{coal} = 90\,^{\circ}C$; $\Delta G^{\neq} = 18.8$ kcal mol^{-1}). The energy barrier for inversion is concentration independent, which indicates a dissociative mechanism that involves Ca–C_α bond breaking (Scheme 2). Adding small amounts of THF[14] also results in fast inversion of the chiral center at room temperature by THF-assisted bond breaking (Scheme 2).

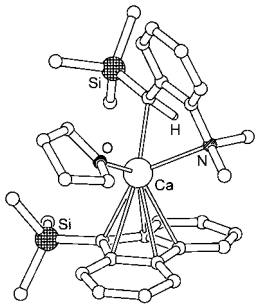
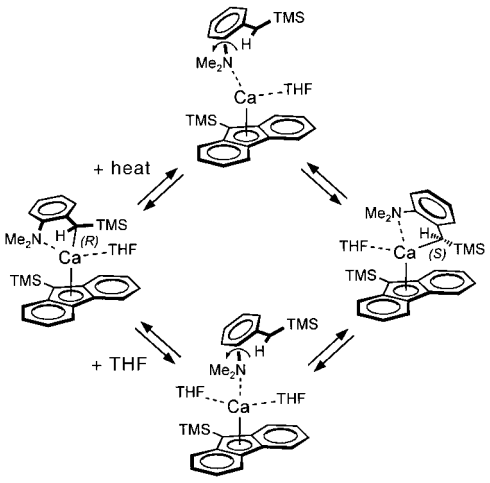


Figure 1. The crystal structure of **3** (only one of the two crystallographical independent but isostructural molecules is depicted). Hydrogen atoms (except for the benzylic hydrogen) have been omitted for clarity. Selected bond lengths [Å] for both independent molecules: Ca-C_α: 2.501(2) and 2.510(2); Ca-N: 2.462(2) and 2.470(2); Ca-O 2.305(2) and 2.310(2); Ca-fluorenyl contacts: 2.690(2), 2.733(2), 2.736(2), 2.785(2), 2.789(2) and 2.683(2), 2.732(3), 2.724(2), 2.771(2), 2.778(2).



Scheme 2.

The dibenzylcomplex (**2**) can be used as an initiator for the living polymerization of styrene.[13] The benzylic TMS substituent and the intramolecular coordinating Me_2N group stabilize the initiator thermodynamically as well as kinetically. The consequence is a sluggish initiation step compared to initiation with *sec*-butyllithium. This effect results in a tailing in the low molecular-weight range of the polymer obtained (Figure 2).[15] Polystyrene obtained with the heteroleptic

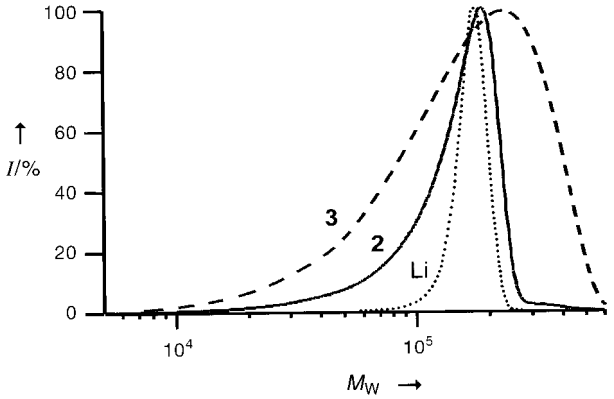


Figure 2. GPC traces of polystyrene obtained with a *sec*-butyllithium initiator (•••• $M_n = 1.091 \times 10^5$, P.D. = 1.039), the homoleptic dibenzylcalcium initiator (**2**) (—— $M_n = 1.093 \times 10^5$, P.D. = 1.369), and the heteroleptic fluorenyl-benzylcalcium initiator (**3**) (- - - -, $M_n = 0.996 \times 10^5$; P.D. = 2.262).

benzylcalcium complex (**3**) shows an even more extensive tailing in the low molecular weight part of the gel permeation chromatography (GPC) trace and consequently a relatively high polydispersion index. The observed tailing could also be explained by chain termination, however, several characteristics suggest living polymerization: a) good agreement between observed and calculated molecular weights (around 100000), b) linear pseudo first-order kinetic plots are obtained (Figure 3) c) the polymerization reactions were monitored by NMR spectroscopy: addition of new monomer after completed polymerization results in renewed styrene insertion, d) stepwise addition of styrene at certain time intervals shows no significant chain termination and polymers of the

 © WILEY-VCH Verlag GmbH, D-69451 Weinheim, 2001 1433-7851/01/4022-4262 $ 17.50+.50/0

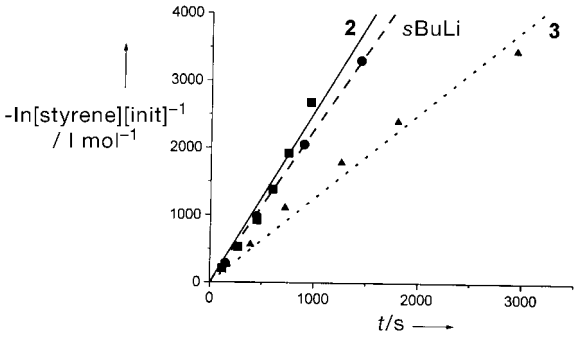


Figure 3. Graphical presentation of (ln[styrene])/[initiator] as a function of the polymerization time (estimated rate constants: (**2**) 2.55 L mol^{-1} s^{-1}, *sec*-BuLi 2.28 L mol^{-1} s^{-1}, and (**3**) 1.26 L mol^{-1} s^{-1}).

final calculated molecular weight are obtained, e) block copolymers with isoprene can be prepared.

The tacticity of the obtained polystyrene was checked by ^{13}C NMR spectroscopy (Figure 4). Polymer obtained with the heteroleptic benzylcalcium complex differs only slightly from the atactic material arising from alkyllithium initiation.

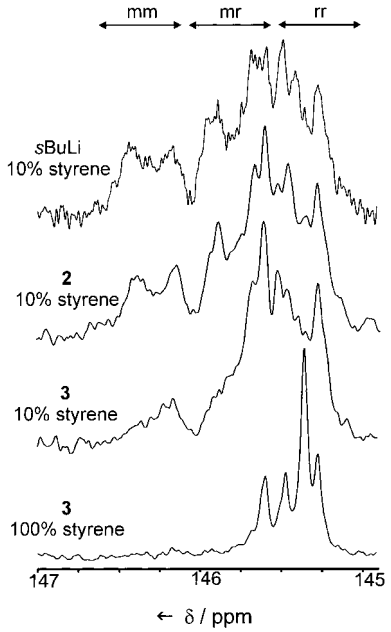
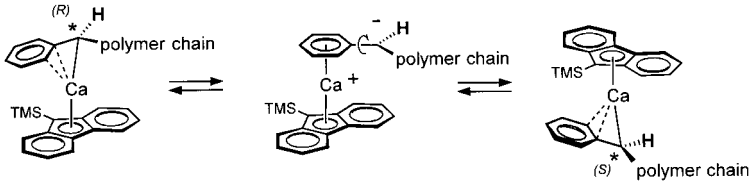


Figure 4. ^{13}C NMR signals of the phenyl C_{ipso} atom in the obtained polystyrene materials ([D$_2$]tetrachloroethane, $T = 100\,^{\circ}$C).

Although there is hardly preference for a syndiotactic insertion, a slight reduction of isotactic and atactic sequences is clearly evident (polymer obtained with heteroleptic benzylbarium complexes never showed any difference to material obtained by alkyllithium initiation). Polymerization at lower temperatures ($-20\,^{\circ}$C instead of the standard temperature of $+70\,^{\circ}$C) only shows a small increase of syndiotactic sequences.

Poor stereocontrol in the polymerization reactions might be a result of the configurationally instability of the chiral anionic chain-end. The barrier for inversion of the anionic chain end is probably lower than that of the chiral carbanion in **3**, which is stabilized by strong intramolecular N$\cdots$Ca coordination.[16] Inversion of the chiral chain end possibly proceeds without complete cleavage of the anion–cation bond: the Ca^{2+} ion binds to the phenyl ring followed by a rotation around the C_{ipso}–C_{α} bond (Scheme 3).

Inversion of the chain end results in racemization of the chiral centers and the formation of atactic polymer. To increase the polymerization rate in respect to the inversion rate, polymerizations in pure styrene were performed. Styrene as a solvent will hardly effect the inversion rates, but a 10-fold increase in insertion rates is expected with respect to the standard polymerization conditions (10% styrene in cyclohexane). NMR spectroscopic analyses of the polymer shows a drastic decrease of isotactic and atactic sequences. The largest



Scheme 3.

signal can be assigned to the pure syndiotactic pentad (rrrr; r = racemic dyad) and the three minor signals are related to polystyrene with high syndiotacticity (overall analysis: 76% rr, 84% r, 22% mr; m = meso dyad). Isotactic sequences are nearly non-existent (less than 2% mm). A slight improvement can be obtained by polymerization at $-20\,^{\circ}$C. All the polymers prepared show a homogenous syndiotacticity and can not be fractionated by extraction with methylethylketone (only minor amounts of low molecular weight chains were extracted). Polymerization experiments with variable intermittent styrene concentrations (in the range 10–100%) show a gradual improvement of stereocontrol with the styrene concentration. Polymerization experiments with 10% styrene in benzene as a solvent, show the same results as polymerization reactions in cyclohexane. Therefore, the increased syndiotacticity on increasing the styrene concentration is not a solvent effect. The results reported here confirm that the insertion step is syndiotactic to a high degree and inversion of the carbanionic chain end leads to stereo errors.

Currently we are also exploring the scope of using the heteroleptic benzylcalcium complex (**3**) in stereocontrolled polymerization of other monomers.

Experimental Section

All experiments were carried out under argon using predried solvents and Schlenk techniques. Styrene polymerizations were performed in a thermostated 100 mL stainless steel reactor at normal pressure (cyclohexane, 50 °C; unless stated otherwise) and quenched with oxygen-free methanol.

Synthesis of **3**: Crystalline bis(2-Me$_2$N-α-Me$_3$Si-benzyl)calcium · (THF)$_2$[13] (4.10 g, 6.86 mmol) and 9-Me$_3$Si-fluorene (1.63 g, 6.84 mmol) were dissolved in benzene (35 mL) and heated at 65 °C for 90 min. The solvent and volatiles of the orange-red solution were removed under oil-pump vacuum at 65 °C for 60 min. The remaining orange solid (after cooling) was obtained NMR pure in quantitative yield. Subsequent crystallization from benzene (15 mL) at 5 °C gave orange crystalline blocks in 73% yield (2.80 g, 5.03 mmol). The crystals contain benzene solvent which can be removed under vacuum. ^{1}H NMR (600 MHz, C_6D_6, 20 °C): $\delta = 0.34$ (s, 1H;

 © WILEY-VCH Verlag GmbH, D-69451 Weinheim, 2001 1433-7851/01/4022-4263 $ 17.50+.50/0

CH(TMS)), 0.42 (s, 9H; TMS-benzyl), 0.59 (s, 9H; TMS-fluorenyl), 0.95 (mb, 4H; THF), 1.93 and 1.96 (2 s, 6H; NMe_2), 2.59 (mb, 4H; THF), 6.12 (t, $^3J(H,H) = 7.5$ Hz, 1H; benzyl), 6.27 (d, $^3J(H,H) = 7.8$ Hz, 1H; benzyl), 6.31 (t, $^3J(H,H) = 7.5$ Hz, 1H; benzyl), 6.88 (d, $^3J(H,H) = 8.4$ Hz, 1H; benzyl), 7.04 (t, $^3J(H,H) = 7.5$ Hz, 1H; fluorenyl), 7.09 (t, $^3J(H,H) = 7.5$ Hz, 1H; fluorenyl), 7.24 (t, $^3J(H,H) = 7.2$ Hz, 1H; fluorenyl), 7.31 (t, $^3J(H,H) = 7.5$ Hz, 1H; fluorenyl), 7.93 (d, $^3J(H,H) = 7.8$ Hz, 1H; fluorenyl), 8.03 (d, $^3J(H,H) = 8.4$ Hz, 1H; fluorenyl), 8.14 (d, $^3J(H,H) = 8.4$ Hz, 1H; fluorenyl), 8.17 (d, $^3J(H,H) = 7.8$ Hz, 1H; fluorenyl); ^{13}C NMR (600 MHz, C_6D_6, 20 °C): $\delta = 2.43$ (TMS), 2.44 (TMS), 24.9 (THF), 41.8 (NMe), 44.5 (NMe), 44.9 (CH(TMS)), 68.5 (THF), aromatics: 87.0, 112.8, 116.5, 116.8, 119.4, 121.2, 121.4, 121.7, 121.9, 123.3, 124.2, 124.3, 124.4, 126.4, 128.3, 135.0, 140.7, 140.9, 147.0.

Crystal structure determination of **3**: Crystals grown from benzene solution contain up to three equivalents of benzene per Ca atom and crack upon cooling resulting in broad peak profiles and poor diffraction. Crystals grown from warm hexane also show solvent incorporation but remain stable upon cooling. Measurement on an Enraf Nonius CAD4 diffractometer at −90 °C, $Mo_{K\alpha}$, $2\theta_{max} = 50°$, 13501 independent reflections ($R_{int} = 0.011$), 10658 reflections observed with $I > 2\sigma(I)$. Crystal data: $C_{32}H_{45}CaNOSi_2$ triclinic, space group $P\bar{1}$, $a = 13.5981(13)$, $b = 16.8236(12)$, $c = 18.2031(15)$ Å, $\alpha = 70.779(6)$, $\beta = 77.084(7)$, $\gamma = 82.671(7)°$, $V = 3826.1(6)$ Å^3, $Z = 4$, $R = 0.0456$, $wR2 = 0.1466$, GOF = 1.08, $\rho_{max} = 0.57$ e Å^{-3}, $\rho_{min} = -0.44$ e Å^{-3}. The unit cell contains a hole with two severely disordered hexane molecules (confirmed by NMR analysis). Disorder was treated with the bypass method using the program SQUEEZE[17] incorporated in PLATON.[18] Crystallographic data (excluding structure factors) for the structure reported in this paper have been deposited with the Cambridge Crystallographic Data Centre as supplementary publication no. CCDC-165023. Copies of the data can be obtained free of charge on application to CCDC, 12 Union Road, Cambridge CB2 1EZ, UK (fax: (+44) 1223-336-033; e-mail: deposit@ccdc.cam.ac.uk).

Received: July 4, 2001 [Z17423]

[1] K. Knoll in *Kunststoff Handbuch 4: Polystyrol* (Eds.: H. Gausepohl, R. Gellert), Hanser, München, **1996**, pp. 67–82; J. R. Wünsch in *Kunststoff Handbuch 4: Polystyrol* (Eds.: H. Gausepohl, R. Gellert), Hanser, München, **1996**, pp. 82–104.

[2] H. H. Brintzinger, D. Fischer, R. Mülhaupt, B. Rieger, R. M. Waymouth, *Angew. Chem.* **1995**, *107*, 1255; *Angew. Chem. Int. Ed. Engl.* **1995**, *34*, 1134; G. W. Coates, *Chem. Rev.* **2000**, *100*, 1223; L. Resconi, L. Cavallo, A. Fait, F. Piemontesi, *Chem. Rev.* **2000**, *100*, 1253.

[3] G. Natta, P. Pino, P. Corradini, F. Danusso, E. Mantica, G. Mazzanti, G. Moraglio, *J. Am. Chem. Soc.* **1955**, *77*, 1708.

[4] N. Ishihara, M. Kuramoto, M. Uoi, *Macromolecules* **1986**, *21*, 2464.

[5] M. Malanga, *Adv. Mater.* **2000**, *12*, 1869.

[6] R. J. Kern, *Nature* **1960**, *187*, 410.

[7] D. J. Worsfold, S. Bywater, *Makromol. Chem.* **1963**, *65*, 245.

[8] L. Cazzaniga, R. E. Cohen, *Macromolecules* **1989**, *22*, 4125.

[9] T. Makino, T. E. Hogen-Esch, *Macromolecules* **1999**, *32*, 5712.

[10] M. Kawabe, M. Murata, K. Soga, *Macromol. Rapid Commun.* **1999**, *20*, 569.

[11] C. Lambert, P. v. R. Schleyer, *Angew. Chem.* **1994**, *106*, 1187; *Angew. Chem. Int. Ed. Engl.* **1994**, *33*, 1129.

[12] A. Weeber, S. Harder, H. H. Brintzinger, K. Knoll, *Organometallics* **2000**, *19*, 1325.

[13] S. Harder, F. Feil, A. Weeber, *Organometallics* **2001**, *20*, 1044.

[14] Circa 4–5 equivalents result in fast inversion at room temperature. Addition of larger amounts of THF result in the crystallization of the solvent-separated ion pair: $[Me_3Si\text{-fluorenyl}^-]_2[Ca^{2+}(THF)_6]$.

[15] Polymerizations with the analogue but more reactive strontium complex show faster initiation and consequently less tailing (polydispersity (P.D.) = 1.218): F. Feil, S. Harder, *Organometallics* **2001**, accepted.

[16] Intramolecular chelation enhances the stability of carbanionic stereogenic centers: C. Strohmann, B. C. Abele, D. Schildbach, K. Strohfeldt, *Chem. Commun.* **2000**, 865.

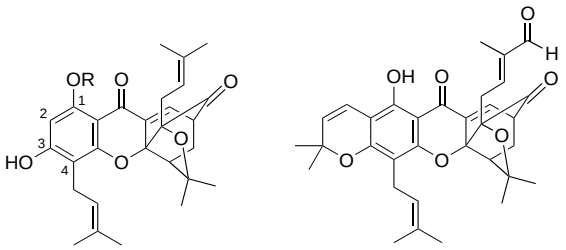
[17] P. A. van der Sluis, A. L. Spek, *Acta Crystallogr. Sect. A* **1990**, *46*, 194.

[18] A. L. Spek, *PLATON, A Multipurpose Crystallographic Tool*, Utrecht University, Utrecht, The Netherlands, **2000**.

"Biomimetic" Cascade Reactions in Organic Synthesis: Construction of 4-Oxatricyclo-[4.3.1.0]decan-2-one Systems and Total Synthesis of 1-*O*-Methylforbesione via Tandem Claisen Rearrangement/Diels–Alder Reactions**

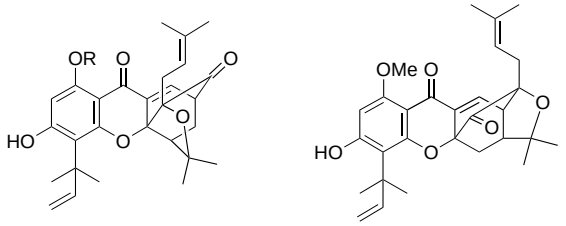
K. C. Nicolaou* and Jim Li

The intriguing 4-oxatricyclo[4.3.1.0]decan-2-one ring system is found in a growing class of biologically active natural products isolated from the genus *Garcinia* of the Guttiferae family of plants. Among the members of this class of compounds are forbesione (**2**, isolated from *Garcinia forbesii*),[1] morellin (**3**, from *G. morella*),[2] and the cytotoxic agents



1: R = Me: 1-*O*-methylforbesione
2: R = H: forbesione

3: morellin



4: R = H: bractatin
5: R = Me: 1-*O*-methylbractatin

6: 1-*O*-methylneobractatin

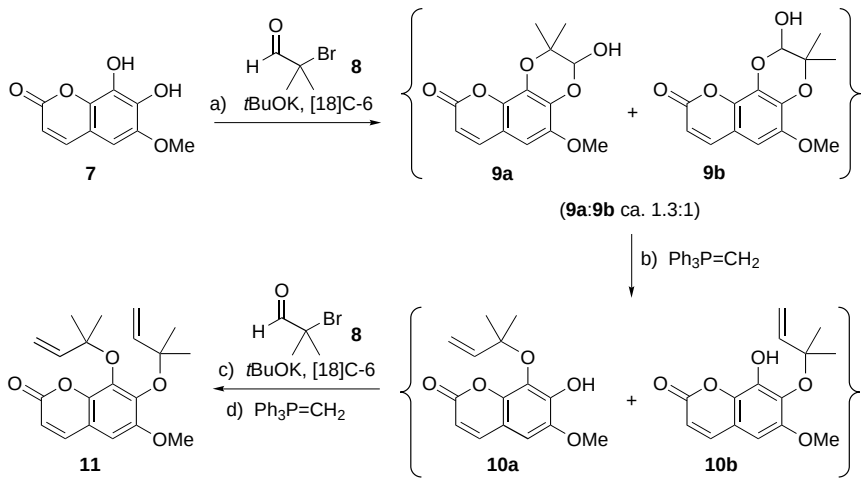
bractatin (**4**), 1-*O*-methylisobractatin (**5**), and 1-*O*-methylneobractatin (**6**), all of which were found in the species *G. bracteata*,[3] as well as lateriflorone (from *G. lateriflora*),[4]

[*] Prof. Dr. K. C. Nicolaou, J. Li
Department of Chemistry and The Skaggs Institute for Chemical Biology
The Scripps Research Institute
10550 North Torrey Pines Road, La Jolla, CA 92037 (USA)
Fax: (+1) 858-784-2469
and
Department of Chemistry and Biochemistry
University of California, San Diego
9500 Gilman Drive, La Jolla, CA 92093 (USA)
E-mail: kcn@scripps.edu

[**] We thank Drs. D. H. Huang, G. Siuzdak, and R. Chadha for NMR spectroscopic, mass spectrometric, and X-ray crystallographic assistance, respectively. This work was financially supported by the National Institutes of Health (USA), The Skaggs Institute for Chemical Biology, a graduate fellowship from The Skaggs Institute for Research (to J.L.), and grants from Abbott Laboratories, ArrayBiopharma, Boehringer Ingelheim, DuPont, Hoffmann-La-Roche, Merck, Pfizer, and Schering Plough.

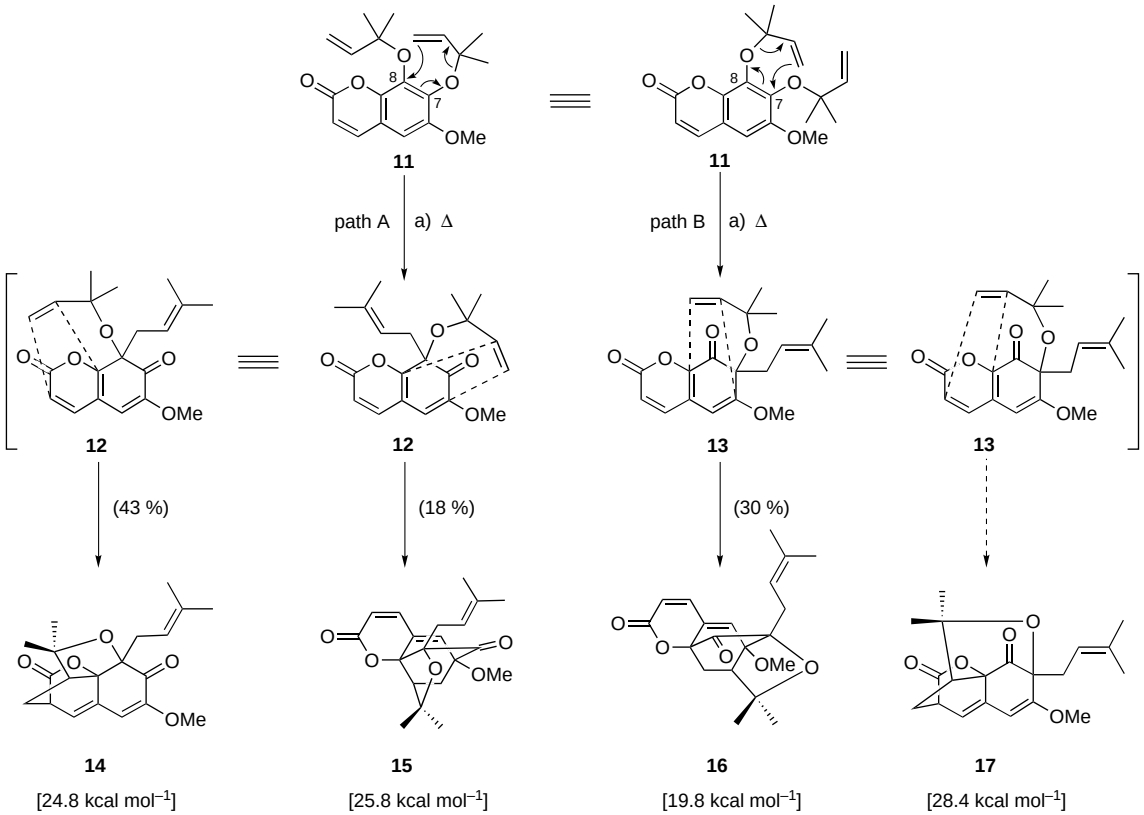
Supporting information for this article is available on the WWW under http://www.angewandte.com or from the author.

hanburin (from *G. hanburyi*),[5] and the gaudichaudiones and gaudichaudiic acids (from *G. gaudichaudii*).[6] An elegant proposal for the biosynthesis of morellins was put forward by Quillinan and Scheinmann over 30 years ago.[7] This biosynthetic hypothesis, in which a Claisen rearrangement followed by an intramolecular Diels–Alder reaction was postulated, was supported by the results of a model study involving unsubstituted allyl ethers which led to rearranged products upon prolonged heating in refluxing decalin in unspecified yields. Here we report the development of this Claisen rearrangement/intramolecular Diels–Alder cascade into a useful strategy for the construction of the fully substituted polycyclic systems found in the two types of natural products represented by the aforementioned compounds. In addition to providing credence to the proposed biogenetic origin of these natural products, the described new synthetic technology found application in the first total synthesis of 1-*O*-methylforbesione (**1**).



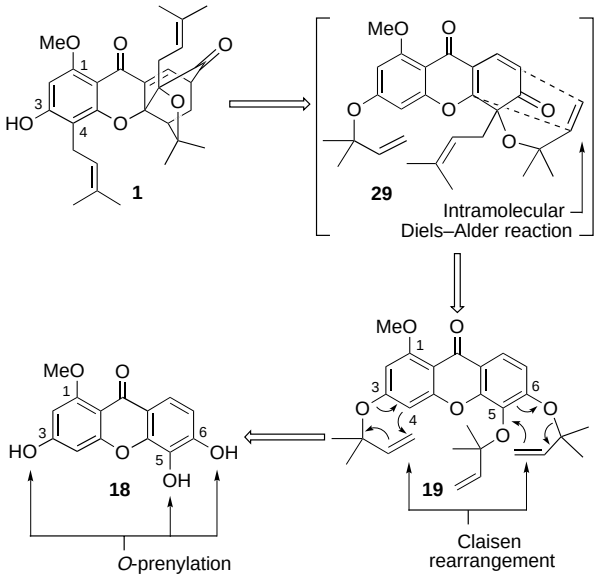
Scheme 1. Synthesis of cascade precursor **11**. a) *t*BuOK (2.1 equiv), THF, 0 °C, 30 min; then concentrated under reduced pressure and suspended in MeCN; [18]C-6 (1.5 equiv), 15 min, 0 °C; **8** (2.5 equiv), 0 →40 °C, 2 h, 92 %; b) $CH_3PPh_3^+Br^-$ (2.0 equiv), NaHMDS (2.0 equiv), THF, 0 →25 °C, 96 %; c) *t*BuOK (1.1 equiv), THF, 0 °C, 30 min, then concentrated under reduced pressure and suspended in MeCN; [18]C-6 (1.0 equiv), 15 min, 0 °C; **8** (1.5 equiv), 0 °C, 1 h; d) $CH_3PPh_3^+Br^-$ (2.0 equiv), NaHMDS (2.0 equiv), THF, 0 °C, 87 % for two steps. NaHMDS = sodium bis(trimethylsilyl)amide.

Coumarin **7** (Scheme 1) was chosen as the entry point to our explorations of the Claisen rearrangement/intramolecular Diels–Alder reaction cascade not only because of the commercial availability of this compound, but also due to the opportunities for molecular diversity it presented. Specifically, it was anticipated that a precursor such as compound **11**, synthesized from **7**, could engage in two possible Claisen rearrangement pathways (A and B, Scheme 2) to furnish the two intermediates **12** and **13**. These two intermediates could then undergo two different intramolecular Diels–Alder reactions as shown in Scheme 2 which would lead to a maximum of four possible final products (**14**–**17**). Molecular



Scheme 2. One-pot cascade Claisen rearrangement/intramolecular Diels–Alder reaction of precursor **11**. a) decalin, 125 °C, 15 min; **14**, 43 %; **15**, 18 %; **16**, 30 %. Energies given in square brackets are differences of strain energies relative to precursor **11**.

 © WILEY-VCH Verlag GmbH, D-69451 Weinheim, 2001 1433-7851/01/4022-4265 $ 17.50+.50/0

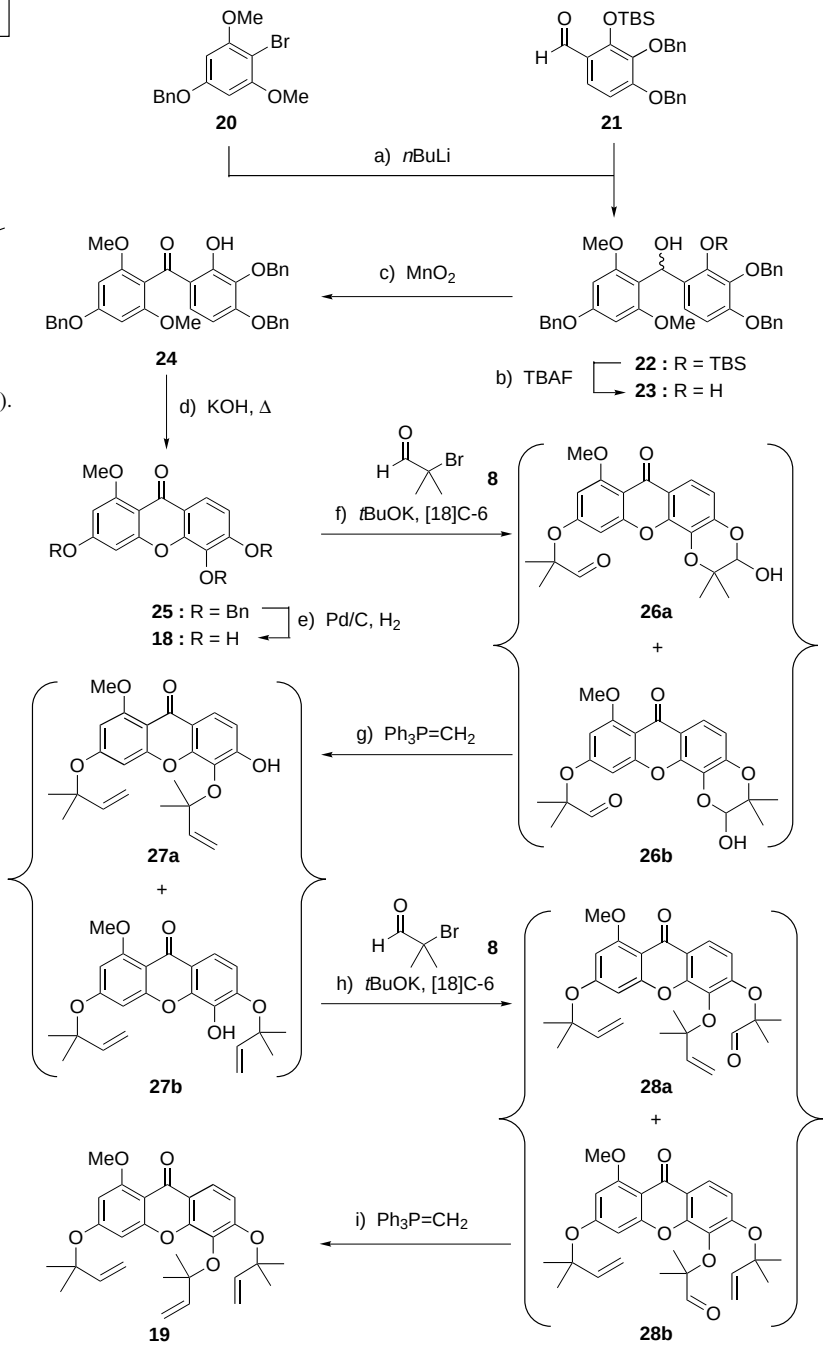


Scheme 3. Retrosynthetic analysis of 1-*O*-methylforbesione (**1**).

mechanics calculations on these cagelike compounds revealed the following relative (to precursor **11**) strain energies: 24.8, 25.8, 19.8, and 28.4 kcal mol^{-1} for compounds **14**, **15**, **16**, and **17**, respectively.[8]

The synthesis of the required precursor **11** from **7** was not trivial given the challenge associated with the construction of the crowded *ortho*-bis-(α,α-dimethylallyl) aryl ethers.[9] Indeed, early attempts to directly allylate or propargylate the catechol system of **7** failed,[10] which prompted us to develop a stepwise approach involving initial reaction of the phenoxide anions of **7** with α-bromoisobutyraldehyde (**8**) followed by Wittig olefination (Scheme 1). This sequence turned out to be both efficient and general as demonstrated by several examples.[11] For the case at hand, the di-potassium salt of **7** reacted with aldehyde **8** in acetronitrile and in the presence of [18]crown-6[12] to afford a mixture of the two regioisomeric lactols **9a**:**9b** (ca. 1.3:1 ratio) in 92% total yield. Treatment of this mixture with 2 equiv of $Ph_3P{=}CH_2$ gave a mixture of mono-olefins **10a** and **10b** (ca. 1.3:1 ratio) in 96% yield. Reiteration of this two-step *O*-alkylation procedure with this mixture resulted in the installation of the second allyl group (87% overall yield) to furnish the desired cascade precursor **11** (Scheme 1).

Heating compound **11** in decalin[13] at 125 °C for 15 min furnished cleanly three products, **14** (43%), **15** (18%), and **16** (30%), which were chromatographically separated and fully characterized by spectroscopic means and X-ray crystallographic analysis.[14] None of the fourth possible structure (**17**) was formed, undoubtedly as a consequence of its highly strained nature relative to the other three products (**14**–**16**, see Scheme 2). These results were both rewarding in terms of confirming the Quillinan–Scheinmann biosynthetic hypothesis[7] and encouraging in terms of possibly facilitating a "biomimetic" total synthesis of a number of natural products. We consequently selected 1-*O*-methylforbesione (**1**) as a



Scheme 4. Synthesis of cascade precursor **19**. a) *n*BuLi (1.05 equiv), THF, −78 °C, 15 min; then aldehyde **21** (1.0 equiv) in THF, −78 → 0 °C, 45 min; b) TBAF (1.2 equiv), THF, 0 °C, 15 min, 92% for two steps; c) MnO_2 (10.0 equiv), CH_2Cl_2, 25 °C, 4 h; d) KOH (10.0 equiv), MeOH, reflux, 6 h, 86% for two steps; e) 10% Pd/C (10% wt/wt), H_2 (1 atm), 25 °C, 45 min, 98%; f) *t*BuOK (3.2 equiv), THF, 0 °C; then concentrated and suspended in MeCN; [18]C-6 (3.0 equiv), 15 min, 0 °C; **8** (4.0 equiv), 0 → 40 °C, 2 h, **26a**:**26b** (ca. 1:2), 73%; g) $CH_3PPh_3^+Br^-$ (3.0 equiv), NaHMDS (3.0 equiv), THF, 0 °C, 1 h, 87%, **27a**:**27b** (ca. 1:2); h) *t*BuOK (1.2 equiv), THF, 0 °C; then concentrated and suspended in MeCN; [18]C-6 (1.0 equiv), 15 min, 0 °C; **8** (1.5 equiv), 0 °C, 2 h, **28a**:**28b** (ca. 1:2), 94%; i) $CH_3PPh_3^+Br^-$ (2.0 equiv), NaHMDS (2.0 equiv), THF, 0 °C, 1 h, 92%. TBS = *tert*-butyldimethylsilyl, Bn = benzyl, TBAF = tetrabutylammonium fluoride.

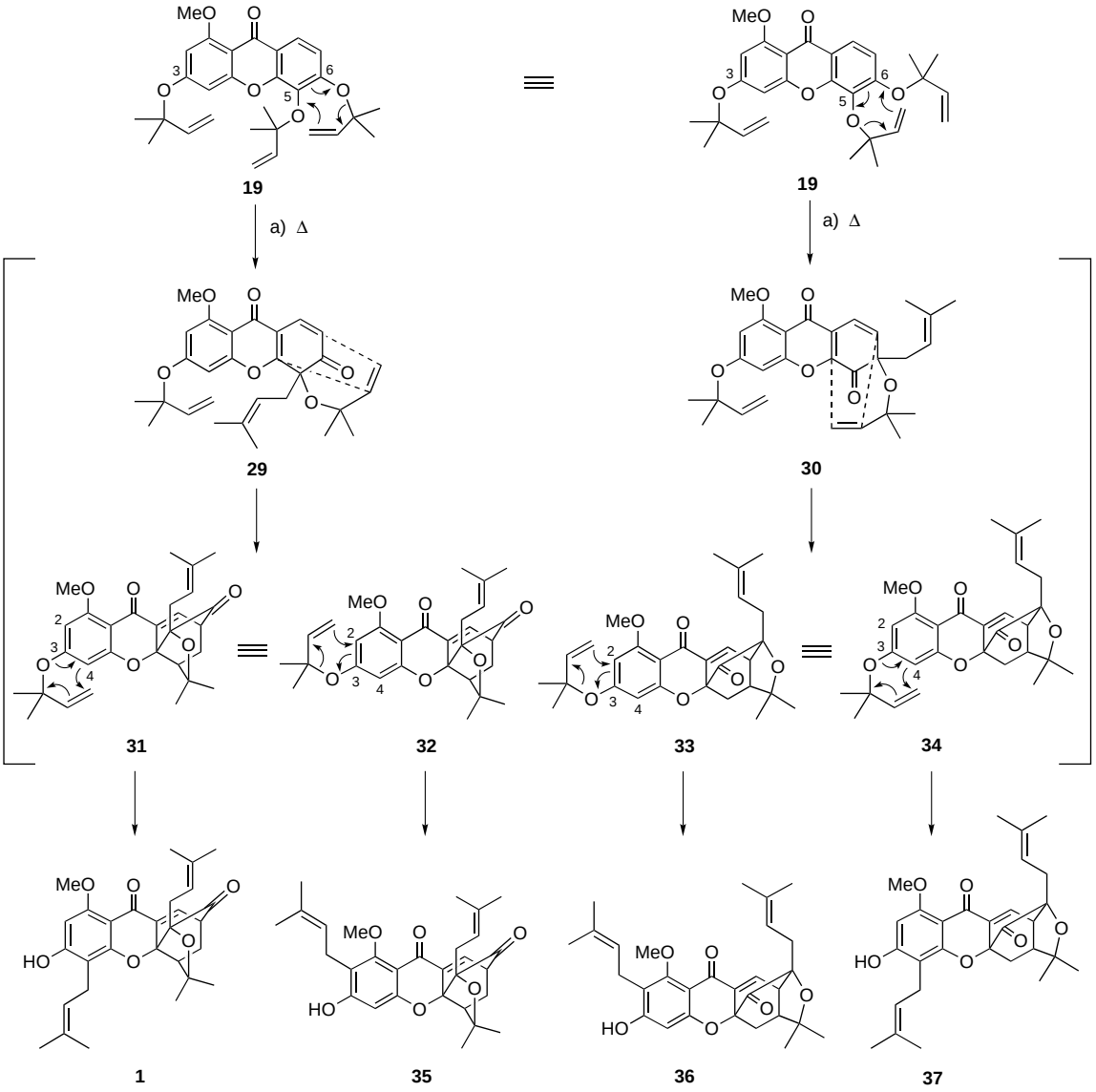
 © WILEY-VCH Verlag GmbH, D-69451 Weinheim, 2001 1433-7851/01/4022-4266 $ 17.50+.50/0 *Angew. Chem. Int. Ed.* **2001**, *40*, No. 22

synthetic target to demonstrate the applicability of this cascade-based synthetic technology to natural product synthesis.

The structure of forbesione contains a xanthone skeleton, two apparent prenyl groups, and a tricyclo[4.3.1.0]decan-2-one system, a cagelike structure which hides a third prenyl moiety. Relying on the one-pot Claisen rearrangement/intramolecular Diels–Alder reaction cascade just described, the tris-(α,α-dimethylallyl) aryl ether **19** may be retrosynthetically defined as a possible precursor to the targeted methyl derivative of forbesione (**1**) (Scheme 3). Compound **19** may, in turn, be derived via the above described two-step allylation protocol from xanthone **18** whose origins can be traced back to benzenoid systems **20** and **21** (Scheme 4).

Coupling of the lithium derivative of **20**[15] with aldehyde **21**[16] followed by desilylation (92% overall yield) and MnO_2 oxidation furnished benzophenone **24** via intermediates **22** and **23** (Scheme 4). Exposure of **24** to KOH in refluxing MeOH led, after hydrogenolysis, to trihydroxy xanthone **18** (85% overall yield) which was subjected to α,α-dimethylallylation as shown in Scheme 1. Thus, treatment of **18** with 3.2 equiv *t*BuOK in THF at 0 °C followed by solvent exchange (THF → MeCN) and sequential addition of [18]crown-6 and α-bromoisobutyraldehyde (**8**) furnished a mixture of aldehyde–lactols (**26a**:**26b** ca. 1:2) in 73% yield. Wittig olefination ($Ph_3P{=}CH_2$) of this mixture then led to a mixture of hydroxy di-olefins (**27a**:**27b**, ca. 1:2, 87% yield) which was allylated further by reiteration of this two-step sequence to afford the targeted precursor **19** (86% over yield) via aldehyde mixture **28a**:**28b**.

Gratifyingly, upon heating prenylated xanthone **19** in DMF at 120 °C for 20 min, the expected compound, 1-*O*-methylforbesione (**1**), was indeed obtained as the major product (63% yield), presumably by the anticipated double Claisen rearrangement followed by an intramolecular Diels–Alder reaction, as outlined in Scheme 5. Accompanying **1** were its isomers **35** (2% yield), **36** (<1% yield, presumed structure[17]), and **37** (26% yield), presumably formed via the



Scheme 5. Synthesis of 1-*O*-methyl forbesione (**1**), and 4-oxatricyclo[4.3.1.0]decan-2-ones **35**, **36** and **37** via a "biomimetic" double Claisen rearrangement/intramolecular Diels–Alder cascade reaction. a) DMF, 120 °C, 20 min; **1**, 63%; **35**, 2%; **36**, <1%; **37**, 26%.

 © WILEY-VCH Verlag GmbH, D-69451 Weinheim, 2001 1433-7851/01/4022-4267 $ 17.50+.50/0

pathways outlined in Scheme 5. The timing of the two Claisen rearrangements has not been determined and the sequences shown in Scheme 5 are simply for purposes of convenience.[18] The structure of 1-*O*-methylforbesione (**1**) was confirmed by both spectroscopic means (see Table 1) and X-ray crystallographic analysis[14] (see Figure 1), whereas those of **35**–**37** were based on spectroscopic evidence and comparisons of their NMR spectra to those of model systems **14**–**17** (Scheme 2) and those reported for the bractatins.[3]

Table 1. Selective analytical data for 1-*O*-methylforbesione (**1**).

Light yellow solid; mp = 192–196 °C (dec.) (ethyl acetate/hexanes, 2:1); R_f = 0.31 (silica gel, ethyl acetate/hexanes, 2:1); ^{1}H NMR (600 MHz, $CDCl_3$): δ = 7.31 (d, J = 8.23 Hz, 1H), 6.26 (bs, 1H), 6.10 (s, 1H), 5.23 (m, 1H), 4.51 (m, 1H), 3.85 (s, 3H), 3.46 (m, 2H), 3.41 (m, 1H), 2.55 (m, 1H), 2.45 (m, 2H), 2.26 (dd, J = 16.05, 5.68 Hz, 1H), 1.81 (s, 3H), 1.76 (d, J = 1.19 Hz, 3H), 1.65 (s, 3H), 1.37 (s, 3H), 1.31 (dd, J = 15.31, 11.55 Hz, 1H), 1.25 (s, 3H), 1.08 (s, 3H); ^{13}C NMR (150 MHz, $CDCl_3$): δ = 204.1, 174.9, 162.0, 161.3, 160.1, 136.4, 135.8, 134.5, 132.3, 121.2, 117.6, 106.4, 104.6, 93.9, 90.6, 84.5, 83.0, 56.2, 49.0, 46.7, 30.2, 29.1, 28.8, 26.0, 25.8, 25.6, 22.6, 18.0, 17.0; HR-MS (MALDI-FT): calcd for $C_{29}H_{34}O_6$ [M+H$^+$]: 479.2428; found: 479.2417

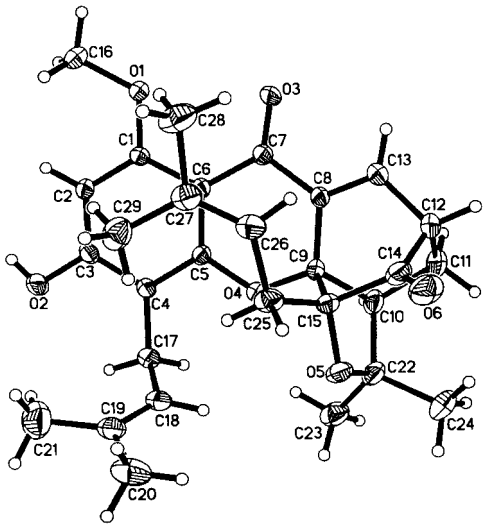


Figure 1. X-Ray crystallographic structure of 1-*O*-methylforbesione (**1**) in ORTEP representation.

The development of the Claisen rearrangement/intramolecular Diels–Alder cascade reaction as a powerful and practical method for the construction of complex molecules is a further demonstration of the value of "biomimetically" inspired synthetic strategies toward natural products. The described expedient total synthesis of racemic 1-*O*-methylforbesione (**1**) bodes well for further applications of this synthetic technology to other members of this constantly expanding class of natural products containing the 4-oxatricyclo[4.3.1.0]decan-2-one ring framework and related systems.

Received: July 27, 2001 [Z17615]

[1] Y.-W. Leong, L. J. Harrison, G. J. Bennett, H. T.-W. Tan, *J. Chem. Res. (S)* **1996**, 392.

[2] a) W. D. Ollis, M. V. J. Ramsay, I. O. Sutherland, S. Mongkolsuk, *Tetrahedron* **1965**, *21*, 1453, and references therein; b) G. Kartha, H. N. Ramachandran, H. B. Bhat, P. M. Nair, V. K. V. Raghavan, K. Venkataraman, *Tetrahedron Lett*. **1963**, 459; c) C. G. Karanjgaonkar, P. M. Nair, K. Venkataraman, *Tetrahedron Lett*. **1966**, 687; d) H. B. Bhat, P. M. Nair, K. Venkataraman, *Indian J. Chem*. **1964**, *2*, 402.

[3] O. Thoison, J. Fahy, V. Dumontet, A. Chiaroni, C. Riche, M. V. Tri, T. Sévenet, *J. Nat. Prod*. **2000**, *63*, 441.

[4] S. Kosela, S.-G. Cao, X.-H. Wu, J. J. Vittal, T. Sukri, Masdianto, S.-H. Goh, K.-Y. Sim, *Tetrahedron Lett*. **1999**, *40*, 157.

[5] a) L. J. Lin, L. Z. Lin, J. M. Pezzuto, G. A. Cordell, N. Ruangrungsi, *Magn. Reson. Chem*. **1993**, *31*, 340; b) J. Asano, K. Chiba, M. Tada, T. Yoshii, *Phytochemistry* **1996**, *41*, 815.

[6] a) S. G. Cao, X. H. Wu, K.-Y. Sim, B. H. K. Tan, J. T. Pereira, W. H. Wong, N. F. Hew, S. H. Goh, *Tetrahedron Lett*. **1998**, *39*, 3353; b) S. G. Cao, V. H. L. Sng, X. H. Wu, K.-Y. Sim, B. H. K. Tan, J. T. Pereira, S. H. Goh, *Tetrahedron* **1998**, *54*, 10915; c) X.-H. Wu, B. H. K. Tan, S.-G. Cao, K.-Y. Sim, S. H. Goh, *Nat. Prod. Lett*. **2000**, *14*, 453; d) V. Rukachaisirikul, W. Kaewnok, S. Koysomboom, S. Phongpaichit, W. C. Walter, *Tetrahedron* **2000**, *56*, 8539; e) Y. J. Xu, S. C. Yip, S. Kosela, E. Fitri, M. Hana, S. H. Goh, K.-Y. Sim, *Org. Lett*. **2000**, *2*, 3945.

[7] A. J. Quillinan, F. Scheinmann, *Chem. Commun*. **1971**, 966.

[8] Computational studies on compounds **11** and **14**–**17** were performed using the program DISCOVER packaged in Insight II software on a SGI workstation. High temperature (1000 K) molecular dynamics (MD) was used to generate conformations of each compound. Molecular mechanics potentials (AMBER force field) were determined relative to **11**.

[9] To the best of our knowledge (SciFinder and Beilstein databases), this type of highly hindered *ortho*-bis-(α,α-dimethylallyl) aryl ether has not been previously reported.

[10] Classical methods involving copper-catalyzed phenolic propargylation proved unsuccessful with the present catechol substrates. The Trost palladium-catalyzed phenolic allylation method [B. M. Trost, D. Toste, *J. Am. Chem. Soc.* **1998**, *120*, 815] also failed to provide an entry into the desired aryl ethers in this instance.

[11] Further details of this two-step sequence for the preparation of various aryl allyl ethers will be reported in due course.

[12] Applications of crown ethers in organic synthesis can be found in the following selected references: a) D. Dehm, A. Padwa, *J. Org. Chem.* **1975**, *40*, 3139; b) F. Terrier, G. Ah-Kow, M. Pouet, M. Simonnin, *Tetrahedron Lett*. **1976**, 227; c) C. L. Liotta, H. P. Harris, M. McDermott, T. Gonzalez, K. Smith, *Tetrahedron Lett*. **1974**, 2417.

[13] Among several solvents evaluated for this one-pot cascade reaction, decalin was found to be the most suitable in terms of yields and convenience.

[14] Crystallographic data (excluding structure factors) for the structures reported in this paper have been deposited with the Cambridge Crystallographic Data Centre as supplementary publication nos. CCDC-168029 (**14**), -168031 (**15**), -168028 (**16**), and -168030 (**1**). Copies of the data can be obtained free of charge on application to CCDC, 12 Union Road, Cambridge CB2 1EZ, UK (fax: (+44) 1223-336-033; e-mail: deposit@ccdc.cam.ac.uk).

[15] Aryl bromide **20** was prepared from 3,5-dimethoxyphenol by bromination with NBS in CH_2Cl_2 followed by benzylation with BnBr and K_2CO_3 in refluxing acetone.

[16] Compound **21** was prepared from 2,3,4-trihydroxybenzaldehyde by benzylation with BnBr and K_2CO_3 in refluxing acetone, followed by selective debenzylation at C2 with $MgBr_2 \cdot OEt_2$, and silylation of the resulting phenolic group with TBSCl.

[17] Owing to the low yield in which this presumed product was formed, its full characterization is still pending.

[18] A small amount of intermediate **31** isolated in some experiments suggested the indicated order of events in the conversion of **19** to **1** as illustrated in Scheme 5.

 © WILEY-VCH Verlag GmbH, D-69451 Weinheim, 2001 1433-7851/01/4022-4268 $ 17.50+.50/0

First Example of Coexistence of Thermal Spin Transition and Liquid-Crystal Properties

Yury Galyametdinov,* Vadim Ksenofontov, Andrej Prosvirin, Igor Ovchinnikov, Galina Ivanova, Philipp Gütlich,* and Wolfgang Haase

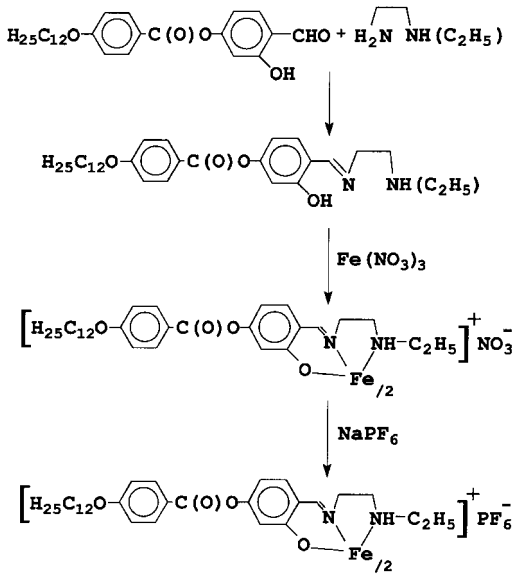
Dedicated to Professor Weyrich on the occasion of his 60th birthday

Flexibility in the synthesis of molecular assemblies based on molecular units is an important factor in achieving synergy of various interesting physical properties in modern materials. The fascinating peculiarities of spin-crossover (SC) compounds[1] stimulated the idea of combining liquid-crystalline (LC) and SC behavior in a single material, which to the best of our knowledge has not yet been achieved.

To obtain highly ordered materials we chose the LC state as a basis for the elaboration of supramolecular organized systems with controlled physical properties.[2] Earlier, similar approaches were used for the easy alignment by magnetic fields of LC compounds[3] containing lanthanide ions with large magnetic moments and anisotropy.[4] Liquid-crystalline materials with giant magnetic anisotropy were thus obtained.

The realization of synergistic SC and LC properties should lead to a combination of the sensitivity of the LC state to electromagnetic fields with the magnetic and optical properties of SC compounds, with their well-known characteristic responses to physical perturbation.[1] The practical application of SC materials with LC properties as active media for memory storage and optical devices is appealing, and the whole traditional variety of LC technologies and techniques can be applied.

As model building blocks for systems with spin-variable properties we chose a complex of Fe^{3+} with an *N*-alkyloxysalicylidenyl-*N*′-ethyl-*N*-ethylenediamine ligand. Spin-crossover behavior for similar complexes was found and investigated previously.[5] Pseudooctahedral complexes of Fe^{3+} with an N_4O_2 coordination core were prepared in a similar way to that described in ref. [5]. Schiff base ligands with elongated substituents were employed to provide the rodlike geometry and hence the LC properties of the complex, which was prepared from the condensation product of 4-(dodecyloxybenzoyloxy)-2-hydroxybenzaldehyde with *N*-ethylethylenediamine (Scheme 1). The synthesis of the complex was carried out without isolation of the intermediate products. The PF_6^- salt was obtained as black microcrystals by metathesis of the NO_3^- salt in CH_3OH, and its composition was confirmed by elemental analysis.



Scheme 1. Synthesis of the liquid-crystalline Fe^{3+} complexes with an LC Schiff base ligand.

Liquid-crystalline properties were confirmed in the crystal state and mesophase by polarizing optical microscopy, differential scanning calorimetry (DSC), and X-ray scattering. The sample contains rodlike molecules (Figure 1) and, in the range 388–419 K, exhibits the fan-shaped texture usually attributed to the smectic A mesophase.



Figure 1. Computer simulation of the molecular structure of the LC Fe^{3+} complex (counterion omitted).

Proposed molecular packing in crystal and mesophase states, based on X-ray scattering data, are shown in Figure 2. The sharp reflection in the small-angle region ($d = 21.5$ Å) detected at room temperature corresponds to the length of $l = 22.6$ Å of the rigid part of the molecule. Drastic changes

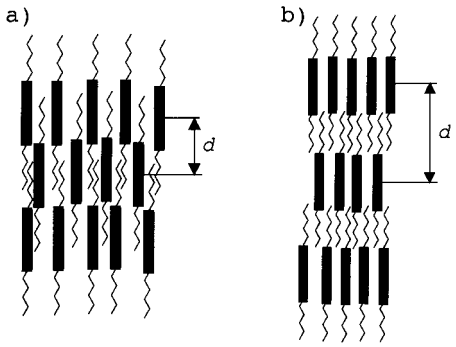


Figure 2. Proposed molecular packing of the Fe^{3+} complex in the crystal and mesophase states at different temperatures: a) starting material, crystal state: $T = 303$ K, $d = 21.5$ Å; b) S_A phase, $T = 391$ K, $d = 33.6$ Å.

[*] Prof. Dr. Y. Galyametdinov, Dr. A. Prosvirin, Prof. Dr. I. Ovchinnikov, Dipl.-eng. G. Ivanova
Kazan Physical Technical Institute, Russian Academy of Science
Sibirsky Tract 10/7, 420029 Kazan (Russia)
Fax: (+7) 84-32-76-50-75
E-mail: galyametdinov@sci.kcn.ru
Prof. Dr. P. Gütlich, Dr. V. Ksenofontov
Institut für Anorganische Chemie und Analytische Chemie
Johannes-Gutenberg-Universität
Staudinger Weg 9, 55099 Mainz (Germany)
Fax: (+49) 6131-39-22990
E-mail: p.guetlich@uni-mainz.de
Prof. Dr. W. Haase
Institute of Physical Chemistry, Darmstadt University of Technology
Petersenstraße 20, 64287 Darmstadt (Germany)

 © WILEY-VCH Verlag GmbH, D-69451 Weinheim, 2001 1433-7851/01/4022-4269 $ 17.50+.50/0

appear at 398 K. At this temperature the formation of the smectic layers is complete. A sharp reflection in the small-angle region ($d = 33.6$ Å) is detected at this temperature. This X-ray pattern indicates a disordered smectic phase. The length of the Schiff base complex, calculated by molecular modeling, is 55.3 Å. The difference between the calculated and experimental data can be explained by interpenetration of alkyl chains of the layers (Figure 2). Alternatively, the smaller experimental smectic layer distances can be explained by strong thermal motion of the alkyl chains on heating in the mesophase and/or bilayer lamellar structure of the mesophase.

Magnetic properties were investigated in the temperature range 4.5 – 460 K (Figure 3). Clearly, the compound exhibits a gradual spin-crossover transition. According to the magnetic

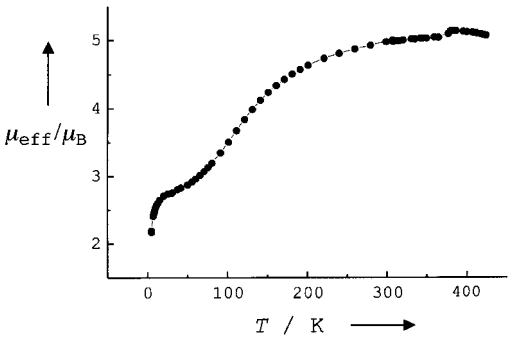


Figure 3. Temperature dependence of the effective magnetic moments μ_{eff} [μ_B] of the Fe^{3+} complex.

susceptibility data, the transition should be almost complete both at high and low temperatures. The value of the effective magnetic moment per Fe ion, μ_{eff}, is 5.14 μ_B at 400 K, instead of the 5.9 μ_B expected for an Fe^{3+} complex in a high-spin state. A fraction of about 88 % of low-spin Fe^{3+} follows from the magnetic susceptibility measured at $T = 4.6$ K. The ^{57}Fe Mössbauer spectra measured in the range $4.2 < T < 293$ K reveal Fe^{3+} in high-spin (HS) and low-spin (LS) states and confirm the occurrence of thermal spin crossover between these states. The room-temperature spectrum (Figure 4a) corresponds to the HS state only, whereas the Mössbauer spectrum measured at $T = 4.2$ K (Figure 4c) reveals two kinds of Fe^{3+} species and confirms the incompleteness of spin crossover at this temperature. The LS fraction of 86 % is in good agreement with that derived from magnetic measurements; the rest is the HS fraction. The isomer shift and quadrupole splitting values at 4.2 K are $\delta = 0.26$ mm s^{-1}, $\Delta E_q = 0.72$ mm s^{-1} for the HS state and $\delta = 0.01$ mm s^{-1}, $\Delta E_q = -2.90$ mm s^{-1} for the LS state. The fractions of the HS and LS components, derived from the spectrum at $T =$ 125 K (Figure 4b), are 52 and 48 %, respectively. This means that the spin transition temperature $T_{1/2}$, at which both spin states are present to 50 %, is around 125 K. Equal areas of both components of the LS spectra rule out the Goldanskii – Karyagin[6] effect or texture influence. The observed pronounced asymmetry of the LS quadrupole doublet is caused by spin – spin relaxation, for which the observed temperature independence of the asymmetry is typical in the range 1.5 – 4.2 K. The relaxation effects are responsible for the broadening of lines of the HS component, too. The large quadrupole splitting for Fe^{3+} (LS) indicates strong distortion of the local N_2O_4 coordination environment of iron, which contributes to the electric field gradient in addition to a noncubic valence electron distribution in the split t_{2g} manifold.

A specific feature in the magnetic behavior of the studied system is the jump in the magnetic moment at $T = 380$ K associated with the crystal – liquid crystal phase transition. To clarify the reason for the observed magnetic anomaly, the compound was studied in the temperature range $293 < T <$ 425 K. The sample was heated in an external magnetic field of 1.5 T through the crystal – smectic phase transition. The jump of μ_{eff} from 5.04 to 5.14 μ_B occurs in the range of crystal – smectic phase transition. Further heating leads to a decrease of μ_{eff} to 5.05 μ_B in the isotropic phase. This value was preserved when the sample was cooled to room temperature in the presence of a magnetic field. Cooling in zero magnetic field led to the value of the magnetic moment at room temperature measured at the beginning of the experiment. The described feature was completely reproducible. Heating the sample in the temperature range $300 < T < 360$ K in a magnetic field of 1.5 T caused a gradual increase in the magnetic moment. This may be explained by increasing orientation of microcrystalline particles with anisotropic paramagnetic susceptibility, as the viscosity of intergrain boundaries in pretransitional regions decreases. This effect is similar to the known phenomenon of magnetic field induced texture formation (thermomagnetic processing) in paramagnetic powder samples.[7] The orientation effect reaches its maximum in the vicinity of the transition from the crystalline (Cr) to smectic (S_A) phase because of a drastic decrease in viscosity in the pre-

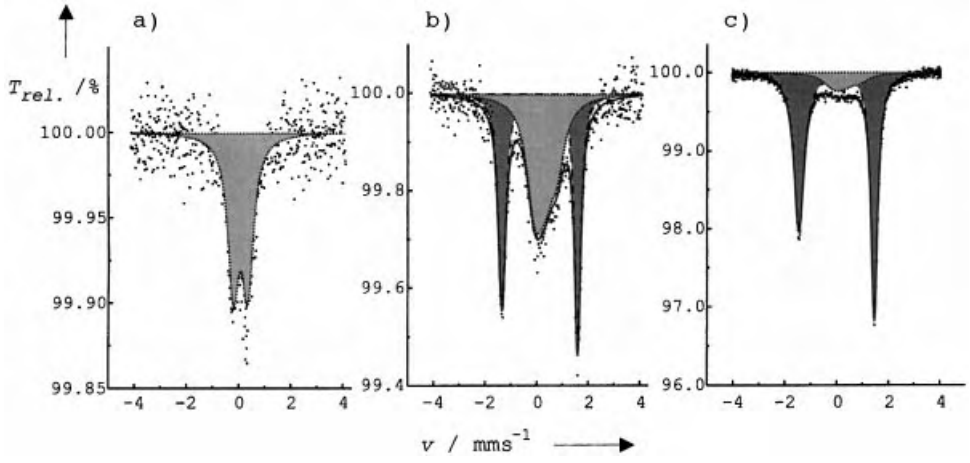


Figure 4. Mössbauer spectra at room temperature (a), 125 K (b), and 4.2 K (c). Shaded subspectra correspond to Fe^{3+}(HS) (••••) and Fe^{3+}(LS) (- - - -).

 © WILEY-VCH Verlag GmbH, D-69451 Weinheim, 2001 1433-7851/01/4022-4270 $ 17.50+.50/0

transitional temperature range. In the smectic phase increasing temperature leads to the disappearance of long-range order, and hence the susceptibility decreases. The behavior of the magnetic susceptibility on cooling in a magnetic field of 1.5 T, with a change from the isotropic to liquid-crystalline phase (Figure 5) may be explained by magnetic anisotropy

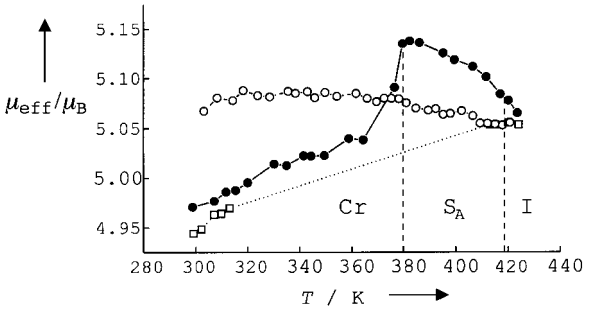


Figure 5. Effective magnetic moment μ_{eff} versus temperature for the Fe^{3+} complex in an applied magnetic field of 1.5 T. ● heating run; ○ cooling run at 1.5 T; □ cooling run at zero magnetic filed. Cr: crystal, S_A: smectic A, I: isotropic phases.

caused by magnetic field induced orientation of the molecules. During the alignment of the molecules, the axis of maximum magnetic anisotropy orients itself parallel to the director in the smectic phase, and a macroscopic orientation of the sample appears. One cannot exclude the possibility that this process is accompanied by a change of the HS/LS ratio because of possible changes of elastic properties of the compound that occur during the rearrangement of the molecular packing.

In conclusion, the possibility of coexistence of spin crossover and liquid-crystalline properties in a single compound has been demonstrated. Our efforts are directed towards enhancing the synergy between SC and LC phenomena. To achieve this we intend to chemically modify the system to increase the SC transition temperature and simultaneously decrease the transition temperature to the liquid-crystalline state. Furthermore, SC compounds containing thermochromic Fe^{2+} will be studied. Due to the presence of paramagnetic ions, the material reported here exhibits enhanced magnetic anisotropy and can be aligned by a magnetic field in the mesophase of a liquid crystal.

Experimental Section

N-ethylethylenediamine, $Fe(NO_3)_3 \cdot 9H_20$, and KPF_6 were used as received from Aldrich. Aldehyde **1** was prepared according to the literature procedure.[3]

2: *N*-Ethylethylenediamine (0.046 g, 0.52 mmol) was added in small portions to **1** (0.208 g, 0.52 mmol) in EtOH (30 mL). The mixture was heated for 20 min at 100 °C, and NaOH (0.021 g, 0.52 mmol) in H_2O (1 mL) was added. $Fe(NO_3)_3 \cdot 9H_20$(0.1 g, 0.53 mmol) in EtOH (5 mL) was added to the resulting orange solution with stirring. A twofold excess of KPF_6 in methanol was added to the resulting suspension of the complex, which was then heated to reflux for 15 min. The product was filtered from the hot mixture. The brown precipitate was washed with methanol and dried in vacuo. Yield: 0.25 g (42 %). Elemental analysis (%) calcd for $C_{56}H_{78}N_4O_8PF_6Fe$: C 59.21, H 6.87, N 4.93; found: C 59.02, H 6.94, N 5.11.

The temperatures and textures of phase transitions were determined with a polarization microscope, equipped with a hot stage and with temperature control of better than ± 0.05 K. Differential scanning calorimetry measurements were carried out on a Perkin-Elmer DSC-2M differential scanning calorimeter (scan rate of 5 K min^{-1}).

The high-temperature X-ray measurements where obtained with a STOE STADI 2 diffractometer, equipped with a linear position-sensitive detector (STOE mini PSD). Monochromatic $Cu_{K\alpha}$ radiation was obtained by using a curved germanium detector (111 plane). The temperature-dependent susceptibilities in the range 4.2 – 450 K of the powdered metallomesogen were recorded by using a Faraday-type magnetometer, equipped with an enhanced heating device operating in the range 300 – 450 K and an applied field of 1.5 T.[8]

Received: July 3, 2001 [Z 17417]

[1] P. Gütlich, A. Hauser, H. Spiering, *Angew. Chem.* **1994**, *106*, 2109 – 2141; *Angew. Chem. Int. Ed. Engl.* **1994**, *33*, 2024 – 2054.
[2] A. Reichert, H. Ringsdorf, P. Schuhmaher, W. Baumeister, T. Scheybani in *Comprehensive Supramolecular Chemistry*, *Vol. 5* (Eds.: J. L.Atwood, J. E. D. Davies, D. D. MacNicol, F. Vogtle, K. S. Suslick), Pergamon, Oxford, **1996**, pp. 313 – 350.
[3] Yu. Galyametdinov, M. Athanassopoulou, K. Griesar, O. Kharitonova, E. Soto-Bustamante, L. Tinchurina, I. Ovchinnikov, W. Haase, *Chem. Mater.* **1996**, *8*, 922 – 926.
[4] K. Binnemans, Yu. Galyametdinov, R. Van Deun, D. Bruce, S. Collinson, A. Polishchuk, I. Bikchantaev, W. Haase, A. Prosvirin, L. Tinchurina, I. Litvinov, A. Gubajdullin, A. Rakhmatullin, K. Uytterhoeven, L. Van Meervelt, *J. Am. Chem. Soc.* **2000**, *122*, 4335 – 4344.
[5] M. S. Haddad, M. W. Lynch, W. D. Federer, D. N. Hendrickson, *Inorg. Chem.* **1981**, *20*, 123 – 132.
[6] V. I. Goldanskii, E. F. Makarov in *Chemical Applications of Mössbauer Spectroscopy* (Eds.: V. I. Goldanskii, R. H. Herber), Academic Press, New York, **1968**, pp. 102 – 107.
[7] D. L. Nagy, K. Kulcsár, G. Ritter, H. Spiering, H. Vogel, R. Zimmermann, I. Dézsi, M. Pardavi-Horváth, *J. Phys. Chem. Solids* **1975**, *36*, 759 – 767.
[8] L. Merz, W. Haase, *J. Chem. Soc. Dalton Trans.* **1980**, 875 – 879.

Assembly of Encapsulated Transition Metal Catalysts**

Vincent F. Slagt, Joost N. H. Reek,* Paul C. J. Kamer, and Piet W. N. M. van Leeuwen

There is considerable interest in the encapsulation of guest molecules in the hollow framework of spherical host molecules. The first examples of containerlike molecules were obtained by performing the synthesis in the presence of the guest molecule.[1] More recent strategies involve the construction of spherical hosts consisting of two self-complementary units held together by hydrogen bonds[2–4] and multicomponent assembly of capsules by using metal – ligand interactions.[5, 6] Initially, only small guest molecules were

[*] Dr. J. N. H. Reek, V. F. Slagt, Dr. P. C. J. Kamer, Prof. Dr. P. W. N. M. van Leeuwen
Institute of Molecular Chemistry, University of Amsterdam
Nieuwe Achtergracht 166, 1018 WV Amsterdam (The Netherlands)
Fax: (+31) 20-525-6456
E-mail: reek@anorg.chem.uva.nl

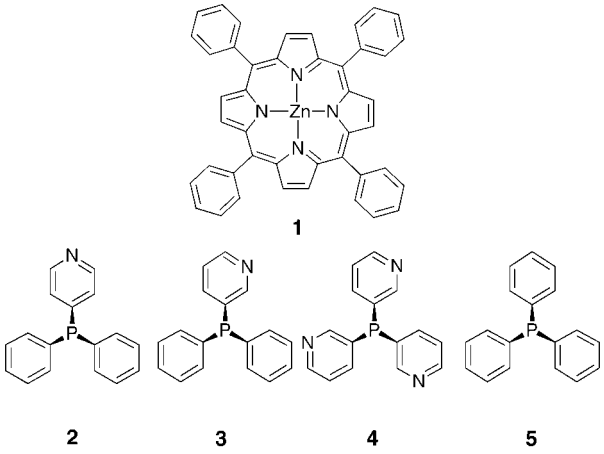
[**] The NRSCC is kindly acknowledged for financial support.

Supporting information for this article is available on the WWW under http://www.angewandte.com or from the author.

encapsulated, but systems based on functionalized calixarenes serve as self-assembled hosts for large guests such as adamantane and fullerenes.[4] The templated assembly of molecular capsules based on structurally self-complementary bis-porphyrins was recently reported.[7]

An intriguing challenge is to use these supramolecular structures as molecular reaction vessels by performing a reaction inside the capsule. For example, Diels–Alder reactions are accelerated when they take place in self-assembled capsules or metallocages.[8, 9] Many reactions of interest require a transition metal catalyst, but so far the encapsulation of transition metal catalysts in molecular capsules has not been reported. The formation of encapsulated transition metal catalysts would lead to a new class of functional assemblies with catalytic properties that depend on the catalyst site and the structure of the molecular reactor created by encapsulation. Here we report on such a strategy using simple building blocks such as porphyrins[10,11] and pyridylphosphanes.[12] These novel catalyst assemblies show enhanced activity in the palladium-catalyzed Heck reaction[13] and rhodium-catalyzed hydroformylation.[14]

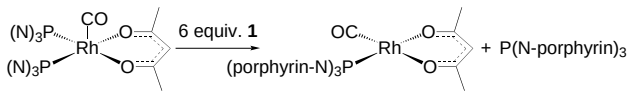
First, the coordination behavior of the pyridylphosphane ligands **2**–**5** towards zinc(II) tetraphenylporphyrin (**1**; Scheme 1) was investigated by NMR and UV/Vis spectroscopy.[15, 16] Job-plot analysis proved the formation of 1:1 complexes between monopyridylphosphanes **2** and **3** and **1**, with binding constants of $K_{1\text{-}2} = 6.1 \times 10^3\,\text{M}^{-1}$ and $K_{1\text{-}3} = 2.3 \times 10^3\,\text{M}^{-1}$. Building block **4** has three nitrogen donor atoms that enable the formation of larger assemblies. Job-plot analysis indicated that indeed three zinc(II) porphyrin units were coordinated to the pyridyl units of **4** (see Supporting Information). This implies that a hemispherical assembly was formed that encapsulates the phosphane ligand in its center.



Scheme 1. Zinc(II) tetraphenylporphyrin and phosphane ligands for catalyst assemblies.

The binding of these building blocks through the nitrogen donor atom is very selective. Triphenylphosphane (**5**) did not coordinate to **1** ($K < 50\,\text{M}^{-1}$). This implicates that the P atom is available for coordination to catalytically active transition metals. After mixing of two equivalents of **1** and $[PdCl_2(\mathbf{2})_2]$ an assembly was formed in which the transition metal is sandwiched between the two porphyrin building blocks. The associated porphyrin units do not have a large impact on the ligand coordination in $[PdCl_2(\mathbf{2})_2]$. The influence of the complexation of three porphyrin units **1** on the coordination behavior of the phosphane moiety of **4** was expected to be much larger, due to the enormous increase in steric bulk and the encapsulation of the phosphane. Indeed, after addition of six equivalents of **1** to a solution of preformed $[PdCl_2(\mathbf{4})_2]$ the ^{1}H and ^{31}P NMR spectra showed the formation of a monophosphane palladium complex due to steric crowding. In addition one equivalent of dissociated $\mathbf{4}(\mathbf{1})_3$ was formed (enforced ligand dissociation).

Similar reactions with $[Rh(acac)(CO)(\mathbf{4})_2]$ (**6**; acac = acetylacetonato) resulted in ligand dissociation and formation of the mono-phosphane rhodium complex **7** (Scheme 2). Addition of a solution of ligand **4** to $[Rh(acac)(CO)_2]$ gives the expected rhodium complex with two coordinated phosphane ligands, whereas in the presence of **1** only mono-phosphane rhodium complex **7** was observed. Molecular modeling studies on the rhodium complexes indicated that the rhodium center is completely encapsulated by the porphyrin assembly (Figure 1). The formation of a bis-phosphane complex is prohibited by steric interactions between the assembled porphyrin units. This implicates that the catalytically active species located at the center of the assembly differs from that of the nonencapsulated complex.



Scheme 2. The assembly of porphyrins on the pyridylphosphane ligands enforces mono-phosphane coordination on the rhodium atom. $P(N)_3$ = tris(*m*-pyridyl)phosphane (**4**), porphyrin = zinc(II) tetraphenylporphyrin (**1**), $P(N\text{-porphyrin})_3$ = three zinc(II) porphyrins assembled on tris(*m*-pyridyl)phosphane $[\mathbf{4}(\mathbf{1})_3]$.

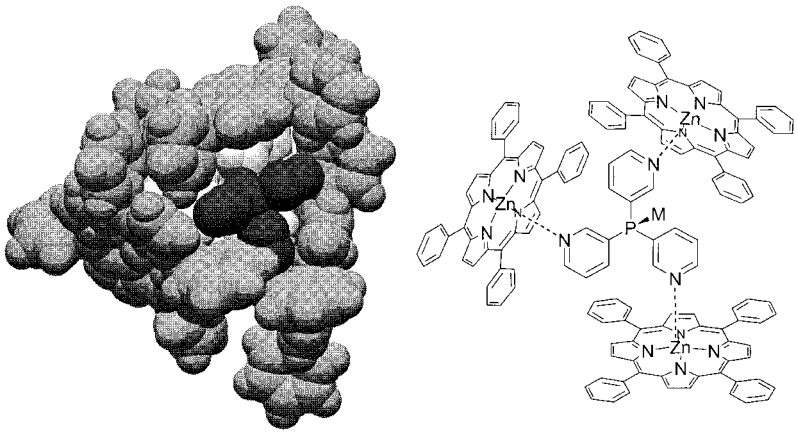


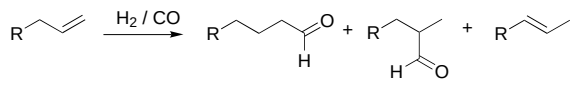
Figure 1. Modeled structure of an encapsulated transition metal catalyst consisting of porphyrin **1** (gray), tris(*m*-pyridyl)phosphane (**4**) (white) and M = [RhH(CO)$_3$] (dark gray).

 © WILEY-VCH Verlag GmbH, D-69451 Weinheim, 2001 1433-7851/01/4022-4272 $ 17.50+.50/0

The encapsulated palladium catalysts were studied in the Heck reaction[13] of iodobenzene and styrene. Three palladium tetrakis-phosphane complexes were prepared as catalyst precursors: [Pd(**4**)$_4$], [Pd(**5**)$_4$], and [Pd(**2**)$_4$].[17] Figure 2 plots the formation of the product as a function of time for the catalyst precursors in the presence and absence of **1**. The identical results of the catalytic reaction with [Pd(**5**)$_4$] in the presence and absence of **1** show that the porphyrin does not disturb the reaction. The presence of **1** when [Pd(**2**)$_4$] was used as precursor also did not change the reaction rate significantly. This sandwich complex does not introduce much steric hindrance, and the catalytically active species remains unchanged. In contrast, the impact of **1** on [Pd(**4**)$_4$] is enormous. In the absence of **1** almost no activity was observed, whereas in presence of **1** the product was rapidly formed. The assembly of **1** on the pyridyl units of the phosphanes leads to the formation of a mono-phosphane complex, and this results in fast oxidative addition of iodobenzene and subsequent reaction with styrene.

The second reaction studied with an encapsulated catalyst was the rhodium-catalyzed hydroformylation of 1-octene (Table 1).[14] Zinc(II) porphyrin **1** does not interfere with the rhodium-catalyzed hydroformylation, since using triphenylphosphane **5** in the presence and absence of **1** gave the same results. The catalyst formed by ligand **3** hardly showed any change in rate or selectivity when **1** was added. This shows that two porphyrin units can be assembled to form a sandwich-type complex without changing the performance of the active catalyst. In contrast, the assembly of three porphyrin units with ligand **4** significantly altered the performance of the catalyst. At 80 °C the catalyst was almost twice as active, and the selectivity had changed (l:b = 1.5 vs 2.8). At room temperature there was an even larger difference between the porphyrin-encapsulated catalyst and the non-encapsulated analogue; the former gave a tenfold higher activity, and the branched product was now even the favored product (l:b = 0.6). The higher activity and isomerization rate in combination with a higher selectivity for the formation of the branched product indicate that the active catalyst is a mono-phosphane rhodium species.[18, 19] This is in accordance with a high-pressure IR spectroscopic study on the catalytically active species and an NMR spectroscopic study on the [Rh(**4**)$_2$(acac)] precursor, which showed only the presence of mono-phosphane complexes after the addition of **1**. These results clearly show that the performance of the rhodium catalyst can be regulated by the assembly of porphyrin building blocks with the pyridylphosphane rhodium complex.

Table 1. Hydroformylation of 1-octene with various rhodium catalyst assemblies.[a]



Ligand[b]	T [°C]	TOF[c]	l:b[d]	Isomers [%][e]
3	80	2.2×10^3	2.9	0.9
3+**1**	80	2.1×10^3	2.8	1.1
4	80	2.8×10^3	2.8	3.8
4+**1**	80	4.5×10^3	1.5	8.3
5	80	1.7×10^3	2.7	1.5
5+**1**	80	1.7×10^3	2.7	1.2
3	25	6	2.8	3.2
3+**1**	25	6	2.8	0.8
4	25	43	2.8	3.4
4+**1**	25	400	0.6	1.0
5	25	4	3.0	1.5
5+**1**	25	4	3.0	1.2

[a] [Rh(acac)(CO)$_2$] 0.084 mmol L^{-1}, $p = 20$ bar (CO:H$_2$ = 1:1); for detailed conditions, see Supporting Information. [b] P:Rh = 25, porphyrin:P = 3. [c] TOF = turnover frequency = (mol aldehyde) (mol Rh)$^{-1}$ h^{-1}; the reaction was stopped after 1 h. [d] l/b = linear/branched. [e] = Percentage isomerization.

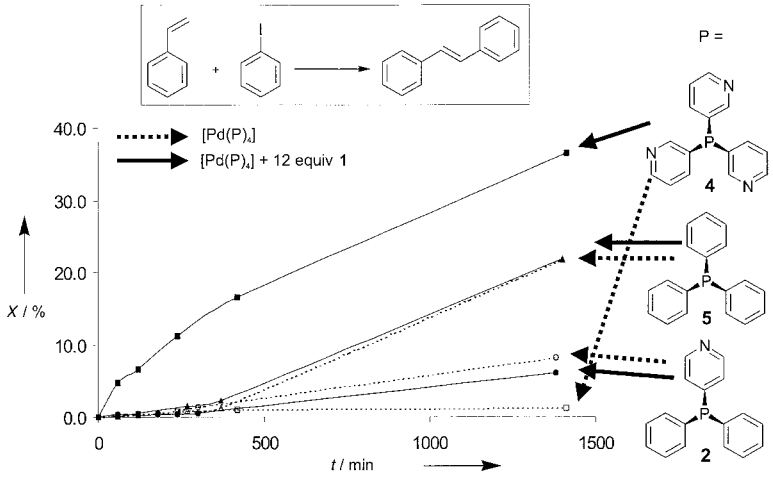


Figure 2. Conversion of styrene in the Heck reaction with various assembled palladium catalysts. The lines through the points are drawn for clarity. X = conversion.

In conclusion, we have shown that hemispherical assemblies that encapsulate well-defined transition metal catalysts can be prepared by using simple pyridylphosphane and porphyrin building blocks. The self-assembled structures are based on selective coordination of pyridyl groups to zinc porphyrins with a transition metal pyridylphosphane complex as the template. The catalytic performance of the encapsulated transition metal complex was differed significantly in selectivity and activity. So far we have only used porphyrin **1** and template ligands **2**–**4** to form the assemblies, but many other building blocks can be envisaged. This will lead to new nano-objects with interesting catalytic properties.

Received: July 12, 2001 [Z17492]

[1] a) D. J. Cram, *Science* **1983**, *219*, 1177–1183; b) J.-M. Lehn in *Supramolecular Chemistry: Concepts and Perspectives*, VCH, Weinheim, **1995**.
[2] a) J. Rebek, Jr., *Chem. Soc. Rev.* **1996**, *25*, 255–264; b) M. Morgan, J. Rebek, Jr., *Chem. Rev.* **1997**, *97*, 1647–1668.
[3] R. Wyler, J. de Mendoza, J. Rebek, Jr., *Angew. Chem.* **1993**, *105*, 1820–1821; *Angew. Chem. Int. Ed. Engl.* **1993**, *32*, 1699–1701.
[4] a) J. Rebek, Jr., *Chem. Commun.* **2000**, 637–643; b) M. Yanase, T. Haino, Y. Fukazawa, *Tetrahedron Lett.* **1999**, *40*, 2781–2784.
[5] a) N. Takeda, K. Umemoto, K. Yamaguchi, M. Fujita, *Nature* **1999**, *398*, 794–796; b) A. Jasat, J. C. Sherman, *Chem. Rev.* **1999**, *99*, 931–967; c) B. Olenyuk, J. A. Whiteford, A. Fechtenkötter, P. J. Stang, *Nature* **1999**, *398*, 796–799.

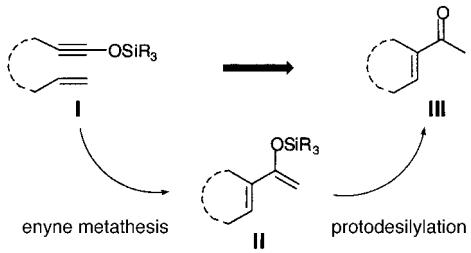
 © WILEY-VCH Verlag GmbH, D-69451 Weinheim, 2001 1433-7851/01/4022-4273 $ 17.50+.50/0

[6] a) L. R. MacGillivray, J. L. Atwood, *Angew. Chem.* **1999**, *111*, 1080–1096; *Angew. Chem. Int. Ed.* **1999**, *38*, 1018–1033; b) C. J. Jones, *Chem. Soc. Rev.* **1998**, *27*, 289–299.
[7] a) J. N. H. Reek, A. P. H. J. Schenning, A. W. Bosman, E. W. Meijer, M. J. Crossley, *Chem. Commun.* **1998**, 11–12; b) R. A. Haycock, A. Yartsev, U. Michelsen, V. Sundström, C. A. Hunter, *Angew. Chem.* **2000**, *112*, 3762–3765; *Angew. Chem. Int. Ed.* **2000**, *39*, 3616–3619.
[8] a) J. M. Kang, J. Santamaria, G. Hilmersson, J. Rebek, Jr., *J. Am. Chem. Soc.* **1998**, *120*, 7389–7390; b) J. M. Kang, J. Rebek, Jr., *Nature* **1997**, *385*, 50–52.
[9] a) M. Fujita, N. Fujita, K. Ogura, K. Yamaguchi, *Nature* **1999**, *400*, 52–55 (6739); b) L. G. Mackay, R. S. Wylie, J. K. M. Sanders, *J. Am. Chem. Soc.* **1994**, *116*, 3141.
[10] a) T. Imamura, K. Fukushima, *Coord. Chem. Rev.* **2000**, *198*, 133–156; b) J. Wojaczynski, L. Latos-Grazynski, *Coord. Chem. Rev.* **2000**, *204*, 113–171.
[11] C. H. Lee, J. S. Lindsey, *Tetrahedron* **1994**, *50*, 11427.
[12] a) R. J. Bowen, A. C. Garner, S. J. Berners-Price, I. D. Jenkins, R. E. Sue, *J. Organomet. Chem.* **1998**, *554*, 181–184; b) A. Buhling, P. C. J. Kamer, P. W. N. M. van Leeuwen, *J. Mol. Catal. A* **1995**, *98*, 69–80; c) G. R. Newkome, *Chem. Rev.* **1993**, *93*, 2067–2089.
[13] I. P. Beletskaya, A. V. Cheprakov, *Chem. Rev.* **2000**, *100*, 3009–3066.
[14] P. W. N. M. van Leeuwen, C. Claver in *Rhodium Catalyzed Hydroformylation*, Kluwer Academic, Dordrecht, **2000**.
[15] a) U. Michelsen, C. A. Hunter, *Angew. Chem.* **2000**, *112*, 780–783; *Angew. Chem. Int. Ed.* **2000**, *39*, 764–767; b) G. Szintay, A. Horvath, *Inorg. Chim. Acta* **2000**, *310*, 175–182.
[16] P. N. Taylor, H. L. Anderson, *J. Am. Chem. Soc.* **1999**, *121*, 11538–11545.
[17] Synthesized by using a procedure similar to J. E. Bäckvall, J. E. Nyström, R. E. Nordberg, *J. Am. Chem. Soc.* **1985**, *107*, 3676–3686.
[18] B. Breit, *Chem. Commun.* **1996**, 2071–2072.
[19] B. Breit, R. Winde, K. Harms, *J. Chem. Soc. Perkin Trans. 1* **1997**, 2681–2682.

Siloxyalkyne–Alkene Metathesis: Rapid Access to Highly Functionalized Enones**

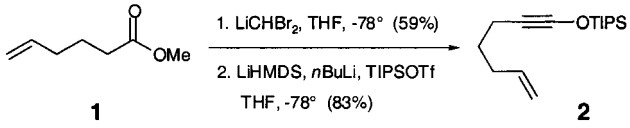
Michael P. Schramm, D. Srinivasa Reddy, and Sergey A. Kozmin*

The advent of structurally defined metal alkylidenes capable of promoting π-bond metathesis under mild conditions, with high efficiency and functional group compatibility, has had a profound effect on modern organic synthesis.[1] Among a range of synthetically useful transformations, the enyne metathesis is particularly noteworthy for the ability to assemble two carbon–carbon bonds in a single step starting from appropriate alkyne and alkene components.[2] However, elaboration of the full synthetic potential of this process has been limited largely to the use of simple, unactivated enyne precursors.[3] We report here a mechanistically intriguing example of the participation of siloxyalkynes in the intramolecular Ru-catalyzed metathesis with terminal alkenes, which resulted in the development of a new method for the synthesis of highly functionalized enones **III** starting from readily accessible acyclic precursors **I** (Scheme 1).[4] Furthermore, this approach represents a novel method for the construction of silyldienol ethers **II** starting directly from enyne **I**, conceptually different from the conventional enol silylation of carbonyl compounds.



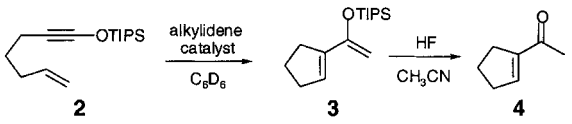
Scheme 1. Projected outcome of the siloxyalkyne–alkene metathesis.

Our studies began with the preparation of a model cyclization substrate **2** (Scheme 2). Construction of siloxyalkyne **2** was accomplished according to a modified Kowalski protocol[5] entailing the initial conversion of ester **1** to the corresponding dibromoketone, followed by generation of the ynolate anion (LHMDS, *n*BuLi) and silylation with TIPSOTf to afford enyne **2**.



Scheme 2. Preparation of siloxyalkyne **2**. LiHMDS = lithium bis(trimethylsilyl)amide, TIPSOTf = triisopropyl trifluoromethanesulfonate.

We next systematically examined several olefin metathesis catalysts in order to achieve the desired conversion of siloxyalkyne **2** to the corresponding diene **3** [Eq. (1)]. Following the unsuccessful attempts to employ either the



(1)

original Grubbs Ru-complex **5**[6] or the Schrock Mo-catalyst **6**[7] (Table 1, entries 1 and 2), we turned our attention to the recently developed Ru-complexes bearing highly nucleophilic imidazolylidene ligands.[8] To our delight, both **7**[9] and **8**[10] were found to promote the desired transformation, nevertheless they displayed a noticeable difference in reactivity.[11] The reaction proceeded to completion in the presence of **8** (5 mol%) over a period of 13 h at 20 °C, and within minutes at 60 °C (entries 4, 5). The cyclization employing complex **7** was

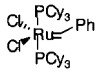
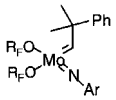
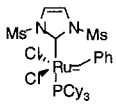
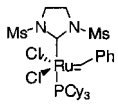
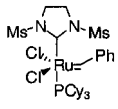
[*] Prof. Dr. S. A. Kozmin, M. P. Schramm, D. S. Reddy
Department of Chemistry
University of Chicago
5735 South Ellis Avenue
Chicago, IL 60637 (USA)
Fax: (+1) 773-702-0805
E-mail: skozmin@uchicago.edu

[**] This work was supported by the University of Chicago. M.P.S. is a recipient of the NIH predoctoral training grant.

Supporting information for this article is available on the WWW under http://www.angewandte.com or from the author.

 © WILEY-VCH Verlag GmbH, D-69451 Weinheim, 2001 1433-7851/01/4022-4274 $ 17.50+.50/0

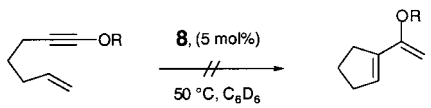
Table 1. Siloxyalkyne – alkene metathesis: initial catalyst evaluation.

Entry	Catalyst[a]	mol %	Conditions	Conv. [%]
1	 **5**	10	60 °C, 6 h	< 5
2	 **6**	10	60 °C, 12 h	< 5
3	 **7**	5	60 °C, 12 h	85
4	 **8**	5	20 °C, 13 h	95
5	 **8**	5	60 °C, 15 min	98

[a] Cy = cyclohexyl, Ar = 2,6-diisoprophylphenyl, $OR_F = OCMe(CF_3)_2$, Ms = methanesulfonyl.

considerably slower requiring 12 h at 60 °C to reach 85 % conversion (entry 3); no reaction was observed at 20 °C. Treatment of the crude reaction mixture (entry 5) with a dilute solution of HF gave acetylcyclopentene **4** as a sole reaction product.

Interestingly, subjection of either ethoxyalkyne **9**[12] or alkynyl phosphate **10**[13] to catalyst **8** did not lead to any detectable amounts of the corresponding diene even under forcing conditions (Scheme 3). This result is particularly intriguing since Clark and co-workers demonstrated that alkynyl ethers with an internal oxygen tether were found to undergo Ru-catalyzed enyne metathesis with good efficiency.[4b]

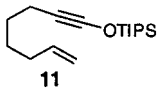
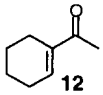
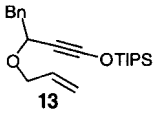
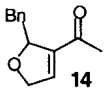
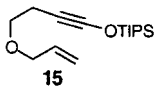
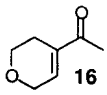
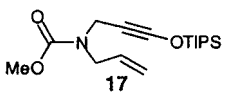
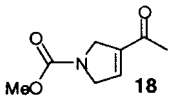
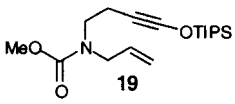
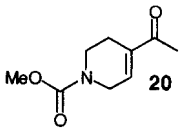
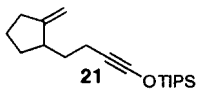
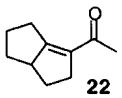
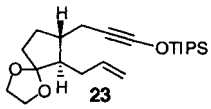
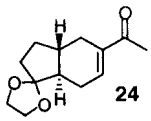
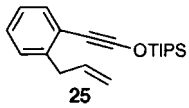
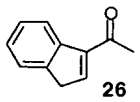
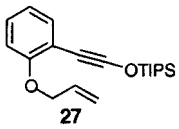
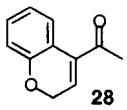
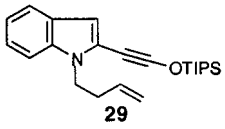
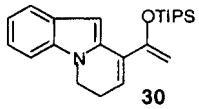


9: R = Et
10: R = P(O)(OEt)$_2$

Scheme 3. Unsuccessful enyne metatheses of alkynyl ether **9** and alkynyl phosphate **10**.

Having established a functional protocol, we next examined the scope of this process (Table 2). All of the siloxyalkynes used in this study were prepared according to the Kowalski protocol,[5] which illustrates the generality of this method. Formation of acetyl cyclohexene **12** proceeded with comparable efficiency (81 % yield, entry 1). Ether and carbamate functional groups were found compatible and afforded the corresponding five- and six-membered heterocycles (entries 2 – 5). The alkyl substitution at the position directly adjacent to the alkyne was well tolerated (86 % yield, entry 2).

Table 2. Siloxyalkyne – alkene metathesis: substrate scope.[a]

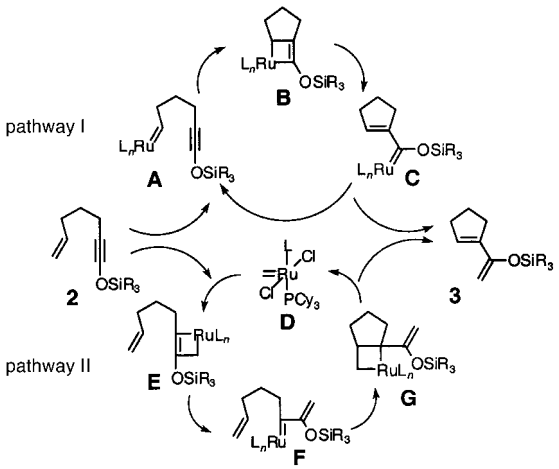
Entry	Siloxyalkyne	Product	Yield [%]
1	 **11**	 **12**	81
2	 **13**	 **14**	86
3	 **15**	 **16**	88
4	 **17**	 **18**	91
5	 **19**	 **20**	95
6	 **21**	 **22**	50[b]
7	 **23**	 **24**	68[c]
8	 **25**	 **26**	88
9	 **27**	 **28**	80
10	 **29**	 **30**	92

[a] General procedure: A solution of the respective siloxyalkyne in benzene (0.1 M) was treated with catalyst **8** (3 – 10 mol %), and warmed to 50 – 60 °C. Upon disappearance of the starting material (15 – 60 min), the reaction mixture was concentrated, treated with 1.0 M solution of HF in MeCN (1.5 – 2 equiv) for 30 min, and purified by chromatography on silica gel. [b] The catalyst loading was 20 mol %. [c] Protodesilylation was conducted by using tetrabutylammonium fluoride to prevent the acetal hydrolysis.

Notably, the siloxyalkyne – alkene metathesis provides a powerful alternative to the existing methods for the preparation of cyclic enones, as this approach avoids the potential β-elimination or regioselectivity problems associated with intramolecular aldol condensation or with Friedel – Crafts acylation. Furthermore, this process offered rapid access to a variety of bicyclic ring systems, that is, diquinane **22**[14] and hydrindane **24**. Arene-conjugated siloxyalkynes **25** and **27** successfully underwent enyne reorganization to yield indene **26** and benzopyran **28**, respectively. In addition, cyclization of the indole-containing siloxyalkyne **29** afforded the tricyclic

diene **30** in 92% yield. Interestingly, multiple attempts to protodesilylate diene **30** proved unsuccessful, presumably because of the instability of the corresponding enone, which suggests the difficulty in the preparation of this siloxydiene by conventional enol silylation approach. The above data collectively illustrate that the siloxyalkyne–alkene metathesis offers a mild and efficient method for the assembly of a wide range of highly functionalized enones representing valuable synthetic intermediates.

Apart from the preparative utility of siloxyalkyne–alkene metathesis, this process raises several mechanistically relevant issues. Whereas bond reorganization of enyne **2** (see Scheme 4) exhibits strong thermodynamic preference for the



Scheme 4. Proposed mechanism of siloxyalkyne–alkene metathesis.

conversion to silyldienol ether **3**,[15] the formation of the observed product is less apparent from a mechanistic standpoint, as two alternative catalytic cycles can be postulated.[16] Among the two pathways, we strongly favor pathway I that involves initial formation of Ru-alkylidene **A**, [2+2] annulation to give metallacyclobutene **B**, and structural reorganization to afford vinyl carbene **C**. Transfer of the methylene unit from substrate **2** results in the formation of diene **3** and regeneration of alkylidene **A**. Although pathway II can not be ruled out entirely at this point, the dominance of pathway I was strongly supported by several NMR experiments. These involved the competition between siloxyalkyne **31** and terminal alkene **32** in the presence of a stoichiometric amount of Ru-benzylidene **8** ($\delta = 19.61$, Figure 1A). Addition of **8** to a solution of alkyne **31** resulted in no reaction after 30 min at 57 °C (Figure 1B). On the other hand, treatment of benzylidene **8** with alkene **32** at 57 °C immediately afforded a new signal corresponding to the Ru-alkylidene ($\delta = 18.35$, Figure 1C).[17] Finally, mixing of the three components **8**, **32**, and **31** (Figure 1D) led to the disappearance of the benzylidene resonance with a concomitant formation of the alkylidene signal; the siloxyalkyne remained unchanged. While this experiment clearly indicated a more facile reaction of benzylidene **8** with terminal alkene component of the enyne **2**, a starting point in pathway I, the intermediacy of a stabilized siloxycarbene **C** (Scheme 4) is less apparent, as this carbene would be expected to display a decreased metathesis reactivity due to the electron-donating nature of the siloxy substituent. We believe, however, that the activating nature of the perhydroimidazolylidene ligand combined with the overall thermodynamically favored release of diene **4**[15] overrides the unfavorable electronic effect of the siloxy group and results in productive catalytic turnover.

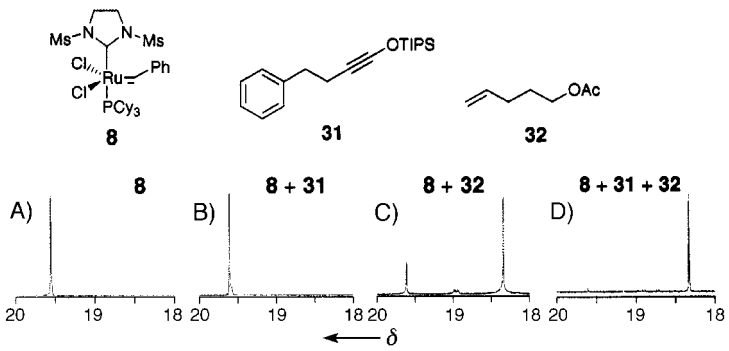


Figure 1. ^{1}H NMR (400 MHz) competition experiments carried out in [D_6]benzene with stoichiometric quantities of reaction partners.

In closing, we have demonstrated the first example of an efficient participation of siloxyalkynes in the intramolecular metathesis with terminal alkenes. This process resulted in the development of a simple and efficient approach to highly functionalized enones starting from readily accessible acyclic precursors. It further expands the synthetic potential of the enyne metathesis. Additional studies on the mechanism and utility of this technology for the construction of highly diverse chemical libraries are in progress and will be reported in due course.

Received: July 23, 2001 [Z17553]

[1] a) T. M. Trinka, R. H. Grubbs, *Acc. Chem. Res.* **2001**, *34*, 18–29; b) R. R. Schrock, *Tetrahedron* **1999**, *55*, 8141–8153; c) R. H. Grubbs, S. Chang, *Tetrahedron* **1998**, *54*, 4413–4450; d) A. Fürstner, *Angew. Chem.* **2000**, *112*, 3140–3172; *Angew. Chem. Int. Ed.* **2000**, *39*, 3012–3043.

[2] For representative examples, see: a) T. J. Katz, T. M. Sivavec, *J. Am. Cem. Soc.* **1985**, *107*, 737–739; b) B. M. Trost, G. J. Tanoury, *J. Am. Chem. Soc.* **1991**, *110*, 1636–1638; d) S.-H. Kim, N. Bowden, R. H. Grubbs, *J. Am. Chem. Soc.* **1994**, *116*, 10801–10802; e) N. Chatani, T. Morimto, T. Muto, S. Murai, *J. Am. Chem. Soc.* **1994**, *116*, 6049–6050; f) A. Kinoshita, N. Sakaibara, M. Mori, *J. Am. Chem. Soc.* **1997**, *119*, 12388–12389; g) W. J. Zuercher, M. Scholl, R. H. Grubbs, *J. Org. Chem.* **1998**, *63*, 4291–4298; h) A. Fürstner, H. Szillat, B. Gabor, R. Mynott, *J. Am. Chem. Soc.* **1998**, *120*, 8305–8314; i) R. Stragies, U. Voigtmann, S. Blechert, *Tetrahedron Lett.* **2000**, *41*, 5465–5468; j) J. Renaud, C.-D. Graf, L. Oberer, *Angew. Chem.* **2000**, *112*, 3231–3234; *Angew. Chem. Int. Ed.* **2000**, *39*, 3101–3104.

[3] For a review, see: M. Mori, *Top. Organomet. Chem.* **1998**, *1*, 133–154.

[4] For participation of enol ethers, see: a) S. Watanuki, N. Ochifigi, M. Mori, *Organometallics* **1995**, *14*, 5062–5067. For enyne metathesis involving ynol ethers with internal oxygen tether, see: b) J. S. Clark, G. P. Trevitt, D. Boyall, B. Stammen, *Chem. Commun.* **1998**, 2629–2630.

[5] C. J. Kowalski, M. S. Haque, K. W. Fields, *J. Am. Chem. Soc.* **1985**, *107*, 1429–1430. For a preparative modification of the original procedure, see: A. B. Smith III, S. A. Kozmin, D. V. Paone, *J. Am. Chem. Soc.* **2000**, *122*, 4984–4985.

[6] S. T. Nguyen, L. K. Johnson, R. H. Grubbs, J. W. Ziller, *J. Am. Chem. Soc.* **1992**, *114*, 3974–3975.

[7] R. R. Schrock, J. S. Murdzek, G. C. Bazan, J. Robbins, M. DiMare, M. O'Regan, *J. Am. Chem. Soc.* **1990**, *112*, 3875–3886.

[8] W. A. Herrmann, C. Köcher, *Angew. Chem.* **1997**, *109*, 2256–2282; *Angew. Chem. Int. Ed. Engl.* **1997**, *36*, 2162–2187.

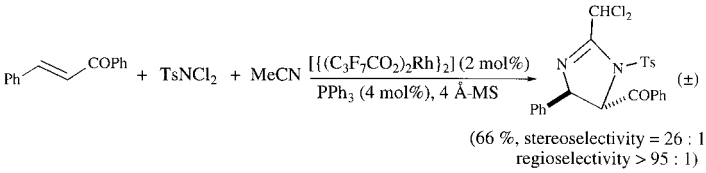
 © WILEY-VCH Verlag GmbH, D-69451 Weinheim, 2001 1433-7851/01/4022-4276 $ 17.50+.50/0

[9] a) M. Scholl, T. M. Trnka, J. P. Morgan, R. H. Grubbs, *Tetrahedron Lett.* **1999**, *40*, 2247 – 2250; b) J. P. Huang, E. D. Stevens, S. P. Nolan, J. L. Petersen, *J. Am. Chem. Soc.* **1999**, *121*, 2674 – 2678.
[10] M. Scholl, S. Ding, C. W. Lee, R. H. Grubbs, *Org. Lett.* **1999**, *1*, 953 – 956.
[11] For a recent account on the reactivity of various imidazolylidene-substituted Ru-complexes in the ring-closing olefin metathesis and enyne metathesis, see: A. Fürstner, L. Ackermann, B. Gabor, R. Goddard, C. W. Lehmann, R. Mynott, F. Stelzer, O. R. Thiel, *Chem. Eur. J.* **2001**, *7*, 3236 – 3253.
[12] Alkyne **9** was prepared by alkylation of ethoxyacetylene with 5-bromo-1-pentene (*n*BuLi, THF, – 78 °C; 76 % yield).
[13] For preparation of alkynyl phosphates, see: a) P. J. Stang, *Acc. Chem. Res.* **1991**, *24*, 304 – 310; b) V. V. Zhdankin, P. J. Stang, *Tetrahedron Lett.* **1993**, *34*, 1461 – 1462.
[14] For an alternative synthesis of **22**, see: L. A. Paquette, G. J. Wells, K. A. Horn, T.-H. Yan, *Tetrahedron* **1983**, *39*, 913 – 924.
[15] DFT calculations (pBP/DN*; MacSpartan Pro 1.0.2) indicated that diene **3** was 44 kcal mol^{-1} lower in energy than the starting enyne precursor **2**.
[16] Previously, depending on the substitution pattern of the enyne precursor, either pathway I[16b,c] or pathway II[16a,d] were postulated to operate: a) A. Kinoshita, M. Mori, *Synlett* **1994**, 1020 – 1022; b) S.-H. Kim, W. J. Zuercher, N. B. Bowden, R. H. Grubbs, *J. Org. Chem.* **1996**, *61*, 1073 – 1081; c) T. R. Hoye, S. M. Donaldson, T. J. Vos, *Org. Lett.* **1999**, *1*, 277 – 279; d) T. Kitamura, Y. Sato, M. Mori, *Chem. Commun.* **2001**, 1258 – 1259.
[17] This outcome is fully consistent with prior results reported by Grubbs and co-workers: P. Schwab, R. H. Grubbs, J. W. Ziller, *J. Am. Chem. Soc.* **1996**, *118*, 100 – 110.

A Novel Electrophilic Diamination Reaction of Alkenes**

Guigen Li,* Han-Xun Wei, Sun Hee Kim, and Michael D. Carducci

Electrophilic addition reactions of olefins have been of fundamental importance in organic chemistry[1] because these reactions can convert inexpensive petroleum alkenes into chemically and biologically useful compounds. At present, olefinic additions involving three or more components in a single operation are rare,[2, 3] which is probably because of the fact that only a few electrophilic addition intermediates enable multistep transformations.[4, 5] Recently, we developed several new eletrophilic addition reactions, aminohalogenation, and α,β-differentiated diamination reactions by using *N*-halogenosulfonamides as the electrophiles.[6, 7] The regio- and stereochemical features of the resulting haloamine and diamine products have unambiguously proven the formation of *N*-(*p*-tosyl),*N*-haloaziridinium or *N*-(*o*-nosyl),*N*-haloaziridinium species during the reaction processes. In our continuing research on this topic we have now discovered a novel three-component reaction (Scheme 1) which provides access to imidazolines[8] and α,β-diamino derivatives.[9, 10]



Scheme 1. Chalcone-based electrophilic diamination reaction.

The current study was initiated by attempts to render the parent version of the aminohalogenation reaction asymmetric and catalytic.[6] Unfortunately, the success of this effort has been seriously limited thus far. For most of the cases we examined the reaction was either significantly deactivated or poor enantiomeric excesses resulted when chiral amine ligands were employed together with copper or zinc ions. Therefore, the search for other metal alternatives or metal – ligand complexes became necessary. When rhodium compounds were examined[11] (for example, rhodium(II) acetate dimer, rhodium(II) trifluoroacetate dimer, and rhodium(II) heptafluorobutyrate dimer) the reaction of methyl cinnamate with $TsNCl_2$ (Ts = tosyl = toluene-4-sulfonyl) led to the formation of complexes and a major side product. This side product was isolated in a yield varying between 18 – 25 % when the above catalysts were employed, although the haloamine product was generated predominantly. The subsequent X-ray structural analysis revealed that this new side product is essentially a multifuctionalized imidazoline derivative (Figure 1).

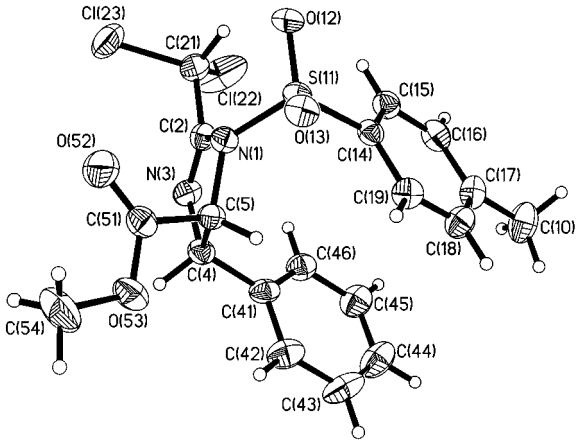


Figure 1. X-ray structure of 1-*p*-toluenesulfonyl-2-dichloromethyl-4-phenyl-5-methyloxycarbonylimidazoline.

[*] Prof. Dr. G. Li, Dr. H.-X. Wei, S. H. Kim
Department of Chemistry and Biochemistry
Texas Tech University, Lubbock, TX 79409-1061 (USA)
Fax: (+1) 806) 742-1289
E-mail: qeggl@ttu.edu
Dr. M. D. Carducci[+]
Department of Chemistry
University of Arizona, Tucson, AZ 85721 (USA)
[+] To whom X-ray analysis data should be addressed.

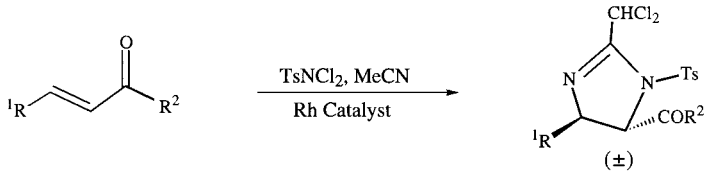
[**] We gratefully acknowledge the National Institutes of Health (GM-R15-60261), the Robert A. Welch Foundation (D-1361) for their generous support, and the National Science Foundation for their partial support of the NMR facility. We thank Mr. Subramanian Karur and Mr. Jason D. Hook for their assistance. The preliminary results of this work have been presented at the 221st ACS National Meeting, San Diego, CA, April 2001.

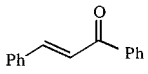
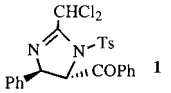
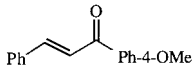
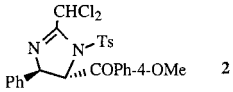
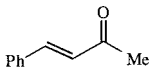
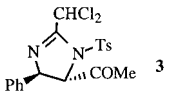
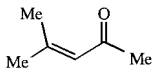
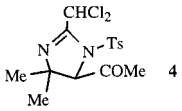
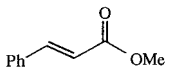
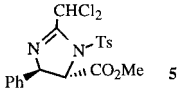
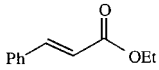
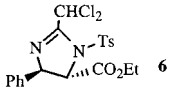
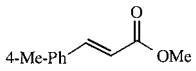
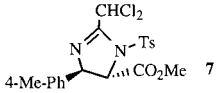
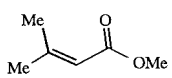
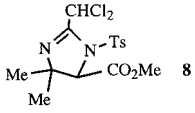
 © WILEY-VCH Verlag GmbH, D-69451 Weinheim, 2001 1433-7851/01/4022-4277 $ 17.50+.50/0

Encouraged by the importance of imidazolines and their imidazole derivatives, as well as diamino acids, for biomedical research,[8–10] we sought to make this side reaction the main reaciton. Of the above rhodium compounds the rhodium(II) heptafluorobutyrate dimer proved to be the catalyst which best favored formation of the imidazoline, and was thus chosen as the lead candidate for examining the effects of the reaction conditions. The model reaction was again based on the use of methyl cinnamate as the substrate (entry 5 of Table 1). Molecular sieves (4 Å) were initially found to increase the formation of imidazolines, as revealed by crude ^{1}H NMR spectroscopic analysis or thin-layer chromatography. In fact, the yield of the imidazoline product increased to nearly 35 % in the presence of 4-Å molecular sieves. Next, our attention was turned to employing ligands that would coordinate with the rhodium(II) center so as to change the catalytic reactivity of the rhodium(II) heptafluorobutyrate dimer. It was found that the Ph_3P–rhodium(II) complex generated by treating 2.0 mol % of the rhodium(II) heptafluorobutyrate dimer with 4.0 mol % of triphenylphosphane can completely inhibit the formation of haloamines. Concurrently, the yield of the imidazoline product rose to 45 %, and then to 51 % when the *N*,*N*-dichloro-*p*-toluenesulfonamide was added to the reaction system in two portions.[12]

Similar to our previous aminohalogenation systems, this reaction is also very easy to perform. Essentially, it can be conducted at room temperature in any convenient vessel of appropriate size, without the need of inert atmosphere protection. Although α,β-unsaturated esters were initially utilized and resulted in successful examples, most of these substrates did not perform as well as the α,β-unsaturated ketones in this system as shown by the low yields (45 %–51 %) realized (entries 5–7). Only in the aliphatic ester case (entry 8) was a good yield (69 %) obtained. However, the yields and selectivities were improved when α,β-unsaturated ketones were used as the substrates. Both aromatic and aliphatic ketones worked well (66–82 % for entries 1–4). Interestingly, the terminal disubstituted substrates (entries 4 and 8) resulted in the highest yields (82 and 69 %, respectively) for both ketone and ester substrate categories. No minor regioisomers were observed in the eight cases exam-

Table 1. PPh_3-[{$(C_3F_7CO_2)_2Rh$}$_2$]-catalyzed cyclic diamination.



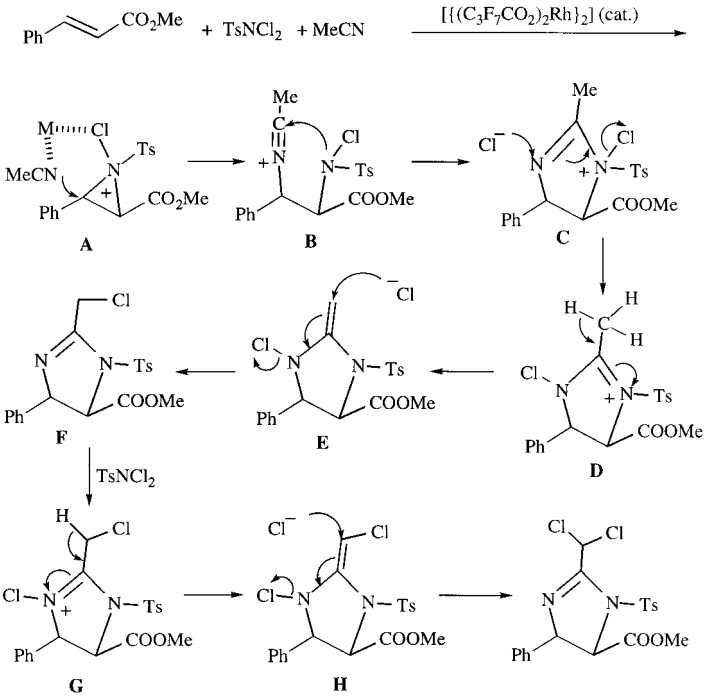
Entry	Substrates	Product (±)	m.p. [°C]	Stereoselectivty (*anti*:*syn*)[a]	yield [%][b]
1		 **1**	130–131	26:1	66
2		 **2**	58–59	40:1	68
3		 **3**	oil	50:1	66
4		 **4**	oil	–	82
5		 **5**	126–127	20:1	51
6		 **6**	102–104	25:1	49
7		 **7**	oil	25:1	45
8		 **8**	134–136	–	69

[a] Estimated by crude ^{1}H NMR determination. [b] Yields after purification by column chromatography.

 © WILEY-VCH Verlag GmbH, D-69451 Weinheim, 2001 1433-7851/01/4022-4278 $ 17.50+.50/0

ined. The diastereoselectivity is good to excellent (*syn*:*anti* = 20:1 – 50:1).

Scheme 2 outlines the mechanistic proposal for the reaction. The first step is the electrophilic addition to form the *N*-(*p*-tosyl),*N*-chloroaziridinium intermediate (**A**).[13, 14] Rhodium, as well as zinc and copper, can catalyze this transformation. The Ritter-type nucleophilic attack by MeCN that

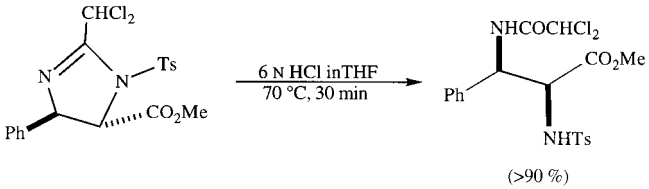


Scheme 2. Possible mechanism of diamination.

effects ring opening gives nitrilium intermediate (**B**). Since the *anti* configuration of methyl cinnamate is retained in the product, the opening of the aziridinium ring by acetonitrile clearly proceeds in a *syn* manner. It seems that the coordination of MeCN to the rhodium center occurs prior to the aziridinium ring opening. The Lewis basic moieties used in this coordination could be either the *N*-chlorine atom or the sulfonyl oxygen atom of the Ts group. The cyclization of intermediate **B** gives rise to the 1*N*-(*p*-tosyl),1*N*-chloroimidazolinium **C**, which then undergoes a 1,3-displacement of the 1*N*-chlorine atom to give 1*N*-(*p*-tosyl),3*N*-chloroimidazolinium **D**. Deprotonation of the 2-methyl group of **D** gives the methylene scaffold **E**, which enables the second S_N2'-type displacement to afford **F**. Chlorination of the 3*N* site of intermediate **F**, which gives rise to **G**, is followed by the second deprotonation of the 2-methyl group to yield **H**. At the final step, the third 1,3-displacement of chlorine results in 1-*p*-toluenesulfonyl-2-dichloromethyl-4-phenyl-5-methyloxycarbonylimidazoline.

The above mechanistic hypothesis can also account for the fact that at least two equivalents of $TsNCl_2$ are needed for the complete conversion. To further confirm the nucleophilic mechanism of forming the 2-dichloromethyl group on the imidazoline ring, the reaction (entry 1 of Table 1) was carried out in carefully degassed acetonitrile in the absence of light. The reaction rate, the yield, and stereochemical outcomes are almost the same as those obtained under normal conditions. The careful analysis of the resulting products also revealed that no chlorination occurs at the 4- and/or 5-positions of the imidazoline ring, hence a possible radical pathway can be ruled out.

Our current investigation has been extended to examine the hydrolysis of 1-*p*-toluenesulfonyl-2-dichloromethyl-4-phenyl-5-methyloxycarbonylimidazoline by treating it with a 6 N HCl solution in THF to give the α,β-differentiated diamino ester *syn*-methyl N^{α}-(4-Ts),N^{β}-dichloroacetyl diaminophenylpropionate (Scheme 3). Other synthetic properties, such as the functionalization of the $CHCl_2$ group and olefination to give 4,5-multifunctionalized imidazoles, will be studied in the future.



Scheme 3. Transformation of imidazoline to α,β-differentiated diamine.

Experimental Section

Triphenylphosphane (5.60 mg, 0.021 mmol), rhodium(II) heptafluorobutyrate dimer (10.9 mg, 0.010 mmol), and freshly distilled acetonitrile (2.50 mL) were added into a dry vial. The mixture was stirred at room temperature for 40 min before 4-Å molecular sieves (200 mg, predried in the oven at 200 °C overnight) were added. The resulting mixture was stirred for 10 min and loaded with chalcone (106 mg, 0.50 mmol; entry 1 of Table 1) and the first portion of *N*,*N*-dichloro-*p*-tolunesulfonamide (60 mg, 0.25 mmol). Stirring was continued for 4 h at RT and followed by the addition of the second portion of *N*,*N*-dichloro-*p*-toluenesulfonamide (240 mg, 1.0 mmol). The resulting light yellow slurry was stirred at RT for 40 h in the capped vial without argon protection. The 4-Å molecular sieves and other solid precipitates were filtered off and washed with EtOAc (3 × 5 mL). The organic solution was directly concentrated without quenching, purified by flash chromatography (with hexane and EtOAc (v/v = 5/1) as the eluent) to give **1** (0.162 g, 66 %) as a colorless solid. m.p. 130 – 131 °C. ^{1}H NMR (300 MHZ, $CDCl_3$): δ = 7.80 – 7.74 (m, 4H), 7.64 – 7.61 (m, 1H), 7.49 – 7.44 (m, 2H), 7.32 – 7.23 (m, 6H), 6.90 (dd, J = 1.4, 8.0 Hz, 2H), 5.56 (d, J = 4.9 Hz, 1H), 5.01 (d, J = 4.9 Hz, 1H), 2.45 (s, 3H); ^{13}C NMR (75 MHz, $CDCl_3$): δ = 193.3, 156.7, 145.7, 138.7, 134.4, 134.3, 133.5, 130.1, 129.0(2), 128.8, 128.7, 128.0, 126.6, 72.3, 71.9, 61.4, 21.7; HR-MS (matrix-assisted laser desorption/ionization (MALDI) FT-MS): m/z [M^++1] found: 487.0644, calcd for $C_{24}H_{20}O_3N_2SCl_2$: 487.0644.

2: ^{1}H NMR (300 MHz, $CDCl_3$): δ = 7.78 (d, J = 8.6 Hz, 2H), 7.74 (d, J = 8.8 Hz, 2H), 7.22 (s, 1H), 6.92 (dd, J = 2.0, 6.8 Hz, 4H), 5.53 (d, J = 5.0 Hz, 1H), 5.01 (d, J = 5.0 Hz, 1H), 3.88 (s, 3H), 2.45 (s, 3H); ^{13}C NMR (75 MHz, $CDCl_3$): δ = 191.7, 164.5, 156.7, 145.6, 138.8, 134.5, 131.2, 130.0, 129.0, 128.6, 128.0, 126.6, 126.4, 114.2, 72.6, 71.5, 61.5, 55.6, 21.7; HR-MS (MALDI-FTMS): m/z [M^++1] found: 517.0768, calcd for $C_{25}H_{22}O_4N_2SCl_2$: 517.0750.

3: ^{1}H NMR (300 MHz, $CDCl_3$): δ = 7.55 (d, J = 8.4 Hz, 2H), 7.32 (s, 1H), 7.18 – 7.14 (m, 3H), 7.10 – 7.08 (m, 2H), 6.69 (d, J = 8.4 Hz, 2H), 5.14 (d, J = 4.3 Hz, 1H), 4.28 (d, J = 4.3 Hz, 1H), 2.40 (s, 3H), 2.39 (s, 3H); ^{13}C NMR (75 MHz, $CDCl_3$) δ 206.0, 156.8, 146.0, 139.6, 132.6, 130.3, 128.6, 127.5, 127.4, 125.6, 75.5, 71.5, 61.8, 26.6, 21.6; HR-MS (MALDI-FTMS): m/z [M^++1] found: 425.0500, calcd for $C_{19}H_{18}O_3N_2SCl_2$: 425.0488.

4: ^{1}H NMR (300 MHz, $CDCl_3$): δ = 7.75 (d, J = 8.5 Hz, 2H), 7.41 (d, J = 8.5 Hz, 2H), 7.21 (s, 1H), 3.99 (s, 1H), 2.47 (s, 3H), 2.23 (s, 3H), 1.21 (s, 3H), 0.89 (s, 3H); ^{13}C NMR (75 MHz, $CDCl_3$): δ = 205.5, 153.5, 146.1,

133.2, 130.4, 127.6, 70.4, 61.7, 30.7, 27.8, 23.2, 21.7; HR-MS (MALDI-FTMS): m/z [M^++1] found: 337.0484, calcd for $C_{15}H_{18}O_3N_2SCl_2$: 337.0488.

5: ^{1}H NMR (300 MHz, $CDCl_3$): $\delta = 7.69$ (d, $J = 8.4$ Hz, 2H), 7.26 – 7.18 (m, 6H), 6.88 (d, $J = 8.4$ Hz, 2H), 5.21 (d, $J = 4.4$ Hz, 1H), 4.56 (d, $J = 4.4$ Hz, 1H), 3.81 (s, 3H), 2.42 (s, 3H); ^{13}C NMR (75 MHz, $CDCl_3$): $\delta = 169.7$, 156.6, 145.7, 139.2, 133.8, 130.1, 128.8, 128.0, 127.7, 125.8, 72.0, 69.2, 61.4, 53.1, 21.6; HR-MS (MALDI-FTMS): m/z [M^++1] found: 441.0446, calcd for $C_{19}H_{18}O_4N_2SCl_2$: 441.0437.

6: ^{1}H NMR (300 MHz, $CDCl_3$): $\delta = 7.70$ (d, $J = 8.4$ Hz, 2H), 7.26 – 7.19 (m, 6H), 6.90 (d, $J = 8.4$ Hz, 2H), 5.20 (d, $J = 4.3$ Hz, 1H), 4.55 (d, $J = 4.3$ Hz, 1H), 4.23 (q, $J = 7.1$ Hz, 2H), 2.42 (s, 3H), 1.29 (t, $J = 7.1$ Hz, 3H); ^{13}C NMR (75 MHz, $CDCl_3$): $\delta = 169.3$, 156.6, 145.7, 139.3, 133.9, 130.0, 128.8, 128.0, 127.7, 125.8, 72.1, 69.3, 62.3, 61.5, 21.6, 14.0; HR-MS (MALDI-FTMS): m/z [M^++1] found: 455.0587, calcd for $C_{20}H_{20}O_4N_2SCl_2$: 455.0594.

7: ^{1}H NMR (300 MHz, $CDCl_3$): $\delta = 7.70$ (dd, $J = 1.8$, 6.6 Hz, 2H), 7.27 – 7.24 (m, 2H), 7.18 (s, 1H), 6.90 (d, $J = 8.2$ Hz, 2H), 6.77 (d, $J = 8.0$ Hz, 2H), 5.17 (d, $J = 4.4$ Hz, 1H), 4.54 (d, $J = 4.4$ Hz, 1H), 3.79 (s, 3H), 2.43 (s, 3H), 2.30 (s, 3H); ^{13}C NMR (75 MHz, $CDCl_3$): $\delta = 169.8$, 156.4, 145.7, 137.9, 136.3, 133.9, 130.0, 129.4, 127.7, 125.7, 71.9, 69.2, 61.4, 53.1, 21.6, 21.1; HR-MS (MALDI-FTMS): m/z [M^++1] found: 455.0597, calcd for $C_{20}H_{20}O_4N_2SCl_2$: 455.0594.

8: ^{1}H NMR (300 MHz, $CDCl_3$): $\delta = 7.83$ (dd, $J = 1.9$, 6.6 Hz, 2H), 7.38 (dd, $J = 1.9$, 6.6 Hz, 2H), 7.05 (s, 1H), 4.33 (s, 1H), 3.68 (s, 3H), 2.46 (s, 3H), 1.26 (s, 3H), 1.12 (s, 3H); ^{13}C NMR (75 MHz, $CDCl_3$): $\delta = 168.$ 5, 153.3, 145.6, 134.3, 130.0, 127.8, 70.9, 69.5, 61.4, 52.3, 29.3, 23.1, 21.7; HR-MS (MALDI-FTMS): m/z [M^++1] found: 393.0437, calcd for $C_{15}H_{18}O_4N_2SCl_2$: 393.0449.

Received: June 18, 2001 [Z17296]

[1] a) E. Block, A. L. Schwan in *Comprehensive Organic Synthesis*, *Vol. 4* (Eds.: B. M. Trost, I. Fleming, M. F. Semmelhack), Pergamon, Oxford, **1991**, pp. 329 – 362; b) L. S. Hegedus in *Comprehensive Organic Synthesis*, *Vol. 4* (Eds.: B. M. Trost, I. Fleming, M. F. Semmelhack), Pergamon, Oxford, **1991**, pp. 551 – 570.

[2] a) B. M. Trost, A. B. Pinkerton, *J. Am. Chem. Soc.* **2000**, *122*, 8081 – 8082; b) B. M. Trost, A. B. Pinkerton, *Angew. Chem.* **2000**, *112*, 368 – 370; *Angew. Chem. Int. Ed.* **2000**, *39*, 360 – 362.

[3] For leading reviews of multicomponent reaction, see a) A. Dömling, I. Ugi, *Angew. Chem.* **2000**, *112*, 3300 – 3344; *Angew. Chem. Int. Ed.* **2000**, *39*, 3169 – 3210; b) S. Kobayashi, *Chem. Soc. Rev.* **1999**, *28*, 1 – 26. For episulfonium and episelenium ions, see refs. [4] and [5].

[4] J. Winkler, M. Finck-Estes, *Tetrahedron Lett.* **1989**, *30*, 7293 – 7296.

[5] a) A. Bewick, J. M. Mellor, W. M. Owton, *J. Chem. Perkin Trans. 1* **1985**, 1039 – 1044; b) A. Bewick, D. E. Coe, G. B. Fuller, J. M. Mellor, *Tetrahedron Lett.* **1980**, *21*, 3827 – 3828.

[6] a) G. Li, H.-X. Wei, S. H. Kim, M. Neighbors, *Org. Lett.* **1999**, *1*, 395 – 397; b) G. Li, H.-X. Wei, S. H. Kim, *Org. Lett.* **2000**, *2*, 2249 – 2252.

[7] G. Li, H.-X. Wei, S. H. Kim, *Tetrahedron Lett.* **2000**, *41*, 8699 – 8701.

[8] M. R. Grimmett in *Comprehensive Heterocyclic Chemistry*, *Vol. 5* (Eds.: A. R. Katritzky, C. W. Rees), Pergamon, Oxford, **1984**, pp. 345 – 457.

[9] D. Lucet, T. Le Gall, C. Mioskowski, *Angew. Chem.* **1998**, *110*, 2724 – 2772; *Angew. Chem. Int. Ed.* **1998**, *37*, 2580 – 2627.

[10] a) E. J. Corey, D.-H. Lee, S. Sarshar, *Tetrahedron: Asymmetry* **1995**, *6*, 3 – 6; b) A. O. Chong, K. Oshima, K. B. Sharpless, *J. Am. Chem. Soc.* **1977**, *99*, 3420 – 3426; c) M. Reetz, R. Jaeger, R. Drewlies, M. M. Hübel, *Angew. Chem.* **1991**, *103*, 76 – 78; *Angew. Chem. Int. Ed.* **1991**, *30*, 103 – 105; d) T. Hayashi, E. Kishi, V. A. Soloshonok, Y. Uozumi, *Tetrahedron Lett.* **1996**, *37*, 4969 – 4972; e) M. E. Solomon, C. L. Lynch, D. H. Rich, *Tetrahedron Lett.* **1995**, *36*, 4955 – 4958.

[11] a) M. P. Doyle, *Chem. Rev.* **1986**, *86*, 919 – 939; b) M. P. Doyle, *Aldrichimica Acta.* **1996**, *29*, 3 – 11; c) H. M. L. Davies, *Aldrichimica Acta* **1997**, *30*, 107 – 114.

[12] The common quenching treatment with aqueous Na_2SO_3 for *N,N*-dichlorosulfonamide-based reactions was not used to avoid some unknown side products. The loading of triphenylphosphane and the rhodium(II) heptafluorobutyrate dimer at 4.0 and 2.0 mol%, respectively, turned out to be near the turnover point since the reaction was not further accelerated in the presence of larger amounts of the catalyst. On the other hand, both the reaction rate and yield were diminished when a reduced amount of catalyst was used. Attempts to further optimize the reaction conditions were also made by using a variety of cosolvents of MeCN with other solvents, such as $CHCl_3$, CH_2Cl_2, toluene, and THF, in different ratios, but success was limited. An excess amount of $TsNCl_2$ (2.2 equiv) proved to be necessary for the complete consumption of the olefin starting materials. With the combination of rhodium/phosphane/4-Å MS in hand, we then went back to examine the combination of triphenylphosphane with the original rhodium compounds ($[Rh(OAc)_2]_2$ and $[Rh(OOCCF_3)_2]_2$), but failed to achieve any improvements. Surprisingly, when the triphenylphosphane ligand was replaced by tributylphosphane, only a tiny amount of the expected imidazolidine product was afforded, as revealed by crude ^{1}H NMR analysis.

[13] L. I. Krimen, D. J. Cota, *Org. React.* **1969**, *17*, 213 – 325.

[14] S.-J. Chang, *Org. Process Res. Dev.* **1999**, *3*, 232 – 234.

Efficient, Catalytic, Aerobic Oxidation of Alcohols with Octahedral Molecular Sieves**

Young-Chan Son, Vinit D. Makwana, Amy R. Howell, and Steven L. Suib*

The oxidation of alcohols to carbonyl compounds is of great interest to the fine chemicals industry and academia. Recently, catalytic oxidations of alcohols in which oxygen is the secondary oxidant have been the focus in many laboratories.[1–6] Alcohol oxidations using Ru,[2] Co,[3] Cu,[4] Pd,[5] and Pt[6] metal catalysts with additives, such as potassium carbonate, sodium bicarbonate, pyridine, molecular sieves, and phenanthroline, have been reported.

Stoichiometric metal oxidants such as chromates and active manganese dioxide have also been widely used.[7] In fact, conventional active manganese oxide has been most commonly used for allylic and benzylic oxidations. The reactivity of active manganese oxide is dependent on preparation methods, compositions, and structure.[7b, 8] Complicated preparation methods are often necessary, and the use of freshly made active manganese oxide is required. Moreover, five to fifty equivalents of this reagent are required to obtain oxidation products, which results in large amounts of nonreusable, toxic waste.

The problems associated with active manganese oxides prompted us to examine octahedral molecular sieves (OMS) as potential catalysts for alcohol oxidations. OMS materials

[*] Prof. S. L. Suib
U-3060, Department of Chemistry
Department of Chemical Engineering and Institute of Materials Science
University of Connecticut, Storrs, CT 06269 (USA)
Fax: (+1) 860-486-2981
E-mail: suib@uconnvm.uconn.edu
Y.-C. Son, V. D. Makwana, Prof. A. R. Howell
U-3060, Department of Chemistry, University of Connecticut
Storrs, CT 06269-3060 (USA)

[**] We acknowledge support of the Geosciences and Biosciences Division, Office of Basic Energy Sciences, Office of Science, U.S. Department of Energy. We also thank Professor Mark E. Davis, Dr. Francis Galasso, and Dr. Lixin Cao for helpful discussions.

 © WILEY-VCH Verlag GmbH, D-69451 Weinheim, 2001 1433-7851/01/4022-4280 $ 17.50+.50/0

are inexpensive, easy to make, and have received a great deal of attention because of their catalytic properties.[9] The K^+ ion form of hollandite (known as cryptomelane) is a microporous manganese oxide with a composition of $KMn_8O_{16} \cdot n\,H_2O$.[10] Synthetic cryptomelane octahedral molecular sieves (OMS-2) consist of structural units of MnO_6 octahedra, which are edge and corner shared. The structure of these materials contains 4.6×4.6 Å tunnels as a result of the 2×2 arrangement of octahedra; potassium ions are present in the tunnels with a small amount of water (Figure 1). The average manganese

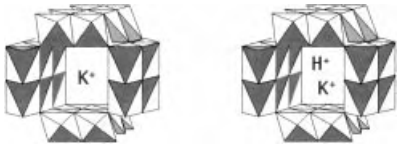


Figure 1. Structures of K-OMS-2 and H-K-OMS-2.

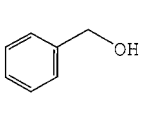
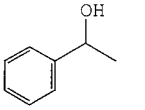
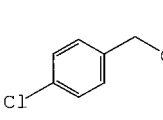
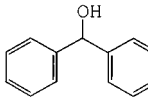
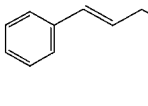
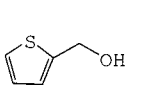
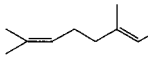
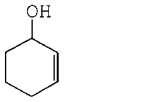
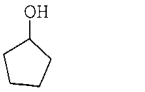
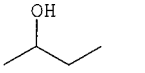
oxidation state of 3.8 of K-OMS-2 arises from the presence of a mixture of Mn^{4+}, Mn^{3+}, and Mn^{2+} ions.[10] This mixed valency of K-OMS-2, along with its one-dimensional tunnel structure, can give rise to interesting oxidation properties.[11] Pore size distribution studies show that a broad range of micropores are present, with diameters ranging from ~4.5 to 7 Å.[12] Herein, we report an evaluation of these materials as inexpensive, efficient, environmentally friendly, selective, aerobic, and heterogeneous catalysts, which do not require any additional co-oxidants for the oxidation of alcohols into carbonyl compounds. K-OMS-2 gave excellent conversions and 100% selectivities for benzylic alcohols without any additives (Table 1, Entries 1–3). However, K-OMS-2 did not provide a high conversion for relatively large substrates (Entry 4) or for allylic alcohols (Entries 5–8). Adding doping materials, such as Cr^{3+}, Ni^{2+}, and Co^{2+} ions, into the K-OMS-2 or using bases as additives decreased conversion.

The use of H-K-OMS-2 (Figure 1) significantly enhanced conversion (Table 1). This result suggests that alcohol oxidations catalyzed by OMS-2 are accelerated by Brønsted acids. Benzylic (Entries 1–4) and allylic alcohols (Entries 5–8) undergo oxidation into the corresponding ketones and aldehydes with H-K-OMS-2. The catalyst is selective, even with sulfur heterocycles (Entry 6), geraniol gave geranial without any isomerization (Entry 7). For alkyl alcohols, the conversion was lower (Entry 9), and a greater amount of H-K-OMS-2 is required.

The reaction is also effective on a 20-mmol scale with no change in the conversion or reactivity. In addition, these OMS-2 materials are very stable and can be stored for a long time (activity retained after two years). Over oxidation did not occur with K-OMS-2 or H-K-OMS-2. Air can be used instead of more expensive oxygen, although oxygen shortens the reaction time and increases conversion.[13] When nitrogen was used instead of air, the conversion significantly decreased to 10%. This is because the catalyst is used without pretreatment and there is a significant amount of adsorbed oxygen on the surface.

After the oxidation reaction, filtered H-K-OMS-2 was washed with methanol and water and heated to 300 °C and could then be reused as a catalyst without any appreciable loss of activity for oxidation. Water, which is the only side product produced from the oxidation reaction, poisons the catalyst. The catalyst can also physically absorb the aldehydes formed in the reaction. X-ray diffraction (XRD) and infrared (IR) spectroscopy studies indicated that after being heated to 300 °C the catalyst returned to its original composition and structure. Temperature-programmed desorption studies of used catalysts show only desorption of H_2O, reactant, or product. The standard Mn leaching experiment[14] was per-

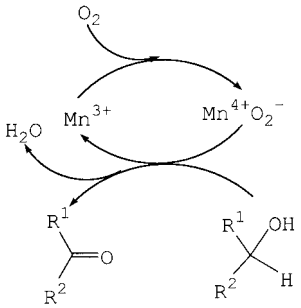
Table 1. The oxidation of various alcohols catalyzed by OMS-2 in the presence of air.[a,b]

Entry	Substrate	Product	Catalyst	Conversion [%][c]
1			K-OMS-2	90(85)[d]
			H-K-OMS-2	97(93)[d]
2			K-OMS-2	93
			H-K-OMS-2	99
3			K-OMS-2	95
			H-K-OMS-2	99
4			K-OMS-2	35
			H-K-OMS-2	100
5			K-OMS-2	50
			H-K-OMS-2	95
6			K-OMS-2	40
			H-K-OMS-2	100
7			K-OMS-2	5
			H-K-OMS-2	95
8			K-OMS-2	30
			H-K-OMS-2	90
9			K-OMS-2	35[e]
			H-K-OMS-2	67[e]
10			H-K-OMS-2	35[f]

[a] Reactions were performed at 110 °C, under toluene reflux and air for 4 h. [b] The selectivity of all oxidation reactions is 100%. [c] The conversion was measured by gas chromatography and ^1H NMR spectroscopy using internal standard methods. [d] Yield of isolated product. [e] The reaction time was 20 h. [f] The reaction time was 16 h.

formed to ascertain if the reaction is truly heterogeneous: Conversion did not change after filtering off the catalyst at reaction temperature and letting the reaction continue. This result demonstrates that the reaction is heterogeneous. Any manganese that leached into solution is not an active homogeneous catalyst. A minimum turnover number based on total moles of manganese and H^+ ions, is approximately 80. A minimum turnover number based on total moles of H^+ ions is 400. The surface area of OMS-2 was varied from 20–250 $m^2 g^{-1}$, and no correlation of activity and surface area was observed (no change in rates). In fact, K-OMS-2 with a larger surface area (97 $m^2 g^{-1}$) was less active than H-K-OMS-2, which has a smaller surface area of 85 $m^2 g^{-1}$. The pore size distributions of K-OMS-2 and H-K-OMS-2 are the same.

The active sites of OMS-2 may be derived from Mn^{3+} ions in tunnel sites in the OMS-2 materials. This can be inferred from the lower reactivity towards large substrates such as 1-acenaphthenol (conversion of $<5\%$ after 24 h). A redox mechanism is considered to involve alcohol oxidation by $Mn^{4+}O_2^-$, which is reduced to Mn^{3+} ions only to be reoxidized by dioxgen (Scheme 1). The formation of dioxygen–manganese complexes may be considered to produce activated oxygen.



Scheme 1. Proposed outline of the mechanism of alcohol oxidation with OMS-2. $R^1 = R^2$; $R^1 \neq R^2$; full list of substrates shown in Table 1.

Mechanistic studies such as kinetic modeling and ^{18}O labeling experiments point to a Mars–van Krevelen mechanism of oxidation rather than the Langmuir–Hinshelwood–Hougen–Watson (LHHW) rate law of heterogeneous catalysis. The Mars–van Krevelen mechanism can be described by Equations (1) and (2) where M=O is the oxidized catalyst, S is an organic substrate, and M is the reduced catalyst. According to this mechanism, lattice oxygen of OMS-2 participates in the oxidation reaction and is later replenished by fluid-phase oxygen. The active species is presumably the O_2^- ion, this indicates a simultaneous transfer of two electrons and not a stepwise electron donation.

$$M{=}O + S \longrightarrow M + S{=}O \quad (1)$$

$$2M + O_2 \longrightarrow 2M{=}O \quad (2)$$

In conclusion, to our knowledge, this is the first example of acid-catalyzed alcohol oxidations with inexpensive, crystalline manganese oxides as catalysts. Octahedral molecular sieves (K-OMS-2 and H-K-OMS-2) without the use of additives catalyzed the oxidation of alcohols to the corresponding aldehydes and ketones under mild conditions. H-K-OMS-2 gave excellent conversions and very high selectivity in the oxidation of alcohols. H-K-OMS-2 is an efficient, selective, easily regenerable and environmentally friendly catalyst. H-K-OMS-2 is inexpensive to make and requires no co-oxidants.

Experimental Section

Preparation of synthetic cryptomelane (OMS-2):[10] Potassium permanganate solution (225 mL, 0.4 M) was added to a 500 mL round-bottomed flask containing a mixture of manganese sulfate hydrate solution (67.5 mL, 1.75 M) and concentrated nitric acid (6.8 mL). The dark brown slurry was heated under reflux for 24 h, then filtered and washed with deionized water several times. The catalyst was dried at 120 °C overnight before use.

H-K-OMS-2: K-OMS-2 was stirred in a 1 M solution of nitric acid for several hours at 60–70 °C, forming H-K-OMS-2. After the washing and drying procedure outlined above, the catalyst was ready for use. Elemental analysis showed that H-K-OMS-2 has the formula $H_{0.2}K_{0.8}Mn_8O_{16} \cdot n\,H_2O$.

A typical procedure for the alcohol oxidation: Toluene (10 mL) and the alcohol (1 mmol) were first added to a round-bottomed flask containing K-OMS-2 (0.05 g; ~0.5 equiv, one manganese was considered to be one active site), represented by $KMn_8O_{16} \cdot n\,H_2O$ ($n = 0.5–10$). The mixture was then stirred under reflux (110 °C) in air. After 4 h, the reaction mixture was cooled, K-OMS-2 was removed by filtration, and the filtrate was analyzed using gas chromatography/mass spectrometry (GC/MS), ^1H NMR, and IR spectroscopy.

Received: May 15, 2001
Revised: August 24, 2001 [Z17113]

[1] a) G.-J. ten Brink, I. W. C. E. Arends, R. A. Sheldon, *Science* **2000**, *287*, 1636–1639; b) K. Kaneda, M. Fujii, K. Morioka, *J. Org. Chem.* **1996**, *61*, 4502–4503; c) T. Nishimura, T. Onoue, K. Ohe, S. Uemura, *Tetrahedron Lett.* **1998**, *39*, 6011–6014; d) B. M. Choudary, M. L. Kantam, A. Rahman, C. V. Reddy, K. K. Rao, *Angew. Chem.* **2001**, *113*, 785–788; *Angew. Chem. Int. Ed.* **2001**, *40*, 763–766; e) I. E. Markó, M. Tsukazaki, P. R. Giles, S. M. Brown, C. J. Urch, *Angew. Chem.* **1997**, *109*, 2297–2299; *Angew. Chem. Int. Ed. Engl.* **1997**, *36*, 2208–2210.

[2] a) I. E. Markó, P. R. Giles, M. Tsukazaki, I. Chellé-Regnaut, C. J. Urch, S. M. Brown, *J. Am. Chem. Soc.* **1997**, *119*, 12661–12662; b) K. Kaneda, T. Yamashita, T. Matsushita, K. Ebitani, *J. Org. Chem.* **1998**, *63*, 1750–1751; c) K. Yamaguchi, K. Mori, T. Mizugaki, K. Ebitani, K. Kaneda, *J. Am. Chem. Soc.* **2000**, *122*, 7144–7145.

[3] S. R. Cicoo, M. Latronico, P. Mastrorilli, G. P. Suranna, C. F. Nobile, *J. Mol. Catal. A* **2001**, *165*, 135–140.

[4] I. E. Markó, P. R. Giles, M. Tsukazaki, S. M. Brown, C. J. Urch, *Science* **1996**, *274*, 2044–2046.

[5] a) K. P. Peterson, R. C. Larock, *J. Org. Chem.* **1998**, *63*, 3185–3189; b) K. Kaneda, Y. Fujie, K. Ebitani, *Tetrahedron Lett.* **1997**, *38*, 9023–9026; c) T. Nishimura, T. Onoue, K. Ohe, S. Uemura, *J. Org. Chem.* **1999**, *64*, 6750–6755.

[6] A. F. Lee, J. J. Gee, H. J. Theyers, *Green Chem.* **2000**, *2*, 279–282.

[7] R. A. Lee, D. S. Donald, *Tetrahedron Lett.* **1997**, *38*, 3857–3860; b) A. J. Fatiadi, *Synthesis* **1976**, 65–104; A. J. Fatiadi, *Synthesis* **1976**, 133–166.

[8] I. M. Goldman, *J. Org. Chem.* **1969**, *34*, 1979–1981; b) L. A. Carpino, *J. Org. Chem.* **1970**, *35*, 3971–3972.

[9] S. L. Brock, N. Duan, Z. R. Tian, O. Giraldo, H. Zhou, S. L. Suib, *Chem. Mater.* **1998**, *10*, 2619–2628.

[10] a) R. N. DeGuzman, Y. F. Shen, E. J. Neth, S. L. Suib, C. L. O'Young, S. Levine, J. M. Newsam, *Chem. Mater.* **1994**, *6*, 815–821; b) Y. G. Yin, W. Q. Xu, R. N. DeGuzman, S. L. Suib, C. L. O'Young, *Inorg. Chem.* **1994**, *33*, 4384–4389; c) N. G. Duan, S. L. Suib, C. L. O'Young, *J. Chem. Soc. Chem. Commun.* **1995**, *13*, 1367–1368.

 © WILEY-VCH Verlag GmbH, D-69451 Weinheim, 2001 1433-7851/01/4022-4282 $ 17.50+.50/0

[11] a) J. M. Thomas, R. Raja, G. Sankar, R. G. Bell, *Nature* **1999**, *398*, 227–230; b) A. Clearfield, *Chem. Rev.* **1988**, *88*, 125–148; c) Y. F. Shen, R. P. Zerger, R. N. DeGuzman, S. L. Suib, L. McCurdy, D. I. Potter, C. L. O'Young, *Science* **1993**, *260*, 511–515; d) Z. R. Tian, W. Tong, J. Y. Wang, N. G. Duan, V. V. Krishnam, S. L. Suib, *Science* **1997**, *276*, 926–930.

[12] C. L. O'Young, R. A. Sawicki, S. L. Suib, *Microporous Mater.* **1997**, *11*, 1–8.

[13] Although we did not experience any incidents during the alcohol oxidation studies using our catalyst, adequate precautions need to be taken against explosion hazards associated with toluene–oxygen vapors at the high reaction temperature. This is so because the lower limit of flammability of toluene is a meager 1.2% by volume in air.

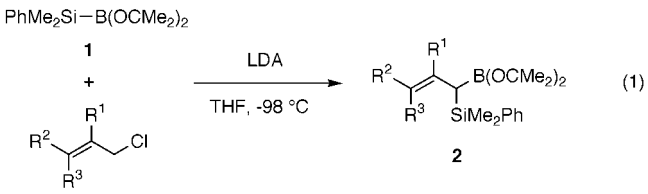
[14] R. A. Sheldon, M. Wallau, I. W. C. E. Arends, U. Schuchardt, *Acc. Chem. Res.* **1998**, *31*, 485–493.

1-Silyl-1-boryl-2-alkenes: Reagents for Stereodivergent Allylation Leading to 4-Oxy-(*E*)-1-alkenylboronates and 4-Oxy-(*Z*)-1-alkenylsilanes**

Masaki Shimizu,* Hirotaka Kitagawa, Takuya Kurahashi, and Tamejiro Hiyama*

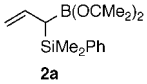
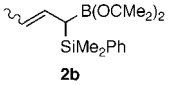
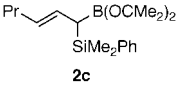
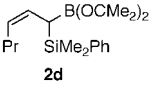
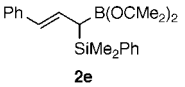
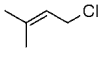
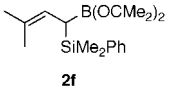
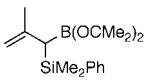
Allylmetal reagents have been widely used in organic synthesis.[1] In addition, allylic boranes[2] and silanes[3] are highly versatile owing to their wide availability, high stability, and low toxicity as well as excellent chemo-, regio-, and stereoselectivities. In sharp contrast, little attention has been paid to 1-silyl-1-boryl-2-alkenes, though such reagents can be regarded as a hybrid of allylic boranes and silanes and are attractive for the construction of stereochemically complex molecules.[4] Yamamoto, Yatagai, and Maruyama prepared α-trimethylsilyl-substituted crotyl-9-BBN (9-BBN = 9-borabicyclo[3.3.1]nonane) by deprotonation of crotyl-9-BBN followed by silylation with chlorotrimethylsilane.[5] Similar boronates were synthesized by Tsai and Matteson by the homologation of alkenylboronates with [chloro(trimethylsilyl)methyl]lithium.[6] Both reagents were found to allylate aldehydes[7] in a manner similar to allylic boranes. Although this methodology is effective for acyclic stereocontrol, allylation with allylic silanes and stereospecificity in boron-selective allylation remained to be explored. Herein we describe the novel stereocontrolled synthesis of 1-silyl-1-boryl-2-alkenes by *gem*-silylborylation of α-chloroallyllithiums and dual stereospecific allylation of aldehydes with silicon or boron functionality of the *gem*-silylboryl reagents.

Recently, the novel *gem*-silylborylation reaction of 1-halo-1-lithio-1-alkenes with (dimethylphenylsilyl)(pinacolato)borane (**1**) was disclosed[8] and is considered to proceed via borate formation followed by 1,2-migration of a silyl group from an ate-type boron to a carbenoid carbon. We envisaged that the title *gem*-silylboryl reagents **2** might be prepared readily by the *gem*-silylborylation with **1** of vinyl-substituted carbenoids [Eq. (1)].[9, 10] Thus, we treated **1**[11] with α-chloroallyllithiums



generated in situ from allylic chlorides and lithium diisopropylamide (LDA) in THF at $-98\,^{\circ}C$. The results are summarized in Table 1. Allyl chloride was converted into **2a** in 82% yield (Entry 1). Substituted allylic chlorides were also *gem*-silylborylated smoothly in good yields irrespective of the substitution pattern (Entries 2–7). No trace of γ-silyl-α-boration by 1,4-migration of a silyl group was observed. Noteworthy is that the olefinic configuration was perfectly retained in compounds **2** (Entries 3–5): stereochemically pure allylic chlorides gave single stereoisomers of **2**.

Table 1. Synthesis of 1-silyl-1-boryl-2-alkenes from allylic chlorides.[a]

Entry	Allylic chloride	Product	Yield [%][b]
1		 **2a**	82
2	 [c]	 **2b**	86[d]
3	 [e]	 **2c**	75[e]
4	 [f]	 **2d**	79[f]
5	 [e]	 **2e**	75[e]
6		 **2f**	72
7		 **2g**	73

[a] allylic chloride (1.0 mol), **1** (1.1 mol), LDA (1.0 mol), THF, $-98\,^{\circ}C$, 10 min then warmed to room temperature. [b] Isolated yields are given. [c] $E/Z = 85:15$. [d] $E/Z = 83:17$. [e] $E/Z = >99:<1$. [f] $E/Z = <1:>99$.

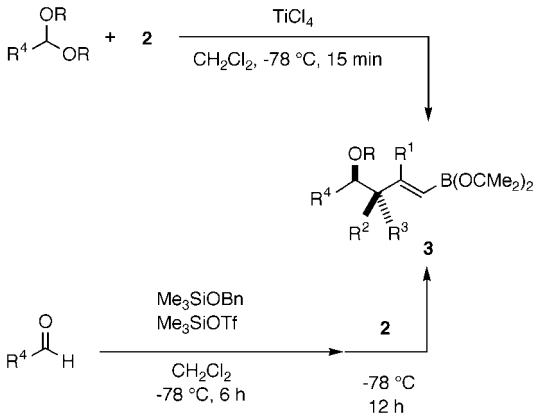
[*] Dr. M. Shimizu, Prof. T. Hiyama, H. Kitagawa, T. Kurahashi
Department of Material Chemistry
Graduate School of Engineering
Kyoto University, Yoshida, Sakyo-ku, Kyoto, 606-8501 (Japan)
Fax: (+81) 75-753-5555
E-mail: thiyama@npc05.kuic.kyoto-u.ac.jp

[**] This work was supported by a Grant-in-Aid for COE Research on Elements Science, No. 12CE2005 from the Ministry of Education, Culture, Sports, Science, and Technology, Japan.

Supporting information for this article is available on the WWW under http://www.angewandte.com or from the author.

 © WILEY-VCH Verlag GmbH, D-69451 Weinheim, 2001 1433-7851/01/4022-4283 $ 17.50+.50/0

We next scrutinized the allylation of **2** taking advantage of allylic silane functionality. After many attempts,[12] we found that compounds **2** allylated acetals in the presence of titanium tetrachloride (Scheme 1).[13, 14] The results are summarized in



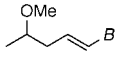
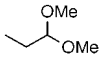
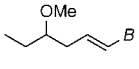
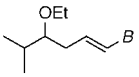
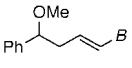
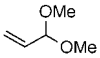
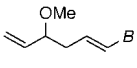
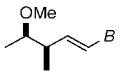
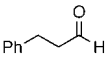
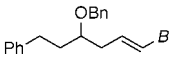
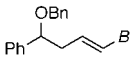
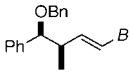
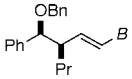
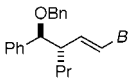
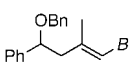
Scheme 1. Allylation of acetals or aldehydes as allylic silanes. Bn = benzyl, OTf = trifluoromethanesulfonate.

Table 2. Aliphatic, aromatic, and α,β-unsaturated acetals reacted with **2** to produce alkenylboronates **3a**–**f** in good yields with high (*E*)-selectivity (Entries 1–6). Moreover, reagents **2** were shown to allylate an oxonium ion in situ generated from an aldehyde, Me_3SiOBn, and Me_3SiOTf, to give the corresponding (*E*)-benzyl ether **3g**–**l** stereoselectively (Entries 7–12).[15] High (*E*)-selectivity of **3** is observed irrespective of the olefinic geometry of **2** (Entries 6, 9, 10, and 11).[16] Markedly, allylation by 1-silyl-(*E*)- and (*Z*)-2-hexenyl boronates **2c** and **2d** proceeded stereospecifically with high (*E*, *erythro*) and (*E*, *threo*) selectivities, respectively (Entries 10 and 11).[17] These results are the first demonstration of silicon-selective allylation over boron in **2**.

Allylation of aldehydes with allylic borane reagents **2a**, **2c**, and **2d** was also studied [Eq. (2)]. Some of results are summarized in Table 3. Both aliphatic and aromatic aldehydes were allylated by **2a** upon heating at 100 °C in the absence of any additive to yield the corresponding alkenylsilanes **4a** and **4b** in moderate to good yields with high *Z*-selectivity (Entries 1 and 2). Comparing with the results of pinacol α-trimethylsilyl allylboronate,[6] the selectivity slightly increased because of the bulkier dimethylphenylsilyl group. Stereochemically pure (*E*)-2-hexenyl boronate **2c** reacted with benzaldehyde to give **4c** in a (*E*, *threo*)/(*Z*, *threo*) ratio of 7:93 (Entry 3), whereas (*E*, *erythro*) isomer **4d** was produced by using **2d** with 94% selectivity (Entry 4). The stereospecific outcome is in accord with chairlike six-membered transition states.[5, 6]

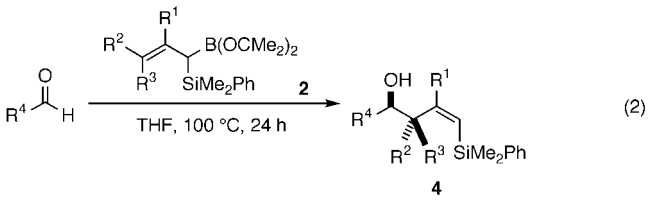
Further synthetic elaboration of the allylated products with the aid of the remaining inorganic functional group and deprotection of benzyl group in **3** are illustrated in Scheme 2. Suzuki–Miyaura coupling[18] of **3d** with iodobenzene gave (*E*)-homoallylic ether **5**, while methoxyethoxymethylation of **4c** with methoxyethoxymethyl chloride (MEMCl) followed by acetal-vinylsilane cyclization mediated by titanium tetra-

Table 2. Allylation of acetals or aldehydes with **2** as an allylic silane.[a]

Entry	2	Electrophile	Product	Yield [%][b]	Isomer ratio[c]
1	**2a**		 **3a**	78 (3)[d]	94:6[e]
2	**2a**		 **3b**	77	95:5[e]
3	**2a**		 **3c**	85	–[f]
4	**2a**		 **3d**	69	97:3[e]
5	**2a**		 **3e**	62	> 95: < 5[e]
6	**2b**[g]		 **3f**	81	73:24:3[h]
7	**2a**		 **3g**	85	> 95: < 5[e]
8	**2a**		 **3h**	88 (73)[i]	> 95: < 5[e]
9	**2b**[g]		 **3i**	81	84:16[j]
10	**2c**		 **3j**	83	95:5[j]
11	**2d**		 **3k**	94	9:91[j]
12	**2g**		 **3l**	70	> 95: < 5[e]

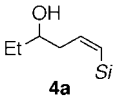
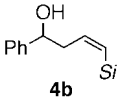
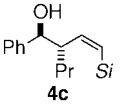
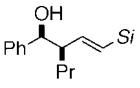
[a] For acetals: **2** (1.0 mol), acetal (2.0 mol), $TiCl_4$ (1.5 mol), CH_2Cl_2, −78 °C, 15 min. For aldehydes: aldehyde (1.0 mol), Me_3SiOBn (1.3 mol), Me_3SiOTf (1.0 mol), CH_2Cl_2, −78 °C, 6 h, then **2** (1.0 mol), −78 °C, 12 h; $B = B(OCMe_2)_2$. [b] Isolated yields are given. [c] Determined by ^1H NMR of a crude product mixture. [d] (*E*)-**3a**: 78% yield; (*Z*)-**3a**: 3% yield. [e] Ratios of *E*/*Z*. [f] The ratio was not determined. [g] *E*/*Z* Mixture of **2b** was used (*E*/*Z* = 83:17). [h] Ratio of (*E*, *erythro*):(*E*, *threo*):others. [i] 88%: Me_3SiOTf (1.0 mol); 73%: Me_3SiOTf (0.1 mol). [j] Ratio of (*E*, *erythro*):(*E*, *threo*).

 © WILEY-VCH Verlag GmbH, D-69451 Weinheim, 2001 1433-7851/01/4022-4284 $ 17.50+.50/0 *Angew. Chem. Int. Ed.* **2001**, *40*, No. 22

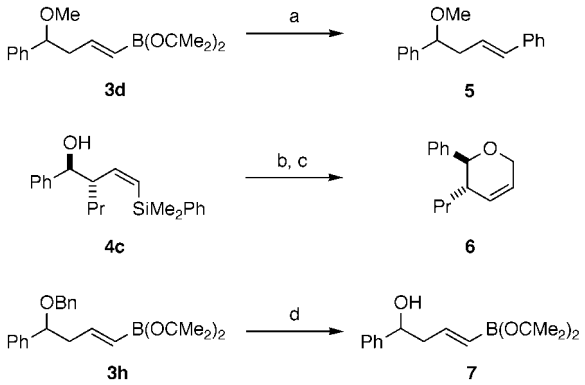


(2)

Table 3. Allylation of aldehydes with **2** as an allylic borane.[a]

Entry	2	Aldehyde	Product	Yield [%][b]	Isomer ratio[c]
1	**2a**		 **4a**	74 (17)	15:85[d]
2	**2a**		 **4b**	89 (0)	9:91[d]
3	**2c**		 **4c**	87 (10)	7: 93[e]
4[f]	**2d**		 **4d**	46 (20)	94:6[g]

[a] **2** (1.0 mol), aldehyde (1.1 mol), THF, 100 °C, 24 h. *Si* = $SiMe_2Ph$. [b] Isolated yields are given. The values in parentheses are recovery of **2**. [c] Determined by ^1H NMR. [d] Ratio of *E*/*Z*. [e] Ratio of (*E*, *threo*):(*Z*, *threo*). [f] Benzaldehyde (3 molar equivalents) was treated at 65 °C for 45 h. [g] Ratio of (*E*, *erythro*):(*Z*, *threo*).



Scheme 2. Synthetic applications of allylated products **3d**, **3h**, and **4c**. a) PhI (1.1 mol), $[Pd(PPh_3)_4]$ (4.9 mol%), aq. KOH (3.0 mol), dioxane, 100 °C, 86% yield; b) NaH (5.1 mol), MEMCl (6.1 mol), THF, RT, 55% yield; c) $TiCl_4$ (3.0 mol), CH_2Cl_2, −78 °C, 82% yield; d) Me_3SiI (1.3 mol), CH_2Cl_2, RT, 73% yield.

chloride gave *trans*-6-phenyl-5-propyl-5,6-dihydro-2*H*-pyran (**6**).[19] Debenzylation of **3h** was carried out in good yield by treatment with Me_3SiI with retention of the (*E*)-alkenylboryl moiety.[20]

In summary, we have demonstrated that *gem*-silylborylation of stereochemically defined α-chloroallyllithiums with silylborane **1** constitutes a new method for the stereocontrolled synthesis of 1-silyl-1-boryl-2-alkenes **2**. Furthermore, stereospecific allylation of aldehydes with **2** was achieved with either the silicon- or boron-functionality, and was demonstrated that under appropriate conditions the corresponding adducts are readily converted into substituted (*E*)- or (*Z*)-homoallylic alcohols.

Experimental Section

Full experimental details and analytical data can be found in the Supporting Information.

2a, *gem*-silylborylation of allyl chloride: A solution of LDA (3.3 mmol) in THF (8 mL) was added to a solution of allyl chloride (0.26 mL, 3.2 mmol) and (dimethylphenylsilyl)(pinacolato)borane (**1**) (0.92 g, 3.5 mmol) in THF (20 mL) at −98 °C. The reaction mixture was stirred for 10 min at −98 °C and then allowed to gradually warm to room temperature. The solution was stirred overnight followed by quenching with saturated aq. NH_4Cl solution. The aqueous layer was extracted with diethyl ether (20 mL). The organic layer was dried over anhydrous $MgSO_4$, and concentrated in vacuo to give the crude product. Purification by column chromatography on silica gel (hexane/ethyl acetate = 9/1) afforded **2a** as a colorless oil (0.79 g, 82% yield); TLC: $R_f = 0.45$ (hexane/ethyl acetate = 9/1); ^1H NMR (200 MHz, $CDCl_3$): $\delta = 0.34$ (s, 3H), 0.35 (s, 3H), 1.13 (s, 6H), 1.16 (s, 6H), 1.79 (d, $J =$ 10.5 Hz, 1H), 4.74 (ddd, $J = 16.8$, 2.2, 0.6 Hz, 1H), 4.78 (dd, $J = 10.5$, 2.2 Hz, 1H), 5.85 (ddd, $J = 16.8$, 10.5, 10.5 Hz, 1H), 7.28–7.38 (m, 3H), 7.48–7.60 (m, 2H); ^{13}C NMR (50 MHz, $CDCl_3$): $\delta = -3.2$, −3.2, 24.7, 24.8, 82.8, 112.2, 127.4, 128.8, 133.9, 135.3, 138.0; IR (neat): $\tilde{\nu} = 2985$, 1623, 1374, 1339, 1318, 1145, 839 cm^{-1}; MS (EI, 70 eV): *m*/*z* 303 (M^++1, 1), 302 (M^+, 5), 301 (M^+ − 1, 1), 284 (M^+ − Me, 6), 245 (28), 235 (M^+ − Ph, 13), 202 (32), 187 (32), 160 (49), 135 ($PhMe_2Si^+$, 100); elemental analysis (%) calcd for $C_{17}H_{27}BO_2Si$: C 67.55, H 9.00; found: C 67.29, H 8.92.

Allylation of acetaldehyde dimethylacetal with **2a**: A solution of $TiCl_4$ in CH_2Cl_2 (1.0 M, 0.82 mL, 0.82 mmol) was added to a solution of **2a** (0.17 g, 0.55 mmol) and acetaldehyde dimethylacetal (116 μL, 1.10 mmol) in CH_2Cl_2 (6 mL) at −78 °C. The solution was stirred for 15 min at −78 °C before quenching with water (0.50 mL) at −78 °C. The mixture was warmed to room temperature, dried over anhydrous $MgSO_4$, and filtered. The filtrate was concentrated to give a crude product consisting of *E*/*Z* = 94:6 as revealed by ^1H NMR spectra. Purification by silica gel column chromatography (hexane/ethyl acetate = 2/1) afforded (*E*)-**3a** (97 mg, 78% yield) and (*Z*)-**3a** (4.1 mg, 3% yield). (*E*)-**3a**: colorless oil; thin layer chromatography (TLC): $R_f = 0.53$ (hexane/ethyl acetate = 2/1); ^1H NMR (200 MHz, $CDCl_3$): $\delta = 1.15$ (d, $J = 6.0$ Hz, 3H), 1.27 (s, 3H), 2.27 (ddd, $J =$ 14.4, 6.6, 1.5 Hz, 1H), 2.44 (ddd, $J = 14.4$, 6.6, 1.5 Hz, 1H), 3.32 (s, 3H), 3.42 (m, $J = 6.0$ Hz, 1H), 5.50 (dt, $J = 18.1$, 1.5 Hz, 1H), 6.60 (dt, $J = 18.1$, 6.6 Hz, 1H); ^{13}C NMR (50 MHz, $CDCl_3$): $\delta = 19.1$, 24.8, 42.6, 56.0, 75.9, 83.1, 150.3. IR (neat): $\tilde{\nu} = 2980$, 2935, 1640, 1362, 1321, 1146, 998, 972, 852 cm^{-1}. MS (EI, 70 eV): *m*/*z* 225 (M^+ − 1, 0.6), 211 (M^+ − Me, 17), 111 (9), 101 (8.0), 95 (8), 59 (100); elemental analysis (%) calcd for $C_{12}H_{23}BO_3$: C 63.74, H 10.25; found: C 63.62, H 10.41.

Allylation of benzaldehyde with **2a**: A solution of **2a** (0.13 g, 0.42 mmol) and benzaldehyde (47 μL, 0.46 mmol) in THF (4 mL) was stirred at 100 °C (oil bath) for 24 h. The reaction mixture was cooled to room temperature, and then ethanolamine (42 μL) was added to the mixture at room temperature. The resulting milky suspension was stirred for 30 min. Filtration of the insoluble material followed by concentration of the filtrate gave a crude product. Purification by silica gel column chromatography (hexane/ethyl acetate = 4/1) gave **4b** as a colorless oil (0.11 g, 89% yield, *E*/*Z* = 9:91); TLC: $R_f = 0.31$ (hexane/ethyl acetate = 4/1); ^1H NMR (200 MHz, $CDCl_3$): $\delta = 0.38$ (s, 6H), 1.77 (brs, 1H), 2.35–2.65 (m, 2H), 4.64 (dd, $J = 7.4$, 5.6 Hz, 1H), 5.85 (dt, $J = 13.9$, 1.3 Hz, 1H), 6.46 (dt, $J = 13.9$, 7.4 Hz, 1H), 7.16–7.42 (m, 8H), 7.48–7.58 (m, 2H); ^{13}C NMR (50 MHz, $CDCl_3$): $\delta = -1.0$, 1.0, 43.0, 73.6, 125.7, 127.4, 127.8, 128.3, 128.9, 130.6, 133.7, 139.3, 143.8, 145.6. IR (neat): $\tilde{\nu}$3400 (br), 3070, 3035, 2965, 2900, 1608, 1428, 1250, 1114, 1053, 822 cm^{-1}; MS (EI, 70 eV): *m*/*z* 283 (M^+ + 1, 0.3), 282 (M^+, 0.5), 281 (M^+ − 1, 2), 264 (M^+ − H_2O, 13), 249 (M^+ − H_2O − Me, 16), 241 (34), 173 (52), 145 (36), 135 ($PhMe_2Si^+$, 91), 121 (47), 107 ($PhCHOH^+$, 100); elemental analysis (%) calcd for $C_{18}H_{22}OSi$: C 76.54, H 7.85; found: C 76.82, H 7.88.

Received: March 20, 2001
Revised: September 3, 2001 [Z16815]

 © WILEY-VCH Verlag GmbH, D-69451 Weinheim, 2001 1433-7851/01/4022-4285 $ 17.50+.50/0

[1] Reviews on allylmetal reagents: a) Y. Yamamoto, N. Asao, *Chem. Rev.* **1993**, *93*, 2207 – 2293; b) W. R. Roush in *Comprehensive Organic Synthesis*, *Vol. 2* (Eds.: B. M. Trost, I. Fleming, C. H. Heathcock), Pergamon, Oxford, **1991**, pp. 1 – 53; c) R. W. Hoffmann, *Angew. Chem.* **1982**, *94*, 569; *Angew. Chem. Int. Ed. Engl.* **1982**, *21*, 555 – 566.

[2] a) E. Negishi, M. J. Idacavage, *Org. React.* **1985**, *33*, 1 – 246; b) A. Pelter, K. Smith, H. C. Brown, *Borane Reagents*, Academic Press, New York, **1988**, pp. 310 – 323; c) D. S. Matteson, *Stereodirected Synthesis with Organoboranes*, Springer, Berlin, **1995**, pp. 260 – 310.

[3] a) H. Sakurai, *Pure Appl. Chem.* **1982**, *54*, 1 – 22; b) A. Hosomi, *Acc. Chem. Soc.* **1988**, *21*, 200 – 206; c) I. Fleming in *Comprehensive Organic Synthesis*, *Vol. 2* (Eds.: B. M. Trost, I. Fleming, C. H. Heathcock), Pergamon, Oxford, **1991**, pp. 563 – 593; d) I. Fleming, *Org. React.* **1994**, *33*, 1 – 246; e) C. E. Masse, J. S. Panek, *Chem. Rev.* **1995**, *95*, 1293 – 1316.

[4] Reviews of *gem*-dimetallic reagents: a) I. Marek, J.-F. Normant, *Chem. Rev.* **1996**, *96*, 3241 – 3267; b) I. Marek, *Chem. Rev.* **2000**, *100*, 2887 – 2900; other kinds of allyldimetallic compounds: (Si, Al) c) E.-i. Negishi, K. Akiyoshi, *J. Am. Chem. Soc.* **1988**, *110*, 646 – 647; (Si, Si) d) D. M. Hodgson, S. F. Barker, L. H. Mace, J. R. Moran, *Chem. Commun.* **2001**, 153 – 154; e) B. Princet, H. Gardes-Gariglio, J. Pornet, *J. Organomet. Chem.* **2000**, *604*, 186 – 190; f) M. Lautens, P. H. M. Delanghe, *Angew. Chem.* **1994**, *106*, 2557; *Angew. Chem. Int. Ed. Engl.* **1994**, *33*, 2448 – 2450; g) M. Lautens, R. N. Ben, P. H. M. Delanghe, *Tetrahedron* **1996**, *52*, 7221 – 7234; (Si, Zr) h) A. N. Kasatkin, R. J. Whitby, *Tetrahedron Lett.* **1999**, *40*, 9353 – 9357; (Si, Sn) i) M. Lautens, A. H. Huboux, B. Chin, J. Downer, *Tetrahedron Lett.* **1990**, *31*, 5829 – 5832; (Sn, Sn) j) refs. [4f] and [4g]; k) H. J. Reich, J. W. Ringer, *J. Org. Chem.* **1988**, *53*, 455 – 457; l) see also ref. [4i]; m) D. Madec, J.-P. Ferezou, *Tetrahedron Lett.* **1997**, *38*, 6657 – 6660; n) D. Madec, J.-P. Ferezou, *Tetrahedron Lett.* **1997**, *38*, 6661 – 6664.

[5] α-Trimethylsilyl crotyl-9-BBN was obtained as a mixture of *E*/*Z* isomers as a result of the allylic rearrangement. a) H. Yatagai, Y. Yamamoto, K. Maruyama, *J. Am. Chem. Soc.* **1980**, *102*, 4548 – 4550; b) Y. Yamamoto, H. Yatagai, K. Maruyama, *J. Am. Chem. Soc.* **1981**, *103*, 3229 – 3231; see also, c) Y. Yamamoto, Y. Saito, K. Maruyama, *J. Organomet. Chem.* **1985**, *292*, 311 – 318.

[6] A ~2:1 mixture of pinacol (*Z*)- and (*E*)-α-trimethylsilyl crotylboronate was obtained. a) D. J. S. Tsai, D. S. Matteson, *Organometallics* **1983**, *2*, 236 – 241; see also, b) D. S. Matteson, D. Majumdar, *Organometallics* **1983**, *2*, 230 – 236.

[7] Allylation of activated carbonyl pyruvates by α-trimethylsilyl crotyl-9-BBN was also reported. a) Y. Yamamoto, T. Komatsu, K. Maruyama, *J. Chem. Soc. Chem. Commun.* **1983**, 191 – 192; b) Y. Yamamoto, K. Maruyama, T. Komatsu, W. Ito, *J. Org. Chem.* **1986**, *51*, 886 – 891.

[8] T. Hata, H. Kitagawa, H. Masai, T. Kurahashi, M. Shimizu, T. Hiyama, *Angew. Chem.* **2001**, *113*, 812 – 814; *Angew. Chem. Int. Ed.* **2001**, *40*, 790 – 792.

[9] Reviews of heteroatom-stabilized allylanions: a) Y. Yamamoto in *Comprehensive Organic Synthesis*, *Vol. 2* (Eds.: B. M. Trost, I. Fleming, C. H. Heathcock), Pergamon, Oxford, **1991**, pp. 55 – 79; b) A. R. Katritzky, M. Piffl, H. Lang, E. Anders, *Chem. Rev.* **1999**, *99*, 665 – 722; generation and reactions of α-chloroallyllithiums: c) T. L. Macdonald, B. A. Narayanan, D. E. O'Dell, *J. Org. Chem.* **1981**, *46*, 1504 – 1506; d) M. Julia, J.-N. Verpeaux, T. Zahneisen, *Bull. Soc. Chim. Fr.* **1994**, *131*, 539 – 554.

[10] Synthesis of allylic boranes by reactions of α-chloroallyllithiums and organoboron compounds: a) H. C. Brown, M. V. Rangaishenvi, *Tetrahedron Lett.* **1990**, *31*, 7113 – 7114; b) H. C. Brown, M. V. Rangaishenvi, *Tetrahedron Lett.* **1990**, *31*, 7115 – 7118; c) H. C. Brown, M. V. Rangaishenvi, S. Jayaraman, *Organometallics* **1992**, *11*, 1948 – 1954; d) H. C. Brown, S. Jayaraman, *J. Org. Chem.* **1993**, *58*, 6791 – 6794.

[11] M. Suginome, T. Matsuda, Y. Ito, *Organometallics* **2000**, *19*, 4647 – 4649.

[12] For example, $TiCl_4$-promoted allylation of benzaldehyde with **2a** resulted in protodesilylation of **2a** producing 1-propenylboronate as a major isomer in low yield, while the same reaction mediated by Bu_4NF afforded a complex mixture.

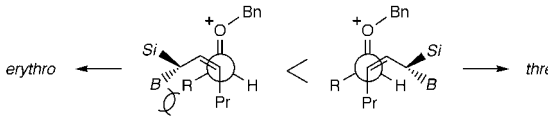
[13] a) Review on coupling reactions of acetals: T. Mukaiyama, M. Murakami, *Synthesis* **1987**, 1043 – 1054; b) A. Hosomi, M. Endo, H. Sakurai, *Chem. Lett.* **1976**, 941 – 942; c) A. Hosomi, M. Ando, H. Sakurai, *Chem. Lett.* **1986**, 365 – 368; d) J. S. Panek, M. Yang, *J. Am. Chem. Soc.* **1991**, *113*, 6594 – 6600.

[14] Reaction of 1-silyl-1-stannyl-2-alkenes with acetals in the presence of $BF_3 \cdot OEt_2$ was reported in which a carbon – tin bond cleaved selectively over a carbon – silicon bond giving rise to (*E*)-alkenylsilanes. See, ref. [4g].

[15] For in situ generation of oxonium ions: a) A. Mekhalfia, I. E. Marko, *Tetrahedron Lett.* **1991**, *32*, 4779; b) J. S. Panek, M. Yang, F. Xu, *J. Org. Chem.* **1992**, *57*, 5790. See also, R. Noyori, S. Murata, M. Suzuki, *Tetrahedron* **1981**, *37*, 3899.

[16] (*E*)-Olefinic selectivity can be explained by *anti*-S_E2' transition states of allylsilanes. See, a) T. Hayashi, M. Konishi, H. Ito, M. Kumada, *J. Am. Chem. Soc.* **1982**, *104*, 4962 – 4963; b) T. Hayashi, M. Konishi, M. Kumada, *J. Am. Chem. Soc.* **1982**, *104*, 4963 – 4965.

[17] Relative stereochemistry between benzyloxy and propyl groups of **3k** being *threo* was confirmed by protodeborylation of **3k** to convert it into 3-[benzyloxy(phenyl)methyl]-1-hexene that was consistent with the product obtained by benzylation and protodesilylation of **4c**. *Erythro* selectivity using the (*E*)-allylic silane may be explained by acyclic *antiperiplanar* transition states (see refs. [13d] and [15b]). However, such a model cannot rationalize *threo* selectivity from the (*Z*)-allylic silane. Although the reason for *threo* selectivity is not clear at present, acyclic *synclinal* transition states (see, ref. [3e]) might be involved considering the steric effect of a boryl group [Eq. (3)].



(3)

[18] N. Miyaura, A. Suzuki, *Chem. Rev.* **1995**, *95*, 2457 – 2483.

[19] L. E. Overman, A. Castaneda, T. A. Blumenkopf, *J. Am. Chem. Soc.* **1986**, *108*, 1303 – 1304.

[20] T. W. Greene, P. G. M. Wuts, *Protective Groups in Organic Synthesis*, 3rd ed., Wiley, New York, **1999**.

Organoclay Derivatives in the Synthesis of Macrocycles

Vasilios Georgakilas, Dimitrios Gournis, and Dimitrios Petridis*

The synthesis of macrocyclic systems is profoundly hindered by reactions of participating components that lead to the formation of mainly oligomeric or polymeric compounds. To overcome this deficiency, template-assisted methods based on metal coordination, electron-donor interactions, hydrogen bonding, and electrostatic interactions have been successfully developed.[1] In these reactions the templating agent plays the essential role of assembling and organizing the participating molecules in a way that makes possible a desirable reaction pathway that would not occur in its absence.[2]

Another potential approach to effectively assemble and organize compounds into well-defined supramolecular arrays

[*] Dr. D. Petridis, Dr. V. Georgakilas, Dr. D. Gournis
Institute of Materials Science
NCSR "Demokritos" Ag. Paraskevi Attikis, Athens (Greece)
Fax: (+30) 1-6519430
E-mail: dpetrid@ims.demokritos.gr

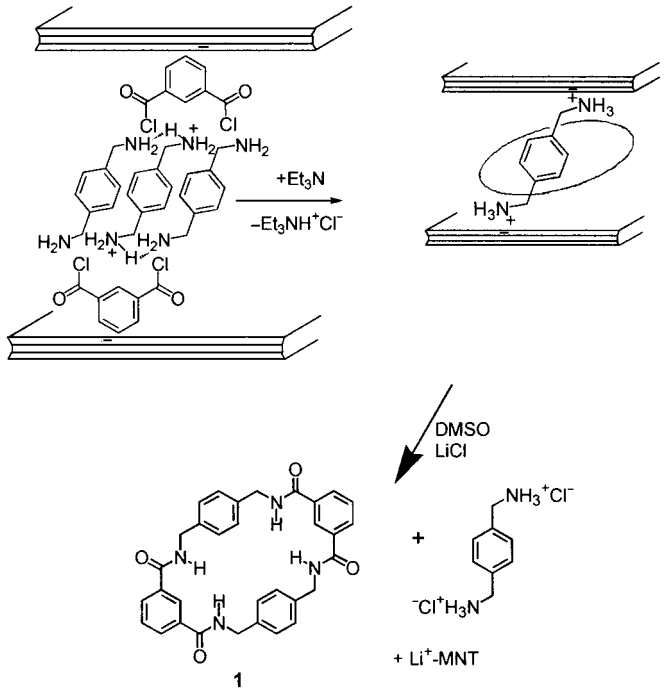
Supporting information for this article is available on the WWW under http://www.angewandte.com or from the author.

 © WILEY-VCH Verlag GmbH, D-69451 Weinheim, 2001 1433-7851/01/4022-4286 $ 17.50+.50/0

is to exploit the intercalation properties of layered solids. Towards this aim, we demonstrate herein that host–guest interactions in lamellar solids offer the means to manipulate the synthesis of macrocycles in a controllable manner.

The host lamellar solid used in our work belongs to the family of 2:1 mica-type layered aluminosilicate minerals and, in particular, to the minerals known as smectite clays. Smectites possess unique swelling, intercalation, and ion-exchange properties that enable their transformation into various classes of derivatives.[3] One such class of easily accessible derivatives results from the uniform insertion of organic cations at the exchange sites of the mineral.[4] A main feature of these organoclay solids is the efficient orientation and alignment of the organic cations in the interlayer zone or galleries of the clay. Apparently, such properties are highly desirable for the active engagement of clay surfaces as templates in the synthesis of macrocycles bearing basic nitrogen substituents.

As an application of these concepts we report the successful synthesis of the tetraamido macrocycle **1** (Scheme 1) on the clay surfaces. The original attempt to synthesize this molecule

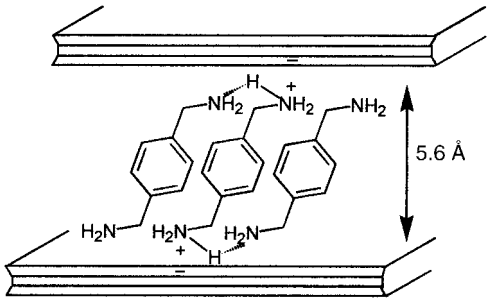


Scheme 1. Proposed pathway for the intergallery formation of macrocycle **1** (– denotes the negative charge of the clay layers).

by direct condensation of *p*-xylylenediamine with isophthaloyl dichloride in $CHCl_3$ gave a [2]-catenane (two interlocked units) as the only isolable product together with other cyclic oligomers and polymers.[5] The macrocycle was successfully synthesized in the form of a rotaxane (28% yield) by the same condensation reaction in the presence of a five-unit molecular axle.[6]

Our synthetic approach to **1** employed the following four steps: a) preparation of a pillared clay from the dihydrochloride salt of *p*-xylylenediamine, b) insertion of neutral *p*-xylylenediamine into the pillared structure, c) reaction of the neutral *p*-xylylenediamine in the layers with the isophthaloyl chloride and formation of the tetramide macrocycle, and d) extraction of the product from the clay.

The first step involves the insertion of the diprotonated *p*-xylylenediamine between the clay layers to give a pillared clay (product **a**) with a basal spacing d_{001} of 13 Å. This distance suggests that there is a single layer of diamine dications lying flat between the clay surfaces. The next step is the introduction of neutral *p*-xylylenediamine into the galleries of the pillared clay. The new organoclay composite (product **b**) was obtained by the addition of a solution of the *p*-xylylenediamine in water (twice the cation-exchange capacity) to a suspension of the pillared clay. The product gave an X-ray diffraction (XRD) pattern with a d_{001} spacing of 15.1 Å. The higher d spacing suggests that the insertion of the neutral diamine into the layers forces the intercalated diamine to adopt a lifted position. Such a position can be explained by assuming that the insertion of diamine between the layers creates an aggregated or a hemisalt structure that arises from hydrogen bonding between the protonated and neutral amino groups (Scheme 2). Similar hemisalt associations in clays has



Scheme 2. Schematic representation of the intergallery *p*-xylylenediamine hemisalt formation (– denotes the negative charge of the clay layers).

been reported for other amines[7] and diamines.[8] Furthermore, after washing **b** with water the d spacing returned to 13 Å, which suggests that the neutral diamine is only weakly held in the layers and therefore is easily eluted into the water phase, leaving behind the protonated diamine cations in a flat orientation. Additional evidence for an interlayer hemisalt formation derives from the FT-IR spectrum of product **b** (Figure 1). The third step is the reaction of isophthaloyl dichloride with a suspension of **b** in CH_3CN in the presence of Et_3N. The intergallery condensation was carried out at room temperature by stirring the suspension for a few hours. The interlayer formation of the cyclic tetramide **1** in Scheme 1 was confirmed by ^1H NMR and FT-IR spectroscopies. The ^1H NMR spectrum[9] contained all the characteristic peaks reported for the authentic macrocycle in the literature[6a] and additional peaks related to the diamine dication pillars. The FT-IR spectrum of the interlayered macrocycle showed the typical amide bands at 1530 and 1635 cm^{-1}. In addition, a strong band at 3000 cm^{-1} indicates that the diamine dications are still maintained in the clay layers, whereas the hydrogen bonds that identify the hemisalt formation have disappeared.

A schematic illustration of the reaction pathway which complies with the observed results is depicted in Scheme 1.

 © WILEY-VCH Verlag GmbH, D-69451 Weinheim, 2001 1433-7851/01/4022-4287 $ 17.50+.50/0

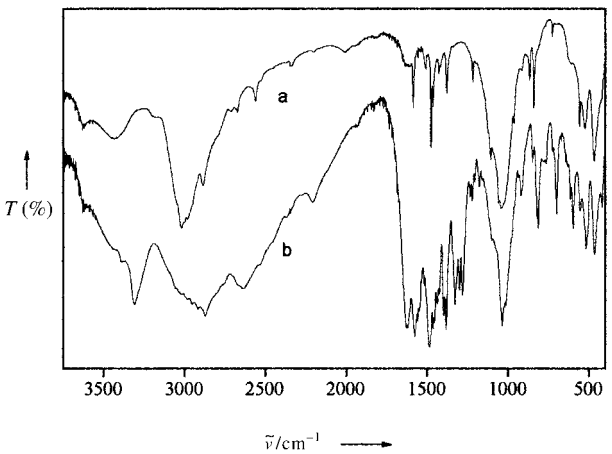


Figure 1. FT-IR spectra (KBr) of: a) the pillared clay (product **a**), b) the clay with the hemisalt in the interlayer space after the intercalation of pillared clay with the neutral diamine (product **b**). The characteristic broad band between 3300 – 2200 cm^{-1} arising from the $[H_2N\text{-}H\cdots NH_2]^+$ hemisalt grouping is replaced in **a** by a strong band near 3000 cm^{-1} which arises from the electrostatically bound $[H_3NCH_2C_4H_4CH_2NH_3]^{2+}$ ions. The spectra are different in the region between 1700 – 1300 cm^{-1} which is associated with the NH_2 scissoring vibrations and the NH_3^+ symmetric deformations.

The isophthaloyl chloride enters the interlayer zone during the synthesis and reacts with the aligned, in-register hydrogen-bonded diamine components to produce the cyclic tetramide. The mode of tetramide formation dictates the wrapping of the molecule around the dicationic organic pillar. The situation is analogous to a rotaxane system, with the mineral layers taking the place of the dumbbell stoppers. Furthermore, the molecular axle, that is, the organic pillar, is rigid and prefixed in the mineral layers. In agreement with the rigid diamine axle, the XRD pattern of the resulting complex shows a basal spacing at 15 Å, which implies that the organic dications maintain their upright position. The interlocked state of the tetramide makes its removal from the clay layers very difficult or even not possible. In fact, although the tetramide is a neutral molecule, it was not eluted into DMSO. One way to overcome this obstacle is to eliminate the diamine pillars. This was accomplished by treating the diamine-pillared clay-macrocycle structure with a concentrated solution of LiCl in DMSO. In this treatment, the Li^+ ions replace the diamine pillars and the macrocycle is simultaneusly liberated into the DMSO solution. The addition of acetone precipitates a mixture of the diamine dihydrochloride salt and the tetraamido macrocycle. The diamine salt is converted into the water-soluble neutral form by treatment with a dilute solution of Na_2CO_3 to leave behind the tetramide as a pure solid in good yield (60 %). The isolation of the pure cyclic tetramide enables its direct identification by ^{1}H NMR spectroscopy and mass spectrometry. Indeed, the ^{1}H NMR spectrum is identical to that reported in the literature,[6a] whereas the mass spectrum shows clearly the molecular ion peak at m/z 532 (see the Supporting Information).

Experimental Section

The clay was a natural Wyoming sodium montmorillonite SWy-1 obtained from the Source Clay Minerals Repository at the University of Missuri, Columbia. It was purified by well-established procedures in clay science. The cationic-exchange capacity (cec) is 80 mequiv per 100 g clay. To prepare the pillared-clay a solution of the *p*-xylylenediamine dihydrochloride salt (125 mg) in water (0.6 mmol, 1.5 × cec) was added to a stirred clay suspension of Na^+-MNT (1 g) in water (20 mL). The mixture was stirred for 1 h, centrifuged, washed with water three times, and air-dried. The dry powder was dispersed in water (30 mL) and a solution of *p*-xylylenediamine (110 mg, 0.8 mmol, 2 × CEC) in water (40 mL) was added. The mixture was stirred for 1 h, and the product was collected by centrifugation and, without washing, was air-dried. A CH_3CN solution (30 mL) containing the isophthaloyl dichloride (490 mg, 2.4 mmol) and Et_3N (242 mg, 2.4 mmol) was added to the dry powder in CH_3CN (30 mL) and the mixture stirred for 24 h. The product was collected by centrifugation and washed with CH_3CN (30 mL). The clay complex was dispersed in LiCl-DMSO solution (20 mL) to remove the organic impurities from the clay. Acetone (50 mL) was added to the organic phase to precipitate the amide tetramer and the *p*-xylylenediamine dihydrochloride salt. The mixture was treated with a diluted Na_2CO_3 solution to convert the diamine salt into the water soluble neutral diamine, thus leaving the tetramide as a pure solid (130 mg, 60 % yield). ^{1}H NMR (300 MHz, $[D_6]$DMSO): $\delta = 4.4$ (s, 8H, CH_2), 7.34 (s, 8H, *p*-xylyl H), 7.56 (t, 2H, isophthaloyl 5-H), 7.9 (d, 4H, isophthaloyl 4-H and 6-H), 8,32 (s, 2H, isophthaloyl 2-H), 9,0 (t, 4H, CONH); FT-IR (KBr): $\tilde{\nu}$: 1635, 1530 cm^{-1} (CONH); EI-MS: m/z: 532 $[M^+]$.

Received: May 25, 2001 [Z 17177]

[1] a) M. C. Thompson, D. H. Busch, *J. Am. Chem. Soc.* **1962**, *84*, 1762 – 1763; b) C. J. Pedersen, *J. Am. Chem. Soc.* **1967**, *89*, 2495 – 2496; c) K. N. Houk, S. Menzer, P. Newton, F. M. Raymo, J. F. Stoddart, D. J. Williams, *J. Am. Chem. Soc.* **1999**, *121*, 1479 – 1487; d) P. L. Anelli, P. R. Ashton, R. Ballardini, V. Balzani, M. Delgado, M. T. Gandolfi, T. T. Goodnow, A. E. Kaifer, D. Philp, M. Pietraszkiewicz, L. Prodi, M. V. Reddington, A. M. Z. Slawin, N. Spencer, J. F. Stoddart, C. Vicent, D. J. Williams, *J. Am. Chem. Soc.* **1992**, *114*, 193 – 218; e) F. M. Raymo, J. F. Stoddart, *Chem. Rev.* **1999**, *99*, 1643 – 1663.

[2] a) C. Seel, F. Vogtle, *Chem. Eur. J.* **2000**, *6*, 21 – 24; b) D. B. Amabilino, J. F. Stoddart, *Chem. Rev.* **1995**, *95*, 2725 – 2828.

[3] a) T. J. Pinnavaia, *Science* **1983**, *220*, 365; b) R. E. Grim, *Clay Mineralogy*, McGraw-Hill, New York, **1968**; c) *Chemistry of Clays and Clays Minerals*, *Mineralogical Society Monograph*, *No. 6* (Ed.: A. C. D. Newman), Longman, London, **1987**.

[4] a) G. Lagaly, *Solid State Ionics* **1986**, *22*, 43; b) "Supramolecular Architecture: Synthetic Control in Thin Films and Solids": C. L. Lin, T. Lee, T. J. Pinnavaia, *ACS Symp. Ser.* **1992**, *499*, 145; c) B. K. G. Thenk, *The Chemistry of Clay—Organic Reactions*, Adam Hilger, London, **1974**.

[5] a) A. G. Johnston, D. A. Leigh, R. J. Pritchard, M. D. Deegan, *Angew. Chem.* **1995**, *107*, 1324 – 1327; *Angew. Chem. Int. Ed. Engl.* **1995**, *34*, 1209 – 1212; b) A. G. Johnston, D. A. Leigh, L. Nazhat, J. P. Smart, M. D. Deegan, *Angew. Chem.* **1995**, *107*, 1327 – 1331; *Angew. Chem. Int. Ed. Engl.* **1995**, *34*, 1212 – 1216.

[6] a) A. G. Johnston, D. A. Leigh, A. Murphy, J. P. Smart, M. D. Deegan, *J. Am. Chem. Soc.* **1996**, *118*, 10662 – 10663; b) D. A. Leigh, A. Murphy, J. P. Smart, A. M. Z. Slawin, *Angew. Chem.* **1997**, *109*, 752 – 756; *Angew. Chem. Int. Ed. Engl.* **1997**, *36*, 728 – 731.

[7] V. C. Farmer, M. M. Mortland, *J. Phys. Chem.* **1965**, *69*, 683 – 687.

[8] P. Cloos, R. D. Laura, *Clays Clay Miner.* **1972**, *20*, 259 – 270.

[9] The ^{1}H NMR (200 MHz, $[D_6]$DMSO) spectra were recorded on an intergallery-formed tetramide using the synthetic clay laponite (from Laponite Industries Ltd.) which is free of paramagnetic centers; see the Supporting Information.

 © WILEY-VCH Verlag GmbH, D-69451 Weinheim, 2001 1433-7851/01/4022-4288 $ 17.50+.50/0

Testing Racemic Chiral Catalysts for Kinetic Resolution Potential**

Beatriz Dominguez, Neil S. Hodnett, and Guy C. Lloyd-Jones*

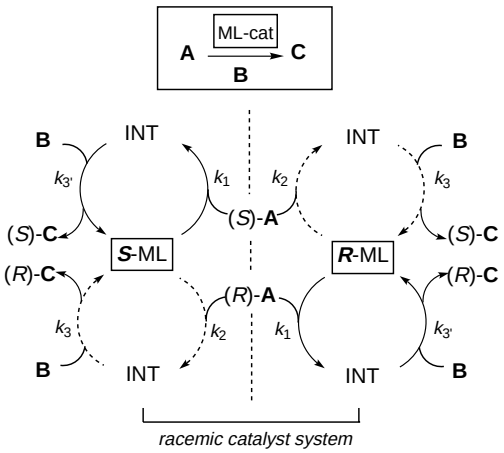
Development of methods for accelerated discovery of asymmetric catalysts has been the subject of much recent attention.[1] Most methods[2] are underpinned by two tactics: 1) the synthesis of diverse sets ("libraries") of novel chiral ligands and 2) rapid ("high-throughput") screening to distinguish selective from nonselective catalysts.

Kinetic resolution is a well known and utilized process in asymmetric catalysis[3] and several novel methods have emerged for rapid screening. Recent examples include the mass spectrometric analysis of pseudoenantiomers[4] and the detection of differential rates between racemic/enantiomerically pure substrates by IR thermography[5] or thermionic resistors.[6]

Despite such advances, a common restriction in the discovery of novel chiral catalysts is the dependence on chiral pool, preexisting asymmetric methodologies, or classical resolution.[7] This reinforces the relationship between ready availability and application. Herein we report on "proof-of-concept" studies for a method that *predicts* whether a catalyst will display significant selectivity in a kinetic resolution reaction. We do this by testing the racemic form, without the need for the preparation of scalemic or enantiomerically pure catalyst.[8] This method differs substantially from asymmetric deactivation ("poisoning"),[9] activation,[10] or complexation[11] of racemic catalysts, since the active catalyst system is racemic.[12]

Kinetic resolution reactions operate through a kinetic match/mismatch relationship (often quantified as "s" $= k_{fast}/k_{slow}$) between the two enantiomers of the substrate and the catalyst. Consider the enantiomeric processes (*R*)-**A** + **B** $\rightarrow$(*R*)-**C**; (*S*)-**A** + **B** $\rightarrow$(*S*)-**C**, where **A** is substrate, **B** is an achiral reagent, and their reaction to give **C** is catalyzed by "ML", a metal complex bearing chiral ligand L (Scheme 1). If there is kinetic diastereoselection between the reaction of "ML" with enantiomers of **A** (i.e. $k_1/k_2\,(=s) > 1$), then kinetic resolution of (±)-**A** will occur if *enantiomerically enriched or pure* "ML" is employed to facilitate turnover of either the left-hand or the right-hand pair of cycles.[13] However, with the racemic catalyst "(±)-ML", enantiomeric catalytic cycles (Scheme 1) will turn over at equal rates and there will be no kinetic resolution.[14]

On the surface it thus appears that the racemic catalyst cannot be tested. However, on closer inspection it emerges that if the reaction velocity does not display a *direct* relationship with the concentration of **A**,[15] then one may gain access to qualitative information regarding the magnitude of s by employing a *scalemic* ($0 < ee < 100$) sample of **A** and monitoring the change in the enantiomeric excess (*ee*) of **A** with conversion. For example, if the catalyst is "perfect" in its selectivity (i.e. $s = \infty$), then enantiomeric catalytic cycles will react exclusively with enantiomeric substrate (**A**). Under a kinetic regime that is pseudo zero-order in [**A**],[15] the enantiomeric catalytic cycles consume **A** at essentially equal rates (i.e. net-*racemic* **A** is converted to **C**) until all of the minor enantiomer of **A** is consumed. Thus the *ee* of the remaining unreacted **A** *increases* throughout reaction[16] and eventually becomes 100%. In contrast, if there is no catalyst selectivity ($s = 1$), then both enantiomers of catalyst react equally proficiently with both enantiomers of substrate. Consequently, the relative rate of consumption of (*R*)-**A** versus that of (*S*)-**A** is solely dependent on their relative concentration (i.e. the enantiomeric ratio) and the *ee* of **A** will remain constant throughout reaction.



Scheme 1. Hypothetical reaction in which (*R*)-**A** is matched with catalyst (*R*)-ML and mismatched with (*S*)-ML (and vice versa for (*S*)-**A**) for conversion to **C** by reaction with **B**. When pure (*R*)-ML or pure (*S*)-ML is employed, kinetic resolution of (±)-**A** will occur.

For the method to be of practical utility, the *ee* of remaining **A** must be measured with reasonable accuracy and thus monitoring changes in *ee* (Δ_{ee}) at lower conversions is preferred. Prior to conducting experiments, we simulated[17] the system in Scheme 1 to study the change in *ee* of **A** with conversion under ideal conditions. The simulation on the left-hand side of Figure 1 indicates that for initial substrate *ee* values (ee_{init}) of 20, 40, 60, and 80%, a selective ($s = 10$),[3c] but

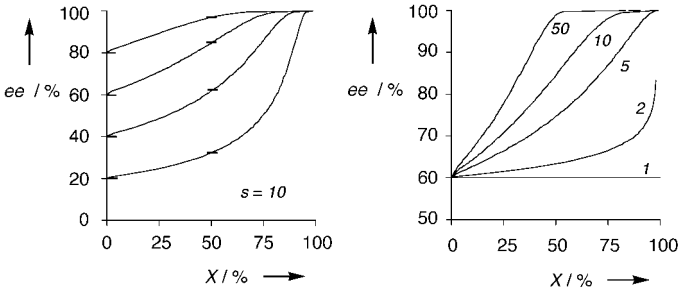


Figure 1. Predicted[17] *ee* of **A** (y axis) as a function of conversion (x axis; X = conversion of **A**) on reaction with **B** catalyzed by racemic catalyst (±)-ML as in Scheme 1. Left-hand graph: $s = 10$ and ee_{init} variable; right-hand graph: $ee_{init} = 60\%$ and s variable.

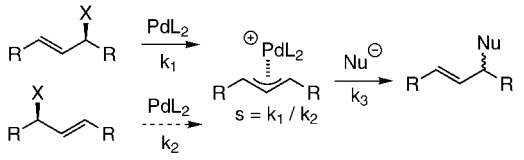
[*] Dr. G. C. Lloyd-Jones, Dr. B. Dominguez, N. S. Hodnett
School of Chemistry, University of Bristol
Cantock's Close, Bristol BS8 1TS (UK)
Fax: (+44) 117-929-8611
E-mail: Guy.Lloyd-Jones@bris.ac.uk

[**] We thank the EPSRC (GR/M83384) for support of this program.

 © WILEY-VCH Verlag GmbH, D-69451 Weinheim, 2001 1433-7851/01/4022-4289 $ 17.50+.50/0

racemic, catalyst system will induce Δ_{ee} values of 12, 21, 24, and 16% respectively after 50% conversion of **A**. For the example of an ee_{init} value of 60%, the right-hand simulation explores the relationships between *ee* and conversion predicted for different selectivity (*s*) values. These simulations demonstrate that it should be feasible to compare racemic catalysts under such conditions and gain some indication of their relative selectivities.

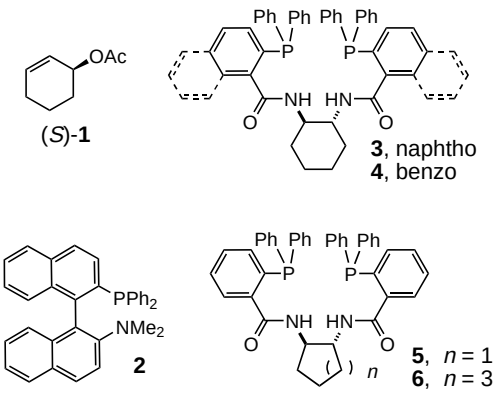
There has recently been considerable interest in Pd-catalyzed kinetic resolution of allylic electrophiles, [Eq. (1)].[18] Since it is common that the rate-limiting step



(1)

involves attack of the nucleophile (most often a stabilized carbanion) on a Pd^{II}-π-allyl intermediate,[19] one may envisage that a pseudo zero-order regime in allylic substrate will hold through a wide range of conversion. Therefore, such a process (e.g. that in Scheme 1, **A** = allylic electrophile; **B** = nucleophile) appeared to be a good candidate for a "proof-of-concept" study in which the *ee* value of an initially scalemic sample of allyl substrate should rise throughout reaction if $s > 1$.

The change in *ee* value of samples of (*S*)-cyclohex-2-enyl acetate (*S*)-**1** (62–64% *ee*) with conversion upon Pd-catalyzed reaction with [$NaCH(CO_2Me)_2$], by employing three well known, but racemic ligands **2**,[20a] **3**,[20b] and **4**,[20c] is given in the left-hand graph in Figure 2. It is evident by comparison with the curves predicted in Figure 1 that the system deviates from ideality. Nonetheless, the magnitude of the Δ_{ee} value does predict **4** to be superior to **2** or **3**. This was indeed found to be the case: the *s* values independently determined under identical conditions with enantiomerically pure samples of (*S*)-**2**, (*R*,*R*)-**3**, and (*R*,*R*)-**4** were 2, 10, and 45 respectively.



To demonstrate the utility of this method, we have prepared and tested analogues of the Trost modular ligand **4**. Unlike *trans*-1,2-diaminocyclohexane (used for the construction of **4**), neither diamine required for construction of ligands **5** and **6** is commercially available. However, racemic ligands (±)-**5** and (±)-**6** were readily prepared in a few steps from cyclopentene and cycloheptene, respectively, and then screened (see right-hand graph in Figure 2). The results clearly suggest that cyclopentyldiamine-derived ligand **5** may have potential utility in enantiomerically pure form.[21]

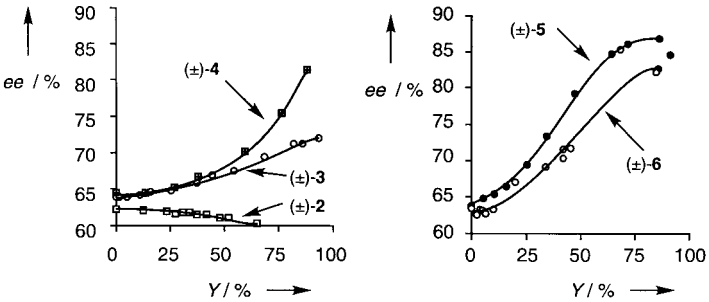


Figure 2. Experimentally observed changes in *ee* (*y* axis) as a function of conversion (*x* axis; *Y* = conversion of **1**) for the Pd-catalyzed reaction of (*S*)-cyclohex-2-enyl acetate ((*S*)-**1**; 62–64% *ee*) with $NaCH(CO_2Me)_2$ in THF at 25 °C. Left-hand graph: using known ligands (±)-**2**, (±)-**3**, and (±)-**4**; right-hand graph: using novel ligands (±)-**5** and (±)-**6**.

In summary, we have demonstrated that the potential efficacy of an enantiomerically pure ligand for a transition metal catalyzed kinetic resolution reaction can be tested by monitoring the reaction of a scalemic substrate by employing a catalyst generated from racemic ligand under pseudo zero-order conditions. The ability to test a racemic ligand *before* enantioselective ligand synthesis or resolution need be developed may prove of significant utility in novel ligand architecture based on axial, planar, helical, or heteroatom (e.g. P) chirality.

Experimental Section

[{Pd(η^3-C_3H_5)Cl}$_2$] (1 mg, 2.5 mmol) and (±)-**5** (5 mg, 7.5 mmol) were dissolved in anhydrous THF (1 mL) and stirred at 25 °C for 15 min to afford a pale yellow solution. In a separate Schlenk tube, (*S*)-**1** (76 mg, 0.50 mmol; 63% *ee*) was added to a solution of dimethylmalonate (164 mg, 1.25 mmol), NaH (60% dispersion in mineral oil, 50 mg, 1.25 mmol), and 4-methylacetophenone (internal standard) in THF (20 mL), immediately followed by the catalyst solution. Aliquots (100–200 μL) of the reaction mixture were periodically withdrawn by cannula, quenched with saturated aqueous NH_4Cl, dried ($MgSO_4$), filtered through a plug of silica, and then analyzed for conversion and *ee* by GC (30 m Chiraldex β-dm column, 123 KPa, 1.4 $cm^3 min^{-1}$, ID 0.25 mm, 90 °C, (*R*)-**1** 9.2 min, (*S*)-**1** 9.5 min) data obtained as shown in Figure 2.

Received: July 12, 2001 [Z17483]

[1] Reviews: a) M. T. Reetz, *Angew. Chem.* **2001**, *113*, 292–320; *Angew. Chem. Int. Ed.* **2001**, *40*, 284–310; b) B. Jandeleit, D. J. Schaefer, T. S. Powers, H. W. Turner, W. H. Weinberg, *Angew. Chem.* **1999**, *111*, 2648–2689; *Angew. Chem. Int. Ed.* **1999**, *38*, 2494–2532; c) H. B. Kagan, *J. Organometal. Chem.* **1998**, *567*, 3–6; d) K. D. Shimizu, M. L. Snapper, A. H. Hoveyda, *Chem. Eur. J.* **1998**, *4*, 1885–1889.

[2] For leading references see: a) K. Mikami, R. Angelaud, K. Ding, A. Ishii, A. Tanaka, N. Sawada, K. Kudo, M. Senda, *Chem. Eur. J.* **2001**, *7*, 730–737; b) H. Wennemers, *Comb. Chem. High Throughput Screening* **2001**, *4*, 273–285; c) R. H. Crabtree, *Chem. Commun.* **1999**, 1611–1616; d) T. Bein, *Angew. Chem.* **1999**, *111*, 335–338; *Angew. Chem. Int. Ed.* **1999**, *38*, 323–326.

 © WILEY-VCH Verlag GmbH, D-69451 Weinheim, 2001 1433-7851/01/4022-4290 $ 17.50+.50/0

[3] Reviews: a) A. H. Hoveyda, M. T. Didiuk, *Curr. Org. Chem.* **1998** *2*, 489 – 526; b) G. R. Cook, *Curr. Org. Chem.* **2000** *4*, 869 – 885; c) J. M. Keith, J. F. Larrow, E. N. Jacobsen, *Adv. Synth. Catal.* **2001**, *343*, 5 – 26.

[4] M. T. Reetz, M. H. Becker, H. W. Klein, D. Stockigt, *Angew. Chem.* **1999**, *111*, 1872 – 1875; *Angew. Chem. Int. Ed.* **1999**, *38*, 1758 – 1761.

[5] M. T. Reetz, M. H. Becker, K. M. Kuhling, A. Holzwarth, *Angew. Chem.* **1998**, *110*, 2792 – 2795; *Angew. Chem. Int. Ed.* **1998**, *37*, 2647 – 2650.

[6] A. R. Connolly, J. D. Sutherland, *Angew. Chem.* **2000**, *112*, 4438 – 4441; *Angew. Chem. Int. Ed.* **2000**, *39*, 4268 – 4271.

[7] See, for example, catalysts for asymmetric acylation: a) G. C. Fu, *Pure Appl. Chem.* **2001**, *73*, 347 – 349; b) A. Spivey, A. Maddaford, T. Fekner, A. J. Redgrave, C. S. Frampton, *J. Chem. Soc. Perkin Trans. 2* **2000**, 3460 – 3468.

[8] As noted by a referee, the method demands availablity of asymmetric protocols for preparation of the enantiomerically enriched substrate and is unsuitable for parallel screening of ligand libraries. However, we envisage that the method will find most utility in screening single novel ligands (in racemic form) in *benchmark* reactions.

[9] See, for example: a) J. W. Faller, D. W. I. Sams, X. Liu, *J. Am. Chem. Soc.* **1996**, *118*, 217 – 218; b) J. W. Faller, *Tetrahedron Lett.* **1993**, *34*, 7359 – 7362.

[10] Reviews: a) K. Mikami, M. Terada, T. Korenaga, Y. Matsumoto, M. Ueki, R. Angelaud, *Angew. Chem.* **2000**, *112*, 3676 – 3701; *Angew. Chem. Int. Ed.* **2000**, *39*, 3532 – 3556; b) K. Mikami, M. Terada T. Korenaga, Y. Matsumoto, S. Matsukawa, *Acc. Chem. Res.* **2000**, *33*, 391 – 401; c) K. Muniz, C. Bolm, *Chem. Eur. J.* **2000**, *6*, 2309 – 2316.

[11] See, for example: J. M. Brown, P. J. Maddox, *Chirality* **1991**, *3*, 345 – 354.

[12] We note that most (but not all) nonlinear effects arise through active "monomer" and inactive aggregate. Leading references: a) C. Girard, H. B. Kagan, *Angew. Chem.* **1998**, *110*, 3088 – 3127; *Angew. Chem. Int. Ed.* **1998**, *37*, 2923 – 2959; b) H. B. Kagan, *Synlett* **2001**, 888 – 899.

[13] For leading references and discussions of the implications of scalemic catalysts in kinetic resolution, see: a) D. G. Blackmond, *J. Am. Chem. Soc.* **2001**, *123*, 545 – 553; b) T. O. Luukas, C. Girard, D. R. Fenwick, H. B. Kagan, *J. Am. Chem. Soc.* **1999**, *121*, 9299 – 9306; c) D. W. Johnson, D. A. Singleton, *J. Am. Chem. Soc.* **1999**, *121*, 9307 – 9312; d) R. F. Ismagilov, *J. Org. Chem.* **1998**, *63*, 3772 – 3774.

[14] Irrespective of the order of "**A**" in the rate equation, comparison of rates of racemic "(±)-**A**" versus enantiomerically pure, for example (*S*)-**A**, will not usually distinguish whether $s > 1$.

[15] "Saturation" or "pseudo zero-order" conditions are quite common in kinetic resolutions (see ref. [3b]). If $k_1[\mathbf{A}][\mathrm{ML}] > k_2[\mathbf{A}][\mathrm{ML}] \gg k_3[\mathbf{B}][\mathrm{INT}]$, Scheme 1, then the "resting state" is INT, $\mathrm{d}[\mathbf{A}]/\mathrm{d}t \propto [\mathbf{B}][\mathrm{INT}]$ and, irrespective of *s*, the *ee* value of **A** will not affect turnover rates.

[16] If the reaction is stereospecific (e.g. (*R*)-**A** gives (*R*)-**C**) then $ee\,\mathbf{C}_{init} < ee\,\mathbf{C}_{final}$ ($= ee\,\mathbf{A}_{init}$).

[17] MacKinetics v0.9.1b, Leipold Associates, USA, **1997**, Scheme 1: $[\mathbf{A}]_0 = [\mathbf{B}]_0 = 1.0$, $[(\pm)\text{-ML}]_0 = 0.02$; $k_1 = 100$, $k_2 = k_1/s$; $k_3 = 1$.

[18] T. Hayashi, A. Yamamoto, Y. Ito, *J. Chem. Soc. Chem. Commun.* **1986**, 1090 – 1092; b) H.-J. Gais, H. Eichelmann, N. Spalthoff, F. Gerhards, M. Frank, G. Raabe, *Tetrahedron: Asymmetry* **1998**, *9*, 235 – 248; c) G. C. Lloyd-Jones, S. C. Stephen, *Chem. Commun.* **1998**, 2321 – 2322; d) S. Ramdeehul, P. Dierkes, R. Aguado, P. C. J. Kamer, P. W. N. M. van Leeuwen, J. A. Osborn, *Angew. Chem.* **1998**, *110*, 3302 – 3304; *Angew. Chem. Int. Ed.* **1998**, *37*, 3118 – 3121; e) J. M. Longmire, B. Wang, X. Zhang, *Tetrahedron Lett.* **2000**, *41*, 5435 – 5439; f) S. R. Gilbertson, P. Lan, *Org. Lett.* **2001**, *3*, 2237 – 2240.

[19] P. B. Mackenzie, J. Whelan, B. Bosnich, *J. Am. Chem. Soc.* **1985**, *107*, 2046 – 2054.

[20] a) Š. Vyskočil, M. Smrčina, V. Hanuš, M. Polášek, P. Kočovský, *J. Org. Chem.* **1998**, *63*, 7738 – 7748; b) B. M. Trost, R. C. Bunt, R. C. Lemoine, T. L. Calkins, *J. Am. Chem. Soc.* **2000**, *122*, 5968 – 5976; c) B. M. Trost, D. L. Van Vranken, C. Bingel, *J. Am. Chem. Soc.* **1992**, *114*, 9327 – 9343.

[21] (*R*,*R*)-**5** was subsequently prepared and tested in the kinetic resolution of (±)-**1** (15 data points, $c = 0 \rightarrow 51\,\%$). Nonlinear regression of $s = \ln[(1-c)(1-ee)]/\ln[(1-c)(1+ee)]$ gave $s = 120 \pm 30$; however, the selectivity increases as the reaction proceeds; for example, $c = 50.7\,\%$; *ee* (**1**) = 99 %; $s = 263$. This selectivity ($s > 100$) is significantly higher than any reported to date in Pd-catalyzed allylic alkylation.[18] We are currently evaluating **5** in other reactions.

 © WILEY-VCH Verlag GmbH, D-69451 Weinheim, 2001 1433-7851/01/4022-4291 $ 17.50+.50/0

PREVIEW 23/2001



REVIEW

Organic Nanoparticles in the Aqueous Phase—Theory, Experiment, and Use — J. Rieger and D. Horn

MINIREVIEW

Self-Complementary Quadruple Hydrogen-Bonding Motifs as a Functional Principle: From Dimeric Supramolecules to Supramolecular Polymers — C. Schmuck and W. Wienand

ESSAY

Chemistry at the Uncertainty Limit — A. H. Zewail

HIGHLIGHT

Recent Progress in the Enantioselective Synthesis of β-Lactams: Development of the First Catalytic Approaches — P. A. Magriotis

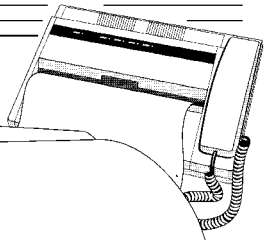
COMMUNICATIONS

The Highly Flexible Bis(hydroxylamine) Ligand $[ON(Me)]_2CH_2^{2-}$ and Its Different Behavior in the Chemistry of Aluminum and Gallium — N. W. Mitzel and C. Lustig

Total Synthesis and Proof of Stereochemistry of Natural and Unnatural Pinnaic Acids: A Remarkable Long-Range Stereochemical Effect in the Reduction of 17-Oxo Precursors of the Pinnaic Acids — S. J. Danishefsky et al.

ORDER FORM REPLY BY FAX

ANGEWANDTE CHEMIE
International Edition



From:

Name _____

Street _____

City _____

State / Zip _____ / _____

To:

WILEY-VCH
P.O. Box 10 11 61
D-69451 Weinheim, Germany

Tel.: +49 6201 - 606 147
Fax: +49 6201 - 606 172
E-mail: subservice@wiley-vch.de

❑ **Please enter my subscription for 2002 (26 issues)**
(Only yearly subscriptions are accepted.) Valid for print or electronic / print and electronic delivery

Simply copy, fill out, and fax.

At the institutional rate:
❑ Europe: € 2158.00/2266.00
❑ Outside Europe: US$ 2878.00/3022.00

at the individual rate* (print only):
❑ Europe: € 228.00
❑ Outside Europe: US$ 318.00

Please tick:
❑ Print
❑ Electronic
❑ Print and electronic

*(Individual rates are available only for bona fide individual orders for personal use, paid for by personal check or credit card. *Rates for personal members of the GDCh outside Germany/Austria/Switzerland)

Method of payment:

❑ Check ❑ VISA ❑ MasterCard ❑ American Express

Account # _____

Exp. Date __ __ ____ Signature X _____

WILEY-VCH

ANGEWANDTE CHEMIE
INTERNATIONAL EDITION
A Journal of the Gesellschaft Deutscher Chemiker
2001
40/23
Pages 4309–4518

COVER PICTURE

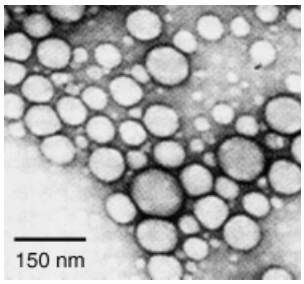
The cover picture shows in the center an electron-density map of the molecular container compound cucurbit[7]uril. The polarizability inside the cavity of this host can be explored through solvatochromic effects on the absorption spectra (bottom right) when probed by the inclusion of an azo chromophore guest (top left). This novel method allows insight into the inner phase of supermolecules. More details about this process is described by Marquiz and Nau on pp. 4387 ff.



REVIEW

Contents

Aqueous, nanodispersed formulations of organic active compounds and effect materials (see electron micrograph) allow a dramatic increase in solubility, an improvement in biological absorption, and the modification of physical properties. The current state of knowledge of the basics of particle formation from homogeneous solution, the influence of the solvent and polymer additives on the morphology, and the supramolecular structure of the nanoparticles, is illustrated with the carotenoids, an industrially interesting class of compounds.



D. Horn, J. Rieger* 4330–4361

Organic Nanoparticles in the Aqueous Phase—Theory, Experiment, and Use

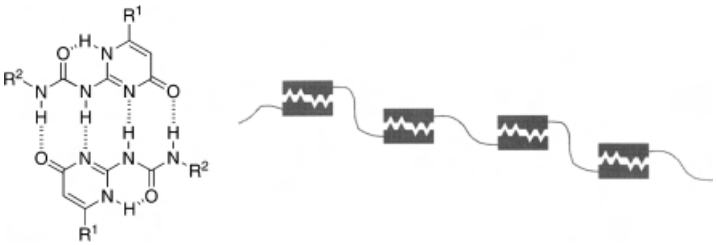
Angew. Chem. **2001**, *113*, 4460–4492

Keywords: carotenoids · disperse systems · nanoparticles · nanostructures · phase transformations

 © WILEY-VCH Verlag GmbH, D-69451 Weinheim, 2001 1433-7851/01/4023-4311 $ 17.50+.50/0

MINIREVIEW

Four linearly arranged hydrogen bonds result in very efficient self-associating systems (left in the picture). Such quadruple hydrogen-bonding motifs offer the opportunity to obtain supramolecular polymers through the self-association of self-complementary monomers (shown schematically on the right). As the formation of noncovalent interactions is reversible and their strength depends on the external conditions, it is possible to influence the macroscopic properties of such polymers through altering the environment.



C. Schmuck,* W. Wienand 4363 – 4369

Self-Complementary Quadruple Hydrogen-Bonding Motifs as a Functional Principle: From Dimeric Supramolecules to Supramolecular Polymers

Angew. Chem. **2001**, *113*, 4493 – 4499

Keywords: dimerizations · heterocycles · hydrogen bonds · molecular recognition · polymers · supramolecular chemistry

ESSAY

Spatial and temporal resolution with, until recently, an unimaginable precision—about 0.01 Å and 10 fs, respectively—are today possible thanks to femtochemistry. However, this atomic-scale resolution raises fundamental questions from quantum mechanics: the Uncertainty Paradox. How is it that this is not an obstacle, and what are the future directions? are the themes of this Essay.

A. H. Zewail* ..... 4371 – 4375

Chemistry at the Uncertainty Limit

Angew. Chem. **2001**, *113*, 4501 – 4506

Keywords: coherence · femtobiology · femtochemistry · spectroscopic methods · ultrafast electron diffraction

VIPs

The following communications are "Very Important Papers" in the opinion of two referees. They will be published shortly (those marked with a diamond will be published in the next issue). Short summaries of these articles can be found on the *Angewandte Chemie* homepage at the address http://www.angewandte.com

Design and Synthesis of a Peptide that Binds Specific DNA Sequences through Simultaneous Interaction in the Major and in the Minor Groove — M. E. Vázquez, A. M. Caamaño,* ◆ J. Martínez-Costas, L. Castedo, J. L. Mascareñas*

Influence of Structural and Rotational Isomerism on the Triplet Blinking of Individual Dendrimer Molecules — T. Vosch, J. Hofkens,* M. Cotlet, ◆ F. Köhn, H. Fujiwara, R. Gronheid, K. Van Der Biest, T. Weil, A. S. Herrmann, K. Müllen, S. Mukamel, M. Van der Auweraer, F. C. De Schryver*

Cesiumauride Ammonia (1/1: $CsAu \cdot NH_3$)—A Crystalline Analogue of Alkali Metals Dissolved in Ammonia? — A.-V. Mudring, M. Jansen,* J. Daniels, S. Krämer, M. Mehring, J. P. Ramalho, A. H. Romero, M. Parrinello

Enantiopure Double-Helical Acetylenic Cyclophanes — D.-L. An, T. Nakano, A. Orita, J. Otera*

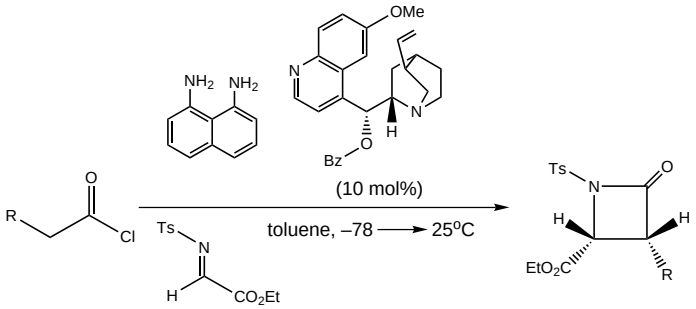
Supramolecular Cluster Catalysis: A Case Study of Benzene Hydrogenation Catalyzed by a Cationic Triruthenium Cluster under Biphasic Conditions — G. Süss-Fink,* M. Faure, T. R. Ward

Syntheses and Crystal Structures of the First Disulfur and Diselenium Complexes of Platinum — K. Nagata, N. Takeda, N. Tokitoh*

Gold-Xenon Complexes — S. Seidel, T. Drews, K. Seppelt*

 © WILEY-VCH Verlag GmbH, D-69451 Weinheim, 2001 1433-7851/01/4023-4312 $ 17.50+.50/0

Two direct catalytic asymmetric syntheses of β-lactams in good yields and high enantio- and diastereoselectivity (up to 96% *ee* and 99:1 d.r.) are described (see reaction scheme for an example). In addition, recent catalytic enantioselective constructions of β-amino acid derivatives en route to enantiomerically pure β-lactams are highlighted.



P. A. Magriotis* ..... 4377 – 4379

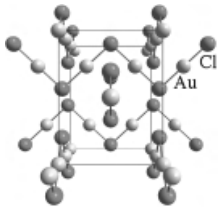
Recent Progress in the Enantioselective Synthesis of β-Lactams: Development of the First Catalytic Approaches

Angew. Chem. **2001**, *113*, 4507 – 4509

Keywords: amino acids · asymmetric catalysis · lactams · Lewis acids · Staudinger reaction

COMMUNICATIONS

Relativistic effects change the symmetry of the solid-state gold halides from a cubic to a chainlike AuX arrangement (X = F, Cl, Br, I; see structure of AuCl) with short Au–Au internuclear distances. The main reason for the relativistic destabilization of the cubic and relativistic stabilization of the chainlike structures is a decrease in ionicity and an increase in covalency in the Au–X interactions.



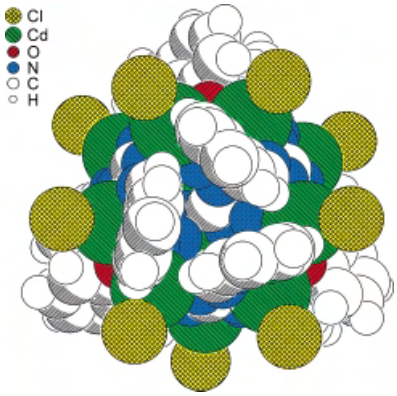
T. Söhnel, H. Hermann, P. Schwerdtfeger* ..... 4382 – 4385

Towards the Understanding of Solid-State Structures: From Cubic to Chainlike Arrangements in Group 11 Halides

Angew. Chem. **2001**, *113*, 4511 – 4515

Keywords: ab initio calculations · density functional calculations · gold · relativistic effects · solid-state structures

A sealed off capsule of composition $[M_{12}(ligand)_4]$ containing a trapped Et_4N^+ ion has the topology of the tetrahedron in which the four nodes are provided by guanidine-based ligands and the six node-to-node connections are provided by pairs of metal centers (see picture).



I. M. Müller, R. Robson,* F. Separovic ..... 4385 – 4386

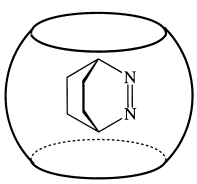
A Metallosupramolecular Capsule with the Topology of the Tetrahedron, 3^3, Assembled from Four Guanidine-Based Ligands and Twelve Cadmium Centers

Angew. Chem. **2001**, *113*, 4519 – 4520

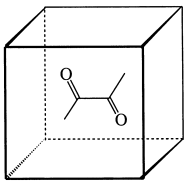
Keywords: cage compounds · coordination chemistry · guanidine · nanostructures · supramolecular chemistry

 © WILEY-VCH Verlag GmbH, D-69451 Weinheim, 2001 1433-7851/01/4023-4313 $ 17.50+.50/0

A polarizability close to the gas phase is measured inside the cavity of the molecular container cucurbit-[7]uril (CB7) by employing 2,3-diazabicyclo[2.2.2]oct-2-ene (DBO) as a solvatochromic guest (CB7 · DBO). Conversely, the previously studied photophysical properties of biacetyl as a guest in a hemicarcerand (HC · biacetyl) indicate an exceptionally high polarizability inside this host cavity. These conclusions can be drawn from the solvatochromism of DBO and biacetyl in different solvents and the gas phase, which reveals correlations with the bulk polarizability. The oscillator strength, that is, the integrated absorption intensity, of the novel probes is not sensitive to the solvent polarity, but responds strongly to the solvent polarizability.



CB7•DBO



HC•biacetyl

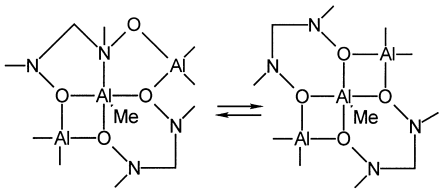
Angew. Chem. **2001**, *113*, 4515 – 4518

C. Marquez, W. M. Nau* ... 4387 – 4390

Polarizabilities Inside Molecular Containers

Keywords: cucurbituril · hemicarcerands · host – guest systems · solvatochromism · solvent effects

Four-, five-, and six-membered rings surround a central five-coordinate aluminum atom in (AlMe)(Al-Me_2)[$(ONMe)_2CH_2$]$_2$ in the solid state, but in solution all eight donor atoms are at some stage involved in bonding to this five-coordinate aluminum center (see scheme). This Al compound is formed from $(HONMe)_2CH_2$ and $AlMe_3$, whereas the reaction with $GaMe_3$ leads to the heteronorbornane $(Me_2GaONMe)_2CH_2$.



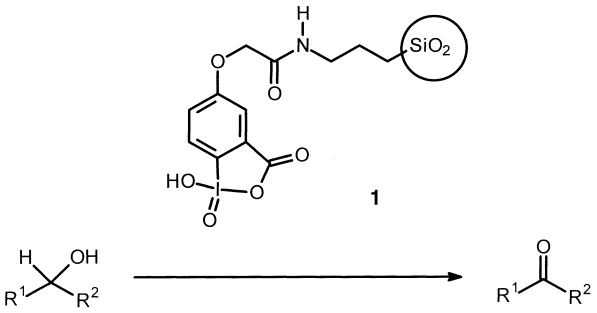
Angew. Chem. **2001**, *113*, 4521 – 4524

C. Lustig, N. W. Mitzel* .... 4390 – 4392

The Highly Flexible Bis(hydroxylamine) Ligand $[ON(Me)]_2CH_2^{2-}$ and Its Different Behavior in the Chemistry of Aluminum and Gallium

Keywords: aluminum · gallium · molecular dynamics · N,O ligands

Primary and secondary alcohols are oxidized smoothly under mild conditions and in high yields to the corresponding aldehydes and ketones by **1** (see scheme), the first polymer-supported IBX.



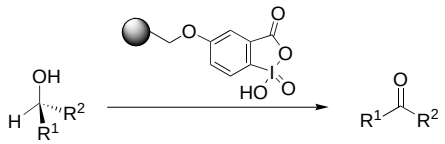
Angew. Chem. **2001**, *113*, 4530 – 4532

M. Mülbaier, A. Giannis* 4393 – 4394

The Synthesis and Oxidative Properties of Polymer-Supported IBX

Keywords: hypervalent compounds · iodine reagents · oxidation · solid-phase synthesis · synthetic methods

The oxidation of various alcohols and cyclization of an olefinic carbamate succeeds with the first polymer-supported iodine(v) reagent (see scheme). The novel oxidizing polymer oxidizes sensitive and complex alcohols, including protected amino alcohols, efficiently in good to excellent yields. In addition, the α,β-dehydration of a ketone is demonstrated.



Angew. Chem. **2001**, *113*, 4532 – 4535

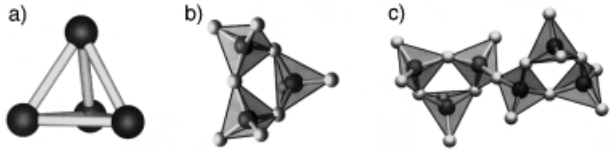
G. Sorg, A. Mengel, G. Jung, J. Rademann* ..... 4395 – 4397

Oxidizing Polymers: A Polymer-Supported, Recyclable Hypervalent Iodine(v) Reagent for the Efficient Conversion of Alcohols, Carbonyl Compounds, and Unsaturated Carbamates in Solution

Keywords: hypervalent compounds · iodine reagents · oxidation · solid-phase synthesis · synthetic methods

 © WILEY-VCH Verlag GmbH, D-69451 Weinheim, 2001 1433-7851/01/4023-4314 $ 17.50+.50/0

The previously unknown silicate ion $[Si_6O_{17}]^{10-}$ (c) and mixed-valent silicon centers that differ by five oxidation states are present in the tetrelide(−1)–tetrelate(+4) compound $Cs_{10}[Si_4][Si_3O_9]$ (anions a and b) and $Rb_{14}[E_4][Si_6O_{17}]$ (E = Si and Ge; anions a and c). The structures of this new class of compounds can be described by chemical twinning of the silicate and Zintl phases $A^I_4[E^{IV}_4]$.



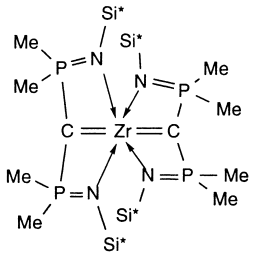
Angew. Chem. **2001**, *113*, 4527–4529

S. Hoffmann, T. F. Fässler,* C. Hoch, C. Röhr* 4398–4400

Alkali Metal Tetrelide–Tetrelates: "Double Salts" With $[E_4]^{4-}$ Zintl Anions (E = Si, Ge) and the First Dimeric Cyclotrisilicate Ions $[Si_6O_{17}]^{10-}$

Keywords: germanides · silicates · silicides · Zintl anions · Zintl phases

Two carbene ligands bound to zirconium: Complex **1** was synthesized under mild conditions by reaction of $CH_2(Me_2P{=}NSiMe_3)_2$ with $[Zr(CH_2C_6H_5)_4]$ in a 2:1 ratio. The resulting complex **1** is the first biscarbene complex of a Group 4 metal. Si* = $SiMe_3$.



1

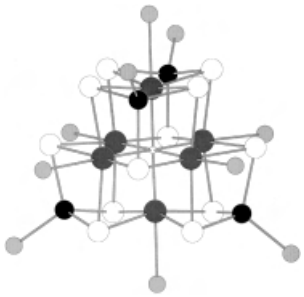
Angew. Chem. **2001**, *113*, 4535–4537

K. Aparna, R. P. Kamalesh Babu, R. McDonald, R. G. Cavell* 4400–4402

The First Biscarbene Complex of a Group 4 Metal: $[Zr\{C(Me_2P{=}NSiMe_3)_2\}_2]$

Keywords: carbene ligands · coordination chemistry · N,P ligands · zirconium

Silylated chalcogenides $(Me_3Si)_2E$ (E = S, Se, Te) grant access to novel Nb–Cu chalcogenido clusters with as yet unknown molecular structures. Dimetallic Nb–Cu selenido clusters $[Cu_4Nb_6Se_{12}O(PMe_3)_{10}][Cu_4NbSe_4Cl_2(PMe_3)_4]$ (the structure of the cation is depicted; Cu: black, Nb: dark gray, P: light gray, Se: white O: small white) and $[Cu_4Nb_2Se_6(PMe_3)_8]$ were isolated from reactions of $(Me_3Si)_2Se$ with Nb-Cu-Se units that were formed in situ. Reactions of CuCl and $NbCl_5$ towards $(Me_3Si)_2S$ or $(Me_3Si)_2Te$ produce the compounds $(NEt_4)[Cu_6Nb_2S_6Cl_5(PEt_3)_6]$ and $[Cu_6NbTe_3(Te_2)_2(PEt_3)_6][CuCl_2]$, respectively.



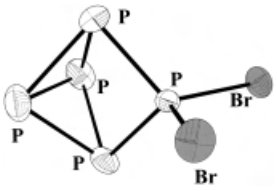
Angew. Chem. **2001**, *113*, 4537–4541

A. Lorenz, D. Fenske* 4402–4406

Syntheses and Structures of Niobium Copper Chalcogenido Clusters: $[Cu_4Nb_6Se_{12}O(PMe_3)_{10}]$-$[Cu_4NbSe_4Cl_2(PMe_3)_4]\cdot 1.5\,DMF$, $[Cu_4Nb_2Se_6(PMe_3)_8]$, $(NEt_4)[Cu_6Nb_2S_6Cl_5(PEt_3)_6]$, and $[Cu_6NbTe_3(Te_2)_2(PEt_3)_6][CuCl_2]$

Keywords: chalcogens · clusters · copper · niobium

Insertion of the intermediately formed carbene-analoguous PX_2^+ ion (X = Br, I) into one of the P–P bonds of the P_4 tetrahedron led to the $P_5X_2^+$ ion (see structure of the Br derivative)—the first example of the previously unknown class of phosphorus-rich binary P–X cations.



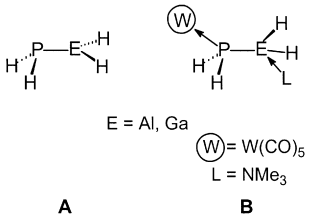
Angew. Chem. **2001**, *113*, 4544–4547

I. Krossing,* I. Raabe 4406–4409

$P_5X_2^+$ (X = Br, I), a Phosphorus-Rich Binary P–X Cation with a C_{2v}-Symmetric P_5 Cage

Keywords: ab initio calculations · cations · halogens · insertion · phosphorus

Neither synthesis nor detection in matrix isolation experiments has been accomplished for the parent compounds of phosphanylalanes and -gallanes of type **A**. H_2 elimination reactions between $[(CO)_5WPH_3]$ and H_3ENMe_3 (E = Al, Ga) have enabled the first synthesis of Lewis acid/base stabilized complexes of the type **B**. Comprehensive density functional theory (DFT) calculations on the aluminum systems verify the high stability of the complexes of type **B**.



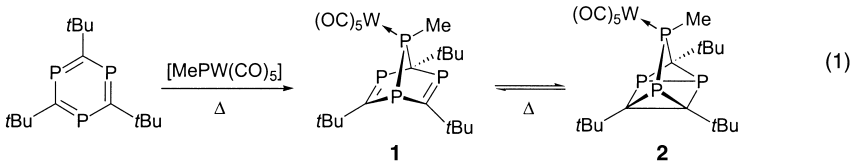
Angew. Chem. **2001**, *113*, 4541–4544

U. Vogel, A. Y. Timoshkin, M. Scheer* 4409–4412

Lewis Acid/Base Stabilized Phosphanylalane and -gallane

Keywords: aluminum · density functional calculations · gallium · Lewis acids · phosphorus

Phosphorus changes stability: Investigation of the phosphorus polycycles **1** and **2**, prepared according to Equation (1), show that the relative stability of the norbornadiene and quadricyclane frameworks is inverted when four of the framework carbon atoms are replaced by phosphorus atoms. These organophosphorus compounds can be isolated at room temperature but are in equilibrium at elevated temperatures. The experimental findings are in agreement with the results of ab initio MO theory calculations.



(1)

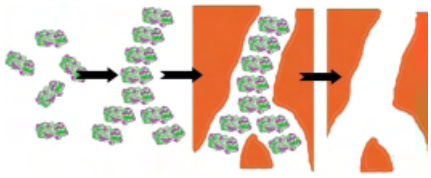
Angew. Chem. **2001**, *113*, 4524 – 4527

M. J. M. Vlaar, A. W. Ehlers, M. Schakel, S. B. Clendenning, J. F. Nixon, M. Lutz, A. L. Spek, K. Lammertsma* ..... 4412 – 4415

Norbornadiene – Quadricyclane Valence Isomerism for a Tetraphosphorus Derivative

Keywords: phosphinidene complexes · phosphorus heterocycles · polycycles · valence isomerism

Self-organization in aqueous media studied indirectly: The aqueous phase is solidified by a silica sol – gel process, and the supramolecular aggregate is 1:1 cast into a solid silica matrix. For the model-system cyclodextrins it was shown that the cyclodextrin molecules self-assemble into "wormlike" aggregates in the porous silica (see scheme). By using this template, porous materials were obtained with promising properties such as a uniform pore system and smooth walls.



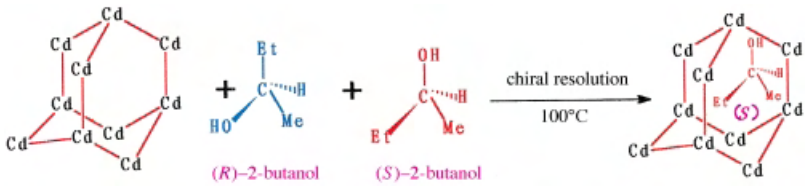
Angew. Chem. **2001**, *113*, 4549 – 4553

S. Polarz,* B. Smarsly, L. Bronstein, M. Antonietti ..... 4417 – 4421

From Cyclodextrin Assemblies to Porous Materials by Silica Templating

Keywords: cyclodextrins · porous materials · self-assembly

Selective inclusion of (*S*)-2-butanol and (*S*)-2-methyl-1-butanol from their racemic mixtures in 98.2 and 98.4 % *ee*, respectively, is obtained with the robust 3D enantiopure hybrid organic – inorganic zeolite analogue $[Cd(QA)_2]$ (see scheme), which is formed by self-assembly of chiral quitenine (HQA) with $Cd(OH)_2$.



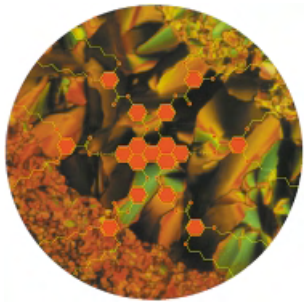
Angew. Chem. **2001**, *113*, 4554 – 4557

R.-G. Xiong,* X.-Z. You, B. F. Abrahams, Z. Xue, C.-M. Che ..... 4422 – 4425

Enantioseparation of Racemic Organic Molecules by a Zeolite Analogue

Keywords: cadmium · crystal engineering · enantioseparation · N ligands · zeolite analogues

Fluorescent liquid crystals: Hydrogen bonding of benzoic acids to azaaromatic receptor groups of diazadibenzoperylene fluorophores induces columnar liquid crystalline mesophases which are highly fluorescent. The structure of a mesogenic supermolecule generated in this way is shown on a background of a polarizing micrograph of the resulting liquid crystalline phase.



Angew. Chem. **2001**, *113*, 4557 – 4560

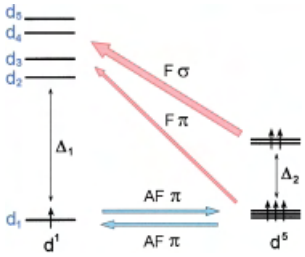
A. Sautter, C. Thalacker, F. Würthner* ..... 4425 – 4428

Control of Liquid Crystallinity of Diazadibenzoperylene Dyes by Covalent and Hydrogen-Bonded Attachment of Mesogens

Keywords: fluorescence · hydrogen bonds · liquid crystals · perylene dyes · supramolecular chemistry

 © WILEY-VCH Verlag GmbH, D-69451 Weinheim, 2001 1433-7851/01/4023-4316 $ 17.50+.50/0

Explaining the magnetism in cyanide-based magnets: The origin of ferromagnetism (F) in the recently synthesized heteronuclear cyanide-bridged clusters and three-dimensional (3D) networks containing octacyanometallates is elucidated. The main factor is the orthogonality of the "magnetic orbitals" of the octametallates to the σ orbitals of all the bridging cyanides, which strongly reduces the antiferromagnetic (AF) contribution to the magnetism of these compounds. The kinetic contribution to the superexchange is shown schematically, the arrows show the direction of the electron transfer.



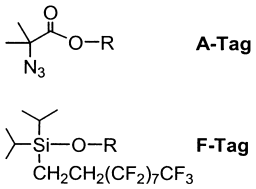
Angew. Chem. **2001**, *113*, 4561 – 4565

L. F. Chibotaru,* V. S. Mironov, A. Ceulemans ..... 4429 – 4433

Origin of Ferromagnetism in Cyano-Bridged Compounds Containing d^1 Octacyanometallates

Keywords: cyanides · magnetic properties · manganese · metal – metal interactions · molybdenum

React or get capped and tagged! Two capping reagents, designated A-Tag and F-Tag, mark unconverted oligosaccharides during automated synthesis for simple separation from the desired products. A-Tagged molecules are removed by an isocyanate scavenger resin after reduction to the amine, and those with an F-tag by filtration through fluorous silica gel. R = oligosaccharide.



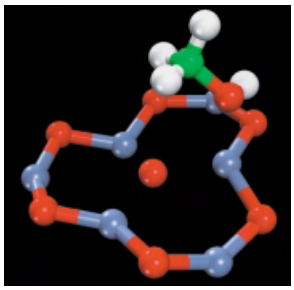
Angew. Chem. **2001**, *113*, 4565 – 4569

E. R. Palmacci, M. C. Hewitt, P. H. Seeberger* ..... 4433 – 4437

"Cap-Tag"—Novel Methods for the Rapid Purification of Oligosaccharides Prepared by Automated Solid-Phase Synthesis

Keywords: oligosaccharides · solid-phase synthesis · synthetic methods

The structures and energetics of the key intermediates in the catalytic conversion of CO_2 into methanol (shown in the figure) are investigated. The polarity of the catalytically relevant $(000\bar{1})$ surface of ZnO gives rise to vacant oxygen sites, which by trapping electrons can promote the reaction. The solid-state embedding method developed is particularly well-suited to studying chemical processes on such localized active sites.



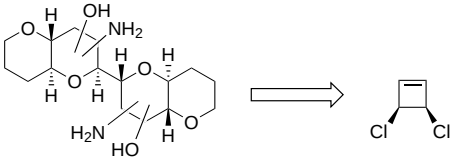
Angew. Chem. **2001**, *113*, 4569 – 4572

S. A. French,* A. A. Sokol, S. T. Bromley, C. R. A. Catlow, S. C. Rogers, F. King, P. Sherwood ..... 4437 – 4440

From CO_2 to Methanol by Hybrid QM/MM Embedding

Keywords: chemisorption · density functional calculations · heterogeneous catalysis · surface chemistry · zinc oxide

An efficient synthesis of cyclic polyether structures (e.g. **1**), which are commonly found in natural products, can be realized from *cis*-3,4-dichlorocyclobutadiene (**2**). The versatility of synthon **2** and a mechanistic rationale for the regio- and stereospecificity of the reactions is discussed.



1 **2**

Angew. Chem. **2001**, *113*, 4573 – 4577

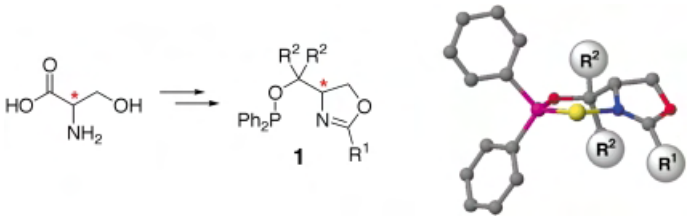
K. C. Nicolaou,* J. A. Vega, G. Vassilikogiannakis ..... 4441 – 4445

cis-3,4-Dichlorocyclobutene as a Versatile Synthon in Organic Synthesis. Rapid Entry into Complex Polycyclic Systems with Remarkably Stereospecific Reactions

Keywords: asymmetric synthesis · cycloalkenes · metathesis · natural products · polycyclic ethers

 © WILEY-VCH Verlag GmbH, D-69451 Weinheim, 2001 1433-7851/01/4023-4317 $ 17.50+.50/0

Both enantiomers are readily prepared of phosphinite–oxazoline ligands **1** from the D and L enantiomers of serine (see Scheme). Iridium complexes derived from these ligands (the structure of one complex is shown) are excellent catalysts for the enantioselective hydrogenation of unfunctionalized alkenes. R^1 = ferrocenyl, aryl; R^2 = alkyl, benzyl.



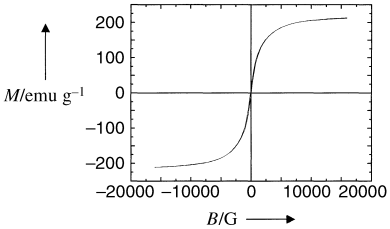
Angew. Chem. **2001**, *113*, 4577–4579

J. Blankenstein, A. Pfaltz* 4445–4447

A New Class of Modular Phosphinite–Oxazoline Ligands: Ir-Catalyzed Enantioselective Hydrogenation of Alkenes

Keywords: asymmetric catalysis · hydrogenation · iridium · ligand design · N,P ligands

A coating of iron carbide and carbon confers air-stability on the nanocrystalline iron particles that were prepared by sonolysis of $[Fe(CO)_5]$ in diphenylmethane followed by annealing of the as-prepared material. The saturation magnetization of this material (222 emu g^{-1}, see picture) is almost as high as that of bulk bcc iron.



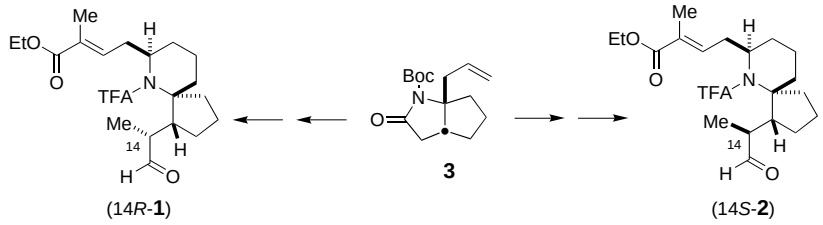
Angew. Chem. **2001**, *113*, 4579–4581

S. I. Nikitenko, Yu. Koltypin, O. Palchik, I. Felner, X. N. Xu, A. Gedanken* 4447–4449

Synthesis of Highly Magnetic, Air-Stable Iron–Iron Carbide Nanocrystalline Particles by Using Power Ultrasound

Keywords: carbides · iron · magnetic properties · nanostructures · sonochemistry

Important intermediates: in an effort to synthesize and determine the stereochemistry of pinnaic acid, C14-epimeric aldehydes **1** and **2** were generated from Meyers' lactam **3**. A key step in the parallel syntheses is a highly stereoselective vinylogous Michael cyclization; Boc = *tert*-butoxy carbonyl, TFA = trifluoroacetic acid.



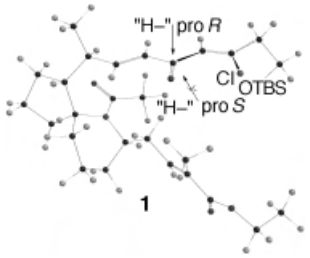
Angew. Chem. **2001**, *113*, 4582–4584

M. W. Carson, G. Kim, M. F. Hentemann, D. Trauner, S. J. Danishefsky* 4450–4452

Concise Stereoselective Routes to Advanced Intermediates Related to Natural and Unnatural Pinnaic Acid

Keywords: alkaloids · asymmetric synthesis · natural products · total synthesis

Build 'em up and knock 'em down: natural pinnaic acid and three of its stereoisomers were synthesized from the aldehydes described in the preceding communication. A key step in the synthesis of natural pinnaic acid was a highly stereoselective reduction of ketone **1**. The stereochemistry was determined by means of degradation studies of the synthetic material; TBS = *tert*-butyldimethylsilyl.



Angew. Chem. **2001**, *113*, 4585–4588

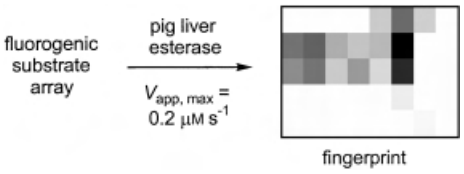
M. W. Carson, G. Kim, S. J. Danishefsky* 4453–4456

Total Synthesis and Proof of Stereochemistry of Natural and Unnatural Pinnaic Acids: A Remarkable Long-Range Stereochemical Effect in the Reduction of 17-Oxo Precursors of the Pinnaic Acids

Keywords: asymmetric synthesis · degradation · natural products · structure elucidation · total synthesis

 © WILEY-VCH Verlag GmbH, D-69451 Weinheim, 2001 1433-7851/01/4023-4318 $ 17.50+.50/0

Differentiation between different enzymes within one class is possible by plotting the relative reaction rates of an enzyme with a series of chromogenic or fluorogenic enzyme substrates as an array of gray-scale squares (see scheme). The characteristic enzyme fingerprints obtained for hydrolytic enzymes such as lipases, esterases, amidases, and epoxide hydrolases are reproducible and enzyme specific. Such fingerprints may be used in quality controls, batch identification, and as screening tools in enzyme discovery programs.



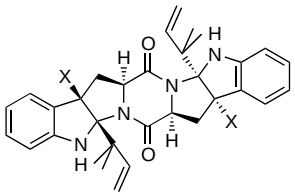
Angew. Chem. **2001**, *113*, 4589 – 4592

D. Wahler, F. Badalassi, P. Crotti, J.-L. Reymond* ..... 4457 – 4460

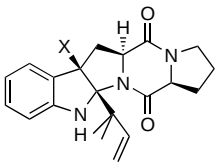
Enzyme Fingerprints by Fluorogenic and Chromogenic Substrate Arrays

Keywords: enzyme assays · enzyme catalysis · high-throughput screening · substrate arrays

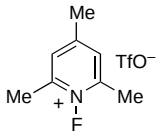
Fluoro-isosteres of natural products containing hexahydropyrazino[1′,2′-1,5]pyrrolo[2,3-*b*]indole-1,4-dione moieties are readily prepared by FP-T300-mediated fluorination – cyclization of cyclo-Trp-AAs (Trp = tryptophan, AA = amino acid). Isosteres **1b** and **2b** of gypsetin (**1a**) and brevianamide E (**2a**), respectively, were thus synthesized.



1a: X = OH
1b: X = F



2a: X = OH
2b: X = F



FP-T300

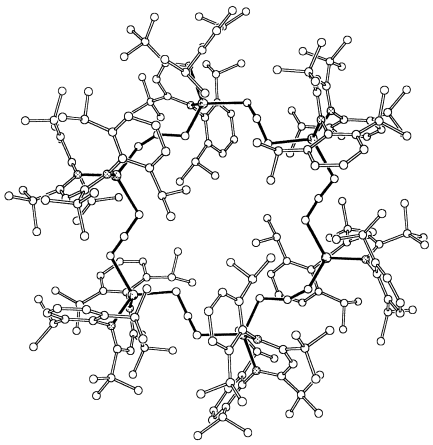
Angew. Chem. **2001**, *113*, 4593 – 4595

N. Shibata,* T. Tarui, Y. Doi, K. L. Kirk ..... 4461 – 4463

Synthesis of Fluorogypsetin and Fluorobrevianamide E by a Novel Fluorination – Cyclization of *cyclo*-L-Trp-L-AAs

Keywords: cyclization · diastereoselectivity · fluorine · natural products · total synthesis

The cyclic hexanuclear species $[\{HC[C(tBu)NAr']_2Mg(C_3H_5)\}_6]$ (see structure) in which the allyl group exhibits μ-η^1:η^1 bonding is formed on thermal treatment of $[HC\{C(tBu)NAr'\}_2Mg(C_3H_5)(thf)]$ under vacuum. Ar′ = 2,6-diisopropylphenyl.



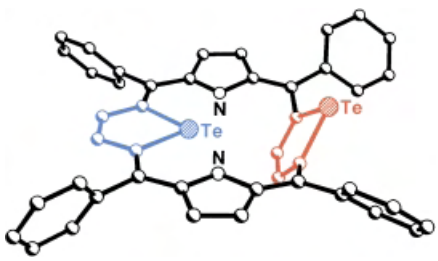
Angew. Chem. **2001**, *113*, 4595 – 4598

P. J. Bailey,* S. T. Liddle,* C. A. Morrison, S. Parsons 4463 – 4466

The First Alkaline Earth Metal Complex Containing a μ-η^1:η^1 Allyl Ligand: Structure of $[\{HC[C(tBu)NC_6H_3(CHMe_2)_2]_2Mg(C_3H_5)\}_6]$

Keywords: allyl ligands · alkaline earth metals · magnesium · N ligands · structure elucidation

The flexible partially inverted structure of an 18-π-electron porphyrin-(1.1.1.1)-like framework is found for 21,23-ditelluraporphyrin (see structure). The dihedral angle between the plane of *meso*-carbon atoms and the inverted tellurophene plane in the solid state is 123.0(2)°, while in solution the porphyrin molecule interchanges between two energetically identical flipped forms.



Angew. Chem. **2001**, *113*, 4598 – 4601

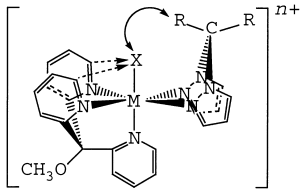
E. Pacholska, L. Latos-Grażyński,* Z. Ciunik ..... 4466 – 4469

An Unorthodox Conformation of [18]porphyrin-(1.1.1.1) Heteroanalogue—21,23-Ditelluraporphyrin with a Flipped Tellurophene Ring

Keywords: heteroporphyrins · nonplanar porphyrins · porphyrinoids · tellurophenes

 © WILEY-VCH Verlag GmbH, D-69451 Weinheim, 2001 1433-7851/01/4023-4319 $ 17.50+.50/0

Stung into action: The largest rate constant to date for ligand substitution at an Ru^{II} center ($110\,M^{-1}s^{-1}$) was observed as a result of a heteroscorpionate ligand effect (see picture; X = H_2O, R = pyrazole, M = Ru) for the substitution of H_2O by CH_3CN.



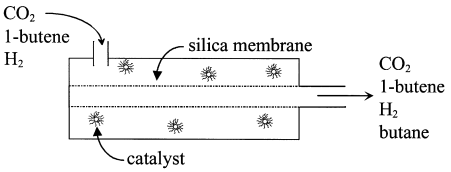
M. H. V. Huynh,* J. Smyth, M. Wetzler, B. Mort, P. K. Gong, L. M. Witham, D. L. Jameson, D. K. Geiger, J. M. Lasker, M. Charepoo, M. Gornikiewicz, J. M. Cintron, G. Imahori, R. R. Sanchez, A. C. Marschilok, L. M. Krajkowski, D. G. Churchill, M. R. Churchill, K. J. Takeuchi* ..... 4469 – 4473

Remarkable Rate Enhancement of Ligand Substitution Promoted by Geometrical Arrangement of Tridentate "Spectator" Ligands

Keywords: kinetics · ligand substitution · N ligands · ruthenium · scorpionates

Angew. Chem. **2001**, *113*, 4601 – 4605

Membrane separation technology is successfully applied for the immobilization of a homogeneous catalyst (a (1*H*,1*H*,2*H*,2*H*-perfluoroalkyl)-dimethylsilyl-substituted derivative of Wilkinson's catalyst) in a continuous process that uses supercritical carbon dioxide as solvent. The catalyst is separated from the products by a microporous silica membrane (see scheme).



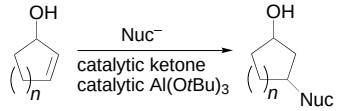
L. J. P. van den Broeke,* E. L. V. Goetheer, A. W. Verkerk, E. de Wolf, B.-J. Deelman, G. van Koten, J. T. F. Keurentjes ..... 4473 – 4474

Homogeneous Reactions in Supercritical Carbon Dioxide Using a Catalyst Immobilized by a Microporous Silica Membrane

Keywords: green chemistry · homogeneous catalysis · hydrogenation · membrane reactors · supercritical fluids

Angew. Chem. **2001**, *113*, 4605 – 4606

Nucleophilic addition to cycloalkenols has been achieved by catalytic electronic activation of the substrate. Catalyzed reversible conversion of the alcohol into a ketone causes electronic activation of the alkene, allowing nucleophilic addition to occur (see scheme).



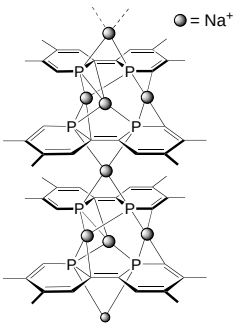
P. J. Black, W. Harris, J. M. J. Williams* ..... 4475 – 4476

Catalytic Electronic Activation: Indirect Addition of Nucleophiles to an Allylic Alcohol

Keywords: aluminum · catalytic electronic activation · homogeneous catalysis · hydrogenation · Michael addition

Angew. Chem. **2001**, *113*, 4607 – 4608

A surprising polymeric structure (see picture) results from the two-electron reduction of a 2,2′-biphosphinine with sodium/naphthalene in dimethoxyethane. When reduction is carried out with lithium in the presence of (2.2.1) cryptand, the reduced ligand adopts a *trans* configuration in the solid state. DFT calculations clearly indicate a phosphaallylic-type structure.



P. Rosa, N. Mézailles, L. Ricard, F. Mathey,* P. Le Floch* .... 4476 – 4479

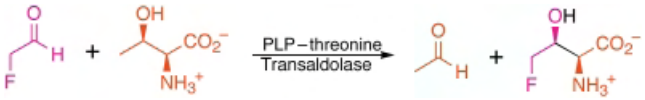
The tmbp Dianion in the Contact Ion Pair $[(tmbp)Na_2(dme)_{1.5}]_n$ and in the Solvent-Separated Ion Pair $[tmbp][(2.2.1)Li]_2$

Keywords: alkali metals · density functional calculations · phosphinines · phosphorus heterocycles · reduction

Angew. Chem. **2001**, *113*, 4608 – 4611

 © WILEY-VCH Verlag GmbH, D-69451 Weinheim, 2001 1433-7851/01/4023-4320 $ 17.50+.50/0

The final enzyme on the biosynthetic pathway to 4-fluorothreonine is identified in *Streptomyces cattleya*. The enzyme catalyzes a pyridoxal phosphate-dependent "transaldose" reaction between L-threonine and fluoroacetaldehyde (see scheme; PLP = pyridoxal 5′-phosphate). Unlike threonine aldolases, glycine is not a substrate for this new type of enzyme.



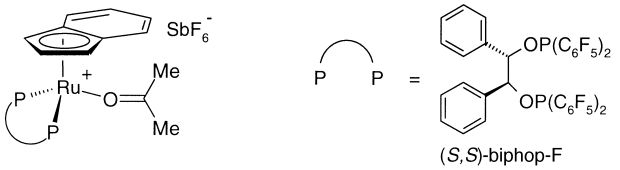
Angew. Chem. **2001**, *113*, 4611 – 4613

C. D. Murphy, D. O'Hagan,*
C. Schaffrath ..... 4479 – 4481

Identification of a PLP-Dependent Threonine Transaldolase: A Novel Enzyme Involved in 4-Fluorothreonine Biosynthesis in *Streptomyces cattleya*

Keywords: biosynthesis · enzyme catalysis · fluorine · natural products · transaldolase

The indenyl roof over the chiral Lewis acid catalyst site of [(indenyl)Ru((*S*,*S*)-biphop-F)]$^+$ (see picture) gives rise not only to high enantioselectivities in Diels – Alder reactions between enals and cyclopentadiene but also affects the *endo*/*exo* diastereoselectivity. The *exo* product is formed preferentially even with acrolein.



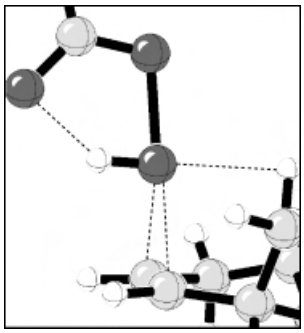
Angew. Chem. **2001**, *113*, 4613 – 4617

E. P. Kündig,* C. M. Saudan, V. Alezra,
F. Viton, G. Bernardinelli 4481 – 4485

[(Indenyl)Ru(biphop-F)]$^+$: A Lewis Acid Catalyst That Controls both the Diene and the Dienophile Facial Selectivity in Diels – Alder Reactions

Keywords: asymmetric catalysis · cycloaddition · Lewis acids · P ligands · ruthenium

Peracids prefer to attack *syn* to an alkyl group as shown by the most stable transition state for the epoxidation of 3-methylcyclohexene (see section of transition state). Computational and experimental evidence explain the origin of this effect and how it might be exploited in synthesis.



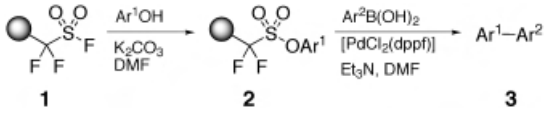
Angew. Chem. **2001**, *113*, 4617 – 4620

I. Washington, K. N. Houk* 4485 – 4488

CH ··· O Hydrogen Bonding Influences π-Facial Stereoselective Epoxidations

Keywords: ab initio calculations · diastereoselectivity · epoxidation · oxidation · peroxides

Three roles for the PFS fluoride resin 1: a linker, a protecting group, and an activating group for phenols. Immobilized "aryl triflates" **2** are generated upon treatment of **1** with phenols. Through a subsequent Suzuki cleavage/cross-coupling reaction an additional aryl group can be appended to the initial phenol to afford biaryls **3** in a "traceless" fashion in high yields.



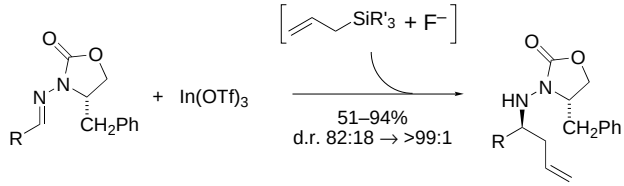
Angew. Chem. **2001**, *113*, 4620 – 4623

Y. Pan, B. Ruhland,
C. P. Holmes* ..... 4488 – 4491

Use of a Perfluoroalkylsulfonyl (PFS) Linker in a "Traceless" Synthesis of Biaryls through Suzuki Cleavage

Keywords: biaryls · C–C coupling · combinatorial chemistry · solid-phase synthesis · synthetic methods

A mild, convenient, and stereoselective addition of allylsilanes to enantiopure *N*-acylhydrazones occurs at room temperature upon complementary activation of both the allylsilane and the hydrazone (see scheme; OTf = trifluoromethanesulfonate). The reaction provides a new mode of acyclic stereocontrol for the asymmetric synthesis of homoallylic amines.



Angew. Chem. **2001**, *113*, 4623 – 4625

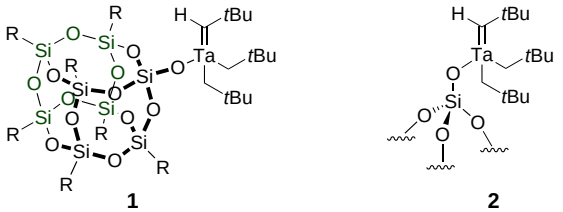
G. K. Friestad,* H. Ding ... 4491 – 4493

Asymmetric Allylsilane Additions to Enantiopure *N*-Acylhydrazones with Dual Activation by Fluoride and $In(OTf)_3$

Keywords: allylation · amines · asymmetric synthesis · chiral auxiliaries · hydrazones

 © WILEY-VCH Verlag GmbH, D-69451 Weinheim, 2001 1433-7851/01/4023-4321 $ 17.50+.50/0

Feher cage analogues, such as **1**, provide easy access to models of surface structures such as **2**, and give a better understanding of surface reactions. In addition, surface complexes such as **2** can be fully characterized by high-resolution 1D and 2D solid-state NMR spectroscopy.



1 **2**

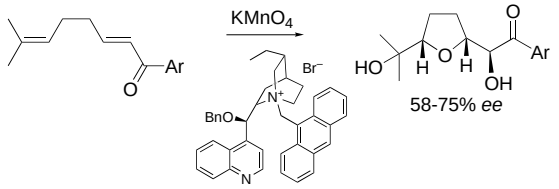
Angew. Chem. **2001**, *113*, 4625 – 4628

M. Chabanas, E. A. Quadrelli, B. Fenet, C. Copéret,* J. Thivolle-Cazat, J.-M. Basset,* A. Lesage, L. Emsley* ..... 4493 – 4496

Molecular Insight Into Surface Organometallic Chemistry Through the Combined Use of 2D HETCOR Solid-State NMR Spectroscopy and Silsesquioxane Analogues

Keywords: NMR spectroscopy · organometallic chemistry · silicates · surface chemistry · tantalum

Up to four new stereocenters are created with control of the relative and absolute stereochemistry in a single step in the unusual phase-transfer-catalyzed oxidative cyclization of achiral dienes with permanganate (see scheme).



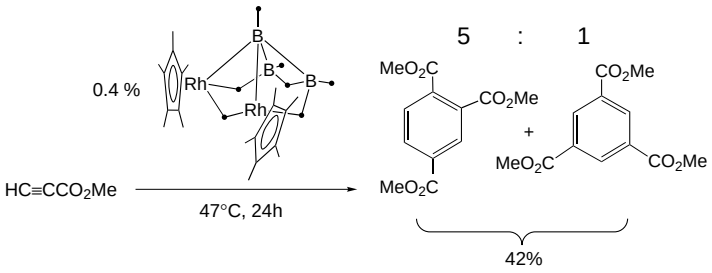
Angew. Chem. **2001**, *113*, 4628 – 4630

R. C. D. Brown,* J. F. Keily 4496 – 4498

Asymmetric Permanganate-Promoted Oxidative Cyclization of 1,5-Dienes by Using Chiral Phase-Transfer Catalysis

Keywords: asymmetric synthesis · cyclization · dienes · diols · phase-transfer catalysis

Catalysis with clusters: Transition metal characteristics control metallaborane reactivity as demonstrated by the reaction of a pair of isoelectronic and nearly isostructural metallaboranes with substituted alkynes. Novel catalytic chemistry of *nido*-[1,2-(Cp*Rh)$_2$B$_3$H$_7$] and *nido*-[2,3-(Cp*Rh)$_2$B$_3$H$_7$] (shown) with alkynes (see scheme) is observed with activities and selectivities that depend on catalyst structure and the alkyne substituents.



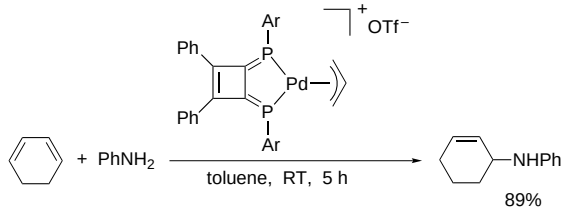
Angew. Chem. **2001**, *113*, 4630 – 4633

H. Yan, A. M. Beatty, T. P. Fehlner* ..... 4498 – 4501

Reactivity of Dimetallapentaboranes—*nido*-[Cp$_2^*$M$_2$B$_3$H$_7$]—with Alkynes: Insertion to Form a Ruthenacarborane (M = RuH) versus Catalytic Cyclotrimerization to Form Arenes (M = Rh)

Keywords: alkynes · boranes · cluster compounds · homogeneous catalysis · transition metals

Room-temperature hydroamination of 1,3-dienes with aniline [Eq. (1)] is efficiently catalyzed by cationic η^3-allyl palladium complexes, prepared by treating [{(η^3-allyl)PdCl}$_2$] with 1,2-diaryl-3,4-bis[(2,4,6-tri-*tert*-butylphenyl)phosphinidene]cyclobutenes and AgOTf in CH_2Cl_2; Ar = 2,4,6-tri-*tert*-butylphenyl.



(1)

Angew. Chem. **2001**, *113*, 4633 – 4635

T. Minami, H. Okamoto, S. Ikeda, R. Tanaka, F. Ozawa,* M. Yoshifuji ..... 4501 – 4503

(η^3-Allyl)palladium Complexes Bearing Diphosphinidenecyclobutene Ligands: Highly Active Catalysts for the Hydroamination of 1,3-Dienes

Keywords: homogeneous catalysis · hydroamination · nucleophilic addition · palladium · P ligands

Supporting information on the WWW (see article for access details).

* Author to whom correspondence should be addressed

 © WILEY-VCH Verlag GmbH, D-69451 Weinheim, 2001 1433-7851/01/4023-4322 $ 17.50+.50/0

BOOKS

Dictionary of Gene Technology	Günther Kahl	*S. Brakmann*	4505
Carobhydrates	Robert V. Stick	*T. Ziegler*	4505
Green Chemical Syntheses and Processes	Paul T. Anastas, Lauren G. Heine, Tracy C. Williamson	*G. Kaupp*	4506
Computational Organometallic Chemistry	Thomas R. Cundari	*T. Strassner*	4508
DNA Arrays	Jang B. Rampal	*C. M. Niemeyer*	4510
Inorganic and Organometallic Polymers	Roland D. Archer	*D. Wöhrle*	4510
Fundaments of Electroanalytical Chemistry	Paul M. S. Monk	*H. H. Girault*	4511
Kinetics of Homogeneous Multistep Reactions	F. G. Helfferich	*D. G. Blackmond*	4512
Heinrich Caro and the Creation of Modern Chemical Industry	Carsten Reinhardt, Anthony S. Travis	*H.-J. Quadbeck-Seeger, S. Becker*	4513

WEB SITES

http://webbook.nist.gov/chemistry	Thermochemistry Standards	*D. Schröder*	4515

SERVICE

- **VIPs** **4312**
- ***Angewandte's* Sister-Journals** **4325 – 4327**
- **Sources** **A137**
- **Vacancies** **A139**
- **Keywords** **4516**
- **Authors** **4517**
- **Preview** **4518**

Issue 22, 2001 was published online on November 16

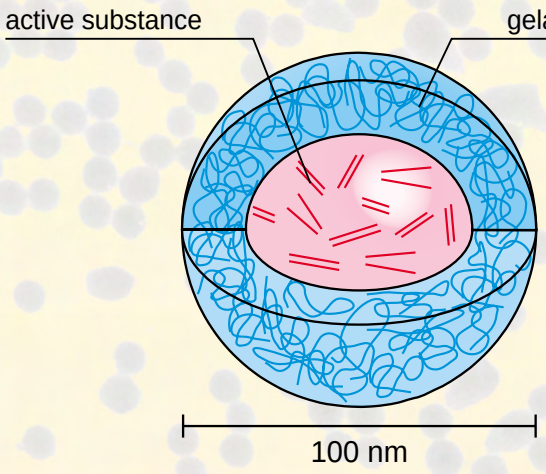
Don't forget all the Tables of Contents from 1998 onwards may be still found on the WWW under: http://www.angewandte.com

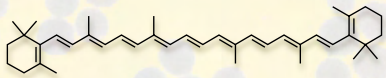
CORRIGENDUM

In the second paragraph of the communication by **D. B. Grotjahn et al.** (*Angew. Chem. Int. Ed.* **2001**, *20*, 3884 – 3887), previous work on complexes of electron-rich or chelating ligands with the CpRuCl fragment was reported (T. Suzuki, M. Tokunaga, Y. Wakatsuki, *Org. Lett.* **2001**, *3*, 735 – 737). The best catalyst in this work was the complex [CpRuCl($Ph_2PCH_2PPh_2$)] and not the complex [CpRuCl($Me_2PCH_2PMe_2$)] given as an example. Thus, the first sentence of the following paragraph should be: "In contrast, here we report that electron-rich or chelating phosphanes are not needed." The authors apologize for the error.

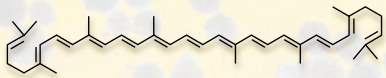
 © WILEY-VCH Verlag GmbH, D-69451 Weinheim, 2001 1433-7851/01/4023-4323 $ 17.50+.50/0

Organic Nanoparticles in Aqueous Phase

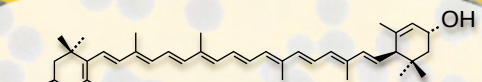




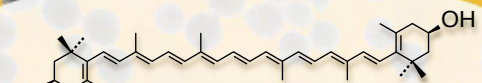
β-carotene $C_{40}H_{56}$



lycopene $C_{40}H_{56}$



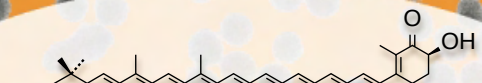
lutein $C_{40}H_{56}O_2$



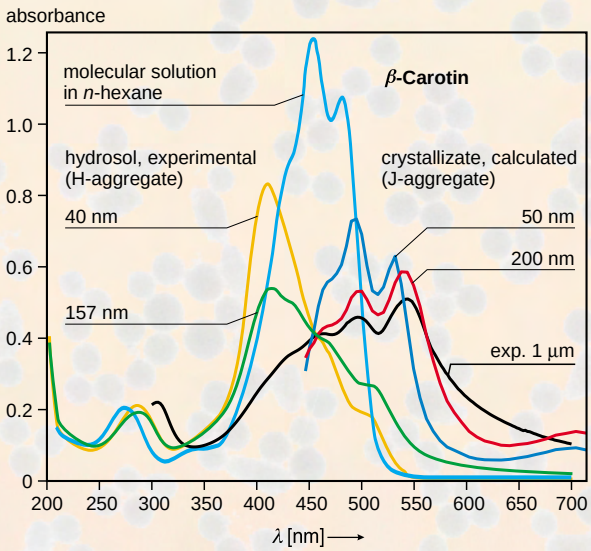
zeaxanthin $C_{40}H_{56}O_2$



canthaxanthin $C_{40}H_{52}O_2$



astaxanthin $C_{40}H_{52}O_4$



ANGEWANDTE CHEMIE © WILEY-VCH

Organic Nanoparticles in the Aqueous Phase—Theory, Experiment, and Use

Dieter Horn and Jens Rieger*

Many active organic compounds and organic effect materials are poorly soluble in water, or even insoluble. Aqueous forms of application thus require special formulation techniques to utilize or optimize the physiological (pharmaceuticals, cosmetics, plant protection, nutrition) or technical (varnishes, printing inks, toners) action. The most interesting properties of nanodispersions of active organic compounds and effect materials include the impressive increase in solubility, the improvement in biological resorption, and the modification of optical, electrooptical, and other physical properties which are achievable only with particle sizes in the middle or lower nanometer range (50 – 500 nm). Hence in addition to economic and ecological constraints there are also technical demands which appear to urgently require the development of new processes for the production of organic nanoparticles as alternatives to the established mechanical milling processes. In this context attention is drawn to the recent increase in research activities which have as their objective the continuous, automatic preparation of nanodispersed systems by precipitation from molecular solution. In this review the current state of knowledge of the fundamentals of particle formation from homogeneous solution and the effect of solvent and polymer additives on the morphology and supramolecular structure of the nanoparticle will be discussed. The practical implementation of this new formulation technology will be explored in detail for the carotenoids, a class of compounds of both physiological and technical interest.

Keywords: carotenoids · disperse systems · nanoparticles · nanostructures · phase transformations

1. Introduction

The importance of nanoparticles, that is, particles with dimensions in the range of about 10 nm to a few hundred nanometers is obvious: they determine our life in the form of protein complexes and other cell components, as viruses, colloidal particles in drinking water, surface water and sea water, and as aerosols; they find use as dispersion colors and as adhesives; in industry they play an important role in the formulation of pigments and in the production of catalysts; numerous attempts are being made to deliver nanoparticulate forms of pharmaceutically active compounds specifically to the desired site of the action in the body; finally nanoparticles find use as quantum dots with special properties for electronic components. Beyond these practical aspects there is scientific interest in nanoparticles owing to their special properties which lie between the properties of molecules and those of bulk material.

[*] Dr. J. Rieger, Dr. D. Horn
BASF AG
Polymer Research, Department of Polymer Physics
67056 Ludwigshafen (Germany)
Fax: (+49) 621-60-92281
E-mail: jens.rieger@basf-ag.de

In a thorough study of the scientific literature on the topic of colloidal systems it became evident that much has been written on inorganic nanoparticles, polymer dispersions, and on the principles of particle formation in general. In contrast, surprisingly little is learnt of the mechanisms of particle formation of organic systems. Moreover, there is a clear gap between that which is reported in many textbooks on particle formation and the current state of knowledge. This unsatisfactory situation was the motivation for this contribution which on the one hand deals with the preparation and properties of organic nanoparticles, and with modern aspects of particle formation on the other.

Organic nanoparticles take on many forms (Figure 1). Here we will limit ourselves to the consideration of pharmaceutically active organic compounds and organic effect materials as they occur, for example in pharmaceuticals applications and in the form of vitamins and pigments. Many of these materials are poorly soluble in water, or even insoluble. Aqueous forms of application thus require special formulation techniques to optimize the physiological (pharmaceuticals, cosmetics, plant protection, nutrition) or technical (varnishes, printing inks, toners) action. An important target in this context is the conversion of the generally coarse crystalline synthesis product into the finest particulate dispersion possible, with

 © WILEY-VCH Verlag GmbH, D-69451 Weinheim, 2001 1433-7851/01/4023-4331 $ 17.50+.50/0

man-made nanoparticles	active substances (pharmaceuticals)	pigments	polymer dispersions	micellar systems	supermolecules and dendrimers	protein aggregates (as nuclei for crystals)
natural nanoparticles	cell components	viruses	environmental colloids (on surfaces, in water, in air)			

Figure 1. Classification of organic nanoparticles.

particle sizes in the range of 10 to 500 nm. In principle two strategies are conceivable for this purpose: 1) the mechanical milling of the raw material by wet or dry milling processes; 2) the conversion of the products or educts dissolved in suitable solvents into nanodispersed systems by precipitation, condensation, or by specific synthesis procedures (Figure 2). In the second case the undesirable solvent must often then be removed. The differentiation between precipitation and condensation processes makes it clear that in the actual precipitation process further additives such as surfactants and polymers assume the role of surface-active colloidal stabilizers; in the condensation process these additives themselves form the nanoparticulate phase (pseudolatexes) which contains the active compound or effect material bound by adsorption or absorption. The synthetic preparation of polymer dispersions[1] as a special class of organic nanoparticles of considerable economic significance will not be discussed here. Other procedures which have also found

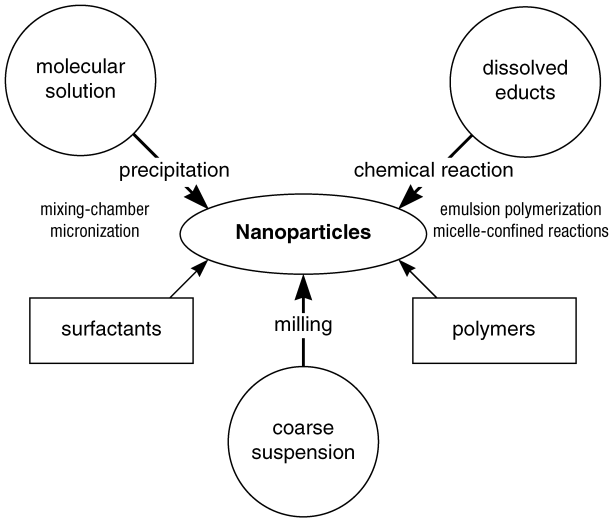


Figure 2. Methods for the preparation of nanoparticles.



D. Horn



J. Rieger

Dieter Horn, born 1936 in Höchst/Odenwald, studied chemistry at the Technical University Darmstadt and the University of Heidelberg, where he gained his doctorate in physical chemistry in 1967 working with Prof. Klaus Schäfer. He then moved to the University of California, Berkeley, where he worked in the physical chemistry group of Prof. George C. Pimentel in the Department of Chemistry. As a member of the NASA Mariner 6 and 7 project team he was responsible for the development and application of analytical methods for the quantitative interpretation of infrared spectroscopic data of the atmosphere and surface of the planet Mars transmitted by the space probes. He joined the main laboratory of BASF AG in autumn 1970 where he first worked on the physics of organic pigments. A colloidal and biophysical work group was built up under his leadership, with research priorities in the preparation of organic nanoparticles and the development of laser optic methods for the characterization of dispersed systems. In 1987 he was appointed head of the polymer physics/solid-state physics research department in the Plastics Laboratory, with research interests in the physics and the physical chemistry of polymeric structural and functional materials, polymeric effect materials, and dispersed active compounds. For his fundamental contributions to applied colloid science he has been awarded the Steinkopff Prize of the Kolloid-Gesellschaft and the Bonhoeffer-Eucken-Scheibe lectureship of the Deutsche Bunsen Gesellschaft für Physikalische Chemie.

Jens Rieger, born 1958, gained his doctorate at the University of the Saarland working with Prof. Arno Holz in theoretical physics on random walks. In 1989 he joined the department for polymer physics/solid-state physics in BASF AG in which, now as senior scientist in charge of the area "Structure Formation", he is working on the following topics: deduction of the structure-property relationships in polymeric, colloidal, and hybrid systems, development of methods for the time-resolved tracking of structure formation processes in complex systems on all length scales, control of crystallization and particle formation processes by polymers. In addition he is exploring the potential of high-performance radiation sources for polymer and colloidal physics (small-angle neutron scattering, X-ray microscopy, SAXS, and WAXS at the synchroton).

extensive use in the preparation of inorganic nanoparticles,[2] such as sol–gel processes,[2, 3] synthesis in microemulsion templates,[2, 4] and aerosol procedures[5] have hitherto played no part in the preparation of organic nanoparticles from the standpoint discussed here. Any discussion of nanoparticles by aggregation of block polymers[6] or by the targeted synthesis of extended molecules such as dendrimers[7] and other branched systems[8] will also be omitted.

To discuss the mechanisms of particle formation it is useful to describe the current state of knowledge—initially independently of the nature of the system formed. Figure 3 gives an initial view of the complexity of particle formation and highlights a number of the outstanding questions. As will become clear, five essential points need to be emphasized within this context.

1. There is a far deeper understanding of the formation of inorganic particles than of organic particles.
2. Interesting advances in protein crystallization have been achieved recently which also affect the classical area of nucleation theory.
3. There is still a considerable need for research in the area of nucleation theory, for example, where the interaction of several components during particle formation is concerned, whether it be the simultaneous precipitation of two materials or the control of particle morphology by the use of additives.
4. Certain particle sizes are necessary to achieve certain effects, these can be obtained either through the "physical chemistry" of the particle-forming system or by the use of additives (protective colloids). For an efficient procedure in both cases the structure-formation processes must be understood on all length scales.
5. Little is known about the molecular processes which take place during the mixing of two starting solutions for producing the state of supersaturation which initiates particle formation.

The preparation of colloidal systems has occupied scientists for a long time.[9, 10] Numerous monographs and review articles have been devoted to this topic, a few of which are mentioned here by way of example.[2, 3, 11–15] Several points arise from a perusal of the literature on this topic: a strongly phenomenological approach is frequently encountered, that is, attempts are made to deduce a mechanism of formation from the structure of the product, often a purely descriptive treatment is considered satisfactory. If one looks beyond textbook knowledge on "supersaturation, nucleation, growth" a "zoo" of theories and interpretations is encountered which must be taken into account if there is a desire to understand at a basic, that is, molecular, level how a nanoparticulate system is formed. This knowledge is of prime importance as only with a knowledge of the mechanistic aspects of particle formation can the process be manipulated specifically, that is, controlled—whether it be by variation of the process parameters or by the use of suitable additive molecules. This area of research is truly interdisciplinary since chemists, physicists, and engineers, each with their specialist knowledge are in demand. However, within academia this cooperation is nowhere near as wide-spread as would appear appropriate for an optimal treatment of this problem.

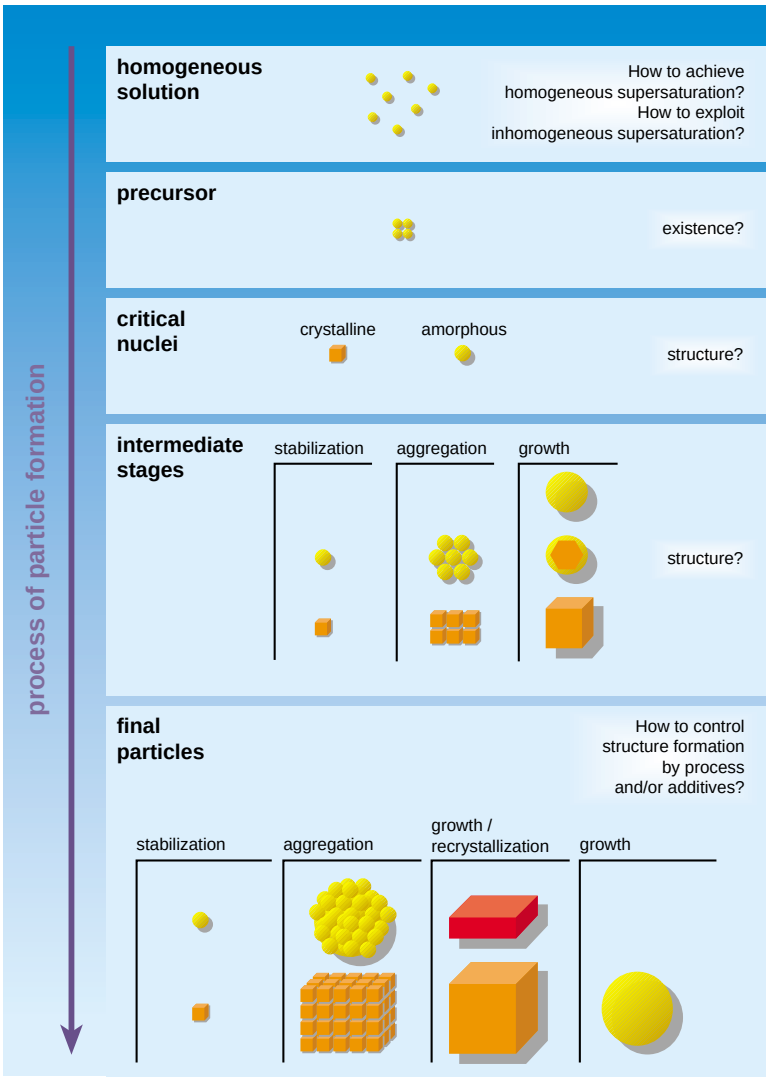


Figure 3. Stages of particle formation and open questions (see text for further explanation).

The article is arranged as follows: in Section 2 the current state of knowledge of the fundamentals of particle formation is discussed, however, the classical theory of nucleation is treated only briefly. Emphasis is placed upon more recent thoughts on mechanisms of particle formation including computer simulations, as well as on the question of to what extent the processes occurring during initiation of particle formation—mainly by the mixing of two educts—are understood? Finally, how the particle formation process can be controlled by the use of (mainly polymeric) additives will be discussed. In Section 3 processes for the preparation of organic nanoparticles are considered. In Section 4 the properties and areas of application of these particles where the nanoparticulate state is a requirement will be introduced. Finally open questions on this topic will again be addressed.

2. Theoretical Approaches

2.1. Classical Nucleation Theory

Textbook knowledge may be summarized in the following way:[11, 14, 16, 17] A multicomponent system exists initially as a single phase. By modification of boundary conditions such as temperature and pressure or by homogenous mixing with a further component the free energy changes in such a way that phase separation is energetically more favorable. The approach taken assumes that particles (atoms, ions, molecules) of the one component coalesce and form nuclei of the separating phase, initially it is immaterial whether it is, for example, the separation of a solid phase in the liquid medium (the subject matter of this article), condensation from the gaseous phase, or bubble formation in a liquid (foaming). The free energy of a spherical nucleus with radius r can be described in respect of the single-phase state to a first approximation as in Equation (1) (the subscripts S and V

$$\Delta G = \Delta G_s + \Delta G_v = 4\pi r^2\gamma + 4/3\pi r^3 \Delta g_v \quad (1)$$

refer to surface and bulk volume, respectively) where γ stands for the surface tension between the two phases and Δg_v for the difference in free energy per unit volume between the two phases. The two terms on the right of the equation have opposite signs so that ΔG as a function of r passes through a maximum (Figure 4). The critical nucleus radius r^* is defined

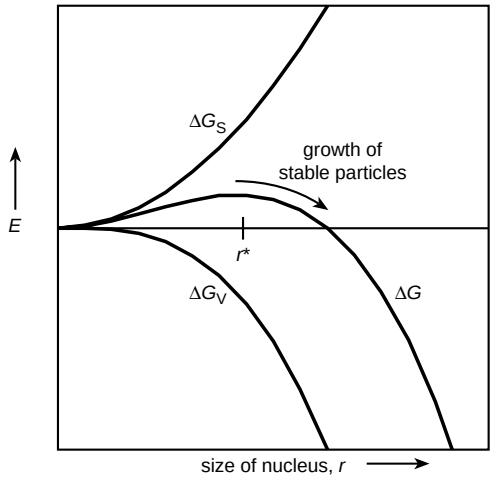


Figure 4. Energy diagram to explane the nucleation process (ΔG: free energy of a particle with radius r, ΔG_s: surface energy, ΔG_v: bulk energy, r^*: radius of the critical nucleus). The particle sizes fluctuate because of statistical processes. Particles with a radius $r < r^*$ redissolve, those with $r > r^*$ grow further.

by the position of the maximum of the free energy and given by Equation (2). Particles with a radius smaller than r^* redissolve, whilst particles which by reason of statistical fluctuations exceed this size are stable and can grow further.

$$r^* = -2\gamma/\Delta g_v \quad (2)$$

Within the scope of a quasi-equilibrium approach (Arrhenius) the rate of nucleation that is, the number of nuclei which form per unit time and volume is described by Equation (3), in which A is determined by the frequency of the molecular

$$J = A\exp(-\Delta G^*/kT) \quad (3)$$

processes and k and T have the usual meanings. The rate of nucleation is thus Equation (4), where in accordance with Equation (5) the supersaturation $S = c(r)/c^*$ is coupled with the particle radius; v is the molecular volume, $c(r)$ denotes the solubility of a particle with radius r, and c^* the equilibrium solubility.

$$J = A\exp(-(16\pi\gamma^3 v^2)/(3k^3T^3[\ln S]^2)) \quad (4)$$

$$kT\ln(S) = 2\sigma v/r \quad (5)$$

In classical colloid chemistry a further model concept is used especially to explain monodispersity in certain systems (Figure 5):[18] the concentration of a dissolved substance continues to rise, for example, by release in a reaction until the critical nucleation concentration is reached. At this point a shower of nuclei are formed which begin to grow. In this way the concentration falls momentarily below the critical threshold so that no new nuclei can form. The nuclei already formed grow until the concentration of the still-dissolved material has fallen to the equilibrium concentration.

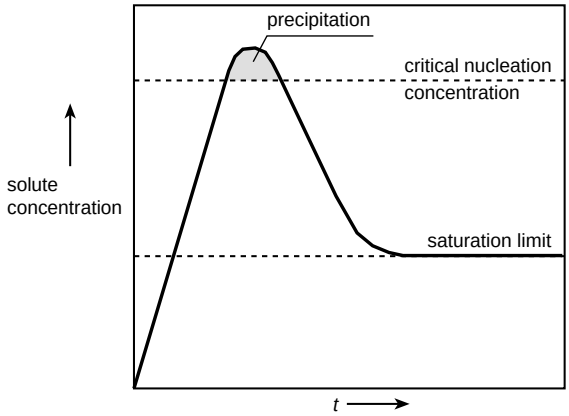


Figure 5. Schematic representation of the concentration relationships in controlled particle formation according to the model representation of LaMer, ref. [18] (for full explanation see text).

2.2. More Recent Knowledge

In the following, new ideas on particle formation from supersaturated systems will be presented in chronological order from the stage of the homogeneous starting state to that of the colloidal particle. An assessment has been intentionally omitted as there is rapid development in this area. For reasons of space complete citation has to be omitted; a comprehensive review of this topic is in preparation.

2.2.1. Precursors

A fundamental assumption of classical nucleation theory is that prior to production of the supersaturation that initiates

particle formation the system can be treated as homogeneous, that is, it is assumed that the components are present in a molecularly dispersed state. Numerous experiments suggest, however, the existence of precursors, that is, species which form from the reacting components, the size of which is still below that of a critical nucleus. This is not meant to suggest transient clusters arising from fluctuations in nucleation, but long-living species which are not considered as part of classical nucleation theory.[11, 19, 20]

2.2.2. The Structure of Clusters and Nuclei

In classical nucleation theory it is assumed that the critical nuclei are spherical and that the structure of the nuclei and their surface can be described by that of the corresponding macroscopic phase, that is, that γ and Δg are defined by the corresponding values of the bulk phase. In many cases this assumption in respect of Δg_v does not apply, most clearly when the nuclei comprise only a small number of molecules, as has been observed with, for example proteins.[21] In turn this point has consequences for the assumptions which are made for the surface tension. Many theories have been proposed for the structure of particle surfaces to take into account that, for example, a density gradient can exist in the transition from particle interiors to the dispersed medium.[22] Moreover, that γ is dependent upon the curvature of the particle surface is not considered in classical nucleation theory. This deficiency was recognized early on and has been redressed in a number of theories.[23, 24] Questions of bulk structure are discussed in detail in Section 2.3. In a few cases the assumption of sphericity also does not apply.[25, 26]

In most theories on particle formation it is assumed that the clusters and nuclei do not interact and that the corresponding rate equations describe particle formation by the incorporation or loss of individual basic elements (atoms, ions, monomers, molecules). There are indications, however that subcritical clusters contribute to nucleation by incorporation and that cluster coagulation plays a role in particle formation.[27]

2.2.3. Spinodal Versus Binodal Decomposition

In the description of the particle formation processes classical nucleation theory is applied almost without exception in the sense that in the phase diagram the supersaturated system exists in the binodal, that is, metastable region (Figure 6). However, with sufficiently high supersaturation the borderline to spinodal decomposition is crossed, and phase separation occurs spontaneously, that is, *without* actual nucleation. That a differentiation must be made between binodal and spinodal demixing (particle formation) is well known in polymer physics.[28] In the case of low molecular systems it has indeed been maintained that: "Spinodal decomposition has never been observed in solutions made up of a solid solute and a liquid solvent because of the large width of the metastable zone that must be crossed without nucleation being induced".[29] It has to be assumed, however, that this citation is attributed to the fact that spinodal demixing in low molecular weight systems is very difficult to detect because of the short time scales involved; the structures formed initially convert rapidly into more compact structures (particles) because of the large surface energy.[28, 30] Investigations in which a particle-forming system was quenched and investigated immediately after establishment of supersaturation supports the assumption that initially during the precipitation of low molecular substances and correspondingly high supersaturation spinodal demulsifying with subsequent conversion into particles also takes place.[31] By simulation of the Brownian movement of particles with suitable interaction potentials it has been shown that dependent upon the level of supersaturation structure-formation mechanisms which are in agreement with the concept of binodal and spinodal demulsifying do occur.[32] The sharp differentiation between binodal and spinodal demulsifying is thus an artifact of highly simplified theories; in most real systems the transition between the two demulsifying mechanisms is gradual.[17, 28]

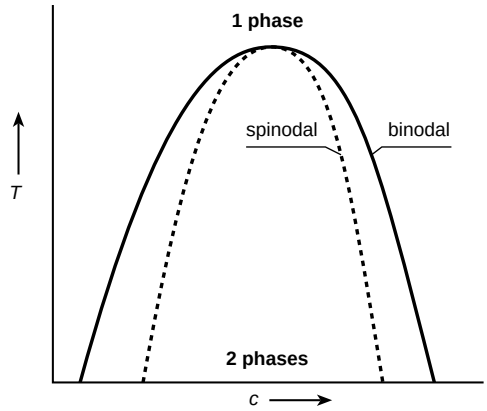


Figure 6. Phase diagram of a two component system with miscibility gap. The region between the binodal and spinodal corresponds to the metastable region in which, according to the classical theories, particle formation takes place through nucleation and growth, whereas the system within the spinodal demixes spontaneously.

2.2.4. Particle Formation in Multicomponent Systems

There is a whole series of more recent theoretical approaches on the formation of multicomponent particles from supersaturated systems. There are, for example discussions on such fundamental questions as to how the surface energy is to be described, how heterogeneous nucleation is influenced, and which pathway the system takes within the realm of the two parameters "number of particles of type A and type B which are contained within the respective critical nucleus".[33] Simulations on the structure of two-component clusters as a function of the interaction parameters are discussed in Section 2.3. In respect to the questions of cardinal interest here, "how surfactants or polymers affect particle formation behavior in the aqueous phase?" the work described is of limited use, however. The points within this context that deserve special attention will be treated in detail in later sections.

2.2.5. What Does Protein Crystallization Teach Us?

In recent years the classical area of particle formation theories has received new stimuli from the area of protein crystallization.[34] With light-scattering experiments it was found that the ability of a whole series of proteins to crystallize (instead of to precipitate amorphously or to gel) correlates with the second virial coefficient.[35, 36] This coefficient is correlated with the interaction potential between individual molecules in solution. It can be shown that the crystallization behavior of the proteins is approximately explained by a simple interaction potential and a study of the resulting complex phase diagrams (see also the discussion in Section 2.3).[34, 36–38]

2.2.6. The Collapse of Polymer Molecules

Owing to the importance for an understanding of the formation of pseudolatex particles, which will be discussed later in the experimental section (Section 3) the collapse transition of individual polymer molecules by changes on solvent quality (by mixing with an antisolvent or by change in temperature) is of interest. The phenomenon is itself well known[39] and—as with low molecular weight systems—may be discussed on the basis of the phase diagram shown in Figure 6,[40] in which, in the case of solvent mixtures, the temperature is replaced by a corresponding quantity which describes the interaction of the polymers with the solvent. That all aspects of the collapse transition are in no way fully known is demonstrated by work carried out in recent years on the dynamics of the collapse transition, the interaction between individual chain collapse and macroscopic phase separation, and conformation statistics at the collapse transition.[41] The relationship between this fundamental work and end-use related experiments on particle formation by the precipitation of polymers[42] is currently not discernible.

2.3. Computer Simulation of the Early Stages of Particle Formation

With the aid of computer simulation it has meanwhile become possible to obtain an insight into structure formation during the early stages—even if initially only with the most idealized systems. For fundamental investigations of the behavior of many-body systems the so-called Lennard–Jones α-β potential (LJ α-β) for the description of the interaction of two particles is widely used [Eq. (6)]. With the help

$$V(r) = -a/r^{\alpha} + b/r^{\beta} \quad (6)$$

of this potential (with $\alpha = 6$ and $\beta = 12$) the homogeneous nucleation of particles from the liquid phase has been studied.[44, 45] With use of the LJ 6-12 potential at moderate cooling, that is, low supersaturation, it has been possible to establish how in the pre-critical phase aggregates with liquid-like structure are formed initially which on exceeding the critical size are present mainly in face-centered cubic (fcc) form. A more precise investigation of the critical nuclei showed that the core exhibits an fcc structure, whereas the shell is liquidlike. In a layer between these two structures a body-centered cubic (bcc) structure is realized. Simulations of this type give an insight into the causes for the so-called Ostwald rule which states that the phase which forms by nucleation is not necessarily that with the thermodynamically most stable (crystal) structure but that which in respect to its free energy is closest to the melt. A series of approaches to explain this phenomenon have been published without as yet any consensus being reached.[12, 46]

In investigations of the LJ 3-6 system with which the phase behavior of protein molecules may be approximately described ten Wolde and Frenkel observed—in addition to phenomena which correspond to the classical ideas of crystalline nucleation—how under modified boundary conditions amorphous nuclei are also formed in which crystalline cores form on further growth.[45, 47] This pathway to particle formation is associated with a lower nucleation barrier. The authors speculate that this result may be put to use to grow better protein crystals for structure determination.

More recently the first attempts to describe the structure of *multicomponent* nuclei have been made. A complete morphology diagram for the structure of two-component clusters as a function of the respective interaction parameters has been determined for LJ 6-12 particles (Figure 7).[48]

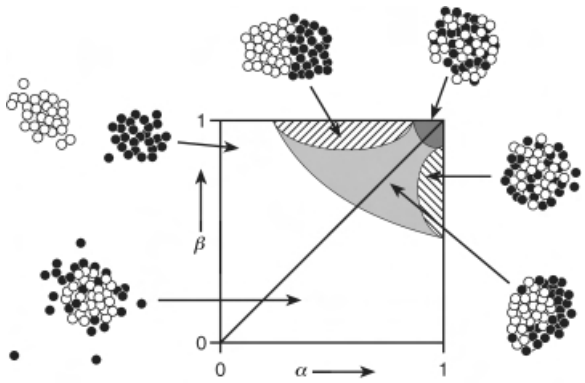


Figure 7. "Morphology diagram" of two-component clusters where α represents the strength of the interaction between the two ("black" and "white") particles and β the strength of cohesion between the "white" particles in comparison to the corresponding value for the "black" particles (according to ref. [48], Copyright©, American Institute of Physics, 1994).

2.4. Particle Growth

2.4.1. Crystallization

The investigation of the growth of crystals is a well established area of research with a countless amount of published work. For this reason reference will be made at this juncture to only two still current books, refs. [11, 49] Beyond this, however, a few points are worth special attention.

1. In the interim it has become possible to follow the growth mechanisms in situ by means of space and time resolved AFM (atomic force microscopy) at moderate supersaturation.[50, 51] In this way a number of model concepts of crystal growth are confirmed, while at the same time new aspects

also come to light, for example, discontinuous growth arising from non-equilibrium effects.[51]

2. During the preparation of oxide films from the aqueous phase it was observed that a film is formed by deposition of crystallites with dimensions in the range of a few nanometers.[52] This gives rise to the question of whether crystal growth at high concentrations takes place according to classical concepts or whether crystals could form by the deposition of preformed precursor crystallites?
3. In the previous Section the Ostwald rule was discussed. For the situation where the transition from one structure to another energetically more favorable takes place by solid-phase transformation the interesting question arises of how this transition may be controlled or suppressed? In the area of biomineralization impressive examples are known of how living organisms regulate these transitions with the aid of proteins, although the details of how this is achieved are not known.[53]

2.4.2 Aggregation

Aggregation phenomena play a critical role in the preparation of many colloidal systems so that for application in general explanations are needed for the conditions under which colloids are stable, or how colloidal particles themselves can be aggregated or flocculated in a targeted manner. Less frequently discussed is the question as to how far the colloidal particles are formed by the aggregation of precursors. There is extensive literature on the "classical" aggregation of colloidal particles, of which just a few, more recent references are cited here.[3, 16, 54, 55] In most of this work it is assumed that the kinetics of formation of aggregate populations are determined by the interaction potential between the particles, the particle size, and the flow conditions within the system. It is intuitively clear that the latter point is complex.[54, 56] However, there are also still unresolved questions of a fundamental nature regarding the interaction between colloidal particles—in contrast to the impression occasionally given in introductory contributions on the stability of colloidal systems. The question as to how far classical theories, for example the frequently used Derjaguin – Landau – Verwey – Overbeek (DLVO) theory, correctly describe interaction effects is under intense discussion.[57]

A number of systems are known in which primary particles with dimension of a few nanometers aggregate to colloidal particles, which are on the one hand compact and astonishingly monodispersed, and on the other exhibit a puzzling anisometry in some cases.[58] Different theoretical approaches have been suggested concerning the mechanisms responsible for monodispersity.[59] The special case of the aggregation step in the formation of monodispersed silica particles in the Stöber process has been discussed in theory in a series of publications.[60]

2.5. Control with Additives

Additives in the form of ions, low molecular weight molecules such as surfactants, and neutral or charged polymers (polyelectrolytes) can dramatically affect the particle formation process, desirably or undesirably. The mechanisms are differentiated as follows: nucleation by individual molecules, heterogeneous nucleation on particles or aggregates present, colloidal stabilization of structures of a mere intermediate nature in the pure particle formation process, and the influencing of crystal growth. In the ideal situation a knowledge of the basic structure – activity relationships can be used for targeted control of the particle formation process. The points described will be discussed individually below.

2.5.1. Nucleation

To what extent individual molecules and especially dissolved polymers can function as nuclei in particle formation is controversial.[61] The relationships in the case of heterogeneous nucleation, that is, nucleation on defined substrates with dimensions >1 nm are more simple.[11, 62] However, the demarcation from the former case is not fixed, for example, during the transition from the dissolved polymer to a particle of collapsed polymer chains as substrate for heterogeneous nucleation.

2.5.2. Colloidal Stabilization by Additives

The investigation of the stability of colloidal particles by adsorbed polymers/surfactants is an extensive and well-established area of research.[63] More recent work which has contributed new facets to previous knowledge will be mentioned here, where primarily electrostatic stabilization by adsorbed polyelectrolytes will be discussed.

The phenomenon of adsorption of polyelectrolytes onto oppositely charged surfaces is still the subject of detailed theoretical investigations even after years of extensive research. It has been shown, for example, how the charge density of a surface under the corresponding boundary conditions can be reduced or even reversed by oppositely charged polyelectrolytes.[64, 65] Whether or not the corresponding counterions are released into the solution during adsorption is dependent upon the physico-chemical parameters of the system.[66] Which adsorption mechanisms occur in the case of specific attractive interactions between copolymers and heterogeneous surfaces has been investigated.[67] Which conformation states may be expected during the "wrapping up" of spheres by polymers has been explained theoretically.[65, 68]

2.5.3. The Influencing of Crystal Growth

In the presence of foreign molecules crystal growth (rate, habit, polymorphism) can be influenced by two different mechanisms, both intentionally and unintentionally: ions/molecules incorporated into the particle influence the precipitation/crystallization behavior at typical concentrations of 0.1 to 1 mmol L^{-1}; ions/molecules interacting with the crystal growth faces are active at concentrations down to 10^{-7} mol L^{-1}.[69] For organic molecular crystals too, numerous instances are known in which crystal modification and habit may be influenced by additives.[70]

In the fundamental discussion on nucleus formation processes and in the discussion of the Ostwald rule the impression may be given that the type of crystal modification produced is dependent only upon the degree of supersaturation. That the nature of the fluid medium in which nucleation and crystallization occur also plays a decisive role is common knowledge in industrial crystallization processes, but described relatively rarely in the literature.[71] In addition to their function as dispersion medium the solvent molecules take on the role of a substance interacting with the growth faces of the crystals.

Also worthy of mention at this point are the possibilities of preventing with the aid of additives an—in general—undesirable Ostwald ripening of the colloidal systems. Ostwald ripening is the growth of larger particles at the expense of smaller, where the necessary material exchange occurs diffusely through the dispersing phase.[12, 72, 73] In the development of dispersed systems in which the solubility of the phase to be dispersed is not especially small one is confronted in all cases by the question of how to prevent Ostwald ripening, that is, how a stable dispersion of small particles may be obtained. There are two approaches to the solution of this problem. Attempts can be made to "seal" the surface of the particle with adsorbing molecules so well that an exchange of the active substance is effectively suppressed. That this approach is possible was demonstrated with a nanoparticulate dispersed dye, which could be effectively stabilized with a suitable mixture of sodium dodecyl sulfate (SDS) and polyvinylpyrrolidone (PVP).[74] This stabilization did not occur with either SDS or PVP alone. Another possibility is to mix the dispersing phase with a second component (2) which is less soluble still in the liquid matrix than the actual active substance (1), but where 2 is soluble in 1.[72, 75] At the start of the ripening process the concentration ratios in all particles are the same. As soon as the particle growth process begins by diffusion of 1 the concentration ratio of 2 to 1 in the smaller particles shifts to greater values, until eventually the associated loss of mixing entropy prevents a further reduction in particle size. Reference is made here to a review article for a detailed discussion of this and other points discussed in this section, ref. [72]

2.6. Particle Formation by Mixing Two Components

The supersaturation necessary for the induction of a precipitation/crystallization reaction may be produced by a variety of methods: 1) change in temperature or pressure, 2) change in the solvent quality of the fluid phase in which the material to be precipitated is initially present by mixing with a second fluid phase which is miscible with the solvent and in which the substance is poorly soluble or insoluble, and 3) by mixing two solvents the dissolved components of which are insoluble in the reacted state. The theoretical approaches described previously do not differentiate in principle between these three cases since *homogeneous* supersaturation is always assumed at the start of the experiment. Within the context discussed here only cases (2) and (3) are of interest. During precipitation by mixing two liquid flows it is often implicitly assumed that the mixing is so intensive and so rapid down to small length scales that the system is homogeneously mixed before particle formation commences. That assumption is clearly only justified when the corresponding time constants are sufficiently different (see below). In practice attempts are made to achieve homogeneity as rapidly as possible by turbulent mixing with high energy input.

The following will describe why an understanding of the mixing behavior is critical for an understanding of the particle formation process, especially when the reaction for phase separation begins during mixing. According to Baldyga the mixing of two liquid flows can be divided into macro-, meso-, and micromixing.[76] The term macromixing includes flow phenomena on length scales of decimeters, such as those that are relevant in stirred vessels. By mesomixing is meant mixing effects on a length scale of millimeters; they are founded upon the breakdown of turbulent vortices into increasingly smaller vortices until viscous processes predominate over inertial forces. The term micromixing encompasses processes in the region of micrometers. In Figure 8 the processes taking place

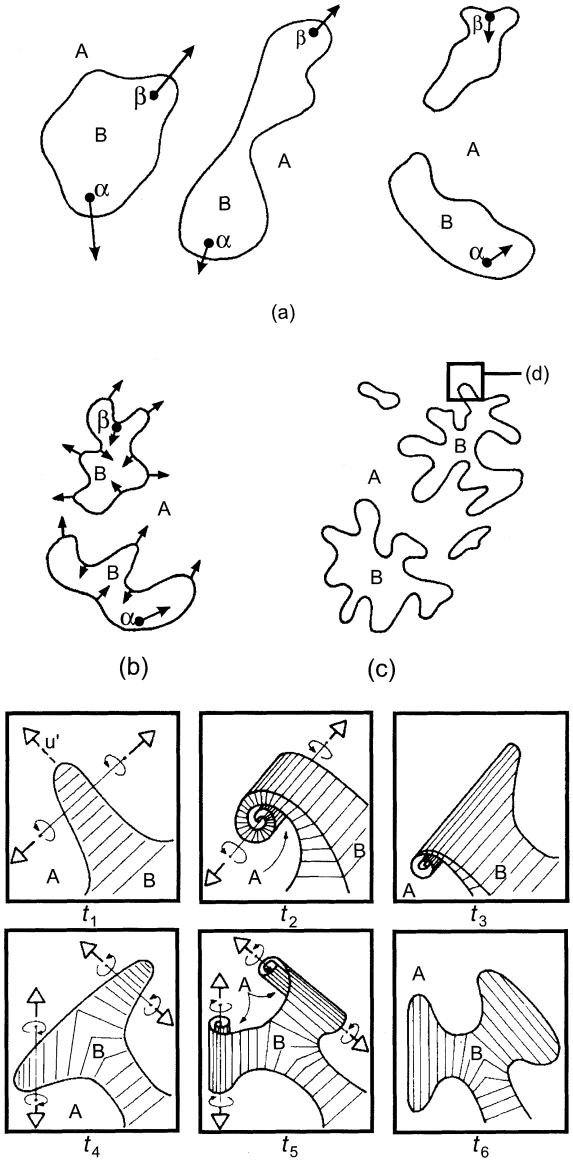


Figure 8. Schematic representation of the mixing processes of two educt flows during turbulent mixing (J. Baldyga[76]).

during turbulent mixing on the scale of micromixing are outlined. Two approaching liquid compartments envelope each other when the layers become increasingly thinner. Locally the two educt flows exist as lamellae. Respective simulations illustrate clearly this effect as well as the inhomogeneity of the turbulence (Figure 9).[77] In each case



Figure 9. Two-dimensional simulation of the mixing of two educt flows under turbulent conditions.[77]

a boundary layer initially exists between the two flows. This boundary layer is initially the site of maximum supersaturation. Whether the rate of particle formation is slower or faster than the time to complete homogeneous mixing, which on small length scales is defined by the rate of diffusion of the molecules, is critical for consideration of the particle formation process. In the first case (slower particle formation) the previously described theories may be used with the named limitations. It is otherwise in the second case (faster particle formation), here the supersaturation profiles and structures that form at the boundary surface between the two mixing educt flows must be explicitly considered. Relatively little is still known experimentally on this point. However, it must be emphasized that in a few cases the phenomenological approaches developed by Baldyga and Bourne and by Franke in the extension to aggregation processes offer a good description of the particle size distributions developing in the precipitation reactions.[76, 78, 79]

The concurrent diffusion and reaction processes have been treated in a series of theoretical studies. Sokolov and Blumen have shown, for example that supersaturation in a system reacting in laminar layers, as is realized locally in the above described liquid vortices, shows a non-classical time course: for extended times the supersaturation is proportional to $t^{-1/4}$.[80] On the basis of classical nucleation theory Dolgonosov calculated supersaturation profiles and particle concentration gradients at reactant boundary interfaces.[81] Similarly Lindberg and Rasmuson proposed that in many of the cases occurring in practice it must be considered that particle formation occurs to a considerable extent in the boundary layer between the educt solutions before the system is fully homogenized by interdiffusion.[82] In all this work it is assumed that particle formation in the boundary layer takes place in a classical manner, that is, by nucleation and growth. For the case of real particle formation processes it still has to be clarified whether or not initially—possibly strongly hydrated—precursors are formed which either aggregate to larger particles with dehydration or partially redissolve in an Ostwald ripening to contribute to actual particle formation on stable nuclei.[83]

In the use of additives for control of the particle formation process the points mentioned gain further in importance; if an additive is added to one of the two educt flows a number of interactions of additive molecules with the particle formation process is conceivable: 1) the additive molecules act as nucleation initiators, 2) the additive molecules complex some of the educt molecules and thus lower the level of supersaturation, which can lead to an increase in the induction time or to a change in the reaction mechanism, 3) the additive molecules are incorporated during particle formation. On the one hand this incorporation can possibly be used to induce a targeted crystal modification during the early stage of particle formation. On the other hand such an incorporation is undesirable when, for example, particles for pharmaceutical purposes need to be prepared in a pure state, 4) the additive molecules coat the surface of the nanoparticles being formed and by efficient dispersing fix a certain particle size distribution.

Which of the mechanisms described comes into effect depends both upon the chemical interaction between the additive molecules with the molecular and particulate species and the time scales upon which the different processes (micromixing, interdiffusion of the reactants and additive molecules, aggregation of precursors, adsorption of the additive molecules to precursors and particles) occur. The significance of these points is familiar from industrial practice. So far they have been examined only sporadically. The speculations of Lannibois-Drean are especially worth a mention.[84] On the basis of experiments on the precipitation of cholesterol acetate from solvents by mixing with water she suggested the following model for the interaction of surfactants with the particles under formation: during the diffusion of water into the solvent phase first of all the solubility of the organic molecules falls so considerably that they precipitate by nucleation. The affinity of the hydrophobic surfactant segment for cholesterol acetate at these water/solvent ratios is not so strong that an irreversible adsorption would occur. This occurs only later when the solvent properties of the water/solvent mixture have further worsened by interdiffusion. During mixing/interdiffusion the system thus passes through successive solubility limits: that of the initially dissolved active substance and that of the surfactant. Clearly in respect of this point there is a need for further research to establish definitively the actual mechanisms and to understand their totality.

It is interesting to observe how different disciplines handle the set of problems described in this Section. Polemically it could be so formulated: chemists are satisfied when they can prepare a defined end state in the form of dispersed nanoparticles under defined experimental conditions. Physicists refer to the problem of turbulent mixing in terms of the final physical questions to be solved.[85] Engineers in contrast have a results-orientated approach to the problem, as documented, for example in the recently published, voluminous work from

Baldyga and Bourne.[76] Finally it is noted that in recent years computer-supported solutions to fluid-dynamics problems are gaining increasingly in importance.[77, 86]

2.7. Experimental Aspects

To understand the stages through which the formation of colloidal particles pass it is necessary to record experimentally the particle formation process by time resolution from the timepoint when supersaturation is realized. That the time-resolved description of processes is in no way trivial is recognized from the limited number of publications in this area. In most cases a description of the mechanism of particle formation is still limited to a retrospective derivation from the structure of the particle formed. That the amount of work published in this problem area is quite limited is because, unlike crystallization, particle formation in precipitation reactions occurs on a clearly shorter time scale, down to the region of milliseconds.

Where time resolution of the chosen measurement method is sufficient the stopped-flow method has proved effective: two educt volumes are led through a mixing cell into a measurement cell. At a predetermined timepoint the flow is interrupted and the particle formation process is measured by a suitable method, for example light scattering or the scattering of intense X-rays. If the measurement method requires longer measurement times the flow reactor or precipitation jet may be used.[31, 87–89] Here, both educt flows are passed through a mixing cell and then through a reactor tube or, after a defined distance, directed as a free beam into a defined atmosphere. Assuming that the system is quasistationary, that is, that over an extended period of time the precipitating system is in the same state at definite positions of the precipitation tube, at a known flow rate v in the tube the detection point x (measured from the mixing cell) at which, for example, spectroscopic or diffractive characterization methods are attached, may be converted into reaction time $\tau = x/v$. Alternatively the tube length may be varied and samples for off-line methods (especially microscopic methods) obtained, for example, by quenching liquid samples at the beam outlet.[31] It is assumed when using these systems that the time scale of the reaction process is longer than the time to homogeneous mixing of the educts in and after the mixing cell; typical mixing times lie in the range of milliseconds for the stopped-flow technique and in the range of microseconds with special flow cells.[88] Hitherto there have been few investigations of processes *during* mixing. More recent experiments show, however, that precursor structures which break down to nanoparticles are already forming at the boundary interface of the two turbulently mixing educt flows.[31]

In the following a number of experimental methods will be described briefly with which particle formation processes may be investigated on length scales of nanometers. Static and dynamic light scattering are established techniques for the investigation of colloidal systems.[90] More recently correlation spectroscopic methods such as fluorescence correlation spectroscopy (FCS) and Raman correlation spectroscopy (RCS) have been developed for the characterization of nanodispersed systems.[91] Concentrated dispersions can also be characterized reliably by fiber optic quasielastic light scattering (FOQELS).[92] Small-angle X-ray and neutron scattering (SAXS and SANS) are also classical methods for the characterization of colloidal systems[93] and have been used in many investigations for the determination of primary particle size and aggregate structures. Investigations on the following systems are cited as examples: lysozyme clusters as precursor for critical nuclei (SANS),[94] precursor formation in zeolite crystallization (SAXS),[95] aggregation and compaction in the formation of SiO_2 and TiO_2 particles (SAXS),[96] hydrolysis and condensation of metal alkoxides,[89] and particle formation in quinacridone and boehmite precipitation,[31] in the latter two cases the above-described precipitation tube technique was used.

UV/Vis spectroscopic methods can be used principally for online analysis of particle size development by means of particle size dependency of turbidity spectra and, where possible absorption spectra (see Section 4.3). A quantitative evaluation is made difficult, however, because model concepts relating to particle size distribution, particle shape, and refractive index differences must be available.

In conclusion a number of techniques for the time-resolved investigation of particle formation processes are listed about which only a few reports are currently available. The earliest stage of particle formation in the hydrolysis of metal alkoxides was studied with the laser-induced liquid beam ionization/desorption (LILBID) technique.[97] An equally exotic technique is X-ray microscopy with which aqueous systems can be investigated under normal pressure with time resolution in the minute range and a space resolution of about 30 nm.[83] Finally an interesting use of the analytical ultracentrifuge[98] has been reported: this method allows the particle size distribution of precursors in the crystallization of lysozyme and CdS to be determined.[99] For completeness the pulse-radio technique is mentioned with which the formation and growth of colloidal metal clusters in an aqueous environment may be studied with a time resolution in the submillisecond range.[100]

3. Preparative Methods for the Production of Organic Nanoparticles

As discussed at the outset, nanodispersed systems can be obtained in two ways (Figure 2): 1) by mechanical milling of the raw material by wet or dry milling processes, or 2) by precipitation or condensation of the products or educts dissolved in solvents with subsequent separation of the unwanted solvent. In both variants additives such as surfactants and polymers take over the function of boundary layer active, colloidal stabilizers or—in the condensation procedure of method (2)—also form the nanoparticulate phase itself which contains the active compound or effect substance, bound by adsorption or absorption.

Milling processes[101] are in principle unsuitable for the production of nanodispersed systems with narrow size distribution since with decreasing particle size it becomes

increasingly more difficult to use the applied mechanical energy in the form of shearing and cavitation forces[102] for particle milling without simultaneously inducing particle agglomeration.[101, 103] Moreover, the unavoidable milling element abrasion which contaminates the end product and is difficult to separate, especially in active compound formulations, is often undesirable or not tolerated.[104] The considerable practical significance of milling processes lies mainly in that in pigment and dyestuffs formulations the achievable particle size distributions in the lower micrometer region, in special cases also below, satisfy technical demands.[101, 105]

In spite of these disadvantages milling processes do find widespread use in the formulation of poorly soluble active compounds[106–108] since alternative technologies which could deliver nanoparticulate products are essentially still in the development stage. These include in particular the described precipitation processes from homogeneous solution which with suitable process control not only allow the preparation of extremely fine particulate dispersions, but also allow a continuous and, in respect of process parameters, easily controllable method of production. These technical advantages also make precipitation processes particularly attractive from an economic viewpoint.

With the theoretical principles discussed in Section 2 in mind the precipitation processes are illustrated below. Various methodological variants for the production of nanodispersed polymer dispersions by physical condensation processes will also be described briefly.[109–111] Figure 10 gives a structured methodical overview of precipitation and condensation processes for the production of organic nanoparticles in aqueous media. Starting from a molecularly dispersed solution of the "active compound" three groups or processes which allow a restriction of particle growth to the nanometer region can be differentiated.

1. With lipophilic solvents (processes I and II) particle dimensioning occurs through an emulsion step as an intermediate stage. The particle size distribution of this oil in water (o/w) emulsion is adjusted mechanically by homogenization.[101, 103, 106] The conversion of the emulsion into a nanodispersion is then carried out by separation of the solvent by evaporation or diffusion procedures. The size distribution of the nanodispersion is determined by that of the o/w emulsion, the mean particle size by the concentration of the substrate in the emulsion phase.
2. If hydrophilic, fully water-miscible solvents are used (processes IV and V) particle formation occurs by precipitation[103] either according to the principles of nucleation and growth outlined in Section 2 or, at extremely high supersaturation, by spinodal phase separation. In each case an agglomeration step can follow these elementary processes (Section 2.4.2).[112]
3. With use of amphiphilic solvents or solvent mixtures (process III) nanoparticle formation takes place through a transient emulsion phase which forms spontaneously and which then transforms into a nanodispersive state.

Only with process groups (2) and (3) is size distribution controlled by the level of the adjustable supersaturation as well as by surfactant additives, which possibly intercede specifically in the elementary steps of nucleation, growth, phase breakdown, and agglomeration. The individual process variants differ in respect of the adjustment of the temporal supersaturation profile as well as in the choice and function of the additives introduced.

In the structuring indicated in Figure 10 only in the limiting cases I and V does particle formation takes place by pure

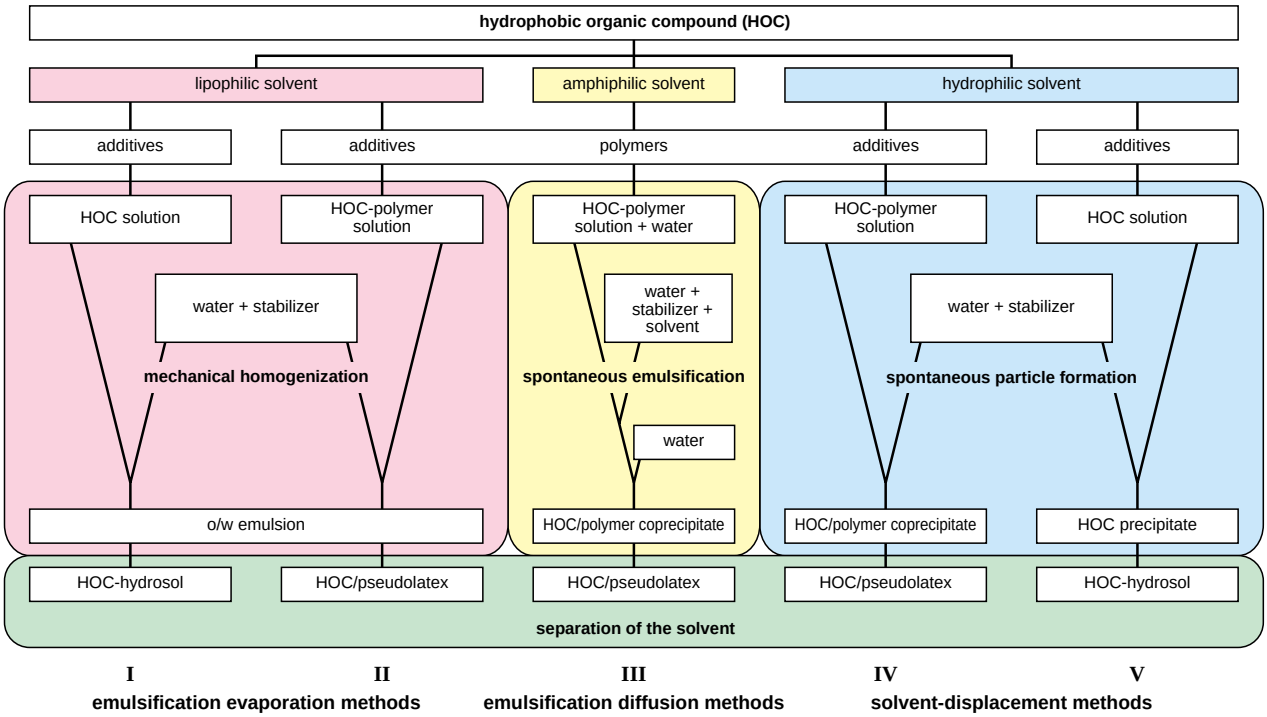


Figure 10. Precipitation and condensation processes for the preparation of organic nanoparticles. More detailed explanations in Figures 11–15 and the text.

precipitation processes (in respect of active compound). In contrast, with variants II, III, and IV processes are described which lead to so-called pseudolatex systems through physical condensation of dissolved macromolecules, that is, the "support" is primarily precipitated.[111] The physico-chemical elementary processes of particle formation and the bonding of dissolved active compounds onto or into the particulate phase are still essentially unexplained. The terms nucleation from a homogeneous supersaturated phase and particle growth normally used in the description of the elemental steps in precipitation reactions are here of limited suitability in describing the complex relationships in particle formation. It should be noted that processes I – III contain an emulsification step prior to the actual particle formation.

Process variants I – V are illustrated below with selected examples. In all processes polymers, surfactants, and surface-active protective colloids play a significant role in particle formation, even if in quite different functions. Detailed knowledge of molecular-specific possibilities for influencing particle formation, especially for the targeted adjustment of particle size and particle morphology, is only available in individual cases.

3.1. Nanoparticle Formation by the Emulsification – Evaporation Process from Lipophilic Solution

3.1.1. Hydrosols of Active Compounds (Process I)

Processes of this type belong to the classical methods for the preparation of water dispersible nanoparticulate hydrosols of water-insoluble active compounds. They were developed especially for the formulation of carotenoids.[113–115] Preparation of the nanoparticles is carried out by dissolving the active compound together with an emulsifier, for example, ascorbyl palmitate, in a suitable solvent, for example, chloroform or methylene chloride, then emulsifying this solution with an aqueous solution of a protective colloid, for example gelatin, and removing the solvent by distillation (Figure 11). The actual precipitation/crystallization takes place in the emulsion droplet during distillation when the solubility limit is crossed. The size of the active compound particle is thus proscribed by the concentration of the active compound solution and the size of the emulsion droplet. The particle size distribution can be adjusted within wide limits by the droplet size distribution of the o/w emulsion through the choice of homogenizer (colloid mill, high pressure homogenizer, ultrasound disperser).[101, 103, 106] A solid nanoparticle which is protected against agglomeration by the suitable choice of the protective colloid is obtained from each emulsion droplet of a well-stabilized emulsion upon removal of the solvent.[116] The particle morphology is usually polycrystalline in the thermodynamically stable crystal structure since the solid formation takes place by evaporation crystallization at low supersaturation.[117] Numerous recipe variants can be realized by the addition of further lipophilic additives to the emulsification formulation. A fundamental difficulty in this process lies in the removal of as much solvent as possible from the final product.

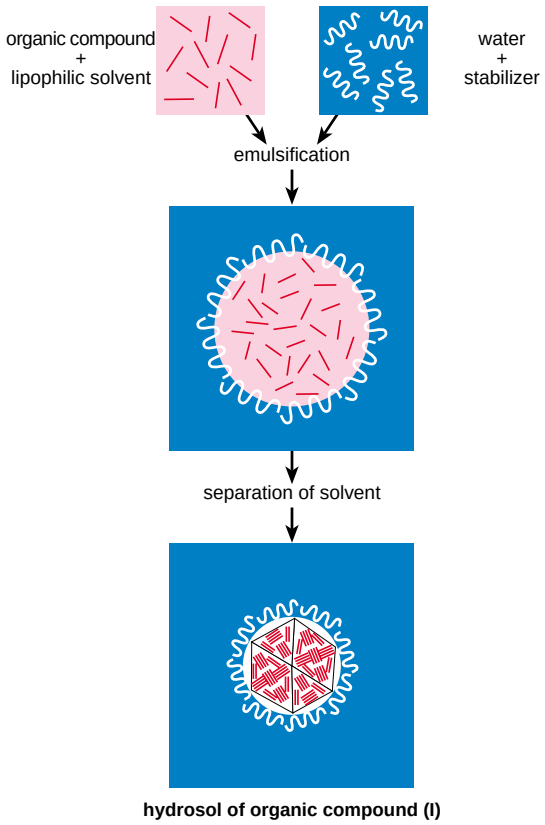


Figure 11. Principle of the preparation of active-compound hydrosol nanoparticles by the emulsification – evaporation process.

3.1.2. Pseudolatex Systems (Process II)

If lipophilic polymers, such as biodegradable polylactides (PLA), poly-β-hydroxybutyrates (PHB), polylactide-co-glycolides (PLGA), polycaprolactones (PCL), or polyalkylcyanoacrylates, are used with the active compound[110, 118–122] nanoparticulate polymer dispersions are obtained which contain the lipophilic active compound either adsorbed or embedded as molecular dispersions or microcrystals (Figure 12).[110, 119, 123] The formulations thus prepared are of increasing interest as parenteral dosage forms (see Section 4.2). A special version of this method for the preparation of protein-loaded polylactide nanoparticles was recently published.[120] In a double emulsion process an aqueous solution of the active protein (protein C plasma inhibitor) was emulsified in a methylene chloride/acetone polylactide solution and this o/w emulsion was then emulsified in an aqueous solution of polyvinyl alcohol (PVA) as protective colloid. After removal of the solvent PLA nanoparticles (200 – 250 nm) were obtained. The protein activity in the nanodispersed formulation could be controlled by the preparation conditions.

On account of the excellent solubilizing properties of chlorohydrocarbons for lipophilic active compounds and galenically interesting additives.[101, 106, 124] The procedure described is in principle widely applicable to the formulation of lipophilic active compounds. However, there is one intrinsic disadvantage in that these toxicologically dubious solvents

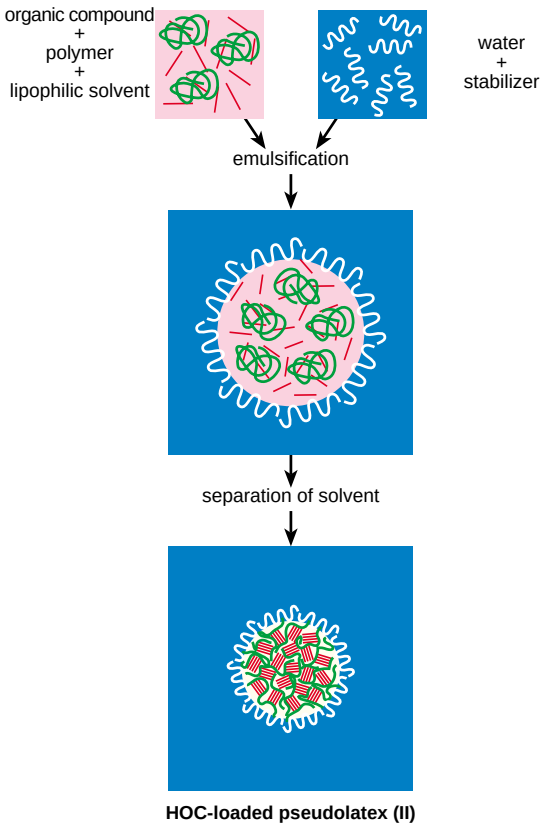


Figure 12. Principle of the preparation of active-compound pseudolatex nanoparticles by the emulsification–evaporation process. HOC = hydrophobic organic compound.

must be fully removed during the workup of the formulation.[106] Therefore, more recently attempts are being made to change the emulsification–evaporation process to the use of more acceptable solvents such as cyclohexane. With the example of cholesteryl acetate as a model compound Sjöström and Bergenstahl were able to show that with an optimized emulsification system it was possible to obtain stable nanodispersed formulations with particle sizes of about 25 nm.[117] Where it is possible in individual cases to find an acceptable solvent the emulsification–evaporation procedure has the advantage in that it should be possible to select suitable protective colloids and emulsifiers on the basis of semi-empirical concepts and thus allow targeted process optimization.[101, 125]

3.2. Nanoparticles by the Emulsification–Diffusion Procedure from Amphiphilic Solution (Process III)

The different process variants are all based upon the use of solvents which are of limited water miscibility and capable of spontaneous emulsion formation (e.g. propylene carbonate, benzyl alcohol, ethyl acetate). This method thus offers the advantage of the use of pharmaceutically acceptable solvents and does not require the use of high-pressure homogenizers for the formation of the o/w emulsion as the preliminary stage of nanoparticle formation.[110, 126, 127] The trick of this process, the physico-chemical principles of which are still not fully clarified, is that the water-saturated solvent phase (+polymer and active compound) and the solvent-saturated aqueous phase (+protective colloid), that is, in thermodynamic equilibrium, are first emulsified by intensive stirring. With the subsequent addition of water to the merely microdispersed o/w emulsion the diffusion equilibrium is disturbed. This induces solvent diffusion into the homogeneous aqueous phase at which point the solubility limits of polymer and active compound are crossed and particle formation commences (Figure 13). Mechanistic investigations with variation in preparation conditions and the use of PLA as polymer and polyvinyl alcohol (PVAL) as protective colloid have shown that each emulsion droplet gives a multiplicity of nanoparticles.[127]

This remarkable finding was explained by the development of concentration fluctuations in the boundary layer region caused by solvent diffusion, when the solubility limit is narrowly exceeded locally and the precipitation of polymer and active material is induced. The interaction of the

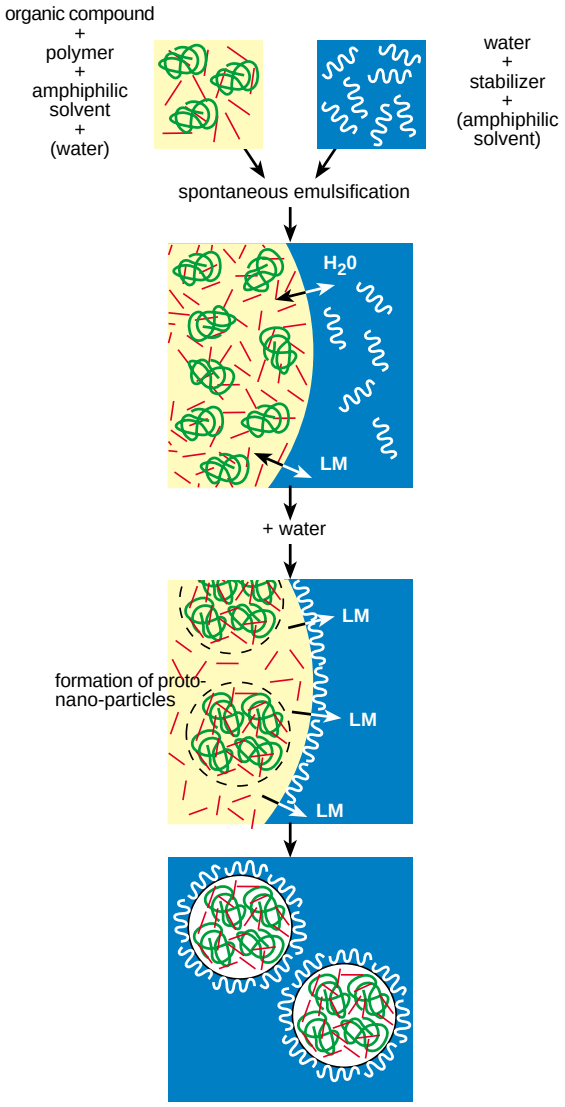


Figure 13. Principle of the preparation of active-compound pseudolatex nanoparticles by the emulsification–diffusion process.

protective colloid molecules present in the aqueous phase with these "proto-nanoparticles" suppresses their further agglomeration and thus determines the achievable particle size distribution of the nanodispersion, which is obtained after removal of the solvent by distillation. According to the mechanism described in Section 2.6 it would also be conceivable that when the solubility limit is crossed during interdiffusion of the two phases, active compound particles which are inhibited in growth by adsorbing protective colloids, and thus colloidally stabilized, form continuously. A process variant which allows a further simplification of the procedure was reported recently.[128] Here the dilution step with water and the separation of the solvent is combined by steam distillation. The process was tested with a series of biodegradable and non-degradable polymers.

A further variant has been used which also manages without a homogenization step, since emulsion formation again occurs spontaneously as a preliminary stage in nanoparticle formation. However, this so-called SESD (spontaneous emulsification solvent diffusion) process[122, 129] suffers from the disadvantage that amphiphilic solvent mixtures with methylene chloride are used as the hydrophobic component. Technically a polymer/active-compound solution, for example PLGA, in acetone/methylene chloride is added with stirring to an aqueous protective-colloid solution (polyvinyl alcohol). A coarse-particle o/w emulsion forms spontaneously the particle size of which is rapidly reduced by diffusive loss of the acetone in the dispersed phase. After evaporation of the solvent PVAL-stabilized polymer particles with incorporated active compound are formed in the nanometer range. The solvent mixture and the polymer-protective colloid combination are so adjusted that clear affinity differences between polymer and protective colloid for the solvent components guarantee phase separation and allow colloidal stabilization.[129] It is clear that in view of the complexity of the individual physico-chemical processes involved in each system a detailed optimization is required to regulate the desired particle size distribution. In this context a modified SESD process has been described by Murakami et al. that uses solvent mixtures without the undesired chlorohydrocarbons.[129] However, since water-miscible solvent mixtures are used the particle formation mechanism must be differentiated from that of the SESD process (Section 3.3.1).

A further variant for the formation of nanodispersed pseudolatex dispersions, possibly loaded with active compound, through an emulsion phase as intermediate stage is the so-called salting-out process.[110, 130] The process is based upon the ability of electrolytes (for example NaCl, $MgCl_2$, $CaCl_2$[110, 131]) or saccharose[132] to salt-out acetone from an aqueous solution. The active compound/polymer solution in acetone is initially emulsified in the aqueous electrolyte or sugar solution in the presence of a protective colloid and then diffusion of acetone into the aqueous phase—with simultaneous formation of nanoparticles—is induced by the addition of water. Here too boundary surface turbulence (initiated by acetone diffusion) or mechanisms as described in Section 2.6 (precipitation during the interdiffusion of the phases) can explain the nanoparticle formation. However, there have been no detailed investigations on the mechanism of particle formation to date. These relationships have proved to be extremely complex. Thus, incorporation of the active compound into the nanoparticle is influenced considerably by the salting-out components.[110, 133, 134] Hitherto only the protective colloids PVAL, polyvinylpyrrolidone (PVP), and hydroxyethylcellulose have demonstrated an adequate effectiveness.[110] The solvent and the salting-out components are separated by distillation or cross-current filtration

3.3. Nanoparticle Formation by Solvent-Displacement Processes from Hydrophilic Solution

The industrial advantages of the processes discussed at this point rest upon the use of water miscible, toxicologically acceptable solvents, (e.g. acetone, short-chain alcohols). The methods were described both for the preparation of nanodispersed pseudolatex transport forms of lipophilic active compounds and for the preparation of pure nanohydrosols of active compounds and effect materials which are poorly soluble or insoluble in water.

3.3.1. Pseudolatex Systems (Process IV)

The modified SESD process (described in Section 3.2) represents a special case of pseudolatex formation by way of a transient emulsion stage.[129] The solvent mixture consists of two water-miscible solvents (acetone/ethanol) with different affinities for the polymer and the protective colloid. In the example used the polymer PLGA has a higher affinity for acetone, whilst the protective colloid PVAL is more soluble in ethanol or methanol. A five-stage model was suggested for the mechanism of particle formation.[129] After mixing the PLGA solution with the aqueous PVAL solution rapid diffusion of the alcohol component first leads to particle size reduction of the transient emulsion intermediate which is formed according to the Marangoni Effect.[135] The preferred diffusion of the alcohol component is explained by the lower affinity of the alcohol for PLGA in the dispersed phase. The likewise occurring acetone diffusion leads to a collapse of the PVAL protective colloid in the boundary layer, accompanied by a PLGA condensation in the increasingly acetone-depleted dispersed phase. Even under mild stirring conditions this spontaneous particle formation process also leads to nanoparticulate pseudolatex dispersions (Figure 14). To what extent this novel process can be extended to other polymer/protective-colloid combinations cannot yet be assessed. Clearly, experience with polymer incorporation of lipophilic active compounds is currently not available.

Fessi et al. showed for the first time that instead of a solvent mixture the use of only one solvent with unlimited water miscibility can also lead to the spontaneous formation of nanoparticulate pseudolatex dispersions.[136] Normally acetone, ethanol,[110, 136–138] or THF[121] are used. In analogy to the modified SESD process the polymer solution, which possibly also contains active compound and other additives, is mixed with the aqueous protective colloid (PVAL) solution. The spontaneous particle formation is again explained by boun-

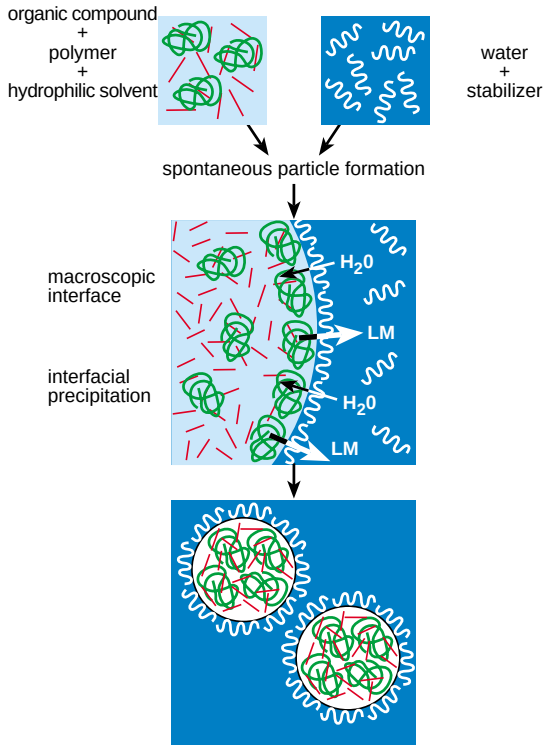


Figure 14. Principle of the preparation of active-compound pseudolatex nanoparticles by the solvent-displacement process.

dary layer turbulence which is initiated by solvent diffusion.[110, 127, 136] According to this model concept boundary layer turbulence leads to breakdown of the nanodimensional solution compartments in which, with increasing diffusive depletion of solvent, polymer and active compound are concomitantly precipitated. Occasionally the term nanoprecipitation is also used to characterize this process.[110, 138–140] The stabilization of the particle by adsorption of the protective colloid is still critical for the nanodimensioning of the particle to prevent a subsequent agglomeration. Here too the question arises whether the assumption of boundary layer turbulence is necessary to explain particle formation. For example, experiments by Lannibois-Drean[84] have shown that even with macroscopic boundary layers between the two educt phases the formation of small particles can be explained by interdiffusion (see also the discussion in Section 2.6).

Wu and co-workers have reported that if the polymer is an ionomer, for example sulfonated polystyrene, a protective colloid can be omitted as electrostatically stabilized nanoparticles are formed.[141, 142] The nanodispersions obtained by precipitation from a THF solution were extremely fine with mean particle sizes in the range 5–12 nm. The particle sizes could be deliberately made smaller with decreasing polymer concentration and increasing degree of sulfonation. The formation of charge-modified PLGA nanoparticles by condensation from an acetone/ethyl acetate solution has also been reported by Kissel and co-workers.[143]

The conversion of these attractive processes into practice is, however, fraught with difficulties as the model concepts on particle formation in the individual case can only supply approximate information as to the optimal composition of the active compound/polymer/solvent/stabilizer system.[110, 144] It appears plausible that the particle size falls with decreasing polymer concentration in the solution phase because of the material balance and the decreasing viscosity.[121, 137, 141, 145–147]

An important requirement for particle formation appears to be that the resulting water/solvent mixture is non-solubilizing for the polymer.[137] The yield of nanoparticles—in addition to the coarse and thus valueless agglomerate—as well as their particle sizes are determined within wide limits by the nature of the solvent and by the mixing ratio with water.[146] In model investigations with hydroxypropylmethylcellulose phthalate (HP55) as polymer and acetone/water mixtures as solvent it was found that the yield of nanoparticles could be increased with increasing water content (up to 30% (v/v)) from a fraction of about 30% to over 90%. This observation was explained by a change in the solvent character from a good to a poor solvent. With the thus associated reduction in chain interaction of the dissolved macromolecule the nanoparticle formation is already predetermined by the structure of the solvent phase (see also Section 2.2.6).[146, 148, 149] Further experimental details have been described recently by Fessi and co-workers.[137] In particular, it was shown in that the usual stirred vessel method for the precipitation of nanoparticles could be developed further by a controlled precipitation in a T-mixer. The objective is a continuous industrial production process. In analogy to the processes described previously a separation of the solvent by distillation is also carried out here, which presumes an adequate colloidal stability of the dispersed system.

The nanoprecipitation process is also suitable for the preparation of nanocapsules. In this case a suitable oil in which the active compound is highly soluble is added to the solution phase. Core-shell particles are then formed with the active compound–oil solution as core.[110, 149, 150]

The motivation for the extensive work on the preparation of nanodispersed pseudolatex systems comes from the demand for aqueous peroral and parenteral (that is, administered by mouth, and for non-intestinal administration) transport forms of lipophilic active compounds. The choice of the hitherto investigated polymer systems is therefore aimed primarily at pharmaceutical-technical acceptance and in individual cases at their biodegradability and tolerance. The particles serve as absorptive or adsorptive active compound supports.[118, 151] This property explains why work is orientated preferentially towards active compound and application-specific areas and a systematic treatment of the complex problem of particle formation based on polymer-physics principles is still essentially absent.[145]

3.3.2. *Active Compound Hydrosols (Process V)*

To date little has been reported on precipitation techniques for the preparation of nanodispersed hydrosols of active compounds (Figure 15),[152–157] in contrast much has been written on precipitation techniques for the preparation of

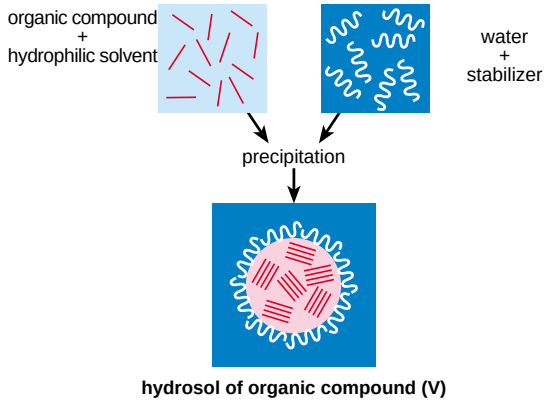


Figure 15. Principle of the preparation of active-compound hydrosol nanoparticles by the solvent-displacement process.

inorganic nanoparticles.[2, 103, 158–162] In particular Matijević and co-workers developed the latter further with the aim of preparing nanodispersed systems with uniform particle size and shape.[2, 161, 162] In contrast, the emphasis of work on the bulk crystallization of organic molecule crystals lay mainly on the production of readily filterable crystal suspensions with particle sizes in the middle micrometer range as the final stage of a synthesis procedure,[163–168] or in a defined crystal modification.[169–171] With organic dyes and pigments and poorly soluble active components further process steps are usually performed, for example, to reduce the particle size by milling or homogenization techniques and thus to modify the color or photoelectric properties or to improve the bioavailability of the active compound.[101] It therefore appears attractive to replace the technically cumbersome mechanical formulation methods by precipitation methods which directly give the active compounds or effect materials with the desired particle size in the nanometer range.

According to the discussion in Section 2 the following conditions must be fulfilled for the preparation of nanodispersed hydrosols by precipitation reactions:

1. nucleation must take place at the highest level of supersaturation possible to maximize the nucleation rate.
2. The limitation of particle growth and the setting of a narrow size distribution require a controlled and rapid reduction in supersaturation subsequent to the nucleation phase, possibly under the influence of specific growth inhibitors.
3. The agglomeration of the primary particles should be prevented or controlled by the presence of viscosity-increasing additives and/or by low molecular weight protective colloids with high surface activity.[172]

If the precipitation of the active material from molecular solutions takes place by the addition of an antisolvent, for example, water, and not by the formation of poorly soluble salts or as result of a chemical reaction, the first condition can be fulfilled by a suitable choice of a solvent which is fully miscible with water and by a highly efficient mixing technique.[164] If it is possible to set high values for supersaturation ($>10^5$) then, according to the most recent investigations of Botet et al., particle formation can also occur by a diffusion-limited aggregation mechanism with active participation of suitable additive molecules, in contrast to the classical model concepts of nucleation and growth.[173] Detailed thermodynamic considerations should show whether or not this is a spinodal separation process (see Section 2.2.3).

The choice of suitable solvents for setting the highest supersaturation possible is naturally limited since in addition to a good solubilizing ability for the active compound, complete miscibility with the antisolvent water, and a lowest possible boiling point for the distillative separation of the solvent from the nanodispersion are necessary. For the formulation of pharmaceutically active compounds toxicological safety is a further limiting parameter. Consequently small-chain alcohols, acetone, or THF are used.

In the mixing methods for the rapid establishment of high supersaturation (Section 2.6) there is need to differentiate between processes with and without back mixing. For preparative work on laboratory scale, processes have been described in which the solution phase is added to the stirred, aqueous protective-colloid solution, either dropwise or by spraying.[154, 165, 174, 175] Precipitation conditions are more readily controlled by the so-called double-jet technique in which the reaction solutions exit the jet pair immersed in protective colloid solution and are mixed at a defined flow angle.[156, 161, 176] In all cases there are hydrodynamically poorly controllable batch processes involved with possible back mixing, so that nanoparticulate systems are only obtained if the precipitation reaction is carried out at sufficiently low active-compound concentration so that a secondary crystallization or particle agglomeration can be held within limits.

A further group of procedures is one in which the active-compound solution and the aqueous protective-colloid solution are vortexed vigorously in a mixing chamber,[152, 153, 163, 164] a static mixer,[154] or a Y- or T-mixer[163, 165, 177] with mixing times down to the millisecond range and particle formation occurring in a subsequent flow tube. Although the hydrodynamic and reactive processes in each of the method-specific mixing zones have in no way been explained (see Section 2.6), the techniques, in particular the non-pulsate delivery of the component flows, allow controllable particle formation with a narrow size distribution by means of varying the mixing conditions and temperature control. Kinetic data on the course of the precipitation reaction can be obtained in certain cases with suitable sensors situated along the flow reactor (see Section 2.7). Furthermore, a particular advantage of this process is that a scale-up from the laboratory apparatus to continuous-production processes is possible.

The method developed by Horn and co-workers for the production of nanodispersed carotenoid hydrosols by precipitation from hydrophilic solution with water uses a continuous mixing chamber process.[152, 153] Figure 16 shows the principle behind the process. Poorly soluble and temperature labile active compounds can also be converted into nanodispersed hydrosols by this method. For this purpose a second mixing chamber is attached in front of the actual precipitation chamber in which a molecularly dispersed solution is produced immediately before precipitation by shock heating of the microdispersed active-compound suspension by turbulent mixing with a hydrophilic solvent at high temperature

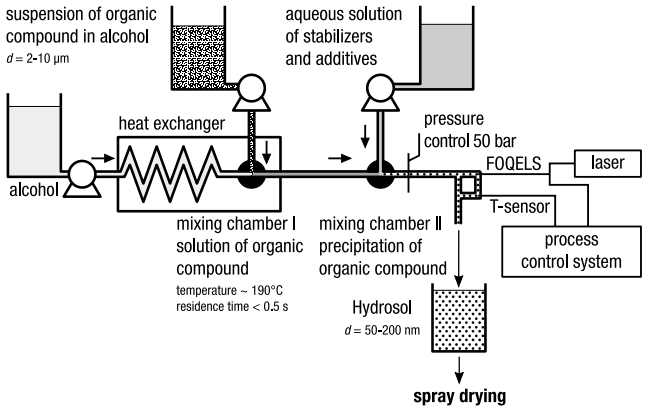


Figure 16. Process scheme of the mixing-chamber process for the preparation of active compound hydrosol nanoparticles by precipitation from hydrophilic solution. Further details in the text.

(ca. 200 °C) and extremely short residence time ($\ll 0.5$ sec). With short-chain alcohols or acetone this method requires a limitation of the system pressure to around 50 bar. The temperature course, residence time, and mixing relationships in the precipitation chamber can be varied within wide limits in a manner specific to the active compound. A laser optic device (FOQELS: fiber-optical quasielastic light scattering) allows online measuring of the mean particle size for process control.[92] As Figure 17 shows, X-ray amorphous, spherical

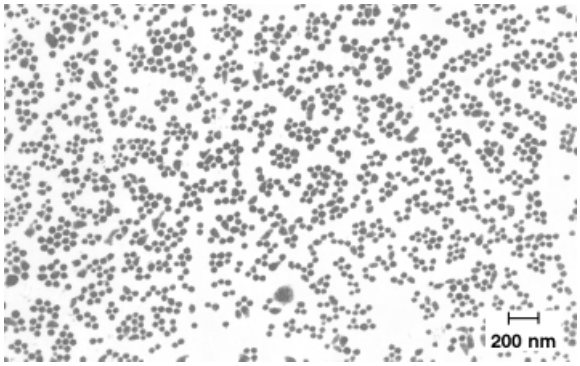


Figure 17. TEM micrograph of a β-carotene hydrosol prepared by the mixing chamber process.

particles of uniform size (in the range 50 – 100 nm) are usually obtained in this way with poorly water soluble or insoluble active materials—in accordance with the Ostwald law and the molecular dynamic model concepts on additive-controlled particle formation of Botet et al.[173]

In agreement with the respective industrial and physiological requirements demanded of hydrosols, biopolymers such as proteins and polysaccharides, or synthetic macromolecules are used as the protective colloids which stabilize the nanoparticles sterically and/or as electrostatically active adsorbate layers.[116, 178] Furthermore, the formulations can be complemented by other industrially or galenically acceptable additives which allow a subsequent conversion of the hydrosols into a redispersible granulate by spray drying or freeze drying (see Section 4). Such a process step can be coupled directly with the continuous hydrosol formation, if as a result of the solvent fractions initially remaining in the precipitation medium there is the risk of particle growth by Ostwald ripening, especially since in accordance with the Kelvin equation (Section 4.1) the apparent solubility of mesoscopic systems increases exponentially with decreasing particle size. This consideration applies particularly to particles with an amorphous solid structure.

Finally, the continuous process for hydrosol formation, that is described here in principle, has the methodological flexibility to make a wide range of nanoparticulate formulations of organic compounds accessible. Thus, for example, polymers and surfactants as well as fats and oils can be introduced by means of the solution phase and in this way novel nanodispersed transport forms for active compounds and effect materials can be prepared (see also Section 4).

3.4. Nanoparticle Formation with Supercritical Fluids

Supercritical fluids (SF) are used in a number of different circumstances for the preparation of micro- to nanodispersed organic systems.[168, 179, 180] Of industrial use are their special solvent properties and the technical feasibility of large temperature gradients.[181] The generation of a sufficiently high supersaturation for the initiation of a precipitation reaction with conventional solvents is on the one hand limited by the generally low dependency of the solubility on temperature, on the other by the difficulty to realize technically the necessary rapid heat exchange. With this in mind one process in which liquid CO_2 is used as cooling agent deserves attention.[182] In this so-called contact cooling process the active compound solution at $-78\,^{\circ}C$ is sprayed into a CO_2 stream and particle formation is induced in the spray droplets by crystallization. Experimental results with an abecarnil/isopropyl acetate system process showed that it was possible to devise systems which also appear to make the formation of nanodispersed precipitates possible.

The use of liquid CO_2 as solvent and precipitating medium for active compounds[183] has been investigated by Larson, King, and other authors.[184] From the viewpoint of toxicological acceptability, the non-combustibility, and the favorable critical data of CO_2 ($p_c = 74$ bar, $T_c = 31\,^{\circ}C$) the so-called RESS process (rapid expansion of supercritical solutions) appears particularly attractive, especially because extra process steps to remove residual solvent may no longer be required. However, SF-CO_2 can act as an oxidizing agent with oxidation-sensitive compounds such as β-carotene and is thus ruled out as a precipitation medium. Consequently, ethane and ethylene were investigated by Chang and Randolph as inert SF precipitation media for β-carotene.[180] In supercritical ethylene ($T_c = 9\,^{\circ}C$, $p_c = 50$ bar) β-carotene shows a change in solubility of about three orders of magnitude to a molar fraction of 10^{-7} in the expansion from a pressure level of 400 bar and a temperature of 50 °C.[180, 181] By immersion of the expansion nozzle into a 10% aqueous gelatin solution stable crystalline solutions could be obtained the mean particle size of which lay at 1 µm, with a fine core fraction

up to 300 nm. In spite of these findings it must be noted that the achievable solubilities of polymers and organic active compounds and effect materials in SF-CO_2, SF-C_2H_4, SF-C_2H_6 are so low that the development of a technically feasible process only appears promising in exceptional cases.

In contrast, in three further process variants, the low SF solubilizing ability for active compounds is used industrially. Both in the GAS process (gas antisolvent process)[185] and in the PCA process (precipitation with compressed fluid antisolvent)[186] SF-CO_2 instead of water serves as the precipitation medium from organic solvents. In the physically related SEDS process (solution enhanced dispersion by supercritical fluid)[183] the organic active-compound solution and the SF-CO_2 are brought into contact in a coaxial mixing nozzle, and thus a rapid extraction of the solvent (e.g. acetone) is possible.[187] However, to date there have only been reports of particle formation in the micrometer range.

Finally, a suggestion from Nakanishi and co-workers deserves attention, namely the preparation of nanoparticles of poorly soluble active compounds and effect materials by precipitation from water-miscible solvents in the supercritical state, if the thermal stability of the compounds permits.[188]. Thus the precipitation of spherical titanylphthalocyanin particles (see also Section 4.3) in the size range of 30–50 nm from SF-acetone at temperatures of 230–330 °C and water as antisolvent was reported.

3.5. Nanoparticles from Polyelectrolyte Complexes

The complex formation of polyanions with polycations in aqueous solution can equally be used for the preparation of nanoparticles under special reaction conditions. They usually take place stoichiometrically by charge compensation,[189] even with structurally very different reaction partners such as globular proteins and linear polyelectrolytes.[190] If the reaction is carried out at sufficiently high dilution, electrically neutral nanoparticles are obtained primarily[189, 191] which, however, because of their hydrophobic nature coagulate to microdispersed agglomerates. The known precipitation reactions for the isolation of proteins from aqueous solution are based upon this secondary reaction.[191, 192]. Electrosterically stabilized primary particles can be obtained when the reaction takes place with a charge-stoichiometric excess of one reaction partner.[189, 193]

Initial experience with nanodimensioned polyelectrolyte complexes in which the reaction partner DNA itself functions as the effect material has been reported recently.[194]

Finally attention is drawn to two more recent developments which represent interesting variants of particle formation with the involvement of polyelectrolytes. In analogy to naturally occurring transport forms of vitamin A by its bonding to specific transport proteins, Thünemann and co-workers[195] have prepared charge stoichiometric vitamin A acid complexes with the polycations poly(L-lysine), poly(L-arginine), and poly(L-histidine) in the form of lamellarly structured nanoparticles (ca. 300 nm) by a special precipitation/redispersion process.[196] The nanoparticles, stabilized with polaxomer 188 poly(ethylene oxide)-poly(propylene oxide) triblock copolymer), could represent an interesting transdermal administration form for vitamin A acid.

Following a procedure described by Decher,[197] Möhwald and co-workers[198] initially formed core–shell hybrid particles by alternating adsorption of polyanions and polycations onto nanosized template particles which were converted into polyelectrolyte capsules after dissolving out the template core. These semipermeable hollow spheres could be used as nanosized precipitation reactors for the preparation of dyestuffs and active compound hydrosols should it prove possible to modify the boundary surface of the hollow space in a substrate-specific manner such that a precipitation reaction takes place preferentially within the hollow spheres.

4. Properties and Areas of Application of Suspensions of Organic Nanoparticles

The emphasis in the application of nanodispersed organic active compounds and effect materials as well as current research and development targets is concerned mainly with the optimization of the bioavailability of active compounds (pharmaceuticals, cosmetics, plant protection) and the control of the optical properties, especially color attributes, by particle size and the supramolecular structure of the particles. In addition, the particle size dependency of the photoelectric properties of organic xerographic photoreceptors is currently the subject of increasing interest in the further technical development of copying processes, in particular laser printers.[199–201] With similar objectives, investigations on nanosized ultrathin layers of such materials have been carried out, but which will not be discussed more closely at this point.[202] In contrast, colloidal-physical aspects of the use of the photovoltaic, photoelectrochemical, and catalytic effects of organic materials have been paid little attention in comparison to inorganic semiconductor materials,[203] in spite of all the hopes which have been placed on this class of materials.[204]

In the next Section the current work and the ensuing products will be reviewed, in which the biological activity and the optical properties of active compounds and effect materials have been optimized by the adjustment of both the particle sizes within the nanometer range and of the supramolecular particle structure.

4.1. Strategies for Increasing the Bioavailability of Poorly Soluble, Organic Active Compounds

By definition, the equilibrium solubility of a substance is understood to be the solubility of the most stable crystal modification in a solvent.[205] This modification is the one with the highest melting point. If, in addition to the melting point T_m (in °C), the octanol/water distribution coefficient, $\log K_{ow}$, is known, then, according to Yalkowsky the molar solubility S_u of an uncharged organic compound, for example, in water, can be estimated with a semi-empirical solubility equation [Eq. (7)].[205] With poorly soluble active compounds a ther-

$$\log S_u = 0.8 - \log K_{ow} - 0.01\,(T_m - 25) \quad (7)$$

modynamically stable increase in solubility by modification of solvent character can be achieved by four alternative methods:[106, 205] 1) Where the active compound is a weak electrolyte the targeted setting of an optimal pH value is obvious. In addition the solubility can be increased by, 2) a change in the solvent polarity (cosolvent), 3) by micelle formation (surfactants), or 4) by active compound complexing (e.g. cyclodextrins).

These measures do not always lead to the objective, since the achievable increase in solubility with acceptable additive concentrations is often insufficient, or, especially for parental administration, the extent of adverse effects does not appear tolerable. Moreover, administration-dependent dilution effects can also lead to unwanted in situ precipitation.[205]

Because of these limitations, methods which are based upon an increase in the apparent solubility and in the rate of dissolution by means of nanoparticulate formulation of the active material, possibly with a simultaneous change in solid structure (metastable crystal modifications) are increasing in importance. According to the Kelvin equation [Eq. (8)][104, 205, 206] where γ represents the boundary surface energy, V the molar

$$\ln(S_{app}/S_0) = (RT)^{-1}2V/r \quad (8)$$

volume, and r the particle radius, at a given temperature T the apparent solubility S_{app} of spherical particles increases exponentially in comparison to the equilibrium solubility S_0 with decreasing particle radius. With values for γ and V which are typical for organic active compounds and effect materials the solubility exhibits a dramatic increase in solubility below a threshold value of $r < 1$ μm. Thus if it is possible to prepare and stabilize a poorly soluble substance in nanoparticulate form an apparently high active material concentration S_{app} can be made available in the dynamic equilibrium.

According to the Noyes – Whitney equation [Eq. (9)][104, 205] a corresponding increased rate of dissolution dM/dt is also correlated as a result where dM/dt stands for the transfer of mass from the solid to the solute state. The high values

$$dM/dt = kA(S_{app} - C(t)) \quad (9)$$

of the specific surface A in a nanoparticulate system also contributes to an increase in the rate of dissolution. The system-specific hydrodynamic relationships of the dissolution process are taken into account in the constant k. In individual cases the solution kinetics are also determined by the temporal change in A and by transient concentration of the solute $C(t)$, as determined by, for example, the resorption kinetics. A further increase in the level of solubility can be achieved by an increase in the boundary surface energy γ if it is possible to prepare the nanoparticles in a metastable crystal modification or as an amorphous particle.[205]

It must be noted, however, that the strategies described for increasing the apparent solubility and the rate of dissolution by nanoparticle formation lead principally to thermodynamically unstable systems which, under the conditions of storage or administration, tend towards recrystallization by Ostwald ripening if the preparation process produces systems with a broad particle size distribution. As already mentioned in Section 3, the mechanical methods of milling or homogenization usually lead to broad particle size distributions the mean particle size of which can lie below 1000 nm. In the area of industrial pharmaceutical research especially, increased activity has been observed recently to improve further the mechanical dispersing procedures with the objective of lowering still further the values of mean particle size and breadth of distribution.[104] As described in Section 3.2.2, significant technical advances have also been made in precipitation processes, which have already led to a broad palette of nanodispersed formulations with improved application properties, particularly in the area of active compounds and foodstuffs colorants.

4.1.1 Active Compounds with Poor Water Solubility

In the search for new active compounds and principles of action, the number of interesting compounds whose potential may be overlooked in standardized screening procedures because of their low solubility or rate of dissolution in water or whose administration in the end fails because of inadequate bioavailability in the normal commercial form of administration is growing. As an alternative to the methods described for the improvement in bioavailability by the addition of cosolvents, micellar and complexing agents, the exploration of the particle size effects has recently become the preferred focus of formulation research and development. The further development of classical milling processes by grinding or homogenizing processes are currently in the foreground of interest—with the development of nanodispersed medical formulations for peroral or parental administration as the objective. R. H. Müller and Liverside et al. have recently reported the preparation and properties of corresponding preparations.[104, 106, 108, 207] In the procedure used by R. H. Müller so-called nanosuspensions were obtained from different active materials with a high-pressure homogenizer; by increasing the number of homogenizer cycles the mean particle size could be reduced to 600 nm in the case of the active material RMKP22, and to around 300 nm with Paclitaxel. The particles obtained were usually X-ray amorphous.

The second procedure is a milling process with ball mills.[108] Because of the use of mechanical milling aids (milling balls of glass, zirconium oxide, etc.) it is unavoidable that with increasing milling time the active compound dispersion is contaminated with milling body fines, which can be a disadvantage for administration, particularly in the area of parenterals.[104, 207] As far as is known the milling products obtained in this way are crystalline nanoparticles, so-called nanocrystals, also with a broad particle size distribution.

The biopharmaceutical aspects of drug formulations accessible by these methods as well as questions of registering have been extensively discussed by R. H, Müller.[104, 207, 208] In addition to the already discussed improvement in bioavailability by increases in apparent solubility and rate of dissolution the improved absorption of poorly soluble active compounds could also be explained by an increased adhesion tendency of the nanoparticles to the wall of the gastrointestinal tract, particularly in formulations for peroral

administration.[207] Furthermore, there are experimental indications that nanoparticles can be absorbed through the GALT system (gut-associated lymphoid tissue.)[209] A further advantage of nanodispersed active compound formulations (< 200 nm) is that sterile filtration techniques can be used without the preparations being subjected to thermal stress.[130] Reference is made here to the extensive literature regarding further details on the status of development and the biopharmaceutical properties of nanodispersed formulations based upon milling and homogenization procedures.[106]

In contrast, there have to date been only isolated reports on the preparation and properties of nanodispersed formulations of poorly soluble active compounds by precipitation reactions. Thus, after extensive investigations Sucker and co-workers[154, 175] were able to prepare X-ray amorphous nanodispersed hydrosols with poorly soluble active materials ($S <$ 10 μg mL^{-1} in water) by controlled precipitation from alcohol solution with water in a static mixer (see Section 3.2). To stabilize the nanoparticles in situ the precipitation reaction was carried out in aqueous solutions of different gelatin types (electrosteric stabilization) or poloxamers (steric stabilization). The hydrosols obtained were transformed by spray drying into storable, redispersible dry powders to prevent particle growth (Ostwald ripening). For this purpose lactose or mannitol were added as spraying aids. With the active compounds israpidin, beclomethasone dipropionate, and cyclosporin, nanodispersed formulations with particle sizes in the range of 200 nm were obtained. In detailed investigations with redispersed cyclosporin hydrosols in animals, concentrations of the active compound similar to those found after the injection of micellar solutions were detected in different tissue types after intravenous injection.[154, 175]

With the active steroid budesonide Matijević and Ruch recently drew attention to the rarely explored industrial potential of the preparation of micro- to nanodispersed active-compound hydrosols by a precipitation reaction from hydrophilic solution.[157]

4.1.2. Water Insoluble Active Materials

The most extensive experience on the improvement of peroral bioavailability of insoluble active compounds by hydrosol formation currently lies with synthetic carotenoids. The carotenoids constitute a class of color pigments widespread in nature with yellow to red color tone nuances.[113, 210, 211] All these compounds are characterized by a structural element consisting of a polyene chain built up from four isoprenyl units the different substitution patterns of which at the chain termini allow an extraordinarily large breadth of variation within the compound class. Today about 600 carotenoids are known.[212] The best known representative, β-carotene, was first isolated from carrots in 1831 and has been produced industrially since 1954.[213] Since then synthetic routes for a whole series of carotenoids have been developed and converted into industrial production processes;[214] a selection is illustrated in Figure 18.

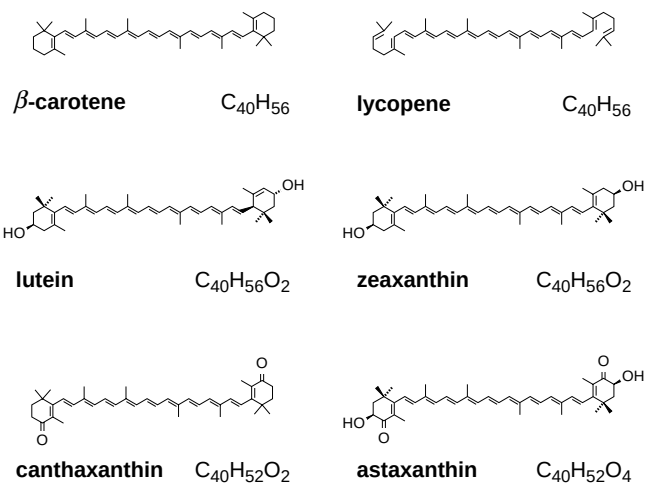


Figure 18. Selection of carotenoids of physiological importance and of interest as foodstuff colorings and for animal nutrition. All the compounds are insoluble in water. Aqueous applications therefore require nanodispersed formulations for optimization of the bioavailability and the coloristic properties.

In addition to the described color the physiological function of carotenoids is of considerable interest. Best known is the action of β-carotene as provitamin A.[211] The practical use of nature-identical synthesis products as active compounds in pharmaceuticals and cosmetics or as coloring agents in the foodstuffs and animal feeds is complicated, however, by the insolubility in water and poor solubility in fats and oils typical of the compound class as a whole.[114, 115, 210, 211] Therefore the conversion of the crystalline synthesis product into nanodispersed formulations is an important requirement, especially for the plethora of forms of administration of the carotenoids in aqueous media. Currently different recipe variants of the mixed chamber process described in Section 3.3.2 are used widely for the production of diverse carotenoid preparations with high color intensity and high bioavailability.[152, 153] Figure 19 gives an overview.

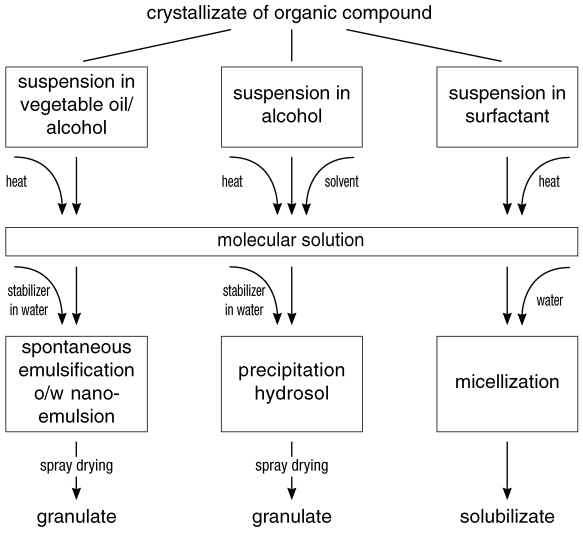


Figure 19. Preparative variants of the mixing-chamber process for the preparation of nanodispersed, water-compatible carotenoid formulations.

Depending on the composition of the active-compound solution produced by temperature shock, nanodispersed hydrosols, emulsions, and micellar solutions are produced for different uses.[152] The effect of particle size and the equally technically controllable supramolecular structure of the dispersed phase on the color are discussed in detail in Section 4.3. Moreover, there are increasing indications that biological absorption is influenced equally extensively by the supramolecular structure of the particles. In feeding experiments with calves and rats it was possible to demonstrate by measurement of the blood-level values or the vitamin A liver-storage values that the biological absorption of β-carotene hydrosols increases significantly with decreasing particle size (see Figure 20).[153, 215] Under comparable experimental conditions milled crystalline products in the micrometer particle size range were practically not absorbed (Figure 21). In other areas of animal nutrition, carotenoids in nanodispersed formulations show an increased bioavailability. Thus nanoparticulate hydrosols from canthaxanthin are widely used in poultry breeding for a natural egg-yolk pigmentation.[115] Analogously astaxanthin, the coloring agent which gives fish and sea food a reddish color, is used as a nanodispersed, amorphous hydrosol formulation in trout and salmon farming.[115]

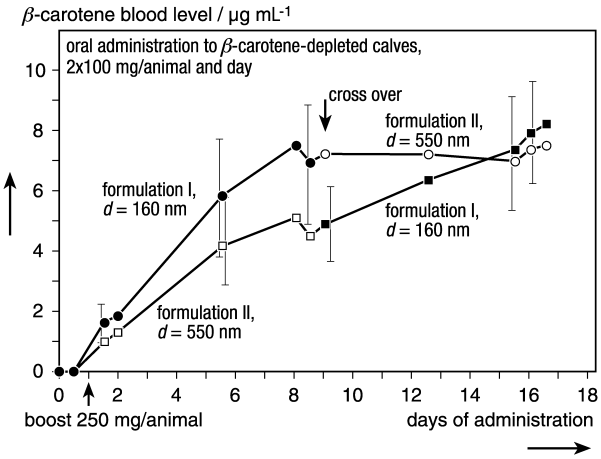


Figure 20. Influence of particle size on the bioavailability of β-carotene hydrosol during oral uptake by calves with minimal β-carotene status. At the cross-over point the feeding to the two calf cohorts was continued after exchange of formulations I and II.

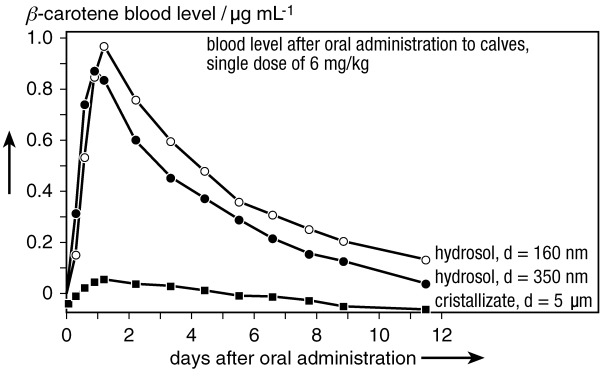


Figure 21. Time course of the β-carotene blood level after single oral administration of β-carotene to calves with minimal β-carotene status. Comparison of nanodispersed formulations with a microdispersed crystallizate.

In all the applications described the nanoprecipitates are used as granulates which are obtained by spray drying procedures. In these formulations the active compound is present in concentrations of 5–10%. The remaining constituents are composed of protective colloids (e.g. gelatin, polysaccharides) and other additives (emulsifiers, antioxidants) typical for precipitation processes as well as further additives (sugar, starch) which enable spray drying and which also contribute to storage stability and redispersibility in the administration medium.[152, 153] The mode of action of the proteins and polysaccharides used as protective colloids are described in detail in ref.[178]. Details on their function in nanodispersed carotenoid formulations are discussed by Horn et al.[152, 153, 216]

In addition to physiological properties of different carotenoid hydrosols described already—the coloring aspects, of interest to the foodstuffs industry, are discussed more closely in Section 4.3—the pointers for further, health-promoting actions of carotenoids are currently increasing. In analogy to the protective action in the plant kingdom, where in the photosynthesis system carotenoids protect chlorophyll from attack by oxygen radicals and singlet oxygen,[217] similar effects are also proposed in other organisms including humans. Thus in patients with low β-carotenoid status there are signs that the risk to health from prostate cancer can be reduced by β-carotene supplementation.[218] The protective action of β-carotene against UV-induced skin changes has been established by Biesalski et al.[219] Other carotenoids which are currently the subject of intense investigation for their health-promoting effects are lycopene,[220] the red colorant in tomatoes, and lutein and zeaxanthin.[221] Recent results suggest that a high lycopene intake by the consumption of tomatoes also reduces the risk of prostate cancer.[222] Lutein and zeaxanthin are the only carotenoids to be concentrated in the yellow spot of the retina and in other ocular tissues and could be involved in the prevention of macula degeneration associated with age[223] and a reduction in the risk of cataract formation.[224]

These are just a few examples of the function of carotenoids in the area of health and nutrition which in the future could extend considerably the use of the nature-identical active compounds. Nanodispersed formulated carotenoids could thus represent important examples for effect-optimized nutraceuticals, that is, nature-identical active materials which manifest their health-promoting, prophylactic action in the boundary between nutrients and pharmaceuticals.

In view of this experience with compounds of the carotenoid class it may also be possible to precipitate poorly soluble hydrophobic active compounds as nanodispersions from hydrophilic solution with appropriate temperature control, contrary to the occasionally expressed opinion.[104] However, it has to be presumed that for an understanding of particle formation in these systems the classical concepts on nucleation and growth as they have been used successfully for the understanding and process development of normal crystallization and precipitation reactions[163–166, 168, 225] play a rather subordinate role in view of the extremely high supersatura-

tions which are achievable, and spinodal separation phenomena possibly dominate in the particle formation process.

Nanoprecipitation processes in association with the exploration of suitable natural and synthetic additives with high active-compound affinity offer attractive prospects for the development of nanodispersed pharmaceutical formulations of lipophilic active compounds which could provide industrial-pharmaceutical research and development with new stimuli.

4.2. Nanodispersed Systems for the Targeted and Controlled Release of Pharmaceutically Active Compounds

In every day industrial-pharmaceutical parlance the term nanoparticle has come to be used to mean nanodispersed polymeric support systems for active compounds.[107, 109, 151, 226–228] They differ fundamentally from the nanosuspensions[106] and hydrosols[154, 175] discussed in Section 3 in which the polymers assume the function of surface-active protective colloids for the colloidal and possibly also the chemical stabilization of the nanodispersed active-compound phase.

Nanoparticles thus represent an alternative to other active-compound transport forms such as microemulsions,[229] niosomes,[230] liposomes,[227, 231] or other so-called SLNs (solid lipid nanoparticles).[208, 232, 233] One of the reasons for the search for alternative, polymer-based transport systems is that an increased stability of the nanodispersed formulation of the active material during storage and administration appears desirable.[151, 234] Moreover, the targeted functionalization of the polymer matrix or the solid-particle surface appears more readily realizable for the controlled and targeted release of the active compound.

Since the pioneering work of Birrenbach and Speiser[235] and Couvreur and co-workers[236] the search for biocompatible polymer materials and methods for their nanodispersed formulation has lead to a flood of publications (see Section 3). In particular, the biopharmaceutical, physiological, and therapeutic properties of such systems have been investigated in extensive studies, including clinical trials. Critical evaluation of the results have been presented recently in reviews[208, 228, 234] and monographs,[106, 151] and already belong to pharmaceutical-technology textbook knowledge.[107] Consequently, a detailed discussion is superfluous at this point especially since nanodimensioning only indirectly affects the properties of the active compound. In summary it must be pointed out, however, that in spite of the considerable research effort which has been expended and the encouraging results in certain areas, nanoparticles as support systems for active pharmaceutical compounds have as yet found no use in medical practice.[208, 228] The reasons given for this include unanswered questions on long-term stability and on the cytotoxicity of polymers and their degradation products—and thus obstacles to medical registration/legislation—as well as industrial production aspects such as the transfer of the laboratory methods described to competitive production processes.[151,208]

4.3. Optical and Electrooptical Properties of Nanodispersed Organic Pigments and Dyestuffs

Crystals of organic molecules are finding numerous technical applications as chromophoric dispersion colloids.[105] Amongst the most important applications are the coloring of lacquers, printing inks, color toners, and a large number of industrial plastics.[101] The most important class of pigments include the phthalocyanins (blue), perylenes (red), and azo dyes (yellow). Special demands are placed on pigments which are used in the coloring of drinks and foodstuffs; the carotenoids as nature-identical pigments are also mentioned in this context. The broad field of relevant technical aspects of respective pigment formulations cannot be undertaken here.[101, 105] Both the coloring properties (color strength, color shade, transparency) and the flow properties of pigmented systems important for processing are influenced quite significantly by the particle size and particle shape at a given pigment concentration.[237]

According to the current state of the art the technical demands placed on the fineness of the pigment and dispersion-dyestuff formulations used in practice are fulfilled by dry and wet milling processes.[101] Usually dispersion colloids with a mean particle size range of around 1 μm are obtained. Work with the aim of a further reduction in particle size down to the nanometer region is currently not of immediate interest from the practical viewpoint. Usually the milled products obtained are subsequently subjected to a so-called formulation or finishing process to obtain a product as uniform as possible in particle size and shape by controlled Ostwald ripening or modification transformation in organic solvents. More recently specific additives which by reason of their molecular structure preferentially occupy individual growth faces and thus enable a specific control of growth kinetics and thus particle habit have been used to control this recrystallization process.[238] Empirical methods of screening are being replaced to an increasing extent by strategic methods of crystal engineering with the use of more powerful computers. Thus with organic molecules it is in some cases already possible to predict their probable packing density in the solid, their orientation in the crystal lattice, and their interaction energies.[239, 240] However, it is to date still not possible to predict quantitatively the particle size dependency of the absorption band structure. The amount of pertinent experimental work is equally sparse, however. Thus hypsochromic shifts of the absorption bands have been observed with ultrathin epitactic layers (1 – 100 nm layer thickness) of perylenes, phthalocyanines, and other pigments, and interpreted as quantum size effects.[202]

Otherwise only isolated reports on investigations into particle size dependencies of optical constants of molecular crystals have appeared.[241–244] In the work of Nakanishi and co-workers the choice of systems investigated was aimed primarily at the potential fields of applications of organic nanocrystals in the area of microelectronics and photonics as alternatives to inorganic systems.[245, 246] Thus, on the basis of the methods described in Section 3.3.2 dispersed systems in the particle size range down to 20 nm were obtained by nanoprecipitation in water of different classes of compounds

(pseudoisocyanines, merocyanines, perylenes, polydiacetylenes) from hydrophilic solution (ethanol, acetone, THF).[174, 245] In the investigations on the perylene system a shift in the absorption band maximum of about 30 nm was found on a reduction in particle size from 200 nm to 50 nm.[242] Recently band shifts of up to 30 nm have also been observed with diphenyl-naphthyl-pyrazoline (DPNP) nanocrystals (400 nm to 20 nm).[244] In explaining these findings a confinement effect was excluded, however, because of the observed particle size range, and a reduction in intermolecular interaction with decreasing particle size through crystal-lattice deformation was discussed as the cause. In investigations on the polydiacetylene system a blue shift of the absorption maximum of about 15 nm was also found with decreasing particle size (150 nm to 70 nm) and similarly interpreted.[243, 247] For a complete explanation of the experimental results, possibly also within the context of confinement effects, an extension of the investigations to particle sizes to 10 nm and below appears necessary. A preparative access to this particle size range was recently demonstrated by the precipitation of organic molecular crystals in inorganic sol–gel templates.[248] The same applies in this respect to a possible increase in the third order non-linear optical susceptibility, $\chi^{(3)}$, by confinement effects in nanodispersed particulate systems.[246, 247, 249] In organic systems the expectations refer in particular to the polydiacetylene class of compounds.[243, 247] However, an experimental confirmation of corresponding theoretical predictions is currently unavailable.[246, 247, 249]

Particle size effects are also receiving increasing attention[250] in connection with the widespread use of organic photoconductors for xerographic copying processes.[201] In the optical production of a graphic electrostatic-charge pattern on a reversibly chargeable carrier, materials are required which at high quantum yield possess high photoconductivity in the visible spectral region—and more recently for use in diode laser printers in the near infrared region too. For this purpose organic semiconductor pigments such as phthalocyanines, perylenes, and azo pigments are converted into nanodispersed systems (20–500 nm) by complex milling processes and incorporated into polymeric support materials in high concentrations.[199, 201, 250] However, here too the relationships between the particle size distribution and the supramolecular particle structure and the technically relevant physical properties such as photoconductivity and charge transport have still been little researched—in spite of the high technical state of development—since the previously described morphological parameters are poorly controllable by milling processes.[199, 200, 201, 250, 251]

In this context particle size effects are significant for two reasons: on the one hand the production of the charge carriers at the boundary surface of the optically active pigment particles takes place by the interaction with the polymer matrix, with additive charge carriers, or also with adsorbed oxygen or water.[200, 201, 250] At a given pigment volume concentration the size of the photooptically active surface increases with decreasing particle size, which is important especially in field strengths of $< 10\ V\,\mu m^{-1}$.[250] On the other hand the photoconductivity of the material, especially with inert polymer supports is determined to a considerable extent by the percolation structure, that is, the mean particle distance and the connectivity of the particle configuration.[200, 250]

Whereas the important technological advances have hitherto been based upon empirical development work,[201] with the example of titanyl phthalocyanin (TiOPc), an especially efficient representative of organic photoconductors, a first step towards a systematic treatment of this problem has been made more recently.[199] The successful preparation of a TiOPc/BBL (BBL = poly(benzobisimidazobenzophenanthrone)) nanocomposite with spherical ($d = 100$ nm), X-ray amorphous TiOPc particles was achieved by in situ hydrolysis of a molecularly dispersed, solid solution of a Lewis acid complex of TiOPc in a polymer matrix (BBL). By subsequent shaping of the films in $CHCl_3$, vapor-phase transformation into the crystalline β-modification with rod-shaped pigment crystals took place.

In addition to the critical influence of crystal structure on the absorption process and thus on the frequency dependency of the photoconductivity with organic molecular crystals,[201] in the case of TiOPc a progressive short-wave shift of the characteristic Q bands (700–900 nm) of the β-modification was observed with controlled reduction in particle size.[199, 252] The photoconductivity found in this wavelength region with nanocomposites containing the equally photoconducting (450–650 nm) BBL support material with crystalline TiOPc lay more than two orders of magnitude above that of comparable materials with amorphous particles.[199, 251]

The process described for the preparation of nanodispersed composites of organic photoconductors with broad spectral sensitivity appears not only interesting from the point of view of basic research on xerography, but it could also open up new industrial methods for the preparation of photoactive materials with possible uses in the storage of solar energy on the basis of photovoltaics and photoconductivity.[199, 253]

The classical particle size effects which are quantitatively describable by the Mie theory in the case of isometric particles must be differentiated in principle from the previously described optical particle size effects, which are based upon a change in the optical constants in nanodimensional crystals with high intermolecular interaction.[254] Accordingly, at a given chemical and crystallographic structure and hence fixed optical constants the particle size determines to a large extent the optical purity and transparency of a pigmented system through the size-dependent balance of absorption and scattering. A special case arises with systems with X-ray amorphous particles recently prepared by the described precipitation reactions. As is shown below with the example of the carotenoids, different supramolecular short-range order structures can be obtained in a targeted manner by variation in the precipitation conditions, which at strong intermolecular dipole interaction leads to marked changes in the absorption spectrum and thus the coloristic properties. Figure 22 summarizes the effects of the different molecular, supramolecular, and solid-state structure on the coloristic properties of a nanodispersed system. In the case of β-carotene the change in particle size and the supramolecular structure, particularly the transition from the crystalline to the amorphous state, has a dramatic effect on the structure of the absorption spectrum.

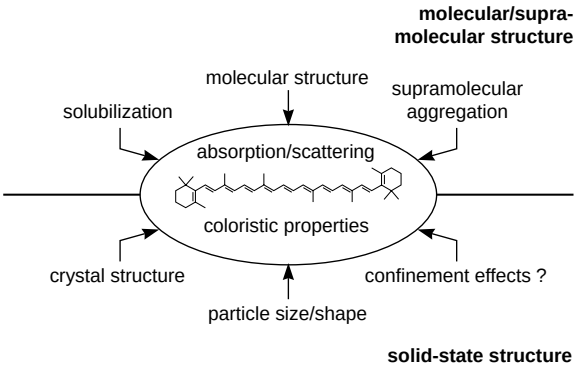


Figure 22. Control of the coloristic properties of nanodispersed carotenoid hydrosols by molecular, supramolecular, and solid-state physical factors.

Figure 23 shows a comparison of absorption spectra of different β-carotene formulations which allow color-tone nuancing from yellow, through orange, to red (see also Figure 24).[152] In comparison to the absorption spectrum of a molecular solution in *n*-hexane the spectra of the amorphous nanoprecipitates show an increasing blue shift with decreasing particle size, whereas a red shift with concomitant change in band structure characterizes the spectra of the crystalline dispersion colloids.[152] According to the most recent experimental and theoretical investigations supramolecular structure and particle size effects participate equally in the development of the complicated band structure.[255]

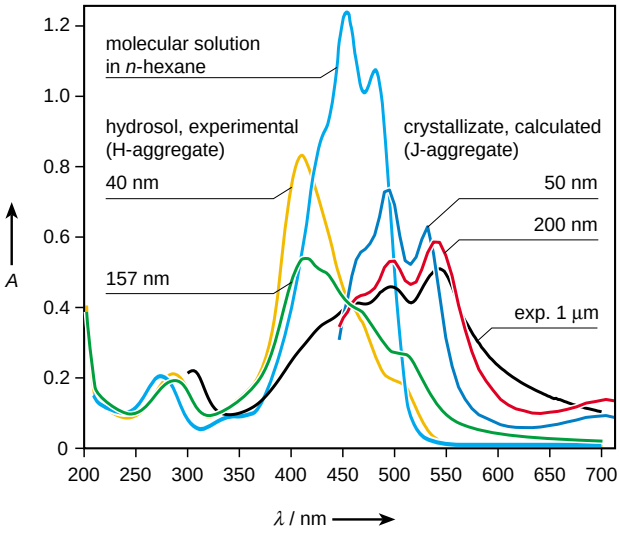


Figure 23. UV/Vis absorption spectra of 5 ppm β-carotene. Influence of aggregate structure and particle size compared with the molecular solution in *n*-hexane.

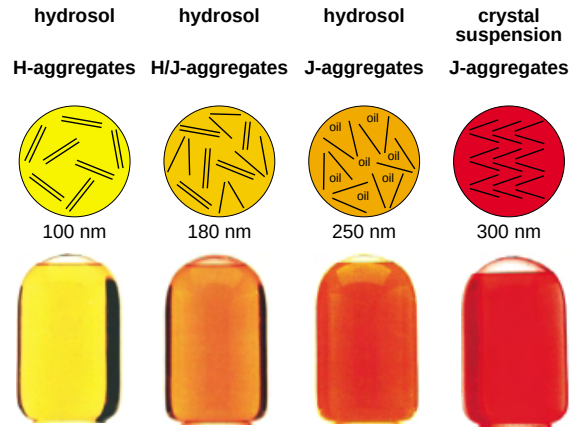


Figure 24. Influence of particle size and aggregation structure on the color tone nuance of nanodispersed β-carotene hydrosols.

In accord with the crystal structure of β-carotene[256] the red shift is explained by a so-called J-aggregate interaction (head-to-tail) of the two β-carotene molecules per unit cell.[152, 257, 258] As yet there has been no exact assignment of the superimposed vibrational coupling structure. The spectrum of a milled crystalline product (mean particle size ca. 1 µm) and the spectra of nanodispersed systems calculated by the Mie theory on the basis of single-crystal spectra[259] show no similarity with the spectra of the products of the same size class obtained by nanoprecipitation. As shown in Figure 25, these products are composed of particles with a core–shell structure which is visualized electron microscopically by the use of specific staining techniques.[152, 153] Details of the function of the gelatin used as protective colloid (type B100, adsorbate film thickness ca. 40 nm) and other protective colloids have been discussed thoroughly elsewhere.[152, 216]

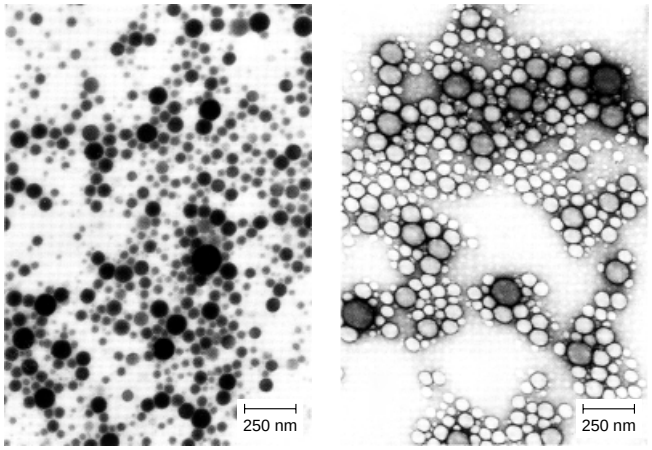


Figure 25. Electron microscopic representation of the core-shell structure of nanodispersed β-carotene hydrosols. The specific staining of the active-compound core (left) was carried out with OsO_4, the gelatin shell (right) with uranyl acetate.

More recent X-ray and theoretical investigations are now providing the first clues on the supramolecular structure of the active compound core and on the significance of the characteristic blue shift of the absorption bands of β-carotene nanoprecipitates.[255] From a simple exciton model[257, 258, 260] and quantum-mechanical molecular-modeling calculations[261] it was possible to show[255] that intermolecular interactions within the context of an H-aggregate structure ("card-stack structure")[152, 257, 258, 262] are consistent with the spectroscopic findings. Hypsochromic band shifts of 44 nm and 40 nm were calculated for an ideal H-aggregate and a tetrameric (2_1_1) aggregate, respectively, which corresponds to a supercell formed from two H-aggregates. In contrast, a band splitting (exciton splitting) is expected for a J-aggregate: in addition to

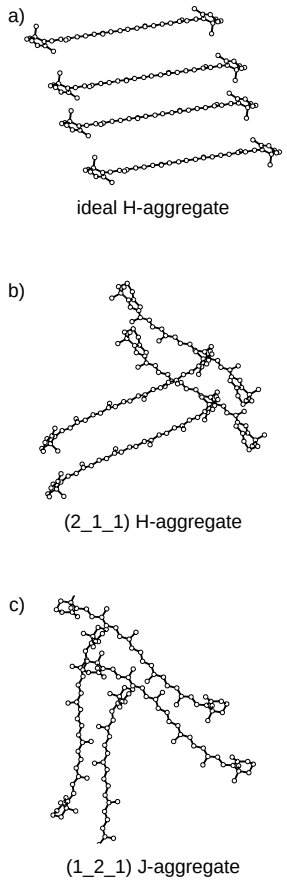


Figure 26. Spatial configuration of different β-carotene tetramers. a) ideal H-aggregate; b) superimposition of two H-aggregates in a (2_1_1) supercell; c) J-aggregate in a (1_2_1) supercell. Quantum chemical calculations give hypsochromically shifted absorption bands of 44 nm and 40 nm for the H-aggregates in (a) and (b), respectively. As expected, an exciton splitting with a bathochromic component (44 nm) and a hypsochromic component (7 nm) is calculated for the J-aggregate.

a bathochromic band shift of 44 nm calculations also gave a component with a 7 nm hypsochromic shift (see Figure 26).[255]

Process and recipe-specific influences on the optical properties of nanoprecipitates can thus be explained by the preferential formation of H- or J-aggregates.[255, 262] Apparently, with decreasing active-compound concentration the formation of H-aggregates is favored during precipitation, whereas small amounts of oil in the recipe induce the formation of J-aggregates. Information on the dimensions of the coherently aggregated supramolecular structures comes from the Bragg profile analysis of the X-ray wide-angle scattering data.[255] According to this the active-compound particles illustrated in Figure 25 are built up of crystalline structural units with dimensions down to about 30 nm in which the molecules of the active compounds are present mainly as H- or J-aggregates, depending upon the selected precipitation conditions. The aggregate sizes correspond to aggregation numbers of up to 10000 molecules. Figure 27 gives a conception of the supramolecular construction of the β-carotene hydrosol particle calculated from the spectroscopic and X-ray data. The thickness of the gelatin adsorbate layer was determined by dynamic light scattering.[216] Whether a morphological construction from crystalline structural units of the named order of magnitude can result in confinement effects is currently unknown

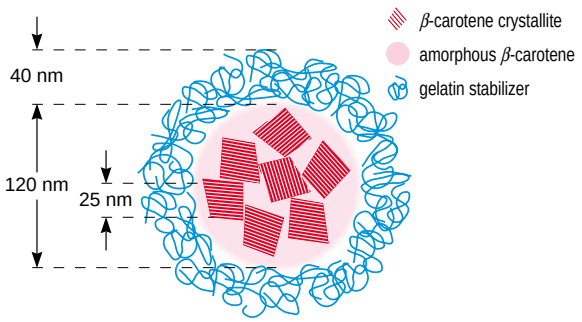


Figure 27. Core-shell structure of the β-carotene hydrosol particle. According to the spectroscopic data and WAXS measurements the active material core consists of H- and J-aggregates with dimensions of up to 30 nm, which corresponds to a maximum aggregation number of 10000 molecules.

5. Discussion and Outlook

A series of tasks may stem from the discussions here, which A) concern fundamental aspects of the nanoparticle formation, and B) which have as their objective the development of industrial processes for the targeted production of nanodispersed formulations of organic active compounds and effect materials. Closely associated with this is C) the evaluation of special physical properties associated with nanoscopic dimensioning with a view to new or improved physiological or industrial properties of organic nanoparticles.

On point A the following problems appear to be in need of special clarification:

1. Which structures are formed at high spontaneous supersaturation? On the one hand it remains to be explained whether—counter to textbook opinion—spinodal demixing phenomena do indeed play a certain role in low molecular weight systems. On the other hand investigations are needed to explain to what extent the structure of the particle exhibits similarity with the bulk structure or whether strongly hydrated, amorphous precursors, or aggregates of nuclei dominate.
2. Are long-lived precursor structures from aggregated molecules present prior to the actual nucleation? If this question is to be answered in the positive the significance that is attributed to these precursors in particle formation needs to be explained.
3. Which structure transformations occur during the transition from the initial nucleus to the observable nanoparticle? This question is of considerable relevance since as shown in Section 2 there are many examples for the particle formation processes which do not run according to the simple nucleation/crystallization scheme.
4. How is the surface of the intermediate stages composed in respect of structure, charge, etc? This point is of great significance in as much as these properties determine the homo- and heteroaggregation behavior.

On point B there are also a number of tasks which need to be addressed.

1. How, with knowledge of the molecular parameters, can the stability and aggregation behavior of nanoparticles be predicted? As was shown in Section 2, in this respect many questions remain unanswered.
2. Is the mean-field description of aggregation process, that is, without consideration of local structure formation and reconstruction processes, sufficient?
3. Can the process in which the production of supersaturated systems is carried out with turbulent or laminar mixing be theoretically described? This task is demanding as several length scales must be considered at the same time. Clearly this question is particularly relevant when the particle

formation processes take place on the same time scale as the mixing processes.

4. How do additives interfere with the particle formation process? This question includes a large number of subsidiary points, for example: nucleation by additives, adsorption/incorporation of the additive molecules into the initially formed nanoparticle, influencing the growth of the nanoparticle with additives, influencing the crystal structure with additives, control of aggregation, and colloidal stabilization with additives.

In view of the described complexity of the, in part competitively occurring, elementary process which take place during particle formation a strategic approach to the selection of suitable additives which, for example, limit particle growth to the nanometer range and stabilize the nanodispersed system against Ostwald ripening and agglomeration appears extremely complicated. Although much is known about the physico-chemical principles of colloidal stabilization of dispersed systems and the surface interactions of polymeric and surfactant additives, little is known of the molecular structure – activity relationships which in certain cases would allow a targeted approach. This explains the observation that the choice of additives has hitherto been made empirically and a mechanistic interpretation of their action is at best qualitative. In most instances technical development work is as a result extremely time consuming and perhaps could be somewhat accelerated by methods of statistical experimental planning.[263] Recent developments in the area of combinatorial materials research could bring advances here. After the successful adaptation of combinatorial synthesis techniques (initially developed for active-compound screening[264]) to inorganic function materials by P. G. Schultz and co-workers[265] the first reports on the combinatorial synthesis of polymer libraries[266] and suitable analytical methods for the rapid screening of such libraries in respect of interesting target parameters have been published.[267] Further development of these techniques would not only make the search for suitable additives more efficient, but there is the hope that with the further development of statistical procedures structure – activity relationships can be derived from analysis of the extensive data sets. Then in the next optimization cycle the discovery of substrate-specific additives could be accelerated still further with this knowledge by means of combinatorial methods.

In regard to the questions concerning the outlook for the innovative application of nanodispersed organic formulations arising from point C, the carotenoid class of compounds, the areas of application of which could be optimized and expanded by nanodispersed formulation, has already been discussed in Section 4. Similarly, new perspectives for the development of oral forms of administration with improved bioavailability and parental administration forms with increased tolerance arise for poorly soluble pharmaceutically active compounds. Moreover, nanodispersed formulations, particularly of thermolabile active compounds, open up the possibility of replacing thermal sterilization processes by a more gentle sterile filtration. In the area of cosmetics the high surface activity of nanodispersed formulations could make the development of new forms of application of active cosmetic and effect materials with improved dose – activity relationship a possibility.

In the area of plant protection as well, alongside the highly expensive search for new active compounds, the development of innovative formulations for the optimization of the effect is gaining in importance. The improvement in bioavailability and the related reduction in potential environmental contamination are therefore part of the crucial development activities of industrial formulation research. Nanodispersed active compound formulations in the form of water redispersible granulates could play an important role in this respect.[268] In addition to the previously described optimization of coloristic effects the improvement of processing and application properties by a nanodispersed formulation is also conceivable in the use of organic pigments, for example, in plastics processing or in ink-jet inks.[269]

Similarly, in regard to the previously discussed solid-state physical and catalytic properties of organic systems, which are of fundamental importance in the promising areas of photonics, electrooptics, and energy storage, theoretical considerations on particle size effects suggest that with nanodispersions of effect materials an improvement in technologically desirable properties may be expected. However, the development work is still in its early stages since until now there has been an absence of technologies which would allow the targeted production of organic effect materials with particle sizes in the desired lower nanometer range.

This review has attempted to present a summary of the numerous and thematically widespread activities in the preparation and use of organic nanoparticles. It is clear that the experimental work on the preparation of nanodispersed systems has been conceived purely empirically and without acknowledgment of the extensive theoretical state of the art. There is clearly an urgent need for action to develop the obviously interdisciplinary field of preparation, characterization, and use of organic nanoparticles more efficiently than before. In the light of the extensive activity in the area of inorganic systems the interest of university research institutes to work in the corresponding area of organic systems appears to be comparatively under developed. This under development is all the more surprising since the problems described deserve considerable attention, both from the viewpoint of basic research as well as in regard to the potential areas of use of nanodispersed active compounds and effect materials which range from biomedical to information technology fields of application.

We thank our BASF colleagues Drs. Helmut Auweter, Peter Erk, Dirk Franke, Erich Hädicke, Robert Heger, Rüdiger Iden, Erik Lüddecke, Frank Runge, Wolfgang Schrof, Horst Weiß, and Harm Wiese for stimulating discussions and comments on the topic presented here.

Received: December 21, 2000 [A 440]

[1] a) D. Distler, *Wäßrige Polymerdispersionen*, Wiley-VCH, Weinheim, **1999**; b) *Polymeric Dispersions* (Ed.: J. M. Asua), Kluwer Academic, Dordrecht, **1997**.

[2] *Fine Particles: Synthesis, Characterization, and Mechanisms of Growth* (Ed.: T. Sugimoto), Marcel Dekker, New York, **2000**.

[3] C. J. Brinker, G. W. Scherer, *Sol-Gel Science*, Academic Press, New York, **1990**.

[4] a) W. F. C. Sager, *Curr. Opin. Colloid Interface Sci.* **1998**, *3*, 276 – 283; b) J. P. Spatz, T. Herzog, S. Mößmer, P. Ziemann, M. Möller, *Adv. Mater.* **1999**, *11*, 149 – 153; c) S. G. Dixit, A. R. Mahadeshwar, S. K. Haram, *Colloid Surf. A* **1998**, *133*, 69 – 75.

[5] T. T. Kodas, M. J. Hampden-Smith, *Aerosol Processing of Materials*, Wiley-VCH, New York, **1999**.

[6] O. Rheingans, N. Hugenberg, J. R. Harris, K. Fischer, M. Maskos, *Macromolecules* **2000**, *33*, 4780 – 4790.

[7] a) B. Voit, *J. Polym. Sci. Part A* **2000**, *38*, 2505 – 2525; b) S. Nlate, J. Ruiz, V. Sartor, R. Navarro, J.-C. Blais, D. Astruc, *Chem. Eur. J.* **2000**, *6*, 2544 – 2553; c) C. Zhisheng, S. L. Cooper, *Adv. Mater.* **2000**, *12*, 843 – 846; d) G. R. Newkome, C. N. Moorefield, F. Vögtle, *Dendritic Molecules—Concepts, Syntheses, Perspectives*, Wiley-VCH, Weinheim, **1996**.

[8] A. Sunder, J. Heinemann, H. Frey, *Chem. Eur. J.* **2000**, *6*, 2499 – 2506.

[9] H. Freundlich, *Kapillarchemie—Eine Darstellung der Chemie der Kolloide und verwandter Gebiete*, Akademische Verlagsgesellschaft, Leipzig, **1909**.

[10] W. Ostwald, *Die Welt der vernachlässigten Dimensionen*, Theodor Steinkopff, Dresden, **1915**.

[11] J. W. Mullin, *Crystallization*, Butterworth-Heinemann, Boston, **1992**.

[12] O. Söhnel, J. Garside, *Precipitation: Basic Principles and Industrial Applications*, Butterworth-Heinemann, Boston, **1992**.

[13] *Fine Particles Science and Technology—From Micro to Nanoparticles* (Ed.: E. Pelizzetti), Kluwer Academic, Dordrecht, **1996**.

[14] M. Takeo, *Disperse Systems*, Wiley-VCH, Weinheim, **1999**.

[15] *Controlled Particle, Droplet and Bubble Formation* (Ed.: D. J. Wedlock), Butterworth-Heinemann, Oxford, **1994**.

[16] J. Schmelzer, G. Röpke, R. Mahnke, *Aggregation Phenomena in Complex Systems*, Wiley-VCH, Weinheim, **1999**.

[17] P. G. Debenedetti, *Metastable Liquids*, Princeton University Press, Princeton, **1996**.

[18] a) V. K. LaMer, R. H. Dinegar, *J. Am. Chem. Soc.* **1950**, *72*, 4847; b) J. D. F. Ramsay in *Controlled Particle, Droplet and Bubble Formation* (Ed. D. J. Wedlock), Butterworth-Heinemann, Oxford, **1994**; c) T. Sugimoto, F. Shiba, T. Sekiguchi, H. Itoh, *Colloid Surf. A* **2000**, *164*, 183 – 203.

[19] A. Randolph, M. A. Larson, *Theory of Particulate Processes*, 2nd ed., Academic Press, New York, **1988**.

[20] J. Stávek, J. Ulrich, *Cryst. Res. Technol.* **1994**, *29*, 465 – 484.

[21] O. Galkin, P. G. Vekilov, *J. Am. Chem. Soc.* **2000**, *122*, 156 – 163.

[22] L. Gránásy, D. W. Oxtoby, *J. Chem. Phys.* **2000**, *112*, 2399 – 2409.

[23] J. Schmelzer, I. Gutzow, J. Schmelzer, Jr., *J. Colloid Interface Sci.* **1996**, *178*, 657 – 665.

[24] a) T. V. Bykov, X. C. Zeng, *J. Chem. Phys.* **1999**, *111*, 10602 – 10610; b) J. Barrett, *J. Chem. Phys.* **1999**, *111*, 5938 – 5946.

[25] V. K. Shen, P. G. Debenedetti, *J. Chem. Phys.* **1999**, *111*, 3581 – 3589.

[26] S.-T. Yau, P. G. Vekilov, *Nature* **2000**, *406*, 494 – 497.

[27] a) G. H. Peters, J. Eggebrecht, *J. Phys. Chem.* **1991**, *95*, 909 – 920; b) H. Arstila, *J. Chem. Phys.* **1997**, *107*, 3196 – 3203; c) V. A. Shneidman, K. A. Jackson, K. M. Beatty, *J. Chem. Phys.* **1999**, *111*, 6932 – 6941.

[28] K. Binder in *Materials Science and Technology*, *Vol. 5 Phase Transformations in Materials* (Ed.: P. Haasen), VCH, Weinheim, **1991**.

[29] A. S. Myerson in *Molecular Modeling—Applications in Crystallization* (Ed.: A. S. Myerson), Cambridge University Press, Cambridge, **1999**.

[30] V. Sofonea, K. R. Mecke, *Eur. Phys. J. B* **1999**, *8*, 99 – 112.

[31] H. Haberkorn, D. Franke, T. Frechen, W. Gösele, J. Rieger, *J. Coll. Interface Sci.*, submitted.

[32] J. F. M. Lodge, D. M. Heyes, *J. Chem. Soc. Faraday Trans.* **1997**, *93*, 437 – 448.

[33] a) B. Gobunov, *J. Chem. Phys.* **1999**, *110*, 10035 – 10045; b) B. E. Wyslouzil, G. Wilemski, *J. Chem. Phys.* **1999**, *110*, 1202 – 1211; c) A. Laaksonen, R. McGraw, H. Vehkamäki, *J. Chem. Phys.* **1999**, *111*, 2019 – 2027; d) H. Vehkamäki, I. J. Ford, *J. Chem. Phys.* **2000**, *113*, 3261 – 3269.

[34] R. Piazza, *Curr. Opin. Colloid Interface Sci.* **2000**, *5*, 38 – 43.

[35] A. George, W. W. Wilson, *Acta Crystallogr. Sect. D* **1994**, *50*, 361 – 365.

[36] D. Rosenbaum, P. C. Zamora, C. F. Zukoski, *Phys. Rev. Lett.* **1996**, *76*, 150 – 153.

[37] P. R. ten Wolde, D. Frenkel, *Science* **1997**, *277*, 1975 – 1978.

[38] C. Haas, J. Drenth, *J. Cryst. Growth* **1999**, *196*, 388 – 394.

[39] A. Y. Grosberg, A. R. Khokhlov, *Statistical Physics of Macromolecules*, AIP, Woodbury, **1994**.

[40] C. Stropnik, V. Musil, M. Brumen, *Polymer* **2000**, *41*, 9227 – 9237.

[41] a) N. Kayaman, E. E. Gürel, B. M. Baysal, F. E. Karasz, *Macromolecules* **1999**, *32*, 8399 – 8403; b) K. Fukui, B. G. Sumpter, M. D. Barnes, D. W. Noid, *Comput. Theor. Polym. Sci.* **1999**, *9*, 245 – 254; c) A. L. Owczarek, T. Prellberg, *Europhys. Lett.* **2000**, *51*, 602 – 607; c) F. J. Solis, M. O. de la Cruz, *J. Chem. Phys.* **2000**, *112*, 2030 – 2035.

[42] E. Plasari, P. Grisoni, J. Villermaux, *Trans. Inst. Chem. Eng. Part A* **1997**, *75*, 237 – 244.

[43] P. W. Atkins, *Physical Chemistry*, 2nd ed., Oxford University Press, Oxford, **1982**.

[44] P. R. ten Wolde, M. J. Ruiz-Montero, D. Frenkel, *Faraday Discuss.* **1996**, *104*, 93 – 110.

[45] a) P. R. ten Wolde, D. Frenkel, *Science* **1997**, *277*, 1975 – 1978; b) P. R. ten Wolde, D. Frenkel, *Phys. Chem. Chem. Phys.* **1999**, *1*, 2191 – 2196.

[46] a) J. Nývlt, *Cryst. Res. Technol.* **1995**, *30*, 443 – 449; b) T. Threlfall, *Org. Proc. Res. Dev.* **2000**, *4*, 384 – 390.

[47] P. R. ten Wolde, D. Frenkel, *Theor. Chem. Acc.* **1999**, *101*, 205 – 208.

[48] A. S. Clarke, R. Kapral, G. N. Patey, *J. Chem. Phys.* **1994**, *101*, 2432 – 2445.

[49] A. Mersmann in *Crystallization Technology Handbook* (Ed.: A. Mersmann), Marcel Dekker, New York, **1995**, pp. 1 – 78.

[50] T. A. Land, A. J. Malkin, Y. G. Kutznesov, A. McPherson, J. J. de Yoreo, *J. Cryst. Growth* **1996**, *166*, 893 – 899.

[51] P. G. Vekilov, J. I. D. Alexander, *Chem. Rev.* **2000**, *100*, 2061 – 2089.

[52] a) T. P. Niesen, M. R. deGuire, J. Bill, F. Aldinger, M. Rühle, A. Fischer, F. C. Jentoft, R. Schlögl, *J. Mater. Res.* **1999**, *14*, 2464 – 2475; b) S. Supothina, M. R. deGuire, T. P. Niesen, J. Bill, F. Aldinger, A. H. Heuer, *Mat. Res. Soc. Symp. Proc.* **1999**, *576*, 203 – 208.

[53] L. Addadi, J. Aizenberg, E. Beniash, S. Weiner in *Crystal Engineering: From Molecules and Crystals to Materials* (Ed.: D. Braga, F. Grepioni, A. G. Orpen), Kluwer Academic, Dordrecht, **1999**, pp. 1 – 22.

[54] a) M. Elimelech, J. Gregory, X. Jia, R. A. Williams, *Particle Deposition and Aggregation*, Butterworth-Heinemann, **1995**; b) O. Atteia, *Colloid Surf. A* **1998**, *139*, 171 – 188.

[55] a) M. Vanni, *J. Colloid Interface Sci.* **2000**, *221*, 143 – 160; b) W. C. K. Poon, M. D. Haw, *Adv. Colloid Interface Sci.* **1997**, *73*, 71 – 126; c) M. Mellema, J. H. J. van Opheusden, T. van Vliet, *J. Chem. Phys.* **1999**, *111*, 6129 – 6135.

[56] a) S. Lu, Y. Ding, J. Guo, *Adv. Colloid Interface Sci.* **1998**, *78*, 197 – 235; b) Y. Adachi, *Adv. Colloid Interface Sci.* **1995**, *56*, 1 – 31.

[57] a) B. W. Ninham, *Adv. Colloid Interface Sci.* **1999**, *83*, 1 – 17; b) S. H. Behrens, D. I. Christl, R. Emmerzael, P. Schurtenberger, M. Borkovec, *Langmuir* **2000**, *16*, 2566 – 2575; c) J. Lyklema, H. P. van Leeuwen, M. Minor, *Adv. Colloid Interface Sci.* **1999**, *83*, 33 – 69; d) S. Ramakrishnan, C. F. Zukoski, *J. Chem. Phys.* **2000**, *113*, 1237 – 1248; e) T. T. Nguyen, A. Y. Grosberg, B. I. Shklovskii, *J. Chem. Phys.* **2000**, *113*, 1110 – 1125; f) O. Spalla, *Curr. Opin. Colloid Interface Sci.* **2000**, *5*, 5 – 12.

[58] a) S.-H. Lee, Y.-S. Her, E. Matijević, *J. Colloid Interface Sci.* **1997**, *186*, 193 – 202; b) L. A. Pérez-Maqueda, L. Wang, E. Matijević, *Langmuir* **1998**, *14*, 4397 – 4401; c) K. Kurumada, H. Nakabayashi, T. Murataki, M. Tanigaki, *Colloid Surf. A* **1998**, *139*, 163 – 170; d) G. Wu, E. Matijević, *J. Dispersion. Sci. Technol.* **1998**, *19*, 903 – 913; e) M. Ocana, M. P. Morales, C. J. Serna, *J. Colloid Interface Sci.* **1999**, *212*, 317 – 323; f) N. Jongen, P. Bowen, J. Lemaître, J.-C. Valmalette, H. Hofmann, *J. Colloid Interface Sci.* **2000**, *226*, 189 – 198.

[59] V. Privman, D. V. Goia, J. Park, E. Matijević, *J. Coll. Interf. Sci.* **1999**, *213*, 36 – 45.

[60] a) G. H. Bogush, C. F. Zukoski, *J. Coll. Interf. Sci.* **1991**, *142*, 19 – 34; b) K. Lee, A. N. Sathyagal, A. V. McCormick, *Coll. Surf. A* **1998**, *144*, 115 – 125.

[61] a) L. Addadi, J. Moradian-Oldak, S. Weiner, *ACS Symp. Ser.* **1991**, *444*, 13 – 27; b) A. P. Wheeler, K. C. Low, C. S. Sikes, *ACS Symp. Ser.* **1991**, *444*, 72 – 84; c) J. P. Candelier, *J. Dispersion. Sci. Technol.* **1993**, *14*, 625 – 644.

[62] a) A. A. Campbell, A. Ebrahimpour, L. Perez, S. A. Smesko, G. H. Nancollas, *Calcif. Tissue Int.* **1989**, *45*, 122 – 128; b) X. Y. Liu, *Proc. 14th Int. Symp. Ind. Cryst.*, *IChemE* (Rugby, computer optical disk), **1999**.

[63] a) G. J. Fleer, M. A. Cohen Stuart, J. M. H. M. Scheutjens, T. Cosgrove, B. Vincent, *Polymers at Interfaces*, Chapman and Hall, London, **1993**; b) M. A. Cohen-Stuart in *Biopolymers at Interfaces* (Ed.: M. Malmsten), Marcel Dekker, New York, **1998**; c) *Colloid-Polymer Interactions* (Eds.: R. S. Farinato, P. L. Dubin), Wiley-Interscience, New York, **1999**; d) E. Killmann in *Adsorption on Silica Surfaces* (Ed.: E. Papirer), Marcel Dekker, New York, **2000**.

[64] a) E. Gurovitch, P. Sens, *Phys. Rev. Lett.* **1999**, *82*, 339 – 342; b) R. Golestanian, *Phys. Rev. Lett.* **1999**, *83*, 2473; c) P. Sens, *Phys. Rev. Lett.* **1999**, *83*, 2474; d) J. F. Joanny, *Eur. Phys. J.* **1999**, *B9*, 117 – 122.

[65] a) S. Y. Park, R. Bruinsma, W. M. Gelbart, *Europhys. Lett.* **1999**, *46*, 454 – 460; b) E. M. Mateescu, C. Jeppesen, P. Pincus, *Europhys. Lett.* **1999**, *46*, 493 – 498.

[66] P. Sens, J.-F. Joanny, *Phys. Rev. Lett.* **2000**, *84*, 8962 – 4865.

[67] a) M. Ellis, C. Y. Kong, M. Muthukumar, *J. Chem. Phys.* **2000**, *112*, 8723 – 8729; b) X. Châtellier, J.-F. Joanny, *Eur. Phys. J. E* **2000**, *1*, 9 – 25.

[68] a) H. Schießel, J. Rudnick, R. Bruinsma, W. M. Gelabrt, *Europhys. Lett.* **2000**, 51, 237 – 243. b) J. W. Jiang, J. M. Prausnitz, *J. Phys. Chem. B* **1999**, *103*, 5560 – 5569; c) K.-K. Kunze, R. R. Netz, *Phys. Rev. Lett.* **2000**, *85*, 4389 – 4392.

[69] D. L. Klug in *Handbook of Industrial Crystallization* (Ed.: A. S. Myerson), Butterworth-Heinemann, Boston, **1993**.

[70] a) R. J. Davey, L. A. Polywka, S. J. Maginn in *Advances in Industrial Crystallization* (Eds.: J. Garside, R. J. Davey, A. G. Jones), Butterworth-Heinemann, Oxford, **1991**; b) I. Weissbuch, M. Lahav, L. Leiserowitz in *Molecular Modeling Applications in Crystallization* (Ed.: A. S. Myerson), Cambridge University Press, Cambridge, **1999**; c) J. K. Guillory in *Polymorphism in Pharmaceutical Solids* (Ed.: H. G. Brittain), Marcel Dekker, New York, **1999**.

[71] a) S. Khoshkoo, J. Anwar, *J. Phys. D* **1993**, *26*, B90 – B93; b) R. Spruijtenberg, *Org. Proc. Res. Dev.* **2000**, *4*, 403 – 406; c) T. Threlfall, *Org. Proc. Res. Dev.* **2000**, *4*, 384 – 390.

[72] P. Taylor, *Adv. Colloid Interface Sci.* **1998**, *75*, 107 – 163.

[73] a) C. Bonafos, B. Garrido, M. Lopez, A. Perez-Rodriguez, J. R. Morante, Y. Kihn, G. Ben Assayag, A. Claverie, *Mat. Sci. Eng.* **2000**, *B69 – 70*, 380 – 385; b) J. Schmelzer, U. Lembke, R. Kranold, *J. Chem. Phys.* **2000**, *113*, 1268 – 1275.

[74] K. Chari, B. Asntalek, J. Kowalczyk, R. S. Eachus, T. Chen., *J. Phys. Chem. B* **1999**, *103*, 9867 – 9872.

[75] K. Landfester, *Macromol. Symp.* **2000**, *150*, 171 – 178; K. Welin-Berger, B. Bergenståhl, *Int. J. Pharm.* **2000**, *200*, 249 – 260.

[76] J. Baldyga, J. R. Bourne, *Turbulent Mixing and Chemical Reactions*, Wiley, Chichester, **1999**.

[77] W. Gerlinger, K. Schneider, H. Bockhorn, *Chem. Ing. Tech.* **2000**, *72*, 618 – 6121.

[78] J. Baldyga, R. Pohorecki, *Chem. Eng. J.* **1995**, *58*, 183 – 195.

[79] D. Franke, W. Gösele, *Chem. Ing. Tech*. **1999**, *71*, 1245 – 1252.

[80] I. M. Sokolov, A. Blumen, *Int. J. Mod. Phys. B* **1991**, *5*, 3127 – 3164.

[81] B. M. Dolgonosov, *Theor. Found. Chem. Eng.* **1995**, *29*, 264 – 2477.

[82] M. Lindberg, Å.C. Rasmuson, *Proc. 14th Int. Symp. Ind. Cryst.*, *IChemE* (Rugby, computer optical disk), **1999**.

[83] J. Rieger, J. Thieme, C. Schmidt, *Langmuir* **2000**, *16*, 8300 – 8305.

[84] "Des Molecules Hydrophobes dans l'Eau: Fabrication de Nanoparticules par Precipitation": H. Lannibois-Drean, Ph.D. Thesis, Université Paris VI, **1995**.

[85] a) V. S. L'vov, *Nature* **1998**, *396*, 519,521; b) L. P. Kadanoff, *Nature* **1996**, *384*, 116 – 117; c) K. R. Sreenisavan, *Rev. Mod. Phys.* **1999**, *71*, S383-S395.

[86] a) R. O. Fox, *Rev. Inst. Fr. Pet.* **1996**, *51*, 215 – 243; b) J. H. Ferziger, M. Peric, *Computational Methods for Fluid Dynamics*, Springer, Berlin, **1999**.

[87] a) J. Rieger, E. Hädicke, I. U. Rau, D. Boeckh, *Tenside Surfactants Detergents* **1997**, *34*, 430 – 435; b) M. R. McDonald, T. X. Wang, M. Gazda, W. M. Scheper, S. W. Evetts, D. W. Margerum, *Anal. Chem.* **1997**, *69*, 3513 – 3520; c) C. P. Bowers, K. D. Fogelman, J. C. Nagy, T. Y. Ridley, Y. L. Wang, S. W. Evetts, D. W. Margerum, *Anal. Chem.* **1997**, *69*, 431 – 438; d) M. Lindén, S. A. Schunk, F. Schüth, *Angew. Chem.* **1998**, *110*, 871 – 873; *Angew. Chem. Int. Ed.* **1998**, *37*, 821 – 823.

[88] C. P. Bowers, K. D. Fogelman, J. C. Nagy, T. Y. Ridley, Y. L. Wang, S. W. Evetts, D. W. Margerum, *Anal. Chem.* **1997**, *69*, 431 – 438.

[89] M. Z.-C. Hu, J. T. Zielke, C. H. Byers, J. S. Lin, M. T. Harris, *J. Mat. Sci.* **2000**, *35*, 1957 – 1971.

[90] a) B. Chu, *Laser Light Scattering*, 2nd ed., Academic Press, Boston, **1991**; b) *Light scattering, Principles and Developement* (Ed.: W. Brown), Clarendon Press, Oxford **1996**.

[91] a) D. Horn, J. Klingler, W. Schrof, K. Graf, *Prog. Colloid Polym. Sci.* **1998**, *111*, 27 – 33; b) W. Schrof, J. Klingler, S. Rozouvan, D. Horn, *Phys. Rev. A* **1998**, *57*, R2523 – R2526.

[92] a) H. Auweter, D. Horn, *J. Colloid Interface Sci.* **1985**, *105*, 399 – 409; b) H. Wiese, D. Horn, *J. Chem. Phys.* **1991**, *94*, 6439 – 6443; c) H. Wiese, D. Horn, *Ber. Bunsenges. Phys. Chem*. **1993**, *97*, 1589 – 1597.

[93] *Neutron, X-Ray and Light Scattering* (Eds.: P. Lindner, T. Zemb), North-Holland, Amsterdam, **1991**.

[94] a) Y. Minezaki, N. Niimura, M. Ataka, T. Katsura, *Biophys. Chem.* **1996**, *58*, 355 – 363; b) O. Vidal, M. C. Robert, F. Boué, *J. Cryst. Growth* **1998**, *192*, 257 – 270.

[95] a) P.-P. E. A. de Moor, T. P. M. Beelen, R. A. van Santen, *J. Phys. Chem. B* **1999**, *103*, 1639 – 1650; b) P.-P. E. A. de Moor, T. P. M. Beelen, B. U. Komanschek, L. W. Beck, P. Wagner, M. E. Davis, R. A. van Santen, *Chem. Eur. J.* **1999**, *5*, 2083 – 2088.

[96] a) H. Boukari, J. S. Lin, M. T. Harris, *J. Colloid Interface Sci.* **1997**, *194*, 311 – 318; b) J.-P. Jalava, E. Hiltunen, H. Kähkönen, H. Erkkilä, H. Härmä, V.-M. Taavitsainen, *Ind. Eng. Chem. Res.* **2000**, *39*, 349 – 361.

[97] F. Sobott, S. A. Schunk, F. Schüth, B. Brutschy, *Chem. Eur. J.* **1998**, *4*, 2353 – 2359.

[98] H. Cölfen, *Crit. Rev. Opt. Sci. Technol.* **1997**, *69*, 525 – 552.

[99] a) J. Behlke, A. Knespel, *J. Cryst. Growth* **1996**, *158*, 388 – 391; b) L. Börger, H. Cölfen, M. Antonietti, *Colloid Surf. A* **2000**, *163*, 29 – 38.

[100] B. G. Ershov, *Russ. Chem. Bull.* **1999**, *48*, 1 – 15.

[101] H. Mollet, A. Grubenmann, *Formulierungstechnik*, Wiley-VCH, Weinheim, **2000**.

[102] D. Peters, *J. Mater. Chem*. **1996**, *6*, 1605 – 1618.

[103] L. G. Lagaly, O. Schulz, R. Zimehl, *Dispersionen und Emulsionen*, Steinkopff, Darmstadt, **1997**.

[104] R. H. Müller, B. H. L. Böhm, M. J. Grau, *Pharm. Ind*. **1999**, *61*, 74 – 78.

[105] R W. Herbst, K. Hunger, *Industrial Organic Pigments*, Wiley-VCH, Weinheim, **1997**.

[106] *Emulsions and Nanosuspensions for the Formulation of Poorly Soluble Drugs* (Eds.: R. H. Müller, S. Benita, B. Böhm), Medpharm, Stuttgart, **1998**.

[107] R. H. Müller, G. E. Hildebrand, *Pharmazeutische Technologie: Moderne Arzneiformen*, WVG, Stuttgart, **1998**.

[108] G. G. Liversidge, K. C. Cundy, *Int. J. Pharm*. **1995**, *125*, 91 – 97.

[109] F. De Jaeghere, E. Doelker, R. Gurny in *Encyclopedia of Controlled Drug Delivery*, *Vol. 2* (Ed.: E. Mathiowitz), Wiley, New York, **1999**, pp. 641 – 664.

[110] D. Quintanar-Guerrero, E. Allémann, H. Fessi, E. Doelker, *Drug Dev. Ind. Pharm.* **1998**, *24*, 1113 – 1128.

[111] J. W. Vanderhoff in *Pharmaceutical Dosage Forms: Disperse Systems*, 2nd ed, *Vol. 1* (Eds.: H. A. Lieberman, M. M. Rieger, G. S. Banker), Marcel Dekker, New York, **1996**, pp. 91 – 152.

[112] A. G. Jones in *Controlled Particle, Droplet and Bubble Formation* (Ed.: D. J. Wedlock), Butterworth-Heinemann, Oxford, **1994**, pp. 61 – 94.

[113] H. Kläui, J. C. Bauernfeind in *Carotenoids as Colorants and Vitamin A Precursors* (Ed.: J. C. Bauernfeind), Academic Press, New York, **1981**, pp. 47 – 317.

[114] H. Kläui, K. Münzel, *Pharm. Acta Helv.* **1965**, *40*, 153 – 164.

[115] U. Manz, *Chimia* **1967**, *21*, 329 – 335.

[116] P. C. Hiemenz, *Principles of Colloid and Surface Chemistry*, Marcel Dekker, New York, **1986**.

[117] B. Sjöström, B. Bergenstahl, *Int. J. Pharm.* **1992**, *88*, 53 – 62.

[118] R. Bodmeier, P. Maincent in *Pharmaceutical Dosage Forms: Disperse Systems*, *Vol. 3* (Eds.: H. A. Lieberman, M. M. Rieger, G. S. Banker), Marcel Dekker, New York, **1998**, pp. 87 – 127.

[119] H. J. Krause, A. Schwarz, P. Rohdewald, *Int. J. Pharm.* **1985**, *27*, 145 – 155.
[120] M. F. Zambaux, F. Bonneaux, R. Gref, E. Dellacherie, C. Vigneron, *J. Controlled Releases* **1999**, *60*, 179 – 188.
[121] M. T. Peracchia, C. Vauthier, D. Desmaële, A. Gulik, J. C. Dedieu, M. Demoy, J. d'Angelo, P. Couvreur, *Pharm. Res.* **1998**, *15*, 550 – 556.
[122] T. Niwa, H. Takeuchi, T. Hino, N. Kunou, Y. Kawashima, *J. Controlled Releases* **1993**, *25*, 89 – 98.
[123] R. Gurny, N. A. Pepers, *Drug Dev. Ind. Pharm.* **1981**, *7*, 1 – 25.
[124] J. A. Ranucci, I. B. Silverstein in *Pharmaceutical Dosage Forms: Disperse Systems*, *Vol. 3* (Eds.: H. A. Lieberman, M. M. Rieger, G. S. Banker), Marcel Dekker, New York, **1998**, pp. 243 – 289.
[125] B. Magenheim, S. Benita in *Microencapsulation* (Ed.: S. Benita), Marcel Dekker, New York, **1996**, pp. 93 – 131.
[126] J. C. Leroux, E. Allémann, E. Doelker, R. Gurny, *Eur. J. Pharm. Biopharm*. **1995**, *41*, 14 – 18.
[127] D. Quintanar-Guerrero, E. Allémann, E. Doelker, H. Fessi, *Colloid Polym. Sci*. **1997**, *275*, 640 – 647.
[128] D. Quintanar-Guerrero, E. Allemann, H. Fessi, E. Doelker, *Int. J. Pharm.* **1999**, *188*, 155 – 164.
[129] H. Murakami, M. Kobayashi, H. Takeuchi, Y. Kawashima, *Int. J. Pharm.* **1999**, *187*, 143 – 152.
[130] Y. N. Konan, E. Allémann, R. Gurny, *Controlled Release Bioact. Mater*. **2000**, *27*, 321 – 322.
[131] E. Allémann, R. Gurny, E. Doelker, *Int. J. Pharm.* **1992**, *87*, 247 – 253.
[132] C. E. Matkovich, *Anal. Chem*. **1973**, *45*, 1915 – 1921.
[133] E. Allémann, J. C. Leroux, R. Gurny, E. Doelker, *Pharm. Res.* **1993**, *10*, 1732 – 1737.
[134] J. C. Leroux, R. Cozens, J. L. Roesel, B. Galli, F. Kubel, E. Doelker, R. Gurny, *J. Pharm. Sci*. **1995**, *84*, 1387 – 1391.
[135] C. V. Sternling, L. E. Scriven, *AIChEJ* **1959**, *5*, 514 – 523.
[136] H. Fessi, F. Puisieux, J. Ph. Devissaguet, N. Ammoury, S. Benita, *Int. J. Pharm*. **1989**, *55*, R1-.R4.
[137] S. Briancon, H. Fessi, F. Lecomte, J. Lieto, *Proc. 14th Int. Symp. Ind. Cryst., IChemE* (Rugby, computer optical disk), **1999**.
[138] S. Stainmesse, A. M. Orecchioni, E. Nakache, F. Puisieux, H. Fessi, *Colloid Polym. Sci*. **1995**, *273*, 505 – 511.
[139] M. J. Alonso, *Drugs Pharm. Sci.* **1996**, *77*, 203 – 242.
[140] J. Molpeceres, M. Guzman, M. R. Aberturas, M. Chacon, L. Berges, *J. Pharm. Sci*. **1996**, *85*, 206 – 213.
[141] M. Li, M. Jiang, C. Wu, *J. Polym. Sci. Polym. Phys. Ed.* **1997**, *35*, 1593 – 1599.
[142] M. Li, M. Jiang, L. Zhu, C. Wu, *Macromolecules* **1997**, *30*, 2201 – 2203.
[143] T. Jung, A. Breitenbach, T. Kissel, *J. Controlled Release* **2000**, *67*, 157 – 169.
[144] J. Kristl, E. Allémann, R. Gurny, *Acta Pharm*. **1996**, *46*, 1 – 12.
[145] a) E. Plasari, P. Grisoni, J. Villermaux, *Trans. Ing. Chem. Eng. Part. A* **1997**, *75*, 237 – 244; b) C. Duclairoir, E. Nakache, H. Marchais, A. M. Orecchioni, *Colloid Polym. Sci.* **1998**, *276*, 321 – 327.
[146] O. Thioune, H. Fessi, J. P. Divissaguet, F. Puisieux, *Int. J. Pharm*. **1997**, *146*, 233 – 238.
[147] P. Wehrle, B. Magenheim,S. Benita, *Eur. J. Pharm. Biopharm*. **1995**, *41*, 19 – 26.
[148] N. Ammoury, H. Fessi, J. P. Devissaguet, M. Dubrasquet, S. Benita, *Pharm. Res.* **1991**, *8*, 101 – 105.
[149] S. S. Guterres, H. Fessi, G. Barrat, J. P. Devissaguet, F. Pusieux, *Int. J. Pharm.* **1995**, *113*, 57 – 63.
[150] *Microencapsulation* (Ed.: F. S. Benita), Marcel Dekker, New York, **1996**.
[151] *Colloidal Drug Delivery Systems* (Ed.: J. Kreuter), Marcel Dekker, New York, **1994**.
[152] D. Horn, E. Lüddecke in *Fine Particles Science and Technology—From Micro to Nanoparticles* (Ed.: E. Pelizzetti), Kluwer, Dordrecht, **1996**, pp. 761 – 775.
[153] D. Horn, *Angew. Makromol. Chem*. **1989**, *166/167*, 139 – 153.
[154] H. Sucker in *Pharmazeutische Technologie: Moderne Arzneiformen* (Eds.: R. H. Müller, G. E. Hildebrand), WVG, Stuttgart, **1998**, pp. 383 – 391.
[155] G. A. Pozarnsky, E. Matijević, *Colloids Surf. A* **1997**, *125*, 47 – 52.
[156] C. Goia, E. Matijević, *J. Colloid Interface Sci.* **1998**, *206*, 583 – 591.
[157] F. Ruch, E. Matijević, *J. Colloid Interface Sci*. **2000**, *229*, 207 – 211.
[158] D. Meisel, *Curr. Opin. Colloid Interface Sci*. **1997**, *2*, 188 – 191.
[159] X. Peng, J. Wickham, A. P. Alivisatos, *J. Am. Chem. Soc*. **1998**, *120*, 5343 – 5344.
[160] R. Pelster, U. Simon, *Colloid Polym. Sci.* **1999**, *277*, 2 – 14.
[161] E. Matijević in *Controlled Particle, Droplet and Bubble Formation* (Ed.: D. J. Wedlock), Butterworth-Heinemann, Oxford, **1994**, pp. 39 – 61.
[162] E. Matijević, *Langmuir* **1994**, *10*, 8 – 16.
[163] A. J. Mahajan, D. J. Kirwan, *J. Phys. D* **1993**, *26*, B176 – B180.
[164] A. J. Mahajan, D. J. Kirwan, *J. Cryst. Growth* **1994**, *144*, 281 – 290.
[165] D. J. Kirwan, C. J. Orella in *Handbook of Industrial Crystallization* (Ed.: A. S. Myerson), Butterworth-Heinemann, Boston, **1993**, pp. 219 – 235.
[166] A. Mersmann, K. Bartosch, B. Braun, A. Eble, Ch. Heyer, *Chem. Ing. Tech.* **2000**, *72*, 17 – 30.
[167] A. Gavezzotti, G. Filippini, *Chem. Commun*. **1998**, 287 – 294.
[168] B. Yu. Shekunov, P. York, *J. Cryst. Growth*, **2000**, *211*, 122 – 136.
[169] S. Khoshkhoo, J. Anwart, *J. Phys. D* **1993**, *26*, B90-B93.
[170] J. Bernstein, *J. Phys. D* **1993**, *26*, B66 – B76.
[171] R. J. Davey, J. Richards, *J. Cryst. Growth* **1985**, *71*, 579 – 601.
[172] P. Mulvaney in *Nanoparticles and Nanostructured Films* (Ed.: J. H. Fendler), Wiley-VCH, Weinheim, **1998**, pp. 275 – 306.
[173] a) H. Lannibois, A. Hasmy, R. Botet, O. A. Chariol, B. Cabane, *J. Phys. II* **1997**, *7*, 319 – 342; b) R. Jullien, R. Botet, *Aggregation and Fractal Aggregates*, World Scientific, Singapore, **1987**.
[174] H. Kasai, H. Singh Nalwa, H. Oikawa, S. Okada, H. Matsuda, N. Minami, A. Kakuta, K. Ono, A. Mukoh, H. Nakanishi, *Jpn. J. Appl. Phys.* **1992**, *31*, L1132 – L1134.
[175] P. Gaßmann, M. List, A. Schweitzer, H. Sucker, *Eur. J. Pharm. Biopharm*. **1994**, *40*, 64 – 72.
[176] K. Zhong, E. Matijević, *J. Mater. Chem*. **1996**, *6*, 443.
[177] C. Heyer, A. Mersmann, *Proc. 14th Int. Symp. Ind. Cryst.*, *IChemE (*Rugby, computer optical disk*)*, **1999**.
[178] J. E. Dickinson, G. Stainsby, *Colloids in Food*, Applied Science Publishers, London, **1982**.
[179] a) J. W. Tom, P. G. Debenedetti, *J. Aerosol Sci*. **1991**, *22*, 555 – 565; b) S. Palakodaty, P. York, *Pharm. Res.* **1999**, *16*, 976 – 985; c) E. Reverchon, *J. Supercrit. Fluids* **1999**, *15*, 1 – 21.
[180] C. J. Chang, A. D. Randolph, *AIChE J.* **1989**, *35*, 1876 – 1882.
[181] J. M. Prausnitz, *Angew. Chem*. **1990**, *102*, 1286 – 1295; *Angew. Chem. Int. Ed. Engl*. **1990**, *29*, 1246 – 1255;.
[182] T. Schleiden, H. Offermann, *Proc. 14th Int. Symp. Ind. Cryst.*, *IChemE (*Rugby, computer optical disk*)*, **1999**.
[183] P. York, M. Hanna, G. O. Humphreys, *Proc. 14th Int. Symp. Ind. Cryst.*, *IChemE (*Rugby, computer optical disk*)*, **1999**.
[184] a) K. A. Larson, M. L. King, *Biotechnol. Prog*. **1986**, *2*, 73 – 79; b) C. Domingo, E. M. Berends, G. M. van Rosmalen, *J. Cryst. Growth* **1996**, *166*, 989 – 995; c) M. Türk, *J. Supercrit. Fluids* **1999**, *15*, 79 – 89.
[185] P. M. Gallagher, M. P. Coffey, V. J. Krukonis, W. J. Hillstrom, *J. Supercrit. Fluids* **1992**, *5*, 130 – 138.
[186] F. E. Wubbolts, O. S. L. Bruinsma, G. M. van Rosmalen, *Proc. 14th Int. Symp. Ind. Cryst.*, *IChemE (*Rugby, computer optical disk*)*, **1999**.
[187] S. Palagodaty, P. York, J. Pritchard, *Pharm. Res.* **1998**, *15*, 1835 – 1843.
[188] Y. Komai, H. Kasai, H. Hirakogo, Y. Hakuta, S. Okada, H. Oikawa, T. Adschiri, H. Inoukata, K. Arai, H. Nakanishi, *Mol. Cryst. Liq. Cryst*. **1998**, *322*, 167 – 172.
[189] H. Dautzenberg, W. Jaeger, J. Kötz, B. Philipp, Ch. Seidel, D. Stscherbina, *Polyelectrolytes*, Hanser, Munich, **1994**.
[190] D. Horn, C.-C. Heuck, *J. Biol. Chem*. **1983**, *258*, 1665 – 1670.
[191] R. R. Fisher, C. E. Glatz, *Biotechnol. Bioeng*. **1988**, *32*, 777 – 785.
[192] K. M. Clark, C. E. Glatz, *Biotechnol. Progr*. **1987**, *3*, 241 – 247.
[193] H. M. Buchhammer, G. Petzold, K. Lunkwitz, *Colloid Polym. Sci.* **2000**, *278*, 841 – 847.
[194] a) K. Roy, J. McGrath, S. C. Kuo, K. W. Leong, *Controlled Release Bioact. Mater*. **2000**, *27*, 842 – 843; b) S. K. Lee, H. J. Yang, K. M. Kim, Y. B. Lee, S. C. Shin, I. J. Oh, *Controlled Release Bioact. Mater*. **2000**, *27*, 834 – 835.
[195] A. F. Thünemann, J. Beyermann, C. von Ferber, H. Löwen, *Langmuir* **2000**, *16*, 850 – 857.
[196] M. Antonietti, J. Conrad, A. F. Thünemann, *Macromolecules* **1994**, *27*, 6007 – 6011.
[197] G. Decher, *Science* **1997**, *277*, 1232 – 1237.

[198] a) E. Donath, G. B. Sukhorukov, F. Caruso, S. Davis, H. Möhwald, *Angew. Chem*. **1998**, 110, 2324 – 2327; *Angew. Chem. Int. Ed.* **1998**, *37*, 2201 – 2205; b) G. Sukhorukov, L. Dähne, J. Hartmann, E. Donath, H. Möhwald, *Adv. Mater*. **2000**, *12*, 112 – 115; c) F. Caruso, *Adv. Mater*. **2001**, *13*, 11 – 22.

[199] S. A. Jenekhe, S. Yi, *Adv. Mater*. **2000**, *12*, 1274 – 1278.

[200] T. Saito, T. Kawanishi, A. Kakuta, *Jpn. J. Appl. Phys.* **1991**, *30*, L1182 – L1185.

[201] K.-Y. Law, *Chem. Rev*. **1993**, *93*, 449 – 486.

[202] a) A. P. Alivisatos, P. F. Barbara, A. W. Castleman, J. Chang, D. A. Dixon, M. L. Klein, G. L. McLendon, J. S. Miller, M. A. Ratner, P. J. Rossky, S. I. Stupp, M. E. Thompson, *Adv. Mater.* **1998**, *10*, 1297 – 1336; b) F. F. So, S. R. Forrest, Y. Q. Shi, W. H. Steier, *Appl. Phys. Lett*. **1990**, *56*, 674 – 676.

[203] A. P. Alivisatos, *MRS Bull.* **1998**, *23(2)*, 18 – 23.

[204] F. Gutmann, L. E. Lyons, *Organic Semiconductors*, Wiley, New York, **1967**.

[205] S. H. Yalkowsky, *Solubility and Solubilization in Aqueous Media*, Oxford University Press, New York, **1999**.

[206] M. Mosharraf, C. Nyström, *Int. J. Pharm.* **1995**, *122*, 35 – 47.

[207] R. H. Müller, B. H. L. Böhm, M. J. Grau, *Pharm. Ind*. **1999**, *61*, 175 – 178.

[208] R. H. Müller, W. Mehnert, *Dtsch. Apoth. Ztg*. **1995**, *135*, 2597 – 2601.

[209] E. Mathiowitz, S. Jacob, Y. S. Jong, C. G. Thanos, K.-P. Yip, M. Sandor, M. Kreitz, D. Abramson, *Controlled Release Bioact. Mater*. **2000**, *27*, 109 – 110.

[210] J. C. Bauernfeind, G. B. Brubacher, H. M. Kläui, W. L. Marusich in *Carotenoids* (Ed.: O. Isler), Birkhäuser, Basel, **1971**, pp. 743 – 769.

[211] *Carotenoids as Colorants and Vitamin A Precursors* (Ed.: J. C. Bauernfeind), Academic Press, New York, **1981**.

[212] O. Straub in *Key to Carotenoids*, 2nd ed., (Ed.: H. Pfauder), Birkhäuser, Basel, **1987**.

[213] O. Isler, H. Lindlar, M. Montavon, R. Rüegg, P. Zeller, *Helv. Chim. Acta* **1956**, *39*, 249 – 259.

[214] J. Paust in *Carotenoids*, *Vol. 2*, *Synthesis* (Eds.: G. Britton, S. Liaaen-Jensen, H. Pfauder), Birkhäuser, Basel, **1996**, pp. 259 – 292.

[215] P. P. Hoppe, F. J. Schöner, *Internationl Symposium on Carotenoids*, Boston, **1987**, Abstr. 53,8.

[216] H. Auweter, V. André, D. Horn, E. Lüddecke, *J. Dispersion. Sci Technol.* **1998**, *19*, 163 – 184.

[217] a) N. J. Krinski, *Pure Appl. Chem*. **1979**, *51*, 649 – 660; b) C. A. Tracewell, J. S. Vrettos, J. A. Bautista, H. A. Frank, G. W. Brudwig, *Arch. Biochem. Biophys.* **2001**, *385*, 61 – 69.

[218] N. R. Cook, M. J. Stampfer, J. Ma, J. E. Manson, F. M. Sacks, J. E. Buring, C. H. Hennekens, *Cancer* **1999**, *86*, 1783 – 1792.

[219] a) H. P. M. Gollnick, W. Hopfenmüller, C. Hemmes, S. C. Chun, C. Schmid, K. Sundermeier, H. K. Biesalski, *Eur. J. Dermatol*. **1996**, *6*, 200 – 205; b) H. K. Biesalski, Ch. Hemmes, W. Hopfenmüller, Ch. Schmid, H. P. M. Gollnick, *Free Radical Res.* **1996**, *24*, 215 – 224.

[220] A. Mortensen, L. H. Skibsted, T. G. Truscott, *Arch. Biochem. Biophys.* **2001**, *385*, 13 – 19.

[221] J. T. Landrum, R. A. Bone, *Arch. Biochem. Biophys.* **2001**, *385*, 28 – 40.

[222] E. Giovannucci, A. Ascherio, E. B. Rimm, M. J. Stampfer, G. A. Colditz, W. C. Willett, *J. Natl. Cancer Inst*. **1995**, *87*, 1767 – 1776.

[223] D. M. Snodderly, *Am. J. Clin. Nutr*. **1995**, *62*, 1448S – 1461S.

[224] L. Brown, E. B. Rim, J. M. Seddon, E. L. Giovannucci, L. Chasan-Taber, D. Spiegelmann, W. C. Willett, S. E. Hankinson, *Am. J. Clin. Nutr.* **1999**, *70*, 517 – 524.

[225] A. Mersmann, M. Löffelmann, *Chem. Ing. Tech*. **1999**, *71*, 1240 – 1244.

[226] P. P. Speiser in *Pharmazeutische Technologie: Moderne Arzneiformen* (Eds.: R. H. Müller, G. E. Hildebrand), WVG, Stuttgart, **1998**, pp. 339 – 356.

[227] L. Yang, P. Alexandridis, *Curr. Opin. Colloid Interface Sci*. **2000**, *5*, 132 – 143.

[228] E. Allémann, *Controlled Release Bioact. Mater*. **2000**, 27, 184 – 185.

[229] D. Attwood in *Colloidal Drug Delivery Systems* (Ed.: J. Kreuter), Marcel Dekker, New York, **1994**, pp. 31 – 71.

[230] J. A. Bouwstra, H. E. J. Hofland in *Colloidal Drug Delivery Systems* (Ed.: J. Kreuter), Marcel Dekker, New York, **1994**, pp. 191 – 217.

[231] D. J. A. Commelin, H. Schreier in *Colloidal Drug Delivery Systems* (Ed.: J. Kreuter), Marcel Dekker, New York, **1994**, pp. 73 – 190.

[232] R. H. Müller, *Controlled Release Bioact. Mater*. **2000**, 27, 188 – 189.

[233] K. Westesen, B. Siekmann in *Microencapsulation* (Ed.: S. Benita), Marcel Dekker, New York, **1996**, pp. 213 – 258.

[234] P. Couvreur, C. Dubernet, F. Puisieux, *Eur. J. Pharm. Biopharm*. **1995**, *41*, 2 – 13.

[235] G. Birrenbach, P. Speiser, *J. Pharm. Sci.* **1976**, *65*, 1763 – 1766.

[236] P. Couvreur, B. Kante, M. Roland, P. Baudhuin, P. Speiser, *J. Pharm. Pharmacol*. **1979**, *31*, 331 – 332.

[237] R. Sappok, *J. Oil Colour Chem. Assoc*. **1978**, *61*, 299 – 308.

[238] R. Iden, *Spektr. Wiss.* **1994**, *8*, 96 – 100.

[239] G. Clydesdale, K. J. Roberts, R. Docherty in *Controlled Particle, Droplet and Bubble Formation* (Ed.: D. J. Wedlock), Butterworth-Heinemann, Oxford, **1994**, pp. 95 – 135.

[240] A. Gavezzotti in *Crystal Engineering: from Molecules and Crystals to Materials* (Ed.: D. Braga, F. Grepioni, A. G. Orpen), Kluwer Academic, Dordrecht, **1999**, pp. 129 – 142.

[241] D. Horn, B. Honigmann, *XII FATIPEC Kongress*, Verlag Chemie, Weinheim, **1974**, pp. 181 – 189.

[242] H. Kasai, H. Kamatani, S. Okada, H. Oikawa, H. Matsuda, H. Nakanishi, *Jpn. J. Appl. Phys.* **1996**, *35*, L221-L223.

[243] H. Katagi, H. Kasai, S. Okada, H. Oikawa, H. Matsuda, H. Nakanishi, *J. Macromol. Sci. A* **1997**, *34*, 2013 – 2024.

[244] a) H.-B. Fu, X.-H. Ji, X.-H. Zhang, S.-K. Wu, J.-N. Yao, *J. Colloid Interface Sci*. **1999**, *220*, 177 – 180; b) H.-B. Fu, J.-N. Yao, *J. Am. Chem. Soc.* **2001**, *123*, 1434 – 1439.

[245] H. Singh Nalwa, H. Kasai, S. Okada, H. Oikawa, H. Matsuda, A. Kakuta, A. Mukoh, H. Nakanishi, *Adv. Mater*. **1993**, *5*, 758 – 760.

[246] E. Hanamura, *Solid State Commun*. **1987**, *62*, 465 – 469.

[247] H. Nakanishi, H. Kasai in *Photonic and Optoelectronic Polymers* (Eds.: S. A. Jenekhe, K. J. Wynne), ACS *Symp. Ser*. **1997**, *672*, 183 – 198.

[248] A. Ibanez, S. Maximov, A. Guiu, C. Chaillout, P. L. Baldeck, *Adv. Mater*. **1998**, *10*, 1540 – 1543.

[249] a) F. S. Spano, S. Mukamel, *Phys. Rev. A* **1989**, *40*, 5783; b) E. Hanamura, *Phys. Rev. B* **1988**, *37*, 1273 – 1279; c) H. Ishihara, K. Cho, *Phys. Rev. B* **1990**, *42*, 1724.

[250] D. M. Pai, B. E. Springett, *Rev. Mod. Phys.* **1993**, *65*, 163 – 211.

[251] T. Saito, W. Sisk, T. Kobayashi, S. Suzuki, T. Iwayanagi, *J. Phys. Chem*. **1993**, *97*, 8026 – 8031.

[252] J. Mizuguchi, G. Rhis, H. R. Karfunkel, *J. Phys. Chem*. **1995**, *99*, 16217 – 16227.

[253] D. Wöhrle, L. Kreienhoop, D. Schlettwein in *Phthalocyanins: Properties and Applications*, *Vol. 4* (Eds.: C. C. Leznoff, A. B. Lever), VCH, Weinheim, **1996**, pp. 219 – 284.

[254] M. Kerker, *The Scattering of Light and other Electromagnetic Radiation*, Academic Press, New York, **1969**.

[255] H. Auweter, H. Haberkorn, W. Heckmann, D. Horn, E. Lüddecke, J. Rieger, H. Weiss, *Angew. Chem*. **1999**, *111*, 2325 – 2328; *Angew. Chem. Int. Ed.* **1999**, *38*, 2188 – 2191.

[256] C. Sterling, *Acta Crystallogr.* **1964**, *17*, 1224 – 1228.

[257] M. Kasha, H. R. Rawls, M. A. El-Bayoumi, *Pure Appl. Chem*. **1965**, *11*, 371 – 393.

[258] L. Dähne, E. Biller, *Adv. Mater*. **1998**, *10*, 241 – 245.

[259] K. Gaier, A. Angerhofer, H. C. Wolf, *Chem. Phys. Lett*. **1991**, *187*, 103 – 109.

[260] H. C. Wolf, *Z. Naturforsch. A* **1956**, *11*, 797 – 800.

[261] a) M. C. Zerner, *ZINDO program*, *QTP*, University of Florida, Gainesville, FL; see also M. C. Zerner, G. H. Loew, R. F. Kirchner, U. T. Müller-Westerhoff, *J. Am. Chem. Soc*. **1980**, *102*, 589 – 599; b) J. Foresman, M. Head-Gordon, J. Pople, M. Frisch, *J. Phys. Chem*. **1992**, *96*, 135 – 149.

[262] a) W. I. Gruszecki, *J. Biol. Phys.* **1991**,*18*, 99 – 109; b) A. V. Ruban, P. Horton, A. J. Young, *J. Photochem. Photobiol. B* **1993**, *21*, 229 – 234.

[263] G. E. Box, N. R. Draper, *Empirical Model-Building and Response Surfaces*, Wiley, New York, **1987**.

[264] F. Balkenhohl, C. von dem Busche-Hünnefeld, A. Lansky, C. Zechel, *Angew. Chem*. **1996**, *108*, 2436 – 2488; *Angew. Chem. Int. Ed. Engl*. **1996**, *35*, 2288 – 2337.

[265] X.-D. Xiang, X.-D. Sun,G Breeno, Y. Lou, K. A. Wang, H. Chang, W. G. Wallace-Freedman, S. W. Chen, P. G. Schultz, *Science* **1995**, *268*, 1738 – 1740.

[266] a) S. Brocchini, K. James, V. Tangpasuthadol, J. Kohn, *J. Am. Chem. Soc*. **1997**, *119*, 4553 – 4554; b) J. M. J. Fréchet, *Polym. Mater. Sci. Eng*. **1999**, *80*, 494; c) B. Jandeleit, D. J. Schaefer, T. S. Powers, H. W. Turner, W. H. Weinberg, *Angew. Chem*. **1999**, *111*, 2648 – 2689; *Angew. Chem. Int. Ed.* **1999**, *38*, 2494 – 2532; ; d) G. Klaerner, A. L. Safir, H.-T. Chang, M. Petro, R. B. Nielsen, *Polym. Prep. (Am. Chem. Soc. Div. Polym. Chem.)* **1999**, *40*, 469; e) J. S. Dordick, D. Kim, X. Wu, *Polym. Prep. (Am. Chem. Soc*, *Div. Polym. Chem.)* **2000**, *41*, 1847 – 1848; f) H. E. Tuinstra, C. H. Cummins, *Adv. Mater*. **2000**, *12*, 1819 – 1822.

[267] R. B. Nielsen, A. L. Safir, M. Petro, T. S. Lee, P. Huefner, *Polym. Mater. Sci. Eng*. **1999**, *80*, 92.

[268] J. Stetter, F. Lieb, *Angew. Chem*. **2000**, *112*, 1792 – 1812; *Angew. Chem. Int. Ed.* **2000**, *39*, 1724 – 1744.

[269] H. J. Spinelli, *Adv. Mater*. **1998**, *10*, 1215 – 1218.

Self-Complementary Quadruple Hydrogen-Bonding Motifs as a Functional Principle: From Dimeric Supramolecules to Supramolecular Polymers

Carsten Schmuck* and Wolfgang Wienand

The self-association of individual molecules can lead to the formation of highly complex and fascinating supramolecular aggregates. However, for binding motifs which rely only on hydrogen bonds, a combination of several such weak interactions is necessary to observe self-association in solution. Systems based on four hydrogen bonds in a linear array can be obtained which efficiently aggregate at least in chloroform. Besides the physical-organic characterization of these aggregates and the factors influencing their stability, such quadruple hydrogen-bonding motifs can also be used in the field of materials science to synthesize, for the first time, supramolecular polymers through the self-association of self-complementary monomers. As the formation of noncovalent interactions is reversible and their strength depends significantly on the chemical environment (for example, solvent, temperature), the macroscopic properties of such polymers can be controlled by variation of these parameters; hence a first step towards intelligent materials with tailor-made properties is made.

1. Introduction

Hydrogen bonds[1] play an important role in determining the three-dimensional structure of chemical and biological systems[2] as a consequence of their specificity and directionality. The formation of one or multiple hydrogen bonds, especially in combination with other noncovalent forces, such as ionic or hydrophobic interactions, can lead to a dramatic change in the micro- and macroscopic properties of the resulting supramolecular assemblies.[3] In contrast to covalent bonds, which once formed are stable under normal conditions and can only be broken by providing sufficient energy, the formation of hydrogen bonds is reversible and their strength depends on the chemical environment, such as the solvent or temperature. Through a variation of the external parameters, this reversibility allows for the direct control of those physical properties of supramolecular assemblies[4] which are determined by the hydrogen bonds. The main drawback of hydrogen bonds is their limited strength; the more polar the solvent is, the weaker the hydrogen bonds are because of the increasing competitive solvation of donor and acceptor sites by solvent molecules.[5] Therefore, a single hydrogen bond possesses a considerable binding energy only in unpolar, aprotic solvents (hexane, toluene). However, stable supramolecular assemblies can also be obtained in more polar solvents, such as chloroform or acetonitrile, by a combination of several such weak interactions in binding motifs with multiple hydrogen bonds.[6]

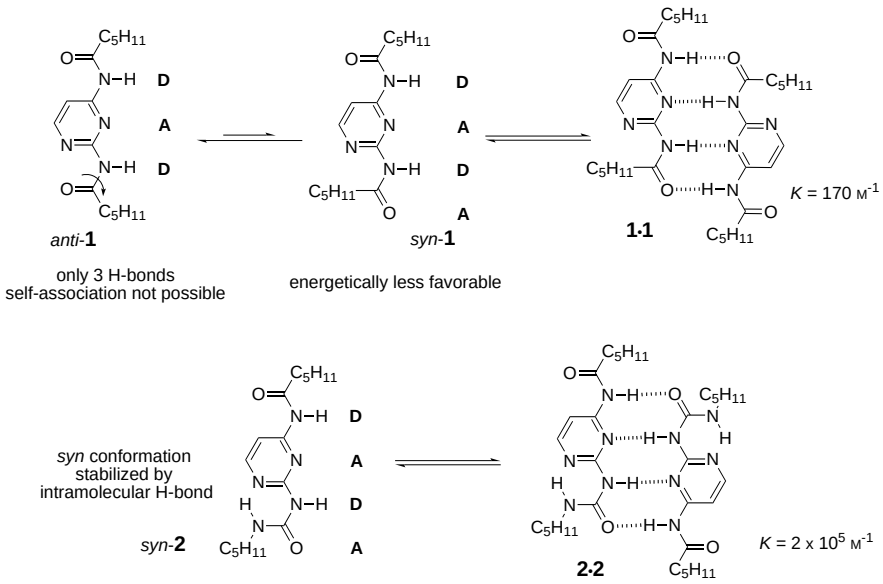
Besides the well-known self-association of molecules with a centrosymmetric AD – DA array of hydrogen-bonding donor (D) and acceptor (A) sites, triple hydrogen-bonding motifs have been studied extensively in the past by the research groups of Whitesides,[7] Zimmermann,[8] and Meijer.[9] Association processes of such triple hydrogen-bonding motifs can only be used for heterodimerization, which requires the synthesis of two different, and yet complementary, molecules. Hence, in recent years research has focused on the exploration of quadruple hydrogen-bonding motifs, which in addition to several arrays that lead only to heterodimerization[10] also give rise to two arrays capable of homodimerization: the ADAD – DADA and AADD – DDAA array.[8] The additional hydrogen bond should also lead to an increased stability of such self-assembled dimers relative to those formed from the triple hydrogen-bonding motifs.[11]

2. The ADAD Binding Motif

Meijer and co-workers were among the first to synthesize self-complementary quadruple hydrogen-bonding motifs with an ADAD array by acylation of diaminotriazines and diaminopyrimidines (Scheme 1).[12] Crystal structure determination of these compounds confirmed the existence of centrosymmetric dimers with the expected ADAD – DADA binding motif. These compounds exhibited pronounced self-association even when dissolved in chloroform. The quantitative determination of the corresponding binding constants for these dimerizations were possible by following the

[*] Dr. C. Schmuck, Dipl.-Chem. W. Wienand
Institut für Organische Chemie
Universität zu Köln
Greinstrasse 4, 50939 Köln (Germany)
Fax: (+49) 221-470-5102
E-mail: carsten.schmuck@uni-koeln.de

 © WILEY-VCH Verlag GmbH, D-69451 Weinheim, 2001 1433-7851/01/4023-4363 $ 17.50+.50/0



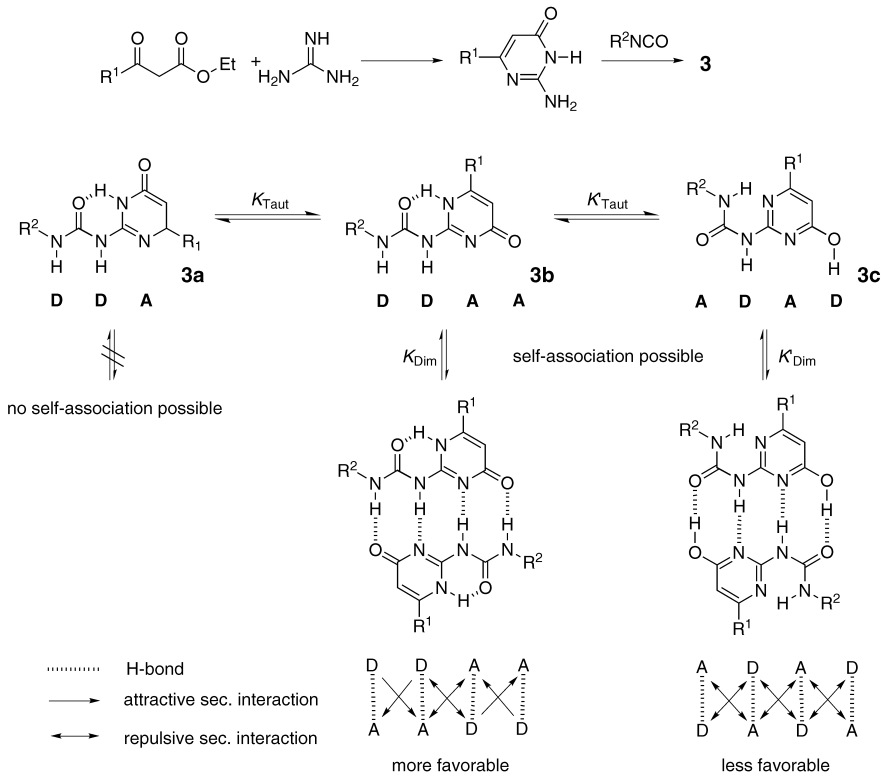
Scheme 1. Diacylpyrimidine **1** and ureidoacylpyrimidine **2** as ADAD bonding motifs according to Meijer and co-workers.

complexation-induced downfield shifts of the NH protons in the ^{1}H NMR spectra, or the shift of the NH stretching frequence to lower wave numbers in the IR spectra.[13] These data showed that the new quadruple hydrogen-bonding motifs have association constants of up to $10^5\,M^{-1}$ in $CDCl_3$ and are, therefore, indeed more stable than the previously studied DAD – ADA hydrogen-bonding arrays ($K \approx 10^2 - 10^3\,M^{-1}$).[8] It was also shown that the conformational flexibility of the molecules has a significant impact on the stability of the aggregates; self-association can only occur if all the hydrogen-bonding donor and acceptor sites are arranged in a linear way and point in the same direction, thereby presenting the necessary ADAD "face" (Scheme 1). This requires a *syn* orientation of the amide groups in the heterocyclic systems developed by Meijer and co-workers. Hence, in the case of the monoacylated derivatives **1** the molecules must first undergo an energetically costly conformational change from the more stable *anti* orientation, which can not dimerize, to the less stable *syn* conformation[14] before self-association can take place. The overall binding energy for the dimerization is, therefore, reduced by the energy which has to be paid for this conformational change. The *syn* conformation of the amide bond in the urea derivatives **2** is already stabilized in the individual molecules by an intramolecular hydrogen bond between the outer ureido NH and the heterocyclic nitrogen atom. This preorganization of the molecule means that dimerization can take place without any prior conformational changes. Therefore, the resulting binding energy is substantially higher in **2**.

3. The AADD Binding Motif

Even more efficient self-assembling quadruple hydrogen-bonding motifs should result from an AADD – DDAA array of donor and acceptor sites according to Jørgensen and co-workers.[15] This proposal can be explained by so-called secondary electrostatic interactions which, in addition to the primary hydrogen bonds, influence the complex stability. Partial negative charges, such as carbonyl oxygen atoms, are electrostatically repulsed by nearby similar negative charges, whereas positive charges, such as amide protons, in proximity have a stabilizing effect. There are thus six repulsive secondary interactions in the ADAD – DADA array besides the four primary hydrogen bonds. However, there are only two such destabilizing interactions in the AADD – DDAA array, but four additional attractive secondary electrostatic interactions. One can thus expect a higher association constant for the AADD – DDAA array relative to the ADAD – DADA one (Scheme 2).

Meijer and co-workers were indeed able to design molecules with such an AADD binding motif based on easily accessible 2-ureido-4-pyrimidones **3** (Scheme 2).[16] Unfortunately, the self-association is complicated by the occurrence of a complex equilibrium of tautomeric forms: the ureidopyr-

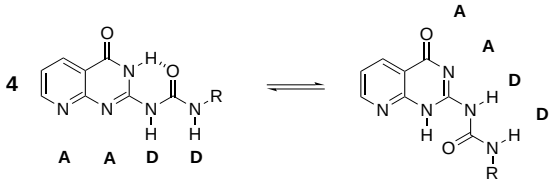


Scheme 2. Synthesis of 2-ureido-4-pyrimidones **3** (top) and the tautomeric and association equilibria observed in solution (bottom).

 © WILEY-VCH Verlag GmbH, D-69451 Weinheim, 2001 1433-7851/01/4023-4364 $ 17.50+.50/0 *Angew. Chem. Int. Ed.* **2001**, *40*, No. 23

imidones can exist in two different lactam forms (**3a** and **3b**) and one aromatic 4-pyrimidinol form (**3c**), of which the 6[1H]-pyrimidone tautomer **3a** is the most stable one. As a consequence of the different arrangements of donor and acceptor sites in these tautomers only the 4[1H]-pyrimidone **3b** and the pyrimidinol **3c** can form self-assembled dimers: In the case of the 4[1H]-pyrimidones **3b** these dimers possess the desired AADD – DDAA binding motif, whereas the pyrimidinols **3c** exhibit a less stable DADA – ADAD array. It was shown by elaborated NMR studies that a complex mixture of all three possible tautomers exists in solution and that the equilibrium composition is determined by the polarity of the solvent, the concentration of the compound, and any substituent present in the 6-position of the pyrimidine ring. Although the 1:1 stochiometry of the dimers and the quadruple hydrogen-bonding motifs with the DDAA – AADD and ADAD – DADA arrays were established by X-ray crystallography of several compounds in this series, quantitative analysis of the association constants was not possible in $CDCl_3$ because the binding constants were too high for a direct determination by ^1H NMR dilution studies. Meijer and co-workers could only estimate a lower limit for the dimerization of the ADAD – pyrimidinol motif **3c** of $K \approx 10^5\,M^{-1}$ and for the AADD – pyrimidone motif **3b** of $K \approx 10^6\,M^{-1}$.[16]

The research group of Meijer chose an indirect method, excimer fluorescence spectroscopy[17] for an experimental determination of the actual association constants. Fluorophoric pyrene groups were attached through an aliphatic linker to the external urea nitrogen atoms of suitable 6-alkyl-substituted pyrimidones which exclusively exist in the tautomeric form **3b**. Dimerization of these ureidopyrimidones results in the formation of excimer homodimers between the two pyrene fluorophors with a significantly red-shifted emission wavelength ($\lambda_{max} = 478$ nm) relative to an isolated pyrene ($\lambda_{max} = 372 - 399$ nm). The intensity of this new fluorescence emission band at 478 nm can, therefore, be used as an indicator for the extent of dimer formation (Figure 1). As pyrene is strongly fluorescent, this method requires much smaller concentrations than those needed for an NMR dilution experiment. From these data Meijer and co-workers could extract a dimerization constant for the AADD array in **3b** of $K = 6 \times 10^7\,M^{-1}$, which is significantly higher than the lower limit estimated from the previous NMR studies. A similar value of $K = 10^7\,M^{-1}$ was determined by Corbin and Zimmermann for their recently developed AADD binding motif **4**.[18] In contrast to the ureidopyrimidones **3** of Meijer and co-workers, dimerization in this case is not hampered by a



tautomeric equilibrium, as all the possible tautomers of **4** possess the same AADD array of hydrogen-bonding donor and acceptor sites and are therefore capable of self-association.[19]

4. Linear Supramolecular Polymers

The extremely efficient self-association of such AADD binding motifs in chloroform now allows for the direct control of the macroscopic physical properties of large supramolecular assemblies.[20] The attachment of more than one such binding motif to oligomer or polymer chains enables new applications in the field of polymer chemistry and material science to emerge. There will again be an extensive self-association of two binding motifs of such "Janus" molecules in chloroform solutions. These binding motifs will not only result in a dimerization but also in a supramolecular linear polymerization, a sort of "supra-polymerization" (Scheme 3).[21] In contrast to conventional polymers, in which the macromolecular chains consist of covalently and hence irreversibly connected monomer units, here supramolecular polymers are obtained which only demonstrate their polymeric properties by the self-association of the corresponding binding motifs.[4, 22, 23] The use of weak and reversible hydrogen bonds to connect different monomer units also provides the first step towards "intelligent", tailor-made polymers. The strength of the interaction between the various monomer units depends on external parameters and can, therefore, be changed by variation of the solvent, pH value, or temperature.

The first reversible polymer based on this principle was obtained by Meijer et al. through the self-association of a bifunctional molecule **5**, in which two ureidopyrimidone binding motifs were covalently linked through an alkyl chain (Scheme 4).[24] Compound **5** shows an association number of more than 500 in chloroform.[25, 26]

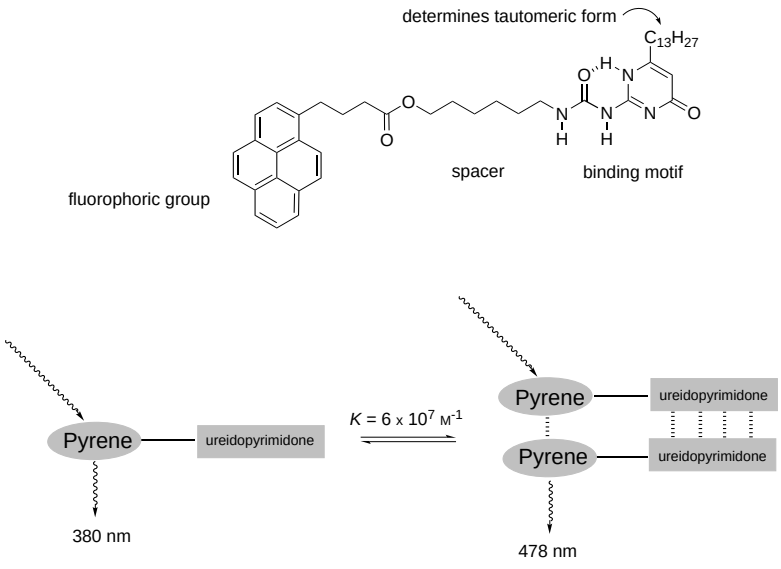
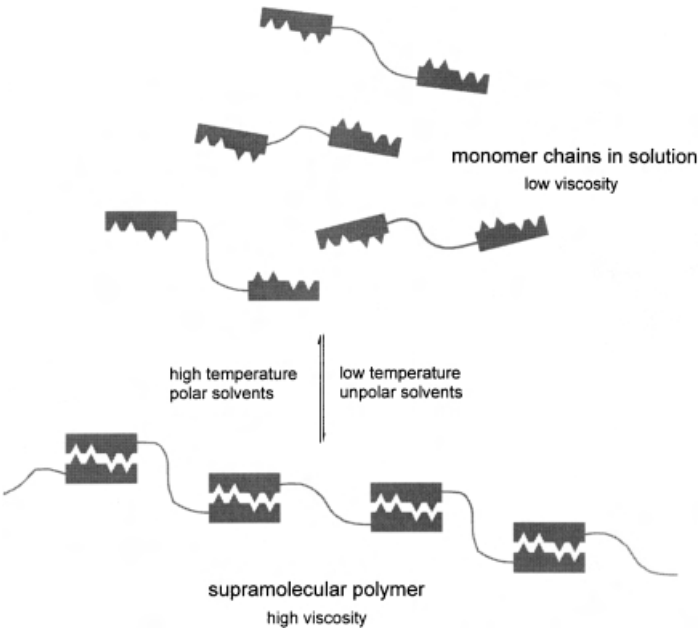
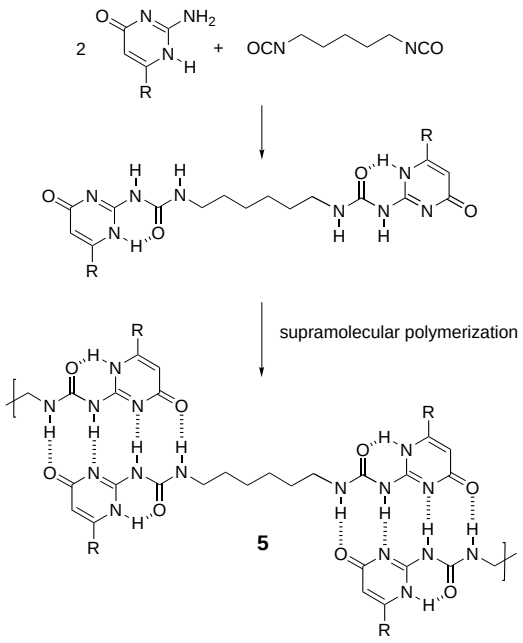


Figure 1. Determination of the dimerization constant for compounds of type **3** by using excimer fluorescence spectroscopy of a pyrene derivative.

 © WILEY-VCH Verlag GmbH, D-69451 Weinheim, 2001 1433-7851/01/4023-4365 $ 17.50+.50/0



Scheme 3. Supra-polymerization of bifunctional "Janus" molecules.



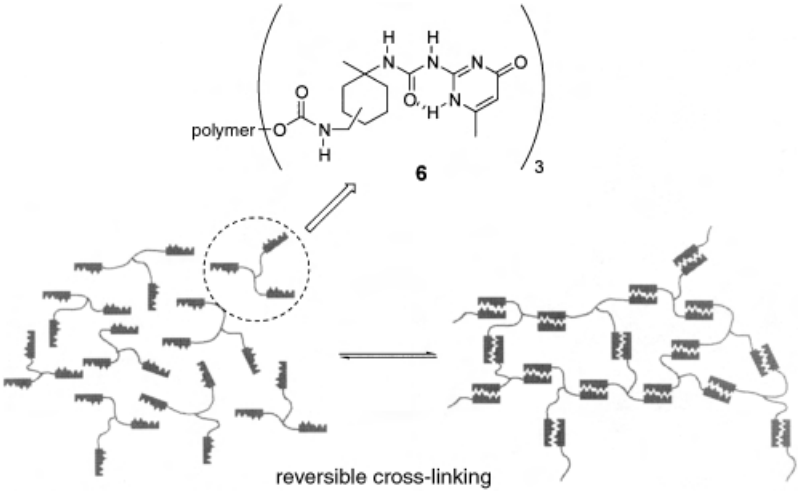
Scheme 4. Synthesis of the first supramolecular homopolymer **5**.

Such solutions are highly viscous and display all the properties of a classical polymer. Noteworthy, however, as this is not found in a conventional polymer, is the strong concentration and temperature dependance of the viscosity. This observation can be explained by the effect of temperature on the strength of the hydrogen bonds between two ureidopyrimidone binding motifs connecting two different chains. The hydrogen bonds are first weakened by increased thermal motion and are finally broken, hence at higher temperatures the material eventually displays only those properties related to the individual monomer units and the solution becomes more fluid and less viscous. The polymeric properties are again restored on decreasing the temperature. Similar effects are observed by the addition of a polar, protic solvent, which also disrupts the hydrogen bonds; the addition of small amounts of trifluoroacetic acid causes a dramatic decrease in the viscosity of the solution.

5. Noncovalently Cross-Linked Polymers

Of course, more than two self-complementary ureidopyrimidone units can also be incorporated into a single molecule. This gives rise to supramolecular 3D networks of type **6** (Scheme 5), which can exhibit completely new properties compared to conventional cross-linked polymers. These materials change with an increasing number of cross-links from a viscous liquid to an elastic solid. The structural composition of covalently cross-linked polymers is normally not precisely defined. The number of cross-links—which is an important parameter for the materials properties—can only be approximately controlled by variation of the polymerization conditions (for example, catalyst concentration, additives).[27] Once formed, the cross-links are irreversible. This situation leads to the trapping of a kinetic polymerization state. The material often contains structural defects such as unreacted functional groups which have an undesired influence on the material properties. This problem does not exist with noncovalently cross-linked polymers. As hydrogen bonds continously dissociate and reform, such a polymer is always close to its thermodynamically favored state. Hence, the density of cross-links in the network is higher and the material becomes stiffer. The application of external pressure, which results in structural defects caused by disruption of hydrogen-bonded cross-links, results in spontaneous reorganization: the material self-heals.

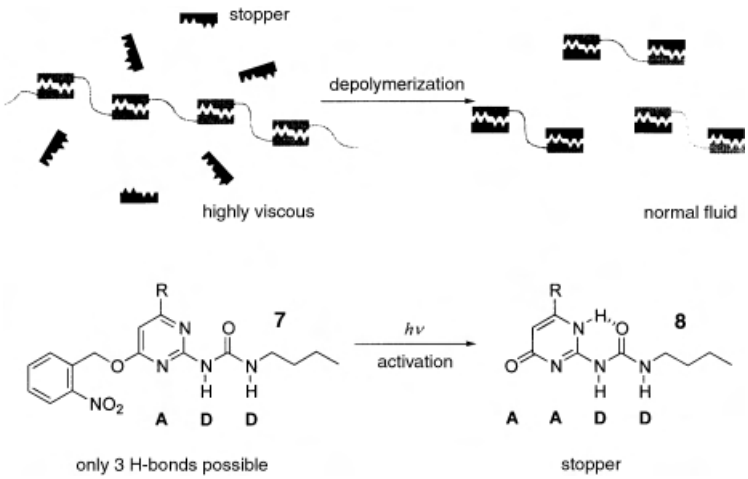
The reversibility of the supramolecular polymerization process can be nicely demonstrated by the addition of a monofunctional ureidopyrimidone stopper **8** to a highly viscous solution of the bifunctional Janus molecule **5**.[25] The stopper **8** interferes with the polymerization through a competitive association with the ureidopyrimidone head



Scheme 5. Reversibly cross-linked supramolecular 3D polymers.

 © WILEY-VCH Verlag GmbH, D-69451 Weinheim, 2001 1433-7851/01/4023-4366 $ 17.50+.50/0

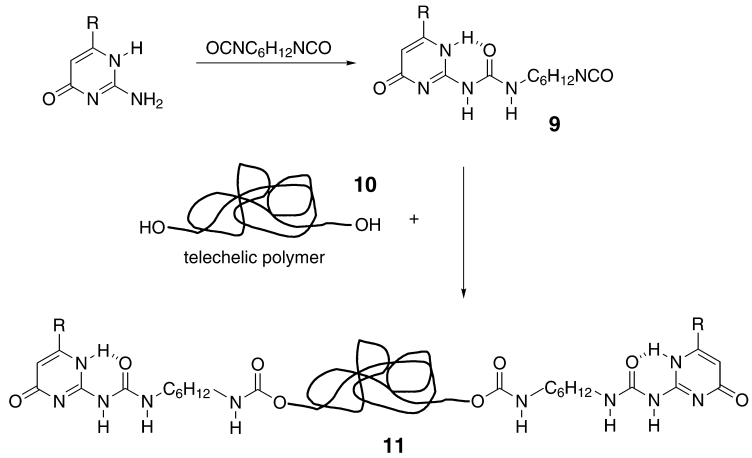
groups of **5** and thus induces rapid depolymerization (Scheme 6). The viscosity of the solution decreases dramatically with increasing concentration of stopper **8**. When the stopper is masked in the form of a photolabile nitrobenzyl ether such as in **7**, the depolymerization can be initiated by external photolysis.[28] The masked stopper with its triple hydrogen-bonding motif does not form dimers with the quadruple hydrogen-bonding motifs in **5** which are stable enough to effectively compete with the polymerization. Photolysis causes the cleavage of the nitrobenzyl ether protecting group and liberates the fourth hydrogen-bonding site, the carbonyl group of the pyrimidone ring. The stopper is now activated and can cause depolymerization. Unfortunately, the process is so far not reversible, and so a complete photochemical switching is not yet possible.



Scheme 6. Depolymerization of a supramolecular polymer induced by addition of a monofunctional stopper **8** (top), which can be liberated photochemically from an inactive precursor **7** (bottom).

6. End Group Modified Telechelic Polymers

New materials with interesting macroscopic properties can be obtained by attaching the ureidopyrimidone binding motif to polysiloxane oligomers or telechelic[29] polymers based on polyethylenes/polybutylenes, polyethers, polycarbonates, or polyesters.[30] For this purpose Meijer et al. developed a general, large-scale synthesis based on *N*-ureidoalkylisocyanates **9** (Scheme 7). Reaction of the isocyanate group with appropriate nucleophiles such as hydroxy or amino groups, which form the end groups of classical telechelic polymers **10**, leads to the corresponding supramolecular polymer units **11** in good yields. Alternatively, alkenyl-substituted ureidopyrimidones can be used directly as monomers for copolymerization with simple alkenes using Ziegler–Natta conditions as was shown recently by Coates and co-workers.[31]



Scheme 7. General synthetic scheme for the end-group modification of telechelic polymers with self-associating hydrogen-bonding motifs.

In contrast to unmodified telechelic polymers, such hybrid materials exhibit improved properties as a result of the self-association which increases their virtual molecular weight.[32] For example, the functionalization of a poly(ethylene/butylene) copolymer with hydroxy end-groups resulted in a macroscopically visible change in the material properties:[30] Whereas the dihydroxy telechelic copolymer is a viscous liquid, the ureidopyrimidone end-group-modified polymer is an elastic solid as a result of the additional supramolecular linking of the individual polymer chains (Figure 2).

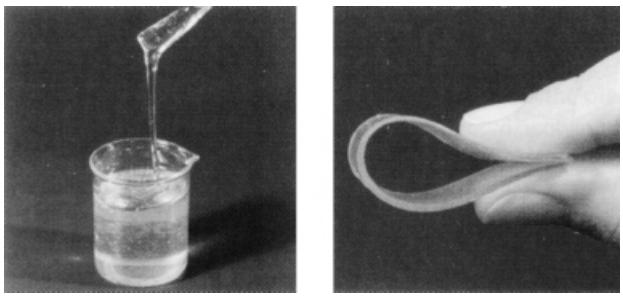
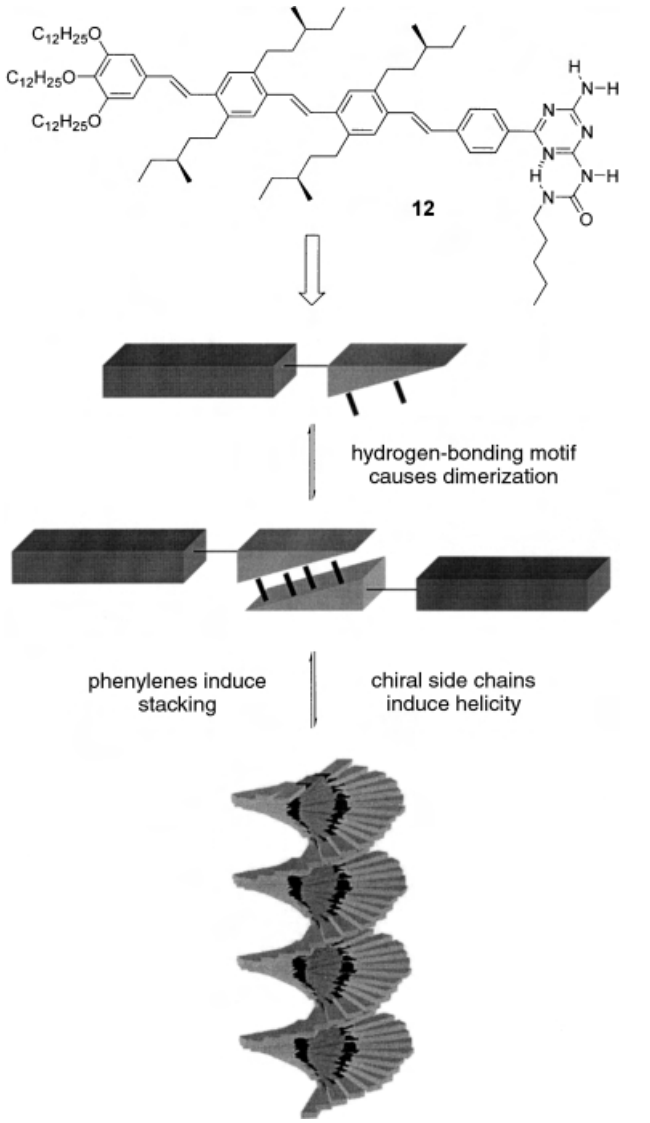


Figure 2. Changing the macroscopic properties of a telechelic poly(ethylene/butylene) copolymer **10** (left) by end-group modification with self-associating hydrogen-bonding motifs **11** (right).[30b]

7. Hierarchical Order in Supramolecular Polymers

Besides linking of the ureidopyrimidone head groups through hydrogen bonds, the mechanical properties of such end group modified supramolecular polymers are also determined by interactions between the polymer chains themselves. This situation opens the way to obtain supramolecular polymers with a higher degree of structural order by incorporation of specific structure-determining groups into the periphery of such systems. For example, the bifunctional ureidopyrimidone **5** forms a supramolecular polymer with a random-coil structure in chloroform. If one modifies the binding motifs by attaching oligo(*p*-phenylenevinylene) groups with chiral side chains, such as in **12**, the resulting supramolecular polymers display a helical superstructure (Scheme 8).[33] In addition to the hydrogen-bonding-based self-association, $\pi-\pi$ interactions between the aromatic rings of the oligo(*p*-phenylenevinylene) groups cause a columnar



Scheme 8. Formation of a helix through $\pi-\pi$ stacking of hydrogen-bonded dimers. Reprinted with permission from the American Chemical Society from ref. [33b].

stacking of the planar head-group dimers. The chiral side chains then induce a helical twist, as could be shown by CD spectroscopy. Again, the extent of the stacking and the helical twist can be controlled by the solvent and the temperature: neither in DMSO nor above 80 °C could any Cotton effect typical of helical structures be observed.

8. Outlook

The first steps toward the supramolecular synthesis of "intelligent" materials with tailor-made properties have been made. However, the exclusive use of hydrogen bonds thus far also limits any potential future application of these systems. The quadruple hydrogen-bonding motifs presented here display their unique and efficient self-association properties only in solvents of low polarity such as chloroform; more polar solvents or even water destroy the hydrogen bonds and, therefore, also their positive effects on the materials properties. Hence, the long-term goal must be to develop new systems, in addition to the binding motifs accessible so far, that also display stable association in aqueous solvents. One possibility in this context is to incorporate additional electrostatic or hydrophobic interactions[34] into self-complementary hydrogen-bonding motifs. Some first and promising examples already do exist and one can look forward to future developments in this field.

Received: June 25, 2001 [M1523]

[1] a) G. A. Jeffrey, *An Introduction to Hydrogen Bonding*, 1st ed., Oxford University Press, New York, **1997**; b) J. Israelachvili, *Intermolecular & Surface Forces*, 2nd ed., Academic Press, London, **1992**.
[2] a) D. Philp, J. F. Stoddart, *Angew. Chem.* **1996**, *108*, 1242–1286; *Angew. Chem. Int. Ed. Engl.* **1996**, *35*, 1154–1196; b) D. S. Lawrence, T. Jiang, M. Levitt, *Chem. Rev.* **1995**, *95*, 2229–2260.
[3] a) G. M. Whitesides, J. P. Mathias, C. T. Seto, *Science* **1991**, *254*, 1312–1319; b) N. B. Bowden, M. Weck, I. S. Choi, G. M. Whitesides, *Acc. Chem. Res.* **2001**, *34*, 231–238; c) C. V. K. Sharma, *J. Chem. Educ.* **2001**, *78*, 617–622; d) D. Rouvray, *Chem. Br.* **2000**, *36*(7), 26–29.
[4] a) F. Vögtle, *Supramolecular Chemistry*, Wiley, Chichester, **1991**; b) J.-M. Lehn, *Supramolecular Chemistry*; *Concepts and Perspectives*, VCH, Weinheim, **1995**; c) J. W. Steed, J. L. Atwood, *Supramolecular Chemistry*, Wiley, Chichester, **2000**.
[5] D. H. Williams, M. S. Westwell, *Chem. Soc. Rev.* **1998**, *27*, 57–64.
[6] For a recent review, see D. C. Sherrington, K. A. Taskinen, *Chem. Soc. Rev.* **2001**, *30*, 83–93.
[7] a) G. M. Whitesides, E. E. Simanek, J. P. Mathias, C. T. Seto, D. N. Chin, M. Mammen, D. M. Gordon, *Acc. Chem. Res.* **1995**, *28*, 37–44; b) C. MacDonald, G. M. Whitesides, *Chem. Rev.* **1994**, *94*, 2383–2420.
[8] S. C. Zimmermann, P. S. Corbin, *Struct. Bonding (Berlin)* **2000**, 63–94.
[9] F. H. Beijer, R. P. Sijbesma, J. A. J. M. Vekemans, E. W. Meijer, H. Kooijman, A. L. Spek, *J. Org. Chem.* **1996**, *61*, 6371–6380.
[10] For a detailed discussion of all the possible geometric arrays of quadruple hydrogen-bonding motifs, see U. Lüning, C. Kühl, *Tetrahedron Lett.* **1998**, 5735–5738.
[11] For a first example of hydrogen-bonding motifs with five or six linear hydrogen bonds, see a) H. Zeng, H. Ickes, R. A. Flowes, B. Gong, *J. Org. Chem.* **2001**, *66*, 3574–3583; b) P. S. Corbin, S. C. Zimmerman, *J. Am. Chem. Soc.* **2000**, *122*, 3779–3780.
[12] F. H. Beijer, H. Kooijman, A. L. Spek, R. P. Sijbesma, E. W. Meijer, *Angew. Chem.* **1998**, *110*, 79–82; *Angew. Chem. Int. Ed.* **1998**, *37*, 75–78.
[13] a) C. S. Wilcox in *Frontiers in Supramolecular Chemistry and Photochemistry* (Eds.: H.-J. Schneider, H. Dürr), VCH, Weinheim, **1990**, pp. 123–144; b) K. A. Connors, *Binding Constants*, Wiley, New York, **1987**, chap. 2 and 5.
[14] A. R. Katritzky, I. Ghiviraga, *J. Chem. Soc. Perkin Trans. 2* **1995**, 1651–1653.
[15] a) W. L. Jørgensen, J. Pranata, *J. Am. Chem. Soc.* **1990**, *112*, 2008–2010; b) J. Pranata, S. G. Wierschke, W. L. Jørgensen, *J. Am. Chem. Soc.* **1991**, *113*, 2810–2819.
[16] F. H. Beijer, R. P. Sijbesma, H. Kooijman, A. L. Spek, E. W. Meijer, *J. Am. Chem. Soc.* **1998**, *120*, 6761–6769.
[17] S. H. M. Söntjens, R. P. Sijbesma, M. H. P. van Genderen, E. W. Meijer, *J. Am. Chem. Soc.* **2000**, *122*, 7487–7493.
[18] P. S. Corbin, S. C. Zimmerman, *J. Am. Chem. Soc.* **1998**, *120*, 9710–9711.
[19] Self-complementary ADAD and AADD binding motifs which are not influenced by a tautomeric equilibrium but which show much weaker binding ($K \approx 10^4\,\text{M}^{-1}$) as a consequence of the absence of stabilizing secondary interactions have been synthesized recently: B. Gong, Y. Yan, H. Zeng, E. Skrzypczak-Jankuum, Y. Wah Kim, J. Zhu, H. Ickes, *J. Am. Chem. Soc.* **1999**, *121*, 5607–5608.
[20] In the meantime, the ureidopyrimidone motif has also been used for the noncovalent linking of two fullerenes: a) M. T. Rispens, L. Sanchez, J. Knol, J. C. Hummelen, *Chem. Commun.* **2001**, 161–162;

 © WILEY-VCH Verlag GmbH, D-69451 Weinheim, 2001 1433-7851/01/4023-4368 $ 17.50+.50/0

b) J. J. Gonzalez, S. Gonzalez, E. M. Priego, C. Luo, D. M. Guldi, J. de Mendoza, N. Martin, *Chem. Commun.* **2001**, 163 – 164.

[21] Self-assembled molecular capsules are formed in a 1:1 dimerization when rigid, concave spacers are used: B. J. B. Folmer, R. P. Sijbesma, H. Kooijman, A. L. Spek, E. W. Meijer, *J. Am. Chem. Soc.* **1999**, *121*, 9001 – 9007.

[22] a) N. Zimmerman, J. S. Moore, S. C. Zimmerman, *Chem. Ind.* **1998**, 604 – 610; b) A. Cifferi, *Supramolecular Polymers*, Marcel Dekker, New York, **2000**.

[23] Rebek and co-workers have designed supramolecular "polycaps", in which the association results from a chloroarene-induced dimerization of calixarene units in unpolar solvents: R. K. Castello, R. Clark, S. L. Craig, C. Nuckolls, J. Rebek, Jr., *Proc. Natl. Acad. Sci. USA* **2000**, *97*, 12 418 – 12 421.

[24] In contrast to this first surpamolecular homopolymer, the polymers designed by the research groups of Lehn, Griffin, as well as Kato and Fréchet at the beginning of the 1990s were based on the hetero-polymerization of two different molecules with complementary binding properties: a) C. Fouquey, J.-M. Lehn, A.-M. Levelut, *Adv. Mater.* **1990**, *2*, 254 – 257; b) J.-M. Lehn, *Makromol. Chem. Macromol. Symp.* **1993**, *69*, 1 – 17; c) C. Alexander, C. P. Jariwala, C. M. Lee, A. C. Griffin, *Makromol. Chem. Macromol. Symp.* **1994**, *77*, 283 – 294; d) C. M. Lee, A. C. Griffin, *Makromol. Chem. Macromol. Symp.* **1997**, *117*, 281 – 290; e) T. Kato, J.-M. Fréchet, *Makromol. Chem. Macromol. Symp.* **1995**, *98*, 311 – 326.

[25] R. P. Sijbesma, F. H. Beijer, L. Brunsveld, B. J. B. Folmer, J. H. Ky Hirschberg, R. F. M. Lange, J. K. L. Lowe, E. W. Meijer, *Science* **1997**, *278*, 1601 – 1604.

[26] Heterodimerization of different ureidopyrimidone motifs can be used for the construction of cyclic aggregates: S. H. M. Söntjes, R. P. Sijbesma, M. H. P. van Genderen, E. W. Meijer, *Macromolecules* **2001**, *34*, 3815 – 3818.

[27] B. Tieke, *Makromolekulare Chemie*, VCH, Weinheim, **1997**.

[28] B. J. B. Folmer, E. Cavini, R. P. Sijbesma, E. W. Meijer, *Chem. Commun.* **1998**, 1847 – 1848.

[29] A telechelic polymer is a low molecular weight polymer or an oligomer with reactive end groups such as hydroxy, amino, carboxy, isocyanate, epoxide, or vinyl.

[30] a) J. H. Ky Hirschberg, F. H. Beijer, H. A. van Aert, P. C. M. M. Magusin, R. P. Sijbesma, E. W. Meijer, *Macromolecules* **1999**, *32*, 2696 – 2705; b) B. J. B. Folmer, R. P. Sijbesma, R. M. Versteegen, J. A. J. van der Rijt, E. W. Meijer, *Adv. Mater.* **2000**, *12*, 874 – 878.

[31] L. R. Rieth, R. F. Eaton, G. W. Coates, *Angew. Chem.* **2001**, *113*, 2211 – 2214; *Angew. Chem. Int. Ed.* **2001**, *40*, 2153 – 2156.

[32] For example, Stadler and co-workers have shown how even weak hydrogen bonds between polymer chains can improve material properties: a) M. Müller, A. Dardin, U. Seidel, V. Balsamo, B. Ivàn, H. W. Spiess, R. Stadler, *Macromolecules* **1996**, *29*, 2577 – 2583; b) M. Müller, U. Seidel, R. Stadler, *Polymer* **1995**, *36*, 3143 – 3150, and references therein.

[33] a) A. El-ghayoury, E. Peeters, A. P. H. J. Schenning, E. W. Meijer, *Chem. Commun.* **2000**, 1969 – 1970; b) J. H. Ky Hirschberg, L. Brunswald, A. Ramzi, J. A. J. M. Vekemans, R. P. Sijbesma, E. W. Meijer, *Nature* **2000**, *407*, 167 – 170; c) A. P. H. J. Schenning, P. Jonkheijm, E. Peeters, E. W. Meijer, *J. Am. Chem. Soc.* **2001**, *123*, 409 – 416.

[34] For some recent examples on the importance of ionic and hydrophobic interactions for supramolecular aggregation in aqueous solution, see a) S. Lahiri, J. L. Thompson, J. S. Moore, *J. Am. Chem. Soc.* **2000**, *122*, 11 315 – 11 319; b) M. Sirish, H. J. Schneider, *J. Am. Chem. Soc.* **2000**, *122*, 5881 – 5882; c) T. Grawe, T. Schrader, M. Gurrath, A. Kraft, F. Osterod, *Org. Lett.* **2000**, *2*, 29 – 32; d) C. Schmuck, *Chem. Eur. J.* **2000**, *6*, 409 – 417; e) C. Schmuck, *Eur. J. Org. Chem.* **1999**, 2397 – 2403; f) L. Isaacs, D. Witt, J. C. Fettinger, *Chem. Commun.* **1999**, 2549 – 2550.

 © WILEY-VCH Verlag GmbH, D-69451 Weinheim, 2001 1433-7851/01/4023-4369 $ 17.50+.50/0

Chemistry at the Uncertainty Limit**

Ahmed H. Zewail*

At the limit of time for chemistry (and biology), the femtosecond time resolution is fundamental for observing atomic-scale dynamics. With quantum uncertainty this paradigm may be questioned, but in fact, because of the powerful concept of coherence in the joint uncertainties, new limits in spatial and temporal resolutions have been reached. In this new regime of dynamics, the scope of applications has proven wide-ranging, encompassing the different areas of molecular sciences. The aim of this Essay is to discuss the concepts—with focus on the world of molecules, simple or complex—and the new knowledge possible at the limit of the uncertainty principle for atomic-scale dynamics.

Knowledge in our universe is not always certain. In everyday life we are familiar with classical mechanics and its description of *macroscopic* systems—the motion of objects with precise knowledge of where the object is (position x) and where it is going (momentum p, or speed v). In contrast, for the *microscopic* world, governed by the laws of quantum mechanics,[2] we cannot predict with the same precision the position and momentum simultaneously; such quantum effects also have a signature in phenomena of the very big, namely in cosmology. Mechanicians of both worlds, classical and quantal, accommodate the difference by recognizing two of the most powerful and uneasy to digest concepts: the uncertainty principle and the particle-wave duality of matter. Particles, even molecules, can behave as waves. The same duality holds for light: waves can behave as particles.

In the nineteenth century Maxwell showed the nature of light to be electromagnetic waves (1864), while Einstein gave light the particle-like description (1905) with a quantum of energy, which was called a photon by G. N. Lewis. (This idea of quanta has its roots in the earlier work (1900) of Planck which relates the energy E to the frequency ν of radiation by $E = h\nu$, where h is Planck's constant.) The connection to matter's duality was made by de Broglie in a brilliant analogy (1924), where he identified the wave character of particles with a wavelength given simply by Equation (1).

$$\lambda_{\text{de Broglie}} = h/p \tag{1}$$

The complementarity of the two descriptions becomes clearer when the concept of coherence is introduced. Two or more waves can produce interference patterns when their amplitudes add up coherently, as shown two centuries ago by Young (1801) in his experiments on light propagating through two holes and resulting in fringes on a screen. This superposition results in a group of waves localized in space (Δx). For all waves, the group generally obeys the relationship $\Delta x \Delta k \approx 1$, where k is the resultant wave number; invoking the duality expression [Eq. (1)] makes $\Delta x \Delta p = \hbar$. For light waves, this behavior, which has also been observed for electrons, is discussed extensively in popular science writings; it embodies many abstract concepts from the microscopic world (such as the superposition of waves, particle and/or wave behavior, quantum measurements, quantum electrodynamics, and the uncertainty principle) and of the connection to macroscopic systems in what is called Schrödinger's cat.

For matter, superpositions analogous to those of light waves can be formed from matter wave functions. The solution of the Schrödinger equation (1926) yields wave functions and their probability distributions which are diffuse over position (x) space. However, if these waves are added up coherently with well-defined phases something remarkable emerges: the probability distribution becomes *localized* in space, as Schrödinger showed in 1926 using the quantum states of a harmonic oscillator. The resultant wave packet and its associated de Broglie wavelength has the essential character of a classical particle: a trajectory in space and time with a well-defined (group) velocity and position—a moving classical marble, but at atomic resolution! For a free particle ($E = p^2/2m$), it is evident that the group velocity of the packet (dE/dp) is simply v, namely the classical speed.

The association of a wave character to a particle motion through de Broglie's relationship, which leads to $\Delta p = \hbar \Delta k$ as discussed above, is entirely consistent with Heisenberg's mechanics (1925) which defines for all quantum systems the uncertainty in measurement—an imprecision in position (with a standard deviation $\sigma_x \equiv \Delta x$) and in momentum (with a standard deviation $\sigma_p \equiv \Delta p$), where both are related by

[*] Prof. A. H. Zewail
Arthur Amos Noyes Laboratory of Chemical Physics
California Institute of Technology
Pasadena, CA 91125 (USA)
Fax: (+1) 626-792-8456
E-mail: zewail@caltech.edu

[**] This contribution is an extended version of a recent commentary published in *Nature*, in the new section Concepts.[1] The invitation by the Editor of *Angewandte Chemie* made me steer the piece towards chemistry questions and provide the experimental – theoretical bridge relevant to molecular dynamics.

 © WILEY-VCH Verlag GmbH, D-69451 Weinheim, 2001 1433-7851/01/4023-4371 $ 17.50+.50/0

$\Delta x \Delta p \geq \hbar/2$. When the equality holds, the packet is termed uncertainty- or transform-limited. Similarly, there is an uncertainty for energy measured over a finite period of time ($\Delta t \Delta E \geq \hbar/2$). This is the crux of the whole matter. With femtosecond resolution it is possible to make $(\Delta x/x) < 1$ and $(\Delta p/p) < 1$. The key concept is the coherent superposition and coherent state (wave packet) probing, in accord with these joint uncertainties (Figure 1).

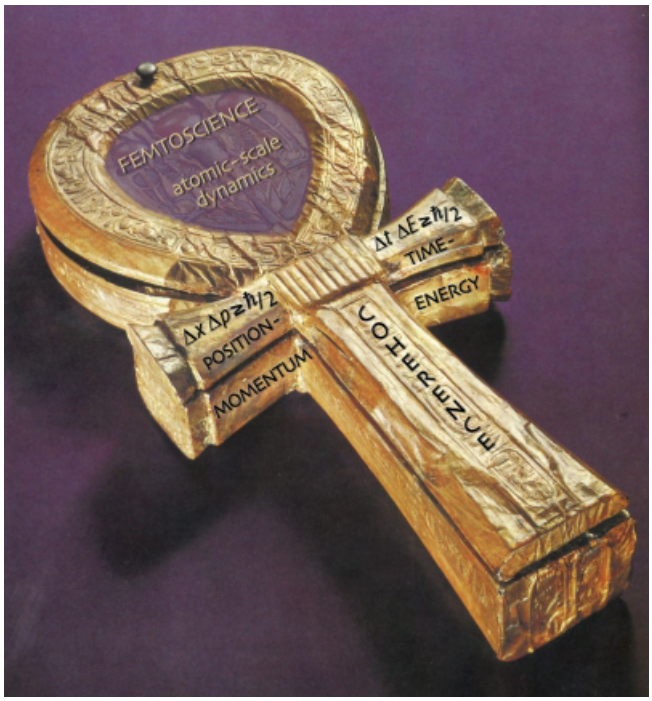


Figure 1. The "ankh", the key of "life" in old Egyption religion—here the key has the codes, coherence and the joint uncertainties, which unlock mysteries of the relationship between quantum uncertainty and femtoscience.

Dynamic processes in chemistry and biology involve motions of atoms in the course of the transformation. The speed of atomic motion is approximately 1 km s^{-1}, and, hence, the time required to record atomic-scale dynamics over a distance of 1 Å is in the range of 100 fs. The very act of such motions as reactions unfold and pass through their transition states—the configurations between reactants and products—cannot be isolated without resolution in space and time on the femtosecond time scale. Thus, only on this time scale can we directly observe the fundamental processes of bond breaking and bond making of molecular structures; this is the central mission of the field of femtochemistry.[3]

If the concepts are clear, what created the perception that quantum uncertainty would limit the importance of femtosecond resolution? Two lines of arguments dominated the thinking.

The first of these is the use of the uncertainty relationship $\Delta t \Delta E \geq \hbar/2$. The energy uncertainty on the femtosecond timescale is "huge" and considered poor by the standards of high-resolution spectroscopy in the energy domain. For example, a 50-fs pulse (full-width at half maximum height) has an energy width ΔE of 294 cm^{-1} ($\sigma_t = 21.2$ fs, $\sigma_E =$ 125 cm^{-1}, and $\sigma_t \sigma_E = \hbar/2$). It seems as though we would be "ruining" the quantized vibrational–rotational states of molecules by using femtosecond excitation or probes! The second issue is that of the spreading of localized wave packets in microscopic systems which was thought to be severe as a result of intra- and intermolecular interactions.

With these two issues in mind, predictions were made in the literature that femtosecond resolution for studies in chemistry and biology would be of limited utility. Had the energy states been prepared incoherently, this would have been true, but clearly it is not. The dispersion in time scales in the energy range of the packet gives a dephasing or spreading time that is longer than that of the nuclear motion—once again the uncertainty is in our favor!

The momentum distribution for a Gaussian-free particle wave packet having the minimum value of the uncertainty product, $\Delta x \Delta p = \hbar/2$, is also Gaussian, and the contribution of the momentum uncertainty to the widening of the packet as it moves is easy to express. We can have a feeling of the time needed for an appreciable spreading (by $\sqrt{2}$ or about 40 %) to take place and express this time by Equation (2), where $t = 0$ is

$$t_s = \Delta x(0)/\Delta v = 2m\Delta x^2(0)/\hbar \qquad (2)$$

the time of minimum uncertainty, m the mass, and $\Delta v = \Delta p/m$. When a free particle wave packet is initiated by an ultrashort light pulse so that it has the minimum value of the $\Delta x \Delta p$ uncertainty product, one can calculate the relationship between the pulse duration and the wave-packet spatial width. It turns out to be quite simple: $\Delta x = \langle v \rangle \Delta t$.

The size of $\hbar$, 1.05457×10^{-34} J s, means that the fuzziness required by the uncertainty principle is imperceptible on the normal scales of size and momentum, but becomes important at atomic scales. For example, if the position of a stationary 200-g apple is initially determined to a small fraction of a wavelength of light, say $\Delta x = 10$ nm, the apple's position uncertainty will spread by about 40 % only after 4×10^{17} s, or 12 billion years, that is, the age of the universe! On the other hand, an electron with a mass 29 orders of magnitude smaller would spread by 40 % from an initial 1-Å localization after only 0.2 fs. Clearly, from the above expression, the much greater masses of atomic nuclei make their wave packets spread orders of magnitude slower than the wave packet of the electron, and in fact this spreading is relatively minor on the femtosecond timescale.

We should recall the consequence of both of our uncertainty relations: A small Δt value is the way to obtain a small Δx value and hence *localization*! What is useful to keep in mind is the relationship of ΔE to the binding energies of atoms—for a 50 fs pulse, ΔE is about 1 kcal mol^{-1}, which is a small fraction of typical binding energies, which are on the order of 70 kcal mol^{-1}.

Experimentally, atomic-scale dynamics of molecules and their reactions have been observed and studied in all phases of matter; they span phenomena from the simple to the very complex, from diatomics to proteins, and from the gas phase to condensed media. The physics can be elucidated using the paradigm case of sodium iodide (NaI, Figure 2). The chemical

 © WILEY-VCH Verlag GmbH, D-69451 Weinheim, 2001 1433-7851/01/4023-4372 $ 17.50+.50/0

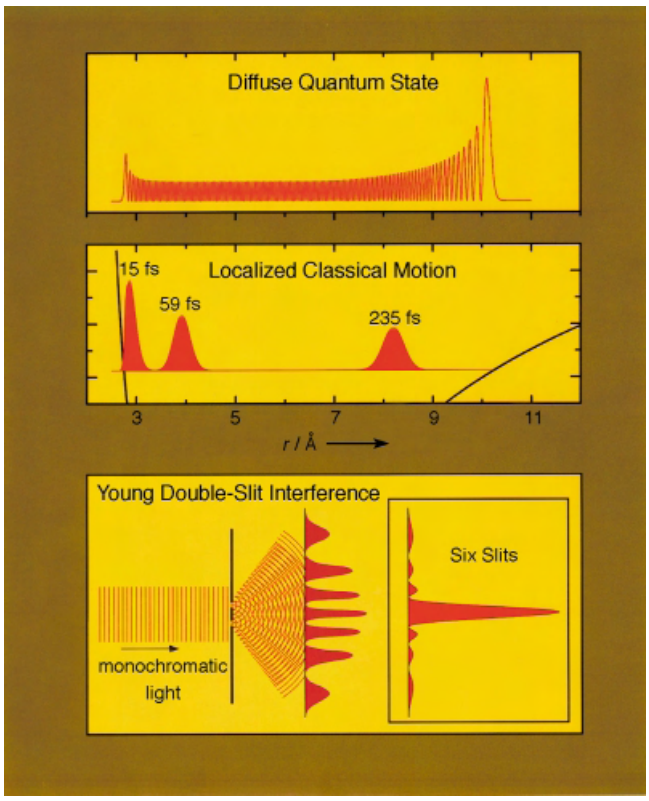


Figure 2. Comparison of localized (wave packet) and diffuse (wave function) representations of molecular systems. Here the results from real quantum calculations made for the NaI system are shown. Top: the stationary-state position probability density at an energy of 5300 cm^{-1}. Middle: the actual wave packet formed at about the same energy and at the same potential—covalent below r = 3 Å and ionic beyond 9 Å (black curves). The wave packet is made by a 15-fs pulse, and its evolution with time is indicated; note the narrow width of the moving wave packet. Bottom: the idea of Young's double-slit interference (1801) and the consequence of replacing two slits by six thin slits but keeping the same total distance. The more the interference channels, the more the localization.[6a]

bond in the diatomic NaI molecule changes character (covalent or ionic) with time, prior to the final breakage to yield atoms of Na and I. The bond also reforms after an electron is transferred.

In experiments at Caltech the wave packet was observed to oscillate periodically (resonance motion) and exhibited a particle-type behavior during the entire course of the reaction. The wave packet was found to be very robust, with relatively minor spreading (dephasing), and the ensemble of molecules behaves in harmony and exhibits "single-molecule" motion. Theoretically—by constructing the superposition of wave functions with their appropriate phases—one confirms that the initial wave packet is indeed highly localized (< 0.3 Å) and remains intact for many periods of its motion. The de Broglie wavelength is also consistent with sub-angström localization: $\lambda \approx 0.1$ Å (from $p = 8.1 \times 10^{-18}$ erg sec cm^{-1} at $E = 5300$ cm^{-1}). This motion conforms to the $\Delta x/x$ criterion given above, with a value of about 0.1. Experiments in the condensed phase and in biological systems can be described with the same concepts, and coherent motions have been observed in all phases of matter.

Why is coherence robust? The observation of motion in real systems requires not only the formation of localized wave packets in each and every molecule, but also a small spread in position among wave packets formed in the typically millions to billions of molecules on which the measurement is performed. The key to achieving this condition is generally provided by the well-defined initial equilibrium configuration of the molecules before excitation and by the "instantaneous" femtosecond launching of the wave packet. The spatial confinement (typically about 0.05 Å) of the initial ground state of the system ensures that all molecules, each with its own coherence among the states which form its wave packet, begin their motion in a bond-length range much smaller than that executed by the actual motion (typically 5 – 10 Å). The femtosecond launching ensures that this narrow range of bond length is maintained during the entire process of preparation. The motion of the ensemble is that of a single-molecule trajectory unless molecular and ensemble coherences are destroyed by intra- and/or intermolecular perturbations.

At the 1972 Welch Conference, in a lively exchange between Eugene Wigner and Edward Teller, the uncertainty paradox was debated for picosecond time resolution. But, as has been seen, the uncertainty paradox is not a paradox even for the shorter timescale of femtoscience and certainly not for the dynamics of physical, chemical, and biological changes. Coherence in the femtosecond time regime, the vibrational timescale of a bond, is essential to the formation of localized, nonequilibrium molecular structures which then evolve with time in complete harmony with the uncertainty principle. At such ultrashort time we recover, by the power of coherence, the classical character of the motion in quantum systems.

Coherence was also not appreciated in the realization of the maser. Charles Townes encountered objections because of concern about the uncertainty principle: the claim was that molecules spend about one ten-thousandth of a second in the cavity of a maser and therefore it is impossible for the frequency of the radiation to be narrowly confined. When recognized, coherence of photons in the stimulated emission-feedback process removed this concern (see for example ref. [4]).

As we cross the femtosecond barrier into the attosecond regime we must recall the vital role of coherence, or otherwise the uncertainty in energy (which is now even larger than that of the femtosecond timescale) might again call into question its utility for electron dynamics, as initially transpired in the femtosecond realm.

Exploring for the Future

With the new limits of spatial and temporal resolutions reached, we are currently witnessing several exciting developments in the studies of the dynamics of complex molecular structures and in the number of molecules detected. One of the most significant advances made in recent years is the development of ultrafast methods for electron and X-ray diffraction to capture the entire molecular structure evolving with time. This approach will have a wide range of applications in chemistry and biology, as it opens up new vistas in the direct linkage of structures to functions.

 © WILEY-VCH Verlag GmbH, D-69451 Weinheim, 2001 1433-7851/01/4023-4373 $ 17.50+.50/0

At Caltech we have focused our effort on the development of ultrafast electron diffraction (UED); for recent references see ref. [5] and citations therein. In UED a femtosecond laser pulse is used to initiate a reaction, but unlike other ultrafast spectroscopies the subsequent laser pulses normally used to probe the progress of the reaction are replaced with ultrashort pulses of electrons. Diffraction patterns are then recorded to provide the evolution of the molecular structure in real time.

A number of experimental challenges had to be overcome for these UED studies to be successful. These include: 1) the problem of determining time zero of the reaction, namely the time of overlap between the pump and probe pulses for clocking the change; this is a nontrivial task as the speed of electrons and photons are different and an in situ detection must be made; 2) the problem of low electron flux required to minimize space-charge-induced temporal broadening of electron pulses; and 3) the problem of low scattering and sensitivity caused by the absence of long-range order (usually present in solids) and the low density of molecules in gases.

Over the past decade UED has been advanced[5] to now allow the direct imaging of transient molecular structures in reactions with a sensitivity to chemical change of about 1% or better. Intermediate and product structures can be observed in real time, with spatial and temporal resolutions of approximately 0.01 Å and 1 ps, respectively; electron pulses as short as 500 fs have been obtained. For example, electrocyclic ring opening of a complex cyclic hydrocarbon (with no heavy atoms) was observed directly upon femtosecond excitation.

Similarly, we studied the reactive transition intermediate in the reaction of ethane to ethylene derivatives, the ligand dissociation in iron pentacarbonyl, the valence isomers of aromatic molecules, and nonequilibrium structures with large amounts of vibrational energy. A paradigm case for this development is that of ring-opening processes in isolated aromatic pyridine. With UED we can observe in real time the disappearance of "old" bonds and the appearance of "new" bonds as the molecular structure transforms from being reactant, to intermediate, and then to products (Figure 3). The progress made in this field demonstrates the new limit achieved in detection sensitivity, versatility, and resolution of UED, as well as the potential for its applications. The extension to even more complex systems, both theoretically and experimentally, represents one of our current research efforts in UED.

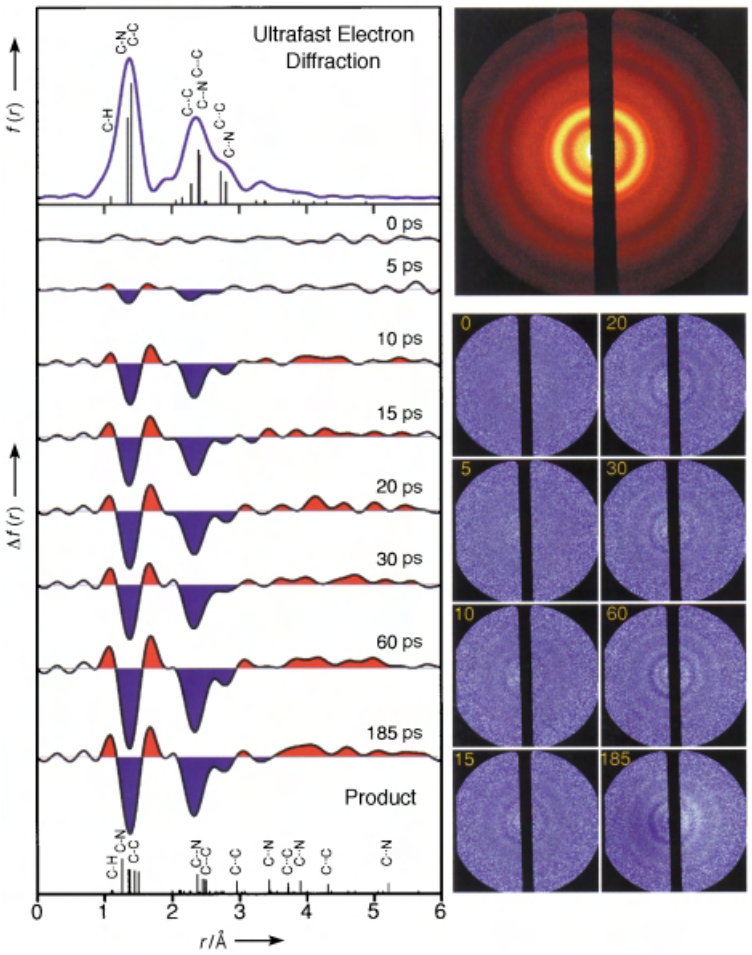


Figure 3. Ultrafast electron diffraction. These experimental images (right) provide the change of the molecular structure studied with time, and shows the evolution during the change. In this case, we directly observe, through the change in the radial distribution function $f(r)$ (left), the depletion of "old" bonds and the making of "new" bonds in the radiationless transition of pyridine molecules during the reaction of ring opening.[6b] Many other systems have been studied similarly using UED.

A second promising area of research is that of complex biological systems, but at the new limits of temporal and spatial resolutions. There have been already important contributions to femtobiology and these include: studies of the elementary steps of vision, photosynthesis, protein dynamics, and electron and proton transport in DNA. In proteins such as those of photosynthetic reaction centers and antennas, hemoglobins, cytochromes, and rhodopsin, a femtosecond event such as bond breaking, twisting, or electron transfer occurs. Global and coherent nuclear motions can be observed in these complex systems.

It is possible that the complexity is not as complicated as we think. For the chemistry and the efficiency to be unique, the system utilizes the organized structure around the "active center" with the necessary restraint on transition states and energy flow. Thus, the early femtosecond events are critical to understanding the function of complex systems as they reflect the important locality in biological dynamics. Our efforts in this direction have so far focused on DNA-twisting dynamics, electron transfer in DNA assemblies, DNA base-pair mimics, and on protein – ligand dynamics. We have recently completed studies on the dynamics of molecular recognition of DNA with drugs, such as anticancer daunomycin (and adriamycin), and of proteins with drugs and vitamins, and observed their elementary steps. For example, the observed charge-separation dynamics of DNA-nucleotides in drug solutions (Figure 4) elucidates the mechanism for the drug's enhanced cytotoxicity with oxygen and with light in experiments with cells—the aim is to provide a molecular basis of clinical observations.

 © WILEY-VCH Verlag GmbH, D-69451 Weinheim, 2001 1433-7851/01/4023-4374 $ 17.50+.50/0

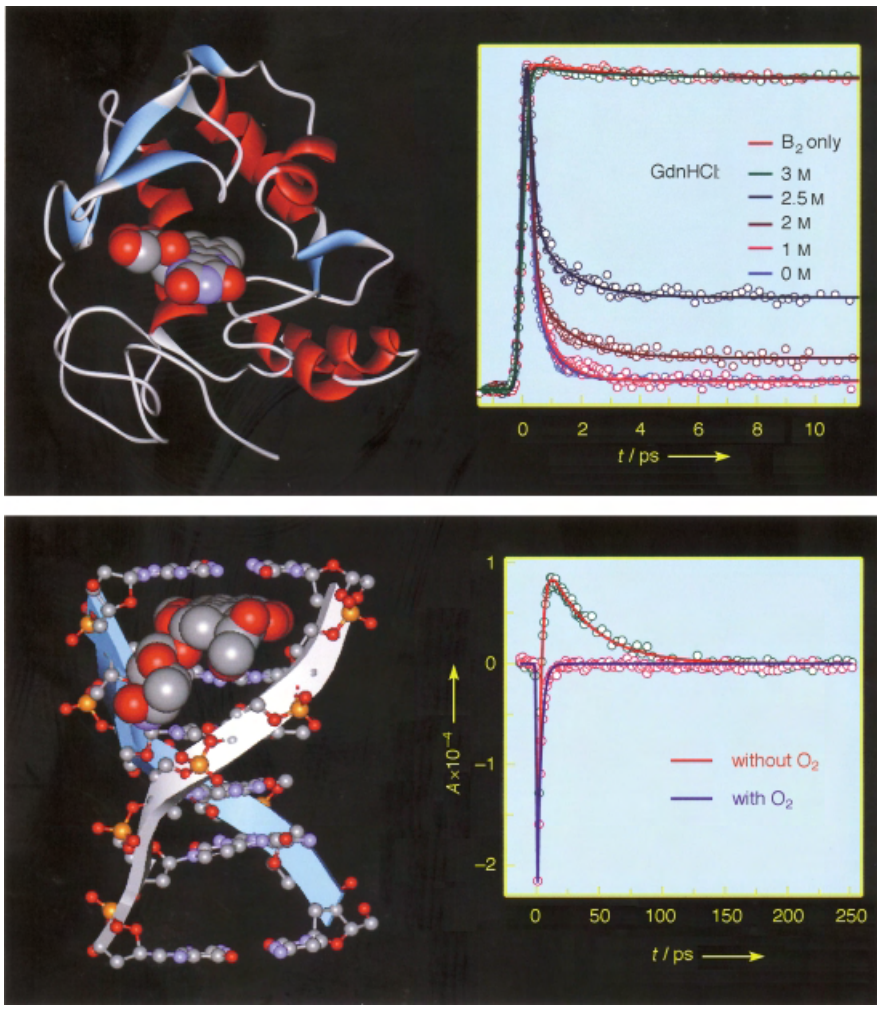


Figure 4. Structures of biological systems studied recently at Caltech: DNA-nucleotide (dGTP) with daunomycin (bottom), and riboflavin (vitamin B_2) with a binding protein (top) in water (buffer) solutions.[6c] The femtosecond transients displayed show the evidence for direct electron transfer and the influence of molecular oxygen. The influence of the denaturant GdnHCL, which unfolds the protein, on the dynamics of charge separation is also shown for the protein system (top).

In the future new extensions are anticipated. The nature and control of enzymatic reactions, the catalytic function of the transition state, and the design of artificial biological functions seem to be areas of great promise for dynamic studies. Also, it is envisaged that the recording of the change of a large biological structure with time and with atomic resolution may be realized. The ultimate goal is the recording of all coordinates in space and time. The impact on problems such as protein folding and molecular recognition is clear.

Finally, we should take advantage of the new limits achieved for applications in research areas such as the following: 1) the control of chemical pathways using prescribed temporal-, phase-, and polarization-specified pulses; 2) the crossing of the barrier to the attosecond regime for studies of electron motion (in 1991 we reported on the proposal of observing such motion in the benzene molecule, and this may be possible in the near future); and 3) extensions of femtochemistry studies to single molecules and at new extremes of pressure and temperature (micro-to-nano-kelvin by laser cooling, or very low temperature using helium clusters) to explore the dynamics outside the ambient conditions of our atmosphere. These are projections based on what we know, but we surely expect uncertainties of the future to bring about unforeseen breakthroughs.

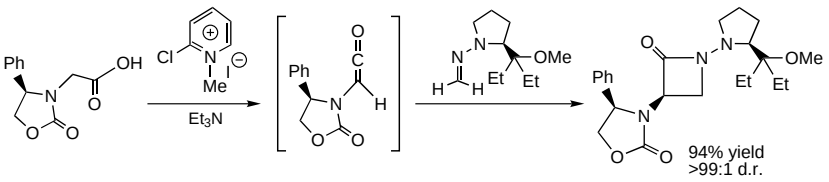
[1] "The Uncertainty Paradox—The fog that was not": A. H. Zewail, *Nature* **2001**, *412*, 279.
[2] F. Hund, *The History of Quantum Theory*, Barnes & Noble, New York, **1974**.
[3] "Femtochemistry: Atomic-Scale Dynamics of the Chemical Bond Using Ultrafast Lasers": A. H. Zewail in *Les Prix Nobel (The Nobel Prizes 1999)*, Almqvist and Wiksell, Stockholm, Sweden, **2000**, pp. 110–203; A. H. Zewail, *Angew. Chem.* **2000**, *112*, 2688–2738; *Angew. Chem. Int. Ed.* **2000**, *39*, 2586–2631.
[4] C. H. Townes, *How the Laser Happened*, Oxford University Press, Oxford, **1999**.
[5] "Direct Imaging of Transient Molecular Structures with Ultrafast Diffraction": H. Ihee, V. Lobastov, U. Gomez, B. Goodson, R. Srinivasan, C. Y. Ruan, A. H. Zewail, *Science* **2001**, *291*, 385.
[6] a) A section of Figure 2 was adapted from ref. [3] and a paper co-authored with J. S. Baskin (J. S. Baskin, A. H. Zewail, *J. Chem. Educ.* **2001**, *78*, 737); b) Figure 3 was adapted from a paper co-authored with V. A. Lobastov, R. Srinivasan, B. M. Goodson, C.-Y. Ruan, and J. S. Feenstra, *J. Phys. Chem. A*, in press; c) Figure 4 was adapted from two papers co-authored with X. Qu, C. Wan, H.-C. Becker, and D. Zhong, *(Proc. Natl. Acad. Sci. USA*, in press); and with D. Zhong (*Proc. Natl. Acad. Sci. USA* **2001**, *98*, 11867). I wish to thank Spencer Baskin, Dongping Zhong, Xiaogong Qu, and Vladimir Lobastov for their help in preparing Figures 2–4.

 © WILEY-VCH Verlag GmbH, D-69451 Weinheim, 2001 1433-7851/01/4023-4375 $ 17.50+.50/0

Recent Progress in the Enantioselective Synthesis of β-Lactams: Development of the First Catalytic Approaches

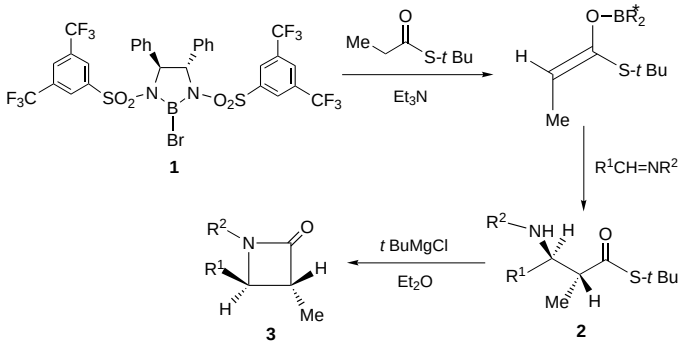
Plato A. Magriotis*

The economic importance of enantiomerically pure compounds[1] and the presence of the azetidin-2-one (β-lactam) ring in several widely used families of antibiotics, such as penicillins, cephalosporins, thienamycins, and monocyclic β-lactams (for example, monobactams),[2] coupled with the recent discoveries that β-lactams can serve as mechanism-based inhibitors of serine proteases[3] and as inhibitors of acyl-CoA cholesterol acyltransferase (ACAT),[4] which is mainly responsible for atherosclerotic coronary heart disease, have stimulated considerable research efforts toward the enantioselective synthesis of β-lactams. Additional impetus for these efforts has been provided by the introduction of the β-lactam synthon methodology, according to which enantiomerically pure β-lactams can be employed as useful intermediates for organic synthesis.[5] Up until recently, the state of the art in this endeavor consisted either of stereocontrolled ketene–imine cycloadditions (Staudinger reaction),[6] which relied on the use of chiral auxiliaries for control, or stereoselective ester enolate–imine condensations (Gilman–Speeter reaction),[7] in which either the ester or the imine component was enantiomerically pure.[8] Interestingly, in a very recent enantioselective example in which both the ketene (Evans–Sjoegren-type ketene)[6b] precursor and the imine (hydrazone in this case)[9b] were enantiomerically pure, the Staudinger reaction proceeded with almost complete diastereoselectivity (Scheme 1).[9a]



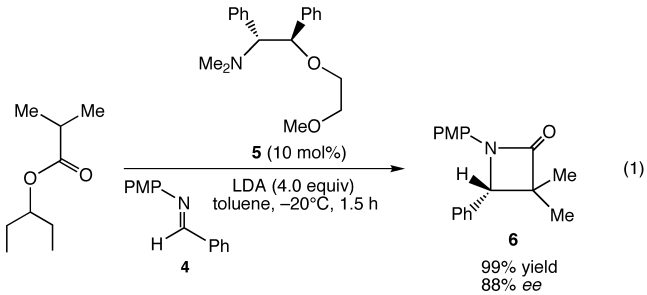
Scheme 1. Matched double diastereoselective Staudinger hydrazone cycloaddition.

The first highly enantio- and diastereoselective example of a Gilman–Speeter-type condensation involving both achiral esters and imines was reported by Corey and co-workers, who employed the chiral nonracemic organoboron Lewis acid **1** (Scheme 2) in yet another application of this useful class of reagents.[10] Treatment of the derived β-amino acid esters **2** with *tert*-butylmagnesium chloride[11] gave rise to 3,4-disubstituted β-lactams **3** (Scheme 2).[12]



Scheme 2. Nonchiral auxiliary-based enantio- and diastereoselective Gilman–Speeter reaction and β-amino ester → β-lactam ring closure.

The first example of a direct catalytic enantioselective synthesis of β-lactams was reported by Tomioka and co-workers who, by capitalizing on previously acquired knowledge on the structure of complexes and mixed aggregates between ester enolates and amide bases,[13] achieved a catalytic asymmetric Gilman–Speeter reaction [Eq. (1); LDA = lithium diisopropylamide, PMP = *p*-methoxyphenyl].[14] Specifically, the reaction of the lithium enolate of



(1)

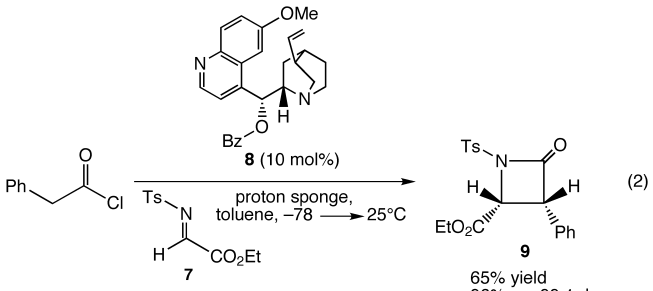
pent-3-yl 2-methylpropanoate with imine **4** in the presence of a catalytic amount of the enantiomerically pure ether ligand **5** resulted in a ternary complex reagent (comprising an achiral

[*] Dr. P. A. Magriotis
Merck & Co. Inc.
126 E. Lincoln Ave., Rahway, NJ 07065 (USA)
Fax: (+1) 732-594-4172
E-mail: pmagriotis@earthlink.net

 © WILEY-VCH Verlag GmbH, D-69451 Weinheim, 2001 1433-7851/01/4023-4377 $ 17.50+.50/0

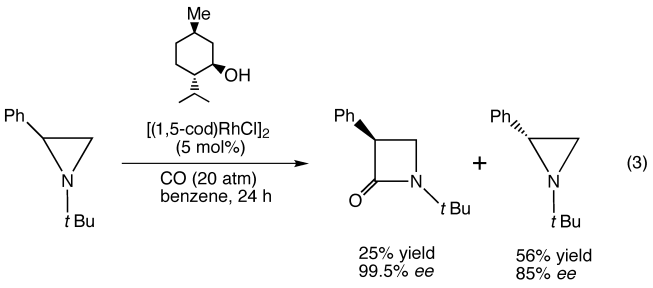
lithium amide (LDA), the ester enolate, and **5**) that afforded β-lactam **6** in high yield and enantiomeric excess (*ee*).[14]

This advance was augmented last year by Lectka and co-workers who first rendered the Staudinger reaction a catalyzed process by making the imine component non-nucleophilic by using **7** [Eq. (2); Bz = benzoyl, Ts = toluene-4-sulfonyl],[15a] and then proceeded to employ a nucleophilic catalyst such as benzoylquinine **8** and obtain *cis*-β-lactam **9** in good yield and with a high *ee* value.[15b]



(2)

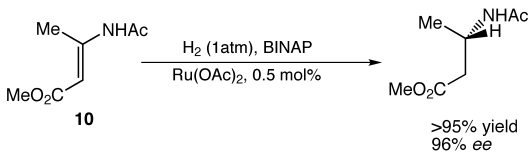
These achievements are significantly more practical and useful than an earlier approach to catalytic asymmetric synthesis of β-lactams, namely a Rh^{I}-catalyzed carbonylation and ring expansion of aziridines [Eq. (3); cod = cyclooctadiene]. This reaction does not result in the creation of a new stereogenic center and is, therefore, merely a kinetic resolution.[15c]



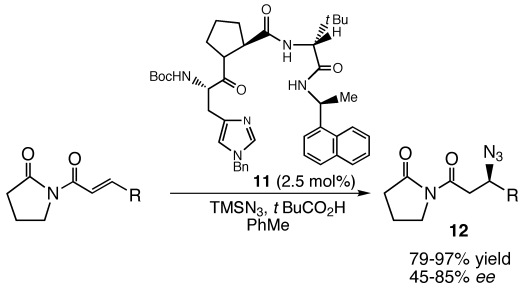
(3)

Since β-amino acids and their derivatives are undoubtedly very important intermediates for the synthesis of β-lactam antibiotics (Scheme 2),[11, 16] much attention has been paid to the preparation of the former compounds in optically active forms.[17]

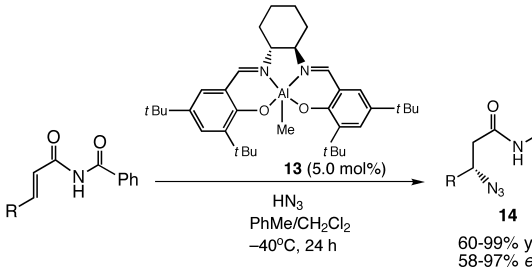
An early approach toward the development of a catalytic enantioselective synthesis of β-amino acids was reported by Noyori and co-workers, who improved upon the original studies of Achiwa and Soga[18a] by demonstrating that BINAP-Ru^{II} metal complexes are excellent catalysts for the enantioselective hydrogenation of β-substituted (*E*)-β-(acetylamino)acrylic acids **10** [Eq. (4); Ac = acetyl, BINAP = 2,2′-bis(diphenylphosphanyl)-1,1′-binaphthyl].[18b] The same objective has been accomplished in three more recent approaches: two asymmetric Michael additions of azide to α,β-unsaturated carbonyl compounds catalyzed by tripeptide **11** and a chiral nonracemic [(salen)Al^{III}] (salen = *N*,*N*′-bis(salicylidene)ethylenediamine anion) complex **13** to provide β-azido amides **12** and **14**, respectively, in excellent yields [Eqs. (5) and (6); Boc = *tert*-butoxycarbonyl, Bn = benzyl, TMS = trimethylsilyl],[18c, 18d] and an enantioselective Mannich-type reaction of



(4)

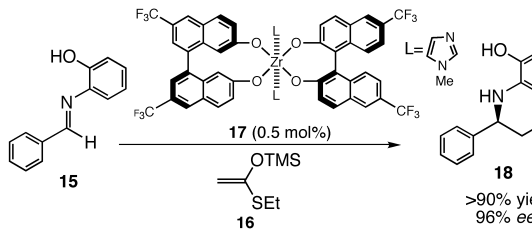


(5)



(6)

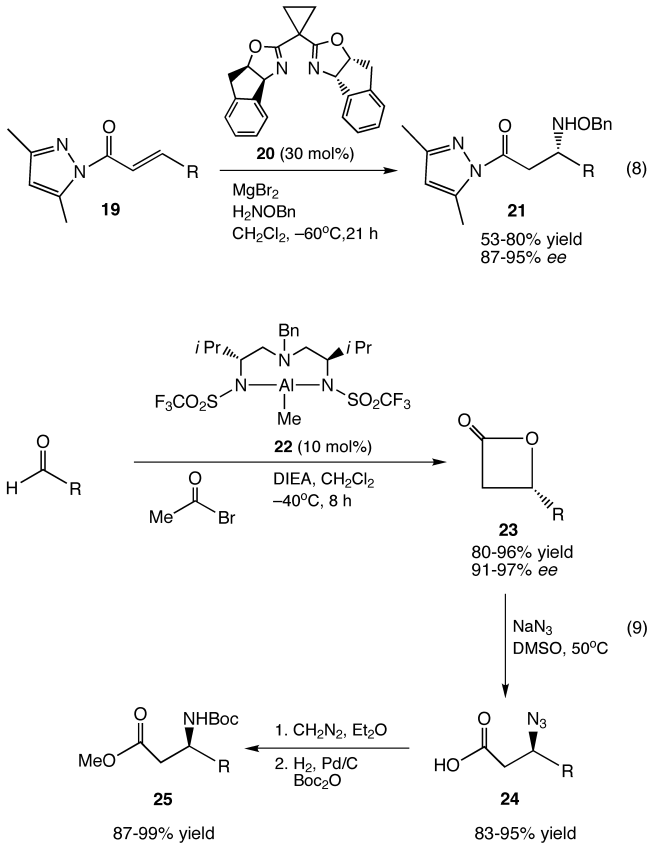
2-aminophenol-derived aldimine **15** with silylketene thioacetal **16** using a novel enantiomerically pure zirconium catalyst **17** to furnish β-amino thioester **18** quantitatively [Eq. (7)].[18e]



(7)

Finally, in related developments, a catalytic asymmetric conjugate addition of *O*-benzylhydroxylamine to unsaturated amides [Eq. (8)] and a catalytic asymmetric acyl halide – aldehyde cyclocondensation [Eq. (9); DIEA = diisopropylethylamine] were reported by the research groups of Sibi and Nelson, respectively, as additional strategies for enantioselective β-amino acid synthesis.[19] Thus, Michael addition of *O*-benzylhydroxylamine to the pyrazole-derived α,β-unsaturated amides **19** in the presence of a chiral nonracemic Lewis acid prepared from $MgBr_2 \cdot OEt_2$ and bisoxazoline **20** yielded β-amino amides **21** of satisfactory enantiomeric purity [Eq. (8)].[19a] On the other hand, ring-opening of the

 © WILEY-VCH Verlag GmbH, D-69451 Weinheim, 2001 1433-7851/01/4023-4378 $ 17.50+.50/0 *Angew. Chem. Int. Ed.* **2001**, *40*, No. 23



β-lactones **23** obtained from the acyl halide-cyclocondensation catalyzed by the Al^{III}-triamine complex **22** gave rise to β-azido acids **24** which were in turn converted into their corresponding *N*-Boc-protected β-amino acid derivatives **25** by using standard procedures [Eq. (9)].[19b]

Upon consideration of the acyl halide – imine **7** and the acyl halide – aldehyde cyclocondensations described in Equations (2) and (9), respectively, it becomes very tempting to speculate on the outcome, as far as the development of a novel catalytic asymmetric synthesis of β-lactams is concerned, of the Staudinger cycloaddition of **7** catalyzed by an enantiomerically pure Lewis acid such as **22** [Eq. (9)] or **1** (Scheme 2) and promoted by an appropriate base for efficient in situ ketene generation.[15b, 19b]

[1] a) S. C. Stinson, *Chem. Eng. News* **2000**, *78*(43), 55; b) S. C. Stinson, *Chem. Eng. News* **1998**, *76*(38), 83; c) S. C. Stinson, *Chem. Eng. News* **1993**, *71*(39), 38; d) S. C. Stinson, *Chem. Eng. News* **1992**, *70*(39), 46.

[2] a) *Chemistry and Biology of β-Lactam Antibiotics*, *Vol. 1–3* (Eds.: R. B. Morin, M. Goldman), Academic Press, New York, **1982**; b) *Antibiotics containing the β-Lactam Structure*, *Parts 1&2* (Eds.: A. L. Demain, N. A. Solomon), Springer, Berlin, **1983**.

[3] a) P. D. Edwards, P. R. Bernstein, *Med. Res. Rev.* ***1994***, *14*, 127; b) O. A. Mascaretti, C. E. Boschetti, G. O. Danelon, E. G. Mata, O. A. Roveri, *Curr. Med. Chem.* **1995**, *1*, 441; c) R. C. Wilmouth, S. Kasamally, N. J. Westwood, R. J. Sheppard, T. D. Claridge, R. T. Alpin, P. A. Wright, G. J. Pritchard, C. J. Schofield, *Biochemistry* **1999**, *38*, 7989.

[4] a) D. A. Burnett, M. A. Caplen, H. R. Davis, Jr., R. E. Burrier, J. W. Clader, *J. Med. Chem.* **1994**, *37*, 1733; b) G. Wu, W. Tornos, *J. Org. Chem.* **1997**, *62*, 6412; c) S. B. Rosenblum, T. Huynh, A. Afonso, H. R. Davis, N. Yumibe, J. W. Clader, D. A. Burnett, *J. Med. Chem.* **1998**, *41*, 973.

[5] a) I. Ojima, F. Delaloge, *Chem. Soc. Rev.* **1997**, *26*, 377; b) I. Ojima, *Acc. Chem. Res.* **1995**, *28*, 383; c) I. Ojima in *The Organic Chemistry of β-Lactams* (Ed.: G. I. Georg), VCH, New York, **1993**, p. 197; d) C. Palomo, J. M. Aizpurua, I. Ganboa, M. Oiarbide, *Pure Appl. Chem.* **2000**, *72*, 1763.

[6] a) H. Staudinger, *Justus Liebigs Ann. Chem.* **1907**, *356*, 51; b) D. A. Evans, E. B. Sjoegren, *Tetrahedron Lett.* **1985**, *27*, 3783; c) G. I. Georg, V. T. Ravikumar in *The Organic Chemistry of β-Lactams* (Ed.: G. I. Georg), VCH, New York, **1993**, p. 295; d) C. Palomo, J. M. Aizpurua, I. Ganboa, M. Oiarbide, *Eur. J. Org. Chem.* **1999**, 3223.

[7] a) H. Gilman, M. Speeter, *J. Am. Chem. Soc.* **1943**, *65*, 2255; b) M. J. Brown, *Heterocycles* **1989**, *29*, 2225; c) D. J. Hart, D.-C. Ha, *Chem. Rev.* **1989**, *89*, 1447; d) M. Benaglia, M. Cinquini, F. Cozzi, *Eur. J. Org. Chem.* **2000**, 563.

[8] a) D. J. Hart, C.-S. Lee, W. H. Pirkle, M. H. Hyon, A. Tsipouras, *J. Am. Chem. Soc.* **1986**, *108*, 6054; b) T. Yamada, H. Suzuki, T. Mukaiyama, *Chem. Lett.* **1987**, 293; c) L. Y. Chen, A. Zaks, S. Chackalamannil, S. Dugar, *J. Org. Chem.* **1996**, *61*, 8341.

[9] a) R. Fernandez, A. Ferrete, J. M. Lassaletta, J. M. Llera, A. Mong, *Angew. Chem.* **2000**, *112*, 3015; *Angew. Chem. Int. Ed.* **2000**, *39*, 2893; b) R. Fernandez, J. M. Lassaletta, *Synlett* **2000**, 1228; for earlier work on double stereodifferentiating Staudinger cycloadditions, see ref. [6d], p. 3227.

[10] E. J. Corey, *Pure Appl. Chem.* **1990**, *113*, 4026.

[11] a) J.-L. Luche, H. B. Kagan, *Bull. Soc. Chim. Fr.* **1971**, 2260; b) T. N. Salzmann, R. W. Ratcliffe, B. G. Cristensen, F. A. Bouffard, *J. Am. Chem. Soc.* **1980**, *102*, 6161.

[12] E. J. Corey, C. P. Decicco, R. C. Newbold, *Tetrahedron Lett.* **1991**, *39*, 5287; for a more recent asymmetric approach to a β-lactam (moderate enantioselectivity) employing a stoichiometric amount of a chiral nonracemic Lewis acid, see F. Zhou, M. R. Detty, R. J. Lachiotte, *Tetrahedron Lett.* **1999**, *40*, 585.

[13] a) D. Seebach, *Angew. Chem.* **1988**, *100*, 1685; *Angew. Chem. Int. Ed. Engl.* **1988**, *27*, 1624; b) Y.-J. Kim, M. P. Bernstein, A. S. Galiano Roth, F. E. Romesberg, P. G. Williard, D. J. Fuller, A. T. Harrison, D. B. Collum, *J. Org. Chem.* **1991**, *56*, 4435; c) P. G. Williard, Q.-Y. Liu, L. Lochmann, *J. Am. Chem. Soc.* **1992**, *114*, 348.

[14] a) K. Tomioka, H. Fujieda, S. Hayashi, M. A. Hussein, T. Kambara, Y. Nomura, M. Kanai, K. Koga, *Chem. Commun.* **1999**, 715; b) T. Kambara, M. A. Hussein, H. Fujieda, A. Iida, K. Tomioka, *Tetrahedron Lett.* **1998**, *39*, 9055; c) H. Fujieda, M. Kanai, T. Kambara, A. Iida, K. Tomioka, *J. Am. Chem. Soc.* **1997**, *119*, 2060.

[15] a) H. Wack, W. J. Drury III, A. E. Taggi, D. Ferraris, T. Lectka, *Org. Lett.* **1999**, *1*, 1985; b) A. E. Taggi, A. M. Hafez, H. Wack, B. Young, W. J. Drury III, T. Lectka, *J. Am. Chem. Soc.* **2000**, *122*, 7831; c) S. Calet, F. Urso, H. Alper, *J. Am. Chem. Soc.* **1989**, *111*, 931.

[16] a) W. B. Wang, E. J. Roskamp, *J. Am. Chem. Soc.* **1993**, *115*, 9417; b) C. Palomo, J. M. Aizpurua, R. Urchegui, M. Iturburu, A. O. de Retana, C. Cuevas, *J. Org. Chem.* **1991**, *56*, 2244; c) N. Miyachi, F. Kanda, M. Shibasaki, *J. Org. Chem.* **1989**, *54*, 5511.

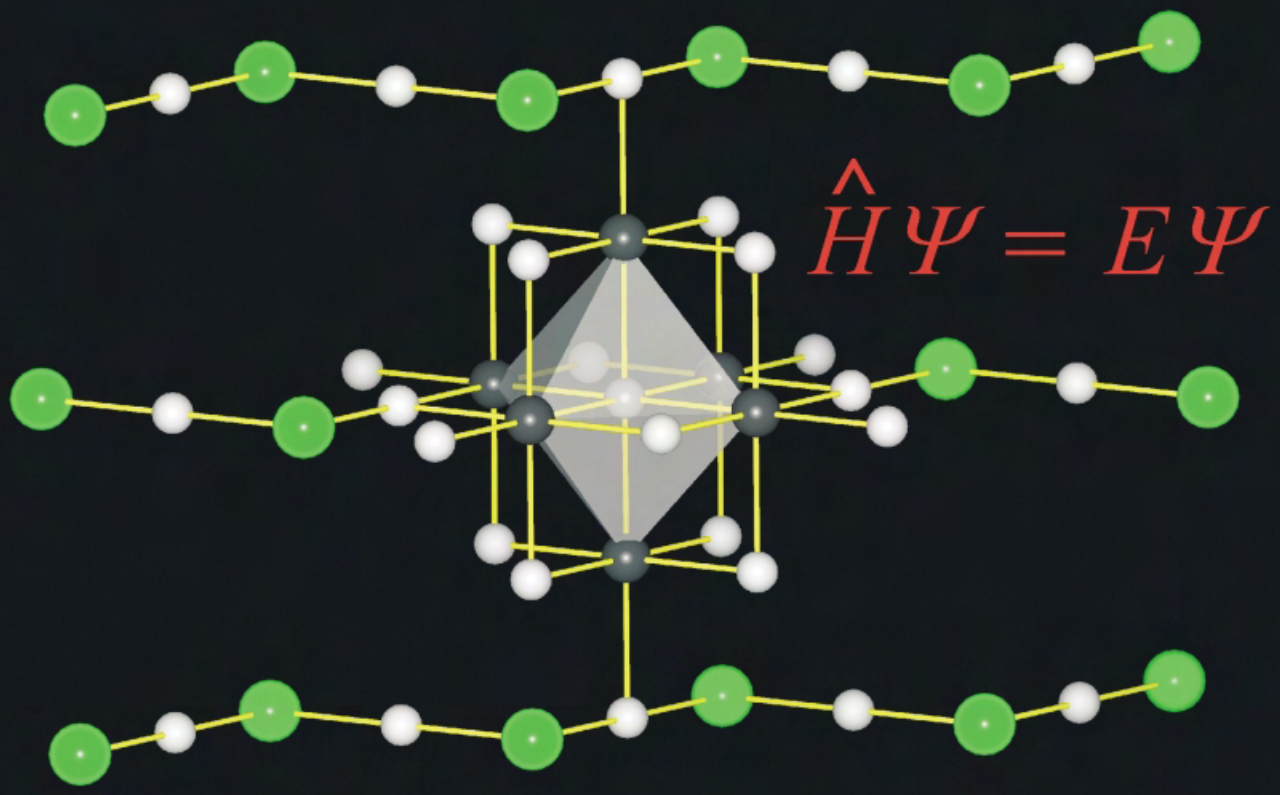
[17] a) E. Juaristi, *Enantioselective Synthesis of β-Amino Acids*, Wiley-VCH, Weinheim, **1997**; b) G. Cardillo, C. Tomasini, *Chem. Soc. Rev.* **1996**, *25*, 117; c) E. Juaristi, D. Quintana, J. Escalante, *Aldrichimica Acta* **1994**, *27*(1), 3; d) D. C. Cole, *Tetrahedron* **1994**, *50*, 9517.

[18] a) K. Achiwa, T. Soga, *Tetrahedron. Lett.* **1978**, *26*, 1119; b) W. D. Lubell, M. Kitamura, R. Noyori, *Tetrahedron: Asymmetry* **1991**, *2*, 543; c) T. E. Horstmann, D. J. Guerin, S. J. Miller, *Angew. Chem.* **2000**, *112*, 3781; *Angew. Chem. Int. Ed.* **2000**, *39*, 3635; d) J. K. Myers, E. N. Jacobsen, *J. Am. Chem. Soc.* **1999**, *121*, 8959; e) H. Ishitani, M. Ueno, S. Kobayashi, *J. Am. Chem. Soc.* **2000**, *122*, 8180; for a very recent and almost identical approach, see S. Xue, S. Yu, Y. Deng, W. D. Wulff, *Angew. Chem.* **2001**, *113*, 2331; *Angew. Chem. Int. Ed.* **2001**, *40*, 2271.

[19] a) M. Sibi, J. J. Shay, M. Liu, C. P. Jasperse, *J. Am. Chem. Soc.* **1998**, *120*, 6615; for a very similar approach, see L. Falborg, K. A. Jorgensen, *J. Chem. Soc. Perkin Trans. 1* **1996**, 2823; b) S. G. Nelson, K. L. Spencer, *Angew. Chem.* **2000**, *112*, 1379; *Angew. Chem. Int. Ed.* **2000**, *39*, 1323; see also S. G. Nelson, T. J. Peelen, Z. Wan, *J. Am. Chem. Soc.* **1999**, *121*, 9742.

 © WILEY-VCH Verlag GmbH, D-69451 Weinheim, 2001 1433-7851/01/4023-4379 $ 17.50+.50/0

Relativistic effects drastically influence solid-state symmetry: copper and silver halides form cubic or hexagonal structures whereas gold halides form chain structures. Calculations with and without relativistic effects (Dirac and Schrödinger equations, respectively) generate the cubic and chain gold halide structures shown here together.



For more information see the following pages.

 © WILEY-VCH Verlag GmbH, D-69451 Weinheim, 2001 1433-7851/01/4023-4381 $ 17.50+.50/0

Towards the Understanding of Solid-State Structures: From Cubic to Chainlike Arrangements in Group 11 Halides**

Tilo Söhnel, Holger Hermann, and Peter Schwerdtfeger*

The prediction of crystal structures for atomic and molecular solids is still very difficult[1] and more or less restricted to ionic compounds with weak covalent bonding character.[2] In contrast to molecular structures which can be rationalized in terms of simple bonding models (VSEPR, hybridization, valence electron rules, ionic/covalent/metallic/Van der Waals bonding etc.), such models do not lead to the successful prediction of crystal structures. This can partly be understood from a many-body expansion of the interaction potential between atoms and molecules, where third- or higher-order effects lead to substantial structural differences in the solid state, especially for the metallic state. Moreover, there are often a number of different modifications (polymorphs) separated by only a few kJ mol^{-1}.

The Group 11 halides are particularly interesting. The low-temperature modifications of the copper halides CuCl (nantokite), CuBr, and CuI (marshite) crystallize in a cubic zinc-blende structure with each copper atom coordinated in a tetrahedral arrangement by four halogen atoms.[3] All the silver halides (except AgI) crystallize in a rock-salt structure (Figure 1A) with silver adopting an octahedral coordination

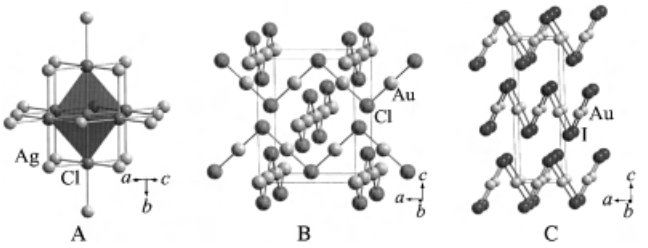


Figure 1. The rock-salt structure of AgCl (A) and the chainlike tetragonal structures of AuCl, chain-I (B), and AuI, chain-P (C).

sphere.[4] AgI crystallizes in three modifications, the cubic zinc-blende structure (γ-AgI, miersite),[5] the hexagonal wurzite structure (β-AgI, iodargyrite),[6] and a cubic high-temperature modification (α-AgI),[7] which incorporates a molten-silver substructure. In all three cases a tetrahedral coordination sphere around silver is found. The gold halides AuX (X = Cl,[8] Br,[9] I[10]), however, are rather unusual in showing chainlike tetragonal structures (Figure 1B, C) of linear AuX_2 units with rather short Au–Au separations attributed to aurophilic interactions.[11]

Relativistic effects are important for Group 11 compounds, especially for gold compounds, and can lead to significant changes in chemical properties.[12] For example, in 1983 Christensen and Kollar pointed out that for CsAu scalar relativistic effects cause a change from a metallic to a semiconducting state with Cs^+Au^- becoming ionic and adopting a rock-salt structure.[13] Geipel and Hess showed that for silver halides in the solid state, relativistic effects cannot be neglected, which leads to a decrease of up to 5.8% in molar volumes and to an increase in cohesive energies by up to 8.9%.[14] On the other hand, Doll et al. pointed out that the rock-salt and chainlike AuCl structures are almost energetically degenerate at the Hartree–Fock level of theory, and that electron correlation effects are mainly responsible for the stabilization of the chainlike structure. From coupled-cluster calculations they conclude that this stabilization originates from excitations out of the Au 5d shells which leads to strong correlation effects between Au–Au pairs.[15] In molecules, strong Au–Au (aurophilic) interactions have been attributed to an interplay of dispersion and relativistic effects.[16]

To investigate the origin of these unusual chainlike structures of gold halides we carried out solid-state calculations for all the Group 11 halides MX (M = Cu, Ag, Au; X = F, Cl, Br, I) by using nonrelativistic and relativistic density functional (DFT) and Hartree–Fock (HF) theory (see Experimental Section).

The calculated sublimation energies MX(s) $\rightarrow$ MX(g) for all known rock-salt, zinc-blende, and wurtzite structures are shown in Figure 2 as a function of the classical dipole–dipole interactions of M^+X^- units. These interactions are obtained from the dipole moments of the free molecules and from the M–X bond lengths in the solid state. In Figure 3 the differences in the sublimation energies versus the dipole moments μ of all the calculated MX (M = Cu, Ag, Au; X = F, Cl, Br, I) structures are shown. A number of important points can be deduced from both figures. The sublimation energy of the cubic and the hexagonal structures correlates nicely with the classical static dipole–dipole interaction, which shows that these solid-state compounds are well described as being of ionic nature (Figure 2). In contrast to the cubic and hexagonal structures the sublimation energies of the chainlike structures do not correlate with the classical dipole–dipole interactions. Clearly, these structures contain large covalent bonding contributions which cannot be neglected.

With the exception of the rock-salt AgF structure (which is known experimentally) both CuF and AuF in zinc-blende and AuF in rock-salt modification show unusually low stabilities compared to that expected from the classical dipole interaction model. In the case of AuF, the very low sublimation energy (ΔE_{sub}) of only 147 kJ mol^{-1} for the rock-salt structure (ΔE_{sub} 140 kJ mol^{-1} for the zinc-blende structure or 182 kJ mol^{-1} for the AuCl chainlike structure; see Figures 2 and 3) is the reason why the disproportionation of AuF(s) into AuF_3(s) and solid gold is assumed to be exothermic.[17] As previously mentioned the relativistic stabilization of solid gold

[*] Prof. Dr. P. Schwerdtfeger, Dr. T. Söhnel, Dr. H. Hermann
Department of Chemistry
University of Auckland
Private Bag 92019, Auckland (New Zealand)
Fax: (64) 9-3737422
E-mail: schwerd@ccu1.auckland.ac.nz

[**] This work was supported by the Alexander von Humboldt Foundation, the Marsden Fund managed by the Royal Society of New Zealand (contract number 96-UOA-PSE-0081), and the Auckland University Research Committee.

 © WILEY-VCH Verlag GmbH, D-69451 Weinheim, 2001 1433-7851/01/4023-4382 $ 17.50+.50/0

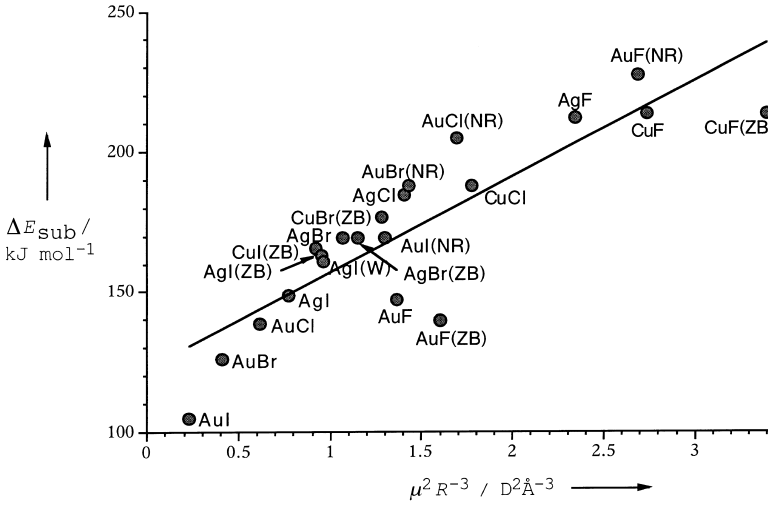


Figure 2. Calculated sublimation energies ΔE_{sub} (zero Kelvin) versus the classical dipole–dipole interactions (ΔE_{sub} [kJ mol^{-1}] $= 35\mu^2 R(MX)^{-3}$(D^2 Å^{-3}) $+ 120$). If not otherwise indicated the rock-salt structure is taken at the relativistic level of theory. ZB: zinc-blende structure, W: wurtzite structure, NR: nonrelativistic structure. Dipole moments μ taken from molecular AuX data (see Experimental Section), M–X bond distances R are from the optimized solid-state geometries.

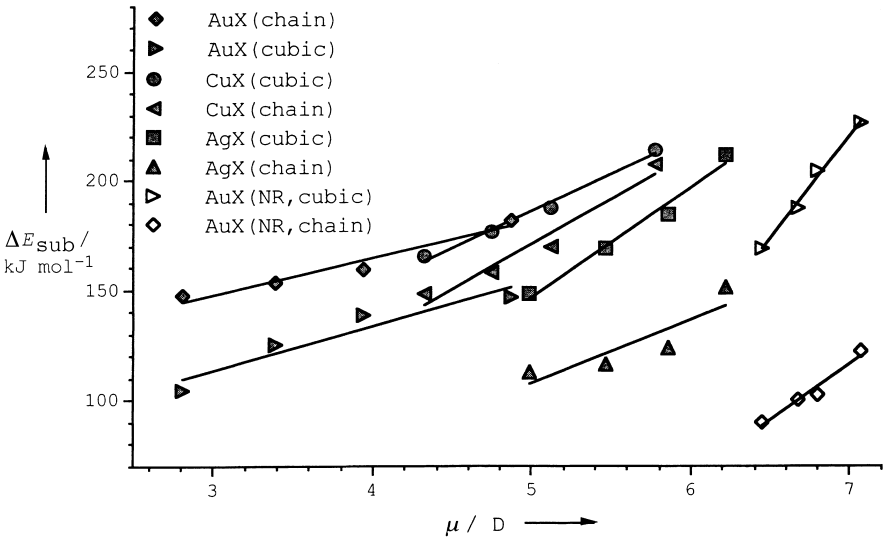


Figure 3. Calculated sublimation energies ΔE_{sub} (zero Kelvin) versus the molecular dipole moment for the cubic and chainlike structures. See Figures 1 and 2 for details.

is partially responsible for this low sublimation energy.[18] Similar arguments may hold for the disproportionation of CuF(s) into CuF_2(s) and solid copper.

The most important conclusion, however, is that all the gold halides AuX in the cubic (rock salt) structure are relativistically destabilized by up to 80 kJ mol^{-1} (more than 30%) compared to the AuX chain structures (Table 1 and Figure 3). This destabilization is a result of the relativistic increase in the gold electronegativity. The molecular AuX compounds are less ionic (reduction of the dipole moment between 2.2 D for AuF and 3.7 D for AuI) and the static dipole–dipole attraction is diminished significantly. In contrast, for the cubic or hexagonal structures at the nonrelativistic level the sublimation energies increase monotonically from copper to silver to gold (Figure 3).

As mentioned before the chainlike structures are the observed stable modifications for the gold halides AuCl, AuBr, and AuI. It is further clear that the energy difference between the cubic and chain modification is far too large to be explained by Au–Au interactions in the chainlike structure only, as the contribution of the aurophilic attraction in the chain is not expected to amount to more than 25–30 kJ mol^{-1}.[16]

The global minima obtained for the different polymorphic forms all agree with the experimental structures obtained at low temperatures, which demonstrates that for such systems the B3LYP functional is capable of producing accurate results. For example, for AuBr the sublimation energy of the rock-salt structure is 125.7 kJ mol^{-1}, for the chain-I structure (Figure 1) 142.5 kJ mol^{-1}, and for the observed chain-P structure 153.9 kJ mol^{-1}. According to the applied model (see Figure 2) the AgI rock-salt structure, which can only be observed experimentally as one of the high-pressure modifications at a pressure of about 0.4 GPa,[19] appears to be less stable than the experimentally observed zinc-blende and wurzite structure types. Similar to experimental findings the zinc-blende and wurzite modifications (with tetrahedral coordination of the silver atoms) are energetically almost degenerate. In contrast to AgI but in agreement with experiment, AgBr is found to be most stable in the rock-salt structure.

Especially striking are the calculated volumes of the unit cells. In all the copper (CuX) and silver (AgX) structures the higher density is found for the experimentally known cubic structures than for the unknown chain structures. In contrast, for the nonrelativistic gold compounds AuX (X = Cl, Br, I) a higher density is found for the chain structures than for the cubic ones. Higher densities are also found for the relativistic chainlike structures, and these are in good agreement with experimental findings, at least for AuCl ($\rho_{exp} = 7.6$ g cm^{-3}) and AuI ($\rho_{exp} = 8.25$ g cm^{-3}).[20] For AuBr ($\rho_{exp} = 8.2$ g cm^{-3}) the densities of the chainlike structures are slightly smaller than for the cubic one. Jansen and Wiegers conclude from differential thermal analysis (DTA) experiments that there may be another modification of AuBr (α-AuBr) at temperatures $T < 85\,^{\circ}$C. From their derived lattice constants it is expected that this structurally unknown modification is related to the chain-I structure.[9]

Table 2 shows Mulliken population analyses for the gold compounds in the solid state and the gas phase. There are two important effects in the solid state caused by relativity in gold compounds. All the AuX compounds show a larger Au(6s) population in the scalar relativistic case than in the nonrelativistic case, this is in agreement with molecular results.[11]

 © WILEY-VCH Verlag GmbH, D-69451 Weinheim, 2001 1433-7851/01/4023-4383 $ 17.50+.50/0

Table 1. Calculated bond distances R [Å], dipole moments μ [D], sublimation energies ΔE_{sub} for AuX(s) $\rightarrow$AuX(g) [kJ mol^{-1}], and bulk densities ρ [g cm^{-3}].[a]

	AuF		AuCl		AuBr		AuI	
molecule	NR	R	NR	R	NR	R	NR	R
R(AuX)	2.162	2.027	2.538	2.354	2.659	2.512	2.816	2.634
μ	7.1	4.9	6.8	3.9	6.7	3.4	6.5	2.8
solid state	NR	R	NR	R	NR	R	NR	R
Cubic								
R(AuX)	2.644	2.601	3.010	2.929	3.143	3.038	3.296	3.232
ΔE_{sub}	227.3	146.9	204.6	138.7	187.7	126.1	173.0	104.8
ρ	9.70	10.20	7.08	7.68	7.41	8.20	7.46	7.97
chainlike								
R(AuX)	2.240	2.136	2.517	2.427	2.672	2.563	2.811	2.707
R(AuAu)	2.997	2.994	3.227	3.226	3.067	3.044	3.077	3.076
	3.154	3.151	3.371	3.370				
ΔE_{sub}	122.6	182.1	102.9	159.4	100.4	153.9	90.2	147.9
ρ	9.01	9.03	7.81	7.81	8.05	8.17	8.27	8.28

[a] For AuF and AuCl the chain-I structure and for AuBr and AuI the chain-P structure were taken (see Figure 1). For AuBr we have ρ = 8.19 g cm^{-3} for the chain-I structure; NR = nonrelativistic, R = relativistic.

Table 2. Mulliken gross atomic charges q and orbital populations n from B3LYP calculations.[a]

	AuF		AuCl		AuBr		AuI	
molecule	NR	R	NR	R	NR	R	NR	R
q	0.70	0.52	0.55	0.33	0.51	0.28	0.42	0.18
n(5d)	10.0	9.87	10.0	9.95	10.0	9.98	10.0	10.0
n(6s)	0.26	0.56	0.37	0.67	0.41	0.69	0.49	0.80
n(6p)	0.04	0.05	0.05	0.05	0.05	0.05	0.05	0.05
solid state	NR	R	NR	R	NR	R	NR	R
Cubic								
q	0.74	0.51	0.64	0.42	0.56	0.32	0.47	0.27
n(5d)	9.99	9.99	10.0	10.0	10.0	10.0	10.0	10.0
n(6s)	0.23	0.46	0.31	0.53	0.38	0.63	0.46	0.68
n(6p)	0.03	0.04	0.04	0.05	0.05	0.06	0.06	0.06
chainlike								
q	0.55	0.40	0.29	0.10	0.19	0.02	0.05	−0.10
n(5d)	9.90	9.76	10.0	9.93	10.0	9.93	10.0	9.97
n(6s)	0.46	0.73	0.61	0.86	0.70	0.94	0.80	1.01
n(6p)	0.08	0.10	0.09	0.11	0.10	0.12	0.11	0.12

[a] For AuF and AuCl the chain-I structure and for AuBr and AuI the chain-P structure were taken (see Figure 1); NR = nonrelativistic, R = relativistic.

This result leads to smaller Au atomic charges in the relativistic than in the nonrelativistic calculations. Because of the decreasing electronegativity from F to I the atomic charge of Au decreases in both the relativistic and nonrelativistic case from F to I. The relativistic and nonrelativistic calculations show a larger 6s, a larger 6p, and a smaller 5d population in the chainlike structures than in the cubic structures. This result suggests that the larger 6s/6p populations enhance the Au−Au interactions in the chains. However, the Au−Au distances in the chainlike structures do not decrease significantly from the nonrelativistic to the relativistic cases contrary to what one expects from strong aurophilic interactions. Another important point is that the 5d and 6p participation in the Au−X bond is increased in the chainlike structures compared to the cubic arrangements which indicates an increased covalency in the Au−X bond.

To examine electron correlation effects we carried out HF calculations for AuCl, AuBr, and AuI. Similar to the findings for AuCl, by Doll et al. the cubic and chainlike structures for all the AuX compounds are almost degenerate at the relativistic HF level of theory (in contrast to the nonrelativistic level): (nonrelativistic HF values are given in parentheses) $\Delta E = E_{sub}(\text{cubic}) - E_{sub}(\text{chain}) = 6.4$ (112.7) kJ mol^{-1} for AuCl, −2.9 (97.8) kJ mol^{-1} for AuBr, −11.6 (93.6) kJ mol^{-1} for AuI.

In summary, we conclude that the unusual chainlike structures found for the gold halides AuCl, AuBr, and AuI can alternatively be explained by relativistic effects (as opposed to correlation effects) leading to an increased covalency in the Au−X interactions.

Experimental Section

All solid-state and molecular calculations were carried out with CRYSTAL98.[21] We used scalar relativistic energy consistent small-core Stuttgart pseudopotentials within the density functional theory (DFT, B3LYP-functional) and Hartree–Fock (HF) formalism to estimate electron correlation effects. In addition we carried out nonrelativistic calculations at the DFT and the HF level of theory for the AuX compounds. At the B3LYP level for the Group 11 metals (Cu, Ag, Au) 5s5p5d uncontracted valence basis sets were fitted while for the halogens (Cl, Br, I) 4s4p valence basis sets were developed. For fluorine we optimized a (7s6p) all-electron basis set at the B3LYP level of theory. The geometries of all the structures were optimized with the program code LoptCG developed by Zicovich-Wilson.[22] CuF and AuF are unknown in the solid state and for both compounds the corresponding structure of the chloride was used as a starting point in the geometry optimizations. The dipole moments of the diatomics were taken from ref. [23] when known, otherwise they were calculated at the coupled-cluster (CCSD(T)) level of theory.

Received: July 24, 2001 [Z17582]

[1] a) J. Maddox, *Nature* **1988**, *335*, 201; b) J. C. Schön, M. Jansen, *Angew. Chem.* **1996**, *108*, 1358–1377; *Angew. Chem. Int. Ed. Engl.* **1996**, *35*, 1286–1304; c) "Crystal Engineering: From Molecules and Crystals to Materials": A. Gavezzotti, *NATO Sci. Ser. Ser. C* **1999**, *538*, 129–142; d) A. Gavezzotti, *Acc. Chem. Res.* **1994**, *27*, 309–314.

[2] A. Grohmann, H. Schmidbaur in *Comprehensive Organometallic Chemistry II*, *Vol. 3* (Eds.: E. W. Abel, F. G. A. Stone, G. Wilkinson), Pergamon, Oxford, **1995**, pp. 1–56.

[3] S. Hull, D. A. Keen, *Phys. Rev. B* **1994**, *50*, 5868–5885.

[4] a) G. L. Bottger, A. L. Greddes, *J. Chem. Phys.* **1972**, *56*, 3735–3739; b) G. S. Nunes, P. B. Allen, J. L. Martins, *Phys. Rev. B* **1998**, *57*, 5098–5105; c) S. Hull, D. A. Keen, *Phys. Rev. B* **1999**, *59*, 750–761.

[5] L. H. Adams, B. L. Davis, *Proc. Natl. Acad. Sci. USA* **1962**, *48*, 983–990.

[6] a) G. Burley, *J. Chem. Phys.* **1963**, *38*, 2807–2812; b) R. J. Cava, F. Reidinger B. J. Wünsch, *Solid State Commun.* **1977**, *24*, 411–416; c) A. Yoshiasa, K. Koto, F. Kanamura, S. Emura, H. Horiuchi, *Acta Crystallogr. Sect. B* **1987**, *43*, 434–440; d) R. O. Piltz, Z. Barnea, *J. Appl. Crystallogr.* **1987**, *20*, 3–7.

[7] a) A. F. Wright, B. E. F. Fender, *J. Phys. C* **1977**, *10*, 2261–2267; b) S. Hoshino, T. Sakuma, Y. Fujii, *Solid State Commun.* **1977**, *22*, 763–765; c) M. J. Cooper, M. Sakata, *Acta Crystallogr. Sect. A* **1979**, *35*, 989–991.

[8] a) E. M. W. Janssen, J. C. W. Folmer, G. A. Wiegers, *J. Less-Common Met.* **1974**, *38*, 71–76; b) J. Strähle, K. P. Lörcher, *Z. Naturforsch. B* **1974**, *29*, 266–267.

[9] a) E. M. W. Janssen, G. A. Wiegers, *J. Less-Common Met.* **1978**, *57*, 47–57; b) E. M. W. Janssen, G. A. Wiegers, *J. Less-Common Met.* **1978**, *57*, 58–67.

[10] H. Jagodzinski, *Z. Kristallogr.* **1959**, *112*, 80–87.

 © WILEY-VCH Verlag GmbH, D-69451 Weinheim, 2001 1433-7851/01/4023-4384 $ 17.50+.50/0

[11] a) P. Pyykkö, *Chem. Rev.* **1997**, *97*, 597 – 636; b) H. Schmidbaur, *Chem. Soc. Rev.* **1995**, 394 – 400.
[12] a) P. Pyykkö, *Chem. Rev.* **1988**, *88*, 563 – 594; b) P. Schwerdtfeger, M. Dolg, W. H. E. Schwarz, G. A. Bowmaker, P. D. W. Boyd, *J. Chem. Phys.* **1989**, *91*, 1762 – 1774.
[13] N. E. Christensen, J. Kollar, *Solid State Commun.* **1983**, *46*, 727 – 730.
[14] N. J. M. Geibel, B. A. Hess, *Chem. Phys. Lett.* **1997**, *273*, 62 – 70.
[15] K. Doll, P. Pyykkö, H. Stoll, *J. Chem. Phys.* **1998**, *109*, 2339 – 2345.
[16] a) P. Pyykkö, N. Runeberg, F. Mendizabal, *Chem. Eur. J.* **1997**, *3*, 1451 – 1457; b) P. Pyykkö, N. Runeberg, F. Mendizabal, *Chem. Eur. J.* **1997**, *3*, 1458 – 1465; c) P. Pyykkö, F. Mendizabal, *Inorg. Chem.* **1998**, *37*, 3018 – 3025; d) P. Pyykkö, T. Tamm, *Organometallics* **1998**, *17*, 4842 – 4852.
[17] W. E. Dasert in *Nonexistent Compounds*, Marcel Dekker, New York, **1965**, pp. 21 – 22.
[18] P. Schwerdtfeger, J. S. McFeaters, M. J. Liddell, J. Hrusak, H. Schwarz, *J. Chem. Phys.* **1995**, *103*, 245 – 252.
[19] G. S. Nunes, P. B. Allen, J. L. Martins, *Phys. Rev. B* **1998**, *57*, 5098 – 5105; S. Hull, D. A. Keen, *Phys. Rev. B* **1999**, *59*, 750 – 761.
[20] R. J. Puddephatt, *The Chemistry of Gold*, Elsevier, Amsterdam, **1978**.
[21] V. R. Saunders, R. Dovesi, C. Roetti, M. Causà, N. H. Harrison, R. Orlando, C. M. Zicovich-Wilson, *Program CRYSTAL98*, University of Torino, Turin (Italy), **1998**.
[22] C. M. Zicovich-Wilson, *Program LoptCG*, Instituto de Technologia Quimica U.P.V.-C.S.I.C., Valencia, Spain, **1998**.
[23] K. P. Huber, G. Herzberg, *Molecular Spectra and Molecular Structure, Constants of Diatomic Molecules*, Van Nostrand, New York, **1979**.

A Metallosupramolecular Capsule with the Topology of the Tetrahedron, 3^3, Assembled from Four Guanidine-Based Ligands and Twelve Cadmium Centers**

Iris M. Müller, Richard Robson,* and Francis Separovic

Coordination chemistry offers scope for the construction by self-assembly of a seemingly limitless range of structures,[1] including cagelike metallosupramolecular species related to polyhedra.[2] We report here a coordinative enclosure with the topology of the tetrahedron in which the four 3-connecting nodes are provided by extensive, approximately flat ligands, each affording three tridentate metal-binding sites, and the six node-to-node connections are provided by pairs of metal centers; the arrangement is represented schematically in Figure 1.

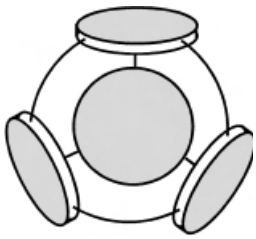
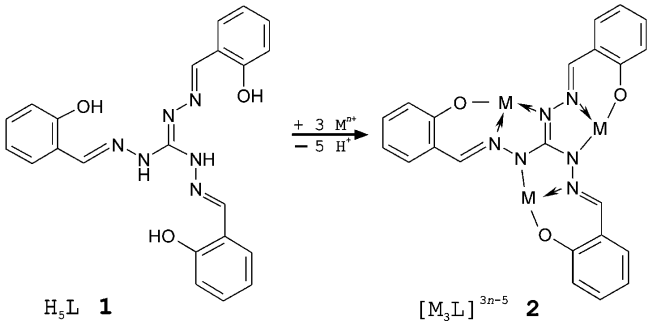


Figure 1. Schematic representation of the cage showing the four almost flat ligands as discs, the central one being at the back. A threefold axis passes throught the center of each disc.

Ligand H_5L (**1**; Scheme 1) is very easy to make and is just one member of a potentially extensive family of Schiff base derivatives of the readily available triaminoguanidine. It has been reported previously that in the presence of appropriate metal cations the central CN_3H_2 core of **1** is readily deprotonated (even by a base as weak as NH_3) to generate a carbonate-like dianionic moiety capable of simultaneously chelating three metal centers in close proximity as in **2** (Scheme 1).[3]

Reaction of the guanidinium chloride salt related to **1**, $[H_6L]Cl$, with cadmium chloride in DMF in the presence of



Scheme 1.

Et_4NOH gives bright yellow rhombic dodecahedral crystals of $(Et_4N)_8[(CdCl)_3L]_4 \cdot 4DMF$ (**3**) in very high yield: the structure was determined by single-crystal X-ray diffraction.[4] Figure 2 shows the immediate environment of one of four symmetry-equivalent ligand units. Four $[L(CdCl)_3]^{2-}$ units are linked by four-membered (-Cd-O-)$_2$ rings to form a cage with the topology of a tetrahedron (Figure 3). All twelve cadmium

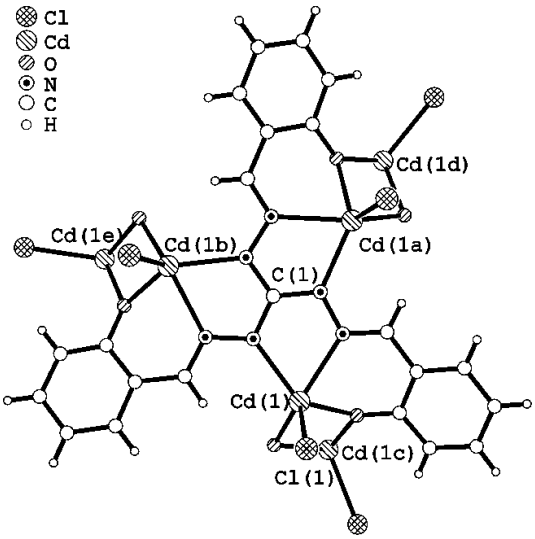


Figure 2. The immediate environment of each of the ligands.

[*] Dr. R. Robson, Dr. F. Separovic
School of Chemistry
University of Melbourne
Parkville, Victoria 3052 (Australia)
Fax: (+61) 3-9347-5180
E-mail: r.robson@chemistry.unimelb.edu.au
Dr. I. M. Müller
Lehrstuhl für Analytische Chemie
NC 4/27, Ruhr-Universität Bochum
44780 Bochum (Germany)
Fax: (+49) 234-321-4420

[**] This work was supported by the "Deutsche Forschungsgemeinschaft" DFG and the Australian Research Council. The authors thank Dr. B. F. Abrahams for help with the X-ray crystallography.

 © WILEY-VCH Verlag GmbH, D-69451 Weinheim, 2001 1433-7851/01/4023-4385 $ 17.50+.50/0

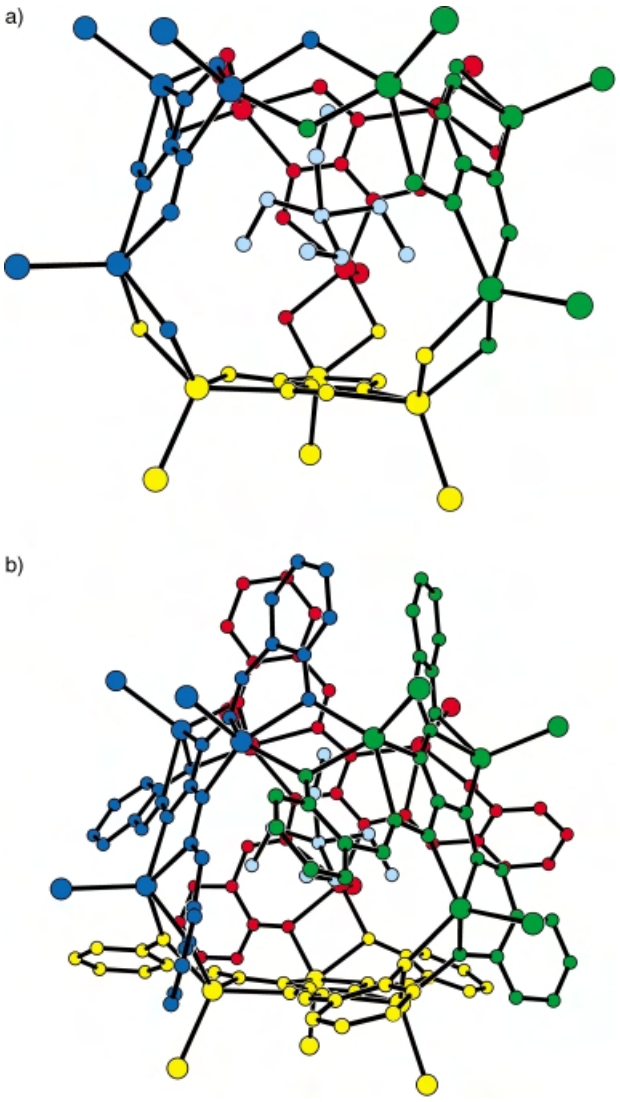


Figure 3. a) Representation of the way in which the four $[(CdCl)_3L]$ units are connected together. For simplicity only the central CN_6 core of each ligand and its three bridging phenoxy oxygen atoms are shown. The entrapped Et_4N^+ ion is also indicated (pale blue). b) View from the same angle as in (a) showing all non-hydrogen atoms in $[\{(CdCl)_3L\}_4 \cdot Et_4N]^{7-}$.

centers are equivalent and are five-coordinate; a chloro ligand is attached to each Cd center on the outside of the cage (Figure 2 and 3). The cage is an octaanion and one of the eight Et_4N^+ countercations is securely locked inside the enclosure; the other seven cations together with the DMF molecules of solvation occupy the spaces in the crystal between the cages in a disordered manner. Individual cages are chiral but the crystal as a whole is racemic.

The solid-state ^{13}C MAS NMR spectrum shows all the features expected for the ligand components, the DMF molecules of solvation, and the Et_4N^+ ions, both trapped and "external". The encaged cations show a methylene signal at $\delta = 59.3$ and a methyl signal at $\delta = 12.5$, whilst the corresponding signals for the "external" cations are at $\delta =$ 53.6 and 9.1, respectively; comparison of CP with single pulse ^{13}C MAS experiments using long recycle times confirmed these assignments. The compound unfortunately has very limited solubility in all solvents tested. However it is sufficiently soluble in $[D_6]$DMSO at 100 °C to afford a ^1H NMR spectrum which reveals that, even under these relatively fierce conditions where it might be suspected that any minimal dissolution might be the result of decomposition, the cage remains intact with its trapped Et_4N^+ ion ($\delta = 0.72$, CH_3) clearly differentiated from the "external" Et_4N^+ ion ($\delta = 1.13$, CH_3); the relative intensities are in the expected 1:7 proportions. The cage would appear to be a very stable entity. As can be seen in Figure 3b salicylaldehyde-derived C_6 rings from three separate ligands make close contact over each face of the imaginary tetrahedron with vertices located at the central guanidine carbon atoms of the four ligands, effectively sealing off the enclosure; the Et_4N^+ prisoner is thereby very securely incarcerated. Analogous products can be isolated with chloride replaced by bromide and with Me_4N^+ encapsulated rather than Et_4N^+.

Experimental Section

$[(C_2H_5)_4N]_8[\{(CdCl)_3(C_{22}H_{15}N_6O_3)\}_4] \cdot 4\,DMF$ (**3**): A solution of tris(2-hydroxybenzylidine)triaminoguanidinium chloride[3] $[H_6L]Cl$ (23.1 mg, 0.051 mmol) in DMF (2 mL) was added to a solution of $CdCl_2 \cdot 2H_2O$ (35.3 mg, 0.161 mmol) in DMF (2 mL). An aqueous solution of Et_4NOH (40 %, 1 mL) was carefully underlayered. Brilliant yellow crystals of **3** were formed over a period of three days. Yield: 56.4 mg (0.012 mmol, 93 %). Elemental analyses (%): calcd: C 37.18, H 5.86, N 9.52, Cd 25.46, Cl 8.03; found: C 37.50, H 5.01, N 9.56, Cd 25.45, Cl 7.78. Solid-state MAS NMR: in addition to signals arising from the ligands (all twelve salicylaldehyde units being equivalent as indicated by the crystallography) at $\delta = 168.0$ (plus shoulder), 147.5, 133.3, 131.7, 125.7, 123.6, 117.7, there are signals arising from DMF at $\delta = 164.0$, 38.6, and 33.6 and signals arising from the trapped Et_4N^+ ion at $\delta = 59.3$ and 12.5 and from "external" Et_4N^+ ions at $\delta = 53.6$ and 9.1.

Crystal structure analysis: Crystals of **3** were small and weakly diffracting. Intensity data were collected on an Enraf-Nonius CAD4 diffractometer employing the ω-2θ scan method, the data were corrected for Lorentz and polarization effects. The structure of **3** was solved by using direct methods (SHELXS-97)[5] and refined by using a full-matrix least-squares refinement procedure (SHELXL-97).[6] Aromatic protons of the ligand were placed at geometrically estimated positions. The atoms of the cage and its trapped Et_4N^+ ion were well defined but the solvent and cations occupying the regions between the cages displayed a high degree of disorder, despite which it was possible to model some of them. Crystallographic data (excluding structure factors) for the structures reported in this paper have been deposited with the Cambridge Crystallographic Data Centre as supplementary publication no. CCDC-165718. Copies of the data can be obtained free of charge on application to CCDC, 12 Union Road, Cambridge CB21EZ, UK (fax: (+44)1223-336-033; e-mail: deposit@ccdc.cam.ac.uk).

Received: June 25, 2001 [Z17351]

[1] G. F. Swiegers, T. J. Malefetse, *Chem. Rev.* **2000**, *100*, 3483.
[2] S. Leininger, B. Olenyuk, P. J. Stang, *Chem. Rev.* **2000**, *100*, 853.
[3] I. M. Müller, R. Robson, *Angew. Chem.* **2000**, *112*, 4527; *Angew. Chem. Int. Ed.* **2000**, *39*, 4357.
[4] Crystal dimensions $0.40 \times 0.37 \times 0.21$ mm^3, cubic, space group $Pn\bar{3}$, $a =$ 21.257(3) Å, $V = 9605(2)$ Å^3, $\rho_{calcd} = 1.532$ g cm^{-3}, $2\theta_{max} = 50°$, $\lambda =$ 0.71073 Å, $T = 130$ K, 1867 measured reflections, 1598 independent reflections ($R_{int} = 0.0355$), numerical absorption correction, $\mu =$ 1.532 mm^{-1}, min./max. transmission factors 0.588/0.653, 128 parameters, $R_1 = 0.0607$, $wR2 = 0.1722$, max. residual electron density 0.609 e Å^{-3}.
[5] G. M. Sheldrick, SHELXS-97, Program for Crystal Structure Solution, Universität Göttingen, **1997**.
[6] G. M. Sheldrick, SHELXL-97, Program for Crystal Structure Refinement, Universität Göttingen, **1997**.

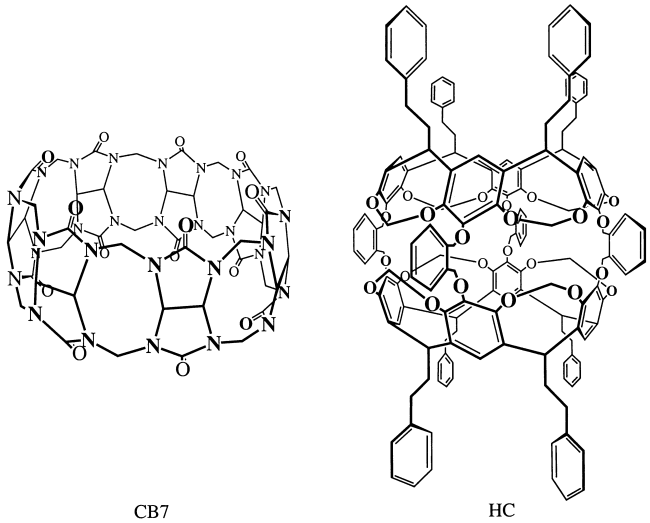
 © WILEY-VCH Verlag GmbH, D-69451 Weinheim, 2001 1433-7851/01/4023-4386 $ 17.50+.50/0

Polarizabilities Inside Molecular Containers**

Cesar Marquez and Werner M. Nau*

In memory of D. J. Cram

Molecular containers or related supramolecular hosts which are sufficiently large to enclose smaller guest molecules are well known to provide a partial or complete protection of the guest from the outside environment. A striking example is the storage of cyclobutadiene in a hemicarcerand (HC), which prevents bimolecular reactions of otherwise transient species.[1] Cram et al. have further suggested that the inside of a HC can be considered as a new phase of matter.[1, 2] This suggestion implies effects beyond mere spatial confinement and chemical isolation, for example, a marked change in the physical bulk properties, such as the polarity or polarizability, of the host cavity. An indication of such a change was obtained by Pina et al., who observed an unusual shift in the phosphorescence maximum of biacetyl when included in a hemicarcerand.[3] We have now examined 2,3-diazabicyclo-[2.2.2]oct-2-ene (DBO) in its complex with cucurbit[7]uril (CB7) and found an unprecedented effect on the UV absorption and fluorescence properties. We can rationalize these unusual observations, ours for CB7 and those of Pina et al. for HC, and provide evidence that the peculiar spectroscopic behavior of the guest molecules results from an extreme polarizability inside these molecular containers that lies close to the gas phase for CB7 and beyond diiodomethane for HC. This evidence supports the view of a new supramolecular phase of matter.



Addition of DBO to an aqueous solution of the molecular container compound CB7—the synthesis of which has been recently reported[4]—results in the immediate formation of a 1:1 inclusion complex, as evidenced by an additional set of NMR signals. The protons of the guest, which show resonances at $\delta = 1.18$ (*syn*-H), 1.63 (*anti*-H), and 5.08 (bridgehead-H) in D_2O, undergo characteristic[5] up-field shifts by 0.77, 0.79, and 0.40 ppm, respectively, upon complexation. UV spectrophotometric and steady-state fluorescence titrations provide a very large binding constant of $(4 \pm 1) \times 10^5\,\text{M}^{-1}$ for this complex, which indicates that there is essentially a perfect fit of the nearly spherical guest in the rigid hollow cavity of the pumpkin-shaped host. The goodness of fit is corroborated by molecular dynamics calculations, which suggest that not even a water molecule can be co-included together with DBO. The cavity of CB7 is thus completely filled by DBO without leaving a larger "empty" space.

Bulk properties such as polarity and polarizability are commonly studied by means of solvatochromic shifts on electronic spectra, such as, effects on absorption, fluorescence, or phosphorescence.[6, 7] The structural variations among the solvents means that a large data set is usually required to expose the underlying relationships of an experimental parameter with the solvent polarity, polarizability, or both. We have used this sensitive and well-accepted method to further characterize the chemical environment of the CB7 cavity sensed by the immersed DBO chromophore. Our solvatochromic studies[8] in the gas phase and in ten solvents reveal that the absorption and fluorescence maximum, the extinction coefficient ε, and the oscillator strength f (the integrated absorption intensity) all depend on the bulk polarizability P of the solvent (Table 1 and Figure 1a). The bulk polarizability is related to the refractive index n of the solvent by the relationship $P = (n^2 - 1)/(n^2+2)$, such that a relationship with n applies as well. A relationship with the solvent polarity is not observed. The dependence of the oscillator strength on the solvent is most pronounced, since it varies systematically over one order of magnitude. For example, perfluorohexane and water are prototypal nonpolar and polar solvents (dielectric constants of 1.57 and 80.2, respectively, at 293 K) but the experimental oscillator strength is nearly the same, as expected from their similar polarizability. Perfluorohexane and carbon disulfide, however, are both nonpolar, but are known for their very low and high polarizability, respectively. Accordingly, these two solvents claim extreme positions in the solvent series, that is, they produce the weakest and strongest oscillator strengths for this absorption. With respect to hydrocarbon solvents, the difference between *n*-hexane and benzene is also in line with the large polarizability of aromatic solvents. It should be noted that a similar correlation with the polarizability is also recognizable for the other solvatochromic parameters: the absorption and fluorescence maximum, and the extinction

[*] Prof. Dr. W. M. Nau, Dipl.-Chem. C. Marquez
Departement Chemie der Universität
Klingelbergstrasse 80, 4056 Basel (Switzerland)
Fax: (+41) 61-267-3855
E-mail: Werner.Nau@unibas.ch

[**] This work was supported by the Swiss National Science Foundation (projects 620-58000.99 and 4047-057552) within the program NFP47 "Supramolecular Functional Materials".

 © WILEY-VCH Verlag GmbH, D-69451 Weinheim, 2001 1433-7851/01/4023-4387 $ 17.50+.50/0

Table 1. Photophysical properties of DBO in different environments.

Environment	P[a]	Absorption			Fluorescence
		λ_{max} [nm]	ε_{max} [$M^{-1}cm^{-1}$]	$f/10^{-4}$[b]	λ_{max} [nm]
gas phase	0.000	374.3	56[c]	3.10[c]	444
CB7[d]	(0.12)[e]	374.0	40	4.87	440
perfluorohexane	0.159	376.3	105	6.79	442
water	0.206	364.4	53	7.30	431
acetonitrile	0.212	378.0	117	8.96	430
n-hexane	0.229	377.9	177	9.38	438
isopropanol	0.231	374.7	101	9.89	431
dichloromethane	0.255	377.4	126	10.33	432
chloroform	0.267	376.6	129	11.11	432
carbon tetrachloride	0.274	376.6	280	18.81	427
benzene	0.295	378.8	274	15.82	430
carbon disulfide	0.355	382.5	493	32.88	420

[a] At 293 K, $P=(n^2-1)/(n^2+2)$. [b] Oscillator strength of the n,π* transition, $f=4.32\times10^{-9}\int_{300\,nm}^{410\,nm}\varepsilon(\tilde{\nu})\,d\tilde{\nu}$. [c] Recorded at 335 K; the gas-phase concentration was calculated from the ideal gas law using the known pressure–temperature dependence (B. S. Solomon, T. F. Thomas, C. Steel, *J. Am. Chem. Soc.* **1968**, *90*, 2249–2258). [d] The data were recorded under conditions of quantitative (>99.9%) complexation (0.5 mM DBO and 4.0 mM CB7). We found that CB7, unlike CB6, is sufficiently water-soluble even in the absence of electrolytes. [e] Interpolated value, see text.

coefficient (Table 1). However, hydrogen-bonding solvents are known to cause an additional hypsochromic shift and band broadening of n,π* transitions,[6, 7] which results in the values for water and isopropanol being apparently too low. Effects arising from band broadening and spectral shift are corrected for when calculating the oscillator strength.

The above solvatochromic effects render DBO an excellent molecular probe for the polarizability of the chemical environment. Strikingly, the oscillator strength of DBO is much lower in the supramolecular complex, that is, inside the CB7 cavity, than in any solvent; for example, the oscillator strength in water is 50% larger than that in CB7. This observation provides spectroscopic evidence that the environment sensed by DBO inside CB7 is characterized by a polarizability even lower than for perfluorohexane. Such an effect of a host on the absorption properties of a guest has not previously been reported. The photophysical properties of DBO inside CB7 are in fact closer to those in the gas phase than to those in solution.

We find a good linear correlation between the inverse of the oscillator strength for DBO and the polarizability ($1/f=3020-8320P$, $r=0.979$, $n=11$, Figure 1a).[9, 10] By employing this equation, we can interpolate a very low polarizability for the CB7 cavity (0.12). A low polarizability of the CB7 cavity is not unexpected. High polarizability of molecules corresponds to high electron density and the ease of moving electrons within the same molecule. These features are facilitated by the presence of heavy atoms, nonpolar σ and in particular π bonds, and easily ionizable lone pairs of electrons. Therefore, iodo and phenyl groups and to some degree also C–H bonds, but much less O–H or C–F bonds, promote a high polarizability of solvents. The CB7 cavity contains only strongly polar bonds, no easily ionizable electron pairs, and no C–H bonds pointing inside.[5] This arrangement is in line with the exceptionally low polarizability detected by the probe.

The opposite is true for hemicarcerands (HCs), and also fullerenes, which possess electron-rich π systems with high electron density inside the cavity. A high polarizability is expected for these types of supramolecular hosts. Motivated by the findings for the CB7 cavity, we have also examined the absorption and phosphorescence characteristics of biacetyl in the gas phase and in 11 solvents[8] and compared it to the known photophysical data for its HC complex.[3] A correlation between the oscillator strength of absorption, as well as the absorption and phosphorescence maximum and the bulk polarizability, also results for biacetyl (Table 2 and Figure 1b). The very weakly polarizable perfluorohexane and the highly polarizable diiodomethane (which could not be assessed for DBO because of its strong UV absorption) result in the lowest and highest solution values for biacetyl.

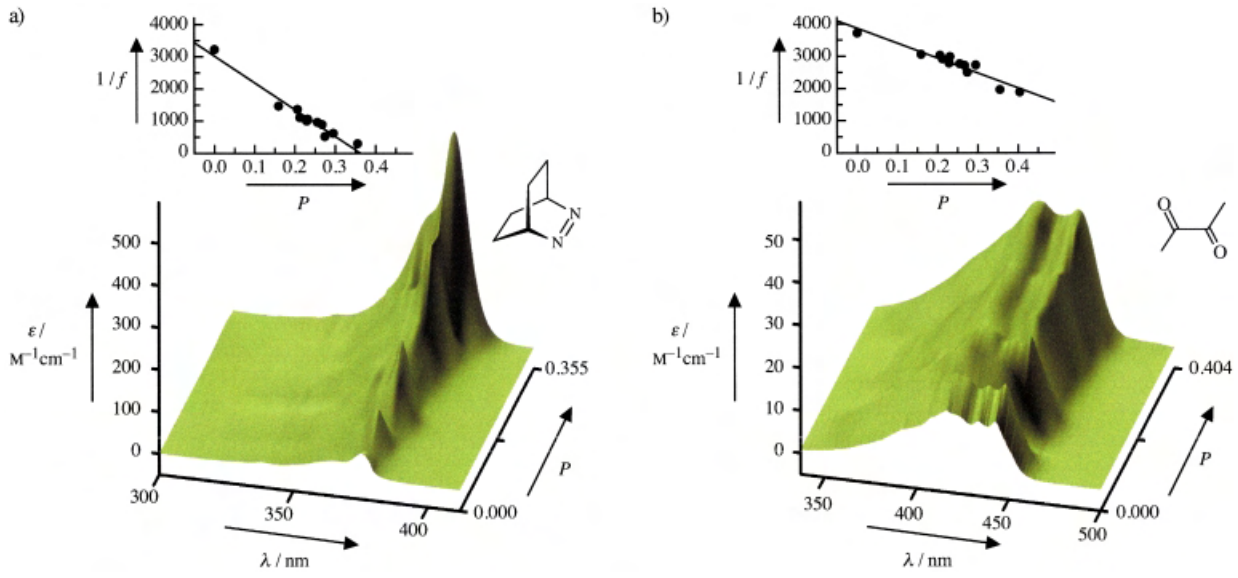


Figure 1. Contour plots of the combined absorption spectra of DBO (a) and biacetyl (b) as a function of the solvent polarizability *P*. Shown on the top are the resulting correlations of the inverse oscillator strength 1/*f*, that is, the integrated absorption intensity versus bulk polarizability.

 © WILEY-VCH Verlag GmbH, D-69451 Weinheim, 2001 1433-7851/01/4023-4388 $ 17.50+.50/0

Table 2. Photophysical properties of biacetyl in different environments.

Environment	P[a]	Absorption			Phosphorescence
		λ_{max} [nm]	ε_{max} [$M^{-1}cm^{-1}$]	$f/10^{-4}$[b]	λ_{max} [nm]
gas phase	0.000	416.6	16.6[c]	2.69[c]	512
perfluorohexane	0.159	418.5	20.1	3.27	514[d]
water	0.206	406.4	17.6[e]	3.30[e]	512
acetonitrile	0.212	415.9	19.8	3.43	515
n-hexane	0.229	421.2	21.9	3.59	519
isopropanol	0.231	419.9	19.2	3.35	518
dichloromethane	0.255	419.8	22.2	3.62	518
chloroform	0.267	420.8	22.2	3.68	519
carbon tetrachloride	0.274	422.6	24.7	4.00	520
benzene	0.295	422.1	22.5	3.67	521
carbon disulfide	0.355	425.7	29.4	5.09	523
diiodomethane	0.404	426.9	30.5	5.30	523
HC	(0.45)[f]	429[g]	–[h]	–[h]	533[g]

[a] At 293 K, $P=(n^2-1)/(n^2+2)$. [b] Oscillator strength of the transition in the visible region, $f=4.32\times10^{-9}\int_{340\,nm}^{500\,nm}\varepsilon(\tilde{\nu})\,d\tilde{\nu}$. [c] The gas-phase concentration was calculated from the ideal gas law using the known pressure–temperature dependence (W. C. Neely, T. D. Hall, *J. Chem. Eng. Data* **1972**, *17*, 294–295). [d] Phosphorescence sensitized by benzophenone. [e] Corrected for the amount of inactive biacetyl hydrate (68%) (H.-J. Buschmann, H.-H. Füldner, W. Knoche, *Ber. Bunsenges. Phys. Chem.* **1980**, *84*, 41–44). [f] Extrapolated value, see text. [g] From ref. [3], in dichloromethane. [h] The accurate intensity of the biacetyl absorption in HC is difficult to determine because of overlap with the host absorption bands and possible impurities (Z. S. Romanova, Ph.D. thesis, Bowling Green State University, USA, **1999**).

A peculiar behavior of biacetyl when included in HC was observed in the previous study[3] and a relationship between the phosphorescence properties and the polarity of the environment was implied in terms of a correlation with the dielectric constant. However, Table 2 reveals that a relationship with polarity does not apply, but rather a relationship with polarizability exists. The gas-phase photophysical properties (Table 2) are also no longer surprising[3] if one employs the polarizability, and not the polarity, for correlation. Since the solvatochromic effects of biacetyl inside HC exceed those in the most polarizable solvents, the conclusion can be drawn that biacetyl inside the HC cavity senses a polarizability even higher than for diiodomethane. Again, linear correlations for the oscillator strength ($1/f=3870-4630\,P$, $r=0.955$, $n=12$, Figure 1b) and for the absorption maximum ($\lambda_{max}=410.3+41.35\,P$, $r=0.918$, $n=11$, excluding the water value) apply, from which a very high polarizability of 0.45 inside the HC cavity can be extrapolated.

In conclusion, the present study establishes DBO and biacetyl as solvatochromic probes for the polarizability of the environment.[10] Evidence was obtained that molecules included in the cavities of molecular containers may experience unusually high or low polarizabilities, depending on the host system. CB7 has a very low polarizability inside its cavity, while HC has a very high one. These results are in agreement with the chemical structures and geometric peculiarities of these hosts.[11] The hypothesis[1, 2] that these cavities may behave like a new phase of matter is therefore confirmed through unexpected, extreme polarizabilities. The question as to what degree such uncommon polarizabilities could be exploited in the context of supramolecular functionality to influence photochemical or thermal chemical reactivity may now be raised. It should be noted that polarizability is considered an important factor in determining the binding strength of host–guest complexes.[12] Moreover, it has been proposed that the polarizability of a host assists supramolecular biomimetic catalysis.[13] This means that the polarizability of a host may become an important supramolecular design criterion, which sheds new light on our findings. Pronounced changes in the so-called "microenvironment" inside supramolecular assemblies are frequently postulated.[14–16] While the polarity of such environments has already been studied in some cases through established probes,[17] their polarizability may be equally important and can now be assessed with the presently introduced solvatochromic probes.

Received: June 21, 2001 [Z17336]

[1] D. J. Cram, M. E. Tanner, R. Thomas, *Angew. Chem.* **1991**, *103*, 1048–1051; *Angew. Chem. Int. Ed. Engl.* **1991**, *30*, 1024–1027.

[2] D. J. Cram, *Nature* **1992**, *356*, 29–36.

[3] F. Pina, A. J. Parola, E. Ferreira, M. Maestri, N. Armaroli, R. Ballardini, V. Balzani, *J. Phys. Chem.* **1995**, *99*, 12701–12703.

[4] J. Kim, I. S. Jung, S. Y. Kim, E. Lee, J. K. Kang, S. Sakamoto, K. Yamaguchi, K. Kim, *J. Am. Chem. Soc.* **2000**, *122*, 540–541.

[5] W. L. Mock in *Comprehensive Supramolecular Chemistry* (Ed.: F. Vögtle), Elsevier, Oxford, **1996**, pp. 477–493.

[6] P. Suppan, N. Ghoneim, *Solvatochromism*, Royal Chemical Society, Cambridge, **1997**.

[7] C. Reichardt, *Solvents and Solvent Effects in Organic Chemistry*, VCH, Weinheim, **1988**.

[8] The solvents and biacetyl used were the highest purity grade (Fluka or Aldrich). Some were purified immediately before use by filtration over aluminum oxide (diiodomethane) or recondensation in vacuum (carbon disulfide). 3 mL of a particular solution were obtained by weighing DBO (490 mg, 1.49 mM) in an aluminum boat or addition of liquid biacetyl (3.00 μL, 11.4 mM) by using a previously calibrated Hamilton GC syringe. Three repeated measurements, measurements at double the concentration, and the use of freshly recondensed biacetyl yielded the same results for ε und f values within an error of 3%. A 1-cm cuvette was used for measurements, except for DBO in the gas phase (10-cm cell). Emission spectra were recorded with a FLS 900 fluorimeter (Edinburgh Analytical Instruments), and UV spectra with a Perkin–Elmer Lambda 19 spectrophotometer (0.1-nm resolution). Samples were degassed by freeze-pump-thaw cycles for the luminescence and gas-phase measurements. Spectra were taken at 22 °C.

[9] An increase in the oscillator strength with solvent polarizability was also found for the forbidden electronic transition of singlet oxygen, see M. Hild, R. Schmidt, *J. Phys. Chem. A* **1999**, *103*, 6091–6096.

[10] We see the origin of this peculiar solvatochromic dependence of the oscillator strength of DBO and biacetyl in a combination of two factors: the forbidden nature of the n,π* electronic transition and the small concomitant decrease in dipole moment upon excitation. According to cases A–D of the theory by Liptay (W. Liptay, *Z. Naturforsch. A* **1966**, *21*, 1605–1618) one expects an increase in the oscillator strength with an increase in refractive index (polarizability) in particular for chromophores with a small dipole moment (case A). This does not apply for DBO (dipole moment 3.5 Debye) and biacetyl (about 1.0 Debye). Furthermore, according to Liptay, a dependence on the dielectric constant dominates for forbidden transitions (case B), which is not observed for DBO and biacetyl. A comprehensive theoretical explanation for the observed solvatochromism is therefore not available at present.

[11] The phenomenon of extreme polarizabilities is not general for all host molecules, but depends on their specific structure. For example, the solvatochromic shifts of DBO in cyclodextrins fall in between those of water and alcohols, which indicates there is a similar polarizability inside the cyclodextrin cavity as in a 2:1 methanol:water mixture. In our previous study (W. M. Nau, X. Zhang, *J. Am. Chem. Soc.* **1999**,

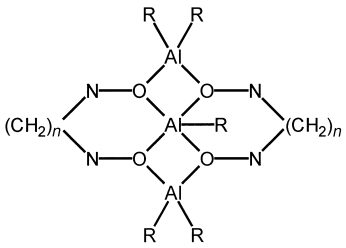
121, 8022 – 8032), we have incorrectly interpreted this effect in terms of polarity.
[12] R. Castro, M. J. Berardi, E. Cordova, M. Ochoa de Olza, A. E. Kaifer, J. D. Evanseck, *J. Am. Chem. Soc.* **1996**, *118*, 10257 – 10268.
[13] A. McCurdy, L. Jimenez, D. A. Stauffer, D. A. Dougherty, *J. Am. Chem. Soc.* **1992**, *114*, 10314 – 10321.
[14] S. Gestermann, R. Hesse, B. Windisch, F. Vögtle in *Stimulating Concepts in Chemistry* (Eds.: F. Vögtle, J. F. Stoddart, M. Shibasaki), VCH, Weinheim, **2000**, pp. 187 – 198.
[15] P. L. Wash, A. R. Renslo, J. J. Rebek, *Angew. Chem.* **2001**, *113*, 1261 – 1262; *Angew. Chem. Int. Ed.* **2001**, *40*, 1221 – 1222.
[16] D. K. Smith, F. Diederich, *Chem. Eur. J.* **1998**, *4*, 1353 – 1361.
[17] C. J. Hawker, K. L. Wooley, J. M. J. Fréchet, *J. Am. Chem. Soc.* **1993**, *115*, 4375 – 4376.

The Highly Flexible Bis(hydroxylamine) Ligand $[ON(Me)]_2CH_2^{2-}$ and Its Different Behavior in the Chemistry of Aluminum and Gallium**

Christian Lustig and Norbert W. Mitzel*

The coordinative flexibility of diolate substituents could be markedly improved if they contained additional donor atoms, preferably in close proximity to the primary donor sites. Such systems are accessible as anions of OH functional bis(hydroxylamines), that is as diolates that contain additional N-heteroatoms in geminal position relative to the metal to be bound. Such diolate ligands with improved flexibility should offer a diverse range of applications, because diolates and other difunctional ligands, in particular those of the salen type, are currently employed in a number of investigations in organoaluminum chemistry.[1] Interest in this area is directed towards the preparation of bimetallic complexes[2] and aluminum cations, which are exceedingly strong Lewis acids and capable of catalyzing reactions such as oxirane oligomerization,[3] where other Lewis acids fail to work. Fundamental investigations have recently produced a number of trinuclear aluminum diolate complexes of the type shown in Scheme 1.[4]

Herein we present the chemistry of the so far neglected tetrafunctional ligand system $[ON(Me)]_2CH_2^{2-}$ with organoaluminum and -gallium compounds. Until now this ligand has only been applied in the coordination chemistry of the nonmetal boron,[5] but not a single metal complex is known. $[HON(Me)]_2CH_2$ is available in high yields using a condensation reaction of *N*-methylhydroxylamine hydrochloride and formaldehyde mediated by potassium carbonate.[6]



Scheme 1. Typical structure of trinuclear diolate complexes of aluminum (and analogously gallium) as obtained from the reaction of AlR_3 with diols. R = alkyl, halogen, H.

The bis(hydroxylamine) $[HON(Me)]_2CH_2$ can be deprotonated with *n*-butyllithium in nonpolar solvents. The resulting suspensions of $[LiON(Me)]_2CH_2$ react with dimethylaluminum and dimethylgallium chloride to afford the heteronorbornane systems $[Me_2MON(Me)]_2CH_2$ (M = Al (**1**), Ga (**2**)); hereby four chemical bonds, including two dative ones, are formed in an one-step reaction. This reaction is completely selective for **2**, but if dimethylaluminum chloride is employed, both products **1** and **3** (see Scheme 2) are possible; subtle changes in conditions switch the selectivity completely to one or the other product. In several runs of this reaction we obtained **3** more often than **1**, but to date we have not been able to establish the conditions under which the selectivity is reliably predictable.

The heteronorbornane systems **1** and **2** parallel our recent findings using the isoelectronic ligand system $[^-CH_2N(Me)]_2CH_2$, which also leads to the heteronorbornane cages $[Me_2MCH_2N(Me)]_2CH_2$.[7] The only organoaluminum hydroxylamide compound published to date is the trimeric $[Me_2AlONMe_2]_3$ compound; its interesting intramolecular Al···N contacts lead to the coordination numbers 4, 5, and 6 in the same molecule.[8]

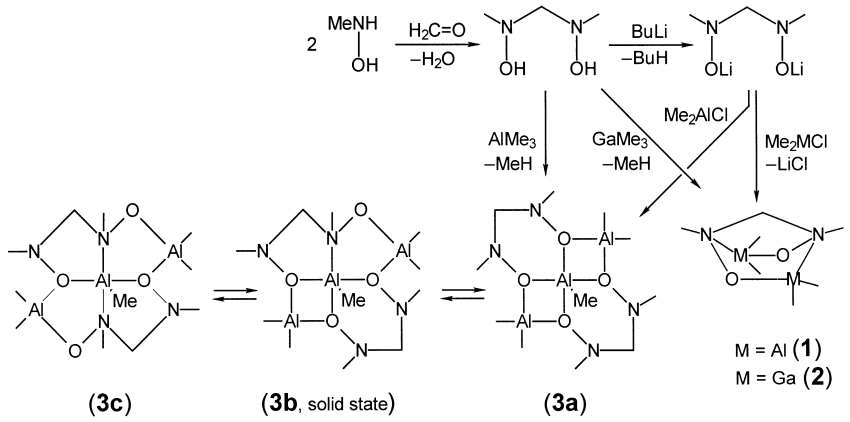
In an attempt to find a simpler synthetic route to the compounds $[Me_2MON(Me)]_2CH_2$ we treated the OH-functional bis(hydroxylamine) $[HON(Me)]_2CH_2$ with trimethylaluminum and -gallium. In the case of trimethylgallium, the product of this reaction was identical to **2**. This is in contrast to the reaction products of $GaMe_3$ with diols, which are usually analogous to the trinuclear aluminum compounds shown in Scheme 1.[2] It is clearly the presence of the nitrogen atoms in geminal position to the gallium atom, which induce this different reaction mode. The reaction with trimethylaluminum afforded colorless crystals of **3a**, which contains four- and five-coordinate aluminum atoms (Scheme 2) as indicated by the two resonance signals in the ^{27}Al NMR spectrum. Crystal structure analyses revealed the two different reaction modes with these earth metal organyl compounds. Both reactions are not sensitive to the stoichiometric ratio of the reagents. Compound **2** is formed even under a stoichiometry of $[HON(Me)]_2CH_2$:$GaMe_3$ of 2:3, while **3** results also from $[HON(Me)]_2CH_2$:$AlMe_3$ mixtures in the ratio 1:2.

The gallium heteronorbornane **2** is aggregated into endless chains in the crystal lattice (Figure 1) through the formation of four-membered Ga_2O_2 rings resulting from two Ga···O contacts (2.332(4) and 2.348(4) Å), which are substantially longer than the Ga–O bond in the norbornane skeleton (1.928(4) Å). The Ga–N distances are 2.256(5) and 2.257(5) Å

[*] Priv.-Doz. Dr. N. W. Mitzel, Dipl.-Chem. C. Lustig
Anorganisch-chemisches Institut
Technische Universität München
Lichtenbergstrasse 4, 85747 Garching (Germany)
Fax: (+49) 89-289-13147
E-mail: N.Mitzel@lrz.tum.de

[**] This work was supported by the Deutsche Forschungsgemeinschaft, the Fonds der Chemischen Industrie, and the Leonhard-Lorenz-Stiftung. We are grateful to Professor Hubert Schmidbaur (Technische Universität München) for generous support.

 © WILEY-VCH Verlag GmbH, D-69451 Weinheim, 2001 1433-7851/01/4023-4390 $ 17.50+.50/0



Scheme 2. Reactions of the bis(hydroxylamine) $[HON(Me)]_2CH_2$ with $AlMe_3$ and $GaMe_3$ and reactions of the dilithiated bis(hydroxylamine) $[LiON(Me)]_2CH_2$ with Me_2GaCl and Me_2AlCl. The latter reaction produces different products upon different reaction conditions. Also shown is the isomerism of the compounds **3a**–**c**.

and correspond to endocyclic N–Ga donor–acceptor bonds, whereby they are longer than those in Me_3Ga–NMe_3 (Ga–N 2.09(3)).[9] The NMR spectra of **2** are consistent with the interpretation of monomeric units in solution and show different resonance signals for the equatorial and axial methyl groups at the gallium centers. This behavior remains unchanged in the temperature range between -90 to $+90\,^{\circ}C$ in $[D_8]$toluene and is the same as that for **1**, for which we could not determine the solid-state structure.

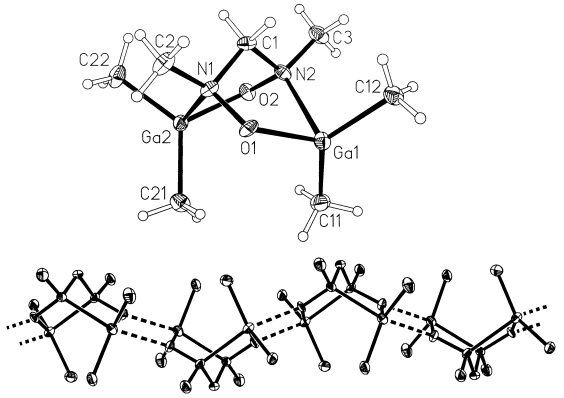


Figure 1. Crystal structure of the monomer of **2** (top) and a plot to illustrate the aggregation into endless chains (bottom). Selected intramolecular distances [Å] and angles [°]: Ga1-O1 1.929(4), Ga1-N2 2.257(5), Ga1-C11 1.940(6), Ga1-C12 1.967(6), O1-N1 1.433(6), N1-C1 1.465(7), N1-C2 1.450(7); Ga1-O1-N1 115.1(3), O1-Ga1-N2 79.2(2), O1-N1-C1 105.5(4), N1-C1-N2 105.0(4), O1-Ga1-C11 115.5(2), O1-Ga1-C12 116.8(2), C11-Ga1-C12 126.8(3), O1-N1-C2 108.1(4), C1-N1-C2 110.1(5). Intermolecular distances [Å] and angles [°]: Ga1-O1′ 2.348(4), Ga2-O2′ 2.332(4); Ga1-O1-Ga1′ 111.4(2), Ga2-O2-Ga2′ 110.8(2), O1-Ga1-O1′ 68.6(2), O2-Ga2-O2′ 69.2(2).

As already indicated in Scheme 2, the crystal structure of **3** (Figure 2) differs from that of the expected symmetrical isomer **3a** and represents the isomer **3b**. In contrast to the 1,3-propanediolates (Scheme 1), both independent molecules in the crystal structure of compound **3** comprise one six-membered, two five-membered, and one four-membered ring arranged about a central five-coordinate Al atom, which has a $AlCO_3N$ connectivity. The difference between the structures **3a** and **3b** is that the central Al atom forms a bond to one of the four nitrogen centers (which were three-coordinate in **3a**), while giving up the connectivity to the neighboring oxygen atom. This demonstrates that switching between two donor centers connected with one another is the reason for the enormous coordinative flexibility of $[ON(Me)]_2CH_2^{2-}$ ligands in comparison to 1,3-propanediolates and other difunctional ligands, which do not possess such donor centers geminal to the metal center.

However, in C_6D_6 solution at ambient temperature we observed NMR signals for ^1H, ^{13}C, and ^{27}Al, which are consistent with

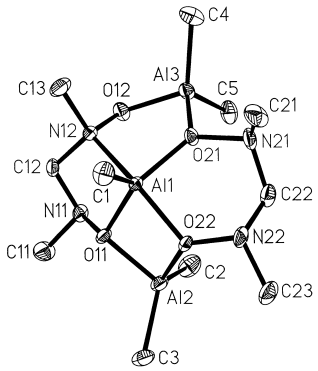


Figure 2. Crystal structure of one of the two independent molecules of **3b**. The other molecule is very similar in geometry but related to the one shown here by inversion symmetry. Selected distances [Å] and angles [°]: Al1-C1 1.945(5), Al1-O11 1.892(3), Al1-O21 1.841(3), Al1-O22 1.874(3), Al1-N12 2.080(3), Al2-O11 1.866(3), Al2-O21 1.856(3), Al3-O12 1.804(3), Al3-O21 1.844(3); C1-Al1-O11 117.6(2), C1-Al1-O21 114.2(2), C1-Al1-O22 108.0(2), C1-Al1-N12 104.1(2), O11-Al1-N12 81.6(1), N12-Al1-O21 84.2(1), O21-Al-O22 90.7(1), O22-Al1-O11 76.0(1), O11-Al2-O22 77.1(1), O12-Al2-O21 91.2(1).

a pseudo C_{2v} structure **3a** (given rotational symmetry of the central methyl group). The seeming difference between solution and solid-state structures are the result of the highly dynamic behavior of **3**, which we studied by ^1H NMR spectroscopy in $[D_8]$toluene in a temperature range between -80 and $+20\,^{\circ}C$ (Figure 3). At $-80\,^{\circ}C$ five signals for the Al-bound methyl groups occur and four for the N-bound ones, clearly indicating the isomer **3b** to be the only species dissolved. Upon warming the solution to $+20\,^{\circ}C$, the spectrum becomes simpler and only three signals for the Al-bound methyl groups and a broad one for the N-bound methyl groups can be observed. This would be consistent with isomer **3a**, but has to be rationalized by a rapid exchange between isomer **3b** and isomer **3a**, which means that averaged over time the five-coordinate aluminum atom interacts with all eight donor centers of the $C_2N_4O_4Al_2$ macrocycle.

The relative energies of the three isomers have been estimated by calculations at the B3LYP/6-31G(d) level of theory, which confirmed **3b** to be the ground state, but **3a** is only 4.5 kJ mol^{-1} higher in energy (the lowest energy con-

 © WILEY-VCH Verlag GmbH, D-69451 Weinheim, 2001 1433-7851/01/4023-4391 $ 17.50+.50/0

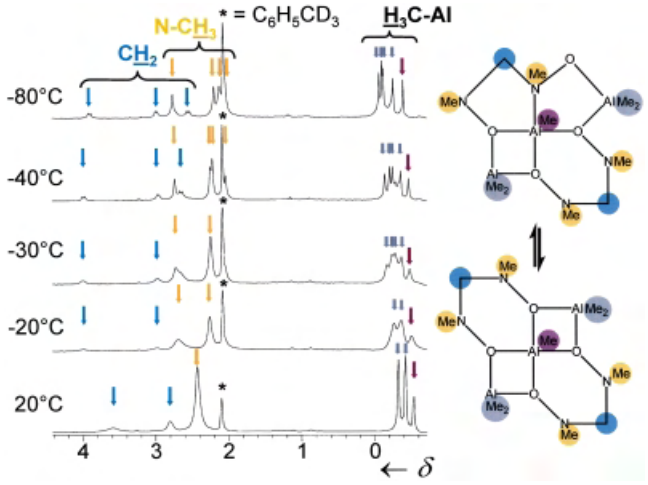


Figure 3. ^{1}H NMR spectra of a solution of **3** in [D$_8$]toluene recorded at temperatures between -80 and $+20\,^\circ$C.

former in each case). The isomer **3c** (Scheme 1), which can be considered as a third possibility, is predicted to be 94 kJ mol^{-1} higher in energy than **3b** and should thus not be observable in solution.

All this demonstrates the enormous flexibility of the $[ON(Me)]_2CH_2^{2-}$ ligand, which is able to adopt and stabilize different coordination modes of the five-coordinate Al atom in **3**; the two isomers **3a** and **3b** have very similar energies allowing the ease of their interconversion. Subtle energy differences are probably also responsible for the different reaction pathways of $[HON(Me)]_2CH_2$ with $AlMe_3$ and $GaMe_3$. The ligand $[ON(Me)]_2CH_2^{2-}$ can thus be expected to become a valuable extension of diolate chemistry, as it can adapt itself to the coordinative requirements of a metal atom to be stabilized, possibly even during a reaction involving this center.

Experimental Section

1: Dimethylaluminum chloride (12.0 mL, 1.0 M solution in hexane, 12 mmol) was slowly added to a suspension of the dilithiated bis(hydroxylamine) in diethyl ether prepared by deprotonation of the free hydroxylamine (0.64 g, 6.0 mmol) with *n*BuLi (7.5 mL of a 1.6 M solution in hexane) at 0 °C, stirred overnight at ambient temperature and filtered to remove lithium chloride. The solvent was removed under reduced pressure and a colorless solid (**1**) was obtained. Yield: 0.52 g (40 %); m.p. 127 °C; ^{1}H NMR (C_6D_6): $\delta = -0.67$ (s, 6H; $AlCH_3$), -0.34 (s, 6H; $AlCH_3$), 1.82 (s, 6H; NCH_3), 2.16 (s, 2H; NCH_2N); ^{13}C{^{1}H} NMR (C_6D_6): $\delta = -10.5$ (s; $AlCH_3$), -9.0 (s; $AlCH_3$), 45.8 (s; NCH_3), 81.2 (s; NCH_2N); ^{27}Al NMR (C_6D_6): $\delta =$ 177.5; elemental analysis correct for $C_7H_{20}Al_2N_2O_2$. The Ga compound **2** can be synthesized in an analogous manner starting from dimethylgallium chloride.

2: The bis(hydroxylamine) $[HON(Me)]_2CH_2$ (0.53 g, 5 mmol) was dissolved in toluene (40 mL) and cooled to 0 °C. A solution of trimethylgallium (1.15 g, 10 mmol) in diethyl ether (15 mL) was added very slowly. During the addition a white solid precipitated. The suspension was stirred overnight, filtered, and stored at $-40\,^\circ$C, whereby **2** formed crystals. Both the crystalline material as well as the precipitate were analytically pure products. Yield: 1.32 g (87 %); m.p. 158 °C (decomp); sublimation point: 73 °C (0.1 mbar); ^{1}H NMR (C_6D_6): $\delta = -0.32$ (s, 6H; $GaCH_3$), 0.17 (s, 6H; $GaCH_3$), 2.25 (s, 6H; NCH_3), 2.63 (s, 2H; NCH_2N); ^{13}C{^{1}H} NMR (C_6D_6): $\delta = -7.2$ (s; $GaCH_3$), -4.1 (s; $GaCH_3$), 43.1 (s; NCH_3), 84.1 (s; NCH_2N); MS (CI): *m*/*z* (%): 304 [M^+] (14), 289 [$M^+ -$ Me] (23); elemental analysis correct for $C_7H_{20}Ga_2N_2O_2$.

3: The bis(hydroxylamine) $[HON(Me)]_2CH_2$ (0.53 g, 5 mmol) was dissolved in diethyl ether (30 mL) and cooled to 0 °C. A solution of trimethylaluminum (10 mL, 1.0 M in hexane, 10 mmol) was slowly added to the solution. After addition, the reaction mixture was allowed to warm to room temperature and stirred overnight, filtered, concentrated to half its volume, and stored at $-78\,^\circ$C. After a week colorless crystals of **3** were formed. Yield: 0.78 g (43 %); m.p. 94 °C; ^{1}H NMR (C_6D_6): $\delta = -0.53$ (s, 3H; $AlCH_3$), -0.45 (s, 6H; $Al(CH_3)_2$), -0.35 (s, 6H; $Al(CH_3)_2$), 2.48 (s, 12H; NCH_3), 2.93 (br s, 2H; NCH_2N), 3.70 (br s, 2H; NCH_2N); ^{13}C{^{1}H} NMR (C_6D_6): $\delta = -11.1$ (s; $AlCH_3$), -8.8 (s; $AlCH_3$), -8.5 (s; $AlCH_3$), 46.1 (s; NCH_3), 83.7 (s; NCH_2N); ^{27}Al NMR (C_6D_6): $\delta = 75$ (s, $\nu_{1/2} =$ 2700 Hz; $AlCH_3$), 149 (s, $\nu_{1/2} = 7500$ Hz; $Al(CH_3)_2$); MS(CI): *m*/*z* (%): 364 [M^+] (92), 349 [$M^+ -$ Me] (23); elemental analysis correct for $C_{11}H_{31}Al_3N_4O_4$.

X-ray crystal structure determinations: The data for **2** [**3**] were collected on a Nonius Turbo CAD4 [Nonius DIP 2020] diffractometer at 123(2) [153(2)] K with graphite-monochromated $Mo_{K\alpha}$ radiation ($\lambda = 0.71073$ Å). The structures were solved by direct methods and refined against F^2 by full-matrix least-squares with SHELXS 97.[10] **2** ($C_7H_{20}Ga_2N_2O_2$): $M_r = 303.69$, monoclinic, space group $P2_1/n$, $a = 7.388(2)$, $b = 10.040(4)$, $c = 16.161(4)$ Å, $\beta = 93.69(2)^\circ$, $V = 1196.3(6)$ Å^3, $Z = 4$, $\rho_{calcd} = 1.686$ g cm^{-3}, $F(000) = 616$, $\mu(Mo_{K\alpha}) = 4.479$ mm^{-1}. A total of 2619 reflections were measured in the range $4.8 \le 2\theta \le 54.0^\circ$, of which 2563 were unique ($R_{int} = 0.093$). Final *R* indices: $R_1 = 0.0605$ ($I > 2\sigma(I)$), $wR_2 = 0.1705$ (all data); max./min. residual electron density 1.23/-1.18 e Å^{-1}. **3** ($C_{11}H_{31}Al_3N_4O_4$): $M_r = 364.34$, triclinic, space group $P\bar{1}$, $a = 9.0333(1)$, $b = 9.4842(2)$, $c = 25.5842(56)$ Å, $\alpha =$ 88.4744(15), $\beta = 83.3769(12)$, $\gamma = 70.4065(15)^\circ$, $V = 2051.0(5)$ Å^3, $Z = 4$, $\rho_{calcd} = 1.180$ g cm^{-3}, $F(000) = 784$, $\mu(Mo_{K\alpha}) = 0.203$ mm^{-1}. A total of 98955 reflections were measured in the range $5.2 \le 2\theta \le 54.6^\circ$, of which 4867 were unique ($R_{int} = 0.044$), Intensity corrections were applied by the program SCALEPACK.[11] Final *R* indices: $R_1 = 0.0861$ ($I > 2\sigma(I)$), $wR_2 =$ 0.1839 (all data); max./min. residual electron density 0.56/-0.36 e Å^{-1}. Crystallographic data (excluding structure factors) for the structures reported in this paper have been deposited with the Cambridge Crystallographic Data Centre as supplementary publication no. CCDC-166900 (**2**) and CCDC-166901 (**3**). Copies of the data can be obtained free of charge on application to CCDC, 12 Union Road, Cambridge CB2 1EZ, UK (fax: (+44) 1223-336-033; e-mail: deposit@ccdc.cam.ac.uk).

Received: July 23, 2001 [Z 17563]

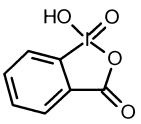
[1] D. A. Atwood, D. Rutherford, *Comments Inorg. Chem.* **1996**, *19*, 25–45.
[2] C. N. McMahon, S. J. Obrey, A. Keys, S. G. Bott, A. R. Barron, *J. Chem. Soc. Dalton Trans.* **2000**, 2151–2161.
[3] D. A. Atwood, J. A. Jegier, D. Rutherford, *J. Am. Chem. Soc.* **1995**, *117*, 6779–6780.
[4] S. Pasynkiewicz, W. Ziemkowska, *J. Organomet. Chem.* **1992**, *423*, 1–4; S. Pasynkiewicz, W. Ziemkowska, *J. Organomet. Chem.* **1992**, *437*, 99–110; W. Ziemkowska, S. Pasynkiewicz, *J. Organomet. Chem.* **1996**, *508*, 243–248; W. Uhl, R. Gerding, A. Vester, *J. Organomet. Chem.* **1996**, *513*, 163–172; J. Lewinski, J. Zachara, *J. Organomet. Chem.* **1998**, *560*, 89–94; W. Ziemkowska, S. Pasynkiewicz, T. Glowiak, *J. Organomet. Chem.* **1998**, *562*, 3–10; W. Ziemkowska, S. Pasynkiewicz, T. Skrok, *Main Group Chem.* **1998**, *21*, 105–111; W. Ziemkowska, S. Pasynkiewicz, R. Anulewicz-Ostrowska, *Main Group Chem.* **2000**, *23*, 169–177.
[5] W. Kliegel, *J. Organomet. Chem.* **1983**, *283*, 9–16; W. Kliegel, S. J. Rettig, J. Trotter, *Can. J. Chem.* **1984**, *62*, 515–520; W. Kliegel, G. Lubkowitz, S. J. Rettig, J. Trotter, *Can. J. Chem.* **1992**, *70*, 2022–2026.
[6] G. Zinner, W. Kliegel, *Chem. Ber.* **1966**, *99*, 2686–2688.
[7] C. Lustig, N. W. Mitzel, *Chem. Commun.* **2000**, 1393–1394.
[8] H. D. Hausen, G. Schmöger, W. Schwarz, *J. Organomet. Chem.* **1978**, *153*, 271–279.
[9] L. M. Golubinskaya, A. V. Golubinskii, V. S. Mastryukov, L. V. Vilkov, V. I. Bregadze, *J. Organomet. Chem.* **1976**, *117*, C4–C6.
[10] SHELXTL, Siemens Analytical X-Ray Instrumentation Inc. Madison, WI, **1995**; refinement: SHELXL93, G. M. Sheldrick, Universität Göttingen, Germany, **1993**.
[11] Z. Otwinowski, W. Minor, *Methods Enzymol.* **1997**, *276*, 307–326.

 © WILEY-VCH Verlag GmbH, D-69451 Weinheim, 2001 1433-7851/01/4023-4392 $ 17.50+.50/0

The Synthesis and Oxidative Properties of Polymer-Supported IBX

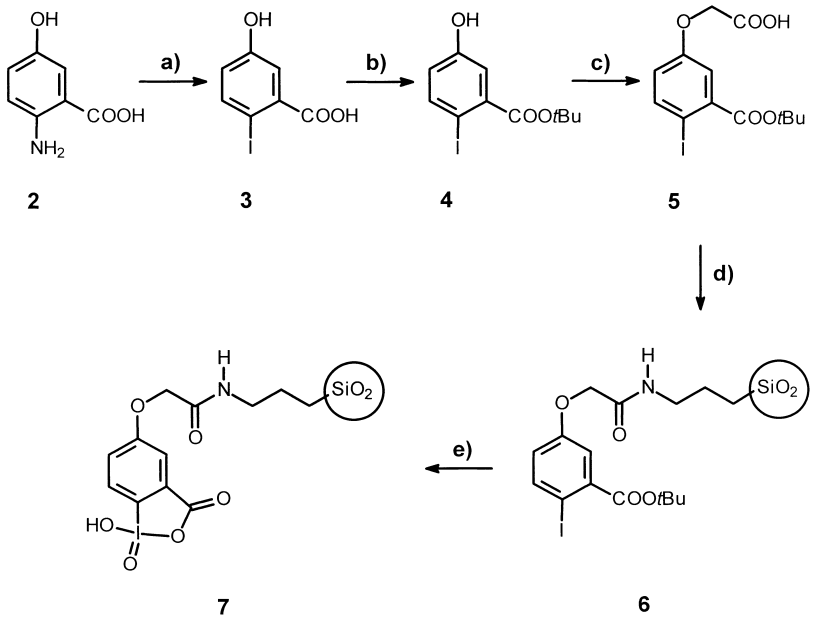
Marcel Mülbaier and
Athanassios Giannis*

In the last 20 years hypervalent iodine reagents have enjoyed an increasing popularity in organic synthesis.[1–6] They can be used for a wide range of chemical transformations, especially as reagents for oxidations.[7–11] For these purposes iodinanes such as (diacetoxyiodo)benzene, [bis(trifluoroacetoxy)iodo]benzene, the Dess–Martin periodinane (DMP), and 1-hydroxy-1,2-benziodoxol-3(1*H*)-one 1-oxide (IBX, **1**) are particularly suitable. The advantages of these reagents are: high efficiency, easy availability, mild reaction conditions, and (with the exception of DMP) stability against moisture and oxygen. Furthermore, they are environmentally safe and can be regenerated. The combination of these properties with the advantages of polymer-supported reagents[12–15] is an attractive and worthwhile aim. Recently, we reported on the synthesis and oxidative properties of two aminomethylpolystyrene-bound (diacetoxyiodo)benzene derivatives.[16] In the context of these investigations we envisaged the development of a polymer-supported IBX reagent. Here we present the synthesis of such an IBX derivative and show that it is a powerful oxidant with broad applicability.



1

The synthesis of reagent **7** was accomplished starting from commercially available 2-amino-5-hydroxybenzoic acid (**2**; Scheme 1). Treatment of compound **2** with $NaNO_2/H_2SO_4$ and excess KI afforded derivative **3**, which was transformed to the *tert*-butyl ester **4** using *N*,*N*-dimethylformamide di-*tert*-butyl acetal.[17] Compound **5** was obtained after alkylation of the phenolic hydroxy group with ethyl α-bromoacetate and subsequent hydrolysis with NaOH. This linker was subsequently coupled to aminopropylsilica gel with DIC/HOBt to give compound **6**. Cleavage of the *tert*-butyl ester with trifluoroacetic acid and oxidation with oxone[18] (potassium peroxymonosulfate) afforded the final reagent **7**.[19]



Scheme 1. Synthesis of **7**: a) $NaNO_2$, H_2SO_4, KI, 90%; b) *N*,*N*-dimethylformamide di-*tert*-butyl acetal 50%; c) NaH, $BrCH_2COOEt$, then NaOH; 84%; d) aminopropylsilica gel, DIC, HOBt, 92%; e) trifluoroacetic acid (10%), then oxone; DIC = diisopropylcarbodiimide, HOBt = 1-hydroxy-1*H*-benzotriazole.

Various primary and secondary alcohols can be oxidized with **7** (Table 1). Whereas DMSO is indispensable as a solvent in the case of IBX, **7** also works in THF; in fact reactions proceed faster in THF than DMSO. Even the presence of water (1–10%) has no negative influence on the yields and reaction times. The products are obtained with high purity and the yields are generally high to excellent. During the oxidation of primary alcohols to the corresponding aldehydes no overoxidation to the carboxylic acid was detected. It is particularly interesting that the oxidation of **4a** leads to **4b** with only the primary hydroxy group oxidized, even if **7** is added in threefold excess.[20] We tried to oxidize menthol and 3-methyl-2-butanol with **7** to get some clues of that remarkable selectivity. The yields of the corresponding ketones were poor (<5%) and cannot be increased even after longer reaction times (48 h). However, 2-methylcyclohexanol (**11a**) is oxidized easily and in high yield to 2-methylcyclohexanone (**11b**). The exact reason for this diverse reactivity is not yet fully understood and is the subject of current investigations.

In summary, we have discovered a powerful and versatile oxidation system[21] which is particularly suitable for the oxidation of alcohols to the corresponding aldehydes and ketones under mild conditions. This method combines the advantages of polymer-supported reagents with the advantages of IBX, which is superior to the Dess–Martin reagent in terms of stability, efficiency, and versatility.[7] The reduced form of **7** is easily separated by simple filtration and can be regenerated by oxidation with oxone.[19] The products are obtained in high purity and side reactions were not detected. Finally our system could be suitable for the polymer-supported synthesis of amino sugars[22] and the cyclization of anilides.[23, 24]

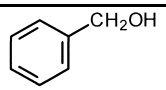
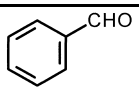
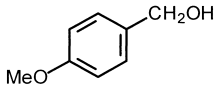
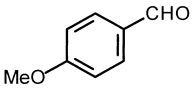
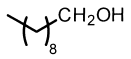
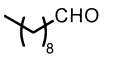
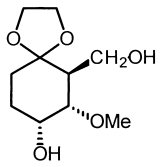
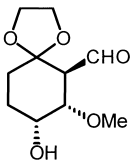
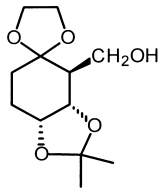
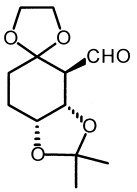
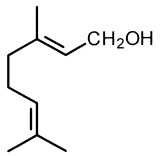
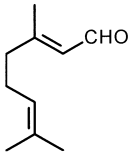
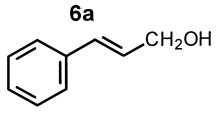
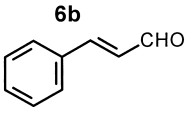
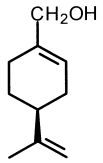
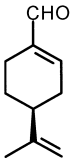
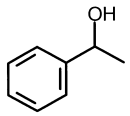
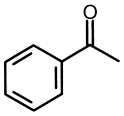
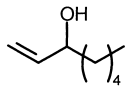
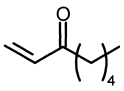
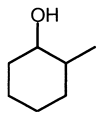
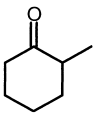
Experimental Section

7: Compound **5** (1.28 g, 3.39 mmol) was dissolved in DMF (5 mL) and HOBt (0.57 g, 3.73 mmol) was added. This mixture was added to a suspension of aminopropylsilica gel (3.00 g, 2.7 mmol, $\approx$0.8 mmol g^{-1} amino groups) in DMF (30 mL). Thereafter, DIC (0.52 mL, 3.39 mmol) was added and the mixture was stirred for 16 h. Pyridine (0.11 mL, 1.35 mmol) and acetic anhydride (0.13 mL, 1.35 mmol) were then added and the mixture was stirred again for 2 h to block any possible free amino groups. Polymer **6** was then filtered, thoroughly washed with DMF and

[*] Prof. Dr. A. Giannis, M. Mülbaier
Institut für Organische Chemie
Universität Karlsruhe
Richard-Willstätter-Allee 2, 76128 Karlsruhe (Germany)
Fax: (+49) 721-608-7652
E-mail: giannis@ochhades.chemie.uni-karlsruhe.de

 © WILEY-VCH Verlag GmbH, D-69451 Weinheim, 2001 1433-7851/01/4023-4393 $ 17.50+.50/0

Table 1. Oxidation of alcohols with reagent **7**.

Entry	Substrate	Product	Purity [%][a]
1	 **1a**	 **1b**	quant.[b]
2	 **2a**	 **2b**	97
3	 **3a**	 **3b**	96
4	 **4a**	 **4b**	86[b]
5	 **5a**	 **5b**	84[b]
6	 **6a**	 **6b**	90[b]
7	 **7a**	 **7b**	94[b]
8	 **8a**	 **8b**	92[b]
9	 **9a**	 **9b**	83[b]
10	 **10a**	 **10b**	80
11	 **11a**	 **11b**	82

[a] Purity estimated by GC-MS. [b] Yield after flash chromatography on silica gel.

methanol, and then dried in vacuo to constant weight. Yield 3.68 g (92%). Derivative **6** was suspended in a mixture of dichloromethane and trifluoroacetic acid (9:1, 30 mL) and was agitated overnight at RT. The obtained compound was then washed thoroughly with methanol and dried in vacuo to constant weight. A solution of oxone (5.0 g, 8.1 mmol) in water (50 mL) was added to the dry polymer. This suspension was stirred at 70 °C for 3 h. The final product **7** was filtered off, washed with water, and dried in vacuo. To determine the activity, compound **7** (100 mg) was suspended in THF (0.5 mL) and benzylic alcohol (6.0 mg, 0.055 mmol) added and this suspension was agitated overnight. The activity was determined by the ratio of starting material to product and is normally in the range of 0.3–0.4 mmol g^{-1}.

IR (drift): $\tilde{\nu} = 3304, 2941, 1661(br), 1573, 1462, 1424, 1100, 950, 799\ cm^{-1}$; elemental analysis (%) calcd for **7**: N 1.1, C 10.8, H 0.9; found: N 0.8, C 10.1, H 1.8.

Oxidation of alcohols: The alcohol was dissolved in THF (5 mL/1 g polymer) and 1.2 equivalents of polymer **7** were added. After agitating the mixture overnight at RT, the reaction mixture was filtered and washed. The combined organic layers were dried over Na_2SO_4 and the solvent was removed in vacuo. If necessary, the products were purified by flash chromatography.

Received: June 13, 2001 [Z17284]
Publication delayed at author's request.

[1] A. Varvoglis, *Hypervalent Iodine in Organic Synthesis*, Academic Press, San Diego, **1997**.
[2] A. Varvoglis, *Tetrahedron* **1997**, *53*, 1179–1255.
[3] A. Varvoglis, S. Spyroudis, *Synlett* **1998**, *3*, 221–232.
[4] P. J. Stang, V. V. Zhdankin, *Chem. Rev.* **1996**, *96*, 1123–1178.
[5] A. Kirschning, *Eur. J. Org. Chem*. **1998**, 2267–2274.
[6] G. Pohnert, *J. Prakt. Chem.* **2000**, *342*, 731–734.
[7] M. Frigerio, M. Santagostino, S. Sputore, G. Palmisano, *J. Org. Chem*. **1995**, *60*, 7272–7276.
[8] M. Frigerio, M. Santagostino, S. Sputore, *J. Org. Chem*. **1996**, *61*, 9272–9279.
[9] M. Frigerio, M. Santagostino, *Tetrahedron Lett.* **1995**, *35*, 8019–8022.
[10] D. B. Dess, J. C. Martin, *J. Org. Chem.* **1983**, *48*, 4156–4158.
[11] E. J. Corey, A. Palani, *Tetrahedron Lett.* **1995**, *36*, 7945–7948.
[12] S. V. Ley, O. Schucht, A. W. Thomas, P. J. Murray, *J. Chem. Soc. Perkin Trans. 1* **1999**, 1251–1252.
[13] J. Clark, D. Macquarrie, *Chem. Commun.* **1998**, 853–860.
[14] S. V. Ley, A. W. Thomas, H. Finch, *J. Chem. Soc. Perkin Trans. 1* **1999**, 669–671.
[15] A. Kirschning, H. Monenschein, R. Wittenberg, *Angew. Chem.* **2001**, *113*, 670–701; *Angew. Chem. Int. Ed.* **2001**, *40*, 650–679.
[16] S. Ficht, M. Mülbaier, A. Giannis, *Tetrahedron* **2001**, *57*, 4863–4866.
[17] U. Widmer, *Synthesis* **1983**, 135–136.
[18] M. Frigerio, M. Santagostino, S. Sputore, *J. Org. Chem*. **1999**, *64*, 4537–4538.
[19] No remarkable loss of activity has been noticed after compound **7** was used four times.
[20] Substrates **4a** and **5a** were kindly provided by Dipl.-Chem. P. Baumhof and Dipl.-Chem. R. Mazitschek. Analytical data for **4b**: ^{1}H NMR (400 MHz, $CDCl_3$): $\delta = 9.80$ (d, $J = 3.1$ Hz, 1H, CHO), 4.21 (d, $J = 3.0$ Hz , 1H, CH), 3.98–3.79 (m, 5H, $2 \times CH_2 + CH$), 3.41 (s, 3H, CH_3), 3.04 (dd, $J = 11$, 3 Hz, 1H, CH), 2.29 (d, $J = 1.6$ Hz, OH), 1.97–1.85 (m, 2H, CH_2), 1.62–1.50 (m, 2H, CH_2); HR-MS (45 °C) calcd: 216.0997, found: 216.0983.
[21] Recently, a new and efficient method for the oxidation of alcohols with oxoammonium resins was published: S. Weik, G. Nicholson, G. Jung, J. Rademann, *Angew. Chem.* **2001**, *113*, 1489–1492; *Angew. Chem. Int. Ed.* **2001**, *40*, 1436–1439.
[22] K. C. Nicolaou, P. S. Baran, Y. Zhong, J. A. Vega, *Angew. Chem*. **2000**, *112*, 2625–2629; *Angew. Chem. Int. Ed.* **2000**, *39*, 2525–2529.
[23] K. C. Nicolaou, Y. Zhong, P. S. Baran, *Angew. Chem*. **2000**, *112*, 636–639; *Angew. Chem. Int. Ed.* **2000**, *39*, 622–625.
[24] K. C. Nicolaou, Y. Zhong, P. S. Baran, *Angew. Chem*. **2000**, *112*, 639–642; *Angew. Chem. Int. Ed.* **2000**, *39*, 625–628.

 © WILEY-VCH Verlag GmbH, D-69451 Weinheim, 2001 1433-7851/01/4023-4394 $ 17.50+.50/0

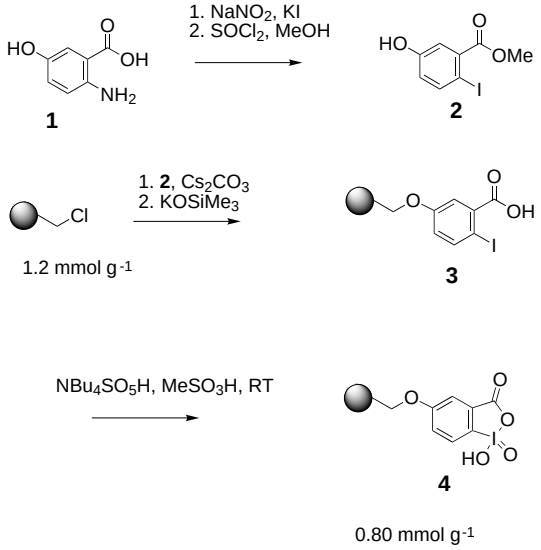
Oxidizing Polymers: A Polymer-Supported, Recyclable Hypervalent Iodine(v) Reagent for the Efficient Conversion of Alcohols, Carbonyl Compounds, and Unsaturated Carbamates in Solution**

Gerhard Sorg, Anne Mengel, Günther Jung, and Jörg Rademann*

Polymer-supported reagents and reactive intermediates can be applied successfully to the parallel conversion of single compounds as well as for the construction of chemical libraries by exploiting the advantages of solution-phase synthesis in combination with those of synthesis on a solid phase.[1–3] The oxidation of alcohols to carbonyl compounds is one of the key transformations in organic synthesis because of the diversity of products that can be obtained from aldehyde and ketone precursors. Recently, polymer-supported oxoammonium salts were demonstrated to be reactive and versatile oxidation reagents.[3a] In contrast to previous methods, oxoammonium salts do not rely on heavy metal salts[3b,c] or on additional co-oxidants.[3d,e] The reactive intermediates derived from 4-alkoxy-2,2,6,6-tetramethylpiperidine-1-oxide (4-TEMPO) were used to oxidize a diverse collection of alcohols, mostly in excellent purity and yield. An extension to even more complex and sensitive substrates, preferably including those with nitrogen functionalities, would be highly desirable.

The chemistry of hypervalent iodine compounds has been reviewed extensively.[4] Iodinanes, that is, iodoso and iodine(III) reagents, have been prepared in a supported fashion by several research groups mainly as the bisacetoxyiodoso derivative[5] or as the respective dihalogeno compounds.[6] Iodoso reagents, however, cannot be used for a general transformation of alcohols to carbonyl compounds. On the contrary, periodinanes (namely, iodoxo and iodine(v) reagents) are widely employed in the oxidation of sensitive and complex alcohols, usually as the 1-hydroxy-(1*H*)-benzo-1,2-iodoxol-3-one 1-oxide (2-iodoxybenzoic acid, IBX)[7] or its acetylation product, the Dess–Martin reagent.[8] Periodinanes have not been prepared on a polymer support so far.

In order to obtain a functional iodine(v) reagent a derivative of 2-iodobenzoic acid was required that was suitable for immobilization and that still retained similar oxidation properties as the parent compound. 4-Hydroxy-2-iodobenzoic acid esters permit efficient immobilization to chloromethyl polystyrene through a phenoxide linker. The alkoxy derivatives have thus been prepared and oxidized to the iodoso and not to the iodoxo derivative.[9] Methyl 5-hydroxy-2-iodobenzoate (**2**) was obtained in two steps from 2-amino-5-hydroxybenzoic acid (**1**) by a Sandmeyer reaction followed by esterification with thionyl chloride in methanol (Scheme 1).[10] Compound **2** was coupled to chloromethylpolystyrene cross-linked with 1% divinylbenzene



Scheme 1. Preparation of polymeric iodine reagent **4**.

(1.20 mmol g^{-1}) by using cesium carbonate as a base. The loading of the resin was determined by elemental analysis and was close to the theoretical loading (98%). Saponification to yield resin **3** was effected by treatment with potassium trimethylsilanoxide in THF.[11] Oxidation of **3** to resin **4** was investigated under various conditions; initial screening for oxidizing activity was conducted by HPLC analysis of the reaction with piperonyl alcohol (**5a**) as the test substrate. The reaction with potassium bromate[8] as well as potassium monopersulfate triple salt[12] (oxone) failed in aqueous solvent mixtures. Traces of the aldehyde **6b** were detected when the phase-transfer catalyst [18]crown-6 was used together with oxone in a triphase system. Tetrabutylammonium oxone[13] in dichloromethane (DCM) was used to avoid the presence of water and to assure proper swelling of the resin. This procedure yielded a low resin activity of 0.05–0.1 mmol g^{-1}. Peroxymonosulfonic acid (Caro's acid) is a stronger oxidant than its anion that is present in oxone and was therefore examined in further oxidation experiments. An equimolar mixture of tetrabutylammonium oxone with methylsulfonic acid (DCM, RT, 3 h) furnished resin **4** with a high activity of 0.8 mmol g^{-1}. Resin **4** was characterized by IR spectroscopy, elemental analysis, and MAS-NMR spectroscopy.[14] Elemental analysis indicated a loading of 0.84 mmol g^{-1}, which corresponded to a yield of 94% in respect to the initial loading and taking into account the mass increase of the resin. No loss of iodine was observed under the strongly acidic reaction conditions. The oxidizing polymer **4** was stable towards air and moisture and it could be stored without loss of activity.

The oxidation properties of periodinane reagent **4** were investigated by reaction with a diverse collection of benzylic,

[*] Dr. J. Rademann, Dipl.-Chem. G. Sorg, Prof. Dr. G. Jung
Institute für Organische Chemie
Universität Tübingen
Auf der Morgenstelle 18, 72076 Tübingen (Germany)
Fax: (+49) 7071-295560
E-mail: joerg.rademann@uni-tuebingen.de
Dr. A. Mengel
Schering AG, 13342 Berlin (Germany)

[**] J.R. gratefully acknowledges generous support from Prof. M. E. Maier, Tübingen, the Strukturfonds of the University of Tübingen, the Fonds der Chemischen Industrie, and the DFG. We thank Graeme Nicholson, Dietmar Schmid, and Daniel Bischoff for analytical support.

 © WILEY-VCH Verlag GmbH, D-69451 Weinheim, 2001 1433-7851/01/4023-4395 $ 17.50+.50/0

allylic, primary as well as secondary alcohols **5a**–**22a**, including the terpene alcohols **11a**, **13a**, and **17a**–**19a**, and the carbamate-protected aminoalcohols **21a** and **22a** (Table 1). All reactions were followed by GC-MS (Figure 1) or by HPLC (214 and 280 nm). The products were identified by NMR spectroscopy and by mass spetrometry (EI, 70 eV); yields were determined by weight. Most alcohols were converted into the respective aldehyde or ketone products in good to excellent yields and purities. Resin **4** that had not been used at elevated temperatures could be recycled by repeated oxidation following extensive washings.

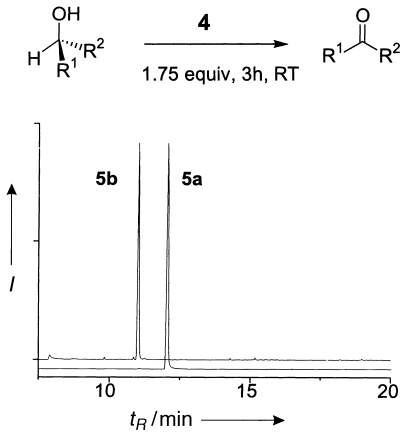


Figure 1. The oxidation of alcohols **5a**–**22a** by polymer **4** (0.8 mmol g^{-1}). The oxidative activity of the polymer reagent was determined using alcohol **5a** as a test substrate; see gas chromatograms.

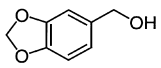
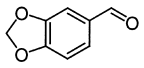
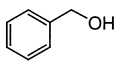
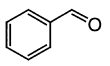
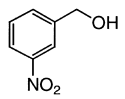
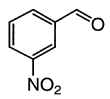
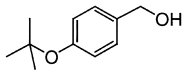
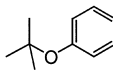
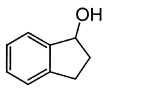
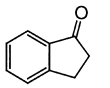
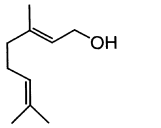
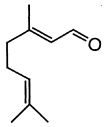
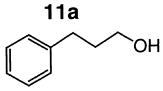
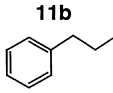
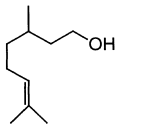
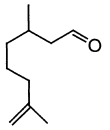
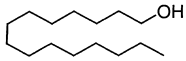
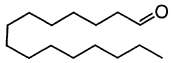
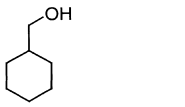
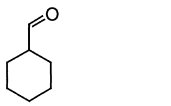
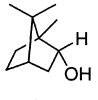
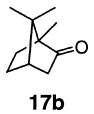
In addition to the oxidation of alcohols, further important transformations effected by IBX were investigated with resin **4**.[15] Cyclohexanol (**16a**) reacted with **4** in a closed vessel (2.3 equiv, DCM, 2 h, 65 °C) to yield the α,β-unsaturated cyclohexenone **16c** via the cyclohexanone **16b** and a postulated iodine–enol ether intermediate.[15a] The unsaturated carbamate **23** was treated with reagent **4** (4 equiv, THF/DMSO (10/1), 90 °C, 16 h) to effect radical cyclization and afforded product **24** in 25 % yield.[15b] It should be noted that at elevated temperatures IBX can oxidize benzylic positions,[15c] which are abundant in the polystyrene backbone of **4** and might account for a competing reaction pathway.

In summary, we have prepared resin **4** as the first polymer-supported periodinane reagent. The resin was obtained with high loading (0.8 mmol g^{-1}) and was capable of converting a diverse collection of alcohols, including complex and sensitivestructures, efficiently and in good to excellent yields into the respective carbonyl compounds. In addition, the α,β-desaturation of carbonyl compounds and the radical cylization of an unsaturated carbamate were demonstrated. The novel reagent is likely to find broad application in polymer-assisted solution-phase synthesis. Furthermore, the new oxidizing resin should be suitable for integration into parallel polymer-supported reaction sequences and for the conversion of compound libraries.

Experimental Section

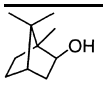
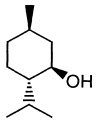
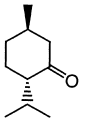
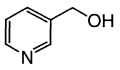
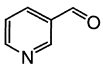
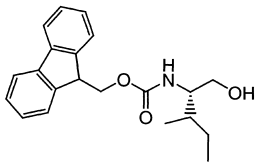
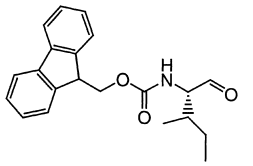
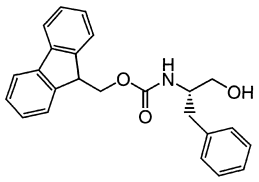
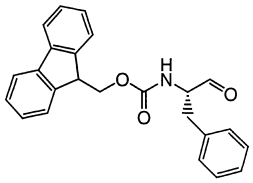
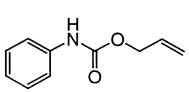
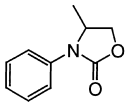
Attachment of **2** to the Merrifield resin: A solution of **2** (500.4 mg, 1.8 mmol) in dry DMF (4 mL) was added to chloromethylated polystyrene

Table 1. Results of the treatment of various alcohols with polymeric reagent **4**.

Starting material	Product	Purity [%][a]
 **5a**	 **5b**	> 95 (84)[e]
 **6a**	 **6b**	> 95
 **7a**	 **7b**	> 95
 **8a**	 **8b**	> 95
 **9a**	 **9b**	95
 **10a**	 **10b**	> 95
 **11a**	 **11b**	90[b]
 **12a**	 **12b**	70
 **13a**	 **13b**	56[c]
 **14a**	 **14b**	69
15a	**15b**	89
 **16a**	 **16b**	67
 **16a**	 **16c**	28[g]
 **17a**	 **17b**	> 95

 © WILEY-VCH Verlag GmbH, D-69451 Weinheim, 2001 1433-7851/01/4023-4396 $ 17.50+.50/0

Table 1. (Continued)

Starting material	Product	Purity [%][a]
 **18a**	 **17b**	> 95
 **19a**	 **19b**	26
 **20a**	 **20b**	66[d]
 **21a**	 **21b**	53[f]
 **22a**	 **22b**	> 95[f] (82)[e]
 **23**	 **24**	25[f, h]

[a] Determined by GC-MS. Reactions with 1.75 equiv of **4**, DCM, 2 h. [b] By-product: 7.5% *Z* isomer. [c] After reduced reaction time (30 min); 36% isopulegol is formed as major product after 2 h. [d] Obtained with 1 equiv of **4**. [e] Yield of isolated product. [f] Purity determined by HPLC. [g] 2.3 equiv of **4**, DCM, 65 °C, 2 h; main product: cyclohexanone (**16b**, 78%). [h] 4 equiv of **4**, THF/DMSO (10/1), 90 °C, 16 h.

resin (0.5 g, 0.6 mmol, 200–400 mesh, cross-linked with 1% divinylbenzene, loading 1.2 mmol g^{-1}). Cs_2CO_3 (390 mg, 1.2 mmol) was added and the reaction mixture was agitated for 3 h at 80 °C. The resin was washed with DMF, THF/AcOH (1/1), MeOH, DCM, MeOH, DCM, Et_2O (six times each) and dried in vacuo. IR: $\tilde{\nu}$ = 1111, 1213, 1244, 1288, 1378, 1561, 1588, 1733 cm^{-1}. Iodine content: 11.73%. Loading: 0.92 mmol g^{-1}. This value corresponds to 98% conversion when the mass increase is taken into account.

Ester hydrolysis: Potassium trimethylsilanoxide in dry THF (4 mL, saturated solution) was added to the resin product (ca. 0.6 mmol). After shaking the resin for 1 h at room temperature and washing with MeOH (5 times), a mixture of THF/AcOH (9/1, 4 mL) was added and the suspension was agitated for 5 h at RT. Finally, the resin was washed (THF, DCM, MeOH, and Et_2O, seven times each) and dried to yield product **3**. IR: $\tilde{\nu}$ = 1707 cm^{-1}, the ester band completely disappeared.

Oxidation of **3**: Resin **3** (100 mg, 0.092 mmol) was treated with a solution of tetrabutylammonium oxone (460 mg, 0.46 mmol, active oxygen ca. 1.6%) and methylsulfonic acid (30 μL, 0.46 mmol) in dry DCM (1.2 mL), and agitated for 3 h at RT. The product was washed thoroughly with DCM, Et_2O, DCM, Et_2O, DCM, and Et_2O (seven times each). The product was dried to yield resin **4**. IR: $\tilde{\nu}$ = 1578, 1602, 1655 cm^{-1}. Iodine content: 10.8%. Loading: 0.85 mmol g^{-1}. This value corresponds to 93% conversion of the chloromethyl groups over three steps when the mass increase is taken into account. The oxidative activity of resin **4** (0.8 mmol g^{-1}) was determined by converting an excess of test substrate **5a**.

Oxidation of alcohols: Solutions of **5a**–**22a** (1 equiv) in dry DCM (15 mM) were treated with resin **4** (1.75 equiv) for 3 h at RT. The resin was filtered off and washed with dry DCM. The volatile compounds in the filtrate were analyzed by GC-MS. The nonvolatile compounds were analyzed by HPLC-MS. For product isolation, the collected filtrates of several washings (DCM, 3 × 2 mL) were evaporated to yield, for 5 mg of starting alcohols **5a** and **22a**: **5b** (4.2 mg, 84%) and **22b** (4.1 mg, 82%), respectively. The purity and identity of the products were determined by GC or HPLC and by NMR spectroscopy.

5b: ^{1}H NMR (400 MHz, CD_3CN): δ = 9.81 (s, 1H, CHO), 6.8–7.5 (m, 3H, aromatic protons), 6.01 (s, 2H, CH_2); ^{13}C NMR (100.6 MHz, CD_3CN): δ = 190.2, 153.6, 148.5, 131.7, 128.2, 108.0, 105.2, 102.3. **22b**: ^{1}H NMR, ^{1}H COSY (400 MHz, [D_6]DMSO): δ = 9.65 (s, 1H, CHO), 7.0–8.0 (m, 13H, aromatic protons), 7.90 (d, ^3J = 7.8 Hz, 1H, NH), 4.3–4.4 (m, 3H, Fmoc-9-H, Fmoc-CH_2), 4.25 (m, 1H, α-CH), 3.25 (dd, ^3J = 6.8, ^2J = 13.9 Hz, 1H, β-CH), 2.82 (dd, ^3J = 10.4 Hz, 1H, β-CH).

Resin recycling: The resin consumed in oxidations was collected, washed, and dried. Oxidation following the procedure described above yielded resin **4** with a restored oxidation activity of 0.8 mmol g^{-1}. Three cycles of resin recycling were investigated.

Received: August 8, 2001 [Z17688]

[1] a) J. Rademann, W. Kraas, B. Dörner, *Nachr. Chem.* **2000**, *48*, 280–283; b) S. V. Ley, I. R. Baxendale, R. M. Bream, P. S. Jackson, A. G. Leach, D. A. Longbottom, M. Nesi, J. S. Scott, R. I. Storer, S. J. Taylor, *J. Chem. Soc. Perkin Trans. 1* **2000**, *23*, 3815–4195; c) A. Kirschning, H. Monenschein, R. Wittenberg, *Angew. Chem.* **2001**, *113*, 670–701; *Angew. Chem. Int. Ed.* **2001**, *40*, 650–679; d) *Combinatorial Chemistry—Synthesis, Analysis, Screening* (Ed.: G. Jung), Wiley-VCH, Weinheim, **1999**.

[2] J. Rademann, J. Smerdka, G. Jung, P. Grosche, D. Schmid, *Angew. Chem.* **2001**, *113*, 390–393; *Angew. Chem. Int. Ed.* **2001**, *40*, 381–385.

[3] S. Weik, G. Nicholson, G. Jung, J. Rademann, *Angew. Chem.* **2001**, *113*, 1489–1492; *Angew. Chem. Int. Ed.* **2001**, *40*, 1436–1439; b) G. Gardillo, M. Orena, S. Sandri, *Tetrahedron Lett.* **1976**, *17*, 3985-3988; c) B. Hinzen, S. V. Ley, *J. Chem. Soc. Perkin Trans. 1* **1997**, 1907–1910; d) C. Bolm, T. Pey, *Chem. Commun.* **1999**, 1795–1796; e) G. Sourkouni-Argirusi, A. Kirschning, *Org. Lett.* **2000**, *2*, 3781–3784.

[4] a) P. J. Stang, V. V. Zhdankin, *Chem. Rev.* **1996**, *96*, 1123–1178; b) A. Varvoglis, *Hypervalent Iodine in Organic Synthesis*, Academic Press, San Diego **1997**; c) T. Wirth, U. H. Hirth, *Synthesis* **1999**, 1271–1287; d) T. Wirth, *Angew. Chem.* **2001**, *113*, 2893–2895; *Angew. Chem. Int. Ed.* **2001**, *40*, 2812–2814.

[5] a) M. L. Hallensleben, *Angew. Makromol. Chem.* **1972**, *27*, 223–227; b) G.-P. Wang, Z.-C. Chen, *Synth. Commun.* **1999**, *29*, 2859–2866; c) S. V. Ley, A. W. Thomas, H. Finch, *J. Chem. Soc. Perkin Trans. 1* **1999**, 669–671; d) S. Ficht, M. Mülbaier, A. Giannis *Tetrahedron* **2001**, *57*, 4863–4866.

[6] a) M. Okawara, Y. Oiji, E. Imoto, *Kogyo Kagaku Zasshi* **1962**, *65*, 1647–1652 [*Chem. Abstr.* **1963**, *58*, 8051d]; b) M. Zupan, A. Pollak, *J. Chem. Soc. Chem. Commun.* **1975**, 715–716.

[7] a) C. Hartmann, V. Meyer, *Chem. Ber.* **1893**, *26*, 1727–1732; b) M. Frigerio, M. Santagostino, *Tetrahedron Lett.* **1994**, *35*, 8019–8022.

[8] D. B. Dess, J. C. Martin, *J. Org. Chem.* **1983**, *48*, 4155–4156.

[9] A. R. Katritzky, B. L. Duell, J. K. Gallos, H. D. Durst, *Magn. Reson. Chem.* **1989**, *27*, 1007–1011.

[10] a) R. A. Moss, K. W. Alwis, J.-S. Shin, *J. Am. Chem. Soc.* **1984**, *106*, 2651–2655; b) H. R. Frank, P. E. Fanta, D. S. Tarbell, *J. Am. Chem. Soc.* **1948**, *70*, 2314–2320.

[11] H.-C. Zhang, B. E. Maryanoff, *J. Org. Chem.* **1997**, *62*, 1804–1809.

[12] M. Frigerio, M. Santagostino, S. Sputore, *J. Org. Chem.* **1999**, *64*, 4537–4538.

[13] B. M. Trost, R. Braslau, *J. Org. Chem.* **1988**, *53*, 532–537.

[14] A. R. Katritzky, G. P. Savage, J. K. Gallos, H. D. Durst, *J. Chem. Soc. Perkin Trans. 2* **1990**, 1515–1518.

[15] a) K. C. Nicolaou, Y.-L. Zhong, P. S. Baran, *J. Am. Chem. Soc.* **2000**, *122*, 7596–7597; b) K. C. Nicolaou, Y.-L. Zhong, P. S. Baran, *Angew. Chem.* **2000**, *112*, 639–642; *Angew. Chem. Int. Ed.* **2000**, *39*, 625–628; c) K. C. Nicolaou, Y.-L. Zhong, P. S. Baran, *J. Am. Chem. Soc.* **2001**, *123*, 3183–3185.

Alkali Metal Tetrelide–Tetrelates: "Double Salts" With $[E_4]^{4-}$ Zintl Anions (E = Si, Ge) and the First Dimeric Cyclotrisilicate Ions $[Si_6O_{17}]^{10-}$**

Stefan Hoffmann, Thomas F. Fässler,* Constantin Hoch and Caroline Röhr*

The inclusion of neutral or charged element clusters in the channels and cavities of zeolite frameworks is a well established method for the preparation of nanostructured materials. Compounds with metal and semiconductor clusters of defined sizes show quantum size effects and can display catalytic properties that are modified by the particle size.[1–4] In general such composites are prepared by the incorporation of the metal or semiconductor unit into an existing zeolite framework by chemical or physical methods. The most common methods are the insertion of molecules and cationic exchange, with subsequent decomposition of the molecules or reduction of the ions within the zeolite framework.[5–8] However, this method is not suitable for the incorporation of the interesting semiconducting elements of Groups 13–15 as the conditions required for the introduction of such ions lead to the degradation of the zeolite structure.[5, 6] The introduction of anions and their subsequent oxidation is, in general, not possible. Herein we describe reactions in which silicate anions with skeleton building potential and semiconductor clusters are simultaneously formed and coexist in the crystal lattice in an "intergrowth" structure.[9, 10]

The extremely air-sensitive black platelike crystals of the title compound were prepared by the reaction of stoichiometric amounts of Si and SiO_2 with the elemental alkali metals (see Experimental Section).

In the crystal structure of $Cs_{10}Si_7O_9$ (**1**),[11a] and corresponding to the ionic formula $Cs_{10}[Si_4][Si_3O_9]$, the Zintl anion $[Si_4]^{4-}$, which is known from the binary Zintl phase A^IE^{IV}[12], and is isosteric and isostructual with white phosphorus (Figure 1a) coexists with the cyclotrisilicate ion $[Si_3O_9]$, known from silicates of the form $A_6[Si_3O_9]$[13]. The two isotypic rubidium compounds $Rb_{14}Si_{10}O_{17}$ (**2a**) and $Rb_{14}Ge_4Si_6O_{17}$ (**2b**)[11b] can also be formally separated into ions in the same way, which, in addition to the silicide known from **1**, and the germanide ion $[E_4]^{4-}$ in the mixed compound, gives the anion $[Si_6O_{17}]^{10-}$, previously unknown for the silicates and composed of two condensed cyclotrisilicate rings (Figure 1b).[14]

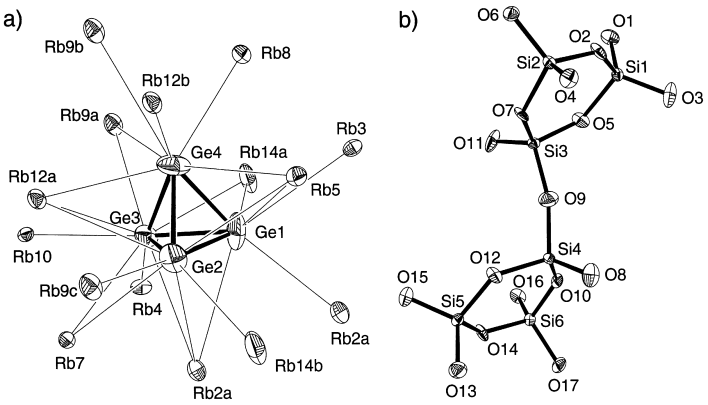


Figure 1. ORTEP plot[18] of the anions in $Rb_{14}Ge_4Si_6O_{17}$: a) germanide ion $[Ge_4]^{4-}$ with the coordination through the Rb centers ($d_{Ge\text{-}Ge}$ = 234–240 (**1**), 236–240 (**2a**), 252–258 (**2b**) pm); b) silicate ion $[Si_6O_{17}]^{10-}$ (range of $d_{Si\text{-}O}$ for **1**, **2a**, and **2b**: $d_{Si\text{-}O_t}$ = 155–161 pm, $d_{Si\text{-}O_b}$ = 163–166 pm).

The structure of the anions and their coordination by the alkali metal cations strongly resembles that of the respective parent compound classes the Zintl phases on the one hand and the oxosilicates on the other: the E–E bonds in the almost perfectly tetrahedral Zintl anions $[E_4]^{4-}$ (Figure 1a) are only slightly shorter than those in the binary Zintl phases RbSi, CsSi, and RbGe.[12] The coordination of the tetrel atoms by the alkali metal cations is also similarly related.[*]

Comparison of the two crystallographically independent trisilicate ions in **1** and the anion $[Si_6O_{17}]^{10-}$ in **2a**/**2b** with the silicate ion in $Cs_6[Si_3O_9]$[13] also shows a good agreement of the bonding parameters: the Si–O bonds to the terminal O atoms (O_t) in each case are significantly shorter than those to the bridging O ligands O_b, the Si–O bonds to the O atoms linking the two rings in **2a**/**2b** are 160(1) and 165(1) pm in **2a**, both bonds are 163(1) pm in **2b**, the bridging angles at the oxygen atoms are 168(1) and 165.8(7)°, respectively.

In both structure types the anions are arranged in alternate layers of silicide/germanide (A) and silicate anions (B) in the pattern …A B A′ B′… that lie perpendicular to the *a b* plane (Figure 2a). By bisecting the double tetrahedral three ring, the stacking pattern of the Rb compound can alternatively be described as…A B1 B2 A′ B1′ B2′…, where the layers indicated with primes are given by inversion, in accord with the concept of "chemical twinning"[9, 10] (Figure 2b). Thus the unit cells of the two types of structure are also closely metric related: the lattice constants perpendicular to the stacking direction (*a* and *b* axis) are similar in each case.

An alternative description of the two structure types can be based on the stacking of layers in the plane of the trisilicate

[*] Prof. Dr.-Ing. C. Röhr, C. Hoch
Institut für Anorganische und Analytische Chemie
Universität Freiburg
Albertstrasse 21, 79104 Freiburg (Germany)
Fax: (+49) 761-2036012
E-mail: caroline@ruby.chemie.uni-freiburg.de
Prof. Dr. T. F. Fässler, S. Hoffmann
Eduard-Zintl-Institut, Anorganische Chemie II
Technische Universität Darmstadt
Petersenstrasse 18, 64287 Darmstadt (Germany)
Fax: (+49) 6151-166029
E-mail: faessler@ac.chemie.tu-darmstadt.de

[**] This work was supported by the Deutsche Forschungsgemeinschaft, the Verband der Chemischen Industrie, the Eidgenössische Technische Hochschule Zürich, the Bundesministerium für Forschung und Technik, and the Adolf-Messer-Stiftung. T.F. and S.H. thank Prof. Dr. D. Günther for the LA-ICP-MS and Dr. V. Shklover (both of the ETH Zürich) for the EDX measurements, C.H. and C.R. thank Mr. M. Idilbi for assistance in the preparative work.

[*] The coordination of the E_4 cluster by 11 of the 14 independent Rb atoms is in very good agreement with the coordination in the cluster in RbGe. In **2a** and **2b** 15 Rb atoms, and in RbSi and RbGe 16 Rb atoms are in direct contact with the four E atoms of the cluster. In **2a** and **2b** there are three μ_3 as well as three μ_2 bonds and in RbGe there are four μ_3 bonds, so that the coordination number for the E_4 cluster in each case is 24.

 © WILEY-VCH Verlag GmbH, D-69451 Weinheim, 2001 1433-7851/01/4023-4398 $ 17.50+.50/0

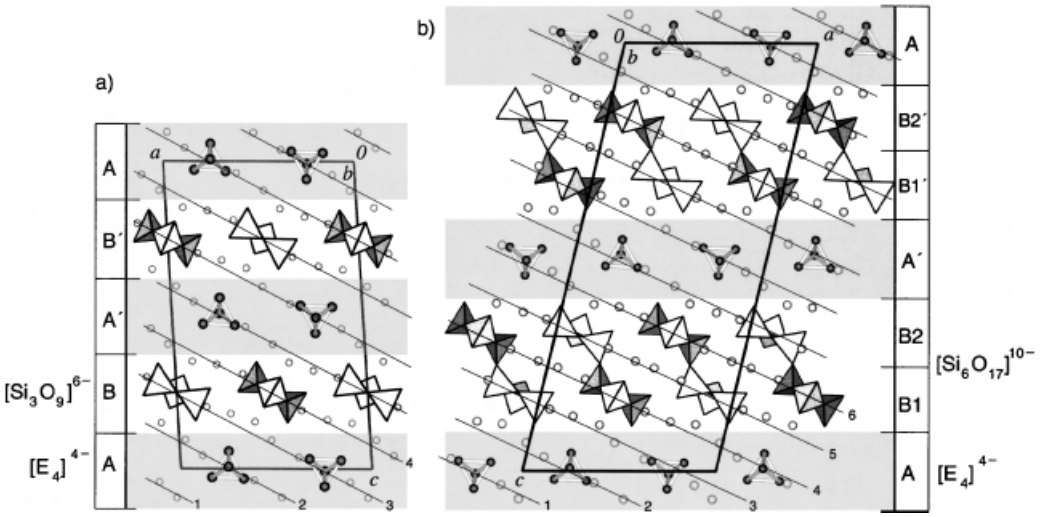


Figure 2. Crystal structures of $Cs_{10}Si_7O_9$ (a) and $Rb_{14}E_{10}O_{17}$ (E = Si, Ge) (b) in the perpendicular projection [010] (Polyhedra: SiO_4-tetrahedra; dark spheres: E; light spheres: Rb, Cs; A: silicide/germanide layers, B: silicate layers).[19]

rings (lines in Figure 2), which are composed of Zintl anions and trisilicate building blocks in the ratio corresponding to the overall composition, that is, 1:1 (**1**) or 1:2 (**2a**/**2b**) and run perpendicular [101] (**1**) and [10$\bar{1}$] (**2a**/**2b**) (identity after four and six layers, respectively).

For the mixed-valent compound **2b** the presence of the very different valence states Ge^- and Si^{4+} can be explained by the somewhat higher electronegativity of Ge compared to Si, the corresponding investigation of the Si system shows that the Zintl anion $[Si_4]^{4-}$ can exist even next to the oxosilicate ions (i.e. Si^{4+}). Thus, mixed-valent compounds can be prepared which contain Si centers in oxidation states that differ by *five* units. The very narrow temperature range for the synthesis and the extreme reactivity of the phases show that a comproportion reaction (for example to "SiO", see Experimental Section) is thermodynamically favorable. Some time ago we prepared the first tetrelide–tetrelate compounds by the reduction of SnO_2 with elemental rubidium, these compounds contain adjacent Zintl anions $[Sn_4]^{4-}$ and stannate(II) ions $[Sn^{II}O_3]^{4-}$[15] and thus a difference in the oxidation states of three. Recently, with the preparation of the alkali metal auride-aurates,[16] similar "intergrowth" structures have been reported for the first time for transition metals.

Experimental Section

$Cs_{10}Si_7O_9$ **1**: Cs (1592.0 mg, 11.978 mmol; Alkalimetall-Handelsgesellschaft Bonn), Si (84.1 mg, 2.995 mmol; Aldrich, 99.95%), and SiO_2 (323.9 mg, 5.390 mmol; Strem, 99.8%) were heated under argon in corundum crucibles in steel autoclaves to 973 K in 2 h, cooled at 100 K h^{-1} to 953 K and subsequently at 2 K h^{-1} to 933 K. After turning off the tube furnace the cooled sample was an almost pure phase of **1**. The X-ray powder diffraction pattern revealed only the weak intensities of elemental silicon. Under the stereomagnifier a small amount of the yellow-ocher X-ray amorphous component of the as yet not fully characterized „SiO" phase could be seen.

$Rb_{14}Si_{10}O_{17}$ **2a**: Stoichiometric amounts of the element/oxide Rb (1026.0 mg, 12.01 mmol; Alkalimetall-Handelsgesellschaft Bonn); Si (36.1 mg, 1.286 mmol; Aldrich, 99.95%); SiO_2 (437.9 mg, 7.288 mmol; Strem, 99.8%) were employed as above and heated at 350 K h^{-1} and annealed for 2 h at 973 K, cooled with 20 K h^{-1} to 773 K and finally rapidly cooled to room temperature. The X-ray powder diffraction pattern of the samples showed, as a small second phase, reflections assigned to the disilicate $Rb_6Si_2O_7$.[13]

$Rb_{14}Ge_4Si_6O_{17}$ **2b**: SiO_2 (35.4 mg; Merck, p.a.), Ge (28.7 mg; ChemPur, 99.99%), and Rb (116 mg; ChemPur, 99.5%) in the ratio 6:4:14 were heated in a welded Nb ampoule over 24 h to 773 K (both heating and cooling with 90 K h^{-1}). As well as reflections corresponding to the title compound the X-ray powder diffraction pattern showed lines resulting from RbGe.[12] In air the crystals decomposed to an orange product. A very small number of single crystals were isolated from a sample containing mostly RbGe, which was obtained when Rb (307 mg; Alpha, 99.8%), Ge (194 mg; Fluka, 99.999%), and Si (35 mg; Alpha, 99.9%) in molar ratio 12:9:4 were employed in a corresponding reaction at 1173 K (heating with 150 K h^{-1}, cooling with 10 K h^{-1}). Small amounts of oxygen are possible as a result of impurities in the starting materials or in the inert gas. In the single crystal the presence of Ge was confirmed by EDX and LA-ICP-MS measurements on a gold coated crystal (EDX = energy dispersive X-ray analysis; LA = laser ablation; ICP = inductive coupled plasma).

Received: July 26, 2001 [Z17612]

[1] V. I. Sradanov, N. P. Blake, D. Markgraber, H. Metiu, G. D. Stucky, *Advanced Zeolite Science and Applications, Studies in Surface Science and Catalysis, Vol. 85*, Elsevier, Amsterdam, **1994**, pp. 115–144.

[2] G. D. Stucky, J. E. MacDougall, *Science* **1990**, *247*, 669–678.

[3] P. Behrens, G. D. Stucky, *Angew. Chem.* **1993**, *105*, 729–732; *Angew. Chem. Int. Ed. Engl.* **1993**, *32*, 696–699.

[4] R. Schöllhorn, *Chem. Mater.* **1996**, *8*, 1747–1757.

[5] C. Huber, K. Moller, T. Bein, *J. Phys. Chem.* **1994**, *98*, 12067–12074.

[6] J. He, Y. Ba, C. I. Ratcliffe, J. A. Ripmeester, D. D. Klug, J. S. Tse, *Appl. Phys. Lett.* **1999**, *74*, 830–832.

[7] H. Miguez, V. Fornes, F. Meseguer, F. Marquez, C. Lopez, *Appl. Phys. Lett.* **1996**, *69*, 2347–2349.

[8] J. L. He, Y. Ba, C. I. Ratcliffe, J. A. Ripmeester, D. D. Klug, J. S. Tse, K. F. Preston, *J. Am. Chem. Soc.* **1998**, *120*, 10697–10705.

[9] B. G. Hyde, S. Andersson, *Inorganic Crystal Structures*, Wiley, New York, **1963**.

[10] E. Parthé, B. Chabot, *Handbook on the Physics and Chemistry of Rare Earth*, Elsevier, Amsterdam, **1985**, p. 113.

[11] a) Crystal data for $Cs_{10}Si_7O_9$ (**1**) at $T = 200(4)$ K: monoclinic, space group $P2/c$ (No. 13), $a = 1487.7(9)$, $b = 819.3(5)$, $c = 2361.6(15)$ pm, $\beta = 93.53(1)^\circ$; $V = 2873(1)$ Å^3, $Z = 4$, $\rho_{calcd} = 3.86$ g cm^3; diffractometer: Bruker AXS CCD (MoK_α radiation, graphite monochromator); $\mu(Mo_{K\alpha}) = 12.85$ mm^{-1}; $2\theta_{max} = 45^\circ$; 16877 measured reflections; 3689 unique reflections; Lorentz, polarization, and multi-scan absorption correction;[11d] structure solution was by direct methods;[11e] least-squares refinement (all Cs atoms anisotropic) with SHELXL-97;[11f] 156 free parameters; GOF = 1.063, *R*-value ($I \geq 2\sigma(I)$): $R1 = 0.096$, $wR2 = 0.2943$; max./min. residual electron density: $5.4/-3.1 \times 10^{-6}$ e$^-$ pm^{-3}.[11c] b) Crystal data for $Rb_{14}Si_{10}O_{17}$ (**2a**)[17]/$Rb_{14}Ge_4Si_6O_{17}$ (**2b**) at 295 K: monoclinic, space group $P2_1/c$ (No. 14), $a = 1455.6(7)$/1455.4(3), $b = 789.2(3)$/792.3(2), $c = 3276.8(9)$/3287.3(7) pm, $\beta = 103.50(1)$/103.50(3)°; $V = 3660(2)$/3686(1) Å^3, $Z = 4$, $\rho_{calcd} = 3.27$/3.47 g cm^{-3}; diffractometer: Bruker AXS CCD/Siemens SMART ($Mo_{K\alpha}$ radiation, graphite monochromator); $\mu(Mo_{K\alpha}) = 18.72$/21.85 mm^{-1}; $2\theta_{max} = 50/42.1^\circ$; 22913/11926 measured reflections; 6509/3855 unique reflections; Lorentz, polarization, and multi-scan absorption correction;[11d] structure solution was by direct methods;[11e] least-squares refinement (all atoms anisotropic) with

SHELXL-97;[11f] 371/370 free parameters; GOF = 0.785/1.074, *R*-value ($I \geq 2\sigma(I)$): $R1 = 0.0723/0.043$, $wR2 = 0.179/0.114$; max./min. residual electron density: $+1.9/+0.9$ and $-1.5/-1.0 \times 10^{-6}$ e$^-$ pm^{-3}, respectively.[11c] c) Further details on the crystal structure investigation(s) may be obtained from the Fachinformationszentrum Karlsruhe, D-76344 Eggenstein-Leopoldshafen, Germany (fax: (+49) 7247-808-666 (Frau S. Höhler-Schlimm); e-mail: crysdata@fiz-karlsruhe.de), on quoting the depository number CSD-411970 ($Cs_{10}Si_7O_9$), -411971 ($Rb_{14}Si_{10}O_{17}$), and -411972 ($Cs_{14}Ge_4Si_6O_9$).d) Bruker AXS, SAINT, and SADABS, **1983**; e) G. Sheldrick, SHELXS-97, Universität Göttingen, **1997**; f) G. Sheldrick, SHELXL-97, Universität Göttingen, **1997**.

[12] E. Busmann, *Z. Anorg. Allg. Chem.* **1961**, *313*, 90 – 106.

[13] C. Hoch, C. Röhr, *Z. Naturforsch. B* **2001**, *56*, 423 – 430.

[14] Dimeric cyclotrisilicate anions were recently found in single crystals of $Rb_{10}Si_6O_{17}$ (space group *Pbca*, $a = 1283{,}7(3)$, $b = 1367{,}1(3)$, $c = 1384{,}6(3)$ pm). S. Hoffmann, T. Fässler, unpublished results.

[15] "Rb/Cs-Stannides, -Stannates and -Stannid-Stannates": C. Hoch, P. Zönnchen, C. Röhr in *20th European Crystallographic Meeting, Prague, Vol. 5*, **1998**, p. 388.

[16] A.-V. Mudring, M. Jansen, *Angew. Chem.* **2000**, *112*, 3194 – 3196; *Angew. Chem. Int. Ed. Engl.* **2000**, *39*, 3066 – 3067.

[17] C. Hoch, C. Röhr, *Z. Kristallogr. Suppl.* **2001**, *18*, 131.

[18] C. K. Johnson, ORTEP-II, Oak Ridge National Laboratory, Oak Ridge, TN, USA, **1976**, ORNL-5138; OPENWINDOWS-Version by N. Yamazaki, Tokyo, Japan, **1991**.

[19] M. Kroeker, L. Finger, DRAWxtl, http://www.lwfinger.net/drawxtl.

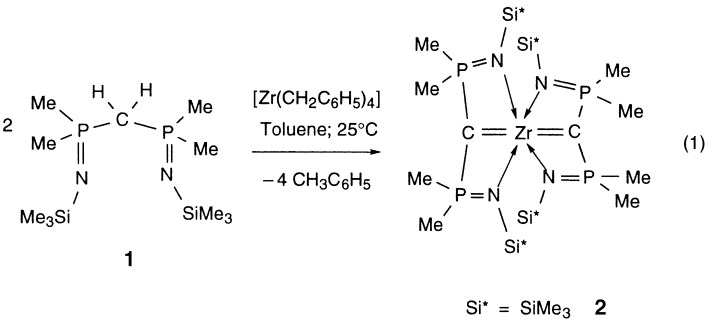
The First Biscarbene Complex of a Group 4 Metal: $[Zr\{C(Me_2P{=}NSiMe_3)_2\}_2]$**

Kasani Aparna, Ruppa P. Kamalesh Babu, Robert McDonald, and Ronald G. Cavell*

The wealth of chemistry demonstrated by metal – carbene species, summarized in a recent set of reviews,[1] illustrates the great versatility that can be expected from these compounds. Carbenes stimulate much interest because of the many applications to catalysis and organic syntheses.[2] We have recently reported on an extensive series of "pincer" and bridged dimer complexes derived from complete deprotonation of the methylene center in bis(iminophosphanyl)-methanes.[3–7] These complexes, which provide an alternative approach to the generation of this reactive metal – carbon center, were assembled in all cases with a metal/carbon combining ratio of 1:1 with only one phosphinimine ligand per metal atom. These complexes possess "carbene" character in that the metal is multiply bound to the carbon center.

These complexes provided a number of Group 4 examples which have been relatively rare[8] in contrast to the extensive examples of conventional Group 5, 6, and 7 metal carbenes.[2, 9–11] The reactivity patterns of these "pincer" carbenes with metals of Group 4 parallel the behavior of alkylidenes.[3, 6] We now report on a novel zirconium biscarbene complex of this ligand system that contains a linear assembly of two of these metal – carbon multiple bond units and is the first example of such a structure. The compound was obtained by a spontaneous double deprotonation of the methylene backbone of two ligands by a tetraalkylzirconium compound in the same fashion as that used previously to make some of the singly derivatized complexes. Biscarbene complexes of early transition metals are exceptionally rare there being only a few structurally characterized examples of biscarbene complexes of Group 5 metals.[12–15]

The reaction of $CH_2(Me_2P{=}NSiMe_3)_2$[16] (**1**) with $[Zr(CH_2C_6H_5)_4]$[17] in a 2:1 ratio in toluene gave the biscarbene complex $[Zr\{C(Me_2P{=}NSiMe_3)_2\text{-}\kappa^3C,N,N'\}_2]$ (**2**) in 30 – 40 % yield as a result of complete deprotonation of the acidic methylene groups of the ligands [Eq. (1)]. Surprisingly, under



1 (1)

Si* = $SiMe_3$ **2**

similar reaction conditions, analogous reactions carried out with the ligands $CH_2(R_2P{=}NSiMe_3)_2$ (R = Ph or Cy) containing Ph or Cy instead of Me groups on the phosphorus center did not yield the desired biscarbene product. This demonstrates the uniqueness of the behavior of this methyl-substituted ligand and suggests that steric factors play a key role in the formation of this biscarbene complex.

The high symmetry of complex **2** is illustrated by the observation of a single sharp resonance signal in the $^{31}P\{^1H\}$ NMR spectrum. The absence of methylene backbone proton signals for the ligand in the ^1H NMR spectrum and the appearance of a positive triplet for the backbone (P-C-P) carbon atoms in the $^{13}C\{^1H\}$ APT spectrum (APT = attached proton test) confirms the double deprotonation of the methylene groups of the ligand. Both in the $^{31}C\{^1H\}$ and the ^1H NMR spectra, the signals of the P-methyl groups appear as "deceptively simple" triplets due to coupling with phosphorus centers that are chemically but not magnetically equivalent, commensurate with the high symmetry of the system.[18]

The molecular structure of **2** (Figure 1) is highly symmetric.[19] The core structure consists of two mutually perpendicular six-membered bicyclic planes, each containing the

[*] Prof. Dr. R. G. Cavell, Dr. K. Aparna, Dr. R. P. Kamalesh Babu, Dr. R. McDonald
Structure Determination Laboratory
Department of Chemistry
University of Alberta
Edmonton, AB, T6G 2G2 (Canada)
Fax: (+1) 780-492-8231
E-mail: Ron.Cavell@Ualberta.ca

[**] We thank the Natural Sciences and Engineering Research Council of Canada, NOVA Chemicals Corp., and the University of Alberta for financial support.

 © WILEY-VCH Verlag GmbH, D-69451 Weinheim, 2001 1433-7851/01/4023-4400 $ 17.50+.50/0

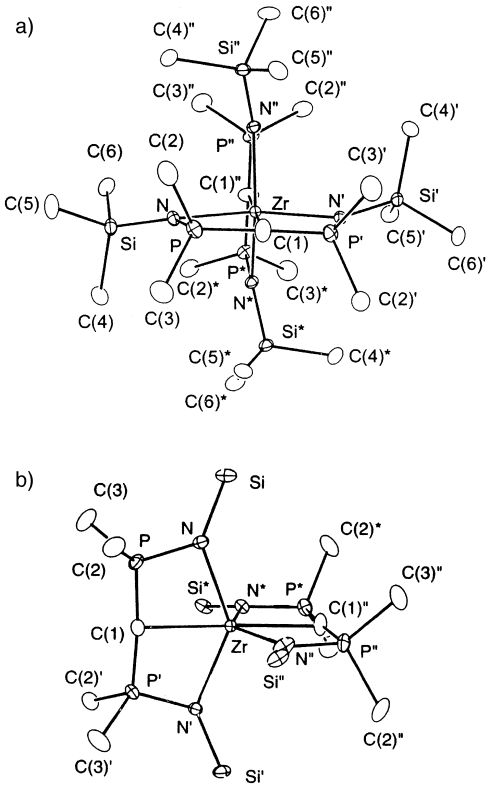


Figure 1. a) Molecular structure of **2** (ORTEP[19] view). All non-hydrogen atoms are represented by Gaussian ellipsoids at the 20% probability level. Hydrogen atoms are not shown. Selected interatomic distances [Å] and angles [°]: Zr-C(1) 2.288(3), Zr-N 2.255(1), P-N 1.630(1), P-C(1) 1.6407(5), P-C(2) 1.811(2), P-C(3) 1.813(2); P-C(1)-P′ 173.9(2), Zr-C(1)-P 93.07(9), N-Zr-N′ 137.63(7), N-Zr-N″ 97.50(2), C(1)-P-N 103.4(1). b) Side view of the core structure of **2**.

tridentate pincer methanediide ligand moiety bound to the central metal center in a spirocyclic fashion. Each of the six-atom planes is formed from the two planar four-membered rings that share a common Zr–C(1) edge. The dihedral angle between these two planar, four-membered rings is 0°; thus, the two ligands are exactly mutually perpendicular and the six-membered bicyclic ring unit is planar. The sum of the angles around the carbene center C(1) is 360°, thus this center is also planar. The C(1)-Zr-C(1)″ angle is exactly 180° by symmetry.

The bonding features within each ligand–metal unit are similar to those which we have encountered in our previously reported systems.[3–7, 20–26] The only major difference between the present biscarbene structure and the monocarbene complex of zirconium is that the six-membered metallacycle in the monoligated structure was not planar but rather subtended a dihedral angle of 11.1(2)° between the two four-membered rings.[7] The Zr–C bond length (2.288(3) Å) in the bis complex is slightly longer than in the mono-ligated analogue,[7] presumably because of the steric crowding at the metal center. However, this M–C distance is shorter than those observed in secondary alkylzirconium derivatives,[27] which supports the assignment of multiple-bond character to the metal–carbene bond.

The bond lengths within the ligand framework of **2** are considerably altered in comparison with those in the free ligands.[28, 29] The P=N bond lengths are elongated and the endocyclic P–C bond lengths are significantly shortened; however, the exocyclic P–C distances are unaffected. The P-C-P bond angle (173.9(2)°) in **2** is considerably wider than in $CH_3CH\{Ph_2P{=}N(Tol)\}_2$ (112.39(19°)[28] and in $H_2C\{Ph_2P{=}NSiMe_3\}_2$ (124.9(2)°).[29] As noted before,[3] comparison of the bond parameters in the six-membered frame with those of similar bis(iminophosphoranyl)methane ligands suggests that there is π-electron delocalization within these frames.

Received: June 15, 2001 [Z17294]

[1] *J. Organomet Chem.* **2001**, *617–618*, 1–754, a special issue on transition metal complexes with carbenes.

[2] a) K. H. Dötz, P. Tomuschat, *Chem. Soc. Rev.* **1999**, *28*, 187–198; b) M. P. Doyle, D. C. Forbes, *Chem. Rev.* **1998**, *98*, 911–935; c) R. R. Schrock, *Acc. Chem. Res.* **1990**, *23*, 158–165; d) W. D. Wulff, *Organometallics* **1998**, *17*, 3116–3134.

[3] R. G. Cavell, R. P. Kamalesh Babu, K. Aparna, *J. Organomet. Chem.* **2001**, *617–618*, 158–169.

[4] R. P. Kamalesh Babu, R. McDonald, S. A. Decker, M. Klobukowski, R. G. Cavell, *Organometallics* **1999**, *18*, 4226–4229.

[5] R. P. Kamalesh Babu, R. McDonald, R. G. Cavell, *Chem. Commun.* **2000**, 481–482.

[6] R. P. Kamalesh Babu, R. McDonald, R. G. Cavell, *Organometallics* **2000**, *19*, 3462–3465.

[7] R. G. Cavell, R. P. Kamalesh Babu, A. Kasani, R. McDonald, *J. Am. Chem. Soc.* **1999**, *121*, 5805–5806.

[8] a) J. D. Meinhart, E. V. Anslyn, R. H. Grubbs, *Organometallics* **1989**, *8*, 583–589; b) P. Binger, P. Müller, R. Benn, R. Mynott, *Angew. Chem.* **1989**, *101*, 647–648; *Angew. Chem. Int. Ed. Engl.* **1989**, *28*, 610–611; c) J. A. van Doorn, H. van der Heijden, A. G. Orpen, *Organometallics* **1995**, *14*, 1278–1283; d) H. van der Heijden, B. Hessen, *J. Chem. Soc. Chem. Commun.* **1995**, 145–146; e) P. Sinnema, L. v. Veen, A. L. Spek, N. Veldman, J. H. Teuben, *Organometallics* **1997**, *16*, 4245–4247; f) R. Baumann, R. Stumpf, W. M. Davis, L.-C. Liang, R. R. Schrock, *J. Am. Chem. Soc.* **1999**, *121*, 7822–7836; g) M. S. Clift, J. Schwartz, *J. Am. Chem. Soc.* **1984**, *106*, 8300–8301, and references therein; h) M. D. Fryzuk, P. B. Duval, S. S. S. H. Mao, M. J. Zaworotko, L. R. MacGillivray, *J. Am. Chem. Soc.* **1999**, *121*, 2478–2487.

[9] K. H. Dötz, H. Fischer, P. Hofmann, F. R. Kreissl, U. Schubert, K. Weiss, *Transition Metal Carbene Complexes*, VCH, Weinheim, **1983**.

[10] J. Feldman, R. R. Schrock, *Prog. Inorg. Chem.* **1991**, *39*, 1–74.

[11] "High-valent Organorhenium Compounds": D. M. Hoffman in *Comprehensive Organometallic Chemistry (II)*, *Vol. 6* (Eds.: E. W. Abel, F. G. A. Stone, G. Wilkinson), Pergamon, Oxford, **1995**, chap. 10, pp. 231–255.

[12] M. R. Churchill, W. J. Youngs, *Inorg. Chem.* **1979**, *18*, 1930–1935.

[13] F. A. Cotton, W. T. Hall, *J. Am. Chem. Soc.* **1979**, *101*, 5094–5095.

[14] J. B. Diminnie, H. D. Hall, Z. Xue, *Chem. Commun.* **1996**, 2383–2384.

[15] B. Hessen, A. Meetsma, F. van Bolhuis, J. H. Teuben, *Organometallics* **1990**, *9*, 1925–1936.

[16] R. P. Kamalesh Babu, R. McDonald, R. G. Cavell, *J. Chem. Soc Dalton* **2001**, 2210–2214.

[17] U. Zucchini, E. Albizzati, U. Giannini, *J. Organomet. Chem.* **1971**, *26*, 357–372.

[18] R. K. Harris, *Can J. Chem.* **1964**, *42*, 2275–2281.

[19] C. K. Johnson, ORTEP-II: A FORTRAN Thermal-Ellipsoid Plot Program for Crystal Structure Illustrations, Oak Ridge National Laboratory, Oak Ridge, TN, Report ORNL-5138, **1976**.

[20] A. Kasani, R. P. Kamalesh Babu, R. McDonald, R. G. Cavell, *Angew. Chem.* **1999**, *111*, 1580–1582; *Angew. Chem. Int. Ed.* **1999**, *38*, 1483–1484.

[21] A. Kasani, R. McDonald, R. G. Cavell, *Organometallics* **1999**, *18*, 3775–3777.

[22] K. Aparna, R. McDonald, M. Ferguson, R. G. Cavell, *Organometallics* **1999**, *18*, 4241–4243.

[23] A. Kasani, R. McDonald, R. G. Cavell, *Chem. Commun.* **1999**, 1993 – 1994.
[24] K. Aparna, M. Ferguson, R. G. Cavell, *J. Am. Chem. Soc.* **2000**, *122*, 726 – 727.
[25] R. P. Kamalesh Babu, K. Aparna, R. McDonald, R. G. Cavell, *Inorg. Chem.* **2000**, *39*, 4981 – 4984.
[26] K. Aparna, R. McDonald, R. G. Cavell, *J. Am. Chem. Soc.* **2000**, *122*, 9314 – 9315.
[27] See for example: a) $[Cp_2Zr(CPh_2H)_2]$: Zr–C 2.379(6), 2.396(6) Å (J. L. Atwood, G. K. Barker, J. Holton, W. E. Hunter, M. F. Lappert, R. Pearce, *J. Am. Chem. Soc.* **1977**, *99*, 6645 – 6652); b) $[Cp_2Zr(CH(CH_3)(6\text{-ethylpyrid-}2\text{-yl})Cl]$: Zr–C 2.421(4) Å (A. S. Guram, D. C. Swenson, R. F. Jordan, *J. Am. Chem. Soc.* **1992**, *114*, 8991 – 8996); c) $[\{Cp_2Zr(CH(Me)CH_2CH_2O)\}_2]$: Zr–C 2.382(11) Å (H. Takaya, M. Yamakawa, K. Mashima, *J. Chem. Soc. Chem. Commum.* **1983**, 1283 – 1284).
[28] M. W. Avis, C. J. Elsevier, N. Veldman, H. Kooijman, A. L. Spek, *Inorg. Chem.* **1996**, *35*, 1518 – 1528.
[29] A. Müller, M. Möhlen, B. Neumüller, N. Faza, W. Massa, K. Dehnicke, *Z. Anorg. Allg. Chem.* **1999**, *625*, 1748 – 1751.
[30] Preparation of **2**. All experimental manipulations were performed under rigorously anaerobic conditions using Schlenk techniques or an argon-filled glovebox. To a pale yellow-brown solution of $[Zr(CH_2C_6H_5)_4]$[17] (0.2 g, 0.44 mmol) in toluene (10 mL) at room temperature was added solid **1** (0.273 g, 0.88 mmol). The reaction mixture was stirred for four days, then concentrated to half of the original volume and finally left at room temperature. After two days a pale brown crystalline solid deposited which was isolated by filtration and washed with few mL of hexane (0.09 g). A second fraction of product (0.02 g) was obtained after cooling the filtrate at $-15\,^{\circ}C$ for 8 h. (Total Yield: 0.11 g, 0.155 mmol, 35.4 %). IR (Nujol mull): $\tilde{\nu}$1457w, 1381s, 1287m, 1278m, 1243s, 1068s, 1038s, 940m, 924s, 897w, 838s, 765s, 751s, 725s, 712w, 685w, 670m, 645m, 615m; ^1H NMR (400.1 MHz, C_6D_6, 298 K): $\delta = 1.58$ (t, $^2J_{P,H} = 6$ Hz, 24 H), 0.39 (s, 36 H; $SiMe_3$); ^{13}C {^1H} NMR (100.6 MHz, C_6D_6, 298 K): $\delta = 77.8$ (t, $^1J_{P,C} =$ 188 Hz, 2 C; PCP), 25.4 (t, $J_{P,C} = 32$ Hz, 8 C; P-CH_3), 4.6 (s, 12 C, CH_3-$SiMe_3$); ^{31}P {^1H} NMR (161.9 MHz, C_6D_6, 298 K): $\delta = 2.9$ (4 P); elemental analysis (%) calcd for $C_{22}H_{60}N_4P_4Si_4Zr$: C 37.31, H 8.54, N 7.91; found: C 37.61, H 8.48, N, 7.64.
[31] Crystal structure analysis for **2**: tetragonal, $P4_2/n$ (no. 86), $a =$ 13.5050(4), $c = 10.5817(5)$ Å, $V = 1929.9(12)$ Å^3, $Z = 2$,. $\rho_{calcd} =$ 1.219 g cm^{-3}, $\mu = 0.593$ mm^{-1} ($Mo_{K\alpha}$, $\lambda = 0.71073$ Å), $T = 193$ K; the structure was solved by direct methods and refined by full-matrix least-squares procedures: $R_1 = 0.0248$ and $wR_2 = 0.0738$ for 1982 reflections with $F_o^2 > 2\sigma(F_o^2)$ and all data respectively. Crystallographic data (excluding structure factors) for the structure reported in this paper have been deposited with the Cambridge Crystallographic Data Centre as supplementary publication no. CCDC-171868. Copies of the data can be obtained free of charge on application to CCDC, 12 Union Road, Cambridge CB2 1EZ, UK (fax: (+44) 1223-336-033; e-mail: deposit@ccdc.cam.ac.uk).

Syntheses and Structures of Niobium Copper Chalcogenido Clusters: $[Cu_4Nb_6Se_{12}O(PMe_3)_{10}][Cu_4NbSe_4Cl_2(PMe_3)_4] \cdot 1.5\,DMF$, $[Cu_4Nb_2Se_6(PMe_3)_8]$, $(NEt_4)[Cu_6Nb_2S_6Cl_5(PEt_3)_6]$, and $[Cu_6NbTe_3(Te_2)_2(PEt_3)_6][CuCl_2]$**

Alexander Lorenz and Dieter Fenske*

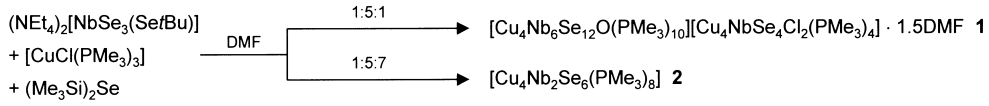
Chalcogenometalates of molybdenum, tungsten, and vanadium, in particular the tetrachalcogenometalates $[ME_4]^{n-}$ (M = Mo, W, $n = 2$, E = S, Se; M = V, $n = 3$, E = S), have been successfully used as complexing ligands for the synthesis of heterodimetallic clusters, since Müller et al. first synthesized $(PPh_4)_2[Ni(WS_4)_2]$[1] in 1971.[2] As a result of the biochemical[3] and industrial[4] interest in the coordination chemistry of chalcogenomolybdates, -tungstenates, and -vanadates, these compounds have been extensively researched, and a multitude of M-M′-E clusters have been synthesized (M = V, Mo, W, M′ = Fe, Cu, Ag, Au, etc., E = S, Se). In contrast, the coordination chemistry of chalcogenoniobates or -tantalates has remained relatively unexplored. Recently, we reported on the reactivity of soluble chalcogenoniobates towards coinage metal salts in which a series of novel Nb – Cu or Nb – Au chalcogenide clusters were prepared by reactions of $Li_3[NbS_4] \cdot 4\,CH_3CN$,[5a,b] $(NEt_4)_4[Nb_6S_{17}] \cdot 3\,CH_3CN$,[5c] and $(NEt_4)_2[NbE_3(E'tBu)]$ (E = S, Se; E′ = S;[5d,e] E = E′ = Se[6]) with copper or gold salts in the presence of phosphane ligands.[6] For example, polynuclear complexes containing a $[Cu_2Nb_2E_4]$ heterocubane unit, such as $[Cu_2Nb_2E_4Cl_2(PMe_3)_6] \cdot DMF$ **I** (E = S, Se, DMF = *N*,*N*-dimethylformamide) with two terminal chloro ligands, can be isolated. Initial attempts to link the cluster units in **I** through bridging Se atoms by the use of $(Me_3Si)_2Se$ (and accompanying loss of Me_3SiCl) have not yet produced crystalline reaction products. However, Wu et al. reported the successful in situ condensation of cluster complexes.[7] Following this concept, we allowed $(NEt_4)_2[NbSe_3(SetBu)]$ and $[CuCl(PMe_3)_3]$ to react in DMF[8] and isolated two novel Nb – Cu cluster compounds, the nature of which was dependent on the amount of $(Me_3Si)_2Se$ added during the reaction. The molecular structures of the ionic compound **1** and the neutral cluster **2** (Scheme 1) were determined by X-ray diffraction.[9] Compound **2** might have been formed by a reaction of intermediate $[Cu_2Nb_2Se_4Cl_2(PMe_3)_6]$ with $[CuCl(PMe_3)_3]$ and $(Me_3Si)_2Se$.

Compound **1** crystallizes in the orthorhombic space group *Pbcn* with eight formula units per unit cell. The ionic compound contains two heterodimetallic Nb-Cu-Se cluster ions, $[Cu_4NbSe_4Cl_2(PMe_3)_4]^{2-}$ and $[Cu_4Nb_6Se_{12}O(PMe_3)_{10}]^{2+}$. The anion is formed by a $[NbSe_4]$ tetrahedron, in which four

[*] Prof. Dr. D. Fenske, Dr. A. Lorenz
Institut für Anorganische Chemie der Universität
Engesserstrasse 15, Geb.-Nr. 30.45, 76128 Karlsruhe (Germany)
Fax: (+49) 721-6088440
E-mail: dieter.fenske@chemie.uni-karlsruhe.de

[**] This work was supported by the Deutsche Forschungsgemeinschaft and the Fonds der Chemischen Industrie.

 © WILEY-VCH Verlag GmbH, D-69451 Weinheim, 2001 1433-7851/01/4023-4402 $ 17.50+.50/0



Scheme 1. Syntheses of the Nb–Cu clusters **1** and **2**.

of the six edges are occupied by two [CuCl] and two $[Cu(PMe_3)_2]^+$ units (Figure 1, top). The copper atoms Cu5–Cu8 surround Nb7 in a slightly distorted square-planar geometry (Cu-Nb-Cu angles: 88.48(7)–91.69(7) and 175.04(8)–175.74(8)°). Cu7 and Cu8 are coordinated in a trigonal-planar fashion, each bound to one Cl^- and two Se^{2-} ligands. In contrast, Cu5 and Cu6 show a distorted tetrahedral coordination geometry, each bound to two Se^{2-} ligands and two P atoms of the PMe_3 ligands. All Se atoms of the $[NbSe_4]$ unit act as μ_3-bridging selenido ligands; Nb–Se distances are 243.7(2)–244.6(2) pm. As expected, Cu–Se bonds involving four-coordinate Cu atoms are significantly longer (247.3(3)–249.2(3) pm) than those involving three-coordinate Cu atoms (238.6(2)–238.9(2) pm). The same observation is made for the Nb–Cu distances that vary even more distinctly (292.0(2) (Nb7–Cu5) or 291.4(2) (Nb7–Cu6) and 275.6(2) (Nb7–Cu7) or 275.8(2) pm (Nb7–Cu8)). Several Nb-Cu-E clusters were synthesized so far that contain tetrahedral $[NbE_4]$ units with two, three, four, five, or six edges of the tetrahedron occupied by copper atoms.[6] The anion in **1** is closely related to these compounds and bridges a gap in the series of these Nb–Cu chalcogenide clusters. A novel molecular cationic structure is observed in **1** (Figure 1, bottom). The metal–chalcogen framework is formed by three concentric deltahedra of either niobium, selenium, or copper atoms, which surround a central O^{2-} ion (Figure 2). The first

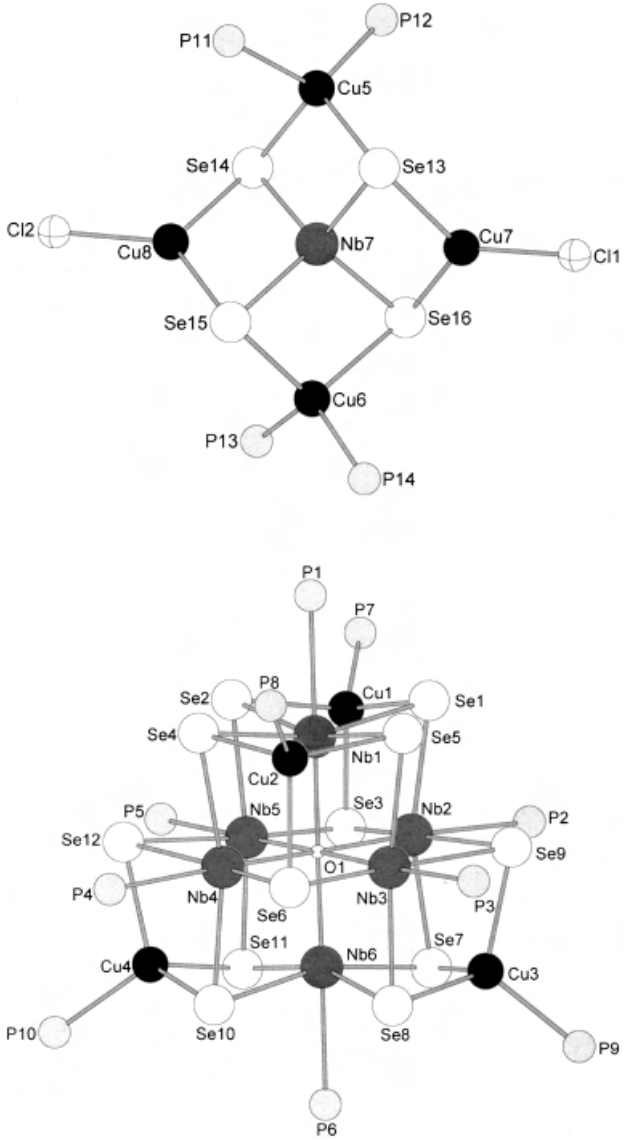


Figure 1. Top: Molecular structure of the $[Cu_4NbSe_4Cl_2(PMe_3)_4]^{2-}$ cluster anion in **1** in the crystal. Selected distance ranges [pm] (CN = coordination number): Nb-Cu(CN 3) 275.6(2)–275.8(2), Nb-Cu(CN 4) 291.4(2)–292.0(2), Nb-Se 243.7(2)–244.6(2), Cu(CN 3)-Se 238.6(2)–238.9(2), Cu(CN 4)-Se 247.3(3)–249.2(3), Cu-P 225.2(6)–226.0(5), Cu-Cl 218.6(4)–218.7(4). Bottom: Molecular structure of the $[Cu_4Nb_6Se_{12}O(PMe_3)_{10}]^{2+}$ cluster cation in **1** in the crystal. Selected distance ranges [pm]: Nb-Nb 310.1(2)–315.8(2), Nb-Cu 302.8(2)–330.0(2), Nb-Se 258.4(2)–264.1(2), Nb-O 219.8(10)–221.9(10), Nb-P 265.4(4)–268.2(4), Cu-Se 237.0(2)–246.1(2), Cu-P 223.1(4)–224.4(4).

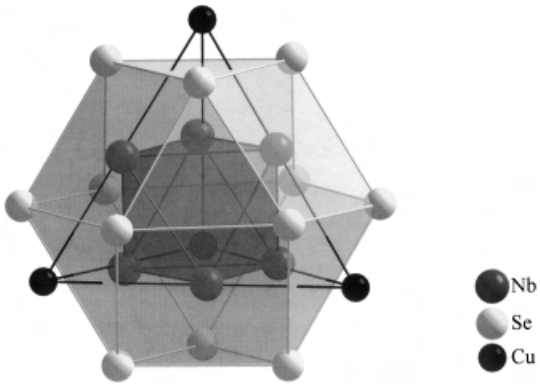


Figure 2. Illustration of the packing of three concentric polyhedra (Nb_6 octahedron, Se_{12} cubooctahedron, Cu_4 tetrahedron) in the cluster cation in **1**.

sphere is represented by a slightly distorted Nb_6 octahedron (Nb1–Nb6) at a mean distance of 220.9 pm from O1. The Nb–Nb distances lie between 310.1(2) and 315.8(2) pm. The second sphere consists of twelve Se atoms (Se1–Se12) that form a cubooctahedron. At distances between 362.1(5) and 366.3(5) pm from O1, the Se_{12} cubooctahedron is on average 65% further away from O1 than the Nb_6 octahedron. Another 10% out from the center, at 387.3(5)–388.8(8) pm from O1, four copper atoms occupy the corners of a tetrahedron (Cu1–Cu4). The latter cap four of the eight triangular faces of the Se_{12} cubooctahedron. A niobium atom is positioned at each of the six edges of the tetrahedron (Cu-Nb-Cu 175.88(6)–179.01(6)°). Alternatively, the cationic substructure of **1** can be described as an oxygen-centered Nb_6 octahedron, in which four of its eight triangular faces are alternately capped by nearly tetrahedral $[Se_3Cu(PMe_3)]$ units. All copper and niobium atoms bind to a terminal PMe_3 ligand. Whereas the copper atoms are four-coordinate, the niobium atoms are six-coordinate. Four Se

 © WILEY-VCH Verlag GmbH, D-69451 Weinheim, 2001 1433-7851/01/4023-4403 $ 17.50+.50/0

atoms, the interstitial oxygen atom O1, and the P atom of the respective PMe_3 ligand surround each Nb center in a distorted octahedral geometry. All twelve Se atoms act as μ_3 bridges. Cu–Se bonds (237.0(2) – 246.1(2) pm) are shorter, and Nb–Se bonds (258.4(4) – 264.1(2) pm) are significantly longer than the respective bonds in the anionic substructure of **1** (Cu–Se 247.3(3) – 249.2(3) pm; Nb–Se 243.7(2) – 244.6(2) pm). All Nb–Cu distances lie between 302.8(2) and 330.0(2) pm. They are longer than those in the molecular structures of the anion or in any Nb-Cu-Se cluster reported so far.

Compound **2** crystallizes in the monoclinic space group *C*2/*c* with four molecules per unit cell. The complex possesses an inversion center and shows a close structural relationship to the cluster observed in **I**. Two of the $[Cu_2Nb_2E_4]$ heterocubane units found in **I** are formally condensed sharing an Nb_2E_2 face (Figure 3). The coordination numbers of Cu as well as those of

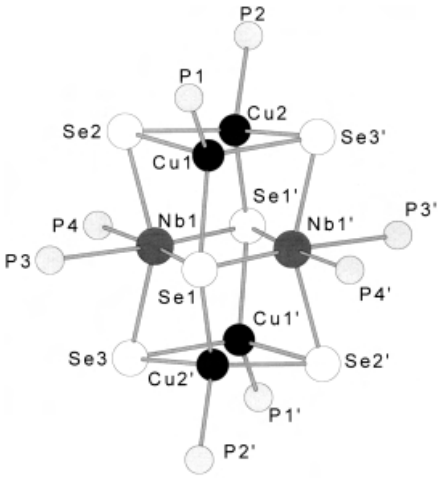
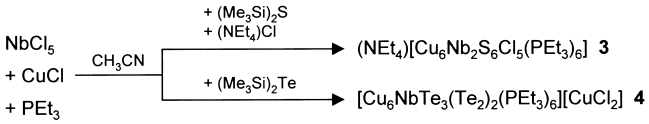


Figure 3. Molecular structure of $[Cu_4Nb_2Se_6(PMe_3)_8]$ (**2**) in the crystal. Selected distance ranges [pm]: Nb-Nb 301.9(7), Nb-Cu 303.0(8) – 305.7(7), Cu-Cu 261.8(7), Nb-μ_3-Se 254.8(7) – 256.6(8), Nb-μ_4-Se 266.3(5) – 264.5(6), Nb-P 269.7(12) – 271.4(11), Cu-μ_3-Se 247.9(6) – 251.2(7), Cu-μ_4-Se 243.4(9) – 246.5(8), Cu-P 224.3(14) – 224.5(16).

Nb atoms remain unchanged during the formal condensation. Se atoms of the Nb_2Se_2 face are now μ_4-bridging ligands (Se1), and therefore show significantly longer distances to neighboring Nb atoms (266.3(5), 264.5(6) pm) than μ_3-bridging Se atoms Se2 and Se3 (254.8(7) and 256.6(8) pm, respectively). However, the bridging mode of the Se atoms has no mentionable effect on the observed Cu–Se bond lengths. The Cu-μ_3-Se bonds (247.9(6) – 251.2(7) pm) are on average 4.4 pm longer than the Cu-μ_4-Se bonds (243.4(9), 246.5(8) pm). This is a result of the significant shortening of the Cu-μ_4-Se bonds perpendicular to the Cu_2E_2 and Nb_2E_2 faces, which has been already observed in **I**. The Nb–Nb distance in **2** (301.9(7) pm) is significantly longer than that observed in **I** (293.6(3) pm). However, although the heterocubane unit is extended in **2** compared to that in **I**, the Cu–Cu distance is 25.8 pm shorter (261.8(7) pm). Under the assumption of a formal oxidation state of +I for the copper centers in the anion in **1** and in **2**, all Nb atoms obtain the formal charge +IV. Preliminary experiments show paramagnetic behavior for **1** and **2**, as expected. Further investigations on the magnetic properties are in progress.

The Nb–Cu chalcogenide clusters can also be synthesized directly by the reaction of $NbCl_5$ with CuCl, PEt_3, and $(Me_3Si)_2E$ (E = S, Te). Orange crystals of the ionic compound **3** are formed upon addition of $(NEt_4)Cl$ in CH_3CN (Scheme 2). However, the analogous reaction of $NbCl_5$ with CuCl, PEt_3, and $(Me_3Si)_2Te$ yields an Nb-Cu-Te cluster **4**. Both compounds were characterized by X-ray diffraction.[9]



Scheme 2. Syntheses of the Nb – Cu clusters **3** and **4**.

Compound **3** crystallizes in the orthorhombic space group *Pnma* with four formular units per unit cell. The cluster anion (Figure 4) has a mirror plane and is formed by two $[Cu_3NbS_3Cl]$ heterocubane units that are linked by three μ_2-bridging chlorine ligands (Cl2, Cl3, Cl4). Such a heterocubane

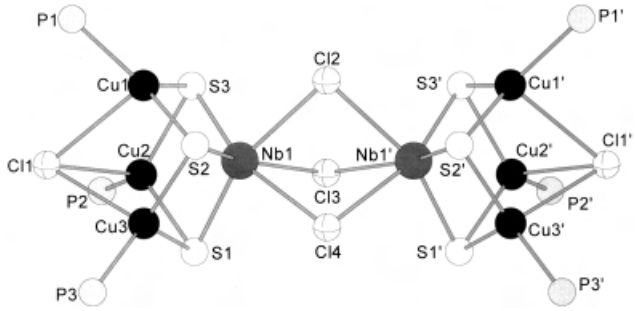


Figure 4. Molecular structure of the $[Cu_6Nb_2S_6Cl_5(PEt_3)_6]^-$ cluster anion in **3** in the crystal. Selected distance ranges [pm]: Nb-Nb 377.5(2), Nb-Cu 272.9(1) – 275.7(2), Cu-Cu 303.8(2) – 305.8(2), Nb-S 233.6(2) – 234.5(3), Nb-Cl 263.9(2) – 265.0(3), Cu-S 224.3(3) – 225.7(3), Cu-P 219.6(3) – 220.7(3), Cu-Cl 263.5(3) – 280.7(3).

unit was already observed in $[Cu_3NbS_3Cl_2(PPh_3)_3(dmf)_2]\cdot 1.5\,DMF$ (**II**).[6] Interatomic distances within the $[Cu_3NbS_3Cl]$ fragment are very similar to those in **II**. However, the bonds between the Cu atoms (Cu1 – Cu3) and the μ_3-Cl ligand (Cl1) are about 8 pm longer in **3** (av 272.4 pm). Additionally, as expected, the bonds from Nb1 to the μ_2-bridging Cl ligands (263.9(2) – 265.0(3) pm) are longer than the Nb–Cl bonds involving terminal Cl ligands in **II** (253.4(2) pm). In **3**, the Nb atoms have the formal charge +V, and the Nb–Nb distance is very large (377.5(2) pm). Several compounds have already been reported that possess two μ_2-Cl-bridged Nb atoms. However, most of them are complexes of Nb^{+III} featuring a metal – metal bond between the Nb centers. Accordingly, one observes significantly shorter Nb–Nb distances (270.8(3) pm) or Nb–μ_2-Cl distances (248.2(5) – 252.4(5) pm) in $(NnBu_4)[Nb_2Cl_7(PEt_3)_2]$.[10]

The ionic compound **4** crystallizes in the triclinic space group $P\bar{1}$ with two formular units in the unit cell. The cation is formed by a distorted, Nb-centered (Nb1) Cu_6 trigonal prism (Figure 5). One of the three edges that define the rectangular

 © WILEY-VCH Verlag GmbH, D-69451 Weinheim, 2001 1433-7851/01/4023-4404 $ 17.50+.50/0

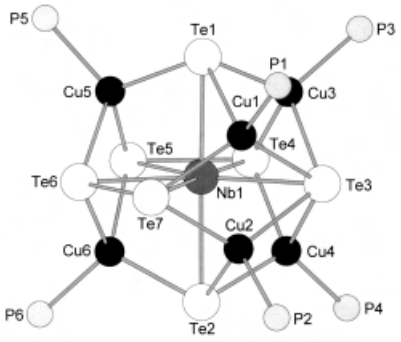


Figure 5. Molecular structure of the $[Cu_6NbTe_3(Te_2)_2(PEt_3)_6]^+$ cluster cation in **4** in the crystal. Selected distance ranges [pm]: Nb-Cu 280.7(4) – 285.1(3), Cu-Cu 260.3(3) – 423.9(4), Te-Te(Te_2^{2-}) 274.9(2) – 279.6(2), Nb-Te 282.3(3) – 351.4(4), Cu-Te 251.4(2) – 274.1(2), Cu-P 221.2(5) – 223.8(5).

faces of the prism is much shorter (Cu1–Cu2 260.3(3) pm) than the other two (365.8(4) and 367.4(4) pm, respectively). The Nb–Cu distances vary slightly (280.7(4) – 285.1(3) pm) and are among the longest observed in Nb–Cu chalcogenide compounds so far. The two triangular faces and one of the distorted rectangular faces of the Cu_6 prism are each capped by a tellurido ligand (Te1, Te2, Te3), the two remaining Cu_4 faces are each capped by a ditellurido ligand (Te4, Te5; Te6, Te7). The atoms Te3 – Te7 describe the equatorial plane of a highly distorted pentagonal Te_7 bipyramid, Te1 and Te2 form the respective vertices (Te ··· Te 274.9(2) – 462.8(5) pm). The Te atoms of the Te_2^{2-} units are bonded to two Cu atoms and the central Nb atom (Nb1), but show different Nb–Te bond lengths. The Nb1–Te5 bond (290.9(3) pm) is about 8 pm longer than the Nb1–Te4 bond (282.3(3) pm); the difference between the Nb1–Te6 and the Nb1–Te7 bond is even greater (Nb1–Te6 298.1(2), Nb1–Te7 351.4(4) pm). Te1 and Te2 are μ_4-bridging ligands and bind to three Cu atoms and the Nb1 atom. In contrast, Te3 acts as μ_5-bridge between four Cu centers and Nb1. In **4**, Nb1 has the coordination number 6+1. The smaller Nb–Te bond lengths lie within the range of the values for $K_6[Nb_4OTe_4(CN)_{12}] \cdot K_2CO_3 \cdot KOH \cdot 8H_2O$[11] (283.2(2) – 285.9(1) pm) and $[Nb_2S(Te_2)(Et_2NCS_2)_4]$[12] (284.2(3) – 285.4(3) pm). The atoms Cu1 – Cu6 each bind to three Te ligands and the P atom of one PEt_3 ligand, and are thus nearly tetrahedrally surrounded. The Cu–Te distances cover a wide range (251.4(2) – 274.1(2) pm). This was also observed in other tellurium-bridged compounds such as $[Cu_{23}Te_{13}(PiPr_3)_{19}]$[13] (253 and 284 pm). A nearly linear coordination geometry around Cu occurs in the counterion $[CuCl_2]^-$ (Cl-Cu-Cl 177.9(3)°). The formation of $[CuCl_2]^-$ ions was reported to occur likewise in the synthesis of other heterodimetallic clusters such as $(PPh_4)_3[MoOS_3(CuCl)_3]$-$[CuCl_2]$.[14]

As in **3**, formal oxidation states of +I(Cu) and +V(Nb) are assigned to the metal centers in **4**. Accordingly, both compounds are diamagnetic. Compounds **1** – **4** are obtained in yields of 45% maximum. Eviently, other soluble compounds are formed during the reactions shown in Schemes 1 and 2, which we have not yet characterized. Compounds **1** – **4** are unsuitable for characterization by further analytical techniques (e.g. NMR spectroscopy), since the crystalline material decomposes as soon as it is dissolved in organic solvents. The products are binary copper and niobium chalcogenides.

Experimental Section

All reaction steps were carried out with strong exclusion of air and moisture in a dry nitrogen atmosphere. Solvents were dried prior to use. C, H, P, and Cu elemental analyses are consistent with the formulas given.

1: $(Me_3Si)_2Se$ (0.065 mL, ca. 0.065 g, ca. 0.290 mmol) was added to a solution of $[CuCl(PMe_3)_3]$ (0.475 g, 1.450 mmol) and $(NEt_4)_2[NbSe_3(SetBu)]$ (0.211 g, 0.290 mmol) in DMF (15 mL), after the solution had been stirred for 90 min. Slow reduction of the volume in vacuum led to the crystallization of reddish black crystals of compound **1** within two weeks. Yield: 0.026 g (17% with respect to Nb).

2: $(Me_3Si)_2Se$ (0.340 mL, ca. 0.338 g, ca. 1.498 mmol) was added to a solution of $[CuCl(PMe_3)_3]$ (0.350 g, 1.070 mmol) and $(NEt_4)_2[NbSe_3(SetBu)]$ (0.155 g, 0.214 mmol) in DMF (12 mL), after the solution had been stirred for 60 min. Black crystals of compound **2** were formed within four weeks. Yield: 0.020 g (12% with respect to Nb).

3: $(Me_3Si)_2S$ (0.103 mL, ca. 0.087 g, ca. 0.487 mmol) was added to a suspension of $NbCl_5$ (0.131 g, 0.485 mmol), CuCl (0.060 g, 0.606 mmol), and PEt_3 (0.215 mL, 0.172 g, 1.455 mmol) in CH_3CN (10 mL), whereafter the reaction mixture was stirred for 60 min. The reaction mixture was then filtered, and $(NEt_4)Cl$ (0.120 g, 0.724 mmol) was added to the dark red filtrate. On stirring the mixture for a few minutes, an orange-red, crystalline precipitate of compound **3** was formed. Yield: 0.080 g (45% with respect to Cu).

4: $(Me_3Si)_2Te$ (0.056 mL, ca. 0.066 g, ca. 0.241 mmol) was added to a suspension of $NbCl_5$ (0.055 g, 0.204 mmol), CuCl (0.020 g, 0.202 mmol) and PEt_3 (0.090 mL, 0.072 g, 0.609 mmol) in CH_3CN (5 mL), whereafter the reaction mixture was stirred for 60 min. The reaction mixture was then filtered, and the reddish black filtrate was reduced to half the volume in vacuum. Slow condensation of Et_2O onto the solution led to the formation of black crystals of compound **4** after three weeks. Yield: 0.012 g (16% with respect to Cu).

Received: July 10, 2001 [Z17461]

[1] a) A. Müller, E. Diemann, *J. Chem. Soc. Chem. Commun.* **1971**, 65; b) A. Müller, E. Diemann, H. Heinsen, *Chem. Ber.* **1971**, *104*, 975 – 980.

[2] a) A. Müller, E. Diemann, R. Jostes, H. Bögge, *Angew. Chem.* **1981**, *93*, 957 – 977; *Angew. Chem. Int. Ed.* **1981**, *20*, 934 – 955; b) A. Müller, E. Diemann, *Coord. Chem. Rev.* **1973**, *10*, 79 – 122.

[3] a) C. F. Mills, *Chem. Ber.* **1979**, *15*, 512 – 520; b) *Molybdenum and Molybdenum Containing Enzymes* (Ed.: M. P. Coughlan), Pergamon, Oxford, **1980**; c) *Molybdenum Enzymes, Cofactors and Model Systems* (Eds.: E. I. Stiefel, D. Coucouvanis, W. E. Newton), American Chemical Society, Washington, **1993**.

[4] C. Bianchini, A. Meli, *J. Chem. Soc. Dalton Trans.* **1996**, 801 – 814.

[5] a) S. C. Lee, R. H. Holm, *J. Am. Chem. Soc.* **1990**, *112*, 9654 – 9655; b) S. C. Lee, J. Li, J. C. Mitchell, R. H. Holm, *Inorg. Chem.* **1992**, *31*, 4333 – 4338; c) J. Sola, Y. Do, J. M. Berg, R. H. Holm, *Inorg. Chem.* **1985**, *24*, 1706 – 1713; d) D. Coucouvanis, S. Chen, B. S. Mandimutsira, C. G. Kim, *Inorg. Chem.* **1994**, *33*, 4429 – 4430; e) B. S. Mandimutsira, S. Chen, R. A. Reynolds III, D. Coucouvanis, *Polyhedron* **1997**, *16*, 3911 – 3920.

[6] A. Lorenz, D. Fenske, *Z. Anorg. Allg. Chem.* **2001**, in press.

[7] J. Guo, X. Wu, W. Zhang, T. Sheng, Q. Huang, P. Lin, Q. Wang, J. Lu, *Angew. Chem.* **1997**, *109*, 2574 – 2576; *Angew. Chem. Int. Ed.* **1997**, *36*, 2464 – 2466.

[8] Compound **I** can be isolated from the reaction of $(NEt_4)_2[NbSe_3(StBu)]$ and $[CuCl(PMe_3)_3]$ (1:5) in DMF. We have so for not been able to crystallize the analogous Nb-Cu-Se compound starting from $(NEt_4)_2[NbSe_3(SetBu)]$.

[9] X-ray structural analyses: STOE-IPDS; data collection and refinement (SHELXS-97, SHELXL-97). **1**: orthorhombic, space group *Pbcn* (no. 60), $Z = 8$, $T = 200$ K, $a = 2216.8(4)$, $b = 2167.3(4)$, $c = 4766.9(10)$ pm, $V = 22902(8) \times 10^6$ pm^3, $\mu(Mo_{K\alpha}) = 74.80$ cm^{-1},

$2\Theta_{max} = 41°$, 57352 reflections collected, 11223 independent reflections ($R_{int} = 0.070$), 9132 observed reflections with $I > 2\sigma(I)$, 733 parameters, max residual electron denisty 0.78×10^{-6} e$^-$ pm^{-3}, $R_1 = 0.055$, $wR_2 = 0.143$. Nb, Cu, Se, Cl, P refined anisotropically. **2**: monoclinic, space group $C2/c$ (no. 15), $Z = 4$, $T = 190$ K, $a = 1806.3(4)$, $b = 1300.4(3)$, $c = 2209.4(4)$ pm, $\beta = 92.73(3)°$, $V = 5183.8(18) \times 10^6$ pm^3, $\mu(Mo_{K\alpha}) = 65.16$ cm^{-1}, $2\Theta_{max} = 40°$, 3536 reflections collected, 1654 independent reflections ($R_{int} = 0.103$), 1183 observed reflections with $I > 2\sigma(I)$, 139 parameters, max residual electron denisty 0.69×10^{-6} e$^-$ pm^{-3}, $R_1 = 0.113$, $wR_2 = 0.256$. Nb, Cu, Se, P refined anisotropically. **3**: orthorhombic, space group *Pnma* (no. 62), $Z = 4$, $T = 190$ K, $a = 2092.5(4)$, $b = 3235.5(7)$, $c = 1228.9(3)$ pm, $V = 8320(3) \times 10^6$ pm^3, $\mu(Mo_{K\alpha}) = 22.20$ cm^{-1}, $2\Theta_{max} = 43°$, 11702 reflections collected, 3621 independent reflections ($R_{int} = 0.035$), 3146 observed reflections with $I > 2\sigma(I)$, 278 parameters, max residual electron denisty 0.83×10^{-6} e$^-$ pm^{-3}, $R_1 = 0.057$, $wR_2 = 0.153$. Nb, Cu, S, Cl, P refined anisotropically. **4**: triclinic, space group $P\bar{1}$ (no. 2), $Z = 2$, $T = 180$ K, $a = 1348.9(8)$, $b = 1532.1(8)$, $c = 1782.7(9)$ pm, $\alpha = 104.33(3)$, $\beta = 105.41(3)$, $\gamma = 100.05(3)°$, $V = 3325(3) \times 10^6$ pm^3, $\mu(Mo_{K\alpha}) = 56.17$ cm^{-1}, $2\Theta_{max} = 42°$, 4338 reflections collected, 3629 independent reflections ($R_{int} = 0.082$), 3366 observed reflections with $I > 2\sigma(I)$, 352 parameters, max residual electron denisty 1.12×10^{-6} e$^-$ pm^{-3}, $R_1 = 0.064$, $wR_2 = 0.169$. Nb, Cu, Te, Cl, P refined anisotropically. Crystallographic data (excluding structure factors) for the structures reported in this paper have been deposited with the Cambridge Crystallographic Data Centre as supplementary publication nos. CCDC-165897 – 165900 (**1** – **4**, respectively). Copies of the data can be obtained free of charge on application to CCDC, 12 Union Road, Cambridge CB21EZ, UK (fax: (+44) 1223-336-033; e-mail: deposit@ccdc.cam.ac.uk).

[10] F. A. Cotton, M. Shang, *Inorg. Chem.* **1993**, *32*, 969 – 976.

[11] V. P. Fedin, I. V. Kalinina, A. V. Virovets, N. V. Podberezskaya, I. S. Neretin, Y. L. Slovokhotov, *Chem. Commun.* **1998**, 2579 – 2580.

[12] M. Sokolov, H. Imoto, T. Saito, V. Fedorov, *J. Chem. Soc. Dalton Trans.* **1999**, 85 – 90.

[13] D. Fenske, J. Steck, *Angew. Chem.* **1993**, *105*, 254 – 257; *Angew. Chem. Int. Ed.* **1993**, *32*, 238 – 242.

[14] W. Clegg, C. D. Garner, J. R. Nicholson, P. R. Raithby, *Acta Crystallogr. Sect. C* **1983**, *39*, 1007 – 1009.

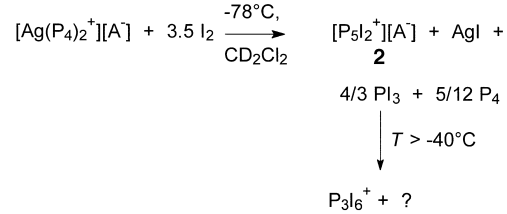
$P_5X_2^+$ (X = Br, I), a Phosphorus-Rich Binary P–X Cation with a C_{2v}-Symmetric P_5 Cage**

Ingo Krossing* and Ines Raabe

Dedicated to Jack Passmore

Our knowledge on simple cations with a polyphosphorus skeleton is still very limited owing to the poor capability of the phosphorus atom to bear positive charge. With mass spectrometric methods naked polyphosphorus cations up to P_{89}^+[1, 2] and binary P–X cations (X = halogen) were shown to exist in the gas phase.[3] Their structures have been elucidated by quantum-chemical methods.[4, 5] In the solid state only the PX_4^+ (X = F – I)[6] and $P_2I_5^+$ ions[7, 8] are known—in contrast to numerous polyphosphorus(Zintl-)anion structures.[9] Classical weakly basic counteranions only led to decomposition.[10] Recently we reported on nonoxidizing, weakly coordinating anions of the type $Al(OR)_4^-$ (OR = polyfluorinated aliphatic alkoxide).[11, 12] These anions stabilize binary Ag – P cations, such as D_{2h}-symmetric $Ag(P_4)_2^+$, $\mathbf{1}^+$.[13, 14] The reaction of $[\mathbf{1}^+][A^-]$ ($A^- = Al[OC(CF_3)_3]_4^-$) with X_2 (X = Br, I) provided evidence for the intermediate formation of the elusive P_5^+ ion but finally only led to the first subvalent binary P – X cation, the C_2-symmetric $P_3I_6^+$ ion with a P_3 backbone.[15]

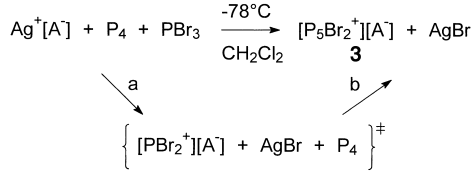
Herein we reinvestigate this reaction by using low-temperature in situ NMR spectroscopy: Reaction of $[Ag(P_4)_2^+][A^-]$ in CD_2Cl_2 with 3.5 equivalents of I_2 at $-78\,°C$ revealed one major product in the in situ ^{31}P NMR spectrum at $-78\,°C$ (see Supporting Information): $[P_5I_2^+][A^-]$ (**2**) (Scheme 1). A



Scheme 1. Reaction pathway for the formation and subsequent decomposition of the $P_5I_2^+$ ion.

scaled-up preparation verified these conclusions (mass balance, Raman spectrum of **2**, PI_3 and P_4 formation). The reaction mixture reacted according to Scheme 1 already at $-40\,°C$ to give $P_3I_6^+$ and other yet unidentified species.[15] The formation and decomposition of $P_5I_2^+$ possibly proceed as follows: it is known that P_4 reacts with iodine to immediately give PI_3 (and only then to give P_2I_4).[16] The PI_3 reacted with the polarizing silver cation of $Ag^+[A^-]$ to give AgI and PI_2^+. This "carbenoid"[5] cation inserted into one P–P bond of the P_4 tetrahedron leading to the formation of $P_5I_2^+$. Upon warming the sample, the excess PI_3 and P_4 react to give P_2I_4 (Raman), which at about $-40\,°C$ becomes slightly soluble and then reacts with $P_5I_2^+$ to form $P_3I_6^+$ and P_4. The latter reaction in CH_2Cl_2 is exergonic by 26 kJ mol^{-1} (COSMO[17, 18] solvation model and MP2/TZVPP[26–29]).

To confirm the PI_2^+ insertion hypothesis, we reacted P_4, PBr_3, and $Ag^+[A^-]$ according to Scheme 2 at $-78\,°C$. Indeed, in situ ^{31}P NMR spectroscopy at $-80\,°C$ showed that $[P_5Br_2^+][A^-]$ (**3**) was the only P-containing product visible after a reaction time of 10 days at this temperature. This confirms the insertion mechanism proposed in the steps a and



Scheme 2. Reaction pathway for the formation of the $P_5Br_2^+$ ion: The intermediate PBr_2^+ ion (a) inserts into the P–P bond of the P_4 cage (b).

[*] Dr. I. Krossing, I. Raabe
Universität Karlsruhe, Institut für Anorganische Chemie
Engesserstrasse Geb. 30.45, 76128 Karlsruhe (Germany)
Fax: (+49) 721-608-48-54
E-mail: krossing@achpc9.chemie.uni-karlsruhe.de

[**] This work was supported by the Deutsche Forschungsgemeinschaft and the Fonds der Chemischen Industrie. We thank Prof. H. Schnöckel for valuable discussions.

Supporting information for this article is available on the WWW under http://www.angewandte.com or from the author.

 © WILEY-VCH Verlag GmbH, D-69451 Weinheim, 2001 1433-7851/01/4023-4406 $ 17.50+.50/0

b in Scheme 2, and is also in agreement with the MP2/TZVPP[26–29] calculated free energy of this reaction in CH_2Cl_2 (COSMO[17] model: $\Delta_r G$(step b, CH_2Cl_2) = −111 kJ mol^{-1}).[18] A scaled-up preparation gave temperature-, air-, and moisture-sensitive crystalline **3** in almost quantitative yield. However, solid **3** is stable for at least two months at −30 °C. The structure of the C_{2v}-symmetric P_5 cage was deduced from the ^{31}P NMR spectrum of the $P_5X_2^+$ ions[19–21] (X = Br, I; see Figure 1 for $P_5Br_2^+$ spectrum).

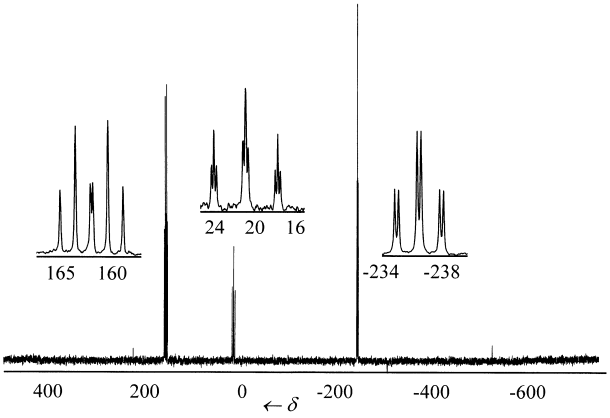


Figure 1. ^{31}P NMR spectrum of **3** in CD_2Cl_2 at 203 K.

The $P_5Br_2^+$ ion is rigid at 298 K according to the ^{31}P NMR spectrum. The crystal structure determination[22] of a colorless monoclinic block of **3** confirmed the presence of the almost C_{2v}-symmetric $P_5Br_2^+$ ion (Figure 2) and the intact $Al[OC(CF_3)_3]_4^-$ ion (see Supporting Information).[23] This P_5 cage is unprecedented and is not found as part of the many polyphosphides or organopolyphosphanes known to date.[24, 25] The P–P bond lengths in the $P_5Br_2^+$ ion (2.150(7) – 2.262(8) Å) are close to the values found in P_4 (2.21 Å) or $Ag(P_4)_2^+$ (2.15 – 2.32 Å),[13] and the P–Br distances lie in the normal range. Ab initio MP2/TZVPP[26–29] and HF-DFT MPW1PW91/6-311G(2df)[30–32] calculations reproduced the solid-state geometry of $P_5Br_2^+$ within 0.024 Å and 1.2°. $P_5Br_2^+$ is a true minimum at both levels of theory; calculated and experimental structural parameters are compared in Table 1. For comparison the $P_5I_2^+$ geometry calculated at the MP2/TZVPP level of theory is also included.

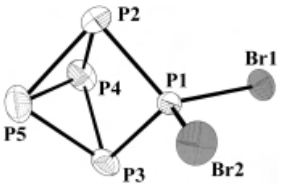


Figure 2. The structure of the $P_5Br_2^+$ ion in **3** at 200 K (25% ellipsoids).

Table 1. Structural parameters of the $P_5X_2^+$ ions (X = Br (**3**), I (**2**)).[a]

Parameter	**3**, Exp.[b]	**3**, MP2[c]	**3**, MPW1PW91[d]	**2**, MP2[c]
P–X	2.140(3)	2.163	2.164	2.383
P1–P2,3	2.156(7)	2.167	2.171	2.181
P2,3–P4,5	2.239(8)	2.259	2.239	2.254
P4–P5	2.211(8)	2.222	2.194	2.229
X-P-X	106.4(2)	105.8	106.1	108.5
P2,3-P1-X	114.7(3)	114.6	115.0	114.2
P2-P1-P3	91.4(3)	92.6	90.9	90.9
P4,5-P2,3-P1	83.0(3)	82.0	83.1	83.1

[a] Distances in [Å], bond angles in [°]. [b] Salt **3** averaged according to C_{2v} symmetry. [c] TZVPP basis set. [d] 6-311G(2df) basis set.

The Mulliken (NBO) charges calculated at the HF-DFT level of theory show that the unipositive charge of the $P_5Br_2^+$ ion is delocalized over the P_5 cage. A partial charge of +0.27 (+0.47) was assigned to P1, +0.16 (+0.15) to P2,3, and +0.14 (+0.13) to P4,5, while the more electronegative atoms Br1,2 remain nearly uncharged (+0.06 or −0.02, respectively). Raman spectroscopy showed that also the bulk material is pure **2** and **3**. Observed and calculated vibrational frequencies of **2** and **3** are collected[30] in Table 2. A total of 10 (**2**) and 13 (**3**) of the 15 expected vibrational bands of the cations were observed and all bands of the P_5 cage are strongly mixed. The symmetric breathing mode of the P_5 cage (A_1, **2**: 541, **3**: 553 cm^{-1}) is slightly weakened compared to the A_1 mode of P_4 (600 cm^{-1}) but higher in energy than the P–P vibrations of red phosphorus (highest energy band at 461 cm^{-1}).[33]

Table 2. Experimental and nonscaled calculated vibrational frequencies ν [s^{-1}] of **2** and **3**.

2, $\nu_{exp.}$ (Int. [%])	**2**, ν_{calcd}[a]	Symmetry	**3**, $\nu_{exp.}$ (Int. [%])	**3**, ν_{calcd} (Int. [%])[b]	Symmetry	Assignment for **3**
796 (21)			797 (34)			Al–O (cf. 798 for $Ag(P_4)_2[A]$)[13]
745 (20)			747 (29)			Al–O (cf. 746 for $Ag(P_4)_2[A]$)[13]
541 (32)	544	A_1	553 (71)	571 (100)	A_1	ν_s; "breathing mode" of the P_5 cage
within A_1 at 541?	537	B_1	534 (20)	557 (7)	B_1	ν_{as}; P2-P1-P3
502 (20)	505	A_1	523 (51)	538 (27)	A_1	ν_s; P_5 cage
within B_1 at 448?	450	B_2	504 (11)	486 (4)	B_2	ν_{as}; P2,3,1 and Br1,2
448 (10)	444	B_1	443 (20)	465 (10)	B_1	ν_{as}; P2,3,4,5
385 (30)	390	B_1	387 (31)	409 (35)	B_2	ν_{as}; P_5 cage
359 (sh)	357	A_2	375 (77)	383 (34)	A_1	ν_s; P2,3,4,5
354 (80)	350	A_1	361 (37)	382 (17)	A_2	ν_{as}; P2,3,4,5
329 (70)	314	A_1	331 (29)	344 (12)	A_1	ν_s; P_5 cage
318 (sh)			321 (24)			anion (cf. 322 for $Ag(P_4)_2[A]$)[13]
234 (4)			234 (8)			anion (cf. 234 for $Ag(P_4)_2[A]$)[13]
under A_1 at 168?	170	B_1	203 (100)	203 (35)	A_1	ν_s; PBr_2 unit
168 (100)	169	A_1	191 (37)	191 (11)	B_2	ν_{as}; PBr_2 unit
126 (4)	132	B_2	150 (20)	148 (5)	B_1	P2-P1-P3 bend
87 (4)	86	A_1	120 (9)	115 (10)	A_1	PBr_2 bend
n.o.[c]	79	A_2	n.b.[c]	84 (3)	A_2	cage deformation
n.o.[c]	56	B_1	n.b.[c]	60 (2)	B_2	cage deformation

[a] MP2/TZVPP frequencies. [b] MPW1PW91/6-311G(2df) frequencies. [c] n.o. = Not observed.

The very weakly basic $Al[OC(CF_3)_3]_4^-$ ion stabilizes, in **1** and **2**, the first binary phosphorus-rich P–X cation (X = halogen, H, organyl) and shows that this class of cations is accessible if a suitable weakly basic and nonoxidizing counterion is provided. In the course of this reaction PX_2^+ ions (X = Br, I), which are isoelectronic to silylene SiX_2 and an interesting class of compounds in their own right, were formed as intermediates and may be used in further reactions with other simple inorganic or organic substrates.

Experimental Section

All manipulations were performed using grease-free Schlenk or dry box techniques and a dinitrogen or argon atmosphere. All apparatus were closed by Young valves and the solvents were rigorously dried over P_2O_5 and degassed prior to use and stored under N_2 on molecular sieves (4 Å). Yellow phosphorus was sublimed prior to use. Full details are disclosed in the Supporting Information.

In situ synthesis of **2**: $Ag(P_4)_2^+[A^-]$ (0.151 g, 0.114 mmol) was weighed into an NMR tube connected to a valve. I_2 (0.101 g, 0.399 mmol) was sublimed onto the solid at 77 K after which CD_2Cl_2 (0.9 mL) was condensed onto the mixture. The NMR tube was sealed and then placed in a dry ice/2-propanol bath and activated with ultrasound at −78 °C for about 10 min. The initial ^{31}P NMR spectra were run 30 min later and the ^{13}C and ^{27}Al NMR spectra after storage at −80 °C one week later (no decomposition visible in the ^{31}P NMR spectrum). ^{13}C NMR (63 MHz, CD_2Cl_2, −90 °C): $\delta = 122.4$ (q, $J(C,F) = 290.1$ Hz; CF_3); ^{27}Al NMR (78 MHz, CD_2Cl_2, −90 °C): $\delta = 39.5$ (s, $\nu_{1/2} = 27$ Hz); ^{31}P NMR (101 MHz, CD_2Cl_2, −90 °C): $\delta = 168.2$ (dt, $^1J(P2,3,P1) = 278.5$ Hz, $^1J(P2,3,\ P4,5) = 152.6$ Hz, 2P), −89.0 (tt, $^1J(P1,P2,3) = 278.5$ Hz, $^2J(P1,\ P4,5) = 26.7$ Hz, 1P), −193.9 (td, $^1J(P4,5,\ P2,3) = 152.6$ Hz, $^2J(P4,5,\ P1) = 26.7$ Hz, 2P). Upon warming the sample to −40 °C, the $P_5I_2^+$ signals vanish quickly and, apart from other unassigned signals of lower intensity, those of $P_3I_6^+$ appear as the major P-containing peaks ^{31}P NMR (−80 °C): $\delta = 89.2$ (d, $^1J(P,P) = 385.5$ Hz, 2P), −4.6 (t, $^1J(P,P) = 385.5$ Hz, 1P).

Synthesis of **2**: $Ag(P_4)_2^+[A^-]$ (1.020 g, 0.765 mmol) was weighed into a two bulbed vessel incorporating a sintered glass frit and stopped by Young valves. I_2 (0.697 g, 2.746 mmol) was sublimed onto the solid at 77 K after which CH_2Cl_2 (5 mL) was condensed onto the mixture. The apparatus was placed in a dry ice/2-propanol bath until the solvent had thawed and was then stored in a −80 °C freezer and heavily shaken every 30 minutes for about one minute (10 ×). After four days at −80 °C the yellow solution over yellow-orange precipitate was filtered at −80 °C. All volatiles were then quickly removed at about 0 °C (expected weight of the material: 1.717 g, found: 1.737 g) and the apparatus immediately transferred into a glove box. Soluble yellow **2** ((0.963 g, 0.700 mmol), expected: 1.052 g; yield: 92 %) and insoluble material (0.611 g; expected: 0.665 g) were isolated, while 0.140 g were not accessible within the flask (total: 0.963 g + 0.611 g + 0.140 g = 1.714 g; expected: 1.717 g). Raman spectra of **2** (Table 2) and the insoluble material (P_4, PI_3, and traces of P_2I_4) were recorded immediately after the sample preparation. A ^{31}P NMR sample of yellow **2** in CD_2Cl_2 gave the same spectrum as the one observed in the in situ reaction described above.

Synthesis of **3**: $Ag^+(CH_2Cl_2)[A^-]$ (0.848 g, 0.731 mmol) was weighed into a two-bulbed glass vessel incorporating a fine sintered glass frit and two Young valves. P_4 (0.086 g, 0.694 mmol) was added to the solid. PBr_3 (0.188 g, 0.066 mL, 0.695 mmol) was added to it at 77 K and CH_2Cl_2 (ca. 10 mL) was condensed onto the mixture and allowed to stir at −78 °C for 8 h. For completion of the reaction the vessel was stored in a −80 °C freezer for 10 days and occasionally heavily shaken. After filtration from the insoluble AgBr a clear colorless solution was obtained. The volume of the solvent was quickly reduced to about 1 mL at 0 °C. Salt **3** crystallized as colorless blocks almost quantitatively from the cooled concentrated filtrate (−30 °C). Yield: 0.752 g (85 %).^{13}C NMR (63 MHz, CD_2Cl_2, −70 °C): $\delta =$ 121.5 (q, $J(C,F) = 292.0$ Hz; CF_3); ^{27}Al NMR (78 MHz, CD_2Cl_2, −70 °C): $\delta = 38.7$ (s, $\nu_{1/2} = 12$ Hz); ^{31}P NMR (101 MHz, CD_2Cl_2, −80 °C): $\delta = 162.0$ (dt, $^1J(P2,3,\ P1) = 320.9$ Hz, $^1J(P2,3,\ P4,5) = 148.7$ Hz, 2P), 20.0 (tt, $^1J(P1,\ P2,3) = 320.9$ Hz, $^2J(P1,\ P4,5) = 25.8$ Hz, 1P), −237.1 (td, $^1J(P4,5,\ P2,3) =$ 148.7 Hz, $^2J(P4,5,\ P1) = 25.8$ Hz, 2P).

Received: July 13, 2001 [Z17496]

[1] a) T. P. Martin, *Z. Phys.* **1986**, *D 3*, 211; b) R. Huang, H. Li, Z. Lin, S. Yang, *J. Phys. Chem.* **1995**, *99*, 1418; c) R. B, Huang, Z. Y. Liu, P. Zhang Y. B. Zhu, F. C. Lin, J. H. Zhao, L. S. Zheng, *Chin. J. Struct. Chem.* **1993**, 180; d) Z. Y. Liu, R. B. Huang, L. S. Zheng, *Z. Phys. D* **1996**, *38*, 171; e) M. D. Chen, J. T. Li, R. B. Huang, L. S. Zheng, C. T. Au, *Chem. Phys. Lett.* **1999**, *305*, 439.

[2] J. A. Zimmerman, S. B. H. Bach, C. H. Watson, J. R. Eyler, *J. Phys. Chem.* **1990**, *95*, 98.

[3] O. A. Mazyar, T. Baer, *Chem. Phys. Lett.* **1998**, *288*, 327.

[4] a) L. Latifzadeh-Masoudipour, K. Balasubramanian, *Chem. Phys. Lett.* **1997**, *267*, 545; b) L. Latifzadeh, K. Balasubramanian, *Chem. Phys. Lett.* **1996**, *258*, 393; c) L. Latifzadeh, K. Balasubramanian, *Chem. Phys. Lett.* **1995**, *241*, 13.

[5] D. Gudat, *Eur. J. Inorg. Chem.* **1998**, 1087.

[6] a) J. Passmore, *J. Chem. Soc. Dalton Trans.* **1978**, 1251; b) C. Aubauer, M. Kaupp, T. M. Klapötke, H. Nöth, H. Pietrowski, W. Schnick, J. Senker, *J. Chem. Soc. Dalton Trans.* **2001**, 1880, and references therein.

[7] S. Pohl, *Z. Anorg. Allg. Chem.* **1983**, *498*, 20.

[8] C. Aubauer, G. Engelhardt, T. M. Klapötke, A. Schulz, *J. Chem. Soc. Dalton Trans.* **1999**, 1729.

[9] M. Baudler, K. Glinka, *Chem. Rev.* **1993**, *93*, 1623.

[10] The very high P–E bond energies (E = F, O) led to the decomposition of the weakly basic counteranions $M_nF_{5n+1}^-$ ($n = 1-4$, M = As, Sb) or SO_3F^-. Reactions of P_4 with $S_2O_6F_2$ furnished elemental sulfur and P,F,O species. The sulfur was then oxidized by excess $S_2O_6F_2$ to give polysulfur cations. Attempts to prepare $P_2I_5^+$ (cf. $[P_2I_5][AlI_4]$) by reacting $I_3^+MF_6^-$ with P_2I_4 in various solvents at −78 °C only led to decomposition and formation of PF_3, MI_3, and elemental iodine (M = As, Sb).[8]

[11] I. Krossing, *Chem. Eur. J.* **2001**, *7*, 490.

[12] S. M. Ivanova, B. G. Nolan, Y. Kobayashi, S. M. Miller, O. P. Anderson, S. H. Strauss, *Chem. Eur. J.* **2001**, *7*, 503.

[13] I. Krossing, *J. Am. Chem. Soc.* **2001**, *123*, 4603.

[14] "Superweak Complexes of tetrahedral P_4 Molecules with the Silver Cation of Innocent Anions": I. Krossing, *Chem. Eur. J.* **2002**, in press.

[15] "Reactions of P_4 and I_2 with $Ag[Al(OC(CF_3)_3)_4]$: From Elusive Polyphosphorous Cations to Subvalent $P_3I_6^+$ and Phosphorus Rich $P_5I_2^+$": I. Krossing, *Dalton Trans.*, accepted.

[16] B. W. Tattershall, N. L. Kendall, *Polyhedron* **1994**, *13*, 1517.

[17] A. Klamt, G. Schürmann, *J. Chem. Soc. Perkin. Trans.* **1993**, *2*, 799.

[18] Including the zero-point energy and thermal corrections to the free energy at 298 K.

[19] The position of the signal of the $P(X_2)$ atom in $P_5X_2^+$ is shifted considerably from $\delta(^{31}P) = +23$ (X = Br) to $\delta(^{31}P) = -89$ (X = I) due to an effective Fermi-contact mechanism[20] which is also responsible for the extreme upfield shift of the PI_4^+ ion ($\delta(^{31}P) = -475$[6, 20, 21]).

[20] M. Kaupp, C. Aubauer, G. Engelhardt, T. M. Klapötke, O. Malkina, *J. Chem. Phys.* **1999**, *110*, 3897.

[21] This is the value of $PI_4^+[A^-]$ (I. Krossing, unpublished results). The signal for solid $PI_4[MF_6]$ appeared at $\delta(^{31}P) = -517$ (M = As) and −519 (M = Sb).[20]

[22] Crystal structure determination of **3**: IPDS (Stoe), graphite-monochromated $Mo_{K\alpha}$ radiation, $T = 200(2)$ K, unit cell determination: 5000 reflections, corrections: Lorentz, polarization, and numerical absorption correction, $\mu = 2.61$ cm^{-1}, direct methods with SHELXS-97, refinement against F^2 with SHELXL-97. Space group: $P2/n$, $Z = 2$, $a = 13.536(3)$, $b = 9.554(2)$, $c = 14.508(3)$ Å, $\beta = 90.15(3)°$, $V =$ 1876.2(6) Å^3, $\rho_{calcd} = 2.269$ g cm^{-1}, $2\theta_{max.} = 52°$, reflections: 14525 collected, 3469 unique, 2323 observed (4σ), 322 parameters, 48 SADI restraints (to fix the anion), $R_1 = 0.0957$, wR_2 (all data) = 0.2823, GooF = 1.082. Upon further cooling a phase transition occurred and all of the 10 tested crystals cracked even when cooled very slowly. Therefore, the rotation of the 12 CF_3 groups could not be frozen out and the agreement factor remained relatively high. Moreover the $P_5Br_2^+$ ion occupies two different positions with a 50 % occupation each (see Supporting Information). Crystallographic data (excluding

 © WILEY-VCH Verlag GmbH, D-69451 Weinheim, 2001 1433-7851/01/4023-4408 $ 17.50+.50/0

structure factors) for the structure reported in this paper have been deposited with the Cambridge Crystallographic Data Centre as supplementary publication no. CCDC-167142. Copies of the data can be obtained free of charge on application to CCDC, 12 Union Road, Cambridge CB2 1EZ, UK (fax: (+44) 1223-336-033; e-mail: deposit@ccdc.cam.ac.uk).

[23] The solid-state arrangement of **3** is derived from a distorted CsCl packing in which the almost spherical $Al(OR)_4^-$ ions form a cubic primitive lattice in which the cubic interstices are occupied by the $P_5Br_2^+$ ion.

[24] A search of the chemical abstracts data base with Scifinder and the Cambridge structural database CSD with the program Conquest did not reveal a precedent of this P_5 cage. However, similar C_{2v}-symmetric MP_4 units (i.e. M = Ir) formally containing a P_4^{2-} unit are known.[25]

[25] M. Scheer, U. Becker, E. Matern, *Chem. Ber.* **1996**, *129*, 721.

[26] Performed with the program TURBOMOLE.[27]

[27] TURBOMOLE, Version 5:a) R. Ahlrichs, M. Bär, M. Häser, H. Horn, C. Kölmel, *Chem. Phys. Lett.* **1989**, *162*, 165; b) M. v. Arnim, R. Ahlrichs, *J. Chem. Phys.* **1999**, *111*, 9183.

[28] F. Weigend, M. Häser, *Theor. Chim. Acta* **1997**, *97*, 331.

[29] a) A. Schäfer, H. Horn, R. Ahlrichs, *J. Chem. Phys.* **1992**, *97*, 2571; b) A. Schäfer, C. Huber, R. Ahlrichs, *J. Chem. Phys.* **1994**, *100*, 5829.

[30] Performed with the program Gaussian98.[31] Vibrational frequencies were assigned based on the visualisation of the modes with the program GaussView.

[31] Gaussian 98 (Revision A.7), M. J. Frisch, G. W. Trucks, H. B. Schlegel, G. E. Scuseria, M. A. Robb, J. R. Cheeseman, V. G. Zakrzewski, J. A. Montgomery, R. E. Stratmann, J. C. Burant, S. Dapprich, J. M. Millam, A. D. Daniels, K. N. Kudin, M. C. Strain, O. Farkas, J. Tomasi, V. Barone, M. Cossi, R. Cammi, B. Mennucci, C. Pomelli, C. Adamo, S. Clifford, J. Ochterski, G. A. Petersson, P. Y. Ayala, Q. Cui, K. Morokuma, D. K. Malick, A. D. Rabuck, K. Raghavachari, J. B. Foresman, J. Cioslowski, J. V. Ortiz, B. B. Stefanov, G. Liu, A. Liashenko, P. Piskorz, I. Komaromi, R. Gomperts, R. L. Martin, D. J. Fox, T. Keith, M. A. Al-Laham, C. Y. Peng, A. Nanayakkara, C. Gonzalez, M. Challacombe, P. M. W. Gill, B. G. Johnson, W. Chen, M. W. Wong, J. L. Andres, M. Head-Gordon, E. S. Replogle, J. A. Pople, Gaussian, Inc., Pittsburgh, PA, **1998**.

[32] C. Adamo, V. Barone, *J. Chem. Phys.* **1998**, *108*, 664.

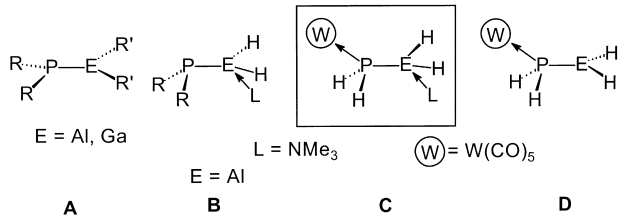
[33] J. R. Durig, J. M. Casper, *J. Mol. Struct.* **1970**, *55*, 351.

Lewis Acid/Base Stabilized Phosphanylalane and -gallane**

Ulf Vogel, Alexey Y. Timoshkin, and Manfred Scheer*

Dedicated to Professor Max Herberhold in occasion of his 65th birthday

Bulky substituents at the main group atoms are necessary for the synthesis of monomeric phosphanylalanes and -gallanes of the type **A**.[1] In contrast to the strong π bonding in B–N, B–P, and B–As derivatives, only very weak π interactions combined with an increase of ionic bond contributions is supposed for the heavier Group 13 elements.[1] Thus, the lone pair of electrons at the heavier Group 15 element and the presence of an adjacent empty orbital at the Group 13 element leads to a head-to-tail dimerization or trimerization if the substituents are not sufficiently bulky. These compounds are mainly synthesized by salt elimination reactions;[1] however, it was shown recently that the cleavage of cyclic oligomers $[R_2PER'_2]_n$ (E = P, As; R = Me; R′ = $SiMe_3$; $n = 2, 3$) by a Lewis base, such as 4-(dimethylamino)-pyridine (DMAP), leads to monomeric complexes.[2] To our knowledge, the parent compounds $[H_2EPH_2]$ (E = Al, Ga) have not yet been synthesized or even detected in matrix isolation experiments,[3a] but ab initio calculations have been carried out for both compounds.[3, 4] It has been suggested that they play important roles in the formation of aluminum phosphide and gallium phosphide semiconductors starting from PH_3 and EH_3, respectively, by chemical vapor deposition (CVD) processes.[5] In 1993 Cowley and Jones reported the synthesis of monomeric base-stabilized phosphanyl- and arsanylalanes of type **B** by a metathetical reaction.[6] In **B** the P atom still contains bulky mesityl substituents, whereas the AlH_2 moiety was stabilized by a Lewis base.



Our interest in this field concerns the synthesis of unsubstituted[7] oligomers and polymers of mixed ligands of elements of Group 13 and 15. By using our general concept of the stabilization of unstable moieties by fixation of the phosphorus lone pair of electrons by metal carbonyl complexes,[8] we report herein on the first synthesis of Lewis acid/base stabilized phosphanylalane and -gallane of type **C**.

According to our denisty functional theory (DFT) calculations[9a] (Table 1), the additional coordination of a Lewis base, such as NMe_3, at $[H_2AlPH_2]$ stabilizes the resulting adduct by 108 kJ mol^{-1}. The additional coordination of a Lewis acid such as $[W(CO)_5]$ leads to a further increase of stabilization by 154 kJ mol^{-1}. On the other hand, if $[H_2AlPH_2]$ is only coordinated by the Lewis acid $[W(CO)_5]$ (compound **D**) the stabilization energy is only −135 kJ mol^{-1}. $[H_2AlPH_2\{W(CO)_5\}]$ (**D**) tends to display an intramolecular (O)C···Al interaction that stabilizes the unsaturated Al center. Therefore, for steric as well as thermodynamic reasons, it seems to be essential for the molecule $[H_2AlPH_2]$ to possess both Lewis base and acid stabilization, as realized in a molecule of type **C**; the stabilization energy of −262 kJ mol^{-1} is higher than the dimerization energy of $[H_2AlPH_2]$ (−147 kJ mol^{-1}; Table 1). Furthermore, it is interesting that the Gibbs energies of H_2 elimination reactions between unprotected AlH_3 and PH_3 [reaction (9)] and between their donor–acceptor complexes [reaction (7)] are similar and, therefore, the presence of the used protecting groups does not change the thermodynamics of the elimina-

[*] Prof. Dr. M. Scheer, Dipl.-Chem. U. Vogel
Institut für Anorganische Chemie der Universität Karlsruhe
76128 Karlsruhe (Germany)
Fax: (+49) 721-608-7021
E-mail: mascheer@chemie.uni-karlsruhe.de
Dr. A. Y. Timoshkin
Philipps-Universität Marburg
35032 Marburg (Germany)

[**] This work was supported by the Deutsche Forschungsgemeinschaft and the Fonds der Chemischen Industrie. A.Y.T. is grateful to the Alexander von Humboldt Foundation for a research fellowship.

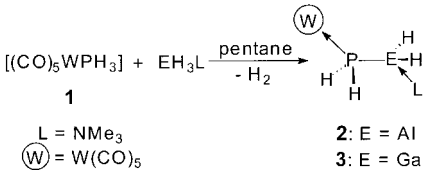
 © WILEY-VCH Verlag GmbH, D-69451 Weinheim, 2001 1433-7851/01/4023-4409 $ 17.50+.50/0

Table 1. Calculated standard enthalpies ΔH^0_{298} [kJ mol^{-1}], Gibbs energies ΔG^0_{298} [kJ mol^{-1}], and entropies ΔS^0_{298} [J K^{-1} mol^{-1}] of gas-phase reactions. B3LYP/6-31G*(ECP on W) level of theory.

Reaction		ΔH^0_{298}	ΔS^0_{298}	ΔG^0_{298}
$2\,H_2AlPH_2 = [H_2AlPH_2]_2$	(1)	− 147.4	− 181.4	− 93.3
$H_2AlPH_2 + NMe_3 = [Me_3N \cdot H_2AlPH_2]$	(2)	− 108.3	− 160.4	− 60.5
$H_2AlPH_2 + [W(CO)_5] = [H_2AlPH_2\{W(CO)_5\}]$	(3)	− 134.9	− 180.6	− 81.1
$H_2AlPH_2 + NMe_3 + [W(CO)_5] = [Me_3N \cdot H_2AlPH_2\{W(CO)_5\}]$	(4)	− 262.2	− 333.6	− 162.8
$AlH_3 + NMe_3 = [Me_3N \cdot AlH_3]$	(5)	− 117.0	− 150.6	− 72.1
$PH_3 + [W(CO)_5] = [H_3P\{W(CO)_5\}]$	(6)	− 129.5	− 138.1	− 88.3
$[Me_3N \cdot AlH_3] + [H_3P\{W(CO)_5\}] = [Me_3N \cdot H_2AlPH_2\{W(CO)_5\}] + H_2$	(7)	− 44.6	− 52.6	− 28.9
$AlH_3 + PH_3 = H_3AlPH_3$	(8)	− 49.4	− 121.3	− 13.3
$AlH_3 + PH_3 = H_2AlPH_2 + H_2$	(9)	− 28.8	− 7.6	− 26.5
$AlH_3 + PH_3 = \frac{1}{2}[H_2AlPH_2]_2 + H_2$	(10)	− 102.5	− 98.3	− 73.2
$[W(CO)_5] + NMe_3 = [Me_3N \cdot W(CO)_5]$	(11)	− 111.5	− 163.2	− 62.9
$[Me_3N \cdot H_2AlPH_2\{W(CO)_5\}] = H_2AlPH_2 + [Me_3N \cdot W(CO)_5]$	(12)	150.7	170.4	99.9

tion reaction, but prevents subsequent reactions of the formed product. Compound $[Me_3N \cdot H_2AlPH_2\{W(CO)_5\}]$ is found to be stable at 298 K with respect to dissociation into the components [reaction (4)] as well as with respect to possible dissociation into $[H_2AlPH_2]$ and $[Me_3N \cdot W(CO)_5]$ [reaction (12)].

Since sterically unprotected Group 13/15 σ-bound compounds are sensitive towards donor solvents such as THF, for the experimental approach to complexes of type **C**, the H_2 elimination reaction[10] appears to us to be the method of choice. Indeed, reactions of $[W(CO)_5PH_3]$ (**1**) with $EH_3 \cdot NMe_3$ in hydrocarbons as solvent lead to the novel complexes $[\{(CO)_5W\}H_2PEH_2 \cdot NMe_3]$ (**2**: E = Al, **3**: E = Ga) in good yields. Experiments to synthesize the corresponding boron-substituted complex in a similar manner have failed so far due to the low reactivity of the borane trimethylamine complex towards **1** [Eq. (13)].



(13)

Compounds **2** and **3** form colorless crystals, which rapidly turn yellowish on exposure to light. They are soluble in hydrocarbon solvents without decomposition at room temperature.[11] The appropriate molecular ion peaks are observed in the mass spectra of both compounds. The ^{31}P NMR spectrum of **2** reveals a broad triplet at $\delta = -250$ (^1J(P,H) = 283 Hz), which is shifted to higher field compared to that of the starting compound $[W(CO)_5PH_3]$ ($\delta = -184$) as one would expect for the substitution of a proton by the electropositive aluminum atom. In accordance with this, the ^{31}P NMR spectrum of **3** shows a triplet of triplets at $\delta = -240$ due to the coupling of the phosphorus atom to the protons at the P and Ga atom, respectively. The Raman spectrum of **2** shows four bands at 1894, 1917, 1966, and 2077 cm^{-1} for the CO stretching frequencies, as well as a band for the P–H vibration mode at 2323 cm^{-1} and one for the Al–H absorption at 1819 cm^{-1}, which are in good agreement with the calculated frequencies.[9b] Furthermore, the broad absorption found at 1680 cm^{-1} indicates the presence of Al–H···Al hydride bridges. This assumption for **2** is confirmed by the X-ray structure analysis, which shows a H-bridged dimer in the solid state (Figure 1, the H atoms on the phosphorus and aluminum atoms could be located and freely refined).

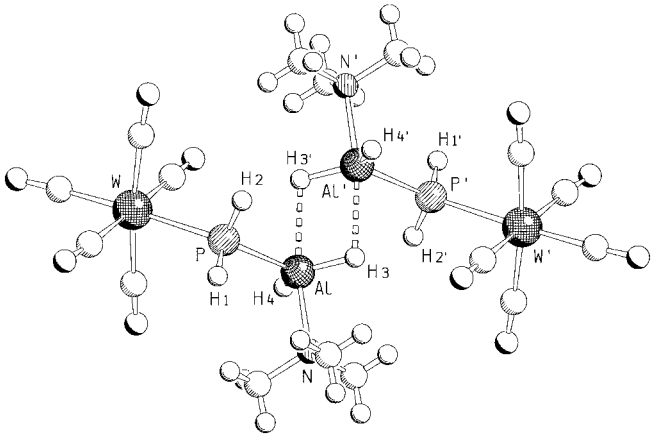


Figure 1. Molecular structure of **2** in the crystal. Selected bond lengths [Å] and angles [°]: Al-P 2.367(1), W-P 2.5491(9), Al-N 2.036(3), Al-H4 1.532, Al-H3 1.553, Al′···H3 2.053; W-P-Al 118.44(4), P-Al-N 103.28(8), W-P-Al-N 118.5, H2-P-Al-H3 11.3.

In the molecular structure of **2**[12] (Figure 1) the aluminum atom adopts a distorted trigonal-bipyramidal coordination sphere (P-Al-N 103.28(8)°) with a Al···H3′ distance to the second molecule of 2.053 Å (compare with 1.553 Å for the intramolecular Al–H3 distance). Similar long hydride bridges were found in the dimer $[H_3Al(NMe_3CH_2Ph)]_2$ (2.07(2) Å).[13] The local geometry around the Al–P axis is almost eclipsed (torsion angle H2-P-Al-H3 11°) and is therefore not consistent with the calculated structure of free $[H_2AlPH_2]$, for which a *gauche* conformation is established with an almost planar geometry around the Al center (torsion angle: 45°). Owing to the weak π interaction combined with the ionic bond contribution, the Al–P bond length in H_2AlPH_2 (2.335 Å[3c]) is shorter than that in **2** (2.377(1) Å), for which such a π interaction is not possible. The Al–P bond length in **2** is close to that in known monomeric compounds with organic substituents, but it is significantly shorter than that in $[(CO)_5CrPPh_2Al(CH_2SiMe_3)_2 \cdot NMe_3]$ (2.485(1) Å),[14] probably due to the steric repulsion of the substituents at the Al and

 © WILEY-VCH Verlag GmbH, D-69451 Weinheim, 2001 1433-7851/01/4023-4410 $ 17.50+.50/0 *Angew. Chem. Int. Ed.* **2001**, *40*, No. 23

P atom, respectively, in the latter compound. In **2** the W–P bond length (2.549(1) Å) and the Al–N bond length (2.036(3) Å) are similar to those in $[W(CO)_5PH_3]$ (**1**) (2.491(2) Å),[15] $[W(CO)_5PMe_3]$ (2.516(2) Å),[16] and $[W(CO)_5PPh_3]$ (2.545(1) Å),[17] and to those in $AlH_3 \cdot N(C_2H_4)_3CH$ (1.991(4) Å)[18] and $[(CO)_5CrPPh_2Al(CH_2SiMe_3)_2 \cdot NMe_3]$ (2.049(3) Å),[14] respectively.

The structural optimization of $[\{(CO)_5W\}H_2PAlH_2 \cdot NMe_3]$ by density functional methods[9] under no symmetry restrictions and tight convergence criteria resulted in the *cis*-orientated isomer being 5 kJ mol^{-1} more stable than the experimentally observed *trans* isomer. Since this difference is very small, the influence of other interactions in the solid-state structure of **2** together with the intermolecular dimerization to form Al···H bridges may play an important role in the preference for the experimentally observed *trans* orientation of the substituents in the solid state.

Like **2** complex **3** also crystallizes in the space group $P2_1/c$. The compounds are, however, not isostructural since **3** is monomeric and lacks intermolecular H bonds. The monomeric nature of **3** leads to a slightly staggered geometry (Figure 2, torsion angle H1-P-Ga-H4 81.4°) in contrast to the

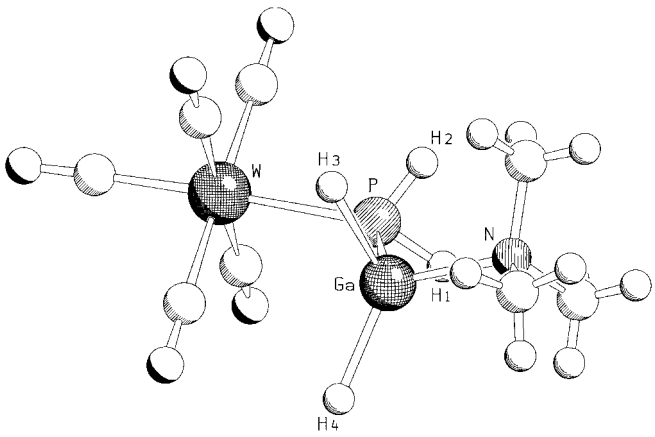


Figure 2. Molecular structure of **3** in the crystal. Selected bond lengths [Å] and angles [°]: Ga-P 2.349(2), W-P 2.537(2), Ga-N 2.039(7); W-P-Ga 114.72(7), P-Ga-N 107.4(2), W-P-Ga-N 158.95, H1-P-Ga-H4 81.4.

eclipsed configuration of the dimeric Al complex **2**. The free $[H_2GaPH_2]$ molecule displays a torsion angle of 44°.[4] The Ga–P bond length in **3** (2.349(2) Å) is slightly longer than the calculated distance in the free molecule $[H_2GaPH_2]$ (2.328 Å) and in the monomeric compounds stabilized by bulky substituents (e.g. tBu$_2$GaP(Mes*)SiPh$_3$, 2.295(3) Å, Mes* = 2,4,6-tri-*tert*-butylphenyl[19]). In the latter compounds the lone pair at the phosphorus atom interacts with the vacant orbital at the planar Ga atom, which is consistent with the flattened geometry at the P center. The Ga–P bond is lengthened if the steric repulsion between the substituents is further increased (e.g. tBu$_2$PGaTmp$_2$, 2.4225(8) Å, Tmp = 2,2,6,6-tetramethylpiperidinate[20]).

The results presented show that Lewis acid/base stabilization is necessary to stabilize the parent compounds of phosphanylalane and -gallane. Owing to their high tendency to lose H_2, the novel compounds open new perspectives for the synthesis of novel substituent-free oligomers comprising the elements of Group 13 and 15 fixed on transition metal centers. Furthermore, their use as molecular precursors in CVD processes could be of interest.

Experimental Section

$[\{(CO)_5W\}H_2PAlH_2 \cdot NMe_3]$ (**2**): $[W(CO)_5PH_3]$ (358 mg, 1.00 mmol)[15] and $AlH_3 \cdot NMe_3$ (89 mg, 1.00 mmol)[21] were refluxed in *n*-hexane (50 mL) under a nitrogen atmosphere until gas evolution ceased (≈2 h). The reaction mixture was filtered and the filtrate was reduced to about 30 mL. After one day at −30 °C **2** (200 mg, 45 %) crystallized as colorless crystals. ^{1}H NMR (300 MHz, [D$_8$]toluene, −40 °C, TMS ext.): $\delta = 1.41$ (s, 9H; NMe_3), 1.70 (d, ^1J(H,P) = 283 Hz, 2H; PH_2); ^{31}P NMR (101 MHz, [D$_8$]toluene, −40 °C, H_3PO_4 ext.): $\delta = -250$ (t, ^1J(P,H) = 283 Hz); MS (FI, 10 kV, 120 °C): m/z: 445 (7) [M^++H]; Raman (solid-state) $\tilde{\nu} = 2941$ (w), 2865 (w), 2803 (w), 2323 (m), 2068 (m), 1975 (sh), 1966 (vs), 1917 (w), 1894 (m), 1819 (w), 1680 (w, br), 460 (m), 438 (m), 103 cm^{-1} (m).

$[\{(CO)_5W\}H_2PGaH_2 \cdot NMe_3]$ (**3**): $[W(CO)_5PH_3]$ (358 mg, 1.00 mmol) and $GaH_3 \cdot NMe_3$ (132 mg, 1.00 mmol)[22] were refluxed in *n*-pentane (50 mL) under a nitrogen atmosphere until gas evolution ceased (≈1 h). The mixture was filtered and the filtrate was reduced to about 30 mL. After crystallization at −30 °C colorless crystals of **3** were obtained, which should be handled under exclusion of light. Yield: 190 mg (39 %). ^{1}H NMR (300 MHz, [D$_8$]toluene, −40 °C, TMS ext.): $\delta = 1.46$ (s, 9H; NMe_3), 1.84 (dt, ^1J(P,H) = 293 Hz, ^3J(H,H) = 3 Hz; PH_2), 4.74 (d br, ^2J(P,H) = 46 Hz; GaH_2); ^{31}P{^{1}H} NMR (101 MHz, [D$_8$]toluene, −40 °C, H_3PO_4 ext.): $\delta = -240$ (s, ^1J(W,P) = 165 Hz; PH_2); ^{31}P NMR (101 MHz, [D$_8$]toluene, −40 °C, H_3PO_4 ext.): $\delta = -240$ (tt, ^1J(H,P) = 293 Hz, ^2J(H,P) = 46 Hz; PH_2); MS (EI, 80 °C): m/z: 488 (0.2) [M^+], 460 (0.2) [$M^+ - CO$], 429 (0.1) [$M^+ - NMe_3$]; Raman (solid state): $\tilde{\nu} = 2942$ (w), 2859 (w), 2806 (w), 2335 (m), 2069 (m), 1971 (vs), 1944 (m), 1919 (m), 1895 (s), 1066 (w), 433 (m), 343 (w), 108 cm^{-1} (s).

Received: July 10, 2001 [Z 17464]

[1] P. P. Power, *Chem. Rev.* **1999**, *99*, 3463–3503.

[2] F. Thomas, S. Schulz, M. Nieger, *Eur. J. Inorg. Chem.* **2001**, 161–166.

[3] a) H.-J. Himmel, A. J. Downs, J. C. Green, T. M. Greene, *J. Chem. Soc. Dalton Trans.* **2001**, 535–545; b) R. D. Davy, H. F. Schaefer III, *J. Phys. Chem. A* **1997**, *101*, 3135–3142; c) calculated at the TZ2P CCSC level.

[4] T. J. Dudley, W. W. Brown, M. R. Hoffmann, *J. Phys. Chem. A* **1999**, *103*, 5152–5160.

[5] a) *CVD of Compound Semiconductors: Precursor Synthesis, Development and Applications* (Eds.: A. C. Jones, P. O'Brien), VCH, Weinheim, **1996**; b) R. L. Wells, W. L. Gladfelter, *J. Cluster Sci.* **1997**, *8*, 217–237.

[6] D. A. Atwood, L. Contreras, A. H. Cowley, R. A. Jones, M. A. Mardones, *Organometallics* **1993**, *12*, 17–18.

[7] free of any organic substituents.

[8] M. Scheer, P. Kramkowski, K. Schuster, *Organometallics* **2000**, *18*, 2874–2883; U. Vogel, G. Stößer, M. Scheer, *Angew. Chem.* **2001**, *113*, 1476–1478; *Angew. Chem. Int. Ed.* **2001**, *40*, 1443–1445; M. Scheer, K. Schuster, U. Becker, *Phosphorus Sulfur Silicon* **1996**, *109–110*, 141–144.

[9] a) DFT calculations have been performed by using the standard Gaussian 98 program suite Gaussian 98 (Revision A.7), M. J. Frisch, G. W. Trucks, H. B. Schlegel, G. E. Scuseria, M. A. Robb, J. R. Cheeseman, V. G. Zakrzewski, J. A. Montgomery, R. E. Stratmann, J. C. Burant, S. Dapprich, J. M. Millam, A. D. Daniels, K. N. Kudin, M. C. Strain, O. Farkas, J. Tomasi, V. Barone, M. Cossi, R. Cammi, B. Mennucci, C. Pomelli, C. Adamo, S. Clifford, J. Ochterski, G. A. Petersson, P. Y. Ayala, Q. Cui, K. Morokuma, D. K. Malick, A. D. Rabuck, K. Raghavachari, J. B. Foresman, J. Cioslowski, J. V. Ortiz, B. B. Stefanov, G. Liu, A. Liashenko, P. Piskorz, I. Komaromi, R. Gomperts, R. L. Martin, D. J. Fox, T. Keith, M. A. Al-Laham, C. Y. Peng, A. Nanayakkara, C. Gonzalez, M. Challacombe, P. M. W. Gill,

B. G. Johnson, W. Chen, M. W. Wong, J. L. Andres, M. Head-Gordon, E. S. Replogle, J. A. Pople, Gaussian, Inc., Pittsburgh, PA, **1998**. B3LYP functional (A. D. Becke, *J. Chem. Phys.* **1993**, *98*, 5648 – 5652; C. Lee, W. Yang, R. G. Parr, *Phys. Rev. B* **1988**, *37*, 785 – 793) has been used together with standard 6-31G* basis set for H, C, N, Al, and P atoms. Effective core potential basis set of Hay and Wadt (P. J. Hay, W. R. Wadt, *J. Chem. Phys.* **1985**, *82*, 299 – 310) was used for W atoms. All structures were fully optimized with subsequent vibrational analysis and correspond to the minimum on the potential energy surface; b) calculated Raman frequencies according to the B3LYP method (compare: A. Y. Timoshkin, H. F. Bettinger, H. F. Schaefer, *J. Am. Chem. Soc.* **1997**, *119*, 5668 – 5678): $\tilde{\nu}$(C – O): 1920, 1938, 1951, 1977, 2048; $\tilde{\nu}$(AlH): 1816, 1836; $\tilde{\nu}$(P – H): 2312, 2316 cm^{-1}.

[10] For H_2 elimination reactions which form bonds between Group 13 and Group 15 elements compare: M. Driess, S. Kuntz, K. Merz, H. Pritzkow, *Chem. Eur. J.* **1998**, *4*, 1628 – 1632.

[11] In toluene and CH_2Cl_2, H_2 elimination reactions occur at room temperature, whereas in donor solvents such as THF these reactions lead to rapid decomposition. The ^{31}P NMR spectra of these solutions in THF indicate an ionic decomposition product of possible formula $[\{(CO)_5W\}_2PH_2]^-$.

[12] Crystal structure analyses of **2** and **3** were performed on a STOE IPDS diffractometer with $Ag_{K\alpha}$ radiation ($\lambda = 0.56087$ Å) for **2** and $Mo_{K\alpha}$ radiation ($\lambda = 0.71073$ Å) for **3**. The structures were solved by direct methods with the program SHELXS-93,[23a] and full matrix least-squares refinement on F^2 in SHELXL-97[23b] was performed with anisotropic displacements for non-H atoms. Hydrogen atoms at carbon atoms were located in idealized positions and refined isotropically according to the riding model. The hydrogen atoms at the phosphorus, aluminum, and gallium atoms were freely refined. **2**: $C_8H_{13}AlNO_5PW$, $M_r = 444.99$, crystal dimensions $0.40 \times 0.20 \times 0.08$ mm^3, monoclinic, space group $P2_1/c$ (no. 14); $a = 6.562(1)$, $b = 13.495(3)$, $c = 17.295(4)$ Å, $\beta = 100.29(3)^\circ$, $T = 210(2)$ K, $Z = 4$, $V = 1506.9(5)$ $Å^3$, $\rho_{calcd} = 1.961$ $Mg\,m^{-3}$, $\mu(Ag_{K\alpha}) = 4.219$ mm^{-1}, 4058 independent reflections ($R_{int} = 0.0435$, $2\theta_{max} = 46.3^\circ$), 3637 observed with $F_o = 4\sigma(F_o)$; 173 parameters, $R_1 = 0.0246$, $wR_2 = 0.0638$. **3**: $C_8H_{13}GaNO_5PW$, $M_r = 487.73$, crystal dimensions $0.50 \times 0.30 \times 0.02$ mm^3, monoclinic, space group $P2_1/c$ (no. 14); $a = 6.629(1)$, $b = 11.533(2)$, $c = 20.112(4)$ Å, $\beta = 90.27(3)^\circ$, $T = 200(1)$ K, $Z = 4$, $V = 1537.4(5)$ $Å^3$, $\rho_{calcd} = 2.107$ $Mg\,m^{-3}$, $\mu(Mo_{K\alpha}) = 9.338$ mm^{-1}, 2912 independent reflections ($R_{int} = 0.1058$, $2\theta_{max} = 52^\circ$), 2623 observed with $F_o = 4\sigma(F_o)$; 161 parameters, $R_1 = 0.0437$, $wR_2 = 0.1137$. Crystallographic data (excluding structure factors) for the structures reported in this paper have been deposited with the Cambridge Crystallographic Data Centre as supplementary publication no. CCDC-166049 (**2**) and CCDC-166050 (**3**). Copies of the data can be obtained free of charge on application to CCDC, 12 Union Road, Cambridge CB2 1EZ, UK (fax: (+44) 1223-336-033; e-mail: deposit@ccdc.cam.ac.uk).

[13] J. L. Atwood, F. R. Bennett, F. M. Elms, C. Jones, C. L. Raston, K. D. Robinson, *J. Am. Chem. Soc.* **1991**, *113*, 8183 – 8185.

[14] C. Tessier-Youngs, C. Bueno, O. T. Beachley, Jr., M. R. Churchill, *Inorg. Chem.* **1983**, *22*, 1054 – 1059.

[15] U. Vogel, M. Scheer, *Z. Anorg. Allg. Chem.* **2001**, *627*, 1593 – 1598.

[16] F. A. Cotton, D. J. Darensbourg, B. W. S. Kolthammer, *Inorg. Chem.* **1981**, *20*, 4440 – 4442.

[17] M. J. Aroney, I. E. Buys, M. S. Davies, T. W. Hambley, *J. Chem. Soc. Dalton Trans.* **1994**, 2827 – 2834.

[18] J. L. Atwood, K. W. Butz, M. G. Gardiner, C. Jones, G. A. Koutsantonis, C. L. Raston, K. D. Robinson, *Inorg. Chem.* **1993**, *32*, 3482 – 3487.

[19] M. A. Petrie, K. Ruhlandt-Senge, P. P. Power, *Inorg. Chem.* **1992**, *31*, 4038 – 4039.

[20] G. Linti, R. Frey, K. Polborn, *Chem. Ber.* **1997**, *130*, 663 – 668.

[21] K. Ruff, *Inorg. Synth.* **1967**, *9*, 30 – 37.

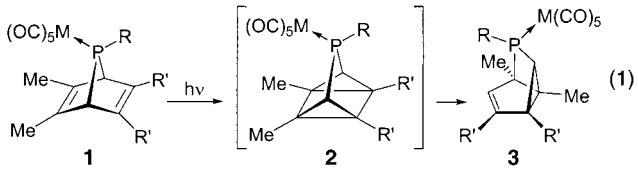
[22] D. F. Shriver, A. E. Shirk, *Inorg. Synth.* **1977**, *17*, 42 – 45.

[23] a) G. M. Sheldrick, SHELXS-93, Universität Göttingen, **1993**; b) G. M. Sheldrick, SHELXL-97, Universität Göttingen, **1997**.

Norbornadiene – Quadricyclane Valence Isomerism for a Tetraphosphorus Derivative**

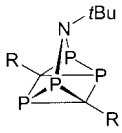
Mark J. M. Vlaar, Andreas W. Ehlers, Marius Schakel, Scott B. Clendenning, John F. Nixon, Martin Lutz, Anthony L. Spek, and Koop Lammertsma*

The photochemically induced valence isomerization of norbornadiene to the higher energy quadricyclane is well established[1] and this is also the case for the 7-oxa- and 7-azanorbornadienes.[2] The related 7-phospha analogue **1** on the other hand undergoes a UV-induced rearrangement to the tricyclic compound **3** [Eq. (1), R = Ph, Me; R′ = CO_2Me; M = W, Cr] presumably via an intermediate quadricyclane **2**, however, this has not been established definitely.[3]



(1)

Recently, we found that tetraphosphaquadricyclane **8** is formed with surprising ease, together with the polycyclic compound **7** (Scheme 1), from the reaction of 2,4,6-tri-*tert*-butyl-1,3,5-triphosphabenzene (**4**) with the transient phosphinidene complex $[PhPW(CO)_5]$,[4, 5] which is generated in situ by thermal degradation of **1** (R = Ph, M = W). The mechanism for the unexpected formation of **8** was not elucidated, but an intramolecular [2+2] cycloaddition of the two P=C units of an intermediate tetraphosphanorbornadiene complex, the 1,4-adduct **6**,[6] was assumed. A similar process has been proposed for the formation of quadricyclane **9**, R = alkyl, but intermediate norbornadiene derivatives were not detected in this case either.[7]



9

Norbornadienes containing two or more P atoms have been proposed as intermediates, mostly in the cyclooligomerization of phosphaalkynes,[7, 8] but to date only one triphospha-7-

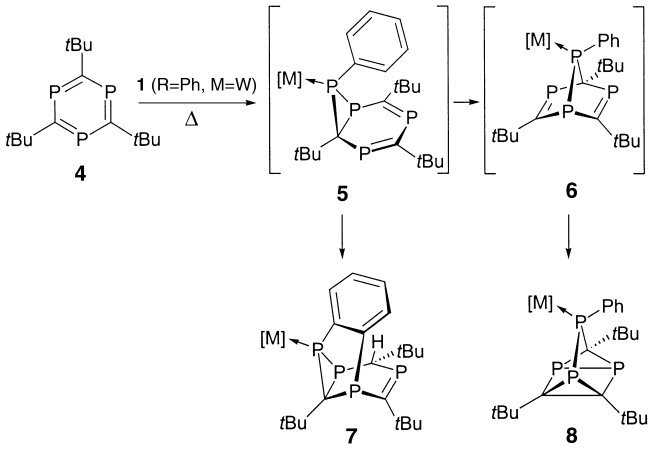
[*] Prof. Dr. K. Lammertsma, M. J. M. Vlaar, Dr. A. W. Ehlers, Dr. M. Schakel
Department of Organic and Inorganic Chemistry
Faculty of Sciences, Vrije Universiteit
De Boelelaan 1083, NL-1081 HV, Amsterdam (The Netherlands)
Fax: (+31) 20-444-7488
E-mail: lammert@chem.vu.nl

S. B. Clendenning, Prof. Dr. J. F. Nixon
The School of Chemistry, Physics and Environmental Science, University of Sussex, Brighton BN1 9QJ (UK)

Dr. M. Lutz, Dr. A. L. Spek
Bijvoet Center for Biomolecular Research
Utrecht University, Padualaan 8, NL-3584 CH, Utrecht (The Netherlands)

[**] The Netherlands Organization for Scientific Research (NOW/CW) is acknowledged for partial support (A.L.S., M.L., K.L.), as are the NSERC of Canada for a scholarship (S.B.C.), and EPSRC for funding phosphaorganometallic chemistry at Sussex University (J.F.N.). Dr. H. Zappey is thanked for the HR-MS spectra and J. C. Slootweg for his initiative.

 © WILEY-VCH Verlag GmbH, D-69451 Weinheim, 2001 1433-7851/01/4023-4412 $ 17.50+.50/0



Scheme 1. Synthesis of **7** and **8**; [M] = $W(CO)_5$.

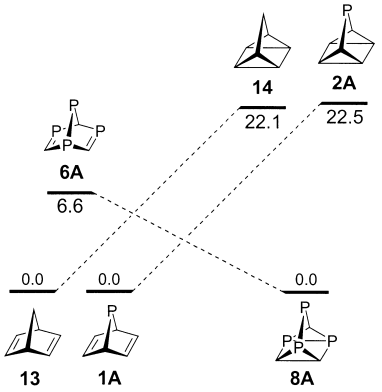
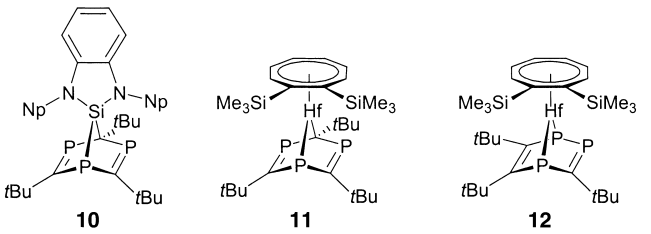


Figure 2. G3(MP2) computed energy difference between **6A** and **8A**, compared to the energy difference between **13** and **14** (experimental)[14] and **1A** and **2A** (MP2/6-31G).[3b]

silanorbornadiene (**10**; Np = CH_2*t*Bu)[9] and two triphospha-7-hafnanorbornadiene complexes (**11** and **12**)[10] have been isolated. While **10** is stable up to 80 °C and does not isomerize to the corresponding quadricyclane, such a quadricyclane intermediate was proposed for the thermal rearrangement of **11** to **12**.[10a]



We evaluated the proposed conversion of **6** into **8** by ab initio MO theory.[11] The MP2/6-31G* optimized geometries for the parent systems (**6A** and **8A**) are depicted in Figure 1. The geometry of quadricyclane **8A** is in good agreement with the experimentally determined molecular structure of **8**.[4] The reduced steric congestion, because of the absence of the bulky $W(CO)_5$ and *t*-butyl groups, is expressed in a shortening of the C1–C2 bond and all the P–C bonds.

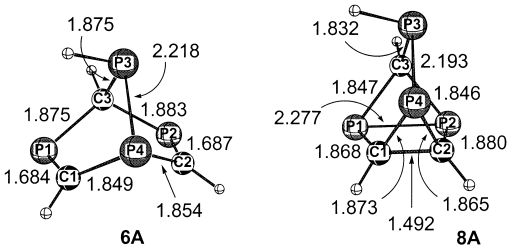
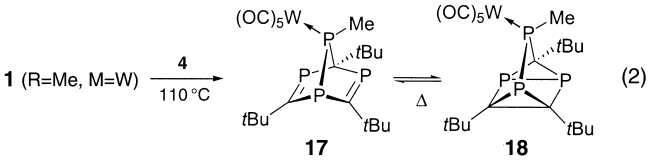


Figure 1. MP2/6-31G* optimized geometries for structures **6A** and **8A**, with selected bond lengths [Å.]

In line with the experimental data, quadricyclane structure **8A** is more stable than its norbornadiene isomer **6A**, by 6.6 kcal mol^{-1} at the G3(MP2) level (Figure 2).[12, 13] This sharply contrasts with the hydrocarbon analogues, since norbornadiene (**14**) is energetically favored over quadricyclane (**13**) by as much as 22.1 kcal mol^{-1} experimentally[14] and by 24.4 and 23.8 kcal mol^{-1} at the G3(MP2)[15] and CCSD(T)//MP2/6-31G* levels,[16] respectively. Likewise, the parent 7-phosphanorbornadiene **1A** is energetically preferred over its quadricyclane isomer **2A** by 22.5 kcal mol^{-1} at the MP2/6-31G* level (Figure 2).[3b]

This inversion of relative stabilities for the tetraphospha compounds, compared with their hydrocarbon analogues, originates from differences in strain energies. Because of their larger number of small hydrocarbon rings quadricyclanes **14** and **2A** are both much more strained than the corresponding norbornadienes **13** and **1A**. However, **8A** is much less strained than hydrocarbon **14** because of the presence of four P atoms in **8A**, phosphorus can accommodate smaller bond angles[17] than carbon and this is reflected in the 6.7 kcal mol^{-1} smaller G2(MP2) strain energy of the three-membered phosphirane ring than that of cyclopropane.[18] A more dramatic illustration is the difference in strain energies for tetraphosphacubane (74.8 kcal mol^{-1})[17, 19] and the all-hydrocarbon cubane (165.1 kcal mol^{-1}).[20] Note that the higher strain energy of **8A** (compared to **6A**), however, is compensated for by the conversion of two of its two highly energetic P=C π bonds (49.4 kcal mol^{-1}) into four P–C σ bonds (66.1 kcal mol^{-1}).[21]

To test the accessibility of valence isomerism for the tetraphospha derivatives experimentally, we treated triphosphabenzene **4** at 110 °C with [MePW(CO)$_5$] [Eq. (2)], generated in situ from **1** (R = Me, M = W).[22] The advantage of



(2)

using the methyl substituted synthon is that no side-products such as **7** can be obtained.[4] Gratifyingly, we indeed obtained a mixture of the expected products **17** and **18** in a 1:8 ratio, as determined from integration of the ^{31}P NMR resonance signals.

 © WILEY-VCH Verlag GmbH, D-69451 Weinheim, 2001 1433-7851/01/4023-4413 $ 17.50+.50/0

The ^{1}H, ^{13}C, and ^{31}P NMR spectra of **18** are very similar to those of **8**.[4] The ^{31}P NMR resonance signals are at $\delta = -112.2$ and -138.1 (CPP ring), $\delta = -122.3$ (CCP ring), and $\delta = 24.2$ (P bridge) and all show multiple P–P couplings. The structure of **17**, the first tetraphosphanorbornadiene compound, is readily deduced from NMR spectroscopy. The phosphaalkene bonds have characteristic downfield ^{31}P NMR resonances ($\delta = 335.3$ and 322.0) and ^{13}C NMR resonances ($\delta = 229.8$ and 226.8),[23] all of which are similar to those reported for **10**.[9] However, the ^{31}P NMR resonance for the bridgehead phosphorus (P4 in Figure 3) at $\delta = 27.3$ is much further downfield than that of **10** ($\delta = -63.8$) and has a typical ^1J(P,P) coupling constant of 174.6 Hz to the neighboring bridging phosphorus (P3, $\delta = 138.8$, ^1J(W,P) = 220.5 Hz), which is shielded by 60.8 ppm relative to the corresponding atom in the 7-phosphanorbornadiene complex **1** (R = Me, M = W).[24]

A single-crystal X-ray diffraction study confirmed the structure of **17** (Figure 3). The two P=C bonds P1–C1 and P2–C2 (1.678(2), 1.676(2) Å), as well as the P3–P4 bond

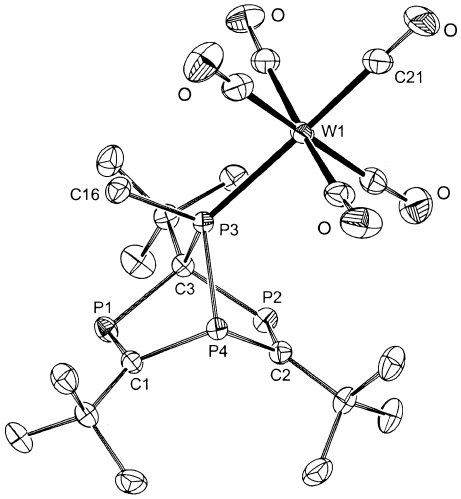


Figure 3. ORTEP plot of **17** with ellipsoids set at the 50% probability level. Hydrogen atoms are omitted for clarity. Selected bond lengths [Å], angles and torsion angles [°]: W1-P3 2.5450(6), P3-C3 1.900(2), P3-P4 2.2078(8), P4-C1 1.861(2), P4-C2 1.861(2), P1-C1 1.678(2), P2-C2 1.676(2), P1-C3 1.892(2), P2-C3 1.878(2), P3-C16 1.846(3); P3-W1-C21 177.79(11), P4-P3-C3 89.68(8), P1-C3-P2 107.86(12), C1-P4-C2 99.67(10), C1-P1-C3 100.08(10), C2-P2-C3 100.24(11), P1-C1-P4 118.46(12), P2-C2-P4 118.46(13), W1-P3-P4 115.14(3), W1-P3-C3 127.48(7), W1-P3-C16 109.15(9), P4-P3-C16 103.77(9), C3-P3-C16 108.28(11), P3-P4-C1 92.27(8), P3-P4-C2 89.67(8); P1-C3-P3 105.16(10), P2-C3-P3 102.87(11), C3-P1-C1-P4 0.39(16), C3-P2-C2-P4 1.31(16).

(2.2078(8) Å), and the P–C single bonds (1.846(3)–1.900(2) Å) are all of the expected lengths. The W1-P3-C16 angle (109.15(9)°) is about 6° smaller than the corresponding angle of tetraphosphaquadricyclane **8**, and reflects an increased steric congestion between the substituents at the bridgehead phosphorus and the *tert*-butyl groups in **17**. The P4-P3-C3 angle for **17** of 89.68(8)° is correspondingly smaller. The MP2/6-31G* optimized geometry of **6A** compares well with the X-ray structure of **17**, when the absence of the W(CO)$_5$, *tert*-butyl, and methyl groups in **6A** is taken into account; most of the P–C single bonds of **6A** are slightly shorter, whereas its P=C bonds are slightly elongated.

Heating a toluene solution of isolated **17** or **18** at 110 °C resulted in both cases in the formation of the same 1:8 mixture of **17** and **18**, as determined by ^{31}P NMR, which suggests these compounds are in thermal equilibrium. Despite some degradation during the isomerization, a Gibbs free energy difference of 2 kcal mol^{-1} could be estimated. This value is 5 kcal mol^{-1} smaller than the G3(MP2) computed energy difference between **6A** and **8A** and is a result of the presence of the stabilizing W(CO)$_5$ fragment[24, 25] and the bulky *tert*-butyl groups.

Whereas concerted [2+2] cycloadditions are Woodward–Hoffman forbidden processes, both head-to-head and head-to-tail thermally induced dimerizations of phosphaalkenes are well known and possibly follow a stepwise reaction path involving ionic or biradical intermediates.[23, 26] However, the photochemically induced [$\pi_s^2+\pi_s^2$] cyclization, which is Woodward–Hoffman allowed, is also feasible for **17**. Thus, full conversion into **18** is observed when a toluene solution of **17** is exposed to daylight for several hours, although extended exposure resulted in complete decomposition.

In conclusion, tetraphospha structures **17** and **18** undergo both thermally and photochemically a norbornadiene–quadricyclane valence isomerism similar to their hydrocarbon analogues, except that the tetraphosphaquadricyclane is the more stable isomer.

Experimental Section

NMR spectra were recorded on a Bruker Avance 250 (^{31}P; 85% H_3PO_4) and an MSL 400 (^{1}H, ^{13}C; TMS) spectrometer, high-resolution mass spectra (HR-MS) on a Finnigan Mat 90, and infrared (IR) spectra on a Mattson 630 Galaxy spectrometer.

Reaction of **4** with [MePW(CO)$_5$]: Complex **1** (R = Me, 0.37 g, 0.66 mmol) and **4** (0.20 g, 0.66 mmol) were heated in refluxing toluene (5 mL) for 18 h. Evaporation to dryness and chromatography over silica with pentane as eluent gave a mixture of **17** and **18** in a 1:8 ratio. Fractional crystallization from a hexane/dichloromethane mixture afforded 0.22 g (49%) of **18** as yellow crystals and 24 mg (6%) of **17** as orange crystals.

17: mp 127–129 °C; ^{31}P NMR ($CDCl_3$, 101.3 MHz): $\delta = 335.3$ (ddd, ^2J(P,P) ≈ ^2J(P,P) ≈ 18 Hz, ^2J(P,P) = 9.1 Hz; C=P), 322.0 (ddd, ^2J(P,P) ≈ ^2J(P,P) ≈ 18 Hz, ^2J(P,P) = 6.5 Hz; C=P), 138.8 (ddd, ^1J(P,P) = 174.6 Hz, ^2J(P,P) = 9.1 Hz, ^2J(P,P) = 6.5 Hz, ^1J(W,P) = 220.5 Hz; W-*P*-P), 27.3 (ddd, ^1J(P,P) = 174.6 Hz, ^2J(P,P) ≈ ^2J(P,P) ≈ 18 Hz; W-P-*P*); ^{1}H NMR ($CDCl_3$ 400.1 MHz): $\delta = 2.16$ (dd, ^2J(H,P) = 6.9 Hz, ^3J(H,P) = 4.2 Hz, 3H; P-CH_3), 1.67 (s, 9H; C(CH_3)$_3$), 1.49 (d, ^4J(H,P) = 1.7 Hz, 9H; C(CH_3)$_3$), 1.46 (d, ^4J(H,P) = 1.8 Hz, 9H; C(CH_3)$_3$); ^{13}C NMR ($CDCl_3$ 100.6 MHz): $\delta = 229.8$ (dddd, ^1J(P,C) ≈ ^1J(P,C) ≈ 56 Hz, ^2J(P,C) ≈ 12 Hz, ^3J(P,C) ≈ 3 Hz; C=P), 226.8 (m; C=P), 197.8 (d, ^2J(P,C) = 24.1 Hz; *trans*-CO), 197.4 (dd, ^2J(P,C) = 5.7 Hz, ^3J(P,C) = 2.6 Hz, ^1J(W,C) = 117.7 Hz; *cis*-CO), 95.8 (dddd, ^1J(P,C) = 67.6 Hz, ^1J(P,C) = 61.1 Hz, ^1J(P,C) = 23.0 Hz, ^2J(P,C) = 6.3 Hz; P$_3$*C*C(CH$_3$)$_3$), 43.2 (ddd, ^2J(P,C) = 56.7 Hz, ^2J(P,C) = 20.2 Hz, ^3J(P,C) = 3.2 Hz; *C*(CH$_3$)$_3$), 43.0 (ddd, ^2J(P,C) = 56.0 Hz, ^2J(P,C) = 19.8 Hz, ^3J(P,C) = 2.6 Hz; *C*(CH$_3$)$_3$), 38.7 (pst, ^2J(P,C) = 15.9 Hz; *C*(CH$_3$)$_3$), 33.1 (m, 2 C(*C*H$_3$)$_3$), 32.6 (dd, ^3J(P,C) = 14.1 Hz, ^3J(P,C) = 7.7 Hz; C(*C*H$_3$)$_3$), 27.8 (dd, ^1J(P,C) = 12.1 Hz, ^2J(P,C) = 6.1 Hz; P-*C*H$_3$); ^{1}H NMR ($CDCl_3$): $\delta =$ 2.16 (dd, ^2J(H,P) = 6.9 Hz, ^3J(H,P) = 4.1 Hz, 3H; P-CH_3), 1.67 (s, 9H; C(CH_3)$_3$), 1.49 (d, ^4J(H,P) = 1.9 Hz, 9H; C(CH_3)$_3$), 1.46 (d, ^4J(H,P) = 2.0 Hz, 9H; C(CH_3)$_3$); HR-MS: calcd for C21H30P4O5W: 670.05536; found: 670.05339; IR (CH_2Cl_2): $\tilde{\nu} = \nu$(CO) 1937 cm^{-1} (s), 2069 cm^{-1} (w).

18: mp 187–188 °C; ^{31}P NMR ($CDCl_3$, 101.3 MHz): $\delta = 24.2$ (dd, ^1J(P,P) = 257.4 Hz, ^2J(P,P) = 15.4 Hz, ^1J(W,P) = 222.6 Hz; W-*P*-P), −112.2 (d, ^2J(P,P) = 47.6 Hz), −122.3 (d, ^1J(P,P) = 257.4 Hz; W-P-*P*), −138.1 (dd, ^2J(P,P) = 47.6 Hz, ^2J(P,P) = 15.4 Hz; P); ^{13}C NMR ($CDCl_3$, 100.6 MHz): $\delta =$ 198.9 (d, ^2J(P,C) = 22.8 Hz; *trans*-CO), 197.5 (dd, ^2J(P,C) = 5.8 Hz, ^3J(P,C) = 4.8 Hz, ^1J(W,C) = 126.0 Hz; *cis*-CO), 69.6 (dddd, ^1J(P,C) =

 © WILEY-VCH Verlag GmbH, D-69451 Weinheim, 2001 1433-7851/01/4023-4414 $ 17.50+.50/0

63.1 Hz, $^1J(P,C) = 58.4$ Hz, $^1J(P,C) = 20.6$ Hz, $^2J(P,C) = 3.4$ Hz; $P_3CC(CH_3)_3$), 55.9 (dddd, $^1J(P,C) = 51.2$ Hz, $^1J(P,C) = 30.6$ Hz, $^2J(P,C) \approx {}^2J(P,C) \approx 4.5$ Hz; CP_2), 51.1 (ddd, $^1J(P,C) = 49.4$ Hz, $^1J(P,C) = 28.5$ Hz, $^2J(P,C) = 4.5$ Hz; CP_2), 37.3 (ddd, $^2J(P,C) = 16.2$ Hz, $^2J(P,C) = 12.4$ Hz, $^2J(P,C) = 3.8$ Hz; $C(CH_3)_3$), 35.1 (dddd, $^2J(P,C) = 18.2$ Hz, $^2J(P,C) = 9.2$ Hz, $^3J(P,C) = 3.2$ Hz, $^3J(P,C) \approx 1$ Hz; $C(CH_3)_3$), 34.7 (dd, $^2J(P,C) = 18.6$ Hz, $^2J(P,C) = 8.2$ Hz; $C(CH_3)_3$), 33.4 (ddd, $^3J(P,C) = 8.7$ Hz, $^3J(P,C) = 6.6$ Hz, $^3J(P,C) = 3.1$ Hz; $C(CH_3)_3$), 31.4 (dd, $^3J(P,C) = 11.4$ Hz, $^3J(P,C) = 6.1$ Hz; $C(CH_3)_3$), 30.9 (dd, $^3J(P,C) = 11.7$ Hz, $^3J(P,C) = 6.9$ Hz; $C(CH_3)_3$), 23.6 (dddd, $^1J(P,C) = 17.2$ Hz, $^2J(P,C) = 7.7$ Hz, $^3J(P,C) = 3.1$ Hz, $^3J(P,C) = 2.3$ Hz; P-CH_3); ^{1}H NMR ($CDCl_3$, 400.1 MHz): $\delta = 2.08$ (dd, $^2J(H,P) = 8.3$ Hz, $^3J(H,P) = 5.3$ Hz, 3H; P-CH_3), 1.30 (s, 9H; $C(CH_3)_3$), 1.26 (s, 9H; $C(CH_3)_3$), 1.25 (s, 9H; $C(CH_3)_3$); HR-MS: calcd for C21H30P4O5W: 670.05536; found: 670.054938; IR (CH_2Cl_2): $\tilde{\nu} = \nu$(CO) 1935 cm^{-1} (s), 2070 cm^{-1} (w).

Crystal structure determination of **17**: $C_{21}H_{30}O_5P_4W$, $Fw = 670.18$, yellow block, $0.30 \times 0.30 \times 0.24$ mm^3, triclinic, $P\bar{1}$ (No. 2), $a = 10.9447(1)$, $b = 11.1640(1)$, $c = 11.3277(1)$ Å, $\alpha = 81.9368(5)$, $\beta = 88.5556(5)$, $\gamma = 76.8724(3)^\circ$, $V = 1334.57(2)$ Å^3, $Z = 2$, $\rho = 1.668$ g cm^{-3}, 28416 measured reflections, 6069 unique reflections ($R_{int} = 0.072$). Intensities were measured on a Nonius KappaCCD diffractometer with rotating anode ($Mo_{K\alpha}$, $\lambda = 0.71073$ Å) at a temperature of 150 K. Absorption correction based on multiple measured reflections using the program PLATON[27] (routine MULABS, $\mu = 4.60$ mm^{-1}, 0.17–0.29 transmission). The structure was solved with automated Patterson methods with the program DIRDIF97[28] and refined with the program SHELXL97[29] against F^2 of all reflections up to a resolution of $(\sin\vartheta/\lambda)_{max} = 0.65$ Å^{-1}. Non-hydrogen atoms were refined freely with anisotropic displacement parameters, hydrogen atoms were refined freely with isotropic displacement parameters. R ($I > 2\sigma(I)$): $R1 = 0.0214$, $wR2 = 0.0497$. R (all data): $R1 = 0.0231$, $wR2 = 0.0505$, $S = 1.041$. Residual electron density between -1.28 and 1.33 e Å^3. The drawings, structure calculations, and checking for higher symmetry was performed with the program PLATON.[27] Crystallographic data (excluding structure factors) for the structures reported in this paper have been deposited with the Cambridge Crystallographic Data Centre as supplementary publication no. CCDC-164106 (**17**). Copies of the data can be obtained free of charge on application to CCDC, 12 Union Road, Cambridge CB21EZ, UK (fax: (+44) 1223-336-033; e-mail: deposit@ccdc.cam.ac.uk).

Received: June 8, 2001 [Z17255]

[1] V. A. Bren, A. D. Dubonsov, V. I. Minkin, V. A. Chenoivanov, *Russ. Chem. Rev.* **1991**, *60*, 451–469.

[2] W. Tochtermann, G. Olsson, *Chem. Rev.* **1989**, *89*, 1203–1214.

[3] a) A. Marinetti, F. Mathey, J. Fischer, A. Mitschler, *Nouv. J. Chim.* **1984**, *8*, 453–457; b) B. Wang, C. H. Lake, K. Lammertsma, *Organometallics* **1997**, *16*, 4145–4149.

[4] M. J. M. Vlaar, A. W. Ehlers, M. Schakel, S. B. Clendenning, J. F. Nixon, M. Lutz, A. L. Spek, K. Lammertsma, *Chem. Eur. J.* **2001**, *7*, 3545–3550.

[5] For reviews on electrophilic phosphinidene complexes see: a) F. Mathey, *Multiple Bonds and Low Coordination in Phosphorus Chemistry* (Eds.: M. Regitz, O. J. Scherer), Thieme, Stuttgart, **1990**, p. 38; b) F. Mathey, *Angew. Chem.* **1987**, *99*, 285–296; *Angew. Chem. Int. Ed. Engl.* **1987**, *26*, 275–286; c) K. D. Dillon, F. Mathey, J. F. Nixon, *Phosphorus: The Carbon Copy*, Wiley, Chichester, **1998**, p. 19.

[6] A related 1,4-adduct has been reported previously for the reaction of [PhPW(CO)$_5$] with [5]metacyclophane. M. J. van Eis, C. M. D. Komen, F. J. J. de Kanter, W. H. de Wolf, K. Lammertsma, F. Bickelhaupt, *Angew. Chem.* **1998**, *110*, 1656–1659; *Angew. Chem. Int. Ed. Engl.* **1998**, *37*, 1547–1550.

[7] F. Tabellion, A. Nachbauer, S. Leininger, C. Peters, M. Regitz, F. Preuss, *Angew. Chem.* **1998**, *110*, 1318–1321; *Angew. Chem. Int. Ed. Engl.* **1998**, *37*, 1233–1235.

[8] a) A. Elvers, F. W. Heinemann, B. Wrackmeyer, U. Zenneck, *Chem. Eur. J.* **1999**, *5*, 3143–3153; b) M. Julino, M. Slany, U. Bergsträßer, F. Mercier, F. Mathey, M. Regitz, *Chem. Ber.* **1995**, *128*, 991–997.

[9] S. B. Clendenning, B. Gehrhus, P. B. Hitchcock, J. F. Nixon, *Chem. Commun.* **1999**, 2451–2452.

[10] a) P. Binger, S. Leininger, K. Günther, U. Bergsträßer, *Chem. Ber.* **1997**, *130*, 1491–1494; b) P. Binger, S. Leininger, J. Stannek, B. Gabor, R. Mynott, J. Bruckmann, C. Krüger, *Angew. Chem.* **1995**, *107*, 2411–2412; *Angew. Chem. Int. Ed. Engl.* **1995**, *34*, 2227–2230.

[11] Gaussian 98 (Revision A.7), M. J. Frisch, G. W. Trucks, H. B. Schlegel, G. E. Scuseria, M. A. Robb, J. R. Cheeseman, V. G. Zakrzewski, J. A. Montgomery, R. E. Stratmann, J. C. Burant, S. Dapprich, J. M. Millam, A. D. Daniels, K. N. Kudin, M. C. Strain, O. Farkas, J. Tomasi, V. Barone, M. Cossi, R. Cammi, B. Mennucci, C. Pomelli, C. Adamo, S. Clifford, J. Ochterski, G. A. Petersson, P. Y. Ayala, Q. Cui, K. Morokuma, D. K. Malick, A. D. Rabuck, K. Raghavachari, J. B. Foresman, J. Cioslowski, J. V. Ortiz, B. B. Stefanov, G. Liu, A. Liashenko, P. Piskorz, I. Komaromi, R. Gomperts, R. L. Martin, D. J. Fox, T. Keith, M. A. Al-Laham, C. Y. Peng, A. Nanayakkara, C. Gonzalez, M. Challacombe, P. M. W. Gill, B. G. Johnson, W. Chen, M. W. Wong, J. L. Andres, M. Head-Gordon, E. S. Replogle, J. A. Pople, Gaussian, Inc., Pittsburgh, PA, **1998**..

[12] G3(MP2): L. A. Curtiss, P. C. Redfern, K. Raghavachari, V. Rassolov, J. A. Pople, *J. Chem. Phys.* **1999**, *110*, 4703–4709.

[13] The G3(MP2) absolute energies (Hartree) are -1480.175672 for **6A** and -1480.186172 for **8A**.

[14] a) D. W. Rogers, L. S. Choi, R. S. Girellini, T. J. Holmes, N. L. Allinger, *J. Phys. Chem.* **1980**, *84*, 1810–1814; b) W. V. Steele, *J. Chem. Thermodyn.* **1978**, *10*, 919–927.

[15] D. W. Rogers, F. J. McLafferty, *J. Phys. Chem. A* **1999**, *103*, 8733–8737.

[16] R. D. Bach, I. L. Schilke, H. B. Schlegel, *J. Org. Chem.* **1996**, *61*, 4845–4847.

[17] S. M. Bachrach, L. M. Perriott, *Tetrahedron Lett.* **1993**, *34*, 6365–6368.

[18] K. Lammertsma, B. Wang, J.-T. Hung, A. W. Ehlers, G. M. Gray, *J. Am. Chem. Soc.* **1999**, *121*, 11650–11651.

[19] S. M. Bachrach, B. D. Gailbraeth, *Tetrahedron Lett.* **1998**, *39*, 4211–4214.

[20] J. D. Cox, G. Pilcher, *Thermochemistry of Organic and Organometallic Compounds*, Academic Press, New York, **1970**.

[21] P. von R. Schleyer, D. Kost, *J. Am. Chem. Soc.* **1988**, *110*, 2105–2109.

[22] A. Marinetti, F. Mathey, *J. Am. Chem. Soc.* **1982**, *104*, 4484–4485.

[23] R. Appel in *Multiple Bonds and Low Coordination in Phosphorus Chemistry* (Eds.: M. Regitz, O. J. Scherer), Thieme, New York, **1990**, pp. 157–219.

[24] A. Marinetti, F. Mathey, J. Fischer, A. Mitschler, *J. Chem. Soc. Chem. Commun.* **1982**, 667–668.

[25] M. J. van Eis, H. Zappey, F. J. J. de Kanter, W. H. de Wolf, K. Lammertsma, F. Bickelhaupt, *J. Am. Chem. Soc.* **2000**, *122*, 3386–3390.

[26] a) L. N. Markovski, V. D. Romanenko, *Tetrahedron* **1989**, *45*, 6019–6090; b) R. Appel, F. Knoll, *Adv. Inorg. Chem.* **1989**, *33*, 259–361.

[27] A. L. Spek, PLATON. A multipurpose crystallographic tool, Utrecht University, The Netherlands, **2001**.

[28] P. T. Beurskens, G. Admiraal, G. Beurskens, W. P. Bosman, S. Garcia-Granda, R. O. Gould, J. M. M. Smits, C. Smykalla, The DIRDIF97 program system, Technical Report of the Crystallography Laboratory, University of Nijmegen, The Netherlands, **1997**.

[29] G. M. Sheldrick, SHELXL-97, Program for crystal structure refinement, University of Göttingen, Germany, **1997**.

From Cyclodextrin Assemblies to Porous Materials by Silica Templating**

Sebastian Polarz,* Bernd Smarsly, Lyudmila Bronstein, and Markus Antonietti

Since the discovery by Beck, Vartuli et al.[1, 2] that ordered mesoporous silicas, such as MCM-41, can be obtained by surfactant templating, the development of new porous materials and porogens as well as the characterization of the resulting structures has become one of the most promising fields in modern materials chemistry.[3–5] Meanwhile, these observations have been extended to a number of techniques by which pore morphology, pore size, and wall material can be varied over a broad range.[6–14]

One of the modifications of the original process relevant here is the "nanocasting" introduced by Attard, Glyde, and Göltner.[15] This is a high-concentration synthesis in which the solidified inorganic compound is a copy of the original phase structure, that is its structure is predetermined by the selection of the template phase. They used lyotropic liquid-crystalline phases, derived from surfactants or—later—block copolymers,[15–17] as templates and obtained the material either as a homogeneous film or as a monolithic object. In addition, this technique also allows the structural characterization of fragile phase structures and transition states of polymers or surfactants by analyzing the well-contrasted solid replica instead of the original soft organic phases.[16, 18]

We extend this approach to supramolecular aggregates of nonpolar cyclodextrins (CDs) in aqueous solution as templates. Our aim is to exploit the use of CDs to generate porous materials, focussing on the fine details of the pore structure and the self-organization of this template. The self-assembly of cyclodextrins has been assumed previously,[19–23] but their organization could—to the best of our knowledge—not be determined in detail.

CDs are cyclic oligosaccharides consisting of covalently linked glucose units (6 units = α-CD, 7 units = β-CD, 8-units = γ-CD); they are characterized by a hydrophilic exterior and a hydrophobic interior[24] the size of which is in the range of 1.5–2 nm. The relatively large number of hydroxy groups per unit area should ideally mediate compatibility with an oxidic inorganic matrix through hydrogen bonding. In fact, this has been proven by three reports in which CDs were employed at low concentrations in a sol–gel process to incorporate functional units such as dyes into a dense and nonporous silica.[25–27]

[*] Dr. S. Polarz, Dr. B. Smarsly, Prof. Dr. M. Antonietti
Max-Planck Institute for Colloids and Interfaces/Research Campus Golm
14424 Potsdam (Germany)
Fax: (+49) 331-5679502
E-mail: polarz@mpikg-golm.mpg.de
Prof. Dr. L. Bronstein
Chemistry Department
Indiana University
800 E. Kirkwood Av., Bloomington, IN 47405 (USA)

[**] We thank the Max-Planck society for funding.

Supporting information for this article is available on the WWW under http://www.angewandte.com or from the author.

So far, CD-containing solutions have been difficult to analyze by standard techniques, thus information about the assembly of CDs in water is still rather limited. We employ nanocasting to investigate the CD assemblies as templates for the silica pore in detail, and we also investigate the driving force for the self-assembly of the cyclodextrin molecules to ordered aggregates.

In a solution of a hydrophilic sugar, such as a cyclodextrin, one would assume that it is moleculary dispersed in the aqueous phase. Nanocasting by a sol–gel process should then result in a porous material in which each pore exhibits the size and shape of a CD molecule, and in which the pores are not mutually ordered. Depending on the concentration, mesoporosity would be achieved by a molecular percolation process at corresponding volume fractions of template to water, but still a disordered pore system would be obtained (as found for instance for polyethyleneglycol solutions[28]).

When a 18 wt% solution of α-CD was templated we observed a different behavior, namely evidence for an ordered aggregation of CDs instead of their molecular dispersion in the silica matrix (see experimental conditions in Table 1 and Supporting Information; all unmodified CDs were templated at a concentration near to their saturation limit in water; the presence of CD in the silica before calcination was verified by IR, thermogravimetric analysis (TGA), and UV/Vis measurements as given in the Supporting Information).[29]

Table 1. Experimental conditions for the preparation of the CD-based silica materials.

Sample name	Amount of CD [g]	Amount of H_2O [g]	Amount of TMOS [g]	Casting temperature [°C]	BET surface [$m^2 g^{-1}$]
α-CD-silica	2	5	4	60	644
β-CD-silica	0.1	5	4	60	2
γ-CD-silica	0.7	5	4	60	–
β-MCD-silica	2	3	4	60	712
β-MCD_*p*-xylene-silica	2.16	3	4	60	596
α-HPCD-silica	2	2	4	60	832
β-HPCD-silica (1)	2	2	4	60	817
β-HPCD-silica (2)	2	3	4	60	873
γ-HPCD-silica	2	2	4	60	763

The CD assembly is expressed in the silica through a bicontinuous "worm-type" pore system with a diameter d of about 1.5 nm (Figure 1). The bicontinuity introduced by the curved and ramified pores, which is apparent in the transmission electron microscopy (TEM) images, is also verified by nitrogen sorption measurements. The material has an internal surface area of 644 $m^2 g^{-1}$, which is too low to be caused by "single CD molecule pores", but is consistent with the observed worm-type pores. A typical N_2 isotherm is given in Figure 2 for a related system (silica obtained with γ-hydroxypropylated CD (γ-HPCD-silica)).

To explain these results, we assume that α-CD self-assembles to "worm-type" aggregates because of its hydrophobic interior and the hydrophilic shell. Maximum contact between the hydrophobic domains and between the hydrophilic domains is given when the flat (uncurved) CD sides are

 © WILEY-VCH Verlag GmbH, D-69451 Weinheim, 2001 1433-7851/01/4023-4417 $ 17.50+.50/0

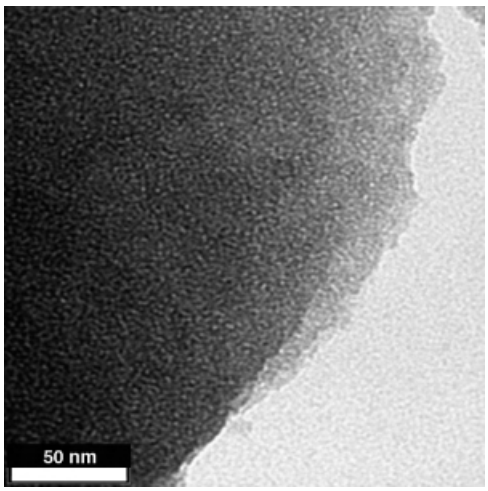


Figure 1. TEM image of α-CD-silica.

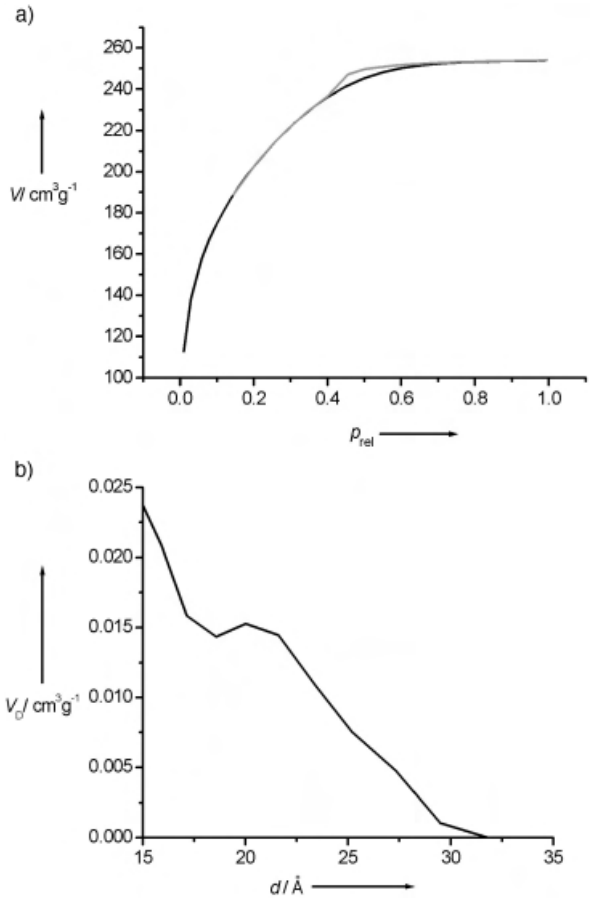


Figure 2. N_2 isotherm of γ-HPCD-silica (a, adsorption printed in black, desorption in gray) and the corresponding DFT pore size distribution (b). V = adsorbed volume, p_{rel} = relative pressure, V_D = differential pore volume, d = diameter.

stacked on top of each other. This situation would be energetically favorable and we assume this to be the driving force for the self-assembly.

This type of amphiphilic organization has little in common with the standard organization of amphiphiles, since the distribution of cohesion energy in CDs has no dipolar or vectorial contributions, but a strong quadrupolar character. Consequently, the aggregation is not seen in surface tension measurements of the concentrated solutions (which behave like classical binary mixtures). Dynamic light scattering, preliminary small-angle X-ray (SAXS) and neutron scattering (SANS) experiments, however, confirm the existence of larger aggregated species already in pure water, that is it is not an artifact of the silica preparation depicted here. The presence of CD assemblies has been proposed by Häusler et al.[19] and Coleman et al.[23] but also mistrusted by Perly et al.[30] Therefore, we conclude that the structures that manifest themselves in the silica pore structure are directly related to the CD organization in pure water and not caused by the presence of silica.

To compare the systems on the basis of equal overall porosities, the more water-soluble statistically hydroxypropylated cyclodextrins (HPCDs; 1.6 hydroxypropyl (HP) groups per CD) were employed, here with 25 wt % of the template in the casting solution. For α-, β-, and γ-HPCD a more disordered pore structure was found (Figure 3a). The statistical evaluation of the TEM images and SAXS data reveals that the pore size correlates nicely with the molecular diameter of the CDs. The obtained values for the pore size are 1.4($\pm$0.3) nm for α-HPCD as a template, 1.6($\pm$0.3) nm for β-HPCD, and 1.8($\pm$0.3) nm for γ-HPCD (molecular diame-

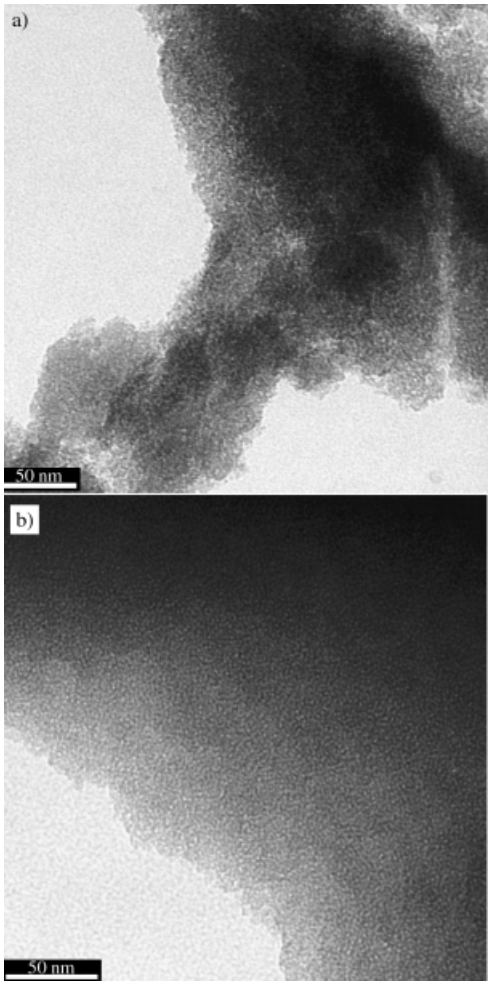


Figure 3. TEM micrographs of β-HPCD-silica (a) and β-MCD_p-xylene-silica (b).

 © WILEY-VCH Verlag GmbH, D-69451 Weinheim, 2001 1433-7851/01/4023-4418 $ 17.50+.50/0

ters for underivatized CDs[31]: 1.37 nm for α-CD, 1.53 nm for β-CD and 1.69 nm for γ-CD).

These values are supported by nitrogen sorption measurements which show characteristics of type I and type IV isotherms (Figure 2; between micro- and mesopores)[32] and pore size distributions (density functional theory (DFT) calculations)[33, 34] with a small maximum at about $2(\pm 0.2)$ nm. The surface areas of the silica materials prepared with the more soluble and disordered HPCDs are in the range of $800-900\ m^2 g^{-1}$ with a porosity of $0.32\ cm^3 g^{-1}$ for all three samples.

β-methylcyclodextrin (β-MCD; also statistically methylated) as a CD of intermediate solubility showed again the wormlike structure typical for unsubstituted CDs, and its BET surface area was lower than the one of the corresponding β-HPCD due to the smoother pore walls. This underlines the influence of the CD substitution pattern on the intermolecular organization of the CD molecules.

To verify the assumption that the quadrupolar amphiphilic character of the CDs is responsible for the alignment to wormlike aggregates, the inclusion compounds of β-MCD with *p*-xylene and naphthalene were prepared, silica-casted, and compared to the structures of the pure β-MCD- and β-HPCD-based silicas. The inclusion leads to a hydrophobized CD pocket. Analytical details about the inclusion compounds are given in the Supporting Information. The resulting silicas were initially investigated by TEM. Figure 3a and b show the TEM results for two extreme cases from the series (β-HPCD (most hydrophilic), β-MCD_*p*-xylene (most quadrupolar amphiphilic)).

In all cases, worm-type pores are observed. A more careful visual inspection, however, reveals that structure, definition, and shape persistence increase with increasing polarity difference within the template (compare Figure 3a and b). Although the TEM images give some indications for the differences in the order of the supramolecular structure, the differences are hard to quantify by electron microscopy solely. The pore structure was additionally characterized by SAXS, which is the appropriate technique to investigate the degree of order of the pore system and to determine the average pore size.

Figure 4a shows the comparison of the SAXS curves of β-HPCD-, β-MCD-, and β-MCD_xylene-silica. To have comparable conditions samples with identical template concentrations were prepared (see Table 1). β-HPCD-silica was therefore analyzed near to its saturation limit (1) and at a standard concentration (2). Already the bare scattering curves indicate a clear difference between the pore systems. For β-$HPCD_{(2)}$, the curve is typical for pores of the size of single CD molecules which are randomly distributed in the silica matrix. Compared to those of β-$HPCD_{(2)}$-silica, the other scattering curves are caused by larger structures than single CD units, since the s^{-4} Porod behavior begins at significantly smaller s values.

The SAXS curves were evaluated by using the concept of "chord length distribution" (CLD), which was previously established to investigate the structure of two-phase systems and, in particular, porous materials.[35, 36] The CLD (which is similar to a pore size distribution) for β-$HPCD_{(2)}$ (Figure 4b)

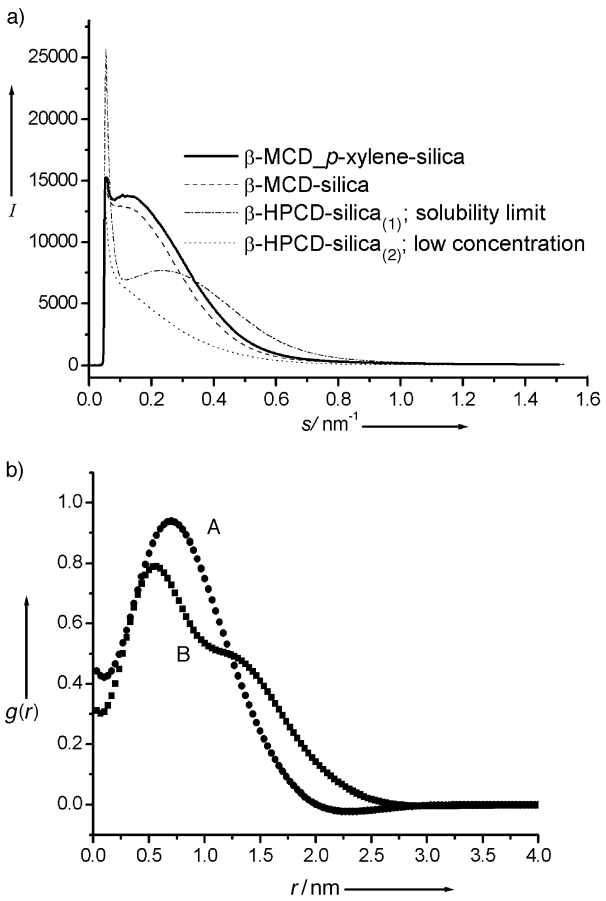


Figure 4. a) SAXS diffractograms of β-HPCD-, β-MCD-, and β-MCD_*p*-xylene-silica, b) corresponding chord length distributions for the two extreme cases β-$HPCD_{(2)}$ (A) and β-MCD_*p*-xylene (B). I = scattering intensity; s = scattering vector; $g(r)$ = chord length distribution function; r = radius.

shows a marked maximum at $r \approx 0.7$ nm and nearly vanishes at $r \approx 2$ nm, related to the cross section and the diameter of the single CD unit. The average chord length of the pores (l_{pore}), which can be regarded as an average pore size D, can be calculated from the Porod length l_p, the first moment of the CLD, through the relation $l_{pore} = l_p/(1-\phi)$, where ϕ is the porosity. Using this approach, for β-HPCD-silica a mean pore size of $D \approx l_{pore} \approx 1.5$ nm is obtained which is in reasonable agreement with the size of a single β-HPCD molecule. Moreover, the CLD starts with a value only slightly above zero which is indicative of a smooth pore/wall interface without angularity and free of very small micropores below 0.5 nm, that is the walls are not porous themselves.[37] Similar results were obtained for the other CD-derived silicas. This differentiates the CD-born silicas from similar structures synthesized with nonionic surfactants and amphiphilic block copolymers.[14, 38, 39] CD-casted porous materials can therefore be regarded as more defined in the monodispersity of their pores. SAXS shows that the more water-soluble HPCDs form essentially disordered molecular pores of the size of the CD, and smooth walls with no disturbing microporosity.

The SAXS curve of β-MCD_*p*-xylene-silica (Figure 4a) differs significantly from that of β-$HPCD_{(2)}$-silica and shows a broad, but significant peak at $s \approx 0.12\ nm^{-1}$ and a downturn at

 © WILEY-VCH Verlag GmbH, D-69451 Weinheim, 2001 1433-7851/01/4023-4419 $ 17.50+.50/0

still smaller s values due to an intermolecular correlation hole which can be interpreted as the ordered packing of large pores. The position of the correlation hole "peak" corresponds to a length scale of about 8 nm, the averaged pore-to-pore distance. From the SAXS curve, no information about the length of the worm-type holes can be obtained, since the packing effect truncates the structure factor towards smaller s values. Furthermore, the CLD for β-MCD_*p*-xylene-silica (Figure 4b) is typical for cylindrical objects for which the first maximum corresponds to the cross section, whereas the tail towards longer distances describes the (here truncated) averaged length of the cylinder. SAXS therefore implies that the pore organization for this silica is given by the copy of a columnar stacking of the CDs where the stacks are mutually correlated, but not long-range ordered. A more detailed κ,ι-analysis of the SAXS data confirmed this conclusion (see Supporting Information).[40–42]

The SAXS curve of β-MCD-silica lies between the two extreme cases (Figure 4a), but is very close to that of the xylene inclusion compound. The latter comparison reveals the influence of a hydrophobic guest in the cavity on the intermolecular order. The difference lies mainly in the region ahead of the peak at $s = 0.12\ \mathrm{nm}^{-1}$ where a stronger downturn is found for the inclusion complex based silica. This behavior is attributed to a higher intercolumnar ordering of the β-MCD_*p*-xylene aggregates compared to β-MCD.

With the SAXS measurements in mind, it is possible to reanalyze the surface area measured by N_2 sorption for the three silicas under consideration (with identical preparation conditions and CD concentrations). β-MCD_*p*-xylene-silica has a surface area of 596 $m^2 g^{-1}$ and a porosity of 0.28 $cm^3 g^{-1}$, the values for β-MCD- and β-HPCD$_{(2)}$-silica are 712 $m^2 g^{-1}$/0.33 $cm^3 g^{-1}$ and 873 $m^2 g^{-1}$/0.40 $cm^3 g^{-1}$, respectively. This tendency is consistent with the trend towards less order and increasing dispersity as the quadrupolar amphiphilicity decreases, as already observed with TEM and SAXS (more disordered pores create higher surface areas due to the higher fraction of moleculary imprinted pores).

β-MCD_naphthalene-silica showed similar features in the TEM images, N_2 sorption, and SAXS as the xylene compound, and no further analytical details for this material are given here.

For a better understanding of the unusual assembly of CD molecules we also performed molecular modeling calculations. First, the structure of a β-CD inclusion complex was calculated with force field (MM2) methods. Our data were in good agreement with those of other calculations.[43] From this starting geometry we calculated the electrostatic potential with the ab initio Hartree–Fock method and a 3-21G basis set. This allowed verification of the proposed quadrupolar gradients in the cyclodextrins. Indeed, a cyclodextrin inclusion complex can be regarded as a cylindrical unit with a hydrophobic core and a hydrophilic exterior (Figure 5a). Then, we investigated the interaction potentials between two CD inclusion units with the semiempirical CNDO method. Three geometries were evaluated with regard to the inter-ring distance (Figure 5b): 1) ideally parallel, 2) staggered parallel, 3) perpendicular orientation of the rings. The interaction of CDs perpendicular to each other is purely repulsive. An

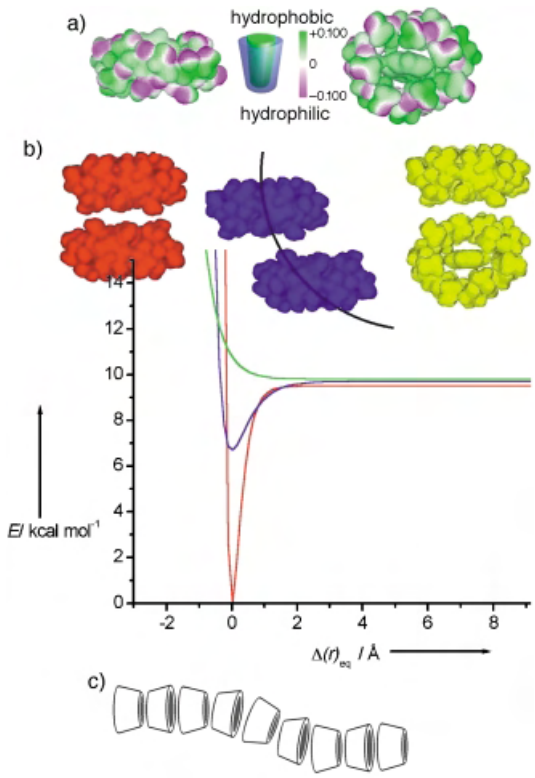


Figure 5. a) MM2-calculated structure of a cyclodextrin inclusion complex and its electrostatic potential distribution from an ab initio Hartree–Fock calculation. b) Calculated energy surfaces as a function of the inter-ring distance for the schematically shown ideally parallel (red), staggered (blue), and perpendicular (yellow) approach. c) Schematic representation of the aggregate structure of α-CD, as revealed by silica nanocasting, dynamic light scattering, and SAXS in solution. Bright: hydrophilic domains; dark: hydrophobic domains. E = energy; $\Delta(r)_{eq}$ = deviance from equilibrium distance.

attractive energy surface is found for the ideally parallel and the staggered parallel arrangement; the minimum of the Morse-type potential is deeper for the ideally parallel orientation.

The energies of the interactions are "soft" and in the range of those of supramolecular organization in agreement with the experimentally found alignment effects. It is energetically favorable for the CD complexes to line up, but slightly bent or staggered geometries (Figure 5c) are also energetically possible, thus resulting in the wormlike structure. A more precise calculational study would need to take into account the solvent and possible entropic effects as well as the influence of hydration and water matrix.

To conclude, cyclodextrins are an alternative to classical amphiphiles as templates for the synthesis of porous materials, for which the pore diameter corresponds exactly to the cyclodextrin size and is in the technically interesting range of 1.5–2.0 nm.

In contrast to all nonionic ethyleneoxide-based surfactants, CDs do not penetrate or mix with the silica walls, that is they create no additional microporosity that would weaken the wall material; such microporosity is one major drawback of previous block copolymer based porous silicas. Only one type of pores is created by the CD route.

 © WILEY-VCH Verlag GmbH, D-69451 Weinheim, 2001 1433-7851/01/4023-4420 $ 17.50+.50/0

Unexpectedly, unsubstituted and partially methylated CDs self-assemble to larger aggregates, mostly of the "wormlike" type. It is argued that the CDs aggregate because of a special distribution of polar and nonpolar sites, which is, however, not dipolar or vectorial as for classical amphiphiles, but rather quadrupolar or discotic in character (a difference between the inside and the outside of the disks). Minimization of the mutual contact areas of hydrophilic and hydrophobic leads to columnar aggregates of CDs and their inclusion complexes (their structures have so far only been studied in the solid state[44]). This model was supported by modeling calculations. When hydrophobic guests are used in inclusion complexes the quadrupolar amphiphilicity changes, and the order formation is enhanced. This results in the interesting situation that the order of the aggregate can be triggered by inclusion of different guest molecules.

In the case of a true casting or a 1:1 copy of a preexisting template structure in water, the silica nanocasting can be seen as a new technique to investigate the solution organization of CDs and possibly other compounds. We will undertake further investigations to elucidate the structure of CDs in pure water and to prove that the organization revealed by the silica pores is a copy of the original state. The use of CDs as templates significantly extends the possibilities of nanocasting, since it enables not only the construction of new porous materials with the help of "quadrupolarly organized" template structures, but also the functionalization or loading of the porous inorganic materials through inclusion complexes.

Experimental Section

All CDs were obtained from Wacker, all other chemicals from Aldrich and used without further purification. The MCD and HPCD were only partially derivatized; statistically 1.6 OH groups per CD molecule were modified.

Preparation of cyclodextrin inclusion compounds: An equimolar amount of *p*-xylene was dispersed in a solution of the CD in water. The mixture was stirred at 50 °C for 24 h in a closed vessel. A sample was isolated for analysis (^{1}H NMR) from the resulting homogeneous phase. The residue was directly used for templating. The naphthalene inclusion complex was prepared according to ref. [45].

General method for the preparation of CD-based silica materials (for the exact amounts and reaction conditions see Table 1): The CD was dissolved in water. Under vigorous magnetic stirring concentrated hydrochloric acid (to adjust pH to 1.7 – 2) and then tetramethylorthosilane were added. After homogenization at room temperature the formed methanol was removed under vacuum at 40 °C. The gels were aged for 24 h at 60 °C, and the resulting silica materials were calcined at 500 °C under oxygen for 15 h.

Details about the characterization methods are given in the Supporting Information.

Received: June 26, 2001,
Revised: September 17, 2001 [Z17368]

[1] C. T. Kresge, M. Leonowicz, W. J. Roth, J. C. Vartuli, J. S. Beck, *Nature* **1992**, *359*, 710.
[2] J. S. Beck, J. C. Vartuli, W. J. Roth, M. E. Leonowicz, C. T. Kresge, K. D. Schmitt, C. T.-W. Chu, D. H. Olson, E. W. Sheppard, S. B. McCullen, J. B. Higgins, J. L. Schlenker, *J. Am. Chem. Soc.* **1992**, *114*, 10834.
[3] M. Linden, S. Schacht, F. Schüth, A. Steel, K. K. Unger, *J. Porous Mater.* **1998**, *5*, 177.
[4] F. Schüth, *Curr. Opin. Colloid Interface Sci.* **1998**, *3*, 174.
[5] U. Ciesla, F. Schüth, *Microporous Mesoporous Mater.* **1999**, *27*, 131.
[6] U. Schubert, G. Kickelbick, N. Hüsing, *Mol. Cryst. Liq. Cryst.* **2000**, *354*, 695.
[7] N. K. Raman, M. T. Anderson, C. J. Brinker, *Chem. Mater.* **1996**, *8*, 1682.
[8] J. S. Beck, J. C. Vartuli, *Curr. Opin. Solid State Mater. Sci.* **1996**, *1*, 76.
[9] T. J. Barton, L. M. Bull, W. G. Klemperer, D. A. Loy, B. McEnaney, M. Misono, P. A. Monson, G. Pez, G. W. Scherer, J. C. Vartuli, O. M. Yaghi, *Chem. Mater.* **1999**, *11*, 2633.
[10] N. Hüsing, U. Schubert, *Angew. Chem.* **1998**, *110*, 22; *Angew. Chem. Int. Ed.* **1998**, *37*, 22.
[11] K. Möller, T. Bein, *Chem. Mater.* **1998**, *10*, 2950.
[12] P. Yang, D. Zhao, D. I. Margolese, B. F. Chmelka, G. D. Stucky, *Nature* **1998**, *396*, 152.
[13] Q. S. Hue, D. I. Margolese, U. Ciesla, P. Y. Feng, T. E. Gier, P. Sieger, R. Leon, P. M. Petroff, F. Schüth, G. D. Stucky, *Nature* **1994**, *368*, 317.
[14] N. A. Melosh, P. Lipic, F. S. Bates, F. Wudl, G. D. Stucky, G. H. Fredrickson, B. F. Chmelka, *Macromolecules* **1999**, *32*, 4332.
[15] G. S. Attard, J. G. Glyde, C. G. Göltner, *Nature* **1995**, *378*, 366.
[16] C. G. Göltner, S. Henke, M. C. Weißenberger, M. Antonietti, *Angew. Chem.* **1998**, *110*, 633; *Angew. Chem. Int. Ed.* **1998**, *37*, 613.
[17] C. Göltner, H. Cölfen, M. Antonietti, *Chem. Unserer Zeit* **1999**, *33*, 200.
[18] E. Krämer, S. Förster, C. Göltner, M. Antonietti, *Langmuir* **1998**, *14*, 2027.
[19] O. Häusler, C. C. Müller-Goymann, *Starch* **1993**, *45*, 183.
[20] P. Tchoreloff, A. Baszkin, M. M. Boisonnade, P. Zhang, A. W. Coleman, *Supramol. Chem.* **1994**, *4*, 169.
[21] A. W. Coleman, I. Nicolis, N. Keller, J. P. Dalbiez, *J. Incl. Phenom. Mol. Recognit. Chem.* **1992**, *13*, 139.
[22] S. Alexandre, A. W. Coleman, A. Kasselouri, J. M. Valleton, *Thin Solid Films* **1996**, *284 – 285*, 765.
[23] C. Derango, P. Charpin, J. Navaza, N. Keller, I. Nicolis, F. Villain, A. W. Coleman, *J. Am. Chem. Soc.* **1992**, *114*, 5475.
[24] W. Sänger, J. Jacob, K. Gessler, T. Steiner, D. Hoffmann, H. Sanbe, K. Koizumi, S. M. Smith, T. Takaha, *Chem. Rev.* **1998**, *98*, 1787.
[25] S. A. Wallington, C. Pilon, J. D. Wright, *J. Sol Gel Sci. Technol.* **1997**, *8*, 1127.
[26] U. Narang, R. A. Dunbar, F. V. Bright, P. N. Prasad, *Appl. Spectrosc.* **1993**, *47*, 1700.
[27] C. Wang, C. Li, Y. Lin, L. Chau, *Appl. Spectrosc.* **2000**, *54*, 15.
[28] B. Smarsly, C. Göltner, M. Antonietti, *Chem. Mater.* **2000**, accepted.
[29] Nanocasting of a saturated β-CD solution results in silica materials with isolated, spherical pores of the size 5 – 10 nm (mesopores). Our only explanation at the moment is that the rather low solubility of β-CD in water is reflected in a spherical aggregate structure. This observation is relevant for all applications of β-CD which employ an aggregated system at the beginning. γ-CD shows a higher solubility, and again, a "worm-type" pore system is found (picture not shown).
[30] N. Azaroualbellanger, B. Perly, *Magn. Reson. Chem.* **1994**, *32*, 8.
[31] S. McCormack, N. R. Russel, J. F. Cassidy, *Electrochim. Acta* **1992**, *37*, 1939.
[32] K. S. W. Sing, D. H. Everett, R. A. W. Haul, L. Moscou, R. A. Pierotti, J. Rouquérol, T. Siemieniewska, *Pure Appl. Chem.* **1985**, *57*, 603.
[33] A. V. Neimark, P. I. Ravikovitch, *Stud. Surf. Sci. Catal.* **2000**, *128*, 51.
[34] J. P. Olivier, *Carbon* **1998**, *36*, 1469.
[35] D. Tchoubar-Vallat, J. Méring, *C. R. Hebd. Seances Acad. Sci.* **1965**, *261*, 3096.
[36] G. Porod, *Small-Angle Scattering of X-Rays*, Gordon and Breach, New York, **1967**.
[37] S. Ciccariello, G. Cocco, A. Benedetti, S. Enzo, *Phys. Rev. B* **1981**, *23*, 6474.
[38] C. G. Göltner, M. Antonietti, *Adv. Mater.* **1997**, *9*, 431.
[39] C. G. Göltner, B. Smarsly, B. Berton, M. Antonietti, *Chem. Mater.* **2000**, *13*, 1617.
[40] S. Ciccariello, A. Benedetti, *Phys. Rev. B* **1982**, *26*, 6384.
[41] S. Ciccariello, R. Sobry, *Acta Crystallogr. Sect. A* **1995**, *51*, 60.
[42] M. A. Micha, C. Burger, M. Antonietti, *Macromolecules* **1998**, *31*, 5930.
[43] K. B. Lipkowitz, *Chem. Rev.* **1998**, *98*, 1829.
[44] M. Morgan, J. Rebek, *Chem. Rev.* **1997**, *97*, 1647.
[45] N. Kobayashi, S. Minato, T. Osa, *Makromol. Chem.* **1983**, *184*, 2123.

 © WILEY-VCH Verlag GmbH, D-69451 Weinheim, 2001 1433-7851/01/4023-4421 $ 17.50+.50/0

Enantioseparation of Racemic Organic Molecules by a Zeolite Analogue**

Ren-Gen Xiong,* Xiao-Zeng You,
Brendan F. Abrahams, Ziling Xue, and Chi-Ming Che

The rational design and construction of hybrid organic–inorganic zeolite analogues (HOIZAs) for enantioseparation and catalysis is of intense current interest. These solids have shown their potential to control the host–guest chemistry of the framework by tailoring or tuning the chemical building blocks from which the network is assembled.[1–6] Through the incorporation of appropriate organic ligands the polarity of an intraframework void may be tuned to attract a range of guest molecules. This potential is not available with pure inorganic zeolites.[1] The inclusion of enantiomerically pure chiral building blocks into microporous materials (zeotypes) for enantiomer separation, as well as chiral synthesis and catalysis, has been a continuing challenge and represents an ambitious goal for chemists.[2–4]

Currently known materials capable of offering enantiomeric separation and catalysis tend to be 2D layer-type structures that are able to intercalate guests.[1, 5] Attempts to resolve enantiomers using zeolite beta, one polymorph of which crystallizes in the chiral space group $P4_122$, have as yet been unsuccessful.[6] It is known that some 3D metal coordination polymers, such as chiral coordination polymers, can reversibly exchange guest molecules while maintaining crystallinity.[7–22] These materials, however, are constructed from achiral building blocks. As a consequence, the product is a racemic mix of crystals, although their single crystals are enantiomeric. Enantiomerically pure HOIZAs with intraframework voids capable of accommodating guest molecules are highly desirable. Ideally, such a 3D framework should have relatively high thermal stability and rigidity, and possess channels that permit reversible inclusion of guests. To the best of our knowledge the existence of chiral 3D HOIZAs capable of resolving racemic guest molecules by the reversible inclusion/removal of guests is unknown. Here we report a robust 3D enantiopure HOIZA capable of resolving racemic mixtures of small organic molecules.

[*] Prof. Dr. R.-G. Xiong, Prof. X.-Z. You
Coordination Chemistry Institute, The State Key Laboratory of Coordination Chemistry
Nanjing University, 210093 Nanjing (P.R. China)
Fax: (+86) 25-3314502 or (+86)-25-3317761
E-mail: xiongrg@netra.nju.edu.cn

Dr. B. F. Abrahams
School of Chemistry, University of Melbourne
Parkville, Victoria 3052 (Australia)

Prof. Dr. Z. Xue
Department of Chemistry, University of Tennessee
Knoxville, Tennessee 37996 (USA)

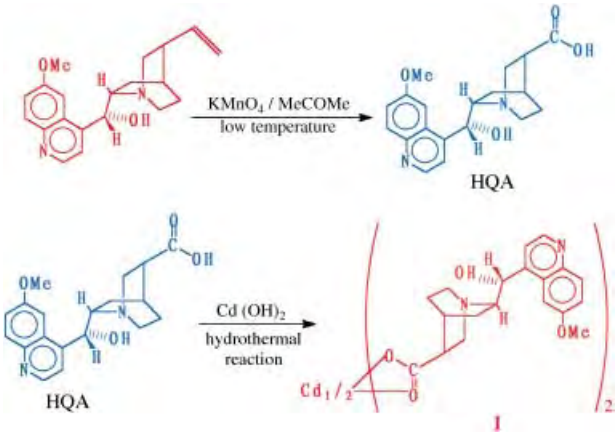
Prof. Dr. C.-M. Che
Department of Chemistry, The University of Hong Kong
Pokfulam Road (Hong Kong)

[**] This work was supported by The Major State Basic Research Development Program (Grant No. G2000077500), the National Natural Science Foundation of China, the Camille Dreyfus Teacher–Scholar Program, the National Science Foundation of the USA (CHE-9904338), and the University of Tennessee SARIF EPPE Fund.

Our strategies employed in preparing such a material involve the rational design and use of functionalized chiral ligands that are capable of bridging metal centers to form an open framework. Specifically, such a framework is produced in a self-assembly process by linking cationic metal centers and an enantiopure chiral bridging ligand containing the following functional groups:

1. A carboxylate binding group that makes the ligand anionic and the framework neutral. This ensures that intraframework voids are not occupied by counterions.
2. A mix of hydrophobic and hydrophilic groups that induce the inclusion of a variety of guests.
3. A pyridyl-type group that is able to satisfactorily complete the coordination sphere of the metal center in the generation of a 3D diamondoid coordination polymer.[23–27]

One candidate that fulfils these requirements is quitenine (6′-methoxyl-(8*S*,9*R*)-cinchonan-9-ol-3-carboxylic acid (HQA)). The enantiopure chiral building block HQA, which is prepared from the off-the-shelf antimalarial alkaloid quinine,[28] reacts with $Cd(OH)_2$ to give HOIZA $[Cd(QA)_2]$ (**1**, Scheme 1) with a homochiral open channel 3D structure.[29] The crystal structure of **1** (Figure 1) shows each Cd^{2+} ion is in a



Scheme 1. Synthesis of quitenine (HQA) and the cadmium complex **1**.

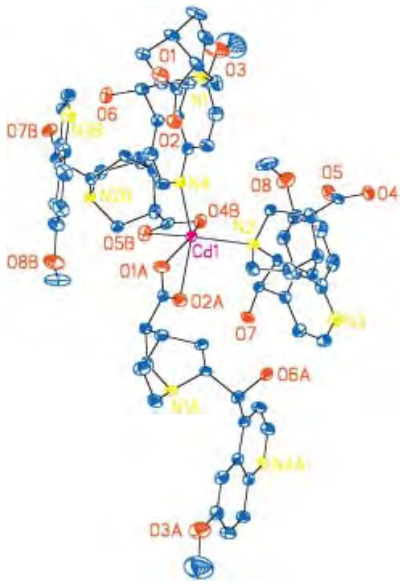


Figure 1. ORTEP view of an asymmetric unit of **1** (30% probability displacement ellipsoids). The H atoms are omitted for clarity.

 © WILEY-VCH Verlag GmbH, D-69451 Weinheim, 2001 1433-7851/01/4023-4422 $ 17.50+.50/0

distorted octahedral geometry and coordinated by two nitrogen atoms and the oxygen atoms of two carboxylate groups. There are two clearly distinct QA^- ligands in **1**. Although both ligands bridge Cd^{2+} centers, they differ significantly in their mode of binding. In both cases the carboxylate groups chelate the metal center but in only one case is the quinoline unit binding to a neighboring Cd^{2+} center. In the other ligand the alipahtic amine coordinates to an adjacent Cd^{2+} ion while the quinoline moiety is uncoordinated. Thus, each Cd^{2+} ion is coordinated by four ligands that bridge to four other symmetry-related Cd^{2+} ions. The Cd^{2+} ions linked by the QA^- ligands that bind through the quinoline group are 10.7 Å apart, while the Cd^{2+} centers bridged by the ligands involving coordination of the aliphatic amine are 7.8 Å apart.

From a topological perspective, each Cd^{2+} ion acts as a four-connecting center in a 3D network. The connectivity of this network (Figure 2) is the same as that found in diamond,

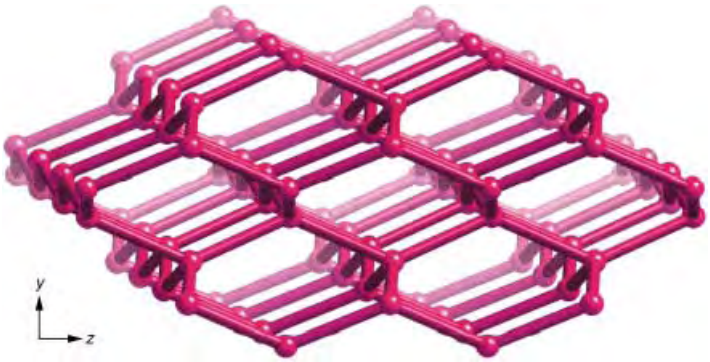


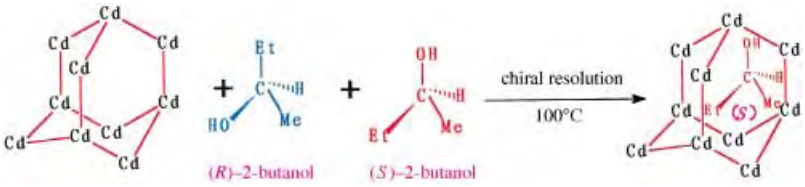
Figure 2. A topological perspective view of **1** in which the straight lines and circles represent the quitenine ligands and Cd atoms, respectively.

although it is somewhat distorted from the ideal cubic structure. As indicated above, the connections between the four-connecting Cd^{2+} centers are not all of the same length and the Cd-Cd-Cd angles fall in the range 98–152°, as compared to the ideal tetrahedral angle of 109.5° found for the C-C-C angles in diamond.

Many coordination networks with open framework structures are interpenetrated by independent networks that fill the intraframework voids. No interpenetration is, however, observed in this structure. The absence of interpenetration results in a lattice with maximum space available for the guest.

Thermogravimetric analysis (TGA) was performed on a polycrystalline sample of **1** to gauge its thermal stability. No clean weight-loss step occurred below 265 °C, which indicates that the network structure is stable below that temperature.

The chirality of the framework suggests that the intraframework voids may provide a chiral environment for guest molecules. Within a diamond network the voids may be considered to lie within adamantane-type cavities (Scheme 2). This asymmetric structural feature in **1** has the potential to allow enantioselective separation of small organic molecules, such as racemic 2-butanol and 2-methyl-1-butanol.



Scheme 2. Inclusion of (*S*)-2-butanol in the adamantane-like cavities of **1**.

In order to investigate whether this coordination polymer allows enantioselective separation, racemic 2-butanol and a powdered sample of $[Cd(QA)_2]$ (**1**) were mixed under solvothermal reaction conditions. A crystalline sample of $((S)\text{-2-butanol}) \subset [Cd(QA)_2]$ (**2**) was obtained. A single-crystal X-ray structural determination[30] clearly shows that (*S*)-2-butanol has been included in **2** (Figure 3). Examination

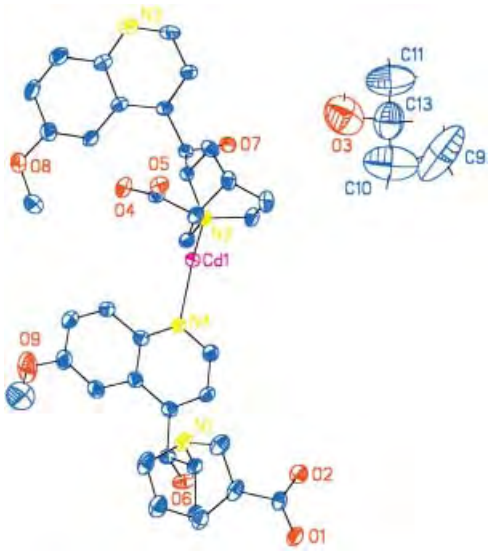


Figure 3. ORTEP view of an asymmetric unit of **2** (30% probability displacement ellipsoids). The H atoms of the frameworks are omitted for clarity.

of the 2-butanol desorbed from **2** showed that it had a specific optical rotation ($[\alpha]_D^{20} = +13.0°$ (neat)) identical to that of a pure (*S*)-2-butanol standard. The *ee* value was estimated to be approximately 98.2%. The adamantane-type cavity within the structure is represented in Figure 4, and it clearly shows the (*S*)-2-butanol lies within the chiral cavity of this network. A TGA of powdered polycrystalline $(S)\text{-2-butanol} \subset [Cd(QA)_2]$ indicated that a weight loss of approximately 8.3% in the 160–204 °C range corresponds to the complete removal of all the (*S*)-2-butanol (calculated 8.51%). The framework is thermally stable up to about 265 °C. This coordination polymer (**2**) is, to our knowledge, the first HOIZA that exhibits enantioselective reversible inclusion of a molecular guest without change to the framework structure. In addition its ability to resolve organic enantiomers is unprecedented.

$(S)\text{-2-methyl-1-butanol} \subset [Cd(QA)_2]$ (**3**), an analogue of **2** with a larger chiral organic guest, was also prepared from racemic 2-methyl-1-butanol by a procedure similar to that

 © WILEY-VCH Verlag GmbH, D-69451 Weinheim, 2001 1433-7851/01/4023-4423 $ 17.50+.50/0

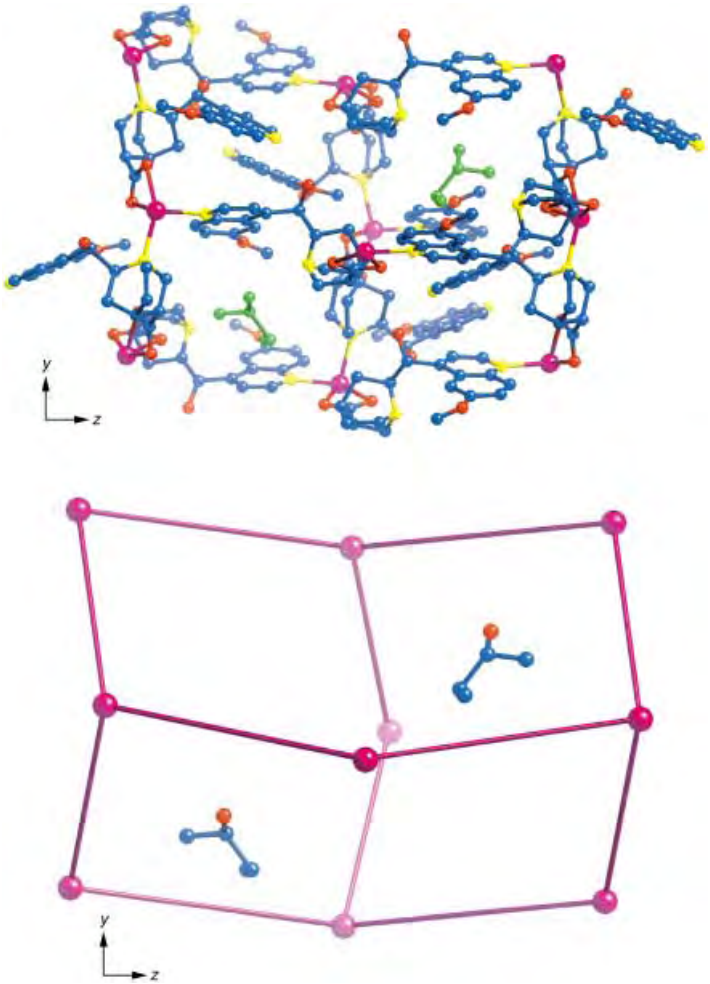


Figure 4. Top: Part of the diamond-like network of **2** including (*S*)-2-butanol. Bottom: A simplified diamond-like network clearly showing the (*S*)-2-butanol sites in the chiral cavity.

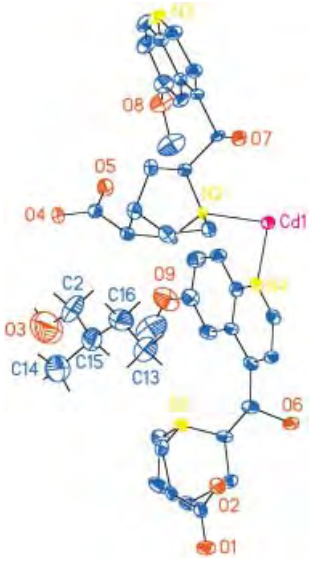


Figure 5. ORTEP view of an asymmetric unit of **3** (30% probability displacement ellipsoids). The H atoms of the frameworks are omitted for clarity.

used in the synthesis of **2**.[31] The solid-state structure (Figure 5) shows that **3** is isostructural with **2**, and that the 2-methyl-1-butanol included is the *S* enantiomer. Similarly, the adamantane-type cavity within the structure is represented in Figure 6, and it clearly shows the (*S*)-2-methyl-1-butanol molecule lies within the chiral cavity of this network. The optical rotation ($[\alpha]_D^{23} = -5.8^\circ$ (neat)) of the 2-methyl-1-butanol desorbed from **3** is identical to the standard (*S*)-2-methyl-1-butanol with an *ee* value of about 8.4%. TGA indicates that **3** begins to lose (*S*)-2-methyl-1-butanol at 80 °C and that the [Cd(QA)$_2$] framework is stable up to about 265 °C. Further investigations on the resolution of other small molecules are currently underway.

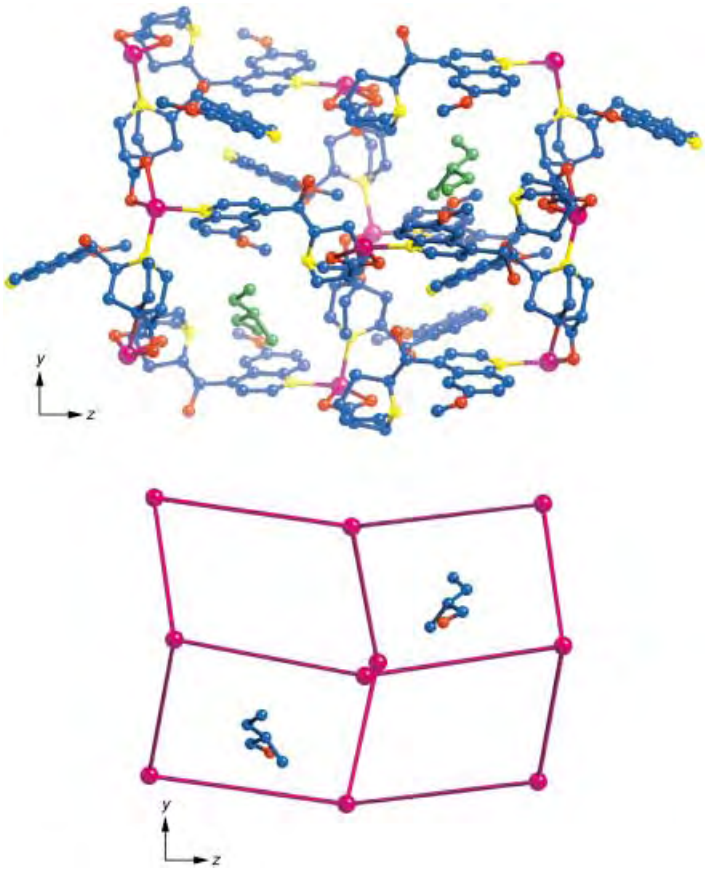


Figure 6. Top: Part of the diamond-like network of **3** including (*S*)-2-methyl-1-butanol. Bottom: A simplified diamond-like network clearly showing the (*S*)-2-methyl-1-butanol sites in the chiral cavity.

Experimental Section

HQA: Slow oxidation of quinine (6.5 g, 20 mmol) with $KMnO_4$ (9.5 g, 60 mmol) in aqueous acetone at 0–5 °C afforded a colorless prismatic crystalline product, which after recrystallization from water and ethanol gave 2.49 g (6.0 mmol, 30% yield) of quitenine · 4 H_2O. Elemental analysis calcd for $C_{19}H_{23}N_2O_4 \cdot 4H_2O$: C 55.06, H 7.30, N 6.76%; found: C 55.11, H 7.31, N 6.81; IR (KBr): $\tilde{\nu}$ = 3395(br, s), 2952(w), 1621(s), 1591(s), 1509 (m), 1473(m), 1435(w), 1369(m), 1242(m), 1025(w), 856(w), 834(w), 718(w), 640(m) cm^{-1}.

1: Hydrothermal treatment of $Cd(OH)_2$ (0.293 g, 2 mmol) and quitenine (1.657 g, 4 mmol) in ethanol for three days at 100 °C afforded 0.954 g (1.2 mmol, 60% yield) of **1** as colorless crystals. Elemental analysis calcd for $C_{38}H_{42}N_4O_8Cd$: C 57.35, H 5.28, N 7.04%; found: C 57.41, H 5.31, N 6.91; IR (KBr): $\tilde{\nu}$ = 3396(br, s), 2945(m), 1623(s), 1543(s), 1513(s), 1474(s), 1410(s), 1244(m), 1228(m), 1103(w), 1029(w), 949(w), 854(w), 832(w), 781(w), 718(w), 642(w), 607(w) cm^{-1}.

2: Hydrothermal reaction of **1** (1.590 g, 2 mmol) with a solution of racemic 2-butanol for three days at 100 °C afforded 0.956 g (1.10 mmol, 55% yield) of **2** as colorless crystalline plates. Elemental analysis calcd for $C_{42}H_{52}N_4O_9Cd$: C 57.98, H 5.98, N 6.44%; found: C 58.04, H 5.86, N 6.51; IR (KBr): $\tilde{\nu}$ = 3416(br, s), 2943(m), 1622(s), 1552(s), 1513(s), 1412(s), 1278(w), 1243(w), 11 228(w), 1104(w), 1030(m), 856(w), 833(w), 717(w), 642(w), 606(w) cm^{-1}.

3: Hydrothermal reaction of **1** (1.590 g, 2 mmol) with a solution of racemic 2-methyl-1-butanol for three days at 100 °C afforded 1.324 g (1.5 mmol, 75% yield) of **3** as colorless crystalline plates. Elemental analysis calcd for $C_{43}H_{54}N_4O_9Cd$: C 58.42, H 6.11, N 6.34%; found: C 58.42, H 6.19, N 6.41;

 © WILEY-VCH Verlag GmbH, D-69451 Weinheim, 2001 1433-7851/01/4023-4424 $ 17.50+.50/0

IR (KBr): $\tilde{\nu}$ = 3360(br, s), 2945(m), 1622(s), 1553(s), 1513(s), 1412(s), 1365(w), 1328(w), 1278(m), 1244(m), 1228(m) 1186(w), 1120(w), 1103(w), 1068(w), 1030(w), 1016(w), 951(w), 918(w), 857(w), 835(w), 780(w), 718(w), 644(w), 605(w) cm^{-1}.

Received: July 16, 2001 [Z17516]

[1] C. Janiak, *Angew. Chem.* **1997**, *109*, 1499 – 1502; *Angew. Chem. Int. Ed. Engl.* **1997**, *36*, 1431 – 1434.
[2] J. S. Seo, D. Whang, H. Lee, S. I. Jun, J. Oh, Y. Jin, K. Kim, *Nature* **2000**, *404*, 982 – 986.
[3] J. Chin, S. S. Lee, K. J. Lee, S. Park, D. H. Kim, *Nature* **1999**, *401*, 254 – 257.
[4] J. M. Rivera, T. Martin, J. Rebek, Jr., *Science* **1998**, *279*, 1021 – 1023.
[5] T. E. Mallouk, J. A. Gavin, *Acc. Chem. Res.* **1998**, *31*, 209 – 217.
[6] M. M. Treacy, J. M. Newsam, *Nature* **1988**, *332*, 249 – 251.
[7] G. B. Gardner, D. Venkataraman, J. S. Moore, S. Lee, *Nature* **1995**, *374*, 792 – 795.
[8] B. F. Abrahams, B. F. Hoskins, D. M. Michail, R. Robson, *Nature* **1994**, *369*, 727 – 729.
[9] O. M. Yaghi, G. Li, H. Li, *Nature* **1995**, *378*, 703 – 706.
[10] H. Li, M. Eddaoudi, M. O'Keeffe, O. M. Yaghi, *Nature* **1999**, *402*, 276 – 279.
[11] S. S.-Y. Chui, S. M.-F. Lo, I. P. H. Charmant, A. G. Orpen, I. D. A. Williams, *Science* **1999**, *283*, 1148 – 1150.
[12] V. A. Russell, C. C. Evans, W. Li, M. D. Ward, *Science* **1997**, *276*, 575 – 579.
[13] M. Fujita, Y. J. Kwon, S. Washizu, K. Ogura, *J. Am. Chem. Soc.* **1994**, *116*, 1151 – 1152.
[14] K. Biradha, C. Seward, M. J. Zaworotko, *Angew. Chem.* **1999**, *111*, 584 – 587; *Angew. Chem. Int. Ed.* **1999**, *38*, 492 – 495.
[15] T. E. Gler, X. Bu, P. Feng, G. D. Stucky, *Nature* **1998**, *395*, 154 – 157.
[16] A. von Zelewsky, O. Mamula, *J. Chem. Soc. Dalton Trans.* **2000**, 219 – 231.
[17] T. Ezuhara, K. Endo, Y. Aoyama, *J. Am. Chem. Soc.* **1999**, *121*, 3279 – 3283.
[18] Z.-F. Chen, R.-G. Xiong, J. Zhang, J.-L. Zuo, X.-Z. You, C.-M. Che, H.-K. Fun, *J. Chem. Soc. Dalton Trans.* **2000**, 4010 – 4012.
[19] W. W. Ellis, M. Schmitz, A. A. Arif, P. J. Stang, *Inorg. Chem.* **2000**, *39*, 2547 – 2557.
[20] J. J. Bodwin, V. L. Pecoraro, *Inorg. Chem.* **2000**, *39*, 3434 – 3435.
[21] L. Carlucci, G. Ciani, D. M. Proserpio, S. Rizzato, *Chem. Commun.* **2000**, 1319 – 1320.
[22] a) F. Grepioni, S. Gladiali, L. Scaccianoce, P. Ribeiro, D. Braga, *New J. Chem.* **2001**, *25* 690 – 695; b) D. Braga, F. Grepioni, G. R. Desiraju, *Chem. Rev.* **1998**, *98*, 1375 – 1406; c) D. Braga, F. Grepioni, *J. Chem. Soc. Dalton Trans.* **1999**, 1 – 8.
[23] S. R. Batten, R. Robson, *Angew. Chem.* **1998**, *110*, 1558 – 1595; *Angew. Chem. Int. Ed. Engl.* **1998**, *37*, 1460 – 1494.
[24] K. A. Hirsch, S. R. Wilson, J. S. Moore, *Chem. Eur. J.* **1997**, *3*, 765 – 771.
[25] a) O. R. Evans, R.-G. Xiong, Z. Wang, G. K. Wong, W. Lin, *Angew. Chem.* **1999**, *111*, 557 – 559; *Angew. Chem. Int. Ed.* **1999**, *38*, 536 – 538; b) R.-G. Xiong, J.-L. Zuo, X.-Z. You, B. F. Abrahams, Z.-P. Bai, C.-M. Che, *Chem. Commun.* **2000**, 2061 – 2062; c) Z.-F. Chen, R.-G. Xiong, B. F. Abrahams, X.-Z. You, C.-M. Che, *J. Chem. Soc. Dalton Trans.* **2001**, 2453 – 2455.
[26] B. L. Chen, M. Eddaoudi, S. T. Hyde, M. O'Keeffe, O. M. Yaghi, *Science* **2001**, *291*, 1021 – 1023.
[27] A. J. Blake, N. R. Champness, S. S. M. Chung, W. S. Li, M. Schroder, *Chem. Commun.* **1997**, 1005 – 1006.
[28] Crystal data for quitenine · 4 H_2O: $C_{19}H_{30}N_2O_8$, orthorhombic, space group $P2_12_12_1$, a = 9.5585(9), b = 10.3410(9), c = 20.8404(19) Å, $\alpha = \beta = \gamma$ = 90.00°, V = 2060.0(3) Å^3, Z = 4, M_r = 414.45, ρ_{calcd} = 1.336 Mg m^{-3}, R_1 = 0.0667, wR_2 = 0.1770, T = 293 K, μ = 1.040 mm^{-1}, S = 1.265, Flack χ = 0.001(2).
[29] Crystal data for **1**: $C_{38}H_{42}N_4O_8Cd$, orthorhombic, space group $P2_12_12_1$, a = 13.8639(8), b = 15.1012(8), c = 19.4313(11) Å, $\alpha = \beta = \gamma$ = 90.00°, V = 4068.0(2) Å^3, Z = 4, M_r = 795.16, ρ_{calcd} = 1.298 Mg m^{-3}, R_1 = 0.0646, wR_2 = 0.1358, T = 293 K, μ = 0.588 mm^{-1}, S = 1.017, Flack χ = 0.01(3).
[30] Crystal data for **2**: $C_{42}H_{52}N_4O_9Cd$, orthorhombic, space group $P2_12_12_1$, a = 13.7818(9), b = 15.0617(10), c = 19.355(13) Å, $\alpha = \beta = \gamma$ = 90.00°, V = 4017.8(5) Å^3, Z = 4, M_r = 869.28, ρ_{calcd} = 1.437 Mg m^{-3}, R_1 = 0.0436, wR_2 = 0.1054, T = 293 K, μ = 0.604 mm^{-1}, S = 0.744, Flack χ = − 0.02(2).
[31] Crystal data for **3**: $C_{43}H_{54}N_4O_9Cd$, orthorhombic, space group $P2_12_12_1$, a = 13.8756(8), b = 15.1162(8), c = 19.2999(10) Å, $\alpha = \beta = \gamma$ = 90.00°, V = 4048.1(4) Å^3, Z = 4, M_r = 883.30, ρ_{calcd} = 1.449 Mg m^{-3}, R_1 = 0.0797, wR_2 = 0.1684, T = 293 K, μ = 0.601 mm^{-1}, S = 1.227, Flack χ = − 0.04(4). The structures were solved with Direct methods using the program SHELXTL (Sheldrick, 1997).[32] All the non-hydrogen atoms were located from the trial structure and then refined anisotropically with SHELXTL using a full-matrix least-squares procedure. The hydrogen atom positions were fixed geometrically at calculated distances and allowed to ride on the parent carbon atoms. The final difference Fourier map was found to be featureless. Crystallographic data (excluding structure factors) for the structures reported in this paper have been deposited with the Cambridge Crystallographic Data Centre as supplementary publication nos. CCDC-166932 – 166935. Copies of the data can be obtained free of charge on application to CCDC, 12 Union Road, Cambridge CB2 1EZ, UK (fax: (+44) 1223-336-033; e-mail: deposit@ccdc.cam.ac.uk).
[32] G. M. Sheldrick, SHELXTL V5.1 Software Reference Manual, Bruker AXS, Inc., Madison, Wisconsin, USA, **1997**.

Control of Liquid Crystallinity of Diazadibenzoperylene Dyes by Covalent and Hydrogen-Bonded Attachment of Mesogens**

Armin Sautter, Christoph Thalacker, and Frank Würthner*

Dedicated to Dr. Günther Seybold on the occasion of his 60th birthday

Functional liquid crystals (LCs) with intrinsic luminescence properties are of great interest in the development of new organic materials, such as anisotropic light emitters, organic lasers, photoconductors, and in LC display technology.[1–3] In contrast to dissolving a fluorescent dye in a LC matrix, fluorescent LCs are thought not only to overcome miscibility and stability problems but also to exhibit novel enhanced optoelectronic properties. To date, only a few examples have been reported such as triphenylenes,[3a–d] benzopyrenes,[3e] hexacatenar compounds,[1a] and perylenes,[2] but the field is

[*] Priv.-Doz. Dr. F. Würthner, Dr. A. Sautter, Dr. C. Thalacker
Abteilung Organische Chemie II
Universität Ulm
Albert-Einstein-Allee 11, 89081 Ulm (Germany)
Fax: (+49) 731-5022840
E-mail: frank.wuerthner@chemie.uni-ulm.de

[**] We thank P. Zell for his assistance in the practical work, Frau G. Dörfner and Prof. U. Thewalt (Sektion Röntgenbeugung, Universität Ulm) and Dr. B. Heise (Abteilung Experimentelle Physik, Universität Ulm) for X-ray diffraction studies. Financial support from the Deutsche Forschungsgemeinschaft (Habilitandenstipendium for F.W.), the Fonds der Chemischen Industrie (Liebig-Stipendium for F.W.), and the Dr. Otto Röhm Gedächtnisstiftung is gratefully acknowledged.

Supporting information for this article is available on the WWW under http://www.angewandte.com or from the author.

rapidly expanding. Here, we report a series of diazadibenzoperylenes **3a–d** that bear mesogenic dodecyloxybenzoyl substituents and aza coordination sites suited for additional control of dye packing by intermolecular interactions. All the compounds **3a–d** exhibit strong luminescence in solution and in the pristine (i.e. solid) states , and **3a–c** form thermotropic columnar liquid crystalline phases in the presence and/or absence of benzoic acids **4a–d**.

Cleavage of all the methoxy ethers of the diazadibenzoperylene **1**[4, 5] with BBr_3 in dichloromethane afforded tetra(*p*-hydroxyphenoxy)diazadibenzoperylene **2** in 95% isolated yield. Esterification reactions of **2** with various dodecyloxy-substituted benzoic acid chlorides in dichloromethane in the presence of triethyl amine led to the title compounds **3a–d** in 42–54% isolated yields (Scheme 1) after purification by chromatography.[5]

All the diazadibenzoperylenes **3a–d** show identical absorption and fluorescence spectra in dichloromethane, with absorption maxima at 495 nm and 464 nm, and a mirror-image fluorescence emission with maxima at 512 nm and 545 nm (Figure 1). The fluorescence quantum yields Φ_F range between 0.65 (**3c**) and 0.83 (**3b**).[6] Aggregation of the molecules in nonpolar solvents, for example methylcyclohexane (MCH), or in the solid state causes pronounced changes in the UV/Vis and fluorescence spectra. For thin films a bathochromic shift of about 10 nm and a pronounced line broadening of the UV/Vis absorption spectra is observed, which implies strong dye–dye interactions in the solid state (Figure 1). As a result of a considerable bathochromic shift of about 100 nm in the fluorescence spectra these films exhibit intense red emission in contrast to the green emission in solution. A spectral fine structure is only observed for **3a** and **b** but not for **3c** which indicates a higher molecular ordering for **3a**, **b** (Figure 1).

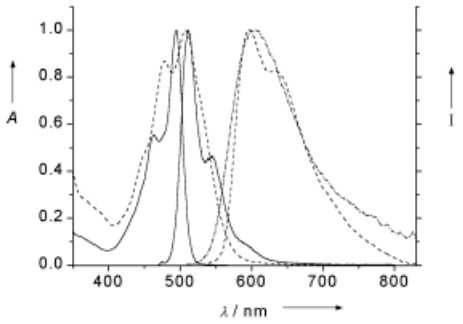


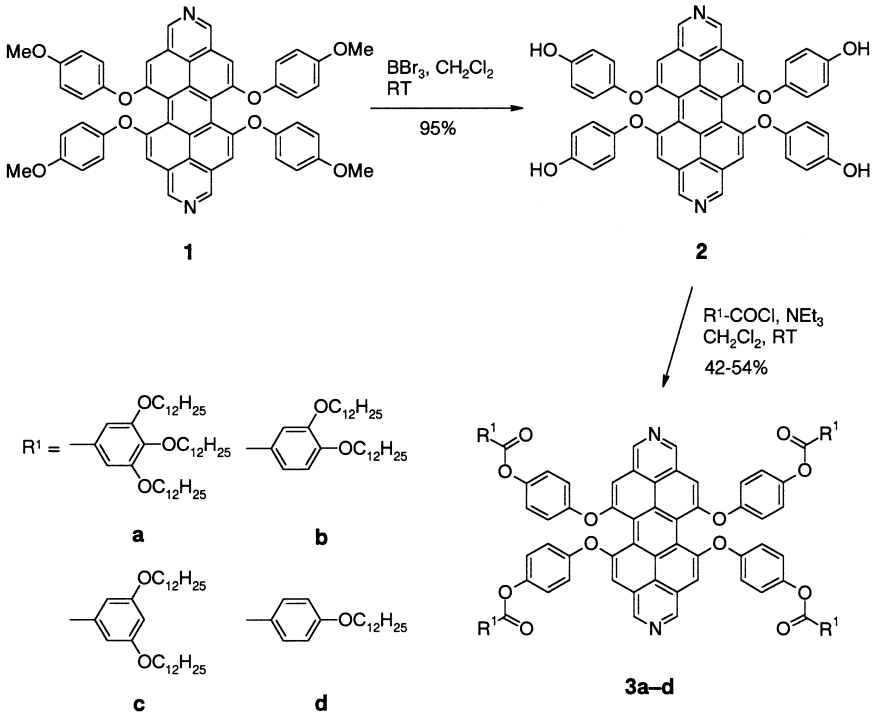
Figure 1. UV/Vis absorption and fluorescence spectra of **3b** in dichloromethane (——) and as thin film (- - - -) on a quartz substrate and film emission spectrum of **3c** (•–•–).

The thermotropic properties of **3a–d** were investigated by optical polarization microscopy (OPM) and differential scanning calorimetry (DSC). Phase-transition temperatures and associated enthalpy values for compounds **3a–d** are given in Table 1. **3d** with only four dodecyloxy chains, melts at 249 °C and crystallizes upon cooling. No LC phase was found for this compound. Compound **3c** which bears (3,5-didodecyloxy)-benzoyl substituents exhibits an unexpected thermotropic behavior. The viscosity of a completely amorphous film of **3c** gradually decrease when the compound is heated and neither a melting point nor a glass transition was observed by OPM and DSC. In contrast, **3b** and **3a** bearing four (3,4-didodecyloxy)- and (3,4,5-tridodecyloxy)benzoyl substituents, respectively, are liquid crystalline from room temperature to their clearing points at 177 °C (**3b**) and 174 °C (**3a**).[7] On slow cooling from the isotropic liquid state large spherulitic textures (ca. 100 μm) can be observed at crossed polarizers by OPM that are characteristic for columnar LC phases (Figure 2a).[8]

Table 1. Phase transition temperatures T [°C] and transition enthalpies ΔH_t [kJ mol^{-1}] (in parentheses) for diazadibenzoperylenes **3a–d**.[a–c]

Compound	T [°C] (ΔH_t [kJ mol^{-1}])
3a	Col 174 (16.3) I
3b	Col 177 (27.3) I
3c	–
3d	Cr 249 (36.5) I

[a] Col = columnar mesophase; [b] I = isotropic liquid; [c] Cr = crystalline solid.



Scheme 1. Synthesis of dodecyloxybenzoyl-substituted diazadibenzoperylenes **3a–d**.

The X-ray crystal structure of a closely related *N*,*N*′-dibutylated diazadibenzoperylene revealed a twisting of the central six-membered ring of the aromatic diazadibenzoperylene backbone by 25°, because of the electrostatic repulsion of the oxygen atoms of the phenoxy substituents.[4] This twisting leads to a propeller-like arrangement of the phenoxy substituents in contrast to most tradi-

 © WILEY-VCH Verlag GmbH, D-69451 Weinheim, 2001 1433-7851/01/4023-4426 $ 17.50+.50/0 *Angew. Chem. Int. Ed.* **2001**, *40*, No. 23

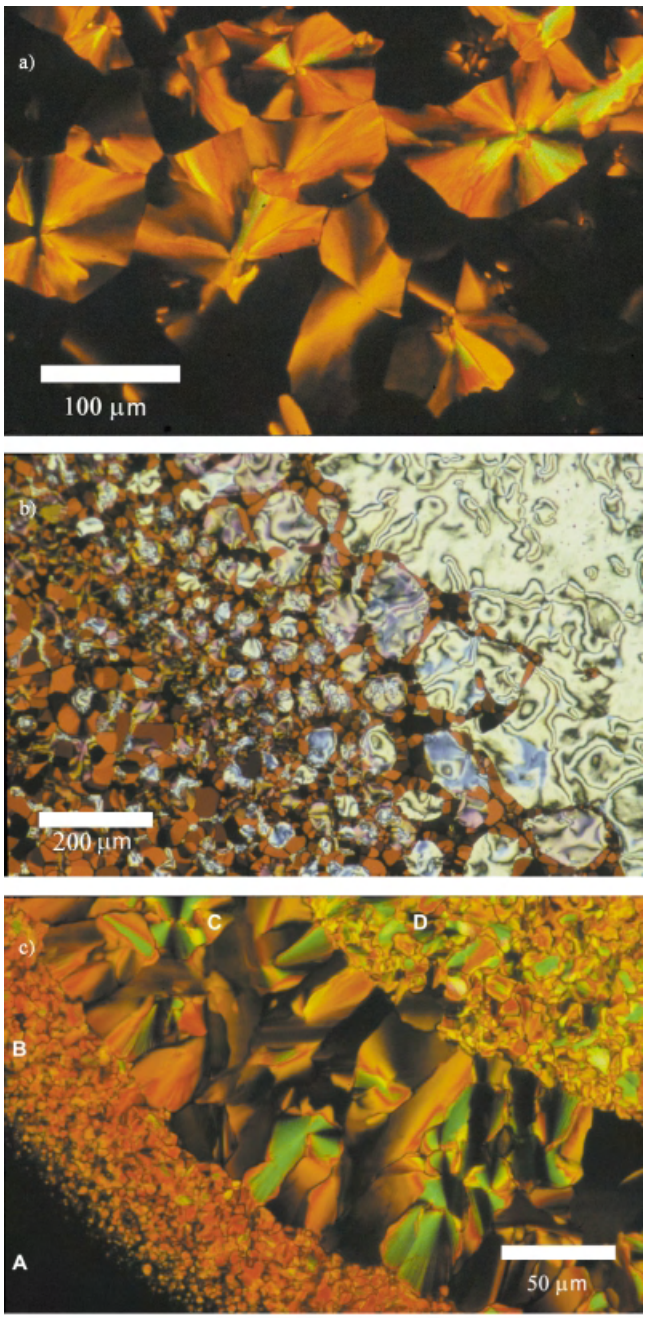
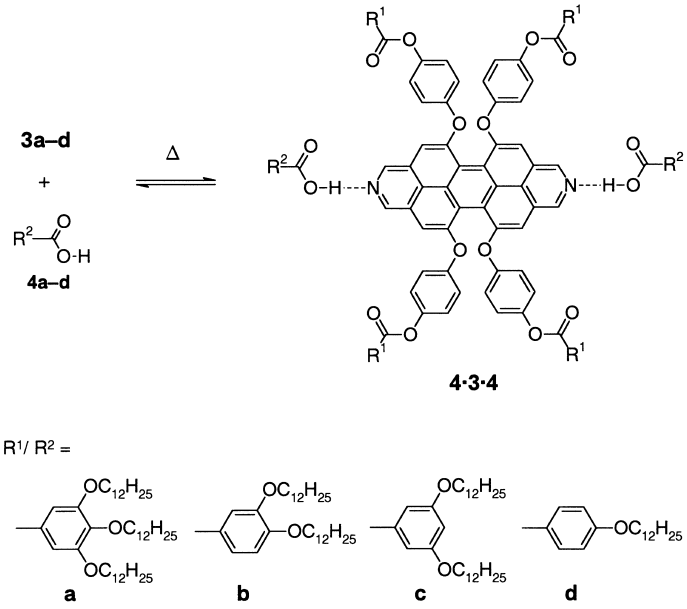


Figure 2. Optical micrographs of the textures of a) the columnar mesophase of **3a** obtained by cooling from the isotropic melt to room temperature; b) the contact region of a melting preparation of the columnar mesogen **3a** and the calamitic mesogen **4d** (top right corner); c) the contact region of a melting preparation of **3c** and **4c**, showing amorphous **3c** (A); a region rich in **3c** (B); complex [**4c**·**3c**·**4c**] (C), and a region with a lower content of **3c** (D). All micrographs were taken at crossed polarizers.

tional columnar mesogens[8] which exhibit disclike central units. Nevertheless, a number of molecules were recently reported that lack a flat core but that are capable of forming columnar mesophases. Here, the main driving force is ascribed to microsegregation,[9] which also plays the crucial role in the formation of columnar mesophases of compounds **3a**, **b** by segregation of the polar diazadibenzoperylene cores from the nonpolar dodecyl chains.

The columnar nature of the mesophase of **3b** was confirmed by X-ray diffraction (XRD) and assigned to a columnar rectangular disordered (Col_{rd}) LC phase with four sharp reflections in the small-angle region at $2\vartheta = 2.04°$, $2.57°$, $4.08°$, and $8.83°$, and a halo in the wide-angle region of the diffractogram.[10] XRD also confirmed the crystalline state of **3d** (abundant sharp reflections) and the amorphous nature of **3c** (only a diffuse reflection at $2\vartheta = 2.73°$ corresponding to 32.3 Å which is about the size of an individual molecule, and a halo in the wide-angle region around $2\vartheta = 20°$).

Compounds **3a**–**d** are distinguished from other mesogens by a unique combination of functionality (optical and redox)[4] and diaza receptor sites suitable for additional control of the supramolecular organization through coordination to carboxylic acid or Lewis-acidic binding partners (e.g. metal ions).[11–13] Here, we will concentrate on hydrogen-bonded complexes between diazadibenzoperylenes **3a**–**d** and the different dodecyloxy-substituted benzoic acids **4a**–**d** (Scheme 2).[12]



Scheme 2. Complex formation between substituted benzoic acids **4a**–**d** and a diazadibenzoperylene **3a**–**d** through hydrogen bonding by melting both compounds together between glass slides or by evaporation of a 1:2 stoichiometric solution of the two components.

For this purpose contact melting preparations were made by melting first a diazadibenzoperylene **3a**–**d** and then a benzoic acid **4a**–**d** between glass slides to give a contact region with a gradient in stoichiometry of the two components. Investigation of the phase behavior of these preparations by repeated heating–cooling cycles on a hot-stage OPM at crossed polarizers revealed crystallinity for all complexes between **3d** and **4a**–**d**, and liquid crystallinity for all complexes formed between **3a**, **b** and **4a**–**d**. For all 1:2 complexes [**4a**–**d**·**3a**, **b**·**4a**–**d**] we observed a decrease in the clearing points between 10 and 30 K with respect to the pure compounds **3a**, **b**. This indicates a destabilization of the columnar mesophases by addition of the benzoic acids which disturb the columnar organization of the mesogenic dyes

 © WILEY-VCH Verlag GmbH, D-69451 Weinheim, 2001 1433-7851/01/4023-4427 $ 17.50+.50/0

3a, **b**. When the calamitic mesogenic benzoic acid **4d** is applied especially beautiful transitions of the mesophases are observed in the contact regions with **3a**, **b** (Figure 2b). Remarkably, all the benzoic acids **4a**–**d** were able to induce columnar LC phases upon coordination to the formerly amorphous diaza ligand **3c** giving rise to well-pronounced textures in the boundary regions of the contact melting preparations. An optical micrograph taken at crossed polarizers for complexation of **3c** with **4c** is depicted in Figure 2c. The left bottom corner (A; the black area), shows amorphous pure **3c**, and the region (B) exhibits small textures which we attribute to an intermediate phase between **3c** and **4c**, rich in **3c**. In the middle region (C) well-pronounced and large textures of complex [**4c**·**3c**·**4c**] with the correct 1:2 stoichiometry can be observed which exhibit a sharp clearing transition at 116 °C. Region (D) has a low **3c** content and the textures become smaller. The same textures as in the middle regions of these contact melting preparations are also observed if complexes [**4a**–**d**·**3c**·**4a**–**d**] are prepared in an exact 1:2 stoichiometry from stock solutions. According to OPM all these mesophases have well-defined clearing points at 111 °C for [**4a**·**3c**·**4a**], 100 °C for [**4b**·**3c**·**4b**], 116 °C for [**4c**·**3c**·**4c**], and 94 °C for [**4d**·**3c**·**4d**] and also here no crystallization is observed upon cooling these samples to room temperature.[14]

In conclusion, we presented a new class of highly fluorescent mesogenic diazadibenzoperylenes **3a**–**c**, the morphological behavior of which could be controlled by hydrogen-bond directed coordination to carboxylic acids. In future work chiral hydrogen-bond donors and metal ions will be applied to induce chiroptical properties by means of the inherently atropisomeric backbone of **3a**–**d** and applications of these supramolecular assemblies in optoelectronics will be addressed.[15]

Received: July 2, 2001 [Z17402]

[1] a) B. P. Hoag, D. L. Gin, *Adv. Mater.* **1998**, *10*, 1546–1551; b) T. Ikeda, O. Tsutsumi, *Science* **1995**, *268*, 1873–1875.

[2] a) R. A. Cormier, B. A. Gregg, *Chem. Mater.* **1998**, *10*, 1309–1319; b) F. Würthner, C. Thalacker, S. Diele, C. Tschierske, *Chem. Eur. J.* **2001**, *7*, 2245–2253; c) I. K. Iverson, S.-W. Tam-Chang, *J. Am. Chem. Soc.* **1999**, *121*, 5801–5802; d) C. Göltner, D. Pressner, K. Müllen, H.-W. Spiess, *Angew. Chem.* **1993**, *105*, 1722–1724; *Angew. Chem. Int. Ed. Engl.* **1993**, *32*, 1660–1662; e) U. Rohr, P. Schlichting, A. Böhm, M. Groß, K. Meerholz, C. Bräuchle, K. Müllen, *Angew. Chem.* **1998**, *110*, 1463–1467; *Angew. Chem. Int. Ed.* **1998**, *37*, 1434–1437; f) T. Hassheider, S. A. Benning, H.-S. Kitzerow, M.-F. Achard, H. Bock, *Angew. Chem.* **2001**, *113*, 2119–2122; *Angew. Chem. Int. Ed.* **2001**, *40*, 2060–2063.

[3] a) D. Adam, P. Schuhmacher, J. Simmerer, L. Häussling, K. Siemensmeyer, K. H. Etzbach, H. Ringsdorf, D. Haarer, *Nature* **1994**, *371*, 141–143; b) J. A. Rego, S. Kumar, H. Ringsdorf, *Chem. Mater.* **1996**, *8*, 1402–1409; c) A. Bacher, C. H. Erdelen, D. Haarer, W. Paulus, H. W. Schmidt, *Adv. Mater.* **1997**, *9*, 1031–1034; d) J. Kopitzke, J. H. Wendorff, *Chem. Unserer Zeit* **2000**, *34*, 4–15; e) A. Beer, G. Scherowsky, H. Owen, H. Coles, *Liq. Cryst.* **1995**, *19*, 565–572.

[4] a) F. Würthner, C. Thalacker, A. Sautter, *Angew. Chem.* **2000**, *112*, 1298–1301; *Angew. Chem. Int. Ed.* **2000**, *39*, 1243–1245; b) A. Sautter, D. G. Schmid, G. Jung, F. Würthner, *J. Am. Chem. Soc.* **2001**, *123*, 5424–5430.

[5] The methoxyphenoxy-substituted diazadibenzoperylene **1** was obtained as previously reported.[4] For synthetic details, characterization, and physical properties of compounds **3a**–**d** refer to the Supporting Information.

[6] a) Determined by the optically dilute method with refractive-index correction, maximum absorptions of the solutions ≤ 0.05. All fluorescence spectra were corrected. Measurements relative to fluorescein in 0.1N NaOH ($\Phi_{ref} = 0.9$); H. G. O. Becker, *Einführung in die Photochemie*, Thieme, Stuttgart, **1983**; b) J. N. Demas, G. A. Crosby, *J. Phys. Chem.* **1971**, *75*, 991–1024.

[7] No crystallization of the compounds could be observed at room temperature over a period of six months.

[8] For a review on polycatenar and phasmidic mesogens see: H.-T. Nguyen, C. Destrade, J. Malthête in *Handbook of Liquid Crystals*, *Vol. 2B: Low Molecular Weight Liquid Crystals II* (Eds.: D. Demus, J. Goodby, G. M. Gray, H.-W. Spiess, V. Vill), Wiley-VCH, Weinheim, **1998**, pp. 865–885.

[9] a) C. Tschierske, *J. Mater. Chem.* **1998**, *8*, 1485–1508; b) A. Pegenau, T. Hegemann, C. Tschierske, S. Diele, *Chem. Eur. J.* **1999**, *5*, 1643–1660; c) X. H. Cheng, S. Diele, C. Tschierske, *Angew. Chem.* **2000**, *112*, 605–608; *Angew. Chem. Int. Ed.* **2000**, *39*, 592–595; d) H. Zheng, T. M. Swager, *J. Am. Chem. Soc.* **1994**, *116*, 761–762; e) L. Douce, A. El-ghayoury, A. Skoulios, R. Ziessel, *Chem. Commun.* **1999**, 2033–2034; f) L. Calucci, S. Zamir, D. Singer, H. Zimmermann, E. J. Wachtel, R. Poupko, Z. Luz, *Liq. Cryst.* **1997**, *22*, 1–9.

[10] The reflections were indexed as the (100), (010), (200), and (230) reflections of a columnar rectangular lattice with lattice constants of $a = 43.2$ and $b = 34.3$ Å (for diffractogram refer to the Supporting Information). The absence of an additional sharp reflection in the wide-angle region suggests a disordered columnar mesophase with no distinct intracolumnar repeat distance as expected for the rather flexible twisted core of the molecules.

[11] Reviews on metallomesogens: a) A.-M. Giroud-Godquin, P. M. Maitlis, *Angew. Chem.* **1991**, *103*, 370–398; *Angew. Chem. Int. Ed. Engl.* **1991**, *30*, 375; b) S. A. Hudson, P. M. Maitlis, *Chem. Rev.* **1993**, *93*, 861–885; c) C. Tschierske, *Angew. Chem.* **2000**, *112*, 2547–2551; *Angew. Chem. Int. Ed*. **2000**, *39*, 2454–2458.

[12] Review on hydrogen-bonded mesogens: a) T. Kato in *Handbook of Liquid Crystals*, *Vol. 2B: Low Molecular Weight Liquid Crystals II* (Eds.: D. Demus, J. Goodby, G. M. Gray, H.-W. Spiess, V. Vill), Wiley-VCH, Weinheim, **1998**, pp. 969–979; for some more papers on the formation of calamitic mesogens by hydrogen-bonding between carboxylic acids and pyridines see: b) H. Bernhardt, W. Weissflog, H. Kresse, *Angew. Chem.* **1996**, *108*, 966–968; *Angew. Chem. Int. Ed. Engl.* **1996**, *35*, 874–876; c) V. A. Mallia, M. George, S. Das, *Chem. Mater.* **1999**, *11*, 207–208.

[13] Hydrogen-bond directed formation of discoid supermolecules which assemble in a columnar mesophase has been reported in a) R. Kleppinger, C. P. Lillya, C. Yang, *J. Am. Chem. Soc.* **1997**, *119*, 4097–4102; b) M. Suárez, J.-M. Lehn, S. C. Zimmerman, A. Skoulios, B. Heinrich, *J. Am. Chem. Soc.* **1998**, *120*, 9526–9532; c) A. Kraft, A. Reichert, R. Kleppinger, *Chem. Commun.* **2000**, 1015–1016; d) D. Goldmann, R. Dietel, D. Janietz, C. Schmidt, J. H. Wendorff, *Liq. Cryst.* **1998**, *24*, 407–411; e) J. H. K. K. Hirschberg, L. Brunsveld, A. Ramzi, J. A. J. M. Vekemans, R. P. Sijbesma, E. W. Meijer, *Nature* **2000**, *407*, 167–170.

[14] The lower clearing temperatures of these supramolecular LCs compared to those of the mesogenic dyes **3a**, **b** and the smaller size of the domains indicate a lower stability of these mesophases. Based on the textures a simple hexagonal or rectangular columnar ordering seems unlikely but further XRD studies are required to reveal the exact type of supramolecular organization.

[15] It is noteworthy that there is no quenching of the diazadibenzoperylene fluorescence upon hydrogen bonding to benzoic acids according to a fluorescence titration experiment in methylcyclohexane.

 © WILEY-VCH Verlag GmbH, D-69451 Weinheim, 2001 1433-7851/01/4023-4428 $ 17.50+.50/0

Origin of Ferromagnetism in Cyano-Bridged Compounds Containing d^1 Octacyanometallates**

Liviu F. Chibotaru,* Vladimir S. Mironov, and Arnout Ceulemans

Giant-spin molecular clusters have attracted much attention in recent years in connection to the design of single-molecule magnets (SMM) based on the phenomenon of blocking of magnetization at low temperatures.[1] One of the requirements for the polynuclear clusters to become a molecular magnet is the high value of the ground-state spin. In this respect, cyano-bridged clusters seem to be promising. Their structural and magnetic properties can easily be tuned by combining $[M(CN)_n]^{m-}$ mononuclear-complex building blocks. As a result, a large variety of cyano-bridged compounds of different dimensionality ranging from clusters to three-dimensional (3D) networks have been synthesized.[2] Among them molecular magnets with high magnetic-ordering temperatures have been obtained on the basis of bimetallic and mixed-valence transition metal cyanides of the Prussian blue family.[3]

Recently, two new groups of heterometallic cyano-bridged compounds have been reported.[4–7] The first corresponds to clusters with fully capped cubane structure (Figure 1) and unusually high ground-state spin. Three compounds of this structure are known to date: they are **1** with $S = 51/2$,[4], **2** with $S = 39/2$,[5] and **3** with $S = 12$.[6]

$[Mn^{II}\{Mn^{II}(MeOH)_3\}_8(\mu\text{-}CN)_{30}\{Mo^{V}(CN)_3\}_6]\cdot 5\,MeOH\cdot 2\,H_2O$ **1**

$[Mn^{II}\{Mn^{II}(EtOH)_3\}_8(\mu\text{-}CN)_{30}\{W^{V}(CN)_3\}_6]\cdot 12\,EtOH$ **2**

$[Ni^{II}\{Ni^{II}(MeOH)_3\}_8(\mu\text{-}CN)_{30}\{Mo^{V}(CN)_3\}_6]\cdot 17\,MeOH\cdot H_2O$ **3**

The second group includes the 3D networks **4** with a ground state spin per formulae unit of $S = 11/2$ (M = Mn), $S = 9/2$ (M = Fe), and $S = 7/2$ (M = Co).[7]

$[Nb^{IV}\{(\mu\text{-}CN)_4M^{II}(H_2O)_2\}_2]\cdot 4\,H_2O$ (M = Mn, Fe, and Co) **4**

[*] Dr. L. F. Chibotaru, Prof. Dr. A. Ceulemans
Department of Chemistry
Katholieke Universiteit Leuven
Celestijnenlaan 200F, 3001 Leuven (Belgium)
Fax: (+32) 16-32-79-92
E-mail: Liviu.Chibotaru@chem.kuleuven.ac.be
Dr. V. S. Mironov
Institute of Crystallography
Russian Academy of Sciences
Leninskii prosp.59 117333 Moscow (Russia)

[**] Financial support by the Belgian National Science Foundation and Flemish Government under the Concerted Action Scheme, the ESF programme on molecular magnets, the Russian Foundation for Basic Research (Grant No. 01-02-32210), and the INTAS Grant 00-00565 are gratefully acknowledged. The authors thank Professor Silvio Decurtins and the members of his group for stimulating discussions and for sending us the structural data on the niobium compound prior the publication, and Dr. Høgni Weihe for useful discussions. We also thank Ken Somers for the help with the Figures.

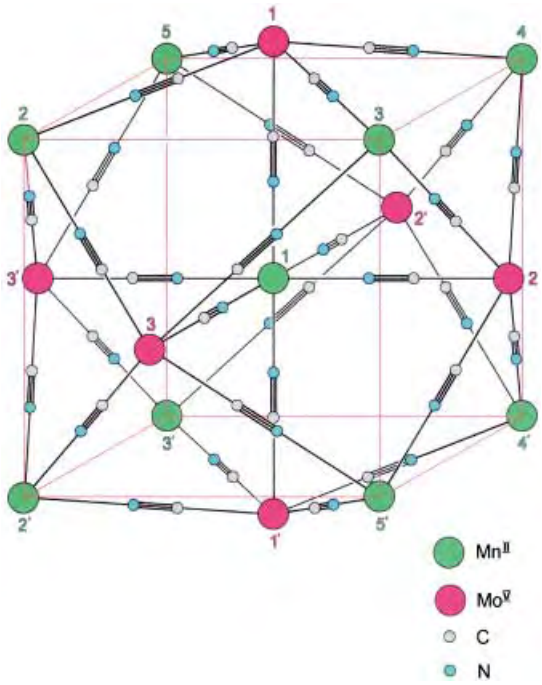


Figure 1. The structure of the $Mo_6^{V}Mn_9^{II}(\mu\text{-}CN)_{30}$ core of the cluster **1** (symmetry group C_2) which contains three nonequivalent molybdenum sites. A similar core is found in **2** (symmetry group S_6), which contains six equivalent tungsten sites, and in **3**.

A common structural feature of **1**–**4** is that they contain octacyanocoordinated Mo^{V}, W^{V}, and Nb^{IV} d^1 metal ions in a high-valent state coupled to low-valent transition metal ions by cyanide bridges. Another distinctive feature is that all the compounds except **2** are ferromagnetic. This result is surprising since no orthogonality of the magnetic orbitals is expected from the structure of these compounds.

Herein, we elucidate the reasons for ferromagnetism in **1**, **3**, and **4** and for the different magnetic behavior of **2**. It is found that these properties are mainly because of the specific symmetry properties of the magnetic orbitals at the octacoordinate ions.

There are two types of coordination for octametallates in the above compounds (Figure 2). The coordination of molybdenum and tungsten in **1**, **2**, and **3** has the geometry close to that of a trigonal dodecahedron (orange frame in Figure 2a). This geometry can be obtained from the cube by compression of one of the two interpenetrating tetrahedra and elongation of the other one, so that the C_4 rotation axis becomes S_4 (green arrow in Figure 2a) and the symmetry lowers from O_h to D_{2d}. In the idealized dodecahedron corresponding to the closest ligand packing, the eight ligands are equidistant from the central metal ion and form polar angles of 36.9° and 69.5° with the S_4 axis. According to the structural data, all the Mo^{V} and W^{V} sites have a nearly regular dodecahedral coordination with angular distortions of less than 3° in **1** and 5° in **2**, and Mo–C and W–C bonds being equal to 2.14 Å within 0.02 Å.[4, 5]

Figure 3a shows the ground d orbital, d_1, on the Mo1 site in **1** calculated with the angular overlap model (AOM). It is predominantly represented by the $d_{x^2-y^2}$ orbital with a small

 © WILEY-VCH Verlag GmbH, D-69451 Weinheim, 2001 1433-7851/01/4023-4429 $ 17.50+.50/0

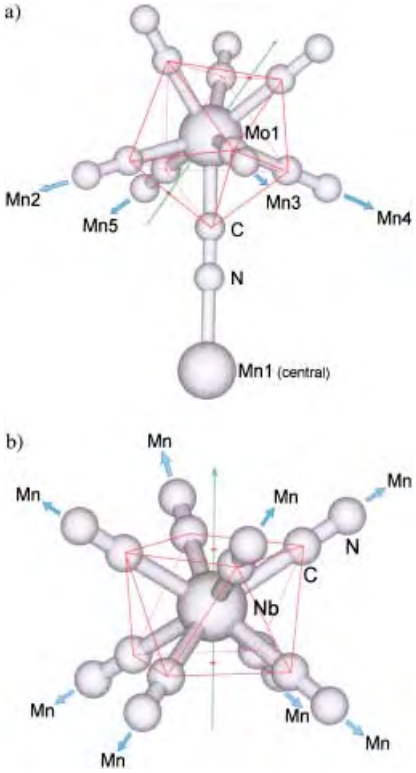


Figure 2. The structure of the octacoordinate metal fragments in the cluster **1** (a) and the compound **4** (b). The fragment in (a) is isostructural to the W site in **2** and the Mo site in **3**. Blue arrows indicate the bridging to the nearest neighbor manganese ions. Green arrows are the main symmetry axes of the orange frames.

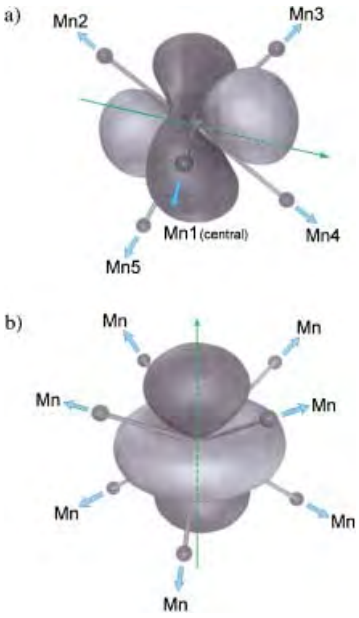


Figure 3. Ground ligand-field orbital d_1 (magnetic orbital) on the Mo1 site in **1** (a) and the Nb site in **4** (b). The arrows have the same meaning as in Figure 2.

admixture of the d_{z^2} orbital arising from small deviations from the strict D_{2d} symmetry of the dodecahedron (in which the z axis coincides with the S_4 axis and x and y with the two C_2 axes). The same is true for the other two non-equivalent molybdenum sites in **1**. Since all the Mo-C-N groups are almost linear, the one σ-and two π-orbital components of the carbon atoms into the corresponding molecular orbitals of the cyanide unit will be directed along and perpendicular to the Mo–C bonds, respectively. Simple symmetry analysis shows that in a D_{2d} dodecahedron the orbital $d_{x^2-y^2}$ is strictly orthogonal to the eight s orbitals pointing from the ligands. This orthogonality is almost fulfilled at all the molybdenum centers in **1** because of the small distortions from the idealized dodecahedral geometry. Indeed, Figure 3a shows that all the Mo–C bonds lie close to the nodal plane of the orbital d_1. An estimation of the overlap of this orbital with s and p cyanide orbitals can be assessed from the projections of d_1 orbital onto the d_σ and d_{π_x}, d_{π_y} components, defined with respect to a given Mo-C-N line (left side of Figure 4).

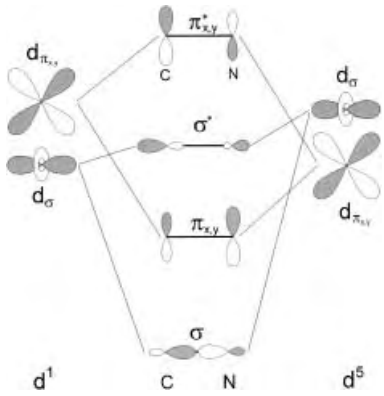


Figure 4. Definition of the d_σ, d_{π_x}, and d_{π_y} orbitals on the 4d(M) and 3d(M′) sites for a given metal pair M-(CN)-M′ (π_y-type orbitals lie in the plane perpendicular to the drawing). The two basic electron-transfer pathways (σ and π) through the cyanide bridge are outlined by the thin oblique lines. The corresponding transfer parameters describe the electron transfer in the chains: $\beta_\sigma = d_\sigma(M)$-σ*,σ(CN)-$d_\sigma(M')$, $\beta_\pi \equiv \beta_{\pi_x} = \beta_{\pi_y} = d_{\pi_x}(M)$-π*,π(CN)-$d_{\pi_x}(M')$.

The square of these components, $F_\sigma(d_1,l_i)^2$ and $F_{\pi_x}(d_1,l_i)^2 + F_{\pi_y}(d_1,l_i)^2$, which define the destabilization of the d_1 orbital by the jth cyanide ligand,[8] are listed in Table 1. The σ overlap is negligibly small compared with the π overlap for all the octametallate sites in the clusters **1** and **2**. The same can be expected for the Mo^V centers in **3** which is structurally similar.

In the 3D networks of **4**, the coordination geometry of the Nb^{IV} ions is close to square antiprismatic (orange frame in Figure 2b). Four ligands are equivalent within the upper and lower planes, but the Nb–C distances and polar angles of upper and lower ligands with respect to the C_4 axis of the antiprism (green arrow in Figure 2b) are somewhat different, so that the symmetry lowers from D_{4d} to C_{4v}. In this geometry, the lowest ligand field orbital d_1 on the niobium ion will be of pure d_{z^2} type (Figure 3b).[9] Noteworthy is that the σ overlap of the d_1 orbital with the cyanide orbital vanishes exactly at the cubic polar angle $\theta_{cub} = 54.7°$. The actual polar angles in the $Nb(CN)_8^{4-}$ fragments, $\theta_2 = 58.2°$, $\pi - \theta_1 = 57.5°$, are very close the closest packing angle $\theta_{c.p.} = 59.2°$ and differ by only a few degrees from θ_{cub}. As a result the directions of the Nb–C bonds for all eight cyanide ligands pass very close to the nodal cones of the d_1 orbital (Figure 3b). That is why in these

 © WILEY-VCH Verlag GmbH, D-69451 Weinheim, 2001 1433-7851/01/4023-4430 $ 17.50+.50/0

Table 1. Angular overlap factors for the ground magnetic orbital d_1 of octametallate sites with respect to σ and π bonds in Mo-CN-Mn, W-CN-Mn, and Nb-CN-Mn pairs in compounds **1**, **2**, and **4**.

Metal pair (i, j)		$F_\sigma(d_1, l_j)^2 \times 10^4$	$F_{\pi_x}(d_1, l_j)^2 + F_{\pi_y}(d_1, l_j)^2$
Mo1	Mn1	10.1	0.331
	Mn2	4.8	0.900
	Mn3	119.0	0.788
	Mn4	57.5	0.442
	Mn5	0.1	0.899
Mo2	Mn1	3.9	0.275
	Mn3	3.3	0.949
	Mn4	61.8	0.723
	Mn4′	8.5	0.951
	Mn5′	59.3	0.541
Mo3	Mn1	0.9	0.279
	Mn2	0.5	0.397
	Mn2′	28.5	0.892
	Mn3	42.5	0.914
	Mn5′	0.01	0.941
W	Mn1	1.2	0.265
	Mn2	1.4	0.940
	Mn3	138.0	0.617
	Mn4	86.3	0.636
	Mn5	10.8	0.944
Nb	Mn1	44.8	0.616
	Mn2	69.7	0.602

octametallates the σ overlap of d_1 is very small too, which is also confirmed by small $F_\sigma(d_1, l_j)^2$ values in Table 1. We can therefore conclude that in the whole series the lowest ligand-field orbital d_1 at the octacyanometallate sites has a *negligible σ overlap* with all the orbitals of the bridging cyanides.

These results have important implications for the magnetism of our compounds. Since d_1 accommodates one electron it also corresponds to a single magnetic orbital at the octametallate centers in **1**–**4**, while the 3d centers contain several magnetic orbitals the unpaired electrons of which form a high-spin ground state (Figure 5). The magnetic coupling (or

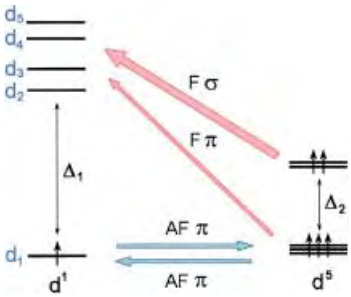


Figure 5. Scheme of the antiferromagnetic (AF; blue) and ferromagnetic (F; pink) kinetic contributions to the superexchange in the (Mo^{V},W^{V},Nb^{IV})-Mn^{II} metal pairs. The arrows indicate the direction of the electron transfer in each contribution.

exchange interaction) between the spins of two centers is described by the conventional Heisenberg spin Hamiltonian $H = -2JS_1S_2$. The spin–spin coupling constant J involves antiferro- and ferromagnetic contributions which are further analyzed within the framework of the kinetic exchange theory.[10]

Figure 5 shows the kinetic contributions to the exchange interaction between spins $S = 1/2$ and $S = 5/2$ in an Mo^{V}-(CN)-Mn^{II} pair. The antiferromagnetic kinetic part [Eq (1)],[10]

$$J_a = -\frac{2}{5}\sum_{\lambda=\pi_x,\pi_y} t_{1\lambda}^2\left(\frac{1}{E_{1\to\lambda}}+\frac{1}{E_{\lambda\to 1}}\right) \quad (1)$$

contains the contributions of the electron transfer from the molybdenum magnetic orbital (d_1) to the manganese magnetic orbitals (d_λ) through the π orbitals of the cyanide bridge and vice versa, described by the transfer parameters $t_{1\lambda}$, with electron promotion energies $E_{1\to\lambda}$ and $E_{\lambda\to 1}$, respectively. Note that in Equation (1) a negative J value favors an antiferromagnetic ground state.

The ferromagnetic kinetic part [Eq. (2)],[10, 11] includes contributions of the electron transfer from the manganese

$$J_f = \frac{2}{5}\sum_{i=2}^{5}\sum_{\lambda=\sigma,\pi_x,\pi_y}\frac{t_{i\lambda}^2}{E_{\lambda\to i}}\frac{I_{1i}}{E_{\lambda\to i}} \quad (2)$$

magnetic orbitals to the molybdenum empty d orbital. I_{1i} describes the intra-atomic exchange interaction between the electron in the magnetic orbital d_1 and the transferred electron to the empty excited orbital d_i on the molybdenum site. The terms $t_{i\lambda}$ are parameters of the electron transfer between three of the manganese half-filled orbitals (λ), involved in the σ, π_x, and π_y through-bridge electron-transfer pathways, and four empty orbitals on the molybdenum site ($i = 2,\ldots5$); $E_{\lambda\to i}$ are the corresponding electron promotion energies. Since the high-spin manganese(II) ion is spherically symmetric, for each cyanide bridge the d orbitals can be defined in such a way that three of them will coincide with d_σ, d_{π_x}, and d_{π_y} orbitals in Figure 4.

The resulting exchange parameter is the sum of J_a and J_f.[12] The competition between these two contributions can be presented in a more simple form. First, the transfer parameters $t_{i\lambda}$ in Equations (1) and (2) for each ligand (l_i) can be expressed by only two independent parameters, β_σ and β_π (Figure 4), multiplied by the corresponding projection coefficients $F_\lambda(d_1, l_j)^2$. Second, one can neglect the ligand-field splitting of the excited d orbitals which is small compared to the leading electron-repulsion contribution into $E_{i\to\lambda}$. By introducing the notations $U_1 = E_{1\to\pi}$, $U_2 = E_{\pi\to 1}$ for Mo→Mn electron transfer between the lowest orbitals and vice versa, the promotion energies for the electron transfer between π and σ orbitals of the manganese to the empty d orbitals of molybdenum become $U_2 + \Delta_1$ and $U_2 + \Delta_1 - \Delta_2$, respectively. Δ_1 and Δ_2 are ligand-field splitting energies on the d^1 and d^5 ions (Figure 5). Third, the parameters I_{1i} in Equation (2) are replaced by their average over the excited d_i orbitals, I.[14] Fourth, using the summation rules for the projection coefficients [Eq. (3)] one can eliminate the summations over the excited d orbitals of the molybdenum site in Equation (2) by expressing them through the relationship given as (4) and (5) below.

$$\sum_{i=1}^{5} F_\sigma(d_i, l_j)^2 = 1, \quad \sum_{i=1}^{5}(F_{\pi_x}(d_i, l_j)^2 + F_{\pi_y}(d_i, l_j)^2)^2 = 2 \quad (3)$$

$$F_\sigma(d_i, l_j)^2 \quad (4)$$

$$C_\pi \equiv F_{\pi_x}(d_1, l_j)^2 + F_{\pi_y}(d_1, l_j)^2 \quad (5)$$

 © WILEY-VCH Verlag GmbH, D-69451 Weinheim, 2001 1433-7851/01/4023-4431 $ 17.50+.50/0

Neglecting the small quantity $F_\sigma(d_i, l_j)^2$ (Table 1) we can finally write down the criterion for ferromagnetism, $J_f > -J_a$, as Equation (6)

$$\frac{\beta_\sigma^2 I}{(U_2 + \Delta_1 - \Delta_2)^2} + (2 - C_\pi) > C_\pi \beta_\pi^2 \left(\frac{1}{U_1} + \frac{1}{U_2}\right) \quad (6)$$

Ligand-field analysis gives $\Delta_1 = 5$ eV and $\Delta_2 = 1.5$ eV, a lowest estimate for $U_1 = 10$ eV.[10a] Given the large difference in valences of molybdenum and manganese ions, U_2 is expected to be 2–3 times smaller than U_1, while I has a value around 1 eV.

The critical ratio of the σ and π transfer parameters for the onset of ferromagnetism under the least-favorable condition $C_\pi = 1$ (Figure 6) decreases with the decrease of U_2 and the increase of I (relative to U_1) and for the estimated values of parameters is found in the range $3.5 < |\beta_\sigma/\beta_\pi| < 4.5$. Hence for ferromagnetism the σ transfer between the manganese magnetic orbitals and the molybdenum empty d orbitals (Figure 5) should be several times stronger than the π transfer between the magnetic orbitals of two metal sites.

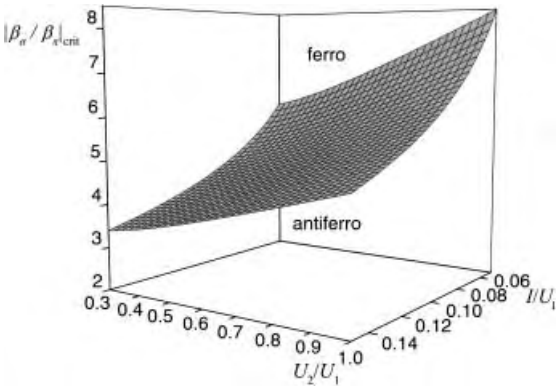


Figure 6. Critical ratio of β_σ and β_π transfer parameters for the onset of ferromagnetism in $4d^1$–$3d^5$ metal pairs.

This is clearly the case for the cyanide bridges where strong covalent admixtures into d_σ are naturally expected because of a close energy position of the σ*(CN) orbital (Figure 4) to the valence d shells of both metal sites. The overlap of the manganese d_σ magnetic orbital with some of molybdenum empty orbitals through the cyanide bridge is significant (Figure 7). As additional evidence, a much stronger σ covalency, compared to the π one, was found in $Cr(CN)_6^{3-}$ ions where about 15% covalent admixture was calculated for the $3d_\sigma(e_g)$ orbitals and only 1% for the $3d_\pi(t_{2g})$ orbitals.[15] Finally, our direct estimations of the transfer parameters in the M-(CN)-M′ pairs within the extended Hückel approach

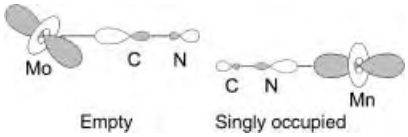


Figure 7. The manganese d_σ magnetic orbital and the molybdenum d_2 empty orbital. The latter also contains admixtures of the cyanide π orbitals (not shown).

give $|\beta_\sigma/\beta_\pi|$ values ranging from 2 to 3. On the other hand it should be noted that Figure 6 presents an upper estimate for the critical value of $|\beta_\sigma/\beta_\pi|$. Indeed, this value should be additionally scaled by a factor $\approx \sqrt{C_\pi}$, which is always smaller than unity (Table 1) because $C_\pi = 1$ would correspond to a perfect overlap of d_1 with the π orbitals of the cyanide. The neglected ferromagnetic contribution from the direct (potential) exchange,[10, 13] will further reduce the critical value of $|\beta_\sigma/\beta_\pi|$.

The above considerations apply directly to the explanation of ferromagnetic exchange in the Mo–Mn and Nb–Mn pairs of **1** and **4**. Passing to M = Fe^{II}, Co^{II} in **4** will merely quench some π antiferromagnetic transfer channels since addition of one and two electrons to the manganese d^5 shell results in the occupation of the d_π orbital. This leads to the increase of ferromagnetism in these compounds. The strongest ferromagnetic effect is expected when M has a completely filled d_π shell and unpaired electrons in the d_σ orbitals. Indeed, the latter do not overlap with the magnetic orbital d_1 at the octametallate site and the antiferromagnetic contribution vanishes [$t_{1\lambda} = 0$ in Eq. (1)]. This is the case for the Mo^V-(CN)-Ni^{II} pairs in **3** which indeed shows the highest ferromagnetic J value of the series.[6] As for the antiferromagnetism in **2**, it can have several causes. A more diffuse 5d shell of tungsten atoms compared to the 4d shell of molybdenum results in smaller intra-atomic exchange interaction (smaller I) and larger $|\beta_\sigma/\beta_\pi|$ critical ratio in Figure 6 for the tungsten ion. Besides, the transfer parameters themselves are expected to change when passing from **1** to **2** because of their high sensitivity to the positions of the d levels on the octametallate sites.

In summary, the exchange interaction in the cyanide complexes with the core $[M_6^V M_9'^{II}(\mu\text{-CN})_{30}]$, M = Mo, W, M′ = Mn, Ni, and 3D networks $[Nb^{IV}\{(\mu\text{-CN})_4 M'^{II}(H_2O)_2\}]$, M′ = Mn, Fe, Co, are analyzed within the Anderson superexchange theory. It is found that the magnetic orbital of each octametallate in these compounds exhibits an almost perfect orthogonality to the σ orbitals of the eight neighboring cyanide ligands despite having a quite different coordination geometry. As a result the antiferromagnetic contribution to the exchange can only be determined by the π transfer between magnetic orbitals, while the ferromagnetic kinetic contribution mainly arises from the σ transfer from the 3d ions. Two factors, the relatively low electron-promotion energy from 3d to 4(5)d ions and the large σ transfer parameter, which exceeds several times the π one, push the balance between the two kinetic exchange contributions towards ferromagnetism. This proposal explains why the compounds **1** and **4** are ferromagnetic in spite of the open π antiferromagnetic channel for electron transfer between magnetic orbitals. In the Mo–Ni cluster **3** the ferromagnetism is additionally stabilized because of absence of the d_π unpaired electrons on the nickel sites.

Received: July 16, 2001 [Z17525]

[1] a) P. D. W. Boyd, Q. Li, J. B. Vincent, K. Folting, H. R. Chang, W. E. Streib, J. C. Huffman, G. Christou, D. Hendrickson, *J. Am. Chem. Soc.* **1988**, *110*, 8537–8539; b) A. Caneschi, D. Gatteschi, R. Sessoli, A. L. Barra, L. C. Brunel, M. Guillot, *J. Am. Chem. Soc.* **1991**, *113*, 5873–5874; c) R. Sessoli, D. Gatteschi, A. Caneschi, M. Novak,

 © WILEY-VCH Verlag GmbH, D-69451 Weinheim, 2001 1433-7851/01/4023-4432 $ 17.50+.50/0

Nature **1993**, *365*, 141 – 143; d) R. Sessoli, H. L. Tsai, A. R. Schake, S. Wang, J. B. Vincent, K. Folting, D. Gatteschi, G. Christou, D. Hendrickson, *J. Am. Chem. Soc.* **1993**, *115*, 1804 – 1816; e) D. D. Awschalom, D. P. Di Vincenzo, *Phys. Today* **1995**, *48*, 43; f) E. D. Dahlberg, J.-G. Zhu, *Phys. Today* **1995**, *48*, 34.

[2] a) T. Mallah, C. Auberger, M. Verdaguer, P. Veillet, *J. Chem. Soc. Chem. Commun.* **1995**, 61 – 62; b) S. M. El Fallah, E. Rentschler, A. Caneschi, R. Sessoli, D. Gatteschi, *Angew. Chem.* **1996**, *108*, 2081 – 2083; *Angew. Chem. Int. Ed. Engl.* **1996**, *35*, 1947 – 1949; c) A. Scuiller, T. Mallah, M. Verdaguer, A. Nivorozhkin, J.-L. Tholence, P. Veillet, *New J. Chem.* **1996**, *20*, 1 – 3; d) J. L. Heinrich, P. A. Berseth, J. R. Long, *J. Chem. Soc. Chem. Commun.* **1998**, 1231 – 1232; e) S. Ferlay, T. Mallah, R. Quahès, P. Veillet, M. Verdaguer, *Inorg. Chem.* **1999**, *38*, 229 – 234; f) T. Mallah, A. Marvilliers, E. Rivière, *Philos. Trans. R. Soc. London Ser. A* **1999**, *357*, 3139 – 3158.

[3] a) W.-D. Griebler, D. Babel, *Z. Naturforsch. B* **1982**, *37*, 832; b) V. Gadet, T. Mallah, I. Castro, M. Verdaguer, P. Veillet, *J. Am. Chem. Soc.* **1992**, *114*, 9213; c) T. Mallah, S. Thiebaut, M. Verdaguer, P. Veillet, *Science* **1993**, *262*, 1554 – 1557; d) S. Ferlay, T. Mallah, R. Quahès, P. Veillet, M. Verdaguer, *Nature* **1995**, *378*, 701; e) S. M. Holmes, G. S. Girolami, *J. Am. Chem. Soc.* **1999**, *121*, 5593.

[4] J. Larionova, M. Gross, M. Pilkington, H. Andres, S. Stoeckli-Evans, H. U. Güdel, S. Decurtins, *Angew. Chem.* **2000**, *112*, 1579 – 1583; *Angew. Chem. Int. Ed*. **2000**, *39*, 1605 – 1609.

[5] Z. J. Zhong, H. Seino, Y. Mizobe, M. Hidai, A. Fijishima, S.-I. Ohkoshi, K. Hashimoto, *J. Am. Chem. Soc.* **2000**, *122*, 2952 – 2953.

[6] F. Bonadio, M. Gross, H. Stoeckli-Evans, S. Decurtins, *Mid-Term Conference on the ESF Programme "Molecular Magnets"* (Davos) **2001**, P22.

[7] P. Franz, L. Keller, M. Pelkington, J. Ensling, S. Decurtins, *Mid-Term Conference on the ESF Programme "Molecular Magnets"* (Davos) **2001**, H4.

[8] A. B. P. Lever, *Inorganic Electronic Spectroscopy*, 2nd ed., Elsevier Science, Amsterdam, **1984**, chap. 1.

[9] J. R. Perumareddi, A. D. Liehr, A. W. Adamson, *J. Am. Chem. Soc.* **1963**, *85*, 249 – 259.

[10] a) P. W. Anderson, *Phys. Rev.* **1959**, *115*, 2 – 13; b) P. W. Anderson in *Magnetism*, *Vol. 2* (Eds.: G. T. Rado, H. Suhl), Academic Press, New York, **1963**, chap. 2.

[11] J. B. Goodenough, *Magnetism and Chemical Bond*, Interscience, New York, **1963**, chap. 5.

[12] It also includes the contribution from the direct (potential) exchange,[10,13] not considered here for simplicity.

[13] O. Kahn, *Molecular Magnetism*, VCH, Weinheim, **1993**, chap. 8.

[14] J. S. Griffith, *The theory of Transition Metal Ions*, Cambridge University Press, Cambridge, **1971**, p. 84.

[15] L. G. Vanquickenborne, L. Haspeslagh, M. Hendrickx, J. Verhulst, *Inorg. Chem.* **1984**, *23*, 1677 – 1684.

"Cap-Tag"—Novel Methods for the Rapid Purification of Oligosaccharides Prepared by Automated Solid-Phase Synthesis**

Emma R. Palmacci, Michael C. Hewitt, and Peter H. Seeberger*

The automated solid-phase synthesis of oligopeptides[1] and oligonucleotides[2] is now routine and has made a major impact on the biochemistry and biotechnology of these biopolymers. Attempts to automate the synthesis of carbohydrates, the most complex class of biopolymers, on solid phase[3] and by computer-assisted planning of solution syntheses[4] have only recently been disclosed. While automated solid-phase synthesis greatly simplifies the assembly process by eliminating the time-consuming purification of intermediates, it is this very feature that often makes the final purification challenging. The removal of sequences deficient by just one unit ($n-1$ products) stemming from incomplete couplings at any stage of the synthesis can be very difficult.

Automated solid-phase synthetic protocols for peptides[5] and nucleic acids[2] often incorporate a capping step in the synthetic cycle to minimize the accumulation of $n-1$ products. Further improvements of this technique are based on the introduction of a capping agent that functions as a unique handle to aid in the purification of the final product.[6]

With the advent of combinatorial chemistry and parallel synthesis, several methods for the expedient purification of a variety of compounds have been reported. Scavenging resins allow byproducts or excess reagents to be removed by reaction of the unwanted moieties with a support-bound functional group, followed by filtration.[7] Affinity labels such as biotin or oligohistidine exploit noncovalent binding and have been extensively used for the rapid purification of tagged biomolecules[8] and synthetic compounds[9] by affinity chromatography. Most recently, the unique behavior of highly fluorinated molecules has been utilized to separate molecules containing a fluorous tag from nonfluorinated compounds by extraction with fluorous solvents or by chromatography on fluorous silica gel.[10]

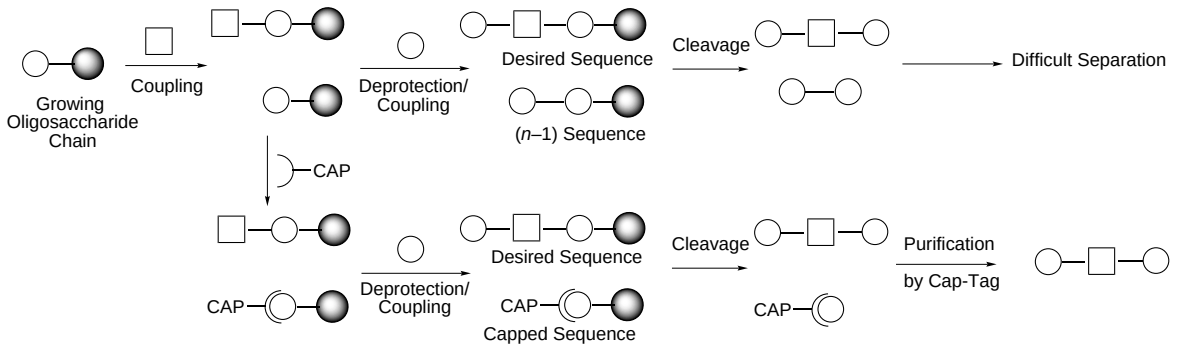
Here we describe two novel capping-and-tagging (cap-tag) methods to aid in the purification of oligosaccharides

[*] Prof. Dr. P. H. Seeberger, E. R. Palmacci, M. C. Hewitt
Department of Chemistry
Massachusetts Institute of Technology
Cambridge, MA 02139 (USA)
Fax: (+1) 617-253-7929
E-mail: seeberg@mit.edu

[**] Financial support from the donors of the Petroleum Research Fund, administered by the ACS (ACS-PRF 34649-G1), Merck (Predoctoral Fellowship for E.R.P.), Boehringer-Ingelheim (Predoctoral Fellowship for E.R.P.), and the NIH (Biotechnology Training Grant for M.C.H.) is gratefully acknowledged. Funding for the MIT-DCIF Inova 501 was provided by the NSF (Award CHE-9808061). Funding for the MIT-DCIF Avance (DPX) 400 was provided by the NIH (Award 1S10RR13886-01). We thank Silicycle (Quebec City, Canada) for the generous gift of fluorous silica gel and isocyanate silica gel scavenger resin. We thank Dr. O. Plante for helpful discussions and help with the automated oligosaccharide synthesizer.

Supporting information for this article is available on the WWW under http://www.angewandte.com or from the author.

 © WILEY-VCH Verlag GmbH, D-69451 Weinheim, 2001 1433-7851/01/4023-4433 $ 17.50+.50/0

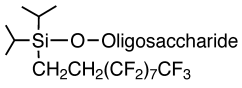


Scheme 1. Schematic overview of the cap-tag approach. Shaded circles = polymer support.

assembled by automated solid-phase synthesis. Following each coupling maneuver unconsumed hydroxyl groups that may give rise to deletion sequences are treated with a capping reagent that renders them silent in subsequent couplings (Scheme 1). The cap-tags also function as a handle that facilitates the separation of all unwanted, capped and tagged, sequences from the desired, untagged products. Two different flavors of cap-tags are introduced: an α-azidoisobutyric ester cap (A-Tag) that can be removed with an isocyanate-functionalized scavenger resin after reduction to the corresponding amine, and a fluorous silyl ether cap (F-Tag) that allows for the removal of tagged sequences by filtration through fluorous silica gel. The introduction of these cap-tags into the automated solid-phase synthesis of oligosaccharides greatly simplifies post-synthetic workup and purification, as demonstrated for three trisaccharide syntheses.



A-Tag

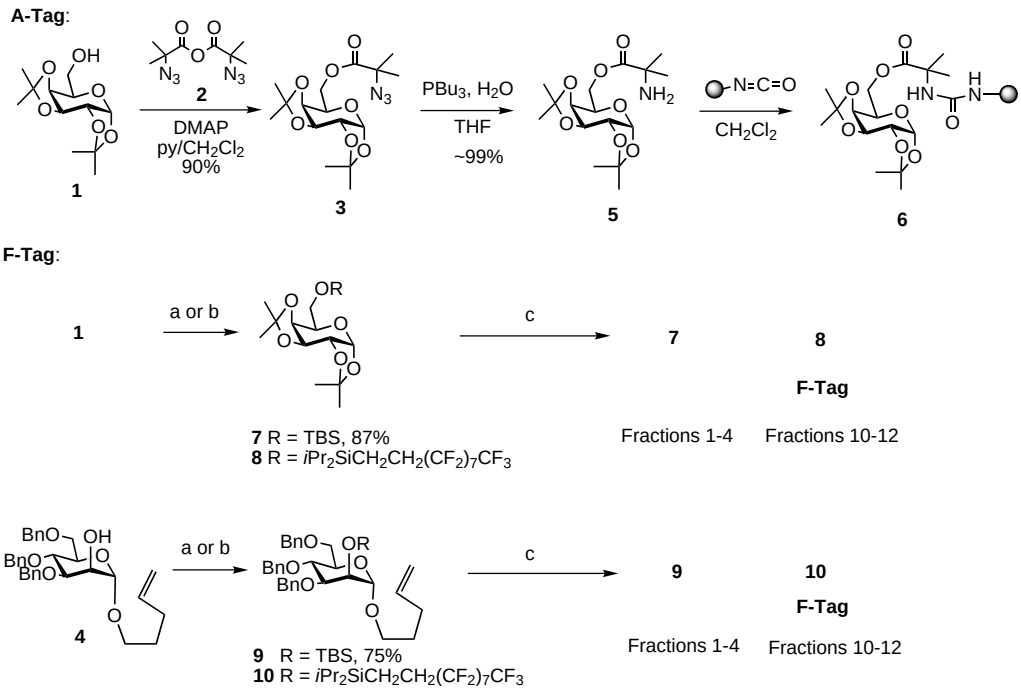


F-Tag

Several issues of critical importance must be considered in the design of cap-tags: 1) the caps must react rapidly and efficiently with hydroxyl groups that were not glycosylated in the previous coupling step; 2) the linkage formed between the hydroxyl group and the cap must be stable during subsequent coupling cycles; 3) cap-tags must be orthogonal to the protecting groups used in the synthesis, and hence different tags may be needed; 4) the cap must contain a unique handle that allows facile separation from full-length products.

Mindful of these design features, we envisioned using the A-Tag as an analogue of the robust pivaloyl ester. Synthesis of the A-Tag capping reagent **2** was straightforward and can be performed on a multigram scale. 2-Azido-2-methylpropionic acid was prepared from commercially available 2-bromo-2-methylpropionic acid,[11] and treatment with dicyclohexylcarbodiimide (DCC) furnished anhydride **2**. Alternatively, the corresponding acid chloride can be prepared and used in place of **2** to introduce the A-Tag.

Initially, we focused on model studies on monosaccharides to examine the properties of the A-Tag (Scheme 2, top). Capping of monosaccharides containing primary (**1**) and secondary (**4**) hydroxyl groups by reaction with **2** in the presence of DMAP afforded esters such as **3** in high yield. With capped monosaccharide **3** in hand, we first determined the stability of the A-Tag to different reaction conditions employed during oligosaccharide synthesis. Monosaccharides containing common temporary protecting groups were com-



Scheme 2. Model monosaccharide synthesis and scavenging. a) 4 equiv (heptadecafluorodecyl)diisopropylsilyl triflate (**11**), 6 equiv 2,6-lutidine in CH_2Cl_2 at RT; b) 1.1 equiv TBSOTf, 2 equiv 2,6-lutidine in CH_2Cl_2 at RT; c) fluorous silica gel ($Si(CH_2CH_2C_6F_{13})_3$), gradient of 80/20% H_2O to 100% MeOH. Bn = benzyl, DMAP = 4-dimethylaminopyridine, py = pyridine; TBS = tBuMe$_2$Si.

 © WILEY-VCH Verlag GmbH, D-69451 Weinheim, 2001 1433-7851/01/4023-4434 $ 17.50+.50/0

bined with **3**, and the protective groups were removed. We found that standard levulinate deprotection conditions (hydrazine in pyridine/AcOH) did not result in removal of the A-Tag. Removal of acetate esters by treatment with sodium methoxide resulted in A-Tag cleavage and thus rendered these groups incompatible.

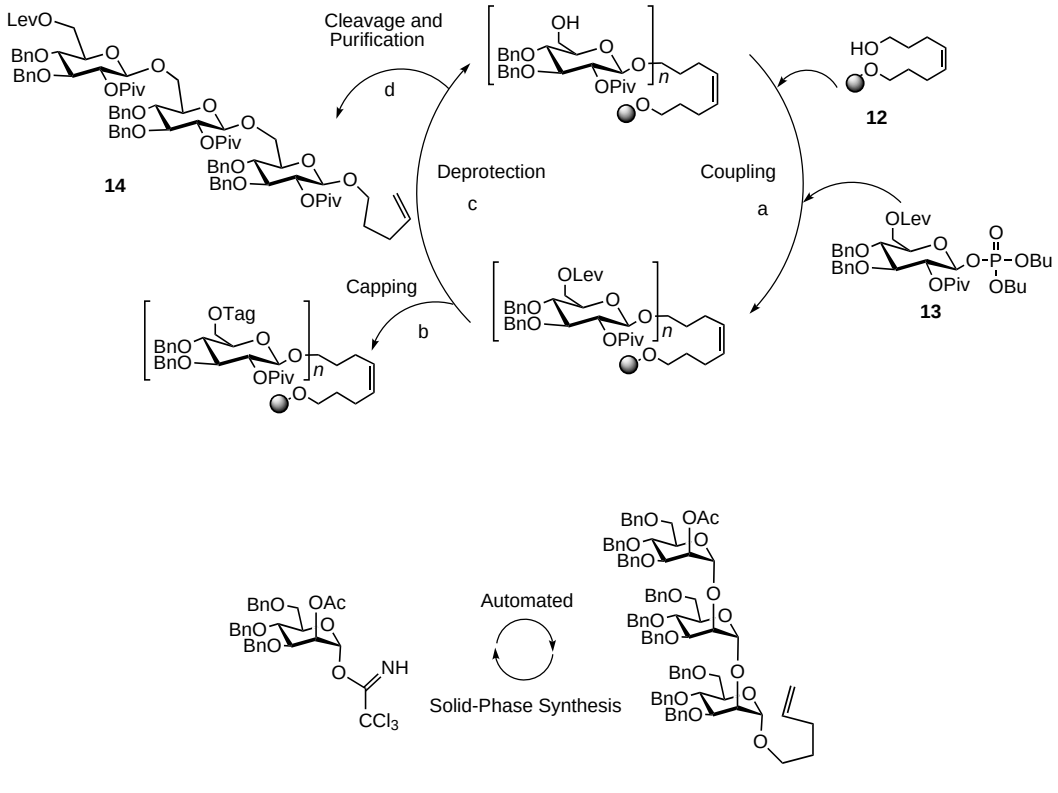
The possibility of removing molecules containing the A-Tag from reactions was also demonstrated on a monosaccharide model (Scheme 2, top). Conversion of azide **3** to amine **5** by treatment with tributylphosphane in water/THF proceeded quickly (< 5 min). Three hours after addition of an isocyanate silica gel scavenging resin to a solution of **5** in CH_2Cl_2, complete consumption of **5** was indicated by failure to detect any amine in a ninhydrin test.

Our second cap-tag incorporates a fluorinated silyl ether tag. Highly fluorinated molecules have been shown to possess unique properties that can be exploited for separating them from very similar fluorine-free compounds.[10] To explore the F-Tag concept on monosaccharide models, (heptadecafluorodecyl)diisopropylsilyl triflate (**11**)[12] was reacted with carbohydrates containing primary (**1**) and secondary (**4**) hydroxyl groups to furnish F-tagged **8** and **10** (Scheme 2, bottom). F-Tag-containing monosaccharides **8** and **10** were completely stable to treatment with sodium methoxide, even after prolonged exposure (24 h).

Silylated monosaccharides **7** and **9** were prepared to demonstrate the separation principle in the cap-tag approach. Equimolar **7**/**8** and **9**/**10** mixtures were applied to columns of tridecafluoro(Si($CH_2CH_2C_6F_{13}$)$_3$)-functionalized silica gel packed in methanol/water (4/1). Unfluorinated monosaccharides **7** and **9** were eluted immediately (fractions 1 – 4), while fluorinated compounds **8** and **10** were eluted in late fractions, only after washing the columns with 100 % methanol.

After establishing that carbohydrates could be tagged and purified with the A-Tag and the F-Tag, we investigated the effectiveness of the cap-tag strategy in the automated solid-phase synthesis of trisaccharides **14** and **16** (Scheme 3). Currently, high yields (ca. 95 % per step) in automated solid-phase oligosaccharide synthesis are ensured by addition of several equivalents of glycosylating agent and repetition of this process (double coupling).[3] To clearly demonstrate the effect of the cap-tags, only single couplings were performed in each cycle, and coupling efficiencies in the range of 85 – 90 % were expected. Syntheses of each oligosaccharide with and without the capping step but with otherwise identical coupling cycles were compared. Resin-bound oligosaccharides prepared with the help of the A-Tag were reduced with tributylphosphane before being cleaved from the solid support. After cleavage, the crude products were treated with isocyanate silica gel scavenger resin. Oligosaccharides prepared without capping were directly cleaved and were not treated with a scavenger resin.

The HPLC traces of the capped and scavenged reaction products (Figure 1) were compared to those of the reaction



Scheme 3. Top: Synthesis of triglucoside **14** in a capping cycle. a) 5 equiv **13**, 5 equiv TMSOTf, − 15 °C, CH_2Cl_2; b) A-Tag: 5 equiv **2**, DMAP, py/CH_2Cl_2; F-Tag: 5 equiv **11**, 2,6-lutidine; c) NH_2NH_2, 15 °C, py/AcOH; d) (1) ethylene, 0.2 equiv Grubbs' catalyst, CH_2Cl_2; (2) A-Tag: PBu_3/THF/water, then isocyanate silica gel scavenger resin; F-Tag: filtration through fluorous silica gel. Shaded circles = polystyrene polymer support. Lev = levulinate, Piv = pivaloyl, TMS = trimethylsilyl. Bottom: Synthesis of trimannoside **16** in a capping cycle. Coupling: 5 equiv **15**, 0.5 equiv TMSOTf, RT, CH_2Cl_2; F-Tag capping: 5 equiv **11**, 2,6-lutidine; deprotection: NaOMe, MeOH, RT; Cleavage: ethylene, 0.2 equiv Grubbs' catalyst, CH_2Cl_2; purification: filtration through fluorous silica gel.

 © WILEY-VCH Verlag GmbH, D-69451 Weinheim, 2001 1433-7851/01/4023-4435 $ 17.50+.50/0

mixture obtained when no cap was used. Significant amounts of mono- and disaccharide deletion sequences were observed close to the desired triglucoside **14** in the synthesis without cap-tag (Figure 1a). These impurities could be almost completely removed by using the A-Tag, which greatly facilitated the purification process (Figure 1b). The F-Tag was similarly effective in the synthesis of **14** when the crude product was filtered through a plug of fluorous silica gel after cleavage from the solid support (Figure 1c).

The efficacy of the F-Tag strategy was also demonstrated for couplings involving secondary hydroxyl acceptors by incorporating a capping step into the solid-phase assembly of trimannoside **16** (Scheme 3 bottom).[13] The disappearance of side products and a significantly improved purity of the crude products can be clearly seen on comparing HPLC and TLC analyses of syntheses performed with and without the F-Tag (Figure 2). The HPLC traces of the crude products clearly reveal the efficiency of the F-Tag in removing unglycosylated C2-hydroxyl-containing deletion sequences (Figure 2a, b). Note that the simultaneous preparation of different oligosaccharide sequences that can be discriminated by introduction of unique F-Tags (containing varying numbers of fluorine atoms) at each stage of the synthesis is within reach.

In summary, we have introduced a new approach to facilitate the purification of oligosaccharides prepared by automated solid-phase synthesis. Incorporation of a capping step allowed for efficient removal of the unwanted side products at the end of the synthesis by use of a scavenger resin or filtration through fluorinated silica gel. The cap-tag method allows oligosaccharides to be obtained without the need for

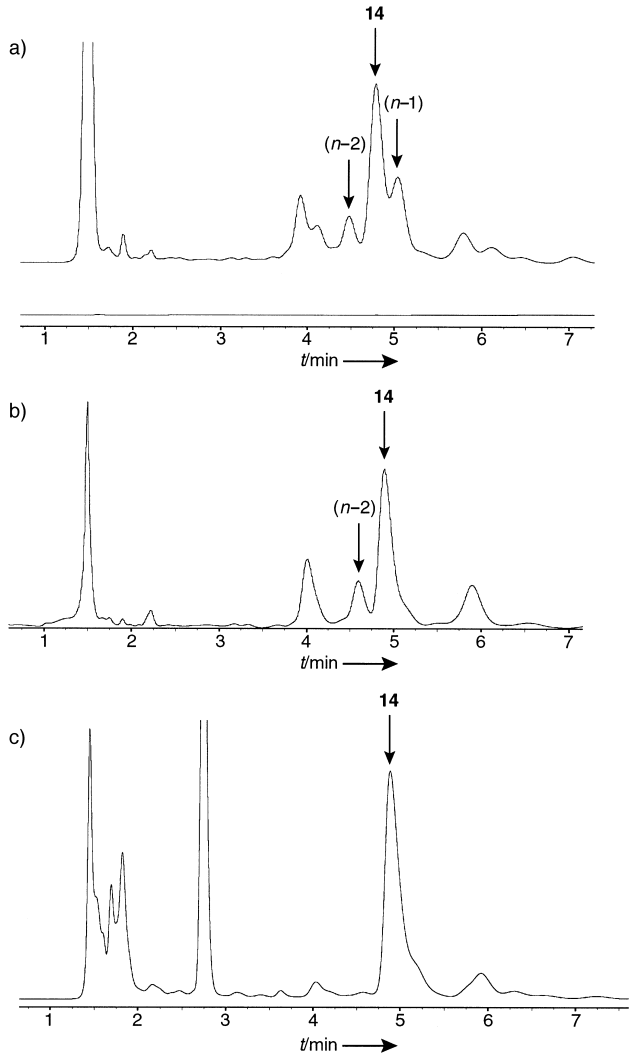


Figure 1. Analytical HPLC of triglucoside **14** syntheses. a) Synthesis without cap-tag; b) synthesis with A-Tag; c) synthesis with F-Tag. The indentity of the unmarked peaks could not be determined. Conditions: 1 mL min^{-1}, 20% EtOAc/hexanes.

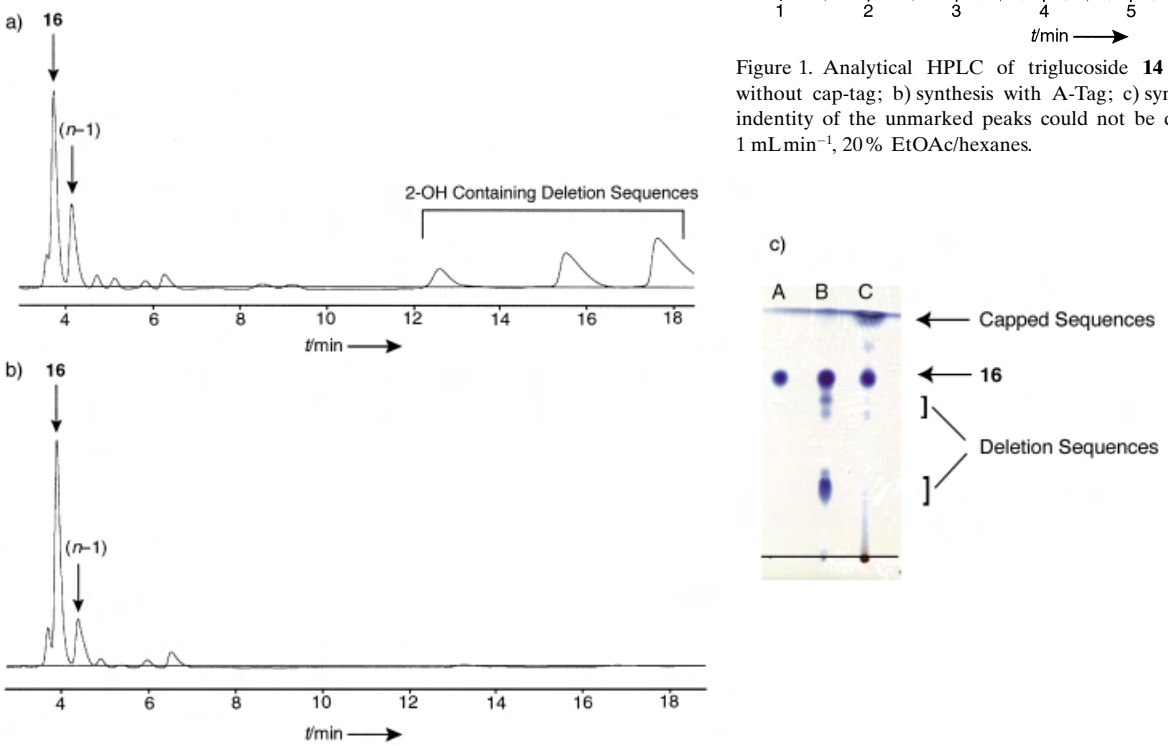


Figure 2. Analytical HPLC of trimannoside **16** syntheses a) without cap-tag (deletion sequences with C2 acetate groups are eluted at about 4 min, and those with C2 hydroxyl groups after 12 min), b) with F-Tag. Conditions: 1 mL min^{-1}, 20% EtOAc/hexanes. c) TLC analysis of trimannoside **16** syntheses. Lane A: pure **16;** lane B: crude **16** prepared without cap; lane C: crude **16** prepared with F-cap. Conditions: 30% EtOAc/hexanes.

 © WILEY-VCH Verlag GmbH, D-69451 Weinheim, 2001 1433-7851/01/4023-4436 $ 17.50+.50/0

double couplings and a large excess of building blocks. The application of the A-Tag and the F-Tag to the automated synthesis of more complex oligosaccharides and other biopolymers is currently being explored.

Experimental Section

General Procedure for the automated synthesis of oligosaccharides incorporating cap-tags: Octenediol-functionalized resin **12** was loaded into a reaction vessel equipped with a cooling jacket and inserted into a modified ABI-433A peptide synthesizer. The resin was glycosylated with donor **13** or **15** (5 equiv) in CH_2Cl_2 (3 mL) with TMSOTf as activator. The suspension was mixed (10 s vortex, 50 s rest) for 15 min. The resin was then washed with CH_2Cl_2 (6×4 mL), and the unglycosylated sites were capped with A-Tag anhydride **2** or F-Tag triflate **11**. The resin was subjected to the appropriate deprotection conditions followed by the washing cycle. The deprotected polymer-bound monosaccharide was then elongated by reiteration of the above glycosylation/capping/deprotection protocol. The final trisaccharide was not deprotected, so that analysis of the products was simplified. For A-Tag, the crude material was treated with tributylphosphine and water, liberated from the resin, then purified with an isocyanate scavenger resin. For F-Tag, the crude material was liberated from the resin and purified with fluorous silica gel.

Received: August 2, 2001 [Z17654]

[1] E. Atherton, R. C. Sheppard, *Solid-Phase Peptide Synthesis: A Practical Approach*, Oxford University Press, Oxford, **1989**.

[2] M. H. Caruthers, *Science* **1985**, *230*, 281 – 285.

[3] O. J. Plante, E. R. Palmacci, P. H. Seeberger, *Science* **2001**, *291*, 1523 – 1527.

[4] a) Z. Zhang, I. R. Ollmann, X.-S. Ye, R. Wischnat, T. Baasov, C.-H. Wong, *J. Am. Chem. Soc.* **1999**, *121*, 734 – 753; b) F. Burkhart, Z. Zhang, S. Wacowich-Sgarbi, C.-H. Wong, *Angew. Chem.* **2001**, *113*, 1314 – 1317; *Angew. Chem. Int. Ed.* **2001**, 40, 1274 – 1277.

[5] S. A. Kates, F. Alberico, *Solid-Phase Synthesis: A Practical Guide*, Marcel Dekker, New York, **2000**.

[6] a) S. Funakoshi, H. Fukada, N. Fujii, *J. Chromatogr.* **1993**, *638*, 21 – 27; b) L. E. Canne, R. L. Winston, S. B. H. Kent, *Tetrahedron Lett.* **1997**, *38*, 3361 – 3364; c) M. A. Shogren-Knaak, B. Imperiali, *Tetrahedron Lett.* **1998**, *39*, 8241 – 8244; d) M. A. Shogren-Knaak, K. A. McDonnell, B. Imperiali, *Tetrahedron Lett.* **2000**, *41*, 827 – 829.

[7] a) J. R. Booth, J. C. Hodges, *Acc. Chem. Res.* **1999**, *32*, 18 – 26; b) for solution-phase tagging of carbohydrates, see V. Pozgay, *Org. Lett.* **1999**, *1*, 477 – 479; c) Y. Ito, O. Kanie, T. Ogawa, *Angew. Chem.* **1996**, *108*, 2691 – 2693; *Angew. Chem. Int. Ed. Engl.* **1996**, *35*, 2510 – 2512.

[8] a) R. Janknecht, G. de Martynoff, J. Lou, R. A. Hipskind, A. Nordheim, H. G. Stunnenberg, *Proc. Natl. Acad. Sci. USA* **1991**, *88*, 8972 – 8976; b) E. Sulkowski, *Trends Biotechnol.* **1985**, *3*, 1 – 7.

[9] S. V. Ley, A. Massi, F. Rodriguez, D. C. Horwell, R. A. Lewthwaite, M. C. Pritchard, A. M. Reid, *Angew. Chem.* **2001**, *113*, 1088 – 1090; *Angew. Chem. Int. Ed.* **2001**, *40*, 1053 – 1055.

[10] a) For a review, see D. P. Curran, *Angew. Chem.* **1998**, *110*, 1230 – 1255; *Angew. Chem. Int. Ed.* **1998**, *37*, 1174 – 1196; b) Z. Luo, Q. Zhang, Y. Oderaotoshi, D. P. Curran, *Science* **2001**, *291*, 1766 – 1769; c) D. P. Curran, Z. Luo, *J. Am. Chem. Soc.* **1999**, *121*, 9069 – 9072.

[11] C. W. Tornoe, H. Sengelow, M. Meldal, *J. Pept. Sci.* **2000**, *6*, 314 – 320.

[12] A procedure for the preparation of **11** was provided by Dr. R. Luo (Fluorous Technologies, Pittsburgh, PA).

[13] R. B. Andrade, O. J. Plante, L. G. Melean, P. H. Seeberger, *Org. Lett.* **1999**, *1*, 1811 – 1814.

From CO_2 to Methanol by Hybrid QM/MM Embedding**

Samuel A. French,* Alexey A. Sokol, Stefan T. Bromley, C. Richard A. Catlow, Stephen C. Rogers, Frank King, and Paul Sherwood

For improvements to be made in long-standing industrial catalytic processes, an understanding of the atomistic mechanisms of the reactions occurring on the surface of the catalyst is required. A variety of experimental techniques can be used to derive information on sorption and reaction processes, but when both the catalyst and reactant mixtures are multicomponent, unambiguous identification of reaction mechanisms is difficult and often controversial. Computational techniques can, however, be used to gain valuable insight and interpret experimental evidence. Herein we show how new methods for modeling surface reactions on oxides can be used to elucidate key steps in a widely studied catalytic process—the conversion of CO_2 to methanol over oxide catalysts.

A large quantity of methanol (in excess of 25 million tonnes worldwide) is produced annually using the multicomponent $Cu/ZnO/Al_2O_3$ catalyst and $CO_2/CO/H_2$ as the feed gas. Many experimental studies of this process have been performed, but no definite reaction mechanism for the production of methanol has been established. However, it has long been acknowledged that the important rate-determining step is the hydrogenation of adsorbed intermediates, for example, the formate ion, at the active sites. Proposed mechanisms for methanol synthesis require the chemisorption of CO_2 before hydrogenation via formate to methanol. Theoretical studies of these systems have been hampered by the difficulty of modeling the catalytically active polar surfaces of ZnO, as well as by problems associated with the restrictions on the size of the system that can be modeled.

The nature of the active site for sorption/catalysis of CO_2 still remains unclear; it has been proposed to use clean oxygen-terminated surfaces of zincite as a test system or model catalyst. Temperature-programmed desorption (TPD) studies have shown that the processes that occur at that

[*] Dr. S. A. French, Dr. A A. Sokol, Dr. S T. Bromley, Prof. C. R. A. Catlow
Davy Faraday Research Laboratory
The Royal Institution of Great Britain
21 Albemarle Street, London, W1S 4BS (UK)
Fax: (+44) 20-7670-2920
E-mail: sam@ri.ac.uk

Dr. S C. Rogers
ICI Strategic Technology Group
Wilton Centre, PO Box 90, Redcar, TS90 8JE (UK)

Dr. F King
Synetix, Belasis Avenue
Billingham, TS23 1LB (UK)

Dr. P Sherwood
CLRC Daresbury Laboratory
Warrington, WA4 4AD (UK)

[**] This work was supported by EU Esprit IV project 25047. S.A.F. is grateful to ICI and Synetix for funding. K. Waugh, L. Whitmore, S. Cristol, and P. Sushko are thanked for their helpful insights. QM/MM = quantum mechanics/molecular mechanics.

 © WILEY-VCH Verlag GmbH, D-69451 Weinheim, 2001 1433-7851/01/4023-4437 $ 17.50+.50/0

particular surface are analogous to those on the industrial Cu/ZnO/Al_2O_3 catalyst.[1] In this study we have therefore concentrated on the polar $(000\bar{1})$ oxygen-terminated surface. The polar character of the surface of a given sample necessitates charge transfer between opposing polar surfaces. One mechanism of quenching the surface polarization is to abstract approximately 25% of the oxygen ions from the surface layer, thus creating *vacant oxygen interstitial surface sites*. The presence of such sites has been confirmed by optical and electron spin resonance (ESR) spectroscopies.[2] They have, moreover, been suggested as the active catalytic sites for methanol synthesis and are, therefore, the focus of the investigation presented here. We have studied the adsorption of important methanol precursors including carbon dioxide, formate, and methoxy ions. We have calculated binding energies, bond lengths, and angles of these and related species to provide insight into the mechanism of methanol synthesis.

In order to pursue these studies a novel solid-state embedding technique has been developed based on a hybrid QM/MM approach by employing molecular embedded cluster methods developed to treat point defects and localized states in ionic materials.[3] At the heart of embedding approaches is a definition of a reference system and a single localized state, which causes only minor long-range perturbation of the reference system. These methods have a rigorous foundation in the many electron theories of localization and separability,[4] and are more appropriate for the present study than are related embedding methods employed in the fields of zeolites and biochemistry.[5]

All ions, but especially anions, are polarizable species. Two major effects are witnessed upon perturbation of the reference system by a localized defect: 1) dramatic short-range effects, (for example, charge transfer and bond breaking) and 2) long-range polarization of electron groups (for example, ions) as a result of the field associated with the defect. Therefore, the model can be treated at two levels of approximation. In the present work the short-range effects are dealt with by fully ab initio methods (density functional theory (DFT)), while the long-range polarization effects are included through the use of the shell model of Dick and Overhauser.[6]

Thus, our structural model is split into two major regions: region 1 being treated by ab initio methods and region 2 with pairwise interatomic potentials. The short- and long-range interactions between regions 1 and 2 require careful attention: the former is handled by an interface between regions 1 and 2, while the latter is described by a mesh of point charges fitted to reproduce the lattice Madelung field at the area of interest.[7] The interface is formed by short-range-localizing model potentials, which act on electrons. In this work such potentials have only been associated with cationic sites, while anionic sites in the interface region were represented simply by point charges and classic interatomic potentials. Relaxation resulting from the defect has been allowed up to a certain cut-off radius, which includes all of region 1 and part of region 2 (typically of the order of 600 atoms; Figure 1).

The methodology described was implemented within ChemShell, which is a computational chemistry environment, based on the Tcl programming language.[7] A DFT treatment,

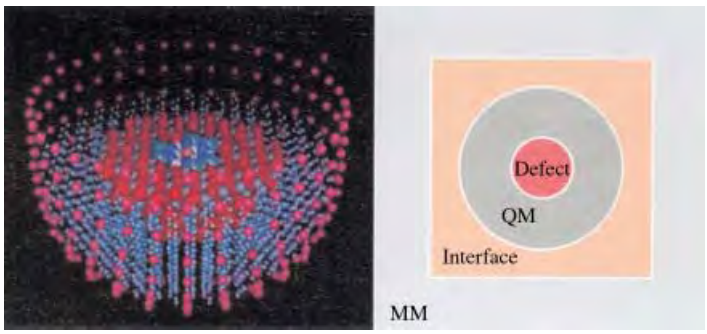


Figure 1. Embedded cluster model used in this work.

as implemented in the GAMESS-UK code, was used.[8] We employed the B97-1[9] exchange correlation functional and TZV2P basis set on O and Zn atoms, which was reoptimized for the ionic state of ZnO (details will be reported elsewhere), along with the standard 6-311 + (2p2d) basis set on all atoms of the adsorbates and a medium quality integration mesh.[8] Interactions in region 2 and at the interface were dealt with using our recently developed atomistic potentials[10] within the GULP code.[11]

Detailed models of the $(000\bar{1})$-0 terminated polar surfaces were investigated using interatomic potentials and the two-dimensional periodic slab model realized within the MARVIN code.[12] Two typical local environments were identified as terrace termination and interstitial vacancy sites; the latter has been used as the active site for the majority of calculations (Figure 2). The atoms highlighted in the figure indicate the

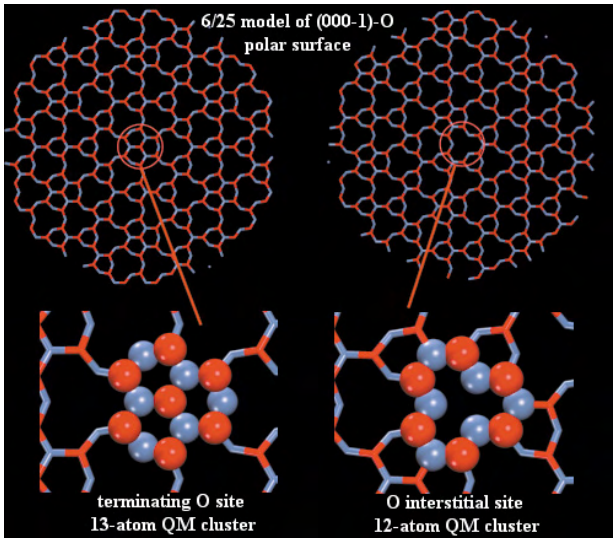


Figure 2. QM regions used for the modeling of vacant oxygen interstitial surface sites. Only the upper surface layer is shown.

surface-embedded quantum region. For the calculations reported, region 1 consists of 12 atoms, the interface has 13 Zn sites, while region 2 comprises approximately 3000 atoms and 250 terminating point charges.

We have undertaken a series of calculations on the reactants, intermediates, and products of methanol synthesis by using the embedding technique described earlier. A

 © WILEY-VCH Verlag GmbH, D-69451 Weinheim, 2001 1433-7851/01/4023-4438 $ 17.50+.50/0

probable reaction sequence for the conversion of the feed gas to methanol has been summarized by Chinchen et al.:[13]

$$H_2(g) \longrightarrow 2H(a) \quad (1)$$

$$CO_2(g) \longrightarrow CO_2(a) \quad (2)$$

$$CO_2(a) + H(a) \longrightarrow HCO_2(a) \quad (3)$$

$$HCO_2(a) + 2H(a) \longrightarrow CH_3O(a) + O(a) \quad (4)$$

$$CH_3O(a) + H(a) \longrightarrow CH_3OH(g) \quad (5)$$

$$CO(g) + O(a) \longrightarrow CO_2(g) \quad (6)$$

$$H_2(g) + O(a) \longrightarrow H_2O(g) \quad (7)$$

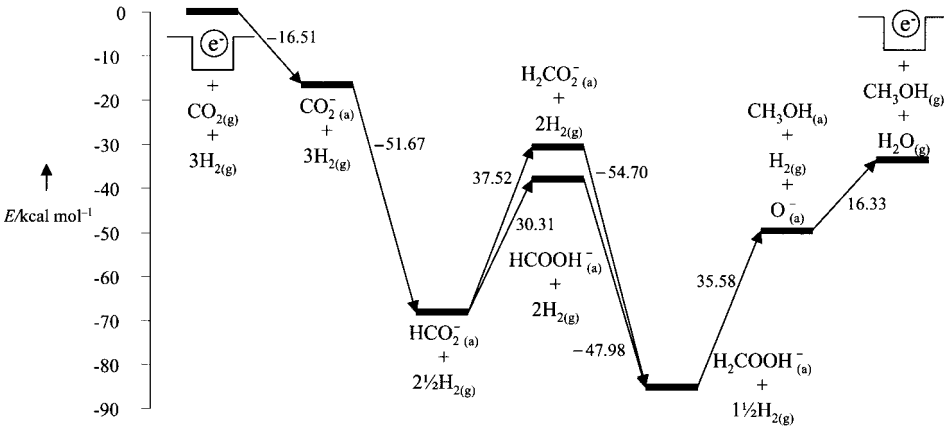


Figure 3. Calculated reaction energy profile for methanol synthesis over ZnO.

The gas-phase and adsorbate species are indicated by (g) and (a), respectively.

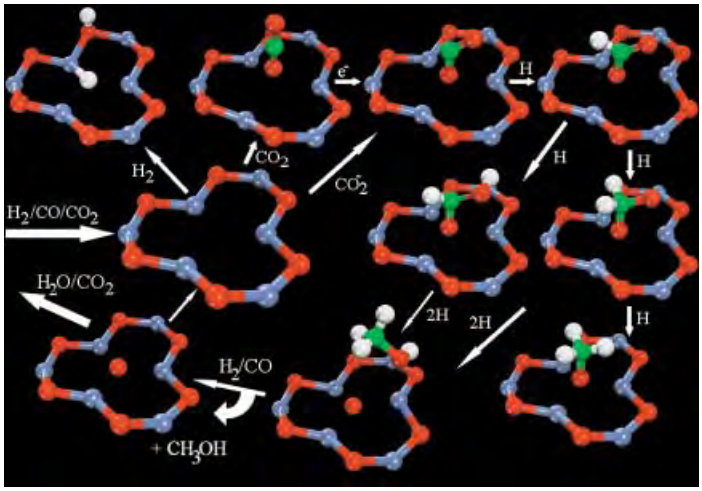
Reaction 4 is a complex process that includes multiple hydrogenation steps, which we have considered separately. The resulting species, which were not considered by Chinchen et al. and others, we find to be stable, although they may possibly be transient and short-lived.

The main catalytically active site that can facilitate the formation of anionic adsorbates is the oxygen interstitial site (as described above and illustrated on the right hand side of Figure 2). This site is able to trap an electron and thus adsorption can occur in two different ways: 1) neutral adsorbates approach the active site at which an electron is trapped and form an anionic surface species, and 2) the transfer of an electron to the neutral active site occurs simultaneously with the adsorption of neutral adsorbates.

The proposed catalytic cycle is summarized in Scheme 1, with the calculated energetics given in Figure 3, which is discussed in greater detail below. We start with the adsorption of CO_2 [Eq. (2)] and H_2 [Eq. (1)]. (Detailed studies of the latter will be reported elsewhere shortly.) CO_2, upon adsorption in a neutral interstitial site, retains the linear structure exhibited in the gas phase. On adding an electron the neutral CO_2 molecule bends and the extra electron populates an antibonding level, which leads to a rearrangement from an sp- to an sp^2-hybridized configuration. (The angle changes from 179.9 to 127.3°.) The interaction with the surface stabilizes the radical CO_2^- species.

The reaction then proceeds by the hydrogenation of the adsorbed CO_2^- species, by surface hydrogen [Eq. (1)], to the formate ion [Eq. (3)].[13] The geometry resulting from our calculations is shown in Scheme 1. The adsorption of hydrogen leads to a closed-shell species. Further hydrogenation can proceed either through the formation of $H_2CO_2^-$ or $HCOOH^-$ (formic acid) as shown in Scheme 1. Temperature-programmed desorption data do not detect these species, which suggests they have a short lifetime and, therefore, high reactivity. Computational techniques allow us to differentiate and investigate these different mechanisms. Further hydrogenation and interactions of the resulting species with the surface and possible surface defects lead to a large variety of possible intermediates. Examples of a methoxy ion [Eq. (4)] (CH_3O^-) chemisorbed onto the surface and physisorbed methanol [Eq. (5)] are also shown in Scheme 1. To complete the catalytic cycle, methanol is removed from the surface and the active site is recycled by desorption of carbon dioxide [Eq. (6)] and water [Eq. (7); Scheme 1].

The structural data are summarized in Table 1. We note that the vacant oxygen interstitial site accommodates both an electron and an oxygen (O^-) anion, thus restoring the terrace-like surface termination. We observe that there is a general trend with the adsorbates for charge transfer towards the



Scheme 1. Catalytic cycle: The geometries of all the reactants are obtained by energy minimization of embedded clusters.

Table 1. Calculated structural parameters of adsorbate species at the vacant oxygen interstitial surface site.

Species	O_a–C [Å]	C–O_b [Å]	O_a-C-O_b [°]	C–H [Å]
CO_2	1.19	1.15	179.9	–
CO_2^-	1.35	1.20	128.3	–
HCO_2^-	1.33	1.23	120.4	1.09
$H_2CO_2^-$	1.43	1.35	112.5	1.11
$HCOHO^-$	1.39	1.38	112.1	1.09
H_3CO^-	1.47	–	–	1.09
H_3COH	3.45	1.44	–	1.09

 © WILEY-VCH Verlag GmbH, D-69451 Weinheim, 2001 1433-7851/01/4023-4439 $ 17.50+.50/0

surface and a corresponding polarization of the chemical bonds in the adsorbate. These effects are shown both in the charge distribution and in the elongation of the lower oxygen–carbon bond relative to those in the gas-phase structures. (In contrast, the alcoholic hydrogen–oxygen bond length has a typical value of 0.97 Å in all the relevant species studied.)

We have calculated the surface adsorption energies by comparing the total energies of the embedded clusters with and without adsorbed species. These calculations are of particular interest as a comparison can be made with experiment. The desorption process considered includes desorption from a neutral and vacant oxygen interstitial site as well as from an adsorbed O^- species. However, as we have concentrated on the catalytically relevant reactants, intermediates, and products, we are only able to compare two models directly with experimental results. The complexity of the preparation of the samples and the reactions, which occur in the adsorption/desorption experimental cycle in the TPD work, prevents us, currently, from making a direct comparison, but this will be addressed in the near future by using calculations that relate directly to the desorption process.

Both experimental desorption energies have been obtained from the low-temperature adsorption of carbon dioxide as reported by Bowker et al.[1b] About 10% of the adsorbed carbon dioxide dissociates to carbon monoxide upon TPD which, therefore, heals the surface defects. We calculate the abstraction of CO_2 from the vacant oxygen interstitial surface site with a trapped electron to be 69 kJ mol^{-1}, which compares to an experimental desorption energy of 109–117 kJ mol^{-1}. The value we calculate provides a lower limit for the adsorption energies as: 1) we neglect the polarization effects beyond a certain cut-off radius (12.5 Å from the QM region), although such effects are likely to be small; and 2) the observed values refer to the free energy, and thus include vibrational contributions, which are omitted from our current study. The energy of desorption of CO is calculated as an energy of cleavage of the O_a–C bond in the CO_2^- adsorbate (as suggested by Bowker et al.) and is found to be 113 kJ mol^{-1}; this value compares favorably to the experimental value of 109 kJ mol^{-1}. The current method slightly overestimates the covalent bonding, which is common to all DFT simulations.

The adsorption energies calculated for other species shown in Scheme 1 allow us to obtain the reaction energies for the full catalytic cycle (Figure 3). The hydrogenation of adsorbates is shown to drive the reaction over the active site, in agreement with experiment. Our calculation uses half of the total energy of gas-phase H_2, thus all our energies are given with respect to molecular gaseous hydrogen as the base line. Two intermediate species are shown to be particularly stable, namely HCO_2^- and H_2COOH^-. The former (the formate ion) is known to be a stable long-lived intermediate,[1b] but the latter has not been experimentally characterized, although it is isomeric with the methoxy species which has been reported.[13]

Our methodology clearly has the ability to elucidate a detailed and quantitative mechanism for the catalytic processes involved in this important reaction. Furthermore, it can be readily extended to include other fields of surface and materials science. Moreover, this approach can be used to calculate electronic, spectroscopic, and other properties of sorbed molecules.

Received: July 23, 2001 [Z17561]

[1] a) V. E. Heinrich, P. A. Cox, *The Surface Science of Metal Oxides*, Cambridge University Press, Cambridge, **1996**; b) M. Bowker, H. Houghton, K. C. Waugh, *J. Chem. Soc. Faraday Trans. 1* **1981**, *77*, 3023; c) K. M. Vandenbusche, G. F. Froment, *App. Catal. A* **1994**, *112*, 37; d) S. Bailey, G. F. Froment, J. W. Snoeck, K. C. Waugh, *Catal. Lett.* **1995**, *30*, 99; e) I. Nakamura, H. Nakano, T. Fujitani, T. Uchijima, J. Nakamura, *Surf. Sci.* **1998**, *404*, 92; f) K. R. Harikumar, C. N. R. Rao, *Appl. Surf. Sci.* **1998**, *125*, 245.

[2] a) K. Vanheusden, C. H. Seager, W. L. Warren, D. R. Tallant, J. Caruso, M. J. Hampden-Smith, T. T. Kodas, *J. Luminescence* **1997**, *75*, 11; b) A. R. Gonzalez-Elipe, J. Soria, *J. Chem. Soc. Faraday Trans. 1* **1988**, *84*, 3961; c) B. Yu, C. Zhu, F. Gan, Y. Huang, *Mater. Lett.* **1998**, *33*, 247.

[3] a) J. H. Harding, A. H. Harker, P. B. Keegstra, R. Pandey, J. M. Vail, C. Woodward, *Physica B* **1985**, *131*, 151; b) A. L. Shluger, E. A. Kotomin, L. N. Kantorovich, *J. Phys. C* **1986**, *19*, 4183; c) Z. Barandiarán, L. Seijo, *J. Chem. Phys.* **1988**, *89*, 5739; d) M. N. Nygren, L. G. M. Petersson, Z. Barandiaran, L. Seijo, *J. Chem. Phys.* **1994**, *100*, 2010; e) P. V. Sushko, A. L. Shluger, C. R. A. Catlow, *Surf. Sci.* **2000**, *450*, 153.

[4] a) S. Huzinaga, A. A. Cantu, *J. Chem. Phys.* **1971**, *55*, 5543; b) R. McWeeny, *Methods of Molecular Quantum Mechanics*, 2nd ed., Academic Press, London, **1992**; c) L. N. Kantorovich, *Int. J. Quantum Chem.* **2000**, *78*, 306.

[5] a) U. Eichler, C. M. Kolmel, J. Sauer, *J. Comp. Chem.* **1996**, *18*, 463; b) M. Sierka, J. Sauer, *Faraday Discuss.* **1997**, *106*, 41; c) J. Gao, *Acc. Chem. Rev.* **1996**, *29*, 298; d) I. Antes, W. Thiel, *J. Phys. Chem. A* **1999**, *103*, 9290.

[6] B. G. Dick, A. Overhauser, *Phys. Rev.* **1958**, *112*, 90.

[7] P. Sherwood, A. H. Devries, S. J. Collins, S. P. Greatbanks, N. A. Burton, M. A. Vincent, I. H. Hillier, *Faraday Discuss.* **1997**, *106*, 79.

[8] GAMESS-UK is a package of ab initio programs written by M. F. Guest, J. H. van Lenthe, J. Kendrick, K. Schoffel, and P. Sherwood, with contributions from R. D. Amos, R. J. Buenker, H. J. J. van Dam, M. Dupuis, N. C. Handy, I. H. Hillier, P. J. Knowles, V. Bonacic-Koutecky, W. von Niessen, R. J. Harrison, A. P. Rendell, V. R. Saunders, A. J. Stone, D. J. Tozer, and A. H. de Vries. The package is derived from the original GAMESS code: M. Dupuis, D. Spangler, J. Wendoloski, *NRCC Software Catalog*, *Vol. 1*, Program No. QG01 (GAMESS), **1980**.

[9] F. H. Hamprecht, A. J. Cohen, D. J. Tozer, N. C. Handy, *J. Chem. Phys.* **1998**, *109*, 6264.

[10] L. Whitmore, A. A. Sokol, C. R. A. Catlow, *Surf Sci.* **2001**, in press.

[11] J. D. Gale, *J. Chem. Soc. Faraday Trans.* **1997**, *93*, 629.

[12] D. H. Gay, A. L. Rohl, *J. Chem. Soc. Faraday Trans.* **1995**, *91*, 92.

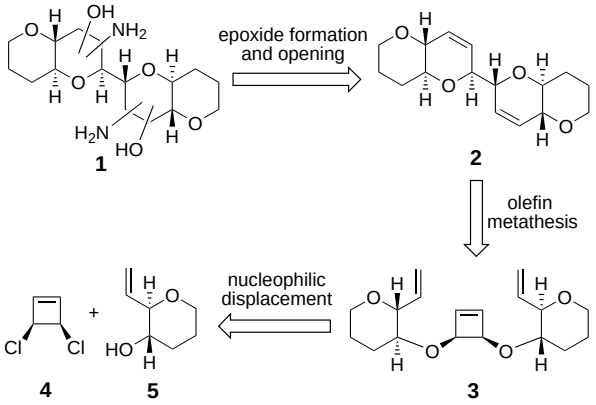
[13] G. C. Chinchen, M. S. Spencer, K. C. Waugh, D. A. Whan, *J. Chem. Soc. Faraday Trans. 1* **1987**, *83*, 2193.

 © WILEY-VCH Verlag GmbH, D-69451 Weinheim, 2001 1433-7851/01/4023-4440 $ 17.50+.50/0

cis-3,4-Dichlorocyclobutene as a Versatile Synthon in Organic Synthesis. Rapid Entry into Complex Polycyclic Systems with Remarkably Stereospecific Reactions**

K. C. Nicolaou,* Juan A. Vega, and Georgios Vassilikogiannakis

The frequent natural occurrence and wide-ranging biological activities of cyclic polyether-type structures has stimulated considerable efforts directed toward their synthesis.[1] Of particular interest are the aminoglycoside antibiotics represented by apramycin[2] and the marine neurotoxins represented by maitotoxin.[3] The former is of current interest by virtue of its RNA-binding properties,[2] whereas the latter constitutes a formidable synthetic challenge owing to its unprecedented molecular complexity and size. Functionalized polyether structures of type **1** (Scheme 1) embody



Scheme 1. Retrosynthetic analysis of structures of type **1**.

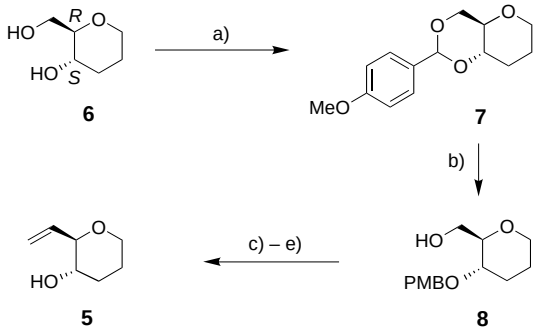
some of the key features found in these natural products, and as such they became targets in our investigations directed toward such complex molecular architectures. Herein we wish to report an expedient entry into these systems from readily available starting materials by means of a series of stereospecific nucleophilic substitutions and an olefin metathesis reaction.

[*] Prof. Dr. K. C. Nicolaou, Dr. J. A. Vega, Dr. G. Vassilikogiannakis
Department of Chemistry and
The Skaggs Institute for Chemical Biology
The Scripps Research Institute
10550 North Torrey Pines Road, La Jolla, CA 92037 (USA)
Fax: (+1) 858-784-2469
and
Department of Chemistry and Biochemistry
University of California, San Diego
9500 Gilman Drive, La Jolla, CA 92093 (USA)
E-mail: kcn@scripps.edu

[**] We thank Drs. D. H. Huang and G. Siuzdak for their assistance with NMR spectroscopy and mass spectrometry, respectively. This work was financially supported by the National Institutes of Health (USA) and The Skaggs Institute for Chemical Biology, a postdoctoral fellowship from the Skaggs Institute for Research (to V.G.), and grants from Abbott, Amgen, ArrayBiopharma, Boehringer-Ingelheim, Glaxo, Hoffmann-La Roche, DuPont, Merck, Novartis, Pfizer, and Schering Plough.

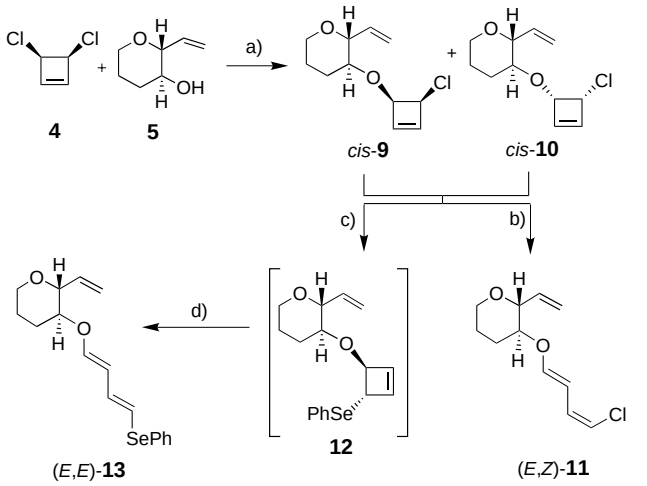
cis-3,4-Dichlorocyclobutene (**4**, Scheme 1) is a readily available building block whose synthetic utility remains largely unexplored despite the early and elegant mechanistic studies of Kirmse et al.[4] which pointed out its potential to undergo highly stereospecific displacement reactions. It was our intention to connect this simple synthon **4** to complex structures such as **1** through an expedient and stereospecific route. Scheme 1 outlines the retrosynthetic plan devised to accomplish this goal. Thus it was anticipated that structures of type **1** could be derived from diolefin **2** by epoxidation, followed by nucleophilic opening of the resulting epoxides. Whereas stereospecificity during the epoxide openings was highly desirable, random formation of these moieties was preferred, at least initially, for optimal molecular diversity. Diolefin **2** could, in turn, be obtained by tandem ring opening/ring closing olefin metathesis of cyclobutene derivative **3** (see Table 1 for physical properties) whose origin from *cis*-3,4-dichlorocyclobutene (**4**) and the hydroxytetrahydropyran system **5** was evident. Such a route constitutes a rapid and flexible access to complex molecular frameworks, which could easily be modified to produce tailor-made intermediates for total synthesis or compound libraries for biological screening purposes.

This strategy proceeded smoothly and, most importantly, revealed a number of interesting reactivity patterns and synthetic opportunities beyond the intended pathway. Hydroxytetrahydropyran **5** was prepared in enantiomerically pure form from **6** by a modification of a previously published sequence.[5] Thus, benzylidine formation followed by regioselective reduction with DIBAL-H, Swern oxidation, Wittig olefination, and DDQ-induced deprotection converted **6** into **5** in good overall yield (Scheme 2).

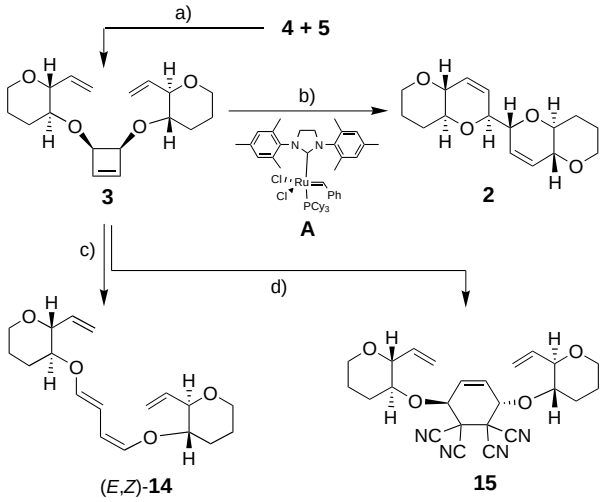


Scheme 2. Synthesis of **5**. Reagents and conditions: a) $MeOC_6H_4CH_2(OMe)_2$ (1.1 equiv), CSA (1.1 equiv), MeCN, 25 °C, 10 h, 82 %; b) DIBAL-H (3.0 equiv), THF, −40 °C, 5 h, 80 %; c) $(COCl)_2$ (1.1 equiv), DMSO (1.1 equiv), Et_3N (1.2 equiv), CH_2Cl_2, −78 °C, 25 °C, 2 h, 91 %; d) CH_3PPh_3Br (1.1 equiv), NaHMDS (1.1 equiv), THF, 0 →25 °C, 1 h; then aldehyde, 25 °C, 6 h, 75 %; e) DDQ (1.2 equiv), CH_2Cl_2:H_2O (10:1), 25 °C, 1 h, 95 %. CSA = 10-camphorsulfonic acid; DIBAL-H = diisobutylaluminum hydride; DMSO = dimethyl sulfoxide; NaHMDS = sodium bis(trimethylsilyl)amide; DDQ = 2,3-dichloro-5,6-dicyano-1,4-benzoquinone.

The reaction of *cis*-3,4-dichlorocyclobutene (**4**) with hydroxy tetrahydropyran compound **5** was then explored. Exposure of **4** to 1.1 equivalents of the sodium alkoxide derived from **5** at 60 °C in THF resulted in the formation of the diastereomeric monosubstituted cyclobutene derivatives **9** and **10** (Scheme 3; 80 % yield, ca. 6:4 ratio). Heating of **9** or **10** or a mixture of the two in refluxing toluene resulted in a clean



Scheme 3. Displacement reactions of *cis*-3,4-dichlorocyclobutene (**4**) (*syn* S_N2' vs. *anti* S_N2'). Reagents and conditions: a) (*syn* S_N2') NaH (2.0 equiv), THF, 25 °C, 1 h; then **4** (1.1 equiv), 60 °C, 10 h, 80 %; b) (conrotatory) toluene, 110 °C, 3 h, 85 %; c) (*anti* S_N2') PhSeCl (1.2 equiv), NaH (2.2 equiv), DMF, 25 °C, 0.5 h, then **9** or **10**, 25 °C, 6 h, 85 %; d) (conrotatory). DMF = *N*,*N*-dimethylformamide.



Scheme 4. Tandem ring opening/ring closing metathesis reaction and conrotatory ring-opening Diels–Alder reaction of cyclobutene derivative **3**. Reagents and conditions: a) **5** (1.0 equiv), NaH (2.0 equiv), THF, 25 °C, 1 h; then **4** (0.5 equiv), 60 °C, 15 h, 85 %; b) **A** (Grubbs' catalyst; 5 mol %), toluene, 45 °C, 12 h, 80 %; c) toluene, 110 °C, 3 h, 90 %; d) TCNE (5.0 equiv), toluene, 110 °C, 3 h, 72 %.

conrotatory opening of the cyclobutene ring, thus leading to the *E*,*Z*-chlorodiene system **11** (85 % yield), whose geometry was confirmed by ^{1}H NMR spectroscopy (J_{cis} = 7.0 Hz, J_{trans} = 12.1 Hz).[4] This thermally induced reaction required relatively high temperatures and was in accordance with the expected *cis* stereochemistry of the cyclobutene derivatives **9** and **10**. Therefore, the displacement of chloride from **4** must have followed a *syn* S_N2' mechanism[4] in which the nucleophile approached the cyclobutene ring from the same side as the departing chloride ion. In contrast, the *anti* S_N2' attack[6] of the phenylselenyl anion on chlorobutene derivative **9** or **10** or a mixture of the two to furnish directly the *E*,*E*-phenylselenodiene **13** (85 % yield) is inferred on the basis of the known propensity of *trans*-cyclobutene derivatives to open through a conrotatory process at much lower temperatures than their *cis* counterparts.[7] No phenylselenocyclobutene derivative **12** was detected in this displacement reaction, which suggests both the *anti* S_N2' mode of reactivity of $PhSe^-$ with the chlorocyclobutenes **9** and **10** and the rapid conrotatory opening of the presumed *trans*-1,2-phenylselenocyclobutene **12** to the *E*,*E*-phenylselenodiene **13** at ambient temperature.

Treatment of **4** with two equivalents of the sodium alkoxide derived from **5** at 60 °C for 15 h gave **3** in 85 % yield (Scheme 4; Table 1). The cyclobutene derivative **3** was then exposed to the third-generation Grubbs' catalyst (**A**)[8] in toluene at 45 °C to afford the desired tetracycle **2** in 80 % yield. Despite close precedent for this olefin metathesis reaction with less sterically hindered substrates,[9] the first-generation Grubbs′ catalyst [$(Cy_3P)_2Cl_2Ru$=CHPh] failed to induce the desired reaction. To explore the chemistry of intermediates encountered on the way to the main target, a solution of compound **3** in toluene was heated at reflux in the absence and in the presence of tetracyanoethylene (TCNE). As expected from the *cis* stereochemistry of the cyclobutene derivative **3**, the *E*,*Z* diene system **14** was the only product of this conrotatory ring-opening reaction (90 % yield) in the absence of TCNE, whereas the C_2-symmetric Diels–Alder product **15** was formed exclusively in 72 % yield in the presence of TCNE, again as a consequence of the stereospecificity of the reactions.

The diolefin **2** was epoxidized in the desired random way by reaction with methyl(trifluoromethyl)dioxirane, which was generated in situ (CH_3CN, 0 → 25 °C),[10] to furnish all four possible epoxides **16**–**19** (Scheme 5) in 90 % total yield and in a ratio of approximately 1:1:1:1. Upon chromatographic separation, three of these epoxides (**16**, **17**, and **19**) crystallized

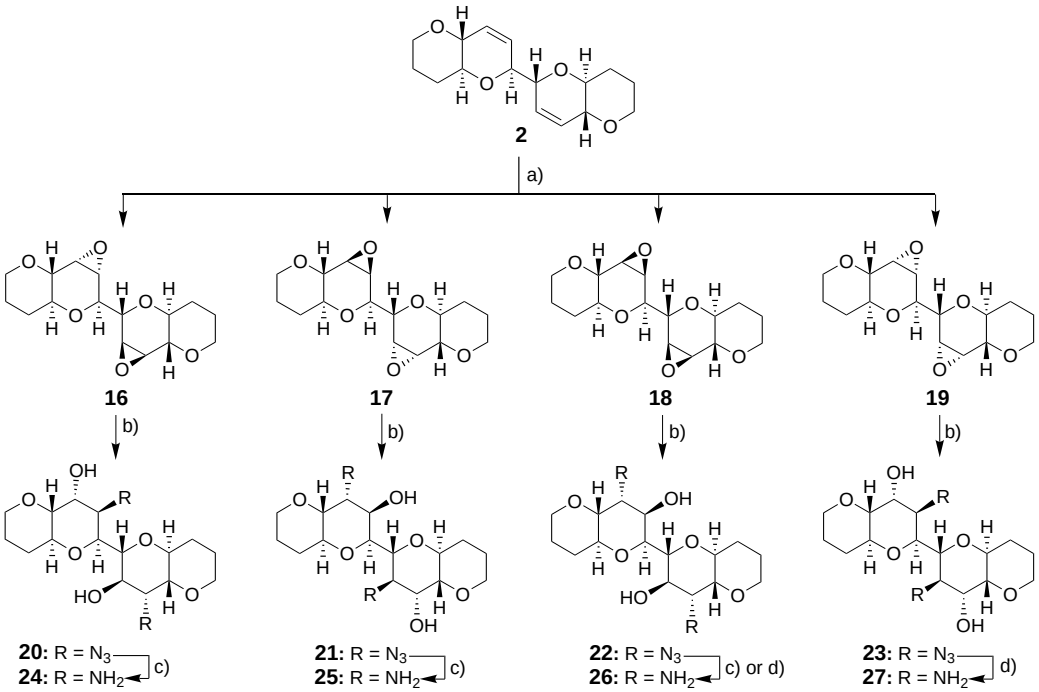
Table 1. Selected physical properties of compounds **3**, **16**, and **22**.

3: Colorless syrup; R_f = 0.37 (silica gel, Et_2O/hexane 1:1); $[\alpha]_D^{25}$ = +50.8 (c = 3.2, $CHCl_3$); IR (film): $\tilde{\nu}_{max}$ = 2931, 2848, 1725, 1437, 1331, 1272, 1161, 1084, 990, 931, 831 cm^{-1}; ^{1}H NMR (500 MHz, $CDCl_3$): δ = 6.29 (m, 2H), 6.09 (ddd, J = 17.2, 11.7, 6.6 Hz, 1H), 6.02 (ddd, J = 17.2, 11.7, 6.6 Hz, 1H), 5.35 (dt, J = 17.2, 1.7 Hz, 2H), 5.19 (m, 2H), 4.65 (t, J = 2.4 Hz, 1H), 4.61 (t, J = 2.6 Hz, 1H), 3.93 (m, 2H), 3.64 (m, 2H), 3.38 (m, 2H), 3.23 (m, 1H), 3.11 (m, 1H), 2.20 (m, 2H), 1.66 (m, 4H), 1.53 (m, 2H); ^{13}C NMR (125 MHz, $CDCl_3$): δ = 142.7, 141.8, 137.0, 136.6, 116.3, 116.2, 81.5, 81.4, 81.0, 80.8, 77.8, 77.2, 67.3 (2 C), 30.7, 30.6, 25.4, 25.2; HRMS (MALDI): calcd for $C_{18}H_{26}O_4$ [M+Na$^+$]: 329.1723, found: 329.1727

16: Colorless crystals; m.p. 146–149 °C (Et_2O/hexane 1:1); R_f = 0.55 (silica gel, Et_2O/hexane 4:1); $[\alpha]_D^{25}$ = +10.4 (c = 0.61, MeOH); IR (film): $\tilde{\nu}_{max}$ = 2942, 2855, 1440, 1266, 1135, 1092, 1023, 955, 837, 793, 725 cm^{-1}; ^{1}H NMR (500 MHz, $CDCl_3$): δ = 4.15 (d, J = 10.2 Hz, 1H), 3.99 (m, 3H), 3.63 (d, J = 4.4 Hz, 1H), 3.45 (m, 6H), 3.30 (d, J = 3.6 Hz, 1H), 3.07 (m, 2H), 1.98 (m, 2H), 1.72 (m, 4H), 1.41 (m, 2H); ^{13}C NMR (125 MHz, $CDCl_3$): δ = 77.8, 75.4, 72.1, 71.0, 69.4, 68.9, 68.8, 68.7, 55.2, 55.1, 52.3, 50.4, 29.2, 29.0, 25.6, 25.5; HRMS (MALDI): calcd for $C_{16}H_{22}O_6$ [M+Na$^+$]: 333.1309, found: 333.1302

22: Colorless crystals; m.p. 99–101 °C (Et_2O/hexane 1:1); R_f = 0.17 (silica gel, Et_2O); $[\alpha]_D^{25}$ = +39.4 (c = 0.53, MeOH); IR (film): $\tilde{\nu}_{max}$ = 3412, 2931, 2860, 2096, 1325, 1261, 1090, 1043, 726 cm^{-1}; ^{1}H NMR (500 MHz, $CDCl_3$): δ = 4.38 (d, J = 10.6 Hz, 1H), 4.24 (t, J = 3.4 Hz, 1H), 4.00 (m, 4H), 3.85 (dd, J = 5.5, 4.0 Hz, 1H), 3.71 (d, J = 10.6 Hz, 1H), 3.50 (m, 6H), 3.14 (d, J = 6.2 Hz, 1H), 2.94 (d, J = 4.7 Hz, 1H), 2.10 (m, 1H), 2.00 (m, 1H), 1.74 (m, 4H), 1.43 (m, 2H); ^{13}C NMR (125 MHz, $CDCl_3$): δ = 76.6, 75.4, 75.2, 72.5, 70.8, 68.4 (2C), 67.1, 67.0, 66.8, 61.5, 60.6, 29.4, 29.1, 25.2, 25.1; HRMS (MALDI): calcd for $C_{16}H_{24}N_6O_6$ [M+Na$^+$]: 419.1649, found: 419.1634

 © WILEY-VCH Verlag GmbH, D-69451 Weinheim, 2001 1433-7851/01/4023-4442 $ 17.50+.50/0



Scheme 5. Epoxidation of diolefin **2**, regiospecific epoxide openings and synthesis of dihydroxy-diamino compounds **24**–**27**. Reagents and conditions: a) Na_2EDTA (4×10^{-4} M (aq.), 0.3 mol%), CF_3COMe (40 equiv), $NaHCO_3$ (30 equiv), oxone (20 equiv), MeCN, 0 → 25 °C, 3 h, 90%; b) NaN_3 (3.0 equiv), NH_4Cl (3.0 equiv), MeOH/H_2O (7:1), 80 °C, 8 h, 88–92%; c) Et_3P (5.0 equiv), CH_3CN/H_2O (9:1), 25 °C, 48 h, 85–91%; d) H_2, Pd/C (10%), Et_3N (5.0 equiv), EtOH, 25 °C, 24 h, 77–81%. Na_2EDTA = ethylenediaminetetraacetic acid disodium salt.

from diethyl ether/hexane. The shown stereostructures were assigned unambiguously by means of X-ray crystallographic analysis (see Figure 1 for **16** and crystallographic data in ref. [11] for **17** and **19**).

Although the random formation of these epoxides (**16**–**19**) was not unexpected, their opening reactions with NaN_3 proved remarkably regio- and stereospecific. Thus, each of these diepoxides (**16**–**19**) opened up in a unique way (Scheme 5) in the presence of NaN_3 and NH_4Cl in MeOH/H_2O (7:1) at 80 °C and led stereospecifically to a single product (88–92% yield). In each reaction, the azide nucleophile apparently attacked from the less sterically hindered trajectory. As graphically depicted in Figure 1, the favorable trajectories (a and b) for the opening of diepoxide **16** led to the formation of diazide **20**. The unfavorable 1,2-diaxial interaction of the incoming azide nucleophile with the hydrogen at C5 (trajectory c) and the 1,2-pseudodiaxial interaction with the bulky group at C9 (trajectory d) were most probably responsible for the observed regiospecificity. Application of the same rationales to diepoxides **17**–**19** provides an explanation for the observed regiospecific outcome of these openings. The structures of these diazides were fully established on the basis of spectroscopic and X-ray crystallographic analysis of **20**, **21**, and **23** (see ORTEP drawing in Scheme 6 for **20** and crystallographic data in ref. [11] for **21** and **23**). The expected structure of diazodiol **22** was fully confirmed by HMQC experiments on the corresponding bis(*p*-bromobenzoate) derivative, which was easily prepared from diol **22** (4-bromobenzoyl chloride, Et_3N, 4-dimethylaminopyridine, 25 °C, 4 h, 93%). Each of the diazides obtained (**20**–**23**) was finally converted into the targeted diaminodiols[12] (**24**–**27**, Scheme 5) in good yield by either catalytic hydrogenation (10% Pd/C) or Et_3P/H_2O-facilitated reduction.

The observed exclusivity in the azide openings of epoxides **16**–**19** prompted us to examine this nucleophilic attack further. Thus, the use of less reagent (1.5 equiv NaN_3) in a shorter time (2 h) in the reaction of epoxide **16** resulted in the

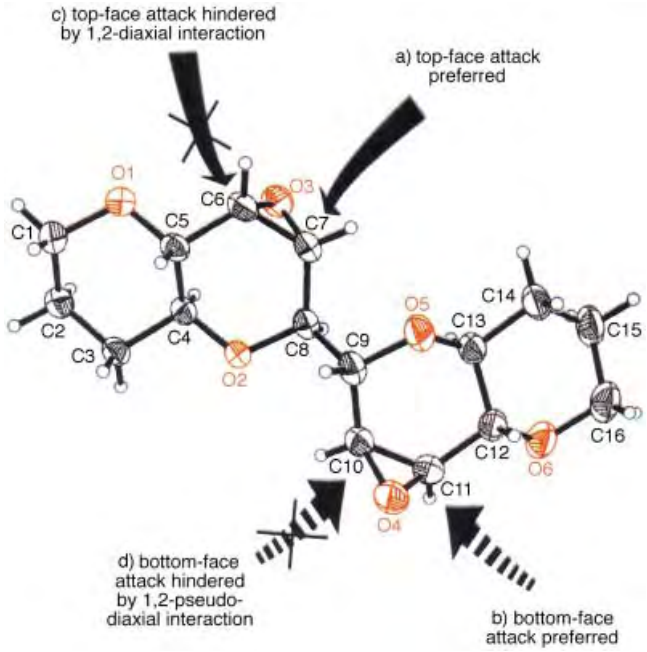
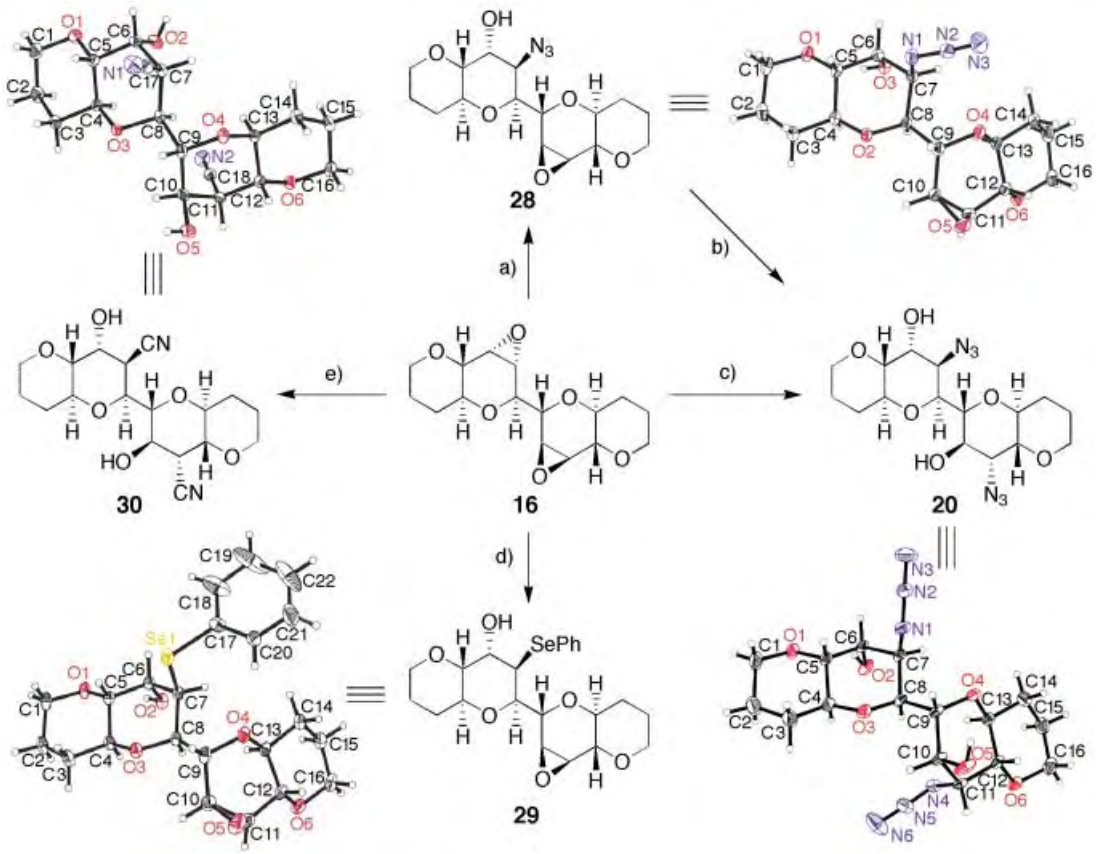


Figure 1. Postulated mechanistic rationale for the regiochemical outcome of the NaN_3 opening of diepoxide **16**. Trajectories a and b are preferred over trajectories c and d owing to less steric congestion. The conformation derived from the X-ray crystallographic analysis of **16** is used.

 © WILEY-VCH Verlag GmbH, D-69451 Weinheim, 2001 1433-7851/01/4023-4443 $ 17.50+.50/0



Scheme 6. Further regiospecific openings of diepoxide **16** with different nucleophiles, and ORTEP drawings of products. Reagents and conditions: a) NaN_3 (1.5 equiv), NH_4Cl (1.5 equiv), MeOH/H_2O (7:1), 80 °C, 2 h, 79 %; b) NaN_3 (1.5 equiv), NH_4Cl (1.5 equiv), MeOH/H_2O (7:1), 80 °C, 6 h, 90 %; c) NaN_3 (3.0 equiv), NH_4Cl (3.0 equiv), MeOH/H_2O (7:1), 80 °C, 8 h, 80 %; d) NaH (2.2 equiv), PhSeCl (2.2 equiv), DMF, 100 °C, 2 h, 79 %; e) Et_2AlCN (8.0 equiv), toluene, 0 °C, 0.5 h, 75 %.

regiospecific formation of mono-azide **28** in 79 % yield (Scheme 6). Thus the sequence of attack on this diepoxide was elucidated (trajectory a is more favorable than trajectory b; Figure 1), which confirms the steric factors that govern this reaction. The structure of **28** was confirmed by X-ray crystallographic analysis[11] (see ORTEP drawing in Scheme 6). Azide **28** was converted into the previously obtained diazide **20** by further reaction (6 h) with NaN_3 (1.5 equiv) at 80 °C (90 % yield). Increasing the steric demand in the reaction by employing the bulkier phenylselenyl anion [$PhSe^-$, generated in DMF from PhSeCl and NaH] led to the same regiochemical outcome as demonstrated by X-ray crystallographic analysis of the resulting monoselenide **29** (see ORTEP structure in Scheme 6). Finally, to probe the question of possible metal coordination effects in these epoxide openings, epoxide **16** was exposed to excess Et_2AlCN in toluene at 0 °C. The result of this experiment, in which complexation forces between the aluminum and the oxygen atoms of the substrate were expected to play a role, was again a highly regio- and stereospecific diepoxide opening, which led to dicyanodiol **30** in 75 % yield. The structure of **30** was proven by X-ray crystallographic analysis (see ORTEP structure in Scheme 6), which again underscores the dominant role of steric effects within these diepoxide structures in their behavior toward nucleophilic reagents.

In conclusion, we have demonstrated the versatility of *cis*-3,4-dichlorocyclobutene (**4**) as a useful building block in organic synthesis and devised a short and highly efficient route to complex and functionalized polyether systems starting from **4**. The methodology is expected to be useful in synthetic applications and in the construction of molecular diversity for biological screening.

Received: August 20, 2001 [Z 17754]

[1] For an adventure in total synthesis directed towards one of these compounds, brevetoxin B, see: K. C. Nicolaou, *Angew. Chem.* **1996**, *108*, 644 – 664; *Angew. Chem. Int. Ed. Engl.* **1996**, *35*, 589 – 607.

[2] a) S. O'Connor, L. K. T. Lam, N. D. Jones, M. O. Chaney, *J. Org. Chem.* **1976**, *41*, 2087 – 2092; b) S. Perzynski, M. Cannon, E. Cundliffe, S. B. Chahwala, J. Davies, *Eur. J. Biochem.* **1979**, *99*, 623 – 628; c) R. Q. Thompson, E. A. Presti, *Antimicrob. Agents Chemother.* **1967**, *7*, 332 – 340; d) R. Ryden, B. J. Moore, *J. Antimicrob. Chemother.* **1977**, *3*, 609 – 613.

[3] a) M. Murata, T. Iwashita, A. Yokoyama, M. Sasaki, T. Yasumoto, *J. Am. Chem. Soc.* **1992**, *114*, 6594 – 6596; b) M. Murata, H. Naoki, T. Iwashita, S. Matsunaga, M. Sasaki, A. Yokoyama, T. Yasumoto, *J. Am. Chem. Soc.* **1993**, *115*, 2060 – 2062; c) M. Murata, H. Naoki, S. Matsunaga, M. Satake, T. Yasumoto, *J. Am. Chem. Soc.* **1994**, *116*, 7098 – 7107; d) M. Satake, S. Ishida, T. Yasumoto, *J. Am. Chem. Soc.* **1995**, *117*, 7019 – 7020; e) M. Sasaki, N. Matsumori, T. Maruyama, T. Nonomura, M. Murata, K. Tachibana, T. Yasumoto, *Angew. Chem.* **1996**, *108*, 1782 – 1785; *Angew. Chem. Int. Ed. Engl.* **1996**, *35*, 1672 – 1675; f) T. Nonomura, M. Sasaki, N. Matsumori, M. Murata, K. Tachibana, T. Yasumoto, *Angew. Chem.* **1996**, *108*, 1786 – 1789; *Angew. Chem. Int. Ed. Engl.* **1996**, *35*, 1675 – 1678; g) W. Zheng, J. A.

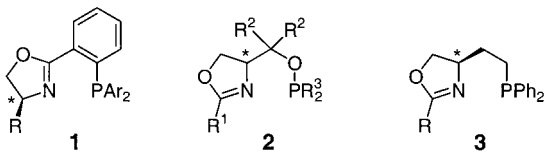
 © WILEY-VCH Verlag GmbH, D-69451 Weinheim, 2001 1433-7851/01/4023-4444 $ 17.50+.50/0

DeMattei, J.-P. Wu, J. J.-W. Duan, L. R. Cook, H. Oinuma, Y. Kishi, *J. Am. Chem. Soc.* **1996**, *118*, 7946 – 7968.
[4] W. Kirmse, F. Scheidt, H.-J. Vater, *J. Am. Chem. Soc.* **1978**, *100*, 3945 – 3946.
[5] K. C. Nicolaou, C.-K. Hwang, B. E. Marron, S. A. DeFrees, E. A. Couladouros, Y. Abe, P. J. Carroll, J. P. Snyder, *J. Am. Chem. Soc.* **1990**, *112*, 3040 – 3054.
[6] For previous reports of such reactions see: a) G. Stork, W. N. White, *J. Am. Chem. Soc.* **1956**, *78*, 4609 – 4624; b) G. Stork, A. F. Kreft III, *J. Am. Chem. Soc.* **1977**, *99*, 3850 – 3851; c) R. M. Magid, O. S. Fruchey, *J. Am. Chem. Soc.* **1977**, *99*, 8368 – 8370.
[7] G. Maier, A. Bothur, *Eur. J. Org. Chem.* **1998**, 2063 – 2072.
[8] For the preparation of this catalyst see: M. Scholl, S. Ding, C. W. Lee, R. H. Grubbs, *Org. Lett.* **1999**, *1*, 953 – 956.
[9] a) W. J. Zuercher, M. Hashimoto, R. H. Grubbs, *J. Am. Chem. Soc.* **1996**, *118*, 6634 – 6640; for selected reviews on the olefin metathesis reaction, see: b) T. M. Trnka, R. H. Grubbs, *Acc. Chem. Res.* **2001**, *34*, 18 – 29; c) R. H. Grubbs, S. Chang, *Tetrahedron* **1998**, *54*, 4413 – 4450; d) T. J. Katz, *Adv. Organomet. Chem.* **1977**, *16*, 283 – 317.
[10] D. Yang, M.-K. Wong, Y.-C. Yip, *J. Org. Chem.* **1995**, *60*, 3887 – 3889.
[11] Crystallographic data (excluding structure factors) for the structures reported in this paper have been deposited with the Cambridge Crystallographic Data Centre as supplementary publication no. S CCDC-168813 – 168821. Copies of the data can be obtained free of charge on application to CCDC, 12 Union Road, Cambridge CB2 1EZ, UK (fax: (+44) 1223-336-033; e-mail: deposit@ccdc.cam.ac.uk).
[12] Interestingly, the spectroscopic data of diaminodiols **24** – **27** reveal the complexation with one molecule of either Et_3N or Et_3P, depending on the protocol used for their preparation (10% Pd/C, Et_3N or Et_3P/H_2O).

A New Class of Modular Phosphinite – Oxazoline Ligands: Ir-Catalyzed Enantioselective Hydrogenation of Alkenes**

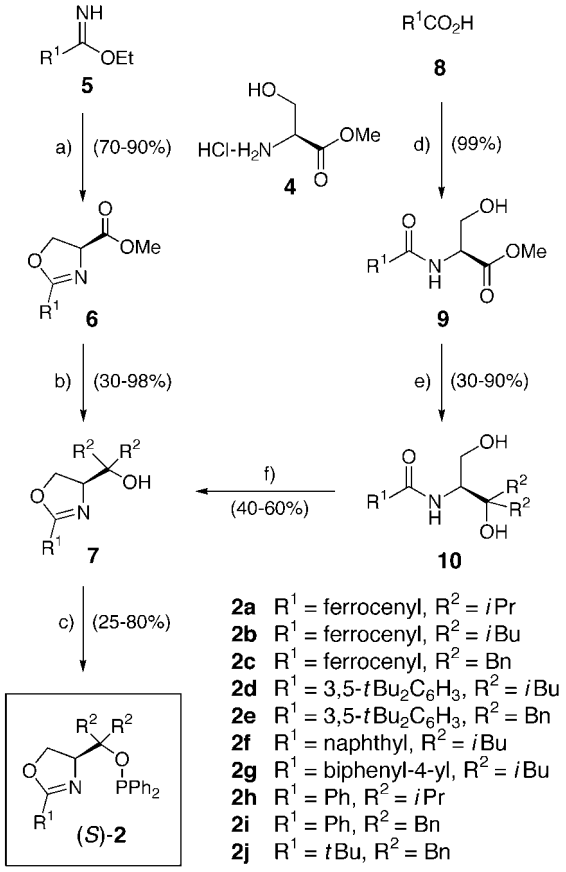
Jörg Blankenstein and Andreas Pfaltz*

Phosphinooxazolines **1** (phox ligands) have been successfully applied in many different enantioselective metal-catalyzed processes.[1] We have recently found that iridium – phox complexes are efficient catalysts for the enantioselective hydrogenation of unfunctionalized alkenes,[2] a class of substrates that gives unsatisfactory results with other catalysts.[3] The best enantioselectivities (up to 99% *ee*) have been observed for 1-alkyl-1,2-diaryl-substituted alkenes, while other alkenes such as monoaryl-1,2-dimethyl-substituted alkenes are converted with only moderate enantiomeric excesses. Here we report a new class of ligands, the phosphinite – oxazolines **2**, which induce high enantioselectivity with a much broader range of alkenes and, thus, significantly enhance the scope of Ir-catalyzed hydrogenation.



1 2 3

Both enantiomers of the phosphinite – oxazoline ligands **2** are readily prepared in three to four steps, starting from imidates **5** or carboxylic acids **8** and L-serine methyl ester hydrochloride (**4**) or the corresponding D isomer (Scheme 1). Special precautions had to be taken in the peptide coupling (step d) to avoid racemization.[4] The addition of Grignard reagents to **9** sometimes gave complex mixtures, so that in general the (hydroxymethyl)oxazolines **7** were preferentially synthesized by means of the imidate route.[5] The modular nature of **2** with its three permutable structural units (R^1, R^2, and the P-substituents) is an attractive feature of these ligands. Especially the selection of the R^1 group, which is derived from a carboxylic acid, is essentially unlimited.



Scheme 1. Synthesis of compounds **2** for which $R^3 = Ph$. a) **4**, $ClCH_2CH_2Cl$, reflux; b) R^2MgX, $-78\,^\circ C$; c) *n*BuLi, NEt_3, $ClPPh_2$, $-78\,^\circ C$; d) **4**, EDC, HOBT, CuCl, DMF; e) R^2MgX, $-78\,^\circ C$; f) (1) NEt_3, TsCl, (2) H_2O. EDC = *N*-(3-dimethylaminopropyl)-*N'*-ethylcarbodiimide hydrochloride, HOBT = 1-hydroxybenzotriazole.

[*] Prof. A. Pfaltz, Dr. J. Blankenstein
Department Chemie
Universität Basel
St.-Johanns-Ring 19, 4056 Basel (Switzerland)
Fax: (+41) 61-2671103
E-mail: andreas.pfaltz@unibas.ch

[**] We thank Dr. Martin Studer and Dr. Benoît Pugin (Solvias AG, Basel) for fruitful discussions, and Prof. Kevin Burgess (Texas A&M University) for preprints of related unpublished work. Financial support by the Swiss National Science Foundation is gratefully acknowledged.

Supporting information for this article is available on the WWW under http://www.angewandte.com or from the author.

Structurally related ligands **3** have been recently synthesized by Burgess et al.; in Ir-catalyzed hydrogenations they were found to give results similar to those of the phox ligands **1**.[6]

For evaluating the phosphinite–oxazoline ligands in Ir-catalyzed hydrogenations, a set of ten derivatives **2a–j** (see Scheme 1) was synthesized from six different precursors of either type **5** or **8** and three different Grignard reagents (R^2MgX). The corresponding Ir complexes were prepared by using the standard procedure developed for Ir–phox catalysts.[2]

Single crystals could be obtained from the iridium complex **11e**-PF_6, and the result of the X-ray structure analysis is shown in Figure 1.[7] Comparison with the structure of the

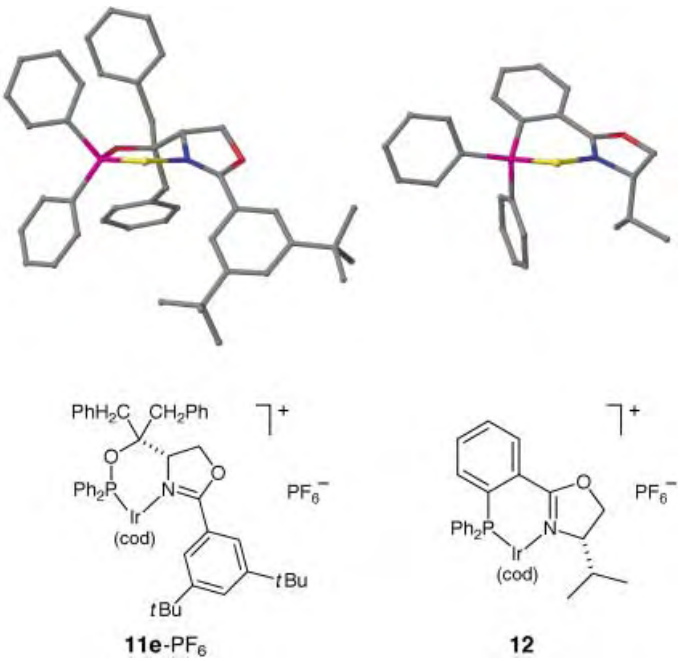
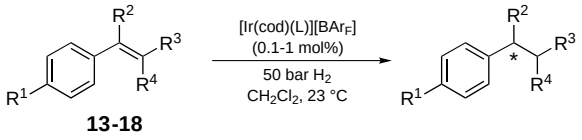


Figure 1. Structures of the iridium complex **11e** (as PF_6 salt) and the analogous phox complex **12** in the crystal (H atoms, PF_6^- ions, and cod ligands have been omitted for clarity).

analogous Ir–phox complex **12**[8] reveals two distinct differences. In contrast to the typical axial–equatorial disposition of the two P-phenyl groups in Ir–phox complexes, the two P–Ph bonds in complex **11e** form a nearly symmetrical arrangement with respect to the coordination plane defined by the P-Ir-N core (dihedral angles N-Ir-P-C: 111° and 126°). In the phox complex **12**, the substituent at the stereogenic center is quite remote from the Ir atom, whereas the bis(*tert*-butyl)phenyl group in complex **11e** extends towards the coordination sphere and, therefore, is expected to interact with reactants bound at the adjacent coordination sites. This implies that the chiral environment of the Ir atom is substantially different in the two complexes.

In initial studies [Ir(cod)L][BAr_F] complexes **11**-BAr_F (L = **2a–j**; cod = cyclooctadiene, BAr_F = tetrakis[3,5-bis(trifluoromethyl)phenyl]borate) were tested in the hydrogenation of alkene **13** [Eq. (1)]. The counterion BAr_F was chosen because of its beneficial effect on catalyst reactivity and stability.[2] In general the reactions were run in CH_2Cl_2 under 50 bar of H_2;



(1)

in toluene very similar results were obtained. With enantioselectivities ranging from 89–98% *ee* for the hydrogenation of **13**, the new ligands proved to be as effective as the phox ligands **1**[2] (Table 1). The ferrocenyl- and 3,5-bis(*tert*-butyl)-

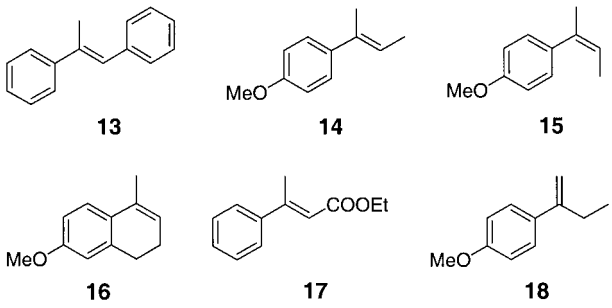
Table 1. Hydrogenation of substrates **13–17**.[a]

Substrate	Ligand	Cat. [mol%]	Conv. [%][b]	*ee* [%][c]
13	**2a**	0.1	100	97 (*R*)
13	**2e**	0.4	100	98 (*R*)
14	**2a**	1.1	100	93 (*R*)
14	**2c**	0.1	100	96 (*R*)
14	**2e**	1.0	100	95 (*R*)
15	**2a**	0.4	100	85 (*S*)
15	**2e**	0.4	100	77 (*S*)
16	**2a**	0.5	100	85 (*S*)
16	**2e**	0.5	100	81 (*S*)
17	**2b**	0.5	100	90 (*R*)
17	**2e**	0.3	100	62 (*R*)

[a] Conditions: see Equation (1); experimental procedures: see ref. [2]. [b] Determined by GC (Restek RTX-1701). [c] Determined by HPLC: for substrates **13**, **14**, **15**, **17** see ref. [2], for **16** Chiracel OD-H was used (0.46 × 25 cm, 20 °C, 0.5 mL min^{-1}, heptane/*i*PrOH 99.8:0.2, $R_f(R) = 12.6$, $R_f(S) = 14.8$ min).

phenyl-substituted ligands **2a–e** proved to be superior to the other derivatives. These differences became more pronounced in the hydrogenation of the monoaryl-substituted alkenes **14–17** (for **14** the enantioselectivity ranged from 45–96% *ee* for **2a–j**). The structure of the backbone substituents (R^2) had a minor but still significant influence; however, no general trend could be derived from the data. With 96% *ee* for the hydrogenation of **14** and 85–90% *ee* for **15–17**, the new ligands clearly outperform the phox ligands **1** (maximum enantioselectivity for reactions of **14**: 61% *ee*, **15**: 42% *ee*, **16**: 61% *ee*, **17**: 84% *ee*).[9]

Terminal alkenes such as **18** are particularly demanding substrates. The highest selectivity for the hydrogenation of **18** has been observed with an *ansa*-bis(cyclopentadienyl)lanthanide catalyst (64% *ee* at 25 °C, 96% *ee* at −80 °C).[10] With



ruthenium-diphosphane complex (Ru-(MeDuPhos)) catalyst in the presence of *t*BuOK, Noyori et al. recently obtained 81–89% *ee* for the hydrogenation of 2-phenylbutene and several

 © WILEY-VCH Verlag GmbH, D-69451 Weinheim, 2001 1433-7851/01/4023-4446 $ 17.50+.50/0 *Angew. Chem. Int. Ed.* **2001**, *40*, No. 23

m- and *p*-substituted derivatives.[11] In our studies with the (phosphinite–oxazoline)Ir complexes **11** a strong dependence of the enantioselectivity on the hydrogen pressure was observed (Table 2). The highest enantioselectivities (up to 88% *ee*) were obtained at ambient pressure, which compares favorably with the best results reported to date.[3, 10, 11]

Table 2. Hydrogenation of 2-(4-methoxyphenyl)butene (**18**).[a]

Ligand	Cat. [mol%]	H_2 [bar]	*ee* [%][b]
2a	0.2	50	46 (*S*)
2a	0.2	10	59 (*S*)
2a	0.1	1	78 (*S*)
2e	0.2	50	53 (*S*)
2e	0.2	10	77 (*S*)
2e	0.1	1	88 (*S*)

[a] Conditions: see Equation (1); 100% conversion in all reactions; experimental procedures: see ref. [2]. [b] Determined by HPLC, see ref. [2].

The new phosphinite–oxazoline ligands **2** significantly expand the scope of enantioselective hydrogenation to classes of substrates for which no efficient catalysts were previously available. The modular construction and the facile synthesis of these ligands should make it possible to tailor their structure for other substrates and other metal-catalyzed reactions.

Received: July 16, 2001 [Z17524]

[1] G. Helmchen, A. Pfaltz, *Acc. Chem. Res.* **2000**, *33*, 336–345.

[2] A. Lightfoot, P. Schnider, A. Pfaltz, *Angew. Chem.* **1998**, *110*, 3047–3050; *Angew. Chem. Int. Ed.* **1998**, *37*, 2897–2899. D. G. Blackmond, A. Lightfoot, A. Pfaltz, T. Rosner, P. Schnider, N. Zimmermann, *Chirality* **2000**, *12*, 442–449. Promising results have also been obtained recently with Ir catalysts derived from chiral imidazolylidene ligands: M. T. Powell, D.-R. Hou, M. C. Perry, X. Cui, K. Burgess, *J. Am. Chem. Soc.* **2001**, *123*, 8878–8879.

[3] a) R. L. Halterman in *Comprehensive Asymmetric Catalysis*, *Vol. 1* (Eds.: E. N. Jacobsen, A. Pfaltz, H. Yamamoto), Springer, Berlin, **1999**, chap. 5.2, p. 183–195; b) although titanocene and zirconocene catalysts can induce high enantioselectivity, the turnover numbers and frequencies are low: R. D. Broene, S. L. Buchwald, *J. Am. Chem. Soc.* **1993**, *115*, 12569–12570; M. V. Troutman, D. H. Appella, S. L. Buchwald, *J. Am. Chem. Soc.* **1999**, *121*, 4916–4917.

[4] T. Miyazawa, T. Otomatsu, Y. Fukui, T. Yamada, S. Kuwata, *J. Chem. Soc. Chem. Commun.* **1988**, 419–420.

[5] For experimental procedures see Supporting Information.

[6] a) D.-R. Hou, J. H. Reibenspies, K. Burgess, *J. Org.Chem.* **2001**, *66*, 206–215; D.-R. Hou, J. H. Reibenspies, T. A. Colacot, K. Burgess, *Chem. Eur. J.*, in press; b) after submission of our paper, phosphinite–oxazoline ligands of the same type (**2**, $R^2 = H$) were reported: G. Jones, C. J. Richards, *Tetrahedron Lett.* **2001**, *42*, 5553–5555.

[7] X-Ray crystal structure analysis of **11e**: crystallized from CH_2Cl_2/Et_2O/pentane, formula: $C_{53}H_{62}Cl_2F_6Ir_1N_1O_2P_2$, $M = 1184.15$ ($[C_{52}H_{60}IrN_1O_2P] \cdot PF_6 \cdot Cl_2CH_2$), orange crystal $0.08 \times 0.11 \times 0.19$ mm, $a = 14.7714(3)$, $b = 14.9908(2)$, $c = 23.7541(5)$ Å, $\alpha = 90.0^\circ$, $V = 5260.0$ Å^3, $\rho_{calcd} = 1.495$ g cm^{-3}, $\mu = 2.762$ mm^{-1}, $F(000) = 2386.186$, $Z = 4$, orthorhombic, space group $P2_12_12_1$, $Mo_{K\alpha}$ radiation ($\lambda = 0.71073$ Å, graphite monochromator), $T = 293$ K, Θ scan range $1.00 < \Theta < 27.00^\circ$. 32529 reflections collected ($\pm h$, $\pm k$, $\pm l$), 11878 independent reflections, 9652 observed reflections [$I = 2\sigma(I)$], 633 refined parameters. $R = 0.0411$, $Rw = 0.0494$, max. residual electron density $-1.57(1.99)$ e$^-$ Å^{-3}, located near the metal center. Restraints were applied to parts of the *tert*-butyl group, which was split due to disorder. Hydrogen atoms were calculated and refined as riding atoms. Data collection was performed with a Kappa CCD diffractometer. Programs used: structure solution: SIR92 (A. Altomare, G. Cascarano, C. Giaccovazzo, A. Gualgliardi, M. C. Burla, G. Polidori, M. Camalli, *J. Appl. Crystallogr.* **1994**, *27*, 435), structure refinement: CRYSTALS (D. J. Watkin, *Crystals, Issue 11*, Chemical Crystallography Laboratory, Oxford, **2001**), weighting scheme: Chebychev polynominal (J. R. Carruthers, D. J. Watkin, *Acta Crystallogr. Sect. A* **1979**, *35*, 698). Crystallographic data (excluding structure factors) for the structures reported in this paper have been deposited with the Cambridge Crystallographic Data Centre as supplementary publication no. CCDC-167319. Copies of the data can be obtained free of charge on application to CCDC, 12 Union Road, Cambridge CB2 1EZ, UK (fax: (+44) 1223-336-033; e-mail: deposit@ccdc.cam.ac.uk). We thank M. Neuburger and Dr. P. Mukherjee (University of Basel) for solving the crystal structure.

[8] P. Schnider, G. Koch, R. Prétôt, G. Wang, F. M. Bohnen, C. Krüger, A. Pfaltz, *Chem. Eur. J.* **1997**, *3*, 887–892.

[9] For the hydrogenation of **16** a selectivity of 92% *ee* was obtained with a Pyr(phox) derivative, an analogue of **1** with a pyrrole backbone (P. G. Cozzi, N. Zimmermann, R. Hilgraf, S. Schaffner, A. Pfaltz, *Adv. Synth. Catal.* **2001**, *343*, 450–454); for **17**, we recently achieved 92% *ee* with Pyr(phox) and another P,N ligand (R. Hilgraf, A. Pfaltz, *Synlett* **1999**, 1814–1816). For **14**, **15**, and **18**, however, these ligands lead to only modest enantioselectivities.

[10] V. P. Conticello, L. Brard, M. A. Giardello, Y. Tsuji, M. Sabat, C. L. Stern, T. J. Marks, *J. Am. Chem. Soc.* **1992**, *114*, 2761–2762; M. A. Giardello, V. P. Conticello, L. Brard, M. R. Gagné, T. J. Marks, *J. Am. Chem. Soc.* **1994**, *116*, 10241–10254.

[11] G. S. Forman, T. Ohkuma, W. P. Hems, R. Noyori, *Tetrahedron Lett.* **2000**, *41*, 9471–9475.

Synthesis of Highly Magnetic, Air-Stable Iron–Iron Carbide Nanocrystalline Particles by Using Power Ultrasound**

Sergei I. Nikitenko, Yuri Koltypin, Oleg Palchik, Israel Felner, Xiao N. Xu, and Aharon Gedanken*

Coated magnetic nanoparticles may have important applications as materials for magnetic data storage, xerography, and magnetic resonance imaging.[1] A protective layer on the surface of the particles prevents interactions between closely

[*] Prof. Dr. A. Gedanken, Dr. Yu. Koltypin, O. Palchik
Department of Chemistry, Bar-Ilan University
Ramat-Gan 52900 (Israel)
Fax: (+972) 3-5351250
E-mail: gedanken@mail.biu.ac.il

Prof. Dr. I. Felner
Racah Institute of Physics, Hebrew University
Jerusalem (Israel)

Dr. S. I. Nikitenko
Institute of Physical Chemistry, RAS
Leninskii Pr.31, 117915 Moscow (Russia)

Dr. X. N. Xu
Department of Physics, Nanjing University
Nanjing 210093 (China)

[**] A. Gedanken is grateful for the support of the German Ministry of Science through the Deutsche-Israeli DIP program. I. Felner and A. Gedanken thank also the Israeli Ministery of Science, Culture and Sport for an infrastructure grant. S. I. Nikitenko thanks the Bar-Ilan Research Authority for his fellowship. The authors also thank Dr. Shifra Hochberg for editorial assistance.

spaced magnetic bits and provides oxidation resistance.[2] Coated iron nanoparticles are of particular interest, since iron has the highest magnetic moment among the ferromagnetic transition metals. Many different processes for obtaining carbon-coated iron nanoparticles have been tested, such as carbon arc, flowing gas plasma, laser-induced pyrolysis, mechanosynthesis, and thermal carbonization.[3] Recently, iron nanoparticles coated with gold,[4a] phosphate,[4b] and silica[4c] were prepared by reverse-micelle reduction and sol–gel techniques. These processes yield unstable iron nanoparticles, and the saturation magnetization of materials thus prepared does not exceed 120 emu g^{-1}.

Uncoated iron nanoparticles have been prepared by using high-intensity ultrasound to decompose [$Fe(CO)_5$] in alkane solutions.[5] The chemical effect of ultrasound is related to acoustic cavitation, that is, the formation, pulsation, and implosive collapse of microbubbles in liquids or other media with elastic properties. The bubble collapse generates transient temperatures of several thousand Kelvin and local pressures of one hundred atmospheres.[6] Such drastic conditions lead to homolytic dissociation of the molecules within the cavitating bubbles.

Iron nanoparticles obtained sonochemically from alkane solutions are not stable in contact with air. To prepare coated iron nanoparticles we studied the sonochemical decomposition of [$Fe(CO)_5$] in diphenylmethane (DPhM), an aromatic solvent with physicochemical properties (m.p. 25 °C, b.p. 265 °C, vapor pressure 1 hPa at 77 °C)[7] that are suitable for sonochemistry. Recently, we revealed that sonolysis of neat DPhM forms a polymerlike solid product. We assumed that small amounts of this product generated in situ would coat the surface of iron nanoparticles formed simultaneously from [$Fe(CO)_5$].

During sonication, the color of the solution changed rapidly from yellow to black. After sonication, the solution was transferred under argon into an inert glove box. The pyrophoric solid product was then removed by centrifugation, washed with pentane, dried under vacuum, and kept in the glove box. The as-prepared material contained 17.6 wt % C and 1.5 wt % H. The reaction yield was 53 % with respect to iron.

The presence of a significant amount of carbon and hydrogen indicates that as-prepared material contains the sonolytic decomposition products of DPhM. The FTIR spectrum reveals the presence of absorption bands at 3060–3020, 2900–2850, and 1100–1000 cm^{-1}, which were assigned to C–H stretching vibrations of aromatic and aliphatic groups and *p*-substituted phenyl groups, respectively.[8] It can be assumed that the structure of the sonopolymer is close to that of polystyrene. Further studies on the polymeric product are in progress.

The XRD diagram (Figure 1 a) showed that the as-prepared material is X-ray amorphous. According to low-resolution transmission electron microscopy (TEM; Figure 2 a), it consists of nanosized globular agglomerates in which very small (ca. 5 nm) dense particles are dispersed. It can be assumed that iron nanoparticles formed from [$Fe(CO)_5$] are included in a globular matrix of DPhM sonication products. As-prepared material is superparamagnetic ($M = 88$ emu g^{-1} at 15 kG external field). This observation confirms that the iron particles are smaller than 10 nm.[5]

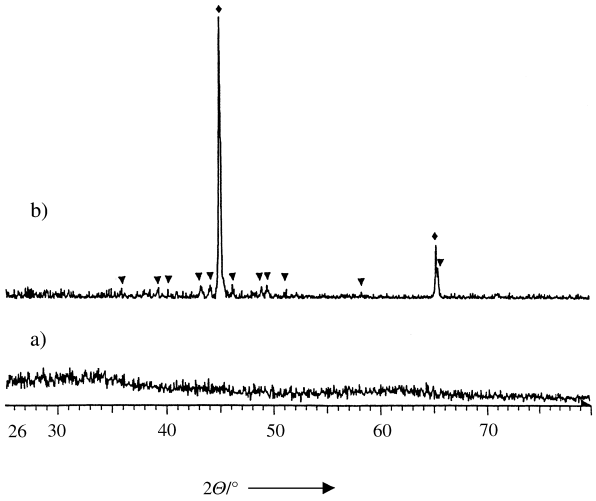


Figure 1. XRD diagrams of as-prepared (a) and annealed materials (b). ◆ bcc Fe, ▼ Fe_3C.

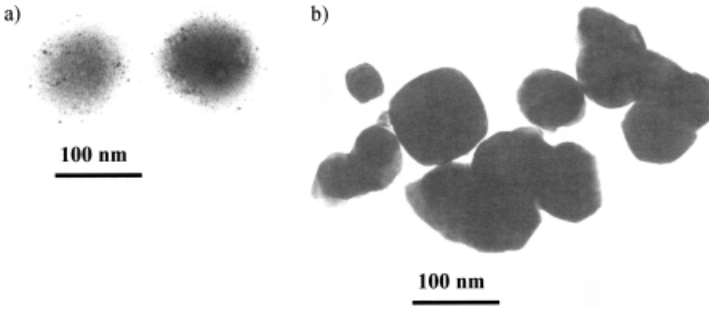


Figure 2. Low-resolution TEM images of as-prepared (a) and annealed materials (b).

An air-stable, dark gray magnetic powder is formed after annealing of the as-prepared pyrophoric sample at 700 °C in argon. The annealed material contains 5.6 wt % C and 0.08 wt % H. The low-resolution TEM image (Figure 2 b) showed that the annealed material consists of tetragonal and round nanoparticles with a particle size in the range of 20–100 nm. The Mössbauer spectrum (Figure 3) revealed the

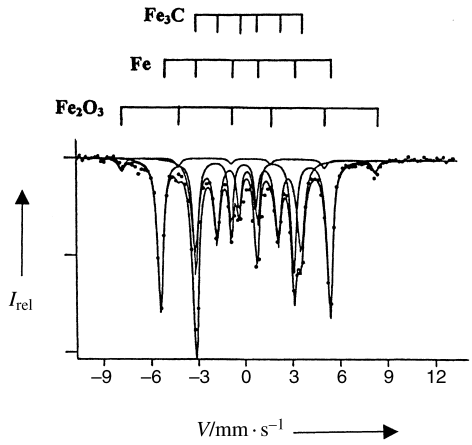


Figure 3. Mössbauer spectrum of annealed material at room temperature.

 © WILEY-VCH Verlag GmbH, D-69451 Weinheim, 2001 1433-7851/01/4023-4448 $ 17.50+.50/0

presence of bcc Fe, iron carbide Fe_3C (I.S. = 0.20 mm s^{-1} and $H_{eff} = (208 \pm 5)$ kOe), and small amounts of Fe_2O_3 (ca. 3 atom %). The ratio of Fe to Fe_3C is close to 4:1. The XRD patterns shown in Figure 1b confirm the presence of bcc Fe and Fe_3C.

The annealed material is ferromagnetic, as follows from the magnetization curve presented in Figure 4. The saturation magnetization M_s and coercive force H_c are 212 emu g^{-1} and 40 Oe, respectively. The M_s value of the material is unexpectedly high and is close to that of bulk bcc Fe (222 emu g^{-1}[9]). Since the M_s value of bulk Fe_3C is small (14 emu g^{-1}[9]), the magnetization of the nanocomposite would be expected to be considerably lower than that of bcc Fe. Further studies are required to explain the high M_s value of the nanocomposite.

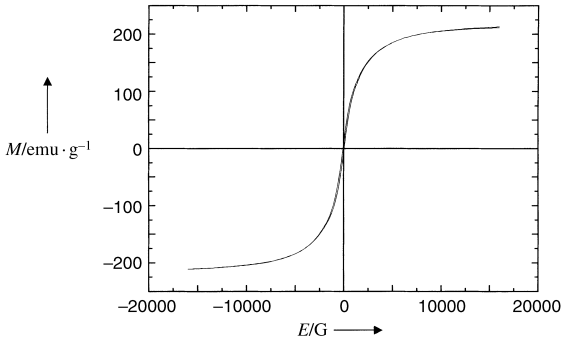


Figure 4. Magnetization curve of annealed material.

The nanocrystalline particles exhibit strong resistance to oxidation with oxygen. The Mössbauer spectrum, XRD data, and magnetic properties of the annealed material did not change after at least four months of contact with air (monthly measurements). The high stability of the nanoparticles could be related to the protective shell formed on the surface. The high-resolution TEM image (Figure 5) shows that iron particles are coated by a crystalline shell with a thickness of about 3 nm. The shell does not exhibit the layered structure typical of graphite. It can be assumed that the coat consists of Fe_3C or a mixture of Fe_3C and C.

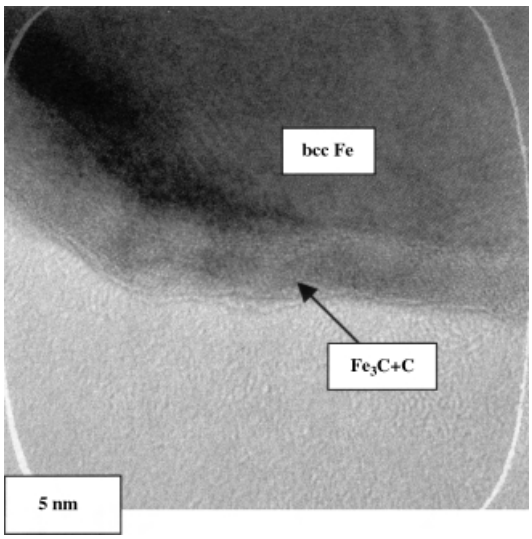


Figure 5. High-resolution TEM image of annealed particles.

Experimental Section

A 0.50 M solution of $[Fe(CO)_5]$ in DPhM was sonicated for 3 h in argon with a Sonics and Materials device ($f = 20$ kHz, $P_{el} = 600$ W, $S = 1$ cm^2, $P_{ac} = 0.45$ W cm^{-3}, measured by the thermal-probe method[6a]). The temperature was kept at 30 °C during sonication. The solids were annealed in an argon stream (99.996 %).

The XRD diagrams were recorded on a Bruker AXS D* Advanced Powder X-ray Diffractometer ($Cu_{K\alpha}$ radiation, $\lambda = 0.15418$ nm). Low-resolution TEM images were obtained with a JEOL-JEM100SX electron microscope with 80 kV accelerating voltage. High-resolution TEM images were obtained by employing a JEOL-3010 device with 300 kV accelerating voltage. Magnetization loops were measured with a Quantum Design MPMS SQUID magnetometer. Mössbauer spectra were recorded on a conventional constant-acceleration spectrometer (50 mCi ^{57}Co(Rh) source). FTIR spectra were recorded in KBr pellets on an Impact 410 Nicolet spectrometer. Elemental analysis was carried out in an Eager 200 CHN analyzer.

Received: May 7, 2001
Revised: September 3, 2001 [Z17054]

[1] P. J. F. Harris, *Carbon Nanotubes and Related Structures*, Cambridge University Press, New York, **1999**.
[2] J. Jiao, S. Seraphin, X. Wang, J. C. Withers, *J. Appl. Phys.* **1996**, *80*, 103.
[3] a) M. E. McHenry, S. A. Majetich, E. M. Kirpatrick, *Mater. Sci. Eng. A* **1995**, *204*, 19; b) S. Iwama, T. Fukaya, K. Tanaka, K. Ohshita, Y. Sakai, *Nanostruct. Mater.* **1999**, *12*, 241; c) B. Gunguly, G. P. Huffman, F. E. Huggins, M. Endo, P. C. Eklund, *J. Mat. Res.* **1993**, *8*, 1666; d) X. Q. Zhao, Y. Liang, Z. Q. Hu, B. X. Liu, *J. Appl. Phys.* **1996**, *80*, 5857; e) T. J. Goodwin, S. H. Yoo, P. Matteazzi, J. R. Groza, *Nanostruct. Mater.* **1997**, *8*, 559; f) E. P. Yelsukov, S. F. Lomayeva, G. N. Konygin, G. A. Dorofeev, V. I. Povstugar, S. S. Mikhailova, A. V. Zagainov, *Nanostruct. Mater.* **1999**, *12*, *Part A* (special issue), 483; g) S. Hirano, S. Tajima, *J. Mater. Sci.* **1990**, *25*, 4457; h) W. Teunissen, J. W. Geus in *Science and Technology in Catalysis* (Eds.: B. Delmon, J. T. Yates), **1999**, p. 185.
[4] a) J. Wiggins, E. E. Carpenter, C. J. O'Connor, *J. Appl. Phys.* **2000**, *87*, 5651; b) S. Rebeyrat, J. L. Grosseau-Poussard, J. F. Dinhut, P. O. Renault, *Thin Solid Films* **2000**, *379*, 136; c) T. Lutz, C. Estournes, J. L. Guille, *J. Sol–Gel Sci. Technol.* **1998**, *13*, 929.
[5] K. S. Suslick, M. Fang, T. Hyeon, *J. Am. Chem. Soc.* **1996**, *118*, 11960.
[6] a) T. J. Mason, *Chemistry with Ultrasound*, Elsevier, Oxford, **1990**, p. 342; b) K. S. Suslick in *Kirk–Othmer Encyclopedia of Chemical Technology*, 4th ed., Supplement, Wiley, New York, **1998**.
[7] *Beilstein Handbook*, *Vol. 5*, 588, I 277.
[8] K. Nakanishi, P. H. Solomon, *Infrared Absorption Spectroscopy*, Holden–Day, San Francisco, **1982**.
[9] *Metals Handbook*, 9th ed., Vol. 9: *Metallography and Microstructures*, Metal Park, Ohio, **1985**.

 © WILEY-VCH Verlag GmbH, D-69451 Weinheim, 2001 1433-7851/01/4023-4449 $ 17.50+.50/0

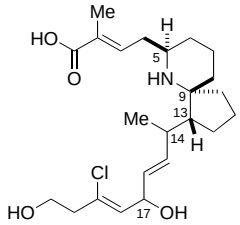
Concise Stereoselective Routes to Advanced Intermediates Related to Natural and Unnatural Pinnaic Acid**

Matthew W. Carson, Guncheol Kim, Martin F. Hentemann, Dirk Trauner, and Samuel J. Danishefsky*

This paper is dedicated to Professor A. I. Meyers for his continuing accomplishments in organic chemistry.

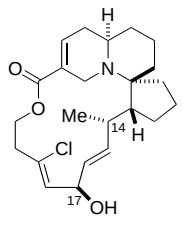
The phospholipase A_2 (PLA_2) family consists of lipolytic enzymes whose constituents catalyze the hydrolysis of intra- and extracellular membrane phospholipids.[1] Cytosolic 85-kDa phospholipase ($cPLA_2$)[2] is an important member of the PLA_2 family since it plays a significant role in the generation of free arachidonic acid from the *sn*-2 position of cellular phosholipids in most mammalian cells.[3] The released arachidonic acid can mediate the biosynthesis of eicosanoids, prostaglandins, leukotrienes, and thromboxanes.[4] These biological messengers govern critical phenomena such as cell proliferation and inflammatory responses. Accordingly, selective $cPLA_2$ inhibitors are promising targets for the development of novel anti-inflammatory drugs.

Two such agents were identified in 1996 when Uemura and co-workers isolated the structurally similar alkaloids pinnaic acid and halichlorine from the Okinawan bivalve *Pinna muricata* and the sponge *Halichondria okadai* Kadota, respectively.[5, 6] Both compounds mediate anti-inflammatory properties, albeit by different mechanisms. Thus, pinnaic acid inhibits $cPLA_2$ in vitro ($IC_{50} = 0.2$ mM) whereas halichlorine is a vascular cell-adhesion molecule-1 (VCAM-1) antagonist.[5, 6] Although pinnaic acid and halichlorine are reported to inhibit different target proteins, cursory inspection reveals that these alkaloids share a novel azaspiro core. Not surprisingly, these compounds have garnered much attention from the synthetic community.[7] Our group has recently reported the total synthesis of halichlorine[8] and suggested a conformational switch mediated by the macrolactone moiety to distinguish it from pinnaic acid.[9] To further our program, which seeks to gain access to natural product inspired non-steroidal privileged structures of potential interest with respect to inflammation, we embarked on the total synthesis of pinnaic acid (see **1**).



pinnaic acid

Proposed **1**: (14*R*, 17 (?))

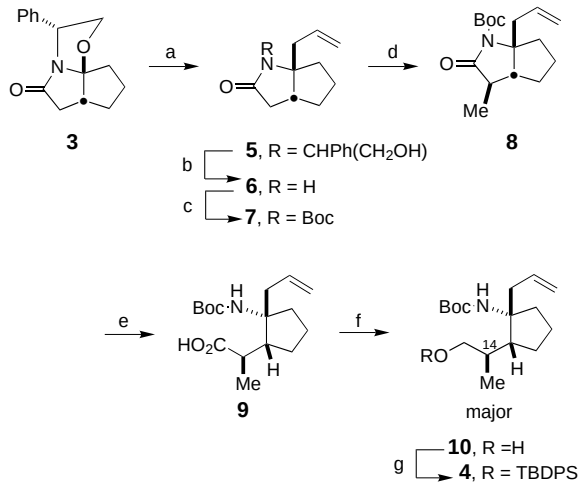


halichlorine

2: (14*S*, 17*R*)

Uemura and co-workers had formulated the relative and absolute stereochemistry of halichlorine as shown in **2**.[6, 10] With only negligible quantities of pinnaic acid available through isolation, the relative stereochemistry at both C14 and C17 of this compound could not be assigned with complete confidence, even after extensive magnetic resonance experiments.[5] However, a preference for (14*R*)-**1** was expressed by Uemura and co-workers. The stereochemistry thus had to be verified by means of total synthesis.

Given the significant homology in the azaspiro core of halichlorine and pinnaic acid, it seemed at the outset that the hard-won lessons of the halichlorine campaign would simplify our objective.[8] In the end, although significant lessons were learned from the total synthesis of halichlorine, extensions to pinnaic acid were far from uneventful. Prior art demonstrated that the Meyers' lactam **3** could be readily converted into protected amino alcohol **4** (Scheme 1).[8, 11] The synthesis of



Scheme 1. Reagents and Conditions: a) $Me_3SiCH_2CH{=}CH_2$, $TiCl_4$, CH_2Cl_2, $-78 \rightarrow 25\,^{\circ}C$, 18 h, 98%; b) Na, EtOH, NH_3/THF, $-33\,^{\circ}C$, 1.0 h, 88%; c) Boc_2O, DMAP, THF, $25\,^{\circ}C$, 18 h, 93%; d) LiHMDS (1.1 equiv), hexanes/THF, $-78 \rightarrow -40\,^{\circ}C$, 1.5 h, then MeI (1.3 equiv), $-40\,^{\circ}C$, 1 h; e) LiOH, THF/H_2O, $25\,^{\circ}C$, 18 h; f) $ClCO_2Et$, NEt_3, THF, $-10\,^{\circ}C$, 1 h, then $NaBH_4$, MeOH, $0 \rightarrow 25\,^{\circ}C$, 1 h, 39% over three steps; g) TBDPSCl, NEt_3, DMAP (10 mol%), $0 \rightarrow 25\,^{\circ}C$, 96%. Boc = *tert*-butoxy carbonyl; DMAP = dimethylaminopyridine; HMDS = 1,1,1,3,3,3-hexamethyldisilazane; TBDPS = *tert*-butyldiphenylsilyl.

[*] S. J. Danishefsky, M. W. Carson, G. Kim,[+] M. F. Hentemann,[++] D. Trauner[+++]
Laboratory for Bioorganic Chemistry
Sloan-Kettering Institute for Cancer Research
1275 York Avenue, New York, NY 10021 (USA)
Fax: (+1) 212-772-8691
and
Department of Chemistry, Columbia University
Havemeyer Hall, New York, NY 10027 (USA)
E-mail: s-danishefsky@ski.mskcc.org

[+] Present address: Department of Chemistry, College of Natural Science
Chungnam National University, Taejon (South Korea)

[++] Present Address: Bayer Corporation
West Haven, CT, 06513 (USA)

[+++] Present Address: Department of Chemistry, University of California Berkeley, CA 94720 (USA)

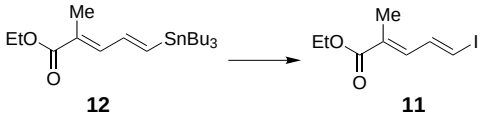
[**] This work was supported by the National Institutes of Health (Grant Numbers: CA28824). Postdoctoral Fellowship support is gratefully acknowledged by M.W.C. (U.S. Army BCRP, DAMD17-98-1-8154), M.F.H. (5T32 CA62948-05), and D.T. (Schering Research Foundation, Berlin). We thank Dr. George Sukenick of the MSKCC NMR Core Facility for NMR and mass spectral analyses.

 © WILEY-VCH Verlag GmbH, D-69451 Weinheim, 2001 1433-7851/01/4023-4450 $ 17.50+.50/0

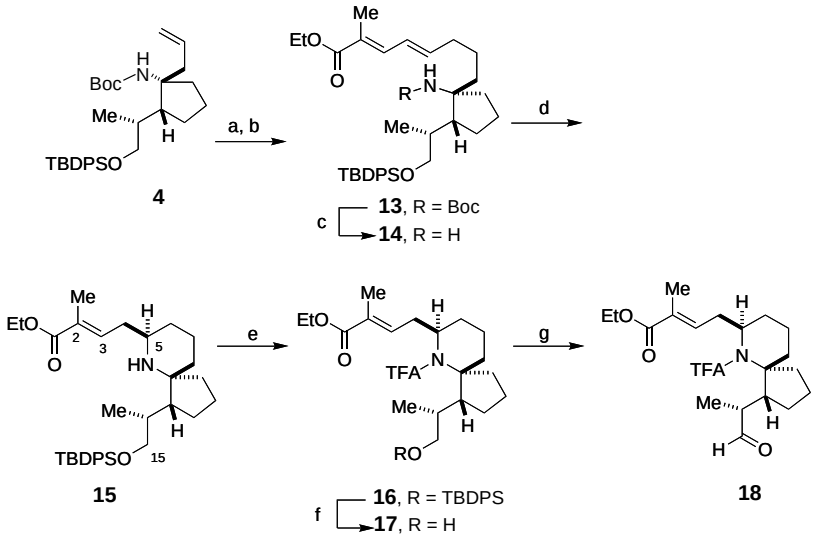
pinnaic acid commenced with the asymmetric allylation of lactam **3** to provide bicyclic lactam **5**. The nitrogen atom was protected, and subsequent highly stereoselective alkylation of the lithium enolate of **7** with methyl iodide led to **8**. Base-induced hydrolysis of **8** followed by reduction of the derived anhydride of **9** gave alcohol **10**.[12]

Given the less than rigorous grounds for assigning the *R* configuration at C14 in pinnaic acid (cf. **1**), we regarded it as unlikely that the two compounds, pinnaic acid and halichlorine, would differ at this center. Accordingly, we took compound **10** forward first. At the stage of **10**, the configuration of the secondary methyl center corresponds to the *S* configuration at C14 of **1**.[13] Protection of alcohol **10** delivered protected amino alcohol **4**, which contains chirality imprints that correspond to those suggested for C9, C13, and C14 of pinnaic acid (**1**).

Our attention was then directed at the azaspiro core of the target. We envisioned coupling an alkylborane derived from **4** with vinyl iodide **11**.[14] The latter was generated in a straightforward manner from known vinyl stannane **12** ([Eq. (1)]; I_2, CCl_4, 25 °C, 2 h).[15] Vinyl iodide **12** was coupled



successfully with the alkylborane of **4** to give **13** in 75% yield (Scheme 2). We then focused on the formation of the piperidine ring through an intramolecular vinylogous (1,6-addition) Michael reaction. Initial experiments showed that



Scheme 2. Reagents and Conditions: a) 9-BBN, THF, 25 °C, 1.5 h; b) **11**, Pd(dppf)$Cl_2 \cdot CH_2Cl_2$, $AsPh_3$, Cs_2CO_3, DMF/H_2O, 25 °C, 3 h, 75%; c) CF_3CO_2H, CH_2Cl_2, 25 °C, 1 h; d) DBU, 25 °C, 18 h, 81% over two steps; e) TFAA (20 equiv), Hünigs base (20 equiv), 1,2-CH_2ClCH_2Cl, 0 °C, 5 min, 88%; f) HF–pyridine, THF/pyridine, 0 → 25 °C, 18 h, 91%; g) TPAP (5 mol%), NMO (2.0 equiv), 3-Å molecular sieves, MeCN, 0.5 h, 84%. 9-BBN = 9-borabicyclo[3.3.1]nonane; DBU = 1,8-diazabicyclo[5.4.0]undec-7-ene; dppf = 1,1′-bis(diphenylphosphinyl) ferrocene; Hünig's base = diisopropylethylamine; NMO = *N*-methylmorpholine *N*-oxide; TFAA = trifluoroacetic anhydride; TPAP = tetrapropylammonium perruthenate.

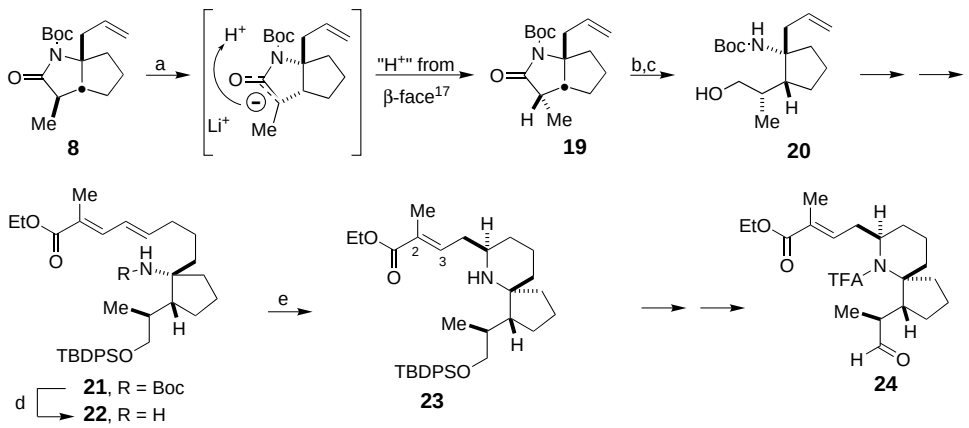
the lithium anion of **13** did not cyclize under a variety of conditions. We surmised that the bulk of the Boc protecting group may impede the N–C bond formation. Indeed, as shown in Scheme 2, upon removal of the Boc group, the resulting free amine **14** underwent smooth based-induced cyclization to afford piperidine **15** in good yield and with excellent diastereoselectivity. Equally important was the fact that the piperidine moiety **15** was generated exclusively as the correct *E* isomer at C2–C3.[16] Thus, in a few steps we were able to complete the bicyclic core of **1** by means of a Suzuki reaction and a stereoselective 1,6 Michael-type cyclization.

Continuing on the path toward pinnaic acid with the *S* configuration at C14 (natural or unnatural), the C15 alcohol of **15** was exposed by cleavage of the TBDPS group. At this point, considerable difficulties were encountered. The first of these was an inability to oxidize **15** to the corresponding aldehyde at C15. The situation here was clearly more complex than in the case of halichlorine, since the proximal nitrogen atom in pinnaic acid must emerge eventually as an NH group. This is in contrast to halichlorine in which the synthetic target mandates the tertiary character of the nitrogen atom at a comparable point. The choice of a proper protecting group for the NH group of **15** turned out to be critical. It would be necessary for this group to enable a diverse set of reactions and to be responsive to deprotection in a straightforward way at one of several stages. After many frustrations with various groups, we settled on the trifluoroacetyl derivative to form **16**. Deprotection of the TBDPS group gave **17**, which was oxidized to aldehyde **18**.

We then set out to form the C14 epimer (*S* configuration) building block of aldehyde **18**, anticipating a synthesis of the *R* version[5] of pinnaic acid. For this purpose, we returned to the methylated Meyers' lactam **8**. Deprotonation of **8** (LiHMDS) and kinetic quenching (2,6-di-*tert*-butyl-4-methylphenol) gave rise to **19** as the major product.[17] Forward processing of **19**, as shown in Scheme 3, afforded, after careful column chromatography, pure primary alcohol **20** (58%, 2 steps). Alcohol **20** was converted into **21**, the *S* version of the spirocyclization precursor. Indeed, deprotection of the Boc group of **21**, followed by treatment of the resultant **22** with DBU, provided **23**, which is the *S* epimer of **15** at C14. Progression of **23** as before afforded aldehyde **24**, the *S* epimer of **18** at C14.

In summary, we have secured the basis for synthesizing the C14 stereocongeners of pre-pinnaic acid building blocks by highly stereoselective sequences. In the following paper, we demonstrate how this chemistry set the stage for the total synthesis of natural and unnatural pinnaic acids in a fashion which elucidates their relative and absolute stereochemistry in rigorous detail.

Received: August 3, 2001 [Z17666]



Scheme 3. Reagents and Conditions: a) LiHMDS (1.2 equiv), THF, −40 °C, 1.5 h, then BHT (1.2 equiv), −78 °C, 1.0 h, 82 %; b) LiOH, THF/H_2O, 25 °C, 18 h; c) $ClCO_2Et$, NEt_3, THF, −10 °C, 1 h, then $NaBH_4$, MeOH, 0 →25 °C, 1 h, 58 % over two steps; d) TFA, CH_2Cl_2, 25 °C, 1 h; e) DBU, 25 °C, 18 h, 76 % over two steps. BHT = 2,6-di-*tert*-butyl-4-methylphenol; TFA = trifluoroacetic acid.

[1] a) J. D. Clark, A. R. Schievella, E. A. Nalefski, L.-L. Lin, *J. Lipid Mediators Cell Signalling* **1995**, *12*, 83; b) E. A. Dennis, *J. Biol. Chem.* **1994**, *269*, 13057; c) I. Kudo, M. Murakami, S. Hara, K. Inoue, *Biochem. Biophys. Acta* **1993**, *177*, 217; d) E. J. Ackerman, E. A. Dennis, *Biochim Biophys. Acta.* **1995**, *1259*, 125; e) H. van den Bosch, *Biochim Biophys. Acta.* **1980**, *604*, 191.

[2] a) M. S. Hixon, A. Ball, M. H. Gelb, *Biochemistry* **1998**, *37*, 8516; b) M. Mosior, D. A. Six, E. A. Dennis, *J. Biol. Chem.* **1998**, *273*, 2184; c) B. Huang, B.-Z. Yu, J. Rogers, I.-J. L. Byeon, K. Sekar, X. Chen, M. Sundaralingam, M.-D. Tsai, M. K. Jain, *Biochemistry* **1996**, *35*, 12164; d) J. Balsinde, E. A. Dennis, *J. Biol. Chem.* **1997**, *272*, 16069; e) Z. Huang, P. Payette, K. Abdullah, W. A. Cromlish, B. P. Kennnedy, *Biochemistry* **1996**, *35*, 3712; f) S. Glover, M. de Carvalho, T. Bauburt, M. Jones, E. Chi, C. C. Leslie, M. H. Gelb, *J. Biol. Chem.* **1995**, *270*, 15359.

[3] a) C. C. Leslie, *J. Biol. Chem.* **1997**, *272*, 16709; b) J. D. Sharp, D. L. White, X. G. Chiou, T. Goodson, G. C. Gamboa, D. Mc Clure, S. Burgett, J. Hoskins, P. L. Skatrud, J. R. Sportsman, G. W. Becker, L. H. Kang, E. F. Roberts, R. M. Kramer, *J. Biol. Chem.* **1991**, *266*, 14850; c) J. D. Clark, L.-L. Lin, R. W. Kriz, C. S. Ramesha, L. A. Sultzman, A. Y. Lin, N. Milona, J. L. Knopf, *Cell* **1991**, *65*, 1043.

[4] a) W. Smith, D. DeWitt, *Adv. Immunol.* **1996**, *62*, 166; b) B. Samuelsson, S. E. Dhalen, J. A. Lindgren, C. A. Rouzer, C. N. Serhan, *Science* **1987**, *237*, 1171.

[5] T. Chou, M. Kuramoto, Y. Otani, M. Shikano, K. Yazawa, D. Uemura, *Tetrahedron Lett.* **1996**, *37*, 3871.

[6] M. Kuramato, C. Tong, K. Yamada, T. Chiba, Y. Hayashi, D. Uemura, *Tetrahedron Lett.* **1996**, *37*, 3867.

[7] For reports on synthetic studies toward pinnaic acid and/or halichlorine, see: a) S. P. Keen, S. M. Weinreb, *J. Org. Chem.* **1998**, *63*, 6739; b) H. Arimoto, S. Asano, D. Uemura, *Tetrahedron Lett.* **1999**, *40*, 3583; c) S. Lee, Z. Zhao, *Org. Lett.* **1999**, *1*, 681; d) S. Lee, Z. Zhao, *Tetrahedron Lett.* **1999**, *40*, 794; e) D. L. J. Clive, V. S. C. Yeh, *Tetrahedron Lett.* **1999**, *40*, 8503; f) J. L. Koviach, C. J. Forsyth, *Tetrahedron Lett.* **1999**, *40*, 8529; g) D. L. Wright, J. P. Schulte II, M. A. Page, *Org. Lett.* **2000**, *2*, 1847; h) J. D. White, P. R. Blackmore, E. A. Korf, A. F. T. Yokochi, *Org. Lett.* **2001**, *3*, 413; i) M. Shindo, Y-I Fukuda, K. Shishido, *Tetrahedron Lett.* **2000**, *41*, 929; j) W. Yokoto, M. Shindo, K. Shishodo, *Heterocycles* **2001**, *54*, 871.

[8] a) D. Trauner, S. J. Danishefsky, *Tetrahedron Lett.* **1999**, *40*, 6513; b) D. Trauner, J. B. Schwartz, S. J. Danishefsky, *Angew. Chem.* **1999**, *111*, 3756; *Angew. Chem. Int. Ed.* **1999**, *38*, 3542.

[9] D. Trauner, S. J. Danishefsky, *Helv. Chim. Acta* **2000**, *83*, 2344.

[10] H. Arimoto, I. Hayakawa, M. Kuramoto, D. Uemura, *Tetrahedron Lett.* **1998**, *39*, 861.

[11] J. A. Ragan, M. C. Claffey, *Heterocycles* **1995**, *41*, 57; b) M. D. Ennis, R. L. Hoffman, N. B. Ghazal, D. W. Old, P. A. Money, *J. Org. Chem.* **1996**, *61*, 5813; for comprehensive reviews on the chemistry of bicyclic lactams, see: c) A. I. Meyers, G. P. Brengel, *Chem. Commun.* **1997**, 1; d) D. Romo, A. I. Meyers, *Tetrahedron* **1991**, *47*, 9503; for a recent example of the application of chiral bicyclic lactams to synthesis, see: e) A. Degnan, A. I. Meyers, *J. Am. Chem. Soc.* **1999**, *121*, 2762.

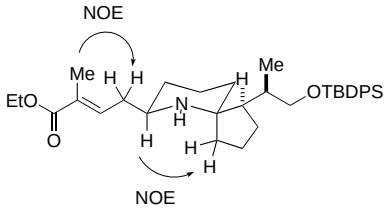
[12] A number of by-products were isolated, including an isomer of **10**, which is epimeric at the secondary methyl center (7 %, 3 steps). The minor stereoisomer was most likely generated by the partial epimerization of (14*R*)-Me-**9** during the basic hydrolysis, and nominally intersects in the synthesis of pinnaic acid (natural or unnatural) that has the *R* configuration at C14 (see below).

[13] As a consequence of the *R* and *S* stereonomenclature systems, the priority rankings change at the secondary methyl center from **10** to the putative pinnaic acid.

[14] For comprehensive reviews of the Suzuki reaction, see: a) S. R. Chemler, D. Trauner, S. J. Danishefsky, *Angew. Chem./Angew. Chem. Int. Ed.*, in press; b) N. Miyaura, A. Suzuki, *Chem. Rev.* **1995**, *95*, 2457; c) A. Suzuki, *J. Organomet. Chem.* **1999**, *576*, 147.

[15] D. A. Evans, J. R. Gage, J. L. Leighton, *J. Am. Chem. Soc.* **1992**, *114*, 9434.

[16] The configurations at C5 and at the C2−C3 double bond were assigned as *R* and *E*, respectively, according to diagnostic NOESY cross peaks:



15

[17] The kinetic quench resulted in a mixture of lactams **19** and **8** (>9:1).

 © WILEY-VCH Verlag GmbH, D-69451 Weinheim, 2001 1433-7851/01/4023-4452 $ 17.50+.50/0

Total Synthesis and Proof of Stereochemistry of Natural and Unnatural Pinnaic Acids: A Remarkable Long-Range Stereochemical Effect in the Reduction of 17-Oxo Precursors of the Pinnaic Acids**

Matthew W. Carson, Guncheol Kim, and Samuel J. Danishefsky*

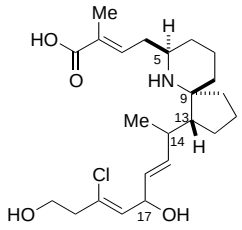
This paper is dedicated to professor Uemura for his discovery of many fascinating natural products

The extraordinary powers of spectroscopic methods and crystallography in elucidating structural, configurational, and conformational issues of small as well as larger (bio size) molecules are well appreciated by practicing chemists. It is rare that total synthesis contributes to the process of structural determination of natural products.[1]

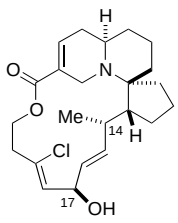
The potentially important pinnaic acid (**1**), isolated in trace quantities from the Okinawan bivalve, *Pinna muricatta* appeared to be an exception.[2] The configuration at C14 of pinnaic acid was assigned to be *R* on grounds which were not rigorous.[2] Furthermore, the configuration at C17 was not assigned at all. We viewed the *R* designation of C14 in pinnaic acid with particular reservation. In the seemingly related halichlorine (**2**), isolated from the sponge *Halichondra okadain*, the configuration of this center was determined to be *S*,[3] which was corroborated by total synthesis.[4]

In the previous communication,[5] we charted a stereoselective route to aldehydes **3** and **4**, differing only in their configuration at C14. The thought was that a total synthesis from these intermediates would allow us to determine which C14 epimer would (following an appropriate outcome at C17) give rise to pinnaic acid. We were not confident that the configuration at C17 would be subject to stereocontrol. Furthermore, even if pinnaic acid were obtained from a particular C14 epimer, we would not necessarily be in a position to define its configuration at C17. It was only a combination of total synthesis and degradation that provided an unambiguous answer.

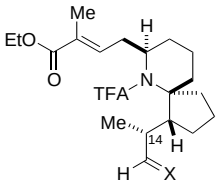
Herein we report: 1) the first total synthesis of pinnaic acid; 2) the rigorous deduction of the stereochemistry of natural pinnaic acid by a combination of total synthesis and chemical degradation; 3) the synthesis and rigorous assignments of the three C14, C17 stereocongeners of pinnaic acid by systematic permutation of the configurations at these carbons; and 4) the discovery of a remarkably stereospecific reduction at C17 en route to pinnaic acid and the dependency of this selectivity on the stereochemistry at C14.



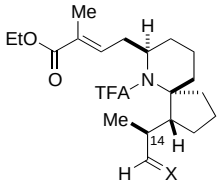
pinnaic acid
Proposed **1**: (14*R*, 17 (?))



halichlorine
2: (14*S*, 17*R*)



3: X = O
8: X = H, OH



4: X = O
12: X = H, OH

As shown in Scheme 1, the opening step, that is, base-mediated reaction of aldehyde **3** with known phosphonate **5**,[6] turned out to be the most complicated element of the synthetic sequence.[7] The reaction did not go to completion, and separation of product **6** from starting material **3** was quite difficult. Instead, the mixture of **6** and **3** was carried forward. Remarkably, reduction of **6** with either (*R*)- or (*S*)-alpine hydride (lithium β-isopinocamphenyl-9-bora-bicyclo[3.3.1]-nonyl hydride)[8] gave a large excess of **7**. Compound **7** was obtained in approximately 30% yield (over two steps), after separation from **8** (the reduction product of **3**; ca. 50% recovery). Deprotection of the silyl group from **7** gave rise to **9**. Concurrent cleavage of the trifluoroacetyl and ethyl ester functions produced a compound whose high field NMR spectrum was quite similar to that reported by Uemura and co-workers.[2] The difficulty arose in that there was no sample of pinnaic acid available for a direct comparison of the synthetic and natural products.

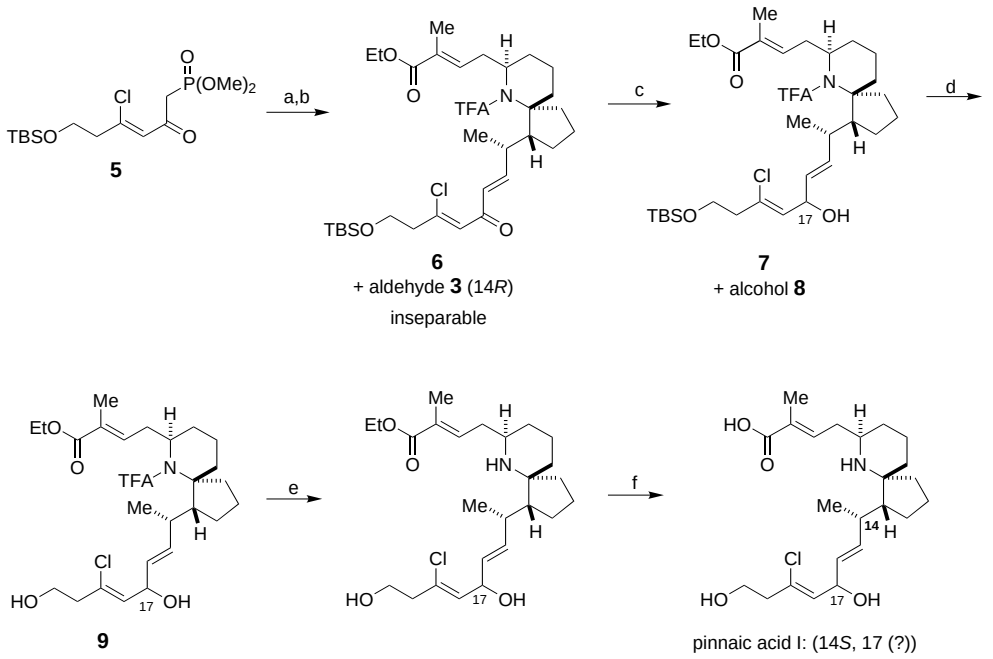
We could not be sure if even the high field NMR spectra would distinguish stereocongeners that only differed at C17 (or C14, see below). Fortunately, the reduction of **6** with sodium borohydride gave useful amounts of **10** (Scheme 2). We used **10** to provide access to another pinnaic acid, which differed from the compound derived from **7** only with respect to the configuration at C17. Compound **10** was desilylated and the trifluoroacetyl and ethyl ester protecting groups were removed (Scheme 2) to afford a pinnaic acid congener. The high field NMR spectrum of this compound differed in rather

[*] S. J. Danishefsky, M. W. Carson, G. Kim[+]
Laboratory for Bioorganic Chemistry
Sloan-Kettering Institute for Cancer Research
1275 York Avenue, New York, NY 10021 (USA)
Fax: (+1) 212-772-8691
and
Department of Chemistry, Columbia University
Havemeyer Hall, New York, NY 10027 (USA)
E-mail: s-danishefsky@ski.mskcc.org

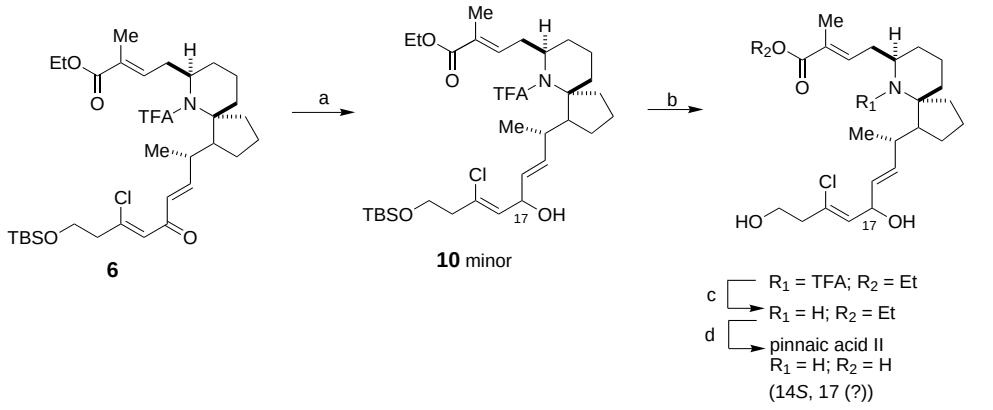
[+] Present address: Department of Chemistry, College of Natural Science
Chungnam National University, Taejon (South Korea)

[**] This work was supported by the National Institutes of Health (Grant Numbers: CA28824). Postdoctoral Fellowship support is gratefully acknowledged by M.W.C. (U.S. Army BCRP, DAMD17-98-1-8154). We thank Dr. George Sukenick of the MSKCC NMR Core Facility for NMR and mass spectral analyses. We would like to thank professor Nakanishi for his supportive interest in the project.

 © WILEY-VCH Verlag GmbH, D-69451 Weinheim, 2001 1433-7851/01/4023-4453 $ 17.50+.50/0



Scheme 1. Reagents and Conditions: a) LiHMDS (1.1 equiv), THF, −78 °C, 0.5 h; b) **3**, THF/HMPA, −78 →25 °C, 2 d; c) (*R*) or (*S*)-alpine hydride, 30% over two steps; d) HF–pyridine, THF/pyridine, 0 °C, 1 h, 95%; e) $NaBH_4$, EtOH, 25 °C, 18 h, 93%; f) LiOH, THF/MeOH/H_2O, 4 h, 40 °C, 90%. HMDS = 1,1,1,3,3,3-hexamethyldisilazane; HMPA = hexamethylphosphoramide; TFA = trifluoroacetic acid.



Scheme 2. Reagents and Conditions: a) $NaBH_4$, $CeCl_3 \cdot 7H_2O$, MeOH, 25 °C, 0.5 h, 23% (**7** + **10**) over two steps; b) HF–pyridine, THF/pyridine, 0 °C, 1 h, 71%; c) $NaBH_4$, EtOH, 25 °C, 18 h, 90%; d) LiOH, THF/MeOH/H_2O, 4 h, 40 °C, 97%.

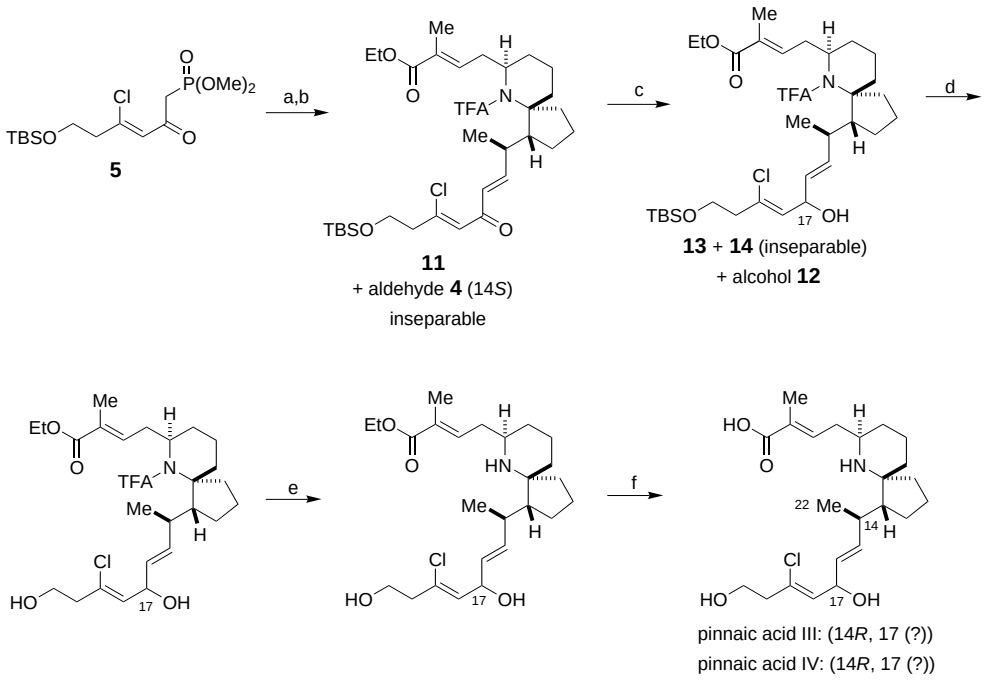
clear ways from the spectrum of natural pinnaic acid.[9] We refer to the final acid derived from **7** as pinnaic acid I and that from the less abundant **10** as pinnaic acid II; the former appeared more likely to be the natural structure.

To use the spectra of the pinnaic acid I synthesized from aldehyde **3** as a basis for structural deduction, it is critical that the NMR spectra of neutral pinnaic acid and its C14 epimer be distinguishable, or else C14 of natural pinnaic acid could not be assigned the *S* configuration with any certainty. To this end, pinnaic acid-like congeners with established *R* configurations at C14 were prepared from aldehyde **4** (see below).[10]

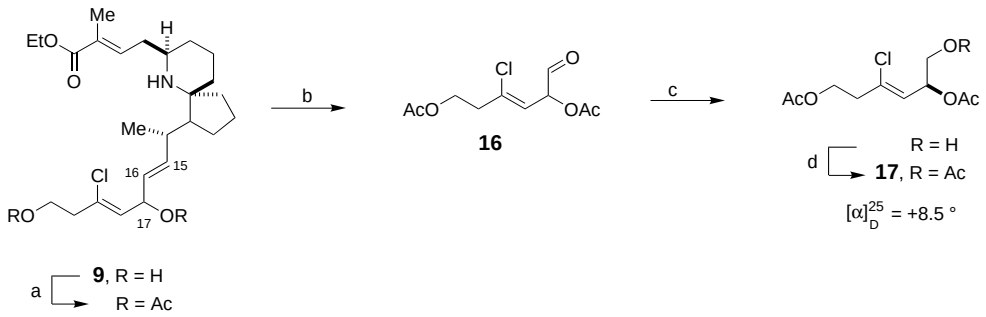
Reaction of the lithium anion of **5** with **4** as above, gave rise to **11**, again mixed with unreacted **4** (Scheme 3).[7] Reduction of the mixture of unreacted **4** and **11** gave rise to a separable mixture of **13** and **14** (1.7:1) as well as alcohol **12**, the reduction product of **4**. These compounds were used individually to obtain pinnaic acids III and IV by methods comparable to those used in the synthesis of pinnaic acids I and II from their precursors, **7** and **10**, respectively. Once again, there were strong homologies in the high field NMR spectra of the end products, but there are clear differences in the readout of these compounds relative to pinnaic acids I and II.[11] At this point it was very clear that only in the case of pinnaic acid I, is there complete correspondence between the high field ^1H NMR spectrum of pure, synthetic product and that reported for the less than homogeneous natural acid.

We had established that pinnaic acid I corresponds to the natural product, and that it has the *S* configuration at C14, since it had been derived from aldehyde **3**. We had not in fact determined rigorously the configuration at C17 of the synthetic material, and therefore of the natural product. Given the noncrystallinity of any of the intermediates, it was necessary for us to undertake an unusual course, that is, the degradation of our synthetic material. For this purpose, it would be necessary to manipulate the C15–C16 double bond in such a way that C17 remains intact in the degradation product. Diol **9** was exposed to acetic anhydride/pyridine in the presence of catalytic DMAP for two hours at room temperature. This treatment served to cap the hydroxy groups at C17 and C21. We hoped that ozonolysis of the C15=C16 bond would occur preferentially to a potentially competitive degradation at the C18=C19 bond containing the chlorine atom. Careful ozonolysis of the diacetate of **9** gave rise to the chloro aldehyde **16**. Reduction of the aldehyde and acetylation of the resultant alcohol produced **17** (Scheme 4). The two enantiomers, **17** and **18** had previously been synthesized by Uemura and coworkers.[3b, 12] It was clear that the degradation product derived from **9** is indeed **17**, which corresponds to the *R* configuration at C17 of pinnaic acid I. Thus the stereochemistry of pinnaic acids I and II (**19** and **20**, respectively) was fully assigned, and **19** corresponds to natural pinnaic acid.

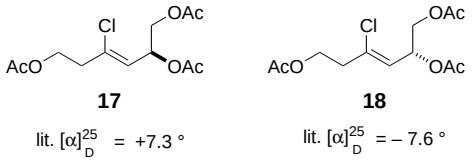
 © WILEY-VCH Verlag GmbH, D-69451 Weinheim, 2001 1433-7851/01/4023-4454 $ 17.50+.50/0



Scheme 3. Reagents and Conditions: a) LiHMDS (1.1 equiv), THF, −78 °C, 0.5 h; b) **4**, THF/HMPA, −78 →25 °C, 2 d; c) (*R*)-or (*S*)-alpine hydride, 25% over two steps; d) HF–pyridine, THF/pyridine, 0 °C, 1 h, 99%, 3 steps; e) $NaBH_4$, EtOH, 25 °C, 18 h, 88%; f) LiOH, THF/MeOH/H_2O, 2.5 h, 40 °C, 91%.



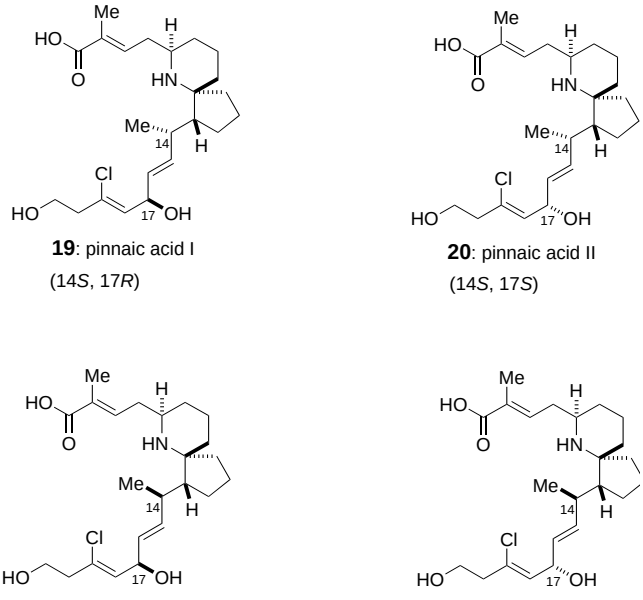
Scheme 4. Reagents and Conditions: a) Ac_2O, pyridine, cat. DMAP, 25 °C, 2 h, 80%; b) O_3, MeOH, −40 °C, then Me_2S; c) $NaBH_4$, $CeCl_3 \cdot H_2O$, MeOH; d) Ac_2O, NEt_3, 25 °C, 35% over three steps. DMAP = dimethylaminopyridine.



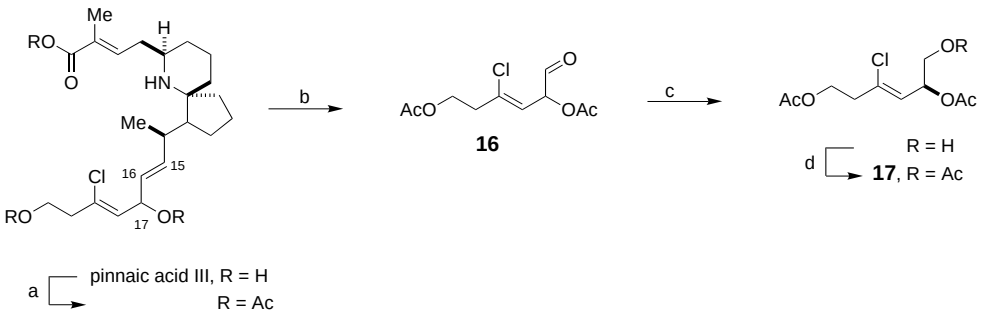
A similar degradation was conducted on pinnaic acid III (Scheme 5). After acetylation at C17, C21, and at the carboxy group, the resultant compound (presented as the mixed anhydride) underwent the procedure described above (cf. Scheme 4). Chiral-phase HPLC analysis showed that the degradation led once again to antipode **17**. Thus pinnaic acids III and IV correspond to **21** and **22**, respectively.

During this work, a remarkable case of long-range stereochemical transmission was discovered. Thus, the reduction of ketone **6** with large reducing agents (alpine boranes) is highly stereospecific towards the alcohol with the *R* configuration at C17. This stereospecificity is not dependent on the chirality of the two boranes. By contrast, the reduction of the C17 ketone moiety in **11** with the same boranes is not stereospecific and gave only a minor preference for **13**. It seems unlikely that the C14 substituent can influence the path of attack of the hydride donor.

We propose that in the case of **6** there is a synergy between the directing influences of the methyl group at C14 and the total molecular environment of the spirocyclic ring system, which results in the control of the reactive conformation that brings with it a high selectivity in the sense of reduction. It seems likely that the configurations at C9 and C5 as well as the *E* C2–C3 side chain serve to dominate the presentation of the C1–C4 side chain. The nature of the C14–C19 side chain follows from the configurations at C13 and C14, and the *trans* double bonds at C15–C16 and C18–C19. An additional constraining factor could be the preference of the methyl group at C14 to be orthogonal to the plane of C15–C19 dienone linkage. This set of preferences coincides, in the case of **6**, with an *anti* relationship of the hydrogen atoms at C13 and C14. Such an *anti* preference of the corresponding hydrogens is



 © WILEY-VCH Verlag GmbH, D-69451 Weinheim, 2001 1433-7851/01/4023-4455 $ 17.50+.50/0



Scheme 5. Reagents and Conditions: a) Ac_2O, NEt_3, 25 °C, 2 h, 72 %; b) O_3, MeOH, −40 °C then Me_2S; c) $NaBH_4$, $CeCl_3 \cdot H_2O$, MeOH; d) Ac_2O, NEt_3, 25 °C, h, chiral-phase HPLC analysis.

seen in the one known X-ray crystal structure, currently available, of a *seco*-halichlorine.[4c] The synergy of these conformational preferences is suggested by the MM2 model depicted in Figure 1. In such a conformer, a strong preference for the delivery of the hydride from the pro-*R* face would be expected, and would lead to the observed product, pinnaic acid I (**19**).

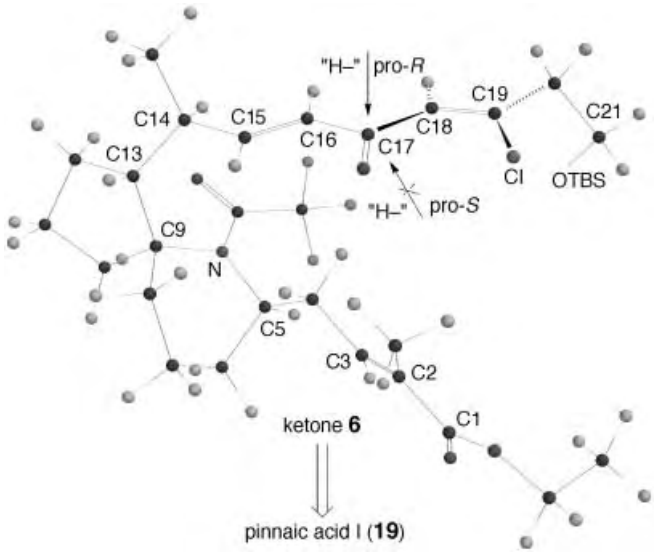


Figure 1. Calculated lowest energy conformer of ketone **6**. The calculations were performed with Macromodel V.6.5 (Monte Carlo simulation, MM2 force field).

By contrast, one (or more) of these preferences are not found in **11** (the C14 epimer of **6**). For instance, simple interchange of the methyl and H substituents at C14, leaving everything else intact, would create a potentially serious eclipsing interaction between the C14 methyl group and the C15–C16 double bond. Presumably, the point mutation at C14 in compound **11** brings with it a major conformational change in the C14–C19 moiety, in which the face preference for reduction of the C17 ketone is diminished. The concept that remote functional groups might profoundly influence a stereochemical outcome (such as face selectivity) by modulating the reacting (Curtin–Hammett[13]) conformer is a fascinating and little-probed aspect of stereochemical control.[14]

With the configurations of the pinnaic acids and halichlorine established by virtue of our synthesis program, we have a sound basis with which to evaluate their biological activity.[15]

Received: August 3, 2001 [Z17667]

[1] The synthesis of himastatin is a recent example in which total synthesis was used to determine the stereochemical assignment of a natural product: T. M. Kamenecka, S. J. Danishefsky, *Angew. Chem.* **1998**, *110*, 3166; *Angew. Chem. Int. Ed.* **1998**, *37*, 2995.
[2] T. Chou, M. Kuramoto, Y. Otani, M. Shikano, K. Yazawa, D. Uemura, *Tetrahedron Lett.* **1996**, *37*, 3871.
[3] a) M. Kuramato, C. Tong, K. Yamada, T. Chiba, Y. Hayashi, D. Uemura, *Tetrahedron Lett.* **1996**, *37*, 3867; b) H. Arimoto, I. Hayakawa, M. Kuramoto, D. Uemura, *Tetrahedron Lett.* **1998**, *39*, 861.
[4] a) D. Trauner, S. J. Danishefsky, *Tetrahedron Lett*. **1999**, *40*, 6513; b) D. Trauner, J. B. Schwartz, S. J. Danishefsky, *Angew. Chem.* **1999**, *111*, 3756; *Angew. Chem. Int. Ed.* **1999**, *38*, 3542; c) D. Trauner, S. J. Danishefsky, *Helv. Chim. Acta* **2000**, *83*, 2344.
[5] M. W. Carson, G. Kim, M. F. Hentemann, D. Trauner, S. J. Danishefsky, *Angew. Chem.* **2001**, *113*, *23*; *Angew. Chem. Int. Ed.* **2001**, *40*, 4450.
[6] S. P. Keen, S. M. Weinreb, *J. Org. Chem.* **1998**, *63*, 6739.
[7] Aldehyde **3** was recovered in good yield, even when excess reagent was used. It seems likely that the aldehyde function is co-opted during the reaction and recovered on workup. Several possible scenarios could be advanced to explain this phenomenon.
[8] a) S. Krishnamurthy, F. Vogel, H. C. Brown, *J. Org. Chem.* **1977**, *42*, 2534. For recent examples see: b) H.-C. Zhang, B. D. Harris, M. J. Costanzo, E. C. Lawson, C. A. Maryanoff, *J. Org. Chem.* **1998**, *63*, 7964; c) H.-C. Zhang, B. D. Harris, C. A. Maryanoff, B. E. Maryanoff, *Tetrahedron Lett.* **1996**, *37*, 7897; d) H.-C. Zhang, M. J. Costanzo, B. E. Maryanoff, *Tetrahedron Lett.* **1994**, *35*, 4891; e) G. L. Jeyaraj, W. R. Porter, *J. Heterocycl. Chem.* **1985**, *22*, 535.
[9] Inspection of the ^{1}H NMR spectra for pinnaic acid II and natural pinnaic acid revealed that the peaks in the ranges of 1.5–3.5 ppm (various azaspiro ring protons, as well as C20 and C21 side chain protons) and 5.6–5.8 ppm (C15, C16, and C18 vinyl protons) for pinnaic acid II display significantly different chemical shifts and couplings than the patterns displayed by natural pinnaic acid.
[10] We note that as a consequence of the *R* and *S* stereonomenclature systems, the priority rankings change at C14 in going from **3** and **4** to the various pinnaic acids.
[11] The C22 methyl ^{1}H NMR doublets in pinnaic acid III ($\delta = 1.13$, $J = 6.8$ Hz) and pinnaic IV ($\delta = 1.16$, $J = 6.8$ Hz) serve as diagnostic peaks and clearly show that neither pinnaic acid III nor pinnaic IV exist as natural pinnaic acid ($\delta = 1.08$, $J = 7.0$ Hz).
[12] We thank Professor Uemura for providing us with these compounds.
[13] a) F. A. Carey, R. J. Sunberg, *Advanced Organic Chemistry Part A: Structure and Mechanisms*, 3rd ed., Plenum, New York, **1990**, p. 215.
[14] For recent synthetic examples of remote stereochemical control from our group, see: a) D. Meng, S. J. Danishefsky, *Angew. Chem.* **1999**, *111*, 1582; *Angew. Chem. Int. Ed.* **1999**, *38*, 1485; b) D. Meng, Q. Tan, S. J. Danishefsky, *Angew Chem.* **1999**, *111*, 3393; *Angew Chem. Int. Ed.* **1999**, *38*, 3197; c) C. R. Harris, S. D. Kuduk, A. Balog, K. Savin, P. W. Glunz, S. J. Danishefsky, *J. Am. Chem. Soc.* **1999**, *121*, 7050.
[15] For a discussion of the biological background of these natural products and the proteins that they inhibit, see refs. [2–5], and references therein.

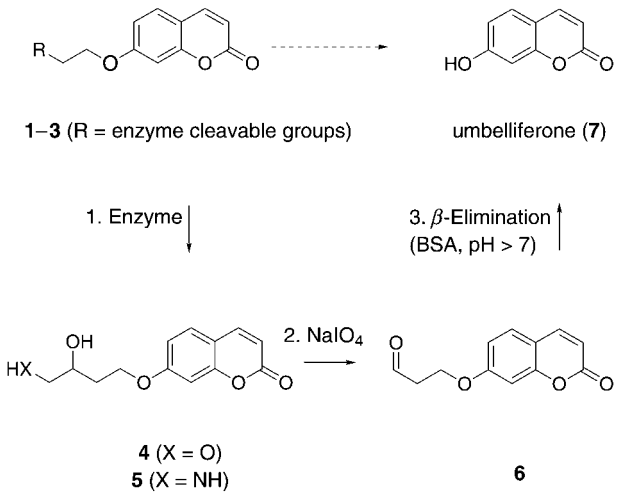
 © WILEY-VCH Verlag GmbH, D-69451 Weinheim, 2001 1433-7851/01/4023-4456 $ 17.50+.50/0

Enzyme Fingerprints by Fluorogenic and Chromogenic Substrate Arrays**

Denis Wahler, Fabrizio Badalassi, Paolo Crotti, and Jean-Louis Reymond*

Enzymes are finding numerous uses as mild, environmentally benign, and selective catalysts in a variety of settings, such as consumer products, diagnostics, laboratory kits, and in the production of fine chemicals.[1] This broad variety of uses is made possible by the tremendous diversity of enzymes available either from the biosphere or by in vitro evolution of known enzymes.[2] Besides enzyme discovery, the problem arises of being able to differentiate between similar enzymes—either to better identify interesting new enzymes or for quality control purposes. An enzyme sample can be checked for purity by electrophoresis and for identity by mass spectrometry.[3] Its actual catalytic function, however, can only be assessed by testing a proper chemical reaction for catalysis. While active-site-specific reagents have been used for cysteine proteases,[4] serine hydrolases,[5] or the proteasome,[6] the most convenient and direct method consists of measuring the reaction of a chromogenic or fluorogenic substrate,[7] sometimes in combination with an electrophoretic separation.[8] The information can be refined using several fluorogenic or chromogenic substrates simultaneously. Microorganisms can be unequivocally identified using a series of 19 chromogenic substrates known as the API ZYM system, in which each substrate reacts selectively with one type of enzyme.[9] Libraries of fluorogenic or chromogenic peptide substrates have been used to characterize the cleavage specificity of proteases.[10] Herein we report arrays of chromogenic and fluorogenic substrates tailored for hydrolytic enzymes, such as esterases, lipases, amidases, and epoxide hydrolases. These arrays allow closely related enzymes to be differentiated and relate to the enzyme's catalytic potential for hydrolyzing synthetically relevant functional groups in a variety of steric and stereochemical environments.

We recently reported a versatile fluorogenic assay for hydrolytic enzymes based on a new type of fluorogenic substrates, such as **1**–**3**.[11] Enzymic reactions on these substrates release a vicinal diol **4** or aminoalcohol **5** as a primary reaction product, which is then processed in situ to the strongly fluorescent product umbelliferone (**7**). The reaction proceeds via the intermediate aldehyde **6** following an oxidation/β-elimination sequence (Scheme 1).[12] Since the



Scheme 1. Principle of periodate-coupled fluorescence assay (see Scheme 2 for R groups).

enzyme-labile functional groups in these substrates are chemically nonactivated, their spontaneous hydrolysis rate is negligible in the absence of a specific catalyst. We reasoned that it might therefore be possible to reliably profile the specific activity of a given enzyme by using an array of such substrates without dealing with nonspecific effects. The general applicability of the oxidation/β-elimination scheme enabled us to readily obtain structural variations close to the reaction center of the substrates. We hoped that the identity of a given hydrolytic enzyme would reveal itself not only by its reaction with a particular functional group, but also by its selectivity pattern among a family of structurally diverse, but functionally related, substrates.

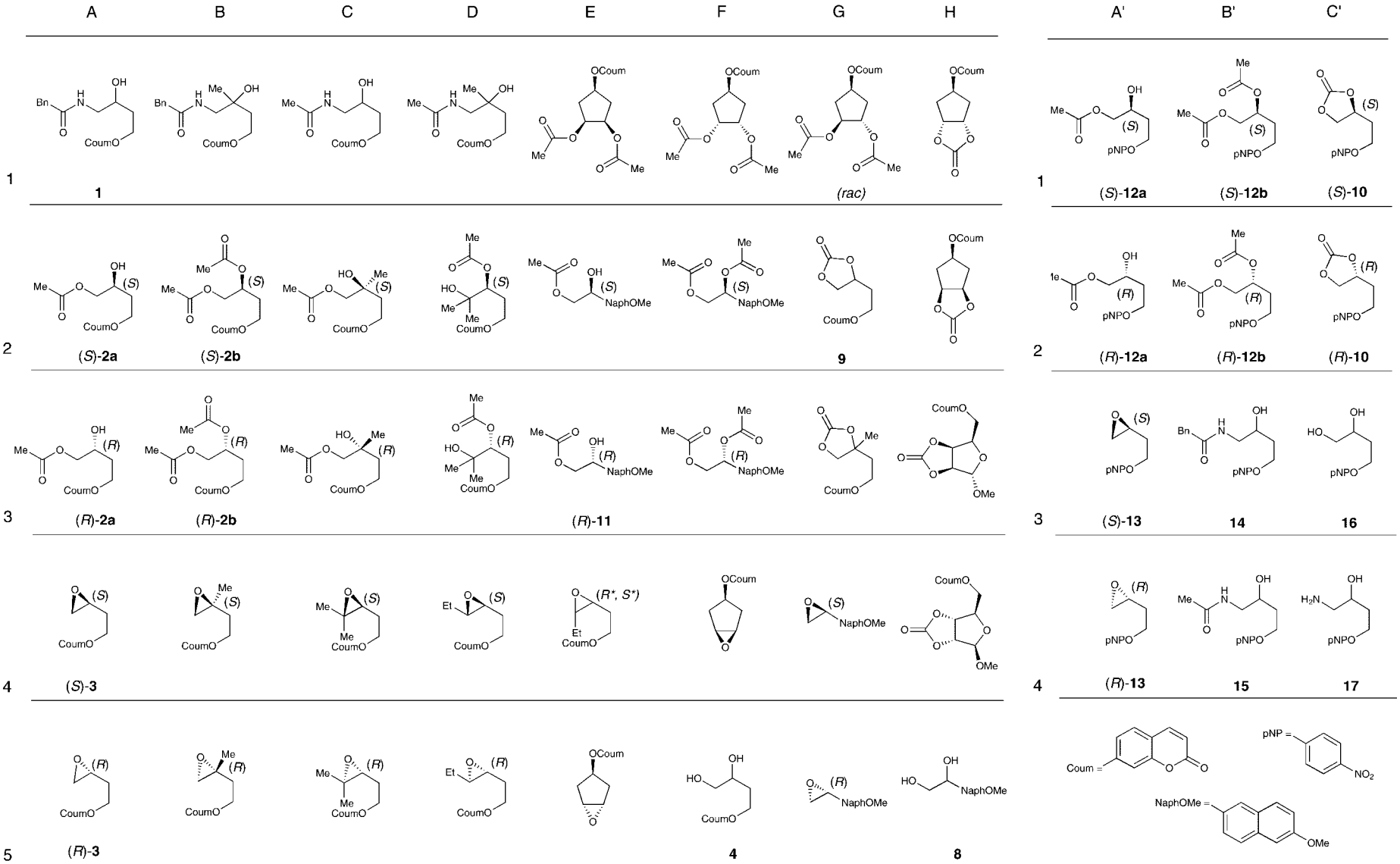
Various amides, epoxides, esters, and carbonates related to **1**–**3** were prepared as components of our substrate arrays. Such functional groups would react with the large family of hydrolase enzymes, many of which share an Asp-His-Ser[13] or Asp-His-Asp[14] catalytic triad. The substrates were assembled in arrays layed out in wells of microtiter plates (Scheme 2). Our fluorogenic substrate array consisted of 40 samples distributed as a 5×8 grid. This array also included substrates releasing fluorescent 6-methoxynaphthaldehyde by oxidation of diol **8** as the primary enzyme reaction product.[15] A chromogenic 4×3 array was prepared with analogues of some of the umbelliferone-derived substrates with *p*-nitrophenol as the chromogenic leaving group. Each array included two diol or aminoalcohol reaction products as positive controls.[16]

We used our arrays to measure a series of hydrolytic enzymes. Reactions were initiated by adding a prediluted solution of the enzyme in buffer containing $NaIO_4$ and bovine serum albumin (BSA) to each substrate stock solution. One array was measured without enzyme to provide the reference

[*] Prof. J.-L. Reymond, D. Wahler
Department of Chemistry & Biochemistry
University of Bern
Freiestrasse 3, 3012 Bern (Switzerland)
Fax: (+41) 31-631-80-57
E-mail: jean-louis.reymond@ioc.unibe.ch
F. Badalassi, Prof. P. Crotti
Dipartimento di Chimica Bioorganica e Biofarmacia
Università di Pisa, 56126 Pisa (Italy)

[**] We would like to thank Prof. R. Furstoss and Dr. A. Archelas at the Faculté des Sciences de Luminy, Marseille, France, for providing a sample of *Aspergillus niger* EH, and Dr. C. Weijers at the Department of Food Technology and Nutrition Sciences, Wageningen University, the Netherlands, for providing a sample of *Rhodotorula glutinis* EH. This work was supported by the University of Bern, the European COST program (Action D12), the Swiss Office Fédéral de l'Education et de la Science, Protéus SA (Nîmes, France), the Ministero della Università e della Ricerca Scientifica e Tecnologica (MURST), and Consiglio Nazionale delle Ricerche (CNR) (Roma). P.C. gratefully acknowledges Merck for generous financial support from a 2000 ADP Chemistry Award.

 © WILEY-VCH Verlag GmbH, D-69451 Weinheim, 2001 1433-7851/01/4023-4457 $ 17.50+.50/0



Scheme 2. Arrays of fluorogenic and chromogenic substrates for hydrolytic enzymes (for clarity, only the compounds cited directly in the text and figure have been numbered).

© WILEY-VCH Verlag GmbH, D-69451 Weinheim, 2001

1433-7851/01/4023-4458 $ 17.50+.50/0 *Angew. Chem. Int. Ed.* **2001**, *40*, No. 23

rates for the very slow spontaneous hydrolysis of the substrates (negative controls) and for the fast oxidation of reference products (positive controls). All reactions were followed over two hours by using the corresponding microtiter plate reader instrument. The recorded signals (Figure 1) were converted into product concentrations by using calibration curves, and the steepest linear portion of each reaction profile was used to calculate the apparent reaction rate in each well. For each enzyme array, the rates measured in the reference plate without enzyme were substracted from the apparent rates, and the resulting net rates plotted in gray-scale relative to the maximum net rate observed in the array, which was set as black. The gray-scale rendering allowed the reactivity pattern of each enzyme to be displayed in an easily identifiable, visual manner. A selection of representative fingerprints is shown in Figure 2.

The analysis for both the fluorogenic and the chromogenic substrate arrays results in activity patterns which clearly differentiate between the different enzymes tested (Figure 2). Enzyme classes, such as esterases and lipases, amidases, and epoxide hydrolases, stand out by their preferential reactivity with the corresponding substrates. Furthermore, the array analysis allows the differentiation between enzymes within one class, with each enzyme displaying a unique pattern. The preferential reactivity of *Rhizopus niveus* lipase with the carbonates **9** and (*S*)-**10**, and the apparent reactivity of elastase with acetate (*R*)-**11** are noteworthy.

The patterns observed are reproducible within less than 10% in the apparent reaction rate at the array positions. These patterns therefore may be considered as fingerprints for the enzyme samples. In each case the question arises as to whether the fingerprint reveals the catalytic action of a single enzyme or whether it combines activities stemming from enzyme impurities not related to the listed main component. In the present set, the fingerprint recorded with *Aspergillus niger* epoxide hydrolase (AEH) is probably enzyme specific since the sample, although not highly purified, only reacts with epoxide substrates, which is an unusual type of reactivity. By contrast, the chemoselectivity observed for lipases and esterases towards esters and carbonates should not be interpreted as a purity indicator because of the ubiquity of this reactivity type. In the general case, the fingerprints could well be specific to the particular preparation or even to a particular enzyme batch.

The substrate arrays shown here are small compared to the peptide libraries developed for proteases.[10] Nevertheless,

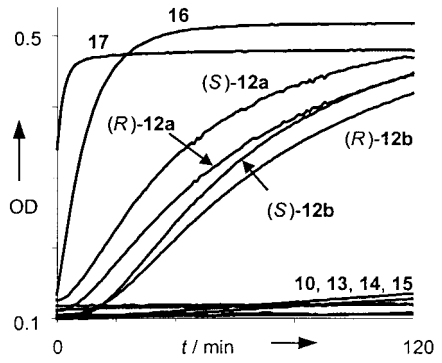


Figure 1. Time course of optical density (OD, at $\lambda = 405$ nm) observed for the reaction of *Pseudomonas fluorescens* lipase with the chromogenic substrate array. Conditions: 0.1 mg mL^{-1} enzyme, 100 μM substrate, 20 mM aq borate pH 8.8, 2.5% v/v DMF, 26 °C, 2 mg mL^{-1} BSA, 1 mM $NaIO_4$. The rates derived from these curves for the different substrates are: **17**: 209300 pM s^{-1}, **16**: 130800 pM s^{-1}, (*S*)-**12a**: 31800 pM s^{-1}, (*S*)-**12b**: 25500 pM s^{-1}, (*R*)-**12a**: 25000 pM s^{-1}, (*R*)-**12b**: 22000 pM s^{-1}, **15**: 4000 pM s^{-1}, (*R*)-**10**: 2600 pM s^{-1}, (*S*)-**10**: 2300 pM s^{-1}, **14**: 1600 pM s^{-1}, (*S*)-**13**: 1400 pM s^{-1}, (*R*)-**13**: 1300 pM s^{-1}. See text and Experimental Section for more information.

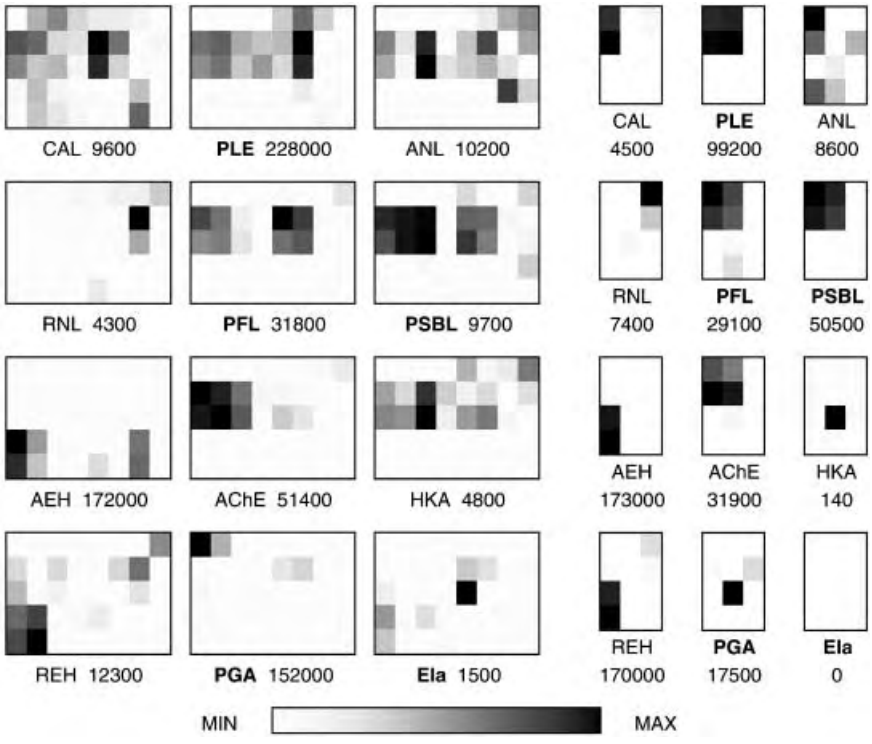


Figure 2. Enzyme fingerprints with fluorogenic and chromogenic substrate arrays. Below each array are given enzyme code and the apparent maximum rate in pM s^{-1}, which is set as black in each array. Enzymes marked in bold appear homogeneous (>90%) by sodium dodecyl sulfate–polyacrylamide gel electrophoresis (SDS-PAGE) analysis. Substrates are positioned as shown in Scheme 2. Conditions: 0.1 mg mL^{-1} enzyme, 100 μM substrate, 20 mM aq. borate pH 8.8 with 2.5% v/v DMF, 26 °C, 2 mg mL^{-1} BSA, 1 mM $NaIO_4$. See text for data treatment. Codes for enzymes: CAL = *Candida antarctica* lipase F62299, PLE = pig liver esterase F46058, ANL = *Aspergillus niger* lipase A39,043-7, RNL = *Rhizopus niveus* lipase F62310, PFL = *Pseudomonas fluorescens* lipase F62321, PSBL = *Pseudomonas* sp. type B lipoprotein lipase F62336, AEH = *Aspergillus niger* epoxide hydrolase, AChE = *Electrophorus electricus* acetylcholine esterase F01023, HKA = hog kidney acylase I F01821, REH = *Rhodotorula glutinis* epoxide hydrolase, PGA = *Escherichia coli* penicillin G acylase F76427, Ela = porcine pancreatic elastase Se20929. Suppliers: F = Fluka, A = Aldrich, Se = Serva. Fingerprints were recorded for a total of 45 different enzymes: 17 lipases, 4 lipoprotein lipases, 10 esterases, 12 amidases (proteases and acylases), and 2 epoxide hydrolases. The following enzymes did not show significant reactivity with any of the substrates: subtilisin, papain, trypsin, chymotrypsin, clostripain, and pepsin.

 © WILEY-VCH Verlag GmbH, D-69451 Weinheim, 2001 1433-7851/01/4023-4459 $ 17.50+.50/0

our arrays provide fingerprints that differentiate between closely related hydrolytic enzymes. In theory, the amount of information recorded in an array with only a few tens of data points should be sufficient to encode for thousands of different enzymes. The practical realization of a differentiating array depends mainly on the choice of the palette of substrates with which different enzymes react differently. The excellent differentiation observed here might depend on the fact that the structural variations between the different substrates are very close to their enzyme-reactive group.

The concept of enzyme fingerprinting as shown here should be quite general. Arrays could include substrates for other enzyme classes and should also be easily realizable using other high-throughput screening (HTS) assays,[7] provided that these produce simple photometric signals that can be recorded in a highly parallel manner, for example by pH[17] or pM[18] indicators. Fingerprint analyses with substrate arrays might prove useful in quality control, batch identification procedures, as well as in enzyme discovery programs by helping to point out novel enzymes with unusual reactivities.[19]

Experimental Section

Synthesis: All substrates and reference products were prepared by functionalization of the parent olefins starting either with epoxidation or with dihydroxylation. Optically pure compounds were obtained from diols prepared by using Sharpless asymmetric dihydroxylation as described before.[11] Substrates in array positions H3 and H4 were derived from D-lyxose and D-ribose, respectively. All new compounds gave satisfactory spectral data and elemental analysis or HR-MS data. Optical purities were checked by chiral-phase HPLC and had $>95\,\%$ *ee* values in all cases.

Measurements: Substrates and reference products were diluted from 2 mM stock solutions in 50 % aqueous *N*,*N*-dimethylformamide (DMF). These solutions were stored at $+4\,^{\circ}C$. Fluorogenic reactions were carried out in round-bottom polypropylene 96-well plates (Costar) and monitored using a Cytofluor II fluorescence plate reader (Perseptive Biosystems, filters $\lambda_{ex} = 360 \pm 20$, $\lambda_{em} = 460 \pm 20$ nm). Chromogenic reactions were carried out in half-area flat-bottom polystyrene 96-well cell culture plates (Costar) and monitored using a Spectramax 250 microplate spectrophotometer (Molecular Devices, $\lambda = 405$ nm). Each well of the array was filled with 5 μL of a substrate stock solution following the layout shown in Scheme 2. The reactions were initiated by adding 95 μL of a freshly prepared solution containing enzyme (0.1 mg mL^{-1}, weighed in from the supplied solid), BSA (2 mg mL^{-1}), and $NaIO_4$ (1 mM) in 20 mM aqueous borate at pH 8.8 to each well of the array. The reactions were recorded over a period of 2 h. See text and figure legend for data treatment.

Received: July 30, 2001 [Z17628]

[1] A. T. Bull, A. W. Bunch, G. K. Robinson, *Curr. Opin. Microbiol.* **1999**, *2*, 246 – 251.

[2] a) B. Marrs, S. Delagrave, D. Murphy, *Curr. Opin. Microbiol.* **1999**, *2*, 241 – 245; b) W. P. C. Stemmer, *Proc. Natl. Acad. Sci. USA* **1994**, *91*, 10747 – 10751; c) W. P. C. Stemmer, *Nature* **1994**, *370*, 389 – 391; d) L. You, F. H. Arnold, *Protein Eng.* **1996**, *9*, 77 – 83; e) M. T. Reetz, K.-E. Jaeger, *Chem. Eur. J.* **2000**, *6*, 407 – 412.

[3] a) S. P. Gygi, G. L. Corthals, Y. Zhang, Y. Rochon, R. Aebersold, *Proc. Natl. Acad. Sci. USA* **2000**, *97*, 9390 – 9395; b) K. H. Lee, *Trends Biotechnol.* **2001**, *19*, 217 – 222.

[4] a) K. Brocklehurst, D. Kowlessur, M. O'Driscoll, G. Patel, S. Quenby, E. Salih, W. Templeton, E. W. Thomas, F. Willenbrock, *Biochem. J.* **1987**, *244*, 173 – 181; b) M. Bogyo, S. Verhelst, V. Bellingard-Dubouchaud, S. Toba, D. Greenbaum, *Chem. Biol.* **2000**, *7*, 27 – 38; c) D. Greenbaum, K. F. Medzihradszky, A. Burlingame, M. Bogyo, *Chem. Biol.* **2000**, *7*, 569 – 581.

[5] a) Y. Liu, M. P. Patricelli, B. F. Cravatt, *Proc. Natl. Acad. Sci. USA* **1999**, *96*, 14694 – 14699; b) D. Kidd, Y. Liu, B. F. Cravatt, *Biochemistry* **2001**, *40*, 4005 – 4015.

[6] T. Nazif, M. Bogyo, *Proc. Natl. Acad. Sci. USA* **2001**, *98*, 2967 – 2972.

[7] a) M. T. Reetz, *Angew. Chem.* **2001**, *113*, 292 – 320; *Angew. Chem. Int. Ed.* **2001**, *40*, 284 – 310; b) D. Wahler, J.-L. Reymond, *Curr. Opin. Chem. Biol.* **2001**, *5*, 152 – 158; c) F. Beisson, A. Tiss, C. Rivière, R. Verger, *Eur. J. Lipid Sci. Technol.* **2000**, 133 – 153.

[8] a) M. S. Lantz, P. Ciborowski, *Methods Enzymol.* **1994**, *235*, 563 – 594; b) C. U. Hellen, *Methods Enzymol.* **1994**, *241*, 46 – 58; c) C. L. Barbieri, *Exp. Parasitol.* **1988**, *67*, 159 – 166.

[9] a) M. W. Humble, A. King, I. Phillips, *J. Clin. Pathol.* **1977**, *30*, 275 – 277; b) E. Gruner, A. Von Graevenitz, M. Altwegg, *J. Microbiol. Methods* **1992**, *16*, 101 – 118; c) P. Garcia-Martos, P. Marin, J. M. Hernandez-Molina, L. Garcia-Agudo, S. Aoufi, J. Mira, *Mycopathologia* **2001**, *150*, 1 – 4.

[10] a) K. Breddam, M. Meldal, *Eur. J. Biochem.* **1992**, *206*, 103 – 107; b) D. Lee, J. L. Adams, M. Brandt, W. E. DeWolf, Jr., P. M. Keller, M. A. Levy, *Bioorg. Med. Chem. Lett.* **1999**, *9*, 1667 – 1672; c) P. M. St. Hilaire, M. Willert, M. A. Juliano, L. Juliano, M. Meldal, *J. Comb. Chem.* **1999**, *1*, 509 – 523; d) J. E. Sheppeck II, H. Kar, L. Gosink, J. B. Wheatley, E. Gjerstad, S. M. Loftus, A. R. Zubiria, J. W. Janc, *Bioorg. Med. Chem. Lett.* **2000**, *10*, 2639 – 2642; e) B. J. Backes, J. L. Harris, F. Leonetti, C. S. Craik, J. A. Ellman, *Nature Biotechnol.* **2000**, *18*, 187 – 193; f) N. Dekker, R. C. Cox, A. Kramer, M. R. Egmond, *Biochemistry* **2001**, *40*, 1694 – 1701.

[11] F. Badalassi, D. Wahler, G. Klein, P. Crotti, J.-L. Reymond, *Angew. Chem.* **2000**, *112*, 4233 – 4236; *Angew. Chem. Int. Ed.* **2000**, *39*, 4067 – 4070.

[12] a) G. Klein, J.-L. Reymond, *Helv. Chim. Acta* **1999**, *82*, 400 – 407; b) R. Pérez Carlòn, N. Jourdain, J.-L. Reymond, *Chem. Eur. J.* **2000**, *6*, 4154 – 4162.

[13] a) C. W. Wharton in *Comprehensive Biological Catalysis*, *Vol. I* (Ed.: M. Sinnott), Academic Press, London, **1998**, pp. 345 – 380; b) D. M. Quinn, S. R. Feaster in *Comprehensive Biological Catalysis*, *Vol. I* (Ed.: M. Sinnott), Academic Press, London, **1998**, pp. 455 – 482.

[14] A. Archelas, R. Furstoss, *Curr. Opin. Chem. Biol.* **2001**, *5*, 112 – 119.

[15] a) B. L. Vallee, US Patent 5162203, **1992** [*Chem. Abstr.* **1993**, *118*, 55103w]; b) B. List, C. F. Barbas, R. A. Lerner, *Proc. Natl. Acad. Sci. USA* **1998**, *95*, 15351 – 15355.

[16] The alcohols and aminoalcohols that are the primary enzyme reaction products were found to release their colored or fluorescent product rapidly ($t_{1/2} < 15$ min) in aqueous buffer in the presence of sodium periodate and bovine serum albumin. Only the D-lyxose- and D-ribose-derived diols, which are released by substrates in positions H3 and H4, respectively, have an unusually slow rate of fluorescence release as a result of the resistance of the intermediate aldehyde to β-elimination ($t_{1/2} > 2$ h). The signal is nevertheless still strong enough in these cases to give good data points.

[17] a) L. E. Janes, R. J. Kazlauskas, *J. Org. Chem.* **1997**, *62*, 4560 – 4561; b) L. E. Janes, A. C. Löwendahl, R. J. Kazlauskas, *Chem. Eur. J.* **1998**, *4*, 2324 – 2331.

[18] G. Klein, J.-L. Reymond, *Angew. Chem.* **2001**, *113*, 1821 – 1823; *Angew. Chem. Int. Ed.* **2001**, *40*, 1771 – 1773.

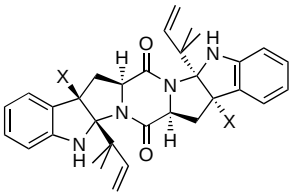
[19] Reactivity with a particular substrate can be assayed reliably when testing individual substrates separately as shown here in the arrays. Chemo-, enantio-, or stereoselectivity, by contrast, might be masked if a crude enzyme extract containing several enzymes with complementary selectivites is tested. Nevertheless, many well-known enzyme mixtures give useful selective transformations, for example, pig liver esterase; see C.-H. Wong, G. M. Whitesides, *Enzymes in Synthetic Organic Chemistry*, Pergamon, Elnsford, NY, **1994**, pp. 66 – 68.

 © WILEY-VCH Verlag GmbH, D-69451 Weinheim, 2001 1433-7851/01/4023-4460 $ 17.50+.50/0

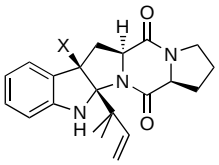
Synthesis of Fluorogypsetin and Fluorobrevianamide E by a Novel Fluorination – Cyclization of *cyclo*-L-Trp-L-AAs**

Norio Shibata,* Takanao Tarui, Yasuhiro Doi, and Kenneth L. Kirk

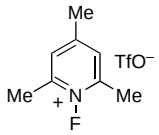
The design of metabolically stable analogues of natural products that have comparable or enhanced biological activity relative to the parent compounds is an important area of research in medicinal chemistry. The incorporation of fluorine atoms into a molecule to inhibit metabolism and/or to alter physicochemical and physiological properties continues to be an important strategy in this research.[1] The replacement of a hydroxyl group by fluorine represents an important and general part of this strategy,[1] and it results in analogues that are often regarded as isosteres of the parent molecules.[2] Thus, the electronegativity and van der Waals radius of fluorine are 4.0 and 1.47 Å, respectively, values that are similar to those of oxygen (3.5 and 1.52 Å).[1, 3a] The C_{sp^3}–F bond of 1.40 Å is slightly shorter than the C_{sp^3}–OH bond (1.43 Å).[3b] Although there are many examples of the effective use of selective fluorination to produce valuable biochemical tools and medicinal agents,[1, 4] examples of fluorine-containing molecules in which a fluorine atom is bound to an asymmetric center are rather limited.[5] In fact, despite the considerable recent progress[6, 7] that has been made in the development of procedures for the enantioselective introduction of fluorine into simple carbonyl compounds, there is concern that application of these procedures to more complex molecules may have serious limitations. Catalytic asymmetric fluorination procedures developed by Hintermann and Togni based on catalysis by chiral Lewis acids,[6d] and by us based on cinchona alkaloids,[7] are new tools to approach this problem. As a part of our research into the development of new methods for the preparation of fluorine-containing biologically active compounds,[7, 8] we have developed a fluorination – cyclization reaction that provides a simple method for the selective introduction of fluorine into complex molecules. To illustrate the utility of this procedure, we report here on the synthesis of fluorogypsetin (**1b**) and fluorobrevianamide E (**2b**) by FP-T300-mediated fluorination – cyclization.



gypsetin (**1a**); X=OH
fluorogypsetin (**1b**); X=F



brevianamide E (**2a**); X=OH
fluorobrevianamide E (**2b**); X=F



FP-T300

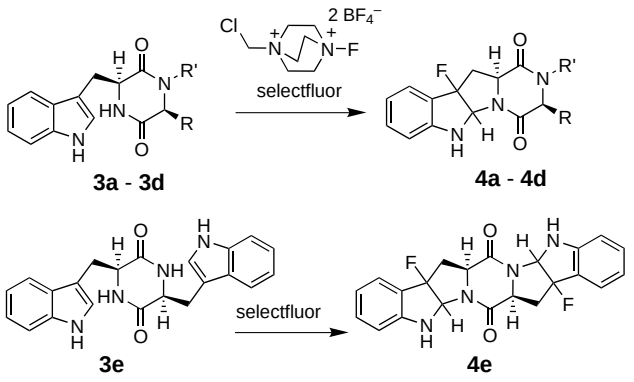
The hexahydropyrazino[1′,2′-1,5]pyrrolo[2,3-*b*]indole-1,4-dione moiety is present in a wide range of natural products. Examples are gypsetin (**1a**),[9] brevianamide E (**2a**),[10] and sporidesmins,[11a,b] compounds that have attracted considerable attention due to their molecular complexity and potent biological activity. A similar structural unit also occurs in himastatin,[11c] fumiquinazoline A,[11d] and asperlicin.[11e,f] Gypsetin (**1a**), a promising competitive inhibitor of acyl-CoA:cholesterol acyltransferase, has evoked particular interest as an important lead in drug discovery. After Danishefsky et al. disclosed the first total synthesis of **1a**,[9c,d] we focused on **1b**, an isostere of **1a**, as an attractive synthetic target. We also became interested in the synthesis of the structurally related **2b**. Since the hydroxyl group of **2a**[10] plays an important role in the biosynthesis of brevianamides,[12] **2b** could serve as a useful probe to gain information about biosynthetic processes of the brevianamide family, in addition to having potentially interesting biological activity. Earlier, we reported the selectfluor-mediated oxidative fluorination of indoles to furnish 3-fluorooxindoles.[8a] Since electrophilic attack of fluorine at the 3-position of the indole ring appears to facilitate nucleophilic addition at the 2-position, we reasoned that a suitably positioned internal nucleophile could attack the 3-position to give a cyclized product. To explore this possibility, we initially investigated the reaction of selectfluor with *cyclo*-L-Trp-L-AAs (**3a**–**d**; Trp = tryptophan, AA = amino acid) as a method to produce fluorohexahydropyrazino[1′,2′-1,5]pyrrolo[2,3-*b*]indole-1,4-diones **4** by fluorination – cyclization (Scheme 1, Table 1).

Investigation of the reaction conditions for the selectfluor-mediated cyclization of *cyclo*-L-Trp-L-Ala (**3a**; Ala = alanine) revealed that the choice of solvent is critical. Performing the reaction in MeCN gave a complex mixture (entry 1). The reason for this poor result seemed to be the low solubility of substrate **3a** in MeCN. Therefore, the addition of co-solvents was investigated. The reaction of **3a** in MeCN/DMSO (1/1) gave a 44% yield of fluorinated compound **4a**; addition of THF instead of DMSO gave a similar result (entries 2 and 3). Fluoropyrazinopyrroloindole **4a** was obtained as a 1/1 mix-

[*] Dr. N. Shibata, T. Tarui, Y. Doi
Faculty of Pharmaceutical Sciences
Toyama Medical and Pharmaceutical University
Sugitani 2630, Toyama 930-0194 (Japan)
Fax: (+81) 76-434-4656
E-mail: nozshiba@ms.toyama-mpu.ac.jp
Dr. K. L. Kirk
Laboratory of Bioorganic Chemistry
National Institute of Diabetes and Digestive and Kidney Diseases
National Institutes of Health, Bethesda, MD 20892 (USA)

[**] This work was supported by a Grant-in-Aid for Scientific Research from the Ministry of Education, Science, Sports and Culture, Japan. N.S. wishes to thank the Novartis Foundation (Japan) for the Promotion of Science for support. We thank Prof. Yoshio Takeuchi very much for generously sharing his facilities, for very kind encouragement and for giving us the opportunity to study in the field of fluorine chemistry. We also thank F-TECH INC. for a gift of FP-T300.

Supporting information for this article is available on the WWW under http://www.angewandte.com or from the author.



a: R=Me, R'=H; **b**: R=*i*Pr, R'=H; **c**: R=Bn, R'=H;
d: R=R'=$CH_2CH_2CH_2$

Scheme 1. Conversion of *cyclo*-L-Trp-L-AAs **3** into fluorohexahydropyrazino[1′,2′-1,5]pyrrolo[2,3-*b*]indole-1,4-diones **4**. For details see Table 1.

Table 1. Fluorination–cyclization of compounds **3** with selectfluor (Scheme 1).[a]

Entry	Substrate **3**	Solvent	Product **4**	Yield [%]
1	**3a**	MeCN	**4a**	–
2	**3a**	MeCN/DMSO (1/1)	**4a**	44
3	**3a**	MeCN/THF (1/1)	**4a**	48
4	**3b**	MeCN/DMSO (1/1)	**4b**	29
5	**3b**	MeCN/THF (1/1)	**4b**	40
6	**3c**	MeCN/DMSO (1/1)	**4c**	34
7	**3c**	MeCN/THF (1/1)	**4c**	42
8	**3d**	MeCN/THF (1/1)	**4d**	27
9	**3e**	MeCN/THF (1/1)	**4e**	44

[a] The reactions were performed at −40 °C for several hours. The products **4** are mixtures of *syn* and *anti* isomers (1/1), with the exception of **4e**, which is a mixture of three isomers (*syn*,*anti*/*syn*,*syn*/*anti*,*anti* = 2/1/1).[13]

ture of diastereomers in which the fluorine atom is *syn* and *anti* with respect to the proton corresponding to the α-position of L-Trp.[13] To demonstrate the generality of the fluorination–cyclization, we extended the procedure to other *cyclo*-L-Trp-L-AAs **3b**–**e**, including *cyclo*-L-Trp-L-Pro (**3d**; Pro = proline) and *cyclo*-L-Trp-L-Trp (**3e**) (Table 1). In all cases, conversion to **4** proceeded in modest yield. Interestingly, **3e** was converted to the corresponding heptacyclic product **4e** with an efficiency comparable to those of the other reactions, despite the requirement for a crucial double fluorination–cyclization (entry 9). Although an attempted halogenation–cyclization of a *cyclo*-Trp-Ala derivative mediated by *tert*-butyl hypochlorite has been reported,[14] as far as we know, this is the first example of fluorination–cyclization of tryptophan derivatives.

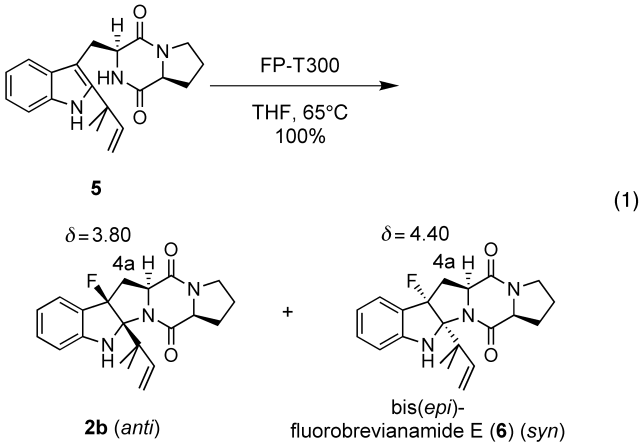
At this point we were gratified that we had succeeded in the first construction of fluoropyrazinopyrroloindoles **4** using a new selectfluor-mediated fluorination–cyclization reaction. However, the yields did not meet our requirements for our planned syntheses of the more challenging molecules **1b** and **2b**. The bulky "reverse-prenyl" substituents present in **1b** and **2b** could present additional problems during the cyclization and thus result in a further decrease in yield. Accordingly, before proceeding with the more challenging syntheses, we conducted a survey of additional electrophilic fluorinating agents. We found that the fluoropyridinium salt FP-T300 was very effective in this process, and produced **4** in good to high yields (Table 2). In the best case, **4b** was formed in 88% yield.

Table 2. Fluorination–cyclization with FP-T300.[a]

Entry	Substrate **3**	Product **4**	Yield [%]
1	**3a**	**4a**	67
2	**3b**	**4b**	88
3	**3c**	**4c**	74
4	**3d**	**4d**	71
5	**3e**	**4e**	74

[a] All reactions were carried out in MeCN at 65 °C for several hours. The products **4** are mixtures of *syn* and *anti* isomers (1/1) except for **4e** (*syn*,*anti*/*syn*,*syn*/*anti*,*anti* = 2/1/1).[13]

Having established the validity of our approach, we now focused on the syntheses of **1b** and **2b**. Under the optimized conditions given above, treatment of reverse-prenylated *cyclo*-L-Trp-L-Pro (**5**), available by total synthesis,[9d] with 1.5 equiv of FP-T300 in THF at 65 °C [Eq. (1)] led to complete



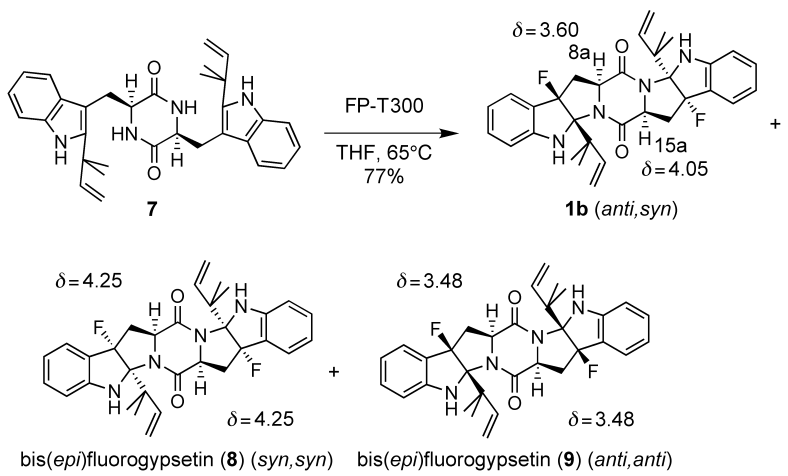
(1)

conversion to give **2b** as a 1:1.6 mixture with the fluorinated bis(*epi*)brevianamide E (**6**). The configuration of each compound was easily determined from the ^{1}H NMR chemical shift of H-4a. Because of the high electronegativity of the *syn*-fluoro substituent, the signal for H-4a of **6** appears at a lower field than that of H-4a of the *anti* isomer **2b** [see Eq. (1)]. This phenomenon is well documented in stereochemical studies on **2a** and its bis-*epi* isomer. In this case the *syn*-proton is similarly deshielded by the *syn*-hydroxyl group.[10c]

On treatment with 3.0 equiv of FP-T300, reverse-prenylated *cyclo*-L-Trp-L-Trp (**7**)[9d] also underwent efficient fluorination–cyclization to give fluorogypsetin (**1b**) and the two bis(*epi*)fluorogypsetins, *syn*,*syn* isomer **8** and *anti*,*anti* isomer **9** (**1b**:**8**:**9** = 2:1:1). Since the *anti*,*syn* isomer is identical to the *syn*,*anti* isomer, the apparent predominant formation of **1b** actually reflects nonselective electrophilic attack of the fluorinating agent from either side of the indole ring with concomitant *trans* addition of nitrogen. Similar to the effects seen with the fluorinated bis(*epi*)brevianamides E, deshielding due to the *syn*-fluorine atom induces a downfield shift of H-15a relative to H-8a. Thus, the ^{1}H NMR chemical shifts of H-8a and H-15a of **1b** were observed at $\delta = 3.60$ and 4.05, respectively [Eq. (2)].

In conclusion, we have developed a general method for the construction of novel fluorohexahydropyrazino[1′,2′-1,5]pyr-

 © WILEY-VCH Verlag GmbH, D-69451 Weinheim, 2001 1433-7851/01/4023-4462 $ 17.50+.50/0 *Angew. Chem. Int. Ed.* **2001**, *40*, No. 23



(2)

rolo[2,3-*b*]indole-1,4-diones based on an electrophilic fluorination–cyclization sequence. We have demonstrated the utility of this procedure by the efficient syntheses of **1b** and **2b**. The biological activities of these alkaloid isosteres will be evaluated and reported subsequently. In addition, we plan to extend application of this new methodology to the synthesis of fluorinated analogues of other indole alkaloids, including himastatin and asperlicin.

Received: June 28, 2001 [Z17385]

[1] a) *Biomedical Aspects of Fluorine Chemistry* (Eds.: R. Filler, Y. Kobayashi), Kodansha/Elsevier Biomedical, Tokyo, **1982**; b) "Biomedical Frontiers of Fluorine Chemistry": *ACS Symp. Ser.* **1996**, *639*; c) *Fusso & Yakugaku* (Eds.: Y. Kobayashi, I. Kumadaki, T. Taguchi), Hirokawa, Tokyo, **1992**; d) J. T. Welch, *Tetrahedron* **1987**, *43*, 3123–3197.

[2] B. E. Smart in *Organofluorine Chemistry: Principles and Commercial Applications* (Eds.: R. E. Banks, B. E. Smart, J. C. Tatlow), Plenum, New York, **1994**, chap. 3, pp. 57–88.

[3] a) A. Bondi, *J. Phys. Chem.* **1964**, *68*, 441–451; b) F. H. Allen, O. Kennard, D. G. Watson, L. Brammer, A. G. Orpen, R. Taylor in *International Tables for Crystallography*, *Vol. C* (Ed.: A. J. C. Wilson), Kluwer, Dordrecht, **1995**, pp. 653–844.

[4] Recent examples: a) J. Lin, P. J. Toscano, J. T. Welch, *Proc. Natl. Acad. Sci. USA* **1998**, *95*, 14020–14024; b) T. Nakano, M. Makino, Y. Morizawa, Y. Matsumura, *Angew. Chem.* **1996**, *108*, 1082–1084; *Angew. Chem. Int. Ed. Engl.* **1996**, *35*, 1019–1021.

[5] J. Fried, E. F. Sabo, *J. Am. Chem. Soc.* **1954**, *76*, 1455–1456; b) D. S. VanViliet, Y. Tachibana, K. F. Bastow, E. Huang, K. Lee, *J. Med. Chem.* **2001**, *44*, 1422–1428.

[6] a) F. A. Davis, H. Qi, G. Sundarababu in *Enantiocontrolled Synthesis of Fluoro-organic Compounds* (Ed.: V. A. Soloshonok), Wiley, Chichester, **1999**, pp. 1–32; b) *Enantiocontrolled Synthesis of Fluoro-organic Compounds* (Ed.: V. A. Soloshonok), Wiley, Chichester, **1999**; c) D. Cahard, C. Audouard, J.-C. Plaquevent, N. Roques, *Org. Lett.* **2000**, *2*, 3699–3701; d) L. Hintermann, A. Togni, *Angew. Chem.* **2000**, *112*, 4530–4533; *Angew. Chem. Int. Ed.* **2000**, *39*, 4359–4362.

[7] a) N. Shibata, E. Suzuki, T. Asahi, M. Shiro, *J. Am. Chem. Soc.* **2001**, *123*, 7001–7009; b) N. Shibata, E. Suzuki, Y. Takeuchi, *J. Am. Chem. Soc.* **2000**, *122*, 10728–10729.

[8] a) Y. Takeuchi, T. Tarui, N. Shibata, *Org. Lett.* **2000**, *2*, 639–642; b) Y. Takeuchi, T. Shiragami, K. Kimura, E. Suzuki, N. Shibata, *Org. Lett.* **1999**, *1*, 1571–1573.

[9] Isolation: a) C. Shinohara, K. Hasumi, Y. Takei, A. Endo, *J. Antibiot.* **1994**, *47*, 163–167; b) B. Nuber, F. Hansske, C. Shinohara, S. Miura, K. Hasumi, A. Endo, *J. Antibiot.* **1994**, *47*, 168–172; synthesis: c) J. M. Schkeryantz, J. C. G. Woo, S. J. Danishefsky, *J. Am. Chem. Soc.* **1995**, *117*, 7025–7026; d) J. M. Schkeryantz, J. C. G. Woo, P. Siliphaivanh, K. M. Depew, S. J. Danishefsky, *J. Am. Chem. Soc.* **1999**, *121*, 11964–11975.

[10] Isolation: a) A. J. Birch, J. J. Wright, *J. Chem. Soc. Chem. Commun.* **1969**, 644–645; synthesis: b) T. Kametani, N. Kanaya, M. Ihara, *J. Am. Chem. Soc.* **1980**, *102*, 3974–3975; c) T. Kametani, N. Kanaya, M. Ihara, *J. Chem. Soc. Perkin Trans. 1* **1981**, 959–963; d) J. F. Sanz-Cervera, T. Glinka, R. M. Williams, *Tetrahedron* **1993**, *49*, 8471–8482.

[11] Synthesis: a) Y. Kishi, S. Nakatsuka, T. Fukuyama, M. Havel, *J. Am. Chem. Soc.* **1973**, *95*, 6493–6495; b) R. Plate, M. A. J. Akkerman, H. C. J. Ottenheijm, *J. Chem. Soc. Perkin Trans. 1* **1987**, 2481–2490; c) T. M. Kamenecka, S. J. Danishefsky, *Angew. Chem.* **1998**, *110*, 3164–3166; *Angew. Chem. Int. Ed.* **1998**, *37*, 2993–2995; d) T. M. Kamenecka, S. J. Danishefsky, *Angew. Chem.* **1998**, *110*, 3166–3168; *Angew. Chem. Int. Ed.* **1998**, *37*, 2995–2998; e) B. B. Snider, H. Zeng, *Org. Lett.* **2000**, *2*, 4103–4106; f) F. He, B. M. Foxman, B. B. Snider, *J. Am. Chem. Soc.* **1998**, *120*, 6417–6418.

[12] For examples see: a) E. M. Stocking, R. M. Williams, J. F. Sanz-Cervera, *J. Am. Chem. Soc.* **2000**, *122*, 9089–9098; b) J. F. Sanz-Cervera, T. Glinka, R. M. Williams, *J. Am. Chem. Soc.* **1993**, *115*, 347–348.

[13] For details of the determination of the stereochemistry of **4**, see Supporting Information.

[14] A chlorinated compound proposed as an intermediate underwent rapid dehydrochlorination to give a pyrrolo[2,3-*b*]indole derivative. M. Ohno, T. F. Spande, B. Witkop, *J. Am. Chem. Soc.* **1970**, *92*, 343–348.

The First Alkaline Earth Metal Complex Containing a μ-η^1:η^1 Allyl Ligand: Structure of $[\{HC[C(tBu)NC_6H_3(CHMe_2)_2]_2Mg(C_3H_5)\}_6]$**

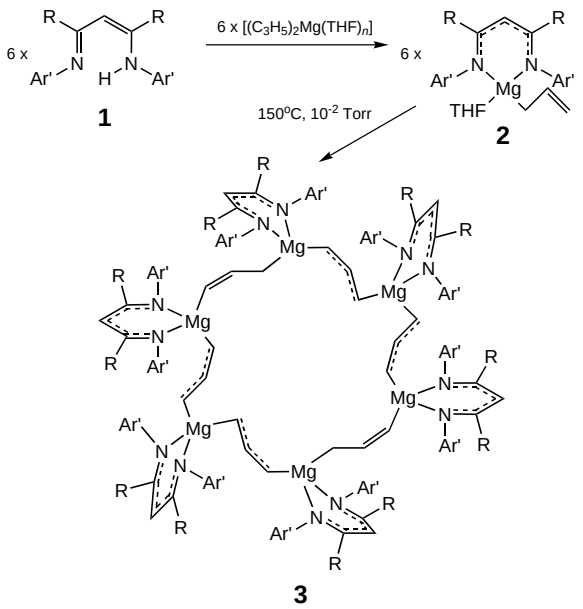
Philip J. Bailey,* Stephen T. Liddle,*
Carole A. Morrison, and Simon Parsons

Recent times have witnessed a surge of interest in the use of β-diketiminates[1] as ancillary ligands in transition metal[2] and main group[3] coordination chemistry. The flexible steric and electronic properties of β-diketiminate ligands, such as **1** (see Scheme 1), make them ideal candidates for the synthesis of well-defined magnesium monoalkyl [(L-X)-Mg-R] complexes; an area that has been recently highlighted as relatively undeveloped,[4] and one which we,[3d, 3g] and others,[3i] have been addressing. Given that there is precedent for the oligomerization and polymerization of ethene by diakylmag-

[*] Dr. P. J. Bailey, Dr. S. T. Liddle, Dr. C. A. Morrison, Dr. S. Parsons
Department of Chemistry
University of Edinburgh
West Mains Road, Edinburgh, EH9 3JJ (UK)
Fax: (+44) 131-6504743
E-mail: Philip.Bailey@ed.ac.uk

[**] The financial support of the UK EPSRC (S.T.L., S.P.) and The Royal Society (C.A.M.) is gratefully acknowledged.

Supporting information for this article is available on the WWW under http://www.angewandte.com or from the author.



Scheme 1. Synthesis of **2** and **3**. Ar′ = 2,6-diisopropylphenyl, R = *t*Bu.

nesium compounds,[5] we have embarked upon a study of well-defined magnesium monoalkyl compounds with β-diketiminate ancillary ligands as potential catalytic agents. As part of this study we have investigated allyl complexes in the hope that they might protect a vacant coordination site without preventing reaction with ethene. A further incentive for this avenue of work is that, outside of transition metal coordination chemistry, there is a dearth of allyl complexes. Indeed, there are relatively few structurally characterized p-block metal allyl compounds,[6] and only a handful of Group I[7] and Group II[8] complexes. Herein we report the synthesis and characterization of the mono-THF solvated β-diketiminate magnesium allyl complex **2** , and its solvent-free form **3**, which adopts a remarkable cyclic hexanuclear structure, in which the allyl ligand adopts a μ-η^1:η^1 coordination mode that is unprecedented for alkaline-earth metal chemistry (Scheme 1).

$[HC\{C(t\text{Bu})NAr'\}_2Mg(C_3H_5)(thf)]$ **2**

$[\{HC[C(t\text{Bu})NAr']_2Mg(C_3H_5)\}_6]$ **3**

Treatment of **1** with one equivalent of $[(C_3H_5)_2Mg(THF)_n]$ in toluene gave a yellow solution (Scheme 1). Upon standing at 5 °C overnight crystals formed, which were identified as **2** by NMR spectroscopy. A single-crystal X-ray structure analysis[9] of these crystals confirmed that **2** is a monomeric species in which the allyl ligand is bound to the four-coordinate magnesium center in a η^1 mode; a chelating β-diketiminate ligand and a molecule of THF complete the coordination sphere of the magnesium atom.

Thermal treatment of **2** (150 °C, 10^{-2} Torr) resulted in an orange oil (Scheme 1). Storage of a concentrated solution of this oil in toluene at −30 °C over three days gave crystals of **3**, which were shown by NMR spectroscopy to be free of THF. Although the best crystals of **3** that could be obtained diffracted only weakly, the essential features of the complex were determined unambiguously by an X-ray structure analysis,[10] which revealed that **3** is a hexanuclear cyclic species, in which magnesium centers are linked by *trans* μ-η^1:η^1 allyl groups. A chelating β-diketiminate ligand completes the coordination sphere of each magnesium center (Figure 1). Within transition metal coordination chemistry η^3 and η^1 coordination by allyl dominates. Although a relatively small number of complexes displaying *cis* μ-η^1:η^1 coordination are known,[11] there are very few examples of *trans* μ-η^1:η^1 coordination known for allyl.[12] Within main group chemistry there is only one example of *trans* μ-η^1:η^1 coordination, namely the tetramethylethylenediamine (TMEDA) solvate of allyllithium.[7e] Hence the coordination mode of allyl in **3** is, to the best of our knowledge, unprecedented in alkaline earth metal chemistry. The observed N-Mg-N chelate bite angles range between 95.4(2) and 97.2(2)°; a modest increase from

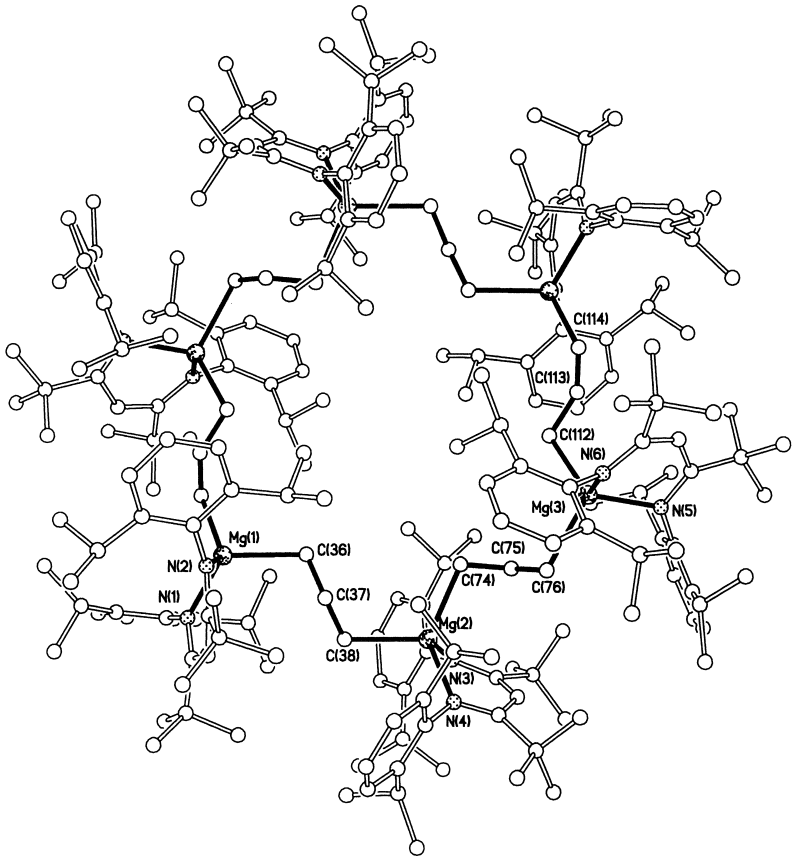


Figure 1. Crystal structure of **3;** hydrogen atoms are omitted for clarity. Only symmetry unique atoms are labeled. Selected bond lengths [Å] and angles [°]: Mg(1)-N(1) 2.056(5), Mg(1)-N(2) 2.067(5), Mg(1)-C(36) 2.327(5), Mg(1)-C(114) 2.328(16), Mg(2)-N(3) 2.039(5), Mg(2)-N(4) 2.075(4), Mg(2)-C(38) 2.290(5), Mg(2)-C(74) 2.308(6), Mg(3)-N(5) 2.058(5), Mg(3)-N(6) 2.048(5), Mg(3)-C(76) 2.304(5), Mg(3)-C(112) 2.252(6); Mg(1)-C(36)-C(37) 106.0(4), Mg(1)-C(114)-C(113) 111.5(10), Mg(2)-C(38)-C(37) 111.7(4), Mg(2)-C(74)-C(75) 107.6(4), Mg(3)-C(76)-C(75) 108.9(4), Mg(3)-C(112)-C(113) 109.4(4).

 © WILEY-VCH Verlag GmbH, D-69451 Weinheim, 2001 1433-7851/01/4023-4464 $ 17.50+.50/0 *Angew. Chem. Int. Ed.* **2001**, *40*, No. 23

that observed in **2**.[9] The substitution of THF by additional allyl coordination results in angles at each magnesium center close to the tetrahedral ideal. The six-membered chelate rings adopt a distorted cyclohexane boat conformation in which the magnesium atom and central backbone carbon atoms deviate by mean distances of 0.3377 and 0.2488 Å, respectively, from the mean plane of the ring. The observed Mg–N bond lengths (mean 2.057(5) Å) are unremarkable and the Mg–C bonds range between 2.214(12) and 2.327(5) Å; these are correspondingly longer bonds than reported for the TMEDA solvate of allylmagnesium chloride (Mg–C bond length of 2.1793(3) Å),[8] the only other structurally reported allylmagnesium species, in which the allyl group bonds in an η^1 mode. Inspection of the allyl C–C bond lengths reveals that four of the six allyl groups are present as resonance-delocalized ligands with essentially identical C–C bond lengths (mean 1.396(7) Å), whereas the other two exhibit more localized long and short C–C bonds (C(112)–C(113) 1.4145(8), C(113)–C(114) 1.2901(11) Å). However, irrespective of internal allyl C–C bond lengths, the Mg-C-C bond angles span a narrow range (107.6(4) – 111.7(4)°) close to the tetrahedral ideal. The allyl groups in **3** could be regarded as β-carbocations in which a negative charge is localized on each sp^2-hybridized CH_2 group. Although the Mg-C-C bond angles suggest sp^3 hybridization of the CH_2 groups, the requirement for conjugative stabilization of the carbocationic β-carbon atom would preclude such an arrangement, and we rationalize the electronic structure on the basis of sp^2 hybridization with distorted coordination caused by the steric demands of the β-diketiminate ligand.[13] Despite the structural data, NMR spectroscopic experiments at room temperature reveal that all allyl ligands are equivalent for **3**, with CH_2 hydrogen atoms appearing as a doublet at $\delta = 2.37$ and the β-CH hydrogen atom as a quintet at $\delta = 5.44$. The differences between the allyl ligands found in the solid state as outlined above must therefore be attributed to solid-state effects, and this is supported by preliminary density functional theory (DFT) calculations on a model system which show equivalent C–C bond lengths.[13]

Our aim in undertaking this work was to induce η^3 coordination of allyl groups to magnesium centers to protect the fourth coordination site by weak β-intramolecular ligation. However, the reluctance of magnesium to partake in π bonding results in an unusual μ-η^1:η^1 coordination mode in which the Mg–C bonding may be regarded as effectively σ in nature.

Experimental Section

2: Diallylmagnesium (0.23 g, 5.0 mmol) in THF (3.5 mL) was added dropwise to a solution of **1** in toluene (30 mL) at room temperature and was stirred for 2 h. The solution was filtered and concentrated to about 10 mL. Storage of the solution at 5 °C overnight gave **2** as colorless blocks in 44% yield. M.p. 141 – 144 °C. ^{1}H NMR (360 MHz, $C_6D_5CD_3$, 293 K): $\delta = 1.28$ (s, 18H; $C(CH_3)_3$), 1.31 (m, 4H; CH_2-THF), 1.42 (d, ^3J(H,H) = 6.8 Hz, 12H; $CH(CH_3)_2$), 1.48 (d, ^3J(H,H) = 6.8 Hz, 12H; $CH(CH_3)_2$), 2.75 (d, ^3J(H,H) = 11.1 Hz, 4H; CH_2-allyl), 3.44 (spt, ^3J(H,H) = 6.8 Hz, 4H; $CH(CH_3)$), 3.89 (m, 4H; OCH_2-THF), 5.48 (s, 1H; CH), 6.16 (quin, ^3J(H,H) = 11.1 Hz, 1H; C*H*-allyl), 7.22 (t, ^3J(H,H) = 5.6 Hz 4H; *meta*-CH), 7.26 (d, ^3J(H,H) = 5.3 Hz, 2H; *para*-CH); satisfactory C, H, and N analyses.

3: Crystals of **2** (1.278 g, 2.0 mmol) were heated to 150 °C under vacuum (10^{-2} Torr) for 1 h to give **3** as an orange oil in quantitative yield. Crystals of **3** were grown from a solution in toluene at −30 °C; yield 38%. M.p. 138 – 140 °C. ^{1}H NMR (360 MHz, $C_6D_5CD_3$, 293 K): $\delta = 1.21$ (s, 108H; $C(CH_3)_3$), 1.28 (d, ^3J(H,H) = 6.5 Hz, 72H; $CH(CH_3)_2$), 1.30 (d, ^3J(H,H) = 6.5 Hz, 72H; $CH(CH_3)_2$), 2.37 (d, ^3J(H,H) = 11.2 Hz, 24H; CH_2-allyl), 3.24 (spt, ^3J(H,H) = 6.8 Hz, 24H; $CH(CH_3)$), 5.38 (s, 6H; CH), 5.44 (quin, ^3J(H,H) = 11.2 Hz, 6H; C*H*-allyl), 7.04 (t, ^3J(H,H) = 6.2 Hz, 12H; *meta*-CH), 7.13 (d, ^3J(H,H) = 6.3 Hz, 24H; *para*-CH); satisfactory C, H, and N analyses.

Received: July 6, 2001 [Z17442]

[1] Also termed β-aminoiminate and diazapentadienyl.

[2] For some recent examples see: a) P. G. Hayes, W. E. Piers, L. W. M. Lee, L. K. Knight, M. Parvez, M. R. J. Elsegood, W. Clegg, *J. Am. Chem. Soc.* **2001**, *123*, 2533; b) V. C. Gibson, C. Newton, C. Redshaw, G. A. Solan, A. J. P. White, D. J. Williams, *Eur. J. Inorg. Chem.* **2001**, 1895; c) L. W. M. Lee, W. E. Piers, M. R. J. Elsegood, W. Clegg, M. Parves, *Organometallics* **1999**, *18*, 2947; d) M. Rahim, N. J. Taylor, S. Xin, *Organometallics* **1998**, *17*, 1315; e) P. H. M. Budzelaar, A. B. van Oort, A. G. Orpen, *Eur. J. Inorg. Chem.* **1998**, 1485; f) P. H. M. Budzelaar, A. W. Gal, *Organometallics* **1998**, *17*, 4121; g) V. C. Gibson, P. J. Maddox, C. Newton, C. Redshaw, G. A. Solan, A. J. P. White, *Chem. Commun.* **1998**, 1651.

[3] For some recent examples see: a) M. Stender, B. E. Eichler, N. J. Hardman, P. P. Power, J. Prust, M. Noltmeyer, H. W. Roesky, *Inorg. Chem.* **2001**, *40*, 2794; b) Y.-L. Huang, B.-H. Huang, B.-T. Ko, C.-C. Lin, *J. Chem. Soc. Dalton Trans.* **2001**, 1359; c) B. M. Chamberlin, M. Cheng, D. R. Moore, T. M. Ovitt, E. B. Lobkovsky, G. W. Coates, *J. Am. Chem. Soc.* **2001**, *123*, 3229; d) P. J. Bailey, R. A. Coxall, C. M. Dick, S. Fabre, S. Parsons, *Organometallics* **2001**, *20*, 798; e) M. H. Chisholm, J. C. Huffman, K. Phomphrai, *J. Chem. Soc. Dalton Trans.* **2001**, 222; f) N. Kuhn, S. Fuchs, M. Steinmann, *Eur. J. Inorg. Chem.* **2001**, 359; g) P. J. Bailey, C. M. E. Dick, S. Fabre, S. Parsons, *J. Chem. Soc. Dalton Trans.* **2000**, 1655; h) P. B. Hitchcock, M. F. Lappert, M. Layh, D.-S. Liu, R. Sablong, T. Shun, *J. Chem. Soc. Dalton Trans.* **2000**, 2301; i) V. C. Gibson, J. A. Segal, A. J. P. White, D. J. Williams, *J. Am. Chem. Soc.* **2000**, *122*, 7120.

[4] F. Bickelhaupt *Grignard Reagents: New Developments* (Ed: H. G. Richey), Wiley, Chichester, UK, **2000**, pp. 299 – 328, and references therein.

[5] a) L. H. Shepherd, Jr., (Ethyl Corp.), US 3597487, **1971** [*Chem. Abstr.* **1971**, *75*, 118398n]; b) L. H. Shepherd, Jr., (Ethyl Corporation), US 3670038, **1970** [*Chem. Abstr.* **1972**, *77*, 88645n]; c) L. H. Shepherd, Jr., (Ethyl Corporation), DE 2008602, **1970**; d) A. Sen (Exxon-Mobil), WO 0073359, **2000**; e) H. E. Podall, W. E. Foster, *J. Org. Chem.* **1958**, *23*, 1848.

[6] For examples see: a) M. Stradiotto, M. A. Brook, M. J. McGlinchey, *New J. Chem.* **1999**, *23*, 317; b) J. M. White, S. Jones, *Acta Crystallogr. Sect. C* **1999**, *55*, 962; c) J. B. Lambert, C. L. Stern, Y. Zhao, W. C. Tse, C. E. Shawl, K. T. Lentz, L. Kania, *J. Organomet. Chem.* **1998**, *568*, 21; d) G. S. Zaitseva, S. S. Karlov, E. S. Alekseyeva, L. A. Aslanov, E. V. Automonov, J. Lorberth, *Z. Naturforsch. B.* **1997**, *52*, 30.

[7] a) D. Jacoby, S. Isoz, C. Floriani, K. Schenk, A. Chiesi-Villa, C. Rizzoli, *Organometallics* **1995**, *14*, 4816; b) W. Uhl, J. Wagner, *J. Organomet. Chem.* **1992**, *427*, 151; c) U. Schümann, E. Weiss, H. Dietrich, W. Mahdi, *J. Organomet. Chem.* **1987**, *322*, 299; d) Z. Huang, M. Chen, W. Qiu, W. Wu, *Inorg. Chim. Acta* **1987**, *139*, 203; e) H. Köster, E. Weiss, *Chem. Ber.* **1982**, *115*, 3422.

[8] M. Marsch, K. Harms, W. Massa, G. Boche, *Angew. Chem.* **1987**, *99*, 706; *Angew. Chem. Int. Ed. Engl.* **1987**, *26*, 696.

[9] P. J. Bailey, S. T. Liddle, S. Parsons, unpublished results.

[10] Crystal data for $\mathbf{3}\cdot 4C_6H_5CH_3$: $C_{232}H_{348}N_{12}Mg_6\cdot 4C_6H_5CH_3$, $M_r = 3771.58$, triclinic, space group $P\bar{1}$, $a = 18.028(6)$, $b = 20.271(7)$, $c = 21.948(7)$ Å, $\alpha = 110.365(4)$, $\beta = 98.789(5)$, $\gamma = 109.543(5)°$, $V = 6749.0(4)$ Å^3, $Z = 1$, $\rho_{calcd} = 0.928$ g cm^{-3}; $Mo_{K\alpha}$ radiation, $\lambda = 0.71073$ Å, $\mu = 0.065$ mm^{-1}, $T = 150$ K. A total of 38910 data (17554 unique, $R_{int} = 0.0998$, $\theta < 22.52°$, reflections at higher angle were very weak or absent due to the severe disorder of solvent molecules; see below) were collected on a Bruker SMART APEX CCD diffractometer equipped with a Bruker Monocap capillary optic using narrow

frames (0.3° in ω) and were corrected semiempirically for absorption (transmission 0.709–0.928). The structure was solved by direct methods and refined by full-matrix least-squares on F^2 values of all to give $wR2 = \{\Sigma[w(F_o^2 - F_o^2)^2]/\Sigma[w(F_o^2)^2]\}^{1/2} = 0.2202$ conventional $R = 0.0830$ for F values of 6700 reflections with $F_o^2 > 2\sigma(F_o^2)$, $S = 0.927$ for 1159 parameters. Residual electron density extremes were 0.267 and -0.221 e Å^{-3}. Highly disordered toluene solvent molecules were treated by the SQUEEZE procedure of PLATON (A. L. Spek, University of Utrecht, The Netherlands, **2000**), which indicated the correct total electron density for four molecules of toluene per molecule of **3**. Crystallographic data (excluding structure factors) for the structures reported in this paper have been deposited with the Cambridge Crystallographic Data Centre as supplementary publication no. CCDC-166394 (**3**). Copies of the data can be obtained free of charge on application to CCDC, 12 Union Road, Cambridge CB2 1EZ, UK (fax: (+44) 1223-336-033; e-mail: deposit@ccdc.cam.ac.uk).

[11] For recent examples see: a) F. A. Cotton, C. A. Murillo, M. A. Petrukhina, *J. Organomet. Chem.* **2001**, *593*, 1; b) T. Nakajima, A. Ishiguro, Y. Wakatsuki, *Angew. Chem.* **2000**, *112*, 1175; *Angew. Chem. Int. Ed. Engl.* **2000**, *39*, 1131; c) T. Chihara, H. Kubota, M. Fukumoto, H. Ogawa, Y. Yamamoto, Y. Wakatsuki, *Inorg. Chem.* **1997**, *36*, 5488.

[12] a) T. B. Gunnoe, P. S. White, J. L. Templeton, *Organometallics* **1997**, *16*, 3794; b) M. Laing, J. R. Moss, J. Johnson, *Chem. Commun.* **1977**, 656.

[13] Preliminary DFT calculations (B3LYP/6–31G*) for the simplified model system $[\{HC(CHNH)_2MgCH_3\}_2(\mu\text{-}\eta^1\text{:}\eta^1\text{-}C_3H_5)]^-$ were performed to obtain supporting evidence for sp^2 hybridization of the allyl CH_2 groups. The C–C bond lengths (1.403 Å) obtained clearly indicate an unsaturated bonding environment; in addition Mulliken charge assignments yield a positive charge to the central CH group, and negative charges to the neighboring CH_2 groups. The highest occupied molecular orbital (HOMO) can be largely attributed to p-type character orbitals located on the CH_2 carbon atoms, pointing in the direction of the Mg centers. Further details are provided in the Supporting Information.

An Unorthodox Conformation of [18]porphyrin-(1.1.1.1) Heteroanalogue—21,23-Ditelluraporphyrin with a Flipped Tellurophene Ring**

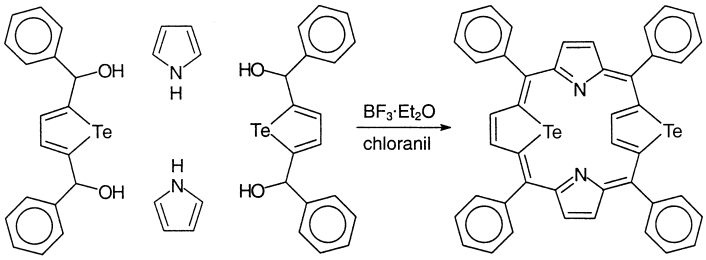
Ewa Pacholska, Lechosław Latos-Grażyński,* and Zbigniew Ciunik

Conformational flexibility of tetrapyrrole macrocycles is currently appreciated as an important factor in the fine-tuning of porphyrin and metalloporphyrin properties.[1] Thus, introduction of sterically demanding residues (including nitrogen atom protonation) in the porphyrin core or at the outer rim (alkylation, arylation), as well as coordination of metal ions, can result in a nonplanar porphyrin conformation. Core-modified porphyrins, formed by replacement of one or more nitrogen atoms by other heteroatom(s), also demonstrate severe nonplanar arrangements once the size and/or number of heteroatoms in the core increases, even though the basic framework of the porphyrin skeleton is preserved.[2] On the whole, [18]porphyrins-(1.1.1.1) and their heteroanalogues contain a similar framework of four essentially planar five-membered rings linked by methine carbon atoms with all the nitrogen atoms or other heteroatoms pointing toward the center of the macrocycle. Even the most severe distortion of a macrocycle preserves such an "in"-macrocycle orientation of the five-membered rings.[1]

An enlargement of the macrocycle by the addition of heterocyclic moiety(s) and/or methine carbon atoms introduces a novel structural motif. Thus a five-membered ring—axiomatic for porphyrins (heteroporphyrins)—can be oriented in such a way that one nitrogen or other heteroatom is located at the outer perimeter and two β-atoms are found in the core or just over the center. An inversion of this type has been detected for the following expanded porphyrins and expanded heteroporphyrins:[3] tetrathia[22]porphyrin-(2.2.2.2),[4] tetrathia[24]porphyrin-(2.2.2.2),[5] *meso*-substituted [22]pentaphyrin-(1.1.1.1.0) (sapphyrins)[6] and its heteroanalogues,[7, 8] [26]hexaphyrin-(1.1.1.1.1.1),[9] heteroanalogues of [26]hexaphyrin-(1.1.0.1.1.0) (rubyrin),[3, 10] and heteroanalogues of [30]heptaphyrins-(1.1.0.0.1.1.0) and [30]heptaphyrins-(1.1.0.1.0.1.0).[11] The lowest limit of the macrocycle size permitting the flipped geometry is exemplified by [18]annulene bridged by three sulfur atoms (which formally may be named trithia[18]porphyrin-(2.2.2)), but it behaves only as an array of isolated thiophene units which are totally out of plane in the solid state.[5] It was also postulated that a 180° rotation of the *N*-confused pyrrole ring of 2-aza-21-carbaporphyrin is necessary to produce the "fused" porphyrin.[12] The conformation of 2-aza-21-carbaporphyrin with the flipped pyrrole ring is energetically accessible as demonstrated by DFT calculations.[13]

Here we report on the synthesis and characterization of 5,10,15,20-tetraphenyl-21,23-ditelluraporphyrin (Te_2TPP, **2**) which is the first heteroanalogue of [18]porphyrin-(1.1.1.1) with the nonplanar macrocyclic conformation containing the flipped five-membered ring.

The 21,23-ditelluraporphyrin **2** was synthesized by condensation of pyrrole and 2,5-bis(phenylhydroxymethyl)tellurophene[14c] (**1** Scheme 1). This procedure follows the methodology previously used for the preparation of 5,10,15,20-



1 **2**

Scheme 1. Synthesis of Te_2TPP.

[*] Prof. Dr. L. Latos-Grażyński, Dr. E. Pacholska, Dr. Z. Ciunik
Department of Chemistry
University of Wrocław
ul. Joliot-Curie 14
50 383 Wrocław (Poland)
Fax: (+71) 32-823-48
E-mail: llg@wchuwr.chem.uni.wroc.pl

[**] Financial support from the State Committee for Scientific Research KBN of Poland (Grant: 3 T09A 155 15) and the Foundation for Polish Science is gratefully acknowledged.

 © WILEY-VCH Verlag GmbH, D-69451 Weinheim, 2001 1433-7851/01/4023-4466 $ 17.50+.50/0

tetraaryl-21,23-diheteroporphyrins.[14] The product was obtained in 11 % yield after chromatographic workup.

Te_2TPP has been characterized by X-ray crystallography.[15, 16] The size of the tellurium atoms is instrumental in the remarkable distortion of macrocycle **2**. One of the tellurophene moieties (Te23) is essentially coplanar with two adjacent pyrrole rings while the second tellurophene ring is flipped and the Te21 atom is directed away from the center of the macrocycle. The geometry is apparent from the views of the macrocycle in Figure 1. The extent of distortion is reflected by a dihedral angle between the plane of *meso*-carbon atoms (C5-C10-C15-C20) and the tellurophene plane (Te21-C1-C2-C3-C4) of 123.0(2)°.

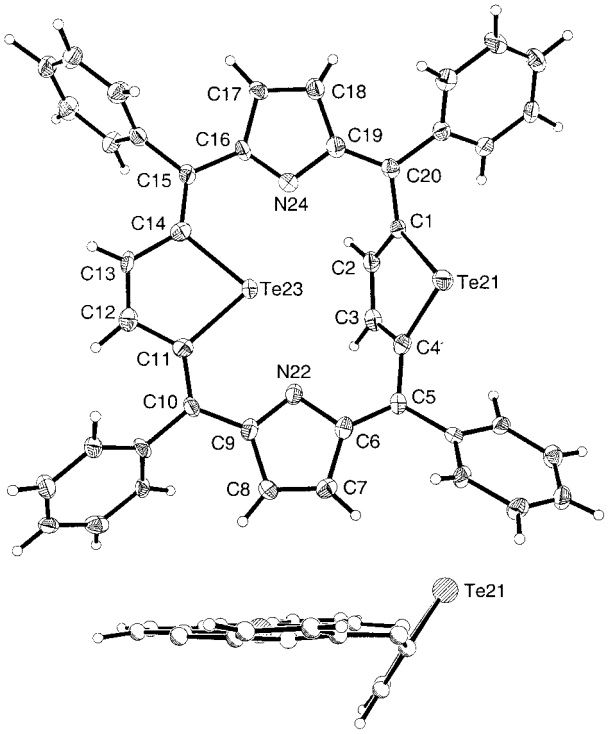


Figure 1. The crystal structure of Te_2TTP (top: perspective view; bottom: side view—the phenyl groups are omitted for clarity). The vibrational ellipsoids represent 50 % probability. (Selected bond lengths [Å]: Te21-C1 2.087(8), Te21-C4 2.088(8), C1-C2 1.37(1), C2-C3 1.42(1), C3-C4 1.36(1), Te23-C11 2.107(8), Te23-C14 2.092(9), C11-C12 1.43(1), C12-C13 1.36(1), C13-C14 1.44(1)).

The electronic spectrum of **2** shows three major bands of comparable intensities at 348, 464, and 668 nm, but the distinct intense Soret-like band typical for aromatic heteroporphyrins is absent (Figure 2). The electronic spectrum of $[(Te_2TPP)H_2]^{2+}$ (**2**-H_2^{2+}), shows the presence of a Soret-like band at 490 nm which is accompanied by a less-intense band at 767 nm. The change in the spectrum is explained by the more aromatic nature of the protonated form.

The remarkable flipped structure of **2** detected in the solid state is preserved in solution, as determined by ^{1}H NMR studies. Unambiguous assignments of the resonances were obtained by a selective deuteration of pyrrole fragments to get $[D_4]Te_2TPP$, as well as by 2D ^{1}H NMR COSY and ROESY experiments. The ^{1}H NMR spectrum of **2** (210 K) exhibits one AB pattern centered at $\delta = 7.8$ ($^3J_{HH} = 4.5$ Hz, Figure 3 A),

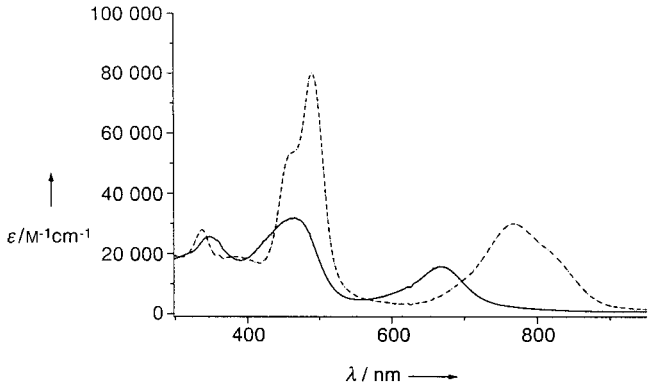


Figure 2. The electronic spectra of Te_2TTP (solid line) and $[(Te_2TTP)H_2]^{2+}$ (dashed line) in dichloromethane.

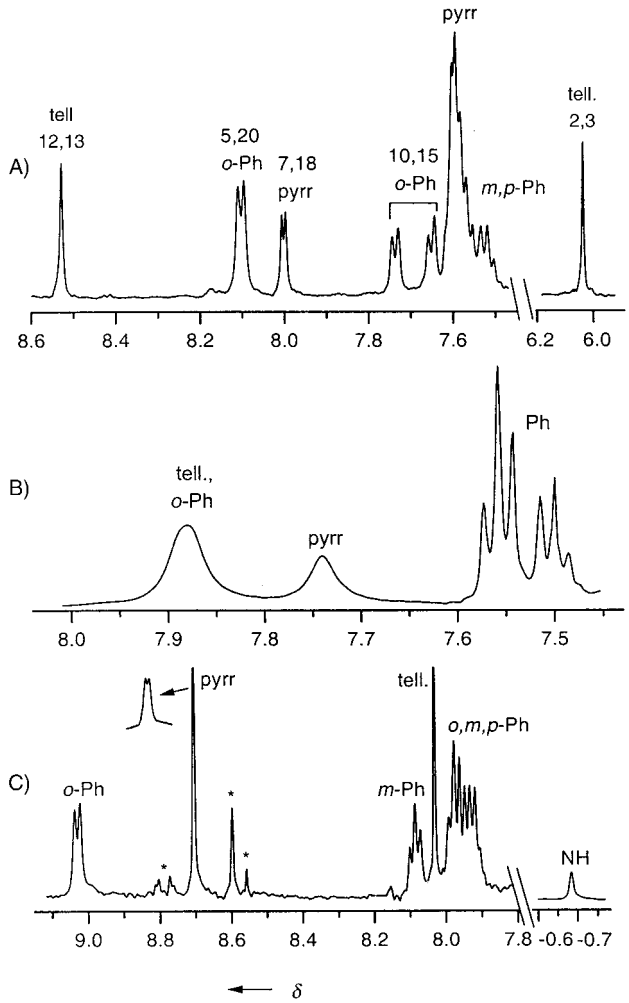


Figure 3. Partial ^{1}H NMR spectra in $CDCl_3$: A) Te_2TTP (210 K); B) Te_2TTP (298 K); C) $[(Te_2TTP)H_2]^{2+}$ (20 equiv of TFA; 210 K). Peak labels follow the systematic position numbering of the porphyrin ring or denote proton groups: *o*, *m*, *p* positions of the *meso*-phenyl groups.

which was readily assigned to the pyrrole ring. The definitive determination of the flipped conformation was provided by the diagnostic shifts of the tellurophene protons at $\delta = 8.53$ and 6.08, which were assigned to the regular and flipped rings, respectively. The aromatic ring current effect is small because of the severe distortion, as reflected here by the difference in

 © WILEY-VCH Verlag GmbH, D-69451 Weinheim, 2001 1433-7851/01/4023-4467 $ 17.50+.50/0

shift between the inner and outer β-H tellurophene resonances ($\delta_{12} - \delta_2 = 2.45$).

Titration with trifluoroacetic acid (TFA) triggers a profound change in the geometry involving a rearrangement toward the "regular" (**R**) structure in which the Te21 and Te23 tellurophene atoms are simultaneously directed toward the center of the macrocycle (Scheme 2). A strong puckering of the macrocycle with large displacements of both tellurophene rings from the mean plane is expected because of the steric crowding. The "regular" structure of **2**-H_2^{2+} is evident in the ^{1}H NMR spectrum as two lines assigned to the tellurophene ($\delta = 8.03$) and pyrrole ($\delta = 8.71$, $^4J_{\text{H-NH}} = 1.5$ Hz) resonances (Figure 3C). The NH resonance located in the upfield region ($\delta = -0.7$) indicates the marked ring current effect. The puckering of the dication is confirmed by the very large differentiation in the *ortho* (ca. $\Delta\delta = 1$) and *meta* (ca. $\Delta\delta =$ 0.15) resonances of the *meso*-phenyl groups.

The well-defined ^{1}H NMR signals of **2** measured in $CDCl_3$ at 210 K (Figure 3A) broaden, coalesce (Figure 3B, 298 K), and finally give one sharp peak for each position. These sharp peaks indicates there is a fast exchange process at 320 K (tellurophene: $\delta = 7.88$, pyrrole: $\delta = 7.74$). In fact, the "in" and "out" arrangements of the two inequivalent tellurophene rings of **2** are exchangeable even at 210 K, as proven by the EXSY correlation in the ROESY map. The Te_2TPP molecule interchanges between two energetically and structurally identical flipped forms **F**-1 and **F**-2 as shown in Scheme 2.

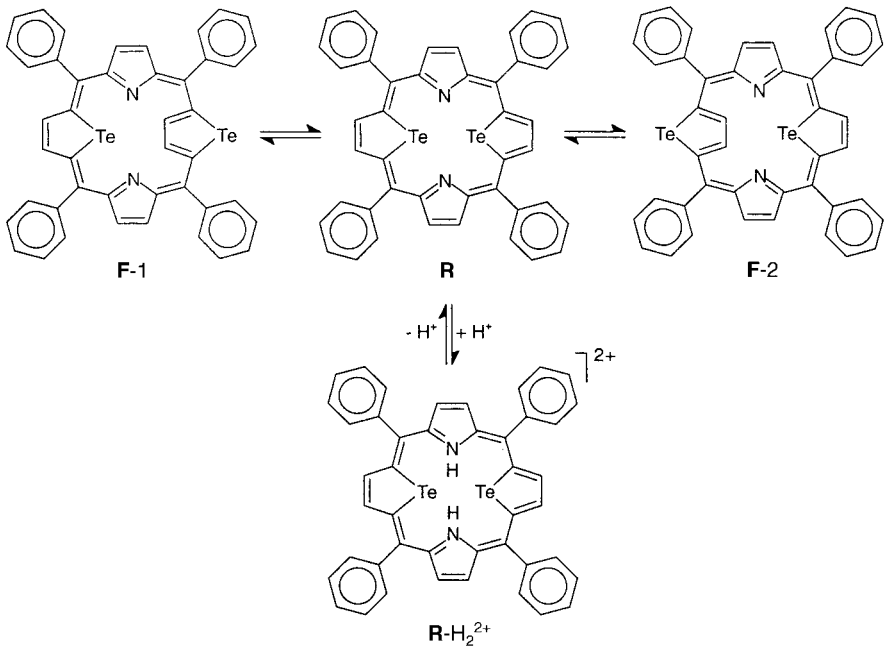
This mechanism implies a sequence of two steps which involves an approximate 180° rotation of the flipped (Te21) tellurophene ring of **F-**1 to form the regular conformation **R**, followed by the analogous flip of the Te23 tellurophene ring to form **F-**2. The Te_2TPP **R** form is not merely transient, but it makes a meaningful contribution to the thermodynamic equilibrium. Consequently, at 320 K the resonance positions differ from these expected for a two-site, equally populated exchange mechanism, namely, β-H tellurophene at $\delta = 7.30$ and β-H pyrrole at $\delta = 7.78$.

Attempts to broaden the basis of heteroporphyrin chemistry has stimulated interest in 21,23-ditelluraporphyrin, which has heretofore escaped all efforts of synthesis.[14c, 17] 21,23-Ditelluraporphyrin provides the first example of the inverted structure of the 18-π electron porphyrin-like frame with four five-membered rings linked by four methine carbon atoms.

Experimental Section

2: Pyrrole (65 mg, 0.97 mmol), **1** (0.37 g, 0.94 mmol), and freshly distilled CH_2Cl_2 (400 mL) were placed in a 1000-mL flask with a reflux condenser. Nitrogen was bubbled through the solution for 20 min, then $BF_3 \cdot Et_2O$ (0.3 mL) and triethyl orthoformate (0.3 mL) were added, and the mixture was stirred for 1 h under nitrogen. Chloranil (0.71 g, 2.9 mmol) was added and the solution was refluxed for 45 min. The solvent was partly evaporated and the reaction mixture was purified by column chromatography on basic alumina. The first fraction (bright green product **2**) was eluted with CH_2Cl_2 and was subjected to a second chromatography (basic alumina, CH_2Cl_2). The product was recrystalized from CH_2Cl_2 with CH_3OH or hexane to yield **2** as a dark green solid in a yield of 11%. UV/Vis (CH_2Cl_2): λ_{max} (logε) = 348 (4.4), 464 (4.5), 668 nm (4.2); for **2**-H_2^{2+} (with TFA): λ_{max} (logε) = 337 (4.4), 457 (sh), 490 (4.9), 767 (4.5), 825 nm (sh); ^{1}H NMR (500 MHz, $CDCl_3$, 210 K): $\delta = 8.53$ (s 2H, tell., 12,13), 8.10 (d, ^3J(H,H) = 7.3 Hz, 4H, *o*-Ph), 8.00 (d, ^3J(H,H) = 4.5 Hz, 2H, pyrr), 7.74 (d, ^3J(H,H) = 7.3 Hz, 2H, *o*-Ph), 7.65 (d, ^3J(H,H) = 7.1 Hz, 2H, *o*-Ph), 7.56 (m, 14H, pyrr) 7.59 (d, ^3J(H,H) = 4.5 Hz, *m*,*p*-Ph), 6.08 (s, 2H, 2H,3H-tell.); for **2**-H_2^{2+} (20 equiv TFA): $\delta =$ 9.03 (d, ^3J(H,H) = 7.2 Hz, 4H, *o*-Ph), 8.71 (d, ^4J(H,H) = 1.5 Hz, 4H, pyrr), 8.09 (t, 2H, *m*-Ph), 8.03 (s, 4H, tell.), 7.95 (m, 12H, *o*,*m*,*p*-Ph), −0.70 (br s, 2H, NH); HR-MS: *m*/*z*: 844.0391; *m*/*z* calcd for $C_{44}H_{28}N_2{}^{130}Te_2$: 844.0381; elemental analysis: calcd for $C_{44}H_{28}N_2Te_2 \cdot 2CH_3OH$: C 61.12, H 4.01, N 3.10; found: C 61.13, H 3.89, N 3.26.

Received: July 12, 2001 [Z17488]



Scheme 2. Regular (**R**) and flipped (**F**) forms of Te_2TPP in conformational equilibrium.

[1] M. Senge in *The Porphyrin Handbook*, *Vol. 1* (Eds.: K. M. Kadish, K. M. Smith, R. Guilard), Academic Press, New York, **2000**, p. 239.

[2] a) E. Vogel, P. Röhrig, M. Sicken, B. Knipp, A. Herrmann, M. Pohl, H. Schmickler, J. Lex, *Angew. Chem.* **1989**, *101*, 1683; *Angew. Chem. Int. Ed. Engl.* **1989**, *28*, 1651; b) E. Vogel, M. Pohl, A. Herrmann, T. Wiss, C. König, J. Lex, M. Gross, J. P. Gisselbrecht, *Angew. Chem.* **1996**, *108*, 1677; *Angew. Chem. Int. Ed. Engl.* **1996**, *35*, 1520; c) E. Vogel, C. Fröde, A. Breihan, H. Schmickler, J. Lex, *Angew. Chem.* **1997**, *109*, 2722; *Angew. Chem. Int. Ed. Engl.* **1997**, *36*, 2609; d) L. Latos-Grażyński, J. Lisowski, L. Szterenberg, M. M. Olmstead, A. L. Balch, *J. Org. Chem.* **1991**, *56*, 4043.

[3] J. S. Sessler, A. Gebauer, S. J. Weghorn, in *The Porphyrin Handbook*, *Vol. 2* (Eds.: K. M. Kadish, K. M. Smith, R. Guilard), Academic Press, New York, **2000**, p. 55.

[4] R. D. Schall, Ph.D. thesis, University of Cologne, Germany, **1993**; F. Jörrens, Ph.D. thesis, University of Cologne, Germany, **1994** (see footnotes 43 and 50 in ref. [3]).

[5] a) A. Strand, B. Thulin, O. Wennerström, *Acta Chem. Scand. Ser. B* **1977**, *31*, 521; b) Z. Hu, J. L. Atwood, M. P. Cava, *J. Org. Chem.* **1994**, *59*, 8071.

[6] a) P. J. Chmielewski, L. Latos-Grażyński, K. Rachlewicz, *Chem. Eur. J.* **1995**, *1*, 68; b) K. Rachlewicz, N. Sprutta, L. Latos-Grażyński, P. J. Chmielewski, L. Szterenberg, *J. Chem. Soc. Perkin Trans. 2* **1998**,

 © WILEY-VCH Verlag GmbH, D-69451 Weinheim, 2001 1433-7851/01/4023-4468 $ 17.50+.50/0

959; c) L. Szterenberg, L. Latos-Grażyński, *Theochem.* **1999**, *490*, 33; c) C. Brückner, E. D. Sternberg, R. W. Boyle, D. Dolphin, *Chem. Commun*. **1997**, 1689.

[7] a) K. Rachlewicz, N. Sprutta, P. J. Chmielewski, L. Latos-Grażyński, *J. Chem. Soc. Perkin Trans. 2* **1998**, 969; b) N. Sprutta, L. Latos-Grażyński, *Org. Lett.* **2001**, *3*, 1933; c) A. Srinivasan, S. K. Pushpan, M. R. Kumar, S. Mahajan, T. K. Chandrashekar, R. Roy, P. Ramamurthy, *J. Chem. Soc. Perkin Trans. 2* **1999**, 961; d) A. Srinivasan, V. G. Anand, S. J. Narayanan, S. K. Pushpan, M. R. Kumar, S. Mahajan, T. K. Chandrashekar, *J. Org. Chem.* **1999**, *64*, 8693; e) S. K. Pushpan, S. J. Narayanan, A. Srinivasan, S. Mahajan, T. K. Chandrashekar, R. Roy, *Tetrahedron Lett.* **1998**, *39*, 9249.

[8] S. J. Narayanan, B. Sridevi, T. K. Chandrashekar, A. Vij, R. Roy, *J. Am. Chem. Soc.* **1999**, *121*, 9053.

[9] a) R. Charrière, T. A. Jenny, H. Rexhausen, A. Gossauer, *Heterocycles* **1993**, *36*, 1561; b) M. G. P. M. S. Neves, R. M. Martins, A. C. Tomé, A. J. D. Silvestre, A. M. S. Silva, V. Félix, M. G. B. Drew, J. A. S. Cavaleiro, *Chem. Commun.* **1999**, 385.

[10] a) A. Srivasan, S. Mahajan, S. K. Pushpan, M. Ravikumar, T. K. Channdrashekar, *Tetrahedron Lett.* **1998**, *39*, 1961; b) A. Srinivasan, V. M. Reddy, S. J. Narayanan, B. Sridevi, S. K. Pushpan, M. Ravikumar, T. K. Chandrashekar, *Angew. Chem.* **1997**, *109*, 2710; *Angew. Chem. Int. Ed. Engl.* **1997**, *36*, 2598.

[11] V. R. G. Anand, S. K. Pushpan, A. Srinivasan, S. J. Narayanan, B. Sridevi, T. K. Chandrashekar, R. Roy, B. S. Joshi, *Org. Lett.* **2000**, *2*, 3829.

[12] a) H. Furuta, T. Ishizuka, A. Osuka, T. Ogawa, *J. Am. Chem. Soc.* **1999**, *121*, 2945; b) H. Furuta, T. Ishizuka, A. Osuka, T. Ogawa, *J. Am. Chem. Soc.* **2000**, *122*, 5748.

[13] L. Szterenberg, L. Latos-Grażyński, *J. Porphyrins Phthalocyanines* **2001**, *5*, 474.

[14] a) A. Ulman, J. Manassen, *J. Am. Chem. Soc.* **1975**, *97*, 6540; b) A. Ulman, J. Manassen, F. Frolow, D. Rabinovich, *Tetrahedron Lett*. **1978**, 167; c) A. Ulman, J. Manassen, F. Frolow, D. Rabinovich, *Tetrahedron Lett*. **1978**, 1885; d) P. J. Chmielewski, L. Latos-Grażyński, M. M. Olmstead, A. L. Balch, *Chem. Eur. J.* **1997**, *3*, 268.

[15] Data collection: the measurement was performed on a Kuma KM4CCD diffractometer using $Mo_{K\alpha}$ radiation ($\lambda = 0.71073$ Å), $T =$ 90 K, in ω scan mode, $2\theta_{max} = 50$. **2**: crystals were prepared by the slow diffusion of CH_3OH into a solution of **2** in CH_2Cl_2 to yield a dark green crystal of $C_{44}H_{28}N_2Te_2$, crystal dimensions $0.07 \times 0.07 \times 0.18$ mm^3, monoclinic, space group $P2_1/n$, $a = 11.579(2)$, $b =$ 12.609(2), $c = 23.035(3)$ Å, $\beta = 99.11(1)^\circ$, $V = 3320.8(8)$ Å^3, $\rho_{calcd} =$ 1.680, $Z = 4$; total no. of reflections collected: 18630; no. of independent reflections: 5824 of which 3988 were included in the refinement of 433 parameters; an absorption correction based on a least-squares fit against $|F_c| - |F_o|$ differences was applied:[18] $\mu =$ 1.793 mm^{-1}, $A_{min.} = 0.8456$, $A_{max.} = 1.21949$. The structure was solved by using direct methods with SHELXS-97 and refined against $|F^2|$ using SHELXL-97 (G. M. Sheldrick, University of Göttingen, Germany, **1997**), final R_1/wR_2 indices (for $I > 2\sigma(I)$): 0.0810/0.0662; max./min. residual electron density: $+0.716/-0.597$ e A^{-3}; H atoms were fixed. Crystallographic data (excluding structure factors) for the structures reported in this paper have been deposited with the Cambridge Crystallographic Data Centre as supplementary publication no. CCDC-166826. Copies of the data can be obtained free of charge on application to CCDC, 12 Union Road, Cambridge CB2 1EZ, UK (fax: (+44) 1223-336-033; e-mail: deposit@ccdc.cam.ac.uk).

[16] The X-ray crystal structure of $Te_2TPP \cdot CHCl_3$, although of poor quality, confirmed the shape of **2**.

[17] L. Latos-Grażyński, E. Pacholska, P. J. Chmielewski, M. M. Olmstead, A. L. Balch, *Angew. Chem.* **1995**, *107*, 2467; *Angew. Chem. Int. Ed. Engl.* **1995**, *34*, 2252.

[18] P. Starynowicz, COSABS99, program for absorption correction, University of Wrocław, **1999**.

Remarkable Rate Enhancement of Ligand Substitution Promoted by Geometrical Arrangement of Tridentate "Spectator" Ligands**

My Hang V. Huynh,* Jennifer Smyth, Modi Wetzler, Brendan Mort, Paul K. Gong, Laura M. Witham, Donald L. Jameson, David K. Geiger, Joanne M. Lasker, Mina Charepoo, Michelle Gornikiewicz, Jose M. Cintron, Gretchen Imahori, Roberto R. Sanchez, Amy C. Marschilok, Lynn M. Krajkowski, David G. Churchill, Melvyn Rowen Churchill, and Kenneth J. Takeuchi*

Dedicated to Dr. Thomas J. Meyer on the occasion of his 60th birthday

The reactivity exhibited by transition metal complexes depends on the oxidation state of the metal center[1] and on stereoelectronic (steric and electronic) effects of the ligands.[2] Since the initial development of poly(pyrazol-1-yl)alkanes[3] and poly(pyrazol-1-yl)borates[4] by Trofimenko, these so-called "scorpionate" ligands have been used in coordination, organometallic, and bioinorganic chemistry.[5–6] Utilizing these scorpionate ligands and different geometrical arrangements of tridentate "spectator" ligands, we observe a dramatic 1.9×10^7 rate increase for ligand substitution at a supposedly inert ruthenium(II) center. To explain these unexpected results, ligand substitution kinetics for complexes having different ligand geometries are compared. Scheme 1 depicts two systems, one in which the active site lies in the plane of the

[*] Dr. M. H. V. Huynh, J. Smyth, M. Wetzler, B. Mort, P. K. Gong, L. M. Witham, J. M. Lasker, M. Charepoo, M. Gornikiewicz, J. M. Cintron, G. Imahori, R. R. Sanchez, L. M. Krajkoski, Dr. M. R. Churchill
Director-Funded Postdoctoral Fellow
Chemistry Division MS J514, Los Alamos National Laboratory
Los Alamos, NM 87545 (USA)
Fax: 1-505-667-3314
E-mail: huynh@lanl.gov

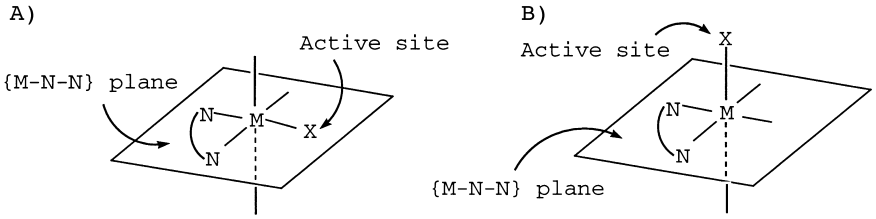
Dr. K. J. Takeuchi, A. C. Marschilok, D. G. Churchill
Department of Chemistry
State University of New York at Buffalo
Buffalo, New York 14260 (USA)
Fax: (+1) 716-645-6963
E-mail: takeuchi@nsm.buffalo.edu

Dr. D. L. Jameson
Chemistry Department, Gettysburg College
Gettysburg, PA 17325 (USA)

Dr. D. K. Geiger
Chemistry Department SUNY Geneseo, Geneseo, NY 14454 (USA)

[**] K.J.T. acknowledges Arco Chemical and the National Science Foundation for support of this research. M.H.V.H. gratefully acknowledges postdoctoral fellowship support from the Director's Office of Los Alamos National Laboratory. Los Alamos National Laboratory is operated by the University of California for the U.S. Department of Energy under Contract W-7405-ENG-36. M.H.V.H. also thanks Dr. Beverly K. Hartline (Deputy Laboratory Director, Argonne National Laboratory), Dr. Donald G. Lee (Chemistry Professor, University of Regina, Saskatchewan, Canada, S4S0A2), Dr. R. Thomas Baker (Los Alamos National Laboratory), and Dr. David E. Morris (Los Alamos National Laboratory) for their suggestions and discussions.

Supporting information for this article is available on the WWW under http://www.angewandte.com or from the author.

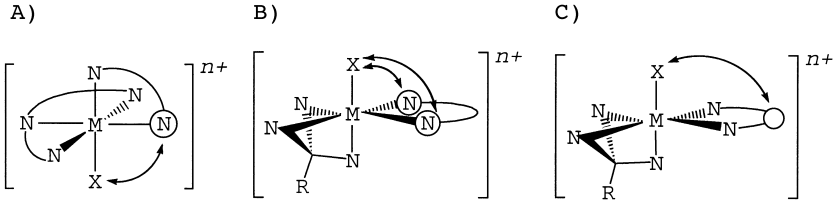


Scheme 1. A) In-plane ligand effect (IPLE) and B) out-of-Plane ligand effect (OPLE).

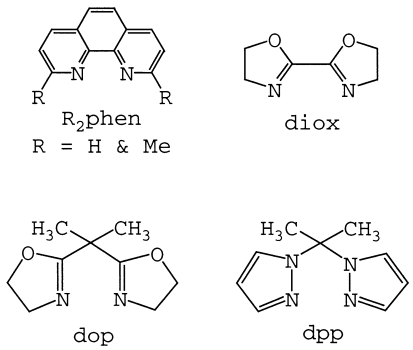
metal center and the bidentate ligand (the in-plane ligand effect (IPLE)), the other in which the active site does not lie in the same plane as the metal and the bidentate ligand (out-of-plane ligand effect (OPLE)).

The tridentate (L_3) meridional 2,2′:6′,2″-terpyridine (trpy) ligand and the facial tridentate tris(pyrid-2-yl)methoxymethane (tpmm) ligand[7] are used in the IPLE and OPLE systems, respectively (Scheme 2).

Bidentate ligands (L_2), shown in Scheme 3, were used for the study of ligand effects. They were judiciously chosen to include rigid ligands (phenanthroline = phen and 2,9-dimethylphenanthroline = Me_2phen), a non-rigid ligand (di(1,3-oxazoline) = diox),[8a–c] a non-aromatic flexible ligand (2,2-di(1,3-oxazolinyl)propane = dop),[8d] and an aromatic flexible ligand ((2,2-dipyrazol-1-yl)propane = dpp).[9]



Scheme 2. Possible arrangements of bidentate and tridentate Ligands: A) IPLE, B) OPLE: *cis*/*cis* interaction, and C) OPLE: backbone interaction.



Scheme 3. Bidentate ligands used in the study.

Reactions occur between $[Ru(Cl)_3(L_3)]$ (L_3 = tpmm = **1** and L_3 = trpy = **2**) and L_2 in a refluxing solvent mixture of 70:30 (v/v) EtOH:H_2O containing two equivalents of NEt_3 and LiCl under N_2 to give the ruthenium(II) chloro products ($[Ru^{II}\text{-}Cl]^+$), $[Ru^{II}(Cl)(L_2)(L_3)]^+$. These $[Ru^{II}\text{-}Cl]^+$ products are further converted into the corresponding ruthenium(II) aqua $[Ru^{II}\text{-}H_2O]^{2+}$ and ruthenium(II) acetonitrile $[Ru^{II}\text{-}NCCH_3]^{2+}$ complexes. They are isolated either as the tetrafluoroborate (BF_4^-) or the perchlorate (ClO_4^-)[10] salts and fully characterized by cyclic voltammetry, elemental analysis, and ^{1}H NMR and UV/Vis spectroscopy.[11a–b] Several $[Ru^{II}\text{-}Cl]^+$ and $[Ru^{II}\text{-}H_2O]^{2+}$ complexes were additionally characterized by X-ray crystallography.[12]

As shown by UV/Vis monitoring at 25.0 ± 0.1 °C in aqueous solution (pH 2.00 and μ = 0.1 M in $NaNO_3/HNO_3$) under pseudo first-order conditions, the ligand substitution reaction according to Equation (1) is first order in both CH_3CN and $[Ru^{II}\text{-}H_2O]^{2+}$.

$$[Ru^{II}(H_2O)(L_2)(L_3)]^{2+} + CH_3CN \longrightarrow [Ru^{II}(NCCH_3)(L_2)(L_3)]^{2+} + H_2O \quad (1)$$

Plots of k_{obs} versus $[CH_3CN]$ for $[Ru^{II}(H_2O)(dpp)(tpmm)]^{2+}$ and $[Ru^{II}(H_2O)(dpp)(trpy)]^{2+}$ and for $[Ru^{II}(H_2O)(dpp)(tpmm)]^{2+}$ and $[Ru^{II}(H_2O)(dop)(tpmm)]^{2+}$ were linear with zero-intercepts consistent with well behaved second-order kinetics.[11c–d] The electronic spectra of all ligand substitution reactions show isosbestic behavior,[11e] and all rate constants are measured as a function of $[CH_3CN]$.[11f] The rate constants of ligand substitution (the averages of at least three or more independent experiments) for all $[Ru^{II}\text{-}H_2O]^{2+}$ complexes in this study are listed in Table 1.

Our previous investigation of $[Ru^{II}\text{-}H_2O]^{2+}$ octahedral complexes revealed that the mechanism of ligand substitution was dissociative interchange (I_d),[13] which was in agreement with that of other ruthenium(II) complexes studied by the groups of Taube,[14] Creutz,[15] and Walsh.[16] In this I_d mechanism, an aqua–ruthenium(II) bond weakens because of stereoelectronic interaction resulting in an increase in the rate constant of aqua–ligand substitution. The activation parameters ($\Delta H^{\neq}$ and $\Delta S^{\neq}$) obtained from the temperature dependence of k_{ls} for $[Ru^{II}(H_2O)(dpp)(tpmm)]^{2+}$ (**12B**$^{2+}$) and $[Ru^{II}(H_2O)(dpp)(trpy)]^{2+}$ (**7B**$^{2+}$) over the temperature range

Table 1. Rate constants for the ligand substitution kinetics of $[Ru^{II}(H_2O)(L_3)(L_2)]^{2+}$ ions.[a]

Entry	$[Ru^{II}(H_2O)(L_2)(L_3)]^{2+}$	IPLE system L_3 = trpy k_{ls} [$M^{-1}s^{-1}$]	OPLE system L_3 = tpmm k_{ls} [$M^{-1}s^{-1}$]
1	$[Ru^{II}(H_2O)(phen)(L_3)]^{2+}$	$(6.2 \pm 0.1) \times 10^{-5}$ (**3B**$^{2+}$)	$(3.9 \pm 0.1) \times 10^{-5}$ (**8B**$^{2+}$)
2	$[Ru^{II}(H_2O)(Me_2phen)(L_3)]^{2+}$	$(4.1 \pm 0.1) \times 10^{-2}$ (**4B**$^{2+}$)	$(2.9 \pm 0.1) \times 10^{-5}$ (**9B**$^{2+}$)
3	$[Ru^{II}(H_2O)(diox)(L_3)]^{2+}$	$(1.4 \pm 0.1) \times 10^{-4}$ (**5B**$^{2+}$)	$(2.9 \pm 0.1) \times 10^{-5}$ (**10B**$^{2+}$)
4	$[Ru^{II}(H_2O)(dop)(L_3)]^{2+}$	$(4.6 \pm 0.1) \times 10^{-5}$ (**6B**$^{2+}$)	$(1.0 \pm 0.1) \times 10^{-2}$ (**11B**$^{2+}$)
5	$[Ru^{II}(H_2O)(dpp)(L_3)]^{2+}$	$(5.9 \pm 0.1) \times 10^{-6}$ (**7B**$^{2+}$)	$(1.1 \pm 0.1) \times 10^{2}$ (**12B**$^{2+}$)

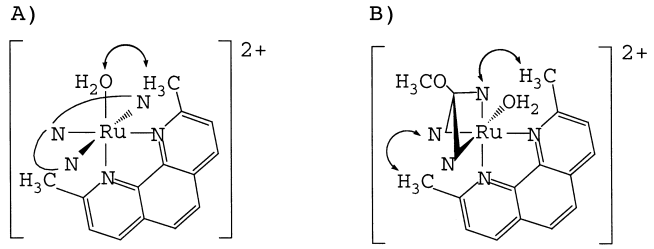
[a] In $NaNO_3/HNO_3$ solution (pH 2.00 and μ = 0.1 M) under pseudo first-order kinetics at 25.0 ± 0.1 °C.

 © WILEY-VCH Verlag GmbH, D-69451 Weinheim, 2001 1433-7851/01/4023-4470 $ 17.50+.50/0

5–65 °C indicated that the ligand substitution was enthalpically and entropically favored, consistent with a dissociative interchange mechanism. $\Delta H^{\neq}$ for $\mathbf{12B}^{2+}$ is 5.9 ± 0.1 kcal mol^{-1} smaller than that for $\mathbf{7B}^{2+}$, and $\Delta S^{\neq}$ of $\mathbf{12B}^{2+}$ is 10.1 ± 0.1 cal K^{-1} mol^{-1} more positive than that for $\mathbf{7B}^{2+}$. These results are consistent with our recent report on activation parameters for the complex $\mathbf{12B}^{2+}$ in a pH = 6.86 solution.[17]

From entries 1 and 2 in Table 1, k_{ls} for $\mathbf{4B}^{2+}$ is enhanced by a factor of 660 relative to that for $\mathbf{3B}^{2+}$ in the IPLE system when the protons are replaced by the methyl groups in the rigid bidentate phenanthroline ligand.[18] In the OPLE system, there is a rate decrease of 0.7 when k_{ls} for $\mathbf{8B}^{2+}$ is compared to that for $\mathbf{9B}^{2+}$.

As shown in Scheme 4 A, the bulkier methyl group on C(2) of the Me_2phen ligand in $\mathbf{4B}^{2+}$ points directly at the H_2O ligand, and this geometry facilitates substitution. In contrast



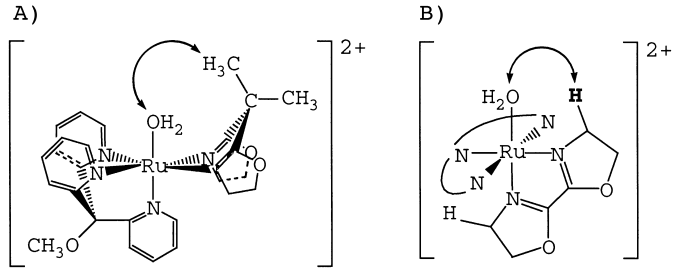
Scheme 4. Arrangements of 2,9-Me_2phen at the ruthenium center by: A) the tpy ligand and B) the tpmm ligand.

as shown in Scheme 4 B, the bulky substituent on C(2) of the Me_2phen ligand in $\mathbf{9B}^{2+}$ points to the two pyridyl rings of the tpmm ligand rather than to the H_2O ligand. As a result, the synthesis of the $[Ru^{II}(Cl)(Me_2phen)(tpmm)]^+$ precursor is more difficult than that of the $[Ru^{II}(Cl)(Me_2phen)(trpy)]^+$ analogue, but there is not any dramatic change in k_{ls} because of the lack of directional interaction with the H_2O ligand.

Based on entries 3 and 4, the propane backbone makes the dop ligand quite different from the diox ligand. In the OPLE system, the inclusion of the propane backbone accelerates k_{ls} for $\mathbf{11B}^{2+}$ by a factor of 345 relative to that for $\mathbf{10B}^{2+}$; however in the IPLE system, the presence of the propane backbone favors k_{ls} for $\mathbf{5B}^{2+}$ by a factor of 3.04. In the OPLE system, as shown in Scheme 5 A, the methyl group on the flexible carbon bridgehead exerts a greater effect on the H_2O ligand, whereas in the IPLE as shown in Scheme 5 B, the proton on C(5) of the five-heteroatom oxazolinyl ring of the diox ligand is too far from the active site to cause any effect on the H_2O ligand.

In contrast to the rigid phen and Me_2phen ligands, the non-aromatic flexible dop ligand exerts a reverse effect in the IPLE and OPLE systems, that is, with dop and trpy the reaction is slower than that with dop and tpmm.

To further investigate the effect exerted by the flexible backbone framework, the two non-aromatic oxazolinyl rings were replaced by the two aromatic pyrazolyl rings. According to the data from entries 4 and 5, the change from non-aromatic oxazolinyl rings to aromatic pyrazolyl rings results in a rate enhancement of 1.1×10^4 (from 1.0×10^{-2} M^{-1} s^{-1} for $\mathbf{11B}^{2+}$ to 1.1×10^2 M^{-1} s^{-1} for $\mathbf{12B}^{2+}$) in the OPLE system and a

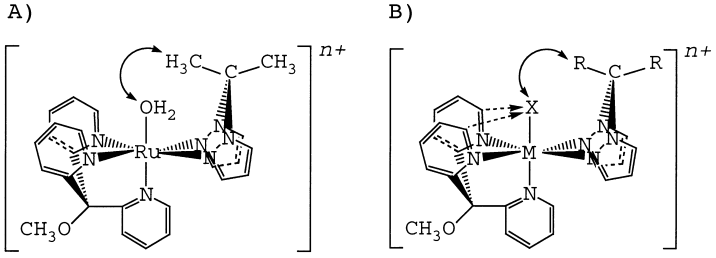


Scheme 5. A) Arrangement of the dop ligand at the ruthenium center by the tpmm ligand and B) arrangement of the diox ligand at the ruthenium center by the tpy ligand.

tenfold decrease of rate constant (from 4.6×10^{-5} M^{-1} s^{-1} for $\mathbf{6B}^{2+}$ to 5.9×10^{-6} M^{-1} s^{-1} for $\mathbf{7B}^{2+}$) in the IPLE system. It is clear that the combination of the flexible propane backbone and the aromaticity of the pyrazolyl rings is the key to the dramatic rate enhancement.

Entries 2 and 5 indicate that replacement of the tpmm ligand in $\mathbf{9B}^{2+}$ by the trpy ligand in $\mathbf{4B}^{2+}$ gives rise to a rate enhancement of 1.4×10^3 in the IPLE system, but the change from the trpy ligand in $\mathbf{7B}^{2+}$ to the tpmm ligand in $\mathbf{12B}^{2+}$ promotes a remarkable rate enhancement of 1.9×10^7 in the OPLE system! Notably, the rate constant of $(1.1 \pm 0.1) \times 10^2$ M^{-1} s^{-1} at pH 2.00 is significantly larger than those of typical ruthenium(II)–aqua complexes by four to eight orders of magnitude.[19] To our knowledge, it is the largest rate constant reported for ligand substitution reactions at a ruthenium(II) center and consistant with our report of a rate constant for $\mathbf{12B}^{2+}$ of 66 M^{-1} s^{-1}.[17]

Although the dop and dpp ligands have two five-membered rings containing two heteroatoms and the propane backbone (as shown in Scheme 3), the aromaticity of the pyrazolyl rings allows the dpp ligand to form the deeper "boat conformation" upon coordination to the metal center, and this conformation allows the methyl group on the carbon bridgehead (C2) to approach closer to the H_2O ligand.[11g] As a consequence, the dpp ligand is a heteroscorpionate ligand, rather than just a simple flexible bidentate ligand, as illustrated in Scheme 6 A.[5]



Scheme 6. Heteroscorpionate ligand effect, where R = pyrazole.

Detailed investigation of the effects caused by the backbone framework and the substituents are pictorially provided in the Supporting Information.[11h]

The X-ray crystal structures of $[Ru^{II}(Cl)(dpp)(tpmm)]BF_4$ (Figure 1 A) and $[Ru^{II}(Cl)(dpp)(trpy)]ClO_4$ (Figure 1 B) illus-

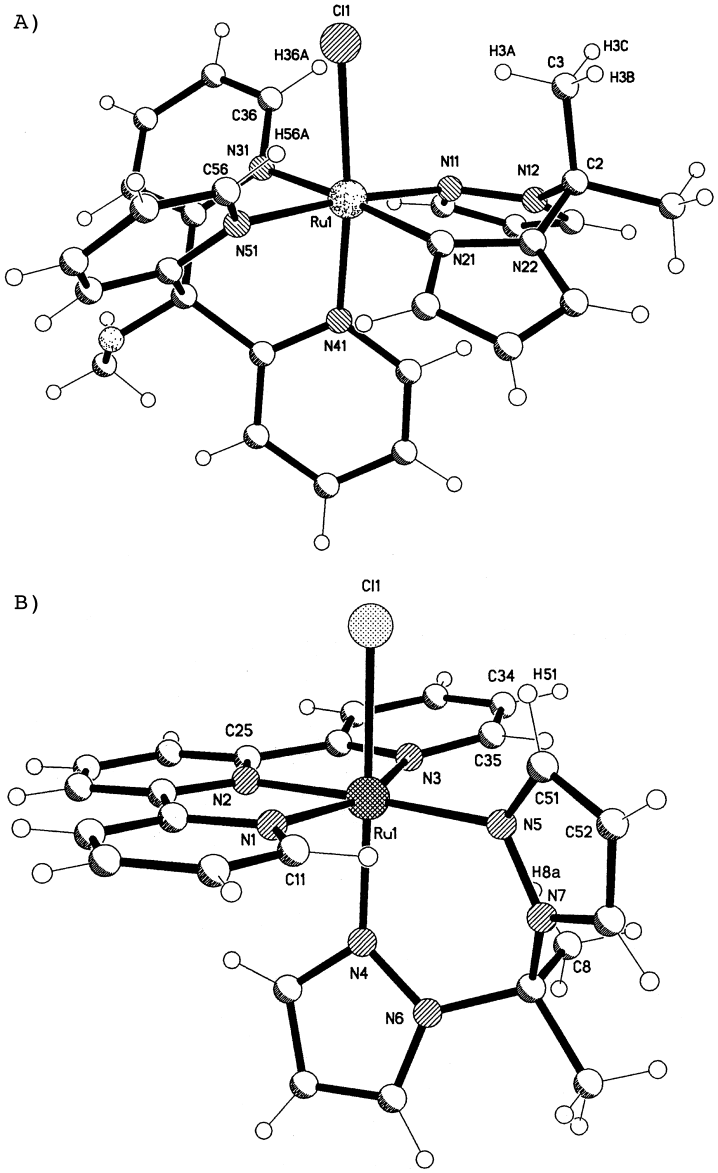


Figure 1. A) ORTEP diagram of the $[Ru^{II}(Cl)(dpp)(tpmm)]^+$ ion (thermal ellipsoids set at 30% probability). B) ORTEP diagram of the $[Ru^{II}(Cl)(dpp)(trpy)]^+$ ion (thermal ellipsoids set at 30% probability) .

trate the bifunctional behavior of the dpp ligand which depends upon its geometrical arrangement, this inturn depends upon the coordination of the tridentate ligand. In the $[Ru^{II}(Cl)(dpp)(tpmm)]BF_4$ complex, the Cl1 $\cdots$ H3a interatomic distance of 2.466 Å is unusually short, which confirms the heteroscorpionate effect of the dpp ligand in **12B**$^{2+}$ in the OPLE system. The structure of the $[Ru^{II}(Cl)(dpp)(trpy)]ClO_4$ complex (Figure 1B) provides evidence for the lack of steric interaction at the chloride ligand. The distances of 3.055 Å between Cl1 and H8a (the proton on one of the methyl groups on the carbon bridgehead) and of 2.771 Å between Cl1 and H51 (the proton on C51 of the pyrazolyl ring) are much longer than the equivalent distances in the tpmm complex (Figure 1a). As supported by the structural data from the $[Ru^{II}(Cl)(dpp)(L_3)]^+$ complexes, the dpp ligand behaves as a heteroscorpionate ligand in the OPLE system, but like a rigid bidentate ligand in the IPLE system.

This study gives a systematically comparison of ligand effects among the three different geometrical arrangements of bidentate ligands. Our results provide the first documented example of three important phenomena: 1) an extraordinarily large rate constant for a ligand substitution at a ruthenium(II) center ($(1.1 \pm 0.1) \times 10^2\,M\,s^{-1}$), 2) an extremely large rate enhancement for ligand substitution in octahedral transition metal complexes (1.9×10^7), primarily because of the nature of bidentate ligands and geometrical arrangements of tridentate "spectator" ligands, and 3) a remarkable rate enhancement for ligand substitution at a supposedly inert ruthenium(II) center, primarily a result of steric interaction.

The unusual heteroscorpionate ligand effect holds great promise for the development of new reagents and catalysts. As indicated in Scheme 6B and indicated in Figure 1A, the heteroscorpionate ligand effect can be explored further by utilizing heteroscorpionate ligands with various curving tails (pseudoaxial R) and with a bulky substituent at the ortho position of the two pyridyl rings of the tpmm ligand (the substituents at C36 and C56 in Figure 1A) that are *cis* relative to the active site of the ruthenium "prey".

Received: June 18, 2001
Revised: September 12, 2001 [Z17297]

[1] a) M. H. V. Huynh, El.-S. El-Samanody, P. S. White, T. J. Meyer, *Inorg. Chem.* **1999**, *38*, 3760–3761; b) C. S. Slone, C. A. Mirkin, G. P. A. Yap, I. A. Guzei, A. L. Rheingold *J. Am. Chem. Soc.* **1997**, *119*, 10743–10753; c) F. Calderazzo, G. Pampaloni, *J. Organomet. Chem.* **1995**, *500*, 47–60.

[2] a) P. Tole, C. Lim, *ACS Symp. Ser.* **1993**, *539*, 240–255; b) L. Acemoglu, J. M. J. Williams, *Adv. Synth. Catal.* **2001**, *343*, 75–77; c) D. Woska, A. Prock, W. P. Giering, *Organometallics* **2000**, *19*, 4629–4638; d) V. J. Catalano, R. A. Heck, C. E. Immoos, A. Ohman, M. G. Hill, *Inorg. Chem.* **1998**, *37*, 2150–2157.

[3] S. Trofimenko, *J. Am. Chem. Soc.* **1966**, *88*, 1842–1844.

[4] S. Trofimenko, *J. Am. Chem. Soc.* **1967**, *89*, 6288–6294.

[5] S. Trofimenko, *Chem. Rev.* **1993**, *93*, 943–980, and references therein.

[6] S. Trofimenko, *Scorpionates: the Coordination Chemistry of Polypyrazolylborate Ligands*, Imperial College Press, London, **1999**.

[7] R. T. Jonas, T. D. P. Stack, *Inorg. Chem.* **1998**, *37*, 6615–6629.

[8] a) L. Knorr, P. Rossler, *Ber.* **1903**, *36*, 1278; b) H. Wenker, *J. Am. Chem. Soc.* **1938**, *60*, 2152; c) I. Butula, G. Karlovic, *Leibigs Ann. Chem.* **1976**, 1455–1464; d) M. Gomez, G. Muller, M. Rocamora, *Coord. Chem. Rev.* **1999**, *195*, 769–835, and references therein.

[9] M. R. Churchill, D. G. Churchill, M. H. V. Huynh, K. J. Takeuchi, R. K. Castellano, D. L. Jameson, *J. Chem. Crystallogr.* **1996**, *26*, 179–183.

[10] Caution! Although we have not detected shock or heat sensitivity of the perchlorate salts examined, other perchlorate salts are known to detonate under some conditions.

[11] a) Supporting Information; b) Supporting Information Table 1; c) Supporting Information Figure 1; d) Inset of Supporting Information Figure 1; e) Supporting Information Figure 2A–E; f) Supporting Information Table 2; g) Supporting Information Figure 3; h) Supporting Information Table 3.

[12] Crystallographic data (excluding structure factors) for the structures reported in this paper have been deposited with the Cambridge Crystallographic Data Centre as supplementary publication no. CCDC-165389 $[Ru^{II}(Cl)(phen)(tpmm)]BF_4 \cdot 1\frac{1}{2}CH_2Cl_2$; -165388 $[Ru^{II}(H_2O)(dop)(tpmm)](ClO_4)_2 \cdot H_2O$; -165386 $[Ru^{II}(Cl)(dpp)(tpmm)]BF_4 \cdot CH_2Cl_2$; -165387 $[Ru^{II}(Cl)(dpp)(trpy)](ClO_4) \cdot \frac{1}{2}C_6H_5CH_3$. Copies of the data can be obtained free of charge on

 © WILEY-VCH Verlag GmbH, D-69451 Weinheim, 2001 1433-7851/01/4023-4472 $ 17.50+.50/0

application to CCDC, 12 Union Road, Cambridge CB2 1EZ, UK (fax: (+44) 1223-336-033; e-mail: deposit@ccdc.cam.ac.uk).
[13] R. A. Leising, J. S. Ohman, K. J. Takeuchi, *Inorg. Chem.* **1988**, *27*, 3804 – 3809.
[14] a) R. E. Shepherd, H. Taube, *Inorg. Chem.* **1973**, *12*, 1392 – 1401; b) S. S. Isied, H. Taube, *Inorg. Chem.* **1976**, *15*, 3070 – 3075.
[15] T. Matsubara, C. Creutz, *Inorg. Chem.* **1979**, *18*, 1956 – 1966.
[16] L. R. Allen, P. R. Craft, B. Durham, J. Walsh, *Inorg. Chem.* **1987**, *26*, 53 – 56.
[17] M. H. V. Huynh, J. M. Lasker, M. Wetzler, B. Mort, L. F. Szczepura, L. M. Witham, J. M. Cintron, A. C. Marschilok, L. J. Ackerman, R. K. Castellano, D. L. Jameson, M. R. Churchill, A. J. Jircitano, K. J. Takeuchi, *J. Am. Chem. Soc.* **2001**, *123*, 8780 – 8784.
[18] C. A. Bessel, J. A. Margarucci, J. H. Acquaye, R. S. Rubino, J. Crandall, A. J. Jircitano, K. J. Takeuchi, *Inorg. Chem.* **1993**, *32*, 5779 – 5784.
[19] a) Typically, rates of aqua-ligand exchange in ruthenium(II) and ruthenium(III) complexes range from 1×10^{-6} M^{-1}s^{-1} to 1×10^{-2} M^{-1}s^{-1}; b) L. Mønsted, O. Mønsted, *Coord. Chem. Rev.* **1989**, *94*, 109 – 150.

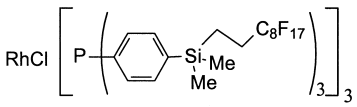
Homogeneous Reactions in Supercritical Carbon Dioxide Using a Catalyst Immobilized by a Microporous Silica Membrane

Leo J. P. van den Broeke,* Earl L. V. Goetheer, Arjan W. Verkerk, Elwin de Wolf, Berth-Jan Deelman, Gerard van Koten, and Jos T. F. Keurentjes

Although homogeneous catalysis offers many advantages over heterogeneous catalysis in terms of catalytic selectivity and activity, the difficult separation of the catalyst from the products and the use of environmentally harmful organic solvents are two major drawbacks.[1, 2] The problem of catalyst separation has been addressed by several groups, and a number of new concepts for immobilization of homogeneous catalysts have been developed.[3] With respect to the use of more environmentally friendly solvents, the application of high-density gases such as supercritical carbon dioxide ($scCO_2$; $T_c = 304.2$ K and $P_c = 73.8$ bar) has some clear advantages.[2, 4] Supercritical solvents are completely miscible with gaseous reagents, and, therefore, avoid possible diffusion limitation in gas – liquid reactions. An important issue for successful operation of homogeneous catalysis in $scCO_2$ is the solubility of the catalyst, which can be achieved by attaching perfluoroalkyl groups to the ligands.[5]

Herein, we present a solution that overcomes these drawbacks. We employ a continuous reactor for homogeneous catalysis in $scCO_2$ that allows an integrated catalyst separation by immobilization of a perfluoroalkylated catalyst on one side of a microporous silica membrane. The low cohesive energy density of perfluoroalkyl groups is used to realize the required solubility of the catalyst in $scCO_2$, and simultaneously the increased size ensures effective retention of the catalyst in the membrane reactor. The reactants and products, which are also dissolved in the $scCO_2$, can diffuse through the membrane.

The principle is demonstrated by using a (1*H*,1*H*,2*H*,2*H*-perfluoroalkyl)dimethylsilyl-substituted derivative of Wilkinson's catalyst, **1**[6] and a supported microporous silica



1

membrane with an average pore size of 0.6 nm.[7] The mechanical strength of ceramic silica membranes allows the use of relatively harsh reaction conditions. As a model reaction the hydrogenation of 1-butene was first carried out in $scCO_2$ in a batch reactor[8] at 200 bar and 353 K. The catalyst **1** was prepared in situ from $[RhCl(cod)]_2$ (cod = *cis*,*cis*-1,5-cyclooctadiene) and six equivalents of P(*p*-(Si$Me_2CH_2CH_2C_8F_{17}$)C_6H_4)$_3$. In the batch reactor the turnover frequency (TOF) at 25 % conversion was found to be 9400 h^{-1}. The high solubility of hydrogen in $scCO_2$, as compared to the solubility in conventional solvents,[6] is responsible for the 10-fold higher activity. For the sake of comparison, the solublity of hydrogen in toluene is 2.7 mM (at 1 bar and 298 K) and in fluorous solvents, like *c*-$C_6F_{11}CF_3$, it is 6.1 mM (at 1 bar and 298 K).

In the continuous membrane set-up (Figure 1), permeation and reaction experiments were typically conducted with a feed pressure of 200 bar and a transmembrane pressure between 0.5 and 10 bar.[9] Experiments have been performed with different pressure differences across the membrane to study the effect of the residence time on the conversion.

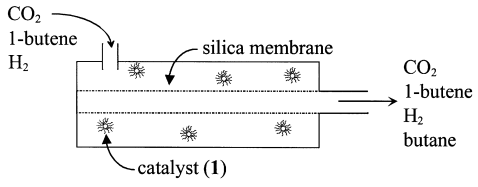


Figure 1. Continuous reaction and separation concept. The membrane reactor is operated in a dead-end configuration.

Up to a feed side pressure of 200 bar high fluxes of carbon dioxide were obtained through the microporous membrane. An overview of the characteristics of the membrane reactor is given in Table 1.

[*] Dr. L. J. P. van den Broeke, E. L. V. Goetheer, A. W. Verkerk,[+] Prof. Dr. J. T. F. Keurentjes
Process Development Group
Department of Chemical Engineering and Chemistry
Eindhoven University of Technology
PO Box 513, 5600 MB Eindhoven (The Netherlands)
Fax: (+31) 40-244-6104
E-mail: l.j.p.van.den.broeke@tue.nl
[+] Dutch Polymer Institute
PO Box 513, 5600 MB Eindhoven (The Netherlands)
E. de Wolf, Dr. B.-J. Deelman,[++] Prof. Dr. G. van Koten
Debye Institute, Department of Metal-Mediated Synthesis
Utrecht University
Padualaan 8, 3584 CH Utrecht (The Netherlands)
[++] ATOFINA Vlissingen BV
PO Box 70, 4380 AB Vlissingen (The Netherlands)

 © WILEY-VCH Verlag GmbH, D-69451 Weinheim, 2001 1433-7851/01/4023-4473 $ 17.50+.50/0

Table 1. Characteristics of the membrane reactor.

Property	
thickness selective silica layer	200 nm
length membrane	0.30 m
outer diameter ceramic membrane	0.014 m
membrane reactor volume	35.0 mL
CO_2 permeance[a] (200 bar, 353 K)	3.0×10^{-3} mol m^{-2} s^{-1} bar^{-1}

[a] Flux divided by the pressure difference across the membrane.

In the continuous process[10] about two permeated reactor volumes were needed to reach a constant conversion of about 40 % (Figure 2). In the experiment a pressure difference of

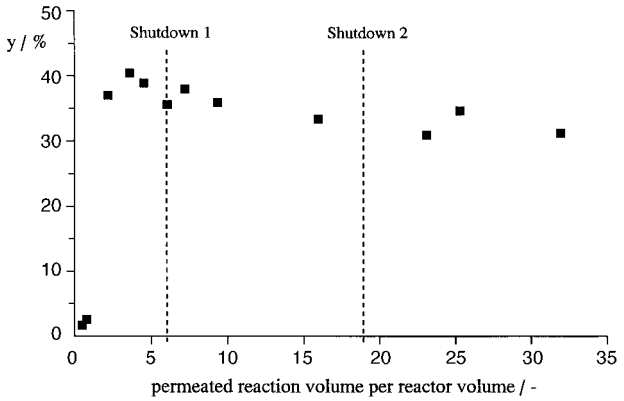


Figure 2. Conversion, y [%], of 1-butene to butane versus permeated volume per reactor volume, for the continuous reaction/separation process.

3 bar is applied, and this corresponds to a residence time of 62 min. The TOF, based on the initial amount of catalyst added, is 4000 h^{-1}, which is about 60 % lower than in the batch experiment (TOF = 9400 h^{-1}). Overnight the pressure of the system was reduced to 60 bar, leaving no pressure difference between the feed and the permeate side of the membrane. During the depressurization of the membrane reactor the catalyst precipitated and no further reaction occurred. The precipitated catalyst was used for a new cycle by pressurization of the membrane reactor. The shutdown procedure was carried out twice to check the stability of the catalyst under those conditions. At the start of a new cycle, the system was first pressurized to 200 bar for 2 h to dissolve the catalyst before creating a transmembrane pressure difference. At the end of the third run a conversion of about 33 % was obtained (TOF = 3000 h^{-1}). An overall turnover number of about 1.2×10^5 was obtained (in 32 h), and a total of 32 reactor volumes had permeated through the membrane. The overall operating time, including start-ups, reaction cycles, and shutdowns, was approximately 75 h.

In Figure 2 an 18 % decrease in conversion is observed (from 40 % to 33 %). Analysis of the permeate stream by UV/Vis spectroscopy[11] and by inductively coupled plasma atomic absorption spectrometry (ICP-AAS) showed that there was no transport of the catalyst or of the free ligand through the membrane; thus, it can be concluded that complete retention of **1** occurred. Even if the decrease in conversion would have been caused by leaching of the catalyst, the retention of the catalyst per permeated reactor volume is still over 99 %. The latter appears highly unlikely since the size of **1**, as obtained from a MMFF94 molecular mechanics structural optimization (4 nm) and dynamic light scattering (2 nm in c-$C_6F_{11}CF_3$), was found to be much larger than the average pore size of the membrane (0.6 nm). Oxidation of **1** due to residual traces of oxygen in the carbon dioxide or the feed is a more likely explanation for the observed decrease in activity.

In conclusion, we have demonstrated the successful application of membrane separation technology for the immobilization of homogeneous catalysts in a continuous process using a supercritical solvent. It is clear that the methodology presented here could be highly relevant for the further development of clean chemical processes based on homogeneous catalysis carried out in environmentally friendly high-density gases.

Received: July 5, 2001 [Z17434]

[1] P. G. Jessop, T. Ikariya, R. Noyori, *Chem. Rev.* **1999**, *99*, 475.
[2] D. Adams, *Nature* **2000**, *407*, 938.
[3] M. G. L. Petrucci, A. K. Kakkar, *Adv. Mater.* **1996**, *8*, 251; J. W. Knapen, A. W. van der Made, J. C. Wilde, P. W. N. M. van Leeuwen, P. Wijkens, D. M. Grove, G. van Koten, *Nature* **1994**, *372*, 659; W. A. Herrmann, C. W. Kohlpainter, *Angew. Chem.* **1993**, *105*, 1588; *Angew. Chem. Int. Ed. Engl.* **1993**, *32*, 1524; E. de Wolf, G. van Koten, B.-J. Deelman, *Chem. Soc. Rev.* **1999**, *28*, 37.
[4] *Chemical synthesis using supercritical fluids* (Eds.: P. G. Jessop, W. Leitner), Wiley-VCH, Weinheim, **1999**; S. L. Wells, J. DeSimone, *Angew. Chem.* **2001**, *113*, 534; *Angew. Chem. Int. Ed.* **2001**, *40*, 518; B. Lin, A. Akgerman, *Ind. Eng. Chem. Res.* **2001**, *40*, 1113.
[5] S. Kainz, D. Koch, W. Baumann, W. Leitner, *Angew. Chem.* **1997**, *109*, 1699; *Angew. Chem. Int. Ed. Engl.* **1997**, *36*, 1628.
[6] B. Richter, A. L. Spek, G. van Koten, B.-J. Deelman, *J. Am. Chem. Soc.* **2000**, *122*, 3945; B. Richter, E. de Wolf, G. van Koten, B.-J. Deelman, *J. Org. Chem.* **2000**, *65*, 3885.
[7] M. K. Koukou, N. Papayannakos, N. C. Markatos, M. Bracht, H. M. Veen, A. Roskam, *J. Membr. Sci.* **1999**, *155*, 241.
[8] The batch reactor, with a volume of 26 mL, consists of two saffire windows for UV/Vis monitoring. The volume of the reactor can be controlled with a piston, which assures sampling without disturbing the reaction conditions. The concentration of **1** was 1.0×10^{-6} mol L^{-1}, and 1-butene and hydrogen were present in a concentration of 0.02 and 0.08 mol L^{-1}, respectively, at a total pressure of 200 bar.
[9] For the permeation experiments and the hydrogenation reaction in the membrane reactor the same high-pressure set-up was used. The catalyst was first synthesized in situ in a high-pressure reactor. The catalyst was introduced into the system by gently flushing CO_2 through the high-pressure reactor. The reaction was started by the addition of the 1-butene and hydrogen to the membrane module. The membrane was pressurized at the feed and permeates side up to 200 bar with the reaction mixture, by using a LKB HPLC pump and was monitored by a Meyvis 802-C pressure module. The permeate needle valve was opened to create a transmembrane pressure varying between 0.5 to 10 bar. The composition of the permeate was monitored by GC and by GC-MS.
[10] During the continuous reaction experiments the concentration of **1** was 1.0×10^{-6} mol L^{-1}, and 1-butene and hydrogen were present in a concentration of 0.02 and 0.08 mol L^{-1}, respectively.
[11] A 2.2 mL high-pressure viewing cell was used in combination with a spectrophotometer; measurements recorded at 280 and 410 nm.

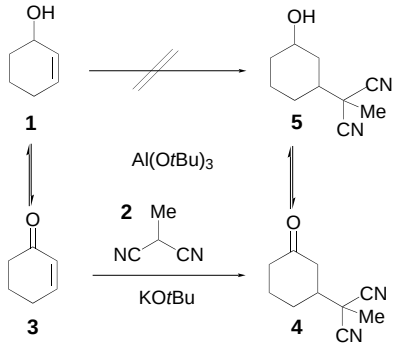
 © WILEY-VCH Verlag GmbH, D-69451 Weinheim, 2001 1433-7851/01/4023-4474 $ 17.50+.50/0

Catalytic Electronic Activation: Indirect Addition of Nucleophiles to an Allylic Alcohol**

Phillip J. Black, William Harris, and Jonathan M. J. Williams*

As a general principle, nucleophiles are able to add to electron-deficient alkenes, but are reluctant to react with electron-rich alkenes.[1] This is readily demonstrated by a comparison of the reactivity of 2-cyclohexen-1-ol (**1**) and 2-cyclohexen-1-one (**3**) towards the nucleophile derived from methylmalononitrile (**2**).[2] Whilst **1** was found to be unreactive even after 11 days, **3** underwent facile conjugate addition (4 h, RT, THF, 83 %; see Scheme 1).

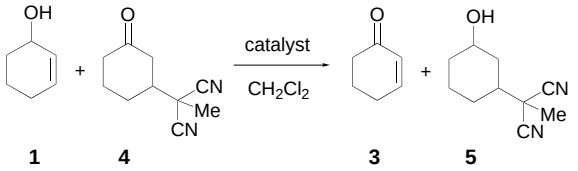
With increasing worldwide interest in domino and cascade reactions,[3] we have considered the possibility of temporarily converting an unreactive allylic alcohol **1** into the electronically activated α,β-unsaturated ketone **3**. The electronically activated substrate would then undergo conjugate addition, followed by a restoration of the alcohol functional group from the conjugate addition product **4**. Overall this would lead to an indirect addition of nucleophiles to allylic alcohols to give the addition product **5** (Scheme 1).



Scheme 1. Catalytic electronic activation of **1** permits conjugate addition followed by subsequent reduction.

For this one-pot approach to be successful, the following criteria must be met: 1) the interconversion of alcohol and ketone must be rapid and reversible; 2) the method for alcohol/ketone interconversion must be compatible with the conjugate addition reaction. The success of the overall catalytic electronic activation principle depends on these requirements.

The most straightforward process for alcohol/ketone interconversion is arguably transfer hydrogenation and there is plenty of scope in this area for choice of catalyst.[4] However, for some rhodium and ruthenium catalysts double-bond migration of allylic alcohols is a known process, affording the saturated ketone by isomerization.[5] It is for this reason that we have chosen to explore aluminum (Meerwein–Ponndorf–Verley (MPV)) catalysts[6] for their ability to effect transfer hydrogenation between 2-cyclohexen-1-ol (**1**) and ketone **4** (Scheme 2).

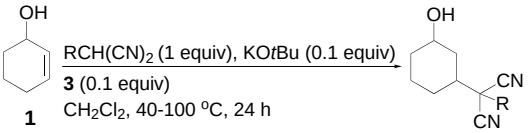


10 mol% $Al(OtBu)_3$, 40 °C, 6 h > 95 % conv.
10 mol% Me_2AlCl, 25 °C, 6 h > 95 % conv.

Scheme 2. Oppenauer/MPV crossover.

These data clearly demonstrate that the equilibrium position for the transfer hydrogenation reaction lies firmly to the right, that is towards the thermodynamically more favorable conjugated ketone. This is beneficial for ensuring a constant supply of enone ready for conjugate addition. Surprisingly, both catalysts exhibit excellent activities at substoichiometric levels; a property not normally associated with MPV-type systems.[6d]

Based on the conditions needed for conjugate addition and for transfer hydrogenation we attempted an indirect nucleophilic addition of methylmalononitrile (**2**) and benzylmalononitrile (**6**)[2] to 2-cyclohexen-1-ol (**1**) and 2-cyclopenten-1-ol (**7**) (Scheme 3, Method A; Table 1).



Method A $Al(OtBu)_3$ (1.0 equiv) R = Me **5a**
Method B $Al(OtBu)_3$ (0.1 equiv) R = Ph **5b**

Scheme 3. Typical procedure for the domino Oppenauer/Michael addition/MPV process.

Although good yields were obtained for cyclohexyl-derived substrates (Table 1, entries 1 and 5), poor results occurred by using substoichiometric amounts of catalyst (Table 1, entries 2 and 4) and for the cyclopentyl system (Table 1, entries 6 and 7). To address these problems the reactions were studied at elevated temperatures using Ace-Pressure tubes (Scheme 3, Method B).

Therefore, we were delighted with the realization of a fully catalytic reaction (Table 2, entries 1 and 2) when higher reaction temperatures were employed; even when using

[*] Prof. Dr. J. M. J. Williams, P. J. Black
Department of Chemistry
University of Bath
Claverton Down
Bath BA2 7AY (UK)
Fax: (+44) 1225-826231
E-mail: j.m.j.williams@bath.ac.uk
W. Harris
Roche Discovery Welwyn
40 Broadwater Road
Welwyn Garden City
Hertfordshire AL7 3AY (UK)

[**] This work was supported by the University of Bath and Roche Discovery (P.J.B.).

 © WILEY-VCH Verlag GmbH, D-69451 Weinheim, 2001 1433-7851/01/4023-4475 $ 17.50+.50/0

Table 1. Indirect nucleophilic addition to cycloalkenols **1** and **7**.[a]

Entry	Substrate	Nucleophile	Catalyst [mol %]	t[b] [h]	Yield[c,d] [%]
1	**1**	**2**	$Al(OtBu)_3$(100)	24	90[e]
2	**1**	**2**	$Al(OtBu)_3$(10)	24	< 5
3	**1**	**2**	Me_2AlCl(100)[f]	24	45
4	**1**	**2**	Me_2AlCl(10)	24	< 5
5	**1**	**6**	$Al(OtBu)_3$(100)	24	81
6	**7**	**2**	$Al(OtBu)_3$(100)	24	27
7	**7**	**6**	$Al(OtBu)_3$(100)	24	19

[a] The reactions were carried out on a 1 mmol scale in dichloromethane (5 mL) at reflux ($Al(OtBu)_3$); or at room temperature (Me_2AlCl). [b] Rate studies indicated that the reaction reached near completion after 6–8 h. [c] Yield of isolated product after column chromatography. [d] The maximum expected yield is 90%. [e] Reaction carried out on a 5 mmol scale. [f] Tetrabutylammonium bromide (4 mol %) added to increase dissolution of methylmalononitrile salt.

Table 2. Catalytic indirect nucleophilic addition to cycloalkenols **1** and **7**.[a]

Entry	Substrate	Nucleophile	$Al(OtBu)_3$ [mol %]	t [h]	Yield[b] [%]
1	**1**	**2**	10	24	90
2	**1**	**2**	10	24	70[c]
3	**1**	**6**	10	24	64
4	**7**	**2**	100	24	60
5	**7**	**6**	100	24	21

[a] The reactions were carried out on a 1 mmol scale in dichloromethane (3 mL) at 100 °C. [b] Yield of isolated product after column chromatography. [c] Cyclohexanone (10 mol %) used as oxidant.

cyclohexanone as an alternative catalytic oxidant (Table 2, entry 2).

However, the increase in temperature does not provide an enhancement in the yields obtained for the cyclopentyl system that we would have anticipated (Table 2, entries 4 and 5). Further experiments using scandium triflate and cerium chloride heptahydrate additives to activate 2-cyclopenten-1-one proved equally unsuccessful. It is suspected that the lower recovered yield at these temperatures is attributed to a competing side reaction (e.g. Pinner[7] reaction).

In summary, we have demonstrated that whilst nucleophiles will not normally add to allylic alcohols, this reaction becomes possible by a procedure involving catalytic electronic activation of the substrate.[8] We anticipate that the concept of catalytic electronic activation could be applied to other reactions that are more successful for electron-deficient alkenes than for electron-rich alkenes.

Experimental Section

Typical procedure for the domino Oppenauer/Michael addition/MPV process: Compounds **1** (0.098 g, 1.0 mmol) and **3** (0.009 g, 0.1 mmol) were added to a suspension of **6** (0.156 g, 1.0 mmol) and KO*t*Bu (0.011 g, 0.1 mmol) in CH_2Cl_2 (3 mL). The solution was heated to reflux under nitrogen and aluminum *tert*-butoxide (0.246 g, 1.0 mmol) in CH_2Cl_2 (2 mL) was added dropwise. After 24 h, the reaction was cooled, diluted with diethyl ether (50 mL), and washed with 10% v/v aqueous HCl (25 mL). The aqueous phase was separated and extracted with diethyl ether (3 × 50 mL). The combined organic extracts were washed with brine, dried ($MgSO_4$), and concentrated in vacuo. Purification by flash column chromatography (SiO_2, 50% petroleum ether/diethyl ether) gave **5b** (0.206 g, 81% yield). $\mathbf{5b}_{\text{axial alcohol}}$: m.p. 106–108 °C; ^{1}H NMR (500 MHz, C_6D_6, 25 °C): $\delta = 0.35$ (br s, 1H; OH), 0.81 (app. ddt, $^3J(H,H) = 2$ Hz, $^3J(H,H) = 4$ Hz, $^2J(H,H) = 13.5$ Hz, 1H; H_{6ax}), 0.96 (app. dq, $^3J(H,H) = 4$ Hz, $^2J(H,H) = 13$ Hz, 1H; H_{4ax}), 1.12 (app. dt, $^3J(H,H) = 2$ Hz, $^2J(H,H) = 13$ Hz, 1H; H_{2ax}), 1.17–1.21 (m, 1H; H_{5eq}), 1.25 (br d, $^2J(H,H) = 14$ Hz, 1H; H_{6eq}), 1.37 (app. tq, $^2J(H,H) = 4$ Hz, $^3J(H,H) = 13$ Hz, 1H; H_{5ax}), 1.64 (br d, $^2J(H,H) = 12.5$ Hz, 1H; H_{4eq}), 1.70 (br d, $^2J(H,H) = 13$ Hz, 1H; H_{2eq}), 1.99 (app. tt, $^3J(H,H) = 3$ Hz, $^3J(H,H) = 12$ Hz, 1H; H_{3ax}), 2.41 (d, $^2J(H,H) = 14$ Hz, 1H; C*H*Ph), 2.51 (d, $^2J(H,H) = 14$ Hz, 1H; C*H*Ph), 3.53 (br s, 1H; H_{1eq}), 7.02–7.25 (m, 5H; Ph); IR (C_6D_6): $\tilde{\nu} = 2282$ (C≡N), 3592 cm^{-1} (O–H); MS (70 eV): m/z (%): 254 [$M^{+\cdot}$], 91 (100) [$PhCH_2^+$].

Received: August 13, 2001 [Z17716]

[1] P. Perlmutter in *Conjugate Addition Reactions in Organic Synthesis*, *Vol. 9* (Eds.: J. E. Baldwin, P. D. Magnus), Pergamon, Oxford, **1992**.

[2] E. Díez-Barra, A. la Hoz, A. Moreno, P. Sánchez-Verdú, *J. Chem. Soc. Perkin Trans. 1*. **1991**, 2589–2592.

[3] a) L. F. Tietze, *Chem. Rev.* **1996**, *96*, 115–136; b) L. F. Tietze, *J. Heterocycl. Chem*. **1990**, *27*, 47; c) F. Ziegler, *Chem. Rev.* **1988**, *88*, 1423; d) G. H. Posner, *Chem. Rev*. **1986**, *86*, 831; e) L. F. Tietze in *Selectivity A Goal for Synthetic Efficiency* (Eds.: W. Bartmann, B. M. Trost), VCH, Weinheim, **1984**, p. 299.

[4] a) R. A. W. Johnstone, A. H. Wilby, I. D. Entwistle, *Chem. Rev*. **1985**, *85*, 129; b) G. Brieger, T. J. Nestrick, *Chem. Rev*. **1974**, *74*, 567.

[5] a) B. M. Trost, R. J. Kulawiec, *J. Am. Chem. Soc*. **1993**, *115*, 2027; b) J.-E. Bäckvall, U. Andreasson, *Tetrahedron Lett*. **1993**, *34*, 5459.

[6] a) A. L. Wilds, *Org. React*. **1944**, *2*, 178–223; b) C. Djerassi, *Org. React*. **1951**, *6*, 207–235; c) H. Lehmann, *Methoden Org. Chem*. (*Houben-Weyl) 4th ed. 1952–, Vol. 4/1b* **1975**, p. 901; d) C. F. de Graauw, J. A. Peters, H. van Bekkum, J. Huskens, *Synthesis* **1994**, 1007–1017.

[7] F. C. Schaffer, G. A. Petters, *J. Am. Chem. Soc*. **1961**, *83*, 412–418.

[8] Although the domino Oppenauer/Michael addition/MPV process has not previously been reported in the literature, a tandem ene-Oppenauer reaction has been reported: B. B. Snider, B. E. Goldman, *Tetrahedron* **1986**, *42*, 2951–2956; and more recently a tandem Michael addition/MPV reduction: M. Node, K. Nishide, Y. Shigeta, H. Shiraki, K. Obata, *J. Am. Chem. Soc*. **2000**, *122*, 1927–1936.

The tmbp Dianion in the Contact Ion Pair $[(tmbp)Na_2(dme)_{1.5}]_n$ and in the Solvent-Separated Ion Pair $[tmbp][(2.2.1)Li]_2$**

Patrick Rosa, Nicolas Mézailles, Louis Ricard, François Mathey,* and Pascal Le Floch*

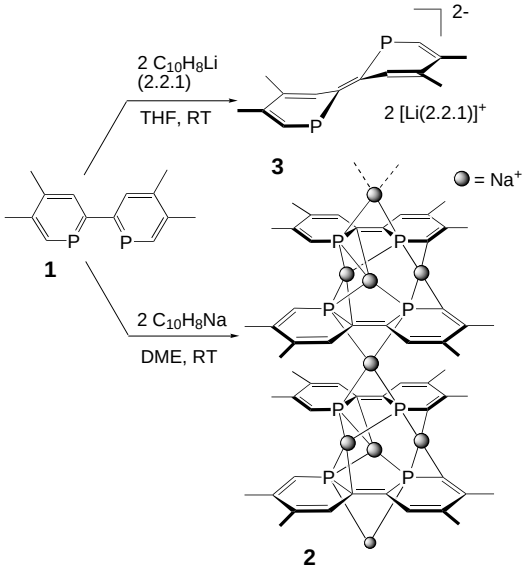
Multiple reductions of unsaturated π systems generally provide important information on delocalization processes. Furthermore they often yield fascinating structures that illustrate aggregation and solvation phenomena of cations,[1] and constitute good models for the modification of solid

[*] Prof. F. Mathey, Dr. P. Le Floch, Dr. P. Rosa, Dr. N. Mézailles, Dr. L. Ricard
Laboratoire Hétéroéléments et Coordination
UMR CNRS 7653, Ecole Polytechnique
91128 Palaiseau Cedex (France)
Fax: (+33) 016-933-3990
E-mail: francois.mathey@polytechnique.fr
lefloch@poly.polytechnique.fr

[**] This work was supported by the CNRS and the Ecole Polytechnique; tmbp = 4,4′,5,5′-tetramethyl-2,2′-biphosphinine, DME = 1,2-dimethoxyethane.

 © WILEY-VCH Verlag GmbH, D-69451 Weinheim, 2001 1433-7851/01/4023-4476 $ 17.50+.50/0

surfaces by adsorption of alkali metals.[2] Whereas reduction processes of unsaturated carbon[3] and nitrogen derivatives are now well documented,[4] that of sp^2-hybridized phosphorus-based molecules and their related transition metal complexes constitute a new field.[5] Recently, we have shown that 2,2′-biphosphinine dianions[6a] could be used efficiently to synthesize highly reduced transitions metal complexes through their reactions with various metal precursors;[6] herein we shed some light on their very peculiar geometrical and electronic structures. The twofold reduction of 4,4′,5,5′-tetramethyl-2,2′-biphosphinine (**1**; tmbp)[7a] was studied in THF and dimethoxyethane at room temperature with lithium naphthalene or sodium naphthalene with and without cryptands. From dimethoxyethane (DME), a polymeric structure of general formula $[(tmbp)Na_2(dme)_{1.5}]_n$ (**2**) crystallized,[8] whereas reaction with lithium in THF in the presence of cryptand (2.2.1) yielded the monomeric complex $[(tmbp)][Li(2.2.1)]_2$ (**3**; Scheme 1).[9]



Scheme 1. Synthesis of polymeric $[(tmbp)Na_2(dme)_{1.5}]_n$ and monomeric $[(tmbp)][Li(2.2.1)]_2$ salts.

The structure of **2** is highly unusual (Figure 1). The 2,2′-biphosphinine ligand adopts a cisoid configuration and the Na2, Na2′, and Na3 cations, which are each coordinated by one DME ligand, link two (tmbp) dianionic units. These two units are stacked to columns by Na1 cations. Relatively long distances (>3.45 Å) indicate that no contact occurs between all these cations and their most noticeable feature is their coordination mode. Indeed, the two cations Na2 and Na2′ are bound both to the two P atoms of one molecule (2.925(2)–3.096(1) Å) and in an η^2-mode to the P1–C5 bond (Na2–C5 = 2.63(3) Å) of the second molecule. These relatively long bond lengths suggest that the bonding between sodium cations and the reduced ligand is mainly electrostatic. This particular geometrical arrangement implies that weak contacts also occur between these two cations and the C4 and C6 carbon atoms (average 3.025 Å). Interestingly, the third cation Na3 is only coordinated on one side of the dimeric unit to the two

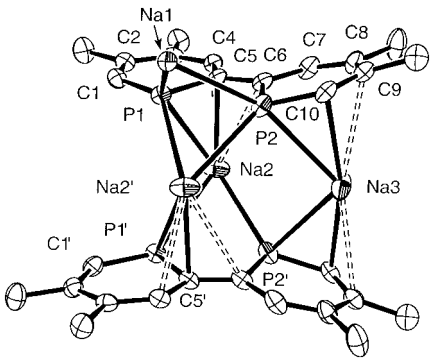


Figure 1. ORTEP view of two units of $[tmbp][Na_2(dme)_{1.5}]_n$ (**2**). The DME ligands have been omitted for clarity. Selected bond lengths [Å] and angles [°]: P1–C1 1.773(3), C1–C2 1.357(4) C2–C3 1.446(4), C3–C4 1.363(4), C4–C5 1.439(4), C5–P1 1.815(3), C5–C6 1.401(4), C6–C7 1.425(4), C7–C8 1.363(4), C8–C9 1.447(4), C9–C10 1.367(4), C10–P2 1.772(3), Na1–P1 2.996(2), Na1–P2 3.011(2), Na2′–P1 3.018(2), Na2′–P2 2.927(2), C5–Na2 2.631(3), Na3–P2 3.068(2), Na3–C10 2.759(3); C1-P1-C5 100.1(1), P1-Na1-P2 61.02(4), P1-Na2′-P2 60.77 (3).

external P2–C10 bonds and a contact with the two C9 carbon atoms (3.097(3) pm). As a consequence of the loss of aromaticity in each phosphinine subunit, the ligand adopts a curved shape. A similar distorsion was observed upon coordination of **1** to a triosmium core.[10] Intramolecular bond lengths are dramatically affected and the connection between the two rings is short (1.401(4) vs 1.49 Å in **1**)[7b] as are the C3–C4 and C7–C8 bonds (1.363(4) Å). Conversely, the internal P=C bonds P1–C5 (1.815(3) Å) and P2–C6 (1.821(3) pm) are significantly lengthened adopting a single-bond character. All these data are in good agreement with the filling of the π* LUMO of the neutral tmbp ligand.[6c, d]

In **3**, the ligand adopts a transoid configuration (Figure 2). The overall geometry of **3** is highly distorted and the C5–C5′ connection deviates out of the plane defined by the other carbon atoms of the ring (C1-C2-C3-C4) and the phosphorus atom ($\Theta = 11°$).[10] Except for this distorsion, bond lengths and bond angles are very similar to those of compound **2**.

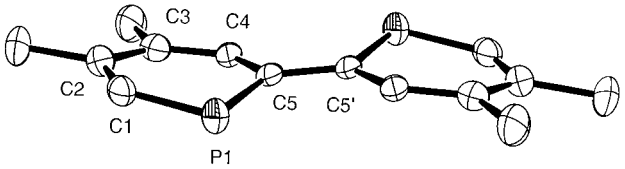
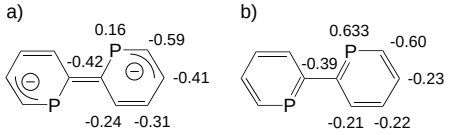


Figure 2. ORTEP view of one molecule of tmbp in **3**. Theoretical data obtained from calculations are given in parentheses. Selected bond lengths [Å] and angles [°]: P1–C1 1.760(7) [1.77], C1–C2 1.36(1) [1.36], C2–C3 1.44(1) [1.43], C3–C4 1.364(8) [1.38], C4–C5 1.431(8) [1.44], C5–P1 1.827(6) [1.87], C5–C6 1.40(1) [1.40]; C5-P1-C1 99.3(3) [100.9], P1-C1-C2 130.1(5) [127.7], C1-C2-C3 119.7(6) [129.9]; C2-C3-C4, 122.1(6) [124.2], C3-C4-C5 129.2(6) [127.7], C4-C5-P1 117.7(4) [117.1].

To assess the effects of the two-electron reduction of **1**, density functional theory (DFT) calculations were carried out on the constituent dianion in **3** (B3LYP/6-31 + G* level of theory).[11] A scan of the potential-energy surface indicated the presence of two minima, a *cis* and a *trans* structure, the former being slightly higher in energy ($E_{cis} - E_{trans} =$ 2.02 kcal mol^{-1}, MP2/6-311 + G(2d,p)//B3LYP/6-31 + G* level

of theory). Though the energy difference between the two configurations is small, all our crystallization attempts using (2.2.1) crytand yielded the *trans*-configuration product. This clearly shows that the loss of energy *trans* → *cis* in **2** is compensated by the Na–C_π and P_π interaction. The calculated geometry of the *trans* structure perfectly matches the experimental data, even reproducing the out of plane distorsion of the C–C bridge ($\Theta_{theo} = 10.5^\circ$). Additionally, the natural bond order (NBO) analysis[12] shows that the phosphorus atom still behaves as a strong donor towards the carbocyclic system and the natural charge at the phosphorus center in **2** (+0.160; c.f. +0.663 in **1**) compares with those calculated for other delocalized anionic structures such as $(CH_2{=}CH)_2P^-$ (+0.142) and the phospholide anion $C_4H_4P^-$ (+0.227).[13, 14] This observation indicates that dianions **2** and **3** should not be regarded as classical phosphides.[15] Indeed, the negative charge in the two rings is mainly delocalized over the P–Cα–Cβ part of the ring. These different data lead us to propose the pseudo-allylic structure in Scheme 2.



Scheme 2. Comparison between natural charges in computed dianionic (a) and free (b) biphosphinine.

Received: July 5, 2001 [Z17433]

[1] See for example: a) C. Lambert, P. v. R. Schleyer, *Angew. Chem.* **1994**, *106*, 1187; *Angew. Chem. Int. Ed. Engl.* **1994**, *33*, 1129; b) D. Hoffmann, W. Bauer, P. v. R. Schleyer, U. Pieper, D. Stalke, *Organometallics* **1993**, *12*, 1193.

[2] See for example: a) C. Janiak, R. Hoffmann, P. Sjövall, B. Kasemo, *Langmuir* **1993**, *9*, 3427; b) P. Wang, Y. Marayuma, R. M. Metzger, *Langmuir* **1996**, *12*, 3932.

[3] a) *Lithium Chemistry: A theoretical and Experimental Overview* (Eds.: A.-M. Sapse, P. v. R. Schleyer), Wiley, New York, **1994**; b) E. Weiss, *Angew. Chem.* **1993**, *105*, 1565; *Angew. Chem. Int. Ed. Engl.* **1993**, *32*, 1501; c) C. Janiak, H. Hemling, *Chem. Ber.* **1994**, *127*, 1251; d) H. Bock, T. Hauck, C. Näther, Z. Havlas, *Angew. Chem.* **1997**, *109*, 650; *Angew. Chem. Int. Ed. Engl.* **1997**, *36*, 638; e) C. Näther, H. Bock, Z. Havlas, T. Hauck, *Organometallics* **1998**, *17*, 4707; f) C. D. Stevenson, J. R. Noyes, R. C. Reiter, *J. Am. Chem. Soc.* **2000**, *122*, 12905; g) P. B. Hitchcock, M. F. Lappert, A. V. Protchenko, *J. Am. Chem. Soc.* **2001**, *123*, 189.

[4] See for example: H. Bock, J.-M. Lehn, J. Pauls, S. Holl, V. Krenzel, *Angew. Chem.* **1999**, *111*, 1004; *Angew. Chem. Int. Ed.* **1999**, *38*, 952.

[5] See for recent examples: a) A. Steiner, D. Stalke, *J. Chem. Soc. Chem. Commun.* **1993**, 444; b) S. Sasaki, F. Murakami, M. Yoshifuji, *Angew. Chem.* **1999**, *111*, 351; *Angew. Chem. Int. Ed.* **1999**, *38*, 340; c) S. Loss, A. Magistrato, L. Cataldo, S. Hoffmann, M. Geoffroy, U. Röthlisberger, H. Grützmacher, *Angew. Chem.* **2001**, *113*, 749; *Angew. Chem. Int. Ed.* **2001**, *40*, 723; d) M. Pfeiffer, T. Stey, H. Jehle, B. Klüpfel, W. Malisch, V. Chandrasekhar, D. Stalke, *Chem. Commun.* **2001**, 337; e) L. Cataldo, S. Choua, T. Berclaz, M. Geoffroy, N. Mézailles, L. Ricard, F. Mathey, P. Le Floch, *J. Am. Chem. Soc.* **2001**, *123*, 6654.

[6] a) P. Rosa, N. Mézailles, L. Ricard, F. Mathey, P. Le Floch, *Organometallics* **1999**, *18*, 348; b) P. Rosa, N. Mézailles, L. Ricard, F. Mathey, P. Le Floch, *Angew. Chem.* **2000**, *112*, 1893; *Angew. Chem. Int. Ed.* **2000**, *39*, 1823; c) S. Choua, H. Sidorenkova, T. Berclaz, M. Geoffroy, P. Rosa, N. Mézailles, L. Ricard, F. Mathey, P. Le Floch, *J. Am. Chem. Soc.* **2000**, *122*, 12227; d) N. Mézailles, P. Rosa, L. Ricard, F. Mathey, P. Le Floch, *Organometallics* **2000**, *19*, 2941; e) P. Rosa, N. Mézailles, L. Ricard, F. Mathey, P. Le Floch, Y. Jean, *Angew. Chem.* **2001**, *113*, 1291; *Angew. Chem. Int. Ed.* **2001**, *40*, 1251.

[7] a) P. Le Floch, D. Carmichael, L. Ricard, F. Mathey, *J. Am. Chem. Soc.* **1991**, *113*, 667; b) P. Le Floch, D. Carmichael, L. Ricard, F. Mathey, A. Jutand, C. Amatore, *Organometallics* **1992**, *11*, 2475.

[8] Preparation and single-crystal growth of **2**: In a dry box a solution of naphthalene/Na (0.2 mmol) in a DME/Et_2O mixture (8:2), was added to solid tmbp (25 mg, 0.1 mmol) under argon. The dark green solution was then transferred to a glass tube which was subsequently sealed. Deep purple crystals of **2** of X-ray quality deposited within a week at room temperature. The tube was taken back into a dry box and the crystals collected on a fine frit, yield (75%). The high sensitivity of the product towards oxygen precluded the determination of elemental analyses. Single crystals of **2** were protected with paratone oil for handling. Crystal structure determination: formula: $C_{46}H_{80}Li_2N_4O_{10}P_2$, dimensions $0.08 \times 0.08 \times 0.04$ mm, monoclinic, space group $P2/n$, $a = 8.440(5)$, $b = 12.760(5)$, $c = 21.340(5)$ Å, $\alpha = 89.970(5)$, $\beta = 90.190(5)$, $\gamma = 89.980(5)^\circ$, $V = 2298.2(17)$ Å^3, $Z = 4$, $\rho_{calcd} = 1.235$ g cm^{-3}, $\mu = 0.243$ cm^{-1}, $F(000) = 908$, $\Theta_{max} = 24.40^\circ$, h,k,l ranges, −9 to 8, −14 to 14, −24 to 24; 11266 reflections collected of which 3793 were unique ($R_{int} = 0.0602$), 2899 reflections with $I > 2\sigma(I)$, and 252 parameters refined, GOF(F^2) = 1.130, final R indices: $R_1 = 0.0468$, $wR_2 = 0.1402$, max./min. residual electron density 0.582(0.167)/−0.466(0.167) e Å^{-3}. For data collection see ref. [9]. In this structure, Na1 and Na3 atoms both sit on twofold axes. The dimer shown in Figure 1 is obtained by a twofold (55502) rotation of the tmbp dianion about Na3 and applying operation 65501 and 45502 to Na2 (ORTEP notation). The symmetry of the dimer is C_2.

[9] Preparation and single-crystal growth of **3**: In a dry box a solution of naphthalene/Li (0.2 mmol) in DME was added to a mixture of solid tmbp (25 mg, 0.1 mmol) and Kryptofix (2.2.1) (66 mg, 0.2 mmol) under argon. The deep purple solution obtained was then sealed in a glass tube and small X-ray quality crystals deposited within a week at room temperature. The tube was taken back into a dry-box and the crystals collected on a fine frit, yield (65%). The high sensitivity towards oxygen precluded the determination of elemental analyses. Single crystals of **3** were protected with paratone oil for handling. Crystal structure determination: formula: $C_{30}H_{48}LiN_2O_5P_2$, dimensions $0.22 \times 0.22 \times 0.16$ mm, triclinic, space group $P\bar{1}$, $a = 10.639(5)$, $b = 10.703(5)$, $c = 12.503(5)$ Å, $\alpha = 100.590(5)$, $\beta = 106.250(5)$, $\gamma = 11.240(5)^\circ$, $V = 1207.6(9)$ Å^3, $Z = 1$, $\rho_{calcd} = 1.272$ g cm^{-3}, $\mu = 0.150$ cm^{-1}, $F(000) = 500$, $\Theta(max) = 20.81^\circ$, h,k,l ranges, −10 to 10, −10 to 10, −11 to 12; 4330 reflections collected of which 2515 were unique ($R_{int} = 0.0347$), 2201 reflections with $I > 2\sigma(I)$, and 252 parameters refined, GOF(F^2) = 1.272, final R indices: $R_1 = 0.0797$, $wR_2 = 0.2185$, max./min. residual electron density 0.476(0.099)/−0.423(0.099) e Å^{-3}. The dianion has a C_i symmetry. Figure 2 shows the assembly resulting from an inversion center at 66602. Data collection for structures **2** and **3**: Nonius Kappa CCD diffractometer, φ and ω scans, $Mo_{K\alpha}$ radiation ($\lambda = 0.71073$ Å), graphite monochromator, $T = 150$ K, structure solution with SIR97,[16] refinement against F^2 (SHELXL97[17]) with anisotropic thermal parameters for all non-hydrogen atoms, calculated hydrogen positions with riding isotropic thermal parameters. Crystallographic data (excluding structure factors) for the structures reported in this paper have been deposited with the Cambridge Crystallographic Data Centre as supplementary publication no. CCDC-166429 (for **2**) and CCDC-166430 (for **3**). Copies of the data can be obtained free of charge on application to CCDC, 12 Union Road, Cambridge CB2 1EZ, UK (fax: (+44) 1223-336-033; e-mail: deposit@ccdc.cam.ac.uk).

[10] M. J. Bakker, F. W. Vergeer, F. Hartl, K. Goubitz, J. Fraanje, P. Rosa, P. Le Floch, *Eur. J. Inorg. Chem.* **2000**, 843.

[11] Calculations were carried out using Gaussian 98 (Revision A.7), M. J. Frisch, G. W. Trucks, H. B. Schlegel, G. E. Scuseria, M. A. Robb, J. R. Cheeseman, V. G. Zakrzewski, J. A. Montgomery, R. E. Stratmann, J. C. Burant, S. Dapprich, J. M. Millam, A. D. Daniels, K. N. Kudin, M. C. Strain, O. Farkas, J. Tomasi, V. Barone, M. Cossi, R. Cammi, B. Mennucci, C. Pomelli, C. Adamo, S. Clifford, J. Ochterski, G. A. Petersson, P. Y. Ayala, Q. Cui, K. Morokuma, D. K. Malick, A. D. Rabuck, K. Raghavachari, J. B. Foresman, J. Cioslowski, J. V. Ortiz, A. G. Baboul, B. B. Stefanov, G. Liu, A. Liashenko, P. Piskorz, I. Komaromi, R. Gomperts, R. L. Martin, D. J. Fox, T. Keith, M. A. Al-

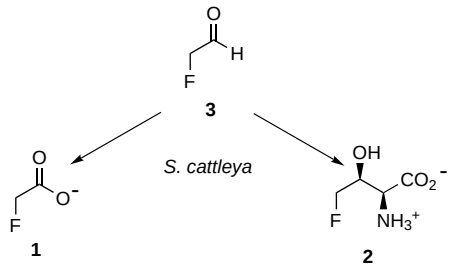
 © WILEY-VCH Verlag GmbH, D-69451 Weinheim, 2001 1433-7851/01/4023-4478 $ 17.50+.50/0

Laham, C. Y. Peng, A. Nanayakkara, C. Gonzalez, M. Challacombe, P. M. W. Gill, B. G. Johnson, W. Chen, M. W. Wong, J. L. Andres, M. Head-Gordon, E. S. Replogle, J. A. Pople, Gaussian, Inc., Pittsburgh, PA, **1998**.
[12] A. E. Reed, L. A. Curtis, F. Weinhold, *Chem. Rev.* **1988**, *88*, 889.
[13] All these structures were computed at the same level of theory.
[14] Comparatively, anions which lack π delocalization exhibit a higher negative charge at P: H_2P^- (−0.883), Me_2P^- (−0.226) computed at the B3LYP/6-31 + G* level of theory.
[15] a) G. Becker, B. Eschbach, D. Käshammer, O. Mundt, *Z. Anorg. Allg. Chem.* **1994**, *620*, 29; b) J. D. Smith, *Angew. Chem.* **1998**, *110*, 2181; *Angew. Chem. Int. Ed.* **1998**, *37*, 2071; c) M. Driess, *Acc. Chem. Res.* **1999**, *32*, 1017.
[16] SIR97: A. Altomare, M. C. Burla, M. Camalli, G. L. Gascarno, C. Giacovazzo, A. Guagliardi, A. G. G. Molterni, G. Polidiri, R. Spagna, *J. Appl. Crystallogr.* **1999**, *32*, 115.
[17] G. M. Sheldrick, SHELXL-97, Universität Göttingen, Germany, **1997**.

Identification of a PLP-Dependent Threonine Transaldolase: A Novel Enzyme Involved in 4-Fluorothreonine Biosynthesis in *Streptomyces cattleya***

Cormac D. Murphy, David O'Hagan,* and Christoph Schaffrath

Fluorinated natural products are extremely rare in nature. Fluoroacetate (**1**) is the most widely distributed of this group of natural products and has been identified as a toxin in a range of tropical and sub-tropical plants[1] and in the actinomycete *Streptomyces cattleya*.[2, 3] In this bacterium fluoroacetate is co-produced with 4-fluorothreonine (**2**), the only naturally occurring fluorinated amino acid which has been identified to date. The biosynthetic pathways leading to fluoroacetate and 4-fluorothreonine have been investigated by using ^{13}C- and ^{2}H- enriched precursors.[4–6] These experiments have revealed that the carbon substrate for fluorination is closely related to an intermediate of the glycolytic pathway between glycerol and pyruvate. Furthermore, the labeling studies demonstrated that fluoroacetate and the C-3 and C-4 atoms of 4-fluorothreonine have the same biosynthetic origin and that there is a single fluorination enzyme. Most recently[7] fluoroacetaldehyde (**3**) has been identified as the common precursor of both fluorometabolites (Scheme 1) and the aldehyde dehydrogenase responsible for the oxidation of fluoroacetaldehyde to fluoroacetate has been isolated and purified.[8] Herein we describe the nature of the biotransformation of fluoroacetaldehyde to 4-fluorothreonine. Sanada et al.,[2] who first reported fluorometabolite production by *S. cattleya*, suggested that 4-fluorothreonine may arise by the direct condensation of fluoroacetaldehyde with glycine in a classical aldolase reaction. However, when [2-^{13}C]glycine was incubated with resting cell cultures of the bacterium,[6] the 4-fluorothreonine produced was doubly labeled in the C-1 and C-2 positions. Thus glycine does not directly contribute to 4-fluorothreonine biosynthesis, but is probably metabolized by serine hydroxymethyl transferase. We now report that L-threonine is the amino acid that condenses with fluoroacetaldehyde in *S. cattleya* to generate 4-fluorothreonine in a transaldolase-mediated reaction.



Scheme 1. Fluoroacetaldehyde is the common precursor of fluoroacetate and 4-fluorothreonine.

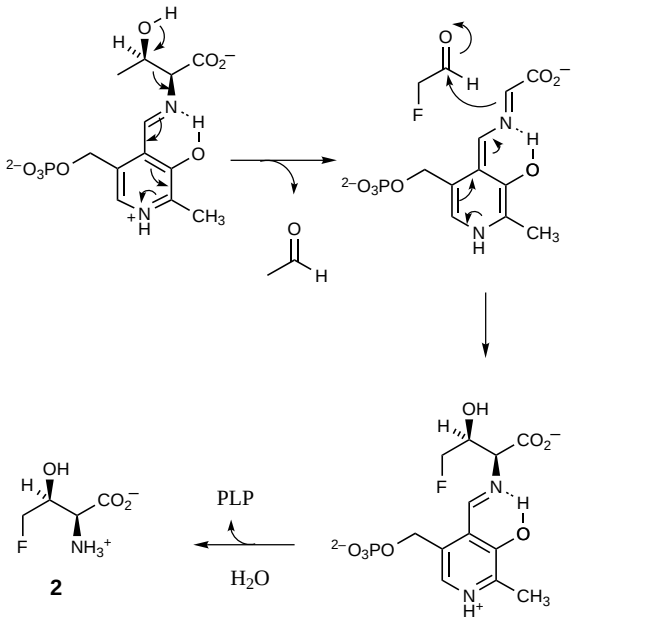
Upon incubation of a cell-free extract of *S. cattleya* with L-threonine, pyridoxal 5'-phosphate (PLP), and fluoroacetaldehyde, 4-fluorothreonine (ca. 0.25 mM) was detected by ^{19}F NMR spectroscopy. When the assay was conducted in the absence of PLP or L-threonine, or with boiled cell-free extract, there was no production of 4-fluorothreonine. When [1-^{2}H]fluoroacetaldehyde was used, a high level (61%) of isotopic label was detected in the (C-2 – C-4) fragment of 4-fluorothreonine by GC-MS analysis, which indicates the direct incorporation of this unit into 4-fluorothreonine generated in vitro. This result is consistent with our previous observation in whole cells.[7] The enzyme was partially purified by ammonium sulfate precipitation and assayed with a range of amino acids (glycine, L-serine, L-cysteine, L-aspartate, L-alanine, and L-*allo*-threonine) instead of threonine. In none of the assay mixtures was 4-fluorothreonine production detected. The key observation that glycine is not a substrate for this enzyme is consistent with whole cell studies with [2-^{13}C]glycine.[6] The requirement for PLP and L-threonine suggests that a novel threonine transaldolase activity is responsible for 4-fluorothreonine production in the bacterium (Scheme 2).

The enzyme was purified further by anion-exchange chromatography. Experiments were conducted by using [1,2,2,2-$^{2}H_4$]acetaldehyde and DL-[4,4,4-$^{2}H_3$]threonine to explore the PLP-transaldolase aspect of the enzyme. After incubation of the enzyme with [1,2,2,2-$^{2}H_4$]acetaldehyde, PLP, and L-threonine, GC-MS analysis revealed a 20% incorporation [M+4] of isotope into the threonine pool. No labeled threonine was detected in a control experiment in which threonine was substituted with glycine. Thus the enzyme – PLP complex accepted acetaldehyde as a substrate and generated a new molecule of L-threonine in a neutral

[*] Prof. D. O'Hagan, Dr. C. D. Murphy, Dipl.-Ing. (FH) C. Schaffrath
University of St. Andrews
School of Chemistry, Centre for Biomolecular Sciences
North Haugh, St. Andrews, Fife, KY16 9ST (UK)
Fax: (+44) 1334-463808
E-mail: do1@st-andrews.ac.uk

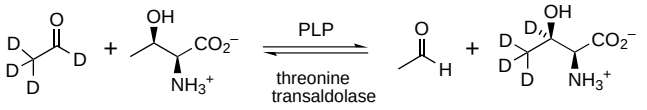
[**] This work was supported by the Biotechnological and Biological Sciences Research Council and the University of St Andrews.

Supporting information for this article is available on the WWW under http://www.angewandte.com or from the author.



Scheme 2. Proposed mechanism for the enzymatic formation of 4-fluorothreonine by threonine transaldolase.

crossover reaction (Scheme 3). A proposed mechanism for the formation of 4-fluorothreonine from fluoroacetaldehyde and threonine is shown in Scheme 2. This mechanism was further supported by the detection of [2-$^2H_3$]acetate after



Scheme 3. The threonine transaldolase mediates a neutral crossover reaction with acetaldehyde as a substrate.

incubation of the enzyme with DL-[4,4,4-$^2H_3$]threonine, PLP, and fluoroacetaldehyde. The labeled acetate was detected after the [2-$^2H_3$]acetaldehyde generated in the assay was oxidized in situ by yeast aldehyde dehydrogenase and NAD^+. Derivitization using 4-(bromoacetyl)biphenyl followed by GC-MS analysis revealed 40% isotope incorporation [*M*+3] into the resultant acetate. A comparatively small amount of labeled acetate (ca. 8%) was detected in control experiments with no fluoroacetaldehyde, which suggests that a small amount of threonine cleavage had occurred in the absence of added aldehyde.

When the enzyme was incubated with L-threonine, PLP, and chloroacetaldehyde instead of fluoroacetaldehyde, 4-chlorothreonine was detected by GC-MS. 4-Chlorothreonine has been identified as a metabolite of several bacteria, either as a free amino acid[9] or as part of a larger peptide structure.[10, 11] It is possible that an enzyme similar to that described above catalyzes the formation of 4-chlorothreonine in these other microorganisms. Consistent with this suggestion is the observation that a radiolabel from [U-^{14}C]threonine is incorporated into the 4-chlorothreonine moiety of the lipodepsipeptide, syringomycin, in *Pseudomonas syringae*.[10]

The PLP-dependent threonine transaldolase has been purified[12] and a monomer of approximately 60 000 kDa was detected (sodium dodecyl sulfate polyacrylamide gel electrophoresis (SDS-PAGE)). Passage of the native enzyme through a gel filtration column (Hiload 16/60 Superdex 200) indicated a molecular weight of 120 kDa, thus the enzyme is probably a dimer. In conclusion, we have identified a threonine transaldolase in *S. cattleya* that is distinct from more classical threonine aldolases in that it does not use glycine as a substrate. The enzyme uses fluoroacetaldehyde and threonine to generate 4-fluorothreonine and acetaldehyde. It can convert chloroacetaldehyde into 4-chlorothreonine, which is suggestive of the mode of biosynthesis of this metabolite in other organisms. Clearly this enzyme is important in the biosynthesis of 4-fluorothreonine in *S. cattleya*. However, it is less clear if the reversible interconversion of L-threonine and acetaldehyde has any metabolic significance to the organism's amino acid biochemistry.

Experimental Section

Streptomyces cattleya NRRL 8057 was grown in 500-mL flasks containing medium (90 mL) of the composition described in reference [3]. After 6 days incubation the cells were harvested and washed with potassium phosphate buffer (50 mM, pH 7) and resuspended in the same buffer (0.5 g wet cell weight per mL). Cell-free extract was prepared by sonication and centrifugation. Threonine transaldolase activity was assayed in a final volume of 1 mL by incubating cell-free extract (910 μL) with L-threonine (2 mM), PLP (0.1 mM), and fluoroacetaldehyde (2 mM) for 16 h at 26 °C. ^{19}F NMR spectra were recorded using a Varian Inova 500 MHz NMR spectrometer (^{19}F, 470.551 MHz); $\delta(D_2O) = -230.4$ (dt, $J = 47$, 25 Hz).

The enzyme activity was partially purified by adding solid $(NH_4)_2SO_4$ to the cell-free extract to 25% saturation and removing the precipitate by centrifugation. The supernatant was adjusted to 45% saturation with solid $(NH_4)_2SO_4$ and the precipitate collected after centrifugation. The pellet was resuspended in tris(hydroxymethyl)aminomethane (Tris) buffer (50 mM, pH 8) and eluted from a Hi-Trap desalting column attached to an AKTA Prime system (Pharmacia). The enzyme was then applied to a Hi-Trap Q XL anion-exchange column (Pharmacia) and the activity eluted with a linear gradient of 0 to 1M KCl in Tris buffer over 25 mL.[12]

DL-[4,4,4-$^2H_3$]Threonine was prepared according to the method described in reference; [13] by GC-MS the label was about 89% [*M*+3] and 7% [*M*+2]. GC-MS analyses of isotopic label incorporation were performed by using an Agilent 6890 gas chromatograph connected to an Agilent 5973 mass-selective detector. The methods used for analysis were similar to those described in reference [6]. 4-Fluorothreonine, threonine, and 4-chlorothreonine were analyzed as the per-trimethylsilyl derivatives. The mass spectrometer was operated in the selected ion monitoring (SIM) mode for determination of the isotopic label in 4-fluorothreonine and threonine. Ion currents *m*/*z* 236 [*M*] and 237 [*M*+1] were monitored for isotope incorporation into (C-2–C-4) of 4-fluorothreonine and ion currents *m*/*z* 320 [*M*], 321 [*M*+1], 322 [*M*+2], 323 [*M*+3], and 324 [*M*+4] were monitored for incorporation of ^{2}H into threonine. The mass spectrometer was operated in the scan mode for identification of 4-chlorothreonine and a compound was detected that had the same mass spectrum as previously reported [9].

Acetate was analyzed by GC-MS as the phenylphenacyl derivative,[6] with the mass spectrometer operated in the SIM mode and at ion currents *m*/*z* 254 [*M*], 255 [*M*+1], 256 [*M*+2], and 257 [*M*+3].

Received: August 28, 2001 [Z 17807]

[1] D. B. Harper, D. O'Hagan, *Nat. Prod. Rep.* **1994**, *11*, 123–133.
[2] M. Sanada, T. Miyano, S. Iwadare, J. M. Williamson, B. H. Arison, J. L. Smith, A. W. Douglas, J. M. Liesch, E. Inamine, *J. Antibiot.* **1984**, *39*, 259–265.

 © WILEY-VCH Verlag GmbH, D-69451 Weinheim, 2001 1433-7851/01/4023-4480 $ 17.50+.50/0

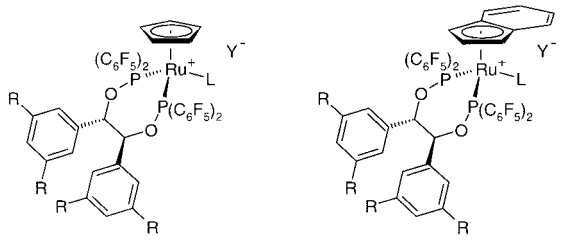
[3] K. A. Reid, J. T. G. Hamilton, R. D. Bowden, D. O'Hagan, L. Dasaradhi, M. R. Amin, D. B. Harper, *Microbiology* **1995**, *141*, 1385 – 1393.
[4] J. T. G. Hamilton, M. R. Amin, D. B. Harper, D. O'Hagan, *Chem. Commun*. **1997**, 797 – 798.
[5] J. Neischalk, J. T. G. Hamilton, C. D. Murphy, D. B. Harper, D. O'Hagan, *Chem. Commun*. **1997**, 799 – 800.
[6] J. T. G. Hamilton, C. D. Murphy, M. R. Amin, D. O'Hagan, D. B. Harper, *J. Chem. Soc. Perkin Trans. 1* **1998**, 759 – 767.
[7] S. J. Moss, C. D. Murphy, J. T. G. Hamilton, W. C. McRoberts, D. O'Hagan, C. Schaffrath, D. B. Harper, *Chem. Commun*. **2000**, 2281 – 2282.
[8] C. D. Murphy, S. J. Moss, D. O'Hagan, *Appl. Environ. Microbiol*. **2001**, *67*, 4919 – 4921.
[9] H. Yoshida, N. Arai, M. Sugoh, J. Iwabuchi, K. Shiomi, M. Shinose, Y. Tanake, S. Omura, *J. Antibiot.* **1994**, *47*, 1165 – 1166.
[10] I. Grgurina, F. Mariotti, *FEBS Lett*. **1999**, *462*, 151 – 154.
[11] H. Lackner, I. Bahner, N. Shigematsu, L. K. Pannell, A. B. Mauger, *J. Nat. Prod*. **2000**, *63*, 352 – 356.
[12] The transaldolase was purified to homogeneity by ammonium sulfate precipitation, anion-exchange chromatography, hydroxyapatite chromatography, and gel filtration.
[13] M. R. Amin, D. B. Harper, J. M. Moloney, C. D. Murphy, J. A. K. Howard, D. O'Hagan, *Chem. Commun*. **1997**, 1471 – 1472.

[(Indenyl)Ru(biphop-F)]$^+$: A Lewis Acid Catalyst That Controls both the Diene and the Dienophile Facial Selectivity in Diels – Alder Reactions**

E. Peter Kündig,* Christophe M. Saudan, Valérie Alezra, Florian Viton, and Gérald Bernardinelli

Cationic arene and cyclopentadienyl complexes of iron and ruthenium incorporating chiral bidentate ligands have been shown to be efficient Lewis acid catalysts for the asymmetric Diels – Alder reaction between enals and dienes.[1–5] Our research in this area has focused on cyclopentadienyliron and -ruthenium complexes, the former giving higher rates and enantiomeric excesses and the latter being more stable and easily recycled.[2] Enantioselectivity in the Ru complexes was strongly increased on changing the aryl groups in the ligand backbone, that is by using **3** rather than **2** as precatalysts.[2a]

The structurally characterized complex [CpRu(biphop-F)-(methacrolein)][SbF_6] (**1d**; biphop-F = 1,2-bis[bis(pentafluoro-



1 R = H, L = $CH_2C(Me)CHO$
2 R = H, L = Me_2CO
3 R = Me, L = Me_2CO

4 R = H, L = $CH_2C(Me)CHO$
5 R = H, L = Me_2CO
6 R = Me, L = Me_2CO

Y = OTf (**a**), BF_4 (**b**), PF_6 (**c**), SbF_6 (**d**), TFPB (**e**)

phenyl)phosphanyloxy]-1,2-diphenylethane)has provided a detailed picture of the catalyst/substrate interaction and of the influence of the anion on the rate of catalysis.[2b] Evidence from the solid-state structure of **1d** and from F/H NMR correlation spectra in solutions of the BF_4^- and the PF_6^- analogues (**1b** and **1c**, respectively) point to ion pairs in which the anion interacts with both the bound substrate and the cationic catalyst.[2a, b] We concluded that the anion slows down product/substrate exchange at the catalyst site. Consequently, complex **1e**, which incorporates the tetrakis[3,5-bis(trifluoromethyl)phenyl] borate anion (TFPB) whose bulk renders this proximity impossible, showed the highest activity. Another way to bring about a larger separation of the anion from the enal group in the catalyst site is to increase the size of the catalyst's capping ligand, for example by changing from the cyclopentadienyl to the indenyl complexes. With an indenyl ligand the question of preferred rotamers arises. Moreover, the propensity of the indenyl ligand to undergo a slip/fold rearrangement[6] risks the occurrence of a different mode of enal binding and reactivity than the desired single coordination site Lewis acid.

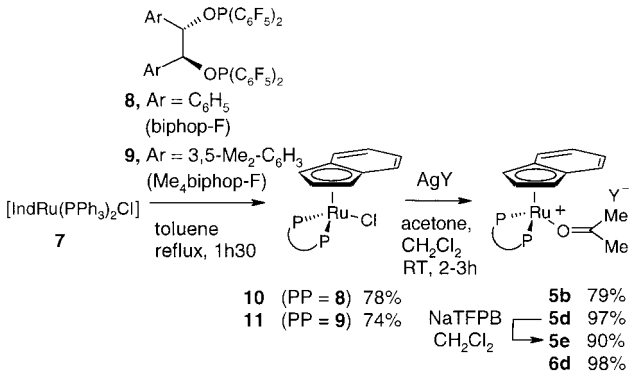
The results described herein provide answers to these questions. The properties of the indenyl complexes are indeed significantly altered from those of the cyclopentadienyl analogues, and diastereoselectivities not previously encountered in the Diels – Alder reaction of enals with dienes are realized. We also note that despite the detailed attention that indenyl complexes of Group 8 metals have received, asymmetric catalytic reactions with this family of compounds have not been reported.[7]

Given that the reaction of [$Ru_3(CO)_{12}$] with indene affords a low yield of the resultant complex,[8] we opted for the thermal substitution of the two PPh_3 ligands in [IndRu-(PPh_3)$_2$Cl][9](**7**) by the bidentate biphop-F[2c, 10](**8**) and Me_4biphop-F (**9**)[2a] ligands to give the Ru complexes **10** and **11** respectively (Scheme 1).

This reaction was complete in 1.5 h, whereas with the cyclopentadienyl analogue the reaction with the very similar ligand 1,2-bis[bis(pentafluorophenyl)phosphanyloxy]cyclopentane (cyclop-F)[2d] took one week to complete. In analogy to the mechanism established in reactions of [$IndRh(CO)_2$], the higher reactivity of the indenyl complex could be ascribed to a reversible η^5/η^3 slippage of the ligand in an associative mechanism (indenyl effect).[11] However, phosphane substitu-

[*] Prof. Dr. E. P. Kündig, Dr. C. M. Saudan, Dr. V. Alezra, F. Viton
Department of Organic Chemistry
University of Geneva
30 Quai Ernest Ansermet, 1211 Geneva 4 (Switzerland)
Fax: (+41) 22-328-7396
E-mail: Peter.Kundig@chiorg.unige.ch
Dr. G. Bernardinelli
Laboratory of Crystallography
University of Geneva
24 Quai Ernest Ansermet, 1211 Geneva 4 (Switzerland)

[**] This work was supported by the Swiss National Science Foundation (FNS grant 20-59374.99) and The Ministère des Affaires Etrangères from France (Lavoisier grant to V.A.). biphop-F = 1,2-bis[bis(pentafluorophenyl)phosphanyloxy]-1,2-diphenylethane.



Scheme 1. Synthesis of indenyl (Ind) complexes.

tion in the Ru complex **7** has been shown to be dissociative, and rate enhancement in going from the cyclopentadienyl to the indenyl complex in this reaction has been attributed to the indenyl moiety acting as an electron reservoir toward the metal fragment thus favoring Ru–P bond cleavage and/or stabilization of the 16-electron intermediate.[12] The X-ray crystal structure of (*S*,*S*)-**10** (Figure 1)[13] shows an arrangement of the [IndRu((*S*,*S*)-biphop-F)] core that closely matches

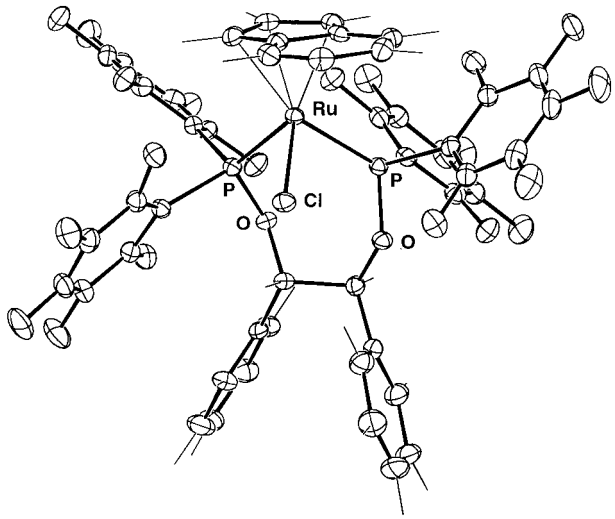


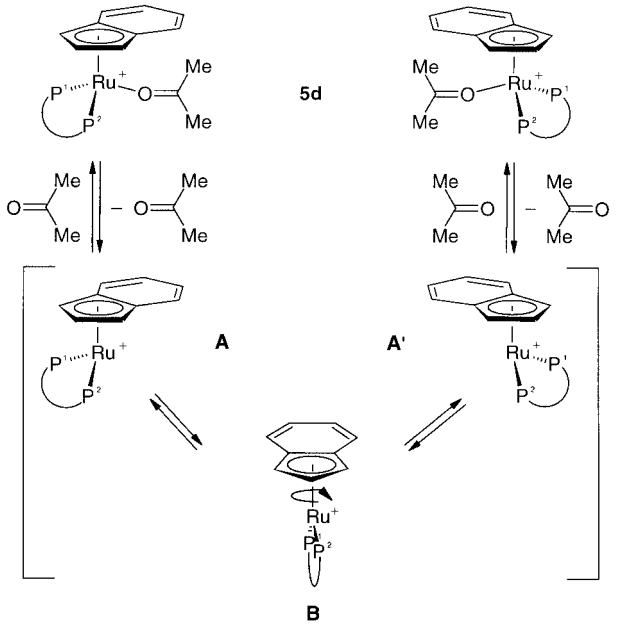
Figure 1. X-ray crystal structure of (*S*,*S*)-**10** (ORTEP view; ellipsoids are represented at the 40% probability level).

that of complex (*S*,*S*)-**1d**[2b] except for the extension of the η^5 ligand. The indenyl ligand in **10** is η^5-coordinated in the solid state[14] and, according to ^{13}C NMR data, also in solution.[15] Rotation of the indenyl ligand should be sterically impeded by the pentafluorophenyl groups. The structure also shows that the indenyl arene ring occupies the same space as the SbF_6 anion in the [CpRu((*S*,*S*)-biphop-F)(methacrolein)][SbF_6] complex (*S*,*S*)-**1d**.[2b] The consequence of this structural change will become apparent when discussing the results of Diels–Alder reactions.

Reaction of a solution of **10** or **11** in acetone with the appropriate silver salt generated the air-stable cationic complexes **5b, d**[16] and **6d** (see Scheme 1). Complex **5e** was obtained from **5d** by anion metathesis[17] with sodium tetrakis[3,5-bis(*m*-trifluoromethyl)phenyl]borate (NaTFPB).[18]

Like their cyclopentadienyl analogues, the indenyl complexes **5** and **6** are stable in solution at room temperature. In CH_2Cl_2, methacrolein readily displaced the coordinated acetone in **5d** to give complex **4d**. The ^{1}H NMR spectrum of **4d** in CD_2Cl_2 was of particular interest because it showed coordinated ($\delta =$ 8.66) and free methacrolein ($\delta = 9.52$). This unusual formyl proton downfield shift (in **1d**, $\delta = 9.74$[2b]) is attributed to the magnetic anisotropy of the indenyl ring.[19] The ^{31}P NMR spectrum of **5d** in [D_6]acetone at room temperature was different from that of the cyclopentadienyl analogue in that it showed a singlet for the two diastereotopic P nuclei of the bidentate ligand. The possibility of coincidental overlap was excluded by the observation of the usual AB quartet at $-80\,^\circ$C.

While we cannot rule out at this stage a Ru–P bond breaking/bond making process, we favor the alternative mechanism shown in Scheme 2. Dissociation of acetone in **5d** leads to the 16-electron intermediate **A**. In the singlet state,



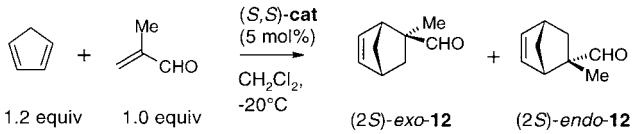
Scheme 2. Proposed pathway for phosphorus site exchange.

A should be pyramidal at the metal center because of the σ-donor and π-acceptor properties of the bidentate ligand biphop-F.[20–22] Inversion of the pyramidal geometry at the metal center through a pendulum movement of the bidentate ligand then gives **A′**. This is accompanied by rotation of the indenyl ligand at point **B**. The process is completed by coordination of acetone. Because of the C_2 symmetry of the ligand, **A** and **A′** are identical.[23] The ^{31}P NMR singlet indicates that at room temperature this process occurs rapidly on the NMR time scale, thus rendering the two phosphorus atoms equivalent.[24] In view of the use of **5d** in catalysis, we note that ligand exchange occurs more rapidly with the indenyl complexes than with the cyclopentadienyl analogues. With regards to asymmetric induction, the pendulum movement of the biphop-F ligand in **5d** is not expected to lead to an erosion of product enantioselectivity because an identical

 © WILEY-VCH Verlag GmbH, D-69451 Weinheim, 2001 1433-7851/01/4023-4482 $ 17.50+.50/0 *Angew. Chem. Int. Ed.* **2001**, *40*, No. 23

stereochemical environment exists in the catalyst–substrate complex at all times.

Diels–Alder reaction of methacrolein with cyclopentadiene catalyzed by (*S*,*S*)-**5d** (5 mol%, CH_2Cl_2, −20 °C) gave the corresponding cycloadduct (*S*)-**12** in 85% yield (see Figure 2) with a diastereomeric ratio of 99.7:0.3 (*exo*:*endo*) and an enantioselectivity of 88% *ee* (*exo*). The chiral cyclopentadienyl and the indenyl complexes afforded the products



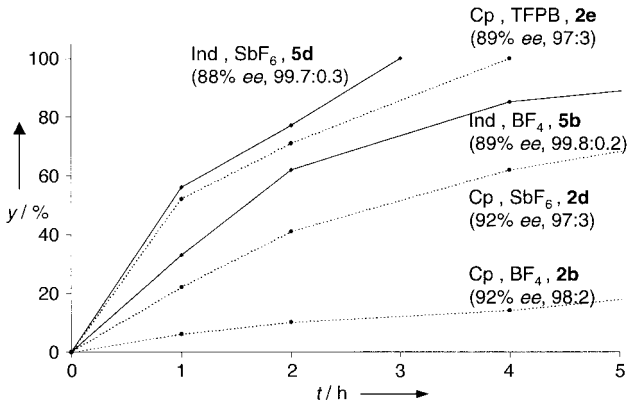


Figure 2. Plot of GC yield (y) as a function of reaction time (t) for the reaction of methacrolein with cyclopentadiene in the presence of (*S*,*S*)-**2b, d, e** (••••) or (*S*,*S*)-**5b, d** (——). In parentheses: *ee* value of the *exo*-cycloadduct **12**, *exo*:*endo* ratio.

with the same sense of asymmetric induction and we take this as an indication that the reaction occurs through an identical diene approach.[2b] Diels–Alder reactions with the indenyl catalysts were faster than with the cyclopentadienyl analogues (Table 1, compare entries 4 and 2 or 5 and 3). Fine-tuning of the ligand backbone by switching from biphop-F (**8**) to Me_4biphop-F (**9**) results in higher asymmetric induction as previously found for cyclopentadienyl complexes (Table 1, entries 4 and 5).

Selected results for the Diels–Alder reaction of methacrolein with cyclopentadiene catalyzed with indenyl (Ind) complexes **5** and analogous cyclopentadienyl (Cp) complexes **2** are presented in Figure 2. The same trend is observed in both cases, that is the rate of Diels–Alder reaction varies with the catalyst counteranion and it increases in the order $BF_4 < SbF_6 <$ TFPB (for clarity, we have omitted the curve for **5e** (TFPB), which is very close to that of **5d**). However the range of rate variations in the indenyl complexes is significantly reduced compared to that for the cyclopentadienyl complexes, and the large change in reactivity found with the TFPB anion in the cyclopentadienyl complex is not observed with the indenyl catalyst.

In the cyclopentadienyl complexes, the anion effect is due to competition between the anion and the aldehyde substrate for the Lewis acid coordination site (with OTf^-), and cooperative binding of the anion to both the aldehyde product and the catalyst (with BF_4^-, PF_6^-, SbF_6^-). The latter modifies the rate of product release and thereby affects the turnover frequency.[2a,b] In the indenyl complexes the anion is further away from the coordination site because of the indenyl arene ring and both phenomena are reduced. A further consequence of the higher efficiency of product/substrate exchange is a switch in the rate-determining step. In contrast to the cyclopentadienyl analogue, changing the ratio of diene:dienophile from 1.2:1 to 5:1 resulted in a faster reaction with indenyl complex **5d** (reaction of methacrolein and cyclopentadiene with 5 mol% of **5d** was completed in 1 h instead of 2.5 h). We take this as an indication that cycloaddition has become the rate-determining step with the indenyl catalyst, whereas it was the product/substrate exchange in the cyclopentadienyl complexes.

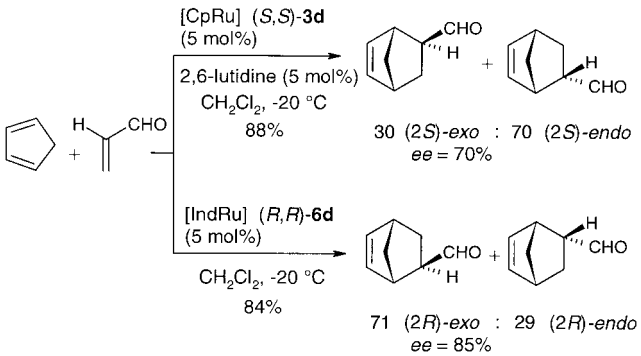
The most remarkable feature of the indenyl catalyst, however, is the increased diastereoselectivity that favors the *exo* cycloadduct by an order of magnitude over that of the cyclopentadienyl catalyst (Table 1, entries 4 and 5). We selected the Diels–Alder reaction of acrolein with cyclopentadiene to further investigate this characteristic. This reaction is known to always give the *endo* cycloadduct as the major product.[26] With **6d** as catalyst, the reaction afforded the *exo* cycloadduct as major product with an *exo*:*endo* ratio of 71:29—a complete inversion of the diastereoselectivity compared to that obtained with the cyclopentadienyl catalyst **3d** (Scheme 3).

To our knowledge, this is the first Diels–Alder reaction of acrolein with cyclopentadiene that favors the *exo* cycloadduct.

Table 1. Reaction of methacrolein with cyclopentadiene.[a]

Entry	Catalyst	Reaction time [h]	Yield [b] [%]	*exo*:*endo*	*ee* [c] [%]	ref.
1	[CpFe((*R*,*R*)-biphop-F)][SbF_6][d]	1	85	98:2	97 (*R*)	[2a]
2	(*S*,*S*)-**2d**	22	91	97:3	92 (*S*)	[2b]
3	(*S*,*S*)-**3d**	22	87	97:3	97 (*S*)	[2a]
4	(*S*,*S*)-**5d**	2.5	85	99.7:0.3	88 (*S*)	
5	(*S*,*S*)-**6d**	4	80	99.8:0.2	95 (*S*)	

[a] Reactions were carried out with 1 mmol methacrolein, 1.2 mmol cyclopentadiene and 5 mol% catalyst in dichloromethane (1 mL) at −20 °C. [b] Yield of cycloadduct isolated. [c] The enantiomeric excess of the *exo* cycloadduct was determined by GC analysis of the diastereomeric acetals obtained by reaction with (2*R*,4*R*)-pentanediol.[25] [d] Reaction was carried out with 1 mmol methacrolein, 5 mmol cyclopentadiene, 5 mol% catalyst, and 5 mol% 2,6-lutidine in dichloromethane (1 mL) at −20 °C.



Scheme 3. Diels–Alder reaction of acrolein with cyclopentadiene catalyzed by (*S*,*S*)-**3d** and (*R*,*R*)-**6d**, respectively: inversion of diastereoselectivity.

As shown in Figure 3, we ascribe the selectivity to an unfavorable *endo* approach of the cyclopentadiene. The cause is the indenyl arene ring that interferes with C(2)–H and C(3)–H of the approaching cyclopentadiene. In the *exo* approach, the envelope shape of the diene places the methylene group further away from this catalyst site capping ligand and this is therefore the favored pathway.

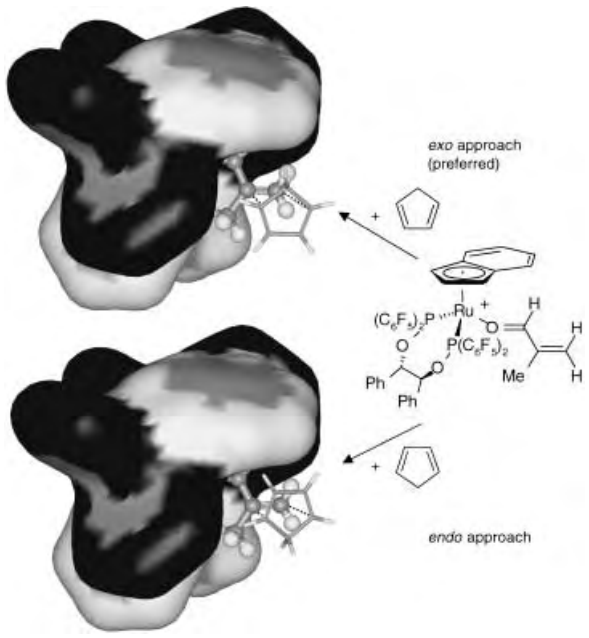


Figure 3. Model of the transition state for the Diels–Alder reaction of methacrolein and cyclopentadiene catalyzed by (*S*,*S*)-**5d**. Top: cyclopentadiene *exo* approach to the methacrolein C_α-*Re* face. Bottom: cyclopentadiene *endo* approach to the methacrolein C_α-*Re* face.

In conclusion, we have synthesized new chiral indenyl ruthenium complexes and have shown their efficiency as Lewis acids in Diels–Alder reactions. They exhibit unprecedented levels of *exo* selectivity, and reach the rates of the usually more active Fe catalysts. The room-temperature stable catalysts can be recovered in high yield.

Experimental Section

(*S*,*S*)-**10**: An orange solution of $[IndRu(PPh_3)_2Cl]$[9] (1.16 g, 1.50 mmol) and (*S*,*S*)-biphop-F (**8**)[2c] (1.42 g, 1.50 mmol) in dry and N_2 saturated toluene (120 mL) was refluxed under N_2 for 1.5 h. After evaporation of the solvent under vacuum, the crude product was purified by flash chromatography on silica gel (pentane:CH_2Cl_2 2:1 to 1:2). Recrystallization from CH_2Cl_2/MeOH afforded compound (*S*,*S*)-**10** as dark red crystals (1.41 g, 78%). ^{1}H NMR (400 MHz, CD_2Cl_2, 20 °C, TMS): $\delta = 7.41-7.34$ (m, 2H; H_{ind}), 7.15–7.00 (m, 7H; 1 H_{ind} + 6 H_{ar}), 6.97 (m, 2H; H_{ar}), 6.63 (bs, 2H; H_{ar}), 6.60 (d, ^3J(H,H) = 8.3 Hz, 1H; H_{ind}), 6.26 (dd, ^3J(H,P) = 14.3 Hz, ^3J(H,H) = 8.5 Hz, 1H; CH-O-P), 5.19 (s, 1H; H_{ind}), 4.90 (dd, ^3J(H,P) = 5.6 Hz, ^3J(H,H) = 8.5 Hz,1H; CH-O-P), 4.81 (s, 1H; H_{ind}), 4.36 (s, 1H; H_{ind}); ^{13}C NMR (100.6 MHz, CD_2Cl_2, 20 °C, TMS): $\delta = 136.1$ (d, J(C,P) = 7.5 Hz, 1C; *i*C (C_6H_5)), 135.6 (s, 1C; *i*C (C_6H_5)), 130.3 (s, 1(CH); $C(5,6)_{Ind}$), 128.9 (s, 1(CH); C_6H_5), 128.8 (s, 1(CH); C_6H_5), 128.3 (s, 4(CH); C_6H_5), 128.2 (s, 2(CH); C_6H_5), 128.0 (s, 1(CH); $C(5,6)_{Ind}$), 127.6 (s, 2(CH); C_6H_5), 124.4 (s, 1(CH); $C(4,7)_{Ind}$), 123.7 (s, 1(CH); $C(4,7)_{Ind}$), 115.8 (d, J(C,P) = 3.3 Hz, 1C; $C(3a,7a)_{Ind}$), 108.0 (d, J(C,P) = 7.5 Hz, 1C; $C(3a,7a)_{Ind}$), 85.7 (dd, J(C,P) = 10.0, 3.3 Hz, 1(CH); CH-O-P), 85.2 (s, 1(CH); $C(2)_{Ind}$), 83.7 (d, J(C,P) = 4.1 Hz, 1(CH); CH-O-P), 74.4 (d, J(C,P) = 10.0 Hz, 1(CH); $C(1,3)_{Ind}$), 72.6 (d, J(C,P) = 6.6 Hz, 1(CH); $C(1,3)_{Ind}$); ^{31}P NMR (202.5 MHz, CD_2Cl_2, 20 °C, H_3PO_4): $\delta = 127.6$ (d, ^2J(P,P) = 65 Hz), 121.2 (d, ^2J(P,P) = 65 Hz).

(*S*,*S*)-**5d**: A solution of $AgSbF_6$ (168 mg, 0.49 mmol) in dried CH_2Cl_2 (4.9 mL) was added to (*S*,*S*)-**10** (478 mg, 0.40 mmol) in dried acetone (6 mL). The mixture was stirred at room temperature for 3 h. After evaporation of the solvent under vacuum, the residue was filtered through celite with acetone. After evaporation of volatiles under vacuum, the product was purified by dissolution in acetone and precipitation by addition of Et_2O to give compound (*S*,*S*)-**5d** as an orange solid (564 mg, 97%). ^{1}H NMR (400 MHz, [D_6]acetone, 20 °C, TMS): $\delta = 7.78$ (d, ^3J(H,H) = 8.6 Hz, 1H; H_{ind}), 7.64 (t, ^3J(H,H) = 7.6 Hz, 1H; H_{ind}), 7.51–7.44 (m, 2H; H_{ind}), 7.14–7.07 (m, 4H; H_{ar}), 7.04–6.96 (m, 4H; H_{ar}), 6.87 (d, ^3J(H,H) = 7.0 Hz, 2H; H_{ar}), 5.63–5.57 (m, 1H; CH-O-P), 5.48 (s, 1H; H_{ind}), 5.32 (dd, ^3J(H,P) = 14.0 Hz, ^3J(H,H) = 7.5 Hz, 1H; CH-O-P), 5.22 (s, 1H; H_{ind}), 4.89 (s, 1H; H_{ind}); ^{13}C NMR (100.6 MHz, [D_6]acetone, 20 °C, TMS): $\delta = 135.5$ (t, J(C,P) = 4.1 Hz, 1C; *i*C (C_6H_5)), 135.2 (s, 1C; *i*C (C_6H_5)), 133.7 (s, 1(CH); $C(5,6)_{Ind}$), 131.0 (s, 1(CH); $C(5,6)_{Ind}$), 129.8 (s, 2(CH); C_6H_5), 129.1 (s, 2(CH); C_6H_5), 128.9 (s, 2(CH); C_6H_5), 128.6–128.4 (m, 1(CH); $C(4,7)_{Ind}$), 128.36 (s, 2(CH); C_6H_5), 128.3 (s, 2(CH); C_6H_5), 123.4 (s, 1(CH); $C(4,7)_{Ind}$), 119.6 (s, 1C; $C(3a,7a)_{Ind}$), 110.9 (s, 1C; $C(3a,7a)_{Ind}$), 86.6 (s, 1(CH); CH-O-P), 86.2 (s, 1(CH); CH-O-P), 83.6 (s, 1(CH); $C(2)_{Ind}$), 70.3 (t, J(C,P) = 7.0 Hz, 1(CH); $C(1,3)_{Ind}$), 68.6 (s, 1(CH); $C(1,3)_{Ind}$); ^{31}P NMR (162 MHz, [D_6]acetone, 20 °C, H_3PO_4): $\delta = 131.0$ (s); ^{31}P NMR (162 MHz, [D_6]acetone, −100 °C, H_3PO_4): $\delta = 129.9$ ($q_{A,B}$, $\Delta\tilde{\nu}_{A,B} = 510$ Hz, $J_{A,B} = 77$ Hz).

12: Methacrolein (0.082 mL, 1.00 mmol) and cyclopentadiene (0.100 mL, 1.22 mmol) were successively added to (*S*,*S*)-**5d** (72 mg, 0.05 mmol) in dried CH_2Cl_2 (1 mL) at −20 °C. After the mixture had been stirred at −20 °C for 2.5 h, acetone (0.4 mL) and water (0.1 mL) were added and the mixture was stirred for 5 min at room temperature. The solution was partially concentrated. Hexane (10 mL) was then added and the mixture filtered through celite. Chromatography on silica gel (pentane/CH_2Cl_2 8:1) gave cycloadduct (*S*)-**12** as a deliquescent white solid (116 mg, 85%) with an *exo*:*endo* ratio of 99.7:0.3 (determined before chromatography) and 88% *ee* (*exo*). Catalyst recovery: the precipitate was eluted from the celite with acetone and the solvent was evaporated under vacuum. After three cycles of dissolution in dried acetone and evaporation under vacuum, the acetone complex (*S*,*S*)-**5d** was recovered quantitatively.

Received: July 23, 2001 [Z17565]

[1] a) D. Carmona, M. P. Lamata, L. A. Oro, *Coord. Chem. Rev.* **2000**, *200–202*, 717–772; b) C. M. Saudan, E. P. Kündig in *Handbook of Lewis acids* (Ed.: H. Yamamoto), Wiley, Weinheim, **2000**, pp. 597–652; c) E. J. Corey, A. Guzman-Perez, *Angew. Chem.* **1998**, *110*, 402–415; *Angew. Chem. Int. Ed.* **1998**, *37*, 388–401; d) L. C. Dias, *J. Braz. Chem. Soc.* **1997**, *8*, 289–332.

[2] a) E. P. Kündig, C. M. Saudan, F. Viton, *Adv. Synth. Catal.* **2001**, *343*, 51–56; b) E. P. Kündig, C. M. Saudan, G. Bernardinelli, *Angew. Chem.* **1999**, *111*, 1298–1301; *Angew. Chem. Int. Ed.* **1999**, *38*, 1220–1222; c) M. E. Bruin, E. P. Kündig, *Chem. Commun.* **1998**, 2635–2636; d) E. P. Kündig, B. Bourdin, G. Bernardinelli, *Angew. Chem.* **1994**, *106*, 1931–1934; *Angew. Chem. Int. Ed. Engl.* **1994**, *33*, 1856–1858.

[3] a) D. Carmona, C. Cativiela, R. García-Correas, F. J. Lahoz, M. P. Lamata, J. A. López, M. P. López-Ram de Víu, L. A. Oro, E. San José, F. Viguri, *Chem. Commun.* **1996**, 1247–1248; b) D. Carmona, C. Cativiela, S. Elipe, F. J. Lahoz, M. P. Lamata, M. P. López-Ram de Víu, L. A. Oro, C. Vega, F. Viguri, *Chem. Commun.* **1997**, 2351–2352; c) D. Carmona, F. J. Lahoz, S. Elipe, L. A. Oro, M. P. Lamata, F. Viguri, C. Mir, C. Cativiela, M. P. López-Ram de Víu, *Organometallics* **1998**, *17*, 2986–2995.

[4] a) D. L. Davies, J. Fawcett, S. A. Garratt, D. R. Russell, *Chem. Commun.* **1997**, 1351–1352; b) A. J. Davenport, D. L. Davies, J. Fawcett, S. A. Garratt, L. Lad, D. R. Russell, *Chem. Commun.* **1997**, 2347–2348.

[5] a) J. W. Faller, J. Parr, *Organometallics* **2001**, *20*, 697–699; b) J. W. Faller, B. J. Grimmond, D. J. D'Alliessi, *J. Am. Chem. Soc.* **2001**, *123*, 2525–2529; c) J. W. Faller, B. J. Grimmond, *Organometallics* **2001**, *20*, 2454–2458.

[6] a) M. J. Calhorda, L. F. Veiros, *Coord. Chem. Rev.* **1999**, *185*, 37–51; b) J. M. O'Connor, C. P. Casey, *Chem. Rev.* **1987**, *87*, 307–318.

 © WILEY-VCH Verlag GmbH, D-69451 Weinheim, 2001 1433-7851/01/4023-4484 $ 17.50+.50/0

[7] V. Cadierno, J. Diez, M. Pilar Gamasa, J. Gimeno, E. Lastra, *Coord. Chem. Rev.* **1999**, *193–195*, 147–205.

[8] M. S. Loonat, L. Carlton, J. C. A. Boeyens, N. J. Coville, *J. Chem. Soc. Dalton Trans.* **1989**, 2407–2414.

[9] L. A. Oro, M. A. Ciriano, M. Campo, C. Foces-Foces, F. H. Cano, *J. Organomet. Chem.* **1985**, *289*, 117–131.

[10] V. Alezra, E. P. Kündig in *Electronic Encyclopedia of Reagents for Organic Synthesis* (Ed.: L. Paquette), Wiley, Chichester, in press.

[11] M. E. Rerek, F. Basolo, *J. Am. Chem. Soc.* **1984**, *106*, 5908–5912.

[12] M. P. Gamasa, J. Gimeno, C. Gonzalez-Bernardo, B. M. Martin-Vaca, D. Monti, M. Bassetti, *Organometallics* **1996**, *15*, 302–308.

[13] Crystal structure determination of (*S*,*S*)-**10**: $[(C_9H_7)(C_{38}H_{12}O_2F_{20}P_2)\text{-RuCl}]\cdot(CH_4O)_2$; $M_r = 1258.2$; $\mu = 0.58\ mm^{-1}$, $\rho_{calcd} = 1.76\ g\,cm^{-3}$, monoclinic, $P2_1$, $Z = 2$, $a = 10.7173(6)$, $b = 12.4521(8)$, $c = 17.7987(10)$ Å, $\beta = 94.465(7)^\circ$, $V = 2368.1(2)$ Å^3, from 7998 reflections ($4.4^\circ < 2\Theta < 51.9^\circ$), red prism $0.14 \times 0.15 \times 0.15$ mm mounted on a quartz fiber with RS3000 oil to prevent degradation. Cell dimensions and intensities were measured at 170 K on a STOE IPDS diffractometer with graphite-monochromated $Mo_{K\alpha}$ radiation ($\lambda = 0.71069$ Å). $-13 < h < 13$; $-15 < k < 15$; $-21 < l < 21$; 29958 measured reflections, 9236 unique reflections of which 8264 were observable ($|F_o| > 4\sigma(F_o)$); R_{int} for equivalent reflections 0.027. Data were corrected for absorption (T_{min}, $T_{max} = 0.9119$, 0.9408). The structure was solved by direct methods using hte program MULTAN 87,[27] all other calculations used the XTAL[28] system and ORTEP[29] programs. Full-matrix least-squares refinement based on F using weight of $1/[\sigma^2(F_o) + 0.0002(F_o)^2]$ gave final values $R = 0.026$, $wR = 0.029$ and $S = 1.87(2)$ for 700 variables and 8264 contributing reflections. Flack parameter $x = -0.01(2)$. Hydrogen atoms were placed in calculated positions except those of the hydroxy groups that were observed and refined with a fixed value of isotropic displacement parameters ($U = 0.05$ Å^2). The final $\Delta\rho$ showed a maximum of $+0.50$ and a minimum of $-0.29\ e\,Å^{-3}$. Crystallographic data (excluding structure factors) for the structure reported in this paper have been deposited with the Cambridge Crystallographic Data Centre as supplementary publication no. CCDC-167480 ((*S*,*S*)-**10**). Copies of the data can be obtained free of charge on application to CCDC, 12 Union Road, Cambridge CB21EZ, UK (fax: (+44) 1223-336-033; e-mail: deposit@ccdc.cam.ac.uk).

[14] For the comparison of solid-state structures the distortion parameters used by Taylor and Marder have been chosen: 1) the slip parameter (Δ) defined as the difference in the average bond lengths of the metal to the ring junction carbons C(3a), C(7a), and of the metal to adjacent carbon atoms of the five-membered ring, C(1), C(3); 2) the hinge angle (HA) defined as the angle between the planes defined by C(1), C(2), and C(3) and C(1), C(3), C(3a), and C(7a). a) S. A. Westcott, A. K. Kakkar, G. Stringer, N. J. Taylor, T. B. Marder, *J. Organomet. Chem.* **1990**, *394*, 777–794; b) A. K. Kakkar, S. F. Jones, N. J. Taylor, S. Collins, T. B. Marder, *J. Chem. Soc. Chem. Commun.* **1989**, 1454–1456. For (*S*,*S*)-**10**, the HA values of 3.5° and the Δ value of 0.12 Å clearly indicate a η^5 coordination of the indenyl ligand.

[15] The parameter $\Delta\delta$ (C3a,7a) = δ(C3a,7a; η^x-indenyl complex) – δ(C3a,7a; sodium indenyl) has been proposed as a measure of the indenyl distortion. Values in the range -20 to -40 ppm are typical for a planar η^5-indenyl ligand, -10 to -20 ppm for a partially slipped η^5-coordination mode and $+5$ to $+30$ ppm for a η^3-coordination mode: R. T. Baker, T. H. Tulip, *Organometallics* **1986**, *5*, 839–845. The $\Delta\delta$ (C3a,7a) value of -18.8 ppm in (*S*,*S*)-**10**, indicates a weak distortion of the indenyl ligand.

[16] A $\Delta\delta$ (C3a,7a) value of -15.4 ppm was found for (*S*,*S*)-**5d**, indicating a weak distortion of the indenyl ligand.

[17] For precedence, see: a) P. V. Bonnesen, C. L. Puckett, R. V. Honeychuck, W. H. Hersh, *J. Am. Chem. Soc.* **1989**, *111*, 6070–6081; b) B. J. Boone, D. P. Klein, J. W. Seyler, N. Q. Méndez, A. M. Arif, J. A. Gladysz, *J. Am. Chem. Soc.* **1996**, *118*, 2411–2421.

[18] S. R. Bahr, P. Boudjouk, *J. Org. Chem.* **1992**, *57*, 5545–5547.

[19] For precedence of large ring-current shifts produced by the indenyl six-membered ring, see: a) J. W. Faller, C. C. Chen, M. J. Mattina, A. Jakubowski, *J. Organomet. Chem.* **1973**, *52*, 361–386; b) J. W. Faller, B. V. Johnson, *J. Organomet. Chem.* **1975**, *88*, 101–113; c) J. W. Faller, B. V. Johnson, C. D. Schaeffer Jr., *J. Am. Chem. Soc.* **1976**, *98*, 1395–1400; d) J. W. Faller, R. H. Crabtree, A. Habib, *Organometallics* **1985**, *4*, 929–935.

[20] T. W. Ward, O. Schafer, C. Daul, P. Hofmann, *Organometallics* **1997**, *16*, 3207–3215.

[21] E. P. Kündig, C. Dupré, B. Bourdin, A. Cunningham, Jr., D. Pons, *Helv. Chim. Acta* **1994**, *77*, 421–428.

[22] A triplet ground state must also be considered with a probable planar geometry at the metal center. For precedent see: K. Costuas, J.-Y. Saillard, *Organometallics* **1999**, *18*, 2505–2512.

[23] Literature precedents: a) H. Kurosawa, H. Asano, Y. Miyaki, *Inorg. Chim. Acta* **1998**, *270*, 87–94; b) D. L. Davies, J. Fawcett, S. A. Garratt, D. R. Russel, *Organometallics* **2001**, *20*, 3029–3034.

[24] The quantitative analysis of the described processes is currently being carried out using a combination of ^{31}P and ^{17}O NMR spectroscopy and density functional theory (DFT) calculations.

[25] K. Furuta, S. Shimizu, Y. Miwa, H. Yamamoto, *J. Org. Chem.* **1989**, *54*, 1481–1483.

[26] D. A. Evans, J. S. Johnson in *Comprehensive Asymmetric Catalysis, Vol. III* (Eds.: E. N. Jacobsen, A. Pfaltz, H. Yamamoto), Springer, Berlin, **1999**, pp. 1177–1235.

[27] P. Main, S. J. Fiske, S. E. Hull, L. Lessinger, G. Germain, J.-P. Declercq, M. M. Woolfson, *A System of Computer Programs for the Automatic Solution of Crystal Structures from X-Ray Diffraction Data*, University of York, England, and Louvain-la-Neuve, Belgium, **1987**.

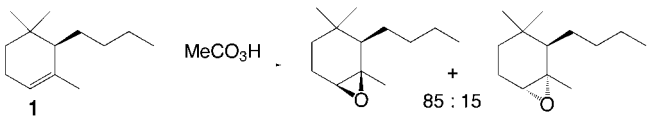
[28] *XTAL3.2 User's Manual* (Eds.: S. R. Hall, H. D. Flack, J. M. Stewart), Universities of Western Australia and Maryland, **1992**.

[29] C. K. Johnson, ORTEP II, Oak Ridge National Laboratory, Oak Ridge, TN, USA, **1976**, ORNL-5138.

CH ··· O Hydrogen Bonding Influences π-Facial Stereoselective Epoxidations**

Ilyas Washington and K. N. Houk*

Epoxidations of α-cyclogeranyl systems,[1] such as **1** [Eq. (1)], occur *syn* to the alkyl group at C3, contrary to expectation based upon steric effects. To determine the origin and scope of



(1)

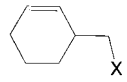
this effect, transition structures have been located for oxygen transfer from peracetic acid to several substituted cyclohexenes (**2**–**4**) with quantum-mechanical methods. An explanation of the anomalous stereoselectivity of epoxidations of **1** was obtained and predictions were made about the

[*] Prof. Dr. K. N. Houk, I. Washington
Department of Chemistry and Biochemistry
University of California
Los Angeles, CA 90095-1569 (USA)
Fax: (+1) 310-206-1843
E-mail: houk@chem.ucla.edu

[**] We are grateful to the National Institute of General Medical Sciences, National Institutes of Health (GM-36700) for financial support of this research and the National Computational Science Alliance (Illinois) for computer time and support.

Supporting information for this article is available on the WWW under http://www.angewandte.com or from the author.

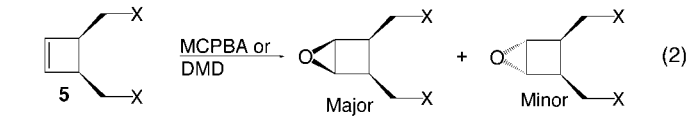
stereoselectivities of epoxidations of cyclohexenes **2**–**4** (OMs = methylenesulfonyloxymethyl). These predictions have been verified experimentally.



2: X= OMs, **3**: X = Br, **4**: X = CN

syn-Directing hydrogen-bonding groups that are able to differentiate diastereotopic faces of a C–C double bond for epoxidations have been widely used in synthesis.[2] Stabilizing hydrogen-bonding interactions between a –OH substituent on the alkene and the peracid oxygen atoms favor epoxidation *syn* to allylic and homoallylic alcohols.[3] A variety of other groups, such as, carboxamides,[4] sulfonamides,[5] carbamates,[6] amido,[7] urethano,[8] ureido,[9] unsaturated acetals,[10] sulfones,[11] sulfoxides,[12] phosphorus oxides,[13] and ammonium salts[14] have all been reported to show similar *syn*-directing effects. These observations have been associated with hydrogen bonding involving the alkene substituent and the peracid.

Surprisingly, the α-cyclogeranyl derivative **1**, which possesses no functionality near the reactive double bond, undergoes epoxidation by peracetic acid to yield the corresponding epoxides with a *syn* to *anti* ratio of 85:15 [Eq. (1)].[1] This observation has been rationalized based on the conformational preference for the axial half-chair conformation as well as on the electrostatic interactions between the peracid and the more electron-rich π face.[1] Similarly, *cis*-3,4(CH_2X)-substituted-cyclobutenes (**5**) [Eq. (2)] have also been reported to undergo selective *syn* epoxidation by *meta*-chloroperbenzoic acid (MCPBA) and dimethyldioxirane (DMD).[15] This has been explained by alkene pyramidalization and electrostatic interactions,[15a] as well as by attractive dipole–dipole interactions.[15b]



X = MsO-, OH, TsO-, MeO-, AcO-

Figure 1 shows four B3LYP/6-31G(d)[16, 17] calculated transition states for the epoxidation of 2,3,4,4-tetramethylcyclohexene (a model for **1**) by peracetic acid. The tetrasubstituted cyclohexene has two half-chair conformations, with the C3 methyl group in axial or equatorial conformations. The conformation with an equatorial methyl group was calculated to be 0.7 kcal mol^{-1} higher in energy than that with an axial methyl group, which was attributed to $A^{1,2}$ strain.[18] In **A**, attack *syn* to the methyl group at C3 has the lowest activation energy, in accord with the experimental preference for the analogous reaction of **1**. In **A** the oxygen that is transferred (O1) is 2.57 Å from a hydrogen atom on the C3 methyl group. The sum of O and H van der Waals radii is 2.6 Å. Transition states with shorter H···O distances (**B** and **C**) or with an equatorial methyl group (**D**) and no H···O contact are higher in energy than **A**.

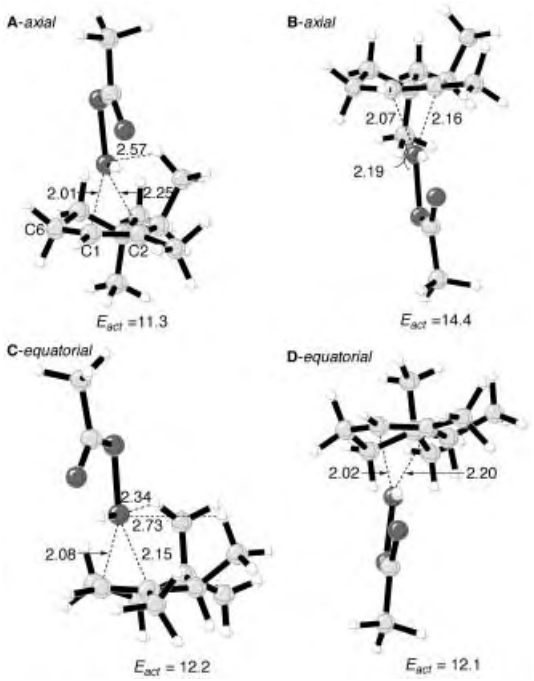


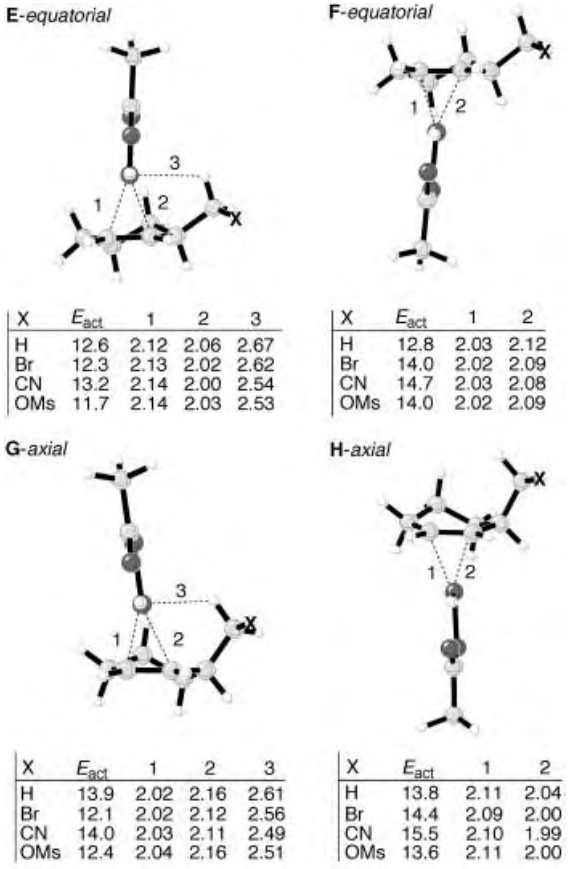
Figure 1. B3LYP/6-31G(d) transition states for epoxidation of 2,3,4,4-tetramethylcyclohexene by peracetic acid. Distances in Angstroms. Energies in kcal mol^{-1}.

Favored transition states **A** and **D** are more asynchronous than **B** and **C**. The C2 methyl group causes C1 to be more nucleophilic in all cases, but in **B** and **C** the forming O1–C1 bond and the axial C6–H bond are eclipsed, resulting in lengthening of the forming O1–C1 bond and a more synchronous transition state.[19] Calculations of the transition states for epoxidation of 1-methylcyclohexene, where the same eclipsing-synchronous and noneclipsing-asynchronous transition states were found, gave activation energies of 11.1 kcal mol^{-1} for the two transition states.

The lower energy of transition states **A** and **C** suggests that there is a slight attractive interaction between the C3 methyl group with the O1 atom of the peracid. Presumably, in **B** the H···O distance of 2.19 Å leads to repulsion. The C3 methyl group contains the C–H bond nearest to the atom O1; this C–H bond is 0.3 mÅ shorter than the other two C–H bonds of the methyl group. C–H bond contraction on the order of 0.2–0.5 mÅ is observed in documented cases of CH···O hydrogen bonding.[20]

Further support for a small attractive CH···O interaction was found in transition states calculated for the epoxidation of 3-methylcyclohexene by peracetic acid at the B3LYP/6-31+G(d,p)//B3LYP/6-31G(d)[21] level of theory (Figure 2). The half-chair conformation with an equatorial methyl group for the reactant is favored by 0.8 kcal mol^{-1} over the conformation with an axial methyl group. The transition state involving *syn* attack (**E**) on the conformation with an equatorial methyl group is 0.2 kcal mol^{-1} lower in energy than **F**. The energy difference of 0.2 kcal mol^{-1} in favor of **E** over **F** is similar to estimates of attractive interactions between CH···O in other systems (0.3–0.7 kcal mol^{-1}).[22] The effect is very small, and a nearly equal mixture of the *cis* and *trans* epoxides are formed experimentally.[23]

 © WILEY-VCH Verlag GmbH, D-69451 Weinheim, 2001 1433-7851/01/4023-4486 $ 17.50+.50/0 *Angew. Chem. Int. Ed.* **2001**, *40*, No. 23



X	E_{act}	1	2	3
H	12.6	2.12	2.06	2.67
Br	12.3	2.13	2.02	2.62
CN	13.2	2.14	2.00	2.54
OMs	11.7	2.14	2.03	2.53

X	E_{act}	1	2
H	12.8	2.03	2.12
Br	14.0	2.02	2.09
CN	14.7	2.03	2.08
OMs	14.0	2.02	2.09

X	E_{act}	1	2	3
H	13.9	2.02	2.16	2.61
Br	12.1	2.02	2.12	2.56
CN	14.0	2.03	2.11	2.49
OMs	12.4	2.04	2.16	2.51

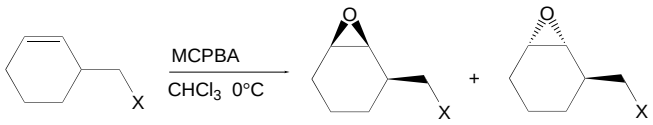
X	E_{act}	1	2
H	13.8	2.11	2.04
Br	14.4	2.09	2.00
CN	15.5	2.10	1.99
OMs	13.6	2.11	2.00

Figure 2. B3LYP/6-31 + G(d,p)//B3LYP/6-31G(d) transition states for epoxidation of 3-substituted cyclohexenes by peracetic acid. The structures shown are from the calculations for X = H.

The $CH_3 \cdots$ peracid hydrogen bonding in the epoxidation of 3-methylcyclohexene is not strong enough for significant differentiation of the two faces of the π bond. However, electronegative substituents on the methyl group could increase the attractive $CH \cdots$ peracid interaction to allow asymmetric epoxidation. Transition states were computed for epoxidations of the electronegatively substituted derivatives of 3-methylcyclohexenes. The results are shown in Figure 2. The conformation containing an equatorial bromomethyl group is favored by 0.1 kcal mol^{-1} over that containing an axial bromomethyl group. The preference for *syn* attack (**E** and **G**) over *anti* attack (**F** and **H**) is now very large (see Figure 2). In the *syn* transition state of **3**, the distances between the methyl hydrogen atom and the oxygen atom of the peracetic acid are 0.05 Å shorter than for 3-methylcyclohexene. The bromine atom increases the electronegativity at the carbon atom making it a better hydrogen bond donor.[24]

Cyano and methylenesulfonyloxymethyl (OMs) groups showed a similar effect (Figure 2). The conformations containing an equatorial cyanomethyl or an equatorial methylenesulfonyloxymethyl group are favored by 0.5 and 0.3 kcal mol^{-1}, respectively, over the axial conformations. For the equatorial and axial cyanomethyl half-chair conformations, *syn* attack is favored by 1.5 kcal mol^{-1} over *anti* attack. For **2**, *syn* attack is preferred by 2.3 kcal mol^{-1} in the equatorial conformation and by 1.2 kcal mol^{-1} in the axial conformation. While the calculated $CH \cdots O$ interaction energies are smaller than that of similar $OH \cdots$ peracid interaction energies (which were calculated to be 2.8 kcal mol^{-1} for epoxidation of 2-cyclohexene-1-ol at the B3LYP/6-311 + G(d,p)//B3LYP/6-31G(d)[25] level) the difference in predicted activation energies between *syn* and *anti* attack for **2**–**4** are substantial enough for π-facial selectivity.

The predictions were tested by experimental epoxidations of **2**–**4** with MCPBA. Epoxidation of **2**–**4** gave quantitative yields of epoxides, stereochemical results are shown in Scheme 1. Compounds **3** and **4** gave *cis* and *trans* epoxide



	X = H[23]	50	50
3:	X = Br	70	30
4:	X = CN	80	20
2:	X = OMs	93	7

Scheme 1. Ratios of stereoisomers obtained from epoxidations of 3-substituted cyclohexenes with MCPBA.

isomers in a ratio of 70:30 and 80:20, respectively, as measured by GC/MS of the crude reaction mixture. The stereochemistry of the major and minor epoxides was assigned by comparison of GC/MS retention times and ^{1}H NMR and ^{13}C NMR data for the reaction mixtures with data for the pure *cis*-3-bromomethyl-1,2-epoxycyclohexane and *trans*-3-cyanomethyl-1,2-epoxycyclohexane synthesized independently (see Experimental Section and Supporting Information). Epoxidation of **2** gave a *cis*:*trans* epoxide ratio of 93:7 as measured by GC/MS of the crude reaction mixture. The stereochemistry of the products was determined by ^{1}H NMR spectroscopy on the isolated epoxides.[26] Although the predicted stereoselectivity is overestimated, the experimentally determined preference for the *cis* epoxide is consistent with $CH \cdots O$ interactions in the transition state.

We have shown a new general effect that peracids prefer to attack *syn* to a homoallylic methyl group, a result of $CH \cdots O$ hydrogen-bonding. Although, the preference is small in the case of the unactivated methyl group, this *syn* preference increases for alkenes with electron-withdrawing substituents. With appropriate electron-withdrawing groups, this interaction may be exploited for stereoselective synthesis.

Experimental Section

General procedure for epoxidation of **2**–**4**: To a flask was added **2**, **3**, or **4**, dry $CHCl_3$, and MCPBA (0.9 equivalents, washed with pH 7 phosphate buffer, crystallized from diethyl ether/hexanes (1:3) and dried at 0.5 mmHg for 12 h). The mixture was stirred for 12 h at 0 °C. Additional MCPBA (0.3 equiv) was added and the mixture was stirred for 2 h at 0 °C, and then KF (to precipitate remaining MCPBA and *meta*-chlorobenzoic acid (MCBA),[27] 1.4 equiv) was added. Epoxide ratios were determined by

 © WILEY-VCH Verlag GmbH, D-69451 Weinheim, 2001 1433-7851/01/4023-4487 $ 17.50+.50/0

GC/MS on the crude reaction mixtures. Stereochemistry determination and all other experimental procedures are given in the Supporting Information.

Received: July 6, 2001
Revised: September 24, 2001 [Z17449]

[1] C. Fehr, *Angew. Chem.* **1998**, *110*, 2509; *Angew. Chem. Int. Ed.* **1998**, *37*, 2407.
[2] For a review on substrate-directed epoxidations see: a) A. H. Hoveyda, *Chem. Rev.* **1993**, *93*, 1307.
[3] a) M. Freccero, R. Gandolfi, M. S. Amade, A. Rastelli, *J. Org. Chem.* **1999**, *64*, 3853; b) R. D. Bach, C. M. Estezez, J. E. Winter, M. N. Glukhovtsev, *J. Am. Chem. Soc.* **1998**, *120*, 680.
[4] A. Hasegawa, H. Z. Sable, *J. Org. Chem.* **1966**, *31*, 4154.
[5] a) B. Zipperer, K. H. Muller, B. Gallenkamp, R. Hildebrand, M. Fletschinger, D. Burger, M. Philat, D. Hunkler, L. Knothe, H. Fritz, H. Prinzbach, *Chem. Ber.* **1988**, *121*, 757; b) H. E. Schink, H. Pettersson, J. E. Backvall, *J. Org. Chem.* **1991**, *56*, 2769.
[6] a) A. Jenmalm, W. Berts, K. Luthman, I. Csoregh, U. Hacksell, *J. Org. Chem.* **1995**, *60*, 1026; b) P. Kococovsky, I. Stary, *J. Org. Chem.* **1990**, *55*, 3226.
[7] a) S. Winstein, R. Boschan, *J. Am. Chem. Soc.* **1950**, *72*, 4669; b) J. Joska, F. Sorm, Collect. Czech. *Chem. Commun.* **1995**, *21*, 745; c) L. Goodman, S. Wienstein, R. Boschan, *J. Am. Chem. Soc.* **1958**, *80*, 4312; d) K. Ponsold, W. Preibach, *J. Prakt. Chem.* **1964**, *25*, 26; e) K. Ponsold, *J. Prakt. Chem.* **1964**, *25*, 32; f) A. Hasegawa, H. Z. Sable, *J. Org. Chem.* **1966**, *31*, 4154; g) G. Lukacs, D. K. Fukushima, *J. Org. Chem.* **1969**, *34*, 2707.
[8] a) W. R. Roush, J. A. Straub, R. Brown, *J. Org. Chem.* **1987**, *52*, 5127; b) H. Kogen, T. Nishi, J. *Chem. Soc. Chem. Commun.* **1987**, 311; c) J. R. Luly, J. F. Dellaria, J. J. Plattner, N. Y. Soderquist, *J. Org. Chem.* **1987**, *52*, 1486; d) K. Hori, Y. Ohfune, *J. Org. Chem.* **1988**, *53*, 3886; e) M. M. Campbell, A. J. Floyd, T. Lewis, M. F. Mahon, R. J. Oglivie, *Tetrahedron Lett.* **1989**, *30*, 1993; f) D. P. Rotella, *Tetrahedron Lett*. **1989**, *30*, 1913; g) S. Julia, B. Furer, *Bull. Soc. Chim. Fr.* **1966**, 1106.
[9] D. K. Fukushima, M.Smulowitz, J. S. Liang, G. Lukacs, *J. Org. Chem.* **1969**, 34, 2702.
[10] I. Honda, A. Ori, G. Tsuchihashi, *Chem. Lett*. **1986**, 1417.
[11] S. A. Hardinger, P. L. Fuchs, *J. Org. Chem.* **1987**, *52*, 2739.
[12] R. P. Joyce, J. A. Galnor, S. M. Weinreb, *J. Org. Chem.* **1987**, *52*, 1177.
[13] J. Clayden, E. W. Collington, E. Egert, A. B. McElroy, S. Warren, *J. Chem. Soc. Perkin Trans. 1* **1994**, 2801.
[14] G. Asensio, C. B. Bernardini, C. Andreu, M. E. G. Nunez, R. Mello, J. O. Edwards, B. Carpenter, *J. Org. Chem.* **1999**, *64*, 4705.
[15] a) M. Freccero, R. Gandolfi, M. S. Amade, *Tetrahedron* **1999**, *55*, 11309; b) R. W. Murray, M. Singh, B. L. Williams, H. M. Moncrieff, *J. Org. Chem.* **1996**, *61*, 1830.
[16] Studies of performic acid, dioxirane, peroxynitrous acid, and oxiziridine epoxidations have shown that B3LYP/6-31G(d) calculations provide transition structure and energies in accord with available experimental data and quadratic configuration interaction (QCI) calculations see: a) K. N. Houk, J. Liu, N. C. DeMello, K. R. Condroski, *J. Am. Chem. Soc.* **1997**, *119*, 10147; b) C. Jenson, J. Liu, K. N. Houk, W. L. Jorgensen, *J. Am. Chem. Soc.* **1997**, *119*, 12982; c) R. D. Bach, M. N. Glukhovtsev, C. Gonzalez, *J. Am. Chem. Soc.* **1998**, *120*, 9902.
[17] Gaussian 98 (Revision A.7), M. J. Frisch, G. W. Trucks, H. B. Schlegel, G. E. Scuseria, M. A. Robb, J. R. Cheeseman, V. G. Zakrzewski, J. A. Montgomery, R. E. Stratmann, J. C. Burant, S. Dapprich, J. M. Millam, A. D. Daniels, K. N. Kudin, M. C. Strain, O. Farkas, J. Tomasi, V. Barone, M. Cossi, R. Cammi, B. Mennucci, C. Pomelli, C. Adamo, S. Clifford, J. Ochterski, G. A. Petersson, P. Y. Ayala, Q. Cui, K. Morokuma, D. K. Malick, A. D. Rabuck, K. Raghavachari, J. B. Foresman, J. Cioslowski, J. V. Ortiz, B. B. Stefanov, G. Liu, A. Liashenko, P. Piskorz, I. Komaromi, R. Gomperts, R. L. Martin, D. J. Fox, T. Keith, M. A. Al-Laham, C. Y. Peng, A. Nanayakkara, C. Gonzalez, M. Challacombe, P. M. W. Gill, B. G. Johnson, W. Chen, M. W. Wong, J. L. Andres, M. Head-Gordon, E. S. Replogle, J. A. Pople, Gaussian, Inc., Pittsburgh, PA, **1998**.
[18] All activation energies were calculated relative to separated reactants in their lowest energy conformations. Zero-point corrections calculated for epoxidation of 3-methylcyclohexene did not change relative energies of the four transition states and are not included in any reported activation energies.
[19] M. J. Lucero, K. N. Houk, *J. Org. Chem*. **1998**, *63*, 6973, and references therein.
[20] Y. Gu, T. Kar, S. Scheiner, *J. Am. Chem. Soc.* **1999**, *121*, 9411.
[21] Studies on epoxidation of allylic alcohols have shown that the B3LYP/6-31G(d) level accurately reproduces structure and energies in accord with available experimental data.[2] Studies show that the B3LYP/6-31+G(d,p) level accurately describes F_nCH_{3-n} interactions with water, methanol, and formaldehyde.[20]
[22] a) J. J. Nova, F. Mota, *Chem. Phys. Lett.* **1997**, *266*, 23; b) D. E. Woon, P. Zeng, D. R. Beck, *J. Chem. Phys.* **1990**, *93*, 7808; c) M. M. Szczesniak, G. Chalasinski, S. M. Cybulski, P. Cieplak, *J. Chem. Phys.* **1993**, *98*, 3078; d) J. J. Novoa, P. Lafuente, F. Mota, *Chem. Phys. Lett.* **1998**, *290*, 519.
[23] G. Bellucci, G. Berti, M. Ferrett, G. Ingrosso, E. Mastoroilli, *J. Org. Chem.* **1978**, *43*, 422.
[24] For 4-fluoro-1-butene the addition of another fluorine atom (4,4-difluorobutene) did not increase the *syn* preference; this is probably due to electrostatic repulsion in the *syn* transition state, between the oxygen atoms of the peracid and the two fluorine atoms.
[25] M. Freccero, R. Gandolfi, M. Sarzi-Amade, A. Rastelli, *J. Org. Chem.* **2000**, *65*, 8948.
[26] M. Chini, P. Crotti, F. A. Lee, C. Gardelli, M. Franco, *J. Org. Chem.* **1992**, *57*, 1713, and references therein.
[27] F. Camps, J. Coll, A. Messeguer, F. Pujol, *J. Org. Chem.* **1982**, *47*, 5402.

Use of a Perfluoroalkylsulfonyl (PFS) Linker in a "Traceless" Synthesis of Biaryls through Suzuki Cleavage

Yijun Pan, Beatrice Ruhland, and Christopher P. Holmes*

Solid-phase synthesis has attracted increasing attention from the scientific community and particularly from the pharmaceutical industry in an effort to speed up drug discovery.[1] A key component in solid-phase synthesis is the linker that is used to attach the molecules to the solid support. There has been significant interest in recent years to develop "traceless" linkers[2] which afford compounds suitable for biological assays lacking any extraneous functionality that may limit their usefulness as drug leads.

We recently reported the preparation of a perfluoroalkylsulfonyl (PFS) fluoride resin, **1** (see Scheme 1, in essence a triflate resin), and its application for the traceless synthesis of arenes using a palladium-mediated reductive deoxygenation.[3] We sought to extend application of this linker to a

[*] Dr. C. P. Holmes, Dr. Y. Pan, Dr. B. Ruhland
Department of Chemistry, Affymax Research Institute
4001 Miranda Avenue, Palo Alto, CA 94304 (USA)
Fax: (+1) 650-424-9860
E-mail: chris_holmes@affymax.com

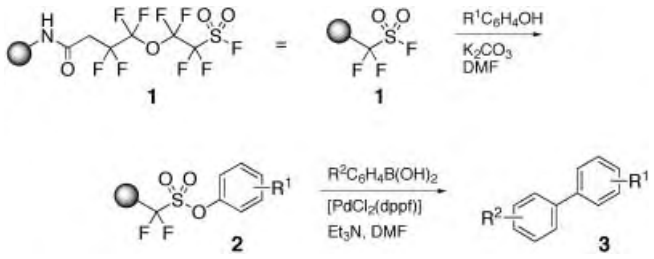
Supporting information for this article is available on the WWW under http://www.angewandte.com or from the author.

 © WILEY-VCH Verlag GmbH, D-69451 Weinheim, 2001 1433-7851/01/4023-4488 $ 17.50+.50/0

cross-coupling strategy whereby additional functionality could be appended to the aryl ring during the cleavage step. Several methods describing the formation of new C–C and C–N bonds upon cleavage of products from the resin have been reported. Recently, an elegant approach to biarylmethanes derived from polymer-supported benzylsulfonium salts was reported by Mioskowski et al.[4] Bräse and Schroen created several types of molecules starting with a resin-bound triazene formed by coupling diazonium salts to an amine resin,[5] whereas separately the research groups led by Carboni[6] and Burgess[7] have treated immobilized boronic acids with various electrophilic species. Reitz et al. reported the preparation of phenethylamines by means of a C–N bond forming reaction by displacing a resin-bound alkylsulfonate with amines.[8]

Our strategy of coupling phenols to the electrophilic sulfonyl fluoride resin **1** to create an aryltriflate species avoids the limitations of the existing methods, which rely on relatively uncommon starting materials or preactivation steps to prepare a linker–substrate conjugate prior to attachment to the support. Aryl triflates have been widely used as substrates to introduce diverse functionality on an aromatic group through palladium-mediated cross-coupling reactions.[9] The Suzuki, Heck, and Stille reactions are among the most powerful methods for C–C bond formation and have been shown to proceed in excellent yield on solid support.[10] We report herein that a Suzuki cleavage/cross-coupling reaction of perfluoroalkylsulfonate resin **2** (see Scheme 1) affords high yields of biaryls.

A variety of phenols were attached to resin **1**[11] through the formation of the polymer-bound perfluoroalkylsulfonates **2**, by using K_2CO_3 as base in dimethylformamide (DMF) at room temperature (Scheme 1). These conditions are very mild



Scheme 1. Attachment and subsequent Suzuki cleavage/cross-coupling reaction of phenols bound to the PFS linker **1** as "aryl triflates" **2** to generate biaryls **3**.

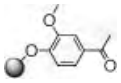
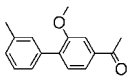
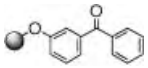
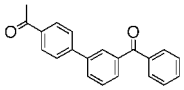
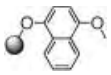
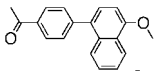
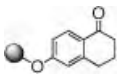
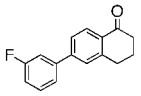
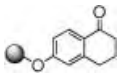
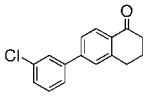
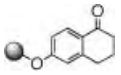
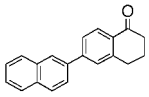
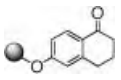
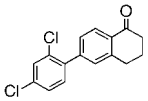
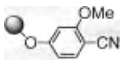
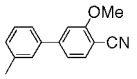
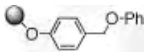
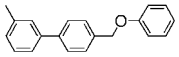
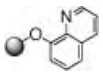
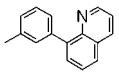
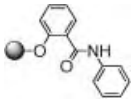
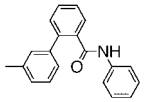
and compatible with a wide range of functionalized compounds such as aldehydes, carboxylic acids, alcohols, and ketones without the need for protecting groups. Loading levels were determined by elemental analysis and could be monitored by the disappearance of the SO_2F signal in the gel-phase ^{19}F NMR spectrum.[3] Others have reported the use of gel-phase ^{19}F NMR spectroscopy to monitor reactions and to determine resin loadings.[12] Although several reports have been published on the Suzuki coupling of aryl triflates, these methods require different sets of conditions (catalyst, base, solvent) depending on the substrates. Our objective was to identify mild reaction conditions employing a single catalyst system that would be suitable for the synthesis of a wide range of biaryl compounds. In our initial studies we tested a variety of catalyst systems including $[Pd_2(dba)_3(PtBu_3)]$ (dba = dibenzylideneacetone), $[Pd(PPh_3)_4]$, and $[Pd(OAc)_2(PCy_3)]$ with different bases (K_3PO_4, K_2CO_3, KF), by varying the solvent and the temperature. However, none of those catalyst systems was of broad applicability, giving inconsistent yields of the desired biaryl products and often considerable amounts of reduction products.[13] We were pleased to discover that our original conditions for the resin-based Suzuki coupling of aromatic iodides proved to be the most general.[14] Treating the polymer-supported aryl perfluoroalkylsulfonate species **2** with a variety of arylboronic acids in the presence of $[PdCl_2(dppf)]$ (dppf = 1,1′-bis(dipenylphosphanyl)ferrocene) and Et_3N in DMF at 80 °C for 8 h afforded the biaryl compounds **3** in good yield and purity (Scheme 1). The desired products were easily isolated by two-phase extraction and purified to homogeneity by preparative thin-layer chromatography. Based on the initial loading of the resin, the biaryl products were isolated in yields of 62–89 %. As shown in Table 1, arylboronic acids and phenols containing both electron-poor and electron-rich substituents participated effectively. Phenols with *ortho* substituents also reacted effectively (entries 1, 10, 11). More remarkably, the *ortho*-substituted and somewhat electron-deficient 2,4-dichlorophenylboronic acid coupled very efficiently giving the biaryl product in 82 % yield (entry 7). It appears that the linker **1** behaves as a polymer-supported triflate species as desired.

Next, we further explored the generality of the traceless Suzuki cleavage/cross-coupling strategy by synthesizing a small library of eleven biarylamides **7** employing reductive amination and acylation steps (Scheme 2). Thus, 4-hydroxybenzaldehyde was tethered to PFS support **1** to generate the resin-bound sulfonate **4**. Aldehyde **4** was split into three aliquots, which were separately subjected to reductive amination with isobutylamine, furfurylamine, and isopropyl amine in the presence of $Na(CN)BH_3$ and HOAc in THF. The resulting benzylamines **5** were further partitioned into aliquots and separately treated with four acid chlorides (benzoyl chloride, *p*-toluoyl chloride, isobutyryl chloride, and 2-furoyl chloride) to give the N-acylated products **6**. Each resin was then individually cleaved as described above with an arylboronic acid to liberate the biarylamides **7a–k** (Scheme 3), which would have been difficult to prepare with other reported solid-phase linkers. In agreement with our previous results,[3] the compounds were of sufficient purity to be submitted directly to biological screening after filtration through silica gel. After purification, the biaryl compounds **7a–k** were isolated in 65–90 % yield based on the original resin loading. While not extremely diverse, the small library did allow us to demonstrate that the intermediates were stable and could be manipulated without degradation; further exploitation and optimization of this process for the preparation of larger libraries is currently underway.

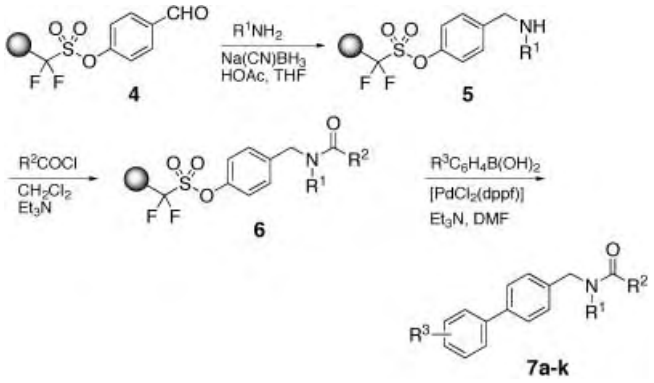
What is noteworthy is that the PFS linker serves as a linker, a protecting group, and an activating group for phenols. The polymer-supported aryl sulfonates appear to be stable to a variety of reaction conditions common in library synthesis

 © WILEY-VCH Verlag GmbH, D-69451 Weinheim, 2001 1433-7851/01/4023-4489 $ 17.50+.50/0

Table 1. Suzuki cleavage/cross-coupling of resin-bound aryl perfluoroalkylsulfonates **2**.

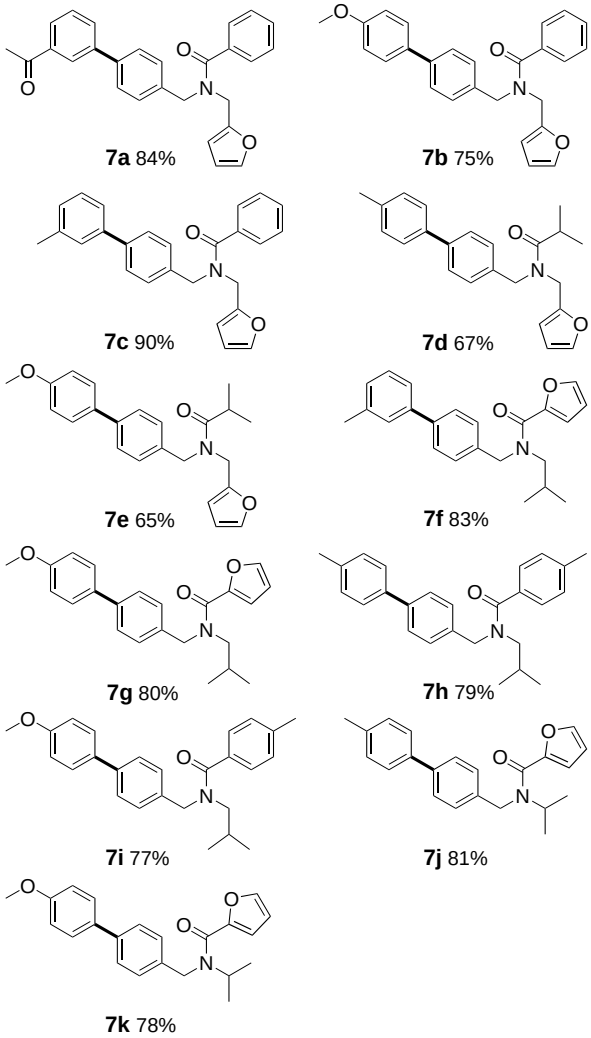
Entry	Resin **2**	$R^2C_6H_4B(OH)_2$[a]	Product **3**	Yield [%][b]
1		A		76
2		B		62
3		B		73
4		C		74
5		D		80
6		E		78
7		F		82
8		A		85
9		A		89
10		A		88
11		A		84

[a] The boronic acids used were A: 3-tolyl-, B: 4-acetylphenyl-, C: 3-fluorophenyl-, D: 3-chlorophenyl-, E: 2-naphthyl-, F: 2,4-dichlorophenylboronic acid. [b] Yields were based on the measured loading of resin **2**.



Scheme 2. Reaction sequence to create a library of biarylamides using **1** as a tethering and activating group.

such as reductive amination and acylation, while affording a high degree of activation in palladium-based reactions. The single-catalyst system $[PdCl_2(dppf)]/Et_3N$ was found to be



Scheme 3. Structures and yields of Suzuki cleavage/cross-coupling products **7** with the newly formed bond in bold.

suitable for the cross-coupling of a variety of substituted phenols and boronic acids. Considering the number of commercially available phenols, the traceless cleavage/cross-coupling strategy using a key Suzuki reaction should serve as a powerful method to generate vast numbers of diverse compounds for drug discovery programs.

Experimental Section

A mixture of polymer-supported aryl perfluoroalkylsulfonate **2** (200 mg, 0.07 mmol), $[PdCl_2(dppf)]$ (7.2 mg), boronic acid (0.26 mmol), and Et_3N (88 μL, 0.62 mmol) in DMF (1.5 – 2.0 mL) was placed in a vial under an N_2 atmosphere. The vial was sealed and magnetically stirred at 90 °C for 8 h. The resin was filtered and washed with Et_2O, and the combined organic phases were washed with 10 % aqueous Na_2CO_3 and water, and evaporated to dryness. The residue was dissolved in Et_2O and eluted through a short bed of silica gel to removed inorganic residues. The crude products were purified by preparative TLC to give the desired products in > 98 % purity.

Received: July 30, 2001 [Z17624]

[1] a) S. E. Hall, *Annu. Rep. Comb. Chem. Mol. Diversity* **1999**, *2*, 15; b) I. Sucholeiki, *Annu. Rep. Comb. Chem. Mol. Diversity* **1999**, *2*, 9; c) W.-C. Haase, P. H. Seeberger, *Curr. Org. Chem.* **2000**, *4*, 481; d) B. Kundu, S. K. Khare, S. Rastogi, *Prog. Drug Res.* **1999**, *53*, 89; e) A. J.

 © WILEY-VCH Verlag GmbH, D-69451 Weinheim, 2001 1433-7851/01/4023-4490 $ 17.50+.50/0

Mendonca, X.-Y. Xiao, *Med. Res. Rev.* **1999**, *19*, 451; f) K. Gordon, S. Balasubramanian, *Curr. Opin. Drug Discovery Dev.* **1999**, *2*, 342; g) C. Watson, *Angew. Chem.* **1999**, *111*, 2025; *Angew. Chem. Int. Ed.* **1999**, *38*, 1903; h) S. Kobayashi, *Chem. Soc. Rev.* **1999**, *28*, 1; i) S. Booth, P. H. H. Hermkens, H. C. J. Ottenheijm, D. C. Rees, *Tetrahedron* **1998**, *54*, 15385; j) P. Hodge, *Chem. Soc. Rev.* **1997**, *26*, 417.

[2] a) F. Zaragoza, *Angew. Chem.* **2000**, *112*, 2158; *Angew. Chem. Int. Ed.* **2000**, *39*, 2077; b) A. B. Reitz, *Curr. Opin. Drug Discovery Dev.* **1999**, *2*, 358; c) C. J. Andres, D. L. Whitehouse, M. S. Deshpande, *Curr. Opin. Chem. Biol.* **1998**, *2*, 353; d) I. W. James, *Tetrahedron Lett.* **1999**, *55*, 4855.

[3] Y. Pan, C. P. Holmes, *Org. Lett.* **2001**, *3*, 2769.

[4] C. Vanier, F. Lorgé, A. Wagner, C. Mioskowski, *Angew. Chem.* **2000**, *112*, 1745; *Angew. Chem. Int. Ed.* **2000**, *39*, 1679.

[5] S. Bräse, M. Schroen, *Angew. Chem.* **1999**, *111*, 1139; *Angew. Chem. Int. Ed.* **1999**, *38*, 1071.

[6] C. Pourbaix, F. Carreaux, B. Carboni, *Org. Lett.* **2001**, *3*, 803.

[7] W. Li, K. Burgess, *Tetrahedron Lett.* **1999**, *40*, 6527.

[8] J. K. Rueter, S. O. Nortey, E. W. Baxter, G. C. Leo, A. B. Reitz, *Tetrahedron Lett.* **1998**, *39*, 975.

[9] a) K. Ritter, *Synthesis* **1993**, *8*, 735; b) W. J. Scott, J. E. McMurry, *Acc. Chem. Res.* **1988**, *21*, 47; c) I. L. Baraznenok, V. G. Nenajdenko, E. S. Balenkova, *Tetrahedron* **2000**, *56*, 3077.

[10] R. Franzén, *Can. J. Chem.* **2000**, *78*, 957; see also references compiled in F. Zaragoza Dörwald, *Organic Synthesis on Solid Phase*, Chapter 5, Wiley-VCH, Weinheim, **2000**.

[11] Support **1** bearing the PFS linker was prepared from Tentagel-NH_2 resin (RAPP Polymere, loading 0.43 mmol g^{-1}) with the loading measured by elemental analysis being typically 0.33 mmol g^{-1}.

[12] a) D. Stones, D. J. Miller, M. W. Beaton, T. J. Rutherford, D. Gani, *Tetrahedron Lett.* **1998**, *39*, 4875; b) A. Svensson, K.-E. Bergquist, T. Fex, J. Kihlberg, *Tetrahedron Lett.* **1998**, *39*, 7193.

[13] In the absence of a suitable nucleophile, reduction to the parent arene is often observed during palladium-mediated reactions of aryl species.

[14] B. Ruhland, A. Bombrun, M. A. Gallop, *J. Org. Chem.* **1997**, *62*, 7820.

Asymmetric Allylsilane Additions to Enantiopure *N*-Acylhydrazones with Dual Activation by Fluoride and $In(OTf)_3$**

Gregory K. Friestad* and Hui Ding

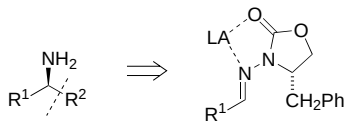
Chiral α-branched amines are common features of biologically active compounds. Direct asymmetric amine synthesis by addition to the C=N bond of carbonyl imino derivatives holds promise for improved access to these substructures by introducing a stereogenic center and a carbon–carbon bond in one step. However, the use of strongly basic organometallic reagents for this purpose[1] can result in competitive metalloenamine formation.[2] Development of alternative milder methods for the construction of C–C bonds is therefore of considerable importance.[3]

[*] Prof. G. K. Friestad, H. Ding
Department of Chemistry, University of Vermont
Burlington, VT 05405 (USA)
Fax: (+1) 802-656-8705
E-mail: gregory.friestad@uvm.edu

[**] We thank the National Science Foundation (Vermont EPSCoR) and the University of Vermont for generous support.

Supporting information for this article is available on the WWW under http://www.angewandte.com or from the author.

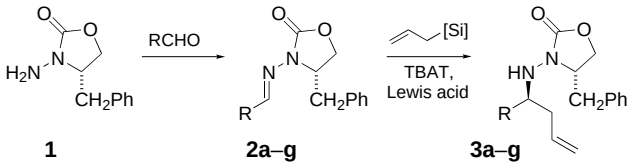
Previously we found that in the presence of Zn^{II} or In^{III} salts, chiral *N*-acylhydrazones (Scheme 1) underwent highly stereoselective radical additions[4] in which Lewis acid activation and restriction of rotamer populations were key design



Scheme 1. Retrosynthetic carbon–carbon bond disconnection of chiral α-branched amines to a Lewis acid activated chiral *N*-acylhydrazone precursor.

elements. We sought to exploit this design further with other reaction types that would broaden the variety of accessible chiral amines. An allyl group is particularly useful for subsequent synthetic manipulations, so extensive efforts have been directed toward the stereoselective allylation of chiral imines, iminium ions, and related C=N electrophiles.[5] We envisioned a novel dual activation protocol in which both the allyl donor and acceptor would be activated in a complementary fashion to promote C–C bond construction under relatively mild conditions. We hypothesized that the fluoride-promoted addition of an allylsilane to *N*-acylhydrazones in the presence of a Lewis acid would achieve this goal with excellent stereocontrol. There are surprisingly few examples of the Sakurai-like fluoride-promoted addition of allylsilanes to C=N bonds,[6] perhaps because of a prevailing perception that allylsilanes are rather unreactive toward imines without the use of strong Lewis acids.[7] We report herein convenient, highly stereoselective additions of allylsilanes to chiral *N*-acylhydrazones at room temperature with dual activation by fluoride and indium(III) trifluoromethanesulfonate.

Our initial studies examined the reaction of allyltrimethylsilane with chiral hydrazone **2a**[4] (Scheme 2). The use of a fluoride ion source required careful consideration of experimental protocols to avoid its potential incompatibility with



Scheme 2. Addition of allylsilanes to enantiopure hydrazones with dual activation by Lewis acid and fluoride ion (**a**: R = Ph; **b**: R = *p*-tolyl; **c**: R = *m*-nitrophenyl; **d**: R = 2-naphthyl; **e**: R = 2-furyl; **f**: R = CH=CHPh; **g**: R = CH_2CH_3; for [Si] see Table 1).

Lewis acids. Eventually, we found that the soluble, air-stable, nonhygroscopic fluoride source tetrabutylammonium triphenyldifluorosilicate (TBAT)[8] could effectively promote allyltrimethylsilane addition to the complex formed by mixing **2a** with a Lewis acid, to provide **3a** [Scheme 2] with good stereoselectivity. The optimal protocol entailed mixing a slight excess of allylsilane with TBAT in CH_2Cl_2 while preparing a mixture of **2a** and a Lewis acid in CH_2Cl_2. After 4 h, these solutions were combined at room temperature, followed by a

 © WILEY-VCH Verlag GmbH, D-69451 Weinheim, 2001 1433-7851/01/4023-4491 $ 17.50+.50/0

normal workup after completion of the reaction. Indium(III) trifluoromethanesulfonate ($In(OTf)_3$) was chosen from a broad range of Lewis acids screened ($ZnCl_2$, $InCl_3$, $In(OAc)_3$, $TiCl_4$, $SnCl_4$, $Sc(OTf)_3$, $Yb(OTf)_3$, $Cu(OTf)_2$, TMSOTf, $BF_3 \cdot OEt_2$).

Variations to the substituents on the silicon atom were examined next (Table 1). Although allyltrialkoxysilanes and various allylchlorosilanes were ineffective under these conditions, allyl(diisopropylamino)dimethylsilane led to a significant improvement and provided **3a** in high yield and stereoselectivity. Commercially available tetraallylsilane proved to be a superior allyl donor and gave **3a** in 78% yield with excellent stereocontrol (d.r. > 99:1).

Table 1. Variation of Silicon Substituents in TBAT/$In(OTf)_3$-Promoted Addition of Allylsilanes to Hydrazone **2a** (Scheme 2).

[Si] of allylsilane	Yield of **3a**[a]	d.r.[b]
$SiMe_3$	58%	94:6
$SiPh_3$	n.r.	–
$Si(OMe)_3$	n.r.	–
$SiCl_3$	n.r.	–
$SiMeCl_2$	n.r.	–
$SiMe_2Cl$	n.r.	–
$SiMe_2N(iPr)_2$	81%	95:5
$Si(allyl)_3$	78%	> 99:1

[a] Yields of isolated purified diastereomer mixtures (n.r.: no reaction). [b] Diastereomer ratio determined by means of HPLC (Microsorb-MV C8, 2-PrOH/hexane).

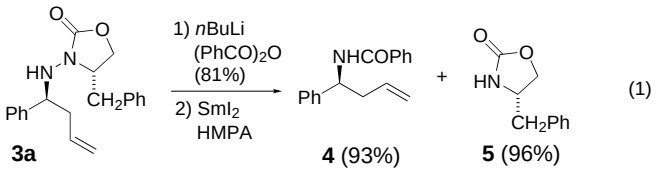
With effective reaction conditions in hand, a brief survey of the scope of the reaction was undertaken by using a series of hydrazones prepared from the corresponding aldehydes (Table 2). Aromatic aldehyde hydrazones **2b–e** generally gave homoallylic amines in good yield with excellent stereoselectivity, and α,β-unsaturated hydrazone (*E*)-**2f** underwent chemoselective addition to the C=N bond. Although propionaldehyde hydrazone **2g**[4] also participated in the reaction, the stereoselectivity was modest.

Table 2. Preparation of Various Aldehyde Hydrazones **2** and TBAT/$In(OTf)_3$-Promoted Addition of Tetraallylsilane (Scheme 2).

Hydrazone	Yield[a]	Allyl adduct	Yield[b]	d.r.[c]
2b	94%	**3b**	94%	98:2
2c	91%	**3c**	71%	> 99:1
2d	92%	**3d**	82%	98:2
2e	92%	**3e**	58%	96:4
(*E*)-**2f**	97%	**3f**	60%	95:5
2g	92%	**3g**	51%	82:18

[a] Yield of isolated hydrazone. [b] Yields of isolated purified diastereomer mixtures. [c] Diastereomer ratio determined by means of HPLC.

To determine the stereochemistry, the auxiliary was removed reductively from the *N*-benzoyl derivative of **3a** to give benzamide **4** [Eq. (1)], which was shown by means of optical rotation to have the *S* configuration.[9] Saturation of the allyl group of **3g** (H_2, Pd/C) gave a known derivative of (*R*)-3-aminohexane.[10] For insight into the mechanism, control experiments were conducted with **2a**:



3a **4** (93%) **5** (96%) (1)

1) Reaction in the absence of $In(OTf)_3$: 15% yield, d.r. 67:33.
2) Reaction without TBAT: 30% yield, d.r. 94:6.
3) Neither $In(OTf)_3$ nor TBAT: no reaction.
4) Additional $In(OTf)_3$ in the TBAT/allylsilane mixture prior to mixing with the $In(OTf)_3$–hydrazone complex: 66% yield, d.r. > 99:1.
5) However, after > 12 h, the mixture of $In(OTf)_3$, TBAT, and allylsilane behaves differently: 22% yield, dr 95:5.

Accordingly, ^1H NMR spectroscopy experiments (500 MHz, CD_2Cl_2, 27 °C) showed that tetraallylsilane is essentially unchanged after 4 h in the presence of TBAT, and when $In(OTf)_3$ is added, consumption of the tetraallylsilane requires at least a further 14 h. Transmetallation to an allylindium species therefore appears to be slow, and hence the reaction of a hypervalent silicate with the Lewis acid complexed hydrazone seems more likely.[11] Furthermore, the variation in the reactivity and selectivity upon changing the silicon ligands suggests the presence of silicon in the transition state of the addition. The improved yield and selectivity with tetraallylsilane over allyltrimethylsilane may be attributed to a more electrophilic silicon atom, which leads to greater fluoride ion affinity, increased hypervalent silicate population, and a later transition state.[12] Stereochemical results are consistent with the chelate structure in Scheme 1, in which restriction of rotamer populations facilitates steric blocking of the *Re* face.

In summary, highly stereoselective allylsilane addition to enantiopure *N*-acylhydrazones occurs in the presence of easily handled, air-stable TBAT and $In(OTf)_3$, which appear to induce complementary dual activation of both reactants. To our knowledge, these are the first examples of useful auxiliary acyclic stereocontrol in allylsilane addition to stable, isolable imino derivatives. Considering the ubiquity of chiral amines and the synthetic versatility of the allyl group, applications to complex targets may be envisioned.

Experimental Section

Allyl addition: A solution of allylsilane (3 equiv) and TBAT (3 equiv) in CH_2Cl_2 (0.75 M), and a solution of $In(OTf)_3$ (1.3 equiv) and hydrazone **2a** in CH_2Cl_2 (0.1 M) were prepared separately. After 4 h at approximately 25 °C, the allylsilane/TBAT mixture was transferred by syringe to the hydrazone/$In(OTf)_3$ mixture. After 2 d at approximately 25 °C, the reaction mixture was washed with water, dried ($MgSO_4$), concentrated, and purified by flash chromatography.

Hydrazone formation: Aldehyde (0.4 mmol), **1** (0.25 mmol), $MgSO_4$ (200 mg), *p*-toluenesulfonic acid (catalytic amount) were heated in toluene (10 mL) at reflux for 10 min.

Received: August 1, 2001 [Z17653]

[1] Reviews: a) S. Kobayashi, H. Ishitani, *Chem. Rev.* **1999**, *99*, 1069; b) R. Bloch, *Chem. Rev.* **1998**, *98*, 1407; c) D. Enders, U. Reinhold, *Tetrahedron Asymmetry* **1997**, *8*, 1895; d) S. E. Denmark, O. J.-C. Nicaise, *Chem. Commun.* **1996**, 999.

[2] a) Aza-enolization of imines with Grignard reagents: G. Stork, S. R. Dowd, *J. Am. Chem. Soc.* **1963**, *85*, 2178; G. Wittig, H. D. Frommeld, P. Suchanek, *Angew Chem.* **1963**, *75*, 978; *Angew. Chem. Int. Ed. Engl.*

 © WILEY-VCH Verlag GmbH, D-69451 Weinheim, 2001 1433-7851/01/4023-4492 $ 17.50+.50/0

1963, *2*, 683; b) less basic organocerium reagents also exhibit azaenolization: D. Enders, E. Diez, R. Fernandez, E. Martin-Zamora, J. M. Munoz, R. R. Pappalardo, J. M. Lassaleta, *J. Org. Chem.* **1999**, *64*, 6329.

[3] For selected recent examples, see: a) review of asymmetric Strecker-type reactions: L. Yet, *Angew. Chem.* **2001**, *113*, 900; *Angew. Chem. Int. Ed.* **2001**, *40*, 875; b) for asymmetric Mannich reactions, see: W. Notz, K. Sakthivel, T. Bui, G. Zhong, C. F. Barbas III, *Tetrahedron Lett.* **2001**, *42*, 199; B. List, *J. Am. Chem. Soc.* **2000**, *122*, 9336; S. Saito, K. Hatanaka, H. Yamamoto, *Org. Lett.* **2000**, *2*, 1891; K. Miura, K. Tamaki, T. Nakagawa, A. Hosomi, *Angew. Chem.* **2000**, *112*, 2034; *Angew. Chem. Int. Ed.* **2000**, *39*, 1958.

[4] a) G. K. Friestad, J. Qin, *J. Am. Chem. Soc.* **2000**, *122*, 8329; b) G. K. Friestad, J. Qin, *J. Am. Chem. Soc.* **2001**, *123*, 9922.

[5] For reviews of allyl organometallic addition to C=N bonds, see: Y. Yamamoto, N. Asao, *Chem. Rev.* **1993**, *93*, 2207; E. F. Kleinman, R. A. Volkmann in *Comprehensive Organic Synthesis*, *Vol. 2* (Eds.: B. M. Trost, I. Fleming), Pergamon, New York, **1991**, pp. 975–1006; see also ref. [1]. For selected recent examples, see: a) allyltin: H. Nakamura, K. Aoyagi, J.-G. Shim, Y. Yamamoto, *J. Am. Chem. Soc.* **2001**, *123*, 372; F. M. Guerra, M. R. Mish, E. M. Carreira, *Org. Lett.* **2000**, *2*, 4265; J. A. Marshall, K. Gill, B. M. Seletsky, *Angew. Chem.* **2000**, *112*, 983; *Angew. Chem. Int. Ed.* **2000**, *39*, 953; b) allylboron: K. Watanabe, S. Kuroda, A. Yokoi, K. Ito, S. Itsuno, *J. Organomet. Chem.* **1999**, *581*, 103; c) allyltitanium: X. Teng, Y. Takayama, S. Okamoto, F. Sato, *J. Am. Chem. Soc.* **1999**, *121*, 11916; d) allylmagnesium: S. Maiorana, C. Baldoliu, P. D. Buttero, E. Licandro, A. Papagni, M. Lanfranchi, A. Tiripicchio, *J. Organomet. Chem.* **2000**, *593–594*, 380; A. G. Steinig, D. M. Spero, *J. Org. Chem.* **1999**, *64*, 2406; e) allylsamarium: R. Yanada, M. Okaniwa, A. Kaieda, T. Ibuka, Y. Takemoto, *J. Org. Chem.* **2001**, *66*, 1283; f) allylindium: H. M. S. Kumar, S. Anjaneyulu, E. J. Reddy, J. S. Yadav, *Tetrahedron Lett.* **2000**, *41*, 9311; T. H. Chan, W. Lu, *Tetrahedron Lett.* **1998**, *39*, 8605; g) allylgermanium: T. Akiyama, J. Iwai, Y. Onuma, H. Kagoshima, *Chem. Commun.* **1999**, 2191.

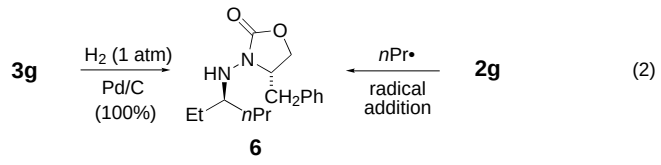
[6] a) X. Fang, M. Johannsen, S. Yao, N. Gathergood, R. G. Hazell, K. A. Jorgensen, *J. Org. Chem.* **1999**, *64*, 4844; b) D.-K. Wang, Y.-G. Zhou, Y. Tang, X.-L. Hou, L.-X. Dai, *J. Org. Chem.* **1999**, *64*, 4233; c) A. S. Pilcher, P. DeShong, *J. Org. Chem.* **1996**, *61*, 6901.

[7] a) Sluggish reactivity of allylsilanes toward neutral imines has been noted: see refs. [1] and [5a]; b) although allylsilane addition to iminium ions is effective, a strong Lewis acid such as $TiCl_4$ or $BF_3 \cdot Et_2O$ is often required; for a review, see: I. Fleming, J. Dunogus, R. Smithers, *Org. React.* **1989**, *37*, 57; recent examples: J. V. Schaus, N. Jain, J. S. Panek, *Tetrahedron* **2000**, *56*, 10263; T. Akiyama, M. Sugano, H. Kagoshima, *Tetrahedron Lett.* **2001**, *42*, 3889.

[8] A. S. Pilcher, H. L. Ammon, P. DeShong, *J. Am. Chem. Soc.* **1995**, *117*, 5166; C. J. Handy, Y.-F. Lam, P. DeShong, *J. Org. Chem.* **2000**, *65*, 3542.

[9] The optical rotation of **4** ($[\alpha]_D^{20} = -2.0$ ($c = 3.4$ in $CHCl_3$)) was within experimental error of an authentic sample ($[\alpha]_D^{20} = -2.2$ ($c = 3.4$ in $CHCl_3$)) prepared from the known homoallylic amine: T. Basile, A. Bocoum, D. Savoia, A. Umani-Ronchi, *J. Org. Chem.* **1994**, *59*, 7766.

[10] Hydrogenation of **3g** gives **6**, identical to that from *n*-propyl radical addition to **2g** [Eq. (2)]. See ref. [4b].



(2)

[11] The allylsilane addition fails in 10:1 CH_2Cl_2/water, which would not likely interfere with allylindium addition (see ref. [5f]).

[12] Similar explanations have been advanced regarding the enhanced reactivity of bis(allyl)silanes. A. Shibato, Y. Itagaki, E. Tayama, Y. Hokke, N. Asao, K. Maruoka, *Tetrahedron* **2000**, *56*, 5373.

Molecular Insight Into Surface Organometallic Chemistry Through the Combined Use of 2D HETCOR Solid-State NMR Spectroscopy and Silsesquioxane Analogues**

Mathieu Chabanas, Elsje Alessandra Quadrelli, Bernard Fenet, Christophe Copéret,* Jean Thivolle-Cazat, Jean-Marie Basset,* Anne Lesage, and Lyndon Emsley*

The structural characterization of heterogeneous catalysts remains difficult. In the late eighties, Feher and later others showed that polyhedral oligomeric silsesquioxanes (POSS) can be used to model the surface structure of partially dehydroxylated silica and therefore infer information about the coordination sphere of metal complexes directly supported on oxides such as silica.[1] This approach can also provide mechanistic insights on surface chemistry processes. However, no direct comparison between these models and their related surface complexes has been reported.

We have recently shown that the reaction of tris(neopentyl)neopentylidene tantalum, $[Ta(=CH\textit{t}Bu)(CH_2\textit{t}Bu)_3]$ (**1**) with $SiO_{2\text{-}(500)}$ gives a mixture of mono-$[\equiv SiO\text{-}Ta(=CH\textit{t}Bu)(CH_2\textit{t}Bu)_2]$ and bisgrafted surface complexes $[(\equiv SiO)_2Ta(=CH\textit{t}Bu)(CH_2\textit{t}Bu)]$,[2a] while its reaction with a $SiO_{2\text{-}(700)}$ provides the monografted species $[\equiv SiO\text{-}Ta(=CH\textit{t}Bu)(CH_2\textit{t}Bu)_2]$ ($\mathbf{2_s}$) as the sole surface species. The characterization was based on elemental analysis, the evolution of neopentane during grafting of **1**, and solvolysis of $\mathbf{2_s}$ as well as infrared (IR) spectroscopy.[2b]

We report here the use of high-resolution solid-state one-dimensional (1D) and two-dimensional (2D) NMR spectroscopy to study $\mathbf{2_s}$ and the use of high-resolution solution-state 1D and 2D NMR spectroscopy of its molecular analogue $[(c\text{-}C_5H_9)_7Si_7O_{12}Si{-}O{-}Ta(=CH\textit{t}Bu)(CH_2\textit{t}Bu)_2]$ ($\mathbf{2_m}$) to define the structure of $\mathbf{2_s}$ at a molecular level and to investigate the reaction pathway leading to the grafted species.

[*] Dr. C. Copéret, Dr. J.-M. Basset, M. Chabanas, Dr. J. Thivolle-Cazat
Laboratoire de Chimie Organométallique de Surface
UMR-9986 CNRS – ESCPE Lyon, 43 blvd du 11 Novembre 1918
69626 Villeurbanne Cedex (France)
Fax: (+33) 4-7243-1795

Dr. E. A. Quadrelli
Dipartimento di Chimica e Chimica Industriale
Via Risorgimento 35, 56100 Pisa (Italy)

B. Fenet
Centre de RMN UCB Lyon 1 – ESCPE Lyon
43 bd du 11 Novembre 1918, 69626 Villeurbanne Cedex (France)

Dr. L. Emsley, Dr. A. Lesage
Laboratoire de Stéréochimie et des Interactions Moléculaires
UMR-117 CNRS – ENS Lyon, Ecole Normale Supérieure de Lyon
69364 Lyon Cedex (France)

[**] We are also indebted to the CNRS, ENS Lyon, and ESCPE Lyon for financial support. M.C. is grateful to the French ministry of education, research, and technology (MENRT) for a pre-doctoral fellowship. E.A.Q. gratefully acknowledges Università di Pisa and S.N.A.M. for financial support. 2D HETCOR = two-dimensional heteronuclear correlation.

Supporting information for this article is available on the WWW under http://www.angewandte.com or from the author.

As previously described, the surface complex $\mathbf{2_s}$, was prepared by treating a solution of $[Ta(=CHtBu)(CH_2tBu)_3]$ in pentane (1.1 equivalents with respect to surface silanols; 0.7–0.8 accessible OH nm^{-2}) with $SiO_{2\text{-}(700)}$.[2b] After workup, $\mathbf{2_s}$ was obtained as a yellow powder typically containing 4.2 % wt of Ta. Noteworthy is the rapid (within 1 min) coloration of silica and discoloration of the supernatant solution upon addition of the pentane solution of **1** to $SiO_{2\text{-}(700)}$. All the observations and chemical analyses are consistent with the proposed structure of $\mathbf{2_s}$ [Eq. (1)], but further corroboration at the molecular level has been sought using both solid-state NMR spectroscopy of the grafted species and solution NMR spectroscopy of molecular model species.

$$\mathbf{1} + \underset{SiO_{2\text{-}(700)}}{\equiv SiOH} \longrightarrow \underset{\mathbf{2_s}}{[\equiv SiO{-}Ta(=CHtBu)(CH_2tBu)_2]} + NpH \qquad (1)$$

To improve the signal-to-noise ratio in the solid-state NMR spectra of **2**, the complex was partially ^{13}C enriched at the α-position by reaction of $[Ta(=C^*HtBu)(C^*H_2tBu)_3]$ (**1***) with $SiO_{2\text{-}(700)}$, which yielded $[\equiv SiO{-}Ta(=C^*HtBu)(C^*H_2tBu)_2]$ ($\mathbf{2_s^*}$). The solid-state ^1H NMR spectrum of $\mathbf{2_s^*}$ shows two broad resonance signals at $\delta = 4.2$ and 1.0 (see the Supporting Information),[3] and its ^{13}C solid-state cross polarization/magic angle spinning (CP/MAS) NMR spectrum displays strong signals at $\delta = 246$, 96.5, and 33.5 (Figure 1a). Moreover, the 2D HETCOR solid-state NMR spectra provided an unequivocal assignment for $\mathbf{2_s^*}$ (see Supporting Information for experimental details). The 2D NMR spectrum, recorded with a contact time of 2 ms (Figure 1c), shows clear correlations between the signals at $\delta = 4.2$ and 1.0 in the ^1H dimension (F_1) with those at $\delta = 246$ and 33.5, respectively, in the carbon dimension (F_2). The signal at $\delta = 96.5$ also correlates with the peak centered at $\delta = 1.0$, strongly suggesting that the methylene protons are buried under this massive signal (the chemical shifts of the corresponding protons for the surface model $\mathbf{2_m}$ are indeed around 1 ppm, see Table 1 and below).

A reaction intermediate can be detected if the preparation of $\mathbf{2_s^*}$ involves a rather short (5 min or less) or a cold (below 15–20 °C) drying step; under such conditions, an extra signal appears in the solid-state NMR spectrum at $\delta = 110$ (Figure 1b), which readily disappears upon treating the sample under vacuum or under heat. During this step, neopentane is evolved. All these observations suggest that the intermediate observed in the reaction of $[Ta(=CHtBu)(CH_2tBu)_3]$ with $SiO_{2\text{-}(700)}$, is the tetraalkyl derivative $[\equiv SiO{-}Ta(CH_2tBu)_4]$ ($\mathbf{3_s}$) which is formed under kinetic control. The intermediate $\mathbf{3_s}$ rapidly releases neopentane, to finally yield $\mathbf{2_s}$ as the sole surface complex.

To corroborate the assignments proposed above and to gain further insight in the reaction mechanism suggested by the detection of intermediate $\mathbf{3_s}$, we have prepared a molecular model of $\mathbf{2_m}$ using the silsesquioxane (c-$C_5H_9)_7Si_7O_{12}SiOH$ (**4**) a Feher-cage analogue,[1d,f] that can mimic an isolated silanol of a silica surface partially dehydroxylated at 700 °C. The thermodynamic product of the reaction between the monosilanol **4** and $[Ta(=CHtBu)(CH_2tBu)_3]$ is $\mathbf{2_m}$ (for characteristic data, see Table 1) alongside one equivalent of neopentane.[4]

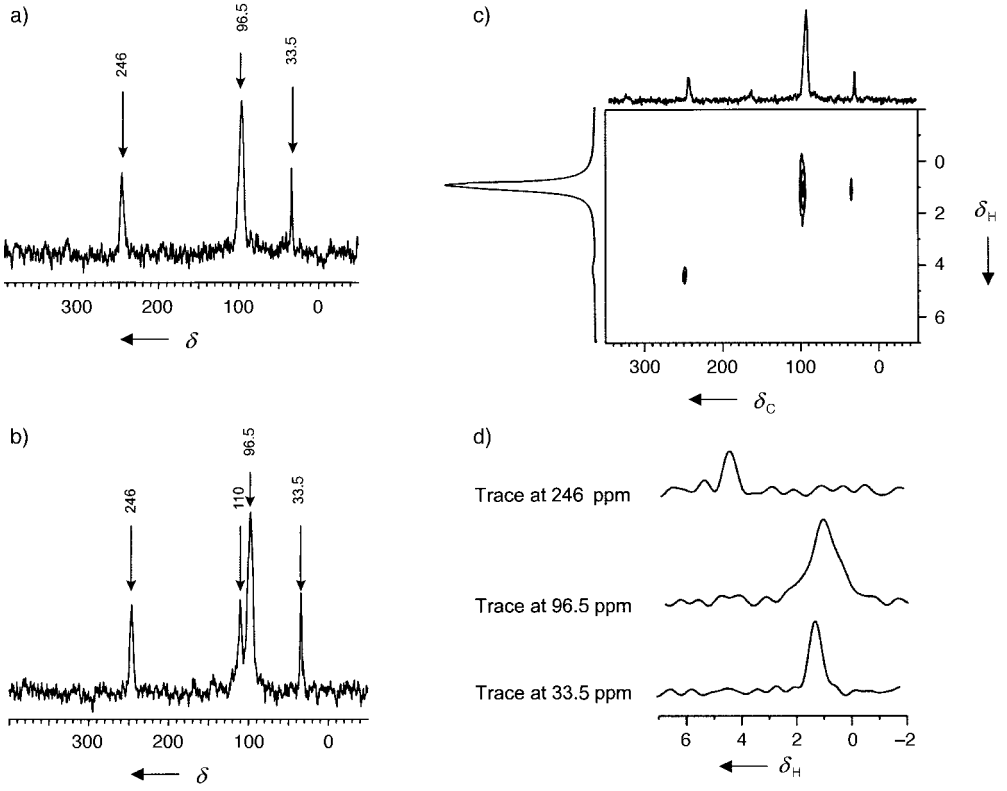


Figure 1. a) CP/MAS ^{13}C solid-state NMR spectra of $\mathbf{2_s^*}$, b) $\mathbf{2_s^*}$ and $\mathbf{3_s^*}$, c) 2D ^1H-^{13}C HETCOR solid-state NMR spectra of $\mathbf{2_s^*}$ (2 ms of contact time). d) Proton traces of the signals at $\delta = 246$, 96.5, and 33.5 in the 2D ^1H–^{13}C NMR spectrum.

The NMR spectroscopy data obtained for $\mathbf{2_m}$ are in good agreement with those of its solid-state counterpart, $\mathbf{2_s}$. Based on NMR spectroscopy data, the reaction is under kinetic control and reaches completion after 48 h. The kinetic monitoring of the reaction shows that a colorless intermediate, $[(c\text{-}C_5H_9)_7Si_7O_{12}SiOTa(CH_2tBu)_4]$ ($\mathbf{3_m}$) is formed immediately upon mixing of the reagents. The long-lived intermediate $\mathbf{3_m}$ ($\tau_{1/2} = 9$ h) has been characterized by 1D and 2D solution NMR spectroscopy, which yields data in good agreement with those obtained for its solid counterpart $\mathbf{3_s}$ (Table 1). The decomposition path of complex $\mathbf{3_m}$ consists of the elimination a neopentane unit by means of α-H abstraction to yield the orange complex $\mathbf{2_m}$.

The combination of the data obtained in the solid state for the synthesis of $\mathbf{2_s}$ and in solution for $\mathbf{2_m}$ allows a mechanistic pathway to be proposed for the reaction:

 © WILEY-VCH Verlag GmbH, D-69451 Weinheim, 2001 1433-7851/01/4023-4494 $ 17.50+.50/0

Table 1. ^{1}H and ^{13}C chemical shifts of **1**, $\mathbf{2_m}$, and $\mathbf{3_m}$ in C_6D_6.

Complex	^{1}H NMR [δ] resonance[a]	assignement	^{13}C NMR [δ] resonance	assignement
1	0.81	$CH_2C(CH_3)_3$	34.7	$=CHC(CH_3)_3$
	1.14	$CH_2C(CH_3)_3$	34.95	$CH_2C(CH_3)_3$
	1.45	$=CHC(CH_3)_3$	35.05	$CH_2C(CH_3)_3$
	1.89	$=CHC(CH_3)_3$	47.0	$=CHC(CH_3)_3$
			113.75	$CH_2C(CH_3)_3$
			249.9	$=CHC(CH_3)_3$
$\mathbf{2_m}$	1.1 – 2.1(m)[b]	$(c\text{-}CH(CH_2)_4)$	22.6, 22.65	$(c\text{-}CH(CH_2)_4)$
			27.4, 27.45, 27.85, 27.9	$(c\text{-}CH(CH_2)_4)$
	1.03(d)[c]	$CH_aH_bC(CH_3)_3$	33.95	$CH_2C(CH_3)_3$
	1.20(d)[c]	$CH_aH_bC(CH_3)_3$	34.4	$=CHC(CH_3)_3$
	1.20	$CH_2C(CH_3)_3$	34.75	$CH_2C(CH_3)_3$
	1.41	$=CHC(CH_3)_3$	45.55	$=CHC(CH_3)_3$
	4.77	$=CHC(CH_3)_3$	95.6	$CH_2C(CH_3)_3$
			245.2	$=CHC(CH_3)_3$
$\mathbf{3_m}$	1.1 – 2.1(m)[b]	$(c\text{-}CH(CH_2)_4)$	22.7, 22.6,	$c\text{-}CH(CH_2)_4)$
	1.34	$CH_2C(CH_3)_3$	22.55	
	1.87	$CH_2C(CH_3)_3$	27.45, 27.55, 27.75, 27.9	$(c\text{-}CH(CH_2)_4)$
			–[d]	$CH_2C(CH_3)_3$
			35.2	$CH_2C(CH_3)_3$
			108.7[b]	$CH_2C(CH_3)_3$

[a] multiplicity in parenthesis; singlets are not specified. [b] broad signal. [c] $J = 14.0$ Hz. [d] Not detected.

addition of the silanol to the alkylidene moiety of **1** (**1**→$\mathbf{3_s}$) followed by an α-H abstraction ($\mathbf{3_s}$→$\mathbf{2_s}$; Scheme 1).[5]

The reactivities of **4** and $SiO_{2\text{-}(700)}$ are relatively similar (immediate reaction of **1** with silanols and a subsequent slower α-H abstraction step), which is probably because of similar pKa values[6] and steric crowding. Finally, 2D HETCOR solid-state NMR spectroscopy is an important tool to unequivocally assign ^{1}H and ^{13}C chemical shifts for surface complexes, and will be important in the future development of surface organometallic chemistry. In conclusion, these data taken together show, besides the analogy between surface and solution chemistry, that the combined use of high-resolution solid state NMR and solution NMR spectroscopy to investigate molecular analogues, is a powerful tool in surface organometallic chemistry, and enables the identification of end products, and determination of the grafting-reaction mechanism. Moreover, we have shown that the Feher cage analogue **4**, is a good model for $SiO_{2\text{-}(700)}$, a silica partially dehydroxylated at 700 °C, which contains mainly isolated silanols, and provides a good estimation of the chemical shifts for surface complexes and can help in understanding elementary steps of surface reactions.

Received: April 2, 2001
Revised: September 18, 2001 [Z16881]

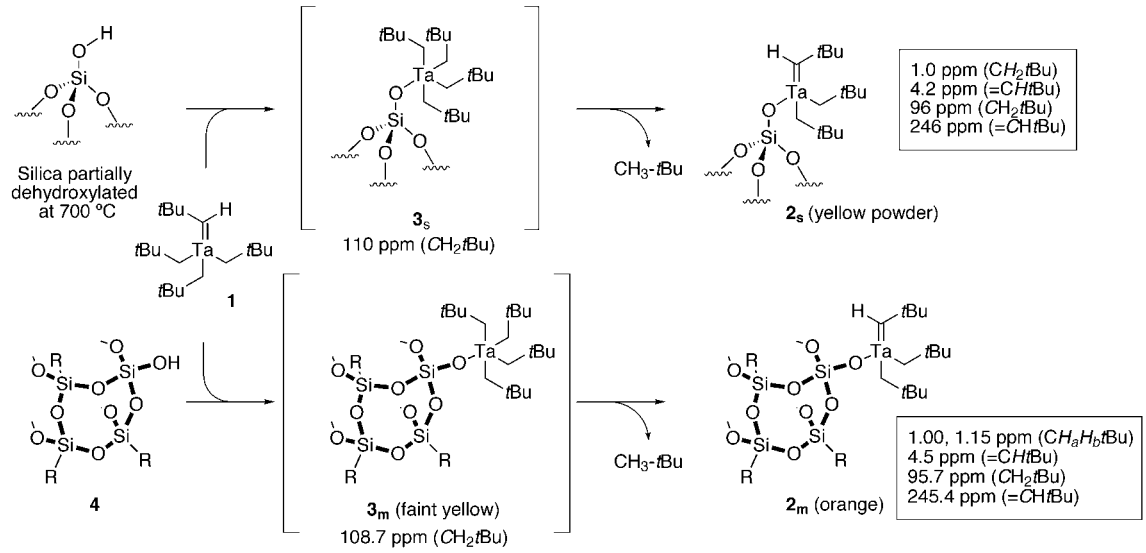
[1] For some examples on the preparation of Feher cages or analogues (POSS) and their reactivity with organometallics, see: a) F. J. Feher, D. N. Newman, J. F. Walzer, *J. Am. Chem. Soc.* **1989**, *111*, 1741; F. J. Feher, D. N. Newman, *J. Int. Biomed. Inf. Data* **1990**, *112*, 1931; b) F. J. Feher, K. J. Weller, J. J. Schwab, *Organometallics* **1995**, *14*, 2009; c) F. J. Feher, T. A. Budzichowski, *Polyhedron* **1995**, *14*, 3239; d) R. Duchateau, H. C. L. Abbendhuis, R. A. Van Santen, S. K.-H. Thiele, M. F. H. Van Tol, *Organometallics* **1998**, *17*, 5222; e) R. Duchateau, H. C. L. Abbendhuis, R. A. Van Santen, A. Meetsma, S. K.-H. Thiele, M. F. H. Van Tol, *Organometallics* **1998**, *17*, 5663; f) R. Duchateau, U. Cremer, R. J. Harmsen, S. I. Mohamud, H. C. L. Abbendhuis, R. A. Van Santen, A. Meetsma, S. K.-H. Thiele, M. F. H. Van Tol, M. Kranenburg, *Organometallics* **1999**, *18*, 5447; g) for a review on various surface models other than POSS, see: R. Murugavel, A. Voigt, M. G. Walawalkar, H. W. Roesky, *Chem. Rev.* **1996**, *96*, 2205.

[2] a) V. Dufaud, G. P. Niccolai, J. Thivolle-Cazat, J.-M. Basset, *J. Am. Chem. Soc.* **1995**, *117*, 4288 – 4294; b) L. Lefort, M. Chabanas, O. Maury, D. Meunier, C. Copéret, J. Thivolle-Cazat, J.-M. Basset, *J. Organomet. Chem.* **2000**, *593 – 594*, 96.

[3] The natural abundance ^{13}C NMR spectrum displays three signals at $\delta =$ 33.5 ($C(CH_3)_3$), 96.5 ($CH_2C(CH_3)_3$), and 246 ($=CH-C(CH_3)_3$), albeit with a poor signal/noise ratio, especially for the latter. Therefore, $\mathbf{2_s}$ was partially ^{13}C enriched at the α-position to the metal, $\mathbf{2_s^*}$, by reaction of $[Ta(=C^*HtBu)(C^*H_2tBu)_3]$ (**1***) with $SiO_{2\text{-}(700)}$.

[4] These values are different from those obtained by Wolczanski and coworkers for $[(tBu)_3SiOTa(=CHtBu)(CH_2tBu)_2]$:R. E. Lapointe, P. T. Wolczanski, G. D. Van Duyne, *Organometallics* **1985**, *4*, 1810. This illustrates the dramatic effects on the NMR data of substituents on Si and the necessity of the oxygen atoms around the Si centers.

[5] This was in fact indirectly shown in the studies of the formation of the surface complexes, see ref. [2a]. Noteworthy is the reaction of HCl on



Scheme 1. Comparison of the reaction of silica partially dehydroxylated at 700 °C ($SiO_{2\text{-}(700)}$) versus $(c\text{-}C_5H_9)_7Si_7O_{12}SiOH$.

[Ta(=CH*t*Bu)(CH_2*t*Bu)$_3$] which yields Cl–Ta(CH_2*t*Bu)$_4$: R. R. Schrock, J. D. Fellmann, *J. Am. Chem. Soc.* **1978**, *100*, 3359.

[6] a) For comprehensive information on the pK_a values of silicas, see: *The Surface Properties of Silicas* (Ed.: A. P. Legrand), Wiley, New York, **1998**, chapter 4B; b) for related comments on **4**, see ref. [1f].

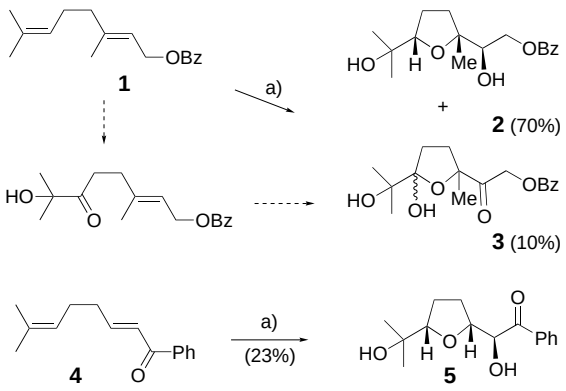
Asymmetric Permanganate-Promoted Oxidative Cyclization of 1,5-Dienes by Using Chiral Phase-Transfer Catalysis**

Richard C. D. Brown* and John F. Keily

2,5-Bis(hydroxymethyl)-substituted tetrahydrofurans (THF diols) are an important structural unit found in many natural and synthetic, biologically active molecules.[1] An elegant approach to the synthesis of THF diols is by the permanganate-promoted oxidative cyclization of 1,5-dienes, which leads to the stereospecific formation of up to four new stereocenters and the THF ring.[2–6] The same transformation has been carried out using other metal–oxo reagents and catalysts.[7, 8] In the permanganate-promoted oxidative cyclization reaction, control of absolute stereochemistry has been achieved with chiral auxiliaries;[4a,b] however, preparation of enantiomerically enriched THF diols by oxidative cyclizations of achiral 1,5-dienes has not been reported. Herein we report the novel high-yielding phase-transfer permanganate-promoted oxidation of geranyl benzoate (**1**) to the corresponding THF diol **2** (Scheme 1), and a procedure for the asymmetric oxidative cyclization of phenone dienes to produce enantiomerically enriched THF diols.

The use of phase-transfer conditions in permanganate-promoted oxidations is well known,[9] although we were not aware of application to the oxidative cyclization of 1,5-dienes. Therefore before attempting to develop an asymmetric process, we investigated the phase-transfer oxidative cyclization of a readily available substrate **1** using achiral tertiary ammonium salts (Scheme 1).[10]

Oxidation of diene **1** with potassium permanganate (2 equiv) in diethyl ether buffered with ethanoic acid gave the best yield of THF diol **2** (70%) when Adogen 464 (0.1–1 equiv) was employed (entry 4, Table 1). Oxidation of enone **4** under the same conditions gave the desired THF diol **5**,



Scheme 1. Oxidative cyclization of dienes **1** and **4**. a) 0.4 M $KMnO_4$ (2 equiv), AcOH (4 equiv), Adogen 464 (0.4 equiv)/Et_2O. Bz = benzoyl.

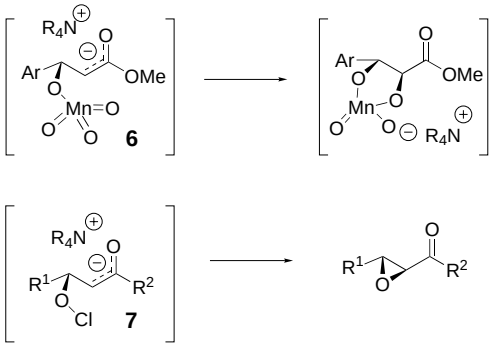
Table 1. Oxidative cyclization of geranyl benzoate (**1**) (see Scheme 1).[a]

Entry	Solvent	Phase-transfer agent	Yield of **2** [%]	Yield of **3** [%]
1	CH_2Cl_2[b]	TBAB	8[c]	not recorded
2	CH_2Cl_2	TBAB	44[d]	21[d]
3	Et_2O	TBAB	40[d]	7[d]
4	Et_2O	Adogen 464	70[d]	10[d]

[a] Reactions were conducted on a 0.19 mmol scale. TBAB = tetrabutylammonium bromide. [b] No AcOH added to the reaction mixture. [c] Yield estimated by HPLC. [d] Yields represent analytically pure isolated material.

albeit in lower yield (Scheme 1). We then returned to our primary goal of developing an asymmetric oxidative cyclization.

Studies on the oxidation of cinnamate esters by quaternary ammonium permanganates led Lee et al. to conclude that the transition state was electron-rich, and they proposed an enolate-like structure **6** with stabilization due to interaction with the ammonium ion (Scheme 2).[11] The similarity of **6** and the initial adduct **7** formed in the phase-transfer-catalyzed nucleophilic epoxidation of enones suggested that chiral catalysts developed for the epoxidation reaction might also be applied to the oxidative cyclization.[12]



Scheme 2. Possible reaction pathways for the permanganate-promoted oxidation of electron-poor olefins (top), and the nucleophilic epoxidation of α,β-enones with ClO^- (bottom).

Oxidative cyclization of geranyl benzoate (**1**) in the presence of **8** in dichloromethane/water/ethanoic acid at

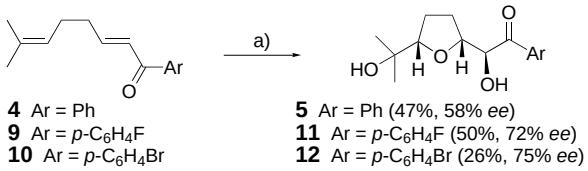
[*] Dr. R. C. D. Brown, J. F. Keily
Department of Chemistry
University of Southampton
Highfield, Southampton SO17 4BJ (UK)
Fax: (+44) 23-80596805
E-mail: rcb1@soton.ac.uk

[**] This work was supported by the EPSRC (J.F.K.) and the Royal Society (R.C.D.B.). We thank Dr. Barry Lygo (University of Nottingham) for helpful discussions, and Syngenta and Merck Sharp and Dohme for unrestricted grants.

Supporting information for this article is available on the WWW under http://www.angewandte.com or from the author.

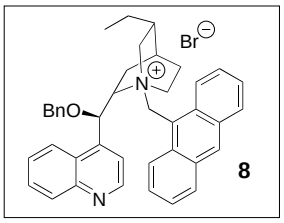
 © WILEY-VCH Verlag GmbH, D-69451 Weinheim, 2001 1433-7851/01/4023-4496 $ 17.50+.50/0

room temperature gave the THF diol **2** with <3% *ee*. Gratifyingly, oxidation of α,β-enone **4** under the same conditions afforded **5** with an encouraging enantiomeric excess (38% *ee*, 14% yield; Scheme 3). A range of solvents



4 Ar = Ph
9 Ar = *p*-C_6H_4F
10 Ar = *p*-C_6H_4Br

5 Ar = Ph (47%, 58% *ee*)
11 Ar = *p*-C_6H_4F (50%, 72% *ee*)
12 Ar = *p*-C_6H_4Br (26%, 75% *ee*)



Scheme 3. Asymmetric oxidative cyclization of 1,5-dienes **4**, **9**, and **10**. a) $KMnO_4$ (powder) (1.6 equiv), AcOH (6.5 equiv), **8** (0.1 equiv)/CH_2Cl_2, $-30\,^{\circ}C$.

were screened for the asymmetric liquid–liquid phase-transfer reaction, and two trends emerged, namely that the yield of **5** improved with solvent polarity, and its enantiomeric excess decreased. Repeating some of the reactions without the phase-transfer catalyst confirmed that a background oxidation was occurring in more polar solvents. The highest level of asymmetric induction observed for the liquid–liquid phase-transfer reaction (40% *ee*) occurred in toluene when **8** (30 mol%) was used as catalyst.

Additional improvements to the yield and enatiomeric excess of **5** (47%, 58% *ee*) were achieved in dichloromethane at $-30\,^{\circ}C$. Importantly, the amount of the tertiary ammonium salt **8** could be reduced to 5 mol% without lowering the enatiomeric excess of **5**, but further reduction to 1 mol% gave **5** with only 26% *ee*. The identities of the compounds that make up the remainder of the mass balance remain unclear; however, they are likely to be highly polar, water-soluble or volatile substances given the high purity of the crude product **5** after the usual work-up, as judged from the ^1H NMR spectrum prior to chromatography.

The asymmetric oxidative cyclization of *para*-substituted systems **9** and **10** afforded the THF diols **11** and **12**, respectively, with slightly higher enatiomeric excesses although oxidation of the *para*-bromo compound **10** was incomplete under the same conditions, explaining the lower yield. The level of asymmetric induction obtained here (58-75% *ee*) is already comparable with the diastereoselectivity obtained for the oxidative cyclization of dienes bearing the Oppolzer sultam chiral auxiliary (80% *de*).[4a]

The relative stereochemistry of the products **5**, **11**, and **12** was determined by X-ray crystallography, and the presence of a heavy atom in **12** allowed its absolute stereochemistry to be established from enantiomerically pure crystals.[13] The observed stereochemical outcome is accounted for by a model presented for the nucleophilic epoxidation of α,β-enones by hypochlorite.[12e] The lack of enantioselectivity observed for the oxidative cyclization of geranyl benzoate (**1**), which is oxidized more rapidly at the C6–C7 double bond, is also in accord with the model.

In conclusion, very promising levels of enantioinduction have been achieved in a novel phase-transfer-catalyzed oxidative cyclization of 1,5-dieneones by permanganate with as little as 5 mol% **8**. The reaction is unusual in that up to four new stereocenters are created with control of relative and absolute stereochemistry in a single synthetic step from an achiral starting material.

Received: August 24, 2001 [Z17790]

[1] a) F. Q. Alali, X. X. Liu, J. L. McLaughlin, *J. Nat. Prod.* **1999**, *62*, 504–540; b) C. J. Dutton, B. J. Banks, C. B. Cooper, *Nat. Prod. Rep.* **1995**, *12*, 165–181; c) S. T. Jan, C. Mao, A. O. Vassilev, C. S. Navara, F. M. Uckun, *Bioorg. Med. Chem. Lett.* **2000**, *10*, 1193–1197; d) H. Wagner, K. Harms, U. Koert, S. Meder, G. Boheim, *Angew. Chem.* **1996**, *108*, 2836–2839; *Angew. Chem. Int. Ed.* **1996**, *35*, 2643–2646; e) J. J. Fernandez, M. L. Souto, M. Norte, *Nat. Prod. Rep.* **2000**, *17*, 235–246.

[2] For early papers describing the oxidative cyclization of 1,5-dienes: a) E. Klein, W. Rojahn, *Tetrahedron.* **1965**, *21*, 2353–2358; b) D. M. Walba, M. D. Wand, M. C. Wilkes, *J. Am. Chem. Soc.* **1979**, *101*, 4396–4397.

[3] For mechanistic discusions of the oxidative cyclization see ref. [2b] and: a) J. E. Baldwin, M. J. Crossley, E.-M. M. Lehtonen, *Chem. Commun.* **1979**, 918–920; b) S. Wolfe, C. F. Ingold, *J. Am. Chem. Soc.* **1981**, *103*, 940–941.

[4] For asymmetric oxidative cyclization of 1,5-dienes: a) D. M. Walba, C. A. Przybyla, C. B. Walker, *J. Am. Chem. Soc.* **1990**, *112*, 5624–5625; a) P. J. Kocienski, R. C. D. Brown, A. Pommier, M. Procter, B. Schmidt, *J. Chem. Soc. Perkin Trans. 1*. **1998**, 9–39.

[5] For application towards the synthesis of natural products see reference [4] and: a) D. M. Walba, P. D. Edwards, *Tetrahedron Lett.* **1980**, *21*, 3531–3534; b) C. Spino, L. Weiler, *Tetrahedron Lett.* **1987**, *28*, 731–734; c) R. C. D. Brown, R. M. Hughes, J. Keily, A. Kenney, *Chem. Commun.* **2000**, 1735–1736.

[6] For general reviews on the synthesis of tetrahydrofurans: a) T. L. B. Boivin, *Tetrahedron* **1987**, *43*, 3309–3362; b) J.-C. Harmange, B. Figadere, *Tetrahedron: Asymmetry* **1993**, *4*, 1711–1754; c) R. Hoppe, H. D. Scharf, *Synthesis* **1995**, 1447–1464; d) U. Koert, *Synthesis* **1995**, 115–132.

[7] a) P. H. J. Carlsen, T. Katsuki, V. S. Martin, K. B. Sharpless, *J. Org. Chem.* **1981**, *46*, 3936–3938; b) M. de Champdore, M. Lasalvia, V. Piccialli, *Tetrahedron Lett.* **1998**, *39*, 9781–9784; c) T. J. Donohoe, J. J. G. Winter, M. Helliwell, G. Stemp, *Tetrahedron Lett.* **2001**, *42*, 971–974; d) V. Piccialli, N. Cavallo, *Tetrahedron Lett.* **2001**, *42*, 4695–4699.

[8] a) For related cyclizations of hydroxyalkenes: a) D. M. Walba, G. S. Stoudt, *Tetrahedron Lett.* **1982**, *23*, 727–730; b) S. Tang, R. M. Kennedy, *Tetrahedron Lett.* **1992** *33*, 5299–5302; c) S. Tang, R. M. Kennedy, *Tetrahedron Lett.* **1992**, *33*, 5303–5306; d) F. E. McDonald, T. B. Towne, *J. Am. Chem. Soc.* **1994**, *116*, 7921–7922; e) F. E. McDonald, T. B. Towne, *J. Org. Chem.* **1995**, *60*, 5750–5751; f) L. J. D'Souza, S. C. Sinha, S. F. Lu, E. Keinan, S. C. Sinha, *Tetrahedron* **2001**, *57*, 5255–5262.

[9] D. G. Lee in *Oxidation in Organic Chemistry*, (Ed.: W. S. Trahanovsky), Academic Press, New York, **1982**, pp. 147–206.

[10] R. J. Armstrong, L. Weiler, *Can. J. Chem.* **1983**, 2530–2539.

[11] a) D. G. Lee, K. C. Brown, *J. Am. Chem. Soc.* **1982**, *104*, 5076–5081; b) D. G. Lee, K. C. Brown, H. Karaman, *Can. J. Chem.* **1986**, *64*, 1054–1059; c) J. F. Perez-Benito, D. G. Lee, *J. Org. Chem.* **1987**, *52*, 3239–3243.

[12] a) J. C. Hummelen, H. Wynberg, *Tetrahedron Lett.* **1978**, 1089–1092; b) R. Helder, J. C. Hummelen, R. W. P. M. Laane, J. S. Weiring, H. Wynberg, *Tetrahedron Lett.* **1976**, 1831–1834; c) B. Lygo, P. G. Wainwright, *Tetrahedron Lett.* **1998**, *39*, 1599–1602; d) B. Lygo, P. G. Wainwright, *Tetrahedron* **1999**, *55*, 6289–6300; e) E. J. Corey, F. Y.

Zhang, *Org. Lett.* **1999**, *1*, 1287–1290; f) B. Lygo, D. C. M. To, *Tetrahedron Lett.* **2001**, *42*, 1343–1346.

[13] M. B. Hursthouse, M. E. Light, S. J. Coles, Department of Chemistry, University of Southampton, personal communication.

Reactivity of Dimetallapentaboranes—*nido*-$[Cp^*_2M_2B_3H_7]$—with Alkynes: Insertion to Form a Ruthenacarborane (M = RuH) versus Catalytic Cyclotrimerization to Form Arenes (M = Rh)**

Hong Yan, Alicia M. Beatty, and Thomas P. Fehlner*

A significant fraction of modern chemistry incorporates the use of transition metals to modify and control the reactivity of main group moieties, for example, organometallic chemistry, and the use of ligands to modify and control the reactivity at metal sites, for example, supramolecular chemistry. Relative to the other p-block elements, the chemistry of carbon is dominant, however, in principle, a similar wealth of chemistry exists for the other p-block elements.[1] In fact, transition metal promoted main group chemistry[2] and main group element promoted transition metal chemistry[3] has generated more interest recently.

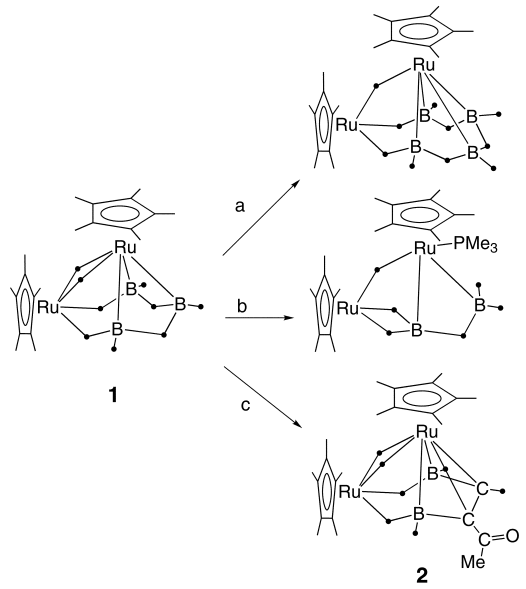
Since developing a practical synthetic route to a class of metallaboranes containing metals ranging from Group 5–9,[4] we have begun to examine the systematic reaction chemistry of these compounds. Thus, thermal elimination reactions as well as reactions with metal fragments, monoboranes, and Lewis bases have been described.[5–11] In these reactions, the distinctive electronic contributions of metal and borane fragments to the cluster structure are seen to be expressed in the overall reactivity. In one case, a new class of metallaborane was revealed, the hypoelectronic rhenaboranes.[12]

In the early days of organometallic chemistry, the reaction of metal species with alkynes yielded a wealth of compounds that helped define structural possibilities.[13] Likewise, the reaction of alkynes with boranes gave rise to carboranes[14] and a subsequent bountiful chemistry of these heteroboranes with metals[15] including catalytic applications.[16] Here we report the comparative reactivity of two isoelectronic *nido*-dimetallapentaboranes with alkynes and demonstrate that a change from Group 8 to Group 9 metal drives a change in the reaction from alkyne insertion to catalytic cyclotrimerization. The latter reaction shows that, with the proper choice of metal, metallaborane clusters provide access to a novel catalytic pathway.

[*] Prof. T. P. Fehlner, Dr. H. Yan, Dr. A. M. Beatty
Department of Chemistry and Biochemistry
University of Notre Dame
Notre Dame, IN 46556 (USA)
Fax: (+1) 219-631-6652
E-mail: fehlner.1@nd.edu

[**] This work was supported by the National Science Foundation. Cp* = η-C_5Me_5.

The chemistry of $[1,2\text{-}(Cp^*RuH)_2B_3H_7]$ (**1**; $Cp^* = C_5Me_5$), has been explored by our group[8] and that of Shimoi.[17–19] The results pertinent to this work are shown in Scheme 1 and illustrate a) cluster expansion and b) cluster degradation. Reaction of **1** with $HCCCO_2Me$ leads to $[1,2\text{-}(Cp^*RuH)_2\text{-}3,4\text{-}CHC(CO_2Me)B_2H_4]$ (**2**; Figure 1),[20] which results from combined cluster degradation and expansion (path c in Scheme 1). This reaction is analogous to the reaction of **1** with phosphanes except that ultimately the alkyne base is incorporated into the borane framework rather than coordinated to a metal site. Thermal reaction of metallaboranes with alkynes



Scheme 1. Reactions of **1** with a) monoborane to give cluster expansion, b) with PMe_3 to give cluster degradation, and c) with $HCCCO_2Me$ to yield **2**. The structures shown are schematic representations, for clarity only the H-bridge of the H-bridged bonds is shown, ● = H.

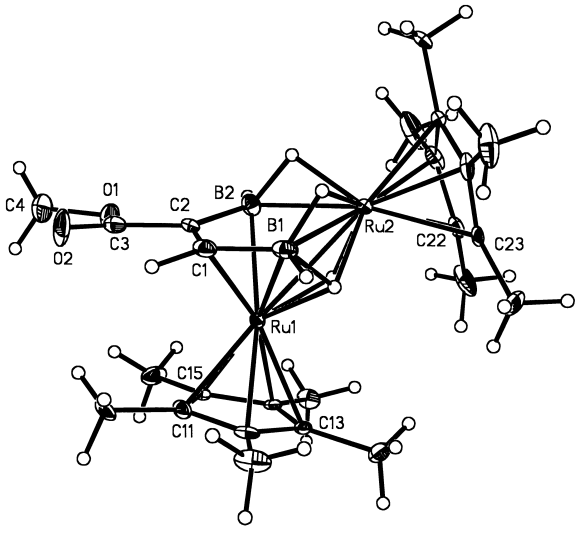
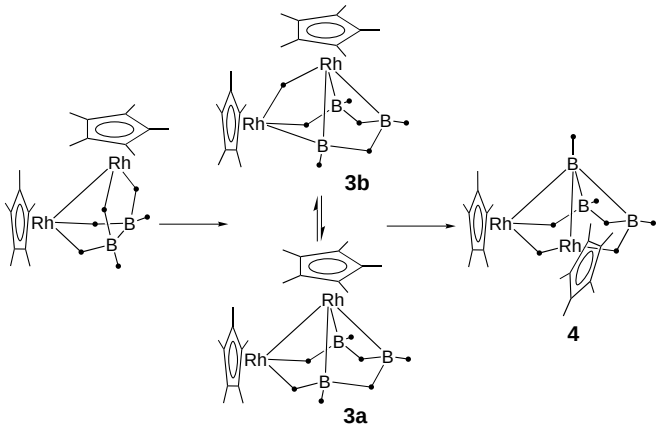


Figure 1. Molecular structure of **2**. Selected bond lengths [Å]: Ru1–Ru2 2.9424(10), Ru1–C1 2.170(8), Ru1–C2 2.180(8), Ru1–B1 2.358(10), Ru1–B2 2.360(10), Ru2–B2 2.385(10), Ru2–B1 2.399(10), B1–C1 1.508(14), B2–C2 1.557(13), C1–C2 1.391(12), C2–C3 1.493(12), O1–C3 1.352(11), O1–C4 1.448(11), O2–C3 1.208(11).

 © WILEY-VCH Verlag GmbH, D-69451 Weinheim, 2001 1433-7851/01/4023-4498 $ 17.50+.50/0

to form metallacarboranes is known[21, 22] as is the metal-catalyzed formation of polyhedral vinyl boranes, which can be precursors to carboranes.[23]

The synthesis of [2,3-$(Cp^*Rh)_2B_3H_7$] (**4**) has been reported.[8, 24] Further work has led to the isolation of [1,2-$(Cp^*Rh)_2B_3H_7$] (**3**; Figure 2)[20] which cleanly converts into **4** on heating. As illustrated in Scheme 2, **3** exists in solution as a equilibrium mixture of two tautomers that differ solely in the placement of one endo hydrogen atom. Isomer **3a**, a direct analogue of B_5H_9, has an RhHB bridge (abundance 40%) whereas **3b** has a structurally unusual apical–basal RhHRh bridge (abundance 60%).



Scheme 2. Formation of **4**, from [$(Cp^*Rh)_2B_2H_6$] and monoboranes via the intermediate **3** which exists in two tautomeric forms in solution.

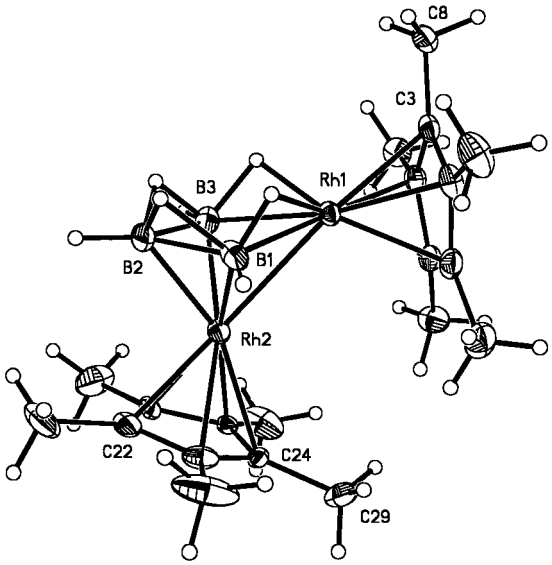


Figure 2. Molecular structure of **3a**. Selected bond lengths [Å]: Rh1–Rh2 2.6892(3), Rh1–B3 2.292(4), Rh1–B1 2.308(3), Rh2–B2 2.061(4), Rh2–B1 2.062(3), Rh2–B3 2.075(4), B1–B2 1.841(5), B2–B3 1.838(5).

The net result of the reaction of either **3** or **4** with a selection of alkynes (Table 1) is the formation of mixtures of 1,2,4- and 1,3,5-substituted benzenes without observable degradation of the rhodaborane. Rates and turnover numbers are modest. Decreasing activities for RC≡CPh, R = H, Me, Ph, suggest a significant steric factor in the reaction. Comparison of rates for $HCCCO_2Me$, catalyzed by **3** and **4** under identical conditions, establishes that **3** is ≈6 times more active at room temperature. The difference in selectivity between **3** and **4** (compare MeC≡CR, R = Ph vs CO_2Me) supports catalysis by the rhodaboranes rather than by a fragment derived from degradation. Partial inhibition of the catalysis by triphenylphosphane and pyridine, neither of which degrades the rhodaboranes under the reaction conditions, suggests competition between the alkyne and added Lewis base for the active site on the rhodaborane.

In contrast to, for example, 16 electron rhodium cyclotrimerization catalysts containing chelating carborane ligands,[25] compounds **3** and **4** are formally saturated and have no labile ligands. Hence, the observed catalytic activity may seem puzzling, however, cluster species of this type are intrinsically Lewis acidic relative to non-cluster compounds with saturated electronic structures. Both base-catalyzed framework rearrangements in pentaborane(9)[26, 27] and ligand substitutions in a metal cluster[28] involve addition of a base to open the cluster thereby facilitating rearrangement before base dissociation and cluster closing. Incorporation of this cluster "breathing" process into the "common" mechanism for alkyne cyclotrimerization[29] leads to a reasonable catalytic cycle shown in abbreviated form for **4** (**3** exists as two tautomers each with two different metal sites) in Scheme 3.

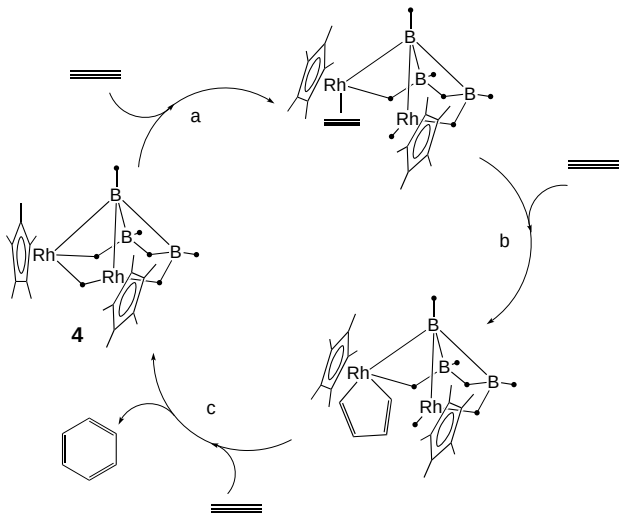
The presence of two Cp*RuH fragments in a pentaborane cluster framework leads to insertion whereas Cp*Rh fragments generate catalytic cyclotrimerization. Catalysis by clusters has been an attractive area since its inception[30] but one that has often been frustrated by facile cluster degradation.[31] A metallaborane is electronically, as well as geometrically, similar to a metal cluster of the same nuclearity. Thus, the borane fragment supports the metal atoms in a cluster environment and provides a reaction pathway not available to, for example, an 18 electron organometallic complex.

Table 1. Comparison of selected catalytic data.[a]

Substrate	**3**[a]					**4**[a]				
	Cat:substrate	t[h]	T [°C]	yield [%]	product ratio	Cat:substrate	t [h]	T [°C]	yield [%]	product ratio
HC≡CPh	1:143	24	22	27	1:3	1:36	24	22	39	1:4
MeC≡CPh	1:84	70	22	3	[b]	1:70	24	70	36	[b]
PhC≡CPh	1:12	48	22	NR		1:10	36	70	NR	
HC≡CCO_2Me	1:77	48	22	85	1:3	1:260	24	47	42	1:5
MeC≡CCO_2Me	1:100	68	22	22	1:1	1:70	24	65	10	3:1

[a] Catalyst to substrate ratio, reaction time, reaction temperature, total yield, ratio of 1,3,5- to 1,2,4-trisubstituted benzene, NR = no reaction. [b] 1,2,4-trimethyl-3,5,6-triphenylbenzene only.

 © WILEY-VCH Verlag GmbH, D-69451 Weinheim, 2001 1433-7851/01/4023-4499 $ 17.50+.50/0



Scheme 3. Proposed catalytic cycle for the cyclotrimerization of alkynes by **4**.

Experimental Section

2: [1,2-(Cp*RuH)$_2$B$_3$H$_7$] (125 mg, 0.24 mmol)[8] in hexane(20 mL) and methyl acetylene monocarboxylate (0.2 mL, 2.24 mmol) were stirred for 8 h at ambient temperature. A yellow solid formed and the suspension became orange. The reaction mixture was concentrated and chromatography (silica gel 60–200) with hexane:toluene = 10:1 afforded the known *nido* cluster [1,2-(Cp*Ru)$_2$(μ-H)B$_4$H$_9$] (8.6 mg, 7%) and with hexane:ether (10:1) the yellow [1,2-(Cp*RuH)$_2$-3,4-CHC(CO$_2$Me)B$_2$H$_4$] (**2**; 74.4 mg, 53%): ^{1}H NMR ([D$_6$]benzene, 22 °C, 600 MHz): δ = 5.53 (s, br, 1H, CH), 3.58 (s, 3H, OMe), 2.72 (br, 2H, B-Ht), 1.78 (s, 15H, Cp*), 1.74 (s, 15H, Cp*), −11.59 (s, 1H, Ru-H-Ru), −11.69 (s, 1H, Ru-H-Ru), −12.25 (s, br, 1H, Ru-H-B), −12.42 (s, br, 1H, Ru-H-B); ^{11}B NMR ([D$_6$]acetone, 22 °C, 128 MHz): δ = −14.2, −15.2 (1:1); ^{13}C NMR ([D$_6$]acetone, 22 °C, 125 MHz): δ = 175.4 (CO), 124.9 (br, *C*=CH), 96.6 (br, C=*C*H), 93.4 (Cp*), 88.8 (Cp*), 50.8 (OMe), 12.1 (Cp*), 10.8 (Cp*); EI-MS: 586.1290 (M^+, found), 586.1297 (calcd); IR (KBr): $\tilde{\nu}$ = 2468(ν_{B-H}), 1604, 1373, and 1222($\nu_{COO}{}^{-1}$) cm^{-1}.

3: LiBH$_4$ (0.45 mL, 0.90 mmol) was added to a stirred orange suspension of [Cp*RhCl$_2$]$_2$ (100 mg, 0.16 mmol) in THF (20 mL) at −20 °C. The release of H$_2$ accompanied the formation of a yellow solution (ca. 0.5 h) which was warmed to room temperature for 0.5 h and then heated to 70 °C for 6.5 h. After removal of solvent, the residue was dissolved in hexane and applied to a silica gel column (2 × 10 cm). Elution with hexane:toluene (10:1) gave a red band which contained an inseparable 1:1.25 mixture of *nido*-[-1,2-(Cp*Rh)$_2$B$_3$H$_7$] (**3a**) and *nido*-[-1,2-(Cp*Rh)$_2$(μ-H)B$_3$H$_6$] (**3b**; 30.5 mg, 37% based on Rh). Further elution with hexane:toluene (1:1) afforded **4** (21.4 mg, 26% based on Rh): ^{1}H NMR ([D$_6$]benzene, −60 °C, 400 MHz): **3a**: δ = 3.95 (br, 1H, B-Ht), 3.66 (br, 2H, B-Ht), 2.07 (s, 15H, Cp*), 1.53 (s, 15H, Cp*), −3.05 (s, 2H, B-H-B), −12.04 (s, 2H, B-H-Rh); **3b**: 5.72 (br, 1H, B-Ht), 4.19 (br, 1H, B-Ht), 2.73 (br, 1H, B-Ht), 1.94 (s, 15H, Cp*), 1.70 (s, 15H, Cp*), −0.16 (s,1H, B-H-B), −3.35 (s, 1H, B-H-B), −14.54 (s, 1H, B-H-Rh), −15.04 (dd, J_1 = 22.1 Hz, J_2 = 28.3 Hz, 1H, Rh-H-Rh); ^{11}B ([D$_6$]benzene, 22 °C, 128 MHz): δ = 5.66, 8.17, 11.02, 22.34 (br); EI-MS: 516.1304 (M^+, 100%, found), 516.1272 (calcd).

Catalytic reactions: In a typical reaction, **4** (8 mg, 15.5 × 10^{-3} mmol) was dissolved in THF (15 mL) and methyl acetylene monocarboxylate (0.36 mL, 4.04 mmol) was added. The resulting reaction mixture was stirred at room temperature for 24 h gradually generating a white solid on the flask wall. After removal of solvent, the residue was purified by chromatography on silica gel. Elution with hexane:CH$_2$Cl$_2$ (3:1) gave **4** (5 mg) and elution with acetone gave a 5:1 mixture of 1,2,4-and 1,3,5-trimethylbenzenetricarboxylates (142.5 mg, 42%). Data on the trimers (^{1}H, ^{13}C NMR spectroscopy, high resolution mass spectroscopy) corresponded to published spectra.

Received: August 16, 2001 [Z17738]

[1] *Inorganometallic Chemistry* (Ed.: T. P. Fehlner), Plenum, New York, **1992**.
[2] H. Chen, S. Schlecht, T. C. Semple, J. F. Hartwig, *Science* **2000**, *287*, 1995.
[3] H. Tobita, K. Hasegawa, J. J. G. Minglana, L.-S. Luh, M. Okazaki, H. Ogino, *Organometallics* **1999**, *18*, 2058.
[4] T. P. Fehlner, *Organometallics* **2000**, *19*, 2643.
[5] J. Ho, K. J. Deck, Y. Nishihara, M. Shang, T. P. Fehlner, *J. Am. Chem. Soc.* **1995**, *117*, 10292.
[6] H. Hashimoto, M. Shang, T. P. Fehlner, *Organometallics* **1996**, *15*, 1963.
[7] S. Aldridge, H. Hashimoto, K. Kawamura, M. Shang, T. P. Fehlner, *Inorg. Chem.* **1998**, *37*, 928.
[8] X. Lei, M. Shang, T. P. Fehlner, *J. Am. Chem. Soc.* **1999**, *121*, 1275.
[9] X. Lei, M. Shang, T. P. Fehlner, *Chem. Eur. J.* **2000**, *6*, 2653.
[10] S. Ghosh, X. Lei, M. Shang, T. P. Fehlner, *Inorg. Chem.* **2000**, *39*, 5373.
[11] X. Lei, M. Shang, T. P. Fehlner, *Organometallics* **2000**, *19*, 5266.
[12] S. Ghosh, M. Shang, Y. Li, T. P. Fehlner, *Angew. Chem.* **2001**, *113*, 1159; *Angew. Chem. Int. Ed.* **2001**, *40*, 1125.
[13] C. Elschenbroich, A. Salzer, *Organometallics*, VCH, New York, **1989**.
[14] R. N. Grimes, *Carboranes*, Academic Press, New York, **1970**.
[15] M. F. Hawthorne, *J. Organomet. Chem.* **1975**, *100*, 97.
[16] R. T. Baker, M. S. Delaney, R. E. King III, C. B. Knobler, J. A. Long, T. B. Marder, T. E. Paxson, R. G. Teller, M. F. Hawthorne, *J. Am. Chem. Soc.* **1984**, *106*, 2965.
[17] Y. Kawano, H. Matsumoto, M. Shimoi, *Chem. Lett.* **1999**, 489.
[18] L. N. Pangan, Y. Kawano, M. Shimoi, *Organometallics* **2000**, *19*, 5575.
[19] L. N. Pangan, Y. Kawano, M. Shimoi, *Inorg. Chem.* **2001**, *40*, 1985.
[20] Crystallographic data (excluding structure factors) for the structures reported in this paper have been deposited with the Cambridge Crystallographic Data Centre as supplementary publication no. CCDC-168355 (**2**) and -168356 (**3**). Copies of the data can be obtained free of charge on application to CCDC, 12 Union Road, Cambridge CB2 1EZ, UK (fax: (+44) 1223-336-033; e-mail: deposit@ccdc.cam.ac.uk).
[21] R. Weiss, J. R. Bowser, R. N. Grimes, *Inorg. Chem.* **1978**, *17*, 1522.
[22] E. J. Ditzel, X. L. R. Fontaine, N. N. Greenwood, J. D. Kennedy, Z. Sisan, B. Stibr, M. Thornton-Pett, *J. Chem. Soc. Chem. Commun.* **1990**, 1741.
[23] R. Wilczynski, L. G. Sneddon, *Inorg. Chem.* **1982**, *21*, 506.
[24] X. Lei, M. Shang, T. P. Fehlner, *J. Am. Chem. Soc.* **1998**, *120*, 2686.
[25] M. Herberhold, H. Yan, W. Milius, B. Warckmeyer, *Organometallics* **2000**, *19*, 4289.
[26] D. F. Gaines, *Acc. Chem. Res.* **1973**, *6*, 416.
[27] D. F. Gaines in *Boron Chemistry-4* (Eds: R. W. Parry, G. Kodama), Pergamon, Oxford, **1980**, p. 73.
[28] K. Knoll, G. Huttner, L. Zsolnai, I. Jibril, M. Wasincionek, *J. Organomet. Chem.* **1985**, *294*, 91.
[29] N. E. Schore, *Chem. Rev.* **1988**, *88*, 1081.
[30] E. L. Muetterties, T. N. Rhodin, E. Band, C. F. Brucker, W. R. Pretzer, *Chem. Rev.* **1979**, *79*, 91.
[31] W. L. Gladfelter, K. J. Roesselet in *The Chemistry of Metal Cluster Complexes* (Eds: D. F. Shriver, H. D. Kaesz, R. D. Adams), VCH, New York, **1990**, p. 329.

 © WILEY-VCH Verlag GmbH, D-69451 Weinheim, 2001 1433-7851/01/4023-4500 $ 17.50+.50/0

(η^3-Allyl)palladium Complexes Bearing Diphosphinidenecyclobutene Ligands: Highly Active Catalysts for the Hydroamination of 1,3-Dienes**

Tatsuya Minami, Hideyuki Okamoto, Shintaro Ikeda, Rika Tanaka, Fumiyuki Ozawa,* and Masaaki Yoshifuji

Dedicated to Prof. François Mathey on the occasion of his 60th birthday

The catalytic hydroamination of unsaturated hydrocarbons is a useful means of synthesizing nitrogen-containing organic molecules.[1] Intramolecular cyclization of aminoalkenes is efficiently catalyzed by lanthanide complexes,[2] and amine-induced telomerization of butadienes[3] and oxidative 1,4-addition of amines to dienes[4] are successfully conducted with palladium catalysts. In contrast, simple intermolecular 1:1 addition of amines to alkenes or dienes is a rather difficult process and has been conducted at high temperature.[5, 6] Hartwig et al. recently reported a significantly improved catalyst, generated from $[Pd(PPh_3)_4]$ and CF_3CO_2H, which performs 1:1 addition of aniline to 1,3-dienes at room temperature.[7] However, even in this case, the reaction takes about a day for completion. Here we report that more efficient catalysts can be prepared by using sp^2-hybridized phosphorus ligands, namely, 1,2-diaryl-3,4-bis[(2,4,6-tri-*tert*-butylphenyl)phosphinidene]cyclobutenes.[8]

sp^2-Hybridized phosphorus compounds have a marked propensity to engage in metal-to-phosphorus π backbonding and have a strong π-acceptor property, comparable to that of the carbonyl ligand.[9] Since the catalytic addition of an amine to a 1,3-diene probably involves nucleophilic attack of the amine on an (η^3-allyl)palladium(II) or palladium(II) diene complex,[7a] we expected that diphosphinidenecyclobutene ligands may effectively enhance the electrophilicity of palladium intermediates and thus give highly active catalysts. Although transition metal complexes of sp^2-hybridized phosphorus compounds have been extensively prepared in the last decade,[9] their application to catalysis has been extremely limited,[10] except for phosphaaromatic compounds such as phosphabenzene and phosphaferrocene.[11, 12]

Complexes **1**–**3** were synthesized by treating $[\{Pd(\eta^3\text{-allyl})Cl\}_2]$[13] with the corresponding diphosphinidenecyclobutene ligand and silver trifluoromethanesulfonate (AgOTf) in CH_2Cl_2 at room temperature, and isolated as yellowish orange solids in 66–96% yields.[14] They are fairly stable towards air in solution and as solids; the solid materials can be stored at room temperature for months without notable decomposition.

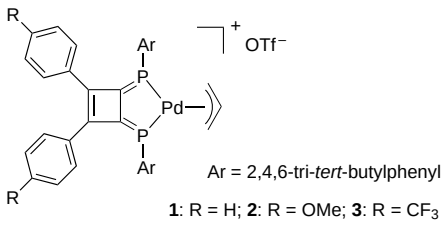


Figure 1 shows the molecular structure of **1**.[15] The diphosphinidenecyclobutene ligand chelates the (η^3-allyl)palladium moiety through two phosphorus atoms. The aryl rings C and D on the phosphorus atoms are nearly perpendicular to the main framework A, whereas the almost parallel arrangement of phenyl groups E and F and the cyclobutene ring B suggests partial π conjugation between them. The C(53)–C(54) and C(54)–C(55) bond lengths (1.383(8) and 1.376(8) Å) and the C(53)-C(54)-C(55) angle (119.9(5)°) are in the typical ranges for η^3-allyl ligands. The three Pd–C distances (2.168(5)–2.178(4) Å) are comparable to those of diphosphane analogues (2.168–2.201 Å).[16]

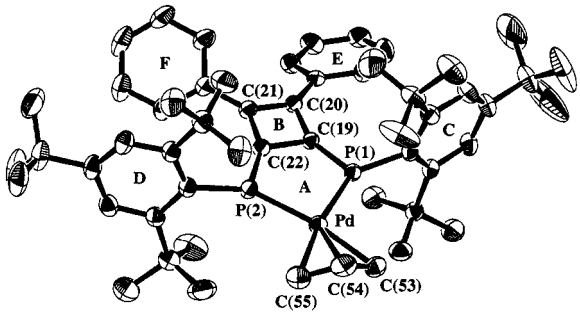
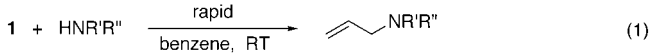


Figure 1. Molecular structure of the cation in crystals of $\mathbf{1}\cdot 2C_6H_6$. Thermal ellipsoids are drawn at the 30% probability level. Triflate anion, benzene molecules (solvent of crystallization), and hydrogen atoms are omitted for clarity. Selected bond lengths [Å] and angles [°]: Pd-P(1) 2.326(1), Pd-P(2) 2.322(1), Pd-C(53) 2.168(5), Pd-C(54) 2.168(5), Pd-C(55) 2.178(4), P(1)-C(19) 1.667(4), P(2)-C(22) 1.671(4), C(19)-C(20) 1.476(5), C(19)-C(22) 1.499(5), C(20)-C(21) 1.406(5), C(21)-C(22) 1.464(5), C(53)-C(54) 1.383(8), C(54)-C(55) 1.376(8); P(1)-Pd-P(2) 85.50(4), Pd-P(1)-C(19) 107.6(1), Pd-P(2)-C(22) 107.4(1), P(1)-C(19)-C(22) 119.6(3), C(20)-C(19)-C(22) 87.8(2), P(2)-C(22)-C(19) 119.9(3), C(19)-C(22)-C(21) 88.5(3), C(19)-C(20)-C(21) 91.7(3), C(20)-C(21)-C(22) 91.9(3), C(53)-C(54)-C(55) 119.9(5). Dihedral angles between least-squares planes [°]: [A]-[B] 2.3(1), [A]-[C] 93.2(1), [A]-[D] 100.3(1), [B]-[E] 28.2(2), [B]-[F] 147.8(2).

Complex **1** is extremely reactive towards amines [Eq. (1)]. Treatment of **1** with diethylamine (10 mol equiv) in benzene



(1)

at room temperature led to instant formation of 3-(*N*,*N*-diethylamino)propene in 82% yield. Similarly, the reaction with aniline afforded a 45% yield of 3-(*N*-phenylamino)pro-

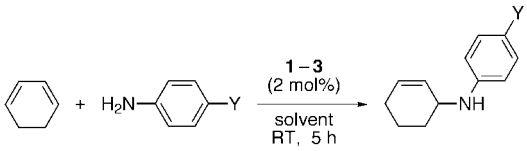
[*] Prof. Dr. F. Ozawa, Dr. T. Minami, H. Okamoto, S. Ikeda, R. Tanaka
Department of Applied Chemistry
Graduate School of Engineering
Osaka City University
Sumiyoshi-ku, Osaka 558-8585 (Japan)
Fax: (+81) 6-6605-2978
E-mail: ozawa@a-chem.eng.osaka-cu.ac.jp
Prof. Dr. M. Yoshifuji
Department of Chemistry
Graduate School of Science
Tohoku University
Aoba, Sendai 980-8578 (Japan)

[**] This work was supported by a Grant-in-Aid for Scientific Research from the Ministry of Education, Science, Sports and Culture, Japan.

Supporting information for this article is available on the WWW under http://www.angewandte.com or from the author.

pene within a few minutes.[17] In contrast, the diphosphane analogues [Pd(η^3-allyl)(dppe)]OTf (dppe = 1,2-bis(diphenylphosphanyl)ethane) and [Pd(η^3-allyl)(dppf)]OTf (dppf = 1,1′-bis(diphenylphosphanyl)ferrocene) were totally unreactive towards aniline under the same reaction conditions.

The high reactivity of **1** was also demonstrated in the catalytic hydroamination of 1,3-cyclohexadiene with anilines [Eq. (2)]. A typical procedure follows: Aniline (0.18 mL, 1.98 mmol) was added to a solution of **1** (21.0 mg, 0.020 mmol)



(2)

and 1,3-cyclohexadiene (0.10 mL, 1.05 mmol) in toluene (2 mL) under nitrogen. The mixture was stirred at room temperature for 5 h. Analysis by GLC revealed complete consumption of the diene. The reaction mixture was concentrated to dryness by pumping, and the residue purified by column chromatography (SiO_2, hexane/AcOEt 100/1) to give 162 mg (89 % yield) of 3-(*N*-phenylamino)cyclohexene.

Representative results are listed in Table 1. The catalytic activity significantly decreased with increasing solvent polarity (entries 1–5). Toluene was among the best solvents examined. The reaction did not proceed in DMF, and precipitation of palladium black occurred. Complex **2** (R = OMe) showed catalytic activity comparable to that of **1** (entry 6), whereas CF_3-substituted **3** was less active (entry 9).[18] Hydroamination with *para*-substituted anilines was also successful (entries 7 and 8).

Table 1. Hydroamination of 1,3-cyclohexadiene with anilines catalyzed by **1**–**3** [Eq. (2)].[a]

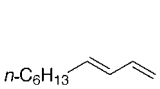
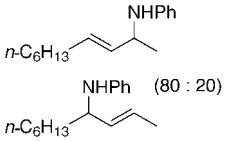
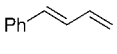
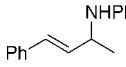
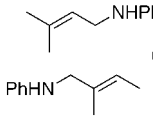
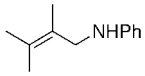
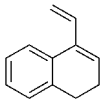
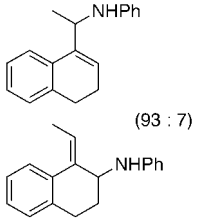
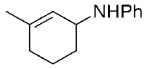
Entry	Catalyst	Y	Solvent	Yield [%][b]
1	**1**	H	toluene	89
2	**1**	H	THF	59
3	**1**	H	dioxane	30
4	**1**	H	CH_2Cl_2	2
5	**1**	H	DMF	0
6	**2**	H	toluene	91
7	**2**	F	toluene	90
8	**2**	OMe	toluene	88
9	**3**	H	toluene	58

[a] All reactions were conducted at room temperature for 5 h with diene (1.0 mmol), aniline (2.0 mmol), catalyst (0.02 mmol), and solvent (2 mL). [b] Yield of isolated product.

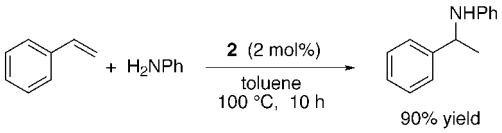
A variety of 1,3-dienes could be hydroaminated with aniline in good to excellent yields (Table 2). All reactions proceeded smoothly at room temperature, except for entry 6, in which about 30 % of unconsumed diene starting material was recovered. 1,2-Addition to a terminal vinyl group is preferred when one of the termini of the diene unit is substituted (entries 1, 2, and 5). Otherwise, 1,4-addition to the diene takes place exclusively (entries 3, 4, and 6).

The present catalysts were also effective for 1,2-addition of aniline to styrene at 100 °C [Eq. (3)]. Complex **2** gave the best result: a 90 % yield of {1-(*N*-phenylamino)ethyl}benzene.

Table 2. Hydroamination of dienes with aniline catalyzed by **2**.[a]

Entry	Diene	Time [h]	Product(s)[b]	Yield [%][c]
1		6	 (80 : 20)	80
2		5		92
3		3	 (88 : 12)	92
4		5		96
5		6	 (93 : 7)	85
6		24		68

[a] All reactions were conducted at room temperature in toluene (2 mL) with diene (1.0 mmol), aniline (2.0 mmol), and catalyst (0.02 mmol). [b] The ratio of isomers was determined by ^{1}H NMR analysis. [c] Yield of isolated product.



(3)

In conclusion, we have found highly active catalysts for the hydroamination of 1,3-dienes with aniline. The reactions readily proceed at room temperature to give the corresponding 1,2- or 1,4-addition products in high yields. The use of diphosphinidenecyclobutene ligands with sp^2-hybridized phosphorus atoms having strong π-acceptor ability is of particular importance for the catalytic activity.

Received: July 26, 2001 [Z17610]

[1] For reviews, see a) R. Taube in *Applied Homogeneous Catalysis with Organometallic Compounds*, *Vol. 1* (Eds.: B. Cornils, W. A. Herrmann), VCH, Weinheim, **1996**, p. 507; b) T. E. Müller, M. Beller, *Chem. Rev.* **1998**, *98*, 675.

[2] a) M. R. Gagné, C. L. Stern, T. J. Marks, *J. Am. Chem. Soc.* **1992**, *114*, 275; b) S. Tian, V. M. Arredondo, C. L. Stern, T. J. Marks, *Organometallics* **1999**, *18*, 2568.

[3] J. Tsuji, *Transition Metal Reagents and Catalysts*, Wiley, Chichester, **2000**, p. 169.

[4] a) J. E. Bäckvall, *Acc. Chem. Res.* **1983**, *16*, 335; b) J. E. Bäckvall, *Pure Appl. Chem*. **1992**, *64*, 429.

[5] a) M. Beller, H. Trauthwein, M. Eichberger, C. Breindl, J. Herwig, T. E. Müller, O. R. Thiel, *Chem. Eur. J.* **1999**, *5*, 1306; b) M. Beller, H. Trauthwein, M. Eichberger, C. Breindl, T. E. Müller, *Eur. J. Inorg. Chem.* **1999**, 1121; c) U. Radhakrishnan, M. Al-Masum, Y. Yamamoto,

 © WILEY-VCH Verlag GmbH, D-69451 Weinheim, 2001 1433-7851/01/4023-4502 $ 17.50+.50/0

Tetrahedron Lett. **1998**, *39*, 1037; d) M. Al-Masum, M. Meguro, Y. Yamamoto, *Tetrahedron Lett.* **1997**, *38*, 6071; e) R. Dorta, P. Egli, F. Zurcher, A. Togni, *J. Am. Chem. Soc.* **1997**, *119*, 10857; f) L. Besson, J. Góre, B. Cazes, *Tetrahedron Lett.* **1995**, *36*, 3857; g) R. W. Armbruster, M. M. Morgan, J. L. Schmidt, C. M. Lau, R. M. Riley, D. L. Zabrowski, H. A. Dieck, *Organometallics* **1986**, *5*, 234; h) K. Takahashi, A. Miyake, G. Hata, *Bull. Chem. Soc. Jpn.* **1972**, *45*, 1183.

[6] For the 1:1 addition of amines to activated alkenes such as enones, see a) M. J. Gaunt, J. B. Spencer, *Org. Lett.* **2001**, *3*, 25; b) M. Kawatsura, J. F. Hartwig, *Organometallics* **2001**, *20*, 1960; c) X. Cheng, K. K. Hii, *Tetrahedron* **2001**, *57*, 5445.

[7] a) O. Löber, M. Kawatsura, J. F. Hartwig, *J. Am. Chem. Soc.* **2001**, *123*, 4366; b) M. Kawatsura, J. F. Hartwig, *J. Am. Chem. Soc.* **2000**, *122*, 9546.

[8] a) R. Appel, V. Winkhaus, F. Knoch, *Chem. Ber.* **1987**, *120*, 243; b) G. Märkl, P. Kreitmeier, H. Nöth, K. Polborn, *Angew. Chem.* **1990**, *102*, 958; *Angew. Chem. Int. Ed. Engl.* **1990**, *29*, 927; c) M. Yoshifuji, K. Toyota, M. Murayama, H. Yoshimura, A. Okamoto, K. Hirotsu, S. Nagase, *Chem. Lett.* **1990**, 2195; d) K. Toyota, K. Tashiro, M. Yoshifuji, S. Nagase, *Bull. Chem. Soc. Jpn.* **1992**, *65*, 2297; e) M. Yoshifuji, Y. Ichikawa, N. Yamada, K. Toyota, *Chem. Commun.* **1998**, 27.

[9] For reviews, see a) P. Le Floch, F. Mathey, *Coord. Chem. Rev.* **1998**, *179/180*, 771; b) F. Mathey, *Acc. Chem. Res.* **1992**, *25*, 90; M. Yoshifuji, *J. Chem. Soc. Dalton Trans.* **1998**, 3343.

[10] a) K. Toyota, K. Masaki, T. Abe, M. Yoshifuji, *Chem. Lett.* **1995**, 221; b) S. Ikeda, F. Ohhata, M. Miyoshi, R. Tanaka, T. Minami, F. Ozawa, M. Yoshifuji, *Angew. Chem.* **2000**, *112*, 4686; *Angew. Chem. Int. Ed.* **2000**, *39*, 4512.

[11] a) F. Mathey, P. Le Floch, *Chem. Ber.* **1996**, *129*, 263; b) F. Knoch, F. Kremer, U. Schmidt, U. Zenneck, P. Le Floch, F. Mathey, *Organometallics* **1996**, *15*, 2713; c) B. Breit, *Chem. Commun.* **1996**, 437; d) B. Breit, *J. Mol. Catal. A* **1999**, *143*, 143; e) B. Breit, R. Winde, T. Mackewits, R. Paciello, K. Harms, *Chem. Eur. J.* **2001**, *7*, 3106.

[12] a) X. Sava, L. Ricard, F. Mathey, P. Le Floch, *Organometallics* **2000**, *19*, 4899; b) C. Ganter, C. Glinsböckel, B. Ganter, *Eur. J. Inorg. Chem.* **1998**, 1163; c) R. Shintani, M. M.-C. Lo, G. C. Fu, *Org. Lett.* **2000**, *2*, 3695; d) K. Tanaka, S. Qiao, M. Tobisu, M. M.-C. Lo, G. C. Fu, *J. Am. Chem. Soc.* **2000**, *122*, 9870.

[13] Y. Tatsuno, T. Yoshida, S. Otsuka, *Inorg. Synth.* **1990**, *28*, 343.

[14] Complexes **1**–**3** were characterized by NMR spectroscopy and elemental analysis: see Supporting Information.

[15] A single crystal of dimensions ca. $0.40 \times 0.25 \times 0.15$ mm was grown by slow evaporation of the benzene solution at room temperature. Crystallographic data for $\mathbf{1} \cdot 2C_6H_6$: $C_{68}H_{85}O_3P_2SF_3Pd$, $M_r = 1207.82$, orthorhombic, space group *Pbca* (no. 61), $a = 29.3798(4)$, $b = 27.9193(4)$, $c = 16.6779(2)$ Å, $V = 13680.3(5)$ Å^3, $Z = 8$, $\rho_{calcd} = 1.173\ g\,cm^{-3}$, $\mu(Mo_{K\alpha}) = 3.98\ cm^{-1}$, $T = 296$ K, $2\theta_{max} = 55.0^\circ$; of the 116497 reflections collected, 15690 were independent ($R_{int} = 0.044$) and used for the structure refinement (625 parameters); $R_1 = 0.044$, $R(F^2) = 0.073$, $R_w(F^2) = 0.133$ for 8198 data with $I > 3\sigma(I)$; $R(F^2) = 0.085$, $R_w(F^2) = 0.158$ for all data. Crystallographic data (excluding structure factors) for the structure reported in this paper have been deposited with the Cambridge Crystallographic Data Centre as supplementary publication no. CCDC-167652. Copies of the data can be obtained free of charge on application to CCDC, 12 Union Road, Cambridge CB2 1EZ, UK (fax: (+44) 1223-336-033; e-mail: deposit@ccdc.cam.ac.uk).

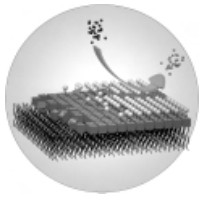
[16] a) T. Hayashi, A. Yamamoto, Y. Ito, E. Nishioka, H. Miura, K. Yanagi, *J. Am. Chem. Soc.* **1989**, *111*, 6301; b) S. L. James, A. G. Orpen, P. G. Pringle, *J. Organomet. Chem.* **1996**, *525*, 299.

[17] After rapid formation in the initial phase, the reaction became significantly slower, probably due to simultaneous decomposition of palladium species (precipitation of palladium-black was noted). The yield of 3-(*N*-phenylamino)propene reached 72% after prolonged reaction time (24 h).

[18] It was confirmed that the diphosphane complexes [Pd(η^3-allyl)(dppe)]OTf and [Pd(η^3-allyl)(dppf)]OTf were inactive towards the catalytic reaction of Equation (2) at room temperature.

 © WILEY-VCH Verlag GmbH, D-69451 Weinheim, 2001 1433-7851/01/4023-4503 $ 17.50+.50/0

PREVIEW 24/2001



REVIEWS

The *B*-Alkyl Suzuki–Miyaura Cross-Coupling Reaction: Development, Mechanistic Study, and Applications in Natural Product Synthesis — S. J. Danishefsky et al.

Oxygen Binding, Activation, and Reduction to Water by Copper Proteins — E. I. Solomon et al.

MINIREVIEW

Enantioselective Construction of Quaternary Stereocenters — J. Christoffers and A. Mann

ESSAYS

Coping with Fritz Haber's Somber Literary Shadow — R. Hoffmann and P. Laszlo

The "Rocky" Road to Literary Fame: Marcel Proust and the Diamond Synthesis of Professor Moissan — O. Krätz

HIGHLIGHT

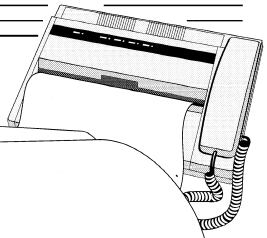
Ru- and Rh-Catalyzed Asymmetric Hydrogenations: Recent Surprises from an Old Reaction — K. Rossen

COMMUNICATIONS

The Total Synthesis of Nominal Diazonamides — P. G. Harran et al.

ORDER FORM REPLY BY FAX

ANGEWANDTE CHEMIE
International Edition



From:

Name _____

Street _____

City _____

State / Zip _____ / _____

To:

WILEY-VCH
P.O. Box 10 11 61
D-69451 Weinheim, Germany

Tel.: +49 6201 - 606 147
Fax: +49 6201 - 606 172
E-mail: subservice@wiley-vch.de

❑ **Please enter my subscription for 2002 (26 issues)**
(Only yearly subscriptions are accepted.) Valid for print or electronic / print and electronic delivery

Simply copy, fill out, and fax.

At the institutional rate:
❑ Europe: € 2158.00/2266.00
❑ Outside Europe: US$ 2878.00/3022.00

at the individual rate* (print only):
❑ Europe: € 228.00
❑ Outside Europe: US$ 318.00

Please tick:
❑ Print
❑ Electronic
❑ Print and electronic

*(Individual rates are available only for bona fide individual orders for personal use, paid for by personal check or credit card. *Rates for personal members of the GDCh outside Germany/Austria/Switzerland)

Method of payment:

❑ Check ❑ VISA ❑ MasterCard ❑ American Express

Account # _____

Exp. Date _____ Signature X _____

WILEY-VCH

ANGEWANDTE CHEMIE

A Journal of the Gesellschaft Deutscher Chemiker

INTERNATIONAL EDITION

2001
40/24
Pages 4519 – 4882



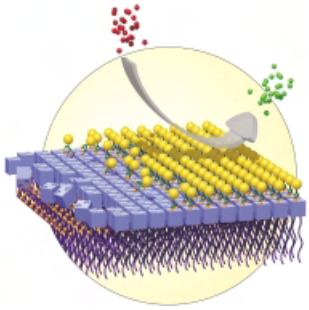
Cover Picture of the Year
Cast your vote at
www.angewandte.com
and win a great book!



The editorial staff and the publishers thank all readers, authors, referees, and advertisers for their interest and support over the past year and wish them all a happy new year.

COVER PICTURE

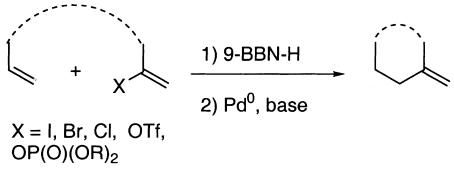
The cover picture shows the process of building functional amphiphilic protein–polymer hybrids in a modular fashion. Monolayers of biotinylated polystyrene (purple) bind the protein streptavidin (blue), resulting in the formation of giant amphiphiles. The remaining free binding sites are subsequently used to associate biotinylated biomacromolecules (yellow), such as the iron-storage protein ferritin. The use of covalent conjugates of streptavidin and horseradish peroxidase leads to the formation of reactive surfaces, which are capable of catalyzing organic reactions. Further details on these giant amphiphiles are reported by Nolte and co-workers on p. 4732 ff.



REVIEWS

Contents

An extremely attractive method for forming C(sp^3)–C(sp^2) bonds in complex molecular settings is the *B*-alkyl Suzuki – Miyaura reaction (see scheme; 9-BBN-H = 9-borabicyclo[3.3.1]nonane; the dashed line indicates that intramolecular reactions are also possible). The regio-, chemo-, and stereoselective nature of this reaction has been used in a number of syntheses of natural and non-natural compounds. An intricate knowledge of the mechanism of this reaction provides the basis for future advancements in this field.



S. R. Chemler, D. Trauner, S. J. Danishefsky* ..... 4544 – 4568

The *B*-Alkyl Suzuki – Miyaura Cross-Coupling Reaction: Development, Mechanistic Study, and Applications in Natural Product Synthesis

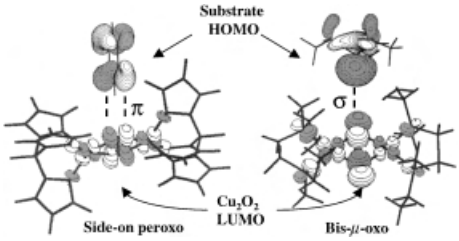
Angew. Chem. **2001**, *113*, 4676 – 4701

Keywords: boranes · C–C coupling · cross-coupling · Suzuki – Miyaura coupling · synthetic methods

© WILEY-VCH Verlag GmbH, D-69451 Weinheim, 2001

1433-7851/01/4024-4521 $ 17.50+.50/0

Copper enzymes are involved in dioxygen binding, activation, and reduction to water. The oxygen intermediates in these enzymes exhibit unique spectroscopic features, which reflect new geometric and electronic structures that play key roles in catalysis. Structure/function correlations are developed and reaction mechanisms are defined on a molecular level. The figure shows the calculated frontier orbitals of the μ-η^2:η^2-side-on bridged-peroxo Cu_2^{II} and the bis-μ-oxo-Cu_2^{III} intermediates, which activate π and σ electrophilic attack on substrates, respectively.



Angew. Chem. **2001**, *113*, 4702 – 4724

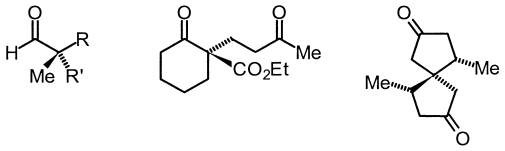
E. I. Solomon,* P. Chen, M. Metz, S.-K. Lee, A. E. Palmer ..... 4570 – 4590

Oxygen Binding, Activation, and Reduction to Water by Copper Proteins

Keywords: bioinorganic chemistry · copper · electronic structure · metalloenzymes · oxygen activation · reaction mechanisms

MINIREVIEW

The synthesis of optically active natural products and pharmaceuticals with quaternary stereocenters is a particular challenge. The potential of new stoichiometric and catalytic asymmetric reactions can be proved by their suitability for the enantioselective generation of such fully substituted carbon centers, such as, for example, in the compounds shown.



Angew. Chem. **2001**, *113*, 4725 – 4732

J. Christoffers,* A. Mann ... 4591 – 4597

Enantioselective Construction of Quaternary Stereocenters

Keywords: asymmetric catalysis · C–C coupling · chiral auxiliaries · enantioselectivity · synthetic methods

VIPs

The following communications are "Very Important Papers" in the opinion of two referees. They will be published shortly (those marked with a diamond will be published in the next issue). Short summaries of these articles can be found on the *Angewandte Chemie* homepage at the address http://www.angewandte.com

Cesiumauride Ammonia (1/1), $CsAu \cdot NH_3$: A Crystalline Analogue of Alkali Metals Dissolved in Ammonia? — A.-V. Mudring, M. Jansen,* J. Daniels, S. Krämer, M. Mehring, J. P. Prates Ramalho, A. H. Romero, M. Parrinello ◆

Enantiopure Double-Helical Alkynyl Cyclophanes — D.-L. An, T. Nakano, A. Orita, J. Otera* ◆

Supramolecular Cluster Catalysis: Benzene Hydrogenation Catalyzed by a Cationic Triruthenium Cluster under Biphasic Conditions — G. Süss-Fink,* M. Faure, T. R. Ward ◆

The First Disulfur and Diselenium Complexes of Platinum: Syntheses and Crystal Structures — K. Nagata, N. Takeda, N. Tokitoh* ◆

Gold – Xenon Complexes — T. Drews, S. Seidel, K. Seppelt*

Iron-Catalyzed Polyethylene Chain Growth on Zinc: Linear α-Olefins with a Poisson Distribution — G. J. P. Britovsek, S. A. Cohen, V. C. Gibson,* P. J. Maddox, M. van Meurs*

 © WILEY-VCH Verlag GmbH, D-69451 Weinheim, 2001 1433-7851/01/4024-4522 $ 17.50+.50/0

ESSAYS

Contents

Picture(s) of Fritz Haber: Rolf Hochhuth, Tony Harrison, and André Malraux—three very different writers—have portrayed Fritz Haber in their novels and plays. The picture may not please chemists. Several biographies and an essay by the historian Fritz Stern have also dealt with Haber's tragic life. Should we accept these as literary portraits, if they are not to our liking? Or struggle with them? And in Haber's case would this be justified?

Angew. Chem. **2001**, *113*, 4733 – 4739

R. Hoffmann, P. Laszlo .... 4599 – 4604

Coping with Fritz Haber's Somber Literary Shadow

Keywords: chemists in the literature · Haber, Fritz · history of chemistry · scientific ethics

What connects the author Marcel Proust, the Chemistry Nobel Laureate Henri Moissan, and the fraudulent engineer Henri François Lemoine? Moissan was obsessed with the idea of preparing artificial diamonds, Lemoine alleged that he had improved the Moissan technique, which only produced diamond dust, and Proust first invested a part of his wealth in the alleged diamond synthesis and then exploited the scandal in a literary work.

Angew. Chem. **2001**, *113*, 4739 – 4745

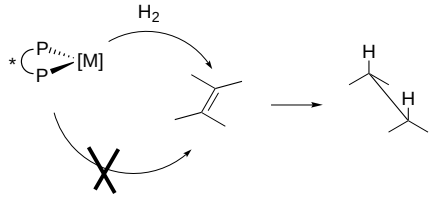
O. Krätz* ..... 4604 – 4610

The "Rocky" Road to Literary Fame: Marcel Proust and the Diamond Synthesis of Professor Moissan

Keywords: artificial diamonds · history of chemistry · Moissan, Henri

HIGHLIGHT

Far from being a well-understood reaction, the enantioselective hydrogenation of prochiral olefins with Rh– and Ru – bisphosphane catalysts (see picture, M = Rh, Ru) has recently shown some surprises. Among them are a catalytic cycle featuring initial addition of hydrogen to the catalyst and not the catalyst – substrate complex as well as a purely ionic mechanism.



Angew. Chem. **2001**, *113*, 4747 – 4749

K. Rossen* ..... 4611 – 4613

Ru- and Rh-Catalyzed Asymmetric Hydrogenations: Recent Surprises from an Old Reaction

Keywords: hydrogenation · P ligands · reaction mechanisms · rhodium · ruthenium

CORRESPONDENCE

Which scaling connects the number of conformers of a protein with the number of residues? The authors both explore this question and van Gunsteren et al. produce additional arguments to those in their original paper. Although the authors do not agree on the "scaling law", they both acknowledge the importance of finding the correct answer as it has a great influence on the chance of simulating protein folding with reasonably good models.

Angew. Chem. **2001**, *113*, 4751 – 4752

Angew. Chem. **2001**, *113*, 4753 – 4754

A. R. Dinner, M. Karplus* 4615 – 4616

Comment on the Communication "The Key to Solving the Protein-Folding Problem Lies in an Accurate Description of the Denatured State" by van Gunsteren et al.

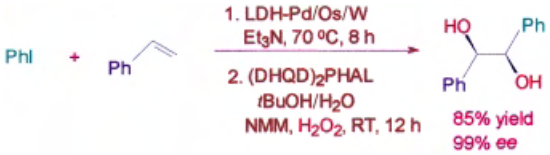
W. F. van Gunsteren,* R. Bürgi, C. Peter, X. Daura ..... 4617 – 4618

Reply

Keywords: computer chemistry · correspondence · molecular dynamics · peptides · protein folding

 © WILEY-VCH Verlag GmbH, D-69451 Weinheim, 2001 1433-7851/01/4024-4523 $ 17.50+.50/0

A transition metal based biomimic approach is used to realize multistep reactions, composed of multicomponent systems, in a single-pot synthesis of chiral diols mediated by a trifunctional (Pd, Os, W) catalyst anchored to a single matrix (see scheme; LDH = layered double hydroxide, $(DHQD)_2PHAL$ = 1,4-bis(9-*O*-dihydroquinidinyl)phthalazine, NMM = *N*-methylmorpholine).



Angew. Chem. **2001**, *113*, 4755 – 4759

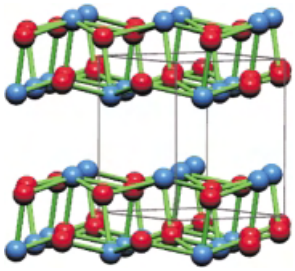
B. M. Choudary,* N. S. Chowdari, S. Madhi, M. L. Kantam ... 4619 – 4623

A Trifunctional Catalyst for the Synthesis of Chiral Diols

Keywords: asymmetric synthesis · heterogeneous catalysis · immobilization · oxidation · transition metals

---

Even under a pressure of 46 GPa, the low-symmetry lone-pair structures of isoelectronic TlF and PbO (see picture for β-PbO), classic examples of systems with a stereochemically active lone pair, resist transformation into the corresponding high-symmetry NaCl and CsCl structures. Ab initio calculations allowed a simple bonding picture for lone-pair structures involving inert-pair elements to be developed.



Angew. Chem. **2001**, *113*, 4760 – 4765

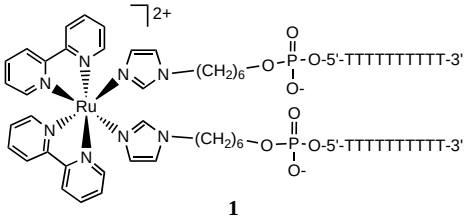
U. Häussermann,* P. Berastegui, S. Carlson, J. Haines, J.-M. Léger ..... 4624 – 4629

TlF and PbO under High Pressure: Unexpected Persistence of the Stereochemically Active Electron Pair

Keywords: ab initio calculations · bond theory · high-pressure chemistry · layered compounds

---

The branched DNA structure 1, in which a transition metal center resides at the branch point and joins two parallel DNA strands, was synthesized by a convergent solid-phase approach. Complex **1** efficiently hybridizes with complementary DNA to generate transition metal linked DNA duplexes. This opens the door to using the geometries of transition metal complexes to direct the association of DNA into novel motifs.



1

Angew. Chem. **2001**, *113*, 4765 – 4768

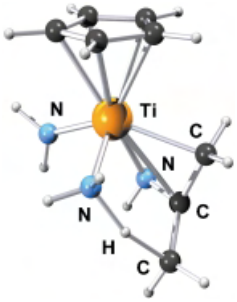
I. Vargas-Baca, D. Mitra, H. J. Zulyniak, J. Banerjee, H. F. Sleiman* 4629 – 4632

Solid-Phase Synthesis of Transition Metal Linked, Branched Oligonucleotides

Keywords: DNA recognition · DNA structures · oligonucleotides · ruthenium

---

Proton transfer from ammine or amide ligands to vinylamine-type π systems in intermediary titanacycles (see picture) of allene and alkyne hydroamination reactions is predicted by DFT model calculations. The weaker coordination of alkenes to the Ti=N fragment, the lack of a π system in the titanacycle, and thus the necessity of direct Ti–C bond protonation rationalize a higher barrier for alkene hydroamination.



Angew. Chem. **2001**, *113*, 4768 – 4771

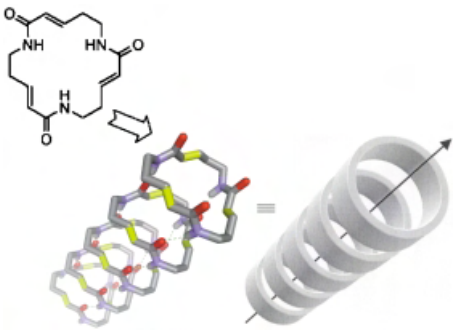
B. F. Straub,* R. G. Bergman* 4632 – 4635

The Mechanism of Hydroamination of Allenes, Alkynes, and Alkenes Catalyzed by Cyclopentadienyltitanium – Imido Complexes: A Density Functional Study

Keywords: density functional calculations · homogeneous catalysis · hydroamination · metallacycles · titanium

---

***C*$_3$-symmetric lactams in a tube**: Specially designed rigid disc-shaped macrolactams self-assemble as endless tubes by means of backbone – backbone hydrogen bonds and van der Waals contacts (see scheme). All the tubes with very strong dipoles further aggregate in a parallel fashion and all the dipoles are still oriented in the same direction.



Angew. Chem. **2001**, *113*, 4771 – 4774

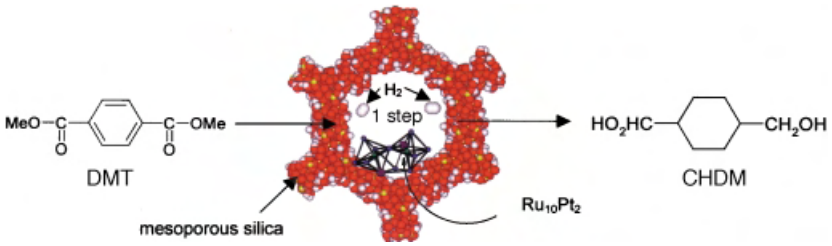
D. Gauthier, P. Baillargeon, M. Drouin, Y. L. Dory* ..... 4635 – 4638

Self-Assembly of Cyclic Peptides into Nanotubes and Then into Highly Anisotropic Crystalline Materials

Keywords: lactams · nanotubes · peptides · self-assembly · supramolecular chemistry

 © WILEY-VCH Verlag GmbH, D-69451 Weinheim, 2001 1433-7851/01/4024-4524 $ 17.50+.50/0

Pores for cluster catalysts: Nanoparticles of both Ru_5Pt and $Ru_{10}Pt_2$, uniformly distributed along the inner walls of mesoporous silica, exhibit high catalytic performance in the single-step hydrogenation of dimethyl terephthalate (DMT, to 1,4-cyclohexanedimethanol (CHDM); see scheme), of benzoic acid (to cyclohexane carboxylic acid), and of naphthalene (in the presence of sulfur) to *cis*-decalin.



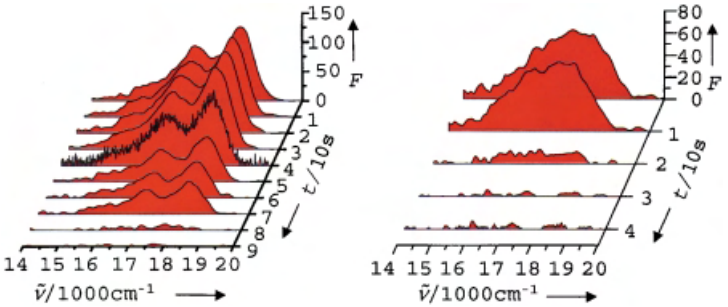
Angew. Chem. **2001**, *113*, 4774 – 4778

R. Raja, T. Khimyak, J. M. Thomas,* S. Hermans, B. F. G. Johnson* ..... 4638 – 4642

Single-Step, Highly Active, and Highly Selective Nanoparticle Catalysts for the Hydrogenation of Key Organic Compounds

Keywords: cluster compounds · heterogeneous catalysis · hydrogenation · platinum · ruthenium

Collective on/off behavior and different spectral behavior has been identified for individual molecules of different isomers (see for example the fluorescence spectra for two isomers as a function of time) with three perylenedicarboximide chromophores. In 8% of the dendrimer molecules, the chromophores interact to form an excimer-like structure which possess a higher rate of intersystem crossing than the rest of the molecules. This is the first time that this phenomenon has been proven experimentally at the single-molecule level.



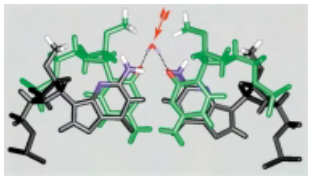
Angew. Chem. **2001**, *113*, 4779 – 4784

T. Vosch, J. Hofkens,* M. Cotlet, F. Köhn, H. Fujiwara, R. Gronheid, K. Van Der Biest, T. Weil, A. Herrmann, K. Müllen, S. Mukamel, M. Van der Auweraer, F. C. De Schryver* ..... 4643 – 4648

Influence of Structural and Rotational Isomerism on the Triplet Blinking of Individual Dendrimer Molecules

Keywords: chromophores · dendrimers · fluorescence spectroscopy · isomers · single-molecule spectroscopy

The simple replacement of 2′-OH by 2′-OMe groups leads, in certain RNA structures, to a significant strengthening of important solute – solvent interactions. Molecular dynamics simulations uncover the complexity of effects associated with the insertion of hydrophobic groups into hydrophilic systems (the arrow indicates a long-lived bridging water molecule located in the shallow groove of a 2′-OMe(GpC) base pair step). Green = skeleton of cytosine, black = skeleton of guanine, red = oxygen atoms of water and of shallow groove carbonyl groups, blue = shallow groove nitrogen atoms, cyan = hydrogen atoms of OMe groups.



Angew. Chem. **2001**, *113*, 4784 – 4786

P. Auffinger,* E. Westhof* 4648 – 4650

Hydrophobic Groups Stabilize the Hydration Shell of 2′-*O*-Methylated RNA Duplexes

Keywords: computer chemistry · hydrophobic effect · molecular dynamics · nucleic acids · solvent effects

 © WILEY-VCH Verlag GmbH, D-69451 Weinheim, 2001 1433-7851/01/4024-4525 $ 17.50+.50/0

Copper gets into the ring: A decanuclear cyclic Cu^{II} complex is synthesized by direct treatment of $CuCl_2$ with a fluorinated amino alcoholate containing one secondary and one tertiary nitrogen donor (see space-filling diagram; Cu light blue, Cl yellow, O red, N dark blue, C gray). Possible factors that lead to the self-assembly of the unique molecular wheel are discussed.



C.-H. Chang, K. C. Hwang, C.-S. Liu, Y. Chi,* A. J. Carty,* L. Scoles, S.-M. Peng,* G.-H. Lee, J. Reedijk* ..... 4651 – 4653

Formation and Stabilization of a Decanuclear Cu^{II} Wheel Linked by Chloride and O···H–N Hydrogen Bonds

Angew. Chem. **2001**, *113*, 4787 – 4789

Keywords: copper · hydrogen bonds · magnetic properties · N,O ligands · self-assembly

Rational design of a malaria vaccine may result from the structure – immunogenicity relationship of analogues of peptide 1585, a protein sequence located at the N-terminal end of the *P. falciparum* 42-kDa merozoite surface protein-1. Altering a few amino acids in peptide 1585 (left) induces immunogenicity and protectivity, and changes the 3D structure, as shown for one of the analogues synthesized (right).



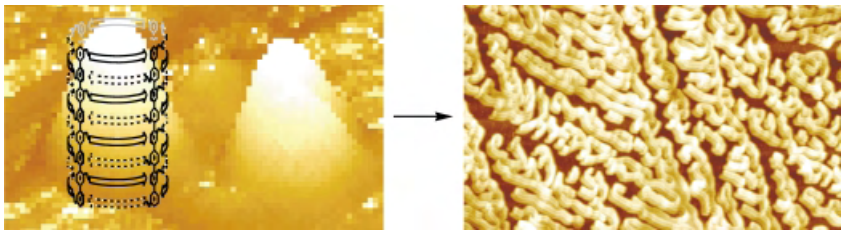
F. Espejo,* M. Cubillos, L. M. Salazar, F. Guzman, M. Urquiza, M. Ocampo, Y. Silva, R. Rodriguez, E. Lioy, M. E. Patarroyo* ..... 4654 – 4657

Structure, Immunogenicity, and Protectivity Relationship for the 1585 Malarial Peptide and Its Substitution Analogues

Angew. Chem. **2001**, *113*, 4790 – 4793

Keywords: immunochemistry · malaria · NMR spectroscopy · protein modification · protein structures

Delightful order and beauty is exhibited by novel supramolecular architectures constructed from preorganizing rigid-rod molecules which first self-assemble into β-barrel tertiary structures (left) and then transform into higher-order quaternary structures (right), that is, "rigid-rod β-fibrils".



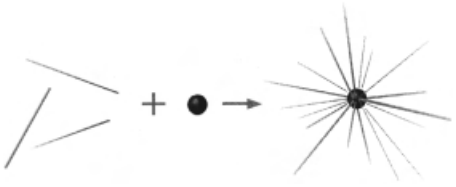
G. Das, L. Ouali, M. Adrian, B. Baumeister, K. J. Wilkinson, S. Matile* ..... 4657 – 4661

β-Fibrillogenesis from Rigid-Rod β-Barrels: Hierarchical Preorganization Beyond Microns

Angew. Chem. **2001**, *113*, 4793 – 4797

Keywords: atomic force microscopy · nanostructures · oligomers · protein models · supramolecular chemistry

A star is born: Size-selected, end-functionalized single-walled carbon nanotubes react with amine-terminated dendrimers to form star-shaped objects (see schematic representation). Analysis of the nanotube stars by atomic force microscopy and scanning electron microscopy show that they exhibit a peculiar response to electron beams.



M. Sano,* A. Kamino, S. Shinkai ..... 4661 – 4663

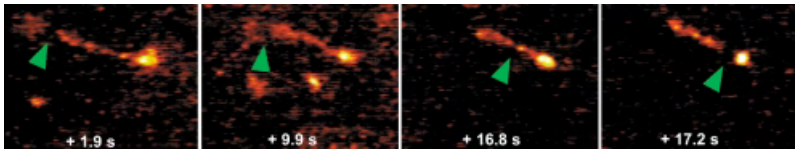
Construction of Carbon Nanotube "Stars" with Dendrimers

Angew. Chem. **2001**, *113*, 4797 – 4799

Keywords: dendrimers · nanostructures · nanotubes · scanning probe microscopy

 © WILEY-VCH Verlag GmbH, D-69451 Weinheim, 2001 1433-7851/01/4024-4526 $ 17.50+.50/0

A slice of life: Individual, fluorescently labeled DNA molecules are cut by a restriction enzyme into a sequence-specific fingerprint-like pattern and the time course of the reaction is analyzed by fluorescence microscopy. As shown in the picture, all the cuts occur one after another from one end to the other along the DNA molecule.



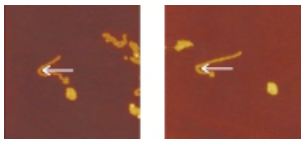
Angew. Chem. **2001**, *113*, 4799 – 4802

B. Schäfer, H. Gemeinhardt, K. O. Greulich* ..... 4663 – 4666

Direct Microscopic Observation of the Time Course of Single-Molecule DNA Restriction Reactions

Keywords: DNA restriction · enzyme catalysis · fluorescence microscopy · optical tweezers · single molecules

Moving individual molecules: Up to 250-nm long polystyrene chains with fourth generation dendrons at each repeat unit were synthesized, individualized on highly oriented pyrolytic graphite (HOPG), and manipulated into a stretched linear conformation by a scanning force microscope tip (see images, arrow indicates direction of movement).



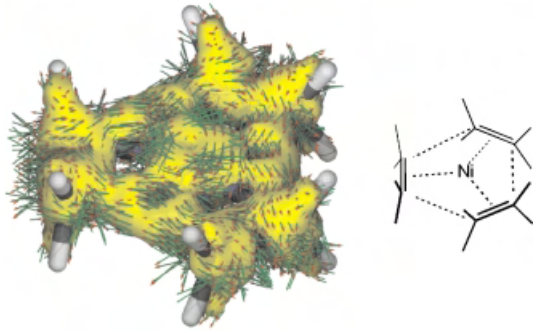
Angew. Chem. **2001**, *113*, 4802 – 4805

L. Shu, A. D. Schlüter,* C. Ecker, N. Severin, J. P. Rabe* ..... 4666 – 4669

Extremely Long Dendronized Polymers: Synthesis, Quantification of Structure Perfection, Individualization, and SFM Manipulation

Keywords: amines · dendrimers · polymerization · scanning force microscopy

An ACID test for aromaticity: A number of criteria prove that tris(ethylene)-nickel(0) and tris(ethyne)nickel(0) are aromatic compounds. The ligands strongly interact in the periphery and are "on the way" to trimerizing to cyclohexane and benzene, respectively. The electronic structure of these complexes (see picture, which shows the current density vectors plotted onto the ACID surface of the nickel ethylene complex) sheds light upon the role of Ni^0 as a catalyst in cyclooligomerization reactions. ACID = anisotropy of the induced current density; a method for visualizing the density of delocalized electrons and for quantifying conjugation effects.



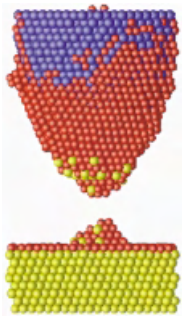
Angew. Chem. **2001**, *113*, 4809 – 4813

R. Herges,* A. Papafilippopoulos ..... 4671 – 4674

Homoaromaticity in Tris(ethylene)nickel(0) and Tris(ethyne)nickel(0)

Keywords: aromaticity · electronic structure · magnetic properties · nickel · through-space interactions

The fabrication of small metal clusters with a scanning tunneling microscope in an electrochemical environment has been simulated with a computer. (The picture shows the copper-covered tip of the scanning tunneling microscope above the Au(111) surface, which is covered by copper.) In the case of copper deposition on Au(111), Cu – Au clusters were formed that are more stable than pure copper. The simulations suggest that the formation of stable clusters by this method can only succeed if the deposited metal and the substrate form a stable alloy.



Angew. Chem. **2001**, *113*, 4807 – 4809

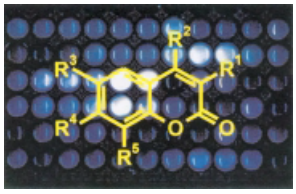
M. G. Del Pópolo, E. P. M. Leiva,* W. Schmickler* ..... 4674 – 4676

On the Stability of Electrochemically Generated Nanoclusters—A Computer Simulation

Keywords: alloys · cluster compounds · electrochemistry · molecular dynamics · scanning tunneling microscopy

 © WILEY-VCH Verlag GmbH, D-69451 Weinheim, 2001 1433-7851/01/4024-4527 $ 17.50+.50/0

"Hits" with high quantum yields: The screening of the chromophores of a coumarin library for optical properties allowed the identification of "hits" with high fluorescence quantum yields (see picture) which could be used as fluorescence labels and laser dyes. The generation of the library was facilitated by an efficient method involving the parallel synthesis utilizing Pd-catalyzed cross-coupling reactions.



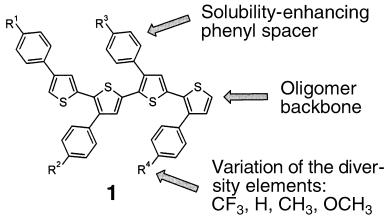
Angew. Chem. **2001**, *113*, 4813 – 4816

M.-S. Schiedel, C. A. Briehn, P. Bäuerle* ..... 4677 – 4680

Single-Compound Libraries of Organic Materials: Parallel Synthesis and Screening of Fluorescent Dyes

Keywords: coumarins · combinatorial chemistry · cross-coupling · fluorescence · high-throughput screening

256 oligomers make up the quaterthiophene library of compounds **1** which was prepared by a combination of parallel and "mix-and-split" syntheses. An automated screening process for the recording of cyclic voltammetric data and subsequent data analysis allowed the development of structure – property relationships on which to base the future design of π-conjugated oligomers.



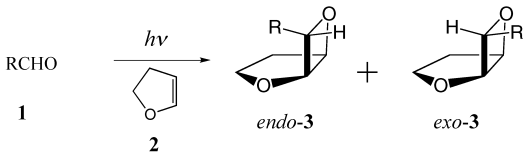
Angew. Chem. **2001**, *113*, 4817 – 4820

C. A. Briehn, M.-S. Schiedel, E. M. Bonsen, W. Schuhmann, P. Bäuerle* ..... 4680 – 4683

Single-Compound Libraries of Organic Materials: From the Combinatorial Synthesis of Conjugated Oligomers to Structure – Property Relationships

Keywords: combinatorial chemistry · conducting materials · cross-coupling · cyclic voltammetry · high-throughput screening

The multiplicity of the excited state controls the product distribution in the formation of *endo*/*exo*-oxetane **3** in the photocycloaddition of aldehydes **1** (R = Ph, Et, Me, *i*Bu) with dihydrofuran **2** (Paternò – Büchi reaction). Whether the singlet or triplet channel dominates is strongly dependent on the temperature, which is therefore critical for the selectivity of the reaction.



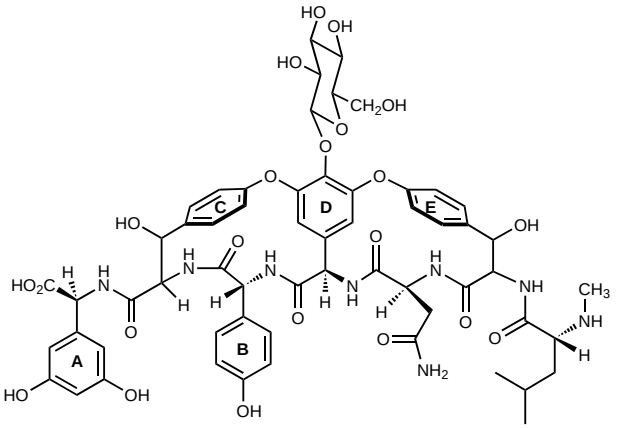
Angew. Chem. **2001**, *113*, 4828 – 4832

A. G. Griesbeck,* S. Bondock, M. S. Gudipati* ..... 4684 – 4687

Temperature and Viscosity Dependence of the Spin-Directed Stereoselectivity of the Carbonyl – Alkene Photocycloaddition

Keywords: diastereoselectivity · isoinversion principle · photochemistry · photocycloaddition · radical reaction

Linear and bicyclic glycopeptides occur as intermediates in the biosynthesis of the aglycon of glycopeptide antibiotics of the type shown. Considering the structures of these peptides and those of previously isolated analogues, the sequence of the three oxidative ring-closing steps can be deduced for type-I and type-II glycopeptide antibiotics. Thus, comprehensive insight into the assembly of the aglycon is achieved for the first time.



Angew. Chem. **2001**, *113*, 4824 – 4827

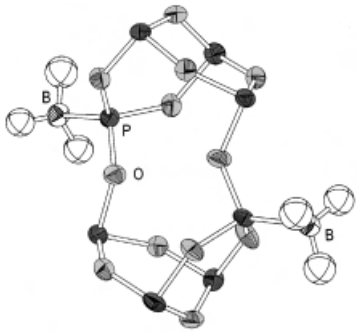
D. Bischoff, S. Pelzer, B. Bister, G. J. Nicholson, S. Stockert, M. Schirle, W. Wohlleben, G. Jung, R. D. Süssmuth* ..... 4688 – 4691

The Biosynthesis of Vancomycin-Type Glycopeptide Antibiotics—The Order of the Cyclization Steps

Keywords: antibiotics · balhimycin · biosynthesis · glycopeptides · vancomycin

 © WILEY-VCH Verlag GmbH, D-69451 Weinheim, 2001 1433-7851/01/4024-4528 $ 17.50+.50/0

Ambivalent chemical reactivity is characteristic for molecular phosphorus oxides: They either react in a vigorous and uncontrolled manner or they are practically inert, for example, in attempts at controlled ring-opening reactions. Thus, the spontaneous dimerization of $P_4O_6 \cdot BH_3$ to give $P_8O_{12} \cdot 2\,BH_3$ (see crystal structure) is a real surprise.



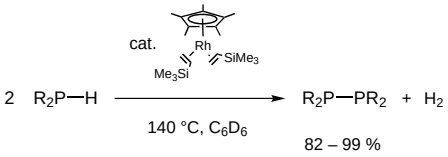
A. Tellenbach, M. Jansen* 4691 – 4694

Dimerization of Molecular Phosphorus Oxides

Angew. Chem. **2001**, *113*, 4838 – 4840

Keywords: cage compounds · mass spectrometry · phosphorus · phosphorus oxides · solid-state structures

Two reaction protocols have been developed for the catalytic dehydrocoupling of secondary phosphanes by the rhodium(I) complex $[Cp^*Rh\{CH_2{=}CH(TMS)\}_2]$: In the presence of an olefin, transfer hydrogenation occurs to give the corresponding alkane and the diphosphane. Without the addition of an olefin, the reaction proceeds by loss of dihydrogen but more elevated reaction temperatures must be used [Eq. (1)].



(1)

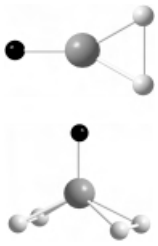
V. P. W. Böhm, M. Brookhart* ..... 4694 – 4696

Dehydrocoupling of Phosphanes Catalyzed by a Rhodium(I) Complex

Angew. Chem. **2001**, *113*, 4832 – 4834

Keywords: homogeneous catalysis · phosphanes · P–H activation · P–P coupling · rhodium

A photolytically induced reaction of AlF with O_2 in an argon matrix afforded the first peroxo and bis-superoxo complexes of aluminum: $FAlO_2$ and $FAl(O_2)_2$ (see picture). The compounds were identified and characterized by IR spectroscopy and density functional theory (DFT) as well as ab initio calculations.



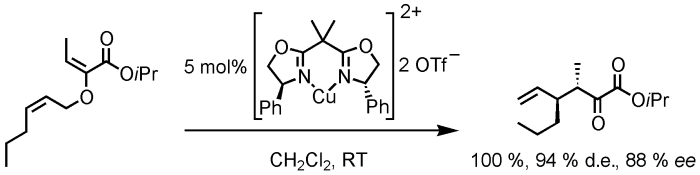
J. Bahlo, H.-J. Himmel, H. Schnöckel* ..... 4696 – 4700

The First Dectection of Peroxo and Bis-superoxo Complexes of Aluminum: $FAlO_2$ and $FAlO_4$

Angew. Chem. **2001**, *113*, 4820 – 4824

Keywords: aluminum · matrix isolation · peroxo ligands · photolysis · superoxo ligands

Almost 90 years after it was first described by Ludwig Claisen, a catalyzed enantioselective Claisen rearrangement has been implemented for the first time. Chiral copper(II) bis(oxazolines) catalyzed the Claisen rearrangement of 2-alkoxycarbonyl-substituted allyl vinyl ethers with enantiomeric excesses of 80 – 90 % (see scheme).



L. Abraham, R. Czerwonka, M. Hiersemann* ..... 4700 – 4703

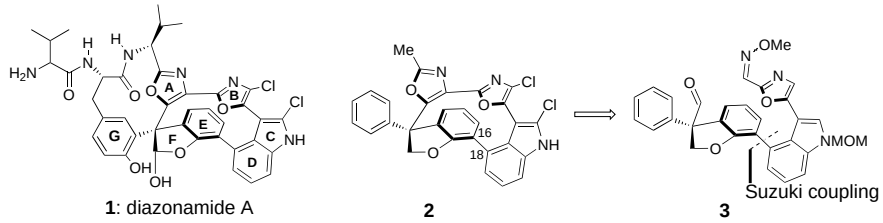
The Catalytic Enantioselective Claisen Rearrangement of an Allyl Vinyl Ether

Angew. Chem. **2001**, *113*, 4835 – 4837

Keywords: asymmetric catalysis · enantioselectivity · ketones · copper · rearrangements

 © WILEY-VCH Verlag GmbH, D-69451 Weinheim, 2001 1433-7851/01/4024-4529 $ 17.50+.50/0

One of the most enticing natural products isolated in recent years and a serious challenge to synthetic chemists is represented by the potent anticancer agent diazonamide A (**1**). By utilizing a highly convergent approach, the ABCDEF macrocycle **2** was constructed in only 16 linear steps based on a key intermolecular Suzuki coupling reaction to generate the C_{16}–C_{18} biaryl linkage and a remarkable SmI_2-induced hetero pinacol coupling cascade sequence.



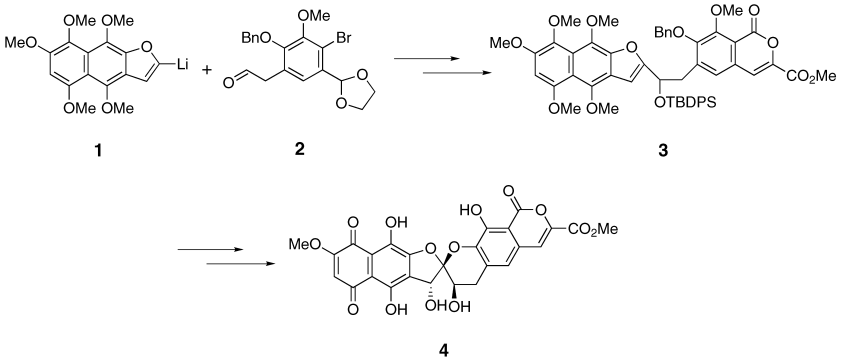
Angew. Chem. **2001**, *113*, 4841 – 4845

K. C. Nicolaou,* X. Huang, N. Giuseppone, P. Bheema Rao, M. Bella, M. V. Reddy, S. A. Snyder 4705 – 4709

Construction of the Complete Aromatic Core of Diazonamide A by a Novel Hetero Pinacol Macrocyclization Cascade Reaction

Keywords: C–C coupling · cyclization · heterocycles · natural products · samarium diiodide

A strategy for the synthesis of heliquinomycin, a selective helicase inhibitor, hinges on the spirocyclization of precursor **3**. Naphthofuran **1** and aldehyde **2** were readily prepared and used in the synthesis of **3**. The key steps in the total synthesis of heliquinomycinone (**4**) include the regioselective dihydroxylation of **3**, and a novel spirocyclization under Mitsunobu conditions.



Angew. Chem. **2001**, *113*, 4845 – 4849

Angew. Chem. **2001**, *113*, 4849 – 4852

D. Qin, R. X. Ren, T. Siu, C. Zheng, S. J. Danishefsky* ..... 4709 – 4713

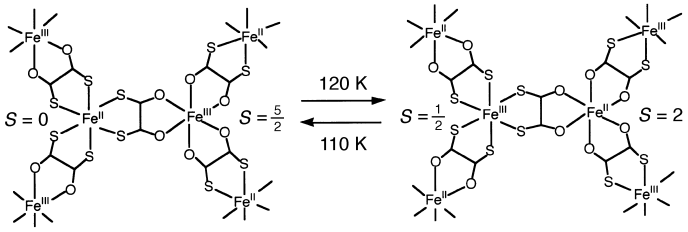
Studies in the Total Synthesis of Heliquinomycinone: Proof of Concept and Assembly of a Fully Mature Spirocyclization Precursor

T. Siu, D. Qin, S. J. Danishefsky* ..... 4713 – 4716

The Total Synthesis of Heliquinomycinone

Keywords: antitumor agents · dihydroxylation · quinones · spiro compounds · total synthesis

Not a classical spin-crossover: The heat capacity of the mixed-valence complex $\{[(n\text{-}C_3H_7)_4N][Fe^{II}Fe^{III}(dto)_3]\}_\infty$ (dto = dithiooxalato, see scheme) exhibits a phase transition at 122.4 K as a result of electron transfer, and gives insight into the cooperative phenomena exhibited by the multifunctional material.



Angew. Chem. **2001**, *113*, 4852 – 4855

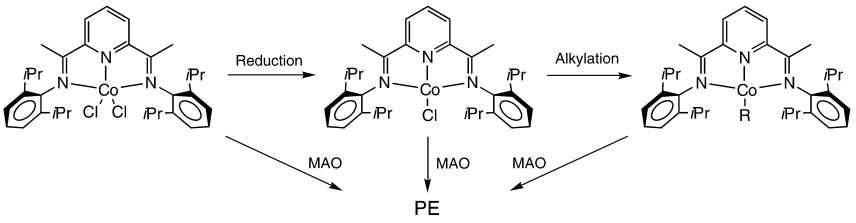
T. Nakamoto, Y. Miyazaki, M. Itoi, Y. Ono, N. Kojima,* M. Sorai* ..... 4716 – 4719

Heat Capacity of the Mixed-Valence Complex $\{[(n\text{-}C_3H_7)_4N][Fe^{II}Fe^{III}(dto)_3]\}_\infty$, Phase Transition because of Electron Transfer, and a Change in Spin-State of the Whole System

Keywords: electron transfer · iron · mixed-valence compounds · O,S ligands · phase transitions

 © WILEY-VCH Verlag GmbH, D-69451 Weinheim, 2001 1433-7851/01/4024-4530 $ 17.50+.50/0

Activated by reduction: On treatment with methylaluminoxane (MAO), the Brookhart/Gibson cobalt-based polymerization precatalyst [$LCo^{II}Cl_2$] is first reduced to [$LCo^{I}Cl$], subsequently alkylated to [$LCo^{I}Me$], and finally converted into the (as yet unknown) active species (see scheme, PE = polyethene).



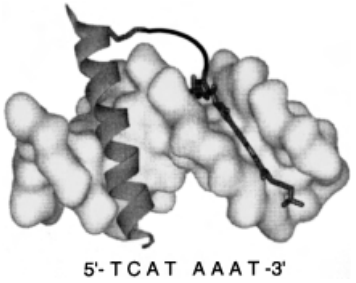
Angew. Chem. **2001**, *113*, 4855 – 4858

T. M. Kooistra, Q. Knijnenburg, J. M. M. Smits, A. D. Horton, P. H. M. Budzelaar, A. W Gal* ..... 4719 – 4722

Olefin Polymerization with [{bis(imino)pyridyl}$Co^{II}Cl_2$]: Generation of the Active Species Involves Co^{I}

Keywords: alkylation · cobalt · homogeneous catalysis · N ligands · polymerization

A bivalent system capable of binding to hybrid DNA sites through simultaneous interaction in the major and the minor groove (see schematic representation) is formed by appropriate linking of the basic region of a b-ZIP protein (GCN4) to a tripyrrole related to the antibiotic distamycin.



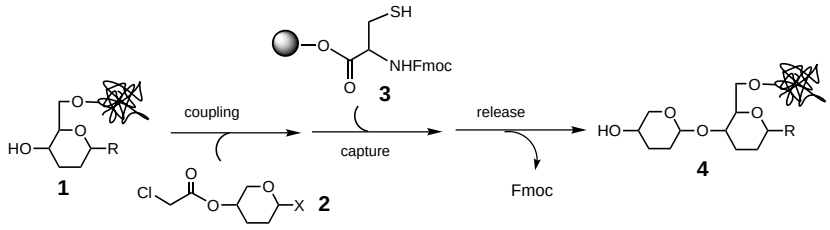
Angew. Chem. **2001**, *113*, 4859 – 4861

M. E. Vázquez, A. M. Caamaño, J. Martínez-Costas, L. Castedo, J. L. Mascareñas* ..... 4723 – 4725

Design and Synthesis of a Peptide That Binds Specific DNA Sequences through Simultaneous Interaction in the Major and in the Minor Groove

Keywords: antibiotics · DNA recognition · peptides

A highly simplified synthesis of a tetrasaccharide was possible by a repeated coupling/capture – release cycle. In the first cycle, a glycosyl acceptor (**1**) bound to a soluble polymer reacted with a glycosyl donor (**2**) having a chloroacetyl group as a temporary protecting group. Solid-phase capture by a resin-bound thiol group (in **3**) was followed by Fmoc removal, which released the polymer-bound disaccharide **4** into the solution phase. Fmoc = 9-fluorenylmethoxycarbonyl.



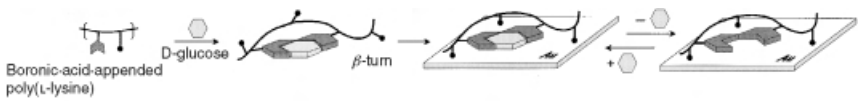
Angew. Chem. **2001**, *113*, 4861 – 4864

H. Ando, S. Manabe, Y. Nakahara, Y. Ito* ..... 4725 – 4728

Solid-Phase Capture – Release Strategy Applied to Oligosaccharide Synthesis on a Soluble Polymer Support

Keywords: glycosylation · oligosaccharides · polymer support · solid-phase synthesis

The dominant solution-phase conformation of a polymer can be fixed to a surface (see scheme). Boronic acid appended poly(L-lysine) assumes different conformations in the presence of D-glucose or D-fructose. When the polymer – glucose complex is anchored to a gold surface, an imprinted interface with "molecular memory" for glucose over fructose can be prepared.



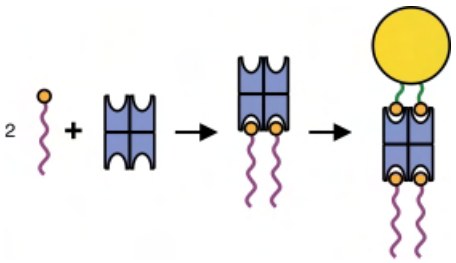
Angew. Chem. **2001**, *113*, 4865 – 4867

A. Friggeri, H. Kobayashi, S. Shinkai,* D. N. Reinhoudt* ..... 4729 – 4731

From Solutions to Surfaces: A Novel Molecular Imprinting Method Based on the Conformational Changes of Boronic-Acid-Appended Poly(L-lysine)

Keywords: molecular recognition · carbohydrates · surface chemistry

Association of streptavidin and two biotinylated polystyrene chains to form protein–polymer hybrids results in "giant amphiphiles" (see first step of schematic representation). Functionality can be introduced by the complexation of other biotinylated molecules to the remaining binding sites of streptavidin (second step).



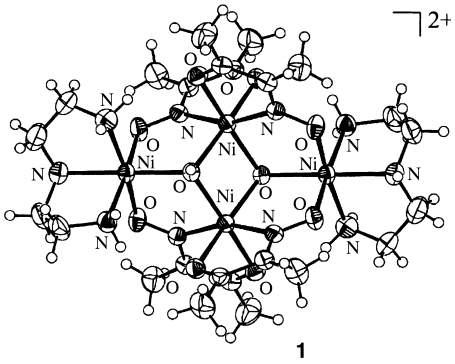
Angew. Chem. **2001**, *113*, 4868–4870

J. M. Hannink, J. J. L. M. Cornelissen, J. A. Farrera, P. Foubert, F. C. De Schryver, N. A. J. M. Sommerdijk, R. J. M. Nolte* 4732–4734

Protein–Polymer Hybrid Amphiphiles

Keywords: aggregation · amphiphiles · monolayers · polymers · proteins

A Ni_4O_2 core based on a "chair" topology forms the central unit of the tetranuclear nickel(II) complex **1**, which possesses μ_3-OH^- and butane-2,3-dione-monooximate bridges and displays fascinating magnetic properties. The major Ni–Ni interactions in **1** are antiferromagnetic in nature, and the large Ni_{core}-O-$Ni_{terminal}$ angle in the core is responsible for driving all the Ni_{core} spins parallel.



1

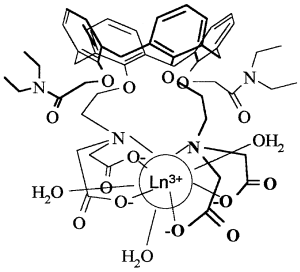
Angew. Chem. **2001**, *113*, 4870–4873

V. V. Pavlishchuk,* S. V. Kolotilov, A. W. Addison,* M. J. Prushan, D. Schollmeyer, L. K. Thompson, E. A. Goreshnik 4734–4737

A Tetrameric Nickel(II) "Chair" with both Antiferromagnetic Internal Coupling and Ferromagnetic Spin Alignment

Keywords: magnetic properties · nickel · oximes

Contrasting calixarenes: Thermodynamically stable and water-soluble calix[4]arene–Ln^{III} (see picture) complexes may represent a new class of relaxation (Ln = Gd) or luminescent (Ln = Eu, Tb) probes for biomedical studies. The first complete characterization of one of these complexes in water is reported. The Gd^{III} chelate shows a strong binding affinity with human serum albumin as a result of the cooperative effects of hydrophobic interaction and coordination by donors groups on the protein.



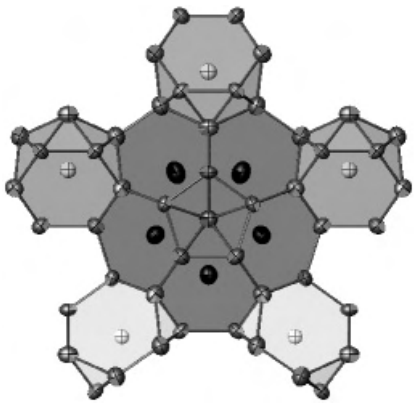
Angew. Chem. **2001**, *113*, 4873–4875

S. Aime, A. Barge, M. Botta,* A. Casnati,* M. M. Fragai, C. Luchinat, R. Ungaro 4737–4739

A Calix[4]arene Gd^{III} Complex Endowed with High Stability, Relaxivity, and Binding Affinity to Serum Albumin

Keywords: calixarenes · contrast agents · coordination chemistry · lanthanides · NMR spectroscopy

A pseudo-pentagonal kernel is the central unit in the new quaternary intermetallic phase $Li_{10}Mg_6Zn_{31}Al_3$ (see structure). This unit can form the basis for decagonal and, possibly, icosahedral quasicrystals. The synthesis, crystal structure, and bonding of $Li_{10}Mg_6Zn_{31}Al_3$ are discussed in detail.



Angew. Chem. **2001**, *113*, 4876–4878

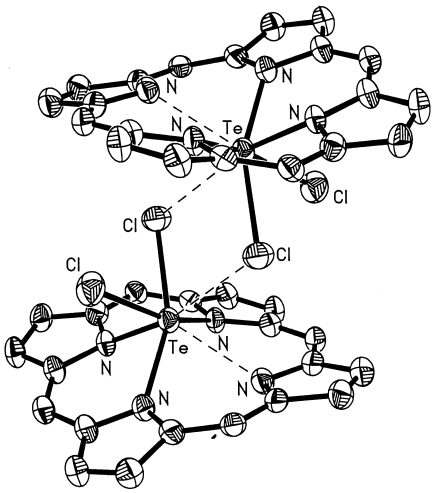
C.-S. Lee, G. J. Miller* 4740–4742

$Li_{10}Mg_6Zn_{31}Al_3$: A New Intermetallic Phase Containing Building Blocks for Decagonal Quasicrystals

Keywords: electronic structure · intermetallic phases · quasicrystals · solid-state structures

 © WILEY-VCH Verlag GmbH, D-69451 Weinheim, 2001 1433-7851/01/4024-4532 $ 17.50+.50/0

An unusual bonding mode for a porphyrin ligand is seen in the tellurium porphyrin complex prepared by treatment of $TeCl_4$ with dilithio *meso*-tetra(*p*-tolyl)porphyrin $[Li_2(ttp)]$. The structure of $[Te(ttp)Cl_2]$ (see picture) has a five-coordinate, square-pyramidal geometry involving a distorted tridentate porphyrin ligand and *cis*-dichloride ligands.



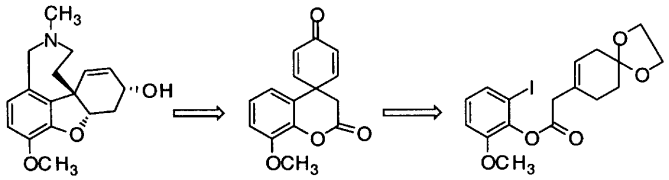
Angew. Chem. **2001**, *113*, 4879 – 4881

D. S. Grubisha, I. A. Guzei, N. Al-Salim, P. D. W. Boyd, P. J. Brothers,* L. K. Woo* ..... 4743 – 4745

Novel Coordination in the First Tellurium Porphyrin Complex: Synthesis and Crystal Structure of $[Te(ttp)Cl_2]$

Keywords: coordination chemistry · macrocyclic ligands · porphyrinoids · structure elucidation · tellurium

Intramolecular Heck reaction of **3** generates a spiro quaternary C atom—a key step in an efficient synthesis of galanthamine (**1**). Galanthamine can be readily obtained from the spiro tricyclic dienone **2**, which was prepared by nonclassical dehydrogenation of the corresponding α,β-unsaturated ketone.



1 2 3

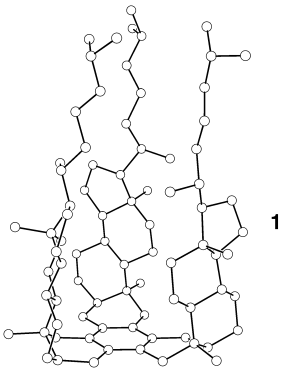
Angew. Chem. **2001**, *113*, 4881 – 4882

C. Guillou,* J.-L. Beunard, E. Gras, C. Thal* ..... 4745 – 4746

An Efficient Total Synthesis of (±)-Galanthamine

Keywords: alkaloids · Heck reaction · natural products · spiro compounds · total synthesis

Starting from coprostanone with a *cis* A/B ring fusion, the basis for a new class of enantioselective hosts has been established. The trimerization by $TiCl_4/ZnCl_2$ gave the tri-steroid **1**, a C_3-symmetric hydrocarbon that, according to X-ray analysis, contains a deep, chiral cleft.



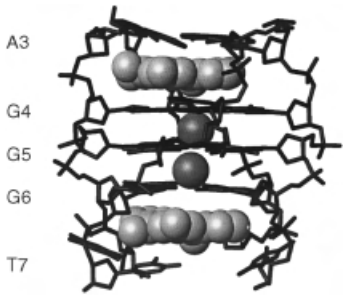
Angew. Chem. **2001**, *113*, 4882 – 4884

R. A. Pascal, Jr.,* M. S. Mathai, X. Shen, D. M. Ho ..... 4746 – 4748

Trimerization of a Steroid Ketone To Form a Chiral Molecular Cleft

Keywords: chirality · cyclotrimerization · polycycles · steroids

Guided by 24 drug – DNA NOEs, the complex formed between RHPS4 (a novel fluorinated polycyclic methylacridinium salt with potent telomerase activity) and $d(TTAGGGT)_4$ has been modeled by using MD simulations with drug molecules intercalated at the ApG and GpT steps. A low-energy structure for the 2:1 complex has a partial positive charge on the acridine 13-N atom (which acts as a pseudo potassium ion) positioned above the center of the G-tetrad (see picture).



Angew. Chem. **2001**, *113*, 4885 – 4887

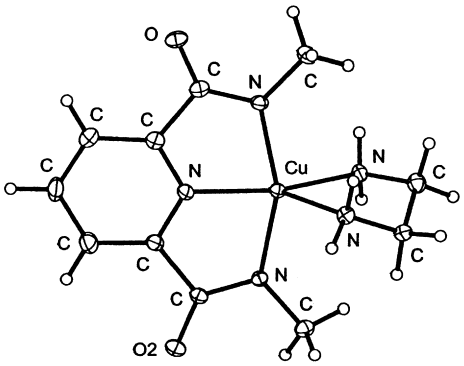
E. Gavathiotis, R. A. Heald, M. F. G. Stevens, M. S. Searle* ..... 4749 – 4751

Recognition and Stabilization of Quadruplex DNA by a Potent New Telomerase Inhibitor: NMR Studies of the 2:1 Complex of a Pentacyclic Methylacridinium Cation with $d(TTAGGGT)_4$

Keywords: DNA recognition · G-quadruplex · NMR spectroscopy · telomerase

 © WILEY-VCH Verlag GmbH, D-69451 Weinheim, 2001 1433-7851/01/4024-4533 $ 17.50+.50/0

Acetonitrile might not be an "innocent" solvent after all: The monomeric Cu^{II} complex [Cu(dmppy)(en)] (see structure) readily cleaves the C–C bond of acetonitrile under ambient conditions. Previously, heterolytic cleavage of the C–C bond of acetonitrile had only been achieved by phosphane complexes of metals in low oxidation states. $dmppyH_2$ = *N*,*N*′-dimethylpyridine-2,6-dicarboxamide, en = ethylenediamine.



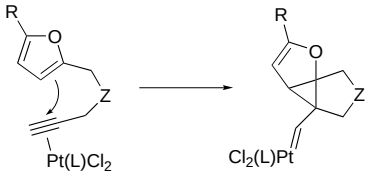
Angew. Chem. **2001**, *113*, 4888 – 4890

D. S. Marlin, M. M. Olmstead, P. K. Mascharak* ..... 4752 – 4754

Heterolytic Cleavage of the C–C Bond of Acetonitrile with Simple Monomeric Cu^{II} Complexes: Melding Old Copper Chemistry with New Reactivity

Keywords: acetonitrile · cleavage reaction · copper · cyanides · N ligands

A platinum cyclopropyl carbene complex, formed by *anti* attack of the furan ring on an (η^2-alkyne)platinum complex (see scheme), is the key intermediate in the intramolecular reaction of furans with alkynes according to experimental studies and density functional calculations.



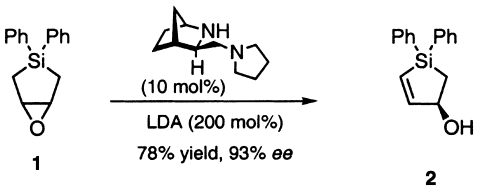
Angew. Chem. **2001**, *113*, 4890 – 4893

B. Martín-Matute, D. J. Cárdenas, A. M. Echavarren* ..... 4754 – 4757

Pt^{II}-Catalyzed Intramolecular Reaction of Furans with Alkynes

Keywords: alkynes · cycloaddition · density functional calculations · heterocycles · platinum

A versatile precursor for the assembly of a range of polyol-containing fragments is the silacyclic alcohol **2** that results from the highly enantioselective, catalytic isomerization of diphenylsilacyclopentene oxide (**1**). The use of this precusor is illustrated with the efficient and highly diastereoselective assembly of acyclic tetraol motifs.



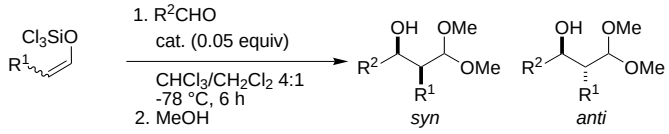
Angew. Chem. **2001**, *113*, 4893 – 4895

D. Liu, S. A. Kozmin* ..... 4757 – 4759

Catalytic Enantioselective Isomerization of Silacyclopentene Oxides: New Strategy for Stereocontrolled Assembly of Acyclic Polyols

Keywords: amides · base catalysis · epoxides · polyols · silanes

The most basic of aldol constructions, namely the controlled stereoselective self-condensation of aldehydes, has finally found a general solution. Geometrically defined trichlorosilyl enolates of aldehydes display excellent reactivity, near perfect diastereoselectivity, and good (albeit variable) enantioselectivity in their addition to a wide range of aldehydes under catalysis by a chiral bisphosphoramide (see scheme).



Angew. Chem. **2001**, *113*, 4895 – 4898

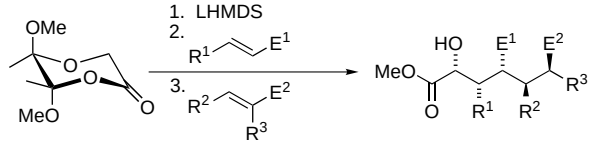
S. E. Denmark,* S. K. Ghosh ..... 4759 – 4762

The First Catalytic, Diastereoselective, and Enantioselective Crossed-Aldol Reactions of Aldehydes

Keywords: aldol reaction · diastereoselectivity · enantioselectivity · Lewis base catalysis

 © WILEY-VCH Verlag GmbH, D-69451 Weinheim, 2001 1433-7851/01/4024-4534 $ 17.50+.50/0

Up to five new stereogenic centers (see **2**) can be formed in one-pot consecutive three- and four-component coupling reactions starting from a butane diacetal desymmetrized glycolic acid derivative **1**. Highly functionalized α-hydroxy acid derivatives are obtained in an easy, fast, clean, and efficient way. LHMDS = lithium hexamethyldisilazide.



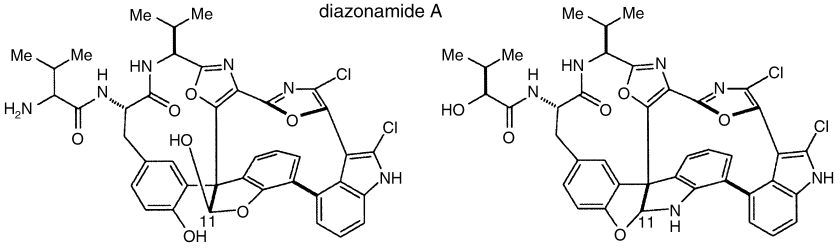
Angew. Chem. **2001**, *113*, 4899 – 4901

D. J. Dixon, S. V. Ley,*
F. Rodríguez ..... 4763 – 4765

Consecutive Three- and Four-Component Coupling Reactions with Anions Generated from a Butane Diacetal Desymmetrized Glycolic Acid Derivative

Keywords: acetals · asymmetric synthesis · C–C coupling · Michael addition · synthetic methods

Unable to bear the weight of scrutiny, the original structure proposed for (−)-diazonamide A (**1**) must be revised. A convergent, stereocontrolled total synthesis provided **1**, which shows altered physical and spectroscopic characteristics relative to those of a sample of the natural product. Reinterpretation of reported data and new insight indicate that the actual structure of diazonamide A is the aminal-containing (*S*)-α-hydroxy isovaleric acid conjugate **2**. Gratifyingly, a synthetic C11 acetal congener of **2** is, by all biological measures examined, similarly potent and functionally equivalent to the antimitotic natural product.



Angew. Chem. **2001**, *113*, 4901 – 4904

J. Li, S. Jeong, L. Esser, P. G. Harran* ..... 4765 – 4769

Total Synthesis of Nominal Diazonamides—Part 1: Convergent Preparation of the Structure Proposed for (−)-Diazonamide A

Angew. Chem. **2001**, *113*, 4905 – 4909

J. Li, A. W. G. Burgett, L. Esser, C. Amezcua, P. G. Harran* 4770 – 4773

Total Synthesis of Nominal Diazonamides—Part 2: On the True Structure and Origin of Natural Isolates

Keywords: antitumor agents · natural products · photochemistry · rearrangements · total synthesis

Supporting information on the WWW (see article for access details).

* Author to whom correspondence should be addressed

SERVICE

• **VIPs**	**4522**	• **Authors**	**4775**
• ***Angewandte's* Sister-Journals**	**4539 – 4541**	• **Preview**	**4776**
• **Vacancies**	**A143**	• **Indexes**	**4779**
• **Keywords**	**4774**		

Issue 23, 2001 was published online on November 28

Don't forget all the Tables of Contents from 1998 onwards may be still found on the WWW under: http://www.angewandte.com

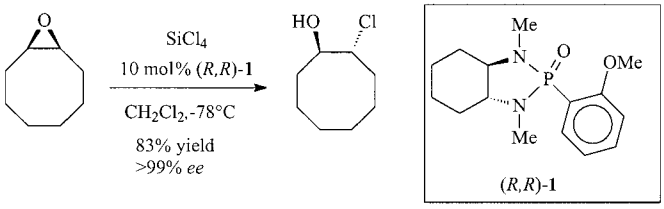
 © WILEY-VCH Verlag GmbH, D-69451 Weinheim, 2001 1433-7851/01/4024-4535 $ 17.50+.50/0

WITHDRAWAL

On the Beneficial Effect of *ortho*-Methoxy Groups in the Asymmetric Ring Opening of *meso* Epoxides with Silicon Tetrachloride Catalyzed by Chiral *ortho*-Methoxyphenyldiazaphosphonamide Lewis Bases**

Gérard Buono*

We published in this journal a communication on the enantioselective opening of *meso* epoxides with silicon tetrachloride in the presence of a catalytic amount of chiral phosphonamides.[1] In that paper we reported the asymmetric ring opening of cyclooctene oxide with $SiCl_4$ in the presence of 10 mol% of chiral phophonamide base (*R*,*R*)-**1** as a catalyst (Scheme 1).



Scheme 1.

For this reaction, we described up to 83% yield and enantiomeric excess higher than 99%. This spectacular result attracted the attention of Professor Scott E. Denmark, who pioneered this research field,[2] because it was found that cyclooctene oxide is one of the slowest acting epoxides in this catalytic system and produced the racemic chlorohydrin. However, Denmark et al. did not succeed in reproducing the results we disclosed and submitted a rebuttal to our paper.[3] We were then contacted by the Editor and Prof. Denmark and prompted to elucidate the origin of such a striking discrepancy. At this stage, I asked my co-workers[4] to check the experimental procedures and analytical conditions and to try to reproduce the described results. I was provided with experimental data and material that fully confirmed our original claims. On the basis of these results we sent a first answer to the rebuttal published in *Angewandte Chemie*, an answer that could not explain why our observation differed from Prof. Denmark's. One month later, we received a letter from the Editor who required further complementary analytical data and information. When I had these new data from my co-workers in hand, I noticed several inconsistencies with the analytical material they had previously provided. Therefore, I decided to reproduce *personally* and *independently* the whole experimental procedures from the very beginning. I was unable to observe the opening of cyclooctene oxide under the described conditions and to reproduce the analytical data (for example, NMR, retention times in chiral GPC and HPLC analyses) provided by my co-workers. Instead, I obtained results similar to those reported by Denmark et al. in their rebuttal.[3] A cross-check undertaken by several colleagues led to identical results. To date, my co-workers[4] have been unable to provide an appropriate scientific rationale for the non-reproducibility of the former results and analyses. Under these circumstances, although our communication presented several other *meso* epoxide openings with fair to high enantioselectivities, which require experimental verification, I wish to withdraw that communication.[1] Other pieces of work based on related experimental results that were published elsewhere will also be withdrawn.[5, 6]

[*] Prof. Dr. G. Buono
UMR CNRS 6516, Faculté de St Jérôme
ENSSPICAM, Avenue Escadrille Normandie Niemen
13397 Marseille, Cedex 20 (France)
Fax: (+33) 4-91-02-77-76
E-mail: buono@spi-chim.u-3mrs.fr

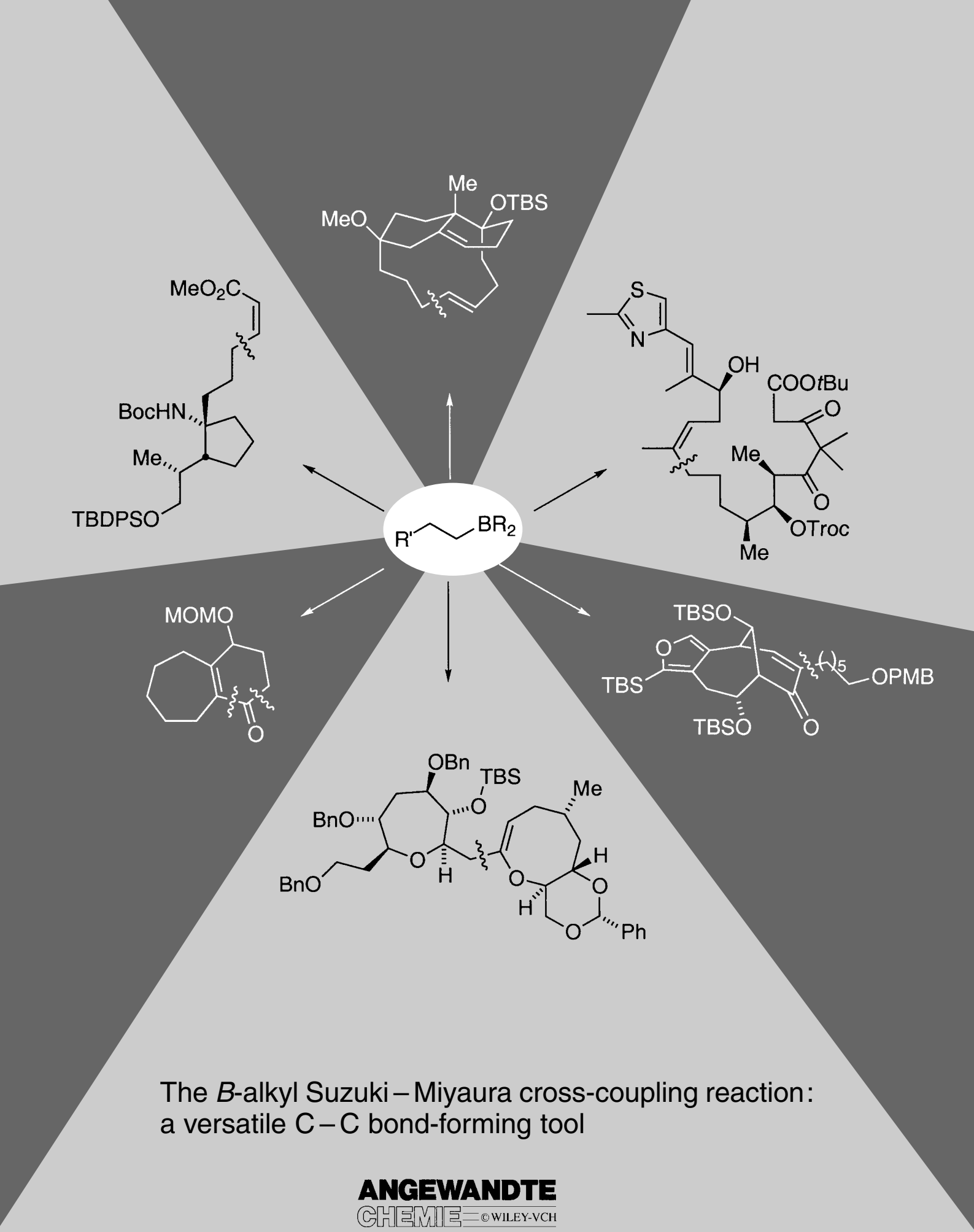
[**] A Response to the correspondence by Professor Scott E. Denmark et al.[3]

[1] J. M. Brunel, O. Legrand, S. Reymond, G. Buono, *Angew. Chem.* **2000**, *112*, 2654; *Angew. Chem. Int. Ed.* **2000**, *39*, 2554.
[2] S. E. Denmark, P. A. Barsanti, K.-T. Wong, R. A. Stavenger, *J. Org. Chem.* **1998**, *63*, 2428.
[3] S. E. Denmark, T. Wynn, B. G. Jellerichs, *Angew. Chem.* **2001**, *113*, 2315; *Angew. Chem. Int. Ed.* **2001**, *40*, 2255.
[4] Except O.L. who left my group in July 1999.
[5] S. Reymond, J. M. Brunel, G. Buono, *Tetrahedron: Asymmetry* **2000**, *11*, 4441.
[6] S. Reymond, O. Legrand, J. M. Brunel, G. Buono, *Eur. J. Org. Chem.* **2001**, 2819.

APOLOGY

In the Communication "A Lewis Acid Catalyst Anchored on Silica Grafted with Quaternary Alkylammonium Chloride Moieties" by **M. V. Landau et al**. the authors made no reference to their thematically related communication "A comparative study of an MCM-41 anchored quaternary ammonium chloride/$SnCl_4$ catalyst and its silica gel analogue" (T. M. Jyothi, M. L. Kaliya, M. Herskowitz, M. V. Landau, *Chem. Commun.* **2001**, 992–993) and vice versa, even though both manuscripts were submitted to their respective journals at the same time. The authors apologize for this oversight.

 © WILEY-VCH Verlag GmbH, D-69451 Weinheim, 2001 1433-7851/01/4024-4536 $ 17.50+.50/0



The *B*-alkyl Suzuki–Miyaura cross-coupling reaction: a versatile C–C bond-forming tool

ANGEWANDTE
CHEMIE
© WILEY-VCH

The *B*-Alkyl Suzuki–Miyaura Cross-Coupling Reaction: Development, Mechanistic Study, and Applications in Natural Product Synthesis**

Sherry R. Chemler, Dirk Trauner, and Samuel J. Danishefsky*

Dedicated to Professor Akira Suzuki

The development of new reactions that facilitate the creative and efficient synthesis of molecular structures with desirable properties continues to fascinate chemists. The test of a significant contribution is its acceptance over time by the scientific community. The *B*-alkyl Suzuki–Miyaura cross-coupling reaction appears to be one such reaction. Since its disclosure by Suzuki and Miyaura in 1986, this reaction has been an attractive solution to challenging synthetic problems.

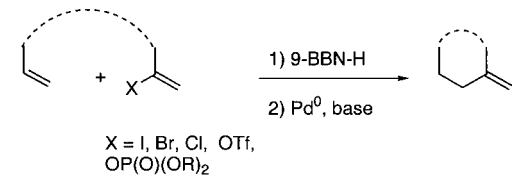
Keywords: boranes · C–C coupling · cross-coupling · Suzuki–Miyaura coupling · synthetic methods

1. Introduction

Transition metal mediated cross-coupling reactions have revolutionized organic synthesis. Many highly efficient and mild protocols for bond construction have emerged by mastery of such reactions, particularly in multifunctional settings.[1, 2] Perhaps the most utilized C–C bond-forming cross-coupling reactions are the Heck,[1] Stille,[3, 4] and Suzuki–Miyaura reactions.[5, 6] In recent years, the olefin metathesis reaction has also emerged as a particularly powerful method, especially for ring formation.[7–12] The *B*-alkyl Suzuki–Miyaura reaction is distinguished from other Suzuki–Miyaura cross-coupling reactions in that a reaction occurs between an alkyl borane (as opposed to a vinyl or aryl borane) and an aryl or vinyl halide, triflate, or enol phosphate. We will show that this important variation, which involves an sp^3 carbon in the coupling event, fills a growing niche. This reaction, which occurs in the presence of a base and a Pd^0 catalyst, was first reported by Suzuki and Miyaura in 1986.[13]

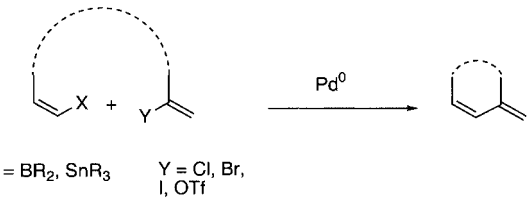
The various transformations that are accessible through these valuable cross-coupling methods are depicted in Equations (1)–(4) (the dashed lines represent intramolecular variations).

B-alkyl Suzuki–Miyaura reaction



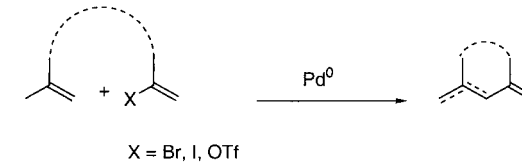
(1)

Suzuki–Miyaura, Stille reactions



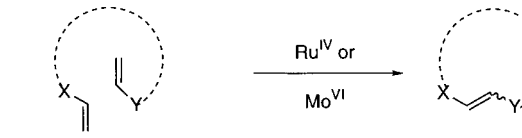
(2)

Heck reaction



(3)

olefin metathesis



(4)

[*] Prof. S. J. Danishefsky, Dr. S. R. Chemler
Laboratory of Bioorganic Chemistry, Sloan-Kettering Institute for Cancer Research
1275 York Ave., Box 106, New York, NY 10021
Fax: (+1) 212-772-8691
E-mail: s-danishefsky@ski.mskcc.org
and
Department of Chemistry, Columbia University
Havemeyer Hall, New York, NY 10027 (USA)
Prof. D. Trauner
Department of Chemistry, University of California, Berkeley
Berkeley, CA 94720 (USA)

[**] A list of abbreviations can be found at the end of the article.

 © WILEY-VCH Verlag GmbH, D-69451 Weinheim, 2001 1433-7851/01/4024-4545 $ 17.50+.50/0

Other cross-coupling methods for $C(sp^3)-C(sp^2)$ bond formation are available,[1, 2, 14] most notably the Negishi protocol,[15–19] which utilizes an alkylzinc derivative as the organometallic component. By comparison, the strength of the *B*-alkyl Suzuki–Miyaura cross-coupling lies in the mild and versatile methods for the synthesis of the alkyl borane component, the ease of incorporation of nontransferable boron ligands, and the manageable toxicity of the boron-derived by-products (e.g. $R_2B(OH)_2^-$).[20] Another advantage of this reaction over similar methods is its tolerance of water, which is often a beneficial additive.

Our interest in the *B*-alkyl Suzuki–Miyaura reaction first emerged in our program involving the synthesis of natural products with challenging structures. As will be demonstrated in Section 11, we have often found this reaction to be a rather valuable resource for the coupling of complex molecular fragments. In this review, a detailed account of the mechanism of the *B*-alkyl Suzuki–Miyaura reaction is presented. Factors that affect its rate, and thereby its efficiency, are summarized. The application of this coupling method to the development of new synthetic protocols as well as illustrations of its growing use in natural product synthesis are highlighted.

2. Synthesis of the Alkyl borane Component

The alkyl borane component of the *B*-alkyl Suzuki reaction can be derived from the hydroboration of the corresponding olefin [Eqs. (5) and (6)][21] or, less frequently, from the alkylation of a boron-based electrophile with an alkyllithium or Grignard reagent [Eqs. (7) and (8)].[22–24] More generally one takes advantage of the fact that alkyl boranes can be synthesized in a highly chemo-, regio-, and diastereoselective manner by means of the hydroboration reaction. In the hydroboration route, the terminal alkyl borane regioisomer is the highly favored adduct (anti-Markovnikov addition). The


S. J. Danishefsky

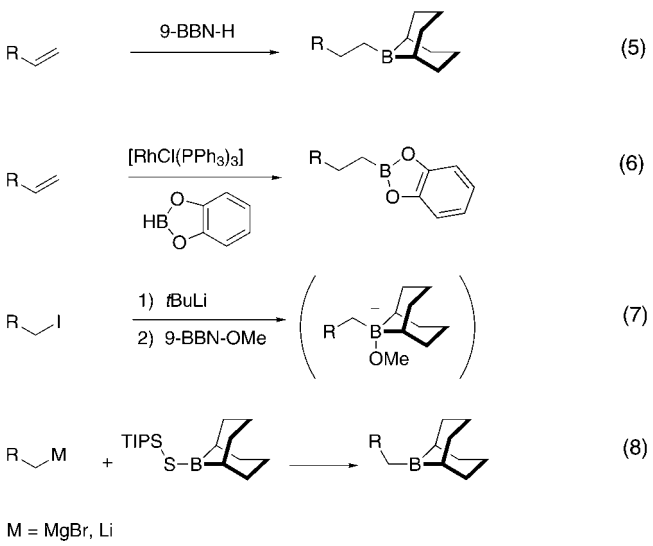

S. R. Chemler


D. Trauner

Samuel J. Danishefsky was born in 1936. Under the tutelage of his father, he was exposed at an early age to the elements of logical though and critical analysis through the study of the Talmud. He received a B.S. degree at Yeshiva University (1956). In keeping with the example of an older brother, Isadore, he took an interest in chemistry at college. A life-long fascination with organic chemistry followed from absorption of two introductory treatments of the subject–one by Rayond Brewster and the other by Louis and Mary Fieser. This exposure led him to pursue organic studies at Harvard University where he received a Ph.D. (1962) under the direction of Professor Peter Yates. From 1961–1963 he was an NIH-sponsored Postdoctoral Fellow at Columbia University under the mentorship of Gilbert Stork. His first independent academic position, which started in 1963, was at the University of Pittsburgh where he became Professor in 1971 and University Professor in 1979. In 1980 he moved to Yale University and served as chairman of the department from 1981–1987. He was named Eugene Higgins Professor in 1984 and Sterling Professor in 1990. In 1993 he returned to New York as Professor of Chemistry at Columbia University and as Kettering Professor and first Head of the Laboratory for Bioorganic Chemistry at the Memorial Sloan–Kettering Cancer Center. His research interests have been in the areas of synthetic strategy, cytotoxic natural products, and, most recently, fully synthetic carbohydrate-based tumor antigens. In 1996 he shared the Wolf Prize in Chemistry with Gilbert Stork.

Sherry R. Chemler was born in Chicago, Illinois, in 1972. She received a B.A. from Boston University in 1994 and a Ph.D. in 1999 from Indiana University. Her doctoral research, under the guidance of Prof. William R. Roush, focused on the development of methodology for the synthesis of polypropionate-derived natural products. As an NIH Postdoctoral Fellow with Professor Danishefsky at the Memorial Sloan–Kettering Cancer Center, she has undertaken the total synthesis of phomactin A. Her research interests include the design and study of novel chemical reactions and the synthesis of molecules with beneficial functional properties.

Dirk Trauner was born in Linz, Austria, in 1967. He received his Diplom in 1994 from the Freie Universität in Berlin, Germany. In 1997 he obtained a Ph.D. from the University of Vienna, Austria, where he worked with Professor Johann Mulzer on the synthesis of alkaloids. He held an Ernst Schering Research Foundation postdoctoral fellowship at the Memorial Sloan–Kettering Cancer Center, where he completed a synthesis of halichlorine under the supervision of Professor Danishefsky. He is currently an assistant professor of chemistry at the University of California, Berkeley. His interests include neurochemistry, the total synthesis of biologically active natural products, and the development of new synthetic methods based on transition metal catalysis.



rate of hydroboration is sensitive to electronic as well as steric factors, although steric effects tend to predominate. Electron-rich, unhindered olefins generally react most rapidly. Thus, a substrate that contains two different olefin moieties often undergoes hydroboration at one double bond, with a high degree of selectivity (Figure 1).[25–27]

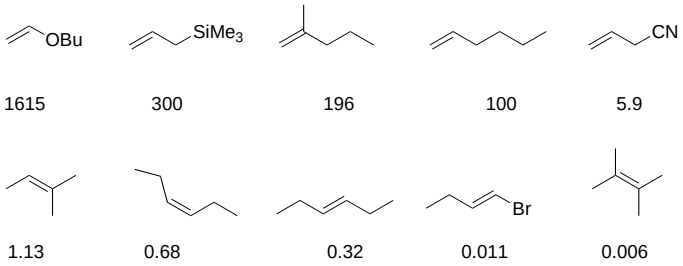


Figure 1. Relative rate of hydroboration with 9-BBN-H.

3. Catalytic Cycle

As in other cross-coupling reactions, the catalytic cycle of the Suzuki–Miyaura reaction is thought to involve a sequence consisting of an oxidative addition, a transmetalation, and a reductive elimination (Figure 2).[5, 28]

The oxidative addition is often the rate-limiting step in a cross-coupling catalytic cycle. Under appropriate reaction conditions, alkenyl, alkynyl, allyl, benzyl, aryl, and alkyl halides may participate in the Suzuki–Miyaura cross-coupling reaction. Aryl and 1-alkenyl halides that are activated by electron-withdrawing groups are more reactive to the oxidative addition step than those with electron-donating groups. Through a competition reaction, Oh-e et al. found bromobenzene to be 2.2 times more reactive than phenyl triflate as a coupling partner in the *B*-alkyl Suzuki reaction with 9-octyl-9-BBN, whereas iodobenzene was consumed exclusively in the presence of phenyl triflate.[29] In a separate study, Molander and Ito determined that the reaction of *p*-ClC_6H_4OTf with a benzyl borate led to exclusive coupling at the triflate position.[20] Therefore, the order of reactivity of the electrophilic partner has been established as:[30]

$$I \gg Br > OTf \gg Cl$$

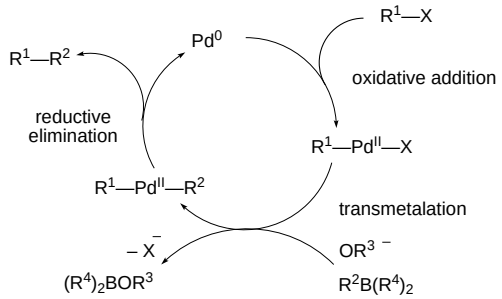


Figure 2. General Suzuki–Miyaura catalytic cycle.

Although alkyl halides that have a hydrogen atom in the β position are considered to be problematic substrates as a result of potentially competing β-hydride elimination processes,[5] $C(sp^3)$–$C(sp^3)$ and carbonylative coupling reactions of alkyl iodides with alkyl boranes have been reported.[31, 32, 101] The nature of the organoborane, the aryl, vinyl, or alkyl halide, the palladium catalyst, and the base all influence the overall rate of the cross-coupling reaction.[33–37]

4. Experimental Factors that Affect the *B*-Alkyl Suzuki–Miyaura Reaction

In the initial reaction development reports, Suzuki and coworkers surveyed various conditions (solvent, base, temperature, and catalyst) for the cross-coupling reaction of *B*-octyl-9-BBN with iodobenzene (Table 1).[13, 21]

4.1. Influence of the Catalyst

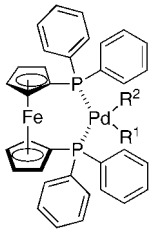
Substoichiometric amounts (3 mol%) of $[PdCl_2(dppf)]$ or $[Pd(PPh_3)_4]$ were found to be viable catalysts for the *B*-alkyl Suzuki–Miyaura reaction (Table 1). Subsequent to these initial studies, complexes with an electron-rich Pd^0 center, or precursors thereof, continued to be the most widely used catalysts for this reaction.[5]

Table 1. Cross-coupling reactions of *B*-octyl-9-BBN with iodobenzene under varying conditions.[a]

Entry	Catalyst	Base [equiv]	Solvent	Temp. [°C]	Yield [%]
1	$[PdCl_2(dppf)]$	NaOH (3)	THF/H_2O (5:1)	65	99
2	$[PdCl_2(dppf)]$	TlOH (1.5)	THF/H_2O (5:1)	20	79
3	$[PdCl_2(dppf)]$	NaOMe (1.5)	THF	65	98
4	$[PdCl_2(dppf)]$	NaOMe (1.5)	THF/MeOH (5:1)	65	18
5	$[PdCl_2(dppf)]$	K_2CO_3 (2)	DMF	50	98
6	$[PdCl_2(dppf)]$	K_3PO_4 (2)	DMF	50	94
7	$[Pd(PPh_3)_4]$	NaOH (3)	THF/H_2O (5:1)	65	84
8	$[Pd(PPh_3)_4]$	NaOH (3)	Benzene/H_2O	80	97

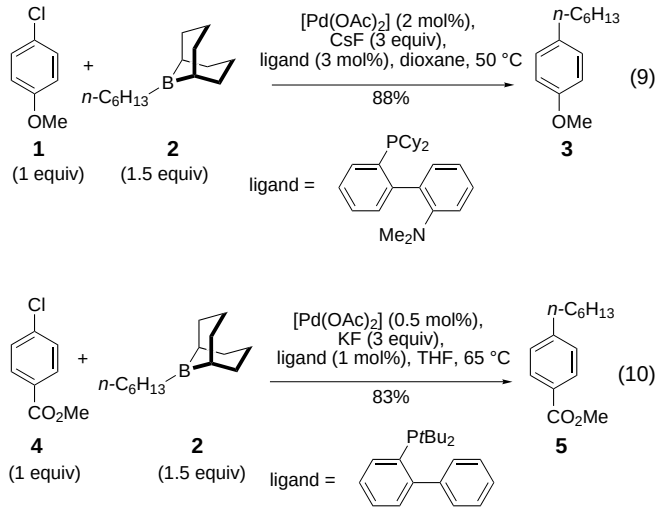
[a] Reactions were carried out for 16 h with 3 mol% catalyst.

One problem commonly associated with the coupling reactions of organometallic compounds that are metalated at sp^3 C atoms and that possess hydrogen atoms in the β position, is the proclivity of the alkyl–palladium complex to undergo β-hydride elimination instead of reductive elimination.[13] The bidentate bis(diphenylphosphino)ferrocene ligand on the palladium catalyst [$PdCl_2$(dppf)] is thought to help favor reductive elimination by enforcing a *cis* geometry between the vinyl and alkyl groups on the square-planar Pd^{II} complex. Thus, this catalyst would be most effective if the reductive elimination process is part of the rate-determining step in the coupling reaction. (If the reactive groups are initially *trans* to each other on the Pd^{II} complex, the complex must rearrange to a *cis* geometry before reductive elimination can occur.) The "bite angle" of the bidentate ligand also affects the rate of the reductive elimination: a large bite angle of the ligand forces the two alkyl groups closer to each other about the Pd^{II} center, thus promoting the reductive elimination process.[35]



Recent studies by Buchwald and co-workers on the effects of ligand structure on the rate of oxidative addition have led to the development of reaction protocols that enable the coupling of alkyl boranes with aryl chlorides. These were previously an unreactive class of substrates [(Eqs. (9) and (10)].[38, 39]

Fürstner and Leitner have also developed a ligand for such coupling partners.[40]



4.2. Influence of the Base and Solvent

A carefully selected base is essential in the projected applications of the *B*-alkyl Suzuki–Miyaura reaction. The base has been proposed to be involved in several steps of the catalytic cycle, most notably the transmetalation process (see Section 5). Miyaura and co-workers found that stronger bases such as NaOH, TlOH, and NaOMe performed well in THF/H_2O solvent systems, whereas weaker bases such as K_2CO_3 and K_3PO_4 were more successful in DMF (Table 1).[13, 21] These reactions were generally conducted at 50–80 °C, although the use of TlOH as the base made the reaction viable at 20 °C (Tl_2CO_3 and TlOEt are commercial available and are thus more commonly used than TlOH). Other research groups have subsequently introduced their own variations on the reaction conditions (base, solvent, ligand additives) in their applications of this reaction to methodologies and natural product syntheses (see Sections 7–11).

4.3. Influence of the Borane Substituents

Generally, unhindered electron-rich organoboranes and electron-deficient vinyl or aryl halides or triflates are the most reactive partners for the *B*-alkyl Suzuki reaction. A survey on the effect of various borane substituents on the coupling reaction is presented in Table 2.[21, 41] A variety of hydroborating reagents such as 9-BBN-H, disiamylborane, dicyclohexylborane, and borane can be used in this reaction (Table 2, entries 1–4), although 9-BBN-H is the most commonly used. The rate of transmetalation of a primary alkyl group on boron is much higher than that of a secondary alkyl group. The coupling reactions between secondary alkyl boron compounds and iodobenzene can occur in moderate yields when

Table 2. Coupling of iodobenzene with alkyl boranes.[a]

Entry	Organoborane	Base (equiv)	Solvent	Yield [%][b]
1		NaOH (3)	THF/H_2O	99
2		NaOH (3)	THF/H_2O	82
3		NaOH (3)	THF/H_2O	93
4		NaOH (3)	THF/H_2O	98
5		KOH (3)	THF/H_2O	40[c]
6		KOH (3)	THF/H_2O	65[c]
7		KOH (3)	THF/H_2O	55[c]
8		KOH (3) Tl_2CO_3 (1.5) TlOH (3)	THF/H_2O THF Benzene/H_2O	75 60 93[d]
9		KOH (3) TlOEt (3) Tl_2CO_3 (1.5) TlOH (3)	THF/H_2O THF/H_2O THF Benzene	trace 41 93 84[e]
10		TlOH (3) Tl_2CO_3 (1.5)	THF/H_2O THF	34 trace
11	octyl–B(OH)$_2$	TlOH (3)	THF/H_2O	trace

[a] Reactions were carried out at 50 °C with [$PdCl_2$(dppf)] catalyst (3 mol %), organoborane (1.1 equiv), and iodobenzene (1.0 equiv) unless otherwise noted. [b] yields (GC) based on iodobenzene. [c] Biphenyl was also obtained as a by-product (10–30 %). [d] [$PdCl_2$(dppe)] was used as the catalyst. [e] [$PdCl_2$(dppf)] was used as the catalyst.

aqueous KOH (3 M) is used as the base (Table 2, entries 5–7). However, there are no examples of *B*-alkyl Suzuki reactions that involve secondary alkyl boranes in preparative synthetic organic chemistry.

Alkyl boronic esters can also be viable substrates in the Suzuki reaction when thallium salts such as TlOH or Tl_2CO_3 are used as the base (Table 2, entries 8–11).[41] In contrast, other bases such as KOH are ineffective in these reactions. The special rate-enhancing effect of thallium salts in the $C(sp^2)$–$C(sp^2)$ Suzuki reaction was first observed by Kishi and co-workers.[42] Thallium salts have since provided a useful solution for difficult Suzuki couplings in numerous instances.[5, 43–45] Unfortunately, the toxicity of the thallium salts restricts their widespread use.

5. Reaction Mechanism of the Suzuki–Miyaura Reaction

5.1. Stereochemistry of the Oxidative Addition

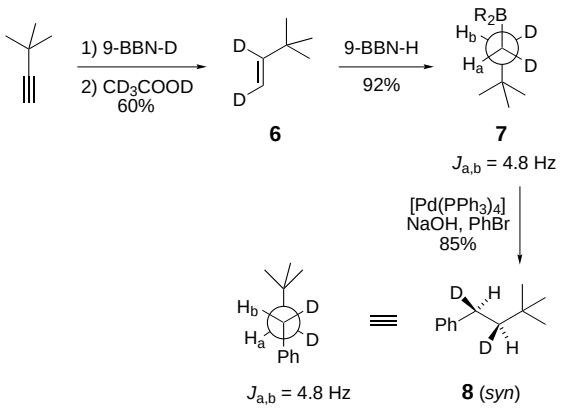
The oxidative addition process in the Suzuki–Miyaura cross-coupling reaction is thought to proceed through the broadly applicable mechanistic framework that accompanies many other cross-coupling processes. The oxidative addition of alkyl and alkenyl halides occurs with retention of configuration, whereas inversion of configuration is observed in the case of allylic and benzylic halides.[2, 31, 46, 47]

5.2. Stereochemistry of the Transmetalation Step

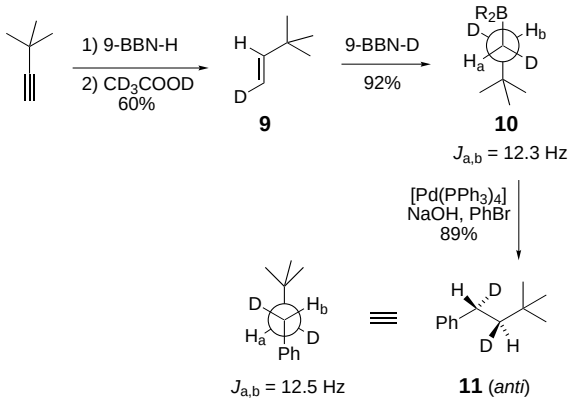
Independent studies by the groups of Soderquist[33] and Woerpel[34] revealed that transmetalation (R–B →R–Pd) occurs with retention of stereochemistry. Both groups used an NMR spectroscopic technique that takes advantage of the preference of bulky substituents on 1,2-disubstituted ethanes to adopt an antiperiplanar conformation.[48] The stereochemistry can then be determined by analysis of the coupling constants of the vicinal protons.

Soderquist and co-workers prepared the known *syn* and *anti* derivatives of *t*BuCHDCHDPh, **8** and **11** (Schemes 1 and 2).[49] Hydroboration of 3,3-dimethyl-1-butyne with 9-BBN-D, followed by treatment with CD_3CO_2D gave the dideuterated olefin **6**. Subsequent hydroboration of **6** with 9-BBN-H followed by Suzuki coupling with PhBr gave **8**, whose H_a–H_b coupling constant of 4.8 Hz is consistent with *syn* stereochemistry (Scheme 1). Hydroboration is a *syn* addition process,[50] and reductive elimination of the Pd intermediate is known to occur with retention of stereochemistry.[51] Soderquist and co-workers thus concluded that the transmetalation step also occurs with retention of stereochemistry. By reversing the order in which the reagent is added, the *anti* isomer **11** was produced; the H_a–H_b coupling constant of 12.5 Hz confirms that transmetalation occurred with retention of configuration (Scheme 2).

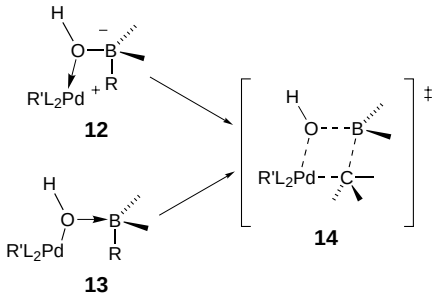
Soderquist and co-workers argued that the four-centered μ_2-hydroxo-bridged transition state model **14** (Scheme 3) is consistent with a transmetalation that proceeds with retention



Scheme 1. Soderquist and co-workers demonstrated that hydroboration of a *cis* dideuterated olefin followed by cross-coupling gives a *syn* adduct.

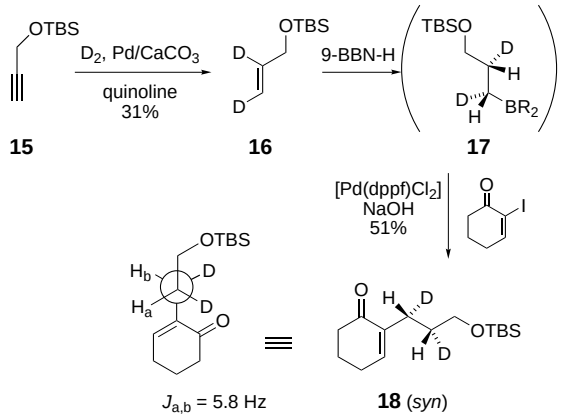


Scheme 2. The hydroboration of a *trans* dideuterated olefin followed by cross-coupling gives the *anti* adduct. These studies show that transmetalation occurs with retention of configuration at the carbon atom.

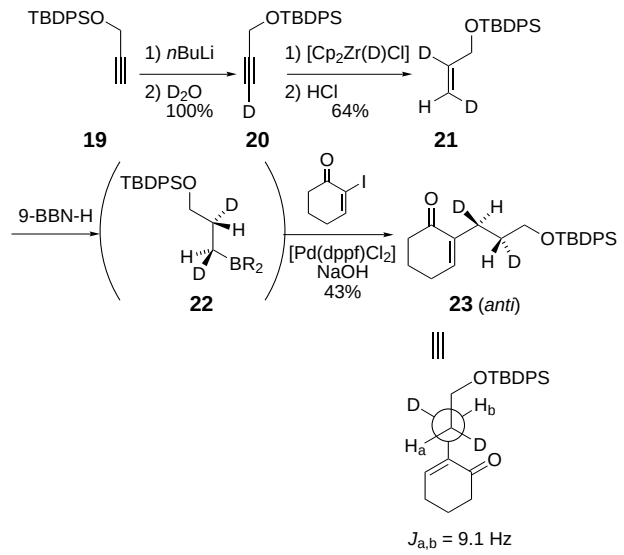


Scheme 3. Mechanism of the transmetalation.

of configuration. The transition state can arise from either the hydroxyborate–palladium complex **12** or the borane–palladium hydroxide complex **13**. Both structures had previously been suggested as possible intermediates by Miyaura and Suzuki.[5] Soderquist and co-workers determined that the mechanism depends on the Lewis acidity of the organoborane (see Section 5.3). In a concurrent and similar study, Woerpel and Ridgway also concluded that transmetalation occurs with retention of stereochemistry (Schemes 4 and 5).



Scheme 4. Woerpel and co-workers also demonstrated that the hydroboration of a *cis*-dideuterated olefin followed by cross-coupling gives a *syn* adduct.

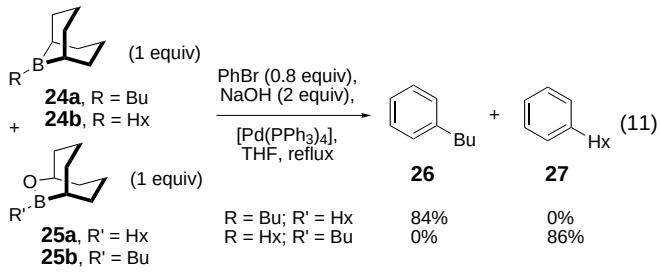


Scheme 5. The hydroboration of a *trans* dideuterated olefin followed by cross-coupling provides the *anti* adduct. These studies also demonstrate that transmetalation occurs with retention of configuration at the carbon atom.

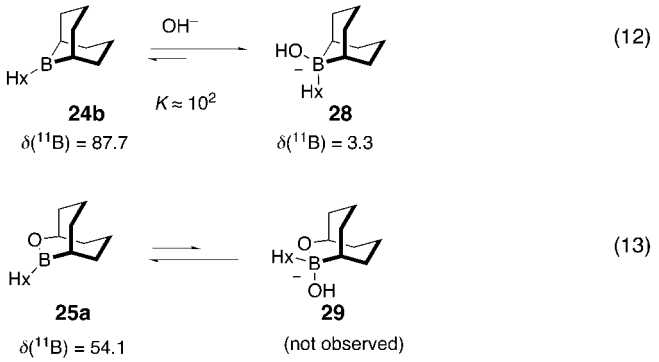
5.3. Role of the Boron Substituents in the Coupling Process

To evaluate the effects of the boron substituents on the rate of the coupling reaction, Soderquist and co-workers performed a competition experiment between the *B*-alkyl-9-BBN derivative **24** and its *B*-alkyl OBBD counterpart **25** [Eq. (11)]. The 9-BBN derivative **24** was found to be significantly more reactive than the R-OBBD derivative **25**, as shown by the exclusive formation of phenylbutane (**26**) in an experiment in which **24a** (R = butyl) and **25a** (R′ = hexyl) competed for bromobenzene. This finding was supported by the exclusive formation of phenylhexane (**27**) in the analogous competition reaction with **24b** (R = hexyl) and **25b** (R′ = butyl).

Soderquist and co-workers hypothesized that the difference in reactivity between the two boranes was related to their different Lewis acidity. This proposal was tested by the study



of the borane ⇄ borate equilibria [Eqs. (12) and (13)]. The boranes were titrated with NaOH and the changes in chemical shift in their ^{11}B NMR spectra were noted. It was found that one equivalent of NaOH shifts the ^{11}B NMR signal of the



9-BBN derivative **24b** from $\delta = 87.7$ to $\delta = 12.0$, two equivalents causes a shift to $\delta = 6.0$, and three equivalents shifts the signal to $\delta = 3.3$ (the spectrum did not change with additional NaOH). In contrast, titration of the OBBD derivative **25a** with NaOH led to no observable change in the ^{11}B NMR spectrum. These studies support the assertion that the 9-BBN derivative **24b** is much more Lewis acidic than **25a**. Thus, under the Suzuki reaction conditions, it is highly probable that the species involved in the transmetalation step in the case of **24b**, is its corresponding borate **28**, whereas the OBBD species **25a** is probably involved in the transmetalation step, rather than its borate derivative **29**. This then implies that transmetalation of the 9-BBN derivative **24a** occurs via intermediate **12**, whereas the transmetalation of the OBBD derivative **25a** occurs via **13** (Scheme 3).

5.4. Role of Base in the Coupling Process

Soderquist and co-workers have shown that the base is involved in as many as five mechanistically distinct events in the *B*-alkyl Suzuki reaction. Arguably the most essential role of the base is the conversion of the alkyl 9-BBN species into the more reactive borate species [R-9-BBN-OH]$^-$. The other four roles include: 1) hydrolysis of the $Pd^{II}X$ intermediate to the more reactive $Pd^{II}OH$ species; 2) complexation of $HOBR_2$ by-products that can compete for base with the trialkyl borane (hence the need for two equivalents of base in the reaction); 3) accelerated coupling rates for the OBBD derivatives; and 4) regeneration of the catalyst.

Based on such studies, Soderquist and co-workers proposed a more detailed catalytic cycle for the *B*-alkyl Suzuki reaction that includes the important role played by the base both for the 9-BBN derived organoborane manifold (top cycle of Figure 3) as well as for the OBBD organoboranes (bottom cycle of Figure 3).

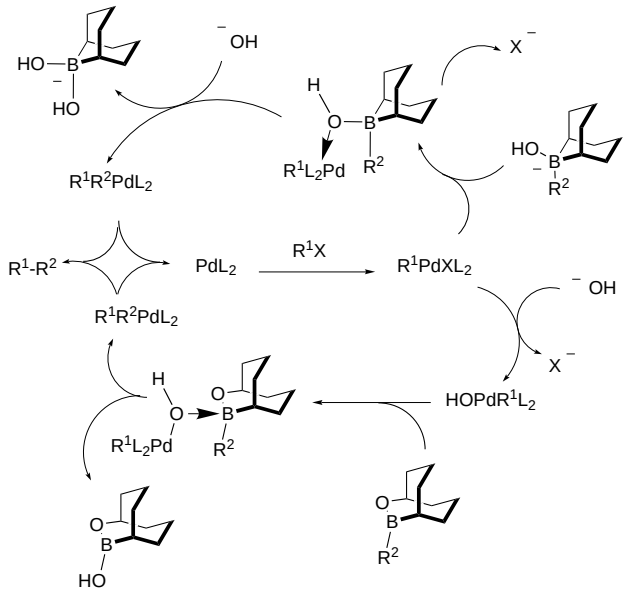
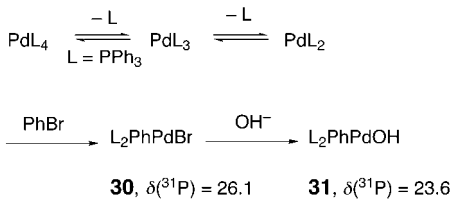


Figure 3. Modified Suzuki – Miyaura catalytic cycle.

Direct evidence for the hydrolysis of a $Pd^{II}X$ intermediate to a $Pd^{II}OH$ intermediate was observed by means of ^{31}P NMR spectroscopy. As shown in Scheme 6, the $[Pd(PPh_3)_4]$ (broad singlet, $\delta = 18.0$) reacts cleanly with PhBr to produce the oxidative addition adduct $[BrPdPh(PPh_3)_2]$ (**30**; $\delta = 26.1$) and PPh_3 ($\delta = -3.2$). When this mixture was treated with two equivalents of NaOH, **30** was partially converted into the hydrolysis product $[HOPdPh(PPh_3)_2]$ (**31**; $\delta = 23.6$). Also, the amount of triphenylphosphane oxide ($\delta = 27.0$) in the mixture increased significantly after addition of the base, a consequence of $Pd^{II} \rightarrow Pd^0$ reduction. Heating the mixture at reflux (THF) increased the rate of conversion of **30** into **31**.



Scheme 6. Evidence for the hydrolysis of the $Pd^{II}Br$ intermediate was obtained by means of ^{31}P NMR spectroscopy.

5.5. Reaction Kinetics

Soderquist and co-workers also determined the kinetics of the reaction for both Bu-9-BBN and Bu-OBBD. For the reaction of PhBr with $[(HO)Bu\text{-}9\text{-}BBN]^-$, they determined that the reaction rate was independent of the concentration of the borate, but was first order in [PhBr]. Therefore, the oxidative addition step in the catalytic cycle is rate limiting for the coupling of Bu-9-BBN derivatives with PhBr. In contrast, the rate of the reaction of Bu-OBBD with PhBr was found to be independent of [PhBr] and [Bu-OBBD], but first order in base. Therefore, the hydrolysis of $[BrPdPh(PPh_3)_2]$ is rate-determining for the coupling of Bu-OBBD with PhBr.

6. Substrate Generality

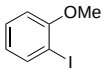
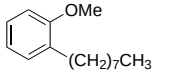
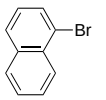
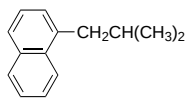
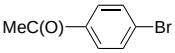
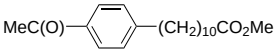
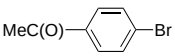
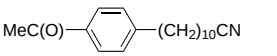
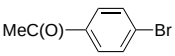
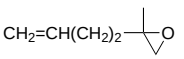
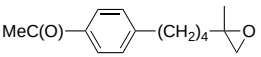
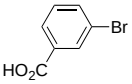
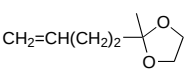
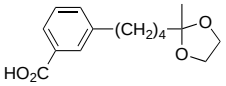
6.1. Cross-Coupling Reactions of Vinyl or Aryl Halides

In their original studies,[13] Miyaura and co-workers found that a combination of $[PdCl_2(dppf)]$ and sodium hydroxide in refluxing THF/water provides adequate cross-coupling conversions, as long as there were no base-sensitive functional groups on either the alkyl boranes or on the aryl halides (Table 3, entries 1 – 2). Potassium carbonate or phosphate suspended in DMF at 50 °C provided superior results for base-sensitive substrates (Table 3, entries 3 – 6).

The study included the cross-coupling reactions of alkyl boranes with a variety of vinyl bromides (Table 4).[42, 52] These reactions again occur with complete retention of olefin geometry.

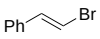
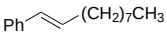
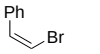
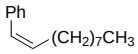
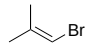
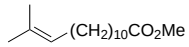
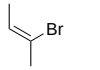
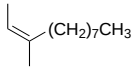
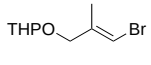
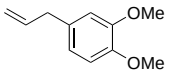
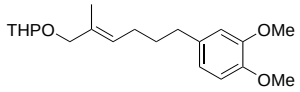
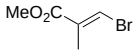
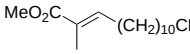
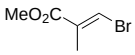
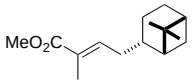
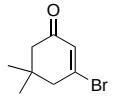
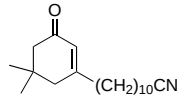
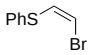
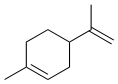
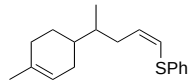
The high degree of chemo- and stereoselectivity of the initial hydroboration phase is efficiently utilized in the *B*-alkyl

Table 3. Cross-coupling reactions of aryl halide substrates with 9-alkyl-9-BBN.[a]

Entry	Aryl halide	Alkene	Product	Yield [%]
1		1-octene		90, 71[b]
2				88, 71[b]
3		$CH_2{=}CH(CH_2)_8CO_2Me$		88[c]
4		$CH_2{=}CH(CH_2)_8CN$		98[c]
5				52[c]
6				77[c]

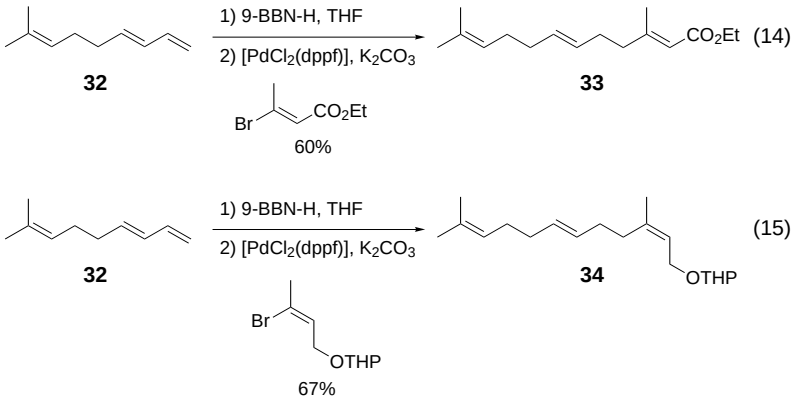
[a] Reactions were run as follows unless otherwise noted: 1) alkene (1 equiv) in THF was treated with 9-BBN-H (1.1 equiv); 2) the borane was added to a solution of aryl halide (1 equiv), $[PdCl_2(dppf)]$ (3 mol %), and NaOH (3 equiv) in THF, and the solution was heated at reflux. [b] NaOMe (1.5 equiv) was used instead of NaOH. [c] K_2CO_3 (2 equiv) was used instead of NaOH and the reaction was conducted in DMF/THF at 50 °C.

Table 4. Cross-coupling reaction of vinyl bromides with 9-alkyl-9-BBN.[a]

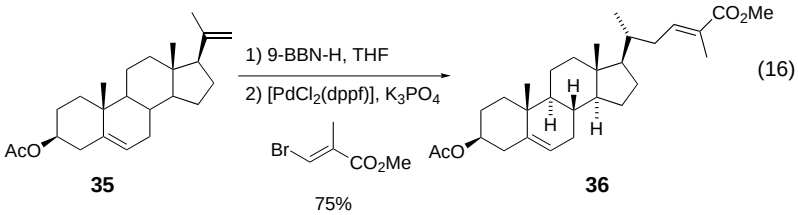
Entry	Vinyl bromide	Alkene	Product	Yield [%]
1		1-octene		85
2		1-octene		90
3		$CH_2{=}CH(CH_2)_8CO_2Me$		92,[c] 69[b]
4		1-octene		98
5				80
6		$CH_2{=}CH(CH_2)_8CN$		80[b]
7				73,[b] 79[c]
8		$CH_2{=}CH(CH_2)_8CN$		81,[b] 72[c]
9				90

[a] Reactions were run as follows unless otherwise noted: 1) alkene (1 equiv) in THF was treated with 9-BBN-H (1.1 equiv); 2) the borane was added to a solution of vinyl halide (1 equiv), [$PdCl_2$(dppf)] (3 mol%), and NaOH (3 equiv) in THF and the solution was heated at reflux. [b] K_2CO_3 (2 equiv) was used instead of NaOH, and the reaction was conducted in DMF/THF at 50 °C. [c] K_3PO_4 (1 equiv) was used instead of NaOH, and the reaction was conducted in DMF/THF at 50 °C.

Suzuki reaction. As an example of chemoselective hydroboration, coupling products derived from triene **32** are obtained in good yields [Eqs. (14) and (15)].[21]



The stereoselective hydroboration of 20-(21)-methylene steroid **35**, which in turn was derived from pregnenolone acetate, produced predominantly the (20*R*)-21-boryl steroid intermediate.[53, 54] This intermediate was cross-coupled with ethyl (*E*)-β-bromomethacrylate to give **36** in 75% yield [Eq. (16)].[21] (For another example, see Table 4, entry 7.) Corey and Roberts have also conducted a study on the synthesis of trisubstituted double bonds through the cross-coupling reactions of alkyl boranes and vinyl iodides.[55]



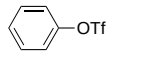
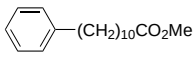
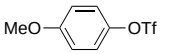
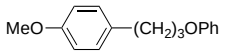
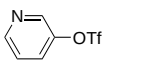
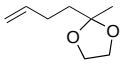
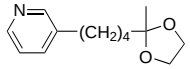
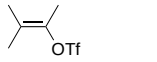
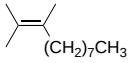
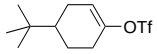
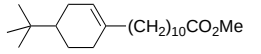
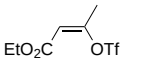
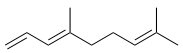
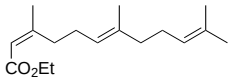
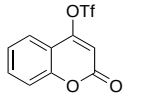
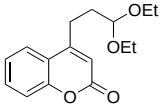
6.2. Cross-Coupling Reactions with Aryl or Vinyl Triflates

Organoboranes can also undergo cross-coupling reactions with aryl or vinyl triflates.[29] Such triflates can be easily accessed from phenols or enolates.[56, 57] A representative substrate pool is shown in Table 5. These cross-coupling reactions are catalyzed by [$Pd(PPh_3)_4$] or [$PdCl_2$(dppf)] in the presence of K_3PO_4 in dioxane or THF.

Molander and Ito recently reported the coupling reactions of aryl or vinyl triflates with potassium alkyl trifluoroborates (Table 6).[20] The potassium alkyl trifluoroborates are solid, crystalline, air- and water-stable reagents that are easily prepared from the corresponding alkyl boronic acids or esters. They undergo Suzuki–Miyaura coupling with the vinyl or aryl triflates in the presence of [$PdCl_2$(dppf)] and Cs_2CO_3 in refluxing THF/H_2O. As shown in Table 6, a variety of functional groups are tolerated.

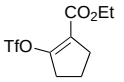
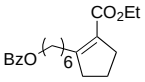
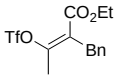
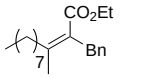
In a particularly challenging coupling reaction of an azulene-derived triflate, Danheiser and co-workers found the Buchwald ligand (*o*-biphenyl)PCy_2 to be essential for its cross-coupling reaction with *B*-ethyl-9-BBN [Eq. (17)].[58] Occhiato et al. found that vinyl triflates derived from six- and seven-membered *N*-alkoxycarbonyl lactams undergo cross-coupling with allyl or alkyl boronic acids and esters (Table 7). Whereas the allyl boronic esters underwent coupling under standard conditions (substoichiometric [$(Ph_3P)_2PdCl_2$], Na_2CO_3, THF, H_2O, reflux), the alkyl boronic acids required the addition of Ag_2O for an acceptable rate of conversion. Interestingly, the six-membered lactam-derived triflates gave much higher yields than the corresponding seven-membered triflates.[59]

Table 5. Aryl or vinyl triflates cross-coupling with 9-alkyl-9-BBN.[a]

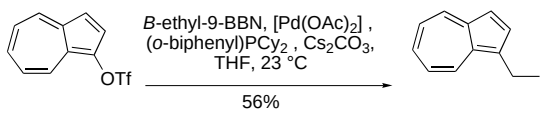
Entry	Triflate	Alkene	Product	Yield [%]
1		$CH_2{=}CH(CH_2)_8CO_2Me$		87, 82[b]
2		$CH_2=CHCH_2OPh$		92, 70[b]
3				65
4		1-octene		67[b]
5		$CH_2{=}CH(CH_2)_8CO_2Me$		89, 86[b]
6				65
7				64

[a] Reactions were run as follows, unless otherwise noted: 1) alkene (1 equiv) in THF was treated with 9-BBN-H (1.1 equiv); 2) the borane was added to a solution of triflate (1 equiv), [$PdCl_2$(dppf)] (2.5 mol%), and K_2PO_4 (1.5 equiv) in dioxane, and the solution was heated at 85 °C. [b] The reaction was carried out in THF at reflux.

Table 6. Cross-coupling of organic halides and triflates with potassium alkyl trifluoroborates.[a]

Entry	Alkyl borane	Triflate	Product	Yield [%]
1[b]	$PhCH_2BF_3K$	*p*-IC_6H_4OTf	*p*-$TfOC_6H_4CH_2Ph$	16
2[b]	$PhCH_2BF_3K$	*p*-BrC_6H_4OTf	*p*-$TfOC_6H_4CH_2Ph$	70
3[b]	$PhCH_2BF_3K$	*p*-ClC_6H_4OTf	*p*-$ClC_6H_4CH_2Ph$	57
4[c]	$NC(CH_2)_5BF_3K$	*p*-$NO_2C_6H_4OTf$	*p*-$NO_2C_6H_4(CH_2)_5CN$	73
5[c]	$Me(CO)(CH_2)_4BF_3K$	*p*-AcC_6H_4OTf	*p*-$AcC_6H_4(CH_2)_4(CO)Me$	79
6[c]	$CH_3(CH_2)_7BF_3K$	*m*-CNC_6H_4OTf	*m*-$CNC_6H_4(CH_2)_6Br$	65
7[c]	$Br(CH_2)_6BF_3K$	*p*-AcC_6H_4OTf	*p*-$AcC_6H_4(CH_2)_6Br$	61
8[c]	$BzO(CH_2)_6BF_3K$			68
9[c]	$CH_3(CH_2)_7BF_3K$			75

[a] The potassium alkyl trifluoroborate (1 equiv) was treated with the triflate (1 equiv) in the presence of [$Pd(Cl_2)$(dppf)] (9 mol%) and Cs_2CO_3 (3 equiv) in THF/H_2O, and the mixture was heated at reflux for 18 h. [b] Borates were prepared by using the corresponding Grignard reagent. [c] Borates were prepared by means of the catalytic hydroboration method.

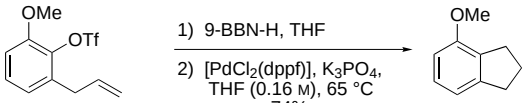


37 **38** (17)

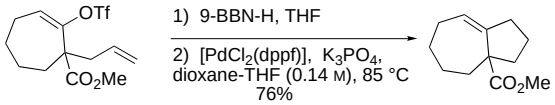
6.3. Intramolecular Cross-Coupling

Miyaura and co-workers demonstrated that five- and six-membered rings can be accessed through the *B*-alkyl Suzuki reaction of aryl or vinyl halides that are functionalized with terminal olefins (Table 8).[21] The cross-coupling reactions were carried out in THF/H_2O solution (0.2 M) by using catalytic [$PdCl_2$(dppf)] and NaOH (3 equiv). The authors did note, however, that they were unable to gain access to larger rings by using this cyclization protocol. Clearly, competing oligomerization processes constitute risk factors that complicate prospects for cyclization. As will be shown in Section 6.4, the macrocyclization reaction can be achieved at lower substrate concentration (thus favoring intramolecular over intermolecular cross-coupling). Oh-e et al. subsequently found that both aryl and vinyl triflates are also good substrates for the intramolecular *B*-alkyl Suzuki reaction [Eqs. (18) and (19)].[29]

Compounds that contain vinyl halide and terminal olefin functional groups linked through a two- or three-carbon tether can also be cyclized to form five- and six-membered exocyclic alkenes (Table 9).[60] In an interesting extension of this idea, Soderquist and co-workers developed a protocol which couples vinyl geminal dibromides with symmetrical bis-boranes, which are derived from the corresponding bis-olefins

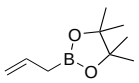
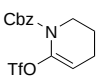
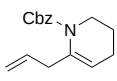
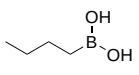
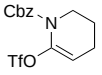
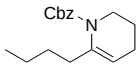
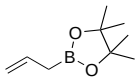
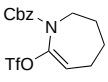
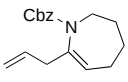
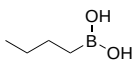
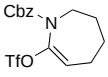
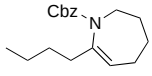


39 **40** (18)



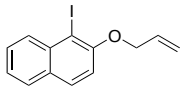
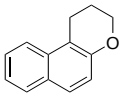
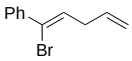
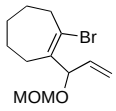
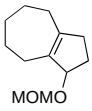
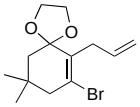
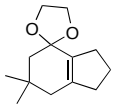
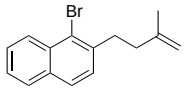
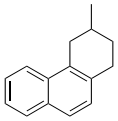
41 **42** (19)

Table 7. Suzuki coupling of piperidine and azepine-derived vinyl triflates.

Entry	Borate	Triflate	Product	Yield [%]
1[a]				65
2[b]				93
3[a]				27
4[b]				22

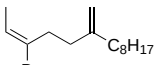
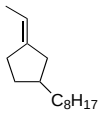
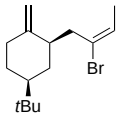
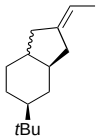
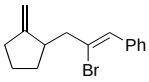
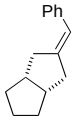
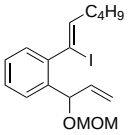
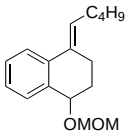
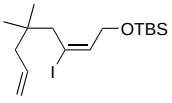
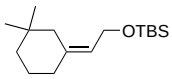
[a] The reactions were run at 80 °C in THF/ Na_2CO_3 (aq., 2 M) with the vinyl triflate (1 equiv) and the borate (1.5 equiv) in the presence of [$(Ph_3P)_2PdCl_2$] (5 mol%). [b] The reactions were run in toluene at 80 °C with the vinyl triflate (1 equiv) and the borate (2 equiv) in the presence of K_2CO_3 (3 equiv), Ag_2O (2 equiv), and [$PdCl_2$(dppf)] (3 mol%).

Table 8. Intramolecular *B*-alkyl Suzuki reactions.[a]

Entry	Substrate	Product	Yield [%]
1			70
2			67
3			68
4			84
5			77

[a] Conditions: 1) Olefin (1 equiv), 9-BBN-H (1.05 equiv), THF, 0 →23 °C; 2) [$PdCl_2$(dppf)] (1.5 mol %), NaOH (3 equiv), THF/H_2O (0.2 M).

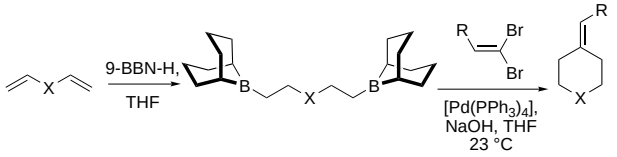
Table 9. Synthesis of exocyclic alkenes

Entry	Alkyl halide	Product	Yield [%]
1			71,[a] 80[b]
2			68[a,c]
3			83,[a] 72[b]
4			51,[a] 69[b]
5			60[a]

[a] 1) 9-BBN-H (1.05 equiv), THF, 0 →23 °C; 2) [$PdCl_2$(dppf)] (1.5 mol %) and NaOH (3 M, 3 equiv) in THF (0.14 M) at 60 °C. [b] Hydroboration as above, followed by [$Pd(PPh_3)_4$] (3 mol %), K_3PO_4 (1.5 equiv), dioxane/THF (0.12 M), 60 °C. [c] Diastereomeric mixture (3:7).

(Table 10).[61] This process involves tandem intermolecular–intramolecular cross-coupling reactions. The authors noted that attempts to apply the methodology to the synthesis of five-membered ring systems starting from 1,4-dienes were unsuccessful.

Table 10. Synthesis of exocyclic alkenes with bisboranes.[a]



Entry	X	R	Yield [%]
1	CH_2	phenyl	56
2	CH_2	*p*-biphenylyl	42
3	CH_2	*p*-tolyl	34
4	CH_2	*p*-anisyl	76
5	CH_2	*p*-butyl	44
6	$Si(CH_3)_2$	phenyl	45
7	$Si(CH_3)_2$	*p*-biphenylyl	60
8	$Si(CH_3)_2$	2-furyl	36
9	$Si(CH_3)_2$	*p*-tolyl	25
10	$Si(CH_3)_2$	*p*-anisyl	41
11	$Si(CH_3)_2$	*n*-butyl	45
12	C(H)OTBS	phenyl	38
13	C(H)OTBS	methyl	64

[a] The olefin (1 equiv) was treated with 9-BBN-H in THF at 25 °C. This solution was subsequently treated with vinyl bromide (1 equiv), NaOH (4 equiv), THF/H_2O (0.09 M), and [$Pd(PPh_3)_4$] (6 mol %) at 25 °C.

In an extension of this cyclization protocol, Cho and Shibasaki reported the asymmetric synthesis of cyclopentanes **45** and **48** by using chiral ligands **49** and **50**, respectively, in the *B*-alkyl Suzuki–Miyaura reaction [Eqs. (20) and (21)].[62] Although the level of asymmetric induction is moderate (28 and 31 % *ee*, respectively), this work constitutes a significant advancement in the field.

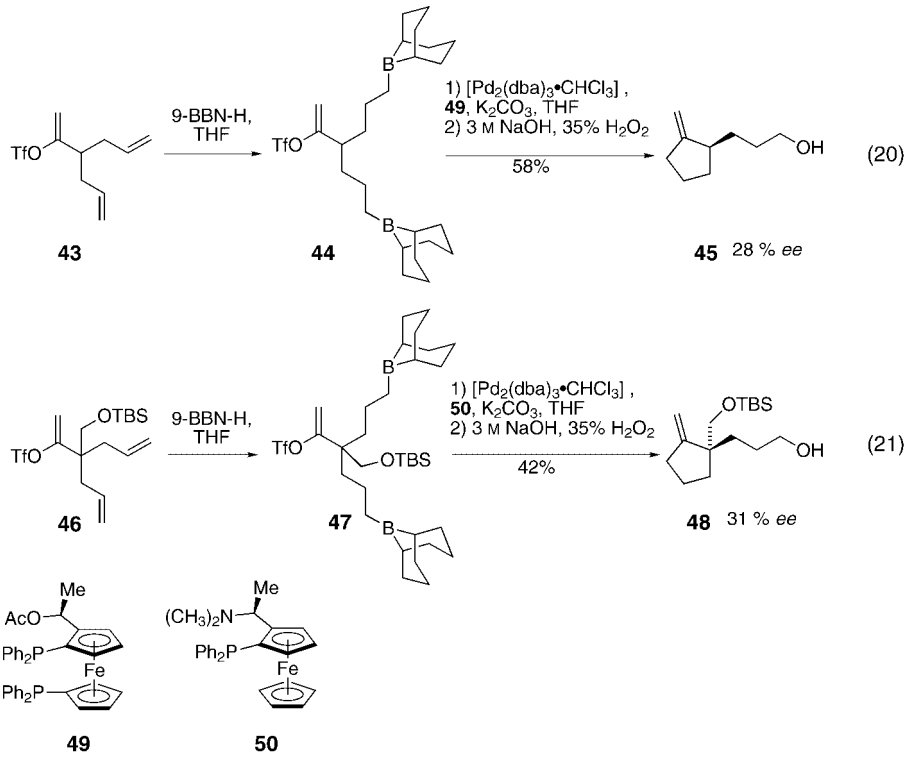
6.4. Macrocyclizations

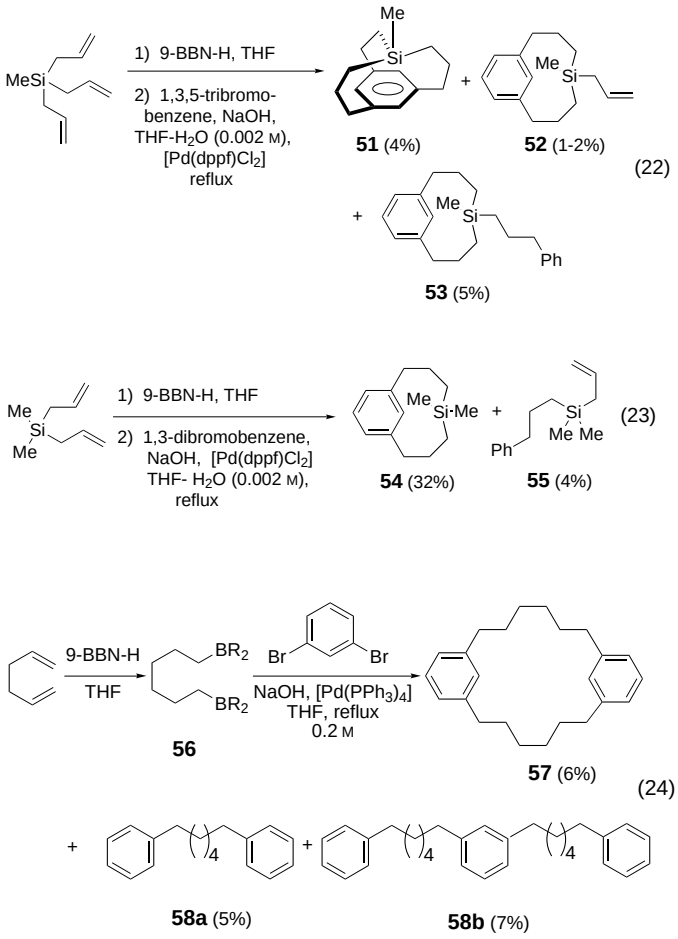
The first moderately successful cyclizations to form rings with more than six members by means of the *B*-alkyl Suzuki–Miyaura reaction were reported by Kwochka and co-workers en route to silametacyclophanes [Eqs. (22) and (23)] and [6.6]metacyclophanes [Eq. (24)].[63, 64]

The hydroboration of methyltriallylsilane followed by coupling with 1,3,5-tribromobenzene gave the target 4-methyl-4-sila[$3^{4,10}$][7]metacyclophane **51** in 4 % yield [Eq. (22)]. Silacycles **52** (1–2 %) and **53** (5 %) were obtained as undesired side products. A higher yield of macrocyclization adduct **54** was achieved in the coupling reaction of diallyldimethylsilane with 1,3-dibromobenzene [Eq. (23)]. Kwochka et al. noted that neither 1,2- nor 1,4-dibromobenzene yielded the corresponding silacyclophanes under similar conditions. Compounds **51**–**54** were used to study anisotropic effects by means of NMR spectroscopic analysis.

In an analogous study, coupling of the bis-borane **56** with 1,3-dibromobenzene led to the desired [6.6]metacyclophane **57** in 6 % yield, with adducts **58a** and **59b** as side products [Eq. (24)].

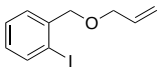
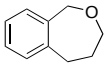
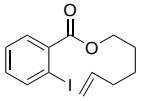
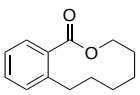
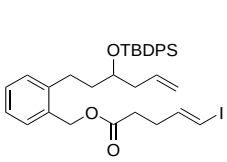
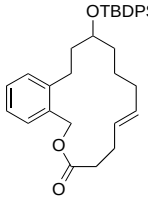
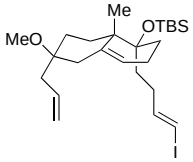
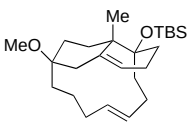
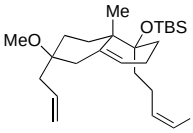
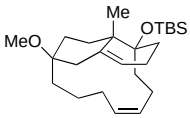
A macrocyclization study which is potentially more relevent to natural product synthesis was subsequently carried out by Danishefsky and Chemler (Table 11).[45] These reactions were carried out under dilute conditions (0.003 M) and with





slow addition of the alkyl borane intermediates to the catalyst solution. In the first set of reaction conditons, the borane was added to a dilute solution of Cs_2CO_3, [$PdCl_2$(dppf)], and $AsPh_3$ in THF/DMF/H_2O.[65] Under a second set of reaction conditions, the borane was treated with TlOEt and the resulting mixture was added dropwise to a dilute solution of [$PdCl_2$(dppf)] and $AsPh_3$ in THF/DMF/H_2O.[43, 44] Although *ortho*-iodobenzenes gave relatively poor yields of cyclization adducts (Table 11, entries 1 and 2), the yields could be improved by extending the centers of reactivity away from the aryl ring and by increasing the ring size (Table 11, entry 3). Transannular macrocyclization was also a viable process (Table 11, entries 4 and 5), especially when TlOEt was used as the base. Apparently, the rate enhancement offered by the thallium base increased the rate of the desired macrocyclization reaction relative to competing oligomerization processes.

Table 11. *B*-alkyl Suzuki macrocyclizations.[a]

Entry	Substrate	Product	Yield [%]
1			22[b]
2			23
3			41
4			40, 60[b]
5			46[b]

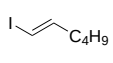
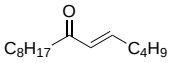
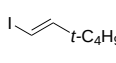
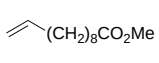
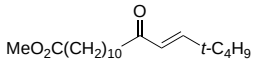
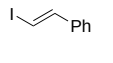
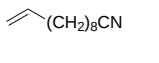
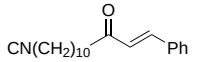
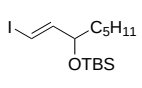
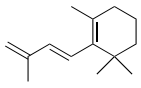
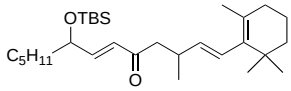
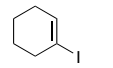
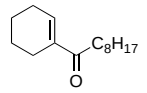
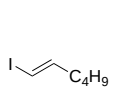
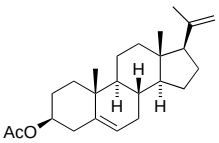
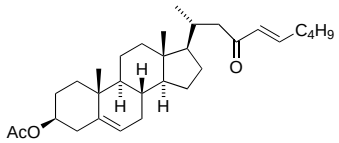
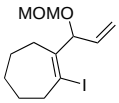
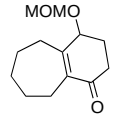
[a] All reactions were carried out as follows, unless otherwise noted: 1) The terminal olefins were hydroborated with 9-BBN-H (1.5 equiv) for 1.5 h at 23 °C in THF (0.5 M); 2) the borane solution was diluted with THF and added over 3–5 h by means of a syringe pump to a solution of [$PdCl_2$(dppf)] (0.2 equiv), $AsPh_3$ (0.2 equiv), Cs_2CO_3 (3 equiv), and H_2O (40 equiv) in a 10:1 THF/DMF solution (0.003 M with respect to the substrate). [b] Water (5 equiv) and TlOEt (3 equiv) were added to the borane solution prior to the addition to the catalyst solution (Cs_2CO_3 and additional H_2O were omitted from these reactions).

6.5. Carbonylative Cross-Coupling Reactions

Another important application of the *B*-alkyl Suzuki reaction is the synthesis of unsymmetrical ketones by means of the palladium-catalyzed reaction of alkyl boranes and vinyl or alkyl halides under a carbon monoxide atmosphere.[31, 32] The synthesis of α,β-unsaturated ketones by means of the carbonylative cross-coupling reaction of alkyl boranes and vinyl iodides proceeded smoothly in benzene or dioxane under a carbon monoxide atmosphere (1 – 3 atm), when K_3PO_4 was used as the base and either $[Pd(PPh_3)_4]$ or $[PdCl_2(PPh_3)_2]$ as the catalyst (Table 12).[32] Iodobenzene and benzyl bromide are also feasible partners in the carbonylative coupling with 9-octyl-9-BBN (82 and 72% yields, respectively, not shown).

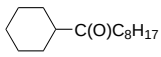
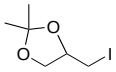
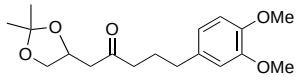
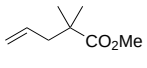
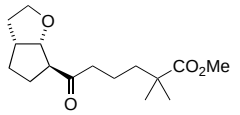
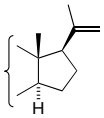
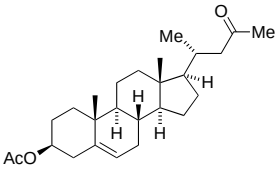
Alkyl iodides are viable substrates for the carbonylative Suzuki coupling reaction with alkyl boranes (Table 13).[31] These reactions were efficiently conducted in the presence of K_3PO_4 and substoichiometric ammounts of $[Pd(PPh_3)_4]$ in dioxane under a carbon monoxide atmosphere. The reaction is greatly accelerated by visible light (100-W tungsten lamp), which suggests that a radical process may be involved in the oxidative addition. Generally, cross-couplings of alkyl halides that have a hydrogen atom in the β position often suffer from competitive side reactions such as β-hydride elimination, thus leading to alkenes or to the isomerization of alkyl groups. However, the carbonylative couplings do not suffer from these problems, probably because the CO insertion is very fast.

Table 12. Carbonylative cross-coupling with alkyl boranes.

Entry	Vinyl iodide	Alkene	Product	Yield [%]
1				99[a]
2				78[b]
3				68[b]
4				53[b]
5				90[c]
6				48[a]
7				77[a]

[a] Reactions conditions: 1) The alkene (1.1 equiv) was treated with 9-BBN-H (1.1 equiv) in THF, 0 °C → RT; 2) benzene, iodoalkene (1 equiv), K_2PO_4 (3 equiv), and $[Pd(PPh_3)_4]$ (5 mol%) were added, and the reaction was conducted under CO (1 atm). [b] Same conditions as above except in dioxane under CO (3 atm).

Table 13. Carbonylative cross-coupling reaction of 9-alkyl-9-BBN with alkyl iodides.[a]

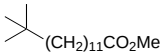
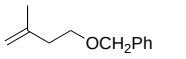
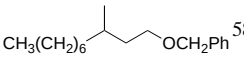
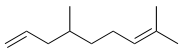
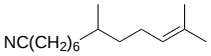
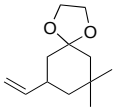
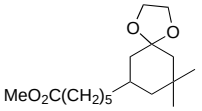
Entry	Alkyl iodide	Alkene	Product	Yield [%]
1	$C_6H_{13}I$	1-octene	$C_6H_{13}C(O)C_8H_{17}$	67
2		1-octene		65
3	tBuCH$_2$I	1-octene	tBuCH$_2$C(O)C$_8$H$_{17}$	69
4		4-allylveratrole		73
5				65
6	$MeO_2C(CH_2)_3I$	$CH_2{=}CH(CH_2)_8CN$	$MeO_2C(CH_2)_3C(O)(CH_2)_{10}CN$	65
7	MeI			50

[a] Reaction conditions: 1) the alkene (1 equiv) in THF was treated with 9-BBN-H (1.05 equiv); 2) the borane was added to a solution of iodoalkene (1.5 equiv), CO (1 atm), $[Pd(PPh_3)_4]$ (3 mol%), and K_3PO_4 (3 equiv) in benzene, and the solution was irradiated with a 100-W tungsten lamp for 24 h.

6.6. C(sp^3)–C(sp^3) Cross-Coupling Reactions

Alkyl halides are not common substrates for the Suzuki reaction as a result of their slow rate of oxidative addition and their fast β-hydride elimination from the derived σ-alkylpalladium intermediate. However, Ishiyama and co-workers found that iodoalkanes react with alkyl boranes in the presence of K_3PO_4 and catalytic amounts of $[Pd(PPh)_4]$ in dioxane to generate the corresponding coupled adducts in moderate to good yields (45 – 71%, Table 14). They noted that $[PdCl_2(dppf)]$ did not act as an efficient catalyst in these reactions. Also, this reaction was not enhanced by light.

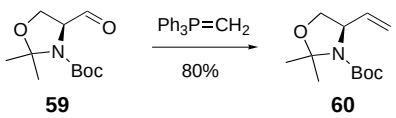
Table 14. Cross-coupling reaction of 9-alkyl-9-BBN with alkyl iodides.[a]

Entry	Alkyl iodide	Alkene	Product	Yield [%]
1	MeI	$CH_2{=}CH(CH_2)_8CO_2Me$	$CH_3(CH_2)_{10}CO_2Me$	71
2	$CH_3(CH_2)_5I$	$CH_2{=}CH(CH_2)_5CH_3$	$C_{14}H_{30}$	64
3		$CH_2{=}CH(CH_2)_8CO_2Me$		45
4	$CH_3(CH_2)_5I$			58
5	$CH_3(CH_2)_3I$	$CH_2{=}CH(CH_2)_8CO_2Me$	$CH_3(CH_2)_{15}CO_2Me$	54
6	$CN(CH_2)_3I$			61
7	$MeO_2C(CH_2)_3I$			57

[a] Reactions conditions: 1) the alkene (1 equiv) in THF was treated with 9-BBN-H (1.0 equiv); 2) this solution was diluted with dioxane and treated with $[Pd(PPh_3)_4]$ (3 mol%), K_3PO_4 (3 equiv), and the alkyl iodide (1.5 equiv), and the solution was heated at 60 °C.

7. Synthesis of Non-natural Amino Acids

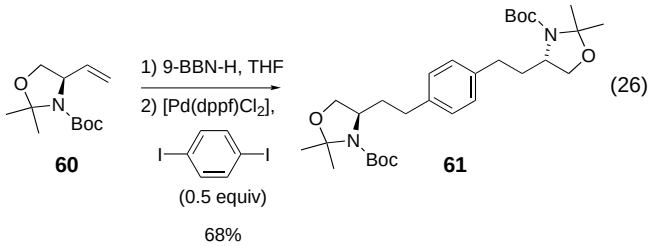
The *B*-alkyl Suzuki reaction has been used effectively in the synthesis of non-natural amino acids. Taylor and co-workers were first to recognize the usefulness of this sort of construction.[66] Starting amino olefin **60** was prepared by means of Wittig olefination of the Garner aldehyde (**59**), which in turn can be obtained from the corresponding L- or D-serine [Eq. (25)]. Hydroboration of **60** with 9-BBN-H followed by Suzuki–Miyaura coupling of the derived alkyl



59 **60** (25)

borane with a variety of vinyl bromides, iodides, and triflates gave the corresponding non-natural amino acid synthons in good yields (Table 15).

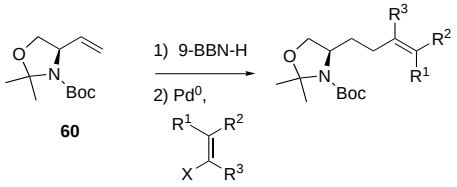
para-Diiodobenzene was coupled twice with **60** as well, to yield diamide **61** in 68% yield [Eq. (26)]. Some of the cross-coupled adducts were converted into their methyl ester amino



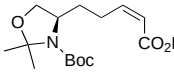
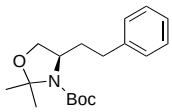
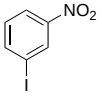
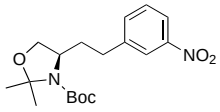
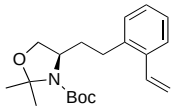
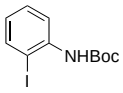
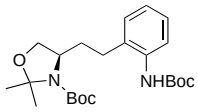
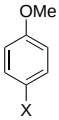
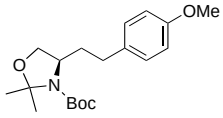
60 **61** (26)

acid derivatives by treatment with Jones' reagent followed by methylation of the resulting acids with diazomethane, for example, [Eq. (27)].

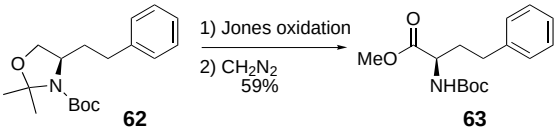
Table 15. Suzuki coupling of amino acid synthons (1).[a]



60

Entry	Substrate	Product	Yield [%]
1			70
2			79 (X = I)
3			72 (X = Br)
4			69
5			76
6			ca. 70
7			72 (X = I)
8			11 (X = OTf)

[a] 1) The olefin (1 equiv) in THF (0.22 M) was treated with 9-BBN-H (2 equiv) at 0 °C, and then warmed to room temperature; 2) the solution was treated with aqueous K_2PO_4 (3 M, 2.1 equiv), vinyl or aryl halide (1.1 equiv) in DMF, and $[PdCl_2(dppf)]$ (5 mol%).



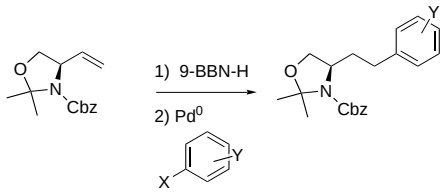
62 **63** (27)

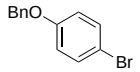
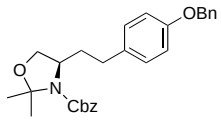
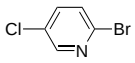
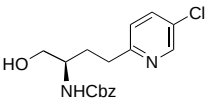
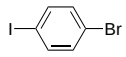
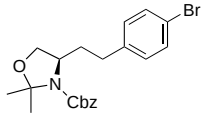
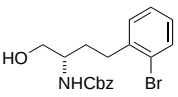
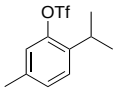
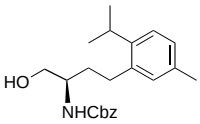
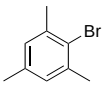
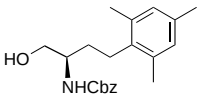
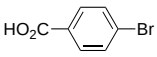
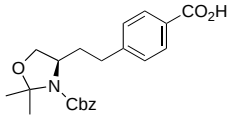
Sabat and Johnson subsequently reported a similar method for the synthesis of α-amino acids and α-amino alcohols that contain a variety of side chains that do not occur naturally.[67] Yields for the coupling of various aryl iodides and bromides ranged from 66–89% (Table 16). The rate of coupling of iodides is much faster than that of bromides (Table 16, entries 3 and 4). All these adducts could be converted into their corresponding amino acid derivatives.

8. Methods for the Synthesis of Phenethyl and Homoallylic Amines

Along similar lines, Overman and Kamatani reported an efficient β-aminoethylation procedure with the *B*-alkyl Suzu-

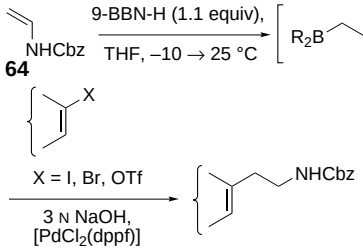
Table 16. Suzuki coupling of amino acid synthons (2).[a]



Entry	Substrate	Product	Yield [%]
1			89
2			81[b]
3			80
4			81[b]
5			73[b]
6			68[b]
7			66

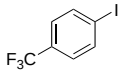
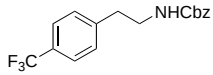
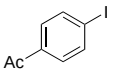
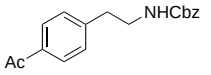
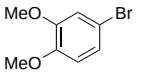
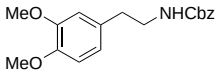
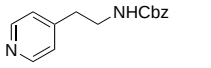
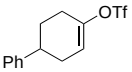
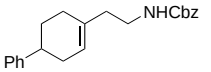
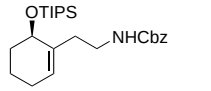
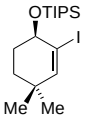
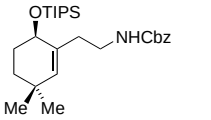
[a] 1) 9-BBN-H, toluene, 80 °C; 2) NaOH (3.2 N), $[Pd(PPh_3)_4]$ (3 mol %), 99 °C. [b] The product mixture was subsequently treated with *p*-toluenesulfonic acid in MeOH.

ki – Miyaura reaction, starting from benzyl vinyl carbamate **64** (Scheme 7).[68] Vinyl carbamate **64**, in turn, was prepared by means of a Curtius rearrangement of acryloyl chloride. Hydroboration of **64** (1.1 – 1.5 equiv) with 9-BBN-H in THF followed by cross-coupling with the aryl or vinyl halide/triflate component (1 equiv) in the presence of a substoichiometric amount of $[PdCl_2(dppf)]$ and excess aqueous NaOH (3 M)



Scheme 7. β-Aminoethylation starting from benzyl vinyl carbamate precursors.

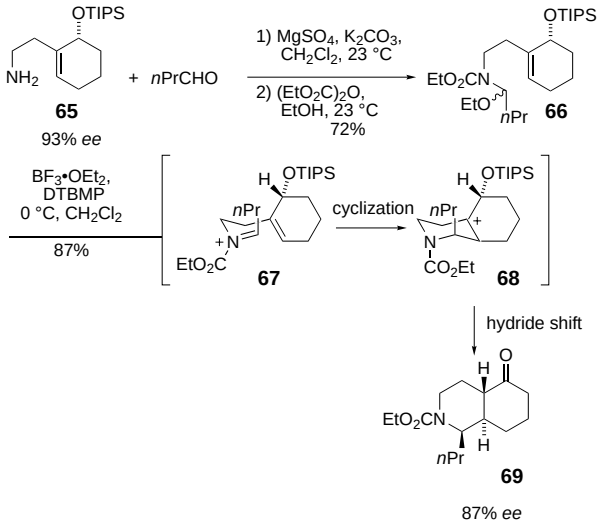
Table 17. Aminoethylation of arenes and alkenes.[a]

Entry	Substrate	Product	Yield [%]
1			87
2			80
3			94
4			88
5			97
6			94
7			77

[a] The coupling reactions were conducted in THF at 25 °C with the borane (1.1 – 1.5 equiv), the vinyl or aryl halide/triflate (1 equiv), and $[PdCl_2(dppf)]$ (9 – 15 mol %) for 1 – 24 h. The borane residues were then oxidized by treatment of the reaction mixtures with buffered aqueous H_2O_2 (30 %).

produced a variety of homoallylic amines in excellent yields (77 – 97 %, Table 17).

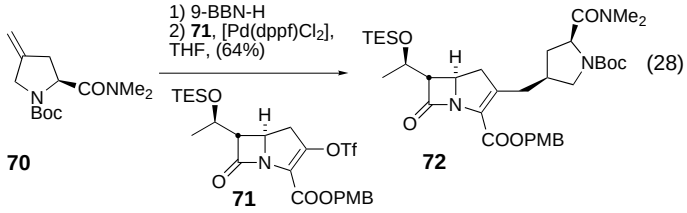
The products obtained by using this method have been used in the synthesis of decahydroisoquinoline rings, which are structural components of isoquinoline alkaloids.[69] Condensation of the primary amine **65** with *n*-butanal under Lewis acid catalysis and ethylation/ethoxycarbonylation of the resulting imine was followed by a pinacol rearrangement. The subsequent hydride migration generated the *trans*-decahydroquinoline **69** (87 % *ee*) with an axial substituent at C1 (Scheme 8).



Scheme 8. Synthesis of *trans*-hydroquinolines by Overman and co-workers.

9. Carbapenemes

Narukawa et al. have demonstrated the used of the *B*-alkyl Suzuki–Miyaura coupling for the preparation of highly functionalized carbapeneme antibiotics.[70] In one example, a stereoselective hydroboration of proline derivative **70** set the stage for a coupling with enol triflate **71** to afford **72** [Eq. (28)]. Other functionalized alkenes have also been employed. The hydroboration step generates a secondary stereocenter in this case.

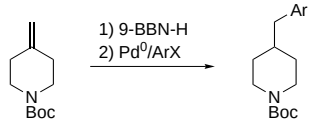


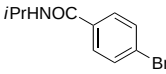
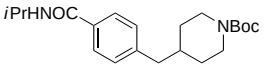
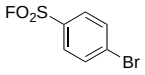
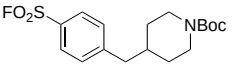
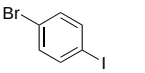
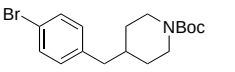
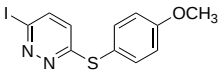
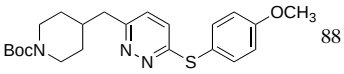
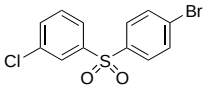
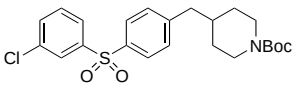
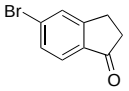
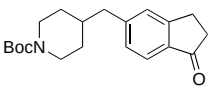
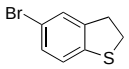
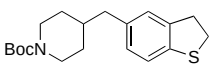
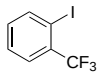
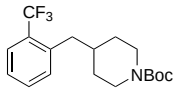
(28)

10. (4-Arylmethyl)piperidines

An interesting study of the *B*-alkyl Suzuki–Miyaura coupling for the synthesis of 4-arylmethyl piperidines was performed by Vice et al. at Schering-Plough Research Institute en route to pharmacologically active compounds.[71] Many functional groups are tolerated under the reaction conditions (Table 18).

Table 18. (4-Arylmethyl)piperidines through Suzuki–Miyaura coupling.[a]



Entry	ArX	Product	Yield [%]
1			98
2			82
3			60
4			88
5			87
6			77
7			80
8			72

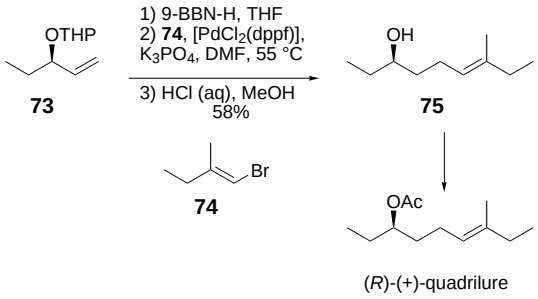
[a] All reactions were run as follows: The unsaturated piperidine (1 equiv) was treated with 9-BBN-H (1 equiv) in THF and heated at reflux for 1 h. The resulting borane was added to a mixture of the aryl halide (0.91 equiv), $[PdCl_2(dppf)]$ (3 mol%), and K_2CO_3 (3 equiv) in DMF, and the mixture was heated at 60 °C for 3 h.

11. Application of the *B*-Alkyl Suzuki–Miyaura Reaction in the Total Syntheses of Natural Products

The *B*-alkyl Suzuki–Miyaura reaction has proven to be of considerable value in natural product syntheses, especially in the coupling reactions of complex fragments. This review will conclude with a comprehensive summary of such synthetic applications and covers the timespan 1990–2001. The synthetic applications are organized according to the sp^2-hybridized coupling partner: aryl or vinyl halides, triflates, and finally, enol phosphates.

11.1. (*R*)-(+)-Quadrilure

Mori and Puapoomchareon reported the first application of the *B*-alkyl Suzuki–Miyaura coupling reaction to the synthesis of (*R*)-(+)-quadrilure in 1990.[72] (*R*)-(+)-Quadrilure is an aggregation pheromone produced by the square-necked grain beetle. Hydroboration of the olefin moiety of intermediate **73** with 9-BBN-H, followed by Pd^0-mediated coupling with vinyl bromide **74** and subsequent removal of the THP protecting group afforded alcohol **75** in 58% yield. Acetylation of alcohol **75** provided the natural product (Scheme 9).

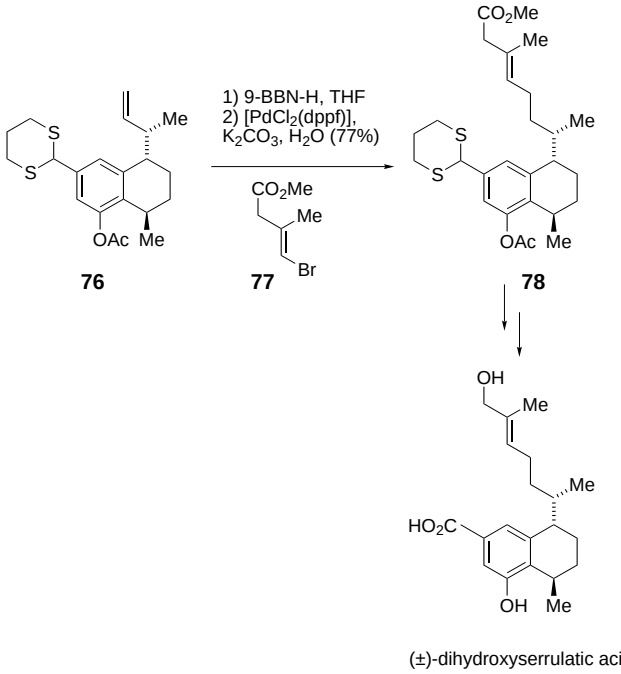


Scheme 9. Mori and co-workers were the first to demonstrate the utility of the *B*-alkyl Suzuki–Miyaura reaction in natural product synthesis.

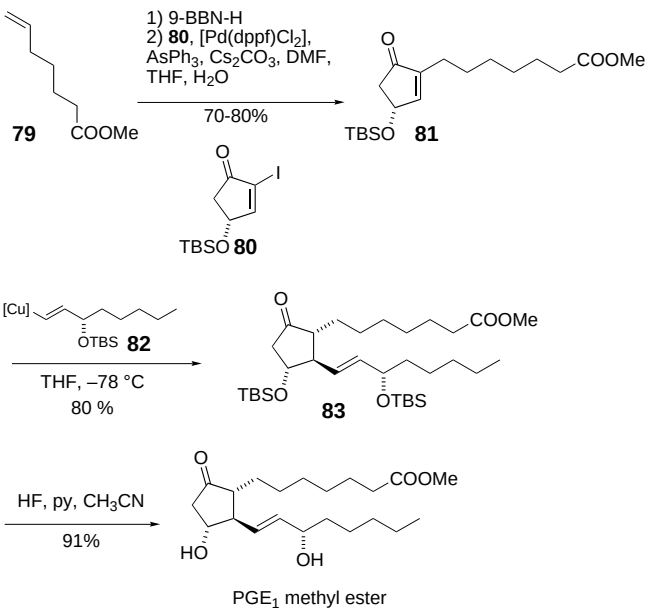
11.2. (±)-Dihydroxyserrulatic Acid

Also in 1990, Uemura and co-workers used the *B*-alkyl Suzuki–Miyaura cross-coupling reaction as a key step in the synthesis of (±)-dihydroxyserrulatic acid,[73, 74] which is a member of the serrulatane class of diterpenoids. The diterpenoids are known for their potent anti-inflammatory and analgesic properties. Hydroboration of the advanced intermediate **76** with 9-BBN-H, followed by cross-coupling with

(*E*)-methyl *β*-bromomethacrylate (**77**) in the presence of [$PdCl_2$(dppf)], K_2CO_3, and H_2O afforded **78** in 77% yield (Scheme 10). Subsequent functional group manipulations transformed intermediate **78** into the natural product.



Scheme 10. Synthesis of (±)-dihydroxyserrulatic acid (Uemura and co-workers).



Scheme 11. Mild cross-coupling conditions were used in the synthesis of PGE_1 methyl ester by Johnson and co-workers.

11.3. Prostaglandin E_1

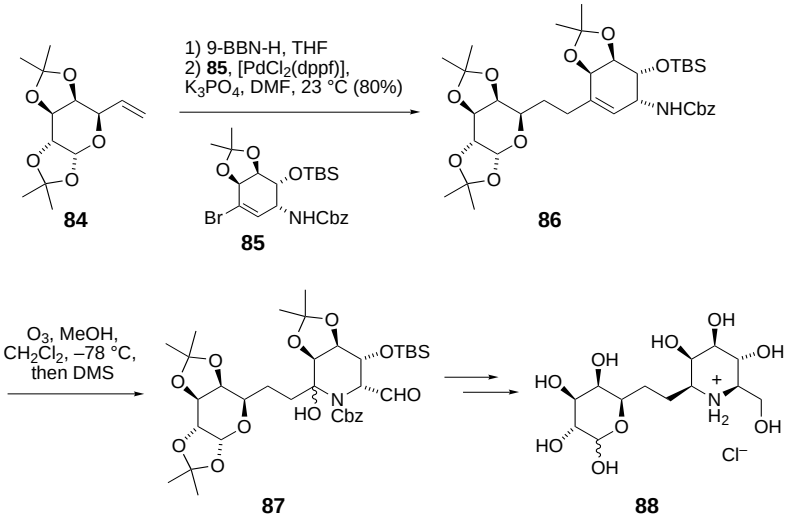
The *B*-alkyl Suzuki–Miyaura cross-coupling was incorporated into a new variant of the three-component synthesis of prostaglandins by Johnson and co-workers in 1993. They used very mild conditions ([$PdCl_2$(dppf)], $AsPh_3$, Cs_2CO_3, DMF/H_2O) to effect a highly efficient coupling of vinyl iodide **80** with the alkyl borane derived from olefin **79** (Scheme 11).[65] Subsequent stereoselective conjugate addition of cuprate **82** to enone **81** afforded **83**, which was then converted into prostaglandin E_1. The Johnson protocols for the Suzuki–Miyaura reaction were used in the majority of later applications of this reaction in the synthesis of natural products.

11.4. Aza-*C*-disaccharides

In 1994, Johnson and co-workers reported the synthesis of an aza-*C*-disaccharide **88**, a potential glycosidase inhibitor, by means of the *B*-alkyl Suzuki–Miyaura method.[75] This class of sugar mimetics, in which the oxygen atom of the glycoside is replaced by a methylene unit, could potentially preserve the binding properties of the parent azasugar, but be more inert to acidic or enzymatic hydrolysis. The key disaccharide coupling step involved the alkyl borane derived from olefin **84** (obtained in several steps from D-galactose) and vinyl bromide **85**. Oxidative cleavage of the resulting olefin by means of ozonolysis, followed by reduction and deprotection, afforded the desired mimetic **88** (Scheme 12).

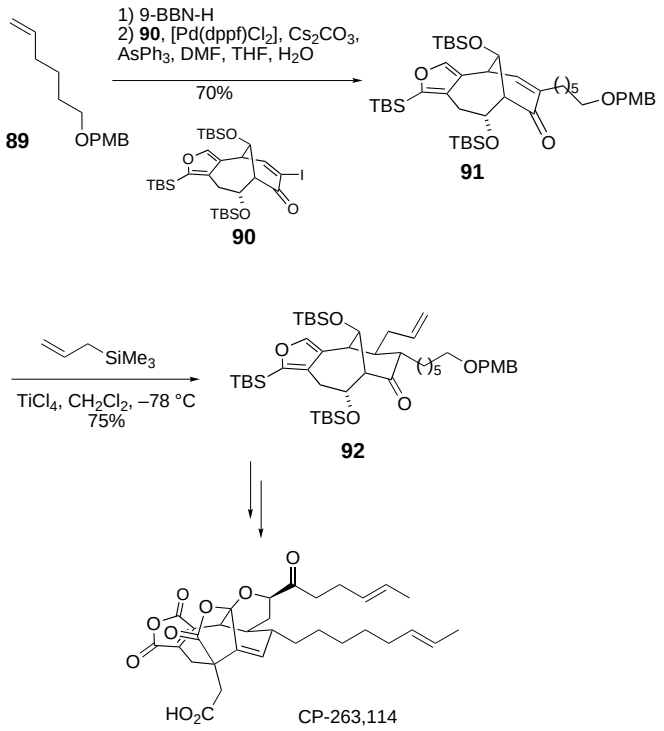
11.5. CP-263,114

Danishefsky and co-workers employed a sequence similar to the Johnson prostaglandin work in the synthesis of CP-263,114, which is a structurally unique fungal metabolite that inhibits squalene synthase and farnesyl transferase.[76, 77] Coupling of iodo-enone **90** with the borane derived from



Scheme 12. Synthesis of aza-*C*-disaccharides by Johnson and co-workers.

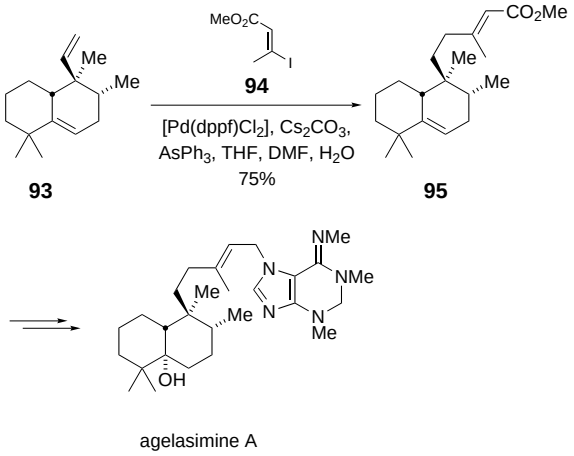
alkene **89** afforded enone **91**. A Sakurai-type conjugate addition then introduced a handle for the second side chain and installed the desired *trans* relative stereochemistry of the side chains. The resulting intermediate **92** was subsequently converted into CP-263,114 (Scheme 13).



Scheme 13. Synthesis of CP-263,114 (Danishefsky and co-workers).

11.6. Agelasimine A

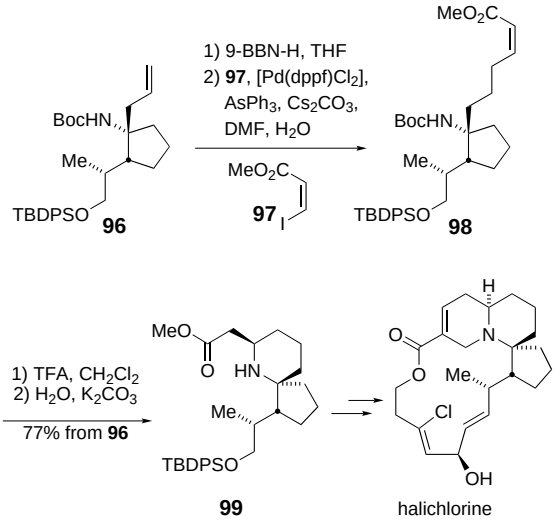
The *B*-alkyl Suzuki coupling served as a key step in the synthesis of the marine diterpenoid agelasimines A by Ohba et al.[78] A key step involved the elongation of the vinyl side chain in compound **93** (Scheme 14). Although the hydroboration of the neopentyl vinyl group with 9-BBN-H required harsh conditions (THF, reflux, 2 h), it proceeded with a high degree of chemoselectivity with respect to the even more hindered trisubstituted double bond. Subsequent palladium-catalyzed cross-coupling with (*E*)-iodoalkenoate **94** then gave α,β-unsaturated ester **95**, which was transformed into agelasimin A in a series of straightforward steps.



Scheme 14. Synthesis of agelasimine A (Ohba and co-workers).

11.7. (+)-Halichlorine

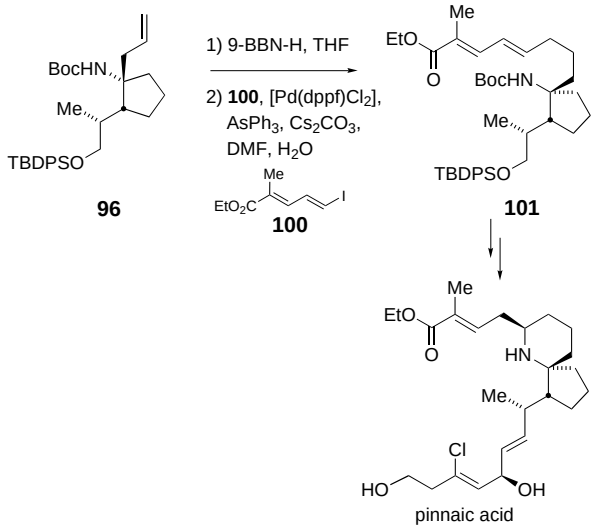
The elongation of an unsaturated side chain by *B*-alkyl Suzuki coupling set the stage for a key step in a synthesis of the marine alkaloid (+)-halichlorine by Danishefsky and Trauner.[79, 80] Contrary to the case in the synthesis of agelasimin A (Section 11.6), the alkene delivered by the vinyl iodide partner was not retained but served as an acceptor in a subsequent conjugate addition. Hydroboration of the protected amino alkene **96**, followed by palladium-mediated Suzuki-coupling with methyl (*Z*)-3-iodoacrylate (**97**), afforded α,β-unsaturated ester **98** (Scheme 15). Upon deprotection of the amino function with TFA and subsequent basification, **98** underwent a highly stereoselective intramolecular 1,4-addition to afford piperidine **99** as the only isolated isomer. Intermediate **99** was subsequently converted into the VCAM-1 inhibitor (+)-halichlorine in eight steps (VCAM = Vascular Cell Adhesion Molecule).



Scheme 15. Synthesis of halichlorine (Danishefsky and co-workers).

11.8. Pinnaic Acid

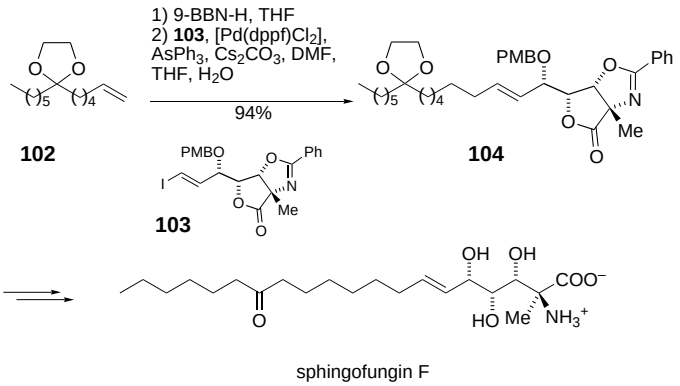
The strategy described in Section 11.7 was expanded further in a synthesis of the related marine natural product pinnaic acid, an inhibitor of cytosolic phospholipase A_2.[81] Hydroboration of **96** followed by coupling with iododienoic ester **100** afforded compound **101** in excellent yield. This intermediate was subsequently converted into pinnaic acid (Scheme 16).



Scheme 16. Synthesis of pinnaic acid (Danishefsky and co-workers).

11.9. Sphingofungin F

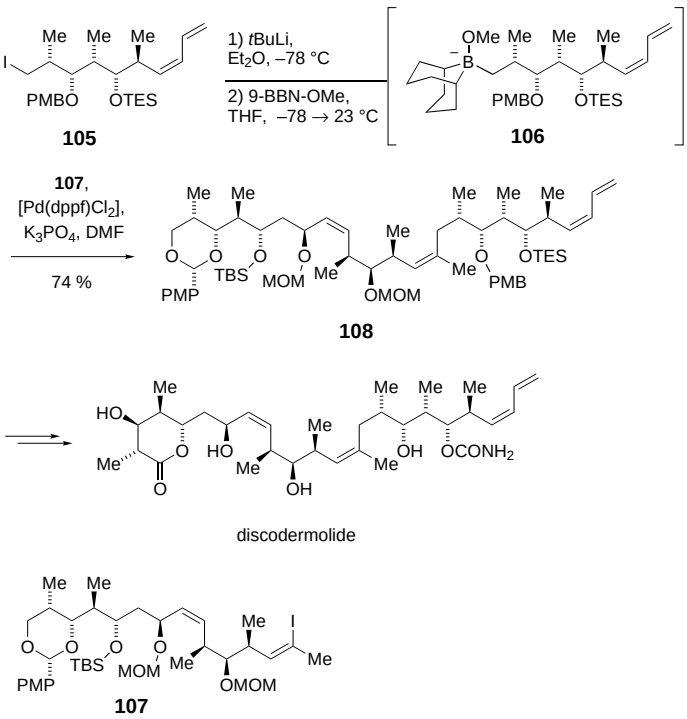
Trost and Lee used the *B*-alkyl Suzuki coupling in a synthesis of the serin palmitoyl transferase inhibitor sphingofungin F.[82] Hydroboration of the terminal alkene **102** and cross-coupling with the densely functionalized (*E*)-iodoalkene **103** gave **104**. Global deprotection of this intermediate then yielded the natural product (Scheme 17). A synthesis of sphingofungin E that uses a similar Suzuki–Miyaura cross-coupling sequence was subsequently reported by Nakamura and Shiozaki.[83]



Scheme 17. Synthesis of sphingofungin F (Trost and co-workers).

11.10. Discodermolide

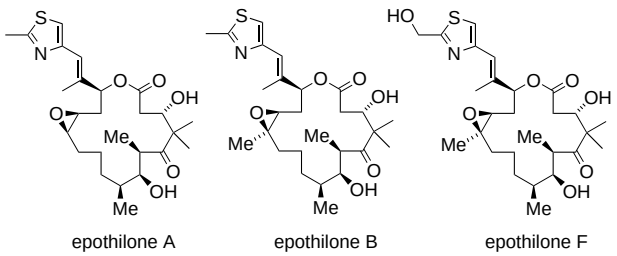
An alternative version of the *B*-alkyl Suzuki coupling was used by Marshall and Johns in an elegant synthesis of the immunosuppressant discodermolide.[22] Lithiation of primary iodide **105**, followed by addition of 9-methoxy-BBN gave the intermediate borate **106**, which was coupled with the trisubstituted iodoalkene **107** in high yield (Scheme 18). An alternative synthesis of the alkyl borane by means of hydroboration of the corresponding 1,1-disubstituted alkene would not have been compatible with the (*Z*,*E*)-diene functionality in **105**. This efficient coupling enabled a highly convergent synthesis of discodermolide.



Scheme 18. Synthesis of discodermolide with an alkyl borate derived from a primary iodide (Marshall and co-workers).

11.11. Epothilones

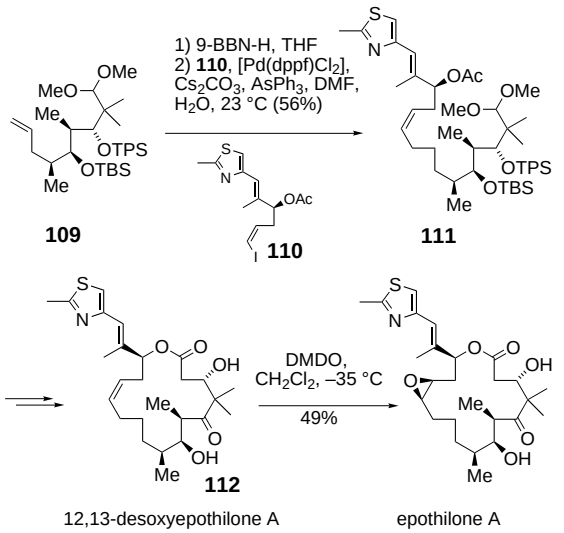
B-alkyl Suzuki coupling reactions were used extensively by Danishefsky and co-workers in the syntheses of the anticancer agents epothilone A, B, and F.[84–88]



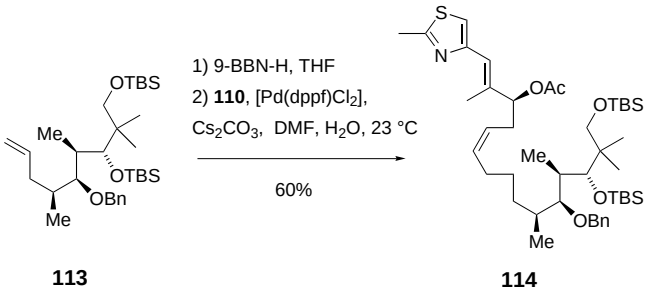
During an early approach to epothilone A, vinyl iodide **110** was coupled with an organoborane derived from alkene **109**. The product **111** was converted into 12,13-desoxyepothilone A by using an intramolecular aldol addition. Chemo- and stereoselective epoxidation then gave epothilone A (Scheme 19).

A closely related reaction was used by Zhu and Panek in the synthesis of epothilone A (Scheme 20).[89]

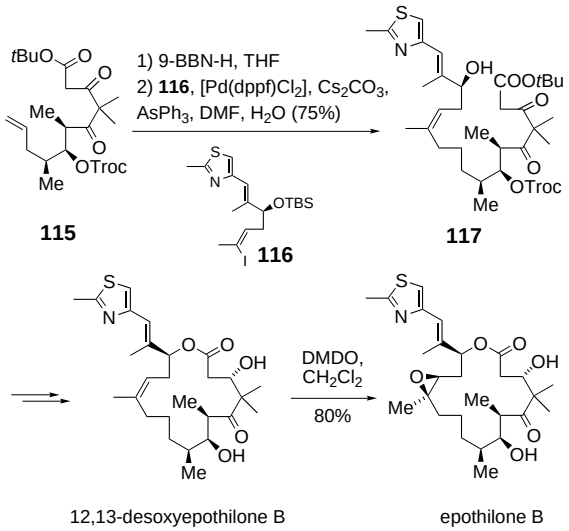
In later syntheses of the epothilones by Danishefsky and co-workers, this chemistry was extended to more elaborate and sensitive substrates (Scheme 21). Hydroboration of **115** and



Scheme 19. An early synthesis of epothilone A (Danishefsky and co-workers).

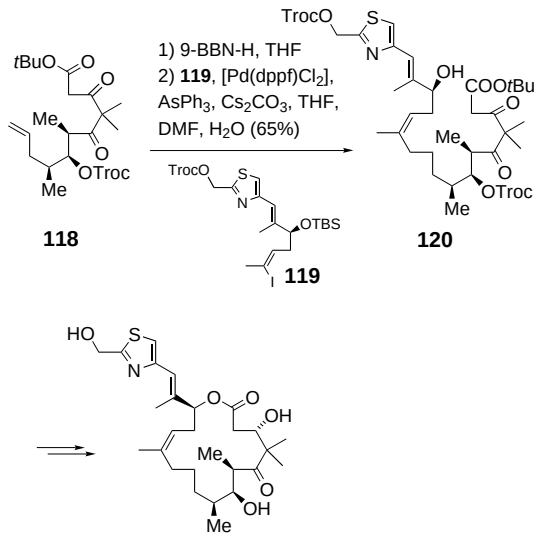


Scheme 20. Panek and co-workers used a similar method in their synthesis of epothilone A.



Scheme 21. Synthesis of epothilone B (Danishefsky and co-workers).

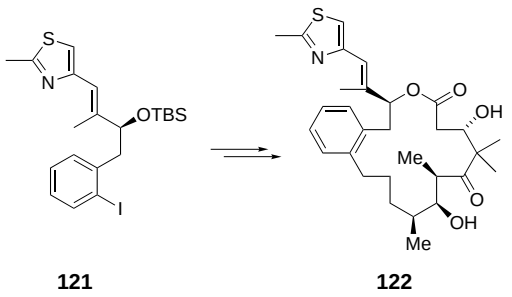
coupling with **116**, followed by treatment of the crude product with dilute hydrochloric acid afforded **117**. The two carbonyl groups and the ester functionality remain unaffected under these conditions. Stereoselective reduction of the β-ketone (relative to the ester moiety), macrolactonization, and subsequent deprotection gave 12,13-desoxyepothilone B, whose selective epoxidation finally afforded epothilone B. A similar sequence was later used in the synthesis of epothilone F (Scheme 22).[90]



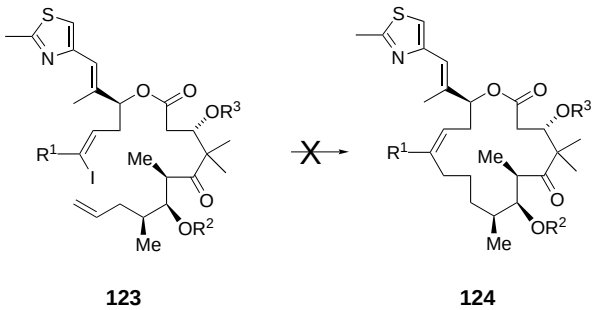
12,13-desoxyepothilone F

Scheme 22. Synthesis of 12,13-desoxyepothilone F (Danishefsky and co-workers).

Aryl iodides were successfully used in related coupling reactions. Compound **121** was converted into epothilone derivative **122** by using the same overall strategy (Scheme 23).[84] Unfortunately, several attempts to effect Suzuki-macrocyclizations in this context (e.g. **123**→**124**) have thus far been unsuccessful (Scheme 24).



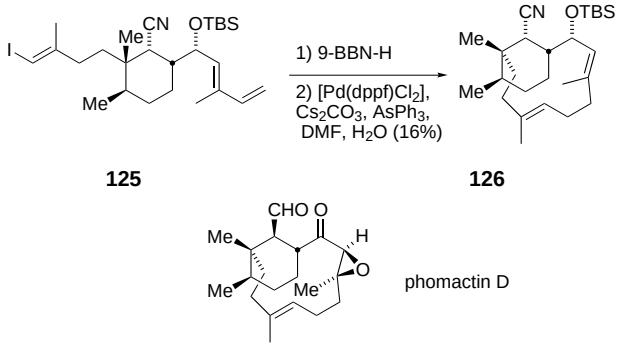
Scheme 23. Synthesis of an epothilone analogue.



Scheme 24. Macrocyclization by means of a *B*-alkyl Suzuki–Miyaura coupling failed in the synthesis of epothilones.

11.12. Phomactin D

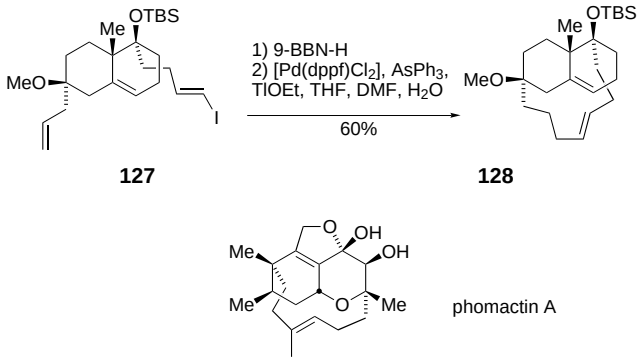
The application of a ring-closing intramolecular *B*-alkyl Suzuki couplings in natural product synthesis was recently described by the Halcomb group.[91] Regioselective hydroboration of the diene moiety in **125** followed by intramolecular cross-coupling afforded the bicyclic product **126**. A highly strained 12-membered ring is formed in the process (Scheme 25). Compound **126** is a possible intermediate en route to phomactin D, which is an antagonist of platelet activating factor (PAF).



125 **126**

Scheme 25. Halcomb and co-workers used a *B*-alkyl Suzuki–Miyaura macrocyclization in their work towards the synthesis of phomactin D.

Simultaneously, a related model study was undertaken by Danishefsky's group to assess whether this chemistry is suitable for the synthesis of the related natural product phomactin A (**127** → **128**, Scheme 26).[45]

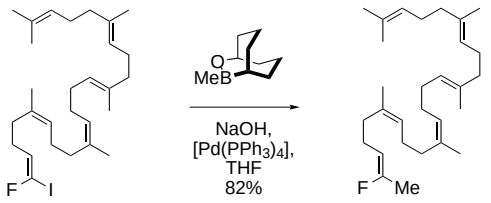


127 **128**

Scheme 26. Danishefsky and co-workers used a transannular *B*-alkyl Suzuki–Miyaura coupling in their work towards the synthesis of phomactin A.

11.13. Squalene Epoxidase Inhibitor

As a final example of the Suzuki–Miyaura coupling reactions between alkyl boranes and vinyl halides, Moore et al. demonstrated that vinyl iodide **129**, which has a geminal fluoride substituent, couples with methyl-OBBD to generate the squalene epoxidase inhibitor **130** in good yield (Scheme 27).[92]

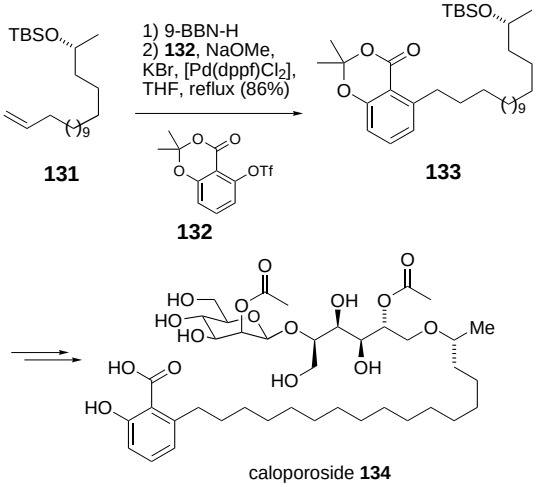


129 **130**

Scheme 27. Moore and co-workers used methyl-OBBD to complete the synthesis of a squalene epoxidase inhibitor.

11.14. Caloporoside

Fürstner and Konetzki used the *B*-alkyl Suzuki coupling in a synthesis of the phospholipase C inhibitor caloporoside (**134**).[93] The (16*R*)-hydroxyheptadecylsalicylic acid part of the natural product was efficiently prepared by means of a palladium-catalyzed cross-coupling: aryl triflate **132** was coupled with the 9-BBN derivative of alkene **131**, to give **133** (Scheme 28).



131 **132** **133**

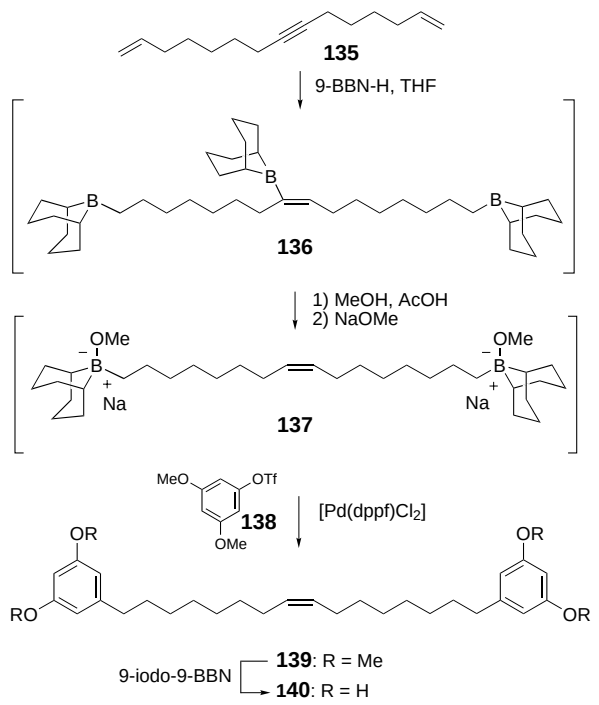
Scheme 28. Synthesis of caloporoside (Fürstner and co-workers).

11.15. 5-Alkylresorcinols

Fürstner's group also described very concise syntheses of several biologically active 5-alkylresorcinols.[94] For example, threefold hydroboration of dienyne **135** afforded the trisborane **136** (Scheme 29). Selective hydrolysis of the less stable vinylic borane and activation of the two remaining alkyl boranes as borate complexes to form **137** then set the stage for a twofold Suzuki coupling with 3,5-dimethoxyphenol triflate (**138**). Overall, this stereoselective one-pot transformation yielded aromatic tetra-*O*-methyl ether **139**. Subsequent deprotection afforded bis-resorcinol **140**, a natural product with DNA-cleaving properties.

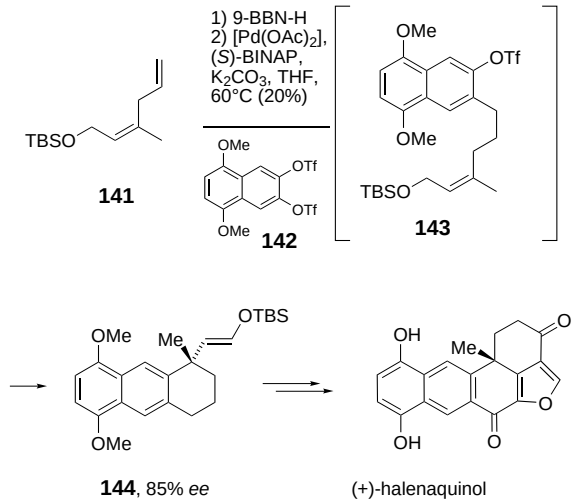
11.16. Halenaquinol

In an elegant synthesis of the bioactive sponge metabolite halenaquinol, Shibasaki and co-workers demonstrated that an



Scheme 29. Fürstner and co-workers used the *B*-alkyl Suzuki – Miyaura coupling in the synthesis of a C_2-symmetric resorcinol derivative.

intermolecular *B*-alkyl Suzuki – Miyaura coupling can be combined with an asymmetric intramolecular Heck-reaction (Scheme 30).[95] Selective hydroboration of diene **141** followed by Pd-mediated cross-coupling with the symmetrical

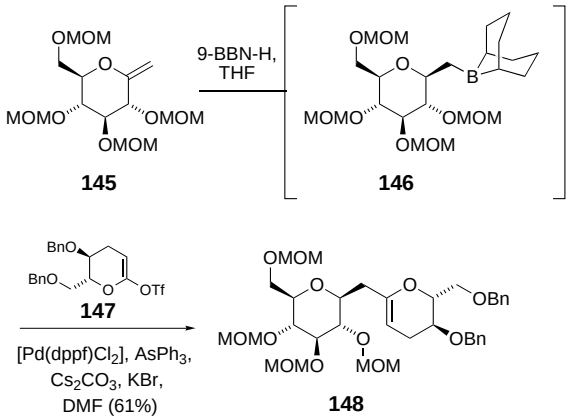


Scheme 30. The first tandem Suzuki – Heck reaction was used by Shibasaki and co-workers in their synthesis of halenaquinol.

aromatic bis-triflate **142** gave intermediate alkene **143**, which immediately underwent cyclization to afford enol ether **144**. In the presence of a chiral phosphane (BINAP), this reaction afforded the cyclization product (85 % *ee*). Although the chemical yield is still unsatisfactory, this is the first example of a tandem reaction that involves a Suzuki coupling. Since many other useful reactions (e.g. allylic alkylations or cycloisomerizations) are catalyzed by Pd^0, further applications and other combinations can be expected to appear in the literature.

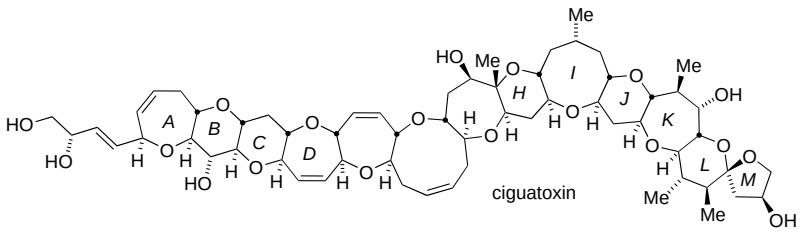
11.17. Ciguatoxin

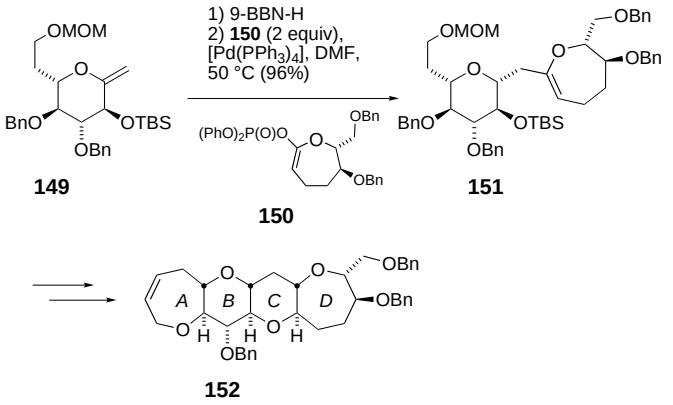
Recently, Sasaki, Tachibana, and co-workers began to apply the *B*-alkyl Suzuki reaction to the synthesis of complex marine polycyclic ethers such as the brevetoxins, ciguatoxin, or gambierol (Schemes 31 – 33).[96–99] This work is unusual in several respects. On the one hand, an exocyclic enol ether, typically derived from a sugar, is used as a borane precursor. Its stereoselective hydroboration proceeds *syn* to the α-alkoxy or α-silyloxy group and generates a tertiary stereocenter. On the other hand, cyclic ketene acetal triflates or phosphates serve as coupling partners. Thus, hydroboration of enol ether **145** furnished **146**. This borane was coupled with ketene acetal triflate **147** to afford the endocyclic enol ether **148** (Scheme 31).



Scheme 31. Sasaki and co-workers relied heavily on the *B*-alkyl Suzuki – Miyaura coupling for the synthesis of polyether natural products.

A considerable portion of the marine-derived polycyclic ether ciguatoxin has been synthesized by using this chemistry. The method has been extended to the synthesis of seven- and eight-membered rings (Schemes 32 and 33). Rings *A* – *D* of this molecule were constructed as shown in Scheme 32. The hydroboration of **149** followed by palladium-mediated coupling with enol phosphate **150** gave compound **151**, which was converted into tetracycle **152** in a few steps. Rings *G* – *M* of ciguatoxin were assembled in a similar way (Scheme 33).

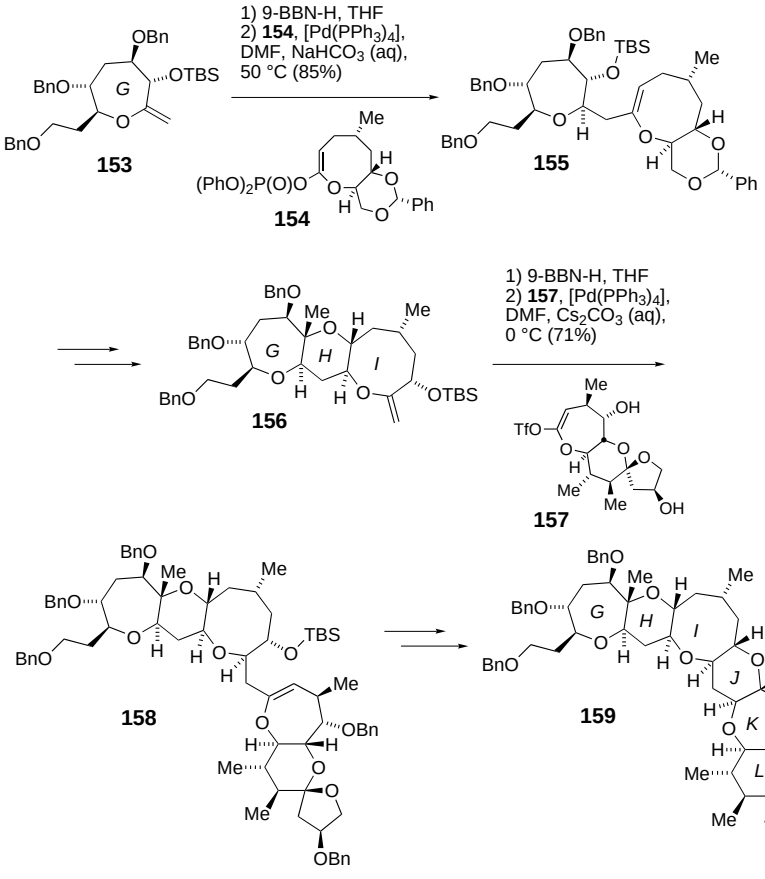




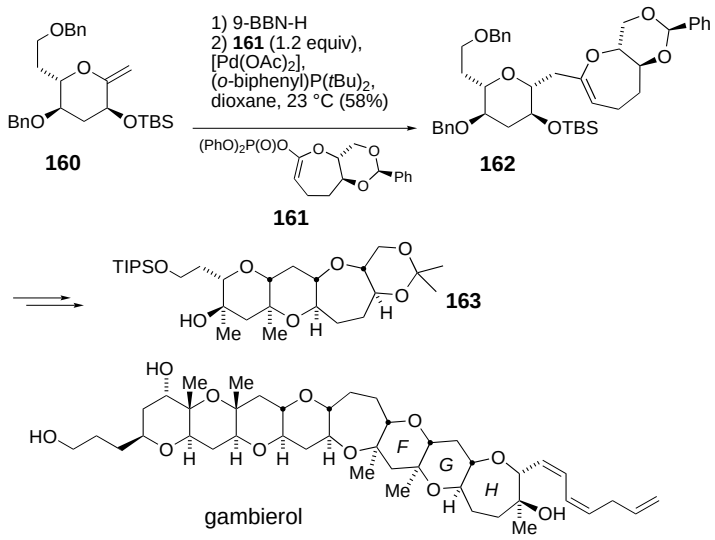
Scheme 32. Synthesis of rings *A* – *D* of ciguatoxin (Sasaki and co-workers).

11.18. Gambierol

The application of this general strategy to the synthesis of the marine polyether toxin gambierol is shown in Scheme 34.[100] Hydroboration of **160** and palladium-catalyzed reaction with the seven-membered cyclic ketene acetal phosphate **161** afforded the coupling product **162**. This intermediate was converted into tetracycle **163**, an intermediate of the *F* – *H* portion of gambierol. The Buchwald ligand (*o*-biphenyl)P(*t*Bu)$_2$ greatly improves the efficiency of the coupling reaction.



Scheme 33. Synthesis of rings *G* – *M* of ciguatoxin (Sasaki and co-workers).



Scheme 34. Work towards the synthesis of gambierol.

12. Summary and Outlook

As demonstrated throughout this review, the *B*-alkyl Suzuki – Miyaura cross-coupling reaction has proven to be an extraordinarily useful tool for the construction of carbon frameworks. These products may ultimately be converted into useful compounds, including biologically active natural and non-natural products. It is probable that this area will develop further. Potential developments include the incorporation of reagent-directed asymmetry in the hydroboration reaction, improvement in catalyst-derived asymmetry in the C–C bond-forming step, improvement of coupling yields, and synthetic applications for secondary and even tertiary alkyl boranes.

Note added in proof: Impressive sp^3 – sp^3 *B*-alkyl Suzuki – Miyaura couplings between alkyl boranes and alkyl bromides were published by Fu and co-workers shortly after this review was prepared.[101]

Abbreviations

9-BBN-H	9-borabicyclo[3.3.1]nonane
BINAP	2,2′-bis(diphenylphosphanyl)-1,1′-binaphthyl
Bn	benzyl
Boc	*tert*-butoxycarbonyl
Bz	benzoyl
Cbz	carbobenzoxy (benzyloxycarbonyl)
Cp	cyclopentadienyl
dba	dibenzylideneacetone
DMDO	dimethyldioxirane
DMS	dimethyl sulfide
dppe	bis(diphenylphosphanyl)ethane
dppf	bis(diphenylphosphanyl)ferrocene

DTBMP	2,6-di-*tert*-butyl-4-methylpyridine
Hx	hexyl
MOM	methoxymethyl
OBBD	9-oxa-10-borabicyclo[3.3.2]decane
PMB	*p*-methoxybenzyl
PMP	*p*-methoxyphenyl
py	pyridine
TBDPS	*tert*-butyldiphenylsilyl
TBS	*tert*-butyldimethylsilyl
TES	triethylsilyl
Tf	trifluoromethanesulfonyl
TFA	trifluoro acetic acid
THP	tetrahydropyranyl
TIPS	triisopropylsilyl
TPS	triphenylsilyl
Troc	trichloroethoxycarbonyl

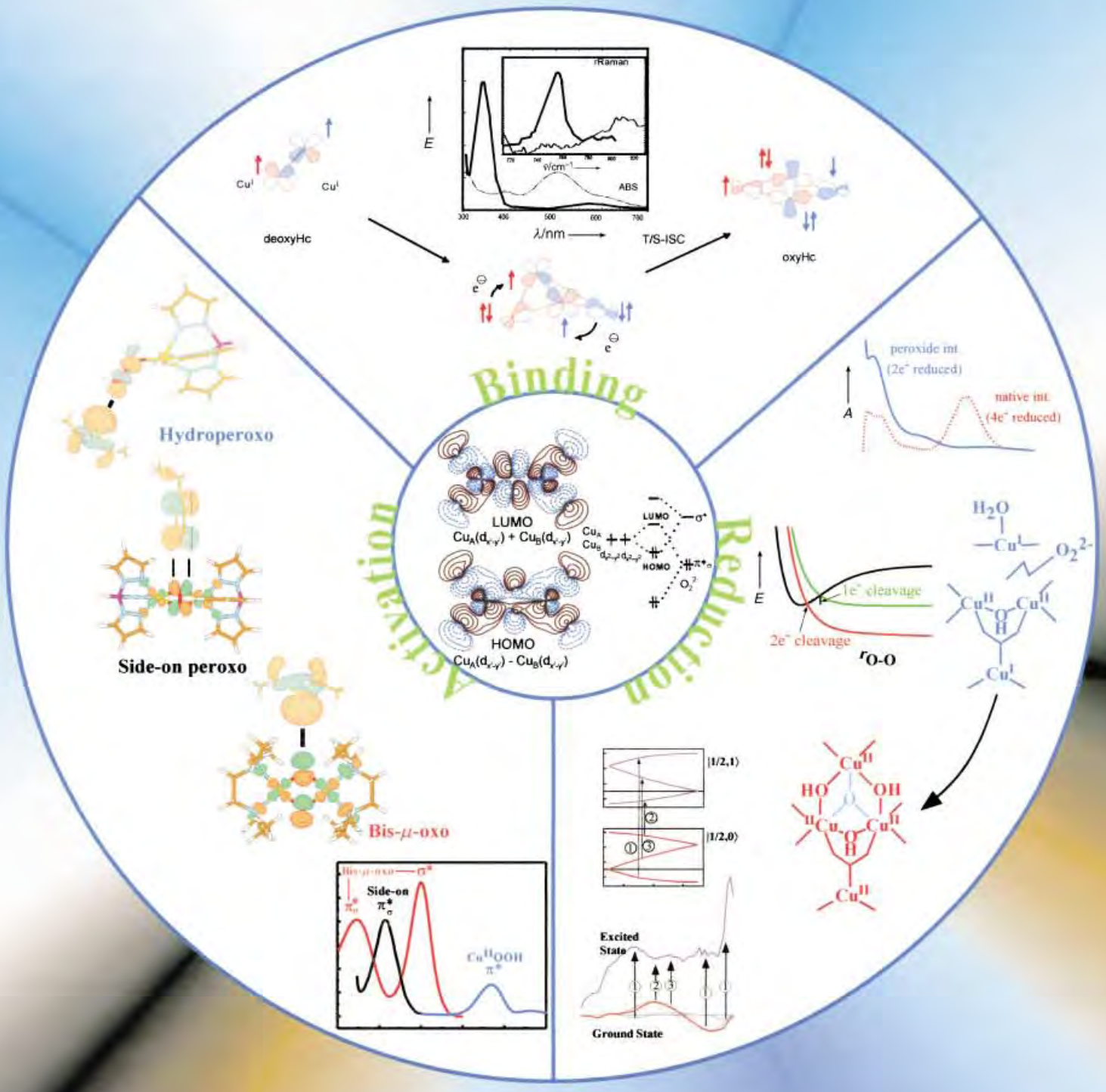
We acknowledge the financial support of the National Institutes of Health (postdoctoral fellowship to S.R.C.) and the Schering Research Foundation, Berlin (postdoctoral fellowship to D.T.).

Received: May 23, 2001 [A 474]

[1] F. Diederich, P. J. Stang, *Metal-catalyzed Cross-coupling Reactions*, Wiley-VCH, Weinheim, **1998**.
[2] L. S. Hegedus, *Transition Metals in the Synthesis of Complex Organic Molecules*, 2nd ed., University Science Books, Sausalito, **1999**.
[3] J. K. Still, *Angew. Chem.* **1986**, *98*, 504; *Angew. Chem. Int. Ed. Engl.* **1986**, *25*, 508 – 524.
[4] T. N. Mitchell, *Synthesis* **1992**, 803 – 815.
[5] N. Miyaura, A. Suzuki, *Chem. Rev.* **1995**, *95*, 2457 – 2483.
[6] A. Suzuki, *J. Organomet. Chem.* **1999**, *576*, 147 – 168.
[7] R. H. Grubbs, S. Chang, *Tetrahedron* **1998**, *54*, 4413 – 4450.
[8] A. Fürstner, *Alkene Metathesis in Organic Synthesis*, Springer, Berlin, **1998**.
[9] A. Fürstner, *Angew. Chem.* **2000**, *112*, 3140 – 3172; *Angew. Chem. Int. Ed.* **2000**, *39*, 3012 – 3043.
[10] M. Schuster, S. Blechert, *Angew. Chem.* **1997**, *109*, 2124 – 2145; *Angew. Chem. Int. Ed. Engl.* **1997**, *36*, 2036 – 2055.
[11] A. Fürstner, *Top. Catal.* **1997**, *4*, 285 – 299.
[12] K. J. Ivin, J. C. Mol, *Olefin Metathesis and Metathesis Polymerization*, 2nd ed., Academic Press, New York, **1997**.
[13] N. Miyaura, T. Ishiyama, M. Ishikawa, A. Suzuki, *Tetrahedron Lett.* **1986**, *27*, 6369 – 6372.
[14] K. Tamao, *Coupling Reactions Between sp^3 and sp^2 Carbon Centers*, in *Comprehensive Organic Synthesis*, *Vol. 3* (Eds.: B. M. Trost, I. Fleming), Pergamon Press, Oxford, **1991**.
[15] M. Kobayashi, E.-i. Negishi, *J. Org. Chem.* **1980**, *45*, 5223 – 5225.
[16] E.-i. Negishi, Z. Owczarczyk, *Tetrahedron Lett.* **1991**, *32*, 6683 – 6686.
[17] E.-i. Negishi, M. Ay, Y. V. Gulevich, Y. Noda, *Tetrahedron Lett.* **1993**, *34*, 1437 – 1440.
[18] A. B. Smith, Y. Qui, D. R. Jones, K. Kobayashi, *J. Am. Chem. Soc.* **1995**, *117*, 12011 – 12012.
[19] D. R. Williams, W. S. Kissel, *J. Am. Chem. Soc.* **1998**, *120*, 11198 – 11199.
[20] G. A. Molander, T. Ito, *Org. Lett.* **2001**, *3*, 393 – 396.
[21] N. Miyaura, T. Ishiyama, H. Sasaki, M. Ishikawa, M. Satoh, A. Suzuki, *J. Am. Chem. Soc.* **1989**, *111*, 314 – 321.
[22] J. A. Marshall, B. A. Johns, *J. Org. Chem.* **1998**, *63*, 7885 – 7892. See also new Highlight article: M. Kalesse, *ChemBioChem* **2000**, *1*, 171 – 175.
[23] J. A. Soderquist, J. C. Justo de Pomar, *Tetrahedron Lett.* **2000**, *41*, 3537 – 3539.
[24] D. S. Matteson, *Tetrahedron* **1989**, *45*, 1859 – 1885.
[25] D. L. Boger, *Modern Organic Synthesis*, TSRI Press, La Jolla, **1999**.
[26] K. Smith, A. Pelter in *Hydroboration of C=C and C≡C*, *Vol. 8* (Eds.: K. Smith, A. Pelter), Pergamon, Oxford, **1991**, pp. 703 – 731.
[27] D. J. Nelson, P. J. Cooper, R. Sounddararajan, *J. Am. Chem. Soc.* **1989**, *111*, 1414 – 1418.
[28] V. Farina, V. Krishnamurthy, W. J. Scott, *Organic Reactions*, Wiley, New York, **1997**.
[29] T. Oh-e, N. Miyaura, A. Suzuki, *J. Org. Chem.* **1993**, *58*, 2201 – 2208.
[30] A. F. Littke, C. Dai, G. C. Fu, *J. Am. Chem. Soc.* **2000**, *122*, 4020 – 4028.
[31] T. Ishiyama, N. Miyaura, A. Suzuki, *Tetrahedron Lett.* **1991**, *32*, 6923 – 6926.
[32] T. Ishiyama, N. Miyaura, A. Suzuki, *Bull. Chem. Soc. Jpn.* **1991**, *64*, 1999 – 2001.
[33] K. Matos, J. A. Soderquist, *J. Org. Chem.* **1998**, *63*, 461 – 470.
[34] B. H. Ridgway, K. A. Woerpel, *J. Org. Chem.* **1998**, *63*, 458 – 460.
[35] J. E. Marcone, K. G. Moloy, *J. Am. Chem. Soc.* **1998**, *120*, 8527 – 8528.
[36] A. L. Casado, P. Espinet, *J. Am. Chem. Soc.* **1998**, *120*, 8978 – 8985.
[37] A. L. Casado, P. Espinet, A. M. Gallego, *J. Am. Chem. Soc.* **2000**, *122*, 11771 – 11782.
[38] D. W. Old, J. P. Wolfe, S. L. Buchwald, *J. Am. Chem. Soc.* **1998**, *120*, 9722 – 9723.
[39] J. P. Wolfe, R. A. Singer, B. H. Yang, S. L. Buchwald, *J. Am. Chem. Soc.* **1999**, *121*, 9550 – 9561.
[40] A. Fürstner, A. Leitner, *Synlett* **2001**, *2*, 290 – 292.
[41] M. Sato, N. Miyaura, A. Suzuki, *Chem. Lett.* **1989**, 1405 – 1408.
[42] J. Uenishi, J.-M. Beau, R. W. Armstrong, Y. Kishi, *J. Am. Chem. Soc.* **1987**, *109*, 4756 – 4758.
[43] J. M. Humphrey, J. B. Aggen, A. R. Chamberlin, *J. Am. Chem. Soc.* **1996**, *118*, 11759 – 11770.
[44] S. A. Frank, H. Chen, R. K. Kunz, M. J. Schnaderbeck, W. R. Roush, *Org. Lett.* **2000**, *2*, 2691 – 2694.
[45] S. R. Chemler, S. J. Danishefsky, *Org. Lett.* **2000**, *2*, 2695 – 2698.
[46] J. K. Kochi, *Organometallic Mechanisms and Catalysis*, Academic Press, New York, **1978**.
[47] R. H. Crabtree, *The Organometallic Chemistry of the Transition Metals*, 2nd ed., Wiley, New York, **1994**.
[48] P. L. Bock, D. J. Boschetto, J. R. Rasmussen, J. M. Demers, G. M. Whitesides, *J. Am. Chem. Soc.* **1974**, *96*, 2814 – 2825.
[49] G. W. Kabalka, R. J. J. Newton, J. Jacobus, *J. Org. Chem.* **1979**, *44*, 4185 – 4187.
[50] G. W. Kabalka, N. S. Bowman, *J. Org. Chem.* **1973**, *38*, 1607 – 1608.
[51] D. Milstein, J. K. Stille, *J. Am. Chem. Soc.* **1979**, *101*, 4981 – 4991.
[52] Y. Hoshino, T. Ishiyama, N. Miyaura, A. Suzuki, *Tetrahedron Lett.* **1988**, *29*, 3983 – 3986.
[53] J. Bottin, M. Fetizon, *J. Chem. Soc. Chem. Commun.* **1971**, 1087 – 1088.
[54] M. M. Midland, Y. C. Kwon, *J. Org. Chem.* **1981**, *46*, 229 – 230.
[55] E. J. Corey, B. E. Roberts, *Tetrahedron Lett.* **1997**, *38*, 8919 – 8920.
[56] P. J. Stang, M. Hanack, L. R. Subramanian, *Synthesis* **1982**, 85 – 126.
[57] D. L. Comins, A. Dehghani, *Tetrahedron Lett.* **1992**, *33*, 6299 – 6302.
[58] J. L. J. Kane, K. M. Shea, A. L. Crombie, R. L. Danheiser, *Org. Lett.* **2001**, *3*, 1081 – 1084.
[59] E. G. Occhiato, A. Trabocchi, A. Guarna, *J. Org. Chem.* **2001**, *66*, 2459 – 2465.
[60] N. Miyaura, M. Ishikawa, A. Suzuki, *Tetrahedron Lett.* **1992**, *33*, 2571 – 2574.
[61] J. A. Soderquist, G. Leon, J. C. Colberg, I. Matrinez, *Tetrahedron Lett.* **1995**, *36*, 3119 – 3122.
[62] S. Y. Cho, M. Shibasaki, *Tetrahedron: Asymmetry* **1998**, *9*, 3751 – 3754.
[63] W. R. Kwochka, R. Damrauer, M. W. Schmidt, M. S. Gordon, *Organometallics* **1994**, *13*, 3728 – 3732.
[64] B. B. Smith, W. R. Kwochka, *J. Org. Chem.* **1997**, *62*, 8589 – 8590.
[65] C. R. Johnson, M. P. Braun, *J. Am. Chem. Soc.* **1993**, *115*, 11014 – 11015.
[66] A. D. Campbell, T. M. Raynham, J. K. Taylor, *Tetrahedron Lett.* **1999**, *40*, 5263 – 5266.
[67] M. Sabat, C. R. Johnson, *Org. Lett.* **2000**, *2*, 1089 – 1092.
[68] A. Kamatani, L. E. Overman, *J. Org. Chem.* **1999**, *64*, 8743 – 8744.
[69] A. Kamatani, L. E. Overman, *Org. Lett.* **2001**, *3*, 1229 – 1232.
[70] Y. Narukawa, K. Nishi, H. Onoue, *Tetrahedron* **1997**, *53*, 539 – 556.

[71] S. Vice, T. Bara, A. Bauer, C. A. Evans, J. Ford, H. Josien, S. McCombie, M. Miller, D. Nazareno, A. Palani, J. Tagat, *J. Org. Chem.* **2001**, *66*, 2487 – 2492.
[72] K. Mori, P. Puapoomchareon, *Liebigs Ann. Chem.* **1990**, 159 – 162.
[73] M. Uemura, H. Nishimura, Y. Hayashi, *Tetrahedron Lett.* **1990**, *31*, 2319 – 2322.
[74] M. Uemura, H. Nishimura, T. Minami, Y. Hayashi, *J. Am. Chem. Soc.* **1991**, *113*, 5402 – 5410.
[75] C. R. Johnson, M. W. Miller, A. Golebiowski, H. Sundram, M. B. Ksebati, *Tetrahedron Lett.* **1994**, *35*, 8991 – 8994.
[76] a) D. Meng, S. J. Danishefsky, *Angew. Chem.* **1999**, *111*, 1582 – 1585; *Angew. Chem. Int. Ed.* **1999**, *38*, 1485 – 1488; b) D. Meng, Q. Tan, S. J. Danishefsky, *Angew. Chem.* **1999**, *111*, 3393 – 3397; *Angew. Chem. Int. Ed.* **1999**, *38*, 3197 – 3201.
[77] For a new Highlight article on this topic, see: J. T. Starr, E. M. Carreira, *Angew. Chem.* **2000**, *112*, 1473 – 1478; *Angew. Chem. Int. Ed.* **2000**, *39*, 1415 – 1421.
[78] M. Ohba, N. Kawase, T. Fujii, *J. Am. Chem. Soc.* **1996**, *118*, 8250 – 8257.
[79] D. Trauner, S. J. Danishefsky, *Tetrahedron Lett.* **1999**, *40*, 6513 – 6516.
[80] D. Trauner, J. B. Schwartz, S. J. Danishefsky, *Angew. Chem.* **1999**, *111*, 3756 – 3758; *Angew. Chem. Int. Ed.* **1999**, *38*, 3542 – 3545.
[81] M. W. Carson, G. Kim, M. F. Hentemann, D. Trauner, S. J. Danishefsky, *Angew. Chem.* **2001**, *113*, 4582 – 4584; *Angew. Chem. Int. Ed.* **2001**, *40*, 4450 – 4452; M. W. Carson, G. Kim, S. J. Danishefsky, *Angew. Chem.* **2001**, *113*, 4585 – 4588; *Angew. Chem. Int. Ed.* **2001**, *40*, 4453 – 4456.
[82] B. M. Trost, C. B. Lee, *J. Am. Chem. Soc.* **1998**, *120*, 6818 – 6819.
[83] T. Nakamura, M. Shiozaki, *Tetrahedron Lett.* **2001**, *42*, 2701 – 2704.
[84] C. R. Harris, S. D. Kuduk, A. Balog, K. Savin, P. W. Glunz, S. J. Danishefsky, *J. Am. Chem. Soc.* **1999**, *121*, 7050 – 7062.
[85] A. Balog, C. Harris, K. Savin, G. Zhang, T.-C. Chou, S. J. Danishefsky, *Angew. Chem.* **1998**, *110*, 2821 – 2824; *Angew. Chem. Int. Ed.* **1998**, *37*, 2675 – 2678.
[86] D. Meng, P. Bertinato, A. Balog, D.-S. Su, T. Kamenecka, E. Sorensen, S. J. Danishefsky, *J. Am. Chem. Soc.* **1997**, *119*, 10073 – 10092.
[87] D.-S. Su, A. Balog, D. Meng, P. Bertinato, S. J. Danishefsky, Y.-H. Zheng, T.-C. Chou, L. He, S. B. Horwitz, *Angew. Chem.* **1997**, *109*, 2178 – 2181; *Angew. Chem. Int. Ed. Engl.* **1997**, *36*, 2093 – 2096.
[88] A. Balog, D. Meng, T. Kamenecka, P. Bertinato, D.-S. Su, E. J. Sorensen, S. J. Danishefsky, *Angew. Chem.* **1996**, *108*, 2976 – 2978; *Angew. Chem. Int. Ed. Engl.* **1996**, *35*, 2801 – 2803.
[89] B. Zhu, J. S. Panek, *Org. Lett.* **2000**, *2*, 2575 – 2578.
[90] C. B. Lee, T.-C. Chou, X.-G. Zhang, Z.-G. Wang, S. K. Kuduk, M. Chappell, S. J. Stachel, S. J. Danishefsky, *J. Org. Chem.* **2000**, *65*, 6525 – 6533.
[91] N. C. Kallen, R. L. Halcomb, *Org. Lett.* **2000**, *2*, 2687 – 2690.
[92] W. R. Moore, G. L. Schatzman, E. T. Jarvi, R. S. Gross, J. R. McCarthy, *J. Am. Chem. Soc.* **1992**, *114*, 360 – 361.
[93] A. Fürstner, I. Konetzki, *J. Org. Chem.* **1998**, *63*, 3072 – 3080.
[94] A. Fürstner, G. Seidel, *J. Org. Chem.* **1997**, *62*, 2332 – 2336.
[95] A. Kojima, T. Takemoto, M. Sodeoka, M. Shibasaki, *J. Org. Chem.* **1996**, *61*, 4876 – 4877.
[96] H. Takakura, K. Noguchi, M. Sasaki, K. Tachibana, *Angew. Chem.* **2001**, *113*, 1124 – 1127; *Angew. Chem. Int. Ed.* **2001**, *40*, 1090 – 1093.
[97] M. Sasaki, H. Fuwa, M. Inoue, K. Tachibana, *Tetrahedron Lett.* **1998**, *39*, 9027 – 9030.
[98] M. Sasaki, H. Fuwa, M. Ishikawa, K. Tachibana, *Org. Lett.* **1999**, *1*, 1075 – 1077.
[99] M. Sasaki, K. Noguchi, H. Fuwa, K. Tachibana, *Tetrahedron Lett.* **2000**, *41*, 1425 – 1428.
[100] H. Fuwa, M. Sasaki, K. Tachibana, *Tetrahedron Lett.* **2000**, *41*, 8371 – 8375.
[101] M. R. Netherton, C. Dai, K. Neuschütz, G. C. Fu, *J. Am. Chem. Soc.* **2001**, *123*, 10099 – 10100.

Cu_m/O_2 Bioinorganic Chemistry



ANGEWANDTE CHEMIE
©WILEY-VCH

Oxygen Binding, Activation, and Reduction to Water by Copper Proteins

Edward I. Solomon,* Peng Chen, Markus Metz, Sang-Kyu Lee, and Amy E. Palmer

Copper active sites play a major role in biological and abiological dioxygen activation. Oxygen intermediates have been studied in detail for the proteins and enzymes involved in reversible O_2 binding (hemocyanin), activation (tyrosinase), and four-electron reduction to water (multicopper oxidases). These oxygen intermediates exhibit unique spectroscopic features indicative of new geometric and electronic structures involved in oxygen activation. The spectroscopic and quantum-mechanical study of these intermediates has defined geometric- and electronic-structure/function correlations, and developed detailed reaction coordinates for the reversible binding of O_2, hydroxylation, and H-atom abstraction from different substrates, and the reductive cleavage of the O–O bond in the formation water.

Keywords: bioinorganic chemistry · copper · electronic structure · metalloenzymes · oxygen activation · reaction mechanisms

1. Introduction

Copper, along with iron active sites dominate the field of biological oxygen chemistry[1] and play important roles in homogeneous[2] and heterogeneous catalysis.[3, 4] Copper proteins are involved in reversible dioxygen binding (hemocyanin),[5] two-electron reduction to peroxide coupled to oxidation of substrates (amine, galactose, and catechol oxidases),[6] activation for hydroxylation (dopamine β-hydroxylase, peptidylglycine α-hydroxylating monooxygenase, tyrosinase, and particulate-methane monooxygenase),[6, 7] and the four-electron reduction to water coupled to substrate oxidation (laccase, ascorbate oxidase, ceruloplasmin and Fet3p)[7] or proton pumping (cytochrome c oxidase, which also contains heme–iron centers).[8] The known copper proteins which are involved in dioxygen binding, activation, and reduction are given in Scheme 1, which is organized based on active-site structural type. Key structural features from the Protein DataBank (PDB) are given in Figure 1.[9–16]

Amine oxidase and galactose oxidase catalyze the two-electron reduction of O_2 to peroxide at a single copper center, which can provide only one electron.[6] As shown in Figure 1A this is accomplished with the aid of an additional redox-active functional group, a topa-quinone in amine oxidase and a tyrosine ligand covalently linked to a cysteine residue through a thioether bond in galactose oxidase. Both functional groups are generated by the post-translational modification of a protein residue by the copper center. In the case of amine oxidase, this involves hydroxylation of a tyrosine by O_2 and involves a single copper center in a reaction that to date is not defined, but may involve tyrosine activation by Cu^{II} centers.[17, 18]

Dopamine β-hydroxylase (DβH) and peptidylglycine α-hydroxylating monooxygenase (PHM) have noncoupled binuclear copper sites,[6] where "coupling" refers to magnetic interactions between the copper centers. This absence of coupling indicates that the Cu^{II} centers of the resting enzyme active site are at least 7 Å apart with no bridging ligation, which is consistent with the crystallographic study on peptidylglycine α-hydroxylating monooxygenase (Figure 1B).[15, 16] The enzyme has one copper center (referred to as Cu_M since it has a methionine ligand[19]) involved in catalysis which is thought to proceed through hydrogen-atom abstraction from the substrate (the benzylic hydrogen in DβH or the α-carbon hydrogen in PHM) by an as-yet unobserved hydroperoxide–Cu^{II}_M complex.[6] The second electron to form the hydroperoxide is derived from Cu_H (the copper with all histidine ligands). Since the copper centers are not coupled (i.e. there is no bridge) the mechanism of transporting the second electron to Cu_M is unclear and has been proposed to involve either a new electron-transfer pathway formed by the substrate bridging the two distant copper centers[16] or by O_2 reduction to superoxide at Cu_H and superoxide channeling to Cu_M.[20]

The coupled binuclear copper proteins include hemocyanin, tyrosinase, and catechol oxidase.[5, 7] The binuclear copper centers in these proteins are strongly coupled through a bridging ligand which provides a direct mechanism for the

[*] Prof. Dr. E. I. Solomon, P. Chen, Dr. M. Metz, Dr. S.-K. Lee, A. E. Palmer
Department of Chemistry
Stanford University
Stanford, CA 94305 (USA)
Fax: (+1) 650-725-0259
E-mail: Edward.Solomon@stanford.edu

 © WILEY-VCH Verlag GmbH, D-69451 Weinheim, 2001 1433-7851/01/4024-4571 $ 17.50+.50/0

two-electron reduction of dioxygen. In oxy-hemocyanin (Figure 1 C) this bridge is the dioxygen unit which binds reversibly to deoxy-hemocyanin ($2\,Cu^{I}$) as peroxide in a side-on bridged (μ-η^2:η^2) structure.[14, 21] This is the most stable oxygen intermediate in copper proteins and exhibits unique spectral features. These features are indicative of a novel electronic structure for the side-on peroxo – Cu^{II}_2 structure which plays a key role in reactivity (Section 2).[5] The spectral/structural features of oxy-hemocyanin and related model complexes provide the reference for oxygen intermediates in the other


E. I. Solomon


P. Chen


M. Metz


A. Palmer


S.-K. Lee

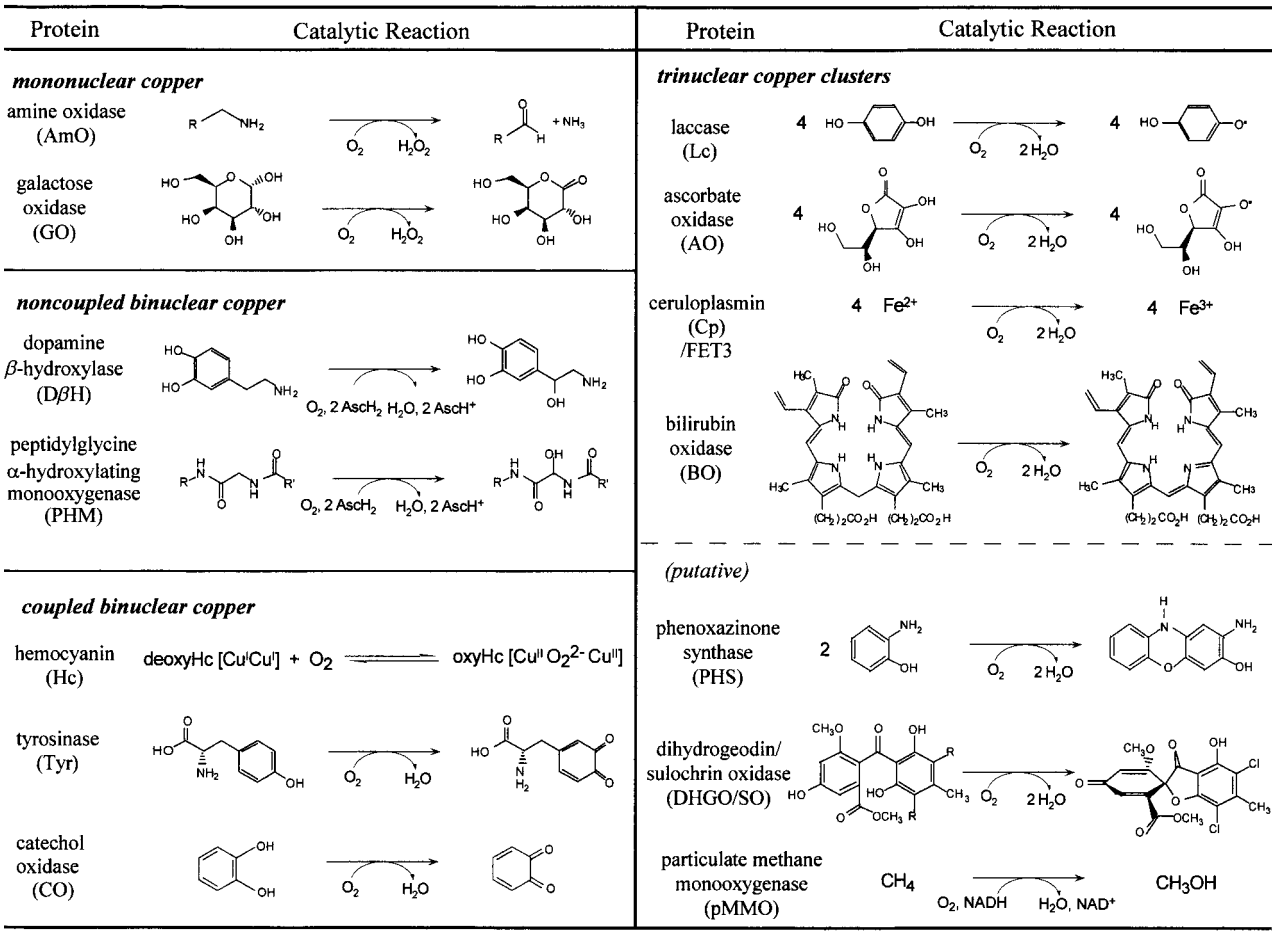
Edward I. Solomon grew up in North Miami Beach, FL, received his Ph.D. from Princeton University (with Donald S. McClure), and was a postdoctoral fellow at the H. C. Ørsted Institute (with Carl J. Ballhausen) and then at Caltech (with Harry B. Gray). He was a professor at MIT until 1982. He then moved to Stanford University where he is now the Monroe E. Spaght Professor of Humanities and Sciences. His research is in the fields of physical-inorganic and bioinorganic chemistry with emphasis on the application of a wide variety of spectroscopic methods to elucidate the electronic structures of transition metal complexes and their contributions to physical properties and reactivity. He has presented numerous named lectures including the First Glen Seaborg Lectures at the University of California, Berkeley, and has been an invited professor at the Tokyo Institute of Technology, Japan, University of Paris, Orsay, France, Tata Institute, Bombay, India, Xiamen University, China, and La Plata University, Argentina. He is a Fellow of the American Academy of Arts and Sciences and the American Association for the Advancement of Sciences and has received a range of awards including the Ira Remsen Award from the Maryland Section of the American Chemical Society, the G. W. Wheland Medal from the University of Chicago and the ACS National Award in Inorganic Chemistry for 2001.

Peng Chen grew up in Jiangsu, China and received his B.S. from Nanjing University in 1997. After spending a year at University of California at San Diego learning organic synthesis with Prof. Yitzhak Tor, he moved to Stanford University where he is the Gerhard Casper Stanford Graduate Fellow working toward his Ph.D. degree in Prof. Edward I. Solomon's group. His research focuses on electronic-structure studies of biologically related copper sites involved in oxygen activation by using a combination of spectroscopic methods and theoretical calculations.

Markus Metz received his Diploma in Chemistry from the Bayerische Julius-Maximilians-Universität Würzburg, Germany, and completed his Ph.D. under the supervision of Prof. Peter Hofmann at he the Ruprecht-Karls-Universität, Heidelberg, on theoretical elucidation of organometallic reaction mechanisms. From 1999 to 2001 he was a DAAD postdoctoral fellow with Professor Edward I. Solomon carrying out theoretical studies on oxygen binding to multinuclear copper proteins. He is a computational chemist at AnorMED Inc. designing metal-based therapeutics.

Amy Palmer received her B.A. in biophysical chemistry in 1994 from Dartmouth College where she studied the molecular mechanism of chromium carcinogenicity with Professor Karen E. Wetterhahn. In 1995, she moved to Stanford University and joined the group of Professor Edward I. Solomon. Her research involves spectroscopic and kinetic studies aimed at elucidating the mechanism of substrate oxidation and O_2 reduction in multicopper enzymes. She is the Franklin Veatch Memorial Fellow at Stanford.

Sang-Kyu Lee, a native of Korea, received his B.S. degree in biochemistry from Lehigh University in 1989 and his Ph.D. degree in biochemistry from the University of Minnesota, Minneapolis, in 1998. His Ph.D studies with Prof. John D. Lipscomb focused on the enzyme reaction mechanism of methane monooxygenase and led to the discovery of reactive intermediates P and Q. He continued his pursuit of metalloprotein enzymology in his postdoctoral research with Prof. Edward I. Solomon through detailed spectroscopic characterization of key intermediates in the reduction of dioxygen to water by multicopper oxidases.



Scheme 1. Copper proteins involved in oxygen binding and activation.

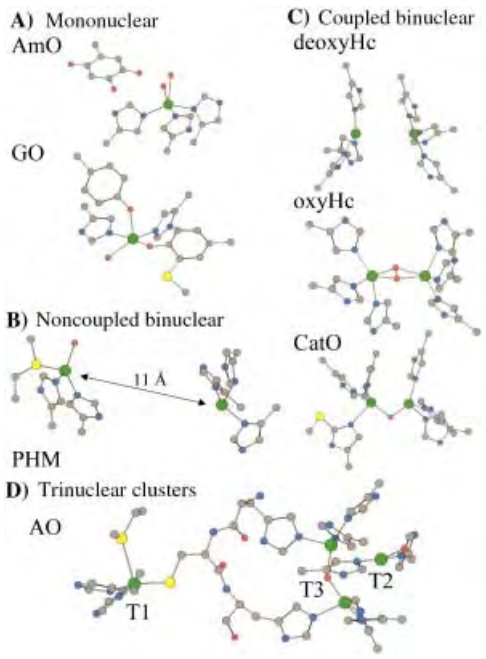


Figure 1. Crystal structures of copper proteins: A) copper amine oxidase (AmO, PDB code *1KSI*), galactose oxidase (GO, PDB code *1GOG*), B) peptidylglycine α-hydroxylating monooxygenase (PHM, PDB code *1PHM*), C) deoxygenated form of hemocyanin (deoxyHc, PDB code *1LLA*), oxygenated form of hemocyanin (oxyHc, PDB code *1OXY*), catechol oxidase (CatO, PDB code *1BT3*), D) ascorbate oxidase (AO, PDB code 1*AOZ*).

copper enzymes which perform different reactions, and allow geometric- and electronic-structure correlations with function in copper chemistry. While a crystal structure is not yet available for tyrosinase, from its spectral features oxy-tyrosinase has a very similar active site to oxy-hemocyanin, the side-on peroxo–Cu_2^{II} structure.[22] However, in the case of oxy-tyrosinase, the site catalyzes the electrophilic oxygenation of phenol to catechol and the two-electron oxidation of catechol to quinone. We have shown that an important difference between hemocyanin and tyrosinase is that the substrate can access and directly coordinate to the copper active site in tyrosinase but not in hemocyanin.[22] The generally accepted mechanism for this reaction is shown in Figure 2.[7] An important question in the monophenolase cycle is whether the side-on bridged peroxo form directly hydroxylates the phenol or whether a bis-μ-oxo Cu_2^{III} structure is also present which carries out this reaction. The side-on peroxo/bis-μ-oxo isomerization was observed and studied in detail in Cu_2O_2 model chemistry.[23] The electronic structures of the side-on peroxo–Cu_2^{II},[24] the bis-μ-oxo Cu_2^{III},[25] and the Cu^{II}–hydroperoxo intermediate[26] indicated above for the noncoupled binuclear copper enzymes will be described and correlated with electrophilic hydroxylation and hydrogen-atom abstraction reactivity in Section 3. The diphenolase mechanism in Figure 2 has been supported by the recent crystal structure of the met (i.e. oxidized, $2\,Cu^{II}$) or resting form of catechol oxidase.[10] The crystal structure also supports

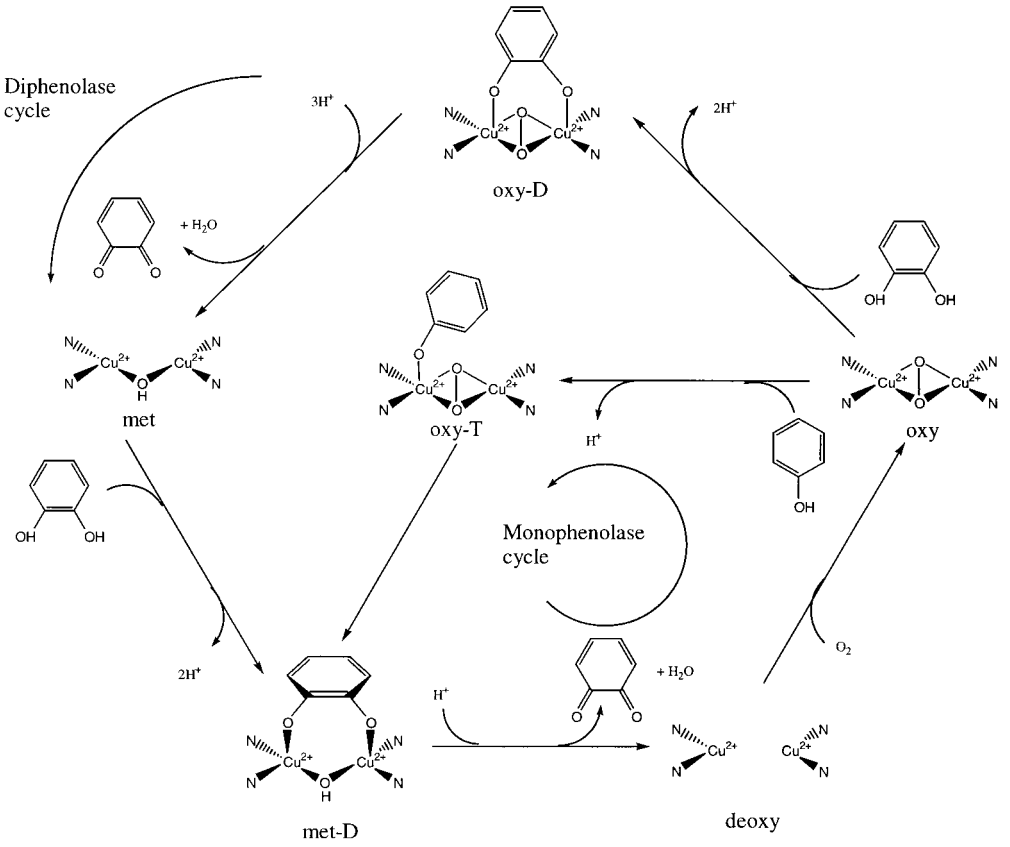


Figure 2. Molecular mechanism for catalysis by tyrosinase. For clarity, the axial ligand on each copper is not included. Reproduced from ref. [27].

the idea of substrate access and coordination to the copper center in catechol oxidase and tyrosinase but not hemocyanin. While both enzymes oxidize catechol to quinone only tyrosinase can hydroxylate phenol. The structural origin of this difference in reactivity is not yet clear but may relate to different structural requirements for the different reactions. Spectral data on the binding of competitive inhibitors to the binuclear Cu site in tyrosinase indicate that a trigonal-bipyramidal rearrangement is involved in phenol hydroxylation (monophenolase cycle, oxy-T $\rightarrow$met-D, Figure 2) but not catechol oxidation (diphenolase cycle).[27]

The final class of structural types in biological Cu/O_2 chemistry is the trinuclear copper cluster found in the multicopper oxidases[7, 28] and potentially in other enzymes including particulate-methane monooxygenase.[29] Laccase and Fet3p[30] are the simplest of the multicopper oxidases. These enzymes contain a trinuclear copper cluster (comprising a hydroxide-bridged coupled binuclear Cu^{II} center called type 3, T3[31] and a three-coordinate mononuclear Cu^{II} center called type 2, T2) and an additional blue, or type 1 (T1), copper center. The type 1 Cu center is >13 Å from the trinuclear cluster but linked to it through an electron-transfer pathway (T1 – Cys – His – T3) (Figure 1D).[9] Ascorbate oxidase is basically a dimer of laccase, and ceruloplasmin contains two additional remote type 1 copper centers.[9, 32] Substrate oxidation occurs at the type 1 center and electrons are transferred rapidly over the >13 Å electron-transfer pathway to the trinuclear copper cluster where dioxygen is reduced to water. An oxygen intermediate, known as the native intermediate, is trapped in the reduction of O_2 by fully reduced (i.e. $4Cu^{I}$) laccase.[7, 33–35] If the type 1 center is replaced by a redox-inactive mercuric ion[36] (the T1Hg derivative) and the reduced trinuclear copper cluster is treated with O_2, a less-reduced oxygen intermediate, the peroxide intermediate, is generated.[37] These intermediates have been studied in detail and this has led to the molecular mechanism for the four-electron reduction of dioxygen to water and a general model for the reductive cleavage of the O–O bond.[38] These studies are presented in Section 4.

The research described below demonstrates the power of combining spectroscopy with density functional theory (DFT) in developing geometric- and electronic-structure/function correlations in biological systems.

2. Dioxygen Binding

2.1. Unique Electronic Structure of Oxy-Hemocyanin

As indicated in the introduction, oxy-hemocyanin and structurally equivalent μ-η^2:η^2 side-on peroxo-bridged binuclear copper model complexes exhibit unique spectral features.[1, 5, 7, 39] First consider peroxide end-on bound in a mononuclear tetragonal Cu^{II} complex as a reference. The key valence orbitals are the high-energy, half-occupied $d_{x^2-y^2}$ orbital on the copper center and the doubly degenerate π^* HOMO on the peroxide.[5] As shown in Figure 3A, one π^* orbital will form a σ bond with the Cu $d_{x^2-y^2}$ orbital and be stabilized (the π^*_σ) whereby the $d_{x^2-y^2}$ half-occupied HOMO will be destabilized, while the other π^* orbital is perpendicular to the Cu-O-O plane (the π^*_v, v = vertical) and only weakly interacts with the copper center. As charge-transfer absorption intensity reflects orbital overlap, the peroxide σ-donor bond produces one intense charge-transfer (CT) transition, the peroxo $\pi^*_\sigma \rightarrow$Cu $d_{x^2-y^2}$ charge transfer. This transfer is observed experimentally in an end-on bound peroxo – Cu^{II} model complex as an absorption band at around 500 nm with $\varepsilon \approx 5800\,M^{-1}cm^{-1}$ (Figure 3B).[40] Also included in Figure 3B is the absorption spectrum of oxy-hemocyanin which exhibits the peroxide $\pi^*_\sigma \rightarrow Cu^{II}$ charge-transfer transition at much higher energy and with about four times the intensity ($\lambda = 350$ nm, $\varepsilon \sim 20000\,M^{-1}cm^{-1}$).[40, 41] Resonance Raman spectra obtained by excitation into these peroxide

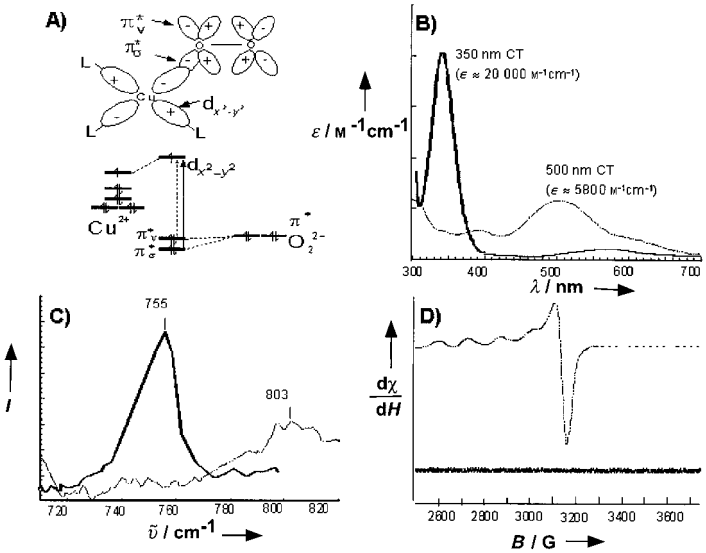


Figure 3. A) Electronic structure of the peroxide – Cu^{II} bond of an end-on bound peroxy – Cu^{II} model complex. Adapted from ref. [5], B) absorption spectra of oxy-hemocyanin (——) and a peroxy – Cu^{II} model complex (- - - -); CT = charge transfer, C) resonance Raman spectra of the intra-peroxide stretch of oxy-hemocyanin (——) and the peroxy – Cu^{II} model complex (——), D) EPR spectra of the oxy-hemocyanin (lower spectrum) and of a tetragonal Cu^{II} model complex. Adapted from ref. [7].

charge-transfer transitions (Figure 3C) show an O–O stretch at about 800 cm^{-1} for the end-on bound peroxide – Cu^{II} model complex, while for oxy-hemocyanin this vibration is at 750 cm^{-1} reflecting an extremely weak O–O bond.[40, 42] Finally, in contrast to mononuclear tetragonal Cu^{II} complexes which exhibit the "normal" EPR spectrum shown in Figure 3D, oxy-hemocyanin has no EPR signal because of the magnetic coupling between the two Cu^{II} centers, mediated by the peroxide bridge.[7] From SQUID (superconducting quantum-interference device) magnetic susceptibility measurements there is a strong antiferromagnetic coupling (two Cu^{II} centers with $S = ½$ couple to form a singlet and a triplet) with the singlet ground state below the triplet by more than 600 cm^{-1}.[43]

We have shown that these unique spectral features reflect the novel electronic structure of the side-on peroxo-bridged Cu_2^{II} complex in Figure 1C.[24, 44] As shown in Figure 4, the HOMO and LUMO for the binuclear Cu^{II} complexes are formed if one takes the symmetric and antisymmetric linear combinations of the half occupied $d_{x^2-y^2}$ orbitals of the two copper centers and allows these to interact with the peroxide valence orbitals in the side-on structure. The dominant interaction again involves the π_σ^* orbital and its bonding with the symmetric combination of $d_{x^2-y^2}$ orbitals to form the LUMO. As with the end-on bound peroxo – Cu^{II} complex in Figure 3A a peroxide σ-donor bond is formed, however, the bonding/antibonding interaction is much larger. The origin of this strong σ-donor interaction can be observed in the contours of the LUMO, where, in the side-on bridged structure, the peroxide has four σ-donor bonds to the two copper centers. This very strong σ-donor interaction leads to the high energy of the peroxide $\pi_\sigma^* \rightarrow Cu^{II}$ charge-transfer transition of oxy-hemocyanin and to its high intensity which reflects the orbital overlap and hence the strength of the σ-donation. An additional bonding interaction is observed in oxy-hemocyanin which is not present in the end-on peroxo – Cu^{II} monomer. This interaction involves stabilization of the antisymmetric combination of $d_{x^2-y^2}$ orbitals by a small bonding interaction with the high-energy unoccupied σ* orbital on the peroxide (Figure 4, HOMO contour). This in turn leads to some π backbonding of electron density from the copper center into the σ* orbital of the peroxide, which is strongly antibonding with respect to the O–O bond. This leads to a very weak peroxide bond and the low O–O stretching frequency in the resonance Raman spectrum of oxy-hemocyanin (Figure 3C).[45] Finally, since in dimers the bridging ligand causes the HOMO/LUMO splitting which is the origin of the antiferromagnetic coupling, the combination of very strong σ donation (destabilization of the LUMO) and π backbonding (stabilization of the HOMO) leads to the large stabilization of the singlet ground state in oxy-hemocyanin.[24]

From the bonding description of oxy-hemocyanin (Figure 4) the key occupied valence orbitals (peroxide π_σ^* and the HOMO ($d_{x^2-y^2} - d_{x^2-y^2}$)) are lowered in energy which gives a very strong peroxide – Cu_2^{II} bond. This stabilizes oxy-hemocyanin from loss of peroxide, which would produce an oxidized (i.e. met) site which can no longer function in dioxygen binding, and greatly contributes to the energetics of O_2 binding to hemocyanin as presented in Section 2.2.

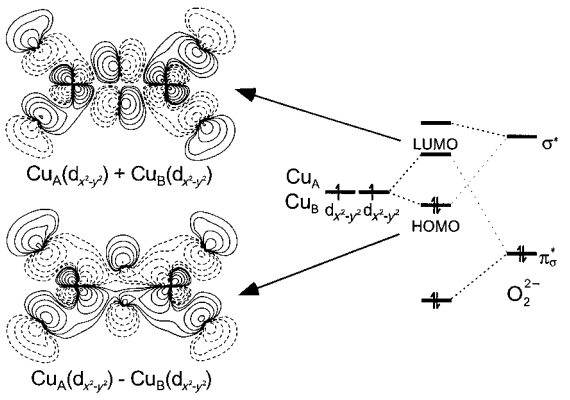


Figure 4. Electronic structure of the peroxide – Cu^{II} bond of oxy-hemocyanin. Adapted from ref. [1].

2.2. The Reaction Coordinate

The unique spectral features for oxy-hemocyanin described above and the more limited data available for deoxy-hemocyanin (two Cu^{I} centers with d^{10} configurations) have been used to evaluate and calibrate hybrid-DFT calculations (at the B3LYP/Lanl2dz level)[46–50] which include time-dependent DFT[51, 52] to correlate to spectral data. These results will not be discussed here except to indicate that the calculations of structural and spectroscopic data and the general bonding description obtained are reasonable, but the oxy-hemocyanin site is calculated to be too covalent and this will effect energetic considerations (see below).[53] These calculations give the change in electronic structure on O_2 binding to deoxy-hemocyanin (Figure 5). The HOMO of

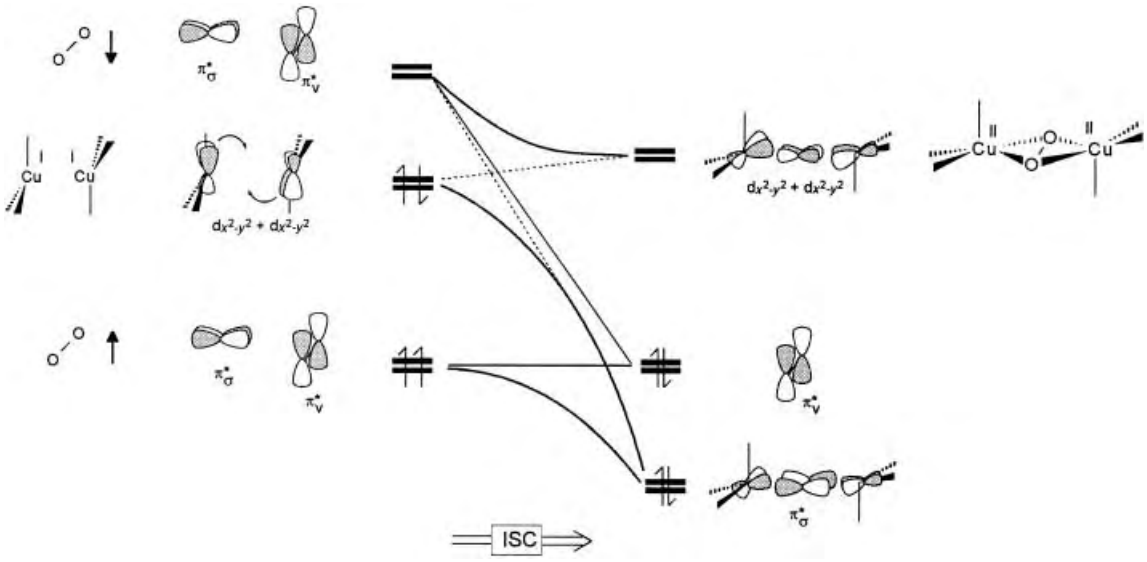


Figure 5. Orbital correlation diagram for O_2 binding to deoxy-hemocyanin. Adapted from ref. [53].

deoxy-hemocyanin has $d_{x^2-y^2}$ orbitals perpendicular to the Cu–Cu vector (each copper(I) unit has an approximately trigonal-planar structure). On O_2 binding these $d_{x^2-y^2}$ orbitals are destabilized and rotate to donate two electrons into the π^* orbital set of O_2 reducing the dioxygen to peroxide and producing the copper-centered LUMO (Figure 5, right, and Figure 4).[53] Thus, O_2 binding involves two-electron transfer and intersystem crossing (ISC) from triplet dioxygen to the singlet ground state of oxy-hemocyanin.

We have used these experimentally calibrated electronic-structure calculations to evaluate the reaction coordinate of oxygen binding to hemocyanin.[53] Figure 6 shows the structures obtained as the peroxide of oxy-hemocyanin is displaced

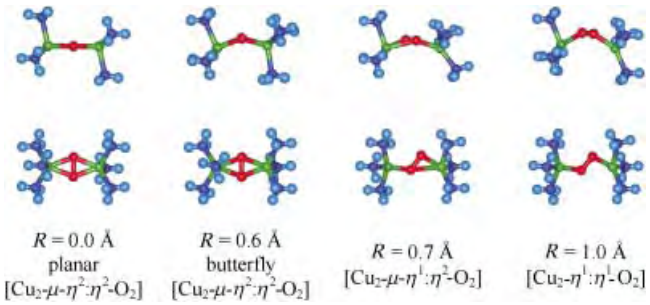


Figure 6. The reaction coordinate of O_2 coordination/release by Hemocyanin. Top: view along the O–O bond in $[Cu_2(\mu\text{-}\eta^2\text{:}\eta^2O_2)]$; Bottom: molecules rotated around the copper – copper vector by 90°. Adapted from ref. [53].

by an amount R above the molecular plane and the geometry is partially optimized on going to the deoxy site with O_2 release. First, the site distorts to a butterfly structure, then to an asymmetrically bridged $\mu\text{-}\eta^1\text{:}\eta^2$, then to an end-on bridged $\mu\text{-}\eta^1\text{:}\eta^1$ structure, and finally loss of O_2 (not shown in Figure 6). This reaction coordinate reflects that maximizing metal – ligand overlap plays a dominant role in determining the coordination mode and shows that even though a nonsymmetric coordination mode does occur, it is energetically favorable to bridge the two copper centers of the binuclear active site.

Figure 7 presents the change in charge along this reaction coordinate. As the peroxide is displaced from the molecular plane, the positive charge on the copper center and the

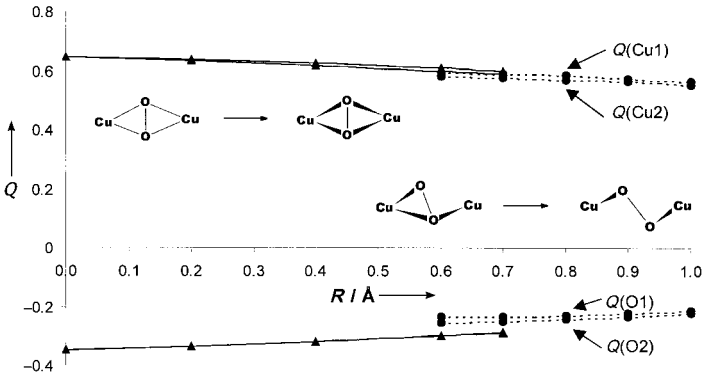


Figure 7. Changes of partial charges (Q) of the copper and oxygen atoms during O_2 release from oxy-hemocyanin in the singlet state with $\mu\text{-}\eta^2\text{:}\eta^2\text{-}O_2$ coordination (——) and in the triplet state with nonsymmetric O_2 coordination (- - - -). R is the distance between the center of the O – O and Cu – Cu vectors. Adapted from ref. [53].

negative charge on the peroxide oxygen atoms continually decrease, consistent with charge transfer to form dioxygen and the reduced site. The charge is donated equivalently to both copper centers even in the non-symmetric $\mu\text{-}\eta^1\text{:}\eta^2$ coordination mode. Thus, simultaneous two-electron transfer is thermodynamically favorable for the peroxide-bridged binuclear copper site. The continuous charge flow in the singlet state prepares the complex for ISC.

We have been particularly interested in understanding how hemocyanin overcomes the spin-forbidden O_2 binding.[53] Figure 8 shows that along the reaction coordinate for O_2 release, as the peroxide is raised above the molecular plane in the butterfly distorted structure the singlet/triplet splitting

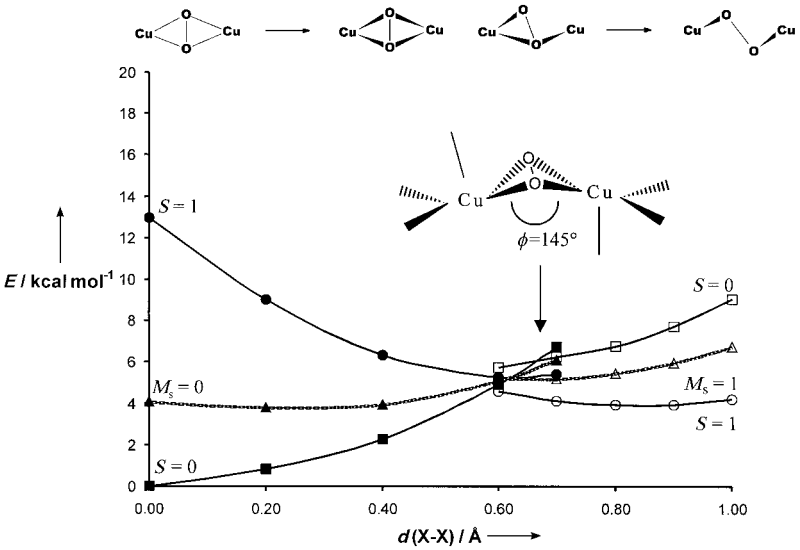


Figure 8. Potential-energy surfaces for the interconversion of oxy-hemocyanin and deoxy-hemocyanin. Filled patterns: symmetric O_2 coordination (μ-η^2:η^2); open patterns: non-symmetric O_2 coordination (μ-η^1:η^2 and μ-η^2:η^2); triplet state: $S=1$; broken symmetry state: magnetic spin quantum number $M_s=0$; singlet state ($S=0$) is spin-projected. The term d(X-X) is the distance between the center of the O–O and the Cu–Cu vectors. Adapted from ref. [53].

greatly decreases and there is ISC at $R \sim 0.6$ Å. As the peroxide is displaced out of the Cu_2O_2 plane, the π^*_σ becomes less σ bonding and the π^*_v becomes involved in σ overlap. These events bring the π* set of orbitals on the peroxide bridge energetically close together and allows them to orient along individual Cu-$\eta^2O_2^{2-}$ planes (Figure 9). As shown in Figure 9B, this produces close to an orthogonal magnetic-orbital pathway between the two Cu^{II} centers which eliminates the superexchange coupling and leads to the triplet ground state. The reduced antiferromagnetic interaction is also apparent from the small contribution of the second copper center to the LUMO (Figure 9B). From Scheme 2 for the triplet ground state, electron transfer results in a spin-up electron in each orthogonal π* orbital of the peroxide which correlates with the $^3\Sigma_g^-$ ground state of O_2 and leads to further energetic stabilization of the triplet ground state by single-center electron exchange.

The energetics of O_2 binding to deoxy-hemocyanin are summarized in Figure 10 and compared to those of mononuclear Cu model systems. The O_2 binding is found to be exothermic by about 16 kcal mol^{-1} which is approximately twice that determined by experiment and reflects that the B3LYP/Lanl2dz calculations overestimate the covalency of the bonds in oxy-hemocyanin. The calculations reproduce the change in energy of O_2 binding observed between the tense and the relaxed quaternary structures of hemocyanin,[1, 54] where the relaxed deoxy site has a shorter Cu^I–Cu^I distance (3.5 Å vs. 4.6 Å for the tense site) and a higher affinity for O_2.[14] Importantly, the calculations show that O_2 binding to isolated Cu^I monomers to form the μ-η^2:η^2 $O_2^{2-}Cu^{II}_2$ dimer is less favorable, which reflects that the protein destabilizes the deoxy site by holding the two Cu^I centers only a short distance apart. This proximity produces a repulsive interaction and increases the exothermicity of O_2 binding to the binuclear copper site in the protein and also provides a mechanism for the protein to regulate the O_2 affinity (i.e. cooperativity) by changing the Cu–Cu distance in deoxy-hemocyanin.[53] (In model complexes this reaction is made more favorable by strained multidentate ligands which destabilize the Cu^I site.[55, 56])

In summary (Figure 11), when triplet O_2 binds to deoxy-hemocyanin, charge is transferred from the copper centers which shifts the unpaired spin density onto the separate metal centers reducing the exchange stabilization of the $^3\Sigma_g^-$ ground state of dioxygen. The reaction coordinate then turns on the superexchange pathway through the bridging peroxide which leads to antiferromagnetic coupling and thus stabilization of the singlet state. This appears to be a general mechanism utilized to overcome the spin-forbidden O_2 binding by coupled binuclear metal sites in metalloproteins.[53]

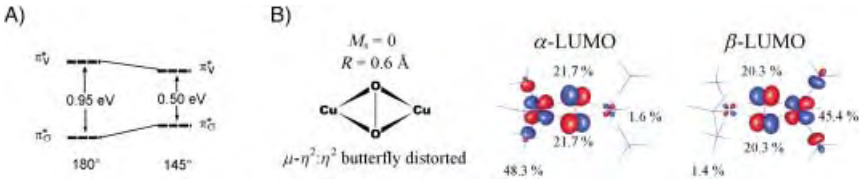
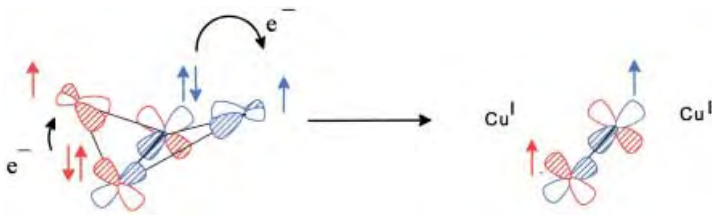


Figure 9. A) Reduction of the energy difference between the two π* peroxide orbitals from butterfly distortion of the [Cu_2(μ-η^2:η^2O_2)] core (spin-orbital energies are averaged), B) contour surface plots of the α and β LUMO obtained from broken-symmetry calculations on the butterfly structure (Figure 8). The Cu and O orbital contributions are obtained from Mulliken population analysis. Adapted from ref. [53].



Scheme 2. Electron transfer out of orthogonal π* peroxide orbitals in the triplet state. Adapted from ref. [53].

3. O_2 Activation by Copper Enzymes and Related Model Complexes

As presented in the introduction, a mononuclear Cu^{II}–hydroperoxide complex (Scheme 3A) is thought to be the catalytic intermediate in H-atom abstraction from substrates in the noncoupled binuclear copper enzymes DβH and PHM.[6] In the coupled binuclear copper enzyme tyrosinase which catalyzes the electrophilic hydroxylation of phenol (Figure 2), a side-on peroxide-bridged

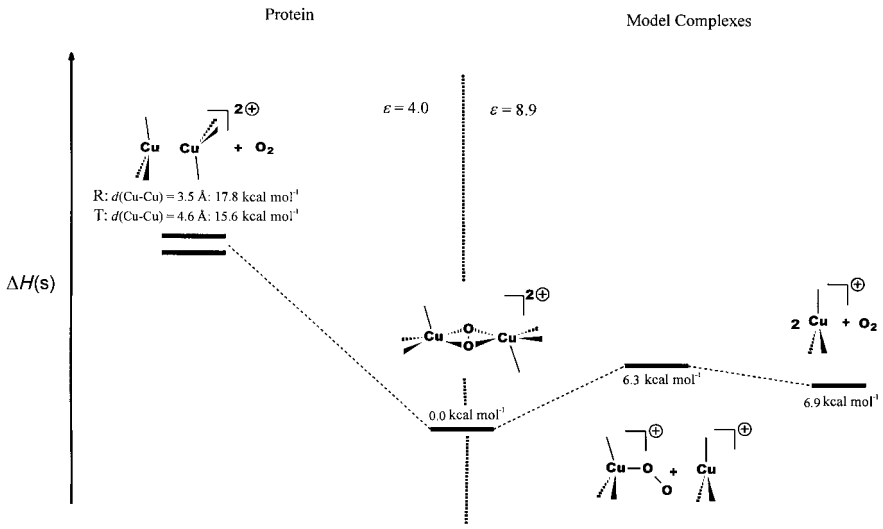
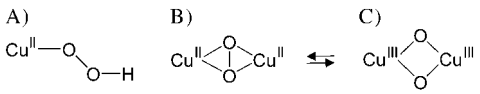


Figure 10. Energy minima of the binuclear (left: protein) and mononuclear model complexes (right) at different stages of O_2 reduction. A mononuclear superoxo complex is included which is not found for the binuclear models. Energy values are derived from spin-projection, frequency, and PCM (polarized continuum model) calculations. For clarity the NH_3 ligands are indicated by lines; R = relaxed structure, T = tense structure, ε = dielectric constant. Adapted from ref. [53].



Scheme 3. Key Cu/O_2 species involved in the dioxygen activation.

binuclear Cu_2^{II} intermediate equivalent to oxy-hemocyanin is present (Scheme 3B).[7] In copper model complexes this side-on peroxo–Cu_2^{II} structure can be in rapid equilibrium with the bis-μ-oxo Cu_2^{III} isomer (Scheme 3C).[23] As presented in section 2.1 for the side-on peroxo–Cu_2^{II} structure, we have used spectroscopy combined with DFT calculations to elucidate the electronic structures of the three peroxo species in Scheme 3.[24–26] Here we consider how these electronic structures contribute to peroxide activation for electrophilic hydroxylation and H-atom abstraction and define electronic differences related to differences in reactivity.

We first consider the binuclear Cu–XYL model system $[Cu_2^I(NO_2\text{-XYL})]$ from Karlin et al (Scheme 4; XYL = *N*,*N*,*N*′,*N*′-tetra(2-pyridylethyl)-3,5-di-(aminomethyl)phenyl) which has been shown to hydroxylate the aromatic ring of the ligand through an electrophilic mechanism very similar to that of tyrosinase.[57] At low temperature with an electron withdrawing $R = NO_2$ group on the ring *para* to the position being hydroxylated, the oxygen intermediate can be stabilized; its absorption spectrum (Figure 12A) is very similar to that of the side-on peroxide-bridged Cu_2^{II} site of oxy-hemocyanin and oxy-tyrosinase but with an additional feature at around 430 nm (ca. 25250 cm^{-1}) which could be contributed by bis-μ-oxo Cu_2^{III} isomer. This possibility could be evaluated experimentally through resonance Raman spectroscopy of this band (Figure 12B).[58] The bis-μ-oxo Cu_2^{III} species would

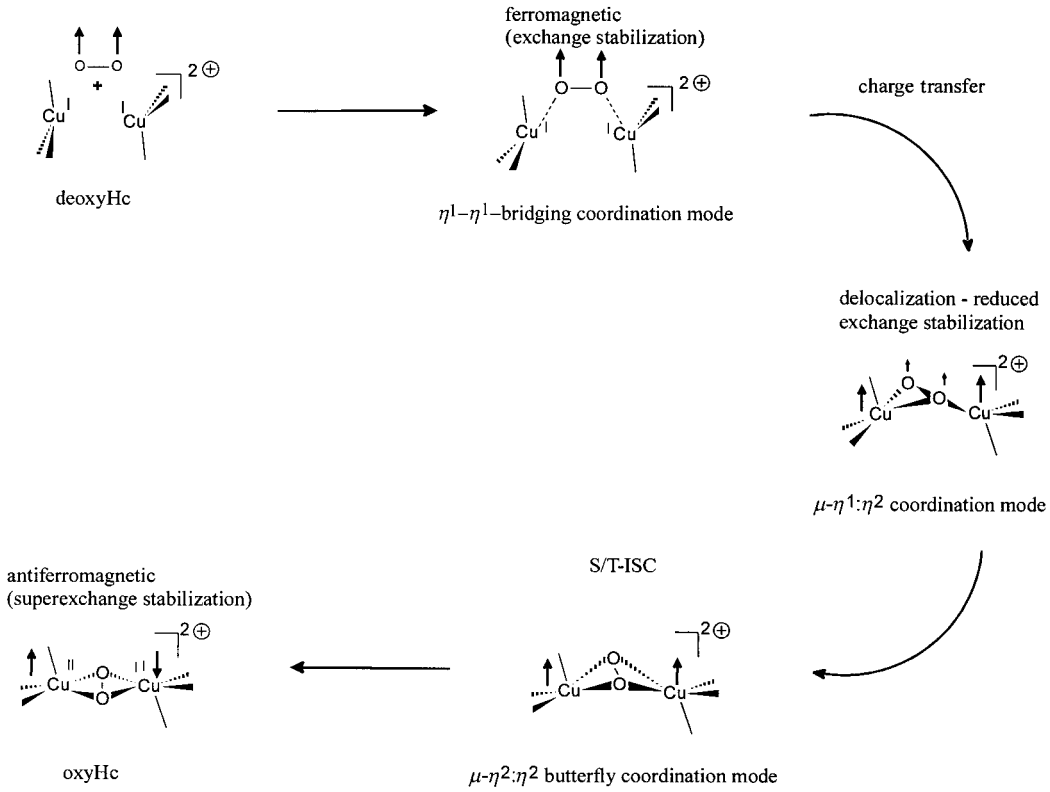
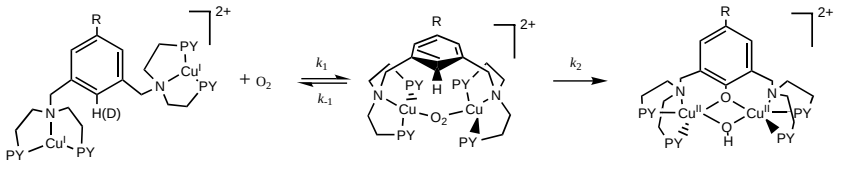


Figure 11. Illustration of the relevant steps for O_2 binding to deoxy-hemocyanin. Localization of unpaired electrons is indicated by arrows (up:α; down:β); S/T-ISC = singlet/triplet intersystem crossing. Adapted from ref. [53].



$[Cu^{I}_{2}(R\text{-}XYL)]^{2+}$ $[Cu_2(R\text{-}XYL)(O_2)]^{2+}$ $[Cu^{II}_{2}(R\text{-}XYL\text{-}O\text{-})(OH)]^{2+}$

Scheme 4. Electrophilic aromatic hydroxylation reaction, PY = pyridinyl. Reproduced from ref. [58].

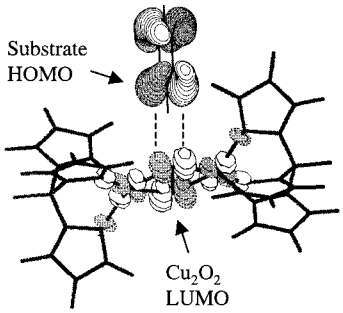


Figure 13. Frontier molecular orbitals showing π overlap of the benzene HOMO and side-on bridged μ-η^2:η^2 peroxo–Cu^{II}_2 LUMO. The side-on complex is modeled by the $[Cu_2(HBPz_3)_2](O_2)$ molecule in the DFT calculation; HBPz3 = hydrotris(3,5-dialkyl-1-pyrazolyl)borate.

exhibit an intense Cu_2O_2 core vibration at approximately 600 cm^{-1} which is not present in Figure 12B, which indicates that the absorption band at about 400 nm is in fact associated with the side-on peroxo–Cu^{II}_2 structure and is derived from a butterfly distortion of the $Cu_2(O_2)$ core.[59] From the noise level of the Raman spectrum (Figure 12B) an upper limit of $<0.1\,\%$ can be determined for the amount of this bis-μ-oxo Cu^{III}_2 species present in the Cu–XYL system.

The side-on peroxo species has a O–O vibration at 747 cm^{-1} which was used to monitor the time course of the hydroxylation reaction. From Figures 12C and D the ν(O–O) band disappears as the ν(C–O) band associated with the hydroxylated ring grows. Thus, either the side-on peroxo directly hydroxylates the ring or it is in a rapid equilibrium with the bis-μ-oxo structure. But as the bis-μ-oxo structure is present at $<0.1\,\%$, this species would have to be several orders of magnitude more reactive than the side-on peroxo species, for it to be responsible for the hydroxylation.

The relative reactivities of the side-on peroxo, bis-μ-oxo, and Cu^{II}-OOH structures (Scheme 3) could be evaluated using frontier molecular orbital (FMO) theory.[25, 26, 58] As shown in Figure 13 an electrophilic mechanism involves the interaction of the HOMO of the donor substrate with the LUMO of the acceptor which in the Cu–XYL case is the Cu_2O_2 core.[58] Electrophilic attack on the aromatic ring of the XYL model complex in Scheme 4 requires good π overlap of the valence orbitals. This in turn requires oxygen π character in the LUMO of the metal site. As shown in Figure 4 and described in Section 2.1 for the side-on peroxo core, π character in the LUMO is derived from the strong donor interaction of the peroxide π^*_σ orbital with the $d_{x^2-y^2}$ derived LUMO of the copper center (Figure 14, middle). The lower the energy of the LUMO and higher the coefficient of mixing of the peroxide π^*_σ orbital into this LUMO the greater the activation for aromatic electrophilic hydroxylation. The energy and π^*_σ character of this orbital is directly reflected in the energy and intensity, respectively, of the O_2^{2-} $\pi^*_\sigma \rightarrow Cu^{II}$ charge-transfer transition as discussed in Section 2.1 for the side-on peroxo structure and included in Figure 15. We have performed equivalent spectroscopic/electronic-structure

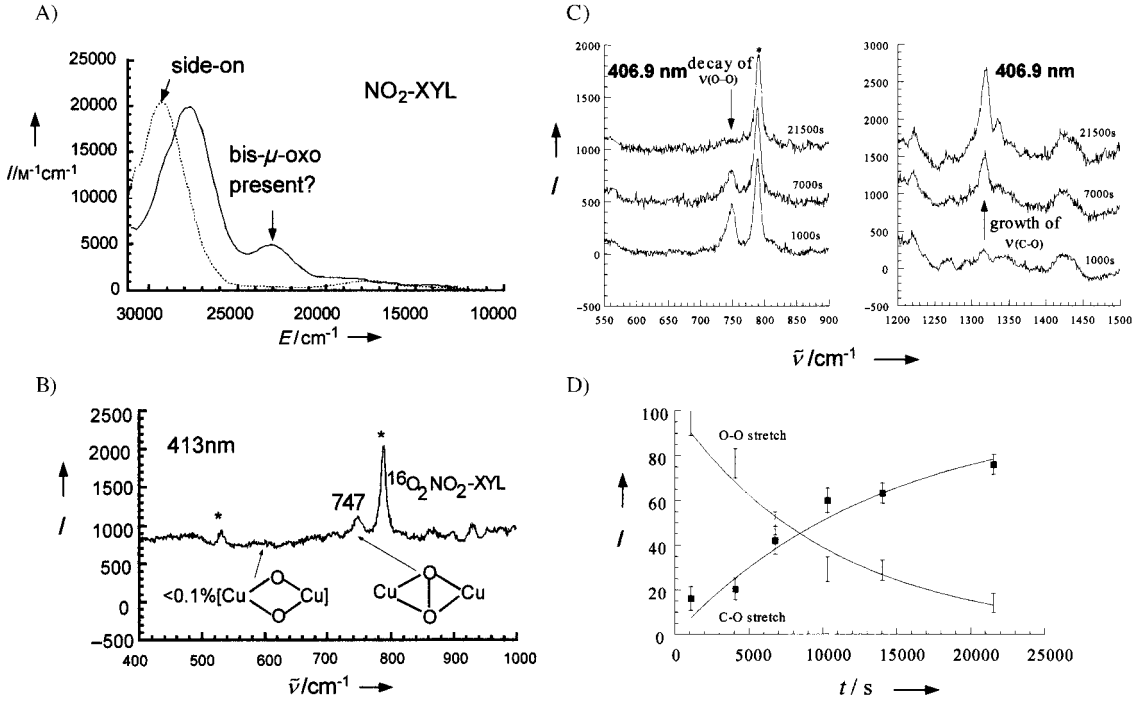


Figure 12. A) Absorption spectra of $[Cu_2(NO_2\text{-}XYL)(O_2)]^{2+}$ and the side-on bridged μ-η^2:η^2 peroxo–Cu^{II}_2 models, B) resonance Raman spectrum of $[Cu_2(NO_2\text{-}XYL)(O_2)]^{2+}$ excited at 413 nm, C) time dependence of resonance Raman signals of $[Cu_2(NO_2\text{-}XYL)(O_2)]^{2+}$ ions during the hydroxylation reaction. D) Correlation of O–O and C–O vibrations in the resonance Raman spectra of $[Cu_2(NO_2\text{-}XYL)(O_2)]^{2+}$ ions. Reproduced from ref. [58].

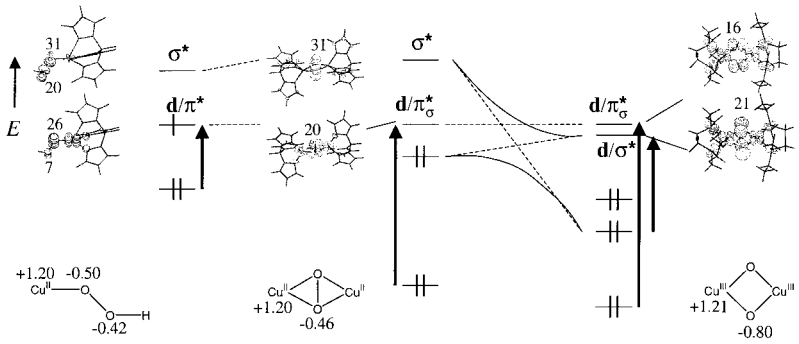


Figure 14. Valence molecular-orbital energy diagrams of copper hydroperoxo, side-on peroxo, and bis-μ-oxo species. Atomic contributions are labeled next to individual MOs (upper). Atom charges are labeled on the chemical structure (lower). Molecular orbitals are labeled by their dominant fragment contributions, thus, d/π^* is a copper d-based orbital with a significant peroxide π^* contribution. The model complexes used are $[Cu(HBPz_3)(OOH)]$, $[Cu_2(HBPz_3)_2(O_2)]$, and $[(L_{ME})_2Cu_2O_2]^{2+}$; $L_{ME} = N,N'$-dimethyl-N,N'-diethylcyclohexyldiamine.

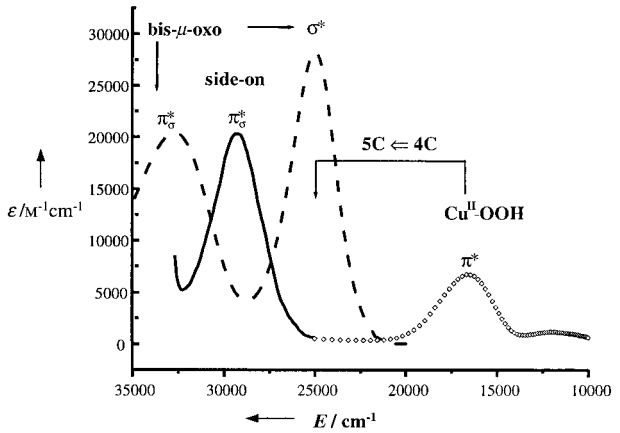


Figure 15. Absorption spectra of side-on peroxo – Cu_2^{II}, bis-μ-oxo Cu_2^{III}, and hydroperoxo – Cu^{II} complexes. Note that the spectrum for the hydroperoxo – Cu^{II} complex is that of a four-coordinate species while the other species are five coordinate. Charge-transfer transitions blue shift by around 8000 – 10000 cm^{-1} in changing from four coordinate to five coordinate as indicated by the arrow for the hydroperoxo – Cu^{II} complex.

studies on the Cu^{II} – hydroperoxide[26] and bis-μ-oxo Cu_2^{III} structures[25] in model complexes leading to the electronic structures at the left and right, respectively, in Figure 14. Their charge-transfer absorption spectra are included in Figure 15. For equivalent ligation, the energies of the LUMOs of all three species are similar. However, for the hydroperoxide – Cu^{II} complex the LUMO contains very little π^* character on the noncoordinated oxygen that would be available for attack on the substrate. Thus, the hydroperoxide – Cu^{II} species should not be effective for electrophilic π attack on aromatic substrates (Figure 16). Alternatively, both the side-on peroxo and the bis-μ-oxo structures have similar π^*_σ peroxide character in their LUMOs and should be similarly activated for electrophilic aromatic hydroxylation. However, in frontier molecular orbital theory there is also a charge term and since the oxygen of the bis-μ-oxo structure are more negative (i.e. more oxide character) this would disfavor the bis-μ-oxo structure relative to the side-on peroxo structure in aromatic hydroxylation (Figure 16). Thus, for the Karlin Cu – XYL system, it is clear that the side-on peroxo-bridged Cu_2^{II} species is responsible for the aromatic hydroxylation. Its concentration is greater than that of the bis-μ-oxo species by more than three orders magnitude and it should be more reactive because of the difference in charge on the oxygen atom. These studies are now being extended to oxy-tyrosinase to determine whether substrate coordination affects the nature of the oxygen species involved in the hydroxylation of the phenol ring.

Figure 14 shows that there is an additional electronic pathway for electrophilic attack on substrates by these copper – oxygen species involving the LUMO+1. Protonation of the peroxide in Cu^{II} – OOH and the large charge donation to the copper centers in the side-on peroxo structure greatly lower the energy of the peroxide σ^* orbital.[26, 60] This reduction in energy leads to the backbonding in the side-on peroxo structure (see Section 2.1). In the bis-μ-oxo species the backbonding cleaves the O–O bond and the σ^* orbital is dramatically lowered in energy to correlate with the LUMO which contains significant σ^* character.[25] This effect can be observed in the charge-transfer spectra of the bis-μ-oxo species (Figure 15) where the new intense low-energy band at $\sim$25000 cm^{-1} reflects the σ^* character in the LUMO. The σ^* pathway (Figure 17) requires good σ overlap with substrates and would be active in reactions, for example, involving oxo transfer to the electron lone pair on a phosphane. From Figure 17 it can be seen that both the hydroperoxide – Cu^{II} and side-on peroxo-bridged Cu_2^{II} species are activated to a similar extent for a σ electrophilic attack, as is observed experimentally.[26, 61]

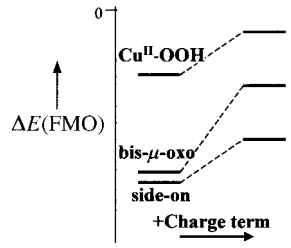


Figure 16. Qualitative frontier molecular-orbital analysis of relative reactivities (more negative ΔE = more reactive) of the different Cu/O_2 species in terms of π^* electrophilic attack (left, the FMO term; right, with inclusion of charge term).

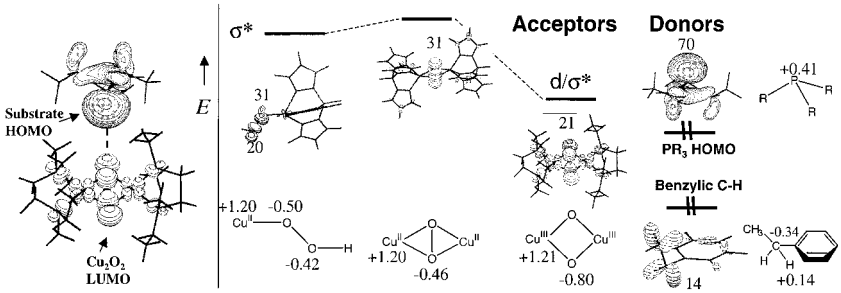


Figure 17. Left: Frontier molecular orbitals indicating σ overlap of the phosphane HOMO and bis-μ-oxo Cu^{III}_2 LUMO. Right: Valence molecular orbital energy diagrams of Cu hydroperoxo, side-on peroxo, and bis-μ-oxo species, and relevant substrates showing the σ^* pathway. Atomic contributions are labeled next to individual MOs. Atom charges are labeled on the chemical structure.

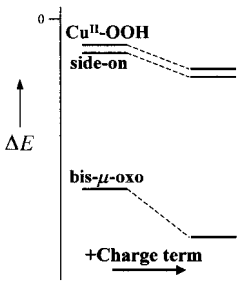


Figure 18. Qualitative frontier molecular-orbital analysis of relative reactivities of different Cu/O_2 species in terms of σ* electrophilic attack (left, the FMO term; right, with inclusion of charge term).

The low energy of the σ*-containing LUMO of the bis-μ-oxo Cu_2^{III} structure makes electrophilic attack more favorable. This effect is further enhanced (Figure 18) by the charge term as the P atom in PR_3 has partial positive character. Comparison of Figure 17 with Figure 18 indicates a large difference in the electrophilic reactivity of these copper–oxygen species for σ- versus π-donor substrates.[62]

Steric factors would limit the σ interaction of bulky substrates with the compact bis-μ-oxo Cu_2^{III} core.[62] However, this would be less of a limitation for H-atom abstraction which would involve the same σ-LUMO pathways shown in Figure 17, thus predicting parallel reactivities for the different copper–oxygen species (Figure 18). The bis-μ-oxo would be most effective as it has the lowest lying σ* LUMO and the most favorable charge term. From frontier molecular orbital theory, the side-on peroxo species should be less active, and there should be a large additional Franck–Condon activation barrier associated with the one-electron reductive cleavage of the O–O bond (Figure 19, considered further in section 4.2.3).[25] Finally H-atom abstraction by the Cu^{II}–OOH species is found to be energetically unfavorable (Figure 20 A).[26] This situation results from the fact that a Cu^{II}–oxyl species would be produced which would only be stabilized by one π-bonding interaction between the Cu and the O centers (see LUMO in Figure 20 B). Thus, for Dβ H and PHM either there is further stabilization of the Cu^{II}–oxyl/Cu^{III}–oxo intermediate which could arise from the complex geometry or the presence of the methionine ligand on Cu_M, or an alternative mechanism for the hydroxylation of the substrates by these enzymes is operative. These possibilities are now being evaluated.

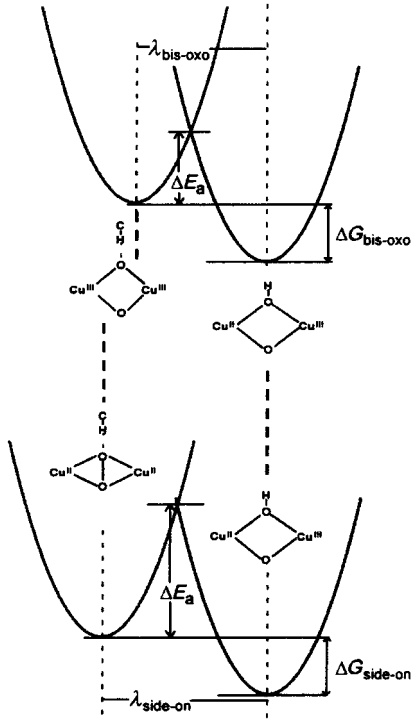
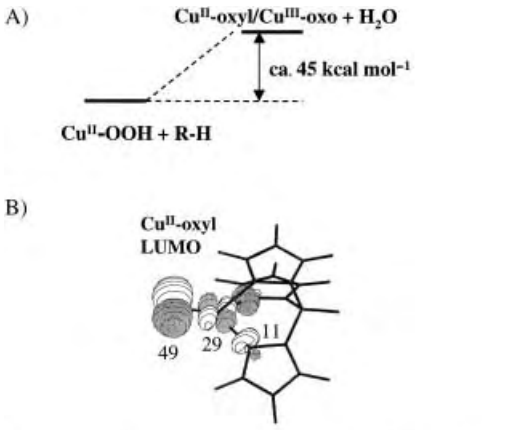


Figure 19. Representation of Franck–Condon barriers of bis-μ-oxo (top) and side-on peroxo (bottom) species for H-atom abstraction; λ = geometric distortion. Adapted from ref. [25].



	Cu	Pz^{ax}	O	OH	Pz^{eq} × 2	BH
Cu^{II}-OOH	1.20	−0.41	**−0.51**	0	−0.37	0.44
Cu^{II}-oxyl	1.25	−0.40	**−0.64**	-	−0.33	0.44
Cu^{II}-oxide	0.79	−0.45	**−0.83**	-	−0.45	0.38

Figure 20. A) Calculated energy change for the H-atom abstraction by Cu^{II}OOH, B) B3LYP calculated LUMO of formally Cu^{II}–oxyl species formed by H-atom abstraction. Atomic contributions are labeled. Table gives calculated atom charges *Q* for relevant species. In the calculation the Cu^{II}–oxyl was modeled by the [Cu(HBPz$_3$)]–oxyl complex.

4. O_2 Reduction to H_2O

4.1. The Trinuclear Copper-Cluster Active Site

As indicated in the introduction, the multicopper oxidases contain three types of copper (types 1–3) with type 3 being a coupled binuclear copper pair.[7] In our early studies we demonstrated that the type 2 and type 3 centers form a trinuclear copper cluster which plays a key role in the reduction of dioxygen to water by the multicopper oxidases.[63, 64] This result has now been strongly supported by X-ray crystallography for the three multicopper oxidases, fungal laccase,[65] ceruloplasmin,[32] and ascorbate oxidase.[9] These studies further showed that the distant type 1 Cu center is linked to the trinuclear copper cluster through the Cys–His electron-transfer pathway (Figure 1 D). The T1Hg derivative,[36] where the type 1 copper is replaced by the redox and spectroscopically inactive mercury ion, has allowed the results from spectroscopy to be correlated with those from crystallography to gain an insight into the electronic structure of the trinuclear copper-cluster site.[66] Low-temperature magnetic circular dichroism (MCD) spectroscopy is sensitive to paramagnetic centers, thus it can selectively probe the ligand-field

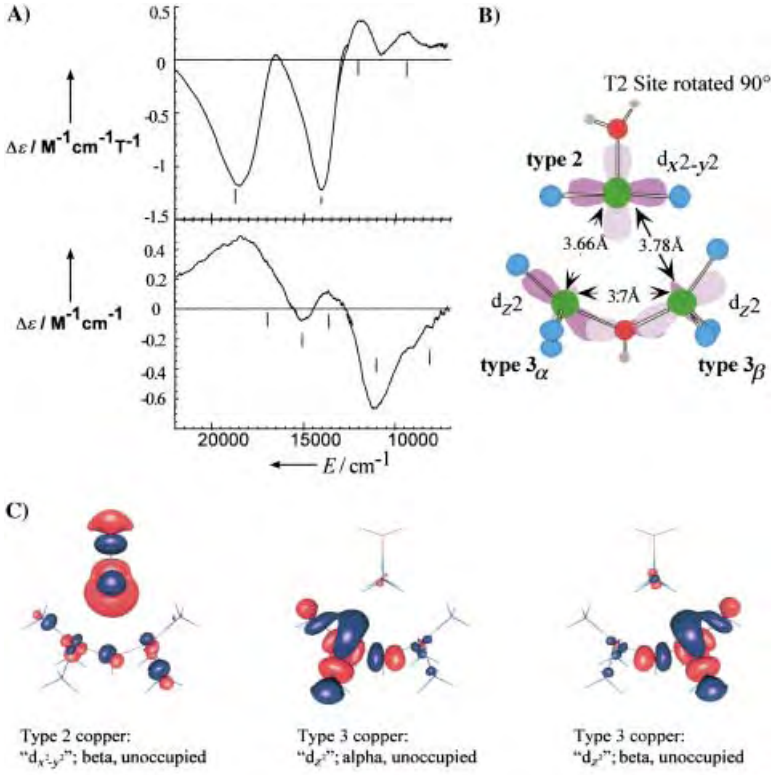


Figure 21. A) Ligand-field transitions (energies indicated by vertical lines) of the trinuclear cluster (top: low-temperature MCD depicts the type 2 Cu transitions, bottom: room-temperature CD depicts the type 3 Cu transitions). Note that there are more than four ligand-field transitions in the CD spectrum indicating that the two type 3 Cu centers are inequivalent, B) ligand-field derived electronic structure of the trinuclear cluster. The HOMO of each Cu center is displayed. Reproduced from ref. [67], C) surface plots of unoccupied MOs obtained from unrestricted DFT calculations. Superposition of these MOs is consistent with the ligand-field result presented in (B) with additional 4p mixing along the coordinatively unsaturated positions of each type 3 copper center.

transitions of the type 2 copper centers ($S = ½$; Figure 21 A, top). Reduction of the type 2 center in the T1Hg derivative results in no change in the circular dichroism (CD) spectrum indicating that the spectral features observed in CD (Figure 21 A, bottom) are ligand-field transitions of the two oxidized type 3 copper centers. These transitions are relatively intense in absorption/CD spectrum because of the distorted geometry of the type 3 copper (see below) but do not contribute to the low-temperature MCD spectrum as these copper centers are magnetically coupled to produce a diamagnetic $S = 0$ ground state. Through ligand-field calculations, the transition energies in Figure 21 A give the description of the electronic structure of the trinuclear copper cluster in Figure 21 B.[67] The three-coordinate type 2 copper center (2 His, 1 H_2O ligand) has a $d_{x^2-y^2}$ ground state and has a square-planar copper environment with an open coordination position oriented toward the two type 3 copper centers. Whereas the type 3 copper centers are four-coordinate (3 His, 1 μ-OH ligand), their electronic structures can best be described as trigonal bipyramidal with open coordination positions in their equatorial planes oriented toward the type 2 copper. Both type 3 copper centers have d_{z^2} ground states, which are oriented for strong antiferromagnetic coupling through the bridging OH^- ion. Thus, the trinuclear copper cluster is ideally configured to react with dioxygen to generate bridged intermediates. Recent DFT calculations support this description (Figure 21 C). Note that these are spin-unrestricted broken-symmetry calculations where the three unoccupied orbitals pictured together reflect the spin distributions on the three copper centers of the trimer, that is, the two T3 Cu centers are antiferromagnetically coupled and the T2 Cu center only weakly interacts with them. In addition, these calculations show 4p mixing for the two type 3 copper centers along the coordinatively unsaturated positions, which could make an important contribution to ligand binding. As with hemocyanin (Section 2.2), one role of the protein is to hold the copper centers of the cluster together which leads to repulsive interactions that would stabilize anionic oxygen intermediates binding within the cluster.[68]

4.2. O_2 Reduction

Reaction of fully reduced native laccase (reduced type 1, reduced trinuclear cluster) and the fully reduced T1Hg laccase derivative (reduced trinuclear cluster) with dioxygen produces different intermediates, namely the native and T1Hg intermediate, respectively, with the absorption spectra given in Figure 22 A.[35, 37, 69, 70] The native enzyme, in contrast to the T1Hg derivative, has a redox-active type 1 center which is oxidized in this reaction (the type 1 absorption band at about 600 nm grows at the same rate as the feature at

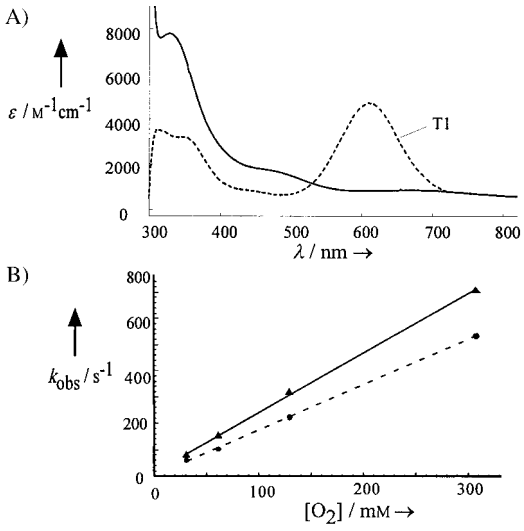


Figure 22. A) Absorption spectra of the peroxide intermediate (——) in T1Hg laccase and native intermediate (- - - -) in native laccase. The 600 nm band in the native intermediate is from the presence of the type 1 Cu center, B) rate of formation of the peroxide (▲, ——) and native intermediates (●, - - - -) as a function of O_2 concentration. Adapted from ref. [66]. The second-order rate constant for the peroxide intermediate is $2.2 \times 10^6\ M^{-1}s^{-1}$ and for native intermediate is $1.7 \times 10^6\ M^{-1}s^{-1}$.

360 nm assigned to the oxygen intermediate). Thus, in the native intermediate the dioxygen is at least one electron further reduced than in the T1Hg intermediate. However, as shown in Figure 22B, the native intermediate and the T1Hg oxygen intermediate have essentially the same rates of formation ($k \sim 2 \times 10^6\,\text{M}^{-1}\text{s}^{-1}$).[71] This similarity indicates that the formation of the T1Hg oxygen intermediate can be the rate-limiting step in the reduction of O_2 and that the rate of electron transfer from the distant type 1 through the >13 Å long Cys–His pathway to the trinuclear copper cluster is very fast ($>10^3\,\text{s}^{-1}$). Spectroscopy has shown (summarized in Section 4.2.1) that the T1Hg oxygen intermediate consists of a peroxy species bound to the trinuclear copper cluster and has a different geometric and electronic structure to that of oxy-hemocyanin. In Section 4.2.2, we extend these studies to define the nature of the native intermediate, which is shown to be a fully oxidized form of the enzyme and is different from the fully oxidized resting state. These studies lead to a proposal for the molecular mechanism of the four-electron reduction of dioxygen to water and insight into the reductive cleavage of the O–O bond (Section 4.2.3).

4.2.1. Peroxy Intermediate: Comparison to Oxy-hemocyanin

Results from isotope-ratio mass spectrometry (IRMS), show that both the O atoms from the O_2 molecule are present in the T1Hg oxygen intermediate, which indicates that the intermediate is a superoxo or peroxo species. These possibilities could be distinguished using the ligand-field region of the CD/MCD spectra (Section 4.1). Figure 23A shows that all the ligand-field transitions of the type 3 copper centers are present in the CD spectrum of the T1Hg intermediate, therefore both type 3 copper centers are oxidized. However, the low-temperature MCD spectrum of the intermediate (Figure 23B) exhibits no type 2 feature (consistent with the lack of a type 2 EPR signal) indicating that the type 2 copper is reduced. Two electrons have been transferred to O_2 from the type 3 copper centers, thus the intermediate is a peroxide species.[37]

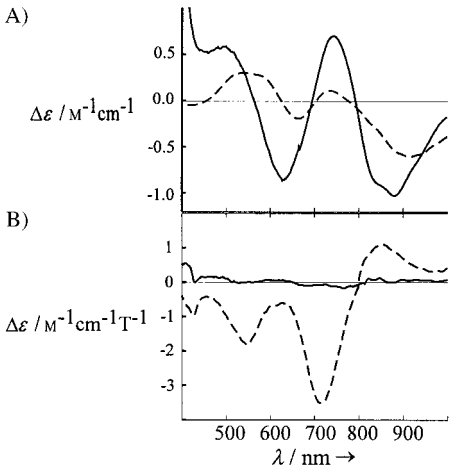


Figure 23. Comparison of the ligand-field transitions in the peroxide intermediate (——) and resting T1Hg laccase (- - - -). A) Ligand-field transitions of the type 3 Cu center, obtained by room-temperature CD and, B) ligand-field transitions of the type 2 Cu center, obtained by low-temperature MCD. Adapted from ref. [37].

SQUID magnetic-susceptibility measurements were used to define the magnetic interactions between the two oxidized type 3 copper centers of this peroxide intermediate. From saturation magnetization and Curie plots (referenced to the fully oxidized T1Hg derivative), the two oxidized type 3 centers of the peroxide intermediate were found to be strongly antiferromagnetically coupled with $-2J > 200\,\text{cm}^{-1}$. This exchange-coupling requires the presence of a bridging ligand between the two type 3 Cu^{II} centers. The bridging ligation was explored by X-ray absorption spectroscopy (XAS) of the T1Hg peroxy intermediate. The Fourier transform of the EXAFS spectrum of the intermediate has an intense outer-shell peak at a $\sim$3.4 Å (phase-shift corrected; Figure 24) which is not present in the oxidized resting (or reduced) trinuclear copper cluster. This result requires the presence of a tightly bound bridging ligand between two copper centers that cannot be the μ-hydroxide present in the oxidized trinuclear copper site (Figure 21B), since this does not have the favorable Debye–Waller factor required for the observation of an outer-shell peak. Thus, two copper centers of the peroxy intermediate of T1Hg laccase are tightly bridged together (Cu–Cu distance of 3.4 Å) by the peroxide.[37]

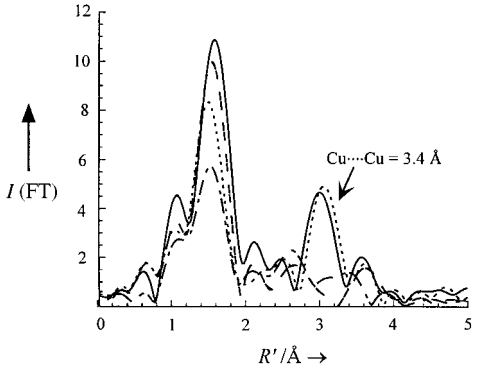


Figure 24. EXAFS spectra (I(FT) = intensity of the Fourier transformed signal) of oxidized T1Hg laccase (– – –), the peroxide intermediate (••••), the peroxide adduct (——), and reduced T1Hg laccase (•–•–). Reproduced from ref. [67].

The antiferromagnetism indicates that the two oxidized type 3 copper centers have a bridging ligand. The possibility of bridging between the type 3 and type 2 copper centers is more difficult to probe in the peroxy intermediate as the type 2 copper center is reduced. However, peroxide binds to the oxidized trinuclear copper cluster in the resting T1Hg derivative producing the peroxy adduct.[67] This adduct has the same intense outer-shell EXAFS peak as the T1Hg peroxy intermediate (Figure 24) indicating a similar peroxide bridging mode. However, in the peroxy adduct, the type 2 copper center is oxidized and paramagnetic and thus can be studied spectroscopically by low-temperature MCD (see Section 4.1), EPR, and other methods. From the EPR data in Figure 25A, the coordination environment of the type 2 Cu^{II} center

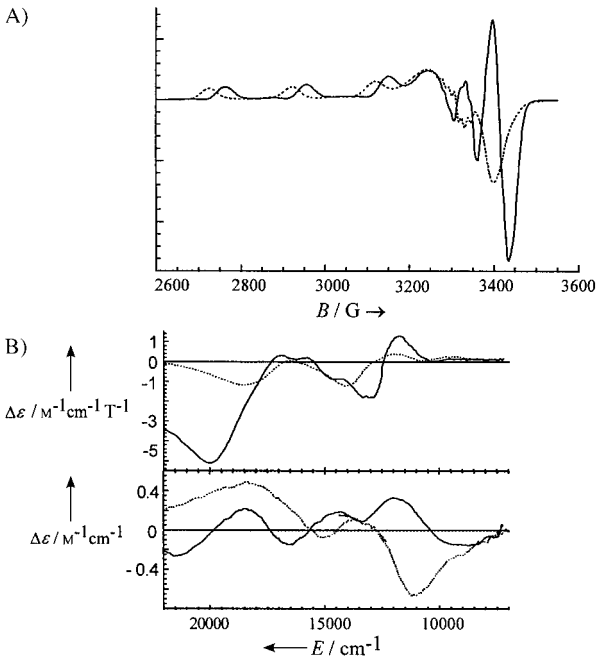


Figure 25. Comparison of the peroxide adduct of T1Hg laccase (——) and resting T1Hg laccase (- - - -). A) EPR and B) low-temperature MCD of the type 2 Cu center and room-temperature CD of the type 3 Cu center. Reproduced from ref. [67].

dramatically changes from rhombic to axial upon peroxide binding to the oxidized trinuclear Cu^{II} cluster. A ligand-field analysis indicates that the type 2 Cu^{II} site becomes four coordinate in the peroxy-bound form. This analysis is supported by the large change in the ligand-field transitions of the type 2 center in the low-temperature MCD spectrum (Figure 25B, top). In addition, there is a peroxide $\rightarrow Cu^{II}$ charge-transfer feature in the peroxide adduct at 400 nm, which has a large low-temperature MCD signal indicating that peroxide is bound to the type 2 Cu^{II} center. The changes in the ligand-field CD features (Figure 25B, bottom) and the fact that there is a peroxide $\rightarrow Cu^{II}$ charge-transfer transition in the absorption spectrum of the peroxide adduct with no associated low-temperature MCD feature (see reference [67]) requires that the peroxide also binds to the type 3 center thus forming a bridge between the type 2 and the type 3 copper centers.

The above studies lead to the two possible descriptions of the peroxide intermediate of the trinuclear copper cluster in the multicopper oxidases shown in Figure 26. In one model, the peroxide internally bridges the type 2 to the type 3 copper centers with the magnetic coupling between the oxidized

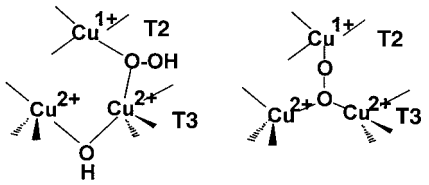


Figure 26. Possible structural models of the peroxide intermediate in the multicopper oxidases where the peroxide intermediate bridges the type 2 and type 3 Cu centers.

type 3 Cu^{II} centers arising from antiferromagnetic coupling through the peroxy bridge. Alternatively, the type 3 Cu^{II} centers could be linked by the hydroxide bridge which is present in the resting site (Figure 21B) and the peroxide could externally bridge the type 2 Cu^{I} and the type 3 Cu^{II} centers as hydroperoxide. Electronic-structure calculations are underway to distinguish between these possibilities. However, it is important to emphasize that both possibilities have a fundamentally different geometric and electronic structure than the μ-η^2:η^2 side-on peroxide bridged structure of oxy-hemocyanin (Figures 3 and 4). This difference can be seen from comparison of the charge-transfer spectra of the peroxide intermediate and oxy-hemocyanin (Figure 27). While the charge-transfer transition of the peroxy intermediate is comparably high in

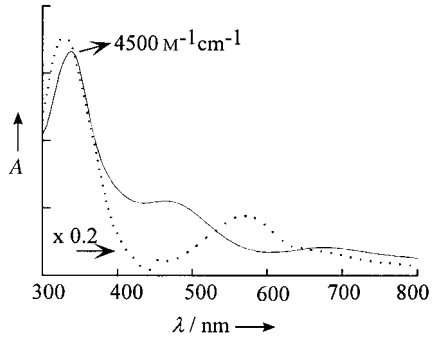


Figure 27. Comparison of the absorption spectra of the peroxide intermediate in T1Hg laccase (——) and the side-on peroxy site in oxy-hemocyanin (- - - -). The 330 nm peak in the oxy-hemocyanin spectrum is scaled down by on fifth to facilitate comparison.

energy at 340 nm, it has less than one fifth of the intensity of that of the oxy-hemocyanin. Such high energy but low intensity requires strong bonding interactions of the peroxide with nonchromophoric atoms (i.e. not Cu^{II}), either the proton in the μ-hydroperoxide arrangement or the type 2 Cu^{I} center in the μ-$(\eta^1)_3$ structure in Figure 26. The low charge-transfer intensity indicates a weak electron-donor interaction with the oxidized copper centers (in contrast to oxy-hemocyanin) which stabilizes the peroxide intermediate at the trinuclear copper-cluster site against the reversible loss of O_2. Further, the protonation of the peroxide (and/or its bonding interaction with the reduced type 2 copper) lowers the energy of the peroxide σ* orbital which activates it for the reductive cleavage of the O–O bond. This reaction is very slow in the peroxy intermediate of T1Hg laccase (0.0003 s^{-1} at pH 7.5) even though the peroxide is bridged to a reduced type 2 copper.[38] MCD studies have shown that the slow reductive cleavage of the peroxide intermediate in T1Hg generates a native intermediate-like species.[37] However, in the native enzyme the native intermediate is generated at a rate of $10^6\,M^{-1}s^{-1}$ (Figure 22B) indicating that the reduction of a peroxy species to form the native intermediate must be very fast ($>350\,s^{-1}$). The nature of the native intermediate is defined below where this difference in reactivity is found to reflect the one- versus two-electron reductive cleavage of the O–O bond.

4.2.2. Native Intermediate: Comparison to the Resting Enzyme

Figure 22 A shows the T1 copper center is oxidized in the native intermediate, thus O_2 must be at least one-electron further reduced than in the T1Hg peroxy intermediate. This combined with the facts that no EPR signal corresponding to type 2 centers is present and that a new broad EPR signal is observed (see below) which further broadens with the use of $^{17}O_2$ led researchers to describe the native intermediate as a three-electron reduced oxyl or hydroxyl species with the type 2 copper center still reduced.[35, 69] The oxidation state of the copper centers in the native intermediate could be directly determined by X-ray absorption edge studies,[72] where we have shown that there is a 1s →4p peak at 8984 eV characteristic of reduced but not oxidized copper. The X-ray edge of the native intermediate of laccase is superimposable with that of the fully oxidized resting enzyme indicating that all the copper centers are oxidized in the native intermediate (Figure 28 A).[73] Thus, O_2 is reduced by four electrons to the $H_2O/OH^-/O^{2-}$ level.[34] Further, the Fourier transform of the EXAFS spectrum of the native intermediate (Figure 28 B shows an outer-shell peak, which is not present in the resting site, that can only be fit to a Cu – Cu interaction at a distance of 3.3 Å.[73]

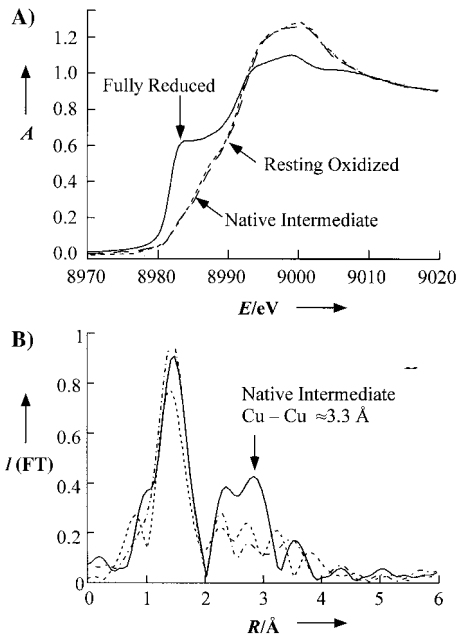


Figure 28. A) Cu_K-edge data for reduced (——), fully oxidized (– – –), and renormalized native intermediate (- - - -; corrected for unreacted reduced laccase); A = normalized absorption, B) nonphase-shift corrected Fourier transforms of the EXAFS data for reduced (•–•–), fully oxidized (- - - -), and native intermediate (——) forms of laccase; I(FT) = intensity of the Fourier transformed signal. Adapted from ref. [73].

While the native intermediate has a fully oxidized trinuclear copper cluster, it has a very different EPR signal from that of the resting oxidized trinuclear cluster, which exhibits the normal EPR signal of the localized type 2 Cu^{II} center (Figure 25 A).[35, 73, 74] The EPR signal of the native intermediate (Figure 29 A with the oxidized type 1 spectrum subtracted) is very broad with low g values including two below 2.00. From the frequency dependence of the g values the ground state has $S = ½$.[73] The EPR signal rapidly relaxes and cannot be observed above 20 K (Figure 29 B). This rapid relaxation suggests the presence of a low-lying excited state and from an Orbach analysis of the temperature dependence of the power saturation, the energy of this state could be estimated at $\sim 150\ cm^{-1}$ above the ground state (Figure 29 C).[73]

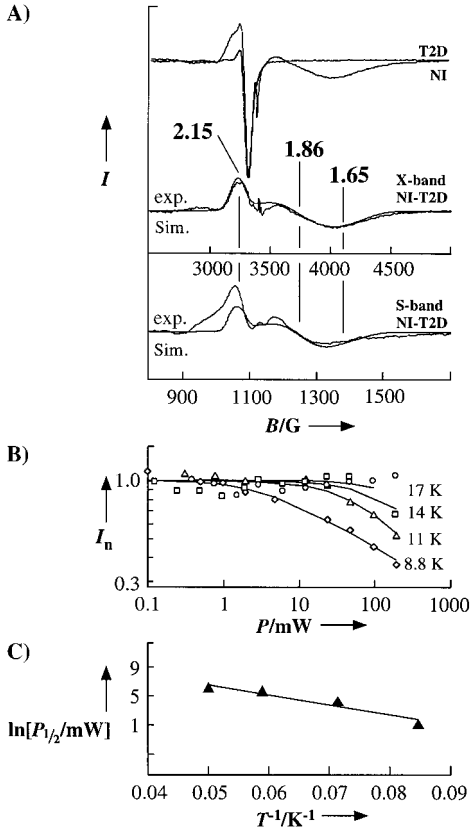


Figure 29. A) Top: the X-band EPR spectra of the native intermediate (NI) and T2D laccase at 200 mW and 10 K, bottom: the X-band and S-band EPR spectra measured T2D subtracted native intermediate (NI – T2D). Simultaneous simulations of the spectra giving g values of 2.15, 1.86, and 1.65 are included (Sim.), B) power saturation studies of the native intermediate. The normalized EPR intensities of the native intermediate at a resonance position around 4000 Gauss are plotted against microwave power varying from 0.1 to 200 mW at (◇) 8.8 K, (△) 11 K, (□) 14 K, and (○) 17 K, C) replot of the $\ln[P_{1/2}]$ against the inverse of temperature, which shows a linear response indicating a low-lying excited state at approximately 140 cm^{-1}. Adapted from ref. [73].

Further insight into the ground and excited states of the oxidized trinuclear copper cluster in the native intermediate could be obtained from the temperature and field dependence of its MCD spectrum. In addition to the 600 nm absorption feature of the type 1 center, the native intermediate exhibits absorption features at 365 and 318 nm (Figure 30 A), which correspond to oxo or hydroxo charge-transfer transitions to the Cu^{II} centers of the trinuclear copper cluster.[73] At low temperature these show a large derivative-shaped MCD signal (Figure 30 A, bottom).[34, 73] The field dependence of these MCD features at low temperature give a saturation

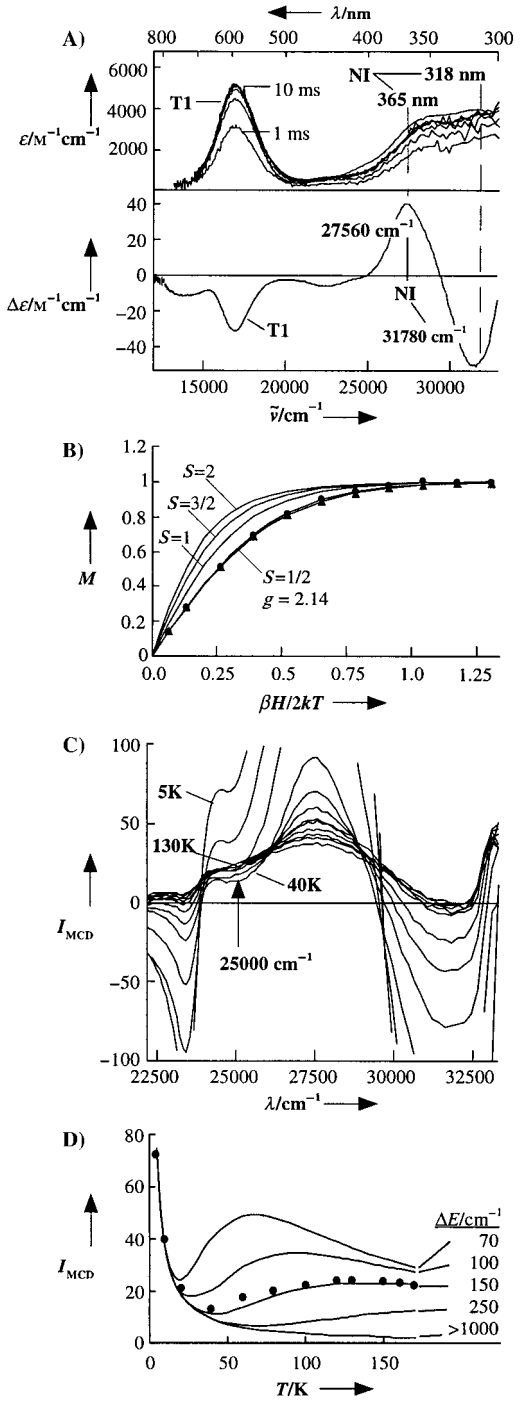


Figure 30. A) Top: formation of the native intermediate (NI) monitored using rapid scan stopped-flow absorption spectroscopy at pH 7.5 and 4 °C. The first scan is taken at 1.28 ms and each successive scan is taken every 2.56 ms up to 11.52 ms. Bottom: the low-temperature MCD spectrum of the native intermediate measured at 7 T and 1.8 K, B) saturation magnetization of the native intermediate MCD spectrum measured at 27560 cm^{-1} (▲) and 31780 cm^{-1} (●) at 1.8 K. Solid lines are simulations based on the different possible spin states indicated. M = normalized magnetization, C) the temperature dependence of the native intermediate MCD spectrum in expanded charge-transfer region (1.8–160 K at 7 T). Note that the MCD signal does not simply decrease as $1/T$; this indicates population of an excited state with a different MCD spectrum, D) the temperature dependence of the native intermediate MCD spectrum taken at 25000 cm^{-1} (●, arrow in part C). The signal intensity decreases between 5 K and 40 K but rises again at higher temperatures, 50–150 K. The solid lines are simulations with different excited-state splitting (best fit ca. 150 cm^{-1}). Adapted from ref. [73].

magnetization curve (Figure 30B) which can be described by a Brillouin function corresponding to an $S = ½$ ground state.[73] The temperature dependence of the high-field MCD spectrum is shown in Figure 30C for the charge-transfer region of the trinuclear copper cluster. For mononuclear $S = ½$ systems, the MCD signal simply decreases with increasing temperature (proportional to $1/T$). However, from the data in Figure 30 the spectra of the native intermediate *change* with increasing temperature indicating Boltzmann population of an excited state with a different MCD spectrum from that of the ground state. For example, the data taken at the 25000 cm^{-1} (arrow, Figure 30C) show that the MCD signal first decreases from 5 to 40 K and then increases with increasing temperature (Figure 30D). Fitting the energy for the excited state being thermally populated gives an energy of 150 cm^{-1}, in agreement with the Orbach analysis of the EPR data.[73]

Thus, the oxidized trinuclear copper cluster site in the native intermediate has an $S = ½$ ground state and a low-lying excited state at around 150 cm^{-1}. We now consider the exchange coupling associated with bridging-ligand interactions between the three Cu^{II} $S = ½$ ions which will reproduce these ground-state features. The exchange coupling of two Cu^{II} centers (Cu_a and Cu_b) associated with the bridging ligand gives a singlet ground state and triplet excited state split in energy by $2J$ (Figure 31). The third Cu^{II} $S = ½$ vector couples to this to produce an $S_{tot} = ½$ ground state ($|S = ½,0\rangle$) and $S_{tot} = ½$ and ⅜ excited states at $2J$. Allowing for a second bridging interaction between copper centers Cu_b and Cu_c splits the energy of the excited ½ and ⅜ states with the $|S = ½,1\rangle$ in Figure 31B being the state observed at

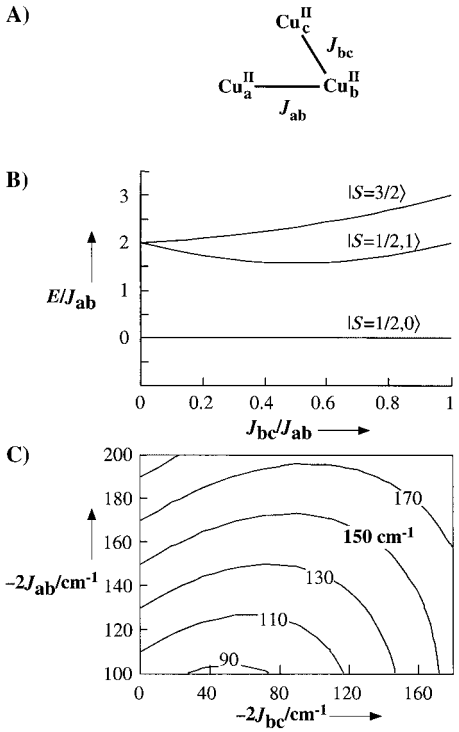


Figure 31. A) Scheme of two-bridge model, B) energy diagram of the two-bridge model as a function of the exchange-coupling ratio, C) solution space for the 150 cm^{-1} separation of the ground state and the first excited state as a function of the two exchange-coupling values based on the two bridge-model. Adapted from ref. [73].

$\sim 150\ cm^{-1}$. A search of the solution space giving an $|S=½,0\rangle/|S=½,1\rangle$ state splitting of $150\ cm^{-1}$ with two bridging ligands (Figure 31C) indicates that the maximum value of J that can be associated with either bridge is approximately $170\ cm^{-1}$.[73] However, the EXAFS data in Figure 28B show that there is a bridged Cu–Cu distance of 3.3 Å. Magneto-structural correlations have been developed for hydroxide-bridged Cu^{II} dimers,[75, 76] which show that at this distance the exchange coupling should be about $520\ cm^{-1}$. This value should be even larger for an oxo bridge (see below, Figure 32). To have an excited state at $150\ cm^{-1}$ with this large exchange coupling (required by the Cu–Cu distance), there must be a third bridge (between Cu_a and Cu_c) which would lead to spin frustration and lower the energy of the $|S=½,1\rangle$ excited state.

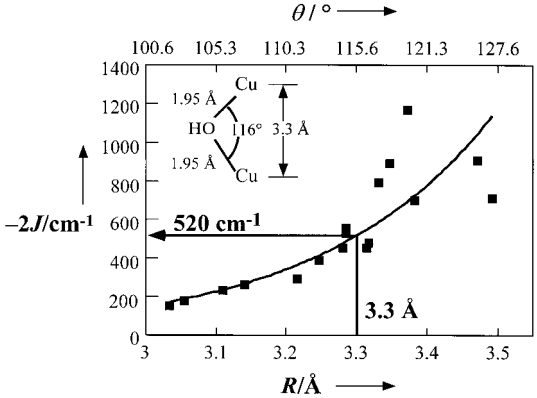


Figure 32. Magneto-structural correlation of the Cu–Cu distance R and the Cu-O-Cu angle (θ) with coupling constants for OH-bridged binuclear Cu^{II} model complexes. Note that there is a nonlinear relationship between the Cu-O-Cu angle and the Cu–Cu distance. Data taken from ref. [76].

Figure 33B presents the solution space giving an $|S=½,0\rangle/|S=½,1\rangle$ energy splitting of $150\ cm^{-1}$ as a function of the three different J values. Fixing $-2J_{ab}$ at $520\ cm^{-1}$ for the Cu–Cu distance of 3.3 Å, the other J values are also required to be large and within ⅔ of this value. The specific J values can be determined from the relative couplings of the three Cu^{II} $S=½$ centers of the trinuclear cluster to the ground $|S=½,0\rangle$ and excited $|S=½,1\rangle$ state wavefunctions; this was obtained experimentally from a comparison of the excited to ground state MCD spectra, where the former was obtained from the temperature dependence of the spectrum in Figure 30C.[73] From Figure 33D, the bands labeled ① correspond to charge-transfer transitions to a Cu^{II} center which change their MCD sign between the ground and excited state, while the band labeled ② goes from strong positive to weak positive and the band labeled ③ goes from weak positive to strong positive in the ground to excited state MCD spectrum. These behaviors reflect the coupling coefficients of the three Cu^{II} centers to the ground and excited $S=½$ states for specific values of $-2J$ (Figure 33C). (Bands ① are charge-transfer transitions to Cu^{II}_b, ② to Cu^{II}_c, and ③ to Cu^{II}_a.) Fitting the experimental MCD data in Figure 33D to Figure 33C gives the three J values which are included in Figure 33A and shows that the unusual spectra of the native intermediate are associated with a fully oxidized trinuclear copper cluster but with all three

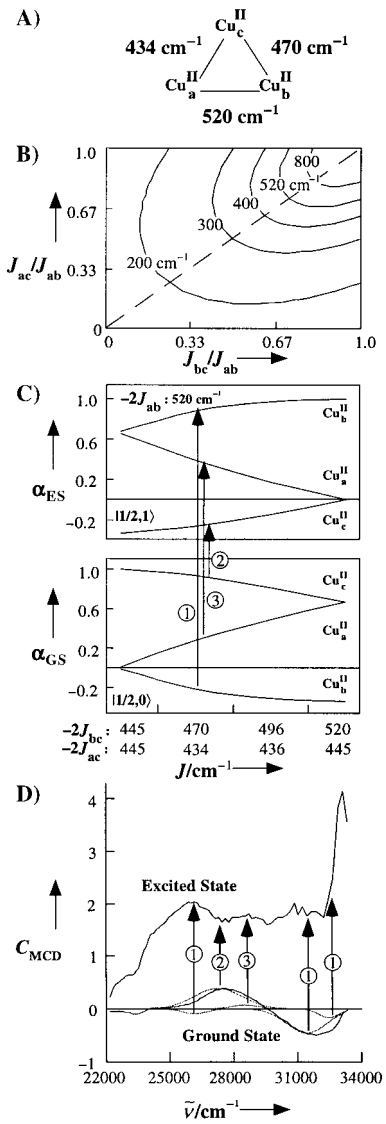


Figure 33. A) Three-bridge model with established coupling constants for the native intermediate, B) solution space for the first excited state at $150\ cm^{-1}$ as a function of the ratio of coupling constants with the third coupling constant fixed at the energy indicated, C) coupling coefficients of the individual copper centers of the trinuclear Cu^{II} cluster in the ground state and excited state wavefunctions; α_{ES} = excited state coefficient, α_{GS} = ground state coefficient (see ref. [73]), D) the ground and excited state MCD spectra of the native intermediate. Bands are grouped together (①, ②, and ③) according to their different temperature dependencies, which correlate with the change in coupling constants indicated in part (C). Gaussian simulation of the ground state spectrum is shown in gray. Adapted from ref. [73].

copper centers involved in strong bridging interactions.[73] This situation leads to the two possible structure models of the native intermediate (NI) shown in Figure 34 where the four-electron reduction of dioxygen has either produced two additional OH^- bridges or one μ_3-oxo bridge.

In summary, the studies of the native intermediate described above show that all four copper centers are oxidized and that this is a four-electron O^{2-}/OH^- product and not a three-electron O^-/OH intermediate. However, the native intermediate is different from the resting enzyme because all the copper centers of the oxidized trinuclear copper cluster

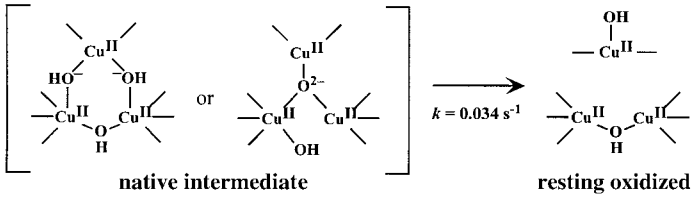


Figure 34. Structural model of the native intermediate, and its decay to the resting oxidized state.

are bridged. The decay of the native intermediate to form the resting enzyme is very slow ($k = 0.034\ s^{-1}$).[77] ^{18}O IRMS combined with ^{17}O EPR studies of the reaction of the reduced enzyme with labeled O_2, show that one oxygen atom of the O_2 unit is present in the resting enzyme. This atom is bound terminally to the type 2 copper center and lies outside the trinuclear cluster (Figure 34).[78, 79] Thus, the slow decay of the native intermediate to the resting oxidized enzyme is consistent with a large structural change that would be associated with the rearrangement of the oxygen atom, from the O_2 molecule, from inside to outside the cluster. Finally it should be emphasized that both the rate of decay of the native intermediate and the rate of reduction of the oxidized trinuclear copper cluster of the resting enzyme are too slow to be consistent with the catalytic turnover.[80–83] Alternatively, the reduction of the native intermediate is rapid indicating that this is the fully oxidized form of the enzyme which is active in catalysis.[7] It is possible that the bridge(s) to the type 2 copper center of the cluster couple this center into the electron-transfer pathway allowing rapid reduction by electrons entering at the type 1 copper center (through the Cys–His pathway to the type 3 center in Figure 1D). This possibility is under investigation.

4.2.3. Molecular Mechanism: Reductive Cleavage of the O–O Bond

The definition of the intermediates in the reduction of O_2 to H_2O in the multicopper oxidases leads to the molecular mechanism for this four-electron process given in Figure 35.

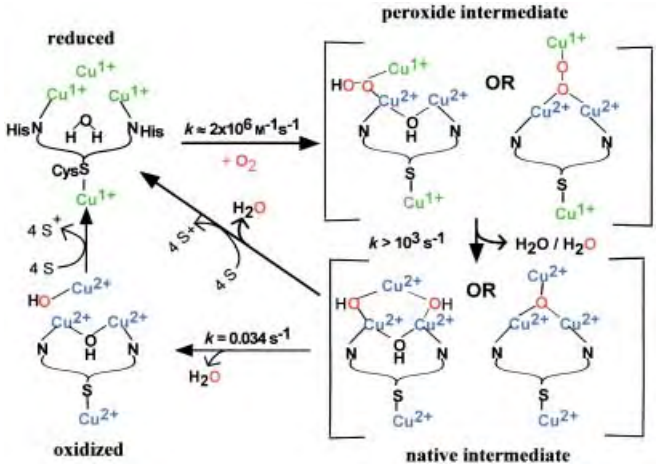


Figure 35. Molecular mechanism for the reduction of O_2 to H_2O in the multicopper oxidases.

The reduced enzyme reacts with dioxygen to generate a two-electron reduced peroxide intermediate with the peroxide bridging an oxidized type 3 copper pair and a reduced type 2 copper center. This peroxide intermediate is reduced in a second two-electron step, thus oxidizing the type 2 and the distant type 1 center to generate the "native intermediate" which is, in fact, an oxo or hydroxo product bridged between the oxidized type 3 and now oxidized type 2 copper centers of the trinuclear cluster. This intermediate is either rapidly reduced by substrate in the catalytic reaction, or, in the absence of substrate, slowly decays to the resting site which contains one oxygen atom of the O_2 terminally bound as H_2O to the type 2 copper. This rearrangement uncouples the trinuclear copper cluster and removes the resting enzyme from the catalytic cycle.

Thus, the reduction of O_2 to H_2O involves two, two-electron steps and from the kinetics shown in Figure 22B, the first step is rate determining and the second is very fast. It is important to note that the second step involves the reductive cleavage of the O–O bond and there is a large Franck–Condon barrier associated with this distortion. We were able to experimentally study this barrier through the temperature dependence of the decay of the peroxide intermediate in the T1Hg laccase, which involves the one-electron (electron from the reduced type 2 center) reductive cleavage of the O–O bond.[38] From the $k(^{16}O_2)/k(^{18}O_2)$ kinetic oxygen isotope effect of 1.10 ± 0.05, the rate-determining step in this reaction is O–O bond cleavage. The experimental barrier we find is quite large ($\sim 9\ kcal\,mol^{-1}$) which is consistent with a slow rate of decay ($3 \times 10^{-4}\ s^{-1}$). From the Marcus theory for electron transfer, the rate for this reduction should depend on the electronic-coupling matrix element (H_{DA}; D = donor, A = acceptor), the thermodynamic driving force (ΔG°), and the reorganization energy (λ). Since the peroxide in the T1Hg intermediate is bound to the type 2 copper center, H_{DA} should be large. The redox potential of the type 2 center in the resting enzyme is 0.37 V,[84] which is close to the E° for the one-electron reduction potential of H_2O_2 (0.38 V), and therefore ΔG° is small and the reaction is thermo-neutral. For an isoenergetic process, the reorganization energy associated with the cleavage of the O–O bond should be around one quarter of the dissociation energy of the bond,[85] which has been estimated to be between 34 and 50 $kcal\,mol^{-1}$ for peroxide.[86–88] This value predicts an activation energy of 8.5–12.5 $kcal\,mol^{-1}$ which is in good agreement with experiment. That the peroxide intermediate is not observed in the native enzyme indicates that the conversion of the peroxide intermediate into the native intermediate is fast relative to its formation (the rate of formation of the peroxide intermediate in T1Hg is $2 \times 10^6\ M^{-1}\,s^{-1}$). Kinetic modeling of the general reaction scheme [Eq. (1)], places a lower limit of $\sim 350\ s^{-1}$ on

$$\text{reduced enzyme} + O_2 \longrightarrow \text{peroxide intermediate} \longrightarrow \text{native intermediate} \longrightarrow \text{resting enzyme} \quad (1)$$

the conversion of the peroxide intermediate into the native intermediate which is $\sim 10^6$ times faster than the one-electron reductive cleavage of the O–O bond in the T1Hg intermediate.[38]

However, in the native enzyme this reaction involves a two-electron transfer, one electron from the type 2 and one from the type 1 copper centers (through the Cys–His pathway), which produces the fully oxidized native intermediate. The E° of the type 1 center is 0.39 V which is similar to that of the type 2 center.[84] Importantly, the potential for two-electron reduction of peroxide is 1.37 V which is one volt ($\sim$46 kcal mol^{-1} for $n=2$ in the Nernst equation) more favorable than the one-electron reduction. This adds a large thermodynamic driving force which greatly lowers the activation barrier (to around 1 kcal mol^{-1}). The difference in activation energy for the 1e$^-$ versus 2e$^-$ reductive cleavage of peroxide is shown in Figure 36. This large difference in activation energy would lead to a 10^7-fold increase in the peroxide reduction rate in the native enzyme, consistent with experiment and the reaction mechanism in Figure 35; O_2 is reduced in two two-electron steps, the second being very rapid because of the large driving force for this reaction.

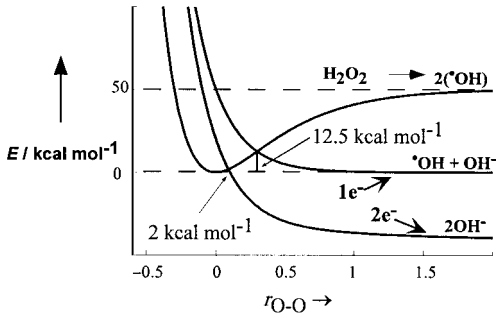


Figure 36. Potential-energy surfaces for the one versus two-electron reductive cleavage of the O–O bond of peroxide. Morse potentials are used to model the reactant (H_2O_2) and product (1e$^-$ and 2e$^-$ cleavage of H_2O_2). The product curve for the 2e$^-$ reductive cleavage is shifted to lower energy by 46 kcal mol^{-1}.

Figure 36 provides general insight into strategies for the reductive cleavage of O–O bonds in biology. Because of the large Franck–Condon barrier associated with this cleavage, there has to be a large thermodynamic driving force for the rapid rate required by most biological processes. This can be achieved either by the stability of the M=O product formed in the one-electron process (e.g. Fe^{IV}=O) or by the one volt more favorable two-electron reduction of peroxide.

5. Summary and Outlook

The unique spectral features of copper/dioxygen intermediates are generally understood and reflect new electronic structures which make major contributions to reactivity. These studies have defined geometric- and electronic-structure/function correlations and led to molecular mechanisms for the reversible binding of oxygen by hemocyanin, oxygen activation by tyrosinase, and the four-electron reduction of oxygen to water by the multicopper oxidases. They have further provided general insight into the reductive cleavage of the O–O bond, an important problem in many areas of biology. Fundamental questions still remain including the nature of the substrate interactions in the different enzymes, how mutations perturb the active sites and change their reactivity, the nature of the oxygen intermediates in the noncoupled binuclear copper enzymes, and in the biosynthesis of the organic cofactors, how the oxygen intermediates in the multicopper oxidases relate to those in cytochrome c oxidase, and how the type 1 copper center couples to the trinuclear copper cluster through the Cys–His pathway in the multicopper oxidases. We look forward to many exciting new insights in the field of copper/O_2 chemistry in the years ahead.

E.I.S. thanks his collaborators and past students as indicated in the references cited for their outstanding contributions to this field. This research was generously funded by the National Institute of Health (DK31450). The following fellowships are gratefully acknowledged: Peng Chen, Gerhard Casper Stanford Graduate Fellowship, Markus Metz, DAAD Postdoctoral Fellowship, Amy Palmer, Franklin Veatch Memorial Fellowship.

Received: April 2, 2001 [A 462]

[1] R. H. Holm, P. Kennepohl, E. I. Solomon, *Chem. Rev.* **1996**, *96*, 2239.
[2] I. E. Marko, M. Tsukazaki, P. R. Giles, S. M. Brown, C. J. Urch, *Angew. Chem.* **1997**, *109*, 2297; *Angew. Chem. Int. Ed. Engl.* **1997**, *36*, 2208.
[3] E. I. Solomon, P. M. Jones, J. A. May, *Chem. Rev.* **1993**, *93*, 2623.
[4] J. B. Reitz, E. I. Solomon, *J. Am. Chem. Soc.* **1998**, *120*, 11467.
[5] E. I. Solomon, F. Tuczek, D. E. Root, C. A. Brown, *Chem. Rev.* **1994**, *94*, 827.
[6] J. P. Klinman, *Chem. Rev.* **1996**, *96*, 2541.
[7] E. I. Solomon, U. M. Sundaram, T. E. Machonkin, *Chem. Rev.* **1996**, *96*, 2563.
[8] S. Ferguson-Miller, G. T. Babcock, *Chem. Rev.* **1996**, *96*, 2889.
[9] A. Messerschmidt, R. Ladenstein, R. Huber, M. Bolognesi, L. Avigliano, R. Petruzzelli, A. Rossi, A. Finazzi-Agro, *J. Mol. Biol.* **1992**, *224*, 179.
[10] T. Klabunde, C. Eicken, J. C. Sacchettini, B. Krebs, *Nat. Struct. Biol.* **1998**, *5*, 1084.
[11] V. Kumar, D. M. Dooley, H. C. Freeman, J. M. Guss, I. Harvey, M. A. McGuirl, M. C. J. Wilce, V. M. Zubak, *Structure* **1996**, *4*, 943.
[12] B. Hazes, K. A. Magnus, C. Bonaventura, J. Bonaventura, Z. Dauter, K. H. Kalk, W. G. Hol, *Protein Sci.* **1993**, *2*, 597.
[13] N. Ito, S. E. V. Phillips, C. Stevens, Z. B. Ogel, M. J. McPherson, J. N. Keen, K. D. S. Yadav, P. F. Knowles, *Nature* **1991**, *350*, 87.
[14] K. A. Magnus, B. Hazes, H. Ton-That, C. Bonaventura, J. Bonaventura, W. G. J. Hol, *Proteins: Struct. Funct. Genet.* **1994**, *19*, 302.
[15] S. T. Prigge, A. S. Kolhekar, B. A. Eipper, R. E. Mains, L. M. Amzel, *Science* **1997**, *278*, 1300.
[16] S. T. Prigge, A. S. Kolhekar, B. A. Eipper, R. E. Mains, L. M. Amzel, *Nat. Struct. Biol.* **1999**, *6*, 976.
[17] P. F. Knowles, D. M. Dooley, *Met. Ions Biol. Syst.* **1994**, *30*, 361.
[18] D. M. Dooley, D. E. Brown, H. C. Freeman, J. M. Guss, H. Matsunami, W. S. McIntire, C. E. Ruggiero, K. Tanizawa, M. Wilce, H. Yamaguchi, *FASEB J.* **1997**, *11*, 79.
[19] N. J. Blackburn, F. C. Rhames, M. Ralle, S. Jaron, *J. Biol. Inorg. Chem.* **2000**, *5*, 341.
[20] S. Jaron, N. J. Blackburn, *Biochemistry* **1999**, *38*, 15086.
[21] N. Kitajima, K. Fujisawa, Y. Moro-oka, *J. Am. Chem. Soc.* **1989**, *111*, 8975.
[22] R. S. Himmelwright, N. C. Eickman, C. D. LuBien, K. Lerch, E. I. Solomon, *J. Am. Chem. Soc.* **1980**, *102*, 7339.
[23] J. A. Halfen, S. Mahapatra, E. C. Wilkinson, S. Kaderli, V. G. Young, Jr., L. Que, Jr., A. D. Zuberbühler, W. B. Tolman, *Science* **1996**, *271*, 1397.
[24] P. K. Ross, E. I. Solomon, *J. Am. Chem. Soc.* **1990**, *112*, 5871.

[25] M. J. Henson, P. Mukherjee, D. E. Root, T. D. P. Stack, E. I. Solomon, *J. Am. Chem. Soc.* **1999**, *121*, 10332.
[26] P. Chen, K. Fujisawa, E. I. Solomon, *J. Am. Chem. Soc.* **2000**, *122*, 10177.
[27] D. E. Wilcox, A. G. Porras, Y. T. Hwang, K. Lerch, M. E. Winkler, E. I. Solomon, *J. Am. Chem. Soc.* **1985**, *107*, 4015.
[28] M. D. Allendorf, D. J. Spira, E. I. Solomon, *Proc. Natl. Acad. Sci. USA* **1985**, *82*, 3063.
[29] H. H. T. Nguyen, A. K. Shiemke, S. J. Jacobs, B. J. Hales, M. E. Lidstrom, S. I. Chan, *J. Biol. Chem.* **1994**, *269*, 14995.
[30] D. J. Kosman, R. Hassett, D. S. Yuan, J. McCracken, *J. Am. Chem. Soc.* **1998**, *120*, 4037.
[31] Note that herein we reserve the term T3Cu for the hydroxo bridged binuclear Cu component of the trinuclear Cu cluster. This has a different geometric and electronic structure from the coupled binuclear Cu sites in hemocyanin, tyrosinase, and catechol oxidase (sometimes also called T3 in the literature).
[32] I. Zaitseva, V. Zaitsev, G. Card, K. Moshov, B. Bax, A. Ralph, P. Lindley, *J. Biol. Inorg. Chem.* **1996**, *1*, 15.
[33] L.-E. Andréasson, R. Brändén, B. G. Malmström, T. Vanngard, *FEBS Lett.* **1973**, *32*, 187.
[34] P. A. Clark, E. I. Solomon, *J. Am. Chem. Soc.* **1992**, *114*, 1108.
[35] R. Aasa, R. Brändén, J. Deinum, B. G. Malmström, B. Reinhammar, T. Vanngard, *FEBS Lett.* **1976**, *61*, 115.
[36] M. M. Morie-Bebel, M. C. Morris, J. L. Menzie, D. R. McMillin, *J. Am. Chem. Soc.* **1984**, *106*, 3677.
[37] W. Shin, U. M. Sundaram, J. L. Cole, H. H. Zhang, B. Hedman, K. O. Hodgson, E. I. Solomon, *J. Am. Chem. Soc.* **1996**, *118*, 3202.
[38] A. E. Palmer, S.-K. Lee, E. I. Solomon, *J. Am. Chem. Soc.* **2001**, *123*, 6591.
[39] E. I. Solomon, M. J. Baldwin, M. D. Lowery, *Chem. Rev.* **1992**, *92*, 521.
[40] J. E. Pate, R. W. Cruse, K. D. Karlin, E. I. Solomon, *J. Am. Chem. Soc.* **1987**, *109*, 2624.
[41] N. C. Eickman, R. S. Himmelwright, E. I. Solomon, *Proc. Natl. Acad. Sci. USA* **1979**, *76*, 2094.
[42] T. B. Freedman, J. S. Loehr, T. M. Loehr, *J. Am. Chem. Soc.* **1976**, *98*, 2809.
[43] E. I. Solomon, D. M. Dooley, R. H. Wang, H. B. Gray, M. Cerdonio, F. Mogno, G. L. Romani, *J. Am. Chem. Soc.* **1976**, *98*, 1029.
[44] P. K. Ross, E. I. Solomon, *J. Am. Chem. Soc.* **1991**, *113*, 3246.
[45] M. J. Baldwin, D. E. Root, J. E. Pate, K. Fujidawa, N. Kitajima, E. I. Solomon, *J. Am. Chem. Soc.* **1992**, *114*, 10421.
[46] A. D. Becke, *J. Chem. Phys.* **1993**, *98*, 5648.
[47] T. H. J. Dunning, P. J. Hay in *Modern Theoretical Chemistry*, *Vol. 3* (Ed.: H. F. Schaefer III), Plenum, New York, **1976**, p. 1.
[48] P. J. Hay, W. R. Wadt, *J. Chem. Phys.* **1985**, *82*, 270.
[49] P. J. Hay, W. R. Wadt, *J. Chem. Phys.* **1985**, *82*, 299.
[50] W. R. Wadt, P. J. Hay, *J. Am. Chem. Soc.* **1985**, *82*, 284.
[51] M. E. Casida, *Recent Adv. Comput. Chem.* **1995**, *1*, 155.
[52] R. E. Stratmann, G. E. Scuseria, M. J. Frisch, *J. Chem. Phys.* **1998**, *109*, 8218.
[53] M. Metz, E. I. Solomon, *J. Am. Chem. Soc.* **2001**, *123*, 4938.
[54] M. Brouwer, C. Bonaventura, J. Bonaventura, *Biochemistry* **1978**, *17*, 2148.
[55] A. Berces, *Inorg. Chem.* **1997**, *36*, 4831.
[56] A. Berces, *Int. J. Quantum Chem.* **1997**, *65*, 1077.
[57] K. D. Karlin, J. C. Hayes, Y. Gultneh, R. W. Cruse, J. W. McKown, J. P. Hutchinson, J. Zubieta, *J. Am. Chem. Soc.* **1984**, *106*, 2121.
[58] E. Pidcock, H. V. Obias, C. X. Zhang, K. D. Karlin, E. I. Solomon, *J. Am. Chem. Soc.* **1998**, *120*, 7841.
[59] E. Pidcock, H. V. Obias, M. Abe, H.-C. Liang, K. D. Karlin, E. I. Solomon, *J. Am. Chem. Soc.* **1999**, *121*, 1299.
[60] D. E. Root, M. Mahroof-Tahir, K. D. Karlin, E. I. Solomon, *Inorg. Chem.* **1998**, *37*, 4838.
[61] P. P. Paul, Z. Tyeklar, R. R. Jacobson, K. D. Karlin, *J. Am. Chem. Soc.* **1991**, *113*, 5322.
[62] P. Chen, E. I. Solomon, *J. Inorg. Biochem.*, in press.
[63] D. J. Spira-Solomon, M. D. Allendorf, E. I. Solomon, *J. Am. Chem. Soc.* **1986**, *108*, 5318.
[64] J. L. Cole, G. O. Tan, E. K. Yang, K. O. Hodgson, E. I. Solomon, *J. Am. Chem. Soc.* **1990**, *112*, 2243.
[65] V. Ducros, A. M. Brzozowski, K. S. Wilson, S. H. Brown, P. Østergaard, P. Schneider, D. S. Yaver, A. H. Pedersen, G. J. Davies, *Nat. Struct. Biol.* **1998**, *5*, 310.
[66] J. L. Cole, P. A. Clark, E. I. Solomon, *J. Am. Chem. Soc.* **1990**, *112*, 9534.
[67] U. M. Sundaram, H. H. Zhang, B. Hedman, K. O. Hodgson, E. I. Solomon, *J. Am. Chem. Soc.* **1997**, *119*, 12525.
[68] M. Metz, E. I. Solomon, unpublished results.
[69] R. Aasa, R. Brändén, J. Deinum, B. G. Malmström, B. Reinhammar, T. Vanngard, *Biochem. Biophys. Res. Commun.* **1976**, *70*, 1204.
[70] L. E. Andréasson, R. Brändén, B. Reinhammar, *Biochim. Biophys. Acta* **1976**, *438*, 370.
[71] J. L. Cole, D. P. Ballou, E. I. Solomon, *J. Am. Chem. Soc.* **1991**, *113*, 8544.
[72] L. S. Kau, D. J. Spira-Solomon, J. E. Pennerhahn, K. O. Hodgson, E. I. Solomon, *J. Am. Chem. Soc.* **1987**, *109*, 6433.
[73] S.-K. Lee, S. D. George, W. E. Antholine, B. Hedman, K. O. Hodgson, E. I. Solomon, *J. Am. Chem. Soc.*, submitted.
[74] H. W. Huang, T. Sakurai, S. Maritano, A. Marchesini, S. Suzuki, *J. Inorg. Biochem.* **1999**, *75*, 19.
[75] V. H. Crawford, H. W. Richardson, J. R. Wasson, D. J. Hodgson, W. E. Hatfield, *Inorg. Chem.* **1976**, *15*, 2107.
[76] S. S. Tandon, L. K. Thompson, M. E. Manuel, J. N. Bridson, *Inorg. Chem.* **1994**, *33*, 5555.
[77] L.-E. Andréasson, B. Reinhammar, *Biochim. Biophys. Acta* **1976**, *445*, 579.
[78] R. Brändén, J. Deinum, *FEBS Lett.* **1977**, *73*, 144.
[79] R. Brändén, J. Deinum, M. Coleman, *FEBS Lett.* **1978**, *89*, 180.
[80] O. Farver, I. Pecht, *Proc. Natl. Acad. Sci. USA* **1992**, *89*, 8283.
[81] P. Kyritsis, A. Messerschmidt, R. Huber, G. A. Salmon, A. G. Sykes, *J. Chem. Soc. Dalton Trans.* **1993**, 731.
[82] T. E. Meyer, A. Marchesini, M. A. Cusanovich, G. Tollin, *Biochemistry* **1991**, *30*, 4619.
[83] L.-E. Andréasson, B. Reinhammar, *Biochim. Biophys. Acta* **1979**, *568*, 145.
[84] B. R. M. Reinhammar, *Biochim. Biophys. Acta* **1972**, *275*, 245.
[85] J.-M. Savéant, *Adv. Electron Transfer Chem.* **1994**, *4*, 53.
[86] A. C. Baldwin in *The Chemistry of Peroxides* (Ed.: S. Patai), Wiley, New York, **1983**, p. 97.
[87] R. D. Bach, P. Y. Ayala, H. B. Schlegel, *J. Am. Chem. Soc.* **1996**, *118*, 12758.
[88] X. Luo, P. R. Flemming, T. R. Rizzo, *J. Chem. Phys.* **1992**, *96*, 5659.

Enantioselective Construction of Quaternary Stereocenters

Jens Christoffers* and Alexander Mann

The stereoselective formation of C–C bonds is of great importance for the synthesis of enantiomerically pure natural products and pharmaceuticals. A broad repertoire of chiral auxiliaries, reagents, and catalysts can be utilized for the reliable generation of tertiary stereocenters. In contrast, the synthesis of organic compounds with quaternary stereocenters is a much more demanding and challenging task. Every enantioselective synthetic method can demonstrate its value through the generation of a fully substituted carbon center. In this Minireview examples of newer stoichiometric and catalytic methods are summarized which have proved their suitability for the enantioselective construction of quaternary stereocenters.

1. Introduction

In the past twenty years impressive progress has been made in the field of organic synthesis.[1] The basis for this development was the enlargement and improvement of the repertoire of transformations available for synthetic organic chemists. In particular, the development of stereoselective[2] and atom-economic[3] techniques for efficient syntheses of enantiomerically pure compounds has been of central importance in this context. Methods for the direct asymmetric coupling of C–C bonds nowadays play a key role in the preparation of complex natural products and pharmaceuticals. The enantioselective construction of carbon centers with four non-hydrogen substituents, that is, quaternary carbon centers, is still a challenge.

The latter problem has been the subject of a number of review articles,[4] and catalytic asymmetric reactions were summarized by Corey and Guzman-Perez a few years ago.[4a] This Minireview collects recent work that has been published since then. Completeness is not claimed, but examples were subjectively selected according to their originality. Moreover, this review focuses on quaternary carbon centers without any heteroatom substituents. Apart from catalytic asymmetric procedures, which are commonly of central interest, the use of chiral auxiliaries is also considered, since they are—despite their stoichiometric application—of great practical relevance.[5]

[*] Prof. Dr. J. Christoffers, Dr. A. Mann
Institut für Organische Chemie der Universität Stuttgart
Pfaffenwaldring 55, 70569 Stuttgart (Germany)
Fax: (+49) 711-685-4269
E-mail: jchr@po.uni-stuttgart.de

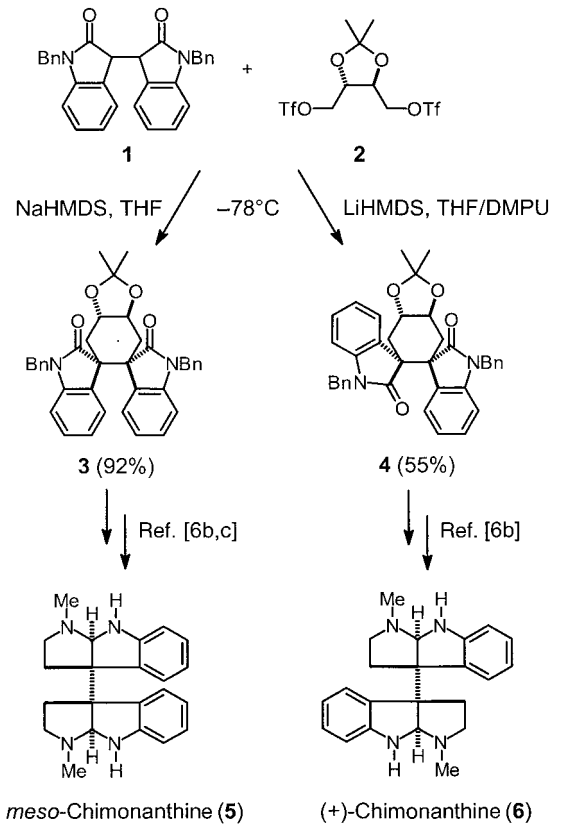
2. Alkylations

Asymmetric alkylations with chiral auxiliaries or catalysts are frequently used and are reliable reactions for the synthesis of quaternary carbon centers. The enantioselective construction of two vicinal quaternary stereocenters, however, is very difficult.

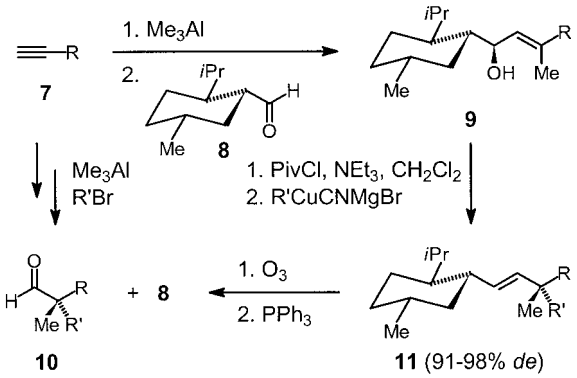
Recently, Overman et al. reported on a new synthesis of the indole alkaloids *meso*-chimonanthine (**5**) and (+)-chimonanthine (**6**) as basic representatives of polypyrroloindoline alkaloids with a hexacyclic 3a,3a′-bispyrrolidino[2,3-*b*]indoline substructure (Scheme 1).[6] The key synthetic step is the dialkylation of dihydroisoindigo **1** (prepared from oxoindole and isatin)[6c] with the chiral bistriflate **2** derived from tartaric acid. Double deprotonation of **1**, followed by alkylation of the achiral dienolate with the dielectrophile **2** furnished two quaternary centers in a single step. The relative configuration of the two stereocenters was tuned by the proper choice of the metal dienolate counterion and the solvent system: With Na^+ as the counterion a chelated intermediate yielded the *cis* product **3**. The use of 1,3-dimethylhexahydro-2-pyrimidinone (DMPU) as cosolvent prevented the chelation of the corresponding lithium enolate and furnished the *trans* product **4**. The generation of two vicinal quaternary stereocenters in one step and the control of their relative configuration make this example particularly striking.

A completely different approach to the synthesis of carbonyl compounds with a chiral quaternary α-center was reported by Spino and Beaulieu.[7] Common strategies for the generation of such carbon centers are the alkylation of chiral enolates or the application of chiral electrophiles. In contrast, this auxiliary-based method utilizes an allylic-substitution reaction (Scheme 2). The auxiliary **8** was prepared in two steps by Wittig olefination of (–)-menthone with methoxymethylphosphonium ylide and subsequent acidic hydrolysis. The sequence started with the synthesis of allylic alcohol **9** by vinylation of aldehyde **8** with a vinylalane derived from alkyne **7** by zirconium-catalyzed carboalumination.[8] The addition

 © WILEY-VCH Verlag GmbH, D-69451 Weinheim, 2001 1433-7851/01/4024-4591 $ 17.50+.50/0



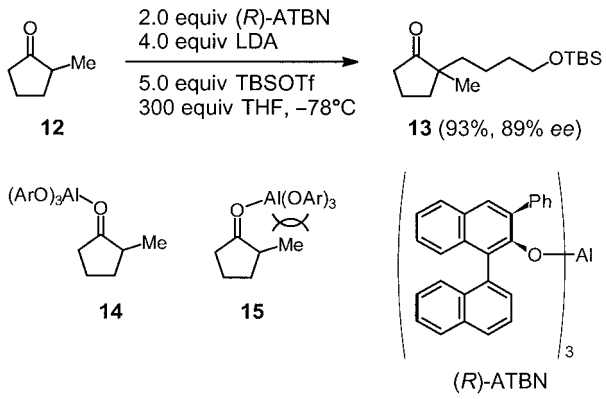
Scheme 1. Construction of vicinal quaternary stereocenters by dialkylation with an optically active dielectrophile. Bn = benzyl; OTf = triflate = trifluoromethanesulfonate; HMDS = 1,1,1,3,3,3-hexamethyldisilazanide; DMPU = 1,3-dimethylhexahydro-2-pyrimidone.



Scheme 2. Auxiliary-mediated synthesis of α-chiral aldehydes by allylic substitution. Piv = pivaloyl = Me_3CCO.

resulted in Felkin product **9** in good yield and diastereoselectivity after separation from the minor diastereoisomer by chromatography. Allylic alcohol **9** was activated as the pivaloate and converted with alkylcuprates of the general type R′CuCNMgBr (R′ = Alkyl) to yield the quaternary stereocenter in the S_N2' products **11** in very good yields and with high diastereoselectivities. Subsequent ozonolysis afforded aldehydes **10** and regenerated auxiliary **8**.

Another methodology for the stereoselective generation of carbonyl compounds with quaternary α-chiral centers was developed by Yamamoto and co-workers (Scheme 3).[9a,b] After precomplexation of the cyclopentanone **12** by the chiral



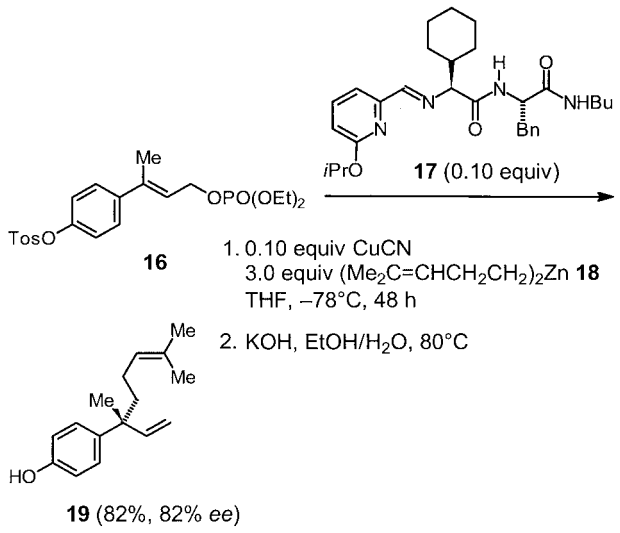
Scheme 3. α-Alkylation of cycloalkanones with THF/TBSOTf in the presence of a chiral Lewis acid. LDA = lithium diisopropylamide; TBS = *tert*-butyldimethylsilyl.

Lewis acid aluminum (*R*)-tris(3-phenyl-1,1′-binaphthoxide-2) ((*R*)-ATBN)[9c,d] and subsequent generation of the enolate, a regioselective alkylation with TBSOTf-activated THF at the sterically more hindered α-site took place. The alkylating reagent TBSOTf/THF had previously been used by Lohray and Enders for the diastereoselective formation of tertiary α-centers by using (*S*)- and (*R*)-*N*-amino-2-methoxymethylpyrrolidine hydrazones (SAMP and RAMP hydrazones, respectively).[10] *O*-Silyltetrahydrofuranium triflate was postulated to be the actual alkylating species. The largeness of the Lewis acid and the resulting steric hindrance in the complexed intermediate **15** was used to explain the high regioselectivity of the reaction ($\geq$20:1). The more stable conformer **14** is siloxybutylated to yield product **13**. In a similar concept, γ-aldolizations of α,β-unsaturated carbonyl compounds ("directed aldol reaction") were successfully achieved by applying an achiral aluminum Lewis acid.[11] The best example out of the original publication is shown in Scheme 3. A variation in the ring size significantly lowered the yields and enantioselectivities. The use of an excess of the chiral reagent currently prevents a broad application and offers an incentive for further improvement of this method.

3. Allylations

Apart from new asymmetric palladium-catalyzed vinylations[12a] and arylations,[12b] particularly of keto-enolates, palladium-catalyzed allylic substitution has become a flexible and established reaction to give quaternary carbon centers.[13] Recently, Hoveyda and co-workers reported on the first copper-catalyzed, enantioselective allylic substitution for the synthesis of quaternary centers (Scheme 4).[14] Modular, nonsymmetric pyridyl-dipeptides, such as **17**, with an aldimine moiety were identified as suitable chiral ligands by multistage parallel screening of ligand libraries. The potential of structurally related compounds as ligands in transition metal catalysis, for example, in asymmetric Strecker reactions or in 1,4-additions to cyclic enones, has already been proved.[15] Di- or trisubstituted allylphosphates such as **16** were used as substrates, and dialkylzinc compounds such as **18**, namely non-stabilized ("hard") alkylation reagents,[16] were used as

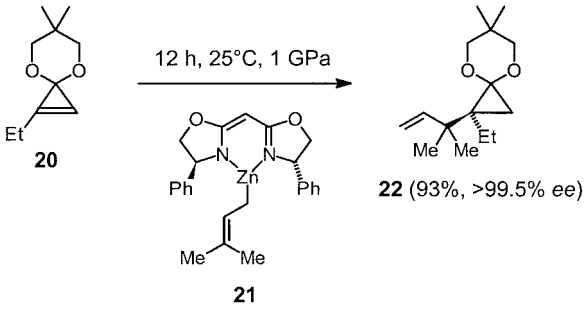
 © WILEY-VCH Verlag GmbH, D-69451 Weinheim, 2001 1433-7851/01/4024-4592 $ 17.50+.50/0 *Angew. Chem. Int. Ed.* **2001**, *40*, No. 24



Scheme 4. Copper-catalyzed allylic substitution. Tos = *p*-tosyl = *p*-toluenesulfonyl.

nucleophiles. In this way, tertiary centers were generated with 66–75% *ee* and quaternary centers with 78–90% *ee*. The synthesis of the fish deterrent (−)-sporochnol (**19**) is shown as an example in Scheme 4.

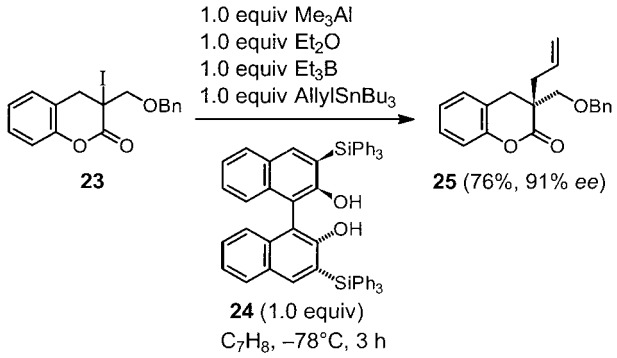
There are to date very few examples of enantioselective allylmetalations of isolated double bonds. As recently reported by Nakamura et al., quaternary stereocenters are generated by allylzincation of the olefin moiety of cyclopropenonacetals such as **20** with excellent enantioselectivities at ambient temperature (Scheme 5).[17] The chiral allylzinc



Scheme 5. Auxiliary-mediated allylzincation.

reagent **21** was prepared in situ by conversion of the corresponding allylzinc bromide, with an anionic bisoxazoline ligand (BOX)[18] being an auxiliary in this case. The ligand-controlled allylzincation of **20** took place regioselectively at the higher substituted carbon atom of the cyclopropene unit. Two vicinal quaternary carbon centers in compound **22** were obtained by application of the prenylzinc derivative **21** and subsequent hydrolysis. At ambient pressure the carbometalation proceeded very slowly, but with good selectivity (for **22** at 1 atm, 72 h: 19% yield, >99.5% *ee*). Application of a high-pressure technique accelerated the process and resulted in an improved yield together with an excellent stereoselectivity.

Although asymmetric C–C bond formations by radical processes have received increasing attention in the past few years, they are still relatively rare compared to other methods.[19] Besides chiral auxiliaries or chiral organotin compounds, chiral Lewis acids play an important role in this field. To date, the only radical reaction for the generation of a quaternary carbon center was introduced by Hoshino and co-workers (Scheme 6).[20] Products such as **25** were obtained in good yield (75–85%) and with high enantioselectivity (75–91% *ee*) by the conversion of α-alkyl-α-iodolactones such as **23** with allyltributylstannane at −78 °C in the presence of a stoichiometric amount of a chiral Lewis acid. Scheme 6 illustrates the best example of the original publication. The Lewis acid was generated in situ from $AlMe_3$ and the binaphthol derivative **24** in the presence of Et_2O as an



Scheme 6. Asymmetric radical-mediated allylation.

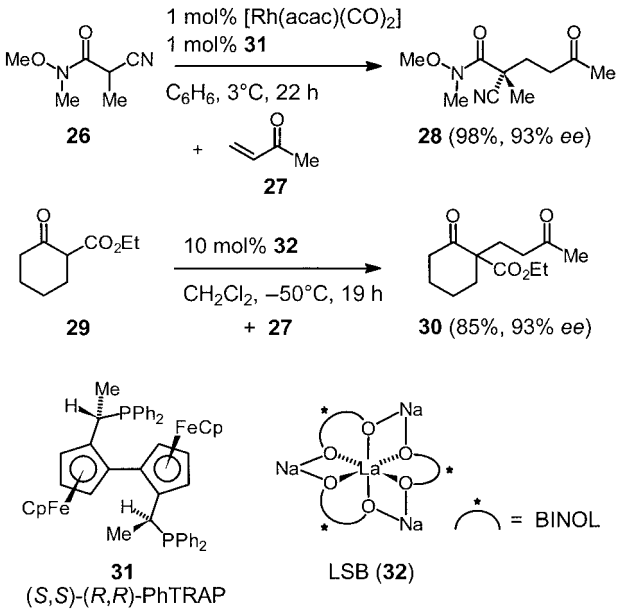
additive, with triethylborane used to initiate the reaction. As was shown by the authors, conversion also proceeded with a catalytic amount of the Lewis acid, but with lower selectivity (for **25** with 0.1 equiv catalyst: 78% yield, 71% *ee*).

4. Conjugate Additions

4.1. Asymmetric Catalysis

Conjugate additions (1,4-additions) of carbon nucleophiles to acceptor-activated C–C multiple bonds belong to the most important and versatile reactions for the synthesis of quaternary and tertiary carbon centers.[21] Recently, such catalytic enantioselective Michael reactions have been the subject of a detailed review article.[21a] Therefore, only two important examples are discussed here.

As early as 1992 Ito and co-workers reported on rhodium-catalyzed Michael reactions of α-methyl-substituted cyanoacetates with vinyl ketones and acrolein.[22b,c] The rhodium catalyst was generated in situ from $[RhH(CO)(PPh_3)_3]$ and the chiral bis(ferrocenylphosphane) ligand 2,2′′-bis[1-(diphenylphosphanyl)ethyl]-1,1′′-biferrocene ((*S*,*S*)-(*R*,*R*)-PhTRAP, **31**).[22a] This diphosphane, bearing planar as well as central stereogenic elements, forms *trans* chelate complexes with rhodium. Cyanoacetamides such as **26** (Weinreb amide)[23] which acted as Michael donors were reported to be alkylated in the α-position by vinyl ketones or acrolein under the reaction conditions used.[22d] Scheme 7 shows the conversion with methyl vinyl ketone (**27**) as an example. In this case, the



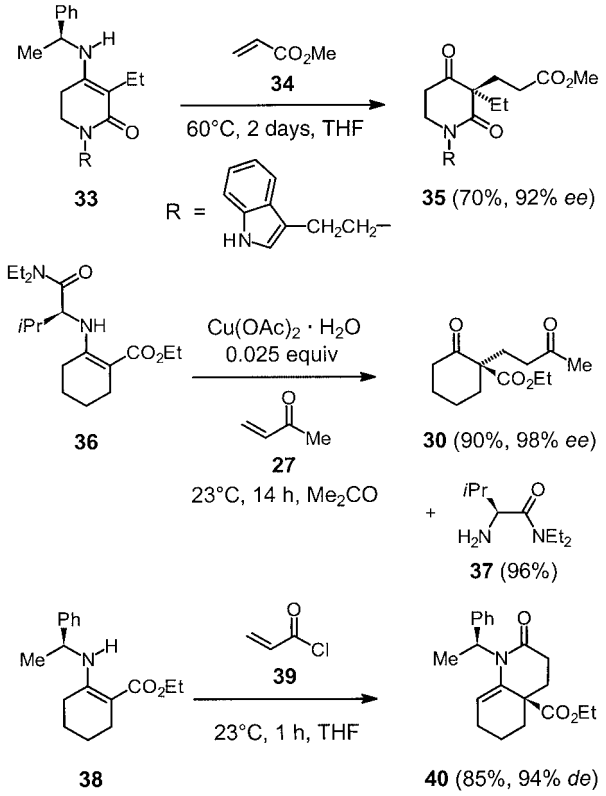
Scheme 7. Rhodium- and heterobimetal-catalyzed Michael reactions. acac = acetyl acetonate; Cp = cyclopentadienyl.

catalyst was generated in situ from the phosphane-free $[Rh(acac)(CO)_2]$ complex. The product **28** was obtained in excellent yield and selectivity, and can be readily transformed into other carbonyl derivatives.

The actual breakthrough in the field of catalytic enantioselective Michael reactions was achieved in 1994 by Shibasaki and co-workers. They introduced a new class of heterobimetallic catalysts, which also turned out to be very versatile for a number of other C–C bond-forming reactions.[21, 24] Tertiary, as well as quaternary stereocenters, are generated with high enantioselectivity by the conversion of different Michael donors with cyclic or open-chain Michael acceptors when catalyzed by a lanthanum-sodium-BINOL complex (LSB, **32**), prepared from $La(OiPr)_3$ and three equivalents each of BINOL (2,2′-dihydroxy-1,1′-binaphthyl) and NaO*t*Bu. In the course of the reaction the acceptor is activated by coordination to the Lewis acidic metal center (La^{3+}), while the Brönstedt basic Na-BINOLate moiety deprotonates and coordinates to the Michael donor. The actual C–C bond-forming step takes place in the coordination sphere of the metal center. Whereas tertiary carbon centers are constructed with high enantioselectivities at ambient temperature, the synthesis of quaternary centers requires lower reaction temperatures, as shown in Scheme 7 for the conversion of the cyclic β-keto ester **29** with methyl vinyl ketone (**27**).[25]

4.2. Application of Chiral Auxiliaries

Auxiliary-mediated asymmetric Michael reactions are also significant since they often tolerate a broad range of substrates and functional groups, and proceed under comparatively mild and neutral reaction conditions.[26] The use of 1-phenylethylamine (first reported in 1985 by Pfau and d'Angelo) as a readily available and universal auxiliary is established in this field.[26b] The new C–C bond is formed from an enamine–Michael reaction, with a cyclic transition state being mechanistically related to an aza–ene reaction.[26a] In some cases, increased reaction temperatures are required, and in particular for the conversion of simple vinyl ketones that are acting as Michael acceptors, a stoichiometric amount of a Lewis acid or high-pressure techniques are necessary.[27] The key intermediate **35** for the total synthesis of (+)-vincamin, the main alkaloid of periwinkle with cerebroprotective activity, was prepared by d'Angelo and co-workers as shown in Scheme 8.[28] Enaminolactam **33** was converted at elevated temperature with two equivalents of methyl acrylate (**34**) to yield the Michael product **35** in 70% yield and with an enantiomeric excess of 92% after cleavage of the auxiliary.



Scheme 8. Asymmetric Michael reactions of optically active enamines.

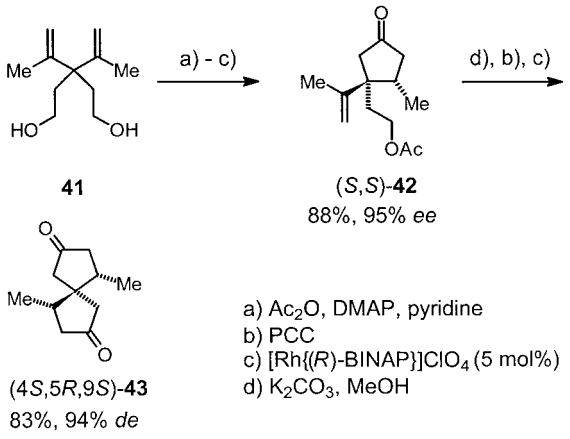
α-Aminocarboxamides such as **37** were recently introduced as an alternative to phenylethylamine in copper-catalyzed asymmetric Michael reactions.[29, 30] The conversion of the corresponding enamines (for example, **36**) with simple vinyl ketones such as **27** proceeds in the presence of a catalytic amount of $Cu(OAc)_2 \cdot H_2O$ at ambient temperature in acetone (Scheme 8). Products such as **30** were obtained with selectivities up to 99% *ee* after cleavage of the auxiliary. Similar enantioselectivities were achieved with open-chain 1,3-dicarbonyl compounds as donors.[31] The auxiliaries, such as **37**, are readily prepared from natural α-amino acids and can be recovered almost quantitatively after workup. In contrast to other transition metal catalyzed reactions, quaternary stereocenters are generated at ambient temperature in excellent selectivities and high yields under very mild reaction conditions by applying this procedure.

 © WILEY-VCH Verlag GmbH, D-69451 Weinheim, 2001 1433-7851/01/4024-4594 $ 17.50+.50/0 *Angew. Chem. Int. Ed.* **2001**, *40*, No. 24

A sequence of N-acylation of the enamino ester **38** with acryloyl chloride (**39**) and subsequent intramolecular enamine–Michael reaction was reported by Stille and coworkers to access δ-lactam derivatives such as **40** (Scheme 8).[32] Phenylethylamine was used as a chiral auxiliary for the enamine–Michael reaction and, moreover, as the nitrogen source of the lactam moiety.[32c] The aza-annulation product **40** was obtained in good yield (85%) and with good diastereoselectivity (94% *de*).

5. Rhodium-Catalyzed Hydroacylation

Rhodium-catalyzed intramolecular asymmetric hydroacylations of γ,δ-unsaturated aldehydes[33] provide access to optically active cyclopentanones bearing a quaternary and a vicinal tertiary carbon center.[34a,b] Tanaka, Suemune, and coworkers developed a remarkable strategy consisting of a double intramolecular hydroacylation of a bispentenal to synthesize chiral asymmetric spirocycles (Scheme 9).[34c] Intramolecular hydroacylation of a prochiral 4-pentenal, prepared from precursor **41**, in the presence of [Rh{(*R*)-BINAP}]ClO_4 as the catalyst yielded the cyclopentanone **42** at room temperature in 95% *ee* and 88% yield. The spiro[4.4]nonane **43** was obtained with very high stereoselectivity after saponification of the ester and subsequent oxidation of the resulting alcohol in a second hydroacylation step. The introduced sequence provides flexible access to spirocenters with two vicinal tertiary stereocenters.



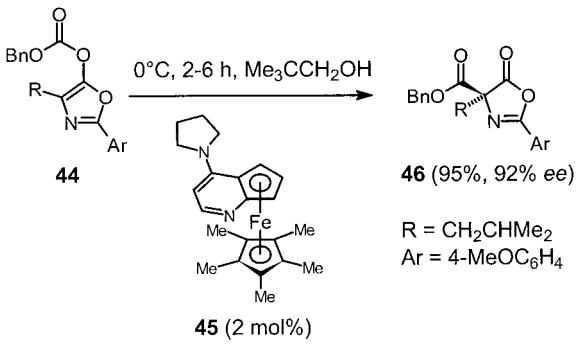
Scheme 9. Synthesis of chiral spiro compounds by double intramolecular rhodium-catalyzed hydroacylation (the yields refer to step c). DMAP = 4-dimethylaminopyridine; PCC = pyridinium chlorochromate.

6. Rearrangements

Rearrangements belong to the most important C–C bond-formating reactions in organic synthesis. Together with cycloaddition reactions, they are definitively atom-economic processes. Since most sigmatropic rearrangements proceed via a well-defined cyclic transition state, they are highly stereospecific and stereoselective.[35] Consequently, such processes provide excellent preconditions for the concurrent construction of more than one stereocenter.

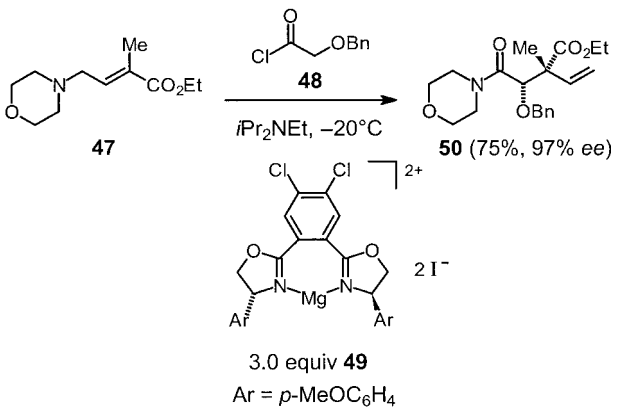
6.1. Asymmetric Catalysis

As already shown by Steglich and Höfle in 1970, the rearrangement of O-acylated azlactones to the corresponding C-acylated oxazolinones is catalyzed by 4-dimethylaminopyridine (DMAP).[36] The first asymmetric version of this 1,2-acyl shift was introduced by Ruble and Fu (Scheme 10).[37a] Substrates such as **44** are converted in the presence of the planar-chiral DMAP derivative **45** (PPY), which acts as the nucleophilic catalyst, in very good yield (93-95%) and with high enantioselectivity (88–92% *ee*) into the oxazoline derivatives **46**, which are interesting precursors for α,α-dialkylated α-aminocarboxylic acid derivatives. Analogous pyrido-annulated ferrocene derivatives with planar chirality were used by the same authors for the stereoselective synthesis of tertiary stereocenters by kinetic resolutions of secondary alcohols and for the additions of alcohols to ketenes.[37b]



Scheme 10. Steglich rearrangement catalyzed by planar-chiral DMAP.

Recently, MacMillan and co-workers reported on the first Lewis acid catalyzed asymmetric version of an acyl–Claisen rearrangement (Scheme 11).[38] The substrates were *N*-allylmorpholine derivatives, such as **47**, which were acylated with a ketene generated in situ from benzyloxyacetyl chloride **48** and iPr_2NEt. The resulting intermediate underwent a [3,3] sigma-

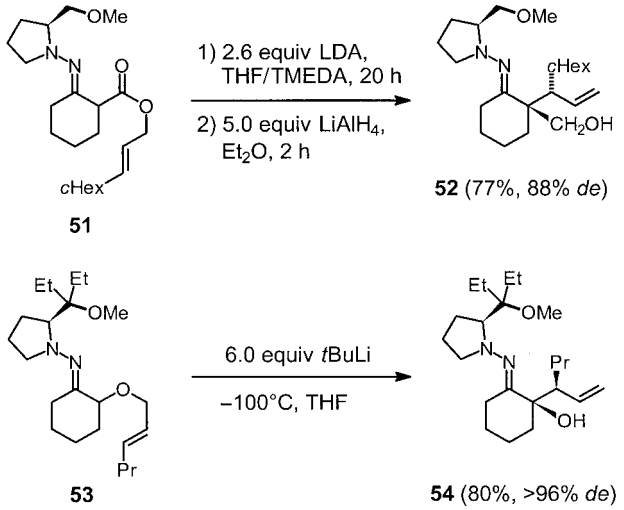


Scheme 11. Acyl–Claisen rearrangement catalyzed by a chiral Lewis acid.

tropic rearrangement to **50** in the presence of the optically active Lewis acid **49**. The *syn* diastereomer (*syn*:*anti* = 94:6) was obtained with high enantioselectivity (97% *ee*) and in good yield (75%). A vicinal tertiary carbon center was generated in addition to the quaternary stereocenter. MgI_2 in combination with a C_2-symmetrical bisoxazoline ligand (Arbox ligand) was used to generate the chiral Lewis acid **49**. An excess amount of the Lewis acid (three equivalents) is required, which thus prevents a broader application of this method.

6.2. Application of Chiral Auxiliaries

Since sigmatropic rearrangements proceed mostly with high stereospecifity, the conversion of enantiomerically pure substrates with tertiary carbon centers can result in the generation of quaternary carbon centers in the product. Consequently, the application of chiral auxiliaries is an attractive strategy.[5, 35] An asymmetric version of the Carroll rearrangement was published by Enders et al. (Scheme 12).[39] The



Scheme 12. Carroll rearrangement and [2,3] Wittig-rearrangement with optically active methoxymethylpyrrolidine derivatives as auxiliaries. *c*-Hex = cyclohexyl; TMEDA = *N*,*N*,*N*′,*N*′-tetramethylethylenediamine.

pyrrolidine derivative (*S*)-*N*-amino-2-methoxymethylpyrrolidine (SAMP) served as the auxiliary. This auxiliary belongs to a class of chiral *N*-aminopyrrolidine derivatives developed by Enders et al. which has proved its versatility in a number of C–C bond-forming reactions.[40] After deprotonation, the SAMP hydrazones, such as **51**, derived from β-keto esters underwent a [3,3] sigmatropic rearrangement. Alcohols **52** were obtained with good diastereoselectivity (94:0:6) after reduction of the carboxylic acid moiety. The auxiliary was cleaved from **52** and the keto function regenerated by ozonolysis. This sequence allows the synthesis of a cycloalkanone with a quaternary α and a tertiary β stereocenter starting from a β-keto allyl ester.

Enders and co-workers also reported on the preparation of chiral α-hydroxy ketones by [2,3] Wittig rearrangements using the optically active pyrrolidine derivative (*S*)-*N*-amino-2-(1-ethyl-1-methoxypropyl)pyrrolidine (SAEP).[41a,b] Quaternary products were obtained starting from an α-allyloxycyclohexanone to give the corresponding SAEP hydrazone **53** (Scheme 12).[41c] The homoallyl alcohol **54** was obtained as the *anti* product (*anti*:*syn* = 91:9) from a [2,3] sigmatropic rearrangement after deprotonation of the starting material **53** with an excess of *t*BuLi. The auxiliary was cleaved from the product **54** by ozonolysis to yield a carbonyl compound with a quaternary O-substituted center and a vicinal tertiary stereocenter.

7. Conclusion

Several new methods and strategies for the enantioselective synthesis of quaternary carbon centers have been developed in the recent years. Only a small selection from a very active area of research has been presented. Despite these new developments, there is still a great demand for new processes and for optimization of the known ones, since they do not always meet the requirements of modern synthetic organic chemistry. In particular, flexibility and versatility with regard to substrates and functional groups, atom-economy, efficiency, and simple performance are standards a modern synthetic method ought to fulfill. Moreover, chiral auxiliaries and ligands should be readily accessible. The development of catalytic asymmetric reactions suitable for the generation of quaternary stereocenters remains a particular challenge.

Received: July 13, 2001 [M1526]

[1] Reviews: a) K. C. Nicolaou, E. J. Sorensen, *Classics in Total Synthesis*, VCH, Weinheim, **1996**; b) K. C. Nicolaou, D. Vourloumis, N. Winssinger, P. S. Baran, *Angew. Chem.* **2000**, *112*, 46–126; *Angew. Chem. Int. Ed.* **2000**, *39*, 44–122.

[2] *Catalytic Asymmetric Synthesis*, 2nd ed. (Ed.: I. Ojima), Wiley-VCH, New York, **2000**.

[3] Review on atom-economy: B. M. Trost, *Angew. Chem.* **1995**, *107*, 285–307; *Angew. Chem. Int. Ed. Engl.* **1995**, *34*, 259–281.

[4] Reviews: a) E. J. Corey, A. Guzman-Perez, *Angew. Chem.* **1998**, *110*, 402–415; *Angew. Chem. Int. Ed.* **1998**, *37*, 388–401; b) K. Fuji, *Chem. Rev.* **1993**, *93*, 2037–2066; c) S. F. Martin, *Tetrahedron* **1980**, *36*, 419–460.

[5] Reviews: a) P. O'Brien, *J. Chem. Soc. Perkin Trans. 1* **2001**, 95–113; b) J. Seyden-Penne, *Chiral Auxiliaries and Ligands in Asymmetric Synthesis*, Wiley, New York, **1995**.

[6] a) L. E. Overman, J. F. Larrow, B. A. Stearns, J. M. Vance, *Angew. Chem.* **2000**, *112*, 219–221; *Angew. Chem. Int. Ed.* **2000**, *39*, 213–215; b) L. E. Overman, D. V. Paone, B. A. Stearns, *J. Am. Chem. Soc.* **1999**, *121*, 7702–7703; c) J. T. Link, L. E. Overman, *J. Am. Chem. Soc.* **1996**, *118*, 8166–8167.

[7] a) C. Spino, C. Beaulieu, *Angew. Chem.* **2000**, *112*, 2006–2008; *Angew. Chem. Int. Ed.* **2000**, *39*, 1930–1932; b) C. Beaulieu, C. Spino, *Tetrahedron Lett.* **1999**, *40*, 1637–1640; c) C. Spino, C. Beaulieu, *J. Am. Chem. Soc.* **1998**, *120*, 11832–11833.

[8] Review: E.-I. Negishi, D. Y. Kondakov, *Chem. Soc. Rev.* **1996**, *25*, 417–426.

[9] a) S. Saito, M. Nakadai, H. Yamamoto, *Synlett* **2000**, 1107–1110; b) S. Saito, M. Ito, K. Maruoka, H. Yamamoto, *Synlett* **1997**, 357–358; c) K. Maruoka, S. Saito, H. Yamamoto, *J. Am. Chem. Soc.* **1995**, *117*, 1165–1166; review: d) S. Saito, H. Yamamoto, *Chem. Commun.* **1997**, 1585–1592.

[10] B. B. Lohray, D. Enders, *Synthesis* **1993**, 1092–1094.

 © WILEY-VCH Verlag GmbH, D-69451 Weinheim, 2001 1433-7851/01/4024-4596 $ 17.50+.50/0

[11] Review: S. Saito, H. Yamamoto, *Chem. Eur. J.* **1999**, *5*, 1959 – 1962.
[12] a) A. Chieffi, K. Kamikawa, J. Åhman, J. M. Fox, S. L. Buchwald, *Org. Lett.* **2001**, *3*, 1897 – 1900; b) J. Åhman, J. P. Wolfe, M. V. Troutman, M. Palucki, S. L. Buchwald, *J. Am. Chem. Soc.* **1998**, *120*, 1918 – 1919.
[13] Recent work: a) S.-L. You, X.-L. Hou, L.-X. Dai, X.-Z. Zhu, *Org. Lett.* **2001**, *3*, 149 – 151; b) B. M. Trost, G. M. Schroeder, *J. Am. Chem. Soc.* **1999**, *121*, 6759 – 6760; c) B. M. Trost, X. Ariza, *J. Am. Chem. Soc.* **1999**, *121*, 10727 – 10737; review on palladium-catalyzed asymmetric allylic alkylation: d) G. Helmchen, A. Pfaltz, *Acc. Chem. Res.* **2000**, *33*, 336 – 345; e) B. M. Trost, D. L. Van Vranken, *Chem. Rev.* **1996**, *96*, 395 – 422.
[14] C. A. Luchaco-Cullis, H. Mizutani, K. E. Murphy, A. H. Hoveyda, *Angew. Chem.* **2001**, *113*, 1504 – 1508; *Angew. Chem. Int. Ed.* **2001**, *40*, 1456 – 1460.
[15] Selected examples: a) M. S. Sigman, P. Vachal, E. N. Jacobsen, *Angew. Chem.* **2000**, *112*, 1336 – 1338; *Angew. Chem. Int. Ed.* **2000**, *39*, 1279 – 1281; b) C. A. Krueger, K. W. Kuntz, C. D. Dzierba, W. G. Wirschun, J. D. Gleason, M. L. Snapper, A. H. Hoveyda, *J. Am. Chem. Soc.* **1999**, *121*, 4284 – 4285; c) S. J. Degrado, H. Mizutani, A. H. Hoveyda, *J. Am. Chem. Soc.* **2001**, *123*, 755 – 756.
[16] Asymmetric synthesis of tertiary stereocenters by copper-catalyzed allylic substitution with diorganozinc reagents: a) F. Dübner, P. Knochel, *Tetrahedron Lett.* **2000**, *41*, 9233 – 9237; b) F. Dübner, P. Knochel, *Angew. Chem.* **1999**, *111*, 391 – 393; *Angew. Chem. Int. Ed.* **1999**, *38*, 379 – 381.
[17] a) M. Nakamura, T. Inoue, A. Sato, E. Nakamura, *Org. Lett.* **2000**, *2*, 2193 – 2196; b) M. Nakamura, M. Arai, E. Nakamura, *J. Am. Chem. Soc.* **1995**, *117*, 1179 – 1180; c) K. Kubota, M. Nakamura, M. Isaka, E. Nakamura, *J. Am. Chem. Soc.* **1993**, *115*, 5867 – 5868.
[18] A. K. Gosh, P. Mathiavanan, J. Cappiello, *Tetrahedron: Asymmetry* **1998**, *9*, 1 – 45.
[19] Selected examples: a) C. C. Gonzales, A. R. Kennedy, E. I. Leon, C. Riesco-Fagundo, E. Suarez, *Angew. Chem.* **2001**, *113*, 2388 – 2390; *Angew. Chem. Int. Ed.* **2001**, *40*, 2326 – 2328; b) M. P. Sibi, Y. Asano, J. B. Sausker, *Angew. Chem.* **2001**, *113*, 1333 – 1336; *Angew. Chem. Int. Ed.* **2001**, *40*, 1293 – 1269; c) A. Gansäuer, T. Lauterbach, H. Bluhm, M. Noltemeyer, *Angew. Chem.* **1999**, *111*, 3122 – 3114; *Angew. Chem. Int. Ed.* **1999**, *38*, 2909 – 2910; d) M. P. Sibi, J. Ji, *J. Org. Chem.* **1997**, *62*, 3800 – 3801; e) M. P. Sibi, J. Ji, *J. Am. Chem. Soc.* **1996**, *118*, 9200 – 9201; review: f) T. Wirth, *Angew. Chem.* **1998**, *110*, 2179 – 2181; *Angew. Chem. Int. Ed.* **1998**, *37*, 2069 – 2071.
[20] M. Murakata, T. Jono, Y. Mizuno, O. Hoshino, *J. Am. Chem. Soc.* **1997**, *119*, 11713 – 11714.
[21] Reviews: a) N. Krause, A. Hoffmann-Röder, *Synthesis* **2001**, 171 – 196; b) M. P. Sibi, S. Manyem, *Tetrahedron* **2000**, *56*, 8033 – 8061.
[22] a) M. Sawamura, H. Hamashima, Y. Ito, *Tetrahedron: Asymmetry* **1991**, *2*, 593 – 596; b) M. Sawamura, H. Hamashima, Y. Ito, *J. Am. Chem. Soc.* **1992**, *114*, 8295 – 8296; c) M. Sawamura, H. Hamashima, Y. Ito, *Tetrahedron* **1994**, *50*, 4439 – 4454; d) M. Sawamura, H. Hamashima, H. Shinoto, Y. Ito, *Tetrahedron Lett.* **1995**, *36*, 6479 – 6482.
[23] J. Singh, N. Satyamurthi, I. S. Aidhen, *J. Prakt. Chem.* **2000**, *342*, 340 – 347.
[24] a) H. Sasai, T. Arai, M. Shibasaki, *J. Am. Chem. Soc.* **1994**, *116*, 1571 – 1572; b) H. Sasai, T. Arai, Y. Satow, K. N. Houk, M. Shibasaki, *J. Am. Chem. Soc.* **1995**, *117*, 6194 – 6198; c) T. Arai, H. Sasai, K.-I. Aoe, K. Okamura, T. Date, M. Shibasaki, *Angew. Chem.* **1996**, *108*, 103 – 105; *Angew. Chem. Int. Ed. Engl.* **1996**, *35*, 104 – 106; d) T. Arai, Y. M. A. Yamada, N. Yamamoto, H. Sasai, M. Shibasaki, *Chem. Eur. J.* **1996**, *2*, 1368 – 1372; reviews: e) M. Shibasaki, H. Sasai, *Pure Appl. Chem.* **1996**, *68*, 523 – 530; f) M. Shibasaki, H. Sasai, T. Arai, *Angew. Chem.* **1997**, *109*, 1290 – 1310; *Angew. Chem. Int. Ed. Engl.* **1997**, *36*, 1236 – 1256.
[25] H. Sasai, E. Emori, T. Arai, M. Shibasaki, *Tetrahedron Lett.* **1996**, *37*, 5561 – 5564.
[26] Reviews: a) J. Leonard, E. Díez-Barra, S. Merino, *Eur. J. Org. Chem.* **1998**, 2051 – 2061; b) J. d'Angelo, D. Desmaële, F. Dumas, A. Guingant, *Tetrahedron: Asymmetry* **1992**, *3*, 459 – 505.
[27] A. Guingant, H. Hammami, *Tetrahedron: Asymmetry* **1991**, *2*, 411 – 414.
[28] D. Desmaële, K. Mekouar, J. d'Angelo, *J. Org. Chem.* **1997**, *62*, 3890 – 3901.
[29] a) J. Christoffers, A. Mann, *Angew. Chem.* **2000**, *112*, 2871 – 2874; *Angew. Chem. Int. Ed.* **2000**, *39*, 2752 – 2754; b) J. Christoffers, U. Rößler, T. Werner, *Eur. J. Org. Chem.* **2000**, 701 – 705.
[30] Reviews: a) J. Christoffers, *Synlett* **2001**, 723 – 732; b) J. Christoffers, *Eur. J. Org. Chem.* **1998**, 1259 – 1266.
[31] J. Christoffers, A. Mann, *Chem. Eur. J.* **2001**, *7*, 1014 – 1027.
[32] a) P. Benovsky, G. A. Stephenson, J. R. Stille, *J. Am. Chem. Soc.* **1998**, *120*, 2493 – 2500; b) N. S. Barta, A. Brode, J. R. Stille, *J. Am. Chem. Soc.* **1994**, *116*, 6201 – 6206; c) J. d'Angelo, A. Guingant, C. Riche, A. Chiaroni, *Tetrahedron Lett.* **1988**, *29*, 2667 – 2670.
[33] a) K. Sakai, J. Ide, O. Oda, N. Nakamura, *Tetrahedron Lett.* **1972**, 1287 – 1290; review and mechanism: b) B. Bosnich, *Acc. Chem. Res.* **1998**, *31*, 667 – 674.
[34] a) M. Tanaka, M. Imai, M. Fujio, E. Sakamoto, M. Takahashi, Y. Eto-Kato, X. M. Wu, K. Funakoshi, K. Sakai, H. Suemune, *J. Org. Chem.* **2000**, *65*, 5806 – 5816; b) M. Takahashi, M. Tanaka, E. Sakamoto, M. Imai, K. Funakoshi, K. Sakai, H. Suemune, *Chem. Pharm. Bull.* **2000**, *48*, 1822 – 1825; c) M. Tanaka, M. Takahashi, E. Sakamoto, M. Imai, A. Matsui, M. Fujio, K. Funakoshi, K. Sakai, H. Suemune, *Tetrahedron* **2001**, *57*, 1197 – 1204.
[35] Review on sigmatropic rearrangements: D. Enders, M. Knopp, R. Schiffers, *Tetrahedron: Asymmetry* **1996**, *7*, 1847 – 1882.
[36] W. Steglich, G. Höfle, *Tetrahedron Lett.* **1970**, 4727 – 4730.
[37] a) J. C. Ruble, G. C. Fu, *J. Am. Chem. Soc.* **1998**, *120*, 11532 – 11533; review on planar-chiral DMAP derivatives: b) G. C. Fu, *Acc. Chem. Res.* **2000**, *33*, 412 – 420.
[38] a) T. P. Yoon, D. W. C. MacMillan, *J. Am. Chem. Soc.* **2001**, *123*, 2911 – 2912; b) T. P. Yoon, V. M. Dong, D. W. C. MacMillan, *J. Am. Chem. Soc.* **1999**, *121*, 9726 – 9727.
[39] a) D. Enders, M. Knopp, J. Runsink, G. Raabe, *Liebigs Ann.* **1996**, 1095 – 1116; b) D. Enders, M. Knopp, J. Runsink, G. Raabe, *Angew. Chem.* **1995**, *107*, 2442 – 2445; *Angew. Chem. Int. Ed. Engl.* **1995**, *34*, 2278 – 2280.
[40] Review on applications in natural product synthesis: D. Enders, C. Thiebes, *Pure Appl. Chem.* **2001**, *73*, 573 – 578.
[41] a) D. Enders, D. Backhaus, J. Runsink, *Angew. Chem.* **1994**, *106*, 2167 – 2170; *Angew. Chem. Int. Ed. Engl.* **1994**, *33*, 2098 – 2100; b) D. Enders, D. Backhaus, J. Runsink, *Tetrahedron* **1996**, *52*, 1503 – 1528; c) D. Enders, M. Bartsch, D. Backhaus, J. Runsink, G. Raabe, *Synthesis* **1996**, 1438 – 1442.

 © WILEY-VCH Verlag GmbH, D-69451 Weinheim, 2001 1433-7851/01/4024-4597 $ 17.50+.50/0

Coping with Fritz Haber's Somber Literary Shadow**

Roald Hoffmann* and Pierre Laszlo*

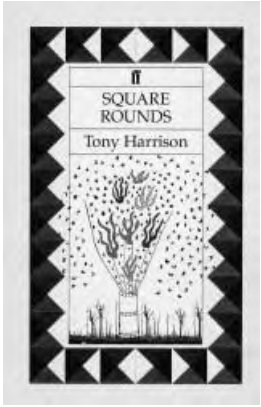
Chemists are legitimately distressed by the chemophobia of the public. One of its manifestations (hardly the only one) is the stereotyped presentation of a chemist as an amoral character, having sold his soul to the Devil. The implicit sin is more than Faustian, for the betrayal is not only personal, but that of humanity. Fritz Haber is often this scapegoat.

Is this stereotyping deserved? And might we, collectively and individually, do something about it? We approach the issue here by way of an attentive reading of a selection[1] of the literary pieces featuring Haber, whether under his own name or in transparent disguise, and of recent biographies of Haber.

The Fictional Haber

1

The British poet and occasional playwright Tony Harrison has written a genuinely funny musical play, *Square Rounds*, in which Fritz Haber has a most prominent role.[2] First performed at the Olivier Theatre in London in 1992, the play evokes very much a puppet show in the manner of Alfred Jarry's *Ubu Roi*. It features a nearly all-female cast of "Munitionettes," that is, of workers producing TNT during World War I. The women also impersonate the main characters, who include Fritz Haber and his wife Clara Immerwahr, Sir Hiram Maxim (the inventor of the machine gun and of an anti-poison gas inhaler), his brother Hudson Maxim (of Maximite TNT charge fame), Justus von Liebig (one of the icons of our profession, entering the play as the pioneering agricultural chemist), and Sir William Crookes (who foresaw the need for nitrogen fixation).



Tony Harrison has done his homework well, his documentation is unimpeachable. Fritz Haber's way to gas warfare is perceptively evoked, making Haber say:

> *"Out of the industry which gives the world its dyes*
> *I can chemically concoct a new shock from the skies. (…)*
> *I'm off to devise a little surprise*
> *something that's certain to stun*
> *all those who thought that war's only fought*
> *with things like that vulgar gun. (…)*
> *My gas will break the deadlock, make the war much shorter*
> *and therefore save millions from the slaughter.*"

Harrison has his characters speak in rhymed verse, a nice touch: Haber indeed versified as a hobby—Stoltzenberg's biography[8] has some choice examples. Harrison has Haber declare:

> *"After the mental struggle of nitrogen fixation*
> *I turn to verse as an effortless relaxation.*"

One of the few male characters in the play is the remarkable folksy sweeper Mawes, whom the "Hun Haber" draws into a hilarious verse competition. The fertilizer theme is the source of much scatological farce. Tony Harrison's inventive verse and talent for repartee, a match for William S. Gilbert of Gilbert and Sullivan fame, leavens and at times threatens to run away from the underlying anti-technological theme. The play has much literal magic, inventive fun with ribbons and costumes color-coded for the chemical elements, a song about N and O, and even a trinitrotoluene canon! And pathos, as in a dramatic Fritz Haber-Clara Haber confrontation.

The reader should not imagine, however, that this verse play is a paean to Haber. In fact, Harrison's wit is marshalled to paint a picture of Haber as devastatingly immoral.

2

Rolf Hochhuth, the German writer of strongly politically focused, well-documented plays, such as *Soldiers*, *The Representative* or *The Deputy* (about the silence by Pius XII during

[*] Prof. R. Hoffmann
Department of Chemistry
Baker Laboratory
Cornell University, Ithaca NY 14853-1301 (USA)
E-mail: rh34@cornell.edu
Fax: (+1)-607-255-5707
Prof. P. Laszlo[+]
Institut de chimie
Université de Liège au Sart-Tilman
4000 Liège (Belgium)
and Département de chimie, Ecole polytechnique, F-91128 Palaiseau (France)
E-mail: clouds-rest@wanadoo.fr
pierrelaszlo@usa.net
[+] Mailing address: POB 665, Pinehurst NC 28370 (USA)

[**] We are grateful to the reviewers of this paper for their provocative comments.

 © WILEY-VCH Verlag GmbH, D-69451 Weinheim, 2001 1433-7851/01/4024-4599 $ 17.50+.50/0

persecution of Jews in Nazi Germany), also invents a dramatic dialogue between Clara and Fritz Haber in the hour preceding her death. This is one of the 13 scenes in his *Sommer 14: Ein Totentanz. (Summer 14: A Dance of Death.)*[3] Actually (and as Hochhuth knew), the event took place in 1915, not 1914. Fritz and Clara begin the scene at the standing desks at which they used to work. Haber is aptly described in the stage directions—photographs bear this out—as looking like a toned-down Georg Grosz caricature. Clara Haber's agony, her understandable qualms about the unethical nature of her husband's war work, is quickly broached. No verse here. Haber is more human than in Harrison's play. But he just doesn't fathom Clara's concerns, nor is he able to hear her determination to kill herself. The day after her death he returned to the front, since this was what he saw as his patriotic duty. Or it was a way to escape his pain? But in that escape he left a thirteen year old son without a father as well as well as a mother.

3

Fritz Haber's figure makes an appearance in a book by André Malraux, *Les Noyers de l'Altenburg* (*The Walnut Trees of the Altenburg*, originally published in 1943).[4] Renamed Hoffmann, he sports a "*clean-shaven face, which was rare at that time, all hooked and angular, like certain Aryan faces that look like Jewish faces, only sharper*.[*]"[5] His concern with the chemical weapon is exclusively technical, the direction and strength of the wind, and clinical,

> *"gas constitutes the most humane method of warfare. For gas, mind you, announces its presence! The opaque cornea first goes blue, the breath starts to come in hisses, the pupil—it's really very odd!—becomes all black*."[5][**]

Whether or not Malraux has handed-on to us an authentic portrait of Fritz Haber or not is of little import. The third part of *Les Noyers de l'Altenburg* (which he wrote at the zenith of his already superb talent as a novelist; it is also his very last novel) contains a description of the attack with chemical weapons that occurred on the Eastern front on June 12, 1915. Malraux follows very closely the narrative of a contemporary witness, Max Wild, a German secret agent.[6]

Malraux's text is memorable; it ranks with the best in French literature. It is reminiscent of Victor Hugo's *Les Misérables*, in epic breath and in documentary accuracy alike. With a collage technique, Malraux inserts snippets of conversations between ordinary soldiers, which he had himself overheard and jotted down, at the beginning of the Second World War. He also makes masterly use of understatement—which brings this part of the novel to the level of Louis-Ferdinand Céline's *Voyage au bout de la nuit*, 1932 and of Erich-Maria Remarque's *Im Westen Nichts Neues* (*All Quiet on the Western Front*), 1929—in conveying the horrors of World War I. Interestingly, Malraux's novel was written during the beginning of World War II, in 1940–41.

Malraux prepares the pages on the use of chemical weapons with an apparently unrelated scene (moral outrage is the unstated, implicit link): an officer in the German Secret Service interrogates a woman suspected of being a Russian spy. He applies psychological torture, confronting her unexpectedly with her young son, convinced that she will break down and confess. But he is thwarted, the logical course of events does not unfold…

Neither does it in the gas attack. This is the feature in the real-life event which attracted the novelist's attention in the first place. It had a bizarre and wonderful outcome, such as only a pacifist writer (Romain Rolland) or a charismatic socialist leader (Jean Jaurès) could have dreamt. Fraternization occurred. In a manifestation of the universal brotherhood of man, in an "assault of pity," the German infantrymen carried on their shoulders back to their own lines all the gassed Russian survivors for medical treatment.

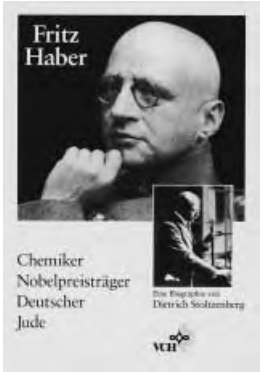
Haber in Biography

Three writers of talent and stature, three views of Haber, with some understanding, but none complimentary… "Could it be otherwise?" the cynical connoisseur of chemophobia will say.

The sweep and complexity of Fritz Haber's life is too great to be summarized here. And elements of it are familiar to our readers. Before attempting to answer the above cynic's question, let us look at some recent biographies of Haber, or of people close to him.[7]

1

We owe the first authoritative biography of Haber published in German in 1994 (an abbreviated English version will soon appear),[8] to Dietrich Stoltzenberg, the son of a Haber co-worker, a distinguished industrial chemist himself. Haber's chemistry is indeed authoritatively and exhaustively treated in Stoltzenberg's book, but that the author is a chemist does not mean that this is just a "scientific biography." The title of the book—*Fritz Haber: Chemist, Nobel Prize Laureate, German, Jew*—is apt, for it evokes the polarities in the physical chemist's life.



Stoltzenberg's meticulously researched biography contains some fascinating new material, for instance Haber's involvement in chemical-warfare research after World War I, carried out in secret, illegal experiments in which the German and Soviet military cooperated. In an indication of the book's success, German reviewers of very different ideological persuasion have used reviews of the book for their own purposes, while uniting in praise of Stoltzenberg's perception and moral tone.

[*] "*Visage rasé, ce qui était rare à l'époque, tout en angles crochus comme certains visages aryens qui semblent des visages juifs plus aigus.*"

[**] "*les gaz constituent le moyen de combat le plus humain. Car le gaz s'annonce, notez! la cornée opaque devient d'abord bleue, la respiration commence à siffler, l'iris—c'est même très curieux!—passe presque au noir.*"

 © WILEY-VCH Verlag GmbH, D-69451 Weinheim, 2001 1433-7851/01/4024-4600 $ 17.50+.50/0 *Angew. Chem. Int. Ed.* **2001**, *40*, No. 24

2

Margit Szöllösi-Janze[9] *Fritz Haber 1868–1934. Eine Biographie*, came out four years after Stoltzenberg's book, and draws first hand on many of the same sources. This excellent biography is especially assured when the author is dealing with contradictory sources, as in her account of Haber's conversion, or the death of his first wife. Both events are wrapped in legend. And even when the testimony of contemporaries is extant, that is colored by the normal human restructuring of memory. In the first case (the conversion) Szöllösi-Janze paints an authoritative canvas of varying attitudes toward acculturation, assimilation, and conversion in 19th Century Germany. In the latter instance she insists on looking at the facts, and does not shy away from questioning unreliable accounts.



Both Szöllösi-Janze and Stoltzenberg are sensitive to the ideological climate of the times, the social responsibility of scientists, and the complexities of Haber as a person. These exemplary biographies, like Walter Moore's life of Schrödinger,[10] or David Cassidy's life of Heisenberg,[11] show that it is possible to write engagingly and in-depth of the science, the person, and the times.

3

There has also appeared recently an attractive account of just one episode in Haber's life, his futile search for gold in the sea in the aftermath of World War I. This is Ralf Hahn's *Gold aus dem Meer*.[12] The complexity of Haber emerges even in the short time frame described. On the 14th of January, 1925, Fritz Haber writes to his co-worker Hans Eisner, (the father, incidentally, of a great neurobiologist and entomologist, Tom Eisner) from aboard a steamship somewhere between China and Indonesia:

"Today I have had the opportunity of crossing the equator for the second time. Which has drawn me to write to you, reviving the memory of our companionship. For you belong to the eleven people whom I've known in my 56 years with whom it is still a pleasure to think of traveling, even when the temperature is over 90 °F.

The sky is hazy, the sea like glass
I feel but weary hate
for life and all striving.
A quick, cool, sound burial!

In China I couldn't do anything about our gold project…"[*]

4

Clara Haber, *née* Immerwahr, is the subject of a biography, *Der Fall Clara Immerwahr (The Case of Clara Immerwahr)*.[13] von Leitner's account evokes well the social background of both Haber and Haber's wife, before they met, that of assimilated or converted Jewish German families (not without some analogy to the New Christians—Christian baptized Jews—in post 1492 Spain and Portugal). The author is also strong in describing the feminist work and the achievements of women's associations in Germany. She traces admiringly Clara Immerwahr's heroic struggle to carve for herself a career in chemistry. Hers was one of the first Ph.D.s granted to a woman in chemistry in Germany. This career she sacrificed for Fritz Haber. Willingly? Did he influence her to drop out?

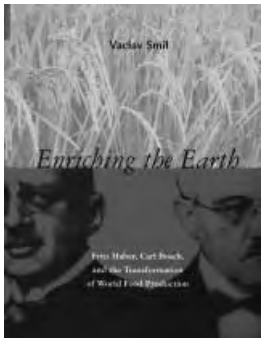


Haber himself is an evil presence in von Leitner's book, who is indiscriminate in her rage against him. To her, ammonia is just an "environmental poison!" The biography falters as Clara Immerwahr's life moves to its tragic end, making much of what we know little. Fritz Haber concealed or even destroyed his wife's suicide note and other documents that would have shed light on a private drama. Not the only one, for Hermann Haber, Fritz and Clara's son, also committed suicide at a later time.

von Leitner may have an obvious anti-Haber bias, but all the evidence shows Fritz Haber to have been unfeeling and unsupportive of his gifted first wife.

5

Vaclav Smil has recently published *Enriching the Earth: Fritz Haber, Carl Bosch, and the Transformation of World Food Production*.[14] This fascinating book, full of clear diagrams, is an encomium, detailed, reasoned and deserved, to the ammonia synthesis.



Wilhelm Ostwald carried out the initial research on the problem at the turn of the twentieth century. He applied in March 1900 for a patent for ammonia synthesis at elevated temperatures and pressures on an iron catalyst (!). But when Carl Bosch, at the time only 25 and at BASF already, checked the results, they were an artifact from hydrogenolysis of iron nitride. Henry Le Chate-

[*] *"Heute hat der Equator mir eine zweite ‚vorsichtige' Überschreitung gestattet und das Ereigniss drängt mich Ihnen im Gedächtnis der ersten zu schreiben, die durch die Reisegemeinschaft mit Ihnen mir in besonders angenehmer Erinnerung ist. Denn Sie gehören zu den elf Menschen die ich in 56 Jahren kennengelernt habe mit denen es oberhalb von 90° Fahrenheit noch ein Vergnügen bereitet zusammen zu reisen.*
Der Himmel ist dunstig, das Meer wie Glass
In meinem Gemüte ist müder Hass
Gegen das Leben und letztes Erstrebniss
Schnelles, kühles, gesundes Begräbniss!
Ich habe in China nichts in unserer Goldsache thun können;

lier also attempted to synthesize ammonia, but an explosion destroyed his laboratory in 1901 and he dropped out of the field.

Fritz Haber got started on the problem consulting for a chemical company in Vienna. He brought to bear on it his unique, very broad training as a chemist. As Smil nicely puts it (p. 69) "*as he was not narrowly specialized, he was not easily deterred by a discouraging result*." Nor by a prestigious senior scientist disparaging his contribution in no uncertain terms: when Walther Nernst heard of Haber's first results at the Bunsen Society conference, held in Hamburg May 9 – 12, 1907, he termed them grossly inaccurate (*stark unrichtigen Zahlen*). Haber was naturally upset; he developed digestive and skin problems, and… went into overdrive. And prevailed. We will reluctantly leave the compelling story of how this was accomplished for this book, or the Stoltzenberg and Szöllösi-Janze biographies. The tale is full of superb science, the most ingenious technical skill, and personal drama. Just imagine the Reichsgericht patent claim hearing in Leipzig in 1912 in which Walther Nernst (a nice BASF honorarium could not have hurt) supports Haber patents against Ostwald's counterclaim.

Actually, Smil's book is really not a biography of Haber (nor Bosch). Nor does it pretend to be—Smil writes in a postscript "*…the lives of the two protagonists exited the story shortly after the commercialization of the ammonia synthesis.*" The book *is* a biography, not of men, but of the element nitrogen as it has, does, and will wend its way through the world.

Smil certainly knows whereof he writes—he has 15 books under his belt on global, agricultural, and environmental issues. Here he gives us an integrated account of the world's preindustrial agriculture, and (in a broader view) of the great nitrogen cycles. Here's a startling fact: in Europe and the US about 40% of the nitrogen atoms in our bodies have seen the inside of a Haber – Bosch process factory. In China, the figure is closer to two thirds. Need one more evidence of the enormous consequences of the ammonia synthesis for life on earth?

6

Fritz Stern, who understands the soul of Germany better, we think, than any other modern historian, has studied Haber's life, and written of it at least twice.[15, 16] There is a family connection too—Stern's father was Haber's personal physician and friend.



Stern's second essay is the centerpiece of his recent book, *Einstein*'s *German World*. It is entitled "Together and Apart: Fritz Haber and Albert Einstein," Indeed it is a study of the two men, whose friendship was founded on great mutual respect and survived the most serious differences during World War I. Even if Einstein and Haber remained on formal "Sie" terms in their letters, one cannot but feel the friendship of the two. Perhaps their unhappy marriages shaped part of a bond, their mutual achievements in their respective fields another.

Stern sees Haber and Einstein as two extremes of the German Jews' relationship with Germany. Their cultural roots and literary referents were deeply German. But in contrast to the great patriot, Haber, Einstein was always suspicious of the anti-Semitism lurking underneath. Fritz Stern's analysis is truly thought-provoking—his writing is history at its best.

Representing a Human Being

From the biographies, we of course get a better overall picture of Haber. Not a consistent one, to be sure—what a long way between the von Leitner caricature and Stern's nuanced setting of Haber in the twentieth century! And biography is an art, too.[17, 18] The secret to writing a successful biography is to find and espouse a systole – diastole rhythm, the same as friendship demands: oscillating between empathy and irony, to love and admire one's subject but not to take him or her too seriously.

We urge our fellow chemists not to grow defensive about literary portrayals of our profession. Out there are all these fine writers, from Harrison to Stern. All are read, or not. Writers make choices, just as we do in our research. No writer of value is likely to be a carbon copy of us. Hochhuth had all the right in the world to write not of Haber's electrochemistry but of an imagined conversation between Fritz and Clara Haber the night before her suicide. The reader and the world are in charge of striking balances, not a writer.

As individuals we make distressing emotional decisions, as part of the choices we all face. Haber's life was full of these—from his conversion, to his struggles with Nernst, to his choice to direct gas-warfare efforts, to his difficulties with his wives, to his response to the first weeks of the Nazi regime. Haber's life is the life of one German Jew in 20th century Germany. His drama is the stuff of life. And his life is drama.

G. Frenking, Marburg, Germany, a reviewer of our paper has written:

> *"…not only in chemistry but in all other areas of science and general life such as arts, politics, and humanities, important figures of the past are portrayed as heroes, while people who did bad things are portrayed as evil. Although we know that all human beings have positive and negative sides, we tend to look at only one side when we describe people who did something outstanding. People like Haber, who excelled in two categories are often described with total blindness for one of the two sides. There seems to be a strong tendency to condemn a person, or to worship him, and it seems difficult to realize that sometimes people behave in both ways. We should learn, particularly we as scientists, to reach for understanding of the whole by considering all important aspects of a person's actions.*"

This is well said. Portrayals (our own) of the leaders of our profession are too often unidimensional and uncritical. We would add that representation of scientists partakes of

 © WILEY-VCH Verlag GmbH, D-69451 Weinheim, 2001 1433-7851/01/4024-4602 $ 17.50+.50/0 *Angew. Chem. Int. Ed.* **2001**, *40*, No. 24

features of representation in chemistry.[19] The skills we draw upon in presenting molecular models, which are familiar to all of us, we ought to extend to human beings, when these sit, so-to-speak, as models for their portrait. It should not be forgotten, furthermore that what any representation produces is an image, not so much of the model, but of the very process by which it is being represented!

Representing molecules in our papers, representing human beings in our books, we indeed share a heritage with the visual arts. The portrait painter has a divided loyalty, to the person portrayed and to the public, in the widest sense. Some portrait painters held in very high regard during their lifetime (we are thinking of Philip de Laszlo (1869–1937), if their loyalty is only of the first kind, are forgotten in the shifting quicksands of time. Other portraitists, who did not shy from depicting their subjects almost as caricatures if need be—Dürer, the Holbeins, father and son, and Goya jump to mind—their work is for posterity.[20] We feel that it is our duty, both as chain-reaction carriers for the chemical culture, and as teachers, to see and to portray the great chemical innovators, warts and all, as the complex human beings they were.

Context

Context has become one of the latest catchwords. Understandably, it is a rallying point where historians of science meet with sociologists of science. The downside is that context may become a smokescreen for relativism, and especially for moral relativism. Fritz Haber's tragic ordeal is an excellent illustration. Well-meaning people (including one of our reviewers) plead that he be assessed in context, that he not be judged from the standpoint of the post-Holocaust and post-Hiroshima present. We beg to differ. The context is sensitively set out in Fritz Stern's essay. And still Haber falls very much short, in our opinion. Though neither of us is a pacifist, we personally would find the same shortcoming in Hiram Maxim and the machine gun, Louis Fieser and napalm, and those who decided to drop the atomic bomb on both Hiroshima and Nagasaki.

Indeed, one might make a case for removing oneself from context as an excellent way to take a moral stand. Chamberlain, when he signed the Munich Agreement, was very much in context. Churchill removed himself from context.[21] Closer to Fritz Haber, both Willstätter and Schlenk had no qualms stepping resolutely outside the context of Nazi Germany.[22]

To step out of context is one way to enter history, true—often with terrible consequences to the individual who chooses this path. Neither Fritz Haber nor, at a later time, Werner Heisenberg had the sensitivity nor the courage to do so. Hence, it should come as no surprise if, in the judgment of history, they are seen as morally lacking—however outstanding their remarkable achievements as scientists.

What Can We Do?

How can we deal with the cruel and damning assimilation of chemistry as a whole, with Haber taken as an emblematic figure? By refusing it as a stereotype of a science. By coming to peace, not sweeping under the carpet of "Oh, that's his personal life," with the neurotic elements very much evident in Haber's personality. As an individual. This is not an attempt to condemn Haber or to absolve him of his moral failings, but to accept him as a person.

Can we be allowed some admittedly crude psychological conjectures? Fritz Haber lost his mother when he was two days old. There had to have been an element of rejection from his father, perhaps holding the infant responsible, to some extent, in his mother's death. Such a surmise would appear to have been borne out, latter in life, by Haber's counter-rejection of his father, when he refused to take-up a position in the family business (Haber senior was a major importer into Germany of indigo dye) and when, very much against his father's wishes, Haber abjured his Jewishness and converted to Protestantism.

Young Fritz Haber was raised by a stepmother ten years older than himself, and by maids and governesses. Because he lacked the loving care of a mother during his young years, he may have made himself into a fortress, putting up what a psychiatrist might term massive defenses, and hyperintellectualizing from an early age the world and the people around him.

Not card-carrying analysts, we still reach for an understanding of a human being in his inner life. Maybe we're simplistic, but where else shall we look? And we know, that even if such an explanation were to make emotional sense, it would not excuse the instances of Haber's amoral to callous behavior, toward his wife or towards Germany's enemies…

To turn to another aspect of the story, has the issue of women in chemistry truly advanced that much since Clara Haber's time? Yes and no. There are recent eloquent stories, such as the belated recognition of Stephanie Kwolek for her invention of aramides (Kevlar) at DuPont. In the US nearly 30% of chemistry Ph.D.'s are women. But, with blatant exceptions such as Portugal, readily understood from the scant salaries of academics there, women to this day remain dramatically under-represented on chemistry faculties in Europe, Japan, and the Americas.[23] Each one of us can make a difference, in that area as well.

Most of us are also teachers. We have to do better than the usual, traditional technical presentation of the ammonia synthesis, invoking it as a fine illustration of Le Chatelier's Principle. We have to talk also about Haber, the historical figure and the person. Fritz Stern does so beautifully; his essay should be assigned reading for that unit of introductory chemistry. If we have become beset and smothered with the stereotype of Haber as a re-enactment of Dr. Frankenstein's hubris, it is to a large extent because of our collective failure to present the great chemical innovators as fallible men and women, with their idiosyncrasies and with their full human depth.

We have in our science, in Haber, a figure worthy of Greek tragedy. Haber faced (and failed to face) questions that confront all of us. His choices and agony are a part of us.

What else can we do? Get involved. This is what Einstein did, speaking against injustice throughout the world. He did so consistently and forcefully. His involvement in all aspects of

 © WILEY-VCH Verlag GmbH, D-69451 Weinheim, 2001 1433-7851/01/4024-4603 $ 17.50+.50/0

public life was unstinting. And this in fact was Einstein's greatest achievement, when the flow of his science abated. He remains an example to all of us, even when we are not in the position where our views are solicited, as Einstein's (the mystical embodiment of wisdom in the 20th Century) were. We have an obligation as human beings to speak out.

[1] We omit, for instance, one novel based on Haber's life: H. H. Wille, *Der Januskopf*, Buch Club 65, Berlin, **1970**. A very readable account of the treatment of chemistry in the literature of the last century is "Die Chemie im Spiegel der Literatur des 20. Jahrhundert": Otto Krätz, *Chem. Unserer Zeit* **1991**, *25*, 44 – 50.

[2] T. Harrison, *Square Rounds*, Faber and Faber, London, **1992**.

[3] R. Hochhuth, *Sommer 14: Ein Totentanz*, Rohwolt, Reinbek, **1989**.

[4] A. Malraux, *Œuvres complètes*, *Vol. 2*, Gallimard, Paris, **1996**, pp. 617 – 815 (coll. La Pléiade).

[5] Quoted in the translation by A. W. Fielding:A. Malraux, *The Walnut Trees of the Altenburg*, Howard Fertig, New York, **1989**.

[6] M. Wild, *Mes aventures dans le service secret, 1914 – 1918*, Payot, Lausanne, **1932**.

[7] We omit an earlier English language biography of Haber: M. Goran, *The Story of Fritz Haber*, University of Oklahoma, Norman, **1967**.

[8] D. Stoltzenberg, *Fritz Haber: Chemiker, Nobelpreistrager, Deutscher, Jude*, VCH, Weinheim, **1994**.

[9] M. Szöllösi-Janze, *Fritz Haber 1868 – 1934. Eine Biographie*, Beck, München, **1998**.

[10] W. J. Moore, *Schrödinger: Life and Thought*, Cambridge University Press, Cambridge, **1989**.

[11] D. C. Cassidy, *Uncertainty. The Life and Science of Werner Heisenberg*, W. H. Freeman, New York, **1992**.

[12] R. Hahn, *Gold aus dem Meer: Die Forschungen des Nobelpreisträgers Fritz Haber in den Jahren 1922 – 1927*, GNT-Verlag, Berlin, **1999**.

[13] G. von Leitner, *Der Fall Clara Immerwahr: Leben für eine humane Wissenschaft*, Beck, München, **1993**.

[14] V. Smil, *Enriching the Earth. Fritz Haber, Carl Bosch, and the Transformation of World Food Production*, MIT Press, Cambridge, MA, **2001**.

[15] F. Stern, *Dreams and Delusions: The Drama of German History*, Columbia University Press, New York, **1987**.

[16] F. Stern, *Einstein's German World: Essays in European History*, Princeton University Press, Princeton, pp. 60 – 164, **1999**.

[17] P. M. Kendall, *The Art of Biography*, George Allen and Unwin, London, **1965**.

[18] S. Schiff, *The American Scholar* **1999**, *68*, 51 – 60.

[19] "Representation in Chemistry": R. Hoffmann, P. Laszlo. *Angew. Chem.* **1991**, *103*, 1 – 16; *Angew. Chem. Int. Ed. Engl.* **1991**, *30*, 1 – 16.

[20] "L'acteur d'Harcourt": R. Barthes in *Mythologies*, Le Seuil, Paris, **1957** wrote a definitive indictment of hagiographic portraiture of the first kind.

[21] "Winston Churchill" in I. Berlin, *The Proper Study of Mankind. An anthology of essays*, Farrar Straus Giroux, New York, **2000**, pp. 605 – 627; this essay was first published in *The Atlantic Monthly*, **1949**, *184*, No. 3.

[22] R. Willstätter, *Aus Meinem Leben*, Verlag Chemie, Weinheim, **1973**; see also F. Litten, *Der Rücktritt Richard Willstätters 1924/25 und seine Hintergründe. Ein Münchener Universitätsskandal?*, Institut für Geschichte der Naturwissenschaften, Munich, **1999**; "Wilhelm Schenk: The Man Behind the Flask": T. T. Tidwell, *Angew. Chem.* **2001**, *113*, 343 – 349; *Angew. Chem. Int. Ed. Engl.* **2001**, *40*, 331 – 337.

[23] "A "Title IX" challenge to academic chemistry. Or, "Isn't a millennium of affirmative action for white men sufficient" ": D. R. Rolison, *Women in the Chemical Workforce*, National Academy Press, Washington, DC, **2000**, chap. 6, pp. 74 – 88; http://cheminfo.chem.ou.edu/faculty/djn/diversity/rolison.html.

The "Rocky" Road to Literary Fame: Marcel Proust and the Diamond Synthesis of Professor Moissan

Otto Krätz*

"Diamond: Many argue that it is nothing more than simply carbon. Someday man will even prepare it artificially! If a diamond were to be discovered in its original form one wouldn't even bother to pick it up." Gustave Flaubert, Dictionary of Received Ideas.[1]

Introduction: Observations Regarding an Altogether Too Pleasant Place

It has been said about the French literary figure Charles-Augustin Sainte-Beuve that with his expression "tour d'ivoire"—ivory tower—he provided a label for the true abode of a great many intellectuals. In any event, the latter quickly adopted the new term, and with gratitude. Gustave Flaubert, in particular, never tired of extolling through vivid images the fragility of this imaginary structure, threatened as it always is by the fierce storms within our world.[2]

Chemists, too, have gladly sought refuge here. Far from the tumult of the evil world, behind protective ivory walls, it became fashionable to complain bitterly about the ingratitude of the masses in the face of the endless benefits conferred by chemistry. In this isolated state relatively little attention was directed to how often the reverse has applied as well. With surprising frequency chemists remained—and remain still today—unappreciative and too often utterly disinterested in the face of cultural and social consequences of their research. Admittedly, Henri Moissan's early death prevented him from reflecting deeply on cultural effects resulting from his fluorine chemistry, as well as his improvements in the recovery of the element chromium and the revolution in lighting technology attributable to acetylene. However, this still does not explain the astonishing fact that the consequences of Moissan's life's work have apparently never been examined by the chemical scientific community with respect to Art Nouveau interior design and the dramatic ascent of chromium, which has

[*] O. Krätz
Alter Berg 19
82319 Starnberg (Germany)

 © WILEY-VCH Verlag GmbH, D-69451 Weinheim, 2001 1433-7851/01/4024-4604 $ 17.50+.50/0

caused it to rise to a status comparable to that of a "guide fossil" for the art of design in the 20th century. The fact that art historians are almost completely oblivious of such abstruse subjects as hydrogen fluoride and high-temperature chemistry almost goes without saying.

Marcel Proust and the Glass Artistry of Emile Gallé

A true Proustian not only indulges in the peculiar-tasting linden blossom tea—nearly obligatory for a Proust fan—and simultaneously nibbles on incredibly crumbly madeleines,[3] he or she also views the world around through the eyes of the admiring master (Figure 1). Snow and ice remind him (or her) of Art Nouveau glass as it would have emerged from the



Figure 1. Marcel Proust in about 1895. The photograph is reprinted with permission from Suhrkamp Verlag.

atelier of Emil Gallé, adorned with the enveloping snow effects that inspired the poet in "Search for A Lost Era" to an image filled with emotional appeal: "Soon winter; in the corner of the window a solidly frozen vein of snow, as on a glass by Gallé".[4] Proust probably knew relatively little about the ingenious techniques—the complex interplay of glass and enamel fluxes and entrapped air bubbles, the incorporation of colored oxide particles, overlaying with other colored glasses, and the various abrasive and etching techniques—with which the great glass artisans of the day, Gallé and Lalique, created such wonderful works. Proust was in fact closely acquainted with the glass artists Gallé and Lalique. Both were frequent visitors to the house of the writer Robert Comte de Montesquiou-Fezensac, who wrote the stylistically instructive essay "Orfèvre et verrier. Gallé et Lalique" (1897). Montesquiou made a significant contribution to the popularization of Art Nouveau glass, at the same time influencing Proust's understanding of art.[5] Strangely enough, the technique of etching glass, which results in a matte surface more reminiscent of snow, had a significant impact on Proust's life, albeit by way of several detours. Etching glass with the aid of gaseous hydrogen fluoride had actually been known for about a hundred years, but the procedure was time-consuming and awkward.[6] Since hydrogen fluoride is a highly toxic gas, it was necessary that the glass surface in question be secured with wax to the mouth of a developing vessel, which was filled with fluorspar and sulfuric acid. After the etching process was complete the wax seal was once again melted, as was wax that had been laid down on the glass surface to protect areas which were to be left unetched. Much more convenient were newer procedures perfected in the last decade of the 19th century whereby a liquid mixture of anhydrous hydrofluoric acid and fluorine-containing salts such as ammonium fluoride was either spread directly on a glass object or applied to a glass plate in a process rather like flexographic printing, to be washed off after etching was complete.[7] However, extensive application of such procedures presupposed the availability of an efficient chemical industry capable of supplying sufficient quantities of fluorine compounds. This was also the technique that permitted participants in the Art Nouveau movement to overrun extensive glass surfaces with meandering matte ornamentation. Window panes, glass doors, and mirrors etched with hydrogen fluoride soon became important stylistic features of the architecture of that period.[8]

Henri Moissan

The singular blossoming of fluorine chemistry around 1900, especially in France, was a consequence of research by Henri Moissan (1852–1907), who subsequently was awarded the Nobel Prize.[9] The son of a clockmaker, he began his studies at the venerable National Museum of Natural History in Paris. Moissan later became a professor at the École supérieure de Pharmacie, and ultimately had a chair in chemistry at the Sorbonne. In 1884 he observed that certain fluorine salts dissolve in anhydrous hydrofluoric acid—the important prerequisite for the new method for etching glass. He succeeded for the first time in 1886 in preparing elemental fluorine, an extremely aggressive gas, by the electrolysis of anhydrous hydrofluoric acid in a platinum vessel. On the basis of this discovery, which broke new chemical ground and made Moissan world famous, he established a broad research program in the area of fluorine compounds and their properties which, in 1900 (roughly 100 years ago) culminated in the publication of his monograph "Le Fluor et ses composés".[10]

Moissan's appearance bore only a crude resemblance to the public vision of a chemistry professor (Figure 2). He loved to carry out his experiments on a pilot plant scale—almost an industrial scale. Accordingly, he wore to work not a laboratory coat, but instead, like a factory worker, a set of utterly unbecoming, tattered old clothes over which he fastened a

 © WILEY-VCH Verlag GmbH, D-69451 Weinheim, 2001 1433-7851/01/4024-4605 $ 17.50+.50/0

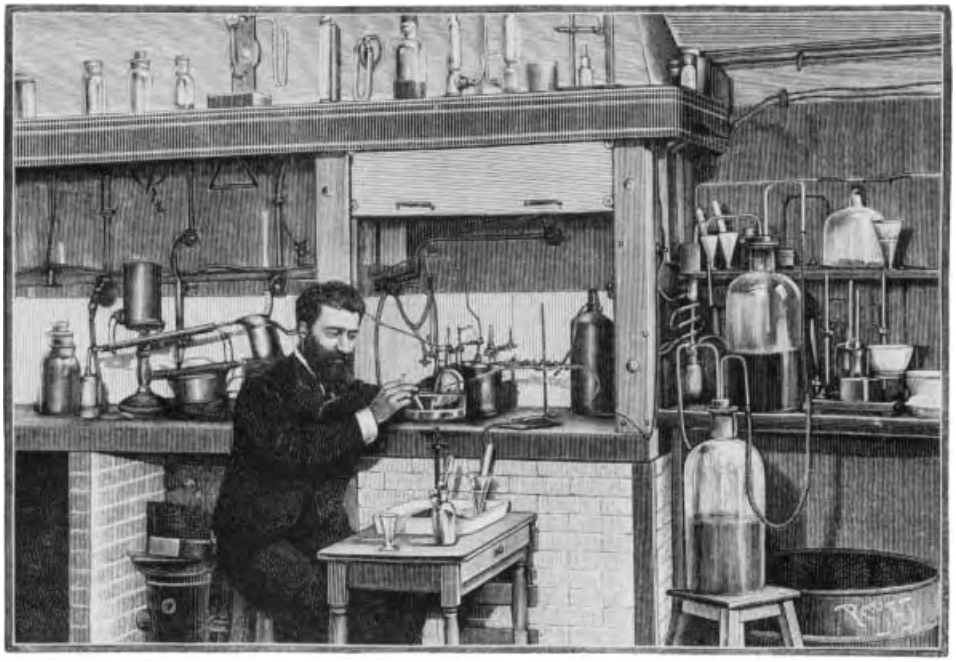


Figure 2. This illustration of Henri Moissan in his laboratory at the École supérieure de Pharmacie in Paris was published in the journal *La Nature* in February 1890. The picture is reprinted with permission from the Deutsches Museum in Munich.

leather or rubber apron. German visitors found it strange that he never—even while carrying out chemical experiments—removed the leather sash of the Legion of Honor.[11] This outfit was crowned by a once noble—but now worn out and dirty—medium-high, round cap, which conferred an oriental look upon his remarkable southern French looking head with its shaggy, bifurcated full beard.[10]

Moissan's Pursuit of a Way to Make Diamonds

Scientists enjoy trying to convince the public that their research is always conducted in an absolutely rational way and subject only to the laws of the strictest logic. However, even the brains of researchers are plagued by will-o'-the-wisp irrational yearnings for recognition and wealth. Moissan's fluorine chemistry seduced him to partake of an academic fad of his day: the quest for a diamond synthesis, a way of preparing artificial diamonds. One of his chemical triumphs had been the synthesis of the unstable fluorocarbon CF_4. Shouldn't this material, under extreme reaction conditions, be capable of undergoing explosive decomposition to crystalline carbon, namely, diamond? The only things Moissan managed to harvest in this way, however, were soot and shattered apparatus. However, at the same time he contracted a passion for the hunt.[12]

In 1891 a nickel–iron meteorite was discovered in Devil's Canyon in Arizona, and it was alleged that it contained diamonds. Moissan managed to acquire a fragment of this meteorite and actually succeeded in confirming the presence of diamonds, although the largest was only 0.7 mm across. The chemist in him thereupon constructed a theory. The cooling of a very hot sample of carbon-containing molten iron, essentially a solution of carbon in liquid iron, must, because of the high pressures generated in the interior, have caused amorphous carbon to crystallize in the form of diamond. Nevertheless, he failed even at the 1500 °C temperature of an oxyhydrogen torch to induce sufficient carbon to dissolve in his molten iron. The only logical course of action seemed to be increasing the temperature of the melt. To this end he developed a simple, but extremely successful, device: Moissan's high-temperature kiln (Figure 3). Even before Moissan, attempts had been made—initially with only modest success—to take industrial advantage of the energy released by Siemens' and Edison's electric generators. But it was Moissan who first succeeded in harnessing the high temperatures associated with an electric arc for use on a laboratory scale in scientific ex-

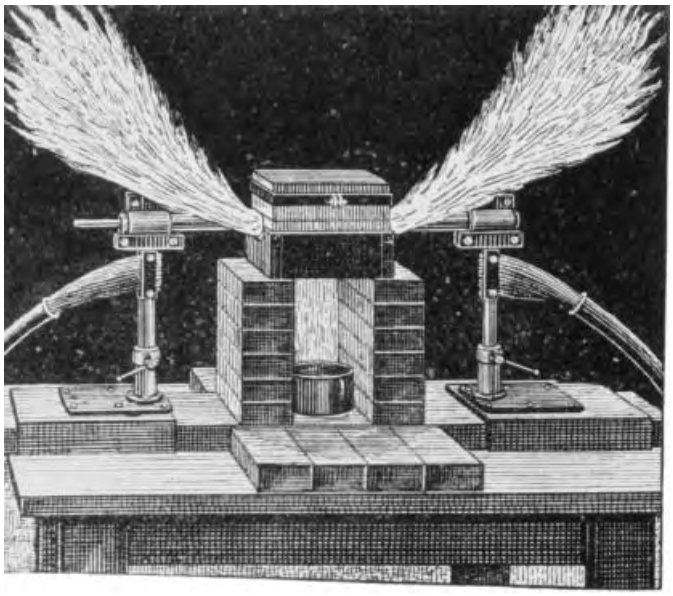


Figure 3. In his attempts to synthesize diamonds, Moissan used an electric furnace made of limestone, in the base of which there was a cylindrical opening; the anode was hollow and contained a cylindrical channel with a diameter of 18 mm in which an iron rod could easily be moved back and forth. The oven rested on two supports, and below it there was placed an iron kettle containing a 10 cm layer of mercury and a layer of water twice that deep. Moissan directed an electrical current of 1000 amps and 60 volts to this oven, and when the appropriate temperature had been reached, that is, when the lime began to distil, the iron rod was slowly pushed forward. As the metal approached the arc it melted, became saturated with carbon, and fell in the form of drops out of the oven, through the water, and into the mercury, where they cooled. This granulated mass, now floating on the surface of the mercury, contained numerous flattened ellipsoids displaying considerable regularity in form and a completely homogeneous character, but with a maximum diameter of 1 cm. From these Moissan was able to isolate transparent diamonds in the form of very tiny crystals 0.016 mm in length (see ref. [10]).

 © WILEY-VCH Verlag GmbH, D-69451 Weinheim, 2001 1433-7851/01/4024-4606 $ 17.50+.50/0

perimentation, thereby opening the way to new lines of research.

Moissan's "Four Électrique"

Moissan first demonstrated his famous "four électrique" at the Académie des Sciences on 12 December 1892. Inside it there was a small combustion chamber with walls constructed from firebricks, within which an electric arc could be struck between two adjustable carbon electrodes to give temperatures between 2000 and 3500 °C depending on the current applied. This device, powered by a large generator built by Edison, permitted Moissan to make a number of singular discoveries, which led to his being regarded as the founder of high-temperature chemistry. Thus, he managed to evaporate materials that previously had been considered incapable even of melting. Several elements heretofore classified as heat-resistant or refractory were found at arc temperatures to undergo reactions with oxygen. Moissan vaporized silicon, copper, silver, nickel, cobalt, manganese, iron, uranium, gold, and the platinum metals, and he also developed the technique of preparing ultrapure metals by distillation.[13]

The Triumphal March of Chromium

Moissan worked especially diligently on the production of chromium, which through his work was transformed from a laboratory curiosity into a commercially exploitable raw material,[14] the senseless mass incorporation of which into jewelery and furniture (later also automobiles) elevated it by the mid-20th century to the stature of a typical guide fossil for everyday culture. It was Lalique who had the remarkable brainstorm to devise artistic etched glass ornamentation for automobiles.[15] This particular innovation failed to make a significant impact—for obvious reasons!—but starting in the 1930s decorative chrome-plated radiator emblems such as the veil-waving "Emily" of Rolls-Royce and the trademark Mercedes star acquired the status of cherished collector's items (the earliest examples were instead plated with nickel). Chrome-plated steel-tube furniture evolved into a symbol of modern living in the 1940s.[16]

Acetylene: A New Source of Light

Despite the inventive genius of men such as Edison, it proved difficult at first to build any substantial market for electric current. The light output provided by the first bulbs was too meager, and the bulbs themselves were too fragile and had too short a lifetime. For this reason, two additional discoveries by Moissan attained enormous significance. In 1892 he observed the formation of calcium carbide in his oven, and he quickly recognized that he had encountered a new class of chemical compounds. In order to obtain pure, homogeneous calcium carbide (CaC_2), Moissan in 1894 heated an intimate mixture containing 12 parts marble lime and 7 parts sugar charcoal for 15 minutes in a carbon crucible in his electric oven, with a current of 1000 amperes at 60 volts. Further experimentation over the course of many years enabled him to extend the procedure to use ordinary commercial quarried limestone and coal directly from the mine.[17]

Among the host of chemical reactions he found calcium carbide to undergo, one promised to be especially interesting from a commercial standpoint: treatment of CaC_2 with water, which led to calcium hydroxide with the evolution of pure acetylene. The latter was found to burn with a bright, luminous flame.[18] This finding initiated a triumphal journey to find a new source of illumination. Electric current could be used in an electrochemical facility to produce calcium carbide and acetylene, two commodities that in those days were more readily transportable than electricity itself. Acetylene lighting gained rapid acceptance, especially for automobiles, which, like the earlier carriages, were initially illuminated using thick candles.[19]

Marcel Proust[20] created an oft-cited monument to this marvelously brilliant illuminating gas in 1907 in his essay "Days in an Automobile,"[21] even though in this context the significance of acetylene had never previously been acknowledged. The author had rented a car from the firm Taximètres Unic de Monaco, operated by his friend Jacques Bizet, a son of the composer, which he allowed his own chauffeur to drive. In the course of an evening visit at Château Glisolle, the hostess invited him to come the next morning in daylight to see her famous rose garden. Instead, Proust told his chauffeur immediately to light the lamps in his car. From a photograph we know that this awe-inspiring heavy vehicle was equipped with four massive, detachable acetylene lamps.[22] Thus, the Marquise de Clermont-Tonnerre was probably the first knowingly to observe her roses by artificial illumination, and she was delighted. "They looked like beauties one has awakened from their sleep," she wrote.[23]

In another excursion with his taxi, Proust arrived at his destination, the Cathedral of Notre Dame in Lisieux, only after nightfall, a consequence of an untimely breakdown. Despite the darkness, he attempted nevertheless to view the famous stone seedling forest of the cathedral's entry portal. "But as I was feeling my way forward, it was suddenly flooded with brightness; trunk by trunk, columns emerged out of the darkness, and from the background shadows there appeared in full light the generous modeling of the stony leaves. It was my chauffeur, the imaginative Agostinelli, who conferred upon these ancient sculptures a greeting from the present, an illumination that only permitted lessons from the past to be read more precisely. Once he realized what it was I wanted to see, he pointed the car's headlights at all the various segments of the portal, one after another."[24]

It must be noted, however, that working with such acetylene lamps was not easy. First, carbide needed to be introduced, and the flow of water had to be regulated. In wind and bad weather it could be difficult to light the flame, even with the aid of storm matches. If too much unburned acetylene were already present, the was a high risk that an explosive flame would result. The resulting heat often caused windows and lenses of the lamps to burst. After use, it was necessary that one cleaned such a burner with a steel brush, removed the calcium hydroxide solution, and much more. Acetylene devices for the illumination of rural ballrooms had a disturbing habit of suddenly exploding. It is thus no wonder

 © WILEY-VCH Verlag GmbH, D-69451 Weinheim, 2001 1433-7851/01/4024-4607 $ 17.50+.50/0

that in the late 1920s it was electric lighting that ultimately displaced all competitors.

The Engineer Lemoine and the Diamond Affair

In fact, Moissan actually did manage to synthesize diamonds in his oven.[25] Unfortunatelly, they remained as small as their precursors from Devil's Canyon. Nevertheless, Moissan acquired a great deal of fame. In 1906 he became the first Frenchman to be awarded the Nobel Prize in chemistry. However, his chemical activities with the aggressive gas fluorine had undermined his health. Aged and weakened prematurely, he succumbed a year after the Nobel Prize ceremony to a rather mild inflammation of the appendix. He was thus able to experience only from the sidelines how his diamond procedure figured in one of the most sensational swindles of the day, thereby acquiring a certain measure of fame.[26]

This swindle which involved the engineer Lemoine, who was allegedly one of Moissan's assistants, together with his supposed discovery of a method for preparing large artificial diamonds also had its effects on Marcel Proust. In fact it cost Proust a significant share of his wealth, so it is not surprising that he was tempted to exploit the scandal related to the synthetic diamond process in a literary way. "One evening I selected this rather meaningless legal affaire, which at the time nevertheless aroused so much public opinion, as a general theme for a series of prose pieces. Here my intent was to try to imitate the styles and manners of a certain number of other authors." Thus did Proust express himself with some understatement in 1919 in the preface to the book edition of "Pastiches et Mélanges."[27] These "pastiches" (derived from the Italian *pasticcio* (pastry) and employed in French in the sense of parody) consisted of a series of nine precious examinations of the Lemoine Affair, each composed in the style of one of Proust's great and revered predecessors, examples, and sources of inspiration: Balzac, Flaubert, the man of letters and critic Sainte-Beuve, the poet Régnier, Edmond de Goncourt, the historian Michelet, the critic Faguet, Ernest Renan, and Duke Saint-Simon. The set of parodies first appeared in the literature supplement to *Le Figaro* in 1908. These pastiches were eminently significant in Proust's development into a great novelist. He "found himself" as an unbridled stylist for the first time in the course of this literary jest. "For me, the whole thing was a matter of hygiene," he admitted to a friend surprisingly drastically in 1919, "one must purge oneself of the natural burden of mimicking."[28]

The Diamond Maker Lemoine

Back to the chemical and historical background to the affair: In the summer of 1905 the engineer Henri François Lemoine met together with Sir Julius Charles Wernher, president of the company De Beers. De Beers Consolidated Mines Ltd., founded in 1880 by Cecil Rhodes in Kimberley, South Africa, retains even today a near monopoly position in the international diamond market. Lemoine contended that he had improved the Moissan process, which until then had produced only diamond dust. Unfortunately, for further development of his apparatus and the production of significantly larger diamonds, he needed additional capital. Sir Julius and Lemoine met in the basement of a Paris department store. Presumably this was the site of a generator capable of providing the necessary high level of electric current. Much to Wernher's surprise, Lemoine carried out his experiment in the nude—as proof that he wasn't hiding any diamonds on his person. He introduced his reaction mixture into a large Moissan electric furnace, and when he removed the formless mass somewhat later it was found indeed to contain 25 relatively large diamonds![29] One must of course bear in mind that the value of a diamond increases far more than proportionately as its carat count rises.[30]

The stones were genuine. The De Beers people were worried that some competitor might license this process and thereby break their monopoly. Consequently, a contract was signed with Lemoine according to which he would place a sealed copy of the process in the vault of a London bank, to be opened only in the event of his death. In exchange, a laboratory was outfitted at Argelès in the Pyrenees, perhaps because it was assumed that enough water power would be available there to run the generator, but it may also have been regarded as a secure location with respect to curious spies. Lemoine submitted huge expense reports to De Beers, culminating in one for more than £64 000—roughly half a million Euros in present-day terms. Gradually the company became suspicious. Secret inquiry revealed that Lemoine was primarily engaged in running a generating plant and selling electricity. This prosaic activity seemed singularly inconsistent with the secretive flair of a diamond maker. It was agreed that another demonstration experiment should be carried out in the presence of an especially shrewd manager from De Beers. The latter flicked into the oven, immediately before the current was switched on, a small South African diamond that he had concealed in his hand. According to Lemoine—who was an engineer, not a chemist—the oven temperature was so high that a normal diamond, in contrast to a synthetic one, would decompose to ash. However, when Lemoine's back was turned, the manager fished his original diamond out once again. It had survived the heat untouched. The De Beers manager thus came to the conclusion that his company was the victim of an out-and-out swindle.

Lemoine was arrested and taken to court. He was released later on bail, and escaped to Constantinople. Wernher managed to inspect the contents of the envelope set aside for safekeeping, which supposedly provided a description of the secret process, but it proved to be fraudulent. Lemoine in the meantime returned secretly but quite calmly to France, where he was again arrested and the trial resumed. It eventually turned out that his "process" was nothing more than sleight of hand. He had acquired some natural diamonds from De Beers through a dealer, hidden them in crevices in the oven walls, and then smuggled them into the reaction mass as he removed it from the oven. On 6 July 1909 he was sentenced to six years of hard labor for fraud.[31]

The world enjoyed a good laugh over Wernher and his company. Perhaps unjustifiably so. A rumor persisted around the stock exchanges that Wernher and De Beers had in fact

 © WILEY-VCH Verlag GmbH, D-69451 Weinheim, 2001 1433-7851/01/4024-4608 $ 17.50+.50/0 *Angew. Chem. Int. Ed.* **2001**, *40*, No. 24

detected the fraud very early on, in order to take such advantage of the rapidly and steeply fluctuating stock values during the four-year affair and trial that the millions squandered by Lemoine in the Pyrenees would be insignificant. The fact is, that among the stockholders who lost a bundle in this speculative venture was Proust. He was actually related to successful stockbrokers on his mother's side of the family, who had left him an impressive legacy, but—consistent with the old saying that the third generation loses what the first generation earns—the writer had apparently not inherited the family mercantile skills.

Proust with Others' Pens

For Proust, confronting the literary styles of those who were to serve as his models was of course more important than chemical principles underlying the scandal described above. Nevertheless, the first pastiche, in the style of Honoré de Balzac,[32] provides insight into the low regard in which the natural sciences were—and perhaps still are—held by the upper reaches of society. In the world of Balzac, chemical knowledge would not be viewed with disgust exactly, but it certainly was not something one chose to display: "'Madame, the secret of producing diamonds has just been discovered.' … 'But I would have thought people had always made some,' replied Léontine naively. As a lady of taste, Madame de Cadignan was careful not to make any comment, where ladies of the middle class would have plunged right into the conversation as a way of bragging in the silliest way about their chemical knowledge."[33]

The ironic pastiche in the style of the famed diaries of Edmond de Goncourt[34] is especially imaginative, a work in which Proust actually brings himself into the scene: "21 December 1907" … And in the course of dessert, Lucien (Daudet, a friend of Proust) tossed out to us the fact … that a certain Lemoine had discovered the secret of making diamonds. In view of the potential loss in value of stocks of unsold diamonds, a single raging agitation held sway in the business world, eventually infecting the judicial system as well, which might have led to this Lemoine's having spent the rest of his days in some dungeon for having offended the brotherhood of jewelers."[35] Proust's fictitious Edmond de Goncourt—the real one had been dead twelve years when this pastiche was devised—decides to write a theatrical work based on this singular situation. Goncourt's somewhat prickly vanity was captured in a delightful way: "As a final bouquet, Lucien brings the news that provides me with the solution for the previously sketched piece: her friend Marcel Proust has committed suicide as a consequence of the slump in diamond prices, a slump that has destroyed part of his fortune. 'A remarkable being, this Marcel Proust,' observed Lucien, 'a man who should live in complete ecstasy, in the sacral trashing of certain landscapes … '"[36] Apparently there were moments in which Proust in true greatness was able to laugh about himself and his ecstatically described hawthorn hedge with its red and white blossoms—a typical example of the cult of entwined flowers in the Art Nouveau and Jugendstil eras—also with its "sexual odor," its "bittersweet almond scent."

But the real point of the Goncourt pastiche is yet to come. "22 December … I awake from my four o'clock nap with a premonition of bad news, because I had dreamed that the tooth that caused me so much pain five years ago when Cruet extracted it had grown back (Cruet was in truth a physician whose work in hygiene had been published by Proust's father, also a physician). And at that moment Pélagie (Goncourt's actual housekeeper) entered with this piece of news brought by Lucien Daudet, news that she had not delivered earlier so as not to disturb my nightmare. Marcel Proust had not committed suicide, Lemoine had in fact discovered absolutely nothing and was supposed to be only a conjurer, and not a particularly gifted one at that, a sort of one-armed Robert Houdin (a very famous magician of the day). That is our misfortune!"[37]

Proust presumably never imagined as he drafted this pastiche that, at the suggestion of Léon Daudet (brother of Lucien, mentioned above), he would in 1919 be awarded the "Prix Goncourt" endowed by Edmond de Goncourt. Proust's financial losses did indeed correspond to the facts. Nevertheless, it should be noted (as a consolation for the reader) that the poet salvaged enough, despite frequently recurring money problems later, to present his chauffeur and friend Alfred Agostinelli in 1914 with an airplane worth 27000 Francs. But Agostinelli died in a crash before he was able to take possession of the gift—the fuselage of which was inscribed with Mallarmé's sonnet "The Swan."[38]

In another pastiche, "VIII. By Ernest Renan", Proust offers a prophecy: "Patience, mankind, patience! Fire up again tomorrow the furnace that has already been extinguished a thousand times, the furnace from which a diamond may someday emerge! In high spirits perfect that crucible in which you will be able to raise carbon to temperatures unknown to Lemoine and Berthelot, so that eternity may envy you."[39] Actually, Moissan's name belongs here rather than Berthelot's. However, Marcelin Berthelot (1827–1907),[40] arguably the greatest French chemist of that era, was a close friend of Ernest Renan, a student of religious history and economics. Berthelot was among the regular guests at the salon of Princess Mathilde Bonaparte, a cousin of Napoleon III,[41] as was Proust himself at a later date. Here Berthelot advised the Goncourt brothers,[42] as he also did Flaubert concerning chemical matters, particularly with respect to Flaubert's last novel: "Bouvard et Pécuchet".[43]

It should be noted here that Proust's prediction proved not quite accurate. An increase in pressure, not temperature, ultimately provided the crucial breakthrough in synthesizing diamonds by the Moissan approach. It was not until 1953 that the Swedish firm Almanna Svenska Elektriska Aktiebolaget successfully synthesized diamonds in molten metal at 2760 °C and 90000 atü, a feat also later accomplished by a group from General Electric at 100000 atü. Both processes were bought up by De Beers and merged with the company's own research efforts into Ultra High Pressure United Inc. It is now possible to prepare diamond crystals several centimeters in size in this way.[44]

In the hope that something like a great beyond exists, from which one is enabled to look down upon this world, and in view of Proust's complicated aestheticism, there may be

 © WILEY-VCH Verlag GmbH, D-69451 Weinheim, 2001 1433-7851/01/4024-4609 $ 17.50+.50/0

reason to take special note of the claim on the part of De Beers that synthetic diamonds are used only for technological purposes (for example, in saws, drills, and milling machines for rocks and minerals), and that the only diamonds cut for the jewelry market are natural stones.

Received: May 8, 2001 [E 30023]

[1] G. Flaubert, *Wörterbuch der Gemeinplätze. debatte 12*, Matthes & Seitz, München, **1985**, p. 41.

[2] G. Flaubert, *Ivan Turgenev. Briefwechsel 1863–1880*, Friedenauer Presse, Berlin, **1989**, p. 63. See also: Flaubert to Louise Colet, 22 November 1852; 20 June 1853, and 29 January 1854; included in: G. Flaubert, *Die Briefe an Louise Colet*, Haffmanns, Zürich, **1995**, pp. 549, 714, and 918.

[3] J.-B. Naudin, A. Borrel, A. Senderens, *Zu Gast bei Marcel Proust. Der große Romancier als Gourmet*, 4th ed., Wilhelm Heyne, München, **1992**, the chapter "Der Wohlgeschmack der Kindheit", p. 15.

[4] M. Proust in *Auf der Suche nach der verlorenen Zeit 3. Guermantes. Frankfurter Ausgabe* (Ed.: L. Keller), Werke II, Bd. III, Suhrkamp, Frankfurt am Main, **1996**, p. 551.

[5] M. Proust in *Essays, Chroniken und andere Schriften. Frankfurter Ausgabe* (Ed.: L. Keller), Werke I, Bd. 3, pp. 192, 287, and 582. Based on the chapter "Orfèvre et verrier—Gallé et Lalique" in R. Comte de Montesquiou-Fezensac, *Les Roseaux pensants*, Paris, **1897**.

[6] J. Bersch, *Chemisch-technisches Lexikon*, 3rd ed., A. Hartleben's, Wien and Leipzig, no date, p. 55. For the complex history of the discovery of techniques for etching glass, see "Aus der Kindheit des Glasätzens. Die Glashütte": O. Vogel, *Das Emaillierwerk* **1942**, *72*, 37–42; "Neue Aspekte zur Entdeckung des Ätzens von Glas": H. Cassebaum, *Silikattechnik* **1983**, *34*, 213–214.

[7] With respect to the difficulties, see "Arbeiter- und Nachbarschutz in Glasätzereien": Gutmann, *Glastech. Ber.* **1926**, *4*, 394–395. For an illustration of the breadth of application of this technique, see "Beitrag zur Eisblumierung": H. Freytag, *Glastech. Ber.* **1942**, *20*, 71–75.

[8] a) G. Fahr-Becker, *Jugendstil*, Könemann, Köln, no date, for example, p. 146; b) J. P. Midant, *L'Art Nouveau. Jugendstil in Frankreich*, ECO, Köln/Eltville am Rhein, **1999**. Especially attractive examples: c) F. Borsi, E. Godoli, *Pariser Bauten der Jahrhundertwende. Architektur und Design der französischen Metropole um 1900*, Nikol, Hamburg, no date. Regarding etched window panes in the Parisian street scene: d) E. Atget, *Paris 1857–1927* (Ed.: H. C. Adam), Benedikt, Köln, **2000**. Particularly fine examples among those included here: Café à l'Homme Armée, p. 169; e) E. Atget, *Paris*, Schirmer/Mosel, München, **1998**; f) R. Toman, G. Zugmann, A. Bednorz, *Wien. Kunst und Architektur*, Könemann, Köln, **1999**. Otto Wagner Hauptpavillon der Stadtbahn, p. 283. Numerous examples in: g) P. Roberts-Jones, *Brüssel. Fin de Siècle, EVERGREEN*, Benedikt, Köln, **1999**.

[9] J. R. Partington, *A History of Chemistry*, *Vol. 4*, MacMillan, London, **1964**, p. 911.

[10] a) "Zur Erinnerung an Henri Moissan": A. Gutbier, *Sitzungsber. Phys.-Med. Soz. Erlangen* **1907**, *39*, 298–560. b) "Das Leben und Wirken Henri Moissans": A. Gutbier, *Verhandlungen des Vereins zur Beförderung des Gewerbefleißes* **1910**, *89*, 95–130.

[11] See ref. [9], p. 912.

[12] A. Alter, P. Testard-Vaillant, *Guide du Paris Savant*, Edition Belin, Paris, **2000**, p. 230.

[13] K. Hoffmann, *Glitzerndes Geheimnis. Gauner*, *Gaukler*, *Gelehrte und Großmachtpolitiker. Ein Kriminalreport über parawissenschaftliche Hochstapeleien*, Urania, Leipzig, Jena, Berlin, **1988**, p. 88 and ref. [16].

[14] H. Moisson, *Le Four électrique*, Paris, **1897** and ref. [10].

[15] René Lalique often attempted to combine his glass artistry with the most modern techniques of the times. Thus, in 1929 he outfitted the Cote d'Azur Pullmann Express cars of the famous Train Bleu, Paris–Nice with tryptiches that depicted bacchants through the application of etching and cutting techniques on white matte glass: Jean de Cars u. Caracalla, *Train Bleu und die großen Riviera-Expresszüge*, *Edition Denoel Paris*, Orell Füssli, Zürich und Wiesbaden, **1989**, pp. 78, 86, and 87.

[16] J. Fiedler, P. Feierabend, *Bauhaus*, Könemann, Köln, **1999**, pp. 320, 329. See also: C. Fiell, P. Fiell, *Design des 20.Jahrhunderts*, Benedikt, Köln, **2000**. For an example related to the keyword International Style, see p. 344.

[17] See ref. [10] as well as ref. [9], p. 913.

[18] Ref. [10a], p. 410.

[19] Ref. [9], p. 920.

[20] Concerning Proust's life in general: a) R. Hayman, *Marcel Proust. Die Geschichte seines Lebens*, Insel, Frankfurt am Main and Leipzig, **2000**. b) R. Wiggershaus, *Proust. Leben und Werk in Bildern. insel taschenbuch 1348*, Insel, Frankfurt am Main and Leipzig, **1992**. c) A. de Botton, *Wie Proust Ihr Leben verändern kann. Eine Anleitung. Fischer Taschenbuch 13734*, Fischer, Frankfurt am Main, **2000**.

[21] The complete title is: Marcel Proust, *Zum Gedenken an die gemordeten Kirchen, I. Die geretteten Kirchen. Die Kirchtürme von Caen. Die Kathedrale von Lisieux. Tage im Automobil.* ref. [29], pp. 87–95, 335.

[22] N. Beauthéac, F.-X. Bouchart, *Auf den Spuren von Marcel Proust. Normandie, Ile de France, Genfer See*, Gerstenberg, Hildesheim, **1999**, p. 108. Regarding the problems associated with acetylene illumination for automobiles of the day: a) A. Stukenbrok Einbeck, *Illustrierter Hauptkatalog 1912*, Nachdruck, Olms, Hildesheim, **1979**, pp. 22–29. b) A. Stukenbrok Einbeck, *Illustrierter Hauptkatalog 1926*, Nachdruck, Olms, Hildesheim, **2000**, pp. 36–40.

[23] See ref. [20a], p. 334.

[24] See ref. [21], p. 91.

[25] See ref. [10a], p. 473.

[26] S. Kanfer, *Das Diamanten-Imperium. Aufstieg und Macht der Dynastie Oppenheimer*, Carl Hanser, München, Wien, **1994**. See the chapter: "Gespenster, Gaunereien und Satjagraha", p. 211 as well as ref. [20], p. 88.

[27] See ref. [29], p. 11.

[28] See ref. [29], p. 306.

[29] See ref. [39], p. 219.

[30] *Le Diamant. Mythe-Magie-Realité* (Ed.: R. Maillard), Flammarion, Paris, **1979**, p. 192. See also: *Diamanten, Faszination, Mythos und Technik* (Ed.: C. Weise), München, **1994**.

[31] See ref. [13], p. 222.

[32] See ref. [18], p. 11.

[33] See ref. [18], p. 16.

[34] See ref. [18], p. 34.

[35] See ref. [18], p. 35.

[36] See ref. [18], p. 35.

[37] See ref. [18], p. 37.

[38] P. Michel-Thiriet, *Das Marcel Proust Lexikon*, *suhrkamp taschenbuch 3049*, Suhrkamp, Frankfurt am Main, **1999**, p. 37.

[39] see ref. [18], p. 51.

[40] a) J. Jacques, *Berthelot. Autopsie d'un mythe. Un savant*, *un époque*, Belin, Paris, **1987**. b) D. Langlois, *Berthelot. Un savant engagé*, J. C. Lattüés, no location, **2000**.

[41] J. des Cars, *La Princesse Mathilde. L'amour*, *la gloire et les arts*, Librairie Académique Perrin, no location, **1996**.

[42] See the in-part word-for-word agreement in the characterization of chemistry by Berthelot on 5 December 1873 "Devant le feu … de fumoir chez la Princesse …" in E. de Goncourt, J. de Goncourt, *Journal. Mémoire de la vie littéraire. II. 1866–1886. Robert Lafont*, Fasquelle and Flammarion, Paris, **1956**, pp. 556, 557, on the one hand, and a scene from "Juliette Faustin" in: E. de Goncourt, *Die Brüder Zemgano. Juliette Faustin. Zwei Romane*, Dieterich'sche Verlagsbuchhandlung, Leipzig, **1989**, p. 298.

[43] It greatly displeased Flaubert when Berthelot was subjected to public attack. See: Flaubert's letter to Maupassant of 23 July 1876 in G. Flaubert, *Der Briefwechsel mit Guy de Maupassant*, Haffmans, Zürich, **1997**. In addition, the frequently common references to Berthelot and Flaubert in the journals of the Goncourt brothers as well as Flaubert's delightful description of a disastrous explosion in a chemical laboratory: G. Flaubert, *Bouvard und Pécuchet. insel taschenbuch 373*, Insel, Frankfurt am Main, **1979**, pp. 101, 102.

[44] a) "Juwelen aus der Retorte": K. Bachmann in *Geo. Das Neue Bild der Erde* **2000**, *7*, 88–106. b) G. van der Schrick, *Le diamant synthétique et le diamant industriel*, ref. [43], p. 276.

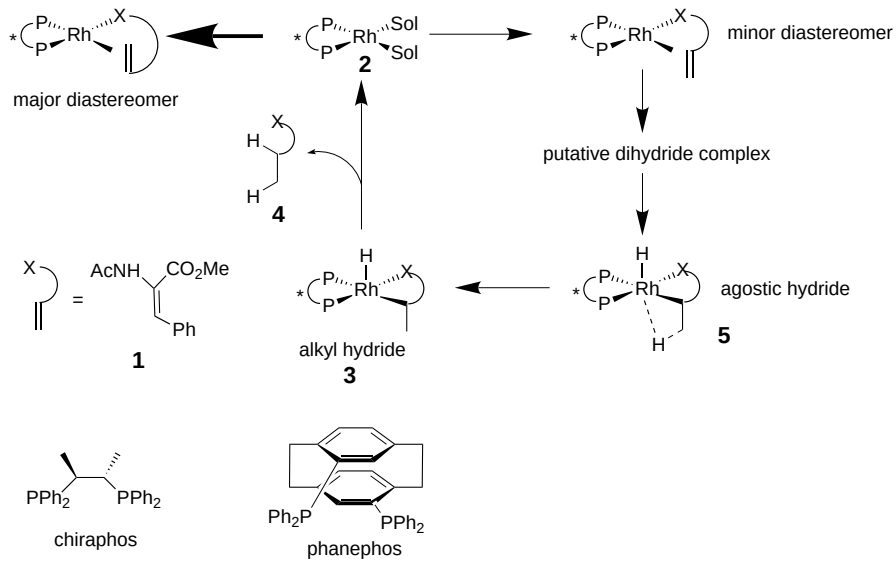
 © WILEY-VCH Verlag GmbH, D-69451 Weinheim, 2001 1433-7851/01/4024-4610 $ 17.50+.50/0

Ru- and Rh-Catalyzed Asymmetric Hydrogenations: Recent Surprises from an Old Reaction

Kai Rossen*

There is an increasing demand for efficiently prepared, enantiomerically pure building blocks, for example as intermediates in the production of pharmaceuticals.[1] Asymmetric catalysis holds the promise of efficiently setting up chirality and has turned into one of the most important fields at the interface between organic synthesis and organometallic chemistry.[2]

Although amazing progress has been made in the last few decades, there is still a clear need for more selective and active catalysts. The use of combinatorial and high through-put techniques has become fashionable lately, but combinatorial methods cannot be a substitute for understanding the reason behind the success or failure of a given catalyst system.[3] Ultimately, detailed mechanistic studies have to be undertaken, not only to satisfy scientific curiosity, but also to provide the understanding that is essential for the field to move ahead.[4]



Scheme 1. The classical mechanism for the hydrogenation of [Rh(bisphosphane)]$^+$. Sol = solvent.

Recently, a number of spectacular results have been published on the mechanism of Rh- and Ru-catalyzed asymmetric hydrogenations. While the classic studies of Rh-catalyzed reactions are now taught as textbook examples for the elegant elucidation of mechanisms, the field is clearly not free from surprises.[5] These unexpected results come from the groups of Brown and Bargon[6b, 7] as well as Gridnev and Imamoto.[8] A common feature of these groups is the extensive use of NMR techniques, demonstrating the extreme power of this tool.

The Rh-catalyzed hydrogenation of dehydroamino acids leading to enantiomerically pure α-amino acids is considered to be a thoroughly understood reaction based on work carried out in the research groups of Halpern and Brown.[6] However, the most recent results clearly show that we are still far from a clear understanding.

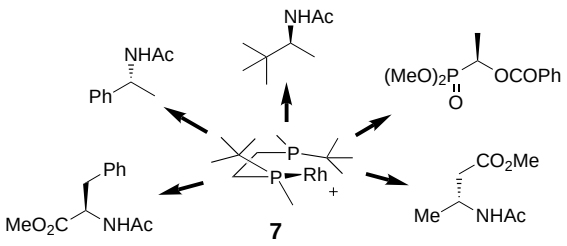
[*] Dr. K. Rossen
Degussa AG, Fine Chemicals Division
PO Box 1345, 63403 Hanau (Germany)
Fax: (+49) 6181-59-4874
E-mail: kai.rossen@degussa.com

The mechanism elucidated for the asymmetric reduction of the standard dehydroacetamide substrate methyl (*Z*)-α-acetamidocinnamate (**1**, Scheme 1) using the chiraphos–rhodium catalyst **2** was clearly shown to proceed by binding of the enamide substrate to the cationic Rh–bisphosphane complex.[6] Both the minor and the major diastereomer have been characterized by various techniques. While it could be demonstrated that the minor diastereomer reacts more rapidly with H_2, the reason for this increased reactivity is not understood. Furthermore, the expected dihydride complex has never been observed with the bisphosphane complexes examined, although the analogous compound for the prototypical Wilkinson catalyst [$(Ph_3P)_3RhCl$] is well-characterized. The first intermediate that can be observed is the alkyl monohydride **3**, which then releases the product **4** and the regenerated active catalyst. While numerous attempts have been made to find experimental evidence for the key step of the hydrogenation, which must clearly be the addition of hydrogen to the catalyst, there is little data on species appearing before the alkyl hydride. It is at this point that the groups of Bargon and Brown can combine hydrogenation using para-hydrogen with use of a new ligand (phanephos) which permits reactions at very low temperatures.[7] With this

 © WILEY-VCH Verlag GmbH, D-69451 Weinheim, 2001 1433-7851/01/4024-4611 $ 17.50+.50/0

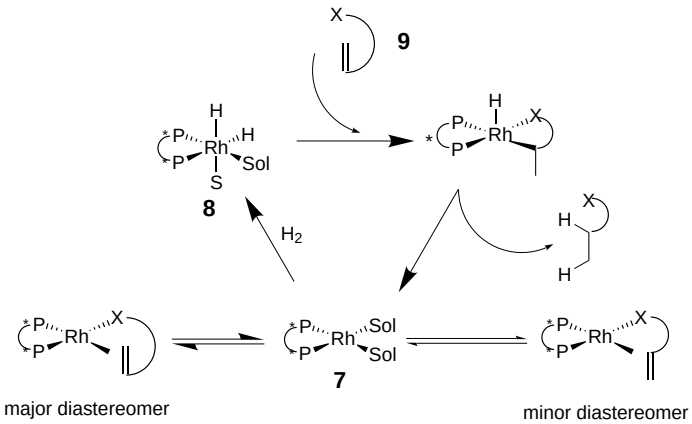
system it becomes possible to identify an agostically bound hydride **5**—that is, a species that could be imagined as lying on the pathway from the dihydrogen complex to the alkyl hydride—and to glimpse for the first time at the initial steps of this reaction. This work thus nicely adds a new facet to our understanding of the classical hydrogenation mechanism.

Recently, the group of Gridnev and Imamoto introduced the electron-rich bisphosphane ligand *t*Bu-BisP* (**6**), which is chiral at P.[8] This ligand adds to the small number of bisphosphane ligands with chirality at P, as opposed to the common attachment of a PPh_2 group onto a chiral backbone. The Gridnev/Imamoto group has demonstrated that the *t*Bu-BisP* – rhodium catalyst **7** (see Scheme 2) can reduce not only α-acetamidoacrylates, but also enamides, (*E*)-β-(acylamino)-acrylates, and protected α,β-unsaturated α-acyloxyphosphonates with high enantioselectivity and reactivity.[8] Thus the catalyst affords a useful entry to the synthesis of enantiomerically highly enriched α-amino acids, amines, β-amino acids, and α-acyloxyphosphonate (Scheme 2).



Scheme 2. Various products obtained with the *t*Bu-BisP* – rhodium catalyst **7** from Gridnev and Imamoto.

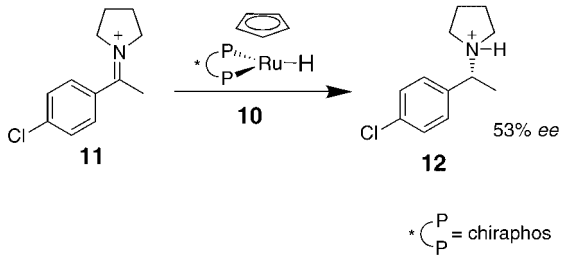
While ligand **6** is clearly an important addition to the repertoire of bisphosphane ligands, the mechanistic work of the inventors is especially notable and surprising.[8] By using their *t*Bu-BisP* ligand, the Gridnev/Imamoto group was able to show that the Rh-catalyzed hydrogenation with this electron-rich system can proceed by an entirely different mechanism (Scheme 3): As expected, the catalyst binds to the substrate, but the authors provide conclusive data that the anticipated oxidative addition of H_2 to this substrate – catalyst complex is not the major pathway. Indeed, the catalytic cycle involves the initial formation of a Rh – hydride species by oxidative addition of hydrogen to the catalyst! Complexation of substrate **9** to the Rh – hydride species **8** initiates the highly enantioselective hydrogenation. It is remarkable how the change from the traditionally used bisphosphane ligands with PPh_2 groups to a trialkylphosphane such as *t*Bu-BisP* induces a fundamental change in the mechanism of the hydrogenation.



Scheme 3. The hydride mechanism of the Gridnev/Imamoto catalyst **7**. Sol = solvent.

Rhodium – bisphosphane catalysts set the benchmark for a number of asymmetric hydrogenations, but the versatility of Ru – bisphosphane catalysts for a wide number of substrates coupled with the markedly lower price of Ru compared to Rh make the Ru-based hydrogenations very attractive. The work of the Noyori group has provided the practical and mechanistic understanding that makes these Ru-based systems probably the most useful family of catalysts for the efficient generation of chirality.[9]

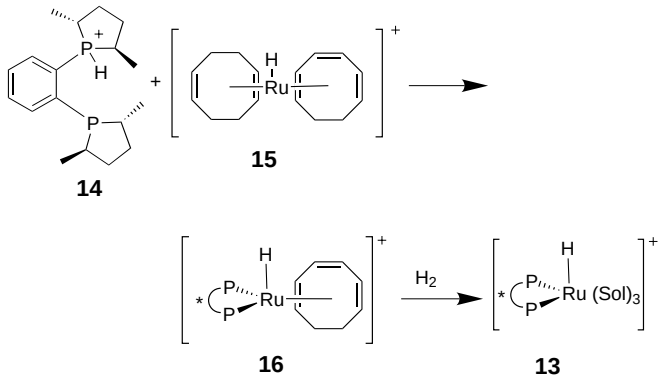
Despite the detailed mechanistic explanation worked out by the Noyori group for a number of these reactions, the mechanism of the "standard" hydrogenation using the bisphosphane – Ru complex is still poorly understood. Additional progress in this area is highly appreciated, and in this context a recent publication by Norton and Magee is important, even though it deals with both a special catalyst and substrate.[10] The Norton group used the bisphosphane – Ru hydride **10** for the hydrogenation of iminium ion **11** (Scheme 4). They showed that the reaction proceeds by an ionic mechanism to give the enantiomerically enriched amine. From a purely practical point of view the obtained enantiomeric excesses show some room for improvement, but more importantly the demonstration of a purely ionic mechanism in the hydrogenation of the iminium ion adds another interesting facet to the myriad of proven mechanisms of Rh- and Ru-based asymmetric hydrogenations.[11]



Scheme 4. Ionic mechanism for the hydrogenation of iminium ion **11** with with the Ru – hydride complex **10**.

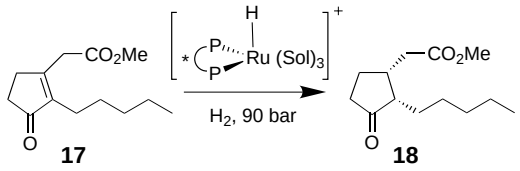
The catalyst system used by Norton and Magee[10] adds to the small number of structurally defined bisphosphane – Ru catalyst systems. That the search for these structures is more than a mere academic exercise has been amply proven by the beautiful work from the collaborators at Firmenich in Switzerland and the University of Alberta.[12] Their work allows access to a number of highly active and well-defined catalysts of the type [Ru(bisphosphane)(H)(solvent)$_3$](BF$_4$) (**13**, Scheme 5). To this end [Ru(1,2:5,6-η-cod)(η^6-cot)] (**15**) is allowed to react with the monoprotio salt of Me-DuPHOS

 © WILEY-VCH Verlag GmbH, D-69451 Weinheim, 2001 1433-7851/01/4024-4612 $ 17.50+.50/0 *Angew. Chem. Int. Ed.* **2001**, *40*, No. 24



Scheme 5. Preparation of the Firmenich/Alberta Ru–hydride catalyst **13**. Sol = solvent.

(**14**) to give the catalyst precursor [Ru(Me-DuPHOS)(H)(η^6-cot)]$^+$ (**16**) (cod = cycloocta-1,5-diene, cot = cycloocta-1,3,5,7-tetraene). Subsequent hydrogenation leads to the active catalyst species **13**. Complex **13** has demonstrated its utility in the highly enantioselective hydrogenation of the difficult to reduce vinylogous β-oxoester **17**, which leads directly to **18**, a commercially important perfume component (Scheme 6).



Scheme 6. Application of the Firmenich/Alberta Ru–hydride catalyst **13** in the hydrogenation of **17**. Sol = solvent.

Just as in the work of the Norton group, the Firmenich/Alberta group prepared and used a Ru–hydride complex. However, while the Norton catalyst is stabilized by the cyclopentadienyl ligand, [Ru(bisphosphane)(H)(solvent)$_3$]$^+$ (**13**) used by Firmenich is reminesicent of the complex [Rh(bisphosphane)(H)(H)(solvent)$_2$]$^+$ (**8**) identified by Gridnev and Imamoto for the right neighbor of Ru in the periodic table. In terms of practicality the Firmenich/Alberta procedure has the advantage of allowing the straightforward synthesis of Ru–bisphosphane complexes with a number of different bisphosphane ligands. This allows the facile screening of ligands for a given hydrogenation substrate with well-defined catalyst systems, a clear prerequisite for understanding the reaction in question.

In summary, recent developments have shown the danger of assuming that the classical mechanism of Rh-catalyzed hydrogenation is valid for all bisphosphane ligands and metal combinations. Furthermore, we now know that the field is not safe from surprises, such as the discovery of a purely ionic reaction mechanism. Stepping back from the individual results, the wide range of observed mechanisms cannot be astonishing: A short look at the complexity of mechanisms for a simple aliphatic nucleophilic substitution would have demonstrated that one cannot expect to describe the far more complex asymmetric hydrogenations—with widely different metals, ligands, and substrates—by a single mechanism. While simple and all-encompassing explanations may have some appeal, mechanistic diversity is also an opportunity to be explored and exploited.

[1] As an example for the importance of the efficient preparation of complex chiral building blocks for pharmaceuticals, note the recent discussions on the cost of providing anti-AIDS drugs in Africa: a) M. Wadman, *Nature* **2001**, *410*, 615–616; b) C. Ezzell, *Sci. Am.* **2000**, *283*, 98–103.

[2] a) G. Helmchen, R. W. Hoffmann, J. Mulzer, E. Schaumann, *Methods of Organic Chemistry (Houben-Weyl) 1st ed.*, Vol. E21, **1995**; b) E. Jacobsen, A. Pfaltz, H. Yamamoto, *Comprehensive Asymmetric Catalysis*, *Vol. 1–3*, Springer, Heidelberg, **1999**; c) I. Ojima, *Catalytic Asymmetric Synthesis*, 2nd ed., Wiley, New York, **2000**.

[3] a) For recent examples with comprehensive lists of references, see P. J. Fagan, E. Hauptman, R. Shapiro, A. Casalnuovo, *J. Am. Chem. Soc.* **2000**, *122*, 5043–5051; b) M. L. Snapper, A. H. Hoveyda, *Comb. Chem.* **2000**, 433–455; c) J. R. Porter, J. F. Traverse, A. H. Hoveyda, M. L. Snapper, *J. Am. Chem. Soc.* **2001**, *123*, 984–985.

[4] For a beautiful example of a catalyst that was discovered by combinatorial methods and is awaiting publication of its mechanistic function, see M. Sigman, E. N. Jacobsen, *J. Am. Chem. Soc.* **1998**, *120*, 4901–4902.

[5] J. P. Collman, L. Hegedus, *Principles and Applications of Organotransition Metal Chemistry*, University Science Books, Mill Valley, **1980**.

[6] a) J. Halpern, *Science* **1982**, *217*, 401–407; b) J. M. Brown, *Chem. Soc. Rev.* **1993**, *22*, 25–41; c) R. Noyori, *Asymmetric Catalysis in Organic Synthesis*, Wiley, New York, **1994**.

[7] R. Giernoth, H. Heinrich, N. J. Adams, R. J. Deeth, J. Bargon, J. M. Brown, *J. Am. Chem. Soc.* **2000**, *122*, 12381–12382.

[8] a) I. D. Gridnev, N. Higashi, T. Imamoto, *J. Am. Chem. Soc.* **2000**, *122*, 10486–10487; b) I. D. Gridnev, N. Higashi, T. Imamoto, *J. Am. Chem. Soc.* **2001**, *123*, 4631–4632; c) I. D. Gridnev, N. Higashi, T. Imamoto, *J. Am. Chem. Soc.* **2000**, *122*, 7183–7194; d) I. D. Gridnev, N. Higashi, T. Imamoto, *J. Am. Chem. Soc.* **2000**, *122*, 7183–7194; e) I. D. Gridnev, M. Yasutake, N. Higashi, T. Imamoto, *J. Am. Chem. Soc.* **2001**, *123*, 5268–5276; f) M. Yasutake, I. D. Gridnev, N. Higashi, T. Imamoto, *Org. Lett.* **2001**, *3*, 1701–1704.

[9] a) R. Noyori, S. Hashiguchi, *Acc. Chem. Res.* **1997**, *30*, 97–102; b) T. Ohkuma, D. Ishii, R. Noyori, *J. Am. Chem. Soc.* **2000**, *122*, 6510–6511; c) R. Noyori, T. Ohkuma, *Pure Appl. Chem.* **1999**, *71*, 1493–1501; d) T. Ohkuma, M. Koizumi, H. Doucet, T. Pham, M. Kozawa, K. Murata, E. Katayama, T. Yokozawa, T. Ikariya, R. Noyori, *J. Am. Chem. Soc.* **1998**, *120*, 13529–13530.

[10] M. P. Magee, J. R. Norton, *J. Am. Chem. Soc.* **2001**, *123*, 1778–1779.

[11] Further ionic hydrogenation mechanisms have been demonstrated: a) R. M. Bullock, M. H. Voges, *J. Am. Chem. Soc.* **2000**, *122*, 12594–12595; b) Y. Shvo, D. Czarkie, Y. Rahamim, D. F. Chodosh, *J. Am. Chem. Soc.* **1986**, *108*, 7400–7401; c) M. Yamakawa, H. Ito, R. Noyori, *J. Am. Chem. Soc.* **2000**, *122*, 1466–1478.

[12] a) D. A. Dobbs, K. P. M. Vanhessche, E. Brazi, V. Rautenstrauch, J.-Y. Lenoir, J.-P. Genet, J. Wiles, S. H. Bergens, *Angew. Chem.* **2000**, *112*, 2080–2083; *Angew. Chem. Int. Ed.* **2000**, *39*, 1992–1995; b) J. Wiles, S. H. Bergens, K. P. M. Vanhessche, D. A. Dobbs, V. Rautenstrauch, *Angew. Chem.* **2001**, *113*, 937–942; *Angew. Chem. Int. Ed.* **2001**, *40*, 914–919.

 © WILEY-VCH Verlag GmbH, D-69451 Weinheim, 2001 1433-7851/01/4024-4613 $ 17.50+.50/0

Comment on the Communication "The Key to Solving the Protein-Folding Problem Lies in an Accurate Description of the Denatured State" by van Gunsteren et al.**

Aaron R. Dinner and Martin Karplus*

In a recent communication,[1] van Gunsteren et al. proposed that the folding of proteins is much easier than has been believed[2] because the number of accessible conformers in the denatured state is only on the order of 10^9 for a 100-residue protein, instead of on the order of 10^{24} to 10^{30} used in previous analyses.[3, 4] This would make it possible for a polypeptide chain to fold to the native state in about 1 s by a random search since the transition from one conformer to another requires about 1 ns.[5] Van Gunsteren et al.[1] based their argument on simulations ranging from 32 to 200 ns of the folding and unfolding of six b and a amino-acid peptides in methanol and water. For these peptides, the number of conformers found by them corresponds to 1.22 to 1.74 conformers per torsional degree of freedom, in the same range as the value 1.33 we found[6] in Monte Carlo simulations with an implicit solvent model of a denatured 16-residue peptide that forms a b-hairpin in the folded state; the simple average of the number of conformers per torsion angle calculated by van Gunsteren et al. for the different peptides is 1.40.

If the number of conformers scales exponentially with the number of amino acids, an estimate of 1.33 (1.40) conformers per backbone torsion angle leads to a denatured state for a 100-residue protein with 1.33^{200} $(1.40^{200}) = 6 \times 10^{24}$ (1.7×10^{29}) accessible conformers,[3, 4] which is many orders of magnitude larger than the value (10^9) suggested by van Gunsteren et al.[1] The essential question concerns not the number of conformers observed in the peptide studies, but the statement that the number of conformers "does not grow exponentially with the length of the peptide" [p. 364/352 of ref. [1]]. It is the latter that leads to their optimistic conclusion concerning the simplicity of the protein folding problem. There is no evidence for or against this claim in their simulations. The peptides studied vary by only a factor of two in size; in fact, there is one short peptide (9 torsion angles) and the five others vary in length only between 16 and 21 torsion angles. Since the number of conformers shows essentially no correlation with the number of torsion angles (the Pearson linear correlation coefficient between the calculated number of conformers and the number of torsion angles is 0.184), it is not possible to draw any conclusion from the data concerning the relation between the length of a peptide chain and the number of conformers. In fact, the only correlation evident in the data is that between the number of conformers and the length of the simulation, independent of the size of the peptide (the Pearson linear correlation coefficient for these data is 0.94). This might suggest that convergence has not been achieved in the reported simulations.

If the length dependence of the number of conformers were nonexponential, this would be very important. Because there are no detailed all-atom simulations for a range of polypeptide sizes that can be used to resolve this question, we consider the results available from simpler models and experimental data. Enumerations of self-avoiding random walks of simple polymers on lattices[7, 8] and analytical models[9] indicate an exponential dependence on chain length. Moreover, experimental estimates[10] for the configurational entropies of proteins obtained by subtracting the entropies of hydration for polar and nonpolar groups from measured entropies of unfolding vary essentially linearly with the length of the sequence (see Table X of ref. [10]), which implies exponential scaling of the number of conformers via the standard Boltzmann definition of the (microcanonical) entropy.

If there are 10^{24} conformers for a 100-residue protein and the interconversion between backbone conformations occurs on a ns time scale (see above), it would take about 2×10^7 years to sample all of them in a random search for the native

[*] Prof. M. Karplus
Department of Chemistry & Chemical Biology
Harvard University
Cambridge, MA 02138 (USA)
Fax: (+1) 617 496-3204
E-mail: marci@tammy.harvard.edu
and
Laboratoire de Chimie Biophysique, ISIS
Université Louis Pasteur
4, Rue Blaise Pascal
67000 Strasbourg (France)
Fax: (+33) 3-90-24-15-62
Dr. A. R. Dinner
Department of Chemistry, University of California
Berkeley, CA 94720 (USA)

[**] We thank Eugene Shakhnovich (Harvard University) for pointing out the references on lattice polymer simulations and very helpful discussions. We also thank Wilfred van Gunsteren for comments on the manuscript. A.R.D. is a Burroughs Wellcome Fund Hitchings–Elion Postdoctoral Fellow. The work done at Harvard was supported in part by the National Institutes of Health.

 © WILEY-VCH Verlag GmbH, D-69451 Weinheim, 2001 1433-7851/01/4024-4615 $ 17.50+.50/0

state. This argument is the essence of the Levinthal paradox. Its resolution is based on the existence of a large enough bias in the effective energy surface to guide the system to the native state, such that only a relatively small fraction of the accessible conformers is sampled along any given trajectory [see ref. [4], and references therein]. For example, in a 27-residue heteropolymer lattice model for a protein, there are a total of 10^{16} possible conformers (taking account of excluded volume). Of these, on the order of 10^{10} conformers (about 2.2 per dihedral angle) are accessible at the fastest folding temperature,[3, 4, 11] while less than 10^6 are sampled in finding the native state. For a 125-residue lattice model, there are about 10^{54} accessible conformers (about 2.7 per dihedral angle),[12] but the folding time for optimized sequences increases by only a factor of $10^2 - 10^3$ over that found for the 27-residue model. These results indicate that in the lattice simulations it is not the number of accessible conformers, but rather the number that are visited during a folding trajectory that determines the folding time. Only a limited search appears to be necessary due to the large number of transition states.

While we agree with van Gunsteren et al.[1] that the denatured ensemble needs to be represented correctly to obtain physically meaningful simulations of folding, the native state has to be represented accurately as well. The stability and the structure of the native state strongly influence the shape of the free energy surface, as evidenced by statistical correlations between these properties and experimentally measured folding rates[13, 14] and by the ability to increase the folding rate for lattice polypeptides by optimizing the native state stability[15, 16] and structure.[17] Whether a molecular dynamics simulation with an accurate force field and a fast supercomputer can fold a protein in the available time, in spite of the 10^{24} or more accessible conformers, depends on the nature of the transition state ensemble obtained, which appears to represent a smaller portion of the configuration space than that in the lattice model studies.[18] With all the effort concentrated on the *two* protein folding problems ("Prediction of Structure from Sequence" on the one hand and "Determination of How a Polypeptide Folds to the Native State" on the other), we look forward to a continuation of the rapid progress made in this area during the recent past.

[1] W. F. van Gunsteren, R. Bürgi, C. Peter, X. Daura, *Angew. Chem.* **2001**, *113*, 363 – 367; *Angew. Chem. Int. Ed.* **2001**, *40*, 351 – 355.
[2] M. Karplus, *Folding Des.* **1997**, *2*, 569 – 576.
[3] C. M. Dobson, A. Šali, M. Karplus, *Angew. Chem.* **1998**, *110*, 908 – 935; *Angew. Chem. Int. Ed.* **1998**, *37*, 868 – 893.
[4] A. R. Dinner, A. Šali, L. J. Smith, C. M. Dobson, M. Karplus, *Trends Biochem. Sci.* **2000**, *25*, 331 – 339.
[5] M. Gruebele, *Annu. Rev. Phys. Chem.* **1999**, *50*, 485 – 516.
[6] A. R. Dinner, T. Lazaridis, M. Karplus, *Proc. Natl. Acad. Sci. USA* **1999**, *96*, 9068 – 9073.
[7] D. S. McKenzie, *Phys. Rep.* **1976**, *27*, 35 – 88.
[8] V. S. Pande, C. Joerg, A. Yu. Grosberg, T. Tanaka, *J. Phys. A* **1994**, *27*, 6231 – 6236; Corrigendum: *J. Phys. A* **1996**, *29*, 4753.
[9] K. A. Dill, *Biochemistry* **1985**, *24*, 1501 – 1509.
[10] G. I. Makhatadze, P. L. Privalov, *Adv. Protein Chem.* **1995**, *47*, 307 – 425.
[11] A. Šali, E. Shakhnovich, M. Karplus, *Nature* **1994**, *369*, 248 – 251.
[12] A. R. Dinner, M. Karplus, *J. Phys. Chem. B* **1999**, *103*, 7976 – 7994.
[13] K. W. Plaxco, K. T. Simons, I. Ruczinski, D. Baker, *Biochemistry* **2000**, *39*, 11177 – 11183.
[14] A. R. Dinner, M. Karplus, *Nat. Struct. Biol.* **2001**, *8*, 21 – 22.
[15] E. I. Shakhnovich, A. M. Gutin, *Proc. Natl. Acad. Sci. USA* **1993**, *90*, 7195 – 7199.
[16] E. I. Shakhnovich, *Phys. Rev. Lett.* **1994**, *72*, 3907 – 3910.
[17] A. R. Dinner, E. Verosub, M. Karplus, *Protein Eng.* **1999**, *12*, 909 – 917.
[18] M. Vendruscolo, E. Paci, C. M. Dobson, M. Karplus, *Nature* **2001**, *409*, 641 – 645.

Reply

Wilfred F. van Gunsteren,* Roland Bürgi, Christine Peter, and Xavier Daura

In their comment,[1] Dinner and Karplus express disagreement with our recent communication to *Angewandte Chemie*[2] based on their interpretation of the latter. They stress that there are indications from lattice model simulations as well as from experiment that the number of conformers of a protein increases exponentially with the number of residues, and they claim that we conclude, based on molecular dynamics simulations of small peptides, that the number of conformations of a protein scales nonexponentially with the number of residues. In this reply, we want to comment on the arguments given by Dinner and Karplus and to repeat our arguments such that it is clear what we observe, what we conclude, and what we suggest.

Dinner and Karplus quote as one source of indications for an exponential dependence of the number of conformers on chain length two studies of "self-avoiding random walks of simple polymers on lattices" (see refs. [7, 8] in their comment) and an analytical model based on lattice statistical mechanics (see ref. [9] in their comment). It is well known that the structural properties of a protein are not only the result of short-range (covalent and repulsive van der Waals) interactions, but to a large extent due to long-range (attractive van

[*] Prof. Dr. W. F. van Gunsteren, R. Bürgi, C. Peter, Dr. X. Daura
Laboratory of Physical Chemistry
Swiss Federal Institute of Technology Zurich
ETH Hönggerberg, 8093 Zurich (Switzerland)
Fax: (+41) 1-632-1039
E-mail: wfvgn@igc.phys.chem.ethz.ch

 © WILEY-VCH Verlag GmbH, D-69451 Weinheim, 2001 1433-7851/01/4024-4616 $ 17.50+.50/0

der Waals and electrostatic) interactions. Self-avoiding random walks model short-range interactions only. Introducing additional nonbonded forces alters the behavior of polymers significantly, as is discussed in ref. [7] of the comment.[1] On the experimental side, the entropies estimated in ref. [10] of the comment[1] include both backbone and side-chain contributions and are therefore very difficult to relate to the number of relevant (low free energy, accessed in "equilibrium folding/unfolding pathways") backbone conformers of a protein. Consequently, we do not consider refs. [7–10] of the comment[1] as proofs of an exponential scaling of the number of equilibrium conformers with respect to chain length.

In their comment and in references therein, Dinner and Karplus calculate the number of conformers per backbone torsional degree of freedom and extrapolate to the number of conformers of an *n*-residue protein by assuming in both cases an exponential scaling. Since we do not want to make assumptions on the nature of the scaling, we did not attempt in our communication to interpolate to the number of conformers per backbone torsional degree of freedom from the peptides studied, nor extrapolate to the number of conformers of an *n*-residue protein.

The exact number of conformers (clusters in our communication[2]) depends not only on the number of residues of the peptide, but also on the intrinsic structural properties of the peptide (hydrogen bonding capacity, steric properties, etc.). It makes no sense to calculate the correlation between the number of clusters and the number of backbone torsional angles for peptides with very similar numbers of degrees of freedom, since the noise will be necessarily big. The only cases where the calculation of this correlation seems appropriate is between the smaller peptide (**A** in our communication) and all the other ones (**B** to **F**), where the number of degrees of freedom duplicates. Considering this, we agree that "the number of conformers shows essentially no correlation with the number of torsion angles", especially not an exponential one.

The exact number of conformers depends also on the clustering algorithm and the clustering criterion. The clustering algorithm used in refs. [3–8] allows for the existence of clusters populated by a single member only, even when they are in structural vicinity of other clusters. These single-member clusters were also counted in Table 1 of our communication. In all simulations we observe a low number of clusters which are significantly populated.[3–8] Increasing the simulation time beyond a given number of folding/unfolding events causes an increase in the number of sparsely populated clusters. The significantly populated clusters, however, remain essentially the same.

The point of our communication is that it is necessary to sample the correct ensemble of low-free-energy equilibrium conformers in order to draw conclusions on polypeptide folding. It goes without saying that "the native state has to be represented accurately as well". Proteins are inhomogeneous molecules. It is precisely this inhomogeneity and the very specific properties of each of the amino acids that makes them biologically important. Therefore, it is extremely important to model the representation of the protein and the interaction functions in such a way that the properties of interest are reproduced. In contrast to the studies cited in the comment,[1] we have shown that the ensembles of structures taken from our simulations accurately reproduce the available NMR data,[3–8] including NMR spectra for one peptide,[9] rather than just reproducing the predominant structure or justifying the simulation results with diffuse qualitative arguments. For the six peptides studied the number of relevant conformers is of the order $10^2 - 10^3$. Considering that these peptides fold in the simulations on a time scale of 10^{-9} s, we *suggest* that a protein that folds in a time scale of 10^{-3} s and shows similar equilibrium properties would access a space of around 10^9 relevant conformers. This estimate is based on the assumption that the number of relevant conformers scales linearly with the folding time, and *not*, as suggested by Dinner and Karplus,[1] by assuming a particular scaling of the number of conformers with respect to the number of backbone torsional angles.

We agree with Dinner and Karplus that it is the number of conformers "that are visited during a folding trajectory that determines the folding time". In contrast to the simulations they quote, our simulations sample an equilibrium of folded and unfolded states. All the conformations we observe are, therefore, part of an "*equilibrium* folding/unfolding pathway". If the reader would like to put it in terms of the protein folding funnel picture[10] this would mean that all conformers sampled belong to the bottom part of the funnel, that is are conformers with a low free energy. Since we do not randomize the conformations during the simulation, they do never leave this region of low free energy. We agree with ref. [11] in the comment[1] that the first stage of folding from a *random* high-free-energy conformation to low-free-energy conformations is fast. However, we consider it plausible that, once this region of low free energy is reached, the conformations are sampled according to their Boltzmann weight. This would imply that the folding time is roughly proportional to the number of accessible equilibrium conformers.

The argument of Dinner and Karplus against the dependence of the folding time on the number of accessible conformers is based on Monte Carlo simulations on a lattice of the folding of a 27-bead and a 125-bead model from random conformations to the "native" state (see refs. [11, 12] in their comment). Interactions are only calculated for nonbonded nearest neighbors. The number of accessible conformers for the smaller model is estimated using the number of native contacts as a coordinate to identify the accessible states; in the case of the larger model two subsets of native contacts are used. As mentioned above (second paragraph), we do not agree with the simplifications used in these models. Furthermore, the use of (subsets of) native contacts as reaction (folding) coordinate leads to a projection which we question. Therefore, we do not consider these calculations valid estimates of the number of equilibrium conformers of a protein of 27 and 125 residues, respectively.

In summary, we do not believe that a definitive scaling law for the number of equilibrium conformers as a function of the number of backbone torsional degrees of freedom can be derived from currently available theoretical or experimental data. Our simulations indicate rather a nonexponential scaling. We want to stress again that, in our opinion, it is

 © WILEY-VCH Verlag GmbH, D-69451 Weinheim, 2001 1433-7851/01/4024-4617 $ 17.50+.50/0

fundamental to describe not only the native state but also the denatured state accurately in order to draw conclusions on the nature and mechanisms of protein folding. Only if the denatured state is well represented, conclusions can be made with respect to folding pathways, time scales, and reaction coordinates.

[1] A. R. Dinner, M. Karplus, *Angew. Chem.* **2001**, *113*, 4751 – 4752; *Angew. Chem. Int. Ed.* **2001**, *40*, 4615 – 4616.

[2] W. F. van Gunsteren, R. Bürgi, C. Peter, X. Daura, *Angew. Chem.* **2001**, *113*, 363 – 367; *Angew. Chem. Int. Ed.* **2001**, *40*, 351 – 355.

[3] X. Daura, B. Jaun, D. Seebach, W. F. van Gunsteren, A. E. Mark, *J. Mol. Biol.* **1998**, *280*, 925 – 932.

[4] X. Daura, K. Gademann, B. Jaun, D. Seebach, W. F. van Gunsteren, A. E. Mark, *Angew. Chem.* **1999**, *111*, 249 – 253; *Angew. Chem. Int. Ed.* **1999**, *38*, 236 – 240.

[5] C. Peter, X. Daura, W. F. van Gunsteren, *J. Am Chem. Soc.* **2000**, *122*, 7461 – 7466.

[6] R. Bürgi, X. Daura, A. Mark, M. Bellanda, S. Mammi, E. Peggion, W. F. van Gunsteren, *J. Peptide Res.* **2001**, *57*, 107 – 118.

[7] X. Daura, K. Gademann, H. Schäfer, B. Jaun, D. Seebach, W. F. van Gunsteren, *J. Am. Chem. Soc.* **2001**, *123*, 2393 – 2404.

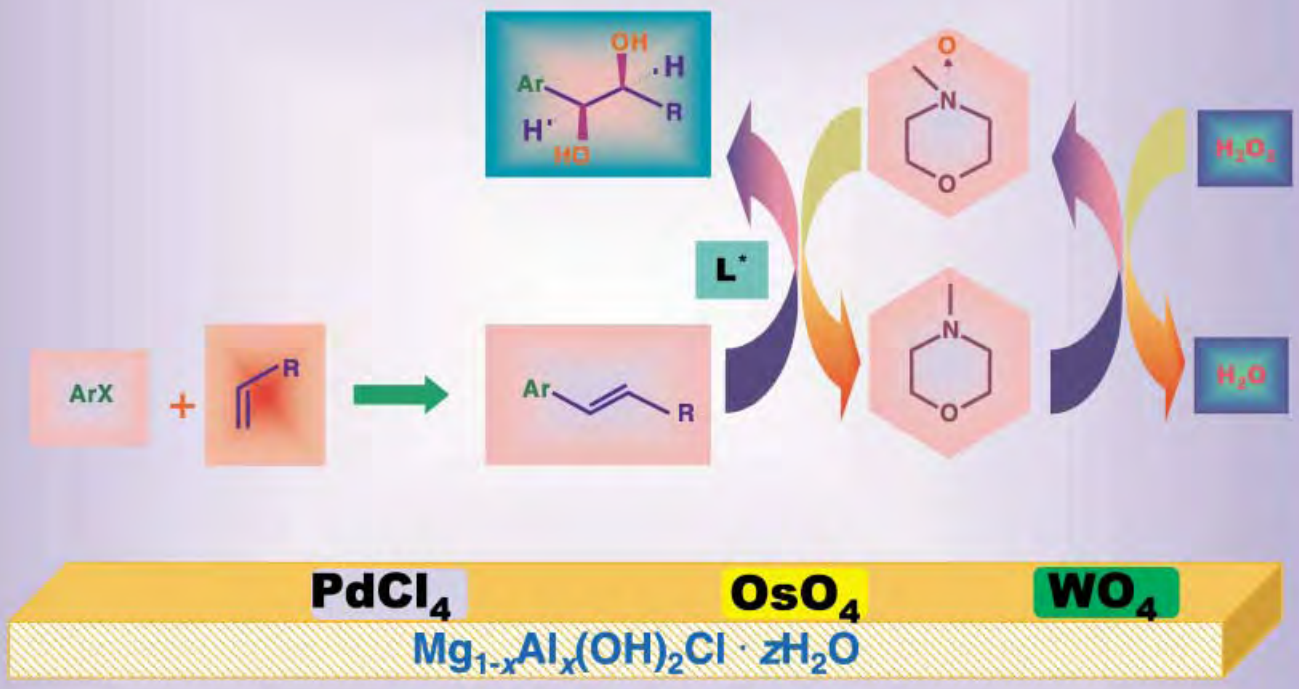
[8] C. Santiveri, M. A. Jiménez, M. Rico, W. F. van Gunsteren, X. Daura, personal communication.

[9] C. Peter, X. Daura, W. F. van Gunsteren, *J. Biomol. NMR* **2001**, *20*, 297 – 310.

[10] P. E. Leopold, M. Montal, J. N. Onuchic, *Proc. Natl. Acad. Sci. USA* **1992**, *89*, 8721 – 8725.

 © WILEY-VCH Verlag GmbH, D-69451 Weinheim, 2001 1433-7851/01/4024-4618 $ 17.50+.50/0

Unique biomimic multicomponent synthesis in a single pot ...



... with a trifunctional catalyst embedded in a single matrix.

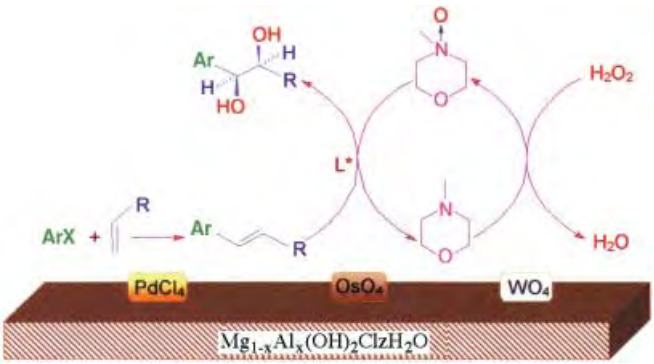
For more information see the following pages.

 © WILEY-VCH Verlag GmbH, D-69451 Weinheim, 2001 1433-7851/01/4024-4619 $ 17.50+.50/0

A Trifunctional Catalyst for the Synthesis of Chiral Diols**

Boyapati M. Choudary,* Naidu S. Chowdari, Sateesh Madhi, and Mannepalli L. Kantam

Many enzymes partake in the intricate construction of complex structures of fascinating stereochemistry from very small molecules in biological systems. The biomimic approach to realize the multistep reactions, composed of multicomponent systems in a single-pot synthesis[1, 2] has been confined to a few examples that include the synthesis of corrin and α-acylaminocarbonamides. Sharpless asymmetric dihydroxylation of olefins offers one of the most efficient methods for the preparation of chiral diols, the key intermediates for many biologically active compounds.[3–5] However, additional upstream operations are required to obtain the desired prochiral olefin, the substrate, and *N*-methylmorpholine *N*-oxide (NMO), the oxidant, employed in molar ratio in asymmetric dihydroxylation. We herein describe an unique single-pot biomimic synthesis of chiral diols mediated by a newly developed trifunctional solid catalyst consisting of active palladium, tungsten, and osmium species embedded in a single layered double-hydroxide matrix to provide the desired prochiral olefins and NMO in situ in a most economical way by Heck coupling and *N*-oxidation of *N*-methylmorpholine (NMM), respectively, for the asymmetric dihydroxylation in a low-cost process (Scheme 1).



Scheme 1. The catalytic cycle in the LDH-PdOsW-catalyzed synthesis of chiral diols using H_2O_2 as the terminal oxidant.

Layered double-hydroxides (LDHs) consist of alternating cationic $M^{II}_{1-x}M^{III}_x(OH)_2^{x+}$ and anionic $A^{n-}\cdot z\,H_2O$ layers.[6] The positively charged layers contain edge-shared metal M^{II} and M^{III} hydroxide octahedra, with charges balanced by A^{n-} ions located in the interlayer spacing or at edges of the lamellae. LDHs have recently received much attention in view of their potential as adsorbents, anion exchangers, and more importantly as catalysts.[7, 8] Small hexagonal LDH crystals of composition $Mg_{1-x}Al_x(OH)_2(Cl)_x\cdot z\,H_2O$ were synthesized following existing procedures ($x = 0.25$; the crystals are 50–100 nm with external surface area of $\sim 100\ m^2\,g^{-1}$).[6] The $PdCl_4^{2-}$ and OsO_4^{2-} ions in the form of Na_2PdCl_4 and K_2OsO_4, respectively, and OsO_4^{2-} and WO_4^{2-} ions as K_2OsO_4 and Na_2WO_4, respectively, are co-exchanged concomitantly onto chloride saturated LDH to obtain bifunctional catalysts, LDH-[$PdCl_4$, OsO_4] (abbreviated as LDH-PdOs) and LDH-[OsO_4, WO_4] (LDH-OsW), respectively. Finally, these bivalent anions are simultaneously exchanged onto a single LDH matrix to yield LDH-[$PdCl_4$,OsO_4,WO_4] (LDH-PdOsW) on interaction with the combined aqueous salt solution. X-ray powder-diffraction patterns of the initial LDH and of the exchanged catalysts hardly differ in the range $2\theta = 3–65°$. The observed basal spacings remain unchanged after the anion exchange, which indicates the position of divalent anions in edge positions of the LDH.

In the FT infrared (IR) spectra of these catalysts, broad absorption bands appear near 830–860 cm^{-1}, assigned to the vibrational asymmetric O=M=O (M = Os and/or W) stretching in contrast to the sharp bands at 819 cm^{-1} in K_2OsO_4 and 831, 857 cm^{-1} in the spectrum of Na_2WO_4. The observation of broad bands in the same region for the catalysts indicates that the osmate and tungstate units are unaffected by exchange onto the support but experience very weak interactions with the support. The Pd–Cl stretching band of the $PdCl_4^{2-}$ ion is observed at 335 cm^{-1} for catalysts LDH-PdOs and LDH-PdOsW. The diffuse reflectance UV/Vis spectra of the catalysts show broad bands with absorption maxima that indicate the presence of related divalent anions in trifunctional and bifunctional catalysts (253 nm WO_4^{2-}, 280 nm $PdCl_4^{2-}$, and 293 nm OsO_4^{2-}). No shift in absorption maxima for these multifunctional catalysts is observed, when compared to the spectra of the pure LDH-complexes (Figure 1). All these studies indicate the retention of the coordination geometries of the specific divalent anions anchored to the LDH matrix in their monomeric form. The Brunauer–Emmet–Teller (BET) surface areas of LDH-PdOs, LDH-OsW, and LDH-PdOsW are found to be 88, 60 and 68 $m^2\,g^{-1}$, respectively.

To understand the in-depth profile of the reactivity of the diversified reaction sequence, the bifunctional catalysts (LDH-PdOs and LDH-OsW) were evaluated in a tandem Heck-asymmetric dihydroxylation reaction and a simultaneous asymmetric dihydroxylation-*N*-oxidation reaction. The tandem Heck-dihydroxylation reaction involved stirring iodobenzene, styrene, and Et_3N at 70 °C for 8 h in the presence of 1 mol% of LDH-PdOs to obtain *trans*-stilbene. After completion of the reaction, as monitored by thin-layer chromatography (TLC), the heating was stopped and a mixture of 1,4-bis(9-*O*-dihydroquinidinyl)phthalazine ($(DHQD)_2PHAL$; 1 mol%) and NMO in *t*BuOH/H_2O (5:1) was introduced and the mixture stirred at room temperature for 6 h to obtain the desired diol in 91% yield with 99% *ee* [Eq. (1)]. The Heck reaction[9] of styrene and iodobenzene in the presence of LDH-PdOs was carried out as above or in acetonitrile or water. The most convenient system to prepare prochiral olefin was the one without any solvent. The

[*] B. M. Choudary, N. S. Chowdari, S. Madhi, M. L. Kantam
Indian Institute of Chemical Technology
Hyderabad 500 007 (India)
Fax: (+91) 40-7170921
E-mail: choudary@iict.ap.nic.in

[**] N.S.C. and S.M. thank the Council of Scientific and Industrial Research, India, for providing research fellowships. We also thank Prof. I. E. Marko for his helpful comments.

 © WILEY-VCH Verlag GmbH, D-69451 Weinheim, 2001 1433-7851/01/4024-4620 $ 17.50+.50/0

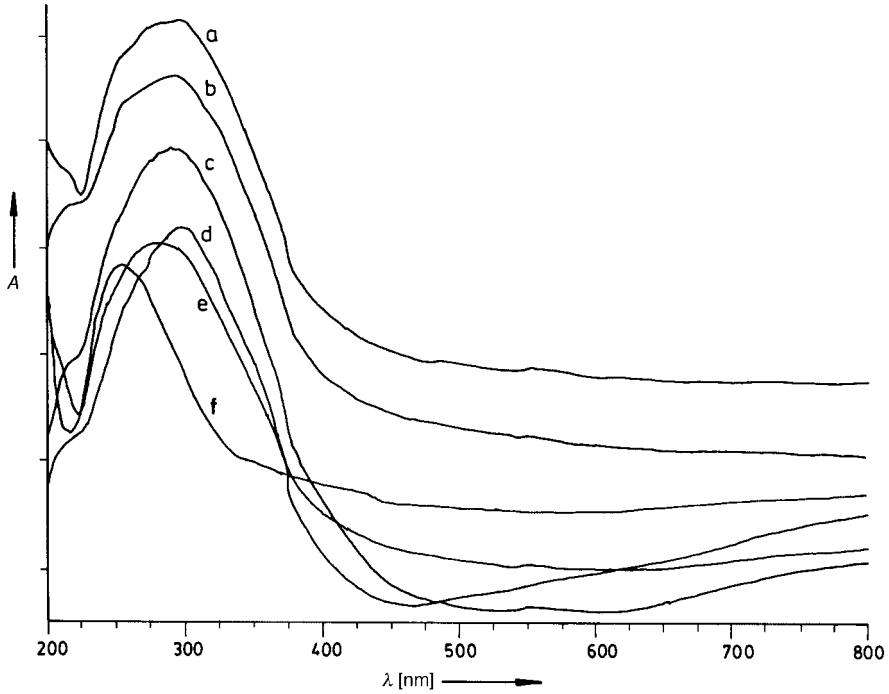
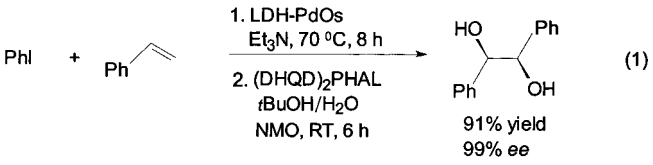


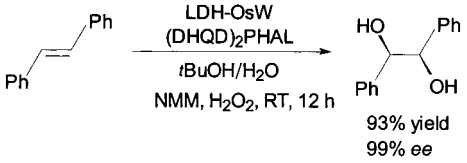
Figure 1. Diffuse-reflectance UV/Vis spectra of a) LDH-PdOsW, b) LDH-OsW, c) LDH-PdOs, d) LDH-Os, e) LDH-Pd, and f) LDH-W.



(1)

methodology described herein uses bulk chemicals such as styrene and acrylates as starting materials to prepare prochiral substrates, stilbenes, and cinnamates in situ and upon dihydroxylation gives chiral diols in a single-pot reaction (Table 1).

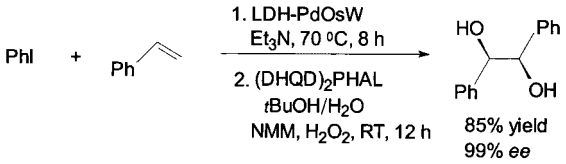
The bifunctional catalyst LDH-OsW was tested in the simultaneous asymmetric dihydroxylation of *trans*-stilbene and *N*-oxidation of NMM in the presence of H_2O_2. The H_2O_2 was added slowly over 12 h to a mixture of 1 mol% of LDH-OsW, $(DHQD)_2PHAL$, *trans*-stilbene, and NMM in *t*BuOH/H_2O (5:1), to afford the desired diol in 93% yield with 99% *ee* [Eq. (2)]. This novel method gave chiral diols by using



(2)

NMM in catalytic amounts and a cheaper oxidant H_2O_2, instead of the NMO currently used in stoichiometric amounts in asymmetric dihydroxylations. This process rivals the one employed by Bäckvall and co-workers, by using flavine, in a biomolecule-induced catalytic oxidation of NMM to NMO in a homogeneous asymmetric dihydroxylation.[4] The homogenous flavine-based process suffers from the problem of difficult catalyst recovery, while the basic advantage of our LDH-OsW process is the recyclability of the catalyst.

The trifunctional catalyst LDH-PdOsW was tested in a Heck-*N*-oxidation-asymmetric dihydroxylation, a multicomponent system in a single-pot reaction. The continuous supply of NMO was ensured in situ though the oxidative cycle of NMM by H_2O_2 as shown in Scheme 1. A mixture of iodobenzene, styrene, and Et_3N in the presence of 1 mol% of LDH-PdOsW was stirred without solvent at 70 °C for 8 h. The heating was stopped and a mixture of $(DHQD)_2PHAL$ (1 mol%) and NMM in *t*BuOH/H_2O (5:1) was added. Subsequently, H_2O_2 was added slowly over 12 h to afford the desired diol in 85% yield with 99% *ee* [Eq. (3)]. In all these multifunctional approaches [Eqs. (1)–(3)], the chiral diols are obtained in good yields with high enantioselectivities (Table 1). Employment of the cheaper raw materials and reduction of number of operations thus favorably influence the economics of the process.

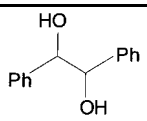
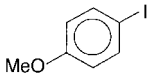
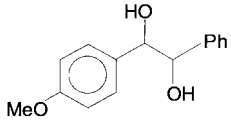
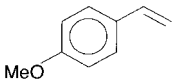
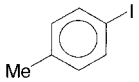
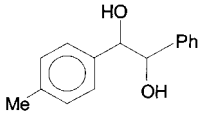
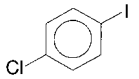
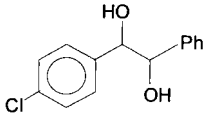
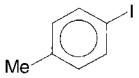
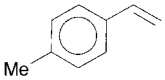
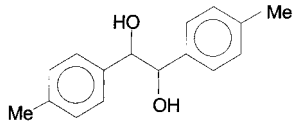
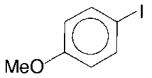
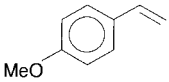
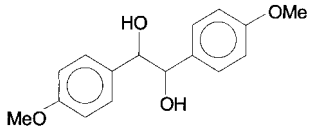
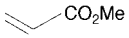
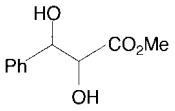
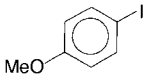
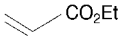
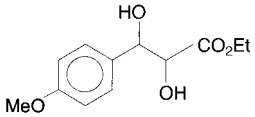


(3)

The LDH-PdOsW was recovered quantitatively by filtration while the chiral ligand was recovered by acid/base extraction (>95% recovery). The recovered catalyst was reused in the multicomponent reaction and following replenishment of the chiral ligand (to make-up 1 mol%) at the appropriate stage, consistent activity was noticed even after 5th cycle. When the reaction was conducted with filtrate obtained by washing of the catalyst with solvent, no product formation was observed. These results and others indicate that the Os and W oxides on the LDH matrix remained bound throughout the reaction, while Pd leached from the support into solution during the reaction and redeposited on the support at the end of the reaction.

The bifunctional and trifunctional catalysts comprising Pd, Os/W performed Heck coupling, *N*-oxidation, and asymmetric dihydroxylation reactions and demonstrated characteristic features of the metal centers in the diverse multifunctional activities of the catalysts. These results substantiate the retention of the coordination geometries of the metal complexes in their monomeric form, a proposal supported by IR and UV/DRS (DRS = diffuse reflectance spectroscopy) spec-

Table 1. The synthesis of chiral diols using heterogeneous multifunctional catalysts LDH-PdOs and LDH-PdOsW.[a]

Entry	Aryl halide	Olefin	Product	Method	Yield	*ee*[b]	Config.[c]
1	PhBr			A	90	99	*R*,*R*
2	PhI			A	91	99	*R*,*R*
3				B	85	99	*R*,*R*
4				A	95	99	*R*,*R*
5				B	85	99	*R*,*R*
6	PhI			A	94	99	*R*,*R*
7				B	88	99	*R*,*R*
8				A	93	99	*R*,*R*
9				B	91	99	*R*,*R*
10				A	90	97	*R*,*R*
11				B	89	97	*R*,*R*
12				A	91	99	*R*,*R*
13				B	86	99	*R*,*R*
14				A	89	99	*R*,*R*
15				B	83	99	*R*,*R*
16	PhI			A	92	95	2*S*,3*R*
17				B	90	98	2*S*,3*R*
18				A	94	95	2*S*,3*R*
19				B	93	96	2*S*,3*R*

[a] Method A and Method B: see Experimental Section. [b] *ee* determined by HPLC analysis on Chiralcel OJ column with 10% isopropanol in hexane as an eluant; flow rate 1 mL min^{-1}; detection UV 220 nm. [c] The absolute configuration was determined by comparison of specific rotations with literature values.[10]

tral data which rule out the formation of bi- or tri-heterometallic species during the exchange process or the dihydroxylation reaction. The superior performance of these catalysts in providing chiral diols with higher yields is ascribed to the large positive electric potential and spatial organization of LDH-PdOs and LDH-PdOsW. These results are in accord with LDH-WO_4 catalyzed oxidative bromination.[8a] The present system composed of new variants, LDH support, Et_3NHX coupled with slow addition of H_2O_2, facilitates the hydrolysis of osmium monogylcolate ester to subdue the formation of bisglycolate ester and thus achieve higher *ee* values.[3d] Further, the higher *ee* values obtained using a bulky chiral ligand, $(DHQD)_2PHAL$ suggest that the OsO_4^{2-} ion is only present on the surface, since the diffusion of the chiral ligand to interact with OsO_4^{2-} ions located in the very small interlamellar space (3 Å) of LDH is very unlikely. This result concurs with the evidence obtained by X-ray diffraction data that the OsO_4^{2-} ions are located at edge positions.

In summary, we have designed and developed a recoverable and reusable LDH-PdOsW trifunctional solid catalyst for the synthesis of chiral diols. The catalyst consists of active palladium, osmium, and tungsten species embedded in a single LDH matrix. This method provides the desired prochiral olefins in situ and chiral diols (which are very valuable intermediates for drugs, such as diltiazem and taxol) from cheaper precursors and NMO by in situ oxidation thus minimizing the number of operations that need to be performed. The high cost and toxicity of osmium, a major obstruction to the use of homogeneous catalysis in industry are addressed by our heterogeneous catalyst.

 © WILEY-VCH Verlag GmbH, D-69451 Weinheim, 2001 1433-7851/01/4024-4622 $ 17.50+.50/0 *Angew. Chem. Int. Ed.* **2001**, *40*, No. 24

Experimental Section

The LDH (Mg-Al-Cl) was obtained using a reported procedure.[8c]

LDH-PdOs: LDH (1 g) was suspended in an aqueous solution (100 mL) of Na_2PdCl_4 and $K_2OsO_4 \cdot 2H_2O$ (0.4 mmol each) and stirred at 25 °C for 12 h under nitrogen atmosphere. The solid catalyst was collected by filtration, washed thoroughly with water (500 mL), and vacuum dried to obtain LDH-PdOs (1.158 g; 0.34 mmol g^{-1} of each Pd and Os).

LDH-OsW: LDH (1 g) was suspended in an aqueous solution (100 mL) of $K_2OsO_4 \cdot 2H_2O$ and $Na_2WO_4 \cdot 2H_2O$ (0.4 mmol each) and stirred at 25 °C for 12 h under nitrogen atmosphere. The solid catalyst was collected by filtration, washed thoroughly with water (500 mL), and vacuum dried to obtain of LDH-OsW (1.172 g; 0.34 mmol g^{-1} of each Os and W).

LDH-PdOsW: LDH (1 g) was suspended in an aqueous solution (100 mL) of Na_2PdCl_4, $K_2OsO_4 \cdot 2H_2O$, and $Na_2WO_4 \cdot 2H_2O$ (0.3 mmol each) and stirred at 25 °C for 12 h under nitrogen atmosphere. The solid catalyst was collected by filtration, washed thoroughly with water (500 mL), and vacuum dried to obtain LDH-PdOsW (1.181 g; 0.25 mmol g^{-1} of each Pd, Os, and W).

General procedure for the synthesis of chiral diols: Method A: LDH-PdOs (29 mg, 0.01 mmol), arylhalide (1 mmol), olefin (1 mmol), and Et_3N (111 mg, 1.1 mmol) were introduced into a round-bottomed flask and stirred at 70 °C for 8–16 h under nitrogen atmosphere. After completion of the Heck coupling as monitored by TLC, the heating was stopped and the reaction mixture was allowed to reach room temperature. A mixture of $(DHQD)_2PHAL$ (7.8 mg, 0.01 mmol) and NMO (175 mg, 1.3 mmol) in *t*BuOH/H_2O (5:1, 5 mL) was added to the reaction mixture and stirred at room temperature. After completion of the diol formation (4–6 h, as monitored by TLC), the catalyst was collected by filtration and washed with ethyl acetate (10 mL). The combined filtrates were extracted with 1N HCl (2 × 5 mL) to recover the chiral ligand from the aqueous layer. The resulting organic phase was further washed with brine solution (5 mL) and the solvent was removed under reduced pressure. The crude material thus obtained was purified by chromatography on silica gel using hexane/ethyl acetate (2:1) as an eluant to afford the corresponding *cis*-diol.

Method B: LDH-PdOsW (40 mg, 0.01 mmol), arylhalide (1 mmol), olefin (1 mmol), and Et_3N (111 mg, 1.1 mmol) were introduced into a round-bottomed flask and stirred at 70 °C for 8–16 h under a nitrogen atmosphere. After completion of the Heck coupling as monitored by TLC, the heating was stopped and the reaction was allowed to reach room temperature. A mixture of $(DHQD)_2PHAL$ (7.8 mg, 0.01 mmol) and NMM (50 mg, 0.5 mmol) in *t*BuOH/H_2O (5:1, 5 mL) was added in one portion to the reaction flask under stirring. H_2O_2 (169 μL, 30% aqueous, 1.5 mmol) was then slowly added over 12 h using a syringe pump. After the addition was complete, the stirring was continued for an additional 1 h and the catalyst was collected by filtration and washed with ethyl acetate (10 mL). The combined filtrates were extracted with 1 N HCl (2 × 5 mL) to recover the chiral ligand from the aqueous layer. The resulting organic phase was further washed with brine solution (5 mL), and the solvent was removed under reduced pressure. The crude material thus obtained was purified by chromatography on silica gel using hexane/ethyl acetate (2:1) as an eluant to afford the corresponding *cis*-diol.

Specific rotations of the diols obtained in method B: entry 3: $[\alpha]_D^{25} = 91.2$ ($c = 1.0$, EtOH) [ref.[10a] 91.0 ($c = 1.11$, EtOH)]; entry 5: $[\alpha]_D^{25} = 93.1$ ($c = 1.0$, EtOH) [ref.[10a] 94.0 ($c = 1.32$, EtOH)]; entry 9: $[\alpha]_D^{25} = 99.2$ (c = 1.0, EtOH) [ref.[10a] 100.0 ($c = 1.11$, EtOH)]; entry 11: $[\alpha]_D^{25} = 119.3$ ($c = 1.0$, EtOH) [ref.[10a] 123.0 ($c = 1.4$, EtOH)]; entry 13: $[\alpha]_D^{25} = 105.8$ ($c = 1.0$, EtOH) [ref.[10a] 107.0 ($c = 1.16$, EtOH)]; entry 15: $[\alpha]_D^{25} = 100.5$ ($c = 1.0$, EtOH) [ref.[10a] 101.0 ($c = 1.15$, EtOH)]; entry 17: $[\alpha]_D^{25} = -10.3$ ($c = 1.0$ $CHCl_3$) [ref.[10b] −10.7 ($c = 1.1$, $CHCl_3$)]; entry 19: $[\alpha]_D^{25} = -5.8$ ($c = 1.0$, $CHCl_3$) [ref.[10c] −6.0 ($c = 0.84$, $CHCl_3$)].

Received: June 8, 2001
Revised: August 14, 2001 [Z17249]

[1] a) C. A. Roessner, A. I. Scott, *Chem. Biol.* **1996**, *3*, 325–330; b) A. Domling, I. Ugi, *Angew. Chem.* **1993**, *105*, 634–635; *Angew. Chem. Int. Ed. Engl.* **1993**, *32*, 563–564; c) P. A. Wender, S. T. Handy, D. L. Wright, *Chem. Ind.* **1997**, 766–769.

[2] For bifunctional catalysts see: a) H.-B. Yu, Q.-S. Hu, L. Pu, *J. Am. Chem. Soc.* **2000**, *122*, 6500–6501; b) S. Yamasaki, M. Kanai, M. Shibasaki, *J. Am. Chem. Soc.* **2001**, *123*, 1256–1257; c) M. Shibasaki, *Chemtracts: Org. Chem.* **1999**, *12*, 979–998; d) G. J. Rowlands, *Tetrahedron* **2001**, *57*, 1865–1882.

[3] a) H. C. Kolb, M. S. VanNieuwenhze, K. B. Sharpless, *Chem. Rev.* **1994**, *94*, 2483–2547; b) I. E. Marko, J. S. Svendsen in *Comprehensive Asymmetric Catalysis II* (Eds.: E. N. Jacobsen, A. Pfaltz, H. Yamamoto), Springer, Berlin, **1999**, pp. 723–787; c) C. Döbler, G. Mehltretter, M. Beller, *Angew. Chem.* **1999**, *111*, 3211–3212; *Angew. Chem. Int. Ed.* **1999**, *38*, 3026–3028; d) J. S. M. Wai, I. E. Marko, J. S. Svendsen, M. G. Finn, E. N. Jacobsen, K. B. Sharpless, *J. Am. Chem. Soc.* **1989**, *111*, 1123–1125.

[4] a) K. Bergstad, S. Y. Jonsson, J.-E. Bäckvall, *J. Am. Chem. Soc.* **1999**, *121*, 10424–10425; b) S. Y. Jonsson, K. Farnegardh, J.-E. Bäckvall, *J. Am. Chem. Soc.* **2001**, *123*, 1365–1371.

[5] a) C. Bolm, A. Gerlach, *Eur. J. Org. Chem.* **1998**, 21–27; b) P. Salvadori, D. Pini, A. Petri, *Synlett* **1999**, 1181–1190; c) D. J. Gravert, K. D. Janda, *Chem. Rev.* **1997**, *97*, 489–509; d) S. Kobayashi, M. Endo, S. Nagayama, *J. Am. Chem. Soc.* **1999**, *121*, 11229–11230.

[6] F. Trifiro, A. Vaccari in *Comprehensive Supramolecular Chemistry*, *Vol. 7*, Pergamon, Oxford, **1996**, p. 251.

[7] a) B. M. Choudary, M. L. Kantam, A. Rahman, C. V. Reddy, K. K. Rao, *Angew. Chem.* **2001**, *113*, 785–788; *Angew. Chem. Int. Ed.* **2001**, *40*, 763–766; b) M. L. Kantam, B. M. Choudary, C. V. Reddy, K. K. Rao, F. Figueras, *Chem. Commun.* **1998**, 763–766; c) B. M. Choudary, M. L. Kantam, B. Kavita, C. V. Reddy, K. K. Rao, F. Figueras, *Tetrahedron Lett.* **1998**, *39*, 3555–3558.

[8] a) B. Sels, D. De Vos, M. Buntinx, F. Pierard, A. Kirsch-De Mesmaeker, P. A. Jacobs, *Nature* **1999**, *400*, 855–857; b) F. V. Laar, D. E. De Vos, D. Vanoppen, B. F. Sels, P. A. Jacobs, A. Del Guerzo, F. Pierard, A. Kirsch-De Mesmaeker, *Chem. Commun.* **1998**, 267–268; c) S. Miyata, *Clays Clay Miner.* **1975**, *23*, 369–375.

[9] a) S. Bräse, A. de Meijere in *Metal-catalysed Cross-Coupling Reactions* (Eds.: F. Diederich, P. J. Stang), Wiley-VCH, Weinheim, **1998**, pp. 99–167; b) I. P. Beletskaya, A. V. Cheprakov, *Chem. Rev.* **2000**, *100*, 3009–3066; c) V. P. W. Bohm, W. A. Herrmann, *Chem. Eur. J.* **2000**, *6*, 1017–1025; d) F. Zhao, B. M. Bhanage, M. Shirai, M. Arai, *Chem. Eur. J.* **2000**, *6*, 843–848; e) A. Biffis, M. Zecca, M. Basato, *Eur. J. Inorg. Chem.* **2001**, 1131–1133; f) M. T. Reetz, E. Westermann, *Angew. Chem.* **2000**, *112*, 170–173; *Angew. Chem. Int. Ed.* **2000**, *39*, 165–168.

[10] a) M. Imuta, H. Ziffer, *J. Org. Chem.* **1978**, *43*, 3319–3323; b) J.-N. Denis, A. Correa, A. E. Greene, *J. Org. Chem.* **1990**, *55*, 1957–1959; c) F. Matsuura, Y. Hamada, T. Shioiri, *Tetrahedron* **1994**, *50*, 9457–9470.

 © WILEY-VCH Verlag GmbH, D-69451 Weinheim, 2001 1433-7851/01/4024-4623 $ 17.50+.50/0

TlF and PbO under High Pressure: Unexpected Persistence of the Stereochemically Active Electron Pair**

Ulrich Häussermann,* Pedro Berastegui,
Stefan Carlson, Julien Haines, and Jean-Michel Léger

It is well known that the post-lanthanide elements thallium and lead display the inert-pair effect, that is, they form compounds in which the oxidation state is two units lower than the corresponding group valency.[1, 2] Frequently, the inert-pair effect is associated with the occurrence of a stereochemically active lone pair which results in an irregular anion environment and low coordination numbers of the cations Tl^+ and Pb^{2+}. As a consequence, open-packed crystal structures are obtained, and it is interesting that the volume required by a lone pair is on the same order as that of an oxygen or fluorine ion.[3] The most prominent examples are the isoelectronic systems PbO and TlF, the layered structures of which are shown in Figure 1.

The room-temperature modification of PbO is red, tetragonal α-PbO (litharge),[4] in which Pb^{2+} ions are situated alternately above and below squares of oxygen ions.[5] The resulting pyramidal layers are easily related to the CsCl structure, which emerges when α-PbO is compressed along the stacking direction until the lead ions of adjacent layers become coplanar, and the Pb^{2+} ions thus form a square net with the same density than that of the O^{2-} ions (Figure 1a). At about 488 °C α-PbO transforms into yellow, orthorhombic β-PbO (massicot).[6] Somewhat unusual for a high-temperature modification, massicot is 3.4% denser than litharge. The structure consists of double layers which correspond to corrugated blocks of the rock salt structure (Figure 1b). The thickness of the blocks is smaller than their separation. Apart from the corrugation, an additional distortion of the massicot double layer with respect to an ideal block of NaCl is the zigzag chain arrangement of the anions. Due to these zigzag chains, the Pb^{2+} ions are, as in litharge, tetracoordinated by anions, although in a folded-square manner.

The ground-state structure of TlF is TlF-II.[7] The structure of TlF-II was only recently unambigously resolved by neutron diffraction, and it was found to be isotypic to β-PbO (Figure 1c).[8] However, there are some delicate differences between the two structures: first, in TlF-II the thickness of the corrugated double layers is slightly larger than their separation, and second the zigzag chain arrangement of the anions within the layers is less pronounced than in massicot. Consequently, the TlF double layers are less distorted with respect to an ideal block of rock salt, and the Tl^+ ions are thus almost fivefold coordinated (4+1) by fluorine anions. At 62 °C TlF-II transforms into tetragonal TlF-I, in which the anion chains within the corrugated blocks are linear and Tl^+ is truly five-coordinate (Figure 1d).[8]

The occurrence of these open-packed structures constructed from ions is fascinating and immediately raises the question of their stability. Compared to the high-symmetry

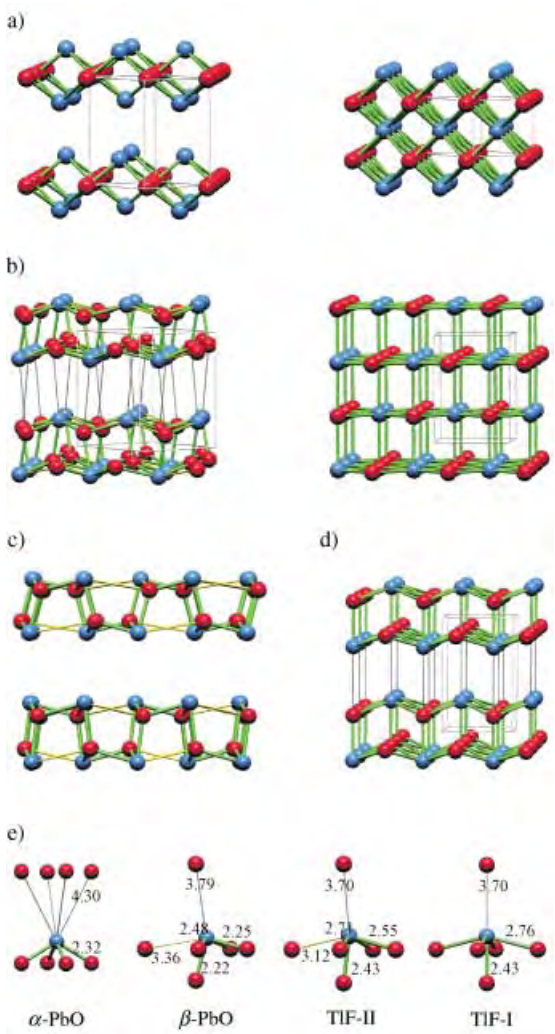


Figure 1. Structures of PbO and TlF. Cations: blue, anions: red. Nearest-neighbor cation – anion contacts are displayed as green (shortest distances), yellow (medium distances), and gray (longest distances) lines. a) The tetragonal α-PbO structure (*P*4/*nmm*) along [110] (left) and its relation to the CsCl structure (right). b) The orthorhombic β-PbO structure (*Pbcm*) approximately along [011] (left) and its relation to the NaCl structure (right). c) Comparison of the double layers (projected along [001]) in the β-PbO (top) and TlF-II structure (bottom). d) The tetragonal TlF-I structure (*P*4/*nmm*) along [100]. e) Cation coordination occurring in these open-packed lone-pair structures. The distances are in Å.

[*] Dr. U. Häussermann, Dr. P. Berastegui
Department of Inorganic Chemistry
Stockholm University
10691 Stockholm (Sweden)
Fax: (+46) 8-152187
E-mail: ulrich@inorg.su.se

Dr. S. Carlson
MAX-laboratory, Lund University
P.O. Box 118, 22643 Lund (Sweden)

Dr. J. Haines
Laboratoire de Physico-Chimie de la Matière Condensée
UMR CNRS 5617
Université Montpellier II, 34095 Montpellier (France)

Dr. J.-M. Léger
Laboratoire des Propriétés Mécaniques et Thermodynamiques des Matériaux
CNRS UPR 9001
Université Paris Nord, Villetaneuse (France)

[**] This work was supported by the Swedish National Science Research Council (NFR) and the Göran Gustafsson Foundation.

 © WILEY-VCH Verlag GmbH, D-69451 Weinheim, 2001 1433-7851/01/4024-4624 $ 17.50+.50/0

structures of NaCl and CsCl, lone-pair structures are clearly unfavorable from an electrostatic point of view. This is firstly manifested in the temperature polymorphism of PbO and TlF, which indicates the presence of competing, energetically close lying, solutions to the ground-state structure, and secondly by the fact that the lone-pair structure is absent in PbS and TlCl, which adopt undistorted NaCl and CsCl structures, respectively. Therefore, under external pressure the open-packed PbO and TlF lone-pair structures might be expected to transform readily into the six-coordinate NaCl or the eight-coordinate CsCl structure. However, recent experiments at relatively low pressures (3.5 and 10.1 GPa for TlF and PbO, respectively)[8, 9] did not reveal such a structural transition. Here we present a structural investigation of TlF and PbO under much higher pressures, with rather surprising results. Additionally, the high-pressure behavior of the two systems was modeled by ab initio calculations. From the theoretical results we were able to extract a simple bonding picture for lone-pair structures involving inert-pair elements. This bonding picture accounts for the occurrence of open-packed ionically bonded structures and their stability relative to "regular" saltlike AB compounds. This issue is of fundamental significance to general chemistry.

The high-pressure structural behavior of TlF and PbO was studied at room temperature in diamond anvil cells (see Methods). The results are displayed in Figure 2. For TlF no structural change is observed, and the TlF-II ground-state structure remains stable up to the highest pressure applied (40 GPa). At this pressure the volume of TlF has dropped to less than 65 % of the ground-state volume V_0 (Figure 2a). The high compressibility of TlF-II, which is reflected in the low bulk modulus (16.0(6) GPa), is typical of layered structures. However, the compressibility along the *a* axis, that is, the stacking direction of the double layers, is lower than those along the *b* and *c* axes, which decrease by approximately the same amount with increasing pressure. The effect of pressure on the structure of TlF-II is minor: relative to the ground-state structure, at a compression of $V/V_0 = 0.65$ the double-layer building blocks are moved closer together, and the longest of the five nearest Tl^+–F^- distances has basically become equal to the four shorter ones to give five-coordinate Tl^+ ions.[10]

The high-pressure behavior of PbO is more complicated (Figure 2b). At 0.9 GPa ground-state litharge transformed into γ-PbO, an orthorhombically distorted variant of tetragonal α-PbO. Massicot was obtained gradually above 3 GPa, and this structure was maintained up to the highest pressure applied (46 GPa). The pressure-induced transition γ-PbO $\rightarrow \beta$-PbO is irreversible, and massicot is retained on decompressing to ambient conditions. The compressibility of massicot (bulk modulus 31(1) GPa) is lower than that of TlF-II. The variation of the lattice parameters under compression (larger decrease in *b* than in *a* and *c*) is interesting, because it indicates that β-PbO develops gradually into the TlF-II structure, whereby the coordination number of Pb^{2+} increases from four to five.[10] Figure 3 summarizes the structural behavior of the investigated systems at high pressure and room temperature.

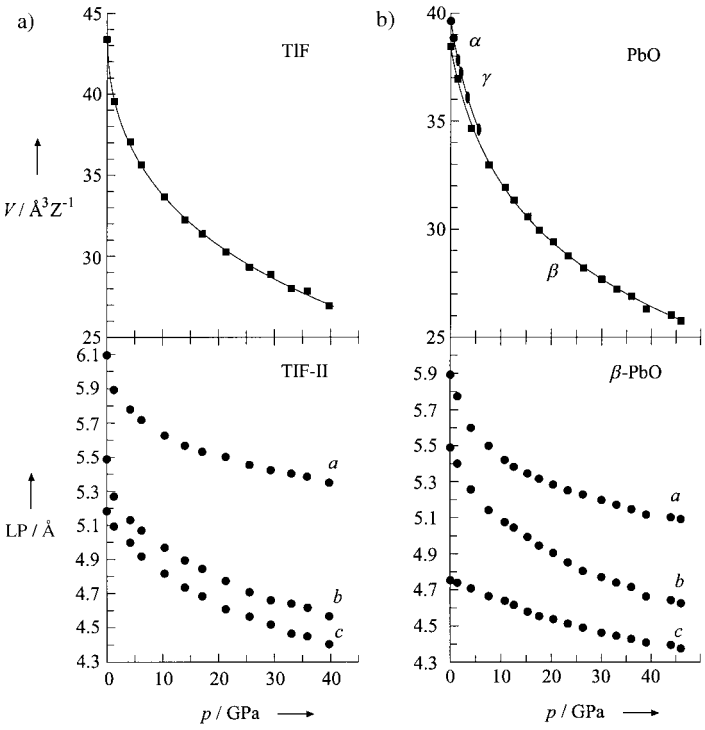


Figure 2. a) Compressibility (top) and evolution of the lattice parameters with pressure (bottom) for TlF-II (space group *Pbcm*). b) Compressibility of PbO (circles: α-PbO, ellipsoids: γ-PbO, squares: β-PbO; top) and evolution of the lattice parameters (LP) with pressure for β-PbO (space group *Pbcm*; bottom).

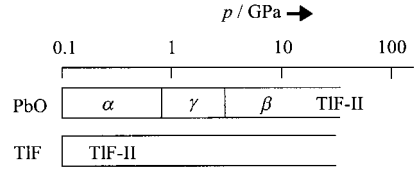


Figure 3. High-pressure structural behavior of PbO and TlF at room temperature.

In conclusion, we observe a remarkable persistence of the low-symmetry lone-pair structures β-PbO and TlF-II at high pressure. It appears surprising that these structures do not transform into the high-symmetry NaCl structure (note the close relationship of β-PbO and TlF-II to this structure) or the more densely packed CsCl structure, because the high-symmetry structures have considerably larger Madelung constants *M* and are thus clearly favored from an electrostatic viewpoint. With increasing pressure this situation becomes rapidly more pronounced, since the difference in electrostatic energy varies approximately as $\Delta M/(V/V_0)^{1/3}$. To solve this puzzle the high-pressure behavior of the systems TlF and PbO was modeled by density functional calculations by employing pseudopotentials and a plane-wave basis set.

We calculated the total energy of TlF and PbO in the structure types α-PbO, β-PbO/TlF-II, TlF-I, CsCl, and NaCl as a function of volume, including a complete relaxation of the open-packed lone-pair structures (see Methods). The results are depicted in Figure 4. We first focus on the structural competition in the low-pressure region ($0.8 < V/V_0 < 1$). For

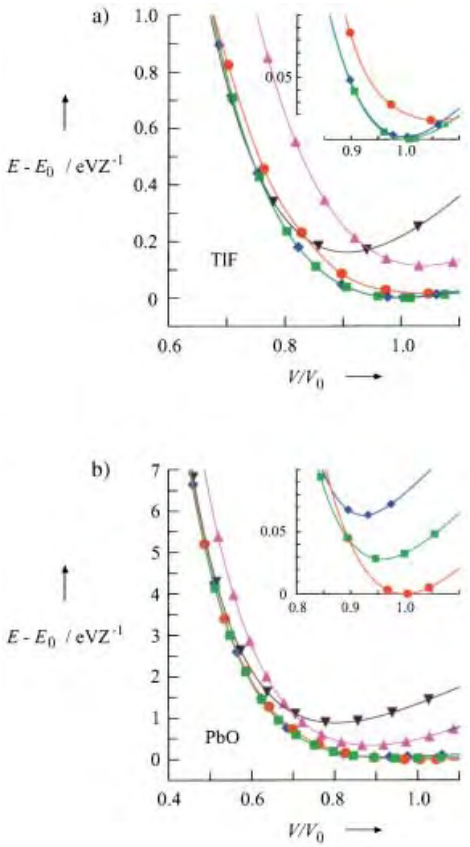


Figure 4. Calculated energy versus volume for TlF (a) and PbO (b) in the structures α-PbO (red circles), β-PbO/TlF-II (green squares), TlF-I (blue diamonds), CsCl (black triangles), and NaCl (pink triangles). E_0 is the energy of the ground state. The insets present a close up of the low-compression region.

both systems the ground-state structures are obtained correctly, although the calculated energy difference between TlF-II and TlF-I is extremely small (about 3 meV Z^{-1}) and virtually disappears under slight compression. For PbO below $V/V_0 = 0.9$ the litharge structure becomes less stable than the massicot structure (the γ modification was not considered in the calculations), and the calculated transition pressure for a direct transformation α-PbO $\rightarrow\beta$-PbO is 3.3 GPa (referring to 0 K).

In the high-compression region of this system, the β-PbO structure remains the most stable down to at least $V/V_0 \approx 0.45$ (corresponding to an external pressure of more than 150 GPa).[11] For the TlF system, however, below $V/V_0 \approx 0.75$ our calculations show the CsCl structure to be more stable than the TlF-II structure, and the transition pressure is about 20 GPa. This is in contradiction with the experimental findings, and the reason for this discrepancy is not yet resolved.[12]

In spite of this, the theoretical calculations confirm the remarkable high-pressure stability of the low-symmetry lone-pair structures and offer the possiblity of explaining their high-pressure persistence by analyzing the electronic structure. For that purpose, the density of states (DOS) of TlF in the TlF-II and CsCl structures and of PbO in the β-PbO and CsCl structures at $V/V_0 = 1$ and $V/V_0 = 0.65$ (corresponding approximately to the effect of the maximum experimental pressure) are depicted in Figure 5.

For the ground-state volume, the DOS curves for both TlF structures display a peculiar three-peak structure of the bands below the Fermi level (labeled A, B, and C in Figure 5a, left). For the PbO structures the DOS has a similar overall shape, although peaks B and C appear to have merged (Figure 5b, left), and the dispersion of the bands is generally larger than for TlF. The band gaps obtained for open-packed TlF-II and β-PbO (2.5 and 2.0 eV, respectively)[13] are considerably larger than those of TlF and PbO in the hypothetical CsCl structure (1.5 and 0.5 eV, respectively).

Under pressure (Figure 5, right) the dispersion of the bands increases, but the threefold partitioning of the DOS is still

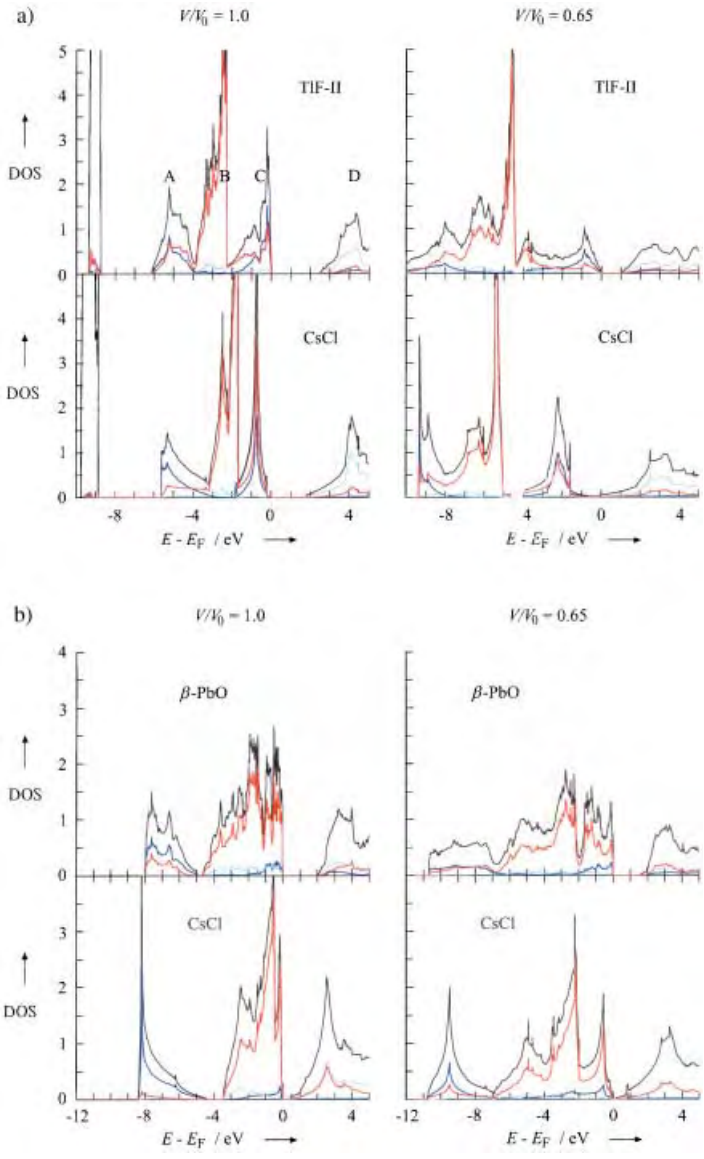


Figure 5. DOS [states/eV Z^{-1}] at the ground-state volume $V/V_0 = 1$ (left) and at a compression of $V/V_0 = 0.65$ (right) for a) TlF in the TlF-II (top) and the CsCl structure (bottom) and b) PbO in the β-PbO (top) and the CsCl structure (bottom). The letters A, B, C, and D in (a) label the different parts of the DOS as discussed in the text. Black lines: total DOS, dark blue lines: cation 6s projected DOS (pDOS), light blue lines: 6p pDOS, red lines: anion 2p pDOS.

 © WILEY-VCH Verlag GmbH, D-69451 Weinheim, 2001 1433-7851/01/4024-4626 $ 17.50+.50/0

recognizable at $V/V_0 = 0.65$. Furthermore, at this compression the band gaps of TlF-II and β-PbO are diminished or have even become closed for TlF and PbO in the CsCl structure (i.e., TlF and PbO would have become metallic if the CsCl structure were attained).

We then tried to understand the characteristic shape of the DOS of these compounds and develop a simple bonding picture for open-packed structures involving inert-pair elements. The buildup of the DOS of TlF and PbO in a high-symmetry structure (NaCl or CsCl) at the ground-state volume is outlined in Figure 6. The inert-pair cations have

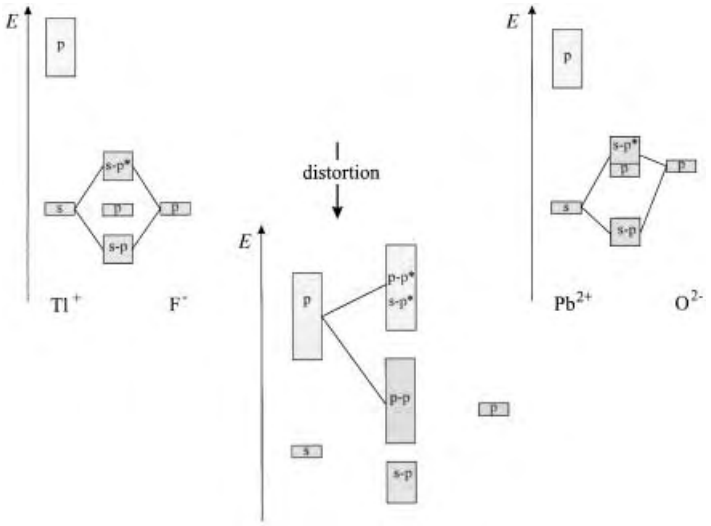


Figure 6. Schematic construction of the DOS of TlF (left) and PbO (right) in a hypothetical high-symmetry structure. Occupied bands are shaded gray. Upon distortion 6p-6s/2p mixing becomes effective, which firstly introduces some p-p bonding between cations and anions and secondly moves partly antibonding s-p states above the Fermi level. Note that in the scheme the consequences of 6p-6s/2p mixing are exaggerated.

the electron configuration $6s^2$, and the separation between the occupied 6s and empty 6p valence states is large.[14] The anions have the valence electron configuration $2p^6$. If we assume that for TlF the energies of the F^- 2p and the Tl^+ 6s states are about the same, the characteristic threefold partitioning of the bands below the Fermi level is a consequence of a strong bonding–antibonding splitting (peak A: 6s-2p bonding, peak B: 2p nonbonding, peak C: 6s-2p antibonding). Additionally the interaction between diffuse 6p orbitals gives rise to an empty band above the Fermi level.

These simple considerations reproduce the calculated DOS curve for TlF in the CsCl structure, as shown in Figure 5, very well, especially with regard to the distribution of the 6s and 2p projected DOS. Analogously, for PbO we obtain a model DOS that fits the calculated DOS under the assumption that the O^{2-} 2p states are somewhat higher in energy than the Pb^{2+} 6s states. Importantly, the closed-shell orbital interactions in TlF and PbO that yield the three-peak pattern of the DOS do not provide any bonding effect, but are instead repulsive. In other words, the ambivalent bonding situation in TlF and PbO involves attractive electrostatic interactions and effective repulsive orbital interactions, and distortion to a low-symmetry structure consequently takes place. The distortion partly removes the repulsive orbital interactions. Empty cation 6p states become available for bonding to a much greater extent than in a high-symmetry structure, because lowering of the symmetry enables 6s- and 2p-based bands to mix (hybridize) over a much larger portion of the Brillouin zone. Additionally, the energetical mismatch between the empty 6p band and the 6s/2p-based bands is diminished because the dispersion of all bands becomes larger when some ions move closer to each other in the distorted structure. The admixture of cation 6p states takes place in peaks B (nonbonding 2p bands become partly bonding) and C (partial release of 6s-2p antibonding states above the Fermi level into peak D) of the DOS.

A consequence of the latter interaction is the stabilization of states below the Fermi level, which leads to an increase in the band gap relative to the high-symmetry structure. The ratio between the number of occupied 6p and 6s states (N_p/N_s, ratio between the integrated 6p and 6s projected DOS up to the Fermi level) provides a "measure of relief" from the $6s^2$-$2p^6$ closed-shell repulsion. Figure 7 shows the N_p/N_s ratios for

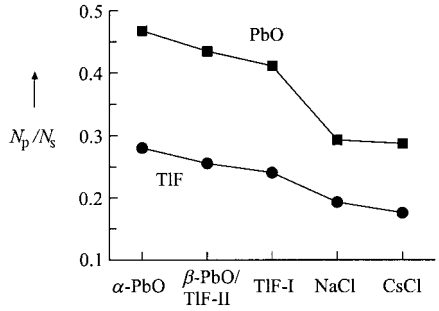


Figure 7. N_p/N_s ratios for TlF and PbO in different structures at the ground-state volume.

TlF and PbO in the considered structures at the ground-state volume. As expected, the more open packed the structure the higher the attained N_p/N_s ratio. Since the relief from the closed-shell repulsion (distortion) is at the cost of less favorable electrostatic interactions, the degree of distortion is a consequence of the balance between the contribution of electrostatic and orbital interactions to the total bonding. The ratio of the two contributions is not changed much under high pressure, because the increasingly unfavorable electrostatic interaction in the open-packed structure is countered by the stabilizing 6p-6s/2p mixing due to the larger band dispersions, which also increase. For PbO the 6p-6s/2s mixing is generally more effective than for TlF because the cation 6p states are closer in energy to the anion 2p state and, in addition, the higher ionic charges imply stronger interactions and hence larger band widths (cf. Figure 5). The apparent contradiction that the formation of a stereochemically active inert lone pair actually requires that the corresponding cation s state is active for bonding was already noted earlier for the PbO system.[15]

In conclusion, the occurrence of a stereochemically active lone pair in crystal structures with inert-pair ions is a consequence of the improvement of an unfavorable bonding situation caused by effective closed-shell repulsion ns^2-np^6. Compounds that crystallize in low-symmetry lone-pair struc-

 © WILEY-VCH Verlag GmbH, D-69451 Weinheim, 2001 1433-7851/01/4024-4627 $ 17.50+.50/0

tures are not particularly stable. This is reflected in the low melting points of TlF and PbO (322 and 897 °C, respectively)[16] compared to RbF and SrO (795 and 2665 °C, respectively).[16] The cation sizes within the pairs Tl^+/Rb^+ and Pb^{2+}/Sr^{2+} are very similar, but RbF and SrO crystallize in a high-symmetry structure (NaCl), and bonding is predominantly based on electrostatic interactions. Additionally, TlF and PbO have lower melting points than TlCl and PbS (431 and 1470 °C, respectively),[16] which adopt high-symmetry structures. This is opposite to the well-known trend observed for "regular" saltlike AB compounds (i.e., alkali metal halides and alkaline earth metal chalcogenides), for which the fluorides and oxides have higher melting points than the chlorides and sulfides. The occurrence of a stereochemically active lone pair in crystal structures with inert-pair ions is decisively dependent on the relative energies of the ionic valence levels. Open-packed lone-pair structures are preferably found for fluorides and oxides because the low-lying anionic 2p states make the closed-shell $n s^2$-$n p^6$ repulsion most effective. For TlCl and PbS, in which the 3p states of the anions are comparably higher in energy, the high-symmetry CsCl and NaCl structures, respectively, are obtained.

Methods

PbO was prepared by dehydration of lead hydroxide in hot 15 N KOH.[9, 17] The powdered α-PbO was mixed with silicone grease as a pressure-transmitting medium and placed in a stainless steel gasket, preindented to a thickness of 120 μm with a 150 μm diameter hole, along with a small amount of ruby powder between the anvils of a diamond anvil cell (DAC). Pressure measurements were based on the shifts of the ruby R_1 and R_2 fluorescence lines.[18] Angle-dispersive X-ray diffraction patterns were obtained at room temperature on an imaging plate placed at between 113.65 and 117.18 mm from the sample by using Zr-filtered Mo radiation from a microfocus tube. A capillary optic was used to obtain a 100 μm diameter beam. Exposure times were typically between 24 and 60 h. The observed intensities on the imaging plates were integrated as a function of 2θ to give conventional one-dimensional diffraction profiles. The individual diffraction peaks were fitted to pseudo-Voigt functions, and the peak positions obtained were used for unit cell refinements with the program U-fit.[19]

A dried powdered sample of TlF of purity >99 % (Alfa Chemicals Ltd.) was loaded with Ar as a pressure-transmitting medium and small ruby crystals (1–2 μm diameter spheres) in a membrane-driven DAC.[20] A preindented stainless-steel gasket with a hole of 125 μm diameter and 30 μm thickness was used. The diffraction experiments were carried out at room temperature at the high-pressure dedicated beamline ID30, European Synchrotron Radiation Facility (ESFR), Grenoble, France. X rays were monochromatized to $\lambda = 0.3738(1)$ Å and the beam was focused to 0.02×0.03 mm^2 spot size at the sample position. The powder diffraction rings were collected with an on-line imaging plate detector.[21] A diffraction pattern of Si was used to determine the sample-to-detector distance (310.042 mm). Corrections for spatial distortion, calculation of imaging plate pixel size (0.07×0.08 mm^2), and subsequent integration over the complete powder rings were performed with the software FIT2D.[22] Unit cell parameters were obtained by indexing and least-square refinement with the program DICVOL91.[23]

Total energy calculations were performed within ab inito density functional theory as implemented in the program VASP.[24] Ultrasoft Vanderbilt-type pseudopotentials[25] were employed, and 5d, 6s, and 6p electrons were considered as valence electrons for Tl and Pb, and 2s and 2p electrons for F and O. The atomic position parameters and lattice parameters of the structure types α-PbO, β-PbO/TlF-II, and TlF-I were relaxed for a set of constant volumes until forces had converged to less than 0.01 eV Å^{-1}. In a second step, we extracted the equilibrium volume V_0 and the ground-state energy E_0 by fitting the E versus V values with a Birch–Murnaghan equation of state. The exchange and correlation energy was assessed by the local-density approximation (LDA).[26] Convergency of the calculations was carefully checked with respect to the plane-wave cutoff and the number of k points used in the summation over the Brillouin zone. A (high) energy value of 500 eV was chosen for the plane-wave cutoff for both systems. The k points were generated by the Monkhorst–Pack method[27] and sampled on grids of $4 \times 4 \times 4$ ($Z = 4$ structures: β-PbO, TlF-II), $6 \times 6 \times 6$ ($Z = 2$ structures: α-PbO, TlF-I), and $8 \times 8 \times 8$ ($Z = 1$ structures: CsCl, NaCl). The integration over the Brillouin zone was performed by the improved tetrahedron method.[28]

Received: June 25, 2001 [Z17348]

[1] N. V. Sidgwick, H. M. Powell, *Proc. R. Soc. London Ser. A* **1940**, *176*, 153.

[2] N. N. Greenwood, A. Earnshaw, *Chemistry of the Elements*, Pergamon, Oxford, **1997**.

[3] J. Galy, G. Meunier, S. Andersson, A. Åström, *J. Solid State Chem.* **1975**, *13*, 142.

[4] Below −85 °C α-PbO transforms into incommensurate α'-PbO (J. Moreau, J. M. Kiat, P. Garnier, G. Calvarin, *Phys. Rev. B* **1989**, *39*, 10296).

[5] J. Leciejewicz, *Acta Crystallogr.* **1961**, *14*, 1304.

[6] a) W. B. White, F. Dachille, R. Roy, *J. Am. Ceram. Soc.* **1961**, *44*, 170; b) R. J. Hill, *Acta Crystallogr. Sect. C* **1985**, *41*, 1281.

[7] C. W. F. T. Pistorius, J. B. Clark, *Phys. Rev.* **1968**, *173*, 692.

[8] P. Berastegui, S. Hull, *J. Solid State Chem.* **2000**, *150*, 266.

[9] D. M. Adams, A. G. Christy, J. Haines, S. M. Clark, *Phys. Rev. B* **1992**, *46*, 11358.

[10] The structures of TlF and PbO at the highest applied pressure could not be refined properly due to the extremely low relative X-ray scattering factor of the anions. Instead, the computationally relaxed structures TlF-II and β-PbO at $V/V_0 = 0.65$ can be used to obtain some information on the structural changes with respect to the ground-state volume. The normalized Tl–F nearest-neighbor distance distribution in TlF-II is: $V/V_0 = 1$: 1.0, 1.023, 1.078 (×2), 1.262, 1.444 (exp: 1.0, 1.044, 1.116 (×2), 1.282, 1.521); $V/V_0 = 0.65$: 1.0, 1.026, 1.065 (×2), 1.130, 1.354. The normalized Pb–O nearest-neighbor distance distribution in β-PbO is: $V/V_0 = 1$: 1.0, 1.012, 1.099 (×2), 1.528, 1.730 (exp: 1.0, 1.013, 1.117 (×2), 1.512, 1.706); $V/V_0 = 0.65$: 1.0, 1.042, 1.079 (×2), 1.138, 1.382.

[11] Above this compression the applied pseudopotentials become unreliable (see Methods).

[12] In contrast to the system PbO, for which calculated and experimental results are in excellent agreement, we observe several deviations for TlF. Apart from the calculated high-pressure transition to the CsCl structure, which is not observed experimentally, these are: 1) the calculated energy difference between the low- (TlF-II) and high-temperature modification (TlF-I) at the ground-state volume is too low; 2) the difference between the calculated and the experimental ground-state volume is considerably higher for TlF (the calculated value is about 8 % too low) than for PbO (the calculated value is about 3 % too low); 3) the relaxed structural parameters for TlF-II at the ground-state volume agree considerably less with experiment than those obtained for β-PbO (cf ref. [10]). The treatment of the exchange–correlation potential with the more advanced generalized gradient approximation (GGA) does not lead to any improvement in the results for TlF. Also, the shortcomings cannot be attributed to the applied method of calculation based on pseudopotentials and a plane-wave basis set, since full-potential techniques give virtually the same structural energy differences for TlF. Finally, one might consider neglected spin–orbit coupling as being responsible for the poorer description of TlF. However, if spin–orbit coupling affected structural stability, this should have been recognized in the PbO system as well. Hence, the discrepancies between theoretical and experimental results for TlF point to an insufficient description of this system by density functional theory, and better agreement may be obtained by a Hartree–Fock-based code. This is currently under investigation.

[13] The band gaps of TlF-II (white) and β-PbO (yellow) are underestimated by about 30 %. The underestimation of band gaps is typical of density functional calculations.

 © WILEY-VCH Verlag GmbH, D-69451 Weinheim, 2001 1433-7851/01/4024-4628 $ 17.50+.50/0

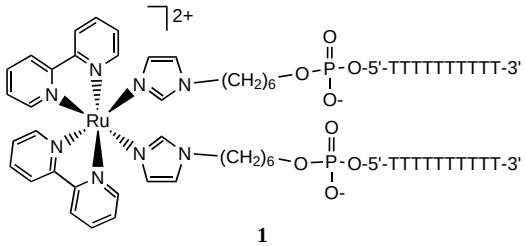
[14] The already large 6s-6p separation in the atoms Tl and Pb is enhanced in the corresponding cations.
[15] a) H. J. Terpstra, R. A. de Groot, C. Haas, *Phys. Rev. B* **1995**, *52*, 11690; b) G. W. Watson, S. C. Parker, G. Kresse, *Phys. Rev. B* **1999**, *59*, 8481.
[16] A. F. Holleman, N. Wiberg, *Lehrbuch der Anorganischen Chemie*, de Gruyter, Berlin, **1995**.
[17] J. R. Schoonover, T. L. Groy, S. H. Lin, *J. Solid State Chem.* **1989**, *83*, 207.
[18] H. K. Mao, J. Xu, P. M. Bell, *J. Geophys. Res.* **1986**, *91B*, 4673.
[19] M. Evain, *U-Fit: a Cell Parameter Refinement Program*, Institut de Matériaux de Nantes, Nantes, France, **1992**.
[20] R. Letoullec, J. P. Pinceaux, P. Loubeyre, *High Pressure Res.* **1988**, *1*, 77.
[21] M. Thoms, S. Bachau, D. Häusermann, M. Kunz, T. Le Bihan, M. Mezouar, D. Strawbridge, *Nucl. Instrum. Methods Phys. Res. Sect. A* **1998**, *413*, 175.
[22] A. Hammersley, *FIT2D V10.3 Reference Manual V4.0* ESFR, Grenoble, France, **1998**.
[23] A. Boultif, D. Louër, *J. Appl. Crystallogr.* **1991**, *24*, 987.
[24] a) G. Kresse, J. Hafner, *Phys. Rev. B* **1993**, *47*, RC558; b) G. Kresse, J. Furthmüller, *Phys. Rev. B* **1996**, *54*, 11169.
[25] a) D. Vanderbilt, *Phys. Rev. B* **1990**, *41*, 7892; b) G. Kresse, J. Hafner, *J. Phys. Condens. Matter* **1994**, *6*, 8245.
[26] J. Perdew, A. Zunger, *Phys. Rev. B* **1981**, *23*, 5048.
[27] H. J. Monkhurst, J. D. Pack, *Phys. Rev. B* **1976**, *13*, 5188.
[28] P. Blöchl, O. Jepsen, O. K. Andersen, *Phys. Rev. B* **1994**, *49*, 16223.

Solid-Phase Synthesis of Transition Metal Linked, Branched Oligonucleotides**

Ignacio Vargas-Baca, Debbie Mitra, Holly J. Zulyniak, Jay Banerjee, and Hanadi F. Sleiman*

Branched oligonucleotides have recently emerged as attractive synthetic targets for the selective recognition of nucleic acids.[1] These molecules have the potential to act as sensitive diagnostic tools for the detection of DNA sequences,[1a,b] and can specifically bind single-stranded DNA/RNA (antisense/antigene strategy).[1c–e] In addition, they can serve as model complexes for the elucidation of the structure and biological role of branched RNA molecules found in nature.[1a,d] In previous branched systems, the DNA strands were linked together through oligonucleotide or small organic-molecule-based vertices.[1, 2] We recently initiated research into the synthesis and properties of a new class of branched oligonucleotides, in which a transition metal acts as the vertex joining two parallel DNA strands. Transition metal centers come in a range of geometries, coordination numbers, and bond angles that are unavailable in carbon chemistry (e.g., octahedral, square planar, trigonal bipyramidal). By combining this varied coordination chemistry with the highly specific interactions of DNA, we expect that these branched metal–DNA complexes will expand the repertoire of DNA structures to novel motifs.[3] This can be achieved both through their binding to single-stranded DNA and RNA, as well as their self-association and formation of DNA "nanostructures".[2] In addition, the rich redox and luminescence properties of metal centers afford a sensitive marker for detecting and monitoring the association of these new structures.

While many transition metal labeled oligonucleotides were reported recently,[4] the metal center is usually tethered as a pendant functional group on a DNA strand, and hence its geometry cannot influence DNA association.[5] Here we report the first synthesis of a transition metal linked branched oligonucleotide (**1**), in which the DNA strands run parallel to each other and the geometry of the metal center can directly influence the orientation of these strands. Furthermore, we have studied the biological behavior of these branched complexes by hybridization to complementary DNA. Thermal denaturation experiments show the formation of novel transition metal linked DNA duplexes with a stability comparable to that of Watson–Crick A/T duplexes.

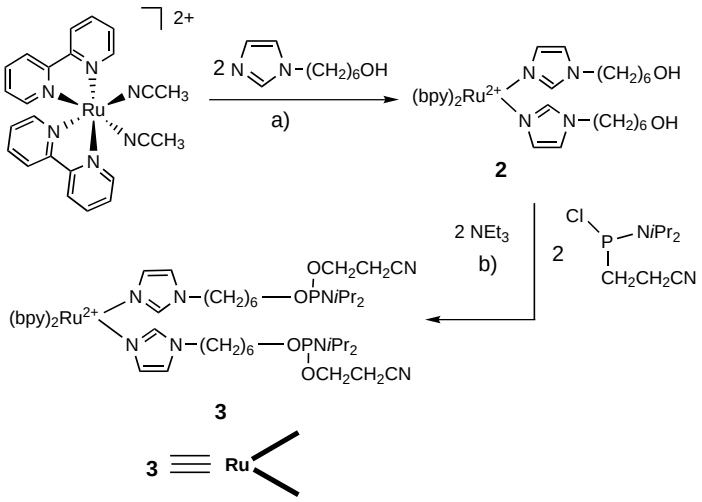


1

In the design of complex **1**, two parallel (5′-3′) oligonucleotide strands are linked to a *cis*-$[(bpy)_2Ru(imidazole)_2]^{2+}$ moiety through *n*-hexyl spacers (bpy = 2,2′-bipyridine). The ruthenium moiety is both redox active and intensely luminescent, and it has been extensively used as a probe of electron transfer processes in proteins.[6] Our convergent solid-phase strategy[7] for the preparation of ruthenium-linked parallel oligonucleotides is outlined in Schemes 1 and 2. This strategy starts with the generation of a ruthenium bis-phosphoramidite branching complex **3**.[8] The reaction of two molar equivalents of 1-(6-hydroxyhexyl)imidazole[9a] with *cis*-$[(bpy)_2Ru(CH_3CN)_2](PF_6)_2$[9b] in refluxing ethanol/water, followed by precipitation with aqueous NH_4PF_6 results in the formation of the *cis*-bis-imidazole ruthenium complex **2** as a deep red solid.[17] The UV/Vis absorption spectrum of **2** shows metal-to-ligand (Ru → bpy) charge transfer (MLCT) bands at 341 and 491 nm.[6a] An interesting feature of this complex is its intense fluorescence, which could prove useful for possible applications as a DNA biosensor. Excitation of the MLCT

[*] Prof. H. F. Sleiman, Dr. I. Vargas-Baca,[+] D. Mitra, H. J. Zulyniak, J. Banerjee
Department of Chemistry, McGill University
801 Sherbrooke St. W., Montreal, Quebec H3A 2K6 (Canada)
Fax: (+1) 514-398-3797
E-mail: hanadi.sleiman@mcgill.ca
[+] Current address:
Department of Chemistry, McMaster University
Hamilton, Ontario L8S 4M1 (Canada)

[**] This work was supported by NSERC (Canada), CFI (Canada) and FCAR (Quebec). The authors gratefully acknowledge Prof. M. J. Damha and his laboratory, McGill University, for helpful discussion.
Supporting information for this article is available on the WWW under http://www.angewandte.com or from the author.



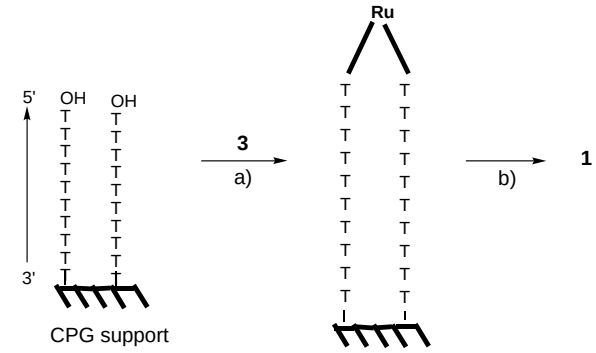
Scheme 1. Synthesis of branching complex **3**. a) Ethanol/water, reflux, 12 h, 86 %; b) CD_2Cl_2, 2 h, quantitative. All complexes are PF_6^- salts.

band at 490 nm in ethanol results in an emission centered at 650 nm.

Complex **2** was functionalized to allow for coupling to DNA by reaction with two molar equivalents of chloro(cyanoethyl)-*N*,*N*-diisopropylphosphoramidite in the presence of triethylamine under an inert atmosphere. The reaction can be monitored by ^{31}P NMR spectroscopy in CD_2Cl_2 and is complete in two hours. The ^{31}P NMR spectrum displays a broad peak at $\delta = 148$ for the phosphoramidite moiety.[10] The bis-phosphoramidite complex **3** is stable in solution at room temperature under an inert atmosphere and was used in the following steps without further purification. One of the attractive features of our conjugation strategy is the compatibility of **3** with the standard protocols for oligonucleotide synthesis. Control experiments on complex **2** showed the stability of the *cis*-$[(bpy)_2Ru(imidazole)_2]^{2+}$ moiety to the conditions of solid-phase DNA synthesis and ammonia cleavage.

In parallel to the synthesis of **3**, the oligonucleotide dT_{10} was assembled on a 500 Å controlled pore glass (CPG) support by using standard solid-phase protocols. To optimize the yield of **1**, our convergent solid-phase strategy requires close proximity of the 5′-OH termini of growing oligonucleotides on the solid support (Scheme 2).[7] Hence, high-density CPG support (56 μmol g^{-1}) was used. Bis-phosphoramidite **3** in CD_2Cl_2 was then added to the solid support under an inert atmosphere, with tetrazole as activator to achieve branching. Subsequent oxidation of the phosphite moiety, cleavage of the oligonucleotide from the solid support in ethanolic ammonia, and evaporation afforded a fluorescent red solid.

The crude mixture was analyzed by denaturing polyacrylamide gel electrophoresis (PAGE) to identify the ruthenium – DNA products (Figure 1 a). The fastest moving band has an electrophoretic mobility identical to that of the control sample of the linear oligonucleotide dT_{10}, and was thus assigned as unmodified DNA. Two slow-moving red fluorescent bands were also visible in the gel. The slowest moving band was attributed to the desired branched ruthenium complex **1** and the next slowest moving band to the mono-



Scheme 2. DNA branching step. a) Tetrazole, RT, 12 h; b) I_2, pyridine, H_2O, then NH_4OH/EtOH, 2 h, RT.

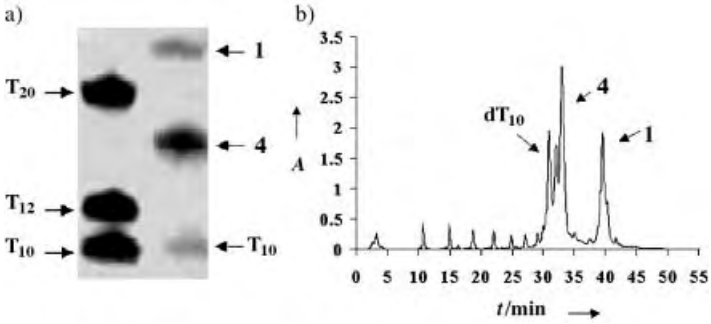


Figure 1. a) Analytical PAGE under denaturing conditions (UV shadowing) of the oligonucleotide mixture obtained according to Scheme 2. b) HPLC (monitoring at 260 nm) of the oligonucleotide mixture. Only the peaks of compounds **1** and **4** show absorbance at 260 and 490 nm. A = absorbance.

stranded ruthenium complex *cis*-$[(bpy)_2Ru^{2+}\{(imidazole)$-$(CH_2)_6O$-5′-$d(T_{10})$-3′$\}\{(imidazole)(CH_2)_6OH\}]$ (**4**; vide infra). The mobility of **1** was significantly lower than that of a 5′-$d(T_{20})$-3′ linear marker, and that of the monostranded complex **4** was lower than that of 5′-$d(T_{10})$-3′, likely due to the presence of the positively charged metal center and the higher molecular weight of these complexes. The intense red color and fluorescence of the ruthenium moiety make it a convenient marker for the identification of the desired ruthenium – DNA complexes.

The products were isolated by ion-exchange HPLC on the crude reaction mixture (Figure 1 b). Monitoring at 260 (DNA π-π* band) and 490 nm (*cis*-$[(bpy)_2Ru(imidazole)_2]^{2+}$ MLCT band) allowed the identification of the fractions containing ruthenium – DNA complexes. Two distinct peaks for such complexes were observed. A MALDI-TOF mass spectrometric analysis of the two isolated samples identified the desired branched ruthenium complex **1** as the fraction with the highest retention time, and the monostranded ruthenium complex **4** as the next-eluting fraction.[11] These results clearly demonstrate the successful synthesis of branched ruthenium – DNA complex **1**, as well as monolabeled complex **4**, by a facile solid-phase approach.

With branched complex **1** in hand, we conducted thermal denaturation experiments[12] to determine its hybridization efficiency with complementary DNA (Figure 2).[13] The melting temperatures were determined for 1:1 and 1:2 mixtures of

 © WILEY-VCH Verlag GmbH, D-69451 Weinheim, 2001 1433-7851/01/4024-4630 $ 17.50+.50/0

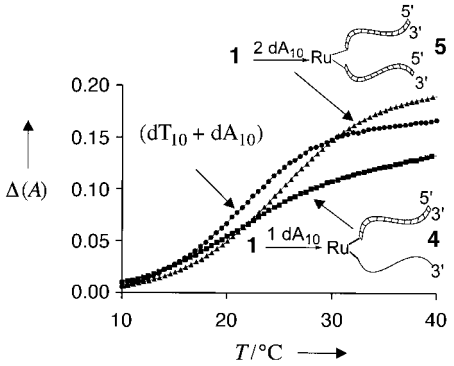


Figure 2. UV absorbance–melting curves at 260 nm. [**1**+dA_{10}] (■); [**1**+2dA_{10}] (▲); (dA_{10}+dT_{10}) (●). Normalized change in absorbance, $\Delta(A)$, was calculated by using $(A_t - A_0)/A_f$, where A_t is the absorbance at a given temperature, A_f is the final absorbance at 90 °C, and A_0 is the initial absorbance at 5 °C. The melting temperatures were calculated to be the maxima of the first derivative plot of the melting curves at 260 nm. % H was calculated using the formula $100[(A_f - A_0)/A_f]$.[1d] The buffer system used was 140 mM KCl, 5 mM Na_2HPO_4, and 1 mM $MgCl_2$, pH 7.2.

1 and dA_{10}. The results for the 1:1 ratio indicated the formation of a duplex involving one of the strands of the branched complex. The thermal denaturation curve at 260 nm showed a monophasic transition at 22.1 °C with a hyperchromicity of 13%. These results are promising as they coincide with the melting temperature of 21.0 °C for a Watson–Crick dA_{10}/dT_{10} duplex in the same buffer system (hyperchromicity 17%). With two equivalents of dA_{10}, a monophasic transition was observed at 26.0 °C with a hyperchromicity of 17%.[14] These results are consistent with hybridization of both strands of **1** and formation of a novel complex **5** (Figure 3), in which a transition metal moiety links two DNA duplexes. Indeed, molecular modeling studies on **5**[15] predict no significant steric or energetic barrier to the formation of this structure (Figure 3). Further characterization of the hybridized complexes by nondenaturing gel electrophoresis and CD spectroscopy is currently underway.

In conclusion, we have prepared the first branched DNA structure **1** containing a transition metal center as the branch point, to which two oligonucleotide strands are attached through monodentate ligands. Importantly, the convergent solid-phase synthesis of **1** allows for the possible incorporation of a range of metal complexes, spacers between the metal atom and DNA, and DNA sequences into the structure.[16] Complex **1** is expected to perform a dual role. It contains luminescent and redox-active *cis*-$[(bpy)_2Ru(imidazole)_2]^{2+}$ that is incorporated into the oligonucleotide and thus can potentially act as a DNA hybridization probe.[4] In addition, analogues of complex **1** containing mixed DNA sequences are expected to associate with their complementary partners to generate a new class of DNA nanostructures. The pioneering work of Seeman[2a] and other recent contributions[2] have elegantly demonstrated the exciting promise of DNA as a building block for nanotechnology. Complexes such as **1** allow the metal-mediated self-assembly of DNA into a new class of photo- and electroactive DNA nanostructures. We are currently investigating the fluorescence response of these complexes to DNA hybridization, as well as their potential for the construction of higher order DNA structures.

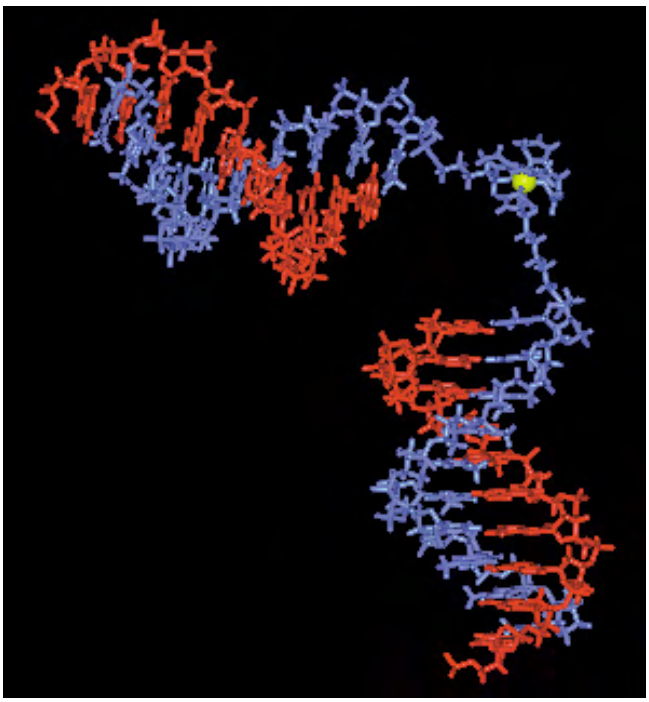


Figure 3. Optimized structure of the expected ruthenium-linked bis(double helical) DNA complex **5**, calculated as a local minimum by the AMBER force-field method.[15] The branched ruthenium complex **1** is shown in blue (ruthenium atom in yellow), and the two dA_{10} strands are shown in red. Because of the flexibility of the hexyl spacer, as well as the influence of solvent and counterions, the structure shown may not be a unique conformation of complex **5**.

Received: July 6, 2001 [Z17443]

[1] a) R. S. Braich, M. J. Damha, *Bioconjugate Chem.* **1997**, *8*, 370–377; b) T. Horn, C. Chang, M. Urdea, *Nucleic Acids Res.* **1997**, *25*, 4835–4841; c) D. Praseuth, A. L. Guieysse, C. Helene, *Biochim. Biophys. Acta* **1999**, *1489*, 181–206; d) R. H. E. Hudson, A. H. Uddin, M. J. Damha, *J. Am. Chem. Soc.* **1995**, *117*, 12470–12477, and references therein; e) M. D. Sorensen, M. Meldgaard, V. K. Rajwanshi, J. Wengel, *Bioorg. Med. Chem. Lett.* **2000**, *10*, 1853–1856, and references therein.

[2] a) N. C. Seeman, *Annu. Rev. Biophys. Biomol. Struct.* **1998**, *27*, 225–248; b) J. J. Storhoff, C. A. Mirkin, *Chem. Rev.* **1999**, *99*, 1849–1862; c) R. P. Fahlman, D. Sen, *J. Am. Chem. Soc.* **1999**, *121*, 11079–11085; d) J. Shi, D. E. Bergstrom, *Angew. Chem.* **1997**, *109*, 70–72; *Angew. Chem. Int. Ed. Engl.* **1997**, *36*, 111–113; e) M. S. Shchepinov, K. U. Mir, J. K. Elder, M. D. Frank-Kamenetskii, E. Southern, *Nucleic Acids Res.* **1999**, *27*, 3035–3041; f) M. Scheffler, A. Dorenbeck, S. Jordan, M. Wustefeld, G. von Kiedrowski, *Angew. Chem.* **1999**, *111*, 3514–3518; *Angew. Chem. Int. Ed.* **1999**, *38*, 3312–3315; g) S. M. Waybright, C. P. Singleton, K. Wachter, C. Murphy, U. H. F. Bunz, *J. Am. Chem. Soc.* **2001**, *123*, 1828–1833.

[3] Metal-mediated self-assembly of peptide structures: a) M. R. Ghadiri, C. Soares, C. Choi, *J. Am. Chem. Soc.* **1992**, *114*, 825–831; b) K. Suzuki, H. Hiroaki, D. Kohda, H. Nakamura, T. Tanaka, *J. Am. Chem. Soc.* **1998**, *120*, 13008–13015.

[4] a) D. J. Hurley, Y. Tor, *J. Am. Chem. Soc.* **1998**, *120*, 2194–2195; b) H. S. Joshi, Y. Tor, *Chem. Commun.* **2001**, 549–550; c) S. I. Khan, A. E. Beilstein, M. W. Grinstaff, *Inorg. Chem.* **1999**, *38*, 418–419, and references therein; d) K. Tanaka, M. Tasaka, H. Cao, M. Shionoya, *Eur. J. Pharm. Sci.* **2001**, *13*, 77–83; e) E. Meggers, P. L. Holland, W. B.

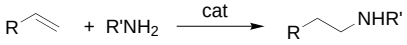
 © WILEY-VCH Verlag GmbH, D-69451 Weinheim, 2001 1433-7851/01/4024-4631 $ 17.50+.50/0

Tolman, F. E. Romesberg, P. G. Shultz, *J. Am. Chem. Soc.* **2000**, *122*, 10714 – 10715.
[5] Three reports have described systems containing branched/difunctional oligonucleotides and metal centers; however, none of these systems has a metal center whose geometry directly influences the orientation of the DNA strands. a) S. Takenaka, Y. Funatu, H. Kondo, *Chem. Lett.* **1996**, 891 – 892; b) F. D. Lewis, S. A. Helvoigt, R. L. Letsinger, *Chem. Commun.* **1999**, 327 – 328; c) see ref. [2g].
[6] a) K. B. Reddy, M. P. Cho, J. F. Wishart, T. J. Emge, S. S. Isied, *Inorg. Chem.* **1996**, *35*, 7241 – 7245; b) T. Pascher, J. R. Winkler, H. B. Gray, *J. Am. Chem. Soc* **1998**, *120*, 1102 – 1103.
[7] M. J. Damha, K. Ganeshan, R. H. E. Hudson, S. V. Zabarylo, *Nucleic Acids Res.* **1992**, *24*, 6565 – 6573.
[8] Selected spectroscopic data of complex **2**: ^{1}H NMR (400 MHz, [D$_6$]acetone): $\delta = 0.85$ (m, 4H), 1.10 (m, 4H), 1.25 (m, 4H), 1.55 (m, 4H), 3.30 (t, 4H), 3.90 (t, 4H), 6.80 (s, 2H), 7.18 (br s, 2H), 7.32 (t, 2H), 7.72 (t, 2H), 7.82 (br s, 2H), 7.89 (t, 2H), 8.10 (m, 4H), 8.45 (d, 2H), 8.54 (d, 2H), 9.13 (d, 2H). FAB-MS: *m*/*z*: 894.9 [$M - PF_6$].
[9] a) K. Iizuka, K. Akahane, Y. Kamijo, D. Momose, Y. Ajisawa, *Brit. UK Pat. Appl.* **1979**, GB 2016452; b) G. M. Brown, R. W. Callahan, T. J. Meyer, *Inorg. Chem.* **1975**, *14*, 1915 – 21.
[10] The expected diastereomers from the chirality of both the *cis*-[(bpy)$_2$Ru(imidazole)$_2$]$^{2+}$ and the phosphoramidite groups could not be resolved at 200 MHz.
[11] Complex **1**: HPLC: 22% of the mixture, MALDI-TOF MS: *m*/*z*: 6861 [M+2Na$^+$]. Complex **4**: HPLC: 54% of the mixture, MALDI-TOF MS: *m*/*z* 3914 [M+2Na$^+$+Li$^+$].
[12] The buffer system used was 140 mM KCl, 5 mM Na_2HPO_4, and 1 mM $MgCl_2$, pH 7.2. This buffer is known to inhibit the formation of a DNA triple helix, which could arise from the association of **1** with one strand of dA_{10}.[1d]
[13] In parallel, control experiments on complex **2** established that the *cis*-[(bpy)$_2$Ru(imidazole)$_2$]$^{2+}$ moiety is stable to the high temperatures required in the melting experiments.
[14] The origin of the observed increase in stability of the duplexes in **5**, as compared to natural dA_{10}/dT_{10} duplexes, is still under investigation. Thermal denaturation studies on monostranded complex **4** with dA_{10} showed a similar increase in T_m,[17] and this suggests that the enhanced stability of the DNA duplexes in these structures may be due to the positively charged metal center. In this respect, the decrease in T_m and hyperchromicity observed for complex **1** with 1 equiv of dA_{10} relative to 2 equiv dA_{10} is also under investigation.
[15] Assuming B-form DNA and fixing the coordinates of the ruthenium moiety according to a reported crystal structure of *cis*-[(bpy)$_2$Ru(imidazole)$_2$]$^{2+}$,[6a] calculations were performed with Hyperchem 6, Hypercube, FL (USA).
[16] Current efforts are focused on the synthesis of analogues of **1** with rigid spacers between imidazole ligands and DNA strands, so that the geometry of the metal center can directly influence the orientation of the strands.
[17] See Supporting Information for experimental details on the synthesis and characterization of complexes **1** – **4**, as well as thermal denaturation studies.

The Mechanism of Hydroamination of Allenes, Alkynes, and Alkenes Catalyzed by Cyclopentadienyltitanium – Imido Complexes: A Density Functional Study**

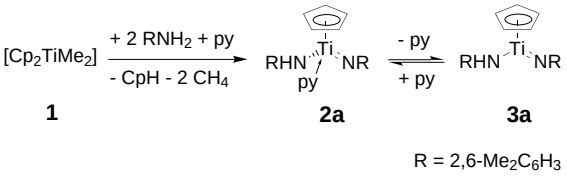
Bernd F. Straub* and Robert G. Bergman*

Considerable effort has been directed towards the development of procedures for hydroamination across carbon – carbon multiple bonds, and several catalytic systems for allene, alkyne, and alkene hydroamination have been investigated.[1] However, a general catalyst for the hydroamination of nonactivated unsaturated hydrocarbons remains elusive. A catalyst for the selective anti-Markovnikov addition of amines to terminal alkenes would be of particular interest [Eq. (1)].



(1)

Recent kinetic studies have been carried out to elucidate the mechanism of hydroamination catalyzed by cyclopentadienyltitanium complexes[2–5] such as the dimethyltitanocene **1** and the imido complex **2a** (Scheme 1).[4, 5] Formation of the active monocyclopentadienyltitanium – imido species [CpTi=NR(NHR)] **3a** (R = 2,6-Me$_2$C$_6$H$_3$) from both the pyridine adduct **2a** and the precatalyst **1** has been established (Scheme 1).[4]



Scheme 1. Generation of [CpTi=NR(NHR)] **3a** from precatalyst [Cp$_2$TiMe$_2$] (**1**) and by equilibration with [CpTi=NR(NHR)py] **2a**.[4]

Titanaazacyclobutenes and titanaazacyclobutanes are proposed as intermediates in the catalytic cycle,[2a, 4, 5] in analogy to the [Cp$_2$Zr(NHR)$_2$]-catalyzed hydroamination of alkynes[6] or the stoichiometric reaction of allenes with zirconium and titanium pyridine imido derivatives.[7] However, the mechanism of the protonation of the titanacycle by the amine is not well understood. Here we report high-level density functional model calculations on the intermediates involved in this step. The origin of the differences between the activation barriers

[*] Dr. B. F. Straub, Prof. R. G. Bergman
Department of Chemistry
University of California
Berkeley, CA 94720-1460 (USA)
Fax: (+1) 510-642-7714
E-mail: bergman@cchem.berkeley.edu
bfstraub@uclink.berkeley.edu

[**] This work was supported by the US National Institutes of Health (grant no. GM-25459 to R.G.B.). B.F.S. gratefully acknowledges a Feodor Lynen research fellowship of the Alexander von Humboldt foundation.

Supporting information for this article is available on the WWW under http://www.angewandte.com or from the author.

 © WILEY-VCH Verlag GmbH, D-69451 Weinheim, 2001 1433-7851/01/4024-4632 $ 17.50+.50/0

in allene and alkyne versus the hypothetical alkene hydroamination catalysis is also explored.

We used the B3LYP functionals,[8] a Hay–Wadt small-core effective-core potential on titanium,[9] and a triple-ζ plus polarization quality basis set[10] for geometry optimization and vibrational frequency analyses.[11] Since total electronic energies are not sufficient for the prediction of barriers for association and dissociation reactions at room or elevated temperature, zero-point vibrational energies and Gibbs free energy corrections have been included for all simplified compounds.

In earlier experimental studies on allene hydroamination, our group observed a first-order dependence on the concentration of catalyst **2a** and allene substrate, a zero-order dependence on the 2,6-dimethylaniline concentration, and an inverse first-order rate dependence on the pyridine concentration.[4] The pyridine adduct **2a** is stable in the presence of 2,6-dimethylaniline towards formation of species such as $[CpTi(NHR)_3]$ (**4a**), dinuclear complexes such as **5a**, and free pyridine.[4] Pohlki and Doye observed that the rate of diphenylacetylene hydroamination depends on both the concentration of precatalyst **1** and 4-methylaniline.[5] Their kinetic analysis postulated the existence of preequilibria that interconvert the active imido species with both titanium amides and dinuclear titanium complexes,[5] and this also explains the low reaction rates of sterically less hindered amines.[3]

We first studied the relative energies of potential catalyst resting states. The preference for pyridine ligation is indeed reproduced by the DFT calculations in the nonsimplified models **2a**–**5a** (Figure 1).

Although the computed strength of pyridine coordination to the simplified {CpTi=NH(NH$_2$)} fragment in **2b** is weaker than the driving force for formation of trisamide **4b** and dimer **5b**, the steric congestion of three 2,6-dimethylanilide ligands at a titanium center inverts the relative stabilities. The computed steric influence of the amine substituents for the stabilities of the titanium species **3** to **5** strongly supports the interpretations of the Doye group.[5]

Next we studied the interaction of these titanium complexes with unsaturated hydrocarbons. The presumed active species **3b** weakly coordinates to allene (Figure 2), ethyne

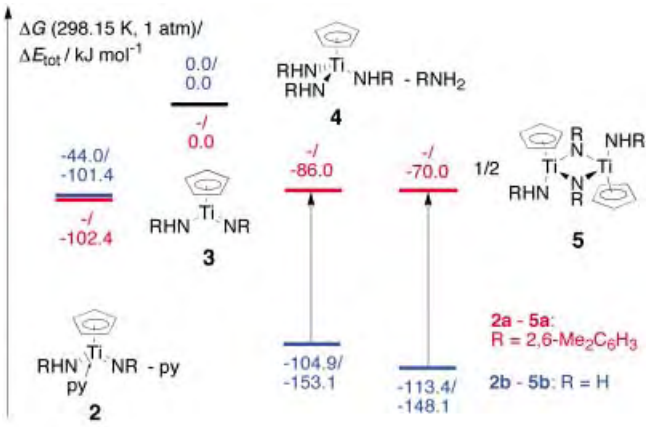


Figure 1. Influence (see arrows) of the amide and imide substituents on the computed relative stabilities of CpTi complexes.

(Figure 3), or ethene (Figure 4), and is predicted to undergo a facile [2+2] cycloaddition with each substrate.

Two pathways for the overall hydroamination reaction have been found for each of the hydrocarbon substrates.

1) Coordination of NH_3 and intramolecular proton transfer from the ammine ligand to a carbon atom (Figure 2 to 4).
2) Proton transfer from an amide ligand to a carbon atom without preceding amine coordination (Figure 5).

The coordination of NH_3 in **11**, **17**, and **23** acidifies the ammine protons compared to those of free ammonia. This is reflected in NBO analyses, which reveal a charge transfer of -0.22 to -0.24 from the ammine ligand to the titanium fragment and a concomitant increase in negative net charge on the C1 carbon atom.[12]

In both the allene and the ethyne pathways, the presence of a vinylamine-type π system facilitates proton transfer. In the allene hydroamination cycle, a proton on the ammine ligand is transferred to the *exo*-methylene group. In a concerted reaction, the Ti–C3 bond cleaves (2.226 Å in **11**, 2.369 Å in **12**), the C1–C2 double bond character vanishes (1.358 Å in **11**, 1.421 Å in **12**), and a C2–C3 double bond is formed (1.475 Å in **11**, 1.426 Å in **12**; see Figure 2 and 3). In the ethyne pathway, coordination of NH_3 distorts the titanaazacyclobutene (**17**) (δ(Ti-C1-C2-N1) = 29.5°, see Figure 3). The

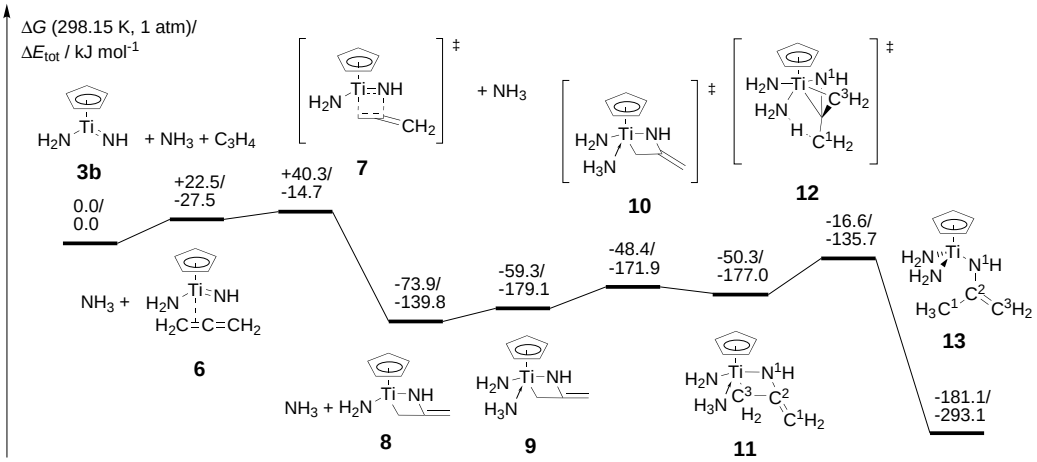


Figure 2. Allene hydroamination pathway: [2+2] cycloaddition, NH_3 coordination, ring inversion via **10**, and intramolecular proton transfer.

 © WILEY-VCH Verlag GmbH, D-69451 Weinheim, 2001 1433-7851/01/4024-4633 $ 17.50+.50/0

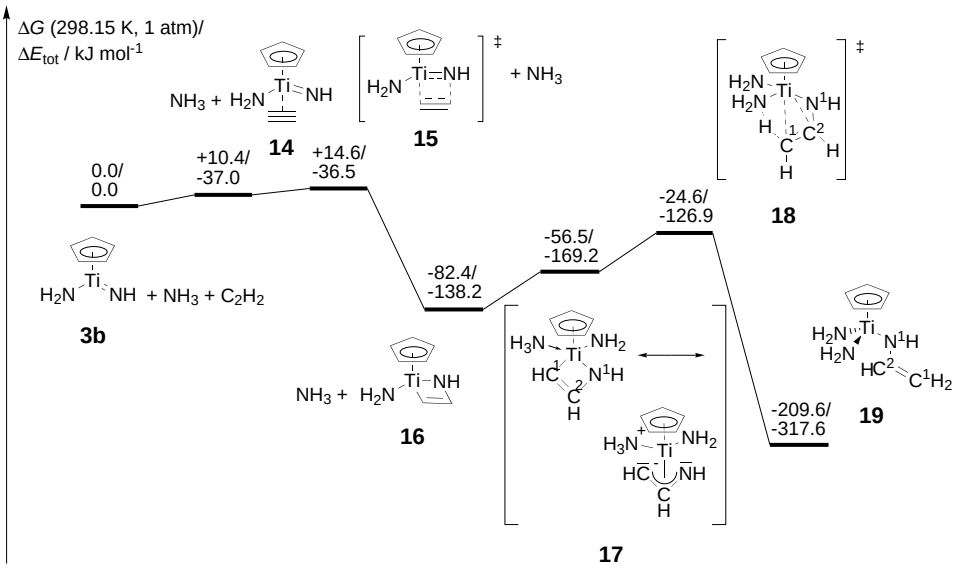


Figure 3. Ethyne hydroamination pathway: [2+2] cycloaddition, NH_3 coordination, and proton transfer.

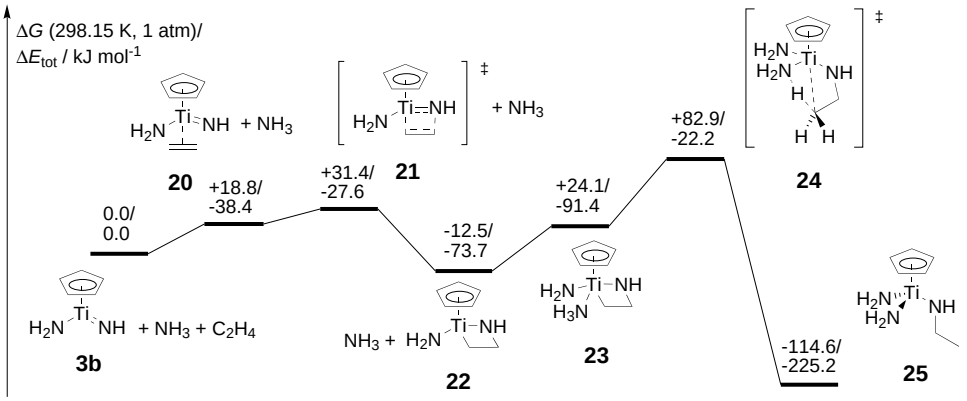


Figure 4. Hypothetical ethene hydroamination pathway: [2+2] cycloaddition, NH_3 coordination, and proton transfer.

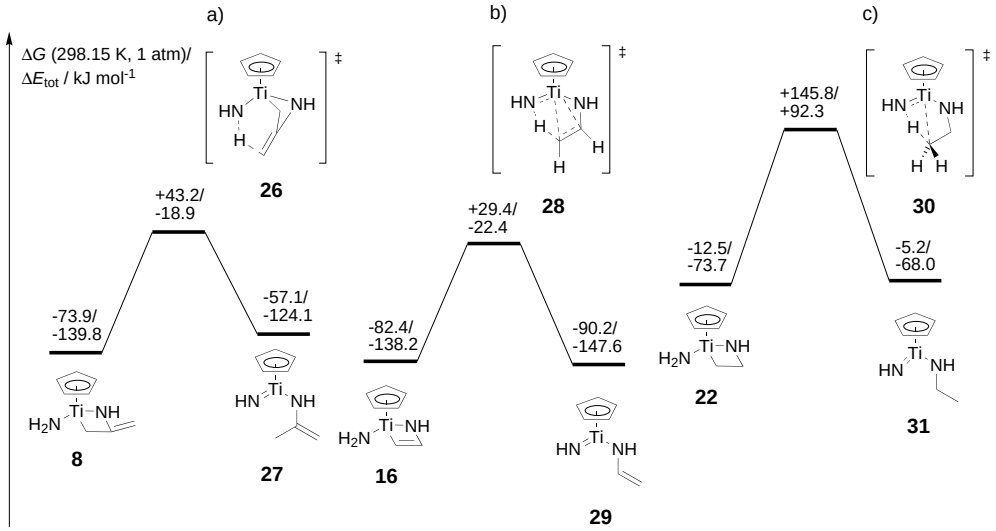


Figure 5. Alternative mechanistic pathways for proton transfer from an amide ligand: hydroamination of (a) allene, (b) ethyne, and (c) ethene.

resulting contribution of a mesomeric structure with a deprotonated dianionic η^3-1-azaallyl ligand facilitates the proton transfer. As in the allene hydroamination pathway, the Ti–C bond is cleaved as the proton transfer proceeds (Figure 3).

We next studied the hypothetical ethene hydroamination. The Gibbs free dissociation energy of ethene from titanacycle **22** is computed to be more than 60 kJ mol^{-1} lower than for the corresponding allene or ethyne dissociation reaction. The NH_3 addition to the ethene adduct **22** is slightly disfavored by 10 to 15 kJ mol^{-1} compared to the NH_3 addition to the allene and ethyne analogues **11** and **17** (Figure 4). Furthermore, no π system is present in the titanacycle **23** and thus the σ Ti–C bond has to be directly protonated. As a consequence, the proton transfer is disfavored by an additional 25 to 30 kJ mol^{-1}. Altogether, the proton transfer step in alkene hydroamination by CpTi–imido complexes is disfavored by about 100 kJ mol^{-1} compared to the corresponding allene and alkyne proton transfer steps.

Since the ammine complexes and their proton transfer transition states possess the highest coordination number at the respective titanium center in the catalytic cycle, they are especially sensitive to steric congestion. As a consequence, bulky amines and sterically demanding unsaturated substrates might support an electronically disfavored and entropically favored pathway without precoordination of amine, but rather with direct proton transfer from an amide ligand to a carbon atom. The computed energetics for these pathways are shown in Figure 5.

The predicted increase in electronic barriers for the amide protonation transfer

 © WILEY-VCH Verlag GmbH, D-69451 Weinheim, 2001 1433-7851/01/4024-4634 $ 17.50+.50/0

compared to the barriers for the respective ammine proton transfer reactions results from the increased distortion of the core structures in the transition states and the lower acidity of the amide protons. Zero point vibration and entropic contributions lower the Gibbs free energy barrier difference between the two pathways to 54 – 63 kJ mol^{-1} by destabilizing the highly ordered ammine proton transfer transition states **12**, **18**, and **24**. This difference could well be overcome by steric congestion induced by bulky substituents of amines and unsaturated hydrocarbon substrates. For comparison, the steric destabilization for complexes with three 2,6-dimethylanilide ligands at a titanium center such as in **4a** and **5a** has been computed to be 67 – 78 kJ mol^{-1}.

In allene and ethyne hydroamination with the simplified [CpTi=NH(NH_2)] system, where proton transfer takes place after initial amine coordination, the transition state for the cycloaddition is the highest point in the catalytic pathway and thus is rate-determining. However, it remains unclear whether the zero-order dependence on the 2,6-dimethylaniline concentration derived from the kinetic data for allene hydroamination[4] results from a rate-determining [2+2] cycloaddition or a rate-determining proton transfer from an amide ligand. A first-order dependence on the amine concentration can occur if the Gibbs free activation energy for the amine coordination plus proton transfer pathway is higher than the barrier for the initial [2+2] cycloaddition, but lower than the barrier for a competing amide proton transfer. A rate-determining amide ligand exchange with free amine could also result in such a rate law (see Supporting Information for computed ligand exchange pathways).

For alkene hydroamination, our model calculations predict that both the ammine and the amide proton transfer to the Ti–C bond have Gibbs free activation energies that are more than 50 kJ mol^{-1} higher than the cycloaddition step (Figure 4 and 5c). This explains the relative ease of allene and alkyne hydroamination compared to alkene hydroamination. Increasing the rate of this proton transfer step as well as stabilizing the metallaazacyclobutane intermediate compared to the catalyst resting state could be the key to making the alkene process successful. We are using these new insights into the hydroamination mechanism to isolate additional intermediates involved in the catalytic cycle, and to tailor more general hydroamination catalysts.

Received: August 9, 2001
Revised: October 5, 2001 [Z17699]

[1] a) T. E. Müller, M. Beller, *Chem. Rev.* **1998**, *98*, 675, and references therein; b) M. Tokunaga, M. Eckert, Y. Wakatsuki, *Angew. Chem.* **1999**, *111*, 3416; *Angew. Chem. Int. Ed.* **1999**, *38*, 3222; c) H. M. Senn, P. E. Blöchel, A. Togni, *J. Am. Chem. Soc.* **2000**, *122*, 4098; d) M. Kawatsura, J. F. Hartwig, *J. Am. Chem. Soc.* **2000**, *122*, 9546; e) M. Kawatsura, J. F. Hartwig, *Organometallics* **2001**, *20*, 1960; f) O. Löber, M. Kawatsura, J. F. Hartwig, *J. Am. Chem. Soc.* **2001**, *123*, 4366; g) H. Schaffrath, W. Keim, *J. Mol. Catal. A* **2001**, *168*, 9; h) M. Nobis, B. Drießen-Hölscher, *Angew. Chem.* **2001**, *113*, 4105; *Angew. Chem. Int. Ed.* **2001**, *40*, 3983.

[2] a) P. L. McGraine, M. Jensen, T. Livinghouse, *J. Am. Chem. Soc.* **1992**, *114*, 5459; b) P. L. McGrane, T. Livinghouse, *J. Am. Chem. Soc.* **1993**, *115*, 11485; c) P. L. McGrane, T. Livinghouse, *J. Org. Chem.* **1992**, *57*, 1323.

[3] a) E. Haak, I. Bytschow, S. Doye, *Angew. Chem.* **1999**, *111*, 3584; *Angew. Chem. Int. Ed.* **1999**, *38*, 3389; b) E. Haak, H. Siebeneicher, S. Doye, *Org. Lett.* **2000**, *2*, 1935.

[4] J. S. Johnson, R. G. Bergman, *J. Am. Chem. Soc.* **2001**, *123*, 2923.

[5] F. Pohlki, S. Doye, *Angew. Chem.* **2001**, *113*, 2361; *Angew. Chem. Int. Ed.* **2001**, *40*, 2305.

[6] a) P. J. Walsh, A. M. Baranger, R. G. Bergman, *J. Am. Chem. Soc.* **1992**, *114*, 1708; b) A. M. Baranger, P. J. Walsh, R. G. Bergman, *J. Am. Chem. Soc.* **1993**, *115*, 2753.

[7] a) Z. K. Sweeney, J. L. Salsman, R. A. Andersen, R. G. Bergman, *Angew. Chem.* **2000**, *112*, 2429; *Angew. Chem. Int. Ed.* **2000**, *39*, 2339; b) A. Bashall, M. McPartlin, P. E. Collier, P. Mountford, L. H. Gade, D. J. M. Troesch, *Chem. Commun.* **1998**, 2555; c) D. J. M. Troesch, P. E. Collier, A. Bashall, L. H. Gade, M. McPartlin, P. Mountford, S. Radojevic, *Organometallics* **2001**, *20*, 3308.

[8] a) A. D. Becke, *J. Chem. Phys.* **1993**, *98*, 5648; b) S. H. Volko, L. Wilk, M. Nusair, *Can. J. Phys.* **1980**, *58*, 1200; c) C. Lee, W. Yang, R. G. Parr, *Phys. Rev. B* **1988**, *37*, 785.

[9] R. Krishnan, J. S. Binkley, R. Seeger, J. Pople, *J. Chem. Phys.* **1980**, *72*, 650.

[10] P. J. Hay, W. R. Wadt, *J. Chem. Phys.* **1985**, *82*, 299.

[11] Jaguar 4.0, release 23, Schrödinger, Inc., Portland, OR, USA, **1998**.

[12] NBO net charge of the hydrogen atoms of NH_3: 0.338; NBO net charge of the hydrogen atoms of the ammine ligand of **11**: 0.386 to 0.414; **17**: 0.379 to 0.402, **23**: 0.383 to 0.389. NBO 4.0. E. D. Glendening, J. K. Badenhoop, A. E. Reed, J. E. Carpenter, F. Weinhold, Theoretical Chemistry Institute, University of Wisconsin, Madison, WI, **1999**.

Self-Assembly of Cyclic Peptides into Nanotubes and Then into Highly Anisotropic Crystalline Materials**

David Gauthier, Pierre Baillargeon, Marc Drouin, and Yves L. Dory*

Syntheses of supermolecules rely on the stabilization provided by noncovalent interactions between recognition sites in each unit.[1–3] The construction of new supramolecular architectures with well-defined shape and size by using tube building blocks is an important subject in organic materials chemistry because novel electronic and photonic properties can result from their three-dimensional (3D) organization (Figure 1a).[2] These tubular structures have also attracted considerable interest because of their utility as models for biological channels.[4–9] It is also thought that in tubes built from stacked cyclic peptides, uniform alignment of amide groups could give rise to a macrodipole moment such as that of an α-helix.[10] Voltage gating and current rectification are important expected new properties for such channel structures.[11]

To date, all attempts to grow crystals of a useful size were frustrated by the inherent insolubility of these materials.[12–15]

[*] Prof. Y. L. Dory, D. Gauthier, P. Baillargeon, M. Drouin
Laboratoire de Synthèse Supramoléculaire, Département de Chimie
Université de Sherbrooke
3001 12e Avenue nord, Fleurimont, J1H 5N4, PQ (Canada)
Fax: (+1) 819-820-6823
E-mail: yves.dory@courrier.usherb.ca

[**] This work was supported by FCAR Québec.

 © WILEY-VCH Verlag GmbH, D-69451 Weinheim, 2001 1433-7851/01/4024-4635 $ 17.50+.50/0

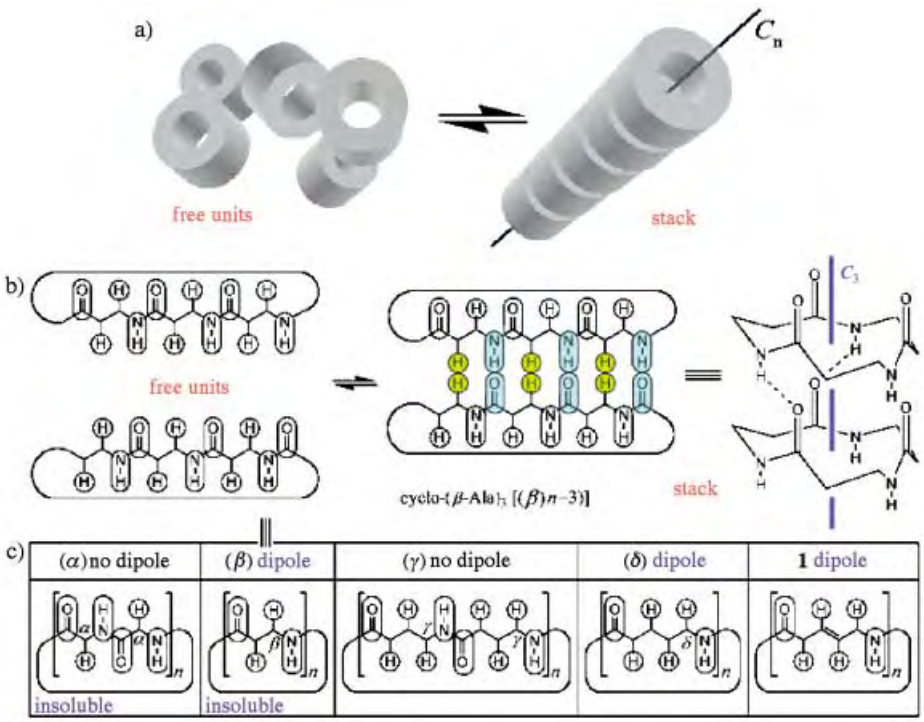


Figure 1. Structure of cyclic peptide nanotubes. a) A modular tube is formed by stacking of free units. b) In the case of cyclo-(β-Ala)$_3$, each free unit associates with the growing stack by means of three H bonds (blue) from amides and three van der Waals contacts (yellow) from pseudo-axial aliphatic hydrogen atoms. c) Types of macrolactams: lactams α and β are notoriously insoluble materials.

Consequently, their tubular structure could not be unequivocally characterized and this undesired insolubility prevented these nanotubes from being practically useful. Here we show how we successfully addressed the critical solubility problem by designing and synthesizing special organic C_n lactam units built from novel amino acids. We could then demonstrate the tubular shape of our supermolecules by X-ray crystallography. Apart from this primary aim, we also managed to extend the dipolar anisotropy of the macromolecular column components to a whole monocrystal to give useful macroscopic properties.

Flat ring-shaped cyclopeptides have the potential to aggregate as "endless" stacks through backbone–backbone H-bond interactions and van der Waals contacts (Figure 1b).[12] In this way, some tubes made from cyclo-(α-amino acid)$_n$ (Figure 1c, α, $n=3$, 4) have been prepared; but they proved difficult to handle because of their strong propensity to aggregate (their structures could only be defined by electron diffraction, calculations, and infrared (IR) spectroscopy of microcrystals).[16–18] The problem was only partially alleviated by using appropriate side chains.[6, 16] The same extreme insolubility was also the main characteristic of tubes made of cyclo-(β-amino acid)$_n$ (β, $n=3$, 4, their structures were obtained by X-ray diffraction analyses of powders, or inferred more indirectly by calculations or IR spectroscopy).[14, 15, 19, 20]

Nothing is known about tubes made of more lipophilic cyclo-(γ-amino acid)$_n$ and cyclo-(δ-amino acid)$_n$ (γ and δ). γ-Amino acids would yield dipole-less tubes and cyclo-(δ-aminopropanoyl)$_3$ would certainly not be rigid enough to retain the necessary tubular shape. However, in the latter case rigidity can be introduced by means of a double bond while lipophilicity would remain unchanged. A structure such as **1** (Figure 1c, $n=3$) is isosteric to cyclohexaglycine (α, $n=3$).[21] Cyclohexaglycine does not crystallize as hollow tubes, rather, two intramolecular H bonds allow the molecule to form two β-turns leaving only two amide groups for stacking along its S_2 axis. On the other hand, **1** can only form one such β-turn, and might still prefer to retain a C_3 symmetrical shape (such as in the hexadepsipeptides eniatins)[18, 22] appropriate for the formation of supramolecular tubes (Figure 2).

The macrocycle **1** was prepared from the thioester **3** with a silver(I) salt in 55% yield.[23] The thioester **3** was

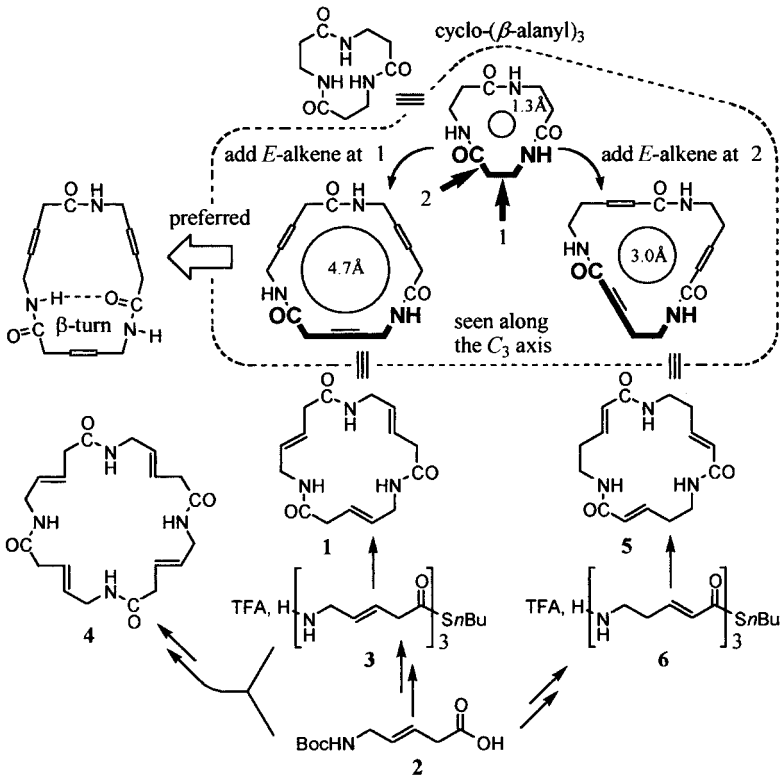


Figure 2. Design and synthesis of lactams **1**, **4**, and **5**. Cyclo-(β-alanyl)$_3$ self-assembles as insoluble "endless" rods (inner diameter of 1.3 Å). *E*-Alkenes inserted at positions 1 and 2 yield more lipophilic lactams **1** and **5** that could stack as tubes with inner diameters of 4.7 Å and 3.0 Å, respectively. However, lactam **1** does not lead to such tubes as it prefers to form a β-turn. The cyclic tetramer **4** was also prepared from **2**; Boc = *tert*-butoxycarbonyl.

 © WILEY-VCH Verlag GmbH, D-69451 Weinheim, 2001 1433-7851/01/4024-4636 $ 17.50+.50/0

obtained from the Boc-protected amino acid **2** in six straightforward steps (overall yield of 83%).[24] The material was easily crystallized by diffusion (ethanol and diethyl ether) and X-ray crystallography showed that **1** and cyclohexaglycine pack in a very similar way. The rectangular shape of **1** is governed by one β-turn and by that two out of three amides are involved in the stacking (Figure 3a).[25–27] We decided to take advantage of the tendency of **1** to form β-turns to create a higher analogue of S_4 symmetry with four β-turns, reminiscent of the backbone of octavalinomycine (Figure 3b).[28] The tetramer **4** was prepared in three steps from **2** and **3** (overall yield of 32%, 67% for the cyclization; Figure 2) and was also crystallized by the same diffusion technique (isopropanol and diethyl ether). However, the crystal structure showed a disclike dipole-less S_2 structure with no intramolecular H bonds (Figure 3c).[26, 27, 29] Despite the overall resemblance to alternating L,D-cyclooctapeptides, no nanotubes are formed since all the units prefer to assemble in a more compact lattice. In that spatial arrangement all eight H-bonding sites are fulfilled, each unit being H bonded to four neighbors (rather than only two in a tubular structure).

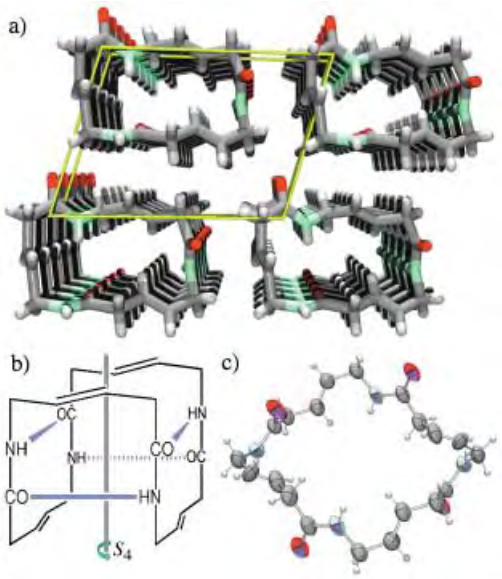


Figure 3. Crystal structures of lactams **1** and **4**. a) The lactam **1** displays one β-turn in the crystal state and self-assembles as flat tubes. b) The cyclic tetramer **4** could also fold by means of β-turns to adopt an S_4-symmetric structure. c) The tetramer **4** is in fact S_2 symmetric, all its amide groups being involved in intermolecular H bonds.

These preliminary results indicated that our systems were still too flexible. To lock the conformation into a more rigid bracelet or crown of C_3 symmetry, it was necessary to prevent β-turns from forming. Our first unit **1** can be seen as cyclo-(β-alanyl)$_3$ in which an *E*-alkene had been inserted at the central bond, position 1 (Figure 2). The resulting 18-membered ring (**1**) is isosteric to cyclohexaglycine and behaves accordingly. However, the *E*-alkene could have been inserted next to the carbonyl of cyclo-(β-alanyl)$_3$ at bond position 2 to afford a new 18-membered lactam **5**. In this new environment, β-turns become impossible and the ring, which now cannot collapse as in structure **1**, has no choice but to adopt a rigid crown structure (Figure 4a). The lactam **5** was then prepared from the thioester **6** in 50% yield.[23] The thioester **6** was obtained from the Boc-protected amino acid **2** in seven steps (overall yield of 34%). The lactam **5** crystallized very easily by diffusion (ethanol and diethyl ether), X-ray data confirmed the expected tubular structure (Figure 4b).[26, 27, 30] However, beyond all expectations, the packing found in the crystal shows all the highly polarized tubes orient in the same direction so that the anisotropy of the units first amplified in the tubes is then further transferred to the whole crystal (Figures 4c and d). The gross dipole of a monocrystal of **5** arising from identical orientation of all amides (Figure 5) should be extremely strong and the resulting material highly anisotropic.

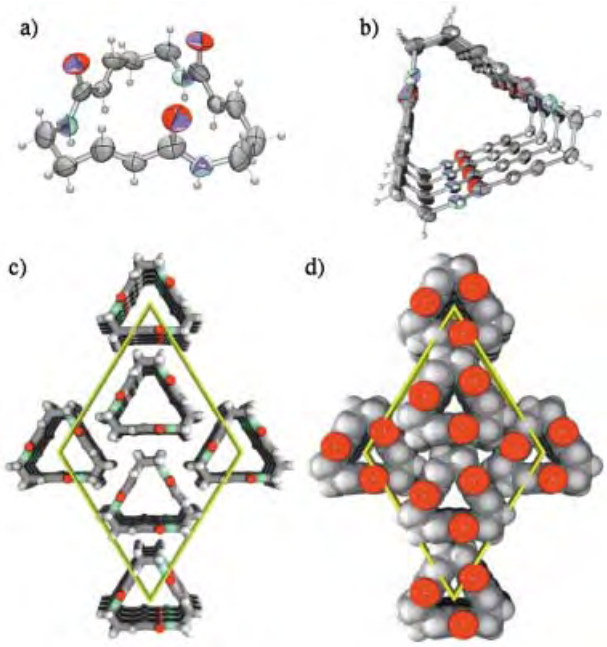


Figure 4. a) The macrocycle **5** adopts a rigid crown structure with all amide groups parallel to the C_3 axis. b) The units stack on top of each other to yield a tube endowed with a very strong dipole. c) The anisotropy is further transferred to the whole crystal since all dipoles remain aligned in the same direction when the tubes aggregate. d) The space-filling diagram shows the very compact packing of the tubes and the parallel channels.

In summary, we have designed special lactam units that were shown to assemble as supramolecular tubes that further

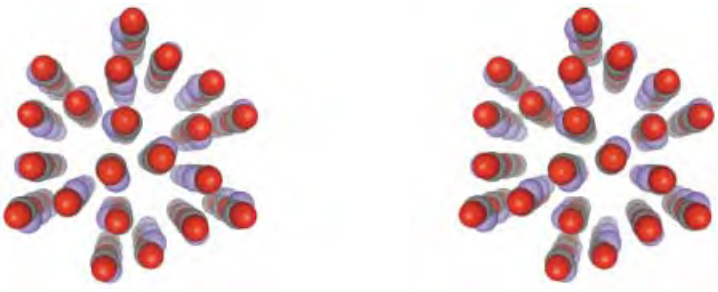


Figure 5. Stereo view of amide groups in the crystal of **5**. The amides in the crystal are perfectly aligned (as in parallel β-sheets). Each resulting "H-bond tape" is separated from its closest intra-tube and inter-tube neighbors by 5.1 Å and 5.0 Å, respectively.

 © WILEY-VCH Verlag GmbH, D-69451 Weinheim, 2001 1433-7851/01/4024-4637 $ 17.50+.50/0

aggregate as bundles. Since all the strong columnar dipoles are oriented in the same direction, intense anisotropy exists that can in principle expand to macroscopic levels. Growing monocrystals of such materials is now possible. We will soon be in a position to find out if highly polarized nanotubes can be used in devices to rectify current or display unexpected properties.[11] Our approach allows us to control precisely the internal diameter of the tube simply by modifying the positions and number of alkenes inside the monomers. We have prepared the higher C_3 symmetric lactam homologue, which incorporates conjugated dienes rather than simple conjugated alkenes; its crystal structure should yield further information about the capacity of conjugation to provide adequate rigidity to the tube units.

Received: June 11, 2001
Revised: October 15, 2001 [Z17261]

[1] J.-M. Lehn, *Pure Appl. Chem.* **1978**, *50*, 871 – 892.
[2] G. M. Whitesides, J. P. Mathias, C. T. Seto, *Science* **1991**, *254*, 1312 – 1319.
[3] K. Müller-Dethlefs, P. Hobza, *Chem. Rev.* **2000**, *100*, 143 – 167.
[4] B. Eisenberg, *Acc. Chem. Res.* **1998**, *31*, 117 – 123.
[5] G. W. Gokel, O. Murillo, *Acc. Chem. Res.* **1996**, *29*, 425 – 432.
[6] M. R. Ghadiri, J. R. Granja, L. K. Buehler, *Nature* **1994**, *369*, 301 – 304.
[7] T. D. Clark, L. K. Buehler, M. R. Ghadiri, *J. Am. Chem. Soc.* **1998**, *120*, 651 – 656.
[8] D. Ranganathan, V. Haridas, C. S. Sundari, D. Balasubramanian, K. P. Madhusudanan, R. Roy, I. L. Karle, *J. Org. Chem.* **1999**, *64*, 9230 – 9240.
[9] D. Ranganathan, C. Lakshmi, I. L. Karle, *J. Am. Chem. Soc.* **1999**, *121*, 6103 – 6107.
[10] D. T. Bong, T. D. Clark, J. R. Granja, M. R. Ghadiri, *Angew. Chem.* **2001**, *113*, 1016 – 1041; *Angew. Chem. Int. Ed.* **2001**, *40*, 988 – 1011.
[11] P. K. Kienker, W. F. DeGrado, J. D. Lear, *Proc. Natl. Acad. Sci. USA* **1994**, *91*, 4859 – 4863.
[12] T. D. Clark, J. M. Buriak, K. Kobayashi, M. P. Isler, D. E. McRee, M. R. Ghadiri, *J. Am. Chem. Soc.* **1998**, *120*, 8949 – 8962.
[13] L. Tomasic, G. P. Lorenzi, *Helv. Chim. Acta* **1987**, *70*, 1012 – 1016.
[14] D. Seebach, J. L. Matthews, A. Meden, T. Wessels, C. Baerlocher, L. B. McCusher, *Helv. Chim. Acta* **1997**, *80*, 173 – 182.
[15] J. L. Matthews, K. Gademann, B. Jaun, D. Seebach, *J. Chem. Soc. Perkin Trans. 1* **1998**, 3331 – 3340.
[16] M. R. Ghadiri, J. R. Granja, R. A. Milligan, D. E. McRee, N. Khazanovich, *Nature* **1993**, *366*, 324 – 327.
[17] J. D. Hartgerink, J. R. Granja, R. A. Milligan, M. R. Ghadiri, *J. Am. Chem. Soc.* **1996**, *118*, 43 – 50.
[18] V. Pavone, E. Benedetti, B. DiBlasio, A. Lombardi, C. Pedone, L. Tomasic, G. P. Lorenzi, *Biopolymers* **1989**, *28*, 215 – 223.
[19] J. Lowbridge, E. Mtetwa, R. J. Ridge, C. N. C. Drey, *J. Chem. Soc. Perkin Trans. 1* **1986**, 155 – 156.
[20] D. N. J. White, C. Morrow, P. J. Cox, C. N. C. Drey, J. Lowbridge, *J. Chem. Soc. Perkin Trans. 2* **1982**, 239 – 243.
[21] I. L. Karle, J. Karle, *Acta Crystallogr.* **1963**, *16*, 969 – 975.
[22] M. Dobler, J. D. Dunitz, J. Krajewski, *J. Mol. Biol.* **1969**, *42*, 603 – 606.
[23] L. Zhang, J. P. Tam, *Tetrahedron Lett.* **1997**, *38*, 4375 – 4378.
[24] R. D. Allan, H. W. Dickenson, G. A. R. Johnston, R. Kazlauskas, H. W. Tran, *Aust. J. Chem.* **1985**, *38*, 1651 – 1656.
[25] Crystal data for **1** (colorless): dimensions $0.15 \times 0.15 \times 0.30$ mm, triclinic, P_1, $a = 4.726(2)$, $b = 7.709$, $c = 11.054(2)$ Å, $\alpha = 72.97(1)$, $\beta = 77.78(1)$, $\gamma = 88.55(1)^\circ$, $V = 306.1$ Å^3, $Z = 1$; $\rho_{calcd} = 1.286$ g cm^{-3}; $2\theta_{max} = 140^\circ$; 1353 reflections (1353 independent, 1193 with $F > 2.0\sigma F$, 1353 used in refinement); 198 parameters were refined; the max. and min. electron density map were 0.241 and -0.207 e Å^{-3}; the final residues were $R(F) = 0.0509$, and $R_w(F^2) = 0.1382$, GoF = 1.042.
[26] The data were collected on a Nonius CAD4 diffractometer; $Cu_{K\alpha}$; $\lambda = 1.54184$ Å; $\omega 2\theta$ scan; 293(2) K; the structure was solved by the application of direct methods and refined using SHELX97 (G. M. Sheldrick, *Acta Crystallogr. Sect. A* **1990**, *46*, 467 – 473); the refinements were against $|F^2|$, the data were reduced using XCAD4 (K. Harms, S. Wocadlo, University of Marburg), all programs included in the WinGX package (L. J. Farrugia, *J. Appl. Crystallogr.* **1999**, *32*, 837 – 838); the H atoms were geometrically placed.
[27] Crystallographic data (excluding structure factors) for the structures reported in this paper have been deposited with the Cambridge Crystallographic Data Centre as supplementary publication no. CCDC-164579 (**1**), -164580 (**4**), and -164581 (**5**). Copies of the data can be obtained free of charge on application to CCDC, 12 Union Road, Cambridge CB2 1EZ, UK (fax: (+44) 1223-336-033; e-mail: deposit@ccdc.cam.ac.uk).
[28] Y. A. Ovchinnikov, V. T. Ivanov, *Tetrahedron* **1974**, *30*, 1871 – 1890.
[29] Crystal data for **4** (colorless): Dimensions $0.05 \times 0.05 \times 0.48$ mm, monoclinic, $P2_1/a$, $a = 9.434(14)$, $b = 10.338(4)$, $c = 11.393(7)$ Å, $\beta = 111.22(6)^\circ$, $V = 1035.8$ Å^3, $Z = 2$; $\rho_{calcd} = 1.246$ g cm^{-3}; $2\theta_{max} = 130^\circ$; 1810 reflections (1725 independent, 967 with $F > 2.0\sigma F$, 1725 used in refinement); 167 parameters were refined; the max. and min. electron density map were 0.366 and -0.217 e Å^{-3}; the final residues were $R(F) = 0.0814$, and $R_w(F^2) = 0.2358$, GoF = 0.931.
[30] Crystal data for **5** (colorless): dimensions $0.08 \times 0.17 \times 0.45$ mm, trigonal, $R3$, $a = 17.299(5)$, $b = 17.299(5)$, $c = 4.819(5)$ Å, $V = 1248.9$ Å^3, $Z = 3$; $\rho_{calcd} = 1.162$ g cm^{-3}; $2\theta_{max} = 130^\circ$; 988 reflections (878 independent, 518 with $F > 2.0\sigma F$, 878 used in refinement); 65 parameters were refined; the max. and min. electron density map were 0.237 and -0.202 e Å^{-3}; the final residues were $R(F) = 0.0937$, and $R_w(F^2) = 0.2556$, GoF = 0.991.

Single-Step, Highly Active, and Highly Selective Nanoparticle Catalysts for the Hydrogenation of Key Organic Compounds**

Robert Raja, Tetyana Khimyak, John Meurig Thomas,* Sophie Hermans, and Brian F. G. Johnson*

More than three quarters of the organic molecular products that are manufactured industrially entail the processes of either hydrogenation or oxidation; and with the impending arrival of the so-called hydrogen economy and the parallel drive towards clean technology this fraction will inevitably rise in the near future, the most desirable agents of conversion

[*] Prof. Sir J. M. Thomas, Dr. R. Raja
The Royal Institution of Great Britain
Davy Faraday Research Laboratory
21 Albemarle Street, London W1S 4BS (UK)
Fax: (+44) 1223-339200
E-mail: has22@cam.ac.uk

Prof. Sir J. M. Thomas
Department of Materials Science and Metallurgy
New Museums Site
Pembroke Street, Cambridge CB2 3QZ (UK)

Prof. B. F. G. Johnson, Dr. R. Raja, T. Khimyak, Dr. S. Hermans
Department of Chemistry, University of Cambridge, Lensfield Road, Cambridge CB2 1EW (UK)
Fax: (+44) 1223-339200

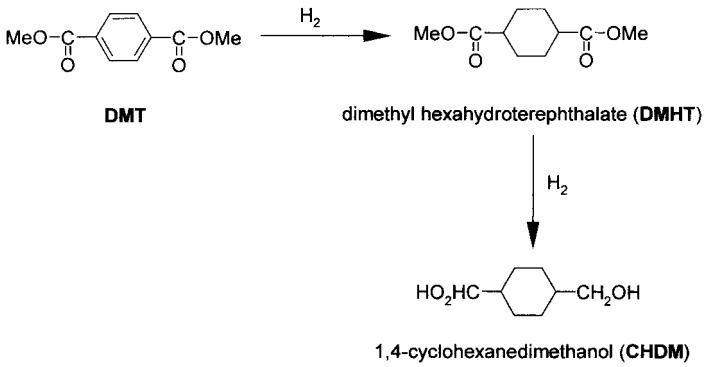
[**] We gratefully acknowledge the support (by a rolling grant to J.M.T. and an award to B.F.G.J.) of EPSRC (UK), of the Cambridge Overseas Trust (Schlumberger research), and ICI (for T.K.), and the award of a research fellowship (for S.H.) from Newnham College, Cambridge.

 © WILEY-VCH Verlag GmbH, D-69451 Weinheim, 2001

being molecular hydrogen and air (or oxygen). But increasing use of these agents requires the further development of robust, new, highly active and selective catalysts that, ideally, should effect single-step conversions under relatively mild and solvent-free conditions.[1] Here we describe the promising performance of two, related new bimetallic nanocatalysts for the hydrogenation of:

1) benzoic acid to cyclohexane carboxylic acid (**1**);
2) dimethyl terephthalate (DMT) to 1,4-cyclohexanedimethanol (CHDM) (**2**);
3) naphthalene in a highly selective manner to *cis*-decalin (**3**).

It is relevant to note that **1**, upon treatment with $NOHSO_4$ in the presence of strong acid (such as oleum) yields caprolactam,[2] the precursor of nylon; that **2** is preferred over ethylene glycol[3] as a stepping stone in the production of polyester fibers for extensive use in photography, antifogging agents, and in other applications involving polycarbonates and polyurethanes;[4] and that **3** is a useful source (and storage medium) for hydrogen. The hydrogenation of only the benzene ring in benzoic acid has scarcely been described.[5] Likewise, the hydrogenation of DMT to dimethyl hexahydroterephthalate (DMHT, Scheme 1) has been achieved to date only with a rhodium complex tethered on silica-supported palladium.[6]



Scheme 1. Hydrogenation of dimethyl terephthalate (DMT).

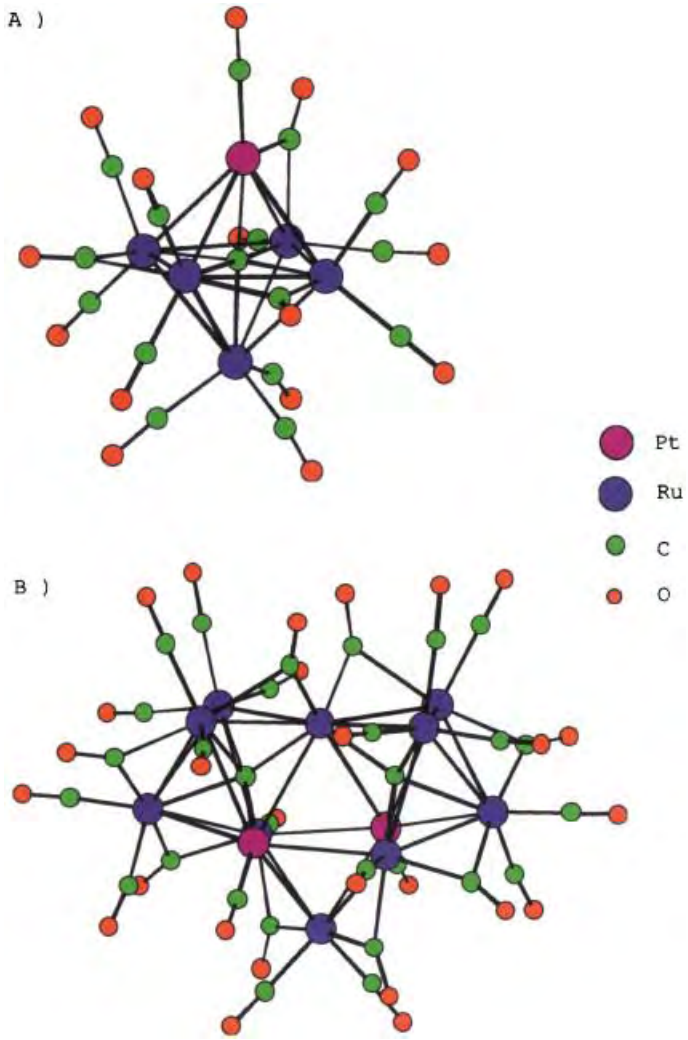


Figure 1. A) Structure of the anion in $[Ph_4P]_2[Ru_5PtC(CO)_{15}]$ (**4**).[18] B) Structure of the anion in $[PPN]_2[Ru_{10}Pt_2C_2(CO)_{28}]$ (**5**; PPN = $[(C_6H_5)_3P{=}N{=}P(C_6H_5)_3]^+$), prepared and fully described as reported elsewhere.[19]

The bimetallic nanoparticle catalysts reported here are discrete anchored clusters, Ru_5Pt and $Ru_{10}Pt_2$, prepared by the gentle decarbonylation of the parent, mixed-metal precursor anions, $[Ru_5PtC(CO)_{15}]^{2-}$ and $[Ru_{10}Pt_2C_2(CO)_{28}]^{2-}$ (Figure 1), after first inserting them, along with their counterions into mesoporous silica, in a manner closely akin to the preparation of anchored Ru_6Sn,[7] Pd_6Ru_6,[8] and of Cu_4Ru_{12},[9] nanoclusters described previously. The diameter of the resulting, well-dispersed, isolated and anchored bimetallic nanoparticles is in the range of approximately 10–20 Å[10, 11] (see below).

A bright-field (BF) scanning transmission electron micrograph (Figure 2A) directly reveals the mesoporosity of the silica (MCM-41) used as host to encapsulate the bimetallic nanoparticle catalysts.[12, 13] And a bright field/high-angle-annular dark field (BF/HAADF) pair (Figure 2B and C) shows clearly the uniform size and distribution of the denuded mixed-metal anion (in this case $Ru_{10}Pt_2$) within the mesopores. These anchored nanoparticle catalysts are readily accessible to all the reactant and product molecules of this investigation.

A preliminary test of the performance of these catalysts was carried out using cyclohexene as the reactant. The results (Table 1) leave little doubt that the catalytic activity and selectivity of both Ru_5Pt and $Ru_{10}Pt_2$ are exceptional. In the hydrogenation of naphthalene again the performance of these two catalysts is exceptional (Table 1): only the fully hydrogenated naphthalenes (decalins) are formed, and the ratio of the *cis* to the *trans* forms is high (ca. 5.5:1 to 8.6:1 depending upon the precise conditions). Moreover, these catalysts are unimpaired in their performance even when substantial amounts of a well-known "sulfur poison" is deliberately introduced—in sharp contrast to the behavior of otherwise good bimetallic nano-catalysts (Pd_6Ru_6, Ru_6Sn, and Cu_4Ru_{12}) previously tested by us.

In the hydrogenation of benzoic acid the efficacy of the two RuPt nanocatalysts again surpasses that of the three, quite distinct bimetallic catalysts that we have previously described (Figure 3).

 © WILEY-VCH Verlag GmbH, D-69451 Weinheim, 2001 1433-7851/01/4024-4639 $ 17.50+.50/0

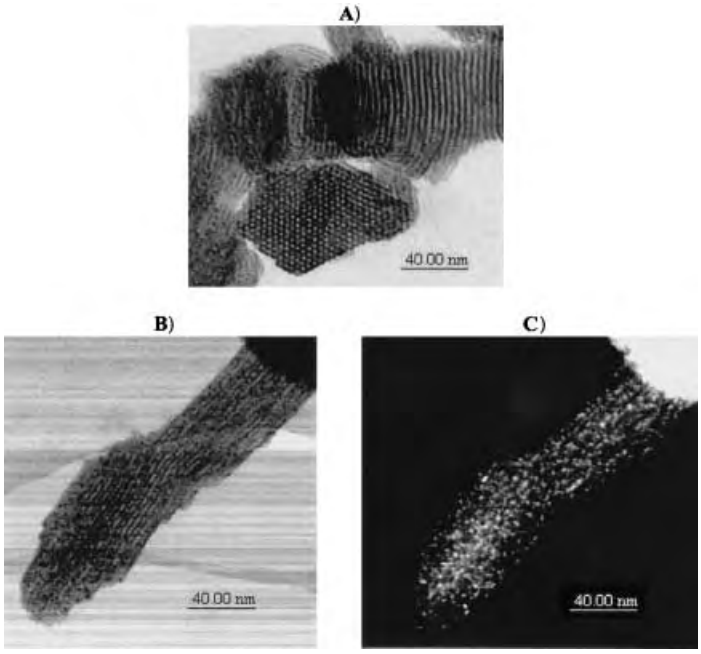


Figure 2. A) BF scanning transmission electron micrograph[7, 12] of a typical group of crystallites of mesoporous silica (ca. 30 Å diameter) onto the inner walls of which nanoparticle arrays have been anchored (not clearly visible, see Figures 2 B and C of $Ru_{10}Pt_2$ catalysts. B) and C) A BF/HAADF pair of another region of the mesopore-encapsulated $Ru_{10}Pt_2$ nanocatalysts. Whereas in (B) many of the nanoparticles are just about visible, in C) they all stand out very clearly and are seen to be aligned along the mesopores (compare Figure 4 of ref. [7]).

The hydrogenation of DMT (see Scheme 1) to the valuable product CHDM (**2**) is carried out industrially in two steps using two reactors.[14] The first, which requires a temperature in the range 160–180 °C and a pressure of 30–48 MPa, uses a supported Pd catalyst. This highly exothermic process yields the intermediate, dimethyl hexahydroterephthalate (DMHT). This, in turn, is converted at about 200 °C and 40 bar (40×10^5 Pa) H_2 over a copper chromite catalyst, into the required CHDM.[14] With our catalysts, one-step conversions of DMHT into CHDM are effected in high yield even after a mere 4 h contact time at 100 °C, a pressure of 20 bar (20×10^5 Pa) H_2, in ethanol as a benign solvent (Table 2). It is noteworthy that the yield of CHDM passes through a maximum, there being cross-linked products such as 4-methyloxymethlhydroxymethylcyclohexane and bis (4-hydroxymethylcyclohexyl) ether formed during the conversion. Other bimetallic nano-catalysts that are less efficient than Ru_5Pt or $Ru_{10}Pt_2$ as straightforward hydrogenation catalysts (see Table 1), species such as Cu_4Ru_{12}, are especially effective in producing good yields of CHDM (see Table 2). Kinetic studies (Figure 4 and Figure 5) reveal the changes more explicitly. It is also noteworthy that the *cis*:*trans* ratio of the CHDM formed is 80:20 for the Cu_4Ru_{12} catalyst, and 65:35 in the case of both the RuPt catalysts. It augurs well here that, in the case of the Cu_4Ru_{12} catalyst, these values are extremely significant for industrial processing (ideally 88:12).[15, 16] Notably, the Pd_6Ru_6 catalyst produces a 50:50 mixture (*cis*:*trans*) of CHDM.

Given the sensitive time dependence of product yields in the (one-step) hydrogenation of DMT there is abundant scope here for the chemical engineer to optimize the production of CHDM. Further work on the structure and catalytic properties of the two compositionally identical, but elementally different, bimetallic nanoparticles, is in progress.

Experimental Section

$[Ph_4P]_2[Ru_5PtC(CO)_{15}]$ (**4**): An excess of KOH (500 mg) was added to a solution of $[Ru_5PtC(CO)_{16}]$ (200 mg, 0.17 mmol) in methanol. The mixture was stirred at room temperature for 2 h after which an excess of Ph_4PCl (160 mg, 0.43 mmol) was added to yield **4** as dark red precipitate. The solid was collected by filtration and washed with hexane, yield: 268 mg (87 %).

Table 1. Hydrogenation of cyclohexene and naphthalene—comparison of catalysts.

Catalyst[a]	Substrate	t [h]	p H_2 [bar][b]	T [K]	Conv [mol %]	TOF [h^{-1}][d]	Product distribution [mol %][e]			
							A	B	C	D
Ru_5Pt/SiO_2	cyclohexene	1.5	10	353	52.5	6860	100	–	–	–
		3	1		96.9	6341	100	–	–	–
$Ru_{10}Pt_2/SiO_2$	cyclohexene	1.5	8	353	75.2	14530	100	–	–	–
		2	0		98.0	14201	100	–	–	–
Pd_6Ru_6/SiO_2	cyclohexene	1.5	15	353	31.3	3250	100	–	–	–
		3	10		55.0	3015	100	–	–	–
Ru_6Sn/SiO_2	cyclohexene	1.5	17	353	15.2	1989	92	–	–	11.5
		3	15		26.5	1734	85	–	–	14.7
Cu_4Ru_{12}/SiO_2	cyclohexene	1.5	17	353	11.5	2015	89	–	–	11
		3	15		21.7	1950	80	–	–	20.2
Ru_5Pt/SiO_2	naphthalene	8	8	373	31.5	792	–	84	15	–
		8[c]	7		32.0	805	–	86.4	13.3	–
$Ru_{10}Pt_2/SiO_2$	naphthalene	8	6	373	44.7	1660	–	89.4	10.2	–
		8[c]	6		45.0	1671	–	88.5	11.3	–
Pd_6Ru_6/SiO_2	naphthalene	8	14	373	7.0	19	–	50	34	15
		8[c]	19			–		no reaction		
Ru_6Sn/SiO_2	naphthalene	8	12	373	9.5	238	–	48.2	45	6.5
		8[c]	18			–		no reaction		
Cu_4Ru_{12}/SiO_2	naphthalene	8	19	373		–		no reaction		
		8[c]	18			–		no reaction		

[a] The mesoporous SiO_2 used here is of the MCM-41 type. Reaction conditions: cyclohexene ≈ 50 g; naphthalene ≈ 8 g (dissolved in 55 g of hexadecane); catalyst = 50 mg; H_2 pressure = 20 bar. [b] Residual H_2 pressure in the reactor. [c] 200 ppm of sulfur was introduced (benzothiophene). [d] TOF = $[(mol_{substr})(mol_{cluster})^{-1}h^{-1}]$. [e] A = cyclohexane; B = *cis*-decalin; C = *trans*-decalin; D = others.

 © WILEY-VCH Verlag GmbH, D-69451 Weinheim, 2001 1433-7851/01/4024-4640 $ 17.50+.50/0 *Angew. Chem. Int. Ed.* **2001**, *40*, No. 24

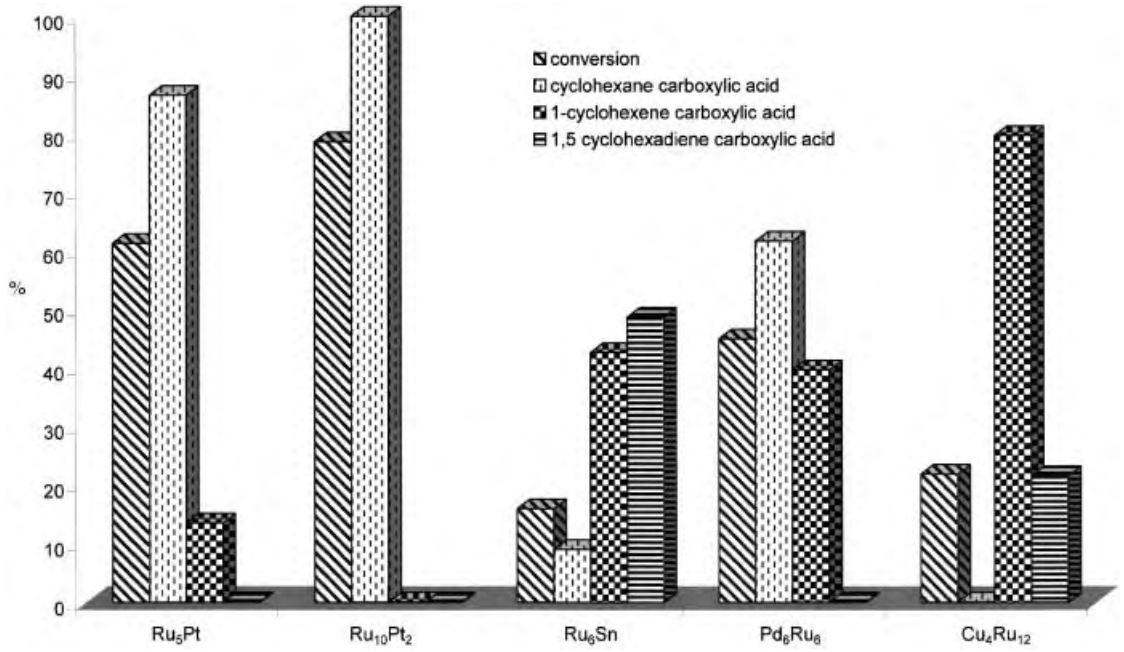


Figure 3. Bar chart of the relative performances and selectivity of the Ru_5Pt and $Ru_{10}Pt_2$ catalysts compared to other bimetallic nanocatalysts, (used by us in our previous studies[7–9]) for the hydrogenation of benzoic acid. Note that the Ru_5Pt and $Ru_{10}Pt_2$ catalysts display a high degree of selectivity for the cyclohexane carboxylic acid in marked contrast to the other bimetallic analogues. Reaction conditions: benzoic acid ≈2.5 g (dissolved in 75 mL of ethanol); catalyst = 50 mg, H_2 pressure = 20 bar, $T = 373$ K; $t = 24$ h.

Table 2. Hydrogenation of dimethyl terephthalate (DMT)—comparison of catalysts.

Catalyst[a]	t [h]	Conv [mol %]	TOF [h^{-1}][b]	Product distribution [mol %][c]			
				A	B	C	D
Ru_5Pt/SiO_2	4	7.5	155	58.7	33.5	–	6.9
	8	18.4	191	55.3	5.2	–	39.4
	24	36.9	138	61.2	–	–	38.7
$Ru_{10}Pt_2/SiO_2$	4	23.3	714	42.6	52.3	–	–
	8	39.5	605	53.6	9.0	–	37.1
	24	67.2	443	51.4	–	–	48.5
Pd_6Ru_6/SiO_2	4	6.2	98	32.9	16.8	–	51.1
	8	15.5	125	22.5	4.2	–	74.2
	24	23.7	64	18.2	–	–	81.5
Ru_6Sn/SiO_2	4	–	–	–	–	–	–
	8	5.3	54	77.2	–	22.6	–
	24	8.0	27	81.0	–	18.6	–
Cu_4Ru_{12}/SiO_2	4	–	–	–	–	–	–
	8	10.4	102	22.2	54.5	23.0	–
	24	14.2	45	25.3	63.2	–	11.3

[a] The mesoporous SiO_2 used here is of the MCM-41 type. Reaction conditions: DMT ≈ 2.5 g (dissolved in 75 mL ethanol); $T = 373$ K; H_2 pressure = 20 bar; catalyst ≈ 50 mg. [b] TOF = $[(mol_{substr})(mol_{cluster})^{-1} h^{-1}]$. [c] A = dimethyl hexahydroterephthalate (DMHT); B = 1,4-cyclohexanedimethanol (CHDM); C = mixture of 4-methyl-4-cyclohexane carboxylic acid methyl ester and 1-hydroxymethyl-4-methylcyclohexane; D = mixture of 4-methyloxymethylhydroxymethylcyclohexane and bis(4-hydroxymethylcyclohexyl) ether.

Elemental analysis calcd (%) for $C_{64}H_{40}O_{15}P_2PtRu_5$: C 42.44, H 2.23, P 3.42; found: C 40.62, H 2.27, P 3.42; IR (CH_2Cl_2): $\tilde{\nu}_{max}$ = (CO) 1975s (br), 1911w (sh), 1823w (br), 1771w (br) cm^{-1}; ^1H NMR (400 MHz, 300 K, CD_2Cl_2): δ = 7.92 – 7.60 (m, 20 H, $P(C_6H_5)_4$); ^{13}C NMR (400 MHz, 300 K, CD_2Cl_2): δ = 201.0 (m, CO), 136.0 – 117.37 (m, C_6H_5); MS: m/z (%): 566 (100) [$M^{2-}/2$], 552 (48) [$M^{2-}/2$ – CO].

The catalytic materials were prepared by standard procedures.[7, 9] The mesoporous silica was loaded with cluster **4** or **5** by making a slurry in diethyl ether/dichloromethane. The mesopore-encapsulated clusters **4** and **5** were activated by heating at 195 °C in vacuo for 2 h. As in earlier preparations,[7] the FT-IR spectra recorded after activation showed no residual peaks corresponding to the carbonyl stretching frequencies.

The electron microscopy characterizations were carried out on a VG HB501 field-emission STEM microscope, and the catalysts dispersed on a holey carbon film supported on a copper grid from a suspension in hexane, as described in ref. [7].

The catalytic reactions were carried out in a high-pressure stainless steel catalytic reactor lined with poly ether ether ketone (PEEK). Dry hydrogen (20 bar (20×10^5 Pa)) was pressurized into the reaction vessel and, using a mini robot liquid-sampling valve, small aliquots of the sample were removed to study the kinetics of the reaction, without perturbing the pressure in the reactor.[17] The products were analyzed (using a suitable internal standard)[7] by gas chromatography (GC, Varian, Model 3400 CX) employing a HP-1 capillary column (25 m × 0.32 mm) and flame ionization detector. The identity of the products was confirmed by injecting authenticated samples and further by liguid chromatography mass spectrometry (LC-MS; Shimadzu, QP 8000) employing a gamma-cyclodextrin dialkyl column (Chiraldex, 20 m × 0.25 mm).

 © WILEY-VCH Verlag GmbH, D-69451 Weinheim, 2001 1433-7851/01/4024-4641 $ 17.50+.50/0

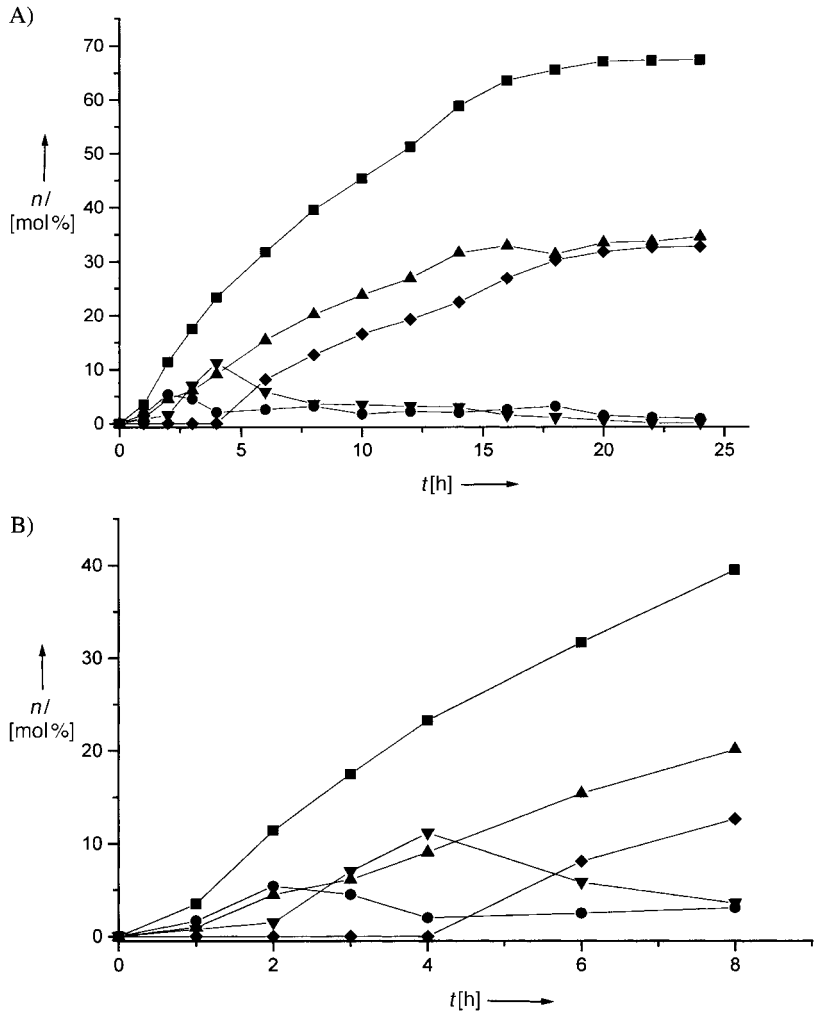


Figure 4. Kinetics of hydrogenation of DMT by using $Ru_{10}Pt_2$ (A). An expanded view of the initial part of the reaction where the formation of CHDM, after 4 h, is clearly detected is shown in (B). The CHDM further reacts in the presence of this catalyst to form coupling by-products as elaborated in Table 2 and in the text. ■ conversion of DMT; ● C (see Table 2 for details); ▲ DMHT; ▼ CHDM; ◆ D (see Table 2 for details).

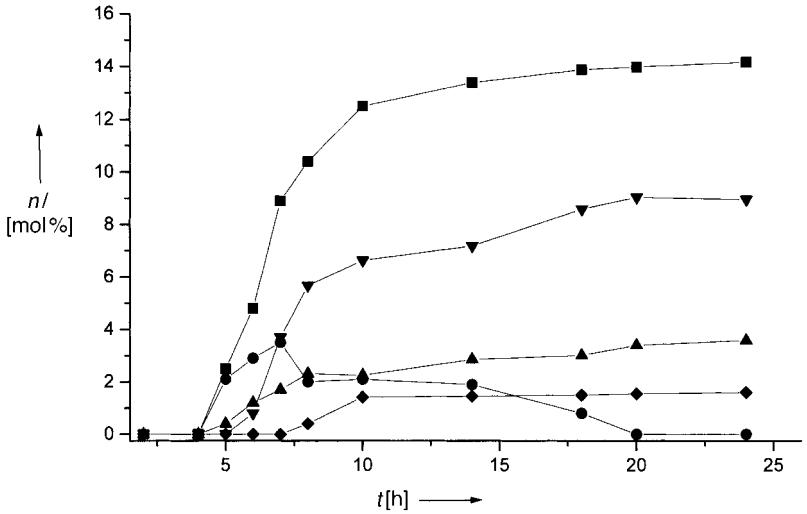


Figure 5. Kinetics of hydrogenation of DMT using Cu_4Ru_{12} as the catalyst. Note that the product distribution is markedly different (c.f. Figure 4) and the formation of by-products is relatively suppressed. The synergistic role of the copper in driving the reaction further (conversion of DMHT into CHDM) is clearly evident here, in stark contrast with what is observed in Figure 4 using the $Ru_{10}Pt_2$ catalyst; ■ conversion of DMT; ● C (see Table 2 for details); ▲ DMHT; ▼ CHDM; ◆ D (see Table 2 for details).

The Ru–Pt catalysts have been re-used three times without appreciable loss in catalytic activity or selectivity. Further, experiments, analogous those reported earlier,[7] were carried out to rule out the possibility of leaching, and analysis of the resulting filtrate at the end of reaction (24 h, for DMT hydrogenation) by ICP (ICP = inductively charged plasma) and atomic absorption spectroscopy (AAS) revealed only trace amounts (< 5 ppb) of dissolved metal ions (Pt, Ru).

Received: August 13, 2001 [Z17719]

[1] J. M. Thomas, R. Raja, G. Sankar, B. F. G. Johnson, D. W. Lewis, *Chem. Eur. J.* **2001**, *7*, 2973.

[2] J. Ritz, H. Fuchs, H. Kieczka, W. C. Morgan, *Ullmanns Encyclopedia of Industrial Chemistry*, Wiley-VCH, Weinheim, Germany, **2001**.

[3] a) T. Mizumoto, H. Kamatani (Toyobo), JP 75142537, **1975** [*Chem. Abstr.* **1976**, *84*, 135183s]; b) B. J. Sublett, G. W. Connell (Eastman Chemical), US-A 5559159, **1995** [*Chem. Abstr.* **1996**, *125*, 277914v].

[4] a) T. K. Debroy, M. Guagliardo, J. P. Pucknat (BASF), EP 262069, **1986** [*Chem. Abstr.* **1988**, *109*, 56675k]; b) R. R. Amborse, J. B. O'Dwyer, B. K. Johnston, D. P. Zielinski, S. Porter, W. H. Tyger (PPG Industries) US-A 4859743, **1988** [*Chem. Abstr.* **1990**, *112*, 38296v].

[5] C. S. Chin, B. Lee, J. Moon, J. H. Song, Y. S. Park, *Bull. Korean Chem. Soc.* **1995**, *16*, 528.

[6] H. Yang, H. R. Gao, R. J. Angelici, *Organometallics* **2000**, *19*, 622.

[7] S. Hermans, R. Raja, J. M. Thomas, B. F. G. Johnson, G. Sankar, D. Gleeson, *Angew. Chem.* **2001**, *113*, 1251–1255; *Angew. Chem. Int. Ed.* **2001**, *40*, 1211–1215.

[8] R. Raja, S. Hermans, D. S. Shephard, S. Bromley, J. M. Thomas, B. F. G. Johnson, T. Maschmeyer, *Chem. Commun*. **1999**, 2131.

[9] D. S. Shephard, T. Maschmeyer, G. Sankar, J. M. Thomas, D. Ozkaya, B. F. G. Johnson, R. Raja, R. D. Oldroyd, R. G. Bell, *Chem. Eur. J.* **1998**, *4*, 1214.

[10] J. M. Thomas, *Angew. Chem.* **1999**, *111*, 3800; *Angew. Chem. Int. Ed.* **1999**, *38*, 3588.

[11] W. Zhou, J. M. Thomas, D. S. Shephard, B. F. G. Johnson, D. Ozkaya, T. Maschmeyer, R. G. Bell, Q. Ge, *Science* **1998**, *280*, 705.

[12] D. Ozkaya, W. Zhou, J. M. Thomas, P. A. Midgeley, V. J. Keast, S. Hermans, *Catal. Lett*. **1999**, *60*, 113.

[13] J. M. Thomas, O. Terasaki, P. L. Gai, W. Zhou, J. Gonzalez-Callet, *Acc. Chem. Res.* **2001**, *34*, 583.

[14] a) M. L. Schlossman (Tevco), US-A 4301046, **1981** [*Chem. Abstr.* **1982**, *96*, 24664c]; b) P. Appleton, M. A. Wood (Eastman Chemical), US 5414159, **1993** [*Chem. Abstr.* **1995**, *123*, 170535d].

[15] P. Werle, M. Morawietz, *Ullmanns Encyclopedia of Industrial Chemistry*, Wiley-VCH, Weinheim, Germany, **2001**.

[16] R. D. Adams, W. Wu, *J. Cluster Sci.* **1991**, *2*, 271–290.

[17] J. M. Thomas, R. Raja, G. Sankar, R. G. Bell, *Acc. Chem. Res.* **2001**, *34*, 191.

[18] The single-crystal X-ray structure of **4** will be reported elsewhere.

[19] B. F. G. Johnson, S. Hermans, T. Khimyak, *Organometallics* **2001**, submitted.

 © WILEY-VCH Verlag GmbH, D-69451 Weinheim, 2001 1433-7851/01/4024-4642 $ 17.50+.50/0

Influence of Structural and Rotational Isomerism on the Triplet Blinking of Individual Dendrimer Molecules**

Tom Vosch, Johan Hofkens,* Mircea Cotlet, Fabian Köhn, Hideki Fujiwara, Roel Gronheid, Koen Van Der Biest, Tanja Weil, Andreas Herrmann, Klaus Müllen, Shaul Mukamel, Mark Van der Auweraer, and Frans C. De Schryver*

The manifestation of the quantum nature of single ions[1] trapped in radiofrequency traps, and of individual molecules immobilized in a matrix, at both cryogenic[2] and room temperature,[3] has been reported. Since the observation of quantum jumps in a single ion it has been predicted that two or more ions trapped close to each other would show collective effects. This scenario was demonstrated by measuring the fluorescence intensity signal of three Ba^+ ions in a trap.[4] The experiment showed a large fraction of simultaneous on/off jumps, far beyond the chance of random coincidence. The presence of collective effects at room temperature has been demonstrated in immobilized single molecules of a conjugated polymer[5] and the light-harvesting complex LH_2[6] containing on average 150 and 27 chromophores, respectively, as well as a multichromophoric dendrimer with 8 chromophores.[7] The collective effect is seen as discrete on/off jumps in the fluorescence time traces of these molecules. VandenBout et al. interpreted the data obtained on a conjugated polymer in terms of an efficient intramolecular energy transfer along the polymer chain, and speculated that a localized polymer defect would quench the excitation along the entire chain.[5] It was demonstrated in an analogous conjugated system that fast energy transfer resulting in collective effects depends on the conformation adopted by the polymer chain.[8] In the case of the dendritic system, an efficient energy transfer of the excitation energy towards the triplet state created in one of the chromophores of the dendrimer was suggested as a mechanism for the collective on/off jumps. The duration of the off periods indeed agrees with the earlier reported triplet lifetime (also from single-molecule measurements in similar conditions) of the chromophore attached to a dendrimer branch.[7] The duration of the off-periods depends strongly on the oxygen concentration, which corroborates the validity of the proposed mechanism as it is known that oxygen is a quencher of the triplet state.[9]

Herein we report on a three chromophoric system. It was possible to obtain three chromophores with a fixed 3D orientation in close proximity by using recent progress made in dendrimer synthesis.[10, 11] The new synthetic approach, based on a Diels–Alder reaction, allows the controlled attachment of a well-defined number of chromophores to the outer rim of the shape-persistent dendritic structure (Figure 1a). Perylenedicarboximide was chosen as the chromophore because of its photostability, its absorption wavelength (around 500 nm), its absorption coefficient ($\varepsilon = 40\,000\ cm^{-1}mol^{-1}L$ in toluene), and its large fluorescence quantum yield ($\varphi_f > 0.9$).[7, 12] The attachment of the chromophores leads to four structural isomers as a result of the asymmetric building blocks used in the synthesis (Figure 1a). Furthermore the rotation of the chromophores, attached in the *meta* position, can lead to two different orientations in space. The fact that the dendrimers (**1**) are spin-coated in a polymer film might freeze out additional rotational isomers. The different isomers might result in differences in the interactions between the chromophores. Two isomers (A and B) of **1** obtained by energy minimization which represent two extreme configurations related to the synthetic uncertainty and with different mutual orientations and distances among the chromophores are presented in Figure 1b and c. These two minimized structures were obtained by using a molecular mechanics optimization method.

Calculations of the electronic transitions and coupling parameters of the two depicted structural isomers of **1** were performed by using the CEO-INDO/S (Collective Electronic Oscillators-Intermediate Neglect of Differential Overlap/Spectroscopic) procedure.[13] The chromophores in isomer A are well separated in space and their center–center distance is 2.86 nm. The calculations indicate that the three chromophores interact and that three exciton states are formed. The transition density matrices of these exciton states are depicted in Figure 2. The density matrix is numbered from chromophore 1 to 3, which means that the first 37 atoms correspond to the atoms of chromophore 1. The coupling between the different chromophores in isomer A is small, with a typical value of about 11 cm^{-1}, and can be either positive or negative, depending on the relative orientation of the individual transition dipoles.

The distances between the three chromophores of isomer B differ (Figure 1c). The distance between pair 2,3 is 1.52 nm, while between pairs 1,3 and 1,2 it is 3.35 and 3.05 nm, respectively. The coupling between the chromophores is

[*] Dr. J. Hofkens, Prof. Dr. F. C. De Schryver, T. Vosch, M. Cotlet, F. Köhn, R. Gronheid, K. Van Der Biest, Prof. Dr. M. Van der Auweraer
Department of Chemistry
Katholieke Universiteit Leuven
Celestijnenlaan 200F, 3001 Heverlee (Belgium)
Fax: (+32) 16-32-7989
E-mail: johan.hofkens@chem.kuleuven.ac.be
frans.deschryver@chem.kuleuven.ac.be

Dr. H. Fujiwara
Research Institute for Electronic Science
Hokkaido University, Sapporo 060-0812 (Japan)

T. Weil, A. Herrmann, Prof. Dr. K. Müllen
Max-Planck-Institut für Polymerforschung
Ackermannweg 10, 55128 Mainz (Germany)

Prof. Dr. S. Mukamel
Chemistry Department, University of Rochester
Rochester, NY 14627-0216 (USA)

[**] J.H. thanks the FWO for a post-doctoral fellowship. T.V. wishes to thank the I.W.T. for a doctoral fellowship. Financial support by the FWO, the DWTC (through IUAP-4-11), and the Flemish Ministry of Education (through GOA/1/2001) is gratefully acknowledged. The EC (through TMR Sisitomas), ESF (through Smarton), and the Volkswagen-Stiftung are also thanked for financial support. Dr. L. Latterini is thanked for the triplet absorption measurements.

Supporting information for this article is available on the WWW under http://www.angewandte.com or from the author.

 © WILEY-VCH Verlag GmbH, D-69451 Weinheim, 2001 1433-7851/01/4024-4643 $ 17.50+.50/0

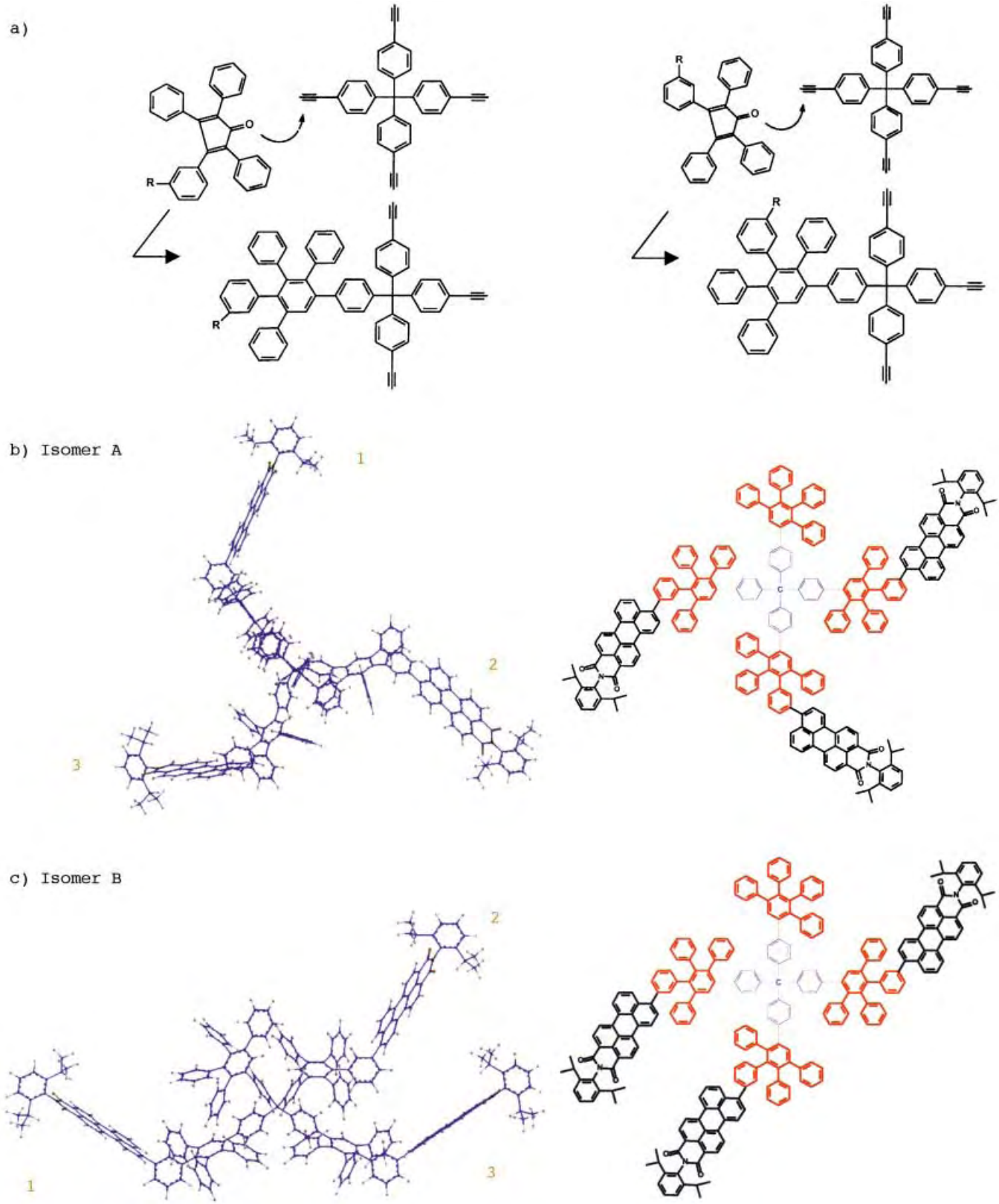


Figure 1. a) Schematic representation of the Diels–Alder reaction that results in the creation of the different structural isomers. b, c) 3D representation of isomers A and B, respectively.

always positive, the coupling in pair 2,3 (90 cm^{-1}) is roughly five times larger than in pairs 1,3 and 1,2. The transition density matrices show that the chromophores in the two isomers are characterized by different interactions.

The knowledge obtained from synthesis-related information together with the results of the calculations that suggested that different structural isomers have different transition density matrices and hence different photophysical

 © WILEY-VCH Verlag GmbH, D-69451 Weinheim, 2001 1433-7851/01/4024-4644 $ 17.50+.50/0

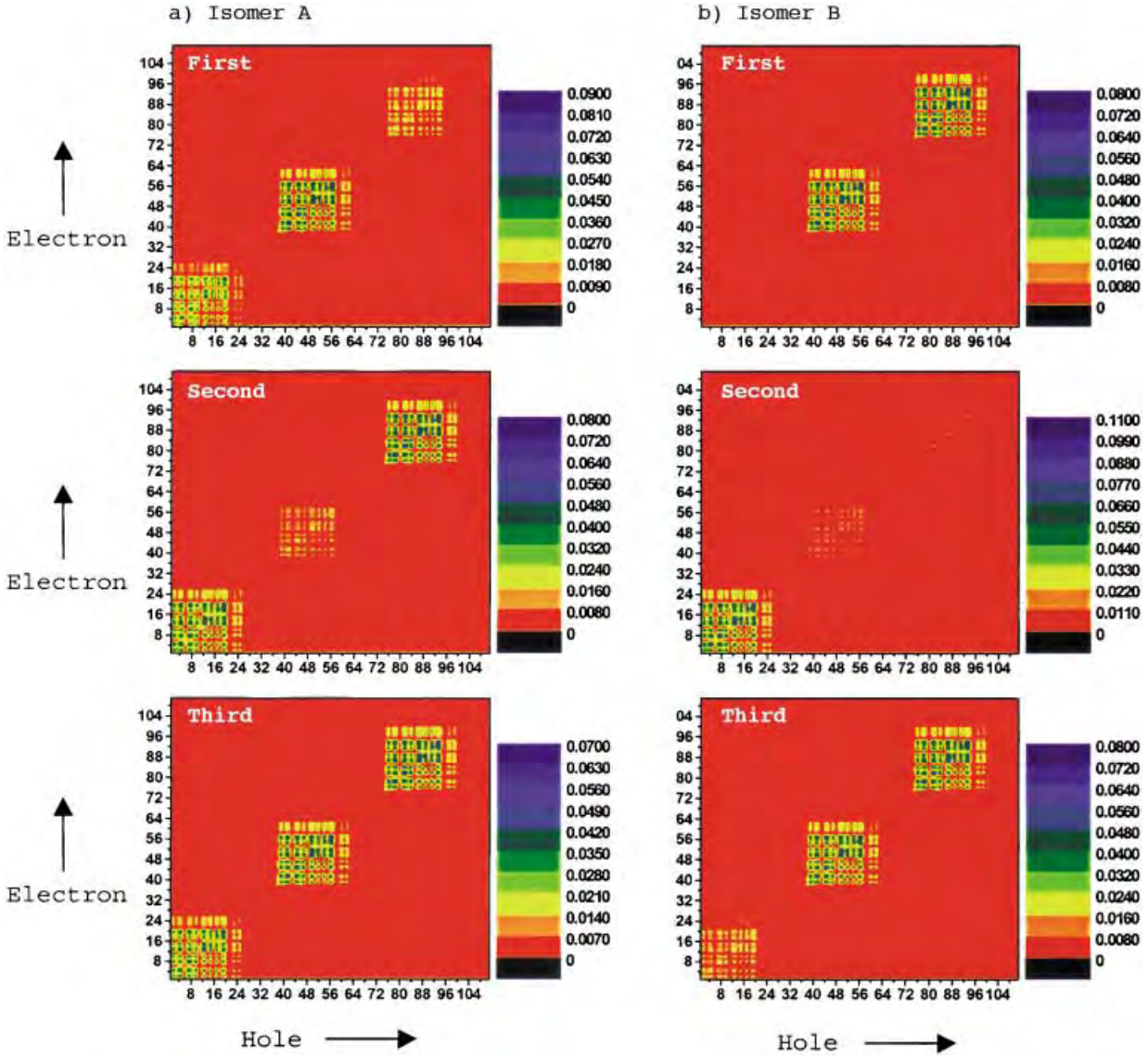


Figure 2. Left column: The three lowest in energy transition density matrices of isomer A. Right column: The three lowest in energy transition density matrices of isomer B.

behavior prompted the investigation of **1** at the single molecule level. Compound **1** was dispersed in a thin polymer film and investigated by confocal fluorescence microscopy at room temperature.[10]

Fluorescence intensity trajectories of one hundred and fifty individual molecules of **1** were recorded. Two clearly distinct types of transients (type I and II) are observed. Type I constitutes 50 % of the total number of transients and has fluorescence intensity trajectories showing stable levels (Figure 3 a). The corresponding emission spectra are structured and show only small fluctuations (spectral diffusion) in the emission maxima (Figure 3 c). Displaying the number of detected photons as a histogram results in three distinct and well-separated peaks and a background peak at five counts (Figure 3 b). The emission spectra show a strong resemblance with the ensemble emission spectrum of both **1** and hexaphenylbenzeneperyleneimide in toluene.[14] The corresponding fluorescence decay measurements yielded decay times of 4.2 ± 0.5 ns. The stepwise changes in fluorescence intensity in the transient can be explained by assuming a stepwise bleaching of the chromophores if the bleached chromophores do not act as a trap for the fluorescence. Transients of the parallel and perpendicular component of the fluorescence were recorded with two independent detectors (polarized transients) to further corroborate this stepwise bleaching. In this way, a trajectory of the degree of polarization (p) can be calculated from Equation (1), where G is a factor that corrects for the different detection efficiencies of both detection channels.

$$p = \frac{I_{par} - G I_{per}}{I_{par} + G I_{per}} \quad (1)$$

Figure 3 d shows an example where three levels in both the polarized fluorescence intensity trajectories can be seen. The p value, however, does not change, which indicates that the polarization of the emission does not change during the entire trajectory. This result means that the emitting chromophore is the last one to photobleach in this case. Figure 3 e, on the

 © WILEY-VCH Verlag GmbH, D-69451 Weinheim, 2001 1433-7851/01/4024-4645 $ 17.50+.50/0

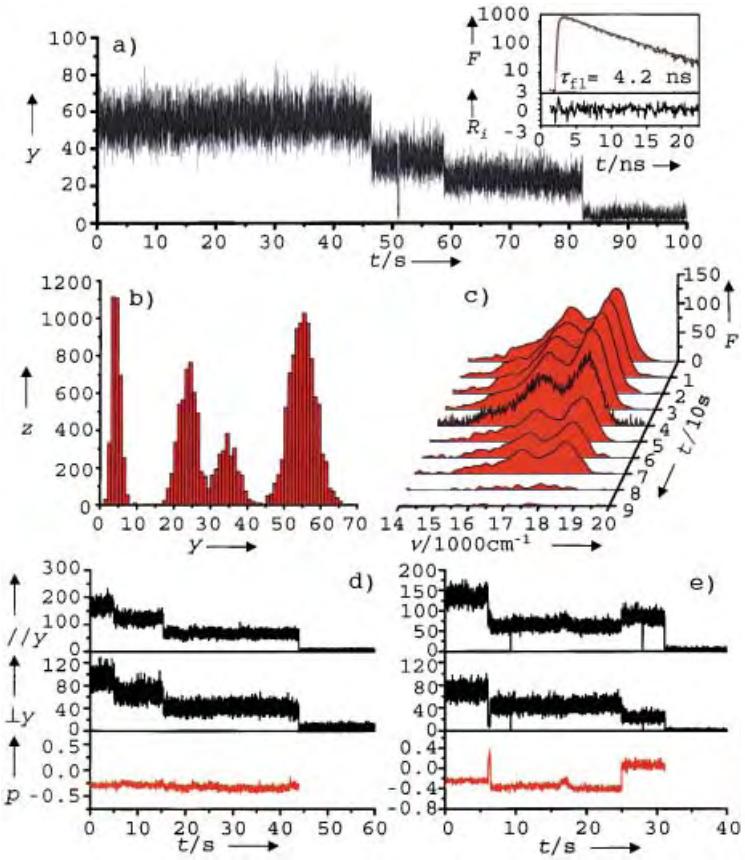


Figure 3. a) Fluorescence intensity trajectory, type I. The inset represents the decay observed during the first 5 s of the transient. b) Frequency histogram of the fluorescence intensity trajectory given in (a). c) The fluorescence spectra as a function of time (10 s integration) of the molecule shown in (a). Both a fitted and a raw spectrum are shown. d, e) Two typically polarized fluorescence intensity trajectories. The upper trace is the parallel channel, while the middle trace shows the perpendicular channel. The lower trace shows the p trajectory. y = number of photons detected in 5 ms; F = fluorescence intensity (in number of detected photons); z = frequency of occurrence; R_i = Residuals.

other hand, shows the p trajectory, and three distinct p values can be distinguished. The variations in the p value coincide with changes in the fluorescence intensity in the trajectory. In this case, the initial emitting chromophore bleaches and a different chromophore starts acting as the fluorescent trap. We propose that emission occurs at all times only from the chromophore that is lowest in energy. This situation implies one chromophore acts as a fluorescent trap while the other chromophores communicate through Förster-type energy transfer. Analysis shows that the p value in 80% of the traces shows three discrete values (as in Figure 3e), while an invariant p value (such as in Figure 3d) is found in 20% of the transients. The invariance of the p value together with a change in the intensity level indicates competition between energy transfer to the fluorescent trap and photobleaching from the singlet excited state. This energy transfer is confirmed by fluorescence anisotropy decay measurements of the ensemble, which is described by a two exponential fitting with parameters of 100 ps and 1.2 ns, where the former relates to energy hopping between the chromophores.[14] Collective on/off jumps occur, but are extremely rare events compared to the previously reported dendrimer system containing eight peryleneimide chromophores.[7] The transient in Figure 3a shows one jump from the second level to the background level and back. The transient displayed in Figure 3d shows no on/off jumps whereas in the transient displayed in Figure 3e three jumps are present (after 7, 10, and 27 s). The collective on/off jumps were explained by the triplet state on one of the chromophores acting as a nonradiative trap and hence quenching all the fluorescence in the molecule. The fluorescence spectrum of **1** and the transient absorption spectrum (T_1-T_n) indeed overlap to a large extent (see inset in Figure 4d), which indicates that a chromophore in a S_1 state and a chromophore in a T_1 state form an almost ideal resonance energy transfer (RET) pair. The idea that the triplet state is indeed involved in the collective behavior was earlier corroborated by the duration of the collective off periods being oxygen dependent.[9] The limited number of collective jumps can be attributed to the extremely low intersystem crossing yield (Y_{ISC}) of the peryleneimide chromophore. When the applied excitation power and the detection efficiency of the setup (10%) are taken into account, and if a diffraction-limited spot of 350 nm is assumed, an average Y_{ISC} value of

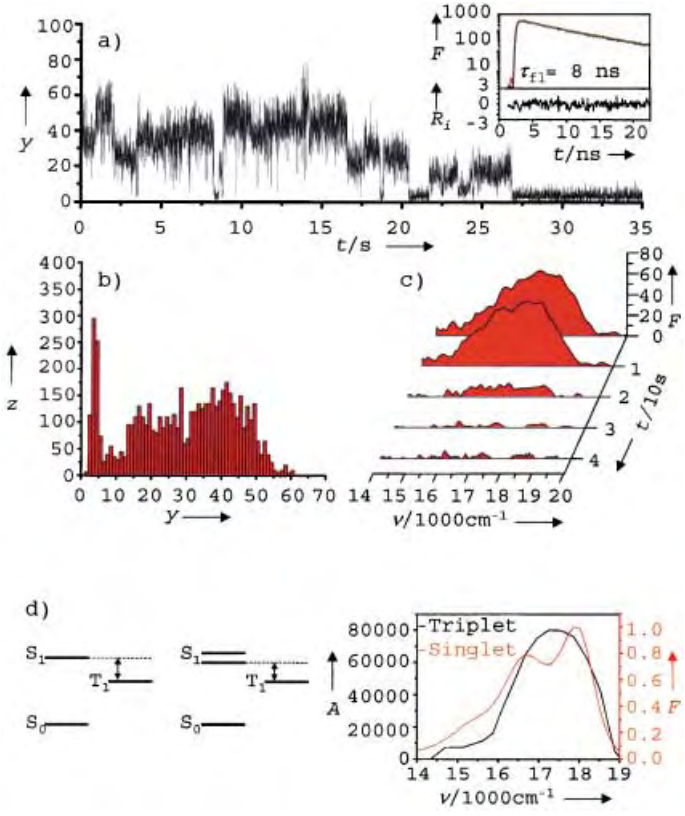


Figure 4. a) Fluorescence intensity trajectory, type II. The inset represents the decay observed during the first 5 s of the transient. b) Frequency histogram of the trajectory in (a). c) The emission spectra corresponding to the transient in (a) are unstructured and red-shifted relative to the solution spectra of **1**. d) Scheme showing that interaction among the chromophores in **1** can result in a smaller energy gap between S_1 and T_1. y = number of photons detected in 5 ms; F = fluorescence intensity (in number of detected photons); z = frequency of occurrence; A = Molar extinction coefficient ($M^{-1}cm^{-1}$); R_i = Residuals.

 © WILEY-VCH Verlag GmbH, D-69451 Weinheim, 2001 1433-7851/01/4024-4646 $ 17.50+.50/0

2×10^{-7} is calculated for the type I transients of **1**. On the basis of the features of the transient, the spectral properties, and the measured decay times, we associate the type I transients with isomers of **1** where the chromophores are equidistantly spaced and the interactions between the chromophores are weak (isomer A in Figure 1).

Roughly 8% of the observed transients display a completely different behavior (Figure 4a). Different intensity levels can be observed for these type II transients, but these levels are not as stable and as well defined as for type I transients. This effect is reflected in the frequency histogram of the number of detected photons (Figure 4b). The reason for these unstable or fluctuating levels might be the binning time of 5 ms. This parameter can create fluctuations in the levels if the on/off processes are faster than the binning time. The corresponding emission spectrum is broad, red shifted by 950 cm^{-1}, and unstructured. We attribute the type II transients to structural isomers where two chromophores are close together, effectively forming a dimer-like or excimer-like structure (isomer B in Figure 1). The difference between the observed shift (950 cm^{-1}) and the calculated exciton coupling (90 cm^{-1}) suggests that considerable relaxation along the interchromophore coordinates occurs after excitation, which justifies our assignment of excimer-like fluorescence.[14] Analysis of simultaneously recorded fluorescence decays results in decay times of about 8 ns. A more stable fluorescence intensity level and a decay time of 4.2 ns without on/off jumps is observed in some of the type II transients after photobleaching of the excimer-like complex.

Ensemble single-photon timing measurements of **1** in toluene indicate the presence of 5% of an excimer-like species at 7.4 ns at an emission wavelength of 725 nm.[14] The ensemble results and single-molecule measurements on **1** match quite well and provide additional evidence for our hypothesis that the unstructured spectra and unstable fluorescence intensity trajectory corresponds to an isomer where two chromophores are spatially close. The average number of emitted photons for the type II transients is less than for type I transients, 5.4 million and 16 million, respectively. This difference in emitted photons could reflect either a difference in survival time, a difference in the quantum yield of emission of the excimer, or enhanced intersystem crossing (see below), or a combination thereof.

The most striking observation in transients of type II is the increased frequency of collective on/off jumps that occur from all intensity levels. If the triplet state is indeed involved in the process of the collective jumps, it implies that the probability of intersystem crossing is higher in type B isomers than in the type A isomers. A similar calculation as for the type I transient (see above) resulted in an average Y_{ISC} value of 1×10^{-5} for type II transients, a change of almost two orders of magnitude.

An explanation is given in Figure 4c for the increased number of on/off jumps and hence increased probability of intersystem crossing. The interaction of two chromophores will result in the formation of two new singlet exciton states, where the lowest one is now energetically closer to the triplet state than to the non-interacting S_1 state. This arrangement results, assuming a constant triplet energy value,[15] in a lower energy gap between the singlet and triplet state and hence in a faster rate for intersystem crossing.[16] The effect was predicted by McRae and Kasha in 1958, but until now never unequivocally proven experimentally at the single-molecule level.[17] According to McRae and Kasha, the S_1 state should be lowered in energy by 1000 cm^{-1} for this effect to have a reasonable influence on the rate of intersystem crossing. The emission maxima of the unstructured spectra are indeed shifted by 950 cm^{-1} relative to the emission maxima of the structured spectra (Figures 3 and 4). This shift is sufficient to explain the increased number of off-states. Indeed one can calculate the rate constant for intersystem crossing (k_{ISC}) for the type I transient by dividing Y_{ISC} with the fluorescence lifetime (4.2 ns). This calculation results in a k_{ISC} value of 50 s^{-1} for the type I transients when the non-radiative decay processes are neglected. An analogous calculation for the type II transients results in a k_{ISC} value of 1250 s^{-1} using a decay time of 8 ns. The difference between the calculated value of 90 cm^{-1} and the value obtained from the spectral shift (950 cm^{-1}) can be explained by assuming that the rather moderate interaction in the ground state of 90 cm^{-1} can increase in the excited state because of a reorientation and relaxation in the attractive part of the interchromophore potential well that exists on the S_1 hypersurface.

The remaining 42% of the transients show enhanced on/off behavior relative to type I transients without the excimer emission of type II and are related to structural and rotational isomers in which the peryleneimides are not overlapping but are nevertheless more strongly coupled than in type I transients. This will be discussed in a separate publication.

In summary we have demonstrated that single-molecule spectroscopy can be used to sort and classify structural isomers of multichromophoric systems. Two distinct subsets of isomers of **1** were identified, which showed profoundly different photophysical properties and resulted in different probabilities of collective on/off jumps. We argued that an increased yield of intersystem crossing is the result of a lower singlet/triplet energy gap in the isomer containing two chromophores that interact in a dimer-like fashion. This finding further corroborates the model we introduced to explain the collective on/off jumps, a triplet state on one of the chromophores quenching the total fluorescence of the multichromophoric entity. Similar effects will influence the photophysical properties and processes in antenna systems where large numbers of chromophores with slightly different interchromophore distances, and hence interactions, exist.

Received: July 19, 2001 [Z17546]

[1] T. Sauter, W. Neuhauser, R. Blatt, P. E. Toschek, *Phys. Rev. Lett.* **1986**, *57*, 1696 – 1698.

[2] J. Bernard, L. Fleury, H. Talon, M. Orrit, *J. Chem. Phys.* **1993**, *98*, 850 – 859; W. E. Moerner, M. Orrit, *Science* **1999**, *283*, 1670 – 1676.

[3] K. D. Weston, P. J.Carson, J. A. DeAro, S. K. Buratto, *Chem. Phys. Lett.* **1999**, *308*, 58 – 64; T. Ha, T. Enderle, D. S. Chemla, P. R. Selvin, S. Weiss, *Chem. Phys. Lett.* **1997**, *271*, 1 – 5; J. A. Veerman, M. F. Garcia Parajo, L. Kuipers, N. F. Van Hulst, *Phys. Rev. Lett.* **1999**, *83*, 2155 – 2158.

[4] T. Sauter, R. Blatt, W. Neuhauser, P. E. Toschek, *Opt. Commun.* **1986**, *60*, 287 – 292.

 © WILEY-VCH Verlag GmbH, D-69451 Weinheim, 2001 1433-7851/01/4024-4647 $ 17.50+.50/0

[5] D. A. VandenBout, W. T. Yip, D. H. Hu, D. K. Fu, T. M. Swager, P. F. Barbara, *Science* **1997**, *277*, 1074 – 1077; J. Yu, D. H. Hu, P. F. Barbara, *Science* **2000**, *289*, 1327 – 1330.
[6] M. A. Bopp, A. Sytnik, T. D. Howard, R. J. Cogdell, R. M. Hochstrasser, *Proc. Natl. Acad. Sci. USA* **1999**, *96*, 11271 – 11276.
[7] J. Hofkens, M. Maus, T. Gensch, T. Vosch, M. Cotlet, F. Köhn, A. Herrmann, K. Müllen, F. C. De Schryver, *J. Am. Chem. Soc.* **2000**, *122*, 9278 – 9288.
[8] T. Huser, M. Yan, L. J. Rothberg, *Proc. Natl. Acad. Sci. USA* **2000**, *97*, 11187 – 11191.
[9] J. Hofkens, W. Schroeyens, D. Loos, M. Cotlet, F. Köhn, T. Vosch, M. Maus, T. Gensch, A. Herrmann, K. Müllen, F. C. De Schryver, *Spectrochim. Acta*, in press
[10] T. Gensch, J. Hofkens, A. Herrmann, K. Tsuda, W. Verheijen, T. Vosch, T. Christ, T. Basché, K. Müllen, F. C. De Schryver, *Angew. Chem.* **1999**, *111*, 3970 – 3974; *Angew. Chem. Int. Ed.* **1999**, *38*, 3752 – 3756.
[11] F. Morgenroth, A. J. Berresheim, M. Wagner, K. Müllen, *Chem. Commun.* **1998**, *10*, 1139 – 1140.
[12] J. Hofkens, L. Latterini, G. De Belder, T. Gensch, M. Maus, T. Vosch, Y. Karni, G. Schweitzer, F. C. De Schryver, A. Herrmann, K. Müllen, *Chem. Phys. Lett.* **1999**, *304*, 1 – 9.
[13] S. Tretiak, V. Chernyak, S. Mukamel, *Chem. Phys. Lett.* **1996**, *259*, 55 – 61; S. Tretiak, C. Middleton, V. Chernyak, S. Mukamel, *J. Phys. Chem. B* **2000**, *104*, 4519 – 4528.
[14] M. Maus, S. Mitra, M. Lor, J. Hofkens, T. Weil, A. Herrmann, K. Müllen, F. C. De Schryver, *J. Phys. Chem. A* **2001**, *105*, 3961 – 3966.
[15] V. Yakhot, M. D. Cohen, Z. Ludmer, *Adv. Photochem.* **1979**, *11*, 489 – 523.
[16] Although the interaction of the S_1 states of two chromophores lead to a splitting and hence lowering of the energy, this does not necessarily hold for the triplet state. The stabilization is related to the extent of the coupling and hence to the oscillator strength of the transition. As the singlet/triplet transition has a low oscillator strength, the splitting of the triplet state will be small.
[17] E. G. McRae, M. Kasha, *J. Chem. Phys.* **1958**, *28*, 721 – 72; W. Siebrand, *J. Chem. Phys.* **1966**, *44*, 4055 – 4057.

Hydrophobic Groups Stabilize the Hydration Shell of 2′-*O*-Methylated RNA Duplexes

Pascal Auffinger* and Eric Westhof*

In memoriam Peter A. Kollman

The higher thermodynamic stability of RNA compared to DNA helices of similar sequence is often ascribed to the 2′-OH group present in RNA and absent in DNA nucleotides. Indeed, the 2′-OH group is involved in specific solute – solvent hydrogen bond acceptor and donor interactions that participate in the stabilization of the RNA hydration shell.[1, 2] Yet, RNA duplexes containing 2′-*O*-methylated nucleotides are structurally more stable than their unmodified counterparts,[1, 3, 4] indicating that the replacement of a hydrophilic 2′-OH by a hydrophobic 2′-OMe group results in additional stabilization of RNA helices. This effect, also observed for DNA and hybrid duplexes containing methylated nucleotides, is commonly explained either by a stiffening of the C3′-*endo* form of the ribose induced by the methyl group, increased stacking of the bases,[5, 6] or favorable lipophilic interactions between consecutive hydrophobic groups.[7] For RNA duplexes, however, explanations based on conformational changes induced by the modified nucleotides are not convincing since NMR studies report that native and entirely methylated duplexes are structurally very similar.[8] It has also been proposed that 2′-*O*-methylations induce a reduction of the hydration of the shallow groove[9] associated with a decrease of the hydration enthalpy.[1] Here, on the basis of two 4.4-ns molecular dynamics (MD) simulations of the natural $r(CpG)_{12}$ and the fully modified 2′-*O*-$Me(CpG)_{12}$ duplexes, we provide computational evidence indicating that, on the contrary, by creating optimal water binding pockets, the 2′-*O*-methylations lead to a significant stabilization of specific nucleotide – water interactions, which could favorably contribute to the enthalpy of hydration.

During the course of the MD simulations, in agreement with crystallographic,[7, 10] NMR,[8] and previous simulation data,[9] it is observed that the 2′-OMe groups are locked into a single orientation (toward the shallow groove, Figure 1), one of the three distinct orientations between which the more mobile 2′-OH groups switch frequently.[2] Despite these local differences the ribose groups of both duplexes retain their initial C3′-*endo* conformation. Thus, conformational restraints imposed by the 2′-OMe groups, which are of importance for flexible mono- and dinucleotides[6] or for methylated DNA strands, do not significantly displace the conformational

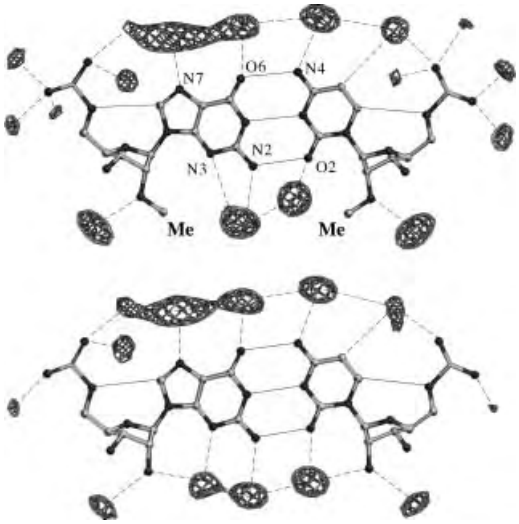


Figure 1. Solvent densities (water molecules and K^+ ions) surrounding 2′-*O*-Me(GC) (top) and r(GC) (bottom) base pairs drawn at a similar contour level.

[*] Dr. P. Auffinger, Prof. E. Westhof
Institut de Biologie Moléculaire et Cellulaire du CNRS
Modélisations et Simulations des Acides Nucléiques, UPR 9002
15 rue René Descartes
67084 Strasbourg Cedex (France)
Fax: (+33) 3-88-60-22-18
E-mail: P.Auffinger@ibmc.u-strasbg.fr
E.Westhof@ibmc.u-strasbg.fr

Supporting information for this article is available on the WWW under http://www.angewandte.com or from the authors.

 © WILEY-VCH Verlag GmbH, D-69451 Weinheim, 2001 1433-7851/01/4024-4648 $ 17.50+.50/0

equilibria observed for RNA helices. Similarly, the stacking patterns determined for CpG and GpC steps are identical for the native and modified duplexes and should not contribute to the observed differences in stability. Thus, the present simulations support the proposal that conformational effects induced by the methylation of the 2′-OH groups are negligible for RNA helices.[8]

Instead, the methyl groups in the modified RNA significantly alter the hydration pattern from that of the native duplex. For the shallow groove of the methylated pairs, two "out-of-plane" hydration sites are observed (Figure 1). Since these hydration sites overlap, a single row of water molecules, similar to that observed in the X-ray structure analysis,[10] connect the base atoms. In the shallow groove of the native duplex, however, three nonoverlapping "in-plane" hydration sites (Figure 1) are seen, which form a row of three water molecules connecting the base atoms and the 2′-OH groups. Overall, it appears that in the modified duplex fewer water molecules contact the shallow-groove hydrophilic atoms than in the native duplex (1.8 vs 2.4; Table 1). Surprisingly, the number of hydrogen bonds formed between shallow-groove hydrophilic atoms and water molecules is similar for the (G)NH_2 and (C)O2 atoms, and slightly reduced for the (G)N3 atoms (the latter are involved, as described below, in asymmetrical hydration patterns). Thus, although the methyl groups do alter the shallow-groove hydration patterns, they do not lead to a significant shielding of the adjacent (C)O2 atoms and the overall accessibility of the (G)N3 atoms is only slightly reduced (see HB %; Table 1).

Table 1. Average number of H_2O/RNA contacts as well as hydrogen bonding percentages (HB %) calculated over the last 3.0 ns of the MD simulation and the twelve central base pairs (for details, see ref. [11]).

	Shallow-groove atoms			
	(G)N3	(G)NH_2	(C)O2	Total[a]
Average contacts				
2′-*O*-Me(GC)	0.4	1.5	0.6	1.8
r(GC)	0.8	1.5	0.9	2.4
Hydrogen bonding percentages (HB %)[b]				
2′-*O*-Me(GC)	40 (18)	84 (2)	85 (4)	
r(GC)	56 (5)	79 (3)	83 (3)	

[a] Due to overlaps between adjacent hydration sites, these numbers do not correspond to the sums of the individual atomic contributions. [b] Numbers in parentheses correspond to standard deviations from the average values.

To obtain information on the solvent dynamics, a comparative analysis of the residence times of the water molecules in the first hydration shell of both duplexes has been performed as described elsewhere.[11] It is observed that for the modified duplex the residence times of shallow-groove water molecules bound to the (G)N3, (G)NH_2, and (C)O2 are much longer than for the native duplex (Figure 2). This effect is most dramatic for the (C)O2 atoms: For the modified duplex residence times exceeding 1 ns are determined, whereas they do not exceed 500 ps for the native duplex. A detailed analysis of the trajectories reveals that, for 2′-*O*-Me(GpC) steps, long-lived water bridges (ca. 1 ns) connect the (C)O2 atoms belonging to adjacent base pairs (Figure 3), while no such long-lived hydration patterns have been observed for the

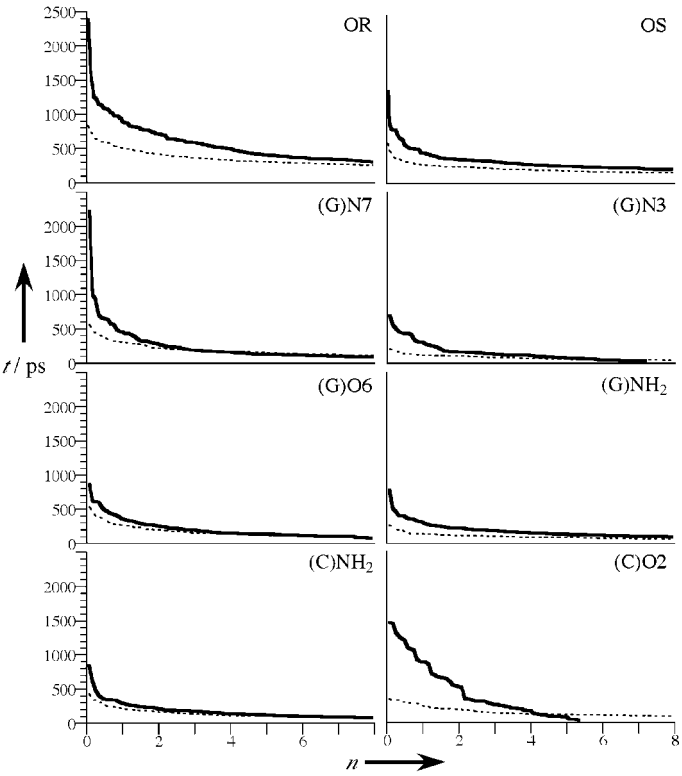


Figure 2. Residence time profiles for water molecules in n(CpG)$_{12}$ (----) and fully modified 2′-*O*-Me(CpG)$_{12}$ (——). The number (n) of atoms bound to selected hydrophilic atoms of the central GC pairs of the native and methylated duplexes is plotted as a function of their hydrogen bonding contact times (t).

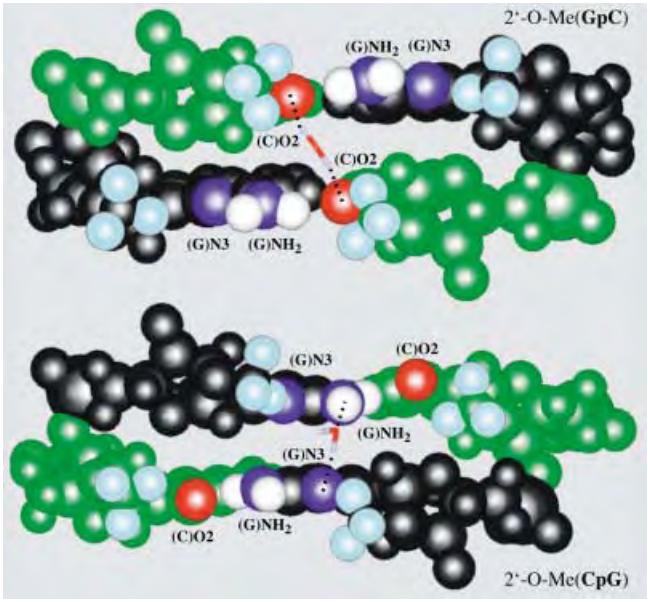


Figure 3. Snapshots extracted from the MD simulations of the methylated RNA duplex. Long-lived shallow-groove water molecules (stick model) bridging adjacent base pairs are shown for GpC (top) and CpG (bottom) steps. Green = skeleton of C, black = skeleton of G, red = shallow groove oxygen atoms and oxygen atoms of water, blue = shallow groove nitrogen atoms, cyan = hydrogen atoms of OMe groups.

native or similar duplexes.[11] For 2′-*O*-Me(CpG) steps, as a result of different stacking interactions, long-lived water bridges (ca. 500 ps) connecting the (G)N3 to the (G)NH_2

 © WILEY-VCH Verlag GmbH, D-69451 Weinheim, 2001 1433-7851/01/4024-4649 $ 17.50+.50/0

group of the adjacent base pair are observed (Figure 3; note that only one of the two N3 atoms participates in this asymmetrical hydration pattern; the other one is shielded by a methyl group). Consequently, long-lived shallow-groove water bridges linking adjacent base pairs are distinctive of the methylated and not the native duplex. Thus, the methyl groups help to delineate, through steric contacts, sequence-dependent hydration pockets in which water molecules optimize their interactions with the hydrophilic (G)N3, (G)NH_2, and C(O2) atoms of the shallow groove.

Interestingly, although no modifications alter the shape of the deep groove, the calculated residence times for bound water molecules in the modified duplex are significantly longer than for those in the native duplex. This is related to the reduced rigidity of the modified duplex induced by both intrinsic conformational factors and cooperative effects associated with the longer lifetimes of the hydration patterns in the shallow groove. Indeed, for the native duplex the average B-factors calculated for all the heavy atoms of the 12 central base pairs are significantly higher ((56 ± 19) Å^2) than those of the methylated duplex ((34 ± 7) Å^2). The presence of methyl groups, therefore, leads to an ordering of the hydration shell, even at a distance from the added hydrophobic groups. It is also observed that ion (K^+) binding is enhanced in the methylated duplex since the longest calculated residence times of an ion in contact with the methylated and native duplex are 2.0 and 1.3 ns, respectively. Indeed, the cooperative effect leading to an increase of the residence times of bound water molecules is linked with that seen for the K^+ ions.

The present MD simulations shed new light on the stabilization mechanisms associated with 2′-*O*-methylation of RNA duplexes. As strong structural effects induced by the modified nucleotides have been ruled out, the effects associated with hydration changes appear central. Here, a combination of steric (OMe), attractive, and repulsive interactions (O2, N3, NH_2) delineates notches in which water molecules fit ideally. As an outcome of the dynamically more stable hydration patterns observed in the shallow groove, the entire structure of the duplex is more rigid and the hydration patterns on the deep groove side are more stable. Although it is very difficult to deconvolute enthalpic and entropic contributions, it is proposed that the reduced mobility of the methylated duplex and of its hydration shell leads to an entropy loss that is overcompensated by a more favorable enthalpy of hydration. Although multiply methylated fragments rarely occur in natural systems, it is inferred that the observed hydration changes are also locally significant for single modifications. Thus, hydration patterns and their dynamics should be considered in the evaluation of the biophysical effects associated with methylation of RNA structures,[12] which are so important for antisense technologies.[1, 3, 13]

More generally, the results give insight into the complexity of effects associated with the insertion of hydrophobic chemical groups into a hydrophilic structure. Usually it is assumed that the addition of hydrophobic groups to a solute in a hydrophilic solvent leads to weakened solute–solvent interactions, resulting in an increase of the solvent entropy and a decrease in the enthalpy associated with solute–solvent interactions. We showed here that the introduction of hydrophobic modifications does not systematically result in a reduction of the binding affinity of the solute for water when the geometrical disposition and surface patterns generated by the hydrophobic and hydrophilic groups are appropriate and such that water molecules can form structured hydrogen bonding networks around the solute.

Computational Details

The simulation protocols and analysis methods are identical to those described in previous work.[11] The AMBER 5.0 simulation package[14] and the Cornell force field[15] have been used for generating the two 4.4-ns MD trajectories of $r(CpG)_{12}$ and 2′-*O*-Me$(CpG)_{12}$ (note that the 4.4-ns MD trajectory of $r(CpG)_{12}$ is an extension of a 2.4-ns trajectory described earlier[11]). The charges of the modified residues have been adapted from those of the native nucleotides. The starting structures are derived from fiber diffraction data.[16] In agreement with X-ray and NMR studies,[8, 10] the 2′-OMe groups have been placed initially so as to point toward the shallow groove. The duplexes were placed in a box containing 5690 (RNA) and 5952 (methylated RNA) water molecules (single point charge/extended (SPC/E)) as well as 72 K^+ and 26 Cl^- ions, resulting in a concentration of added KCl of approximately 0.25 M. The target temperature and pressure were set to 25 °C and 1 atm, respectively. During the course of the simulations, both duplexes remain close to each other and to their initial A-form.

Received: August 2, 2001 [Z17655]

[1] M. Egli, *Angew. Chem.* **1996**, *108*, 2020–2036; *Angew. Chem. Int. Ed. Engl.* **1996**, *35*, 1894–1909.
[2] P. Auffinger, E. Westhof, *J. Mol. Biol.* **1997**, *274*, 54–63.
[3] L. L. Cummins, S. R. Owens, L. M. Risen, E. A. Lesnik, S. M. Freier, D. McGee, C. J. Guinosso, P. D. Cook, *Nucleic Acids Res.* **1995**, *23*, 2019–2024.
[4] E. A. Lesnik, S. M. Freier, *Biochemistry* **1998**, *37*, 6991–6997.
[5] N. Yathindra, M. Sundaralingam, *Biopolymers* **1979**, *18*, 2721–2731.
[6] G. Kawai, Y. Yamamoto, T. Kamimura, T. Masegi, M. Sekine, T. Hata, T. Limori, T. Watanabe, T. Miyazawa, S. Yokoyama, *Biochemistry* **1992**, *31*, 1040–1046.
[7] P. Lubini, W. Zürcher, M. Egli, *Chem. Biol.* **1994**, *1*, 39–45.
[8] M. Popenda, E. Biala, J. Milecki, R. W. Adamiak, *Nucleic Acids Res.* **1997**, *25*, 4589–4598.
[9] K. Kulinska, T. Kulinski, A. Lyubartsev, A. Laaksonen, R. W. Adamiak, *Computer and Chemistry* **2000**, *24*, 451–457.
[10] a) D. A. Adamiak, J. Milecki, M. Popenda, R. W. Adamiak, Z. Dauter, W. R. Rypniewski, *Nucleic Acids Res.* **1997**, *25*, 4599–4607; b) D. A. Adamiak, W. R. Rypniewski, J. Milecki, R. W. Adamiak, *Nucleic Acids Res.* **2001**, *29*, 4144–4153.
[11] a) P. Auffinger, E. Westhof, *J. Mol. Biol.* **2000**, *300*, 1115–1133; b) P. Auffinger, E. Westhof, *J. Mol. Biol.* **2001**, *305*, 1057–1072.
[12] a) T. Hesson, A. Mannarino, M. Cable, *Biochemistry* **2000**, *39*, 2619–2625; b) H. Grosjean, R. Benne, *Modification and Editing of RNA*, American Society for Microbiology, Washington, **1998**; c) H. Bügl, E. B. Fauman, B. L. Staker, F. Zheng, S. R. Kushner, M. A. Saper, J. C. Bardwell, U. Jakob, *Mol. Cell.* **2000**, *6*, 349–360.
[13] S. M. Freier, K. H. Altmann, *Nucleic Acids Res.* **1997**, *25*, 4429–4443.
[14] D. A. Case, D. A. Pearlman, J. W. Caldwell, T. E. Cheatham, W. S. Ross, C. L. Simmerling, T. A. Darden, K. M. Merz, R. V. Stanton, A. L. Cheng, J. J. Vincent, M. Crowley, D. M. Fergusson, R. J. Radmer, G. L. Seibel, U. C. Singh, P. K. Weiner, P. A. Kollman, University of California, San Francisco, **1997**.
[15] W. D. Cornell, P. Cieplak, C. I. Bayly, I. R. Gould, K. M. Merz, D. M. Ferguson, D. C. Spellmeyer, T. Fox, J. W. Caldwel, P. A. Kollman, *J. Am. Chem. Soc.* **1995**, *117*, 5179–5197.
[16] S. Arnott, E. Selsing, *J. Mol. Biol.* **1974**, *88*, 551–553.

 © WILEY-VCH Verlag GmbH, D-69451 Weinheim, 2001 1433-7851/01/4024-4650 $ 17.50+.50/0

Formation and Stabilization of a Decanuclear Cu^{II} Wheel Linked by Chloride and O···H–N Hydrogen Bonds**

Che-Hao Chang, Kuo Chu Hwang, Chao-Shiuan Liu, Yun Chi,* Arthur J. Carty,* Ludmila Scoles, Shie-Ming Peng,* Gene-Hsiang Lee, and Jan Reedijk*

Self-assembly by hydrogen bonding, π–π stacking, and van der Waals interactions are allvery important processes in the formation of biological architectures.[1] These mechanisms are being developed as efficient design tools in material sciences for organizing individual molecular motifs into highly ordered supramolecules.[2] Among these supramolecules, compounds with an unsupported cyclic structure are of particular interest, not only for their unique molecular shapes, but also for their potential as models of infinite one-dimensional chain complexes, and for studies of quantum-size effects.[3] Several of these unusual supramolecules are known;[4] however, major difficulties are how to control the growth of the metal chain along a pre-designated cyclic orientation and how small molecules can be included inside such wheels. Herein, we report a one-pot, high-yield synthesis of the largest known cyclic Cu^{II} cluster complex. The molecular assembly is generated and stabilized by two conventional inter-atomic attractive forces, namely, formation of Cl-Cu-Cl bonds and the ability of the oxygen atom of the amino alkoxide ligand $OC(CF_3)_2CH_2NHCH_2CH_2NMe_2$[5] to form a hydrogen bond to its central, secondary nitrogen atom.

Single-crystal X-ray structural analysis showed that complex **1** $[Cu^{II}ClL]_{10}$ ($L = OC(CF_3)_2CH_2NHCH_2CH_2NMe_2$) crystallizes in the triclinic space group $P\bar{1}$ with two $[Cu^{II}ClL]_{10}$ molecules in the unit cell.[6] One of these two similar molecules is shown in Figure 1. The structure consists of a large $Cu_{10}Cl_{10}$ cyclic framework, with its center on a crystallographic center of inversion. Taken individually, each Cu^{II} center in **1** is coordinated in a distorted square-pyramidal geometry with two nitrogen atoms, one oxygen atom, and one chlorine atom occupying the basal positions, and with a second chlorine atom from the neighboring $[Cu^{II}ClL]$ fragment occupying the axial position and acting as a bridge between two Cu^{II} centers. The Cu–O bonds span the range 1.934–1.944(3) Å, while the Cu–N bonds to the nitrogen atoms (N2, N4, N6, N8, and N10) (1.999–2.024(4) Å) are much shorter than those to the terminal NMe_2 groups (N1, N3, N5, N7, and N9; 2.071–2.089(4) Å). Moreover, the Cu–Cl(basal) bonds (2.248–2.267 Å) are much shorter than the Cu–Cl(axial) bonds (2.573–2.738 Å), but still well within the range expected for significant Cu–Cl coordination.[7]

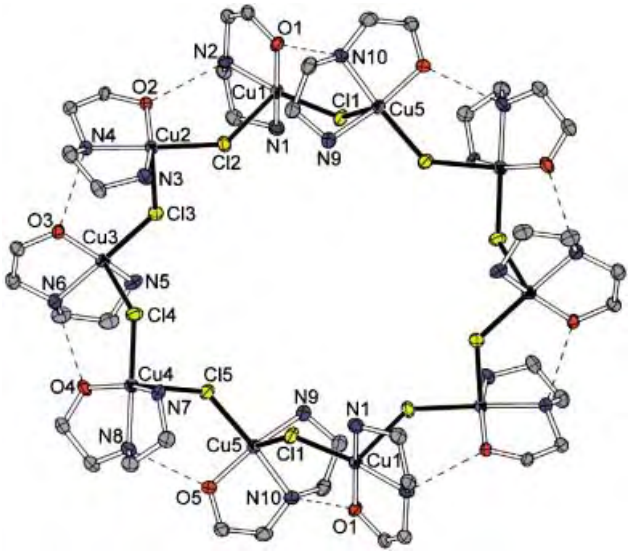


Figure 1. ORTEP drawing of complex **1** (thermal ellipsoids set at the 50% probability); all the CF_3 and Me groups have been omitted for clarity. Selected bond lengths [Å]: Cu1-O1 1.942(3), Cu1-N1 2.078(4), Cu1-N2 1.999(4), Cu1-Cl1 2.267(1), Cu1-Cl2 2.653(1), Cu2-Cl2 2.266(1), Cu2-Cl3 2.573(1), O2···N2 2.834(1).

The oxygen atom of each fluoroalkoxide terminus is located very close to the central N–H group of the neighboring $[Cu^{II}ClL]$ unit (c.f. O2···N2 = 2.834(1) Å and O1···N10 = 2.905(2) Å). These contacts are within the range of values found for medium-strong N–H···O hydrogen bonds observed in metal complexes (O···N = 2.69–2.98 Å).[8] It appears that this N–H···O hydrogen bonding is the intramolecular force that is responsible for holding the amino alkoxide ligand in a perpendicular configuration and simultaneously stabilizing the $Cu_{10}Cl_{10}$ ring structure.

Furthermore, all the CF_3 functional groups reside around the outer periphery, while the methyl substituents of the NMe_2 functional groups point towards the interior of the ring. The ring diameter, defined as the distance between two symmetry related, opposing copper atoms, ranges from 11.98(8) to 13.94(9) Å for the atoms Cu5 and Cu3, respectively. This packing arrangement creates a rectangular hole 3.5 × 6 Å, sufficient to incorporate small molecules such as organic solvents. In fact, and most surprisingly of the two Cu^{II}

[*] Prof. Y. Chi, C.-H. Chang, Prof. K. C. Hwang, Prof. C.-S. Liu
Department of Chemistry
National Tsing Hua University
Hsinchu 30013, Taiwan (Republic of China)
Fax: (+886) 3-572-0864
E-mail: ychi@mx.nthu.edu.tw
Prof. A. J. Carty, L. Scoles
Steacie Institute for Molecular Sciences
National Research Council Canada
100 Sussex Drive, Ottawa, Ontario K1A 0R6 (Canada)
Fax: (+1) 613-957-8850
E-mail: arthur.carty@nrc.ca
Prof. S.-M. Peng, G.-H. Lee
Department of Chemistry and Instrumentation Center
National Taiwan University
Taipei 10764, Taiwan (Republic of China)
Fax: (+886) 2-2363-6359
E-mail: smpeng@mail.ch.nthu.edu.tw
Prof. J. Reedijk
Leiden Institute of Chemistry
Leiden University
PO Box 9502, 2300 RA Leiden (The Netherlands)
Fax: (+)31-71-527-4671
E-mail: reedijk@chem.leidenuniv.nl

[**] We thank the National Science Council of Taiwan, R.O.C. (Grant No. NSC 90-2113-M-007-007) as well as the National Research Council, Canada for providing the financial support.

 © WILEY-VCH Verlag GmbH, D-69451 Weinheim, 2001 1433-7851/01/4024-4651 $ 17.50+.50/0

wheels within the asymmetric unit, one is found to be empty, while the second contains two acetonitrile solvent molecules.

To our knowledge, the molecular arrangement of complex **1** is unique. Only two other, smaller, cyclic molecules with Cu^{II} centers have been reported: one is the "flywheel" complex which contains six inner Cu^{II} metal centers,[9] while the other is an octameric Cu^{II}–pyrazolate complex[10] which possesses a copper-containing, cyclic or metallacrown skeletal arrangement.[11] The wheel structure composed of other transition metal elements has been observed in the Mn^{III} and Fe^{III} salicylhydrazidate complexes,[12] and for Fe^{III} alkoxide and Cr^{III} acetate complexes.[13]

Figure 2 shows the molar effective magnetic moment (μ_{eff}) as a function of temperature. In the temperature range 300–40 K, the μ_{eff} remains nearly constant. At 300 K, the μ_{eff} has a value of 5.76 μ_B, which corresponds to a combination of ten

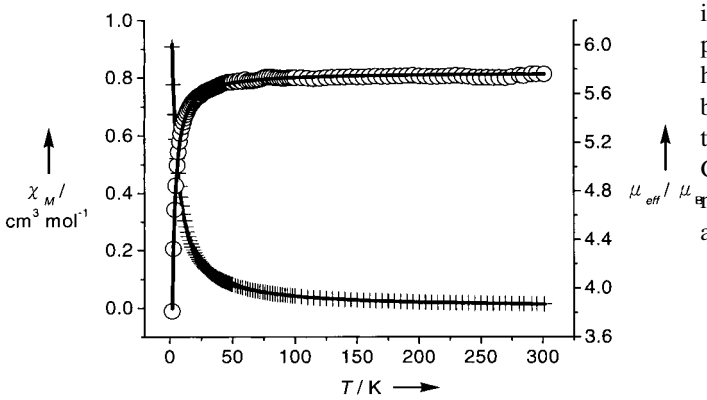


Figure 2. The magnetic susceptibility and effective magnetic moment of **1** are plotted as a function of temperature. The data were obtained from a powder sample of **1** at an external field of 1 Tesla. The solid lines in the magnetic susceptibility are the best-fitting calculated curves to Equation (2).

weakly interacting Cu^{II} centers (S = 1/2, 1.83 μ_B per Cu^{II}, g = 2.112 obtained from ESR measurement of a powder sample at 298 K). Upon cooling below 40 K, the μ_{eff} decreases very quickly, and reaches a value of 3.81 μ_B at 2 K. The decrease in the μ_{eff} at low temperatures is a characteristic of antiferromagnetically coupled metal centers. To deduce the exchange parameter J, the experimental molar magnetic susceptibility χ_M versus temperature T (see Figure 2) was analyzed according to the modified Heisenberg alternating linear-chain model. The spin Hamiltonian, for such a chain is given in Equation (1) where $n = 10$ for ten Cu^{II} nuclei, $\boldsymbol{S}_{11} \equiv \boldsymbol{S}_1$, and $0.4 < \alpha \leq 1.0$.[14]

$$\mathscr{H} = -2J\sum_{i=1}^{n/2}(\boldsymbol{S}_{2i}\boldsymbol{S}_{2i-1} + \alpha\boldsymbol{S}_{2i}\boldsymbol{S}_{2i+1}) \quad (1)$$

The susceptibility[14] used to fit the data is given in Equation (2) where χ_M = molar magnetic susceptibility, $x = |J|/kT$, N = Avogadro number, β = Bohr magneton, k = Boltzmann constant, and T = temperature.

$$\chi_M = 10\frac{Ng^2\beta^2}{kT}\frac{A + Bx + Cx^2}{1 + Dx + Ex^2 + Fx^3} \quad (2)$$

The parameters used in fitting the least-squares curve are: $A = 0.25$, $B = -0.13695 + 0.26387\alpha$, $C = 0.017025 - 0.12668\alpha + 0.49113\alpha^2 - 1.1977\alpha^3 + 0.87257\alpha^4$, $D = 0.070509 + 1.3042\alpha$, $E = -0.0035767 - 0.40837\alpha + 3.4862\alpha^2$-$0.73888\alpha^3$, and $F = 0.36184 - 0.065528\alpha + 6.65875\alpha^2 - 20.945\alpha^3 + 13.585834\alpha^4$. The best least-squares fitting results in a small negative J value of $-1.19\ cm^{-1}$ and $\alpha = 0.9$, which indicates a very weak intramolecular antiferromagnetic coupling between the adjacent Cu^{II} centers. The small negative J value must arise because the unpaired electron on each Cu^{II} center is almost orthogonal to its neighbors. This situation occurs because the chloride bridge is asymmetric, with the long Cu–Cl bond not involved in a magnetic orbital. In the magnetization (M) versus external magnetic field (H_0) experiment recorded at 5 K, the magnetization increases monotonically as H_0 increases. At $H_0 = 5$ Tesla, the magnetization still does not saturate, which is typical behavior of noncoupled systems.

The corresponding bromide analogue [$Cu^{II}BrL$] (**2**) was isolated in 97% yield and a single-crystal X-ray analysis performed.[15] The solid-state structure of **2** consists of a hexanuclear complex, composed of two structurally similar, but crystallographic independent [$Cu^{II}BrL$]$_3$ fragments within the unit cell (Figure 3). In both trinuclear entities, all the Cu–N and Cu–O bonds are regular and their lengths are nearly identical to those of **1**. However, only two Cu^{II} atoms adopt the expected square-pyramidal geometry, while the

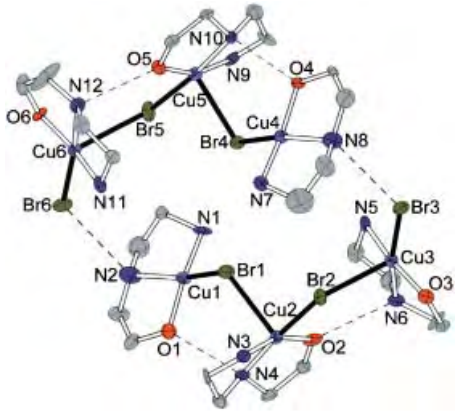


Figure 3. ORTEP drawing of complex **2** (thermal ellipsoids set at 50% probability); all the CF_3 and Me groups have been omitted for clarity. Selected bond lengths [Å]: Cu1-N1 2.02(1), Cu1-N2 2.05(1), Cu1-O1 1.899(9), Cu1-Br1 2.352(2), Cu2-Br1 2.827(2), Cu2-Br2 2.412(2), Cu3-Br2 2.812(2), Cu3-Br3 2.424(2), O1···N4 3.04(2), O2···N6 3.11(1), Cu1···Br6 4.711(2), Cu4···Br3 4.653(2), N2···Br6 3.50(1), N8···Br3 3.43(1).

third has a distorted square-planar arrangement with dihedral angles between the CuN_2 and CuOBr planes of 30.3° at the Cu1 and 27.8° at the Cu4 centers. This tetrahedral distortion results from a lack of Br→Cu apical interactions and the occurrence of Br···H–N hydrogen bonding (Br···N = av 3.47 Å). Such an interaction has also been seen in the cage supramolecule $[Ni_6(atu)_8Br]Br_3$ (Br···N = 3.33–3.40 Å; Hatu = amidinothiourea)[16] where the H bond terminates the growth of the metal chain. In our compounds the average Cu–Br bond is about 0.1 Å longer than the respective Cu–Cl bond in complex **1**, and therefore the lengthening of the Cu-Br-Cu distance also increases the O···N separation between

 © WILEY-VCH Verlag GmbH, D-69451 Weinheim, 2001 1433-7851/01/4024-4652 $ 17.50+.50/0

the adjacent amino alcoholate ligands to 2.95–3.10 Å, which clearly results in weaker interligand hydrogen bonding. It seems that both the tetrahedral distortion and a reduction in the strength of N–H···O bonding are major factors that destabilize the decanuclear configuration, and forms the bis-trinuclear structure.

Both complexes **1** and **2** are highly soluble in polar solvents such as acetone, methanol, and acetonitrile, less soluble in THF, and insoluble in less polar media such as diethyl ether and chlorinated hydrocarbons. Thus, smaller aggregates from the Cu^{II} complex **1** are likely to be present in polar solvent, since polar solvents might disrupt the hydrogen bonding and chloride–metal dative bonding; otherwise, these complexes should exhibit limited solubility if the solid-state structures remain intact. In fact, electrospray mass spectrometry data of **1** in acetonitrile gave a series of fragmentation ions with formula $\{[Cu^{II}ClL]_n-Cl\}$ ($n=2-8$) within the detection limit of the instrument, m/z: 3000. Similar spectral patterns were also obtained with the bromide complex **2**. These observations are consistent with the proposed disintegration of the metal wheel structure in polar solvents.

In summary, these results indicate that the asymmetric amino alkoxide ligand allows the assembly of wheel-shaped supramolecules by utilization of strong interligand O···H–N hydrogen bonds. Variations in the ligand may lead to different wheel sizes and, therefore, to the inclusion of different small molecules. Ongoing studies deal with crystallizations in various solvents and with small molecules. The structural diversity of the supramolecules $[Cu^{II}XL]_n$, X = Cl and Br, is further exemplified by the crystal structure of complexes **1** and **2**. Changing the coordinated anion from chloride to bromide ion can significantly alter the molecular structure and the magnetic properties by increasing the interatomic Cu···Cu distance and decreasing the length and strength of hydrogen bonding. The larger negative exchange parameter in **2** ($J=-3.40\ cm^{-1}$), than **1**, is attributed to the stronger magnetic coupling resulting from the nonorthogonal intersection between the adjacent $[Cu^{II}BrL]$ units.

Experimental Section

Synthesis of the Cu^{II} complexes: The sodium alkoxide of approximate formula [NaL], $L=OC(CF_3)_2CH_2NHCH_2CH_2NMe_2$, was prepared by deprotonation of the amino alcohol LH (4.0 g, 14.9 mmol) with excess sodium hydride (0.43 g, 17.9 mmol) in THF solution at 0 °C. The solution was filtered to remove the sodium hydride. The filtrate was treated with 1.2 equivalents of $CuCl_2$ (2.4 g, 17.9 mmol) at room temperature. After 12 hours, the solution was filtered to remove the insoluble NaCl and the filtrate concentrated to dryness. The residual was purified by recrystallization from a mixture of acetonitrile and diethyl ether, to give the cyclic compound $[Cu^{II}ClL]_{10}$ (**1**, 3.05 g, 0.83 mmol) as a royal blue crystalline solid in 56% yield. The bromide complex **2** was obtained similarly in 97% yield.

The magnetic susceptibility of powder samples was measured in a SQUID magnetometer (Quantum Design, model: HPHS-5) at an external magnetic field of 1 Tesla in the temperature range of 300–2 K. All data were corrected for diamagnetism by using Pascal's constants for all the constituent atoms. Magnetic moments were calculated according to the equation $\mu_{eff}=2.828\sqrt{\chi_M T}$. In the least-squares fitting the residue function R is defined as $R=\Sigma(\chi_{M\,obs}-\chi_{M\,calcd})^2/\Sigma(\chi_{M\,obs})^2$. The least-squares residue value R is 6.39×10^{-5} for the complex **1**, and 1.05×10^{-3} for the complex **2**.

Received: August 15, 2001
Revised: September 17, 2001 [Z17737]

[1] a) G. A. Ozin, *Acc. Chem. Res.* **1997**, *30*, 17; b) S. Mann, G. A. Ozin, *Nature* **1996**, *382*, 313; c) J. Y. Ying, C. P. Melmert, M. S. Wong, *Angew. Chem.* **1999**, *111*, 58; *Angew. Chem. Int. Ed.* **1999**, *38*, 56.

[2] a) J.-M. Lehn, *Angew. Chem.* **1990**, *102*, 1347; *Angew. Chem. Int. Ed. Engl.* **1990**, *29*, 1304; b) M. Munakata, L. P. Wu, T. Kuroda-Sowa, *Adv. Inorg. Chem.* **1998**, *46*, 1973; c) S. Leininger, B. Olenyuk, P. J. Stang, *Chem. Rev.* **2000**, *100*, 853; d) M. J. Zaworotko, *Chem. Commun.* **2001**, 1.

[3] a) A. Caneschi, D. Gatteschi, C. Sangregorio, R. Sessoli, L. Sorace, A. Cornia, M. A. Novak, C. Paulsen, Wernsdorfer, *J. Magn. Magn. Mater.* **1999**, *200*, 182; b) D. Gatteschi, R. Sessoli, A. Cornia, *Chem. Commun.* **2000**, 725; c) J. Bruno, R. J. Silbey, *J. Phys. Chem. A* **2000**, *104*, 596.

[4] a) B. Grossmann, J. Heinze, E. Herdtweck, F. H. Köhler, H. Nöth, H. Schwemk, M. Spiegler, W. Wachter, B. Weber, *Angew. Chem.* **1997**, *109*, 384; *Angew. Chem. Int. Ed. Engl.* **1997**, *36*, 387; b) Y. L. Cho, H. Uh, S.-Y. Chang, H.-Y. Chang, M. G. Choi, I. Shin, K.-S. Jeong, *J. Am. Chem. Soc.* **2001**, *123*, 1258.

[5] This amino alcohol ligand was prepared by combining hexafluoroacetone and diazomethane in diethyl ether, followed by addition of *N*,*N*-dimethylethylenediamine using a modified procedure of that described in literature: a) I.-S. Chang, C. J. Willis, *Can. J. Chem.* **1977**, *55*, 2465; b) P.-F. Hsu, Y. Chi, T.-W. Lin, C.-S. Liu, A. J. Carty, S.-M. Peng, *Chem. Vap. Deposition* **2001**, *7*, 28; c) Y. Chi, S. Ranjan, T.-Y. Chou, C.-S. Liu, S.-M. Peng, G.-H. Lee, *J. Chem. Soc. Dalton Trans.* **2001**, 2462.

[6] Crystal data for **1**: $C_{84}H_{129}Cl_{10}Cu_{10}F_{60}N_{22}O_{11.5}$, $M_r=3760.99$, triclinic, space group $P\bar{1}$, $a=15.3193(9)$, $b=17.899(1)$, $c=29.874(1)$ Å, $\alpha=103.239(1)$, $\beta=101.807(1)$, $\gamma=100.634(1)^\circ$, $V=7571.6(7)$ Å^3, $T=150$ K, $Z=2$, $\mu(Mo_{K\alpha})=1.678\ mm^{-1}$, 70160 reflections collected, 30945 unique ($R_{int}=0.035$), final wR_2(all data) = 0.1555. $R_1[I>2\sigma(I)]=0.0468$. Two acetonitrile molecules and 1.5 water molecules were also located in the unit cell. ESI MS (^{63}Cu): highest m/z 2894, $[Cu^{II}ClL]_8-Cl$. Crystallographic data (excluding structure factors) for the structures reported in this paper have been deposited with the Cambridge Crystallographic Data Centre as supplementary publication no. CCDC-172596 (**1**), and 172597 (**2**). Copies of the data can be obtained free of charge on application to CCDC, 12 Union Road, Cambridge CB2 1EZ, UK (fax: (+44) 1223-336-033; e-mail: deposit@ccdc.cam.ac.uk).

[7] S. Wang, Z. Pang, J. C. Zheng, M. J. Wagner, *Inorg. Chem.* **1993**, *32*, 5975.

[8] S. M. Couchman, J. C. Jeffery, M. D. Ward, *Polyhedron* **1999**, *18*, 2633; K. Sakai, K. Matsumoto, *J. Am. Chem. Soc.* **1989**, *111*, 3074.

[9] V. Tangoulis, C. P. Raptopoulou, S. Paschalidou, E. G. Bakalabassis, S. P. Perlepes, A. Terzis, *Angew. Chem.* **1997**, *109*, 1165; *Angew. Chem. Int. Ed. Engl.* **1997**, *36*, 1083.

[10] G. A. Ardizzoia, M. A. Angaroni, G. La Monica, F. Cariati, S. Cenini, M. Moret, N. Masciocchi, *Inorg. Chem.* **1991**, *30*, 4347.

[11] V. L. Pecoraro, A. J. Stemmler, B. R. Gibney, J. J. Bodwin, H. Wang, J. W. Kampf, A. Barwinski, *Prog. Inorg. Chem.* **1997**, *45*, 83.

[12] S.-X. Liu, S. Lin, B.-Z. Lin, C.-C. Lin, J.-Q. Huang, *Angew. Chem.* **2001**, *113*, 1118; *Angew. Chem. Int. Ed.* **2001**, *40*, 1084.

[13] a) K. L. Taft, C. D. Delfs, G. C. Papaefthymiou, S. Foner, D. Gatteschi, S. J. Lippard, *J. Am. Chem. Soc.* **1994**, *116*, 823; b) A. Caneschi, A. Cornia, S. J. Lippard, *Angew. Chem.* **1995**, *107*, 511; *Angew. Chem. Int. Ed. Engl.* **1995**, *34*, 467; c) C. Benelli, S. Parson, G. A. Solan, R. E. P. Winpenny, *Angew. Chem.* **1996**, *108*, 1967; *Angew. Chem. Int. Ed. Engl.* **1996**, *35*, 1825; d) R. W. Saalfrank, I. Bernt, E. Uller, F. Hampel, *Angew. Chem.* **1997**, *109*, 2596; *Angew. Chem. Int. Ed. Engl.* **1997**, *36*, 2482; e) E. J. L. McInnes, C. Anson, A. K. Powell, A. J. Thomson, S. Poussereau, R. Sessoli, *Chem. Commun.* **2001**, 89.

[14] W. E. Hatfield, *J. Appl. Phys.* **1981**, *52*, 1985.

[15] Crystal data for **2**: $C_{24}H_{39}Br_3Cu_3F_{18}N_6O_3$, $M=1231.95$, monoclinic, space group $P2_1$, $a=12.2885(5)$, $b=20.7306(9)$, $c=17.1578(7)$ Å, $\beta=109.551(1)^\circ$, $V=4119(1)$ Å^3, $T=150$ K, $Z=4$, $\mu(Mo_{K\alpha})=4.563\ mm^{-1}$, 32243 reflections collected, 16143 unique ($R_{int}=0.0605$), final wR_2(all data) = 0.1200. $R_1[I>2\sigma(I)]=0.0506$. Some fluorine and carbon atoms were disordered.

[16] R. Vilar, D. M. P. Mingos, A. J. P. White, D. J. Williams, *Angew. Chem.* **1998**, *110*, 1323; *Angew. Chem. Int. Ed. Engl.* **1998**, *37*, 1258.

 © WILEY-VCH Verlag GmbH, D-69451 Weinheim, 2001 1433-7851/01/4024-4653 $ 17.50+.50/0

Structure, Immunogenicity, and Protectivity Relationship for the 1585 Malarial Peptide and Its Substitution Analogues

Fabiola Espejo,* Marcia Cubillos, Luz Mary Salazar, Fanny Guzman, Mauricio Urquiza, Marisol Ocampo, Yolanda Silva, Raul Rodriguez, Eduardo Lioy, and Manuel Elkin Patarroyo*

Malaria continues to be one of the greatest public health problems in the world. Between 300 and 500 million people are affected annually, which leads to 1.5 to 2.5 million deaths, mainly in children less than 5 years old.[1, 2] Immunoprophylactic method development is the only cost-effective control alternative[3] and currently several malarial vaccines including our SPF-66 have been tested and shown to have limited (but significant)[4] or no efficacy in humans.[5]

The *Plasmodium falciparum* merozoite surface protein-1 (MSP-1) is one of this parasite's most abundant merozoite membrane molecules. It plays a key role in merozoite invasion of human erythrocytes, and is therefore regarded as a promising vaccine candidate.[6] Our objective is to induce an immune response able to block the receptor–ligand interaction responsible for human red blood cell (RBC) invasion.

Our first step was to identify MSP-1 sequences involved in the invasion process; such sequences were then used (unmodified or with single or multiple substitutions) in immunization studies. The changes induced in the lead peptide three-dimensional structure (determined by using NMR spectroscopy) were analyzed by correlating the substitution with the degree of protective immunity in *Aotus* monkeys.

Relevant MSP-1 sequences have previously been identified by their interaction with human RBCs.[7] One of these sequences, located in the N-terminal portion of the 42-kDa MSP-1 fragment (peptide 1585: EVLYLKPLAGVYRSLKKQLE), binds to RBC with an affinity constant of 180 nM. We have chosen the peptide 1585 (which has a conserved sequence in all parasite strains) to avoid the wide genetic variability of *P. falciparum*.[8, 9]

Evidence to date suggests that the conserved protein sequence in *P. falciparum* has poor or no antigenicity (capacity to induce immune response after infection) nor immunogenicity (capacity to induce immune response when used as a vaccine) in humans.[7]

The first step in the design of analogues was to recognize those amino acids critical to the RBC binding process and to determine if residue substitution induced immunogenicity and protectivity. Determination of these residues[10, 11] showed that the L5, K6, P7, A9, and S14 residues of peptide 1585 (EVLY**LKP**L**A**GVYR**S**LKKQLE) are essential to RBC binding (data not shown).

All peptides used in this study were synthesized by a solid-phase multiple peptide synthesis procedure using the *tert*-butoxycarbonyl (Boc) strategy.[12] The final product was characterized by analytical high performance liquid chromatography (HPLC) and mass spectrometry.

Table 1 shows sequences for peptide 1585 and its substitution analogues that were used in immunization studies of *Aotus* monkeys highly susceptible to *P. falciparum* malaria. Humoral immune response and protective efficacy induced by peptide 1585 and its analogues are also shown in Table 1. Humoral immune response was quantified by measuring the level of parasite-specific antibodies in immunized monkey sera by an immunofluorescence assay (IFA).[13]

Immunized and control monkeys were challenged on day 60 by intravenous inoculation of 200 000 freshly infected erythrocytes obtained from a nonimmune donor previously infected with the FVO strain of *P. falciparum*. This dose is known to be 100 % infective for these monkeys.[13]

All control and nonprotected monkeys developed patent parasitaemia (determined by using acridine orange staining and fluorescence microscopy) by day 5; they were treated with quinine when 6 % levels of parasites were reached (usually by days 8–10).

The data presented in Table 1 shows how some amino acid (AA) substitutions render the lead peptide 1585 immunogenic. Group A comprises glycine analogues of peptide 1585: substitution of AAs critical to RBC binding made peptides 5187, 5188, and 5189 immunogenic and protective, whilst noncritical residue substitution (peptides 6187 and 6177) failed to induce sero-conversion and protection in immunized monkeys.

Critical binding residues were substituted by AAs with similar mass but different polarity in Group B analogues. This group presents very high antibody levels associated with full protection for 16 to 50 % of the immunized monkeys. Experiments repeated three times with peptide 11860 resulted in 30 % protective efficacy in 31 monkeys (data not shown).

Group C shows that 12 out of 30 substitution analogues, as well as the lead peptide 1585, did not induce *P. falciparum* parasite antibodies nor protection against experimental challenge.

Sera from monkeys vaccinated with the protective analogues induced parasite-specific antibodies that recognized the denatured 195-kDa MSP-1 protein and its 83-kDa, 42-kDa, 33-kDa, and 21-kDa cleavage products, among them peptide 10014. Monkeys immunized with nonprotective peptides (13454) did not produce such antibodies, as determined by using Western Blott analysis (Figure 1). Table 1 clearly demonstrates that modifications induced by some AA substitutions render the nonimmunogenic peptide 1585 immunogenic and protective.

NMR structure determinations were carried out with the lead peptide 1585 (*EVLY**LKP**L**A**GVYR**S**LKKQLE*), protective analogues 10014 (*EVLY**HV**PLAGVYRSLKKQLE*) and 11860 (*EVLY**HM**PL**G**GVYR**A**LKKQLE*), and the nonpro-

[*] Dr. F. Espejo, Prof. Dr. M. E. Patarroyo, Dr. M. Cubillos, Dr. L. M. Salazar, Dr. F. Guzman, Dr. M. Urquiza, Dr. M. Ocampo, Dr. Y. Silva, Dr. R. Rodriguez, Dr. E. Lioy
Fundación Instituto de Inmunologia de Colombia (FIDIC)
Universidad Nacional de Colombia
Avda. Calle 26 No. 51–60, Bogotá (Colombia)
Fax: (+57) 1-2803999
E-mail: fespejo@hotmail.com
mepatarr@mail.com

 © WILEY-VCH Verlag GmbH, D-69451 Weinheim, 2001 1433-7851/01/4024-4654 $ 17.50+.50/0

Table 1. Humoral immune response and protective efficacy induced by analogues of peptide 1585 in *Aotus* monkeys.[a]

Polymerized peptide No.	Peptide sequence																			IFA titers ≥320			Group
																				II_{15}	III_{20}	Prot	
1585	E	V	L	Y	**L**	**K**	**P**	L	**A**	G	V	Y	R	**S**	L	K	K	Q	L	E	0	0	0/5	
5187	–	–	–	–	**G**	**K**	**P**		**A**	–	–	–	–	**S**	–	–	–	–	–	–	ND.[b]	1(320)	1/4	A
5188	–	–	–	–	**L**	**G**	**P**	–	**A**	–	–	–	–	**S**	–	–	–	–	–	–	ND.[b]	1(320)	1/4	A
5189	–	–	–	–	**L**	**K**	**G**	–	**A**	–	–	–	–	**S**	–	–	–	–	–	–	ND.[b]	1(1280)	1/4	A
6187	–	–	–	–	**L**	**K**	**P**	**G**	**A**		–	–	–	**S**	–	–	–	–	–	–	0	0	0	A
6177	–	–	–	–	**L**	**K**	**P**	–	**A**	–	–	–	–	**G**	–	–	–	–	–	–	0	0	0	A
13450	–	–	–	–	**L**	**L**	**D**		**A**	–	–	–	–	**S**	–	–	–	–	–	–	2(2560)	1(2560)	2/4	B
22806				–	**L**	**L**	**D**	–	**A**	–	–	–	–	**S**	–	–	–	–			3(1280)	1(1280)	2/9	B
10014	–	–	–	–	**H**	**V**	**P**	–	**A**	–	–	–	–	**S**	–	–	–	–	–	–	2(640)	1(640)	2/4	B
22768				–	**H**	**L**	**P**	–	**A**	–	–	–	–	**A**	–	–	–	–			0	1(5120)	1/10	B
11860	–	–	–	–	**H**	**M**	**P**	–	**G**	–	–	–	–	**A**	–	–	–	–	–	–	1(1280)	1(2560)	2/6	B
22770				–	**H**	**L**	**P**		**G**	–	–	–	–	**A**	–	–	–	–			1(1280)	1(280)	2/9	B
13454	–	–	–	–	**L**	**M**	**S**	–	**A**	–	–	–	–	**S**	–	–	–	–	–	–	0	0	0/5	C
14448	–	–	–	–	**H**	**M**	**D**	–	**G**	–	–	–	–	**V**	–	–	–	–	–	–	0	0	0/3	C
14496	–	–	–	–	**H**	**M**	**D**	–	**S**	–	–	–	–	**V**	–	–	–	–	–	–	0	0	0/4	C
13724	–	–	–	–	**H**	**V**	**T**	–	**S**	–	–	–	–	**S**	–	–	–	–	–	–	0	0	0/5	C
12896	–	–	–	–	**H**	**V**	**P**	–	**S**	–	–	–	–	**A**	–	–	–	–	–	–	0	0	0/5	C
12898	–	–	–	–	**H**	**V**	**P**	–	**G**	–	–	–	–	**A**	–	–	–	–	–	–	0	0	0/5	C
15954	–	–	–	–	**L**	**M**	**D**	–	**A**	–	–	–	–	**S**	–	–	–	–	–	–	0	0	0/3	C
15956	–	–	–	–	**L**	**M**	**P**	–	**A**	–	–	–	–	**S**	–	–	–	–	–	–	0	0	0/4	C
15958	–	–	–	–	**L**	**K**	**D**	–	**S**	–	–	–	–	**S**	–	–	–	–	–	–	0	0	0/6	C
15960	–	–	–	–	**L**	**M**	**D**		**S**	–	–	–	–	**S**	–	–	–	–	–	–	0	0	0/4	C
13728	–	–	–	–	**N**	**L**	**D**	–	**G**	–	–	–	–	**S**	–	–	–	–	–	–	0	0	0/5	C
13452	–	–	–	–	**L**	**I**	**D**	–	**A**	–	–	–	–	**S**	–	–	–	–	–	–	0	0	0/5	C
controls																					0	0	0/50	C

[a] Each monkey received three 125-μg subcutaneous polymerized peptide injections[11] on days 1, 20, and 40, homogenized in the first dose with complete Freund's Adjuvant. Incomplete Freund's Adjuvant was used in the second and third doses. Controls received only Freund's Adjuvant on the same days. IFA was carried out to assess humoral immune response 15 days after the second (II_{15}) and 20 days after the third (III_{20}) immunization. Protection was defined as complete parasite absence in immunized monkey blood for 15 days following challenge. [b] Not determined.

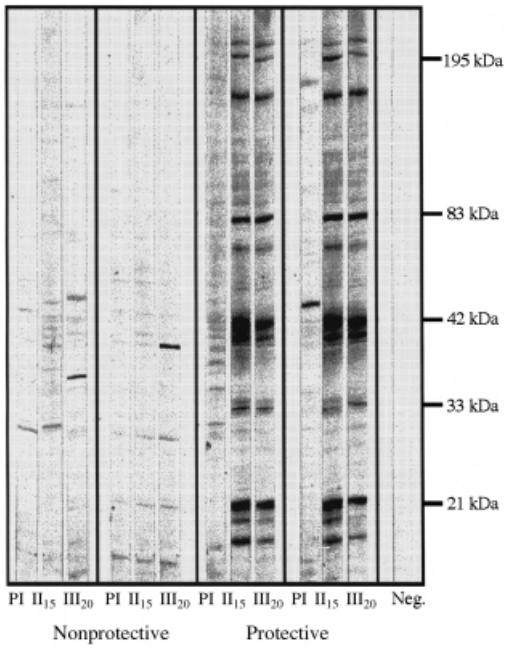


Figure 1. Western Blott analysis for solubilized antigens from late-stage *P. falciparum* schizonts. Sera from *Aotus* monkeys immunized with 13454 nonprotective (left) and 10014 protective (right) peptides were used. PI = Preimmune sera; II_{15}, III_{20} = sera taken 15 or 20 days after the second and third immunization, respectively.

tective 13454 analogue (*EVLYL**MS**LAGVYRSLKKQLE*) to establish the relationship between the three-dimensional structure of relevant substitution analogues and immunogenicity and protective efficacy observed in monkeys.

Peptide samples (8 mM) were dissolved in 25% 2,2,2-trifluoroethanol/water (TFE/H_2O) at pH 4–5.[14] A Bruker DRX-600 spectrometer was used for standard ^1H-^1H two-dimensional experiments (DQF-COSY, TOCSY, and NOESY) using Xwinnmr software. Sequence-specific assignments were made following standard procedures;[15] NOESY spectra recorded at different temperatures (285–315 K) were used to obtain amida temperature coefficients for predicting hydrogen bonds ($-\Delta\delta/T < 4$).

A structural calculation that was consistent with experimental data was carried out using a Molecular Simulations Inc. Software package (Insight II). NOE intensities were partitioned into three categories (strong, medium, and weak), then converted into distance restraints (1.8–2.7, 2.7–3.5 and 3.5–5.0 Å). The ϕ angular constraints were derived from $^3J_{NH\text{-}C\alpha H}$ coupling constants and were constrained to $-70^\circ \pm 30^\circ$ if $^3J_{NH\text{-}C\alpha H} < 6$.

We determined the structure of peptide 1585 in solution by using connectivities (Figure 2) and a database with a total of 251 NOE constraints, 12 ϕ dihedral angle constraints, and 9 hydrogen bond constraints. The 18 best (lowest energy) structures which fulfilled the constraints were selected from the 50 resulting conformers in the refined set and had 0.2 Å maximal distance and 2.4° maximal angular constraint violation. Procheck[16] was used on the refined structures. The root-mean-square deviation (rmsd) for the 18 structures (backbone atoms) versus the consensus structure was 0.17 Å. The results for the other analogues are presented in Table 2.

 © WILEY-VCH Verlag GmbH, D-69451 Weinheim, 2001 1433-7851/01/4024-4655 $ 17.50+.50/0

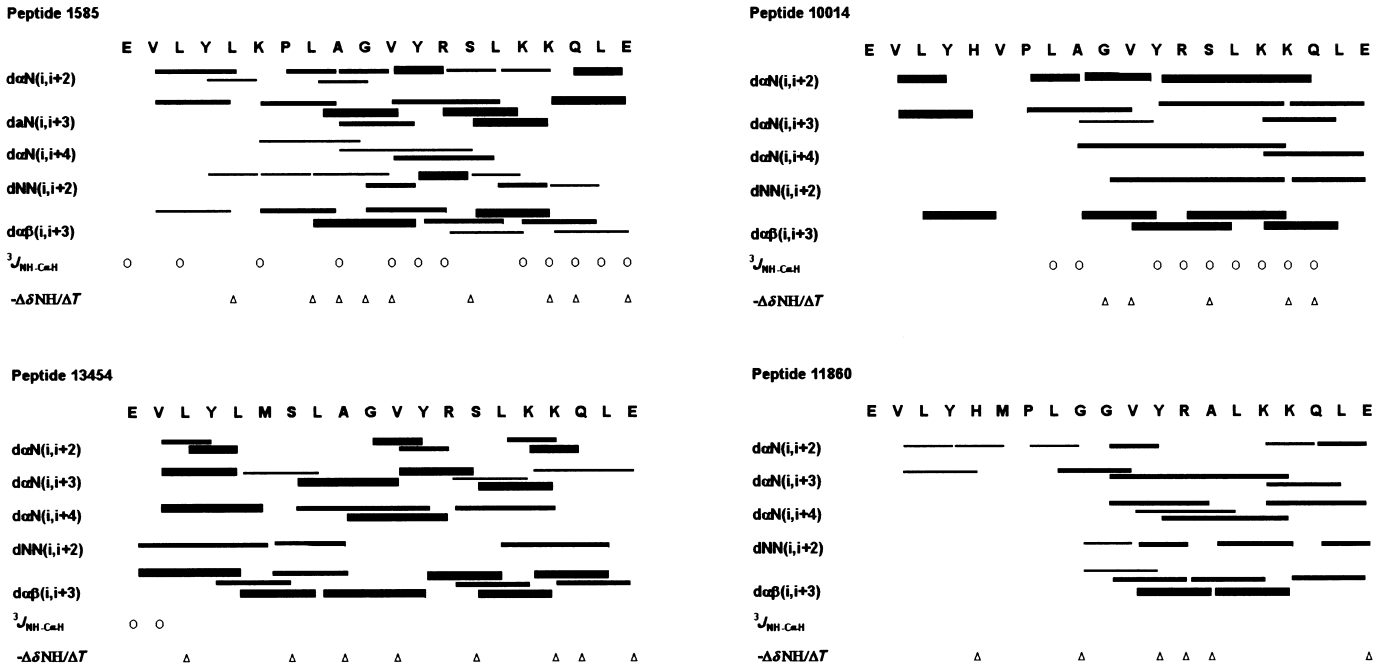


Figure 2. Summary of sequential medium range NOE connectivities (NOE intensities are represented by the line thickness). $^3J_{NH\text{-}C\alpha H}$ coupling constants are indicated by ○ if lower than 6 Hz. NH protons with slow exchange rates (involved in H-bonds $NH_i \cdots O_{i-4}$) are indicated by △.

Table 2. Summary of structure calculation results with the α-helical regions shaded.

Peptide	Helical structure residues	NOE connectivities	Number of structures superimposed out of 50 (helical segments shaded)	Rmsd [Å]	Max NOE violation [Å]	Protection
1585	4–12	251	18 EVL YLKPLAGVY RSLKKQLE	0.17	0.20	nonprotective
13454	5–16	279	33 EVL YLMSLAGVYRSLKKQLE	0.59	0.20	nonprotective
10014	9–18	198	15 EVLYHVPLAGVYRSLKKQLE	0.48	0.30	protective
11860	8–17	244	16 EVLYHMPLGGVYRALKKQLE	0.47	0.40	protective

Figure 3 shows the three-dimensional structures of lead peptide 1585, the nonprotective analogue 13454, as well as the protective 10014 and 11860 analogues.

All the peptides have a partial α-helical structure in 25% TFE, which indicates that each peptide has a strong helix-forming region; however, significant differences were observed in the location and extent of this structural element. In peptide 1585 the α-helical structure extends from residue 4 to 12 and in nonprotective peptide 13454 from residue 5 to 16, so in both cases it includes areas in which critical binding residues are located.

By contrast, immunogenic and protective peptides 10014 (L5 →H and K6 →V modifications) and 11860 (with L5 →H, K6 →M, A9 →G and S14 →A changes) possess a more flexible structure in critical binding residue areas (L5, K6, P7, A9). In these peptides the α-helical portion comprises residues 9–18 and 8–17, respectively, which leaves the N-terminal portion more flexible. These protective peptides may thus access a higher number of possible conformers.

Side chain conformation reliability is limited by relatively high conformational freedom. Nevertheless, a dramatic change in the relative spatial arrangement of the helical central region AA side-chain of peptide 1585 was clearly seen when critical RBC-binding residues were substituted.

Increased flexibility of the critical binding residue in peptides 10014 and 11860 (located next to the relatively rigid helical core) may allow these analogues to fit better into immune system molecules, which explains the induction of protective immunity. Such modifications may increase the

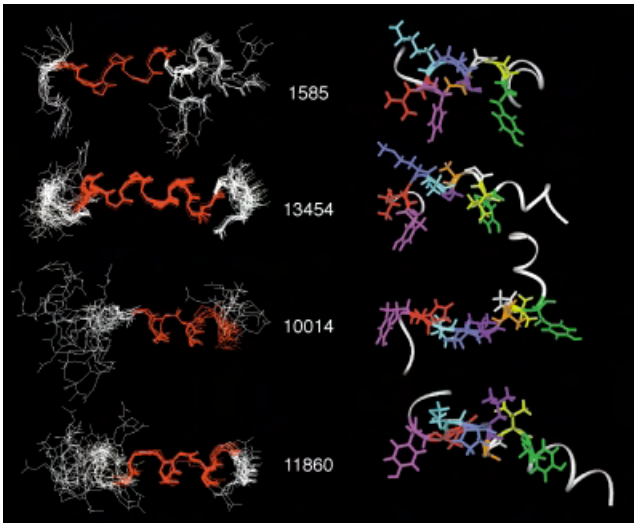


Figure 3. Structures of the nonprotective peptides 1585 and 13454, as well as the protective peptides 10014 and 11860. Left: modified amino acid backbones are shown in red. Right: ribbon representations. Color code: Y4 fuchsia; L5 (1585, 13454), H5 (10014, 11860) red; K6 (1585), M6 (13454, 11860), V6 (10014) pale blue; P7 (1585, 10014, 11860), S7 (13454) dark blue; A9 (1585, 10014, 13454), G9 (11860) brown; V11 yellow; Y12 green.

 © WILEY-VCH Verlag GmbH, D-69451 Weinheim, 2001 1433-7851/01/4024-4656 $ 17.50+.50/0

stability of the complex formed by major histocompatibility complex molecules, altered peptide ligands and T-cell receptors (MHC – altered-peptide-ligand – TCR complex) as recently shown for the altered AH1 tumor peptide, for which increased MHC – peptide – TCR complex stability was correlated with improved immune response.[17] Alternatively, perhaps a T-cell antagonist is converted into an agonist by repair of TCR – peptide – MHC interface defects, as suggested by other research groups.[18]

Herein we were able to correlate immunogenicity (particularly protective efficacy of a synthetic peptide in vivo) with three-dimensional structural features. Understanding the structure-protection relationship will lead to a more rational design of a *P. falciparum* malaria vaccine in the near future and any one of the reported modified peptides could be used as part of a multicomponent subunit malaria vaccine.

Received: June 12, 2001
Revised: October 10, 2001 [Z17274]

[1] K. Marsh, *Parasitology* **1992**, *104*, 553 – 569.
[2] L. H. Miller, M. F. Good, G. Milon, *Science* **1994**, *264*, 878 – 1883.
[3] H. D. Engers, T. Godal, *Parasitol. Today* **1998**, *4*, 56 – 64.
[4] P. Graves, H. Gelband, P. Garner, *Parasitol. Today* **1998**, 219 – 221.
[5] L. H. Miller, S. L. Hoffman, *Nature Med. Vaccine Suppl.* **1998**, *4*, 520 – 524.
[6] A. A. Holder, M. J. Blackman, *Parasitol. Today* **1994**, *10*, 182 – 184.
[7] M. Urquiza, L. E. Rodriguez, J. E. Suarez, F. Guzman, M. Ocampo, H. Curtidor, C. Segura, E. Trujillo, M. E. Patarroyo, *Parasite Immunol.* **1996**, *18*, 515 – 526.
[8] M. Plebanski, A. V. S. Hill, *Curr. Opin. Immunol.* **2000**, *12*, 437 – 441.
[9] M. Aidoo, V. Udhayakumar, *Parasitol. Today* **2000**, *16*, 50 – 56.
[10] L. E. Rodriguez, M. Urquiza, M. Ocampo, J. Suarez, H. Curtidor, F. Guzman, L. E. Vargas, M. Triviños, M. Rosas, M. E. Patarroyo, *Parasitology* **2000**, *120*, 225 – 235.
[11] E. Lioy, J. Suarez, F. Guzman, S. Siegrist, G. Pluschke, M. E. Patarroyo, *Angew. Chem.* **2001**, *113*, 2701 – 2706; *Angew Chem. Int. Ed.* **2001**, *40*, 2631 – 2635.
[12] R. A. Houghten, *Proc. Natl. Acad. Sci. USA* **1985**, *82*, 5131 – 5139.
[13] R. Rodriguez, A. Moreno, F. Guzman, M. Calvo, M. E. Patarroyo, *Am. J. Trop. Med. Hyg.* **1990**, *43*, 339 – 354.
[14] V. Waterhouse, C. Johnson, *Biochemistry* **1994**, *33*, 2121 – 2128.
[15] K. Wüthrich, *NMR of Protein and Nucleic Acids*, Wiley, New York, **1986**.
[16] R. A. Laskowski, M. W. MacArthur, D. S. Moss, J. M. Thorton, *J. Appl. Crystallogr.* **1993**, *26*, 283 – 291.
[17] J. E. Slanky, F. M. Rattis, L. F. Boyd, T. Famhy, E. M. Jaffe, J. Schenk, D. M. Pardoll, *Immunity* **2000**, *13*, 529 – 583.
[18] B. M. Baker, S. J. Gagnon, W. Biddison, D. C. Willey, *Immunity* **2000**, 475 – 484.

β-Fibrillogenesis from Rigid-Rod β-Barrels: Hierarchical Preorganization Beyond Microns**

Gopal Das, Lahoussine Ouali, Marc Adrian, Bodo Baumeister, Kevin J. Wilkinson, and Stefan Matile*

Fibrillogenesis of β-sheet peptides is attracting considerable scientific attention because of its importance in medicine and nanoscience.[1–12] Recent structural studies with synthetic models go beyond pure peptide chemistry.[5–9] These studies were consistently in support of repeated "β-dyads" of polar and apolar amino acid residues as the minimal structural requirement for β-fibrillogenesis[4] (if any),[3] and also supported a universal "cross-β" motif in β-fibrillar quaternary structures. The term cross-β is used for layered β-strands that are oriented perpendicular to the long fibril axis. In this case, one fibril (or protofilament) dimension is defined by the length of the β-strand, the other by the number of stacked, amphiphilic β-bilayers.[1–12] Further self-assembly of β-fibrils produces a quite remarkable, in part transient, polymorphism including formation of helices, ribbons, tubes, and sheets.[1–12] Whereas elegant strategies to inhibit random β-fibril self-assembly[8, 9] and to control two-dimensional organization of β-sheet monolayers[13] have been conceived recently, little is known about how to direct fibril self-assembly toward higher order structures. However, the difficulties with preorganizing β-sheet tertiary structures can be bypassed by using *p*-oligophenyl rods instead of β-sheets as β-barrel "staves".[14–16] The objective of this study was to expand this powerful preorganization strategy from tertiary β-barrel structures to quaternary β-fibril structures. We report, for the first time, the direct observation of "rigid-rod" β-barrels by atomic force microscopy as well as their controlled transformation into unidirectional self-assembled "rigid-rod" β-fibrils of exceptional beauty.

The formation of tetrameric rigid-rod β-barrels **1** is preorganized by rigid-rod "staves" in the monomers **2** (Figure 1). Barrel – stave supramolecule **1** further contains 32 interdigitating β-dyad-pentapeptides that produce hydrophobic outer and hydrophilic inner β-barrel surfaces (Figure 1).[14–16] Structural and functional studies implied that tetramer **1**

[*] Prof. S. Matile, Dr. G. Das, Dipl.-Chem. B. Baumeister
Department of Organic Chemistry
University of Geneva
1211 Geneva (Switzerland)
Fax: (+41) 4122-328-7396
E-mail: stefan.matile@chiorg.unige.ch
Dr. L. Ouali, Dr. K. J. Wilkinson
Analytical and Biophysical Environmental Chemistry (CABE)
University of Geneva, 1211 Geneva (Switzerland)
Dr. M. Adrian
Laboratoire d'Analyse Ultrasructurale (LAU)
Bâtiment de Biologie
Université de Lausanne, 1015 Lausanne (Switzerland)

[**] We thank J. Buffle and J. Dubochet for their fruitful discussions and the Swiss NSF (21-57059.99 (S.M.), 2000-050629.97 (K.J.W.), and the National Research Program "Supramolecular Functional Materials" 4047-057496 (S.M.)) for their financial support.

 © WILEY-VCH Verlag GmbH, D-69451 Weinheim, 2001 1433-7851/01/4024-4657 $ 17.50+.50/0

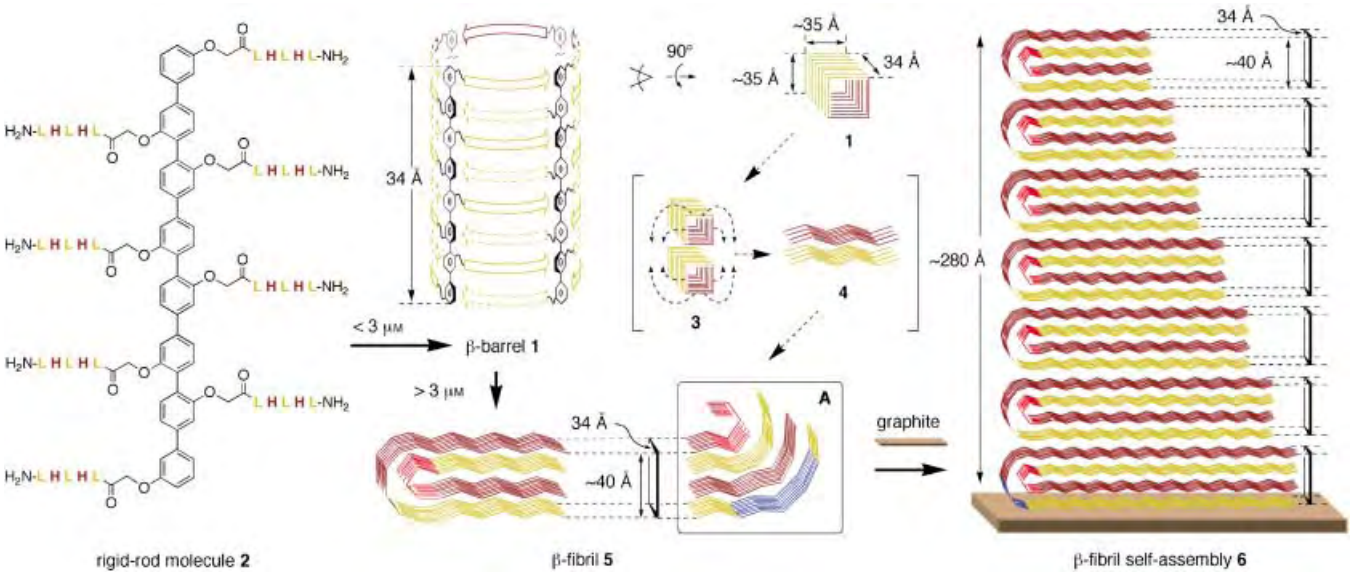


Figure 1. Hierarchical preorganization of tertiary (β-barrel **1**) and tentative quaternary structures (β-fibril **5** and β-fibril heptamer **6**) by rigid-rod molecule **2**. Amino acid residues (one-letter abbreviation, **2**) are in yellow (hydrophobic) and bronze (hydrophilic). β-Strands are depicted with an identical color code, either as arrows pointing to the C-terminus (**1**) or as lines (**1**, **3**–**6**). β-Barrel turns are in red, and fibril curvature induced by surface repulsion in blue. Tentative (transient) structures (and mechanisms) are in brackets (**3**,**4**), frames (A), and dashed arrows. The indicated dimensions are estimates that are compatible with literature[1–12] and experimental values (Figures 2, 4, and 5). The presence of a contracted trimer existing presumably in a pH-dependent equilibrium with tetramer **1** is not shown for clarity.[16]

forms, as expected, in lipid bilayers and, more surprisingly, in water.[16, 17] This previously suspected, but somewhat counterintuitive, formation of rigid-rod β-barrels with hydrophobic exteriors in water is here confirmed at relevant concentrations (< 3 μM, see below) by using atomic force microscopy (AFM). AFM images were obtained by adsorption of β-barrels **1** from dilute aqueous solutions onto mica (Figure 2).

Most of the detected objects have heights that match the length of the *p*-octiphenyl barrel staves within the vertical image resolution of 1.0–2.0 Å[11, 18] (Figure 2A); control experiments unambiguously confirmed that the additional, much smaller "objects" originate from residual 2-(4-morpholinyl)ethanesulfonic acid (MES) buffer. Consistent with the similarity between the diameter and height of tetramer **1** (Figure 1), the significant objects, within the poorer lateral AFM image resolution, had identical mean widths around 40 Å (Figure 2A). Although orientation of the barrels in the vertical direction is expected from interactions of hydrophilic barrel ends (rather than hydrophobic barrel sides) with the hydrophilic mica, no conclusions can be reached concerning the barrel orientation from the AFM images depicted in Figure 2. A conelike rather than a cylindrical barrel shape, without central channels, appeared in surface plots (Figure 2C). This appearance corresponds exactly, however, to the image distortion that is anticipated for scanning with commercial AFM tips with a radius of curvature of approximately 10 nm[6] without further refinements such as tip screening and image averaging.[18]

Rigid-rod β-barrels **1** were as poorly soluble in water as one would expect on the basis of their hydrophobic sides.[14–16] Transformation of β-barrels into β-fibrillar quaternary structures occured at around saturation but before the appearance of turbidity. β-Fibrillogenesis was characterized with thioflavin T (ThT), an amyloid-specific fluorophore (Figure 3).[5]

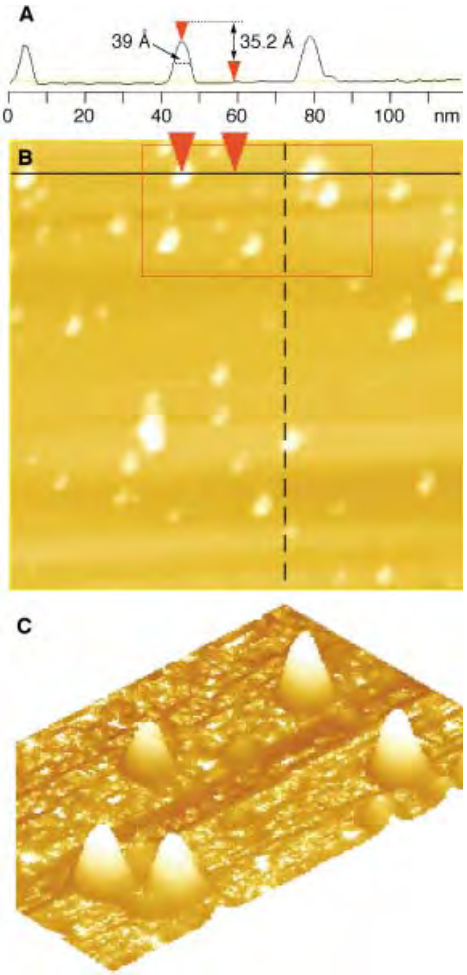


Figure 2. AFM image of rigid-rod β-barrels **1** on mica (1.5 μM **2**, 1.0 mM MES, pH 5.5). A) Heights and widths for β-barrels centered on the solid black line in (B); C) surface plot of the area within the frame in (B).

 © WILEY-VCH Verlag GmbH, D-69451 Weinheim, 2001 1433-7851/01/4024-4658 $ 17.50+.50/0

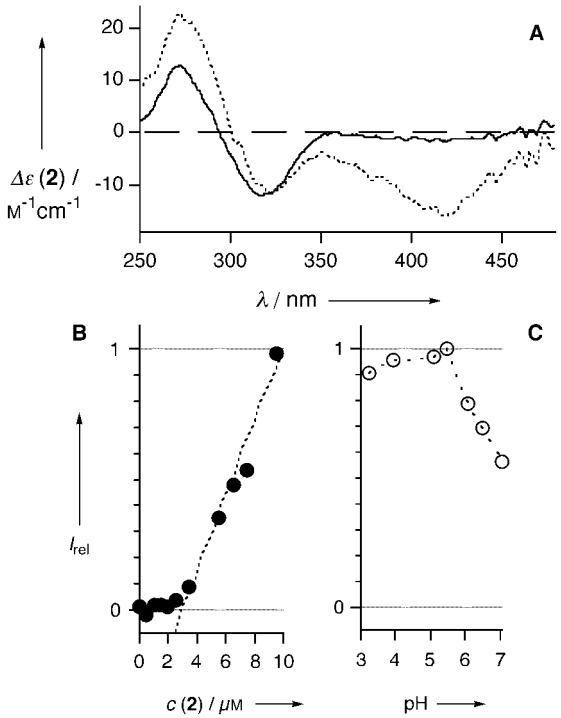


Figure 3. β-Fibrillogenesis from rigid-rod β-barrels **1** characterized by the thioflavin T (ThT) binding assay.[5] A) Circular dichroism (CD) spectra of rigid-rod β-fibrils (5 μM **2**, 10 mM MES, pH 5.5) in the presence (dotted line) and absence (solid line) of ThT (10 μM). B) and C) Changes in the spectroscopic properties of ThT observed by CD (see example in A), fluorescence emission (intensity shown for $\lambda_{ex} = 420$ nm, $\lambda_{em} = 500$ nm), and FRET (intensity at $\lambda_{ex} = 319$ nm, $\lambda_{em} = 500$ nm (depicted) as a function of *p*-octaphenyl concentration (B, pH 5.5) and pH (C, 5 μM **2**).

The appearance of a broad, induced CD Cotton effect (ICD CE) centered at 420 nm was observed in the circular dichroism (CD) spectra of *p*-octiphenyl[14–16] β-fibrils (Figure 3A, solid line) upon addition of ThT (Figure 3A, dotted line). This ICD CE demonstrated the location of ThT chormophores within the chiral environment provided by rigid-rod β-fibrils. The binding of ThT to rigid-rod β-fibrils was further observable by the characteristic increase in ThT emission.[1–12] The presence of ThT emission upon excitation of *p*-octiphenyl rods (319 nm) rather than ThT itself (420 nm) was indicative of fluorescence resonance energy transfer (FRET) from *p*-octiphenyl donors to ThT acceptors. The presence of FRET provided further corroborative evidence for ThT binding to rigid-rod β-fibrils since it operates over short distances only.

The properties of rigid-rod β-fibrils could thus be readily identified from the ICD CE, emission, or FRET related to the ThT fluorophore. The dependence of ThT binding on the concentration of rod **2** suggested that β-fibrillogenesis occurs above a critical barrel concentration $c = 3$ μM (Figure 3B). Maximal β-fibrillogenesis was observed at pH 5.5 (Figure 3C).[16] As for β-amyloid fibrils,[8, 9] this finding suggested intermolecular interactions between protonated and neutral histidines in rigid-rod β-fibrils.

Direct observation of hydrated rigid-rod β-fibrils was possible by using electron cryomicroscopy and cryonegative staining.[12, 19] This method was of interest because it provides access to high-contrast cryomicrographs of intact vitrified structures. Rigid-rod β-fibrils appear white against a background with an enhanced darkness from ammonium molybdate (Figure 4).[12, 19]

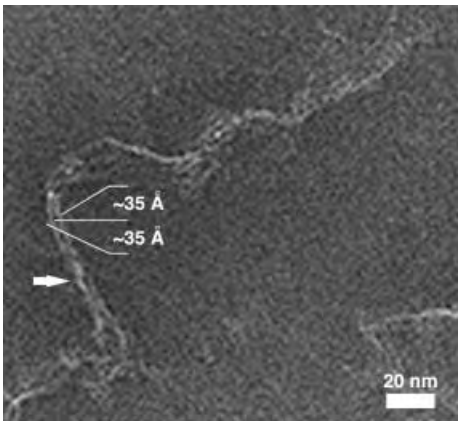


Figure 4. Electron cryomicrograph of rigid-rod β-fibrils (15 μM **2**, 10 mM MES, pH 5.5). Apparent fibril dimensions ca. 3.5×3.5 nm (for tentative structure, see **5** in Figure 1) and a fibril crossover (arrow) are indicated.

Short, fibrillar quaternary structures of about uniform diameter near the resolution limit (ca. 3.5×3.5 nm) were observed at pH 5.5 (Figure 3C and Figure 4). These "rod-like"[12] fibrils self-assembled in a poorly organized manner and included rare fibril crossovers (Figure 4, arrow). Their highly variable overall appearance included some indications of unidirectional fibril self-assembly into meandering, "ribbonlike" quaternary structures and a few less structured, presumably nonfibrillar, subdomains. Some of the vitrified "rigid-rod" β-fibrils were similar to intermediate rather than mature amyloid-β-fibrils.[12] This similarity may be of potential interest because of the likely "noncross-β" structure of rigid-rod β-fibrils (Figure 1, see below). Consistent with increased β-bilayer charge and hydrophobicity upon full histidine protonation and deprotonation, much shorter "mini-fibrils" and amorphous aggregates were detected at pH 4.5 and 6.5, respectively (not shown).

The overall poor self-organization of dilute aqueous rigid-rod β-fibrils was dramatically amplified on graphite. Indeed, AFM images of rigid-rod β-fibrils revealed hierarchical preorganization beyond the micron scale in three dimensions (Figure 5).

β-Fibril self-assemblies on graphite are composed of fibrils with uniform width and height of about 4.0 nm (Figure 5, bottom). Similar fibril dimensions were identified in assemblies observed by using electron cryomicroscopy (Figure 4). A uniform height of approximately 28.0 nm for the assemblies suggests that about seven of these β-fibrils grow one on top of the other, without any irregularities, even at the termini (Figure 5, top). β-Fibril heptamers are further characterized by extensive meandering with some "U-turns" that create lateral, often loose, contact between two β-fibril heptamers. "Dimeric" β-fibril heptamers, however, never cross, twist, touch, or fuse.

Although speculations on possible structures of rigid-rod β-fibrils and β-fibril self-assemblies need appropriate reservation,[1–12] some comments may be constructive for future

 © WILEY-VCH Verlag GmbH, D-69451 Weinheim, 2001 1433-7851/01/4024-4659 $ 17.50+.50/0

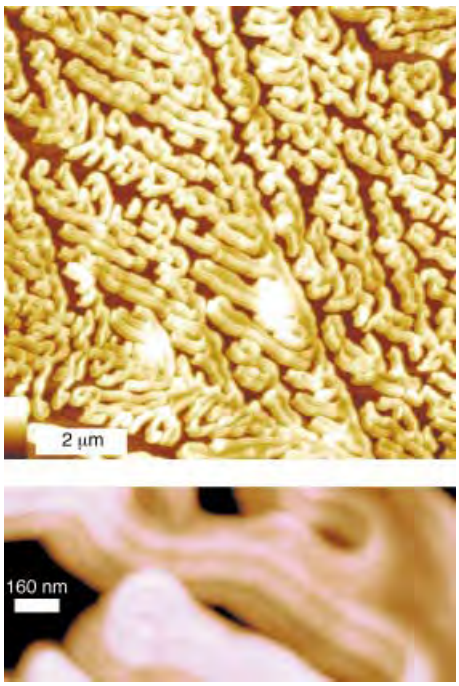


Figure 5. AFM image of rigid-rod β-fibril self-assemblies on graphite at low (top, vertical scale bar = 80 nm) and high magnification (bottom, 5 μM **2**, 3.3 mM MES, pH 5.5; for tentative structure, see **6** in Figure 1).

developments (Figure 1). With direct structural evidence for rigid-rod β-barrels **1** in hand (Figure 2), it is reasonable to propose that β-fibrillogenesis is initiated above the critical barrel concentration of $c = 3$ μM by lateral barrel–barrel contacts between hydrophobic β-faces. Under these partially denaturating conditions,[1–12] β-barrel dimers **3** (or higher oligomers) may transform into transient β-bilayers **4**. Dimerization of β-bilayers **4**, perhaps directed by β-barrel turns (Figure 1, red), gives the tentative rigid-rod β-fibril **5**. Note that in contrast to classical dimeric β-bilayers,[1–12] β-fibril **5** comprises a "noncross-β" motif and, perhaps, terminal and some central β-barrel turns. Dimensions of 3.4 × ca. 4.0 nm estimated for β-fibril **5** roughly match experimental values (Figure 4 and 5). Initiation and termination of unidirectional self-assembly of β-fibril **5** into heptamer **6** (Figure 5) is then similarly preorganized by (transient) nucleating β-barrel turns (Figure 1A, red) and further supported by surface repulsion (Figure 1A, blue). Note that twisting of single fibrils in the tentative heptamer **6** cannot be excluded experimentally.

In conclusion, this report on hierarchical preorganization of β-sheet structures by synthetic rigid-rod "β-dyad" peptides describes a rich tertiary and quaternary structural plasticity of delightful order and beauty. Unprecedented direct structural evidence at the tertiary structural level will increase confidence in efforts to exploit the easily accessible functional plasticity of rigid-rod β-barrels.[14–16] Their controlled transformation into rigid-rod quaternary β-structures with identical promise for structural and functional plasticity dramatically enriches the broad spectrum of applicability of rigid-rod molecules in bioorganic chemistry and beyond.

Methods

Spectroscopic studies: Absorption spectra were recorded on a Varian Cary 1 Bio spectrophotometer, circular dichroism spectra on a JASCO-710 spectropolarimeter, and fluorescence spectra on FluoroMax-2 (Jobin Yvon-Spex), all equipped with injector port, stirrer, and temperature controller (25 °C). Details on routine synthesis, purification (by reverse phase high-performance liquid chromatography (RP-HPLC)) and characterization of **2** will be reported elsewhere (see references [14–17]). Stock solutions were prepared from freshly repurified (RP-HPLC) **2**. An aliquot (usually 20 μL) of a concentrated stock solution in MeOH or dimethyl sulfoxide (DMSO) was added to buffer (usually 2 mL of 10 mM MES, pH as indicated; nearly identical results were obtained for < 100 mM MES, 10–100 mM phosphate, and < 100 mM XCl (X = Na, K)). Rigid-rod fibrils were characterized above the critical barrel concentration (c(**2**) = 3 μM) and below the appearance of minor (c(**2**) = 10 μM) to appreciable sample turbidity (c(**2**) = 15 μM). The binding of thioflavin T (ThT, usually 10 μM, Aldrich) was monitored by addition of an aliquot (usually 20 μL) from a concentrated stock solution in water to fibril samples prepared as above. UV/Vis: $\lambda_{max} = 412$ nm; CD: $\lambda_{max} = 420$ nm (Figure 3A); fluorescence emission: $\lambda_{ex} = 420$ nm, $\lambda_{em} = 500$ nm;[5] FRET: $\lambda_{ex} = 319$ nm,[14–16] $\lambda_{em} = 500$ nm. The following parameters were varied: c(ThT) = 0–14 μM (see, for example, Figure 3A), c(**2**) = 0–25 μM (see, for example, Figure 3B), pH 3.4–7.1 (e.g. Figure 3C), c(guanidinium chloride) = c(NaCl) = 0–2 M (*identical* decrease in intensities, not shown), c(Cu(OAc)$_2$) = 0 → 90 μM (decrease in intensities, not shown), t = 5 min–2 days (negligible change, not shown).

Atomic force microscopy (AFM): Samples were prepared as above and spectroscopically characterized prior to measurement. Barrels (see, for example, Figure 2) were prepared by deposition of 5 μL of an aqueous solution of **2** (1.5 μM, 1 mM MES, pH 5.5) on freshly cleaved mica followed by vibration isolated air-drying. Fibril self-assemblies (see, for example, Figure 5) were prepared by placing 5 μL of an aqueous solution of **2** (5 μM, 3.3 mM MES, pH 5.5) on graphite using otherwise identical procedures. Images were collected on a Nanoscope IIIa multimode scanning probe workstation (Digital Instruments) in tapping mode by using etched silicon tips (NanoProbes, Digital Instruments), a drive frequency of 250–300 kHz, and scanning speed at a line frequency of 1.2–2.2 Hz, at ambient temperature.

Negative-staining electron cryomicroscopy: Samples were prepared as above and spectroscopically characterized prior to measurement. Images were collected following routine protocols.[12, 19] In brief, 5 μL aqueous solutions of **2** (15–20 μM, 10 mM MES, pH 4.5–6.5, 0–90 μM Cu(OAc)$_2$) were dropped on gold-sputtered 200-mesh carbon grids, placed upside down on a drop of saturated ammonium molybdate (10 s), blotted, vitrified with liquid ethane, mounted under liquid nitrogen, examined at ca. –172 °C (Philips CM12 electron microscope, 80 kV, nominal magnification 45000), and recorded (Kodak 4489).

Received: May 29, 2001
Revised: September 9, 2001 [Z17195]

[1] J.-C. Rochet, P. T. Lansbury, Jr., *Curr. Opin. Struct. Biol.* **2000**, *10*, 60.
[2] J. W. Kelly, *Curr. Opin. Struct. Biol.* **1998**, *8*, 101.
[3] M. Fandrich, M. A. Fletcher, C. M. Dobson, *Nature* **2001**, *410*, 165.
[4] M. W. West, W. Wang, J. Patterson, J. D. Mancias, J. R. Beasley, M. H. Hecht, *Proc. Natl. Acad. Sci. USA* **1999**, *96*, 11211.
[5] Y. Takahashi, A. Ueno, H. Mihara, *ChemBioChem* **2001**, *2*, 75.
[6] H. A. Lashuel, S. R. LaBrenz, L. Woo, L. C. Serpell, J. W. Kelly, *J. Am. Chem. Soc.* **2000**, *122*, 5262.
[7] N. Yamada, K. Ariga, M. Naito, K. Matsubara, E. Koyama, *J. Am. Chem. Soc.* **1998**, *120*, 12192.
[8] T. S. Burkoth, T. L. S. Benzinger, D. N. M. Jones, K. Hallenga, S. C. Meredith, D. G. Lynn, *J. Am. Chem. Soc.* **1998**, *120*, 7655.
[9] T. S. Burkoth, T. L. S. Benzinger, V. Urban, D. M. Morgan, D. M. Gregory, P. Thiyagarajan, R. E. Botto, S. C. Meredith, D. G. Lynn, *J. Am. Chem. Soc.* **2000**, *122*, 7883.
[10] A. Lim, A. M. Makhov, M. J. Sanderholm, J. D. Griffith, B. W. Erikson, *Biochem. Biophys. Res. Commun.* **1999**, *264*, 498.

 © WILEY-VCH Verlag GmbH, D-69451 Weinheim, 2001 1433-7851/01/4024-4660 $ 17.50+.50/0

[11] C. Goldsbury, J. Kistler, U. Aebi, T. Arvinte, G. J. S. Cooper, *J. Mol. Biol.* **1999**, *285*, 33.
[12] B. Bohrmann, M. Adrian, J. Dubochet, P. Kuner, F. Müller, W. Huber, C. Nordstedt, H. Döbeli, *J. Struct. Biol.* **2000**, *130*, 232.
[13] H. Rapaport, K. Kjaer, T. R. Jensen, L. Leiserowitz, D. A. Tirrell, *J. Am. Chem. Soc.* **2000**, *122*, 12523.
[14] S. Matile, *Chem. Soc. Rev.* **2001**, *30*, 158.
[15] S. Matile, *Chem. Rec.* **2001**, *1*, 162.
[16] B. Baumeister, N. Sakai, S. Matile, unpublished results.
[17] B. Baumeister, A. Som, G. Das, N. Sakai, S. Matile, unpublished results.
[18] A. Engel, D. J. Müller, *Nat. Struct. Biol.* **2000**, *7*, 715.
[19] M. Adrian, J. Dubochet, S. D. Fuller, J. R. Harris, *Micron* **1998**, *29*, 145.

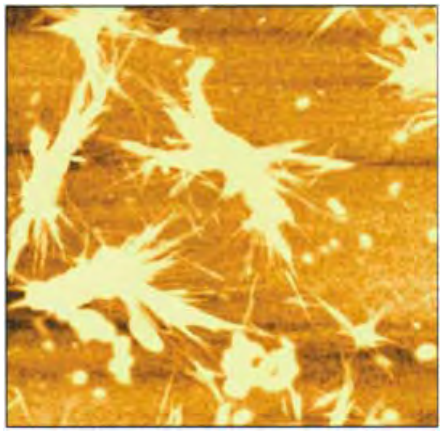


Figure 1. AFM image (5×5 μm) of carbon nanotube stars on mica. The reaction mixture was directly cast on mica without any purification.

Construction of Carbon Nanotube "Stars" with Dendrimers

Masahito Sano,* Ayumi Kamino, and Seiji Shinkai

Since carbon nanotubes are either metallic or semiconducting and exhibit ballistic transport,[1] the positioning of individual nanotubes in a well-defined spatial orientation may produce novel physical properties. By the currently available growth methods, carbon nanotubes are produced only in a stringlike form. Chemical modification is an attractive method for constructing various large-scale structures by positioning stringlike nanotubes. Herein we report the construction of star-shaped structures in which many carbon nanotubes radiate from a dendrimer center. These super-structured carbon nanotubes exhibit a peculiar response to electron beams. The synthesis of the stars was made possible by carefully fractionating the nanotubes by size.

Commercially available single-walled carbon nanotubes (SWNTs) are very long and are difficult to disperse in solution.[2–6] A standard procedure is to apply ultrasonication in strong acids to cut SWNTs into short pieces,[7, 8] followed by light etching to introduce oxygen-containing groups, such as carboxylic acids. Cut SWNTs are fractionated according to their characteristic sizes, as discussed herein. The carboxylic acid groups of the fractionated SWNTs were converted into acid chlorides and were then treated with the tenth generation poly(amidoamine) (PAMAM) starburst dendrimer (G10).

Atomic force microscopy (AFM) on cast films of the reaction mixture on mica reveals star-shaped objects (Figure 1). The average spine length is approximately 0.8 μm, which agrees well with the length of the SWNTs in the fraction. Although acid treatment tends to produce oxygen-containing groups at the side walls as well as at the ends,[9] our findings indicate, as proposed by other studies,[8, 10, 11] that the acid chloride groups at the open ends are more reactive than those at the side walls. Many spines are thicker than several nm and indicates, therefore, that there must be bundles of SWNTs in some burs. We think that many SWNTs simply adhere by van der Waals interactions to those tubes that have reacted with a dendrimer because of local high concentrations of tubes around the dendrimer. Some SWNTs are seen to bridge between two stars, which suggests that both ends of some SWNTs have reacted. Spectroscopic characterization was not possible because of the extremely low molar concentrations of stars that resulted from the initial low concentrations of SWNTs and difficulties in purification. Support that the SWNTs are covalently linked to the dendrimers rather than self-coagulated is provided by the observation that the star structures were completely destroyed after heating the stars for 3 h at 500 °C in N_2.

When the same sample shown in the AFM image of Figure 1 was coated with Pt/Pd and observed by scanning electron microscopy (SEM), star-shaped objects with much thicker burs were imaged. These spines were thicker than would be expected from the mere presence of the Pt/Pd films (Figure 2). Since the number of spines in the SEM image is smaller than that in the AFM image, it is likely that some of the spines in a star adhere together during residual water evaporation and metal deposition when they are placed in a vacuum. Without any metal coating, the acid-treated SWNTs

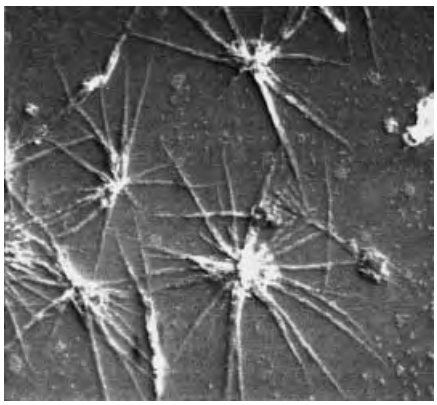


Figure 2. SEM image of the same sample as used to obtain Figure 1, but coated with Pt/Pd.

[*] Dr. M. Sano, A. Kamino, Prof. Dr. S. Shinkai
Chemotransfiguration Project—JST
2432 Aikawa, Kurume, Fukuoka 839-0861 (Japan)
Fax: (+81) 942-39-9012
E-mail: mass@jst.ktarn.or.jp

 © WILEY-VCH Verlag GmbH, D-69451 Weinheim, 2001 1433-7851/01/4024-4661 $ 17.50+.50/0

that are not used for reaction usually give bright contrast on silicon surfaces when examined by SEM. Interestingly, some stars appear very dark when uncoated stars are imaged with the acid-treated SWNTs (Figure 3). It is not clear if all the stars give dark contrast since the acid-treated SWNTs form a network and hide the stars. While the mechanism is not well understood, the SEM results suggest that the star-shaped SWNTs may possess novel response characteristics to incoming electrons.

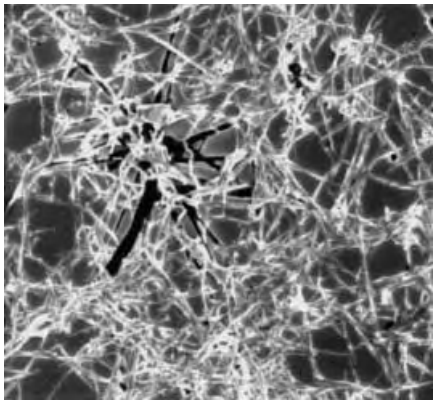


Figure 3. SEM image of a mixture of stars and the acid-treated SWNTs on silicon without any metal coating.

Cutting pristine SWNTs by acid produces SWNTs with a broad size distribution.[8] No star-shaped structures were recognizable by AFM or SEM when the whole distribution was used for the reaction with the dendrimers. This result can be rationalized by the reactivity of the SWNTs being size-dependent. If the number of oxygen-containing groups at both ends of a SWNT is independent of the tube length but the length affects the collision probability of the ends to other reactants, then chemical reactivity is expected to vary with the size of the SWNTs. Dynamic light scattering (DLS) was measured on various fractions collected at different centrifugal forces to ascertain the effect of size on the transport properties of SWNTs.[12] Here, a fraction collected as a supernatant solution with a centrifugal acceleration of G (in a unit of g) is designated G. Figure 4a plots the first cumulant Γ divided by the square of the wave number q as a function of G. In the case of a solid sphere, the initial relaxation rate Γ/q^2 is a translational diffusion constant. The stringlike shape of SWNTs, a broad length distribution within each fraction, and possible bundle formation, however, do not allow simple interpretation of Γ/q^2. Nevertheless, the value of Γ/q^2 reflects the structures and transport properties of SWNTs. The curve shows two regions of increasing Γ/q^2 values (at $G < 3500$ and $G > 12500$) and a plateau region between them. The scattering intensity was 5 to 10 times smaller at $G = 35300$ than for all other fractions.

AFM observations were also made on selected fractions from each region. All the samples show tubular and globular morphology. The measured length (for tubular moieties) or diameter (for globular moieties) exhibit histograms with a peak and a slowly decaying tail to larger sizes. The peak positions are depicted in Figure 4b. The higher the G value is,

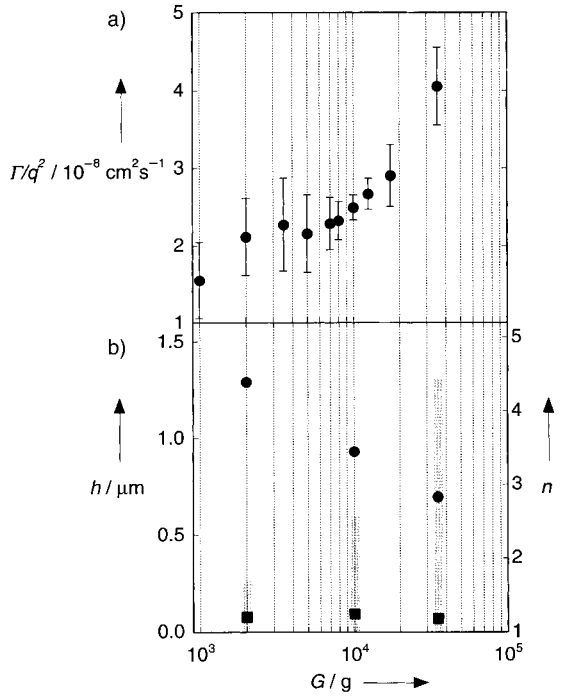


Figure 4. a) A plot of the initial relaxation rates Γ/q^2 obtained by DLS measurements against the centrifugal acceleration G used to fractionate the SWNTs dispersion. b) The most abundant length (circles) and diameter (squares) of the tubular and globular aggregates, respectively, at selected fractions. The vertical bars indicate the ratio of globular aggregates to tubular aggregates found in the AFM images. h = size, n = ratio of globular to tubular aggregates.

the shorter the tubular aggregates become. The globular aggregates have the same size regardless of the G value, but are found more in the higher G fractions. Globular morphology is considered to result from the aggregation of very short tubes during solvent evaporation.

We have shown previously that a SWNT has a persistence length of 0.8 μm.[13] Since this value agrees well with the tube length in the plateau region, the first increase of Γ/q^2 at $G <$ 3500 is most likely caused by a change in tube conformation. Those SWNTs in the region $G > 3500$ are stiff and straight, whereas SWNTs at smaller G values are semiflexible. Although physical factors that cause the second increase of Γ/q^2 at $G > 12500$ are not well understood, the higher G fractions contain larger numbers of very short SWNTs that move faster. The stars, as shown above, were obtained by using only those SWNTs in the plateau region. When the higher G fractions were added, the AFM images appear indistinguishable from those of physical mixtures without reaction. This result suggests that very short tubes reacted with the dendrimers before the longer ones had chance to do so. This study demonstrates the importance of size control for the construction of well-defined nanotube objects.

Experimental Section

SWNTs (a laser-oven product purchased from Tubes@Rice with an average radius of 0.6 nm) were cut by ultrasonication in strong acids and lightly etched in H_2SO_4/H_2O_2,[7, 8] followed by washing on a teflon filter with water until the filtrate became neutral. The SWNTs were dispersed in solvents by ultrasonication for 60 s in a laboratory ultrasonic washing bath (42 kHz,

 © WILEY-VCH Verlag GmbH, D-69451 Weinheim, 2001 1433-7851/01/4024-4662 $ 17.50+.50/0

90 W). Water was used for the DLS measurement and DMF for the reaction. The SWNT dispersion was subjected to a series of centrifugations starting from the largest force. Each time, a supernatant solution was separated from the heavier residue, which was redispersed for further centrifugation. The concentration of each supernatant solution was adjusted to 1.0 $\mu g\,mL^{-1}$. DLS measurements were performed with a wavelength of 632.8 nm and a scattering angle of 90° at 30 °C and the data were analyzed with a cumulant method. Measurements have been repeated several times using different batches of the acid treatments. Subsequent experiments showed that the measurements were performed on SWNTs in the concentration-independent region.

The SWNT fractions in the plateau region were treated with thionyl chloride to produce SWNTs derivatized with acid chloride groups, as reported by others.[8, 10] In the present case, we used centrifugation and decantation cycles to wash the acid chloride-derivitized SWNTs with dry THF and DMF to minimize coagulation. A dispersion of acid chloride-derivatized SWNTs in DMF (10 μL) was added to the dendrimer (G10) dissolved in 10 mM NaOH. The concentration of SWNTs was so low that the solution hardly had any color. This was necessary, since amine-terminated dendrimers act as a glue to stick SWNTs together and coagulate the SWNTs immediately.[14] The mixture was stirred at room temperature for 12 h and the reaction mixture was directly cast on mica or silicon for AFM and SEM studies.

AFM was performed in a noncontact mode in air at room temperature. SEM images were taken with an acceleration voltage of 5.0 kV for Pt/Pd coated samples and 1.0 kV for uncoated samples.

Received: August 13, 2001 [Z17718]

[1] R. Saito, G. Dresselhaus, M. S. Dresselhaus, *Physical Properties of Carbon Nanotubes*, Imperial College, London, **1998**.

[2] P. J. Boul, J. Liu, E. T. Mickelson, C. B. Huffman, L. M. Ericson, I. W. Chiang, K. A. Smith, D. T. Colbert, R. H. Hauge, J. L. Margrave, R. E. Smalley, *Chem. Phys. Lett.* **1999**, *310*, 367 – 372.

[3] B. Z. Tang, H. Xu, *Macromolecules* **1999**, *32*, 2569 – 2576.

[4] K. D. Ausman, R. Piner, O. Lourie, R. S. Ruoff, M. Korobov, *J. Phys. Chem. B* **2000**, *104*, 8911 – 8915.

[5] J. L. Bahr, E. T. Mickelson, M. J. Bronikowski, R. E. Smalley, J. M. Tour, *Chem. Commun.* **2001**, 193 – 194.

[6] A. Star, J. F. Stoddart, D. Stueuerman, M. Diehl, A. Boukai, E. W. Wong, X. Yang, S.-W. Chung, H. Choi, J. R. Heath, *Angew. Chem.* **2001**, *113*, 1771 – 1775; *Angew. Chem. Int. Ed.* **2001**, *40*, 1721 – 1725.

[7] A. G. Rinzler, J. Liu, H. Dai, P. Nikolaev, C. B. Huffman, F. J. Rodríguez-Macías, P. J. Boul, A. H. Lu, D. Heymann, D. T. Colbert, R. S. Lee, J. E. Fischer, A. M. Rao, P. C. Eklund, R. E. Smalley, *Appl. Phys. A* **1998**, *67*, 29 – 37.

[8] J. Liu, A. G. Rinzler, H. Dai, J. H. Hafner, R. K. Bradley, P. J. Boul, A. Lu, T. Iverson, K. Shelimov, C. B. Huffman, F. Rodriguez-Macias, Y.-S. Shon, T. R. Lee, D. T. Colbert, R. E. Smalley, *Science* **1998**, *280*, 1253 – 1256.

[9] D. B. Mawhinney, V. Naumenko, A. Kuznetsova, J. T. Yates, Jr., J. Liu, R. E. Smalley, *Chem. Phys. Lett.* **2000**, *324*, 213 – 216.

[10] J. Chen, M. A. Hamon, H. Hu, Y. Chen, A. M. Rao, P. C. Eklund, R. C. Haddon, *Science* **1998**, *282*, 95 – 98.

[11] Z. Liu, Z. Shen, T. Zhu, S. Hou, L. Ying, Z. Shi, Z. Gu, *Langmuir* **2000**, *16*, 3569 – 3573.

[12] Short SWNTs can be fractionated by chromatography: S. Niyogi, H. Hu, M. Hamon, P. Bhowmik, B. Zhao, S. M. Rozenzhak, J. Chen, M. E. Itkis, M. S. Meier, R. C. Haddon, *J. Am. Chem. Soc.* **2001**, *123*, 733 – 734.

[13] M. Sano, A. Kamino, J. Okamura, S. Shinkai, *Science* **2001**, *293*, 1299 – 1301.

[14] J. Liu, M. J. Casavant, M. Cox, D. A. Walters, P. Boul, W. Lu, A. J. Rimberg, K. A. Smith, D. T. Colbert, R. E. Smalley, *Chem. Phys. Lett.* **1999**, *303*, 125 – 129.

Direct Microscopic Observation of the Time Course of Single-Molecule DNA Restriction Reactions**

Bürk Schäfer, Helgard Gemeinhardt, and Karl Otto Greulich*

While biophysical studies, such as force measurements[1–4] or laser cutting[5] of single DNA molecules can be found in the literature in a large variety of applications, direct light-microscopic detection of DNA single molecule reactions is rare. In most of the latter cases, unstained DNA molecules were coupled to microspheres (beads) and held with optical or magnetic tweezers. The reaction was then observed indirectly by the change of some distance or force, for example, displacement of the sphere reflected the reaction progress.[6–10] In this sense, single DNA-molecule reactions are usually detected in "blind" experiments. One of the exceptions is the direct microscopic observation of the reaction of fluorescently stained *E.-coli*-RNA-polymerase on unstained DNA.[11] One particularly interesting class of reactions are those of restriction endonucleases, since they allow individual DNA molecules to be characterized and distinguished. As many as 3000 different restriction endonucleases of one subclass (type II) are known.[12] The observation of restriction reactions is, however, difficult, since the restriction step is an all-or-none process, that is, cut or non-cut, of the DNA molecule at a given restriction site. To date, single-molecule restriction has been observed by blind cutting of individual fluorescently marked DNA molecules and analyzing the fluorescence bursts of the restriction fragments.[13]

We have already reported the cutting of a single, bead-coupled DNA molecule by the restriction endonuclease Apa 1, which has one cutting site in the target molecule,[14] and the restriction by Sma I and Eco RI with three and five cutting sites.[15] Herein, we introduce temporal resolution and thus information on the kinetics of single DNA-molecule restriction.

Figure 1 shows the restriction of a single DNA molecule by the enzyme Eco RI. In part (g) of Figure 1, the cutting pattern expected from the 48502 base pairs (bp) long sequence of Lambda phage DNA is shown. The molecule is stretched by hydrodynamic flow from bottom right to top left. In the example shown the DNA end with the longest restriction fragment (21226 bp) is attached to the bead. Binding of the short fragment (3530 bp) is also observed, but then usually only one or two cuts can be detected since some restriction sites are in the part of the DNA molecule which is wrapped around the bead. Such wrapping causes the bead fluorescence seen in Figure 1.

At a given time, usually 5 – 20 seconds after injection of the enzyme, the first cut is seen (Figure 1b); this point is then

[*] Prof. Dr. K. O. Greulich, B. Schäfer, H. Gemeinhardt
Institut für Molekulare Biotechnologie
Postfach: 100 813, 07708 Jena (Germany)
Fax: (+49) 3641-656410
E-mail: kog@imb-jena.de

[**] We thank Dr. Werner Wolf for helpful discussions and the VW-foundation, Grant No. I/75099 for supporting this work.

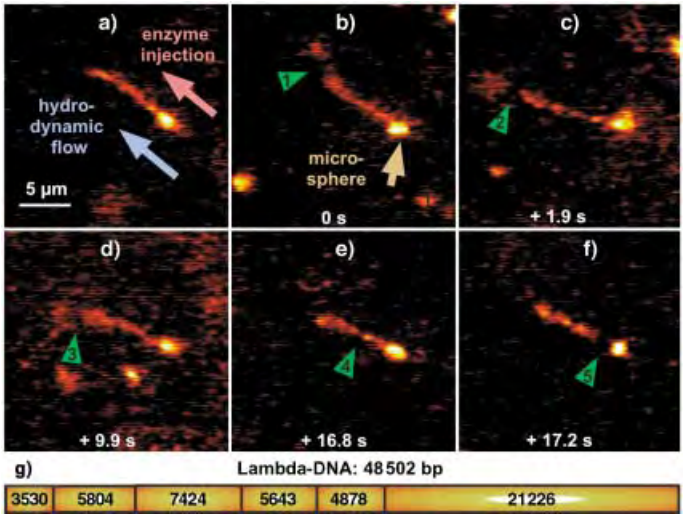


Figure 1. Example of the complete enzymatic digestion of a single hydrodynamically stretched lambda-DNA molecule with the restriction endonuclease EcoR I (a–f). All five expected restriction sites are observed. g) Expected cutting pattern (restriction map) of EcoR I on Lambda phage DNA

defined as zero time. After being cut from the main molecule, the fragment quickly collapses into a globular structure (as any DNA molecule does so when no force is applied) and is transported away with the flow. In steps of several seconds (for the exact times see Figure 1) the other expected cuts can be seen. Two details are important: the first cut occurs at the end of the DNA molecule which is distant from the bead, the second cut is closer to the bead and so on. Obviously, the reaction proceeds against the hydrodynamic flow. Furthermore, the cuts are consecutive, that is, no expected cutting site is omitted. These observations can be most simply explained by the binding of a single enzyme molecule to the distant end and subsequent motion along the DNA molecule towards the bead; this will be discussed in some detail below.

An equivalent observation has been made with the restriction endonuclease Sma I, which has three expected cutting sites in the Lambda phage DNA molecule. In total, ten molecules were investigated with Sma I and ten molecules with Eco RI, this corresponds to a total of 80 restriction events. The features outlined above were observed for more than 50 % of these molecules, in another 30 % restriction sites at one end are omitted, but consecutive cutting is still preserved. Only in four of the 20 molecules the features described above do not hold. This regularity indicates that indeed enzymatic cuts and not just mechanical DNA breaks are seen. A more detailed proof is given by the fact that the fluorescence intensity of the single restriction fragments divided by the total fluorescence of DNA molecules reflects the expected restriction fragment size (see ref.[15]).

From the times at which the cuts are observed, time courses of the reactions can be generated. Figure 2a shows such time courses of six complete Sma I restriction reactions, Figure 2b the corresponding results for five Eco RI reactions. Each curve was measured for an individual DNA molecule.

The observed result becomes even clearer when the reactions between two adjacent cutting sites are represented

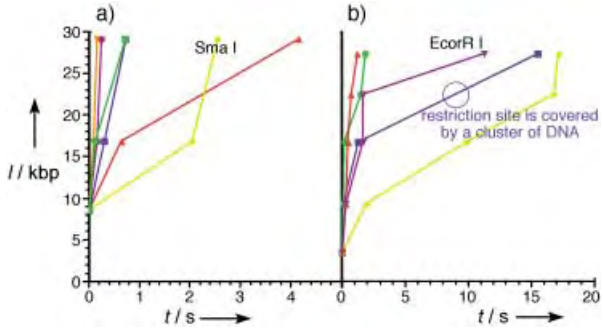


Figure 2. Restriction time courses of Sma I (a) and EcoR I (b) for 11 different molecules. Each curve represents the restriction of one single DNA molecule. Note that the time-axis scales are different for Sma I and Eco RI.

separately (Figure 3). For each enzyme two groups of data are found. Since the slope of each of the straight lines is a measure of the reaction rate, clearly each of the enzymes has a slow and a fast reaction rate and for Sma I this rate is generally faster than for Eco RI. The dotted lines correspond to free diffusion of the enzyme through the solution. Essentially, all rates are slower than the diffusion rate, which indicates that motion along the DNA molecule can, on the one hand, be thermally driven, but, on the other hand, is obviously reduced as if there were friction.

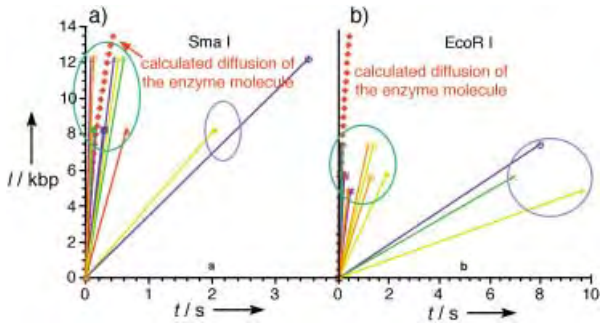


Figure 3. Restriction rates of Sma I (a) and Eco RI (b). The slope of each line reflects the restriction rate between subsequent cuts. Two different groups of restriction rates can be distinguished for each enzyme and are indicated by circles.

Diffusion could also explain why the recognition process between enzyme and DNA cannot require exact binding to the five (Eco RI) or three (Sma I) restriction sites on the 48502 bp long Lambda phage DNA. Both enzymes have six bp long recognition sites. It would require more than 1500 (EcoR I) or 3000 (Sma I) contacts between one enzyme molecule and the DNA molecule to statistically hit one specific site. The concentration of the microinjected enzyme surrounding the DNA is approximately 6×10^4 molecules per pL. The mean rate of contacts between one enzyme molecule and the DNA follows from this concentration to be around 1 contact per second. Thus, 1500 contacts would require half an hour for EcoR I and 3000 contacts for Sma I one hour. To find one restriction site solely by spatial diffusion of the enzyme in the observed time of about one second is impossible.

 © WILEY-VCH Verlag GmbH, D-69451 Weinheim, 2001 1433-7851/01/4024-4664 $ 17.50+.50/0

Together with the above mentioned fact that most of the cuts are consecutive, this suggests that the enzyme molecule binds randomly (statistically) to some site on the DNA molecule, searches for its six-bp restriction site and cuts. Since in all the observed cases where the reaction continues, it does so in the forward direction, often with the same speed, we suggest that the enzyme cuts at the rear (lagging) side of its recognition sequence while already being attached to the forward (leading) side. For Eco RI this is easily conceivable, since its restriction site is 5′..G ↓ AATTC..3′ where the arrow indicates the cut. For Sma I the restriction site is highly symmetric (Sma I: 5′..CCC ↓ GGG..3′) and thus a simple explanation is not possible. Here a differential affinity of the enzyme for G and C tracts has to be invoked. A final answer will probably only be possible once the structure of Sma I is solved.

While the explanation given for the observations may appear plausible, an alternative possibility has to be excluded: that not a single, but several individual enzyme molecules are attached to the DNA molecule and cooperate. However, in this case one would have to invoke a hidden mechanism, which orchestrates these different molecules so that the cuts are consecutive. Such a mechanism is at least much less probable than the mechanism postulated above. In the case of Eco RI, with its five restriction sites, such a multimolecule process is highly improbable.

The observed speeds of enzyme progression along the DNA appear to be high, but can be explained by guided diffusion. Values observed in our experiments are 50 kbp s^{-1} (17 μm s^{-1}) for Sma I and 30 kbp s^{-1}(10 μm s^{-1}) for EcoR I. Other enzyme reaction rates are known for DNA polymerase I (10 bp s^{-1}), T7-DNA polymerase (300 bp s^{-1}) and the DNA polymerase holoenzyme (1.000 bp s^{-1}). Furthermore the reaction rate of RecBCD, a DNA helicase and exonuclease is estimated to be 1.000 bp s^{-1}.[16] All these reaction rates are slower than our measured reaction rates. Polymerases execute a reaction on every base pair and can gain energy from bond cleavage (for example by ATP consumption). In contrast, the linear motion of restriction endonucleases along DNA observed in the present work can only occasionally receive energy from bond cleavage and thus has to take its energy from thermal motion. It was already suggested above that this is possible on the basis of diffusion and thus the mechanism can be explained.

Experimental Section

Biotinylation and staining: Lambda DNA (48,502 bp or 16.5 μm in its stretched form, New England Biolabs, Schwalbach, Germany) was biotinylated by using biotin-16-ddUTP (Roche Diagnostics, Mannheim, Germany). The lambda-DNA molecules in a concentration of 2.5×10^8 molecules per μL together with a 10-fold excess of biotin-16-ddUTP were incubated with terminal transferase (Boehringer Mannheim, Germany) in the recommended buffer (5 × the concentration recomended by the supplier: 1M potassium cacodylate, 125 mM Tris-HCl (Tris = tris(hydroxymethyl)aminomethane), 1.25 mg/ml bovine serum albumin, pH 6.6, Boehringer Mannheim) and 1.5 mM $CoCl_2$ (Boehringer Mannheim) for 20 min at 37 °C. The transferase reaction was terminated by adding EDTA (50 mM; EDTA = ethylendiaminetetraacetate). The biotinylated DNA was diluted at a ratio of 1:20 with H_2O and stained by mixing it with the fluorescent intercalating dye SYBRGreen (Molecular Probes, Oregon, USA). SYBRGreen is not the optimal dye in terms of stability, but, besides DAPI, is the only dye where we could observe an restriction endonuclease activity on stained DNA, so far.[14] Since Molecular Probes does not provide the exact dye concentration in the stock solution, a dilution of 0.08 % was determined empirically to be best suited for the staining procedure

Coupling of DNA to microspheres: In the following step, the stained and biotinylated molecules were coupled to streptavidin coated microspheres (diameter 1 μm, Polysciences, Eppelheim, Germany).[15] DNA preparation still containing residual material from the biotinylation and staining procedures was mixed with the microspheres (10^7 spheres per μL in H_2O) at a ratio of 5:1 and incubated for 15 min in the dark at room temperature. The final solution contained 3×10^5 molecules of DNA per μL in H_2O. Under these conditions, only one or at most a few DNA molecules are expected to bind to one microsphere, and the low ion concentration (for all dilution steps water was used) makes DNA stretching easily possible. For coupling single DNA molecules to polystyrene microbeads, the DNA molecules were end labeled at the 5′position with biotin, while the beads were covered with streptavidin. Because of the high binding constant of streptavidin with biotin, DNA bead binding occurs immediately upon mixing. For details of this procedure see ref. [15]

Handling of DNA molecules by optical tweezers and hydrodynamic flow: For handling of a single DNA molecule the sphere/DNA suspension (5 μL) was dropped onto a microscope cover slide and investigated in the fluorescence microscope. To retard fast photobleaching, an antifade kit (Appligene Oncor, Heidelberg, Germany) was used in a dilution of 2:5. Observation in the bright field shows the microspheres and in the fluorescence mode the DNA. Switching between both modes allowed a microsphere with an attached DNA molecule to be identified and then trapped with optical tweezers.[17, 18] The DNA molecule was stretched by the hydrodynamic force between the DNA molecule and the surrounding buffer which is generated by moving the cover slide while holding the microsphere with the tweezers. When the motion of the slide was stopped, the stretched DNA molecule coiled up within one or two seconds.

Enzymatic Reaction: The restriction endonucleases Sma I and EcoR I (New England Biolabs, Schwalbach, Germany) were used. The enzymes were suspended in a 5 × higher concentration than recommended by the supplier, for the recommended reaction buffers (Sma I: 250 mM potassium acetate, 100 mM Tris acetate, 50 mM magnesium acetate, 5 mM DTT (DTT = 1,4-dithiothreitol), pH 7.9; EcoR I: 250 mM NaCl, 500 mM Tris-HCl, 50 mM $MgCl_2$, 0.125 % Triton X-100, pH 7.5) to provide the necessary ion concentration for the restriction reaction after enzyme injection. Purification requires filtration with 0.22 μm centrifugal filter units (Ultrafree-MC, Millipore, Eschborn, Germany). If a higher concentrated reaction buffer is used, the DNA molecule on the microsphere tends to collapse as a result of the high ionic strength of the mixture even in hydrodynamic flow. A micromanipulator and microinjector device (Eppendorf, Hamburg, Germany) was used to inject the endonuclease and reaction buffer mixture.

The injection capillary was positioned 10 μm in front of the stretched DNA molecule. To start the enzymatic restriction, a volume of 0.1 – 0.2 pL of the prepared enzyme/buffer mixture was microinjected into the DNA solution on the cover slide at room temperature. The enzyme-buffer was thereby diluted by a factor of approximately 1:5 so that it reached its recommended concentration.

Received: June 25, 2001
Revised: October 15, 2001 [Z17349]

[1] T. R. Strick, J. F. Allemand, D. Bensimon, A. Bensimon, V. Croquette, *Science* **1996**, *271*, 1835 – 1837.
[2] S. R. Quake, H. Babcock, S. Chu, *Nature* **1997**, *388*, 151 – 154.
[3] C. G. Baumann, S. B. Smith, V. A. Bloomfield, C. Bustamante, *Proc. Natl. Acad. Sci. USA* **1997**, *94*, 6185 – 6190.
[4] M. D. Wang, H. Yin, R. Landick, J. Gelles, S. M. Block, *Biophys. J.* **1997**, *72*, 1335 – 1346.
[5] N. Endlich, C. Hoyer, A. Harim, S. Monajembashi, K. O. Greulich, *Exp. Tech. Phys.* **1995**, *41*, 303 – 311.
[6] B. Maier, D. Bensimon, V. Croquette, *Proc. Natl. Acad. Sci. USA* **2000**, *97*, 12 002 – 12 007.
[7] A. D. Mehta, M. Rief, J. A. Spudich, D. A. Smith, R. M. Simmons, *Science* **1999**, *283*, 1689 – 1695.

 © WILEY-VCH Verlag GmbH, D-69451 Weinheim, 2001 1433-7851/01/4024-4665 $ 17.50+.50/0

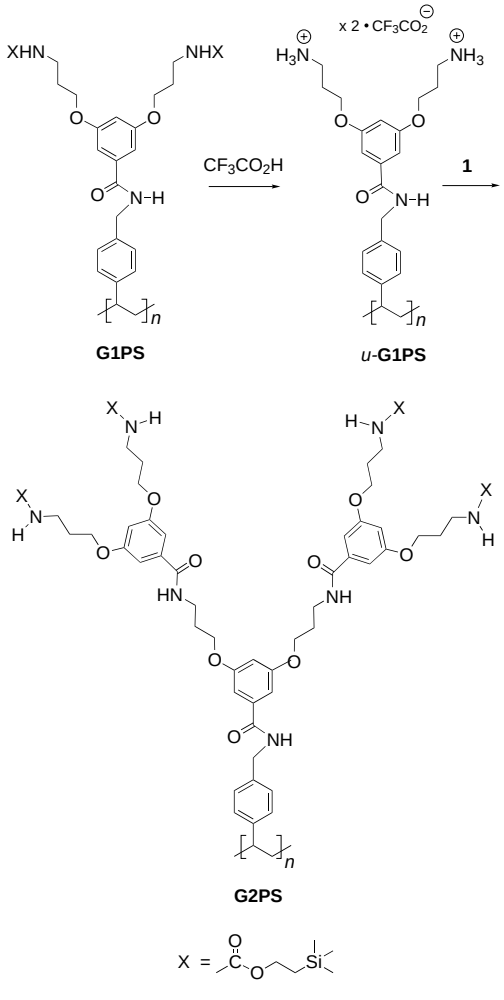
[8] H. Yin, M. D. Wang, K. Svoboda, R. Landick, S. M. Block, J. Gelles, *Science* **1999**, *270*, 1653 – 1657.
[9] M. D. Wang, M. J. Schnitzer, H. Yin, R. Landick, J. Gelles, S. M. Block, *Science* **1998**, *282*, 902 – 907.
[10] G. J. L. Wuite, S. B. Smith, M. Young, D. Keller, C. Bustamante, *Nature* **2000**, *404*, 103 – 106.
[11] Y. Harada, T. Funatsu, K. Murakami, Y. Nonoyama, A. Ishihama, T. Yanagida, *Biophys. J.* **1999**, *76*, 709 – 715.
[12] A. Pingoud, A. Jeltsch, *Nucleic Acids Res.* **2001**, *29*, 3705 – 3727.
[13] A. V. Orden, R. A. Keller, W. P. Ambrose, *Anal. Chem.* **2000**, *72*, 37 – 41.
[14] C. Hoyer, S. Monajembashi, K. O. Greulich, *J. Biotechnol.* **1996**, *52*, 65 – 73.
[15] B. Schäfer, H. Gemeinhardt, V. Uhl, K. O. Greulich, *Single Mol.* **2000**, *1*, 33 – 40.
[16] P. R. Bianco, L. R. Brewer, M. Corzett, R. Balhorn, Y. Yeh, S. C. Kowalczykowski, R. J. Baskin, *Nature* **2001**, *409*, 374 – 378.
[17] A. Ashkin, *Proc. Natl. Acad. Sci. USA.* **1997**, *94*, 4853 – 4860.
[18] K. O. Greulich, *Micromanipulation by Light in Biology and Medicine: The Laser Microbeam and Optical Tweezers*, Birkhäuser, Basel, **1999**.

Extremely Long Dendronized Polymers: Synthesis, Quantification of Structure Perfection, Individualization, and SFM Manipulation**

Lijin Shu, A. Dieter Schlüter,* Christof Ecker, Nikolai Severin, and Jürgen P. Rabe*

The enormously successful top-down approach to nanostructured materials[1] increasingly faces its limitations. For example, it is virtually impossible to both control and determine nanostructures on the atomic scale by cutting and etching. In recent years the alternative bottom-up approach to the nano world has made considerable progress from single atom manipulation[2a] towards rather well defined, more complex structures,[2b] although not enough to make it technologically important at this stage. Complex molecules with predictable shapes on the nanometer-scale were constructed, handled, and characterized and it was possible to individualize and manipulate them[3] or to assemble even more complex functional arrays.[4] The bottom-up approach is closely related to the scanning-probe microscopies which provide particularly important analysis, manipulation, and construction tools. Their consequent application and further methodical development have provided indispensible knowledge about both individualized and assembled properties of molecules, the behavior of molecules at interfaces,[5] and thus laid the foundation for what may become competition for the top-down approach within the next 10 years or so. For resolution reasons, scanning force microscopy (SFM) is useful for larger objects (a few nm in diameter) than scanning tunneling microscopy (STM, a few Å). On the other hand, there are no structural limitations for SFM, whereas STM is restricted to sufficiently thin molecules on conducting substrates. Dendronized polymers have been developed over the last 10 years as nanoscaled molecular objects at the interface between the materials and bio sciences.[5f] Despite considerable effort in many laboratories to date it has not been possible to synthesize such polymers carrying fourth generation (G4) dendrons and having both high molar mass and a functionalized surface for chemical modifications. We here report the divergent synthesis of an extremely high molar mass, surface functionalized, G4 dendronized polystyrene (PS), its individualization and SFM visualization on graphite, and its manipulation with the SFM tip.

Radically initiated polymerization of dendronized vinyl-type macromonomers leads to polymers the number of repeat units of which decreases with increasing dendron genera-

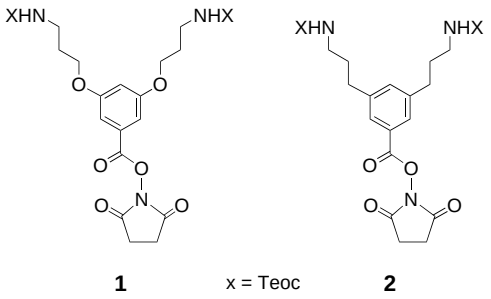


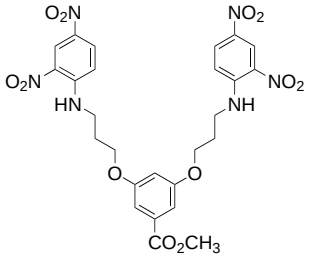
Scheme 1.

[*] Prof. Dr. A. D. Schlüter, Dr. L. Shu
Institut für Chemie
Freie Universität Berlin
Takustrasse 3, 14195 Berlin (Germany)
Fax: (+49) 30-838-53357
E-mail: adschlue@chemie.fu-berlin.de
Prof. Dr. J. P. Rabe, Dipl.-Phys. C. Ecker, Dr. N. Severin
Institut für Physik
Humboldt-Universität zu Berlin
Invalidenstrasse 110, 10115 Berlin (Germany)
Fax: (+49) 30-2093-7632
E-mail: rabe@physik.hu-berlin.de

[**] This work was supported by the Deutsche Forschungsgemeinschaft (Sfb 448, TPs 1 and 5) and the Fonds der Chemischen Industrie; SFM = scanning force microscopy.

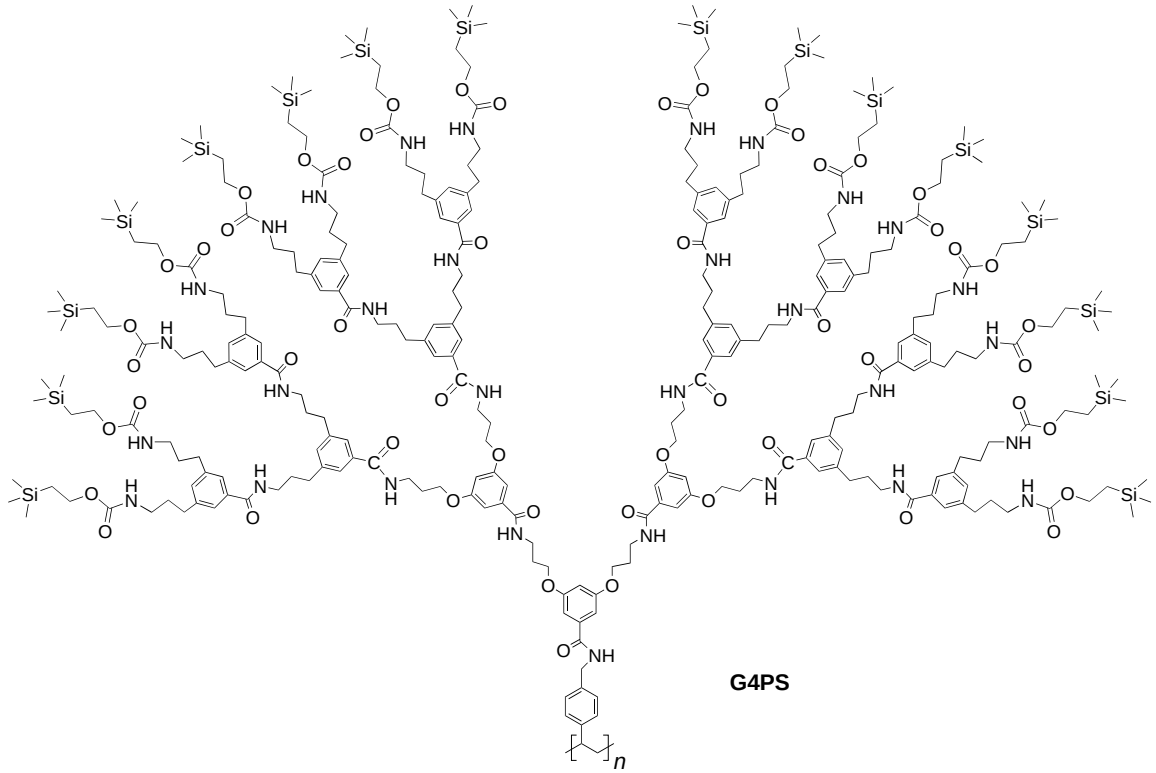
 © WILEY-VCH Verlag GmbH, D-69451 Weinheim, 2001 1433-7851/01/4024-4666 $ 17.50+.50/0





3

tion.[6] If long-chain polymers decorated with high generation dendrons are required, a divergent synthesis starting from a low generation and, thus, high molar mass dendronized polymer must be brought about. Dendrons have to be added stepwise to this scaffold's functional groups, until the desired generation is reached. A well known problem associated with divergent syntheses is the inavoidable increase of structural imperfection with an increasing number of coupling steps.[7] The selection of the optimum coupling chemistry and the method to quantify the coupling efficiency is therefore essential. Given our experience with amide formations, the known **G1PS** with two trimethlysilyl ethyloxy carbonyl (Teoc) protected peripheral amine groups was selected as the starting polymer[8] (Scheme 1) and the activated ester G1 dendrons **1** and **2** as growth reagents.[9] Compounds **1** and **2** were chosen because they can be prepared in large quantities, easily purified, and promised to give very high conversions.[10] Scheme 1 shows the synthetic sequence by which **G1PS** was converted into **G2PS**. Deprotection of **G1PS** to *u*-**G1PS** (u = unprotected) was with trifluoroacetic acid, and in this case and all following ones, could be easily driven to completion (500 MHz NMR). Reaction of *u*-**G1PS** with **1** furnished **G2PS** which was then subjected to the same deprotection/dendronization (with **2**[11]) sequence to give **G3PS**; repetition gave **G4PS**.[12] This sequence was carried out for two samples of **G1PS** which considerably differed in their molar mass (Sample 1: $M_n = 26.000$, $P_n = 40$, polydispersity index (PDI) = 2.8; sample 2: $M_n = 308.000$, $P_n = 460$, PDI = 1.8; average values according to gel permeation chromatography (GPC) in THF versus polystyrene standard[13]). All conditions were optimized for sample 1 and then applied to sample 2. The efficiency of the coupling was determined for each step by treating the remaining nondendronized amine groups of the respective dendronized polymer with 2,4-dinitrofluorobenzene (Sanger's reagent[14])[15] and measuring the UV absorbance referenced to standard **3** resulting from the dinitroaniline derivative formed.[16] The results for the **G3PS**/**G4PS** conversion with sample 1 are: 93.3 % (1.2 equiv of **1**) and 99.2 – 99.4 % (1.8 equiv of **1**, four independent dendronizations)[17] and for the conversions **G1PS**/**G2PS**, **G2PS**/**G3PS**, and **G3PS**/**G4PS** using sample 2 99.8 % (1.8 equiv of **1**), 99.7 %, and 99.4 %, respectively (1.8 equiv of **2**).[18] Thus, if the succinidyl activated ester **1** or **2** is used in 1.8-fold excess per amine

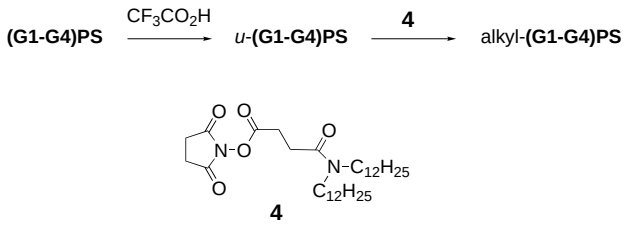


G4PS

 © WILEY-VCH Verlag GmbH, D-69451 Weinheim, 2001 1433-7851/01/4024-4667 $ 17.50+.50/0

function, dendronization is virtually complete even for sample 2 and for the most critical **G3PS/G4PS** conversion in which eight amines per repeat unit need to be dendronized. The homologous series of **(G1–G4)PS**[19] were decorated with two dodecyl chains per amine group by treating the respective deprotected dendronized polymers with active ester **4** (Scheme 2) to increase the adsorption energy on graphite.[20]

Spin-coating from sufficiently diluted solutions (10 μg mL^{-1} at 3000 r.p.m.) of **G2PS** through **G4PS** in THF and drying for about 1 h at 40 °C in air allows the immobilization of individual molecules on the basal plane of highly oriented pyrolytic graphite (HOPG). SFM height-images (e.g., of **G4PS** in Figure 1a) show that the molecules adsorb with the molecular backbones parallel to the surface, but clearly not in a conformation, which is given by a random walk in two dimensions. Instead, there is a tendency of the backbones to fold within the plane. This folding results in a characteristic smallest separation between backbones which increases with the generation of the dendrimer side chains and amounts to about 7.3 ± 0.6 nm for **G4PS**. This value fits well to the assumption that each



Scheme 2.

monomer fills a cylindrical slice where the thickness is given by the length of the repeat unit and the diameter is calculated from an assumed density of approximately $\rho = 1$ g mL^{-1} to be 8.2 nm.

To distinguish single macromolecules from loosely bound molecular aggregates, single objects were moved across the surface by switching the SFM tip at the center of the image from tapping mode to contact mode and then moving the tip in a certain direction across the surface.[21] Figure 1b displays a tapping-mode image after moving the single object sitting left of the center of Figure 1a further to the left (as indicated by the arrow in Figure 1b). The moved object remains one continuous chain which changes its conformation, while the other objects remained completely unaltered (Figure 1b). Figures 1c–d show that the molecule can be almost fully extended (the only fold left is at the molecule's terminus), which indicates a contour length of more than 260 nm which translates into at least 1000 repeating units. Figures 1e and f show that the folds can also be made and removed by manipulating the molecule with the tip, which indicates that the rigidity of the molecule is not sufficient to allow it to be moved across the surface without changing its shape. We are not aware of any published case in which a polymer chain was moved by the SFM on a surface over several 100 nm leaving all the other molecules unaffected.

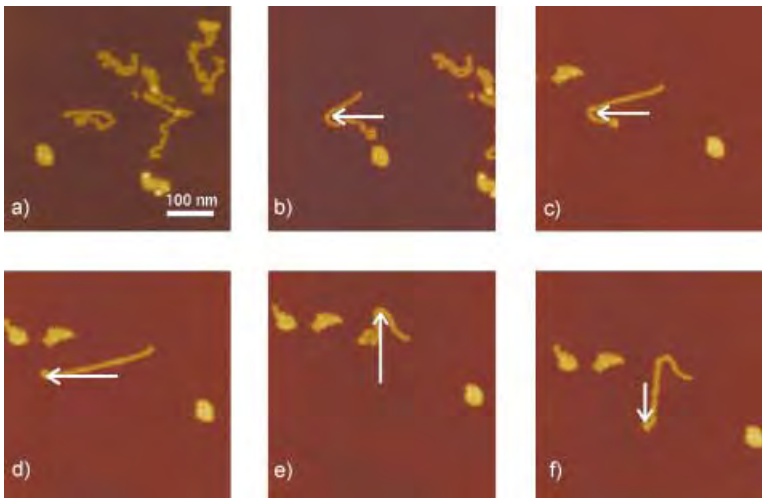


Figure 1. Sequence of SFM height images in tapping mode of **G4PS** spin-coated on HOPG. a) after preparation; b–d) after moving the tip in contact mode in three steps to the left; e) after pushing the molecule together and then moving it up; f) after moving the molecule down. The images (b–f) are centered to fully cover the one object which has been moved.

Figure 2 displays a similar sequence for the alkyl-**G4PS**. Again there are characteristic separations between backbones and also small folds, which, however, are wider than in **G4PS** without alkyl chains (10.4 ± 0.2 nm vs. 7.3 ± 0.6 nm). Again

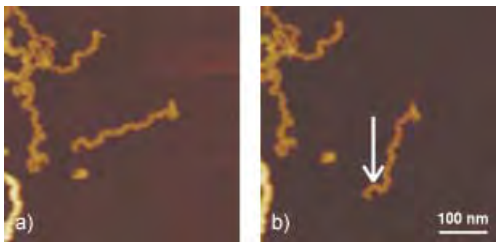


Figure 2. Sequence of SFM height images in tapping mode of alkylated **G4PS** spin-coated on HOPG, a) after preparation; b) after moving the tip in contact mode downwards.

the separations compare well to the diameter of a cylinder with $\rho = 1$ g mL (9.5 nm). After moving a single molecule by sliding the SFM tip from the center of Figure 2a downwards the fold-structure along the backbone remains intact to a large extent (Figure 2b). Basically the molecule has been translated and rotated with a small localized bend at one point along the backbone. This result indicates that the "heavy" alkylation (32 alkyl chains per repeating unit) enhanced the rigidity of the backbone so that it maintains its shape to a large extent upon manipulation across the surface of HOPG. This finding raises many questions about the factors essential for the achievement of conformationally inflexible molecules.

Experimental Section

SFM images were obtained in tapping mode using a Nanoscope IIIa (Digital Instruments, Inc. Santa Barbara, CA). Silicon cantilevers with a force constant of 42 N m^{-1} and a resonance frequency of 300 kHz were used. Manipulation of single macromolecules with the SFM has been performed in the contact mode. The molecules were pushed by the tip while applying a constant force of 1.6 μN towards the substrate.

 © WILEY-VCH Verlag GmbH, D-69451 Weinheim, 2001 1433-7851/01/4024-4668 $ 17.50+.50/0

Dendronization of *u*-**G3PS** to **G4PS**: Triethylamine (300 mg) and **2** (600 mg, 0.97 mmol) were added to a solution of *u*-**G3PS** (260 mg, 0.10 mmol repeating units) in methanol (8 mL). During the first 2 h of stirring at room temperature, CH_2Cl_2 (4 mL) was added continuously. The resulting mixture was stirred for 48 h. After removal of the solvents, CH_2Cl_2 (6 mL), triethylamine (100 mg, 2.0 mmol), and a further portion of **2** (300 mg, 0.50 mmol) were added to the residue. The solution was stirred for another 48 h. After removal of the solvent and base, the residue was then dissolved in THF (4 mL) and precipitated four times into methanol:water (4:1/v:v) and lyophilized from benzene to give 0.54 g (93 %) of polymer **G4PS**.

Modification of *u*-**G4PS** with **4**: *N*,*N*-didodecylsuccinic acid (240 mg, 0.53 mmol), 4-dimethylaminopyridin (DMP) (8 mg), and *N*-hydroxysuccinimide (64 mg) were added to dry CH_2Cl_2 (3 mL). After cooling to 0 °C, dicyclohexylcarbodiimide (DCC; 120 mg, 0.58 mmol) was added and the mixture stirred for 24 h at room temperature. The precipitate and the solvents were removed. The resulting mixture was used without separation (the yield was 65 % according to NMR measurement). To the above mixture methanol (1.5 mL), triethylamine (50 mg), and *u*-**G4PS** (41 mg, 0.007 mmol), dissolved in methanol (0.5 mL), was added and the mixture was stirred for 4 days. After removal of the solvent, the residue was dissolved in THF (1.5 mL) and precipitated into methanol:water (4:1/v:v) and lyophilized from benzene to give 66 mg (91 %) of alkyl-**G4PS**.

Received: July 23, 2001 [Z17560]

[1] "Micromachining and Microfabrication": *SPIE Handbook of Microlithography, Vol. 1* (Ed.: P. Rai-Choudhury), SPIE, Bellingham, WA, **1997**, pp. 139 – 250; D. Natelson, R. L. Willett, K. W. West, L. N. Pfeiffer, *Appl. Phys. Lett.* **2000**, *77*, 1991 – 1993.

[2] a) M. F. Crommie, C. P. Lutz, D. M. Eigler, *Science* **1993**, *262*, 218 – 220; b) R. Dagani, *Chem. Eng. News* **2000**, *78(42)*, 27 – 32; G. Decher, *Science* **1997**, *277*, 1232 – 1237; J. P. Spatz, T. Herzog, S. Mößmer, P. Ziemann, M. Möller, *Adv. Mater.* **1999**, *11*, 149 – 153; M. Gao, C. Lesser, S. Kirstein, H. Möhwald, A. L. Rojach, H. Weller, *J. Appl. Phys.* **2000**, *87*, 2297 – 2302; V. Balzani, A. Credi, F. M. Raymo, J. F. Stoddart, *Angew. Chem.* **2000**, *112*, 3484 – 3530; *Angew. Chem. Int. Ed.* **2000**, 39, 3348 – 3391.

[3] T. A. Jung, R. R. Schlittler, J. K. Gimzewski, H. Tang, C. Joachim, *Science* **1996**, *271*, 181 – 184.

[4] I. Willner, F. Patolsky, J. Wasserman, *Angew. Chem.* **2001**, *113*, 1913 – 1916; *Angew. Chem. Int. Ed.* **2001**, *40*, 1861 – 1864.

[5] a) M. Rief, F. Oesterhelt, B. Heymann, H. E. Gaub, *Science* **1997**, *275*, 1295 – 1297; b) W. Stocker, B. Karakaya, B. L. Schürmann, J. P. Rabe, A. D. Schlüter, *J. Am. Chem. Soc.* **1998**, *120*, 7691 – 7695; c) S. A. Prokhorova, S. S. Sheiko, C.-H. Ahn, V. Percec, M. Möller, *Macromolecules* **1999**, *32*, 2653 – 2660; d) P. Samorí, N. Severin, K. Müllen, J. P. Rabe, *Adv. Mater.* **2000**, *12*, 579 – 582; e) S. S. Sheiko, *Adv. Polym. Sci.* **2000**, *151*, 61 – 174; f) A. D. Schlüter, J. P. Rabe, *Angew. Chem.* **2000**, *112*, 860 – 880; *Angew. Chem. Int. Ed.* **2000**, *39*, 864 – 883.

[6] A. D. Schlüter, *Top. Curr. Chem.* **1998**, *197*, 165 – 191. See also: A. Desal, N. Atkinson, F. Rivera, W. Devonport, I. Rees, S. E. Branz, C. I. Hawker, *J. Polym. Sci. Polym. Chem.* **2000**, *38*, 1033 – 1044.

[7] D. A. Tomalia, A. M. Naylor, W. A. Goddard III, *Angew. Chem.* **1990**, *102*, 119 – 157; *Angew. Chem. Int. Ed. Engl.* **1990**, *29*, 113 – 149.

[8] I. Neubert, A. D. Schlüter, *Macromolecules* **1998**, *31*, 9372 – 9378.

[9] L. Shu, A. Schäfer, A. D. Schlüter, *Macromolecules* **2000**, *33*, 4321 – 4328.

[10] J. F. G. A. Jansen, E. M. M. de Brabander-van den Berg, E. W. Meijer, *Science* **1994**, *266*, 1226 – 1231; J. F. G. A. Jansen, E. W. Meijer, *J. Am. Chem. Soc.* **1995**, *117*, 4417 – 4418.

[11] The solubility of **G3PS** and **G4PS** was higher when **2** instead of **1** was used for the dendronizations.

[12] The mass loss during workup of the homologous series of dendronized polymers (**G2** – **G4**)**PS** was kept below 10 % for each step. The *P*n and *P*w-values should therefore be practically unchanged.

[13] The molar mass of dendronized polymers is underestimated by GPC versus PS: S. Förster, I. Neubert, A. D. Schlüter, P. Lindner, *Macromolecules* **1999**, *32*, 4043 – 4049.

[14] F. Sanger, E. O. P. Thompson, *Biochem. J.* **1953**, *53*, 353.

[15] The conditions for the attachment of the Sanger reagent were modified in a wide range to assure complete reaction: 20 – 60 °C, 2 h – 7 days, 5 – 10 equivalents.

[16] The absorbances of the modified polymers were corrected for the unmodified one.

[17] If **G2PS** is reacted with a G2 activated ester dendron (not shown) the degrees of coverage are somewhat lower.

[18] These numbers are higher than those typically reported for amidation reactions involving activated esters. Note that they resemble conversions more than yields and, thus, can be compared with the high conversions observed in the Merrifield procedure. For a recent quantitative amidation reaction in dendron synthesis, see: Y. Yamakawa, M. Ueda, K. Takeuchi, M. Asai, *Macromolecules* **1999**, *32*, 8363 – 8369. Also, see ref. [10].

[19] Theoretical molar masses of the higher homologues prepared from **G1PS** (sample 2) are: **G2PS**, $M_n = 616\,000$; **G3PS**, $M_n = 1\,336\,000$; **G4PS**, $M_n = 2\,668\,000$; small-angle neutron-scattering investigations are in progress.

[20] For ordered arrays of straight alkyl chains on HOPG reflecting the graphite symmetry axes, see: J. P. Rabe, S. Buchholz, *Science* **1991**, *253*, 424 – 427.

[21] R. Lüthi, E. Meyer, H. Haefke, L. Howald, W. Gutmannsbauer, H.-J. Güntherodt, *Science* **1994**, *266*, 1979 – 1980.

 © WILEY-VCH Verlag GmbH, D-69451 Weinheim, 2001 1433-7851/01/4024-4669 $ 17.50+.50/0

Homoaromaticity in Tris(ethylene)nickel(0) and Tris(ethyne)nickel(0)

Rainer Herges* and Andrea Papafilippopoulos

Since Wilke et al. synthesized tris(ethylene)nickel(0) (**1**) in 1973,[1] the structure of this first binary metal ethylene complex[2] and other nickel(0) alkene and alkyne complexes[3] have been thoroughly investigated. A major motivation of interest in these structures is the fact that Ni^0 complexes catalyze the synthetically and industrially important cyclooligomerization of alkenes and alkynes.[4, 5] A number of comprehensive studies notwithstanding,[6] we are still far from understanding all mechanistic details of these reactions.

There are two conceivable trigonally coordinated, highly symmetrical structures of tris(ethylene)nickel(0), one with the Ni atom and all carbon atoms in a plane (**1a**) and the other with the double bonds perpendicular to the coordination plane (**1b**; see Figure 1). These have been termed "planar" (**1a**) and "upright" (**1b**) by Hoffmann and Rösch.[7] Even though Wilke et al. suggested the correct structure **1a** immediately after synthesis, it is by no means trivial to explain the preference of the "planar" structure. Pitzer and Schaefer III predicted by ab initio calculations that the planar structure is 24 kcal mol^{-1} more stable than the the upright conformer.[8] According to Hoffmann and Rösch the stabilization of **1a** is due to a more efficient interaction of the π^* MOs of the ethylene units with the 3d orbitals of Ni.[7] Pitzer and Schaefer III basically agree with this interpretation.[8] The corresponding parent tris(ethyne)nickel(0) complex (**2**) is not known but planar derivatives were synthesized by Youngs et al.[9] The parent compound **2** is expected not to be completely flat, because of the steric interaction of the acetylene hydrogen atoms.[10]

We have now found a surprisingly strong cyclic homoconjugation between the ethylene units in the planar structure **1a** and between the ethyne ligands in the D_3 structure of tris(ethyne)nickel(0) (**2a**). The C···C distance between the ligands of 2.681 Å in **1a** and 2.703 Å in **2a**[11] is in each case far below the sum of the van der Waals radii of the neighboring sp^2 and sp carbon atoms. Thus, **1a** and **2a** can be designated to be aromatic or "on the way" to trimerizing to cyclohexane and benzene, respectively. This does not only explain the preference of the planar arrangement of the fragments in **1** but also sheds light upon the role of nickel(0) as a catalyst in C–C bond formation processes.

Our results among other methods are based on a recently published method for the investigation of delocalization and conjugation effects in molecules.[12] This ACID (anisotropy of the induced current density) method provides a powerful and general way to visualize the density of delocalized electrons and to quantify conjugation effects. We have shown that the ACID scalar field can be interpreted as the density of delocalized electrons. Even subtle effects such as the homoconjugation in cycloheptatriene and the anomeric effect are clearly visible in the corresponding ACID plots.[12]

Figure 1 presents the ACID plots[12] of planar **1a**, and upright-tris(ethylene)nickel(0) (**1b**) and D_3-tris(ethyne)nickel(0) (**2a**).[13] There is a strong interaction between the central nickel atom and the three ethylene units in the planar structure **1a**. Coordination is much weaker (only visible at lower isosurface values) in upright **1b**. Most interesting, and surprising, however, is the strong cyclic homoconjugation between the three ethylene ligands. We defined the critical isosurface value (CIV) (the lowest ACID value in space between two interacting units) as a measure of the strength of a conjugation.[12] With a CIV of 0.0639 between the ethylene ligands in the planar complex **1a**, this value is in the range of the aromatic transition state of the parent Diels–Alder reaction[14] (0.0686) and only 0.01 lower than the CIV describing the π conjugation in benzene (0.0739). The interaction of the three ethylene units without Ni but fixed in the same geometry as in the planar complex is considerably smaller (CIV = 0.0263), indicating a very weak homoconjugation in the absence of nickel (Figure 1). The ACID value at a naked nickel atom without ligands is exactly zero. Hence, the homoaromaticity arises from the interaction of the three ethylene units with the central nickel atom.

Remaining doubts on an homoaromatic interaction of the three ethylene units in **1a** and **2a** can be eliminated by plotting the current density vectors onto the ACID isosurface (Figure 2). The current density vectors indicate a strong diamagnetic ring current[15] in the periphery which is typical for an aromatic system.[16]

Other magnetic parameters as well point to a considerable degree of aromaticity[17] in **1a** and **2a** (see Table 1). The magnetic susceptibility χ and more importantly the anisotropy of the magnetic susceptibility $\Delta\chi$ have been used as a measure for aromaticity.[18] Both χ and $\Delta\chi$ are more negative in aromatic compounds than in nonaromatic reference structures. For example χ for benzene and fulvene is -46.1 and -34.1 ppm (cgs), respectively; the corresponding values for $\Delta\chi$ are -69.7 and -34.2.[13] A similar trend is found in **1a** and **1b** and in **2a** and **2b**. The planar structures exhibit considerably more negative values for χ and $\Delta\chi$ (Table 1). The size of the effect is typical for aromatic compounds.[18] According to the $\Delta\chi$ values the aromaticity is somewhat less pronounced in **2a** than in **1a**. This might be due to the nonplanar conformation and the resulting less efficient interaction of the acetylene ligands. The large positive value of $\Delta\chi$ in **2b** arises from the anisotropy of the acetylene ligands.

If there is a ring current in **1a** and **2a**, the nickel atoms should exhibit a large upfield NMR shift compared to the nonaromatic counterparts **1b** and **2b** because the nickel atoms are exactly placed in the center of the ring where the shielding induced by the ring current is largest. This is indeed the case. The calculated upfield shift in **1a** versus **1b** is extraordinarily large and amounts to 1847.7 ppm and to 1826.9 ppm in **2a** versus **2b**.[13, 19] Again the aromaticity in **2a** obviously is somewhat lower than that in **1a** (Table 1).

What is the origin of this remarkable homoaromaticity in **1a** and **2a**? A simple and straightforward answer is provided

[*] Prof. Dr. R. Herges, A. Papafilippopoulos
Institut für Organische Chemie
Universität Kiel
Otto Hahn-Platz 4, 24098 Kiel (Germany)
Fax: (+49) 431-880-1558
E-mail: rherges@oc.uni-kiel.de

 © WILEY-VCH Verlag GmbH, D-69451 Weinheim, 2001 1433-7851/01/4024-4671 $ 17.50+.50/0

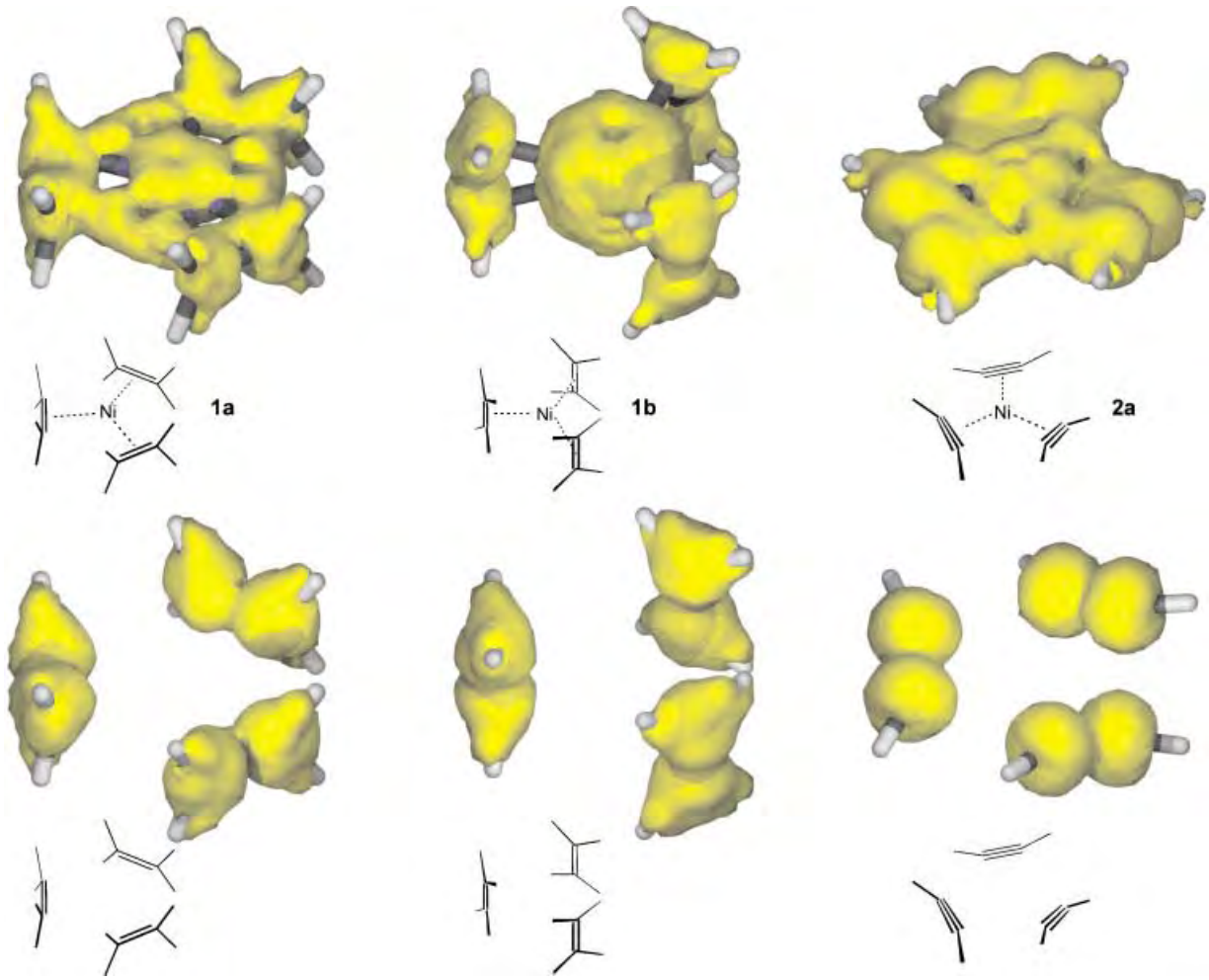


Figure 1. Delocalized electrons in planar and upright-tris(ethylene)nickel(0) (**1a** and **1b**, respectively) and D_3-symmetrical tris(ethyne)nickel(0) (**2a**) (first row).[11] Delocalization in the nickel complexes is compared to conjugation in the free ligands without nickel (second row). The ligands are fixed in the geometry of the complexes. The isosurfaces are plotted using the ACID method[12] at an isosurface value of 0.05. Nickel atoms without ligands exhibit zero ACID (see text).

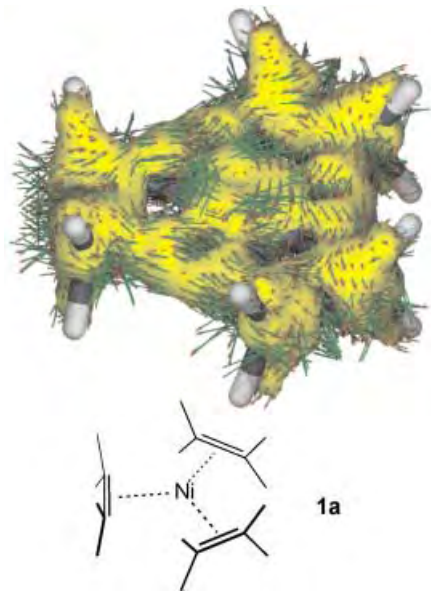


Figure 2. Current density vectors plotted onto the ACID surface of **1a**. The vector of the magnetic field is perpendicular to the coordination plane and pointing upwards.

Table 1. Calculated energies, imaginary frequencies (B3LYP/6-31 + G*) and magnetic properties (CSGT) of planar and upright-tris(ethylene)nickel(0) (**1a** and **1b**, respectively) and D_3- and upright-tris(ethyne)nickel(0) (**2a** and **2b**, respectively).

	1a (D_{3h})	**1b** (D_{3h})	**2a** (D_3)	**2b** (D_{3h})
E_{abs}[a]	− 1743.867904	− 1743.822389	− 1740.170096	− 1740.104356
E_{rel}[b]	0.0	28.4	0.0	41.3
N_{imag}[c]	0	4	0	9
χ[d]	− 82.5	− 26.9	− 65.1	+ 2.11
$\Delta\chi$[e]	− 56.5	− 29.1	− 47.5	+ 85.7
CIV[f]	0.0639	0.0263	0.0565	–[g]
$\delta(^{61}Ni)$[h]	− 1460.7	+ 387.0	− 62.7	+ 1764.2

[a] In a.u. [b] Relative to the planar structures **1a** and **2a** in kcal mol^{-1}. [c] Number of imaginary frequencies, according to a harmonic frequency calculation. [d] Magnetic susceptibility calculated using the CSGT method[20] in ppm (cgs). [e] anisotropy of the magnetic susceptibility calculated from the magnetic susceptibility tensor according to $\Delta\chi = \chi_{zz} - \chi_{xx}$, χ_{zz} is the susceptibility component perpendicular to the ring plane, χ_{xx} and χ_{yy} are identical since **1a,b** and **2a,b** are symmetric tops (molecules with C_n, $n > 2$), the ring plane (xy) is defined by the midpoints of the C–C bonds and the Ni atom. [f] Critical isosurface value between the ligands (see text). [g] Topology of the ACID isosurface representing direct ligand–ligand interaction does not exist. [h] Ni NMR chemical shift relative to that of $[Ni(CO)_4]$, which is the generally accepted standard in ^{61}Ni NMR spectroscopy.

 © WILEY-VCH Verlag GmbH, D-69451 Weinheim, 2001 1433-7851/01/4024-4672 $ 17.50+.50/0

by qualitative MO theory. Hoffmann and Rösch already pointed out that there is an interaction of the π* orbitals of the ethylene ligands with the 3d orbitals of nickel which is more efficient in the planar structure **1a** than in the upright conformer **1b**.[7] More specifically: in **1a** both, the π and π* degenerate set of ethylene orbitals (e′) interact with $3d_{xy}$ and $3d_{x^2-y^2}$ (e′) of nickel (Figure 3). Mixing ethylene π* character

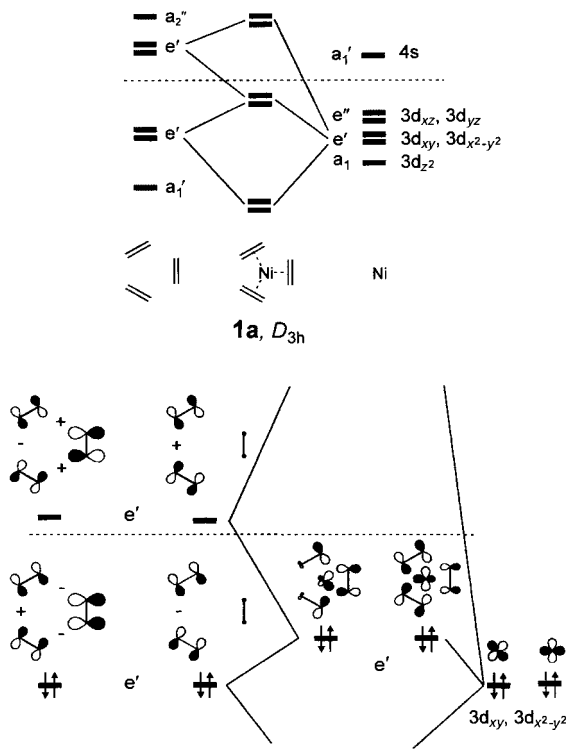
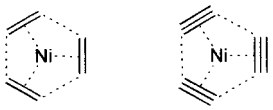


Figure 3. MO diagram for **1a** (top). Only the e′ orbital interaction is shown. The detail from the MO diagram (bottom) illustrates the mixing of π and π* orbitals of ethylene into the bonding orbitals of the complex. The coefficients of the D_{3h}-symmetry-adapted MOs of the ethylene π and π* orbitals correspond to the ethylene units being at an infinite distance. The coefficients of the nickel complex are drawn using the Kohn – Sham orbitals of the density functional theory (DFT) calculation (see text). + signs denote bonding and − signs antibonding character between the ethylene units.

into the bonding orbitals of the complex lowers the bond order of the ethylene double bonds and increases bonding between the ethylene units leading to homoconjugation. Note that the e′ orbital of the D_{3h}-symmetry-adapted orbitals of the π* ethylene units (LUMO, Figure 3, left) has an overall ethylene – ethylene bonding character (two bonding, one antibonding interaction in the left orbital, one bonding interaction in the right orbital of the degenerate set), whereas the π ethylene orbitals (HOMO, Figure 3, left) are ethylene – ethylene antibonding (two antibonding and one bonding interaction in the left e′ orbital and one antibonding interaction in the right e′ orbital). The same is true for the tris(ethyne)nickel complex (**2**).

Thus the central nickel atom not only holds the three π ligands ethylene and ethyne in a favorable position for a trimerization (a_1' orbital interaction, see Figure 3) but also favors the reaction by lowering the π bond order within the ligands and by increasing the bond order between the ligands. For completion of the hypothetical trimerization of ethylene to cyclohexane and the known reaction of ethyne to benzene, the nickel atom has to leave the center of the complex. A concerted cycloaddition process, the strong homoaromaticity not withstanding, thus is unlikely and was not found by an extensive search on the reaction hypersurface. The mechanism in detail, probably is more complicated[5c, 6b–f,21] and will be subject of further theoretical studies.



1a **2a**

To depict the strong homoconjugation, the structural formula of **1a** and **2a** should be written with dashed lines connecting the ligands.

Received: May 28, 2001
Revised: July 27, 2001 [Z17190]

[1] K. Fischer, K. Jonas, G. Wilke, *Angew. Chem.* **1973**, *85*, 620 – 621; *Angew. Chem. Int. Ed. Engl.* **1973**, *12*, 565 – 566.
[2] a) T. Merle-Mejean, C. Cosse-Mertens, S. G. F. Bouchareb, J. Mascetti, M. Tranquille, *J. Phys. Chem.* **1992**, *966*, 9148 – 9158; b) J. Mink, M. Gal, P. L. Goggin, J. L. Spencer, *J. Mol. Struct.* **1986**, *142*, 467 – 472; c) P. Csaszar, P. L. Goggin, J. Mink, J. L. Spencer, *J. Organomet. Chem.* **1989**, *379*, 337 – 349; d) H. Huber, G. A. Ozin, W. J. Power, *J. Am. Chem. Soc.* **1976**, *98*, 6508 – 6511; G. A. Ozin, W. J. Power, T. H. Upton, W. A. Goddard, *J. Am. Chem. Soc.* **1978**, *100*, 4750 – 4760.
[3] For review see: a) G. Wilke, *Angew. Chem.* **1988**, *100*, 190 – 211; *Angew. Chem. Int. Ed. Engl.* **1988**, *27*, 186 – 206; b) M. J. Chetcuti in *Comprehensive Organometallic Chemistry II*, *Vol. 9* (Eds.: E. W. Abel, F. G. A. Stone, G. Wilkinson), Elsevier Science, Oxford, **1994**, pp. 107 – 191.
[4] The first nickel-catalyzed alkene and alkyne trimerizations were observed by Reppe: W. Reppe, W. J. Schweckendieck, *Liebigs Ann. Chem.* **1948**, *560*, 104.
[5] For review see: a) M. Lautens, W. Klute, *Chem. Rev.* **1996**, *96*, 49 – 92; b) N. E. Schore, *Chem. Rev.* **1988**, *88*, 1081 – 1119; c) P. W. Jolly in *Comprehensive Organometallic Chemistry*, *Vol. 8* (Ed.: G. Wilkinson), Elsevier Science, Oxford, **1982**, pp. 649 – 670; d) W. Keim, A. Behr, M. Röper, *Comprehensive Organometallic Chemistry*, *Vol. 8* (Ed.: G. Wilkinson), Elsevier Science, Oxford, **1982**, pp. 371 – 462; P. W. Jolly in *Comprehensive Organometallic Chemistry*, *Vol. 8* (Ed.: G. Wilkinson), Elsevier Science, Oxford, **1982**, pp. 613 – 647.
[6] a) U. Rosenthal, W. Schulz, *J. Organomet. Chem.* **1987**, *321*, 103 – 117; b) J. J. Eisch, J. E. Galle, *J. Organomet. Chem.* **1975**, *96*, C23 – C26; c) H. Hoberg, W. Richter, *J. Organomet. Chem.* **1980**, *195*, 355 – 362; d) J. J. Eisch, J. E. Galle, A. A. Aradi, M. P. Boleslawski, *J. Organomet. Chem.* **1986**, *312*, 399 – 416; e) R. Diercks, L. Stamp, J. Kopf, H. Tom Dieck, *Angew. Chem.* **1984**, *96*, 891 – 895; *Angew. Chem. Int. Ed. Engl.* **1984**, *23*, 893 – 894; f) A. W. Parkins, R. C. Slade, *J. Chem. Soc. Dalton Trans.* **1975**, 1352 – 1356; g) K. Kitaura, S. Sakaki, K. Morokuma, *Inorg. Chem.* **1981**, *20*, 2292 – 2297; h) T. Ziegler, *Inorg. Chem.* **1985**, *24*, 1547 – 1552.
[7] N. Rösch, R. Hoffmann, *Inorg. Chem.* **1974**, *13*, 2656 – 2666.
[8] R. M. Pitzer, H. F. Schaefer III, *J. Am. Chem. Soc.* **1979**, *101*, 7176 – 7183.
[9] a) J. D. Ferrara, C. Tessier-Youngs, W. J. Youngs, *J. Am. Chem. Soc.* **1985**, *107*, 6719 – 6721; b) J. D. Ferrara, A. A. Tanaka, C. Fierro, C. A. Tessier-Youngs, W. J. Youngs, *Organometallics* **1989**, *8*, 2089 – 2098; c) W. J. Youngs, J. D. Kinder, J. D. Bradshaw, C. A. Tessier, *Organometallics* **1993**, *12*, 2406 – 2407.
[10] G. A. Ozin, D. F. McIntosh, W. J. Power, R. P. Messmer, *Inorg. Chem.* **1981**, *20*, 1782 – 1792.
[11] Selected distances [Å] an angles [°] (B3LYP/6-31 + G*): **1a**: Ni-C 2.068, C-C 1.386, C-H 1.088, C ··· C 2.681, H-C-C 120.6, H-C-H 115.3; **1b**: Ni-C 2.165, C-C 1.369, C-H 1.089, C ··· C 3.557, H-C-C 121.3, H-C-H 116.1; **2a**: Ni-C 1.998, C-C 1.249, C-H 1.0737, H ··· H 2.614, C ··· C

 © WILEY-VCH Verlag GmbH, D-69451 Weinheim, 2001 1433-7851/01/4024-4673 $ 17.50+.50/0

2.703, H-C-C 155.85, the acetylene units are twisted by 15° out of the hypothetical coordination plane.
[12] R. Herges, D. Geuenich, *J. Phys. Chem. A* **2001**, *105*, 3214 – 3220.
[13] The structures were optimized and checked by harmonic frequency analysis at the B3LYP/6-31 + G* level of theory using the Gaussian 98 suite of programs. Chemical shifts and magnetic susceptibilities are calculated at the same level of theory using the CSGT method implemented in Gaussian 98 (Revision A.7), M. J. Frisch, G. W. Trucks, H. B. Schlegel, G. E. Scuseria, M. A. Robb, J. R. Cheeseman, V. G. Zakrzewski, J. A. Montgomery, R. E. Stratmann, J. C. Burant, S. Dapprich, J. M. Millam, A. D. Daniels, K. N. Kudin, M. C. Strain, O. Farkas, J. Tomasi, V. Barone, M. Cossi, R. Cammi, B. Mennucci, C. Pomelli, C. Adamo, S. Clifford, J. Ochterski, G. A. Petersson, P. Y. Ayala, Q. Cui, K. Morokuma, D. K. Malick, A. D. Rabuck, K. Raghavachari, J. B. Foresman, J. Cioslowski, J. V. Ortiz, B. B. Stefanov, G. Liu, A. Liashenko, P. Piskorz, I. Komaromi, R. Gomperts, R. L. Martin, D. J. Fox, T. Keith, M. A. Al-Laham, C. Y. Peng, A. Nanayakkara, C. Gonzalez, M. Challacombe, P. M. W. Gill, B. G. Johnson, W. Chen, M. W. Wong, J. L. Andres, M. Head-Gordon, E. S. Replogle, J. A. Pople, Gaussian, Inc., Pittsburgh, PA, **1998**.
[14] R. Herges, H. Jiao, P. von R. Schleyer, *Angew. Chem.* **1994**, *106*, 1441; *Angew. Chem. Int. Ed. Engl.* **1994**, *33*, 1376 – 1378.
[15] For a very thorough review on the concept of the ring current see: P. Lazzaretti, *Prog. Nucl. Magn. Reson. Spectrosc.* **2000**, *36*, 1 – 88.
[16] For a very recent application of current density plots on coronene and corannulene see: E. Steiner, P. W. Fowler, L. W. Jenneskens, *Angew. Chem.* **2001**, *113*, 375 – 379; *Angew. Chem. Int. Ed.* **2001**, *113*, 362 – 366.
[17] P. von R. Schleyer, H. Jiao, *Pure Appl. Chem.* **1996**, *68*, 209 – 218.
[18] W. H. Flygare, *Chem. Rev.* **1974**, *74*, 653.
[19] Experimental ^{61}Ni NMR chemical shifts on tris(ethylene)nickel(**0**) unfortunately are not known. Because of its large quadrupole moment (0.16×10^{-28} m^2), low natural abundance (1.19 %), and low receptivity the ^{61}Ni NMR chemical shifts of only two trigonal-planar Ni^0 complexes ([Ni(cdt)] (cdt = all-trans-1,5,9-cyclododecatriene) and [Ni(C_2H_4)$_2$(PMe_3)]) have been published: a) R. Benn, A. Rufinska, *Angew. Chem.* **1986**, *98*, 851 – 871; *Angew. Chem. Int. Ed. Engl.* **1986**, *25*, 861 – 881. Further data on tetrahedral, zero-valent complexes: b) K. D. Behringer, J. Blümel, *Magn. Reson. Chem.* **1995**, *33*, 729 – 733; c) N. Hao, M. J. McGlinchey, B. G. Sayer, G. J. Schrobilgen, *J. Magn. Reson.* **1982**, *46*, 159 – 162; d) H. Schumann, M. Meißner, H.-J. Kroth, *Z. Naturforsch. B* **1980**, *35*, 639 – 641; e) R. Benn, A. Rufinska, *Magn. Reson. Chem.* **1988**, *26*, 895 – 902.
[20] T. A. Keith, R. F. W. Bader, *J. Chem. Phys. A* **1993**, *99*, 3669 – 3693.
[21] a) K.-R. Pörschke, *Angew. Chem.* **1987**, *99*, 1321 – 1322; *Angew. Chem. Int. Ed. Engl.* **1987**, *26*, 1288; b) K.-R. Pörschke, *J. Am. Chem. Soc.* **1989**, *111*, 5691 – 5699; c) T. Takahashi, F.-Y. Tsai, Y. Li, K. Nakajima, M. Kotora, *J. Am. Chem. Soc.* **1999**, *121*, 11 093 – 11 100.

On the Stability of Electrochemically Generated Nanoclusters—A Computer Simulation**

Mario G. Del Pópolo, Ezequiel P. M. Leiva,* and Wolfgang Schmickler*

The scanning tunneling microscope (STM), operated in an electrochemical environment, offers a precise and cheap way to produce small metal clusters on a foreign substrate. Pioneering work in this area has been performed by Kolb, Ullmann, and Will,[1] who developed the following procedure for the deposition of nanosized copper clusters on single-crystal gold electrodes: The gold electrode is held at a potential a little positive of the deposition potential for copper, while the tip potential is set below this value, so that copper atoms are deposited on the tip surface. The tip is then pressed against the electrode and withdrawn again. As the tip separates from the electrode a metal cluster remains, which typically comprises 20 – 100 atoms, and is a few monolayers high. This method also works for the generation of palladium clusters on Au(111), but not for copper on Ag(111).[1, 2]

The generation of such metal clusters is of great interest, since they are expected to play a major role in future nanotechnologies. The deposition of copper clusters on the Au(111) surface has been investigated most extensively, and is considered as a prototype for the electrochemical fabrication of nanoclusters. Recently, this process has attracted further attention because the copper clusters are stable at a potential at which bulk copper dissolves. This is surprising because generally clusters tend to be less stable than the corresponding bulk material. Kolb, Engelmann, and Ziegler[3] have speculated that this increased stability is caused by quantum confinement: They propose that the electrons in the cluster are separated from the bulk of the electrode by a potential energy barrier, so that the energy levels in the cluster are discrete and not continuous as in bulk metals. The dissolution

[*] Prof. Dr. E. P. M. Leiva, M. G. Del Pópolo
Universidad Nacional de Córdoba
Unidad de Matemática y Física
Facultad de Ciencias Químicas
5000 Córdoba (Argentina)
Fax: (+54) 351-4334189
E-mail: eleiva@fcq.unc.edu.ar
Prof. Dr. W. Schmickler
Abteilung Elektrochemie
Universität Ulm
89069 Ulm (Germany)
Fax: (+49) 731-5025409
E-mail: wolfgang.schmickler@chemie.uni-ulm.de

[**] This work was supported by Consejo Nacional de Investigaciones Científicas y Técnicas (CONICET), by Consejo de Investigaciones Científicas y Tecnológicas de la Provincia de Córdoba (CONICOR), by the Secretaría de Ciencia y Técnica de la Universidad Nacional de Córdoba (SeCyT-UNC; program BID 802/OC-AR PICT Nr. 06-04505) and by the Fundación Antorchas (E.P.M.L and M.G.D.) as well as by the Deutsche Forschungsgemeinschaft under the program "Grundlagen der elektrochemischen Nanotechnologie" (W.S.). Some of the calculations were performed on a Digital workstation financed by the Alexander von Humboldt Stiftung.

Supporting information for this article is available on the WWW under http://www.angewandte.com or from the author.

 © WILEY-VCH Verlag GmbH, D-69451 Weinheim, 2001 1433-7851/01/4024-4674 $ 17.50+.50/0

of a Cu atom to a solvated Cu^{2+} ion would leave two electrons behind, which would have to be accommodated at a level above the Fermi energy. This would be energetically less favorable than the dissolution of bulk copper, for which the remaining electrons stay at the Fermi level, and would thus make the clusters more stable. There are, however, some difficulties with this explanation: There may indeed be a potential energy barrier separating the electrons in a metal cluster from the underlying bulk metal; however, such barriers are small and do not lead to isolated electronic levels in the cluster, but to resonance levels with a lifetime of the order of femtoseconds.[4] Copper dissolution occurs on a much longer timescale, since it involves the solvation of the ion, which takes picoseconds or longer. Therefore there is plenty of time for the dissolving atom to exchange electrons with the substrate. Indeed, the very fact that these clusters can be imaged with an STM shows that there is rapid electron exchange between the cluster and the substrate. Thus the reason for the stability has to lie elsewhere.

To gain further insight into the fabrication and the stability of these copper clusters we have performed extensive molecular-dynamics simulations. The approach of an STM tip to a metal surface in the vacuum has been simulated by the group of Landman;[5] in the cases investigated, it led to an exchange of material between tip and substrate, but did not result in the generation of stable clusters. We have adapted their method to the problem at hand, which has a peculiarity that is often not appreciated: At the potential, at which the copper cluster is formed, the Au(111) surface is already covered by a monolayer of adsorbed copper atoms, a phenomenon that is known as underpotential deposition.

Figure 1 shows a series of snapshots of a typical simulation. The starting configuration (Figure 1 a) shows a platinum STM tip with several layers of deposited copper atoms above the Au(111) surface, which is covered by a copper monolayer; the distance between the surface and the nearest Cu atoms was about 7.6 Å and to the nearest Pt atom about 19.6 Å. The tip was then moved in steps of 0.6 Å towards the surface; after each such step the system was allowed to equilibrate for 300 ps. The "jump-to-contact" process, in which the copper atoms from the tip jump to form a bridge to the substrate, occurred after the tip had been moved by 3.6 Å. This stage is depicted in Figure 1 b; in this instance the bridge consisted of five Cu atoms. The tip was then moved further towards the surface, which began to be deformed. In this particular run the tip was moved another 8.4 Å towards the surface after the jump-to-contact; the closest approach is shown in Figure 1 c. Subsequently the tip was withdrawn from the substrate with the same step size as in the approach. A connective neck began to form, which contained both Cu and Au atoms. After the tip and the substrate have separated, a cluster is left behind on the surface (Figure 1 d). In this particular run the cluster consisted of 26 Cu atoms and 11 Au atoms. Thus the fabricated cluster consists of a mixture of copper and gold, and not of pure copper. In addition, a few Au atoms have been transferred to the tip.

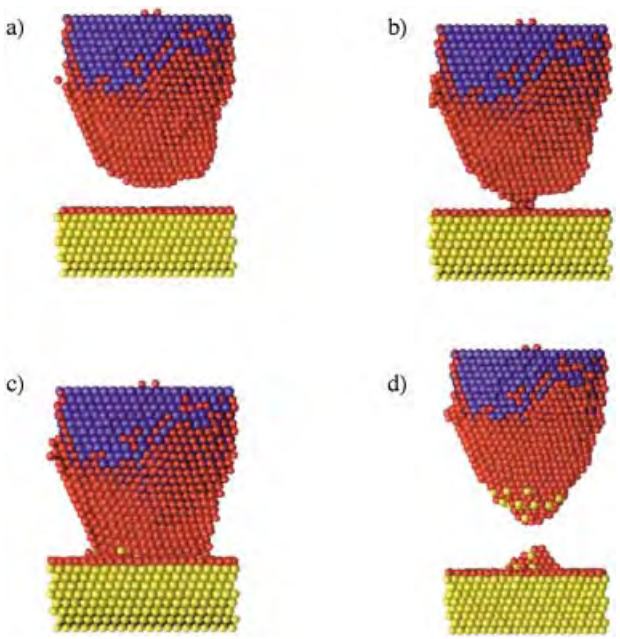


Figure 1. Snapshots of four stages in the fabrication of a metal cluster on Au(111). Yellow spheres: gold atoms; red spheres: copper atoms; blue spheres: platinum atoms.

Until now, we have performed 12 such simulations with various distances of approach. In some simulations the tip was withdrawn in a steady instead of a stepwise manner. Whenever a cluster of more than monomolecular height was formed, it contained both Au and Cu atoms, the gold content varying between 8 and 40 %.

We note in passing that a monolayer of copper deposited on gold has a tendency to form a surface alloy after several hours;[6] this is further evidence for the ease with which these two metals form alloys in an electrochemical environment, even without the impact of a tip.

As a measure of the hardness with which the tip approaches the surface we may use the distance over which the tip is moved towards the surface after the jump-to-contact process.[5] This distance was varied between 2.4 to 8.4 Å. The size of the clusters ranged from 10 to 60 atoms, and their height between two and four monolayers. There was little systematic variation between the distance of furthest approach and the size of the clusters, except that the gentlest approach always produced the smallest clusters. Experimentally, the height of the clusters has been found to increase with the distance of approach,[2] and to reach an average height of about three to fours layers, the same as in our simulations. The experimentally produced clusters seem to contain more atoms than ours, typically about one hundred, but this difference can be attributed to the ideal tip shape in the simulations, and to the small system size. Overall our simulations reproduce the cluster heights and sizes of the experiments quite well.

During the formation of the cluster, Au atoms are moved from the substrate to the cluster and also to the tip. Therefore the surface shows some damage both in the Cu monolayer and in the gold substrate (Figure 2), which typically extends over one to two layers of the substrate. The experimental evidence for such damage is controversial: While Kolb et al.[3] claim that the substrate is left intact, others[7] have observed holes after cluster formation. In any case we would expect such damage to heal rapidly on the timescale on which the experiments are performed, which is seconds to minutes,

 © WILEY-VCH Verlag GmbH, D-69451 Weinheim, 2001 1433-7851/01/4024-4675 $ 17.50+.50/0

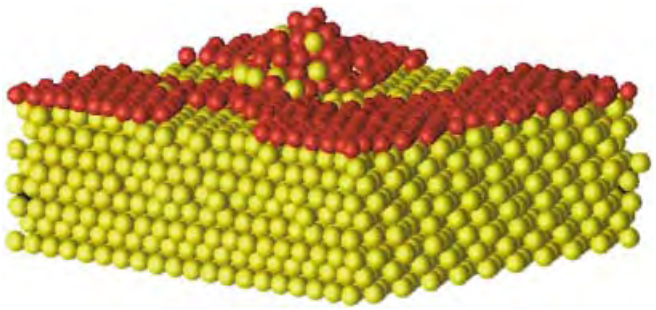


Figure 2. Final stage of the cluster formation.

while our simulations last only a few nanoseconds. The corrugation of the Au(111) surface is small and surface transport fast.

Copper and gold are known to form stable alloys, so we expected our clusters to be more stable than pure copper clusters. To test this hypothesis, we removed the tip from our system and let the cluster and substrate relax to equilibrium. We then determined the cluster atom whose removal requires the least change in energy—obviously, this is always a surface atom. This atom was removed, and the system was again equilibrated. This process was repeated till the cluster had disappeared. This simulation was then repeated for a cluster in which all the gold atoms have been replaced by copper. The sequence of energy increments associated with the removal of the atoms was used along with the master equation for a one-dimensional single-step process to obtain the number of atoms and the cluster height as a function of the chemical potential μ. The cohesive energy of bulk copper is $E_c = -3.54$ eV, so a pure copper cluster would be completely dissolved at chemical potentials below this value.

In electrochemistry the (electro)chemical potential of the copper atoms varies with the electrode potential. Therefore, the scale of chemical potentials for copper can be converted to the electrode potential ϕ according to Equation (1) where the standard equilibrium potential for the copper deposition and dissolution reaction has been taken as zero; the division by two is due to the fact that copper dissolves as a divalent ion.

$$\phi = (E_c - \mu)/2 \quad (1)$$

Figure 3 shows the number of atoms n and the cluster height h both for a typical copper–gold cluster and for a pure copper cluster as a function of the electrode potential. The pure copper cluster dissolves at a potential below the dissolution potential for pure cluster, since its large surface area makes it less stable. In contrast, the copper–gold cluster has still about a third of its original size at a potential of $\phi = 0.05$ V (Figure 3a), and only gradually dissolves at higher values. Interestingly, our simulations reflect the experimental observation by Kolb et al. that the dissolution of the cluster is layer by layer.[2]

Thus our simulations suggest that the stability of the clusters is caused by the formation of a Cu–Au alloy. This hypothesis also explains why copper does not form stable clusters on silver: Copper and silver are immiscible at temperatures below 600 K, and do therefore not form stable

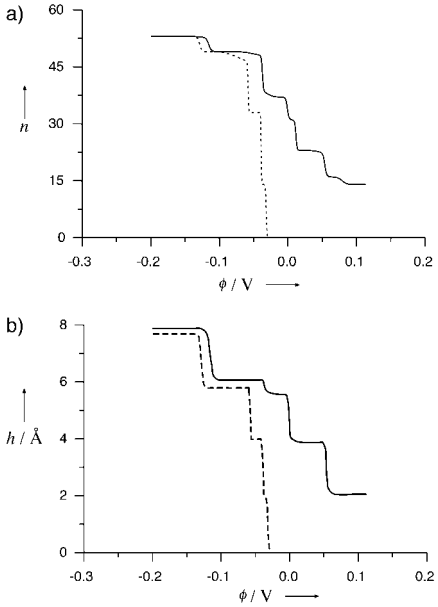


Figure 3. Number of atoms n (a) and cluster height h (b) as a function of electrode potential ϕ; the zero of the potential scale correponds to the dissolution potential for bulk copper. Full lines: Cu–Au cluster, broken line: pure Cu cluster.

Cu–Ag clusters. Indeed, a few test simulations for the deposition of copper on Ag(111) that we have performed never resulted in clusters. In contrast, palladium and gold do mix at room temperature,[8] so the formation of clusters on Au(111) when palladium is deposited with an STM is in line with our arguments; we surmise, that these clusters consist of both palladium and gold atoms.

Therefore it seems that in general this electrochemical technique only results in stable clusters if the substrate and the deposited metal form a stable alloy. Indeed, it is difficult to see how it could be otherwise: At potentials above the equilibrium potential of the deposited metal a pure cluster should either dissolve or relax into an island one monolayer high; at lower potentials the cluster should continue to grow. Only an alloy can remain stable above the dissolution potential for the pure metal.

Received: July 23, 2001 [Z17566]

[1] D. M. Kolb, R. Ullmann, T. Will, *Science* **1997**, *275*, 1097.
[2] D. M. Kolb, R. Ullmann, J. C. Ziegler, *Electrochim. Acta* **1998**, *43*, 2751.
[3] D. M. Kolb, G. E. Engelmann, J. C. Ziegler, *Angew. Chem.* **2000**, *112*, 1166; *Angew. Chem. Int. Ed.* **2000**, *39*, 1123.
[4] R. Otero, A. L. Vazquez de Parga, Rodolfo Miranda, *Surf. Sci.* **2000**, *447*, 143.
[5] "Consequences of Tip-Sample Interactions": U. Landman, W. D. Luedtke in *Scanning Tunneling Microscopy III* (Eds.: R. Wiesendanger, H. J. Güntherodt), Springer, Berlin, **1993**; U. Landman, W. D. Luedtke, N. A. Burnham, R. J. Colton, *Science* **1990**, *248*, 454.
[6] E. Budevski, G. Staikov, W. J. Lorenz, *Electrochemical Phase Formation and Growth*, Wiley-VCH, Weinheim, **1996**, p. 128 ff.
[7] S. Maupai, Ph.D. thesis, Technical University of Erlangen, **2001**.
[8] R. Hultgren, P. D. Desai, D. T. Hawkin, M. Gleiser, K. K. Kelly, *Selected values of the thermodynamic properties of binary alloys*, American Society for Metals, Metals Park, OH, **1973**.

 © WILEY-VCH Verlag GmbH, D-69451 Weinheim, 2001 1433-7851/01/4024-4676 $ 17.50+.50/0

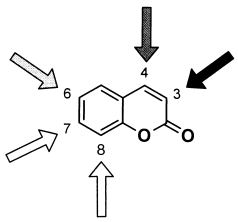
Single-Compound Libraries of Organic Materials: Parallel Synthesis and Screening of Fluorescent Dyes**

Marc-Steffen Schiedel, Christoph A. Briehn, and Peter Bäuerle*

The potential of combinatorial chemistry in the pharmaceutical industry has been demonstrated for lead-structure identification and optimization with numerous examples published.[1] Similar change of paradigm has been seen in the areas of materials and catalyst research.[2] To date the principles of combinatorial chemistry have been applied in the areas of inorganic solid-state materials (e.g. luminescence[3]), homogenous and heterogeneous catalysts, and polymeric materials. The combinatorial concept facilitates the efficient generation of a large number of substances and their screening for desirable properties. These properties are dependent on numerous interdependent parameters.

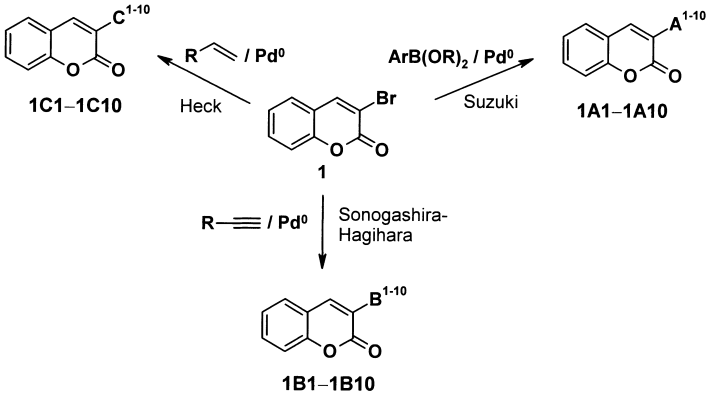
A further field of research in materials science, where structure–property relationships are often not predictable and an empirical identification process is required for the elicitation of lead structures and their further development, is that of organic materials. Consequently, we asked whether the concepts of combinatorial chemistry are applicable to the development of novel organic materials? We report here and in the following correspondence[4] the efficient generation and screening of single-compound libraries containing fluorescent dyes[5] and π-conjugated oligomers; with these studies we show that the concepts of combinatorial chemistry can be successfully applied to organic materials using rapid parallel and mix-and-split synthesis in solution and also on solid supports. For a successful screening and subsequent data analysis highly pure compounds are of the utmost importance. The analysis of the data sets encompassed the structure–property relationships[4] which should make a rational design of novel organic materials with desirable properties possible.

In this study we concentrate on fluorescent dyes of the coumarin type which are of interest not only because of their pharmacological activity[6] but also because of their applications as laser dyes,[7] fluorescent labels[8] (e.g. in biological applications), emission layers in organic light-emitting diodes (OLED),[9] and as optical brighteners.[10] The correlation between optical properties (especially the fluorescence quantum yield) and the molecular structure can currently be described only empirically, since no detailed theoretical predictions are possible. A large number of compounds in a combinatorial library should correlate to a better understanding of the inherent structure–property relationships from which specifically tailored materials can be produced. Consequently, our goal was the development of a fast, parallel synthesis of highly pure coumarins and screening them for optical properties. Through substituent manipulation of the coumarin scaffold at positions 3, 4, 6–8 (Scheme 1) increased diversity is introduced which crucially alters the electronic structure and the associated dye properties.[11]



Scheme 1. Substituent variation on the coumarin scaffold.

Starting from 3-bromocoumarin **1**[12] we introduced substituents at the 3-position of the scaffold which extended the π system of the parent chromophore; this was achieved by Pd-catalyzed cross-coupling reactions. These types of reactions involving coumarin have not been widely published.[13] The efficiency of a combinatorial synthetic approach greatly depends on the compatibility of the coupling components and their suitability with the reaction conditions. Therefore, the initial step requires the optimization of the synthetic method for each individual reaction type. Scheme 2 shows the coupling reactions of compound **1**. Utilizing C–C bond formation reactions of Suzuki, Sonogashira–Hagihara, and Heck type with the coupling components **A1**–**A10**, **B1**–**B10**, and **C1**–**C10** (Scheme 3) facilitated the introduction of arene, ethynylene, and ethenylene moieties.



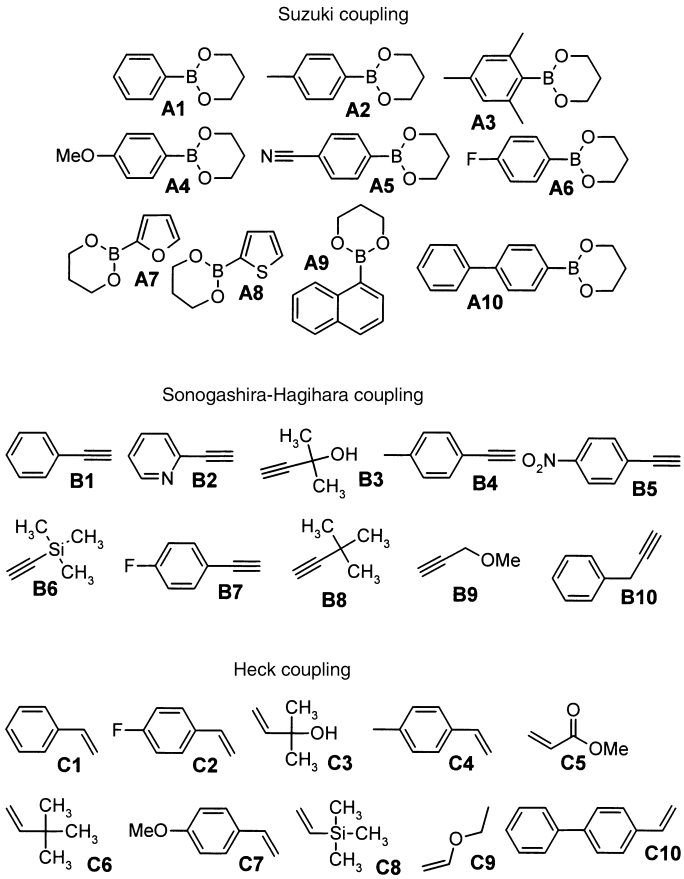
Scheme 2. Cross-coupling reactions with 3-bromocoumarin **1**. The product numbering is derived from the corresponding starting materials (e.g. **1A1** is from **1** and **A1**). For the definitions of **A1**–**C10** see Scheme 3.

First, bromocoumarin **1** was coupled in a parallel synthesizer[14] with the (hetero)aromatic boronic esters **A1**–**A10**, with $[Pd(PPh_3)_4]$ as catalyst and CsF as base. The generation of the boronic esters was accomplished using reported procedures.[15] The coupling products between these boronic esters and compound **1** were pre-purified by parallel filtration with SPE-columns[16] followed by further purification and analysis by sequential automated high-pressure liquid chromatography-mass spectrometry (HPLC-MS).[17] From these parallel reactions we obtained 3-(hetero)aryl substituted coumarins **1A1**–**1A10** in yields of 67–97% with greater than 99% purity. The Sonogashira–Hagihara coupling reactions of coumarin **1** and terminal acetylenes **B1**–**B10** utilizing

[*] Prof. P. Bäuerle, Dipl.-Chem. M.-S. Schiedel, Dr. C. A. Briehn
Abteilung Organische Chemie II (Organische Materialien und Kombinatorische Chemie)
Universität Ulm
Albert-Einstein-Allee 11, 89081 Ulm (Germany)
Fax: (+49) 731 5022840
E-mail: peter.baeuerle@chemie.uni-ulm.de

[**] This work was made possible with funds from Fonds der Chemischen Industrie. We also thank Prof. V. Austel and Dr. E. Mena-Osteritz, University of Ulm, for valuable discussions and general input; Dr. G. Götz, University of Ulm, for photography and also Boehringer Ingelheim, Biberach, for apparatus support.

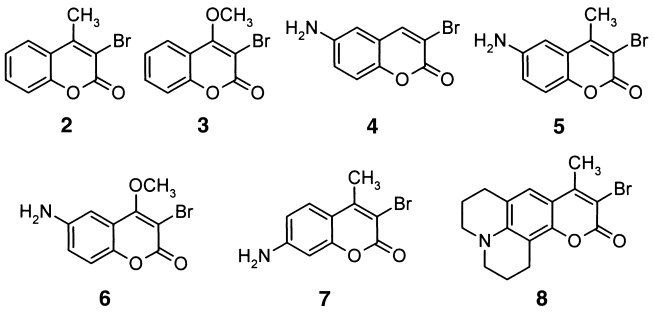
 © WILEY-VCH Verlag GmbH, D-69451 Weinheim, 2001 1433-7851/01/4024-4677 $ 17.50+.50/0



Scheme 3. Coupling components for the Pd-catalyzed parallel syntheses of 3-bromocoumarins **1**–**8**.

the catalytic system of $[Pd(PPh_3)_2Cl_2]$/CuI furnished the 3-ethynylcoumarins **1B1**–**1B10** in yields of 74–95%. Similarly, the Heck coupling with alkenes **C1**–**C10** utilizing the catalytic system $[Pd_2(dba)_3]$/AgOAc (dba = dibenzylideneacetone, OAc = acetate) gave isomerically pure 3-(*E*)-ethenylcoumarins **1C1**–**1C10** in yields of 30–94%. The efficiency of the synthetic methods is shown in that all 30 products were isolated with high purity and in yields sufficient for further screening.

Additionally, seven 3-bromocoumarins **2**–**8** which incorporated functional groups at the 4-, 6-, 7-, and 8-positions were synthesized for the parallel generation of further coumarin



libraries.[18] The aforementioned reaction conditions of the three cross-coupling reactions were optimized for selected combinations of coumarins **2**–**8** and the coupling components **A1**–**A10**, **B1**–**B10**, and **C1**–**C10** and the resulting synthetic method employed for the generation of all possible combinations.[19] From a possible 240 coumarin derivatives 151 (63%) were isolated in >99% purity[20] and of these 127 (84%) were previously unpublished compounds. The remaining compounds could not be isolated in sufficient purity for screening because of low conversions or separation difficulties.

The purified library members were screened for the desired optical properties. The use of a microplate reader allowed the accelerated recording of fluorescence and excitation spectra of the coumarins in ethanol. The determined absorption maxima ($\lambda_{max} = 314-430$ nm) and the emission maxima ($\lambda_{max} = 400-569$ nm) covered a wide range of values. The quantity of the acquired data was sufficient for a detailed correlation between the geometrical and electronic structures of the dyes to be deduced. These results should allow the rational design of dyes which contain specifically desired properties and results pertaining to this will be published in due course.

While the structure–property relationships can be deduced for absorption and fluorescence, the correlation between these factors with respect to the fluorescence quantum yield is still not totally understood. To estimate the quantum yield of the individual compounds, ethanolic solutions of the coumarins were irradiated in microplates with a UV lamp (Figure 1). From the coumarin library 34 derivatives with the most intensive fluorescence (in different emission ranges) were

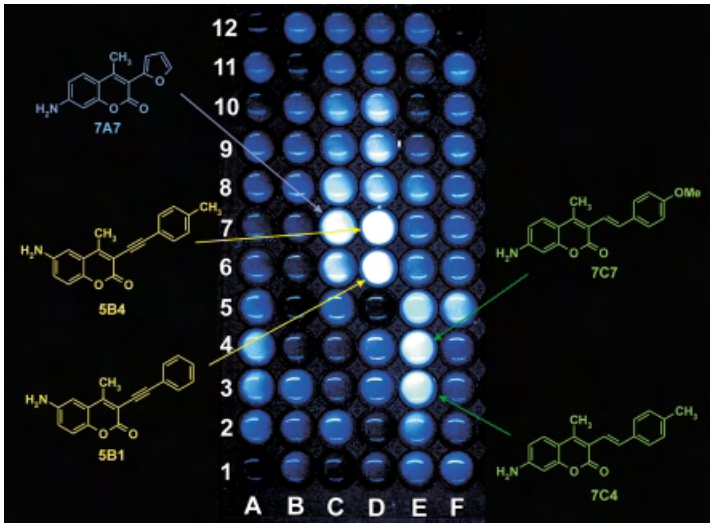


Figure 1. Screening of a coumarin library in a microtiter plate. In the row A–F the coumarins are sorted with respect to their absorption properties.

selected and the fluorescence quantum yield of each was determined by standard procedures (Table 1).[21] The following "hits" were identified (Figure 2): **5A9** ($\phi_f = 0.18$, $\lambda_{abs} =$ 373 nm, $\lambda_{em} = 535$ nm), **8A2** ($\phi_f = 0.90$, $\lambda_{abs} = 395$ nm, $\lambda_{em} =$ 478 nm), **7C4** ($\phi_f = 0.62$, $\lambda_{abs} = 393$ nm, $\lambda_{em} = 480$ nm), and **7B1** ($\phi_f = 0.98$, $\lambda_{abs} = 397$ nm, $\lambda_{em} = 455$ nm). Among these "hits" the 3-phenylethynyl substituted coumarin **7B1** exhibited a higher fluorescence quantum yield than the comparable

 © WILEY-VCH Verlag GmbH, D-69451 Weinheim, 2001 1433-7851/01/4024-4678 $ 17.50+.50/0

Table 1. Absorptions and emission properties of selected coumarins based on the fluorescence quantum yields.

Coumarin	λ_{abs}[a] [nm]	λ_{em}[b] [nm]	ϕ_f[c]	Coumarin	λ_{abs}[a] [nm]	λ_{em}[b] [nm]	ϕ_f[c]
1A4	337	439	0.94	**4A7**	385	553	0.02
1A8	355	442	0.91	**4A8**	394	564	0.02
1A10	334	438	0.72	**4B4**	394	578	0.03
1C1	355	447	0.67	**5A9**	373	535	**0.18**
1C2	354	446	0.66	**5B1**	389	549	0.10
1C4	360	452	0.72	**5B4**	387	548	0.09
1C10	371	463	0.73	**6A5**	382	565	0.12
2A7	341	439	0.25	**6A6**	364	532	0.16
2C2	346	435	0.32	**6A10**	361	530	0.10
2C4	352	441	0.38	**7C4**	393	480	**0.62**
2C7	360	466	0.57	**7C7**	396	485	0.58
7A2	360	449	0.35	**8A2**	395	478	**0.90**
7A5	370	469	0.26	**8A6**	395	479	0.77
7A7	378	481	0.40	**8A7**	411	495	0.73
7A9	363	442	0.70	**8A8**	405	506	0.55
7B1	397	455	**0.98**	**8A9**	394	474	0.84
7C6	369	455	0.38	**8C7**	427	496	0.58

[a] Absorption maxima in ethanol (longest wavelength transition). [b] Maxima of the corrected emission spectra in ethanol. [c] External standard: 9,10-diphenylanthracene ($\phi_f = 0.95$, in cyclohexane).[20]



Figure 2. "Hits" identified by the qualitative and subsequent quantitative screening of the fluorescence quantum yield: **8A2**, **7C4**, **5A9**, and **7B1**.

and commercially available coumarin 120 ($\phi_f = 0.88$, $\lambda_{abs} = 354$ nm, $\lambda_{em} = 435$ nm in ethanol).[22] In view of possible applications of these compounds (e.g. as fluorescent labels in biological systems) the NH_2 substituted derivatives **7B1**, **7C4**, and **5A9** are of interest since these dyes can be linked to a biomolecule through their amino groups. Also, the following step of the combinatorial development process, namely the application of these novel chromophores as active layers in organic light-emitting diodes and their optimization should be possible. The application of combinatorial strategies for the screening and optimization of organic charge-transporting materials in a spatially addressable library of organic light-emitting diodes was recently reported by Schmidt et al.[23]

This work clearly demonstrates that the concepts of combinatorial chemistry can be successfully applied to development and improvement of novel materials. The efficient synthetic method for the parallel execution of Pd-catalyzed cross-coupling reactions yielded a large number of unpublished fluorescent coumarin dyes. Following the automated purification the screening for optical properties identified several "hits" with high fluorescence quantum yields. The development of structure–property relationships based on the collective data sets should allow the rational design of coumarin dyes. This study demonstrates the successful application of a combinatorial approach strategy encompassing the design of the lead structure, development of synthetic routes, efficient library synthesis and purification techniques, screening, and data analysis.

Received: July 25, 2001 [Z17596]

[1] *Combinatorial Chemistry—Synthesis, Analysis, Screening* (Ed.: G. Jung), Wiley-VCH, Weinheim, **1999**.

[2] a) B. Jandeleit, D. J. Schaefer, T. S. Powers, H. W. Turner, W. H. Weinberg, *Angew. Chem.* **1999**, *111*, 2648–2689; *Angew. Chem. Int. Ed.* **1999**, *38*, 2494–2532; b) S. Senkan, *Angew. Chem.* **2001**, *113*, 322–341; *Angew. Chem. Int. Ed.* **2001**, *40*, 312–329.

[3] a) J. Wang, Y. Yoo, C. Gao, I. Takeuchi, X. Sun, H. Chang, X.-D. Xiang, P. G. Schultz, *Science* **1998**, *279*, 1712–1714; b) E. Danielson, M. Devenney, D. M. Giaquinta, J. H. Golden, R. C. Haushalter, E. W. McFarland, D. M. Poojary, C. M. Reaves, W. H. Weinberg, X. D. Wu, *Science* **1998**, *279*, 837–839; c) X.-D. Sun, C. Gao, J. Wang, X.-D. Xiang, *Appl. Phys. Lett.* **1997**, *70*, 3353–3355; d) E. Danielson, J. H. Golden, E. W. McFarland, C. M. Reaves, W. H. Weinberg, X. D. Wu, *Nature* **1997**, *389*, 944–948; e) X.-D. Sun, K.-A. Wang, Y. Yoo, W. G. Wallace-Freedman, C. Gao, X.-D. Xiang, P. G. Schultz, *Adv. Mater.* **1997**, *9*, 1046–1049.

[4] C. A. Briehn, M.-S. Schiedel, E. M. Bonsen, W. Schuhmann, P. Bäuerle, *Angew. Chem.* **2001**, *113*, 4817–4820; *Angew. Chem. Int. Ed.* **2001**, *40*, 4680–4683.

[5] a) German Patent Application 100 12 962.5, March 16, 2000; PCT-Application PCT/EP01/02735, May 15, 2001; b) P. Bäuerle, Seminar at the Conference *Combi Europe: Combinatorial Approaches and High Throughput Screening for New Materials Discovery*, The Knowledge Foundation Inc., Frankfurt am Main, Germany, **2000**.

[6] a) K. R. Romines, J. K. Morris, W. J. Howe, P. K. Tomich, M.-M. Horng, K.-T. Chong, R. R. Hinshaw, D. J. Anderson, J. W. Strohbach, S.-R. Turner, S. A. Miszak, *J. Med. Chem.* **1996**, *39*, 4125–4130; b) *Coumarins—Biology, Applications and Mode of Action* (Eds.: R. O'Kennedy, R. D. Thornes), Wiley, Chichester, **1997**.

[7] a) R. Raue in *Ullmannns Encyclopedia of Industrial Chemistry*, *Vol. A15*, 5th ed. (Eds.: B. Elvers, S. Hawkins, G. Schulz), VCH, Weinheim, **1990**, pp. 155–157; b) R. S. Koefod, K. R. Mann, *Inorg. Chem.* **1989**, *28*, 2285–2290.

[8] a) P. D. Edwards, R. C. Mauger, K. M. Cottrell, F. X. Morris, K. K. Pine, M. A. Sylvester, C. W. Scott, S. T. Furlong, *Bioorg. Med. Chem. Lett.* **2000**, *10*, 2291–2294; b) M. Adamczyk, M. Cornwell, J. Huff, S. Rege, T. V. S. Rao, *Bioorg. Med. Chem. Lett.* **1997**, *7*, 1985–1988; c) C. A. M. Seidel, A. Schulz, M. H. M. Sauer, *J. Phys. Chem.* **1996**, *100*, 5541–5553; d) A. Adronov, S. L. Gilat, J. M. Fréchet, K. Ohta, F. V. R. Neuwahl, G. R. Fleming, *J. Am. Chem. Soc.* **2000**, *122*, 1175–1185; e) K. H. Shaughnessy, P. Kim, J. F. Hartwig, *J. Am. Chem. Soc.* **1999**, *121*, 2123–2132.

[9] a) J. Kido, Y. Lizumi, *Appl. Phys. Lett.* **1998**, *73*, 2721–2723; b) A. Niko, S. Tasch, F. Meghdadi, C. Brandstätter, G. Leising, *J. Appl. Phys.* **1997**, *82*, 4177–4182; c) S. Tasch, C. Brandstätter, F. Meghdadi, G. Leising, G. Froyer, L. Athouel, *Adv. Mater.* **1997**, *9*, 33–36.

[10] A. E. Siegrist, H. Hefti, H. R. Meyer, E. Schmidt, *Rev. Prog. Coloration* **1987**, *17*, 39–55.

[11] Note: Substituent variation at the 3-, 4-, 6-, and 7-positions exhibit an especially strong influence on the electronic properties of the chromophore. a) *Organic Luminescent Materials* (Eds.: B. M. Krasovitskii, B. M. Bolotin), Wiley-VCH, Weinheim, **1988**; b) R. M. Christie, *Rev. Prog. Coloration* **1993**, *23*, 1–18; c) N. A. Kuznetsova, O. L. Kaliya, *Russ. Chem. Rev.* **1992**, *61*, 683-696; d) O. A. Ponmarev, E. R. Vasina, V. G. Mitina, A. A. Sukhorukov, *Russ. J. Phys. Chem.* **1990**, *64*, 518–521.

[12] a) W. H. Perkin, *Justus Liebigs Ann. Chem.* **1871**, *157*, 115–119; b) P. Pfeiffer, *Chem. Ber.* **1915**, *48*, 1048–1058.

 © WILEY-VCH Verlag GmbH, D-69451 Weinheim, 2001 1433-7851/01/4024-4679 $ 17.50+.50/0

[13] a) A. K. Mitra, A. De, N. Karchaudhuri, J. Mitra, *J. Chem. Res. (S)* **1998**, 766 – 767; b) G. M. Boland, D. M. X. Donnelly, J.-P. Finet, M. D. Rea, *J. Chem. Soc. Perkin Trans. 1* **1996**, 2591 – 2597.
[14] Quest 210 Synthesizer, Fa. Argonaut Technologies.
[15] compare with a) W. König, W. Scharrnbeck, *J. Prakt. Chem.* **1930**, *128*, 153 – 170; b) M. S. Wong, J.-F. Nicoud, *Tetrahedron Lett.* **1993**, *34*, 8237 – 8240; c) Y. Kobayashi, R. Mizojiri, E. Ikeda, *J. Org. Chem.* **1996**, *61*, 5391 – 5399; d) A. Finch, J. C. Lockhart, *J. Chem. Soc.* **1962**, 3723 – 3728. The boronic acids **A 7**, **A 9**, and **A 10** are unpublished.
[16] SPE = Solid-phase extraction; for filtration columns with RP-18 material was used in conjunction with a "VacMaster SPE Processing Station" (Separtis IST); mobile phase: acetonitrile/water.
[17] Purification and mass detection were performed on an HPLC-MS (Waters) fitted with a LC/MS detector (Micromass ZMD; electrospray ionization (ESI) mode). Chromatography performed on Xterra RP-18 (analytic: 3.5 μm, 4.6 × 100 mm; semi-preparative: 7.0 μm, 19 × 150 mm) columns (Waters) with an acetonitrile – water gradient.
[18] The following references were utilized for the synthesis of bromocoumarins **2** – **4**, **7**, and **8**: **2**: F. Peters, H. Simonis, *Chem. Ber.* **1908**, *41*, 830 – 837; **3**: K. Takagi, M. Hubert-Habart, *Bull. Soc. Chim. Fr.* **1980**, *2*, 444 – 448; **4**: a) B. B. Dey, K. K. Row, *J. Chem. Soc.* **1923**, *123*, 3375 – 3384; b) B. B. Dey, T. R. Seshadri, *Chem. Zentralbl.* **1926**, *97*, 1648 – 1649; **7**, **8**: N. A. Gordeeva, M. A. Kirpichenok, N. S. Patalakha, I. I. Grandberg, *Chem. Hetreocycl. Compd. (Engl. Transl.)* **1990**, *26*, 1329 – 1337; Bromocoumarins **5** and **6** were available by selective nitration and subsequent reduction starting from coumarin **2** and **3**: KNO_3 (1.22 g, 12 mmol) was added to a solution of coumarin **2** or **3** (10 mmol) in 96 % sulfuric acid (60 mL) at 0 °C. After stirring at 0 °C for 2.5 h, the solution was poured into crushed ice forming a precipitate. This precipitate was collected and washed successively with diluted Na_2CO_3 solution. The pure 6-nitrated derivatives were obtained by recrystallizing from ethanol/water (95/5). For the reduction, the nitro compounds (10 mmol) were dissolved at 100 °C in 80 % acetic acid (200 mL) and treated portionwise with iron powder (3.35 g, 60 mmol). After 10 min the solution was poured into ice and extracted several times with chloroform. The solvent was subsequently removed and the crude product purified by column chromatography on silica (hexane/ethylacetate 50/50; overall yields: 66 % (**5**), 63 % (**6**)).
[19] Representative example for a parallel Suzuki cross-coupling: synthesis of 7-amino-4-methyl-3-*p*-tolyl-chromen-2-one (**7 A 2**): Coumarin **7** (25.4 mg, 0.1 mmol), boronic ester **A 2** (35.2 mg, 0.2 mmol), CsF (121 mg, 0.8 mmol), and $[Pd(PPh_3)_4]$ (5.78 mg, 5 mol %) were heated at 90 °C under argon in dry dioxane for 16 h. The solvent was evaporated and the residue was dissolved in acetonitrile/water. This solution was then filtered through a SPE (RP-18) column and purified by automated HPLC-MS affording the pure product (21.2 mg, 80 %). M.p. 260 – 262 °C; ^{1}H NMR (400 MHz, [D$_6$]DMSO, 25 °C): δ = 7.44 (d, J = 8.7 Hz, 1H), 7.20 (d, J = 7.9 Hz, 2H), 7.12 (d, J = 7.9 Hz, 2H), 6.60 (dd, J = 8.7, 1.9 Hz, 1H), 6.45 (d, J = 1.9 Hz, 1H), 6.07 (broad s, 2H), 2.33 (s, 3H), 2.13 (s, 3H); ^{13}C NMR (100 MHz, [D$_6$]DMSO, 25 °C): δ = 160.8, 154.6, 152.8, 148.6, 136.6, 132.5, 130.5 (2C), 128.7 (2C), 126.8, 119.8, 111.6, 109.4, 98.5, 21.0, 16.3; UV/Vis (ethanol): λ_{max} (ε [L mol^{-1} cm^{-1}]) = 360 nm (22 500); EI-MS (70 eV): m/z (%) : 265 (88) [M^+], 237 (100) [M^+ – CO].
[20] For further structure validation 20 % of the library members were characterized spectroscopically (^{1}H NMR).
[21] Optically dilute measurements with refractive-index corrections, maximal absorption of the solutions ≤ 0.04. Calibrated spectrometer (Perkin Elmer LS 50B); measurements referenced to 9,10-diphenylanthracene (ϕ_f = 0.95); a) *Principles of Fluorescence Spectroscopy*, 2nd ed. (Ed.: J. R. Lakowicz), Kluwer Academic/Plenum Publishers, New York, **1999**; b) J. N. Demas, G. A. Crosby, *J. Phys. Chem.* **1971**, *75*, 991 – 1024.
[22] T. Besson, G. Coudert, G. Guillaumet, *J. Heterocycl. Chem.* **1991**, *28*, 1517 – 1523.
[23] a) C. Schmitz, P. Pösch, M. Thelakkat, H.-W. Schmidt, *Phys. Chem. Chem. Phys.* **1999**, *1*, 1777 – 1781; b) C. Schmitz, M. Thelakkat, H.-W. Schmidt, *Adv. Mater.* **1999**, *11*, 821 – 826.

Single-Compound Libraries of Organic Materials: From the Combinatorial Synthesis of Conjugated Oligomers to Structure – Property Relationships**

Christoph A. Briehn, Marc-Steffen Schiedel, Eva M. Bonsen, Wolfgang Schuhmann, and Peter Bäuerle*

The development process of novel materials is often encumbered by the time-consuming "one-at-a-time" process of material synthesis and evaluation. This situation is particularly true for π-conjugated oligomers which serve as model compounds for conducting polymers and are recognized as materials in their own right.[1] Accordingly, there is a need for novel methods that provide for both rapid compound generation and subsequent evaluation. Combinatorial methodologies that were developed for the high-speed synthesis and high-throughput screening of pharmaceuticals could help to overcome these bottlenecks in the materials development process.[2] Moreover, the rapid generation of data sets provided by combinatorial methods and their subsequent translation into structure – property relationships may enable the rational design of new materials.

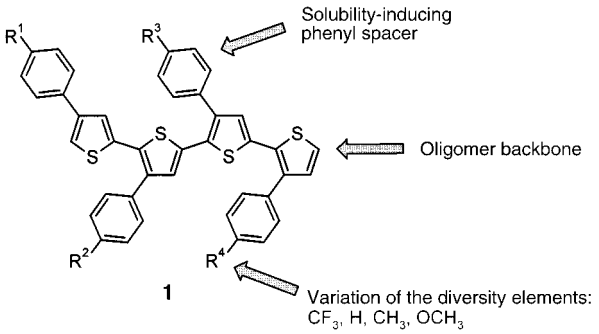
While most of the combinatorial approaches in materials science concentrate on the development of inorganic solid-state materials, polymeric materials, and catalytic systems,[3] we report here and in the preceding correspondence[4] the development of combinatorial strategies for the generation of organic materials. The focus of this study is the combinatorial synthesis and subsequent screening of oligothiophenes which are one of the most examined classes of π-conjugated oligomers.[5] The strategy covers all stages of the combinatorial discovery process: design of the lead structure, elaboration of the synthetic route, generation of the library and purification, screening, and data analysis. We focused on a regioregular head-to-tail coupled quater(3-arylthiophene) as the lead structure (Scheme 1). Because of their defined structure these aryl substituted oligomers, together with the already intensively investigated oligo(3-alkylthiophene)s, are outstanding model compounds for the parent (polydisperse) poly(3-arylthiophene)s and poly(3-alkylthiophene)s.[6] The

[*] Prof. Dr. P. Bäuerle, Dr. C. A. Briehn, Dipl.-Chem. M.-S. Schiedel
Abteilung Organische Chemie II (Organische Materialien und Kombinatorische Chemie)
Universität Ulm
Albert-Einstein-Allee 11, 89081 Ulm (Germany)
Fax: (+49) 731-502-2840
E-mail: peter.baeuerle@chemie.uni-ulm.de
Dr. E. M. Bonsen, Prof. Dr. W. Schuhmann
Analytische Chemie—Elektroanalytik and Sensorik
Ruhr-Universität Bochum, 44780 Bochum (Germany)

[**] This work was made possible with funds donated from Fonds der Chemischen Industrie, the BMBF (Kekulé grant to C.A.B) and the DFG (Schu 929/5-1). We thank Prof. V. Austel, the University of Ulm, for valuable discussions and also Boehringer Ingelheim Pharmaceuticals Inc., Ridgefield (USA), for apparatus support.

Supporting information for this article is available on the WWW under http://www.angewandte.com or from the author.

 © WILEY-VCH Verlag GmbH, D-69451 Weinheim, 2001 1433-7851/01/4024-4680 $ 17.50+.50/0



Scheme 1. Lead structure: quater(3-arylthiophene) **1**.

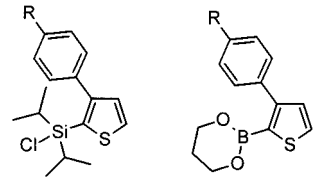
latter are already successfully employed as active components in electronic devices, such as organic field-effect transistors.[7] The oligothiophene **1** is substituted at the 3-position of each thiophene subunit with phenyl groups that are in turn substituted at their *para* positions with four diversity elements of different electronic nature ($R = CF_3$, H, CH_3, OCH_3).

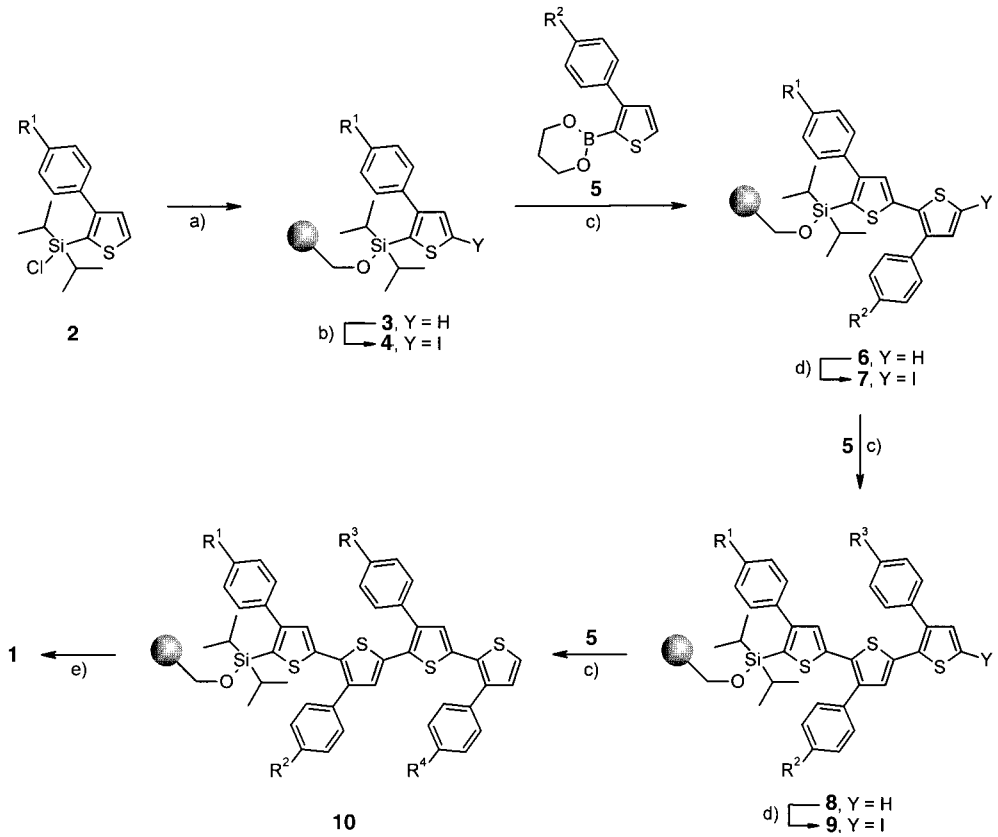
The phenyl spacer should increase the solubility of the oligomers and ensure the electronic communication between the substituents and the oligomer backbone. These four backbone substituents should influence the electronic structure of the quaterthiophenes without greatly changing the overall geometry of the molecule (which is mainly determined by the phenyl groups). The lead structure **1** should therefore permit a systematic investigation of the substitutent influence on the energy levels of the molecular orbitals and the development of structure – property relationships.

As previously demonstrated by several research groups, the utilization of solid-phase synthesis offers substantial advantages for the synthesis of π-conjugated oligomers over solution-phase synthesis.[8] These advantages include quicker and more effective purification techniques and maximized overall yields. The synthesis of the quater(3-arylthiophene)s **1** is based on the recently published solid-phase synthesis of a regioregular head-to-tail coupled quater(3-*p*-tolyl)thiophene (Scheme 2).[8e]

In a stepwise addition approach the first of the four arylthiophenes is anchored to the polymer matrix by a traceless silyl linker; this is realized by treating a (chlorosilyl)thiophene **2** with hydroxymethylated polystyrene. Oligomer growth is accomplished by an iterative sequence of iodination and Suzuki cross-coupling with the thiophene boronic ester **5**. Resin-bound thiophene **3** was halogenated to **4** by metalation with lithium diisopropylamide (LDA) and subsequent reaction with iodine. In contrast, a mercuration – iododemercuration reaction ($Hg(OCOC_5H_{11})_2$ instead of LDA) was required for the selective access to the iodinated bi- and terthiophenes **7** and **9**. The cross-couplings for the preparation of dimer **6**, trimer **8**, and tetramer **1** required a $[Pd(PPh_3)_4]$ catalyst. Finally, quaterthiophene **1** was liberated from the resin by treating the derivatized polymer support with 10% trifluoroacetic acid (TFA) in CH_2Cl_2.

The (chlorosilyl)thiophene **2a – d** and thiophene boronic ester **5a – d** building blocks are needed to introduce diversity in the final quaterthiophenes. These building blocks were synthesized in good yields following literature procedures starting from the corresponding 2-bromo-3-arylthiophenes.[8e, 9] In the optimization studies the electronic influence of these diversity elements on the reactivity of the building blocks and the resin-bound oligomers was readily apparent. For example, the markedly different reactivity between the boronic esters **5a – d** required a further optimization of the reaction conditions for the Suzuki cross-coupling. The C–C bond formation reaction between the





Scheme 2. Solid-phase synthesis of the quater(3-arylthiophene)s **1**: a) hydroxymethylated polystyrene, imidazole, DMF, 20 °C; b) 1. LDA, THF, −60 °C; 2. I_2; c) $[Pd(PPh_3)_4]$, THF/H_2O, $NaHCO_3$ or Na_2HPO_4/NaH_2PO_4; d) 1. $Hg(OCOC_5H_{11})_2$, CH_2Cl_2, 20 °C; 2. I_2, CH_2Cl_2; e) 10% TFA, CH_2Cl_2, 20 °C. Selected spectroscopic data can be found in the Supporting Information.

 © WILEY-VCH Verlag GmbH, D-69451 Weinheim, 2001 1433-7851/01/4024-4681 $ 17.50+.50/0

resin-bound iodinated thiophenes and boronic esters **5b–d** with $NaHCO_3$ as the base gave nearly quantitative conversions. However, under these conditions the trifluoromethyl substituted building block **5a** furnished the coupling product in very low conversions. Therefore, a buffer system of NaH_2PO_4/Na_2HPO_4 was employed and proved to be highly efficient in cross-couplings with the boronic ester **5a**.

With the development and optimization of the synthetic method complete, the oligomer library was constructed by utilizing both the parallel and the "mix-and-split" synthesis. This library included all possible permutations of the four diversity elements (functional groups) resulting in a library of 256 tetramers. The synthesis of the iodobithiophenes **7** was performed in parallel, the subsequent oligomer growth to the quaterthiophenes **1** used the "mix-and-split" technique. In the latter technique, the individual compounds are synthesized in micro-reactors each labeled with a unique radiofrequency tag for identification.[10] Using this procedure a 256-membered quaterthiophene library was synthesized after successful generation of a 16-membered test library.

Since the purity of the compounds is a crucial prerequisite for a meaningful screening, all the oligomers were purified using automated preparative high-pressure liquid chromatography (HPLC).[11] 243 of the 256 library members could be isolated in milligram quantities with purities of greater than 98%. In addition, the integrity and identity of the oligomers could be assessed by coupled mass spectrometry. The quaterthiophenes were available in isolated overall yields of 2–51% which do not reflect the overall reaction conversions but rather display the separation difficulties during the HPLC purification. The ^{1}H NMR spectroscopic analysis of selected raw products revealed an overall conversion of 40–55% (which appeared to be nearly independent of the building blocks employed) corresponding to an average conversion of 89–93% per reaction step.

In view of the technological applications of π-conjugated oligomers and their corresponding polymers the investigation of optical and electrochemical properties is of interest. The screening of the purified oligomers by means of absorption and fluorescence spectroscopy and cyclic voltammetry should allow the development of detailed structure–property relationships which can be used to estimate the properties of similar oligomers and polymers. The screening of optical properties revealed only a marginal influence by the substituents on the absorption maxima ($\lambda_{abs} = 381-392$ nm) and emission maxima ($\lambda_{em} = 492-518$ nm). However, the optical gap which is associated with the energy difference of the frontier orbitals slightly increases with the electron-donating nature of the substituents ($\Delta E = 2.71-2.74$ eV).

The electronic consequences of the oligomer substitution on the relative energy levels of the frontier orbitals were further investigated by cyclic voltammetry. A significant increase of the probe throughput was obtained by using a fully automated screening device. The apparatus constructed for the electrochemical screening is shown in Figure 1. It comprises a 96-well plate (which was used as an array of electrochemical cells), a three-electrode setup (Pt working electrode, Pt counter electrode, and Ag/AgCl reference electrode), a solvent dispenser, a potentiostat, and a computer

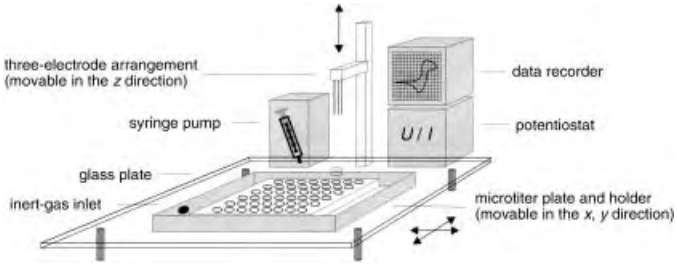


Figure 1. Apparatus for the automated cyclic voltammetry.

for data acquisition. To precisely position the electrode setup into the wells the microtiter plate was fixed to a holder which could be orientated in the *x*,*y* plane and the electrode setup was attached to a holder with *z*-direction mobility. Tailored software[12] allowed the positioning of the electrodes into the cavities of the well plate, the dosing of the electrolyte[13] under exclusion of oxygen using a serially controlled solvent dispenser, and after a predefined delay (which was necessary for solvating the compound) acquisition of the voltammetric data. Cyclic voltammograms for each measurement were stored in a separate file.

By extracting the relevant data from the voltammograms, information on the substituent effects on redox potentials was provided. The first oxidation potentials of the quaterthiophenes (E_1^0) covered a large range of 0.42–0.68 V.[14] A systematic shift to higher oxidation potentials occurred when the substituents had a more pronounced acceptor character. This general trend is illustrated in the color-coded diagram, Figure 2. A similar relationship was found for the second oxidation potentials of the quaterthiophenes (E_2^0), these covered a range of 0.78–0.90 V.

The correlation of the collected redox potentials with the substituent descriptor $\Sigma\sigma_p^+$ (which was defined as sum of the

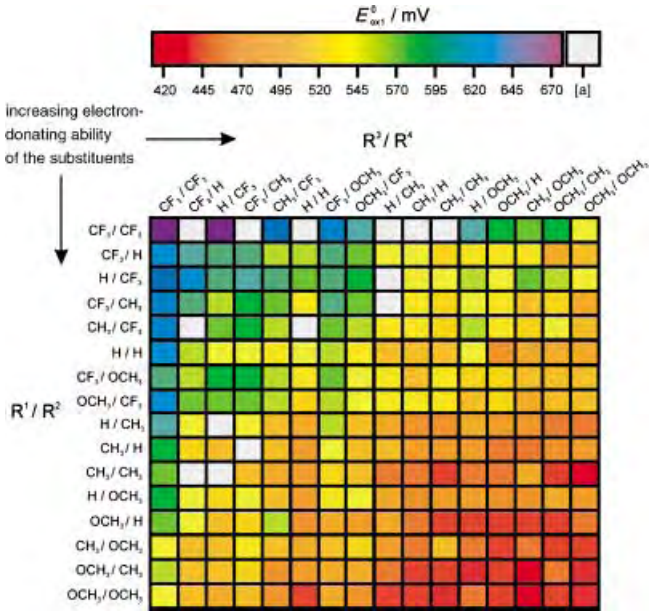


Figure 2. Color-coded matrix of the first oxidation potentials (E_1^0) of the quaterthiophenes **1**. The substituents R^1 and R^2 are arranged along the ordinate, the substituents R^3 and R^4 along the abscissa. [a] Not determined because of sample impurity.

 © WILEY-VCH Verlag GmbH, D-69451 Weinheim, 2001 1433-7851/01/4024-4682 $ 17.50+.50/0

Hammett constants σ_p^+ of the individual substituents[15]) facilitated a detailed analysis of the substituent effects. This descriptor, which numerically reflects the overall contributions of the individual substituents, is plotted in Figure 3 against the first and second oxidation potentials.[16] This plot

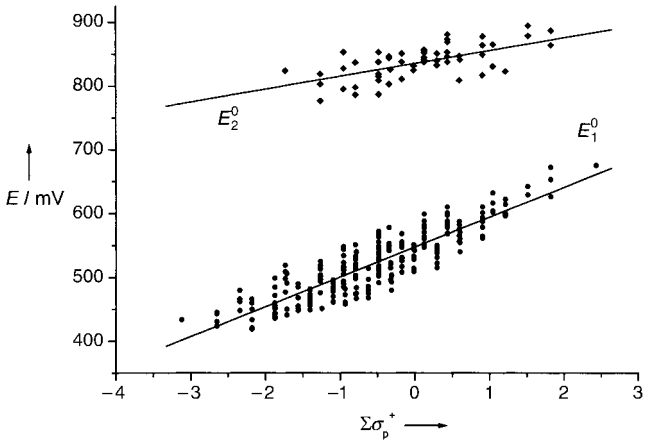


Figure 3. Correlation between the first and second oxidation potentials E_1^0 and E_2^0 of the quaterthiophenes **1** and the substituent descriptor $\Sigma\sigma_p^+$.

displays, on first inspection, a linear correlation between $\Sigma\sigma_p^+$ and the redox potentials. While the potentials reflect the overall electron affinity of the four substituents, the slopes of the trend lines indicate the susceptibility of the oxidation potentials to the electronic influence of the substituents.[17] The first oxidation potential is therefore more influenced by the electronic nature of the substituents than the second. In addition, for some of the oligomers with the same substituent constitution (same $\Sigma\sigma_p^+$ value) a scattering of the oxidation potentials of up to 80 mV (E_1^0) is observed. This fact indicates that, beside their electronic nature, the sequence of the four substituents also influences the oxidation potential. Finally, the electrochemical energy gaps ($\Delta E = 2.84 - 2.91$ V, difference between the first oxidation potential E_1^0 and the reduction potential were determined for some representative quaterthiophenes,[18] these electrochemical energy gaps were found to be in good agreement with the data obtained by the optical analysis.

These results and those of the preceding study[4] clearly demonstrate that the principles of combinatorial chemistry can be utilized for the development of organic materials. The stepwise oligomer growth by solid-phase synthesis and the subsequent screening for optical and electrochemical properties enabled the collection of large data sets which could be used to deduce structure–property relationships. The substitution with the different electronically diverse elements opens the avenue to the effective control and fine-tuning of the optical and electrochemical properties of such π-conjugated oligomers.

Received: July 25, 2001 [Z17597]

[1] a) *Handbook of Conducting Polymers*, 2nd ed. (Eds.: T. A. Skotheim, R. L. Elsenbaumer, J. R. Reynolds), Marcel Dekker, New York, **1998**; b) *Electronic Materials: The Oligomer Approach* (Eds.: K. Müllen, G. Wegner), Wiley-VCH, Weinheim, **1998**.

[2] *Combinatorial Chemistry—Synthesis, Analysis, Screening* (Ed.: G. Jung), Wiley-VCH, Weinheim, **1999**.

[3] For review, see: a) B. Jandeleit, D. J. Schaefer, T. S. Powers, H. W. Turner, W. H. Weinberg, *Angew. Chem.* **1999**, *111*, 2648–2689; *Angew. Chem. Int. Ed.* **1999**, *38*, 2494–2532; b) S. Senkan, *Angew. Chem.* **2001**, *113*, 322–341; *Angew. Chem. Int. Ed.* **2001**, *40*, 312–329.

[4] M.-S. Schiedel, C. A. Briehn, P. Bäuerle, *Angew. Chem.* **2001**, *113*, 4813–4816; *Angew. Chem. Int. Ed.* **2001**, *40*, 4677–4680.

[5] P. Bäuerle in ref. [1b], pp. 105–197.

[6] a) J. P. Ferraris, M. M. Eissa, I. D. Brotherston, D. C. Loveday, *Chem. Mater.* **1998**, *10*, 3528–3535; b) R. D. McCullough, *Adv. Mater*. **1998**, *10*, 93–116.

[7] H. Sirringhaus, J. P. Brown, R. H. Friend, M. M. Nielsen, K. Beechgard, B. M. W. Langeveld-Voss, A. J. H. Spiering, R. A. J. Janssen, E. W. Meijer, P. Herwig, D. M. deLeeuw, *Nature* **1999**, *401*, 685–688.

[8] a) J. C. Nelson, J. K. Young, J. S. Moore *J. Org. Chem.* **1996**, *61*, 8160–8168; b) P. R. L. Malenfant, J. M. J. Fréchet, *Chem. Commun.* **1998**, 2657–2658; c) S. Huang, J. M. Tour, *J. Org. Chem.* **1999**, *64*, 8898–8906; d) T. Kirschbaum, C. A. Briehn, P. Bäuerle, *J. Chem. Soc. Perkin Trans. 1* **2000**, 1211–1216; e) C. A. Briehn, T. Kirschbaum, P. Bäuerle, *J. Org. Chem.* **2000**, *65*, 352–359.

[9] **2a** (73%), **2d** (79%): 1) 2-bromo-3-arylthiophene (aryl = *p*-trifluormethylphenyl or *p*-anisyl), *n*BuLi, Et_2O, −70 °C; 2) $Cl_2Si(iPr)_2$, −30 °C. **5a** (71%): 1) 2-bromo-3-(*p*-trifluormethylphenyl)thiophene, *n*BuLi, THF, −70 °C; 2) *O*,*O*′-bis(2,6-dioxaborinan-1-yl)propane-1,3-diol, −70 °C; 3) BF_3, −30 °C. **5d** (85%): 1) 2-Bromo-3-(*p*-anisyl)-thiophene, Mg, THF; 2) $B(OiPr)_3$, −70 °C; 3) H_2O; 4) 1,3-propandiol, molecular sieve (4 Å). Compounds **2b**, **c** and **5b**, **c** are reported in ref. [8e].

[10] The "AccuTag-System" from IRORI was used for the "mix-and-split" synthesis.

[11] The chromatography was performed on normal phase (nitrophenyl) using CH_2Cl_2/*n*-hexane as the eluant.

[12] The software for the cyclic voltammetry, the control of the stepper motors (for the positioning of the electrodes and samples) and the solvent dispenser was written in Visual Basic 3.0 (W. S.).

[13] 0.1 M Bu_4NPF_6 in CH_2Cl_2 was used as electrolyte. Ferrocene was used as an internal standard.

[14] Potentials are referenced to the ferrocene/ferricinium ion (Fc/Fc^+) redox pair and were determined at a scan rate of $v = 100$ mV s^{-1}.

[15] For review, see: C. Hansch, A. Leo, R. W. Taft, *Chem. Rev.* **1991**, *91*, 165–195; Hammett constants of diversity elements: $\sigma_p^+ = 0.61$ for R = CF_3, 0 for R = H, −0.31 for R = CH_3, −0.78 for R = OCH_3.

[16] Similar correlations of oxidation potentials with Hammett constants: a) D. J. Guerrero, X. M. Ren, J. P. Ferraris, *Chem. Mater.* **1994**, *6*, 1437–1443; b) A.-J. Attias, P. Hapiot, V. Wintgens, P. Valat, *Chem. Mater.* **2000**, *12*, 461–471.

[17] The trend lines were fitted using the method of least squares: for the first oxidation potential: E_1^0 [V] = 0.55 + 0.047 $\Sigma\sigma_p^+$ (correlation coefficient $R = 0.90$, standard deviation 0.02 V); for the second oxidation potential: E_2^0 [V] = 0.84 + 0.020 $\Sigma\sigma_p^+$ (correlation coefficient $R = 0.62$, standard deviation 0.02 V).

[18] For the determination of the electrochemical energy gaps cyclic voltammograms were recorded in acetonitrile (0.1 M Bu_4NPF_6).

 © WILEY-VCH Verlag GmbH, D-69451 Weinheim, 2001 1433-7851/01/4024-4683 $ 17.50+.50/0

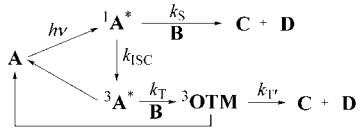
Temperature and Viscosity Dependence of the Spin-Directed Stereoselectivity of the Carbonyl–Alkene Photocycloaddition**

Axel G. Griesbeck,* Samir Bondock, and Murthy S. Gudipati*

The unusual nonlinear temperature dependence of the stereoselectivity of Paternò–Büchi photocycloadditions of electron-rich cycloalkenes with chiral phenyl glyoxylates served as the basis for the development of the isoinversion principle by Scharf and co-workers.[1] The influence of the excited-state spin multiplicity was not observed in these studies as substrates with high intersystem crossing (ISC) rates were used and thus exclusive (bimolecular) triplet reactions were expected.[2] However, the ISC-process from the triplet 1,4-biradical (2-oxatetramethylene),[3] which is necessary to form the closed-shell product, was not discussed as a further possible selection step in the context of the isoinversion principle.

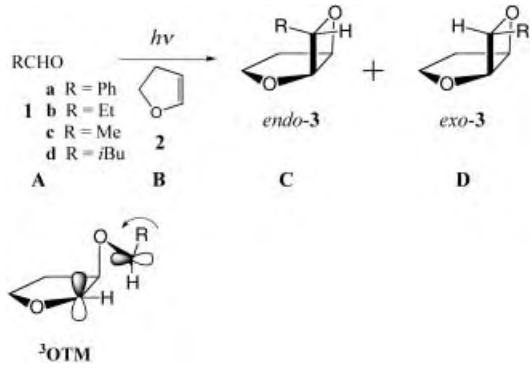
Inversion effects in stereoselectivity/temperature correlations were observed also for other photochemical[4] as well as for a multitude of thermal processes.[5] Despite several attempts to understand these effects theoretically,[1] their origin is still debatable.[6] A simplified model interprets the inversion points in the selectivity/temperature correlation as changes between two selection stages that are controlled to a different by the respective differences in activation enthalpy and entropy degree.[1] Alternatively inversion regions can be postulated which result from a change in the rate-determining step.[7]

In recent years we have analyzed closely the mechanism of the terminal bond-forming step in triplet [2+2] photocycloadditions with an emphasis on the non-induced ("simple") diastereoselectivity.[8] The detection of the concentration dependence of the stereoselectivity of the Paternò–Büchi reaction was essential for demonstrating different simple diastereoselectivities in singlet and triplet routes.[9] Each pair of carbonyl and alkene components exhibited a characteristic substrate concentration at which point a 1:1 ratio of singlet and triplet reactivity, that is, spin selectivity, could be detected. The shape of these concentration/diastereoselectivity correlations reflects the different kinetic contributions to this complex reaction scenario (Scheme 1). The C/D selectivity is controlled by the geometry of the conical intersection in the case of the singlet reaction (k_S)[10] and by the optimal ISC geometry of the 2-oxatetramethylene biradical (^{3}OTM) in the case of the triplet reaction (k_T).[11]



Scheme 1. Mechanism for a photocycloaddition that involves singlet and triplet states.

Our initial assumption was that the activation parameters should strongly differ for these two processes and consequently characteristic nonlinear behavior might occur during temperature variation. Prior to these experiments, solvent viscosity effects in triplet and singlet photocycloadditions were studied to separate these influences from temperature effects. The photocycloaddition of benzaldehyde (**1a**) with 2,3-dihydrofuran (**2**) was investigated as a typical triplet reaction with concentration-independent diastereoselectivity (Scheme 2).[9]



Scheme 2. Photocycloaddition of **2** with **1a–d**.

The variation of the solvent viscosity over a large range ($\eta = 0.3$ to 1500 cP)[12] resulted in a weak but significant increase in *endo* selectivity from 82% to 91% (Table 1, Figure 1).[13] More pronounced effects were detected in the analogous reactions with aliphatic aldehydes **1b–d** and dihydrofuran (1M substrate concentrations). In all cases, the diastereoselectivity increased with increasing solvent viscosity (the value for the reaction of **1b** in glycerol is omitted in Figure 1). In our mechanistic model (Scheme 1), an increase in solvent viscosity should favor the triplet channel as a result of a reduction in the diffusion rate limit (about 4 orders of magnitude in the viscosity range).[14] Thus the viscosity of the medium only slightly influences the diastereoselectivity of the triplet photocycloaddition (k_T) which is controlled by the geometry of the 2-oxatetramethylene triplet 1,4-biradical (^{3}OTM).[8, 11] The influence of the solvent viscosity on the diastereoselectivity of the singlet reaction, which can be estimated from the correlation (Figure 1), is more distinct.

[*] Prof. Dr. A. G. Griesbeck, S. Bondock
Institut für Organische Chemie
Universität zu Köln
Greinstrasse 4, 50939 Köln (Germany)
Fax: (+49) 221-470-5057
E-mail: griesbeck@uni-koeln.de
Priv.-Doz. Dr. M. S. Gudipati
Institut für Physikalische Chemie
Universität zu Köln
Luxemburgerstrasse 116, 50939 Köln (Germany)
Fax: (+49) 221-470-5144
E-mail: murthy.gudipati@uni-koeln.de

[**] This work was funded by the Deutsche Forschungsgemeinschaft and the Fonds der Chemischen Industrie. S.B. thanks the Egyptian government for a Ph.D. grant.

Supporting information for this article is available on the WWW under http://www.angewandte.com or from the author.

 © WILEY-VCH Verlag GmbH, D-69451 Weinheim, 2001 1433-7851/01/4024-4684 $ 17.50+.50/0

Table 1. Viscosity dependence of the diastereoselectivity of the Paternò–Büchi reaction of **2** (1M) with **1a** (1M) and **1b** (1M) at 293 K.

Solvent	η [P]	k_{diff}[a]	k'_{Diff}[b]	*endo*/*exo*[c] for **2**+**1a**	*endo*/*exo* for **2**+**1b**[d]
n-hexane	0.0033	1.8×10^{10}	2.9×10^{10}	82:18	45.3:54.7
acetonitrile	0.0036	1.6×10^{10}	2.6×10^{10}	82:18	45.3:54.7
n-heptane	0.0041	1.4×10^{10}	2.3×10^{10}	85:15	48.6:51.4
methanol	0.0060	9.8×10^{9}	1.6×10^{10}	84:16	49.6:50.4
ethanol	0.012	4.8×10^{9}	7.9×10^{9}	86:14	50.4:49.6
n-propanol	0.023	2.5×10^{9}	4.1×10^{9}	90:10	52.1:47.9
n-butanol	0.029	2.0×10^{9}	3.3×10^{9}	87:13	53.6:46.4
n-octanol	0.085	6.9×10^{8}	1.1×10^{9}	89:11	57.5:42.5
glycol	0.20	2.9×10^{8}	4.7×10^{8}	83:17	59.0:41.0
1,2-propanediol	0.56	1.0×10^{8}	1.6×10^{8}	87:13	60.5:39.5
1,4-butanediol	0.89	6.6×10^{7}	1.1×10^{8}	91:9	72.6:27.4
glycerol	15.0	3.9×10^{6}	6.3×10^{6}	[e]	80.2:19.8

[a] $k_{diff}=2\times10^{5}\,T/\eta$. [b] $k'_{Diff}=8\times RT/2000$ (ref. [12]). [c] Determined by means of NMR spectroscopic analysis of the crude product mixture (±2%). [d] Determined by means of GC analysis of the crude product mixture (±1%). [e] Could not be determined.

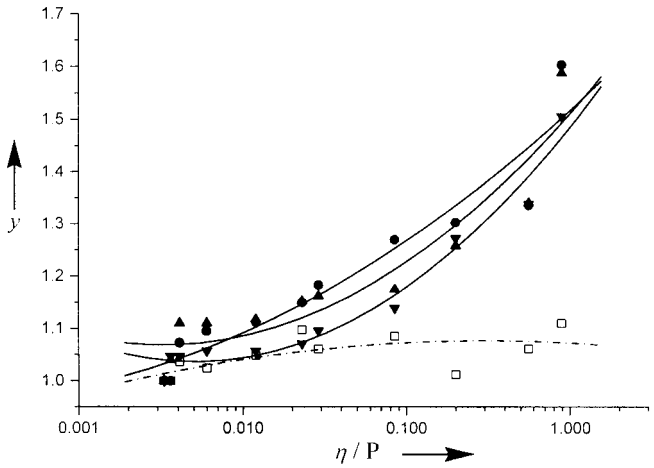


Figure 1. Viscosity dependence of the diastereoselectivity of the Paternò–Büchi reaction of **2** with **1a**–**d** (**1a**: □; **1b**: ●; **1c**: ▲; **1d**: ▼) at 293 K; y = *endo*/*exo*-diastereoselectivity (normalized to 1.0 for the lowest solvent viscosity).

The temperature dependence of the Paternò–Büchi reaction was subsequently studied in the triplet reaction between **1a** and **2**. No influence was detected, within an error margin. The concentration dependence of the Paternò–Büchi reaction at different temperatures was investigated with the standard system propionaldehyde (**1b**) and **2** in *n*-hexane (Figure 2). This substrate combination was used primarily to determine the different simple diastereoselectivities of singlet and triplet photocycloadditions.[9]

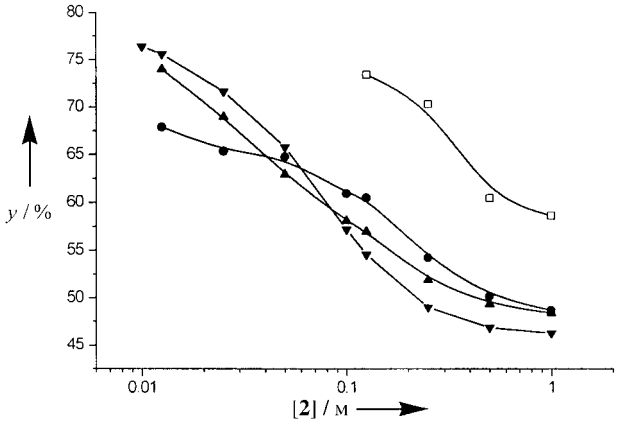


Figure 2. Concentration dependence of the Paternò–Büchi reaction of **2** with **1b** at different temperatures (+25 °C: ●; +10 °C: ▲; −14 °C: ▼; −78 °C: □) in *n*-hexane; y = *endo*-selectivity.

In the temperature region between −14 and +25 °C, the diastereoselectivity/concentration correlation showed only small changes, whereas at lower (−78 °C) temperatures the point of isospinselectivity is shifted significantly to higher concentrations. This shift is not proof for nonlinear temperature dependence, but a clear indication that not only the concentration, but also the temperature influences the diastereoselectivity of photocycloadditions with carbonyl compounds, which can react in their S_1 and T_1 states. In a next series of experiments, the temperature dependence of the *endo*/*exo*-selectivity was investigated at constant concentration (1M). The aliphatic aldehydes **1b**–**d** gave characteristic nonlinear curves with inversion points for **1c** and **1d** (Figure 3).

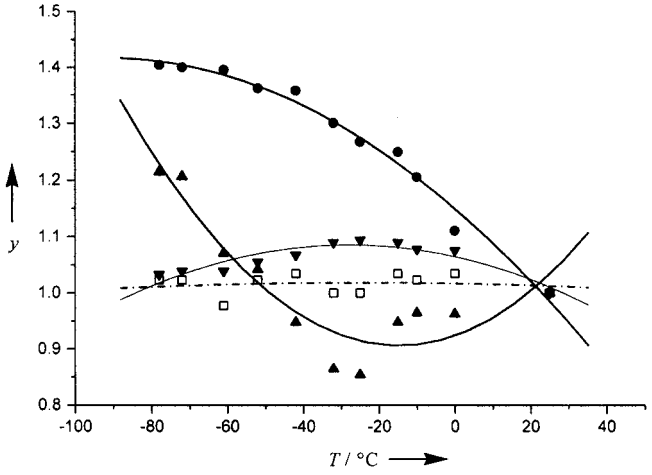


Figure 3. Temperature dependence of the Paternò–Büchi reaction of **2** with **1a**–**d** (**1a**: □; **1b**: ●; **1c**: ▲; **1d**: ▼) in *n*-hexane; y = *endo*/*exo*-diastereoselectivity (normalized to 1.0 for 23 °C).

The **1c**/**2** system shows the strongest deviation from linearity with an inversion temperature of −37 °C. For this specific reaction, we have learned from concentration studies that the acetaldehyde triplet adds to 2,3-dihydrofuran with high *endo* selectivity (up to 85%), whereas the singlet gives the same products with moderate *exo* selectivity (up to

 © WILEY-VCH Verlag GmbH, D-69451 Weinheim, 2001 1433-7851/01/4024-4685 $ 17.50+.50/0

65 %).[9] Thus, the temperature correlation can be interpreted qualitatively as follows: at room temperature under high concentration conditions, the cycloadducts **3c** were formed with low *exo* selectivity, predominantly through the singlet channel. This selectivity increases with decreasing temperature (as intuitively expected) and reaches an inversion point at $-17\,^{\circ}C$ (Figure 3). At this point, the triplet reactivity gains sufficient influence to increase the *endo* selectivity. The rate of the intersystem-crossing process (k_{ISC}) is expected to be nearly temperature independent.[15]

This selectivity reversal could be detected for the **1c**/**2** system in a temperature region that is experimentally accessible. A marginal change in activation parameter, however, catapults this effect out of the experimental window ($+40$ to $-78\,^{\circ}C$). This might have been the reason why we did not see an inversion effect in the propionaldehyde photocycloaddition. If this assumption is true, a change in substrate concentration might shift the inversion region back into the experimentally accessible range. Thus, we measured the temperature dependence of the **1b**/**2** system at 5 M (both substrates) and indeed detected an inversion point at $-27\,^{\circ}C$. Presumably, in this case an increase in concentration led to a low-temperature shift of the inversion region (Figure 4). The reverse should be observed in reactions with their inversion points at low temperatures; which could be shifted to higher temperature with concentration variation. Yet, this effect could not be verified experimentally.

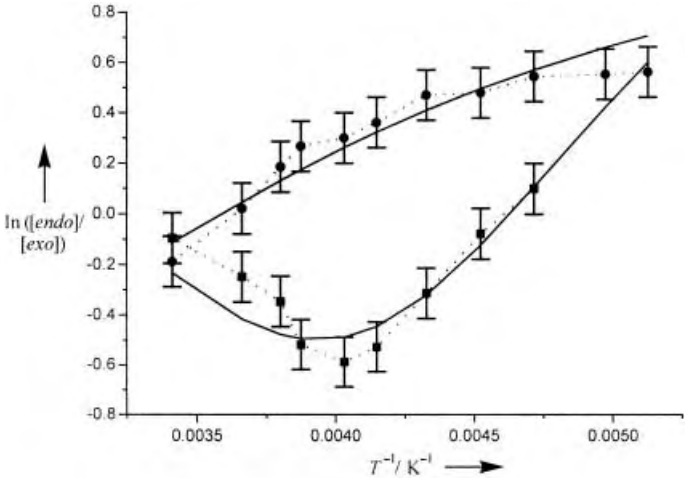


Figure 4. Plots of ln ([*endo*]/[*exo*]) versus $1/T$ for the Paternò–Büchi reaction of **2** with **1b** at concentrations of 1 M (●)and 5 M (■) in *n*-hexane.

To determine the kinetic parameters we simulated the curves shown in Figure 4. The simulations were carried out based on the following considerations: the amount of product P_j formed, which in the present case is either the *exo* or *endo* oxetane **3** from the singlet and triplet channels, is given by Equation 1 (with four channels: *exo* ($j=1$) and *endo* ($j=2$) from the singlet state, as well as *exo* ($j=3$) and *endo* ($j=4$) from the triplet state of the aldehyde).

$$P_j = A_j\, e^{\frac{-E_j}{RT}} \tag{1}$$

Because the lifetime of the S_1 state of aliphatic aldehydes is of the order of ~ 1 ns,[16] the reaction probability from the singlet channel is further restricted by molecular diffusion. Under such conditions, the photophysical deactivation processes compete with the photochemical channels. Thus in dilute solutions the probability of reaction from the singlet channel (R_S) decreases and the probability of triplet population (ϕ_T) increases. On the other hand, when the concentrations of the aldehyde and olefin are increased, though one expects reaction from the singlet channels to dominate, other processes such as collisional quenching of the excited singlet and triplet aldehyde by the ground-state aldehyde cannot be ignored. If the temperature is lowered, a diffusion-controlled decrease in the reaction from the singlet channel is expected. As a result of the $\approx$200-fold longer lifetime of the T_1 state of the aldehyde (200–400 ns)[16] the reaction probability (R_T) from the triplet channel should be less dependent on the temperature.[17] From our previous studies we know that at concentrations above 1 M, the reaction of **1b** and **2** takes place only through the singlet channel at room temperature.[18] Normalized temperature-dependent reaction probabilities from the singlet and triplet channels with respect to room temperature (300 K) can be approximated by Equations 2a and b. The exponent n reflects the nonlinearity of the temperature-dependent contributions from molecular diffusion, viscosity, and concentration.[19]

$$R_S = (T/300\ \mathrm{K})^n \tag{2a}$$

$$R_T = (1 - R_S)\phi_T \tag{2b}$$

From the concentration studies at 300 K, we know the *endo*/*exo* ratios for pure singlet and triplet channels.[9] By using this information we can reduce the number of parameters according to Equations 3 and 4.

$$S^{300\mathrm{K}}_{endo/exo} = \frac{P_2}{P_1} = \frac{A_2}{A_1}\, e^{\frac{-(E_2 - E_1)}{300\mathrm{K}\,R}} \tag{3}$$

$$E_1 = E_2 + 300\mathrm{K}\,R \ln\left(\frac{S^{300\,\mathrm{K}}_{endo/exo} A_1}{A_2}\right) \tag{4}$$

For the triplet channel, the corresponding Equation 5 is used.

$$E_3 = E_4 + 300\,\mathrm{K}\,R \ln\left(\frac{S^{300\,\mathrm{K}}_{endo/exo} A_3}{A_4}\right) \tag{5}$$

Thus, the temperature-dependent overall *endo*/*exo* ratio Σ is given by Equation 6.

$$\Sigma^{T}_{endo/exo} = \frac{R_S P_2 + (1 - R_S)\phi_T P_4}{R_S P_1 + (1 - R_S)\phi_T P_3} \tag{6}$$

The *endo*/*exo* selectivity was simulated with the use of these eight parameters for 1-M and 5-M concentrations of the aldehyde and dihydrofuran (Figure 4).

The reliability of the present simulations (notwithstanding the large number of parameters) comes from the fact that after fitting the experimental data from 5-M solutions, all the other parameters were fixed, and only n and ϕ_T were varied to simulate the curve for the 1-M data. It should be noted that these variable parameters are not independent, but are highly correlated with each other.[20] The "selectivity inversion" can

 © WILEY-VCH Verlag GmbH, D-69451 Weinheim, 2001 1433-7851/01/4024-4686 $ 17.50+.50/0

be interpreted qualitatively: the activation barrier for the formation of the *exo* product (E_1) from the singlet channel is much smaller than for the formation of the *endo* product. However, the pre-exponential factor for the *endo* product is larger than for the *exo* product. With decreasing temperature, the exponential part dominates and more *exo* than *endo* product is formed.

The situation is completely different for triplet channel: the formation of both the *endo* and *exo* products has almost no barrier, whereas the pre-exponential factors favor the formation of the *endo* product. As a result of the lack of activation barrier for both the products, the *endo*/*exo* ratio from the triplet channel should not be temperature dependent. This has been proved experimentally in the case of the photocycloaddition of **1a** with **2** (see Supporting Information). If the reaction probabilities R_S and R_T were not temperature dependent, then no "selectivity inversion" would be observed. The temperature-dependent reaction probabilities R_S and R_T are reflected in the values n and ϕ_T. At the higher concentration (5 M), n is large, thus reflecting a faster decrease in the reaction probability (R_S) from the singlet channel. This may be caused by quenching of the excited singlet aldehyde molecule by the ground-state aldehydes. Similarly, the relative triplet quantum yield (ϕ_T) is very small, which implies that at higher concentrations the majority of the excited singlet aldehyde molecules react or are deactivated. At the lower concentration (1 M), n is small and R_S decreases less steeply with temperature and $(1 - R_S)$ increases correspondingly from the initial value of 0 at 300 K. Simultaneously, the relative triplet population ϕ_T is predicted to be close to 1.0. Thus, both singlet and triplet channels compete with each other at 1 M concentration. With decreasing temperature, the triplet contribution increases. As a result of the larger *endo*/*exo* selectivity from the triplet channels (5.6)[9] with decreasing temperature, the total *endo*/*exo* ratio increases steadily.

The simulations do not indicate an abrupt change in the selectivity correlation as is the case in isoinversion curves,[1] but an inversion region as described by Hale and Ridd.[7] From our model we expect this inversion region to lie outside the experimental window for many substrate combinations, either in photochemical or thermal reactions. Thus, inversion phenomena might often be overlooked. Variations of the substrate concentrations, however, change the inversion region strongly and represent an additional method of shifting the "inversion point" into the experimental region.

Received: June 21, 2001 [Z17334]

[1] H. Buschmann, H.-D. Scharf, N. Hoffmann, M. W. Plath, J. Runsink, *J. Am. Chem. Soc.* **1989**, *111*, 5367 – 5373.

[2] A contrasting behavior was described for aromatic acyl cyanides: C. Zagar, H. D. Scharf, *Chem. Ber.* **1991**, *124*, 967 – 969.

[3] a) S. C. Freilich, K. S. Peters, *J. Am. Chem. Soc.* **1981**, *103*, 6255 – 6257; b) R. A. Caldwell, T. Majima, C. Pac, *J. Am. Chem. Soc.* **1982**, *104*, 629 – 630; c) S. C. Freilich, K. S. Peters, *J. Am. Chem. Soc.* **1985**, *107*, 3819 – 3822. Concerning the customary terminology, the ISI Citation Database lists (1993 to 2001) 1240 references for "biradical" and 886 references for "diradical".

[4] a) N. Braussand, N. Hoffmann, H.-D. Scharf, *Tetrahedron* **1997**, *53*, 14701 – 14712; b) J. Muzart, F. Hénin, J.-P. Pète, A. M'Boungou-M'Passi, *Tetrahedron: Asymmetry* **1993**, *4*, 2531 – 2534; c) J. Muzart, F. Hénin, S. J. Aboulhoda, *Tetrahedron: Asymmetry* **1997**, *8*, 381 – 389; d) T. Bach, K. Jödicke, *Chem. Ber.* **1993**, *126*, 2457 – 2466; e) D. Becker, Y. Cohen-Arazi, *J. Am. Chem. Soc.* **1996**, *118*, 8278 – 8284.

[5] a) H. Buschmann, H.-D. Scharf, N. Hoffmann, P. Esser, *Angew. Chem.* **1991**, *103*, 480 – 518; *Angew. Chem. Int. Ed. Engl.* **1991**, *30*, 477; b) D. Heller, H. Buschmann, H.-D. Scharf, *Angew. Chem.* **1996**, *108*, 1964 – 1967; *Angew. Chem. Int. Ed. Engl.* **1996**, *35*, 1852 – 1854; c) A. Wiegers, H.-D. Scharf, *Tetrahedron: Asymmetry* **1996**, *7*, 2303 – 2312; d) M. A. MeyerStork, D. Haag, H.-D. Scharf, *J. Chem. Soc. Perkin Trans. 2* **1997**, 593 – 595; e) T. Göbel, K. B. Sharpless, *Angew. Chem.* **1993**, *105*, 1417 – 1418; *Angew. Chem. Int. Ed. Engl.* **1993**, *32*, 1329 – 1331; f) G. Cainelli, D. Giacomini, P. Galletti, *Chem. Commun.* **1999**, 567 – 572.

[6] L. Liu, Q.-X. Guo, *Chem. Rev.* **2001**, *101*, 673 – 695.

[7] K. J. Hale, J. H. Ridd, *J. Chem. Soc. Chem. Commun.* **1995**, 357 – 358.

[8] A. G. Griesbeck, H. Mauder, S. Stadtmüller, *Acc. Chem. Res.* **1994**, *27*, 70 – 76.

[9] A. G. Griesbeck, M. Fiege, S. Bondock, M. S. Gudipati, *Org. Lett.* **2000**, *2*, 3623 – 3625.

[10] I. J. Palmer, I. N. Ragazos, F. Bernardi, M. Olivucci, M. A. Robb, *J. Am. Chem. Soc.* **1994**, *116*, 2121 – 2132.

[11] A. Kutateladze, *J. Am. Chem. Soc.* **2001**, *123*, 9279 – 9282.

[12] The η-values were taken from a publication on the photodenitrogenation of azoalkanes: W. Adam, V. Marti, C. Sahin, A. V. Trofimov, *J. Am. Chem. Soc.* **2000**, *122*, 5002 – 5003.

[13] Changes in solvent polarity do not influence the simple diastereoselectivity; however, they strongly change the regioselectivity of the Paternò – Büchi reaction: A. G. Griesbeck, S. Buhr, M. Fiege, H. Schmickler, J. Lex, *J. Org. Chem.* **1998**, *63*, 3847 – 3854.

[14] This is obtained by using the Debye equation: $k_{diff} = 2 \times 10^5\, T/\eta$: P. Debye, *Trans. Electrochem. Soc.* **1942**, *82*, 265; or alternatively by using the modified equation: $k'_{Diff.} = 8 \times RT/2000\eta$. See also: P. J. Wagner, I. Kochevar, *J. Am. Chem. Soc.* **1968**, *90*, 2232 – 2238.

[15] For ISC of azoalkanes, see: M. H. Chang, D. A. Dougherty, *J. Am. Chem. Soc.* **1982**, *104*, 2333 – 2334; N. J. Turro, C. A. Renner, W. H. Waddell, T. J. Katz, *J. Am. Chem. Soc.* **1976**, *98*, 4320 – 4322; for ISC of aromatic hydrocarbons, see: J. B. Birks in *Organic Molecular Photophysics* (Ed.: J. B. Birks), Wiley, New York, **1973**, pp. 39 – 45.

[16] J. Kossanyi, S. Sabbah, P. Chaquin, J. C. Ronfart-Haret, *Tetrahedron* **1981**, *37*, 3307 – 3315.

[17] The quantum yield for the "pure" triplet reaction of **1a** with **2** was determined by means of valerophenone actinometry (benzene; extrapolation to 0% conversion): $\phi = 0.48$; see: P. J. Wagner, A. E. Kemppainen, *J. Am. Chem. Soc.* **1972**, *94*, 7495 – 7499; for applications to Paternò – Büchi reactions, see: M. Abe, E. Torii, M. Nojima, *J. Org. Chem.* **2000**, *65*, 3426 – 3431.

[18] The Stern – Volmer analysis of the fluorescence quenching of propionaldehyde by 2,3-dihydrofuran resulted in $k_q = 2.2 \times 10^9\,M^{-1}s^{-1}$ with $\tau(S_1) = 1.8 \times 10^{-9}$ s.

[19] Attempts to express this dependence numerically led to less accurate results as a result of an increase in the number of unknown parameters.

[20] Parameters for simulation of the reaction of **2** with **1b**: $E_1 = 157$, $E_2 = 8992$, $E_3 = -12.5$, and $E_4 = 5.8\,J\,mol^{-1}$; $A_1 = 0.054$, $A_2 = 1.599$, $A_3 = 0.057$, $A_4 = 0.327$; at 5 M: $n = 8.99$, $\phi_T = 0.0079$; at 1 M: $n = 0.88$, $\phi_T = 0.9975$. Only relative values for the preexponential factors resulted from the simulation.

 © WILEY-VCH Verlag GmbH, D-69451 Weinheim, 2001 1433-7851/01/4024-4687 $ 17.50+.50/0

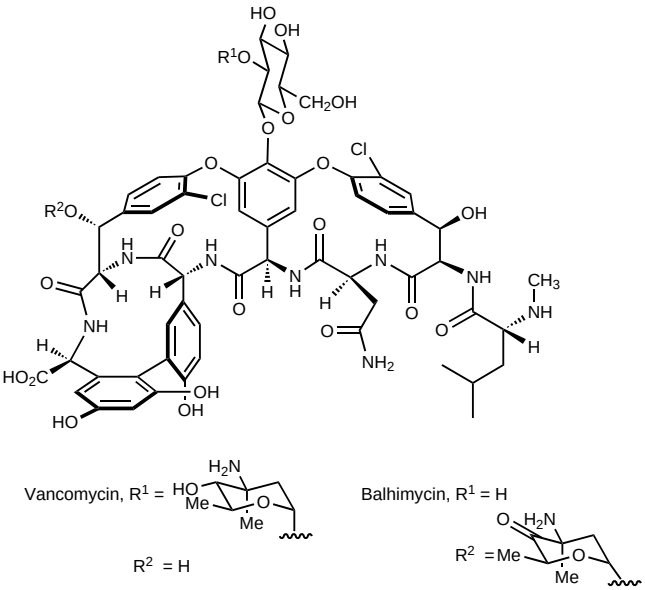
The Biosynthesis of Vancomycin-Type Glycopeptide Antibiotics—The Order of the Cyclization Steps**

Daniel Bischoff, Stefan Pelzer, Bojan Bister, Graeme J. Nicholson, Sigrid Stockert, Markus Schirle, Wolfgang Wohlleben, Günther Jung, and Roderich D. Süssmuth*

Dedicated to Professor K. Barry Sharpless on the occasion of his 60th birthday

Vancomycin (Scheme 1),[1] a glycopeptide antibiotic produced by *Amycolatopsis orientalis*, is the most prominent representative of a family comprising several hundred natural products with common structural features. A tremendous amount of work has been focused on the elucidation of its structure, mode of action, and on the total synthesis.[1, 2] The potency of vancomycin against methicillin-resistant *Staphylococcus aureus* strains (MRSA) has led to its widespread application as an antibiotic of last resort.[3] Until recently, little work has been done on the molecular biology of the glycopeptide biosynthesis, with the exception of a few biochemical studies.[4] The sequencing of the chloroeremomycin biosynthesis gene cluster of *A. orientalis* provided first insights into the genes participating in the glycopeptide biosynthesis.[5] However, the nature and sequence of many essential biosynthesis steps and the structures of biosynthesis intermediates remained unknown. The identification of the balhimycin gene cluster in *A. mediterranei*[6] and the development of a host–vector system for the balhimycin producer[7] enables the biosynthesis to be manipulated for the first time.

Our work addresses the question of how nature assembles the unique aglycon structure. This moiety confers antibiotic activity and its assembly thus represents a key step in the glycopeptide antibiotic biosynthesis. Therefore, we focused our attention on three oxygenases (OxyA, OxyB, and OxyC) in the glycopeptide biosynthesis gene cluster of the balhimycin producer *A. mediterranei DSM5908*. These are presumably involved in the three oxidation steps leading from a linear precursor peptide to the side chain cyclized aglycon.



Scheme 1. Structures of the glycopeptide antibiotics vancomycin and balhimycin.

From an integration mutant within the oxygenase region we characterized hexa- and heptapeptides, which we suggested to be linear intermediates of the aglycon.[6, 8] In a subsequent study we isolated the first monocyclic peptides from a gene replacement mutant in the *oxyA* gene, the ring closure of which possibly represents the first step in the three oxidative bridging reactions.[9] Herein, we report the first bicylic peptides. These structures allow us to deduce the sequence of the three oxidative bridging steps of the aromatic side chains leading to the formation of the aglycon.

From the culture filtrate of a gene replacement mutant SPoxyBcat (Figure 1), two compounds, SP-901 (**1**) and SP-1066 (**2**) with molecular masses of 901.3 and 1066.4 Da, respectively, were isolated. Full structural analysis showed that they were the linear dechlorinated analogues of compounds previously described (Scheme 2).[8]

From the culture filtrate of a second gene replacement mutant SPoxyCcat of *A. mediterranei* (Figure 1), three compounds SP-911 (**3**), SP-1073 (**4**), and SP-1238 (**5**) with molecular masses of 911.3, 1073.4, and 1238.4 Da, respectively, were isolated (Scheme 3). As in the case of compounds **1** and **2**, the isotopic pattern of the $[M+H]^+$ signals of compounds **3**–**5** indicated the absence of chlorine atoms. By means of chiral amino acid analysis, D-*N*-methylleucine (MeLeu), L-Asx, and D-4-hydroxyphenylglycine (Hpg) were identified as constituents for all compounds. In the case of compound **5**, L-3,5-dihydroxyphenylglycine (Dpg) was detected additionally. Edman degradation of compounds **3**–**5** gave the sequence ^{1}MeLeu-^{2}-———-^{3}Asn-^{4}-———-^{5}Hpg-^{6}-———.

[*] Dr. R. D. Süssmuth,[+] D. Bischoff, B. Bister, G. J. Nicholson, Prof. Dr. G. Jung
Institut für Organische Chemie
Universität Tübingen
Auf der Morgenstelle 18, 72076 Tübingen (Germany)
Fax: (+49) 7071-29-5560
E-mail: roderich.suessmuth@uni-tuebingen.de
Dr. S. Pelzer, S. Stockert, Prof. Dr. W. Wohlleben
Institut für Mikrobiologie/Biotechnologie
Universität Tübingen
Auf der Morgenstelle 28, 72076 Tübingen (Germany)
Dr. M. Schirle
Institut für Zellbiologie, Abtl. Immunologie
Universität Tübingen
Auf der Morgenstelle 15, 72076 Tübingen (Germany)
[+] Present address:
Department of Molecular Biology
The Scripps Research Institute
10550 North Torrey Pines Road
La Jolla, CA 92037 (USA)

[**] This work was supported by the Deutsche Forschungsgemeinschaft (SFB 323) and by a grant of the EU (MEGATOP, QLK3-1999-00650). R. D. S. gratefully acknowledges the support of a Feodor-Lynen Fellowship granted by the Alexander-von-Humboldt Stiftung. We thank Corina Bihlmaier and Volker Pfeifer for help with transformation and Southern hybridization, J. A. Moss (La Jolla (USA)) for critical comments on the manuscript and Prof. Dr. M. E. Maier and Prof. Dr. H.-P. Fiedler (Tübingen) for generous support.

 © WILEY-VCH Verlag GmbH, D-69451 Weinheim, 2001 1433-7851/01/4024-4688 $ 17.50+.50/0

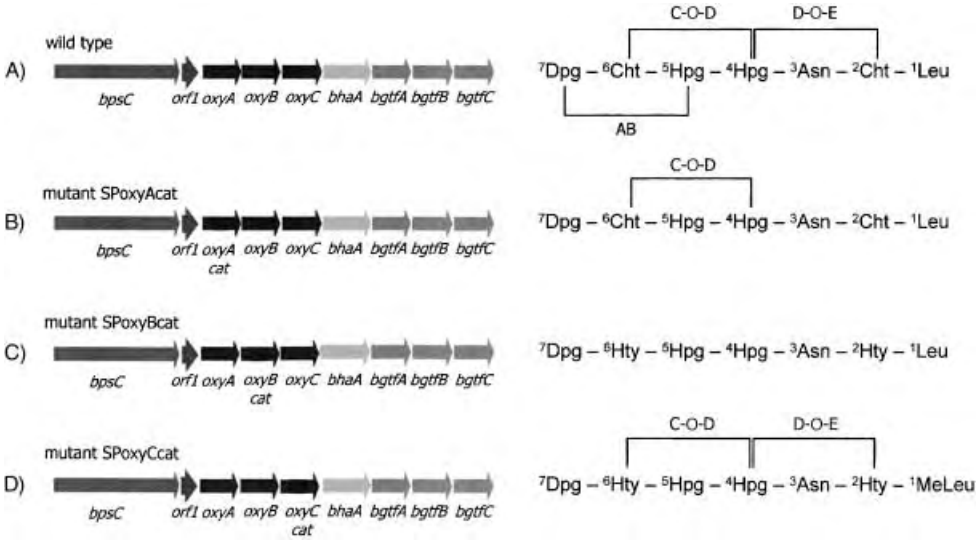
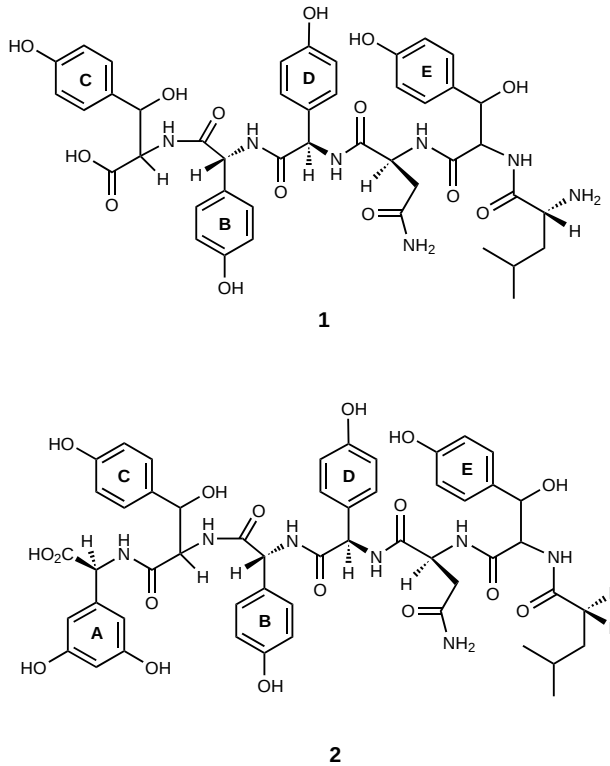
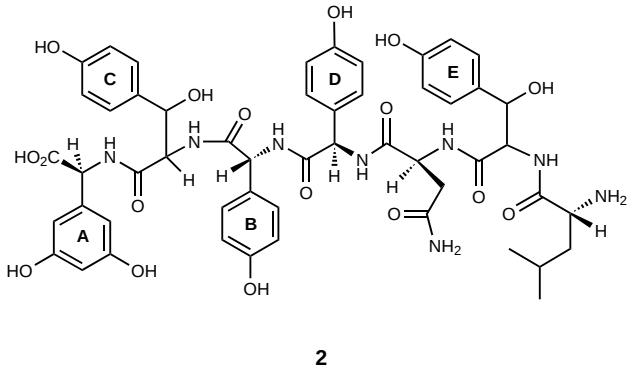


Figure 1. Gene organization of *A. mediterranei* wild type strains and of the corresponding mutants. The degree of cyclization is shown schematically for the example of the characterized heptapeptides. A) Gene organization of a part of the balhimycin biosynthetic gene cluster from *A. mediterranei* wild type. B) *oxyA* gene replacement mutant SPoxyAcat. C) *oxyB* gene replacement mutant SPoxyBcat. D) *oxyC* gene replacement mutant SPoxyCcat. *bpsC*: peptide synthetase gene; *orf1*: Orf with unknown function; *oxyA – C*: oxygenase genes; *bhaA*: halogenase gene; *bgtfA – C*: glycosyltransferase genes. *cat*: chloramphenicol resistance gene; Hty = β-hydroxytyrosine).



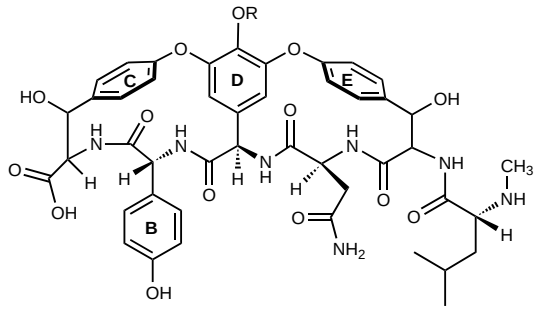
1



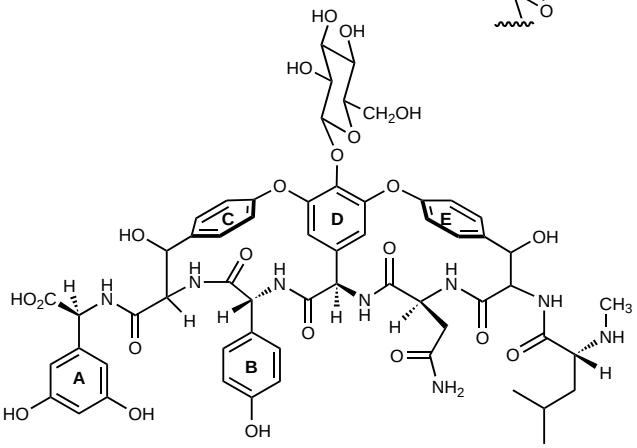
2

Scheme 2. Structures of SP-901 (**1**) and SP-1066 (**2**).

Curiously, Dpg did not appear in cycle 7 of Edman degradation of compound **5**. In accordance with previous data obtained by Edman degradation of SP-1134 (linear) and SP-1132 (monocyclic),[8, 9] cyclization of the C-O-D and the D-O-E ring systems was found for **3** – **5** (Table 1). Sugar analysis by GC-MS revealed D-glucose for compounds **4** and **5**. 2D-NMR experiments (COSY, TOCSY, NOESY, HSQC, HMBC) on **5** (Table 2) confirmed these results and revealed the structure of **5**[10] with β-glycosylation at ^{4}Hpg as shown in Scheme 3.



3 R=H **4** R=



5

Scheme 3. Structures of SP-911 (**3**), SP-1073 (**4**), and SP-1238 (**5**).

Compounds **1** – **5** as well as those characterized in previous studies[8, 9] all contain β-hydroxylated tyrosine groups at positions 2 and 6. This confirms our former suggestion that

Table 1. Results of Edman degradation of intermediates isolated from different *A. mediterranei* mutants.

Peptide	Degradation cycle[a]						
	1	2	3	4	5	6	7
SP-1134[b]	Leu	Cht	Asn	Hpg	Hpg	Cht	Dpg
SP-1132[c]	Leu	Cht	Asn	–	Hpg	–	Dpg
SP-1238[d]	MeLeu	–	Asn	–	Hpg	–	n.d.
Aglycon	MeLeu	–	Asn	–	–	–	–

[a] – = no amino acid identified; n.d. = assignment ambiguous. [b] Linear heptapeptide SP-1134.[8] [c] Monocyclic heptapeptide SP-1132.[9] [d] Newly identified bicyclic heptapeptide SP-1238.

β-hydroxylation is already present at the linear precursor-peptide stage. In contrast to the linear and the monocyclic peptide intermediates, the bicyclic metabolites **3**–**5** isolated from culture filtrates of SPoxyCcat are N-methylated at ^{1}Leu. These data also show that the early formed bicylic C-O-D-O-E ring intermediate is subject to N-methylation. The results are in accordance with the enzyme assays of the overexpressed *N*-methyltransferase of *A. orientalis*, which showed that the demethylated aglycon and demethylated glycopeptides are clearly favored over linear peptides for the N-methylation.[11] Similarly, the O-glycosylation of ^{4}Hpg in **4** and **5** (β-D-Glc), as found in balhimycin, shows that the bicyclic C-O-D-O-E system is already recognized by a glycosyltransferase of the balhimycin biosynthesis gene cluster. In contrast to the chlorinated peptides from the SPoxyAcat mutant, the unexpected absence of chlorine in peptides **1**–**5**, which were isolated from SPoxyBcat and SPoxyCcat, cannot be explained at the current stage of our investigations. It is conceivable that gene replacement of *oxyB* and *oxyC* also affected expression of *bhaA* which codes for the respective halogenase[12] and which is located directly downstream. Furthermore, it is still unknown why hexapeptides can be isolated, as already shown for the postulated linear biosynthesis precursors.[8]

Finally, the inactivation of oxygenase genes (*oxyA*, *oxyB*, *oxyC*) through replacement mutants reveals peptides with different degrees of cyclization (Figure 1). According to these results, that is the characterization of compounds **1**–**5**, and those described in our previous contribution,[9] we postulate the order of the cyclization steps as follows: 1. Formation of the C-O-D ring system; 2. Formation of the D-O-E ring system; 3. Formation of the biaryl AB system. Thus, the oxygenases act in a stepwise fashion in the sequence OxyB $\rightarrow$OxyA $\rightarrow$OxyC.

The N-methylation of Leu as well as the glycosylation at ^{4}Hpg can partially occur already at the stage of the bicylic intermediate as indicated by the occurrence of compounds **3**–**5** and **4**, **5**, respectively. Since glycosylation in position 6 is not observed, glycosylation at ^{4}Hpg by a glycosyltransferase is considered to be the first step in the glycosylation sequence. These results indicate a relaxed substrate specificity of the participant enzymes and are in agreement with the known biochemical action of the enzymes methyltransferase (Mtf)[11] and glycosyltransferase (Gtf)[13] in the chloroeremomycin and vancomycin gene cluster. We assume that the sequence of the aglycon assembly is representative for type-I and type-II glycopeptide antibiotics.

Experimental Section

The mutants SPoxyBcat and SPoxyCcat of *Amycolatopsis mediterranei DSM5908* were grown in liquid culture. All peptides were purified (yields SPoxyBcat: 8.6 mg L^{-1} (**1**), 10.6 mg L^{-1} (**2**); yields SPoxyCcat: 1.2 mg L^{-1} (**3**), 0.8 mg L$^-$ (**4**), and 0.5 mg L^{-1} (**5**)) and analyzed according to procedures described previously.[8, 9]

Received: July 12, 2001 [Z17490]

[1] a) M. K. McCormick, W. M. Stark, G. E. Pittenger, R. C. Pittenger, G. M. McGuire, *Antibiot. Annu.* **1955**–**1956**, 606–611; b) G. M. Sheldrick, P. G. Jones, O. Kennard, D. H. Williams, G. A. Smith, *Nature* **1978**, *271*, 223–225; c) P. J. Loll, A. E. Bevivino, B. D. Korty, P. H. Axelson, *J. Am. Chem. Soc.* **1997**, *119*, 1516–1522; d) C. M. Harris, H. Kopecka, T. M. Harris, *J. Am. Chem. Soc.* **1983**, *105*, 6915–6922; e) S. G. Grdadolnik, P. Pristovsek, D. F. Mierke, *J. Med. Chem.* **1998**, *41*, 2090–2099.

Table 2. ^{1}H and ^{13}C NMR shifts of the peptide SP-1238 (**5**) ([D6]DMSO, 298 K).

		NH, CO	α	β	Others		
^{1}Leu	$\delta(^1$H)	8.93	4.00	1.68/1.57	1.64 (γ), 0.86/0.90 (δ), 2.63 (NCH$_3$)		
	$\delta(^{13}$C)	167.6	59.2	38.7	23.6 (γ), 22.5/22.2 (δ), 31.0 (NCH$_3$)		
^{2}Hty	$\delta(^1$H)	8.62	4.90	5.23	5.86 (OH$^\gamma$), 7.60 (2), 7.22 (3), 7.06 (5), 7.25 (6)		
	$\delta(^{13}$C)	–[a]	58.8	71.2	136.8 (1), 127.5 (2), 154.7 (4), 122.2 (3), 121.2 (5), 128.1 (6)		
^{3}Asn	$\delta(^1$H)	–[a]	4.34	2.58/2.19	7.53/7.07 (δ)		
	$\delta(^{13}$C)	169.7	50.3	36.0	171.5 (γ)		
^{4}Hpg	$\delta(^1$H)	8.00	5.21	–	5.49 (2), 5.78 (6)		
	$\delta(^{13}$C)	166.8	54.7	–	106.3 (2), 132.1 (1), 152.9 (3), 156.4 (4), –[a] (5), 106.6 (6)		
^{5}Hpg	$\delta(^1$H)	8.80	5.18	–	7.11 (2,6), 6.68 (3,5), 9.44 (OH^4)		
	$\delta(^{13}$C)	168.4	55.6	–	128.1 (2,6), 114.8 (3,5), 158.4 (4), –[a] (1)		
^{6}Hty	$\delta(^1$H)	–[a]	4.75	5.44	5.65 (OH$^\gamma$), 7.37 (2), 7.06 (3), 7.16 (5), 7.55 (6)		
	$\delta(^{13}$C)	167.8	58.8	71.0	138.2 (1), 127.6 (2), 121.2 (3), 153.4 (4), 121.9 (5), 126.4 (6)		
^{7}Dpg	$\delta(^1$H)	8.73	5.15	–	6.28 (2,6), 9.35 (OH^{3,5}), 6.15 (4)		
	$\delta(^{13}$C)	171.7	55.9	–	105.2 (2,6), 158.1 (3,5), 101.9 (4), –[a] (1)		
Glc		1′	2′	3′	4′	5′	6′
	$\delta(^1$H)	5.18	3.34	3.26	3.16	3.18	3.72/3.46
	$\delta(^{13}$C)	102.6	73.7	76.3	69.8	77.1	60.8
OH	$\delta(^1$H)	–	–[a]	–[a]	–[a]	–	–[a]

[a] Assignment not determined. Hty = β-hydroxytyrosine.

 © WILEY-VCH Verlag GmbH, D-69451 Weinheim, 2001 1433-7851/01/4024-4690 $ 17.50+.50/0

[2] a) D. H. Williams, B. Bardsley, *Angew. Chem.* **1999**, *111*, 1264 – 1286; *Angew. Chem. Int. Ed.* **1999**, *38*, 1172 – 1193; b) K. C. Nicolaou, C. N. C. Boddy, S. Bräse, N. Winssinger, *Angew. Chem.* **1999**, *111*, 2230 – 2287; *Angew. Chem. Int. Ed.* **1999**, *38*, 2096 – 2152.
[3] R. C. Yao, L. W. Crandall in *Glycopeptide Antibiotics* (Ed.: R. Nagarajan), Marcel Dekker, New York, **1994**, pp. 1 – 21.
[4] a) S. J. Hammond, M. P. Williamson, D. H. Williams, L. D. Boeck, G. G. Marconi, *J. Chem. Soc. Chem. Commun.* **1982**, 344 – 346; b) S. J. Hammond, D. H. Williams, R. V. Nielsen, *J. Chem. Soc. Chem. Commun.* **1983**, 116 – 117.
[5] A. M. A. van Wageningen, P. N. Kirkpatrick, D. H. Williams, B. R. Harris, J. K. Kershaw, N. J. Lennard, M. Jones, S. J. M. Jones, P. J. Solenberg, *Chem. Biol.* **1998**, *5*, 155 – 162.
[6] a) The sequences of *oxyA*, *oxyB*, and *oxyC* have been deposited as part of the balhimycin biosynthesis gene cluster at the EMBL-GenBank under accession number Y16952; b) S. Pelzer, R. Süssmuth, D. Heckmann, J. Recktenwald, P. Huber, G. Jung, W. Wohlleben, *Antimicrob. Agents Chemother.* **1999**, 1565 – 1573.
[7] S. Pelzer, W. Reichert, M. Huppert, D. Heckmann, W. Wohlleben, *J. Biotechnol.* **1997**, *56*, 115 – 128.
[8] R. D. Süssmuth, S. Pelzer, G. Nicholson, T. Walk, W. Wohlleben, G. Jung, *Angew. Chem.* **1999**, *111*, 2096 – 2099; *Angew. Chem. Int. Ed.* **1999**, *38*, 1976 – 1979.
[9] D. Bischoff, S. Pelzer, A. Höltzel, G. J. Nicholson, S. Stockert, W. Wohlleben, G. Jung, R. D. Süssmuth, *Angew. Chem.* **2001**, *113*, 1736 – 1739; *Angew. Chem. Int. Ed.* **2001**, *40*, 1693 – 1696.
[10] The ^{1}H NMR signals of the C-O-D and of the D-O-E ring were assigned according to diagnostic NOE interactions given in the Supplementary Material of:D. L. Boger, S. Miyazaki, O. Loiseleur, R. T. Beresis, S. L. Castle, J. H. Wu, Q. Jing, *J. Am. Chem. Soc.* **1998**, *120*, 8920 – 8926.
[11] D. P. O'Brian, P. N. Kirkpatrick, S. W. O'Brian, T. Staroske, T. I. Richardson, D. A. Evans, A. Hopkinson, J. B. Spencer, D. H. Williams, *Chem. Commun.* **2000**, 103 – 104.
[12] "Nucleic acid fragment and vector containing halogenase and method for the halogenation of chemical compounds": S. Pelzer, P. Huber, R. Süßmuth, J. Recktenwald, D. Heckmann, W. Wohlleben, Patent Wo 00/77182A1, **2000**.
[13] H. C. Losey, M. W. Peczuh, Z. Cheng, U. S. Eggert, S. D. Dong, I. Pelczer, D. Kahne, C. T. Walsh, *Biochemistry* **2001**, *40*, 4745 – 4755.

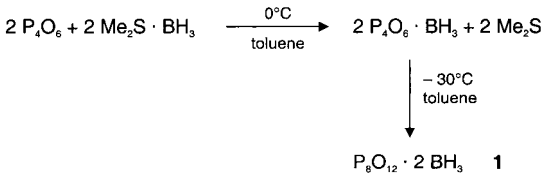
Dimerization of Molecular Phosphorus Oxides

Akbar Tellenbach und Martin Jansen*

Highly symmetric, spatially closed molecular compounds are frequently much less willing to undergo reactions. Such inhibition of a reaction based on its kinetics may have considerable effects in the most diverse fields in chemistry. For instance, in chemical transport reactions involving SiF_4 as a component of the gas phase, the thermodynamically calculated transport rates are not reproduced experimentally, because the reaction back to the solid is strongly inhibited.[1] In addition, SF_6 or CCl_4 are stable towards water at room temperature, although in view of the thermodynamics they should undergo vigorous hydrolysis.[2]

In this respect P_4O_6 appears particularly ambivalent, on the one hand it adds smoothly as donor ligand or reacts rapidly with water giving phosphonic acid, on the other hand it is remarkably resistant to directed ring-opening reactions. Among the few controlled and selective reactions on the adamantane-like P_4O_6 cage are the nitrene insertion[3] and several alcoholyses.[4] In view of this, the observation reported herein of a spontaneous dimerization of the monoborane adduct of P_4O_6 without the need for special activation was unexpected.

In the attempt to crystallize $P_4O_6 \cdot BH_3$,[5, 6] which forms in the stoichiometric reaction of P_4O_6 with $Me_2S \cdot BH_3$, at $-30\,^\circ C$ in a concentrated toluene solution, we obtained instead the dimer $P_8O_{12} \cdot 2BH_3$ (**1**) as crystalline material (Scheme 1). After three months single crystals had formed which were suitable for a crystal structure analysis.[7]



Scheme 1. Synthesis of **1**.

The principal building block of **1** is a novel P_8O_{12} framework, which evidently originates from the fusion of two P_4O_6 cages after cleavage of one P–O bond in each cage. As shown in Figure 1, two $P_4O_6 \cdot BH_3$ units were connected through two common oxygen atoms (O1, O7) in such a manner that the borane groups point in opposite directions (head – tail linkage). The dimer is folded along the two bridging oxygen atoms, resulting in dihedral angles of 151° (P1-O1-O7-P5) and 164° (P4-O7-O1-P8), respectively. The different dihedral

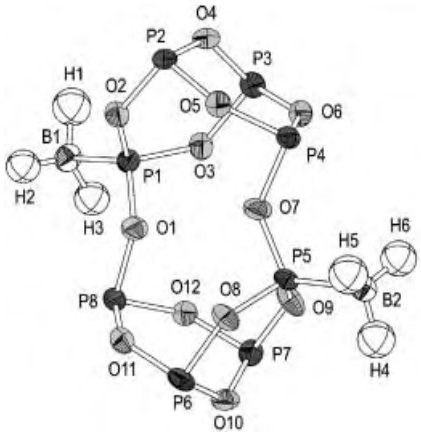


Figure 1. Molecular structure of **1** (ellipsoids for 50% probability). Selected bond lengths [pm] and angles [°]: P1-B1 187.2(2), P1-O1 158.0(2), P1-O2 158.9(2), P1-O3 158.5(2), P2-O2 166.5(2), P2-O4 163.7(2), P2-O5 162.7(2), P3-O3 166.0(2), P3-O4 163.9(2), P3-O6 162.4(2), P4-O5 162.5(2), P4-O6 163.2(2), P4-O7 165.6(2), B1-H1 113(4), B1-H2 101(3), B1-H3 119(3); O1-P1-O2 102.1(1), O1-P1-O3 103.2(1), O2-P1-O3 104.6(1), P1-O1-P8 126.8(1), P1-O2-P2 131.5(1), P1-O3-P3 135.4(1), P2-O4-P3 126.6(1), H1-B1-H2 111(3), H1-B1-H3 117(2), H2-B1-H3 118(2).

[*] Prof. Dr. M. Jansen, Dipl.-Chem. A. Tellenbach
Max-Planck-Institut für Festkörperforschung
Heisenbergstrasse 1, 70569 Stuttgart (Germany)
Fax: (+49) 711-689-1502
E-mail: martin@jansen.mpi-stuttgart.mpg.de

 © WILEY-VCH Verlag GmbH, D-69451 Weinheim, 2001 1433-7851/01/4024-4691 $ 17.50+.50/0

angles reflect an additional twisting about the O4 – O10 axis, which reduces the molecular symmetry to C_1. The P–O bond lengths vary between 157.8 and 167.1 pm and thus lie in the expected range for P–O single bonds. As in the monosubstituted P_4O_6 derivatives P_4O_7,[8] P_4O_6S,[9] and P_4O_6Se, [10] starting from the four-coordinate (pentavalent) phosphorus atom an alternating shortening and lengthening of the P–O bond lengths is observed compared to those in the unsubstituted P_4O_6 molecule (P–O bond lengths 165.3 pm[11]): Looking from P1 or P5, respectively, the first P–O bond lengths are on average 158.3, the second ones 166.3, and the subsequent ones 162.9 pm. The O-P-O bond angles vary between 95.3 and 104.7°; those at the boron-bearing phosphorus atoms tend to be larger than those at the three-coordinate phosphorus atoms. The B-P-O bond angles range between 112.5 and 118.2°, the P-O-P bond angles between 126.6 and 138.6°. The B–P bond lengths (187.2 and 186.8 pm, respectively) are somewhat shorter than those of comparable borane – phosphite adducts $(RO)_3P \cdot BH_3$ (187.9 – 189.5 pm;[12] R = organic group).

The colorless crystals of **1** are stable at room temperature and inert conditions, but decompose in the presence of moist air with vigorous evolution of H_2, and are explosive under pressure even at −80 °C. On warming to 70 °C a remarkable decomposition occurs leading to the formation of an orange-red solid, which is insoluble in toluene, above 250 °C crystalline BPO_4 (tetragonal) is formed. ^{31}P NMR spectra of **1** dissolved in toluene or CH_2Cl_2 demonstrate the immediate and complete fragmentation into two monomer units $P_4O_6 \cdot BH_3$.[13] In the course of the dimerization one of the longest P–O bonds of the monomers is cleaved, and the resulting dangling bonds are saturated intermolecularly. Again, on dissolving the dimer, the longer P–O bonds in the asymmetric P-O-P bridges between the two $P_4O_5 \cdot BH_3$ units represent the expected point of bond cleavage.

The ^{31}P-MAS-NMR spectrum of the compound **1** is in accord with the results of the crystal structure determination, and shows a strong high-field shift for the isotropic phosphorus signals in comparison to the signals of the monomer. All eight crystallographically independent phosphorus positions are resolved in the ^{31}P-MAS-NMR spectrum (162.0 MHz, 298 K, 85 % phosphoric acid as external standard; $\delta = 66.9$, 70.4, 79.0, 80.7, 81.6, 82.2, 82.8, 84.2). Based on cross-polarization from ^1H to ^{31}P spins as well as on the additional splitting through coupling to the ^{11}B nuclei, the signals at $\delta =$ 66.9 and 70.4 can be assigned to the boron-bearing phosphorus atoms. As expected, the ratio between the intensities of these signals and those caused by the uncoordinated phosphorus atoms ranging from $\delta = 79.0$ to 84.2 is 2:6.

The presence of a previously unknown P_8O_{12} framework in **1** was particularly interesting in terms of the possibility of providing a route to synthesize P_8O_{12} as a new molecular phosphorus oxide through thermal or chemical abstraction of the BH_3 groups. Whereas initial preparative approaches in this direction have remained unsuccessful, we were able to detect masses in the mass spectrum of **1** at *m/z* 451.76 and 439.74, which correspond to $P_8O_{12} \cdot BH_3$ and to a P_4O_6 dimer, respectively; in both cases the isotopic patterns observed confirm the assignment (Figure 2).

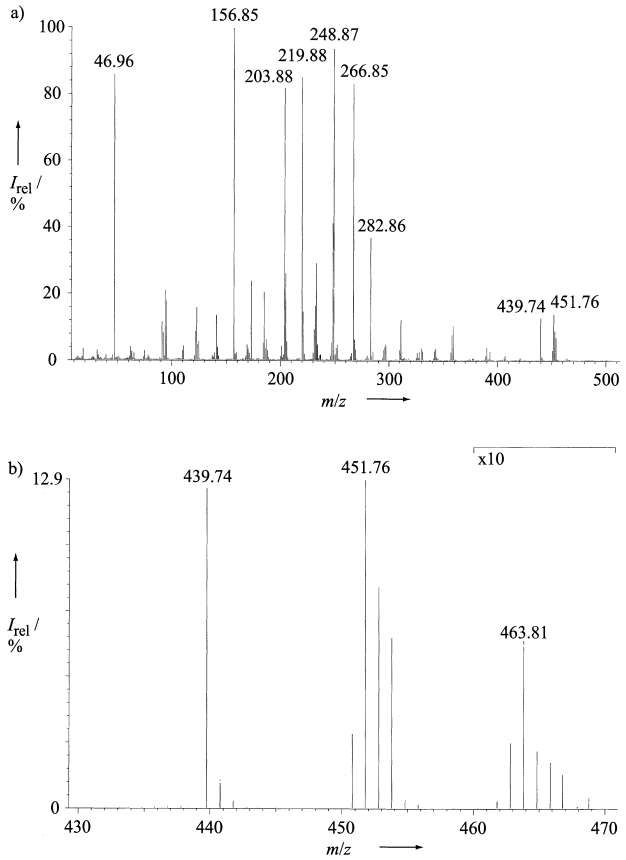


Figure 2. Mass spectrum (EI, 70 eV) of **1** at 373 K. a) Complete mass range. b) Upper mass range (from *m/z* 460 magnified 10-fold). *m/z* (%): 463.81 (0.6) [$P_8O_{12} \cdot 2BH^+$], 451.76 (12.9) [$P_8O_{12} \cdot BH^+$], 439.74 (12.6) [$P_8O_{12}^+$], 282.86 (36.6) [$P_5O_8^+$], 266.85 (83.2) [$P_5O_7^+$], 248.87 (93.7) [$P_4O_7 \cdot BH_2^+$], 219.88 (85.1) [$P_4O_6^+$], 203.88 (82.0) [$P_4O_5^+$], 156.85 (100) [$P_3O_4^+$], 46.96 (86.0) [PO^+].

The discovery of the dimerization of P_4O_6 now offers the opportunity to interpret conclusively previously not understood XANES measurements on compounds such as P_4O_7, P_4O_6S, and P_4O_6Se. At that time, unexplicable fundamental and reversible changes of the spectra were recorded in the gas phase as a function of the temperature. In each case the spectrum calculated for the isolated molecule was only obtained at higher temperatures.[14] By CI mass spectra of P_4O_7 we have now been able to prove that this effect is associated with a dimerization, P_4O_7 exists partially (12.1 % of the base peak, Figure 3) as a dimer in the gas phase at 323 K. Also, the ^{31}P NMR spectrum of a saturated toluene solution of P_4O_7 shows, in addition to the signals of monomeric P_4O_7 molecules, signals of weak intensity, whose relative intensity pattern, complicated multiplet structures, and chemical shifts comparable to those of **1**, suggest analogous P_4O_7 dimers.[15]

The synthesis of **1** provides the first example of a selective linkage of molecular phosphorus oxides leading to the formation of a previously unknown P_8O_{12} framework. The dimerization detected for $P_4O_6 \cdot BH_3$ and P_4O_7 is induced by the characteric distortion of the P_4O_6 cage caused by the attachment of a BH_3 group or an additional oxygen atom, respectively. In this process nine P–O bonds in the cage are significantly shortened, three, in contrast, lengthened. The

 © WILEY-VCH Verlag GmbH, D-69451 Weinheim, 2001 1433-7851/01/4024-4692 $ 17.50+.50/0 *Angew. Chem. Int. Ed.* **2001**, *40*, No. 24

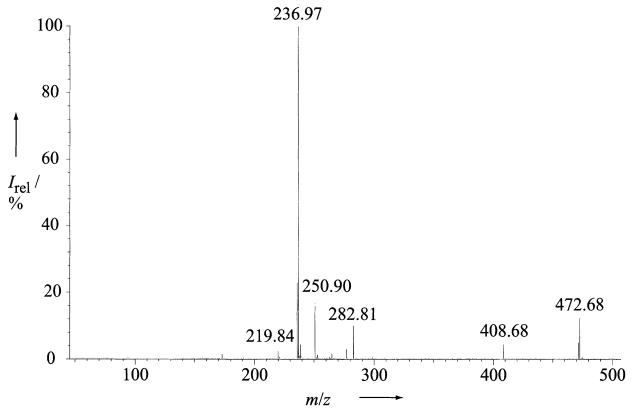


Figure 3. Mass spectrum (CI, methane) of P_4O_7 at 323 K. m/z (%): 472.68 (12.1) $[P_8O_{14}H^+]$, 408.68 (4.3) $[P_7O_{12}^+]$, 282.81 (9.8) $[P_5O_8^+]$, 250.90 (15.7) $[P_5O_6^+]$, 236.97 (100) $[P_4O_7H^+]$, 219.84 (2.1) $[P_4O_6^+]$.

weakening of these P^{III}–O bonds as well as the shift of the electron density to the four-coordinate phosphorus atom enhances the susceptibility of the P^{III} atoms towards nucleophilic attack by oxygen atoms and explains the formation of dimers with the structure observed in **1**. The O-P-O angles in **1** are on average 100.2° and thus remain almost unchanged compared to those of the monomeric compounds P_4O_7,[8] P_4O_6S,[9] and P_4O_6Se[10] (100.0°). In contrast, the average P-O-P bond angle in **1** of 132.8° is significantly larger than the corresponding value of 125.6° in the monomeric P_4O_6 derivatives, approaching the bond angles of about 140° that occur preferentially at the bridging oxygen atoms in strain-free polyphosphates and polysilicates. At the same time this widening of the angle at the oxygen atom facilitates larger P–O double-bond contributions, which is in agreement with the pronounced high-field shift of the phosphorus signals in the ^{31}P-MAS-NMR spectrum of **1** and leads to an additional stabilization of the cage. Since the number of P–O bonds remains unchanged by the dimerization, the thermodynamic driving force is predominantly considered to be the gain of additional bond enthalpy as a consequence of reduced strain in the cage, which at low temperatures evidently overcompensates the loss in entropy associated with the dimerization.

The unexpected observation of the spontaneous dimerization of molecular phosphorus oxides with an adamantane-like framework explains originally uninterpretable spectroscopic findings. Furthermore, they may help to solve other puzzling aspects of the chemistry of molecular phosphorus oxides. For example, the slow disproportionation of even highly pure P_4O_6 samples, observed on storage, could be induced by such a dimerization. The fact that the tendency to dimerize initially increases and then decreases with increasing temperature, which is confusing at first glance, can be readily understood on the basis of the interplay between the thermodynamic driving force, which favors the dimerization at low temperatures, and the kinetic inertness of the spatially closed monomers.

Experimental Section

All manipulations were carried out in glass apparatus predried under vacuum and under inert conditions (argon). P_4O_6 was distilled under reduced pressure, toluene was heated under reflux over P_4O_{10} and freshly distilled prior to use.

$Me_2S \cdot BH_3$ (0.47 mL, 0.38 g, ca. 4.96 mmol; Strem Chemicals, in 5–6% Me_2S excess) was added dropwise under stirring to a cold solution (0 °C) of P_4O_6 (1.2 g, 5.46 mmol) in toluene (1.5 mL). The clear, colorless solution was stirred for 2 h at 0 °C, and subsequently freed from Me_2S at −10 °C under reduced pressure, until the solution stopped boiling. After storage for three months at −30 °C the almost solidified solution was allowed to warm to room temperature; the clear, colorless crystals of **1**, which were up to 1 mm in size with a cuboid-like habit, initially remained undissolved. The crystals were separated from the mother liquor and dried under vacuum at room temperature. The powder diffractogram of the material obtained in this way was consistent with the calculated diffractogram of **1**, and showed no other additional phases.

Caution: Solid $P_8O_{12} \cdot 2BH_3$ is extremely explosive under pressure even under strict inert gas conditions and cooling to −80 °C (friction- and shock-sensitive). We recommend that the solid is neither handled in sealed glass apparatus nor in larger amounts (maximal 1.5 g).

Received: June 1, 2001 [Z17213]

[1] J. Hofmann, R. Gruehn, *Z. Anorg. Allg. Chem.* **1977**, *431*, 105–116.

[2] *Gmelins Handbuch der Anorganischen Chemie*, 8th ed., Schwefel, Teil B, Lieferung 3, Verlag Chemie, Weinheim, **1963**, p. 1723.

[3] M. Jansen, S. Strojek, *J. Chem. Soc. Chem. Commun.* **1995**, 1509–1510; S. Strojek, M. Jansen, *Chem. Ber.* **1996**, *129*, 121–124.

[4] U. Schülke, *Phosphorus Sulfur Silicon* **1990**, *51/52*, 153–156.

[5] According to ^{31}P NMR spectra in solution, the previously reported,[6] however to date not fully characterized, $P_4O_6 \cdot nBH_3$ ($n = 1–3$) compounds are composed of a P_4O_6 cage with phosphorus-bound borane groups.

[6] J. G. Riess, J. R. van Wazer, *J. Am. Chem. Soc.* **1966**, *88*, 2339–2340; J. G. Riess, J. R. van Wazer, *J. Am. Chem. Soc.* **1967**, *89*, 851–856; G. Kodama, H. Kondo, *J. Am. Chem. Soc.* **1966**, *88*, 2045–2046.

[7] Crystal structure analysis of **1**: SMART-1000 diffractometer with a CCD detector (Bruker AXS), crystal dimensions $0.7 \times 0.7 \times 0.7$ mm, $T = 183(1)$ K, orthorhombic, space group *Pbca* (no. 61), $a = 8.606(3)$, $b = 15.686(6)$, $c = 22.960(9)$ Å, $V = 3099(2)$ Å^3, $Z = 8$, $\rho_{ber.} = 2.003$ g cm^{-3}, $2\theta_{max} = 65°$, $\lambda(Mo_{K\alpha}) = 0.71073$ Å, ω scan, 49064 measured reflections, 5604 independent reflections, 4704 observed reflections $[I > 2\sigma(I)]$, $\mu = 0.952$ mm^{-1}, min./max. transmission = 0.3898/0.4991, absorption correction through symmetry-equivalent and redundant reflections (SADABS), structure solution by direct methods (SHELXS-97), struture refinement according to full-matrix least-squares procedures against F^2 (SHELXL-97), 224 parameters, hydrogen atoms refined freely (isotropic), $R_1 = 0.0364$, $wR_2 = 0.0938$ (observed reflections), min./max. residual electron density −0.318/0.762 e Å^{-3}. Further details on the crystal structure investigation may be obtained from the Fachinformationszentrum Karlsruhe, 76344 Eggenstein-Leopoldshafen, Germany (fax: (+49) 7247-808-666; e-mail: crysdata@fiz-karlsruhe.de), on quoting the depository number CSD-411904. Lattice parameters refined from powder data ($T = 298$ K): $a = 8.6163(2)$, $b = 15.6350(3)$, $c = 22.9882(5)$ Å, $V = 3096.8(1)$ Å^3.

[8] M. Möbs, M. Jansen, *Z. Anorg. Allg. Chem.* **1984**, *514*, 39–48; M. Jansen, M. Voss, *Angew. Chem.* **1981**, *93*, 120–121; *Angew. Chem. Int. Ed. Engl.* **1981**, *20*, 100; K. H. Jost, M. Schneider, *Acta Crystallogr. Sect. B* **1981**, *37*, 222–224.

[9] F. Frick, M. Jansen, P. J. Bruna, S. D. Peyerimhoff, *Chem. Ber.* **1991**, *124*, 1711–1714.

[10] J. Clade, M. Jansen, B. Engels, C. M. Marian, *Z. Anorg. Allg. Chem.* **1995**, *621*, 2065–2069.

[11] M. Jansen, M. Möbs, *Inorg. Chem.* **1984**, *23*, 4486–4488; M. Jansen, M. Voss, H.-J. Deiseroth, *Angew. Chem.* **1981**, *93*, 1023–1024; *Angew. Chem. Int. Ed. Engl.* **1981**, *20*, 965.

[12] J. Rodgers, D. W. White, J. G. Verkade, *J. Chem. Soc. A* **1971**, 77–80; J. C. Clardy, D. S. Milbrath, J. G. Verkade, *Inorg. Chem.* **1977**, *16*, 2135–2137; T. Imamoto, E. Nagato, Y. Wada, H. Masuda, K. Yamaguchi, T. Uchimaru, *J. Am. Chem. Soc.* **1997**, *119*, 9925–9926.

 © WILEY-VCH Verlag GmbH, D-69451 Weinheim, 2001 1433-7851/01/4024-4693 $ 17.50+.50/0

[13] ^{31}P NMR (121.5 MHz, 298 K, 85 % phosphoric acid as external standard): $\delta = 117.1$ (d, $^{2}J(P,P) = 27.6$ Hz, q, $^{3}J(P,B) = 0.7$ Hz, 3 P; uncoordinated phosphorus), 90 (m, broadened through the quadrupole moment of boron, 1 P; boron-bearing phosphorus); compare reference [6].

[14] C. Engemann, G. Kohring, A. Pantelouris, J. Hormes, S. Grimme, S. D. Peyerimhoff, J. Clade, F. Frick, M. Jansen, *Chem. Phys.* **1997**, *221*, 189 – 198; C. Engemann, Dissertation, Universität Bonn, **1997**.

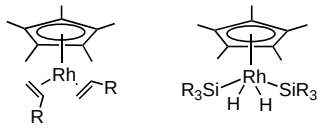
[15] ^{31}P NMR (121.5 MHz, 298 K, 85 % phosphoric acid as external standard): $\delta = 94.0 - 94.6$ (m, 4 P; P^{III} corresponding to P2, P3, P6, P7 in **1**), 79.6 – 80.1 (m, 2 P; P^{III} corresponding to P4, P8 in **1**), – 54.3 – – 53.6 (m, 2 P; P^{V} corresponding to P1, P5 in **1**).

Dehydrocoupling of Phosphanes Catalyzed by a Rhodium(I) Complex**

Volker P. W. Böhm and Maurice Brookhart*

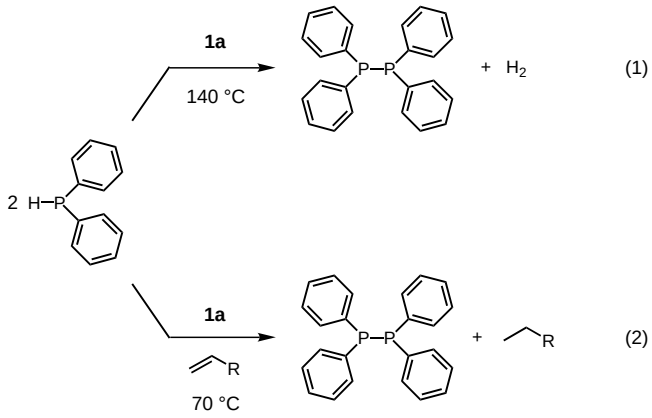
Although catalytic dehydrocoupling of phosphanes has been reported with Group 4 metallocene catalysts $[K(thf)_2][Cp^*_2ZrH_3]$ and $[Cp_2TiMe_2]$ ($Cp^* = C_5Me_5$, $Cp = C_5H_5$), these reactions are limited to the activation of primary phosphanes RPH_2 in the formation of (cyclic) oligomers and the cross-coupling of primary and secondary phosphanes with primary silanes.[1–3] Late transition metal catalysis of these types of reaction has only been reported for the coupling of phosphanes with borane.[4]

Complexes of the type [Cp*Rh(olefin)$_2$] (**1**) are known to activate C–H bonds in arenes,[5] olefins,[6] aldehydes,[7] and alkanes,[6, 8] as well as B–H bonds[8] and such activated species have been incorporated into catalytic cycles. The rhodium(v) catalyst **2** which is a precursor to the fragment [Cp*Rh] has been used similarly for the activation of C–H bonds in arenes and alkanes as well as of Si–H bonds.[9] Owing to the lack of reports on the activation of bonds between hydrogen and Group 15 elements, we became interested in the reactivity of secondary phosphanes towards the complex [Cp*Rh{CH_2=CH(TMS)}$_2$] (**1a**).[10]



1 **2**

Heating diphenylphosphane, $HPPh_2$, in the presence of complex **1a** in C_6D_6 at 140 °C results in an immediate color change of the solution from yellow to red accompanied by the formation of a new compound with a ^{31}P NMR signal at $\delta = -13.6$ which does not exhibit ^{1}J(P,H) coupling. At the same time, the ^{1}H resonance signal for the P-H proton of $HPPh_2$ disappears and a signal for dihydrogen grows in at $\delta = 4.46$ [Eq. (1)]. As a side reaction, vinyltrimethylsilane is partially hydrogenated [Eq. (2)]. The product formed was identified by comparison to an authentic



sample as tetraphenyldiphosphane, Ph_4P_2.[11] Repeating the experiment without complex **1a** leads to the recovery of unchanged $HPPh_2$. When an excess of vinyltrimethylsilane is added to the reaction, the coupling occurs at temperatures as low as 70 °C and hydrogenation of the olefin is observed rather than the evolution of dihydrogen [Eq. (2)].

To investigate the scope of this catalytic reaction, various diaryl- and dialkylphosphanes were employed (Table 1). Reactivity is not sensitive to electronic effects but steric demand plays a decisive role. Mesityl (2,4,6-$Me_3C_6H_2$), *tert*-butyl, and cyclohexyl substituents prevent coupling (Table 1, entries 8, 11, and 13) whereas phenyl, *para*-anisyl, ethyl, and isobutyl groups are well-tolerated (Table 1, entries 5, 7, 9, and 10). Turnover numbers (TON) as high as 1300 mol product per mol Rh were achieved with $HPPh_2$ (Table 1, entry 6). An intermediate behavior is exhibited by dicyclopentylphosphane which reacts only very sluggishly (Table 1, entry 12). The rhodium catalyst **1a** also tolerates ether functionalities (Table 1, entries 7 and 17). $HPPh_2$ can be coupled in good yields at 110 °C in the presence of vinyltrimethylsilane or 3,3-dimethyl-1-butene (Table 1, entries 1 – 4). Lower turnovers in comparison to those achieved in the high-temperature process without added olefin are likely due to increased formation of unreactive 18-electron species bearing olefinic ligands. No hydrophosphination of the olefin is observed in any case.[12] Using phenylphosphane, H_2PPh, and *para*-anisylphosphane in the coupling reaction does not lead to the formation of polymeric or oligomeric polyphosphanes. Instead, the two isomers of diaryldiphosphanes, *rac*- and *meso*-ArHP–PHAr, are formed in equal amounts in low yields (Table 1, entries 14 – 17). Higher turnovers with primary phosphanes could be achieved only if the reaction was run in neat

[*] Prof. Dr. M. Brookhart, Dr. V. P. W. Böhm
Department of Chemistry
University of North Carolina at Chapel Hill
Chapel Hill, NC 27599-3290 (USA)
Fax: (+1) 919-962-2476
E-mail: mbrookhart@unc.edu

[**] We thank the National Institutes of Health (NIH) for financial support and O. Daugulis for samples of dimesitylphosphane and 2,4,6-tri-*tert*-butylphenylphosphane. V.P.W.B. acknowledges a Feodor Lynen fellowship of the Alexander-von-Humboldt-Stiftung (Germany).

Supporting information for this article is available on the WWW under http://www.wiley-vch.de/home/angewandte/ or from the author.

 © WILEY-VCH Verlag GmbH, D-69451 Weinheim, 2001 1433-7851/01/4024-4694 $ 17.50+.50/0

Table 1. Dehydrocoupling of phosphanes catalyzed by **1a**.[a]



Entry	R	R′	[Rh] [mol %]	*t* [h]	*T* [°C]	Olefin[b]	Yield[c] [%]	Conversion[c] [%]
1	C_6H_5	C_6H_5	1.8	17	110	CH_2=CH(TMS)	79	88
2	C_6H_5	C_6H_5	0.3	17	110	CH_2=CH(TMS)	61	63
3	C_6H_5	C_6H_5	7.8	27	70	CH_2=CH*t*Bu	60	63
4	C_6H_5	C_6H_5	0.3	17	110	CH_2=CH*t*Bu	52	57
5	C_6H_5	C_6H_5	2.7	16	140	–	96	99
6	C_6H_5	C_6H_5	0.06	18	140	–	79	80
7	4-$(H_3CO)C_6H_4$	4-$(H_3CO)C_6H_4$	7.8	14	145	–	92	100
8	2,4,6-$(H_3C)_3C_6H_2$	2,4,6-$(H_3C)_3C_6H_2$	1.6	18	140	–	0	1
9	CH_2CH_3	CH_2CH_3	7.1	40	145	–	88	93
10	$CH_2CH(CH_3)_2$	$CH_2CH(CH_3)_2$	2.0	34	140	–	82	84
11	$C(CH_3)_3$	$C(CH_3)_3$	2.0	48	140	–	0	5
12	*cyclo*-C_5H_9	*cyclo*-C_5H_9	5.3	40	145	–	7	14
13	*cyclo*-C_6H_{11}	*cyclo*-C_6H_{11}	4.8	48	140	—	0	6
14	C_6H_5	H	3.1	29	110	CH_2=CH(TMS)	8[d]	10
15	C_6H_5	H	1.1	18	145	–	3[d]	5
16	C_6H_5	H	0.6	26	150	–	30[d,e]	56
17	4-$(H_3CO)C_6H_4$	H	5.8	18	145	–	5[d]	8

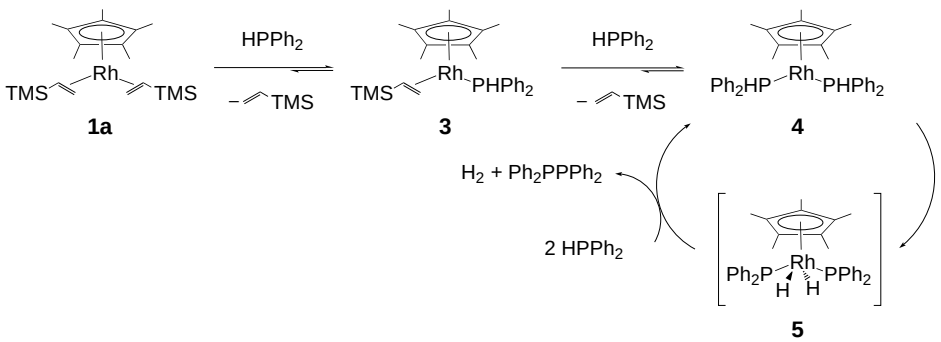
[a] 114 μmol phosphane, 0.7 mL C_6D_6. [b] 1.1 equivalents olefin with respect to phosphane; the olefin serves as the hydrogen acceptor. No olefin added implies release of H_2. [c] Yield and conversion are based on initial phosphane concentration as determined by NMR spectroscopy. [d] Two isomers (*rac* and *meso*) are formed in equal amounts. [e] Reaction in neat phenylphosphane.

phosphane (Table 1, entry 16); however, side reactions giving unassigned products occur under these conditions.

The transformation of $HPPh_2$ was monitored by NMR spectroscopy at 110 °C in [D_8]toluene. At the beginning of the reaction, stepwise exchange of the bound olefins by the phosphane and formation of the complexes **3** and **4** is observed by ^1H and ^{31}P NMR spectroscopy (Scheme 1).[11] The complex [Cp*Rh($PHPh_2$)$_2$] (**4**) is the major resting state of the catalyst during the reaction and accounts for 83 % of the amount of **1a** initially used as determined by integration of ^1H NMR signals. After full conversion of the starting material, three additional unidentified rhodium species build up which are characterized by broad Cp* signals at $\delta = 1.54$, 1.74, and 1.79 in the ^1H NMR spectrum. No doublets in the $^{31}P\{^1H\}$ NMR spectrum could be assigned to phosphorus atoms coordinated to rhodium centers although the product Ph_4P_2 and diphenylphosphide $[Ph_2P]^-$ are known to form complexes with [Cp*Rh] fragments.[13, 14] As the +5 oxidation state for rhodium is well-precedented[15] and as steric demand governs phosphane reactivity, formation of the rhodium(v) intermediate **5** stabilized by phosphide ligands during the catalytic cycle seems plausible (Scheme 1); however, no definitive proof of such a species has been obtained.

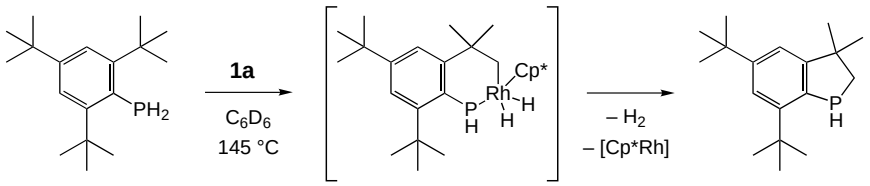
The above-mentioned B–H and Si–H bond activation reactions mediated by catalysts similar to **1a** have been coupled with the activation of C–H bonds, resulting in the catalytic formation of products possessing B–C and Si–C bonds, respectively.[8, 9] However, no cross-coupling with the solvents C_6D_6 or [D_8]toluene is observed during the dehydrocoupling reactions studied here. Additionally, H/D exchange reactions between arenes and olefins usually observed with **1a** in C_6D_6 are also suppressed.[6] However, the formation of $DPPh_2$ in low amounts, as identified in the $^{31}P\{^1H\}$ NMR spectrum, is indicative of the reversible activation of the aromatic solvent and the P–H bond.

While no *intermolecular* P–C bond formation has been seen which might result from dual P–H and C–H bond activation and coupling, we have observed a remarkable catalytic *intramolecular* P–C coupling involving activation of the C–H bond of an unactivated methyl group. Treatment of 2,4,6-tri-*tert*-butylphosphane (supermesitylphosphane; **6**) with **1a** in C_6D_6 at 145 °C results in quantitative formation (93 % yield of isolated product after 4 h) of 3,3-dimethyl-5,7-di-*tert*-butylphosphaindane (**8**; Scheme 2). Such a cyclic phosphane has been observed to form from the phosphinidene 2,4,6-$[(CH_3)_3C]_3C_6H_2P$: by intramolecular C–H insertion;[16] however, this intermediate seems unlikely in the present reaction. Again, a rhodium(v) intermediate **7** is plausible (Scheme 2).



Scheme 1. Proposed mechanism of the dehydrocoupling reaction via rhodium(v) intermediate **5**.

We have shown the late transition metal complex **1a** catalyzes the dehydrocoupling of primary and secondary



6 **7** **8**

Scheme 2. Proposed mechanism for the formation of the cyclic phosphane **8** via rhodium(v) complex **7**.

phosphanes. In particular, the catalytic dehydrocoupling of secondary phosphanes is efficient and has been reported for the first time. Aryl and alkyl substituents are tolerated but reactivity is limited to sterically less demanding substrates. The resting state of the catalyst in the coupling of $HPPh_2$ is the diphosphanerhodium(i) complex **4** that is dominant throughout catalysis. Presumably, the reaction proceeds via a rhodium(v) species such as **5**. This catalytic reaction is advantageous over currently available methods for the synthesis of diphosphanes which produce stoichiometric amounts of salts as by-products.[17]

Received: July 18, 2001 [Z17540]

[1] a) M. C. Fermin, D. W. Stephan, *J. Am. Chem. Soc.* **1995**, *117*, 12645 – 12646; b) N. Etkin, M. C. Fermin, D. W. Stephan, *J. Am. Chem. Soc.* **1997**, *119*, 2954 – 2955.

[2] a) S. Xin, H. G. Woo, J. F. Harrod, E. Samuel, A.-M. Lebuis, *J. Am. Chem. Soc.* **1997**, *119*, 5307 – 5313; b) R. Shu, L. Hao, J. F. Harrod, H.-G. Woo, E. Samuel, *J. Am. Chem. Soc.* **1998**, *120*, 12988 – 12989.

[3] Review: D. W. Stephan, *Angew. Chem.* **2000**, *112*, 322 – 338; *Angew. Chem. Int. Ed.* **2000**, *39*, 314 – 329.

[4] a) H. Dorn, R. A. Singh, J. A. Massey, A. J. Lough, I. Manners, *Angew. Chem.* **1999**, *111*, 3540 – 3543; *Angew. Chem. Int. Ed.* **1999**, *38*, 3321 – 3323; b) H. Dorn, R. A. Singh, J. A. Massey, J. M. Nelson, C. A. Jaska, A. J. Lough, I. Manners, *J. Am. Chem. Soc.* **2000**, *122*, 6669 – 6678, c) H. Dorn, E. Vejzovic, A. J. Lough, I. Manners, *Inorg. Chem.* **2001**, *40*, 4327 – 4331.

[5] C. P. Lenges, M. Brookhart, *J. Am. Chem. Soc.* **1999**, *121*, 6616 – 6623.

[6] C. P. Lenges, P. S. White, M. Brookhart, *J. Am. Chem. Soc.* **1999**, *121*, 4385 – 4396.

[7] C. P. Lenges, M. Brookhart, *Angew. Chem.* **1999**, *111*, 3746 – 3750; *Angew. Chem. Int. Ed.* **1999**, *38*, 3533 – 3537.

[8] H. Chen, S. Schlecht, T. C. Semple, J. F. Hartwig, *Science* **2000**, *287*, 1995 – 1997.

[9] P. I. Djurovich, A. R. Dolich, D. H. Berry, *J. Chem. Soc. Chem. Commun.* **1994**, 1897 – 1898; b) K. Ezbiansky, P. I. Djurovich, M. LaForest, D. J. Sinning, R. Zayes, D. H. Berry, *Organometallics* **1998**, *17*, 1455 – 1457.

[10] For a review on catalytic heteroatom – heteroatom bond formation by heteroatom – hydrogen bond activation see: F. Gauvin, J. F. Harrod, H. G. Woo, *Adv. Organomet. Chem.* **1998**, *42*, 363 – 405.

[11] For details on experimental procedures, spectral data of products, and the preparation of starting materials see the Supporting Information.

[12] Review: L.-B. Han, M. Tanaka, *Chem. Commun.* **1999**, 395 – 402.

[13] For rhodium(i) and rhodium(ii) complexes see: W. Hieber, R. Kummer, *Chem. Ber.* **1967**, *100*, 148 – 159.

[14] For rhodium(ii) and rhodium(iii) complexes see: a) B. Klingert, H. Werner, *J. Organomet. Chem.* **1983**, *252*, C47 – C52; b) B. Klingert, H. Werner, *J. Organomet. Chem.* **1987**, *333*, 119 – 128; c) H. Werner, B. Klingert, A. L. Rheingold, *Organometallics* **1988**, *7*, 911 – 917.

[15] a) M.-J. Fernandez, P. M. Maitlis, *J. Chem. Soc. Chem. Commun.* **1982**, 310 – 311; b) M.-J. Fernandez, P. M. Bailey, P. O. Bentz, J. S. Ricci, T. F. Koetzle, P. M. Maitlis, *J. Am. Chem. Soc.* **1984**, *106*, 5458 – 5463; c) S. B. Duckett, D. M. Haddleton, S. A. Jackson, R. N. Perutz, M. Poliakoff, R. K. Upmacis, *Organometallics* **1988**, *7*, 1526 – 1532.

[16] a) M. Yoshifuji, T. Sato, N. Inamoto, *Chem. Lett.* **1988**, 1735 – 1738; b) A. H. Cowley, F. Gabbaï, R. Schluter, D. Atwood, *J. Am. Chem. Soc.* **1992**, *114*, 3142 – 3144; c) X. Li, D. Lei, M. Y. Chiang, P. P. Gaspar, *J. Am. Chem. Soc.* **1992**, *114*, 8526 – 8531; d) R. A. Aitken, W. Masamba, N. J. Wilson, *Tetrahedron Lett.* **1997**, *38*, 8417 – 8420.

[17] a) K. Sasse, *Methoden Org. Chem. (Houben-Weyl) 4th ed., 1963 –*, Bd. XII/1, **1963**, pp. 182 – 186; b) A. Schmidpeter, G. Burgert, *Phosphorus Sulfur* **1985**, *22*, 323 – 335; c) J. T. Yeh, L. R. Avens, J. L. Mills, *Phosphorus Sulfur Silicon Relat. Elem.* **1990**, *47*, 319 – 323.

The First Dectection of Peroxo and Bis-superoxo Complexes of Aluminum: $FAlO_2$ and $FAlO_4$**

Jan Bahlo, Hans-Jörg Himmel, and Hansgeorg Schnöckel*

Peroxo and superoxo complexes are of major importance because of the role they play as oxygen carrier systems in biology[1] and in preparative chemistry.[2–4] For instance, peroxo complexes of vanadium show insulinomimetic properties[2] and complexes of rhenium are applied in olefin epoxidation.[3, 4] Another example from this class of compounds is hemocyanin, which contains a dinuclear copper site capable of binding O_2 in a μ-η^2:η^2 peroxo complex.[1] Finally, peroxo complexes are potential intermediates or products during the oxidation of metals or metal clusters.[5] Consequently, there is substantial interest in the exploration and isolation of new stable peroxo and superoxo complexes. Herein we report on the photolytically induced reaction of AlF with O_2 in solid argon matrices, which leads to the first known peroxo complexes and bis-superoxo complexes of aluminum, namely $FAlO_2$ and $FAlO_4$.[6] All products were identified and characterized on the basis of their IR absorptions (including the effects of isotopic changes ($^{16}O_2$, $^{18}O_2$, $^{16}O_2/^{18}O_2$, $^{16}O^{18}O$) and of quantum-mechanical calculations (ab initio (UHF and, in some cases, MP2) and density functional theory (DFT) calculations). In addition to their relevance for possible applications,[7] the title compounds show interesting electronic properties. While $FAlO_2$ exists in a singlet electronic ground state,[8] the $FAlO_4$ species exhibits a triplet ground state. The complexation of a second dioxygen molecule to $FAlO_4$ thus represents a spin-allowed process, and dioxygen complexes of this kind might well be of significant relevance as intermediates in oxidation processes.

[*] Prof. Dr. H. Schnöckel, Dipl.-Chem. J. Bahlo, Dr. Dr. H.-J. Himmel
Institut für Anorganische Chemie
Universität Karlsruhe (TH)
Engesserstrasse, Geb. 30.45, 76133 Karlsruhe (Germany)
Fax: (+49) 721-608-4854
E-mail: hg@achpc9.chemie.uni-karlsruhe.de

[**] We thank Professor R. Ahlrichs for fruitful discussions and the Deutsche Forschungsgemeinschaft for the award of an Habilitation grant to H.-J.H.

 © WILEY-VCH Verlag GmbH, D-69451 Weinheim, 2001 1433-7851/01/4024-4696 $ 17.50+.50/0

The reactions of AlF and $(AlF)_2$ with *one* O_2 molecule result in the formation of the peroxo species $FAlO_2$ and $FAl(\mu\text{-}O)_2AlF$, respectively.[9, 10] The presence of a third distinct species in the spectra for experiments with high dioxygen concentrations in the matrix shows that AlF is capable of binding a *second* O_2 moiety to give a molecule with the composition $FAlO_4$. $FAlO_2$ is the dominating species formed in the matrices for *low* O_2 concentrations (1%), while $FAlO_4$ dominates for *high* O_2 concentrations (5–15%).

Figure 1a shows an IR spectrum recorded upon UV photolysis ($\lambda_{max} = 254$ nm) of matrices containing AlF and 5% $^{16}O_2$. Experiments with different oxygen isotopomers and different O_2 concentrations show that the spectrum contains signals attributed to three different reaction products. The first group of signals at 1077.3 and 781.8 cm^{-1} was assigned to product **1**, and the second group at 942.8 and 812.9 cm^{-1} to product **2**. The signals at 892.4 and 705.3 cm^{-1} were attributed to species **3**. For low O_2 concentrations (1%), species **1** and **2** dominated, but species **3** gained intensity relative to **1** and **2** for higher O_2 concentrations (5%). This might imply that **1** and **2** are products of the reaction with one O_2 unit, while **3** is the product of the reaction with two O_2 molecules.

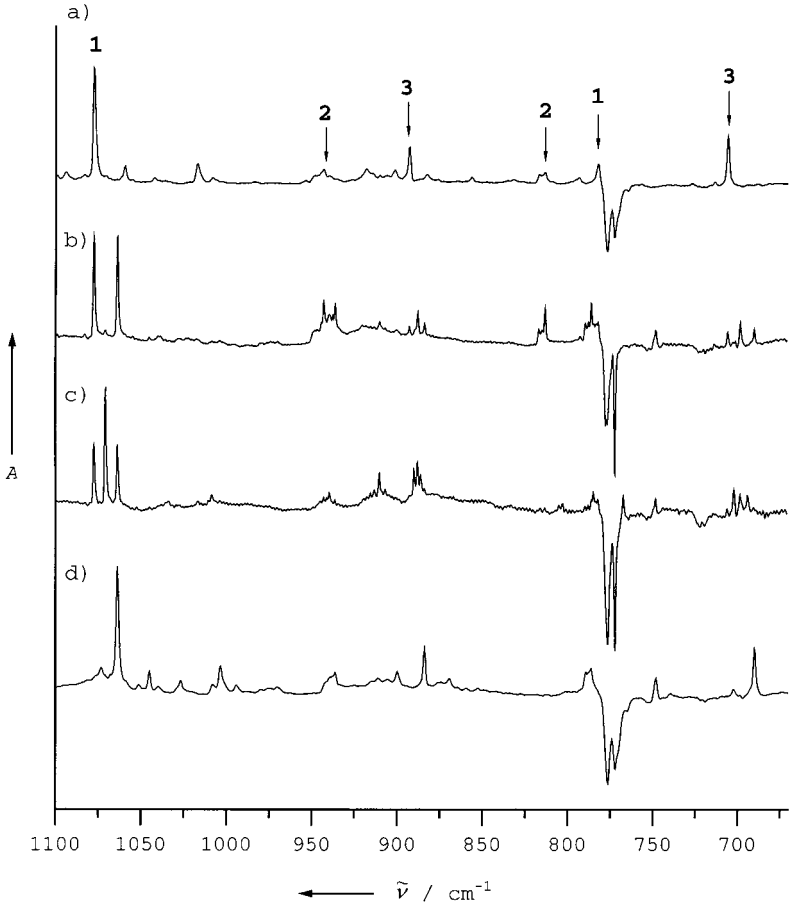


Figure 1. IR spectrum recorded after cocondensation of molecular AlF together with O_2 in a solid argon matrix followed by photolysis of the matrix with UV light ($\lambda_{max} = 254$ nm): a) $^{16}O_2$, b) $^{16}O_2/^{18}O_2$ (1:1 mixture), c) $^{16}O_2/^{16}O^{18}O/^{18}O_2$ (1:2:1 mixture), d) $^{18}O_2$.

Upon $^{16}O/^{18}O$ substitution, the signals due to product **1** were shifted to 1063.6 and 747.9 cm^{-1}, corresponding to $^{16}O/^{18}O$ ratios of 1.0132 and 1.0455, respectively (Figure 1d). The signals due to species **2** exhibited red shifts of 6.6 and 27.3 cm^{-1} ($^{16}O/^{18}O = 1.0065$ and 1.0348, respectively). The absorptions due to product **3** were shifted to 883.7 and 689.9 cm^{-1}, implying $^{16}O/^{18}O$ ratios of 1.0102 and 1.0232, respectively. Other experiments with 1:1 mixtures of $^{16}O_2$ and $^{18}O_2$ revealed that the signals for **1** were found to be the superposition of the signals observed in the experiments using $^{16}O_2$ and $^{18}O_2$ separately (Figure 1b). Two doublet features at 942.8/936.2 and 812.9/785.6 cm^{-1} in experiments with 1:1 mixtures of $^{16}O_2$ and $^{18}O_2$ could be assigned to **2**. Thus, it follows that **1** and **2** contain one O_2 group. By contrast, species **3** gave rise to extra signals that could not be accounted for merely by the superposition of the signals observed in the experiments using $^{16}O_2$ and $^{18}O_2$ separately. Following UV-photolysis two groups of absorptions associated with product **3** were observed to grow in, with three signals in each group. The signals of the first group were located at 892.4/887.6/883.7 cm^{-1}, that of the second group at 705.3/697.9/689.8 cm^{-1}. From this pattern it follows that **3** hosts two O_2 groups. Finally, the experiment was repeated by using 1:2:1 mixtures of $^{16}O_2$, $^{16}O^{18}O$, and $^{18}O_2$. The two vibrational modes of **1** were now both split into triplets positioned at 1077/1070/1063 and 781/767/747 cm^{-1} (Figure 1c). The bands due to **2** also showed triplet patterns, with the signals due to the $^{16}O^{18}O$ form of species **2** appearing at 939.4 and 802.7 cm^{-1}. Species **3** again gave rise to two groups of signals, but this time with as many as five signals in each group (892.4/889.7/887.6/885.9/883.7 and 705.6/701.5/697.9/693.5/689.8 cm^{-1}). This pattern indicates the presence of two pairs of equivalent O atoms.

Herein we will focus the discussion mainly on species **1** and **3**; species **2** will be discussed in detail elsewhere.[9] The results of the experiments indicate that these species have the composition $FAlO_2$ (**1**) and $FAlO_4$ (**3**), which would be better discribed as $FAl(O_2)_2$. Our DFT calculations resulted in the global minimum structures shown for **1** and **3**.



Species **1** and **3** both exhibit C_{2v} symmetry with Al–F distances of 1.6340 and 1.6552 Å, respectively, which are typical values for Al–F bonds found in three-coordinate Al^{III} species (e.g. AlF_3 1.631(3) Å[11]). The O–O bond length in **1** is 1.6637 Å, whereas that in **3** (1.3673 Å) is, as expected, significantly shorter, but in good agreement to the distance expected for O_2^- (1.3519 Å according to DFT calculations with the B3LYP basis set). The O-Al-O angle is 58.4° in **1** and

Table 1. Observed and calculated spectra of FAl($^{16}O_2$), FAl($^{18}O_2$), and FAl($^{16}O^{18}O$) (**1**).[a]

FAl($^{16}O_2$) obs.	FAl($^{16}O_2$) calcd[b] MP2/TZVPP	FAl($^{16}O_2$) calcd[b] B3LYP/6-311G*	FAl($^{18}O_2$) obs.	FAl($^{18}O_2$) calcd[b] MP2/TZVPP	FAl($^{18}O_2$) calcd[b] B3LYP/6-311G*	FAl($^{16}O^{18}O$) obs.	FAl($^{16}O^{18}O$) calcd MP2/TZVPP	FAl($^{16}O^{18}O$) calcd B3LYP/6-311G*	Assignment
1077.3	1087.7 (147)	1114.4 (144)	1063.6	1074.4 (149)	1098.9 (146)	1070.7	1081.2 (148)	1106.8 (145)	ν_1 (a_1)
–[d]	720.4 (13)	739.8 (14)	–[d]	696.6 (9)	715.7 (9)	–[d]	706.6 (12)	724.0 (12)	ν_2 (a_1)
–[d]	525.6 (12)	528.2 (12)	–[d]	501.6 (12)	504.5 (12)	–[d]	513.9 (12)	516.6 (12)	ν_3 (a_1)
–[c]	238.2 (119)	238.5 (121)	–[c]	236.2 (116)	236.6 (118)	–[c]	237.2 (117)	237.6 (120)	ν_4 (b_1)
781.8	810.6 (66)	782.4 (19)	747.9	775.8 (66)	748.1 (20)	766.8	794.8 (65)	768.8 (19)	ν_5 (b_2)
–[c]	224.5 (74)	217.7 (73)	–[c]	220.6 (70)	213.9 (69)	–[c]	222.5 (72)	215.8 (71)	ν_6 (b_2)

[a] Frequencies in cm^{-1}, intensities in $km\,mol^{-1}$ in parentheses. [b] C_{2v} symmetry; geometry (bond lengths in Å, angles in °): MP2/TZVPP: Al–F 1.6430, Al–O 1.7006, O–O 1.6596, O-Al-O 58.4; B3LYP/6-311G*: Al–F 1.6390, Al–O 1.7102, O–O 1.6637, O-Al-O 58.4. [c] Out of range of detection. [d] Too weak to be detected.

Table 2. Observed and calculated spectra of FAl($^{16}O_2$)$_2$, FAl($^{18}O_2$)$_2$, and FAl($^{16}O^{18}O$)$_2$ (**3**).[a]

FAl$^{16}O_4$ obs.	FAl$^{16}O_4$ calcd[b]	FAl$^{18}O_4$ obs.	FAl$^{18}O_4$ calcd[b]	FAl$^{16}O_2{}^{18}O_2$ obs.	FAl$^{16}O_2{}^{18}O_2$ calcd	Assignment
–[d]	1138.6 (2)	–[d]	1074.0 (3)	–[d]	1136.8 (5)	ν_1 (a_1)
892.4	900.6 (151)	883.7	898.9 (149)	887.6	899.8	ν_2 (a_1)
–[d]	506.9 (9)	–[d]	486.0 (10)	–[d]	496.2 (10)	ν_3 (a_1)
–[c]	186.1 (20)	–[c]	178.9 (18)	–[c]	182.5 (19)	ν_4 (a_1)
–[d]	404.7 (0)	–[d]	380.6 (0)	–[d]	390.8 (0)	ν_5 (a_2)
–[c]	69.9 (0)	–[c]	65.9 (0)	–[c]	67.8 (0)	ν_6 (a_2)
–[d]	490.6 (1)	–[d]	467.2 (2)	–[d]	479.9 (1)	ν_7 (b_1)
–[d]	242.5 (50)	–[d]	238.3 (38)	–[d]	240.2 (49)	ν_8 (b_1)
–[c]	176.0 (0.01)	–[c]	166.9 (0.03)	–[c]	171.4 (0.03)	ν_9 (b_1)
–[d]	1135.1 (12)	–[d]	1071.0 (9)	–[d]	1072.5 (6)	ν_{10} (b_2)
705.3	714.3 (179)	689.9	694.2 (175)	697.9	701.5 (177)	ν_{11} (b_2)
–[d]	205.3 (26)	–[d]	199.6 (24)	–[d]	201.8 (24)	ν_{12} (b_2)

[a] Frequencies in cm^{-1}, intensities in $km\,mol^{-1}$ in parentheses. [b] C_{2h} symmetry; geometry (bond lengths in Å, angles in °): B3LYP/6–311G*: Al–F 1.6552, Al–O 1.8562, O–O 1.3673, O-Al-O 43.2. [c] Out of range of detection. [d] Too weak to be detected or IR silent.

43.2° in **3** (for O atoms of the same O_2 unit), and as a consequence, the Al–O distance increases from 1.7006 Å in **1** to 1.8562 Å in **3**.[12]

The calculated vibration frequencies for **1** and **3** are compared with the experimental values in Table 1 and Table 2, respectively.[13] The calculations predict in both cases two of the six or twelve, respectively, modes to carry sufficient intensity to guarantee their detection subject to the molecule being formed in sufficient yields. This is in agreement to the experiments which provide in both cases clear evidence for two strong absorptions. The observed frequencies of these two modes are in good agreement with the calculated values.

The ab initio calculations for **1** at the MP2 level of theory and using a TZVPP type basis set resulted, in agreement with the DFT calculations, in a global minimum structure with C_{2v} symmetry (singlet electronic ground state). The Al–O and O–O distances of 1.7006 and 1.6596 Å, respectively, are somewhat shorter than those predicted on the basis of the DFT calculations. The Al–F bond length and the O-Al-O angle are 1.6430 Å and 58.4°, respectively. The following frequencies (in cm^{-1}) were calculated for FAl$^{16}O_2$ (symmetry assignment and intensity [$km\,mol^{-1}$] in parentheses): 1087.7 (a_1, 147), 810.6 (b_2, 66), 720.4 (a_1, 13), 525.6 (a_1, 12), 238.2 (b_1, 119), 224.5 (b_2, 74).

Ab initio calculations for **3** at the HF level of theory with a 6-311G*-type basis set also gave a triplet electronic ground state, which is now slightly distorted from C_{2v} symmetry, resulting in only C_2 symmetry. Thus two different values are obtained for the Al–O distances of one O_2 (1.8798 and 1.7849 Å). Other geometrical parameters (bond lengths in Å, angles in °) are: Al–F 1.6327, O–O 1.3030, F-Al-O 112.7/120.4, O-Al-O 40.6 (for O atoms of one O_2 unit). As expected, the frequency calculation using the HF method resulted in wavenumbers higher than those calculated using DFT methods. The following frequencies (in cm^{-1}) were calculated for FAl($^{16}O_2$)$_2$ (symmetry assignment and intensity [$km\,mol^{-1}$] in parentheses): 1329.3 (b, 101), 1320.0 (a, 9), 954.1 (a, 185), 797.1 (b, 273), 569.8 (a, 6), 388.2 (b, 51), 300.9 (a, 7), 220.0 (b, 33), 211.8 (b, 22), 199.8 (a, 24), 175.2 (b, 2), 124.2 (a, 0.09). Attempts to calculate the structure and frequencies for **3** using the MP2 method were less successful. The MP2 method appears to be generally less reliable for the computation of O_2-containing molecules such as **3**.

Mode coupling makes an assignment of the absorptions almost impossible. Therefore a normal coordinate analysis was carried out for all molecules. Force constants of 247 and 585 $N\,m^{-1}$ were derived for the O–O stretching force constant f(O–O) of **1** and **3**, respectively, and values of 660 and 190 $N\,m^{-1}$ were calculated for O_2^- and O_2^{2-}, respectively. The stretching force constants f(Al–F) and f(Al–O) of the Al–F and Al–O bonds are 597 and 445 $N\,m^{-1}$, respectively, for **1** and 493 $N\,m^{-1}$ and 193 $N\,m^{-1}$, respectively, for **3**.[14] A detailed analysis of the bonding properties within triplet **3** proved difficult, and so far we were not able to establish a clear picture of the frontier orbitals and the charge distribution. However, the O–O distance and force constant support the presence of O_2^- units coordinated to the aluminum center. This would imply that the unpaired electrons are located at the O_2^- groups with only weak coupling between the two groups.

In the same way,[9] experiments with AlCl and AlBr in place of AlF provided evidence for the generation of $ClAlO_2$, $ClAl(O_2)_2$, $BrAlO_2$, and $BrAl(O_2)_2$ as products of the photolytically induced matrix reaction of AlCl with *one* or *two* O_2 molecules. This observation supports the presented assignment of **1** and **3**.

The characterization of the peroxo and bis-superoxo complexes **1** and **3** provides the opportunity to compare these complexes with previously investigated systems with similar structure: In the peroxovanadium imidazole monoanion O–O distances are 1.475(2) and 1.467(3) Å, which are thus similar

 © WILEY-VCH Verlag GmbH, D-69451 Weinheim, 2001 1433-7851/01/4024-4698 $ 17.50+.50/0 *Angew. Chem. Int. Ed.* **2001**, *40*, No. 24

to the value for the O–O distance in $FAl(O_2)_2$. An example for a peroxorhenium complex is $[CH_3Re(O_2)_2O]$, which has been studied in the gas phase by using electron diffraction[3] and exhibits O–O and Re–O distances of 1.451(6) and 1.67(1) Å, respectively. $[(Ph_3P)_2PtO_2]$ exhibits a O–O bond length of 1.26 Å,[18] which is shorter than the value of 1.3520 Å calculated for O_2^-. In $[\{Cu[HB(3,5\text{-}i\text{Pr}_2pz)_3]\}_2(O_2)]$, which might serve as a model compound for oxohemocyanin,[19] the O–O distance is 1.41 Å and is thus significantly longer than the calculated value for O_2^- (1.3520 Å), but shorter than that for O_2^{2-} (1.6258 Å).

Superoxo and peroxo complexes of main group elements are very rare. The Group 1 elements form ionic MO_2 complexes with C_{2v} symmetry.[20] Of the Group 2 element compounds MgO_2 is known.[21–24] Oxygen compounds of Group 13 have also been frequently studied.[25–29] $FAlO_2$ is also structurally similar to $OSiO_2$ and F_2SiO_2, which have both been charaterized by IR spectroscopy in matrix isolation experiments.[30–32] One of the few examples of a main group element bis-superoxo complex is $Mg(O_2)_2$.[21–24] It is noteworthy that alkali metals are capable of binding not only one but also two dioxygen molecules.[20] All these compounds will be discussed and compared with $XAlO_2$ and $XAl(O_2)_2$ (X = F, Cl, or Br) in detail elsewhere.[9]

In Figure 2 the energies for **1** and **2** are compared relative to molecular AlF and two oxygen molecules. We note that the reaction of AlF with the first O_2 molecule is less exothermic ($\Delta E = -140.5$ kJ mol^{-1}) than the reaction of $FAlO_2$ with the second oxygen molecule to give $FAl(O_2)_2$ ($\Delta E = -152.3$ kJ mol^{-1}).

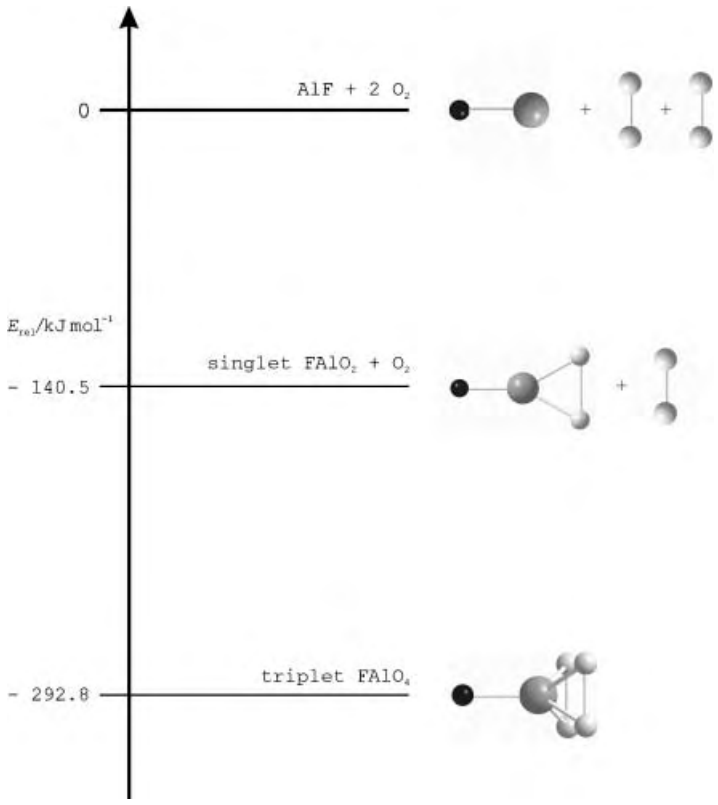
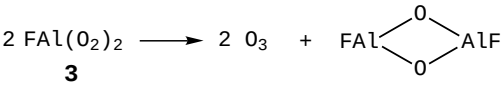


Figure 2. Energies of **1** and **2** relative to the energies of the starting materials AlF and O_2.

We propose that **1** and **3** occur as intermediates in the oxidation of AlF to give solid FAlO. Although the structure of FAlO is unknown, it is expected to show similarities to the structure of isoelectronic SiO_2. This conclusion seems plausible since the reaction (1) has been calculated to be



(1)

exothermic (-81.8 kJ mol^{-1}) and the molecule $FAl(\mu\text{-}O_2)AlF$,[9] like the dimer of SiO_2 ($OSi(\mu\text{-}O_2)SiO$),[33] could be the next intermediate to the solid-state materials FAlO and SiO_2, respectively. Possibly species like **3**, in which two O_2 units are coordinated to the metal atom, may also play a major role as intermediates in many oxidation processes, for example of metal atom clusters or metal surfaces.

Experimental Section

Details of the setup of our matrix apparatus can be found in reference [34]. The subhalogenide AlF was generated in a Knudsen-type graphite cell by passing CHF_3 (Messer, 99.995 %) over Al (Merck, 99.999 %), heated resistively to 900 °C. The AlF molecules produced in this process were deposited together with an excess of O_2-doped argon onto a copper block kept at 13 K by means of a closed-cycle cryostat (Leybold LB 510). Immediately after deposition the matrices were investigated by IR spectroscopy. Subsequently the matrices were photolyzed with UV radiation and the photolytically induced reactions again monitored by IR spectroscopy.

The IR spectra were recorded on a Bruker 113v spectrometer, equipped with an MCT and a DTGS detector. The spectra were recorded with a resolution of 0.5 cm^{-1} (MCT detector) and 1.0 cm^{-1} (DTGS detector).

UV-photolysis ($\lambda_{max} = 254$ nm) was performed with a low-pressure Hg lamp (Gräntzel, Karlsruhe) operating at 200 W.

The chemicals used for the matrix reactions were purchased from the following sources and with the quoted purities: $^{16}O_2$: Messer, 99.9998 %, $^{18}O_2$: Prochem, 99.1 %, Ar: Messer, 99.9998 %.

Ab initio UHF and density functional theory (B3LYP) calculations were carried out with the Gaussian 98 program package[35] and a 6-311G(d)-type basis set was used. Ab initio (MP2) calculations were carried out with the RIMP2 module[36] of the TURBOMOLE program package[37] with a TZVPP-type basis set.

Received: May 9, 2001
Revised: August 24, 2001 [Z17069]

[1] N. Kitajima, Y. Moro-oka, *Chem. Rev.* **1994**, 94, 737.
[2] See for example W. Adam, Y. Y. Chan, D. Cremer, J. Gauss, D. Scheutzow, M. J. Schindler, *J. Org. Chem.* **1988**, *53*, 3007; A. L. Baumstark, P. C. Vasquez, *J. Org. Chem.* **1988**, *53*, 3437.
[3] W. A. Herrmann, *J. Organomet. Chem.* **1995**, *500*, 149.
[4] W. A. Herrmann, R. W. Fischer, W. Scherer, M. U. Rauch, *Angew. Chem.* **1993**, *105*, 1209–1212; *Angew. Chem. Int. Ed. Engl.* **1993**, *32*, 1157.
[5] A. N. Salanov, V. N. Bibin, *Surf. Sci.* **1999**, *441*, 399.
[6] Preliminary results for this reaction have been published previously.[10] However the assignments of the observed frequencies and the conclusions concering the structures of the obtained molecules were not correct.
[7] H.-J. Himmel, W. Schmid, R. Burgard, unpublished results.
[8] The first excited triplet state of $FAlO_2$ exhibits a slightly higher energy (by 38.2 kJ mol^{-1}).[9]
[9] J. Bahlo, H.-J. Himmel, H. Schnöckel, *Inorg. Chem.*, unpublished results.

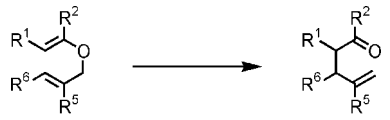
 © WILEY-VCH Verlag GmbH, D-69451 Weinheim, 2001 1433-7851/01/4024-4699 $ 17.50+.50/0

[10] R. Ahlrichs, L. Zhengyan, H. Schnöckel, *Z. Anorg. Allg. Chem.* **1984**, *519*, 155.
[11] G. V. Girichev, A. N. Utkin, N. I. Giricheva, *Izv. Vyssh. Uchebn. Zaved. Khim. Khim. Tekhnol.* **1983**, *26*, 634.
[12] The larger Al–O distance in **3** is in agreement with the values found in other highly coordinated Al compounds. For example, the Al–O bond lengths in the octahedral $[Al(O_2)(acac)_3]$ (acac = acetyl acetonate) complex is 1.89 Å (N. Ya. Turova, V. A. Kozunov, A. I. Yanovskii, N. G. Bokii, Yu. T. Struschkov, B. L. Tarnopolskii, *J. Inorg. Nucl. Chem.* **1979**, *41*, 5).
[13] The calculations give the following frequencies [in cm^{-1}] for the other isotopomers of **3** (with intensity [in $km\,mol^{-1}$] and symmetry assignment in parentheses): 1074.0 (3, a_1), 898.9 (149, a_1), 486.0 (10, a_1), 178.9 (18, a_1), 380.6 (0, a_2), 65.9 (0, a_2), 467.2 (2, b_1), 238.3 (38, b_1), 166.9 (0.03, b_1), 1071.0 (9, b_2), 694.2 (175, b_2), 199.6 (24, b_2) for $FAl(^{18}O_2)_2$, and 1136.8 (5, a_1), 899.8 (150, a_1), 496.2 (10, a_1), 182.5 (19, a_1), 390.8 (0, a_2), 67.8 (0, a_2), 479.9 (1, b_1), 240.2 (49, b_1), 171.4 (0.03, b_1), 1072.5 (6, b_2), 701.5 (177, b_2), 201.8 (24, b_2) for $FAl(^{16}O)_2(^{18}O)_2$.
[14] This relation reflects the influence of the coordination number. For example, f(Al–F) decreases from 501 in FAlO[15] to 200 $N\,m^{-1}$ in AlF_6^{3-}.[16, 17]
[15] H. Schnöckel, *J. Mol. Struct.* **1978**, *50*, 275.
[16] M. J. Reisfeld, *Spectrochim. Acta Part A* **1973**, *29*, 1923.
[17] E. J. Baran, A. E. Lavat, *Z. Naturforsch. A* **1981**, *36*, 677.
[18] C. D. Cook, P.-T. Cheng, S. C. Nyburg, *J. Am. Chem. Soc.* **1969**, *91*, 2123.
[19] N. Kitajima, K. Fujisawa, C. Fujimoto, Y. Moro-oka, S. Hashimoto, T. Kitagawa, K. Toriumi, K. Tatsumi, A. Nakamura, *J. Am. Chem. Soc.* **1992**, *114*, 1277.
[20] R. R. Smardzewski, L. Andrews, *J. Chem. Phys.* **1972**, *57*, 1327.
[21] L. Andrews, J. T. Yustein, *J. Phys. Chem.* **1993**, *93*, 12700.
[22] L. Andrews, J. T. Yustein, C. A. Thompson, R. D. Hunt, *J. Phys. Chem.* **1994**, *98*, 6514.
[23] L. Andrews, G. V. Chertihin, C. A. Thompson, J. Dillon, S. Byrne, C. W. Bauschlicher, Jr., *J. Phys. Chem.* **1996**, *100*, 10088.
[24] L. Andrews, G. P. Kushto, J. T. Yustein, E. Archibong, R. Sullivan, J. Leszczynski, *J. Phys. Chem. A* **1997**, *101*, 9077.
[25] L. V. Serebrennikov, S. B. Osin, A. A. Maltsev, *J. Mol. Struct.* **1982**, *81*, 25.
[26] I. V. Ovchinnikov, L. V. Serebrennikov, A. A. Maltsev, *Khim. Fak. Mosk. Gos. Univ.*, Moscow, **1984**.
[27] L. V. Serebrennikov, A. A. Mal'tsev, *Vestn. Mosk. Univ. Ser. 2: Khim.* **1985**, *26*, 137.
[28] T. R. Burkholder, J. T. Yustein, L. Andrews, *J. Phys. Chem.* **1992**, *96*, 10189.
[29] S. M. Sonchik, L. Andrews, K. D. Carlson, *J. Phys. Chem.* **1983**, *87*, 2004.
[30] B. Tremblay, P. Roy, L. Manceron, M. E. Alikhani, D. J. Roy, *Chem. Phys.* **1996**, *104*, 2773.
[31] A. Patyk, W. Sander, J. Gauss, D. Cremer, *Angew. Chem.* **1989**, *101*, 920; *Angew. Chem. Int. Ed. Engl.* **1989**, *28*, 898.
[32] A. Patyk, W. Sander, J. Gauss, D. Cremer, *Chem. Ber.* **1990**, *123*, 89.
[33] T. Mehner, H. J. Göcke, S. Schunck, H. Schnöckel, *Z. Anorg. Allg. Chem.* **1990**, *580*, 121.
[34] H. Schnöckel, S. Schunck, *Chem. Unserer Zeit* **1987**, *21*, 73.
[35] Gaussian 98 (Revision A.7), M. J. Frisch, G. W. Trucks, H. B. Schlegel, G. E. Scuseria, M. A. Robb, J. R. Cheeseman, V. G. Zakrzewski, J. A. Montgomery, R. E. Stratmann, J. C. Burant, S. Dapprich, J. M. Millam, A. D. Daniels, K. N. Kudin, M. C. Strain, O. Farkas, J. Tomasi, V. Barone, M. Cossi, R. Cammi, B. Mennucci, C. Pomelli, C. Adamo, S. Clifford, J. Ochterski, G. A. Petersson, P. Y. Ayala, Q. Cui, K. Morokuma, D. K. Malick, A. D. Rabuck, K. Raghavachari, J. B. Foresman, J. Cioslowski, J. V. Ortiz, A. G. Baboul, B. B. Stefanov, G. Liu, A. Liashenko, P. Piskorz, I. Komaromi, R. Gomperts, R. L. Martin, D. J. Fox, T. Keith, M. A. Al-Laham, C. Y. Peng, A. Nanayakkara, C. Gonzalez, M. Challacombe, P. M. W. Gill, B. G. Johnson, W. Chen, M. W. Wong, J. L. Andres, M. Head-Gordon, E. S. Replogle, J. A. Pople, Gaussian, Inc., Pittsburgh, PA, **1998**.
[36] K. Eichhorn, O. Treutler, H. Öhm, M. Häser, R. Ahlrichs, *Chem. Phys. Lett.* **1995**, *240*, 283.
[37] O. Treutler, R. Ahlrichs, *J. Chem. Phys.* **1995**, *102*, 346.

The Catalytic Enantioselective Claisen Rearrangement of an Allyl Vinyl Ether**

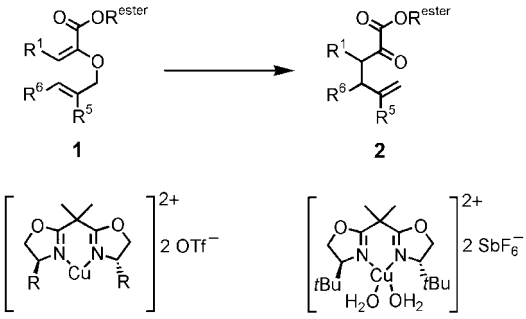
Lars Abraham, Regina Czerwonka, and Martin Hiersemann*

The [3,3]-sigmatropic rearrangement of an allyl vinyl ether was described by Claisen for the first time in 1912.[1] Since then this rearrangement, which was named after him, has been developed into one of the most powerful C–C bond forming methods (Scheme 1).[2] There are various approaches to carry out the Claisen rearrangement and related [3,3]-sigmatropic rearrangements enantioselectively by using chiral reagents.[3, 4] The only catalytic enantioselective [3,3]-sigmatropic rearrangement known to date was described for allyl imidates.[5] Yamamoto et al. used chiral Lewis acids based on Al^{III} for the enantioselective Claisen rearrangement of acyclic, aliphatic allyl vinyl ethers. However, 1–2 equivalents of the chiral Lewis acid are required and the range of substrates is very select.[6]



Scheme 1. The Claisen rearrangement of an allyl vinyl ether. Which catalysts are able to catalyze this process diastereo- and enantioselectively?

In our search for a chiral catalyst for the Claisen rearrangement of 2-alkoxycarbonyl-substituted allyl vinyl ethers **1**, we found the combination of $Cu(OTf)_2$ and a molecular sieve to be suitable.[7] In an extension of this work, we now report the use of chiral copper(II) bis(oxazoline) ([Cu^{II}(box)]) complexes as catalysts for the Claisen rearrangement (Scheme 2).



3 (R = Ph): [Cu{(*S*,*S*)-Ph-box}](OTf)$_2$ **5**: [Cu{(*S*,*S*)-*t*Bu-box}](H$_2$O)$_2$(SbF$_6$)$_2$
4 (R = *t*Bu): [Cu{(*S*,*S*)-*t*Bu-box}](OTf)$_2$

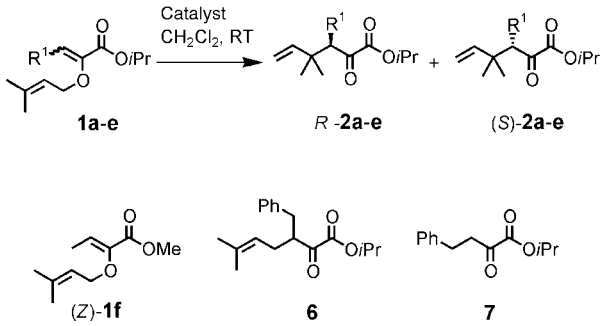
Scheme 2. General substrate structure and the catalysts used.

[*] Dr. M. Hiersemann, L. Abraham, R. Czerwonka
Institut für Organische Chemie
Technische Universität Dresden
01062 Dresden (Germany)
Fax: (+49) 351-463-33162
E-mail: martin.hiersemann@chemie.tu-dresden.de

[**] This work was financially supported by the Deutsche Forschungsgemeinschaft, the Fonds der Chemischen Industrie, and the Dr. Otto Röhm Gedächtnisstiftung. M.H. thanks Prof. P. Metz and Prof. H.-U. Reißig for their support.

 © WILEY-VCH Verlag GmbH, D-69451 Weinheim, 2001 1433-7851/01/4024-4700 $ 17.50+.50/0

Chiral [Cu^{II}(box)] complexes have proven to be suitable catalysts for a large number of reactions.[8, 9] In our investigations, we employed the commercially available Ph-BOX and *t*Bu-BOX ligands (Scheme 2). Initially, we investigated the [Cu^{II}(box)](OTf)$_2$ catalyzed Claisen rearrangement of allyl vinyl ethers in which only one center of chirality is formed during the rearrangement (Scheme 3, Table 1).[10] We could show that the catalyst (*S*,*S*)-**3** was able to catalyze the

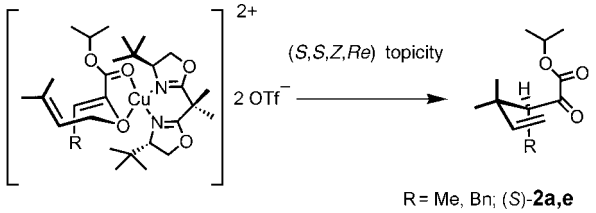


Scheme 3. Catalytic enantioselective Claisen rearrangement. Results are given in Table 1.

Claisen rearrangement of 1-methyl-6,6-dimethyl-substituted allyl vinyl ether **1a** with perfect chemoselectivity and very good enantioselectivity (Table 1, entries 1–5). A change in the configuration of the vinyl ether double bond or the absolute configuration of the catalyst led, as expected, to the reversal of the absolute configuration of the rearrangement product **2a** (Table 1, entries 1, 2, 5).[11] The catalyzed rearrangement was markedly slower with (*S*,*S*)-**4** as the catalyst (Table 1, entry 3). The combination of 4-Å molecular sieves and (*S*,*S*)-**4** showed a satisfactory reactivity and gave the highest enantiomeric excesses (Table 1, entry 4). Remarkably, we observed the same absolute configuration in the rearrangement product **2a** when (*S*,*S*)-**4** and (*R*,*R*)-**3** were used (Table 1, entries 2, 4). This effect was first described for the catalysis of the hetero-Diels–Alder reaction by [Cu^{II}(box)] catalysts.[13]

In addition to the methyl group, other alkyl and alkenyl groups are tolerated on C1 of the allyl vinyl ether (Table 1). The catalyzed rearrangement of the methyl ester (*Z*)-**1f** did not lead to an improvement in the enantioselectivity (Table 1, entry 14). In the catalyzed rearrangement of the 1-benzyl-substituted allyl vinyl ether (*Z*)-**1e**, (*S*,*S*)-**4** in combination with molecular sieves showed the highest enantioselectivity, however with an unacceptable reaction time of three days (Table 1, entry 11). Use of the cationic Cu^{II} complex (*S*,*S*)-**5** resulted in a drastic reduction in the chemoselectivity;[14] in addition to the Claisen rearrangement product **2e**, the [1,3]-rearrangement product **6**, and the α-oxoester **7** were isolated (Table 1, entry 12). Clearly, the more Lewis-acidic catalyst (*S*,*S*)-**5** can cause the dissociation of the allyl vinyl ether (*Z*)-**1e**, which results in the formation of the [1,3]-rearrangement product and can lead to the hydrolysis of the vinyl ether unit. Noteworthy is that the addition of molecular sieves in this case hinders the formation of the α-oxoester **7**. The catalysis of the Claisen rearrangement is also successful on a larger scale: the rearrangement of 4 mmol of the allyl vinyl ether (*Z*)-**1e** was catalyzed with only 0.5 mol% (*R*,*R*)-**3** when the reaction time was increased to 24 h (Table 1, entry 13).

The absolute configuration of the products that results from the use of (*S*,*S*)-**4** can be understood on the basis of known models (Scheme 4):[9] we assume that the allyl vinyl ether is coordinated to the Cu^{II} ion in a bidentate fashion. The formation of a chelate between the [Cu^{II}(box)] catalyst and the substrate is generally accepted as the prerequisite for a high enantioselectivity.[9] This chelation should lead to a relatively rigid, ideally planar arrangement of the box ligand,



Scheme 4. Model for the stereochemical pathway of the catalyzed Claisen rearrangement.

Table 1. Catalytic enantioselective Claisen rearrangements.

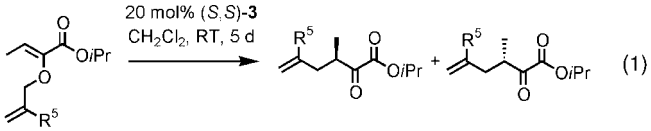
Entry	Substrate	R^1	*Z*:*E*	Catalyst	*t* [h]	Yield [%][a]	*R*:*S*[b]
1	(*Z*)-**1a**	methyl	96:4	5 mol% (*S*,*S*)-**3**	1	100	91:9
2	(*Z*)-**1a**	methyl	96:4	5 mol% (*R*,*R*)-**3**	1	100	9:91
3	(*Z*)-**1a**	methyl	96:4	10 mol% (*S*,*S*)-**4**	24	47[c]	6:94
4	(*Z*)-**1a**	methyl	96:4	10 mol% (*S*,*S*)-**4**[d]	24	99	6:94
5	(*E*)-**1a**	methyl	4:96	5 mol% (*S*,*S*)-**3**	1	99	9:91
6	(*Z*)-**1b**	ethyl	100:0	5 mol% (*S*,*S*)-**3**	2	99	92:8
7	(*Z*)-**1c**	2-propyl	90:10	5 mol% (*S*,*S*)-**3**	24	98	89:11
8	(*Z*)-**1d**	2-propenyl	100:0	5 mol% (*S*,*S*)-**3**	1	100	93:7
9	(*Z*)-**1e**	benzyl	97:3	5 mol% (S,*S*)-**3**	1	99	88:12
10	(*Z*)-**1e**	benzyl	97:3	10 mol% (*S*,*S*)-**4**	72	7[e]	–
11	(*Z*)-**1e**	benzyl	97:3	10 mol% (*S*,*S*)-**4**[d]	72	94[f]	8:92
12	(*Z*)-**1e**	benzyl	97:3	10 mol% (*S*,*S*)-**5**	24	62[g]	27:73
13	(*Z*)-**1e**	benzyl	97:3	0.5 mol% (*R*,*R*)-**3**[h]	24	100	12:88
14	(*Z*)-**1f**	methyl	100:0	5 mol% (*S*,*S*)-**3**	3	99	90:10

[a] Yield of isolated, analytically pure product after removal of the catalyst by filtration through a column of silica gel (4 × 0.5 cm). Reactions were carried out with 0.4 mmol substrate. [b] Determined by HPLC: Chiracel OD 14025, hexane:*i*PrOH 99.9:0.1. [c] In a mixture with 52% substrate. [d] Additionally with 4-Å molecular sieves. [e] In a mixture with 93% substrate. [f] In a mixture with 6% substrate. [g] In a mixture with 24% [1,3]-rearrangement product **6** and 13% α-oxoester **7**. [h] On a 4 mmol scale.

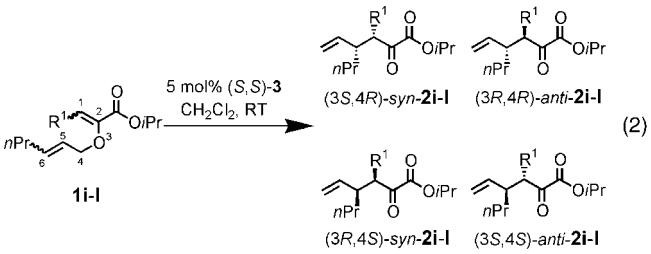
 © WILEY-VCH Verlag GmbH, D-69451 Weinheim, 2001 1433-7851/01/4024-4701 $ 17.50+.50/0

the Cu^{II} ion, and the vinyl ether unit. For a chair-shaped conformation of the allyl vinyl ether, the allyl unit would then approach the vinyl-ether double bond on the side opposite to the *tert*-butyl group of the BOX ligand. This direction of aproach leads to the favored *Re* attack on the *Z*-configured vinyl ether double bond during catalysis with (*S*,*S*)-**4**. Ultimately, this is, an enantiotopos-differentiating reaction in which the catalyst can distinguish between the two enantiotopic lone pairs on the oxygen atom of the allyl vinyl ether.

When we used the allyl vinyl ethers (*Z*)-**1g** and (*Z*)-**1h**, which are not substituted in the 6-position, we found that considerably greater concentrations of catalyst and longer reaction times were necessary, and lower enantioselectivities were obtained [Eq. (1)]. The diasteroselective construction of



two neighboring centers of chirality is one of the strengths of the thermal Claisen rearrangement.[2] Therefore, we investigated the conditions under which the inherent diastereoselectivity of the thermal Claisen rearrangement can be combined with the enantioselectivity of the catalyzed Claisen rearrangement [Eq. (2)]. Once again, in agreement with our results with the $Cu(OTf)_2$/molecular sieve catalyzed Claisen rearrangement, the diastereoselectivity of the Claisen rearrangement was dependent on the configuration of the allyl ether double bond (Table 2). Allyl vinyl ethers with a *Z*-configured allyl ether double bond rearranged with very good diastereo- and enantioselectivities (Table 2, entries 3–5, 7, 9, 10). The relative configuration of the rearrangement product can be determined by the choice of the configuration of the vinyl ether double bond (Table 2, entries 3, 4). The relationship between the configuration of the double bond in the allyl vinyl ether and the relative configuration of the rearrangement product is the same in this case as for the thermal rearrangement ("(*Z*,*Z*) to *syn*" and "(*E*,*Z*) to *anti*").[2] This observation indicates a chair-shaped transition state in the catalyzed Claisen rearrangement of the allyl vinyl ethers **1i**–**l** which have a *Z*-configured allyl ether double bond.



The catalyzed Claisen rearrangement of allyl vinyl ethers with an *E*-configured allyl ether double bond is generally not completely diastereoselective. The extent of the diastereoselectivity is dependent on the configuration of the vinyl ether double bond and on the substituent at C1 (Table 2, entries 1, 2, 6, 8). The preference for the *syn* diastereomer in the catalyzed rearrangement of the *Z*,*E*-configured 1-isopropyl-substituted allyl vinyl ether (*Z*,*E*)-**1k** is particularly remarkable because, on the basis of a chair-type transition state, the formation of an *anti* diastereomer is expected (Table 2, entry 8).[15]

We have presented here the first catalytic enantioselective Claisen rearrangement. We exploited the potential of chiral, Lewis-acidic, [Cu^{II}(box)] catalysts and the ability of our 2-alkoxycarbonyl-sustituted allyl vinyl ethers to complex in a bidentate mode and thus, were able to achieve excellent chemoselectivities and acceptable enantioselectivities. Our current work focuses on the improvement of the enantiomeric excesses and substrate tolerances by variation of the substrate structure and the catalyst.

Experimental Section

General procedure: A mixture of the ligand (6–22 mol%) and $Cu(OTf)_2$ (5–20 mol%) in CH_2Cl_2 (2 mL) was stirred in a round-bottomed flask under argon at room temperature for 1–3 h. Subsequently, the corresponding allyl vinyl ether (0.4 mmol) in CH_2Cl_2 (2 mL) was added. After stirring for a suitable reaction time, the catalyst was removed by filtration of the reaction solution through a short column of silica gel (4 × 0.5 cm). The solvent was removed and the residue dried in a high vacuum to give the rearrangement product, which was generally an analytically pure colorless oil.

Received: August 8, 2001 [Z 17689]

Table 2. Diastereo- and enantioselectivity of the catalyzed Claisen rearrangement.

Entry	Substrate	R^1	Config.	*t* [h][a]	Yield [%][b]	*syn*:*anti*[c]	*ee* [%][d]
1	(*E*,*E*)-**1i**	methyl	1*E*,5*E*	12	100	86:14	82 (*3S,4R*)
2	(*Z*,*E*)-**1i**	methyl	1*Z*,5E	4	100	28:72	72 (*3R,4R*)
3	(*E*,*Z*)-**1i**	methyl	1*E*,5*Z*	38	99	3:97	88 (*3S,4S*)
4	(*Z*,*Z*)-**1i**	methyl	1*Z*,5*Z*	38	98	99:1	84 (*3R,4S*)
5	(*Z*,*Z*)-**1i**	methyl	1*Z*,5*Z*	12[e]	99	96:4	84 (3*R*,4*S*)
6	(*Z*,*E*)-**1j**	benzyl	1*Z*,5*E*	6	100	44:56	n.d.[f]
7	(*Z*,*Z*)-**1j**	benzyl	1*Z*,5*Z*	48	100	95:5	82 (*3R,4S*)
8	(*Z*,*E*)-**1k**	2-propyl	1*Z*,5*E*	7	96[g]	85:15	n.d.[f]
9	(*Z*,*Z*)-**1k**	2-propyl	1*Z*,5*Z*	24[h]	97	94:6	n.d.[f]
10	(*Z*,*Z*)-**1l**	2-propenyl	1*Z*,5*Z*	24	98	92:8	86 (*3R,4S*)

[a] Reaction time not optimized. [b] Yield of isolated, analytically pure product after removal of the catalyst by filtration through a column of silica gel (4 × 0.5 cm). Reactions were carried out with 0.4 mmol substrate. [c] Determined from the ^{1}H NMR spectra. [d] Determined by HPLC: Chiracel OD1 14025, hexane:*i*PrOH 99.9:0.1. Absolute configuration assigned by assumption of a (*S*,*S*,1*Z*,1*Si*) or (*S*,*S*,1*E*,1*Re*) topicity of a chair-shaped transition state. The *ee* value of the minor diastereomer could not be determined. [e] With 10 mol% catalyst. [f] n.d. = not determined. [g] In a mixture with 4% substrate. [h] With 7.5 mol% catalyst.

 © WILEY-VCH Verlag GmbH, D-69451 Weinheim, 2001 1433-7851/01/4024-4702 $ 17.50+.50/0

[1] L. Claisen, *Ber. Dtsch. Chem. Ges.* **1912**, *45*, 3157 – 3166.

[2] Reviews: a) F. E. Ziegler, *Chem. Rev.* **1988**, *88*, 1423 – 1452; b) H. Frauenrath in *Methods Org. Chem.* (*Houben-Weyl*) *4th ed. 1952* – , *Vol. E21d*, **1995**, pp. 3301 – 3756.

[3] T. P. Yoon, D. W. C. McMillan, *J. Am. Chem. Soc.* **2001**, *123*, 2911 – 2912.

[4] Reviews: a) H. Ito, T. Taguchi, *Chem. Soc. Rev.* **1999**, *28*, 43 – 50; b) D. Enders, M. Knopp, R. Schiffers, *Tetrahedron: Asymmetry* **1996**, *7*, 1847 – 1882.

[5] a) Y. Jiang, J. M. Longmire, X. Zhang, *Tetrahedron Lett.* **1999**, *40*, 1449 – 1450; b) Y. Donde, L. E. Overman, *J. Am. Chem. Soc.* **1999**, *121*, 2933 – 2934; c) Y. Uozumi, K. Kato, T. Hayashi, *Tetrahedron: Asymmetry* **1998**, *9*, 1065 – 1072; d) F. Cohen, L. E. Overman *Tetrahedron: Asymmetry* **1998**, *9*, 3213 – 3222; e) T. K. Hollis, L. E. Overman, *Tetrahedron Lett.* **1997**, *38*, 8837 – 8840; f) M. Calter, T. K. Hollis, L. E. Overman, J. Ziller, G. G. Zipp, *J. Org. Chem.* **1997**, *62*, 1449 – 1456.

[6] a) K. Maruoka, H. Banno, H. Yamamoto, *J. Am. Chem. Soc.* **1990**, *112*, 7791 – 7793; b) K. Maruoka, H. Yamamoto, *Synlett* **1991**, 793 – 794; c) K. Maruoka, H. Banno, H. Yamamoto, *Tetrahedron: Asymmetry* **1991**, *2*, 647 – 662.

[7] M. Hiersemann, L. Abraham, *Org. Lett.* **2001**, *3*, 49 – 52.

[8] See the cited literature in W. Zhuang, N. Gathergood, R. G. Hazell, K. A. Jørgensen, *J. Org. Chem.* **2001**, *66*, 1009 – 1013.

[9] Reviews: a) J. S. Johnson, D. A. Evans, *Acc. Chem. Res.* **2000**, *33*, 325 – 335; b) D. A. Evans, T. Rovis, J. S. Johnson, *Pure Appl. Chem.* **1999**, *71*, 1407 – 1415; c) A. K. Gosh, P. Mathivanan, J. Cappiello, *Tetrahedron: Asymmetry* **1998**, *9*, 1 – 45.

[10] The synthesis of the 2-alkoxycarbonyl-substituted allyl vinyl ethers corresponding to our procedure and subsequent separation of the vinyl ether double bond isomers by preparative HPLC: M. Hiersemann, *Synthesis* **2000**, 1279 – 1290.

[11] The absolute configuration was determined for, among others, the rearrangement product **2e** by chemical correlation using the auxiliary method of Evans et al.[12] Alkylation of (*S*)-3-(3,3-dimethyl-pent-4-enoyl)-4-isopropyl-oxazolidine-2-one (lithium diisopropylamide (LDA), THF, $-78\,^{\circ}C$, then benzyl bromide; 76%), and subsequent reductive cleavage of the auxiliary group ($LiAlH_4$), THF, $-78\,^{\circ}C \rightarrow RT$; 16%) gave the alcohol (*S*)-(−)-2-benzyl-3,3-dimethyl-pent-4-en-1-ol with >95% *ee*. The reduction of **2e** (Table 1, entry 13) to the diol ($LiAlH_4$, THF, $-78\,^{\circ}C \rightarrow RT$) and subsequent oxidative cleavage ($NaIO_4$, THF/H_2O, RT, 20 min) followed by a second reduction ($NaBH_4$, EtOH) gave (*S*)-(−)-2-benzyl-3,3-dimethyl-pent-4-en-1-ol with 79% *ee* (85% over the three steps).

[12] D. A. Evans, M. D. Ennis, D. J. Mathre, *J. Am. Chem. Soc.* **1982**, *104*, 1737 – 1739.

[13] a) M. Johannsen, K. A. Jørgensen, *J. Org. Chem.* **1995**, *60*, 5757 – 5762; b) D. A. Evans, J. S. Johnson, C. S. Burgey, K. R. Campos, *Tetrahedron Lett.* **1999**, *40*, 2879 – 2828; b) K. A. Jørgensen, *Angew. Chem.* **2000**, *112*, 3702 – 3733; *Angew. Chem.* **2000**, *39*, 3558 – 3588.

[14] D. A. Evans, S. W. Tregay, C. S. Burgey, N. A. Paras, T. Vojkovsky, *J. Am. Chem. Soc.* **2000**, *122*, 7936 – 7943.

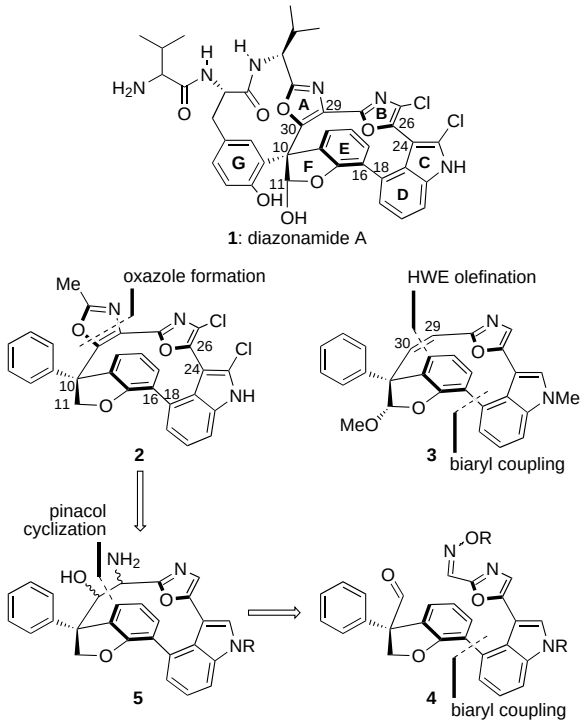
[15] The thermal rearrangement of all the allyl vinyl ethers described here led, with very high to complete diastereoselectivity, to the diastereomer with the relative configuration that can be explained by the assumption of a chair-shaped transition state during the rearrangement.

 © WILEY-VCH Verlag GmbH, D-69451 Weinheim, 2001 1433-7851/01/4024-4703 $ 17.50+.50/0

Construction of the Complete Aromatic Core of Diazonamide A by a Novel Hetero Pinacol Macrocyclization Cascade Reaction**

K. C. Nicolaou,* Xianhai Huang, Nicolas Giuseppone, Paraselli Bheema Rao, Marco Bella, Mali V. Reddy, and Scott A. Snyder

In 1991, Fenical and Clardy disclosed the structure of diazonamide A (**1**, Scheme 1), a secondary metabolite isolated from the colonial ascidian *Diazona chinensis*, whose unprecedented molecular architecture includes a cyclic polypeptide backbone, a strained halogenated heteroaromatic core trapped as a single atropisomer, and a lone quaternary center at the epicenter of the two major macrocyclic subunits.[1] Significant synthetic efforts have been directed towards diazonamide A by a number of laboratories around the world because of the unique challenges posed by this structural framework, its impressive in vitro cytotoxicity, and the inability to harvest additional material from the original source.[2] However, despite much progress, a route to this fascinating compound still remains elusive.



Scheme 1. Structure of diazonamide A (**1**) and retrosynthetic analysis of model system **2**.

To date, the majority of synthetic approaches derive from two distinct retrosynthetic analyses of the diazonamide problem, namely initial synthesis of the peptide framework (the AG macrocycle) with late-stage closure of the C_{16}–C_{18} bond, or alternatively, early introduction of the C_{16}–C_{18} biaryl axis followed by a macrocyclization event to form the crucial C_{29}–C_{30} linkage with subsequent A-ring oxazole synthesis. Although advanced synthetic intermediates have proven recalcitrant in the face of intensive efforts to forge the C_{16}–C_{18} bond in the former approach,[2c] the overall viability of the latter retrosynthetic blueprint has been verified based on studies in which we developed a highly convergent route to **3** (Scheme 1) by calling upon the power of the Suzuki and Horner–Wadsworth–Emmons (HWE) reactions to generate the C_{16}–C_{18} biaryl linkage and the C_{29}–C_{30} alkene, respectively.[3] In addition, an approach in which C_{29}–C_{30} bond formation was accomplished by Dieckmann condensation also realizes this goal.[2b] Herein, we report the elaboration of the previously synthesized **3** to the complete ABCDEF macrocycle as well as the development of a novel and concise hetero pinacol macrocyclization cascade sequence induced by SmI_2/HMPA which enables access to the parent 12-membered diazonamide model system **2** (Scheme 1) in only sixteen linear steps.

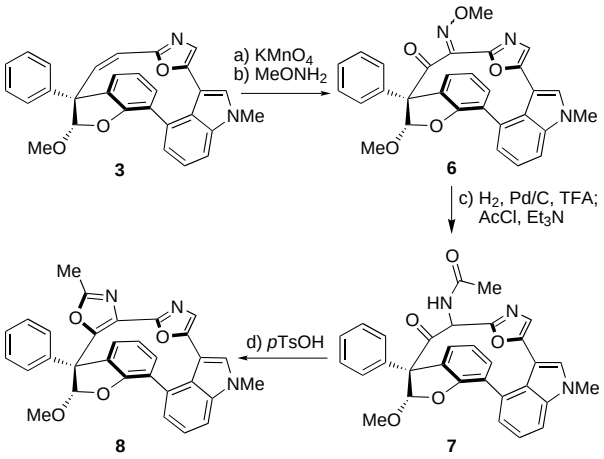
Shortly after our disclosure of **3**,[3] we established that the final A-ring oxazole of the diazonamide skeleton could be fashioned from the C_{29}–C_{30} olefinic residue by following a four step sequence as delineated in Scheme 2. First, exposure of **3** to $KMnO_4$ in acetic anhydride[4] led to the formation of a diketone, which was then transformed to **6** by selective conversion of the more activated and less sterically hindered carbonyl group to its corresponding methoxime derivative. Significantly, although dihydroxylation of the alkene in **3** could readily be achieved using stoichiometric amounts of OsO_4 activated by quinuclidine,[5] the resulting diol proved highly unstable as it decomposed rapidly both in solution and during isolation, which led to the near exclusive formation of benzofuran side products by the cyclofragmentation pathway we have observed frequently in this type of system.[6] With **6** in hand, the oxime function was reductively cleaved through hydrogenolysis in acidified methanol.[7] Subsequent in situ acetylation of the resultant amine using AcCl furnished acetamide **7**. Finally, formation of the desired oxazole ring in **8** was achieved from **7** by Gabriel–Robinson cyclodehydration initiated by *p*TsOH in refluxing benzene (50% yield);[8] significantly, no other condition screened proved equally effective for this oxazole formation.[9]

Overall, although the above route proved successful for completion of the aromatic core of diazonamide A, the

[*] Prof. Dr. K. C. Nicolaou, Dr. X. Huang, Dr. N. Giuseppone, Dr. P. Bheema Rao, Dr. M. Bella, Dr. M. V. Reddy, S. A. Snyder
Department of Chemistry and The Skaggs Institute for Chemical Biology
The Scripps Research Institute
10550 North Torrey Pines Road, La Jolla, CA 92037 (USA)
Fax: (+1) 858-784-2469
and
Department of Chemistry and Biochemistry
University of California San Diego
9500 Gilman Drive, La Jolla, CA 92093 (USA)
E-mail: kcn@scripps.edu

[**] We thank Drs. D. H. Huang and G. Suizdak for NMR spectroscopic and mass spectrometric assistance, respectively. Financial support for this work was provided by The Skaggs Institute for Chemical Biology, the National Institutes of Health (USA), American Biosciences, a predoctoral fellowship from the National Science Foundation (S.A.S.), a postdoctoral fellowship from the Association pour la Recherche sur le Cancer (N.G.), and grants from Abbott, Amgen, Array Biopharma, Boehringer-Ingelheim, Glaxo, Hoffmann-LaRoche, DuPont, Merck, Novartis, Pfizer, and Schering Plough.

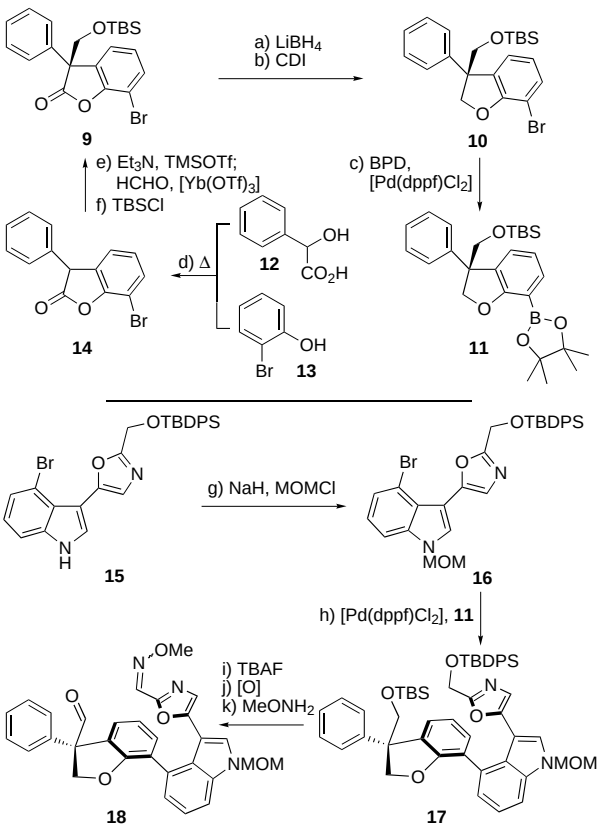
Supporting information for this article is available on the WWW under http://www.angewandte.com or from the author.



Scheme 2. Initial model studies which led to the complete heteroaromatic skeleton (**8**) of diazonamide A: a) $KMnO_4$ (6.0 equiv), Ac_2O, 0 °C, 2 h, 35 %; b) $MeONH_2 \cdot HCl$ (20 equiv), EtOH, 25 °C, 12 h, 95 %; c) Pd/C (10 %, 2.0 equiv), H_2 (3.0 atm), TFA/MeOH (1:20), 25 °C, 12 h; then AcCl (3.0 equiv), Et_3N (3.0 equiv), CH_2Cl_2, 25 °C, 30 min, 80 %; d) *p*TsOH, benzene, 80 °C, 20 h, 50 %. TFA = trifluoroacetic acid, *p*TsOH = *p*-toluenesulfonic acid.

relatively modest yields observed for initial HWE closure to generate **3** as well as for diketone formation suggested that it would be potentially challenging to process sufficient material by using the developed sequence to complete the total synthesis of diazonamide A in the context of a fully elaborated G ring. As such, we sought a second-generation strategy to prepare model system **2** (Scheme 1). Mindful of our previous use of the McMurry reaction to form the challenging eight-membered ring in our total synthesis of Taxol,[10] we hypothesized that we could enlist a hetero pinacol coupling reaction to fashion a fully functionalized C_{29}–C_{30} bond directly suitable for A-ring oxazole formation (**5**, Scheme 1) from a percursor aldehyde – oxime (**4**). Since the pioneering efforts from the groups of Corey, Hart, and Bartlett,[11] which established oximes as highly competent radical acceptors in reductive cyclizations, numerous examples of hetero pinacol coupling reactions of alkyl, vinyl, and ketyl radicals with oxime ethers have been reported in both inter-[12] and intramolecular[13] contexts. To the best of our knowledge, however, this variant of the pinacol reaction has not yet been successfully applied in a macrocyclization reaction to generate a ring size greater than seven, despite precedent for medium-size ring formation in related systems in which dialdehydes were employed.[14] As such, the diazonamide problem offered a unique and challenging test for the power of this synthetic methodology.

To pursue this idea, the requisite synthetic fragments were prepared as shown in Scheme 3, commencing from the previously reported lactone **9** (prepared in nine steps from known starting materials).[3] Complete reduction of the lactone with $LiBH_4$ was followed by the smooth formation of dihydrobenzofuran **10** in 95 % yield upon heating the resultant diol with 1,1′-carbonyldiimidazole in THF at reflux, a result which has been previously reported in related systems except under far more forcing conditions.[15] Subsequent conversion of **10** to boronate **11** was then achieved in 70 % yield by using the conditions developed by Ishiyama et al.[16] For the



Scheme 3. Synthesis of key intermediate **18**: a) $LiBH_4$ (8.0 equiv), THF, 25 °C, 4 h, 95 %; b) CDI (2.0 equiv), THF, reflux, 2 h, 95 %; c) BPD (1.2 equiv), $[Pd(dppf)Cl_2] \cdot CH_2Cl_2$ (0.2 equiv), KOAc (3.0 equiv), DMSO, 90 °C, 6 h, 70 %; d) **12** (1.0 equiv), **13** (1.0 equiv), H_2SO_4 (70 % aq.), 45 min, 42% (95% based on recovered **13**); e) Et_3N (3.0 equiv), TMSOTf (1.2 equiv), CH_2Cl_2, 0 °C, 1 h; then HCHO (37 % in H_2O, 5.0 equiv), $[Yb(OTf)_3]$ (0.1 equiv), THF, 25 °C, 24 h, 78 %; f) TBSCl (3.0 equiv), imidazole (6.0 equiv), DMF, 25 °C, 6 h, 95 %; g) NaH (2.0 equiv), THF, 0 °C, 5 min; then MOMCl (2.0 equiv), THF, 0 °C, 10 min, 94 %; h) **11** (1.0 equiv), $[Pd(dppf)Cl_2] \cdot CH_2Cl_2$ (0.2 equiv), K_2CO_3 (5.0 equiv), DME, 110 °C, 8 h, 66 %; i) TBAF (3.0 equiv), THF, 25 °C, 10 min, 93 %; j) Dess – Martin periodinane (3.0 equiv), $NaHCO_3$ (10 equiv), CH_2Cl_2, 25 °C, 1 h, 88 %; k) $MeONH_2 \cdot HCl$ (10 equiv), DMSO, 25 °C, 10 min, 91 %. CDI = 1,1′-carbonyldiimidazole, BPD = bis(pinacolato)diboron, dppf = (diphenylphosphanyl)ferrocene, LiHMDS = lithium salt of 1,1,1,3,3,3-hexamethyldisilazane, TBS = *tert*-butyldimethylsilyl, TBDPS = *tert*-butyldiphenylsilyl, MOM = methoxymethyl, TBAF = tetrabutylammonium fluoride.

purposes of this model study, lactone **9** was also accessed through initial reaction of mandelic acid (**12**) with 2-bromophenol (**13**) using Padwa's method,[17] followed by facile elaboration of **14** to **9**,[18] which enabled the synthesis of boronate **11** in just six linear synthetic operations.

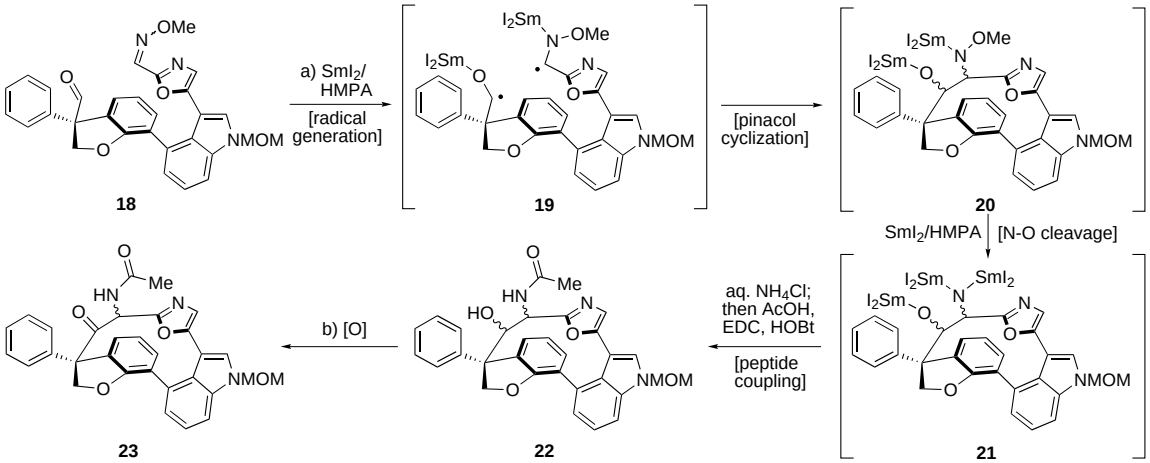
Next, the previously reported indole – oxazole **15**[3] (available in six steps from 4-bromoindole) was protected as its MOM ether (**16**) in 94 % yield by a standard protocol. In a final series of steps, **11** and **16** were smoothly coupled by using $[Pd(dppf)Cl_2]$ and K_2CO_3 in DME at 105 °C[16] to afford **17** in 66 % yield. Finally, a tandem deprotection – oxidation sequence cleanly provided an intermediate dialdehyde, with the more activated benzylic aldehyde selectively engaged as a methyloxime ether upon exposure to excess methoxylamine hydrochloride in DMSO (75 % overall for three steps). With **18** in hand, the stage was set to attempt the critical hetero pinacol macrocyclization.

 © WILEY-VCH Verlag GmbH, D-69451 Weinheim, 2001 1433-7851/01/4024-4706 $ 17.50+.50/0 *Angew. Chem. Int. Ed.* **2001**, *40*, No. 24

In assessing reaction conditions to initially screen, the power of SmI_2[19] seemed uniquely suited for our purposes, and the recent reports of SmI_2-induced scission of the N–O bond of oximes[20] suggested that it might be possible to effect a cascade sequence involving macrocyclization followed by in situ N–O cleavage to generate an amino alcohol such as **5** (Scheme 1) directly. However, despite extensive literature searches, we could find only one isolated example of reductive cyclization with subsequent oxime cleavage in the presence of SmI_2,[21] in which the use of a large excess of SmI_2 (6.0 equiv) followed by prolonged treatment with deoxygenated H_2O[22] led to an amino alcohol product. In light of the fact that there are no other reports of amino alcohol products arising from SmI_2-induced reductive cyclization, in which typically only three to four equivalents of SmI_2 are employed, we hypothesized that only through the use of a gross excess of SmI_2 in conjunction with a donor ligand additive such as HMPA would the desired cascade sequence proceed.

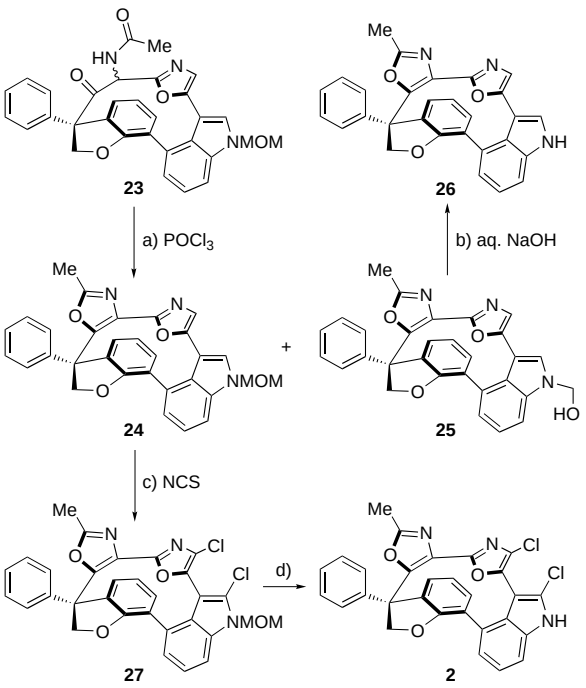
Most gratifyingly, after treatment of aldehyde–oxime **18** with a premixed complex of 9.0 equiv of SmI_2 and 36.0 equiv of HMPA in THF at ambient temperature for 1 h, followed by quenching with aqueous NH_4Cl, extraction, solvent removal, and subsequent peptide coupling with a DMF solution of AcOH, EDC, and HOBt, we observed the formation of compound **22** as a mixture of stereoisomers in 25% overall yield (Scheme 4). In the event, we believe that initial exposure of **18** to SmI_2/HMPA led to the generation of diradical intermediate **19**, which then cyclized to provide **20**. The presence of excess SmI_2 complexed with HMPA then effected N–O cleavage, which first led to intermediate **21**, and then provided the desired amino alcohol upon workup which was trapped as its acetamide (**22**). As such, each step in the cascade proceeded in an average yield of 63%. Although one could also envision solely the generation of a ketyl radical which then engaged the oxime directly to provide **20**, the isolation of noncyclized material with both the aldehyde and oxime reduced suggests that diradical **19** cannot be excluded. In accordance with earlier reports exploring aldehyde–oximes,[13a,e] the macrocyclization did not proceed at all in the absence of HMPA. Significantly, when the ratio of HMPA/SmI_2 was reduced from 4:1 to 2:1 (still with 9.0 equiv of SmI_2), **22** was observed along with significant amounts of cyclized product with the N–O linkage firmly intact, indicating that the presence of a suitable donor ligand in conjunction with excess SmI_2 is the critical combination required for reliable oxime cleavage after reductive cyclization. Moreover, these results suggest that in cases where one wishes to effect only N–O cleavage, the addition of HMPA might greatly facilitate the transformation in cases which prove difficult or low-yielding with SmI_2 alone.[20a,c] This proposition, along with an exploration of the generality of this cascade sequence, is the subject of current investigations. Finally, one should note that the final peptide coupling is a highly general reaction and L-valine amino acids bearing Fmoc, Boc, and Cbz protecting groups were readily coupled in yields comparable to those obtained with AcOH. This procedure represents a step forward in terms of overall synthetic utility, since previous reports have only indicated that products from SmI_2 reactions could be trapped directly with simple acylating reagents.

After the desired cascade sequence, oxidation of **22** to ketoamide **23** was smoothly effected with Dess–Martin periodinane in 94% yield. As shown in Scheme 5, formation of the A-ring oxazole was then accomplished by heating **23** in neat $POCl_3$ at 70 °C for 2 h, providing **24** and **25** in a ratio of 2.4:1 and in an overall yield of 65%.[23] The formation of **25** was significant in that it indicated that MOM cleavage was far more facile with the heterocyclic skeleton completed, since numerous synthetic precursors such as **16** were recovered unscathed under these reaction conditions.[24] Simply treating **25** with aqueous NaOH in THF[25] then readily effected the expulsion of formaldehyde which led to the fully deprotected diazonamide skeleton **26**. Additionally, the A-ring oxazole could also be fashioned from **23** with *p*TsOH in refluxing benzene, albeit in lower yield with prolonged reaction times, whereas the use of the Burgess reagent in refluxing THF[26] afforded **24** exclusively in comparable yield to that obtained with $POCl_3$.



Scheme 4. Novel pinacol coupling cascade sequence to efficiently prepare ketoamide **23**. a) SmI_2 (0.1M in THF, 9.0 equiv), HMPA (36 equiv), THF, 25 °C, 1 h; then saturated aq. NH_4Cl, 25 °C, 1 h; solvent removal; then AcOH (3.0 equiv), EDC (3.0 equiv), HOBt (3.0 equiv), DMF, 25 °C, 4 h, 25% overall, 63% per synthetic operation in the cascade sequence; b) Dess–Martin periodinane (15 equiv), $NaHCO_3$ (50 equiv), CH_2Cl_2, 25 °C, 1.5 h, 94%. HMPA = hexamethylphosphoramide, EDC = 3-(3-dimethylaminopropyl)-1-ethylcarbodiimide, HOBt = 1-hydroxy-1*H*-benzotriazole.

 © WILEY-VCH Verlag GmbH, D-69451 Weinheim, 2001 1433-7851/01/4024-4707 $ 17.50+.50/0



Scheme 5. Completion of the synthesis of the fully elaborated heterocyclic skeleton **2** of diazonamide A (**1**). a) $POCl_3$, 70 °C, 2 h, **24**/**25** (2.4:1), 65 %; b) aq. NaOH (15 %, excess), THF, 25 °C, 10 min, 74 %; c) NCS (3.0 equiv), THF/CCl_4 (1:1), 55 °C, 8 h, 73 %; d) BBr_3 (1.0 M in CH_2Cl_2, 2.0 equiv), CH_2Cl_2, −78 °C, 20 min; then aq. NaOH (15 %, excess), THF, 25 °C, 10 min, 61 %.

In a final study, exposure of **24** to 3.0 equiv of NCS in THF/CCl_4 (1:1) at 55 °C for 10 h cleanly provided dichloro compound **27** as a single atropisomer along the C_{24}–C_{26} biaryl axis. Formation of the ABCDEF macrocycle prior to chlorination was critical for the selectivity of this reaction, as chlorination of earlier synthetic intermediates such as **17** proceeded with equal facility, but provided a 1:1 mixture of atropisomers which could not be interconverted in CD_3CN at 340 K over 30 min. Subsequent use of BBr_3 in CH_2Cl_2 at −78 °C for 20 min led to the exclusive cleavage of the methyl ether linkage of the MOM protecting group in **27**, which upon immediate treatment with aqueous NaOH completed the synthesis of **2** in just sixteen linear steps from known or commercially available starting materials.[27]

In summary, the entire highly strained ABCDEF aromatic core of diazonamide A has been constructed and a novel samarium(II)-based macrocyclization cascade reaction has been developed. Applications of the gathered knowledge and developed technology to the total synthesis of diazonamide A and analogues thereof for chemical biology studies are anticipated.

Received: September 21, 2001 [Z17940]

[1] N. Lindquist, W. Fenical, G. D. Van Duyne, J. Clardy, *J. Am. Chem. Soc.* **1991**, *113*, 2303 – 2304.

[2] a) P. Magnus, C. Lescop, *Tetrahedron Lett.* **2001**, *42*, 7193 – 7196; b) E. Vedejs, M. A. Zajac, *Org. Lett.* **2001**, *3*, 2451 – 2454; c) J. Li, X. Chen, A. W. G. Burgett, P. G. Harran, *Angew. Chem.* **2001**, *113*, 2754 – 2757; *Angew. Chem. Int. Ed.* **2001**, *40*, 2682 – 2685; d) P. Wipf, J.-L. Methot, *Org. Lett.* **2001**, *3*, 1261 – 1264; e) J. D. Kriesberg, P. Magnus, E. G. McIver, *Tetrahedron Lett.* **2001**, *42*, 627 – 629; f) A. Radspieler, J. Liebscher, *Synthesis* **2001**, 745 – 750; g) D. E. Fuerst, B. M. Stoltz, J. L. Wood, *Org. Lett.* **2000**, *2*, 3521 – 3523; h) X. Chen, L. Esser, P. G. Harran, *Angew. Chem.* **2000**, *112*, 967 – 970; *Angew. Chem. Int. Ed.* **2000**, *39*, 937 – 940; i) E. Vedejs, J. Wang, *Org. Lett.* **2000**, *2*, 1031 – 1032; j) E. Vedejs, D. A. Barba, *Org. Lett.* **2000**, *2*, 1033 – 1035; k) P. Magnus, E. G. McIver, *Tetrahedron Lett.* **2000**, *41*, 831 – 834; l) F. Chan, P. Magnus, E. G. McIver, *Tetrahedron Lett.* **2000**, *41*, 835 – 838; m) F. Lach, C. J. Moody, *Tetrahedron Lett.* **2000**, *41*, 6893 – 6896; n) M. C. Bagley, S. L. Hind, C. J. Moody *Tetrahedron Lett.* **2000**, *41*, 6897 – 6900; o) M. C. Bagley, C. J. Moody, A. G. Pepper, *Tetrahedron Lett.* **2000**, *41*, 6901 – 6904; p) H. C. Hang, E. Drotleff, G. I. Elliott, T. A. Ritsema, J. P. Konopelski, *Synthesis* **1999**, 398 – 400; q) P. Magnus, J. D. Kreisberg, *Tetrahedron Lett.* **1999**, *40*, 451 – 454; r) A. Boto, M. Ling, G. Meek, G. Pattenden, *Tetrahedron Lett.* **1998**, *39*, 8167 – 8170; s) P. Wipf, F. Yokokawa, *Tetrahedron Lett.* **1998**, *39*, 2223 – 2226; t) S. Jeong, X. Chen, P. G. Harran, *J. Org. Chem.* **1998**, *63*, 8640 – 8641; u) C. J. Moody, K. J. Doyle, M. C. Elliott, T. J. Mowlem, *J. Chem. Soc. Perkin Trans. 1* **1997**, 2413 – 2419; v) J. P. Konolpelski, J. M. Hottenroth, H. M. Oltra, E. A. Veliz, Z. C. Yang, *Synlett* **1996**, 609 – 611; w) C. J. Moody, K. J. Doyle, M. C. Elliott, T. J. Mowlem, *Pure Appl. Chem.* **1994**, *66*, 2107 – 2110.

[3] K. C. Nicolaou, S. A. Snyder, K. B. Simonsen, A. E. Koumbis, *Angew. Chem.* **2000**, *112*, 3615 – 3620; *Angew. Chem. Int. Ed.* **2000**, *39*, 3473 – 3478.

[4] K. B. Sharpless, R. F. Lauer, O. Repic, A. Y. Teranishi, D. R. Williams, *J. Am. Chem. Soc.* **1971**, *93*, 3303 – 3304.

[5] a) F. He, Y. Bo, J. D. Altom, E. J. Corey, *J. Am. Chem. Soc.* **1999**, *121*, 6771 – 6772; b) E. J. Corey, S. Sarshar, M. D. Azimioara, R. Newbold, M. C. Noe, *J. Am. Chem. Soc.* **1996**, *118*, 7851 – 7852.

[6] K. C. Nicolaou, S. A. Snyder, A. Bigot, J. A. Pfefferkorn, *Angew. Chem.* **2000**, *112*, 1135 – 1138; *Angew. Chem. Int. Ed.* **2000**, *39*, 1093 – 1096.

[7] M. Hudlicky, *Reductions in Organic Chemistry*, ACS Monograph 188, American Chemical Society, **1996**, pp. 149 – 189.

[8] R. L. Parsons, C. H. Heathcock, *J. Org. Chem.* **1994**, *59*, 4733 – 4734.

[9] Use of Martin's sulfurane as well as variants of the Gabriel – Robinson cyclodehydration such as $PPh_3/Cl_6C_2/Et_3N$ (see P. Wipf, C. P. Miller, *J. Org. Chem.* **1993**, *58*, 3604 – 3606) failed to deliver the desired compound. In a related system, *p*TsOH in toluene was the reported condition employed for oxazole formation (see ref. [2d]).

[10] K. C. Nicolaou, Z. Yang, J. J. Liu, H. Ueno, P. G. Nantermet, R. K. Guy, C. F. Claiborne, J. Renaud, E. A. Couladouros, K. Palvannan, E. J. Sorensen, *Nature* **1994**, *367*, 630 – 633.

[11] a) E. J. Corey, S. G. Pyne, *Tetrahedron Lett.* **1983**, *24*, 2821 – 2824; b) D. J. Hart, F. L. Seely, *J. Am. Chem. Soc.* **1988**, *110*, 1631 – 1633; c) P. A. Bartlett, K. L. McLaren, P. C. Ting, *J. Am. Chem. Soc.* **1988**, *110*, 1633 – 1634.

[12] For selected examples, see: a) T. Hanamoto, J. Inanaga, *Tetrahedron Lett.* **1991**, *32*, 3555 – 3556; b) H. Miyabe, R. Shibata, C. Ushiro, T. Naito, *Tetrahedron Lett.* **1998**, *39*, 631 – 634.

[13] For selected examples, see: a) D. Riber, R. Hazell, T. Skrydstrup, *J. Org. Chem.* **2000**, *65*, 5382 – 5390; b) G. E. Keck, T. T. Wager, J. F. D. Rodriguez, *J. Am. Chem. Soc.* **1999**, *121*, 5176 – 5190; c) G. E. Keck, S. F. McHardy, J. A. Murry, *J. Org. Chem.* **1999**, *64*, 4465 – 4476; d) J. Tormo, D. S. Hays, G. C. Fu, *J. Org. Chem.* **1998**, *63*, 201 – 202; e) H. Miyabe, M. Torieda, K. Inoue, K. Tajiri, T. Kiguchi, T. Naito, *J. Org. Chem.* **1998**, *63*, 4397 – 4407; f) G. E. Keck, T. T. Wager, *J. Org. Chem.* **1996**, *61*, 8366 – 8367; g) T. Kiguchi, K. Tajiri, I. Ninomiya, T. Naito, H. Hiramatsu, *Tetrahedron Lett.* **1995**, *36*, 253 – 256; h) P. Camps, M. Font-Bardia, D. Muñoz-Torrero, X. Solans, *Liebigs Ann.* **1995**, 523 – 535; i) T. Shono, N. Kise, T. Fujimoto, A. Yamanami, R. Nomura, *J. Org. Chem.* **1994**, *59*, 1730 – 1740; j) T. Naito, K. Tajiri, T. Harimoto, I. Ninomiya, T. Kiguchi, *Tetrahedron Lett.* **1994**, *35*, 2205 – 2206; k) J. Marco-Contelles, L. Martínez, A. Martínez-Grau, C. Pozuelo, M. L. Jimeno, *Tetrahedron Lett.* **1991**, *32*, 6437 – 6440.

[14] For recent review articles on the application of SmI_2 in organic synthesis, see: a) A. Krief, A.-M. Laval, *Chem. Rev.* **1999**, *99*, 745 – 777; b) G. A. Molander, C. R. Harris, *Tetrahedron* **1998**, *54*, 3321 – 3354; c) G. A. Molander, C. R. Harris, *Chem. Rev.* **1996**, *96*, 307 – 338;

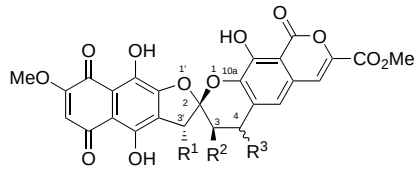
 © WILEY-VCH Verlag GmbH, D-69451 Weinheim, 2001 1433-7851/01/4024-4708 $ 17.50+.50/0

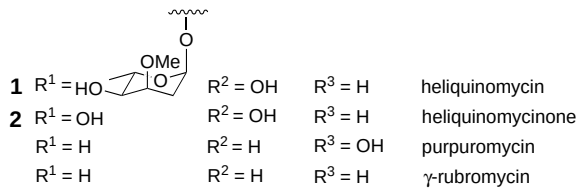
d) T. Skrydstrup, *Angew. Chem.* **1997**, *110*, 355 – 357; *Angew. Chem. Int. Ed. Engl.* **1997**, *36*, 345 – 347.
[15] J. A. Stafford, N. L. Valvano, *J. Org. Chem.* **1994**, *59*, 4346 – 4349. Although one might expect the formation of a seven-membered carbamate upon reaction with 1,1′-carbonyl diimidazole, we hypothesize that in this particular case the formation of five-membered rings is favored exclusively based on considerations of ring strain.
[16] T. Ishiyama, M. Murata, N. Miyaura, *J. Org. Chem.* **1995**, *60*, 7508 – 7510.
[17] A. Padwa, D. Dehm, T. Oine, G. A. Lee, *J. Am. Chem. Soc.* **1975**, *97*, 1837 – 1845.
[18] The addition of HCHO was achieved using the protocol reported by S. Kobayashi, I. Hachiya, *J. Org. Chem.* **1994**, *59*, 3590 – 3596. For a related example, see: P. Bernardelli, O. M. Moradei, D. Friedrich, J. Yang, F. Gallou, B. P. Dyck, R. W. Doskotch, T. Lange, L. A. Paquette, *J. Am. Chem. Soc.* **2001**, *123*, 9021 – 9032.
[19] a) J. L. Namy, P. Girard, H. B. Kagan, *Nouv. J. Chem.* **1977**, *1*, 5 – 7; b) P. Girard, J. L. Namy, H. B. Kagan, *J. Am. Chem. Soc.* **1980**, *102*, 2693 – 2698.
[20] a) G. E. Keck, T. T. Wager, S. F. McHardy, *Tetrahedron* **1999**, *55*, 11755 – 11772; b) J. L. Chiara, C. Destabel, P. Gallego, J. Marco-Contelles, *J. Org. Chem.* **1996**, *61*, 359 – 360; c) G. E. Keck, S. F. McHardy, T. T. Wager, *Tetrahedron Lett.* **1995**, *36*, 7419 – 7422.
[21] J. Marco-Contelles, P. Gallego, M. Rodríguez-Fernández, N. Khiar, C. Destabel, M. Berbabé, A. Martínez-Grau, J. L. Chiara, *J. Org. Chem.* **1997**, *62*, 7397 – 7412. For a preliminary disclosure of the same reductive coupling/N–O cleavage and an example with altered protecting groups, see a) J. L. Chiara, J. Marco-Contelles, N. Khiar, P. Gallego, C. Destabel, M. Bernabé, *J. Org. Chem.* **1995**, *60*, 6010 – 6011; b) S. Bobo, I. Storch de Gracia, J. L. Chiara, *Synlett* **1999**, 1551 – 1554.
[22] The role of H_2O is either as a proton source or, more likely, as a donor ligand which increases the reducing power of SmI_2. For leading references, see: a) S. Hanessian, C. Girard, *Synlett* **1994**, 861 – 862; b) E. Hasegawa, D. P. Curran, *J. Org. Chem.* **1993**, *58*, 5008 – 5010.
[23] Although $POCl_3$/DMF has been reported several times for oxazole formation from ketoamides, use of neat $POCl_3$ is far more rare. For one example, see: R. L. Dow, *J. Org. Chem.* **1990**, *55*, 386 – 388.
[24] In one particularly instructive example, remote substituents played a critical role in the ease of MOM cleavage from an indole substrate: A. I. Meyers, T. K. Highsmith, P. T. Buonara, *J. Org. Chem.* **1991**, *56*, 2960 – 2964.
[25] J. E. Macor, J. T. Forman, R. J. Post, K. Ryan, *Tetrahedron Lett.* **1997**, *38*, 1673 – 1676.
[26] C. T. Brain, J. M. Paul, *Synlett* **1999**, 1642 – 1644.
[27] This protocol represents a new method for MOM cleavage on indoles, particularly for acid-sensitive substrates since typical deprotection procedures utilize HCl at elevated temperatures. Since previous reports have already established the acid-sensitivity of the aryl chlorine atoms on the diazonamide skeleton that bears a free indole (see ref. [2c]), the ability to initially cleave the methyl ether only, followed by basic hydrolysis, is crucial for the survival of the chlorine substituents in **2**.

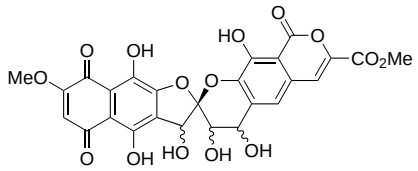
Studies in the Total Synthesis of Heliquinomycinone: Proof of Concept and Assembly of a Fully Mature Spirocyclization Precursor**

Donghui Qin, Rex X. Ren, Tony Siu, Changsheng Zheng, and Samuel J. Danishefsky*

Heliquinomycin (**1**) was isolated by Chino et al. from *Streptomyces sp.* MJ 929-SF2.[1] The structure of its aglycone moiety **2**, which we term heliquinomycinone, is related to structures encountered in the purpuromycin,[2] γ-rubromycin,[3] and griseorhodin antibiotics.[4] Although spiroketal







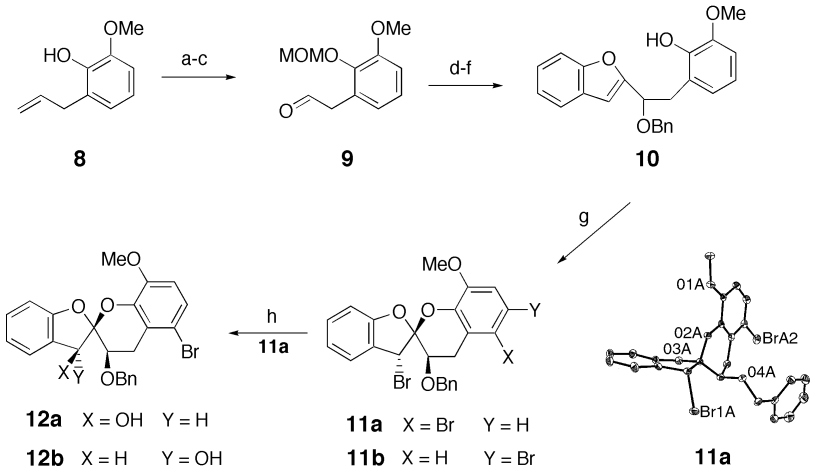
griseorhodin C

linkages in natural products are well known,[5] it is less common that such a moiety is derived from two phenolic hydroxy groups (C2). An arrangement in which the spiroketal core of the hexacyclic structure is linked to a glycoside, in this case to a 2,6-dideoxyhexose (cymarose) sugar, seems to be unique to **1**.

[*] Prof. S. J. Danishefsky,[+] Dr. D. Qin, Dr. R. X. Ren, T. Siu, Dr. C. Zheng
Department of Chemistry, Columbia University
Havemeyer Hall, New York, NY, 10021 (USA)
E-mail: s-danishefsky@ski.mskcc.org
[+] Laboratory for Bioorganic Chemistry
Sloan – Kettering Institute for Cancer Research
1275 York Ave., New York, NY, 10021 (USA)
Fax: (+1) 212-772-8691

[**] This work was supported by the National Institutes of Health (Grant numbers: AI 16943 and HL25848). A Postdoctoral Fellowship is gratefully acknowledged by R.X.R. (NIH, Grant Number IF32EY06750-0181). The authors thank Dr. Daniel Chen for important initial experiments, Dr. Brian Bridgewater and Prof. Ged Parkin of Columbia University for X-ray crystal structure analysis of **11a**, and Yashuiro Itagaki for high-resolution mass spectral analyses.

Adding to the interest level in heliquinomycin, is its inhibition of human DNA helicase, an important enzyme that unwinds double-stranded DNA prior to its replication.[6] It seems reasonable that helicase inhibition could be the basis of action for an anticancer drug:[7] selectivity could arise from the increased proclivity for transformed cells to undergo DNA turnover. The chemistry lessons inherent in attempts to build challenging structures such as **1** and **2**, as well as the opportunity to explore a potentially new type of restraint on uncontrolled cell growth, prompted us to undertake a total synthesis program directed toward these agents. Herein and in the following paper, we record a journey, which after serious difficulties led to a total synthesis of heliquinomycinone (**2**), the aglycone of heliquinomycin.[8]

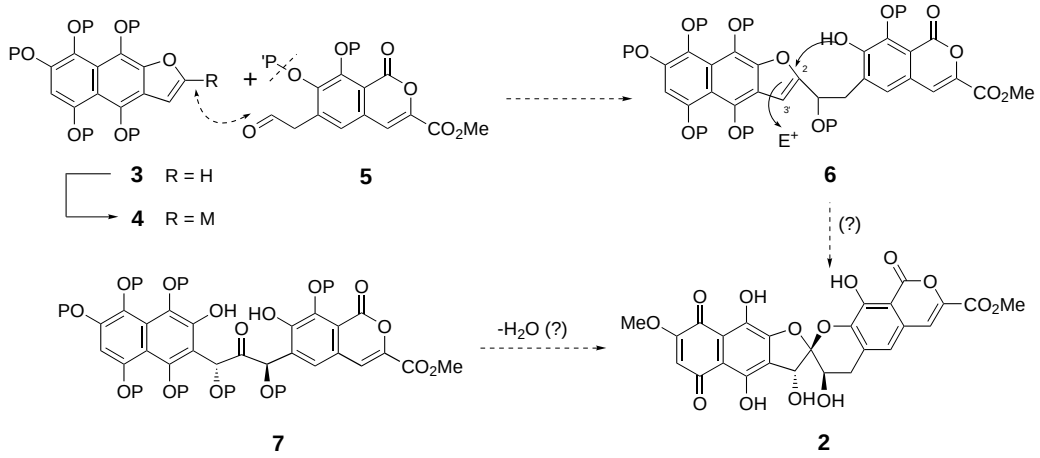


Scheme 2. Reagents and conditions: a) *N*,*N*-diisopropylethylamine, MOMCl, 50 °C, 66 %; b) OsO_4, NMO, acetone/H_2O, 63 %; c) $NaIO_4$, (aq.) $NaHCO_3$, CH_2Cl_2, 99 %, d) 2,3-benzofuran, *n*BuLi, −78 °C, THF; e) KH, BnBr, THF, 70 % (over two steps); f) ethereal HCl (1N), 2-propanol, THF, 93 %; g) NBS, CH_2Cl_2, (**11a**/**11b** 4:5, 85 %); h) AgOTf, wet THF, (**12a**:**12b** 3:1, 81 %). MOM = methoxymethyl; NMO = 4-methylmorpholine *N*-oxide; Bn = benzyl; NBS = *N*-bromosuccinimide.

Our central strategy for the synthesis is shown in Scheme 1: the spiroketal linkage would be fashioned through electrophilic potentiation at C2−C3′ of an appropriate naphthofuran (**6** →**2**). We anticipated that the synthesis of **6** by connecting the required subunits **4** and **5** could well be more straightforward than the assembly of a stereochemically correlated α,α'-difunctionalized ketone **7**, which is a more traditional type of spiroketal precursor. Ring closure of **6** would involve the nucleophilic attack of a proximal suitably differentiated phenolic hydroxy group at C2. It did not escape our attention that if the ring-closing step involved the inversion of the configuration at C2 of the naphthofuranoid system, (in which E^+ is translatable to OH^+), the required anti relationship between the 1,2-spiroketal bond and the putative hydroxy group at C3′ would be assured. Less certain, but still reasonable, was the possibility that the resident hydroxy group at C3 (free or protected), would direct the sense of electrophilic attack of E^+ at the naphthofuran ring. In this way, the nucleophilic cyclization step would also establish the governing configurational relationship between the spiroketal group and the C3 stereogenic center in the pyranoid moiety. In other words, the relative stereochemistry required to reach heliquinomycinone might arise from a structure with only one stereogenic center (C3). Thus if the precursor has the correct absolute configuration at the future C3, the aglycone might be delivered with enantiotopic control.

A model that allowed us to evaluate the concept, albeit at a rather primitive level, was soon assembled (Scheme 2). Various attempts at electrophilic spiroketalization of **10** were initiated. Of these, a favorable result arose only from the bromonium ion induced conversion of **10**.[9] This step was complicated by concurrent and nonspecific bromination of the phenol ring. In spite of this drawback, we took the formation of **11a** (verified by means of X-ray crystal structure analysis) and **11b** to be supportive of the general concept.[10] The benzylic bromine atom was readily replaced through solvolytic displacement by an oxygen-based nucleophile.[9] However, in early studies, compounds **12a** and **12b** were produced in a 3:1 ratio. Clearly, the solvolytic step at C3′ occurred primarily with inversion of configuration.

It was presumed that an appropriately functionalized naphthofuran moiety (substituted with five methoxy or



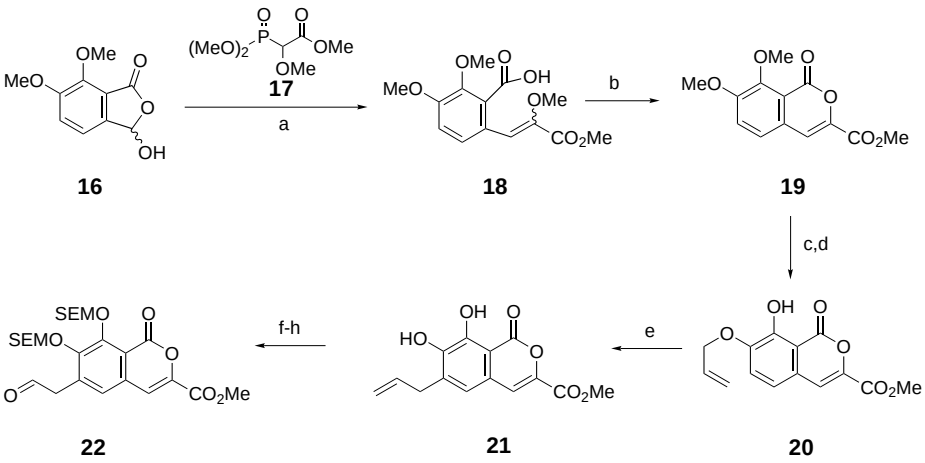
Scheme 1. Strategy for the synthesis of heliquinomycinone (**2**).

 © WILEY-VCH Verlag GmbH, D-69451 Weinheim, 2001 1433-7851/01/4024-4710 $ 17.50+.50/0

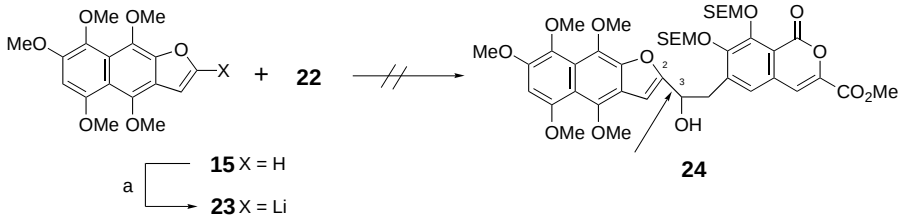
equivalent groups) would be susceptible to a broad range of reagents for realizing the desired integrated oxidative dearomatization and nucleophilic spirocyclization sequence. Accordingly, we set out to assemble functional versions of the two fragments, that is, naphthofuran **3** and aryl acetaldehyde **5**. It was further assumed (naively as it turned out) that a suitable metalo derivative of naphthofuran **4** would couple to **5** to produce a substrate of the type **6**, which we hoped to convert into **2**.

A convergent synthesis of naphthofuran **15** was implemented based on a modified strategy of Perry et al. (Scheme 3).[11] The known nitrile **13**[12] was treated with the dianion of 3-furoic acid to afford furan **14** in 92% yield. Intramolecular Friedel–Crafts acylation, followed by reduction and permethylation[13] provided **15** in moderate yield (44% over two steps).

The synthesis of the aryl acetaldehyde **22**, which includes an isocoumarin moiety, commenced with commercially available opianic acid **16** (Scheme 4). A modified Horner–Emmons reaction of **16** and **17**[14] afforded **18** as a mixture of stereoisomers (98%, 1:1). Cyclization under acidic conditions afforded isocoumarin **19**. Boron tribromide was used for the demethylation of the two aromatic ethers, and selective monoallylation of the resulting compound afforded **20**. Claisen rearrangement of **20** gave rise to product **21** (75% over two steps). The phenol functions were protected as SEM ethers under standard conditions. Cleavage of the double bond in a two-stage dihydroxylation/sodium periodate cleavage[15] provided aldehyde **22**.[16]



Scheme 4. Reagents and conditions: a) NaH, THF, 0° C, 98% (1:1); b) H_2SO_4 (3N), MeOH, reflux, 83%; c) BBr_3, CH_2Cl_2, −78 °C, 98%; d) LiHMDS, DMF, allyl bromide, −40 °C, 84%; e) xylene, 185 °C, 89%; f) SEMCl, DMAP, Et_3N, CH_2Cl_2, 86%; g) OsO_4, NMO, acetone/H_2O, 92%; h) $NaIO_4$, THF/Et_2O, 95%. DMAP = 4-dimethylaminopyridine; SEM = 2-(trimethylsilyl)ethoxymethyl; HMDS = hexamethyldisilazane.

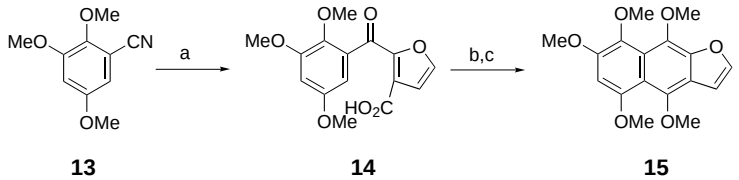


Scheme 5. Reagents and conditions: a) *n*BuLi, THF, −78 °C.

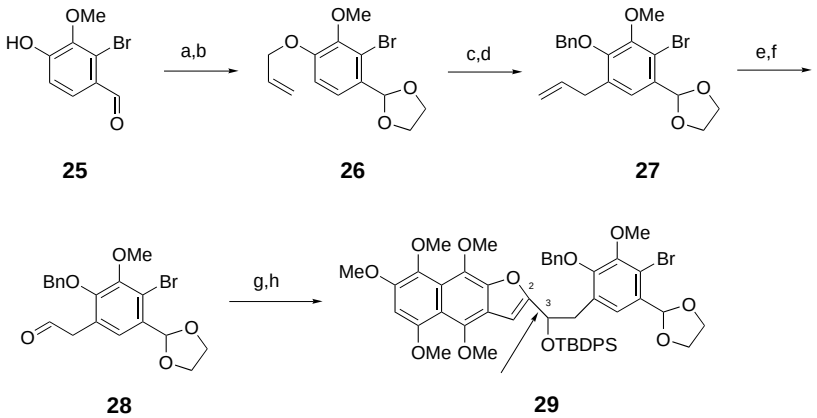
With **22** and **15** in hand, we focused on coupling the two units. Treatment of aldehyde **22** with lithiated naphthofuran **23** did not give any of the desired coupling product **24** (Scheme 5). Instead, naphthofuran **15** and aldehyde **22** were recovered. The formyl group in **22** is not particularly hindered, and thus the failure of the coupling reaction suggested a strong tendency toward proton transfer rather than toward C–C bond formation with the putative nucleophile **23**. Presumably, the ease of deprotonation of the benzylic methylene group of **22** is enhanced by the *para* carbonyl function of the isocoumarin moiety. The effects of cerium[17] and various other metal additives were explored in an attempt to modulate the basicity of the metalated naphthofuran. The inability to form a C–C bond implies that enolization is facile. A striking indication of the difficulty of targeting a carbon nucleophile to the formyl group of **22** is seen in its reaction with *n*-butyllithium. The *n*-butyl group added to the isocoumarin moiety, but left the aldehyde group intact.

Given our interpretation of the role of the C9 isocoumarin carbonyl group in triggering proton transfer between **23** and **22**, and following many failures to accomplish the addition reaction, we reluctantly decided against a fully convergent coupling step. Instead, we would use an aryl acetaldehyde target without a *para* carbonyl group to form the C3–C2 bond. Evidently, it would be necessary to reconstitute the isocoumarin moiety at a later stage in the synthesis. Several suitable aldehydes were examined. Eventually, we decided to couple the *ortho*-bromo dioxolane **28** with the lithio derivative **23**.

Protection of aldehyde **25**[18] and monoalkylation of the phenol afforded **26** in 90% yield (Scheme 6). Claisen rearrangement was induced by heating **26** to 240 °C. The resulting phenol was protected as its benzyl ether to produce **27**. We presumed that the C10a phenol could be exposed at a suitable stage for the oxidative spiroketalization (**6** → **2**). Dihydroxyla-



Scheme 3. Reagents and conditions: a) 3-furoic acid, *n*BuLi (2.2 equiv), THF, −78 °C, then **13**, 92%; b) H_2SO_4, 3 days, 88%; c) $Na_2S_2O_4$, TBABr, KOH, dimethyl sulfate, THF/H_2O, 50%. TBABr = tetrabutylammonium bromide.



Scheme 6. Reagents and conditions: a) ethylene glycol, benzene, reflux, 95%; b) K_2CO_3, allyl bromide, acetone, reflux, 95%; c) decalin, 240°C; d) K_2CO_3, BnBr, acetone, reflux, 57% (over two steps); e) OsO_4, NMO, acetone/H_2O, 97%; f) $NaIO_4$, acetone/H_2O, 88%; g) **23**, THF, −78°C; h) TBDPSCl, imidazole, CH_2Cl_2, 64% (over two steps). TBDPS = *tert*-butyldiphenylsilyl.

tion of the terminal vinyl function of **27** was followed by oxidative cleavage, thus giving the desired aldehyde precursor **28**.

The coupling reaction of **23** with **28** proceeded moderately well. The resulting secondary alcohol (C3) was protected as a silyl ether (**29**, 64% over two steps). We next addressed the formation the isocoumarin from **29** (Scheme 7). For this purpose, the lithio derivative of **29** was carboxylated and the resulting acid was methylated to afford ester **30**. The cyclic ketal was cleaved and the resulting aldehyde was condensed with **31**[14] to form **32**. The TBS silyl ether protecting group in **32** was cleaved with tetrabutylammonium fluoride. The product, which was not completely characterized, was treated with potassium carbonate in methanol to afford **33**. The benzyl group of **33** was cleaved to give phenol **34**, and the stage was set for the spirocyclization step.

Finally, a suitable precursor for **2** was in hand. In the following communication,[19] we show that it was indeed possible to reach heliquinomycinone via **33**, but only after overcoming some unforeseen and serious difficulties.

Received: September 5, 2001 [Z17859]

[1] a) M. Chino, K. Nishikawa, M. Umekia, C. Hayashi, T. Yamazaki, T. Tsuchida, T. Sawa, M. Hamada, T. Takeuchi, *J. Antibiot.* **1996**, *49*, 752; b) M. Chino, K. Nishikawa, T. Tsuchida, R. Sawa, H. Nakamura, K. T. Nakamura, Y. Muraoka, D. Ikeda, H. Naganawa, T. Sawa, T. Takeuchi, *J. Antibiot.* **1997**, *50*, 143.

[2] M. R. Bardone, E. Martinelli, L. F. Zerilli, C. Coronelli, *Tetrahedron* **1974**, *30*, 2747.

[3] H. Brockmann, A. Zeeck, *Chem. Ber.* **1970**, *103*, 1709.

[4] R. M. Stroshane, J. A. Chen, E. A. Rubalcuba, A. L.Garietson, A. A. Aszalos, P. P. Roller, *J.Antibiot.* **1979**, *32*, 197.

[5] F. Perron, K. F. Albizati, *Chem. Rev.* **1989**, *89*, 1617.

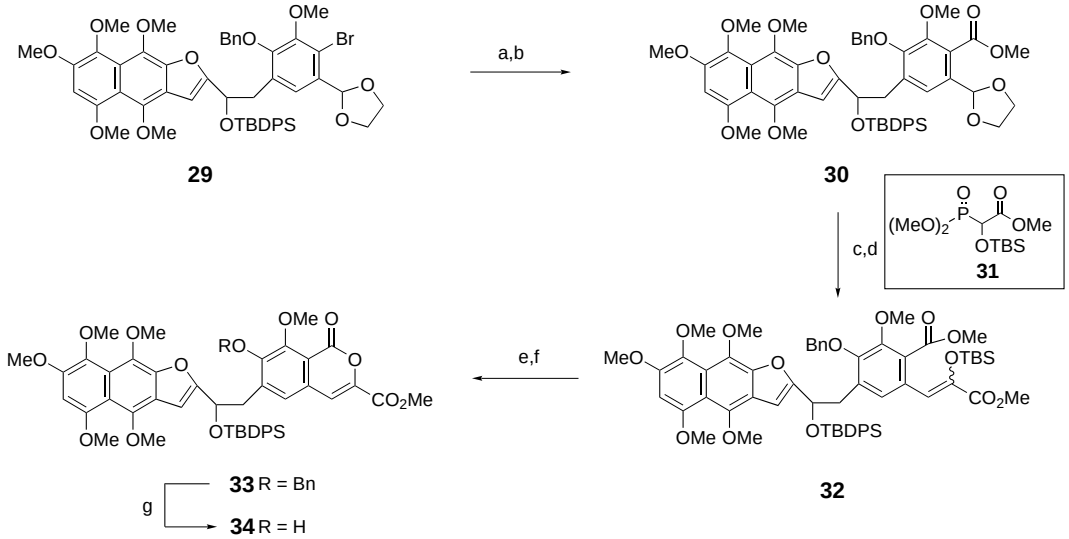
[6] S. W. Matson, K. A. Kaiser-Rogers, *Annu. Rev. Biochem.* **1990**, *59*, 289.

[7] M. Chino, K. Nishikawa, A. Yamada, M. Ohsono, T. Sawa, F. Hanaoka, M. Ishizaka, T. Takeuchi, *J. Antibiot.* **1998**, *51*, 480.

[8] For model studies toward the spiroketal core of heliquinomycin and related structures, see: a) T. Capecchi, C. B. de Koning, J. P. Michael, *Tetrahedron Lett.* **1998**, *39*, 5429; b) T. Capecchi, C. B. de Koning, J. P. Michael, *J. Chem. Soc. Perkin Trans. 1* **2000**, 2681; for syntheses of the isocoumarin subunit, see: c) T. P. Thrash, T. D. Welton, V. Behar, *Tetrahedron Lett.* **2000**, *41*, 29; d) S. P. Waters, M. C. Kozlowski, *Tetrahedron Lett.* **2001**, *42*, 3567; for a synthesis of the naphthalene subunit of heliquinomycin and related structures, see: e) X. Xie, M. C. Kozlowski, *Org. Lett.* **2001**, *3*, 2661.

[9] NBS was previously used for the activation of a benzofuran: G. F. Miknis, R. M. Williams, *J. Am. Chem. Soc.* **1993**, *115*, 536.

[10] Crystallographic data (excluding structure factors) for the structures reported in this paper have been deposited with the Cambridge Crystallographic Data Centre as supplementary publication no. CCDC-169848 (**11a**). Copies of the data can be obtained free of charge on application to CCDC, 12 Union Road, Cambridge CB2 1EZ, UK (fax: (+44) 1223-336-033; e-mail: deposit@ccdc.cam.ac.uk).



Scheme 7. Reagents and conditions: a) *n*BuLi (3.0 equiv), CO_2 (g), −78°C, THF; b) $TMSCHN_2$, MeOH/benzene, 81% (over two steps); c) HCl (3N), acetone/THF, 95%; d) LiHMDS, **31**, THF, −78→25°C, then aldehyde, 96%; e) TBAF (1.0 equiv), THF, 0°C; f) K_2CO_3, MeOH, 72% (over two steps); g) H_2, Pd/C (5%), EtOAc, 92%. TBAF = tetrabutylammonium fluoride; TBS = *tert*-butyldimethylsilyl.

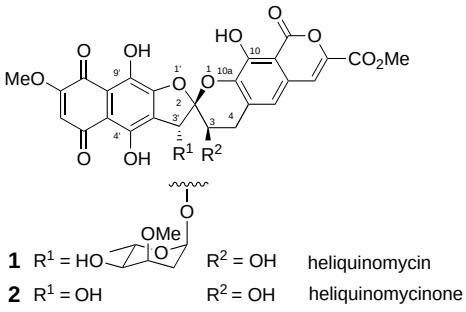
 © WILEY-VCH Verlag GmbH, D-69451 Weinheim, 2001 1433-7851/01/4024-4712 $ 17.50+.50/0

[11] a) P. J. Perry, V. H. Pavalidis, J. H. Hadfield, I. G. C. Coutts, *J. Chem. Soc. Perkin Trans. 1* **1995**, 1085; b) P. J. Perry, V. H. Pavalidis, J. H. Hadfield, *Tetrahedron* **1997**, *53*, 3195.
[12] M. A. Rizzacasa, M. V. Sargent, *J. Chem. Soc. Perkin Trans. 1* **1988**, 2425.
[13] G. A. Kraus, T. O. Man, *Syn. Commun.* **1986**, *16*, 1037.
[14] a) E. Nakamura, *Tetrahedron Lett.* **1981**, *22*, 663; b) D. Horne, J. Gaudino, W. J. Thompson, *Tetrahedron Lett.* **1984**, *25*, 3529.
[15] The Lemieux Johnson protocol was not applicable because under those conditions the only product observed was the benzaldehyde: R. Pappo, D. S. Allen Jr., R. U. Lemieux, W. S. Johnson, *J. Org. Chem.* **1956**, *21*, 478.
[16] Behar and co-workers independently described the synthesis of a related compound by an analogous route; see ref. [8c].
[17] T. Imamoto, N. Takiyama, K. Nakamura, T. Hatajima, Y. Kamiya, *J. Am. Chem. Soc.* **1989**, *111*, 4392.
[18] R. A. Hill, G. W. Kirby, G. J. O'Loughlin, D. J. Robins, *J. Chem. Soc. Perkin Trans. 1* **1993**, 1967.
[19] T. Siu, D. Qin, S. J. Danishefsky, *Angew. Chem.* **2001**, *113*, 4849; *Angew. Chem. Int. Ed.* **2001**, *40*, 4713.

The Total Synthesis of Heliquinomycinone**

Tony Siu, Donghui Qin, and Samuel J. Danishefsky*

In the preceding communication,[1] we described the assembly of intermediate **3**, which was envisioned as a substrate for an oxidative dearomatization-spiroketalization sequence (**3** → **4**, Scheme 1), en route to heliquinomycinone (**2**), the aglycone of the naturally occurring helicase inhibitor



1 R^1 = HO R^2 = OH heliquinomycin
2 R^1 = OH R^2 = OH heliquinomycinone

heliquinomycin (**1**). A large number of reagent combinations were used in attempts to bring about the conversion of **3** into a product of the type **4** (Scheme 1). In particular, we were seeking electrophiles that could be introduced concomitantly with nucleophilic spirocyclization. Unfortunately, even after screening a large number of possibilities, this strategy was not successful. When projected electrophilic cyclizations were attempted by using halonium equivalents such as NBS, NIS, NCS, or iodine in the presence of sodium bicarbonate, oxidative demethylation and quinone formation occurred. Similar results were observed when various epoxidations of the furanoid ring were attempted.[2] An important constraining factor was the electron richness of the pentamethoxynaphthalene moiety present in **3**. This pattern lent itself to ready pairwise oxidative demethylations to produce ring A or ring B quinones, with subsequent deactivation of the furan double bond. Furthermore, no reaction occurred when metal-based reagents such as $Pd(OAc)_2$, $Ti(OAc)_3$, Re_2O_7,[3] and Hg^{II} salts were explored to activate the furan double bond for nucleophilic attack. Even after extensive experimentation, we were unable to carry out the transformation **3** → **4**. In substance, we were unable to overcome the combination of nonreactivity of the furanoid moiety to some reagent combinations, and the high vulnerability of the pentamethoxynaphthalene structure to others.

The one successful oxidation which targeted the furan ring and did not compromise the integrity of the pentamethoxynaphthalene moiety, arose from the action of osmium tetroxide on **5**,[4] which gave a diastereomeric mixture of **6** (Scheme 2, 50–60%). The product was difficult to separate and could not be satisfactorily characterized by means of ^{1}H NMR spectroscopy. Our decision to go forward with this material was based largely on a supportive mass spectrum. Deprotection of the benzyl ether exposed the C10a phenolic function, again as a poorly characterized mixture of diastereomers **7**.

With triol **7** in hand, all that remained to reach hydroquinonoid versions of **2** was acid-induced spiroketalization (Scheme 3). Remarkably, this seemingly attainable goal could not be accomplished. The hydroxy group at the pre-C3′ benzylic position was unexpectedly vulnerable.[5] An attempt at a spirocyclization under Mitsunobu-type conditions was unsuccessful and instead led to the transformation of diastereomers **7** into **9**.[6]

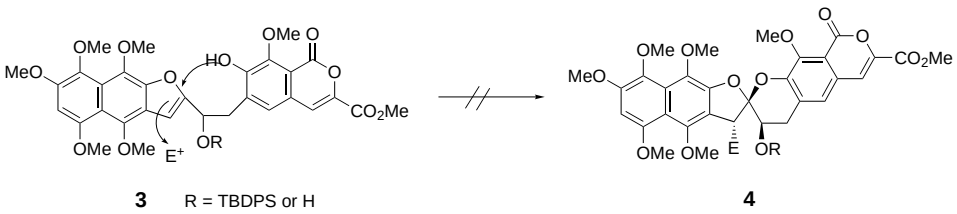
In retrospect, this result reflects the ease of formation of a quinone-methide-like heterolysis product, presumably mediated by the strong electron-donating nature of the five methoxy groups on the naphthalene system. Various protections of C3 and C3′ in the hope of favoring the desired spirocyclization were not productive.

A chance observation proved to be critical in solving the problem. Exposure of diastereomers **6** to air, in the presence of triethylamine/methanol led to oxidation at C3′, thus forming the α-hydroxyketone (Scheme 4).[7] Subsequent debenzylation gave **10** as a 1:1 mixture of anomers. It was hoped that the presence of the ketone would prevent bond formation between the "C10a" phenol and "C3′" (except for that arising from a presumably reversible hemicacetal link). However, the feasibility of spirocyclization in **10**, adjacent to a ketone linkage, was by no means certain.

Under Mitsunobu conditions,[6] the desired cyclization was achieved and mixture **10** afforded compounds **11** and **12** in a 1:1 ratio after removal of the silyl ethers. These products were

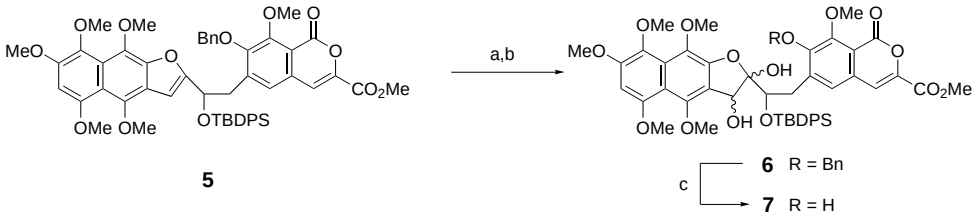
[*] Prof. S. J. Danishefsky,[+] T. Siu, Dr. D. Qin
Department of Chemistry, Columbia University
Havemeyer Hall, New York, NY, 10021 (USA)
E-mail: s-danishefsky@ski.mskcc.org
[+] Laboratory for Bioorganic Chemistry
Sloan–Kettering Institute for Cancer Research
1275 York Ave., New York, NY, 10021 (USA)
Fax: (+1) 212-772-8691

[**] This work was supported by the National Institutes of Health (Grant numbers: AI 16943 and HL25848). The authors thank Dr. Makoto Chino of Nippon Kayaku Co., Ltd. for kindly providing a sample of heliquinomycin, and Yashuiro Itagaki of Columbia University for high-resolution mass spectral analyses.



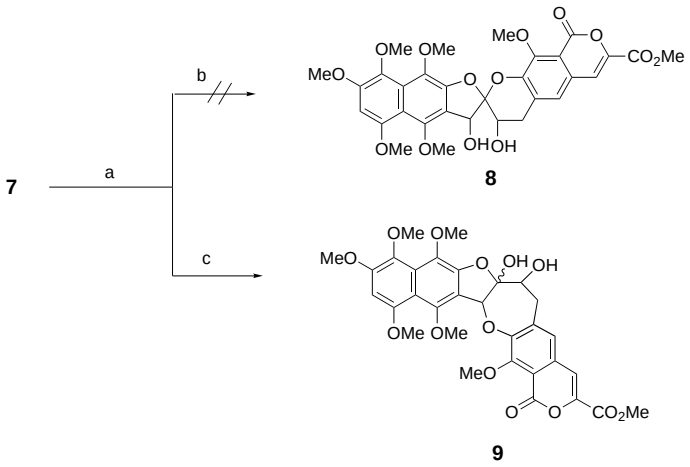
3 R = TBDPS or H **4**

Scheme 1. a) TBDPS = *tert*-butyldiphenysilyl.



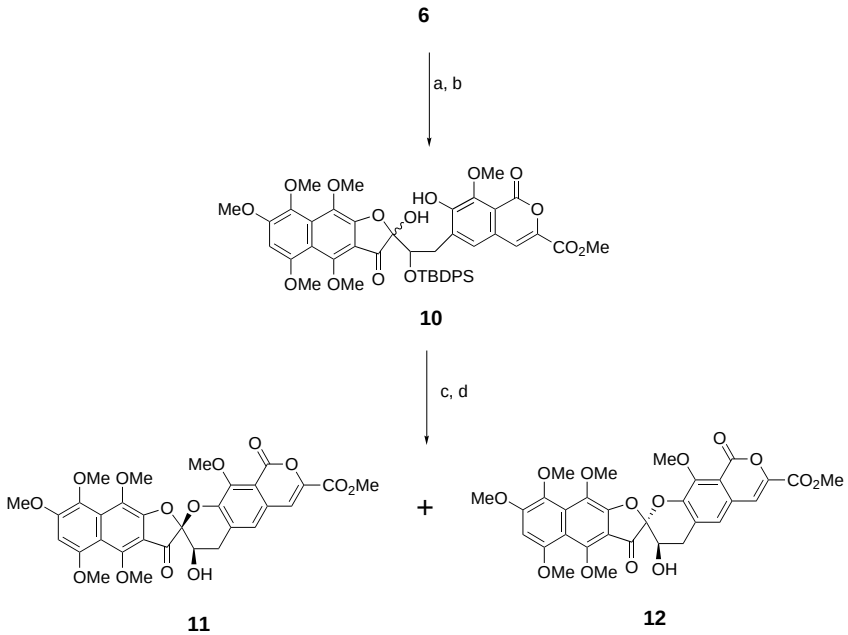
5 **6** R = Bn **7** R = H

Scheme 2. Reagents and conditions: a) OsO_4, pyridine, THF/H_2O; b) $NaHSO_3$, 3 days, 50–60 %; c) H_2, Pd/C (5 %), EtOAc, 95 %. TBDPS = *tert*-butyldiphenylsilyl. Bn = benzyl.



8 **9**

Scheme 3. Reagents and conditions: a) TBAF, THF, 95 %; b) various sources of acid; c) DIAD, PPh_3, CH_2Cl_2, 50 %. TBAF = tetrabutylammonium fluoride; DIAD = diispropylazodicarboxylate.



10 **11** **12**

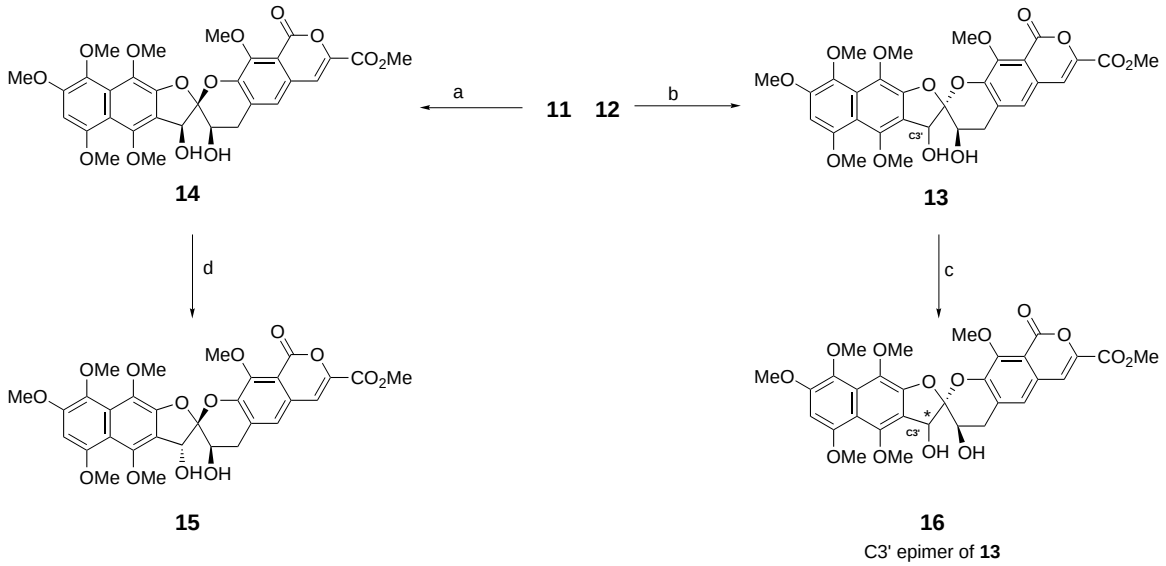
Scheme 4. Reagents and conditions: a) Et_3N, MeOH, 45 %; b) H_2, Pd/C (5 %), EtOAc, 94 %; c) DEAD, PPh_3, CH_2Cl_2, −78→25 °C; d) TBAF, THF, 0 °C, 72 % (over two steps). DEAD = diethylazodicarboxylate; TBAF = tetrabutylammonium fluoride.

separated cleanly and fully characterized. It is unclear whether a given anomer in mixture **10** affords a given spiroketal (**11** or **12**) by inversion, or whether it leads to a mixture of spiroketals via the oxonium ion followed by unselective cyclization.

At this stage, we had no basis to assign the relative configurations unambiguously at C2 and C3 in **11** and **12**. We then studied in detail the reduction of ketones **11** and **12** (Scheme 5). Gratifyingly, each of these ketones underwent highly stereoselective reduction upon treatment with tetramethylammonium triacetoxyborohydride to afford **13** and **14**, respectively.[8] We could not be confident as to the relative configuration of **13** and **14**, and the ^{1}H NMR signals for the aliphatic groups of either product did not correspond with those of heliquinomycin (**1**).[9] Although comparison of **13** and **14** with compounds in the quinone series was somewhat problematic, we came to the tentative conclusion that neither of these two products had the relative configuration at C3, C2, and C3′ which we wanted in our eventual target **2**.

We now reasoned that heterolysis of the C3′ benzylic hydroxyl group, which occurred in the unwanted transformation of **7** into **9**, might allow for solvolytic inversion at C3′ in **13** or **14**. If such a reaction could be realized, and if all structures to date were correct, one of these two emerging diols would be a suitable candidate for progression to heliquinomycinone. Treatment of **13** and **14** with $BF_3 \cdot OEt_2$ in separate reactions gave **16** and **15**, respectively, in moderate yields.[10] At this stage, our prospects improved significantly. The ^{1}H NMR spectrum of **15** corresponded well with that of **1**. Moreover, from a small sample of **1**, we were able to obtain heliquinomycinone (**2**) by hydrolysis of the glycoside link. Again, there was an encouraging similarity in the upfield regions of the ^{1}H NMR spectra of **2** and **15**. In contrast, the upfield region of the ^{1}H NMR spectrum of **16** did not correspond well with that of **1** or **2**.[11] On this basis, we tentatively assigned the relative configuration of heliquinomycinone at C3′, C2, and C3 to diol **15**, and hence to its precursor **14**, as shown. As for **13** and **16** we could assign the relationship of the spiro centers and C3 to be as shown. However, we cannot rigorously assign the configurations at C3′ in

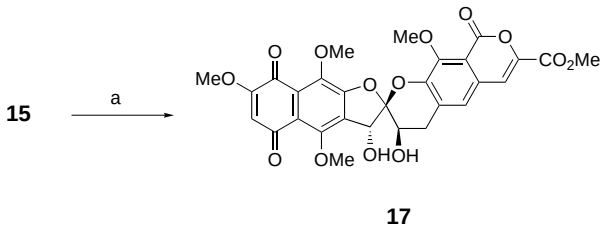
 © WILEY-VCH Verlag GmbH, D-69451 Weinheim, 2001 1433-7851/01/4024-4714 $ 17.50+.50/0 *Angew. Chem. Int. Ed.* **2001**, *40*, No. 24



Scheme 5. Reagents and conditions: a) $Me_4NBH(OAc)_3$ MeCN/acetic acid (5:1), 72%; b) same conditions as a), 69%; c) $BF_3 \cdot OEt_2$ (0.5 equiv), CH_2Cl_2, 64%; d) same conditions as c), 71%.

these epimers, as neither corresponded to the heliquinomycin pattern.

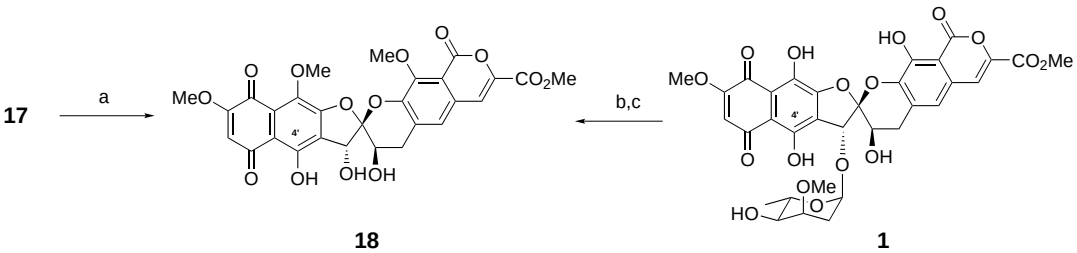
Diol **15**, which was prepared stereospecifically from ketone **11**, was treated with cerium ammonium nitrate to afford the corresponding quinone **17** (Scheme 6). There remained the daunting challenge of tridemethylation of the fully synthetic material. Treatment of **17** with $BBr_3 \cdot Me_2S$ led to initial demethylation at C4′ to form **18**. Presumably, the specificity of demethylation arises from the mediation by the proximal hydroxy group at C3′. As confirmation, compound **18** could be reached from **1** (Scheme 7). Thus, dimethylation of heliquinomycin at C9′ and C10 was carried out as shown. The selectivity must arise from the large proximal glycoside, which hinders methylation at C4′. Deglycosylation of this compound afforded naturally derived **18**. Gratifyingly, the high-field ^{1}H NMR spectra and TLC mobility of the synthetic and naturally derived bis-methyl ethers **18** were identical.



Scheme 6. Reagents and conditions: a) cerium ammonium nitrate, MeCN/H_2O (5:1), 0°C, 77%.

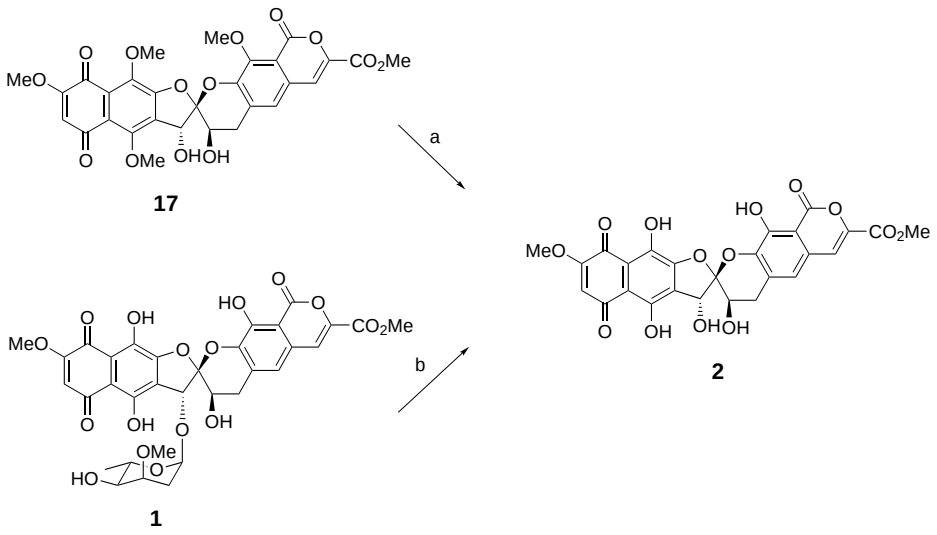
Compound **17** was treated with BBr_3 in dichloromethane, which resulted in the cleavage of the three appropriate methyl ethers to give fully synthetic racemic **2**. Remarkably, the aglycone is much more labile than **1**, which has the cymarose glycoside attachment. Nonetheless, synthetic **2** could be purified by sephadex LH-20 chromatography (Scheme 8). The high-field ^{1}H NMR spectrum of fully synthetic **2** is identical to that of the naturally derived aglycone. Congruity was also seen in comparison of the TLC mobility and the IR and mass spectra of the naturally derived and fully synthetic **2**; thus heliquinomycinone had been fully synthesized in a 23-step sequence, which is highlighted by a remarkable spirocyclization (see formation of **11**).

In retrospect, this total synthesis proved to be far more difficult at several points than had been anticipated. In the end, the failure to synthesize a single diol at the stage of **6** complicated matters because of our inability to rechannel the undesired anomer into the desired series. The dihydroxylation reaction is the only step without stereocontrol. It may yet be possible, when operating in an enantiomerically defined setting, to benefit from a reagent-dominated specific enantiofacial attack on a suitable precursor (cf **5**).[12] The availability of optically defined **10** would allow for clarification of the fascinating spirocyclization under Mitsunobu conditions.



Scheme 7. Reagents and conditions: a) $BBr_3 \cdot Me_2S$ (5 equiv), CH_2Cl_2, 0°C, 64%; b) Ag_2O, MeI, 65°C, $CHCl_3$; c) HCl (1N, 100 equiv), 65°C, THF, 67% (over two steps).

 © WILEY-VCH Verlag GmbH, D-69451 Weinheim, 2001 1433-7851/01/4024-4715 $ 17.50+.50/0



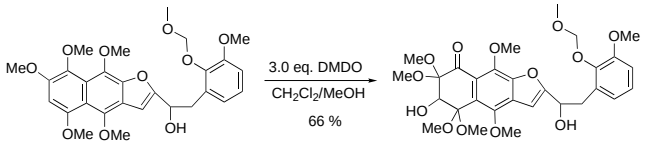
Scheme 8. Reagents and conditions: a) BBr_3 (15 equiv), CH_2Cl_2, $-78\,^{\circ}C$, 52%; b) HCl (1N, 100 equiv), 65 °C, THF, quantitative.

Our longer term goals in the project involve an enantiodefined synthesis of **2**, a synthesis of heliquinomycin itself, and an evaluation of the *anti* helicase activity of the various heliquinomycin analogues that were formed in the project. It is expected that the identification of the complexities of the problem described herein and the synthesis of the aglycone portion, will be of benefit in future synthetic projects.

Received: September 5, 2001 [Z17860]

[1] D. Qin, R. X. Ren, T. Siu, C. Zheng, S. J. Danishefsky, *Angew. Chem.* **2001**, *113*, 4845; *Angew. Chem. Int. Ed.* **2001**, *40*, 4709.

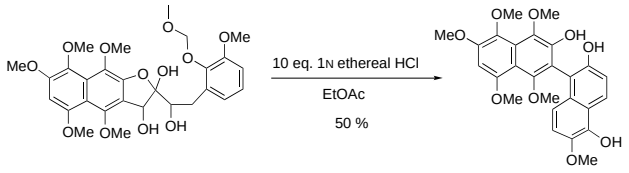
[2] An interesting example of the problems associated with the electron richness of the naphthalene ring in hindering the desired epoxidation of the furan is shown in a model substrate:



[3] a) S. Tang, R. M. Kennedy, *Tetrahedron. Lett*. **1992**, *33*, 5303; b) R. M. Kennedy, S. Tang, *Tetrahedron Lett*. **1992**, *33*, 3729.

[4] For previous examples of dihydroxylations of benzofuran and indole rings, see: a) M. P. Meisinger, F. A. Kuehl, Jr., E. L. Rickes, N. G. Brink, K. Folkers, M. Forbes, F. Zilliken, P. Gyorgy, *J. Am. Chem. Soc.* **1959**, *81*, 4979; b) G. B. Feigelson, M. Egbertson, S. J. Danishefsky, *J. Org. Chem*. **1988**, *53*, 3390.

[5] A demonstration of the vulnerability of the C3′ position even relative to C2 in a model substrate is shown below:



[6] O. Mitsunobu, *Synthesis* **1981**, 1.

[7] H. Ishii, T. Ishikawa, S. Takeda, S. Ueki, M. Suzuki, *Chem. Pharm. Bull.* **1992**, *40*, 1148.

[8] Hydride reduction of protected variants of **11** and **12** that contained bulky protecting groups on the C3 hydroxy function also gave only products **13** and **14**.

[9] Both diastereomers show clear NOE enhancements between the C3 methine and the C3′ methine. No NOE interaction was observed between these two protons in heliquinomycin.

[10] The results of this reaction support a mechanism for epimerization at C3′ rather than the more traditional epimerization at C2 of the spiro center. Had epimerization at C2 occurred, the product of **12** would have corresponded to either one of the products derived from **11**. No such crossover was observed.

[11] The C4 protons of **16** appear as a doublet whereas the C4 protons of naturally derived heliquinomycinone appear as two doublets of doublets.

[12] H. C. Kolb, M. S. van Nieuwenhze, K. B. Sharpless, *Chem. Rev*. **1994**, *94*, 2483.

Heat Capacity of the Mixed-Valence Complex $\{[(n\text{-}C_3H_7)_4N][Fe^{II}Fe^{III}(dto)_3]\}_\infty$, Phase Transition because of Electron Transfer, and a Change in Spin-State of the Whole System**

Tadahiro Nakamoto, Yuji Miyazaki, Miho Itoi, Yuuki Ono, Norimichi Kojima,* and Michio Sorai*

Recently a novel mixed-valence complex $\{[(n\text{-}C_3H_7)_4N][Fe^{II}Fe^{III}(dto)_3]\}_\infty$ (**1**) containing asymmetric ligand dto (dithiooxalato: $C_2O_2S_2^{2-}$) was synthesized by Kojima and coworkers.[1] This complex dispalys ferromagnetic order below ~6 K and exhibits an interesting phenomenon at temperatures between 110 K and 120 K, where a change in the spin state of the whole system occurs as the result of electron transfer. This situation is schematically shown in Figure 1.

[*] Prof. Dr. M. Sorai, Dr. Y. Miyazaki, Dr. T. Nakamoto
Research Center for Molecular Thermodynamics
Graduate School of Science, Osaka University
Toyonaka, Osaka 560-0043 (Japan)
Fax: (+81) 6-6850-5526
E-mail: sorai@chem.sci.osaka-u.ac.jp
Prof. Dr. N. Kojima, M. Itoi, Y. Ono
Graduate School of Arts and Science
The University of Tokyo
Komaba, Tokyo 153-8902 (Japan)
Fax: (+81) 3-5454-4311
E-mail: cnori@mail.ecc.u-tokyo.ac.jp

[**] Contribution No. 48 from the Research Center for Molecular Thermodynamics. This work was partially supported by a Grant-in-Aid for Scientific Research on the Priority Areas of "Metal-Assembled Complexes" (Area No. 401/12023229) from the Ministry of Education, Science, Sports and Culture, Japan; dto = dithiooxalato.

 © WILEY-VCH Verlag GmbH, D-69451 Weinheim, 2001 1433-7851/01/4024-4716 $ 17.50+.50/0

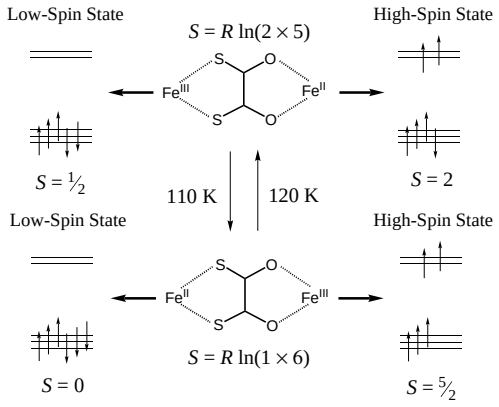


Figure 1. Schematic representation of the electron transfer phenomenon in $\{[(n\text{-}C_3H_7)_4N][Fe^{II}Fe^{III}(dto)_3]\}_\infty$. Symbol S has been used both for the spin quantum number (left and right) and for the entropy arising from the spin multiplicity (center).

Although the structure of the complex has not been determined owing to the lack of suitable single crystals, at room temperature a network structure with an alternating array of Fe^{II} and Fe^{III} ions bridged by dto ligands bonding through the S atoms to Fe^{III} centers and through O atoms to the Fe^{II} centers may be presumed by analogy to bimetallic oxalato complexes.[2] The coordination spheres of both Fe sites are presumed to be twisted trigonal prismatic also by analogy of other dto complexes.[3] The valence and the spin states of each Fe site were determined by ^{57}Fe Mössbauer spectroscopy.[1] At 200 K the FeO_6 site is divalent and in a high-spin (HS) state ($^5T_{2g}$, $S=2$; $S=$ spin quantum number), while the FeS_6 site is trivalent and in a low-spin (LS) state ($^2T_{2g}$, $S=1/2$). At 77 K, however, as a result of the electron transfer, the FeO_6 site becomes trivalent and is in an HS state ($^6A_{1g}$, $S=5/2$) while the FeS_6 site is converted to divalent state and in an LS state ($^1A_{1g}$, $S=0$). On the basis of the magnetic-susceptibility measurement the transition temperature between these two states was determined to be 110 K on cooling and 120 K on heating.[4]

At first glance, this phenomenon seems to be a type of spin crossover because a change in the spin state actually occurs in the whole system. However, there is a crucial difference between this phenomenon and usual spin-crossover phenomenon. No spin crossover has been reported for FeO_6 complexes regardless of the valence state of the Fe center, while several spin-crossover FeS_6 complexes have been found in ferric compounds such as tris(dithiocarbamato) complexes $[Fe^{III}(dtc)_3]$.[5] In the title complex, however, since the Fe^{III} ion in FeS_6 site is already in the LS state at room temperature, temperature-induced spin-crossover phenomenon can no longer be expected at low temperatures. Therefore, neither of two Fe sites can independently cause a temperature-induced spin-crossover phenomenon. Although a great number of spin-crossover systems[6–8] and mixed-valence systems[9–10] are known, a system such as **1** is unknown. Investigation of thermal properties provides us with important information concerning energy and entropy. To shed light on this phenomenon from a thermodynamic viewpoint, we measured heat capacities of **1**. Herein we describe the mechanism of the novel electron transfer transition.

Observed molar heat capacities under constant pressure (C_p) of $\{(n\text{-}C_3H_7)_4N[Fe^{II}Fe^{III}(dto)_3]\}_\infty$ are plotted in Figure 2. A sharp peak at 122.4 K and a broad heat-capacity anomaly centered at 253.5 K are observed. The origin of the latter heat

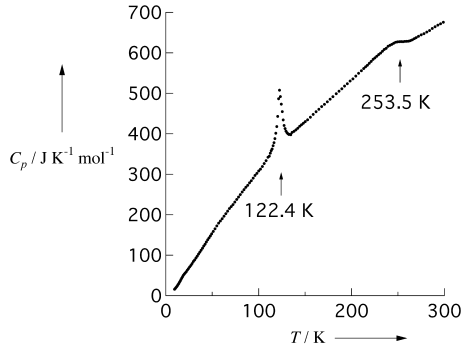


Figure 2. Molar heat capacity of crystalline $\{[(n\text{-}C_3H_7)_4N][Fe^{II}Fe^{III}(dto)_3]\}_\infty$ as a function of temperature.

capacity anomaly can be attributed to an order–disorder type of phase transition of $[(n\text{-}C_3H_7)_4N]^+$ ion, based on similar heat-capacity anomalies observed in the analogous molecule-based magnets such as $\{(n\text{-}C_4H_9)_4N[M^{II}Fe^{III}(ox)_3]\}_\infty$ where M = Fe or Zn.[13] The anomaly at 122.4 K clearly arises from the phase transition resulting from the electron transfer, as the transition temperature agrees well with the temperature at which the anomaly was observed in the magnetic-susceptibility measurements.[4]

In addition, a small heat capacity hump was observed around 20 K. As no event has been found in this temperature region by the magnetic-susceptibility measurement, the origin of this anomaly has not been assigned. The very low-temperature heat capacity of **1** measured by use of a calorimeter with a ^{3}He/^{4}He dilution refrigerator, will be reported, in due course, along with the magnetic heat capacity arising from the ferromagnetic transition at $\sim$6 K[4] together with the analysis of the heat-capacity anomaly observed around 20 K.

Although the phase transition at 122.4 K does not take place isothermally, it should be regarded as first-order phase transition, because supercooling phenomenon have been observed. As shown in Figure 3a, no anomaly was detected in the measurement for the specimen cooled to 110 K. Two small C_p waves, seen in the 120–130 K region, were caused by the experimental condition that we adopted, that is, the rather small temperature increment for C_p determination. The sample cooled to 100 K exhibited a small anomaly. This anomaly became larger as the temperature was lowered. This observation indicates that the transition temperature upon cooling $T_c(\downarrow)$ is about 110 K, which is in good agreement with the $T_c(\downarrow)$ determined by the magnetic-susceptibility measurement.[4]

For determination of the excess heat capacities because of the electron-transfer phenomenon, it is necessary to estimate a normal heat capacity or lattice heat capacity, C_{lat}. For this purpose the effective frequency distribution method[14] is a good approximation. In the present case, however, this procedure seems to be difficult because of the presence of the broad heat capacity anomaly centered at 253.5 K, the starting temperature of which is difficult to determine. In the

 © WILEY-VCH Verlag GmbH, D-69451 Weinheim, 2001 1433-7851/01/4024-4717 $ 17.50+.50/0

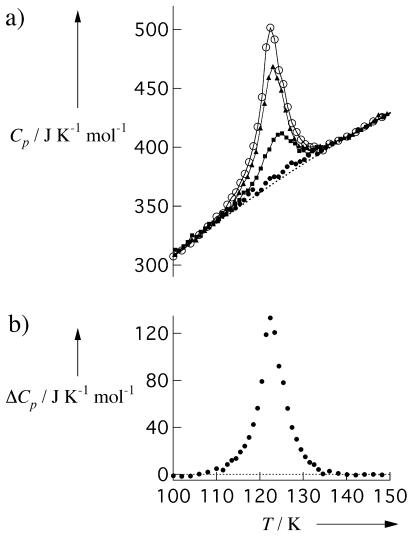


Figure 3. a) Molar heat capacities of crystalline $\{[(n\text{-}C_3H_7)_4N][Fe^{II}Fe^{III}(dto)_3]\}_\infty$ in the vicinity of the phase transition at 122.4 K. (○) are the data shown in Figure 2, which correspond to the heat capacities for the specimen well annealed at 100 K after once cooled to 80 K and then cooled again to 5 K. Filled symbols indicate the data obtained after cooling to the temperatures: (●) 110 K, (■) 100 K, and (▲) 90 K. The solid curves are to aid the eye. The dashed curve shows for the normal heat capacity. b) Excess molar heat capacities because of the phase transition.

present complex, however, the C_p data of the supercooling state seems to coincide well with those of the low-temperature phase below T_c. Therefore the C_{lat} curve was estimated by a least-squares fitting of a polynomial function of temperature, $a\,T^2+b\,T+c$, to the C_p data in the temperature range between 80 K and 160 K. The "best fit" C_{lat} curve thus determined is represented by Equation (1) and shown in Figure 3a by dashed curve.

$$C_{lat}\,[\mathrm{J\,K^{-1}\,mol^{-1}}] = -67.81 + 4.657\,T\,[\mathrm{K}] - 0.008935\,(T\,[\mathrm{K}])^2 \quad (80 < T\,[\mathrm{K}] < 160) \tag{1}$$

The difference between the observed and the normal heat capacities shown in Figure 3b corresponds to the excess heat capacity, ΔC_p. The enthalpy and entropy arising from the electron-transfer phenomenon are determined to be $\Delta_{trs}H = 1.04\ \mathrm{kJ\,mol^{-1}}$ and $\Delta_{trs}S = 9.20\ \mathrm{J\,K^{-1}\,mol^{-1}}$, respectively.

The entropy change is larger than the spin-only value expected for the change in the spin multiplicity $R\ln(10/6) = 4.25\ \mathrm{J\,K^{-1}\,mol^{-1}}$. Should the ligand-field symmetry remain O_h through out the phase transition, then the change in the orbital angular momentum contributes $R\ln[(3\times3)/(1\times1)] = 18.27\ \mathrm{J\,K^{-1}\,mol^{-1}}$ to the entropy gain. If this is the case, the total entropy gain because of the spin and orbital amounts to $22.51\ \mathrm{J\,K^{-1}\,mol^{-1}}$. However, this is not the case because this value is far beyond the experimental entropy. The orbital degeneracy, such as $^5T_{2g}$ and $^2T_{2g}$ encountered in high-spin Fe^{II} and low-spin Fe^{III} systems in an O_h symmetry, is usually lifted by the Jahn–Teller distortion to give a nondegenerate or lower-degenerate ground state. In such a case, the orbital contribution to the entropy becomes small or negligible. In **1**, it is very likely that a trigonal distortion is encountered in the FeO_6 and FeS_6 sites. Under such a situation, the ground terms $^5T_{2g}$ of Fe^{II}(HS) and $^2T_{2g}$ of Fe^{III}(LS) in O_h ligand-filed symmetry are reduced to ^5E and ^2A in a trigonal symmetry,[15] respectively. If this orbital contribution is fully taken into account, the electronic entropy gain from spin and orbital will be $R\ln[(10\times2)/6] = 10.01\ \mathrm{J\,K^{-1}\,mol^{-1}}$. This value is very close to the experimental value of $9.20\ \mathrm{J\,K^{-1}\,mol^{-1}}$ resulting from the electron-transfer phenomenon. Although we discussed the orbital contribution to entropy for octahedral and trigonal ligand fields, there is a possibility that the actual ligand-field symmetry of **1** is lower than trigonal symmetry. In such a case, the orbital contribution to the entropy gain is further reduced. Therefore, the entropy gain expected from the electron transfer is in the range between $R\ln(10/6) = 4.25\ \mathrm{J\,K^{-1}\,mol^{-1}}$ from the spin multiplicity and $R\ln(20/6) = 10.01\ \mathrm{J\,K^{-1}\,mol^{-1}}$ from the spin and the orbital in trigonal symmetry.

Since the observed entropy gain is $9.20\ \mathrm{J\,K^{-1}\,mol^{-1}}$, the entropy originating in intramolecular vibrations is considerably smaller than in normal spin-crossover phenomena. For example, about $35\ \mathrm{J\,K^{-1}\,mol^{-1}}$ was estimated for the vibrational contribution to the entropy change in the spin-crossover phenomenon observed in $[Fe(phen)_2(NCS)_2]$[16] and $37\ \mathrm{J\,K^{-1}\,mol^{-1}}$ for $[Fe(2\text{-}pic)_3]Cl_2\cdot EtOH$.[17]

The magnitude of vibrational entropy crucially depends on the bond lengths between the metal ion and the ligands. The longer the bond length, the greater the vibrational entropy is. The metal–ligand bond length is affected by the spin state of the metal ion: it is longer for the HS state than for the LS state. Therefore, the normal spin-crossover phenomenon always involves a large entropy gain from the metal–ligand skeletal vibrations. In **1**, the FeO_6 site is in the HS state and the FeS_6 site is in the LS state, irrespective of the oxidation state. Therefore, in a strict sense both the Fe sites do not experience the spin-state conversion encountered in normal spin-crossover phenomena. However, since the oxidation states at the FeO_6 and FeS_6 sites are altered by the electron transfer, one can expect a change in vibrational system.

Another factor determining the bond length is the oxidation state of the metal ion. According to Shannon,[18] typical ionic radii of low-spin Fe ions with coordination number six are 75 pm and 69 pm for Fe^{II}(LS) and Fe^{III}(LS), respectively. As shown in Figure 4, the metal–ligand bond lengths are elongated by 13.5 pm at the FeO_6 site at the phase transition while those at the FeS_6 site contracte by 6 pm. When the phase transition as a result of the electron transfer occurs, the FeO_6 site remarkably contributes positively to the vibrational entropy whereas the FeS_6 site has a negative contribution. If the oxidation and reduction sites consisted of identical ligands, these two conflicting contributions to entropy would be canceled out and thus no vibrational entropy would be expected. In the present case, however, since the ligands are not identical and the relative atomic masses are different (O: 15.9994, S: 32.065), a net, though very small, contribution to the vibrational entropy is expected. To confirm experimentally the vibrational contribution to the entropy gain, variable-temperature IR spectroscopy investigations are now in progress.

In the mixed-valence complex **1** the spin state of the whole system dramatically changes by virtue of the electron transfer. At first glance, this phenomenon seems to be a type of spin-

 © WILEY-VCH Verlag GmbH, D-69451 Weinheim, 2001 1433-7851/01/4024-4718 $ 17.50+.50/0 *Angew. Chem. Int. Ed.* **2001**, *40*, No. 24

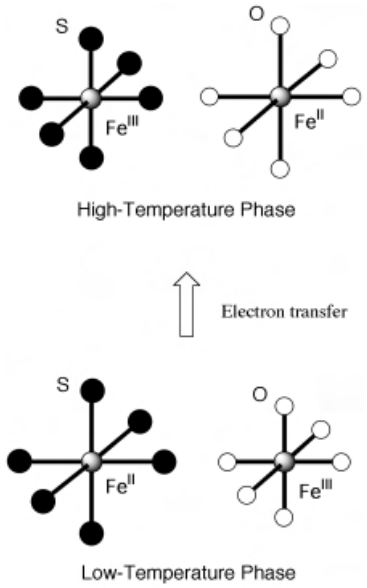


Figure 4. The relationship between the electron transfer and the metal–ligand bond lengths.

crossover phenomenon. However, the present calorimetric study clearly revealed that this novel phenomenon is quite different from usual (or classical) spin-crossover phenomenon.

Experimental Section

Synthesis of **1** is reported elsewhere.[1, 4] Heat capacity measurements between 8 K and 300 K were made with a home-built adiabatic microcalorimeter.[11, 12] The mass of the sample for calorimetry was 0.95853 g (1.4556 mmol). A small amount of He gas was sealed in the calorimeter cell to aid the heat transfer.

Received: May 21, 2001
Revised: August 27, 2001 [Z17145]

[1] N. Kojima, W. Aoki, M. Seto, Y. Kobayashi, Yu. Maeda, *Synth. Met.* **2001**, *121*, 1796–1797.
[2] S. Decurtins, H. W. Schmalle, H. R. Oswald, A. Linden, J. Ensling, P. Gütlich, A. Hauser, *Inorg. Chim. Acta* **1994**, *216*, 65–73.
[3] a) F. J. Hollander, D. Coucouvanis, *Inorg. Chem.* **1974**, *13*, 2381–2386; b) M. Mitsui, H. Okawa, H. Sakiyama, M. Ohba, N. Matsumoto, T. Kurisaki, H. Wakita, *J. Chem. Soc. Dalton Trans.* **1993**, 2991–2994.
[4] N. Kojima, W. Aoki, M. Itoi, Y. Ono, M. Seto, Y. Kobayashi, Yu. Maeda, *Solid State Commun.* **2001**, *120*, 165–170.
[5] K. Ståhl, I. Ymén, *Acta Chem. Scand. Ser. A* **1983**, *37*, 729–737, and references therein.
[6] E. König, *Prog. Inorg. Chem.* **1987**, *35*, 527–622; E. König, *Struct. Bonding* **1991**, *76*, 51–152.
[7] P. Gütlich, A. Hauser, H. Spiering, *Angew. Chem.* **1994**, *106*, 2109–2141; *Angew. Chem. Int. Ed. Engl.* **1994**, *33*, 2024–2054.
[8] O. Kahn, *Molecular Magnetism*, Wiley-VCH, New York, **1993**, chap. 4.
[9] *Mixed-Valence Compounds* (Ed.: D. B. Brown), Reidel, Dordrecht, **1980**.
[10] *Mixed Valency Systems: Applications in Chemistry, Physics and Biology* (Ed.: K. Prassides), Kluwer, Dordrecht, **1991**.
[11] Y. Ogata, K. Kobayashi, T. Matsuo, H. Suga, *J. Phys. E* **1984**, *17*, 1054–1057.
[12] Y. Kume, Y. Miyazaki, T. Matsuo, H. Suga, *J. Phys. Chem. Solids* **1992**, *53*, 1297–1304.
[13] A. Bhattacharjee, Y. Miyazaki, M. Sorai, *J. Phys. Soc. Jpn.* **2000**, *69*, 479–488.
[14] M. Sorai, S. Seki, *J. Phys. Soc. Jpn.* **1972**, *32*, 382–393.
[15] P. Ganguli, V. R. Marathe, *Inorg. Chem.* **1978**, *17*, 543–550.
[16] M. Sorai, S. Seki, *J. Phys. Chem. Solids* **1974**, *35*, 555–570.
[17] K. Kaji, M. Sorai, *Thermochim. Acta* **1985**, *88*, 185–190.
[18] R. D. Shannon, *Acta Crystallogr. Sect. A* **1976**, *32*, 751–767.

Olefin Polymerization with [{bis(imino)pyridyl}$Co^{II}Cl_2$]: Generation of the Active Species Involves Co^{I}**

T. Martijn Kooistra, Quinten Knijnenburg, Jan M. M. Smits, Andrew D. Horton, Peter H. M. Budzelaar, and Anton W Gal*

The independent discovery by the groups of Brookhart and Gibson that bis(imino)pyridyl (N_3) complexes of iron and cobalt (Figure 1) are precursors for active polymerization and oligomerization catalysts[1] has put a new perspective on late transition metals as polymerization catalysts. However, there have been very few reports of successful extension of the system (other than trivial changes of substituents), which indicates that our understanding of this catalytic system is still incomplete.

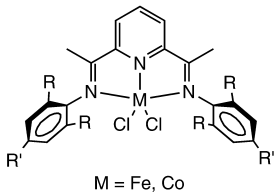


Figure 1. Previously reported bis(imino)pyridyl precatalysts [$N_3^RFeCl_2$] and [$N_3^RCoCl_2$].[1]

The mechanism by which polymerization is believed to proceed is essentially the same as for early transition metals, that is, the active species is a cationic metal(II) alkyl complex. One recent publication contradicts this belief for the iron-based catalyst system.[2] Mechanistic studies are difficult for several reasons. In addition to problems of high activity (and hence low concentration) and the large excess of MAO (MAO = methylaluminoxane) used, the Fe and Co systems are also paramagnetic, which complicates NMR spectroscopy studies. Gibson has mentioned some preliminary studies of iron–alkyl species which appear to support formation of $[N_3FeR]^+$[3] moieties, but so far no reports on the corresponding Co systems have appeared. The groups of Gambarotta[4a]

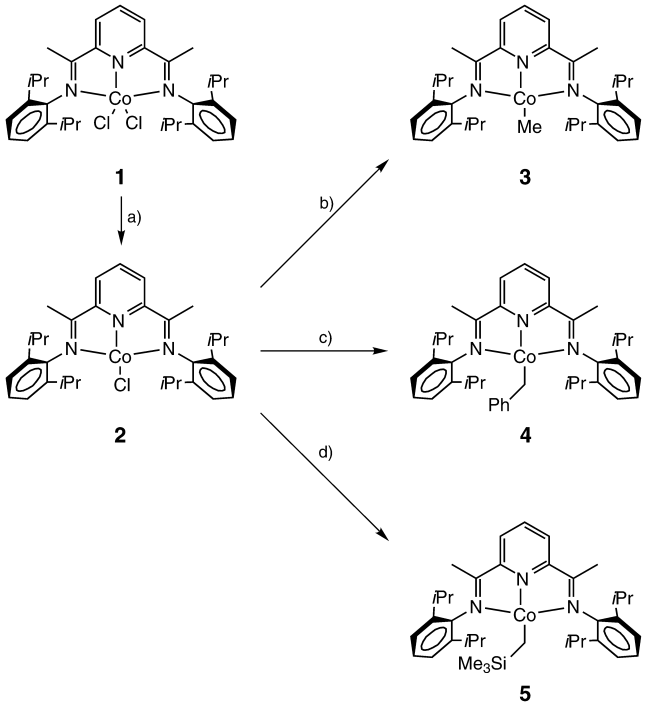
[*] Prof. Dr. A. W Gal, T. M. Kooistra, Q. Knijnenburg, J. M. M. Smits, Dr. P. H. M. Budzelaar
Department of Inorganic Chemistry
University of Nijmegen
Toernooiveld 1, 6525 ED Nijmegen (The Netherlands)
Fax: (+31)24-355-3450
E-mail: gal@sci.kun.nl
Dr. A. D. Horton
Shell International Chemicals B.V.
Shell Research and Technology Centre, Amsterdam
P.O. Box 38000, 1030 BN Amsterdam (The Netherlands)

[**] This research was sponsored by CW/STW and Basell Technology Company.

 © WILEY-VCH Verlag GmbH, D-69451 Weinheim, 2001 1433-7851/01/4024-4719 $ 17.50+.50/0

and Brookhart[4b] have used other metals (V, Rh/Ru) in the same ligand environment to model possible active species. The Fe and Co systems have also been studied theoretically.[5] For Fe, Ziegler and co-workers obtained results in excellent agreement with the experimental data.[5a] For the Co system, however, the predominant termination pathway could not be unambiguously assigned and the calculated olefin-complexation barrier was found to be rather high.[5b] Thus, it is not immediately obvious that the active species in the Co system must be strictly analogous to that in the Fe system. We decided to study the Co system in more detail in the hope of establishing the nature of the active species and to understand the differences with the Fe system. Herein we describe our first results in this area.

Alkylating, $[N_3{}^{i\mathrm{Pr}}Co^{II}Cl_2]$(**1**; $N_3{}^{i\mathrm{Pr}}$ = 2,6-bis-[1-(2,6-diisopropylphenylimino)ethyl]pyridine; Scheme 1) with better defined alkylating agents than MAO (MeLi, Et_2Zn) we found that the Co^{II} chloride was not immediately alkylated, but instead was first reduced to a (presumably square planar) diamagnetic Co^{I} chloride.[6] According to ^{1}H NMR spectroscopy, side products were formed in this reaction, but crystallization from toluene yielded the main product **2** as deep purple crystals.[7]



Scheme 1. Synthesis of $[N_3{}^{i\mathrm{Pr}}Co^{I}]$ complexes. Reagents and conditions: a) 1.2 equiv MeLi, toluene, 5 h or 2 equiv MAO, toluene, instant; b) 1.1 equiv MeLi, diethyl ether, 3 days or 2 equiv MAO, toluene, instant; c) 2.0 equiv Bn_2Mg, toluene, 2 h; d) 1.2 equiv $LiCH_2SiMe_3$, toluene, 10 min.

Complex **2** could be selectively alkylated. Treatment of **2** with a slight excess of MeLi, Bn_2Mg, or $LiCH_2SiMe_3$ resulted in the corresponding neutral (also diamagnetic) Co^{I} alkyl complexes in three days, two hours, and ten minutes, respectively (Scheme 1). The upfield shift of the phenyl signals of the benzyl group in **4**, which results from shielding by the aryl rings of the ligand, indicates that the alkyl moieties are located between the two aryl rings of the ligand. The ^{1}H NMR spectra of all the Co^{I} species showed unusual downfield shifts for the *para* pyridine (Py) hydrogen atom (9.5 – 10.3 ppm) and upfield shifts for the ketimine methyl hydrogen atoms (– 1.2 – 0.1 ppm) that are as yet unexplained.

Crystals of **5** obtained from hexane were suitable for X-ray diffraction. In agreement with NMR spectroscopy data, **5** is a square-planar Co^{I} complex (Figure 2),[8] and is the first structurally characterized Co^{I} – alkyl species with nitrogen

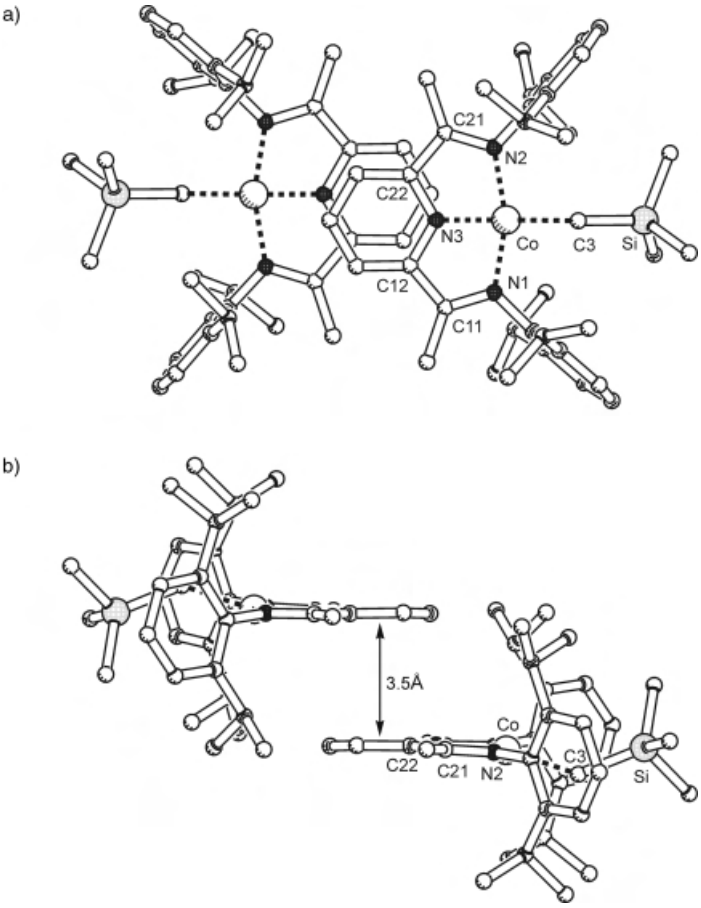


Figure 2. PLUTON[9] drawing of the pairwise arrangement of **5** in the crystal lattice; a) top view, b) side view. Selected bond lengths [Å] and angles [°]: Co–N1 1.9291(17), Co–N2 1.9202(17), Co–N3 1.8369 (16), Co–C3 1.984(2), N1–C11 1.327(3), N2–C21 1.330(3), C11–C12 1.436(3), C21–C22 1.434(3); N1–Co–N2 161.00(7), N3–Co–C3 165.91(9).

donors. All the reported crystal structures of Co^{I} – alkyl complexes combine trimethylphosphane ligands with a π-acceptor ligand.[10] The most notable difference between **5** and the corresponding Co^{II} dichloride[1d] is the shortening of the Co–N bonds by 0.2 – 0.3 Å, caused by the contraction of the cobalt radius because of the transition from high spin to low spin upon reduction from Co^{II} to Co^{I}. Since the bis(imino)-pyridyl ligands are very good π acceptors,[11] the better π-backdonating properties of Co^{I} compared with Co^{II} centers might also play a role. The increased π backdonation is apparent from the long imine double bonds and the short C_{Py}–C_{imine} bonds.[12] In the crystal lattice the molecules occur in pairs related by a center of inversion. The two molecules of

 © WILEY-VCH Verlag GmbH, D-69451 Weinheim, 2001 1433-7851/01/4024-4720 $ 17.50+.50/0 *Angew. Chem. Int. Ed.* **2001**, *40*, No. 24

each pair have parallel pyridine rings in close contact with each other (the distance between ring planes is about 3.5 Å), suggestive of π stacking (Figure 2b). This appears to be a unique feature of complex **5**, since it is not observed in any of the reported crystal structures of iron(II) and cobalt(II) compounds with this type of ligand.

The reaction of **1** with either MeLi or Et_2Zn, to form **2** as described above, was accompanied by a color change from pale brown to deep purple, which is the same color change as initially observed on activation of **1** with 1000 equivalents of MAO. Therefore we investigated whether the Co^I complexes exhibit polymerization activity. Neither to Co^I chloride **2** nor the alkyls **3**–**5** are themselves active in polymerization. On activation with an excess of MAO, however, all of them polymerized ethene at appoximately the same rate as the originally reported $[N_3{}^{i\mathrm{Pr}}Co^{II}Cl_2]$ (**1**) when tested under identical conditions (Table 1).

The unbranched polyethenes (PE) obtained in all five experiments were very similar (as concluded from NMR spectroscopy and differential scanning calorimetry (DSC) analysis). In particular, the gel permeation chromatography (GPC) traces of the major polymer fraction were superimposable (Figure 3) with virtually identical peak molecular weights[13] for the five precatalysts (Table 1). These results are consistent with polymerization involving the same catalyst active species in all cases.

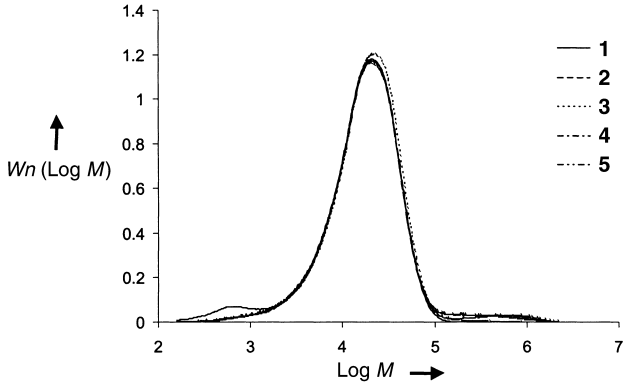


Figure 3. Molecular-weight distribution from GPC analysis of the polymers obtained with complexes **1**–**5** as precatalysts.

Thus, Co^I chlorides and alkyls might be intermediates in the activation mechanism with MAO. Indeed, when two equivalents of MAO were added to **1**, a ^{1}H NMR spectrum of **2** was obtained.[14] Subsequent treatment with another two equivalents of MAO resulted in the spectrum of **3**. Clearly, MAO converts **1** selectively and completely into a Co^IMe complex prior to the actual activation. This result makes the assumption of a Co^{II} active species (e.g.[1d], [5b]) less logical;[18] possibilities involving Co^I or even Co^{III} active species also deserve serious consideration.[19] The unexpected generation of the active species via a Co^I species will have implications for the design of new cobalt polymerization catalysts.

Experimental Section

All reactions were carried out under N_2 using standard Schlenk techniques or in a dry box. NMR spectroscopic measurements were performed on Varian gemini 300 and Inova 400 spectrometers. Compound **1** was synthesized according to literature procedures.[1d]

$[N_3{}^{i\mathrm{Pr}}CoCl]$ (**2**): **1** (1.24 g, 1.83 mmol) and MeLi (46.4 mg, 2.12 mmol, 1.16 equiv) were suspended in toluene (10 mL). After stirring for 5 h at room temperature, the color had changed from pale brown to deep purple and the mixture was filtered over celite. Purple crystals were obtained from the filtrate at −35 °C. Washing with hexane and drying yielded **2** (323 mg, 0.561 mmol; 31 %). ^{1}H NMR (300 MHz, C_6D_6, 298 K): $\delta = 9.53$ (t, 1H, $^3J(H,H) = 7.7$ Hz, Py−H_p), 7.41 (t, 2H, $^3J(H,H) = 7.7$ Hz, Ar−H_p), 7.26 (d, 4H, $^3J(H,H) = 7.8$ Hz, Ar−H_m), 6.91 (d, 2H, $^3J(H,H) = 7.8$ Hz, Py−H_m), 3.33 (sept, 4H, $^3J(H,H) = 6.9$ Hz, C*H*Me$_2$), 1.17 (d, 12H, $^3J(H,H) = 6.9$ Hz, CH*Me*Me), 1.05 (d, 12H, $^3J(H,H) = 6.9$ Hz, CHMe*Me*), 0.05 (s, 6H, N=C*Me*); ^{13}C NMR (100 MHz, C_6D_6, 298 K): $\delta = 167.34$ (N=*C*), 152.79 (Py−C_o), 150.87 (Ar−C_{ip}), 140.75 (Ar−C_o), 127.05 (Ar−C_p), 125.52 (Py−C_m), 123.75 (Ar−C_m), 114.89 (Py−C_p), 29.06 (*C*HMe$_2$), 24.01 (CH*Me*Me), 23.77 (CH*Me*Me), 21.22 (N=C*Me*); elemental analysis calcd (%) for $C_{33}H_{43}N_3ClCo$: C 68.80, H 7.52, N 7.29, Cl 6.15, Co 10.23; found: C 68.92, H 7.55, N 7.22, Cl 6.05, Co 10.06.

$[N_3{}^{i\mathrm{Pr}}CoMe]$ (**3**): **2** (96 mg, 0.17 mmol) and MeLi (4.0 mg, 0.18 mmol, 1.1 equiv) were dissolved in diethyl ether (10 mL). After stirring for 3 days at room temperature, the mixture was filtered over celite. The purple filtrate was evaporated to dryness in vacuo. The residue contained **3** and **2** in a ratio of 5:1, according to ^{1}H NMR spectroscopy. ^{1}H NMR (300 MHz, C_6D_6, 298 K): $\delta = 10.19$ (t, 1H, $^3J(H,H) = 7.7$ Hz, Py-H_p), 7.86 (d, 2H, $^3J(H,H) = 7.8$ Hz, Py−H_m), 7.49 (t, 2H, $^3J(H,H) = 7.7$ Hz, Ar−H_p), 7.37 (d, 4H, $^3J(H,H) = 7.8$ Hz, Ar−H_m), 3.13 (sept, 4H, $^3J(H,H) = 6.9$ Hz, C*H*Me$_2$), 1.18 (d, 12H, $^3J(H,H) = 6.9$ Hz, CH*Me*Me), 0.62 (d, 12H, $^3J(H,H) = 6.9$ Hz, CHMe*Me*), 0.58 (s, 3H, Co*Me*), −1.15 (s, 6H, N=C*Me*).

$[N_3{}^{i\mathrm{Pr}}CoCH_2C_6H_5]$ (**4**): **2** (85 mg, 0.15 mmol) and $Bn_2Mg \cdot 0.5$ dioxane (38 mg, 0.15 mmol, 2.04 equiv) were dissolved in toluene (5 mL). After stirring for 2 h at room temperature, the color had changed from purple to blue. The mixture was filtered over celite and the blue filtrate was evaporated to dryness in vacuo. ^{1}H NMR of the residue showed that the conversion was quantitative. ^{1}H NMR (300 MHz, C_6D_6, 298 K): $\delta = 10.27$ (t, 1H, $^3J(H,H) = 7.8$ Hz, Py−H_p), 7.68 (d, 2H, $^3J(H,H) = 7.8$ Hz, Py−H_m), 7.61 (t, 2H, $^3J(H,H) = 7.8$ Hz, Ar−H_p), 7.45 (d, 4H, $^3J(H,H) = 7.8$ Hz, Ar−H_m), 6.79 (t, 1H, $^3J(H,H) = 7.5$ Hz, Bn−H_p), 6.56 (t, 2H, $^3J(H,H) = 7.5$ Hz, Bn−H_m), 5.60 (d, 2H, $^3J(H,H) = 7.2$ Hz, Bn-H_o) 3.20 (sept, 4H, $^3J(H,H) = 6.6$ Hz, C*H*Me$_2$), 2.50 (s, 2H, Bn−CH_2) 1.15 (d, 12H, $^3J(H,H) = 6.9$ Hz, CH*Me*Me), 0.63 (d, 12H, $^3J(H,H) = 6.9$ Hz, CHMe*Me*), −1.16 (s, 6H, N=C*Me*); ^{13}C NMR (100 MHz, C_6D_6, 298 K): $\delta = 165.99$ (N=*C*), 157.48

Table 1. Polymerization results[a]

Catalyst precursor	Yield of PE [g]	Rate [kg mmole^{-1} bar^{-1} h^{-1}]	Rate relative to **1** [%]	Unsaturated examples[c]	Saturated examples[c]	M_p[d] [$\times 10^{-3}$]	T_{m2}[e] [°C]	ΔH[f] [J g^{-1}]
1	0.884	1.01	(100)	1.3	2.1	20.8	135.4	243.5
2	1.133	1.29	128	[g]	2.4	21.1	133.1	235.7
3 (84 % pure)[b]	0.744	0.85	84	0.9	1.2	22.3	[g]	[g]
4	1.002	1.15	114	0.8	1.6	21.1	[g]	[g]
5	0.818	0.93	92	0.7	1.2	21.7	133.1	232.1

[a] Catalyst (0.5 μmole), MAO (0.5 mmole, 1000 equiv), toluene (40 mL), ethene (7 bar), 15 min. [b] Remainder mostly **2**. [c] End groups per 1000 carbon atoms determined from ^{1}H NMR (unsaturated) and ^{13}C NMR (saturated) spectroscopy. [d] Peak molecular weight determined by GPC methods. [e] Melting temperature determined by DSC (second heating run). [f] Enthalpy of melting determined by DSC (second heating run). [g] Not determined.

 © WILEY-VCH Verlag GmbH, D-69451 Weinheim, 2001 1433-7851/01/4024-4721 $ 17.50+.50/0

(Bn−C_{ip}), 155.61 (Py−C_o), 154.87 (Ar-C_{ip}), 141.39 (Ar−C_o), 127.55 (Bn−C_m, Bn−C_o), 126.93(Ar-C_p), 124.82 (Ar−C_m), 123.98 (Py−C_m), 119.85 (Bn−C_p), 116.43 (Py−C_p), 28.62 (*C*HMe$_2$), 25.75 (N=C*Me*), 24.38 (CHMe*Me*), 23.35 (CH*Me*Me), 1.15 (Bn−*C*H$_2$).

[N$_3^{i\mathrm{Pr}}$CoCH$_2$SiMe$_3$] (**5**): **2** (71 mg, 0.12 mmol) and LiCH$_2$SiMe$_3$ (14 mg, 0.15 mmol, 1.2 equiv) of were dissolved in toluene (5 mL). After stirring for 10 min at room temperature, the mixture was filtered over celite. The purple filtrate was evaporated to dryness in vacuo. ^{1}H NMR spectroscopy of the residue showed that the conversion was quantitative. Purple crystals were obtained from a hexane solution at $-35\,^\circ$C. ^{1}H NMR (300 MHz, C_6D_6, 298 K): $\delta = 9.89$ (t, 1H, ^3J(H,H) = 7.8 Hz, Py−H_p), 7.62 (d, 2H, ^3J(H,H) = 7.5 Hz, Py−H_m), 7.51 (t, 2H, ^3J(H,H) = 7.5 Hz, Ar−H_p), 7.39 (d, 4H, ^3J(H,H) = 7.5 Hz, Ar−H_m), 3.30 (sept, 4H, ^3J(H,H) = 6.9 Hz, C*H*Me$_2$), 1.11 (d, 12H, ^3J(H,H) = 6.9 Hz, CH*Me*Me), 1.04 (d, 12H, ^3J(H,H) = 6.9 Hz, CHMe*Me*), 0.53 (s, 2H, C*H*$_2$SiMe$_3$), −0.54 (s, 9H, CH$_2$Si*Me*$_3$), −0.85 (s, 6H, N=C*Me*); ^{13}C NMR (100 MHz, C_6D_6, 298 K): $\delta = 165.70$ (N=*C*), 155.25 (Ar−C_{ip}), 154.20 (Py−C_o), 140.91 (Ar−C_o), 126.98 (Ar−C_p), 124.70 (Ar−C_m), 123.87 (Py−C_m), 115.90 (Py−C_p), 28.67 (*C*HMe$_2$), 25.19 (N=C*Me*), 24.69 (CHMe*Me*), 24.17 (CH*Me*Me), 3.12 (Si*Me*$_3$), CH_2SiMe$_3$ not visible; elemental analysis calcd (%) for $C_{37}H_{54}N_3CoSi$: C 70.78, H 8.67, N 6.69; found: C 70.66, H8.73, N 6.85.

Received: July 30, 2001
Revised: September 26, 2001 [Z17632]

[1] a) B. L. Small, M. Brookhart, A. M. A. Bennett, *J. Am. Chem. Soc.* **1998**, *120*, 4049–4050; b) G. J. P. Britovsek, V. C. Gibson, B. S. Kimberley, P. J. Maddox, S. J. McTavish, G. A. Solan, A. J. P. White, D. J. Williams, *Chem. Commun.* **1998**, 849–850; c) B. L. Small, M. Brookhart, *J. Am. Chem. Soc.* **1998**, *120*, 7143–7144; d) G. J. P. Britovsek, M. Bruce, V. C. Gibson, B. S. Kimberley, P. J. Maddox, S. Mastroianni, S. J. McTavish, C. Redshaw, G. A. Solan, S. Strömberg, A. J. P. White, D. J. Williams, *J. Am. Chem. Soc.* **1999**, *121*, 8728–8740; e) G. J. P. Britovsek, S. Mastroianni, G. A. Solan, S. P. D. Baugh, C. Redshaw, V. C. Gibson, A. J. P. White, D. J. Williams, M. R. J. Elsegood, *Chem. Eur. J.* **2000**, *6*, 2221–2231.

[2] E. P. Talzi, D. E. Babushkin, N. V. Semikolenova, V. N. Zudin, V. A. Zakharov, *Kinetics and Catalysis* **2001**, *42*, 147–153. Neutral complexes rather than cationic intermediates are suggested to be the active components when [N$_3^{\mathrm{Me}}$FeCl$_2$] is activated with either MAO or AlMe$_3$.

[3] V. C. Gibson, lecture at the *11th International Symposium on Homogeneous Catalysis*, University of St. Andrews, UK, **1998**.

[4] a) D. Reardon, F. Conan, S. Gambarotta, G. Yap, Q. Wang, *J. Am. Chem. Soc.* **1999**, *121*, 9318–9325; b) E. L. Dias, M. Brookhart, P. S. White, *Organometallics* **2000**, *19*, 4995–5004.

[5] a) L. Deng, P. Margl, T. Ziegler, *J. Am. Chem. Soc.* **1999**, *121*, 6479–6487; b) P. Margl, L. Deng, T. Ziegler, *Organometallics* **1999**, *18*, 5701–5708; c) E. A. H. Griffiths, G. J. P. Britovsek, V. C. Gibson, I. R. Gould, *Chem. Commun.* **1999**, 1333–1334; d) D. V. Khoroshun, D. G. Musaev, T. Vreven, K. Morokuma, *Organometallics* **2001**, *20*, 2007–2026.

[6] This reduction is not restricted to N$_3^{i\mathrm{Pr}}$. Preliminary experiments indicate that also complexes of the 2,6-Me$_2$C$_6$H$_3$ and 2,4,6-Me$_3$C$_6$H$_2$ substituted ligands were reduced to the corresponding Co$^{\mathrm{I}}$ chloride when treated with MeLi in toluene.

[7] Unfortunately, these crystals proved not to be suitable for X-ray diffraction.

[8] Crystal size: 0.50 × 0.50 × 0.42 mm. Crystal data: monoclinic, space group $P2_1/n$, $a = 13.5506(3)$, $b = 14.8113(4)$, $c = 17.8299(4)$ Å, $\beta = 95.3671(17)^\circ$, $V = 3562.81(15)$ Å^3, $\rho_{\mathrm{calcd}} = 1.171$ mg m^{-3}, $2\theta_{\max} = 55.06^\circ$, $R = 0.0421$ ($I > 2\mathrm{sigma}(I)$), $wR2$ (all data) = 0.1035. 14766 reflections were measured (8114 independent) and included in the refinement against $|F^2|$, using the SHELXL program[17] (392 parameters). Lorentz and polarization corrections were applied, no absorption correction was performed. Max. residual electron density: 0.607 e Å^{-3}. The hydrogen atoms were placed at calculated positions, and refined isotropically in riding mode. The X-ray diffraction data were collected at 148(2) K on a Nonius Kappa CCD diffractometer with rotating anode using graphite monochromatized Mo$_{K\alpha}$ radiation ($\lambda =$ 0.71073 Å), ϕ en ω scan. The structure was solved by the PATTY option[15] of the DIRDIF program system.[16] Crystallographic data (excluding structure factors) for the structures reported in this paper have been deposited with the Cambridge Crystallographic Data Centre as supplementary publication no. CCDC-167159. Copies of the data can be obtained free of charge on application to CCDC, 12 Union Road, Cambridge CB21EZ, UK (fax: (+44) 1223-336-033; e-mail: deposit@ccdc.cam.ac.uk).

[9] A. L. Spek, Platon, multipurpose crystallographic tool, Utrecht University, Utrecht, The Netherlands, **2001**.

[10] Co$^{\mathrm{I}}$Me: a) H.-F. Klein, K. Ellrich, B. Hammerschmitt, U. Koch, G. Cordier, *Z. Naturforsch.* **1990**, *45*, 1291; b) H.-F. Klein, E. Auer, T. Jung, C. Rohr, *Organometallics* **1995**, *14*, 2725–2732; Co$^{\mathrm{I}}$Ph: c) H.-F. Klein, R. Hammer, J. Gross, U. Schubert, *Angew. Chem.* **1980**, *92*, 835–836; *Angew. Chem. Int. Ed. Engl.* **1980**, *19*, 809; Co$^{\mathrm{I}}$C≡CH: d) G. Stringer, N. J. Taylor, T. B. Marder, *Acta Crystallogr.* **1996**, *52*, 80–82.

[11] B. de Bruin, E. Bill, E. Bothe, T. Weyhermüller, K. Wieghardt, *Inorg. Chem.* **2000**, *39*, 2936–2947.

[12] P. H. M. Budzelaar, B. de Bruin, A. W. Gal, K. Wieghardt, J. H. van Lenthe, *Inorg. Chem.* **2001**, *40*, 4649–4655. Using the method described in this paper, we estimate a backdonation of approximately 0.9 e for **5**, compared to < 0.1 e for **1**.

[13] The presence of trace amounts of low (**1**) or high molecular weight polymers (**2**–**5**) results in a slight broadening of the M_w/M_n values: **1**: 3.4; **2**: 3.7; **3**: 2.5; **4**: 3.2; **5**: 3.1.

[14] The spectrum was partly obscured by the signals of MAO, toluene, and residual THF from the synthesis of **1**.

[15] P. T. Beurskens, G. Beurskens, M. Strumpel, C. E. Nordman in *Patterson and Pattersons* (Eds.: J. P. Glusker, B. K. Patterson, M. Rossi) Clarendon Press, Oxford, **1987**, p. 356.

[16] P. T. Beurskens, G. Beurskens, W. P. Bosman, R. de Gelder, S. Garcia-Granda, R. O. Gould, R. Israel, J. M. M. Smits, DIRDIF-96, a computer program system for crystal structure determination by Patterson methods and direct methods applied to difference structure factors; Crystallography Laboratory, University of Nijmegen, The Netherlands, **1996**.

[17] G. M. Sheldrick, SHELXL-97, program for the refinement of crystal structures; University of Gottingen, Germany, **1997**.

[18] There are, however, still possibilities for re-oxidation of Co$^{\mathrm{I}}$ to Co$^{\mathrm{II}}$ on activation. For example, alkyl abstraction from [N$_3$CoR] could produce [N$_3$Co]$^+$ species, which could oxidize a second molecule of [N$_3$CoR] to the Co$^{\mathrm{II}}$ species [N$_3$CoR]$^+$. Alternatively, [N$_3$Co(C$_2$H$_4$)]$^+$, from ethene capture by [N$_3$Co]$^+$, could be attacked by a Lewis acid A, to give a zwitterionic Co$^{\mathrm{III}}$ species [N$_3$Co(C$_2$H$_4$A)]$^+$ which could comproportionate with [N$_3$CoR] to give the two Co$^{\mathrm{II}}$ complexes [N$_3$CoR]$^+$ and [N$_3$Co(C$_2$H$_4$A)].

[19] One possibility for a Co$^{\mathrm{I}}$ active species would be an [N$_2$CoMe] complex formed by MAO abstraction of an imine group from the metal center; this would be electronically similar to Ni$^{\mathrm{II}}$/Pd$^{\mathrm{II}}$ diimine catalysts. A Co$^{\mathrm{III}}$ active species could be formed by Lewis acid attack on [N$_3$Co(C$_2$H$_4$)]$^+$, as described above.[18]

 © WILEY-VCH Verlag GmbH, D-69451 Weinheim, 2001 1433-7851/01/4024-4722 $ 17.50+.50/0

Design and Synthesis of a Peptide That Binds Specific DNA Sequences through Simultaneous Interaction in the Major and in the Minor Groove**

M. Eugenio Vázquez, Ana M. Caamaño, José Martínez-Costas, Luis Castedo, and José L. Mascareñas*

Most transcription factors (TFs) bind specific DNA sequences using dimeric or multimer motifs, with more or less equal binding energy contributions from each domain and usually strong cooperativity between them.[1] One of the most remarkable examples of bivalent DNA recognition is provided by the bZIP family of TFs, which bind DNA as leucine zipper mediated homo- or heterodimers, with the N-terminal basic region (BR) of each monomer inserting into adjacent DNA major grooves.[2] It has been shown that the leucine zipper unit can be replaced by other noncovalent dimerizing units, or by artificial covalent linkers, without significantly compromising the recognition properties of the system.[3, 4] However, monovalent bZIP BRs exhibit very low DNA binding affinities.[3a, 5] It was recently demonstrated that covalent attachment of one basic region of a bZIP protein (GCN4) to DNA at an appropriate position allows sequence-specific binding.[6] This results suggests that monomeric bZIP-basic region peptides might be able to fold and bind DNA specifically, provided they could be properly delivered to their cognate recognition site. On these grounds we envisaged that suitable tethering of a bZIP-BR domain to a molecule that binds with moderate-to-good affinity in the minor groove of an adjacent sequence might provide for specific binding of the peptide to its cognate major groove site (Figure 1). Most importantly, the resulting conjugate should exhibit higher affinity for its target hybrid DNA site than its individual components have for their target sites.[7] Herein we demonstrate the validity of this approach by reporting the first designed peptide derivative capable of binding to DNA with nanomolar affinity through a bivalent, major–minor groove recognition motif.[8]

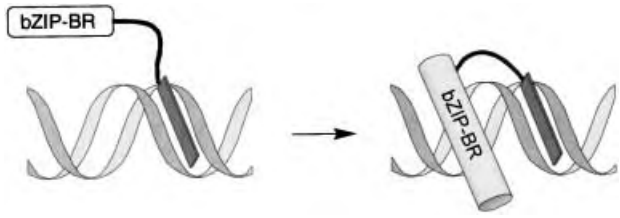


Figure 1. Strategy for DNA recognition.

For minor-groove recognition we used distamycin A,[9] a well known tripyrrole antibiotic that binds DNA preferentially at A–T rich sites. For the major-groove counterpart we chose the basic region of GCN4, a bZIP protein which binds specifically to the cAMP response element site (CRE: 5′-ATGAcgTCAT-3′). From the X-ray structures of the DNA complexes of GCN4[10] and distamycin A,[11] we built an hypothetical model for simultaneous interaction of the GCN4 BR and distamycin with adjacent DNA sites (Figure 2).[12] On

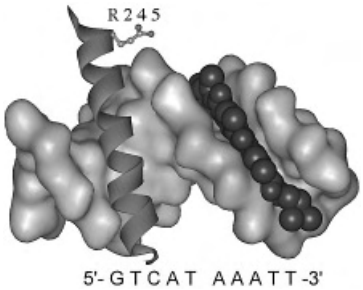


Figure 2. Model for the simultaneous interaction of the GCN4 basic region and distamycin at adjacent sites with DNA

the basis of this model we designed the hybrid **1** (Scheme 1), in which the tether connects the nitrogen atom of the N-terminal pyrrole of a distamycin analogue with the side chain of a glutamic acid. The latter replaces the Arg245 residue of the natural protein. The tether was chosen to span the required distance between the attachment points while allowing for crossover of the phosphate backbone, a process that may be facilitated by the presence of the secondary amine in the chain.

The key step for the synthesis of this hybrid consisted of the coupling of the tripyrrole derivative **2** with the peptide while it was still attached to the resin and fully protected except at the Glu245 residue (Scheme 1).[13]

The DNA binding properties of hybrid **1** were first assessed by circular dichroism, a spectroscopic technique particularly useful for studying DNA–b-ZIP interactions because of the well-established folding of the b-ZIP BRs from random coil to an α-helix upon specific DNA binding.[4] The CD spectrum of compound **1** in the absence of DNA is similar to that of peptide **3** (Figure 3a), which lacks the tripyrrole tether and hence can be used as a control in the binding studies. Unfortunately, addition of an 18 base pair (bp) duplex containing the designated hybrid DNA sequence (T/CRE^{hs})[14] to **1** at 4 °C, did not produce a significant variation of the CD signal at 222 nm, which indicates that the basic region is not inserting into the groove. The considerable

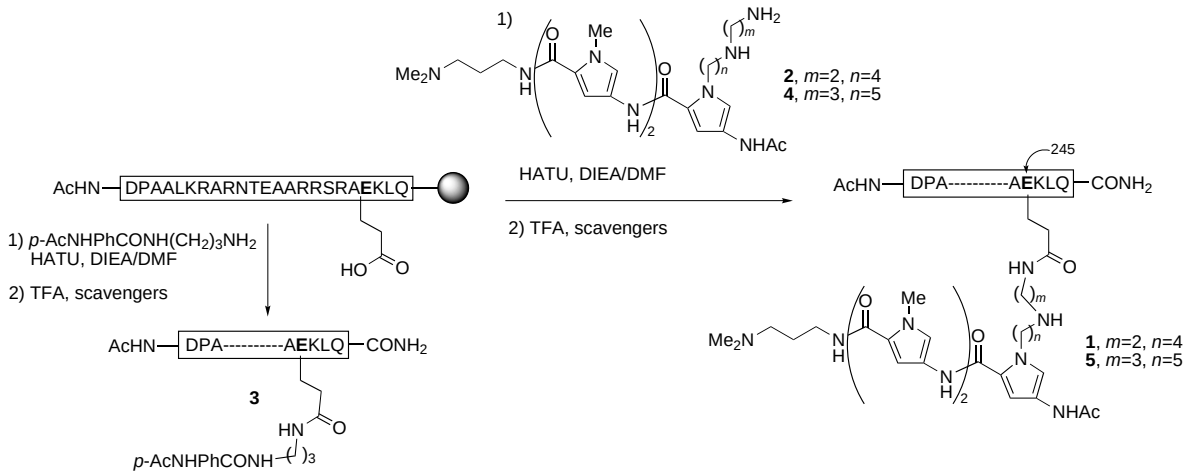
[*] Prof. Dr. J. L. Mascareñas, M. E. Vázquez, A. M. Caamaño, Prof. Dr. L. Castedo
Departamento de Química Orgánica
y Unidad Asociada al CSIC
Universidad de Santiago de Compostela
15782 Santiago de Compostela (Spain)
Fax: (+34) 981-595-012
E-mail: qojoselm@usc.es

Dr. J. Martínez-Costas
Departamento de Bioquímica y Biología Molecular
Universidad de Santiago de Compostela
15782 Santiago de Compostela (Spain)

[**] This work was supported by the Spanish M.E.C. (PB97-0524) and the Xunta de Galicia (PGIDT00PXI20912PR). M.E.V. and A.M.C. thank the Xunta de Galicia and the University of Santiago for their predoctoral fellowships. We are very grateful to Prof. G. L. Verdine for his input and support in the early phases of this work. We also thank Prof. J. Benavente for allowing us to use the radioactivity facilities and Prof. C. Abell for critical reading of the manuscript.

Supporting information for this article is available on the WWW under http://www.angewandte.com or from the author.

 © WILEY-VCH Verlag GmbH, D-69451 Weinheim, 2001 1433-7851/01/4024-4723 $ 17.50+.50/0



Scheme 1. Synthesis of the hybrid peptides. DIEA = diisopropylethylamine, HATU = *N*-[(dimethylamino)-1*H*-1,2,3-triazolo[4.5-*b*]pyridin-1-ylmethylene]*N*-methylmethanaminium hexafluorophosphate oxide, DMF = *N*,*N*-dimethylformamide, TFA = trifluoroacetic acid.

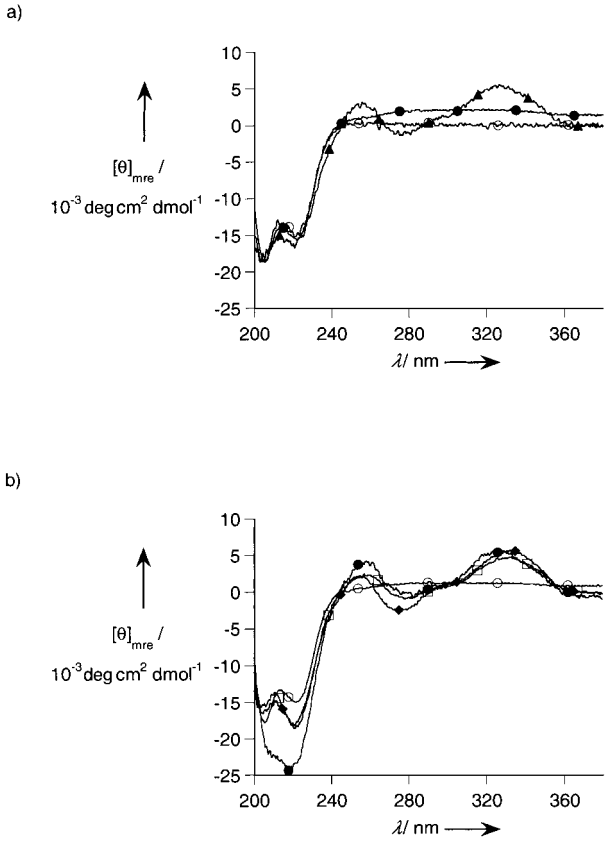


Figure 3. CD spectra of the peptides **1**, **3**, and **5** in the presence or absence of ds-oligonucleotides: a) **3** in the absence of DNA (○), **1** in the absence of DNA (●), **1** in the presence T/CRE^{hs} (▲); b) Spectra of **5** in the absence of DNA (○), in the presence of T/CRE^{hs} (●), in the presence of TcgCRE^{hs} (□), in the presence of T/CRE^{hs}*m* (◆). CD measurements were performed at 4 °C on a JASCO J-715 in a 2-mm cell. Samples contained 10 mM phosphate buffer (pH 7.5), 100 mM NaCl, 5 μM peptide, and 5 μM ds-oligo when present. Spectra of the peptides in the presence of DNA were calculated as the difference between the spectra of the peptide–DNA mixture and the spectrum of free DNA. ds-Oligonucleotides used (the BR subsite (CRE^{hs}) is underlined and the tripyrrole subsite (T) is in italics):

T/CRE^{hs}: 5′-d(CGAACGTCAT*AAAAT*CCT)-3′
3′-d(GCTTGCAGTATTTTAGGA)-5′
TcgCRE^{hs}: 5′-d(CGAACGTCATCG*AAATT*CCT)-3′
3′-d(GCTTGCAGTAGCTTTAAGGA)-5′
T/CRE^{hs}*m*: 5′-d(CGAACGTCGT*AAAAT*CCT)-3′
3′-d(GCTTGCAGCATTTTAGGA)-5′

positive signal at about 330 nm suggests that the tripyrrole does bind at the A–T rich site.[15] Indeed, a similar band was observed upon addition of the same double-stranded(ds) DNA (T/CRE^{hs}) to the tripyrrole **2**.[16] As expected, addition of T/CRE^{hs} to peptide **3** does not induce any change in its CD spectrum (results omitted in Figure 3a for clarity).

We realized from the computer model of the complex that the two parts of **1** are relatively tightly tethered and this might impose some geometric restriction on the required simultaneous binding of both segments. Therefore we synthesized the hybrid **5**, which features a slightly longer connector.[17] Addition of T/CRE^{hs} to peptide **5** induced a remarkable increase in the magnitude of the signal at 222 nm, which indicates that, in this case, the BR peptidic domain is folding and binding to the DNA (Figure 3b). A band at 330 nm in the CD spectrum corresponding to the insertion of the oligopyrrole into the minor groove is also clearly seen. As expected no significant increase in ellipticity was observed upon incubation of **5** with TcgCRE^{hs}, a ds-oligonucleotide including a bp spacing between the binding sites, nor with CRE^{hs} which features a bp mismatch at the BR peptide binding subsite (T/CRE^{hs}*m*).

With these data at hand, we further assessed the DNA-binding properties of the synthetic hybrid peptides by using gel mobility shift analysis, by titrating ^{32}P-end-labeled dsDNAs with increasing concentrations of the peptides. As illustrated in Figure 4, peptide **5** did bind to T/CRE^{hs} with nanomolar affinity, albeit producing two bands, the faster migrating one being slightly more intense. Incubation of peptide **5** with the dsDNA mutated at the BR binding site (T/CRE^{hs}*m*) gave a band with mobility similar to that of the slower migrating one in the preceding experiment. As expected, we could not detect any peptide–DNA complex at concentrations below 100 nM in the presence of a dsDNA containing exclusively the BR peptide binding site (CRE^{hs}). These results together with the CD data indicate that the more intense, faster migrating band obtained upon incubation of **5** with the designated dsDNA corresponds to the expected compact major–minor mode of binding, while the other less intense band results from a complex in which the oligopyrrole is inserted into the groove but the BR peptide

 © WILEY-VCH Verlag GmbH, D-69451 Weinheim, 2001 1433-7851/01/4024-4724 $ 17.50+.50/0

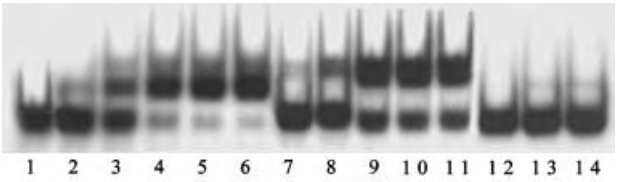


Figure 4. Autoradiograms showing the binding of hybrid **5** to ^{32}P-labeled DNAs. Lanes 1–6: T/CRE^{hs}, **5**: 0, 7.7, 19, 38, 58, 77 nM respectively; Lanes 7–11: T/CRE^{hs}*m*, **5**: 7.7, 19, 38, 58, 77 nM respectively; lanes 12–14: CRE^{hs}, **5**: 38, 77, 154 nM respectively. Binding reactions were performed over 10 min at 4 °C using < 1 nM labeled DNAs in a binding mixture (20 μL) containing 20 mM tris(hydroxymethyl)aminomethane (pH 7.5), 100 mM KCl, 2 mM $MgCl_2$, 2 mM ethylenediaminetetraacetate, 10% glycerol, 0.3 mg mL^{-1} *N,O*-bovine serum albumin (BSA), and 2% NP-40. The products were resolved by polyacrylamide gel electrophoresis using a 10% nondenaturing acrylamide gel and 0.5X TBE (25 mM tris borate and 0.5 mM EDTA) buffer.
CRE^{hs}: 5′-d(CGAC<u>GTCAT</u>CGGAGGTCCT)-3′
3′-d(GCTG<u>CAGTA</u>GCCTCCAGGA)-5′

makes non-specific electrostatic contacts to the phosphate groups.[18]

In conclusion, appropriate linking of a b-ZIP basic region to a minor groove binding tripyrrole allowed for specific binding to its cognate DNA site. The hybrid compound **5** shows considerably higher affinity for its designated target DNA sequence than that of its isolated components for their respective cognate subsites. Although further refinement of the design is necessary to obtain compounds with higher affinities and better specificities, the work described herein confirms the viability of this new type of major–minor groove DNA-binding molecules.

Received: July 23, 2001 [Z17576]

[1] For reviews on DNA-binding proteins, see: a) C. O. Pabo, R. T. Sauer, *Annu. Rev. Biochem.* **1992**, *61*, 1053–1095; b) S. K. Burley, *Curr. Opin. Struct. Biol.* **1994**, *4*, 3–11; c) B. Alberts, D. Bray, J. Lewis, M. Raff, K. Roberts, J. D. Watson, *Molecular Biology of the Cell*, Garland Publishing, New York, **1994**, chap. 9; d) C. Branden, J. Tooze, *Introduction to Protein Structure*, Garland Publishing, New York, **1999**, chap. 8–10; e) D. S. Latchman, *Eukaryotic Transcription Factors*, Academic Press, London, **1998**, chap. 8; f) N. M. Luscombe, S. E. Austin, H. M. Berman, J. M. Thornton, *Genome Biology* **2000**, *1*, 1–37.
[2] H. C. Hurst, *Protein Profile* **1996**, *3*, 1–72.
[3] a) R. V. Talanian, C. J. McKnight, P. S. Kim, *Science* **1990**, *249*, 769–771; b) B. Cuenoud, A. Shepartz, *Science* **1993**, *259*, 510–513; c) T. Morii, M. Shimomura, M. Morimoto, I. Saito, *J. Am. Chem. Soc.* **1993**, *115*, 1150–1151; d) T. Morii, Y. Saimei, M. Okagami, K. Makino Y. Sugiura, *J. Am. Chem. Soc.* **1997**, *119*, 3649–3655; e) Y. Aizawa, Y. Sugiura, T. Morii, *Biochemistry* **1999**, *38*, 1626–1632.
[4] The use of an azobenzene as a dimerizing unit allows the DNA affinity of the peptides to be photomodulated: A. M. Caamaño, M. E. Vázquez, J. Martínez-Costas, L. Castedo, J. L. Mascareñas, *Angew. Chem.* **2000**, *112*, 3234–3237; *Angew. Chem. Int. Ed.* **2000**, *39*, 3104–3107.
[5] Recently Zondlo and Shepparzt have developed a smart strategy for achieving monovalent DNA recognition which is based on grafting the DNA-binding residues into the helix of an *aPP* protein: a) N. J. Zondlo, A. Schepartz, *J. Am. Chem. Soc.* **1999**, *121*, 6938–6939; b) J. W. Chin, A. Schepartz, *J. Am. Chem. Soc.* **2001**, *123*, 2929–2930.
[6] D. Stanojevic, G. L. Verdine, *Nat. Struct. Biol.* **1995**, *2*, 450–457.
[7] This system would somewhat mimick the mode of recognition of a number of transcription factors that bind DNA by interacting with both the major and minor grooves. See for example: a) J.-A. Feng, R. C. Johnson, R. E. Dickerson, *Science* **1994**, *263*, 348–355; b) A. Draganescu, J. R. Levin, T. D. Tullius, *J. Mol. Biol.* **1995**, *250*, 595–608; c) G. Meinke, P. B. Sigler, *Nat. Struct. Biol.* **1999**, *6*, 471–477.
[8] A major–minor groove DNA-binding ligand made of a hairpin polyamide and a 11-mer oligonucleotide has been previously described: J. W. Szewczyk, E. E. Baird, P. B. Dervan, *Angew. Chem.* **1996**, *108*, 1596–1598; *Angew. Chem. Int. Ed.* **1996**, *35*, 1487–1489.
[9] C. Zimmer, U. Wahnert, *Prog. Biophys. Mol. Biol.* **1986**, *47*, 31–112.
[10] T. E. Ellemberger, C. J. Brandl, K. Struhl, S. C. Harrison, *Cell* **1992**, *71*, 1223–1237.
[11] M. Coll, C. A. Frederick, A. H. J. Wang, A. Rich, *Proc. Natl. Acad. Sci. USA* **1987**, *84*, 8385–8389.
[12] The model was constructed by superimposing appropriate base pairs, by using the INSIGHTII software package on a SGI workstation.
[13] The synthesis of **2** and **1** have been previously communicated: M. E. Vázquez, A. M. Caamaño, L. Castedo, D. Gramberg, J. L. Mascareñas, *Tetrahedron Lett.* **1999**, *40*, 3625–3629.
[14] The target site of this sequence does not match exactly with that of the model, but it was used on the basis of the reported preferred (1:1) recognition sites for distamycin, see: D. Rentzeperis, L. A. Marky, T. J. Dwyer, B. H. Geierstanger, J. G. Pelton, D. A. Wemmer, *Biochemistry* **1995**, *34*, 2937. See also reference [15].
[15] F.-M. Chen, F. Sha, *Biochemistry* **1998**, *37*, 11143–11151.
[16] We have calculated an approximate K_d value of 0.8 ± 0.5 μM by CD titration of compound **2** with this dsDNA.
[17] The synthesis of **5** was carried out by using similar procedures as for the synthesis of **1**, and is described in the Supporting Information. Electrospray mass spectrometry: *m/z* [M+H$^+$] found: 3271.4; calcd: 3270.8.
[18] A related mode of interaction has been previously observed with microgonotropens, see: D. Sengupta, A. Blaskó, T. C. Bruice, *Biorg. Med. Chem.* **1996**, *4*, 803–813, and references therein.

Solid-Phase Capture–Release Strategy Applied to Oligosaccharide Synthesis on a Soluble Polymer Support**

Hiromune Ando, Shino Manabe, Yoshiaki Nakahara, and Yukishige Ito*

Advances in the techniques for oligosaccharide synthesis have lagged behind those for other classes of biological oligomers. For the preparation of oligopeptides and oligo-

[*] Dr. Y. Ito, Dr. H. Ando, Dr. S. Manabe
RIKEN (The Institute of Physical and Chemical Research)
and CREST, Japan Science and Technology Corporation (JST)
2–1 Hirosawa, Wako-shi, Saitama 351-0198 (Japan)
Fax: (+81) 48-462-4680
E-mail: yukito@postman.riken.go.jp
Prof. Dr. Y. Nakahara
Department of Applied Biochemistry, Tokai University
and CREST, JST
Kitakaname 1117, Hiratsuka-shi, Kanagawa 259-1292 (Japan)

[**] This work was supported in part by the Mizutani Foundation for Glycoscience (grant to Y.I.), the RIKEN Presidential Fund (grant to S.M.), and the Ministry of Education, Culture, Sports, Science and Technology (Grant-in-Aid for Scientific Research to S.M.). We thank Dr. Teiji Chihara and his staff for the elemental analyses, Ms. Yasuko Tanaka for her contribution at the exploratory stage of this work, and Ms. Akemi Takahashi for her technical assistance.

Supporting information for this article is available on the WWW under http://www.angewandte.com or from the author.

nucleotides, the automated synthesizer has become a routine tool, in which polymer-support synthesis plays a key role.

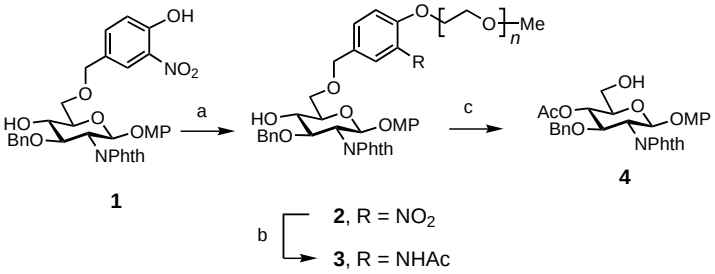
Considering the structural diversity of glycoconjugate-derived oligosaccharides,[1] the potential utility of oligosaccharide synthesis on a polymer support is obvious.[2] This technology would greatly facilitate glycoconjugate synthesis and could possibly reap the benefits of automation.[3] However, several problems must be solved before this goal can be reached: firstly, the difficulty in monitoring reaction progress; secondly, the reduced reactivity of substrates bound to the polymer support; and thirdly, the limitations in scaling up. Addressing these issues, we recently developed a methodology for the monitorable synthesis of oligosaccharides on a soluble polymer support based on the "tag–reporter" concept.[4] It exploited low molecular weight poly(ethylene)glycol (PEG),[5] which served both as a "reporter" in the monitoring of the reaction by matrix-assisted laser desorption/ionization time-of-flight (MALDI-TOF) mass spectrometry and as a "tag" in the separation of support-bound materials from the reaction mixture due to its high polarity.[6, 7]

Although syntheses on polymer supports can indeed be monitored,[4, 8] the success of this method assumes all reactions can be driven to near completion. This seems to be a difficult requirement, considering that typical O-glycosylations proceed in 50–80% yield.[9] Now, we wish to report a refined strategy for the synthesis of PEG-tagged oligosaccharides that circumvents this obstacle.

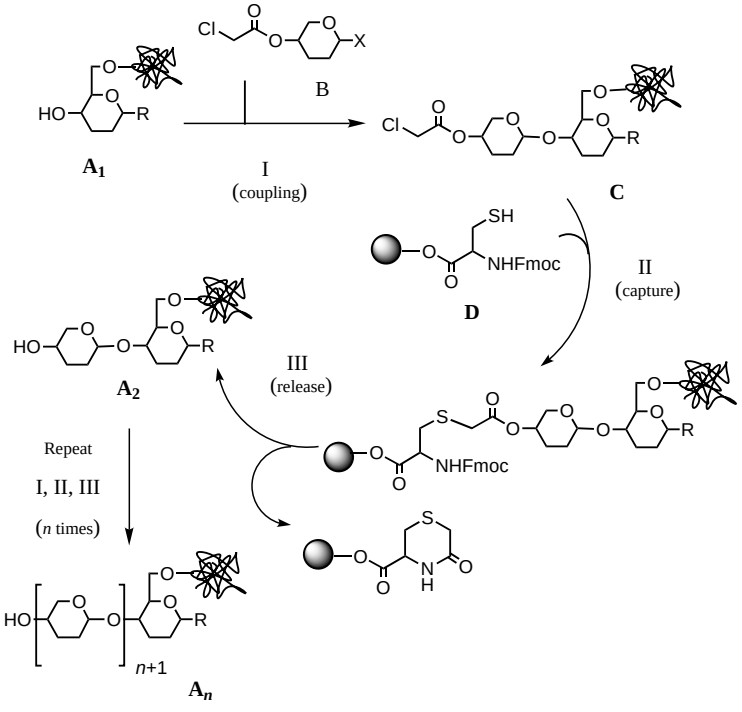
This new approach is based on the concept of resin-aided capture–release (Scheme 1).[10] It employs a glycosyl acceptor bound to a low molecular weight PEG support ($\mathbf{A_1}$) in combination with a chloroacetyl (CA) carrying donor (**B**), as described before.[4] The PEG-bound component can be recovered by filtration through a pad of silica gel. At this stage, excess donor and side product(s) can be removed. The coupled product (**C**), potentially contaminated with unreacted acceptor $\mathbf{A_1}$, is then captured onto solid phase by a chemoselective reaction between CA and a resin-bound thiol group (**D**). After removal of Fmoc, the exposed amine function should cyclize spontaneously to release a disaccharide ($\mathbf{A_2}$), which is now ready for the next coupling. Repetition of this cycle should provide facile access to correctly assembled oligomers $\mathbf{A}_n$.

To examine the adequacy of this strategy, we selected a lactosamine repetition sequence as the target. It is well recognized that polylactosamine [(Galβ1 →4GlcNAcβ1 →3)$_n$] is an important structural motif of Asn-linked[11] and Ser/Thr-linked[12] glycoproteins and of glycosphingolipids.[13]

PEG-supported monosaccharide **2**, which carries the nitro-modified Wang resin-type linker,[14] was prepared as depicted in Scheme 2. Previously reported **1**[4] was treated with PEG



Scheme 2. Preparation of PEG-supported monosaccharide **2**. a) PEG monomethyl ether, DEAD, Ph_3P, THF, RT, 18 h, 99%; b) acetylacetone, Zn/Cu, THF, RT, 16 h, then Ac_2O, Et_3N; c) DDQ, $ClCH_2CH_2Cl/H_2O$, RT, 4 h, 92% overall. DEAD = diethyl azodicarboxylate, DDQ = 2,3-dichloro-5,6-dicyanobenzoquinone, MP = p-$MeOC_6H_4$, Phth = phthaloyl.

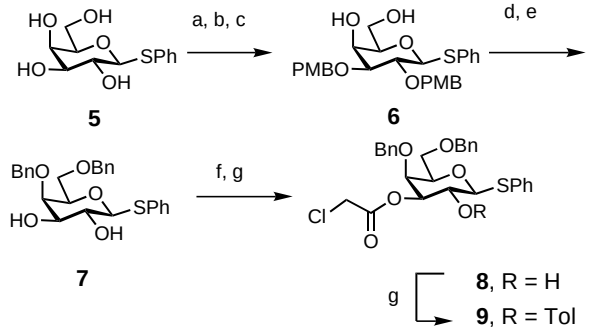


Scheme 1. Capture–release strategy for the synthesis of disaccharides $\mathbf{A_2}$ and oligosaccharides $\mathbf{A}_n$ on a polymer support. Fmoc = 9-fluorenylmethoxycarbonyl.

methyl ether (av $M_w = 550$) under Mitsunobu conditions. Nearly quantitative carbohydrate incorporation was supported by ^{1}H NMR spectroscopy and confirmed by the cleavage experiment performed under the conditions reported by Kusumoto et al. for the removal of the nitrobenzyl group.[15] Namely, the nitro group of **2** was first converted to the acetamido group in **3**, which was then treated with DDQ[16] to afford compound **4** in high overall yield.

Galactosyl donor **9**, which has a chloroacetyl group, was prepared from phenylsulfanylgalactoside **5**[17] via **6**–**8** (Scheme 3). The coupling of **2** and **9** was performed with dimethyl(methylsulfanyl)sulfonium triflate (DMTST)[18] in CH_2Cl_2 (Scheme 4). To evaluate the efficacy of the capture–release process only a substoichiometric amount (0.9 equiv) of **9** was used for this reaction. The reaction progress was monitored by MALDI-TOF mass spectrometry as described previously.[4, 19] The mixture was passed through a pad of silica gel that was first washed with AcOEt, and the PEG-bound component was eluted with AcOEt/MeOH 3:1. Analysis of this fraction by ^{1}H NMR spectroscopy revealed the presence of disaccharide **10** and unreacted acceptor **2** in a ratio of about 10:3 (Figure 1A). This indicates that the

 © WILEY-VCH Verlag GmbH, D-69451 Weinheim, 2001 1433-7851/01/4024-4726 $ 17.50+.50/0 *Angew. Chem. Int. Ed.* **2001**, *40*, No. 24



Scheme 3. Preparation of galactosyl donor **9**. a) $(MeO)_2CMe_2$, CSA, MeCN, RT, 10 min; b) *p*-methoxybenzyl chloride (PMBCl), NaH, DMF, RT, 15 h; c) 60% AcOH, RT, 13 h, 56% overall; d) benzyl bromide, NaH, DMF, RT, 5 h; e) DDQ, CH_2Cl_2/H_2O, RT, overnight, 79% from **6;** f) $(ClCH_2CO)_2O$, pyridine, CH_2Cl_2, $-40\,^{\circ}C$, 3 h, 33%; g) *p*-MeC_6H_4COCl (TolCl), pyridine, CH_2Cl_2, $0\,^{\circ}C \rightarrow RT$, 3 h, 85%. CSA = 10-camphorsulfonic acid, DMF = dimethylformamide.

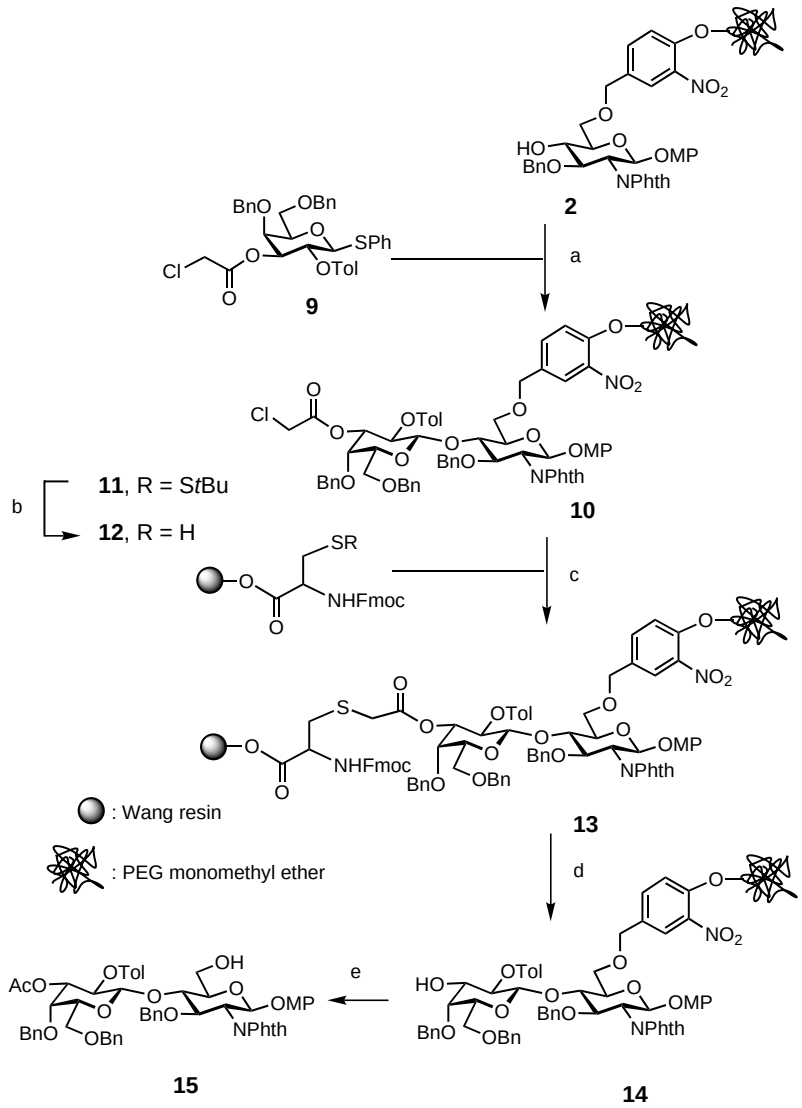
glycosylation proceeded in a highly efficient manner (ca. 85% based on donor **9**) and that the entropic disadvantage inherent to reactions on a polymer support was kept to a minimum through the use of low molecular weight PEG. Additionally, potential contamination by moisture due to the hygroscopic nature of PEG was practically inconsequential.

The mixture of disaccharide **10** and unreacted **2** was then subjected to the capture–release cycle. According to our expectations, thiol-containing resin **12** generated from commercially available S*t*Bu-protected cysteine-loaded Wang resin **11** efficiently captured the coupled product. This step was monitored by chloroacetyl color test with *p*-nitrobenzylpyridine–piperidine.[4, 20] Subsequent release was effected by treatment with 4-(aminomethyl)piperidine[21] to afford **14** with excellent purity. As apparent from ^1H NMR analysis, unreacted acceptor **2** was completely removed (Figure 1B). At this stage, the coupled product was fully characterized as disaccharide **15**, which was obtained from **14** after cleavage from PEG (Scheme 4).

Further chain elongation was performed according to Scheme 5. Namely, the second glucosamine residue was incorporated by using trichloroacetimidate **16**. Crude trisaccharide **17** was then subjected to capture–release to give **18**. After final glycosylation with thioglycoside **9** and capture–release, tetrasaccharide **20** was cleaved from PEG to provide **21**. Complete deprotection was performed in a standard manner to give the free tetrasaccharide Galβ1 $\rightarrow$4GlcNAcβ1 $\rightarrow$3Galβ1 $\rightarrow$4GlcNAcβ1 $\rightarrow$ OMP.

We have developed a resin-aided capture–release strategy for oligosaccharide synthesis on a polymer support. As an initial demonstration of the strategy, we examined the construction of an oligosaccharide consisting solely of synthetically straightforward 1,2-*trans* (β) glycosidic linkages. More systematic studies should prove the generality of this strategy to a wide range of glycoconjugate-derived glycans.

Received: June 1, 2001
Revised: August 13, 2001 [Z17211]



Scheme 4. Capture–release of disaccharide **10**. a) DMTST, MS 4 Å/CH_2Cl_2, $-20 \rightarrow 0\,^{\circ}C$, 14 h, 94%; b) nBu_3P, EtOH/CH_2Cl_2/H_2O (4:6:1), RT, 3 h, 98%; c) **12** (3 equiv), iPr_2EtN (3 equiv), CH_2Cl_2/MeCN (1:1), RT, 14 h; d) 4-(aminomethyl)pyridine (15 equiv), THF, RT, 12 h, then Amberlyst 15E, 82% from **10;** e) acetylacetone, Zn/Cu, THF, RT, 18 h, then Ac_2O, Et_3N; f) DDQ, $ClCH_2CH_2Cl/H_2O$, RT, 3 h, 86% from **14**.

[1] A. Kobata, *Acc. Chem. Res.* **1993**, *26*, 319–324.
[2] Recent reviews: Y. Ito, S. Manabe, *Curr. Opin. Chem. Biol.* **1998**, *2*, 701–708; H. M. I. Osborn, T. H. Khan, *Tetrahedron* **1999**, *55*, 1807–1850; P. M. St. Hilaire, M. Meldal, *Angew. Chem.* **2000**, *112*, 1210–1228; *Angew. Chem. Int. Ed.* **2000**, *39*, 1162–1179; P. H. Seeberger, W.-C. Hasse, *Chem. Rev.* **2000**, *100*, 4349–4393.
[3] O. J. Plante, E. R. Palmacci, P. H. Seeberger, *Science* **2001**, *291*, 1523–1527.
[4] H. Ando, S. Manabe, Y. Nakahara, Y. Ito, *J. Am. Chem. Soc.* **2001**, *123*, 3848–3849.
[5] L. Jiang, R. C. Hartley, T.-H. Chan, *Chem. Commun.* **1996**, 2193–2194.
[6] Review: P. H. Toy, K. D. Janda, *Acc. Chem. Res.* **2000**, *33*, 546–554. For pioneering work on PEG-supported oligosaccharide synthesis: S. P. Douglas,

 © WILEY-VCH Verlag GmbH, D-69451 Weinheim, 2001 1433-7851/01/4024-4727 $ 17.50+.50/0

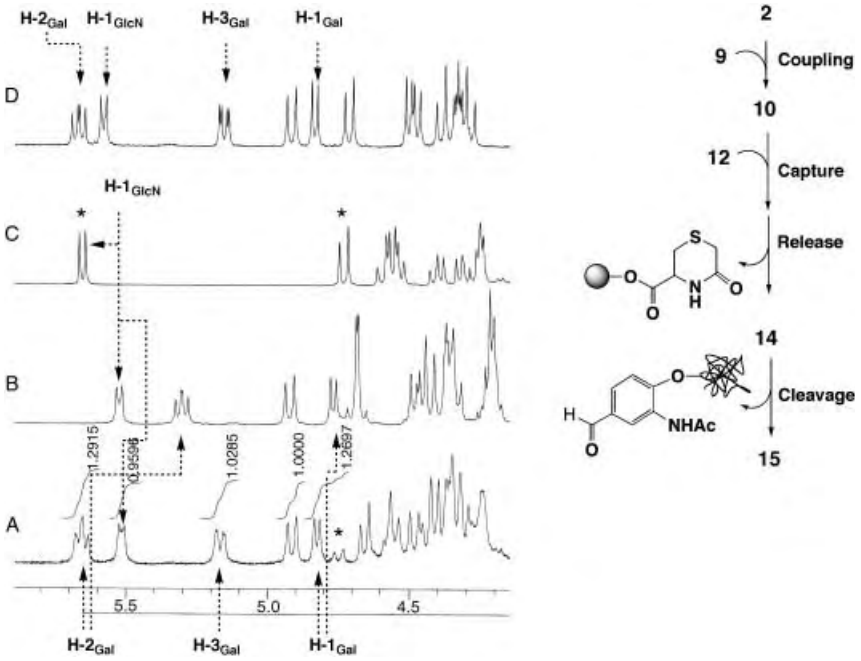
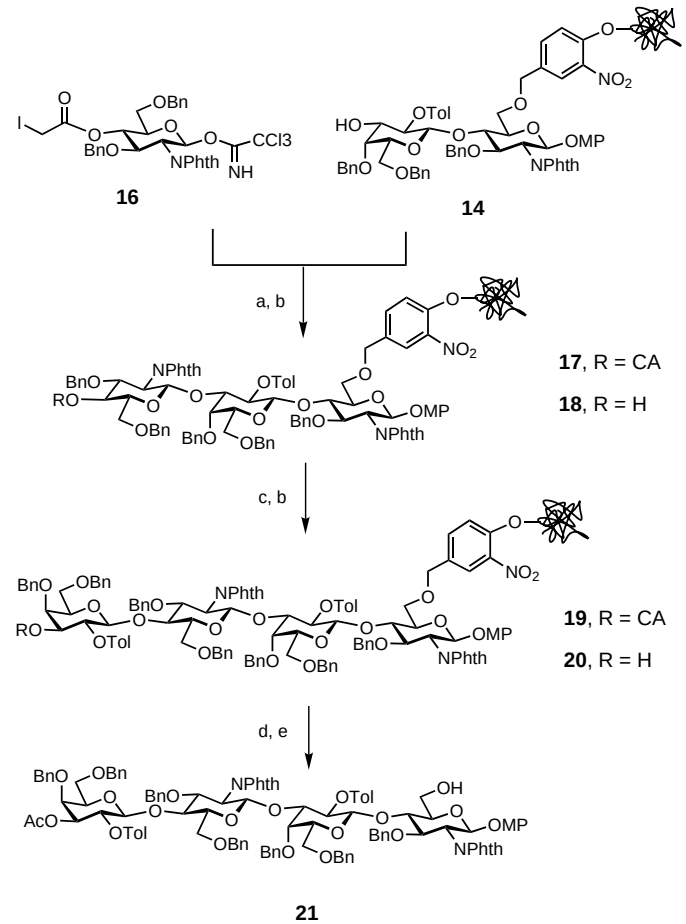


Figure 1. ^{1}H NMR spectra of crude **10** before capture (A), released disaccharide **14** (B), PEG-supported acceptor **2** (C), and disaccharide **15** after cleavage (D), and schematic reaction sequence. The starred signals belong to unreacted **2**.



Scheme 5. Synthesis of tetrasaccharide **21**. a) TMSOTf/CH_2Cl_2, $-20\,^\circ$C, 1 h, 95%; b) **12**, iPr$_2$EtN, MeCN/CH_2Cl_2, RT, then 4-(aminomethyl)pyridine, THF, RT, 79% (**18**), 80% (**20**); c) **9**, DMTST, MS 4 Å, CH_2Cl_2, $0\rightarrow10\,^\circ$C, 5 h, 88%; d) acetylacetone, Zn/Cu, THF, RT, 18 h, then Ac_2O, Et_3N; e) DDQ, $ClCH_2CH_2Cl/H_2O$, RT, 3 h, 72% overall. TMSOTf = trimethylsilyl triflate.

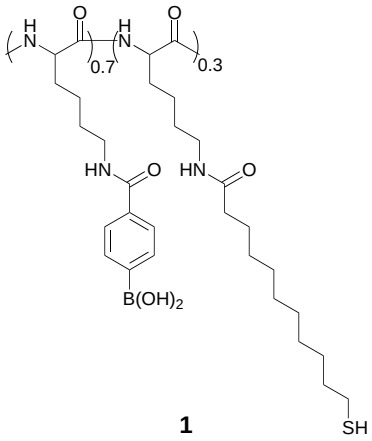
D. M. Whitfield, J. J. Krepinsky, *J. Am. Chem. Soc.* **1995**, *117*, 2116 – 2117.
[7] Recent examples of tag-assisted product isolation: V. Pozgay, *Org. Lett.* **1999**, *1*, 477 – 480; H. Perrier, M. Labelle, *J. Org. Chem.* **1999**, *64*, 2110 – 2113; S.-Q. Zhang, K. Fukase, S. Kusumoto, *Tetrahedron Lett.* **1999**, *40*, 7479 – 7483; K. Itami, K. Mitsudo, T. Kamei, T. Koike, T. Nokami, J. Yoshida, *J. Am. Chem. Soc.* **2000**, *122*, 12013 – 12014; S. V. Ley, A. Massi, F. Rodríguez, D. C. Horwell, R. A. Lewthwaite, M. C. Pritchard, A. M. Reid, *Angew. Chem.* **2001**, *113*, 1088 – 1090; *Angew. Chem. Int. Ed.* **2001**, *40*, 1053 – 1055.
[8] P. H. Seeberger, X. Beebe, G. D. Sukenick, S. Pochapsky, S. Danishefsky, *Angew. Chem.* **1997**, *109*, 507 – 510; *Angew. Chem. Int. Ed. Engl.* **1997**, *36*, 491 – 493; T. Kanemitsu, O. Kanie, C.-H. Wong, *Angew. Chem.* **1998**, *110*, 3574 – 3577; *Angew. Chem. Int. Ed.* **1998**, *37*, 3415 – 3418.
[9] F. Baressi, O. Hindsgaul, *J. Carbohydr. Chem.* **1995**, *14*, 1043 – 1087.
[10] Review: A. Kirschning, H. Monenschein, R. Wittenberg, *Chem. Eur. J.* **2000**, *6*, 4445 – 4450.
[11] M. Hummel, H. C. Hedrich, A. Hasilik, *Eur. J. Biochem.* **1997**, *245*, 428 – 433.
[12] K. Maemura, M. Fukuda, *J. Biol. Chem.* **1992**, *267*, 24379 – 24386.
[13] K. Watanabe, S. Hakomori, R. A. Childs, T. Feizi, *J. Biol. Chem.* **1979**, *254*, 3221 – 3228.
[14] Similar linkers were reported previously: S. Manabe, Y. Nakahara, Y. Ito, *Synlett* **2000**, 1241 – 1244; X. Wu, M. Grathwohl, R. R. Schmidt, *Org. Lett.* **2001**, *3*, 747 – 750.
[15] K. Fukase, T. Yoshimura, M. Hashida, S. Kusumoto, *Tetrahedron Lett.* **1991**, *32*, 4019 – 4022; K. Fukase, K. Egusa, Y. Nakai, S. Kusumoto, *Mol. Diversity* **1996**, *2*, 182 – 188.
[16] Y. Oikawa, T. Yoshioka, O. Yonemitsu, *Tetrahedron Lett.* **1982**, *23*, 885 – 888.
[17] K. C. Nicolaou, N. J. Bockovich, D. R. Carcanague, *J. Am. Chem. Soc.* **1993**, *115*, 8843 – 8844.
[18] P. Fügedi, P. J. Garegg, *Carbohydr. Res.* **1986**, *149*, c9-c12.
[19] Due to the statistical distribution of the length of the PEG chain, which consists of 8 – 20 ethylene glycol units, the progress of the reaction was clearly seen in the mass spectrum by the shift of a group of signals with a characteristic mountainlike shape (m/z 980 – 1450, highest peak at 1212) to a higher molecular weight region (m/z 1570 – 2020, highest peak at 1751).
[20] O. Kuisle, M. Lolo, E. Quiñoá, R. Riguera, *Tetrahedron* **1999**, *55*, 14807 – 14812.
[21] L. Carpino, B. J. Cohen, K. E. Stephens, Jr., S. Y. Sadat-Aalaee, J.-H. Tien, D. C. Langridge, *J. Org. Chem.* **1986**, *51*, 3732 – 3734.

 © WILEY-VCH Verlag GmbH, D-69451 Weinheim, 2001 1433-7851/01/4024-4728 $ 17.50+.50/0

From Solutions to Surfaces: A Novel Molecular Imprinting Method Based on the Conformational Changes of Boronic-Acid-Appended Poly(L-lysine)

Arianna Friggeri, Hideki Kobayashi, Seiji Shinkai,* and David N. Reinhoudt*

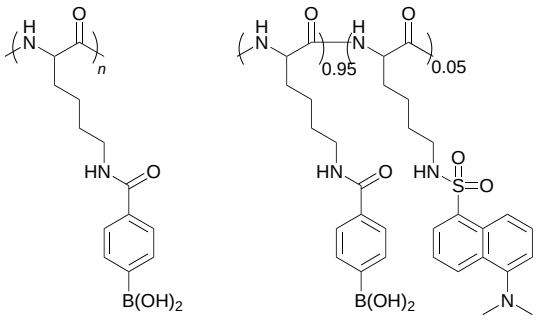
Molecular imprinting is usually defined as a process consisting of the copolymerization of functional and cross-linking monomers in the presence of a template (guest) molecule.[1] Subsequently, the template molecule is removed, revealing well-defined binding sites in which the arrangement of functional groups is particularly suited for binding the template molecule or other structurally related molecules. In the first approach to molecular imprinting, Wulff and co-workers covalently coupled the monomers to the template molecule.[2] Shortly thereafter, Mosbach and co-workers presented an imprinting method relying on noncovalent linkages that allows a wider choice of functional monomers and template molecules.[3] Recently, an imprinting method based on the immobilization of the template on a solid support has been reported.[4] Hitherto, molecular imprinting has usually been carried out in solution,[5] and only a few examples of imprinting at surfaces are known.[6] In this paper we present a novel, solution-to-surface imprinting method based on the different higher-order conformations adopted by boronic-acid-appended poly(L-lysine) **1**, in the presence of



1

sugars. In a three-step procedure the polymer–template complex initially formed in solution is subsequently anchored to a metal surface, which is then rinsed to remove the template molecules, resulting in a glucose-selective, molecularly imprinted interface.

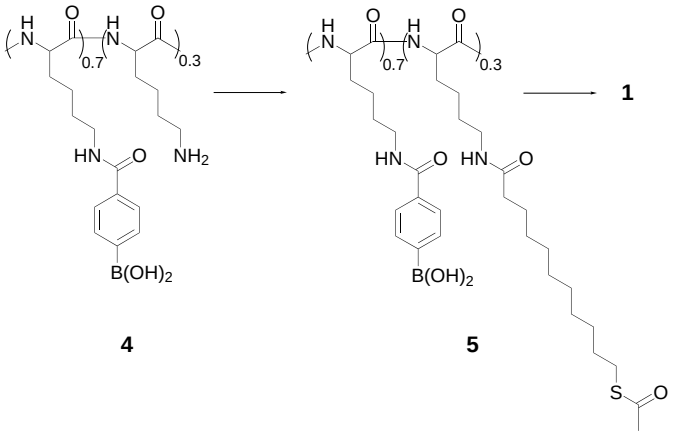
The conformational transitions of poly(L-lysine) are related to very subtle changes in secondary forces such as hydrogen-bonding interactions, electrostatic effects, and hydrophobicity.[7] At neutral pH, poly(L-lysine) assumes a β-sheet structure, in the medium to high pH region, an α-helix, and at even higher pH values, a random coil.[7] In our previous work we found that the addition of monosaccharides to boronic-acid-appended poly(L-lysine) **2** increases the α-helix content of the



2 **3**

polypeptide chain,[8] and the pH at which the maximum α-helix content is usually observed is shifted to a lower pH region in the presence of sugars. Recently, Kobayashi et al.[9] found that at pH > 10 and in the presence of D-glucose, polymer **3** has mainly a β-turn structure. The stabilization of this β-turn is attributed to the capability of D-glucose to bind concomitantly to two boronic acid moieties of the polypeptide chain, thus forming intrapolymeric cross-links.

To take advantage of such sugar-induced conformational changes for the realization of a molecularly imprinted interface, we synthesized poly(L-lysine) derivative **1** according to Equation (1). This polymeric adsorbate contains boronic acid moieties, which can bind to saccharides, and also 10-sulfanyldecyl moieties, which can anchor the polypeptide to a gold surface without hindering its conformational flexibility.



4 **5** **1** (1)

Molecular imprinting of adsorbate **1** was carried out at pH 11 in the presence of a large excess of either D-fructose or D-glucose, since these experimental conditions had previously shown the largest differences in conformation adopted by

[*] Prof. S. Shinkai, Dr. A. Friggeri, H. Kobayashi
Chemotransfiguration Project
Japan Science and Technology Corporation
2432 Aikawa, Kurume, Fukuoka 839-0861 (Japan)
Fax: (+81) 942-39-9012
E-mail: seijitcm@mbox.nc.kyushu-u.ac.jp
Prof. D. N. Reinhoudt
Chemotransfiguration Project
MESA+ Research Institute, University of Twente
P.O. Box 217, 7500 AE Enschede (The Netherlands)
Fax: (+31) 53-489-4645
E-mail: smct@ct.utwente.nl

Supporting information for this article is available on the WWW under http://www.angewandte.com or from the authors.

 © WILEY-VCH Verlag GmbH, D-69451 Weinheim, 2001 1433-7851/01/4024-4729 $ 17.50+.50/0

poly(L-lysine) derivative **3**.[8b, 9, 10] Circular dichroism (CD) spectroscopy in homogeneous solution (Figure 1) confirmed that in the absence of saccharides, **1** adopts a random coil conformation with a small percentage of α-helix structure.[7, 11] The percentage of α-helix content can be estimated by using

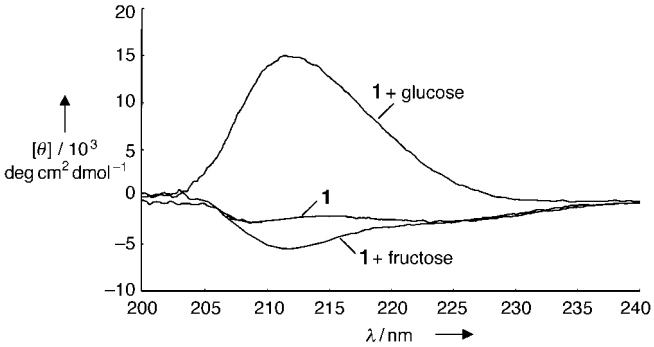


Figure 1. CD spectra of **1**, **1** + D-fructose, and **1** + D-glucose, at pH 11.

the relationship established by Greenfield and Fasman for poly(L-lysine) [Eq. (2)].[11a, 12] CD spectroscopy shows that in the polymer chain of **1** about 13% α-helix is present. The CD spectrum of **1** and D-fructose indicates that the major part of the polypeptide adopts the random coil conformation. However, in the case of **1** and D-glucose, the CD sign is inverted to positive values indicating the expected formation of the β-turn structure along the polypeptide chain, as was previously observed for compound **3**.[9]

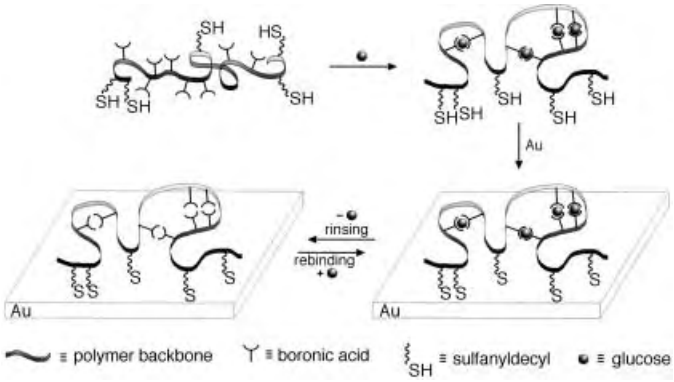
$$\%\ \alpha\text{-helix} = -([\theta]_{208} + 4000)/29000 \qquad (2)$$

An aqueous solution of **1** containing either D-fructose or D-glucose was equilibrated for approximately 20 min, and subsequently a gold-covered quartz crystal microbalance (QCM) resonator was immersed in this solution for 5 h. This treatment allows the polymer, either as a random coil or as a β-turn, depending on the saccharide, to be fixed onto the gold surface by means of the sulfanyl moieties present in **1**.[13] To remove the templating saccharide from the surface-bound polypeptide, the QCM resonator was rinsed thoroughly with acetate-buffered aqueous solution (pH 5). Subsequently, the rebinding of D-glucose and D-fructose by this poly(L-lysine) derivative **1** was monitored by following the changes in frequency (ΔF) of the resonator upon addition of the saccharide guests (Table 1). In the case of a QCM resonator covered with (nonimprinted) polypeptide **1**, addition of 1 mmol of D-fructose caused a significantly larger *decrease* in frequency ($\Delta F = 72 \pm 11$) than the same amount of D-glucose ($\Delta F = 42 \pm 7$).[14] These responses are in accordance with the fact that the interaction between boronic acid and D-fructose ($\lg K_a = 3.64$) is stronger than that between boronic acid and D-glucose ($\lg K_a = 2.04$).[10] However, the opposite was observed when a D-glucose-imprinted QCM resonator was exposed to the same two sugars (see Table 1). These results are indicative of a "molecular memory" effect induced by the imprinting process. Moreover, the QCM resonator covered with D-glucose-imprinted polypeptide **1** could be reused at least three times for the detection of D-glucose, with deviations $\leq 10\%$ of the initial value. The smaller response observed for D-fructose on the D-glucose-imprinted surface, compared to the responses on the nonimprinted polymer **1** surface, might be due to the conformation adopted by the D-glucose-imprinted polymer. D-Glucose can bind to two boronic acid groups and this brings the two boronic acid units in close proximity, giving rise to β-turn structures (Scheme 1).

Table 1. Changes in resonant frequency (ΔF) of QCM resonators covered with nonimprinted and imprinted surfaces of adsorbate **1**, upon addition of D-fructose or D-glucose (1 mmol, pH 8).[a]

Guest	ΔF		
	Nonimprinted	D-Glucose-imprinted	D-Fructose-imprinted
D-fructose	72 ± 11	41 ± 10	69 ± 9
D-glucose	42 ± 7	64 ± 5	33 ± 8

[a] All values correspond to decreases in frequency and are the average of at least three measurements.[14]



Scheme 1. Schematic representation of the solution-to-surface imprinting process based on the conformational changes of **1** in the presence of D-glucose.

If the conformation of the polypeptide is fixed through its adsorption to the gold surface, the boronic acid units will remain in close proximity even after the removal of the D-glucose template molecules (Scheme 1). D-Fructose, however, binds to boronic acid in a 1:1 fashion. The close proximity of two boronic acid moieties in the D-glucose-imprinted polymer might sterically hinder the complexation of two D-fructose molecules and thus lead to a lower ΔF value.

When a QCM resonator covered with D-fructose-imprinted polypeptide **1** was exposed to a D-fructose solution, the signal observed ($\Delta F = 69 \pm 9$) was similar to that obtained when the nonimprinted polymer surface was exposed to the same amount of D-fructose ($\Delta F = 72 \pm 11$; Table 1). Moreover, the addition of D-glucose to the D-fructose-imprinted interface also caused a response in the same range as that of D-glucose on the nonimprinted polymer surface (Table 1). Therefore, the D-fructose-imprinted polymer **1** interface does not show a better selectivity towards D-fructose than the nonimprinted polypeptide interface does. If the interaction of D-fructose with poly(L-lysine) derivative **1** does not cause significant conformational changes to the polypeptide, as indicated by circular dichroism, then it seems likely that the imprinting process will not give rise to a significant "molecular memory" effect. Interestingly, this observation implies that CD spec-

 © WILEY-VCH Verlag GmbH, D-69451 Weinheim, 2001 1433-7851/01/4024-4730 $ 17.50+.50/0

troscopy could be used to predict whether a polymer–template system in solution would result in a successfully imprinted polymer on a surface.

The sensitivity of the D-glucose-imprinted polypeptide **1** layer towards successive additions of D-glucose to the measurement cell was studied as a function of the guest concentration (Figure 2). Saturation behavior was observed,

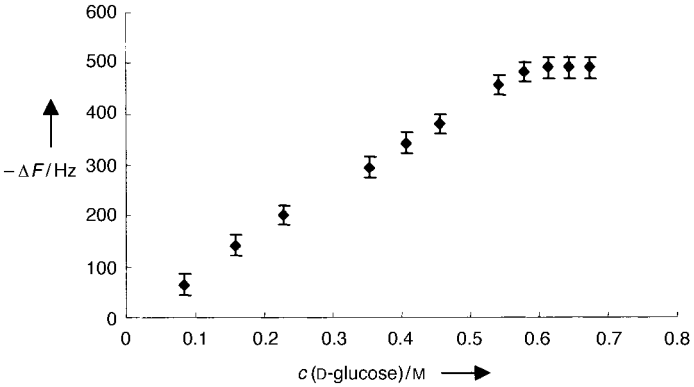


Figure 2. Frequency changes of a QCM with a D-glucose-imprinted polypeptide **1** interface upon successive additions of a D-glucose solution (pH 8).

with a maximum change in frequency corresponding to a 0.67 M concentration of D-glucose in the cell. Further additions of the guest no longer resulted in a decrease of the frequency of the resonator.[15] Moreover, the number of boronic acid recognition sites (3.0×10^{-4}) calculated from the saturation value ($\Delta F = -500$ Hz) of the curve in Figure 2 compares very well to the number of boronic acid units estimated to be present on the polymer adsorbed to the gold surface (between 1.7×10^{-4} and 4.1×10^{-4}).[16]

In conclusion, we have presented a new molecular imprinting method based on the conformational changes of poly(L-lysine) derivative **1**, arising from the interaction between the polymer and the template molecules. Subsequent adsorption of the imprinted polymer onto a gold surface fixes the conformation of the polypeptide, thereby creating a novel molecularly imprinted interface. Furthermore, the application of a D-glucose-imprinted polymer interface for the selective detection of D-glucose over D-fructose has been demonstrated successfully. We hope to extend this novel imprinting concept to other polymer/metal surface systems to create new, selective sensor interfaces for small molecules.

Experimental Section

Synthesis of **1** [Eq. (1)]: **5**: To a solution of 11-acetylsulfanylundecanoic acid (0.025 g, 0.096 mmol) in MeOH/THF (1:3, 15 mL) cooled to 0 °C, were added 1-hydroxybenzotriazole (HOBT; 0.013 g, 0.096 mmol) and 3-(3-dimethylaminopropyl)-1-ethylcarbodiimide (EDC, 0.018 g, 0.096 mmol). The solution was stirred at 0 °C for 1 h and subsequently at room temperature for 1 h. It was then added dropwise to a solution of **4** (0.085 g, 0.477 unit mmol) and *N*-ethylmorpholine (0.1 mL) in MeOH (20 mL), and the reaction mixture was stirred at room temperature for 24 h. The solvent was subsequently removed under reduced pressure and the residue dissolved in a minimum amount of MeOH. Upon addition of acetone (15–20 mL) a white precipitate formed which was filtered off and dried to afford **5** in 50% yield. The content of the boronic acid moieties and the acetylsulfanylundecanoic amide moieties as determined by ^{1}H NMR spectroscopy was found to be 70 and 30 mol%, respectively. ^{1}H NMR (300 MHz, $CDCl_3$:CD_3OD = 4:1, 25 °C): δ = 8.20–7.90 (brs, 4H; ArH), 3.58 (brs, 1H; CH), 3.24 (brs, 2.9H; CH_2N), 2.71 (brs, 0.9H; CH_2S), 2.20 (brs, 0.9H; $C(O)CH_2$ and brs, 1.3H; CH_3), 1.80–1.40 (m, 6H; CH_2 in poly(L-lysine)), 1.13 (m, 6.9H; CH_2 in acetylsulfanylundecanoic amide side chain).

1: To a nitrogen-saturated solution of **5** (0.063 g, 0.230 mmol) in MeOH (20 mL) was added an aqueous solution of K_2CO_3 (0.5 g in 20 mL), and the solution was heated at reflux for 30 min. After the solution had cooled to room temperature, 2N HCl was added (2 mL) and the organic solvent was subsequently removed under reduced pressure. The residue was dissolved in a minimum amount of MeOH, and upon addition of acetone (15–20 mL) a pale yellow precipitate formed, which was then filtered off and dried to afford **1** in 95% yield. ^{1}H NMR (300 MHz, CD_3OD, 25 °C): δ = 8.20–7.90 (brs, 4H; ArH), 3.98 (brs, 1H; CH), 3.25 (brs, 2.9H; CH_2N), 2.73 (brs, 0.9H; CH_2S), 2.22 (brs, 0.9H; $C(O)CH_2$), 2.00–1.20 (m, 6H; CH_2 in poly(L-lysine)), 1.13 (m, 6.9H; CH_2 in acetylsulfanylundecanoic amide side chain).

QCM measurements were carried out as described in the literature.[17] For the preparation of the QCM resonators see the Supporting Information.

Received: July 30, 2001 [Z17631]

[1] K. Haupt, K. Mosbach, *Chem. Rev.* **2000**, *100*, 2495

[2] G. Wulff, *Angew. Chem.* **1995**, *107*, 1958; *Angew. Chem. Int. Ed. Engl.* **1995**, *34*, 1812.

[3] K. Mosbach, O. Ramström, *Bio/Technology* **1996**, *14*, 163.

[4] E. Yilmaz, K. Haupt, K. Mosbach, *Angew. Chem.* **2000**, *112,* 2178; *Angew. Chem. Int. Ed.* **2000**, *39*, 2115.

[5] a) H. Asanuma, T. Hishiya, M. Komiyama, *Adv. Mater.* **2000**, *12*, 1019; b) M. J. Whitcombe, E. N. Vulfson, *Adv. Mater.* **2001**, *13*, 467.

[6] a) O. Chailapakul, R. M. Crooks, *Langmuir* **1995**, *11*, 1329; b) M. Lahav, E. Katz, A. Doron, F. Patolsky, I. Willner, *J. Am. Chem. Soc.* **1999**, *121*, 862; c) H. Shi, W.-B. Tsai, M. D. Garrison, S. Ferrari, B. D. Ratner, *Nature* **1999**, *398*, 593; d) T. Miyahara, K. Kurihara, *Chem. Lett.* **2000**, 1356; e) Y. Okahata, K. Yasunaga, K. Ogura, *J. Chem. Soc. Chem. Commun.* **1994**, 469; f) Y. Kanekiyo, K. Inoue, Y. Ono, M. Sano, S. Shinkai, D. N. Reinhoudt, *J. Chem. Soc. Perkin Trans. 2* **1999**, 2719.

[7] H. A. Scheraga, *Chem. Rev.* **1971**, *71*, 195.

[8] a) T. Nagasaki, T. Kimura, S. Arimori, S. Shinkai, *Chem. Lett.* **1994**, 1495; b) T. Kimura, S. Arimori, M. Takeuchi, T. Nagasaki, S. Shinkai, *J. Chem. Soc. Perkin Trans. 2* **1995**, 1889.

[9] H. Kobayashi, K. Nakashima, Y. Ohshima, I. Hamachi, S. Shinkai, *J. Chem. Soc. Perkin Trans. 2* **2000**, 997.

[10] a) T. D. James, K. R. A. Samankumara Sandanayake, S. Shinkai, *Angew. Chem.* **1996**, *108*, 2038; *Angew. Chem. Int. Ed. Engl.* **1996**, *35*, 1910; b) J. Yoon, A. W. Czarnik, *J. Am. Chem. Soc.* **1992**, *114*, 5874.

[11] a) N. Greenfield, G. D. Fasman, *Biochemistry* **1969**, *8*, 4108; b) E. R. Blout, C. de Loze, S. M. Bloom, G. D. Fasman, *J. Am. Chem. Soc.* **1960**, *82*, 3787.

[12] $[\theta]_{208}$ is the mean residue ellipticity, in deg cm^2 dmol^{-1}, at an extremum of the curve for the α-helix form of poly(L-lysine). See ref. [11].

[13] Considering that the molecular weight of the poly(L-lysine) starting material employed in these experiments is 5000–15000 and that the molecular weight per poly(L-lysine) unit is 208, every polymer chain consists of 24–72 units of which 30% (7–22 units) are surface-anchoring units (i.e. 10-sulfanyldecyl units).

[14] All ΔF values measured are uncorrected for the effect of surface roughness. a) A. Janshoff, H.-J. Galla, C. Steinem, *Angew. Chem.* **2000**, *112*, 4164; *Angew. Chem. Int. Ed.* **2000**, *39*, 4004; b) C. Malitesta, I. Losito, P. G. Zambonin, *Anal. Chem.* **1999**, *71*, 1366.

[15] Although the data in Figure 2 are reminiscent of a Langmuir adsorption isotherm, adsorption of a guest molecule at a given site cannot be considered independent of adsorption occurring at neighboring sites since many of the binding sites (i.e. boronic acid moieties) are located on the same polymer chain, which changes conformation upon binding of the D-glucose guest molecules.

[16] See Supporting Information for details.

[17] Y. Kanekiyo, I. Kazuhiko, Y. Ono, M. Sano, S. Shinkai, D. N. Reinhoudt, *J. Chem. Soc. Perkin Trans. 2* **1999**, 2719.

 © WILEY-VCH Verlag GmbH, D-69451 Weinheim, 2001 1433-7851/01/4024-4731 $ 17.50+.50/0

Protein – Polymer Hybrid Amphiphiles**

Jurry M. Hannink, Jeroen J. L. M. Cornelissen, Joan A. Farrera, Philippe Foubert, Frans C. De Schryver, Nico A. J. M. Sommerdijk, and Roeland J. M. Nolte*

Low molecular weight amphiphilic molecules are known to form a large variety of self-assembled structures, for example monolayers, micelles, vesicles, and rod- and sheetlike structures, in water.[1] Well-defined diblock copolymers—so-called superamphiphiles—such as poly(ethyleneglycol) – poly(benzyl ether) dendrimers, polystyrene – poly(propyleneimine) dendrimers, polystyrene-*block*-poly(2-vinylpyridine)s, and block copolymers of styrene and isocyanopeptides, have been shown to generate these highly ordered structures as well.[2] Herein we describe a new class of amphiphiles, namely "giant amphiphiles", in which a protein or enzyme acts as a polar head group and polymers act as the apolar tails (Figure 1). These biohybrids differ from other protein – polymer systems described in the literature, in the sense that the protein to polymer ratio is predefined and the position of the conjugation site is precisely known.

The hybrid amphiphiles were prepared by the association of two molecules of monobiotinylated polystyrene (**1**; $M_n = 9147$, $M_w/M_n = 1.03/1$, Figure 1a) with streptavidin. This 60-kD protein consists of four identical subunits, each of which can bind one biotin molecule.[3, 4] The affinity between streptavidin and biotin is so high ($K_a \approx 10^{15}\,\text{M}^{-1}$; 21 kcal mol^{-1}) that the complex formation can be regarded as irreversible. The valeric acid carboxyl group of biotin can be used for modification because it does not play a significant role in the binding process.[3, 5] The binding sites are positioned in pairs on opposite faces of the protein, which allows the use of the protein as a versatile modular building block in the construction of supramolecular systems (Figure 1b).[6]

The ability of biotinylated polystyrene **1** to specifically bind streptavidin was ascertained using the HABA – streptavidin assay.[7] In this test the dye HABA (4′-hydroxyazobenzene-2-carboxylic acid) is expelled from the protein binding pocket by the biotin end group of the polymer, which results in changes in the relative intensities of the UV/Vis absorption bands of the dye.

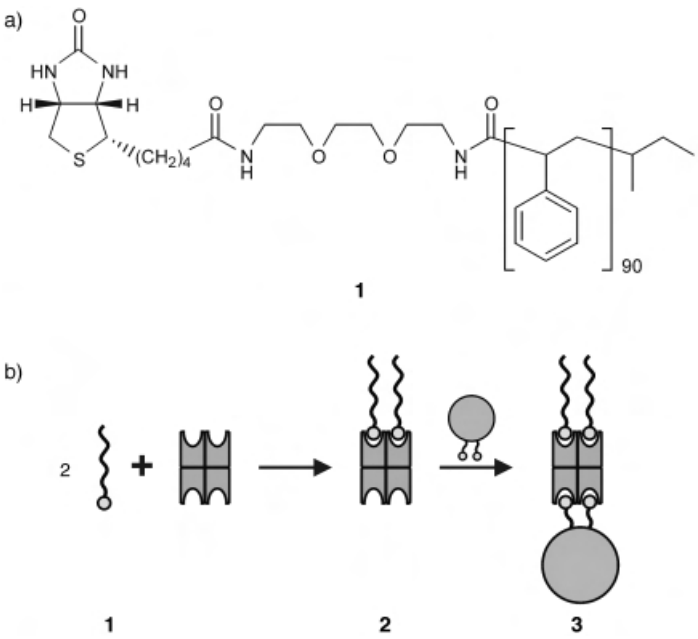


Figure 1. a) Structure of biotinylated polystyrene **1**. b) Schematic representation of giant amphiphile **2** and the modular construction of the functional protein – polymer hybrids **3**.

The protein – polymer hybrids were constructed by making use of a Langmuir trough, which allowed us to monitor the formation of the giant amphiphiles. The biotinylated polymer **1** was spread at the air/water interface, and subsequent compression of the monolayer resulted in the formation of a rigid film. Brewster angle microscopy (BAM) and atomic force microscopy (AFM) revealed that this monolayer was the result of merging separate microscopic domains of biotinylated polymer (Figure 2a). The surface pressure/surface area isotherm of **1** in the absence of streptavidin (Figure 3) showed a lift-off area of 5.2 nm^2 and a molecular area of 3.9 nm^2. A dramatic increase in these two values per biotinylated macromolecule was observed (to 14.8 and 12.0 nm^2, respectively) in the presence of active streptavidin (0.5 equiv). A molecular area of 24 nm^2 was deduced[8] for the amphiphilic complex from the obtained area per polymer chain. This value agrees well with those of 23.5 – 35.7 nm^2 reported for streptavidin in the literature.[9] To confirm that the increase in area is largely a consequence of the specific binding of the protein to the biotinylated polymer, the isotherm of **1** was recorded on a subphase containing deactivated streptavidin (Figure 3). This isotherm showed only slight differences from that of **1** on a buffer solution as a result of unspecific binding of the protein.[10]

Monolayers of the giant amphiphiles, prepared with rhodamine Red-X labeled streptavidin, were transferred to solid substrates by the Langmuir – Schaefer (LS) technique.[11] Confocal fluorescence microscopy ($\lambda_{ex} = 543$ nm) in combination with AFM revealed fluorescent domains with a thickness of 7 nm (Figure 2c,d). Investigation of these do-

[*] Prof. Dr. R. J. M. Nolte, J. M. Hannink, J. J. L. M. Cornelissen
Department of Organic Chemistry, NSR Center
University of Nijmegen
Toernooiveld, 6525 ED Nijmegen (The Netherlands)
Fax: (+31) 24-365-2929
E-mail: nolte@sci.kun.nl
Dr. J. A. Farrera
Departament de Química Orgànica
Universitat de Barcelona, Barcelona (Spain)
P. Foubert, Prof. Dr. F. C. De Schryver
Department of Chemistry
Katholieke Universiteit Leuven, Heverlee (Belgium)
Dr. N. A. J. M. Sommerdijk
Laboratory of Macromolecular and Organic Chemistry
Eindhoven University of Technology, Eindhoven (The Netherlands)

[**] This research was supported by the Netherlands Foundation for Chemical Research (CW-NWO), the EC TMR Sisitomas and ESF Smarton programs, and the Ministerio de Educación y Cultura (Spain). The authors thank H. P. M. Geurts, P. J. H. M. Adams, and J. L. J. van Dongen for experimental assistance.

Supporting information for this article is available on the WWW under http://www.angewandte.com or from the author.

 © WILEY-VCH Verlag GmbH, D-69451 Weinheim, 2001 1433-7851/01/4024-4732 $ 17.50+.50/0

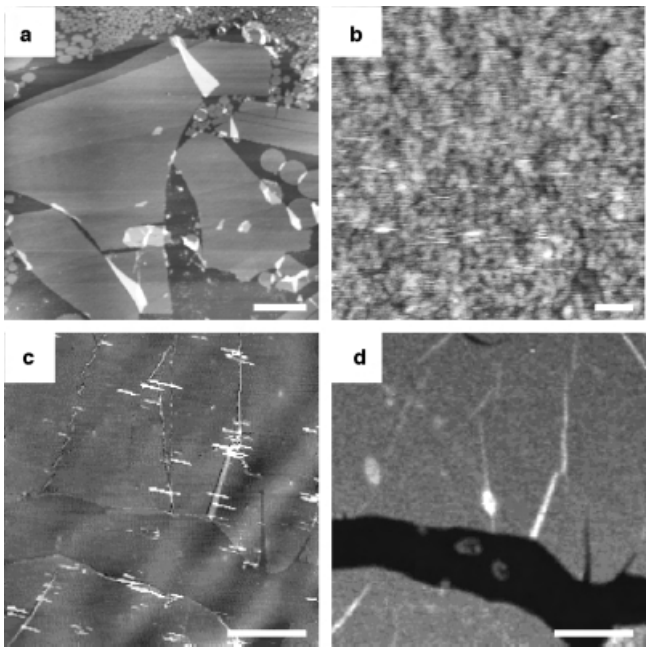


Figure 2. Topographic images of a monolayer of polymer **1** measured with confocal-AFM in water: a) pure polymer (scale bar = 1 μm); b) polymer with bound streptavidin (scale bar = 50 nm). Monolayer of rhodamine Red-X labeled protein–polymer hybrids: c) AFM topographic image (scale bar = 10 μm); d) confocal fluorescence image (λ_{ex} = 543nm, scale bar = 10 μm).

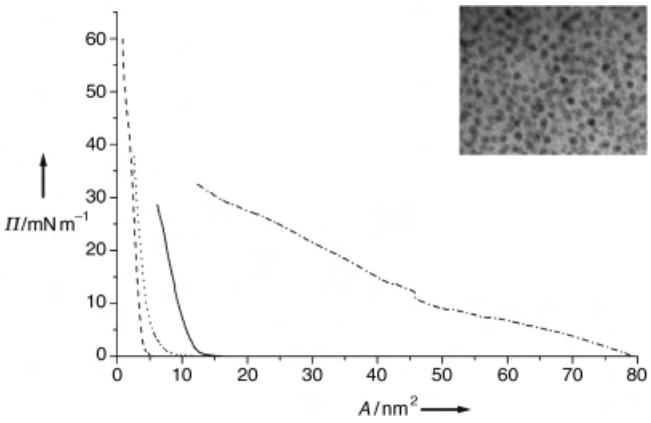


Figure 3. Surface pressure/surface area isotherms of biotinylated polystyrene **1** recorded on a subphase without protein (– – –); a subphase containing streptavidin (——); a subphase containing deactivated streptavidin (····); and a subphase containing streptavidin and biotinylated ferritin (·–·–). The inset shows a transmission electron microscope image of a compressed ferritin-streptavidin–polystyrene monolayer (Π = 35 mN m^{-1}) transferred to a formvar coated electron microscope grid.

mains in a separate experiment demonstrated that the surfaces of these layers consisted of spherical particles. The dimensions of these particles agreed well with those expected for streptavidin (Figure 2b), when AFM tip-broadening effects and the mobile nature of the ethyleneglycol moiety of polymer **1** under the process of liquid imaging are taken into account.[12] To confirm that the pair of binding sites of streptavidin opposite to that occupied by the polymer chains was still available, the sample was incubated in a solution of fluorescein-labeled biotin. Fluorescence imaging (λ_{ex} = 488 nm) suggested that the geographic location of the bound fluorescein indeed corresponded with that of the rhodamine Red-X label of streptavidin.

The ability of the protein–polymer hybrid to complex other biotinylated molecules was tested in the case of the 460-kD iron storage protein ferritin. Biotinylated ferritin was added to the subphase underneath a noncompressed monolayer of streptavidin–polystyrene conjugates. The resulting system could be compressed to a uniformly dense film in which the ferritin molecules are closely packed (Figure 3). The molecular area of the conjugate was estimated from the recorded isotherm to be 126 nm^2 (63 nm^2 per polymer chain), which agrees well with values reported for the cross-sectional area of ferritin (133nm^2).[13]

Enzyme functionalized protein–polymer hybrids could be prepared from a covalent horse radish peroxidase(HRP)–streptavidin (1/1) conjugate by using the approach described above for ferritin. Extensive washing of the subphase was performed to exclude the presence of unbound HRP–streptavidin molecules. The catalytic activity of the resulting polymer–enzyme hybrid system was assessed by using the standard ABTS/H_2O_2 assay.[14] To this end hydrogen peroxide and 2,2′-azino-bis(3-ethylbenzothiazoline-6-sulfonic acid) (ABTS) were injected into the subphase, which was circulated through a UV flowcell. This procedure meant that the reaction could be monitored in real time. The slope of the activity plot proved to be independent of the applied surface pressure, which indicates that the catalytic activity of the enzyme is not influenced by lateral pressure in the range measured (Π = 7–33 mN m^{-1}, Figure 4). Confirmation that

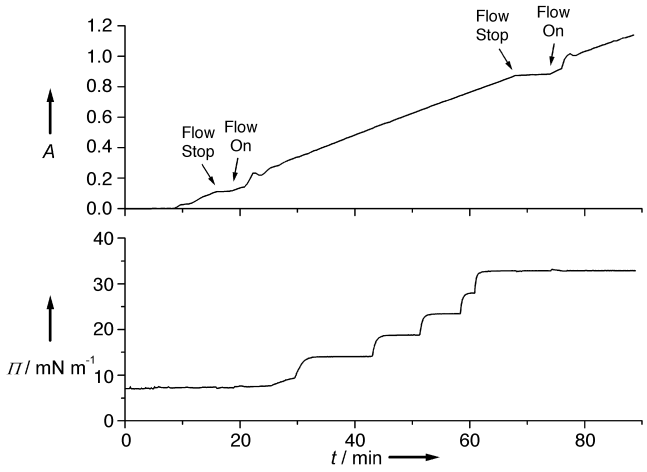


Figure 4. UV absorption at 420 nm of the subphase (top) and the surface pressure of the monolayer (bottom) as a function of time for the HRP–streptavidin–polystyrene hybrid system. The arrows indicate when the circulation of the aqueous subphase through the UV cell was switched on or off.

the oxidation reaction occurred at the monolayer of HRP–streptavidin–polystyrene hybrids and not in the subphase was obtained from the observation that the slope of the curve immediately leveled off when the circulation of the aqueous subphase through the UV cell was stopped.

In summary, we have constructed amphiphilic protein–polymer hybrids by the association of two biotinylated polystyrene molecules **1** and streptavidin. The pair of free

 © WILEY-VCH Verlag GmbH, D-69451 Weinheim, 2001 1433-7851/01/4024-4733 $ 17.50+.50/0

binding sites opposite to that occupied by the polymer chains can be used to bind other biotinylated molecules, as was demonstrated for the iron storage protein ferritin. The giant amphiphiles can also be functionalized with enzymes as was shown with horse radish peroxidase. The resulting hybrids retained their catalytic activity. The precise control over the structure of the giant amphiphiles in principle allows for tuning of their aggregate morphologies. In this way well-defined structures analogous to those reported for low molecular weight surfactants and surfactants derived from block copolymers will become attainable.

Received: June 29, 2001 [Z17397]

[1] M. C. Feiters, R. J. M. Nolte in *Advances in Supramolecular Chemistry*, *Vol. 6* (Ed.: G. W. Gokel), Jai, Stamford, CT, USA, **2000**, pp. 41 – 156.

[2] a) I. Gitsov, K. L. Wooley, J. M. J. Fréchet, *Angew. Chem.* **1992**, *104*, 1282 – 1285; *Angew. Chem. Int. Ed. Engl.* **1992**, *31*, 1200 – 1202; b) J. C. M. v. Hest, M. W. P. L. Baars, D. A. P. Delnoye, M. H. P. v. Genderen, E. W. Meijer, *Science* **1995**, *268*, 1592 – 1595; c) J. P. Spatz, S. Mößmer, M. Möller, *Angew. Chem.* **1996**, *108*, 1673 – 1676; *Angew. Chem. Int. Ed. Engl.* **1996**, *35*, 1510 – 1512; d) J. J. L. M. Cornelissen, M. Fischer, N. A. J. M. Sommerdijk, R. J. M. Nolte, *Science* **1998**, *280*, 1427 – 1430.

[3] N. M. Green, *Adv. Protein Chem.* **1975**, *29*, 85 – 133.

[4] M. Wilchek, E. A. Bayer, *Methods Enzymol.* **1990**, *184*, 5 – 13.

[5] M. Wilchek, E. A. Bayer, *Anal. Biochem.* **1988**, *171*, 1 – 32.

[6] a) W. Müller, H. Ringsdorf, E. Rump, G. Wildburg, X. Zhang, L. Angermaier, W. Knoll, M. Liley, J. Spinke, *Science* **1993**, *262*, 1706 – 1708; b) W. Müller, H. Ringsdorf, E. Rump, G. Wildburg, X. Zhang, L. Angermaier, W. Knoll, J. Spinke, *J. Biomater. Sci. Polym. Ed.* **1994**, *6*, 481 – 495; c) Y. Imanishi, S. Kimura, *Polymer* **1996**, *37*, 4929 – 4935; d) K. Ijiro, H. Ringsdorf, E. Birch Hirschfeld, S. Hoffmann, U. Schilken, M. Strube, *Langmuir* **1998**, *14*, 2796 – 2800.

[7] P. C. Weber, J. J. Wendoloski, M. W. Pantoliano, F. R. Salemme, *J. Am. Chem. Soc.* **1992**, *114*, 3197 – 3200.

[8] The molecular area was deduced by extrapolation of the isotherm slope to zero pressure.

[9] a) S. A. Darst, M. Ahlers, P. H. Meller, E. W. Kubalek, R. Blankenburg, H. O. Ribi, H. Ringsdorf, R. D. Kornberg, *Biophys. J.* **1991**, *59*, 387 – 396; b) D. Vaknin, J. Als-Nielsen, M. Piepenstock, M. Lösche, *Biophys. J.* **1991**, *60*, 1545 – 1552.

[10] R. Blankenburg, P. Meller, H. Ringsdorf, C. Salesse, *Biochemistry* **1989**, *28*, 8214 – 8221.

[11] I. Langmuir, V. J. Schaefer, *J. Am. Chem. Soc.* **1938**, *60*, 1351 – 1360.

[12] M. M. Stevens, S. Allen, W. C. Chan, M. C. Davies, C. J. Roberts, S. J. B. Tendler, P. M. Williams, *Analyst* **2000**, *125*, 245 – 250.

[13] H. Yoshimura, T. Scheybani, W. Baumeister, K. Nagayama, *Langmuir* **1994**, *10*, 3290 – 3295.

[14] N. P. Groome, *J. Clin. Chem. Clin. Biochem.* **1980**, *18*, 345 – 349.

A Tetrameric Nickel(II) "Chair" with both Antiferromagnetic Internal Coupling and Ferromagnetic Spin Alignment**

Vitaly V. Pavlishchuk,* Sergey V. Kolotilov, Anthony W. Addison,* Michael J. Prushan, Dieter Schollmeyer, Laurence K. Thompson, and Eugeny A. Goreshnik

Interest in polynuclear complexes of the 3d metals has been stimulated by the search for new magnetic materials[1, 2] and by demonstration of the occurrence of oligonuclear metal centers in proteins such as urease.[3] Of the relatively small number of reported tetranuclear complexes of $S = 1$ nickel(II) of known structure, the majority have a hemicubane- or "butterfly-" rather than a squarelike core.[4] Of these molecules, just one is entirely antiferromagnetic,[5] while the remainder entail purely ferromagnetic interactions amongst the nickel(II) ions.[6–10] Oximes have shown promise as bridging ligands for the preparation of polynuclear complexes.[11, 12] The reaction of 1,4,7-triazaheptane (diethylenetriamine, Dien) with the monooxime of 2,3-butanedione (ModaH) in the presence of Ni^{II} ions, instead of yielding the anticipated Schiff base derivative, gave the tetranuclear Ni^{II} compound **1** (dark brown crystals; $C_4H_8O_2$ = 1,4-dioxane), containing uncondensed but coordinated ketone and amine groups. Figure 1a shows the structure of the the cation of **1**, while Figure 1b highlights its Ni^{II} core.

$[\{Ni(Dien)\}_2(\mu_3\text{-}OH)_2\{Ni_2(Moda)_4\}](ClO_4)_2 \cdot 2\,C_4H_8O_2 \cdot 2\,H_2O$ **1**

The centrosymmetric $[\{Ni(Dien)\}_2(\mu_3\text{-}OH)_2\{Ni_2(Moda)_4\}]^{2+}$ ion possesses an Ni_4O_2 core based on a "chair" topology.[13] Two central Ni atoms (Ni_c) with pseudo-octahedral N_2O_4 donor ligand sets are bridged by hydroxyl ions to form a central Ni_2O_2 parallelogram (Figure 1b) in which the Ni_c–O(μ) distances are 2.038 Å, the Ni-O-Ni angles are 97.73°, and the Ni_c–Ni_c separation is 3.070 Å. The $Moda^-$ ligands are coordinated to the Ni_c atoms through their ketone-O and oximate-N atoms. The Ni_c–O(ketone) bonds in **1** (2.113 and 2.114 Å) are akin to another recently described[14]

[*] Prof. Dr. V. V. Pavlishchuk, S. V. Kolotilov
L. V. Pisarzhevskii Institute of Physical Chemistry
of the National Academy of Sciences of the Ukraine
Prospekt Nauki 31, Kiev 03039 (Ukraine)
Fax: (+380) 44-265-6216
E-mail: pavlisvv@phyche.freenet.kiev.ua

Prof. Dr. A. W. Addison, Dr. M. J. Prushan
Department of Chemistry, Drexel University
Philadelphia, PA 19104 (USA)
Fax: (+1) 215-895-1265
E-mail: addisona@drexel.edu

Prof. Dr. D. Schollmeyer
University of Mainz (Germany)

Prof. Dr. L. K. Thompson
Memorial University (Canada)

Prof. Dr. E. A. Goreshnik
I. Franko Lvov State University (Ukraine)

[**] A.W.A. and M.J.P. thank Drexel University for support.

 © WILEY-VCH Verlag GmbH, D-69451 Weinheim, 2001 1433-7851/01/4024-4734 $ 17.50+.50/0

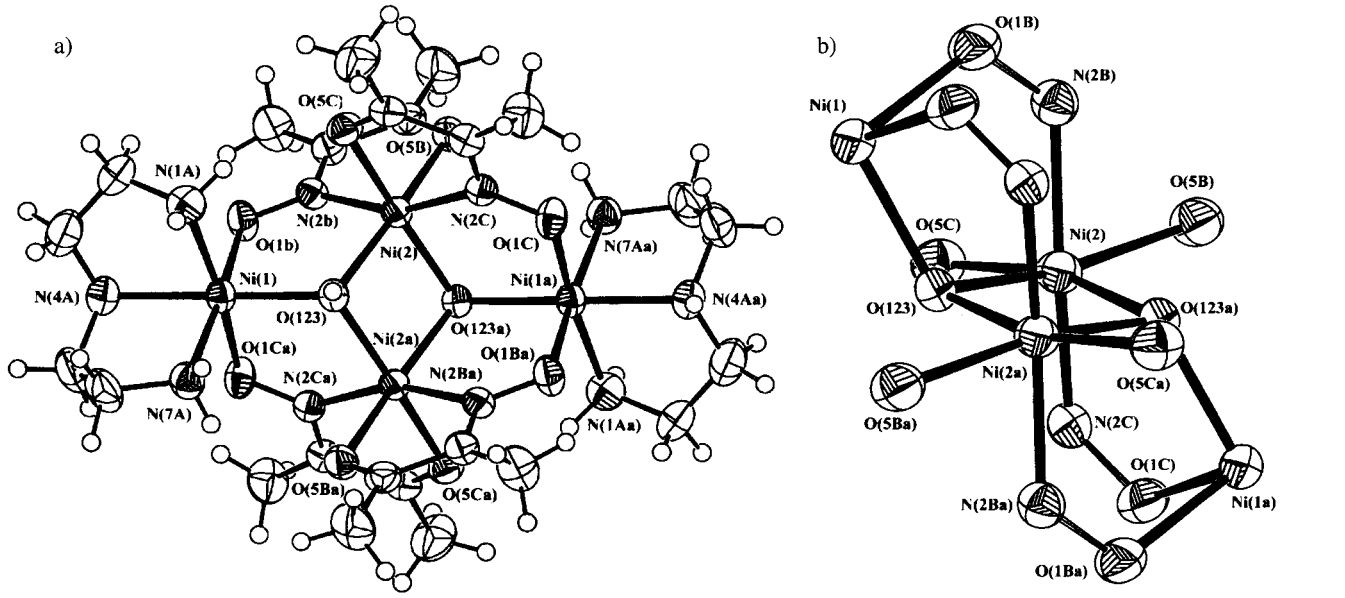


Figure 1. a) Structure of the tetranuclear cation of **1** (ORTEP diagram); b) structure of the coordination core of the tetranuclear complex (ORTEP diagram), displaying the displacement of the terminal nickel ions above and below the central Ni_2O_2 plane. The diagrams are differently scaled.

example of a similarly rare Ni–O(ketone) bond (2.13 Å). The terminal Ni^{II} ions (Ni_t) are bound to opposite sides of the $Ni_{c2}O_2$ parallelogram, each one by a μ_3-OH^- group and two oximate-O atoms (Figure 1b). The pseudo-octahedral N_3O_3 coordination sphere around each Ni_t atom is completed by the three nitrogen donor atoms of a facially coordinated Dien molecule. The Ni_t–Ni_c distances are 3.412 and 3.397 Å, the Ni_t-O-Ni_c angles are 112.37 and 111.61°, and the Ni_t–Ni_t separation is 6.077 Å. The Ni_t atoms lie below and above the $Ni_{c2}O_2$ plane, respectively, the Ni_t–O(hydroxyl) vectors being at 125° to this plane, though the four Ni atoms themselves lie in (another) common plane.

The magnetochemical behavior of a polycrystalline sample of **1** in the temperature range 2–300 K is displayed in Figure 2. The value of $\chi_m T$ decreases with decreasing temperature, from 4.56 ($\mu_{eff} = 3.0\ \mu_B$ per Ni) at 300 K to 0.02 $cm^3 K mol^{-1}$ (0.2 μ_B per Ni) at 2 K. As the value of $\chi_m T$ for a tetranuclear unit of four noninteracting $S = 1$ Ni^{II} ions with $g = 2.0$ would be 4.0 $cm^3 mol^{-1}$ K ($\mu_{eff} = 2.83\ \mu_B$ per Ni), it is clear that the major interactions within **1** are antiferromagnetic in nature. The three different types of Ni–Ni exchange interactions, namely between Ni_c–Ni_t, Ni_c–Ni_c, and Ni_t–Ni_t, may be represented as J_a, J_b, and J_c, respectively (Scheme 1).

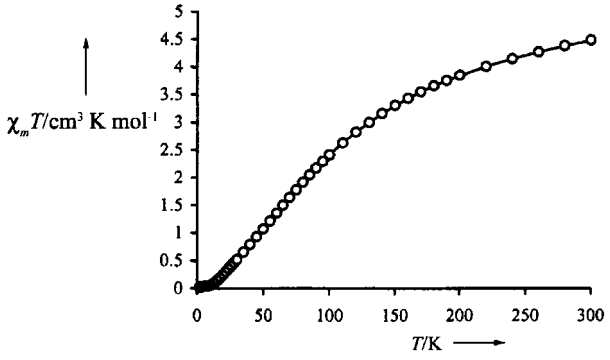
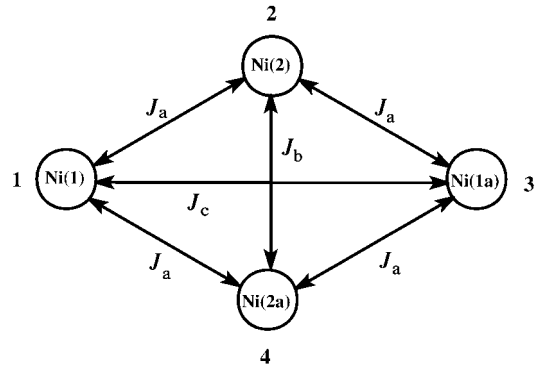


Figure 2. A plot of χT versus T for **1**. The points represent the experimental data, the line the least-squares fit as described in the text.



Scheme 1. Magnetic coupling topology for the tetranuclear complex **1**.

According to Kambe's vector coupling scheme,[15] the total spin S_T steps integrally from 0 to 4 for this tetranickel(II) molecule, while the internal pairwise spin combinations S_{13} (devolving from J_c) and S_{24} (devolving from J_b) correspondingly vary integrally from 0 to 2 for each of these Ni^{II} pairs. Nineteen combinations of S_T, S_{13}, and S_{24} result, designated by (S_T, S_{13}, S_{24}), and at each energy Equation (1) is valid.[16]

$$E_{S_T} = -J_a S_T(S_T+1) - S_{13}(S_{13}+1)(J_c - J_a) - S_{24}(S_{24}+1)(J_b - J_a) + 4J_b + 4J_c \quad (1)$$

Application of the van Vleck equation[17] to the corresponding isotropic exchange Hamiltonian [Eq. (2)][16] yielded the susceptibility expression [Eqs. (3), (4)] to which the variable-temperature magnetic data were fitted.

$$\mathcal{H} = -2J_a(S_1S_2 + S_2S_3 + S_3S_4 + S_1S_4) - 2J_b(S_2S_4) - 2J_c(S_1S_3) \quad (2)$$

$$\chi'_m = \frac{\mathfrak{N}g^2\beta^2}{3kT}[(\Sigma S_T(S_T+1)(2S_T+1)e^{(-E_{S_T}/kT)}]/[\Sigma S_T(2S_T+1)e^{(-E_{S_T}/kT)}] \quad (3)$$

$$\chi_m = \chi'_m(1-\rho) + \frac{2\mathfrak{N}g^2\beta^2\rho}{3kT} + tip \quad (4)$$

This yielded $g = 2.32(2)$, $2J_a = -40.6(5)\ cm^{-1}$, $2J_b = +20(5)\ cm^{-1}$, $\rho = 0.019$, $tip(4Ni) = 1.00 \times 10^{-3}\ cm^3 mol^{-1}$, $R^2 = 1.7 \times 10^{-5}$. No significant improvement in fit was effected by introduction of a nonzero value for the third J parameter (J_c or of intermolecular zJ'); these are expected to be small in any case. As values of $\chi_m T$ are much less responsive to J for ferromagnets ($J > 0$) of low nuclearity than for analogous antiferromagnets ($J < 0$), the dominating effect of J_a results in reduced precision for the estimate of J_b (or J_c). Indeed, the trough for the dependence of R on J_a and J_b in Figure 3 shows

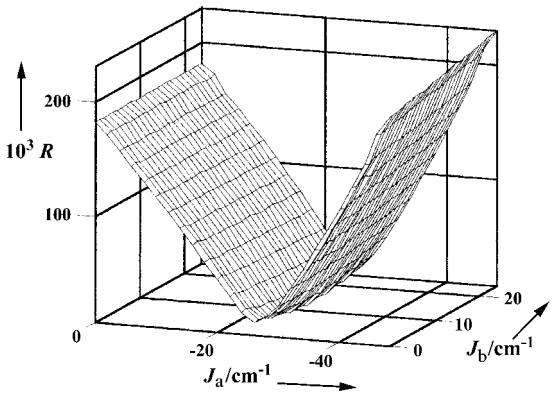


Figure 3. Variation of the residual fit error R (as $\sqrt{R^2}$), as a function of the variation of J_a and J_b about the deduced values for **1**.

how a numerological outcome of the very weak dependence of $\chi_m T$ on $J_b > 0$ is that any estimate of J_b is rendered exceedingly imprecise. An analogous situation with $-J_a \gg J_b$ has been observed for other tetranuclear iron(III) systems,[18, 19] for which spin frustration was proposed. The similar numerological properties of the Ni_4 model render it difficult in such cases to distinguish between intrinsic ferromagnetic coupling between the Ni_c versus the obligatory alignment of their spins to parallel as a consequence of other couplings. However, more recent work[20, 21] appears to mitigate against the spin frustration interpretation and in favor of a *competing spin interaction* outcome. First, a classical spin-frustrated state does not sensibly correspond to an $S_T = 0$ state. A *degenerate frustrated* state may occur if the ground state is (or is at a crossing with) an $S_T > 0$ state.[21] Figure 4a displays the spin ladder corresponding to the fitted parameters. This illustrates the relative isolation of the (0,2,2) ground state (e.g., [Ni1, Ni2, Ni3, Ni4] = [↑ ↑, ↓ ↓, ↑ ↑; ↓ ↓]), while Figure 4b and c, which display the progress of the lowest state energies as a function of J_a and J_b, respectively, reinforce the finding[5] that there is no such crossover in this $J_a < 0$ region. They also illustrate how the E_{S_T} themselves are much more strongly dependent on J_a than on J_b.

One particular aspect of the comparison of **1** with other reported tetranickel(II) systems is revealing with respect to the relationship between the J_a and J_b values. Correlations[22, 23] of J with the angle θ, reinforced by other recent results,[5, 9, 10] quite clearly indicate that J decreases with θ, crossing $J = 0$ at a θ value of about 95–100°. At 112°, this predicts a $2J_a$ value of about -30 to $-60\ cm^{-1}$, while the lesser angle predicts a $2J_b$ value around zero. A value of $2J_a = -40\ cm^{-1}$ fits this correlation well. We conclude that the larger (Ni_c-O-Ni_t) angle is the core's fundamentally causative structural feature, which by setting the larger $-2J$ value, thus drives all the Ni_c spins parallel.[5, 20]

Experimental Section

1: $Ni(ClO_4)_2 \cdot 6H_2O$ (1.46 g, 4 mmol), followed by Et_3N (606 mg, 6 mmol) were added to ModaH (404 mg, 4 mmol) and Dien (206 mg, 2 mmol) in 96% ethanol (5 mL) at room temperature. The brown solid obtained was recrystallized from $MeNO_2$/1,4-dioxane (1:1) to yield **1** as a crystalline product (yield: 1.09 g, 85%). Elemental analysis (%) calcd for $C_{32}H_{72}Cl_2N_{10}Ni_4O_{24}$: C 29.9, H 5.60, N 10.9, Ni 18.3; found: C 29.8, H 5.55, N 10.9, Ni 18.3; FAB mass spectrum: m/z (%): 971 (49) $[\{Ni_4(Dien)_2(OH)_2(Moda)_4\}ClO_4]^+$, 492 (100) $[Ni_3O(Moda)_2ClO_4]^+$.

Crystal data for **1**: $C_{32}H_{72}Cl_2N_{10}Ni_4O_{24}$, $M_r = 1286.74$, monoclinic, $a = 10.4880(7)$, $b = 16.1935(10)$, $c = 16.2944(11)$ Å, $\beta = 106.9580(10)$, $V = 2647.1(3)$ Å^3, $T = 295(2)$ K, space group $P2_1/c$, $Z = 2$, $\rho_{calcd} = 1.614\ g\,cm^{-3}$, $\mu(Mo_{K\alpha}) = 0.71069$ Å, $\mu = 1.589\ mm^{-1}$, $2\theta_{max} = 56.58°$; crystal dimensions $0.18 \times 0.13 \times 0.05$ mm, 24155 reflections measured, 6524 unique reflections ($R_{int} = 0.118$) used for solution (SIR-99) and refinement (SHELX-97) by full-matrix least-squares on F^2; no absorption correction. Final $R_w(F^2) =$

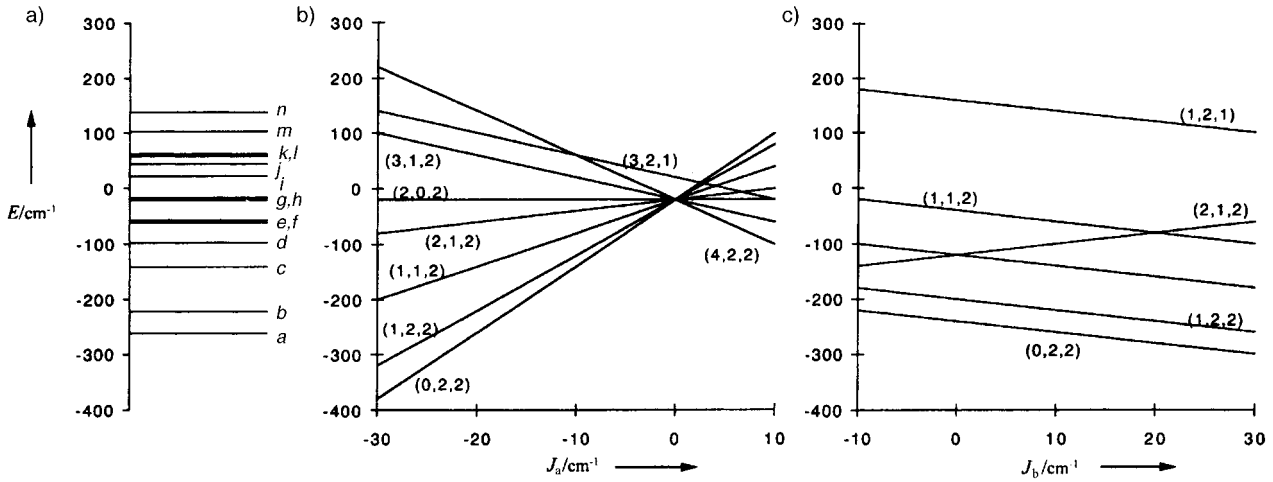


Figure 4. a) Spin ladder for $[\{Ni(Dien)\}_2(\mu_3\text{-}OH)_2\{Ni_2(Moda)_4\}]^{2+}$. The levels are $a = 0,2,2$; $b = 1,2,2$; $c = 2,2,2/1,1,2$; $d = 1,2,1$; $e = 2,1,2$; $f = 0,1,1$; $g = 3,2,2/2,0,2$; $h = 0,1,1$; $i = 2,2,2/1,1,1$; $j = 2,2,0/1,1,0/0,0,0$; $k = 3,1,2$; $l = 2,1,1$; $m = 3,2,1$; $n = 4,2,2$. The 0,2,2 ground state is separated from the next lowest state (1,2,2) by 40 cm^{-1}. b) Effect on the energies of the lowest states at $2J_b = +20\ cm^{-1}$ as a result of the variation in J_a about the experimental value, and c) as a result of the variation in J_b about the experimental value at $2J_a = -40\ cm^{-1}$.

 © WILEY-VCH Verlag GmbH, D-69451 Weinheim, 2001 1433-7851/01/4024-4736 $ 17.50+.50/0

0.110; H atoms treated by a riding model; max. and min. residual electron densities were +0.550 and −0.453, respectively. Crystallographic data (excluding structure factors) for the structure reported in this paper has been deposited with the Cambridge Crystallographic Data Centre as supplementary publication no. CCDC-55327. Copies of the data can be obtained free of charge on application to CCDC, 12 Union Road, Cambridge CB21EZ, UK (fax: (+44) 1223-336-033; e-mail: deposit@ccdc.cam.ac.uk). Susceptibilities from a Pd-standard-calibrated Quantum Design MPMS5S SQUID, at a field of 0.1 T. The diamagnetic correction applied for **1** was $-5.32 \times 10^{-4}\ cm^3\ mol^{-1}$.

Received: January 9, 2001
Revised: October 4, 2001 [Z16393]

[1] D. Gatteschi, *Adv. Mater.* **1994**, *6*, 635.
[2] R. J. Bushby, J.-L. Paillaud in *An Introduction to Molecular Electronics* (Eds.: M. C. Petty, M. R. Bryce, D. Bloor) Edward Arnold, London, **1995**.
[3] a) M. A. Halcrow, G. Christou, *Chem. Rev.* **1994**, *94*, 2421; b) E. Jabri, M. B. Carr, R. P. Hausinger, P. A. Karplus, *Science* **1995**, *268*, 998.
[4] C. J. Matthews, K. Avery, Z. Xu, L. K. Thompson, L. Zhiao, D. O. Miller, K. Biradha, M. J. Zaworotko, C. Wilson, A. E. Goeta, J. A. K. Howard, *Inorg. Chem.* **1999**, *38*, 5266.
[5] a) A. Escuer, R. Vicente, S. B. Kumar, F. A. Mautner *J. Chem. Soc. Dalton. Trans.* **1998**, 3473. b) During preparation of this manuscript, the first mixed-magnetism Ni_4 cubane was reported: J. M. Clemente-Juan, B. Chansou, B. Donnadieu, J.-P. Tuchagues, *Inorg. Chem.* **2000**, *39*, 5515.
[6] J. M. Clemente-Juan, H. Andres, J. J. Borrás-Almenar, E. Coronado, H. U. Güdel, M. Aebersold, G. Kearly, H. Büttner, M. Zolliker, *J. Am. Chem. Soc.* **1999**, *121*, 10021.
[7] C. J. Gómez-García, J. J. Borrás-Almenar, E. Coronado, L. Ouahab, *Inorg. Chem.* **1994**, *33*, 4016.
[8] M. S. El Fallah, E. Rentschler, A. Caneschi, D. Gatteschi, *Inorg. Chim. Acta* **1996**, *247*, 231.
[9] Z. E. Serna, L. Lezama, M. K. Urtiaga, M. I. Arriortua, M. G. Barandika, R. Cortés, T. Rojo, *Angew. Chem.* **2000**, *112*, 352; *Angew. Chem. Int. Ed.* **2000**, *39*, 344.
[10] A. Escuer, M. Font-Bardía, S. J. Kumar, X. Solans, R. Vicente, *Polyhedron* **1999**, *18*, 909.
[11] F. Birkelbach, M. Winter, U. Flörke, H.-J. Haupt, C. Butzlaff, M. Lengen, E. Bill, A. A. X. Trautwein, K. Wieghardt, P. Chaudhuri, *Inorg. Chem.* **1994**, *33*, 3990.
[12] V. V. Pavlishchuk, S. V. Kolotilov, A. W. Addison, M. J. Prushan, R. J. Butcher, L. K. Thompson, *Inorg. Chem.* **1999**, *38*, 1759.
[13] In a strict "butterfly" geometry, the two "wings" are "beating" in-phase, and there is no center of symmetry; this "chair" structure might thus be considered an "out-of-phase butterfly".
[14] V. V. Pavlishchuk, S. V. Kolotilov, A. W. Addison, R. J. Butcher, E. Sinn, *J. Chem. Soc. Dalton Trans.* **2000**, 335.
[15] K. Kambe, *J. Phys. Soc. Jpn.* **1950**, *5*, 48.
[16] E. Sinn, *Coord. Chem. Rev.* **1970**, *5*, 313. Care is required in comparing *J* values: some authors use a "2*J*" exchange integral as here, while others use "*J*".
[17] J. H. van Vleck, *The Theory of Electric and Magnetic Susceptibilities*, Oxford University Press, Oxford, **1932**. ρ is the fraction of the nickel atoms present as paramagnetic impurity, while the other symbols have their usual meanings. $R^2 = \frac{\Sigma(\chi_{obs} - \chi_{calcd})^2}{\Sigma\chi^2_{obs}}$.
[18] J. K. McCusker, J. B. Vincent, E. A. Schmitt, M. L. Mino, K. Shin, D. K. Coggin, P. M. Hagen, J. C. Huffman, G. Christou, D. N. Hendrickson, *J. Am. Chem. Soc.* **1991**, *113*, 3012: $J_a \equiv J_{BW}$, $J_b \equiv J_{BB}$.
[19] R. D. Cannon, U. A. Jayasooriya, R. Wu, S. K. Arapkoske, J. A. Stride, O. F. Nielsen, R. P. White, G. J. Kearley, D. Summerfield, *J. Am. Chem. Soc.* **1994**, *116*, 11869.
[20] O. Kahn, *Molecular Magnetism*, VCH, Weinheim, **1993**.
[21] O. Kahn, *Chem. Phys. Lett.* **1997**, *265*, 109.
[22] K. K. Nanda, L. K. Thompson, J. N. Bridson, K. Nag, *J. Chem. Soc. Chem. Commun.* **1994**, 1337.
[23] M. A. Halcrow, J.-S. Sun, J. C. Huffman, G. Christou, *Inorg. Chem.* **1995**, *34*, 4167.

A Calix[4]arene Gd^{III} Complex Endowed with High Stability, Relaxivity, and Binding Affinity to Serum Albumin**

Silvio Aime, Alessandro Barge, Mauro Botta,* Alessandro Casnati,* Marco Fragai, Claudio Luchinat, and Rocco Ungaro

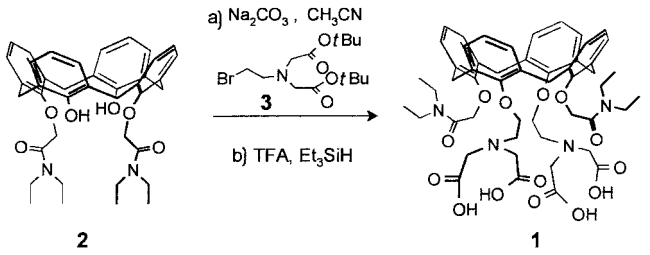
An interesting class of macrocyclic ligands uses calixarenes as a molecular platform. These ionophores[1] are characterized by high lipophilicity and have been mainly used as selective extractants or carriers of alkali,[2] alkaline earth,[3] lanthanide, and actinide metal ions.[4] The complexation of lanthanide ions by calix[4]arene ligands has also been studied with the purpose of developing new luminescent probes.[5] Very little is known on the use of calixarene lanthanide complexes as contrast agents for magnetic resonance imaging (MRI),[6] although this possibility has been envisaged[7] and a recent example has been reported.[8] To develop efficient systems for MRI the problem of water solubility and stability of the complexes has to be solved. Several years ago we reported the luminescent properties of lanthanide complexes of a calix[4]-arene tetraamide derivative in water.[9] However, the complexes were not very stable and after a short time the free ligand precipitated out of the solution. One efficient way to complex hard divalent and trivalent metal ions in water is to use aminopolycarboxylic acid derivatives.[10] Herein we report the synthesis of a new calix[4]arene-based ligand which presents two acetamide and two ethylenaminodicarboxy groups at the lower rim of the macrocycle, able to form complexes with Gd^{III} in water, these complexes are characterized by high values of relaxivity.[6]

The diamide tetraacid derivative **1** was synthesized in 45% overall yield, by alkylation of the diamide of calix[4]arene **2**[11] with Na_2CO_3 and 2-[*N*,*N*-bis(*tert*-butyloxycarbonylmethyl)-amino]-1-bromo-ethane (**3**)[12] in acetonitrile, followed by hydrolysis of *tert*-butyl esters using trifluoroacetic acid (TFA) and triethyl silane (Scheme 1). The ^1H NMR spectrum of **1** in CD_3OD, clearly show that the calixarene ligand is in the cone

[*] Prof. M. Botta
Dipartimento di Scienze e Tecnologie Avanzate
Università del Piemonte Orientale "Amedeo Avogadro"
Corso Borsalino 54, 15100 Alessandria (Italy)
Fax: (+39) 011-6707855
E-mail: botta@ch.unito.it
Prof. A. Casnati, Prof. R. Ungaro
Dipartimento di Chimica Organica e Industriale
Università di Parma
Parco Area delle Scienze 17/A, 43100 Parma (Italy)
Fax: (+39) 0521-905472
E-mail: casnati@ipruniv.cce.unipr.it
Prof. S. Aime, Dr. A. Barge
Dipartimento di Chimica I.F.M.
Università di Torino
Via P. Giuria 7, 10125 Torino (Italy)
Dr. M. Fragai, Prof. C. Luchinat
CERM, University of Florence
Via L. Sacconi 6, 50019 Sesto Fiorentino (Italy)

[**] This work was supported by CNR (Programma M.U.R.S.T. - Chimica Legge 95/95) "Agenti di contrasto, di shift e sonde luminescenti". We thank C.I.M. (Centro Interdipartimentale Misure) dell'Università di Parma for the NMR and mass spectroscopy facilities.

 © WILEY-VCH Verlag GmbH, D-69451 Weinheim, 2001 1433-7851/01/4024-4737 $ 17.50+.50/0



Scheme 1.

conformation: two doublets ($\delta = 4.36$ and 3.25, $J = 13.1$ Hz) for the methylene protons bridging the aromatic nuclei.[13] This conformation also ensures that all potential binding groups are located on the same side of the macrocycle.

The [Gd^{III}(**1**)] complex has a relaxivity of 9.6 $mM^{-1}s^{-1}$ in water, at 20 MHz and 25 °C, which is constant in the pH range 4–9, which indicates that the structure of the complex is stable over a change in proton concentration of five orders of magnitude. This value is about two times higher than that of the monoaquo complexes $[Gd(dota)(H_2O)]^-$ and $[Gd(dtpa)(H_2O)]^{2-}$ (DOTA = 1,4,7,10-tetraazacyclododecane-1,4,7,10-tetraacetic acid, DTPA = diethylenetriaminepentaacetic acid) which suggest a higher hydration of the metal ion in our case.[14] The nuclear magnetic relaxation dispersion (NMRD) profile of [Gd^{III}(**1**)][15] (Figure 1),

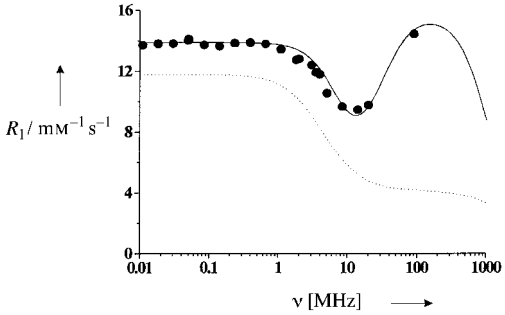


Figure 1. NMRD profile of [Gd^{III}(**1**)] in water at 25 °C and pH 6.8. The solid curve through the experimental data is the best-fit of the equations for inner- and outer-sphere paramagnetic relaxation. The lower dotted curve represents the calculated profile of the commercial MRI contrast agent $[Gd(dota)]^-$.[6a] ν = proton Larmor frequency, R_1 = longitudinal water-proton relaxivity.

confirms this hypothesis as the best fit of the data to the equations for the inner- and outer sphere relaxation yields a hydration number q of 3, a Gd–water protons separation r of 3.1 Å and a reorientational correlation time τ_R of about 150 ps.[16] Thus, the higher relaxivity of the complex compared to that of the commercial MRI contrast agents is because of a higher number of coordinated water molecules and a longer reorientational correlation time, a consequence of its higher molecular weight. This result implies that only two coordinating arms of the ligand are involved in the complexation of the metal ion. Enhanced relaxivities are observed when the reorientational motion of the paramagnetic complex is slowed down upon formation of noncovalent adducts with macromolecular substrates.[14, 17] MRI contrast agents with such a binding capability, in particular towards serum albumin, have been devised as blood-pool agents for angiographic applications.[18] An important requisite is a high thermodynamic (and/or kinetic) stability to ensure integrity of the complex upon binding to the protein and increased retention time in vivo. Our results represents an advance in the design of calixarene–Gd^{III}-based contrast agents with respect to a recently reported example in which the Gd^{III} complex has a stability constant of only $2 \times 10^5\ M^{-1}$.[8] From relaxometric competition experiments we measured a lower limit of the stability constant of $1 \times 10^{13}\ M^{-1}$ for [Gd^{III}(**1**)] in water at pH 6.8, a value sufficiently high to ensure the integrity of the complex in the presence of the protein, although not yet adequate for in vivo use. The binding interaction with human serum albumin (HSA) was investigated by titrating a solution (0.037 mmol L^{-1}) of [Gd^{III}(**1**)] with the protein at 25 °C and monitoring the increase of the proton solvent relaxation rate R_1 at 20 MHz (Figure 2). From the analysis of the data

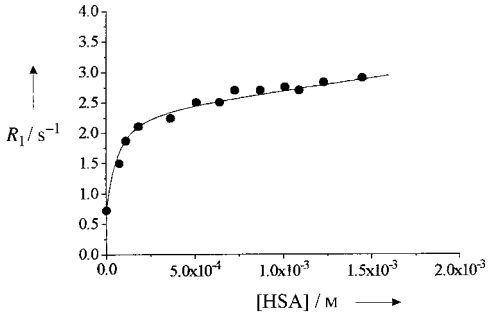


Figure 2. Relaxometric titration of a 0.037 mM solution of [Gd^{III}(**1**)] with HSA at 25 °C, pH 6.8, and 20 MHz. From the analysis of the data a relaxivity as high as 60 $mM^{-1}s^{-1}$ is calculated for the HSA bound adduct of the complex. Details of the general methods and instrumentation used are given in refs. [17b, c]; R_1 = longitudinal water-proton relaxation rate.

according to the equation of the proton relaxation enhancement (PRE),[17c] by assuming the presence of a single class of equivalent binding sites, we calculated an affinity constant K_A of $2.4 \times 10^4\ M^{-1}$ and an enhancement of six of the relaxivity of the macromolecular adduct over that of the free complex. The binding constant is in the upper range found for the noncovalent interaction of suitably functionalized DOTA and DTPA complexes to HSA.[17b, c] However, the NMRD profile of the complex in the presence of an excess of HSA (Figure 3) supports the view of the formation of a ternary complex involving the displacement of one or more coordinated water molecules by the protein, since a reasonable fitting of the data could only be obtained by considering a single coordinated water molecule.[19] In spite of the displacement of two water molecules by HSA, the relaxivity of the adduct reaches a peak of about 50 $mM^{-1}s^{-1}$ at 30 MHz. Interestingly, the calculated value of the residence lifetime τ_M for the coordinated water, approximately 40 ns, is considerably shorter (300 ns) than those for the clinically used MRI contrast agents $[Gd(dtpa)]^{2-}$ and $[Gd(dota)]^-$. This value is near optimal for attaining maximum relaxivities for macromolecular Gd^{III} complexes.[17c] An involvement of the donor groups on the surface of the protein in the coordination of the Gd^{III} ion has been recently reported for a Gd^{III} complex with a functionalized DO3A ligand (DO3A = 1,4,7,10-tetraazacyclododecane-1,4,7-triacetic acid.[20]

 © WILEY-VCH Verlag GmbH, D-69451 Weinheim, 2001 1433-7851/01/4024-4738 $ 17.50+.50/0

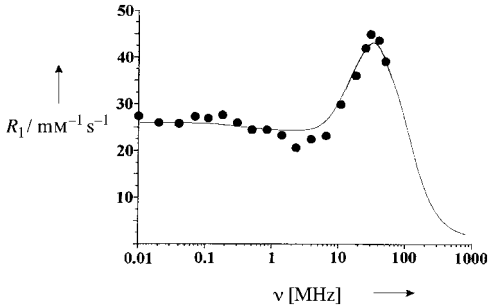


Figure 3. NMRD profile of the [Gd^{III}(**1**)] – HSA adduct 25 °C. The best-fit curve was calculated with the parameters: $\Delta = 0.023$ cm^{-1}, $\tau_R = 1.75$ ns, $\tau_V =$ 12 ps, D(ZFS) = 0.24 cm^{-1}, $\tau_M = 38$ ns, $q = 1$, $r = 3.1$ Å;[19] ν = proton Larmor frequency, R_1 = longitudinal water-proton relaxivity, τ_V = correlation time for electron relaxation, D(ZFS) = static zero-field splitting.

To surmise, the high binding affinity of [Gd^{III}(**1**)] to HSA is the result of a cooperative effect of the hydrophobic interaction brought about by the aromatic macrocyclic moiety and of the coordination of donor groups of the protein (probably Asp or Glu). These preliminary results augurs well for the development of a new class of stable, water soluble MRI contrast agents of enhanced efficacy (Gd^{III} complexes) and luminescent probes (Eu^{III}/Tb^{III} complexes) for biomedical studies.

Experimental Section

Melting points were determined with an electrothermal melting point apparatus in a capillary sealed under nitrogen. ^{1}H NMR spectra were recorded with a Bruker AC 300 spectrometer. Mass spectra were obtained either with a Finnigan MAT SSQ710 spectrometer (desorption chemical ionization (DCI) using methane as ionizing gas) or with a ZMD MICROMASS spectrometer (electrospray ionization (ESI) methanol/dichloromethane = 9/1). All solvents were purified with standard procedures; dry solvents were obtained by literature methods and stored over molecular sieves.

Synthesis of the *tert*-butyl ester of **1**: Na_2CO_3 (15 mL; 0.65 g, 6.15 mmol) and compound **3** (0.32 g, 0.92 mmol) were added under nitrogen atmosphere to a stirred solution of diamide **2** (0.20 g, 0.31 mmol) in dry acetonitrile. After 14 h reflux, the solvent was removed under vacuum and 1N HCl (20 mL) added. The water layer was then extracted with AcOEt (Ac = acetyl), and the organic phase washed twice with water. The tetra-*tert*-butyl ester of **1** was obtained by removing the solvent under vacuum. Yield = 51 %; ^{1}H NMR (300 MHz, $CDCl_3$, 25 °C, TMS): $\delta = 6.60 - 6.54$ (m, 12H; ArH), 4.69 (s, 4H; OCH_2CO), 4.65 (d, $J = 13.6$ Hz, 4H; ArCH_2Ar ax), 4.12 (t, $J = 7.1$ Hz, 4H; OCH_2CH_2N), 3.45 (s, 8H; NCH_2CO), 3.40 – 3.27 (m, 8H; NCH_2CH_3), 3.25 (t, $J = 7.1$ Hz, 4H; OCH_2CH_2N), 3.17 (d, $J =$ 13.6 Hz, 4H; ArCH_2Ar eq), 1.42 (s, 36H; CCH_3), 1.16 – 1.08 (m, 12H; NCH_2CH_3); CI-MS m/z: 1193.8 [$(M+H)^+$].

1: Trifluoroacetic acid (5.9 mL, 62.90 mmol) was added to a solution of the tetra-*tert*-butyl ester of **1** (0.50 g, 0.42 mmol) and triethyl silane (3.3 mL, 20.96 mmol) dissolved in of dry CH_2Cl_2 (10 mL). After stirring at room temperature for 14 h, the solvent was removed under vacuum. Product **1** was obtained by precipitation with Et_2O from the CH_2Cl_2 solution. Yield = 90 %; m.p. 140 – 142 °C; ^{1}H NMR (300 MHz, CD_3OD, 25 °C, TMS) $\delta = 7.17$ (d, $J = 7.4$ Hz, 4H; ArH), 6.97 (t, $J = 7.4$ Hz, 2H; ArH), 6.28 (s, 6H; ArH), 4.54 – 4.51 (m, 8H; OCH_2CO, OCH_2CH_2N), 4.36 (d, $J = 13.1$ Hz, 4H; ArCH_2Ar ax), 4.22 – 4.12 (m, 12H; NCH_2COOH, OCH_2CH_2N), 3.51 – 3.44 (m, 4H; NCH_2CH_3), 3.25 (d, $J = 13.1$ Hz, 4H; ArCH_2Ar eq), 3.30 – 3.21 (m, 4H; NCH_2CH_3), 1.21 – 1.13 (m, 12H; NCH_2CH_3); ESI-MS m/z: 969.8 [$(M+H)]^+$.

Received: August 28, 2001 [Z17811]

[1] a) R. Ungaro, A. Pochini in *Calixarenes, a Versatile Class of Macrocyclic Compounds* (Eds.: J. Vicens, V. Böhmer), Kluwer, Dordrecht, **1991**, p. 127; b) M. A. McKervey, M.-J. Schwing in *Calixarenes, a Versatile Class of Macrocyclic Compounds* (Eds.: J. Vicens, V. Böhmer), Kluwer, Dordrecht, **1991**, p. 149; c) M. A. McKervey, M.-J. Schwing-Weill, F. Arnaud-Neu in *Comprehensive Supramolecular Chemistry*, *Vol. 1* (Ed.: F. Vögtle), Pergamon, Oxford, **1996**, p. 537; d) A. Casnati, R. Ungaro in *Calixarenes in Action* (Eds.: L. Mandolini, R. Ungaro), Imperial College Press, London, **2000**, p. 62.

[2] a) R. Ungaro, A. Casnati, F. Ugozzoli, A. Pochini, J.-F. Dozol, C. Hill, H. Rouquette, *Angew. Chem.* **1994**, *106*, 1551; *Angew. Chem. Int. Ed. Engl.* **1994**, *33*, 1506; b) C. Hill, J.-F. Dozol, V. Lamare, H. Rouquette, B. Tournois, J. Vicens, Z. Asfari, R. Ungaro, A. Casnati, *J. Inclusion Phenom.* **1994**, *19*, 399; c) A. Casnati, A. Pochini, R. Ungaro, F. Ugozzoli, F. Arnaud, S. Fanni, M.-J. Schwing, R. J. M. Egberink, F. de Jong, D. N. Reinhoudt, *J. Am. Chem. Soc.* **1995**, *117*, 2767.

[3] a) J.-F. Dozol, H. Rouquette, R. Ungaro, A. Casnati, Patent FR 93-4566, 930419, **1993**; WO 94-FR432 940418, **1994** [*Chem. Abstr.* **1995**, *122*, 239730]; b) A. Casnati, L. Baldini, N. Pelizzi, K. Rissanen, F. Ugozzoli, R. Ungaro, *J. Chem. Soc. Dalton Trans.* **2000**, 3411; c) G. Arena, A. Contino, A. Magrì, D. Sciotto, J. D. Lamb, *Supramol. Chem.* **1999**, *10*, 5.

[4] a) L. H. Delmau, N. Simon, M. J. Schwing-Weill, F. Arnaud-Neu, J. F. Dozol, S. Eymard, B. Tournois, V. Böhmer, C. Gruttner, C. Musigmann, A. Tunayar, *Chem. Commun.* **1998**, 1627; b) S. Barboso, A. G. Carrera, S. E. Matthews, F. Arnaud-Neu, V. Böhmer, J. F. Dozol, H. Rouquette, M. J. Schwing-Weill, *J. Chem. Soc. Perkin Trans. 2* **1999**, 719; c) A. Arduini, V. Bohmer, L. Delmau, J. F. Desreux, J. F. Dozol, M. A. G. Carrera, B. Lambert, C. Musigmann, A. Pochini, A. Shivanyuk, F. Ugozzoli, *Chem. Eur. J.* **2000**, *6*, 2135.

[5] a) F. J. Steemers, H. G. Meuris, W. Verboom, D. N. Reinhoudt, E. B. van der Tol, J. W. Verhoeven, *J. Org. Chem.* **1997**, *62*, 4229; b) G. Ulrich, R. Ziessel, I. Manet, M. Guardigli, N. Sabbatini, F. Fraternali, G. Wipff, *Chem. Eur. J.* **1997**, *3*, 1815; c) L. Prodi, S. Pivari, F. Bolletta, M. Hissler, R. Ziessel, *Eur. J. Inorg. Chem.* **1998**, 1959; C. Fischer, G. Sarti, A. Casnati, B. Carrettoni, I. Manet, R. Schuurman, M. Guardigli, N. Sabbatini, R. Ungaro, *Chem. Eur. J.* **2000**, *6*, 1026.

[6] a) S. Aime, M. Botta, M. Fasano, E. Terreno, *Chem. Soc. Rev.* **1998**, *27*, 19; b) D. Parker, J. A. G. Williams, *J. Chem. Soc. Dalton Trans.* **1996**, 3613.

[7] a) E. M. Georgiev, D. M. Roundhill, *Inorg. Chim. Acta* **1997**, *258*, 93; b) A. M. Krishnan, R. Lohrmann, WO 95-US14801 [WO 96/14878 A2], **1996** [*Chem. Abstr.* **1995**, *125*, 109099].

[8] L. H. Bryant, Jr., A. T. Yordanov, J. J. Linnoila, M. W. Brechbiel, J. A. Frank, *Angew. Chem.* **2000**, *112*, 1686; *Angew. Chem. Int. Ed.* **2000**, *39*, 1641.

[9] N. Sabbatini, M. Guardigli, A. Mecati, V. Balzani, R. Ungaro, E. Ghidini, A. Casnati, A. Pochini, *J. Chem. Soc. Chem. Commun.* **1990**, 878.

[10] A. Bianchi, L. Calabi, F. Corana, S. Fontana, P. Losi, A. Maiocchi, L. Paleari, B. Valtancoli, *Coord. Chem. Rev.* **2000**, *204*, 309.

[11] A. Casnati, C. Fischer, M. Guardigli, A. Isernia, I. Manet, N. Sabbatini, R. Ungaro, *J. Chem. Soc. Perkin Trans. 2* **1996**, 395.

[12] M. A. Wiliams, H. Rapoport, *J. Org. Chem.* **1993**, *58*, 1151.

[13] C. D. Gutsche, L. J. Bauer, *J. Am. Chem. Soc.* **1985**, *107*, 6052.

[14] a) P. Caravan, J. J. Ellison, T. J. McMurry, R. B. Lauffer, *Chem. Rev.* **1999**, *99*, 2293; b) R. B. Lauffer, *Chem. Rev.* **1987**, *87*, 901; c) S. Aime, M. Botta, M. Fasano, E. Terreno, *Acc. Chem. Res.* **1999**, *32*, 941.

[15] a) S. H. Koenig, R. D. Brown III, *Prog. NMR Spectrosc.* **1990**, *22*, 487; b) C. Luchinat, *Magn. Reson. Chem.* **1993**, *31*, S145.

[16] a) L. Banci, I. Bertini, C. Luchinat in *Nuclear and Electron Relaxation*, VCH, Weinheim, **1991**; b) É. Tóth, L. Helm, A. E. Merbach in *The Chemistry of Contrast Agents in Medical Magnetic Resonance Imaging* (Eds.: É. Tóth, A. E. Merbach), Wiley, Chichester, **2001**, p. 45.

[17] a) S. Aime, M. Botta, M. Fasano, S. Geninatti Crich, E. Terreno, *Coord. Chem. Rev.* **1999**, *185 – 186*, 321; b) S. Aime, M. Botta, M. Fasano, S. Geninatti Crich, E. Terreno, *J. Biol. Inorg. Chem.* **1996**, *1*, 312; c) S. Aime, M. Botta, M. Fasano, E. Terreno in *The Chemistry of Contrast Agents in Medical Magnetic Resonance Imaging* (Eds.: É. Tóth, A. E. Merbach), Wiley, Chichester, **2001**, p. 193.

[18] P. A. Rink, *Magnetic Resonance in Medicine*, Blackwell, Oxford, **1993**.

[19] I. Bertini, O. Galas, C. Luchinat, G. Parigi, *J. Magn. Reson. A* **1995**, *113*, 151.

[20] S. Aime, E. Gianolio, E.Terreno, G. B. Giovenzana, R. Pagliarin, M. Sisti, G. Palmisano, M. Botta, M. P. Lowe, D. Parker, *J. Biol. Inorg. Chem.* **2000**, *5*, 488.

 © WILEY-VCH Verlag GmbH, D-69451 Weinheim, 2001 1433-7851/01/4024-4739 $ 17.50+.50/0

$Li_{10}Mg_6Zn_{31}Al_3$: A New Intermetallic Phase Containing Building Blocks for Decagonal Quasicrystals**

Chi-Shen Lee and Gordon J. Miller*

Dedicated to Professor Hans Georg von Schnering on the occasion of his 70th birthday

Since the discovery of a quasicrystalline structure in the Mn – Al system,[1] the complete structural characterization of a quasicrystal remains an active and vital segment of quasicrystal research. This problem entails finding both the positional coordinates of the atomic network as well as how the network is decorated by the constituent elements. Most quasicrystalline phases involve ternary and quaternary compositions, which create complex structural problems to solve, and also appear to exist for two different regimes: icosahedral and dodecahedral systems.[2] Many strategies to solve these structures utilize related crystalline phases, called approximants, to provide models of atomic arrangements that may exist in the quasicrystal itself.[3] An important class of approximants for icosahedral quasicrystals is the Bergman-phase structure,[4] which occurs for numerous A – M – X (s – p – d) materials (A = Li, Mg; M = Cu, Zn; X = Al). Our own investigations have included detailed experimental and theoretical studies of the structure, phase width, and site preferences for Bergman phases in the Li-Mg-Zn-Al system.[5–7] Herein we report a new compound discovered during this systematic investigation, $Li_{10}Mg_6Zn_{31}Al_3$, whose structure contains a pseudo-pentagonal unit that could be considered as a possible model of decagonal quasicrystalline structures.

$Li_{10}Mg_6Zn_{31}Al_3$ crystallizes in the space group *Cmcm*, with five independent positions (A1 – A5) for Li/Mg atoms and eight positions (M1 – M8) for Zn/Al atoms (Figure 1).[8] The Zn/Al atoms form a three-dimensional (3D) network of truncated tetrahedra (one of the Friauf polyhedra) along with two other polyhedra with 12 and 14 vertices that resemble two different ways to fuse an icosahedron and a truncated tetrahedron. All of these polyhedra encapsulate Li/Mg atoms. The shortest M–M distances range between 2.42 and 2.85 Å. Most of the M sites are 100 % Zn; only the M6 and M8 sites refine as a mixture of Zn and Al atoms (site occupancies are: M6 = 0.93(1) Zn + 0.07 Al; M8 = 0.39(1) Zn + 0.61 Al). As evident in Figure 1 and emphasized in Figure 2, the important structural kernel is a pseudo-pentagonal unit formed by a ring of five truncated tetrahedra, each sharing two hexagonal faces with adjacent polyhedra (shaded dark gray in Figure 1 and 2).

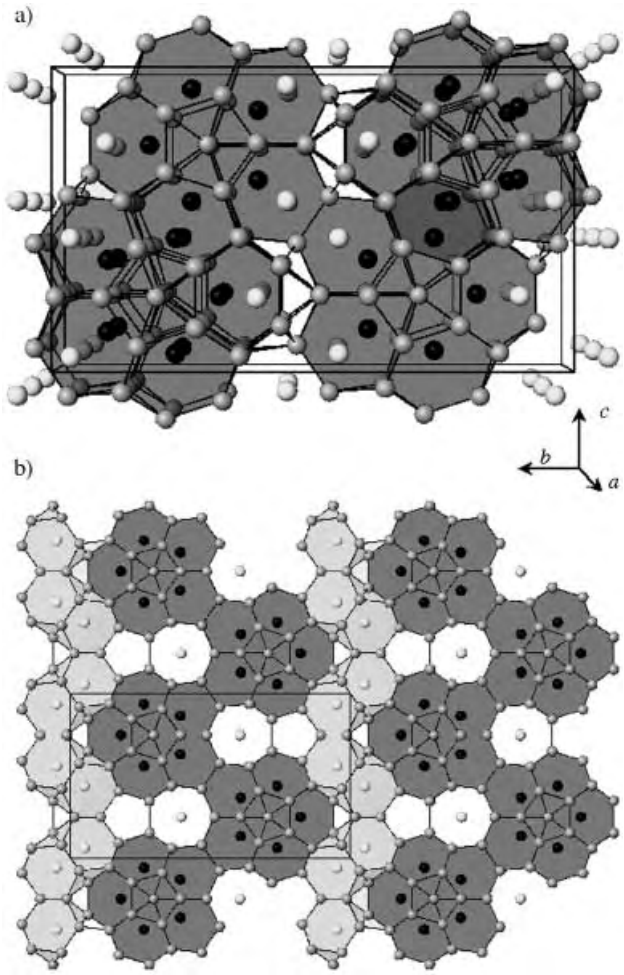


Figure 1. a) The three-dimensional structure of $Li_{10}Mg_6Zn_{31}Al_3$ projected along [100]; black: A1 – A3 sites; white: A4, A5 sites; gray: M1 – M8 sites; b) projection along [100] emphasizing sheets of two different ribbons of edge-sharing Friauf polyhedra running along [001].

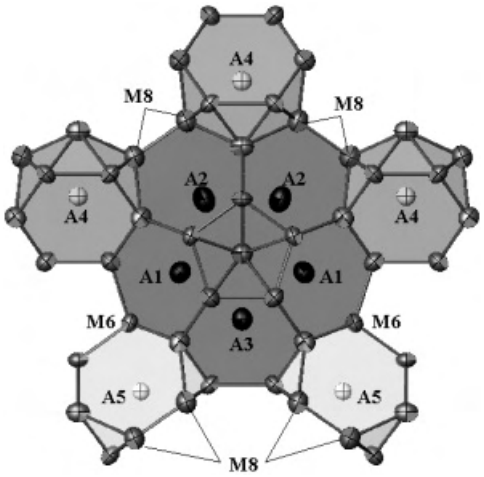


Figure 2. The pseudo-pentagonal motif of shared truncated tetrahedra (dark gray) plus coordination polyhedra around A4 (medium gray) and A5 sites (light gray). A sites and mixed-metal M sites are labeled; sites with no labels are Zn.

This condensation of truncated tetrahedra creates two pentagonal pyramids of Zn/Al atoms (M–M distances range between 2.64 and 2.68 Å) connected by a short distance

[*] Prof. G. J. Miller, C.-S. Lee
Department of Chemistry and Ames Laboratory
US Department of Energy
Iowa State University, Ames, IA 50011-3111 (USA)
Fax: (+1) 515-294-0105
E-mail: gmiller@iastate.edu

[**] The Ames Laboratory is operated for the U.S. Department of Energy (US DOE) by Iowa State University under contract No. W-7405-ENG-82. This work was supported by the Office of Basic Energy Sciences, Materials Chemistry Division of the US DOE. The Bruker CCD-1000 diffractometer was purchased by a grant from the U.S. National Science Foundation, NSF 97-11121.

 © WILEY-VCH Verlag GmbH, D-69451 Weinheim, 2001 1433-7851/01/4024-4740 $ 17.50+.50/0

(2.42 Å) between apical atoms. The A1 – A3 sites (Figure 2) coordinated by the truncated tetrahedra involve different mixtures of Li and Mg atoms (site occupancies: A1 = 0.48(2) Li + 0.52 Mg; A2 = 0.38(2) Li + 0.62 Mg; A3 = 0.24(2) Li + 0.76 Mg). The next shell of polyhedra for this motif consists of two Li-centered $(A5)M_{12}$ (light gray) and three Li-centered $(A4)M_{14}$ cages (medium gray). These pseudo-pentagonal units form zigzag chains along the *c* direction by sharing two 14-vertex cages and the M8 – M8 edges (2.63 Å) that connect them (see Figure 1b). The resulting chains are stitched together in the *b* direction to form layers by sharing hexagonal faces of the Li-centered $(A5)M_{12}$ cages, which also creates chains of these polyhedra along the *c* direction (note: there is a short Li–Li distance of 2.86(5) Å through the shared hexagonal face. This distance lies between the covalent diameter, 2.46 Å, and van der Waals diameter, 3.10 Å of Li). The subsequent layers in the *bc* plane (emphasized in Figure 1) are stacked along the *a* axis with a shift of *b*/2 from one layer to the next. Therefore, the ribbons of pseudo-pentagonal units alternate with the zigzag chains of LiM_{12} cages in each layer.

The site symmetry of the pseudo-pentagonal unit in $Li_{10}Mg_6Zn_{31}Al_3$ is C_{2v} with pseudo-fivefold symmetry along the *a* axis at the M4 sites. The deviations from pentagonal symmetry are slight: all M–M distances and M-M-M angles in the bases of the pentagonal pyramids are 2.67(2) Å and 108.0(5)°, respectively; all A–A distances and A-A-A angles between the truncated tetrahedra are 3.22(2) Å and 108.0(4)°, respectively. A similar pseudo-pentagonal construct is found in the icosahedral approximants, the Bergman phases $Li_{16}Mg_{10}(Zn_xAl_{1-x})_{54}$ $(0.36 \le x \le 0.73)$,[6] with a site symmetry C_s, but these motifs are fused to form the 84-atom Samson cluster, and show substantial deviations from pentagonal symmetry: in the bases of the pentagonal pyramids, three M–M distances are 2.65(1) Å, while two are 2.80(1) Å. The truncated tetrahedra encapsulate slightly different mixtures of Li and Mg atoms, which may influence the observed metrics: among the five A sites, in $Li_{10}Mg_6Zn_{31}Al_3$ there are $2 \times 48(2)$, $2 \times 38(2)$. and $1 \times 24(2)$ % Li; whereas in the quaternary Bergman phases there are $2 \times 75(2)$ and $3 \times 34(2)$ % Li.[6]

Tight-binding, linear muffin-tin orbital atomic sphere approximation (TB-LMTO-ASA) calculations were performed on "$Li_{10}Mg_6Zn_{30}Al_4$" as a model for the observed structure to understand the composition and bonding characteristics of $Li_{10}Mg_6Zn_{31}Al_3$.[11, 12] The total density of states (DOS) curve (Figure 3) shows no band gap at the Fermi level ($E_F = -1.7$ eV) at the valence electron count per atom (vec) of 1.86 e^- per atom for $Li_{10}Mg_6Zn_{31}Al_3$. In fact, it lies just below a distinct minimum in the DOS curve. The crystal orbital Hamilton population (COHP) curves for M–M, M–A, and A–A interactions indicate that none of their orbital populations (i.e., bond orders) are optimized at 1.86 e^- per atom.[13] The COHP for all M–M contacts is optimized at vec = 1.96 e^- per atom (Figure 3), which locates the minimum in the DOS curve and corresponds to the possible compositions $Li_{16-x}Mg_xZn_{34-y}Al_y$ $(x + y = 14)$. The M–A COHP optimizes at an even higher vec value of 2.11 e^- per atom. Attempts to synthesize "$Li_{10}Mg_6Zn_{26}Al_8$" (vec = 1.96 e^- per atom) produced the Bergman phase structure: $x = 0.71$ for

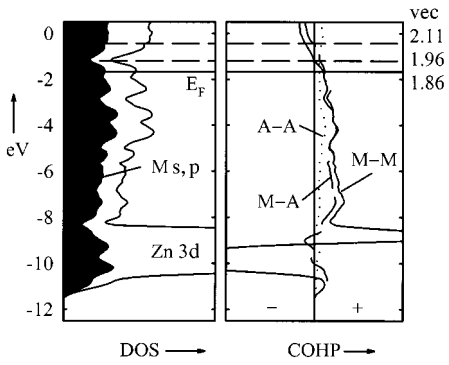


Figure 3. TB-LMTO-ASA DOS and COHP curves for $Li_{10}Mg_6Zn_{30}Al_4$. The contribution from M (Zn, Al) valence s and p orbitals is shaded. The solid line at -1.7 eV denotes the Fermi energy for the observed vec = 1.86 e^- per atom; the two dashed lines at -1.2 and -0.4 eV, respectively, are Fermi levels for optimized M–M (vec = 1.96 e^- per atom) and M–A (vec = 2.11 e^- per atom) contacts.

$Li_{16}Mg_{10}(Zn_xAl_{1-x})_{54}$. The overall compositions of these two phases, $Li_{10}Mg_6Zn_{31}Al_3 \equiv A_{16}M_{34}$ and the Bergman phases $Li_{16}Mg_{10}(Zn_xAl_{1-x})_{54} \equiv A_{26}M_{54} \approx A_{16}M_{33.2}$ are very similar. Since the Li-Mg-Zn-Al Bergman phases are observed for a vec value in the range 2.00 – 2.28 e^- per atom,[5–7] this new quaternary compound prefers to form at lower vec values, that is Zn-rich compositions, when compared to the Bergman phases. Although the TB-LMTO-ASA calculations identify that M–M and M–A interactions are strongest at low vec values, further analysis of interatomic potentials may be needed to elucidate the driving forces for forming this structure.

To understand the elemental site preferences in this intermetallic phase, extended Hückel calculations were performed on a model of $Li_{10}Mg_6Zn_{31}Al_3$ in which all atomic sites were given the same atomic potential.[14, 15] The site preferences for the different elements among the crystallographic sites are compared by their relative Mulliken populations (Figure 4).[6] This method involves placing the same atomic potential at each site and calculating the Mulliken populations relative to the average value for a range of electron counts. It has proved to be very useful in the characterization of site preferences between electropositive and electronegative elements in intermetallic systems such as

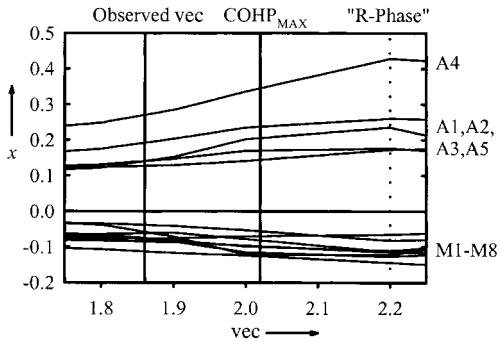


Figure 4. Relative Mulliken populations (x) of the A1 – A5 and M1 – M8 sites versus the vec range from 1.75 to 2.25 e^- per atom. The two solid lines indicate the observed vec (1.86 e^- per atom) and vec for optimized bonding for M–M and M–A contacts together (2.2 e^- per atom; $COHP_{MAX}$). The optimum vec for the Li-Mg-Zn-Al R-phases is shown as a dotted line.

 © WILEY-VCH Verlag GmbH, D-69451 Weinheim, 2001 1433-7851/01/4024-4741 $ 17.50+.50/0

the Bergman phases, ternary α-Mn structures, and complex Ca-Li-Al systems.[6, 7, 16] The computational result indicates that all A sites are positively polarized and all M sites are negatively polarized for the vec range between 1.8 and 2.2 e^- per atom, which are consistent with the relative electronegativities between Li/Mg and Zn/Al.

The pseudo-pentagonal units in the new intermetallic phase $Li_{10}Mg_6Zn_{31}Al_3$ link together to form layers rather than icosahedral-like cages as in the Bergman phases (Figure 5). If we attempt to build layered models with this building block using the principle of self-similarity to form a framework for a

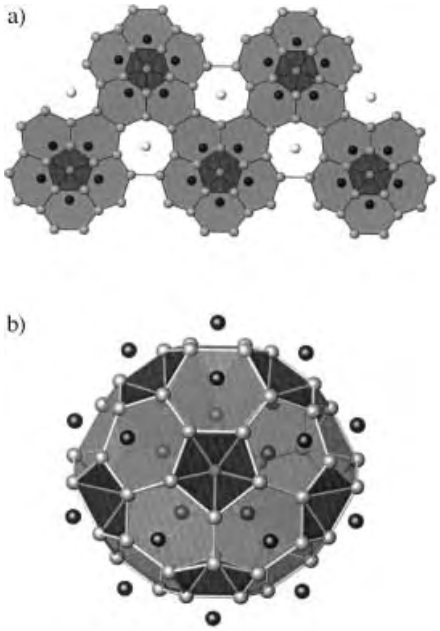


Figure 5. Two observed ways of condensing five face-sharing truncated tetrahedra: a) into ribbons as seen in $Li_{10}Mg_6Zn_{31}Al_3$; and b) into cages as seen in the Bergman phases found in Li-Mg-Zn-Al systems.[5–7] The truncated tetrahedra are shaded light gray and the pentagonal pyramids created by the condensation of these polyhedra are shaded dark gray.

decagonal quasicrystalline phase,[17] two aspects of structural frustration arise: 1) too short M–M distances in polyhedra surrounding A sites; and 2) large void spaces. Nevertheless, the occurrence of five face-sharing truncated tetrahedra in both Bergman-type crystalline approximants as well as the structure of $Li_{10}Mg_6Zn_{31}Al_3$ identifies this motif as an important kernel from which to build models of decagonal and icosahedral quasicrystalline structures.

Experimental Section

$Li_{10}Mg_6Zn_{31}Al_3$ was first obtained from a reaction of the elements in the molar ratio Li:Mg:Zn:Al = 32:20:85:23 to study Bergman-type compounds. The reactants were heated in a sealed Ta tube under dynamic vacuum (ca. 10^{-4} atm) at 1070 K for 2 days, then cooled to room temperature in the furnace. The product contained a mixture of the title compound (major), $MgZn_2$ (minor), and a trace amount of Al. The characteristic silvery rods of $Li_{10}Mg_6Zn_{31}Al_3$ could be manually separated from the product. Single-phase $Li_{10}Mg_6Zn_{31}Al_3$ (>90% according to Guinier X-ray powder diffraction) could be synthesized by mixing the elements in the molar ratio, $10:6:30.75 \pm 0.25:3.25 \pm 0.25$ using the same reaction conditions mentioned above. Several reactions at different (Li/Mg) and (Zn/Al) ratios were performed to study the phase width (Li:Mg:Zn:Al = 10:6:14:20, 10:6:20:14, 10:6:30.5:3.5, 10:6:31:3, and 10:6:34:0). The title phase only occurred for the initial mixture, Li:Mg:Zn:Al = 10:6:31:3. The other reactions yielded mixtures of elements, $MgZn_2$, a Bergman phase, and the title compound, depending on the relative compositions of Li:Mg:Zn:Al. The product is stable in the air for at least two weeks, but decomposes readily in 0.1M HNO_3(aq). Single crystals suitable for X-ray diffraction analysis were selected from crushed products. At least two independent single-crystal data sets were collected for each sample. Further details on the crystal structure investigation may be obtained from the Fachinformationszentrum Karlsruhe, 76344 Eggenstein-Leopoldshafen, Germany (fax: (+49) 7247-808-666; e-mail: crysdata@fiz-karlsruhe.de), on quoting the depository number CSD-411919.

Received: May 21, 2001
Revised: October 4, 2001 [Z17157]

[1] D. Shechtman, I. Blech, D. Gratias, J. W. Cahn, *Phys. Rev. Lett.* **1984**, *53*, 1951.
[2] A. P. Tsai, in *Physical Properties of Quasicrystals* (Ed.: Z. M. Stadnik), Springer, Berlin, **1999**, pp. 1–50.
[3] W. Steurer, T. Haibach, in *Physical Properties of Quasicrystals* (Ed.: Z. M. Stadnik), Springer, Berlin, **1999**, pp. 51–89.
[4] G. Bergman, J. L. T. Waugh, L. Pauling, *Acta Crystallogr.* **1957**, *10*, 254.
[5] C.-S. Lee, G. J. Miller, *J. Am. Chem. Soc.* **2000**, *122*, 4937.
[6] C.-S. Lee, G. J. Miller, *Inorg. Chem.* **2001**, *40,* 338.
[7] G. J. Miller, C.-S. Lee, W.-J. Tsai, *Mat. Res. Soc. Proc.* **2001**, in press.
[8] Crystal data of $Li_{10}Mg_6Zn_{31}Al_3$: $0.07 \times 0.07 \times 0.04$ mm^3; orthorhombic, *Cmcm* ($Z = 2$); $a = 5.1020(19)$, $b = 23.477(9)$, $c = 13.691(5)$ Å; $V = 1639.8(11)$ Å^3; $\rho_{calcd} = 4.704$ g cm^{-3}; $2\theta_{max} = 58.66°$; $Mo_{K\alpha}$, $\lambda = 0.71073$ Å; Smart CCD, three sets of frames with 0.3° scans in ω for an exposure time of 60 s per frame; $T = 298(2)$ K; $N_{meas} = 3015$, $N_{ind} = 1028$ ($I > 2\sigma(I)$); corrections for Lorentz and polarization effects; absorption corrections were based on fitting a function to the empirical transmission surface as sampled by multiple equivalent measurements,[9] $\mu = 22.29$ mm^{-1}; solved by direct methods (SHELXTL-V5.12)[10] and subsequently refined by full-matrix, least-squares calculations based on F^2; all independent atomic sites are assumed to be 100% occupied by (Li/Mg) or (Zn/Al) atoms; thermal parameters for A4 and A5 sites were only refined isotropically due to the unreasonable ellipsoid parameter at U_{11} (A5 only); $\Delta\rho = 1.259$ and -1.388 e$^-$ Å^{-3}, $R_1/wR_2 = 0.0522/0.0884$, GOF = 1.091; detailed results are deposited at the Fachinformationszentrum, Karlsruhe, Germany.
[9] SAINT, Version 4, Siemens Analytical X-ray Instruments, Madison, WI, **1995**.
[10] SHELXTL, Version 5.12, Reference Manual, Siemens Analytical X-ray Systems, Madison, WI, **1996**.
[11] a) O. K. Andersen, *Phys. Rev. B* **1975**, *12*, 3060; b) G. Krier, O. Jepsen, A. Burkhardt, O. K. Andersen, TB-LMTO-ASA Version 47.
[12] "$Li_{10}Mg_6Zn_{30}Al_4$" TB-LMTO-ASA computational parameters: Al at M8 site, Mg at A2, A3 and 50% A1 sites; Wigner–Seitz radii: Li (1.65 Å); Mg (1.80–1.90 Å); Zn (1.40–1.50 Å); Al (1.50 Å); no empty spheres needed to satisfy the overlap criteria; 26 *k* points for Brillouin zone integrations.
[13] a) R. Dronskowski, P. E. Blöchl, *J. Phys. Chem.* **1993**, *97*, 8617; b) T. Hughbanks, R. Hoffmann, *J. Am. Chem. Soc.* **1983**, *105*, 3528.
[14] a) R. Hoffmann, W. N. Lipscomb, *J. Chem. Phys.* **1962**, *36*, 2179; b) R. Hoffmann, *J. Chem. Phys.* **1963**, *39*, 1397; c) J. H. Ammeter, H. B. Bürgi, J. C. Thibeault, R. Hoffmann, *J. Am. Chem. Soc.* **1978**, *100*, 3686; d) M.-H. Whangbo, R. Hoffmann, R. B. Woodward, *Proc. R. Soc. London Ser. A* **1979**, *366*, 23.
[15] Atomic orbital parameters (all single-ζ STO functions) for Al: $H_{ii}(3s) = -12.3$ eV, $H_{ii}(3p) = -6.5$ eV, ζ (3s) = 1.37, ζ (3p) = 1.36; 100 *k* points in the first Brillouin zone with overlaps included through second nearest neighbor unit cells.
[16] a) G. J. Miller, *Eur. J. Inorg. Chem.* **1998**, 523; b) C.-S. Lee, PhD thesis, Iowa State University (USA), **2000**.
[17] C. Janot, *Quasicrystals: A Primer*, Clarendon Press, Oxford, **1994**.

 © WILEY-VCH Verlag GmbH, D-69451 Weinheim, 2001 1433-7851/01/4024-4742 $ 17.50+.50/0

Novel Coordination in the First Tellurium Porphyrin Complex: Synthesis and Crystal Structure of [Te(ttp)Cl_2]**

Desiree S. Grubisha, Ilia A. Guzei, Najeh Al-Salim, Peter D. W. Boyd, Penelope J. Brothers,* and L. Keith Woo*

Despite the wealth of fundamental and applied research on porphyrin complexes of the metallic elements, non-metal porphyrin complexes have been much less extensively studied.[1] Porphyrin complexes of the groups 13–15 elements are well-established, but as yet no porphyrin complex of any group 16 element is known. Gouterman and co-workers reported UV/Vis spectral changes on reaction of free-base porphyrins with $TeCl_4$ and $SeCl_4$, but no well-characterized species were isolated.[2] As part of our continuing studies of main group porphyrin complexes,[3] we have investigated the synthesis, characterization, and molecular structure analysis of the first tellurium porphyrin complex.

The reaction between tellurium(IV) chloride and one equivalent of the dilithium *meso*-tetra-*p*-tolylporphyrin salt, Li_2(ttp), in refluxing hexane yielded a dark green solid of [Te(ttp)Cl_2] (72% yield). [Te(ttp)Cl_2] is moisture sensitive in solution and decomposes on exposure to air within seconds. However, it is stable in the solid state for weeks at ambient temperature in the dark in an inert atmosphere.

The molecular structure of [Te(ttp)Cl_2][4] is presented in Figure 1. The two molecules are related by a crystallographic inversion center. The tellurium coordination sphere is best described as a square pyramid in which the atoms Cl(1), Cl(2), N(1), and N(3) form the square base of the pyramid and are coplanar to within 0.024 Å. The angles at the Te center from the apical atom to the basal atoms range from 78.27(10) to 89.73(8)°. Three of the porphyrin nitrogen atoms occupy one triangular face of the square pyramid, with the apical Te–N(2) bond length significantly shorter than those of the basal Te–N(1) and Te–N(3) bonds. Five-coordinate Te^{IV} complexes are typically square pyramidal with a short bond to the apical atom. Comparable examples with a $TeCl_2N_3$ coordination sphere are difficult to find, but several closely related $TeCl_3N_2$ complexes show basal Te–Cl bond lengths in the range 2.370–2.563 Å, basal Te–N bond lengths in the range 2.185–2.352 Å, and apical Te–N bond lengths in the range 1.996–2.096 Å.[5] The basal Te–Cl, basal Te–N, and apical Te–N bond lengths observed for [Te(ttp)Cl_2] are consistent with these.

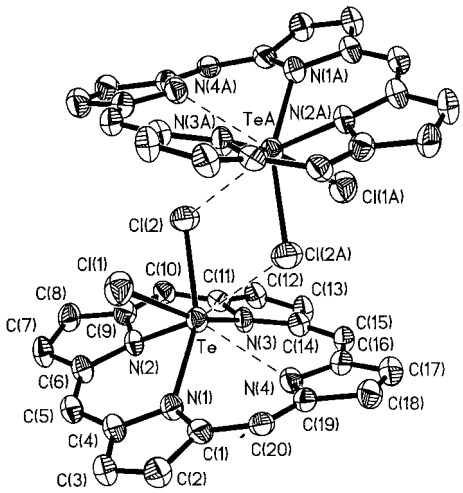


Figure 1. ORTEP plot of [Te(ttp)Cl_2]. The *meso*-tolyl groups and hydrogen atoms are omitted for clarity. Thermal ellipsoids are at the 30% probability level. Selected bond lengths [Å] and angles [°]: Te-N(1) 2.274(3), Te-N(2) 2.094(3), Te-N(3) 2.361(3), Te-N(4) 2.598(3), Te-Cl(1) 2.5108(10), Te-Cl(2) 2.5530(10), Te-Cl(2A) 3.2206(10); N(2)-Te-N(1) 80.53(11), N(2)-Te-N(3) 78.27(10), N(1)-Te-N(3) 118.38(10), N(2)-Te-Cl(1) 89.47(8), N(1)-Te-Cl(1) 78.45(8), N(3)-Te-Cl(1) 156.51(8), N(2)-Te-Cl(2) 89.73(8), N(1)-Te-Cl(2) 157.35(8), N(3)-Te-Cl(2) 78.93(8), Cl(1)-Te-Cl(2) 81.08(4), N(2)-Te-N(4) 122.1(4).

The fourth porphyrin nitrogen atom (N(4)), and a chlorine atom from the symmetry-related molecule (Cl(2A)), are found on the open square face of [Te(ttp)Cl_2] at much longer Te–N and Te–Cl distances. The Te–N(4) separation (2.598(3) Å) considerably exceeds the sum (2.11 Å) of the covalent radii of tellurium and nitrogen atoms but is within the sum of the van der Waals radii (3.61 Å). Similarly, the long Te–Cl(2A) distance is within the sum of the van der Waals radii of Te and Cl atoms (3.81 Å).[6]

The remarkable aspect of the structure of [Te(ttp)Cl_2] is the fact that it adopts five-coordinate geometry with only three coordinated porphyrin nitrogen atoms when the normal situation for [M(Por)X_2] (Por = porphyrin) complexes is six coordination with either *trans* or, less commonly, *cis* geometry.[1] Octahedral, six-coordinate Te^{IV} complexes are well-known, so this geometry is not necessarily precluded. One rationale for the five-coordinate geometry is the VSEPR model for an AX_5E species, in which the Te^{IV} center bears a stereochemically active lone pair of electrons *trans* to the N(2) atom.

Density functional calculations[7] on the [Te(porphyrin)Cl_2] moiety confirm the unusual geometry, with qualitative agreement between the molecular structure observed by X-ray crystallography and the computed structure of the model complex (approximate C_s symmetry). This computed structure also shows square pyramidal geometry with a short apical Te–N bond, tridentate porphyrin coordination, and a long Te–N interaction involving the fourth porphyrin nitrogen atom. A view of the computed structure is given in Figure 2. The principal differences between the molecular structure of [Te(ttp)Cl_2] and the calculated model, [Te(porphyrin)Cl_2], are associated with the porphyrin ring conformation (saddle versus dome) and the effect of the additional weak Te–Cl(2A) interaction from the neighboring complex. A natural bond

[*] Assoc. Prof. P. J. Brothers, Dr. N. Al-Salim, Assoc. Prof. P. D. W. Boyd
Department of Chemistry
University of Auckland
Private Bag 92019, Auckland (New Zealand)
Fax: (+64) 9-373-7599
E-mail: p.brothers@auckland.ac.nz

Assoc. Prof. L. K. Woo, Dr. D. S. Grubisha, Dr. I. A. Guzei
Department of Chemistry
Iowa State University
Ames, IA 50011-3111 (USA)
Fax: (+1) 515-294-0105
E-mail: kwoo@iastate.edu

[**] This work was supported in part by the Research Corporation. ttp = *meso*-tetra-*p*-tolylporphyrin.

 © WILEY-VCH Verlag GmbH, D-69451 Weinheim, 2001 1433-7851/01/4024-4743 $ 17.50+.50/0

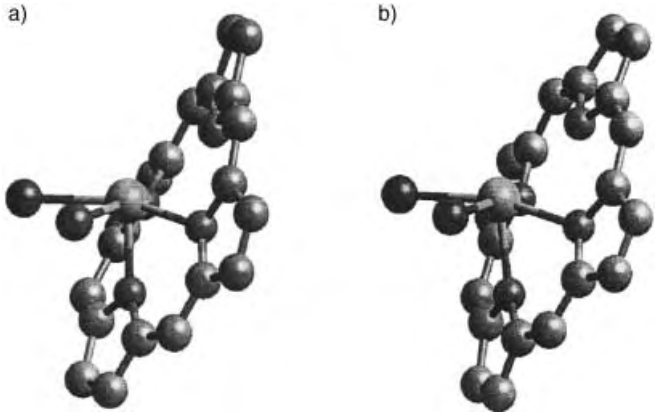


Figure 2. Experimental (a) and calculated (b) [Te(porphyrin)Cl_2] structures. Orientations are arranged to give maximum overlap of the TeN_4Cl_2 atoms in the two structures. The labeling scheme is as for Figure 1. Hydrogen atoms are omitted. Selected bond lengths [Å] and angles [°] in structure (b): Te-N(1) 2.395, Te-N(2) 2.170, Te-N(3) 2.399, Te-N(4) 2.595, Te-Cl(1) 2.515, Te-Cl(2) 2.517; N(2)-Te-N(4) 121.6.

orbital analysis shows the presence of a lone pair of electrons with predominantly *s* character on the tellurium atom.[8]

The ^{1}H NMR spectrum of [Te(ttp)Cl_2] in $CDCl_3$ shows two broad doublets ($\delta = 8.28$ and 8.03) and a doublet of doublets ($\delta = 7.59$) arising from the tolyl protons. These observations indicate that the two faces of the porphyrin macrocycle are chemically different, as expected from the molecular structure. However, the resonances for the β-pyrrole protons ($\delta = 9.20$) and for the tolyl methyl groups ($\delta = 2.72$) both appear as sharp singlets. As a result, the complex has apparent overall C_{4v} symmetry in solution at 25 °C which indicates that the $TeCl_2$ unit must be rapidly migrating around the N_4 porphyrin core. It was not possible to freeze out a static solution structure down to -50 °C.

In summary, the first tellurium porphyrin complex has been prepared. The five-coordinate, square-pyramidal geometry involving only three porphyrin nitrogen atoms represents an unusual bonding mode for the porphyrin ligand.[9] The structure is interesting in light of the relatively poor understanding that exists of the electronic structure and stereochemical effect of the lone pair of electrons in Te^{IV} complexes. Further reactivity studies of [Te(ttp)Cl_2] and a similar complex, [Te(oep)Cl_2] (oep = octaethylporphyrin), are underway.

Experimental Section

A solution of $TeCl_4$ (168 mg, 0.62 mmol) and [Li_2(ttp)(thf)$_2$] (451 mg, 0.52 mmol) in hexane was refluxed for 6 h after which time the dark green suspension was filtered. The residue was recrystallized at -20 °C from a solution of toluene layered with hexane. Filtration yielded microcrystalline green-black [Te(ttp)Cl_2] (325 mg, 72.2 % yield). Elemental analysis calcd for $C_{48}H_{36}Cl_2N_4Te$: C 66.47, H 4.18, N 6.46; found: C 66.68, H 4.72, N 6.36; ^{1}H NMR ($CDCl_3$): $\delta = 9.20$ (s, 8H, β-H), 8.28 (d, 4H, $^3J_{H,H} = 6$ Hz, *meso*-$C_6H_4CH_3$), 8.03 (d, 4H, $^3J_{H,H} = 6$ Hz, *meso*-$C_6H_4CH_3$), 7.59 (dd, 8H, $^3J_{HH} = 6$ Hz, *meso*-$C_6H_4CH_3$), 2.72 (s, 12H, *meso*-$C_6H_4CH_3$); UV/Vis: 458 (Soret), 550, 591, 640 nm.

Received: August 7, 2001 [Z17687]

[1] a) J. K. M. Sanders, N. Bampos, Z. Clyde-Watson, S. L. Darling, J. C. Hawley, H.-J. Kim, C. C. Mak, S. J. Webb in *The Porphyrin Handbook*, *Vol. 3* (Eds.: K. M. Kadish, K. M. Smith, R. Guilard), Academic, San Diego, **1999**, chap. 15; b) R. Guilard, E. Van Caemelbecke, A. Tabard, K. M. Kadish in *The Porphyrin Handbook*, *Vol. 3* (Eds.: K. M. Kadish, K. M. Smith, R. Guilard), Academic, San Diego, **1999**, chap. 21.

[2] P. Sayer, M. Gouterman, C. R. Connell, *Acc. Chem. Res.* **1982**, *15*, 73.

[3] a) W. J. Belcher, M. Breede, P. J. Brothers, C. E. F. Rickard, *Angew. Chem.* **1998**, *110*, 1133; *Angew. Chem. Int. Ed.* **1998**, *37*, 1112; b) W. J. Belcher, P. D. W. Boyd, P. J. Brothers, M. J. Liddell, C. E. F. Rickard, *J. Am. Chem. Soc.* **1994**, *116*, 8416; c) T. Barbour, W. J. Belcher, P. J. Brothers, C. E. F. Rickard, D. C. Ware, *Inorg. Chem.* **1992**, 31, 746; d) J. Chen, L. K. Woo, *Inorg. Chem.* **1998**, *37*, 3269.

[4] Structure determination of **1**: Crystals were obtained from toluene/hexane, $C_{48}H_{36}Cl_2N_4Te$, $M_r = 867.31$, monoclinic, space group $P2_1/n$ (14), $a = 15.1181(9)$, $b = 16.2592(9)$, $c = 19.4662(11)$ Å, $\beta = 109.442(1)$°; $V = 4512.1(4)$ Å^3; $Z = 4$; $\rho_{calcd} = 1.277$ g cm^{-3}; $\mu = 0.813$ mm^{-1}; $F(000) = 1752$. Data collected on a Siemens SMART system at 173(2) K, dark green crystal ($0.42 \times 0.26 \times 0.23$ mm), graphite-monochromated $Mo_{K\alpha}$ radiation ($\lambda = 0.71073$). A total of 28020 reflections ($1.49 < \theta < 26.37$°) were collected; 9180 were considered observed for 500 parameters (final agreement factors: $R = 0.0426$, $R_w = 0.0853$, GOF = 1.007; max/min residual electron density $1.095/-0.529$ e Å^{-3}). The crystal structure was solved and refined using the SHELXTL (version 5.1) program library (G. Sheldrick, Bruker Analytical X-ray Systems, Madison, WI). Direct methods provided most non-hydrogen atoms from the *E* map, while the remaining non-hydrogen atoms were located in an alternating series of full-matrix least-squares cycles and difference Fourier maps. All non-hydrogen atoms were refined with anisotropic displacement parameters. All hydrogen atoms were included in the structure factor calculation at idealized positions and refined as riding atoms with relative isotropic displacement parameters. Several peaks in the electron difference map, attributed to severely disordered solvent molecules, were present in the asymmetric unit. The SQUEEZE filter of the program PLATON (P. van der Sluis, A. L. Spek, *Acta Crystallogr. Sect. A* **1990**, *46*, 194) was used to correct the diffraction data for diffuse scattering effects and to identify the solvate molecules. Approximately 4.6 solvate molecules of toluene and/or hexane were present in the unit. All derived results are based on known contents. No data are given for the diffusely scattering species. Crystallographic data (excluding structure factors) for the structures reported in this paper have been deposited with the Cambridge Crystallographic Data Centre as supplementary publication no. CCDC-168149. Copies of the data can be obtained free of charge on application to CCDC, 12 Union Road, Cambridge CB2 1EZ, UK (fax: (+44) 1223-336-033; e-mail: deposit@ccdc.cam.ac.uk).

[5] a) J. Münzenberg, M. Noltemeyer, H. W. Roesky, *Chem. Ber.* **1989**, *122*, 1915; b) E. Hey, C. Ergezinger, K. Dehnicke, *Z. Naturforsch. B* **1989**, *44*, 205; c) D. K. Kennepohl, H.-G. Schmidt, M. Noltemeyer, H. W. Roesky, *Z. Naturforsch. B* **1992**, *47*, 5; d) T. Chivers, D. D. Doxsee, X. Gao, M. Parvez, *Inorg. Chem.* **1994**, *33*, 5678.

[6] W. W. Porterfield, *Inorganic Chemistry, A Unified Approach*, Addison Wesley, Reading, MA, **1984**.

[7] A full geometry optimization with no symmetry constraints was performed using the Amsterdam density functional program ADF2000.01 (E. J. Baerends, D. E. Ellis, P. Ros, *Chem. Phys.* **1973**, *2*, 41; L. Versluis, T. Ziegler, *J. Chem. Phys.* **1988**, *322*, 88; G. te Velde, E. J. Baerends, *J. Comput. Phys.* **1992**, *99*, 8; C. Fonseca Guerra, J. G. Snijders, G. te Velde, E. J. Baerends, *Theor. Chem. Acc.* **1998**, *99*, 391). Calculations were performed using the LDA description of Vosko, Wilk, and Nusair (S. H. Vosko, L. Wilk, M. Nusair, *Can. J. Phys.* **1980**, *58*, 1200) with gradient corrections of Becke (A. D. Becke, *Phys. Rev. A* **1988**, *38*, 3098) and Lee, Yang, and Parr (C. Lee, C. W. Yang, R. G. Parr, *Phys. Rev. B* **1988**, *37*, 785) for exchange and correlation, respectively. The frozen-core approximation was used. C, H, N, and Cl atoms were described by using a double zeta STO basis with polarization functions and Te atoms by a triple zeta STO basis. Relativistic effects were included by using the ZORA approach (E. van Lenthe, A. E. Ehlers, E. J. Baerends, *J. Chem. Phys.* **1999**, *110*, 8943).

[8] Calculations used the NBO program v3.1 implemented in Gaussian 98 (J. P. Foster, F. Weinhold, *J. Am. Chem. Soc.* **1980**, *102*, 7211; A. E. Reed, F. Weinhold, *J. Chem. Phys.* **1985**, *83*, 1736). A 6-31G* basis was

 © WILEY-VCH Verlag GmbH, D-69451 Weinheim, 2001 1433-7851/01/4024-4744 $ 17.50+.50/0

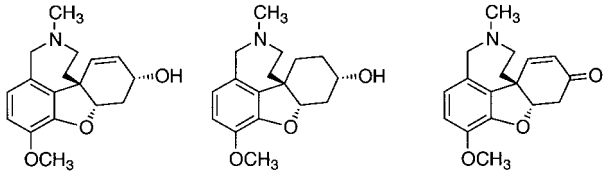
used for C,H,N, and Cl atoms and the SDD pseudopotential and basis was used for Te atoms in the program Gaussian 98. (Gaussian 98 (Revision A.7), M. J. Frisch, G. W. Trucks, H. B. Schlegel, G. E. Scuseria, M. A. Robb, J. R. Cheeseman, V. G. Zakrzewski, J. A. Montgomery, R. E. Stratmann, J. C. Burant, S. Dapprich, J. M. Millam, A. D. Daniels, K. N. Kudin, M. C. Strain, O. Farkas, J. Tomasi, V. Barone, M. Cossi, R. Cammi, B. Mennucci, C. Pomelli, C. Adamo, S. Clifford, J. Ochterski, G. A. Petersson, P. Y. Ayala, Q. Cui, K. Morokuma, D. K. Malick, A. D. Rabuck, K. Raghavachari, J. B. Foresman, J. Cioslowski, J. V. Ortiz, B. B. Stefanov, G. Liu, A. Liashenko, P. Piskorz, I. Komaromi, R. Gomperts, R. L. Martin, D. J. Fox, T. Keith, M. A. Al-Laham, C. Y. Peng, A. Nanayakkara, C. Gonzalez, M. Challacombe, P. M. W. Gill, B. G. Johnson, W. Chen, M. W. Wong, J. L. Andres, M. Head-Gordon, E. S. Replogle, J. A. Pople, Gaussian, Inc., Pittsburgh, PA, **1998**.)

[9] A tridentate porphyrin bonding mode in which the fourth porphyrin nitrogen atom is protonated was proposed for [Re(HTPP)(CO)$_3$] on the basis of its ^{1}H NMR spectrum, but no X-ray crystal structure was obtained: M. Tsutsui, C. P. Hrung, D. Ostfeld, T. S. Srivastava, D. L. Cullen, E. F. Meyer, Jr., *J. Am. Chem. Soc.* **1975**, *97*, 3952.

An Efficient Total Synthesis of (±)-Galanthamine**

Catherine Guillou,* Jean-Luc Beunard, Emmanuel Gras, and Claude Thal*

(−)-Galanthamine (**1**),[1] a tertiary alkaloid isolated from *Amaryllidaceae*, is a centrally acting, competitive, and reversible inhibitor of acetylcholinesterase which enhances cognitive functions in Alzheimer's patients.[2] This drug is available



1 (−)-galanthamine **2** (−)-lycoramine **3** (−)-narwedine

in Austria, and is the most recently approved acetylcholinesterase inhibitor for use in the United States and Europe. However, the botanical supplies of **1** are insufficient for its clinical uses.[3] Galanthamine (**1**) has a spiro quaternary carbon atom. Establishment of this quaternary center is the critical element in the total synthesis of galanthamine-type alkaloids. Most of the reported syntheses of **1** are based on a biomimetic intramolecular phenolic oxidative coupling.[4]

[*] Dr. C. Guillou, Dr. C. Thal, J.-L. Beunard, Dr. E. Gras
Institut de Chimie des Substances Naturelles, CNRS
Avenue de la Terrasse, Gif-sur-Yvette (France)
Fax: (+33) 1-69-07-72-47
E-mail: guillou@icsn.cnrs-gif.fr

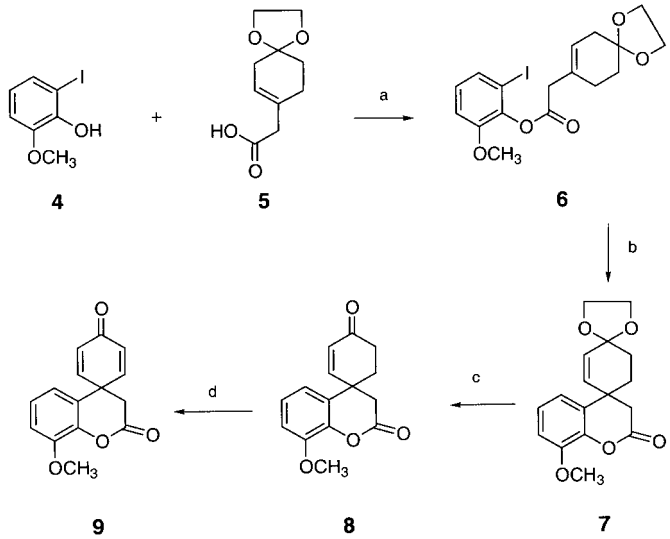
[**] We are grateful to the CNRS for financial support, and the French Ministry of Education and Research for Ph.D grants to J.L.B. and E.G. Professor P. Potier is gratefully acknowledged for his interest in our work.

Supporting information for this article is available on the WWW under http://www.angewandte.com or from the author.

We previously reported the use of an intramolecular Heck reaction as an alternative for creating the spiro quaternary carbon atom of galanthamine-type alkaloids. A formal synthesis of lycoramine (1,2-dihydrogalanthamine; **2**) was thus achieved.[5] Since then, the Heck reaction has been used to access 3-deoxygalanthamine.[6] However, many chemical transformations were required to introduce the allylic alcohol group,[6b] which is essential for anticholinesterase activity. The best total synthesis of galanthamine was achieved in 15 steps with an overall yield of only 1 %.[6b]

An efficient synthesis of (−)-galanthamine (**1**) could be facilitated by a short and efficient synthesis of (±)-narwedine (**3**) or derivatives thereof (e.g., (±)-oxonarwedine (**11**), Scheme 2), since the transformation of (±)-narwedine into its (−) enantiomer has been shown to proceed in high yield.[7] Moreover, (±)-narwedine may be resolved by means of dynamic diastereoisomeric salt formation with di-*p*-toluoyl-D-tartaric acid.[8]

Here we report on an efficient route to (±)-galanthamine (**1**) based on the synthesis of (±)-oxonarwedine (**11**). Our strategy was to form the C12a–C12b bond by an intramolecular Heck reaction to access the spiro tricyclic dienone **9**, which could then be used as a valuable synthetic precursor of **1** and eventually narwedine (**3**). A short synthesis of **9** is summarized in Scheme 1. Esterification of acid **5** with 2-iodo-6-methoxyphenol (**4**)[9] furnished the ester **6** in 80 % yield.



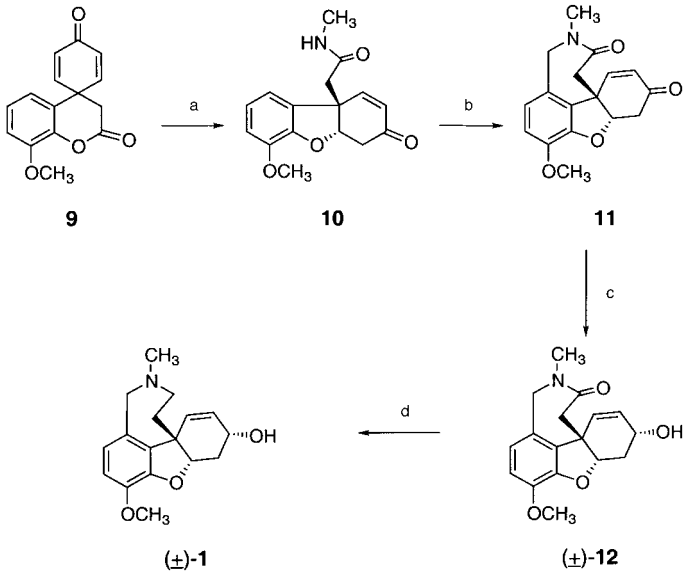
Scheme 1. a) EDCI, DMAP, CH_2Cl_2, 0 → 20 °C, 5 h, 80 %; b) [$Pd_2(dba)_3$], dppe, TlOAC, CH_3CN, reflux, 3 d, 67 %; c) Ph_3CBF_4, CH_2Cl_2, 20 °C, 1 h, 100 %; d) 4 Å molecular sieves, $(PhSeO)_2O$, CH_2Cl_2, reflux, 20 h, 50 %. dba = *trans,trans*-dibenzylideneacetone, DMAP = 4-dimethylaminopyridine, dppe = 1,2-bis(diphenylphosphanyl)ethane, EDCI = *N*′-(3-dimethylaminopropyl)-*N*-ethylcarbodiimide.

Heck cyclization of **6** was accomplished in 65 % yield in the presence of 10 % [$Pd_2(dba)_3$], 20 % dppe, and thallium acetate (1.2 equiv) in acetonitrile. The dioxolane group of **7** was deprotected with triphenylcarbenium tetrafluoroborate to give **8** in quantitative yield. The oxidation of the α,β-unsaturated ketone **8** to the corresponding dienone **9** proved difficult. Previous attempts to achieve this transformation

 © WILEY-VCH Verlag GmbH, D-69451 Weinheim, 2001 1433-7851/01/4024-4745 $ 17.50+.50/0

with an excess of $(PhSeO)_2O$ or 2,3-dichloro-5,6-dicyano-1,4-benzoquinone were unsuccessful.[10] Moreover, it was not possible to introduce a halogen atom α to the ketone group or to prepare the corresponding enol ether in order to obtain the required dienone **9**. We found that the transformation of **8** to **9** can be accomplished by nonclassical oxidation. The dienone **9** was obtained in 50% yield by using $(PhSeO)_2O$ in the presence of 4 Å molecular sieves. A 1/1 mixture of alumina and silica could also be used instead of the molecular sieves. These oxidative systems have not been previously described.

The reaction of **9** with 40% aqueous methylamine at room temperature resulted in the spontaneous Michael addition of the resulting phenol to cyclohexadienone to afford amide **10** in quantitative yield. Compound **10** was cyclized by the action of paraformaldehyde and trifluoroacetic acid to give **11** in 63% yield. Enone **11** was reduced with L-Selectride to give alcohol **12** in 93% yield. Finally, reduction of **12** with $LiAlH_4$ in DME afforded (±)-galanthamine (**1**) in 80% yield (Scheme 2).



Scheme 2. a) 40% $MeNH_2$, THF, 20 °C, 20 min, 100%; b) $(CH_2O)_n$, TFA, $Cl(CH_2)_2Cl$, 60 °C, 20 h, 63%; c) L-Selectride, THF, −78 °C, 1 h, 93%; d) $LiAlH_4$, DME, 50 °C, 12 h, 80%. DME = 1,2-dimethoxyethane, TFA = trifluoroacetic acid.

Thus, (±)-galanthamine was synthesized in eight steps with an overall yield of 12%. This is the shortest and most efficient nonbiomimetic total synthesis of (±)-galanthamine to date. An intramolecular Heck reaction followed by a nonclassical dehydrogenation reaction provided the key intermediate spirocyclohexadienone **9**. Syntheses of compounds related to galanthamine and narwedine (**3**) are in progress.

Received: July 3, 2001 [Z17414]

[1] For reviews, see a) O. Hoshino in *The Alkaloids*, *Vol. 51* (Ed.: G. A Cordell), Academic Press, New York, **1998**, pp. 323–424; b) S. F. Martin in *The Alkaloids*, *Vol. 30* (Ed.: A. Brossi), Academic Press, New York, **1987**, pp. 251–376.

[2] a) U. Thatte, *Curr. Opin. CPNS Invest. Drugs* **1999**, *1*, 357–372; b) M. Weinstock, *CNS Drugs* **1999**, *12*, 307–323; c) A. Nordberg, A. L. Svensson, *Drug Saf.* **1998**, *19*, 465–480; d) K. Unni, *CNS Drugs* **1998**, *10*, 447–460.

[3] a) V. V. Mikhno, *Farm. Zh. (Kiev)* **1966**, *21*, 28–29; b) J. Batisda, F. Viladomat, J. M. Llabres, S. Quiroga, C. Codina, M. Rubiralta, *Planta Med.* **1990**, *56*, 123–124; c) T. Hille, H. R. Hoffmann, M. Kreh, R. Matusch, DE 19,509,663 Lts, Lohmann Thérapie système; *Chem. Abstr.* **1996**, *125*, 230784.

[4] a) D. Krikorian, V. Tarpanov, S. Parushev, P. Mechkarova, *Synth. Commun.* **2000**, *30*, 2833–2846; b) B. Küenburg, L. Czollner, J. Fröhlich, *Org. Process Res. Dev.* **1999**, *3*, 425–431; c) Y. Kita, M. Arisawa, M. Gyoten, M. Nakajima, R. Hamada, H. Tohma, T. Takada, *J. Org. Chem.* **1998**, *63*, 6625–6633; d) L. Czollner, W. Frantsits, B. Küenberg, U. Hedenig, J. Fröhlich, U. Jordis, *Tetrahedron Lett.* **1998**, *39*, 2087–2088; e) D. A. Chaplin, N. Fraser, P. D. Tiffin, *Tetrahedron Lett.* **1997**, *38*, 7931–7932; f) J. Szewczyk, J. W. Wilson, A. H. Lewin, F. I. Caroll, *J. Heterocycl. Chem.* **1995**, *32*, 195–199; e) R. Vlahov, D. Krikorian, G. Spassov, M. Chinova, F. Vlahov, S. Parushev, G. Snatzke, L. Ernst, K. Klieslich, W. R. Abraham, W. S. Sheldrick, *Tetrahedron* **1989**, *45*, 3329–3345; f) K. Shimizu, K. Tomioka, S. I. Yamada, K. Koga, *Chem. Pharm. Bull.* **1978**, *26*, 3765–3771; g) K. Shimizu, K. Tomioka, S. I. Yamada, K. Koga, *Heterocycles* **1977**, *8*, 277–281; h) D. H. R. Barton, G. W. Kirby, *J. Chem. Soc.* **1962**, 806–817; i) M. Node, S. Kodama, Y. Hamashima, T. Baba, N. Hamamichi, K. Nishide, *Angew. Chem.* **2001**, *113*, 3150–3152; *Angew. Chem. Int. Ed.* **2001**, *40*, 3060–3062.

[5] E. Gras, C. Guillou, C. Thal, *Tetrahedron Lett.* **1999**, *40*, 9243–9244.

[6] a) P. J. Parsons, M. D. Charles, D. M. Harvey, L. R. Sumoreeah, A. Shell, G. Spoors, A. L. Gill, S. Smith, *Tetrahedron Lett.* **2001**, *42*, 2209–2211; b) B. M. Trost, F. D. Toste, *J. Am. Chem. Soc.* **2000**, *122*, 11262–11263; c) C. Pilger, B. Westermann, U. Flörke, G. Fels, *Synlett* **2000**, *8*, 1163–1165.

[7] W. C. Shieh, J. A. Carlson, *J. Org. Chem.* **1994**, *59*, 5463–5465.

[8] D. A. Chaplin, N. B. Johnson, J. M. Paul, G. A. Potter, *Tetrahedron Lett.* **1998**, *39*, 6777–6780.

[9] C. Y. Chen, J. P. Liou, M. J. Lee, *Tetrahedron Lett.* **1997**, *38*, 4571–4574.

[10] M. Ishizaki, K. Ozaki, A. Kanmatsu, T. Isoda, O. Hoshino, *J. Org. Chem.* **1993**, *58*, 3877–3885.

Trimerization of a Steroid Ketone To Form a Chiral Molecular Cleft**

Robert A. Pascal, Jr.,* Mary S. Mathai, Xianfeng Shen, and Douglas M. Ho

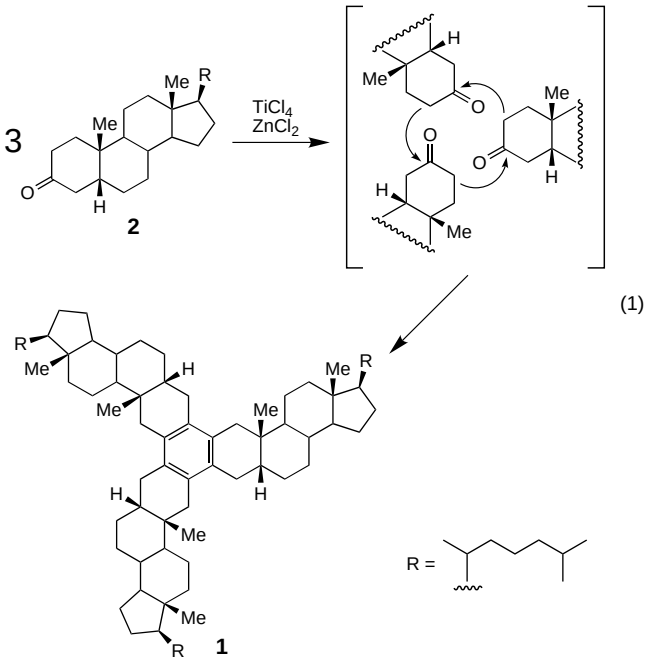
The acid-catalyzed trimerization of cyclic ketones to give hexasubstituted benzenes has long been known, and various acid catalysts have been employed for this transformation.[1] Unlike the trimerization of alkynes, this triple aldol condensation is inherently directional, and, if an enantiomerically pure starting ketone is used, then only a single, enantiomerically pure, C_3-symmetric product will be obtained. We now show that the trimerization of steroid ketones with *cis* A/B ring fusions yields a new class of chiral molecular bowls.

[*] Prof. R. A. Pascal, Jr., Dr. M. S. Mathai, X. Shen, Dr. D. M. Ho
Department of Chemistry
Princeton University
Princeton, NJ 08544 (USA)
Fax: (+1) 609-2586746
E-mail: snake@chemvax.princeton.edu

[**] This work was supported by a National Science Foundation Grant (CHE-0077990).

 © WILEY-VCH Verlag GmbH, D-69451 Weinheim, 2001 1433-7851/01/4024-4746 $ 17.50+.50/0

Molecular mechanics calculations (MMFF[2, 3]) indicate that trimers of *trans* A/B steroids are relatively flat molecules, but trimers derived from *cis* A/B steroids, such as **1**, should



(1)

contain deep, chiral clefts. The one-step synthesis of a new class of chiral bowls was a very attractive prospect, but all attempts to trimerize steroid ketones by using H_2SO_4, HCl/HOAc, $SiCl_4$, and polyphosphoric acid as catalysts were unsuccessful. However, when coprostanone (**2**, 5β-cholestan-3-one) was heated with $TiCl_4$ and $ZnCl_2$ in hexanes, the trimer **1** was obtained in 31% yield [Eq. (1)]. This material was easily purified, and its C_3 symmetry was unambiguously established by its 27-line ^{13}C NMR spectrum. Similar reactions of 5α-cholestan-3-one and 5β-androstan-3-one gave the corresponding steroid trimers in 66% and 29% yields, respectively (data not shown).[4]

Trimer **1** is a remarkable hydrocarbon. Crystals of **1** suitable for X-ray analysis[5] were obtained from $CHCl_3$/EtOH, and the molecular structure of one of the two crystallographically independent molecules is shown in Figure 1. As expected, the B, C, and D rings of the tri-steroid core of **1** define a C_3-symmetric cavity above its aromatic base. This cavity is further extended by the steroid side chains, and it has an overall depth of around 14 Å. The strongly slanting walls of the C_3-symmetric cleft make it impossible to assign a single value to its width, but, for example, the C1 – C64 distance is 5.8 Å (see Figure 1, right). When van der Waals radii are taken into account, the cavity appears to be large enough to accommodate a small alkane guest, although no guest molecule was observed in the crystal.

The experimental structure of compound **1** is significantly more compact than predicted by gas-phase calculations as can be seen from Figure 2. The tight packing of compound **1** in the crystal may explain the difference between the calculated and observed structures. The molecules form columnar dimers

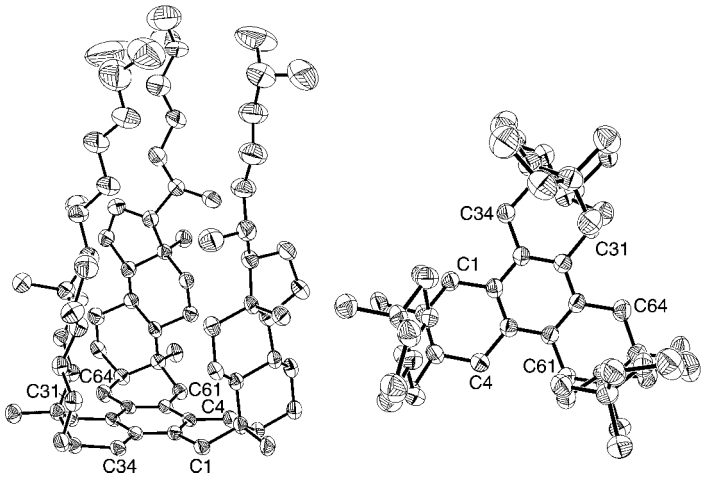


Figure 1. Two views of the molecular structure of one of the two crystallographically independent molecules of compound **1**. Thermal ellipsoids are drawn at the 40% probability level, hydrogen atoms have been omitted for clarity, and in the right structure the steroid side chains have been omitted.

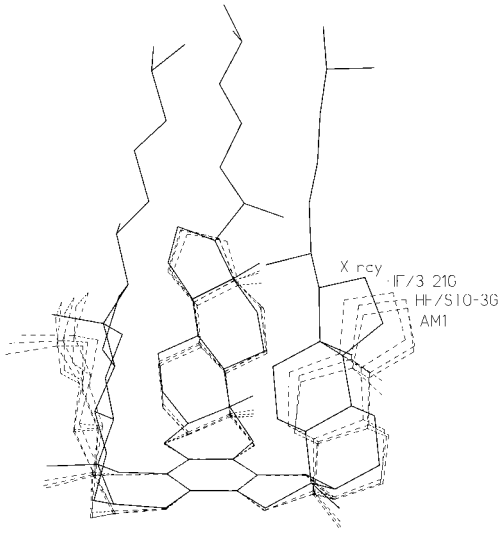


Figure 2. Superposition of the X-ray structure of **1** and the structures of its tri-steroid core calculated by three different computational methods (AM1[9] and low-level ab initio methods[10]).

through interacting side chains, and these dimers stack side by side to form the layered structure illustrated in Figure 3. If nothing else, these results suggest that the relatively rigid cavity in **1** may be able to flex enough to accommodate guest molecules of varying sizes.

It has been argued[11, 12] that the ideal enantioselective host molecule should contain a chiral cavity, strongly complementary to only one enantiomer of the chiral guest, and it should possess a single, clearly defined, minimum energy conformation. Practical applications require that the host should be preparable from readily available starting materials by way of a short, simple synthesis. Compound **1** is the first example of a new class of molecules that may meet these criteria. The C_3-symmetric ground state conformation of its tri-steroid nucleus (ignoring the flexible side chains) is more than 5 kcal mol^{-1} below the next most stable conformation (MMFF), thus the

 © WILEY-VCH Verlag GmbH, D-69451 Weinheim, 2001 1433-7851/01/4024-4747 $ 17.50+.50/0

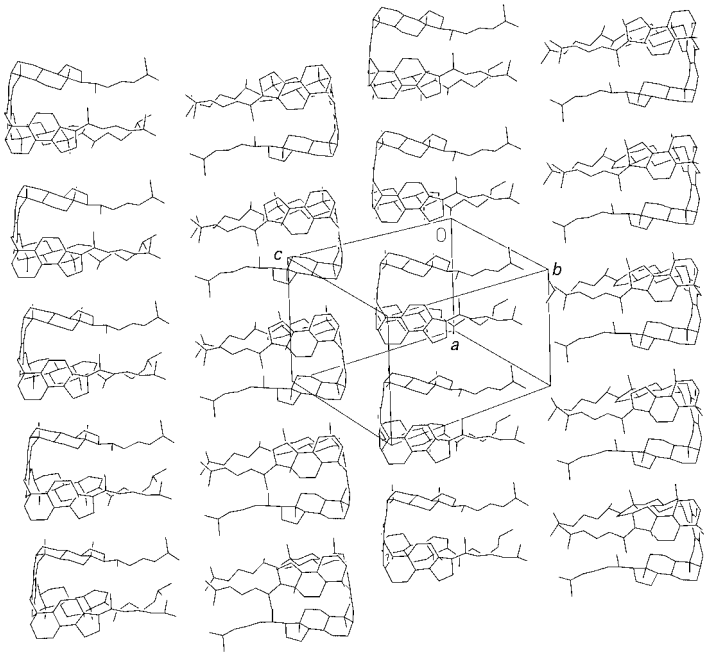


Figure 3. Crystal packing diagram showing one layer of molecules of **1**.

tri-steroid may be considered to be "conformationally homogeneous".[12] Furthermore, the facile synthesis of **1** suggests that similar compounds could be prepared from a variety of naturally occuring ketones, and such trimers may prove to be good frameworks for the construction of new chiral auxilliaries or enantioselective hosts.

Experimental Section

Preparation of **1**: Ketone **2** (468 mg, 1.21 mmol) was dissolved in hexanes (15 mL) in a screw-capped tube. Anhydrous $ZnCl_2$ (165 mg, 1.21 mmol) and $TiCl_4$ (1.21 mL of a 1M solution in CH_2Cl_2) were added to give a light yellow mixture. The tube was placed in an oil bath, heated to 120 °C, and left overnight. After cooling, water was added, and the resulting mixture was extracted twice with CH_2Cl_2. The combined organic layers were washed four times with water, dried over Na_2SO_4, and concentrated to leave a light yellow solid (400 mg). Fractionation of this material by silica gel column chromatography (45:1 hexanes:EtOAc) gave trimer **1** as a white crystalline solid (140 mg, 0.127 mmol, 31 % yield). Melting behavior: 175 °C, begins to darken and shrink; 270 °C, fully melted with decomposition. ^{1}H NMR (500 MHz, $CDCl_3$): $\delta = 0.66$ (s, 9H), 0.849 (d, $J = 7$ Hz, 9H), 0.852 (d, $J = 7$ Hz, 9H), 0.87 (d, $J = 6$ Hz, 9H), 1.12 (s, 9H), 0.9–2.1 (methylene envelope, ca. 80H), 2.49 (dd, $J = 16$ Hz, 7 Hz, 3H), 2.82 (m, 6H); ^{13}C NMR (125.8 MHz, $CDCl_3$): $\delta = 12.2$, 19.0, 21.9, 22.8, 23.0, 23.3, 24.5, 25.1, 26.3, 26.5, 28.2, 28.3, 28.7, 28.9, 34.5, 35.4, 36.6, 38.2, 39.6, 39.8, 40.4, 41.2, 43.0, 56.8, 57.2, 130.4, 131.0 (27 of 27 expected resonances); FAB MS: m/z (%): 1105 (M^+ [$^{12}C_{80}{}^{13}C_1$], 100); $[\alpha]_D^{25} = +45$ ($c = 1$ in $CHCl_3$);[13, 14] UV (cyclohexane): λ_{max} (ε) = 300 (300, sh), 284 (460, sh), 276 (490), 254 (490, sh), 230 (2100, sh), 216 nm (2800); CD (cyclohexane): $[\theta]_{300} = +520$, $[\theta]_{286} = +630$, $[\theta]_{275} = +540$; CD (heptane): $[\theta]_{299} = +500$, $[\theta]_{286} = +620$, $[\theta]_{275} = +500$.

Received: July 30, 2001 [Z17637]

[1] Typical examples of such trimerizations include the following (with the catalyst in parentheses): a) C. Mannich, *Ber. Dtsch. Chem. Ges.* **1907**, *40*, 153–158 (H_2SO_4); b) R. Seka, W. Kellermann, *Ber. Dtsch. Chem. Ges.* **1942**, *75*, 1730–1738 ($ZnCl_2$/HOAc); c) S. S. Elmorsy, A. Pelter, K. Smith, *Tetrahedron Lett.* **1991**, *32*, 4175–4176 ($SiCl_4$/EtOH); d) A. N. Pyrko, *Zh. Org. Khim.* **1992**, *28*, 215–216 ($TiCl_4$); e) R. B. M. Ansems, L. T. Scott, *J. Am. Chem. Soc.* **2000**, *122*, 2719–2724 ($TiCl_4$).

[2] T. A. Halgren, *J. Comput. Chem.* **1996**, *17*, 490–519.

[3] Molecular mechanics, semiempirical, and ab initio calculations were performed by using the SPARTAN program package (Version 5.0; Wavefunction, Inc., Irvine, CA, USA).

[4] M. S. Mathai, PhD thesis, Princeton University (USA), **1994**.

[5] X-ray crystal structure determination for **1**: Formula $C_{81}H_{132}$, $M = 1105.87$, crystal size $0.33 \times 0.23 \times 0.15$ mm, triclinic, $P1$, $a = 11.6885(2)$, $b = 13.2846(3)$, $c = 24.5806(6)$ Å, $\alpha = 87.117(1)$, $\beta = 84.528(1)$, $\gamma = 68.063(1)^\circ$, $V = 3523.9(1)$ Å^3, $Z = 2$, $\rho_{calcd} = 1.042$ Mg m^{-3}, $Mo_{K\alpha}$ radiation ($\lambda = 0.71073$ Å), $2\theta_{max} = 45.1^\circ$, $T = 200(2)$ K, Nonius Kappa CCD diffractometer. A total of 44081 reflections were indexed, integrated, and corrected for Lorentz and polarization effects by using DENZO-SMN and SCALEPACK.[6] Data reduction gave 18424 unique reflections ($R_{int} = 0.053$), of which 13497 had $I > 2\sigma(I)$. The structure was solved by the direct methods program CRUNCH,[7] and it was refined by full-matrix least-squares on F^2 using SHELXTL.[8] All carbon atoms were refined with anisotropic displacement coefficients, and hydrogens were included with a riding model and isotropic displacement coefficients [U(H) = 1.2U(C) or 1.5U(C_{methyl})]. Moderate disorder in two of the steroid side chains warranted the inclusion of a disorder model and some restraints. $R(F) = 0.059$, $wR(F^2) = 0.131$, and $S = 1.07$ for the 13497 reflections with $I > 2\sigma(I)$, and $R(F) = 0.091$, $wR(F^2) = 0.148$, and $S = 1.02$ for all unique reflections, 1522 parameters, and 55 restraints. The residual electron density ranged from -0.16 to 0.35 e A^{-3}. Crystallographic data (excluding structure factors) for the structure reported in this paper have been deposited with the Cambridge Crystallographic Data Centre as supplementary publication no. CCDC-163715. Copies of the data can be obtained free of charge on application to CCDC, 12 Union Road, Cambridge CB2 1EZ, UK (fax: (+44) 1223-336-033; e-mail: deposit@ccdc.cam.ac.uk).

[6] Z. Otwinowski, W. Minor, *Methods Enzymol.* **1997**, *276*, 307–326.

[7] R. de Gelder, R. A. G. de Graaf, H. Schenk, *Acta Crystallogr. Sect. A* **1993**, *49*, 287–293.

[8] G. M. Sheldrick, *SHELXTL* Version 5, Siemens Analytical X-ray Instruments, Madison, WI, USA, **1996**.

[9] M. J. S. Dewar, E. G. Zoebisch, E. F. Healy, J. J. P. Stewart, *J. Am. Chem. Soc.* **1985**, *107*, 3902–3909.

[10] W. J. Hehre, L. Radom, P. von R. Schleyer, J. A. Pople, *Ab Initio Molecular Orbital Theory*, Wiley, New York, **1986**, pp. 63–100.

[11] D. J. Cram, *Angew. Chem.* **1988**, *100*, 1041–1052; *Angew. Chem. Int. Ed. Engl.* **1988**, *27*, 1009–1020.

[12] a) X. Wang, S. D. Erickson, T. Iimori, W. C. Still, *J. Am. Chem. Soc.* **1992**, *114*, 4129–4137; b) J.-I. Hong, S. K. Namgoong, A. Bernardi, W. C. Still, *J. Am. Chem. Soc.* **1991**, *113*, 5111–5112; c) G. Li, W. C. Still, *J. Am. Chem. Soc.* **1993**, *115*, 3804–3805.

[13] We thank Natasha Kagan for determining the specific rotation.

[14] For comparison, the specific rotations of coprostanone and coprostane are +36 and +25, respectively, in $CHCl_3$ (L. F. Fieser, M. Fieser, *Steroids*, Reinhold, New York, **1959**, p. 28).

 © WILEY-VCH Verlag GmbH, D-69451 Weinheim, 2001 1433-7851/01/4024-4748 $ 17.50+.50/0

Recognition and Stabilization of Quadruplex DNA by a Potent New Telomerase Inhibitor: NMR Studies of the 2:1 Complex of a Pentacyclic Methylacridinium Cation with $d(TTAGGGT)_4$**

Evripidis Gavathiotis, Robert A. Heald, Malcolm F. G. Stevens, and Mark S. Searle*

Telomerase is a cellular ribonucleoprotein, consisting of a reverse transcriptase and an endogenous RNA template, that maintains telomere length at the ends of eukaryotic chromosomes.[1] Telomeres consist of double-stranded DNA composed of tandem repeats of guanine-rich sequences (5′-TTAGGG in humans) with a single-stranded 3′-end overhang necessary to ensure complete chromosomal DNA replication, while protecting the chromosome ends from fusion and degradation.[1, 2] The telomeres shorten with each round of cell division, due to incomplete lagging-strand replication, limiting the number of replicative cycles before the cell enters a state of senescence.[3] Telomere length in immortalized cells (e.g. cancer cells) is tightly regulated by the enzyme telomerase whose reverse transcriptase activity allows the addition of 5′-TTAGGG repeats to maintain telomere length through an indefinite number of cell divisions.[4] While telomerase activity is absent in human somatic cells it is detected in the majority of human tumor-derived cell lines. Consequently, telomerase has become a high-profile target for anticancer drug design.[5]

The discovery that the G-rich telomeric repeats are able to assemble into novel four-stranded quadruplex structures, consisting of guanine tetrads stabilized by monovalent cations (Na^+ and K^+) (Figure 1),[6] has focused attention for structure-specific drug design. Since telomerase reverse transcriptase activity depends on a single-stranded DNA primer,[4] small molecules that bind and stabilize the folded quadruplex form of the primer are potential inhibitors of telomerase function. A number of quadruplex-specific ligands have been reported with the common feature of an extended aromatic ring system capable of interacting through extensive π stacking with G-tetrads.[5] However, there has been a paucity of detailed structural data available on the drug–DNA complexes due to intractable NMR spectra arising from extensive drug-induced line broadening.[7] The exception is a dicationic perylene-tetracarboxylic diimide derivative (PIPER), which forms either a sandwich complex bound between the blunt ends of a quadruplex dimer formed from $d(TTAGGG)_4$, or

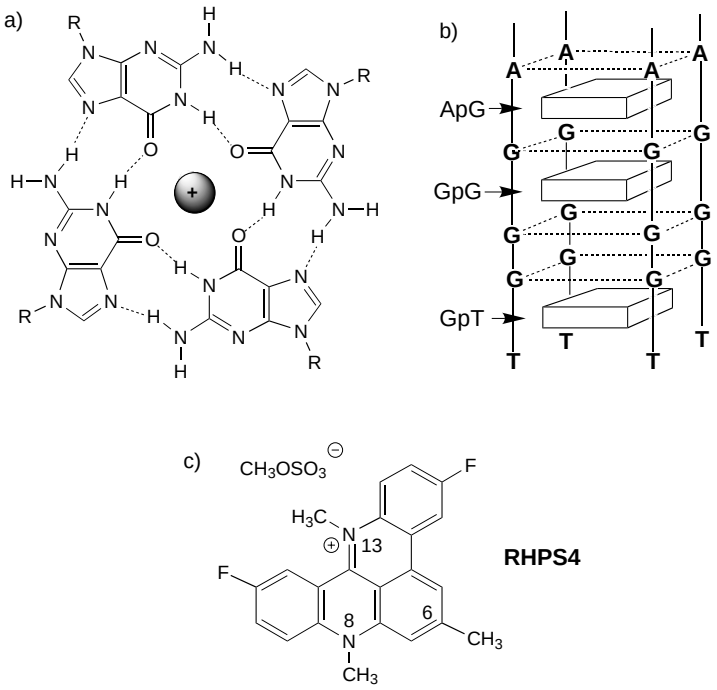


Figure 1. a) Structure of the G-tetrad showing complexation with K^+. b) Schematic of the intermolecular quadruplex showing potential sites of intercalation at ApG, GpG, and GpT sites. c) Structure of **RHPS4**.

intercalates by end-stacking at the GpT step of $d(TAGGGTTA)_4$.[8]

Here we describe the interaction and stabilization of quadruplex DNA by a novel fluorinated polycyclic methylacridinium salt (**RHPS4**; Figure 1c), which shows enhanced binding to higher ordered DNA structures (triplex/quadruplex) over duplex and single-stranded DNA as measured by differential dialysis.[9a,b] **RHPS4** has been shown to inhibit telomerase with an IC_{50} value of 0.33 μM, while decreasing tumor cell proliferation of breast 21NT cells at concentrations as low as 200 nM.[9c,d] **RHPS4** is weakly cytotoxic (mean GI_{50} value in the NCI 60 human tumor cell panel is 13.18 μM), giving a therapeutic index (GI_{50}/IC_{50}) of 40.[9a] This activity does not appear to be associated with Taq polymerase and topoisomerase II inhibition, strongly suggesting that **RHPS4** is an inhibitor of telomerase function. To investigate structural details of the drug–quadruplex interaction we have carried out ^1H NMR spectroscopic studies on the **RHPS4** complex with the intermolecular parallel-stranded quadruplex $d(TTAGGGT)_4$, formed from the human telomeric repeat (Figure 1).

1D and 2D NMR spectra of $d(TTAGGGT)_4$ are extremely well-resolved.[10] The NMR data show that the structure is highly symmetrical with all four strands equivalent.[11] Three imino proton resonances are observed between $\delta = 11-12$, each signal representing equivalent guanine bases within a given tetrad (Figure 2a). We see no resonances attributable to thymine imino protons, which precludes the formation of stable T-tetrads. The pattern and intensity of internucleotide NOEs within the G4G5G6 region is consistent with the results of previous studies of intermolecular quadruplexes, which showed strong base stacking between adjacent G-tetrads. We

[*] Dr. M. S. Searle, E. Gavathiotis
School of Chemistry
University Park, Nottingham NG7 2RD (UK)
Fax: (+44) 115-951-3564
E-mail: mark.searle@nottingham.ac.uk
R. A. Heald, Prof. M. F. G. Stevens
Cancer Research Laboratories
School of Pharmaceutical Sciences
University Park, Nottingham NG7 2RD (UK)

[**] We thank the EPSRC of the UK and AstraZeneca for financial support to E.G. M.F.G.S. and R.A.H. are supported by the Cancer Research Campaign of the UK.

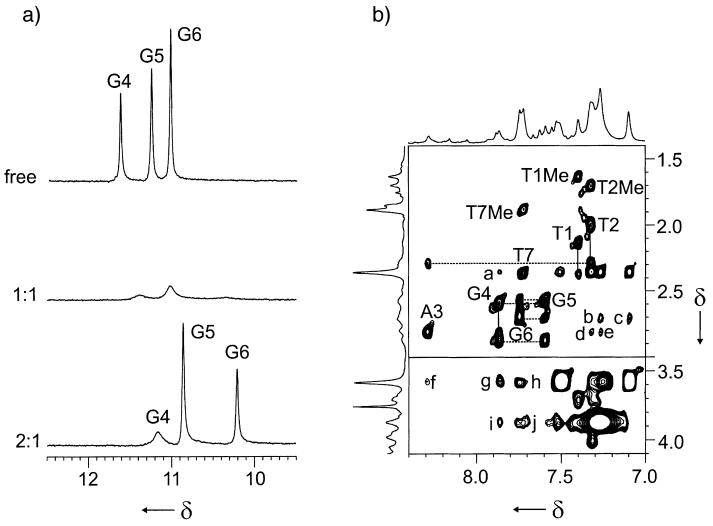


Figure 2. a) 1D ^{1}H NMR data recorded in 90% H_2O solution showing the guanine imino proton resonances for G4, G5, and G6 in d(TTAGGGT)$_4$ (free), the 1:1 complex with **RHPS4**, and the 2:1 complex all at 303 K. b) Portion of the 250 ms NOESY spectrum of the 2:1 complex recorded at 318 K highlighting a number of key NOEs. In the top panel, NOEs labeled T1 through to T7 represent intranucleotide base H6 or H8 to deoxyribose H2′/H2″. Dashed horizontal lines highlight internucleotide NOE connectivities. Thymine methyl to H6 NOEs are also assigned. Key drug–DNA NOEs are labeled as follows: a) 6-Me to G4H8, b) H7 to G6H2′/H2″, c) H5 to G6H2′/H2″, d) H1 or H12 to A3H2′/H2″, e) H7 to A3H2′/H2″, lower panel; f) 8-Me to A3H8, g) 8-Me to G4H8, h) 8-Me to G6H8, i) 13-Me to G4H8, and j) 13-Me to G6H8/T7Me.

observe a number of additional NOEs at the A3–G4 step (G4NH to A3H8 and A3H2) that indicate good stacking interactions between the two sets of purine bases. Further, the amino proton of A3 (A3-NH_2) is readily resolved at $\delta = 7.1$ and exhibits strong NOEs to G4NH and A3H2. The A3-$NH_2 \leftrightarrow$ A3H2 NOE is not expected to arise as an intranucleotide NOE but is consistent with an interaction between adenine bases within an A-tetrad. Quantitative NOE measurements involving sugar H1′ ↔ base H6/H8 confirm that all glycosidic bonds are *anti* including that of A3. This contrasts with the data of Hosur et al. for d(AGGGT)$_4$ where the adenines were shown to form an A-tetrad with the purines in the *syn* conformation, while the T and A residues of d(TAGGGT)$_4$ appeared to have a more flexible conformation resulting in poor stacking interactions.[12] Our data reveal that the A3-NH_2 signal persists at high temperature and shows similar stability to the guanine imino protons. Thus, additional thymines on the 5′-end appear to have a significant effect in stabilizing and modulating nucleotide conformation and base stacking interactions. We have calculated a high-resolution structure of d(TTAGGGT)$_4$ using an NOE-restrained MD protocol with an explicit solvation model.[13] Thus, this initial structure provides a starting point for studies of drug–quadruplex interactions.

Titration of **RHPS4** into d(TTAGGGT)$_4$ results in significant line broadening which we attribute to intermediate exchange of the drug between a number of possible bound conformations and/or a number of sites of similar affinity. The three guanine imino protons are seen to broaden considerably at a drug/quadruplex ratio of 1:1 (Figure 2a). Titrating drug beyond this point up to a 2:1 ratio produces a new set of resonances that are sharper and appreciably shifted by up to 0.8 ppm. Although the imino proton of G4 remains exchange broadened at 298 K, suggestive of drug mobility within the ligand binding site, this resonance sharpens appreciably above 318 K. The spectra were generally of superior quality at higher temperatures where the drug appears to be in fast exchange between binding sites and different bound conformations. The effect of the ligand on quadruplex stability is clearly evident from the intensity of the guanine imino proton resonances which disappear when the free quadruplex is fully melted at 333 K. However, these resonances are still visible in the 2:1 drug complex at temperatures up to 353 K. NOESY data collected at 318 K show the quadruplex structure to be fully formed with full retention of the fourfold symmetry and a largely similar pattern of sequential connectivities along the DNA backbone. Chemical shift analysis shows the thymines T1 and T2 to be unperturbed by ligand binding, however, the base H6 and CH_3 of T7 shift by 0.2–0.35 ppm. The data show that binding affects the A3G4 and G6T7 segments primarily, particularly G4 and G6. Many internucleotide NOEs between G4 and G5, and G5 and G6 indicate that the integrity of the stack of G-tetrads is preserved (Figure 2b). At the A3–G4 step the internucleotide NOEs are weaker but still evident.

Drug resonances are readily assigned from a combination of TOCSY and NOESY data and allow a number of drug–quadruplex interactions to be identified that pinpoint the drug binding sites (Figure 2b). By far the largest number of intermolecular NOEs involve G4 and G6, while none are attributed to G5 at the center of the stack of G-tetrads. NOEs are detected to both purine nucleotides at the A3–G4 site, indicating that the ApG step is a primary intercalation site. A number of NOEs to G6 show that the drug also inserts at the G6–T7 step; however, very few NOEs are observed to T7 despite the perturbations to its chemical shifts. Two very strong NOEs from the drug 8-CH_3 to G4NH and G6NH show that the drug is stacking primarily with the G-tetrads with many other drug–DNA NOEs involving base and sugar protons positioning the edges of the acridine ligand in the grooves. The general effects of ligand binding on line widths means that some weak NOEs observed in the free quadruplex are difficult to detect in the bound state. The 4-NH_2 group of A3 is still visible and stabilized against exchange, as well as being upfield shifted by 0.4 ppm, suggesting that the A-tetrad is still intact, although drug–DNA NOEs to the adenines are generally weak. We conclude that the drug complex is stabilized primarily through extensive π stacking with the G-tetrads.

Guided by 24 drug–DNA NOEs, we have modeled the complex using NOE-restrained MD simulations (100 ps) with drug molecules docked at the ApG and GpT steps. A low-energy structure that satisfies the majority of the distance restraints is shown in Figure 3a, with the partial positive charge on the acridine 13-N acting as a pseudo potassium ion positioned above the center of the G-tetrad.[14] The overlap between the π system of the drug and the complementary G-tetrad of G4 (Figure 3b) suggests several key positions around the acridine ring that may provide future points for ligand substitution to enhance quadruplex affinity and specificity through interactions in the grooves.

 © WILEY-VCH Verlag GmbH, D-69451 Weinheim, 2001 1433-7851/01/4024-4750 $ 17.50+.50/0

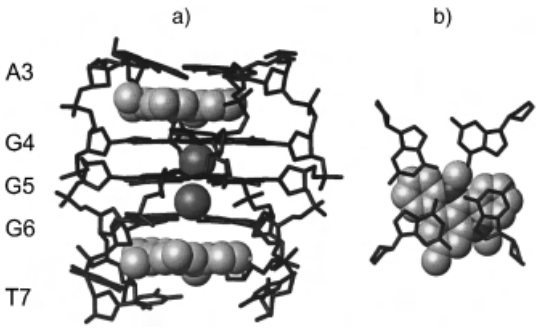


Figure 3. a) Structure of the 2:1 complex with d(TTA*GGG*T)$_4$ showing the AGGGT core with **RHSP4** intercalated at the A3–G4 and G6–T7 sites. b) π Stacking of the drug with the G4 tetrad showing the orientation with respect to the various grooves.

Recent detailed studies of cationic porphyrin–DNA quadruplex interactions have invoked both GpG intercalation and violation of the neighboring site exclusion principle.[15] In contrast, the perylenetetracarboxylic diimide intercalator (PIPER) described by Federoff et al.,[8] and the polycyclic methylacridinium cation reported here, are unable to disrupt the G-tetrad core by insertion at a GpG step and displacement of stabilizing K^+ ions. Instead the drug forms complex-stabilizing interactions by stacking on the ends of the G-quadruplex. Similar conclusions have been drawn from modeling studies of a disubstituted anthraquinone,[5e] and a number of trisubstituted acridine derivatives with the human intramolecular quadruplex where the drug is proposed to bind to the TTA cross-over loop while end-stacking with a G-tetrad.[5f] In the complex of PIPER with d(TAGGGTTA)$_4$, formation of the 1:1 complex appears to favor end-stacking at the GpT step rather than the ApG step, which the authors attribute to the difficulty of disrupting the stronger base stacking between purine tetrads.[8] In contrast, **RHPS4** appears to show relatively little discrimination between these two intercalation sites. The **RHPS4**-d(TTAGGGT)$_4$ complex represents one of a very limited number of drug–quadruplex structures so far characterized. We are currently utilizing this structural information in further rational design and targetting of these higher ordered DNA structures.

Received: August 2, 2001 [Z17661]

[1] a) E. H. Blackburn, *Nature* **1991**, *350*, 569–572; b) V. A. Zakian, *Science* **1995**, *270*, 1601–1604; c) E. H. Blackburn, *Cell* **1994**, *77*, 621–623; d) T. R. Cech, *Angew. Chem.* **2000**, *112*, 34–44; *Angew. Chem. Int. Ed.* **2000**, *39*, 34–43.

[2] a) V. L. Makarov, Y. Hirose, J. P. Langmore, *Cell* **1997**, *88*, 657–666; b) W. E. Wright, V. M. Tesmer, K. E. Huffman, S. D. Levine, J. W. Shay, *Genes Dev.* **1997**, *11*, 2801–2809.

[3] a) T. De Lange, *Proc. Natl. Acad. Sci. USA* **1994**, *91*, 2882–2885; b) C. B. Harley, B. Villeponteau, *Curr. Opin. Genet. Dev.* **1995**, *5*, 249–255.

[4] a) J. Lingner, T. R. Hughes, A. Shevchenko, M. Mann, V. Lundblad, T. R. Chech, *Science* **1997**, *276*, 561–567; b) T. M. Nakamura, G. B. Morin, G. B. Chapman, S. L. Weinrich, W. H. Andrews, J. Lingner, C. B. Harley, T. R. Cech, *Science* **1997**, *277*, 955–959; c) J. Feng, W. D. Funk, S. S. Wang, S. L. Weinrich, A. A. Avillon, C. P. Chiu, R. R. Adams, E. Chang, R. C. Allsop, J. Yu, *Science* **1995**, *269*, 1236–1241.

[5] a) J.-L. Mergny, P. Mailliet, F. Lavelle, J.-F. Riou, A. Laoui, C. Helene, *Anti-Cancer Drug Des.* **1999**, *14*, 327–339; b) P. J. Perry, T. C. Jenkins, *Expert Opin. Invest. Drugs* **1999**, *8*, 1981–2008; c) E. Raymond, J. C. Soria, E. Izbicka, F. Boussin, L. Hurley, D. D. Von-Hoff, *Invest. New Drugs* **2000**, *18*, 123–137; d) H. Han, L. H. Hurley, *Trends Pharm. Sci.* **2000**, *21*, 136–142; e) M. A. Read, S. Neidle, *Biochemistry* **2000**, *39*, 13422–13432; f) M. Read, J. R. Harrison, B. Romagnoli, F. A. Tanious, S. H. Gowan, A. P. Reszka, W. D. Wilson, L. R. Kelland, S. Neidle, *Proc. Natl. Acad. Sci. USA* **2001**, *98*, 4844–4849.

[6] a) C. Kang, X. Zhang, R. Ratliff, R. Moyzis, A. Rich, *Nature* **1992**, *356*, 126–128; b) Y. Wang, D. J. Patel, *Structure* **1993**, *1*, 263–272; c) Y. Wang, D. J. Patel, *J. Mol. Biol.* **1993**, *234*, 1171–1183; d) J. Feigon, K. M. Koshlap, F. W. Smith, *Methods Enzymol.* **1995**, *261*, 225–255; e) K. Phillips, Z. Dauter, A. I. H. Murchie, D. M. J. Liley, B. Luisi, *J. Mol. Biol.* **1997**, *273*, 171–182; f) N. V. Hud, P. Schultze, V. Sklenar, J. Feigon, *J. Mol. Biol.* **1999**, *285*, 233–243.

[7] R. T. Wheelhouse, D. Sun, H. Han, F. X. Han, L. H. Hurley, *J. Am. Chem. Soc.* **1998**, *120*, 3261–3262.

[8] O. Y. Federoff, M. Salazar, H. Han, V. V. Chemeris, S. M. Kerwin, L. H. Hurley, *Biochemistry* **1998**, *37*, 12367–12374.

[9] a) R. A. Heald, C. Modi, J. C. Cookson, I. Hutchinson, C. A. Laughton, S. M. Gowan, L. R. Kelland, M. F. G. Stevens, *J. Med. Chem.* **2001**, in press. b) Fluorescence quenching studies with intermolecular quadruplexes and the human intramolecular form indicate a binding affinity of about $2.2 \times 10^5\,\text{M}^{-1}$; c) S. M. Gowan, R. A. Heald, M. F. G. Stevens, L. R. Kelland, *Mol. Pharmacol.* **2001**, *60*, 981–998; d) **RHPS4** has not been tested on non-tumor cells.

[10] NMR data were collected on a sample of d(TTAGGGT) at a concentration of 6.4 mM single strands in 100 mM KCl and 10 mM K_2HPO_4 on a Bruker DRX500 spectrometer using standard phase-sensitive pulse sequences.

[11] R. Jin, B. L. Gaffney, C. Wang, R. A. Jones, K. J. Breslauer, *Proc. Natl. Acad. Sci. USA* **1992**, *89*, 8832–8836.

[12] P. K. Patel, A. S. R. Koti, R. V. Hosur, *Nucleic Acids Res.* **1999**, *27*, 3836–3843.

[13] Distance restaints (650 DNA-DNA and 24 drug-DNA) were derived from NOESY data collected at mixing times of 75, 100, and 150 ms by extrapolating to zero mixing time (J. Baleja, J. Moult, B. D. Sykes, *J. Mag. Res.* **1990**, *87*, 375–384). NOE-restrained MD simulations, using an explicit solvent model, followed previously reported procedures (E. Gavathiotis, G. J. Sharman, M. S. Searle, *Nucleic Acids Res.* **2000**, 28, 728–735). Structures were displayed and analyzed by using MOLMOL (R. Koradi, M. Billeter, K. Wüthrich, *J. Mol. Graphics* **1996**, *14*, 51–55).

[14] In the final energy minimized structure no restraint violations > 0.3 Å were observed for the DNA, however, three of the 24 drug–DNA NOEs were violated by > 0.3 Å. Although we have modeled a single bound drug conformation at the ApG and GpT intercalation sites, the dynamic nature of the interaction (evident from ^{1}H and ^{19}F temperature-dependent line widths) does not preclude multiple interconverting conformations, all of which will contribute to the average NOE intensity. The analysis of NOEs from a single DNA proton to several drug protons apparently remote from each other on the acridine ring can arise from the drug rotating between the four equivalent stacked conformations, though this is further complicated by the fourfold symmetry of the quadruplex which makes each strand equivalent by NMR. We are currently evaluating a more dynamic modeling approach.

[15] I. Haq, J. O. Trent, B. Z. Chowdhry, T. C. Jenkins, *J. Am. Chem. Soc.* **1999**, *121*, 1768–1779.

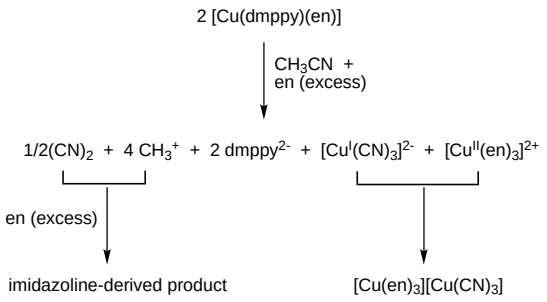
 © WILEY-VCH Verlag GmbH, D-69451 Weinheim, 2001 1433-7851/01/4024-4751 $ 17.50+.50/0

Heterolytic Cleavage of the C–C Bond of Acetonitrile with Simple Monomeric Cu^{II} Complexes: Melding Old Copper Chemistry with New Reactivity**

Dana S. Marlin, Marilyn M. Olmstead, and Pradip K. Mascharak*

The reduction of Cu^{II} ion with cyanide (CN^-) to form stable cyanocopper(I) complexes (such as the trigonal-planar $[Cu(CN)_3]^{2-}$ species) and gaseous cyanogen has been known for quite some time.[1, 2] In this reaction, CN^- in excess acts as both the reductant for the conversion of Cu^{II} to Cu^{I} and as the ligand for Cu^{I}, and is itself oxidized to cyanogen gas, $(CN)_2$. Historically, the rich reaction chemistry of cyanogen (including but not limited to that produced by Cu^{II} and KCN) with various organic compounds such as amines dates back well over a century.[2] The reaction of $(CN)_2$ with aliphatic diamines to produce imidazolines and polymeric amidines among other products is well documented.[2] In addition, the Cu^{I} cyanide complexes mentioned above also have their own interesting chemistry. The Sandmeyer reaction, for example, utilizes CuCN in the formation of aryl nitriles from their corresponding aryl diazonium salts.[3] Also, Cu^{I} cyanide complexes are known to form large extended structures in the presence of amines.[4, 5] Despite the reactivity of Cu^{II} with CN^- (to form $[Cu^{I}(CN)_x]^{x-1}$ complexes), simple Cu^{II} salts in the presence of nitriles (alkyl cyanides) such as acetonitrile (CH_3CN) are generally quite stable, and hence salts of the $[Cu(CH_3CN)_4]^{2+}$ ion are common Cu^{II} starting materials for syntheses of other Cu^{II} complexes.[1] The Cu^{I} salts of CH_3CN are also stable, and the use of $[Cu(CH_3CN)_4]^{+}$ salts in syntheses of Cu^{I} complexes has been equally exploited.[1] In fact, metal-mediated splitting of the C–CN bond in alkyl cyanides (e.g. CH_3CN) has so far only been shown to occur with the aid of reactive low-valent metal complexes such as those containing a Pt^0 or Ni^0 metal center.[6, 7] To our knowledge, the reaction of Cu^{II} with CH_3CN to produce $[Cu^{I}(CN)_3]^{2-}$ (and a methylated product) has not been demonstrated as yet.

We have recently reported the syntheses and structures of several monomeric Cu^{II} complexes coordinated to the deprotonated tridentate ligand *N*,*N*′-dimethylpyridine-2,6-dicarboxamide ($dmppyH_2$, where the H atoms represent the dissociable carboxamido hydrogen atoms), and also commented on the instability of most of these complexes in solution. We speculated that the instability and/or reactivity of $[Cu^{II}(dmppy)(L)]$ complexes in solution may be due to severe out-of-plane distortion of the Cu^{II} ion from the $dmppy^{2-}$ plane.[8] The highly basic nature of the $dmppy^{2-}$ ligand could be another contributing factor for this reactivity. Here we report the synthesis and structure of [Cu(dmppy)(en)] (en = ethylenediamine) and describe its reactivity toward CH_3CN. When [Cu(dmppy)(en)] is added to a mixture of CH_3CN and en, crystalline $[Cu(en)_3][Cu(CN)_3]$ is isolated in nearly quantitative yield (based on Cu) in addition to intact $dmppyH_2$, and a methylated imidazoline-derived polymeric material (Scheme 1). In this chemistry, the formation of the cyanocopper(I) complex $[Cu(CN)_3]^{2-}$ and the methylated polymeric product must be a result of the heterolytic cleavage of CH_3CN into CH_3^+ and CN^-.



Scheme 1. Reaction of [Cu(dmppy)(en)] with CH_3CN in the presence of ethylenediamine initally produces $[Cu(en)_3][Cu(CN)_3]$, $dmppyH_2$, and cyanogen, which slowly reacts to yield a imidazoline-derived product.

The complex [Cu(dmppy)(en)] was synthesized from $[\{Cu(dmppy)(py)\}_2]$[8] and ethylenediamine in DMF. [Cu(dmppy)(en)] has only partial solubility in DMF and crystals suitable for an X-ray structure analysis of this complex are obtained upon careful layering a DMF/en solution onto a solution of $[\{Cu(dmppy)(py)\}_2]$ also in DMF. The structure of [Cu(dmppy)(en)] shows that the $dmppy^{2-}$ ligand coordinates to the Cu^{II} ion in the basal plane of a distorted square-pyramidal geometry; the en ligand occupies the remaining two sites (Figure 1).[9] When [Cu(dmppy)(en)] is suspended in a mixture of CH_3CN and en (10:1 v/v), large

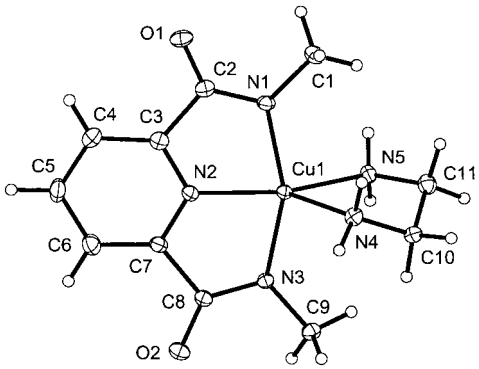


Figure 1. Structure of [Cu(dmppy)(en)] showing 50% thermal ellipsoids and selected atom labels. Selected bond lengths [Å] and angles [°]: Cu1-N1 2.0206(17), Cu1-N2 1.9455(18), Cu1-N3 2.0421(17), Cu1-N4 2.210(3), Cu1-N5 2.073(2); N2-Cu1-N1 79.20(6), N2-Cu1-N3 79.20(6), N1-Cu1-N3 158.23(7), N2-Cu1-N5 148.89(8), N1-Cu1-N5 99.28(9), N3-Cu1-N5 97.81(8), N2-Cu1-N4 127.98, N1-Cu1-N4 95.61(8), N3-Cu1-N4 99.76(8), N5-Cu1-N4 83.12(7).

[*] Prof. Dr. P. K. Mascharak, D. S. Marlin
Department of Chemistry and Biochemistry
University of California, Santa Cruz
Santa Cruz, CA 95064 (USA)
Fax: (+1) 831-459-2935
E-mail: pradip@chemistry.ucsc.edu
Dr. M. M. Olmstead
Department of Chemistry
University of California, Davis
Davis, CA 95616 (USA)

[**] This work was supported by a grant from the National Science Foundation (CHE-9818492).

 © WILEY-VCH Verlag GmbH, D-69451 Weinheim, 2001 1433-7851/01/4024-4752 $ 17.50+.50/0

crystals of $[Cu(en)_3][Cu(CN)_3]$ (Figure 2)[10] appear over a period of 1–2 weeks along with a flocculent white precipitate. Although $[Cu(en)_3][Cu(CN)_3]$ has been synthesized previously,[11] and the structures of the individual ions $[Cu(en)_3]^{2+}$[12, 13] and $[Cu(CN)_3]^{2-}$[14, 15] have been determined separately in other crystal lattices, the structure of $[Cu(en)_3][Cu(CN)_3]$ (Figure 2) as a unit had not been determined until now. The reaction of [Cu(dmppy)(en)] with CH_3CN and ethylenediamine is slow mainly due to its low solubility under the conditions used, and also appears to be quite complex in nature (Scheme 1). Analogous complexes such as [Cu(dmppy)(bpy)],[8] which are soluble in CH_3CN, react faster in the en/CH_3CN mixture and cleave CH_3CN at a faster rate (1–2 days). The isolation of $[Cu(en)_3][Cu(CN)_3]$ indicates that cleavage of CH_3CN must be heterolytic due to the presence of CN^- in the products. As mentioned above, the reduction of Cu^{II} to Cu^{I} and subsequent formation of $[Cu(CN)_3]^{2-}$ is well established. In fact, Cu^{II} complexes of CN^- are not particularly common.[16]

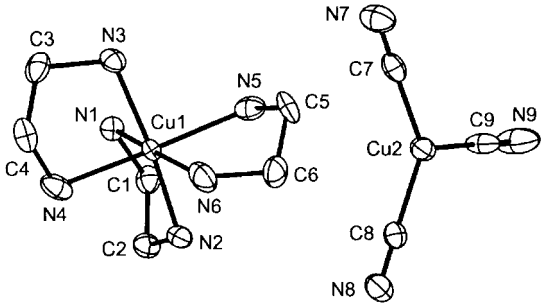
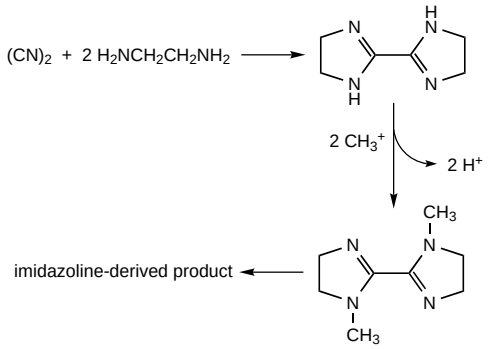


Figure 2. Structure of $[Cu(en)_3][Cu(CN)_3]$ showing 50% thermal ellipsoids and selected atom labels. Selected bond lengths [Å] and angles [°]: Cu1-N1 2.367(4), Cu1-N2 2.047(4), Cu1-N3 2.040(3), Cu1-N4 2.097(4), Cu1-N5 2.120(4), Cu1-N6 2.320(4), Cu2-C7 1.930(5), Cu2-C8 1.934(4), Cu2-C9 1.924(5), C9-N9 1.151(6); N1-Cu1-N6 172.08(14), N4-Cu1-N5 169.48(14), N2-Cu1-N3 170.62(15), C9-Cu2-C7 119.98(17), C9-Cu2-C8 119.95(17), C7-Cu2-C8 120.01(16).

Determination of the exact fate of the CH_3^+ group produced from the heterolytic cleavage of CH_3CN, however, is a less trivial task. We were successful in recovering the intact $dmppyH_2$ ligand from the solution after the reaction was complete.[17] ^1H NMR and mass spectra data reveal that the recovered $dmppyH_2$ ligand does not contain any additional methyl groups derived from the heterolytic cleavage of CH_3CN, as had been initially expected. Cyanogen is known to react with ethylenediamine to yield 2,2′-bis(2-imidazoline) (Scheme 2).[2] Data from ^1H NMR, IR, and mass spectral analysis on the white precipitate[18] led us to conclude that the expected imidazoline product is formed in our case, and that it is also methylated, presumably by the methyl groups from CH_3CN cleavage (Scheme 2). Although we were not able to determine the exact structure of this species, the gradual conversion in the mass spectra of high molecular weight peaks (at m/z 274.7 and 168.1) to a single peak at m/z 83.1, which is consistent with the degredation of a polymeric species to an *N*-methylimidazoline monomer, supports the assignment of a methylated imidazoline. Furthermore, ^1H NMR data reveal only three peak positions in the methyl and methylene region



Scheme 2. Possible scheme for the reaction of cyanogen with ethylenediamine to produce 2,2′-bis(2-imidazoline) which may be subsequently methylated by CH_3^+ and react further to produce the imidazoline-derived product.

($[D_6]$DMSO: $\delta = 2.7$, 2.9, and 3.3). The IR spectrum of this material is dominated by a band at 1592 cm^{-1} which is assigned to the C=N stretching frequency. In addition, absorptions in the range expected for C–H stretches (3452 cm^{-1}) are also present. It should be noted that the reaction depicted in Scheme 2 is only one possibility (or only part of what may be occurring) and this scheme does not account for all the methyl groups produced by CH_3CN cleavage.

In conclusion, we have prepared a very simple Cu^{II} complex that cleaves CH_3CN heterolytically into CN^- and CH_3^+. This reaction is quite novel for Cu^{II}, although the reactivity subsequent to CH_3CN clevage is well established in copper chemistry. The reactivity of [Cu(dmppy)(en)] and related species toward CH_3CN appears to be dictated by the highly basic nature of the $dmppy^{2-}$ ligand.[19] Further work directed at evaluating the mechanism of the CH_3CN cleavage is currently underway in our laboratory.

Experimental Section

[Cu(dmppy)(en)]: A solution of [{Cu(dmppy)(py)}$_2$] (0.10 g, 0.15 mmol) in DMF (3 mL) was carefully layered on a solution of en (0.09 g, 1.5 mmol) in DMF (1 mL). Within 48 h, large blue-green crystalline blocks had formed on the walls of the vial which were filtered off, washed with CH_3CN, and dried under vacuum (0.06 g, 63% yield). Crystals suitable for an X-ray structure determination of [Cu(dmppy)(en)] were grown in a capillary tube by the same method. FT-IR (KBr): $\tilde{\nu} = 3262$ (m), 3173 (m), 2934 (w), 2861 (w), 1619 (m), 1592 (s), 1572 (s), 1384 (m), 1363 (m), 1296 (m), 1068 (m), 1047 (m), 1017 (m), 835 (w), 750 (m), 740 (m), 684 (m), 572 (w); EPR (100 K, DMF/Tol (1:1 v/v), 9.43 GHz): $g_\parallel = 2.22$, $g_\perp = 2.06$, $A_\parallel = 178$ G.

Reaction of [Cu(dmppy)(en)] with en and CH_3CN: en (0.3 mL) was added to a suspension of [Cu(dmppy)(en)] (0.020 g, 0.06 mmol) in CH_3CN (3 mL) and the mixture was sealed and stored at 25 °C for 1–2 weeks. During this time, all the suspended [Cu(dmppy)(en)] had been replaced by large crystals of $[Cu(en)_3][Cu(CN)_3]$ (0.018 g, 80% yield based on copper) and a flocculent white precipitate. The latter was collected by centrifugation and dried under vacuum. FT-IR of $[Cu(en)_3][Cu(CN)_3]$ (KBr): $\tilde{\nu} = 3310$ (s), 3248 (s), 2950 (CN, m), 2884 (m), 2066 (s), 1586 (m), 1323 (w), 1101 (w), 1037 (s), 973 (m), 707 (w), 527 (w).

Received: July 27, 2001 [Z17614]

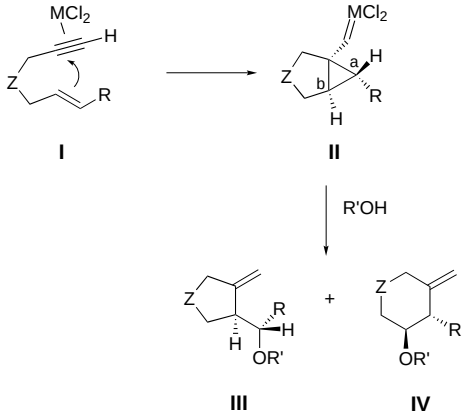
[1] B. J. Hathaway, *Copper: Comprehensive Coordination Chemistry*, *Vol. 5*, Pergomon Press, Oxford, **1987**, p. 533–774.
[2] T. K. Brotherton, J. W. Lynn, *Chem. Rev.* **1959**, *59*, 841–883.

[3] J. March, *Advanced Organic Chemistry: Reactions Mechanisms and Structure*, 4th ed., Wiley, New York, **1992**, p. 723–724.
[4] F. B. Stocker, T. P. Staeva, C. M. Rienstra, D. Britton, *Inorg. Chem.* **1999**, *38*, 984–991.
[5] D. J. Chesnut, J. Zubieta, *Chem. Commun.* **1998**, 1707–1708.
[6] D. H. Gerlack, A. R. Kane, G. W. Parshall, J. P. Jesson, E. L. Muetterties, *J. Am. Chem. Soc.* **1971**, *93*, 3543-
[7] G. Favero, A. Morvillo, A. Turco, *Gazz. Chim. Ital.* **1979**, *109*, 27–28.
[8] D. S. Marlin, M. M. Olmstead, P. K. Mascharak, *Inorg. Chem.* **2001**, *40*, in press.
[9] a) Crystal data for [Cu(dmppy)(en)]: Blue plates of dimensions $0.35 \times 0.13 \times 0.06$ mm^3; monoclinic, space group $P2_1/n$, $a = 7.022(2)$, $b = 16.136(5)$, $c = 11.313(4)$ Å, $\beta = 93.11(2)^\circ$, $V = 1280.0(7)$ Å^3, $Z = 4$, $\rho_{calcd} = 1.634$ Mg m^{-3}, $2\theta_{max} = 63^\circ$, $\mu(Mo_{K\alpha}) = 1.713$ mm^{-1}, ω scans, $\lambda = 0.71073$ Å; the data were collected at 92(2) K on a Bruker SMART 1000 diffractometer; a total of 34867 reflections were measured, of which 9910 were independent ($R_{int} = 0.067$) and included in the refinement; mim./max. transmission = 0.5855/0.9042; solution by direct methods (SHELXS-97, Sheldrick, **1990**); refinement by full-matrix least-squares based on F^2 (SHELXTL 6.1, Sheldrick, **2001**); 175 parameters, $R1 = 0.0641$, $wR2 = 0.1254$ for all data; $R1 = 0.0460$ computed for 7282 observed data ($I > 2\sigma(I)$). b) Crystallographic data (excluding structure factors) for the structures reported in this paper have been deposited with the Cambridge Crystallographic Data Centre as supplementary publication nos. CCDC-167732 [Cu(dmppy)(en)] and CCDC-167733 [Cu(en)$_3$][Cu(CN)$_3$]. Copies of the data can be obtained free of charge on application to CCDC, 12 Union Road, Cambridge CB21EZ, UK (fax: (+44) 1223-336-033; e-mail: deposit@ccdc.cam.ac.uk).
[10] Crystal data for [Cu(en)$_3$][Cu(CN)$_3$]: Blue parallelpiped crystals of dimensions $0.50 \times 0.38 \times 0.28$ mm^3; Monoclinic, space group $P2_1/n$, $a = 7.6690(9)$ Å, $b = 17.2770(19)$ Å, $c = 12.4609(13)$ Å, $\beta = 95.038(9)^\circ$, $V = 1644.7(3)$ Å^3, $Z = 2$, $\rho_{calcd} = 1.557$ Mg m^{-3}, $2\theta_{max} = 55^\circ$, $\mu(Mo_{K\alpha}) = 2.591$ mm^{-1}, ω scans, $\lambda = 0.71073$ Å; the data were collected at 130(2) K on a Siemens P3 diffractometer; a total of 4171 reflections were measured, of which 3769 were independent ($R_{int} = 0.044$) and included in the refinement; mim./max. transmission = 0.3574/0.5307; solution by direct methods (SHELXS-97, Sheldrick, **1990**); refinement by full-matrix least squares based on F^2 (SHELXTL 6.10, XL, Sheldrick, **2000**); 217 parameters, $R1 = 0.0811$, $wR2 = 0.1109$ for all data; $R1 = 0.0463$ computed for 2532 observed data ($I > 2\sigma(I)$).[9b]
[11] M. Wicholas, T. Wolford, *Inorg. Nucl. Chem. Lett.* **1975**, *11*, 157–159.
[12] I. Bertini, P. Dapporto, D. Gatteschi, A. Scozzafava, *J. Chem. Soc. Dalton Trans.* **1979**, 1409–1414
[13] D. L. Cullen, E. C. Lingafelter, *Inorg. Chem.* **1970**, *9*, 1858-
[14] J. Pickardt, B. Staub, K. O. Schäfer, *Z. Anorg. Allg. Chem.* **1999**, *625*, 1217–1224.
[15] P. Chaudhuri, K. Oder, K. Wieghardt, J. Weiss, J. Reedijk, W. Hinrichs, J. Wood, A. Ozarowski, H. Stratemaier, D. Reinen, *Inorg. Chem.* **1986**, *25*, 2951–2958.
[16] M. Wicholas, T. Wolford, *Inorg. Chem.* **1974**, *13*, 316–318.
[17] Solvent from the filtrate was removed under vacuum, and the residue was dissolved in H_2O and extracted with CH_2Cl_2. The organic layer was collected, dried, and solvent removed under vacuum to yield pure dmppyH_2.
[18] The floculent white precipitate formed upon reaction of [Cu(dmppy)(en)] with CH_3CN and ethylenediamine was seperated by centrifugation and dried under vacuum.
[19] One of the reviewers has suggested that a amide-bound Cu^{III} could be involved in the mechanism of the C–C bond cleavage of acetonitrile. Although this appears to be plausible, we do not have any spectroscopic evidence of an intermediate containing trivalent copper at this time.

Pt^{II}-Catalyzed Intramolecular Reaction of Furans with Alkynes**

Belén Martín-Matute, Diego J. Cárdenas, and Antonio M. Echavarren*

The coordination of electrophilic $PtCl_2$ to the C≡C bond of an enyne (**I**, Scheme 1) promotes intramolecular reaction of the alkene to form a cyclopropyl Pt carbene intermediate **II**.[1, 2] Subsequent attack of an alcohol or water at the cyclopropyl carbon atoms C_a and C_b of **II** leads to the formation of five- or six-membered carbo- or heterocyclic rings under catalytic conditions.[1]



Scheme 1. Metal-induced reaction of enynes to yield five- or six-membered rings.

These cyclizations are also catalyzed by $AuCl_3$ and some Ru^{II} complexes.[1] In this regard, the recent finding that the intramolecular reaction of furans with alkynes can be catalyzed by $AuCl_3$ to afford phenols is of considerable interest.[3, 4] The reaction was proposed to proceed by a [4+2] cycloaddition of the furan to the alkyne followed by cleavage of the resulting oxabicyclic adduct.[3] Although this mechanistic proposal is reasonable, the related intramolecular reaction of arenes with alkynes with catalysis by Pt^{II} or Ru^{II}[5] was proposed to take place by electrophilic aromatic substitution with an (η^2-alkyne)metal electrophile.

We have found that 5-furyl-1-alkynes are also cyclized by $PtCl_2$ as catalyst. Several intermediate products could be obtained by conducting the reaction in an aqueous solvent. A clearer picture of the mechanism was obtained by performing

[*] Prof. Dr. A. M. Echavarren, B. Martín-Matute, Dr. D. J. Cárdenas
Departamento de Química Orgánica
Universidad Autónoma de Madrid
Cantoblanco, 28049 Madrid (Spain)
Fax: (+349) 1-3973966
E-mail: anton.echavarren@uam.es

[**] This work was supported by the DGICYT (project PB97-0002) and the MCyT (predoctoral fellowship to B.M.-M.). We also acknowledge Johnson Matthey PLC for a generous loan of $PtCl_2$.

Supporting information for this article is available on the WWW under http://www.angewandte.com or from the author.

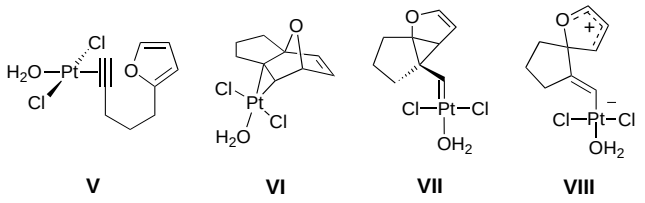
 © WILEY-VCH Verlag GmbH, D-69451 Weinheim, 2001 1433-7851/01/4024-4754 $ 17.50+.50/0

density functional calculations (DFT) on the intramolecular reaction of a furan with an alkyne coordinated to $PtCl_2$.

The cyclization of 2-furylmethyl propargyl ether (**1**) was carried out in the presence of $PtCl_2$ (5 mol%) as catalyst in refluxing acetone to give phenols **2** (44%) and **3** (16%) (Scheme 2).[6] Malonate **4** gave a mixture of phenols **5** (54%) and **6** (16%). Similar results were obtained with $[PtCl_2(MeCN)_2]$ as catalyst. The cyclization of ether **1** with $AuCl_3$ (3 mol%) as catalyst in MeCN at room temperature also afforded a mixture of **2** and **3**, although the yields were lower (30 and 1.5%, respectively). Cyclization of **7** led selectively to phenol **8** (75%).[7]

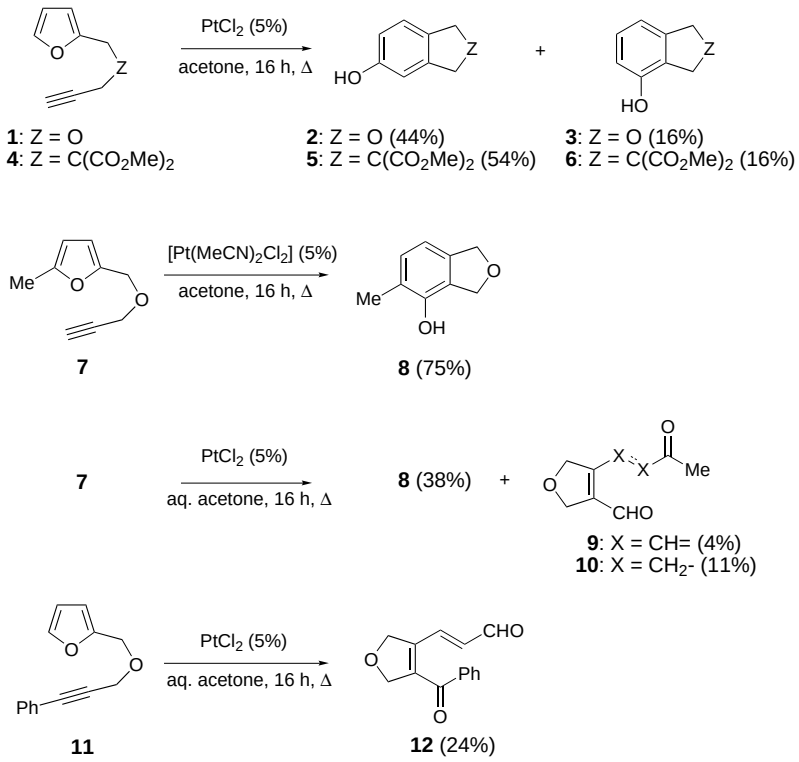
When these reactions were performed in the presence of water, in addition to the phenols, 2,5-dihydrofurans were also obtained in variable yields. Thus, **7** reacted in 10% aqueous acetone under reflux with $PtCl_2$ (5 mol%) to furnish a mixture of phenol **8** (38%), and ketoaldehydes **9** (4%) and **10** (11%). On the other hand, ether **11** with a terminal phenyl group gave ketoaldehyde **12** (24%).

The formation of dicarbonyl compounds **9**, **10**, and **12** cannot easily be accounted for by a [4+2] cycloaddition pathway. To determine the nature of the reaction profile for the intramolecular reaction of alkynes and furans, we therefore performed DFT calculations on a model compound. Several pathways can be envisaged in principle, starting with coordination of the alkyne to the metal center (**V**), which was assumed to be also coordinated by a water molecule. First, a Diels–Alder reaction between the furan and the coordinated alkyne could give intermediate **VI**.[3] Alternatively, formation of a cyclopropyl Pt carbene[1] **VII** by reaction of the alkyne with the C2–C3 double bond of furan could occur. A third plausible mechanism involves a Friedel–Crafts-type reaction of the electron-deficient alkyne at C2 of the furan via **VIII**.[5]



We searched for different reaction products that could be formed from **V**.[8, 9] The Diels–Alder *endo* adduct **VI** (Figure 1) was located as a minimum of higher energy than **V** (+8.5 kcal mol^{-1}). The corresponding transition state $\mathbf{TS_{V\text{-}VI}}$ shows relatively short C–C distances for the bonds that are being formed, especially for that involving the alkyne terminal C atom (2.025 Å) and lies 30.2 kcal mol^{-1} above **V**. The carbon atoms of the coordinated alkene in **VI** are substantially pyramidalized, and the structure resembles a platinacyclopropane. The Cl-Pt-Cl angle diminishes from **V** to **VI** (171.6 to 161.9°) bacause of the steric hindrance imposed by the side chain. Alternatively, the internal C atom of the alkyne might react with the nucleophilic C2–C3 bond of the furan to give the cyclopropylcarbene **VII**. This complex shows a very short C(sp^2)–Pt distance (1.890 Å), in accord with the carbene character. The formation of **VII** is exothermic (−3.4 kcal mol^{-1}), and the activation energy to reach transition state $\mathbf{TS_{V\text{-}VII}}$ is much lower (9.4 kcal mol^{-1}) than that of the Diels–Alder reaction. The attack of the furan takes place on the opposite side to the metal atom through an early asymmetric transition state with very different C–C distances (2.293 and 2.528 Å for Pt-C2′ and Pt-C3′, respectively). This would be the preferred pathway for both thermodynamic and kinetic reasons. The formation of intermediate **VIII** was also considered, but the only minimum-energy structure that could be located when trying to obtain a minimized Friedel–Crafts complex was again **VII**. Apparently, the delocalization of the positive charge in **VIII** is not enough to compensate for the stability of the Pt cyclopropylcarbene.

These findings led to a mechanistic proposal summarized in Scheme 3. The initially formed complex **IX** would evolve exothermically to form key intermediate **X**. Cleavage of the cyclopropane and the dihydrofuran rings would form **XI**, which could be trapped by water to form dicarbonyl compounds such as **9**, **10**, and **12**.[10] An intramolecular [2+2] cycloaddition of the platinum carbene with the carbonyl group could then give **XII**, which would undergo reductive elimination to give epoxide **XIII**.[11] This last intermediate, which explains the formation of the isolated phenols, has also been proposed in the Au^{III}-catalyzed synthesis of phenols.[3]



Scheme 2. Intramolecular reaction of furans with alkynes in the absence and in the presence of water.

 © WILEY-VCH Verlag GmbH, D-69451 Weinheim, 2001 1433-7851/01/4024-4755 $ 17.50+.50/0

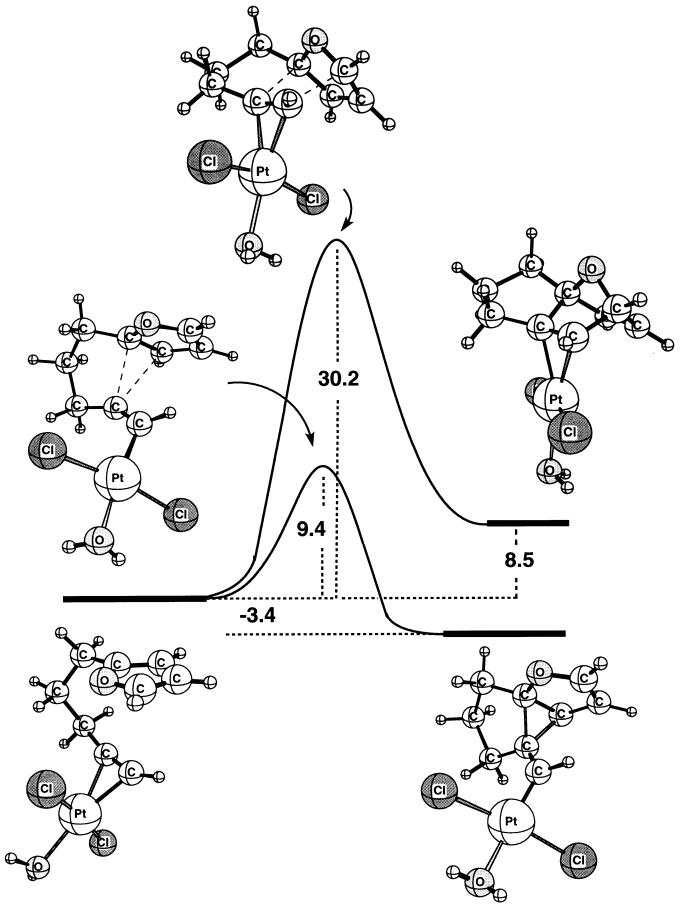
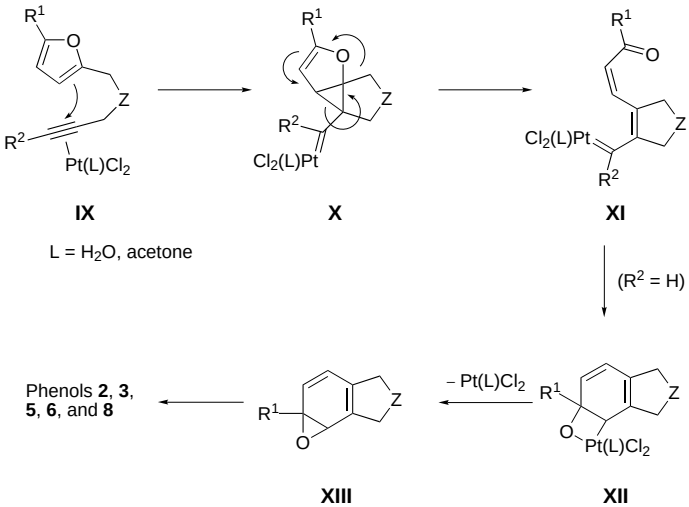
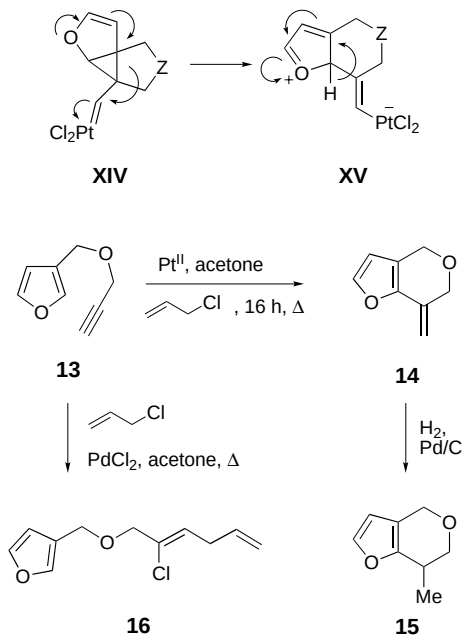


Figure 1. Reaction coordinate for two alternative reaction pathways of Pt^{II} complex **V** to give **VI** or **VII**. Energies in kcal mol^{-1} at the B3LYP/6-31G(d) level including ZPE correction.



Scheme 3. Mechanistic proposal.

Attaching the alkyne-containing chain at C3 of the furan was therefore expected to give **XIV**, which might evolve to form **XV** by cleavage of the cyclopropyl ring, followed by rearomatization (Scheme 4). Alternatively, **XV** could be formed by a direct electrophilic aromatic substitution pathway. In fact, treatment of 3-furylmethyl propargyl ether (**13**)



Scheme 4. Reactions with a 2-substituted furan.

with $PtCl_2$ (5 mol %) led to **14** as the only new product, although the yield of isolated product was low because of its ready polymerization. For this reason, the crude product was immediately hydrogenated to give **15**. Curiously, the best result (34 % overall yield) was realized in the presence of allyl chloride, although the role of this additive is not yet known.[12] In contrast, the use of $[PdCl_2(MeCN)_2]$ (5 mol %) as catalyst (Et_2O, reflux) led only to the chloroallylation of the terminal alkyne to give **16**.[13]

In summary, the intramolecular reaction of furans with alkynes catalyzed by $PtCl_2$ is mechanistically related to that of enynes in polar solvents[1] and is initiated by the nucleophilic attack of the furan on an (η^2-alkyne)platinum(II) complex to form a cyclopropyl platinum carbene. This work suggests that similar transformations could be carried out with other electron-rich heterocycles and alkynes.

Received: August 2, 2001 [Z17658]

[1] a) M. Méndez, M. P. Muñoz, A. M. Echavarren, *J. Am. Chem. Soc.* **2000**, *122*, 11549 – 11550; b) M. Méndez, M. P. Muñoz, C. Nevado, D. J. Cárdenas, A. M. Echavarren, *J. Am. Chem. Soc.* **2001**, *123*, 10511 – 10520.

[2] a) B. M. Trost, M. J. Krische, *Synlett* **1998**, 1 – 16; b) N. Chatani, K. Kataoka, S. Murai, N. Furokawa, Y. Seki, *J. Am. Chem. Soc.* **1998**, *120*, 9104 – 9105; c) A. Fürstner, H. Szillat, F. Stelzer, *J. Am. Chem. Soc.* **2000**, *122*, 6785 – 6786; d) S. Oi, I. Tsukamoto, S. Miyano, Y. Inoue, *Organometallics* **2001**, *20*, in press.

[3] A. S. K. Hashmi, T. M. Frost, J. W. Bats, *J. Am. Chem. Soc.* **2000**, *122*, 11553 – 11554.

[4] For a highlight on the catalytic applications of gold, see G. Dyker, *Angew. Chem.* **2000**, *112*, 4407 – 4409; *Angew. Chem. Int. Ed.* **2000**, *39*, 4237 – 4239.

[5] N. Chatani, H. Inoue, T. Ikeda, S. Murai, *J. Org. Chem.* **2000**, *65*, 4913 – 4918.

[6] See the Supporting Information for experimental details and characterization data.

 © WILEY-VCH Verlag GmbH, D-69451 Weinheim, 2001 1433-7851/01/4024-4756 $ 17.50+.50/0

[7] The reaction of **7** with $AuCl_3$ as catalyst afforded exclusively phenol **8** (69%).[3] In the platinum(II)-catalyzed reaction, traces (ca. 1%) of a phenol tentatively assigned as 1,3-dihydro-6-methyl-5-isobenzofuranol were also obtained.

[8] a) The calculations were performed with Gaussian 98.[8b] The geometries of all complexes were optimized at the DFT level of theory with the generalized gradient approximation and the B3LYP hybrid functional.[8c, d] The standard 6-31G(d) basis set was used for C, H, O and Cl, and the default LANL2DZ pseudorelativistic potential and basis set were used for Pt. Harmonic frequencies were calculated at B3LYP level to characterize the stationary points and to determine the zero-point energies (ZPE). The starting approximate geometry for the transition states (TS) were located graphically; b) Gaussian 98 (Revision A.7), M. J. Frisch, G. W. Trucks, H. B. Schlegel, G. E. Scuseria, M. A. Robb, J. R. Cheeseman, V. G. Zakrzewski, J. A. Montgomery, R. E. Stratmann, J. C. Burant, S. Dapprich, J. M. Millam, A. D. Daniels, K. N. Kudin, M. C. Strain, O. Farkas, J. Tomasi, V. Barone, M. Cossi, R. Cammi, B. Mennucci, C. Pomelli, C. Adamo, S. Clifford, J. Ochterski, G. A. Petersson, P. Y. Ayala, Q. Cui, K. Morokuma, D. K. Malick, A. D. Rabuck, K. Raghavachari, J. B. Foresman, J. Cioslowski, J. V. Ortiz, B. B. Stefanov, G. Liu, A. Liashenko, P. Piskorz, I. Komaromi, R. Gomperts, R. L. Martin, D. J. Fox, T. Keith, M. A. Al-Laham, C. Y. Peng, A. Nanayakkara, C. Gonzalez, M. Challacombe, P. M. W. Gill, B. G. Johnson, W. Chen, M. W. Wong, J. L. Andres, M. Head-Gordon, E. S. Replogle, J. A. Pople, Gaussian, Inc., Pittsburgh, PA, **1998**.; c) P. J. Stephens, F. J. Devlin, C. F. Chabalowski, M. J. Frisch, *J. Phys. Chem.* **1994**, *98*, 11623–11627; d) W. Kohn, A. D. Becke, R. G. Parr, *J. Phys. Chem.* **1996**, *1000*, 12974–12980.

[9] Bond lengths, bond angles, and atomic coordinates for the structures of Figure 1 are given in the Supporting Information.

[10] a) A mechanistic hypothesis for the formation of dihydrofurans from **XI** is outlined in the Supporting Information; b) we have previously observed the formation of an aldehyde from a related platinum carbene intermediate;[1b] c) for the related oxidation of a nickel carbene intermediate, see: S. K. Chowdhury, K. K. D. Amarasinghe, M. J. Heeg, J. Montgomery, *J. Am. Chem. Soc.* **2000**, *122*, 6775–6776.

[11] Rhodium carbenes, generated in situ from $[Rh_2(OAc)_4]$ and diazo compounds, react with aldehydes to form epoxides. See, for example, a) V. K. Aggarwal, H. Abdel-Rahman, R. V. H. Jones, H. Y. Lee, B. D. Reid, *J. Am. Chem. Soc.* **1994**, *116*, 5973–5974; b) M. Hamaguchi, H. Matsubara, T. Nagai, *Tetrahedron Lett.* **2000**, *41*, 1457–1460.

[12] Trapping of an intermediate alkenylmetal intermediate with allyl chloride: C. Fernández-Rivas, M. Méndez, A. M. Echavarren, *J. Am. Chem. Soc.* **2000**, *122*, 1221–1222.

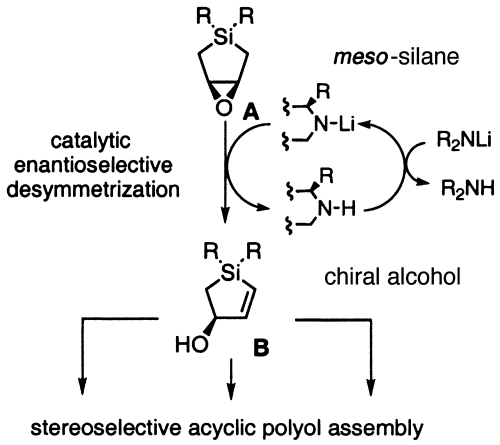
[13] a) K. Kaneda, T. Uchiyama, Y. Fujiwara, T. Imanaka, S. Teranishi, *J. Org. Chem.* **1979**, *44*, 55–63; b) J.-E. Bäckvall, Y. I. M. Nilsson, R. G. P. Gatti, *Organometallics* **1995**, *14*, 4242–4246, and references therein.

Catalytic Enantioselective Isomerization of Silacyclopentene Oxides: New Strategy for Stereocontrolled Assembly of Acyclic Polyols**

Dong Liu and Sergey A. Kozmin*

Creation of molecular chirality by desymmetrization of readily available prochiral precursors is a powerful synthetic strategy.[1] This approach is particularly attractive when a substoichiometric amount of chiral catalyst is utilized to mediate such transformations with high efficiency and enantioselectivity.[2] We have been engaged in the development of new catalytic desymmetrization approaches based on the use of cyclic silicon-containing templates. Herein, we disclose a highly enantioselective base-promoted rearrangement of silacyclopentene oxide, which resulted in the development of a novel strategy for the preparation of acyclic polyol-containing motifs. To our knowledge, enantioselective desymmetrization of cyclic silanes has not been documented prior to this work.[3, 4]

Pioneered by Whitesell and Felman,[5] base-mediated epoxide isomerization utilizing chiral lithium amides has become a valuable method for the preparation of allylic alcohols.[6] With this as a precedent, we devised a strategy for desymmetrization of *meso*-silane **A** (Scheme 1). Enantioselective deprotonation, followed by β-elimination would result in the formation of enantiomerically enriched allylic alcohol **B**. Importantly, the use of a catalytic amount of chiral base in combination with an appropriate agent capable of regenerat-



Scheme 1. General strategy for the desymmetrization of *meso*-silane **A** to give enatiomerically enriched allylic alcohol **B**.

[*] Prof. Dr. S. A. Kozmin, D. Liu
Department of Chemistry
University of Chicago
5735 South Ellis Avenue
Chicago, IL 60637 (USA)
Fax: (+1) 773-702-0805
E-mail: skozmin@uchicago.edu

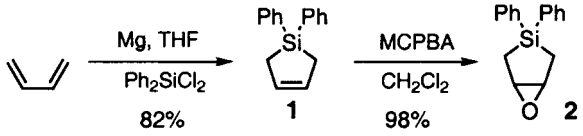
[**] Initial funding of this work was provided by the University of Chicago. We are grateful to the donors of the Petroleum Research Fund for further financial support.

Supporting information for this article is available on the WWW under http://www.angewandte.com or from the author.

 © WILEY-VCH Verlag GmbH, D-69451 Weinheim, 2001 1433-7851/01/4024-4757 $ 17.50+.50/0

ing the active catalyst would result in the development of a catalytic enantioselective process.[7] Silane **B**, which incorporates structural features of both the vinyl silane and allylic alcohol, was envisioned to serve as a versatile precursor for the assembly of a wide range of synthetically valuable acyclic polyol fragments.

Silacyclopentene oxides can be readily assembled on a preparative scale according to the general sequence illustrated in Scheme 2. In the case of the diphenyl-substituted derivative, silylation of magnesium–butadiene,[8] followed by oxidation of the resulting silacyclopentene **1** with 3-chloroperoxybenzoic acid (MCPBA) furnished epoxide **2** in an overall yield of 80% for the two steps.[9]



Scheme 2. Preparation of diphenylsilacyclopentene oxide (**2**).

We anticipated that the presence of the silicon atom would have two beneficial effects on the epoxide rearrangement: 1) α-Si-carbanion stabilization favoring initial deprotonation; and 2) the ability to maximize the level of asymmetric induction by adjusting the exocyclic silicon substituents positioned in the direct proximity to the deprotonation site. Systematic cross-examination of three silacyclopentene oxides and four chiral amide bases (Figure 1) revealed that the

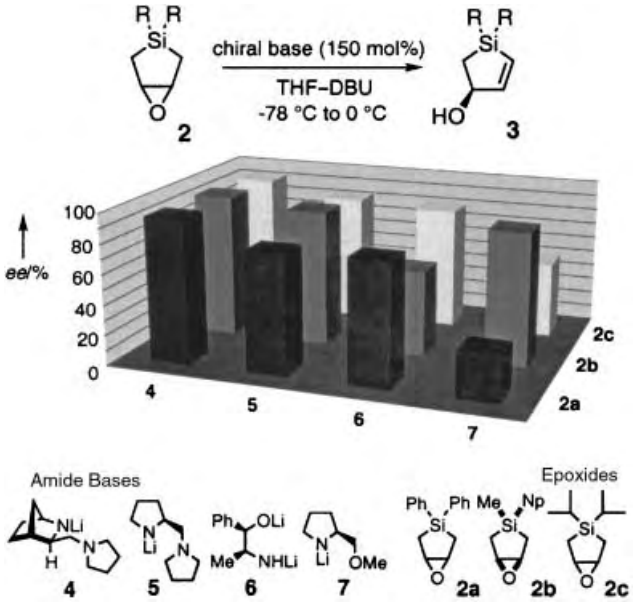
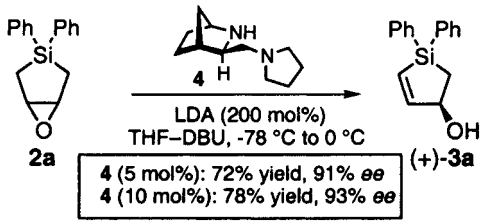


Figure 1. Base-mediated rearrangement of silacyclopentene oxides **2** to give allylic alcohols **3**.

use of diphenylsilacyclopentene oxide **2a** in combination with bicyclic amide **4**[10] resulted in the highest level of enantioselectivity (95% *ee*). Furthermore, we found that the rearrangement can be performed efficiently using a catalytic amount of **4** and two equivalents of lithium disopropylamide (LDA), in agreement with results obtained by Andersson and co-workers for the rearrangement of carbocyclic epoxides.[10] While 91% *ee* was obtained with a 5 mol% loading, the use of 10 mol% of amide **4** resulted in 93% *ee* and 78% yield (Scheme 3).[11, 12]

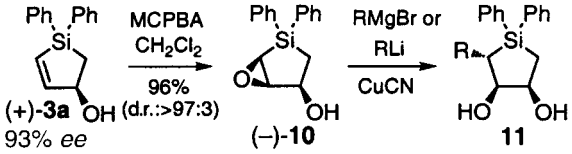


Scheme 3. Catalytic enantioselective isomerization of **2** to give (+)-**3a**.

Having secured an efficient access to alcohol (+)-**3a** in high enantiomeric purity, our subsequent efforts focused on the stereoselective construction of tetraol fragment **12** (see Table 2). The approach commenced with a diastereoselective hydroxy-directed epoxidation of (+)-**3a** to give (−)-**10** (d.r.: >97:3),[9] followed by Si-guided cuprate addition to afford silacyclic diol **11** (Table 1).[13] The latter transformation was found to be highly regioselective and general for incorporating a variety of alkyl, aryl, and alkenyl fragments. Importantly, potential products resulting from either the Peterson elimination or fragmentation were not observed under these highly nucleophilic conditions.

Our studies on the oxidative cleavage of silacyclic diols **11** began with the examination of the Tamao[14] and the Fleming[15] protocols, which generally resulted in incomplete reactions and isolation of multiple products. We soon uncovered that the oxidative cleavage of the silacyclopentane

Table 1. Epoxidation/cuprate addition sequence.[a]

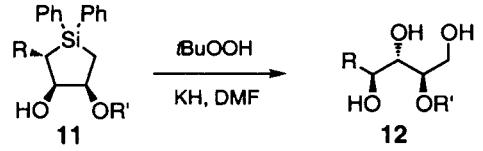


Entry	R	**11**	Yield [%][b]	d.r.
1		(−)-**11a**	91[c]	>97:3
2		(−)-**11a**	72[d]	>97:3
3		(−)-**11b**	78[c]	>97:3
4		(−)-**11c**	92[c]	>97:3
5		(−)-**11d**	87[c]	>97:3
6		(−)-**11e**	92[c]	>97:3
7		(−)-**11f**	86[c]	>97:3
8		(−)-**11g**	91[d]	>97:3
9	 ($LiAlH_4$)	(−)-**11f**	64[e]	>97:3

[a] For detailed experimental procedures and compound characterization, see Supporting Information. [b] Refers to the yield of spectroscopically pure product isolated after silica gel chromatography. [c] Organocuprate was generated from the corresponding Grignard reagent. [d] Organocuprate was generated from the corresponding organolithium reagent. [e] Reduction was carried out on the methoxymethyl(MOM)-protected alcohol (−)-**10** to prevent formation of the *meso* product.

 © WILEY-VCH Verlag GmbH, D-69451 Weinheim, 2001 1433-7851/01/4024-4758 $ 17.50+.50/0

Table 2. Oxidative cleavage of cyclic silanes.[a]



Entry	Silane	R	R′	**12**	Yield [%][b]
1	(−)-**11a**		H	(−)-**12a**	78
2	(+)-**11b**		H	(−)-**12b**	76
3	(+)-**11c**		H	(−)-**12c**	79
4	(−)-**11f**		H	(−)-**12d**	70
5	(−)-**11h**		MOM	(−)-**12e**	74

[a] For detailed experimental procedures and compound characterization, see Supporting Information. [b] Refers to the yield of spectroscopically pure product isolated after silica gel chromatography.

scaffold can be efficiently accomplished according to the Woerpel procedure employing the use of basic *t*BuOOH in DMF.[16] Several representative tetraols **12** were prepared in good yields *with complete overall diastereoselectivity* illustrating the generality of this strategy (Table 2). The occurrence of a polyol motif **12** in a number of bioactive natural products is noteworthy. Representative examples include the side chain portion of bacteriohopanoid.[17a] and the central macrolide segment of herbarumin I, a highly potent phytotoxic agent.[17b]

In summary, we have demonstrated a highly enantioselective catalytic isomerization of silacyclopentene oxide, a pivotal point in our strategy for the stereoselective assembly of acyclic polyols. Development of an arsenal of new asymmetric processes utilizing cyclic silanes is currently in progress.

Received: September 6, 2001 [Z17864]

[1] a) T.-L. Ho, *Symmetry: A Basis for Synthetic Design*, Wiley, New York, **1995**; b) R. S. Ward, *Chem. Soc. Rev.* **1990**, *19*, 1; c) M. C. Wills, *J. Chem. Soc. Perkin Trans. 1* **1999**, 1765.

[2] For selected examples of catalytic enantioselective desymmetrizations, see: a) S. L. Schreiber, T. S. Schreiber, D. B. Smith, *J. Am. Chem. Soc.* **1987**, *109*, 1525; b) W. A. Nugent, *J. Am. Chem. Soc.* **1992**, *114*, 2768; c) L. E. Martinez, J. L. Leighton, D. H. Carsten, E. N. Jacobsen, *J. Am. Chem. Soc.* **1995**, *117*, 5897; d) T. Iida, N. Yamamoto, H. Sasai, M. Shibasaki, *J. Am. Chem. Soc.* **1997**, *119*, 4783; e) M. Lautens, T. Rovis, *J. Am. Chem. Soc.* **1997**, *119*, 11090; f) S. E. Denmark, P. A. Barsanti, K. T. Wong, R. A. Stavenger, *J. Org. Chem.* **1998**, *63*, 2428; g) T. Oriyama, K. Imai, T. Sano, T. Hosoya, *Tetrahedron Lett.* **1998**, *39*, 397; h) S. L. Aeilts, D. R. Cefalo, P. J. Bonitatebus, J. H. Houser, A. H. Hoveyda, R. R. Schrock, *Angew. Chem.* **2001**, *113*, 1500; *Angew. Chem. Int. Ed.* **2001**, *40*, 1452.

[3] For the use of cyclic siloxanes in stereoselective synthesis, see: a) K. Tamao, T. Nakajima, R. Sumiiya, H. Arai, N. Higuchi, Y. Ito, *J. Am. Chem. Soc.* **1986**, *108*, 6090; b) S. H. Bergens, P. Noheda, J. Whelan, B. Bosnich, *J. Am. Chem. Soc.* **1992**, *114*, 2121; c) M. R. Hale, A. H. Hoveyda, *J. Org. Chem.* **1992**, *57*, 1643; d) M. J. Zacuto, J. L. Leighton, *J. Am. Chem. Soc.* **2000**, *122*, 8587; For the use of siliranes, see: e) P. M. Bodnar; W. S. Palmer, J. T. Shaw, J. H. Smitrovich, J. D. Sonnenberg, A. L. Presley, K. A. Woerpel, *J. Am. Chem. Soc.* **1995**, *117*, 10575, and references therein.

[4] For reviews on preparation and properties of cyclic silanes, see: a) J. Hermanns, B. Schmidt, *J. Chem. Soc. Perkin. Trans. 1* **1998**, 2209; b) J. Hermanns, B. Schmidt, *J. Chem. Soc. Perkin. Trans. 1* **1999**, 81.

[5] J. K. Whitesell, S. W. Felman, *J. Org. Chem.* **1980**, *45*, 755.

[6] For reviews, see: a) J. K. Crandall, M. Apparu, *Org. React.* **1983**, *29*, 345; b) D. M. Hodgson; A. R. Gibbs, G. P. Lee, *Tetrahedron* **1996**, *52*, 14361; c) P. O'Brien, *J. Chem. Soc. Perkin Trans. 1* **1998**, 1439.

[7] For a pioneering investigation on catalytic enantioselective isomerization of carbocyclic epoxides, see: M. Asami, T. Ishizaki, S. Inoue, *Tetrahedron: Asymmetry* **1994**, *5*, 793.

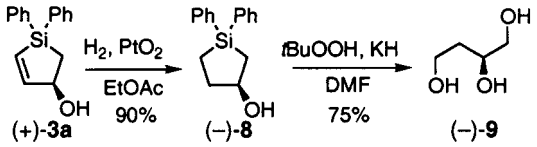
[8] a) W. J. Richter, *Synthesis* **1982**, 1102; b) S. Mignani, D. Damour, J.-P. Bastart, G. Manuel, *Syn. Commun.* **1995**, *25*, 3855.

[9] G. Manuel, R. Boukherroub, *J. Organomet. Chem.* **1993**, *447*, 167.

[10] a) M. J. Södergren, P. G. Andersson, *J. Am. Chem. Soc.* **1998**, *120*, 10760; b) M. J. Södergren, S. K. Bertilsson, P. G. Andersson, *J. Am. Chem. Soc.* **2000**, *122*, 6610.

[11] Determination of the enantiomeric excess was carried out by the Mosher ester ^{1}H NMR analysis; see Supporting Information for details. The attempts to resolve alcohol **3a** using six different chiral HPLC stationary phases proved unsuccessful.

[12] The absolute configuration of silane (*R*)-**3a** was later confirmed by its conversion to the known (*S*)-triol **9**, as illustrated below.



[13] K. Tamao, E. Nakajo, Y. Ito, *J. Org. Chem.* **1987**, *52*, 4414.

[14] K. Tamao, M. Kumada, K. Maeda, *Tetrahedron Lett.* **1984**, 321.

[15] I. Fleming, P. E. Sanderson, *Tetrahedron Lett.* **1987**, *28*, 4229.

[16] J. H. Smitrovich, K. A. Woerpel, *J. Org. Chem.* **1996**, *61*, 6044.

[17] a) N. Zhao, N. Berova, K. Nakanishi, M. Rohmer, P. Mougenot, U. J. Jurgens, *Tetrahedron* **1996**, *52*, 2777; b) J. F. River-Cruz, G. Garcia-Aguirre, C. M. Cerda-Garcia-Rojas, R. Mata, *Tetrahedron* **2000**, *56*, 5337.

The First Catalytic, Diastereoselective, and Enantioselective Crossed-Aldol Reactions of Aldehydes**

Scott E. Denmark* and Sunil K. Ghosh

The apotheosis of the aldol addition reaction is one of the most well-documented chapters of modern organic synthesis; the generality, versatility, and selectivity associated with this process have been the subject of countless reviews and authoritative summaries. Stimulated by the challenge posed by nature, a generation of synthetic organic chemists has constructed an impressive edifice of knowledge which constitutes insightful, elegant, and practical solutions to the structural and stereochemical problems presented by polypropionate-derived natural products. Yet, at this advanced vantage, it is remarkable that the most basic of aldol

[*] Prof. Dr. S. E. Denmark, Dr. S. K. Ghosh
Department of Chemistry, University of Illinois
Urbana, IL 61801 (USA)
Fax: (+1) 217-333-3984
E-mail: denmark@scs.uiuc.edu

[**] We are grateful to the National Science Foundation for generous financial support (NSF CHE 9803124).

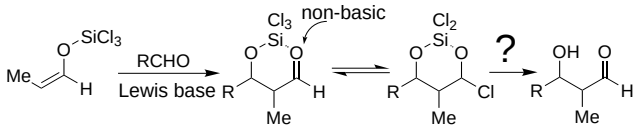
Supporting information for this article is available on the WWW under http://www.angewandte.com or from the author.

 © WILEY-VCH Verlag GmbH, D-69451 Weinheim, 2001 1433-7851/01/4024-4759 $ 17.50+.50/0

constructions, namely the controlled, stereoselective self-condensation of aldehydes, has found no general solution.[1]

Even within the realm of modern enolate chemistry,[2] the problems inherent in this construction are readily apparent: 1) poly-aldolization that results from secondary additions to the aldehyde products, 2) dehydration of the product, which enables Michael-type additions, 3) Tishchenko-type processes, and 4) oligomerization of the product. Superimposed upon these issues is the relatively small size of aldehyde enolates, which renders stereoselection challenging. Nevertheless, a number of notable advances are on record which both overcome and illustrate these problems. Early studies by Heathcock et al. on the *E* and Z lithium enolates of propanal demonstrated the low selectivity and stereochemical convergence in the formation of the (metastable) *syn* and *anti* aldol products.[3] In 1997, Mahrwald et al. reported the crossed addition of aldehydes promoted by $TiCl_4$.[4] Good *syn* selectivity can be obtained with appropriate choice of aldehyde and the products can be isomerized to the more stable *anti* products with $Ti(OiPr)_4$[3b] (also with concomitant Tishchenko reduction[3c]). Aldol addition of trichlorotitanium enolates generated by both reduction and conjugate addition has also been studied by Oshima and co-workers.[5] Stereoselectivity is variable, but highly *syn*-selective processes have been noted. More recently, this group has described the aldol additions of stereodefined *E* and *Z* (tributoxytitanium) enolates of aldehydes.[6] Whereas good yields of aldol products were obtained (also with ketones) the diastereoselectivity was low and weakly dependent on enolate geometry.

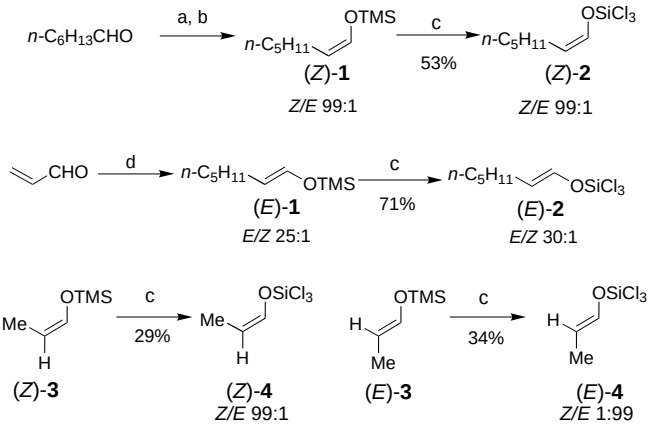
Consideration of the shortcomings outlined above suggested that a potential solution might accrue from the application of our recently developed aldol chemistry of trichlorosilyl enolates[7] of esters,[7b] substituted ketones,[7c] and methyl ketones.[7d] Our mechanistic understanding of this process[8] identifies the crucial role of the Lewis basic oxygen atom of the carbonyl group to associate with the chiral, cationic trichlorosilyl enolate (Scheme 1). Because the aldolate exists



Scheme 1. Formulation of Lewis base catalyzed crossed-aldol reaction of aldehydes.

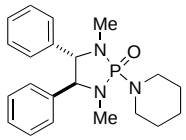
as a chelated complex, the basicity of the carbonyl group of the product is attenuated. Moreover, we expected that the immediate product might exist as a chlorohydrin by analogy with hemiacetal adducts noted by Oshima et al. Finally, in view of the dramatic rate enhancements seen for Lewis base catalysis of these processes, we anticipated that reactions would take place at low temperatures under the influence of chiral phosphoramides. We report herein the successful implementation of this plan which provides the first method of catalytic enantioselective crossed-aldol reactions of aldehydes.

To test the feasibility of this concept first required the generation of stereodefined trichlorosilyl enolates of aldehydes. Although a number of different methods have been described from these laboratories, none were capable of delivering the enoxytrichlorosilanes with high geometrical purity.[9] A new method was therefore devised that has its origins in the Stork–House generation of lithium enolates.[10] Thus, the stereodefined trimethylsilyl enol ethers of heptanal ((*E*)- and (*Z*)-**1**) were prepared by either direct enolization (*Z*/*E* 87:13)[11] followed by chromatographic enrichment or copper-catalyzed conjugate addition of *n*-butylmagnesium chloride to acrolein and trapping with TMSCl[12] (Scheme 2). Cleavage of the TMS enol ethers with MeLi is known to lead to retention of the geometry of the double bond; moreover, after quenching with excess $SiCl_4$ the derived trichlorosilyl enolates (**2**) were found to be highly geometrically enriched. The corresponding trichlorosilyl enolates of propanal ((*E*)-**4** and (*Z*)-**4**) could also be obtained in high geometrical purity by a similar process.[13]



Scheme 2. a) TMSOTf, Et_3N, Et_2O, 56%; b) separate; c) 1. MeLi, Et_2O, 2. $SiCl_4$; d) 1. *n*BuMgCl, $CuBr \cdot Me_2S$, 2. TMSCl, 41%. TMS = Me_3Si; Tf = CF_3SO_2.

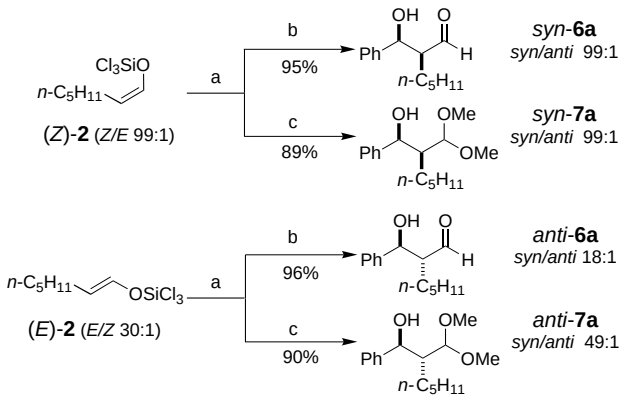
Orienting experiments employed geometrically pure samples of (*Z*)- and (*E*)-**2** in the reaction with benzaldehyde and catalyst (*S*,*S*)-**5**. We were delighted to find that, by using just 5 mol% of catalyst, the aldehyde was consumed at $-78\,^{\circ}C$ within a few hours![14] Quenching the reactions under mildly basic conditions (THF/Et_3N/H_2O 18:1:1) afforded the hydroxy aldehydes **6a** in excellent yield and with extremely high diastereoselectivity (Scheme 3). However, these products were unstable and rapidly formed oligomers on standing.[2, 15] Alternatively, quenching the reactions with dry methanol produced the stable dimethyl acetals **7a** in excellent yield and with similarly high diastereoselectivity. Although the enantioselectivities were poor (see below), the high yields and rigorous relative stereoselection encouraged us to optimize experimental variables and explore the scope of the reaction.



(*S*,*S*)-**5**

Optimization experiments employed a 78:22 mixture of (*E*)-**2** and (*Z*)-**2** with benzaldehyde and catalyst (*S*,*S*)-**5**. A brief examination of solvent and temperature revealed that a 4:1 blend of $CHCl_3$ and CH_2Cl_2 at $-78\,^{\circ}C$ gave faster and

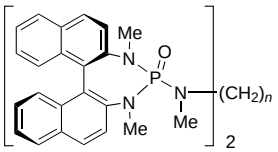
 © WILEY-VCH Verlag GmbH, D-69451 Weinheim, 2001 1433-7851/01/4024-4760 $ 17.50+.50/0 *Angew. Chem. Int. Ed.* **2001**, *40*, No. 24



Scheme 3. a) PhCHO, (*S*,*S*)-**5** (0.05 equiv), CH_2Cl_2, −78 °C; b) THF, Et_3N, H_2O; c) MeOH.

cleaner reactions than CH_2Cl_2 alone. Surprisingly, the reaction rate, yield, and selectivity showed little sensitivity to concentration (0.1 to 1.0 M range) and catalyst loading (0.05 to 1.0 equiv). Accordingly, for the survey of catalyst structure, we employed the most convenient conditions of 0.25 M and only 0.05 equiv of catalyst.

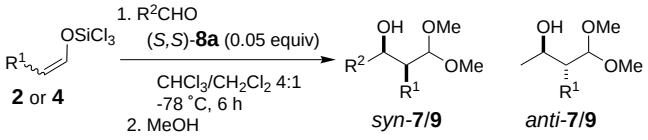
From the wide range of chiral phosphoramides at our disposal[16] several structural motifs were examined and although reactions were effectively catalyzed with excellent diastereoselectivity, the enantiomeric ratios were poor. In view of our recent demonstration that this aldolization process displays a second-order dependence on the phosphoramide[8] we investigated the use of alkyl linked bis-phosphoramides as promoters.[17] Employment of dimeric versions of stilbene-1,2-diamine- and cyclohexyl-1,2-diamine derived catalysts were largely ineffective here. However, we were delighted to find that one structure, namely the dimeric 1,1′-binaphthyl-2,2′diamine-derived phosphoramides **8a** uniquely gave excellent diastereomeric and enantiomeric selectivity. The homologous dimer **8b** was significantly less selective, which further illustrates the sensitivity of this reaction to catalyst structure.[18]



8a: *n* = 5, **8b:** *n* = 6

With an optimized procedure in hand, we could evaluate the substrate generality of the crossed-aldol reaction with enolates **2** and **4** and a variety of aldehydes (Table 1). In all cases, the products were isolated and analyzed as the dimethyl acetals **7** and **9**. With the exception of aliphatic aldehydes as starting material, the aldol products were formed in near quantitative yields as analytically pure acetals. The diastereospecificity for all cases was a near perfect reflection of the geometrical composition of the trichlorosilyl enolate precursors.[19] On the other hand, the enantioselectivity of the process was highly variable and dependent on both the enolate and the aldehyde structure.[20, 21] For example, whereas the reaction of (*Z*)-**2** with benzaldehyde proceeded with very good enantioselectivity, (*E*)-**2** afforded *anti*-**7a** with somewhat attenuated *ee* (Table 1, entries 1 and 2). The effect of enolate structure was immediately apparent in the reactions of (*Z*)-**4** and (*E*)-**4** with benzaldehyde wherein the smaller size of the enolate lead to lower selectivities particularly for (*E*)-**4** (entries 3 and 4). The dependence of enantioselectivity on aldehyde structure was extensively investigated with aromatic, olefinic, acetylenic, and aliphatic aldehydes. In general, the enantioselectivity with

Table 1. Aldol reactions of **2** and **4**.[a]



Entry	Enolate	R^1	R^2	Product	Yield [%][b]	*syn*/*anti*[c]	*ee* [%][c]
1	(*Z*)-**2**	*n*Pent	Ph	**7a**	92	99/1	90
2	(*E*)-**2**	*n*Pent	Ph	**7a**	91	3/97	82
3	(*Z*)-**4**	Me	Ph	**9a**	95	98/2	81
4	(*E*)-**4**	Me	Ph	**9a**	97	1/99	59
5	(*Z*)-**4**	Me	2-naphthyl	**9b**	99	99/1	86
6	(*E*)-**4**	Me	2-naphthyl	**9b**	99	2/98	53
7	(*Z*)-**4**	Me	1-naphthyl	**9c**	97	98/2	54
8	(*E*)-**4**	Me	1-naphthyl	**9c**	97	2/98	70
9	(*Z*)-**4**	Me	(*E*)-PhCH=CH	**9d**	86	99/1	42
10	(*E*)-**4**	Me	(*E*)-PhCH=CH	**9d**	88	1/99	26
11	(*Z*)-**4**	Me	(*E*)-PhCH=C(Me)	**9e**	91	97/3	68
12	(*E*)-**4**	Me	(*E*)-PhCH=C(Me)	**9e**	89	1/99	90
13	(*Z*)-**4**	Me	(*E*)-MeCH=CH	**9f**	85	99/1[d]	5
14	(*E*)-**4**	Me	(*E*)-MeCH=CH	**9f**	91	2/98[d]	52
15	(*Z*)-**4**	Me	PhC≡C	**9g**	98	98/2	7
16	(*E*)-**4**	Me	PhC≡C	**9g**	99	2/98	76
17	(*Z*)-**4**	Me	$PhCH_2CH_2$	**9h**	47	95/5	8
18	(*E*)-**4**	Me	$PhCH_2CH_2$	**9h**	79	1/99	66
19	(*Z*)-**4**	Me	*c*-C_6H_{11}	**9i**	42	97/3[d]	44
20	(*E*)-**4**	Me	*c*-C_6H_{11}	**9i**	69	1/99[d]	19

[a] All reactions run on 1.0 mmol scale. [b] Yield of analytically pure product. [c] Determined by CSP-SFC on Chiralpak columns. [d] Determined by CSP-SFC of the derived benzoates on Chiralpak columns.

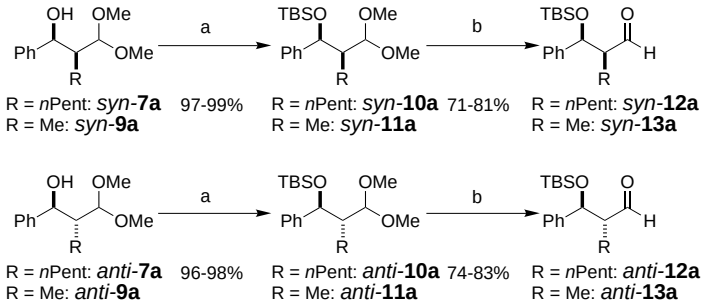
 © WILEY-VCH Verlag GmbH, D-69451 Weinheim, 2001 1433-7851/01/4024-4761 $ 17.50+.50/0

aromatic aldehydes (entries 3–8) was good with the *syn* isomer giving slightly better results. In fact, *syn*-**9b** could be obtained in 66% yield and >99% *ee* after recrystallization. Curiously, 1-naphthaldehyde behaved differently in that the *anti* diastereomer was formed in higher *ee* than the *syn* isomer.

As a class, the unsaturated aldehydes gave overall disappointing enantioselectivities (with the significant exception of 2-methylcinnamaldehdye and (*E*)-**4**) and no trends were immediately apparent (entries 9–14). Here again, the enolate that exhibited the higher enantioselectivity was structure dependent and dramatically so in the case of (*E*)-2-butenal. This behavior was seen in the reaction of phenylpropynal as well. In this case, the *anti* isomer **9g** (from (*E*)-**4**) was formed with good enantioselectivity while *syn*-**9g** (from (*Z*)-**4**) was nearly racemic.

We were pleased to find that (*Z*)-**4** and (*E*)-**4** also reacted with enolizable aliphatic aldehydes although higher temperature (−25 °C) and longer reaction times (20 h) were required (entries 17–20). Hydrocinnamaldehyde reacted in moderate to good yield, but again, the divergence in behavior of the *Z* and *E* enolates is dramatic. Moreover, in the case of cyclohexanecarbaldehyde, (*Z*)-**4** afforded *syn*-**9i** with moderate selectivity whereas (*E*)-**4** now afforded *anti*-**9i** in poor enantioselectivity.

To demonstrate the synthetic utility of the acetals, we converted them to the TBS-protected aldehydes **12a** and **13a** in two high-yielding steps (Scheme 4). These products are stable, chromatographable, distillable liquids that could be obtained in analytically pure form without detectable epimerization.



Scheme 4. a) TBSCl, imidazole, DMF; b) silica gel, oxalic acid (aq), CH_2Cl_2. TBS = tBuMe$_2$Si.

In summary, we have documented the first catalytic enantioselective crossed-aldol reactions of aldehydes. Geometrically defined trichlorosilyl enolates of aldehydes undergo high yielding, diastereoselective additions to a wide range of aldehyde acceptors with good albeit highly variable enantioselectivity. The use of a dimeric chiral Lewis base as the catalyst was critical for achieving useful enantioselectivities. Extension of these studies to other aldehyde enolates and improvements in catalyst design are underway.

Received: August 15, 2001 [Z17734]

[1] The enzyme 2-deoxyribose 5-phosphate aldolase (DERA) does catalyze the aldol addition reaction of acetaldehyde and propanal with various aldehyde acceptors. a) C. F. Barbas III, Y.-F. Wang, C.-H. Wong, *J. Am. Chem. Soc.* **1990**, *112*, 2013; b) L. Chen, D. P. Dumas, C.-H. Wong, *J. Am. Chem. Soc.* **1992**, *114*, 741; c) H. J. M. Gijsen, C.-H. Wong, *J. Am. Chem. Soc.* **1995**, *117*, 7585.

[2] For a recent discourse on the problems of crossed-aldol reactions under acid or base catalysis see: C. H. Heathcock in *Comprehensive Organic Synthesis, Vol. 2, Additions to C-X Bonds, Part 2* (Ed.: C. H. Heathcock), Pergamon, Oxford, **1991**, p. 133.

[3] C. H. Heathcock, C. T. Buse, W. A. Kleschick, M. C. Pirrung, J. E. Sohn, J. Lampe, *J. Org. Chem.* **1980**, *45*, 1066.

[4] a) R. Mahrwald, B. Costisella, B. Gündogan, *Tetrahedron Lett.* **1997**, *38*, 4543; b) R. Mahrwald, B. Costisella, B. Gündogan, *Synthesis* **1998**, 262; c) R. Mahrwald, B. Gündogan, *Chem. Commun.* **1998**, 2273.

[5] a) K. Maeda, H. Shinokubo, K. Oshima, *J. Org. Chem.* **1998**, *63*, 4558; b) S. Uehira, Z. Han, H. Shinokubo, K. Oshima, *Org. Lett.* **1999**, *1*, 1383.

[6] a) K. Yachi, H. Shinokubo, K. Oshima, *J. Am. Chem. Soc.* **1999**, *121*, 9465; b) Z. Han, H. Yorimitsu, H. Shinokubo, K. Oshima, *Tetrahedron Lett.* **2000**, *41*, 4415.

[7] a) S. E. Denmark, R. A. Stavenger, *Acc. Chem. Res.* **2000**, *33*, 432; b) S. E. Denmark, S. B. D. Winter, X. Su, K.-T. Wong, *J. Am. Chem. Soc.* **1996**, *118*, 7404; c) S. E. Denmark, R. A. Stavenger, K.-T. Wong, X. Su, *J. Am. Chem. Soc.* **1999**, *121*, 4982; d) S. E. Denmark, R. A. Stavenger, *J. Am. Chem. Soc.* **2000**, *122*, 8837.

[8] a) S. E. Denmark, X. Su, Y. Nishigaichi, *J. Am. Chem. Soc.* **1998**, *120*, 12990; b) S. E. Denmark, S. M. Pham, *Helv. Chim. Acta* **2000**, *83*, 1846.

[9] S. E. Denmark, R. A. Stavenger, S. B. D. Winter, K.-T. Wong, P. A. Barsanti, *J. Org. Chem.* **1998**, 63, 9517.

[10] a) G. Stork, P. F. Hudrlik, *J. Am. Chem. Soc.* **1968**, *90*, 4464; b) H. O. House, B. M. Trost, *J. Org. Chem.* **1965**, *30*, 2502.

[11] H. Emde, D. Domsch, H. Feger, U. Frick, A. Götz, H. H. Hergott, K. Hofmann, W. Kober, K. Krägeloh, T. Oesterle, W. Steppan, W. West, G. Simchen, *Synthesis* **1982**, 1.

[12] S. Matsuzawa, Y. Horiguchi, E. Nakamura, I. Kuwajima, *Tetrahedron* **1989**, *45*, 349.

[13] For the preparation of (*E*)-**1b** and (*Z*)-**1b**, see Supporting Information.

[14] Control experiments revealed that no addition took place under these conditions in the absence of (*S*,*S*)-**5**.

[15] S. D. Rychnovsky, D. J. Skalitzky, *J. Org. Chem.* **1992**, *57*, 4336.

[16] S. E. Denmark, X. Su, Y. Nishigaichi, D. M. Coe, K.-T. Wong, S. B. D. Winter, J. Y. Choi, *J. Org. Chem.* **1999**, *64*, 1958.

[17] For recent demonstration of the synthetic utility of dimeric phosphoramide promoters see: a) S. E. Denmark, J. Fu, *J. Am. Chem. Soc.* **2000**, *122*, 12021; b) S. E. Denmark, T. Wynn, *J. Am. Chem. Soc.* **2001**, *123*, 6199; c) S. E. Denmark, J. Fu, *J. Am. Chem. Soc.* **2001**, *123*, 9488.

[18] For an analysis of the dependence of the enantioselectivity on catalyst chain length see reference [17a].

[19] The relative configuration of the products was assigned on the basis of the $^3J_{HH}$ couplings in **7** and **9** which displayed the characteristic range of 1.7–3.4 Hz for the *syn* isomers and 6.8–8.8 Hz for the *anti* isomers (see Supporting Information).

[20] The absolute configurations of *syn*-**9a** was assigned by conversion to methyl (−)-3-hydroxy-2-methyl-3-phenylpropanoate which has been unambiguously assigned as the (2*S*,3*S*)-isomer. a) T.-H. Yan, C.-W. Tan, H.-C. Lee, H.-C. Lo, T.-Y. Huang, *J. Am. Chem. Soc.* **1993**, *115*, 2613; b) C. H. Heathcock, C. T. White, J. J. Morrison, D. Van Derveer, *J. Org. Chem.* **1981**, *46*, 1296.

[21] The absolute configuration of *anti*-**9a** was determined by conversion to (−)-3-(*tert*-butyldimethylsiloxy)-2-methyl-3-phenylpropanal which has been unambiguously assigned as the (2*R*,3*S*)-isomer. I. Paterson, D. J. Wallace, C. J. Cowden, *Synthesis* **1998**, 639. We thank Professor Paterson for providing detailed information.

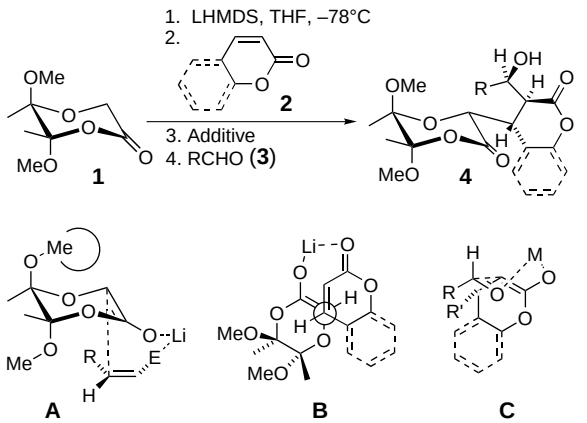
 © WILEY-VCH Verlag GmbH, D-69451 Weinheim, 2001 1433-7851/01/4024-4762 $ 17.50+.50/0

Consecutive Three- and Four-Component Coupling Reactions with Anions Generated from a Butane Diacetal Desymmetrized Glycolic Acid Derivative**

Darren J. Dixon, Steven V. Ley,* and Félix Rodríguez

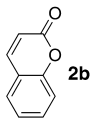
The impressive progress made in the last few years in high-throughput screening of compounds for biological testing has driven synthetic chemists to develop new procedures and technologies for the production of diverse arrays of compounds in a fast, clean, and efficient way. Among these procedures, the sequential coupling reactions (domino or consecutive) offer the opportunity of building up large libraries of complex molecules from simple substrates within a short time and with an important reduction in production costs and in the amount of waste generated.[1] For these reasons, the sequential processes extend far beyond an academic pursuit[2] by providing a rapid solution to the synthesis of new, functionally dense skeletal arrangements which may exhibit desirable biological properties. Notable sequential reactions include the four-component Ugi reaction[3] and the MIMIC chemistry introduced by Posner et al.[4] However, although these methods create desirable functional group density around a central core, more often than not these processes lack stereocontrol and lead to mixtures of diastereomers. Furthermore, such reactions are rarely enantioselective and yield racemic products. Clearly, a significant advancement in this field would be provided by sequential coupling processes in which the products are formed as single diastereomers and enantiomers.[5] To this end we have investigated the use of butane diacetal (BDA) desymmetrized glycolic acid derivative **1** (Scheme 1) for reactions of this type. This was partly a result of the abundance of biologically and pharmacologically significant α-hydroxy acids,[6] but more importantly because of the excellent levels of stereocontrol imparted by this building block in lithium enolate alkylation,[7] aldol,[8] and Michael[9] reactions to give a variety of enantiopure α-hydroxy acids. It was our view that **1** would not only be the sole source of asymmetry but would also govern the relative stereochemistry in the subsequent C–C bond-forming reactions. Herein we report new stereoselective one-pot consecutive reactions starting with anions generated from **1**. This strategy has allowed us to produce, in a single step, α-hydroxy acids with up to five new stereogenic centers in high yield and in high diastereomeric excesses.

Treatment of **1**[7] with one equivalent of lithium hexamethyldisilazide (LHMDS) in THF at $-78\,^{\circ}C$, followed by the addition of one equivalent of α,β-unsaturated lactones **2**, and after 30 min the addition of another electrophile coupling partner (e.g. aldehydes **3**) led to the three-component coupling products **4** as a mixture of only two diastereomers (Scheme 1; Table 1, entries 1, 3, and 5; only the major diastereomer is depicted). Moreover, when the reaction was carried out in the presence of one equivalent of trimethyl borate, the selectivity of the reaction was increased to give compounds **4** with d.r. values as high as 5.2:1 (Table 1, entries 2, 4, and 6).



Scheme 1. α-Hydroxy acid derivatives **4** from the one-pot consecutive Michael–aldol reaction initiated with the enolate derived from **1**. R′ = BDA moiety.

Table 1. Three-component coupling products **4** obtained according to Scheme 1.

Entry	2	R	Additive	Product	Yield [%][a]	d.r.[b]
1	 **2a**	Ph	–	**4a**	74	2.8:1
2	**2a**	Ph	$B(OMe)_3$	**4a**	72	4.0:1
3	**2a**	4-MeO-C_6H_4	–	**4b**	66	2.5:1
4	**2a**	4-MeO-C_6H_4	$B(OMe)_3$	**4b**	63	5.2:1
5	 **2b**	4-MeO-C_6H_4	–	**4c**	73	3.2:1
6	**2b**	4-MeO-C_6H_4	$B(OMe)_3$	**4c**	64	3.3:1

[a] Yield based on starting BDA desymmetrized glycolic acid derivative **1**. [b] Ratio determined by means of ^1H NMR spectroscopy.

The structures of compounds **4** (major and minor diastereomers) were determined by means of NMR spectroscopy and confirmed by X-ray crystal structure analysis.[10] These studies indicate that the only difference between the two diastereomers is the stereochemistry of the carbon atom that bears the hydroxy group formed in the final aldol reaction. Surprisingly, the major diastereomers contain a *syn* β-hydroxycarbonyl structure, which is not the expected product from an aldol reaction between an *E* enolate and an aldehyde, according to the Zimmerman-Traxler chairlike transition-state model.[11] The stereochemical outcome of the reaction can be explained as follows: first, the Michael acceptor approaches the lithium enolate derived from glycolate **1** from

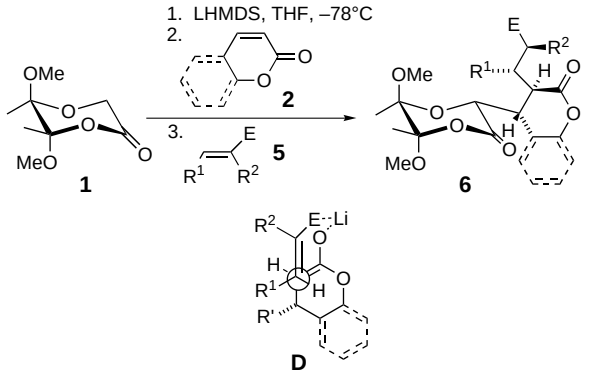
[*] Prof. Dr. S. V. Ley, Dr. D. J. Dixon, Dr. F. Rodríguez
Department of Chemistry, University of Cambridge
Lensfield Road, Cambridge CB2 1EW (UK)
Fax: (+44) 1223-33-6442
E-mail: svl1000@cam.ac.uk

[**] We gratefully acknowledge financial support from the EPSRC (to D.J.D.), the EU (Marie Curie Fellowship to F.R.), and the Novartis Research Fellowship (to S.V.L.). We are also indebted to Dr. John E. Davis for the X-ray crystal structure determinations.

 © WILEY-VCH Verlag GmbH, D-69451 Weinheim, 2001 1433-7851/01/4024-4763 $ 17.50+.50/0

the face opposite the axial 1,3-related methoxy group (see **A** in Scheme 1). Moreover, the configurational assignment of the products is compatible with a combination of the two trigonal centers involved in this reaction according to the model shown in **B** (Scheme 1).[12] This first reaction proceeded with very high diastereoselectivity to give a new lithium enolate intermediate.[13] The reaction of this newly formed enolate with the aldehyde to give mainly the *syn* aldol product can be explained through the closed twist-boat transition state shown in **C** (Scheme 1).[14, 15]

Encouraged by the results obtained in the one-pot Michael–aldol reaction described above and to extend the scope of this methodology, we decided to investigate the one-pot Michael–Michael three-component coupling reaction. Thus, treatment of the enolate derived from **1**, generated as above, with α,β-unsaturated lactones **2**, followed by reaction with a second Michael acceptor **5** gave the highly functionalized α-hydroxy acid derivatives **6** in high yields (Scheme 2). When



Scheme 2. α-Hydroxy acid derivatives **6** from the one-pot consecutive Michael–Michael reaction initiated with the enolate derived from **1**. R′ = BDA moiety.

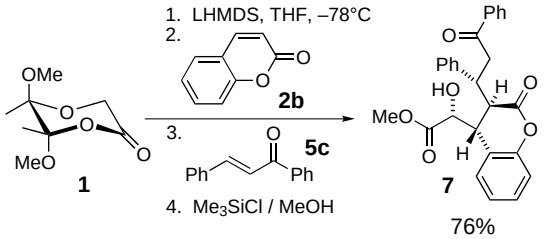
5,6-dihydro-2*H*-pyran-2-one **2a** was used as the first Michael acceptor, a mixture of only two diastereomers was obtained (3:1 ratio; Table 2, entry 1). Pleasingly, when the reaction was carried out with coumarin **2b** as the first Michael acceptor, selectivities higher than 20:1 were observed (Table 2, entries 2–4). The structures of the major and minor diastereomers of **6a**, as well as compounds **6c** and **6d**, were unequivocally determined by X-ray structure analysis.[10] The stereochemical outcome of the process can be explained, in the first steps of the reaction, as previously described for the case of the Michael–aldol reaction (see **A** and **B** in Scheme 1). The second Michael addition seems to occur through the closed (chelated) transition state model shown in **D** (Scheme 2) and previously proposed for related reactions.[12]

We were also intrigued by the possibility of incorporating a new component into the reaction sequence with the concomitant removal of the BDA protecting group. Thus, we investigated the one-pot four-component coupling reaction described in Scheme 3. Consecutive reaction of the enolate derived from **1** with coumarin **2b** followed by reaction with *trans* chalcone **5c** and final treatment with chlorotrimethylsilane in methanol gave α-hydroxy acid derivative **7** in excellent yield (76%) and diastereoselectivity (>20:1) in a single step.

Table 2. Three-component coupling products **6** obtained according to Scheme 2.

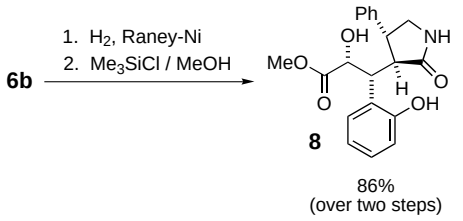
Entry	2	5	Product	Yield [%][a]	d.r.[b]
1	**2a**	**5a**	**6a**	80	3:1
2	**2b**	**5a**	**6b**	81	>20:1
3	**2b**	**5b**	**6c**	90	>20:1
4	**2b**	**5c**	**6d**	95	>20:1

[a] Yield based on **1**. [b] Ratio determined by means of ^{1}H NMR spectroscopy.



Scheme 3. α-Hydroxy ester **7** from the one-pot consecutive Michael–Michael–Michael reaction initiated with the enolate derived from **1**.

The synthetic utility of some of these multicomponent coupling products is illustrated by the transformation of compound **6b** into γ-lactam **8** through the sequential nitro reduction/cyclization process shown in Scheme 4. The highly functional compound **8** is readily prepared and combines α-hydroxy acid, γ-lactam, phenol functionalities, and four stereogenic centers in its structure.[6, 16] Furthermore, these functional groups could be modified to lead to even larger arrays of compounds.



Scheme 4. Highly functionalized γ-lactam **8** from compound **6b**.

 © WILEY-VCH Verlag GmbH, D-69451 Weinheim, 2001 1433-7851/01/4024-4764 $ 17.50+.50/0 *Angew. Chem. Int. Ed.* **2001**, *40*, No. 24

In summary, BDA desymmetrized glycolic acid has proved to be an interesting reagent in one-pot, consecutive, three- and four-component coupling reactions. Highly functionalized α-hydroxy acid derivatives are obtained in good yields and with high diastereoselectivities from simple and readily available starting materials. The simplicity of the method should allow the synthesis of large libraries of compounds with potential biological activity in an easy, fast, clean, and efficient way. Investigations along these lines as well as on the mechanisms of the reactions and the applications of this methodology in the synthesis of natural products are underway in our laboratories.

Experimental Section

Representative procedure for the preparation of **7**: A solution of lithium hexamethyldisilazide in THF (1M, 0.20 mL, 0.20 mmol) was added dropwise to a solution of **1** (0.038 g; 0.20 mmol) in THF (0.5 mL) at $-78\,^{\circ}C$. The resulting pale yellow solution was stirred for 10 min at the same temperature, and then a solution of coumarin **2b** (0.032 g; 0.22 mmol) in THF (0.5 mL) was added dropwise at $-78\,^{\circ}C$. After 30 min, a solution of *trans* chalcone **5c** (0.045 g, 0.22 mmol) was added dropwise. The reaction mixture was stirred for a further 30 min at the same temperature, and then a solution of trimethylsilyl chloride (0.31 mL) in methanol (5 mL) was added at $-78\,^{\circ}C$. The reaction mixture was warmed to room temperature overnight. The solvents were removed in vacuo to give the crude product, which was purified by column chromatography (1:1 petroleum ether/ethyl acetate) to afford pure **7** (0.063 g, 76%): $[\alpha]_D^{25} = +30.5$; ^1H NMR (400 MHz, $CDCl_3$): $\delta = 7.75-6.69$ (m, 14H; ArH), 4.15 (dd, $J = 5.9$, 3.1 Hz, 1H; C*H*OH), 3.61 (s, 3H; OCH_3) 3.48 (d, $J = 6.6$ Hz, 2H; CH_2CO), 3.29 (dt, $J = 11.6$, 6.6 Hz, 1H; CHPh), 3.14 (dd, $J = 11.6$, 1.0 Hz, 1H; $CHCO_2$), 2.88 (d, $J = 3.1$ Hz, 1H; OH), 2.81 (d, $J = 5.9$ Hz, 1H; C*H*CHOH; unresolved coupling to $CHCO_2$); ^{13}C NMR (100 MHz, $CDCl_3$): $\delta = 197.2$, 172.2, 169.2, 152.2, 140.6, 136.7, 133.0, 129.0, 128.4, 127.9, 127.8, 124.6, 117.7, 74.7, 52.6, 49.1, 43.5, 42.9, 39.8; HRMS (EI): calcd for $C_{27}H_{24}O_6NNa$ $[M+Na]^+$: 467.1471, found: 467.1481.

Received: September 5, 2001 [Z17855]

[1] a) L. F. Tietze, *Chem. Rev.* **1996**, *96*, 115; b) L. F. Tietze, U. Beifuss, *Angew. Chem.* **1993**, *105*, 137; *Angew. Chem. Int. Ed. Engl.* **1993**, *32*, 131; c) G. H. Posner, *Chem. Rev.* **1986**, *86*, 831.

[2] a) K. C. Nicolaou, E. W. Yue, T. Oshima in *The New Chemistry* (Ed.: N. Hall), Cambridge University Press, Cambridge, **2001**, p. 168; b) L. F. Tietze, F. Haunert in *Stimulating Concepts in Chemistry* (Eds.: F. Vögtle, J. F. Stoddart, M. Shibasaki), Wiley-VCH, Weinheim, **2000**, p. 39.

[3] A. Dömling, I. Ugi, *Angew. Chem.* **2000**, *112*, 3300; *Angew. Chem. Int. Ed.* **2000**, *39*, 3169.

[4] G. H. Posner, K. S. Webb, E. Asirvatham, S. Jew, A. Del'Innocenti, *J. Am. Chem. Soc.* **1988**, *110*, 4754.

[5] For some recent papers on asymmetric sequential reactions, see: a) J. Barluenga, F. Rodríguez, F. J. Fañanás, E. Rubio, *Angew. Chem.* **1999**, *111*, 3272; *Angew. Chem. Int. Ed.* **1999**, *38*, 3084; b) S. Ikeda, D. Cui, Y. Sato, *J. Am. Chem. Soc.* **1999**, *121*, 4712; c) S. G. Davies, D. R. Fenwick, *Chem. Commun.* **1997**, 565.

[6] G. M. Coppola, H. F. Schuster in *α-Hydroxy Acids in Enantioselective Synthesis*, VCH, Weinheim, **1997**.

[7] E. Díez, D. J. Dixon, S. V. Ley, *Angew. Chem.* **2001**, *113*, 2990; *Angew. Chem. Int. Ed.* **2001**, *40*, 2906.

[8] D. J. Dixon, S. V. Ley, A. Polara, T. Sheppard, *Org. Lett.* **2001**, in press.

[9] D. J. Dixon, S. V. Ley, F. Rodríguez, *Org. Lett.* **2001**, in press.

[10] Crystallographic data (excluding structure factors) for the structures reported in this paper have been deposited with the Cambridge Crystallographic Data Centre as supplementary publication no. CCDC-171362 to -171368. Copies of the data can be obtained free of charge on application to CCDC, 12 Union Road, Cambridge CB2 1EZ, UK (fax: (+44) 1223-336-033; e-mail: deposit@ccdc.cam.ac.uk).

[11] H. E. Zimmerman, M. D. Traxler, *J. Am. Chem. Soc.* **1957**, *79*, 1920.

[12] For some excellent works on the steric course of enolate Michael addition reactions, see: a) K. Suzuki, D. Seebach, *Liebigs Ann. Chem.* **1992**, 51; b) D. A. Oare, M. A. Henderson, M. A. Sanner, C. H. Heathcock, *J. Org. Chem.* **1990**, *55*, 132; c) D. A. Oare, C. H. Heathcock, *J. Org. Chem.* **1990**, *55*, 157.

[13] The first Michael addition reaction was proven to proceed in a 22:1 d.r. in the case of **2a** and 65:1 d.r. in the case of **2b**; see ref. [9].

[14] This kind of transition state has been proposed previously for the aldol reaction between *E* enolates and aldehydes: a) Y. Li, M. N. Paddon-Row, K. N. Houk, *J. Org. Chem.* **1990**, *55*, 481; b) C. Gennari, R. Todeschini, M. G. Beretta, G. Favini, C. Scolastico, *J. Org. Chem.* **1986**, *51*, 612; c) R. W. Hoffmann, K. Ditrich, S. Froesch, *Tetrahedron* **1985**, *41*, 5517.

[15] Although less likely, an "open" (nonchelated) transition state is feasible: a) S. E. Denmark, B. R. Henke, *J. Am. Chem. Soc.* **1991**, *113*, 2177; b) R. Noyori, I. Nishida, J. Sakata, *J. Am. Chem. Soc.* **1981**, *103*, 2106; c) D. Dougherty, *Tetrahedron Lett.* **1982**, 4891.

[16] γ-Lactams and γ-amino acids are important pharmacologically active compounds. For examples, see: a) R. B. Silverman, R. Andruszkiewicz, S. M. Nanavati, C. P. Taylor, M. G. Vartanian, *J. Med. Chem.* **1991**, *34*, 2298; b) H. H. Schneider, R. Schmiechen, M. Brenzinnki, J. Seider, *Eur. J. Pharmacol.* **1986**, *127*, 105; c) B. Lippert, B. W. Metcalf, M. J. Jung, *Eur. J. Biochem*. **1977**, *74*, 441.

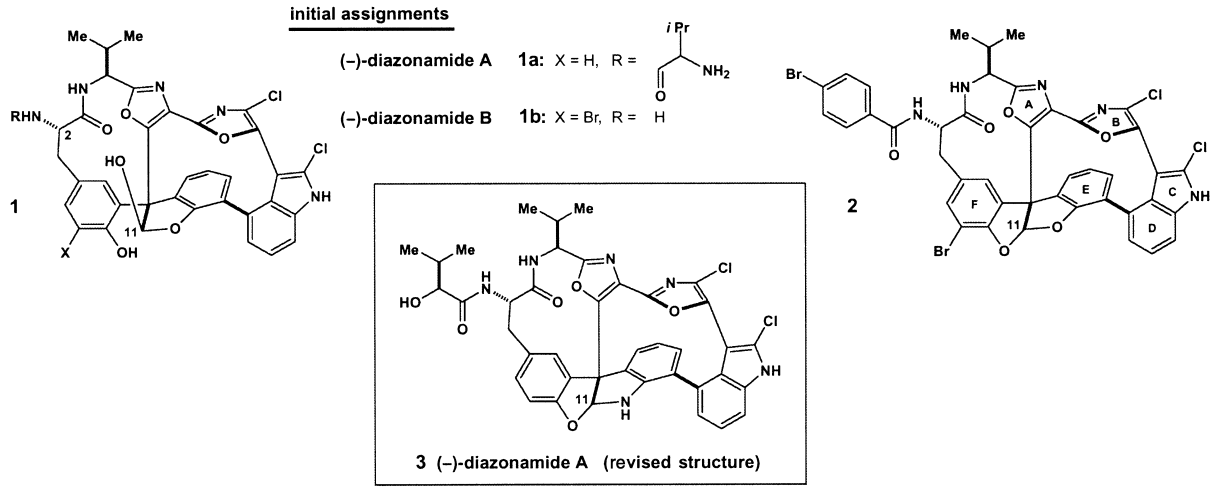
Total Synthesis of Nominal Diazonamides—Part 1: Convergent Preparation of the Structure Proposed for (−)-Diazonamide A**

Jing Li, Susan Jeong, Lothar Esser, and Patrick G. Harran*

In 1991 Fenical, Clardy and co-workers reported the composition and skeletal stereochemistry of two unique toxins extracted from tissues of the marine invertebrate *Diazona angulata*.[1] The structure of the major isolate, termed diazonamide B (**1b**, Scheme 1), was given from X-ray diffraction measurements on a crystal of derived *p*-bromobenzamide **2**. The acylation of **1b** purportedly caused dehydration of its C11 hemiacetal, which leaves the configuration at this position the one noted ambiguity in an analysis that included designation of absolute stereochemistry. The core of the minor metabolite was subsequently assigned by analogy and a complete proposal (**1a**) made more consistent with available

[*] Prof. P. G. Harran, J. Li, S. Jeong
Department of Biochemistry
University of Texas, Southwestern Medical Center at Dallas
Dallas, TX 75390-9038 (USA)
Fax: (+1) 214-648-6455
E-mail: pharra@biochem.swmed.edu
L. Esser[+]
Laboratory of Cell Biology, National Cancer Institute
National Institutes of Health, Bethesda, MD 20892 (USA)
[+] Address correspondence to this author regarding X-ray analyses.

[**] Funding provided by the NIH (RO1-GM60591), the NSF (CAREER 9984282), the Howard Hughes Medical Institute (junior faculty support), the Robert A. Welch Foundation, and the Advanced Research Program of the Texas Higher Education Coordinating Board.

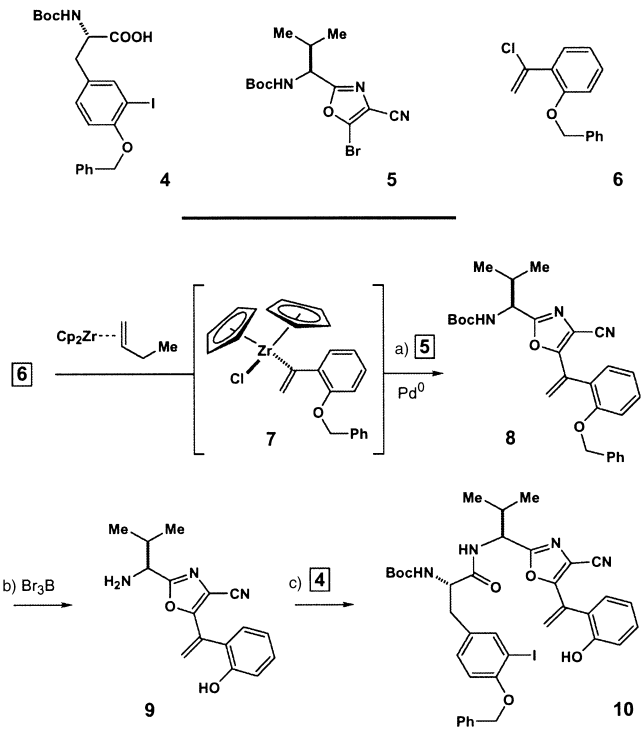


Scheme 1. Diazonamide structure: initial and revised assignments.

data by incorporation of a valine-derived C2-amine appendage (of undetermined configuration).[2] In retrospect, evidence argued against this specification.[3] However, in the excitement of uncovering such a remarkable new class of materials and the finding that one of them (namely, diazonamide A) showed potent antineoplastic activity,[4] certain details were inadvertently overlooked.

In the decade since this report, diazonamide synthesis has become a topic of considerable interest. Numerous laboratories have taken on the architectural problem and important progress has been made in key areas.[5] Our own tactics for constructing a diazonamide ring system have likewise evolved steadily.[6] Herein we describe a culmination of these efforts with the preparation of **1a** and **2**. Our doing so makes it clear for the first time that neither is a natural product (or a derivative). Rather, new evidence suggests that the true structure of (−)-diazonamide A is L-α-hydroxyisovaleric acid conjugate **3** (Scheme 1).[3]

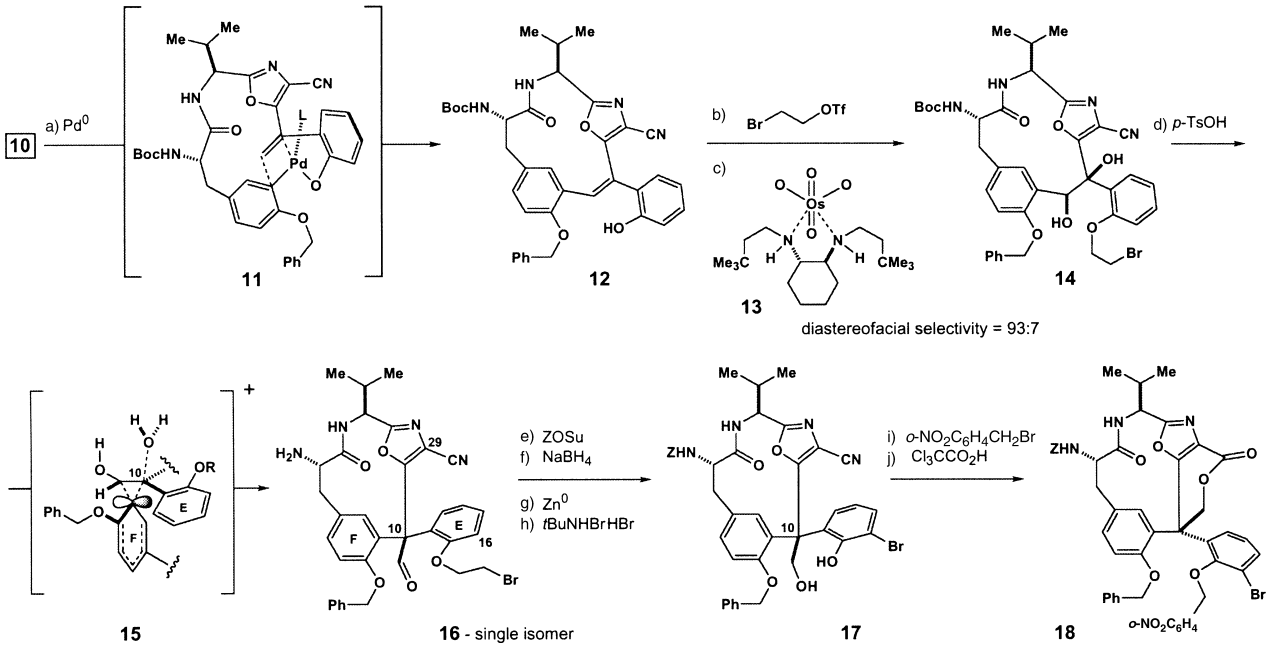
Key design elements in our synthesis respond to stereochemical challenges provided by the structure of diazonamides. These have been described elsewhere.[6a,b] Suffice it to say that the completed effort can be broken down into five segments of comparable size, two of which are commercial products and mole quantities of the other three (**4**–**6**, Scheme 2) are readily accessible.[7] For reasons that will become apparent, the macrolactam harboring the central core of the molecule is built first. This begins by treating dibutylzirconocene[8] with α-chloro styrene **6**. The regiodefined vinyl Zr^{IV} species (**7**, Scheme 2) putatively generated in situ is then cross-coupled with bromide **5** in a process catalyzed by palladium to afford 1,1-disubstituted ethylene **8**. Notably, this variant of Takahashi's modification[9] of a Negishi coupling neither requires nor benefits from a Zr-to-Zn transmetalation prior to addition of the electrophile. The protecting groups on **8** are subsequently removed and the amine produced (**9**) is condensed with tyrosine derivative **4** to afford modified dipeptide **10**. When **10** is exposed to catalytic Pd^0 in the presence of Ag_3PO_4, cyclic triarylethylene **12** is formed at 75 °C (Scheme 3). This Heck endocyclization is pivotal[10] in that **12** has the content of a diazonamide core and



Scheme 2. Reaction conditions: a) [Cp_2ZrCl_2], *n*BuLi, THF, −78 °C, then **6**, −78 °C → RT, 3 h; 3.8 mol% $Pd(OAc)_2$, 3.8 mol% P(*o*-tolyl)$_3$, Ag_3PO_4, **5**, RT, 8 h, (85%); b) 2.5 equiv BBr_3, CH_2Cl_2, −78 → −20 °C, (quant.); c) **4**, *i*Pr_2NEt, TBTU, DMF, RT, (89%). Boc = tert-butoxycarbonyl; TBTU = 2-(1*H*-benzotriazol-1-yl)-1,1,3,3-tetramethyluronium tetrafluoroborate.

needs only to be oxidatively restructured to reveal this feature. After the C16 phenol is derivatized as its 2-bromoethyl ether, oxidation is achieved by exposure to the complex formed between OsO_4 and (1*S*,2*S*)-*N*,*N*′-bis(3,3-dimethylbutyl)-cyclohexane-1,2-diamine (namely, **13**).[11] Decomposition of incipient Os^{VI} glycolates with H_2S provides a 93:7 ratio of diastereomeric *syn*-glycols in which β-isomer **14** is favored—a particularly gratifying outcome for this stereochemically mismatched transformation.[12] With **14** in hand, its

 © WILEY-VCH Verlag GmbH, D-69451 Weinheim, 2001 1433-7851/01/4024-4766 $ 17.50+.50/0 *Angew. Chem. Int. Ed.* **2001**, *40*, No. 24



Scheme 3. Reaction conditions: a) 3 mol % $[Pd_2(dba)_3]$, 6 mol % 2-(di-*tert*-butylphosphanyl)biphenyl, Ag_3PO_4, THF, 75 °C (82 % based on recovered **10**); b) *t*BuOK, THF, 1.2 equiv 2-bromoethyltriflate, 0 °C; c) 1.2 equiv **13**, toluene, $-78 \rightarrow -25$ °C; H_2S(g), THF, -50 °C, (67 % from **12**); d) 3×1 equiv *p*-TsOH, toluene, 95 °C, 40 min; e) ZOSu, DMF, RT, (54 % from **14**); f) $NaBH_4$, $CeCl_3 \cdot 7H_2O$, MeOH; g) Rieke zinc (excess), 3:1 THF/EtOH, 0 °C, (75 % from **16**); h) $tBuNH_2/Br_2$ complex, toluene/THF/CH_2Cl_2, $-78 \rightarrow -20$ °C, 10 h (86 %, *ortho*:*ortho*/*para* = 5:1); i) *o*-nitrobenzyl bromide, K_2CO_3, NaI, DMF, (52 %); j) 4.8 equiv Cl_3CCO_2H, 1 equiv H_2O, toluene, 68 °C, (90 %). dba = *trans*,*trans*-dibenzylideneacetone; Z = benzyloxycarbonyl; Su = *N*-succinimidyl.

restructuring takes the form of a ring-contracting pinacol rearrangement initiated with anhydrous *p*-TsOH. While efficiency is modest for the change, stereochemical communication is near perfect (presumably mediated by phenonium ion **15**)[6b] as triarylacetaldehyde **16** is produced as a single C10 diastereomer. It should be noted that the operations that convert **12** to **16** are our only deliberate stereochemical manipulations. The axial asymmetries of the diazonamide polycycle can now be made an artifact of their assembly.[13] Following carbamoylation of the C2 amine, reduction of the C10 aldehyde, and degradation of the 2-bromoethyl ether, the resultant E-ring phenol is *ortho*-brominated to afford **17**.[14] Reetherification of the more acidic nucleophile in **17** then provides a product that, when warmed with moist Cl_3CCO_2H, generates lactone **18**.

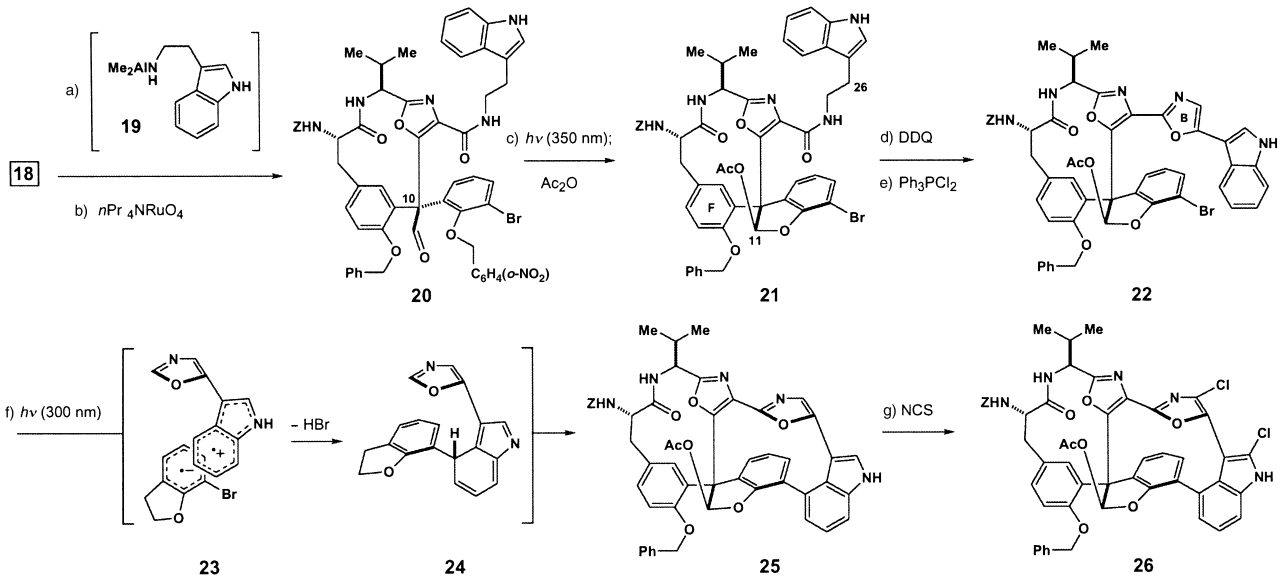
Active ester **18** is now a versatile platform on which to launch attempts at completing a target polycycle. While this goal was elusive for some time, nonproductive forays finally gave way to success. Lactone **18** is opened with dimethylaluminum amide **19** which was derived in situ from tryptamine and $AlMe_3$.[6b] The resultant δ-hydroxy amide is oxidized with $n Pr_4NRuO_4$ and the aldehyde formed (**20**) briefly photolyzed (350 nm) in dilute dioxane solution to provide a crude C11 hemiacetal (Scheme 4). Acylation of this material with Ac_2O affords a single diastereomer of acetate **21**.[15] A two-step oxidation/cyclodehydration[5q] protocol then parlays the acyl tryptamine segment of this molecule into bis(oxazoyl)indole **22**—a structure one-bond removed from the target ring system.

Gratifyingly, UV irradiation of degassed solutions of **22** (300 nm, 5.0×10^{-3} M in 3:1 CH_3CN/H_2O) results in loss of HBr and the formation of internal arylation product **25**. A single regioisomeric biaryl (one atropdiastereomer) is isolated from this reaction although there is competing production of uncyclized materials lacking bromine. One mechanism to interpret this Witkop-type cyclization[16] invokes intramolecular photo-induced electron transfer from the indole chromophore to the adjacent bromo arene. Mesolytic elimination of bromide from the resultant radical-ion pair **23**, biradical collapse, and prototropy in 4*H*-indole **24** would give **25**. A benefit realized by including Li^+ ions into the medium,[17] the inability of 4-methyl-2,6-di(*tert*-butyl)phenol to inhibit the reaction, and the observation that materials chlorinated at C25 and C27 do not photocyclize similarly are consistent with this view.[18]

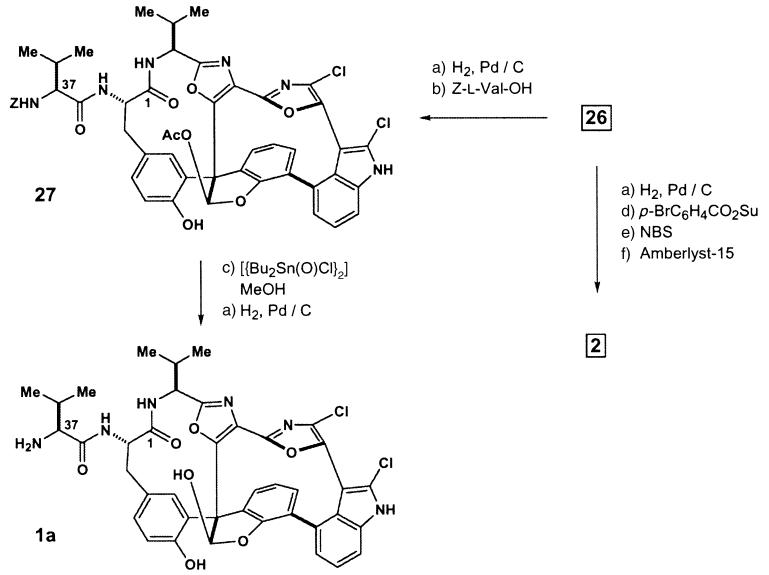
With **25** in hand, completion of a putative diazonamide is straightforward. The right periphery of the molecule is oxidized with *N*-chlorosuccinimide to afford dichloride **26** directly (Scheme 5).[6a] This material is then partially hydrogenolyzed and the product amine reacylated with Z-L-Val-OH. Stannoxane-catalyzed deacetylation of the acetyl hemiacetal[6a] and a final hydrogenolysis provides **1a**—the structure originally proposed for (−)-diazonamide A.[1a]

Remarkably, this material is different from a sample of natural (−)-diazonamide A,[19] particularly by qualitative measures such as its stability to handling[20] and its mobility on a thin-layer chromatography plate. The former issue is most troubling. Mass spectrometry indicates that late synthetic intermediates begin to decompose through net C10 deformylation almost immediately after unmasking a free C11 hemiacetal. The process completes upon attempted preparative HPLC purification of **1a** under conditions identical to those used to isolate natural (−)-diazonamide A.[2] In addition, a second degradation pathway available in this series

 © WILEY-VCH Verlag GmbH, D-69451 Weinheim, 2001 1433-7851/01/4024-4767 $ 17.50+.50/0



Scheme 4. Reaction conditions: a) 1.3 equiv **19**, toluene/CH_2Cl_2, 0°C→RT, (83%); b) 5 mol% nPr_4NRuO_4, 1.5 equiv NMO, 4 Å MS, CH_2Cl_2, (78%); c) *hν* (350 nm), 0.003 M in degassed dioxane; excess Ac_2O, pyridine, DMAP, CH_2Cl_2, (85%); d) 2.2 equiv DDQ, 9:1 THF/H_2O, (89%); e) $(Cl_3C)_2$, Ph_3P, Et_3N, THF, (68%); f) *hν* (300 nm), 2 equiv LiOAc, 3 equiv epichlorohydrin, 0.005 M in 3:1 CH_3CN/H_2O, (32–40%); g) 2 equiv NCS, THF, 32°C, 10 h, (60%). NMO = 4-methylmorpholine-*N*-oxide; DMAP = 4-dimethylaminopyridine; DDQ = 2,3-Dichloro-5,6-dicyano-1,4-benzoquinone; NCS = *N*-chlorosuccinimide.



Scheme 5. Reaction conditions: a) 1 atm H_2, 10% Pd/C, MeOH, RT, (quant.); b) Z-L-Val-OH, TBTU, *i*Pr_2NEt, DMF, (92%); c) 40 mol% $[\{Bu_2Sn(O)Cl\}_2]$, toluene/MeOH 70°C, (80%); d) *p*-$BrC_6H_4CO_2Su$, DMF, RT, (79%); e) NBS, *i*Pr_2NH, CH_2Cl_2/THF, (48%); f) Amberlyst-15, 4 Å MS, 1:4 CH_3CN/CH_2Cl_2 (54–85%). NBS = *N*-bromosuccinimide.

appears as a result of the cleavage of the strained macrolactam ring through diketopiperazine formation that involves the C37 amine and the C1 amide carbonyl.[21] These observations, and compelling spectroscopic data,[3] suggest a misassignment of the C2 amine appendage. However, this is not the whole story. We have synthesized the reported derivative of diazonamide B (**2**, Scheme 5) whose crystallographic characterization formed the basis of initial diazonamide assignments. While fully consistent with our designation, ^{1}H-NMR data for synthetic **2** is subtly different from that reported for material derived from natural (−)-diazonamide B.[2] The X-ray structure of C11 diphenyl acetal **28** (Figure 1)[22] makes it very likely that the heterocyclic skeletons shown for synthetic **1a** and **2** are correct—a result which leaves the true constitution of natural diazonamides in doubt. A solution to this puzzle requires reinterpretation of data collected on natural isolates as well as new insights. The communication directly following this one provides both.[3]

Experimental Section

2 (synthetic): $R_f = 0.72$ (35% EtOAc/benzene); $[\alpha]_D^{25} = -108.8°$ ($c = 0.32$, MeOH); IR (film): $\tilde{\nu} = 3281, 2965, 1660, 1651, 1644, 1538, 1479, 1063, 752\ cm^{-1}$; ^{1}H NMR (400 MHz, [D$_4$]MeOH, 25°C): $\delta = 7.79$ (d, $J = 8.4$ Hz, 2H), 7.66 (d, $J = 8.4$ Hz, 2H), 7.52 (s, 1H), 7.51 (s, 1H), 7.48 (dd, $J = 0.8$, 8.4 Hz, 1H), 7.38 (app t, $J = 8.4$ Hz, 1H), 7.24 (m, 2H), 7.11 (dd, $J = 1.2$, 7.6 Hz, 1H), 6.97 (app t, $J = 7.6$ Hz, 1H), 6.93 (s, 1H), 4.99 (d, $J = 6.0$ Hz, 1H), 4.76 (dd, $J = 2.8$, 12.0 Hz, 1H), 3.60 (app t, $J = 12.0$ Hz, 1H), 2.92 (dd, $J = 3.2$, 12.8 Hz, 1H), 2.36–2.28 (sym 6-line m, 1H), 1.11 (d, $J = 6.8$ Hz, 3H), 1.01 (d, $J = 6.8$ Hz, 3H); ^{13}C NMR (75 MHz, [D$_4$]MeOH, 25°C): $\delta = 174.9, 168.6, 163.4, 159.7, 156.5, 154.8, 152.9, 141.9, 139.9, 136.7, 134.5, 134.4, 133.6, 133.0, 132.7, 130.7, 130.6, 130.6, 130.2, 129.6, 129.2, 128.8, 127.5, 126.4, 125.4, 124.5, 124.17, 124.16, 122.7, 119.5, 112.5, 104.0, 98.0, 63.1, 58.4, 56.6, 37.9, 31.6, 19.5, 18.8$; ES-MS: calcd for $C_{42}H_{27}Br_2Cl_2N_5O_6$ [M^++H]: 925.98, found: 926.04; calcd for $C_{42}H_{27}Br_2Cl_2N_5O_6$ [M^- − H]: 923.96, found: 923.96; HR-FAB-MS: calcd for $C_{42}H_{27}Br_2Cl_2N_5O_6$ [M^++Li]: 931.9865, found: 931.9878.

27: $R_f = 0.25$ (50% EtOAc/benzene); $[\alpha]_D^{25} = -211.8°$ ($c = 0.40$, MeOH); IR (film): $\tilde{\nu} = 3270, 2966, 1766, 1658, 1651, 1514, 1205, 1048, 754\ cm^{-1}$; ^{1}H NMR (400 MHz, [D$_4$]MeOH, 25°C): $\delta = 8.75$ (s, 1H), 7.43 (d, $J = 8.0$ Hz, 1H) 7.38–7.30 (m, 6H), 7.15 (d, $J = 7.6$ Hz, 1H), 7.10 (d, $J = 7.6$ Hz, 1H), 6.84–6.75 (m, 4H), 6.54 (d, $J = 1.2$ Hz, 1H), 5.11 (s, 2H), 4.50 (dd, $J = 2.4$, 11.2 Hz, 1H), 4.47 (d, $J = 8.8$ Hz, 1H), 3.97 (d, $J = 6.8$ Hz, 1H), 3.22 (app t, $J = 12.8$ Hz, 1H), 2.66 (dd, $J = 2.4$, 12.8 Hz, 1H), 2.08–1.98 (m, 2H), 1.84 (s, 3H), 1.07 (d, $J = 6.4$ Hz, 3H), 0.96–0.93 (m, 9H); ^{13}C NMR (75 MHz, [D$_4$]MeOH, 25°C): $\delta = 173.5, 172.3, 169.0, 163.8, 157.4, 156.5, 154.1, 154.0,$

 © WILEY-VCH Verlag GmbH, D-69451 Weinheim, 2001 1433-7851/01/4024-4768 $ 17.50+.50/0

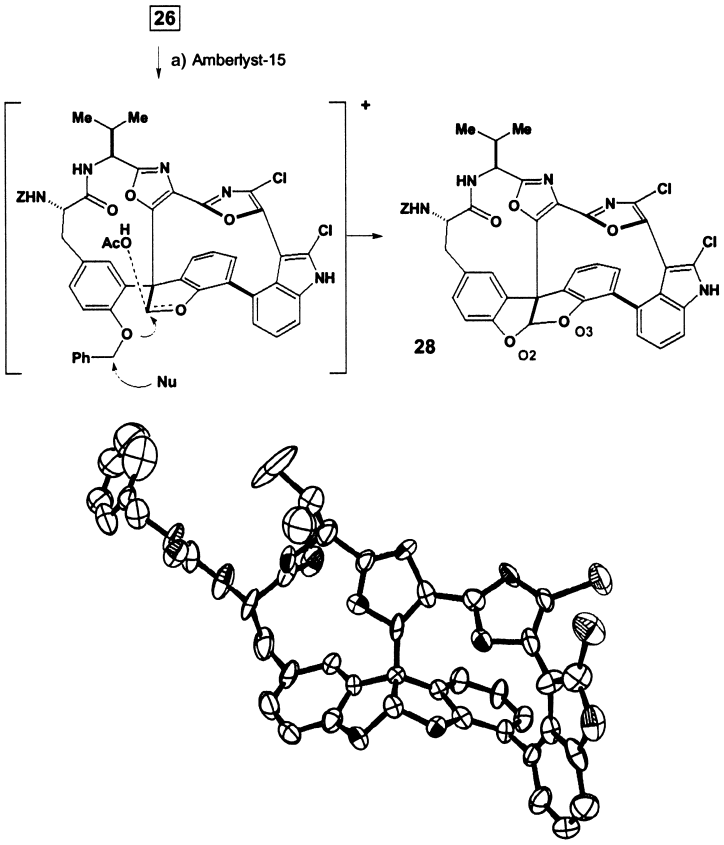


Figure 1. Preparation and X-ray structure (ORTEP; 30% probability thermal ellipsoids) of diphenyl acetal **28**. a) Amberlyst-15, 4 Å MS, 1:4 CH_3CN/CH_2Cl_2.

153.8, 140.9, 137.0, 135.3, 133.5, 132.2, 130.0, 129.1, 128.3, 127.9, 127.8, 127.8, 127.7, 127.1, 126.5, 126.3, 126.0, 124.2, 123.4, 122.8, 122.7, 121.6, 121.3, 117.1, 110.8, 100.7, 97.5, 66.5, 60.7, 59.2, 56.7, 55.2, 37.0, 31.1, 30.2, 19.4, 19.1, 18.4, 18.2, 17.5; ES-MS: calcd for $C_{50}H_{44}Cl_2N_6O_{10}$ $[M^+ + H]$: 959.26, found: 959.25; calcd for $C_{50}H_{44}Cl_2N_6O_{10}$ $[M^- - H]$: 957.24, found: 957.26.

1a: $R_f = 0.10$ (10% MeOH/CH_2Cl_2); ^1H NMR (major C11 epimer; 400 MHz, [D$_6$]DMSO, 25 °C): $\delta = 9.77$ (s, 1H), 8.95 (d, $J = 6.4$ Hz, 1H), 8.26 (br s, 1H), 7.86 (d, $J = 5.6$ Hz, 1H), 7.58 (d, $J = 5.6$ Hz, 1H), 7.46 (d, $J = 8.4$ Hz, 1H), 7.31 (app t, $J = 8.0$ Hz, 1H), 7.10 (d, $J = 7.2$ Hz, 1H), 7.20 (dd, $J = 1.3$, 8.0 Hz, 1H), 6.78 (d, $J = 8.4$ Hz, 1H), 6.73 (dd, $J = 2.0$, 6.8 Hz, 1H), 6.66–6.62 (m, 2H), 6.34 (d, $J = 1.3$ Hz, 1H), 4.47 (app t, $J = 8.4$ Hz, 1H), 4.38 (dd, $J = 6.4$, 8.4 Hz, 1H), 3.16 (br s, 1H), 3.04 (app t, $J = 12.0$ Hz, 1H), ≈2.48 (1H; obscured by residual solvent signal), 1.91–1.96 (m, 2H), 0.97 (d, $J = 6.8$ Hz, 3H), 0.89 (d, $J = 6.8$ Hz, 3H), 0.84 (d, $J = 7.2$ Hz, 3H), 0.82 (d, $J = 7.2$ Hz, 3H); ES-MS: calcd for $C_{40}H_{36}Cl_2N_6O_7$ $[M^+ + H]$: 783.21, found: 783.31; calcd for $C_{40}H_{36}Cl_2N_6O_7$ $[M^- - H]$: 781.20, found: 781.25; HR-FAB-MS: calcd for $C_{40}H_{36}Cl_2N_6O_7$ $[M^+ + Li]$: 789.2183, found: 789.2198.

Received: November 12, 2001 [Z18198]

[1] a) N. Lindquist, W. Fenical, G. D. Van Duyne, J. Clardy, *J. Am. Chem. Soc.* **1991**, *113*, 2303–2304; b) the producing organism, originally classified as *Diazona chinesis*, has since been correctly identified as *Diazona angulata*.

[2] N. Lindquist, Ph.D. thesis, University of California San Diego (USA), **1989**.

[3] J. Li, A. W. G. Burgett, L. Esser, C. Amezcua, P. G. Harran, *Angew. Chem.* **2001**, *113*, 4906–4909; *Angew. Chem. Int. Ed.* **2001**, *40*, 4770–4773.

[4] Diazonamide A is a potent cytotoxin (inducing growth arrest in mitosis) with a mean $GI_{50} = 4.9$ nM against a standardized panel of human cancer cell lines. COMPARE analysis was completed at the NCI on December 1, 1997 (Developmental Therapeutics Program): NSC: D-700089-Y/1. Exp. ID:9712SR87-64.

[5] a) P. Magnus, C. Lescop, *Tetrahedron Lett.* **2001**, *42*, 7193–7196; b) E. Vedejs, M. A. Zajac, *Org. Lett.* **2001**, *3*, 2451–2454; c) J. D. Kreisberg, P. Magnus, E. G. McIver, *Tetrahedron Lett.* **2001**, *42*, 627–629; d) P. Wipf, J. L. Methot, *Org. Lett.* **2001**, *3*, 1261–1264; e) K. C. Nicolaou, S. A. Snyder, K. B. Simonsen, A. E. Koumbis, *Angew. Chem.* **2000**, *112*, 3615–3620; *Angew. Chem. Int. Ed.* **2000**, *39*, 3473–3478; f) D. E. Fuerst, B. M. Stoltz, J. L. Wood, *Org. Lett.* **2000**, *2*, 3521–3523; g) M. C. Bagley, C. J. Moody, A. G. Pepper, *Tetrahedron Lett.* **2000**, *41*, 6901–6904; h) M. C. Bagley, S. L. Hind, C. J. Moody, *Tetrahedron Lett.* **2000**, *41*, 6897–6900; i) F. Lach, C. J. Moody, *Tetrahedron Lett.* **2000**, *41*, 6893–6896; j) E. Vedejs, D. A. Barda, *Org. Lett.* **2000**, *2*, 1033–1035; k) E. Vedejs, J. Wang, *Org. Lett.* **2000**, *2*, 1031–1032; l) P. Magnus, E. G. McIver, *Tetrahedron Lett.* **2000**, *41*, 831–834; m) F. Chan, P. Magnus, E. G. McIver, *Tetrahedron Lett.* **2000**, *41*, 835–838; n) H. C. Hang, E. Drotleff, G. I. Elliott, T. A. Ritsema, J. P. Konopelski, *Synthesis* **1999**, 398–400; o) P. Magnus, J. D. Kreisberg, *Tetrahedron Lett.* **1999**, *40*, 451–454; p) A. Boto, M. Ling, G. Meek, G. Pattenden, *Tetrahedron Lett.* **1998**, *39*, 8167–8170; q) P. Wipf, F. Yokokawa, *Tetrahedron Lett.* **1998**, *39*, 2223–2226; r) T. F. Jamison, Ph.D. thesis, Harvard University, Cambridge, MA (USA), **1997**; s) C. J. Moody, K. J. Doyle, M. C. Elliott, T. J. Mowlem, *J. Chem. Soc. Perkin Trans. 1* **1997**, *16*, 2413–2419; t) J. P. Konopelski, J. M. Hottenroth, H. M. Oltra, E. A. Véliz, Z. C. Yang, *Synlett* **1996**, 609–611; u) C. J. Moody, K. J. Doyle, M. C. Elliott, T. J. Mowlem, *Pure Appl. Chem.* **1994**, *66*, 2107–2110; v) K. C. Nicolaou, X. Huang, N. Giuseppone, P. Bheema Rao, M. Bella, M. V. Reddy, S. A. Snyder, *Angew. Chem.* **2001**, *113*, 4841–4845; *Angew. Chem. Int. Ed.* **2001**, *40*, 4705–4709.

[6] a) J. Li, X. Chen, A. W. G. Burgett, P. G. Harran, *Angew. Chem.* **2001**, *113*, 2754–2757; *Angew. Chem. Int. Ed.* **2001**, *40*, 2682–2685; b) X. Chen, L. Esser, P. G. Harran, *Angew. Chem.* **2000**, *112*, 967–970; *Angew. Chem. Int. Ed.* **2000**, *39*, 937–940; c) S. Jeong, X. Chen, P. G. Harran, *J. Org. Chem.* **1998**, *63*, 8640–8641.

[7] **4**: Prepared in two steps (1. $CuNO_3$; NaOH, BnBr; 2. 2-*tert*-butoxycarbonyloxyimino)-2-phenylacetonitrile) from L-3-iodo-tyrosine. **5**: two steps from N-Boc-L-valine. See Ref. [6c]. **6**: two steps (1. BnBr; 2. PPh_3, $(Cl_3C)_2$, 110 °C) from 2-hydroxy acetophenone.

[8] E. Negishi, F. E. Cederbaum, T. Takahashi, *Tetrahedron Lett.* **1986**, *27*, 2829–2832. A reduced form of $[Cp_2ZrBu_2]$ (in-situ β-hydride elimination and reductive elimination of n-C_4H_9) is shown in Scheme 2 to emphasize that its interaction with **6** is conveniently formulated as an oxidative addition.

[9] T. Takahashi, M. Kotora, R. Fisher, Y. Nishihara, K. Nakajima, *J. Am. Chem. Soc.* **1995**, *117*, 11039–11040.

[10] Successful Heck cyclization requires a free C16 phenol in **10**, an observation which is consistent with on-metal templating (for example, **11**; L = 2-(di-*tert*-butylphosphanyl)biphenyl) to promote olefin carbometalation within the catalytic cycle.[6c]

[11] S. Hanessian, P. Meffre, M. Girard, S. Beaudoin, J.-Y. Sancéau, Y. Bennani, *J. Org. Chem.* **1993**, *58*, 1991–1993.

[12] An intrinsic facial bias in this ring system leads to undesired *syn*-α-glycolate stereochemistry (d.r. ≈ 6:1) upon stoichiometric dioxyosmylation with OsO_4/*p*-(dimethylamino) pyridine in THF solvent.

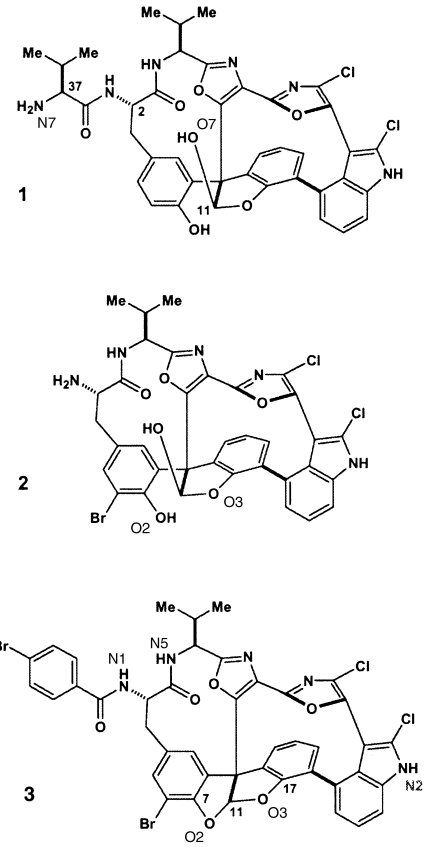
[13] It is possible to assign stereochemistry to each of the three chiral biaryl axes in **1a**. In principle, the structure could exist in 2^3 atropdiastereomeric forms. However, geometry dictates that six of these are prohibitively high in energy. When assembled, only the ring network depicted and its enantiomer are relevant. Our synthetic pathway selects for one.

[14] D. E. Pearson, R. D. Wysong, C. V. Breder, *J. Org. Chem.* **1967**, *32*, 2358–2360.

[15] Stereochemistry at C10 and C11 in advanced intermediates has been confirmed through crystallographic analysis of the DDQ oxidation product of **21**. Details will be included in a later disclosure.

[16] a) O. Yonemitsu, P. Cerutti, B. Witkop, *J. Am. Chem. Soc.* **1966**, *88*, 3941–3945; b) H. G. Theuns, H. B. M. Lenting, C. A. Salemink, H. Tanaka, M. S. Shibata, K. Ito, R. J. J. C. Lousberg, *Heterocycles* **1984**, *22*, 2007–2011; c) for an impressive synthesis of (−)-indolactam V which uses related methodology see: M. Mascal, C. J. Moody, *J. Chem. Soc. Chem. Commun.* **1988**, 589–590.

[17] a) A. H. Fainberg, S. J. Winstein, *J. Am. Chem. Soc.* **1956**, *78*, 2767–2774; b) J. Mattay, *Synthesis* **1989**, 233–252.
[18] A non-chain radical mechanism that involves C16–Br bond homolysis and intramolecular addition of the resultant aryl radical to the indole nucleus cannot, at this point, be ruled out.
[19] We are grateful to Professor William Fenical (Scripps Institute of Oceanography) for a generous gift of natural (−)-diazonamide A.
[20] Synthetic **1a** appears (^{1}H NMR) as an ≈4:1 mixture of C11 epimers. However, unpredictable degradation prevents detailed characterization of these materials. Protected derivative **27** is serviceable with respect to handling and analysis.
[21] Diketopiperazine formation appears to be a competing pathway when a C37 Fmoc-amine-protected congener of **27** is treated with DBU in THF. Fmoc = fluorenylmethyloxycarbonyl.
[22] Crystallographic data (excluding structure factors) for the structure reported in this paper have been deposited with the Cambridge Crystallographic Data Centre as supplementary publication no. CCDC-174087. Copies of the data can be obtained free of charge on application to CCDC, 12 Union Road, Cambridge CB2 1EZ, UK (fax: (+44) 1223-336-033; e-mail: deposit@ccdc.cam.ac.uk).



Scheme 1. Initial diazonamide structure assignments.

Total Synthesis of Nominal Diazonamides—Part 2: On the True Structure and Origin of Natural Isolates**

Jing Li, Anthony W. G. Burgett, Lothar Esser, Carlos Amezcua, and Patrick G. Harran*

In the preceding communication we described a fully synthetic pathway to the structure proposed for (−)-diazonamide A (**1**, Scheme 1).[1] This material is not identical to the natural product, which raises the obvious question: What is the true structure of diazonamide A? Herein we provide an answer. In addition, we report that defined synthetic entity **8** induces, with equal potency, a toxic phenotype in cell culture indistinguishable from that produced by natural (−)-diazonamide A.

Spectroscopic data for the heterocyclic cores of diazonamides A and B are nearly identical.[2] So when the crystal structure of a *p*-bromobenzamide derivative of diazonamide B was reported as **3**,[2a] the diazonamide A assignment seemed only to require reconciling its exact mass (765.1998 amu)[3] within the same framework. The molecular formula $C_{40}H_{35}N_6O_6Cl_2$ is consistent with this mass (Δ − 0.3 ppm) although it was thought to reflect a desiccated form of the molecule as a result of a C11 hemiacetal that loses water during HRMS analysis. Likewise, the C11 diphenylacetal reported in **3** was thought a result of net dehydration occurring during derivatization of diazonamide B with *p*-bromobenzoyl chloride. Hemiacetal functionality was considered a necessary part of both natural products to accommodate a small vicinal coupling between C11H and an exchangeable, one-proton resonance just over $\delta = 7$ in ^{1}H NMR spectra ([D$_6$]DMSO). The diazonamide A assignment (**1**) was then completed by incorporation of a terminal valine residue which emanates from the C2 amine. In the context of a C11 hemiacetal, this designation does coincide with the high resolution mass measurement but, unfortunately, with little else.

Acid digests of diazonamide A do not produce valine.[2b] ^{1}H NMR (360 MHz, [D$_6$]DMSO) indicates the presence of two isopropyl groups in the molecule, but the N7 protons are reported as a sharp, one-proton doublet at $\delta = 5.46$. This resonance is, in turn, coupled (5.9 Hz) to the C37 methine hydrogen at $\delta = 3.75$.[4] In a triacetate derivative, the C37 proton shifts downfield to $\delta = 5.11$, although it now appears as a doublet rather than the more complex pattern one might expect for a C37 acetamide.[5] Moreover, in non-acetylated material, C37 resonates at $\delta = 76.9$ (50 MHz, [D$_4$]MeOH)—considerably downfield from the corresponding carbon atom

[*] Prof. P. G. Harran, J. Li, A. W. G. Burgett, C. Amezcua
Department of Biochemistry
University of Texas, Southwestern Medical Center at Dallas
Dallas, TX 75390-9038 (USA)
Fax: (+1) 214-648-6455
E-mail: pharra@biochem.swmed.edu
L. Esser[+]
Laboratory of Cell Biology, National Cancer Institute
National Institutes of Health, Bethesda, MD 20892 (USA)
[+] Address correspondence to this author regarding X-ray analyses.

[**] Funding provided by the NIH (RO1-GM60591), the NSF (CAREER 9984282), the Howard Hughes Medical Institute (junior faculty support), the Robert A. Welch Foundation, and the Advanced Research Program of the Texas Higher Education Coordinating Board. We are grateful to Professor Michael Roth for his time, insight, and advice.

Supporting information for this article is available on the WWW under http://www.angewandte.com or from the author.

 © WILEY-VCH Verlag GmbH, D-69451 Weinheim, 2001 1433-7851/01/4024-4770 $ 17.50+.50/0

in a typical valine free-base.[6] We believe these observations are consistent with the C37 substituent in natural diazonamide A being an alcohol rather than an amine.[7]

For this to be true, the NH_2 to OH change dictates that a compensatory permutation be made at another position in the structure to rectify the attendant increase by 1 Da in molecular mass.[8] This requires revising the X-ray structure assigned as **3**. Notably, the exact mass of diazonamide B is 743.0340 amu.[2] However, the structure proposed for this material (**2**) has the formula $C_{35}H_{26}N_5O_6Cl_2Br$ and an $[[M^+ + H] - H_2O]$ ion has the calculated mass 744.0416 amu. The formula $C_{35}H_{25}N_6O_4Cl_2Br$ $[[M^+ + H] = 743.0576$ amu] is more consistent with the observed mass ($\Delta = 2.4$ ppm) and this suggests that a protonated nitrogen atom in diazonamide B has been mistaken for oxygen in **3**.

C11 hemiacetals in natural diazonamides are not indicated by mass spectrometry. Moreover, synthetic materials with this functional group (namely, **1**)[1] ionize intact, which makes the O2 or O3 assignment suspect. In the structure assigned as **3**, the observed C7–O2 bond length (1.371 Å) falls within the range typical for aryl C–O bond distances (1.353 – 1.409 Å) and deviates by just 1.5 σ (σ = standard deviation) from the mean value of 1.385 Å (based upon 36 bonds in 20 related substructures found within the Cambridge Crystallographic Database).[9] However, the C17–O3 bond, likewise expected to be an aryl C–O bond, is measured at 1.433(16) Å. This is 0.048 Å (3 σ) longer than the mean and, notably, exceeds the maximal value (1.409 Å) observed for a bond of this type. Atom O3 also displays an unusually large thermal motion for an atom in a rigid group (Figure 1). The average B-factor (B_{eq}) in the core (O3 excluded) is 4.8(3) Å^2 while the temperature factor of O3 itself is 7.42 Å^2—or 8.7 σ above the average.[10] This indicates that the O3 assignment should be changed to an element with fewer electrons and a larger covalent radius.

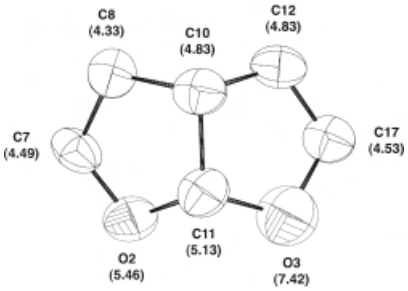
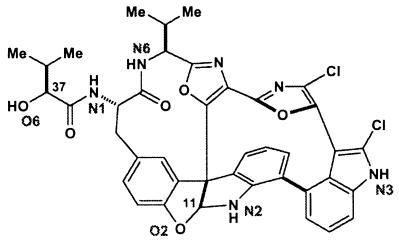
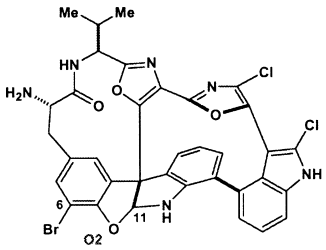


Figure 1. Partial reconstruction (ORTEP; 50% probability thermal ellipsoids) of the X-ray structure refinement assigned as **3** (CCDC ref. code = JIMBUC). Numbers in parentheses are equivalent isotropic displacement coefficients (B_{eq}) in units of Å^2.

When taken together, these data are consistent with the electron density assigned as O3 being a protonated nitrogen atom and, by extension, the actual structure of (–)-diazonamide B being C11 diarylaminal **5** (Scheme 2). This change, in combination with an *S*-configured C37 alcohol,[11] gives **4** as our revised structure of (–)-diazonamide A. We have performed an $^1H/^{15}N$-HSQC experiment on natural diazonamide A that, when interpreted in light of extensive $^1H/^1H$ and $^1H/^{13}C$ correlations obtained for the compound,[2b] clearly



4 (–)-diazonamide A (revised Structure)



5 (–)-diazonamide B (revised Structure)

Scheme 2. Revised structures of (–)-diazonamides A and B.

supports this assignment. The $^1H/^{15}N$-HSQC experiment[12] allows protons attached to nitrogen to be uniquely identified. The two-dimensional spectrum shown in Figure 2[13] indicates four such connectivities in the natural product: $\delta = 12.82$ (N3H); $\delta = 8.66$ (N6H); $\delta = 7.68$ (N1H); $\delta = 7.16$ (N2H). The proton resonance at $\delta = 7.16$ is coupled to C11H (DQF-COSY) and was originally assigned as O7H in **1**. Moreover, the exchangeable one-proton doublet at $\delta = 5.46$, first identified as $N7H_2$, is not coupled to ^{15}N—consistent with our C37 hydroxy model.

To demonstrate these issues further, we have synthesized L-valine and (*S*)-α-hydroxy isovaleric acid conjugates of our synthetic, C11 diphenyl acetal core structure **6**[1] (**7** and **8**, respectively; Scheme 3). Alcohol **8** is >50-fold more potent than amine **7** at inhibiting the growth of human ovarian adenocarcinoma OVCAR-3 in vitro (Table 1). Within experimental error, **8** and natural diazonamide A are equipotent in this assay.[14] Compound **8** is also an antimitotic agent. Populations of OVCAR-3 accumulate as tetraploid (4N) when exposed to low doses of **8** (30 nM). Those cells remaining viable persist with two copies of their genome for the duration of the experiment.[15] The effect is similar to positive antimitotic controls (taxol and vinblastine) and indistinguishable from that produced by 30 nM diazonamide A treatment.

To look for effects on mitosis directly, we synchronize a monkey kidney epithelial cell line (BS-C-1) in S phase, treat individually with **8** and diazonamide A, and image the tubulin cytoskeleton by immunofluorescence microscopy 9 hours later. In contrast to a vehicle-alone control (Figure 3A), a more significant fraction (ca. 30%) of BS-C-1 cells treated with 100 nM **8** or diazonamide A appear mitotic. Moreover, virtually none of these cells are able to construct a normal bipolar mitotic spindle (Figure 3B,C). The phenotype is pleotropic at the level of precise microtubule and chromosomal (data not shown) organization although, importantly, the

 © WILEY-VCH Verlag GmbH, D-69451 Weinheim, 2001 1433-7851/01/4024-4771 $ 17.50+.50/0

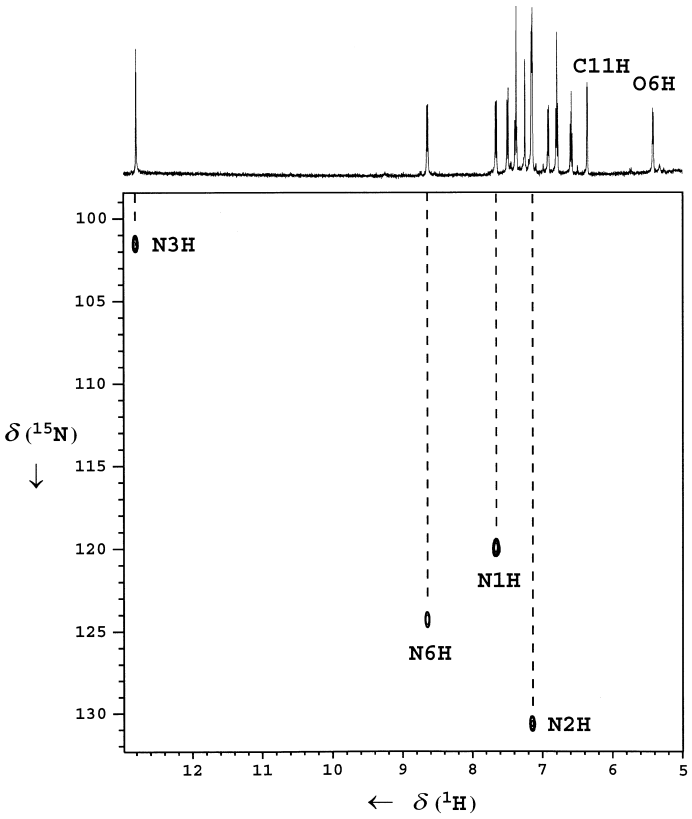
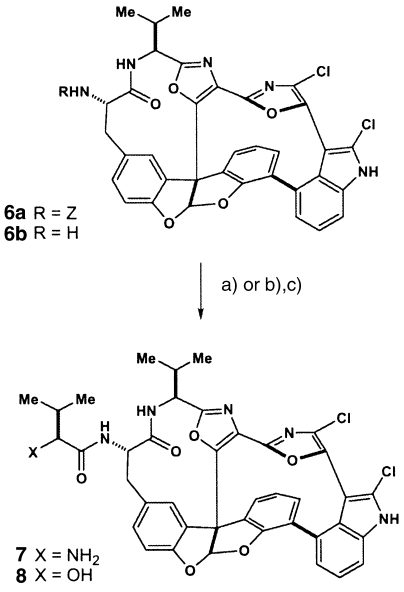


Figure 2. Partial $^{1}H/^{15}N$-HSQC spectrum (500 MHz, $[D_6]$DMSO) of natural diazonamide A.



Scheme 3. Reaction conditions: a) L-α-hydroxy isovaleric acid, $(EtO)_2$-P(O)CN, *N*-methylmorpholine, THF (**8**; 95%); b) Z-L-Val-OH, TBTU, iPr_2NEt, DMF; c) 10% Pd/C, 1 atm H_2 (g), MeOH (**7**; 92%, 2 steps). Z = benzyloxycarbonyl; TBTU = 2-(1H-benzotriazol-1-yl)-1,1,3,3-tetramethyluronium tetrafluoroborate.

range of effects is similar for both compounds. We are confident that, by these preliminary measures, acetal **8** is a functional equivalent of (−)-diazonamide A. This is a key discovery in that it validates the ability of our existing

Table 1. In vitro cytotoxicity assays.[a]

Compound	GI_{50} [nM]
natural diazonamide A	8
8	16
8 (*epi*-C37)	191
7	845
6a	> 10000
3	> 10000
paclitaxel	8

[a] Growth inhibition determined for human adenocarcinoma OVCAR-3 after 48 h compound treatment with the CellTiter-Glo viability assay (Promega).

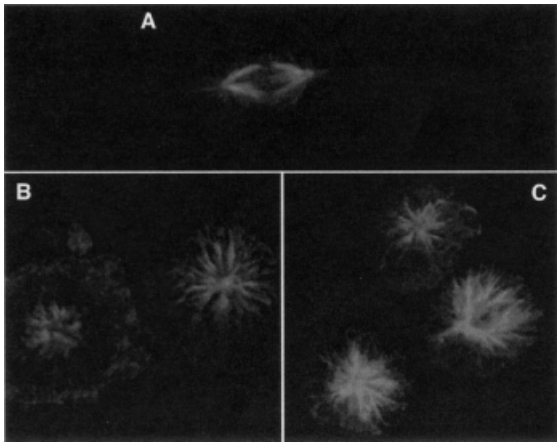
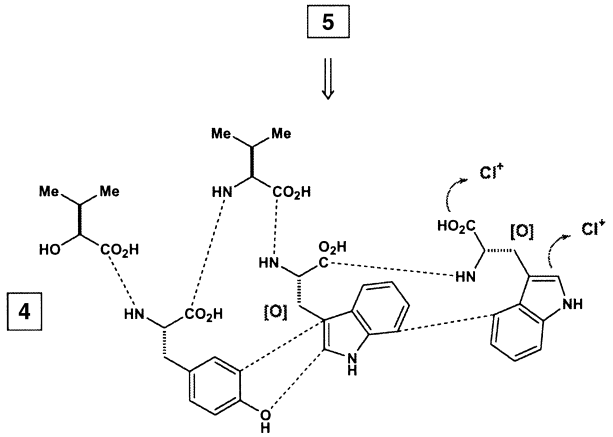


Figure 3. Mitotic BS-C-1 cells 9 hours post release from thymidine block. Confocal immunofluorescence microscopy showing tubulin-based assemblies formed in the presence of: **A**) 0.01% EtOH; **B**) 100 nM **4** (natural diazonamide A), and **C**) 100 nM **8**.

synthesis to fuel more sophisticated biochemical and molecular biological aspects of diazonamide research.

In closing, our structure revisions appear to clarify a biosynthetic lineage between diazonamide polycycles and four common amino acids (Scheme 4). Initial assignments (namely, **1** and **2**) seemed to require invoking an ambiguous hybrid assembly of amino acid and aromatic polyketide segments.[2] Details notwithstanding, the polyheterocyclic core now appears to be a derivative of an oxidized, 4,7-linked ditryptophan unit with the macrolactam ring being formed by



Scheme 4. A plausible biosynthetic origin of revised diazonamide structures.

 © WILEY-VCH Verlag GmbH, D-69451 Weinheim, 2001 1433-7851/01/4024-4772 $ 17.50+.50/0 *Angew. Chem. Int. Ed.* **2001**, *40*, No. 24

a net oxidative cycloaddition between tyrosine and tryptophan. We are not aware of precedent for the latter event although the outcome is generally reminiscent of the production of dehydrodiconiferyl alcohols during lignan biosynthesis.[16]

Experimental Section

8: $R_f = 0.58$ (75% EtOAc/benzene); $[\alpha]_D^{25} = -154.8^\circ$ ($c = 0.47$, MeOH); IR (film): $\tilde{\nu} = 3280$, 2965, 1659, 1652, 1645, 1520, 1490, 1441, 1053, 910, 753 cm^{-1}; ^1H NMR (400 MHz, $[D_4]$MeOH): $\delta = 7.51$ (d, $J = 2.0$ Hz, 1H), 7.47 (dd, $J = 1.2$, 8.0 Hz, 1H), 7.36 (app t, $J = 8.0$ Hz, 1H), 7.27 (dd, $J = 2.0$, 8.4 Hz, 1H), 7.20 (app dd, $J = 1.2$, 7.8 Hz, 2H), 7.07 (dd, $J = 1.2$, 7.6 Hz, 1H), 6.93 (app t, $J = 7.6$ Hz, 1H), 6.88 (d, $J = 8.4$ Hz, 1H), 6.84 (s, 1H), 4.98 (d, $J = 6.0$ Hz, 1H), 4.61 (dd, $J = 3.2$, 11.6 Hz, 1H), 3.89 (d, $J = 4.0$ Hz, 1H), 3.47 (app t, $J = 8.4$ Hz, 1H), 2.81 (dd, $J = 3.2$, 12.8 Hz, 1H), 2.34–2.26 (sym 6-line m, 1H), 2.14–2.06 (sym 10-line m, 1H), 1.10 (d, $J = 6.8$ Hz, 3H), 1.03 (d, $J = 6.8$ Hz, 3H), 0.96 (d, $J = 6.8$ Hz, 3H), 0.92 (d, $J = 6.8$ Hz, 3H); ^{13}C NMR (75 MHz, $[D_4]$MeOH): $\delta = 175.8$, 175.2, 163.2, 159.8, 159.3, 154.9, 153.7, 141.8, 136.7, 132.4, 131.8, 131.3, 131.2, 130.7, 130.4, 129.5, 128.7, 127.9, 127.6, 127.0, 125.2, 124.2, 124.1, 124.1, 122.7, 119.7, 112.5, 111.8, 98.1, 77.0, 62.2, 57.3, 56.5, 39.0, 33.4, 31.6, 19.7, 19.6, 18.7, 16.6; ES-MS: calcd for $C_{40}H_{33}Cl_2N_5O_7$ [M^++H]: 766.18, found: 766.30; calcd for $C_{40}H_{33}Cl_2N_5O_7$ [M^- – H]: 764.16, found: 764.31. HR-FAB-MS calcd for $C_{40}H_{33}Cl_2N_5O_7$ [M^++Li]: 772.1917, found: 772.1962.

Received: November 12, 2001 [Z18199]

[1] J. Li, S. Jeong, L. Esser, P. G. Harran, *Angew. Chem.* **2001**, *113*, 4901–4906; *Angew. Chem. Int. Ed.* **2001**, *40*, 4765–4770.

[2] a) N. Lindquist, W. Fenical, G. D. Van Duyne, J. Clardy, *J. Am. Chem. Soc.* **1991**, *113*, 2303–2304; b) N. Lindquist, Ph.D. thesis, University of California San Diego (USA), **1989**.

[3] The high resolution FAB mass spectrum of diazonamide A shows a cluster of six ions between 765 and 770 amu, the relative intensity of which indicates the presence of two chlorine atoms. Heavy-atom analysis confirms that chlorine is the only halogen present.

[4] The corresponding C37 methine resonance in synthetic **1** appears at $\delta = 3.2$ (400 MHz, $[D_6]$DMSO) and is broadened.

[5] Peracetylated diazonamide A shows three methyl singlets at $\delta = 2.87$, 2.23, 2.16 in its ^1H NMR spectrum (360 MHz, $CDCl_3$) and two new IR absorbances at 1760 cm^{-1} and 1725 cm^{-1}.

[6] BioMagResBank is a searchable database of NMR spectroscopic data on proteins, peptides, and nucleic acids. See: http://www.bmrb.wisc.edu/index.html.

[7] This requires that diazonamide A be a conjugate of α-hydroxy isovaleric acid (HIV). The ^1H NMR spectrum (300 MHz, $[D_6]$DMSO) of HIV (L-form, Fluka) shows that Cα resonates at $\delta = 3.73$ (^{13}C NMR: $\delta = 74.5$) and is weakly coupled to the exchangeable carbinol proton at $\delta = 5.0$.

[8] We initially considered that misassignments were made only in the C2 amine side chain. An α-hydroxy amidine congener of **1** was therefore prepared. This material incorporates a C37 carbinol and does have the same net atomic composition as **1**. However, chromatographic and spectroscopic properties of the compound rule it out as a possibility.

[9] See supporting information.

[10] For comparison, we note that $B_{eq} = 6.00$ and 5.35 $Å^2$, respectively, for O2 and O3 in the X-ray structure refinement of synthetic diphenyl acetal **28**.[1]

[11] ^1H NMR spectra of **8** and its C37 epimer (derived from D-α-hydroxy isovaleric acid) are near identical. We assign C37-*S* stereochemistry in **4** based upon relative potencies in cell-based assays. See Table 1.

[12] L. E. Kay, P. Keifer, T. Saarinen, *J. Am. Chem. Soc.* **1992**, *114*, 10663–10665.

[13] $^1H/^{15}N$-HSQC, $^1H/^{13}C$-HSQC, and DQF-COSY experiments were recorded at 25°C on a 500 MHz Varian Inova spectrometer. Data was processed using NmrPipe and analyzed with NMRView.

[14] The trace amount of natural diazonamide A (ca. 700 μg) available for these experiments makes it likely that weighing error alone could approach a factor of two.

[15] The effect of compound treatment on cell ploidy was evaluated by fluorescence-activated cell sorting (at 4 h intervals over 16 h). Experimental results are provided as supplementary information.

[16] D. R. Gang, M. A. Costa, M. Fujita, A. T. Dinkova-Kostova, H. Wang, V. Burlat, W. Martin, S. Sarkanen, L. B. Davin, N. G. Lewis, *Chem. Biol.* **1999**, *6*, 143–151.

 © WILEY-VCH Verlag GmbH, D-69451 Weinheim, 2001 1433-7851/01/4024-4773 $ 17.50+.50/0